UNIVERSAL
LIBRARY
OU_172201
UNIVERSAL
LIBRARY

EVOLUTION EMERGING

In Two Volumes

VOLUME I: Text

VOLUME II: Illustrations



THE MACMILLAN COMPANY
NEW YORK • BOSTON • CHICAGO
DALLAS • ATLANTA • SAN FRANCISCO

MACMILLAN AND CO., LIMITED
LONDON • BOMBAY • CALCUTTA
MADRAS • MELBOURNE

THE MACMILLAN COMPANY
OF CANADA, LIMITED
TORONTO

EVOLUTION EMERGING

A Survey of Changing Patterns from Primeval Life to Man

WILLIAM KING GREGORY

A Collaborative Work of

THE AMERICAN MUSEUM OF NATURAL HISTORY

and

COLUMBIA UNIVERSITY

VOLUME II

THE MACMILLAN COMPANY

New York

TODAY & TOMORROW'S BOOK AGENCY
74, EASTI HARPHUL SINGH
DELHI.

COPYRIGHT, 1951, BY THE AMERICAN MUSEUM OF NATURAL HISTORY

All rights reserved—no part of this book may be reproduced in any form without permission in writing from the publisher, except by a reviewer who wishes to quote brief passages in connection with a review written for inclusion in magazine or newspaper.

PRINTED IN THE UNITED STATES OF AMERICA

First Printing

The author extends his thanks and acknowledgments to the authors, publishers, and copyright holders whose illustrations or data have served as bases for some of the drawings in Volume II, as noted in the captions, the bibliography and the following list.

Figs. 1.1; 1.2; 1.4; 1.5A,B; 1.6; 1.7; 2.1C; 2.8; 3.4; 3.5D,E; 4.1A,E,F; 4.2; 4.4A,C,D; 4.7A–A2,D; 4.8D–D2; 5.2A1–4; 5.3A2–A4; 5.4C; 5.5A,A1; 5.7A,B; 5.8; 5.11C–E; 5.12A; 5.14A,B; 7.25; 9.3A; 10.10F; 12.47A; 15.3B; 15.6; 19.34D. From T. J. Parker and W. A. Haswell, *A Textbook of Zoology*, Vol. I, First Edition. Copyright 1897 by Macmillan Co., Ltd. Vol. II, Sixth Edition. Copyright 1940 by Macmillan Co., Ltd.

Figs. 1.3; 3.4A,B; 3.5A. From W. Goldring, *New York State Museum Handbook No. 10.* Copyright 1931 by New York State Museum.

Figs. 1.5B1; 5.9A. From W. C. Allee, "The Evolution of the Invertebrates." In *The Nature of the World and of Man* (Ed. H. H. Newman). Second Edition. Copyright 1927 by the University of Chicago.

Figs. 2.2A,B; 2.5E; 2.17A; 2.39; 2.40; 3.5B,C; 4.5A,A1, B1; 4.6A,B; 4.7B–C1; 5.19; 7.1D, 9.113A,B; 12.16B; 12.27D; 13.4A; 13.14C. From Karl A. von Zittel, *Grundzuge der Palaontologie*, Vol. I, Sixth Edition Revised. Copyright 1924 by R. Oldenbourg Verlag. Vol. II, Third Edition Revised. Copyright 1918 R. Oldenbourg Verlag.

Fig. 2.5B. From Maxwell Smith, *East Coast Marine Shells.* Copyright 1937 by Maxwell Smith.

Figs. 2.11A–C; 2.35E. From Shintaro Hirase, *A Collection of Japanese Sea Shells* Sixth Edition. Copyright 1938 by Matsumura Sanshodo.

Figs. 2.18A–E; 2.19F; 2.20A. From William Wenz, "Gastropoda." In Schwindewolf, *Handbuch der Palaozoologie.* Copyright 1938–1940 by Verlagsbuchhandlung Gebruder Borntraeger, now Naturwissenschaftlicher Verlag.

Figs. 2.25A,B; 3.1. From Amadeus W. Grabau, *A Textbook of Geology.* Pt. II. Copyright 1921 by D. C. Heath and Company.

Figs. 2.28A–F; 2.29A–C; 2.30; 2.31B. From Maxwell Smith, *A Review of the Volutidae.* Copyright 1942 by Beal-Maltbie Shell Museum.

Fig. 2.32B. From Paul A. Robert, *Kunstgebilde des Meeres.* Muscheln und Schneckengehäuse. Copyright (no date) by Irisdruck C. Weller and Company, now Iris Verlag.

Figs. 2.35C; 2.36B,F. From Maxwell Smith, *World-wide Sea Shells.* Copyright 1940 by Tropical Photographic Laboratory.

Figs. 3.3; 3.4C,D,F; 4.1C,D,G. From W. Goldring, *New York State Museum Handbook No. 9.* Copyright 1929 by New York State Museum.

Figs. 3.4E; 5.12B,C, 5.15; 5.16A,A1; 5.17; 6.13B; 7.4A. From William Patten, *The Evolution of the Vertebrates and Their Kin.* Copyright 1912 by The Blakiston Company.

Fig. 4.3. From H. F. Osborn, *The Origin and Evolution of Life.* Copyright 1917 by Charles Scribner's Sons.

Figs. 4.4B; 4.5B,C. From E. W. Berry, *Paleontology.* Copyright 1929 by McGraw-Hill Book Company.

Figs. 4.6C; 7.3A. From W. K. Spencer, "Some Aspects of Evolution in Echinodermata." In *Evolution: Essays on Aspects of Evolutionary Biology . . .* Copyright 1938 by The Clarendon Press.

Figs. 5.2; 5.6; 5 10A1,C; 5.16; 5 17; 5.19; 5.20. From W. K. Gregory, "The Roles of Motile Larvae and Fixed Adults in the Origin of the Vertebrates." In *The Quarterly Review of Biology,* V. 21, No. 4, Dec. 1946. Copyright 1946 by The Williams and Wilkins Company.

Figs 5.6C,D,D1. From G. R de Beer, *Embryology and Evolution.* Copyright 1930 by The Clarendon Press.

Figs. 5.13; 6.19A–B; 8.7D; 8.46C,D; 8.54; 9.3B; 9.17C; 9.19A,C; 10.2; 10.3C; 10.10A; 10.17aD. From Edwin S. Goodrich, "Cyclostomes and Fishes." In *A Treatise on Zoology* (Ed. Sir Ray Lankester). Copyright 1909 by A. and C. Black, Ltd.

Fig. 6.2B. From O. Abel, *Die Stamme der Wirbeltiere.* Copyright 1919 by Walter de Gruyter and Company.

Figs. 8.12; 8.20B,C; 8.61. From J. F. Daniel, *The Elasmobranch Fishes.* Second Edition. Copyright 1928 by University of California Press.

Figs. 10.18; 10.19A; 11.3; 11.7–11.10A; 11.11–11.16;

11.25B. From W.K. Gregory and H. C. Raven, "Studies on the Origin and Early Evolution of Paired Fins and Limbs." In *Annals of the New York Academy of Sciences,* Vol. XLII, Art. 3, Nov. 15, 1941. Copyright 1942 by New York Academy of Sciences.

Figs. 12.12a; 16.39. From W. K. Gregory, *Our Face from Fish to Man.* Copyright 1929 by G. P. Putnam's Sons.

Figs. 12.16C; 13.1A; 19.3B,C; 19.9C,E,F; 19.15E; 19.20A1,X; 20.1A,C; 20.17A,D,E; 20.22B,E; 20.26F; 23.30A; 23.33B; 23.39. From Richard Lydekker, *The New Natural History.* Merrill and Baker American edition; undated. Copyright (Royal Natural History) by Frederick Warne and Company, Ltd.

Fig. 12.31E. From H. P. Nierstrasz, "Die Atmungsorgane." In *Vergleichende Anatomie der Wirbeltiere.* Copyright 1927 by Julius Springer Verlag.

Figs. 13.1C; 13.3A; 13.4C,D; 13.5C,D1. From S. W. Williston, *Water Reptiles of the Past and Present.* Copyright 1914 by the University of Chicago.

Figs. 13.12A,B; 13.13A, 13.14A,C; 13.20A; 14.4A–E; 14.5C; 14.6B,C; 14.7C; 14.8D–F; 14.10A,C; 16.36A. From S. W. Williston, *Osteology of the Reptiles.* Copyright 1925 by Harvard University Press.

Figs. 15.3A,B. From H. G. Seeley, *Dragons of the Air.* Copyright 1901 by D. Appleton and Company, now Appleton-Century-Crofts, Inc.

Fig. 15.5A. From W. P. Pycraft, *Birds in Flight.* Copyright 1922 by Gay and Hancock, Ltd., now A. and C. Black, Ltd.

Fig. 15.5B. From F. W. Headley, *The Flight of Birds.* Copyright 1912 by H. F. and G. Witherby, Ltd.

Figs. 15.7; 15.8C; 15.9; 15.15D. From Gerhard Heilmann, *The Origin of Birds.* Copyright 1927 by D. Appleton and Company, now Appleton-Century-Crofts, Inc.

Fig. 15.19A. From A. S. Romer, *Vertebrate Paleontology.* Second Edition. Copyright 1945 by the University of Chicago.

Figs. 16.5H; 16.37J; 16.55a; 16.55b. From Cunningham's *Text-book of Anatomy* (Ed. Arthur Robinson). Fifth Edition revised, 1927. William Wood and Company, now Oxford University Press.

Figs. 16.54; 24.13. From W. K. Gregory, *Man's Place Among the Anthropoids . . .* Copyright 1934 by Oxford University Press.

Figs. 16.11B, 16.13B. From Robert Broom, *Mammal-like Reptiles.* Copyright 1932 by H. F. and G. Witherby, Ltd.

Fig. 16.63. From T. S. Westoll, "The Mammalian Middle Ear." In *Nature,* 114, Jan. 27, 1945. Copyright 1945 by the Macmillan Company, Ltd.

Fig. 16.64. From G. R. De Beer, *The Development of the Vertebrate Skull.* Copyright 1937 by Oxford University Press.

Figs. 16.73G,H. From A. S. Romer, *Man and the Vertebrates.* Third Edition. Copyright 1941 by the University of Chicago.

Figs. 18.1C; 19.38B–D; 22.10B,B1; 22.11; 24.9E1,F1. From Max Weber, *Die Säugetiere.* Bd. II. Copyright 1928 by Gustav Fischer.

Fig. 19.15D. From F. E. Beddard, "Mammalia." In *Cambridge Natural History,* Vol. 10. Copyright 1902 by The Cambridge University Press, now by The Macmillan Company.

Figs. 21.17B; 21.18B; 21.21C. From W. B. Scott, *A History of Land Mammals in the Western Hemisphere.* Revised edition. Copyright 1937 by The American Philosophical Society.

Fig. 21.22. From F. B. Loomis, *The Deseado Formation of Patagonia.* Copyright 1914 by The Trustees of Amherst College.

Fig. 23.80. From W. K. Gregory, *The Origin and Evolution of the Human Dentition.* Copyright 1922 by The Williams and Wilkins Company.

Plate 12.IV. From E. D. Cope, *The Origin of the Fittest.* Copyright 1887 by D. Appleton and Company, now Appleton-Century-Crofts, Inc.

CONTENTS*

VOLUME II

			Page
CHAPTER	I.	The First Living Things	1
CHAPTER	II.	The World of Molluscs	7
CHAPTER	III.	Externally Articulated Animals (Arthropods)	53
CHAPTER	IV.	Coelomate Food-sifters of Diverse Types (Brachiopods, Polyzoa, Echinoderms)	59
CHAPTER	V.	The Prochordates and the Problem of the Origin of the Vertebrates	67
CHAPTER	VI.	The Vertebrates Come Forth: Shell-skinned Ancestors of the Vertebrates and Some of Their Branches	85
CHAPTER	VII.	Early Experiments Among Streamlined Predators (Placoderms)	103
CHAPTER	VIII.	Advanced Predators of the Shark Tribe	121
CHAPTER	IX.	The Branching Tribes of Bony Fishes	173
CHAPTER	X.	The Air-breathers Struggle for Life (Dipnoans, Lobe-fins)	323
CHAPTER	XI.	The Air-breathers Come Up on Land	343
CHAPTER	XII.	From Lowland Marsh to Forest and Desert	377
CHAPTER	XIII.	Back to the Waters and Down to the Sea	445
CHAPTER	XIV.	The Reign of the Archosaurians (Thecodonts, Crocodilians and Dinosaurs)	467
CHAPTER	XV.	Bat-winged Reptiles (Pterosaurs) and the Feather-winged Frame of Birds	521
CHAPTER	XVI.	From Slinking Reptiles to Running Mammals: A Critical Stage in Evolution	547
CHAPTER	XVII.	The Dark Ages of Mammalian History (Mesozoic Mammals)	625
CHAPTER	XVIII.	Branching Evolution in Egg-laying and Marsupial Mammals	647
CHAPTER	XIX.	Rise of the Placental Mammals (The Outer Form and Inner Frame of Insectivores, Edentates, Bats, Rodents)	681
CHAPTER	XX.	Archaic and Modernized Carnivora, Including Seals (Pinnipedia)	727
CHAPTER	XXI.	Outer Form and Inner Frame Among the Hoofed Mammals (Ungulata)	765
CHAPTER	XXII.	Fish-like by Convergence (Cetacea)	889
CHAPTER	XXIII.	Origin, Rise and Development of the Primates	905
CHAPTER	XXIV.	Man's Debt to the Past	991

* See also Volume I Contents, pp. xiii–xxi; also Volume I Index.

CHAPTER I

THE FIRST LIVING THINGS

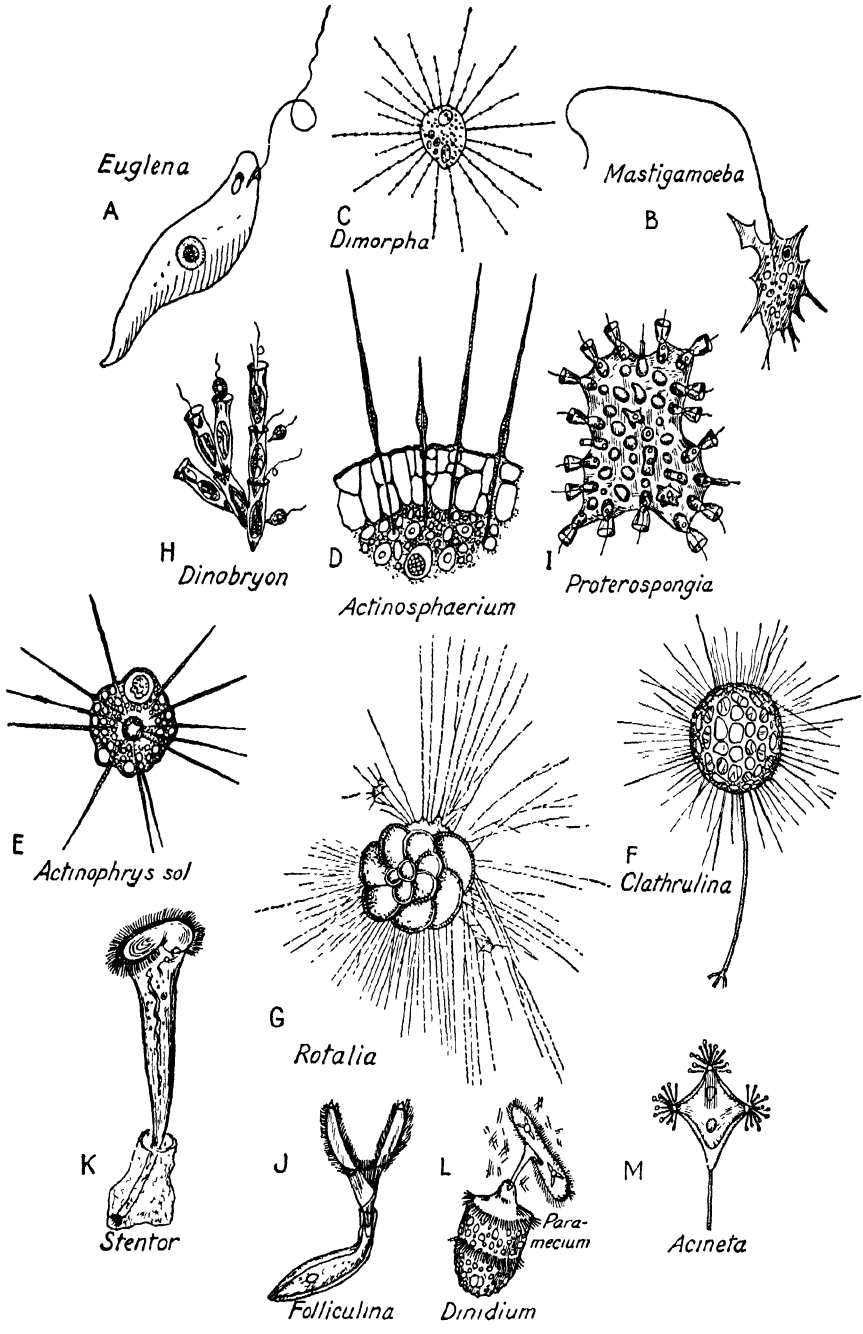
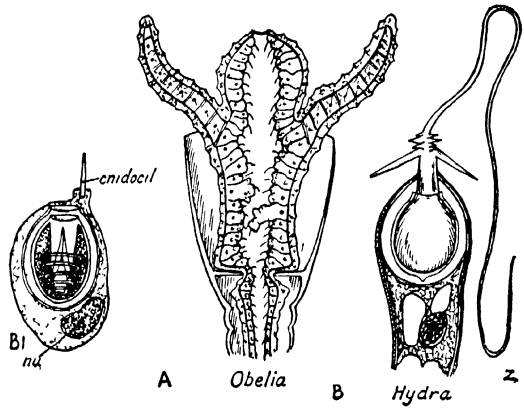


Fig. 1.1. Typical Protozoa. A, a flagellate (class Mastigophora) that retains chlorophyll; B, an amoeba-like flagellate; C–F, Heliozoa, with stiff, radiating axopodia; G, a primitive foraminifer; H, a branching flagellate with bell-like mouths; I, a colonial choano-flagellate with collar cells; J, K, typical ciliates, showing arrangement of cilia to form whorls; L, an aggressive ciliate attacking a *Paramecium*. The latter has discharged its trichocysts (or nematocysts). M, A tentacle-bearing ciliate. All after Parker and Haswell, Vol. I.



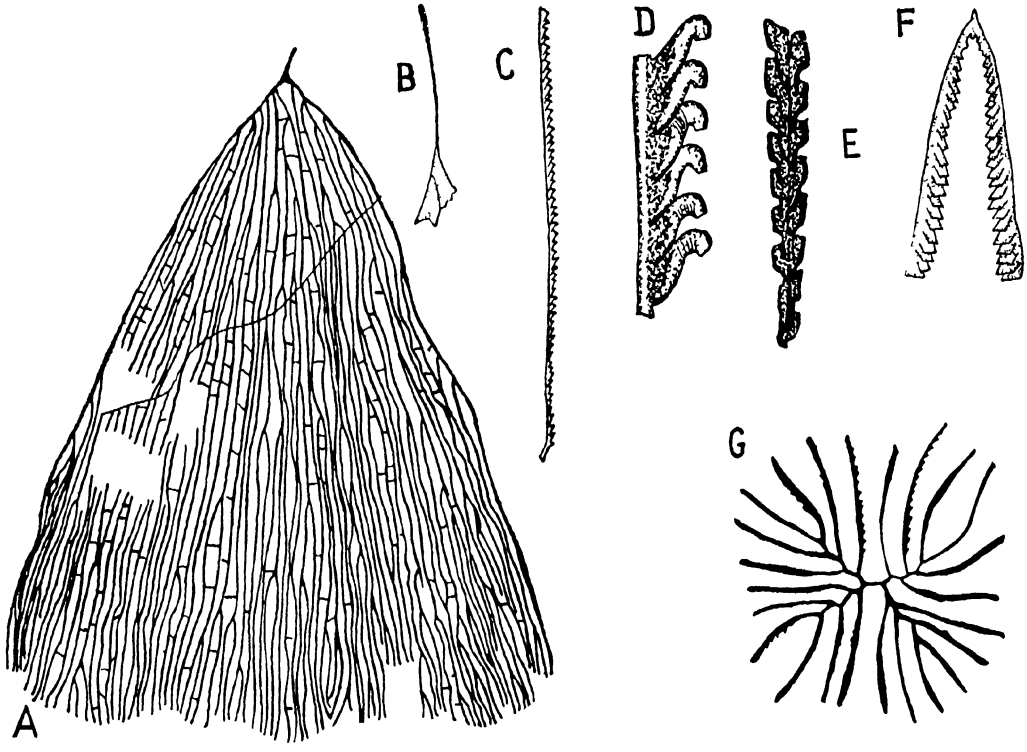
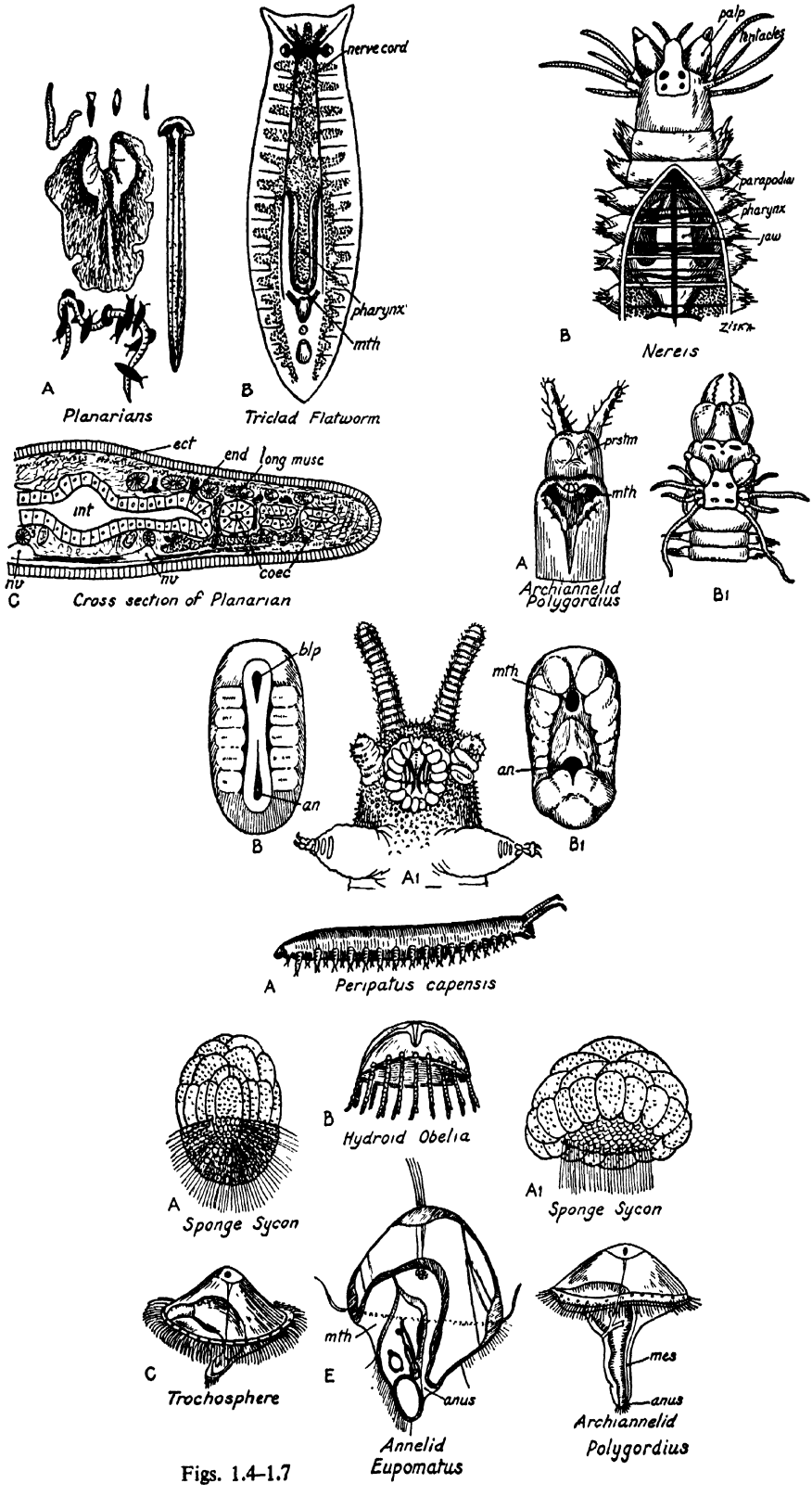


Fig. 1.2. A microscopic monster and its weapons. From Parker and Haswell.

Fig. 1.3. Graptolites. From Goldring, after Ruedemann and Holm. A, A relatively primitive, attached and bush-like colony (*Dictyonema*), X1. B, Sicula, a parent stem of the same, X1. C, One-branched Silurian graptolite (*Monograptus*), X1. The thecae or horny sockets for the minute living animals form a serrated series on one side of a common stalk. D, A bit of the same, much enlarged. E, One-branched form (*Climacograptus*) with two rows of thecae, X7. F, Two-branched form (*Didymograptus*), X1. G, Many-branched form (*Goniograptus*), X1. Courtesy of N. Y. State Museum, Albany, N. Y.


A
Planarians
nerve cord
pharynx
mth
B
Triclad Flatworm
palp
tentacles
parapodia
pharynx
jaw
B
Nereis
ect
end
long musc
int
nv
nv
coel
C
Cross section of Planarian
prstm
mth
A
Archiannelid
Polygordius
B1
blp
an
B
mth
an
B1
A1
A
Peripatus capensis
A
Sponge Sycon
B
Hydroid Obelia
A1
Sponge Sycon
C
Trochosphere
mth
E
anus
Annelid
Eupomatus
mes
anus
Archiannelid
Polygordius

Figs. 1.4–1.7

Fig. 1.4 (top left). Free-living flatworms (A, B), the most primitive of the three-layered animals. C, Cross-section of a planarian (flatworm), showing the endodermal intestine and one of its lateral outgrowths or caeca. The mesodermal muscles and the ducts of the reproductive system are seen between the endo- and ectoderm. All after Parker and Haswell, Vol. I.

Fig. 1.5 (top right). A, head of an archiannelid, *Polygordius*: ventral view, showing mouth, prostomium and tentacles; B, head of typical annelid (*Nereis*), dorsal side with roof of pharynx opened to show retracted jaws. The latter lie in a muscular pouch or proboscis which can be protruded (B1). B, after Parker and Haswell, Vol. I; B1, after Allee.

Fig. 1.6 (center). *Peripatus*, the most primitive of the existing Arthropoda. A, right side of living *Peripatus capensis*; A1, ventral view of head, showing antennae jaws, oral papillae and first pair of legs, B, A stage in the development of *Peripatus capensis*, in which the elongated blastopore is closing up in its middle part; the mesoderm on either side of the blastopore is dividing into segments. B1, a later stage in which the blastopore has given rise to the mouth and the anus and the segments of the head and trunk are better developed. All from Parker and Haswell, after Balfour.

Fig. 1.7 (bottom). Free-swimming embryos and larvae of lower invertebrates. The flatworms (Platyhelminthes) nemertine or proboscis worms (Nemathelminthes), the moss animals (Bryozoa), the molluscs and perhaps the brachiopods all include at least some marine members that have free larvae more or less like C and E below These phyla are therefore sometimes grouped in a superphylum, Trochozoa. (See Allee, 1926, 1927, p. 293.) After Parker and Haswell, Vol. I.

CHAPTER II

THE WORLD OF MOLLUSCS

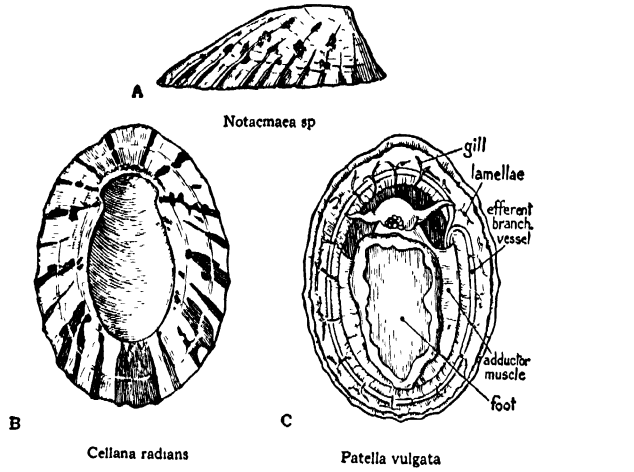


Fig. 2.1 (top). The limpet and his wave-beaten shell-tent. In A, the anterior end is toward the right. C, from Parker and Haswell.

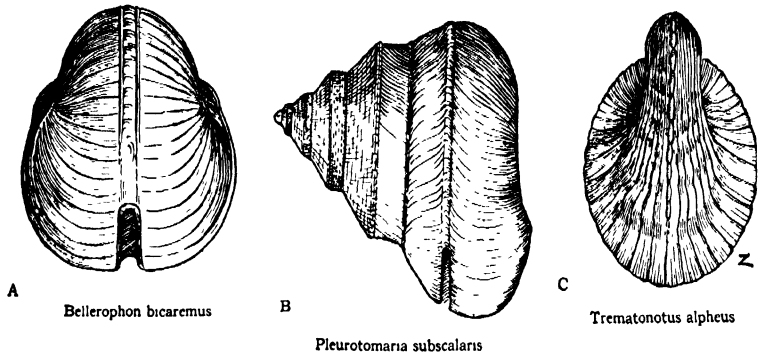


Fig. 2.2. Primitive Palaeozoic slit-shells. After Zittel. A and C form symmetrical spirals; B, a helicoid.

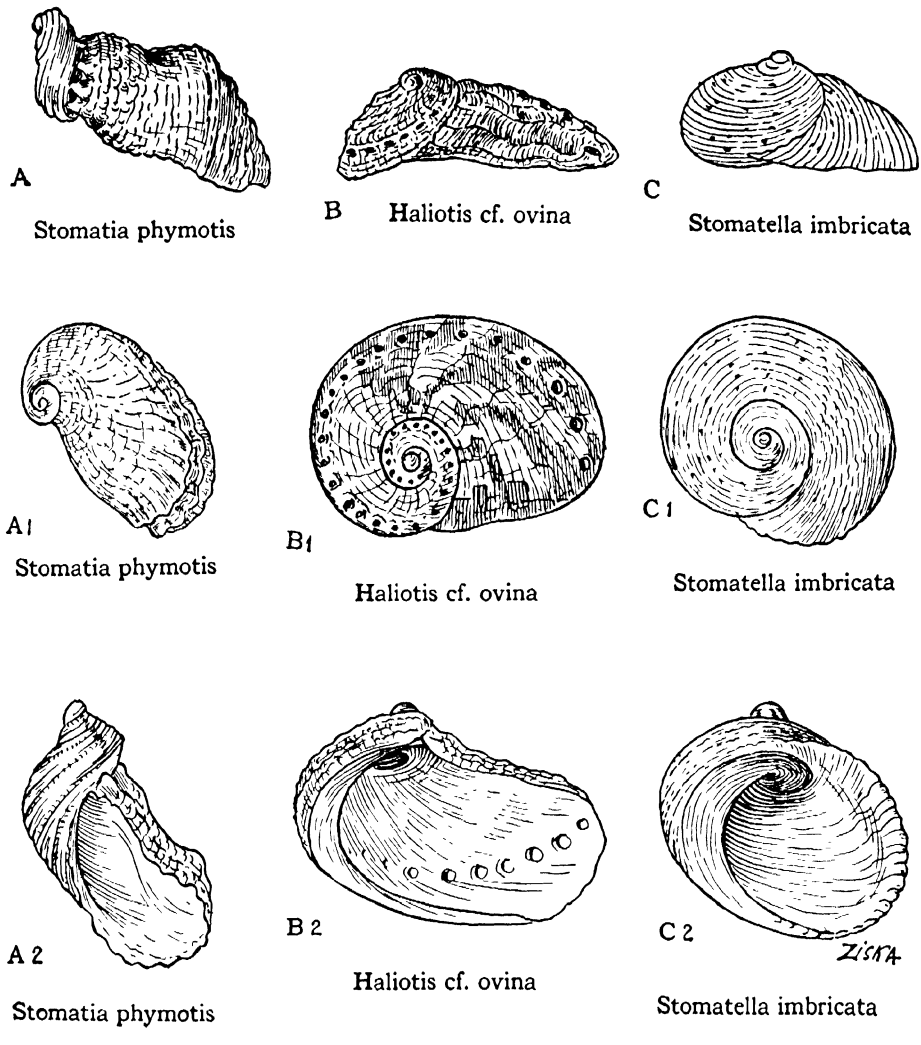


Fig. 2.3. Twisting and radial expansion in stomatellids and haliotids. Front, top and under side views. Author's collection.

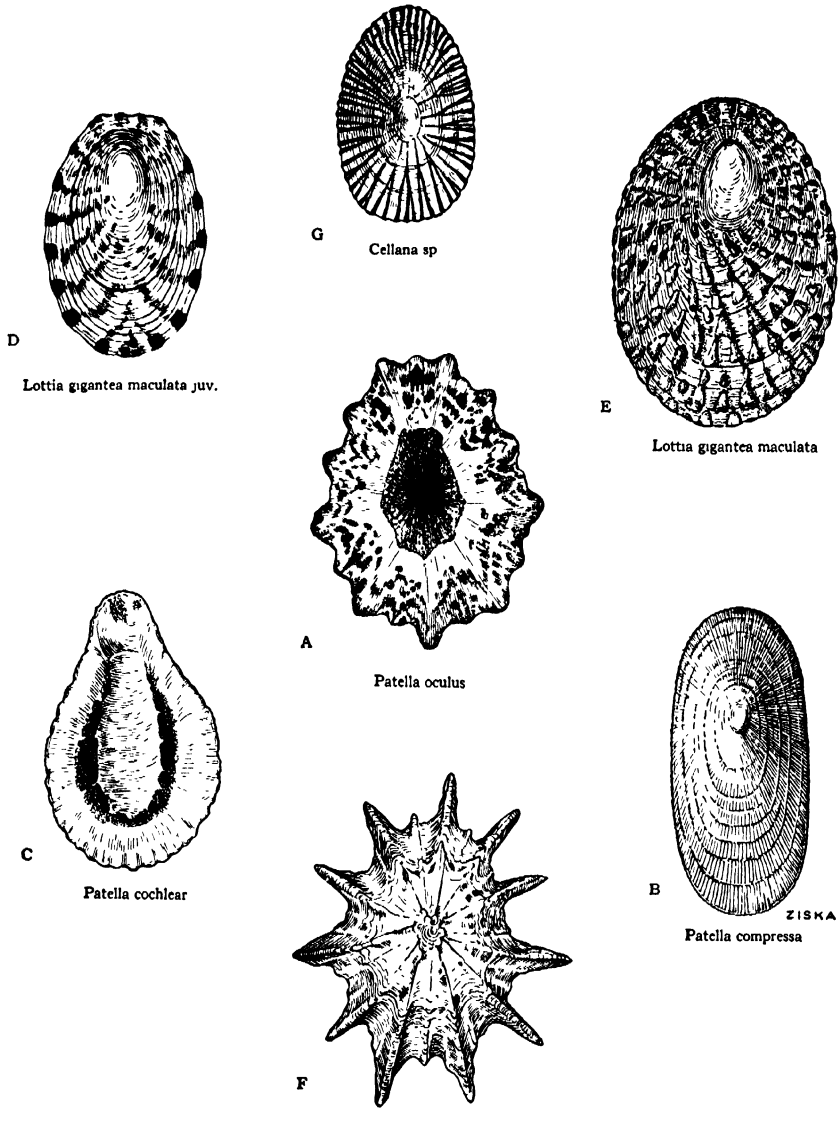
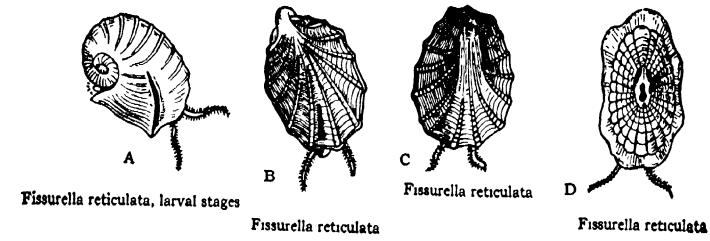
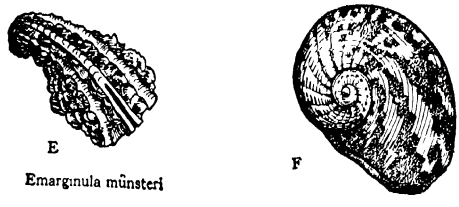
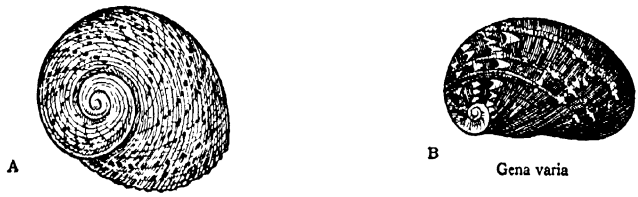
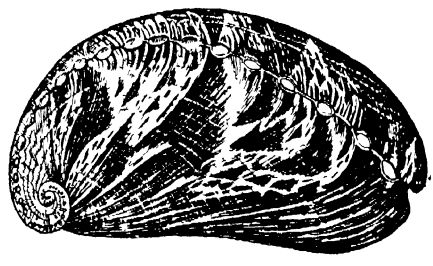


Fig. 2.4. The limpets try for bilaterality. Possibly derived from very remote depressed spiral forms, the limpets have acquired sucker-like habits and an oval or stellate shell with strengthening ribs. A, Represents the under side as seen with transmitted light. The dark area in the middle marks the back and head of the snail. In the "ear-shaped" limpet (C) the dark areas on the under side indicate the attachment of the adductor muscles and heighten the oyster-like appearance. Author's collection.









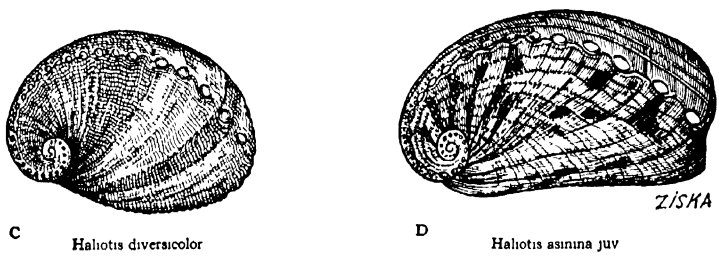


Fig. 2.5 (top). Remnants of the Palaeozoic shell-slit (A, B) in developing keyhole shells (A–E) and in the abalone (F). A, C, D, from Bronn, after Boutan, B, from Maxwell Smith; E, from Zittel; F, author's collection.

Fig 2.6. Comparison of haliotids (C–E) with more primitive shells (A, B), indicating transformation from simple spiral (A) to logarithmic spiral (E), and from revolving dots (A) to curving triangles (E). Author's collection.

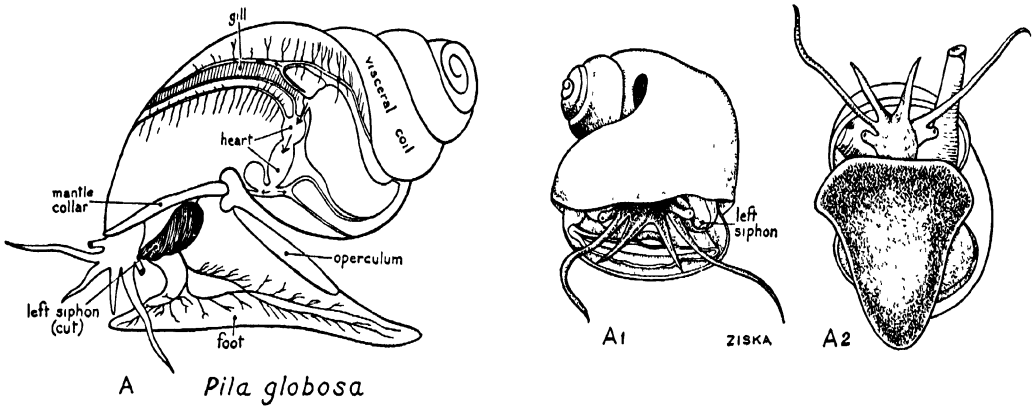


Fig. 2.7a. The snail and its shell. After Prashad. A, left side, after removal of shell; A1, front view; A2, ventral view. In A, the mantle has been removed (except the mantle collar), exposing the heart, the forwardly pointing gill and the visceral coil. The latter is directed toward the rear and projects on the right side (A1). The head points away from the visceral coil and from the spire of the shell. The aperture of the shell is directed downward; when viewed from below, the aperture is to the right of the expanded body whorl and the shell is dextral (see text). After Prashad.

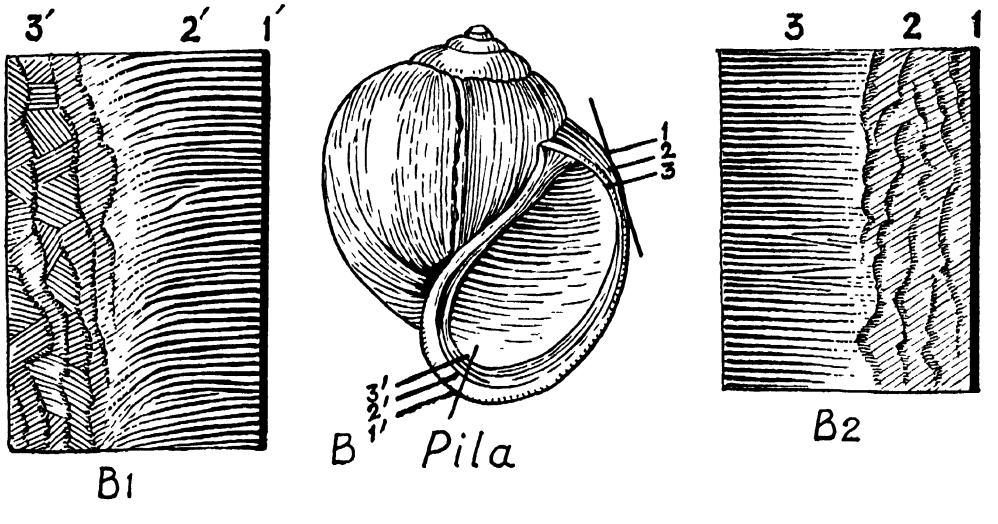


Fig. 2.7b. In B1, the section at right angles to the border of the mantle, the fibres of the ostracum are parallel to the growing mantle, while those of the hypostracum, or deepest layer, are crisscrossed. In B2, the section tangent to the surface, the fibres of the ostracum are oblique, those of the hypostracum are transverse, to the mantle itself. After Prashad.

Fig. 2.8 (facing page). Development of snail, diagram. From Zittel. The faster spiral growth of the left side rotates the gills from the rear to the front, where they point obliquely forward (hence the ordinal name, Prosobranchiata). At the same time the nerve loop is twisted into a figure 8 (streptoneury).

Fig. 2.9 (facing page). Primitive helicoids with slight (D) or moderate (E) radial acceleration in successive whorls. A, B, E, are seen from below and show the open conical umbilicus. The sundial (A), according to Thiele and to Wenz, is related to the cerithiids (fig. 2.16). The conical *Astraea* (B) is related to the trochids (fig. 2.11) but its outer rim extends downward and bears marginal projections. These features are emphasized in *Xenophora* (C), which, however, seems to be related to the stromboid group (fig. 2.18). Author's collection.

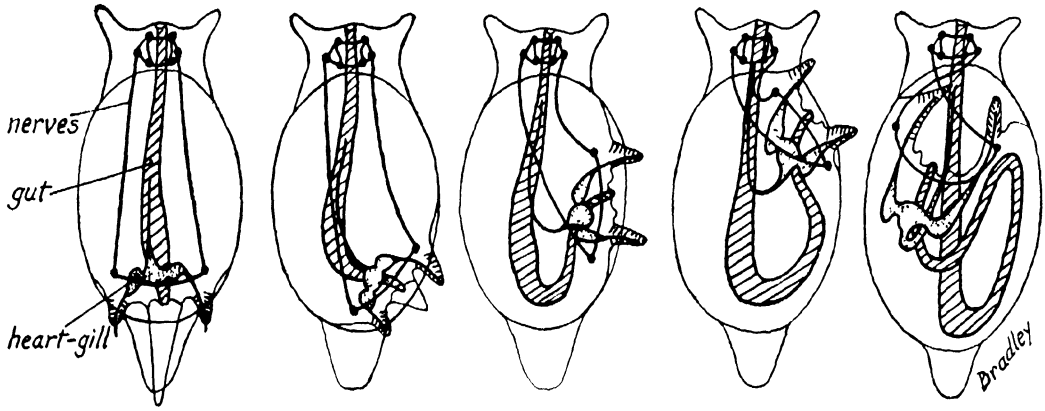
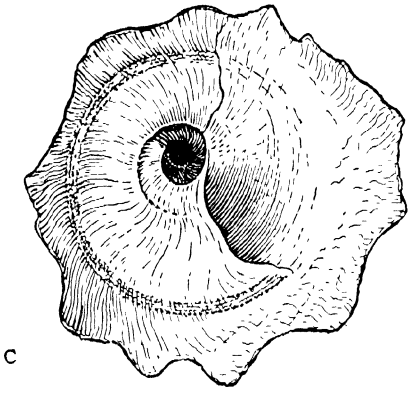
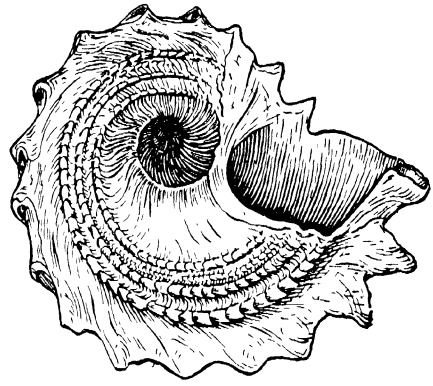


Fig. 2 8



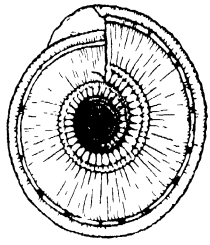
C

Xenophora exusta



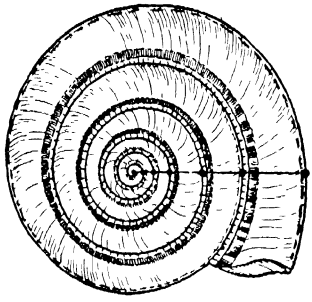
B

Astraea heliotropium



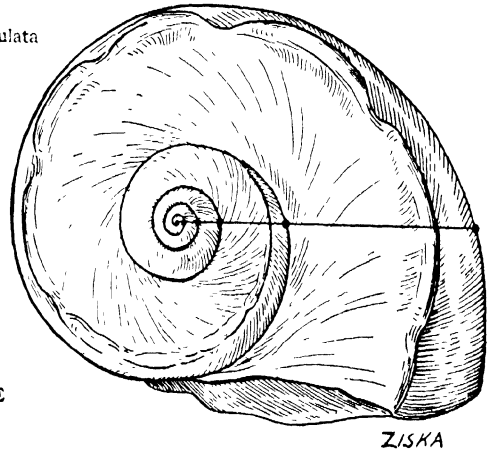
A

Architectonica granulata



D

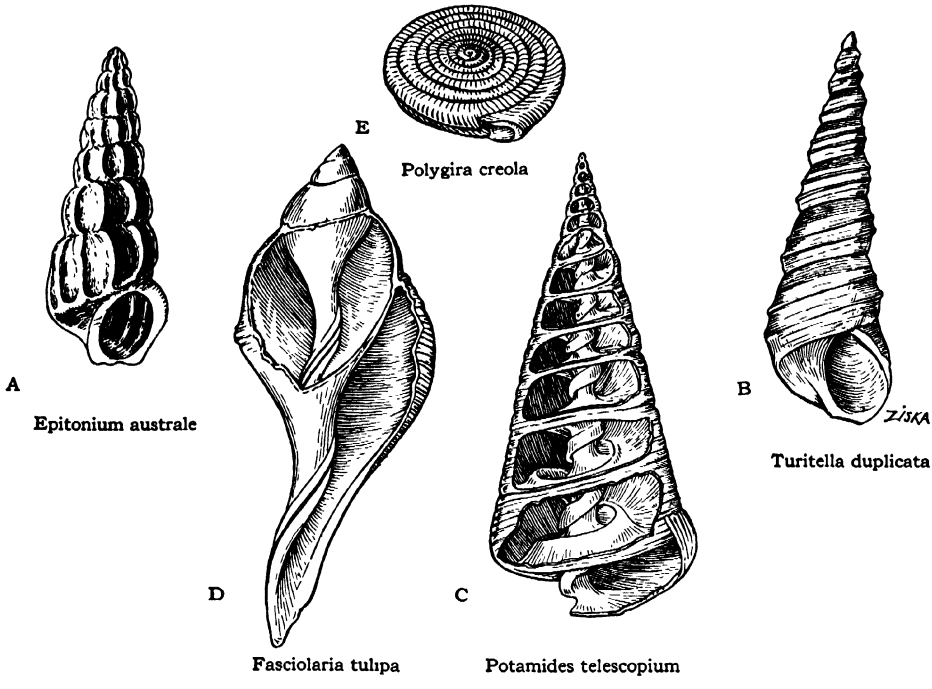
Architectonica granulata



E

Turbo marmoratus

Fig. 2.9



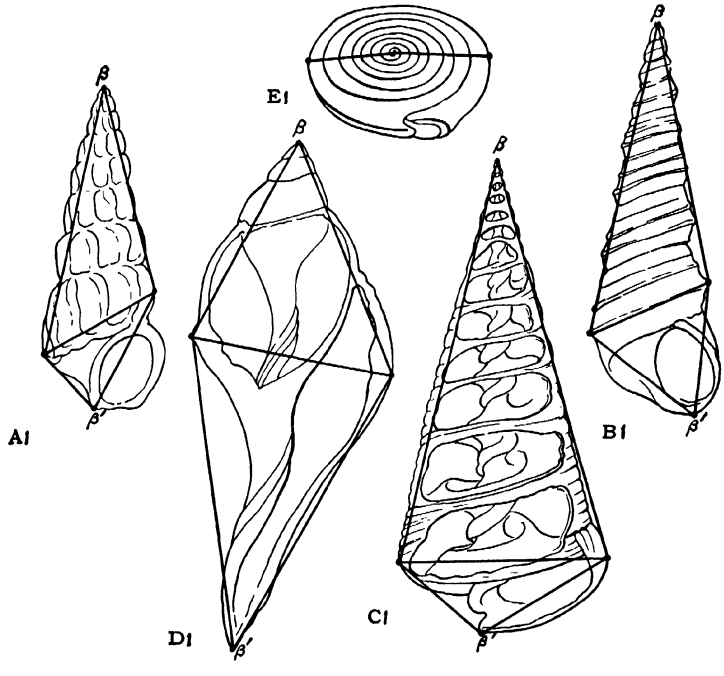


Fig. 2.10. Varying relations between the apical angle (β) and the acceleration of radial growth in successive whorls. Author's collection.

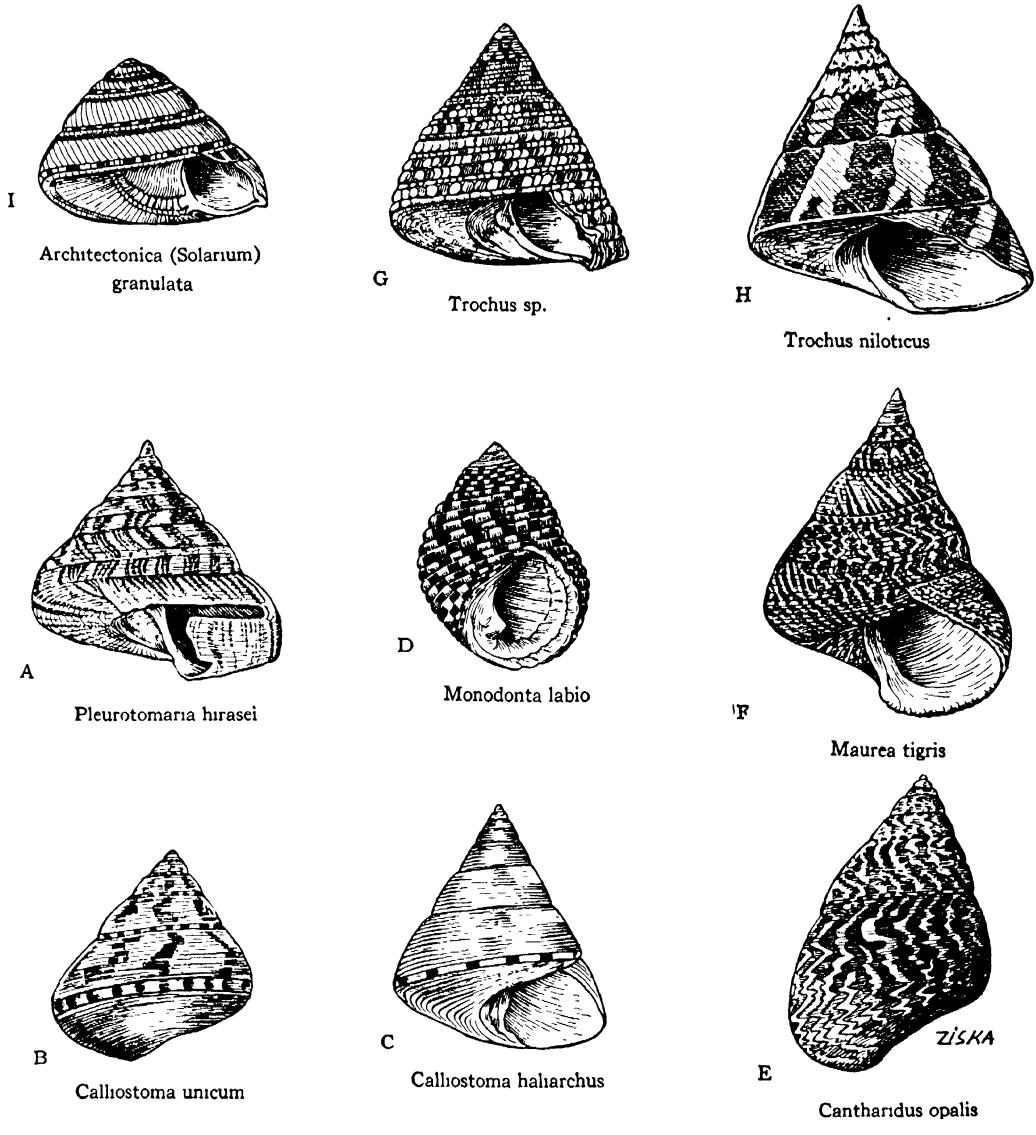


Fig. 2.11. The trochoid theme and its variants. A, slit-shell, a deep-sea survivor of the primitive Palaeozoic *Pleurotomaria* group, B, C, primitive trochoids; D–H, typical trochoids; I, sundial shell. The more primitive trochoids (B, C) retain the conical form of the slit-shells (A). Some of the more advanced trochids become sharply conical (G, H); the globose *Monodonta* (D) resembles both the neritids and the littorinids The color patterns range from simple revolving lines to dot-and-dash, zigzags and broad oblique patches. A–C, after Hirase; D–I, author's collection.

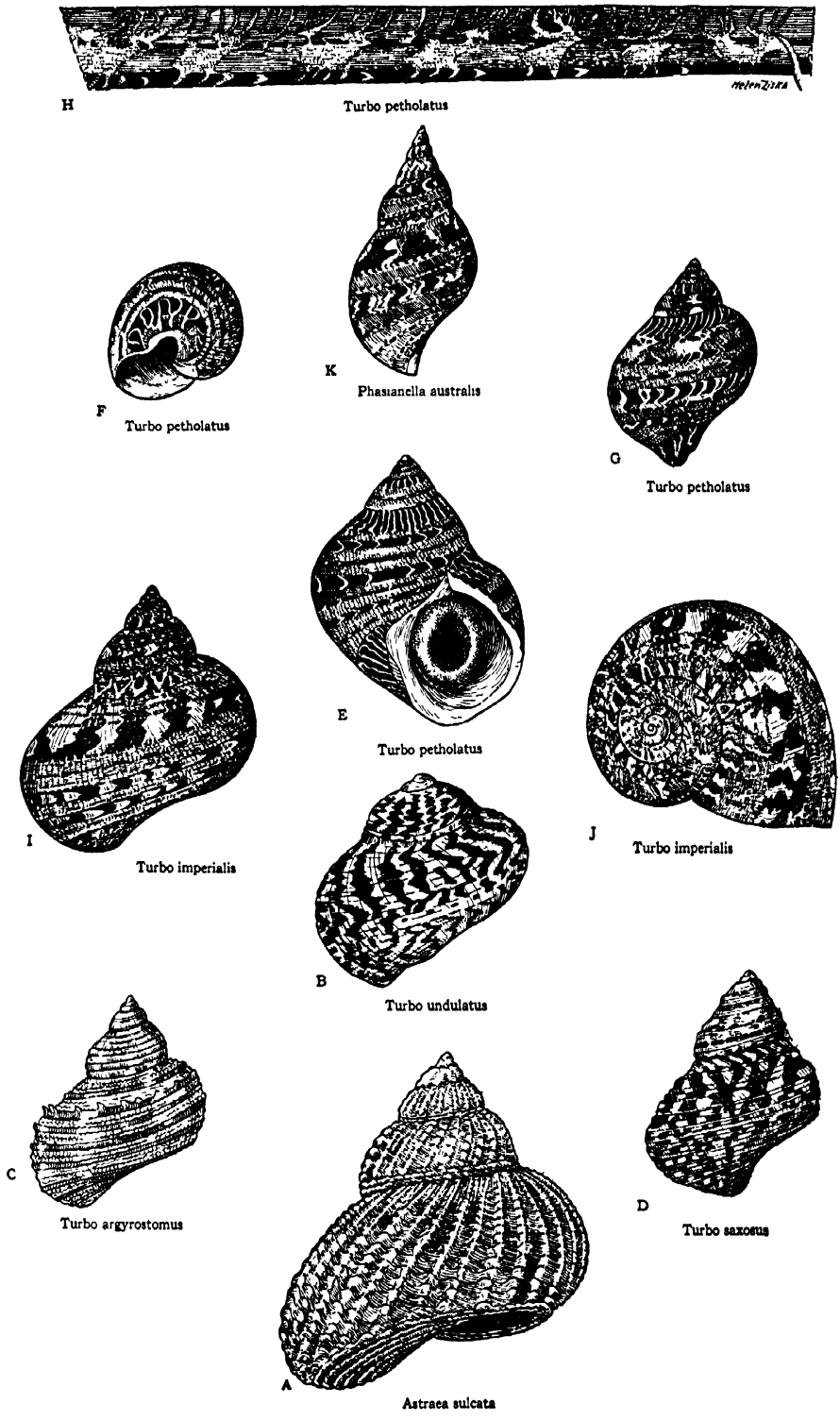

H
Turbo petholatus
K
Phasianella australis
F
Turbo petholatus
G
Turbo petholatus
E
Turbo petholatus
I
Turbo imperialis
J
Turbo imperialis
B
Turbo undulatus
C
Turbo argyrostomus
D
Turbo saxosus
A
Astraea sulcata

Fig. 2.12

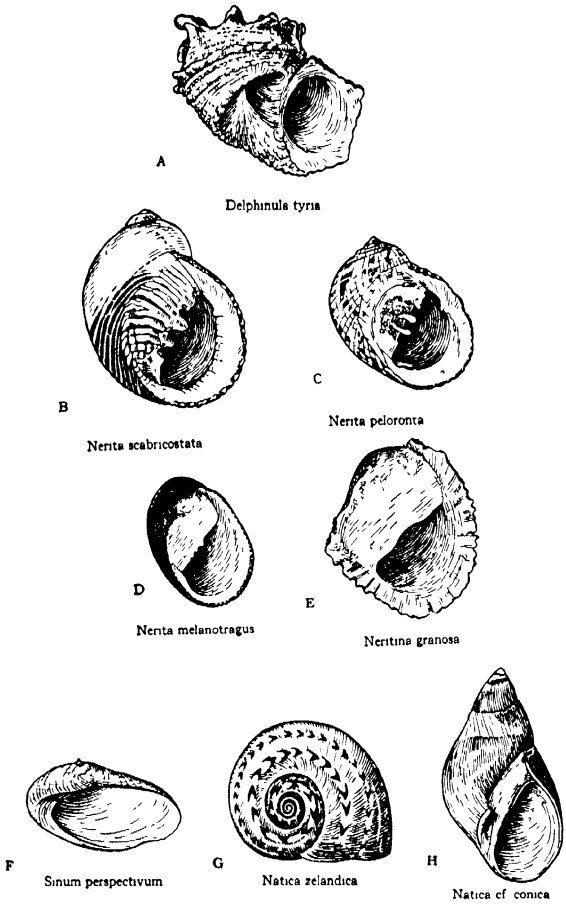


Fig 2 13

Fig. 2.13. Dolphin (A), nerites (B–E), and bull's eye or moon shells (F–H). The dolphin starts as a nearly flat spiral, as do many of its early Palaeozoic relatives, but later its tube spirals downward. The shell-tube of the globose nerites ends in a circular or oval rim. The inner lip is flattened by contact with the folded-back operculum on the back of the foot. The spire is reduced and the body wall globose. The snails cling to the rocks like limpets. The typical *Natica* (G) or bull's-eye shell is nearly globose but there are also some depressed (F) and conical (H) forms. The upper part of the inner lip is reflected over the wall of the shell by a large light callus and the umbilicus is usually conspicuous Author's collection

Fig. 2.14 Comparative morphology of the deck shell (C, C1), indicating the probable derivation of the deck from the surface of the inner lip of the aperture, and of the rim from that of a relatively primitive helicoid (A, A1). The crucible (D, D1) seems to represent an emarginated, folded-up deck. The last traces of the deck may be seen in the paired muscle scars of the cap shells (E, E1) Author's collection.

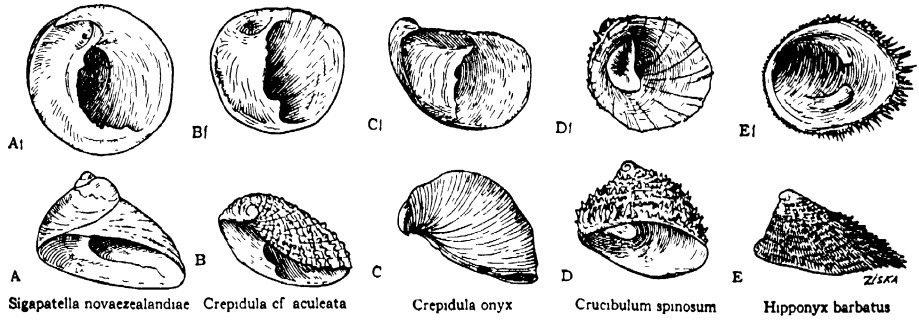


Fig. 2 14

←Fig. 2.12 (facing page). The whirling astraeids, turbans and pheasant shells, showing range from lamellose, undulatory surface (A), to revolving cords (B–D) and smooth porcellanous surface (E–J). Color patterns, originally of simple waves and cords (A–C), pass through the dot-dash (D) and dash-crescent (E) stages and then become exceedingly complex (G) and confused (J). Fortuitous juxtaposition of modified crescents and spots, blotches or different cord lines sometimes gives rise to "letters" (F) and animal-like figures (H). Author's collection.

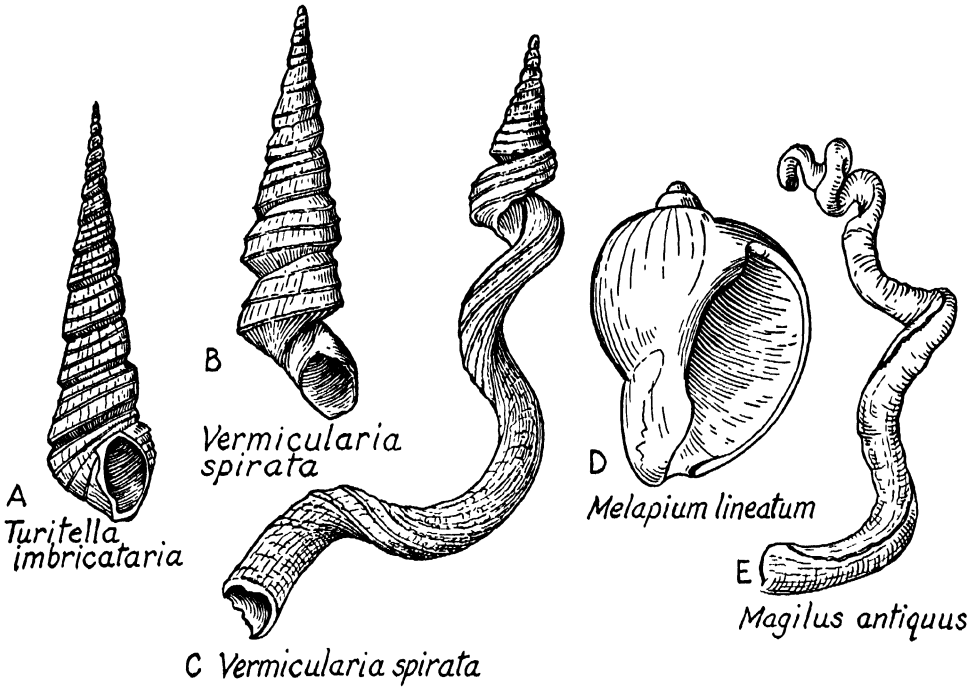


Fig. 2.15. Regular growth of the shell tube in turritellids (A) *versus* aberrant growth in vermetids (B, C) and magilids (D, E). Author's collection.

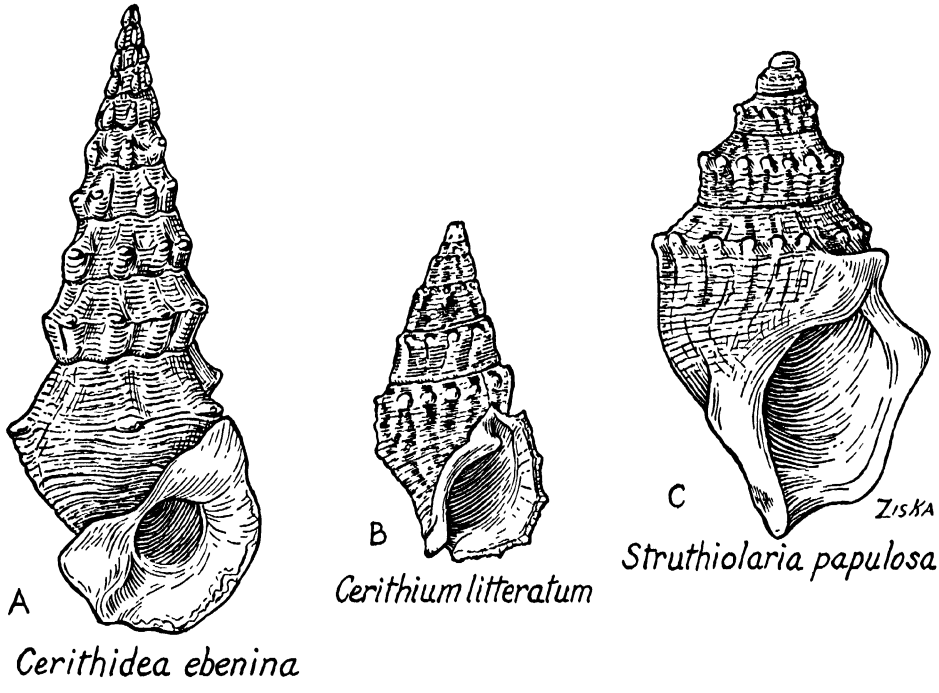


Fig. 2.16. Transition from holostomous (A) to siphonostomous (C) apertures. Author's collection.

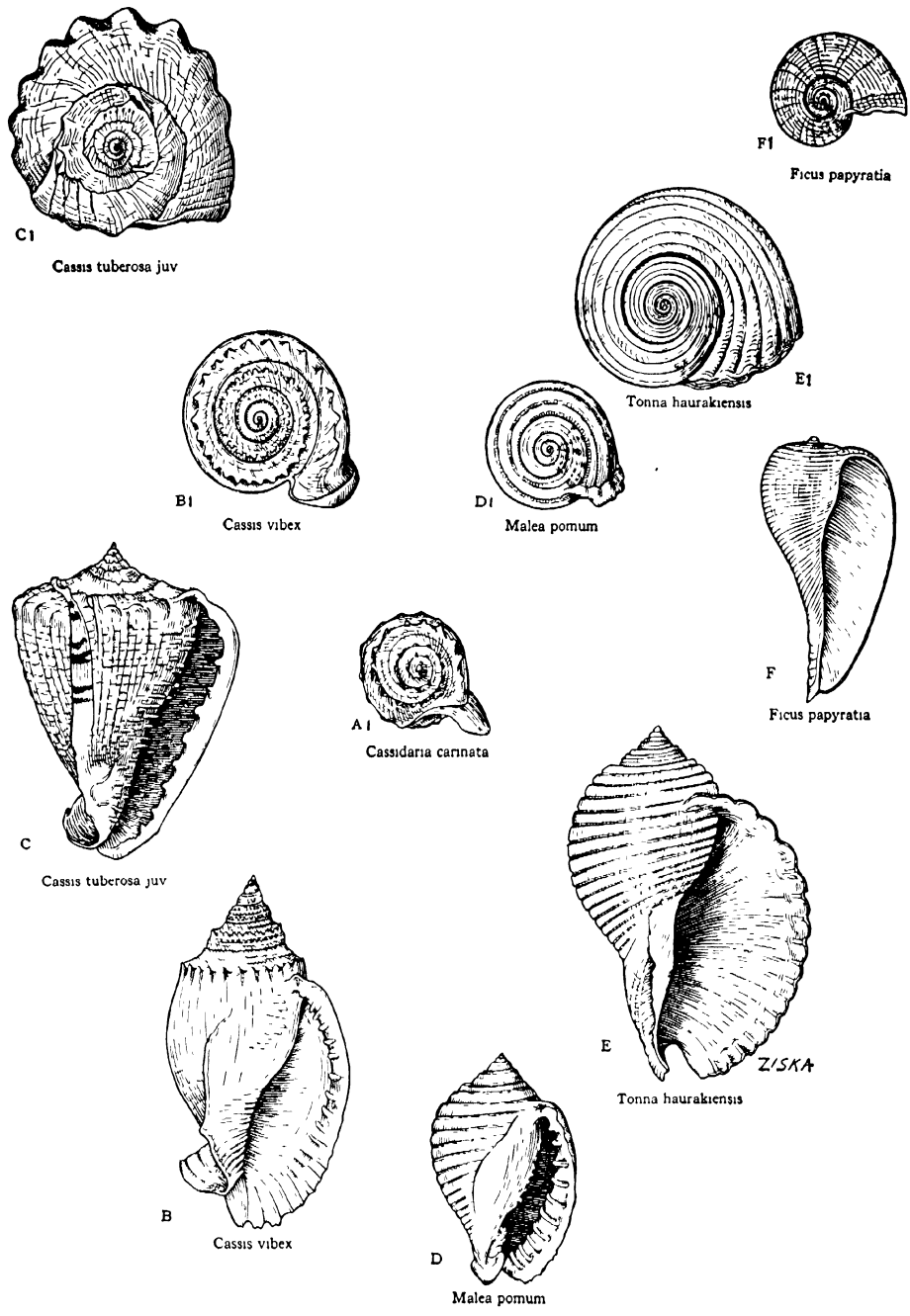
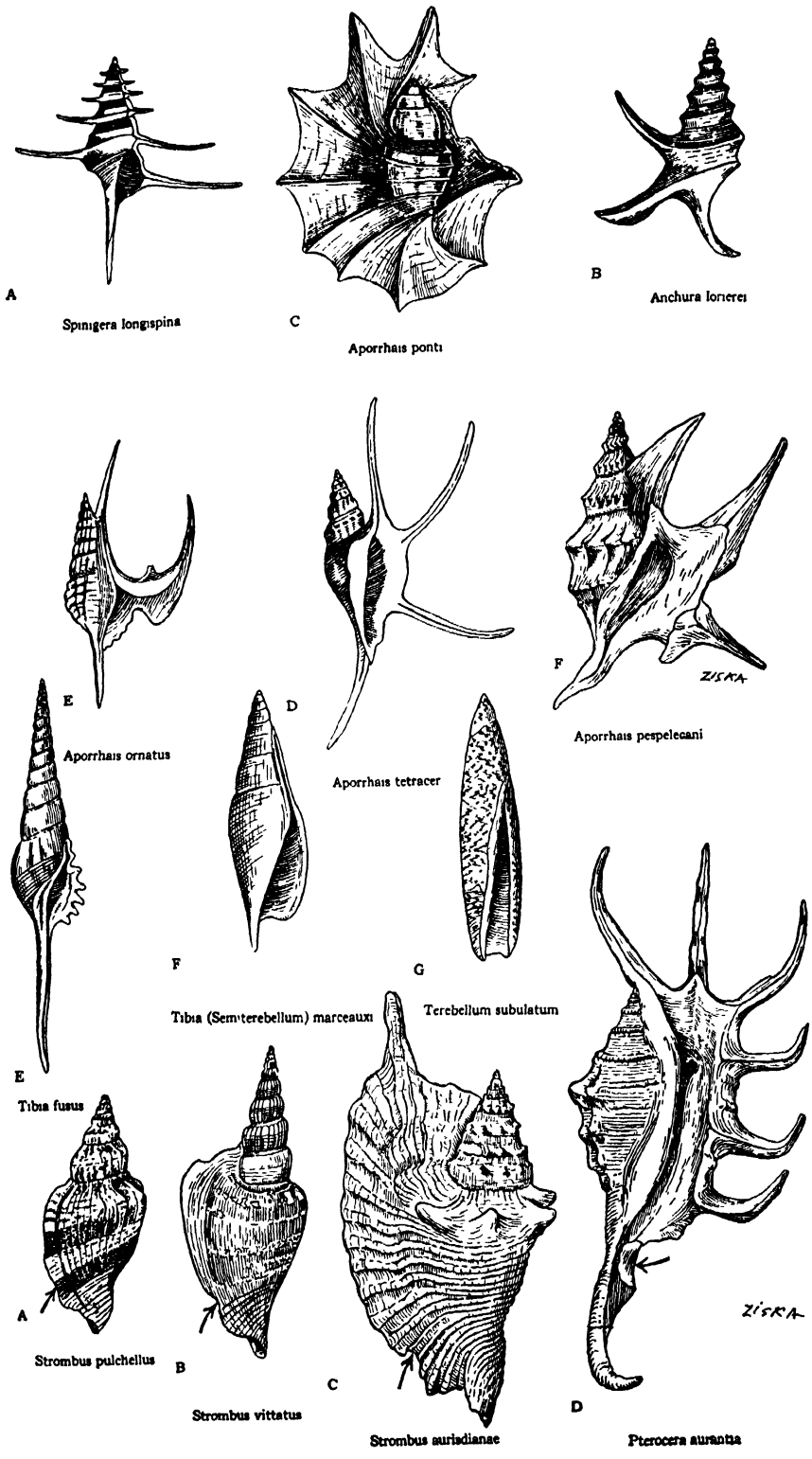


Fig. 2.17a, b. Adaptive branching of the tuns (A, D, E) and helmets (B, C). The most primitive member (A) of the group, from the Eocene of France, bears regular revolving ridges and conical projections in successive whorls, the siphon is deflected as in *Aporrhais* (fig. 2.18F), the outer lip is somewhat reflected. The helmets (C) emphasize the stop-and-go method of growth, while the tuns (E) stress continuous growth. The typical helmets (C) have attained an obconical form, suggesting that of the cones (figs. 2.36, 37), while the tuns (D, E) have become almost globose. In the paper fig shell (F) the spire is much reduced and the stem or siphonal tube has been greatly elongated. A, from Zittel; others from author's collection.


A
Spinigera longispina
C
Aporrhais pomi
B
Anchura lorierei
E
Aporrhais ornatus
D
F
Tibia (Semiterebellum) marceauxi
Aporrhais tetracer
G
Terebellum subulatum
F
ZISKA
Aporrhais pespelecani
E
Tibia fusus
A
Strombus pulchellus
B
Strombus vittatus
C
Strombus aurisdianae
D
ZISKA
Pterocera aurantia

Figs. 2.18, 19

Fig. 2.18 (top). Exuberant growth of the outer margin of the mantle in fossil and recent aporrhaids, producing shelly spines and webs. The primitive aporrhaids resemble the early fusids (fig. 2.25A) in their long spout for the proboscis. The spout is later shortened and curved outward. A, middle Jurassic from Wenz, after Deslongchamps; B, Middle Jurassic, from Wenz, after Orbigny; C, Upper Jurassic, from Wenz, after Brongniart; D, Upper Jurassic, from Wenz, after Orbigny; E, Upper Cretaceous, from Wenz, after Orbigny; F, Recent.

Fig. 2.19. The more primitive strombs of Upper Cretaceous time show a moderate development of the "horns." In recent strombs these may be either reduced (A, B) or greatly emphasized (C, D), with new horns on the outer lip. In the different species of *Tibia* the horns are already reduced (E), finally disappearing (F); but the upward extension of the inner and outer lips and the slit between them remain as a vestige of aporrhaid characters even in the smooth bullet-shaped *Terebellum* (G). A–E, G author's collection; F, from Wenz, after Deshayes.

Fig. 2.20 (facing page). A sample of the cowries and their relatives. The typical cowry shell consists of two flaps which are inrolled toward each other, leaving a narrow slit guarded with tooth-like ridges. This is partly the result of the marked acceleration of the axial dimension of the body whorl and extreme reduction of the spire. The primitive cowry of Upper Jurassic time (A) was already approaching the typical cypraeid characters. Among recent cowries *Trivia* (B) retains most of the ancestral characters, especially clear traces of a revolving cord system. The diverse color patterns of the cowries are due to the activities of the right and left flaps of the mantle, which are reflected up over the surface of the shell. In the "egg" shells (H–J) the ends of the cowry shell are prolonged and the shell rests lengthwise along the branches of gorgonians. A, Upper Jurassic, from Wenz, after Gemmellaro; others from author's collection.

Fig. 2.21 (top). Comparison of one of the helmet shells (A1) with a cowry (B1), showing convergence in the lengthening and inrolling of the outer lip, reduction of the spire and reflection of the mantle up over the left side of the shell. Author's collection.

Fig. 2.22. Tritons and frog shells. During "stop" periods the frog-shells (ranellids or bursids) develop strong folds at the outer margin of the growing mantle (D), thus acquiring prominent axial flanges on opposite sides of the shell. These attain extreme specialization in *Ranella pulchra* (E). The color pattern becomes conspicuous in the noble *Triton* (C), in which "partridge feathers" appear along revolving zones. The highly specialized *Distorsio* (F) is well named from its irregular, contorted contour. Author's collection.

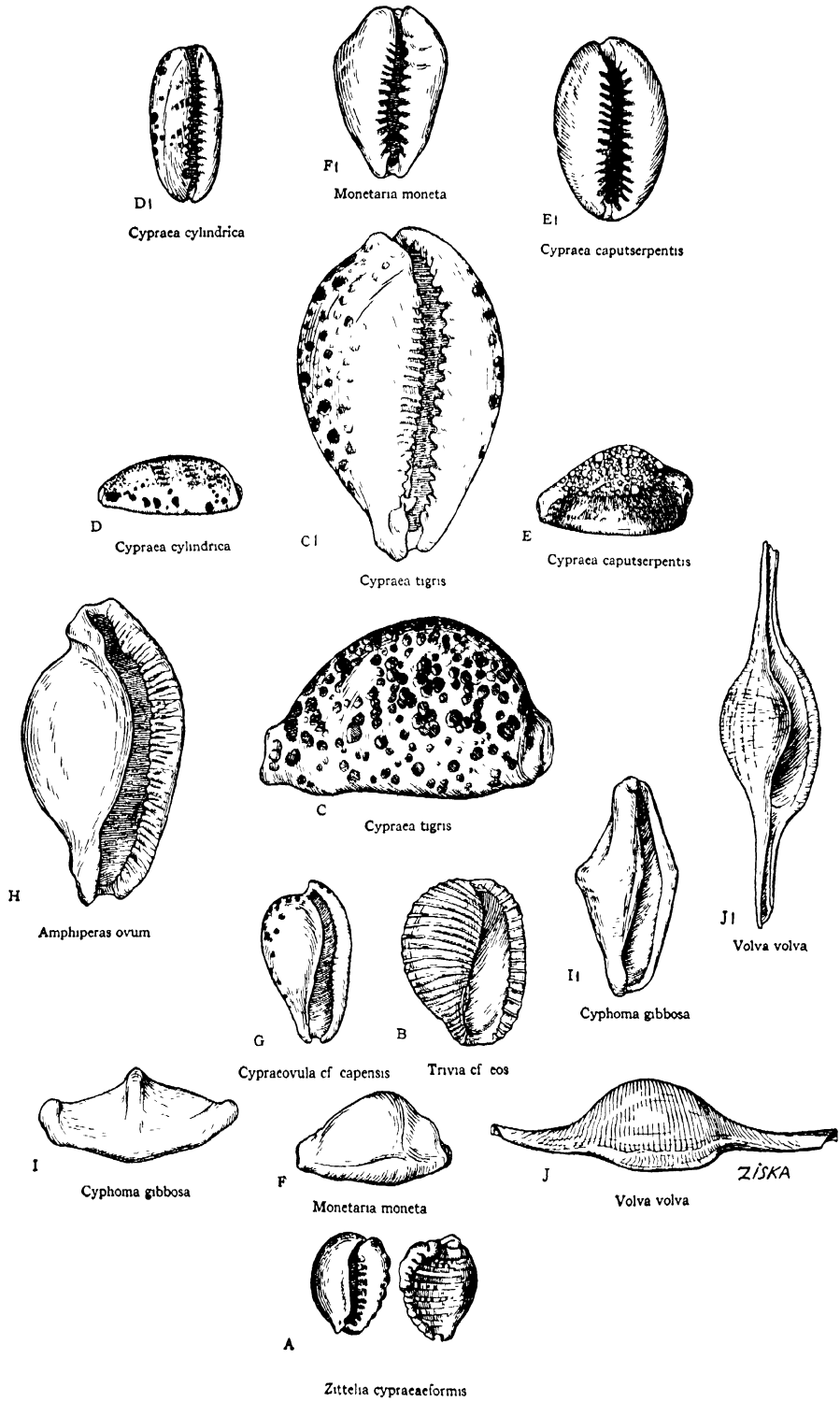
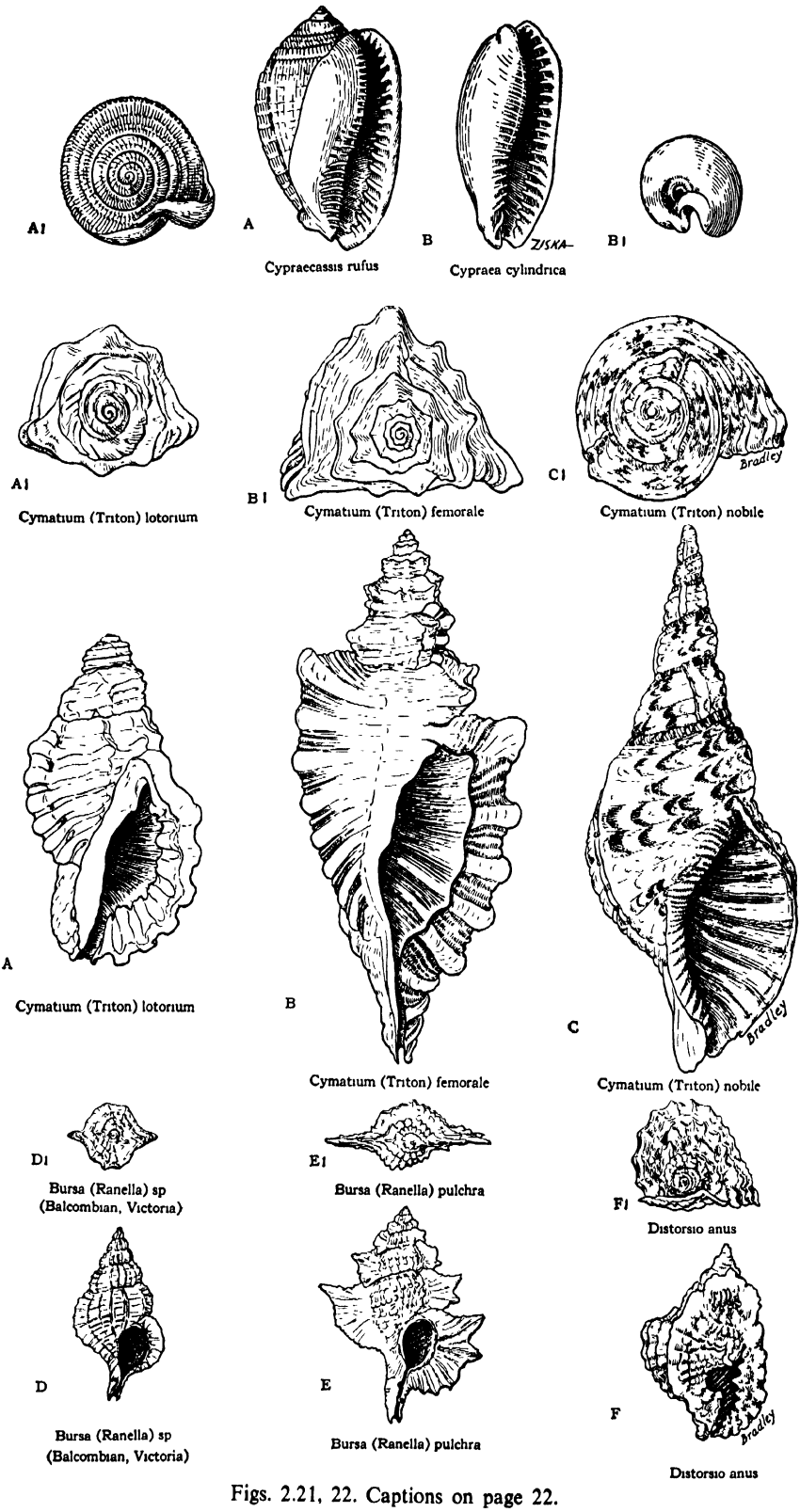

D1
Cypraea cylindrica
F1
Monetaria moneta
E1
Cypraea caputserpentis
D
Cypraea cylindrica
C1
Cypraea tigris
E
Cypraea caputserpentis
H
Amphiperas ovum
C
Cypraea tigris
J1
Volva volva
I1
Cyphoma gibbosa
G
Cypraeovula cf capensis
B
Trivia cf eos
I
Cyphoma gibbosa
F
Monetaria moneta
J
Volva volva
ZISKA
A
Zittelia cypraeaeformis

Fig. 2.20



Figs. 2.21, 22. Captions on page 22.

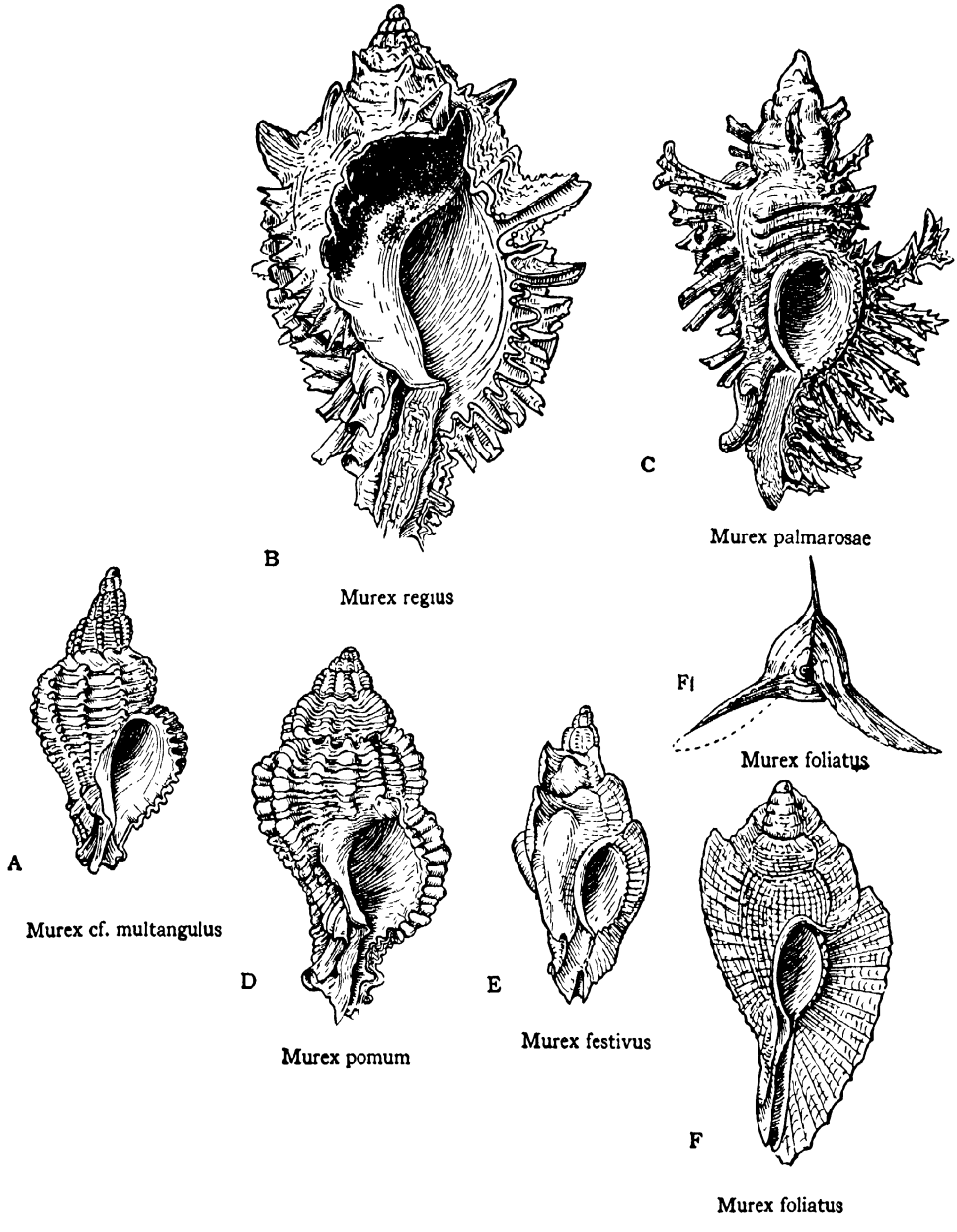


Fig. 2.23. Rock shells. The primitive muricid (A) agrees with the ranellids (fig. 22D) in emphasizing the rounded axial folds on the outer lip of the aperture. In one branch these folds give rise to extended fins (E–F). In other lines (B, C) the folds grow out into crowded stems. Author's collection.

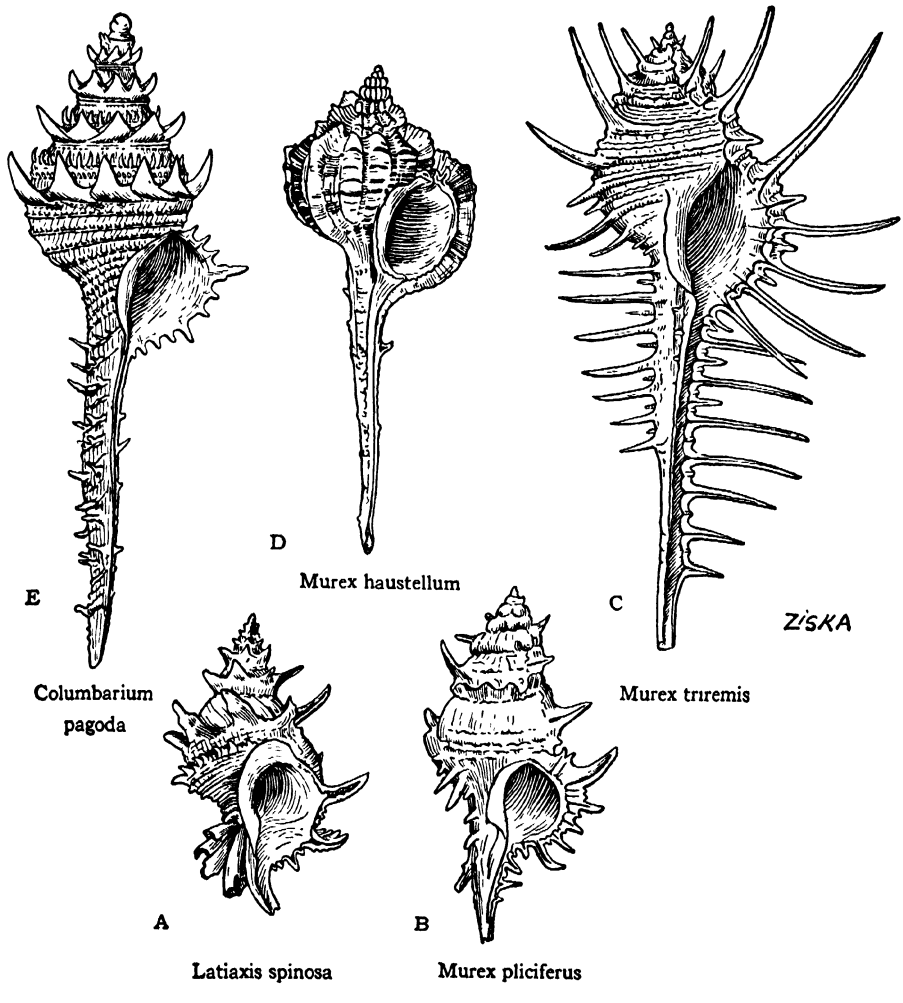


Fig. 2.24. Starting from shells with rounded axial folds (D), one line of the spiny muricids (C) culminates in shells with rows of long spikes. In another direction (E) the spines and well-developed tower form a pagoda-like contour. The relation of this last form to the muricids is by convergence, the pagoda shell being probably related to the turrids (fig. 2.35A, B) and fusids (fig. 2.25A–F). Author's collection.

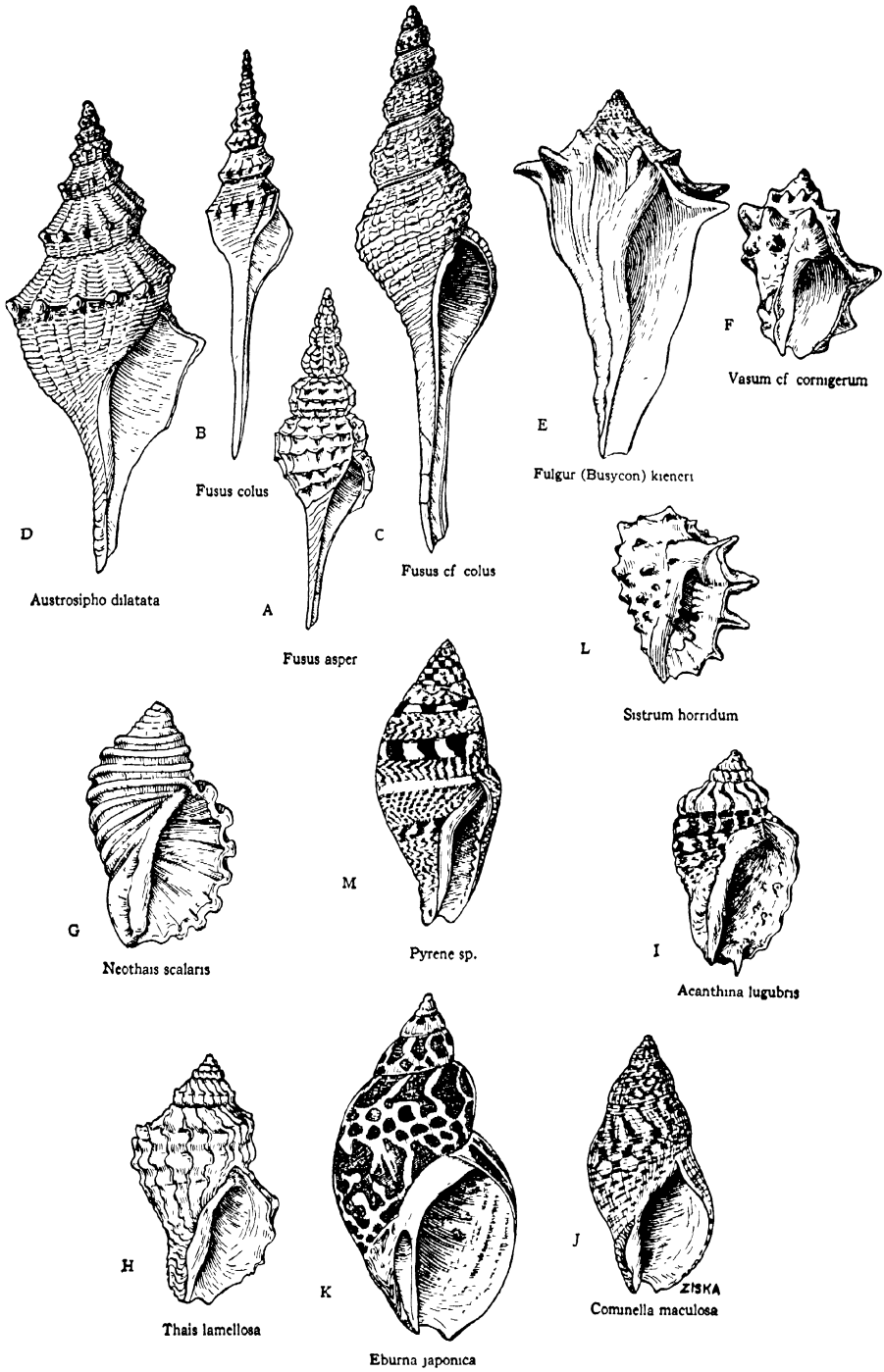
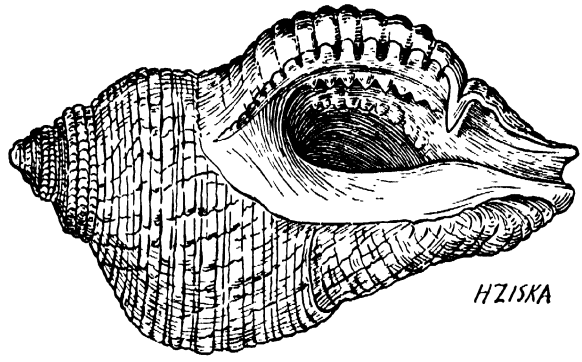
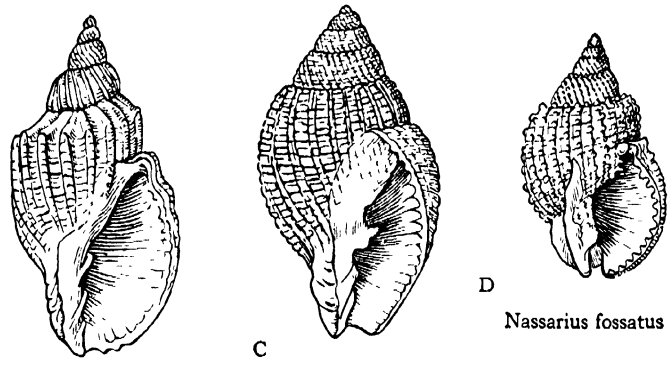


Fig. 2.25. Diverse examples of the Buccinacea, including fusids (A–F) with varying siphons, thaisids (G, H, I, L), cominellids (J, K) and pyrenids (columbellids) (M). Both the surface layers and the color patterns are extremely diversified and specialized in this group. A, B, after Grabau; others from author's collection.



A

Acanthina lapilloides



B

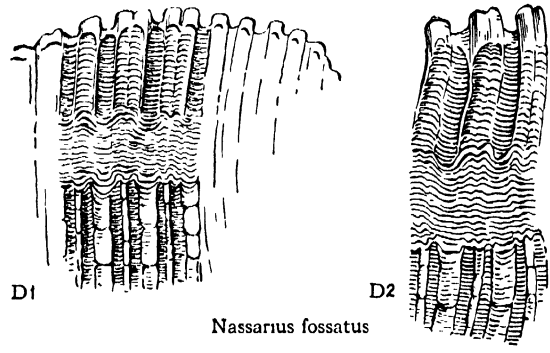
Cancellaria cf. spengleriana

C

Cancellaria reticulata

D

Nassarius fossatus

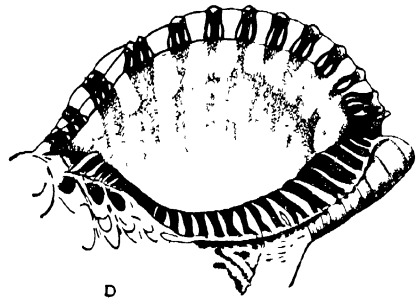


D1

D2

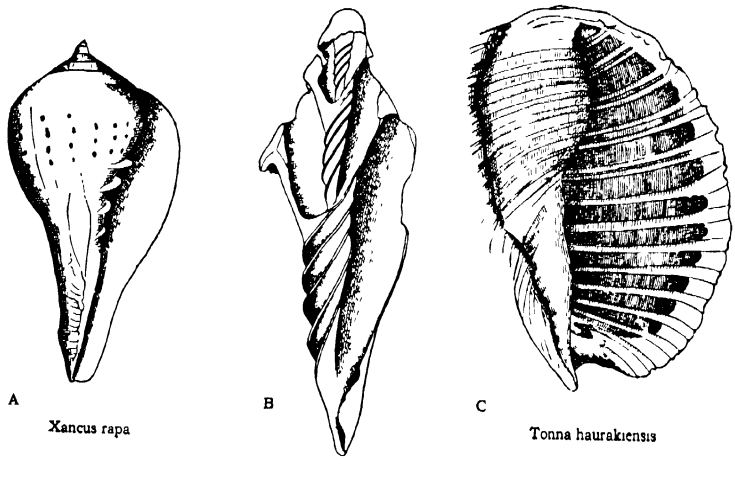
Nassarius fossatus

Fig. 2.26 Thorn shell (A), lattice shell (B, C) and dog whelk (D). The "thorn" of *Acanthina* (A) is an anisomere, evolved by emphasis of one of the many folds (polyisomeres) on the outer lip of the shell. The deepest layer (hypostracum) produces tooth- or bead-like projections on the inside of the outer lip. *Acanthina* belongs in the Buccinacea (cf. fig. 2.25I). The lattice shells (B, C) are so named from the crossing of axial and revolving ridges. They are possibly related to the turrids (fig. 2.35 A, B) and cones (figs. 2.36, 37) and may stand near the base of the Volutacea (cf. 2.28A). The dog whelk (D) represents another widely varying family of the Buccinacea with convergent resemblance to *Cancellaria* (B, C). Its numerous revolving ribs are composed of minute threads (D1, D2). Author's collection.



D

Cymatium (Triton) nobile



A

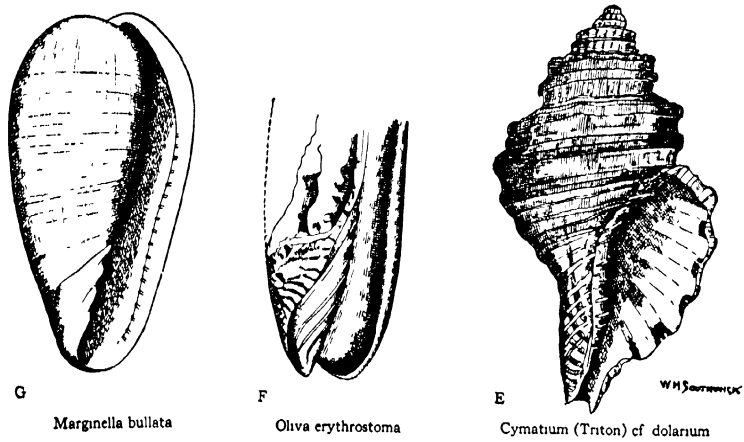
Xancus rapa

B

Alcithoe jaculoides

C

Tonna haurakiensis



G

Marginella bullata

F

Oliva erythrostoma

E

Cymatium (Triton) cf dolarium

Fig. 2.27. Typical polyisomeres. Occurrence of plaits on the columella and marginal folds around the aperture in tuns (C), tritons (D, E) and other families (B, F, G). The grooves between the plaits may serve as channels for tendons of the columella muscle. The genesis of new polyisomeres is illustrated by the curious ridges along the outer lip of the *Triton* (D), which are arranged in folds containing from one to three denticles. Author's collection

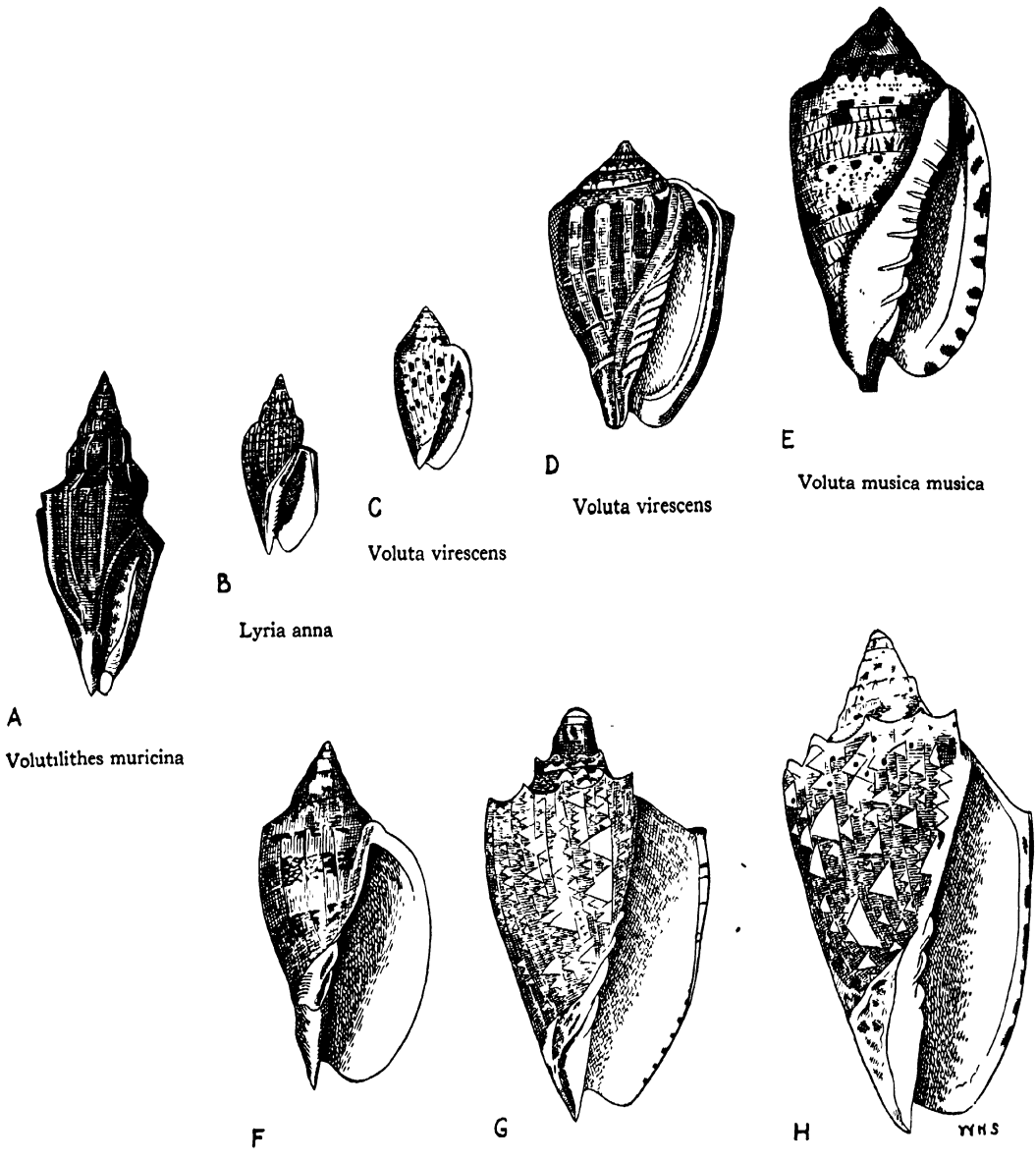


Fig. 2.28. Divergence of the typical volutes into two main lines: one (A–E) culminating in *Voluta musica*, with a pattern of revolving lines and spots; the other (F, H) ending in *Aulica pulchra pulchra*, with panels and decolorate V's combined with ocellus-like spots. A, B, F from Maxwell Smith, 1942; others from author's collection.

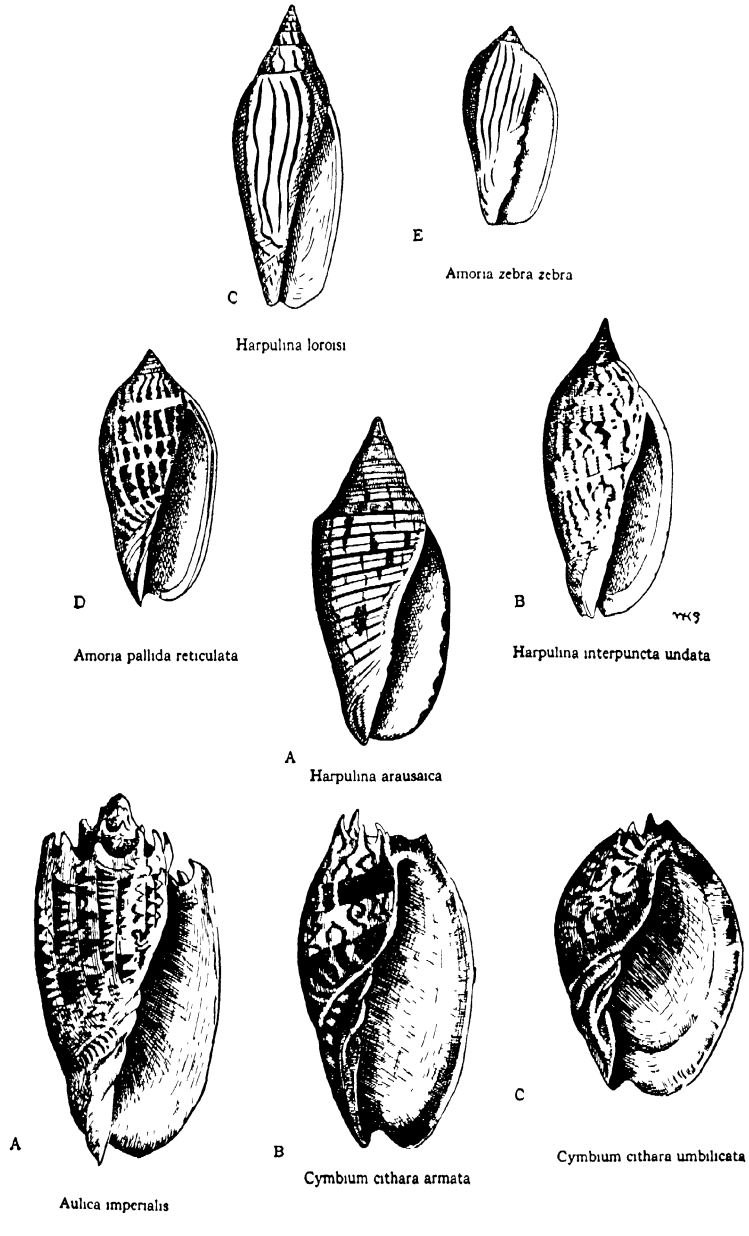


Fig. 2.29 (top). Divergence in the volute *Harpulina* from irregular panels and zigzags (B) to revolving lines (A) and axial stripes (C). This divergence is paralleled in the genus *Amoria* (D, E). A–C, after Maxwell Smith, 1942; D, author's collection.

Fig. 2 30. From some more central type of volute (A) the bailer shells (B, C) have been derived by great widening of the outer lip and shortening of the spire. The color patterns, more regular and understandable in (A), become very irregular in some of the bailers (C). All from Maxwell Smith (1942).

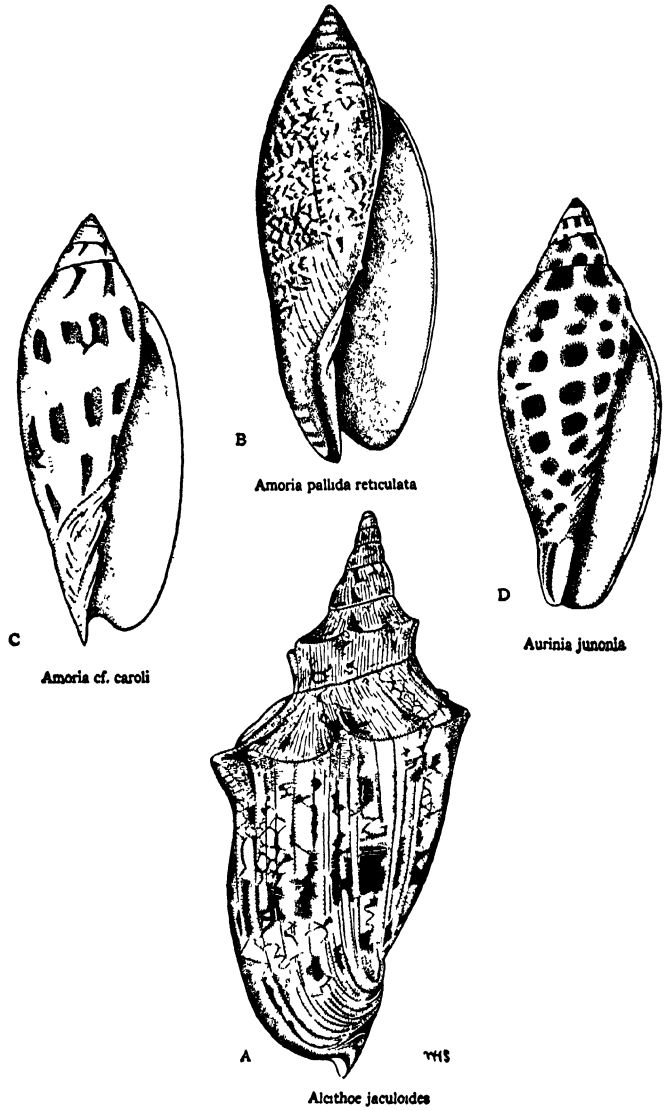


Fig. 2.31. Contrast between a fairly primitive volute (A) with castellated spire and three very specialized forms (B–D) with smooth fusiform contours. Traces of revolving color bands, breaking up into irregular patches (A) and confused V's (B). In C and D the pigment cells have been reorganized and produce rounded blotches (C) or large spots (D). A, author's collection; B, from Maxwell Smith (1942, pl. 5, fig. 42), after Reeve; C, author's collection (Heron Island, Queensland); D, author's collection (cf. Maxwell Smith, 1942, pl. 6, fig. 53).

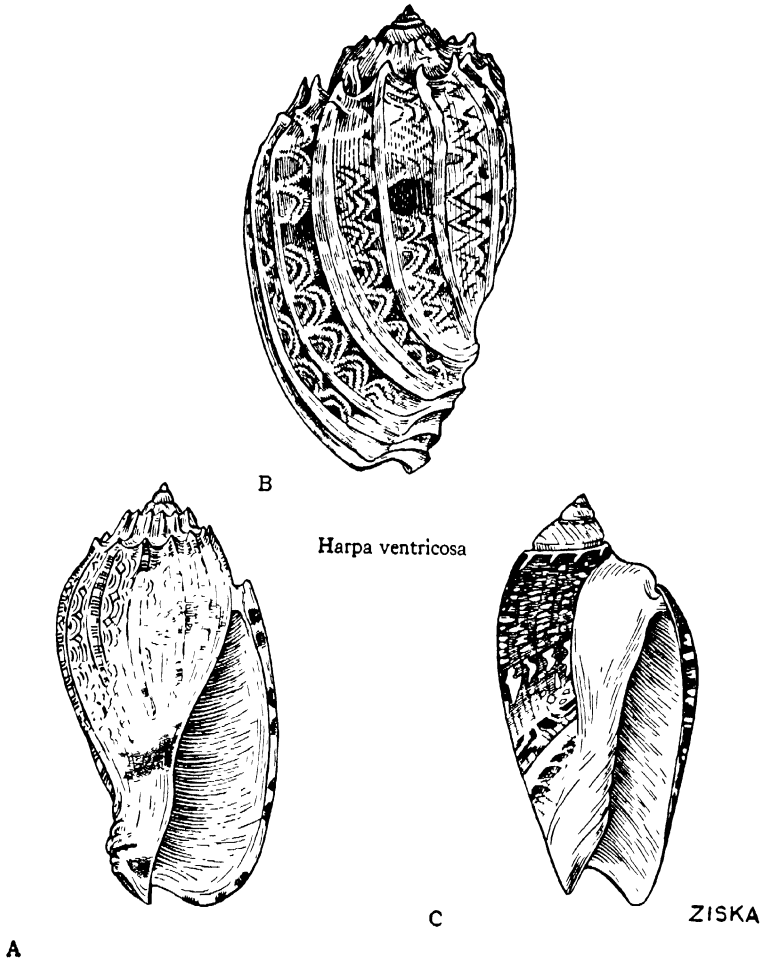


Fig. 2.32. The harps develop a pattern of strong axial ridges, oscillating lines and "partridge feathers." They may be related to the lattice-shells (fig. 2.26 B, C) and are classed with them and with the mitres and olives under the Volutacea. A, C, author's collection; B, partly from an aquarelle by Paul A. Robert.

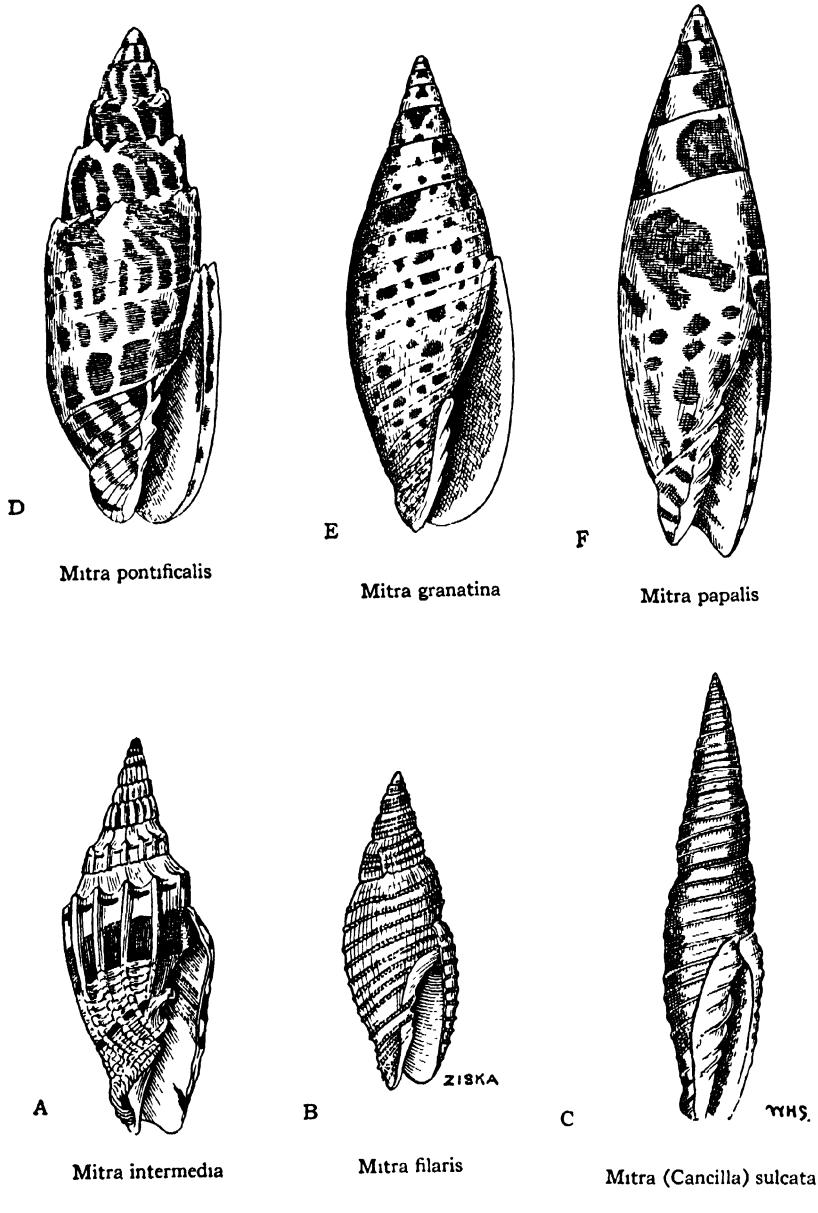


Fig. 2.33. The pontifical mitre and its relatives. Probably the least specilized of the mitres are such castellated forms as *Mitra intermedia* (A), from which may have been derived, on one hand, the imposing *Mitra pontificalis* (D), on the other, the smooth porcellanous surface of *Mitra papalis* (F). The revolving cords are retained in *filaris* (B) and *sulcata* (C). The group may have been derived from the stem of the turrids and it is included in the Volutacea (cf. fig. 2 38). Author's collection.

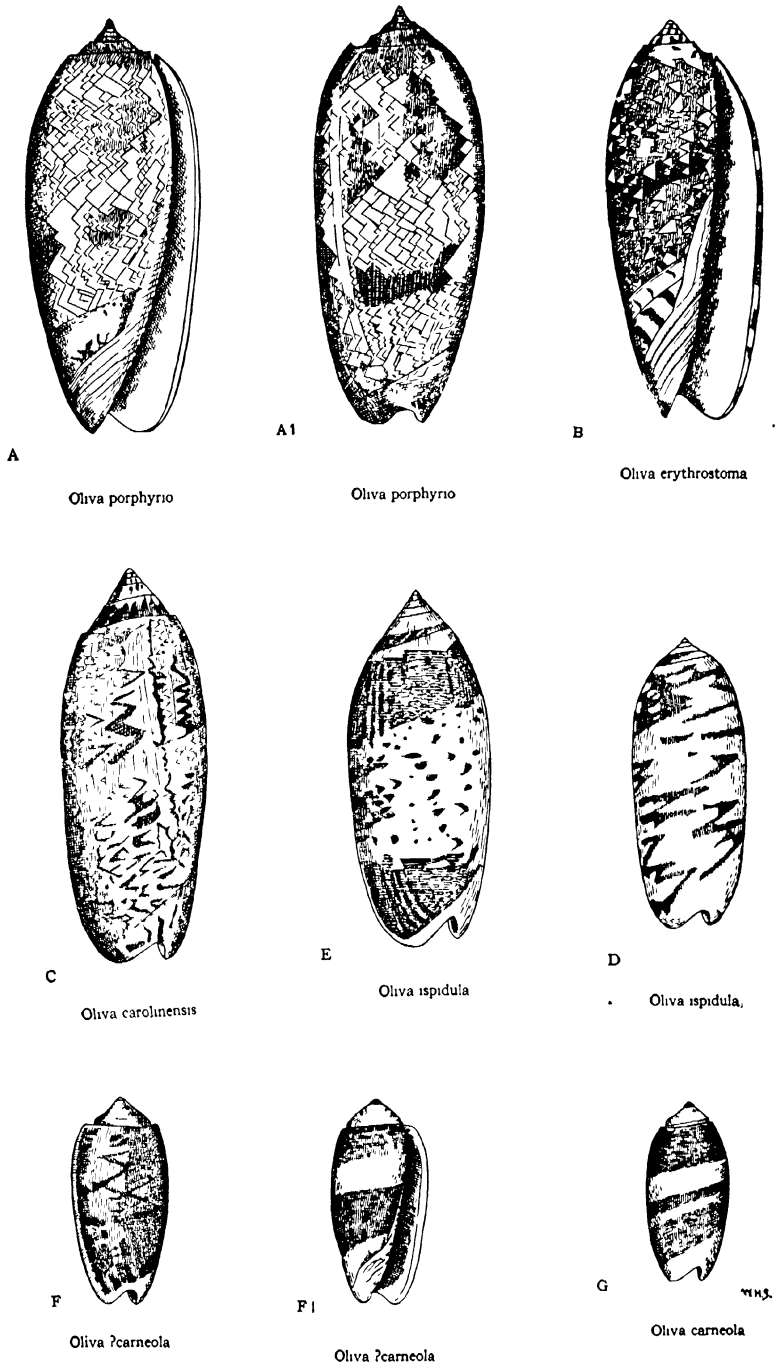


Fig. 2.34. The olives parallel the cowries (fig. 2.20) in developing an almost completely involuted shell with a glistening surface but they do not reduce the spire so much. They are related to the marginellids (fig. 2.27G), mitres (fig. 2.33) and volutes (fig. 2.30). Their color patterns are based on a profusion of small V-shaped polyisomeres, which sometimes combine into color bands but show extremely wide variability in certain species. Author's collection.

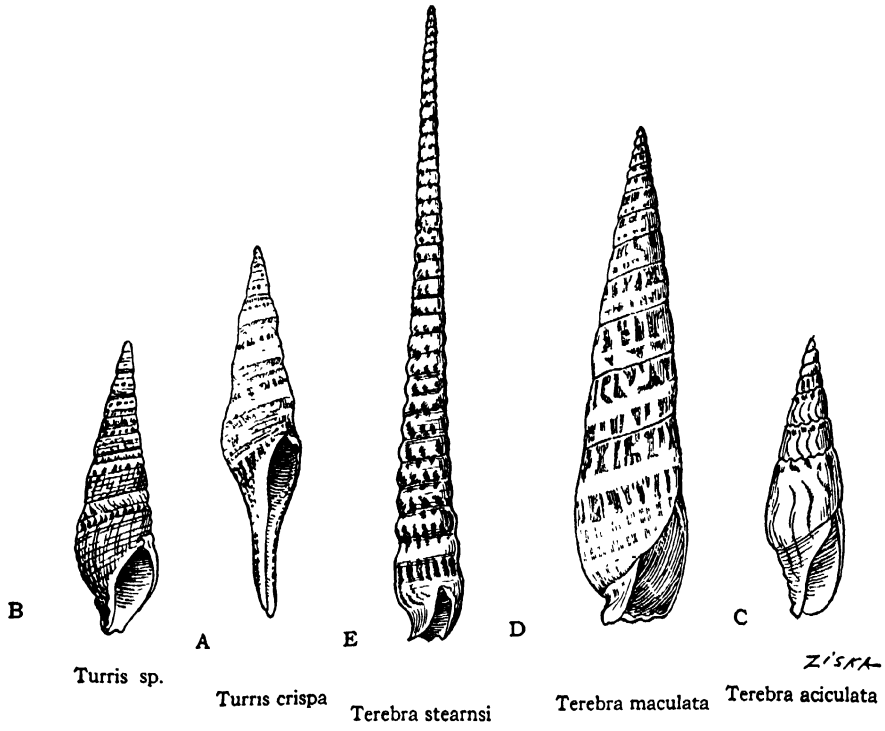


Fig. 2.35. The turrids (A, B) are often called pleurotomids on account of the notch at the upper (posterior) end of the aperture at the side of the body wall. Such a notch is developed also in some of the thaisids (*Iopas*) and nassariids (fig. 2.26D). The typical turrids have a high spire and primitively a long siphonal canal (A) like that of the early fusids. Among the many hundreds of extinct and recent species referred to this family some simulate the shells of different families. The terebrids (C–E) have a short siphonal canal and a spire of moderate to extreme height. Thus they parallel or converge toward the turrids, cerithiids, turritellids, melaniids and others. The very small apical angle of *Terebra stearnsi* (E) indicates a correspondingly low acceleration of growth. E, from Hirase; C, from Maxwell Smith (1940); A, B, D, author's collection.

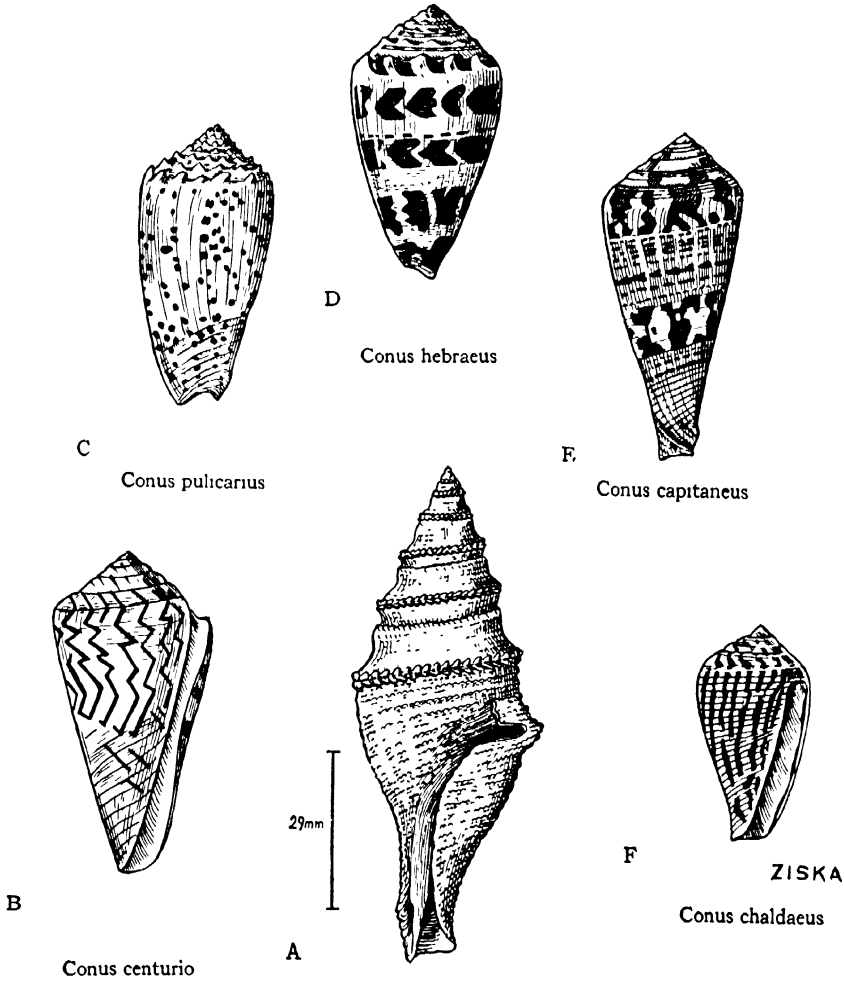


Fig. 2.36. Comparison of various specialized cones (B–F) with a primitive turrid (A) from the Upper Tertiary (Balcombian) of Australia. The abconical form of the cone is readily derived from the biconical form of such a primitive turrid by the shortening of the spire. B, F, from Maxwell Smith (1940); A, C, D, E, author's collection.

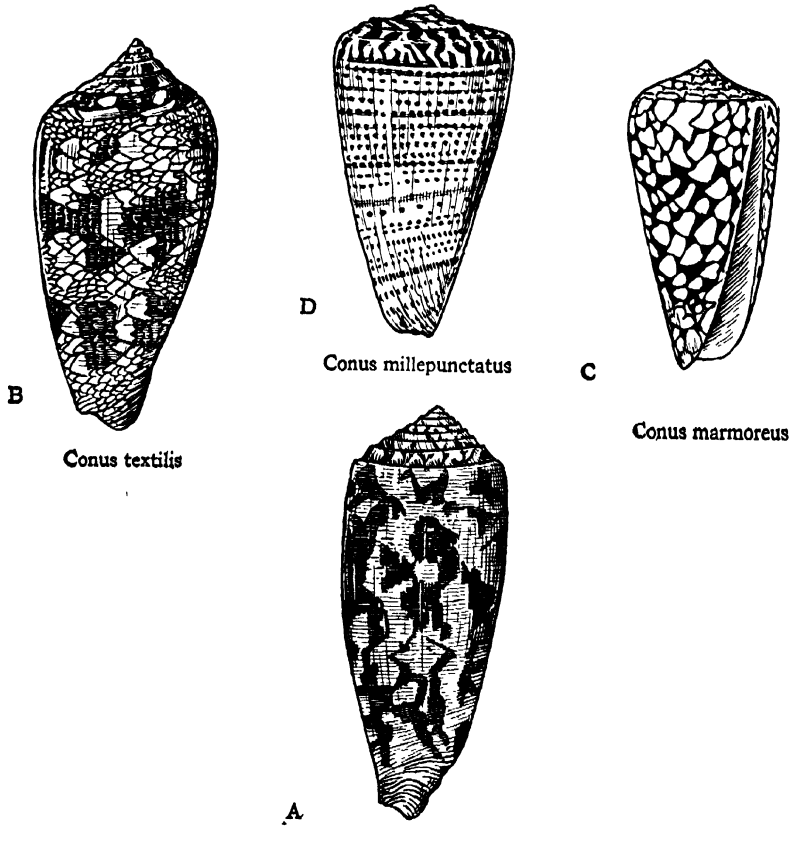
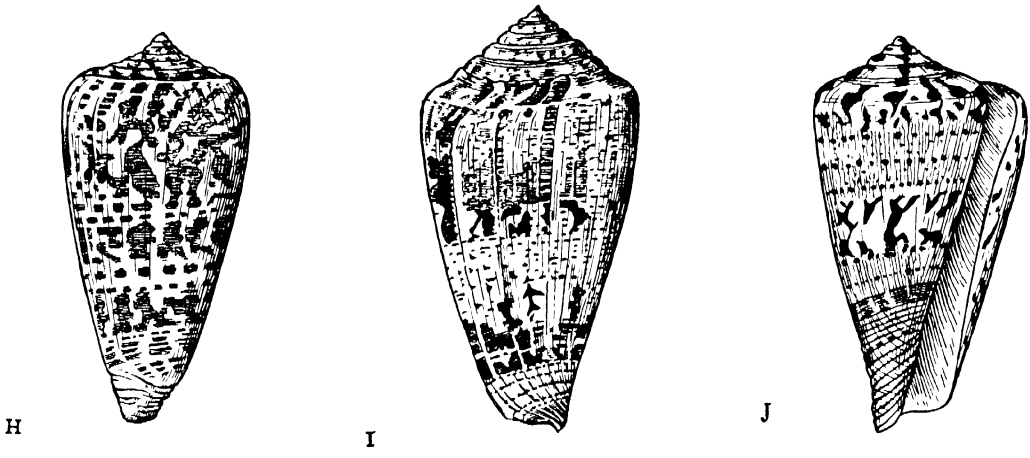


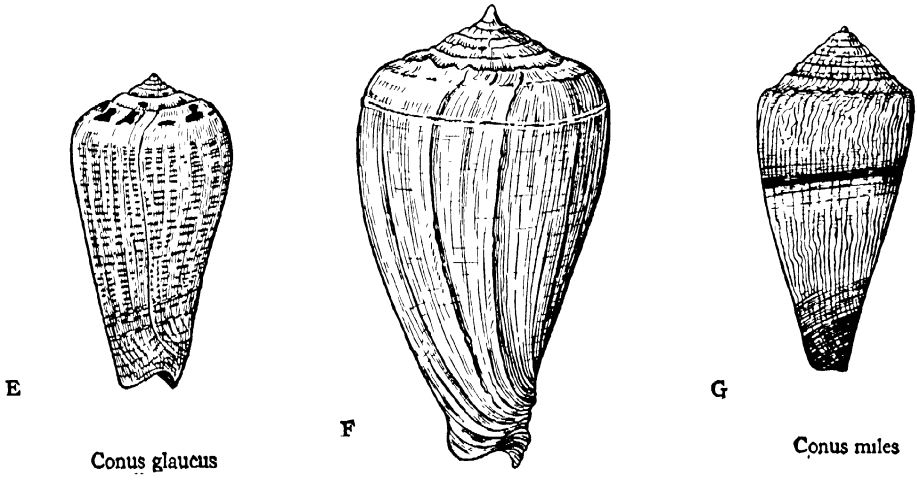
Fig. 2.37a, b. A few samples from the wide range of color patterns in the cones. In the primitive cones, probably derived from the stem of the turrids, the revolving pigment spots were perhaps clustered in two or three color bands, between which were revolving dashes and spots. Breaking up and segregation of the color bands produced interrupted black spots (fig. 2.36D) and confused monsters (figs. 2.37b H; 2.37a A). Temporary cessation of forward growth of the mantle produced panels (fig. 3.37a I) and tended to realign the pigment in vertical (axial) series (fig. 2.37b H, I, J) and even to produce zebra stripes (fig. 2.36F). Contesting revolving and axial factors produced zigzags (fig. 2.36B). Another reorganization of pigment factors produced axial oscillating lines (fig. 2.37b G), confused scales (2.37a B) and obliquely arranged geodetic reticulations (C). Author's collection.



Conus proteus

Conus purpurascens

Conus capitaneus



Conus glaucus

Conus figulinus

Conus miles

Fig. 2.37b

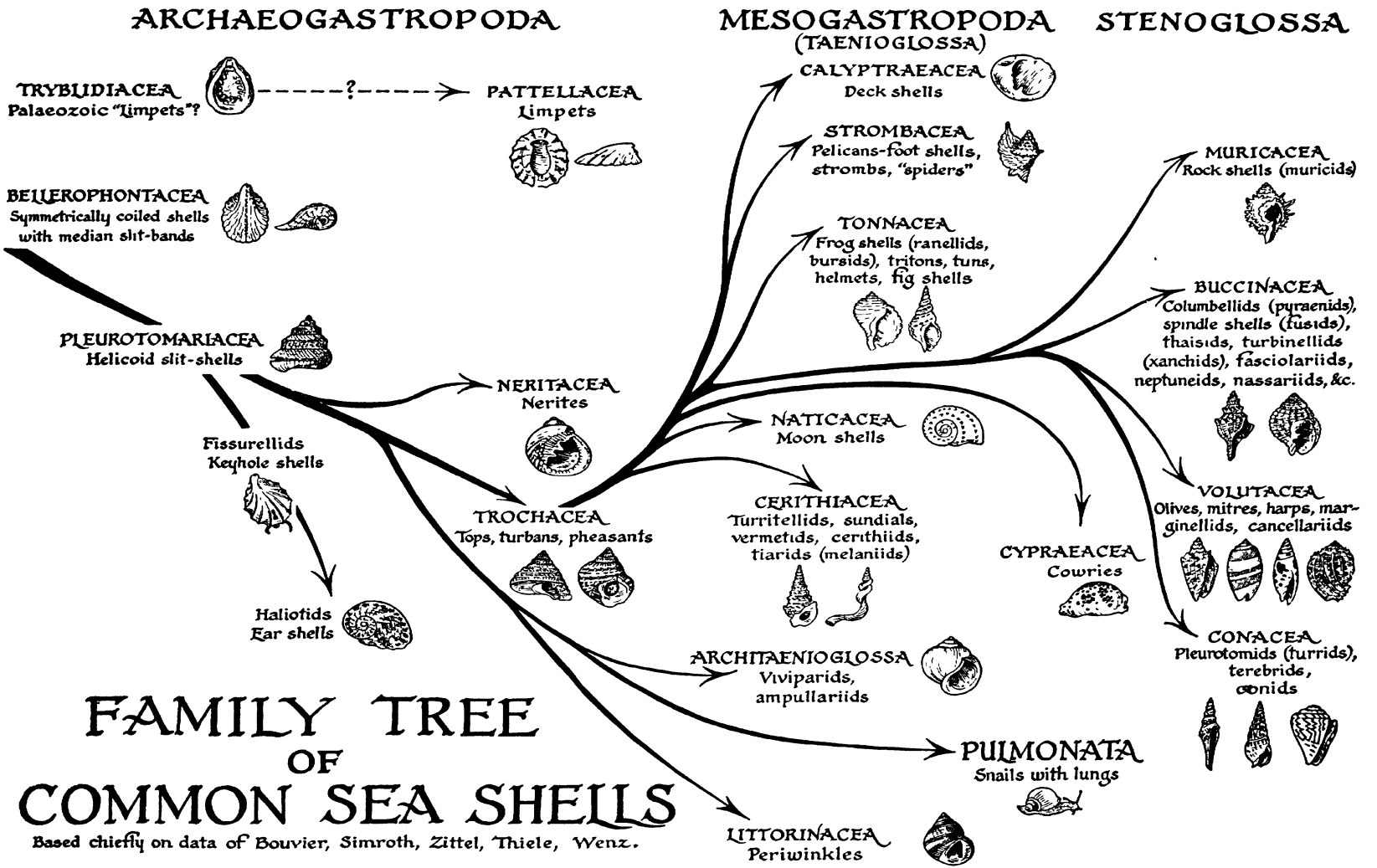

ARCHAEOGASTROPODA
MESOGASTROPODA (TAENIOGLOSSA)
STENOGLOSSA
TRYBLIDIACEA
Palaeozoic "limpets"?
PATTELLACEA
Limpets
BELLEROPHONTACEA
Symmetrically coiled shells with median slit-bands
PLEUROTOMARIACEA
Helicoid slit-shells
Fissurellids
Keyhole shells
Haliotids
Ear shells
NERITACEA
Nerites
TROCHACEA
Tops, turbans, pheasants
CALYPTRAEACEA
Deck shells
STROMBACEA
Pelicans-foot shells, strombs, "spiders"
TONNACEA
Frog shells (ranellids, bursids), tritons, tuns, helmets, fig shells
NATICACEA
Moon shells
CERITHIACEA
Turritellids, sundials, vermetids, cerithiids, tiarids (melaniids)
ARCHITAENIOGLOSSA
Viviparids, ampullariids
LITTORINACEA
Periwinkles
PULMONATA
Snails with lungs
CYPRAEACEA
Cowries
MURICACEA
Rock shells (muricids)
BUCCINACEA
Columbellids (pyraenids), spindle shells (fusids), thaisids, turbinellids (xanchids), fasciolariids, neptuneids, nassariids, &c.
VOLUTACEA
Olives, mitres, harps, marginellids, cancellariids
CONACEA
Pleurotomids (turrids), terebrids, conids
FAMILY TREE
OF
COMMON SEA SHELLS
Based chiefly on data of Bouvier, Simroth, Zittel, Thiele, Wenz.

Fig. 2.38

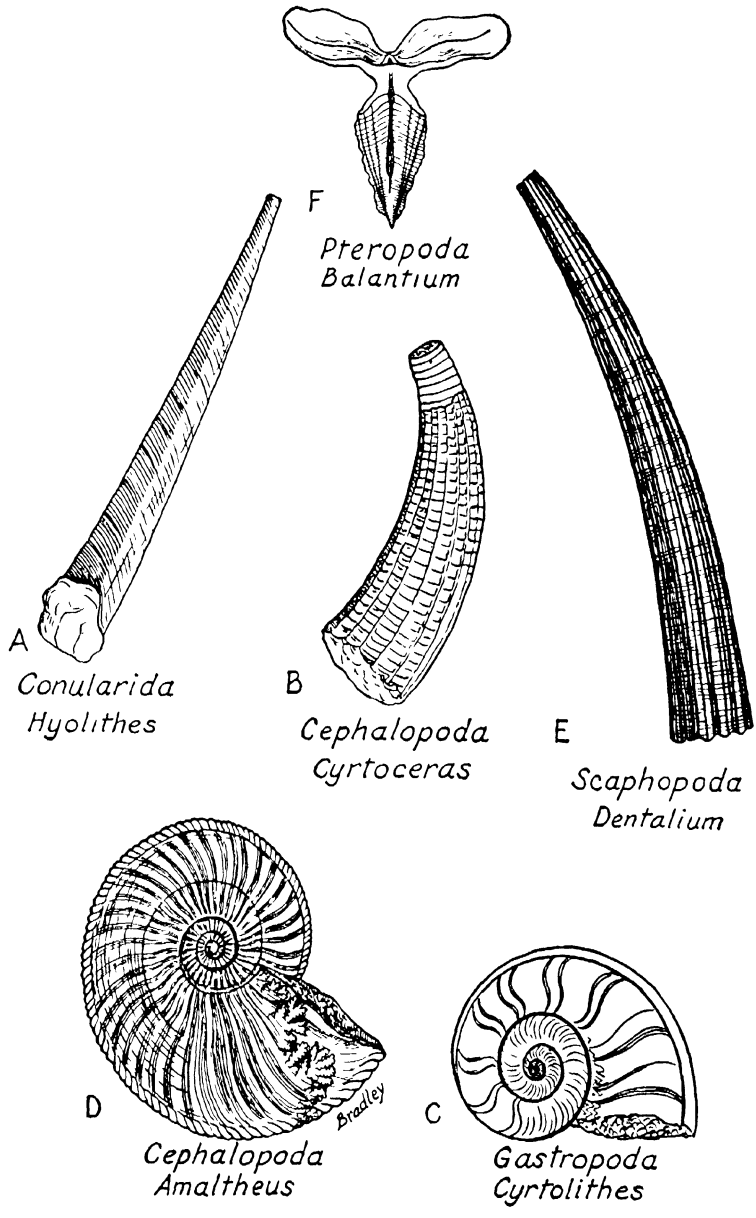


Fig. 2.39. Convergence in horn-like shell form of "conularid" (A), cephalopod (B) and scaphopod (E), and in spiral shell form of gastropod (C) and nautiloid cephalopod (D). A may belong with the pteropod (F). Data from Zittel.

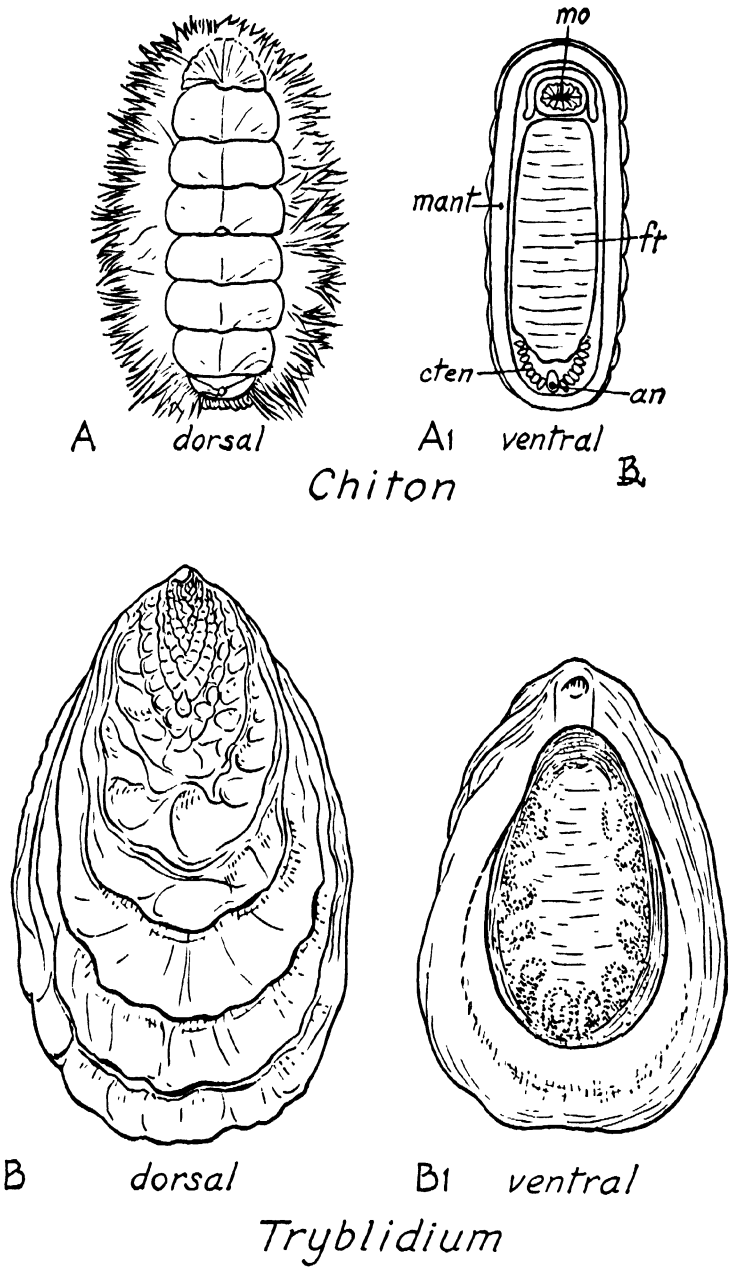


Fig. 2.40. Comparison of oval sucking-disc shell forms (A, A1), the articulated shell of a chiton, and (B, B1) the non-articulated shell of an early limpe Data from Zittel.

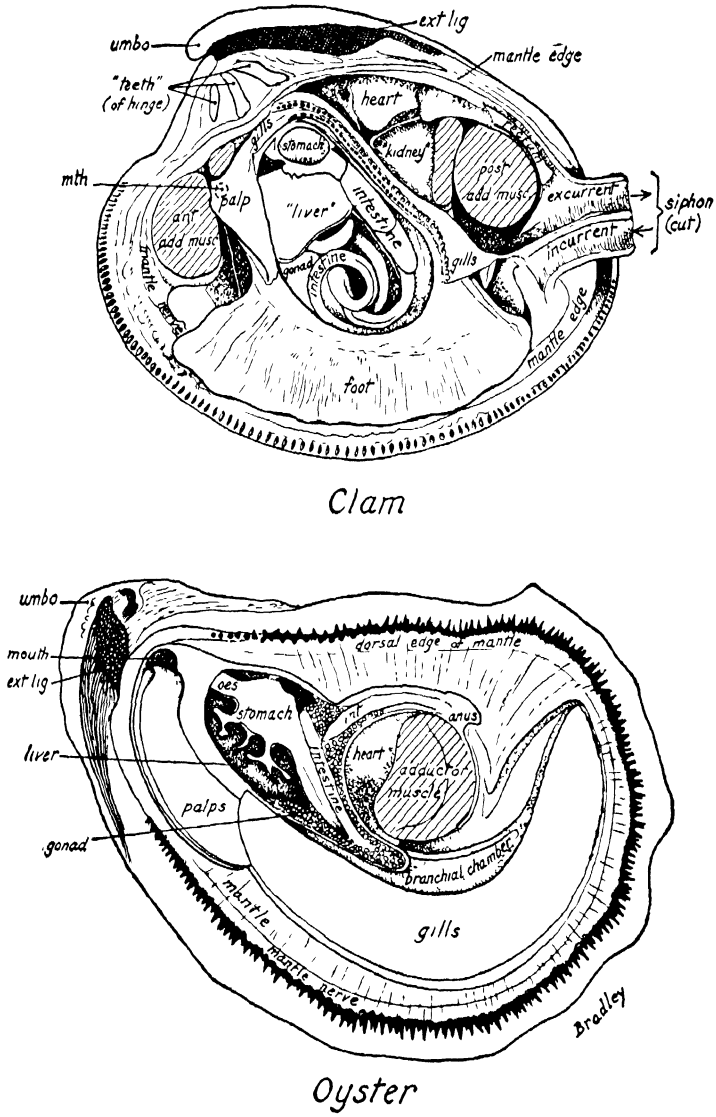
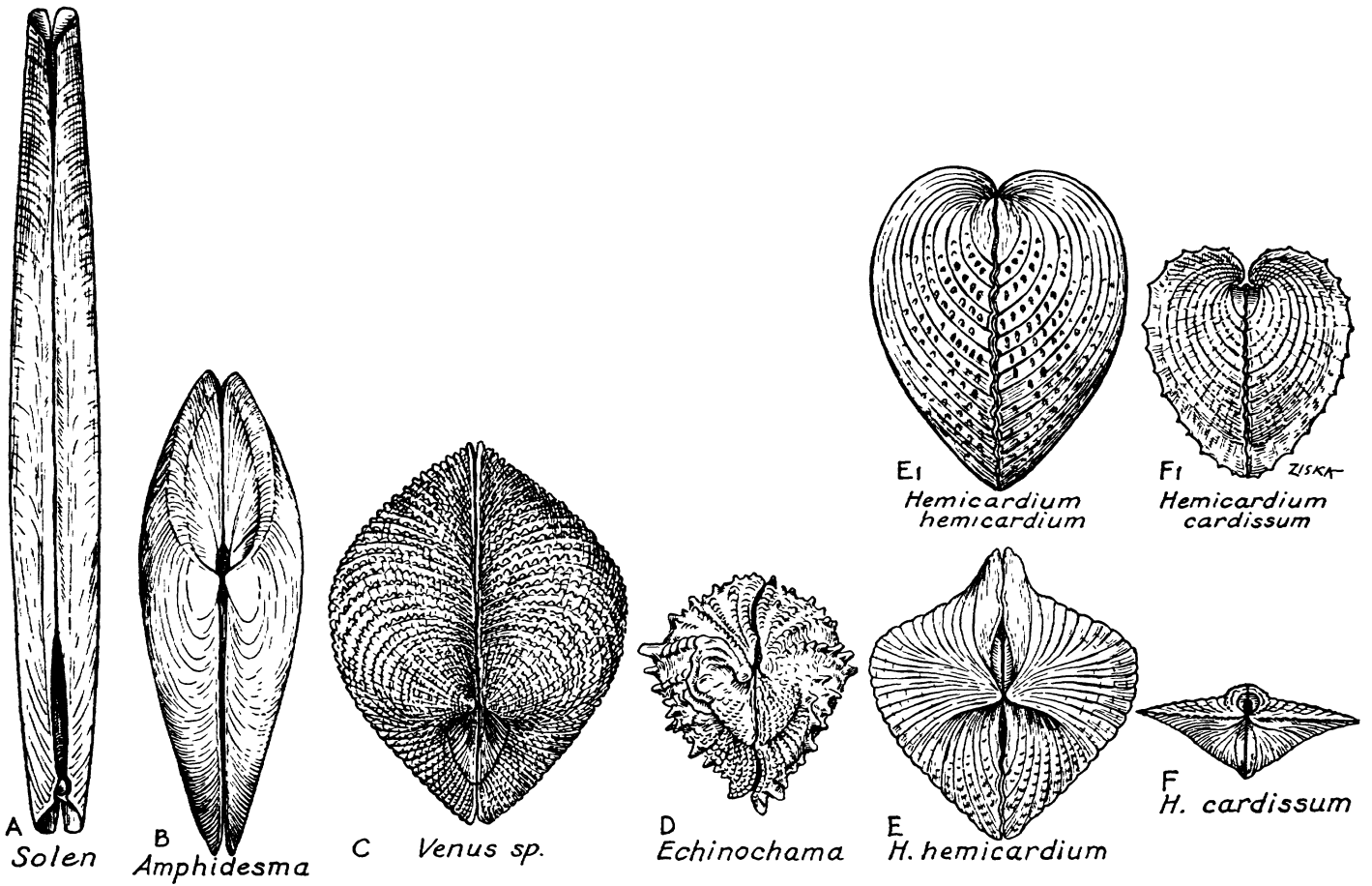


Fig. 2 41. Anatomy of clam and oyster. From enlarged models by Dr. B. E. Dahlgren.



Figs. 2.42, 43. Breadth *versus* length in bivalves. In the relatively primitive clam *Amphidesma* (B) the breadth is about one-third of the length. In the razor clam (A) is has fallen to between one-seventh and one-eighth of the length; in the particular *Venus* clam figured (C) the breadth is about two-thirds of the length, while in *Echinochama* (D) it rises to four-fifths. Extreme breadth is attained in the specialized cockle-shells (E, F) in which the breadth may become more than twice the length. Author's collection.

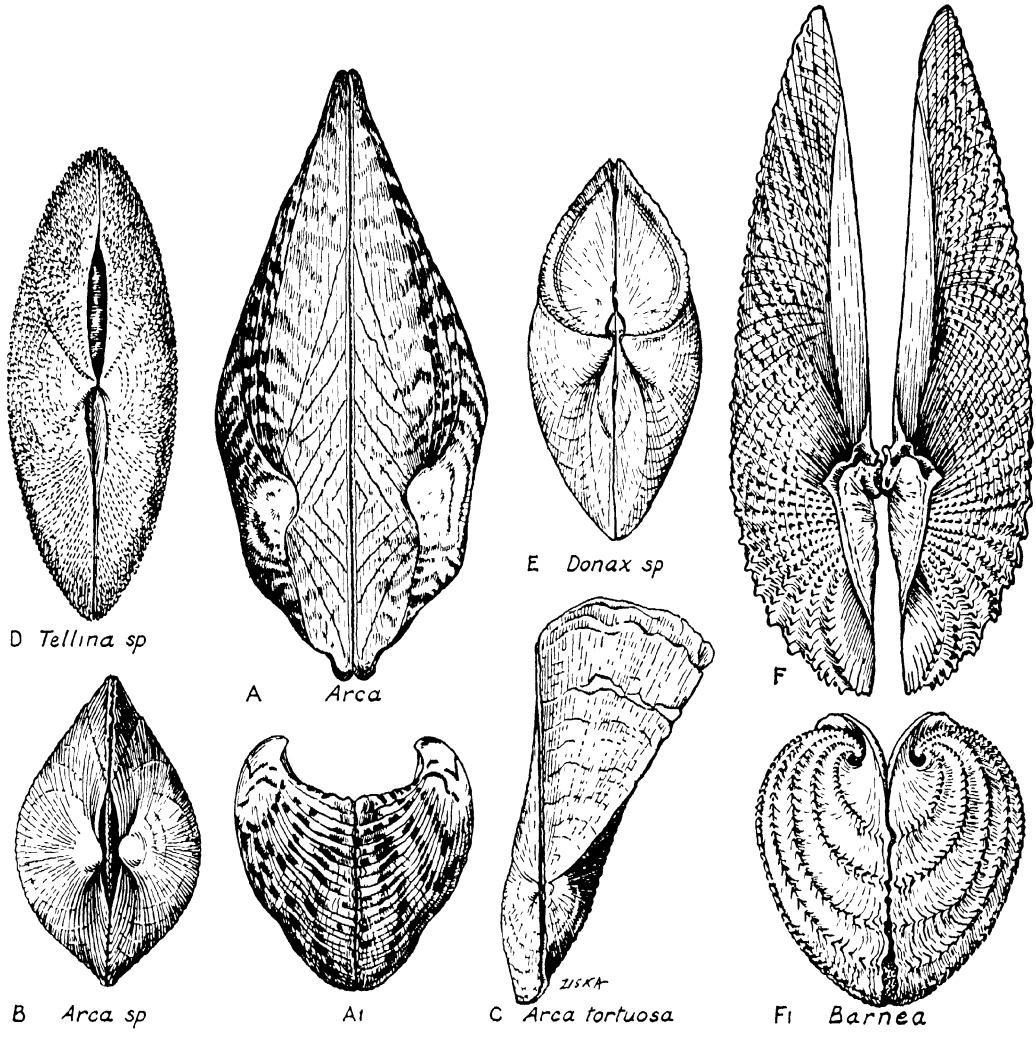


Fig. 2.44. Symmetry (A) and asymmetry (C) in bivalve shells. The valves grow spirally (A1) and radiately away from the tips of the beaks or umbones, above the straight hinge line. Author's collection.

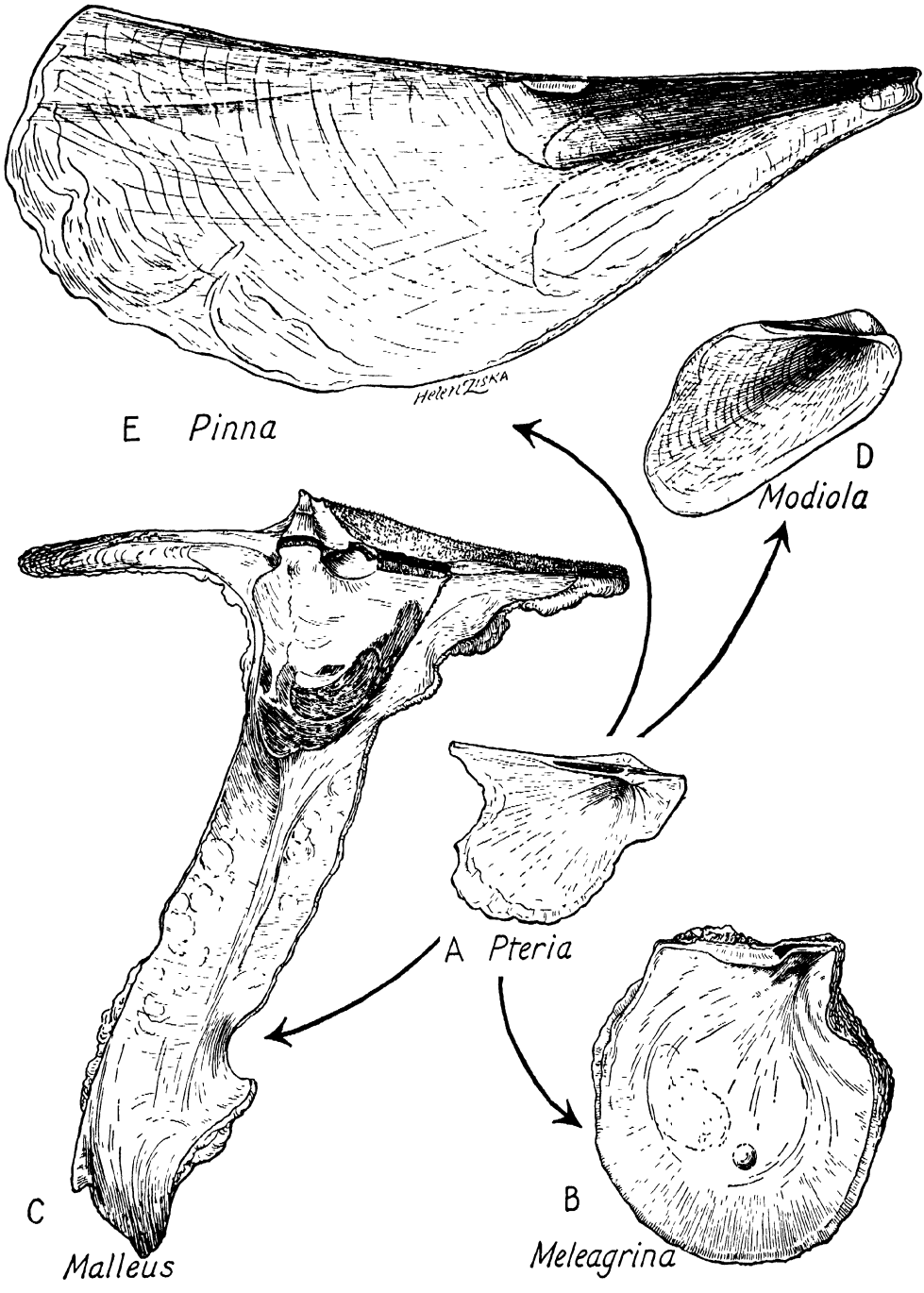


Fig. 2.45. Height *versus* length in bivalves. In the quite primitive *Pteria* (A) the umbo or growth center of each valve remains near the small anterior end, while the shell grows rapidly downward and backward; but the maximum height is less than the length of the hinge line. In the pearl oyster (B) the shell has expanded, especially beneath the front end, so that the height is much greater than the length of the hinge line. In the hammer shell (C) the hinge line has lengthened but the height has become about five times as great as the anteroposterior length of the middle part. The mussels and their allies (D) retain a fairly primitive rounded triangular outline, but in the ear shells (E) the length has become three times as great as the height. Author's collection.

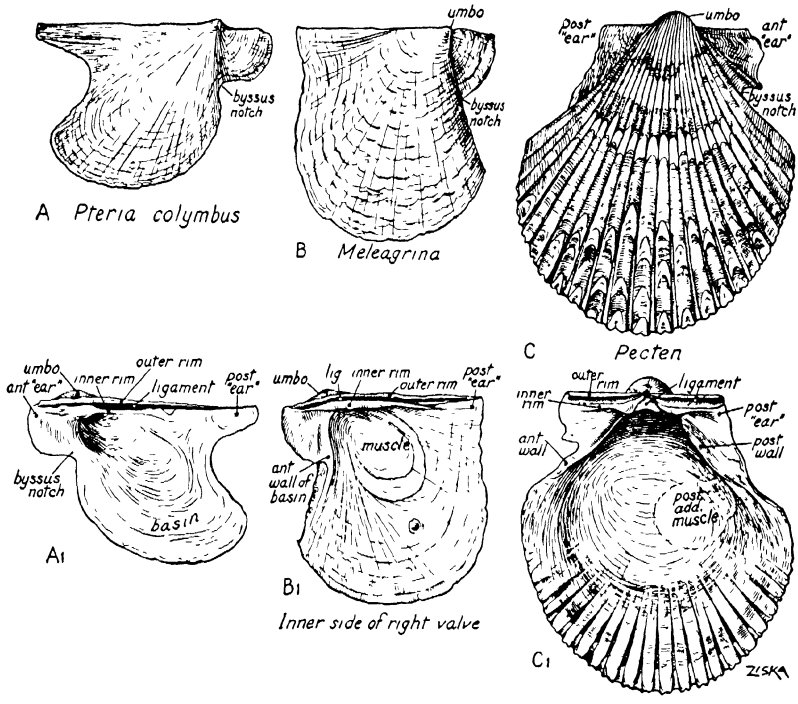


Fig. 2.46a. Aviculoid hingers (A, B) with long straight hinge line and long external ligament Various forms of this hinge type are found in the order Anisomyaria, in which the posterior adductor muscle is enlarged and the anterior reduced or wanting. In the scallops (C1) the middle of the hinge groove is interrupted by a triangular depression for the internal ligament. It is flanked by swellings of the inner rim which seem to represent the two large "teeth" or condyles in *Spondylus*. Author's collection.

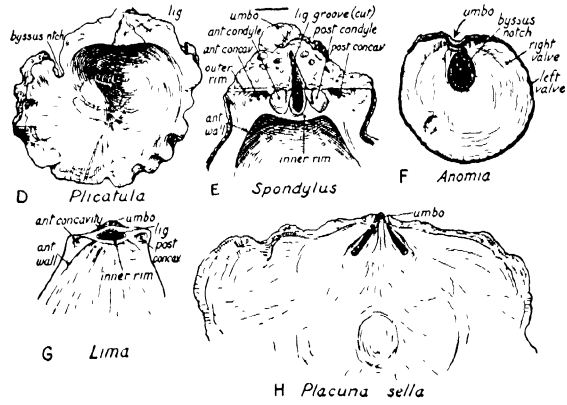


Fig. 2.46b. Specialized derivatives of the aviculoid type (D–H). Interior views of right valves. In *Lima* (G) the groove for the ligament has shortened into a triangular pit, homologous with that of *Pecten* (C1). The paired "condyles" seen in *Spondylus* (E) are wanting on the right valve of *Lima*, but the anterior and posterior concavities receive the projecting "teeth" or swellings of the left valve. *Plicatula* (D) retains the primitive byssus notch on the anterior margin, its triangular pit for the ligament recalls that of *Pecten*. In *Anomia* (F) the huge byssus notch has been displaced to the middle of the border of the right valve, which is tightly appressed to the substratum. In a young *Placuna* (H) both valves are excessively thin and translucent and the shell as a whole is exceedingly thin transversely Inverted V-ridges and grooves form the hinge. Author's collection.

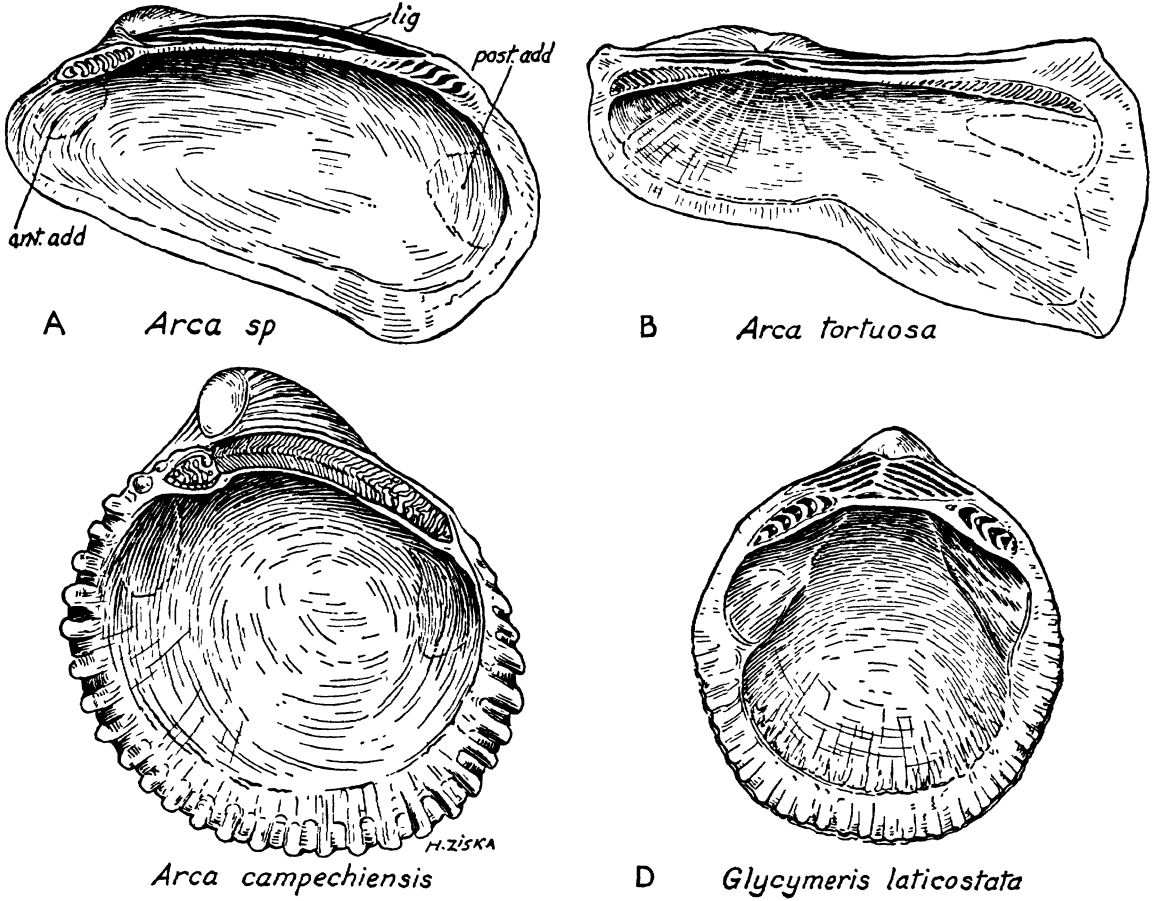


Fig. 2.47. Hinge line and "teeth" in ark shells. In these primitive dimyarians (with well developed anterior and posterior adductor muscles) the anterior and posterior parts of the hinge line bear a series of numerous small "teeth" or projections which fit into corresponding depressions in the opposite valve. The word *taxodont* is applied to this type. The "arks" range from Silurian to Recent times; in the still older *Ctenodonta* (family Nuculidae) of the Lower Silurian the arched row of teeth is not interrupted beneath the umbo. Author's collection.

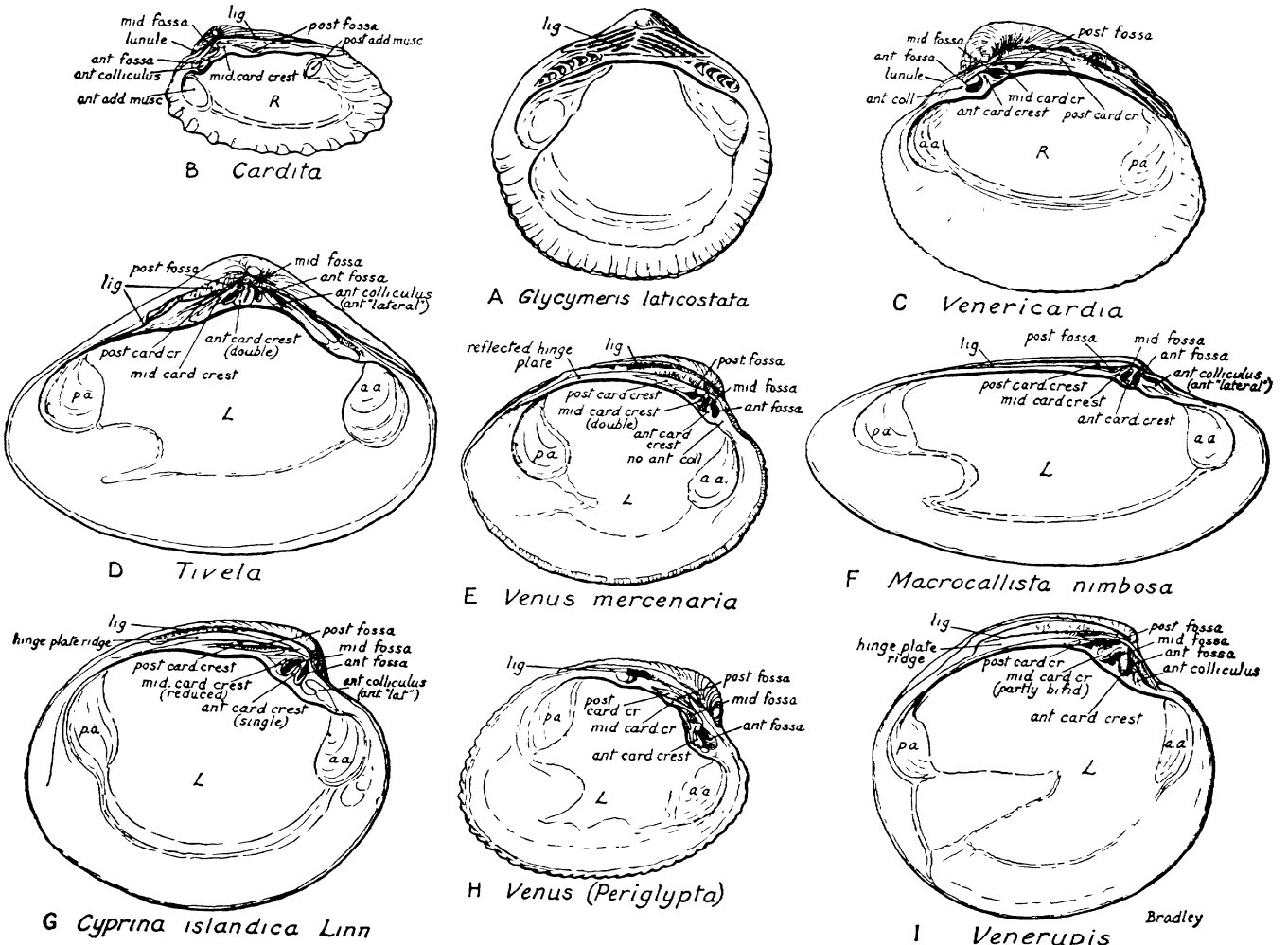


Fig. 2.48. Basic unity and adaptive diversity in taxodont (A) and heterodont (B–I) hinge forms, mainly of venerid clams. Author's collection

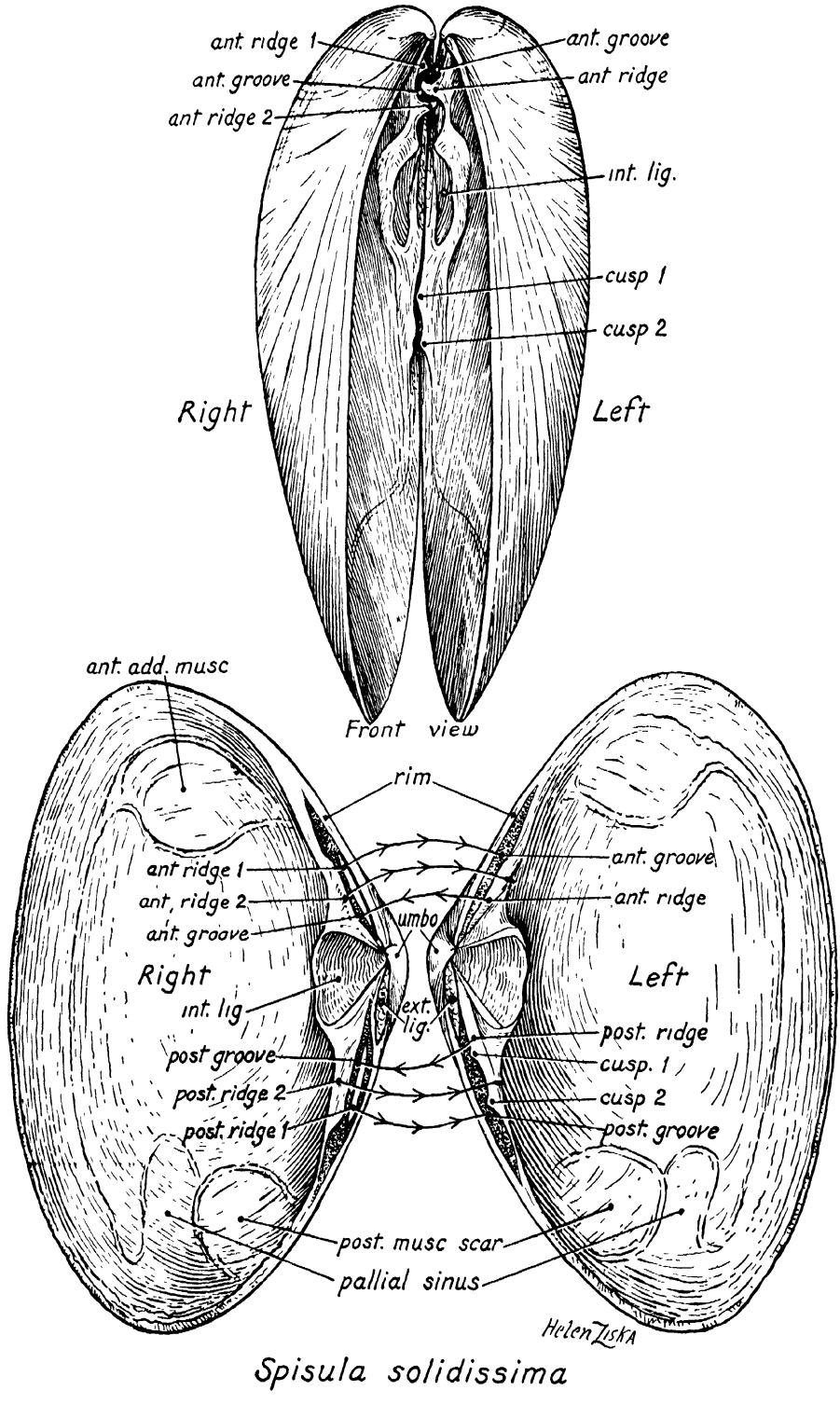


Fig. 2.49. Occlusal relations of the opposite valves in a mactrid ("beach clam"). The mutual fitting of the parts is indicated by the arrows. Author's collection.

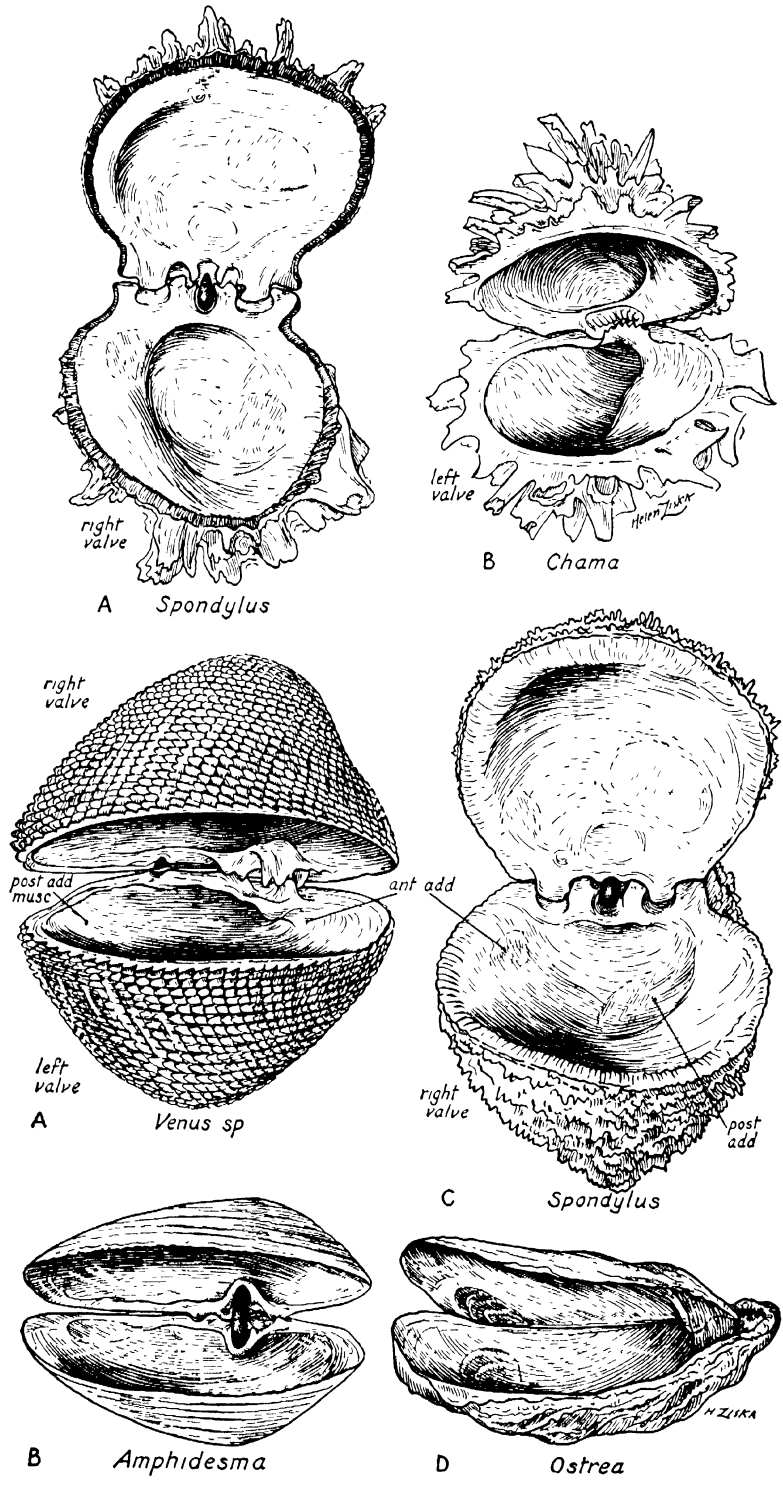


Fig. 2.50 (top). Spinous processes evolved convergently in two shells of widely different families. Author's collection.

Fig. 2.51. Teleodont (A, B) and isodont (C) types, and a "toothless" derivative (D) of the prionodesmodont type. The internal ligament or resilium (B, C) acts as a spring to open the valves when the adductor muscles are relaxed. Author's collection.

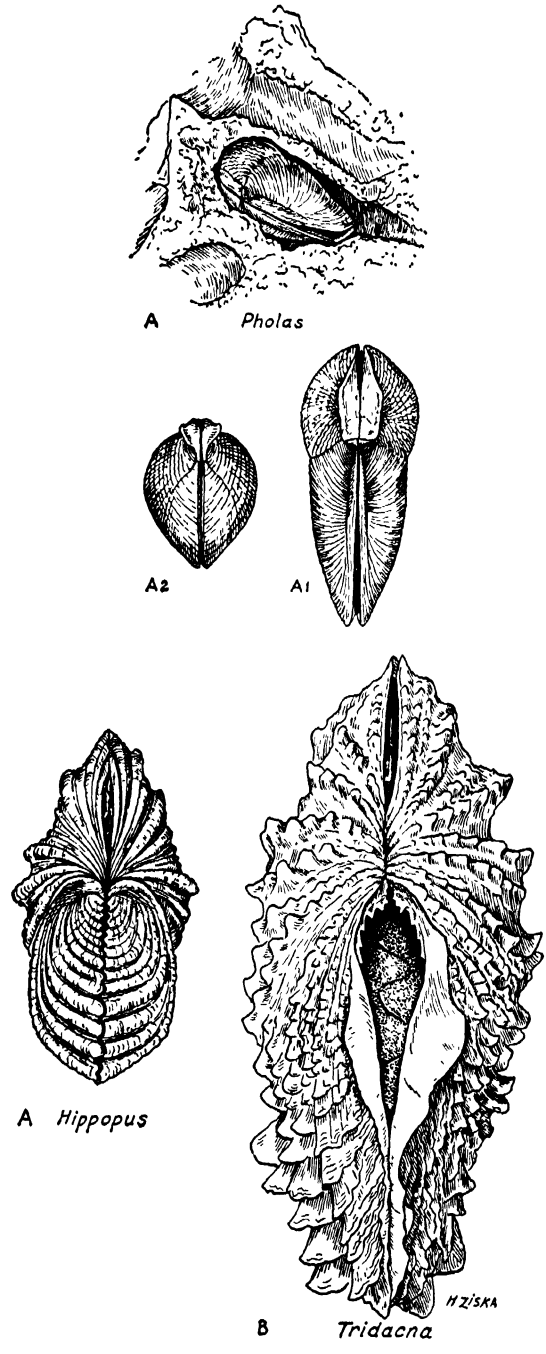


Fig. 2.52 (bottom). Specialized derivatives of the cockle family (Cardiidae). Author's collection.

Fig. 2.53 (top). Rock-boring Piddock (*Pholas*). A, as found in partly consolidated sand, but with burrows opened; A1, top view; A2, front end. Together with the angel-wing (*Barnea*, fig. 2.45) the Pholadidae represent a specialized branch of the order Desmodonta of the Anisomyaria (Zittel). In these the hinge line is short and usually asthenodont, or toothless. The order ranges from the Silurian to the Recent. Author's collection.

CHAPTER III

EXTERNALLY ARTICULATED ANIMALS (ARTHROPODS)

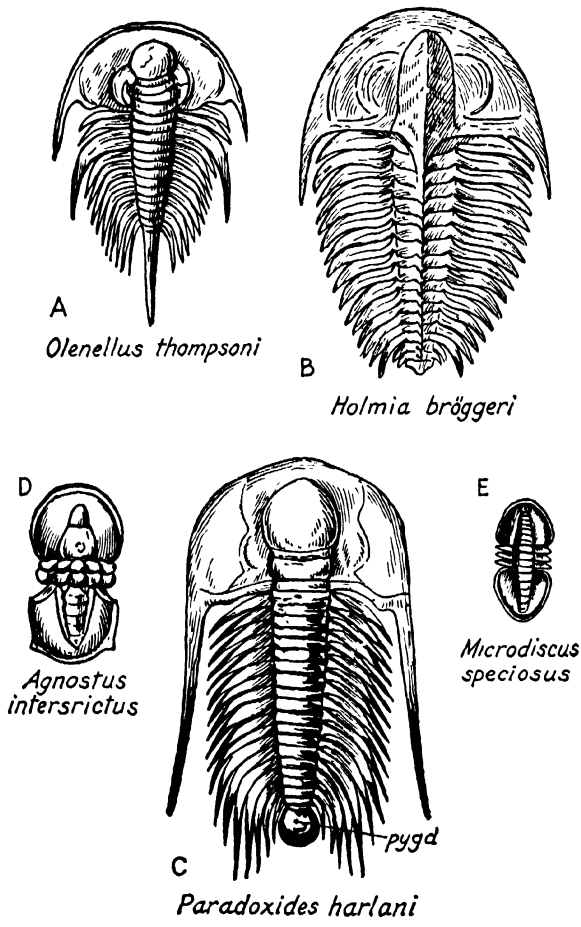


Fig. 3.1. Cambrian Trilobites. From Grabau, after various authors.

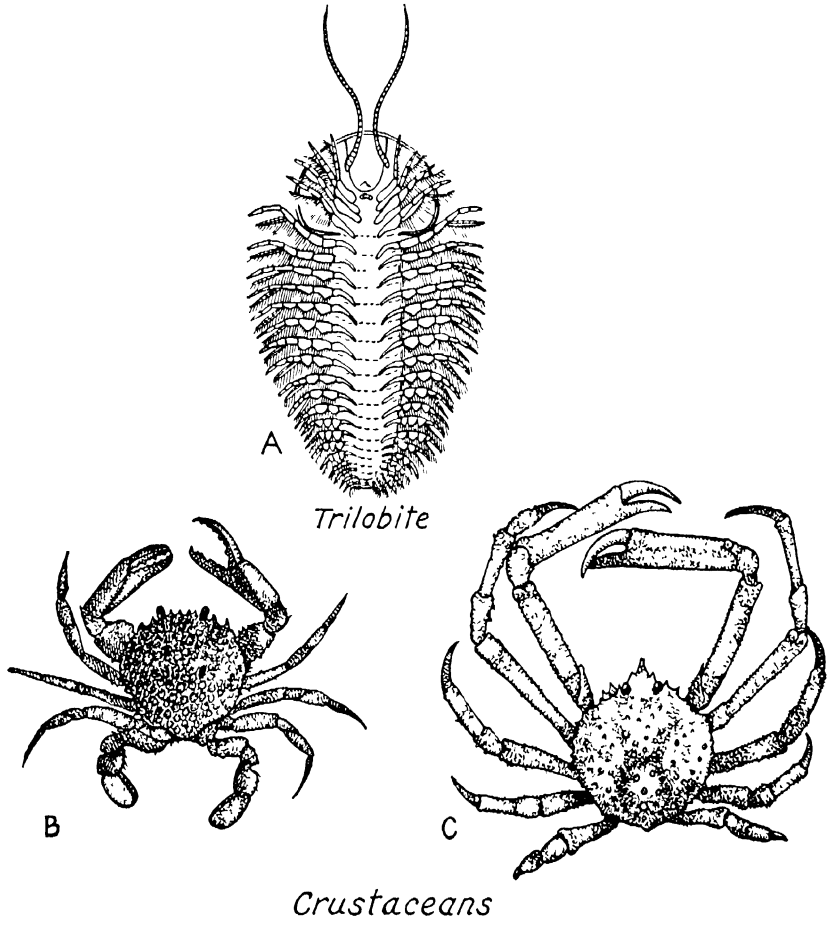


Fig. 3.2. A primitive trilobite and two divergently specialized crustaceans, illustrating the contrasts between primitive polyisomeres (A), specialized anisomeres (B) and secondarily similar polyisomeres (C). A, Cambrian trilobite (*Triarthrus beckii*), ventral side, showing appendages, B, modern crab (*Platyonichus ocellatus*); C, spider crab (*Libinia dubia*). A, from Gregory, after Beecher; B, C, after A. G. Meyer.

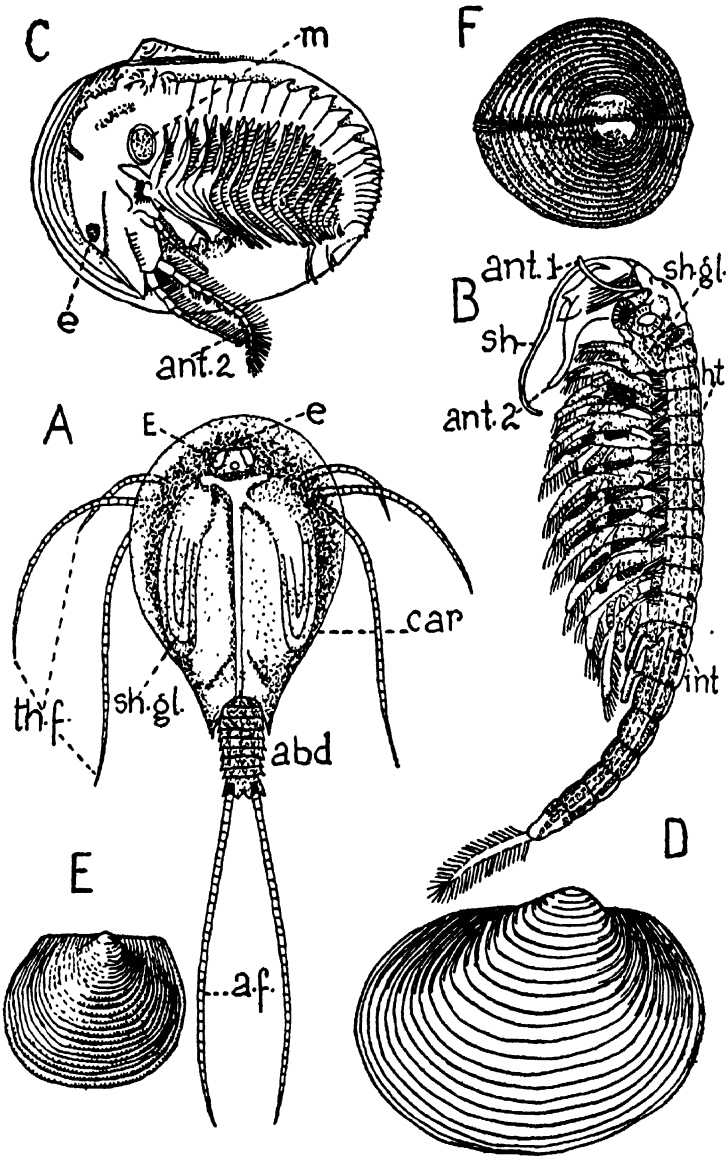


Fig. 3.3. Primitive crustaceans representing modified descendants of the pretrilobite stock. A, *Apus,* dorsal aspect; B, *Branchipus,* lateral view; C, *Estheria,* animal in shell with one valve removed; D, exterior of one valve of same; E, *Estheria* (Upper Devonian); F, *Schizodiscus. abd,* abdomen; *a.f.,* caudal styles (abdominal furca); *ant.* 1, antennule; *ant.* 2, antenna; *car,* carapace; E, paired eye; *e',* median eye; *int.* intestine; *ht,* heart; *m,* adductor muscle; *sh,* shell; *sh.gl.,* shell gland; *th.f.,* thoracic foot. From Goldring.

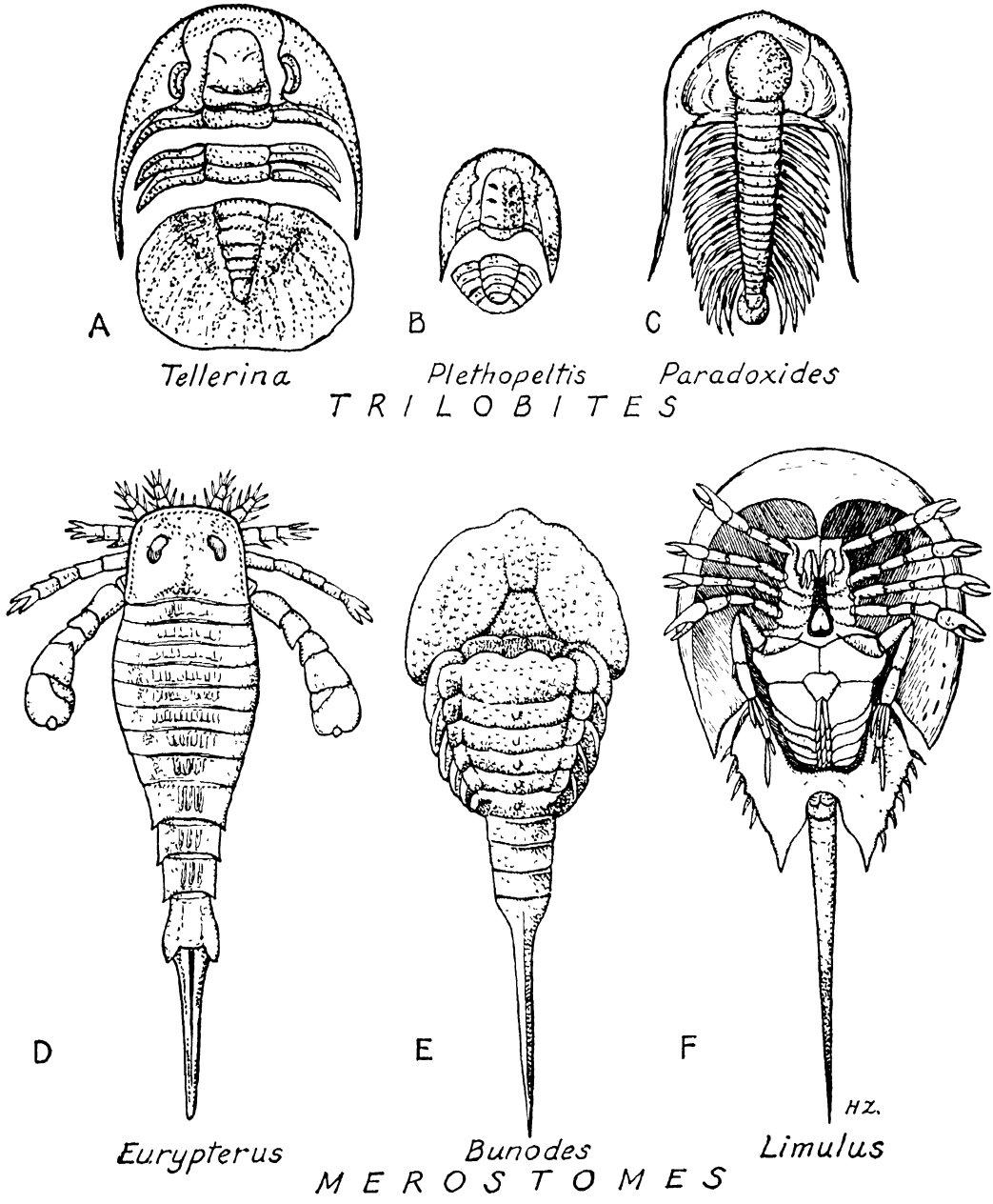


Fig. 3.4. Comparison of trilobites (A–C), eurypterids (D, E) and king crab (F). From Goldring.

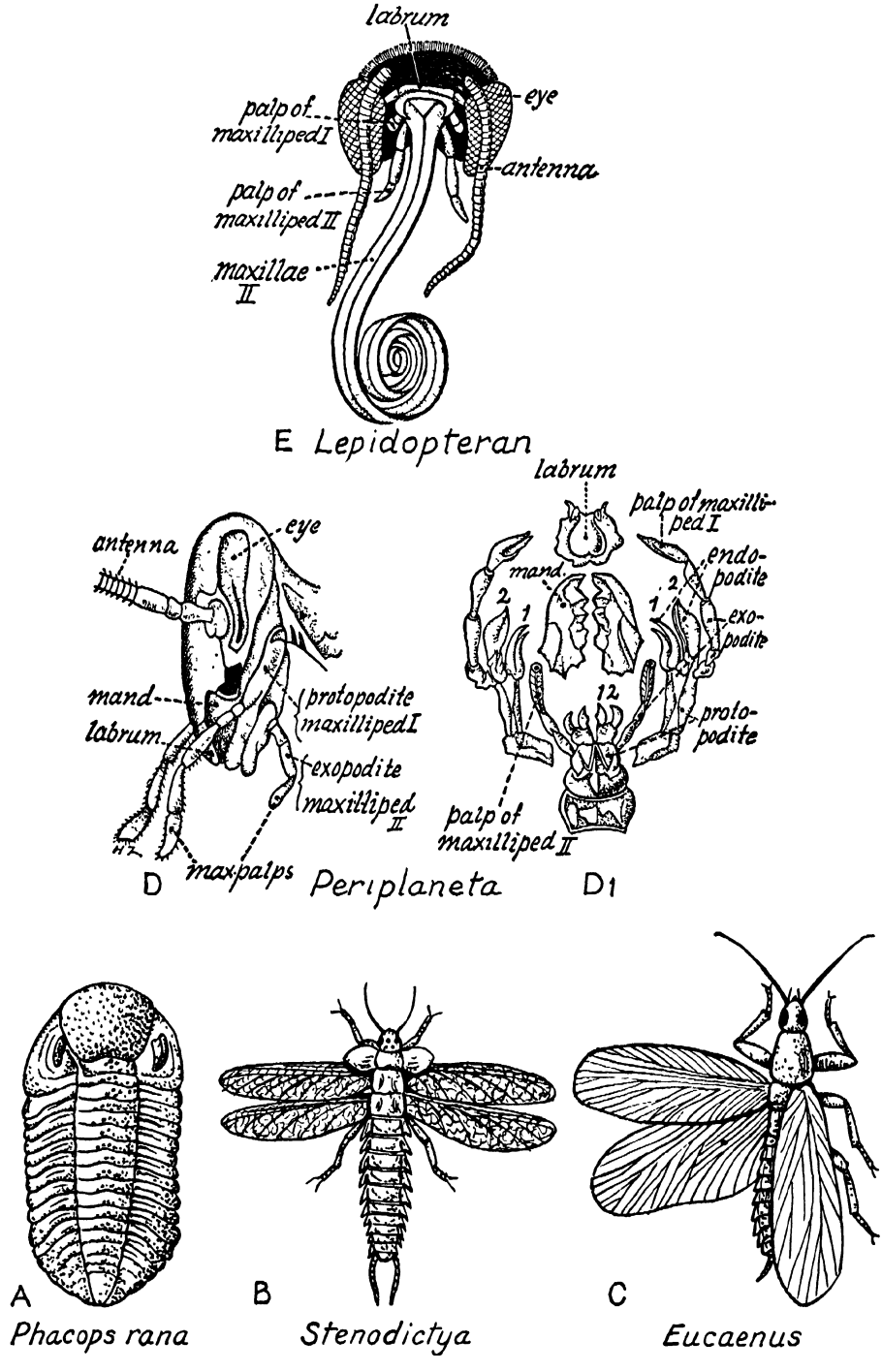
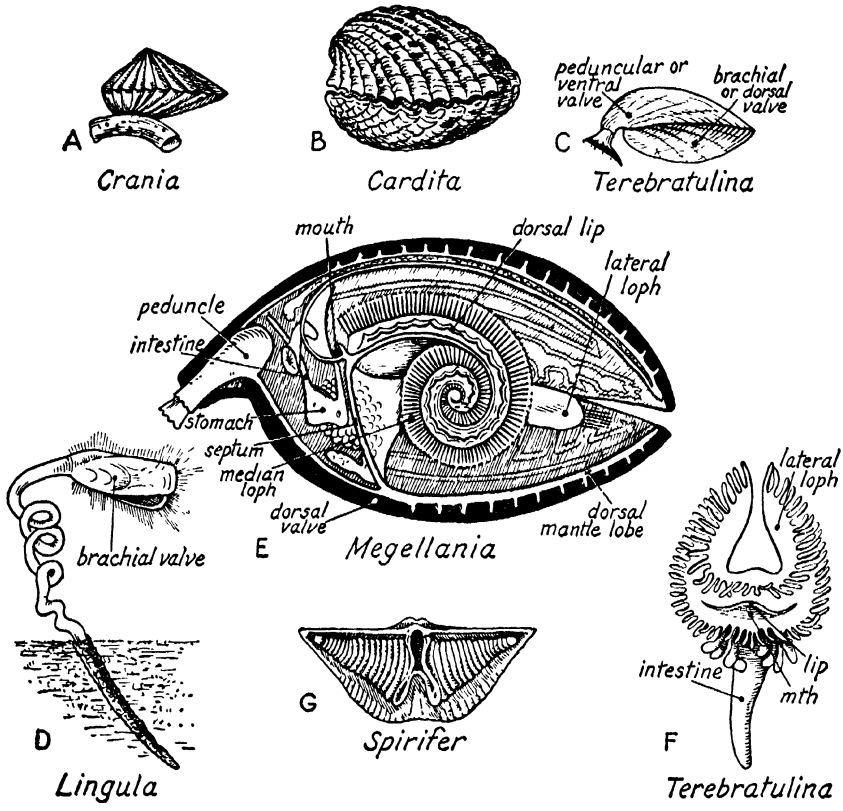


Fig. 3.5. Devonian trilobite (A), Carboniferous primal insect (B), ancestral cockroach (C), head of modern cockroach (D, D1) and moth (E). In the trilobite (A) the dorso-lateral plates or pleurae are primitive polyisomeres. In (B), a primal insect, the first three pairs of pleurae are emphasized as wing-covers and wings. In (C), a primitive insect, the first pair has already disappeared, leaving two pairs of wings. In the modern cockroach (D) the appendages of the mouth parts (D1) recall the cephalic appendages of the trilobite (fig. 3.2A) and are much less specialized than those of the lepidopteran, which have evolved into a proboscis (E). A, after Goldring; B, C, after Zitell; D, E, after Parker and Haswell.

CHAPTER IV

COELOMATE FOOD-SIFTERS OF DIVERSE TYPES (BRACHIOPODS, POLYZOA, ECHINODERMS)



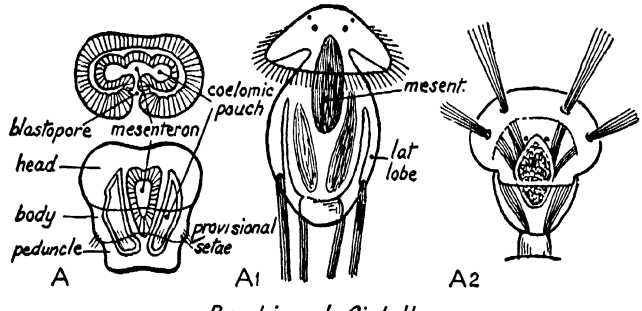


Fig. 4.1 (top). Brachiopods. A, sessile brachiopod, convergently resembling B, bivalve mollusc; C, stalked brachiopod bent over, the peduncular (or true ventral valve) being above the brachial or true dorsal valve; D, brachiopod with a long contractile stalk; E, diagram of anatomy (compare C); F, mouth and lophs (arms) facing toward the stalk; G, Devonian brachiopod with fully developed lateral lophs supported on helicoid "arms." A, E, F, after Parker and Haswell; C, D, G, after Goldring.

Fig. 4.2. Embryonic development of a brachiopod (*Cistella*). A, Three-lobed embryo showing coelomic pouches; A1, free-swimming larva, suggesting a trochophore; the lateral lobes of the mantle point backward. A2, later stage, after fixation; the lateral mantle lobes, reflexed over the head, will give rise to both the lophophore and the shell. From Parker and Haswell, after Balfour, Lang, and Kowalevsky.

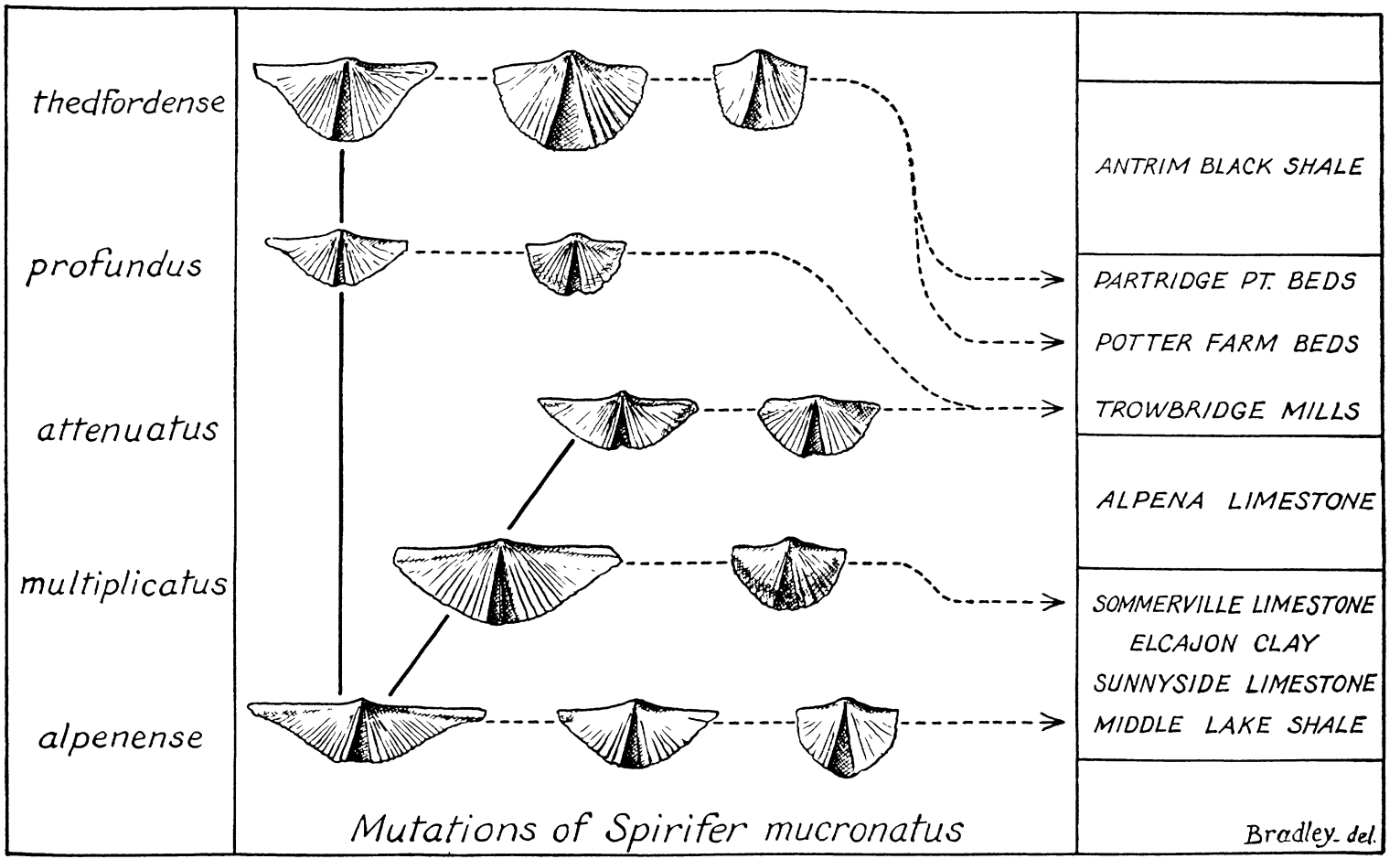


Fig. 4.3. Brachiopods. Successive mutations of a Devonian brachiopod *Spirifer mucronatus*. Specimens from the geologic section at Alpena, Michigan, on the shore of Lake Huron, and from the corresponding section at Thedford across the lake on the Canadian shore; arranged by A. Grabau to show the relationships of the various mutations. From "The Origin and Evolution of Life" by Henry Fairfield Osborn, p. 140.

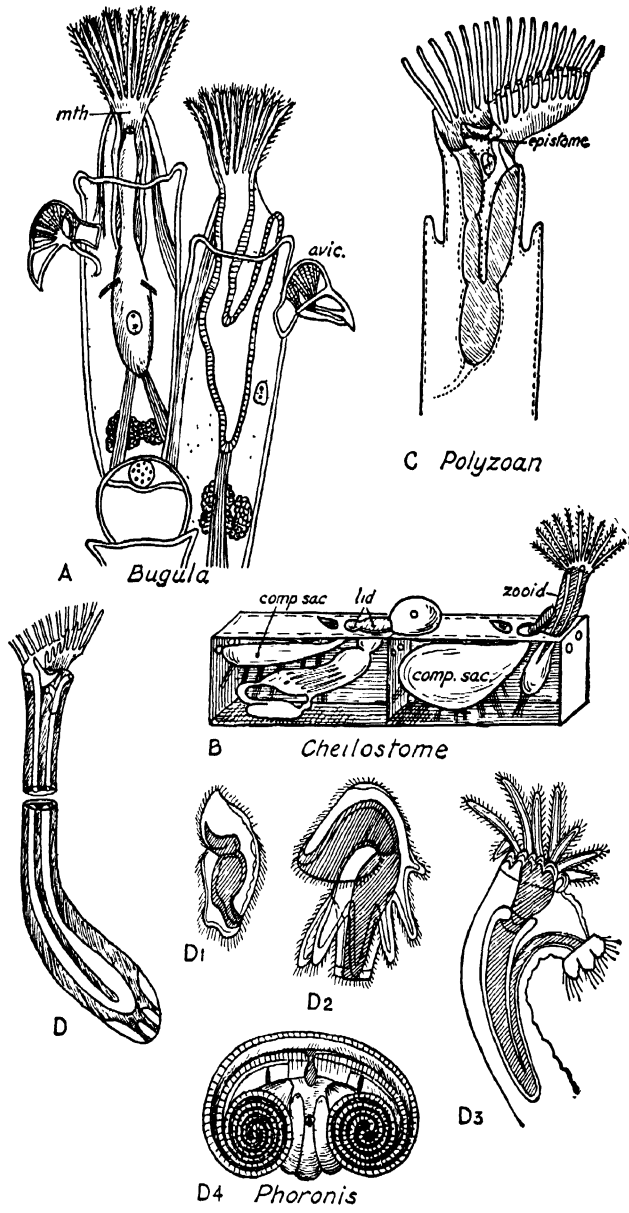


Fig. 4.4. Bryozoans and related forms. A, two "bird's-head coralline" zooids in the extended position. After Parker and Haswell. B, An allied form with one zooid extended, the other retracted into its chamber. From Berry, after Bassler. The compensating sac is part of a hydrostatic system developed only in the order Cheilostomata, suborder Ascophora. Presumably it facilitates the sudden retraction of the zooids and the closure of the double horny lid covering both the zooid and the compensating sac. C, Median sections of a "phylactolaematous polyzoan," i.e., one of the bryozoans with an epistome and (D) of *Phoronis*. Diagrams from Parker and Haswell after Korscheldt and Heider, Cori. D1–D3, larval stages in the development of *Phoronis*. From Parker and Haswell, from Balfour's Embryology. The youngest stage (D1) recalls the trochophore stage of many inverterbrates, including brachiopods. D4, Mouth, spiral lophophores and associated parts in adult *Phoronis*. From Parker and Haswell, after Benham.

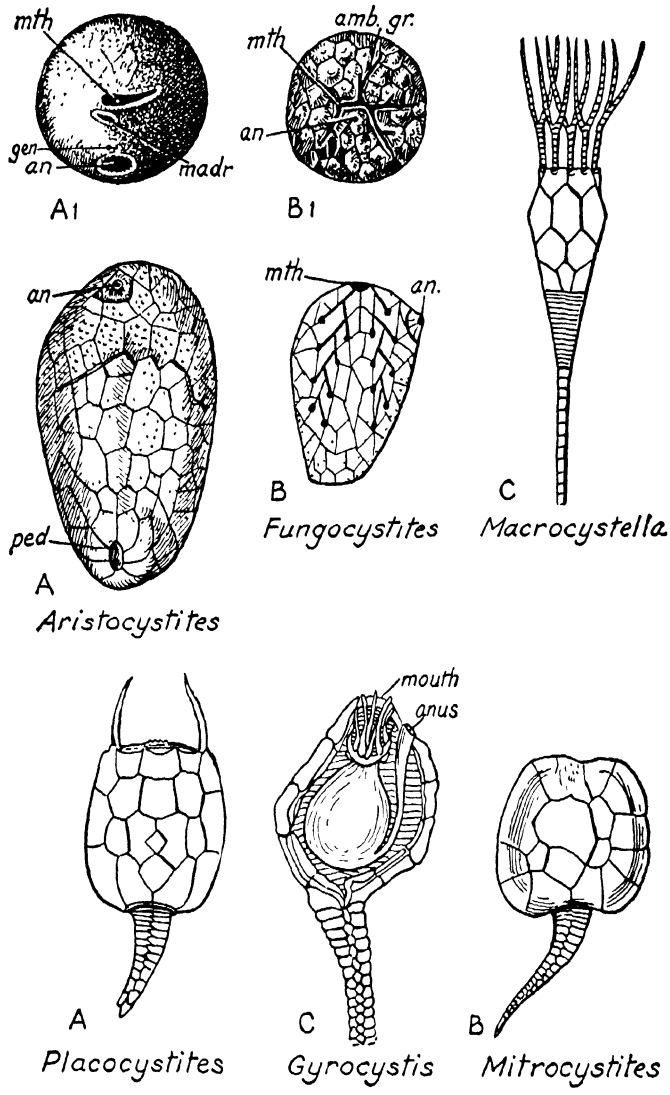


Fig. 4.5 (top). Primitive Palaeozoic echinoderms. A, Lower Silurian ovoidal or pear-shaped sack-like cystoid. B, B1, Branching, ambulacral grooves (*amb. gr.*) with pores leading toward the mouth. The gut was more or less U-shaped, the anus (*an*) being near the mouth (*mth*). C, Stalked cystoid with tentacles or "arms" around the mouth, which faces upward. From Zittel, Berry, after Barrande, Eichwald, Bather.

Fig. 4.6. Ordovician and Silurian cystoids of the order Carpoidea, with strongly distorted quinqueradiate pattern and secondary bilaterality (Cf. fig. 5.19 caption). A, B, from Zittel after Jaekel; C, after Spencer.

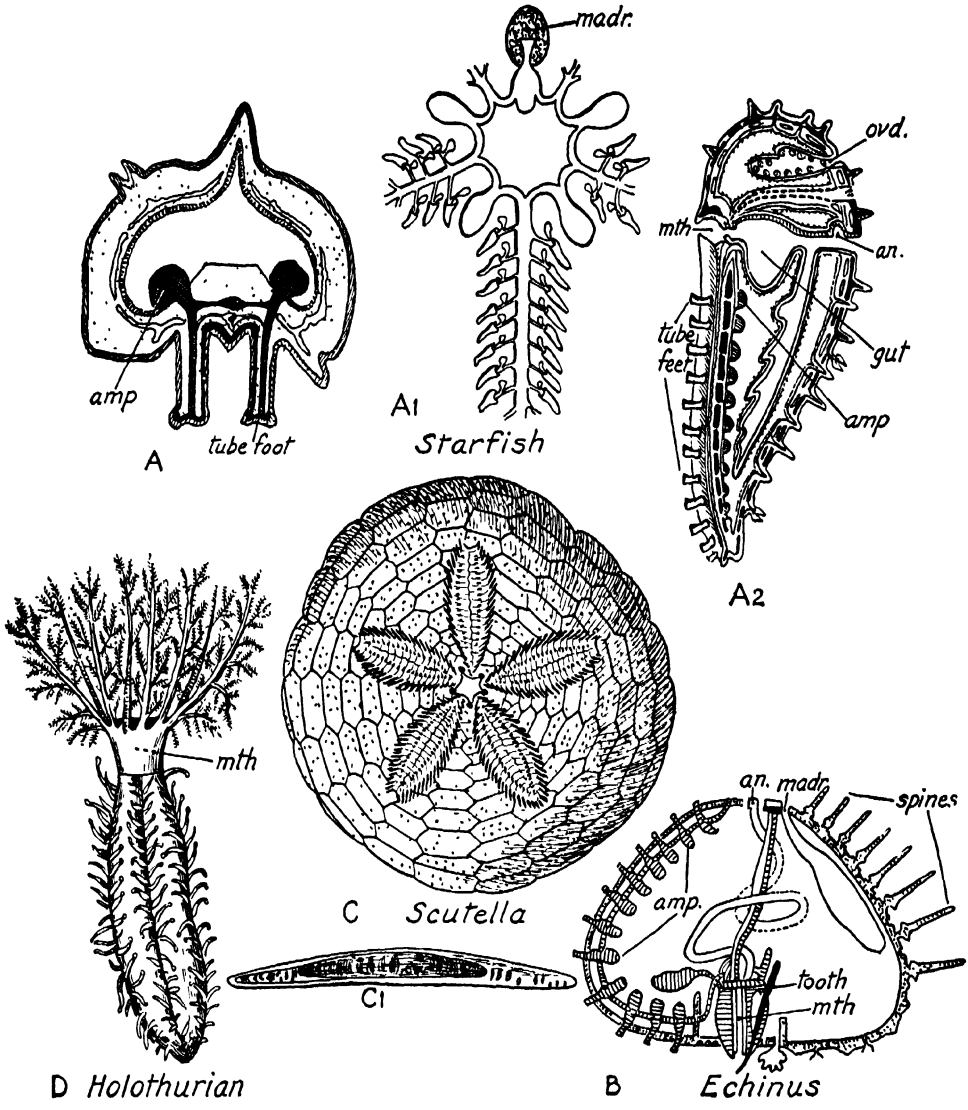


Fig. 4.7. Starfish (A1–A3), sea-urchin (B), sand-dollar (C, C1), and sea-cucumber (D), all with tube-feet. A, Vertical section through an arm of a starfish, showing the tube-feet and their ampullae perforating the body wall and supported by the skeletal tissue. The ambulacral groove lies between the tube-feet. From Parker and Haswell, from Leuckart, after Hamman. A1, Part of the ambulacral or radiate water system of a starfish, showing the tube-feet and their ampullae. The madreporite (*madr.*) is a sieve-like cover of the madreporic canal and is an important landmark among echinoderms. From Parker and Haswell, after Gegenbaur. A2, Diagrammatic vertical section of a starfish, showing the spatial relations of the mouth, tube-feet, intestine, anus, etc. From Parker and Haswell, after Parker's Biology. B, Diagrammatic cross-section of a sea-urchin (*Echinus*), to show the spatial relations of the tube-feet and their ampullae, the mouth, "Aristotle's lantern," the digestive tract, anus, and madreporite. From Zittel, after J. W. Gregory and von Stromer. C, A Miocene spatangoid (sand-dollar) and its cross-section (C1), representing a greatly widened and flattened sea-urchin. From Zittel. D, A holothurian, or sea-cucumber. A distant relative of the starfish and sea-urchin, in which the body has been greatly elongated in the direction of the line joining mouth and anus. The animal lies on one side; its ventral surface bears three ambulacral areas and is the equivalent of the trivium, or three anterior rays of the starfish, the rest of the body representing the bivium (Parker and Haswell, I, p. 369); the tentacles represent enlarged and branched tube-feet. From Parker and Haswell, from Hertwig's Lehrbuch, after Ludwig.

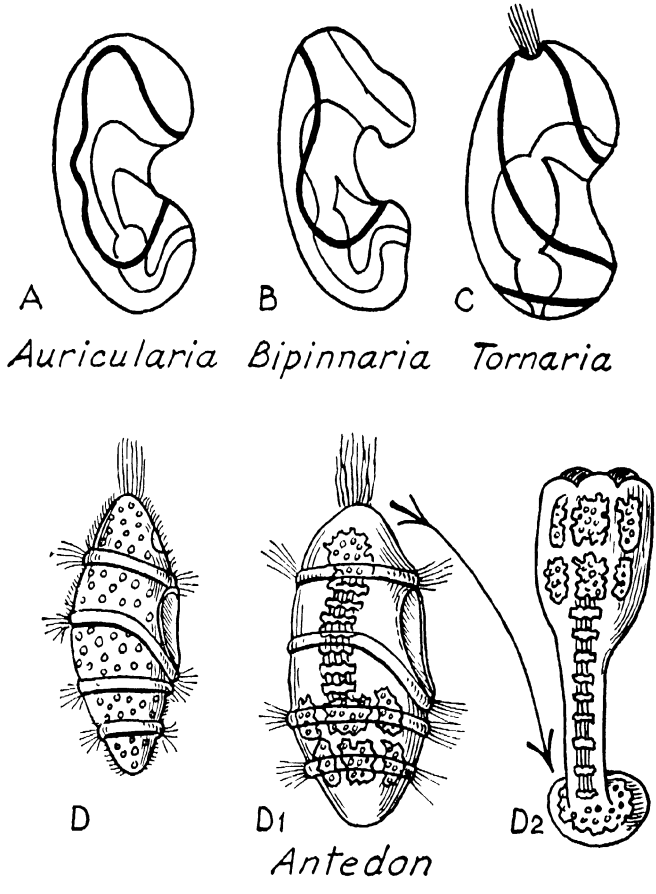


Fig. 4 8 Larval echinoderms (A, B, D) and balanoglossid (C) A, of a holothurian; B, of an asteroid; C, *"Tornaria"* larva of *Balanoglossus*; D–D2, Three larval stages of a crinoid A–C, after Delage and Hérouard; D–D2, after Parker and Haswell.

CHAPTER V

THE PROCHORDATES AND THE PROBLEM OF THE ORIGIN OF THE VERTEBRATES

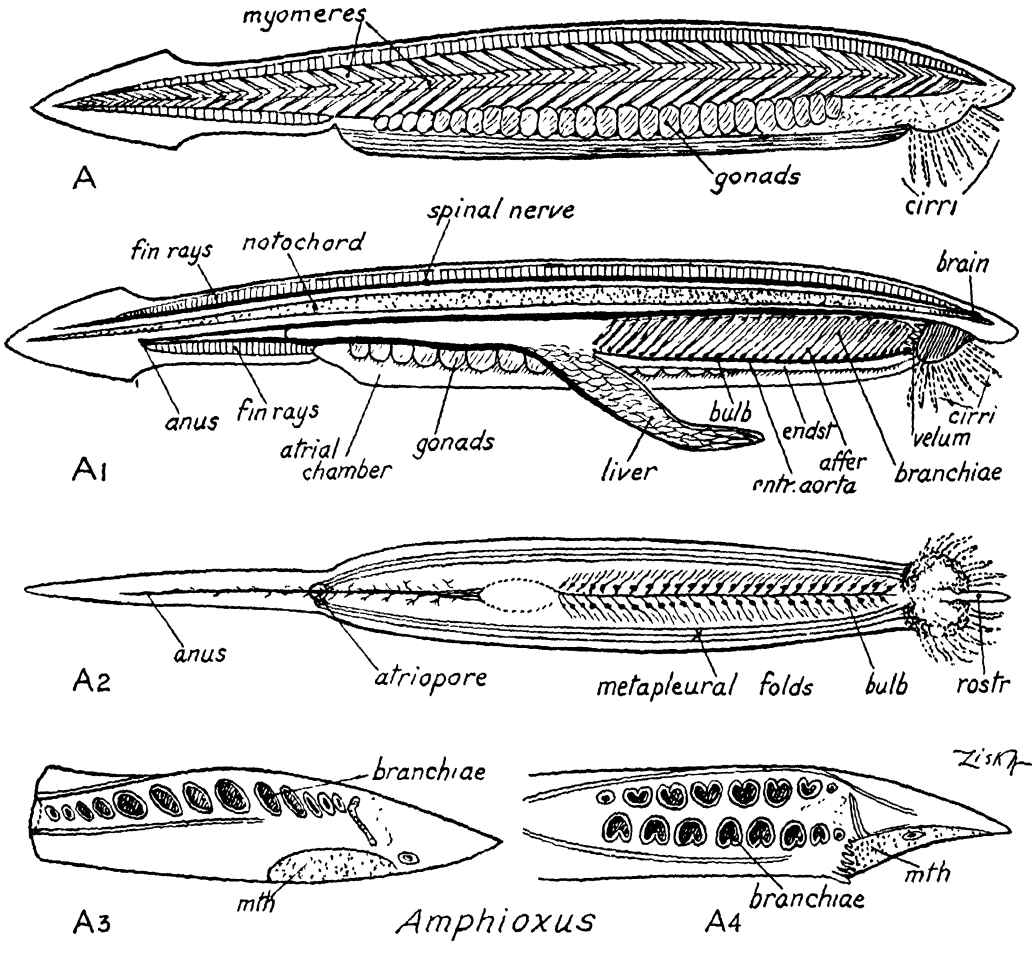


Fig. 5.1. Diagrams of the anatomy of *Amphioxus*. A, the animal as seen from the right side, showing the numerous myomeres or muscle flakes, the gonads (seen through the thin body wall), the buccal cirri, the metapleural folds. From Delage and Hérouard, after Lankester. A1, Sagittal section, showing the interior of the left half of the pharynx with its gill bars, the circulatory system, the branchial chamber, the endostyle, the liver or hepatic coecum, the notochord, the spinal nerve cord, the minute brain, etc. After Delage and Hérouard (Pls. 12, 15). A2, Outline of ventral view, indicating internal ventral vein and the little bulbs at the bases of the afferent arteries. After Delage and Hérouard. A3, Young larval stage, seen from below, showing the large mouth arising on the left side and the row of right gill pouches. After Delage and Hérouard. A4, Later larval stage, seen from below, showing the mouth shifting toward the midventral line, the gill pouches of both sides folding up into anterior and posterior halves.

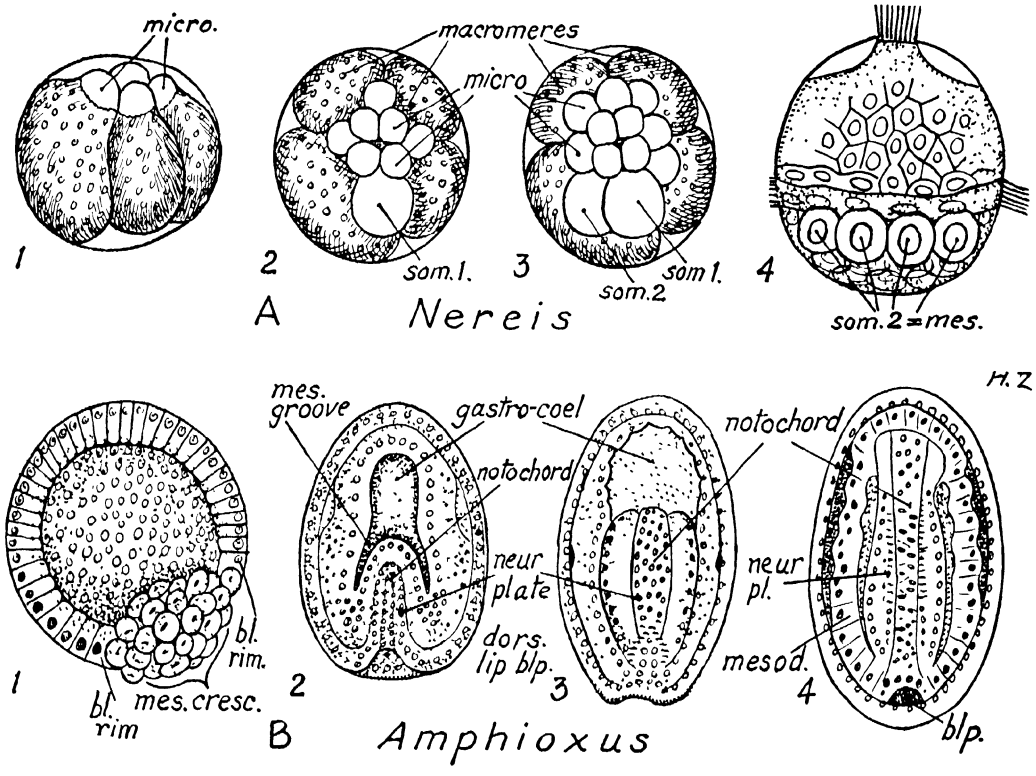


Fig. 5 2. Contrasting development of the mesoderm in a primitive member (A) of the teloblastic (annelid-arthropod) series, and in *Amphioxus* (B), representing the enterocoelic (chordate) series. In (A) the mesoderm arises from a single cell, the second somatoblast; in (B) the mesoderm is derived from the cells of the "mesodermal crescent," which bud from the larger endoderm cells beneath the rim of the blastopore (B1, B2). Later (B3, B4) the cells of the mesoderm crescent grow forward into the cavity of the blastula. The notochordal cells and the ectoderm of the neural plate also take part in this forward growth. The so-called enterocoelic pouches forming the future somites develop their coelomic cavities from the "mesoderm groove" a remnant of the posterior part of the gastrocoele, or cavity of the gastrula. The head cavity is derived from the anterior part of the gastrocoele. A1–A3, from Parker and Haswell, after Westinghausen; A4, from Parker and Haswell, after E. B. Wilson; B1–B4, after Conklin.

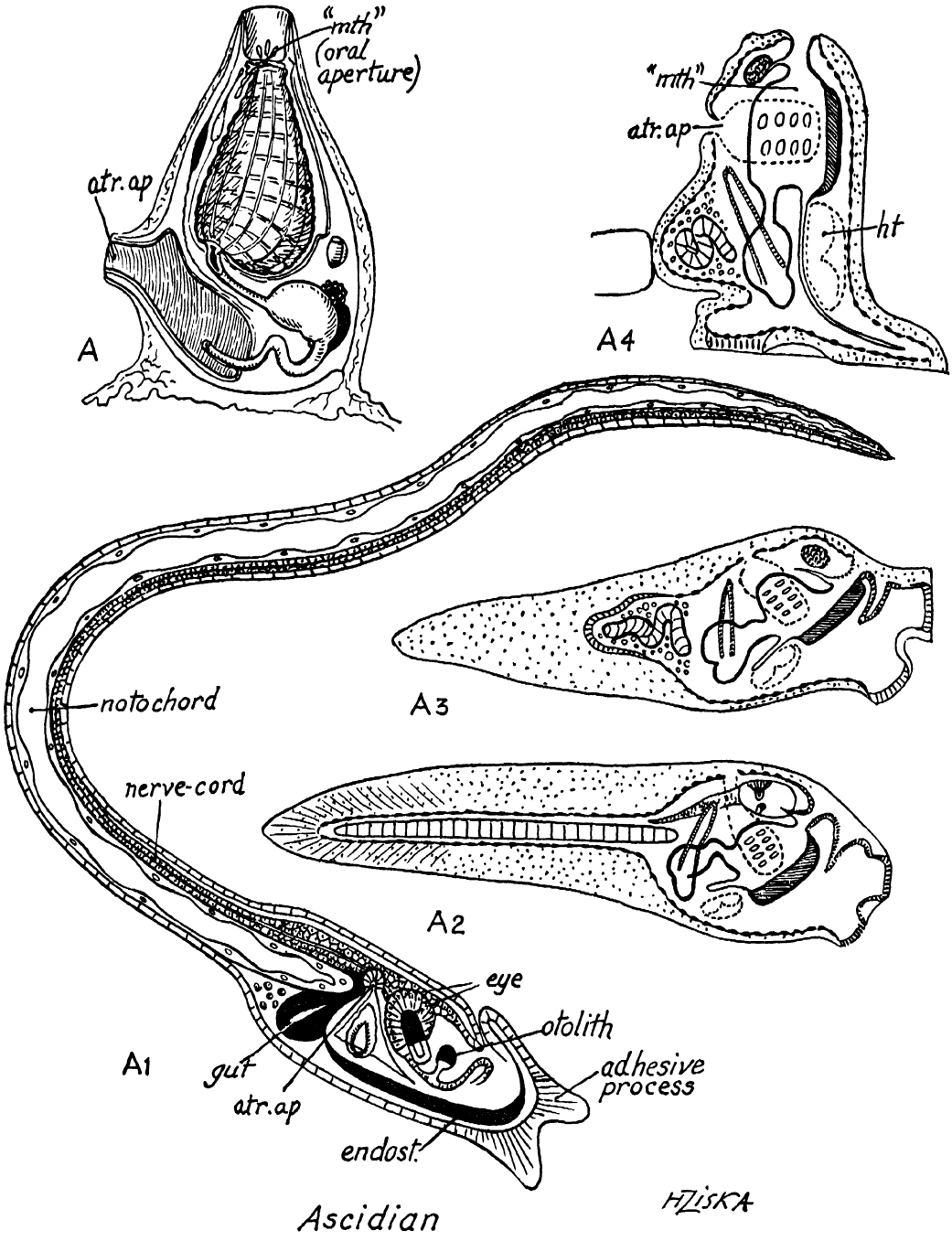


Fig. 5.3. Sessile ascidian and its development from a free-swimming larva. A, A1, from Delage and Hérouard; A2–A4, from Parker and Haswell, from Korscheldt and Heider, after Seeliger. *"Mth,"* functional mouth or oral aperture, probably homologous with the mouth of vertebrates; *atr.ap,* atrial aperture leading to atrial sack.

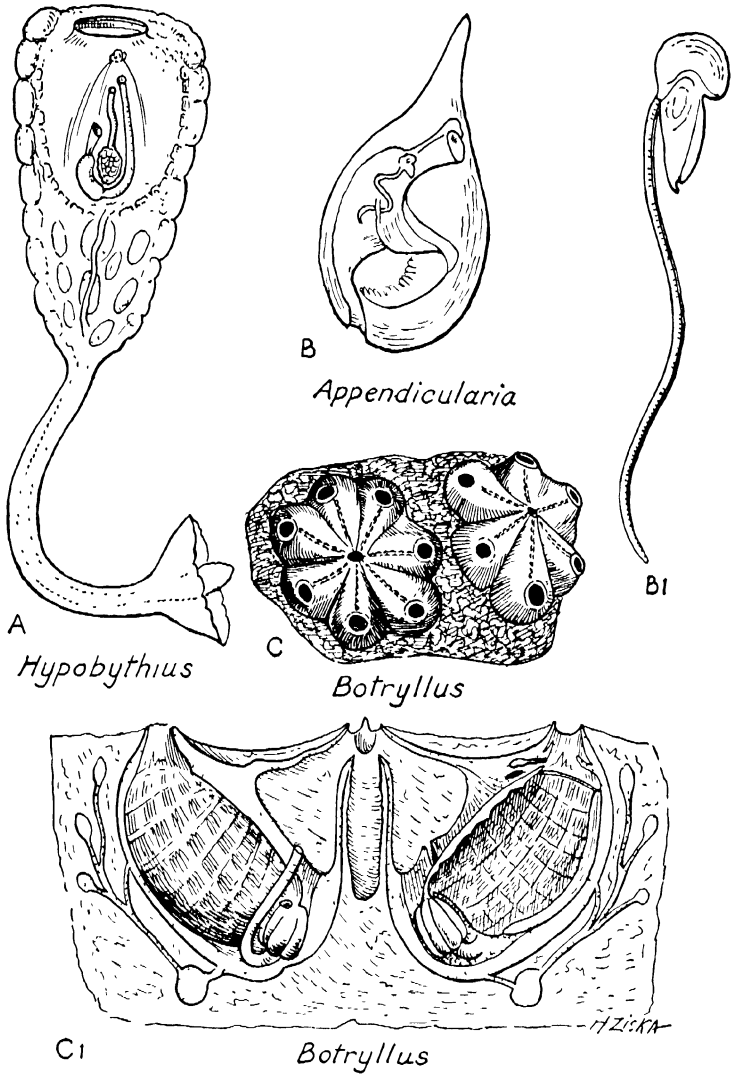


Fig. 5.4. Various ascidians: stalked (A), secondarily floating (B, B1) and sessile, colonial (C, C1). A, B, B1, C1 from Delage and Hérouard, after Herdman; C, from Parker and Haswell, after Milne Edward.

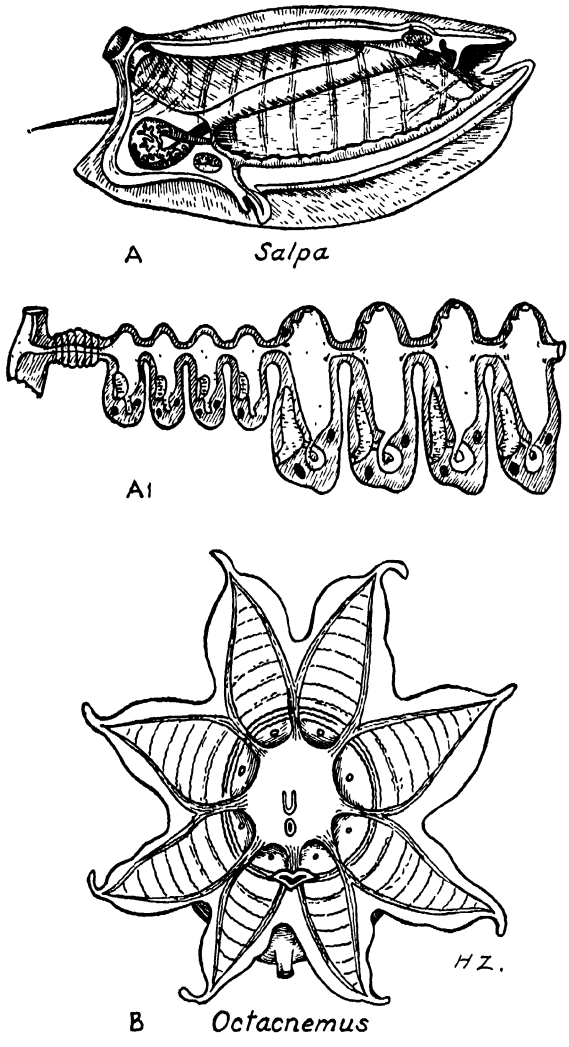


Fig. 5.5. Secondarily free-swimming ascidians: Boat-shaped (A), with chain of buds, or polyanisomeres (A1); medusa-like (B). A, after Parker and Haswell; A1, B, after Delage and Hérouard.

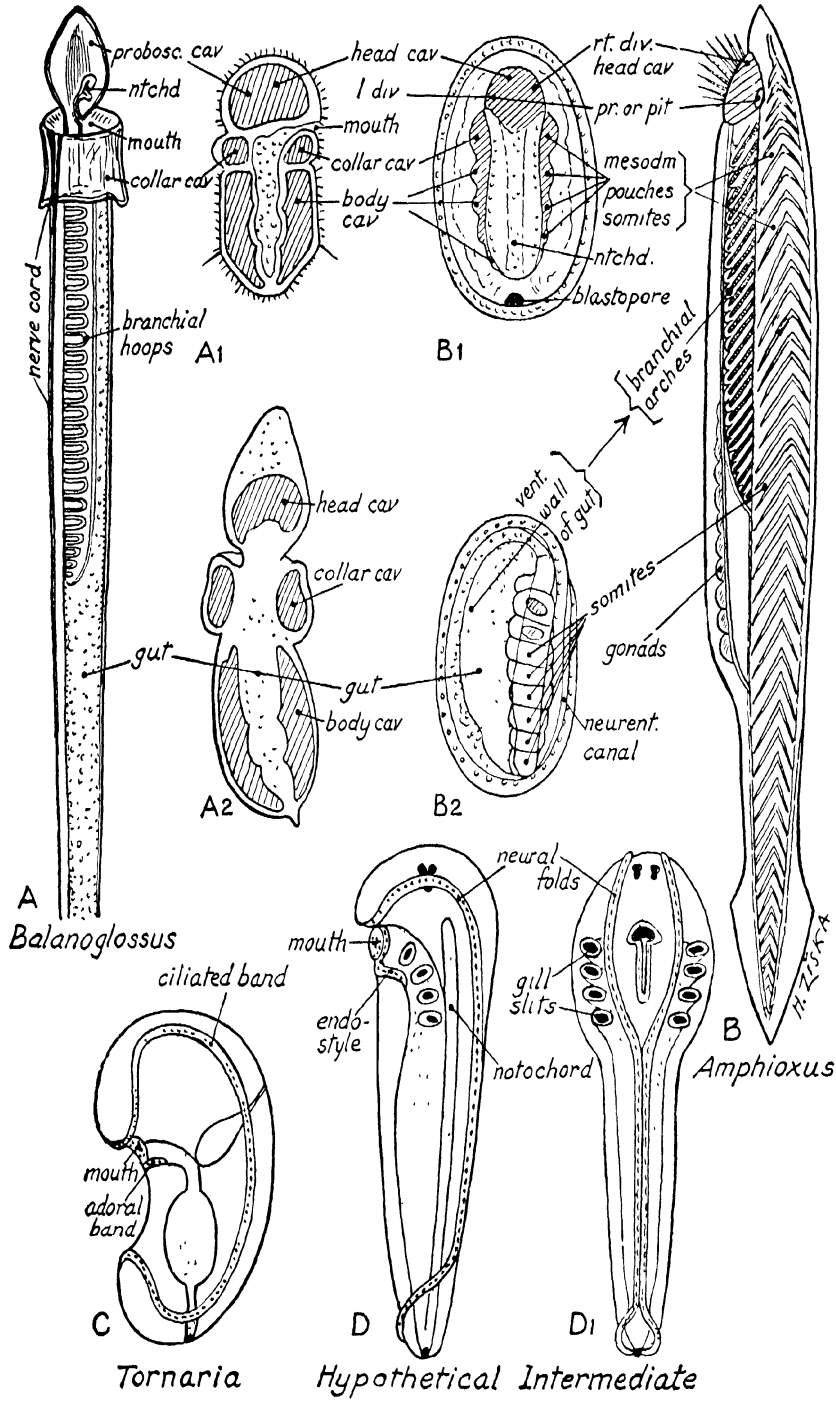


Fig. 5.6. Comparison of *Balanoglossus* and *Amphioxus*, embryonic and adult. According to McBride and others three "primary coelomic cavities" in *Amphioxus* correspond respectively to the proboscis, collar, and body-cavities of *Balanoglossus*. Arrows indicate how, according to Conklin, the various parts of the embryonic gut cavity (B1, B2) in *Amphioxus* give rise to their derivatives in the adult (B). Garstang's theory: Tornaria into chordate (C–D1). A, A1, A2, B, after Delage and Hérouard; B1, B2, after Conklin; C, D, D1, from de Beer, after Garstang.

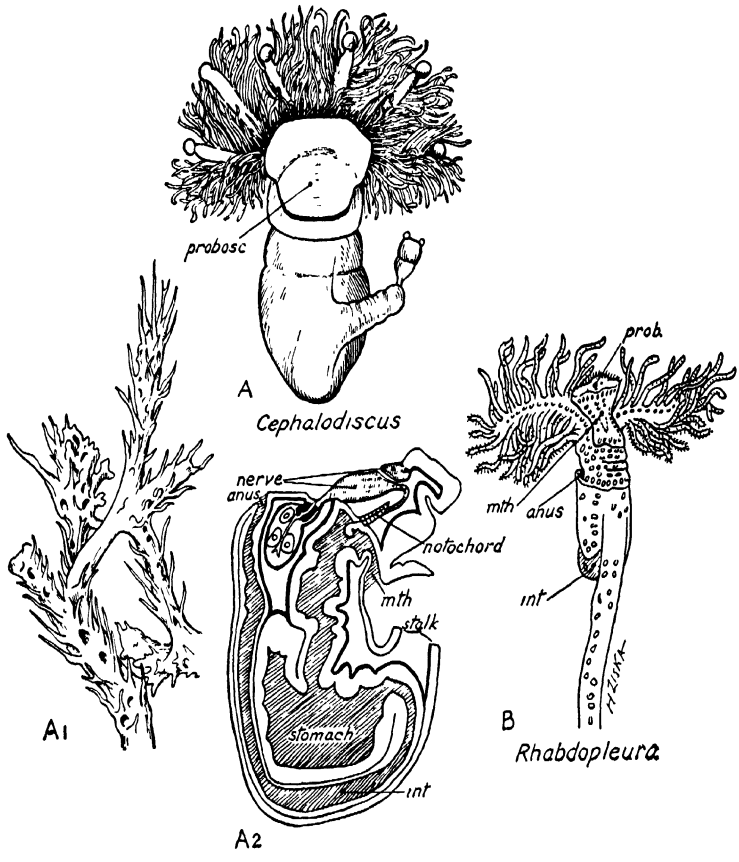


Fig. 5.7 (top). Bryozoa-like prochordates. A, single zooid of *Cephalodiscus* with bud; A1, gelatinous investment with sites of zooids (dark spots); A2, longitudinal section of zooid; B, a stalked relative of *Cephalodiscus*. From Parker and Haswell. A, after McIntosh; A1, A2, after Harmer; B, after Schepotieff.

Fig. 5.8. Comparison of free-swimming ascidian *Appendicularia* (A) with stalked invertebrates, *Phoronis* (B) and *Rhabdopleura* (C). From Parker and Haswell. A, after Herdman, but with the tail twisted into the "morphologic position" (Delage and Hérouard); B, after Balfour; C, after Schepotieff.

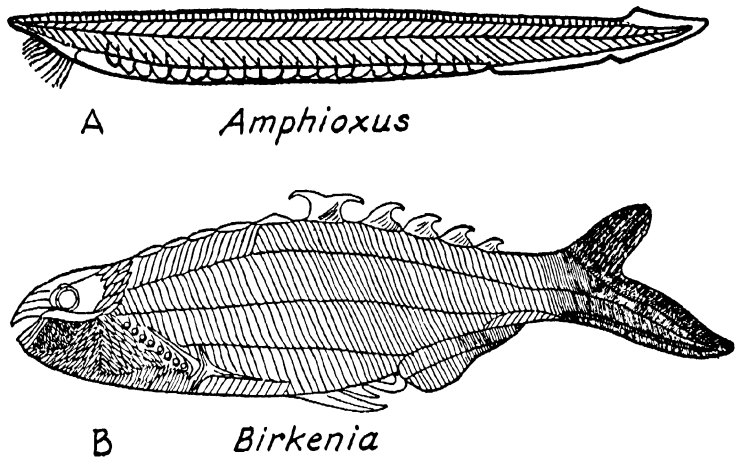


Fig. 5 9. Comparison of Silurian anaspid ostracoderm with *Amphioxus*. A, after Allee, B, after Kiaer.

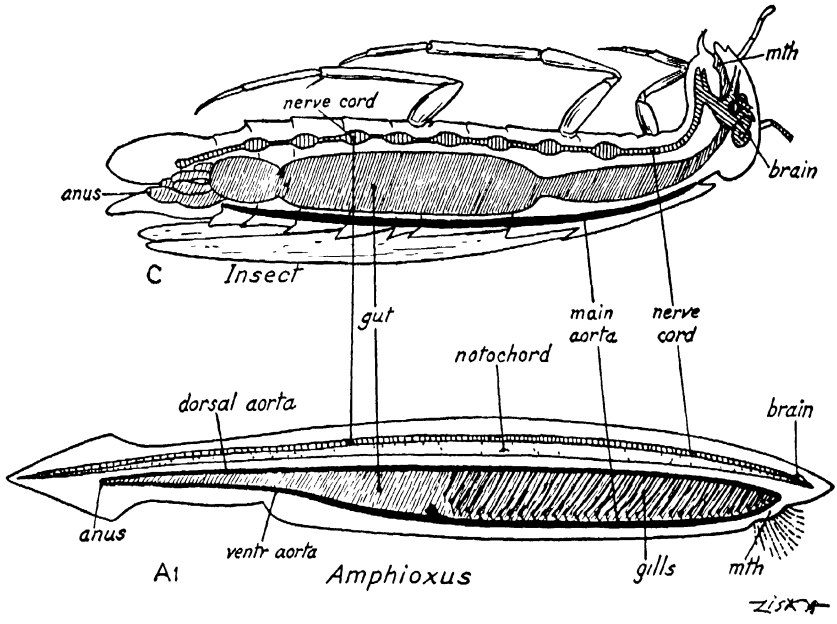


Fig. 5.10. Geoffroy Saint Hilaire's "Notonect" (insect-swimming-on-its-back) compared with *Amphioxus*. By turning the insect on its back we arbitrarily make its nerve cord dorsal and its heart ventral, as they are in chordates. But the diagram also shows how profound are the contrasts between these two phyla.

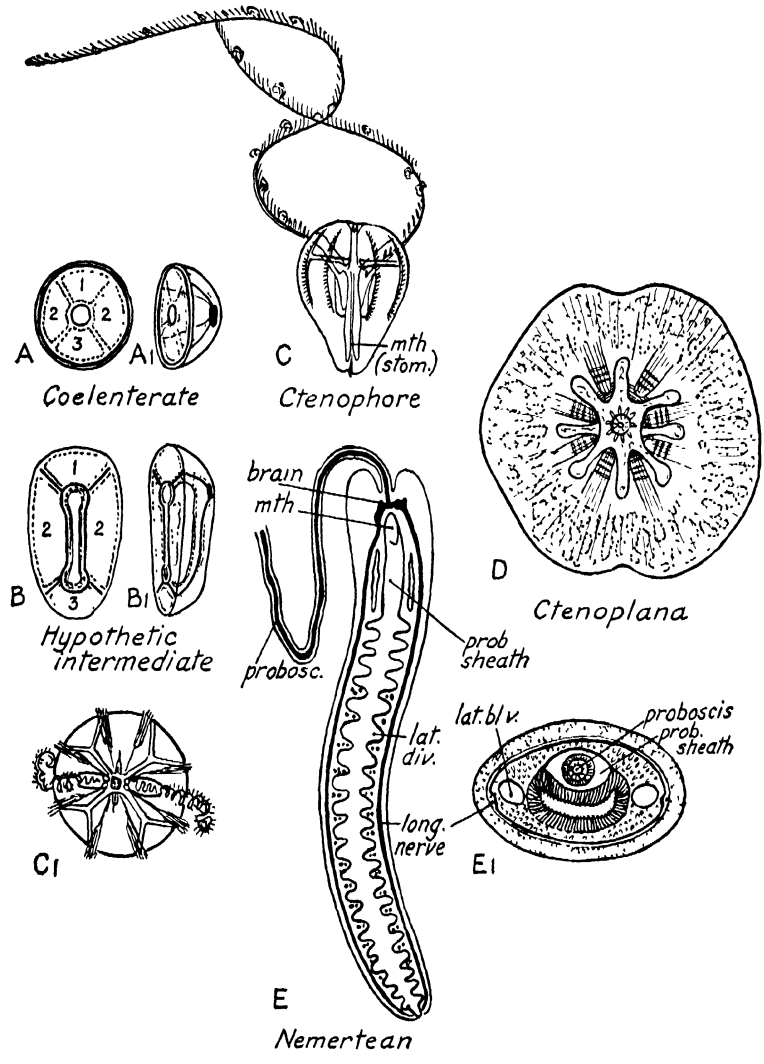


Fig. 5.11. A, B, Supposed transformation of an ancestral coelenterate (A, A1) into a basal chordate (Compare fig. 5.6A1). From Delage and Hérouard, after Masterman. 1, Protomere (=head or proboscis cavity); 2, right and left mesomeres (collar cavity or pharynx); 3, metamere or locomotor mesomere. C, C1, a ctenophore, showing the jellyfish-like habitus combined with the beginnings of mesoderm and other higher features pointing toward the flatworms; D, a creeping ctenophore; E, E1, a nemertean, a three-layered, coelomate "worm." C–E1, after Parker and Haswell.

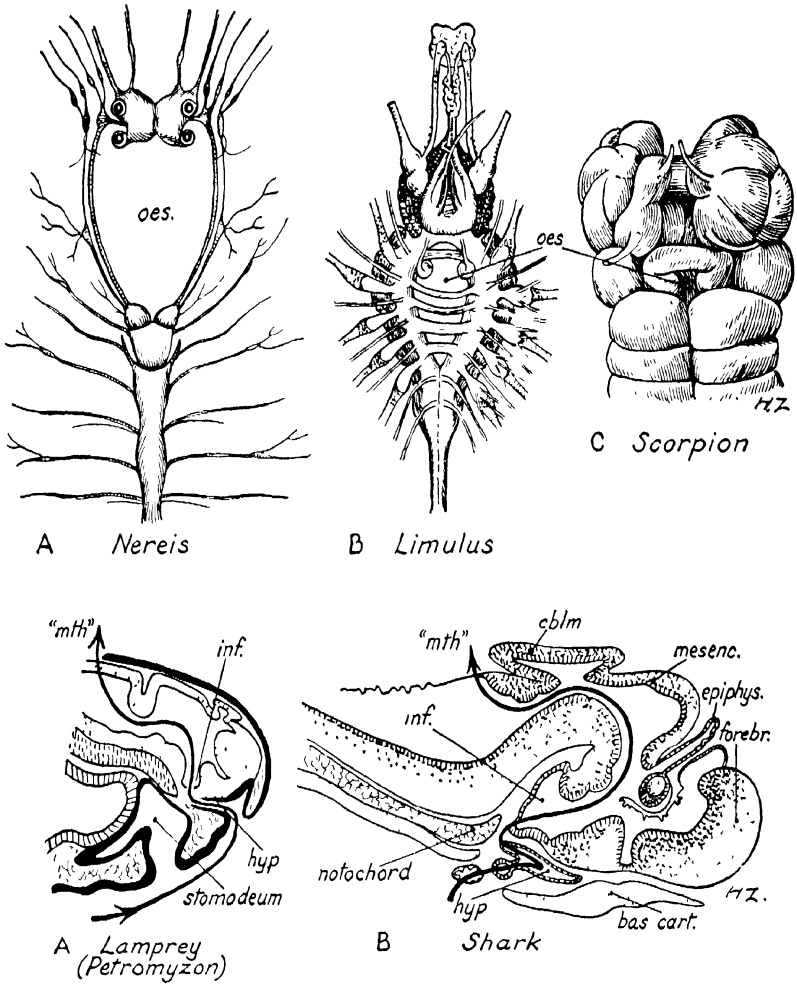


Fig. 5.12 (top). Progressive cephalization (i.e., increase in size and concrescence of neuromeres) in the annelid-arthropod phyla. A, a primitive marine annelid with small brain and slender circumoesophageal commissures surrounding large oeophagus (*oes*); B, intermediate conditions in *Limulus*; C, advanced cephalization with great reduction of oesophagus in embryo scorpion. A, from Parker and Haswell, after Quatrefages; B, C, after Patten.

Fig. 5.13. Median longitudinal sections of the embryonic brain and associated parts in the lamprey (A) and shark (B). The heavy black line shows the imagined ancient pathway from the stomodeum through the hypophysis into the infundibulum of the brain, thence upward and backward through the ventricles and out through the "old mouth" lying between the two halves of the medulla oblongata. A, from Goodrich, after Dohrn; B, from Goodrich, after von Kuppfer.

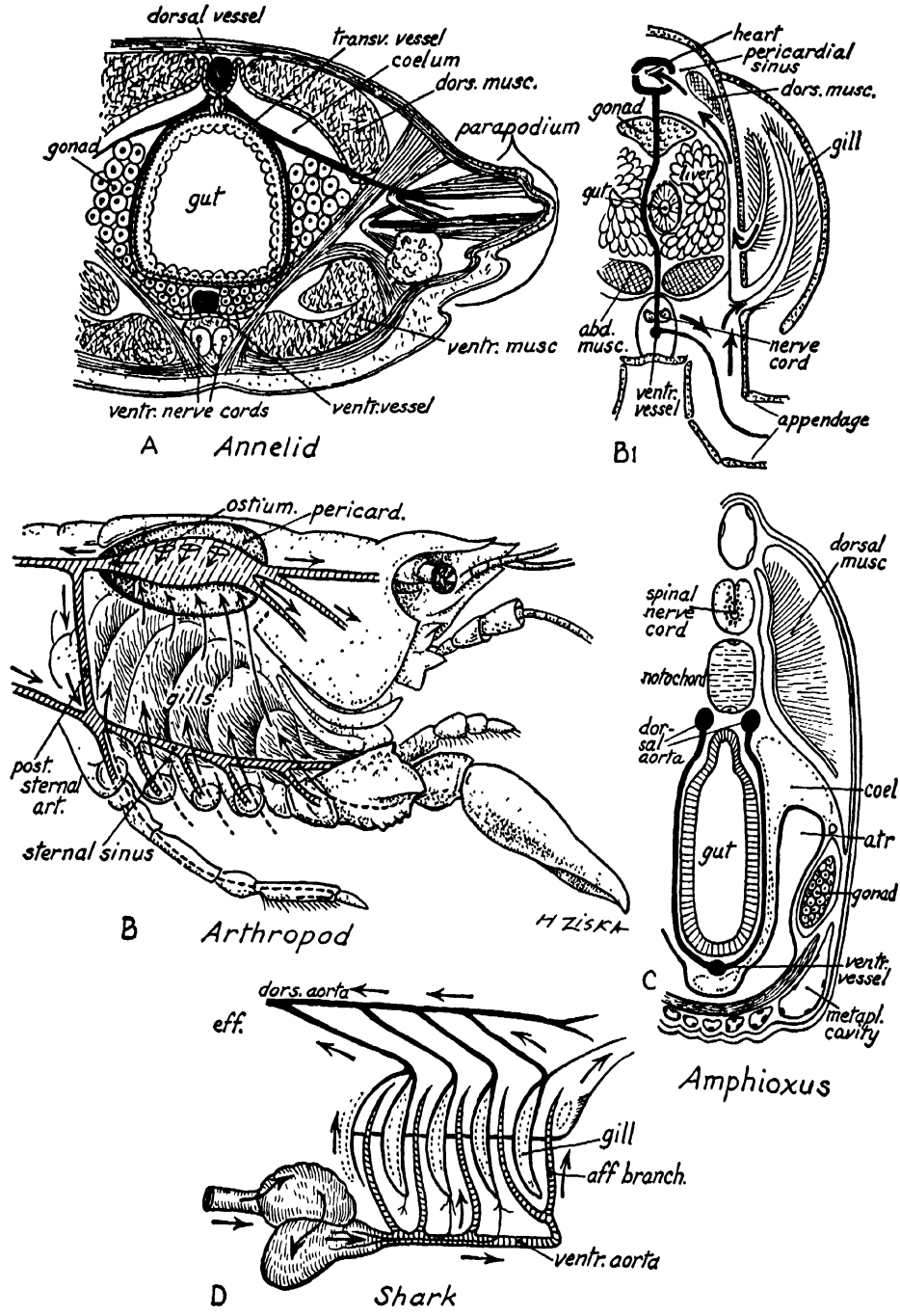


Fig. 5.14. Comparison of cross-sections of annelid (A), crustacean (B) and *Amphioxus* (C), showing basic unity between annelid and crustacean and profound contrast with primitive chordate.

A, from Parker and Haswell; B, from Parker and Haswell, after Lang; C, from Delage and Hérouard, after Bowen and Hatschek. Contrast of circulatory systems between arthropod (B) and shark (D). In the arthropod (B) the blood flows outward from the heart in several directions (forward, backward, downward); from the paired appendages it goes to the gills, thence to the pericardial sinus and so to the heart. In the vertebrate (E) the blood is driven from the heart directly to the gills, thence to the carotids and dorsal aorta and thence to all parts of the body. Data from Parker and Haswell.

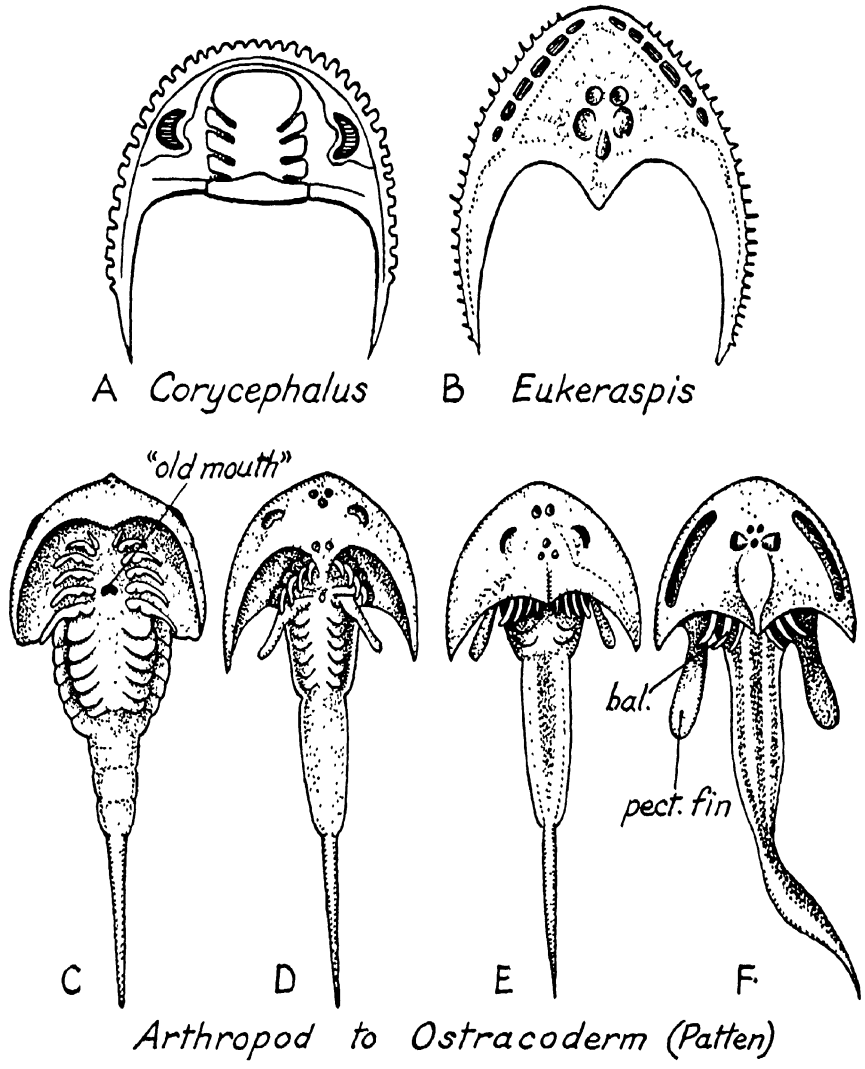


Fig. 5.15. Patten's comparison of trilobite (A) and ostracoderm (B) head-shields, together with his ingenious, hypothetical solution of the problem of transforming an overturned arthropod (C) into a basic vertebrate (F). D and E are completely hypothetical stages. In F, the "balancers" (*bal*) are hypothetically added from the embryos of *Polypterus*, Dipnoi and amphibians. After Patten.

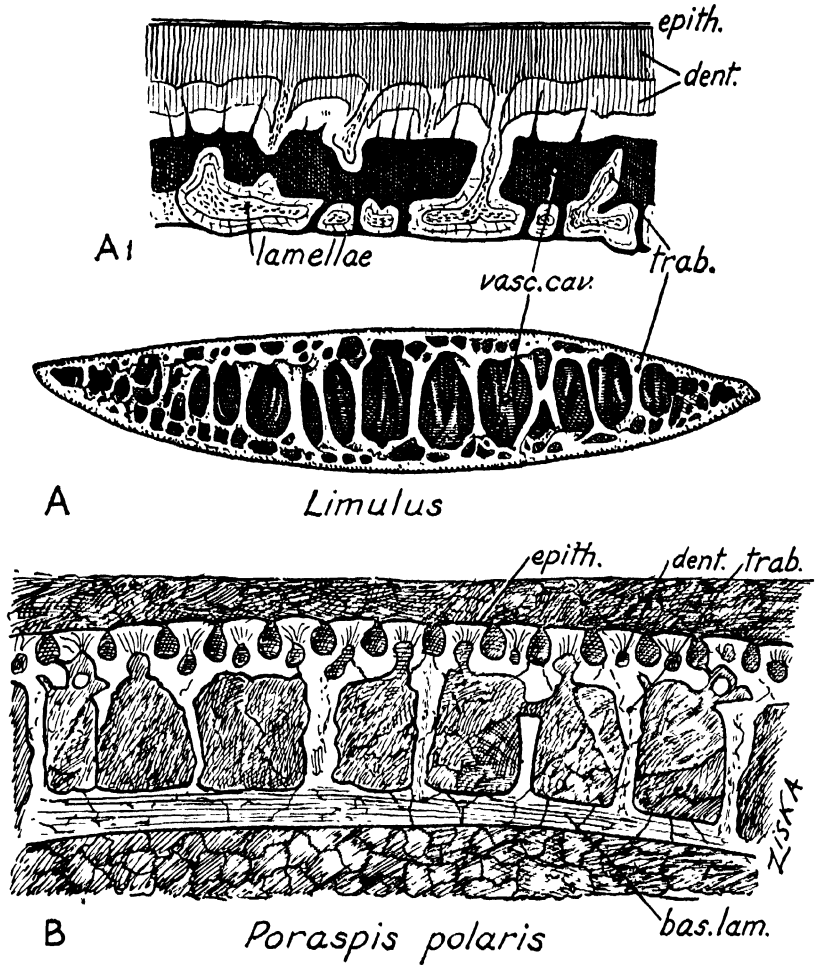


Fig. 5.16. Comparisons of cross-sections of exoskeleton of surving arthropod (A, A1) and Palaeozoic ostracoderm (B). A, A1, after Patten; B, after Kiaer and Heintz. *Epith*, epithelium; *dent*, dentine; *trab*, trabeculae; *bas. lam.*, basal lamellae; *vasc. cav.*, vascular cavity.

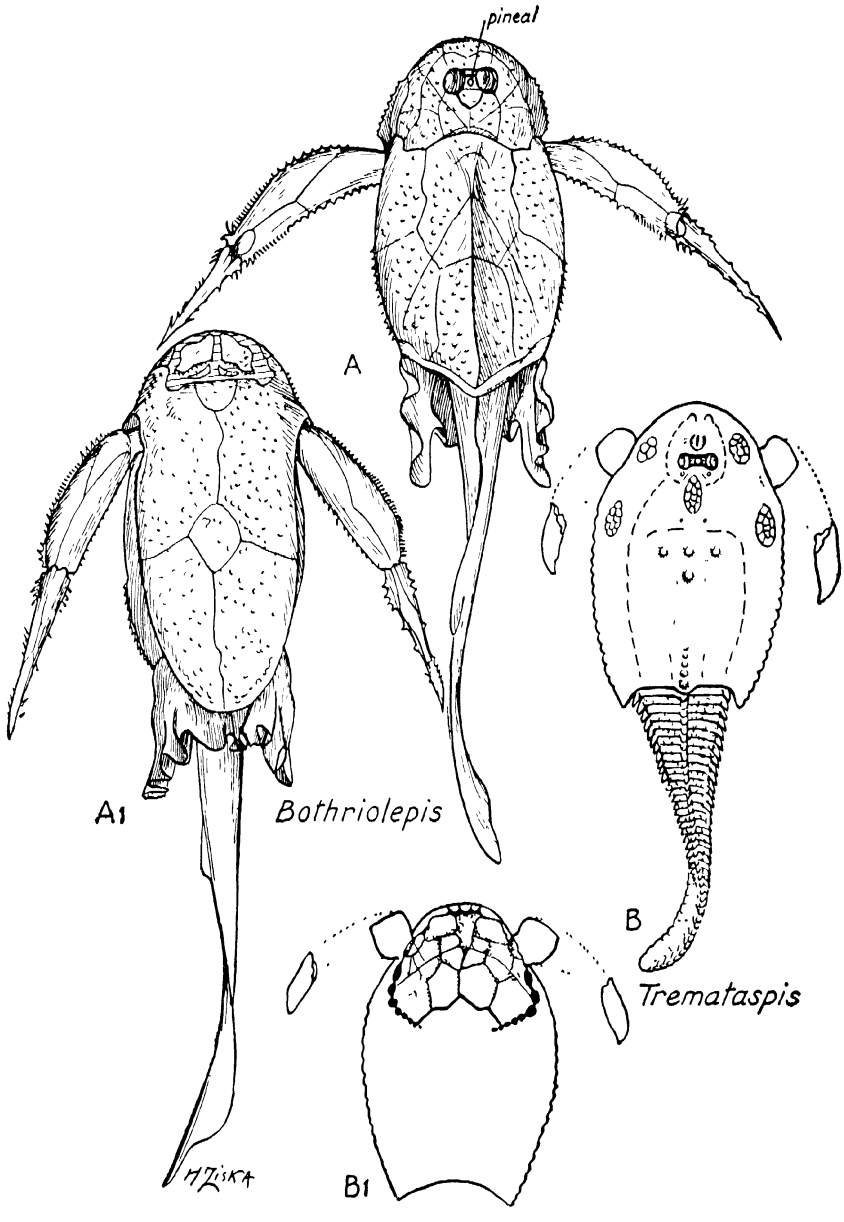


Fig. 5.17. A typical antiarch (*Bothriolepis*, A, A1) compared with a cephalaspid ostracoderm (*Trematapis*). In B, B1, the supposed paired appendages were later identified by Patten himself as displaced dorsal and anal finspines. A, B, dorsal aspect; A1, B1, ventral aspect. All after Patten.

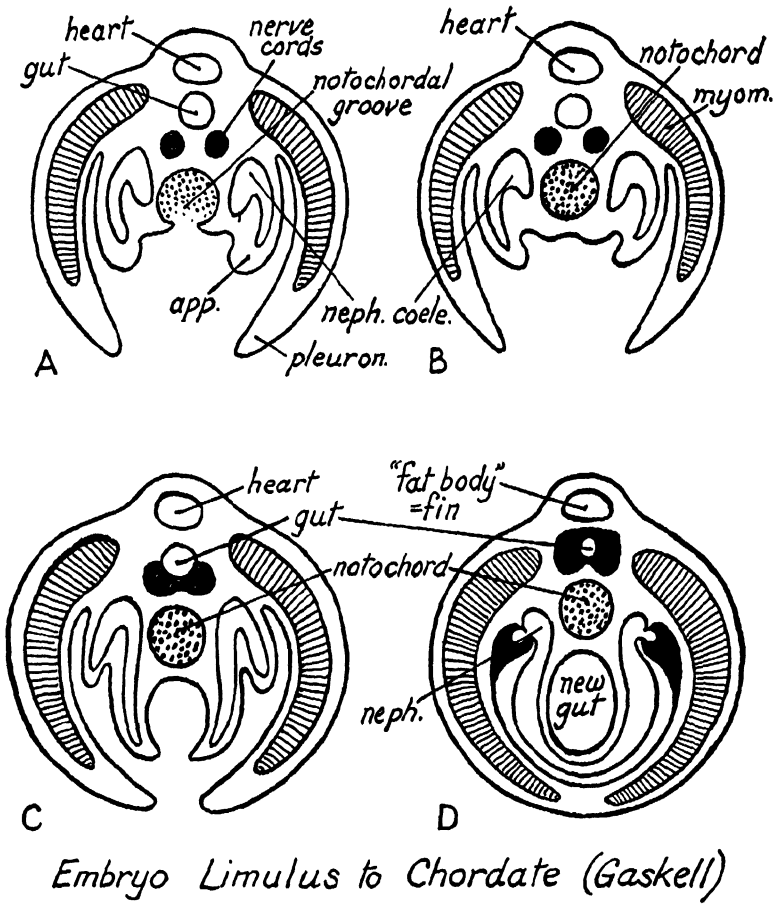


Fig. 5.18. Diagrams illustrating Gaskell's theory of the origin of vertebrates. Simplified cross-sections: A, an embryo *Limulus*; D, an "Ammocoete" larva of a lamprey; B, C, hypothetical intermediate stages. After Gaskell.

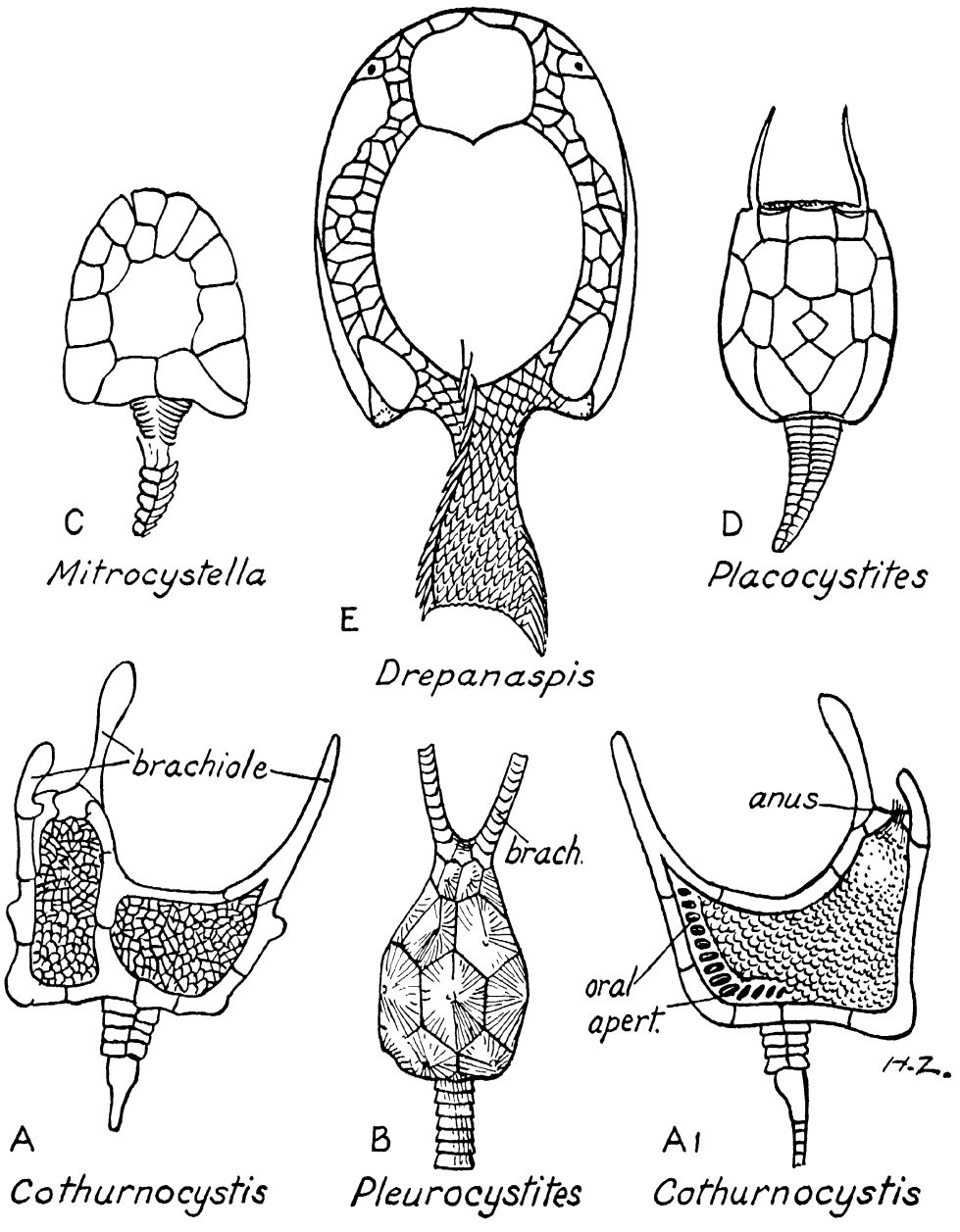


Fig. 5.19 Diverse carpoid echinoderms (A–D) compared with an ostracoderm (E). According to Bather and others the carpoids were *laterally* compressed, C being the right side, D the left. E is *dorsoventrally* compressed. Thus the resemblances between C, D, E would be convergent (J. H. McGregor). A, C, D, after Bather; B, after Jaekel; E, after Traquair.

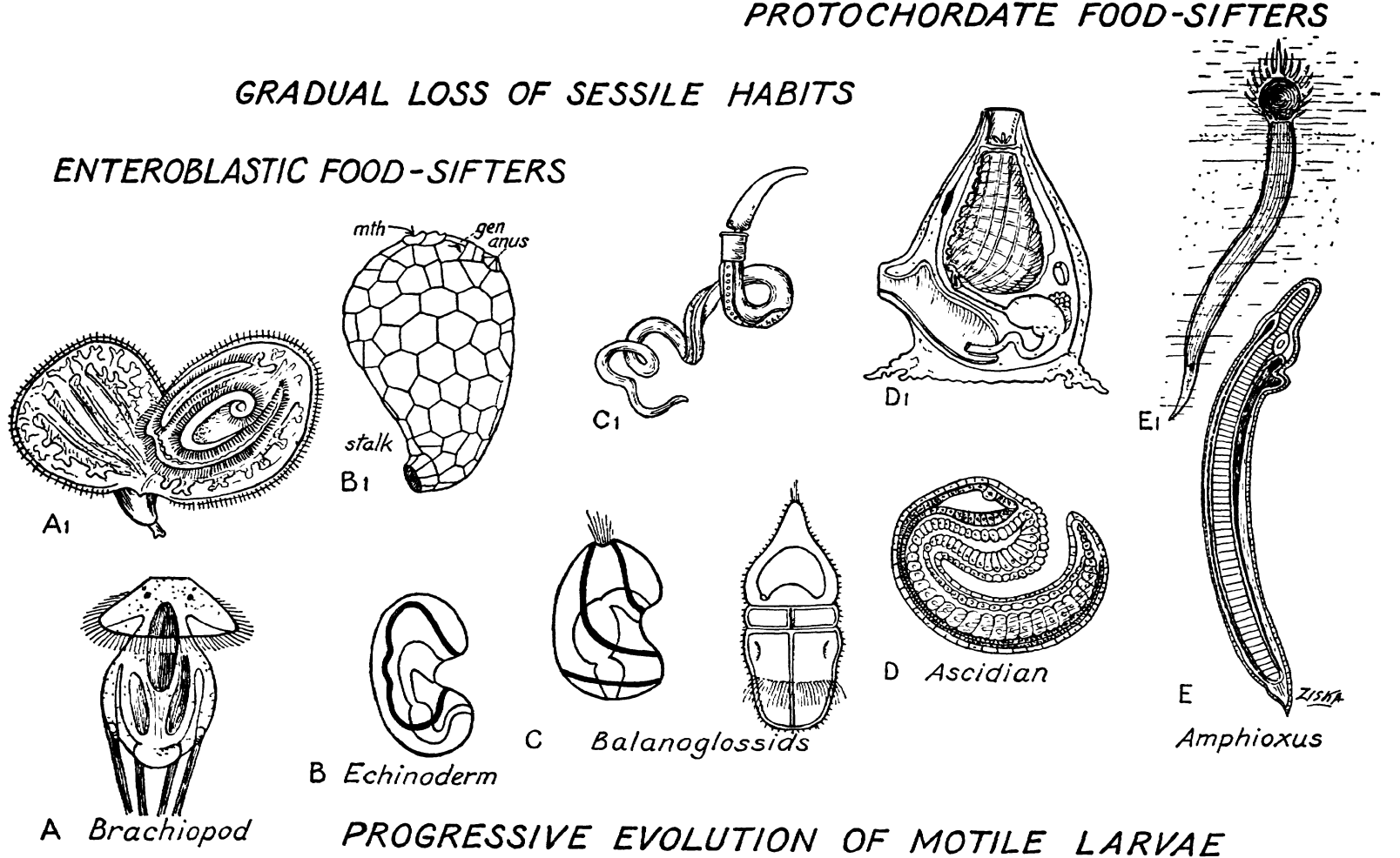


Fig. 5.20. Ascending grades of food-sifters and their free-swimming larvae. In A–D free-swimming larvae give rise to sedentary or slow-moving adults. In E the free-swimming adaptations of the larvae are retained and improved in the adult. For *enteroblastic* read *"enterocoelic."*

CHAPTER VI

THE VERTEBRATES COME FORTH: SHELL-SKINNED ANCESTORS OF THE VERTEBRATES AND SOME OF THEIR BRANCHES

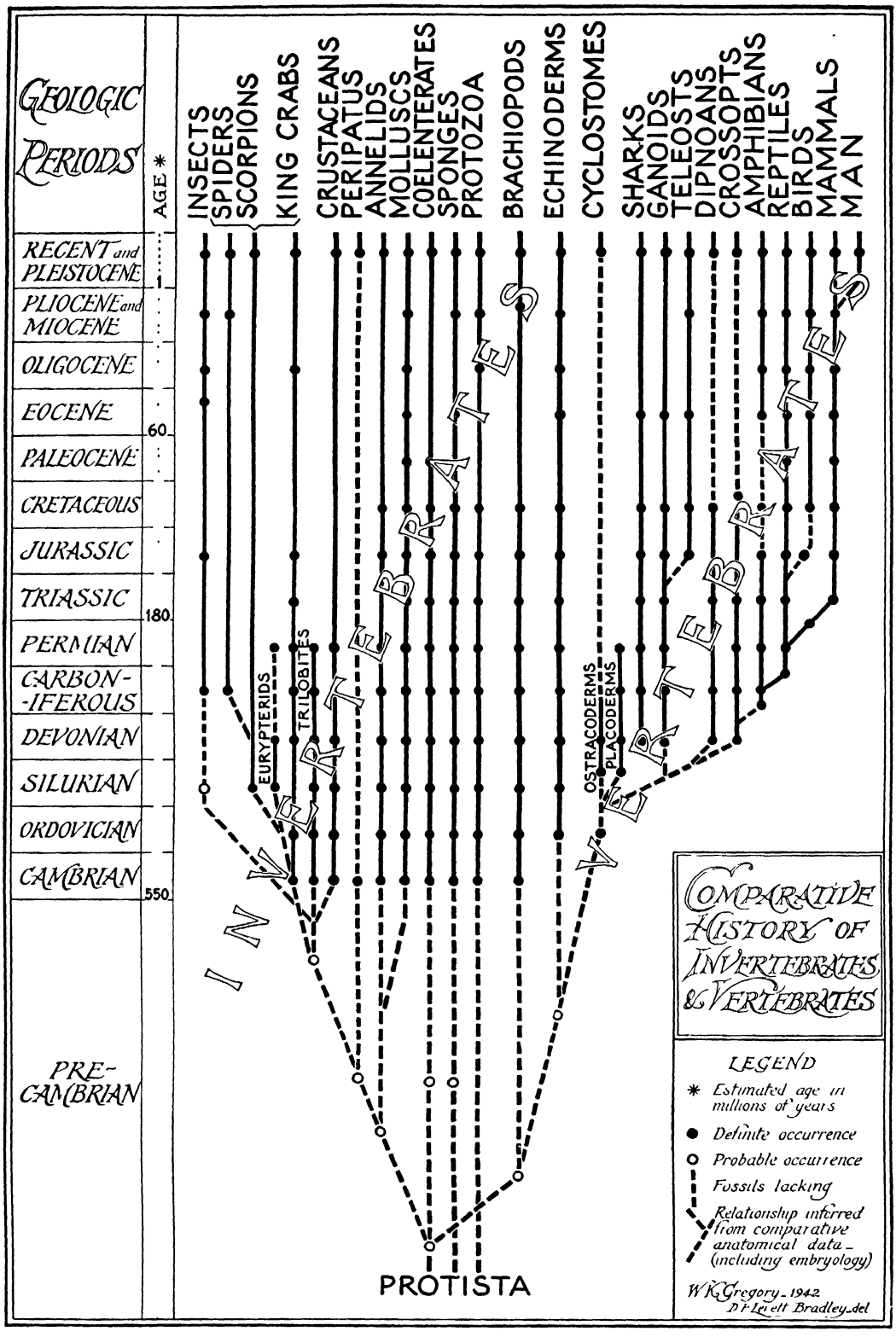
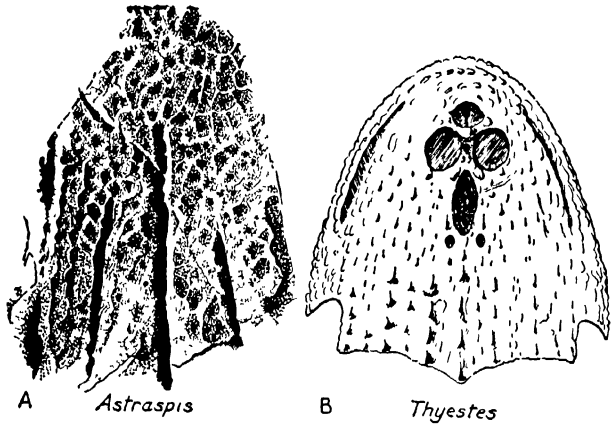

GEOLOGIC PERIODS
AGE *
RECENT and PLEISTOCENE
PLIOCENE and MIOCENE
OLIGOCENE
EOCENE
PALEOCENE
CRETACEOUS
JURASSIC
TRIASSIC
PERMIAN
CARBON-IFEROUS
DEVONIAN
SILURIAN
ORDOVICIAN
CAMBRIAN
PRE-CAMBRIAN
60
180
550
INSECTS
SPIDERS
SCORPIONS
KING CRABS
CRUSTACEANS
PERIPATUS
ANNELIDS
MOLLUSCS
COELENTERATES
SPONGES
PROTOZOA
BRACHIOPODS
ECHINODERMS
CYCLOSTOMES
SHARKS
GANOIDS
TELEOSTS
DIPNOANS
CROSSOPTS
AMPHIBIANS
REPTILES
BIRDS
MAMMALS
MAN
EURYPTERIDS
TRILOBITES
OSTRACODERMS
PLACODERMS
INVERTEBRATES
VERTEBRATES
PROTISTA
COMPARATIVE HISTORY OF INVERTEBRATES & VERTEBRATES
LEGEND
* Estimated age in millions of years
Definite occurrence
Probable occurrence
Fossils lacking
Relationship inferred from comparative anatomical data - (including embryology)
W.K. Gregory - 1942
P.P. Levitt Bradley del

Fig. 6.1



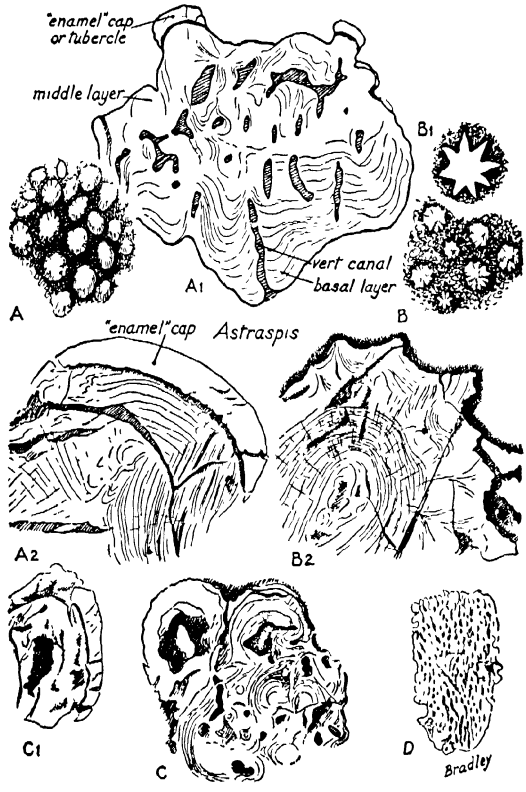


Fig. 6.2 (top). Part of the head-shield of *Astraspis desiderata* (A) compared with the entire head-shield (B) of a later (Upper Silurian) ostracoderm. A, after Bryant, X 6/10; B, after Abel, enlarged.

Fig. 6.3. Microphotographs of *Astraspis* tesserae. After W. L. Bryant, 1936. A, Surface tubercles of the low-crowned oval type, X 6. A1, Single tessera in vertical section, X 22½. A2, Vertical section through an oval tubercle, showing fibrous laminated structure beneath the enamel-like cap, X 105. B, Stellated tubercles with pointed crowns, X 6. B1, Eight-pointed horizontal section of star tip of one tubercle, X 32½. B2, Obliquely horizontal section of grooved tubercle, showing concentric laminae of fibrous structure, X 105. C, Horizontal section through base of tubercles, showing concentric laminae and large pulp cavities. The small openings may be pore canals, X 22½. C1, Vertical section of tubercle, showing large pulp cavity, X 52½. D, Visceral surface of tessera, showing network of perpendicular canals, X 7/2.

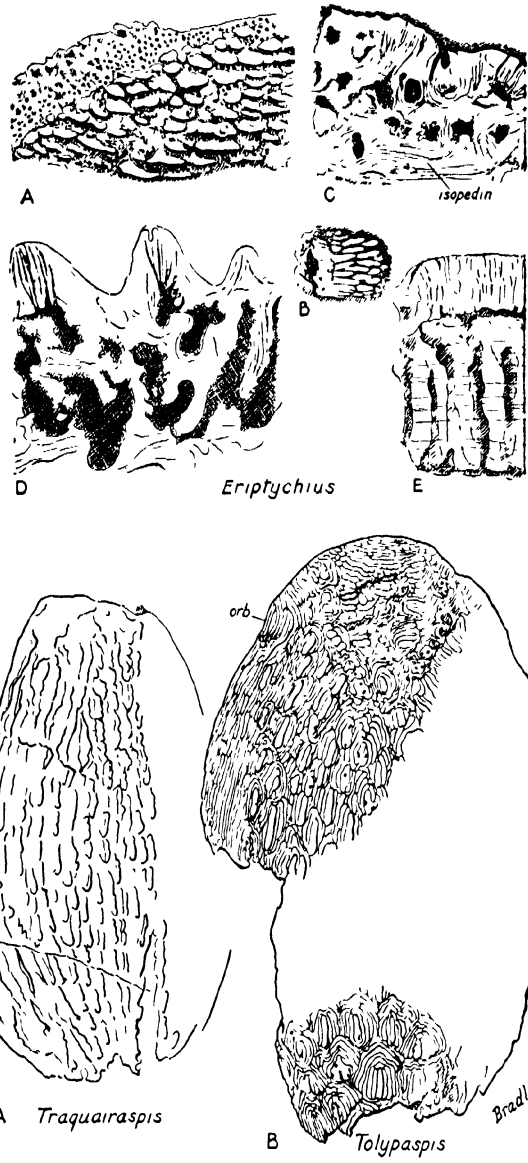


Fig. 6.4 (top). *Eriptychius* scales, from microphotographs. After W. L. Bryant. A, Surface of scale, showing small low-crowned tubercles and subparallel ridges, with area of overlap and its orifices of supposed mucous canals, X 12. B, Another scale, showing area of overlap, X 6. C, Vertical section of scale near margin (X 93) shows: basal layer of isopedin, or tissue lacking bone cell spaces and built up of horizontal laminae; middle layer, perforated by large vascular canals forming a spongy labyrinth; outer layer, "composed of transparent concentric lamellae, penetrated and bound together by minute parallel fibres, disposed at right angles to the laminae." D, Vertical section through middle and superficial layers of scales (X 120) shows vascular and pulp-like cavities, which give off branching "dentine tubules." E, Vertical section of scale cut in a longitudinal direction, X 72. "The basal layer with its wide perpendicular canals is greatly expanded at the expense of the [vascular] middle layer." Beneath the transparent outer layer numerous pulp cavities are fused into one.

Fig. 6.5. Exceptional forms of sculpture on the shields of cyathaspid pteraspids. After Kiaer and Heintz. A, Ventral shield with lines of larger and smaller dentinal ridges. B, Dorsal shield, in which the parallel ridge systems seem to be subdividing into well-ridged scales recalling the more or less separate units in the Ordovician *Astraspis*. The surface ornamentation of *Traquairaspis*, as well as that of the Lower Devonian *Weigeltaspis* of Brotzen (1933, p. 649) recall the parallel ridges on the scales of *Eriptychius* (fig 6.4A).

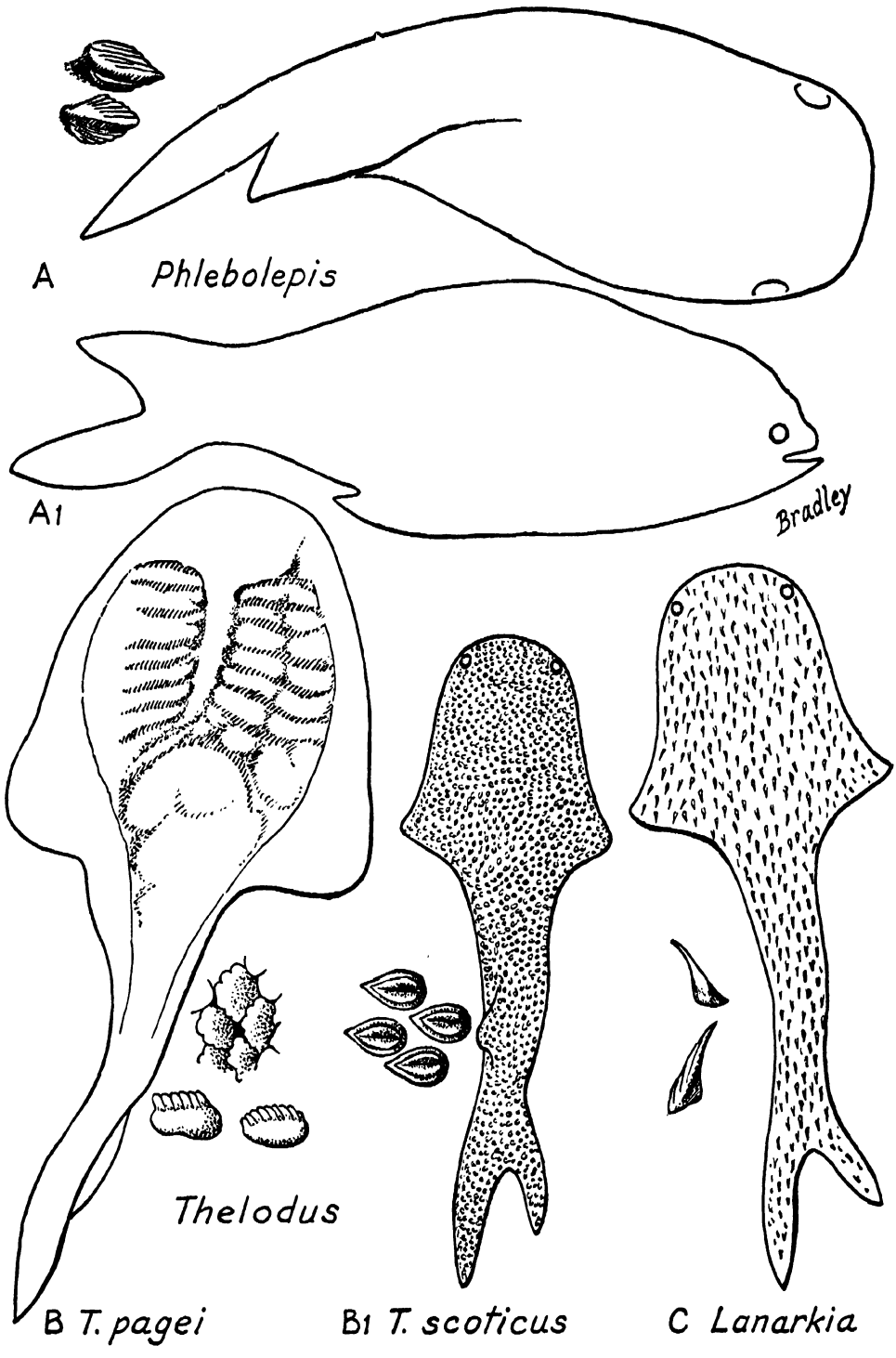


Fig. 6.6. Upper Silurian (A, A1, B1, C) and Lower Devonian (B) thelodonts, with enlarged views of scales. A, A1, after Kiaer (mainly from his pl. III, fig. 1, 1924; tail from pl. IV, fig. 2); B, B1, C, after Traquair. Scales greatly enlarged.

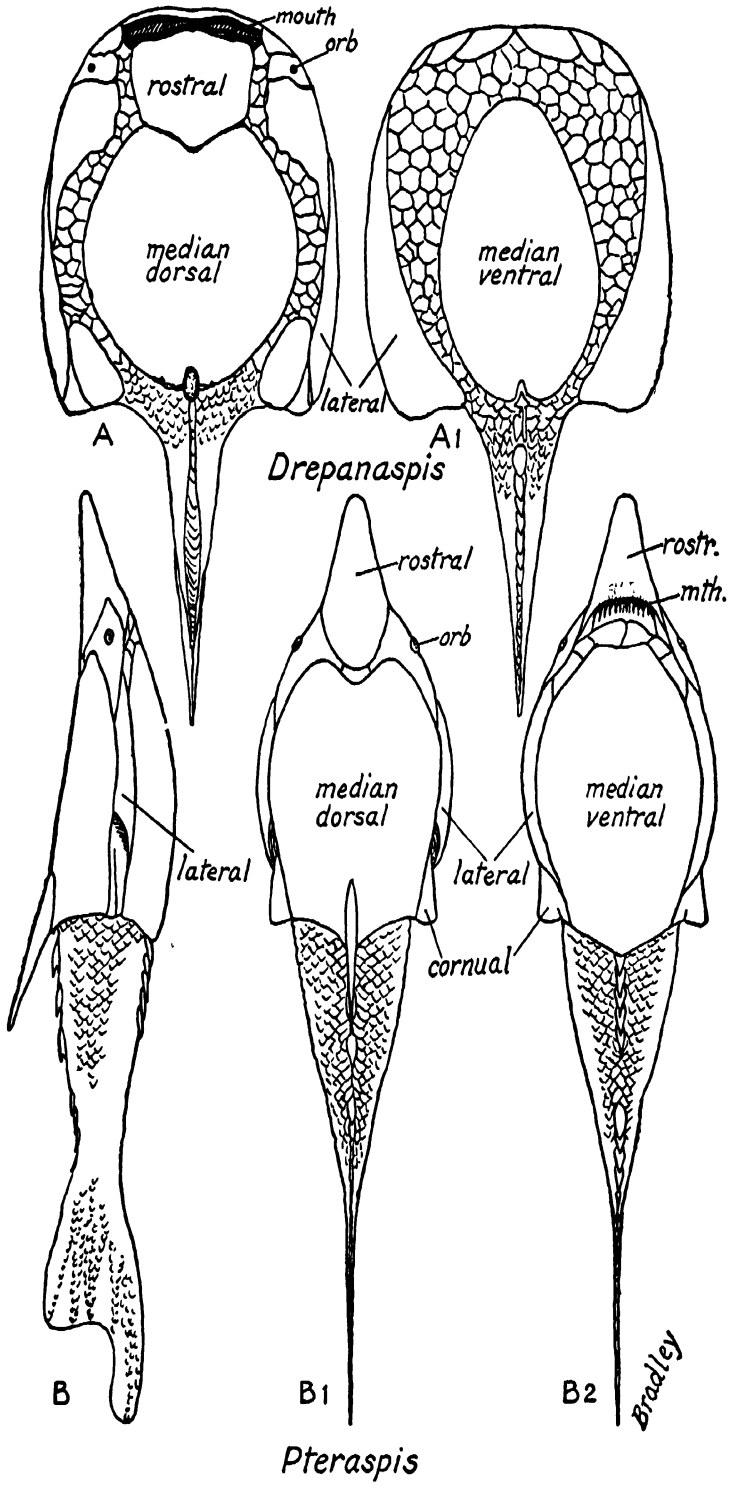


Fig. 6.7. Depressed (A) and fusiform (B) pteraspids. A, After Traquair; B, from E. I. White.

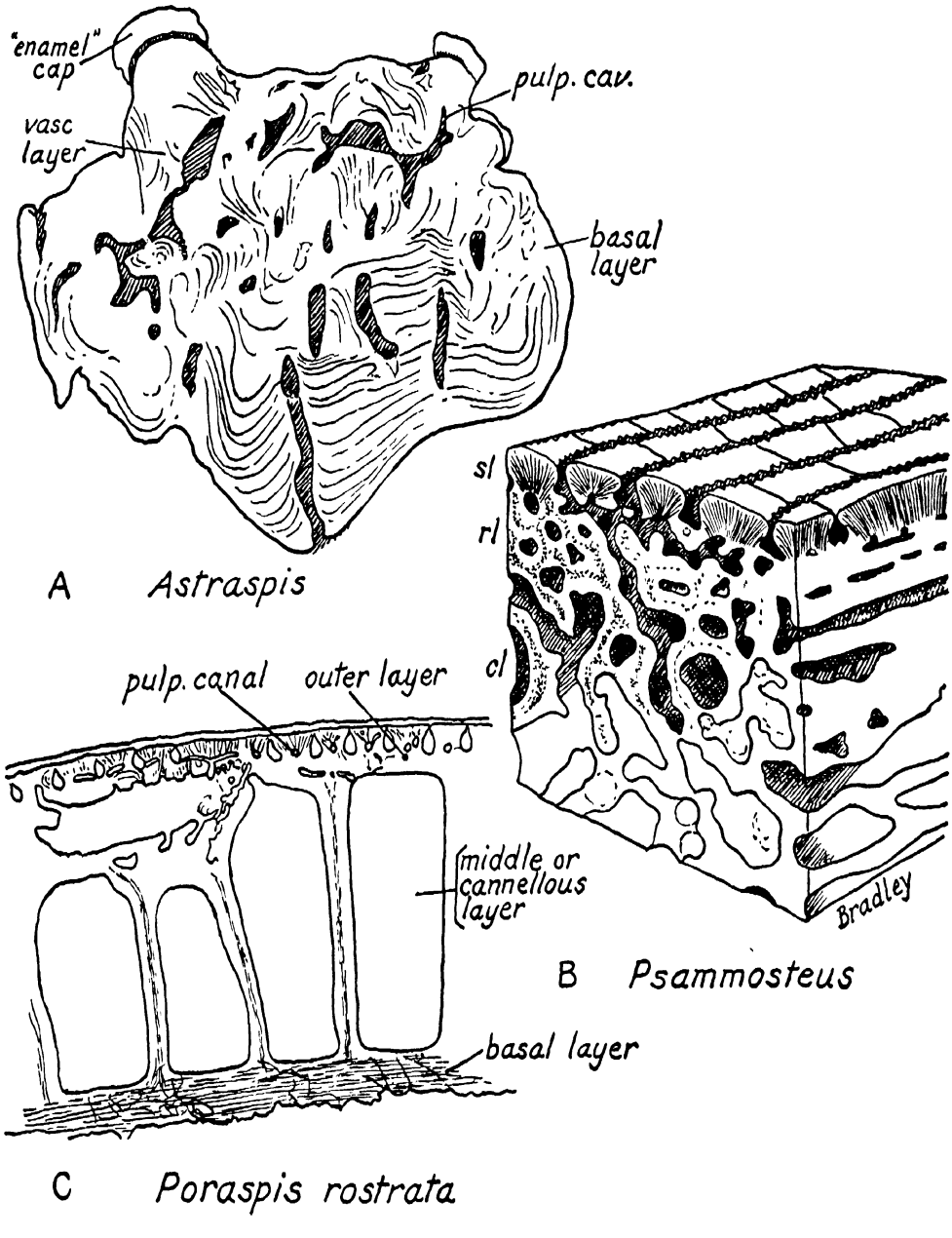


Fig. 6.8. Microsections of exoskeletal pieces in ostracoderms of the order Heterostraci. A, is the oldest and presumably the most primitive. It is irregularly formed with gradual transition from the laminated basal layer to the vascular or middle layer; this in turn passes into the outer layer of dentine-like tubercles, which are covered by a transparent, amorphous enamel-like cap. In B, the parallel dentinal ridges are separated by more or less regularly spaced grooves, which are continuous below with the meandering tubes of the reticular vascular layer and are thought to have lodged mucous canals. The lower stratified layer is not shown in this figure. In C, the middle or cancellous layer has been greatly enlarged and there is a sharp regimentation of similar units in all the layers—apparently indicating a later grade of evolution. A, after Bryant; B, from Stensiö, after Kiaer; C, after Kiaer and Heintz

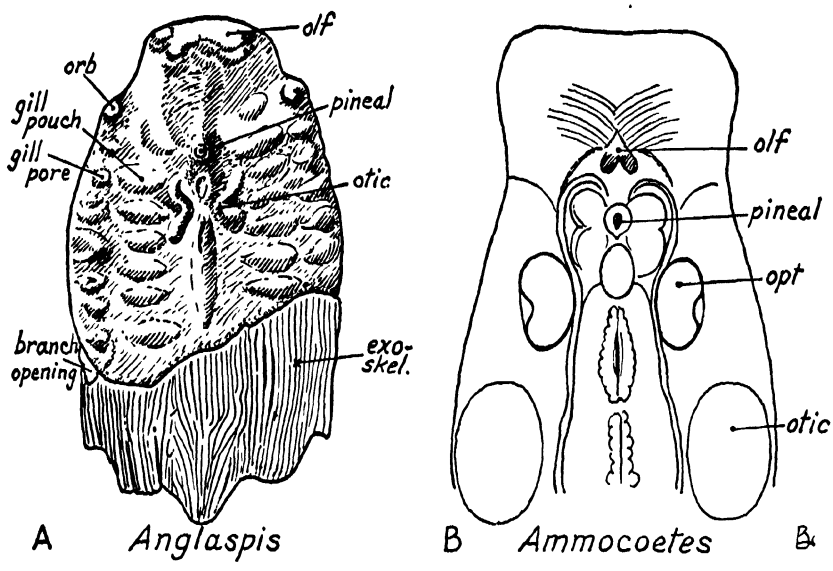


Fig. 6.9. Comparative anatomy of the head in pteraspid (A) and larval lamprey (B). In B, the naso-hypophysial tube has been displaced upward and backward (*olf*), as have also the paired eyes; the otic capsules are enlarged. The gill pouches lie beneath the cranial plane, as in A, but are not shown. A, after Kiaer; B, after Gaskell.

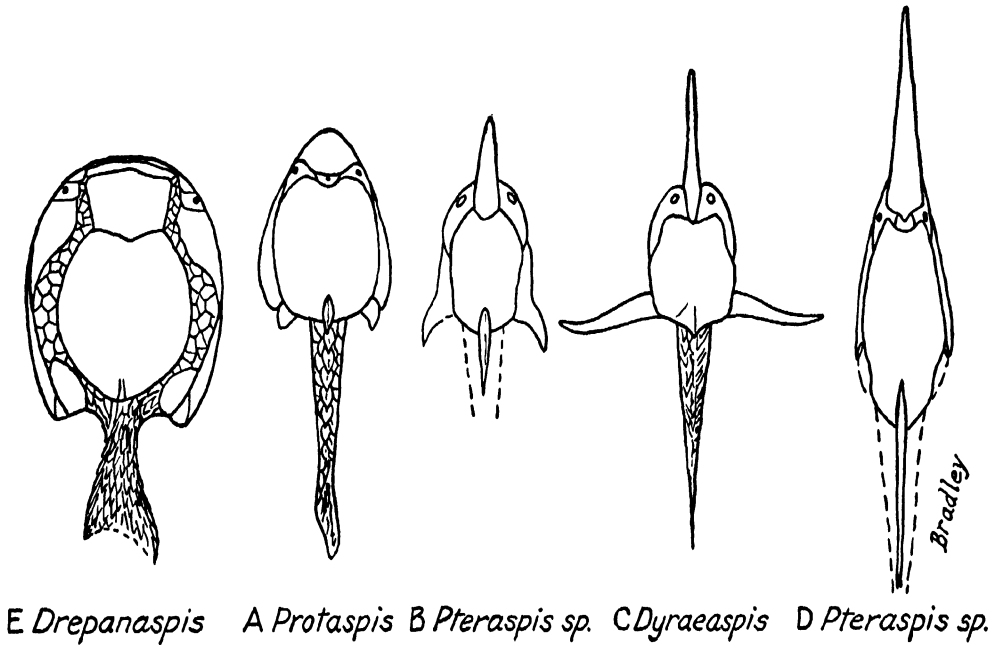


Fig. 6.10. Anisomerism in the head-shields of pteraspids. Based on figures by Heintz and Bryant.

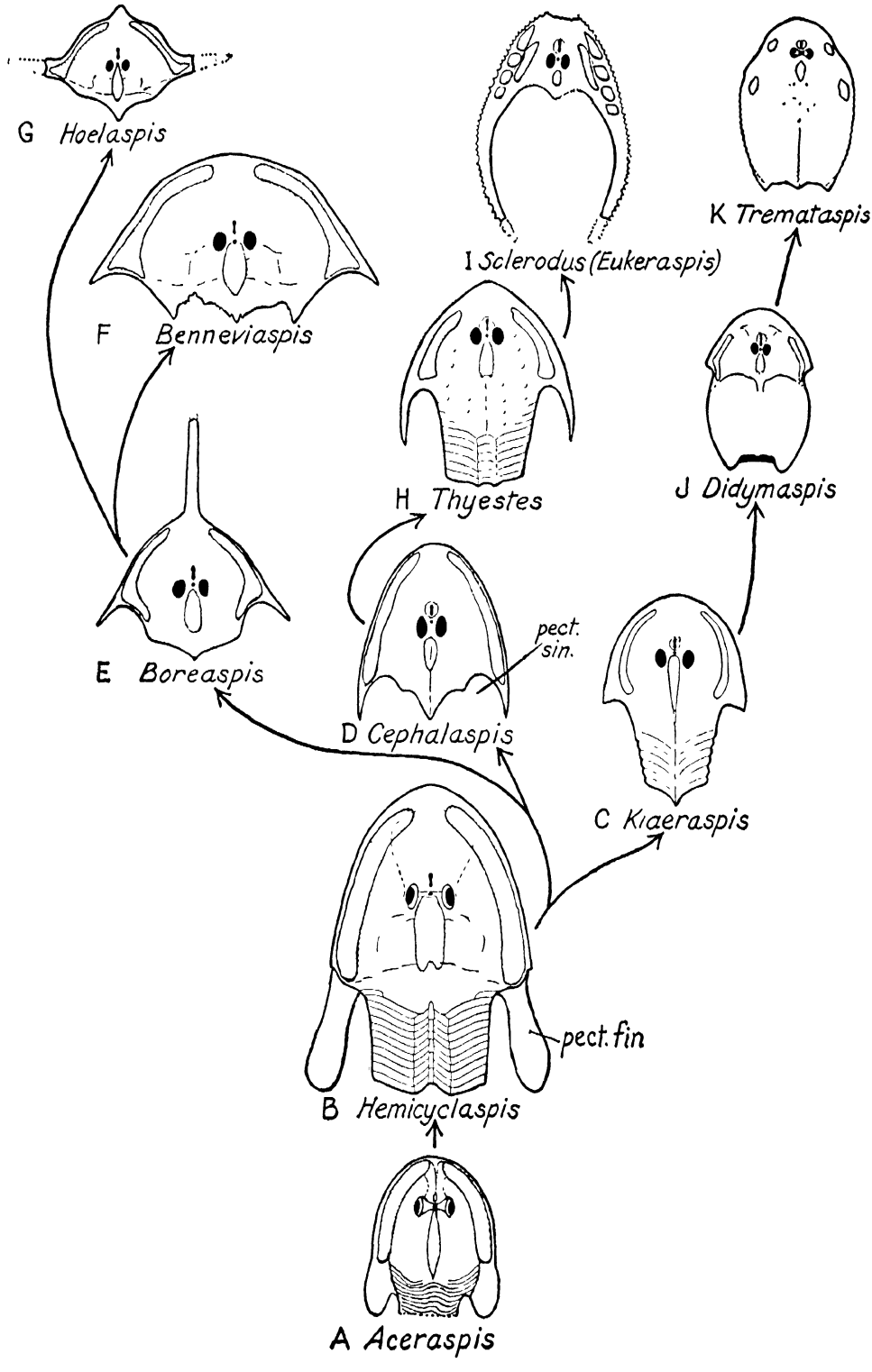


Fig. 6.11. Anisomerism and divergence among the cephalaspids. From Gregory: A, after Heintz; B–J, after Stensiö; K, after Patten.

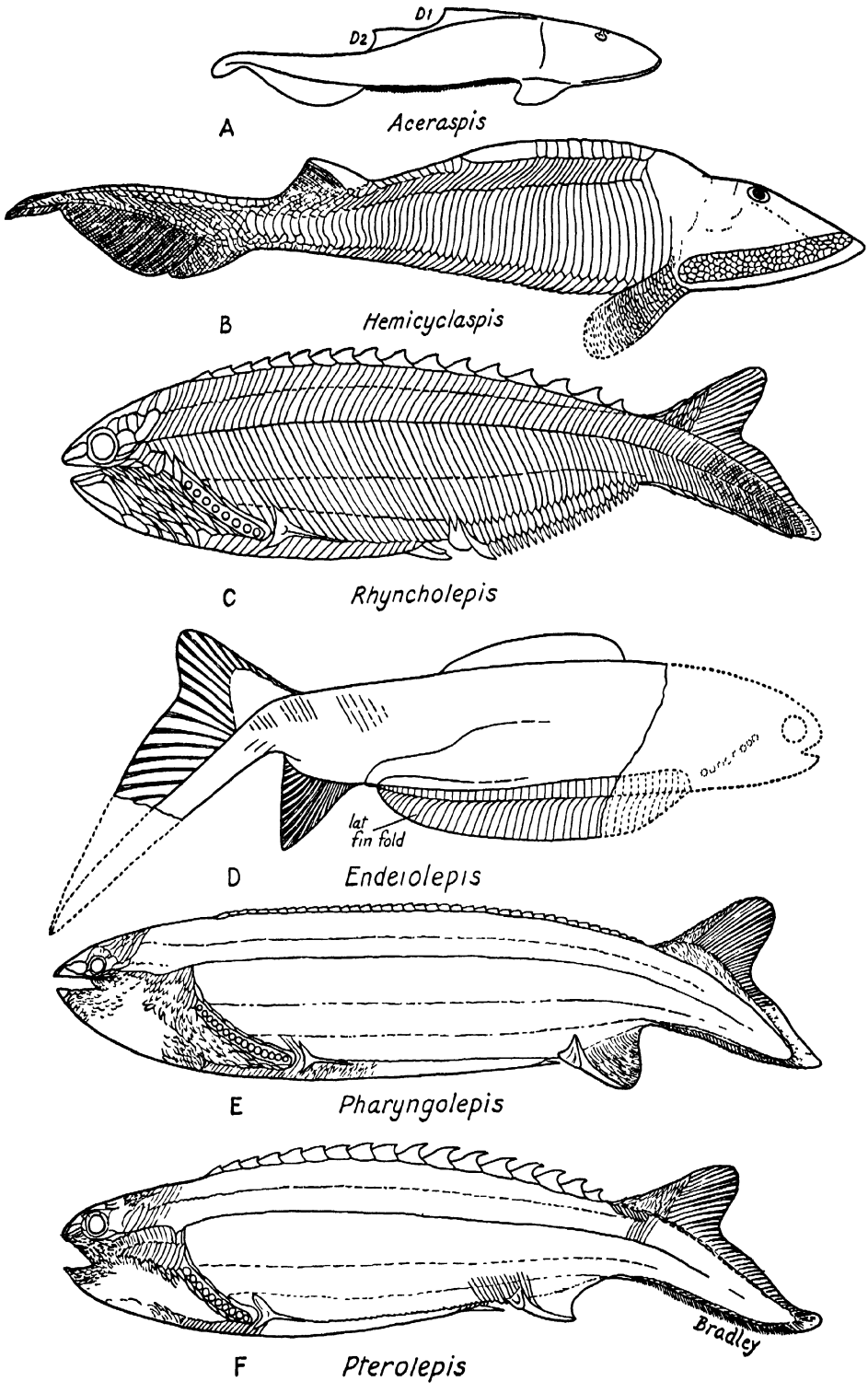
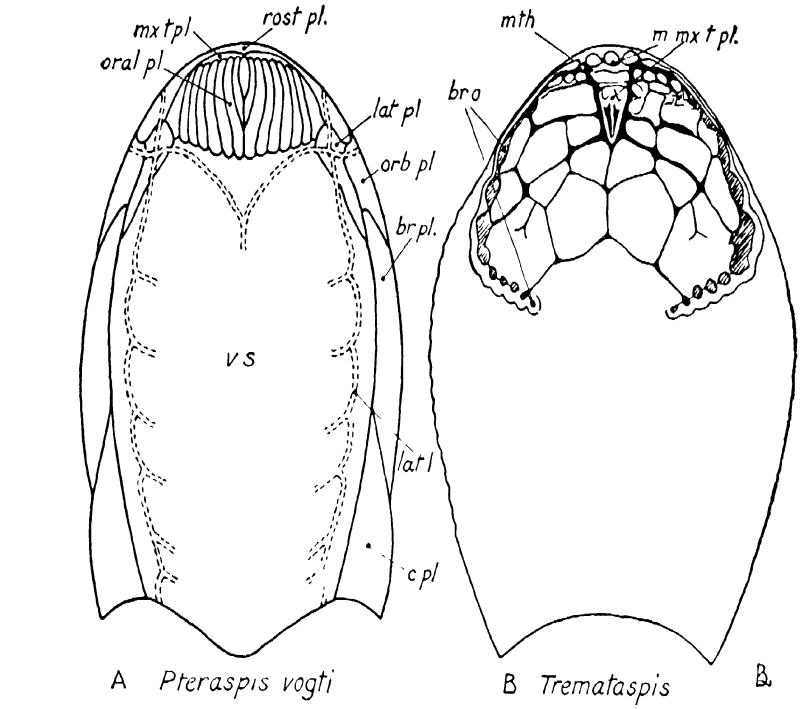


Fig. 6.12. The body form in two cephalaspids (A, B) and four anaspids (C–F). All from the Upper Silurian of Europe. A, after Heintz; B, D, after Stensio; C, E, F, after Kiaer. Not to scale.



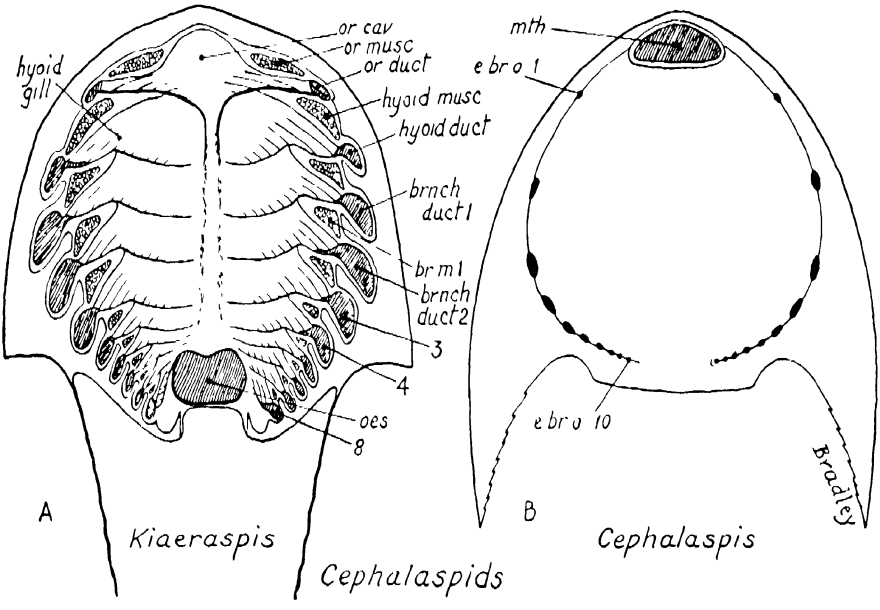


Fig. 6.13 (top). Ventral surface of the shield, showing contrasting arrangement of throat- and mouth-plates in a pteraspid (A) and a cephalaspid (B). A, from Kiaer; B, from Kiaer, after Patten.

Fig. 6.14. Diagrams showing the probable arrangement of the mouth, gill-openings and gills in relation to the known skeletal parts. After Stensiö.

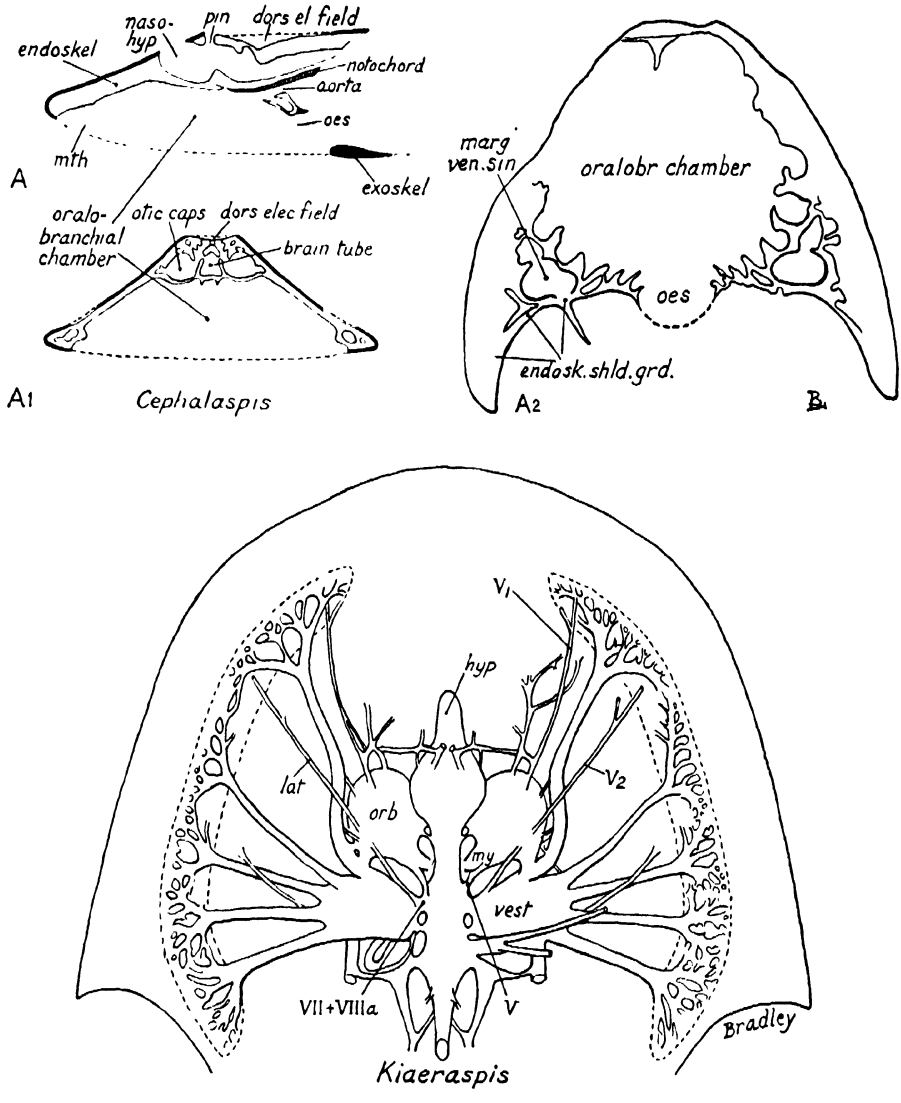


Fig. 6.15 (top). Schematic median sagittal (A) and transverse (A1) sections through the head of a cephalaspid. Section A1 is well behind the orbits and runs through the otic capsule. Endoskeletal tissue, unshaded; exoskeletal parts, black. Horizontal section (A2) of head-shield, dorsal view. Showing relations of the "endoskeletal shoulder girdle" to the oralobranchial chamber. After Stensiö.

Fig. 6.16. Head-shield of a cephalaspid seen from below, showing the branching of the tubes for the so-called electric nerves. After Stensiö.

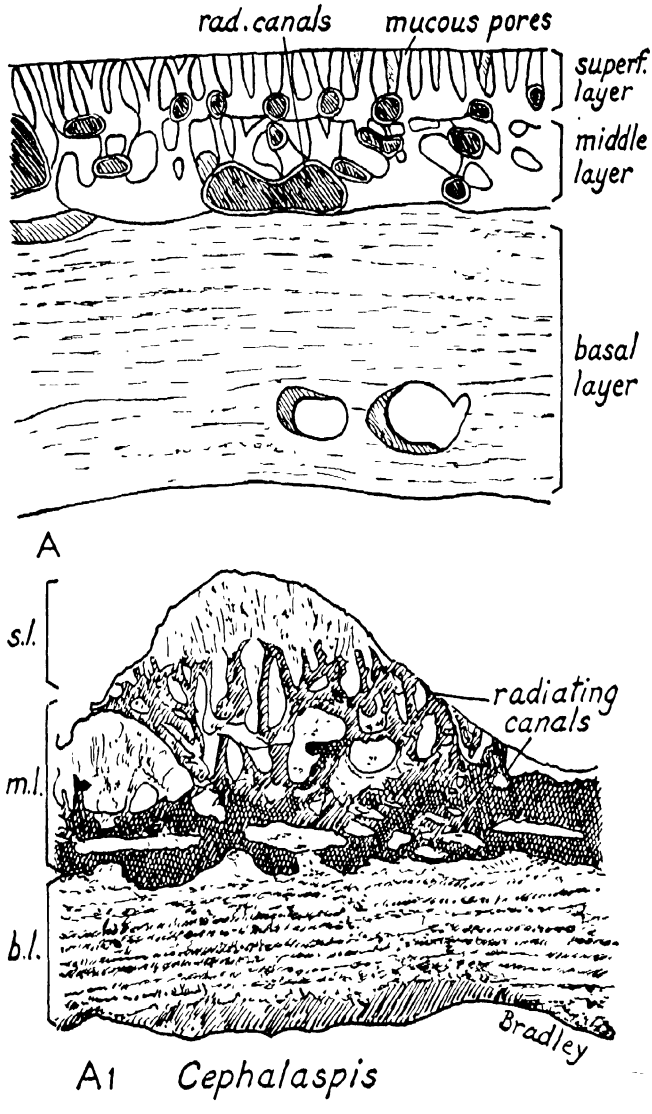


Fig. 6.17. Transverse sections of the exoskeleton. After Stensiö. In A the superficial layer entirely covers the middle layer; in A1, it is alternately heaped up into a tubercle and thinned out or lacking at the bottom of the wide mucous grooves into which the radiating canals probably discharged their mucous.

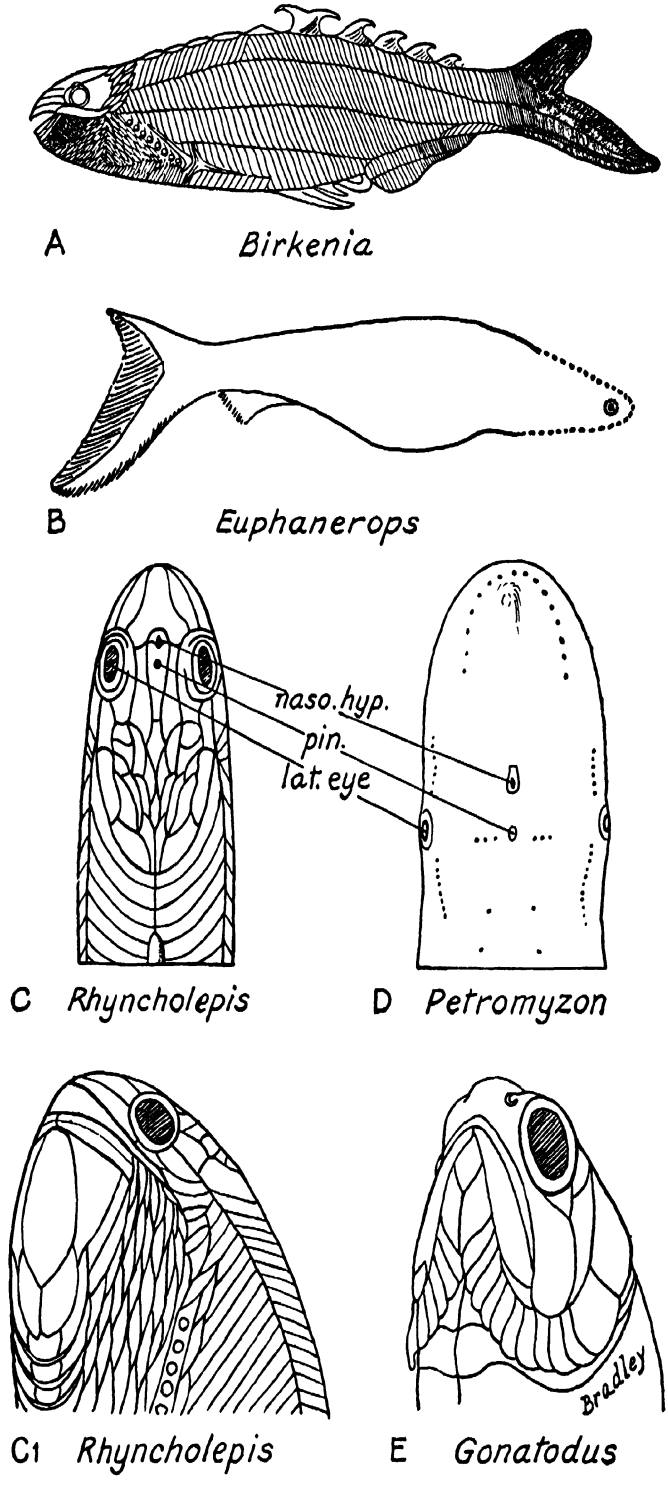


Fig. 6.18. Comparison of anaspids (A, B, C, C1), cyclostome (D) and primitive ganoid (E). A, after Stetson; B, from Stensiö, after A. S. Woodward; C, C1, D, E, after Kiaer.

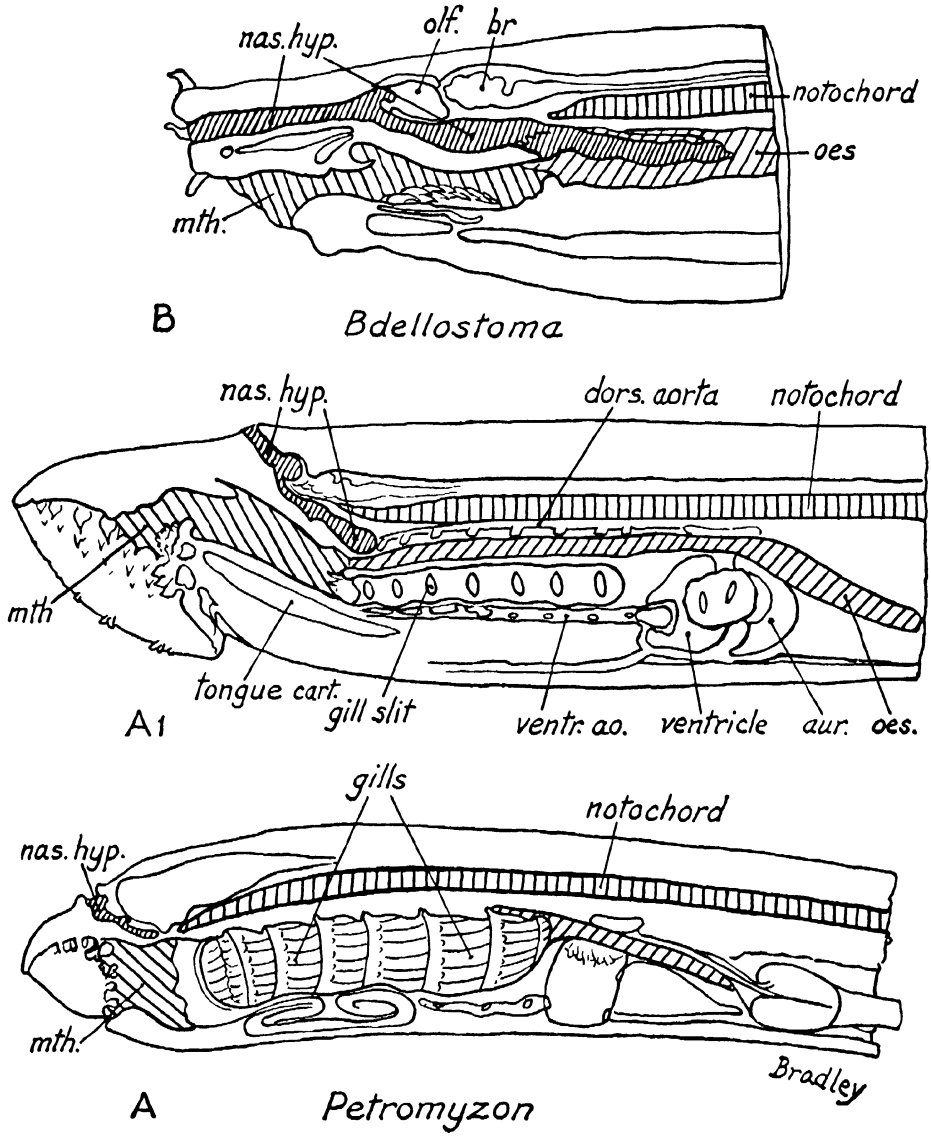


Fig. 6 19. Cephalothorax of modern Agnatha. A, larval stage; A1, adult stage; B, adult hagfish. Simplified from Goodrich.

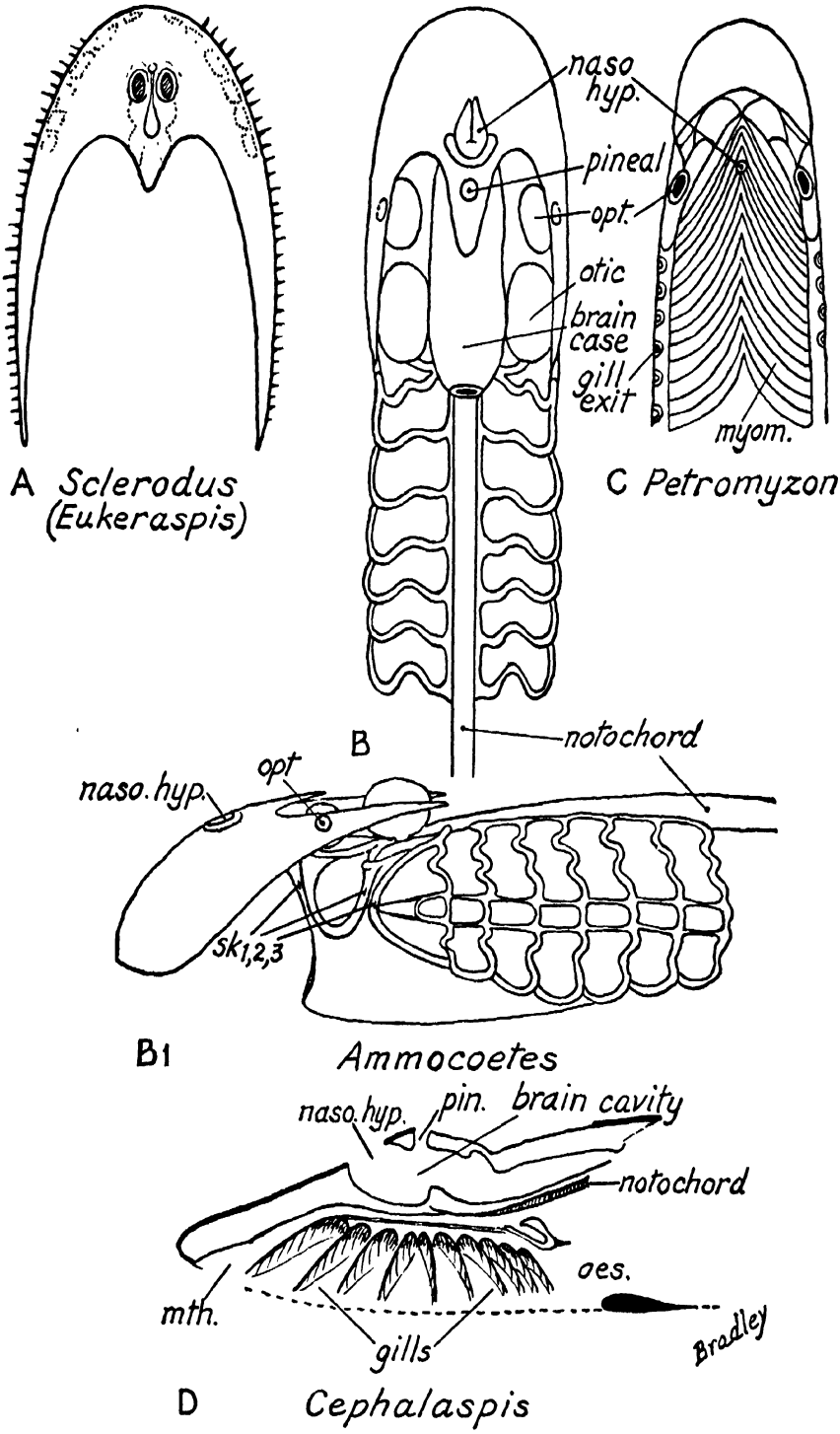


Fig. 6.20. Comparison of ostracoderms and cyclostomes. A, from Gaskell, after Woodward; B, B1, after Gaskell; C, after Gaynor Evans; D, after Stensiö, slightly modified to indicate position of interbranchial septa.

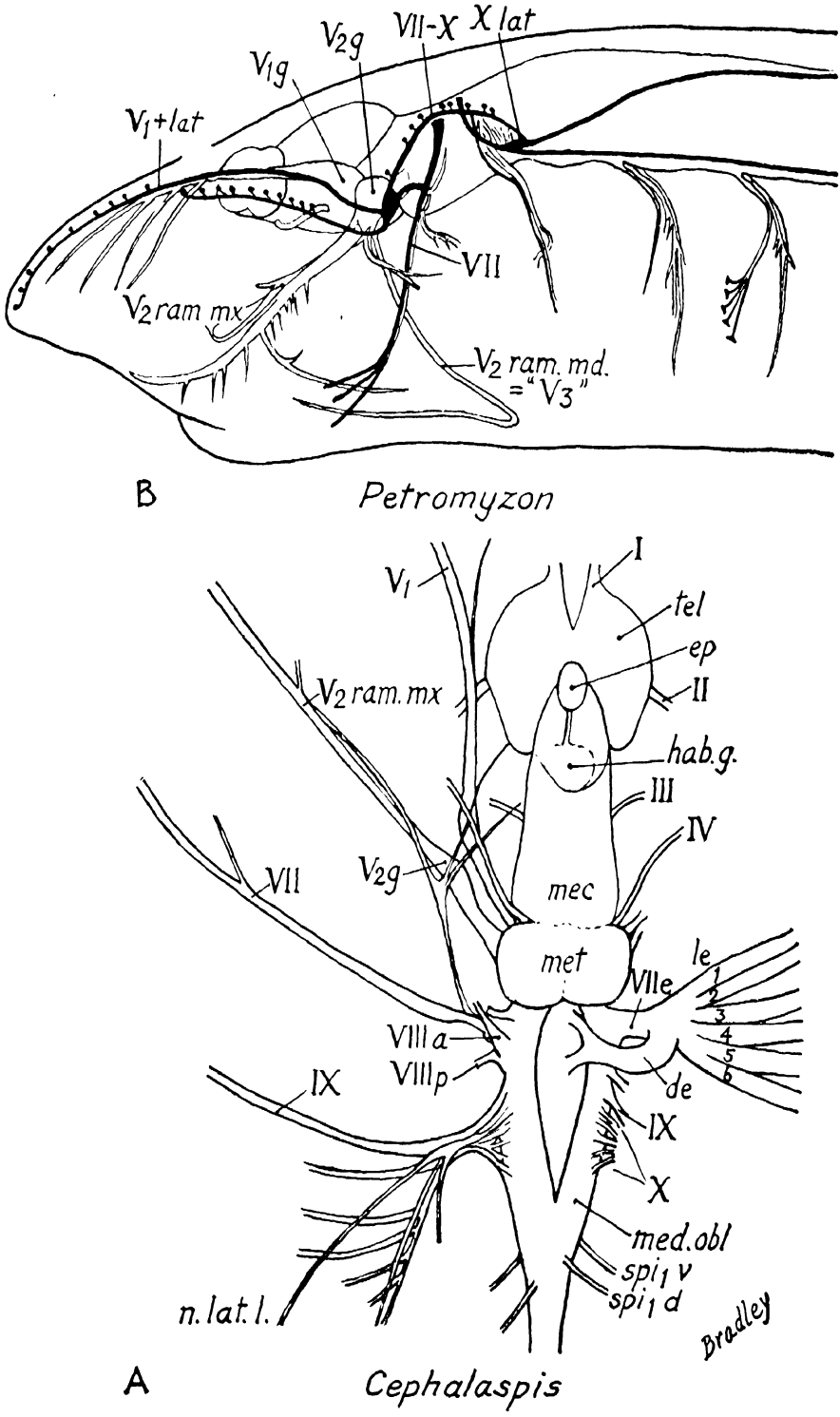


Fig. 6.21. A, Cranial nerves and restored brain of *Cephalaspis*. After Stensiö. B, Relations of the ophthalmic, fifth, seventh and tenth cranial nerves in *Petromyzon*. From Stensiö, after Johnston.

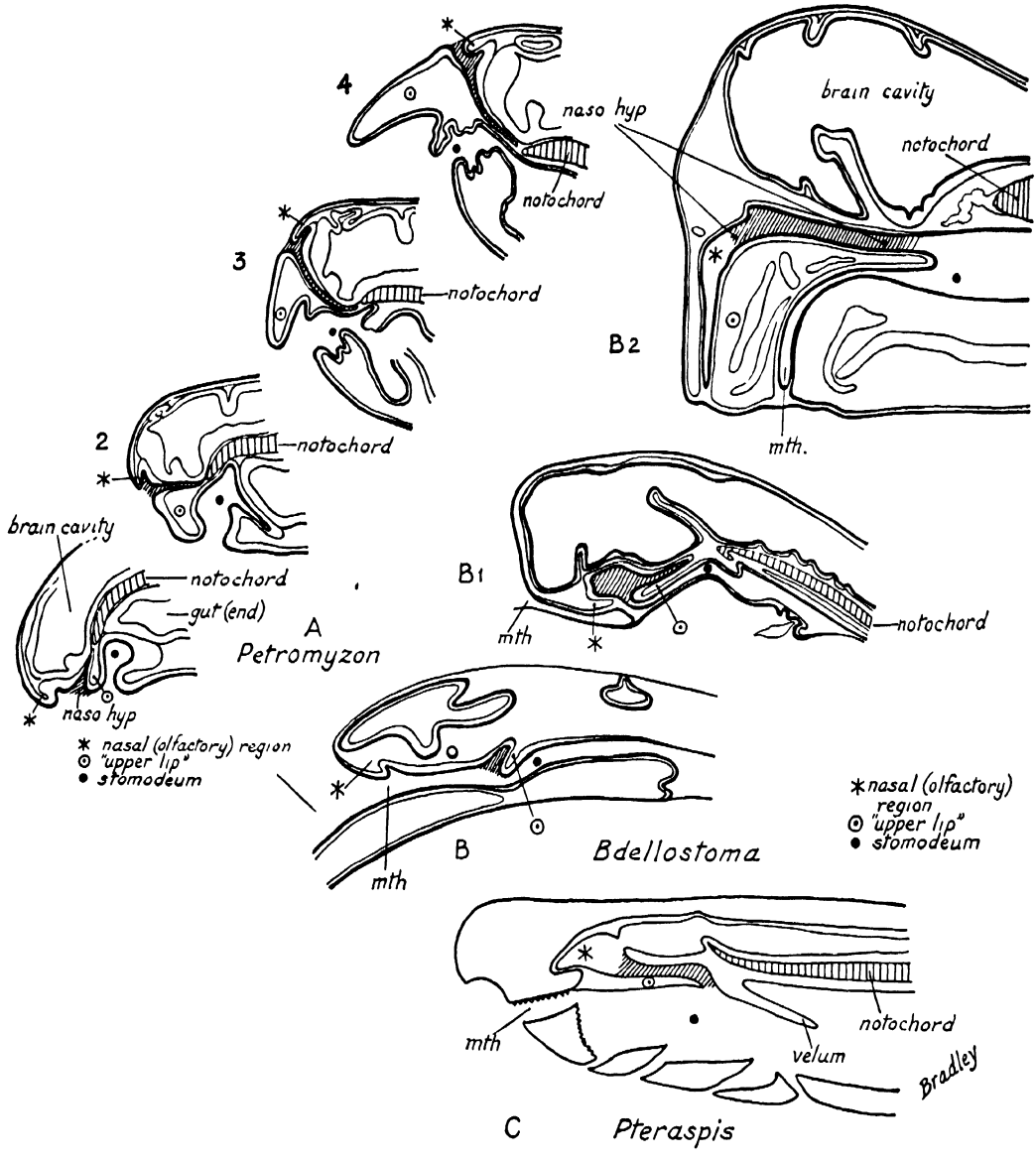


Fig. 6.22. Progressive displacement of the hypophysial fold from the ventral to the dorsal surface in the development of the lamprey (A1–A4). Modified from Stensiö, after Goodrich. Supposed relations of the naso-hypophysial duct in foetal myxinoid (B–B2) and in adult *Pteraspis* (C). B, from Stensiö, after Kupfer; C, after Kiaer.

CHAPTER VII

EARLY EXPERIMENTS AMONG STREAMLINED PREDATORS (PLACODERMS)

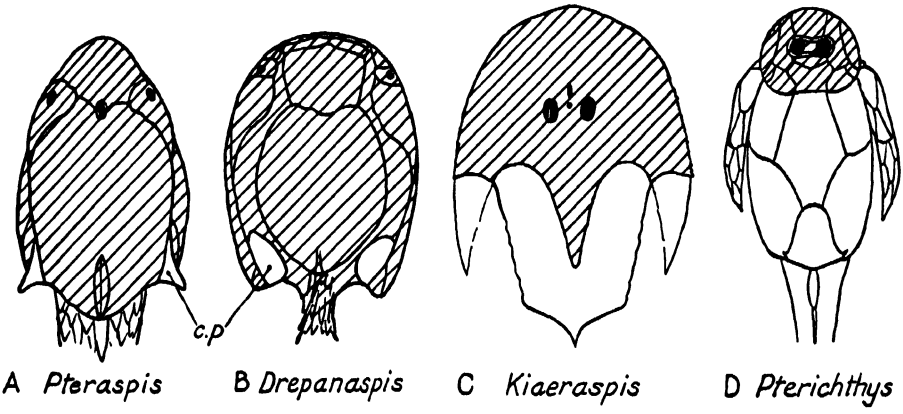


Fig. 7.1 (top). Comparison of the head-shields (cross-hatched) in ostracoderms (A–C) and antiarch (D). In C and D there is also a carapace or shoulder-girdle, behind the head. A, B, after Heintz; C, after Stensiö; D, from Zittel, after Traquair.

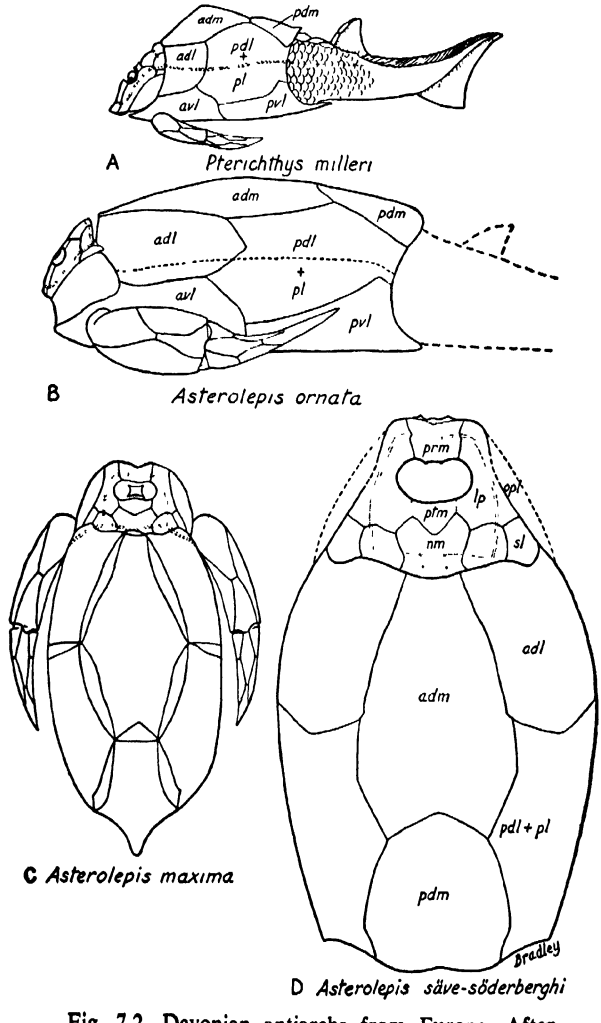


Fig. 7.2. Devonian antiarchs from Europe. After Gross.

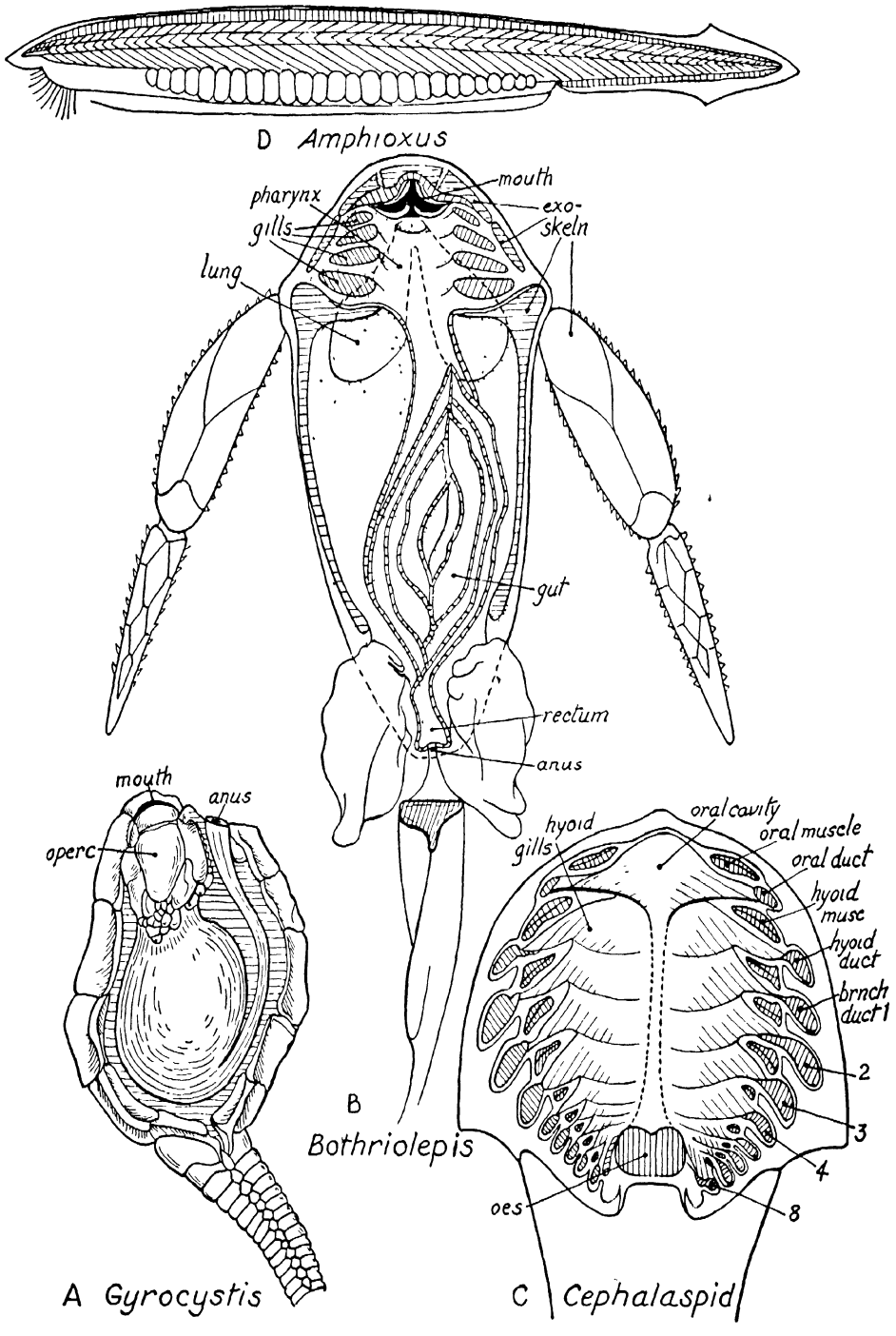


Fig. 7.3. Carpoid echinoderm (A) compared with early chordates (B, C) and *Amphioxus* (D). Showing the already great advance of the early chordates beyond the carpoid grade in the evolution of the oralobranchial organ and in the dominance of the vertebrate locomotor system, with a flexible axis extending to or into the head. A, after W. K. Spencer; B, after Dennison; C, after Stensiö; D, after Delage and Hérouard.

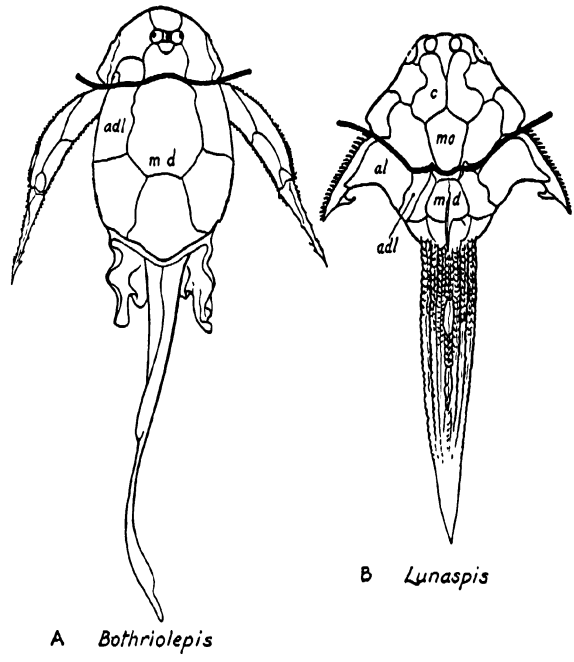


Fig. 7.4. Comparison of antiarch (A) and primitive acanthaspid arthrodire (B). In different ways *Lunaspis* recalls such diverse forms as *Thelodus* (pectoral projections), *Bothriolepis* (pectoral appendages with serrated borders), *Gemündina* (general form of body, skull pattern), *Acanthaspis* (pectoral spines). It agrees with both antiarchs and arthrodires in the sharp division between head and thorax. A, after Patten; B, after Broili.

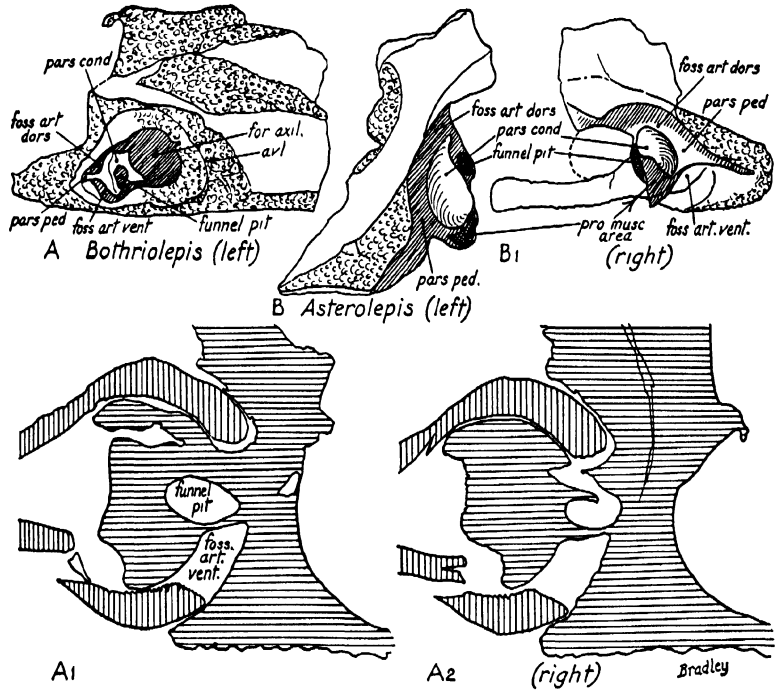


Fig. 7.5. The articulation of the pectoral appendage in antiarchs. A, Left anteroventrolateral with pectoral articular region. The brachial process includes a pars pedalis (which separates the dorsal and ventral parts of the articular fossa) and a pars condylyoidea, which is surrounded by the inner surface of the proximal end of the pectoral appendage (A1, A2). The funnel pit leads medially into a canal and probably transmitted an artery and possibly a nerve to the pectoral appendage (Stensiö, 1931, pp. 96–102). A is a lateral view of the left side. B is an anterior and somewhat dorsomedial view of the left side. B1 is an antero-lateral and somewhat dorsal view of the right side. After Stensiö.

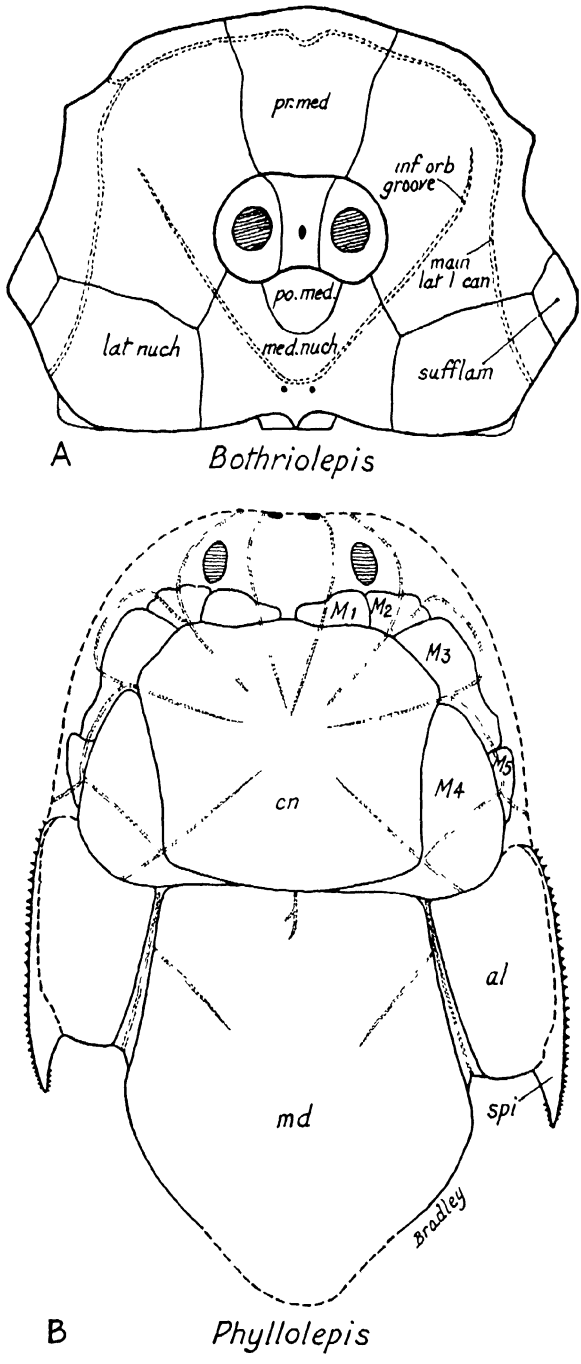


Fig. 7.6. Contrasting patterns in antiarch (A) and phyllolepid (B). The Upper Devonian *Phyllolepis* was formerly referred to the pteraspid ostracoderms, but has been shown by Gross (1934) and by Stensiö to belong among the Placodermi. Stensio (1936, p. 30) also showed that *Phyllolepis* possessed many important characters in common with certain Arthrodira (fig. 7.7) and it is regarded by Stensio (1936) and Moy-Thomas (1939, p. 43) as a highly specialized branch of the Arthrodira. After Stensiö.

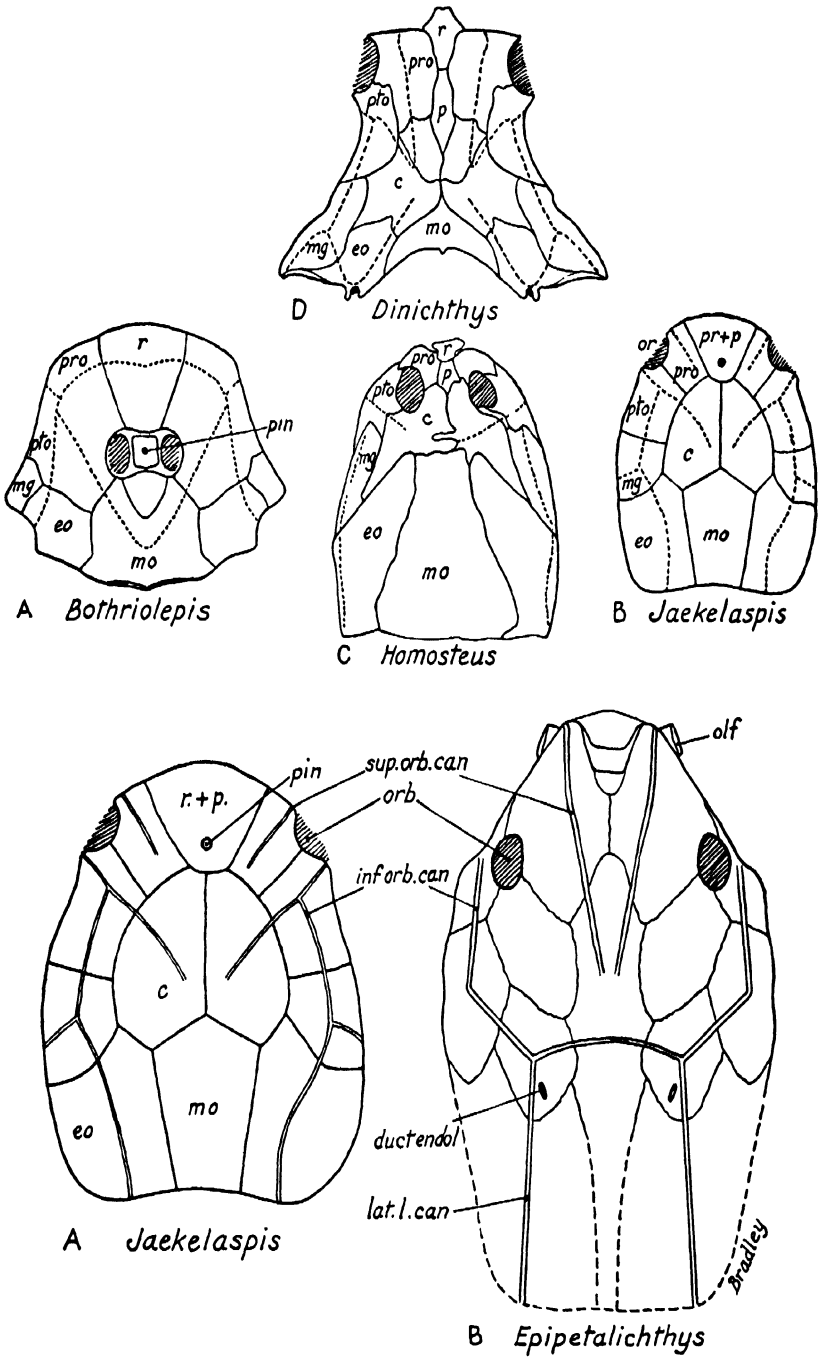


Fig. 7.7 (top). Comparison of head-shields in placoderms, A, C, after Hussakof; B, after Heintz; D, after Eastman.

Fig. 7.8. Comparison of skull top in acanthaspid (A) and stegoselachian, or petalichthyid (B), showing basic agreement, especially in the arrangement of the lateral line canals. The convergence of the lateral line grooves toward the central plates was shown by Dean (1901, pp. 116, 117) to be a basic feature of the macropetalichthyids, coccosteids and dinichthyids. A, after Heintz; B, after Stensiö.

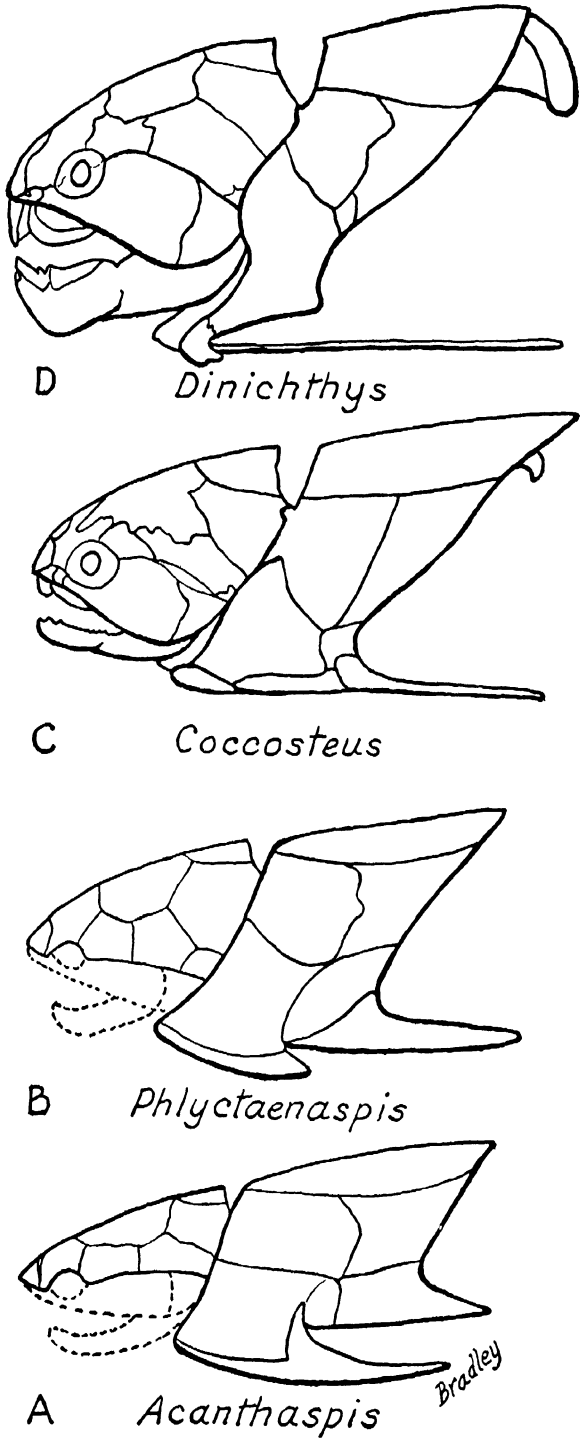
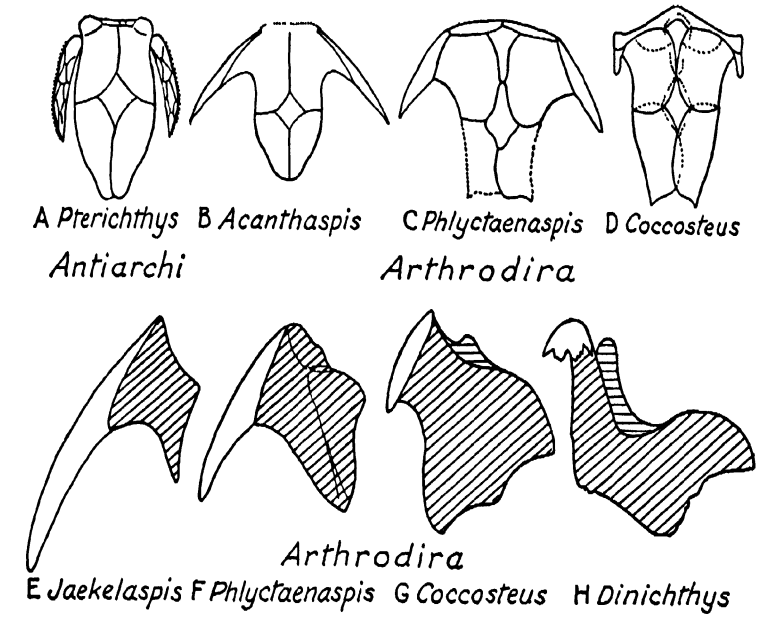


Fig. 7.9. A series of placoderms illustrating stages from small mud-living acanthaspid to gigantic predatory arthrodire. After Heintz.



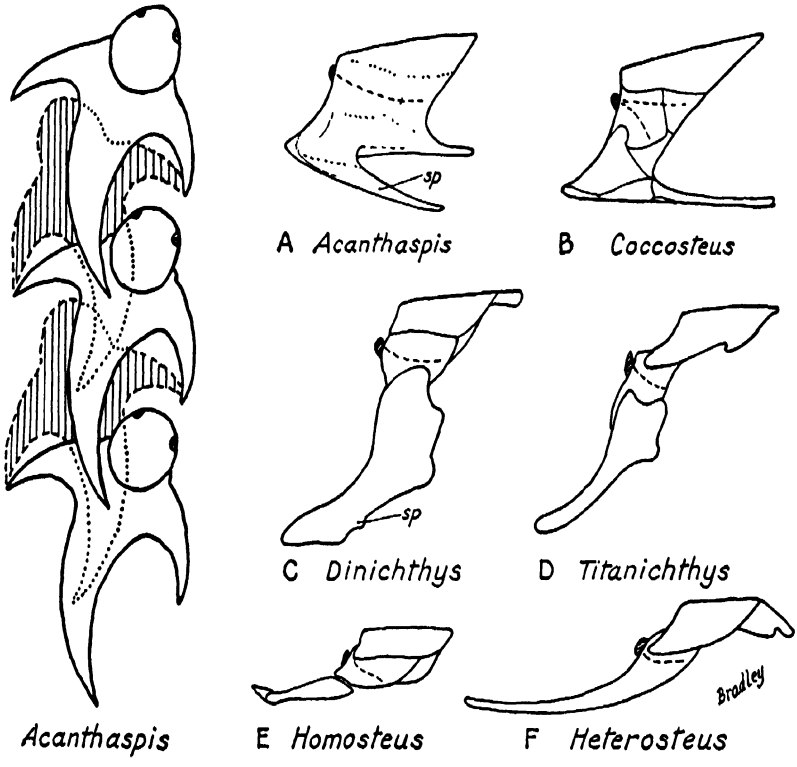


Fig. 7.10 (bottom left). Supposed use of the pectoral spikes in forward locomotion of an acanthaspid. After Heintz.

Fig. 7.11 (top). Reduction of the pectoral spine in Arthrodira. A–D, after Hussakof; E–H, after Heintz.

Fig. 7.12 (bottom right). Reduction of the thoracic shield to a shoulder-girdle in Arthrodira. After Heintz.

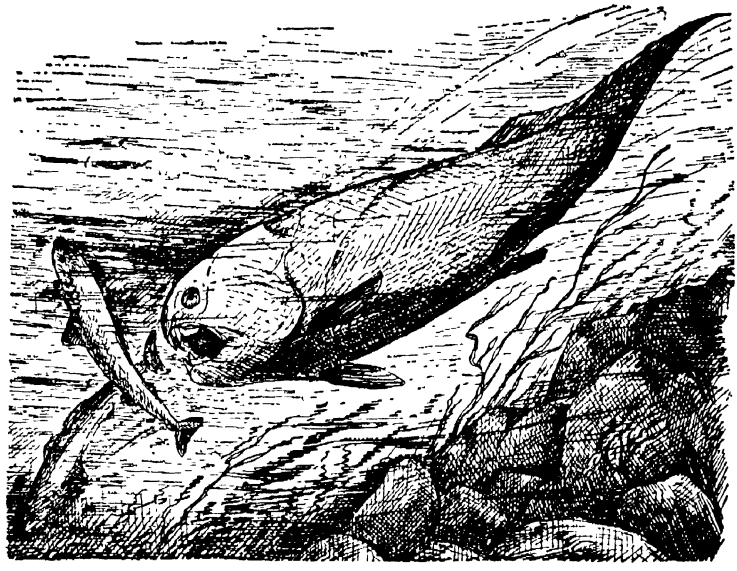


Fig. 7.13. *Dinichthys* pursuing *Cladoselache*. Restoration of the giant free-swimming predator *Dinichthys*. After Heintz.

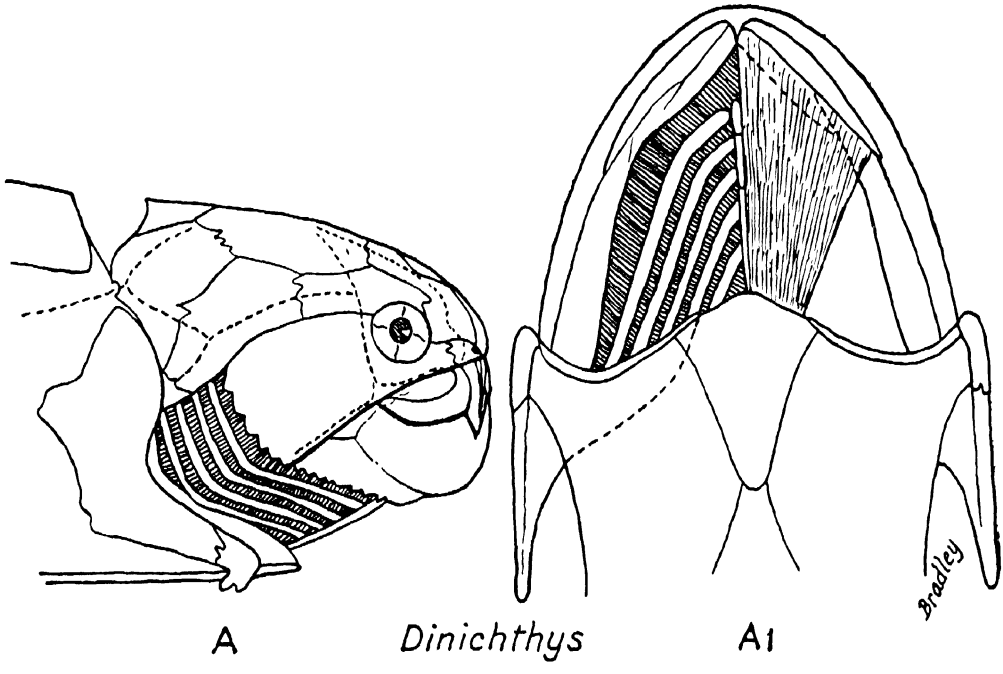
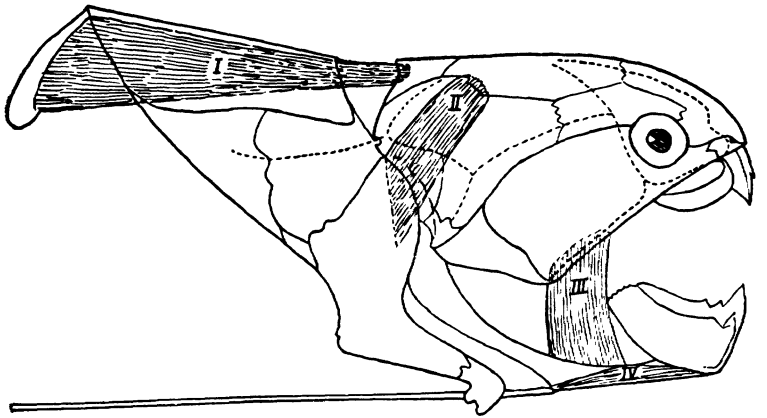


Fig. 7.14. Heintz's restoration of the branchial region of *Dinichthys*. A, from the right side, after removal of part of cheek plates; A1, from beneath.



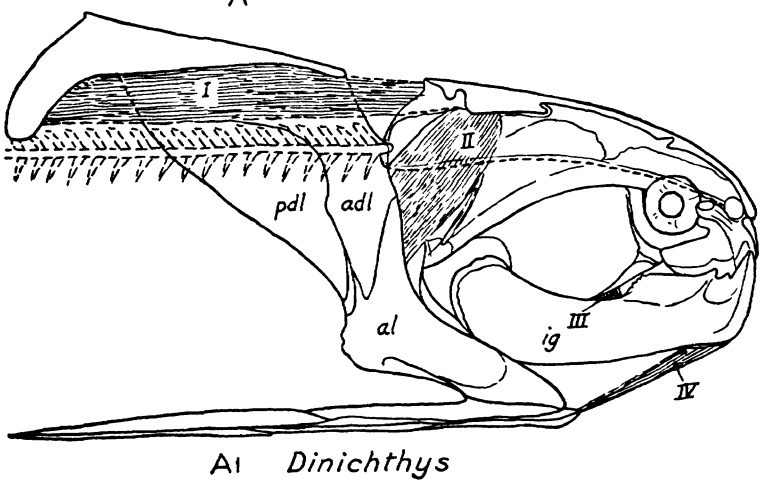
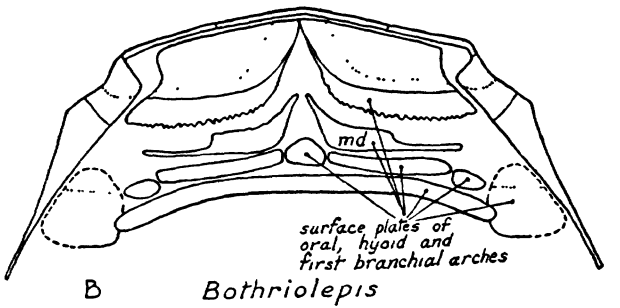


Fig. 7.15. Restoration of the main muscles (I, II, III, IV) of the arthrodiran jaws by Heintz. Stensiö would place III on the inner side of the cheek and mandible, as in sharks and other fishes.



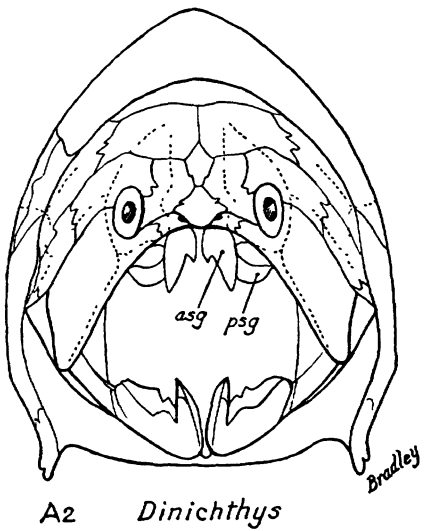


Fig. 7.16. The dermal or surface elements in the jaws of typical antiarch (B) and arthrodire (A2). A2, after Heintz; B, after Stensiö. *Asg*, antero-superognathal; *md*, mandible (inferognathal); *psg*, postero-superognathal; *ig*, mandible.

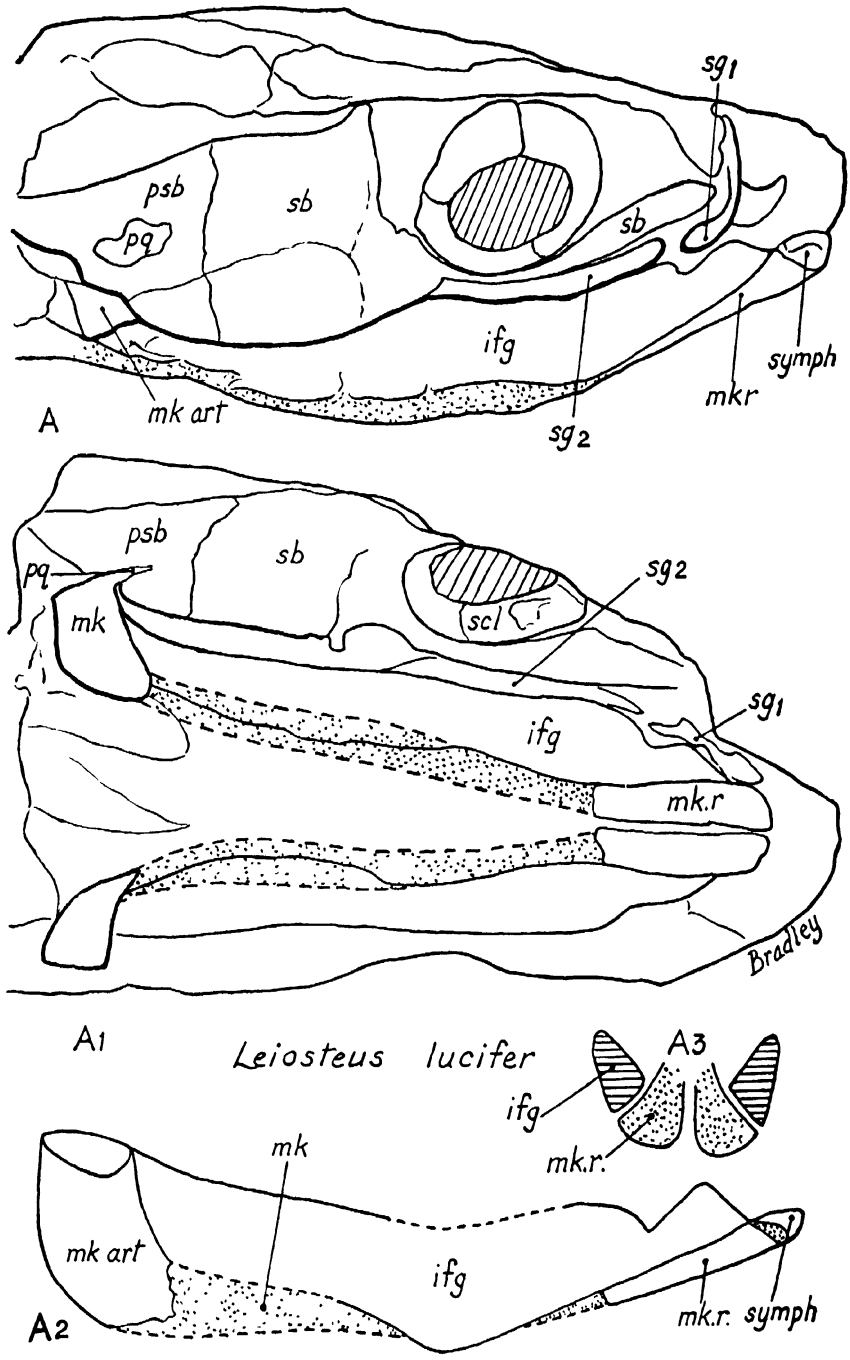


Fig. 7.17. Skull and jaws of an arthrodire indicating the relations of Meckel's cartilage to the bony mandible (*ifg*). A, side view; A1, ventral view; A2, lateral view of right half of mandible; A3, cross-section of rostral end of mandible, showing inferognathals abutting against calcified part of Meckel's cartilages. *Sg1*, *sg2*, superognathals 1, 2; *ifg*, inferognathal; *sb*, suborbital plate; *mk*, cartilaginous part of Meckel's cartilage (restored); *mk.r.*, Meckel's cartilage, right; *mk.art*, articular portion of Meckel's cartilage; *pq*, part of palatoquadrate; *sym*, symphysial cartilage. After Stensiö.

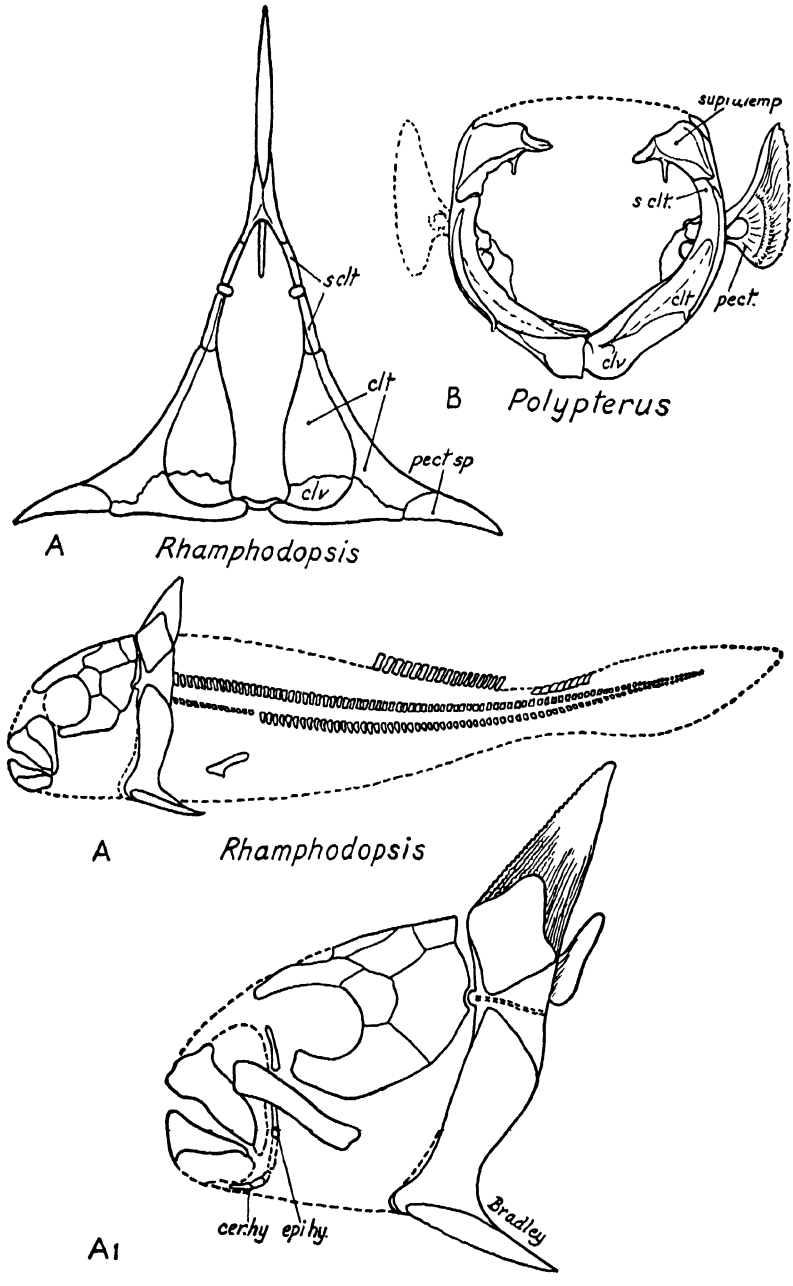


Fig. 7.18. Exoskeletal pectoral girdles of a ptyctodont (A) and a ganoid fish (B), showing general correspondence of parts. A, after Watson.

Fig. 7.19. A Devonian ptyctodont, from the Middle Old Red Sandstone of Scotland. After Watson.

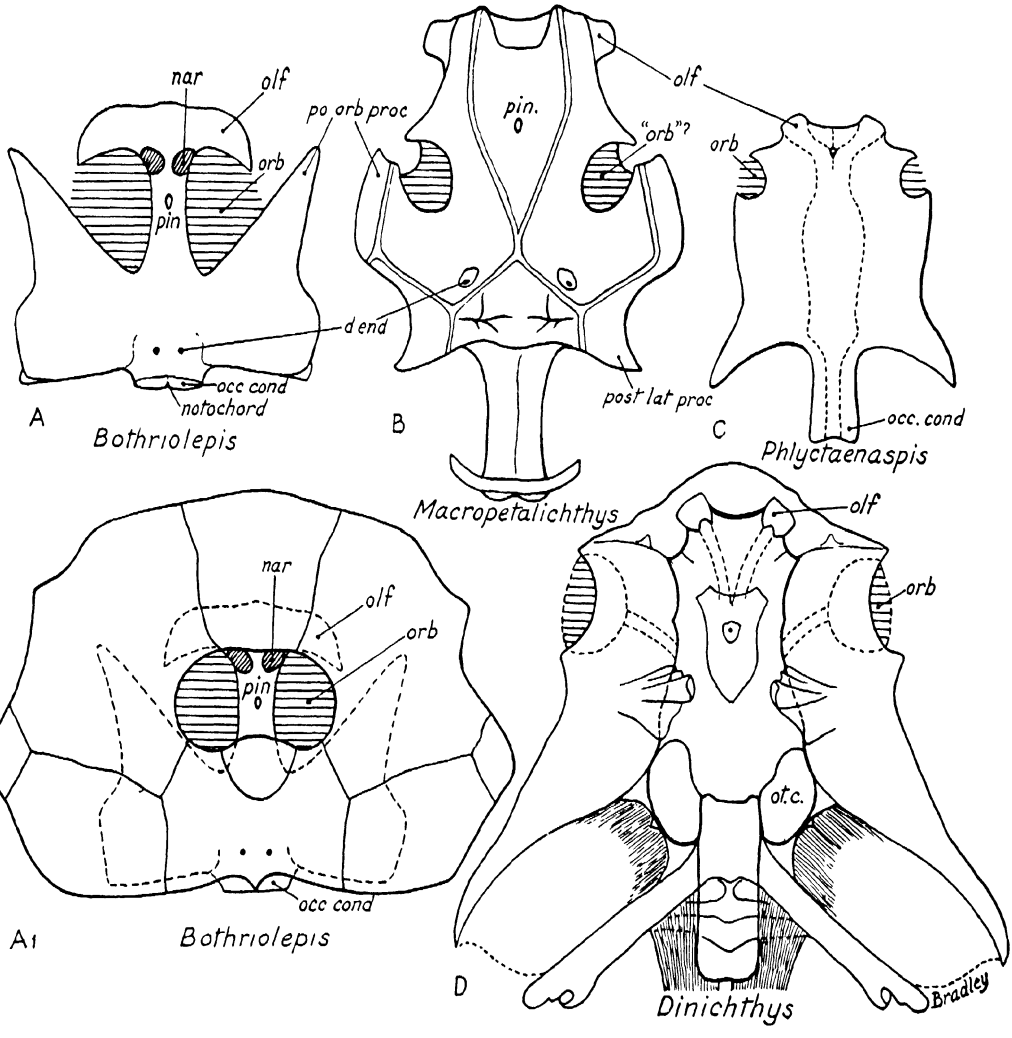
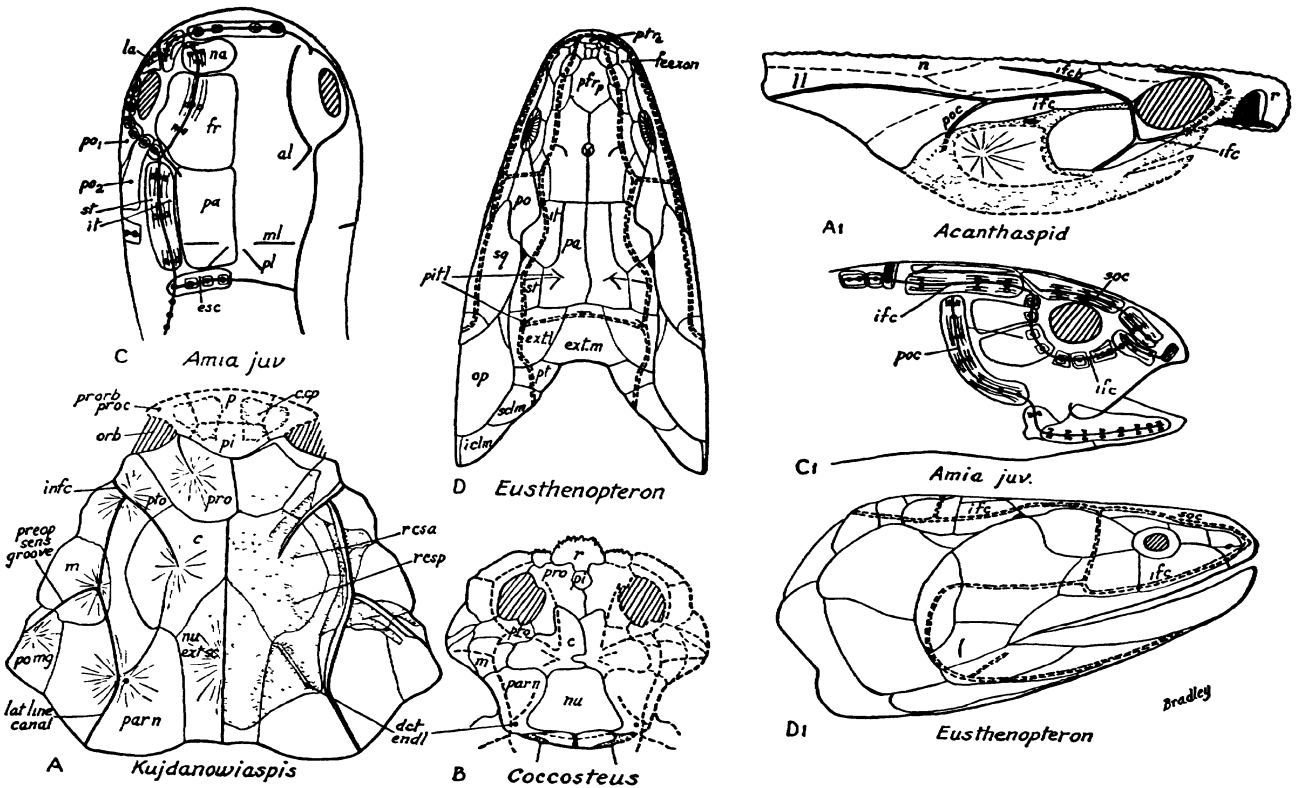
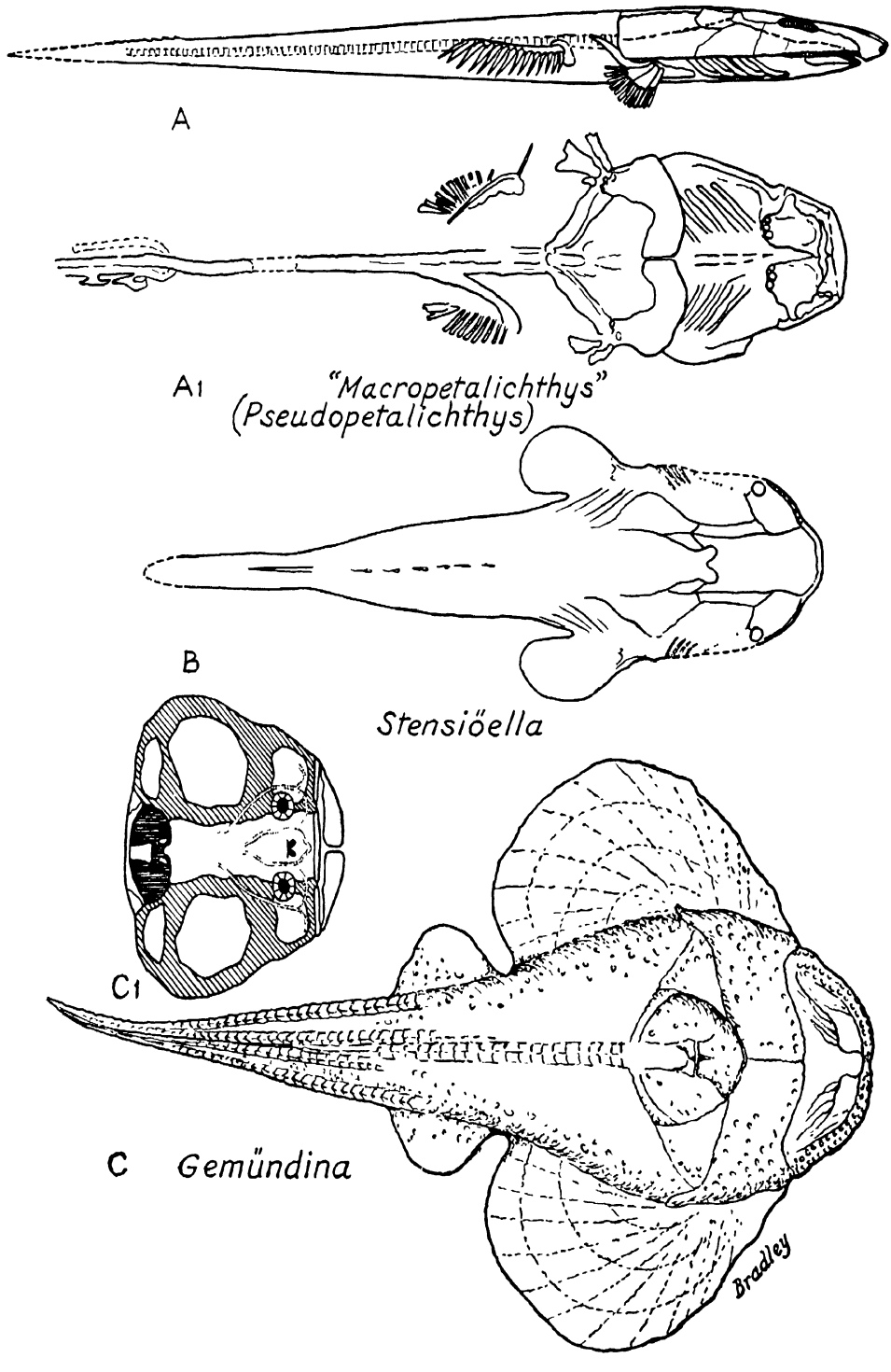


Fig. 7.20. The endocranium and its relations to the dermocranium in antiarch (A, A1), petalichthyid (B), and arthrodires (C, D). D is seen from below, the others from above. The petalichthyids and arthrodires are distinguished by the marked elongation of the skeletal nerve-tube behind the otic capsules. This tube bears a sagittal crest and may have been located between two spinal muscle masses that served to move the body upon the head as a fulcrum. The very short occiput of the antiarch (A) is presumably more primitive and is associated with a different method of locomotion. A, A1, B, C, after Stensio; D, after Heintz.



Figs. 7.21, 22. Dorsal (A–D) and lateral (A1, C1, D1) views of skulls, showing lateral line patterns in: primitive Upper Silurian acanthaspid (A, A1), primitive arthrodire (B), larval ganoid (C, C1), and Devonian crossopterygian (D, D1). All after Sensiö.



Figs. 7.23, 24. Shark-like (A, A1, B) and ray-like (C, C1) placoderms from the lower Devonian of Germany. Restored by Broili.

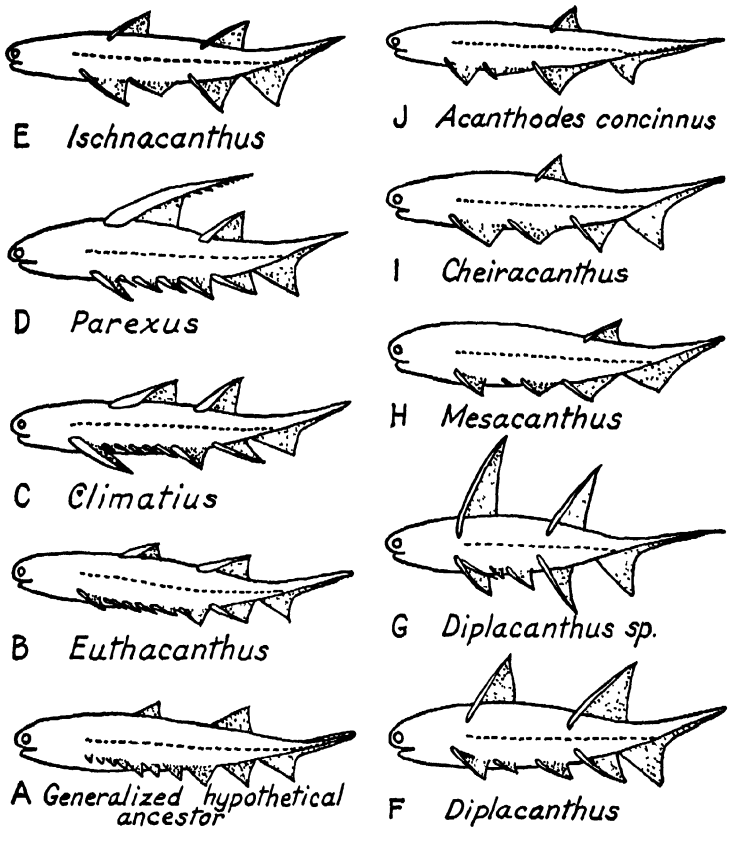


Fig. 7.25 (top). Evolution of the typical acanthodians. From Parker and Haswell, after C. Forster Cooper.

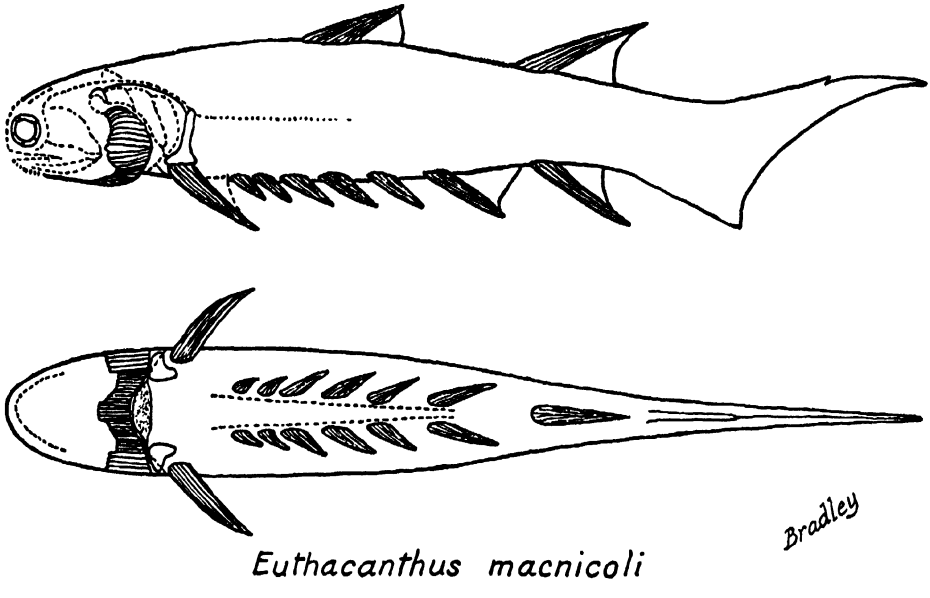


Fig. 7.26. A primitive acanthodian from the Lower Devonian of Britain. After Watson.

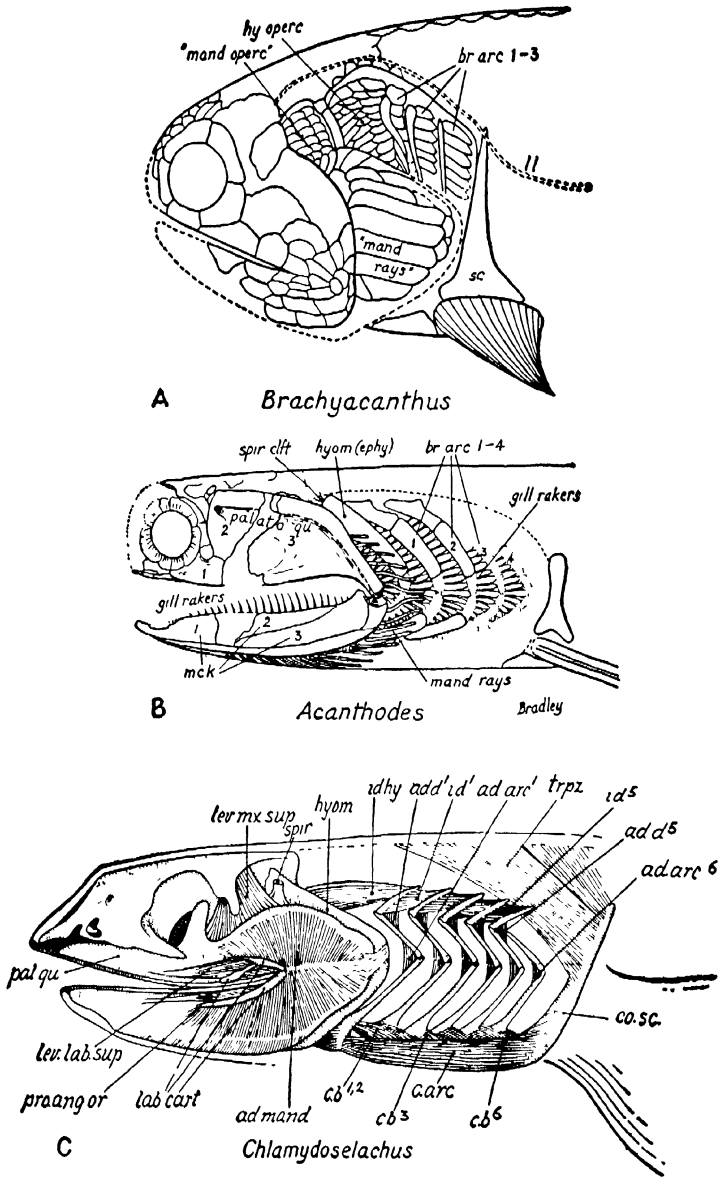


Fig. 7.27. Jaws from gill arches. In the acanthodians (A, B) the oral or mandibular arch supported an enlarged opercular flap (*mand. rays*), which overlapped those of the hyoid and branchial arches. The upper and lower jaws (B) were each subdivided into segments (1, 2, 3) homologous with those of the hyoid and branchial arches. In the living frilled shark (C) the main adductor jaw muscles are in series with the deep adductors (*add. arc.*) of the gill arches. These deep muscles fall into two main groups: extensors of the oral and branchial arches, running anteroposteriorly, and flexors, running vertically. A, B, After Watson; C, after Allis. Abbreviations (Allis): *ad.arc.*, musculi adductores arcuales 1–6; *ad.d.*, adductores dorsales 1–5; *ad.mand.*, adductor mandibulae; *c.arc*, coraco-arcualis; *c b*, coracobranchiales 1–6; *co.sc.*, coracoscapular arch; *hyom*, hyomandibular; *id*, interdorsales 1–5; *id.hy.*, interacualis between hyal and first branchial arch; *lab.cart.*, labial cartilages; *lev.lab. sup.*, levator labii superioris; *lev.mx.sup*, levator maxillae superioris; *pal.qu.*, palatoquadrate; *pro.ang.or.*, protractor anguli oris; *trpz.*, trapezius.

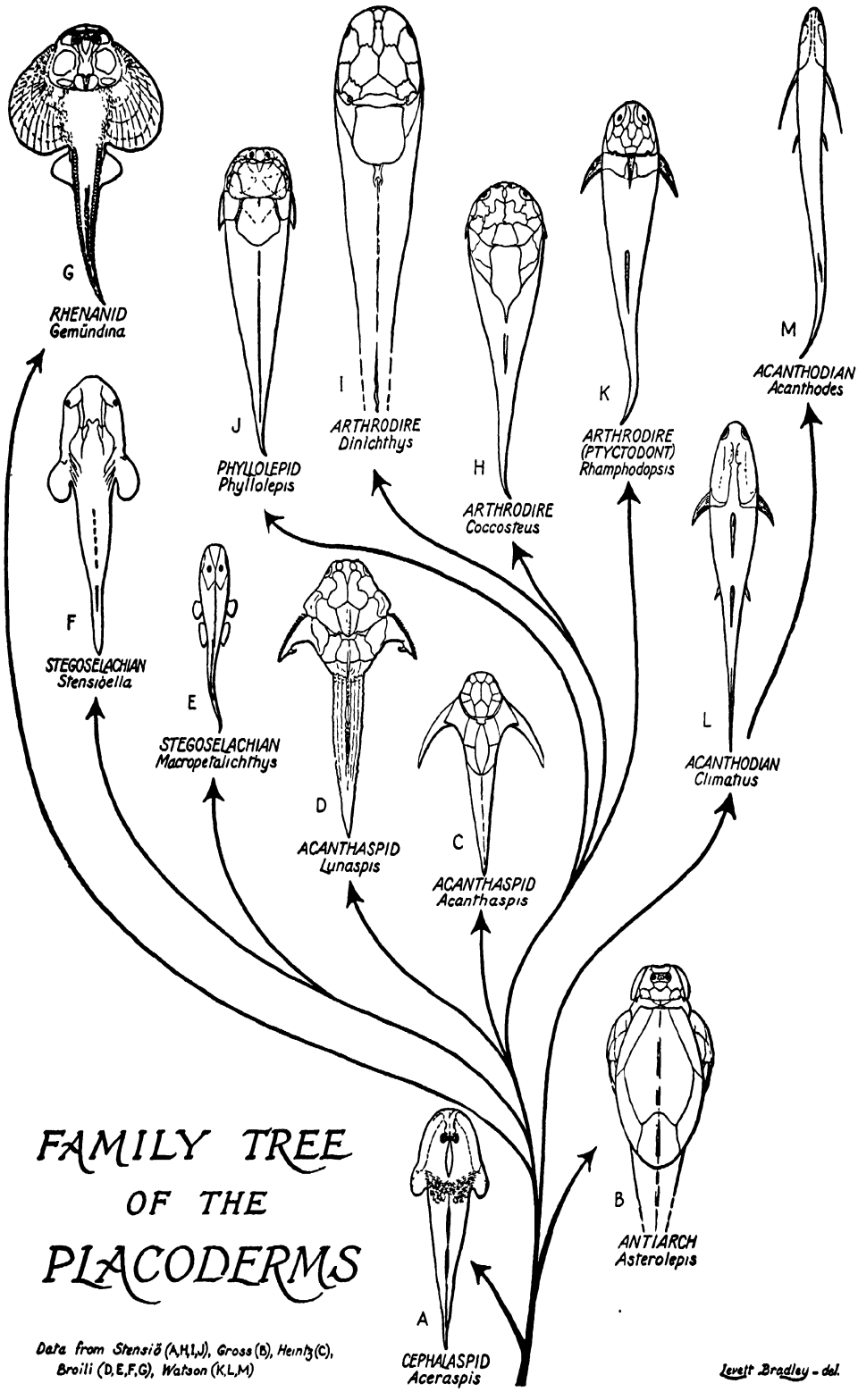

G
RHENANID
Gemündina
J
PHYLLOLEPID
Phyllolepis
I
ARTHRODIRE
Dinichthys
H
ARTHRODIRE
Coccosteus
K
ARTHRODIRE
(PTYCTODONT)
Rhamphodopsis
M
ACANTHODIAN
Acanthodes
F
STEGOSELACHIAN
Stensiöella
E
STEGOSELACHIAN
Macropetalichthys
D
ACANTHASPID
Lunaspis
C
ACANTHASPID
Acanthaspis
L
ACANTHODIAN
Climatius
B
ANTIARCH
Asterolepis
A
CEPHALASPID
Aceraspis
FAMILY TREE
OF THE
PLACODERMS
Data from Stensiö (A,H,I,J), Gross (B), Heintz (C),
Broili (D,E,F,G), Watson (K,L,M)
Leveit Bradley - del.

Fig. 7.28

CHAPTER VIII

ADVANCED PREDATORS OF THE SHARK TRIBE

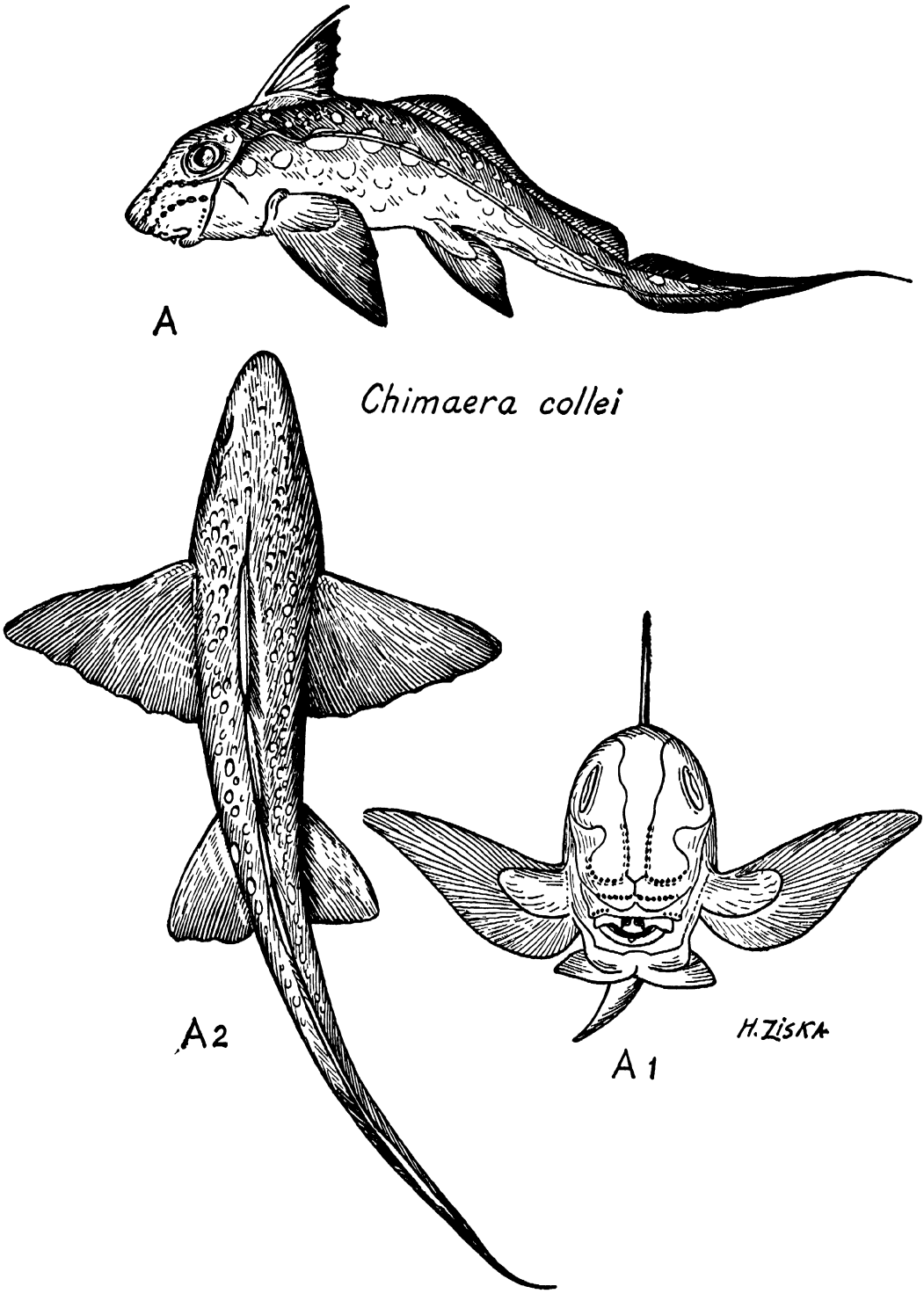


Fig. 8.1. A live *Chimaera collei*. After Bashford Dean.

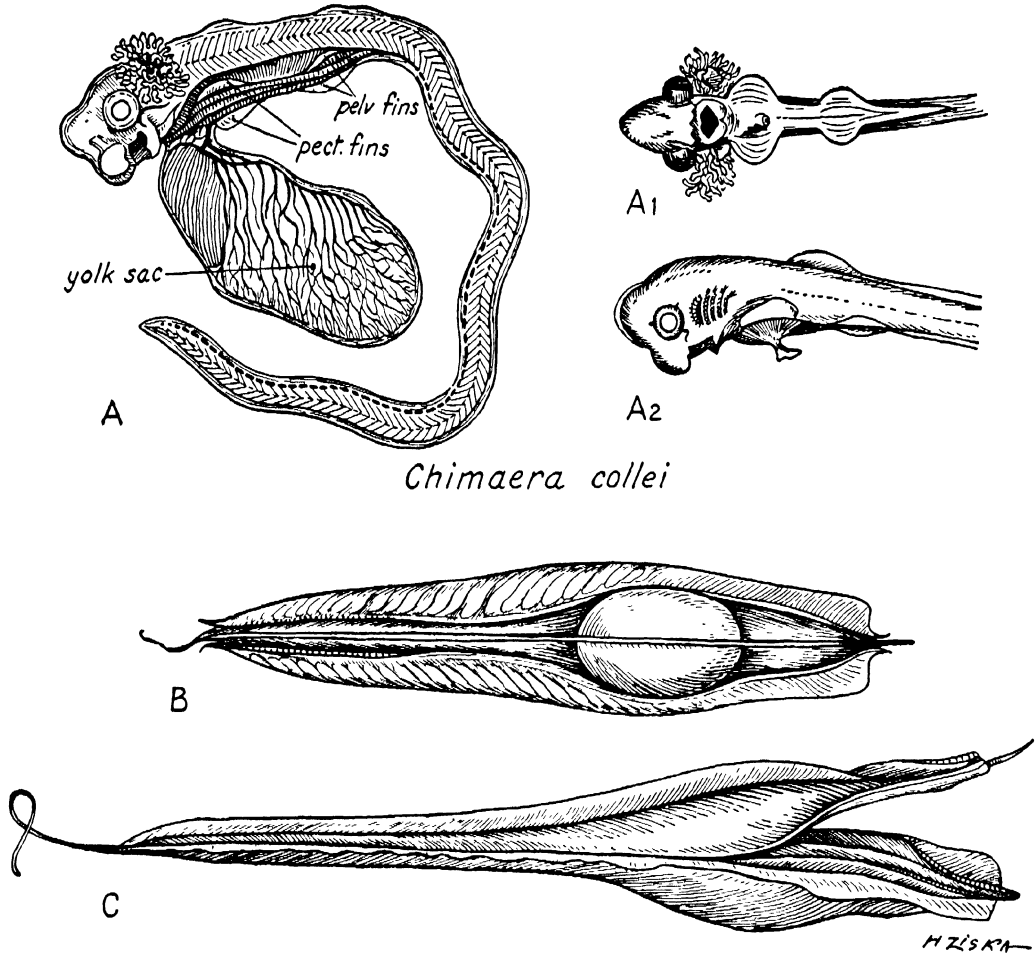


Fig. 8.2. A late embryo of Chimaera collei (A) and two egg capsules (B, C). The Anlagen of the pectoral and pelvic fins appear as finfolds, as does also the dorsal fin. The egg capsules are made of very tough horny material and protect the developing young until the larval stage; then the capsule splits open at the anterior end and permits the larval fish to escape. After Dean.

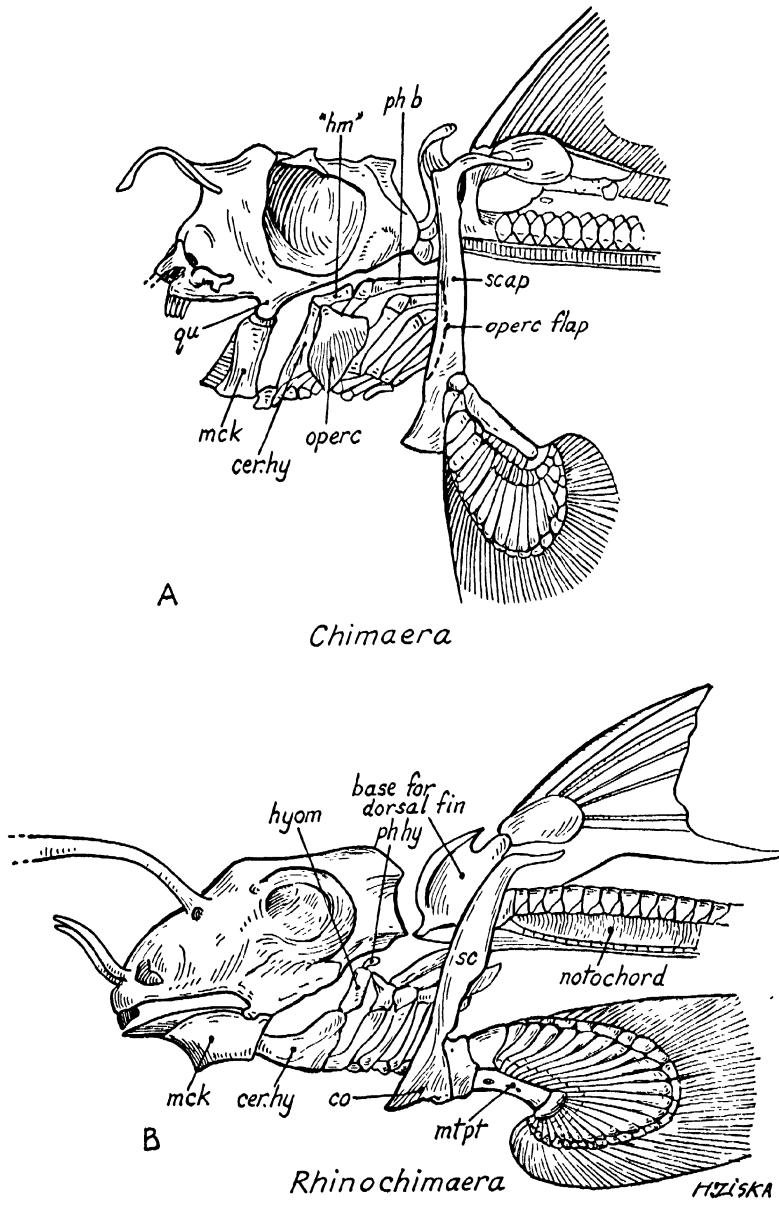


Fig. 8.3. Skeleton of head (rostrum omitted) and forepart of two recent chimaeroids. The shoulder girdle recalls the diminished thoracic girdle of the ptyctodont placoderms (fig. 7.19) from which the chimaeroids may have been derived. After Dean.

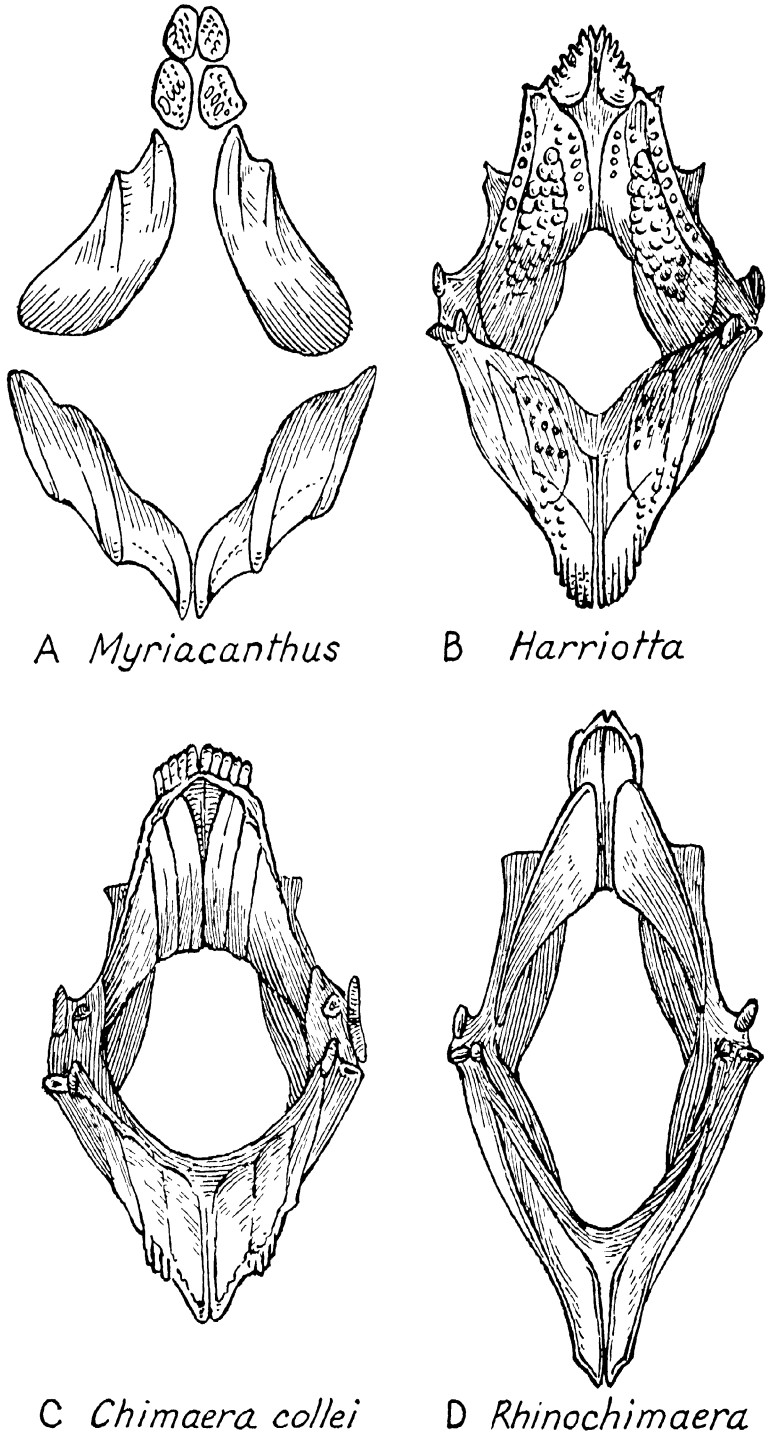


Fig. 8 4. Jaws and tooth plates of Lower Jurassic (A) and modern chimaeroids. After Dean.

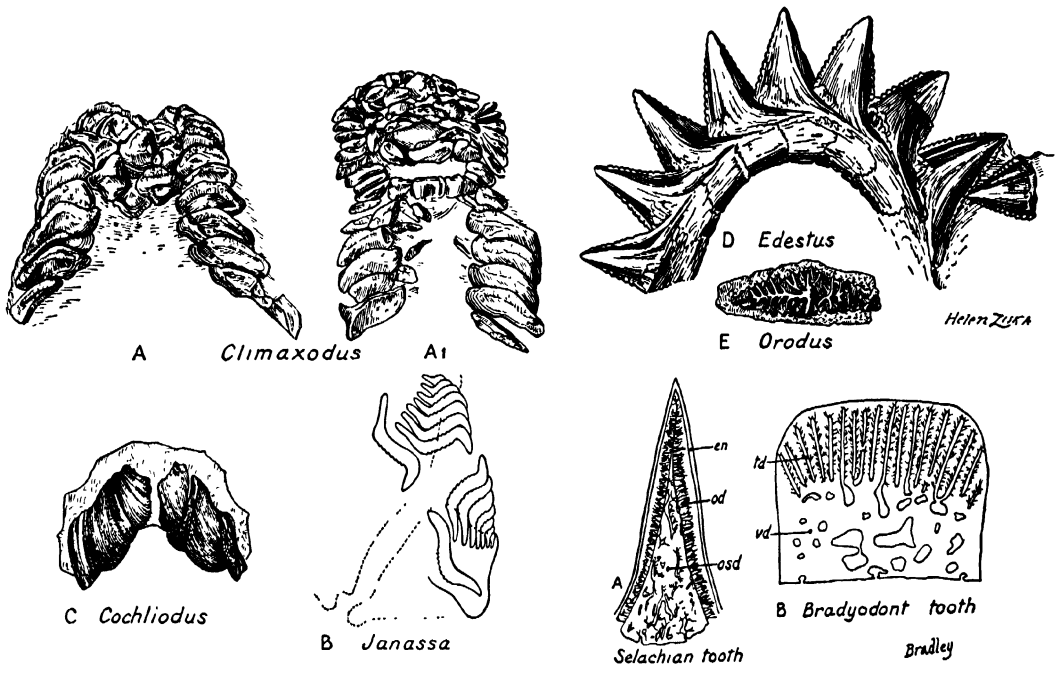


Fig. 8.5 (left). Dentitions of bradyodonts. A, Relatively primitive stage from the Lower Carboniferous of Scotland. A, Upper teeth; A1, lower teeth. B, *Janassa,* from the Upper Permian of Germany. Sagittal section through upper and lower, showing vertical succession. C, *Cochliodus,* from the Carboniferous Limestone of Great Britain. D, Lower teeth of *Edestus,* showing spirally coiled symphysial teeth. E, Mountain-like cheek teeth of *Orodus.* A, C, D, E, after Smith Woodward; B, after Jaekel.

Fig. 8.6. Sections of selachian tooth (A) and bradyodont tooth (B). After Moy-Thomas, 1939. *En,* enamel; *od,* orthodentine; *osd,* osteodentine; *td,* tubular dentine; *vd,* vascular dentine.

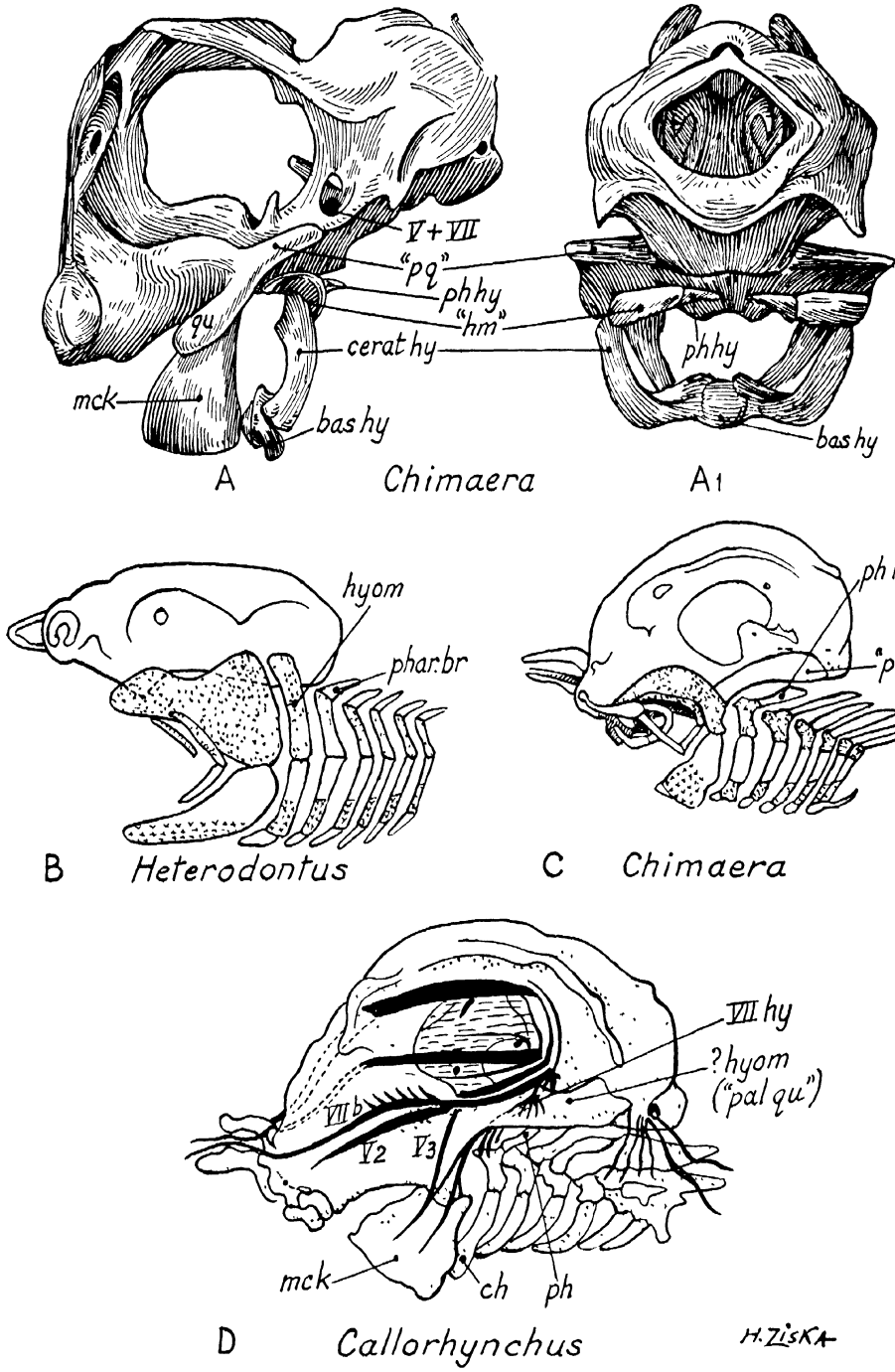


Fig. 8.7. The hyomandibular problem in chimaeroids. Dean's solution (A, A1, B, D). The hyomandibular (*hm*) is distinct from the palatoquadrate; endorsed by de Beer and Moy-Thomas, 1935. A, A1, A wax plate model of the chondrocranium of a late embryo in lateral and occipital view. Goodrich's solution (D): the hyomandibular is more probably fused with the quadrate; endorsed by Watson, 1937.

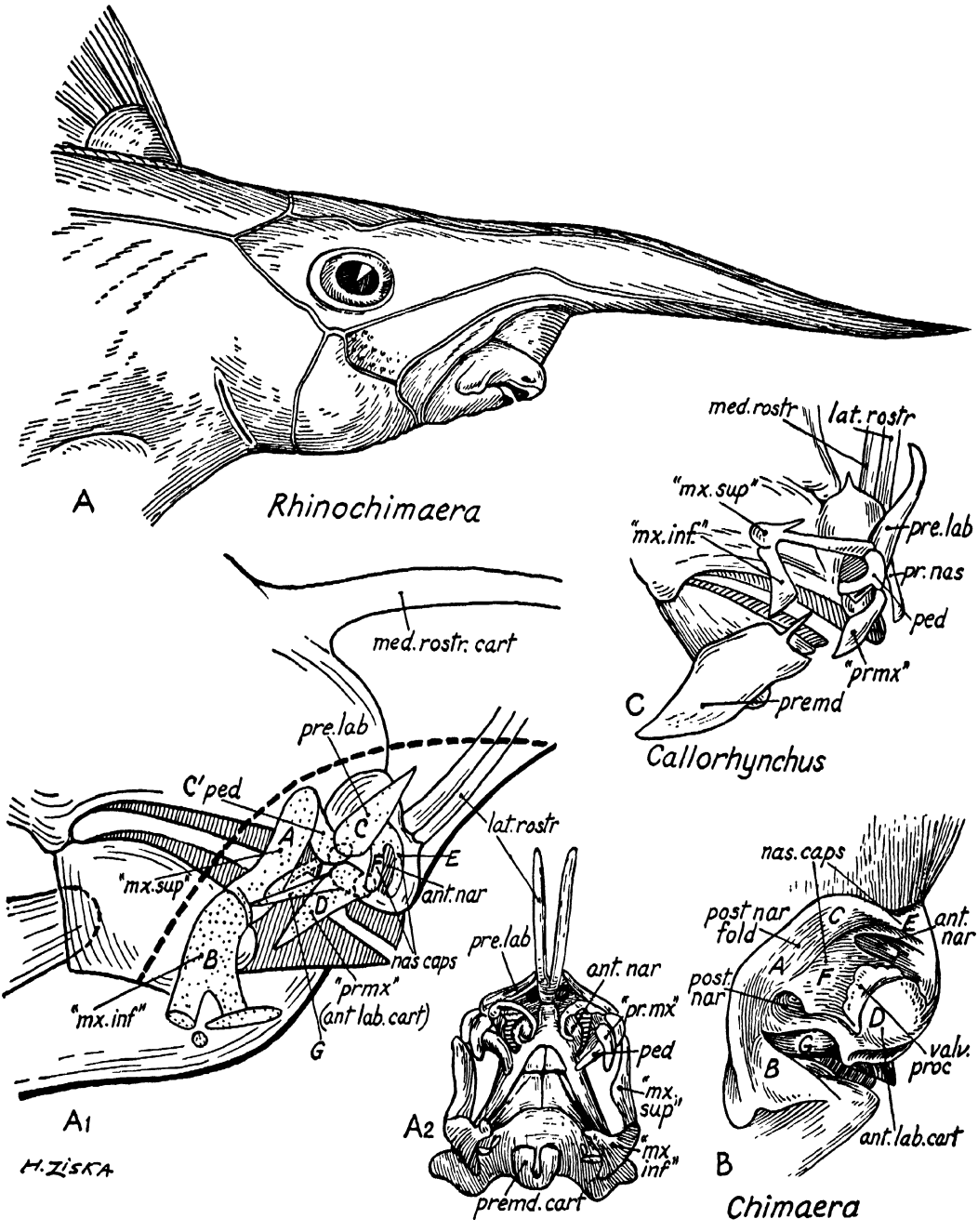


Fig. 8.8a, b. Head (A) and labial cartilages (A1) of *Rhinochimaera*. After Dean. The labial cartilages lie just beneath the skin that covers the jaws and base of the rostrum.

The oronasal folds (B) and labial cartilages (A2, C) of other chimaeroids. A, A1, after Dean; B, after Allis, lettering added; C, A2 (C1) after Holmgren.

BAC, main naso-labial fold (*"mx.sup," "mx.inf"*) covering main nasal cartilages; *C'* (*ped*) hinder arm of *C*, attached proximally to skull by strong ligament; *C* also serves as a link between the lateral rostral cartilages and the labial cartilages; *D*, antero-internal fold, a "valvular process," part of the nasal cartilages; *EF*, nasal capsule covering anterior and posterior nares; *G*, inner fold connecting naso-labial fold with nasal capsule. *G* is connected by ligament to *F* and by fascia to the joint *A–C*. Thus contraction of the retractor muscles behind *A–C* would tend to draw backward both the main naso-labial fold and the "valvular process" *D*.

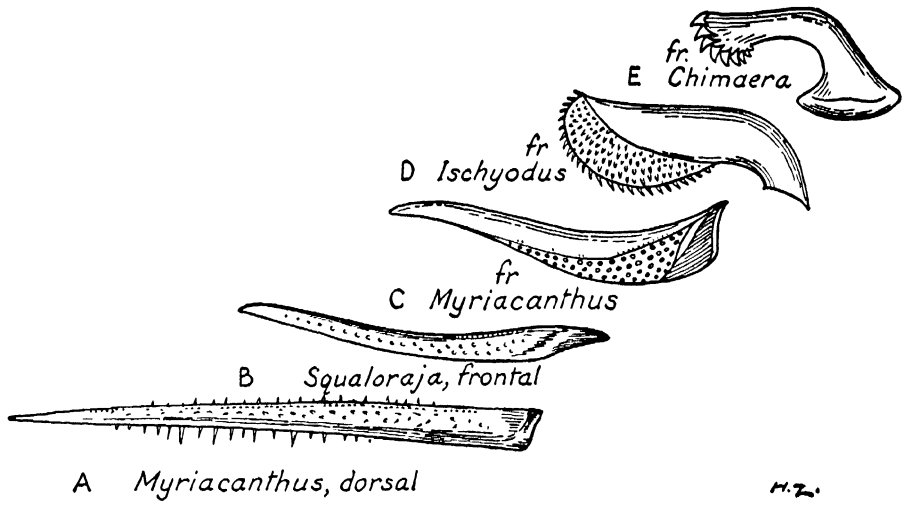


Fig. 8.9. Evolution of the frontal spine in chimaeroids. After Dean.

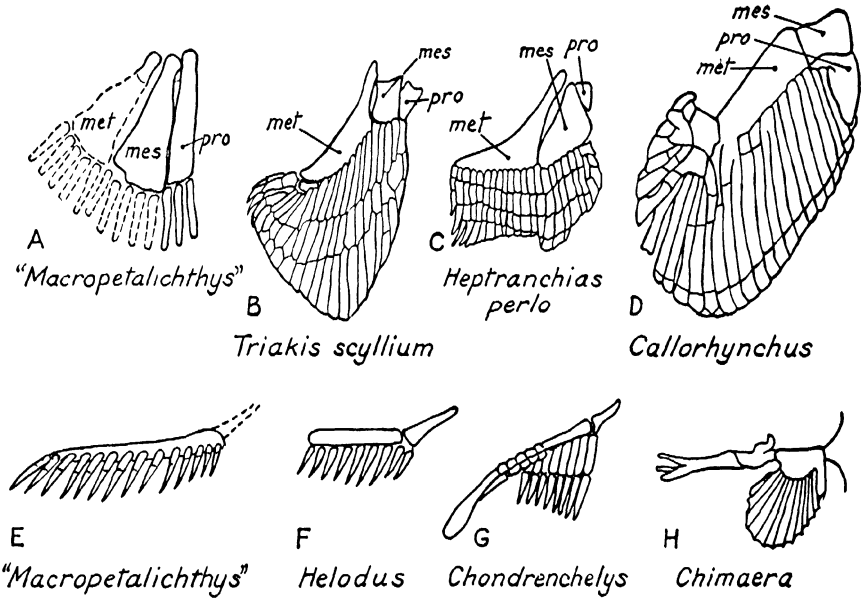


Fig. 8.10. Comparative series of pectoral (A–D) and pelvic (E–H) fins. Skeleton of the right pectoral fins of a stegoselachian (A), recent shark (B, C) and chimaeroid (D), to show the reduction of the propterygium in the latter and the curving of the radials around the distal end of the metapterygium on to the postaxial border. In the pelvic fins the metapterygial rods in males (H) are produced to form claspers. A, E, after Broili; B–D, after E. G. White; F–H, after Moy-Thomas.

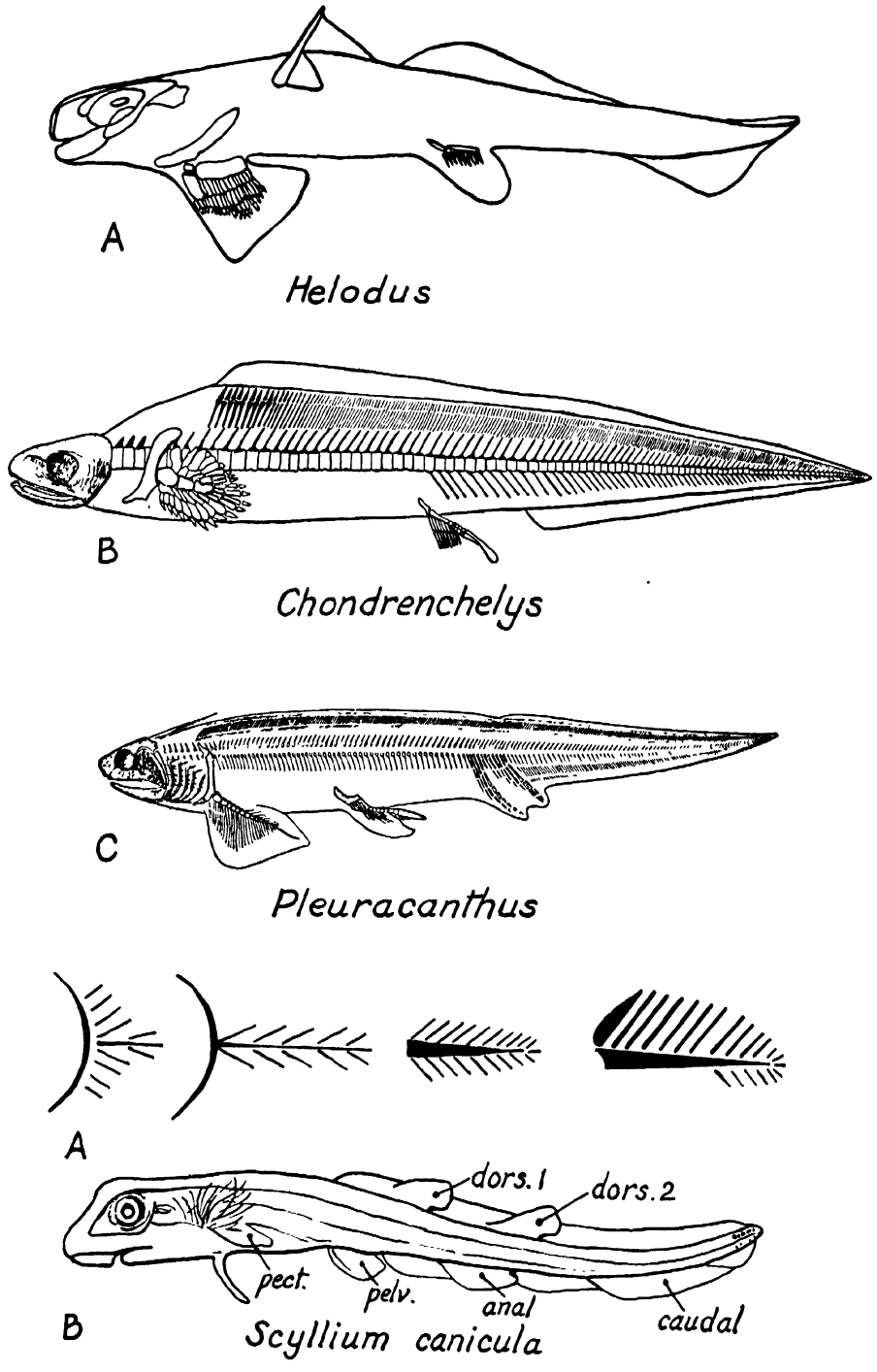


Fig. 8.11 (top). Two bradyodonts and a pleuracanth shark. A, B, restored by Moy-Thomas; C, from Moy-Thomas, after Jaekel. According to Moy-Thomas's earlier view (1935, p. 402), *Chondrenchelys* was regarded as a "descendant of a group connecting the Holocephali with the Pleuracanthia." Later, however (1939, p. 23), he concluded that "the Chondrenchelydi seem to be early bradyodonts which convergently resemble the pleuracanths."

Fig. 8.12. The "archipterygial" (A) and finfold (B) theories of the origin of paired fins. A, from Daniel, after Gegenbaur; B, from Daniel, after Mayer.

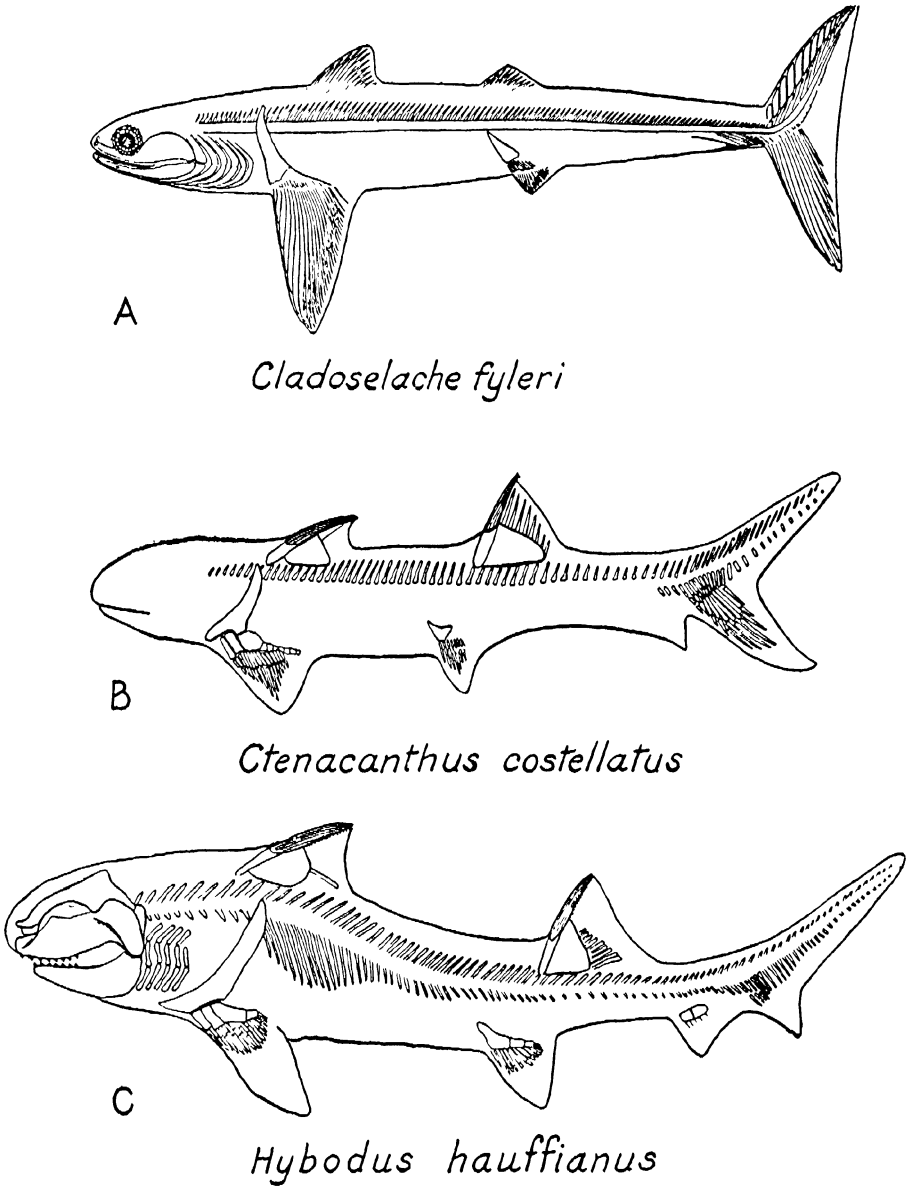


Fig. 8.13. Sharks from the Upper Devonian (A), Lower Carboniferous (B) and Lower Jurassic (C). A, from Moy-Thomas, after Dean; B, C, after Moy-Thomas.

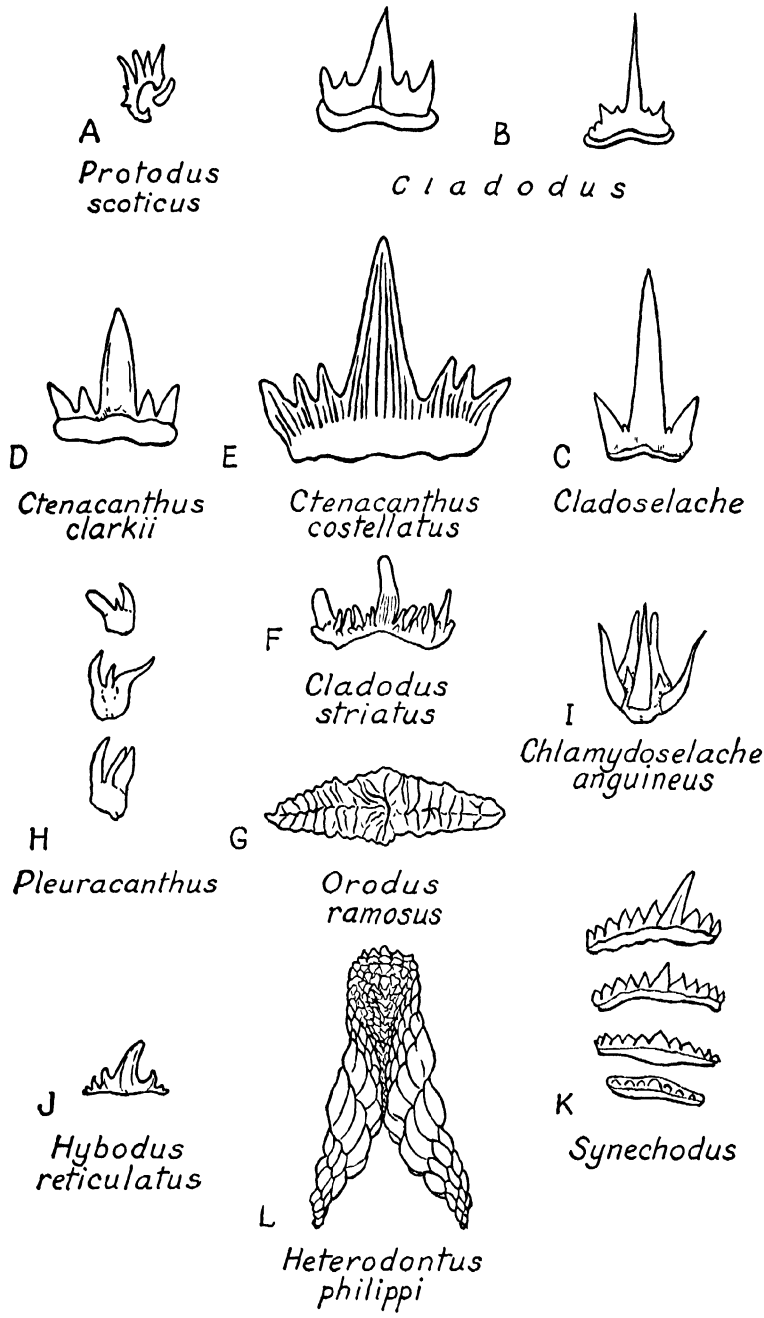


Fig. 8.14. Teeth of some Palaeozoic sharks and their derivatives. In the Protodontidae (A) of the Upper Silurian and Lower Devonian the cuspidate teeth are arranged in transverse series curving round the cartilage of the jaw, those of each series fused together by their expanded bases. Somewhat similar whorls of teeth are found in the earlier acanthodians. "Cladodont" teeth (B, F) from the Upper Devonian are multicuspidate and seem to have given rise to those of ctenacanths (D, E) and cladoselachians (C); probably also to those of pleuracanths (H), frilled sharks (I), orodonts (G), and hybodonts (J). From the latter were derived the heterodonts (K, L). A, from White, after A. S. Woodward; B, F, from White, after Dean; E, after Moy-Thomas; C, D, after Dean; H, from White, after A. S. Woodward; I, from White, after Garman; G, after A. S. Woodward; J, K, L, after A. S. Woodward.

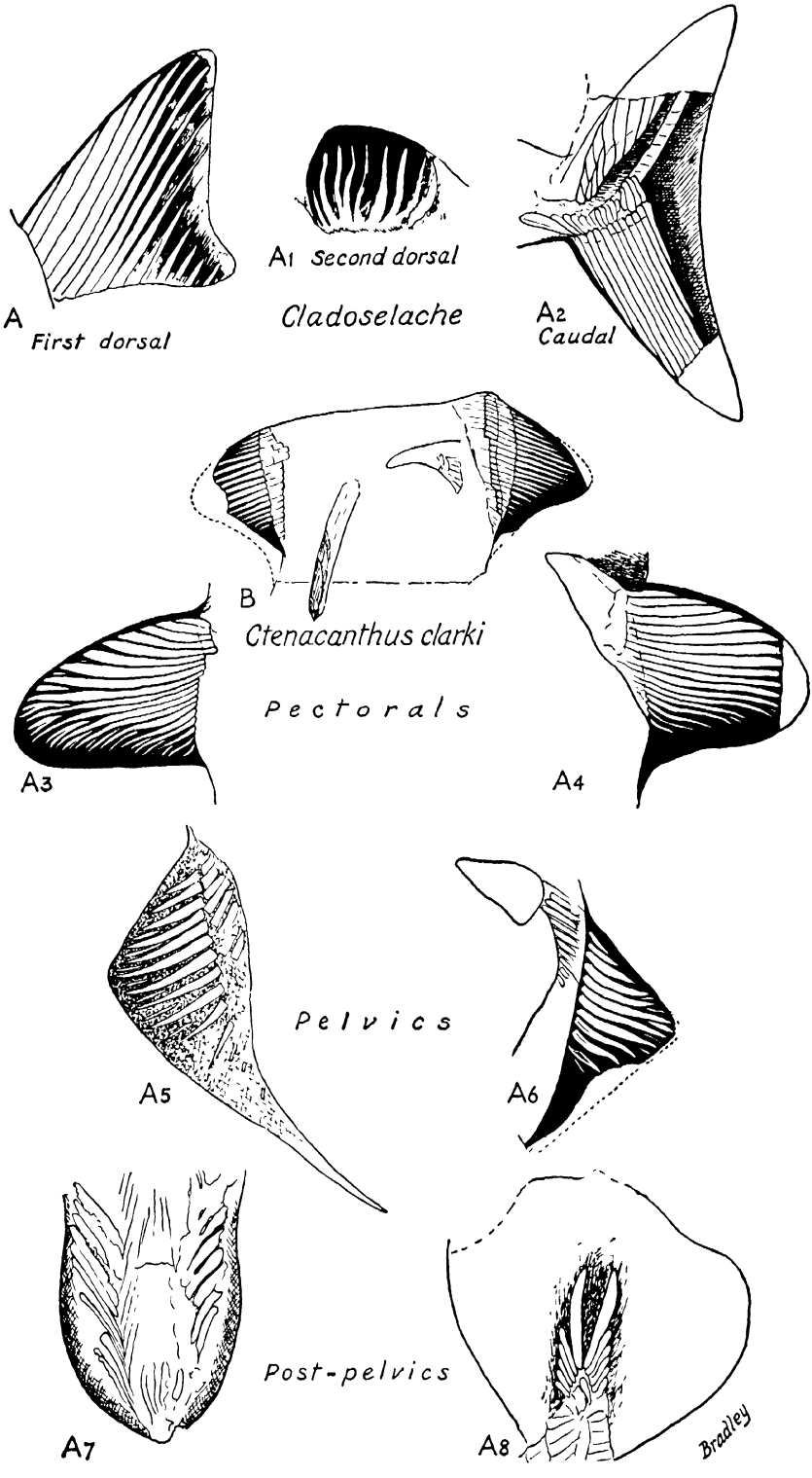
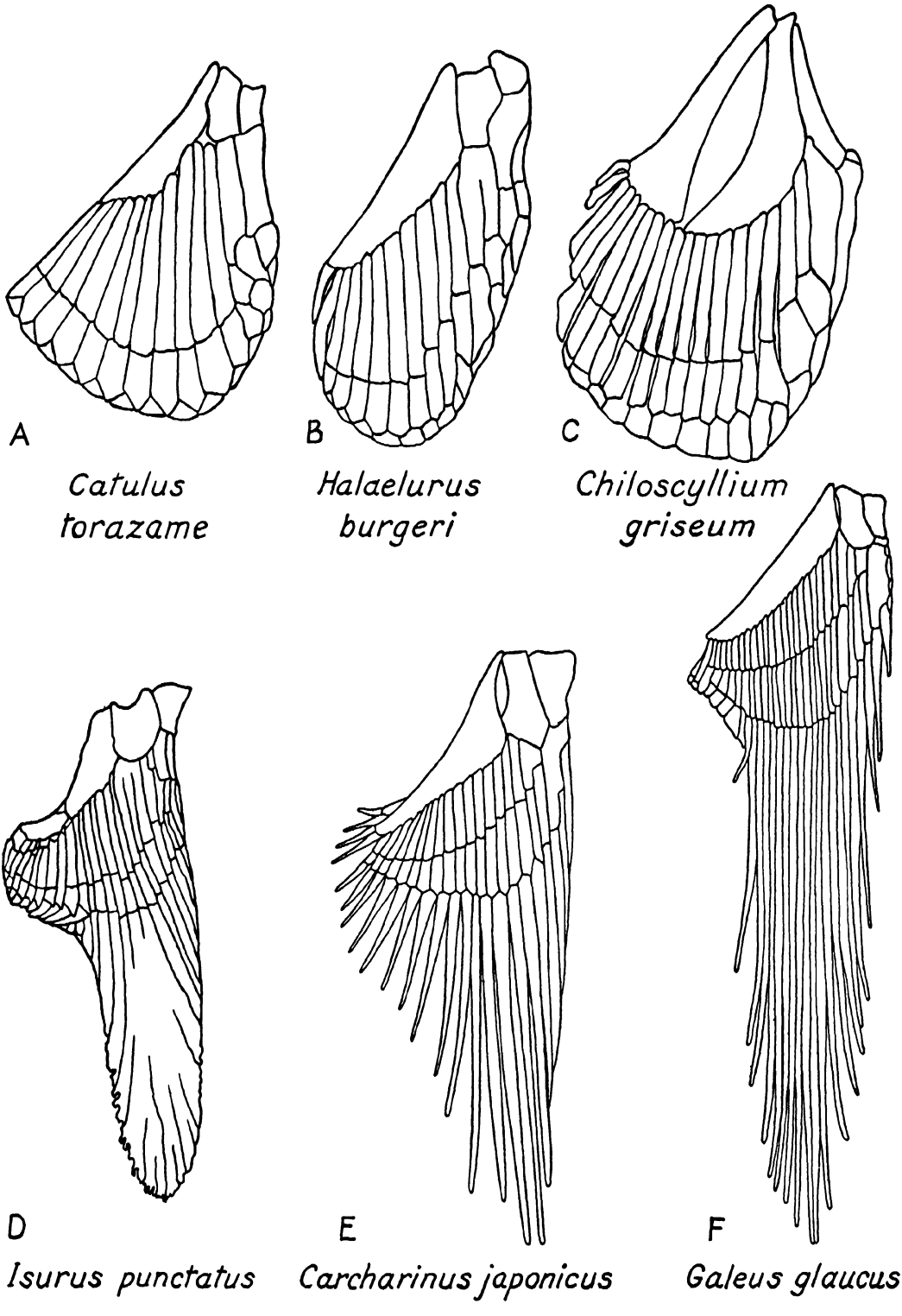
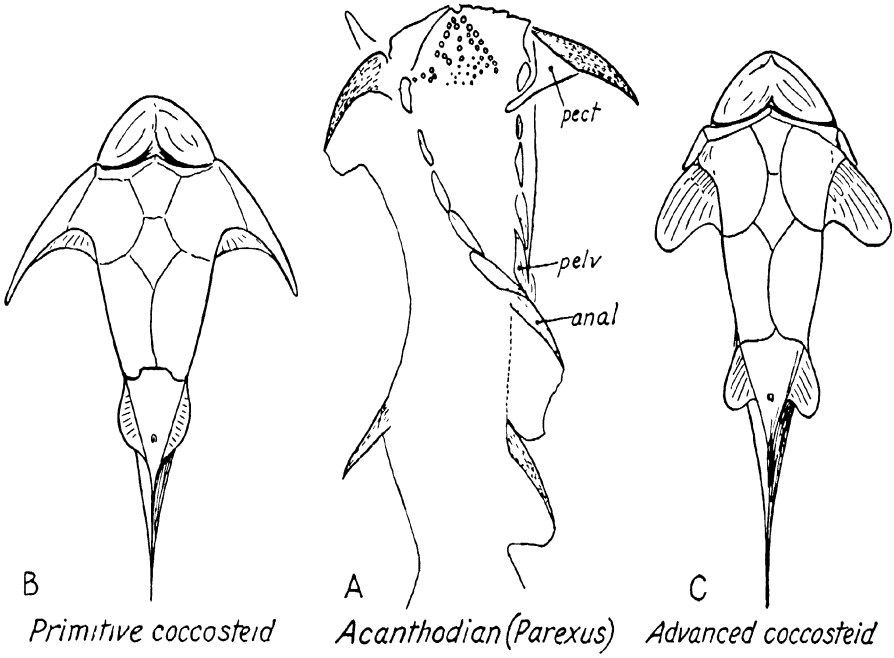


Fig. 8.15. Median (A–A2) and paired (A3–A8) fins of *Cladoselache* and *Ctenacanthus clarki* (B). After Dean.



Figs. 8.16, 17. Pectoral fins of sharks, showing varying prolongation of the radials. After E. G. White.



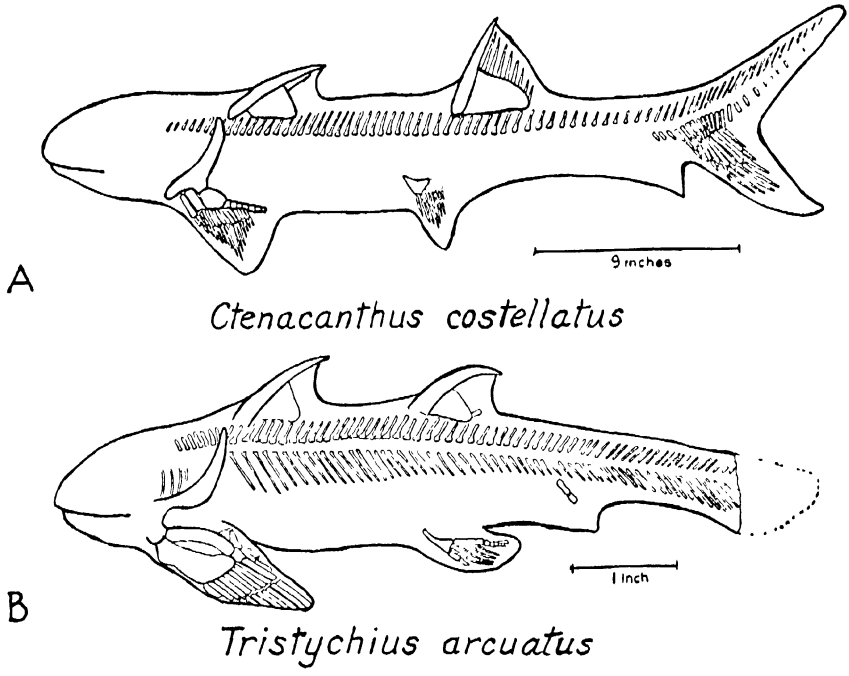


Fig. 8.18 (top). Suggested reduction of pectoral spines and outgrowth of radial rods in placoderms. A, Primitive acanthodian with vigorous development of spines and few or no radial supporting rods. After Dean. B, Primitive and C, advanced cocosteid; tentative reconstructions by Heintz, showing initial slight fin web with initial radials, followed by extension of radials and basals.

Fig. 8.19. Two late Palaeozoic sharks. After Moy-Thomas. A, *Ctenacanthus costellatus,* from the Lower Carboniferous of Scotland; the tribasic pectoral fin bears a jointed metapterygial axis. B, *Tristychius arcuatus* of the same age, with dibasic pectoral.

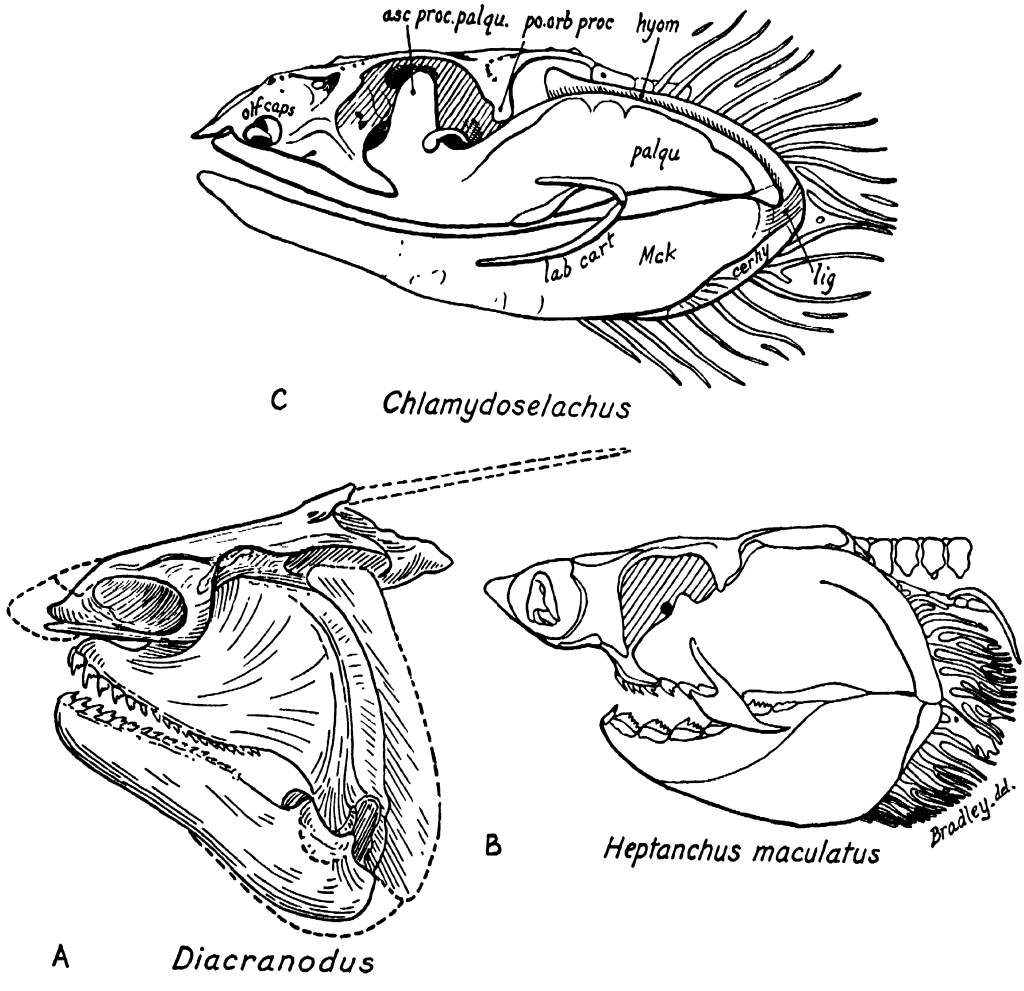


Fig. 8.20. Comparative side views of skulls of pleuracanth (A) and notidanoids (B, C). A, original (see fig. 8.22); B, from Daniel; C, from Daniel, after Allis.

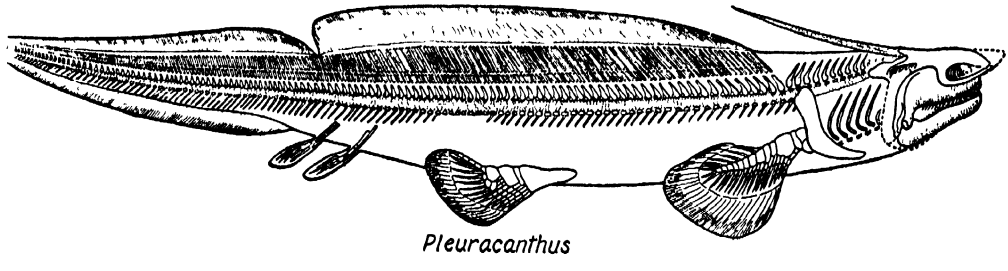


Fig. 8.21. Restoration of *Pleuracanthus* (*Xenacanthus*) *decheni*, from the Permian of Nyran, Czechoslovakia, showing so-called archipterygial pectoral fin with segmented metapterygial axis. From Dean, after Fritsch, but with changes in skull and paired fins.

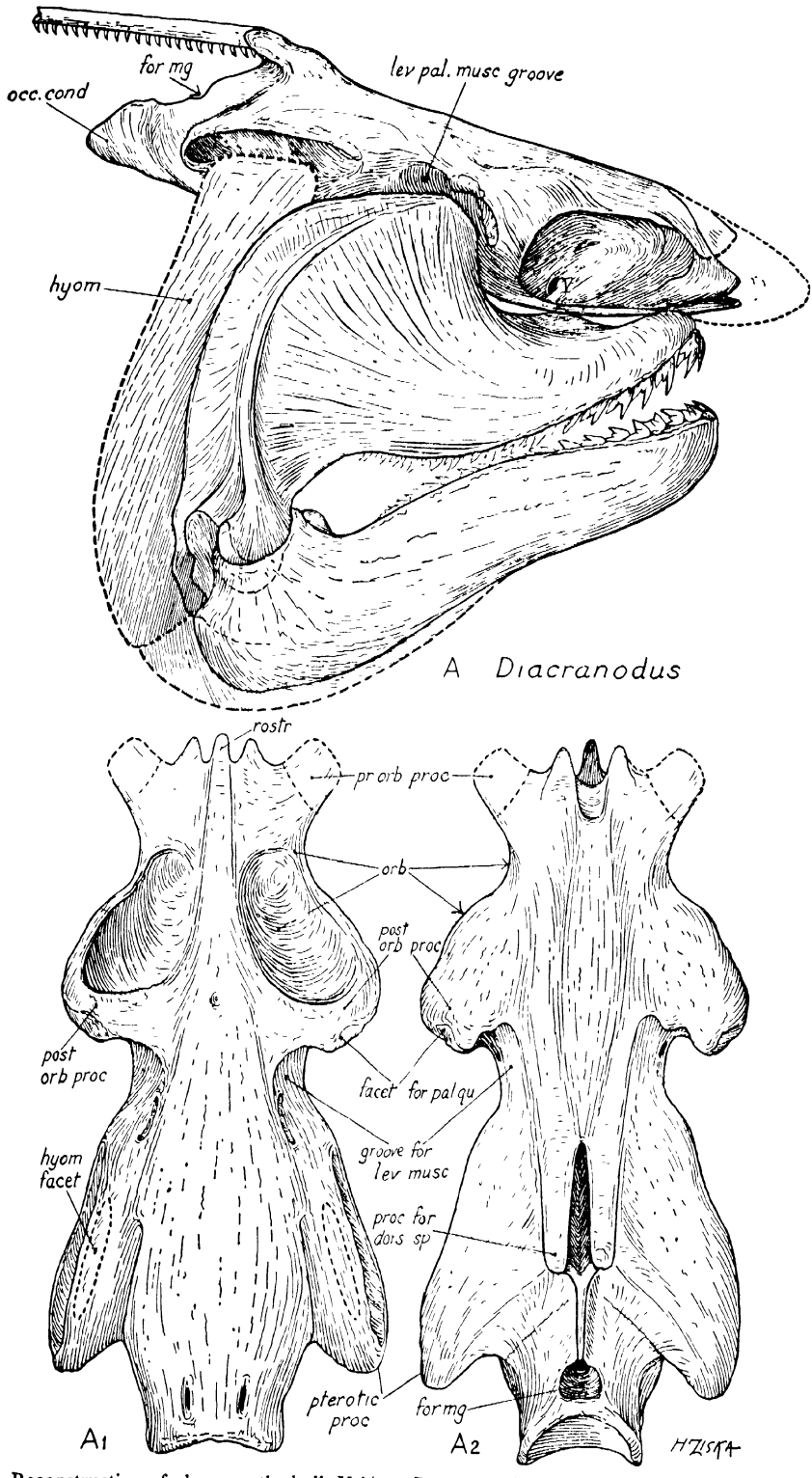


Fig. 8.22. Reconstruction of pleuracanth skull, X ½. Based on various skull parts of *Diacranodus texensis* Cope, from the Permian of Texas; data also from Romer and Price. A1, ventral surface; A2, dorsal surface.

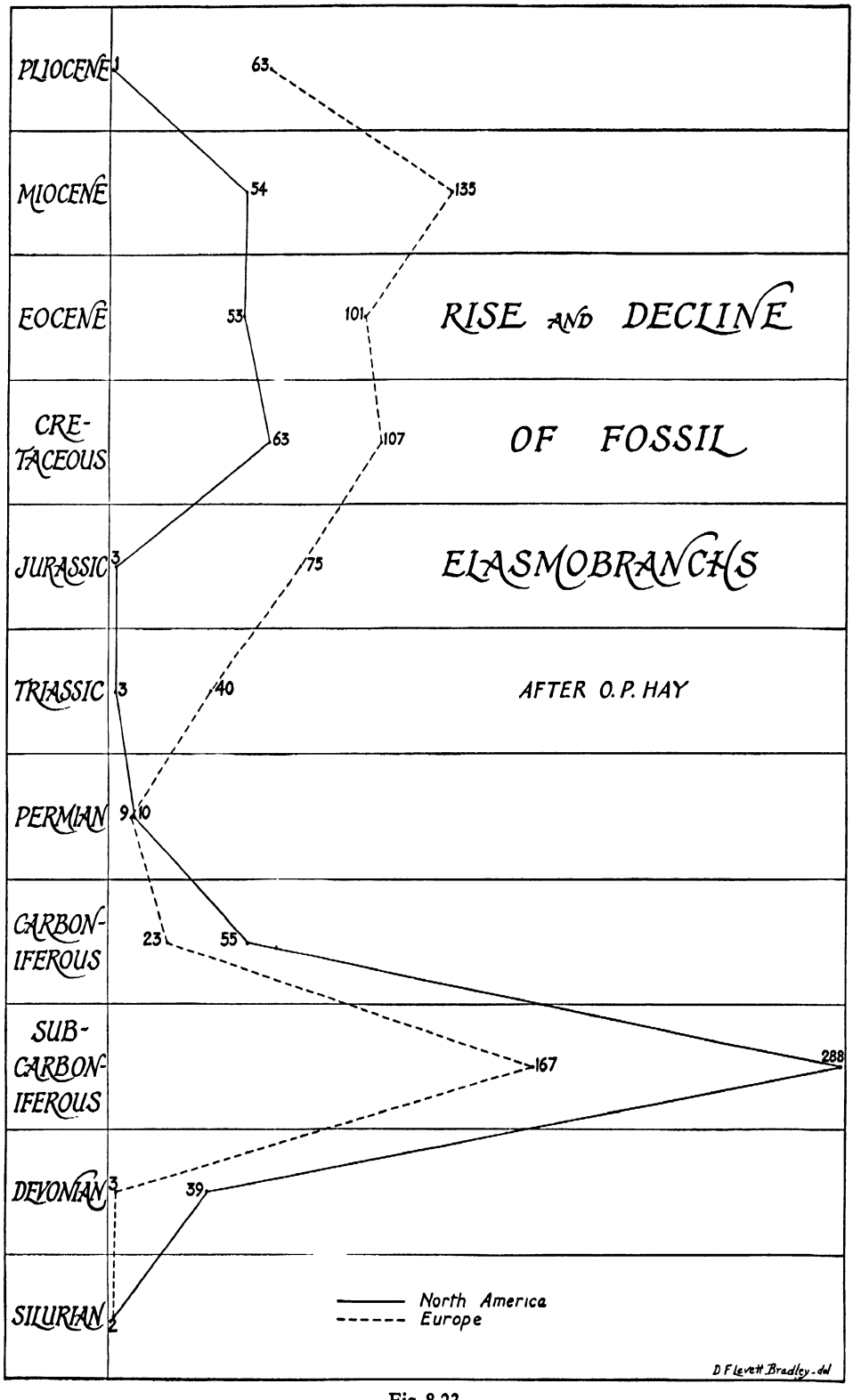

PLIOCENE
MIOCENE
EOCENE
CRE-
TACEOUS
JURASSIC
TRIASSIC
PERMIAN
CARBON-
IFEROUS
SUB-
CARBON-
IFEROUS
DEVONIAN
SILURIAN
1
63
54
135
53
101
63
107
3
75
3
40
9
10
23
55
167
288
3
39
2
RISE AND DECLINE
OF FOSSIL
ELASMOBRANCHS
AFTER O. P. HAY
North America
Europe
D F Leverett Bradley - del

Fig. 8.23

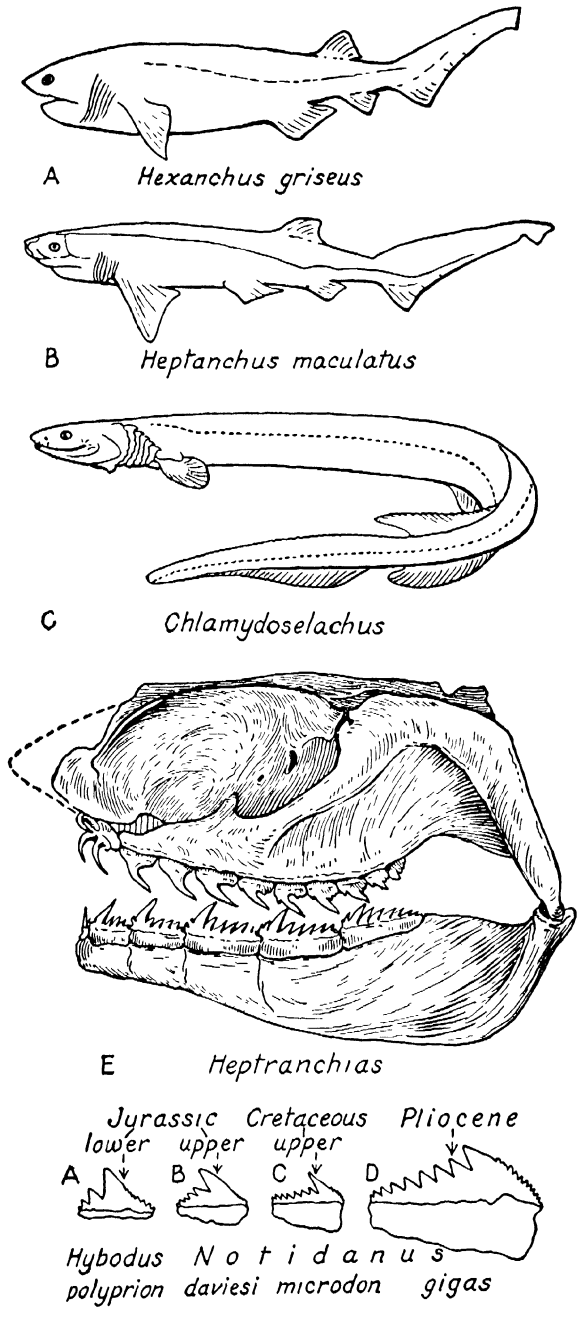


Fig. 8.24 (top). Modern relicts of the Jurassic notidanoids. A, Six-gilled shark, after Jordan and Evermann. B, Seven-gilled shark, after Daniel. C, Frilled shark, from Dean, after Garman; pectoral fin after Gudger.

Fig. 8.25. Evolution of notidanoid lower teeth from the hybodont type (A–D). This series suggests that the saw-like notidanoid lower teeth have been derived ultimately from a cladodont stem (fig. 8.14 B) by emphasis and backward bending of the middle cusp, reduction or suppression of the anterior cusps and multiplication of the posterior cusps. After Smith Woodward. E, Skull of young notidanoid, showing marked difference between upper and lower teeth and great enlargement of posterior part of palatoquadrate, which conceals the slender hyomandibular in the lateral view.

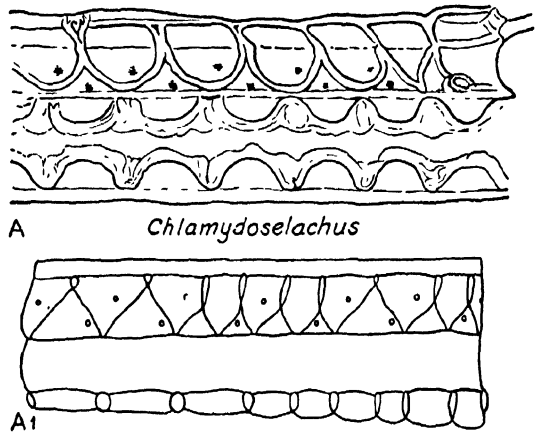


Fig. 8.26. Several thoracic vertebrae of the frilled shark in mesial section. The centra in the frilled shark, as in the notidanoids, consist of narrow-waisted cyclospondylic cylinders of calcified tissue surrounding the notochord. In the thoracic region there is but one centrum to each myotome, but beneath the dorsal fin there is a transitional condition (A1) leading to two centra to each segment. After Garman.

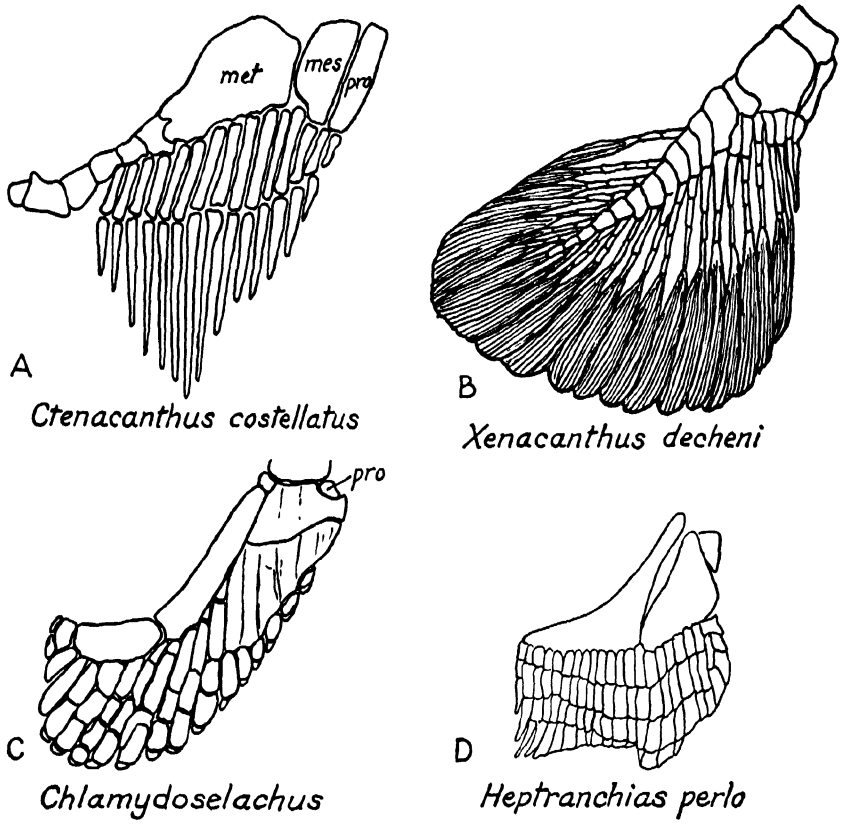


Fig. 8.27. Right pectoral fin of Palaeozoic and archaic modern sharks. A and B retain both the propterygium and the jointed metapterygial axis. In C and D the propterygium is reduced but C retains part of the jointed metapterygian axis. A, Carboniferous ctenacanth, after Moy-Thomas. B, Permian pleuracanth, after Fritsch. C, Modern frilled shark, after Garman. D, Modern notidanoid, from E. G. White.

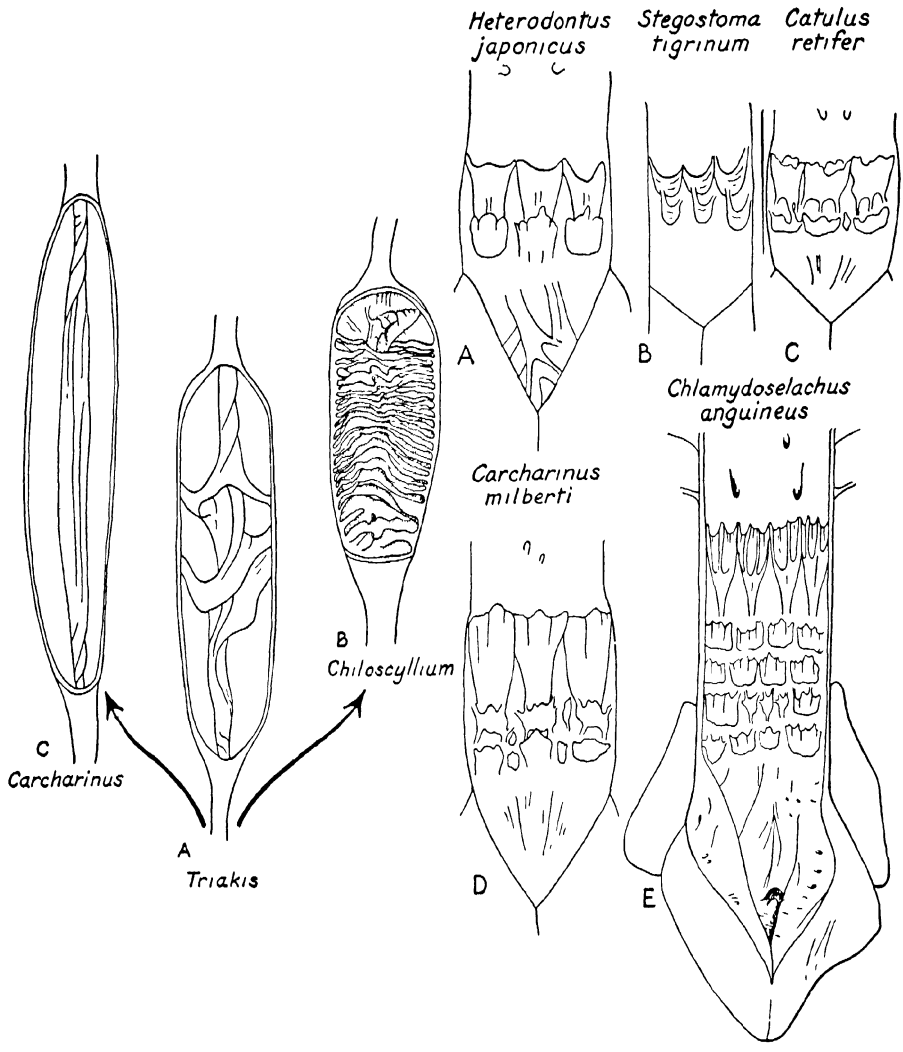


Fig. 8.28. The three main types of intestinal spiral valves. After E. G. White. A, The primitive spiral type (I) with few turns. B, The ring type (II) with more than thirty transverse folds characteristic of the Isurida. The scroll type (III) characteristic of the Carcharinida. Transitional stages connect the three main types.

Fig. 8.29. Another set of variable polyisomeres, the heart valves. After E. G. White. Two rows of valves are found in *Chimaera, Heterodontus, Squalus,* the nurse sharks and the cat sharks, all relatively primitive forms; three rows are characteristic of the carcharinids; the notidanids and the frilled shark have four to five, and certain dasybatoid rays have six or seven.

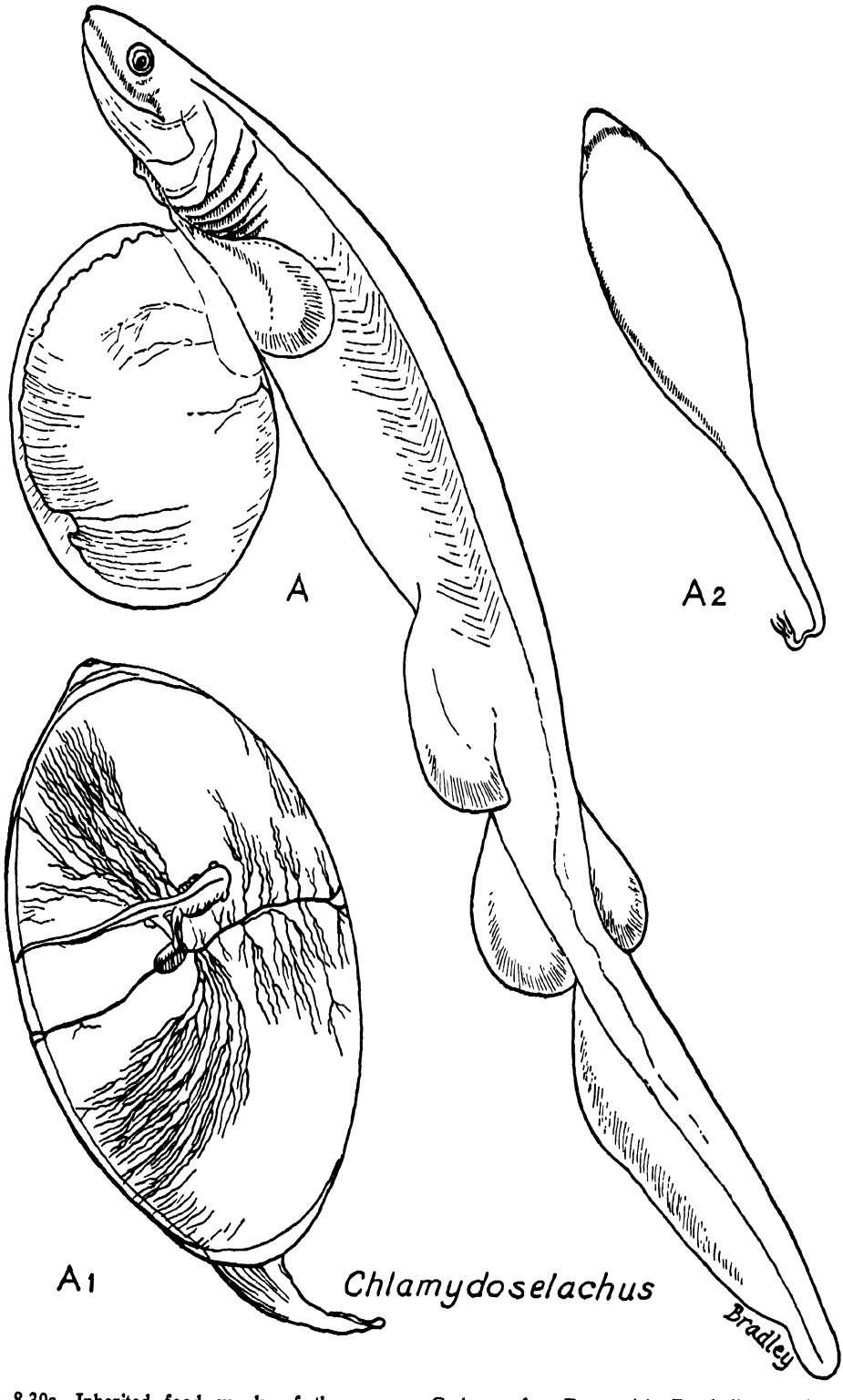


Fig. 8.30a. Inherited food supply of the young frilled shark. From Gudger, after Dean. A, Dean's 390 mm. embryo attached to its reduced egg. From Gudger, after Dean. A1, Eggshell, containing egg (100 x 65 mm.) and embryo. From Gudger, after Nishikawa. A2, An empty egg capsule.

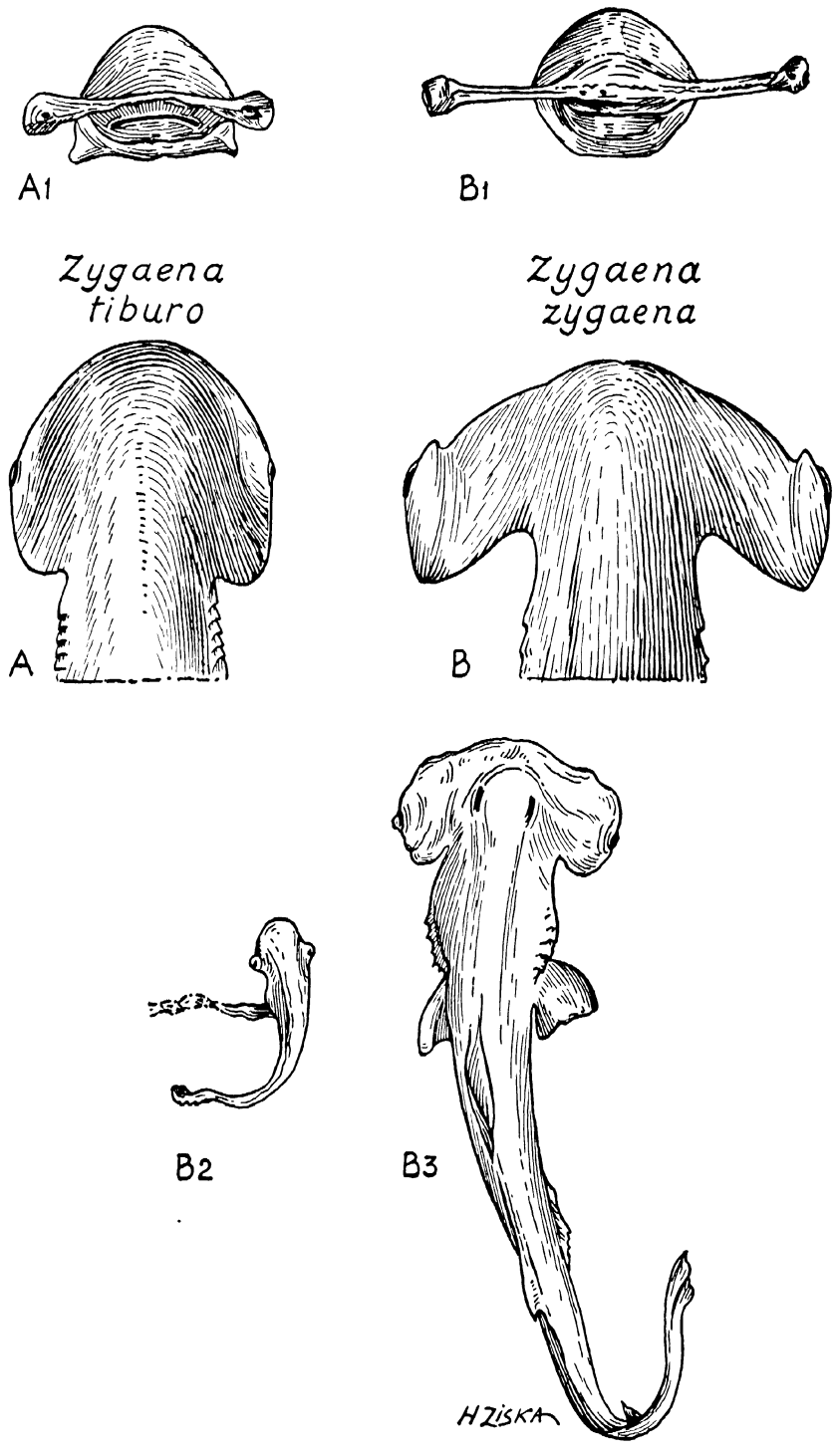


Fig. 8.30b. Heads of Bonnet (A) and Hammer-head (B) sharks. From American Museum models. B2, B3, Embryos of hammer-head. From specimens presented by Lieut. Otis Barton. In the younger stage (B2) the widening of the anterior part of the head is just beginning.

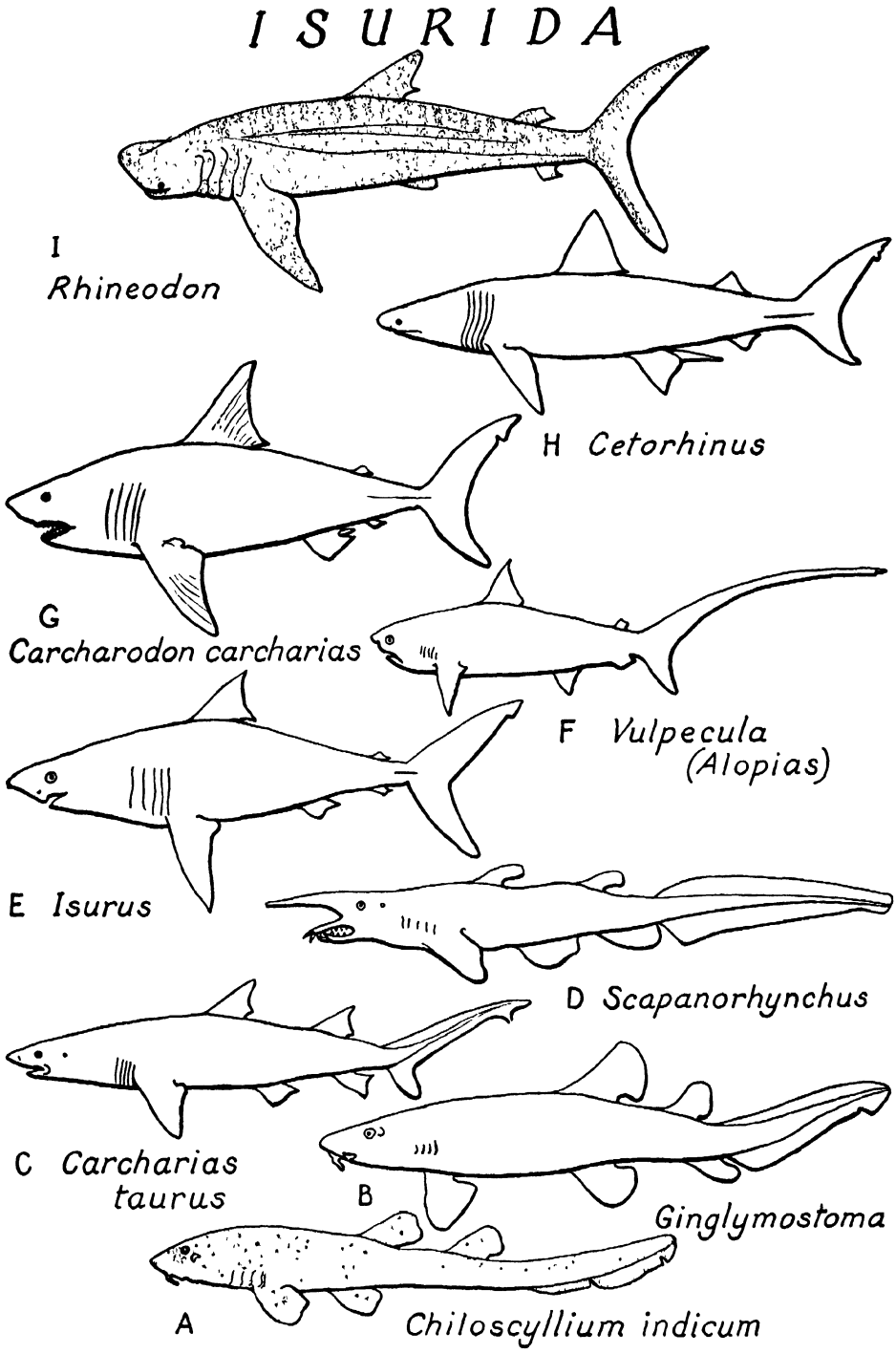


Fig. 8.31. Main types of the suborder Isurida of the order Galea. Arranged in the general order of specialization (A–I). After E. G. White. In the primitive inshore, grovelling types (A, B) the body is elongate and both dorsal fins are placed well to the rear. In the advanced free-swimming, pelagic forms (E–I) the first dorsal is large, at the summit of the back, the second dorsal and anal fins are often reduced.

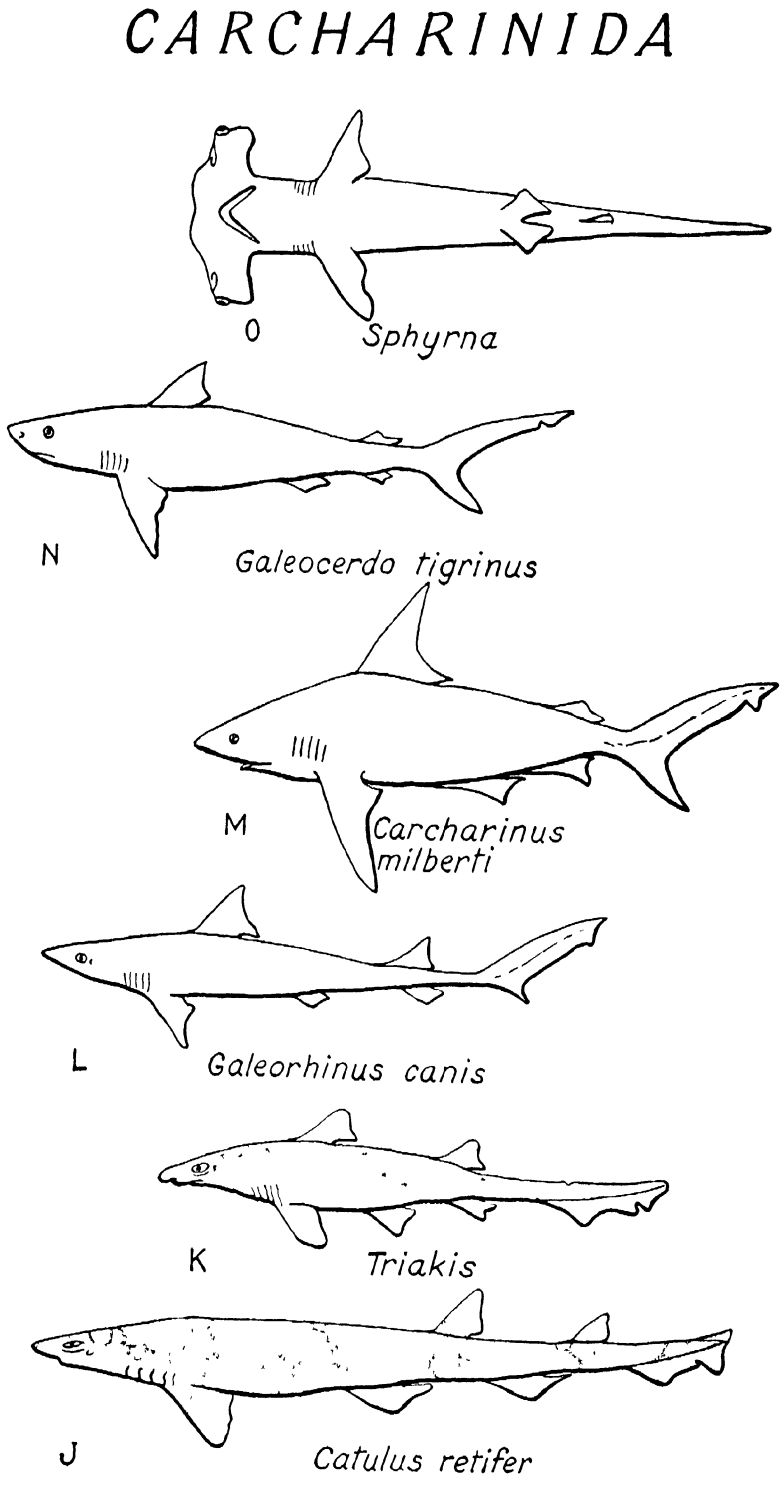


Fig. 8.32. The main types in the suborder Carcharinida of the order Galea. After E. G. White.

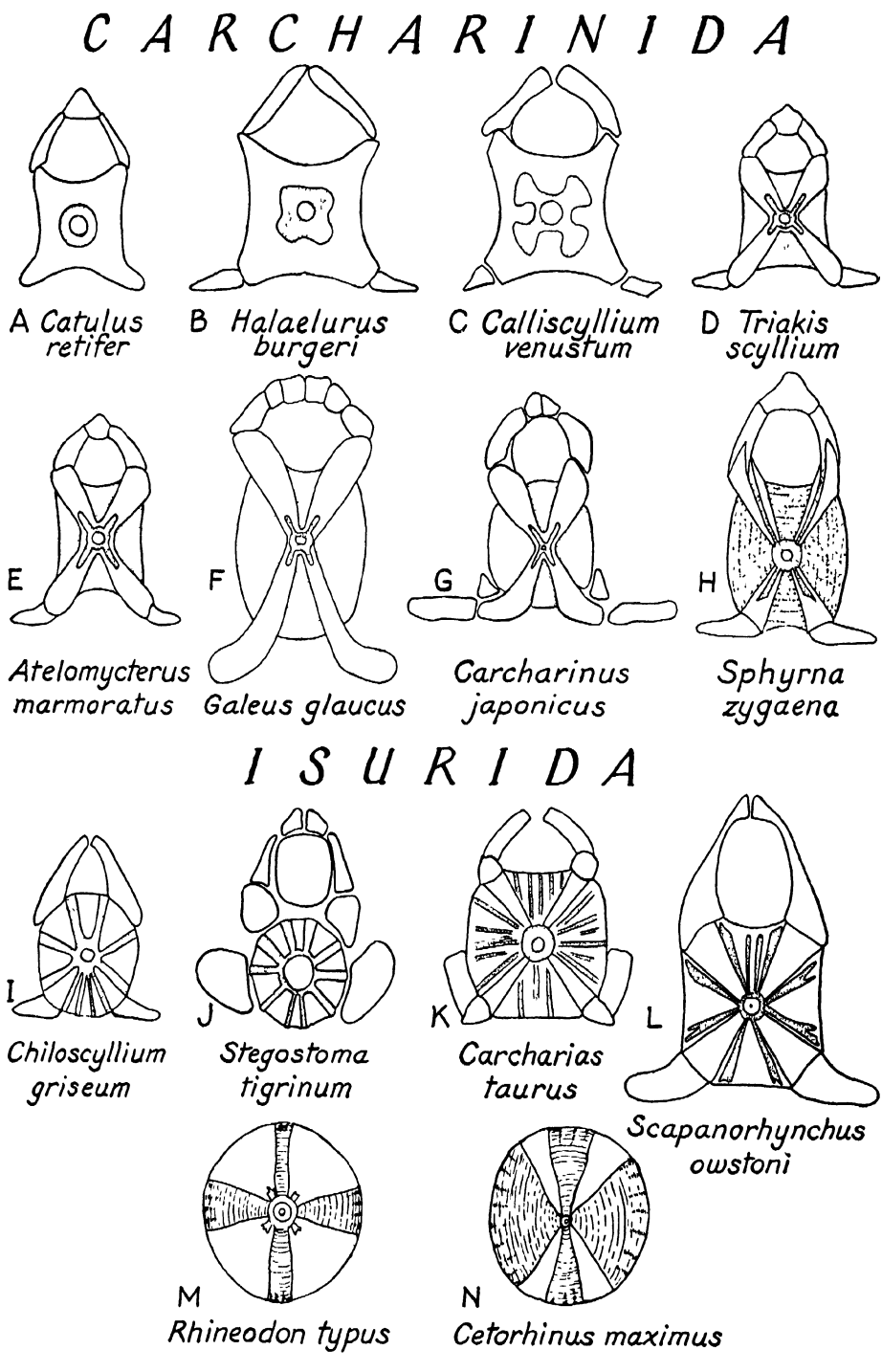


Fig. 8.33. Main types of vertebrae in the order Galea. After E. G. White. A–H, According to White, represent successive morphological stages in the suborder Carcharinida, from the cyclospondylic cat shark (A) through the Maltese cross-stage to the asterospondylic ground shark (G) and hammer-head (H). In I–N, the radiating folds do not form a Maltese cross but tend to multiply irregularly.

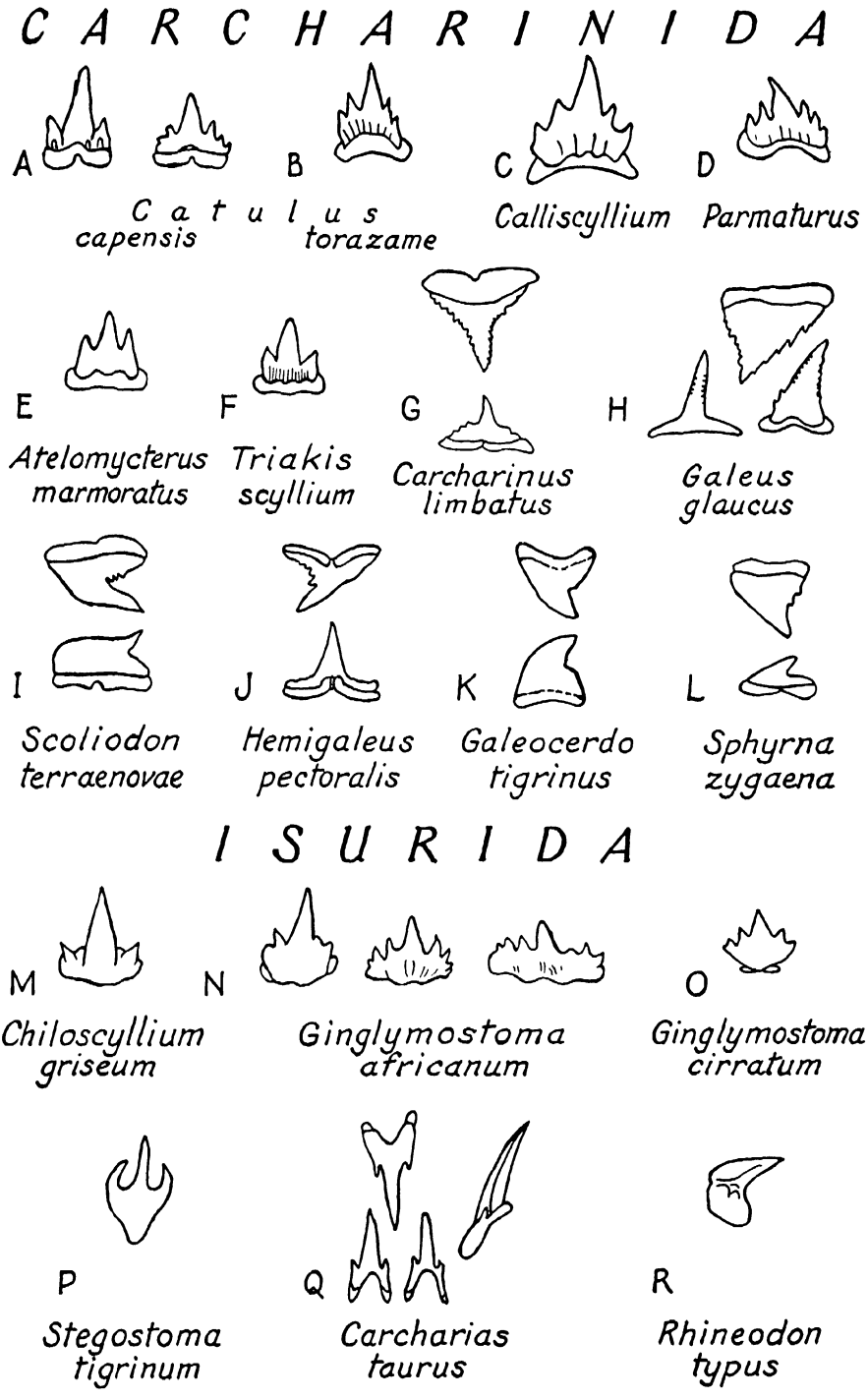


Fig. 8.34. Typical teeth of the suborders Carcharinida and Isurida. After E. G. White. In the cat sharks (A–D) the teeth retain primitive characters and recall those of the Upper Devonian cladodonts (fig. 8.14 B). In the carcharinids (G–H) the upper and lower teeth are often but not always (J, K) unlike, the uppers being triangular, the lower, with narrow main cusps. Among the Isurida, the teeth of the nurse sharks (M–P) are often small, low-crowned, tending to form a dental pavement, those of the sand shark (Q) have long sharp tips with small basal cusps; those of the whale shark (R) reduced, with recurved points.

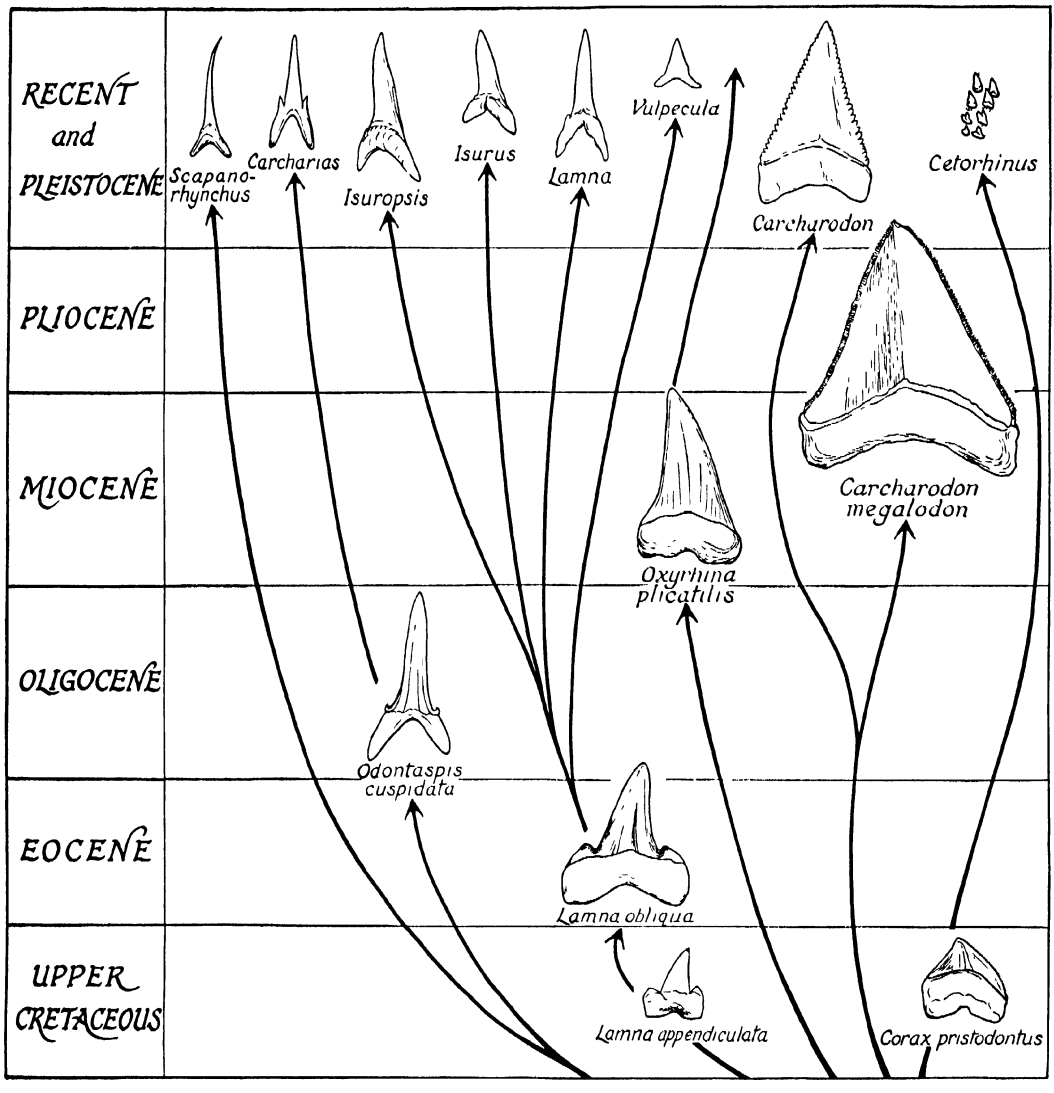


Fig. 8.35. Teeth of modern lamnoids and their predecessors. Fossil teeth after Smith Woodward; recent teeth from specimens. Adaptive branching has led along various lines, from moderately primitive teeth, with one high cusp flanked on either side by low basal cusps in the Upper Cretaceous, to: (1) very long sharply pointed crowns, with little or no basal cusps; (2) wide triangular crowns with serrated edges; (3) degenerate minute triangular crowns. But intergrades often occur even in a single jaw, with large narrow, sharp teeth near the front and minute low, wide triangular teeth at the rear end. Thus the different generic and specific types have been produced merely by altering the rates of growth of their parts.

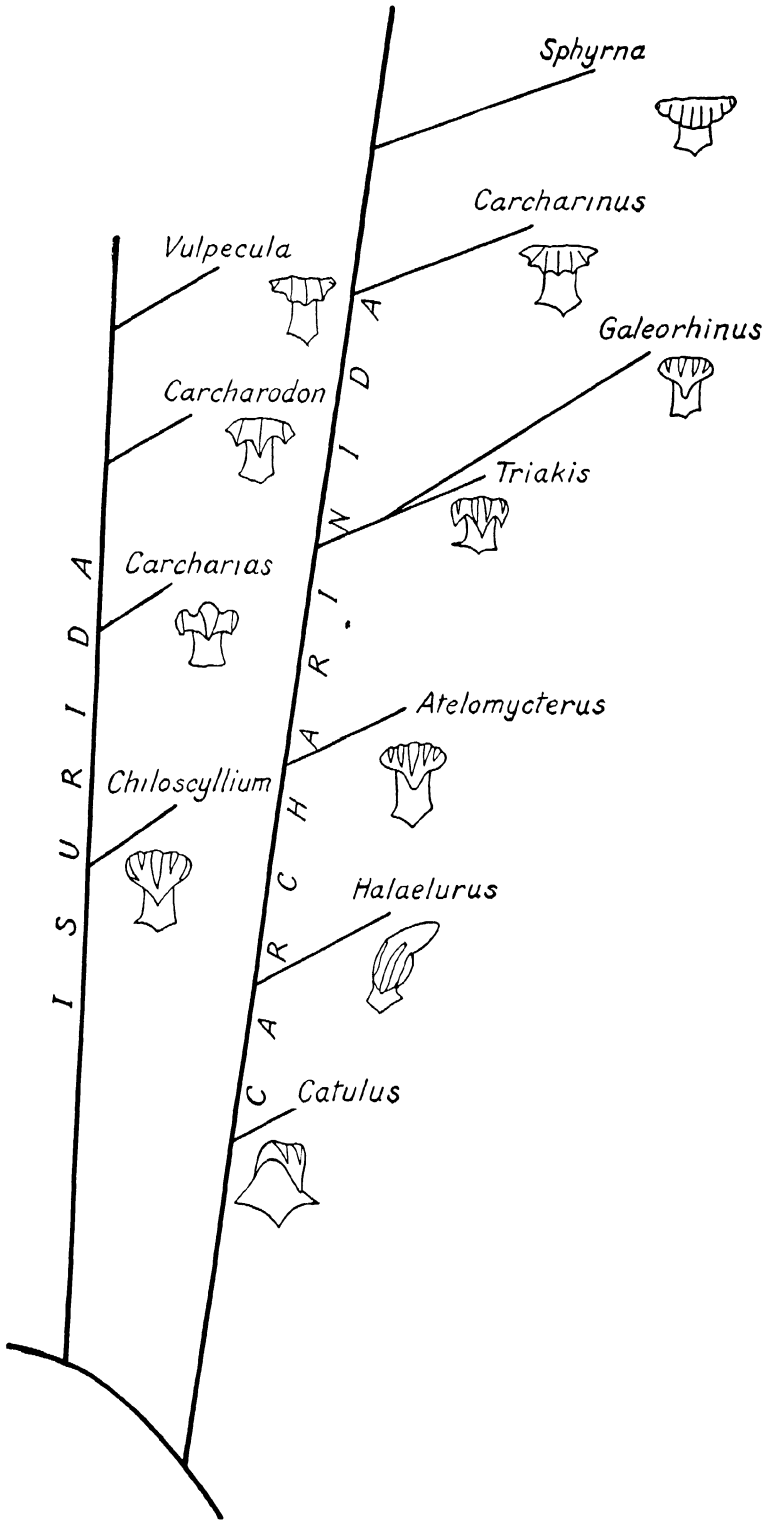


Fig. 8.36. Dermal denticles of Isurida and Carcharinida. After E G. White.

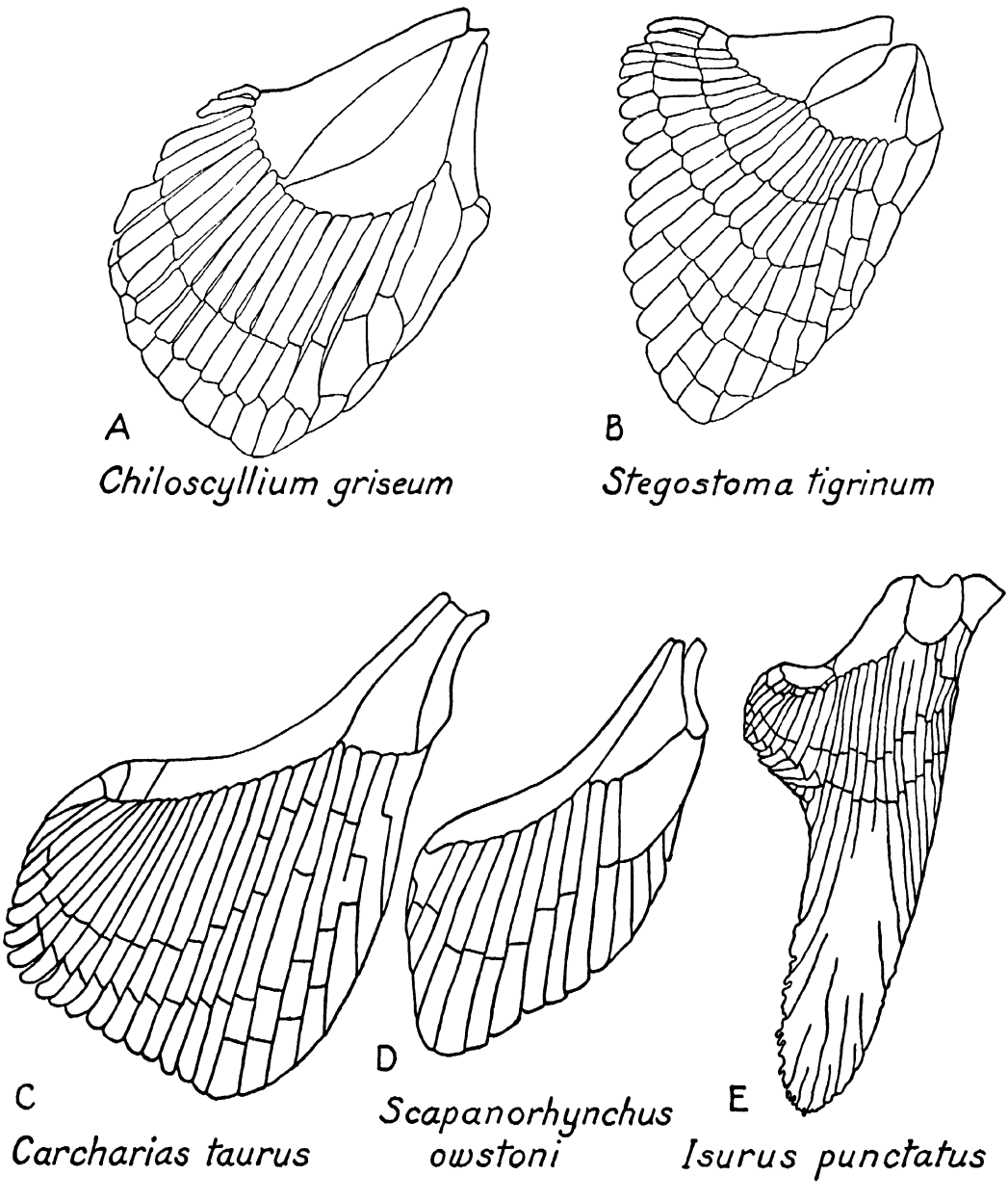


Fig. 8.37. Pectoral fins of the suborder Isurida. After E. G. White. In the more primitive inshore or grovelling forms (A, B) the pectoral fin is short and paddle-like, with large muscular base, short stout radials and broadly convex outer border; in the advanced pelagic, fast-swimming form (E) the muscular base is narrow, the distal rows of radials greatly produced, the anterior margin is prolonged, the outer part of the fin becoming narrow and wing-like.

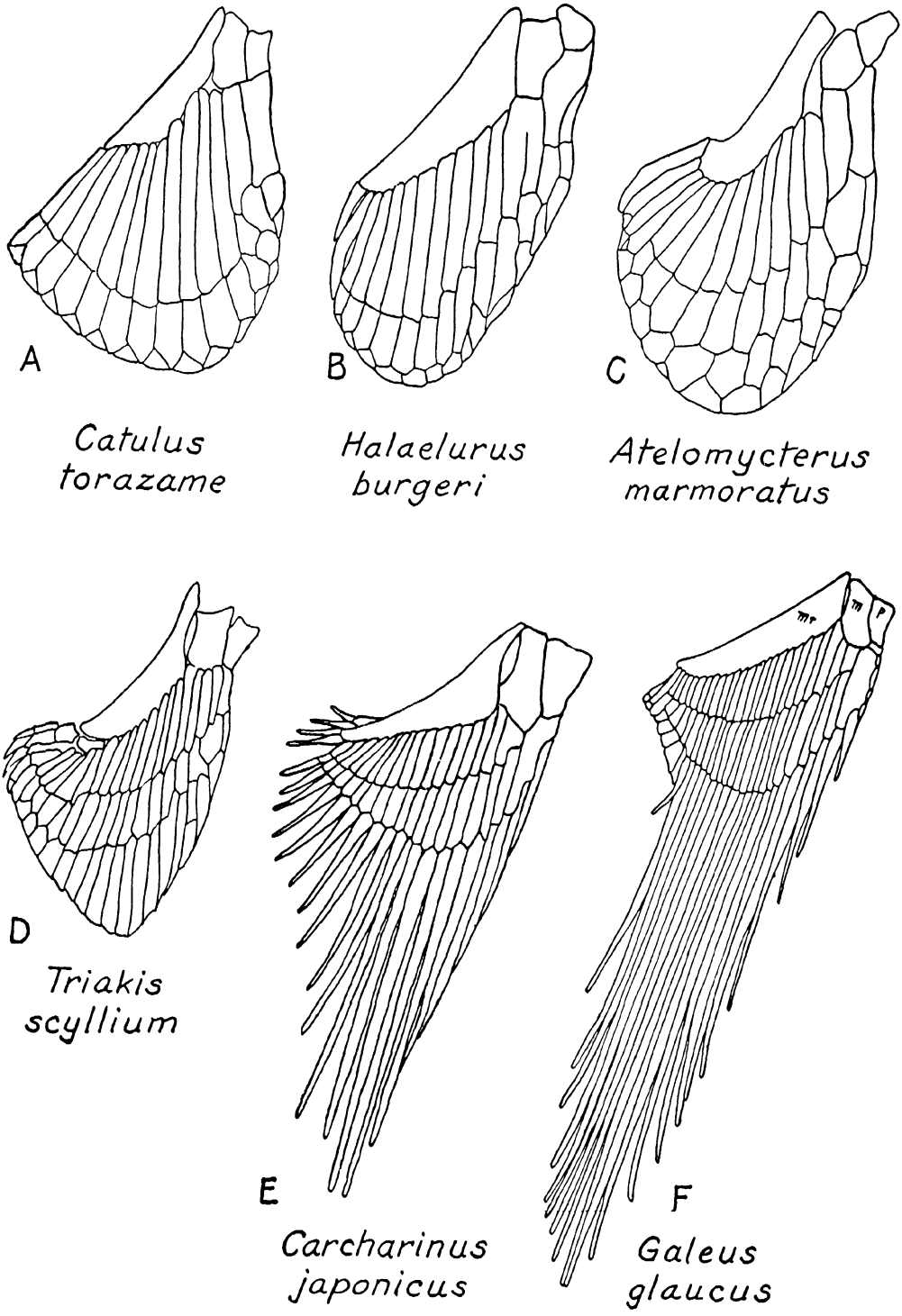


Fig. 8.38. Pectoral fins of the suborder Carcharinida. After E. G. White. In the primitive inshore or grovelling cat sharks (A) the pectoral fin skeleton recalls that of the more primitive nurse sharks (Fig. 8.37 A) in having short stout radials and a convex paddle-like shape; in the pelagic blue shark (F), on the other hand, the radials are greatly elongate and the fin becomes more or less wing-like, as in the wide-ranging pelagic *Isurus* (Fig. 8.37 E). Intermediate stages are seen in B, D, E.

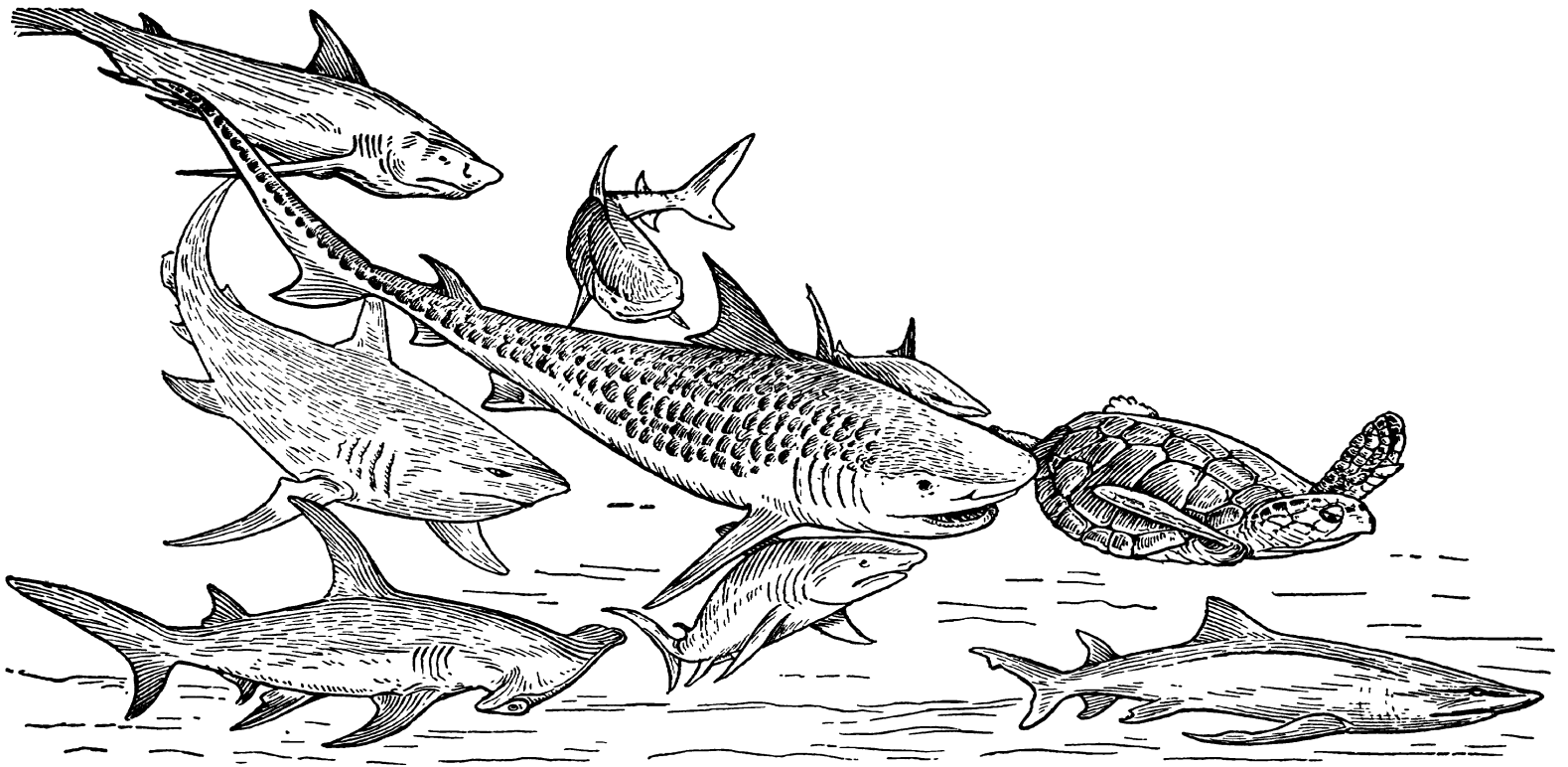


Fig. 8.39. The Sea Rovers. Representatives of the two great competing suborders of the modernized order Galea. The central tiger shark (*Galeocerdo tigrinus*), the three requiem or ground sharks (*Carcharinus*) and the hammer-head (*Sphyrna zygaena*) represent the later (Eocene to Recent) and in some ways less advanced suborder Carcharinida. The sand shark (*Carcharias*, at the lower right, and the huge man-eater or white shark (*Carcharodon*) are members ot the somewhat older (Cretaceous to Recent) suborder Isurida.

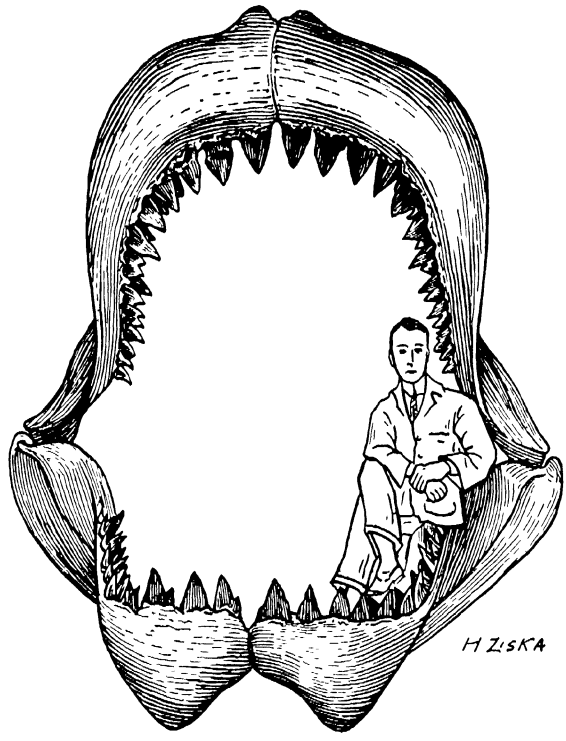


Fig. 8.40 (top). Teeth of giant fossil shark (*Carcharodon megalodon*) from the Tertiary of New Jersey. American Museum exhibit, the jaws enlarged from those of a recent man-eater.

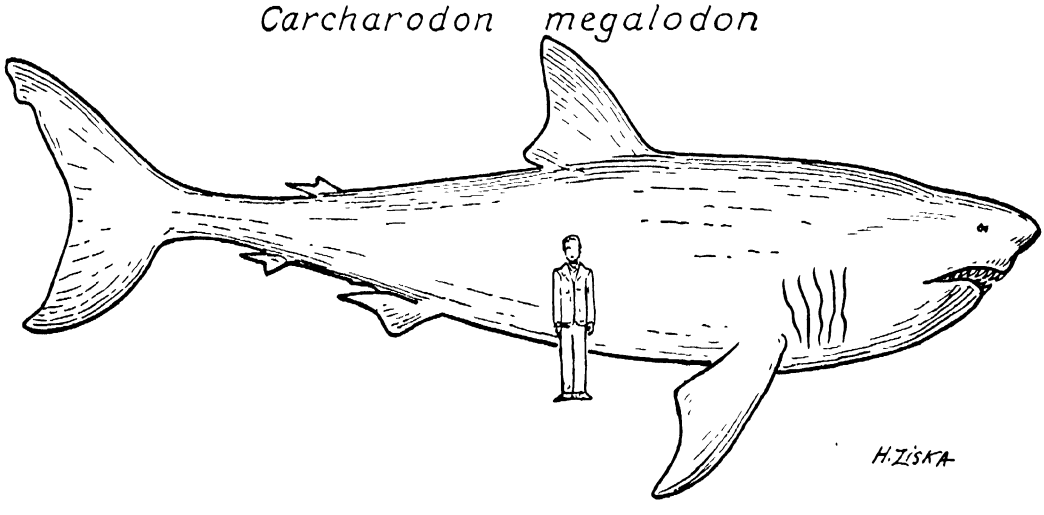


Fig. 8.41. Sketch restoration of extinct *Carcharodon megalodon* with five-foot-eight-inch man for comparison. Estimated over-all length, 41 feet; this is probably much too short for the teeth figured above.

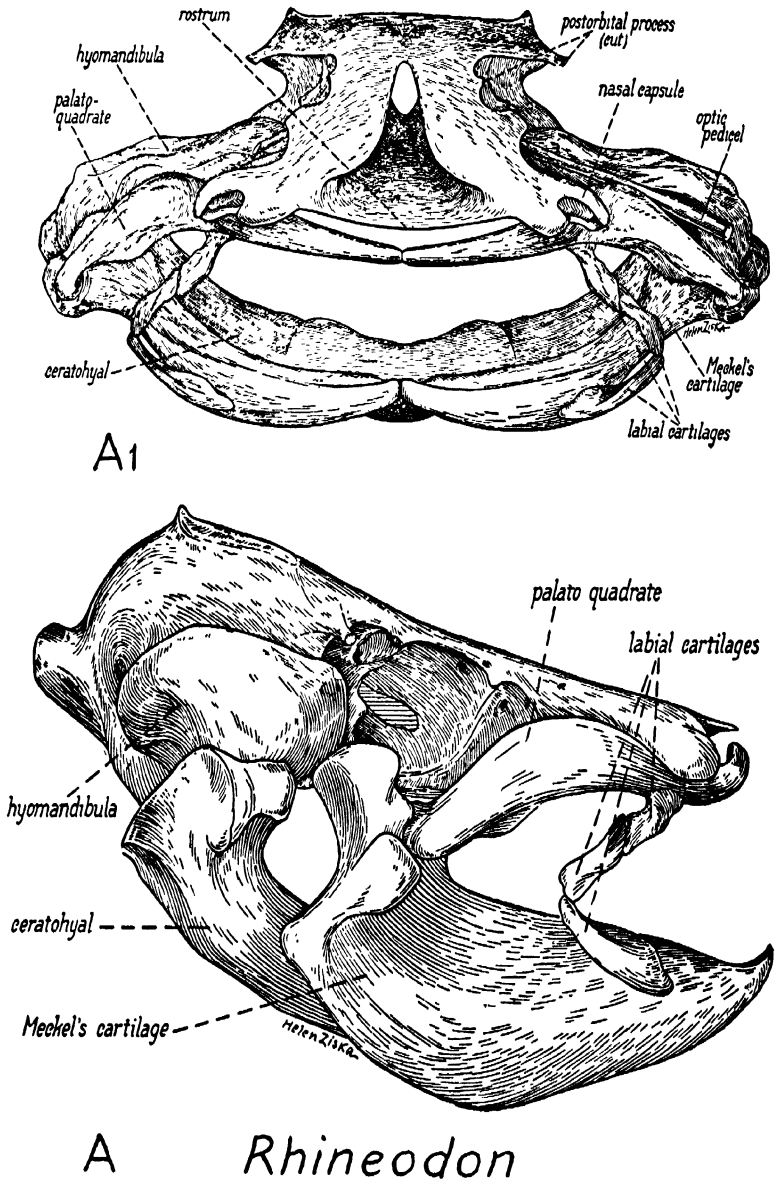
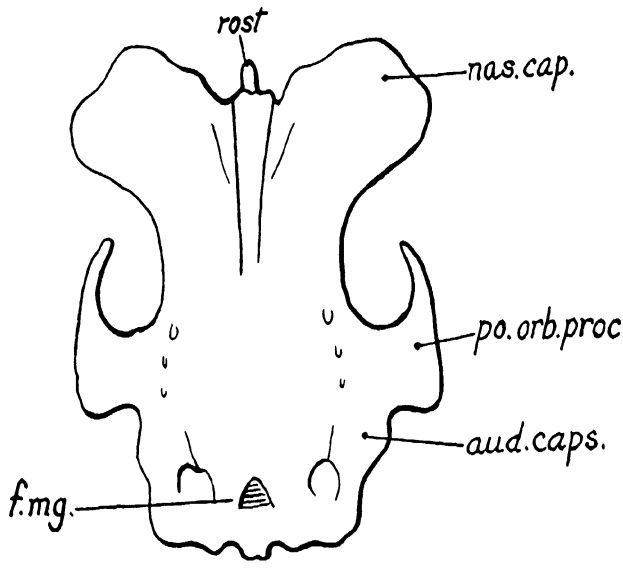
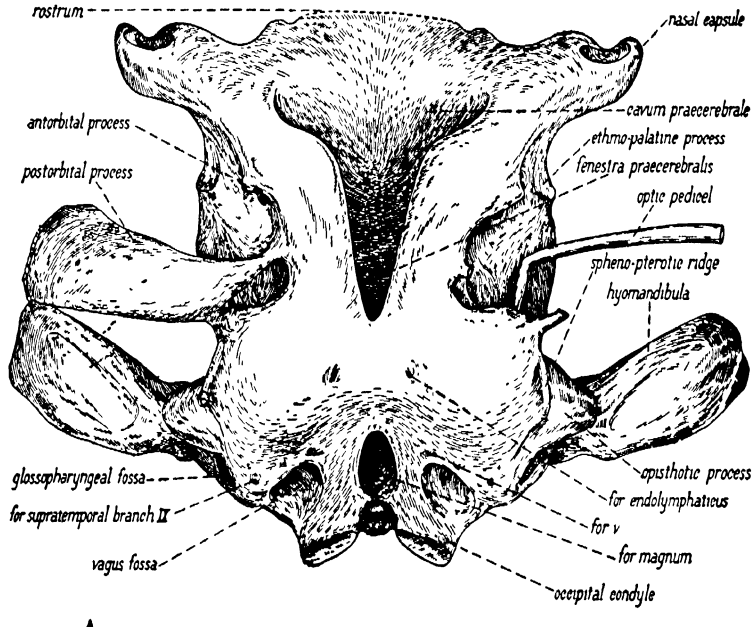


Fig. 8.42, 43. Skull of the whale shark (*Rhineodon*). After Denison. A, side view; A1, front view; B, top view of a nurse shark skull. In correlation with the extreme widening of the mouth, the cranium is also widened and the opposite olfactory capsules are far apart. In A, the postorbital process has been cut off to expose the huge hyomandibular. The endocranium, although fundamentally similar to that of the nurse sharks (B), has lost all but a trace of the rostrum.



B Stegostoma



A2

Fig. 8.43

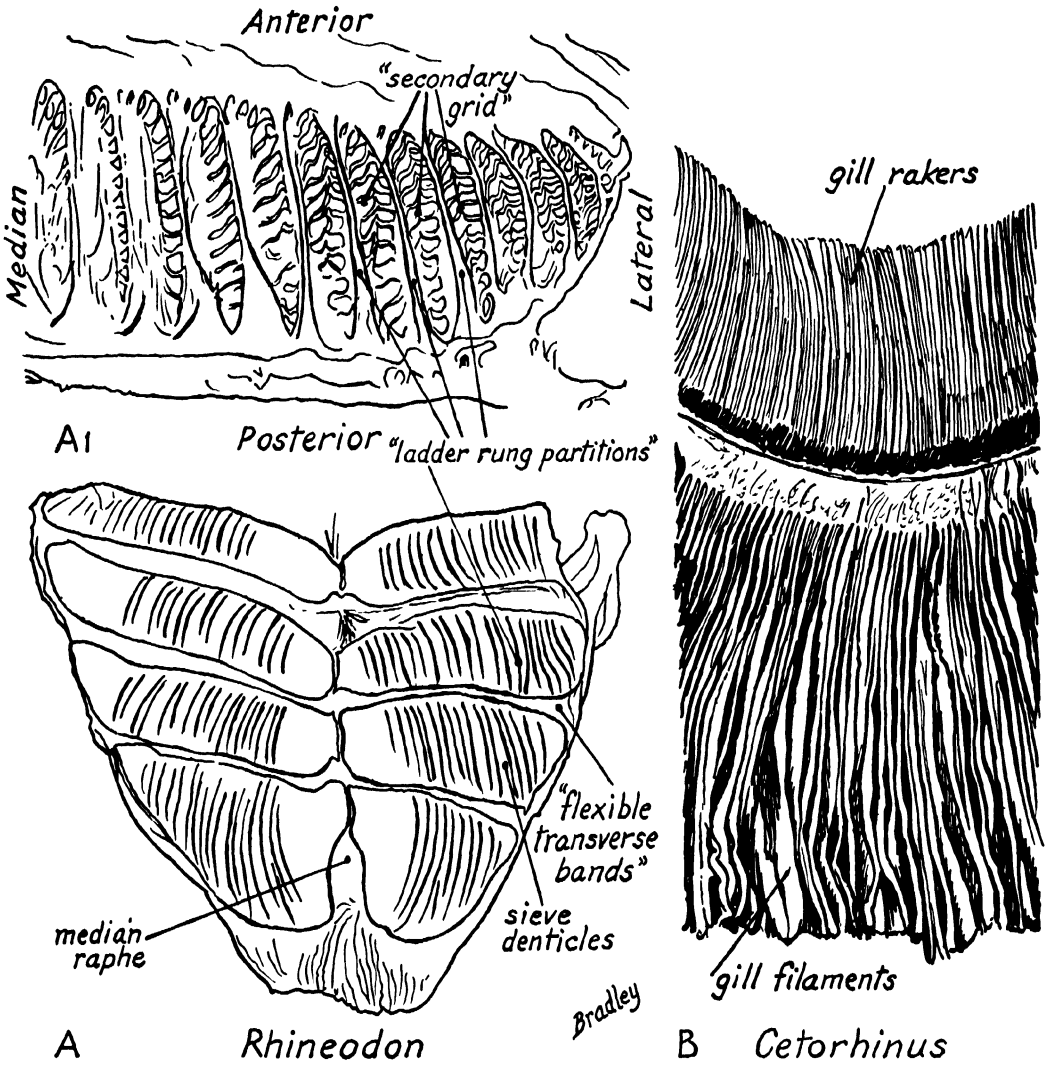


Fig. 8.44. Diverse modifications of the "gill rakers" in the whale shark (A, A1) and the basking shark (B). In *Cetorhinus* the gill rakers are long, narrow and thin plates fastened to the proximal borders of the gill arches and projecting into the pharynx. They are analogous with similar gill rakers in herrings and likewise serve as a strainer to prevent the escape of food and to permit the passage of the water. In the whale shark the complex sieve is located near the bottom of the gill pockets and does not protrude into the pharynx. A, after Gudger; B, after E. G. White.

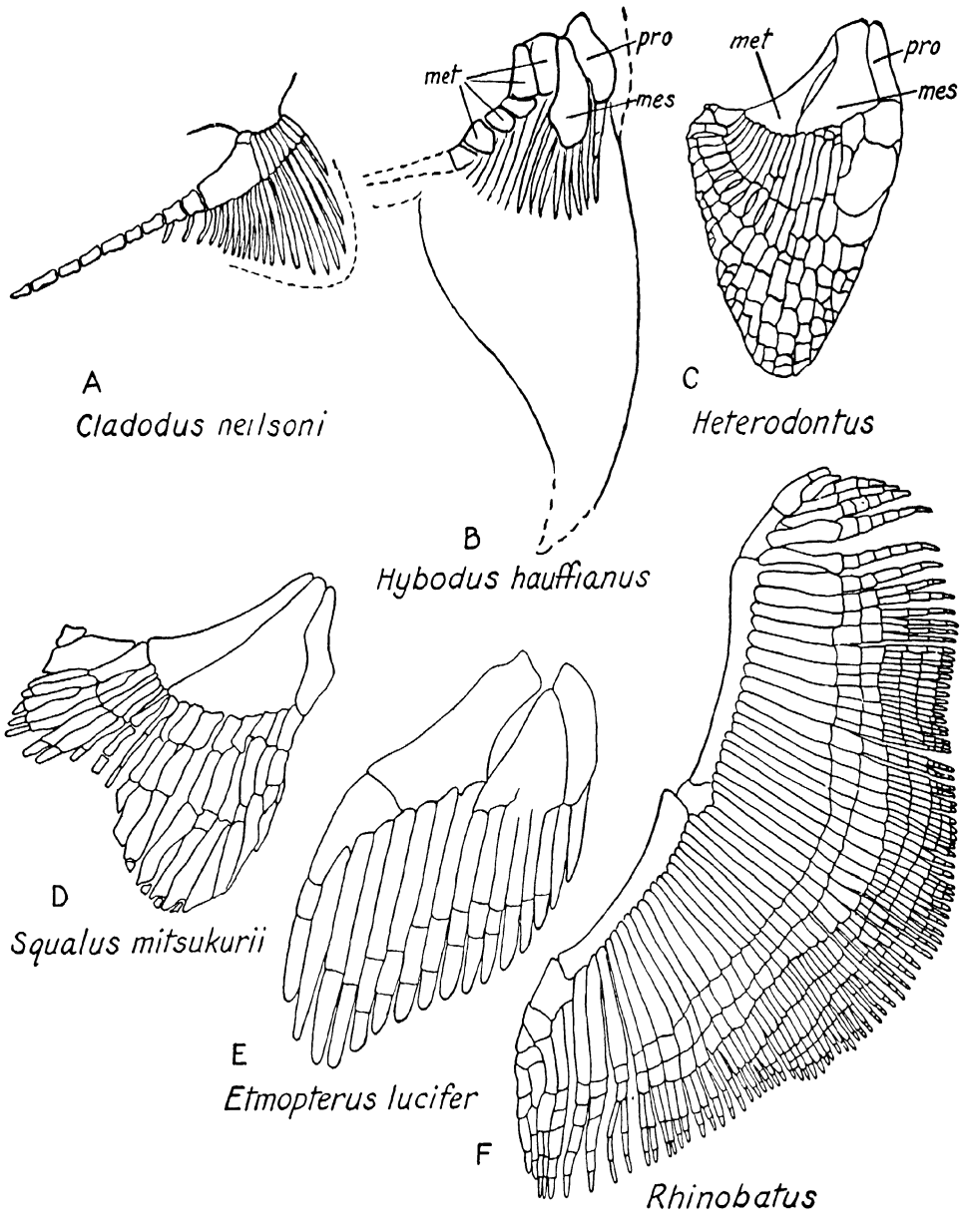


Fig. 8.45. Right pectoral fin skeletons of (A) Lower Carboniferous "cladodont" with prolonged and jointed metapterygium; (B) Lower Jurassic hybodont, retaining a jointed metapterygium Restoration based on the specimens figured by Koken (1907, Taf. I, II). C, Modern bull-head (heterodont) shark with a single metapterygium. D, E, Progressive anteroposterior elongation of the fin in squaloids and primitive batoid. Data from E. G. White.

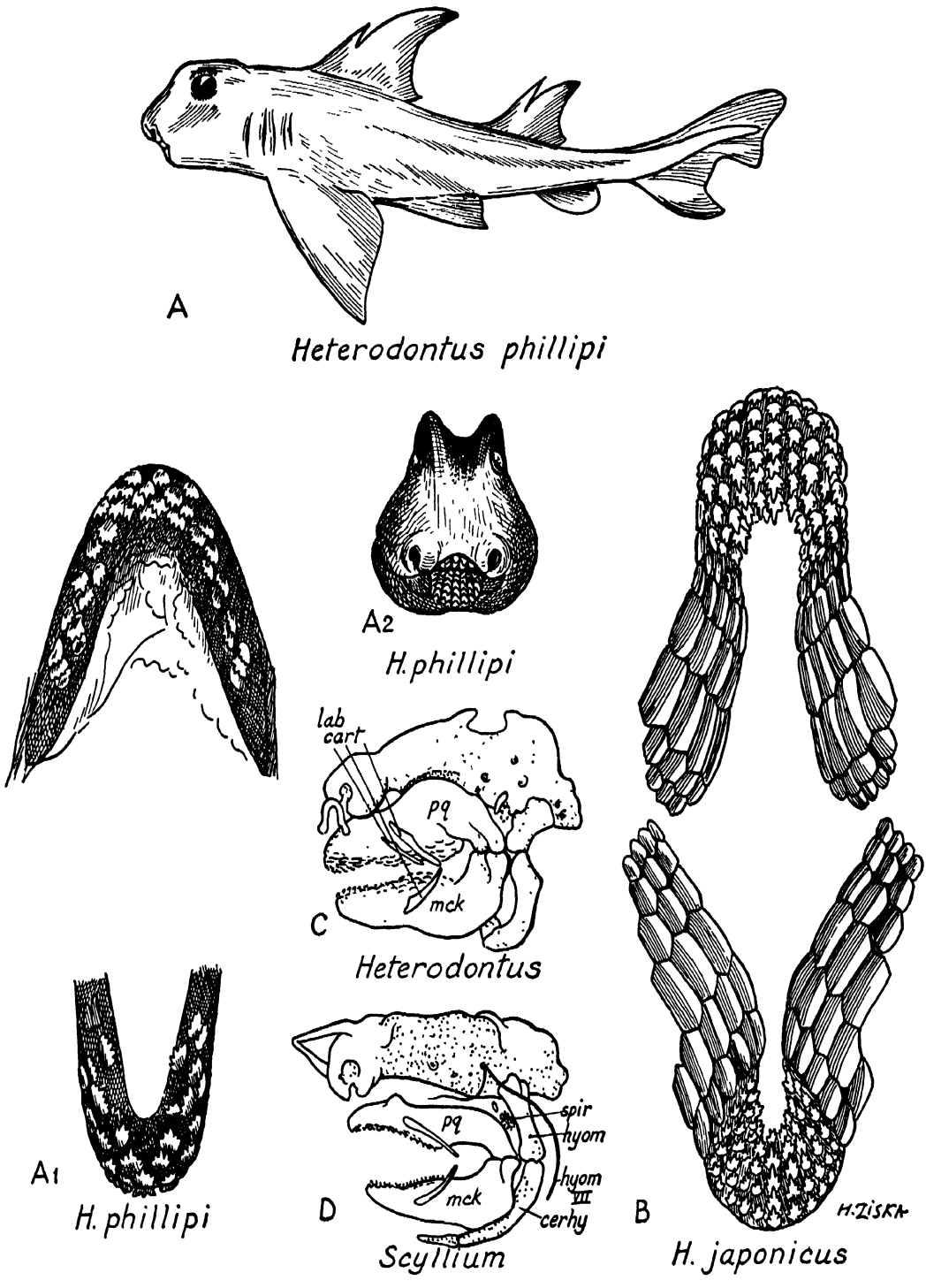


Fig. 8.46a. "Port Jackson" and Japanese heterodont sharks. A, B, from B. G. Smith, after various authors. Contrasting jaw types of heterodont and normal shark. C, after Dean; D, after Goodrich.

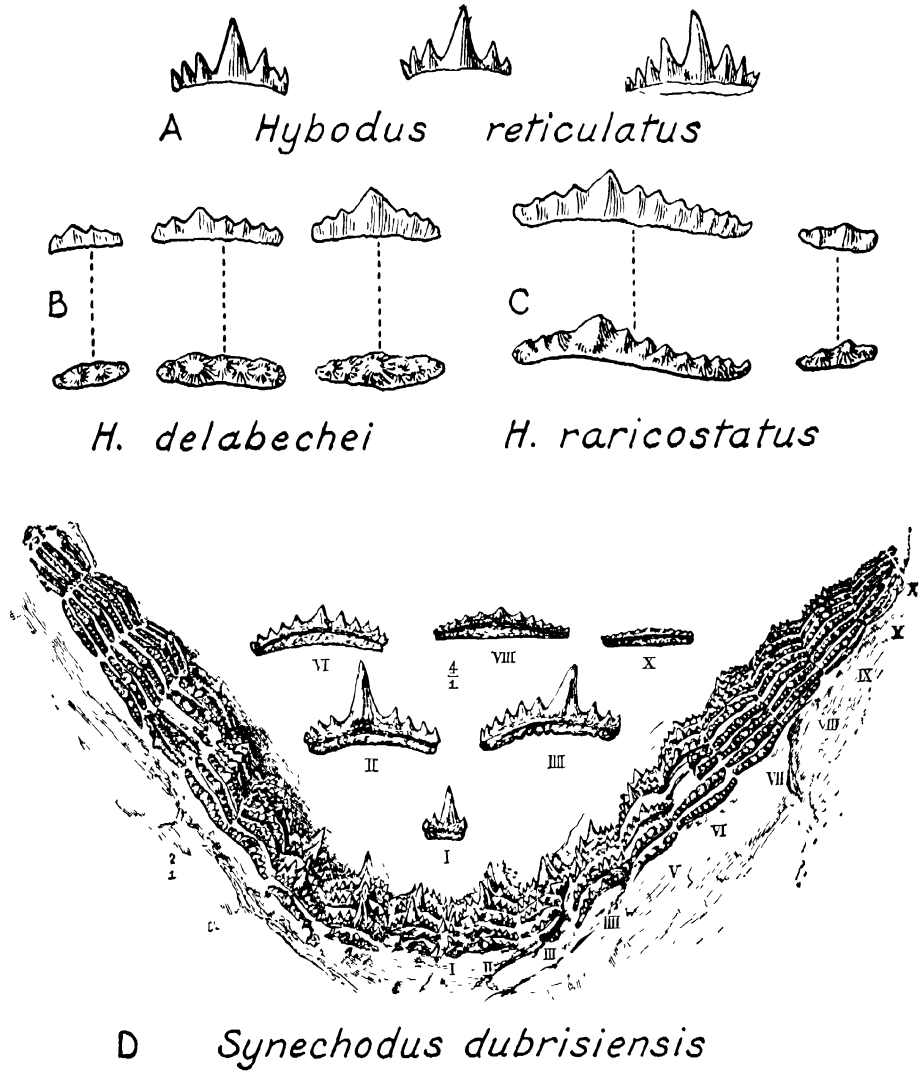


Fig 8 46b. Forerunners of the bull-head (heterodont) sharks. After A. S. Woodward. Showing the many-cusped teeth of the earlier hybodonts (A–C). The more anterior teeth have high central cusps but in the cheek teeth the cusps are reduced and each tooth is equivalent to a rolling tooth plate of the heterodonts (fig. 8.46a B).

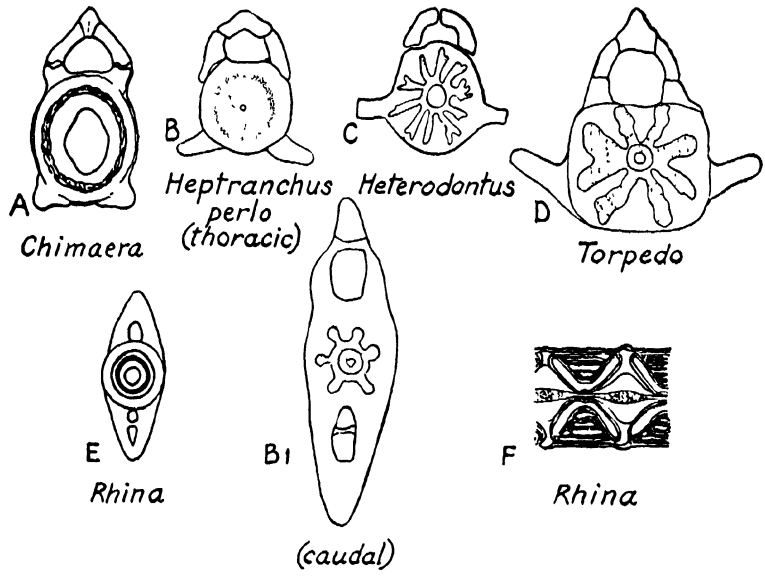


Fig. 8.47. Primitive cyclospondylic (A, B) and subasterospondylic, or pseudasterospondylic centra (C, D). The latter arise by emphasis of the "Maltese cross" system of radiating longitudinal calcified ridges (fig. 8.33 C). C and D are sometimes called tectospondylic but this word is more properly, limited to vertebrae with concentric calcifications (E, F). Data from E. G. White and Hasse.

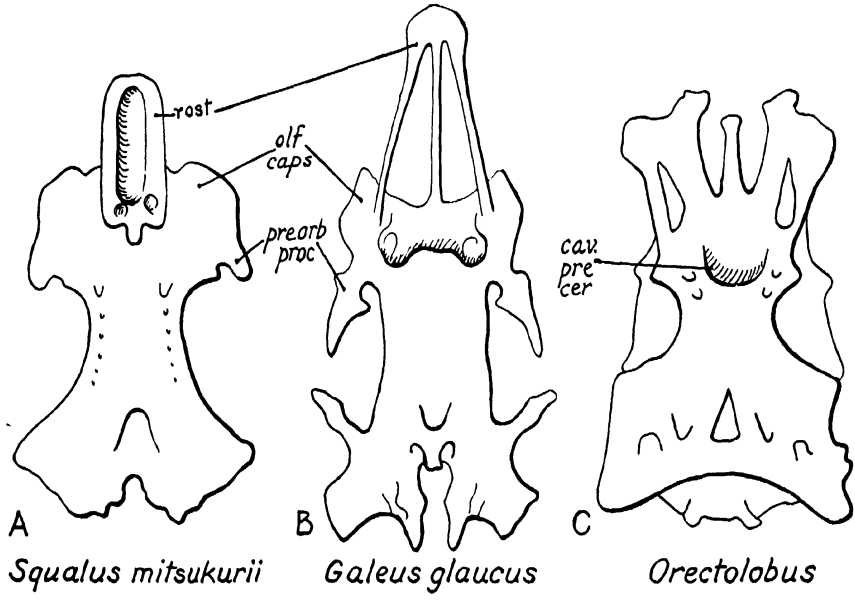


Fig. 8.48. Skulls of modern sharks and rays (in dorsal view) to show differences in the rostrum. After E. G. White. In A, a relatively primitive form, the strong boat-like rostrum is not perforated; in B, the top and sides are open, leaving three narrow bars; in C, the distal part of the tripod is truncated, leaving only the stumps.

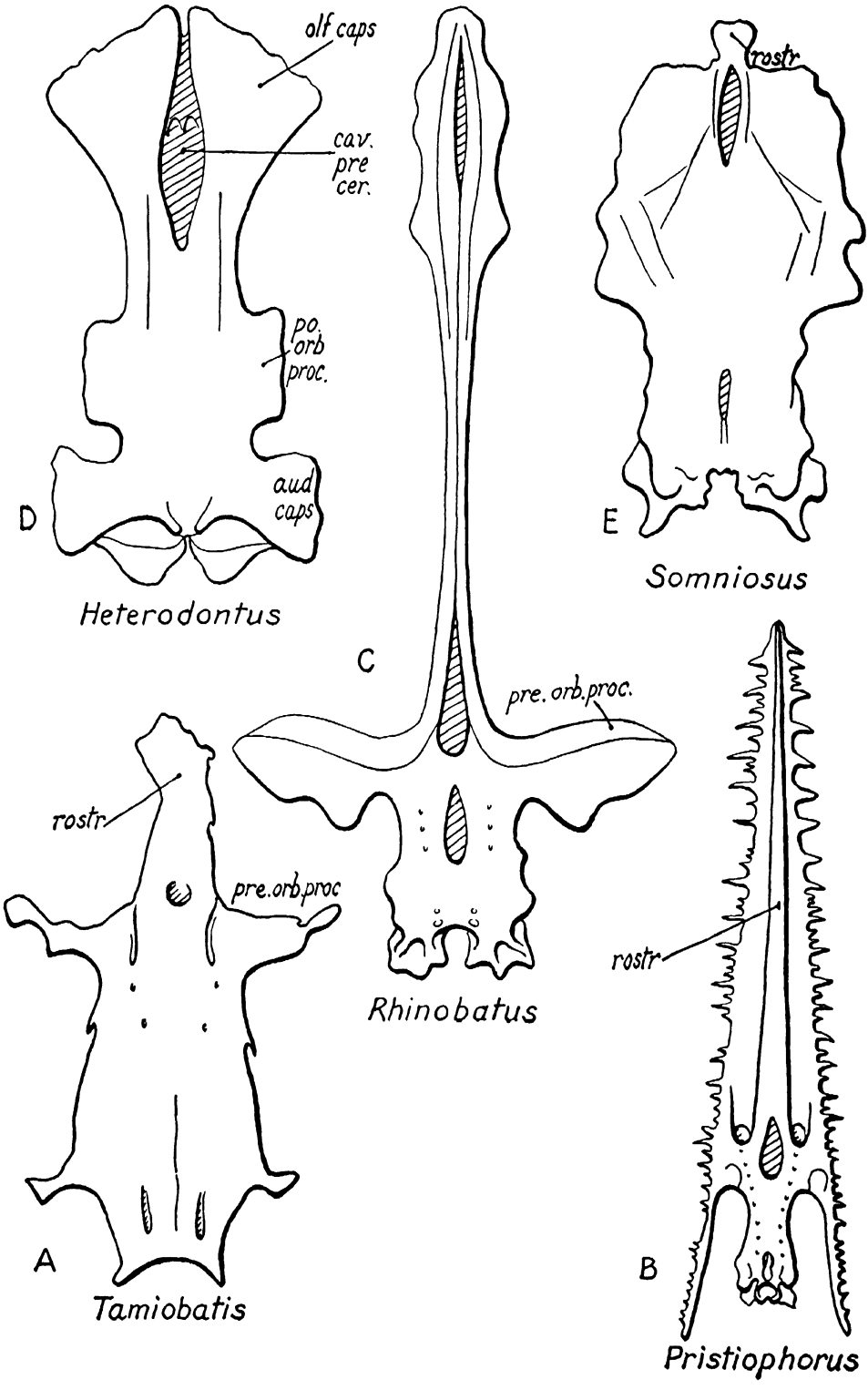


Fig. 8.49. Skull outlines of various elasmobranchs.
A, after Berg; B–E, after E. G. White.

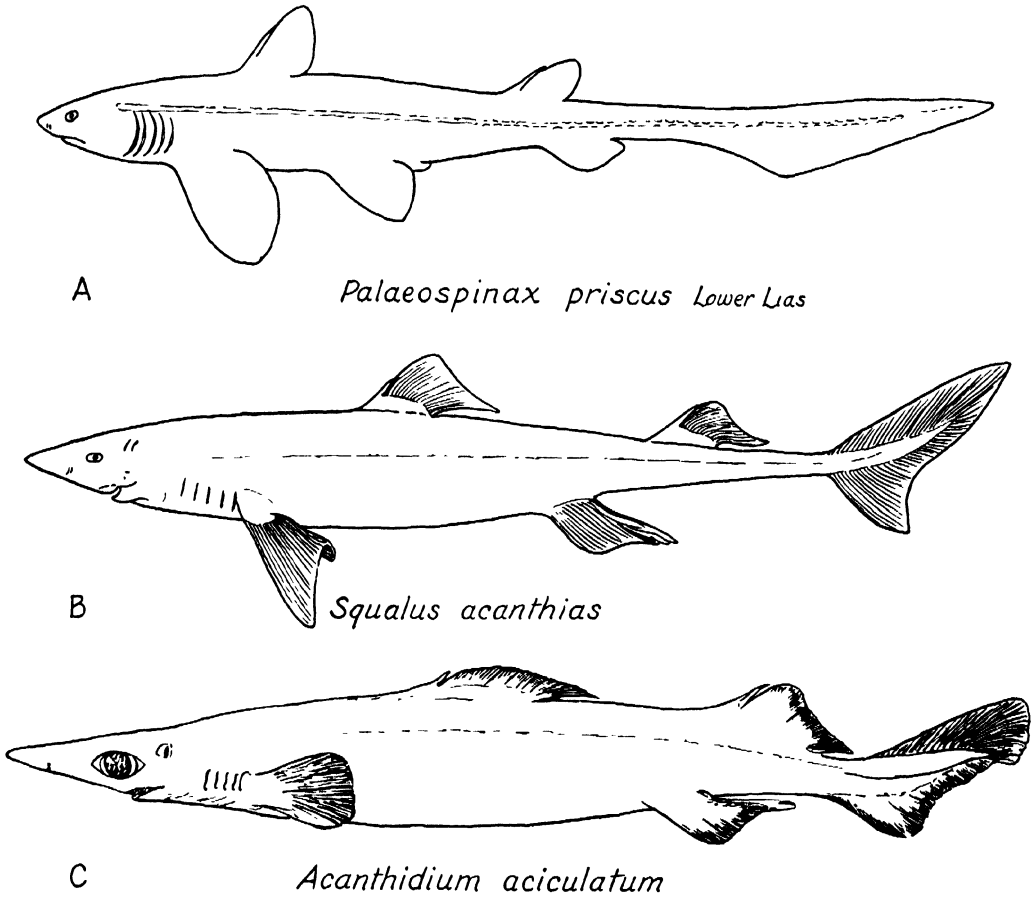
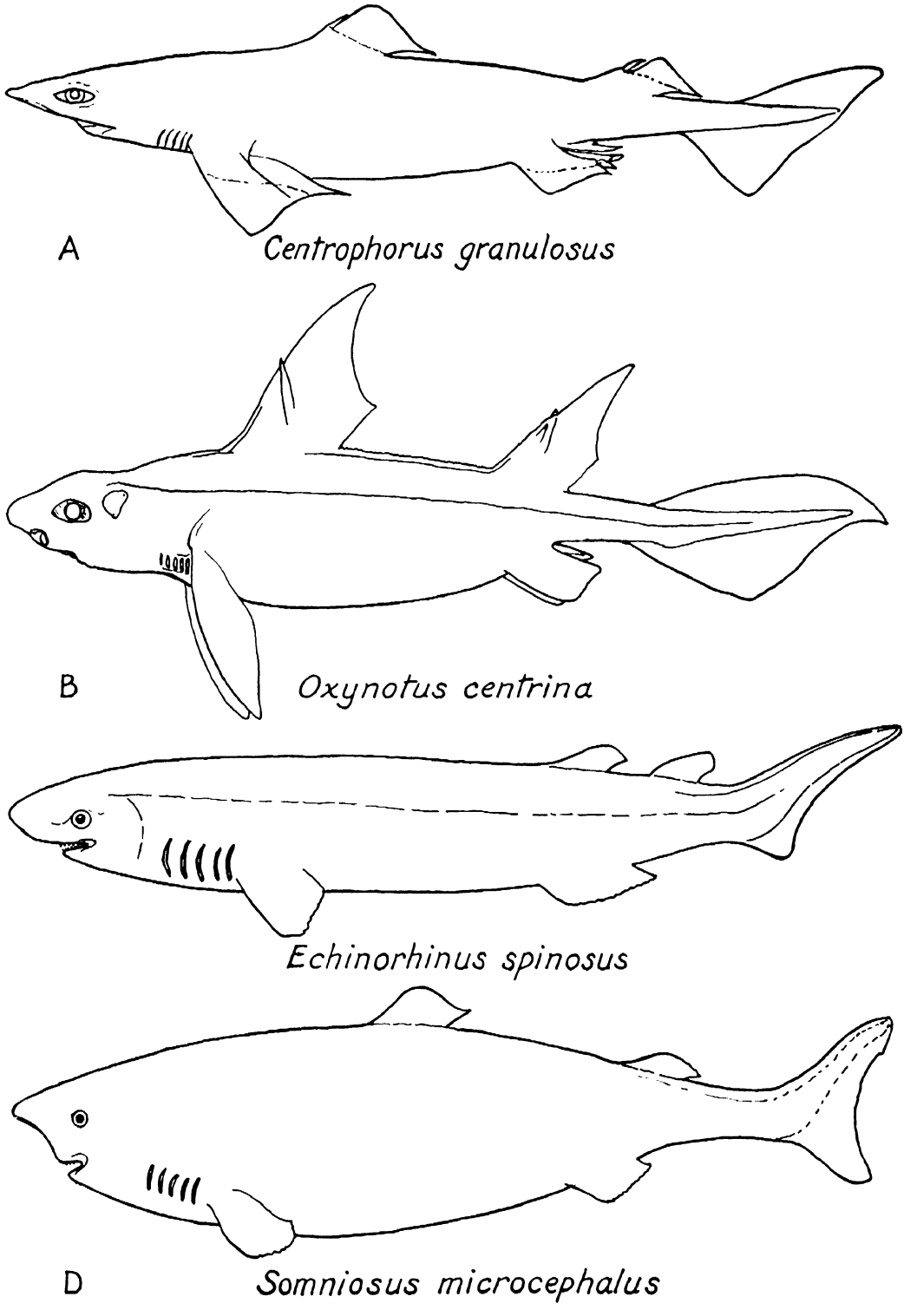
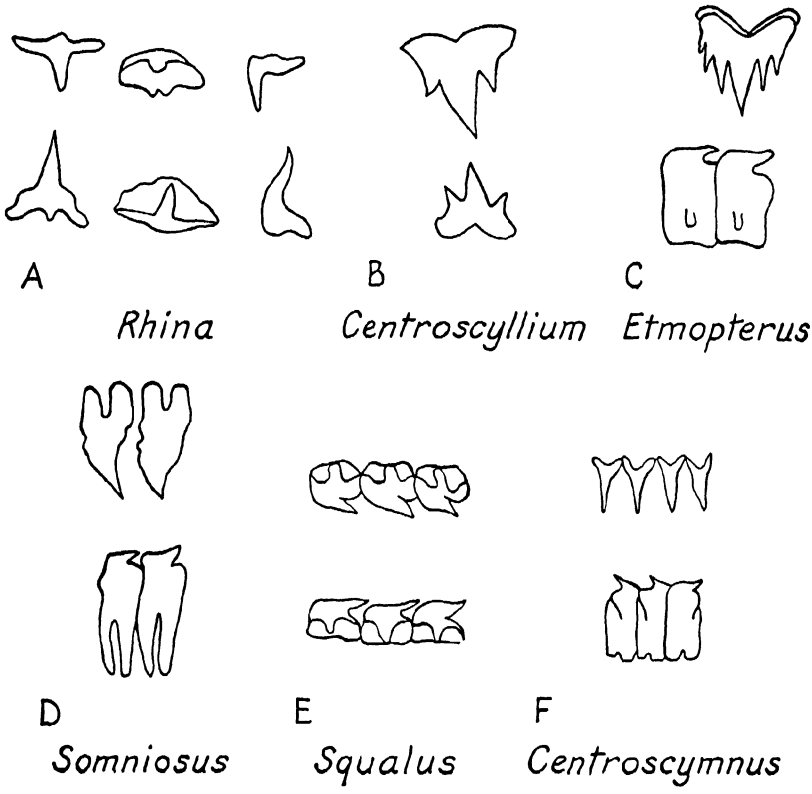


Fig. 8.50. The "spiny dogfish" (B) and its relatives. A, Lower Jurassic predecessor, after Dean. C, Specialized form with a rather long rostrum, after Garman.



Figs. 8.51, 52. More relatives of the spiny dogfish. After Good and Bean.



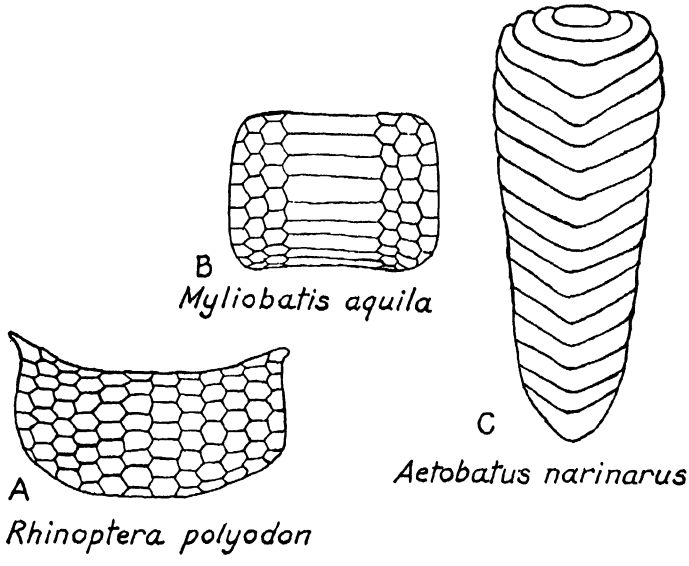


Fig. 8.53 (top). Teeth of squaloids. From E. G. White, after Garman.

Fig. 8.54. Evolution of the dental mill of the eagle ray. Three structural stages illustrating progressive emphasis of the median and reduction of the lateral rows of dental units. Data from Goodrich.

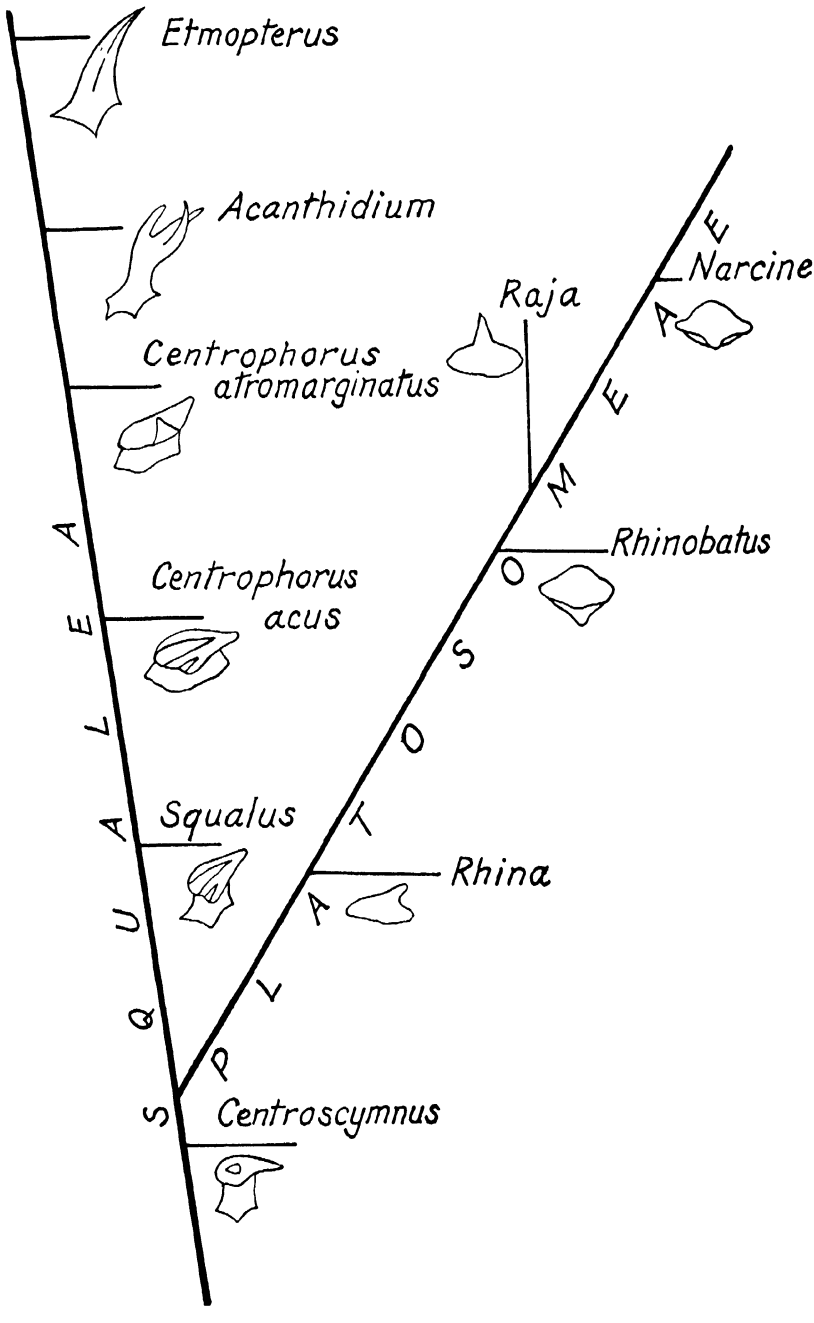


Fig. 8.55. Divergent evolution of dermal denticles in Squalea and Platosomeae (Skates and Rays) After E. G. White.

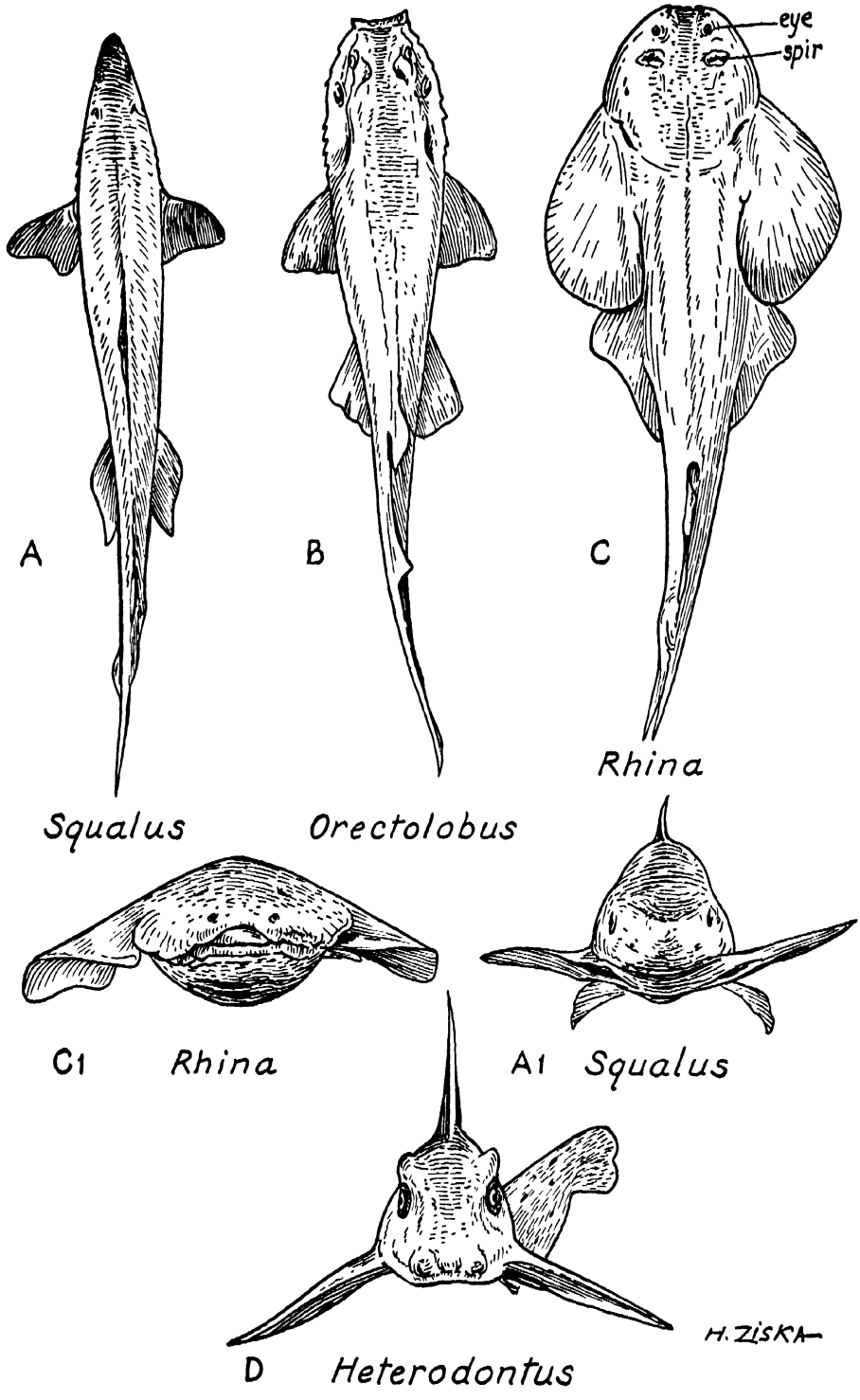


Fig. 8.56. The monkfish (C) compared with more normal sharks (A, B). After Gregory.

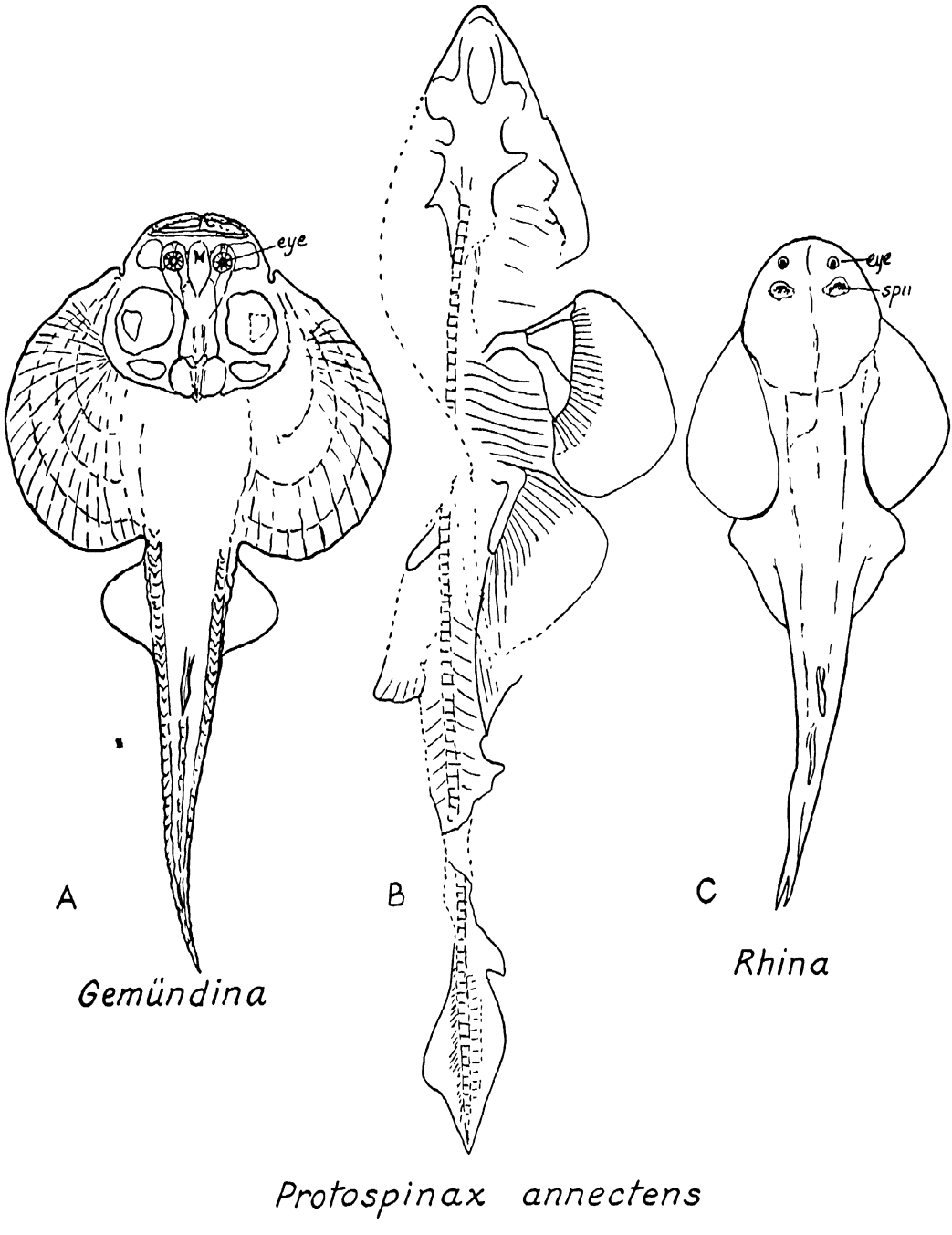


Fig. 8.57. Convergence *versus* consanguinity. It has been usually assumed that the resemblance between the Upper Devonian placoderm *Gemundina* (A) and the modern monkfish (C) is wholly convergent; but it is conceivable that *Rhina, Protospinax* (B) and the modern skates and rays may have been derived directly from *Gemundina* or its Upper Devonian relatives and that the Japanese sawfish (Pristiophoridae) and the Squalidae (fig. 8.60) have also been derived from the *Gemündina* stem. A, after Broili; B, from E. G. White, after A. S. Woodward; C, after Gregory.

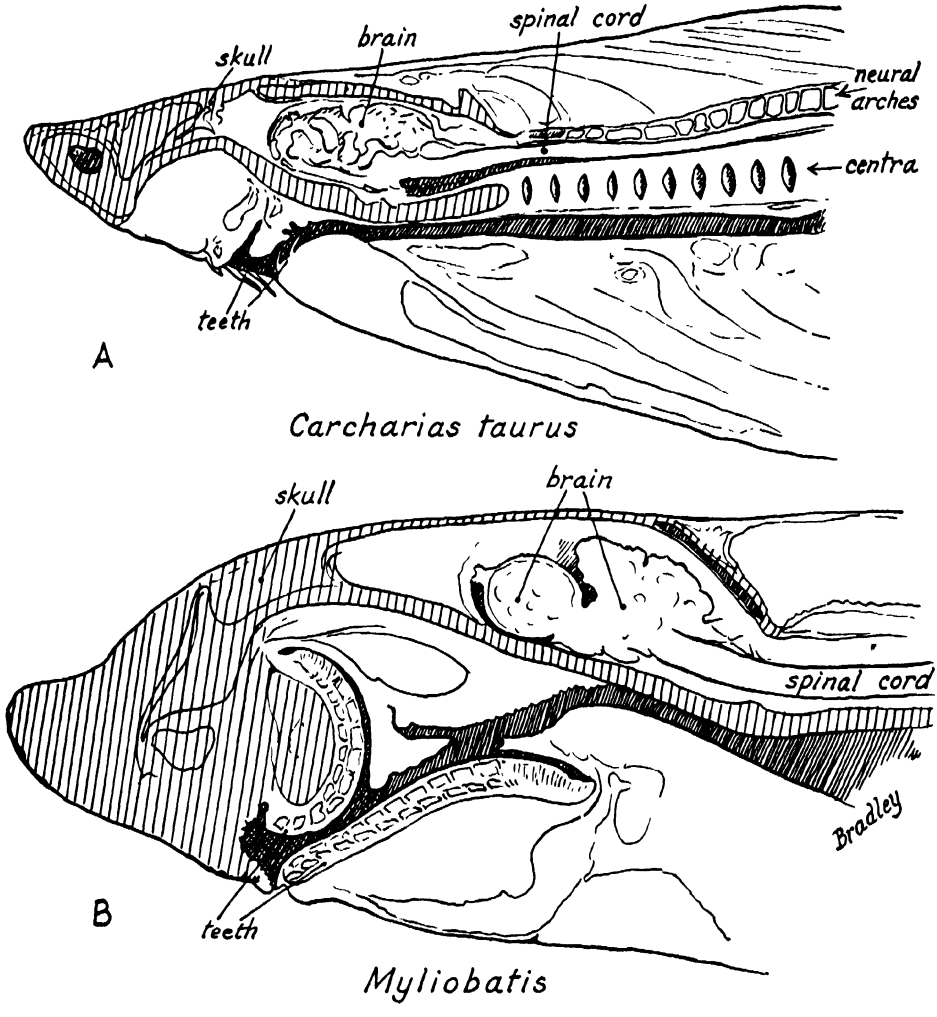


Fig. 8.58. Mesial sections of the jaws and heads of predatory (A) and durophagous (B) elasmobranchs. After Garman.

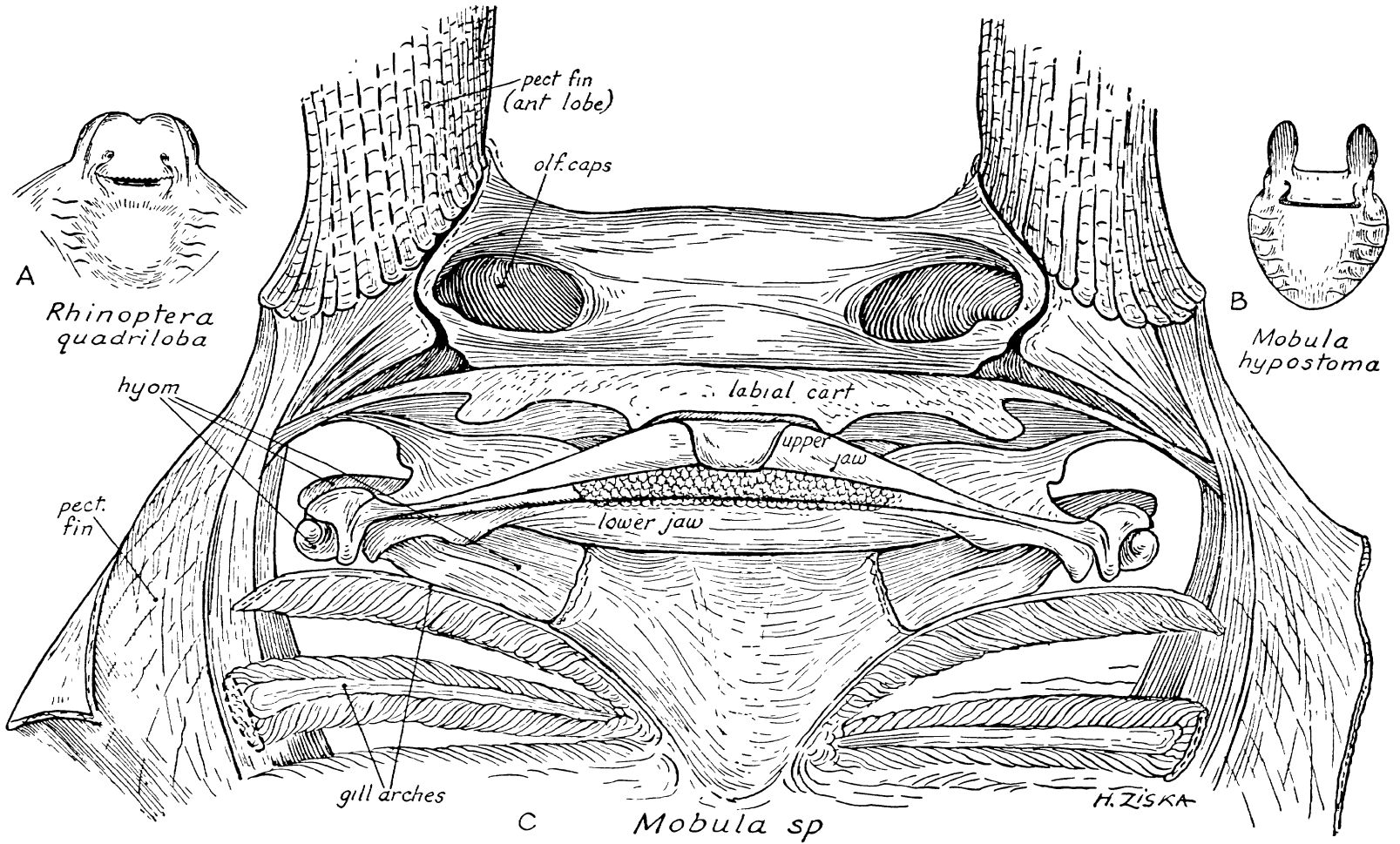


Fig. 8.59. The jaws and neighboring parts in the mantas. A, B, after Garman; C, from a foetal specimen.

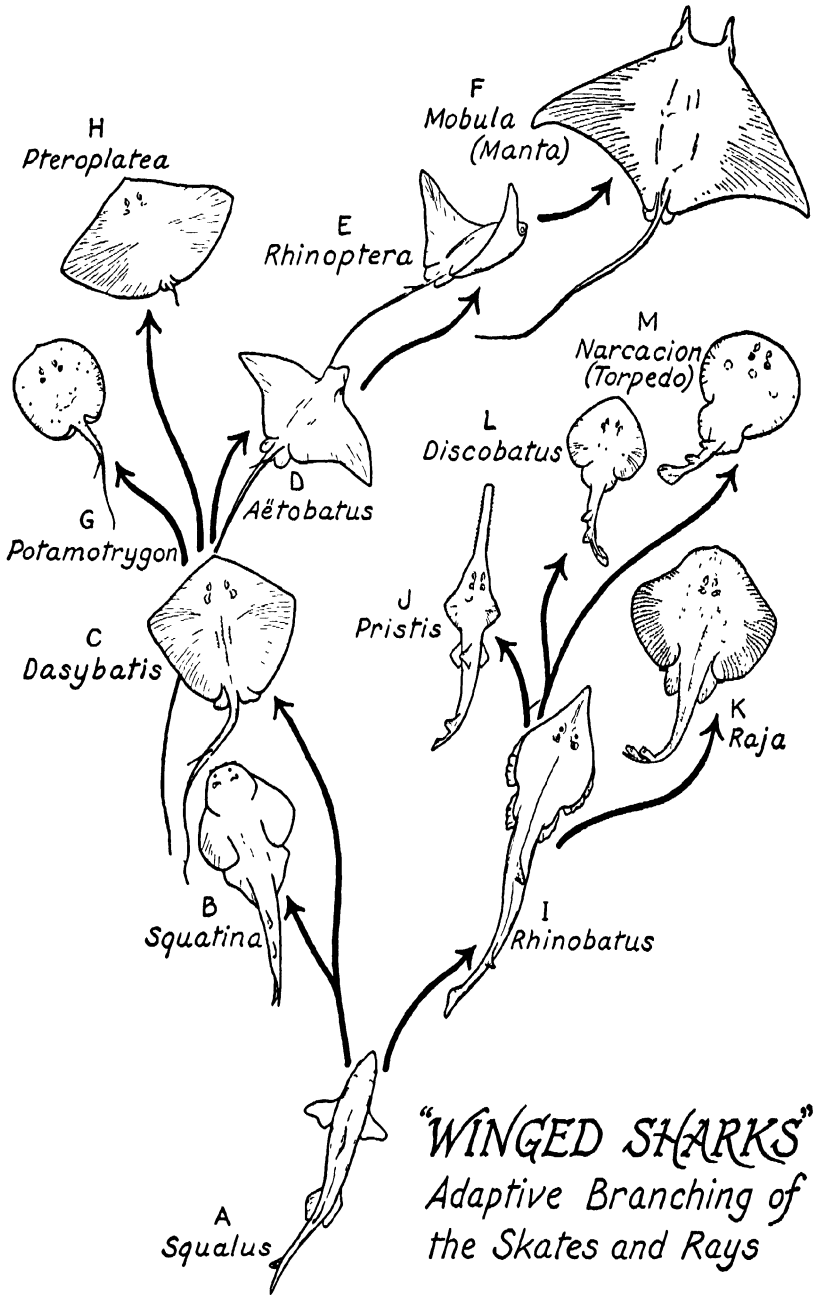


Fig. 8.60. Divergent anisomerism in skates and rays. After Gregory.

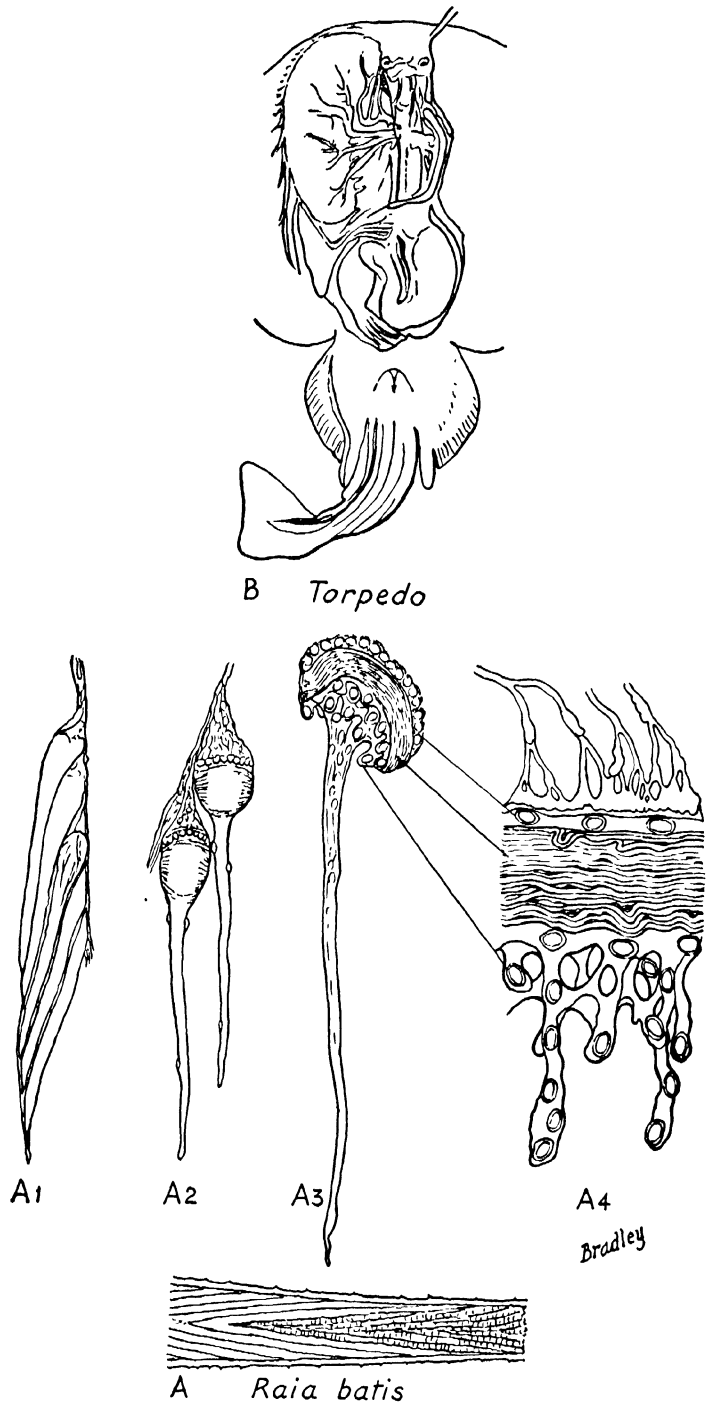


Fig. 8.61. Electric organs in the tail of a skate (A); B, on the pectoral fins of a torpedo ray. A–A4, after Daniel; B, from Daniel, after Schimpekewitsch in Krupki's Atlas. A, The electric organ in place, as a series of modified myomeres including their nerves. A1, modified muscle fibres, greatly enlarged; A2, transitional fibres with electric cells at the distal end; A3, fully developed electric cell; A4, portion of electric organ, greatly enlarged.

CHAPTER IX

THE BRANCHING TRIBES OF BONY FISHES

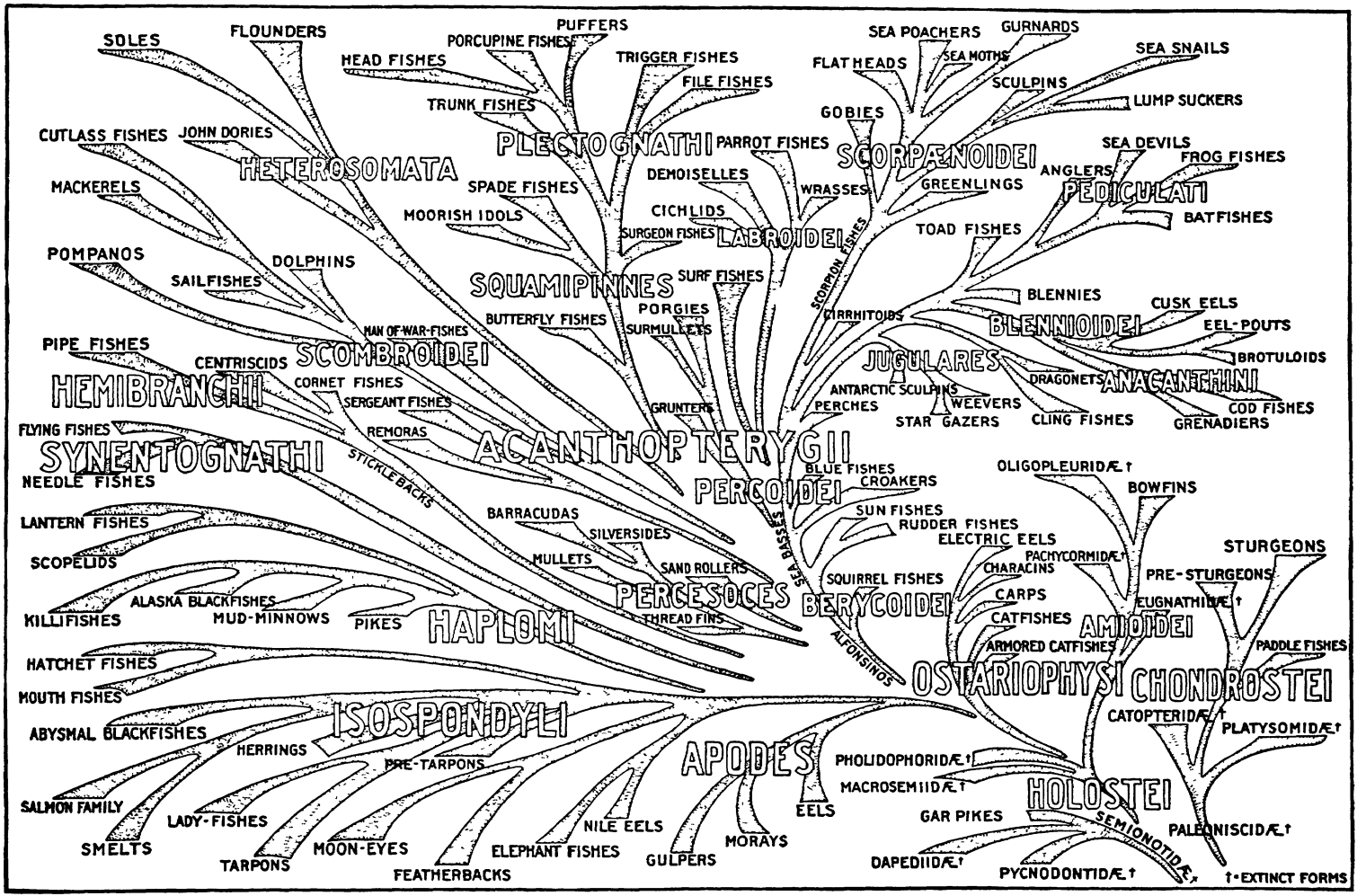

SOLES
FLOUNDERS
PUFFERS
PORCUPINE FISHES
HEAD FISHES
TRIGGER FISHES
FILE FISHES
TRUNK FISHES
SEA POACHERS
GURNARDS
SEA SNAILS
FLAT HEADS
SEA MOTHS
SCULPINS
LUMP SUCKERS
GOBIES
CUTLASS FISHES
JOHN DORIES
PLECTOGNATHI
PARROT FISHES
SCORPÆNOIDEI
SEA DEVILS
FROG FISHES
HETEROSOMATA
DEMOISELLES
ANGLERS
GREENLINGS
PEDICULATI
MACKERELS
SPADE FISHES
WRASSES
MOORISH IDOLS
CICHLIDS
BATFISHES
SURGEON FISHES
LABROIDEI
TOAD FISHES
SCORPION FISHES
POMPANOS
DOLPHINS
SAILFISHES
SQUAMIPINNES
SURF FISHES
BLENNIES
CUSK EELS
PORGIES
GIRRHITOIDS
BUTTERFLY FISHES
BLENNIOIDEI
EEL-POUTS
MAN OF WAR FISHES
SURMULLETS
PIPE FISHES
SCOMBROIDEI
JUGULARES
BROTULOIDS
CENTRISCIDS
CORNET FISHES
HEMIBRANCHII
ANTARCTIC SCULPINS
DRAGONETS
ANACANTHINI
SERGEANT FISHES
GRUNTERS
PERCHES
WEEVERS
COD FISHES
FLYING FISHES
REMORAS
STAR GAZERS
CLING FISHES
GRENADIERS
SYNENTOGNATHI
ACANTHOPTERYGII
STICKLEBACKS
BLUE FISHES
OLIGOPLEURIDÆ †
NEEDLE FISHES
PERCOIDEI
CROAKERS
BOWFINS
SEA BASSES
SUN FISHES
BARRACUDAS
RUDDER FISHES
LANTERN FISHES
SILVERSIDES
ELECTRIC EELS
STURGEONS
PACHYCORMIDÆ †
SCOPELIDS
MULLETS
SAND ROLLERS
CHARACINS
PRE-STURGEONS
SQUIRREL FISHES
PERCESOCES
BERYCOIDEI
CARPS
EUGNATHIDÆ †
ALASKA BLACKFISHES
KILLIFISHES
MUD-MINNOWS
PIKES
HAPLOMI
THREAD FINS
CATFISHES
AMIOIDEI
ALFONSINOS
ARMORED CATFISHES
PADDLE FISHES
HATCHET FISHES
OSTARIOPHYSI
CHONDROSTEI
MOUTH FISHES
CATOPTERIDÆ †
PLATYSOMIDÆ †
ABYSMAL BLACKFISHES
ISOSPONDYLI
APODES
HERRINGS
PHOLIDOPHORIDÆ †
PRE-TARPONS
MACROSEMIIDÆ †
HOLOSTEI
SALMON FAMILY
EELS
GAR PIKES
LADY-FISHES
NILE EELS
SEMIONOTIDÆ †
PALÆONISCIDÆ †
SMELTS
MOON-EYES
MORAYS
DAPEDIIDÆ †
TARPONS
ELEPHANT FISHES
GULPERS
PYCNODONTIDÆ †
FEATHERBACKS
† = EXTINCT FORMS

Fig. 9.1a

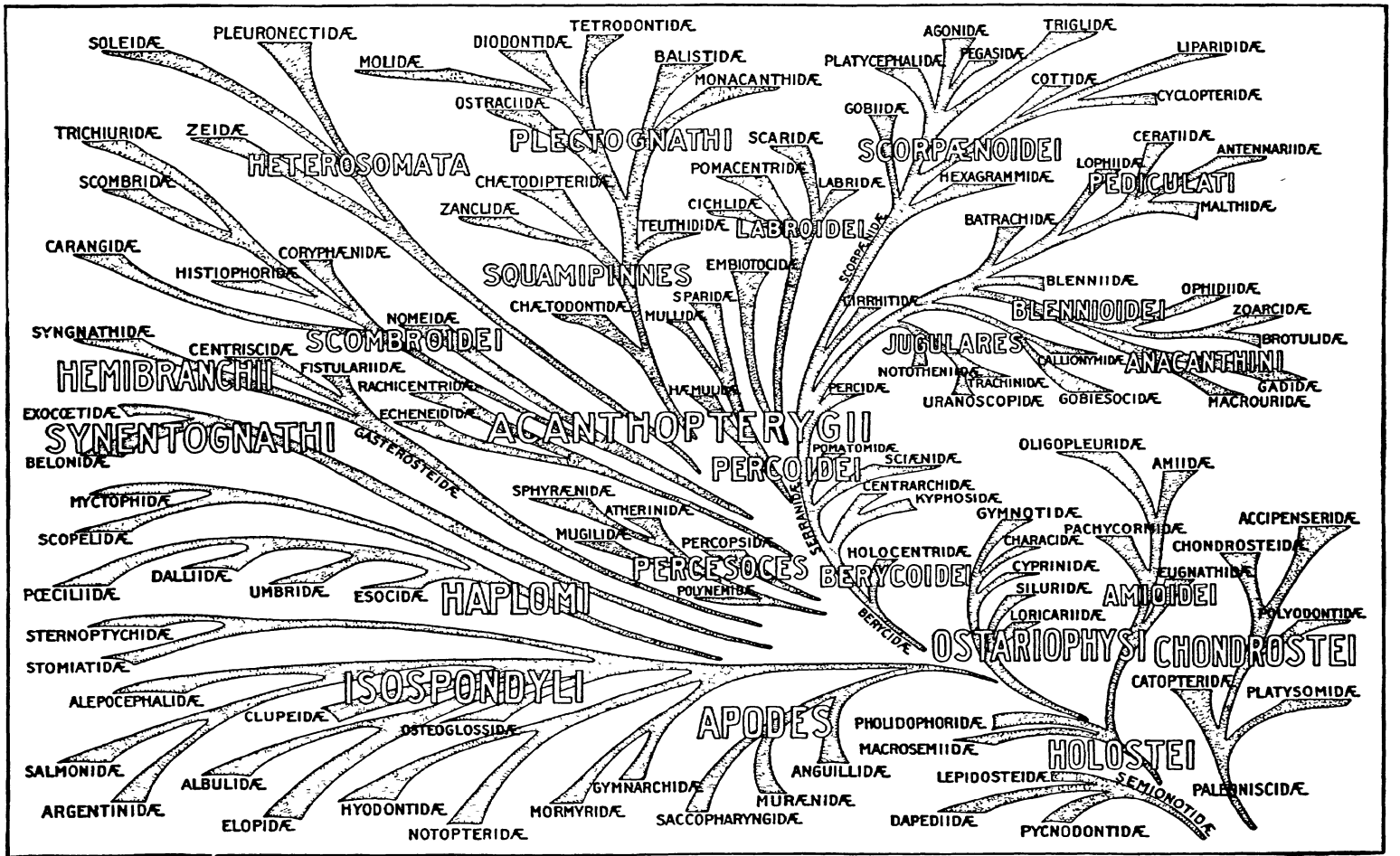


Fig. 9.1a, b. Family Tree of the Ganoids and Teleost Fishes.

Figs 9.1a, b, drawn in 1926, were revised from an earlier one made in 1906 (Gregory, 1907). Subsequent discovery has tended to connect the stem of the higher fishes more closely with those of the amioids, the bony ganoids (Holostei) and the palaeoniscoids.

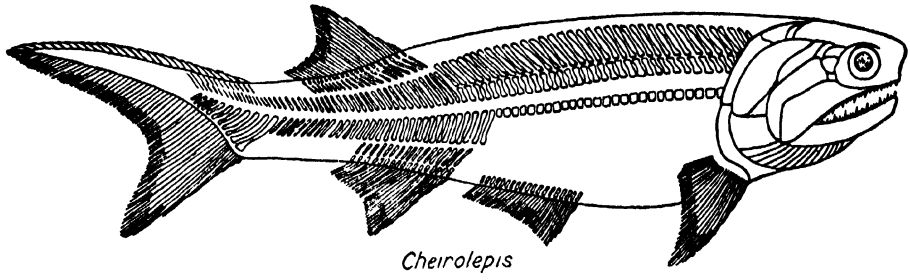


Fig. 9.2. The Founder of the Ganoid-Teleost Hosts, from the middle Devonian of Great Britain. Restoration of the skeleton by A. Smith Woodward.

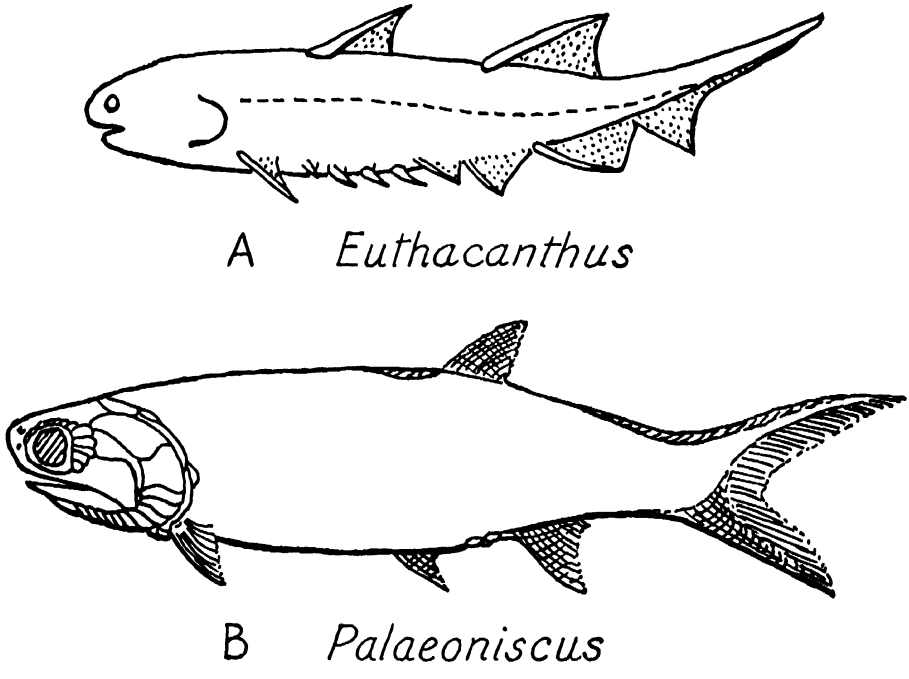


Fig. 9.3. Comparison of the most primitive known Acanthodian (A) from the Lower Old Red Sandstone of Scotland with the type of the Palaeoniscoids (B) from the Lower Permian of Europe. A, after Forster Cooper, B, after Traquair.

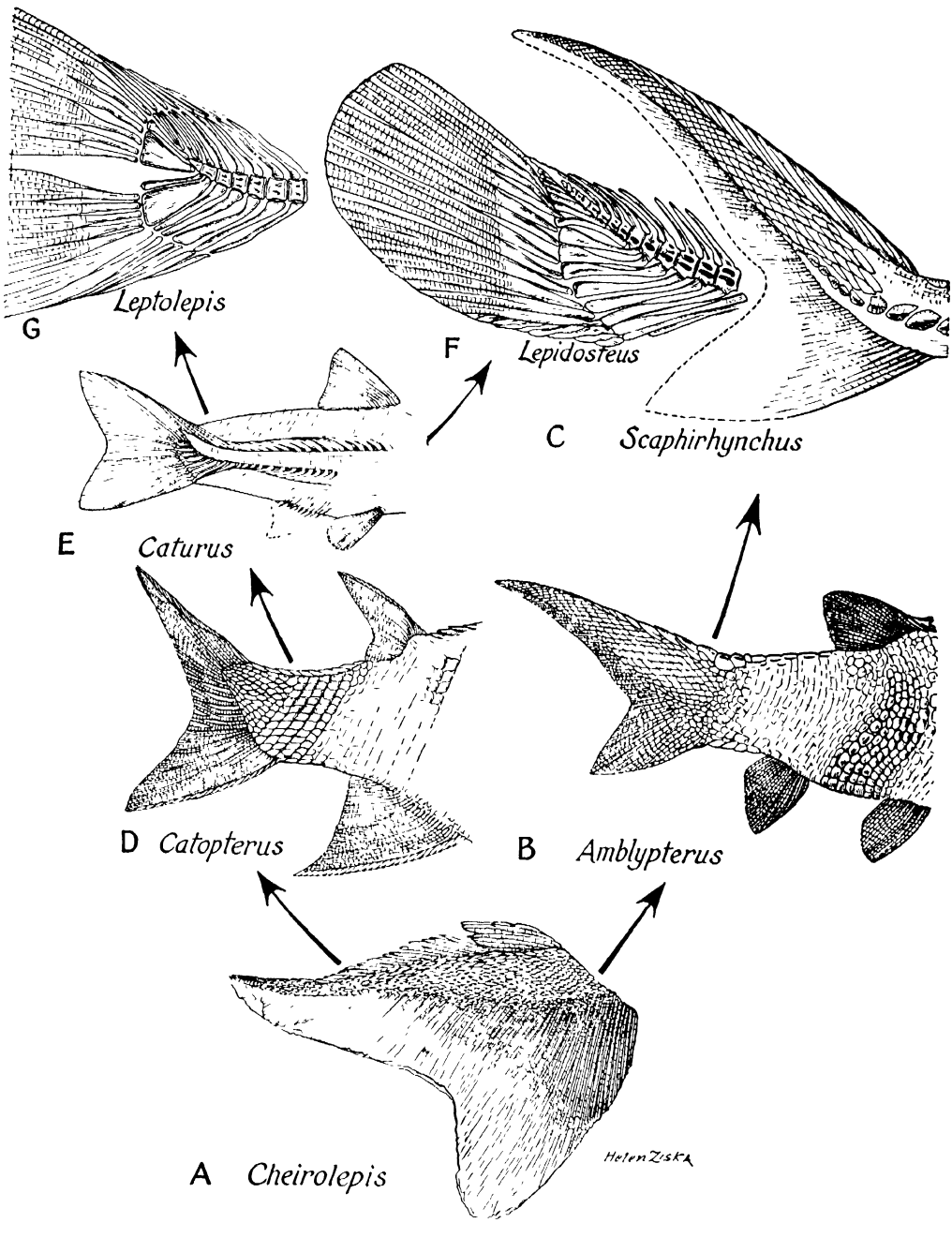


Fig. 9.4. Evolution of the tail in ultraconservative (A–C), moderate (D–F), and advanced forms (G). From specimens. A. *Cheirolepis trailli.* Old Red Sandstone (Middle Devonian) of Scotland. B, *Amblypterus blainvillei.* Carboniferous, Autun, France. C, *Scaphirhynchus platorhynchus.* Recent. D, *Catopterus redfieldi* Triassic, New Jersey, U S.A. E, *Caturus* sp. Lower Jurassic, Bavaria. F, *Lepidosteus* sp. Recent, Mississippi, U S.A. G, *Leptolepis dubius.* Jurassic, Bavaria. Data from A. Smith Woodward.

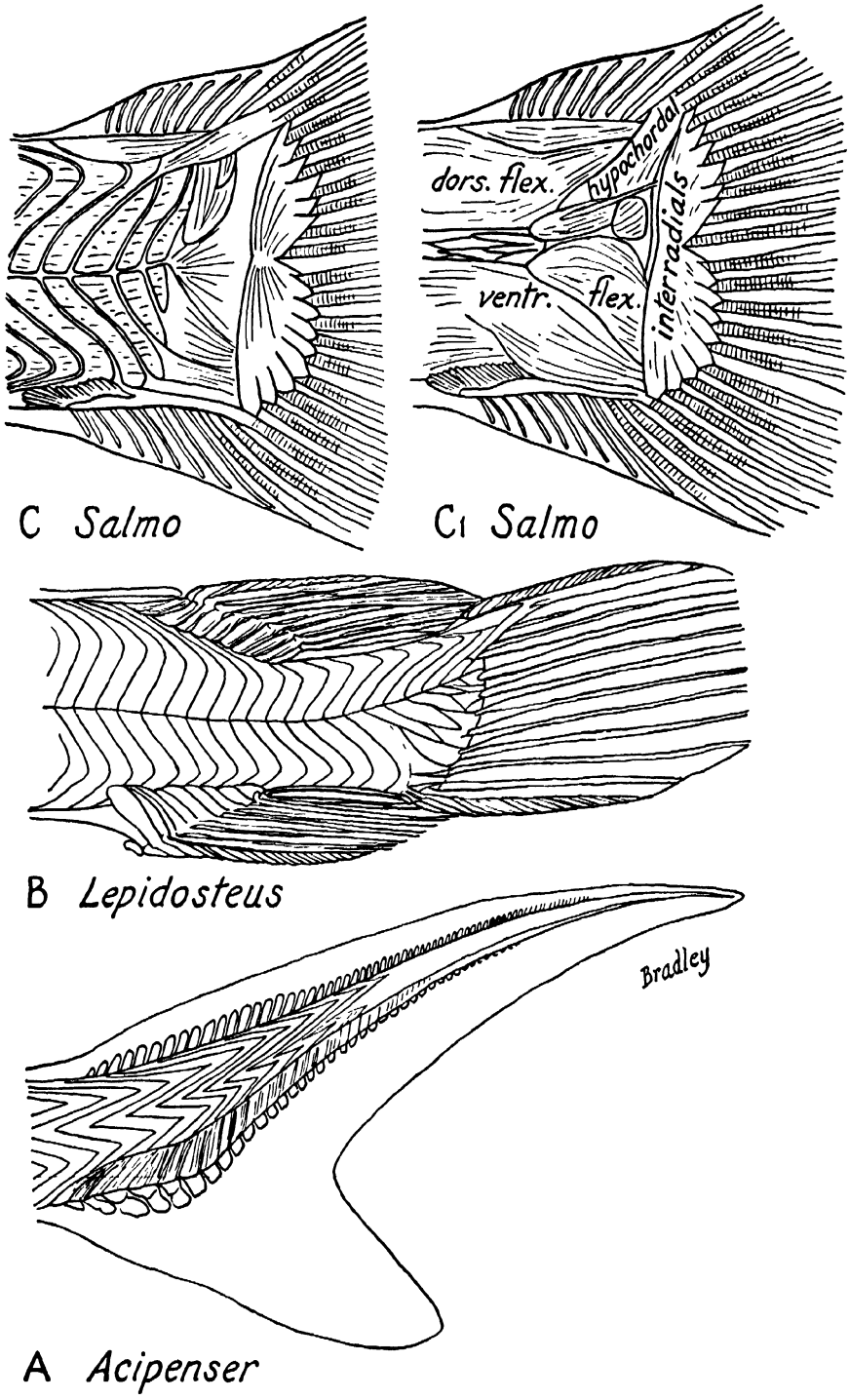


Fig. 9.5. Primitive (A), moderate (B) and advanced (C) stages in the evolution of the tail muscles. After Schmalhausen.

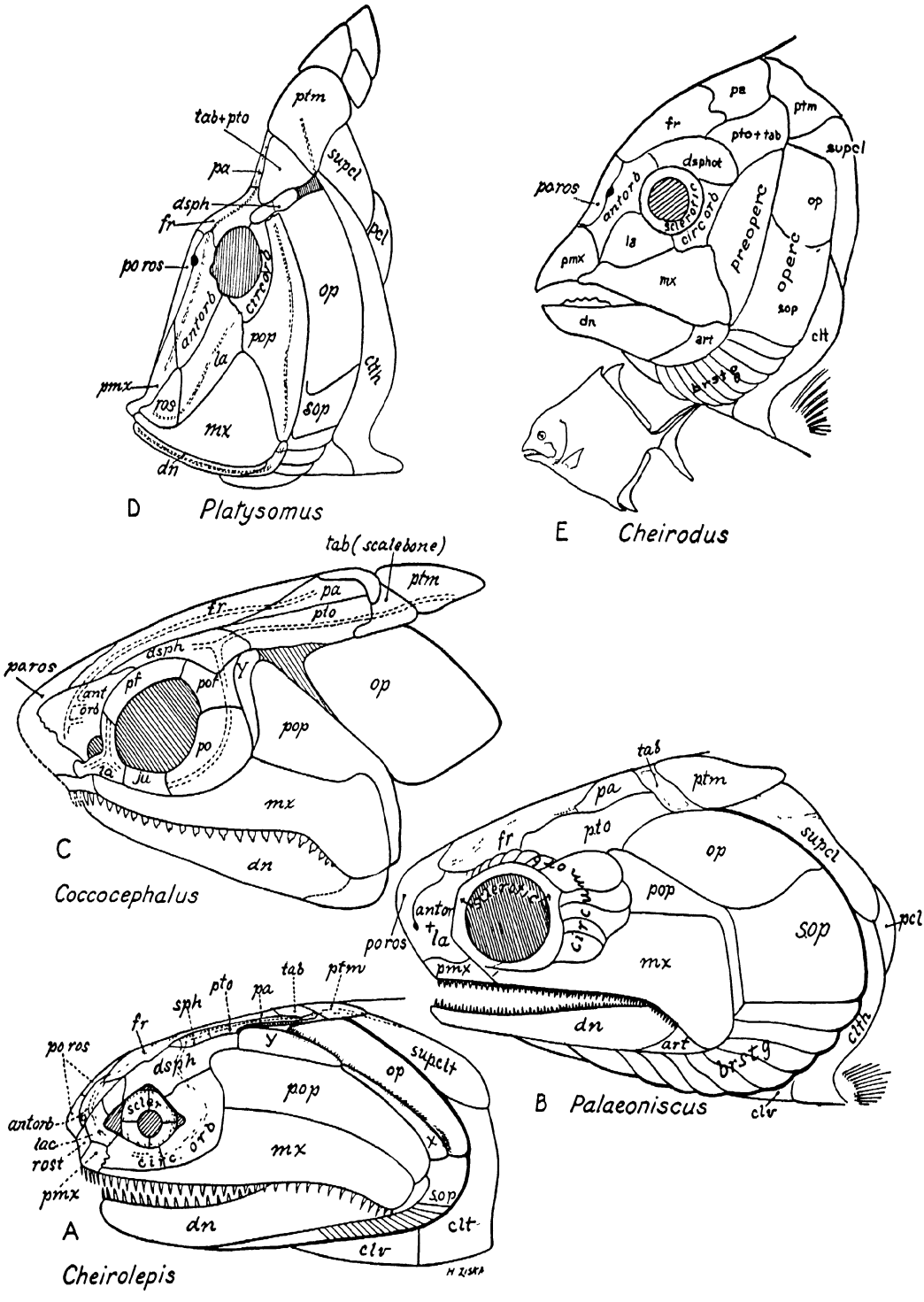


Fig. 9.6. Skull pattern and pectoral girdle in primitive (A–C) and advanced (D, E) palaeoniscoids. A, C, after Watson; B, D, E, after Traquair.

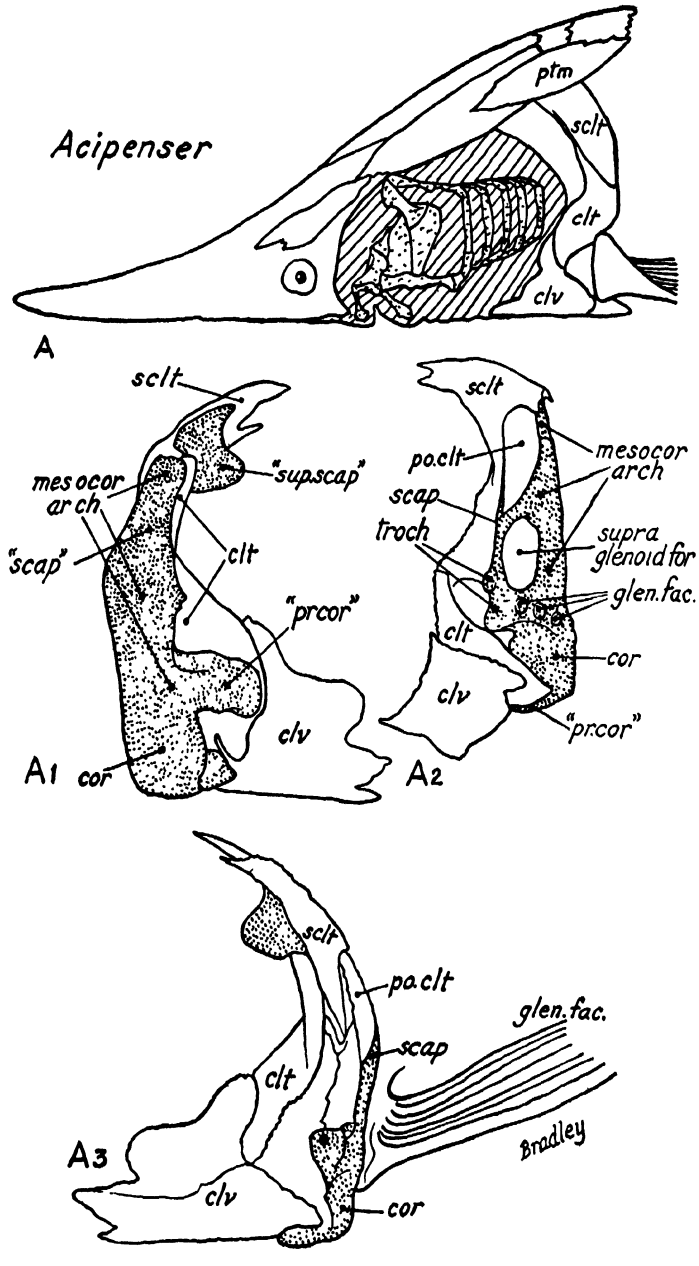


Fig. 9.7. Left half of the shoulder girdle of the sturgeon. A, in its relation to the skull and branchial chamber; A1, inner view; A2, posterior view; A3, outer side. Endoskeletal parts stippled. A, mainly after A. S. Woodward; A1–A3, modified from W. K. Parker (1865).

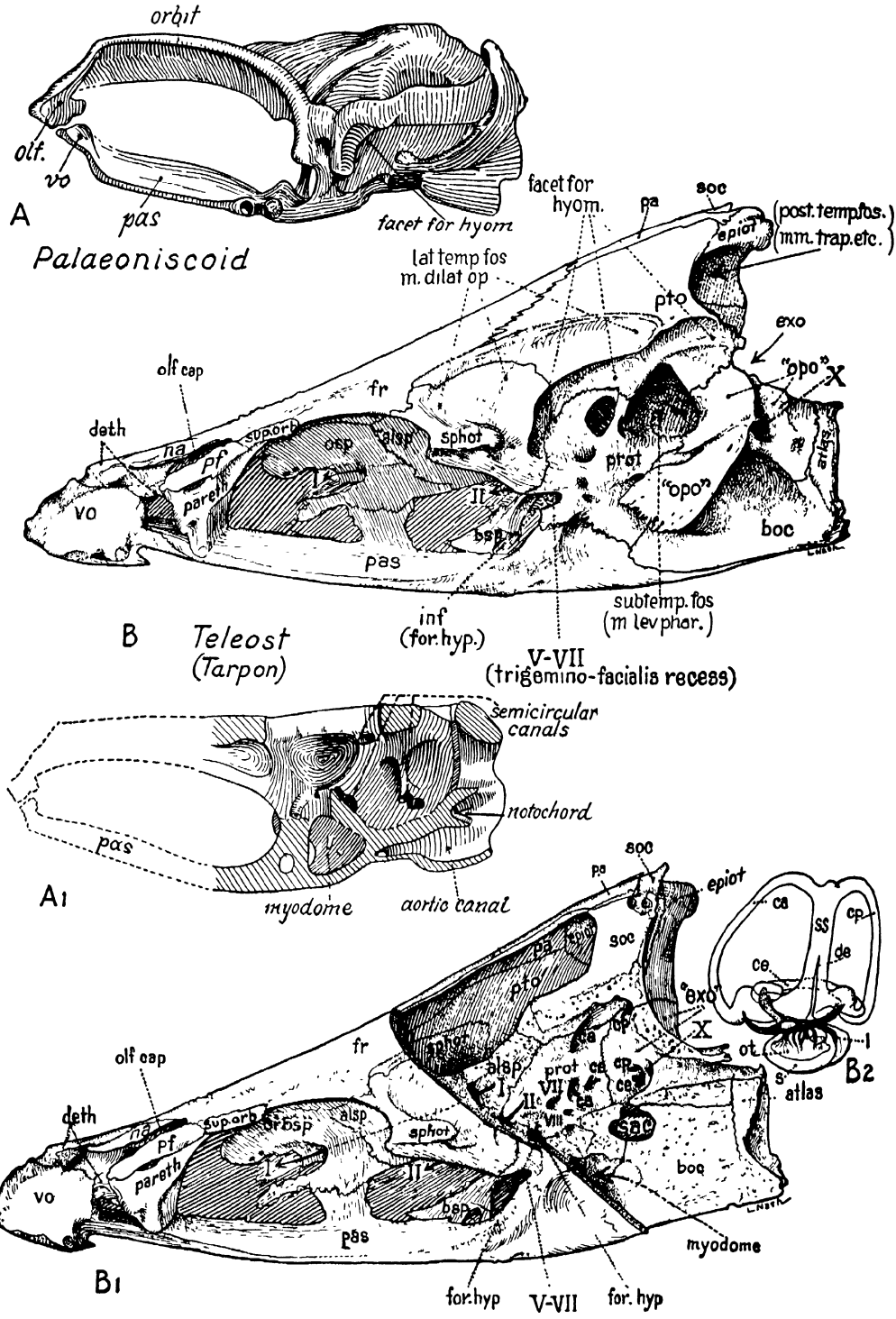


Fig. 9.8. Neurocrania of primitive Palaeozoic palaeoniscoid (A, A1) and conservative modern teleost (B, B1). A, A1, after Watson; B, B1, after Gregory.

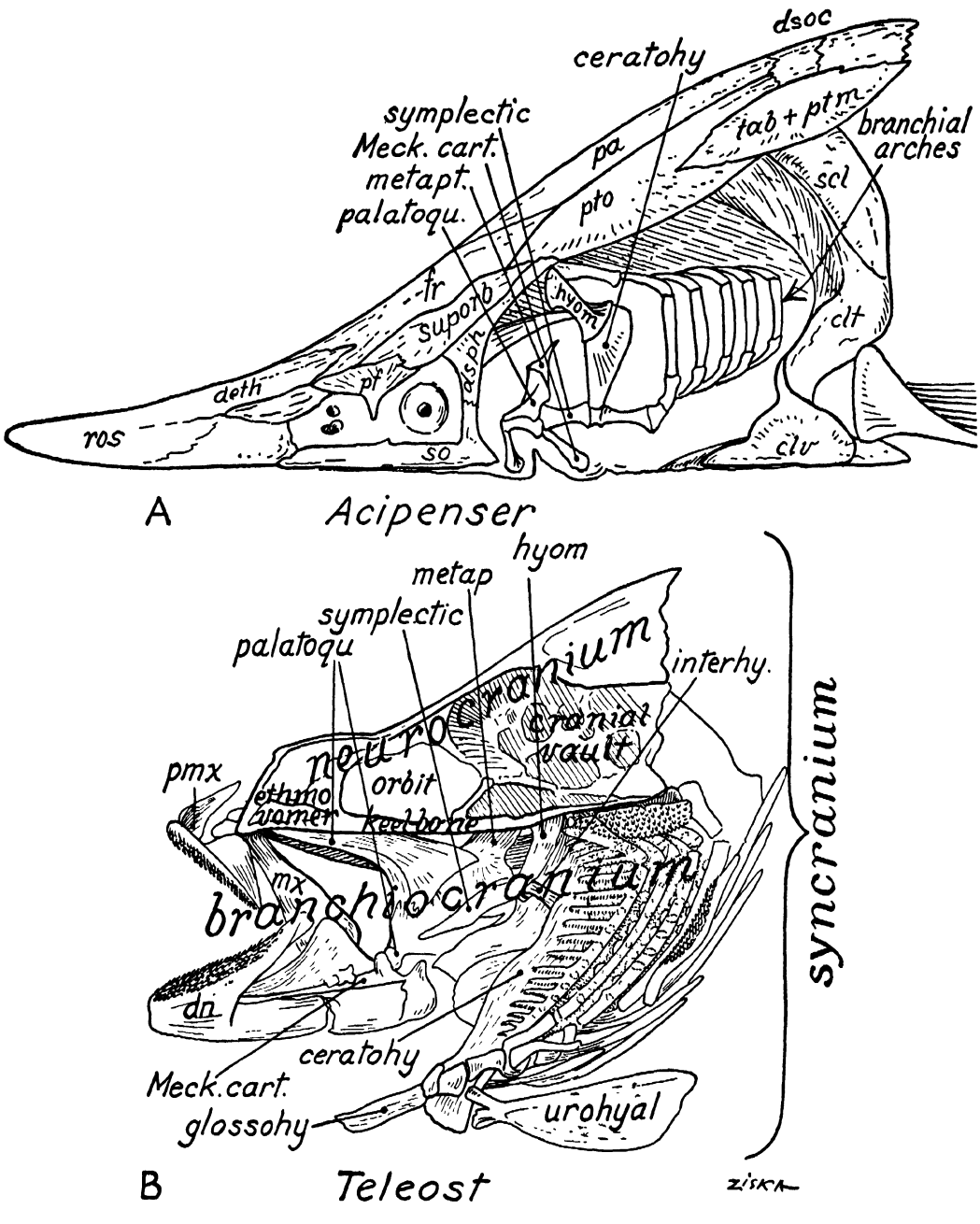


Fig. 9.9. Relations of the neurocranium and the branchiocranium. After Gregory. A, Left side of sturgeon skull, opercular flap removed, after A. S. Woodward. B, Right half of bass skull, medial view, after Lucas, with addition of names of main parts.

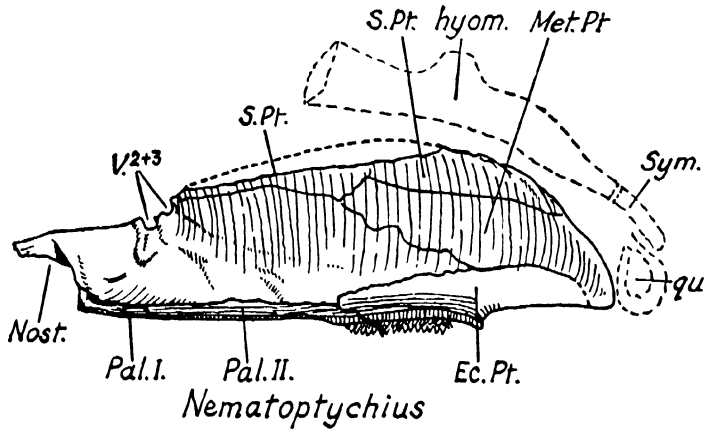


Fig. 9.10. Palatopterygoid complex of a palaeoniscoid. Left side, lateral aspect, after removal of the maxilla. The positions of the quadrate, hyomandibular and symplectic are indicated from another palaeoniscoid. The suprapterygoids represent ossifications in the dorsal flange of the primary upper jaw and include the metapterygoid The latter gives rise to the metapterygoid of later fishes; the other suprapterygoids disappear. After Watson (1925).

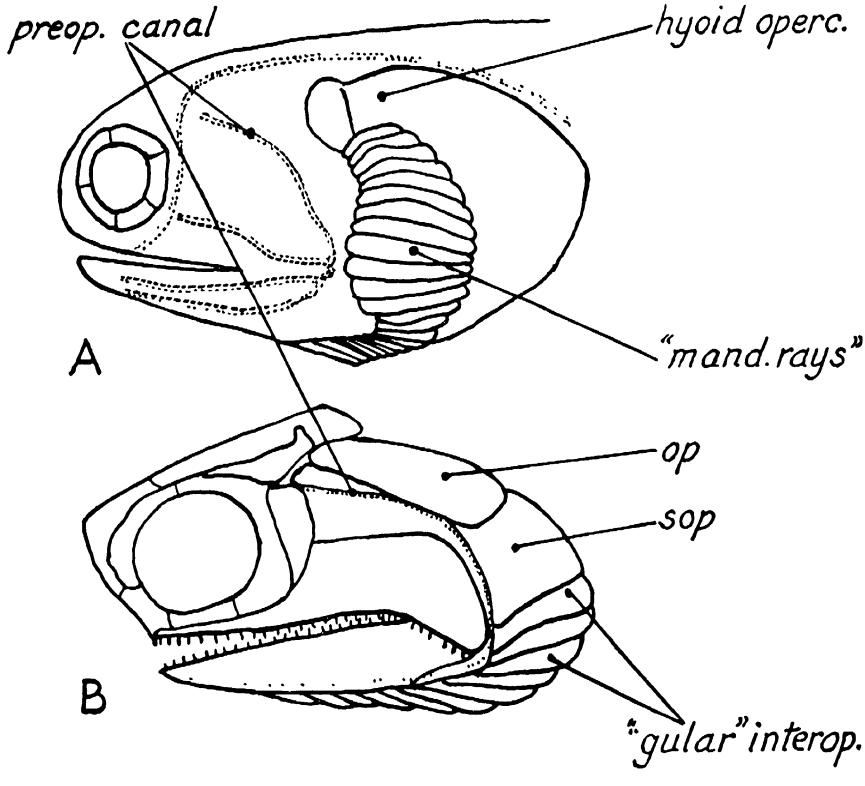


Fig. 9.11. Comparison of opercular region of (A) Acanthodian and (B) Palaeoniscoid. The hyoid opercular fold of the acanthodian may perhaps have given rise to the upper half of the opercular fold of the palaeoniscoid, while the "mandibular rays" of the former may be represented by the interopercular and lateral gular (branchiostegal) plates of the latter. Both from Moy-Thomas, after Watson.

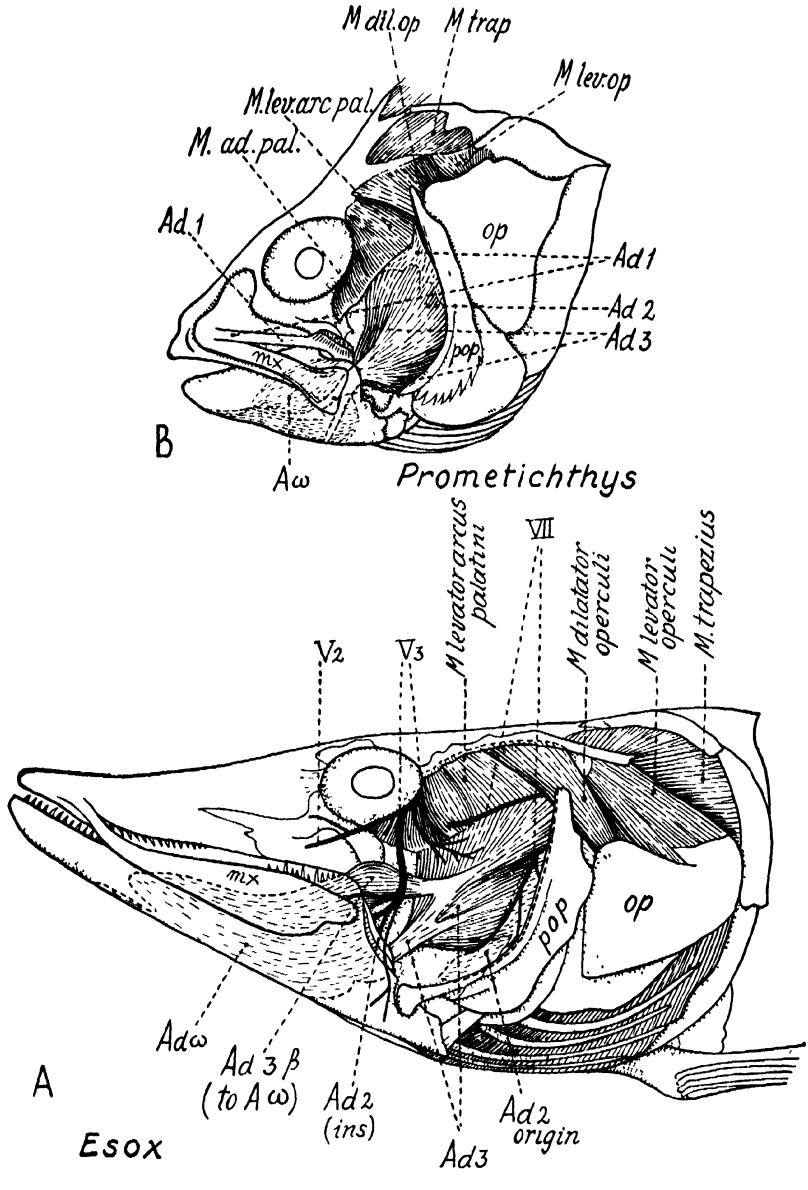


Fig. 9.12. Relations of the muscles of the jaws and operculum to the bones and cranial nerves. After Vetter. The curved anterior border of the preopercular gives a base for part of the adductor muscles (*Ad* 2).

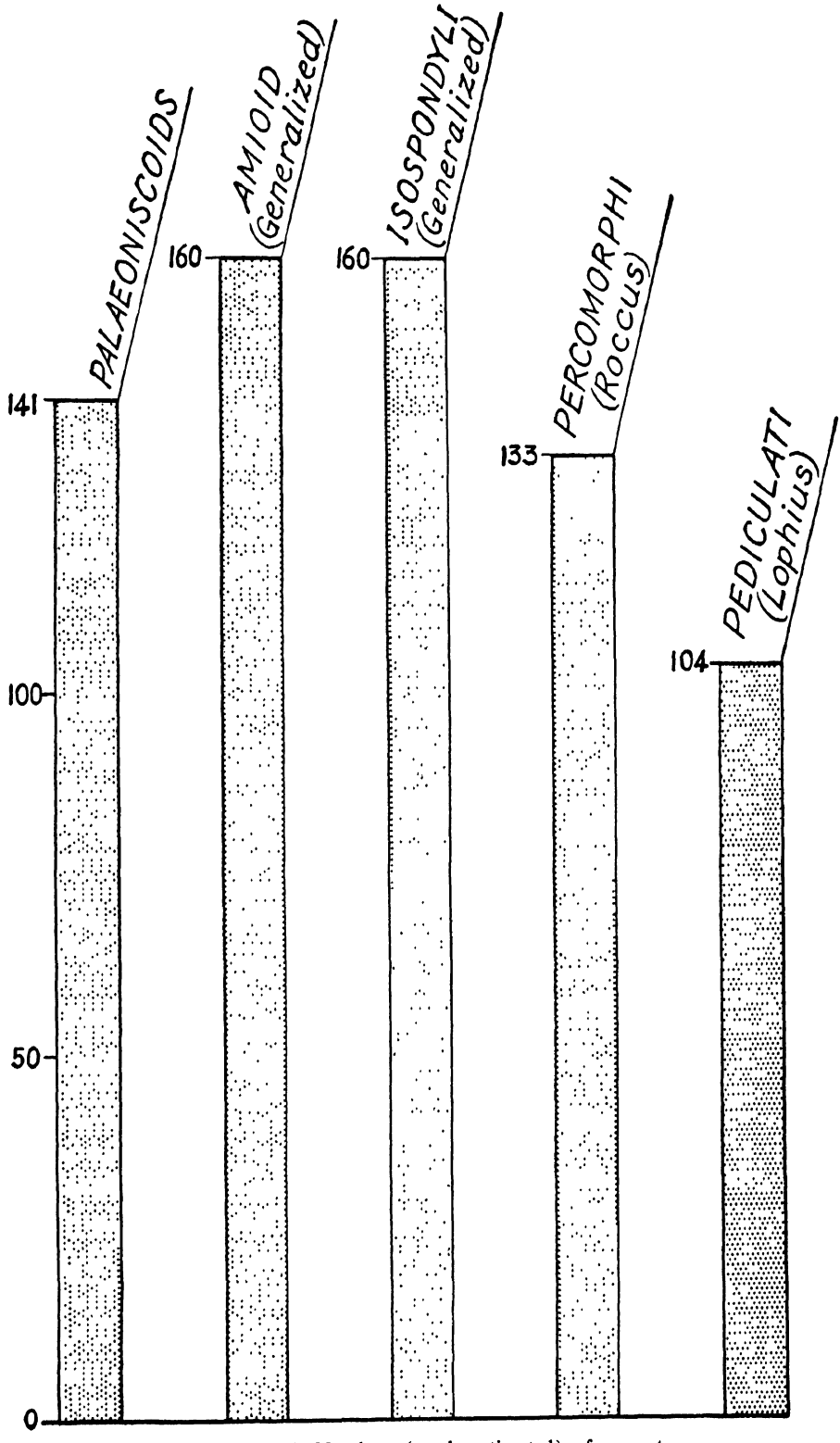


Fig. 9.13. Numbers (partly estimated) of separate bones in the syncrania of successive grades.

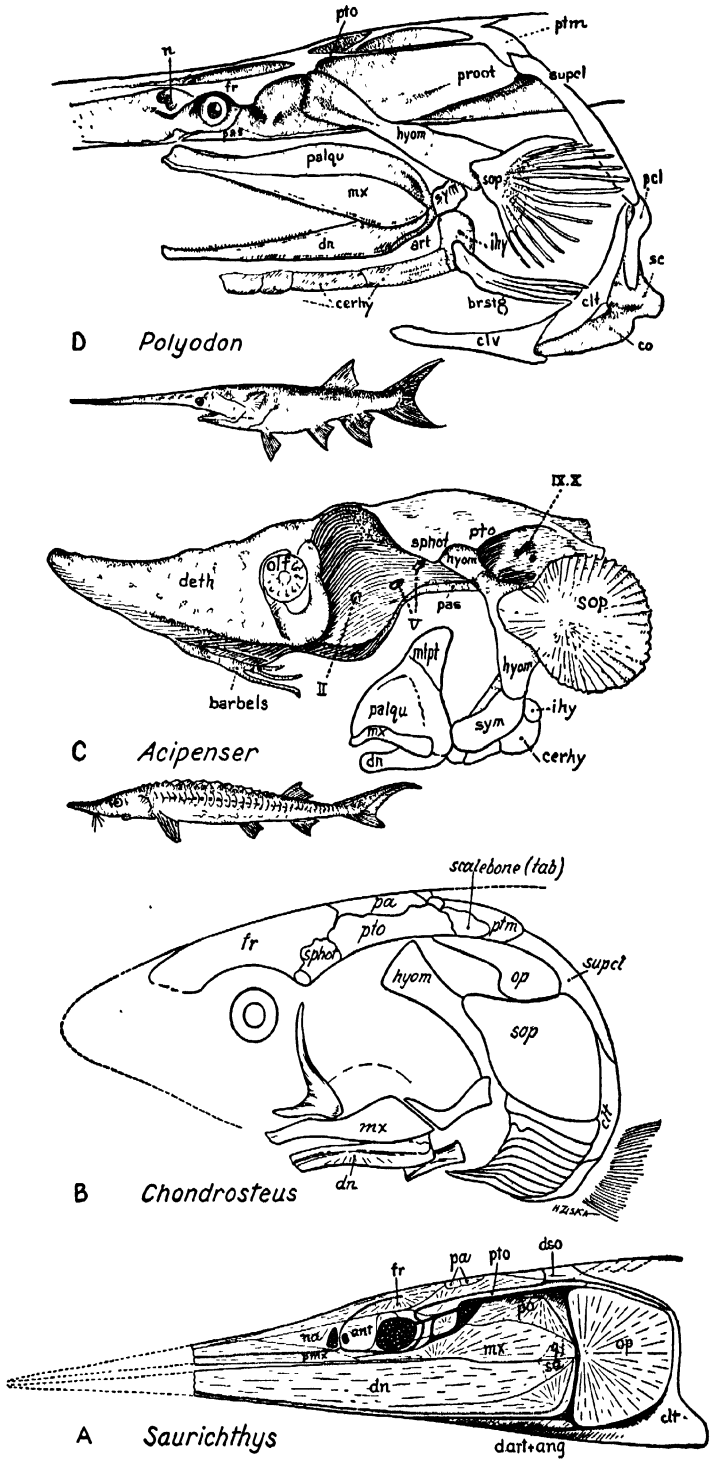


Fig. 9.14. Skulls of Chondrosteans, illustrating retrogression of the primary dermocranium, progressive chondrification (due probably to retention of larval conditions) and (in C) development of secondary polyisomeres in the form of bony scutes. A, after Stensiö; B, after Smith Woodward.

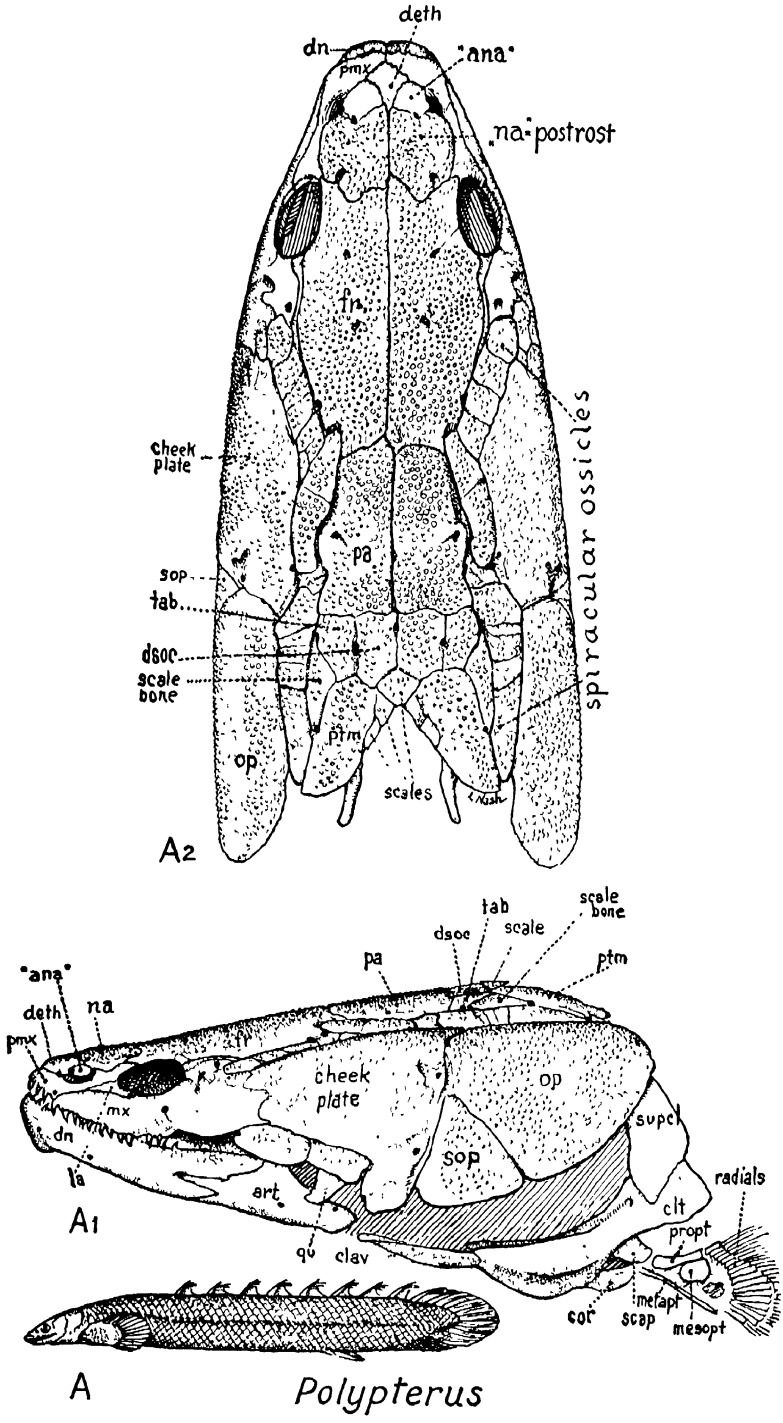


Fig. 9.15. The recent *Polypterus* of Africa, formerly thought to be a survivor of the Palaeozoic Crossopterygians (Lobe-fins), but shown by E. S. Goodrich (1909, 1928) and E. I. White (1939) to be a somewhat specialized descendant of the Palaeoniscoid stock. In its general body form and shortened caudal lobe *Polypterus* is convergent toward the garpike (*Lepidosteus*, fig. 9.17C).

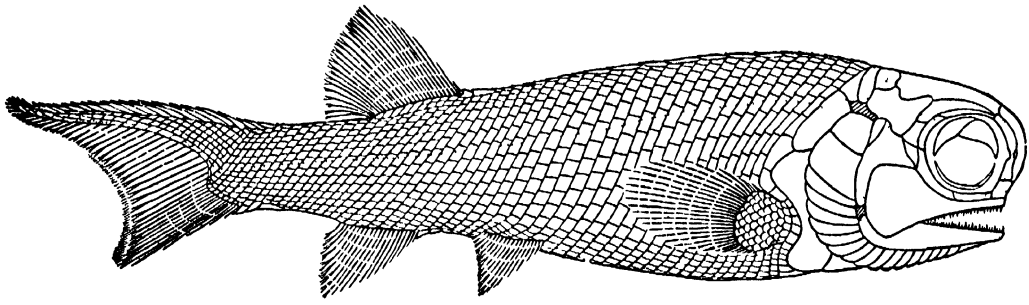


Fig. 9.16. *Cornuboniscus budensis.* After E. I. White (1939, p. 53).

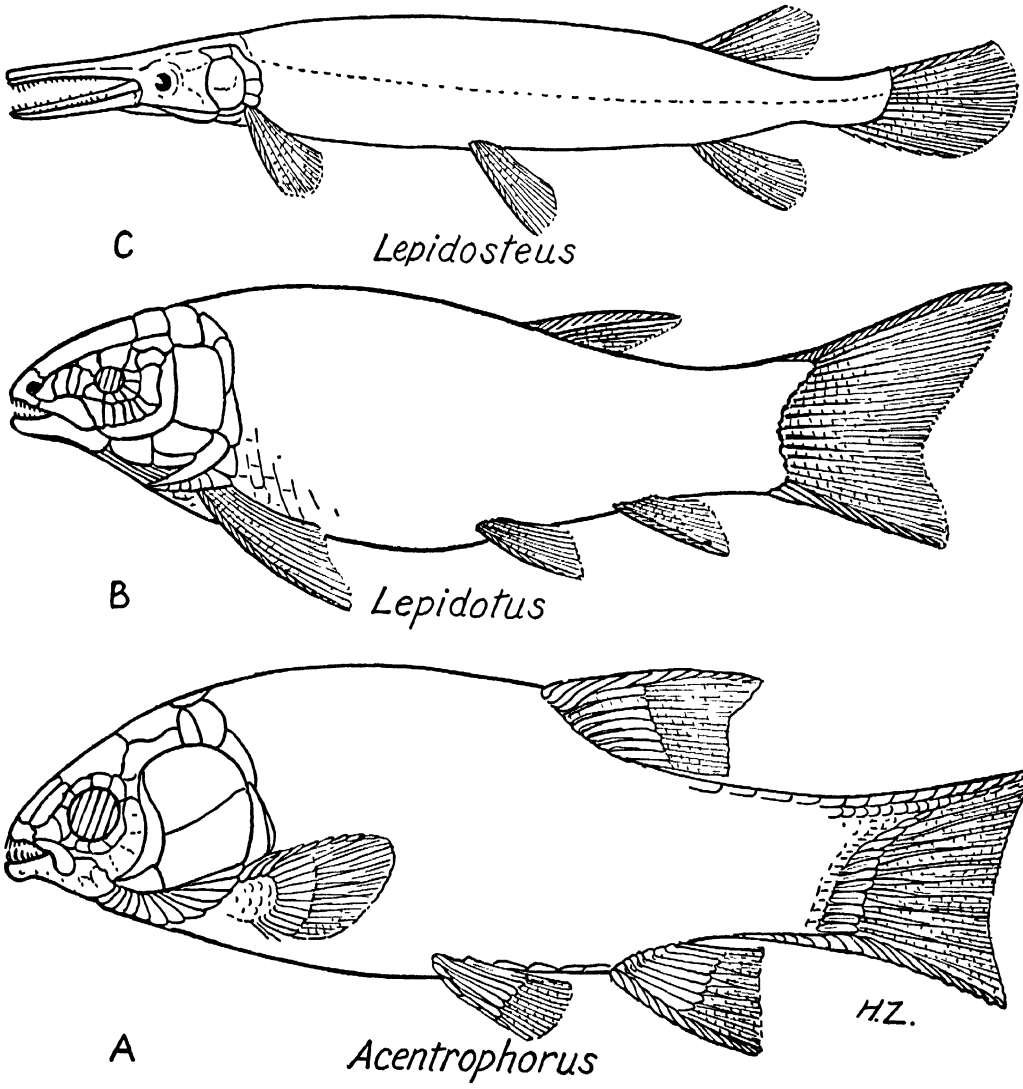
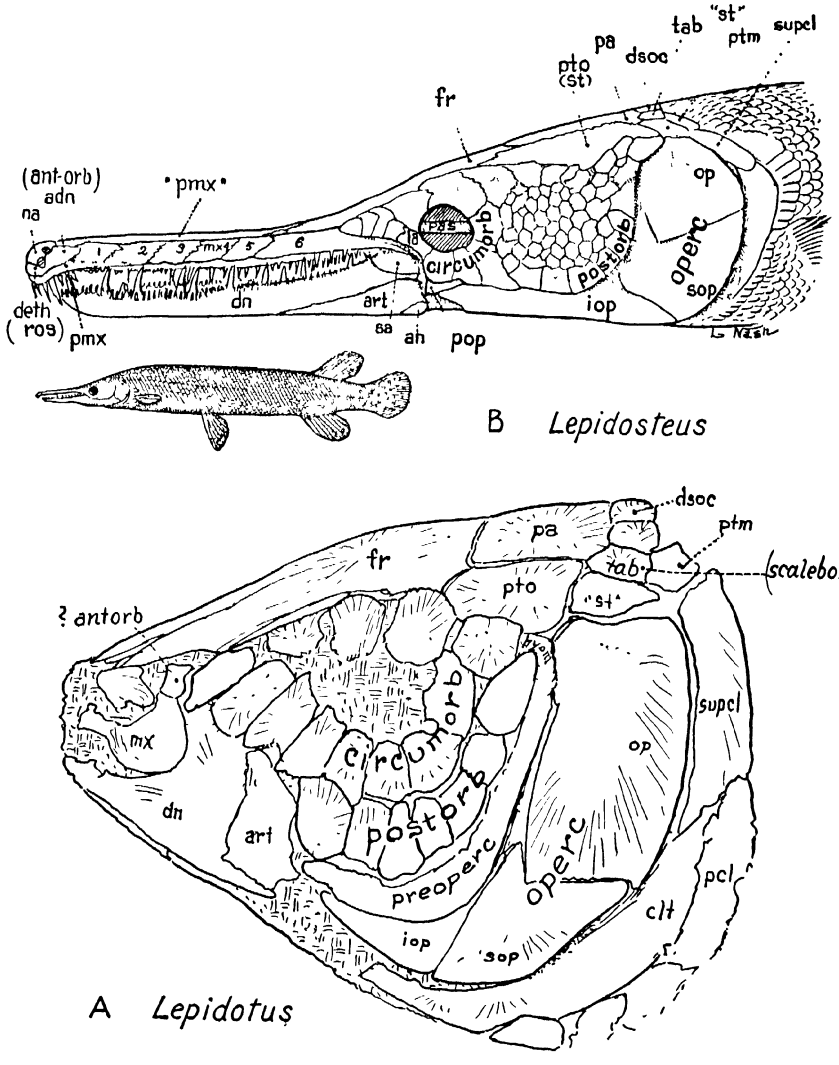


Fig. 9.17



←Fig. 9.17 (facing page). Outlines of two fossil and one recent protospondyl Ganoids. A, Triassic Semionotid, after E. L. Gill. B, Jurassic Semionotid, after Abel. C, Recent Garpike, after Goodrich. All reduced to nearly the same total length to show differences in proportion of head to body. In C the height of the body has decreased, the rostrum lengthened.

Fig. 9.18. The skull of the modern Garpike (B) compared with that of its Jurassic ancestor or relative (A). In *Lepidosteus* the supramaxillary plates (1–6) seem to be secondary polyisomeres, as do also the ossicles covering the cheek. The preopercular has become greatly reduced and the interopercular enlarged (Tate Regan). A, after A. S. Woodward.

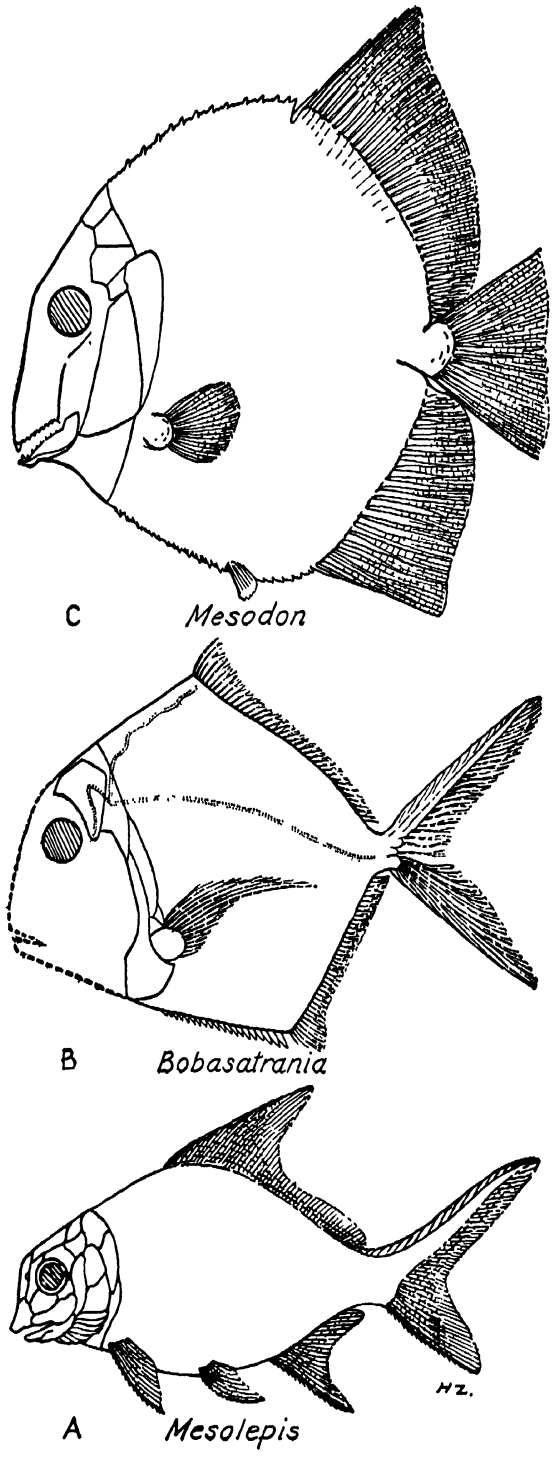


Fig. 9.19. From high-backed to discoid body form. A, Upper Carboniferous Platysomid, from Goodrich, after Traquair. B, Triassic Dorypterid, after Stensiö. C, Jurassic Pycnodontid, from Goodrich, after Traquair.

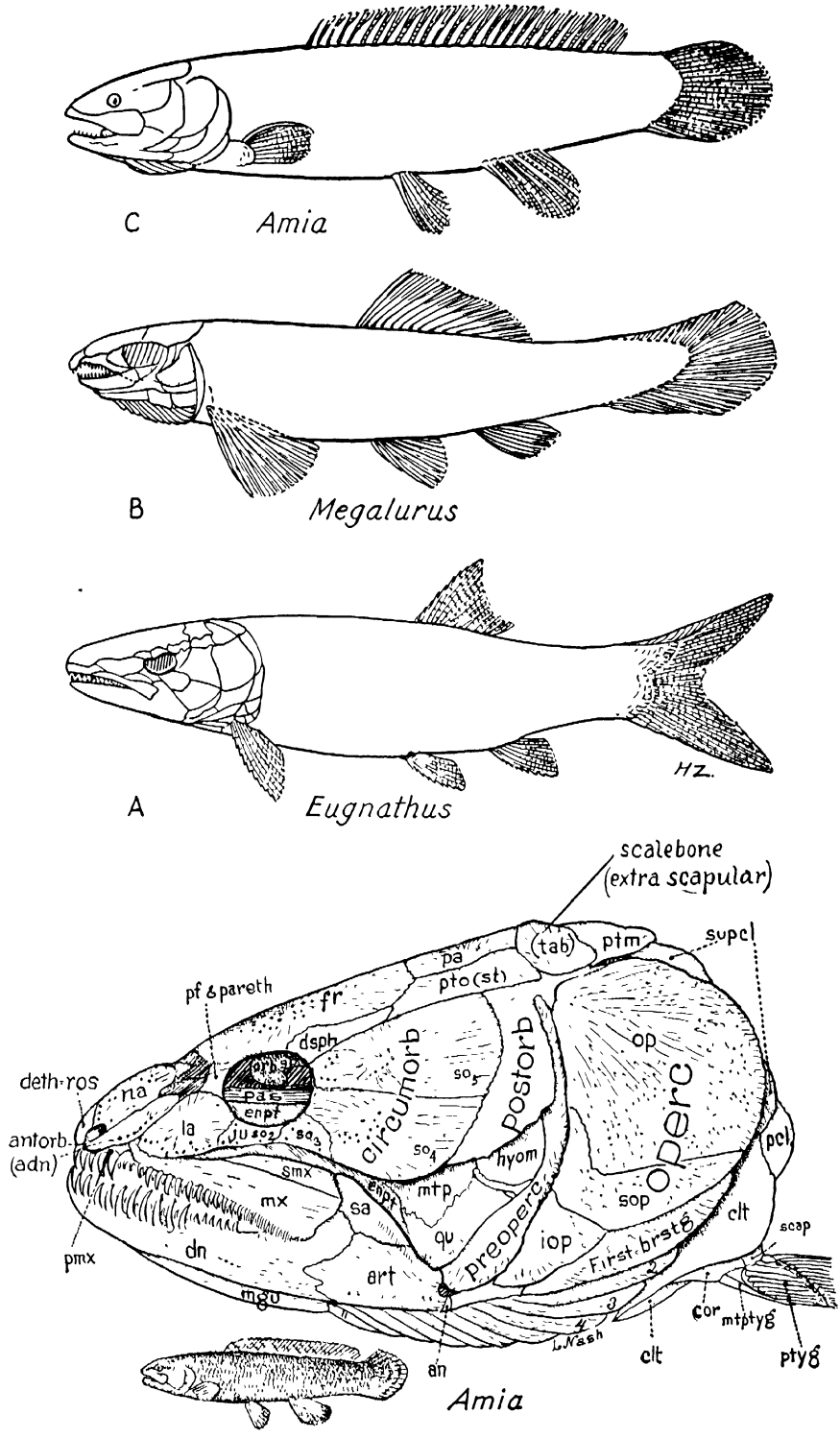


Fig. 9.20 (top). Progressive lengthening of the dorsal fin in the *Amia* line. A, primitive Lower Jurassic Protospondyl; B, moderate or intermediate Jurassic stage; C, advanced or recent stage. A, after A. S. Woodward; B, after Zittel (Eastman); C, after Goodrich.

Fig. 9.21. The only surviving Protospondyl, *Amia*. After Gregory.

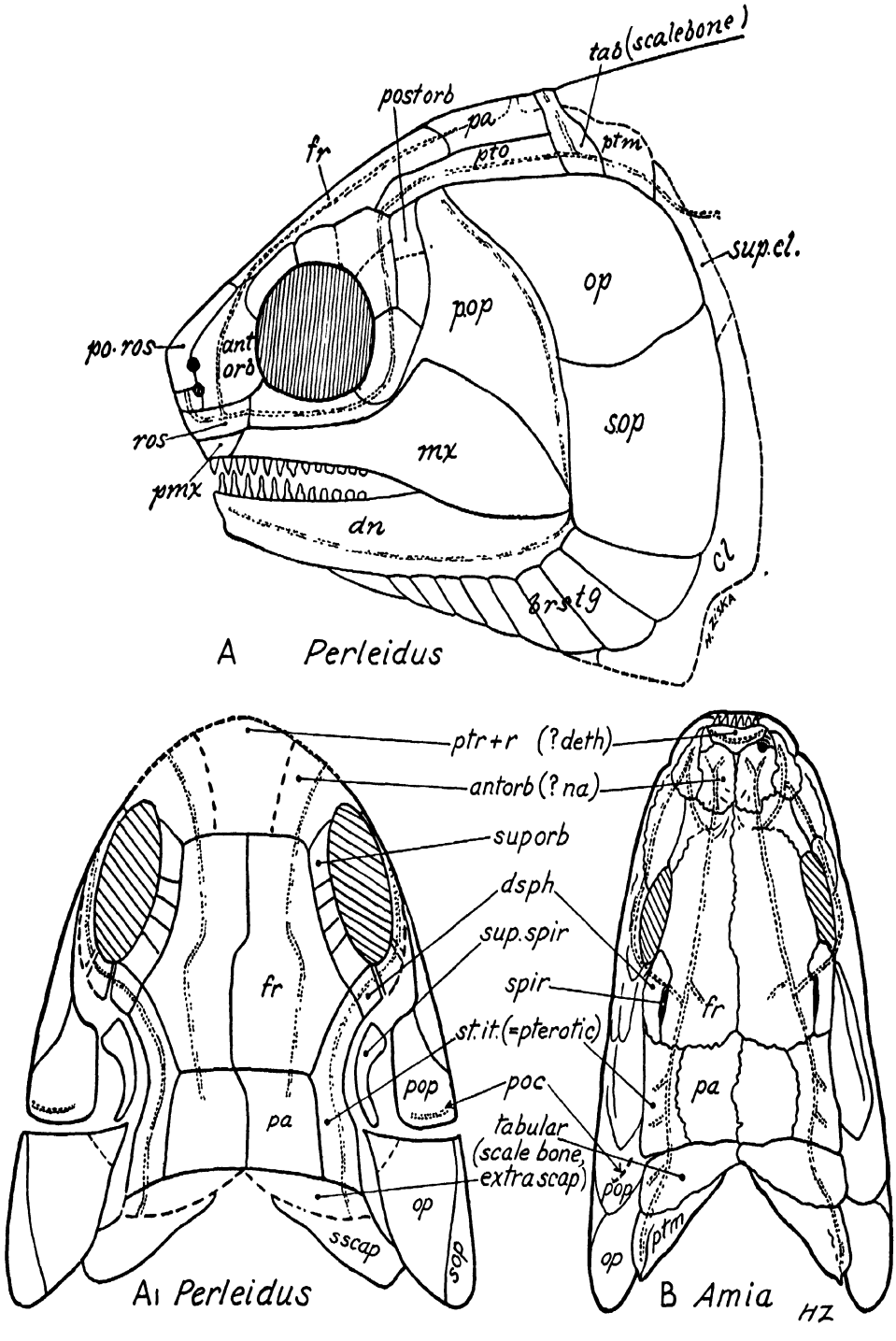


Fig. 9.22. Triassic and modern Amioid skulls. In A1 and B the names used by Stensiö are correlated with the names used by the author (Gregory, 1933). A, A1, after Stensiö. *Ptr*, postrostral; *r*, rostral; *dsph*, dermosphenotic; *sup.spir*, supraspiracular; *st.it.*, supratemporal-intertemporal; *poc*, preopercular canal; *s.scap*, suprascapular (=posttemporal).

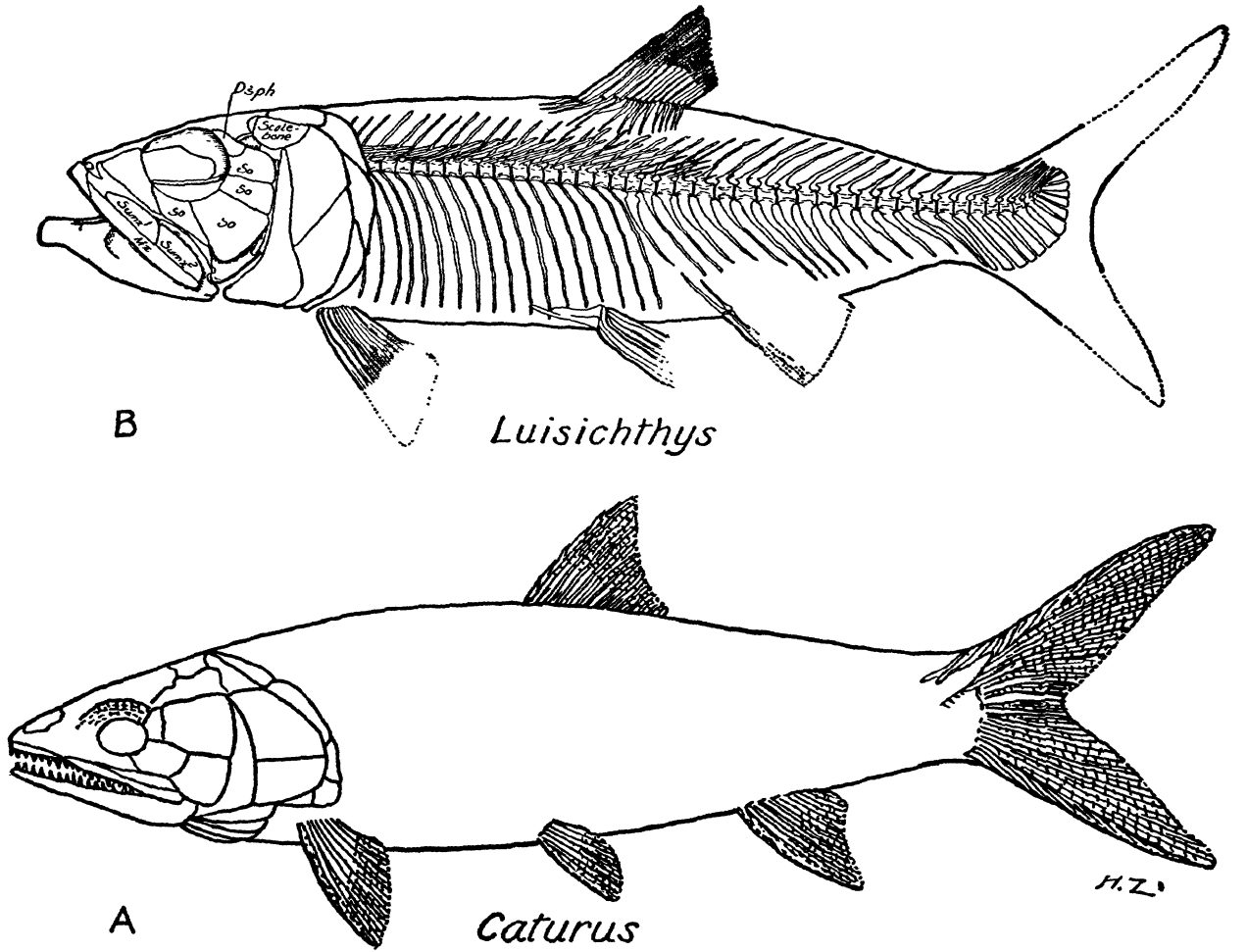


Fig. 9.23. Progressive Jurassic Amioid (A) and primitive Jurassic lepto-lepid Teleost (B). A, after A. S. Woodward; B, after T. E. White.

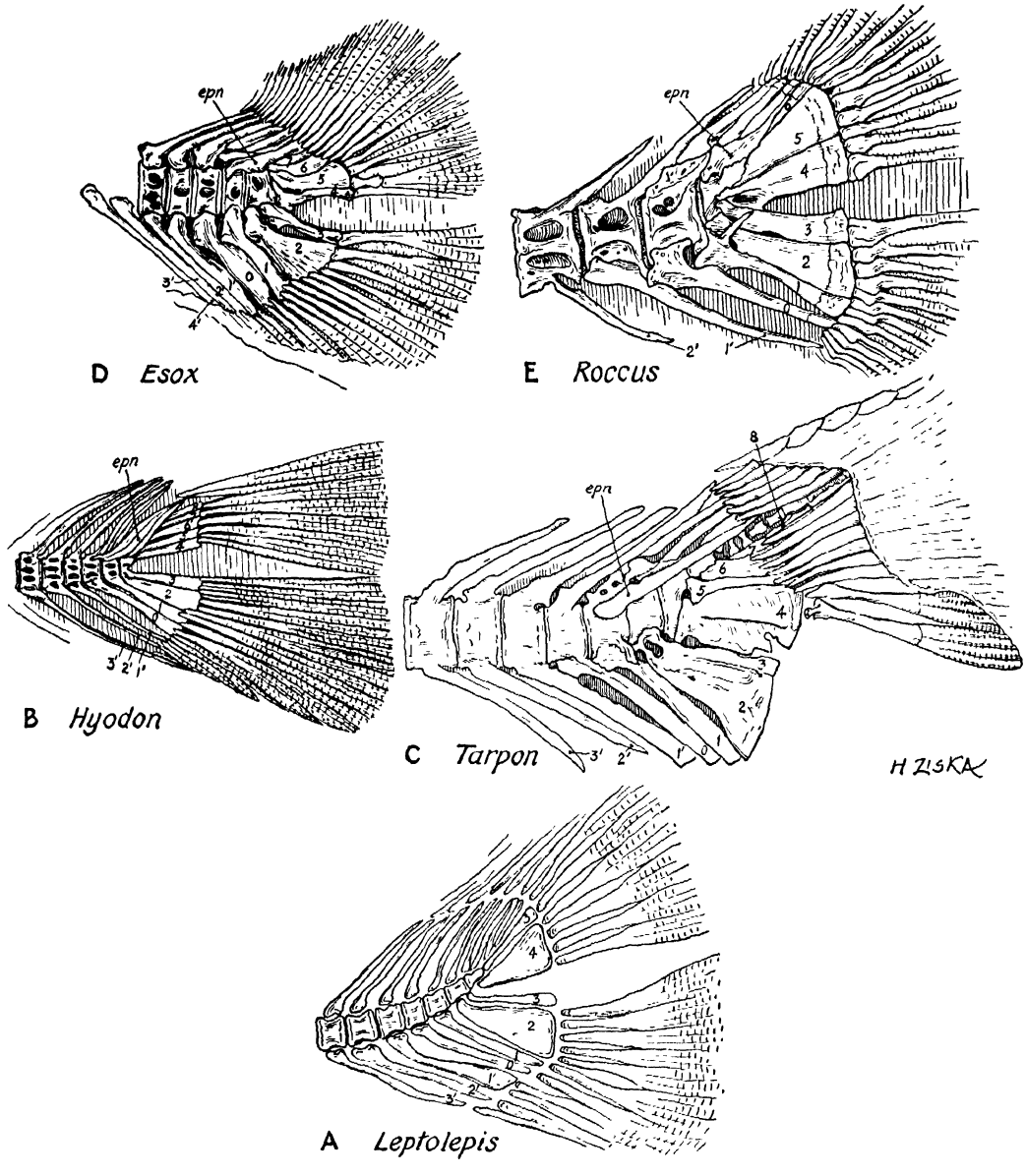


Fig. 9.24. Progressive anisomerism of hypural bones. A, Primitive Jurassic Teleost, after A. S. Woodward. B, C, Surviving Isospondyls, the former more primitive, with less expanded hypurals; the latter with greatly expanded hypurals 2, 4. D, Typical Haploman, with expanded 2, small 4 and moderate 5; transitional between B and E. E, Typical Percoid, with moderately expanded 2, 3, 4, 5. The enumeration of the hypurals 1–8 is adopted from G. Hollister (1936, 1937), although the transition from haemal spines to hypurals is gradual. The former are here numbered 0, 1′, 2′, 3′, 4′.

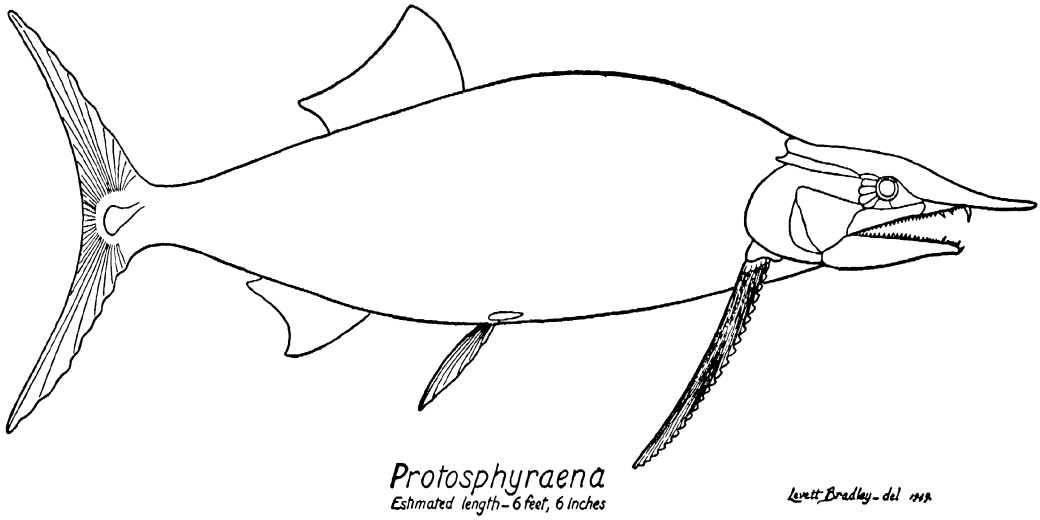


Fig. 9.25. A large Amioid of the Upper Cretaceous. Provisional outline.

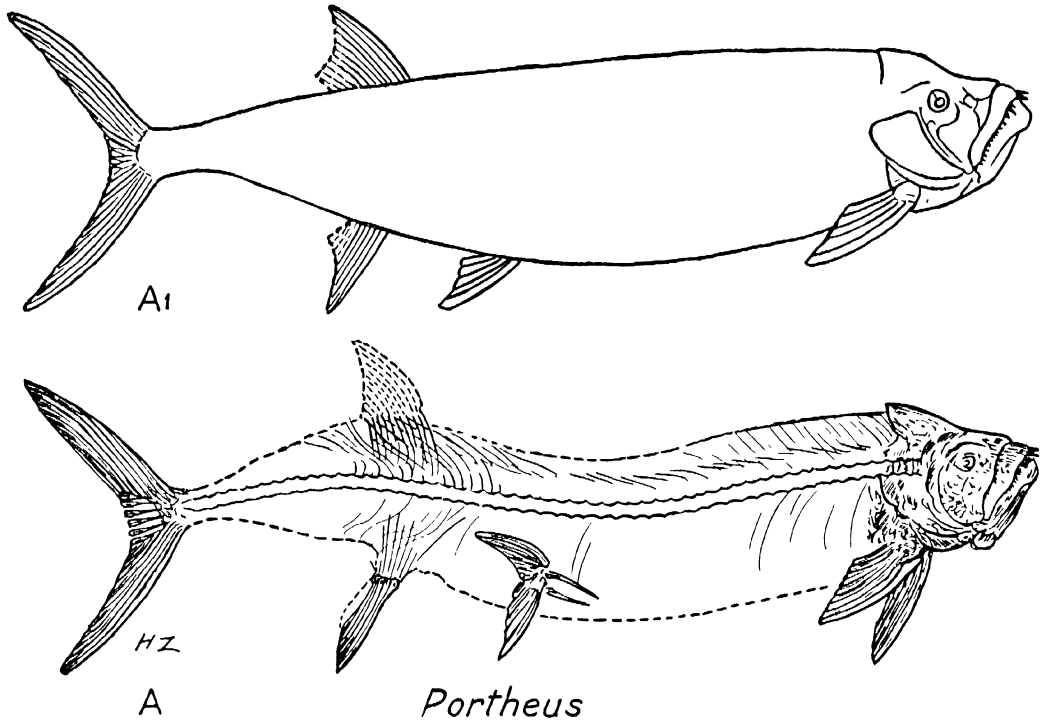


Fig. 9.26. The giant "Bulldog" fish of the American Cretaceous. Sketch (A) of a nearly complete skeleton, 12 feet, 8 inches long, discovered by George F. Sternberg in the Cretaceous of Kansas and prepared by him for the Museum of the Kansas State Teachers College at Hays, Kansas. Provisional outline (A1).

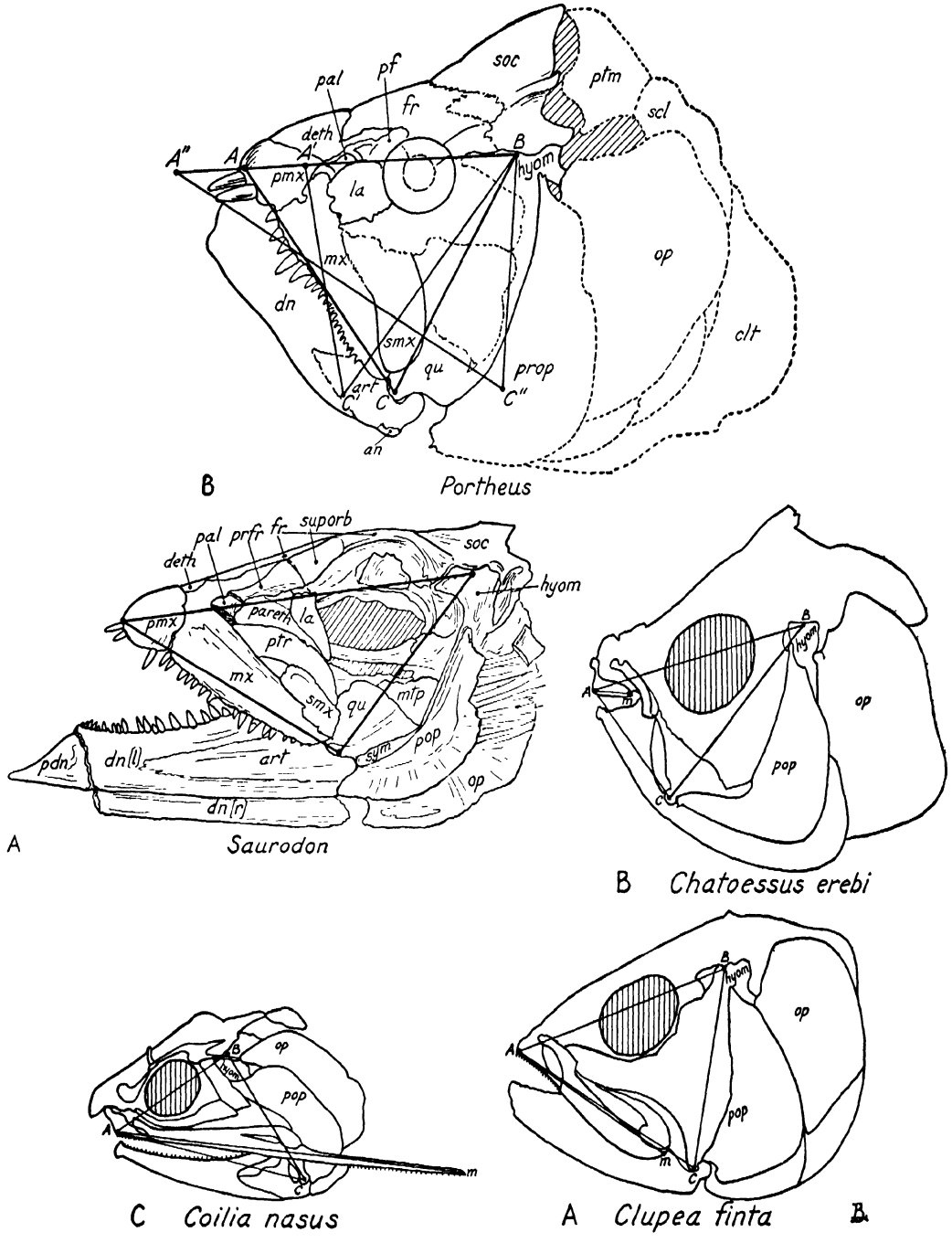
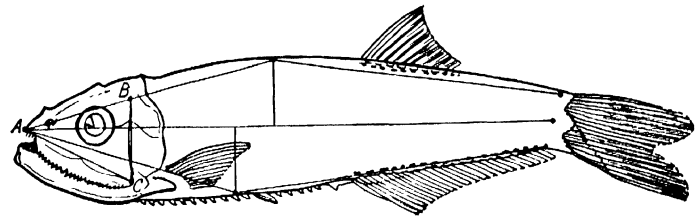
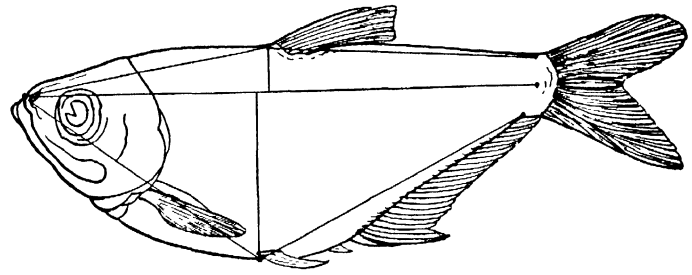


Fig. 9.27 (top). Skulls of two predatory Cretaceous Isospondyls of the family Chirocentridae, illustrating differences in the slope of the upper jaw (*C, C, C', C', A", C"*) which would be occasioned by shifting A and C to new positions. *A*, prosthion; *B*, mid-point of hyomandibular facets; *C*, quadrate-articular facet.

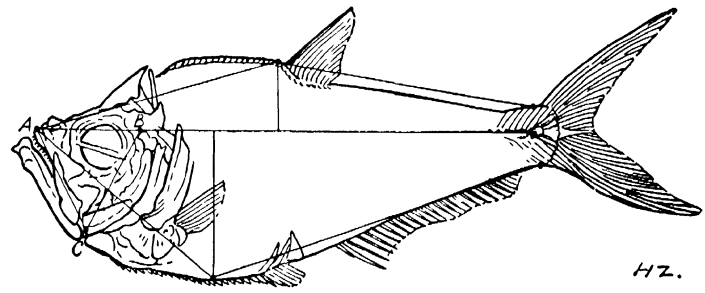
Fig. 9.28. Varying relations of length and inclination (*Am*) of mouth to the suspensorial angle (*ABC*) in primitive (A), small-mouthed (B) and "scoop-net" (C) herrings.



C *Ilisha caribbaea*



B *Ilisha argentata*



A *Diplomystus dentatus*

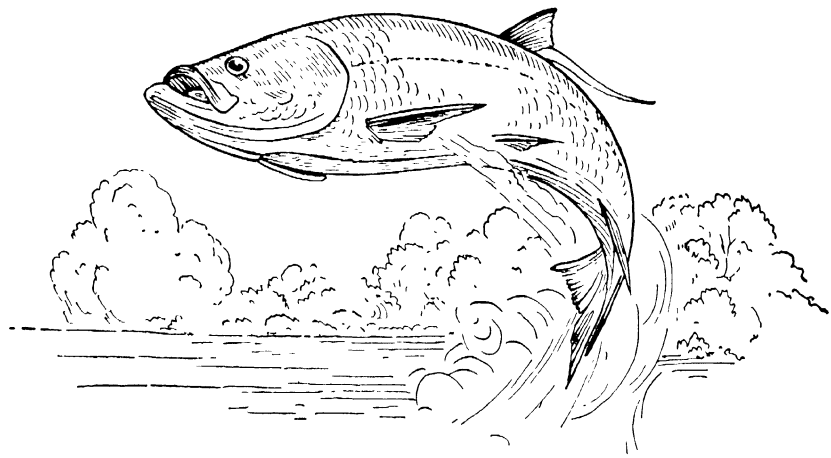


Fig. 9.29 (top). Primitive Eocene herring (A) and its modern relatives (B, C). In the primitive forms of this family the belly is deepened, the quadrate-articular joint is low and the mouth inclines sharply upward; in C the ventral diameter has decreased and with it the depth of the quadrate-articular joint and the inclination of the upper jaw *AC*. A, after Cope; B, C, after Meek and Hildebrand.

Fig. 9.30. Leaping Tarpon. After Gregory and La Monte.

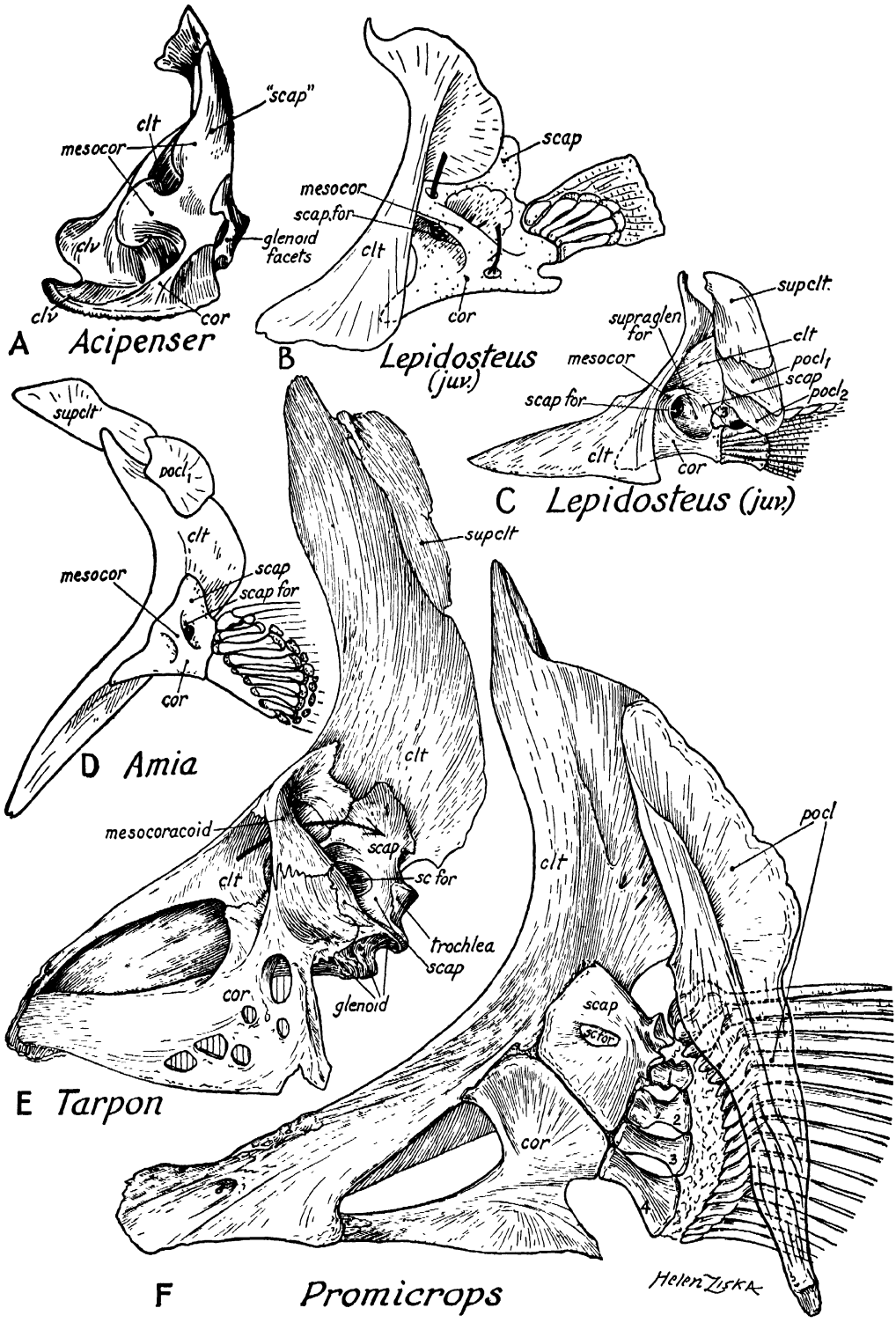


Fig. 9.31. Relations of the scapulo-coracoid to the cleithrum in successive grades of fishes. Mesial view of right half of girdle.

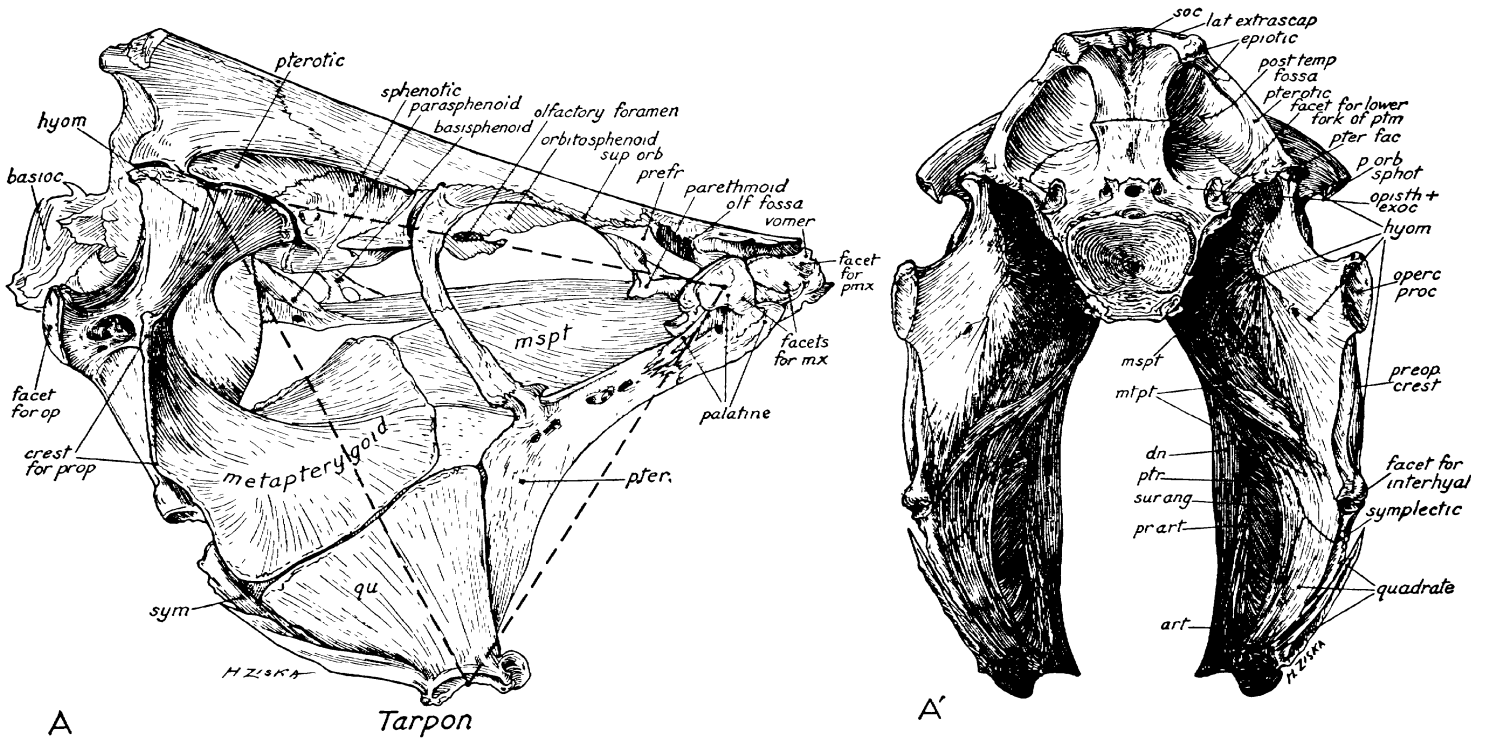


Fig. 9.32a Tarpon skull, showing: (A) inverted truss formed by inner upper jaw (palato-pterygo-quadrate) and suspensorium (hyomandibular + symplectic), (A') rear view, showing all attachments of jaws to skull and bracing of skull to meet thrust from vertebral column.

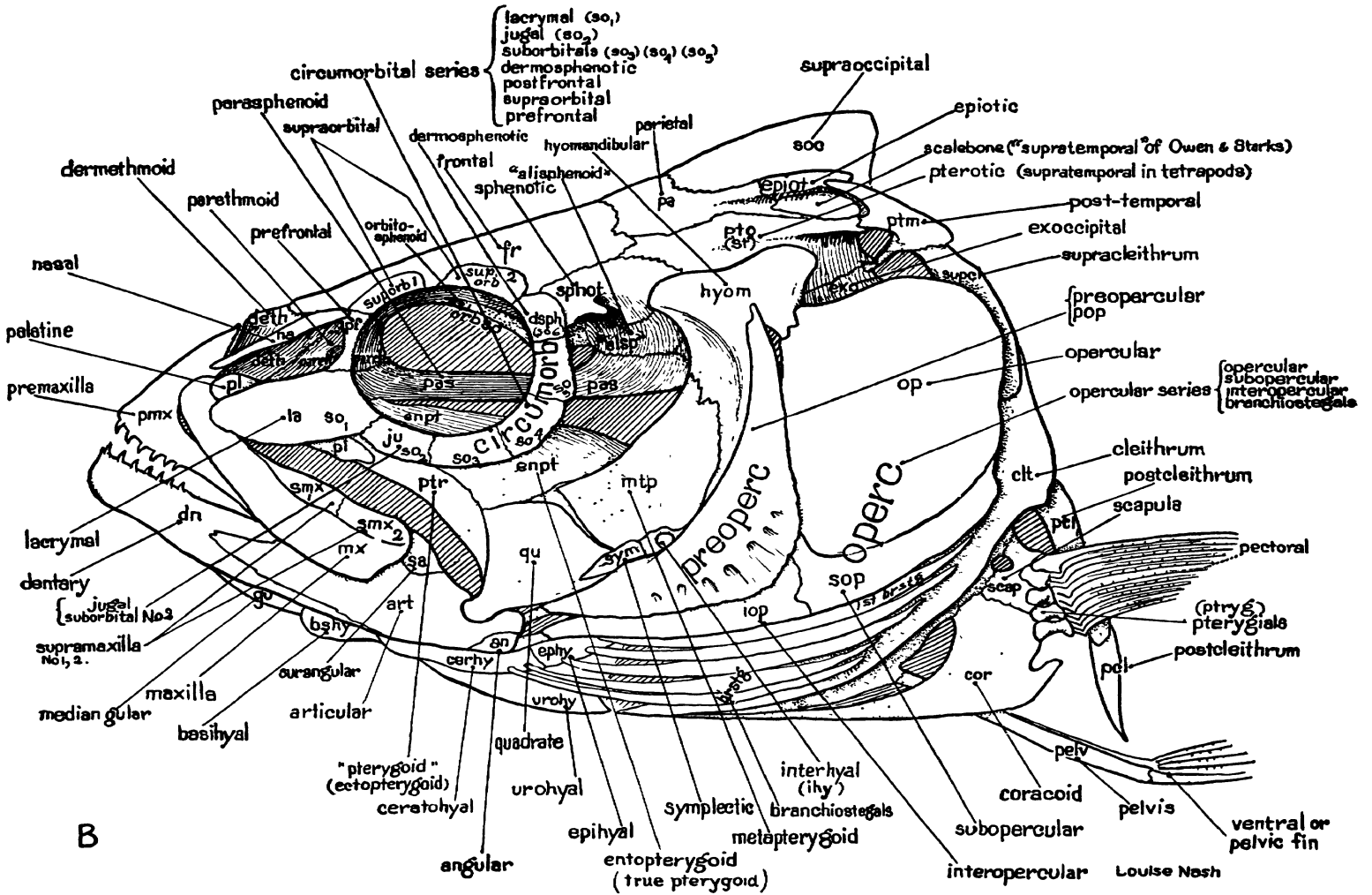

circumorbital series
lacrymal (so1)
jugal (so2)
suborbitals (so3) (so4) (so5)
dermosphenotic
postfrontal
supraorbital
prefrontal
parasphenoid
supraorbital
dermosphenotic
frontal
"alisphenoid"
sphenotic
parietal
hyomandibular
supraoccipital
epiotic
soo
scalebone ("supratemporal" of Owen & Starks)
pterotic (supratemporal in tetrapods)
post-temporal
exoccipital
supracleithrum
dermethmoid
parethmoid
prefrontal
orbito-sphenoid
nasal
palatine
premaxilla
lacrymal
dentary
jugal
suborbital No 2
supramaxilla No 1, 2.
maxilla
median gular
basihyal
articular
surangular
"pterygoid" (ectopterygoid)
ceratohyal
quadrate
angular
urohyal
epihyal
entopterygoid (true pterygoid)
symplectic
metapterygoid
interhyal (ihy)
branchiostegals
interopercular
suboperculars
coracoid
pelvis
ventral or pelvic fin
preopercular
opercular
opercular series
cleithrum
postcleithrum
scapula
pectoral
pterygials
Louise Nash
B

Fig. 9.32b

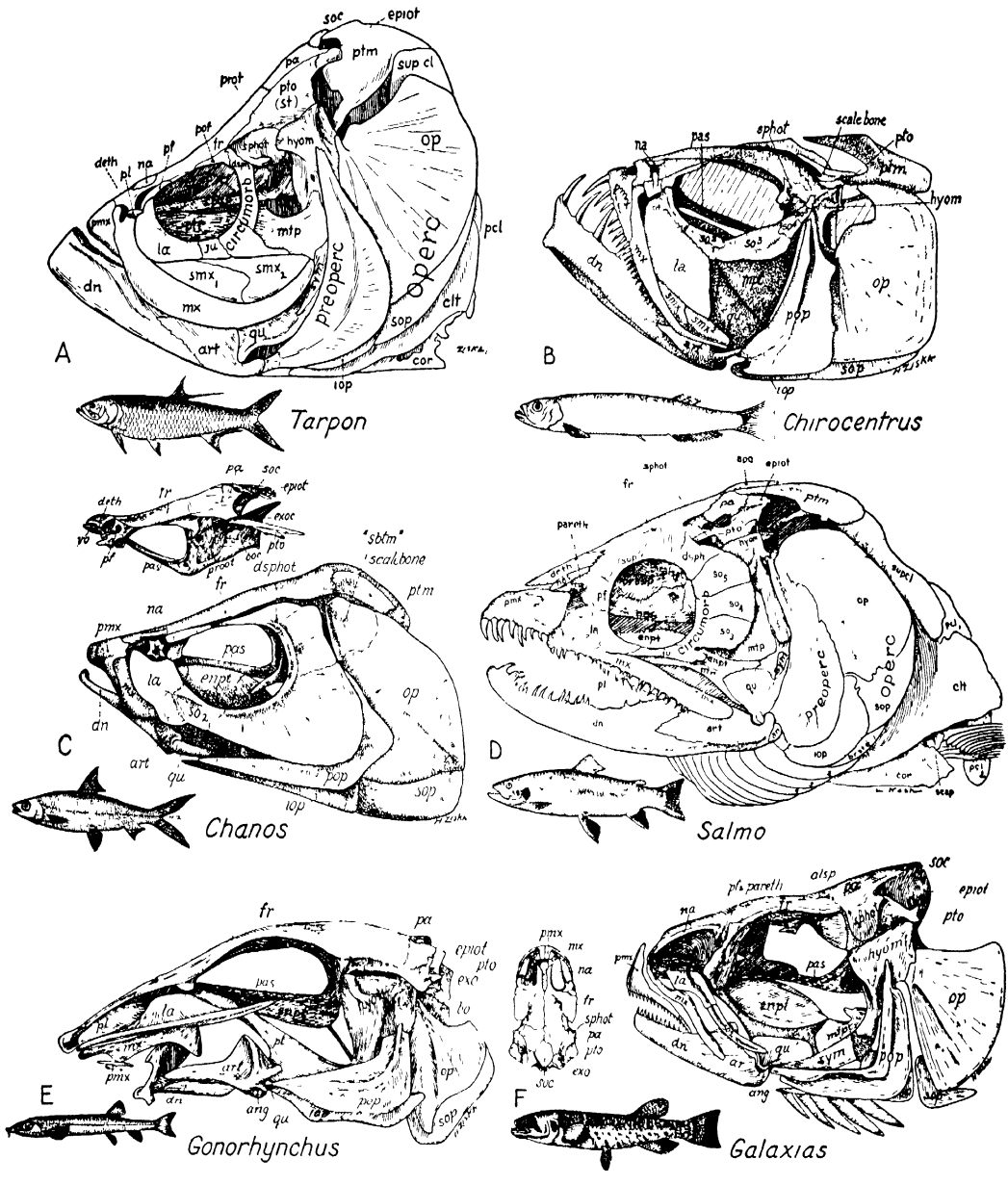


Fig. 9.32b (facing page). Composite diagram of teleost skull, with names and abbreviations here used. Beginning behind the orbit there are five arcs or curved series of surface bones: (1) circumorbital, (2) preopercular, (3) opercular, (4) cleithral, (5) scapulo-coracoid. The postorbitals of ganoids, covering the cheeks, have been lost (fig 9.18A).

Fig 9.33 Selective branching of the skulls, jaws and teeth in Isospondyls, showing range from predaceous (B,D,F) to prehensile (A), edentulous (C), and suctorial (E) stages. E is convergent toward the sturgeons (fig. 9.14C). B,C,E, after Ridewood; F, after Swinnerton.

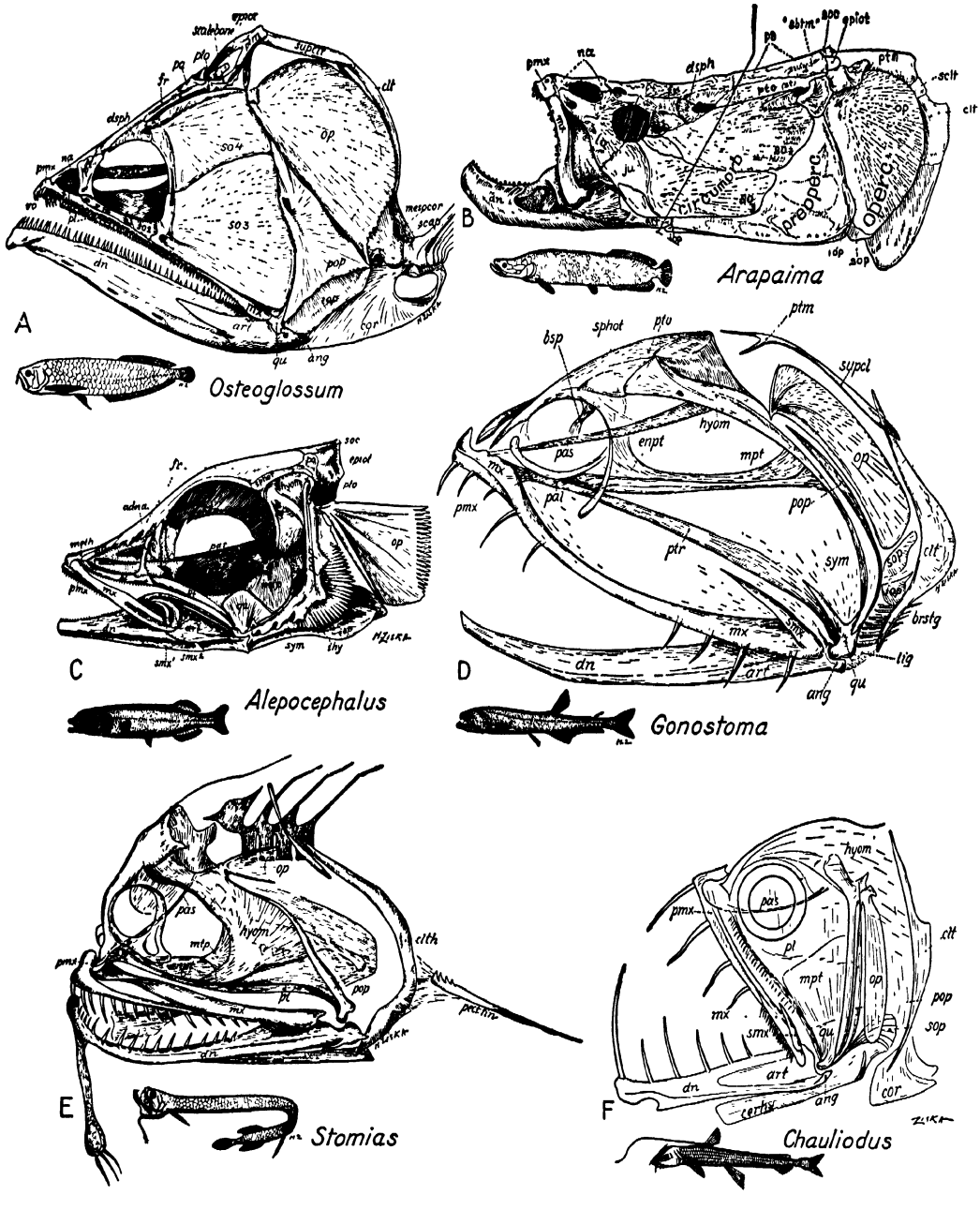


Fig. 9.34. Selective branching of skulls, jaws and teeth in Isospondyls (continued): fresh-water osteoglossids (A, B), alepocephaloid (C), and stomiatoids (D–F). A, B, retain a relatively primitive skull, jaws and teeth; in C the maxilla is edentulous; in E the piercing, needle-toothed type is highly specialized; D–F are from young or immature specimens. After Gregory.

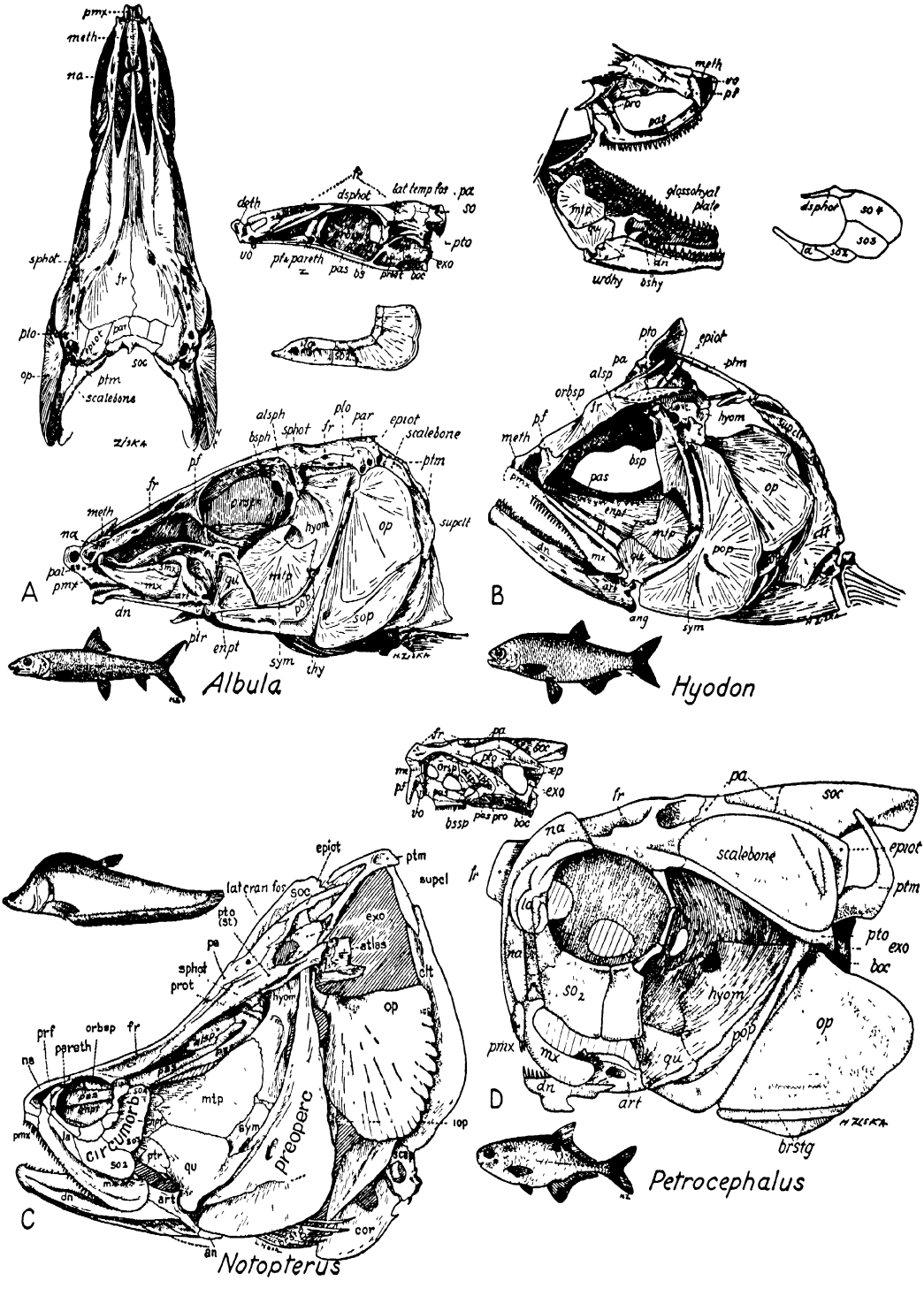


Fig. 9 35. Selective branching of the skull, jaws and teeth in Isospondyls (concluded). In the relatively primitive B and C, the teeth on the maxilla are retained (cf. fig. 9.34 A), but in A and D they are lost. Median rows of teeth on the parasphenoid and glossohyal are shown in B. After Gregory.

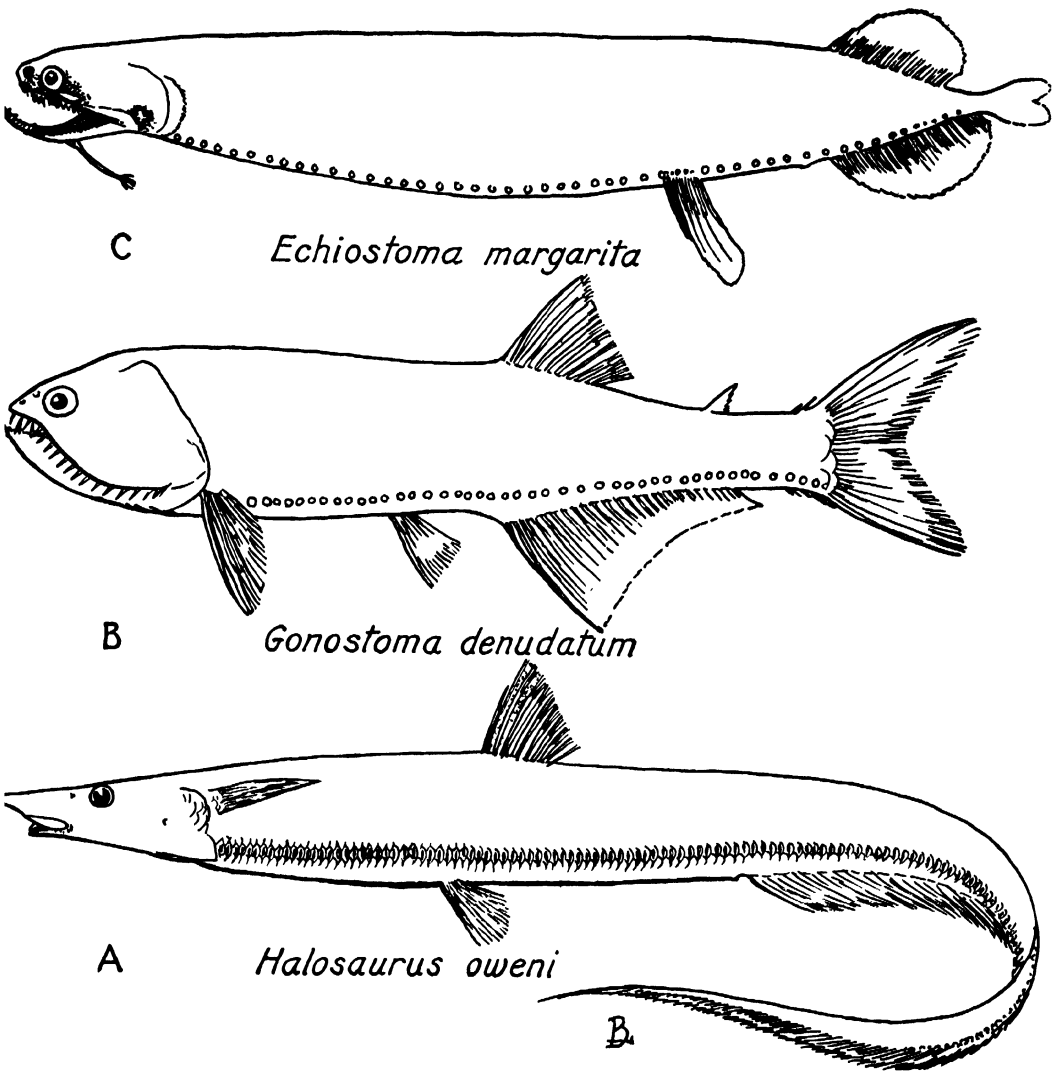


Fig. 9.36. Comparison of rows of photophores (in B, C) with lateral line organs (A) of abyssal fishes.

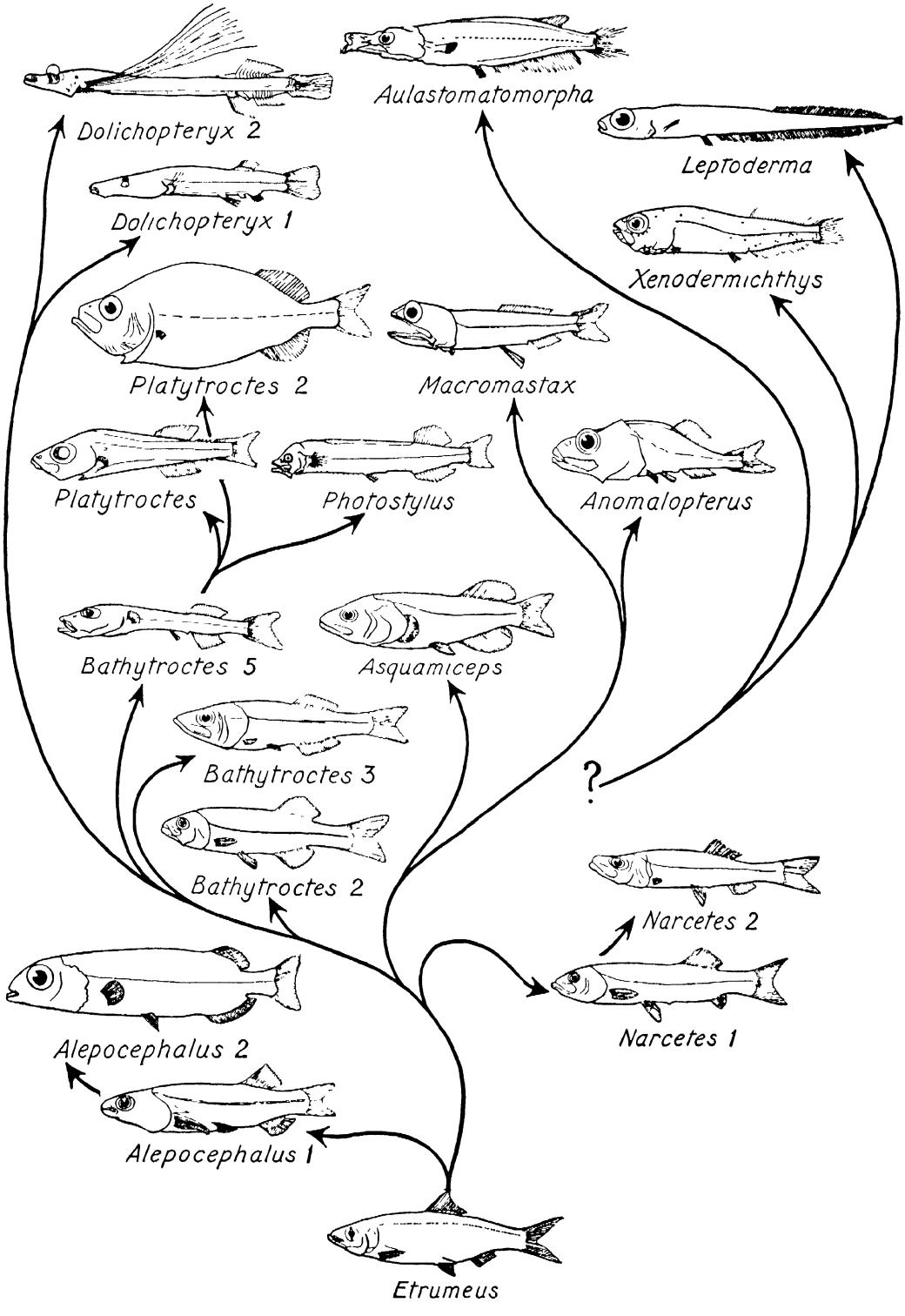


Fig. 9.37. Selective branching of the Alepocephaloidea. Based mainly on data of Beebe and others. Gregory and Conrad, 1936.

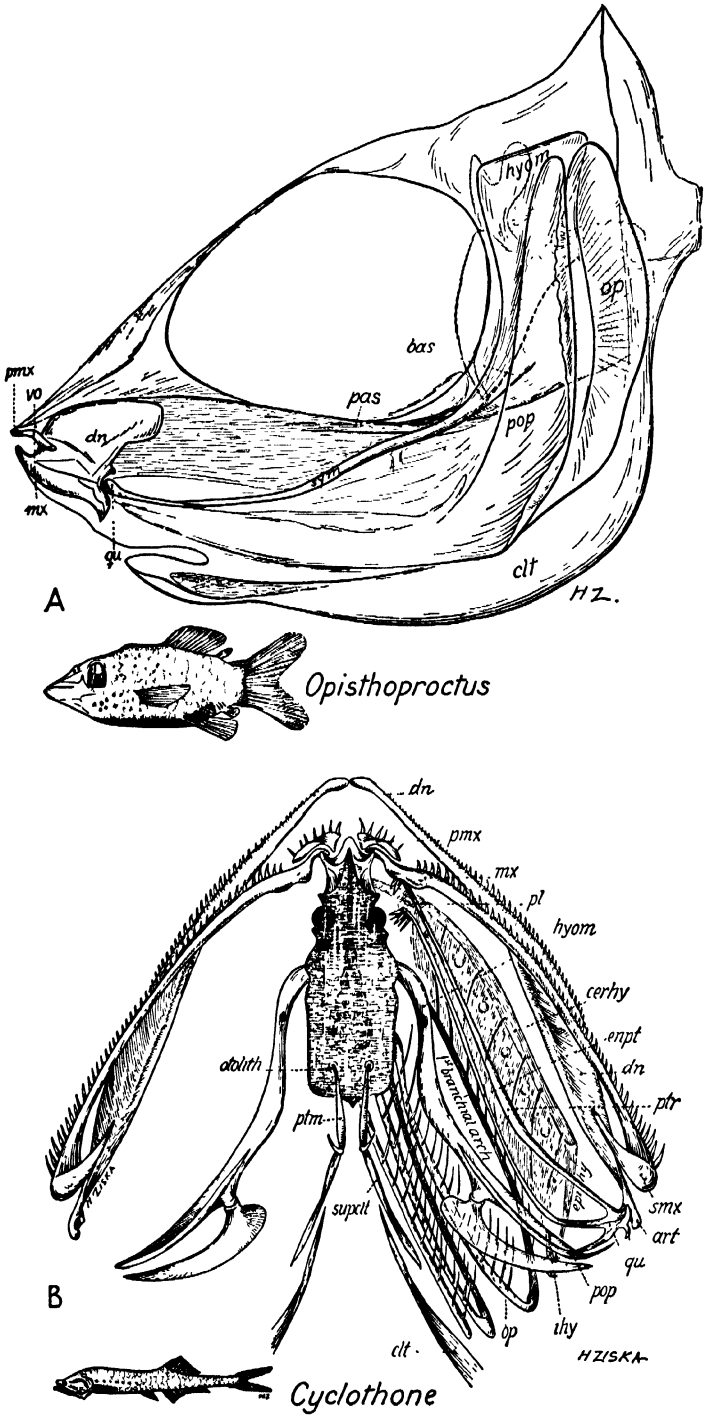


Fig. 9.38. Extremes of skull and jaw form in two deep-sea fishes: A, with very large eyes and minute nibbling jaws; B, with small eyes and slender trap-like jaws. A is from a larval or immature specimen; the eyes and delicate circumorbital plates were not preserved. Otoliths dotted. B shows the luminous organs of the hyoid skin flap and the attenuated bones of the jaws and branchial arches. After Gregory.

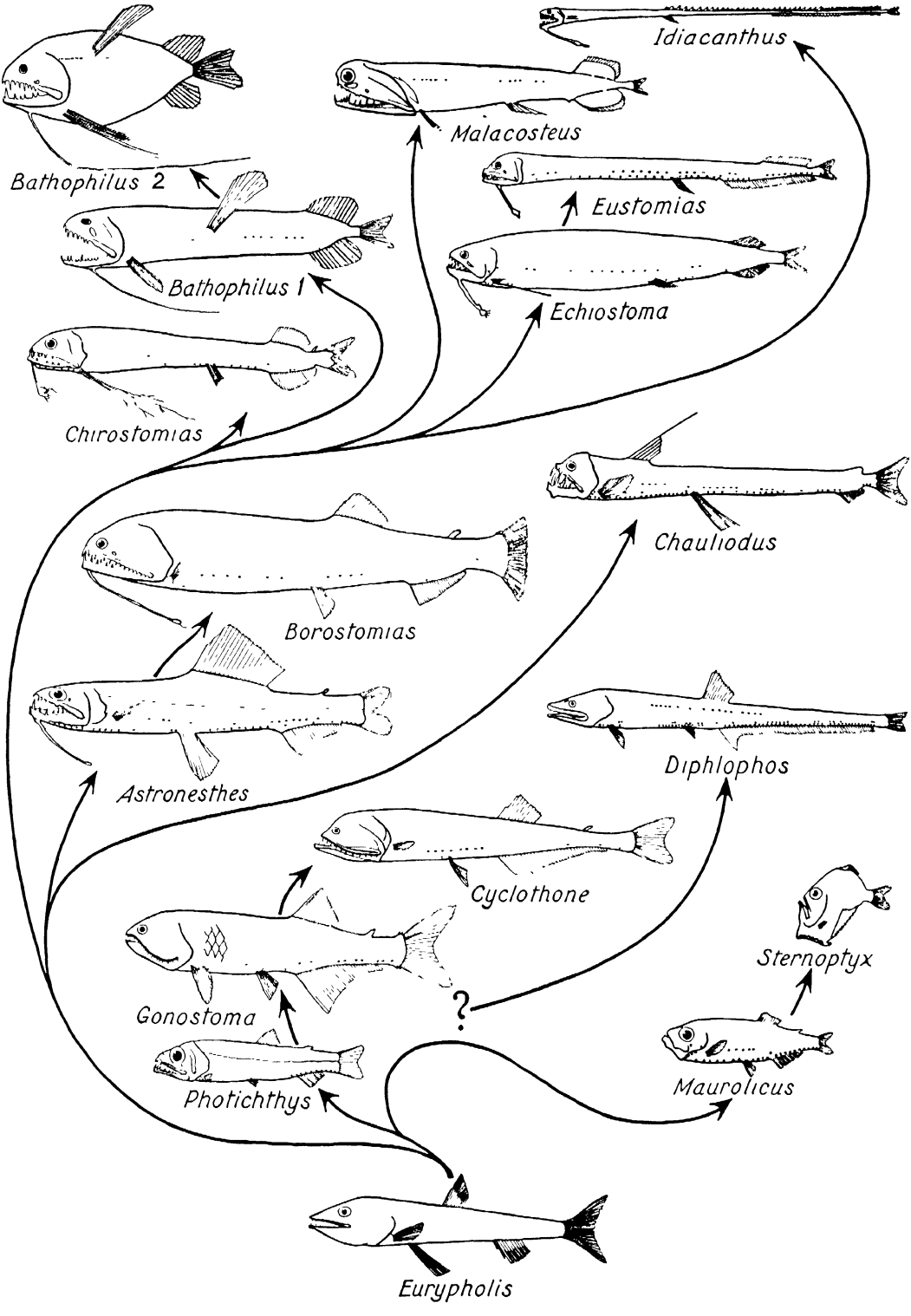


Fig. 9.39. Branching of the Stomiatoids. Based on data from various authors, in Gregory and Conrad (1936).

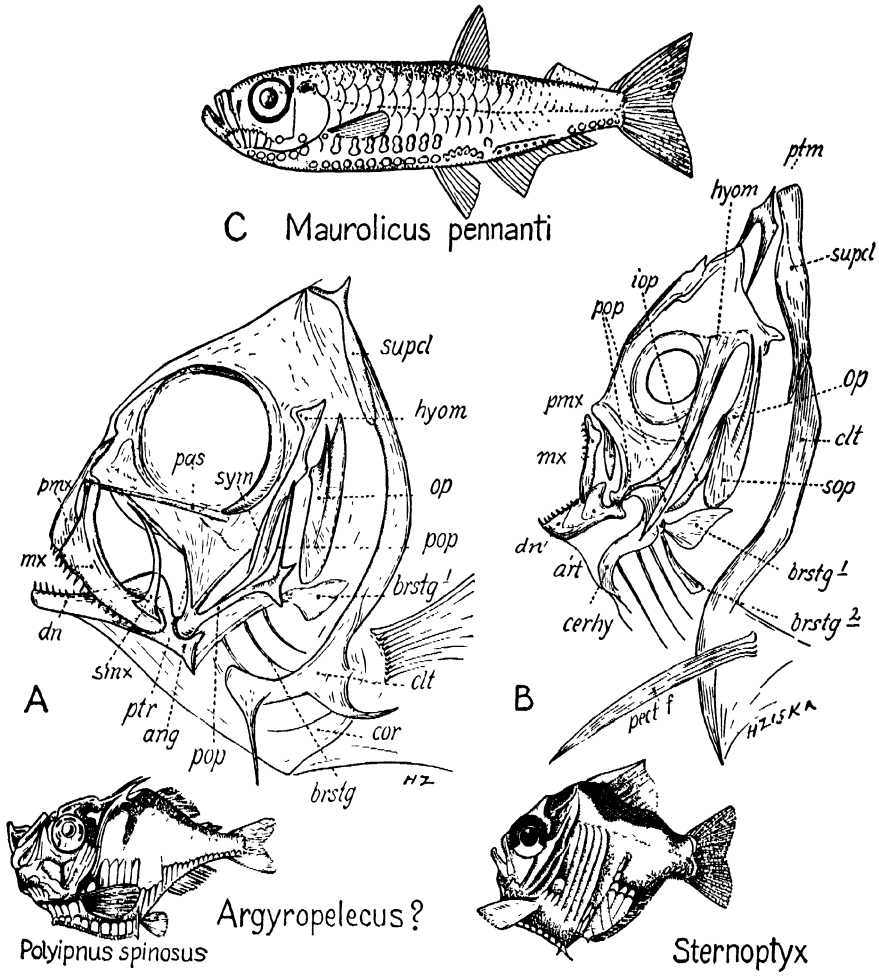


Fig. 9.40 (top). The silver hatchet-fishes, including a primitive (C) and two highly specialized members (A, B). After Gregory.

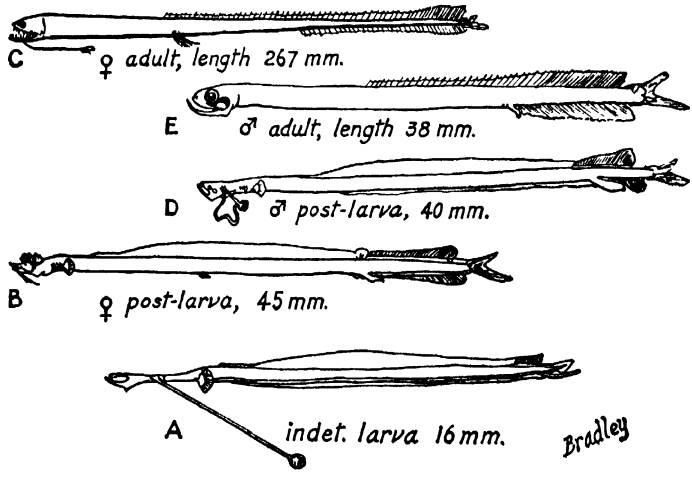


Fig. 9.41. Larval and adult male and female stages of the stomiatoid *Idiacanthus*. After Beebe.

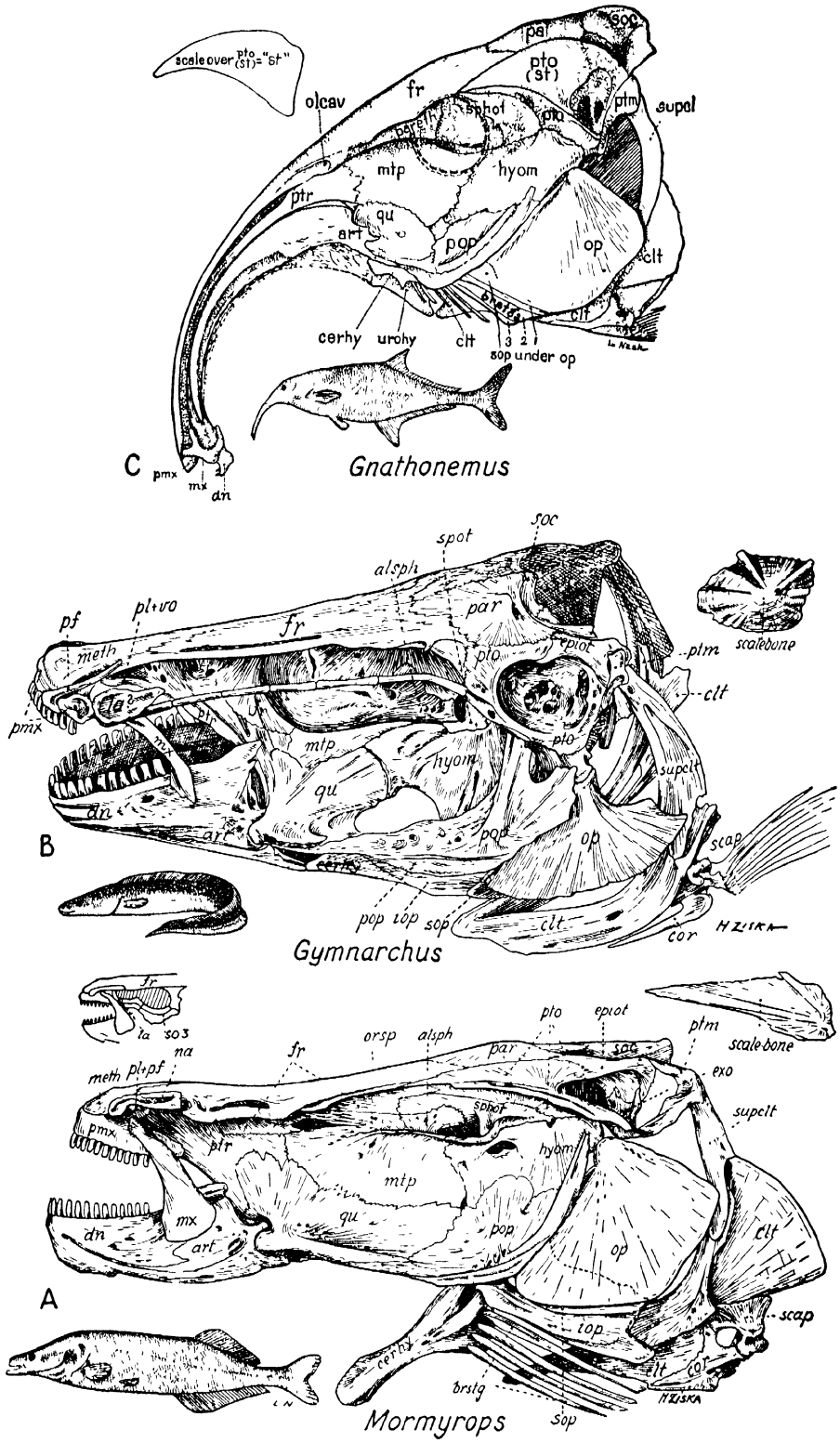


Fig. 9.42. Mormyrids and their strange skulls (see also fig. 9.35 D). After Gregory.

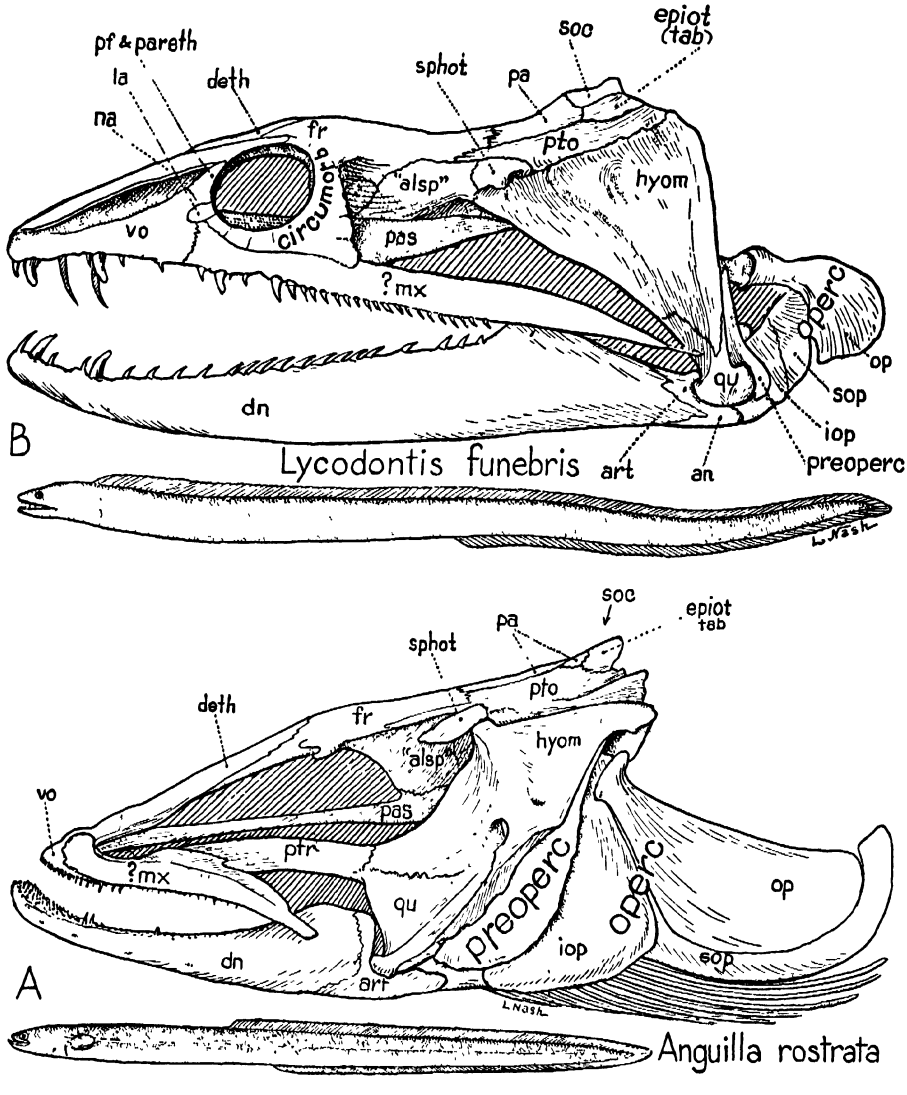


Fig. 9.43. From specialization to superspecialization by anisomerism. In the true eels (A) the skull is already specialized, especially in the loss of the premaxillae and depression of the operculars. In the morays (B) there are also reduction of the opercular elements, great elongation of the jaws, backward swing of the hyomandibular, loss of the pterygoid, etc. After Gregory.

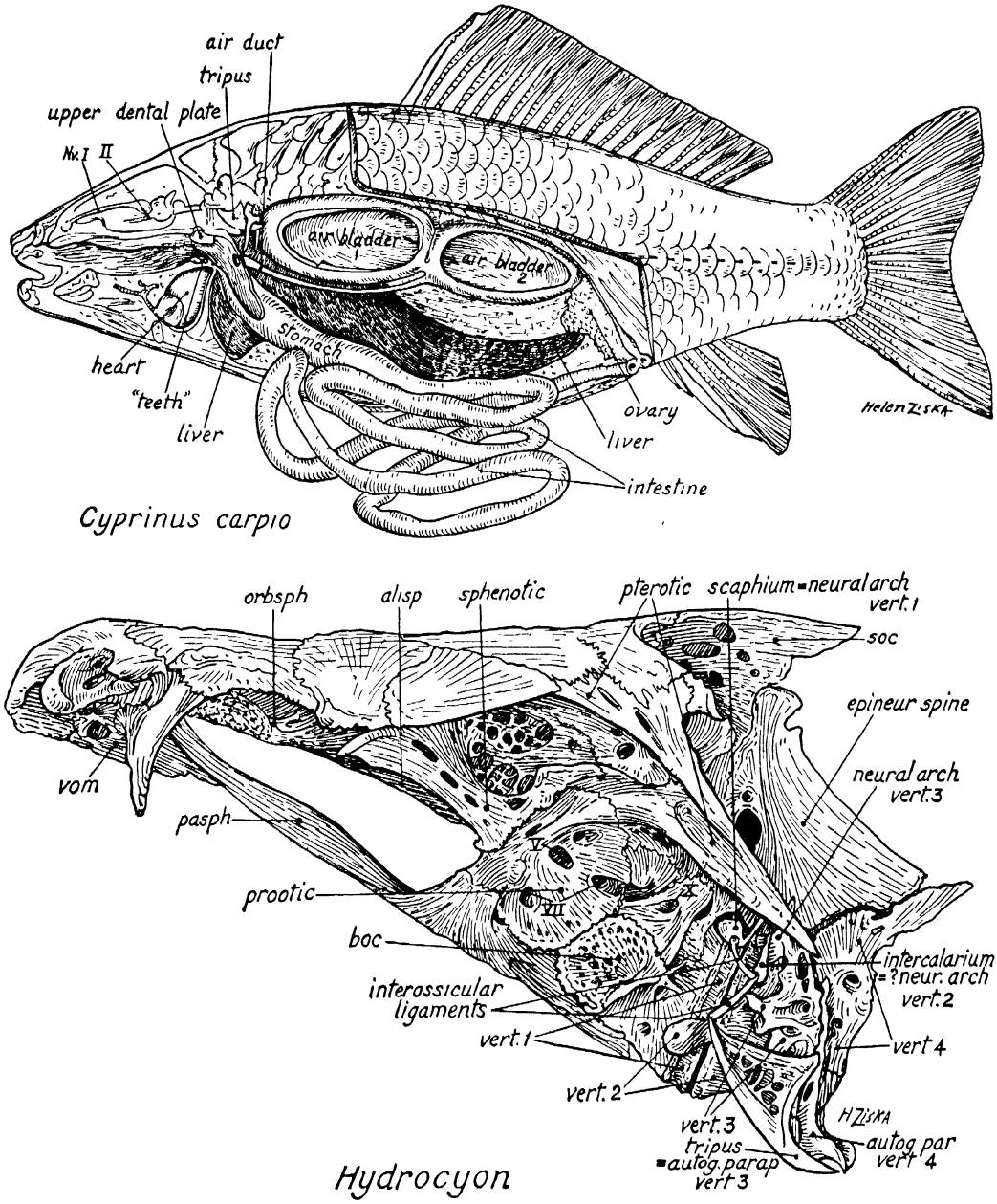


Fig. 9.44 (top). Anatomy of a typical cypriniform. Data from Goodrich and others.

Fig. 9.45. The skull and Weberian bones of a large Characin. The skull itself is of primitive teleost type, retaining the orbitosphenoid but masked by specialization (e.g., cancellous bone). The most anterior of the Weberian ossicles, the claustrum, which was not preserved, would articulate with the dorsal part of the scaphium. It transmits vibrations from the more lateral members of the series to the inner ear. The exact size and position of the intercalarium are somewhat doubtful, as this ossicle was restored from a smaller specimen. The interossicular ligaments are provisionally indicated in the light of data by Krumholz (1943). The inferred homologies of the several ossicles with the parts of the vertebrae are based partly on the literature, especially Goodrich (1909, pp. 372, 373), Kranilof (1927; cited by Berg, 1943, p. 266). According to Kranilof (cf. Berg, 1943, pp. 266, 268), the bone here marked "epineural spine" represents the neural spine of the third vertebra, but it seems, like the supraoccipital, rather to correspond with one of the interneurals or radials.

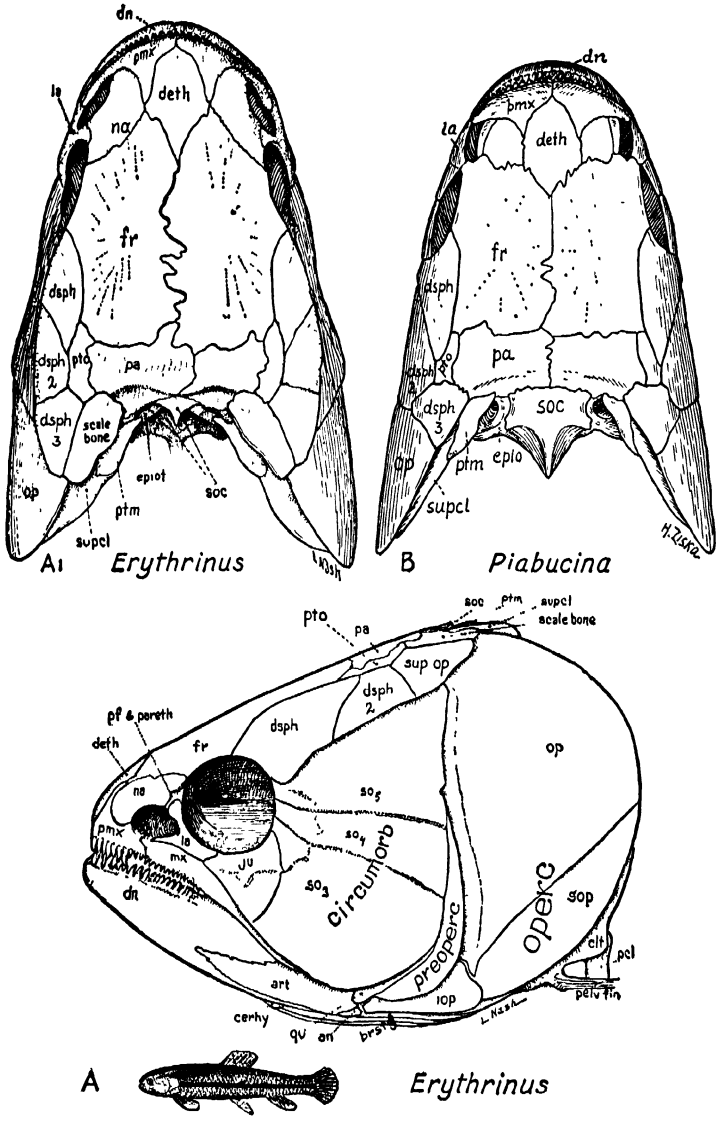


Fig. 9.46. Characins of the South American subfamily Erythrininae. After Gregory and Conrad.

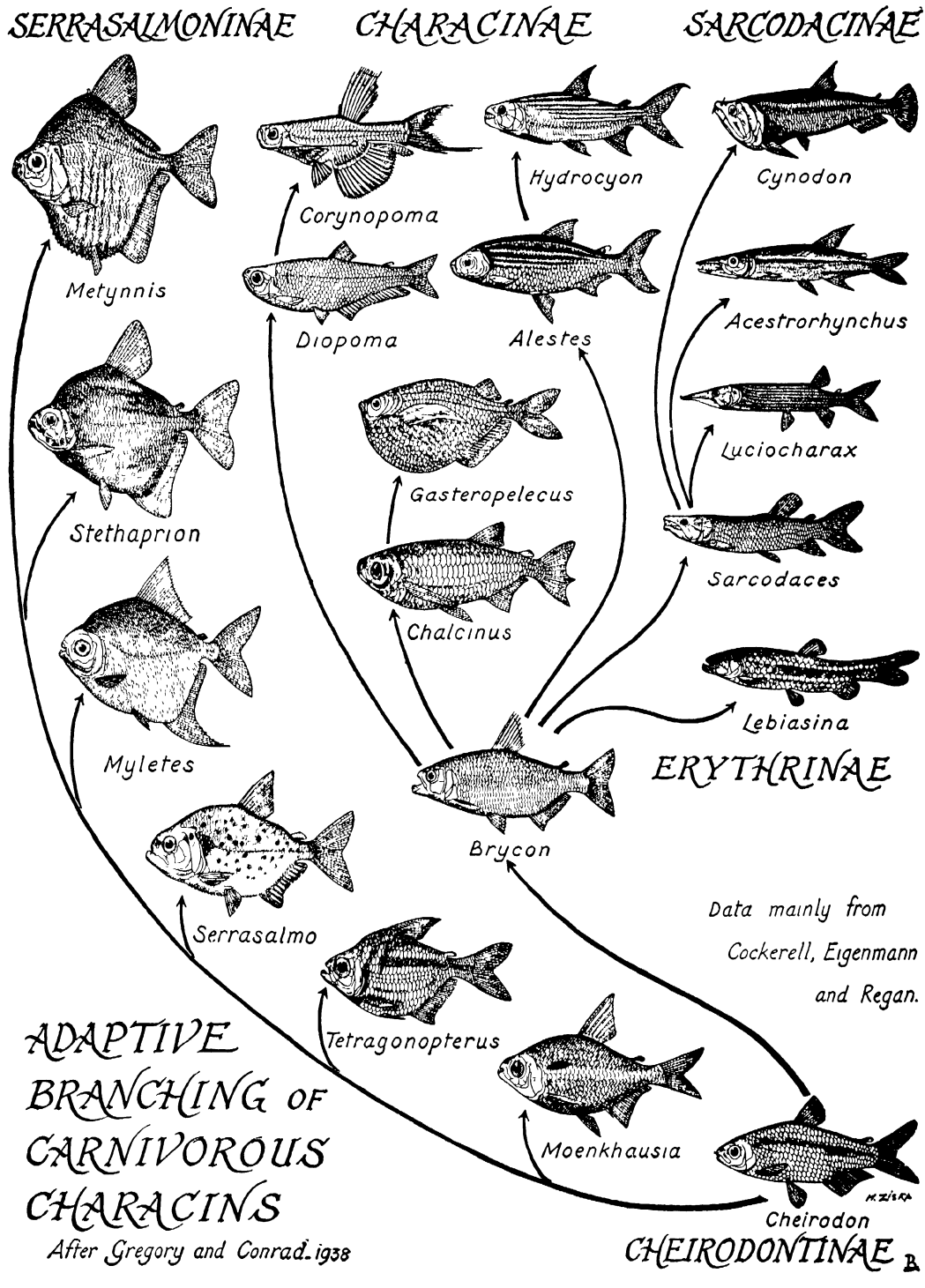

SERRASALMONINAE
CHARACINAE
SARCODACINAE
Metynnis
Corynopoma
Hydrocyon
Cynodon
Diopoma
Alestes
Acestrorhynchus
Luciocharax
Gasteropelecus
Stethaprion
Sarcodaces
Chalcinus
Lebiasina
Myletes
ERYTHRINAE
Brycon
Data mainly from
Cockerell, Eigenmann
and Regan.
Serrasalmo
Tetragonopterus
ADAPTIVE
BRANCHING OF
CARNIVOROUS
CHARACINS
After Gregory and Conrad. 1938
Moenkhausia
Cheirodon
CHEIRODONTINAE

Fig. 9.47

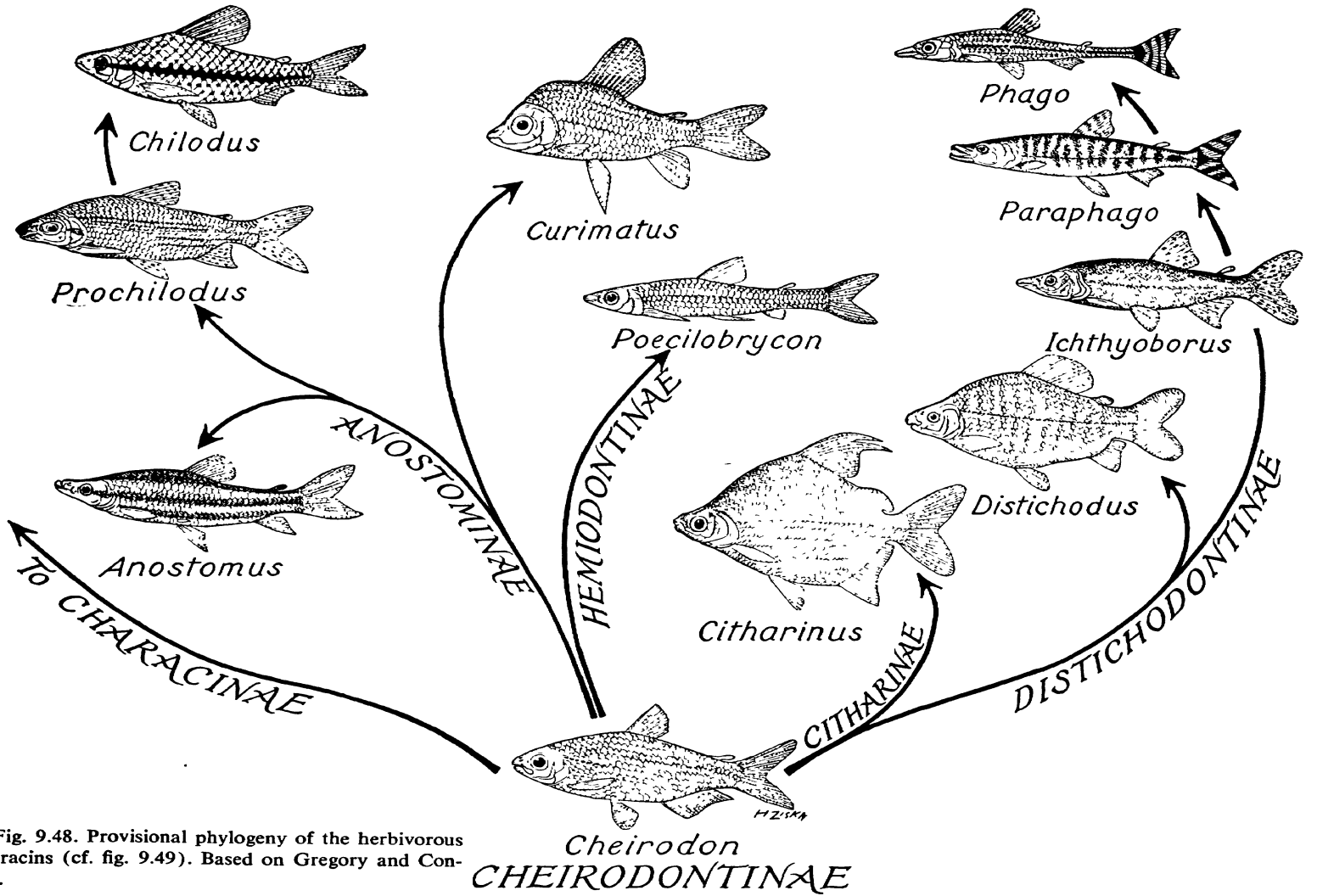


Fig. 9.48. Provisional phylogeny of the herbivorous characins (cf. fig. 9.49). Based on Gregory and Conrad.

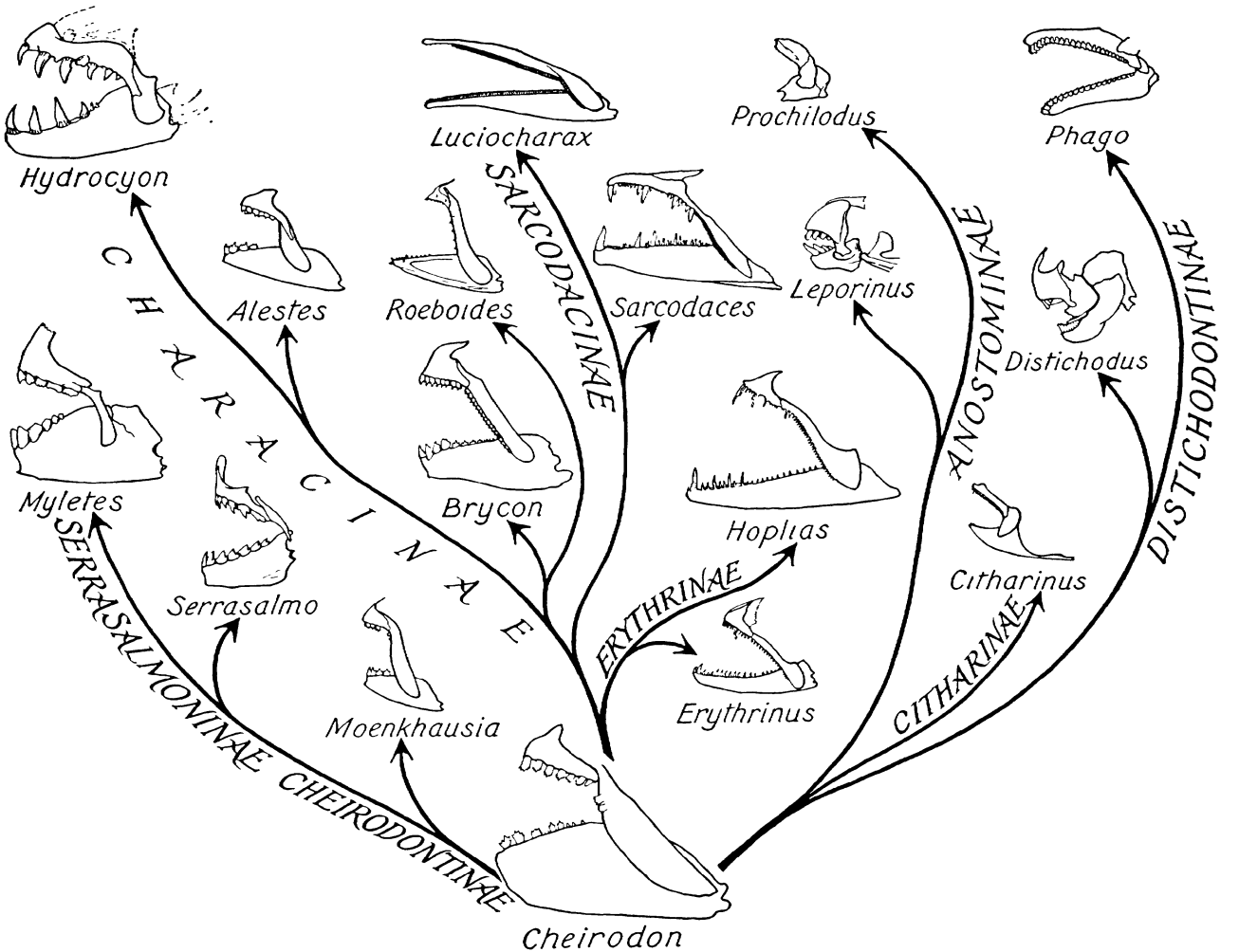


Fig. 9.49. Adaptive branching of the dentition in the subfamilies of Characins. Based on Gregory and Conrad.

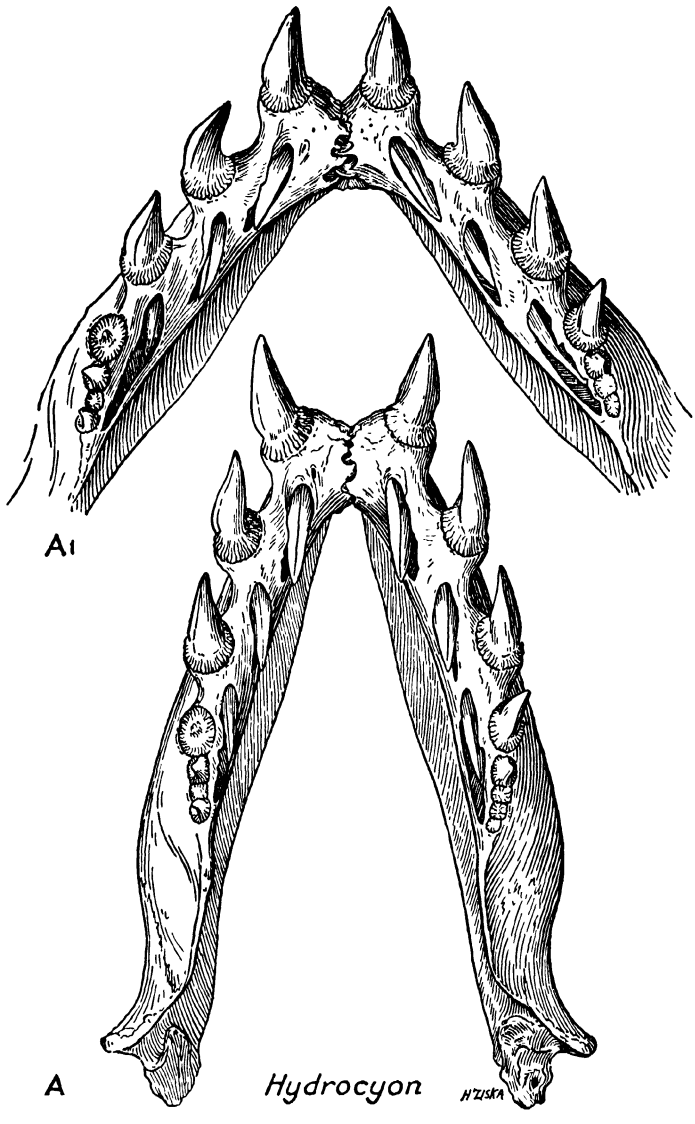


Fig. 9.50. Lower jaw of a large African Characin, with complex hinge at anterior end. After Gregory and Conrad.

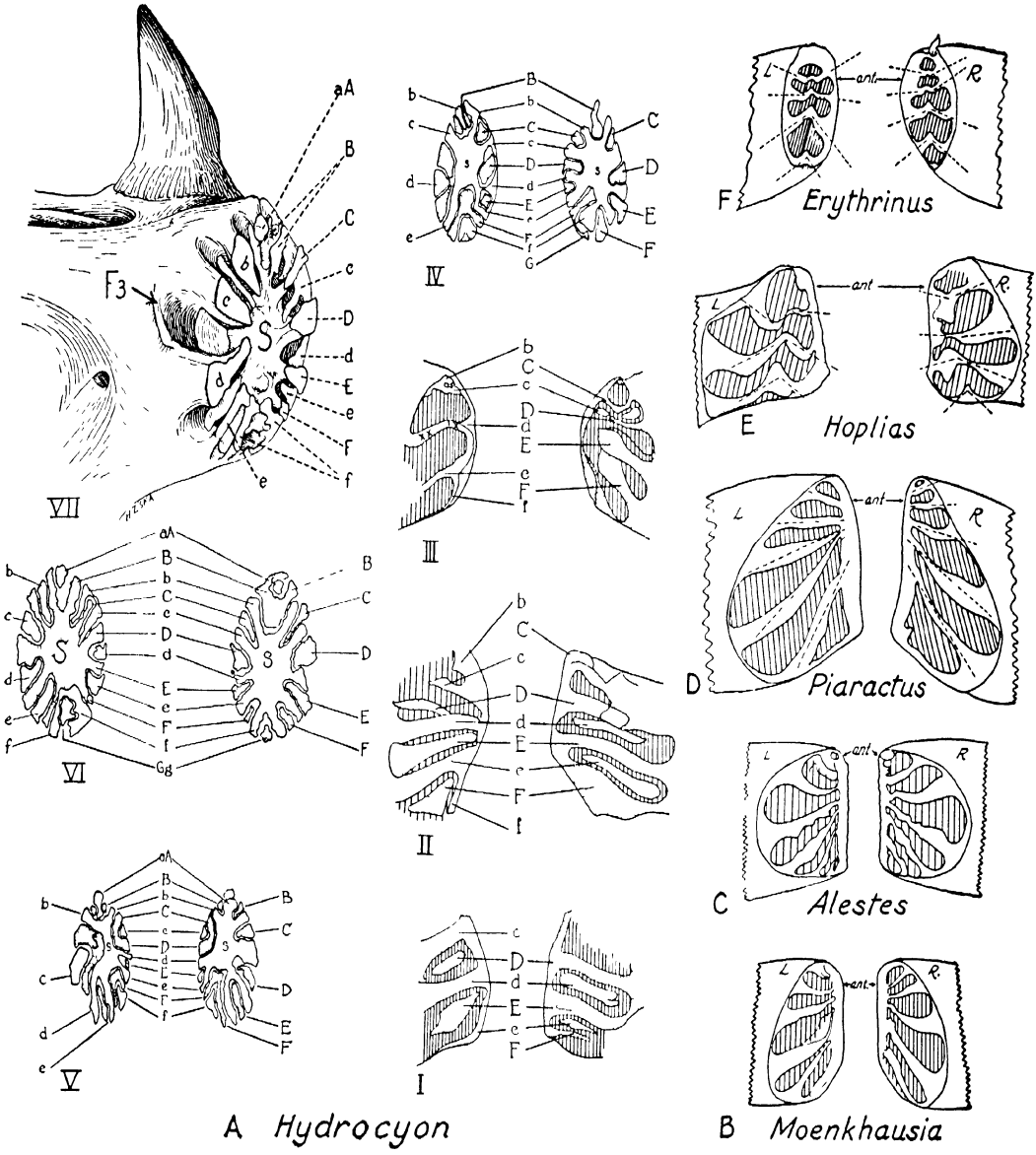


Fig. 9.51. Growth stages of jaw-hinge in *Hydrocyon*, with adult hinges of other genera. After Gregory and Conrad (1937). Capital letters and shaded or stippled areas represent parts of the right half of the mandible; lower case letters and light unshaded areas belong to the left half. In I, II, III, the vertical hatchings indicate cavities.

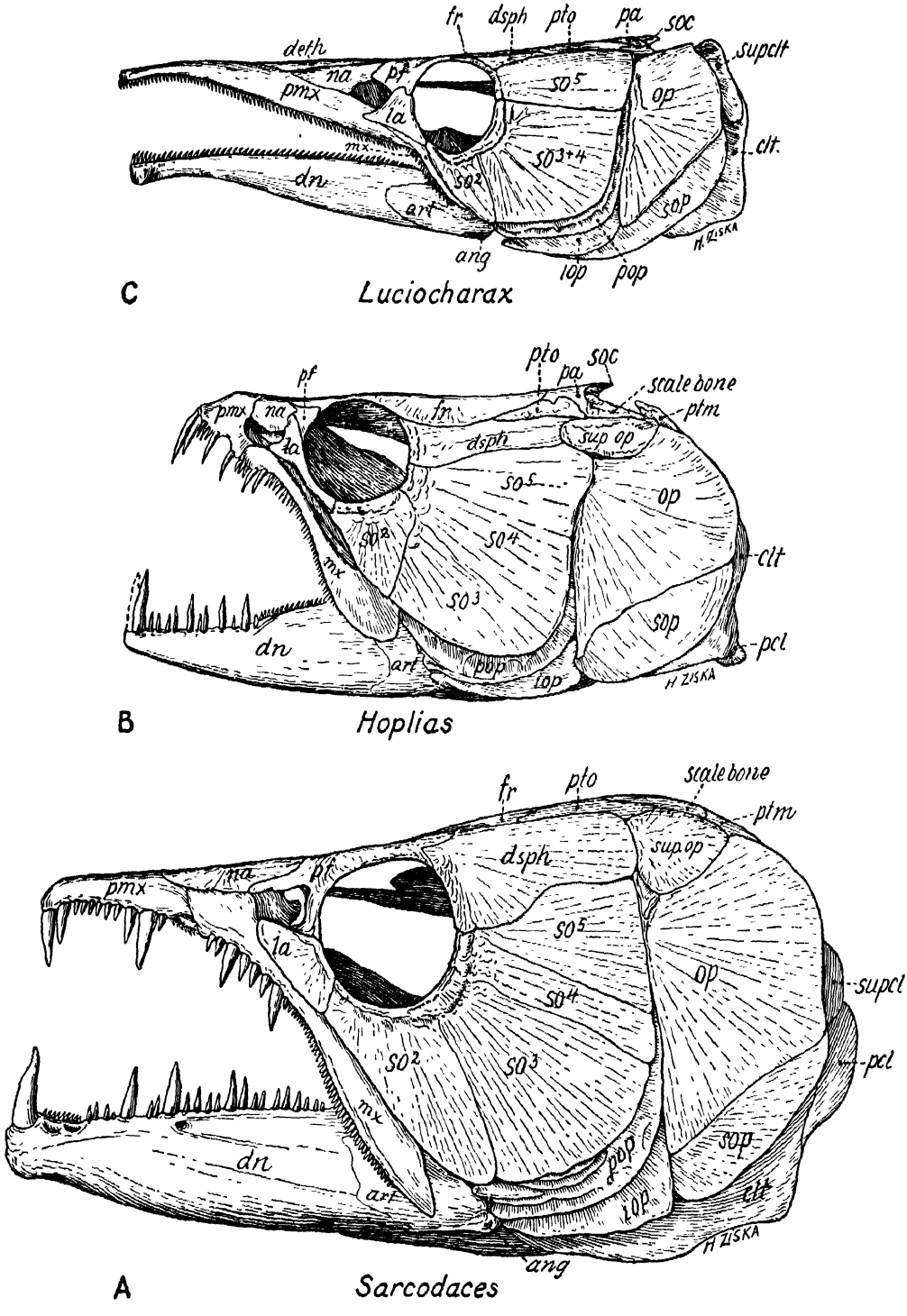


Fig. 9.52. Skulls of pike-like characins of the subfamilies Sarcodacinae (A,C), Erythrinae (B). After Gregory and Conrad (1938).

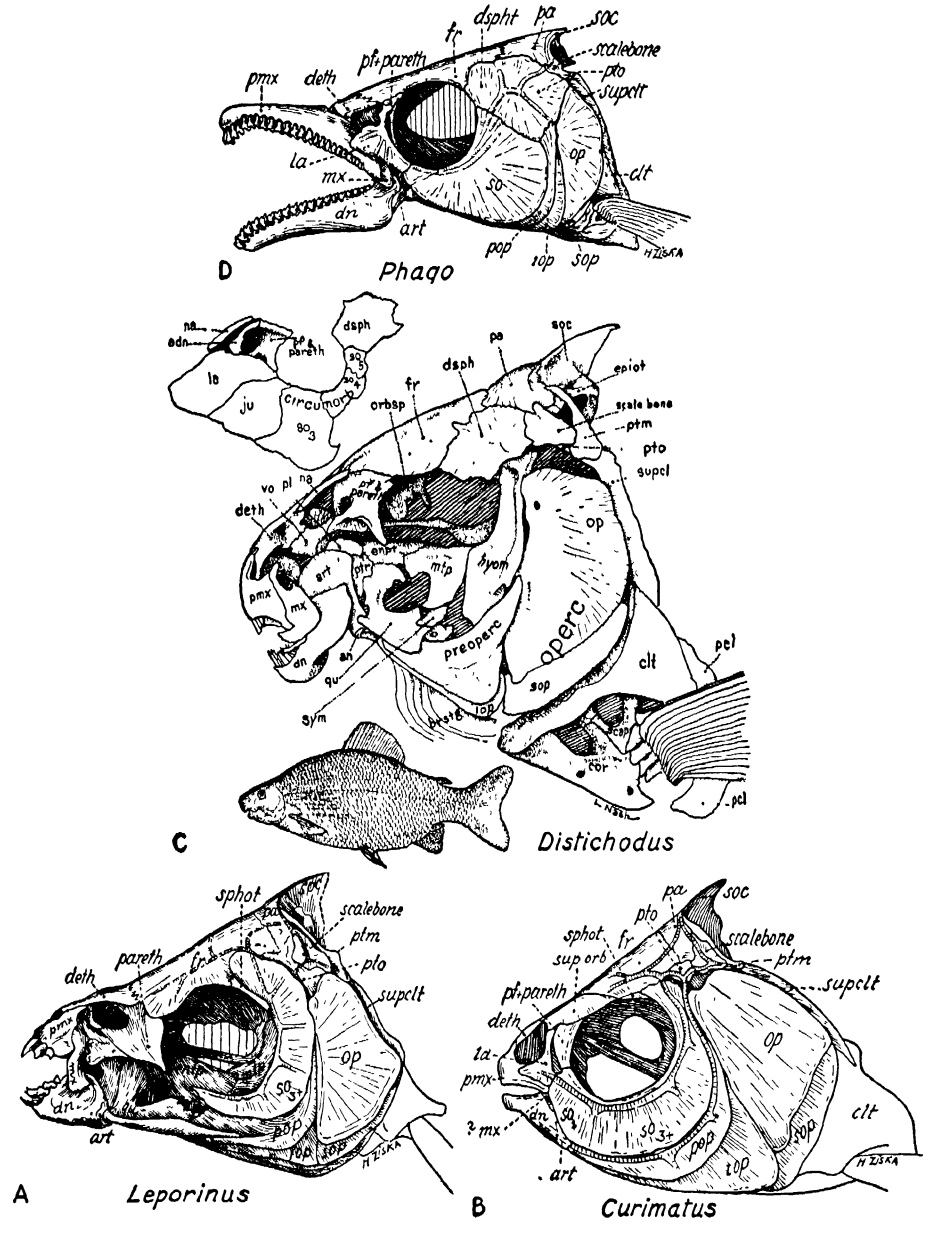


Fig. 9.53. Skulls and dentitions of the nibbling Characins of the subfamilies Anostomatinae (A, B) and Distichodontinae (C, D). After Gregory and Conrad.

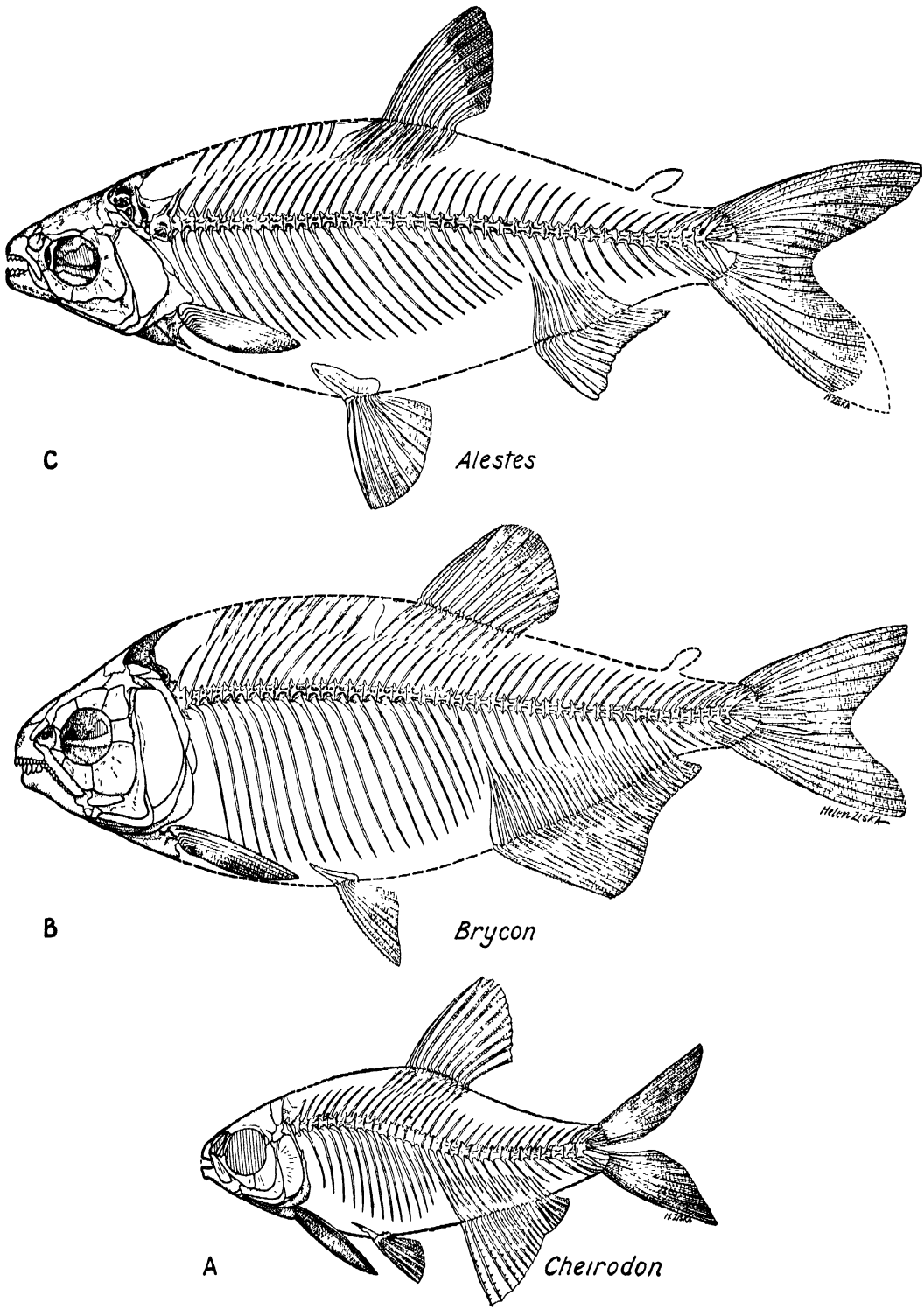


Fig. 9.54. Close relationship in skeletal construction of South American (A,B) and African (C) Characins. After Gregory and Conrad.

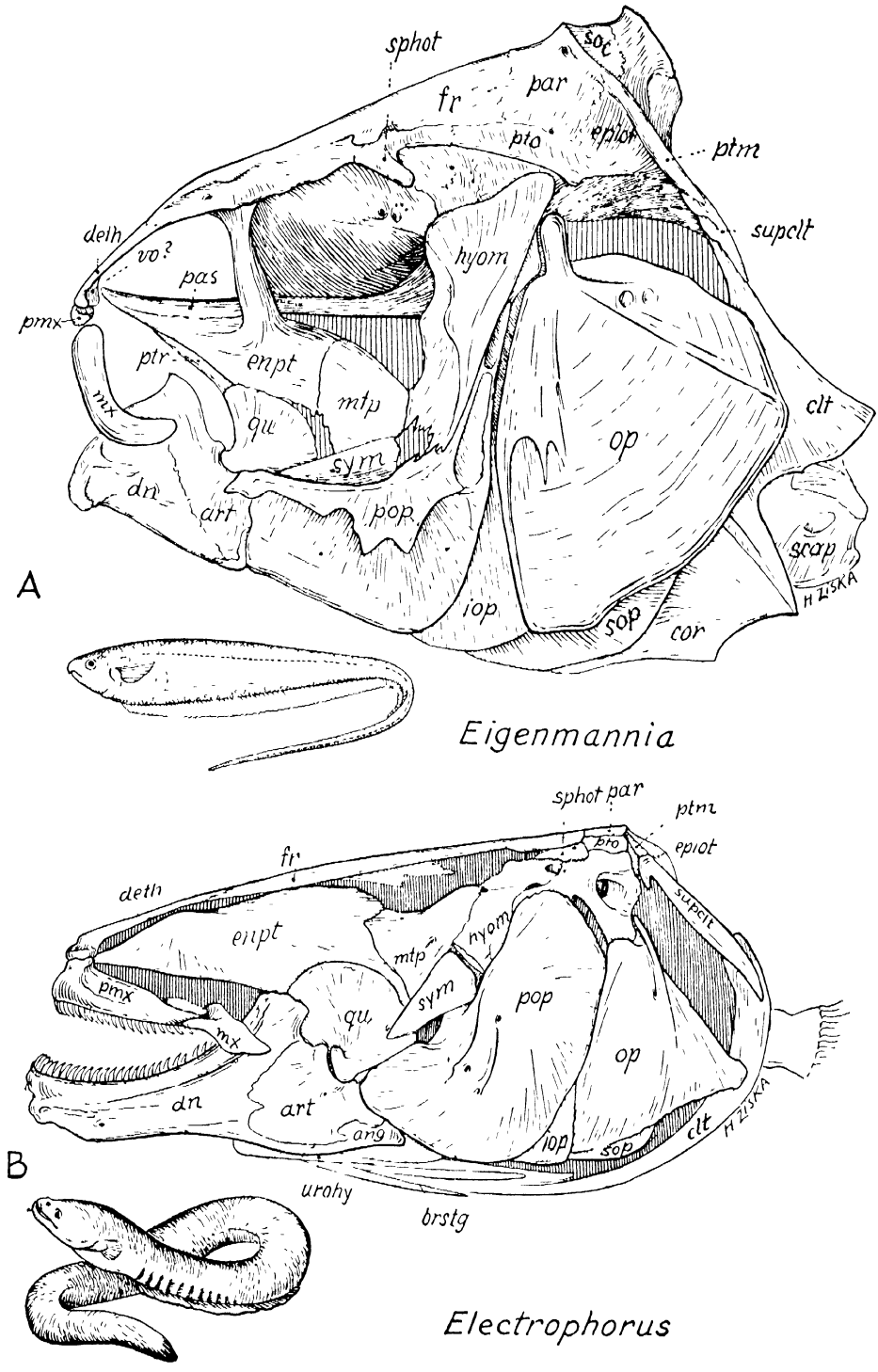


Fig. 9.55. Eel-like Characins. A, after Ellis; B, original.

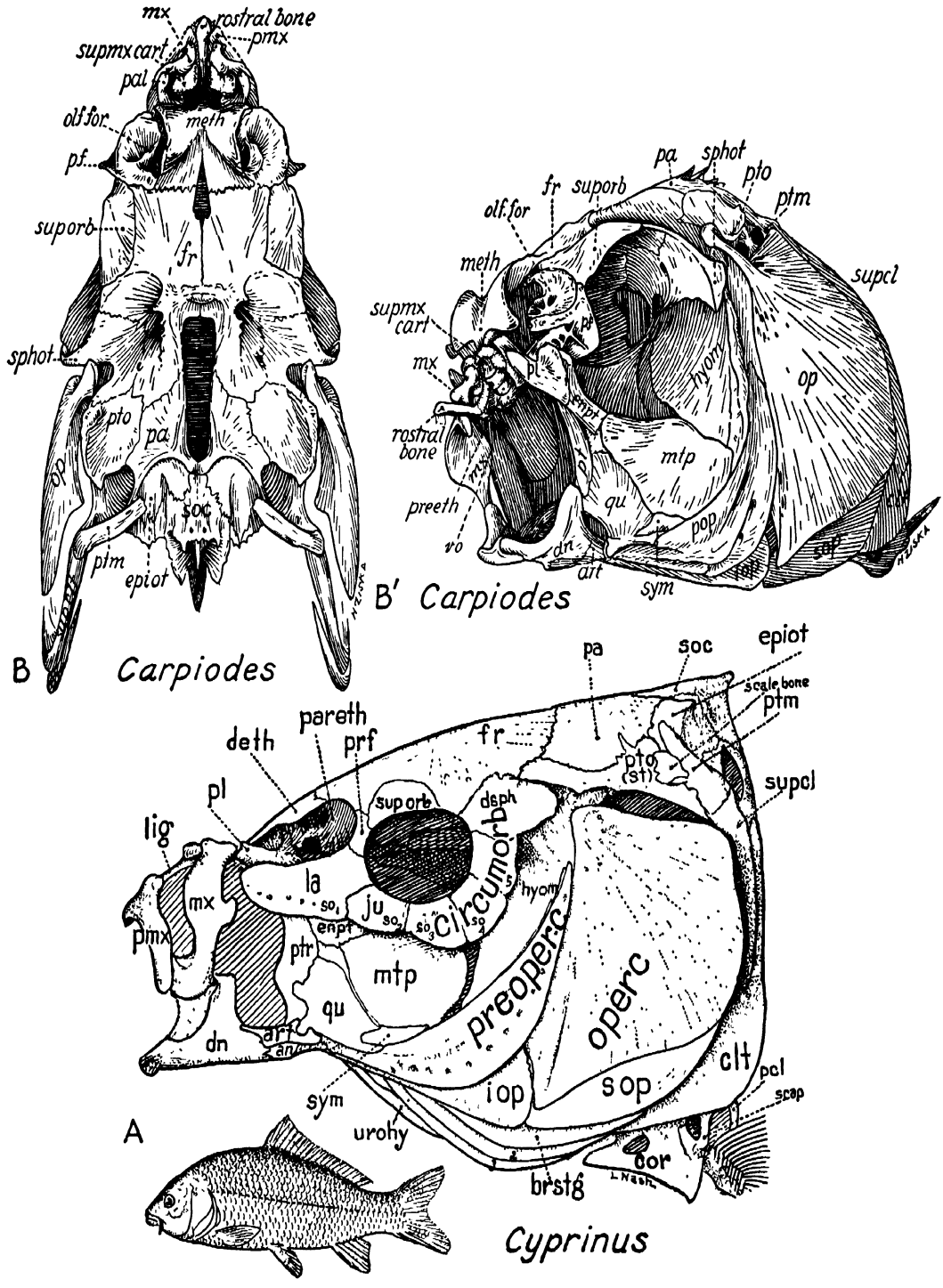
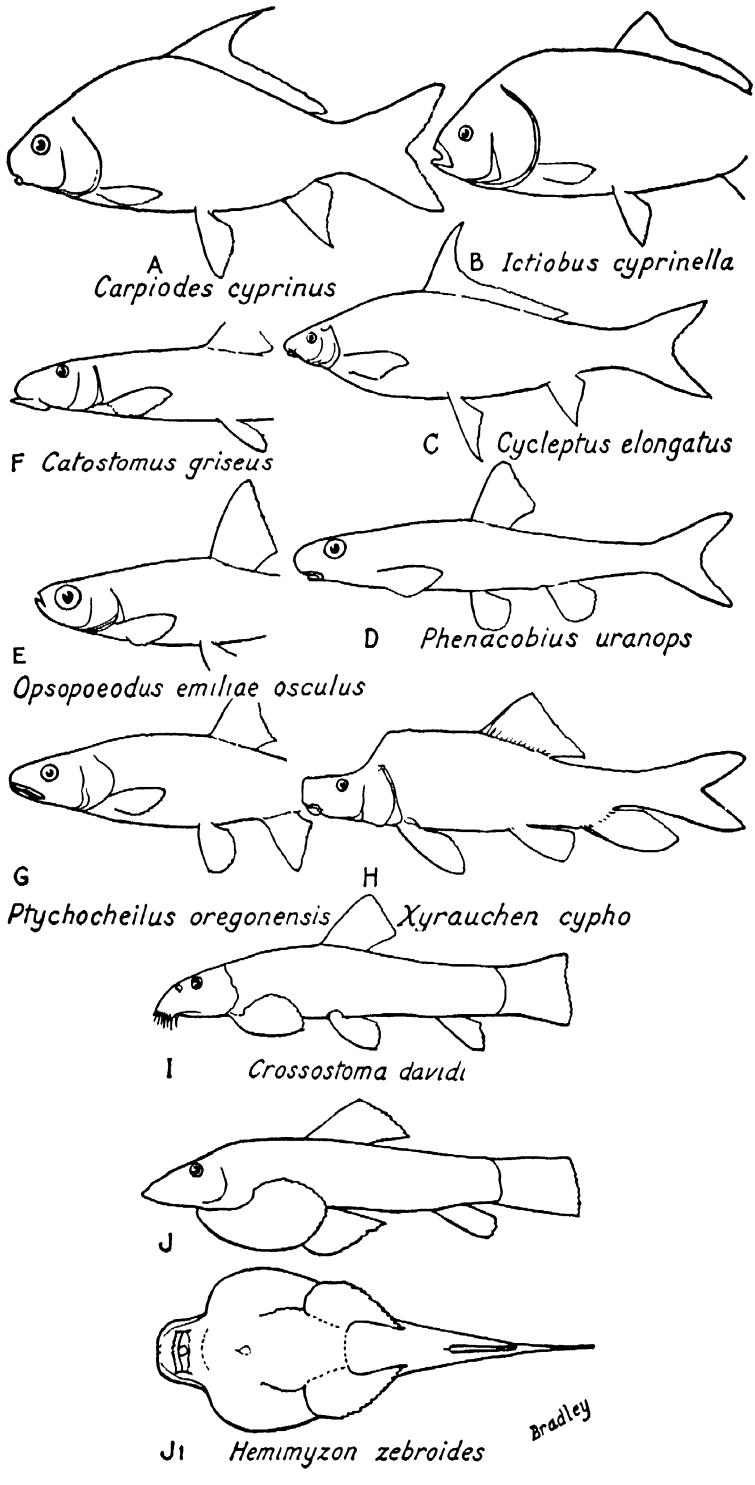


Fig. 9.56. Two American Carps or suckers and their protrusile jaws (for *Cyprinus* read *Ictiobus*).



Figs. 9.57, 58. Range in form of the body, head and mouth in American Cyprinoids and in stream- and bottom-living loaches (I, J). Based on figures by Jordan and Evermann (1896).

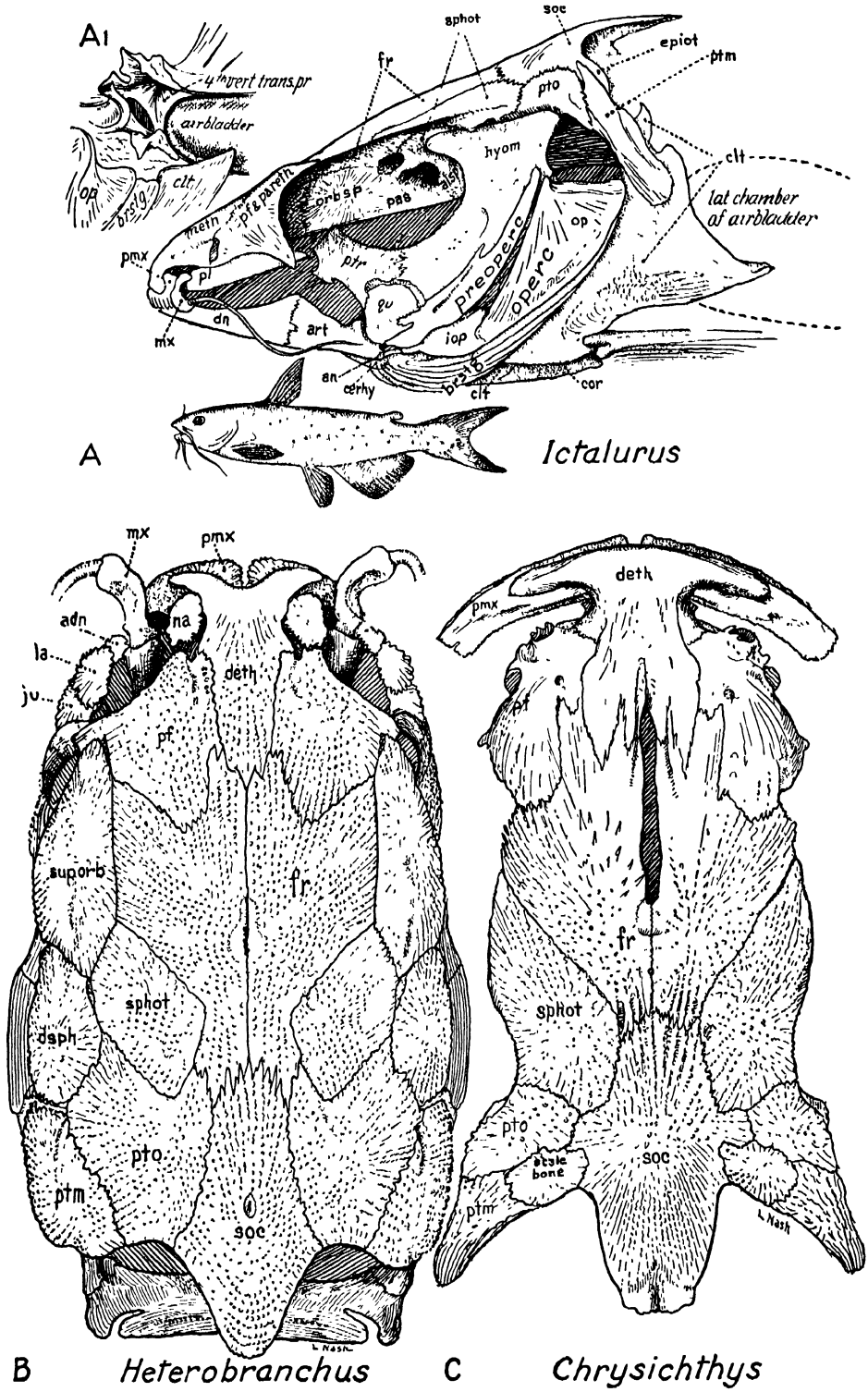


Fig. 9.59. Catfish skulls.

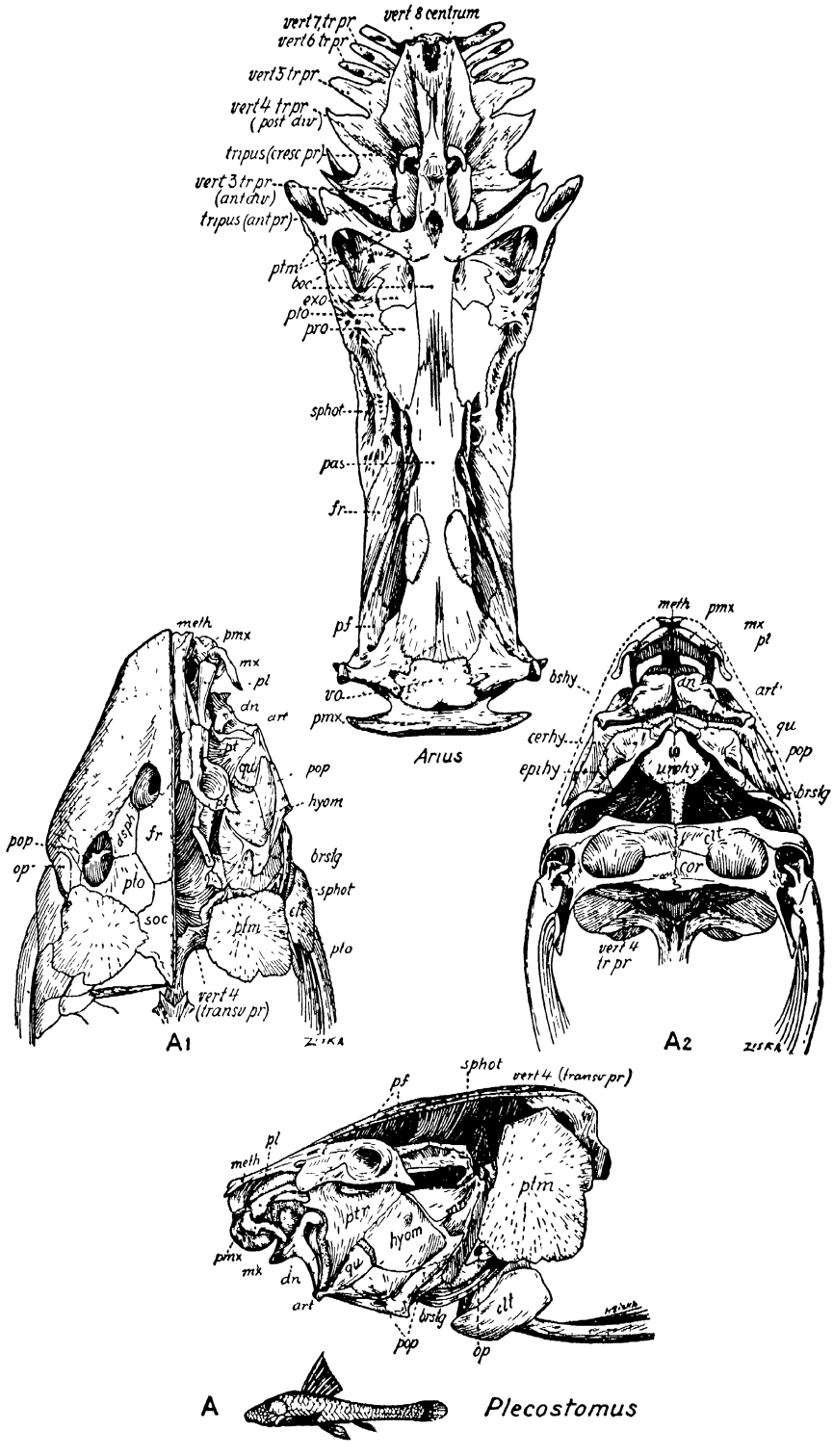


Fig. 9.60 (top). Under side of the skull of the "crucifix fish."

Fig. 9.61. An armored Catfish, showing secondary ossicles covering parts of skull.

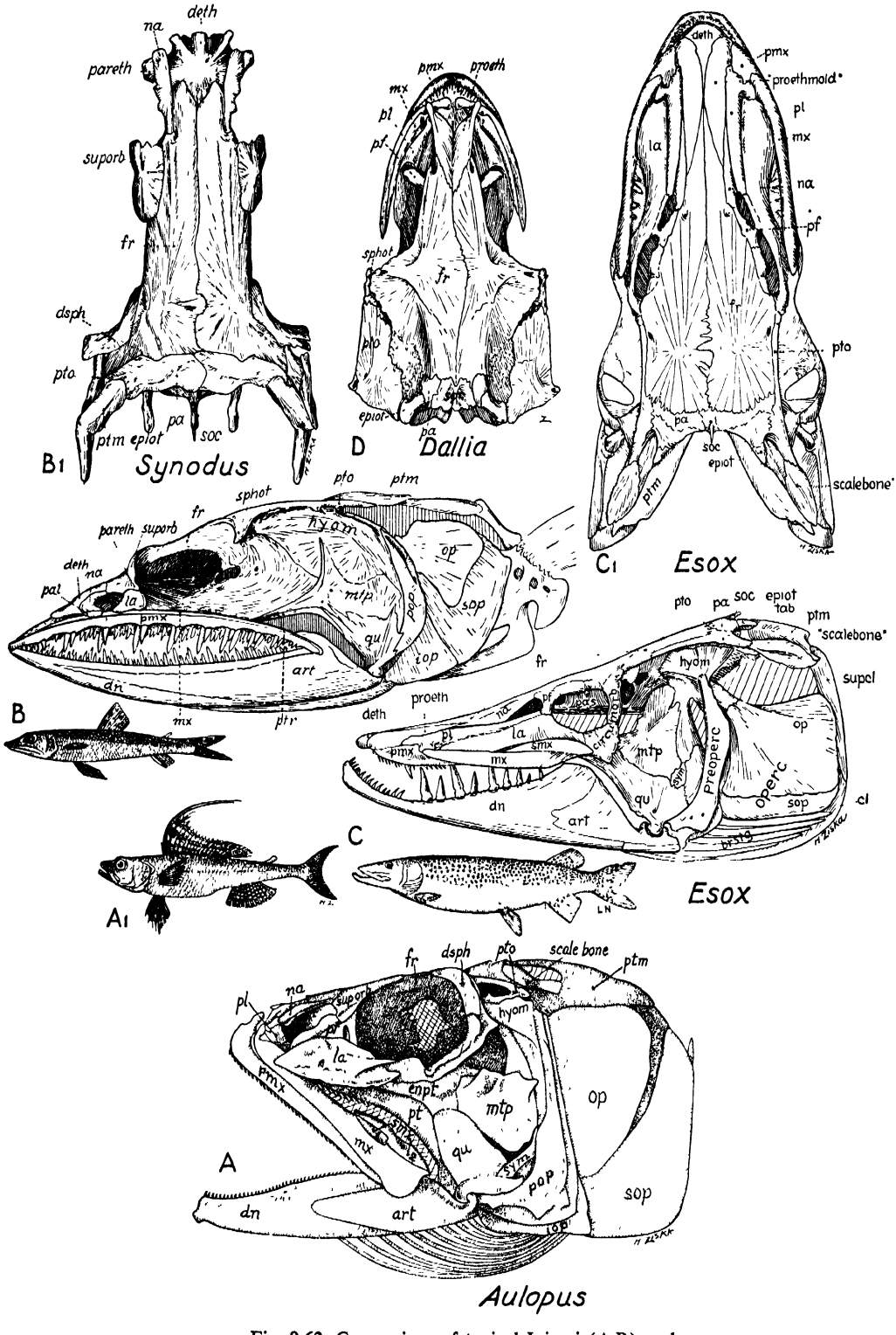


Fig. 9.62. Comparison of typical Iniomi (A,B) and Haplomi (C,D).

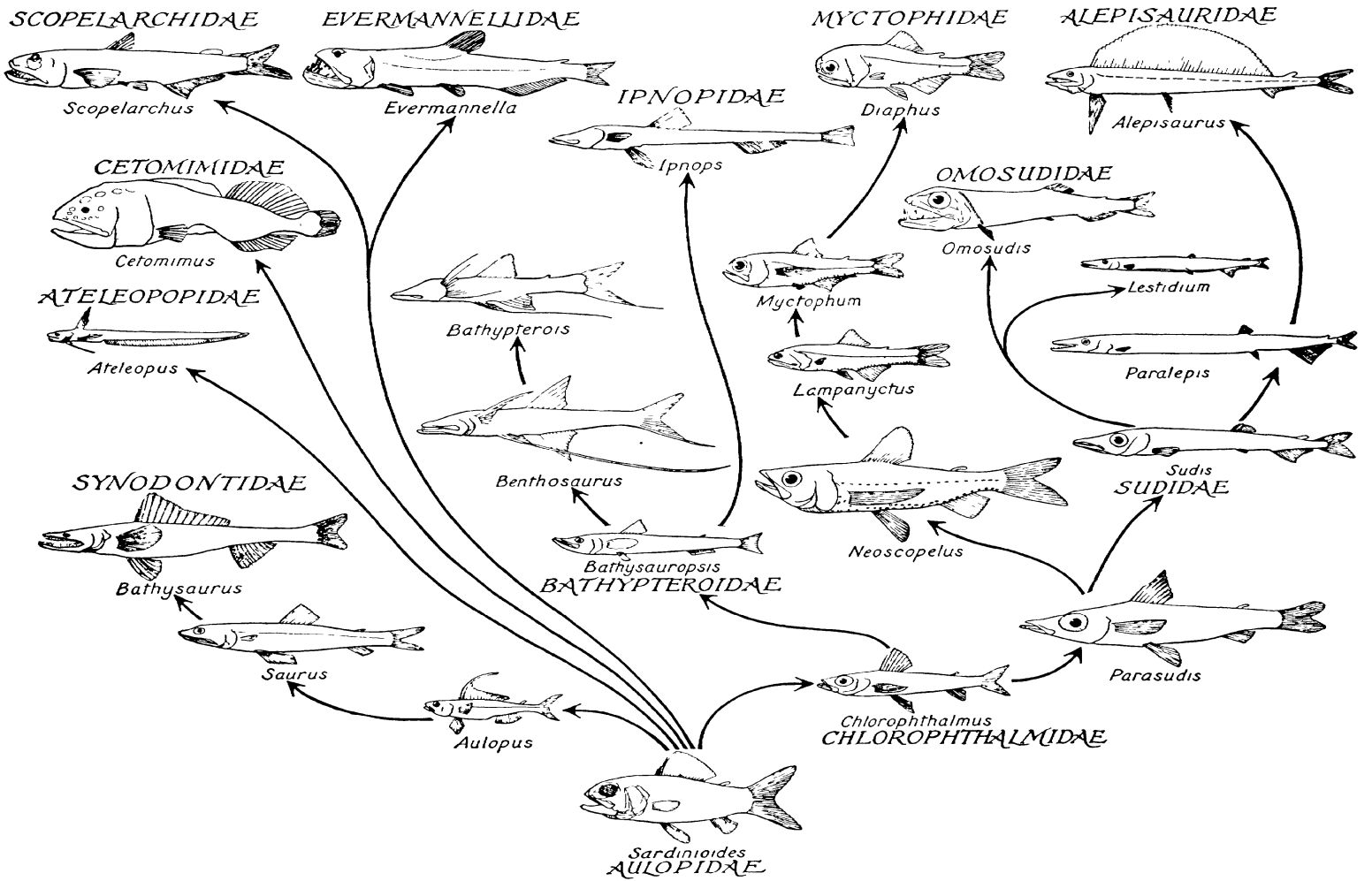
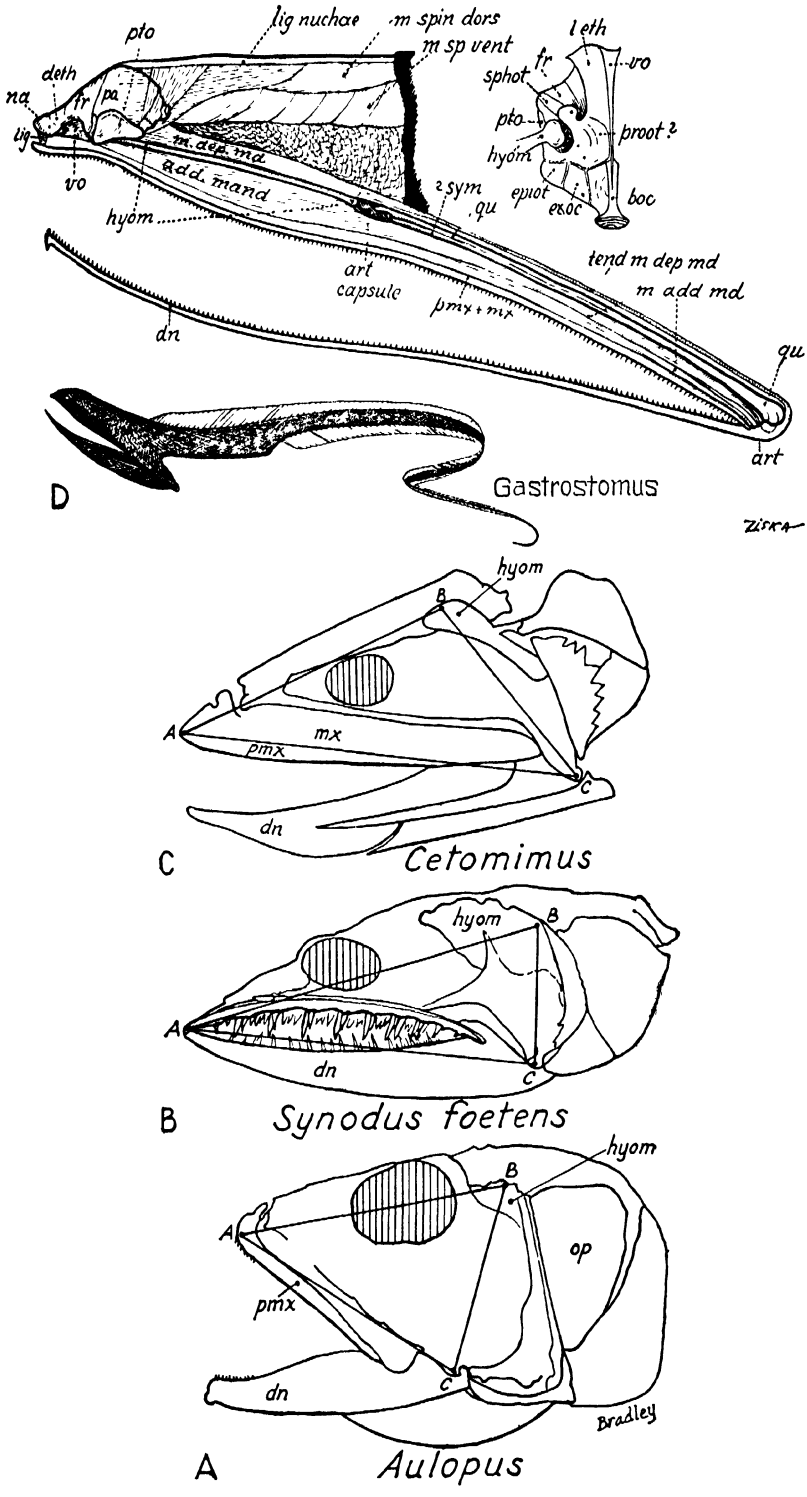


Fig. 9.63. Provisional phylogeny of the Iniomi. After Gregory and Conrad (1936)



Figs. 9.64, 65. Climax of the scoop-net technique. Four grades (A–D) in the backward prolongation of the jaws and suspensorium (*hyom*). In B, the point *B* should have been placed over the *m* in *hyom*. D, from Gregory; data from Nusbaum-Hilarowicz, 1923.

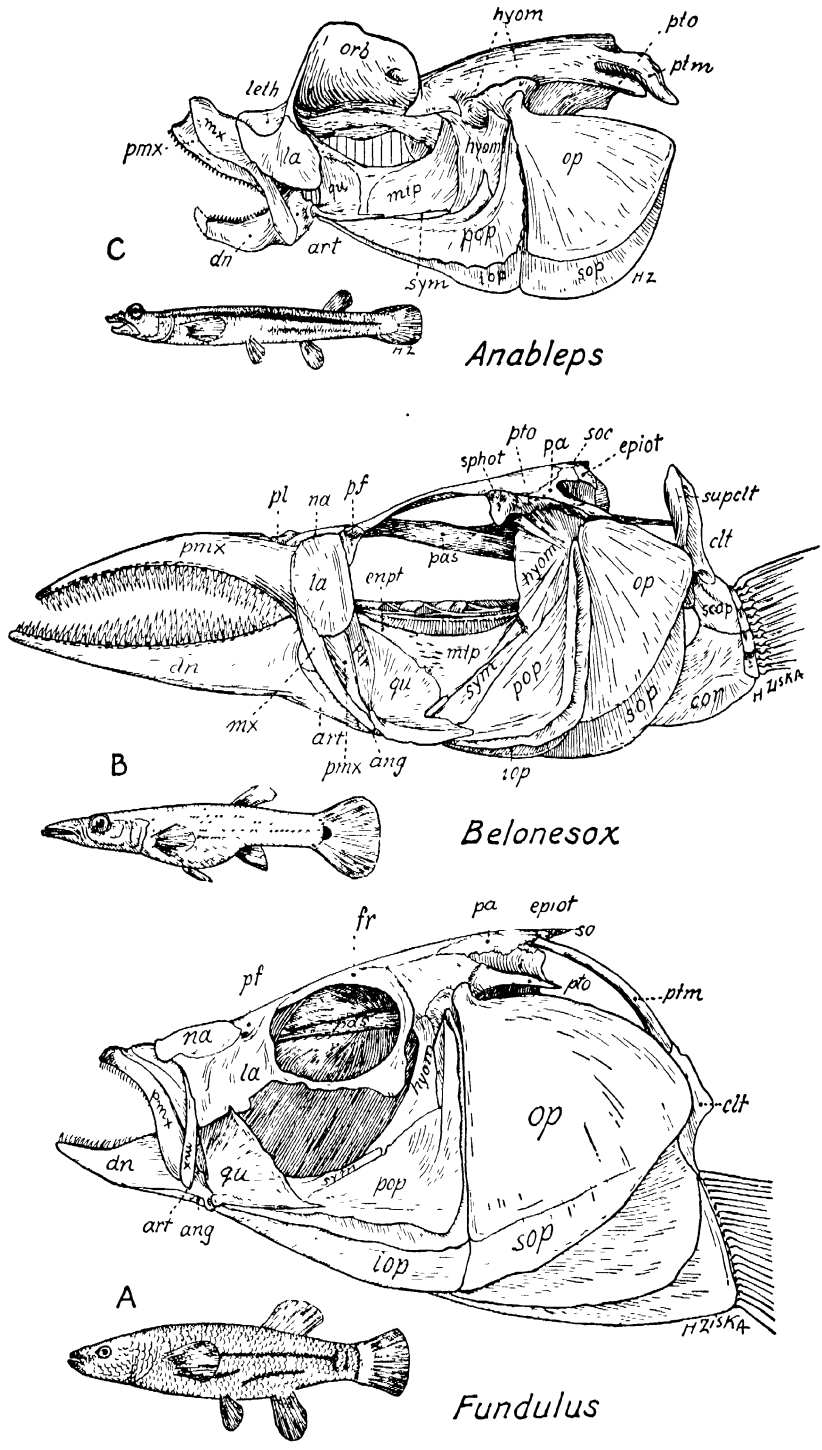


Fig. 9 66. A rather primitive (A) and two diversely specialized (B,C) members of the "toothed carp" order (Microcyprini).

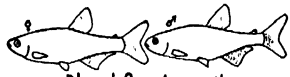
A SIMPLIFIED PICTORIAL CLASSIFICATION

ORDER OSTARIOPHYSI — Characins, Carps and Catfishes

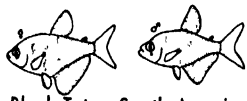
Family Characidae
Characins



Copeina, Brazil
Copeina guttata (Steindachner)



Blood fin, Argentina
Aphyocharax rubripinnis Pappenheim

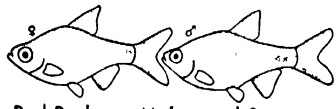


Black Tetra, South America
Gymnocorymbus ternetzi (Boulenger)

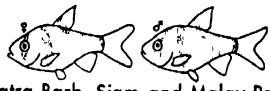
Family Cyprinidae
Carps



Zebra fish, India
Brachydanio rerio (Hamilton-Buchanan)



Red Rasbora, Malay and Sumatra
Rasbora heteromorpha Duncker



Sumatra Barb, Siam and Malay Pen.
Barbus partipentazona Fowler

Family Callichthyidae
Catfishes



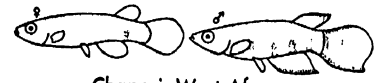
Armored catfish, Trinidad
Corydoras aeneus (Gill)

ORDER CYPRINODONTES — Killifishes, Top-minnows, etc.

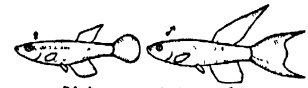
Family Cyprinodontidae
Egg-laying tooth-carps



Top-minnow, S. E. United States
Fundulus chrysotus Holbrook



Chaperi, West Africa
Epiplatys chaperi (Sauvage)



Bivittatum, West Africa
Aphyosemion bivittatum (Loennberg)

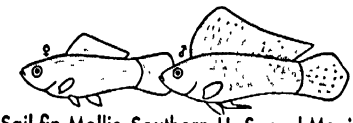
Family Poeciliidae
Live-bearers



Moonfish, Mexico
Platypoecilus maculatus Guenther



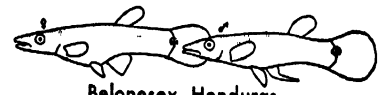
Sword tail, Mexico
Xiphophorus helleri Heckel



Sail-fin Mollie, Southern U. S. and Mexico
Mollienisia latipinna Le Sueur



Guppy, Northern South America
Lebistes reticulatus (Peters)



Belonesox, Honduras
Belonesox belizanus Kner

Fig. 9.67a, b. Killifishes, live-bearers and other aquarium pygmies. From Gregory and La Monte, arranged and drawn by Donald Marcy.

OF THE MORE COMMON AQUARIUM FISHES

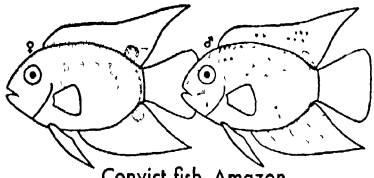
ORDER PERCOMORPHI — ORDER LABYRINTHICI

Cichlids, Nandids, etc. — Anabantids, etc.

Family Cichlidae
Cichlids



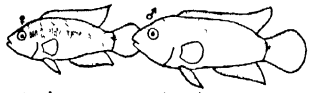
Mouthbreeder, Egypt
Haplochromis multicolor (Hilgendorf)



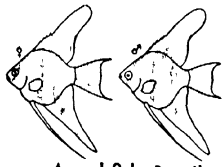
Convict fish, Amazon
Cichlasoma severum (Heckel)



Flag Cichlid, Brazil
Cichlasoma festivum (Heckel)

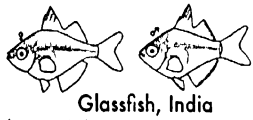


Jack Dempsey, South America
Cichlasoma biocellatum Regan



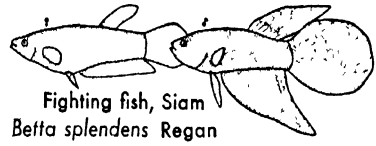
Angel fish, Brazil
Pterophyllum scalare
Cuvier and Valenciennes

Family Ambassidae Ambassids

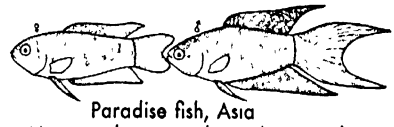


Glassfish, India
Ambassis lala (Hamilton-Buchanan)

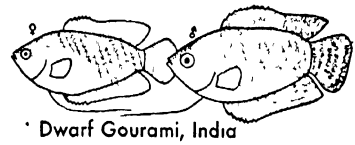
Family Anabantidae
Anabantids



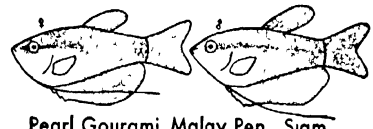
Fighting fish, Siam
Betta splendens Regan



Paradise fish, Asia
Macropodus opercularis (Linnaeus)



Dwarf Gourami, India
Colisa lalia (Hamilton-Buchanan)



Pearl Gourami, Malay Pen., Siam
Trichogaster leeri (Bleeker)



Kissing, Gourami, Malay region
Helostoma temminck Cuvier and Valenciennes



Fig. 9.67b

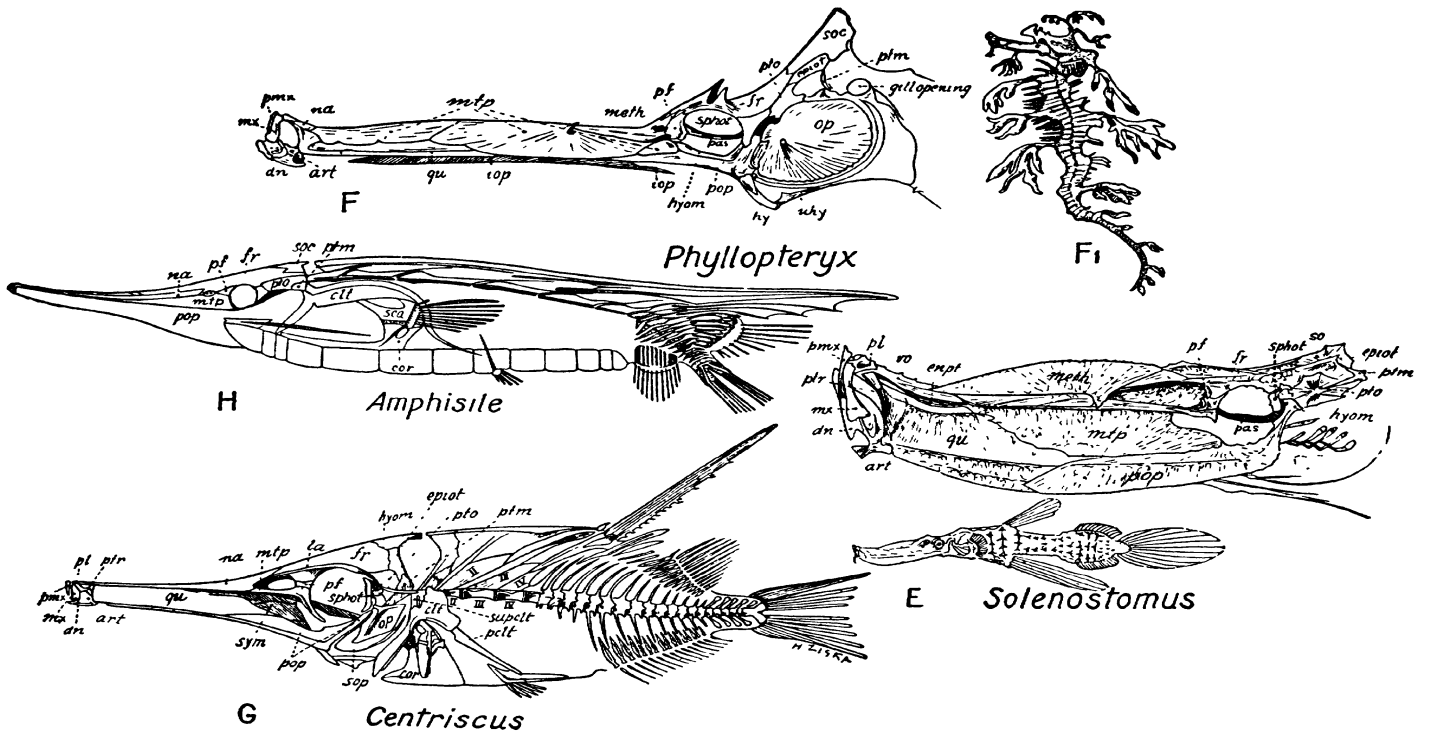
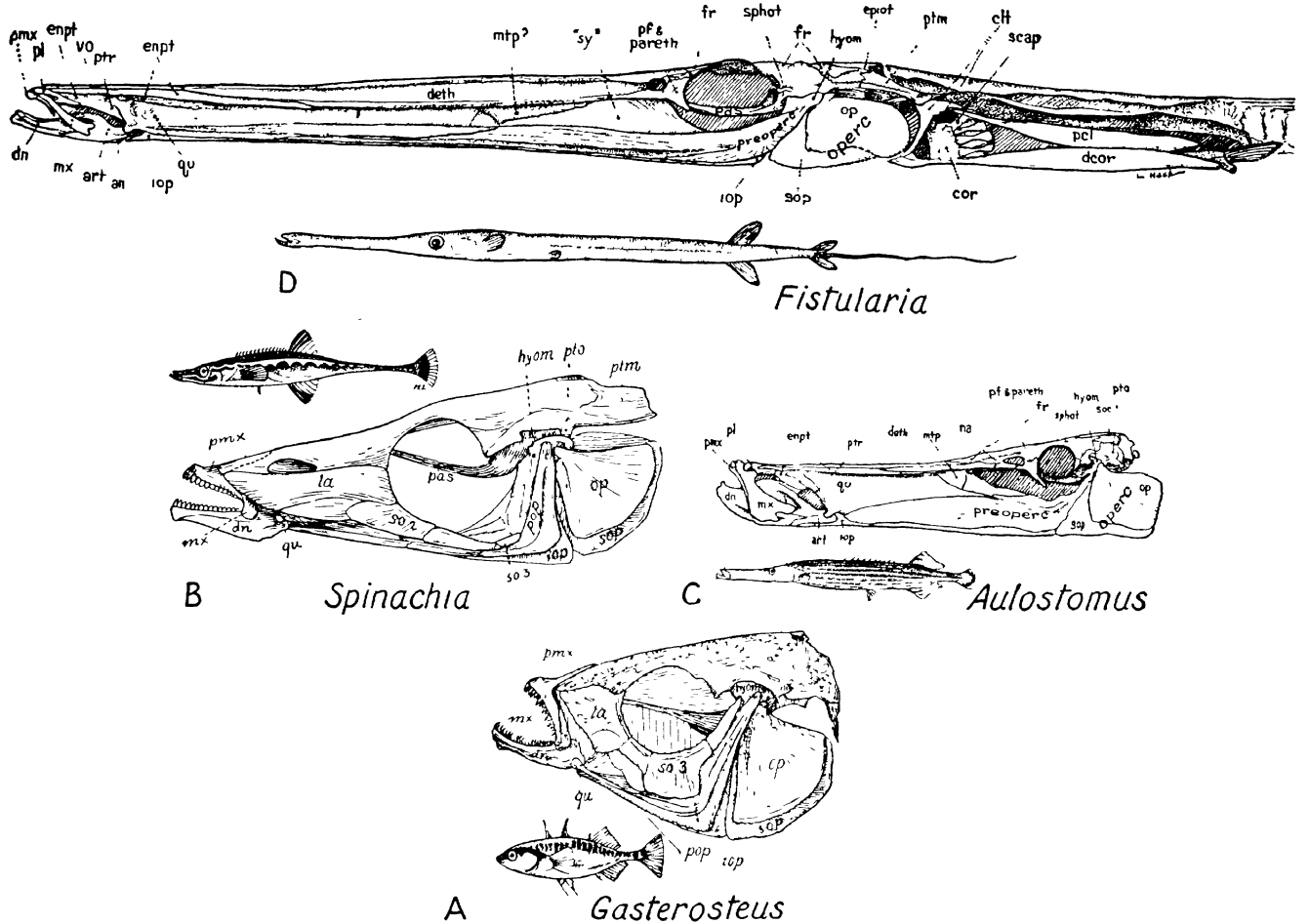


Fig. 9.68



Figs. 9.68, 69. From Sticklebacks (A,B) to flute-mouths (C,D), sea-horses (E,F), and shrimp fishes (G, H). After Gregory.

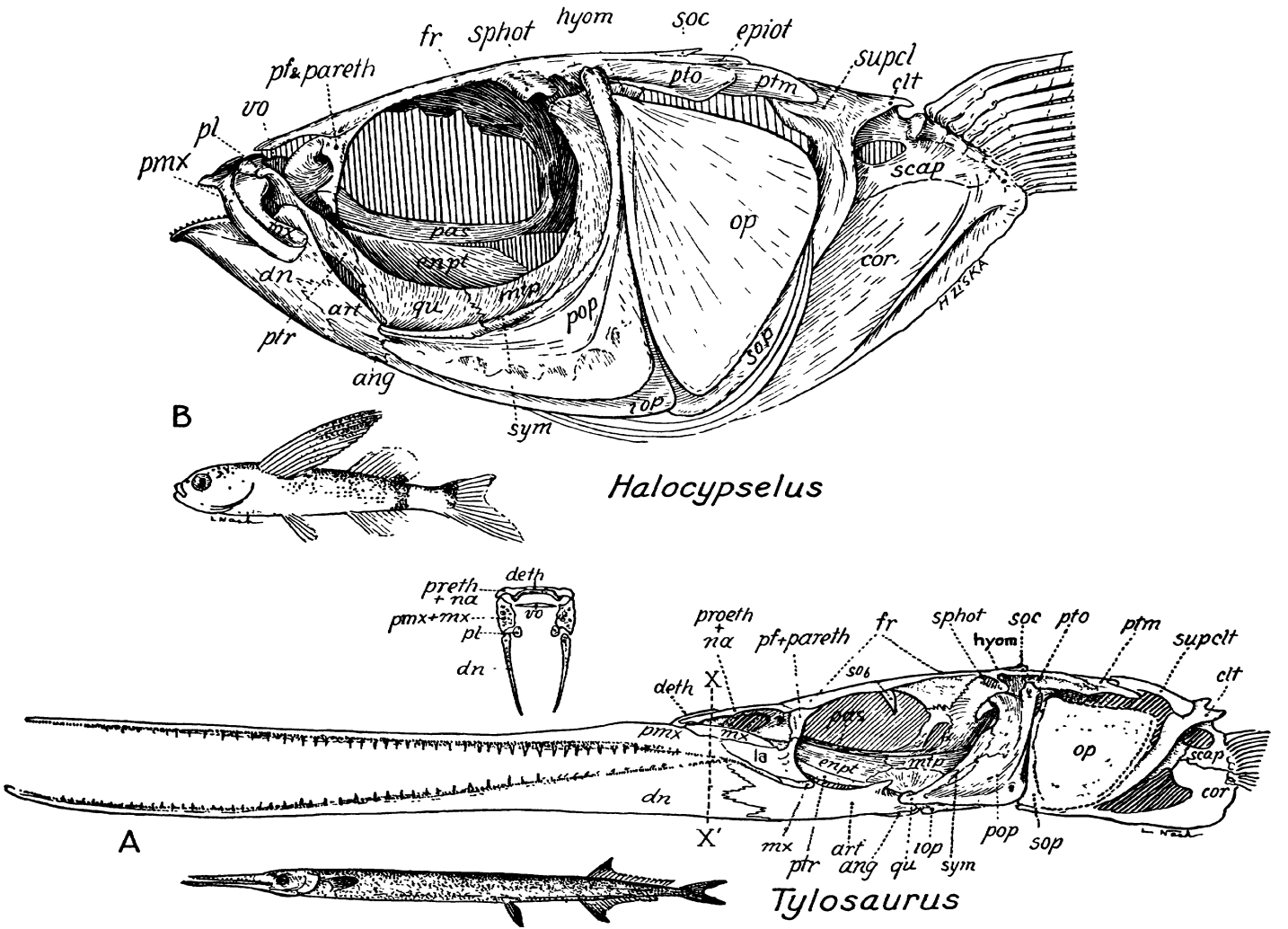

fr
sphot
hyom
soc
epiot
supcl
clt
pf+pareth
pto
ptm
vo
pl
pmx
scap
op
pas
cor
mx
enpt
dn
art
qu
mtp
pop
ptr
sop
ang
iop
sym
B
Halocypselus
preth + na
deth
pmx+mx
vo
pl
dn
proeth + na
pf+pareth
fr
sphot
soc
pto
ptm
supclt
hyom
clt
sob
deth
X
pas
pmx
mx
la
enpt
mtp
op
scap
cor
dn
X'
mx
art
iop
pop
sop
ptr
ang
qu
sym
A
Tylosaurus

Fig. 9.70

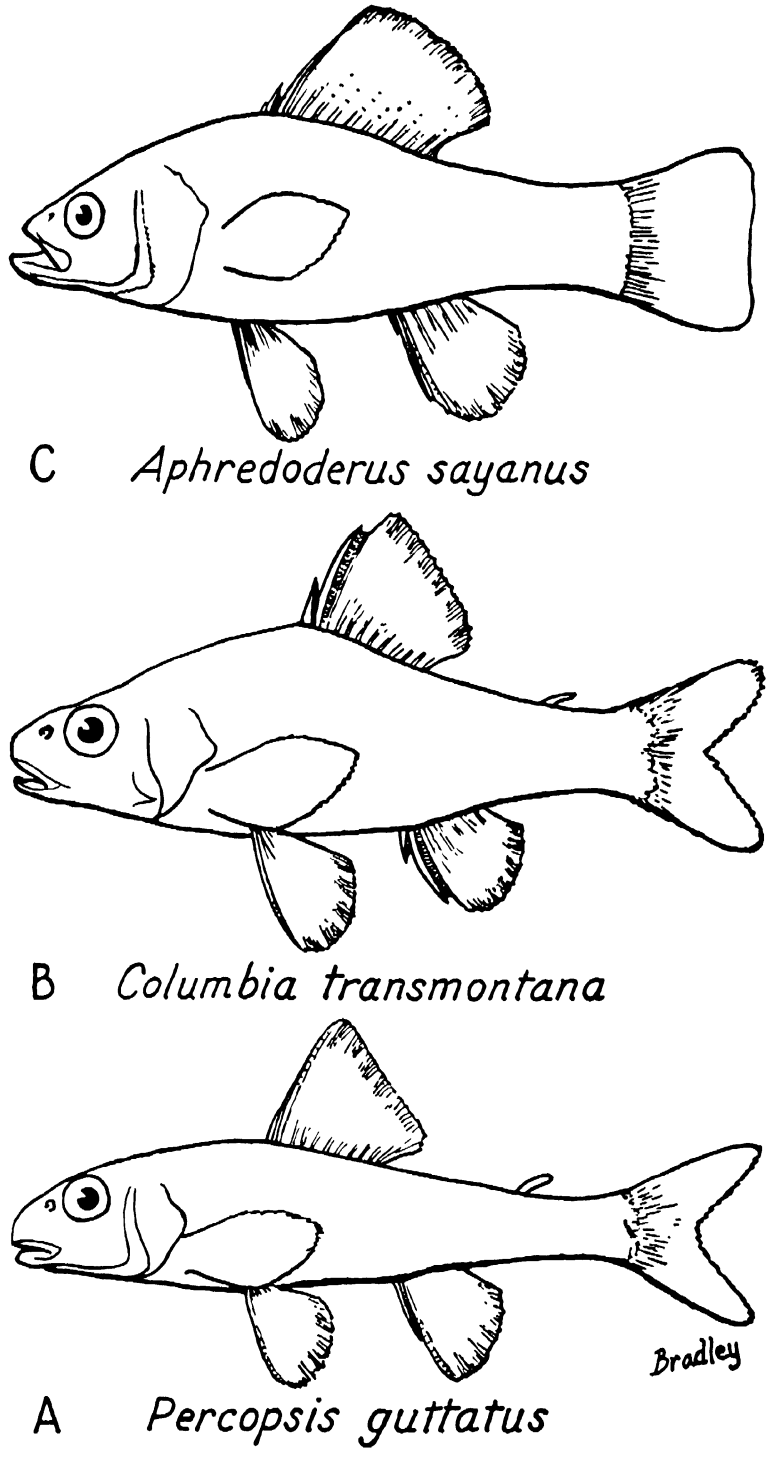


Fig. 9.70 (facing page). Hound fish and flying fish. The skulls are fundamentally similar in spite of extreme difference in length of jaws.

Fig. 9.71. Structural links between soft-rayed and spiny-finned fishes. After Jordan and Evermann.

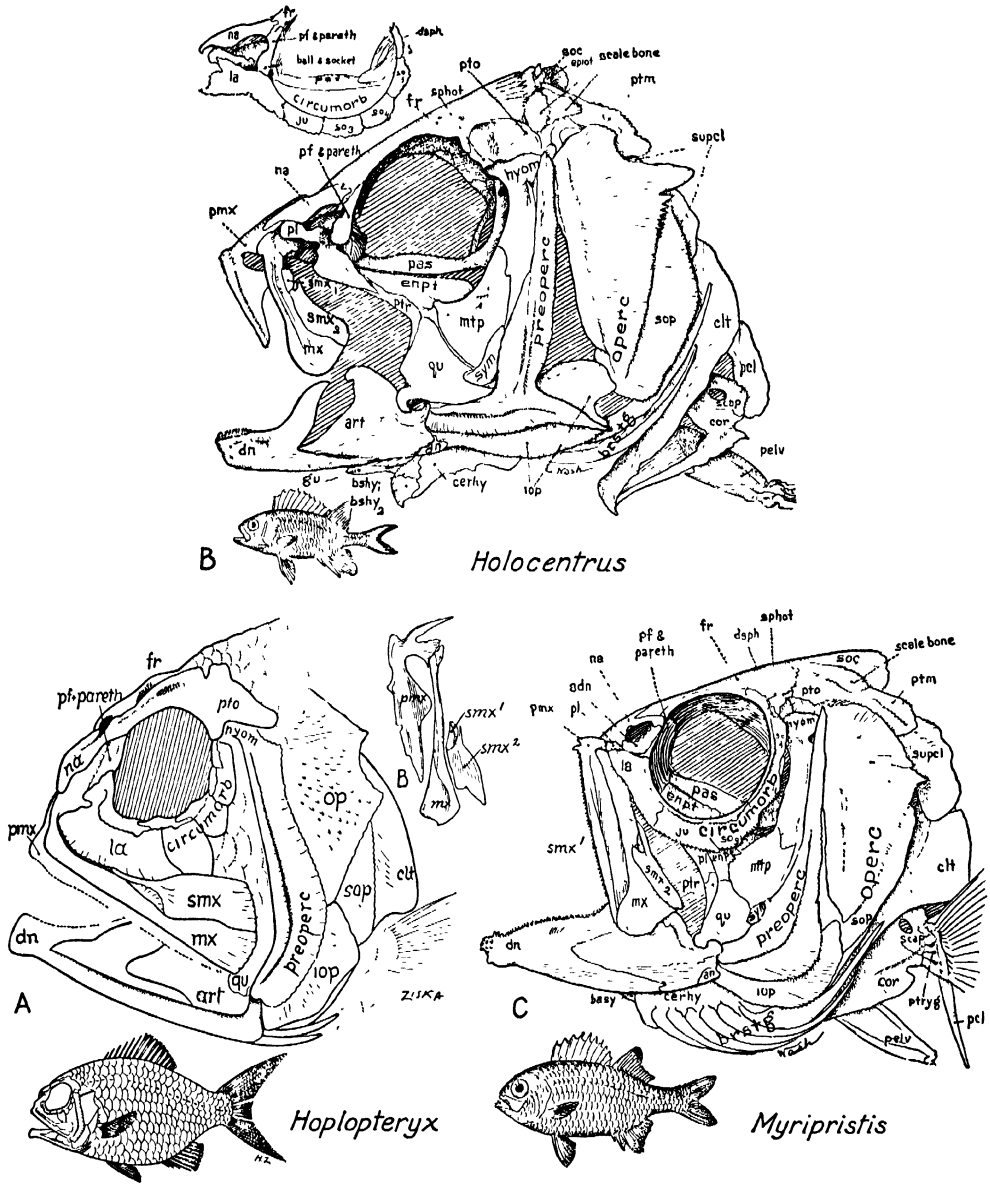


Fig. 9.72. Fossil and recent Berycoids. A, after Smith Woodward; B, C, after Gregory.

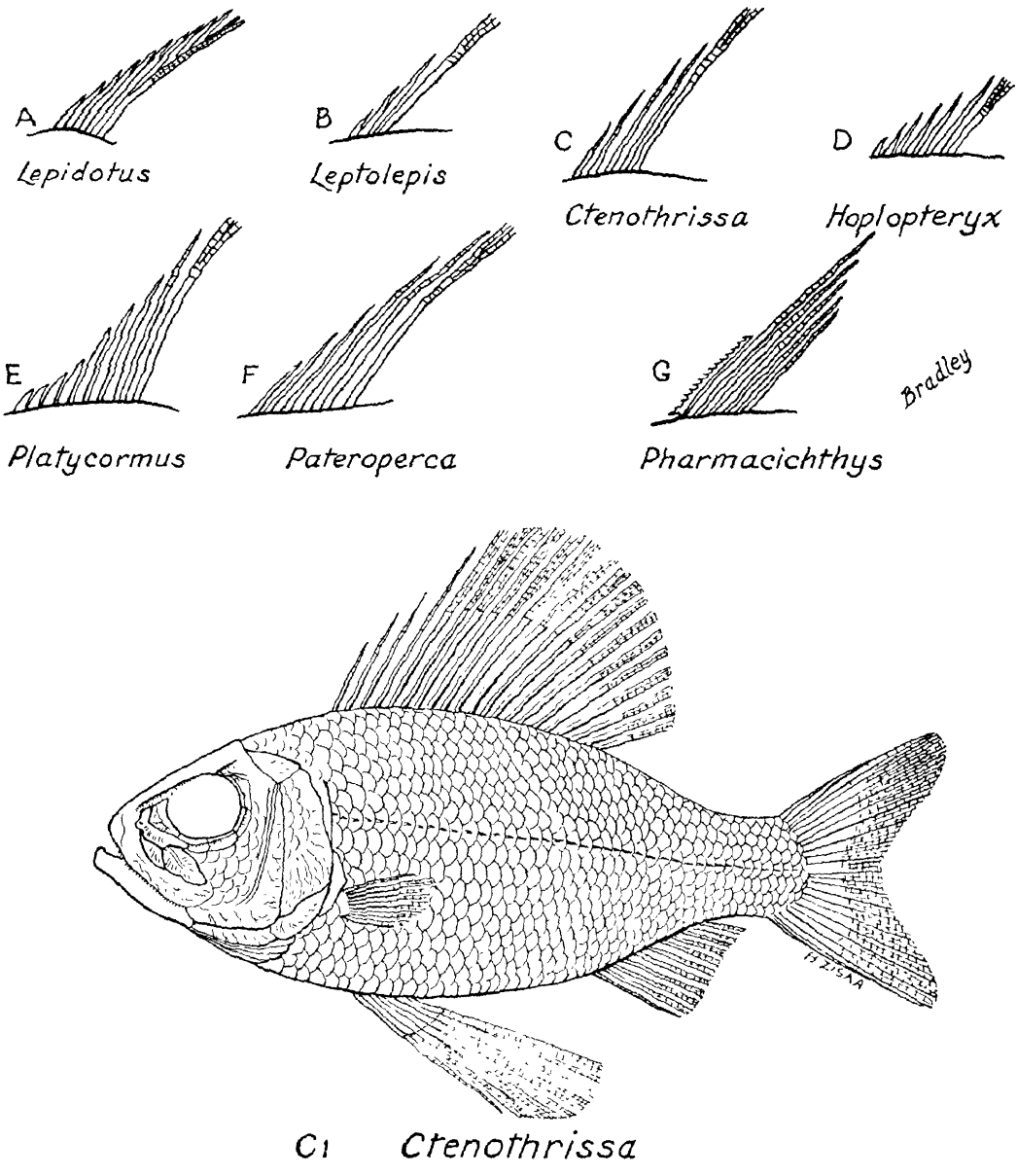


Fig. 9.73. Links between the soft-rayed and the spiny-finned orders, showing origin of spiny rays of dorsal fin from fulera (A,E). After Smith Woodward.

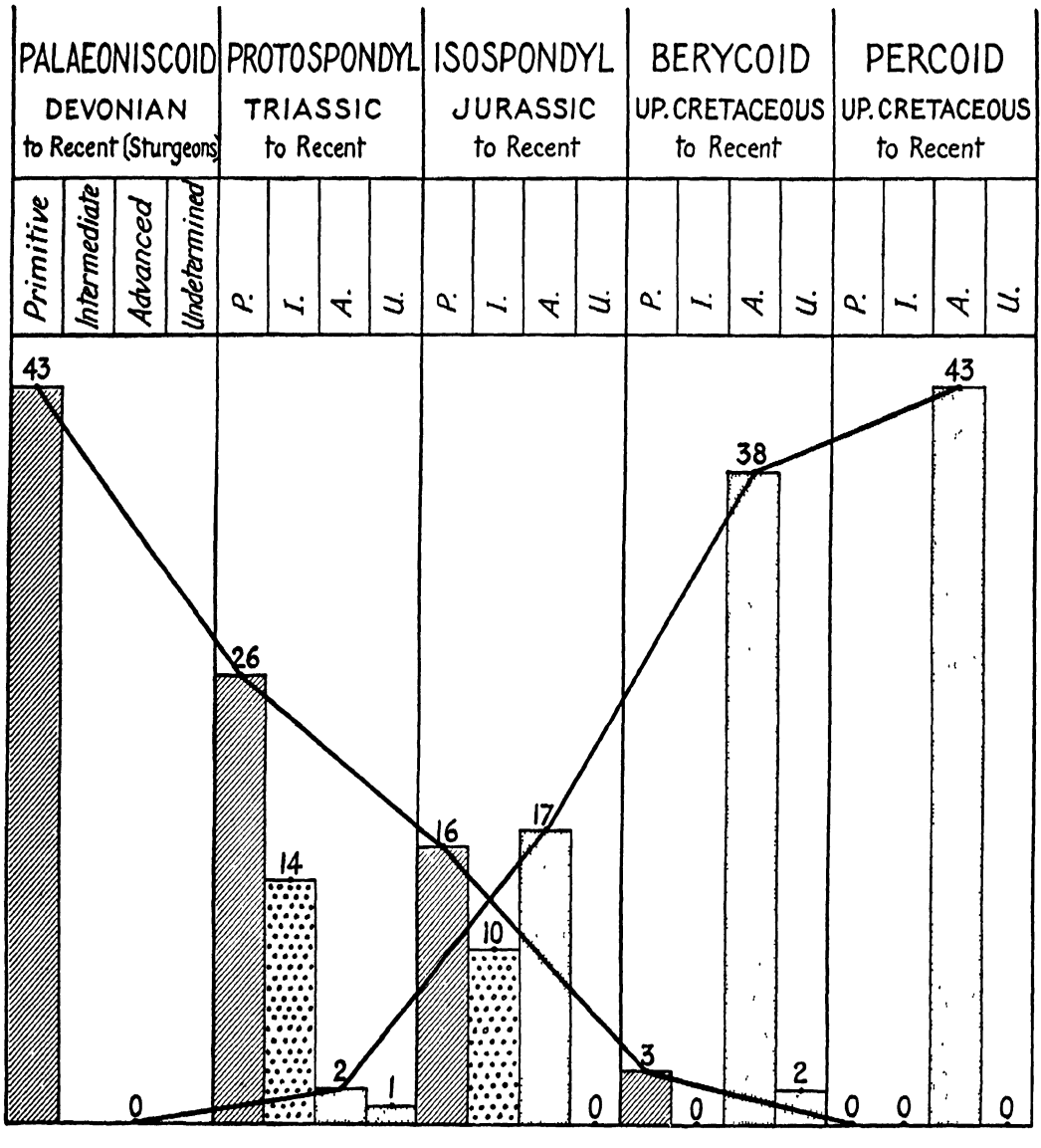


Fig. 9.74. Successive grades of evolution in the bony fishes, showing decline of primitive palaeoniscoid characters and rise of advanced percoid characters.

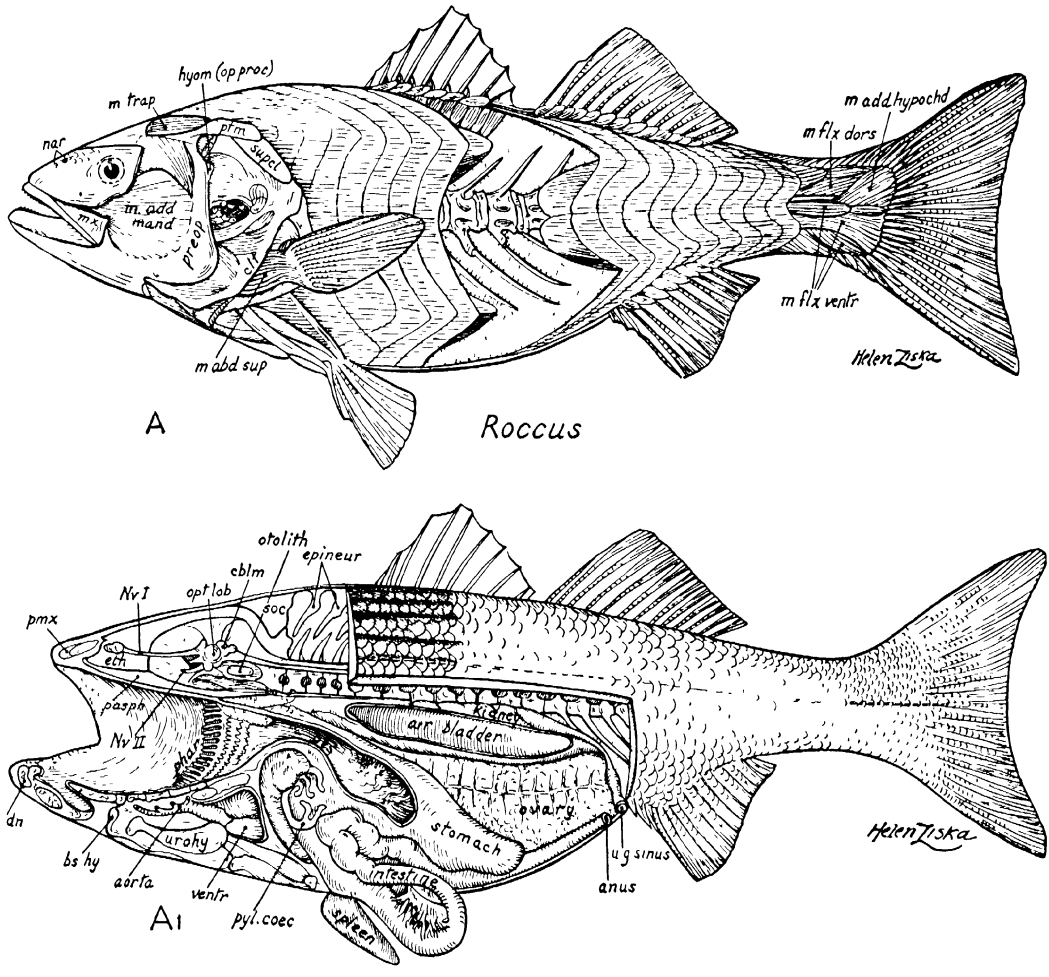


Fig. 9.75 Anatomy of striped bass. Model, based on dissections by Marcelle Roigneau.

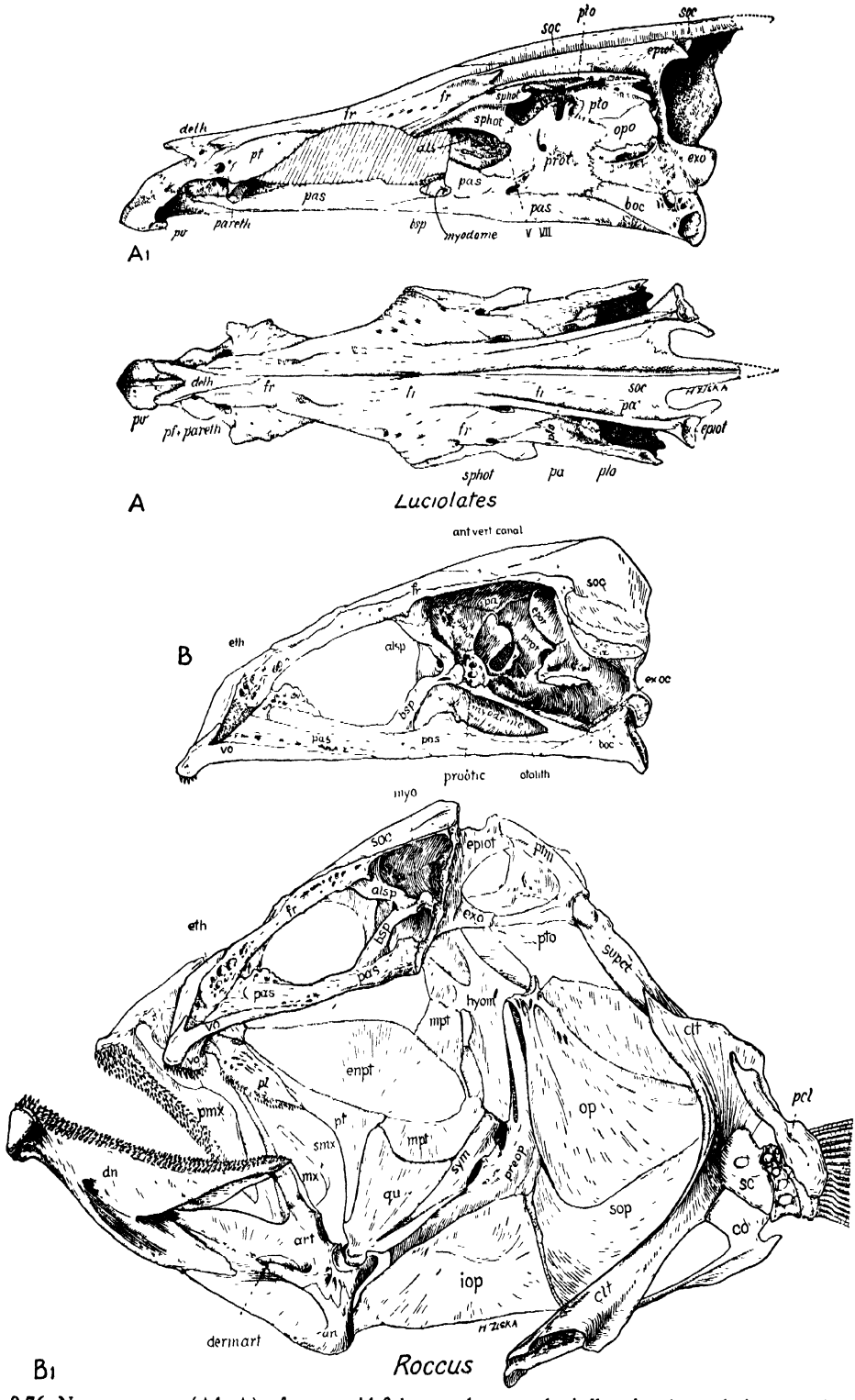
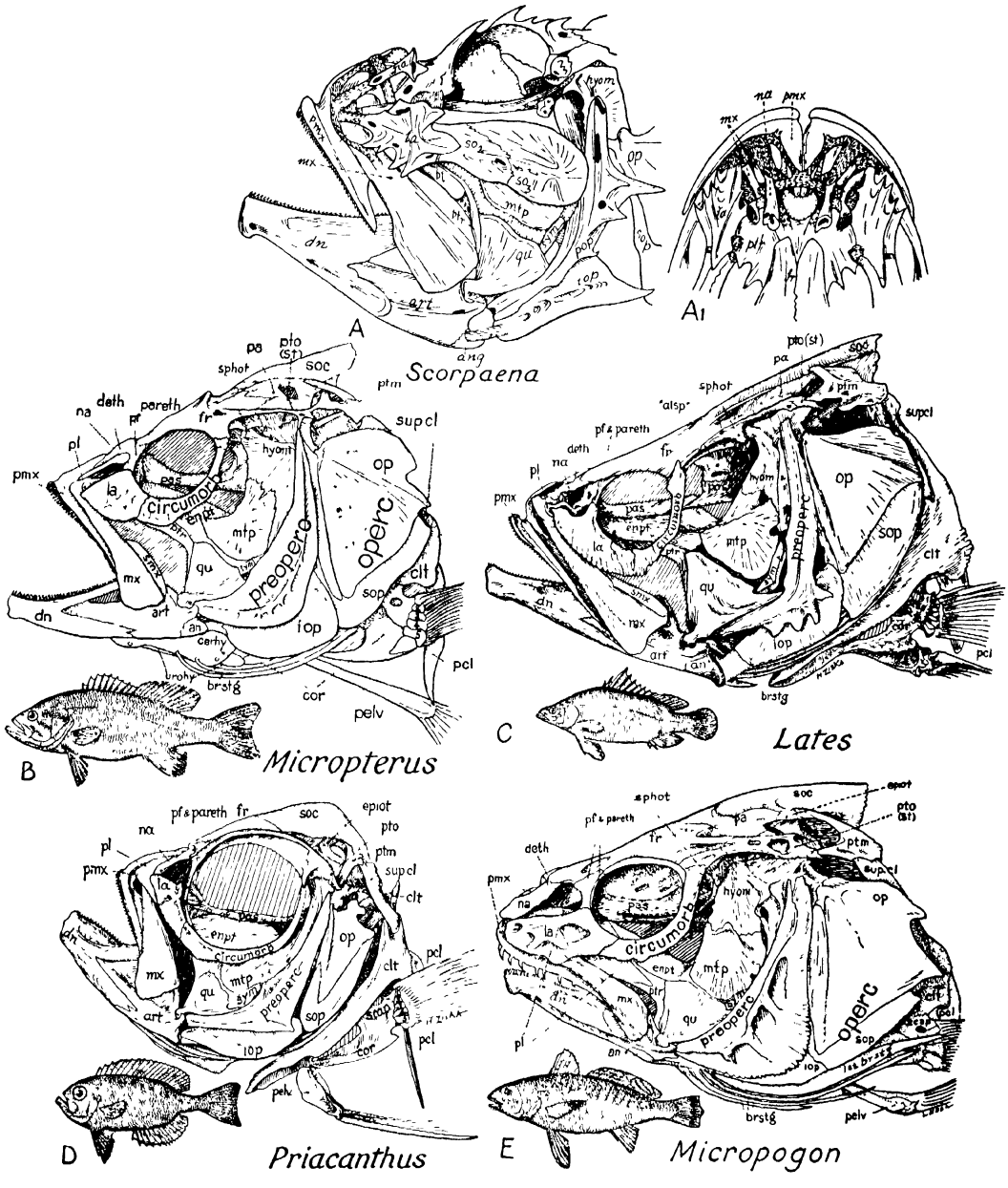


Fig. 9.76. Neurocranium (A1, A) of a percoid fish. Mesial section (B), interior of right side of neurocranium; B1, inner side right half, of jaws, opercular and pectoral girdle, showing relations to the neurocranium and to the three branches of the post-temporal. After Gregory.



Figs. 9.77, 78. Skull of *Scorpaena* (A, A1), showing connections of outer jaw bones with ligaments, skull parts and lateral line tubes. After Allis. Some representative percomorphs and their skulls (B–E), showing adaptive branching of the jaws and dentition. From the central predaceous types (B) were derived the various forms in figs. 9.78–84. A, Scorpaenidae; B, Centraarchidae; C, Serranidae (Centropominae); D, Serranidae (Priacanthinae); E, Sciaenidae, showing large pits for slime glands following the old route of lateral line organs. After Gregory.

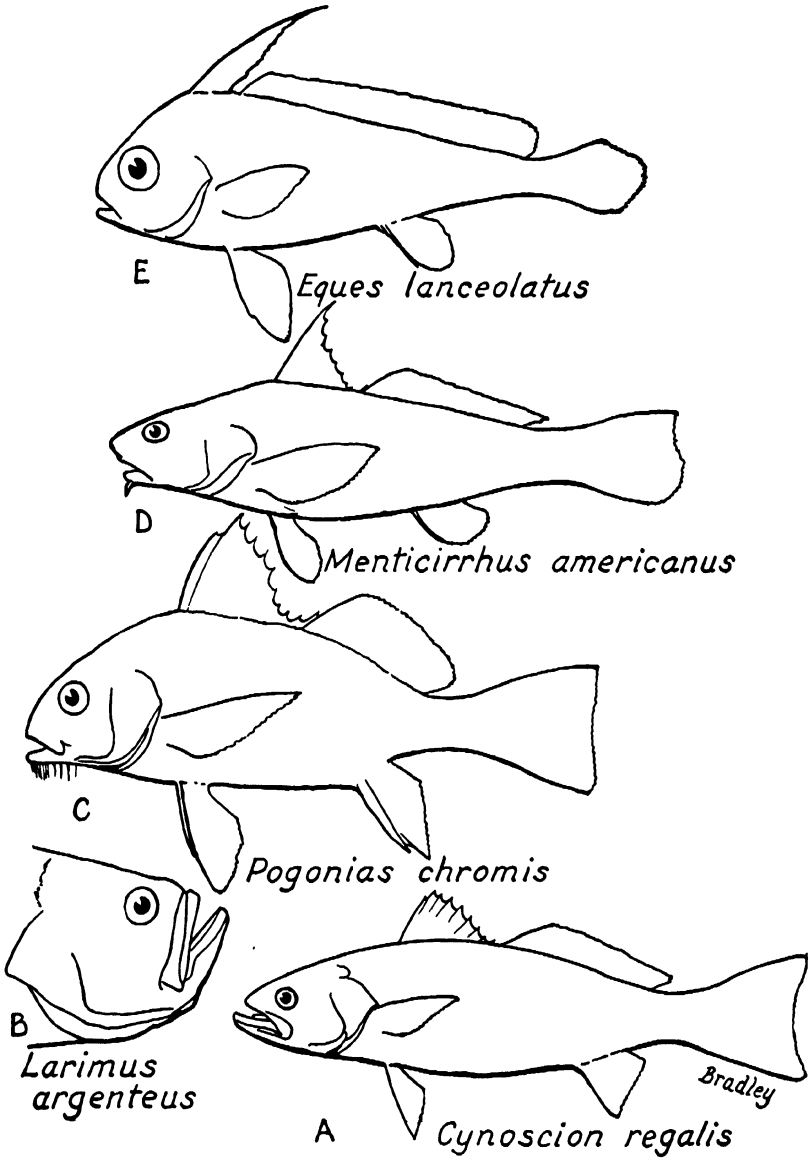
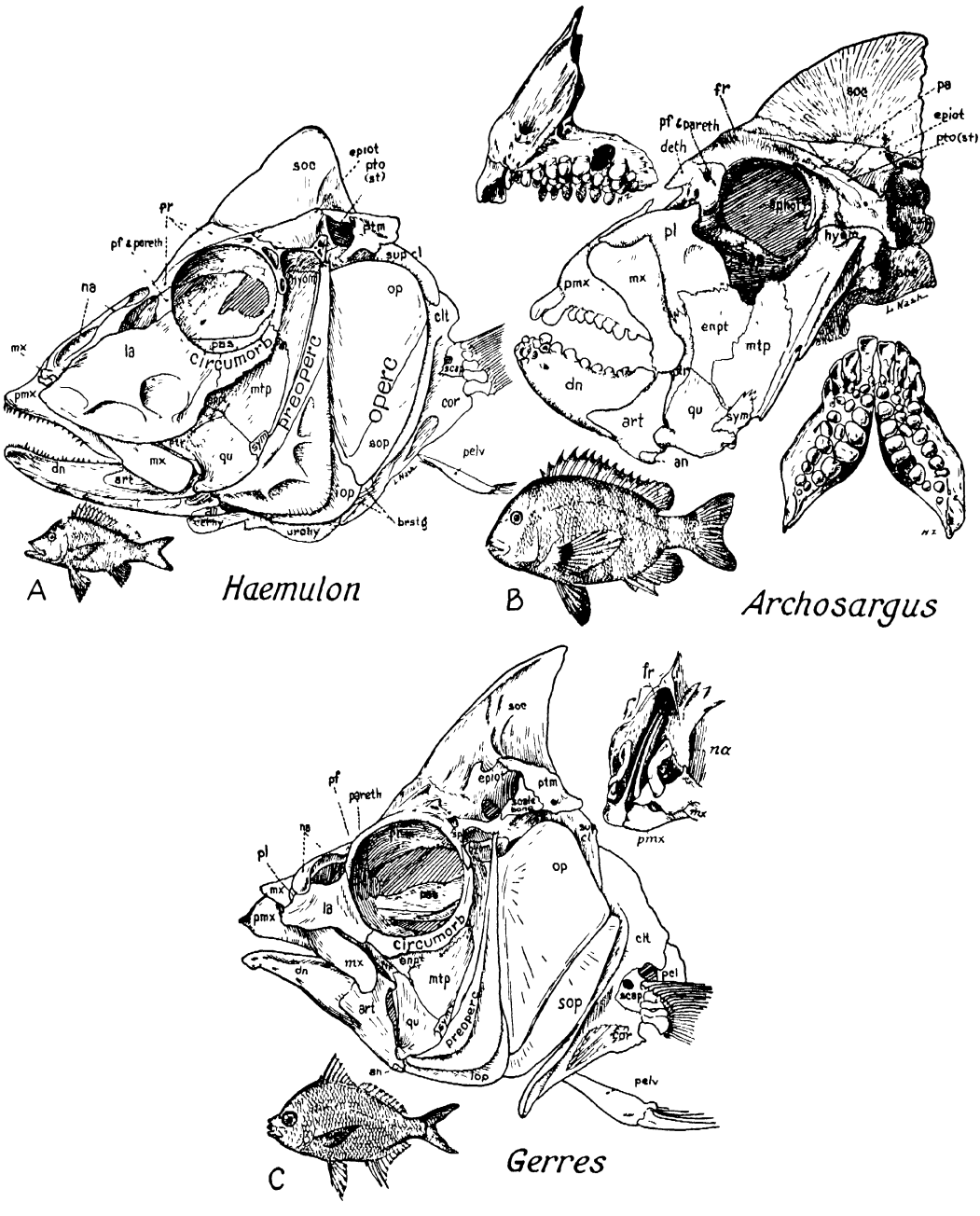


Fig. 9.79. Range of body-form in American Sciaenids. Data from Jordan and Evermann.



Figs. 9.80, 81. A grunt (A) showing enlargement of anterior suborbital (*la*); a sheepshead (B) showing pebble-like crushing teeth and massive jaws. A mojarra (C) with delicate, edentulous jaws. After Gregory.

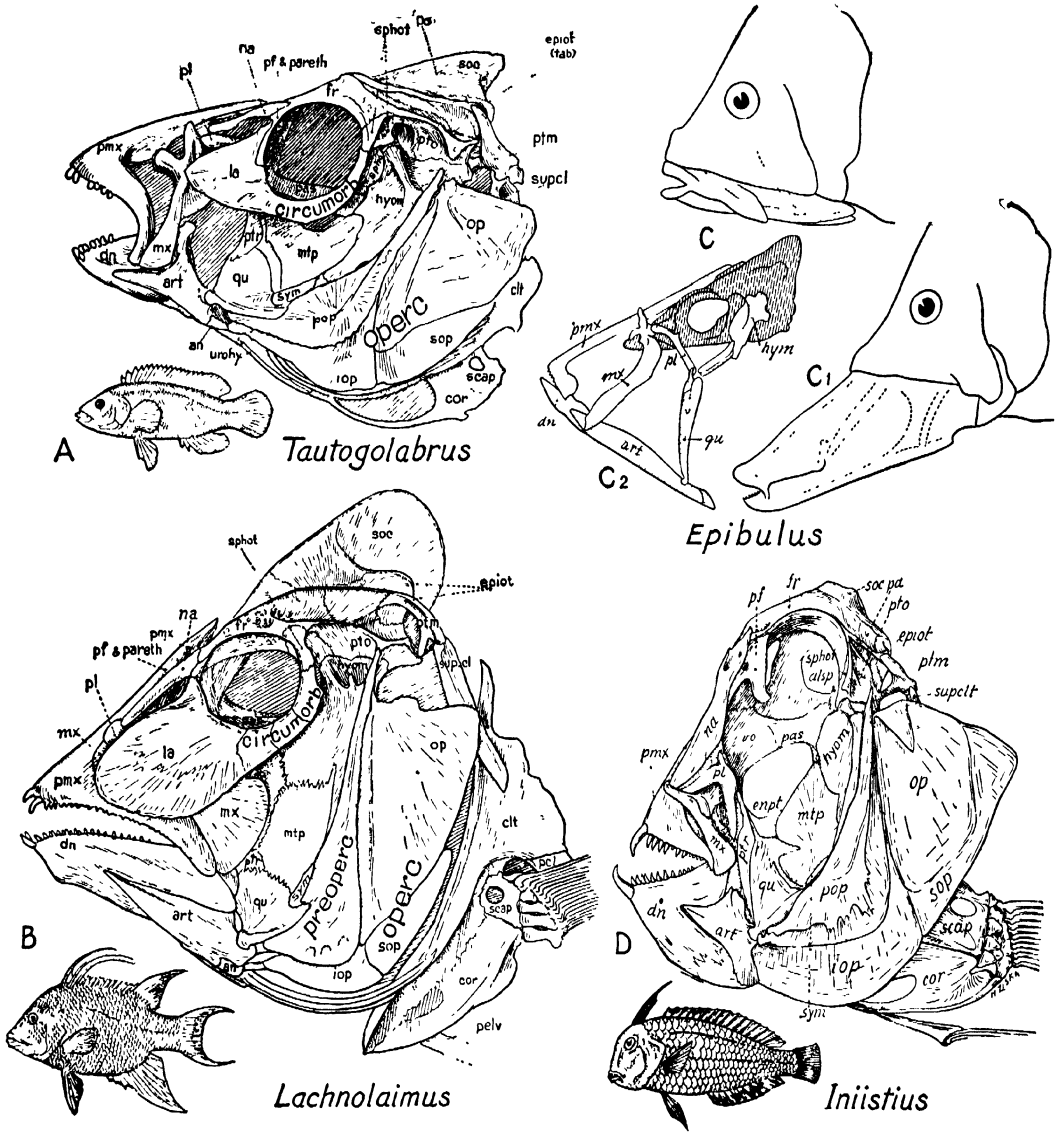
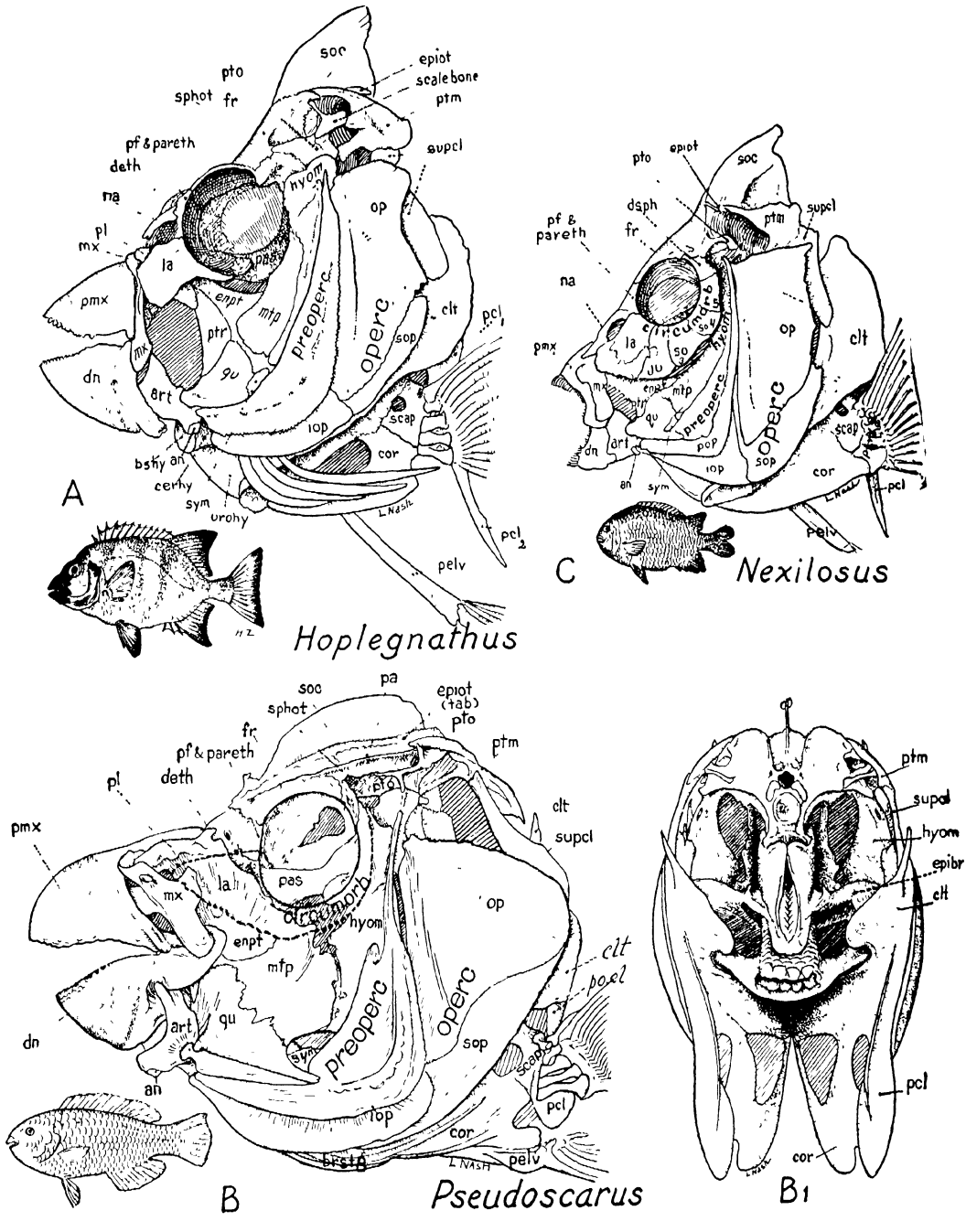
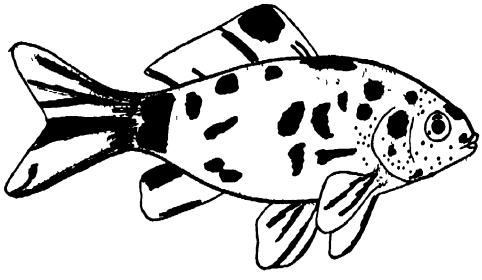


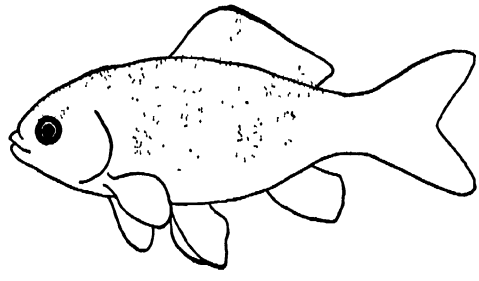
Fig. 9.82. Wrasses and their jaw appratus. A wrasse with strongly projectile jaws (C). A, B, D, after Gregory; C–C2, after Delsman.



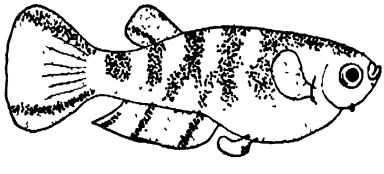
Figs. 9.83, 84 A Percoid with a crushing beak (A); a parrot wrasse (B) and its dental mill (B1) seen from the rear; a demoiselle (C) with small nipping jaws. After Gregory.



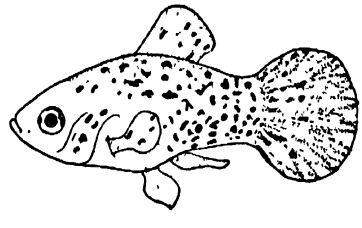
1



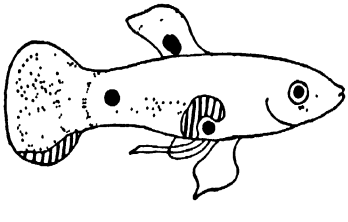
2



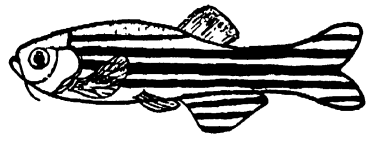
3



4



5



6

Fig. 9.85

Fig. 9.85. Diverse hereditary color patterns in cyprinids, (1, 2, 6) Microcyprini (3, 4, 5). After H. B Goodrich, 1935.

1. The common shubunkin or calico fish, a hybrid between an ordinary goldfish (*Carassius auratus*) and a "colorless shubunkin." The irregular pattern seems to be due to a conflict of opposing tendencies or processes, involving the production and destruction of melanophores. The color patterns of goldfish are produced by the localized destruction of a previously established uniform color (usually dark brown) (Goodrich, 1935, p. 271).

2. A gold and white gold fish, *Carassius auratus* Stippled areas=gold. In this fish "the dark brown melanophores of the young (color due to both melanophores and xanthophores) have partly disintegrated, leaving a pattern of red and white or of red and silver" (Goodrich). "The destruction of color cells proceeds from various centers and sweeps like a wave through the dermis of the skin. . . . Red and black fish are those in which the process has not been completed" (Goodrich, p. 271).

3. Variegated medaka, *Oryzias latipes,* showing pattern of melanophores (coarse stippling) on yellow body (fine stippling). This pattern is due "to differences in the chromogen producing powers of individual cells and not to hormones" (Goodrich, p. 270). In this fish the pattern may be due to embryonic segregation of cells having different capacities of melanin formation followed by cell migration.

4. In the Mexican killifish, *Platypoecilus maculatus* (after Gordon) there is a notable series of color patterns, produced in part by different types of cells, the micro-melanophores, giving rise to stippling, the macro-melanophores to spots. There are no coloreless melanophores in this species (Gordon). The different patterns (one spot, twin spots, crescent, moon) are due to the aggregation of micro-melanophores in well defined areas at the base of the caudal fin, whereas the nigra or black pattern is formed of macro-melanophores. Interaction between the gene for micro-melanophores and the gene for the nigra or black type apparently produces an extension of the black band (Gordon, 1928), while in interspecific crosses between *Platypoecilus* and *Xiphophorus* the interaction of genic and other factors controlling the development of macro-melanophores in some way results in melanotic overgrowth which often become destructive tumors (Gordon, 1931b).

5. A male guppy, *Lebistes reticulatus* (after Winge), showing the color patterns coccineus, vitellinus and maculatus. Solid black=black, stippled=yellow, crossbarred = red. "The studies of Schmidt and Winge * [on this species] have revealed an extraordinary assemblage of color patterns chiefly in the form of spots of varied colors and each apparently controlled by independent genes" (Goodrich, 1935, p. 273).

6. In the zebra fish, *Brachydanio rerio,* "the regions of the future light stripes are at first occupied by a sparse population of melanophores which later disintegrate" (Goodrich and Nichols, 1931). Conditions controlling the localization of stripes are unknown (Goodrich, 1935).

* For references, see Goodrich, 1935.

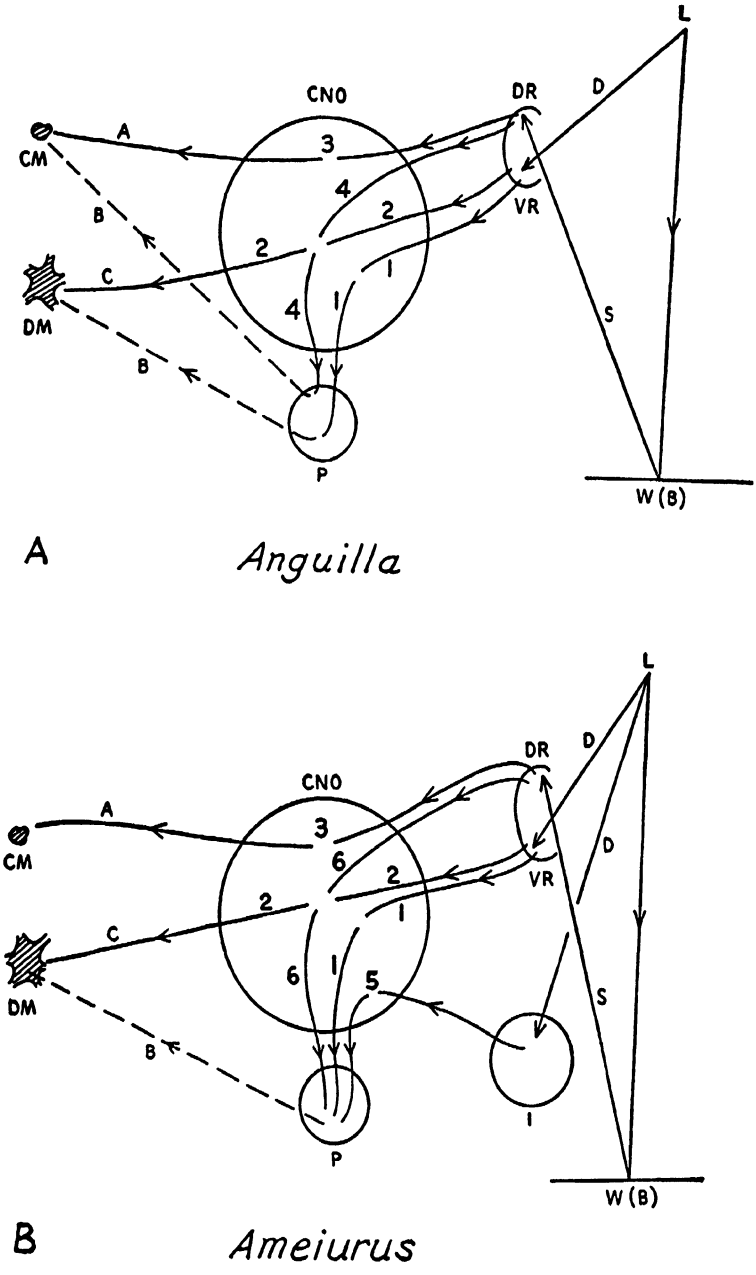


Fig. 9.86. Diagrams of the melanophore system in the Eel (A) and in the Catfish (B). After G. H. Parker (1943).

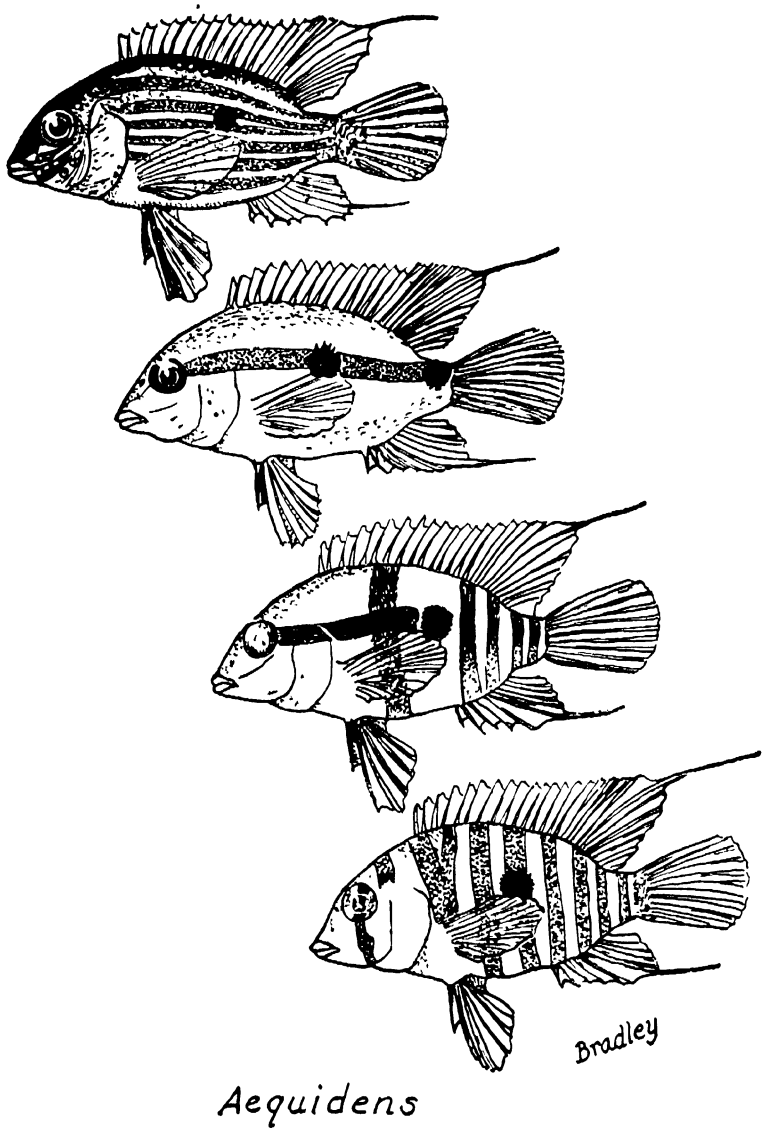


Fig. 9.87. Four of the seven changing patterns, observed within twenty-four hours, in a single living cichlid fish (*Aequidens tetramerus*). After Beebe (1943).

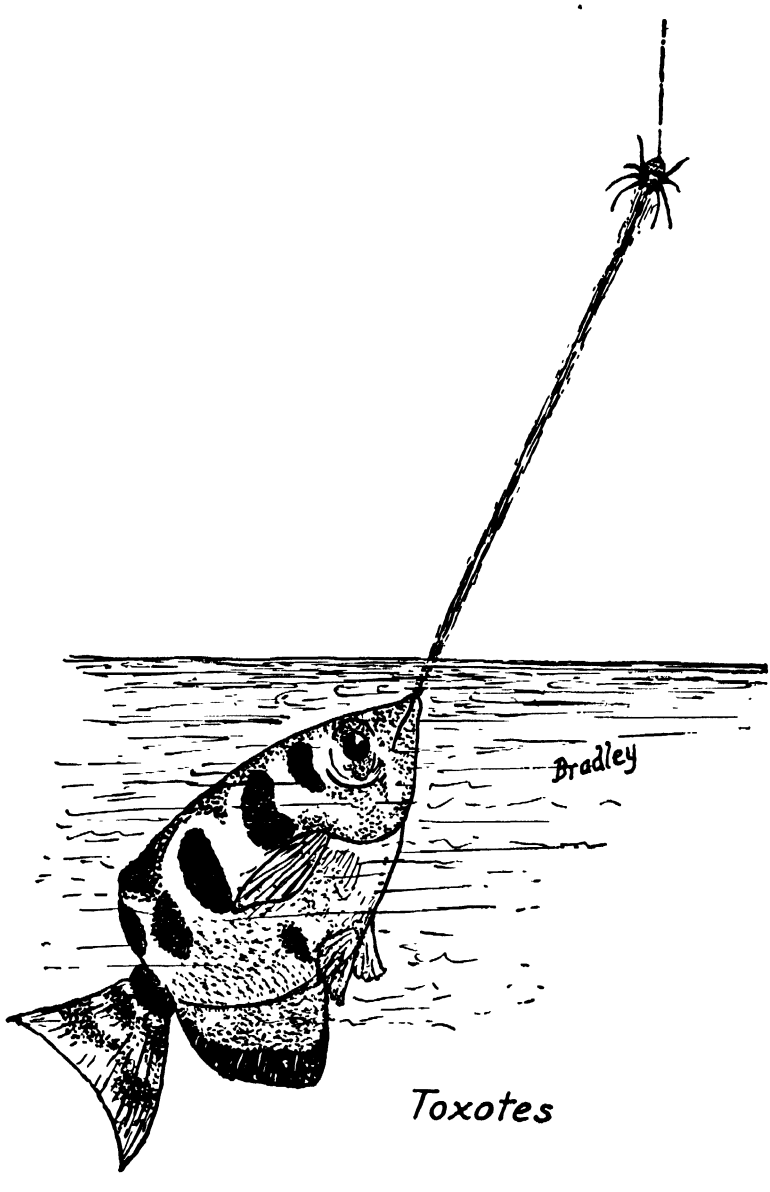
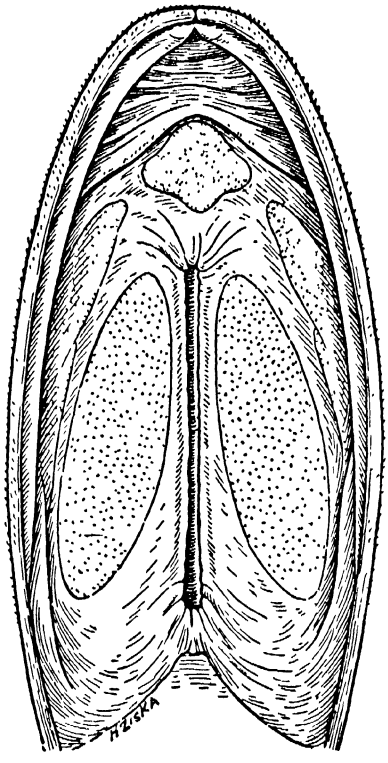
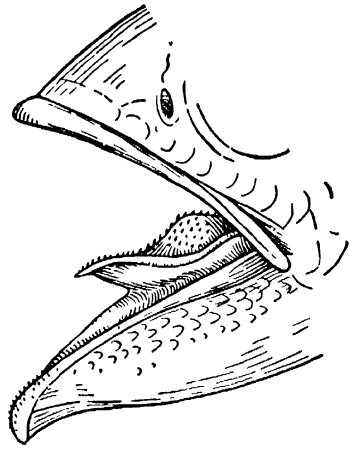
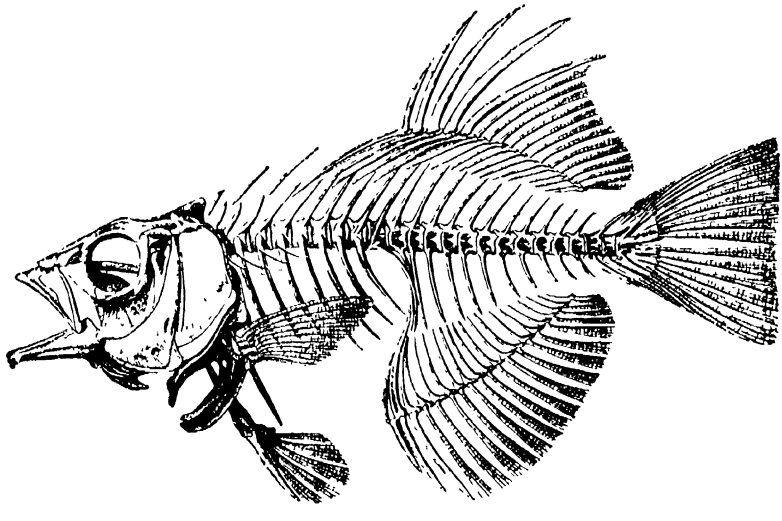


Fig. 9.88. The Archer Fish in action. Photo. N. Y. Zoological Society. After Hugh M. Smith.*







Toxotes

Fig. 9.89 (top). "Blow-pipe" of Archer Fish. After Hugh M. Smith *

"The groove-tube which enables the archer fish to project pellets of water from its mouth is a narrow slot in the roof of the mouth which is closed by the tongue. When the odd-shaped tongue fits against the roof of the mouth a slender tube is formed which is less than a sixteenth of an inch in diameter in a fish that is seven inches long." *

Fig. 9.90. Skeleton of Archer Fish. After Hugh M. Smith. From Agassiz.

* Quotation and figures from *Natural History Magazine*, 1936, vol. 38, no. 6, pp. 2–11.

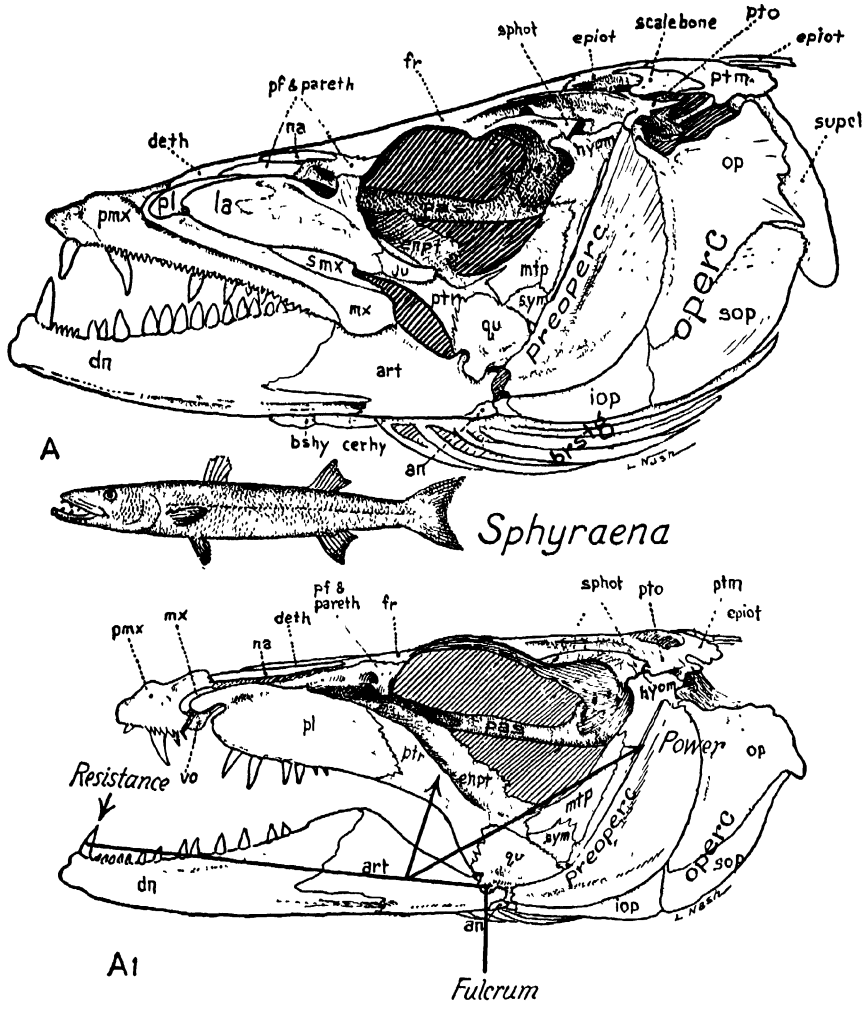


Fig. 9.91. The Barracuda and its skull (A). In A1 the premaxillae and part of the maxillae have been removed to show the palato-quadrate complex, or primary upper jaw. The mandible acts as a lever of the third class, the adductor mandibulae muscles being inserted between the fulcrum and the resistance. After Gregory.

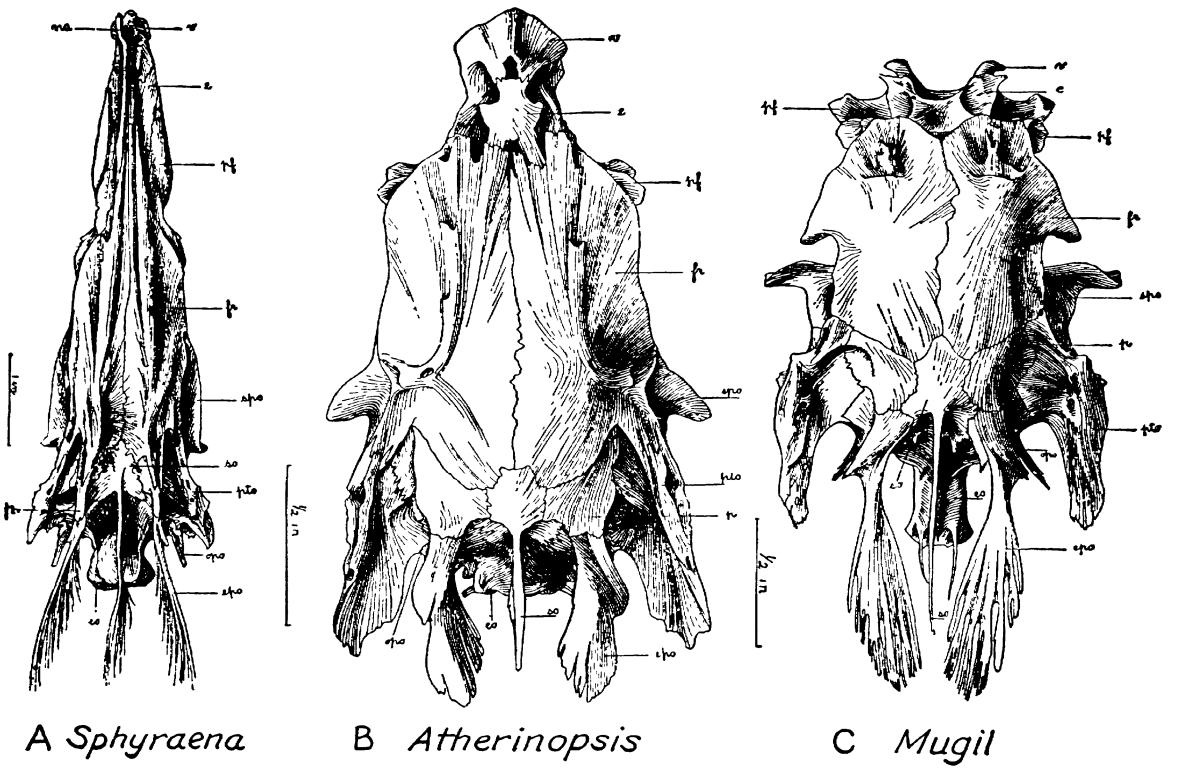


Fig. 9.92. Skull tops of Percesoces, showing divergence in proportions (anisomerism). The brush-like prolongations of the epiotics are probably connected with long tendons of epaxial muscles. After Starks.

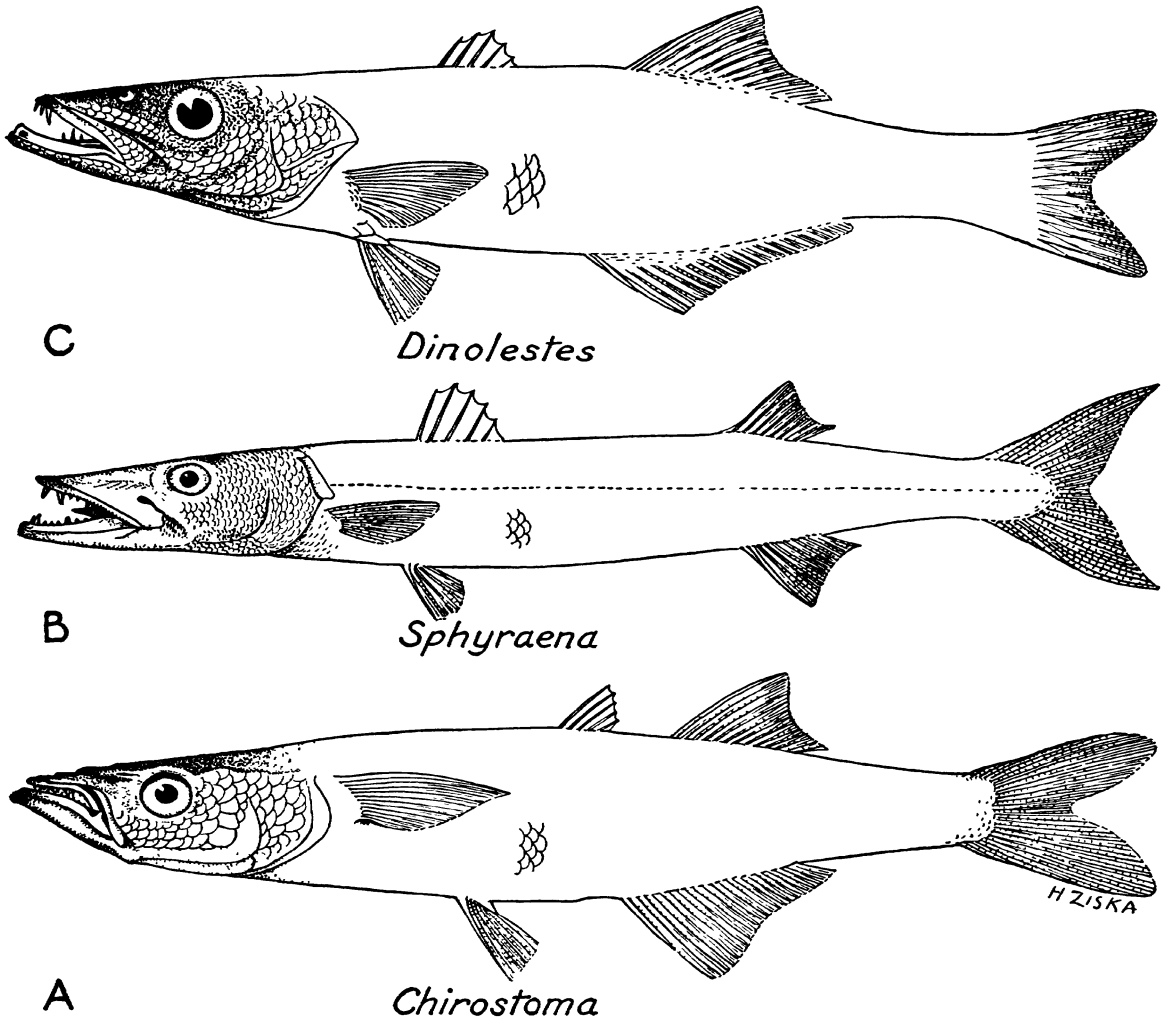
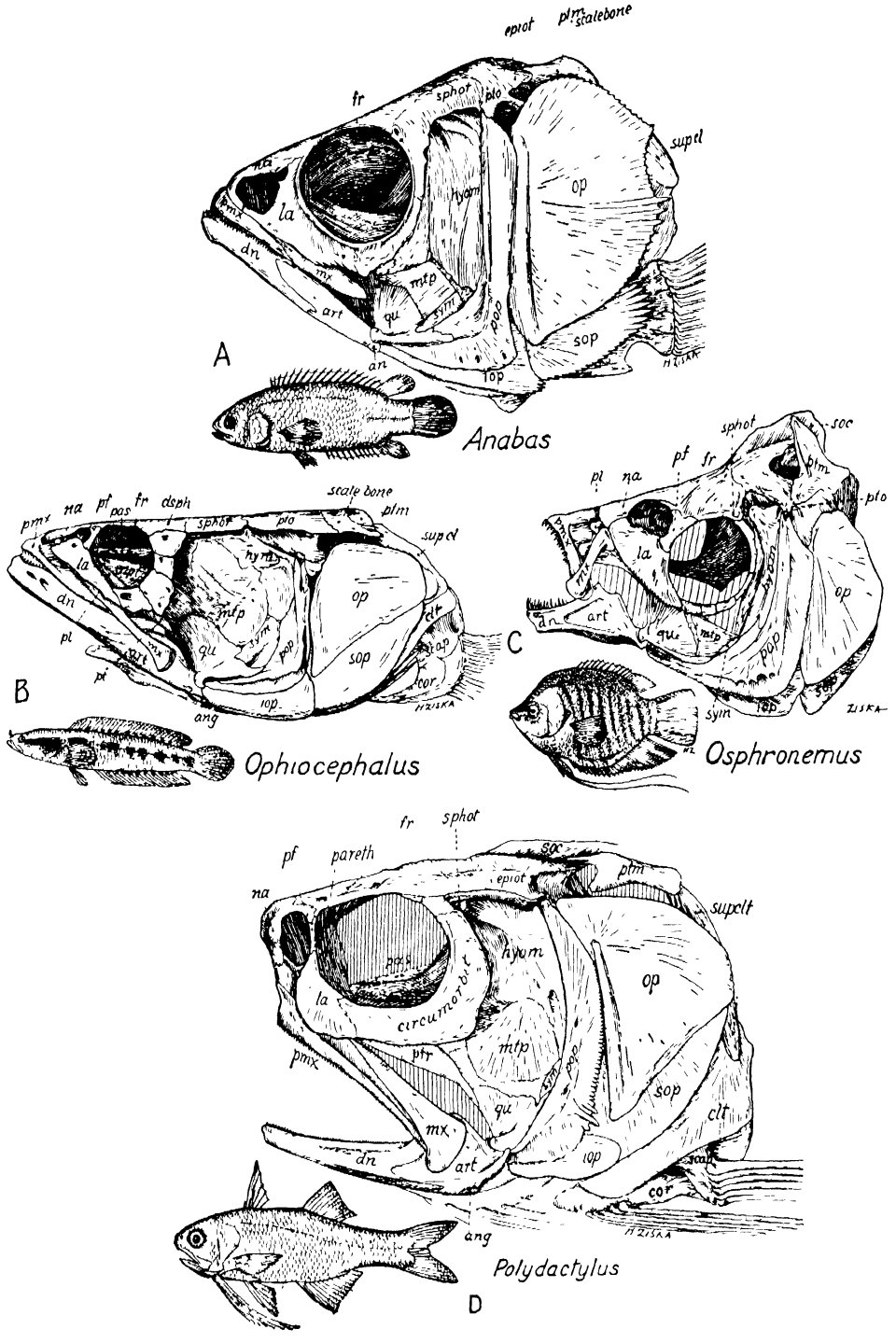
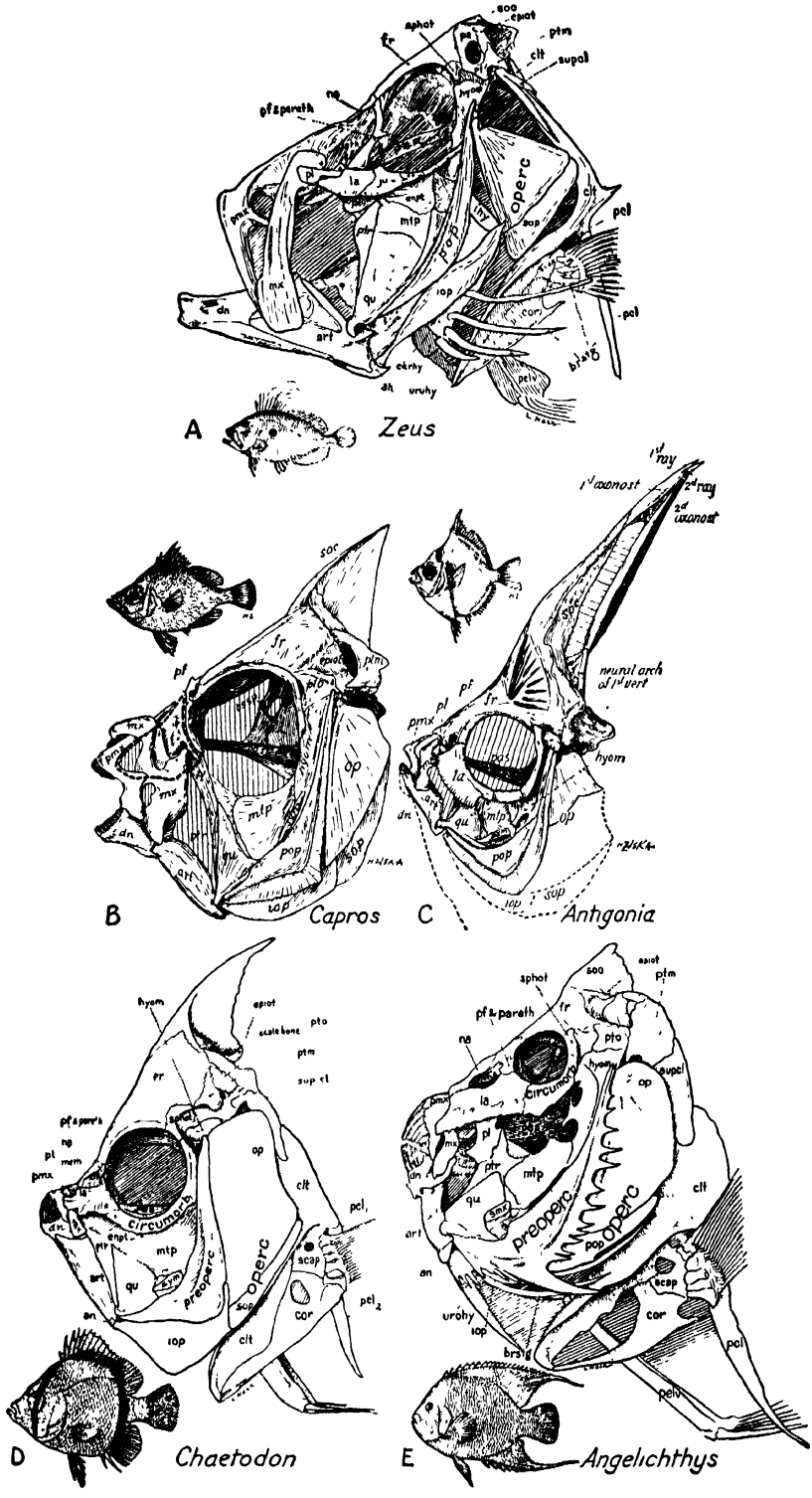


Fig. 9.93



←Fig. 9.93 (facing page). Comparison of Silverside (A), Barracuda (B) and marine Percoid (C). All drawn to the same length. After Starks.

Figs. 9.94, 95. Fishes with an accessory breathing organ (Labyrinthici, A–C). A fish (D) with subdivided pectoral fins. The elongated lower anterior rays may have a sensory function. After Gregory.



Figs. 9.96, 97. Contrasting characters of *Zeus* (A) and Caproids (B, C), Chaetodont (C) and Angelfish (D). After Gregory.

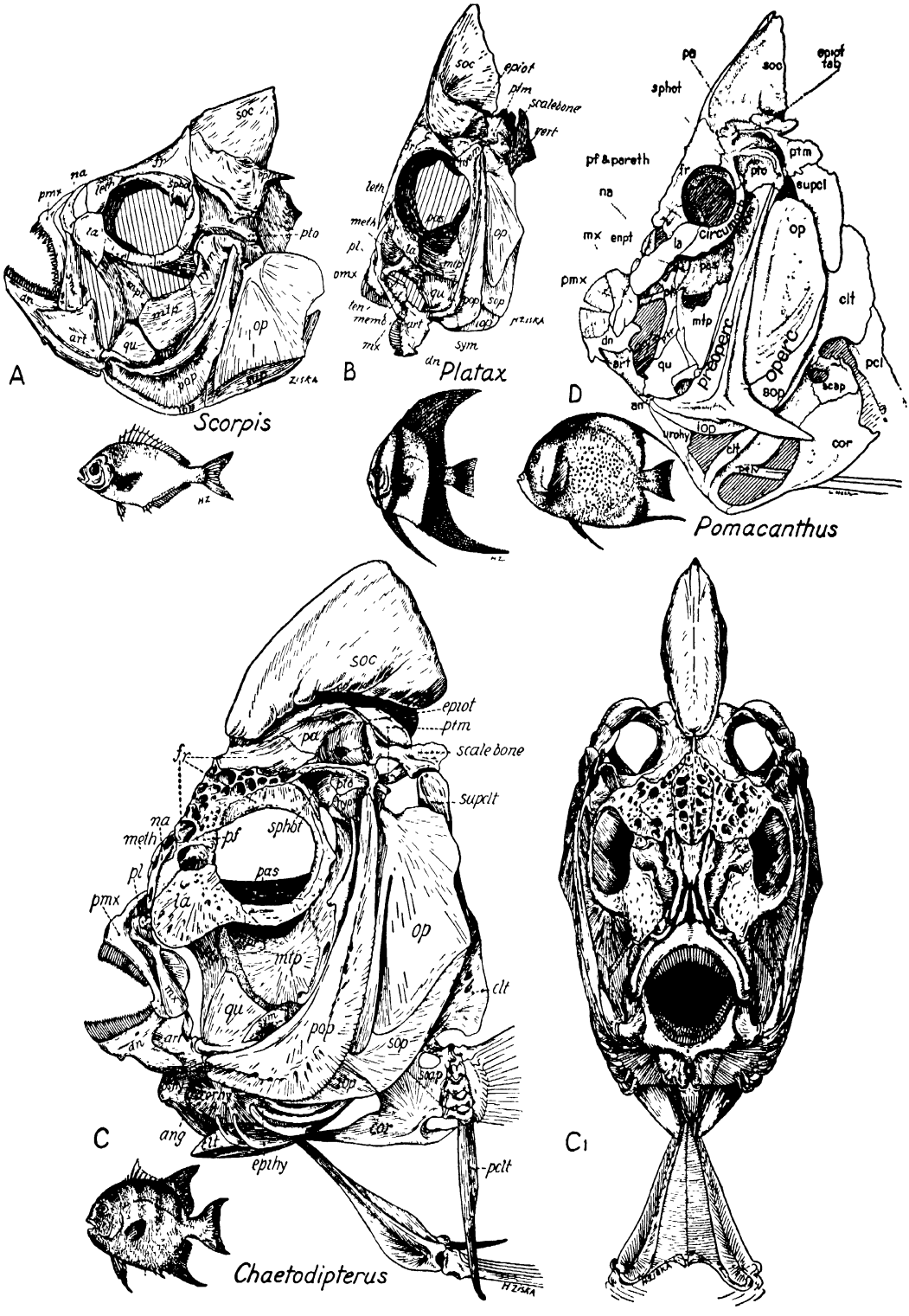


Fig. 9.98. Comparison of rhomboid and subcircular fishes. After Gregory.

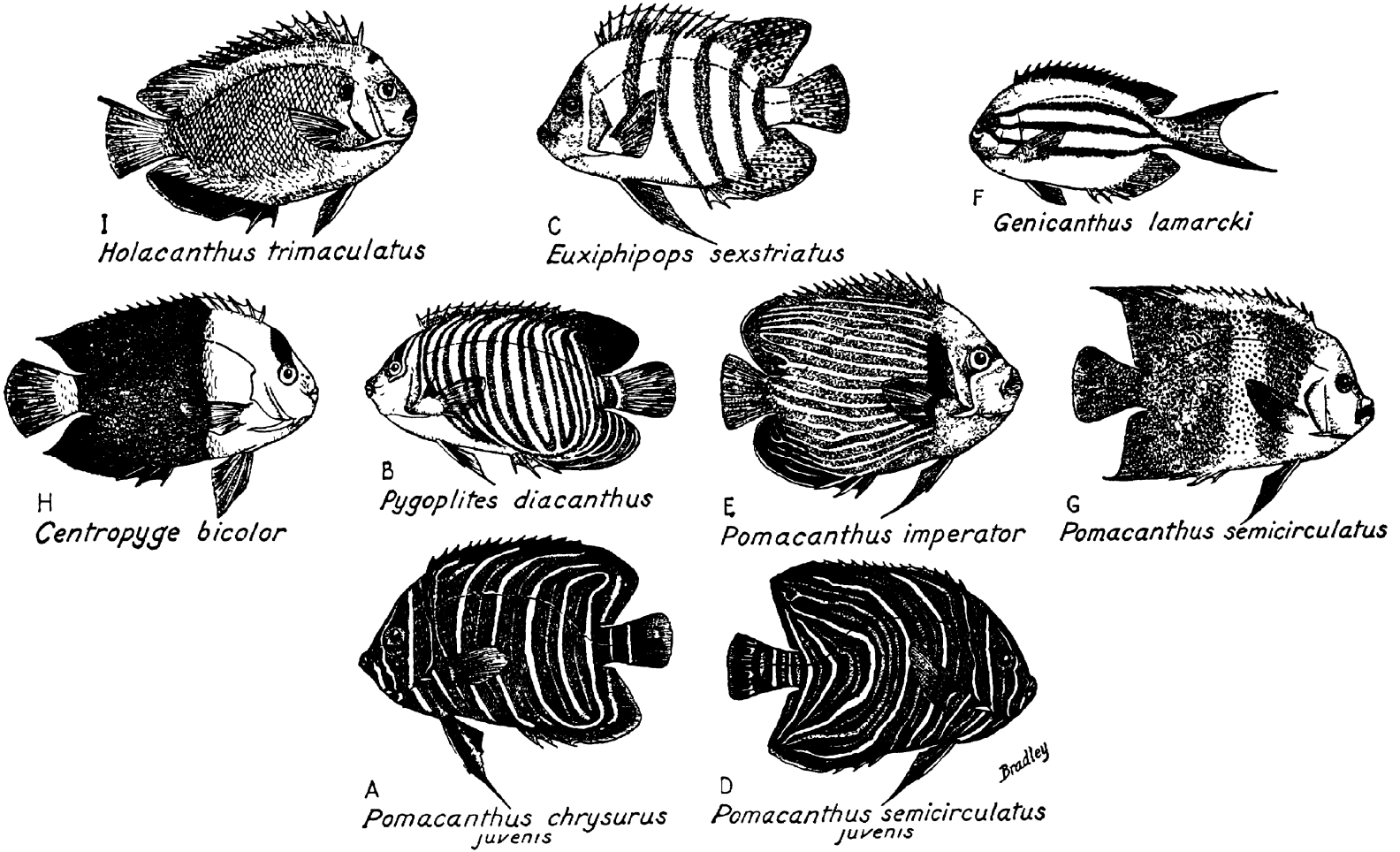


Fig. 9.99. Sample color patterns of Angel fishes. Selected from Weber and De Beaufort's figures (1936).

Fig. 9 100 (below). Divergent color patterns of Chaetodonts. Selected figures from Weber and De Beaufort (1936).

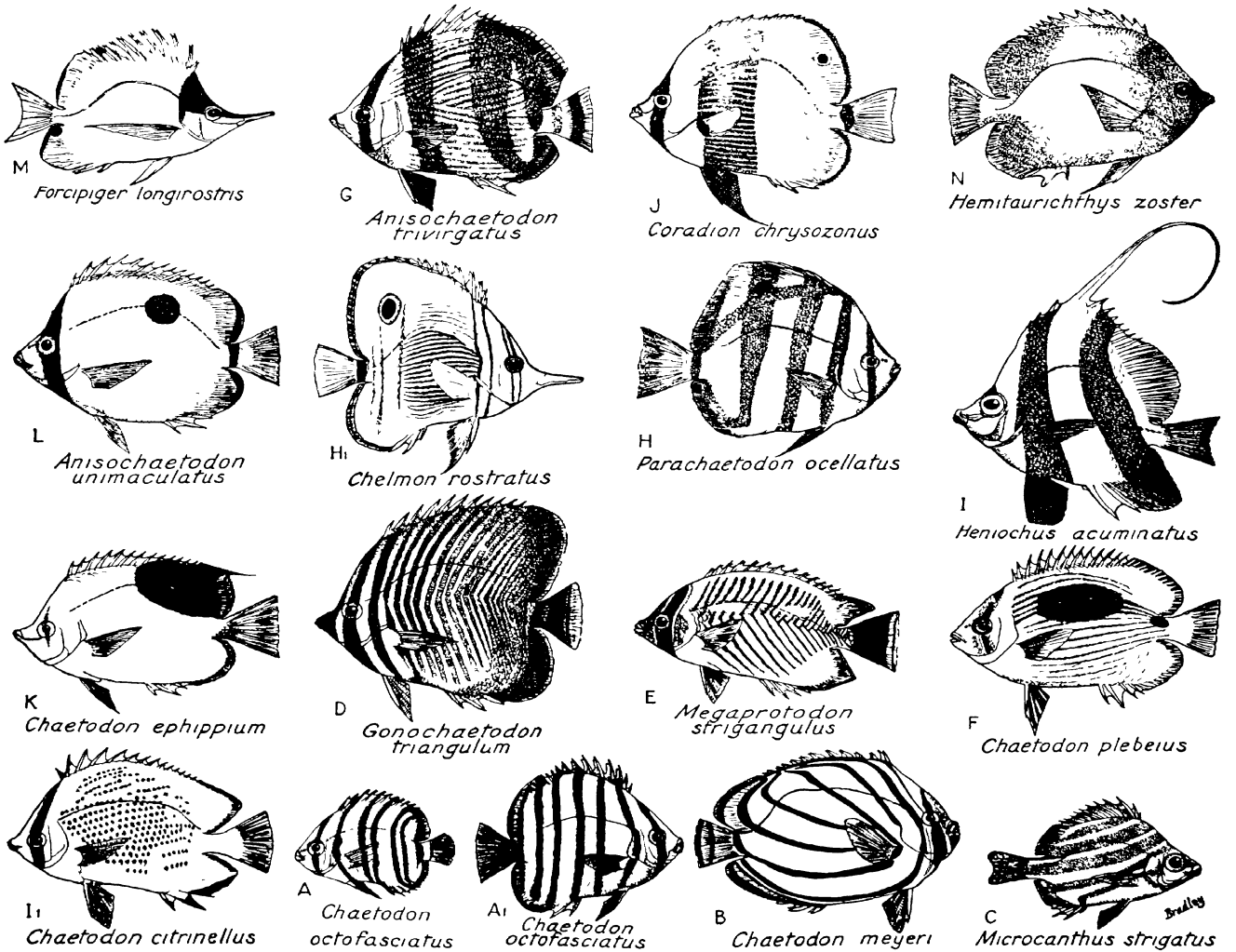

M
Forcipiger longirostris
G
Anisochaetodon trivirgatus
J
Coradion chrysozonus
N
Hemitaurichthys zoster
L
Anisochaetodon unimaculatus
H1
Chelmon rostratus
H
Parachaetodon ocellatus
I
Heniochus acuminatus
K
Chaetodon ephippium
D
Gonochaetodon triangulum
E
Megaprotodon strigangulus
F
Chaetodon plebeius
I1
Chaetodon citrinellus
A
Chaetodon octofasciatus
A1
Chaetodon octofasciatus
B
Chaetodon meyeri
C
Microcanthus strigatus

Fig. 9.100

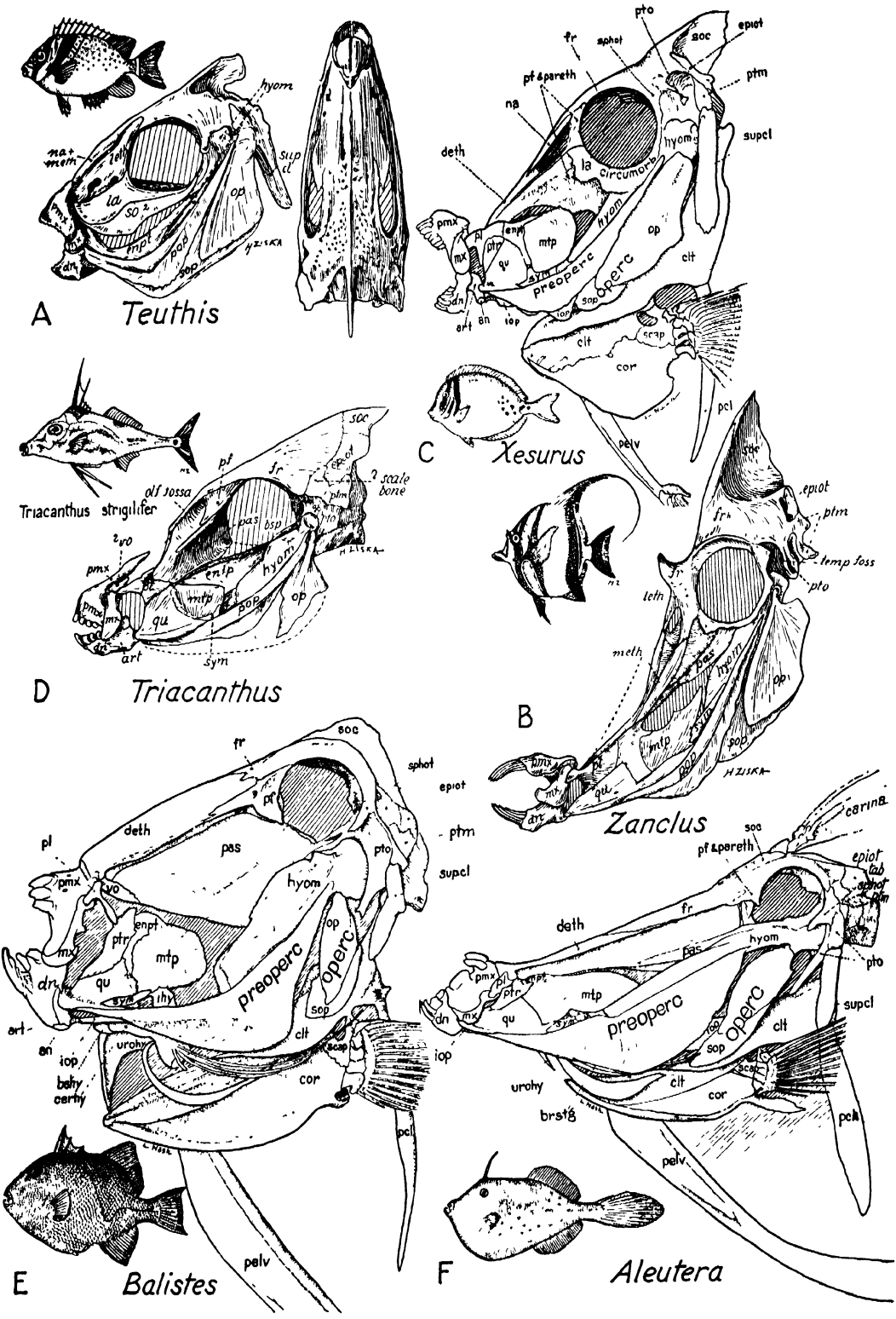


Fig. 9.101. Some nibbling derivatives of the percoid stem. After Gregory.

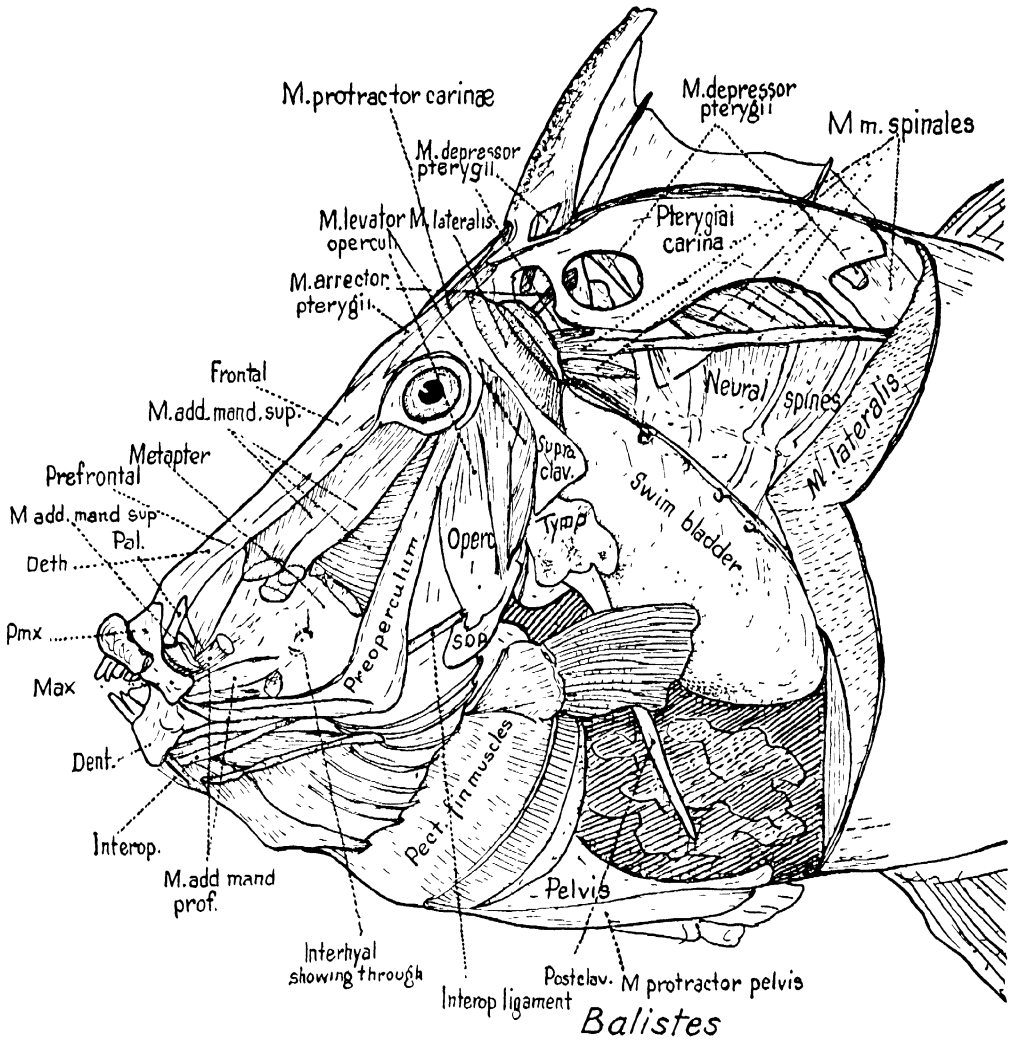


Fig. 9.102. Partial dissection of a Trigger fish. After Gregory.

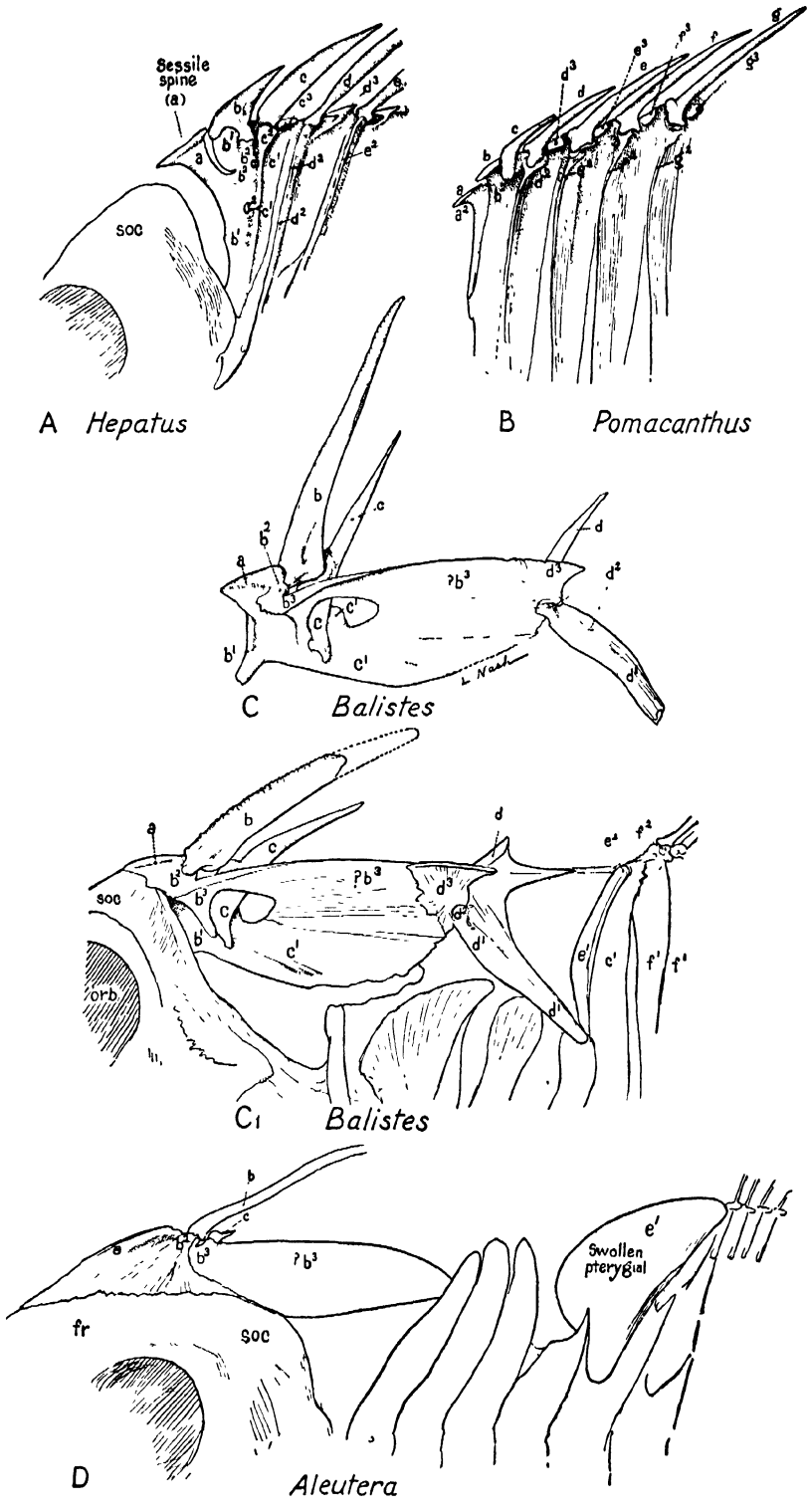


Fig. 9.103. Homologies of the anterior fin spines of the Surgeon (A), Angel (B), and Trigger fishes (C, C1, D).

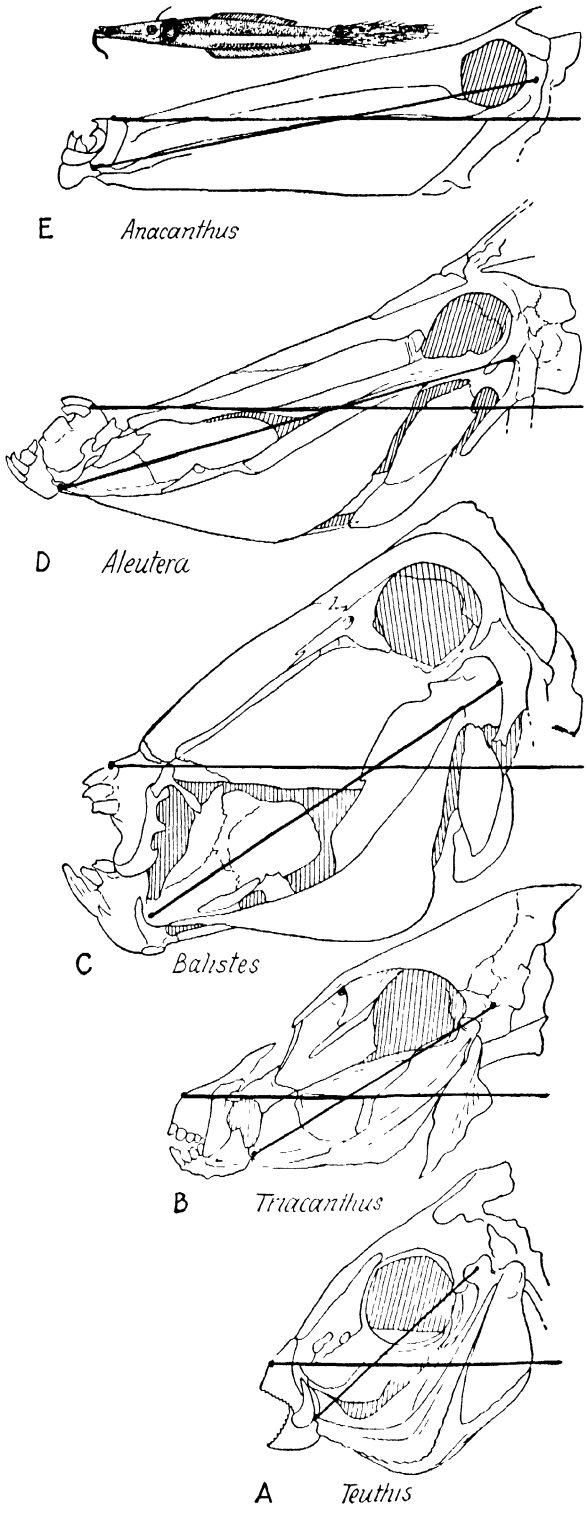
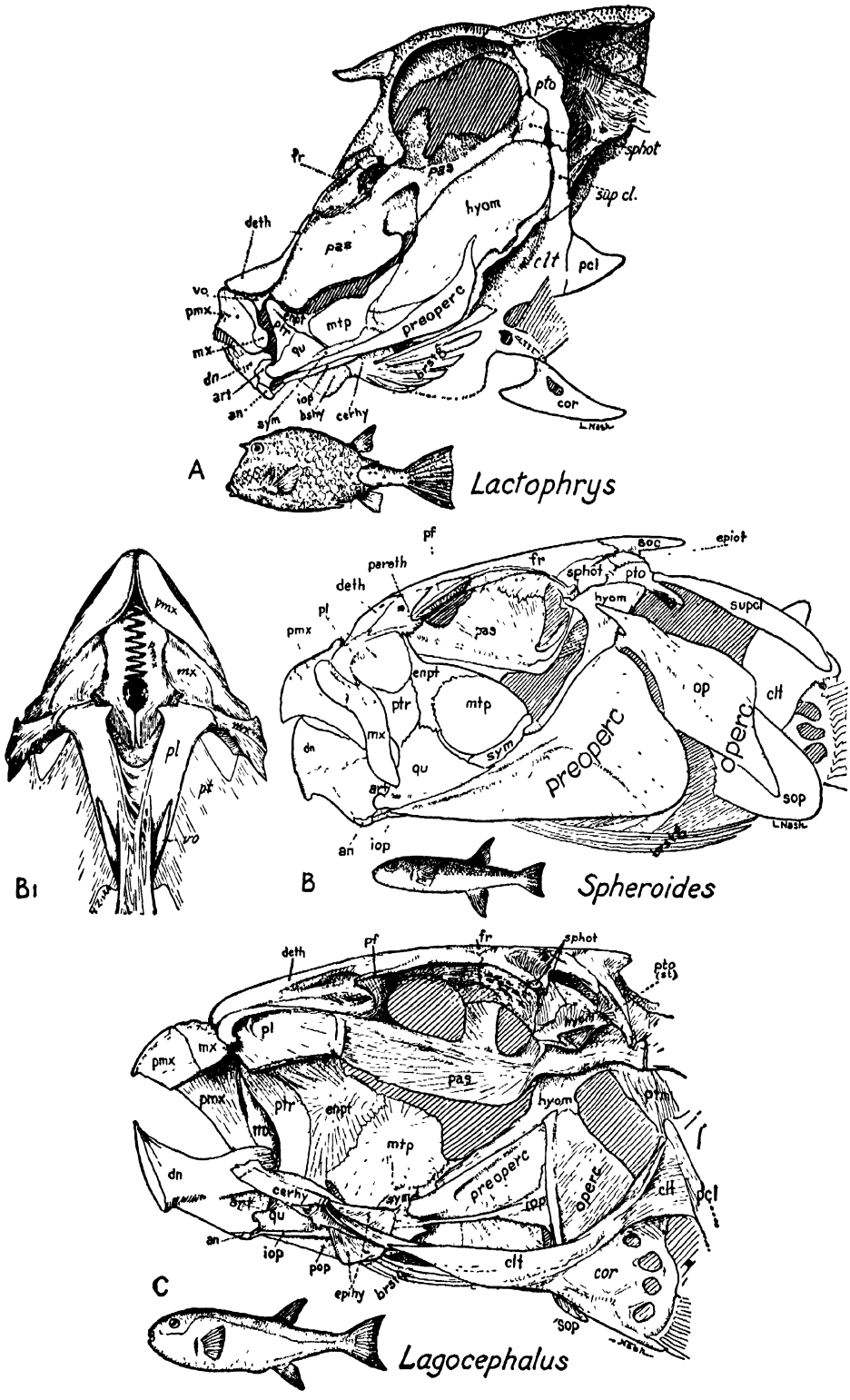


Fig. 9.104. Progressive elongation of the preorbital face in Teuthids (A, B) and Trigger fishes (Balistoids, C–E). After Gregory.



Figs. 9.105, 106. The cowfish (A) and its armor. The puffers (B, B1, C), a well-beaked branch of the Balistoid stock. After Gregory.

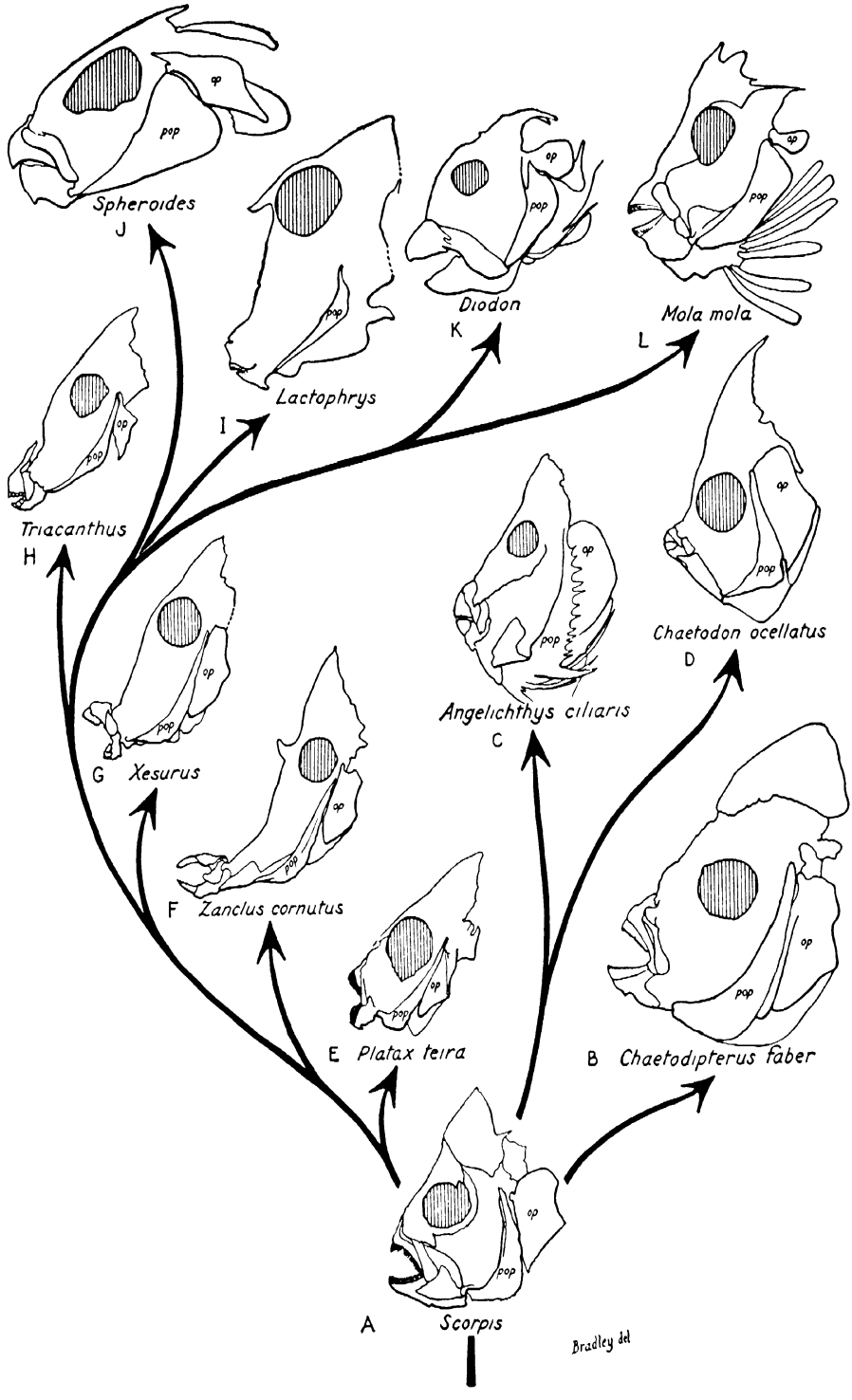


Fig. 9.107. Summary of inferred relationships of the nibbling to beak-like Balistoids and Chaetodontoids.

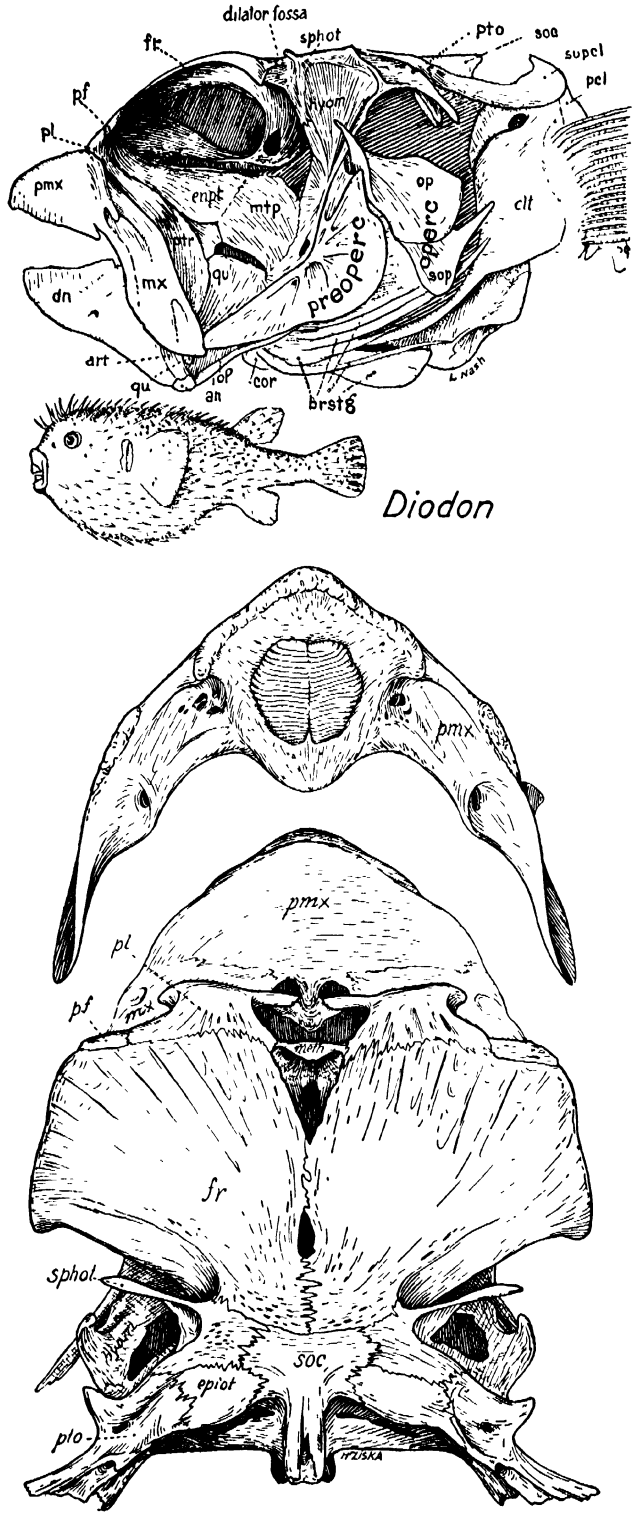


Fig. 9.108. The Porcupine fish and its crushing jaws. fter Gregory.

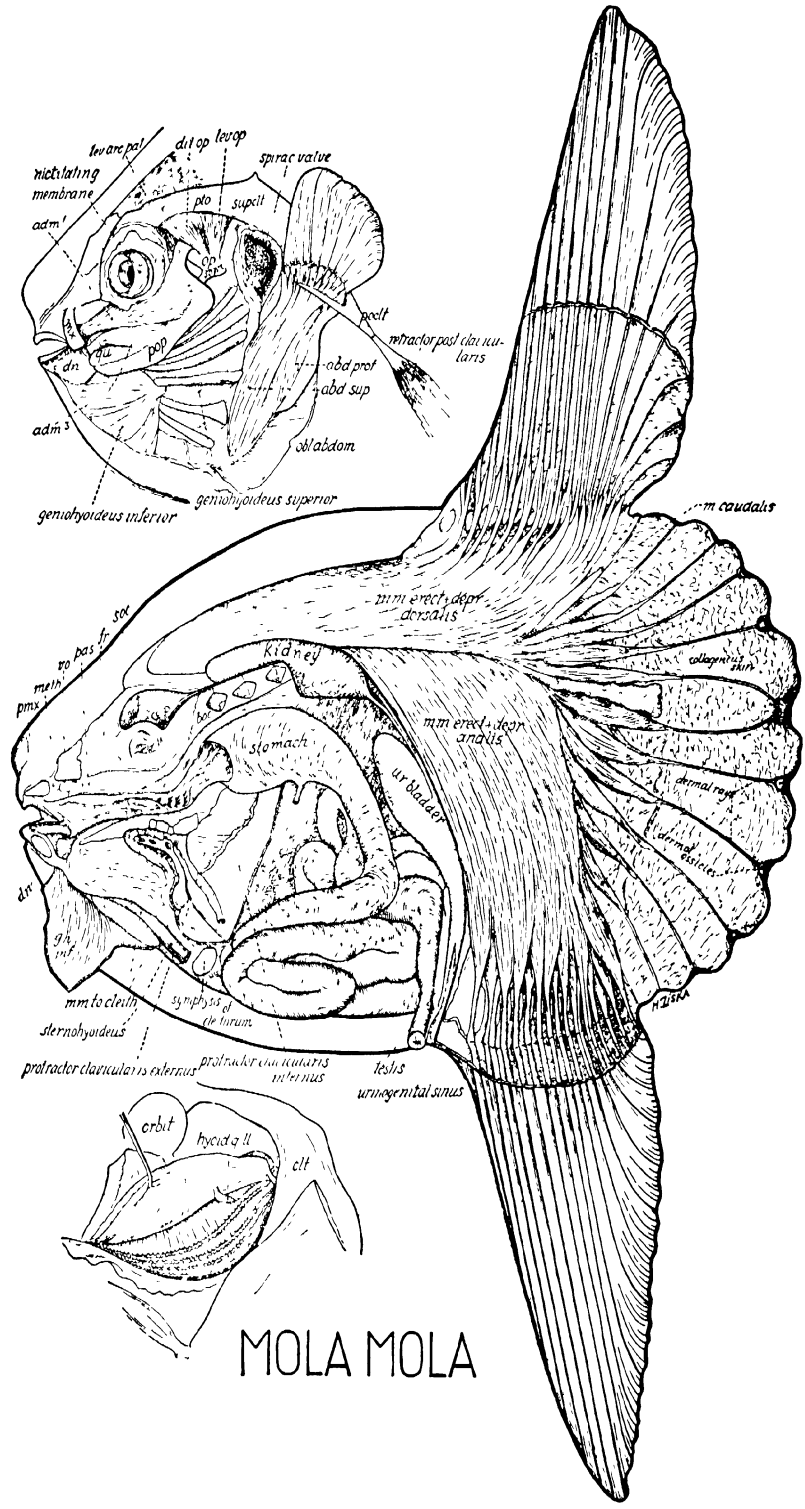


Fig. 9.109. Anatomy of the "Ocean Sunfish." For *m. caudalis*, read *m. pseudocaudalis* (= parts of mm. erector + depressor dorsalis + e d. ventralis). (cf. fig. 9 110) After Gregory and Raven (1934).

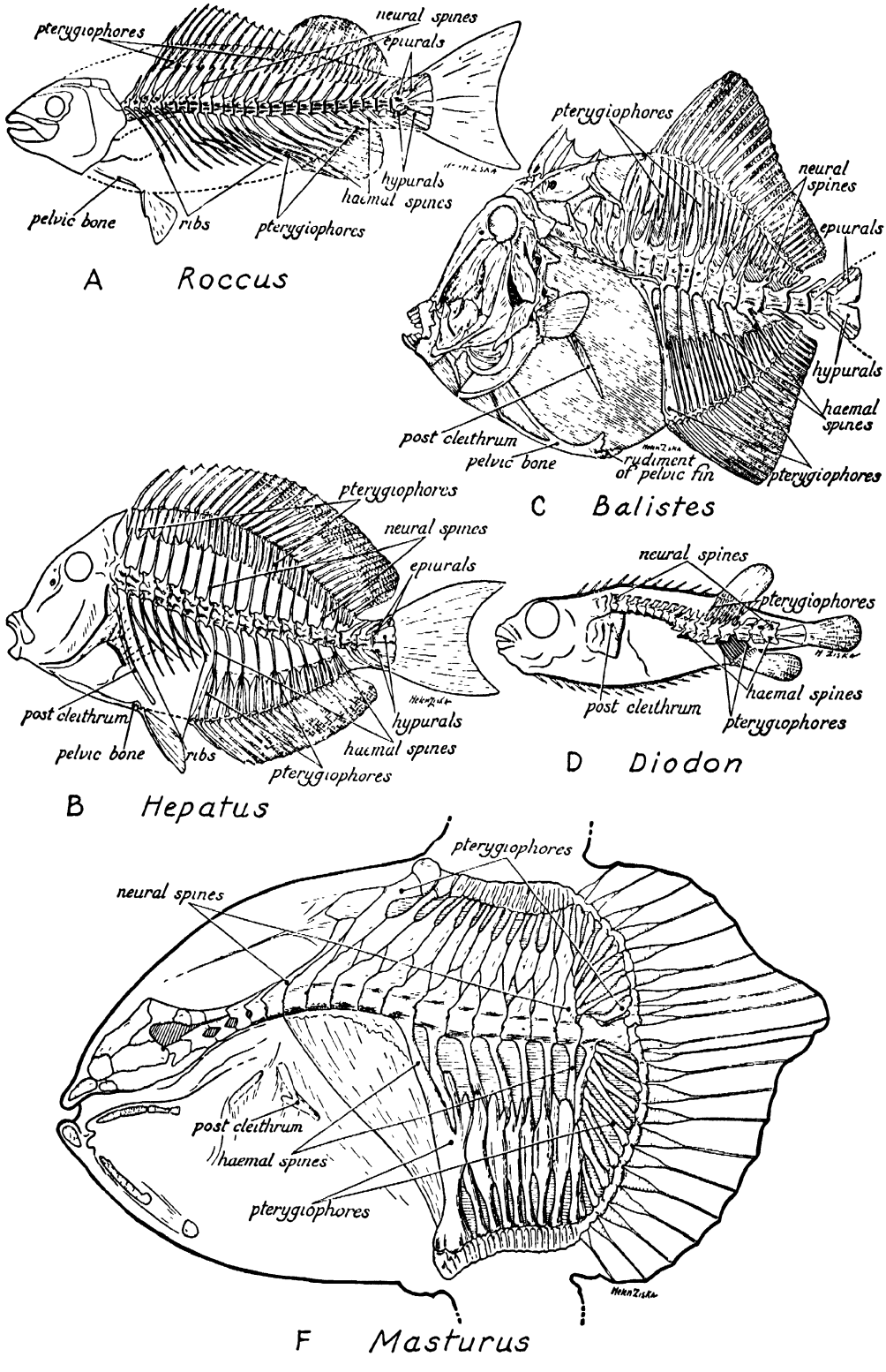
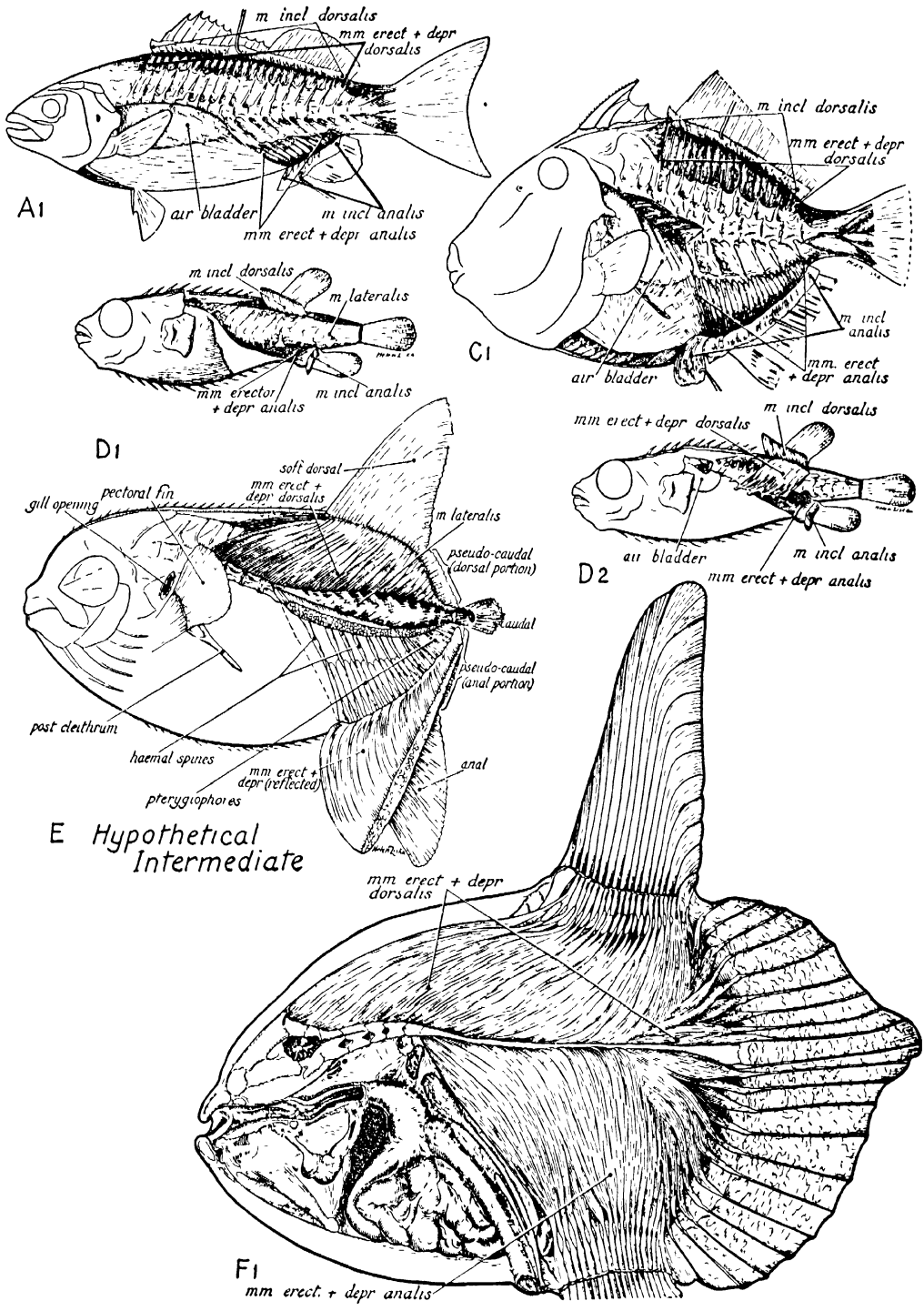

pterygiophores
neural spines
epurals
hypurals
haemal spines
pelvic bone
ribs
pterygiophores
A Roccus
pterygiophores
neural spines
epurals
hypurals
haemal spines
post cleithrum
pelvic bone
rudiment of pelvic fin
pterygiophores
C Balistes
pterygiophores
neural spines
epurals
post cleithrum
hypurals
haemal spines
pelvic bone
ribs
pterygiophores
B Hepatus
neural spines
pterygiophores
haemal spines
post cleithrum
pterygiophores
D Diodon
pterygiophores
neural spines
post cleithrum
haemal spines
pterygiophores
F Masturus

Fig. 9.110a



Figs. 9.110a, b. Comparative series showing evolution of the locomotor apparatus of the Nipple-tailed Ocean Sunfish. After H. C. Raven (1939).

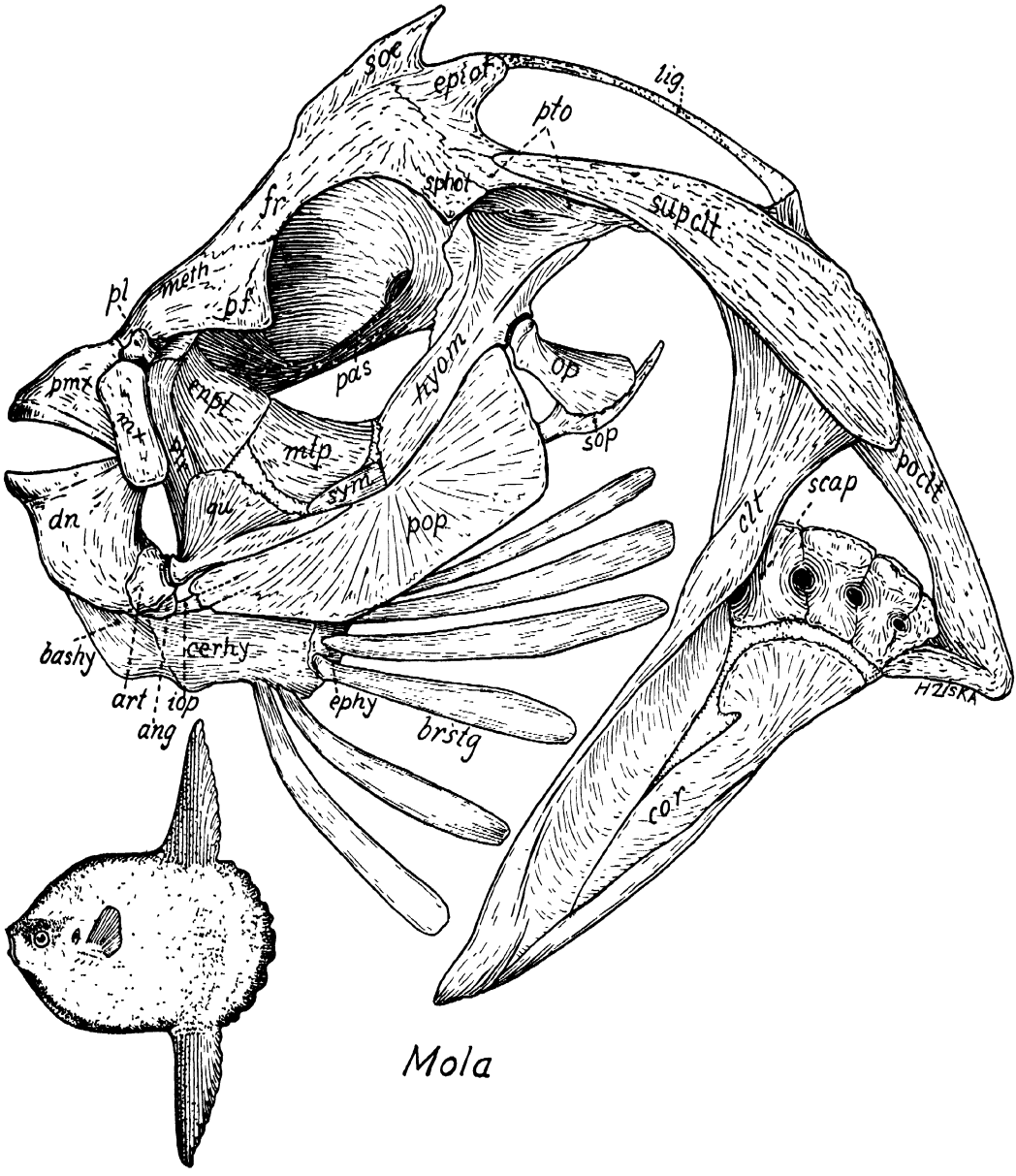


Fig. 9.111. Skull of *Mola*. After Gregory.

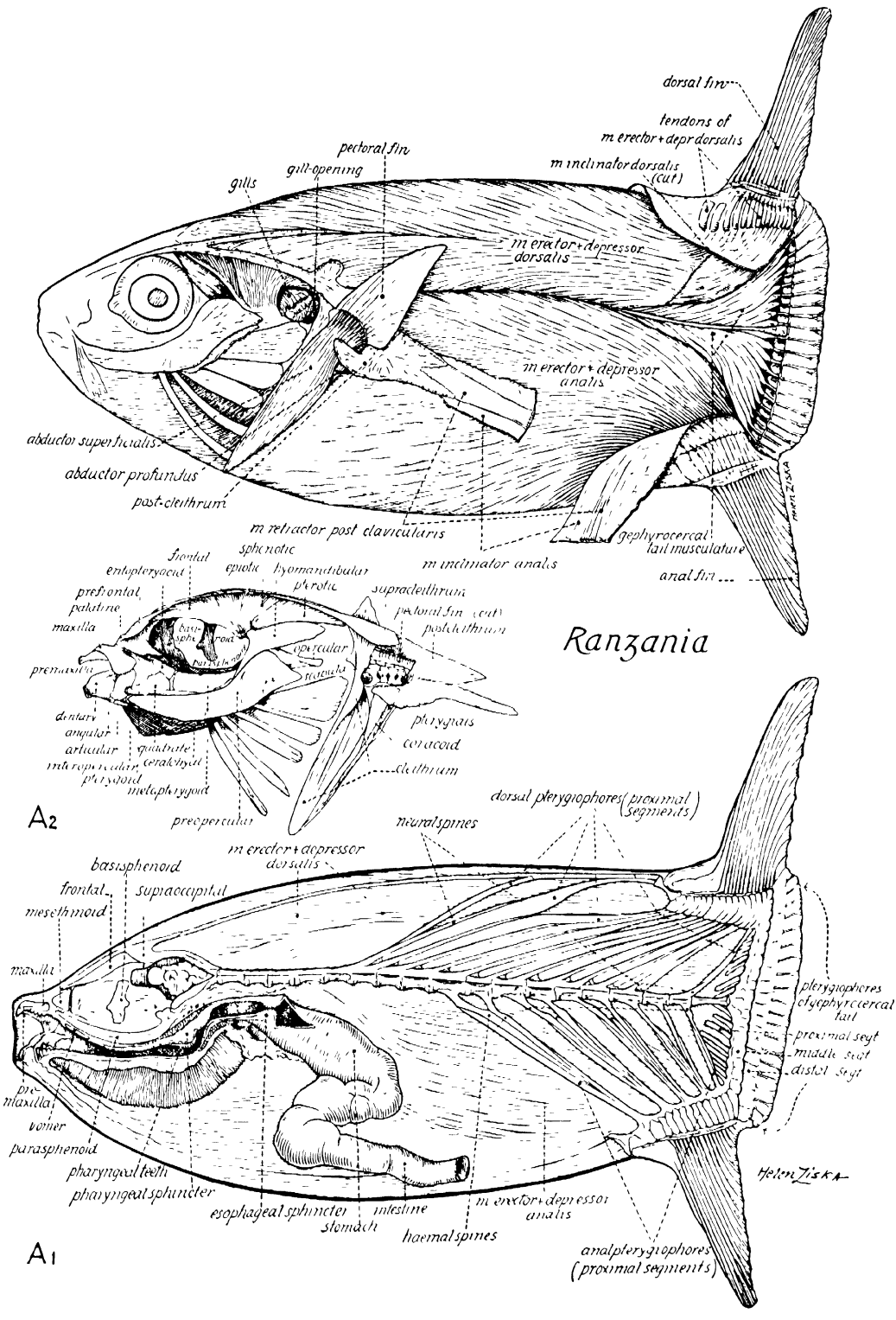


Fig 9 112. Anatomy of *Ranzania* After H C Raven.

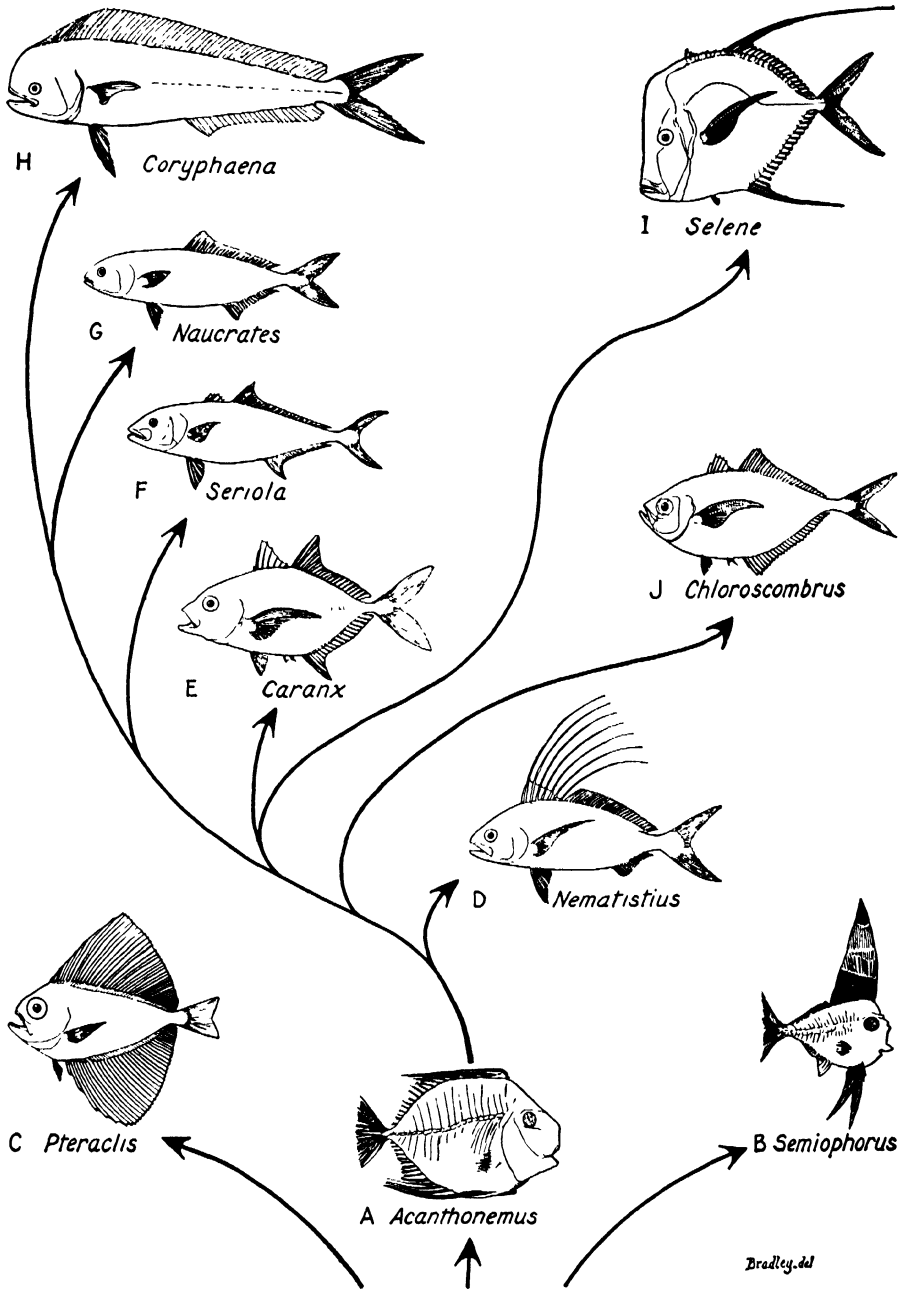


Fig 9.113. Range of body forms in fossil and recent Carangoids. A, B, after Zittel; C, after Good and Bean; D–J, after Jordan and Evermann.

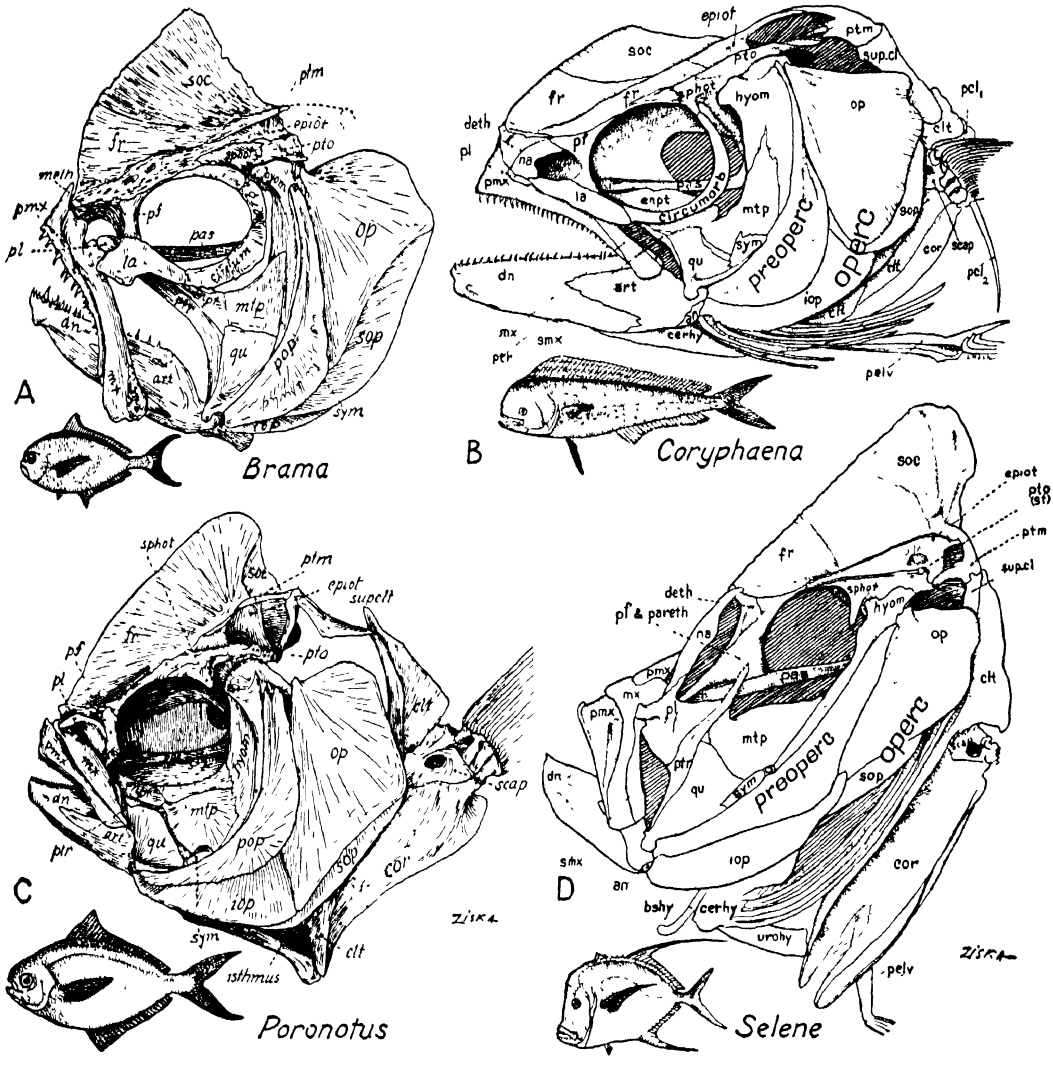


Fig. 9.114. Skull forms of Carangoids. After Gregory.

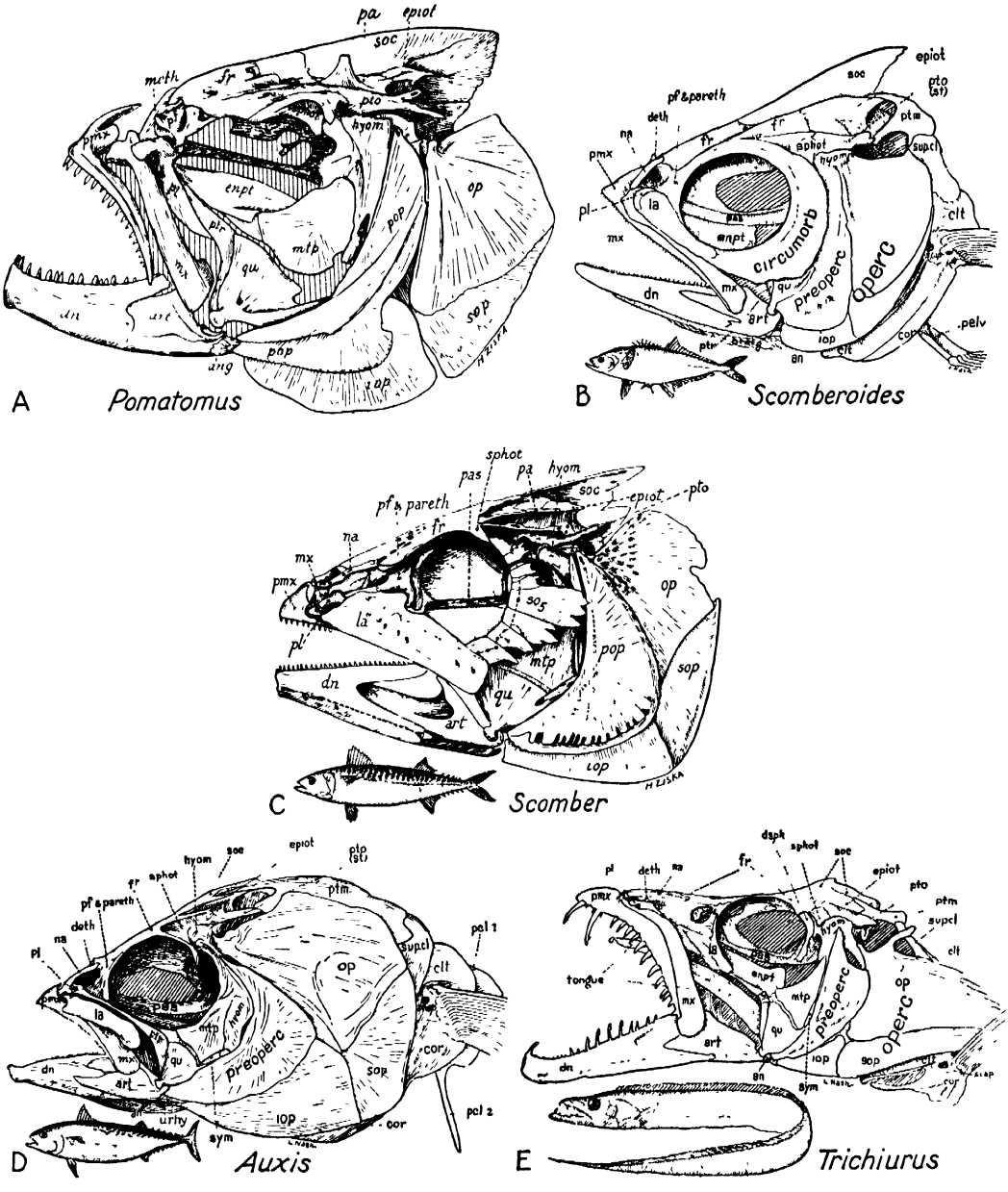


Fig. 9.115. A relatively primitive Percoid (A), a progressive Carangid (B) and three specialized scombroid skull types (C–E). After Gregory.

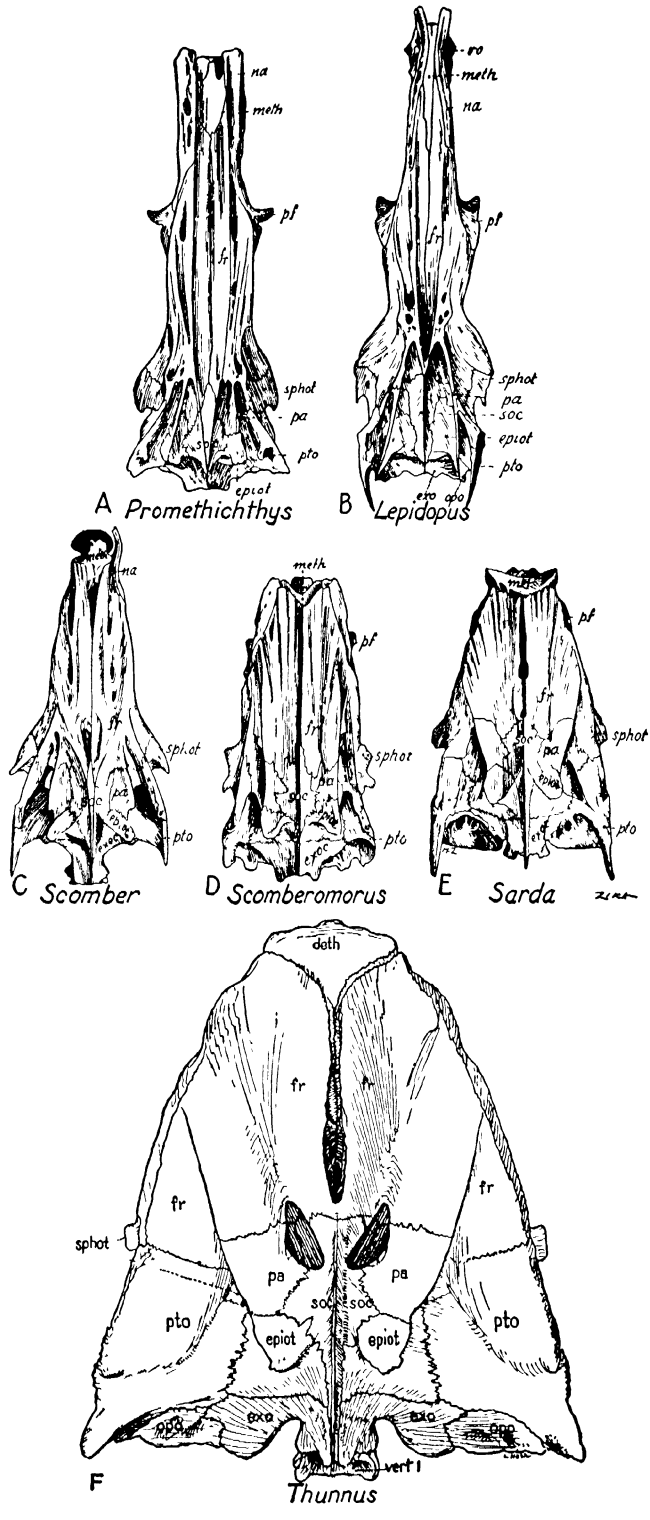


Fig. 9.116. Range in skull form in Scombroids. Top views. A–E, after Starks; F, after Gregory.

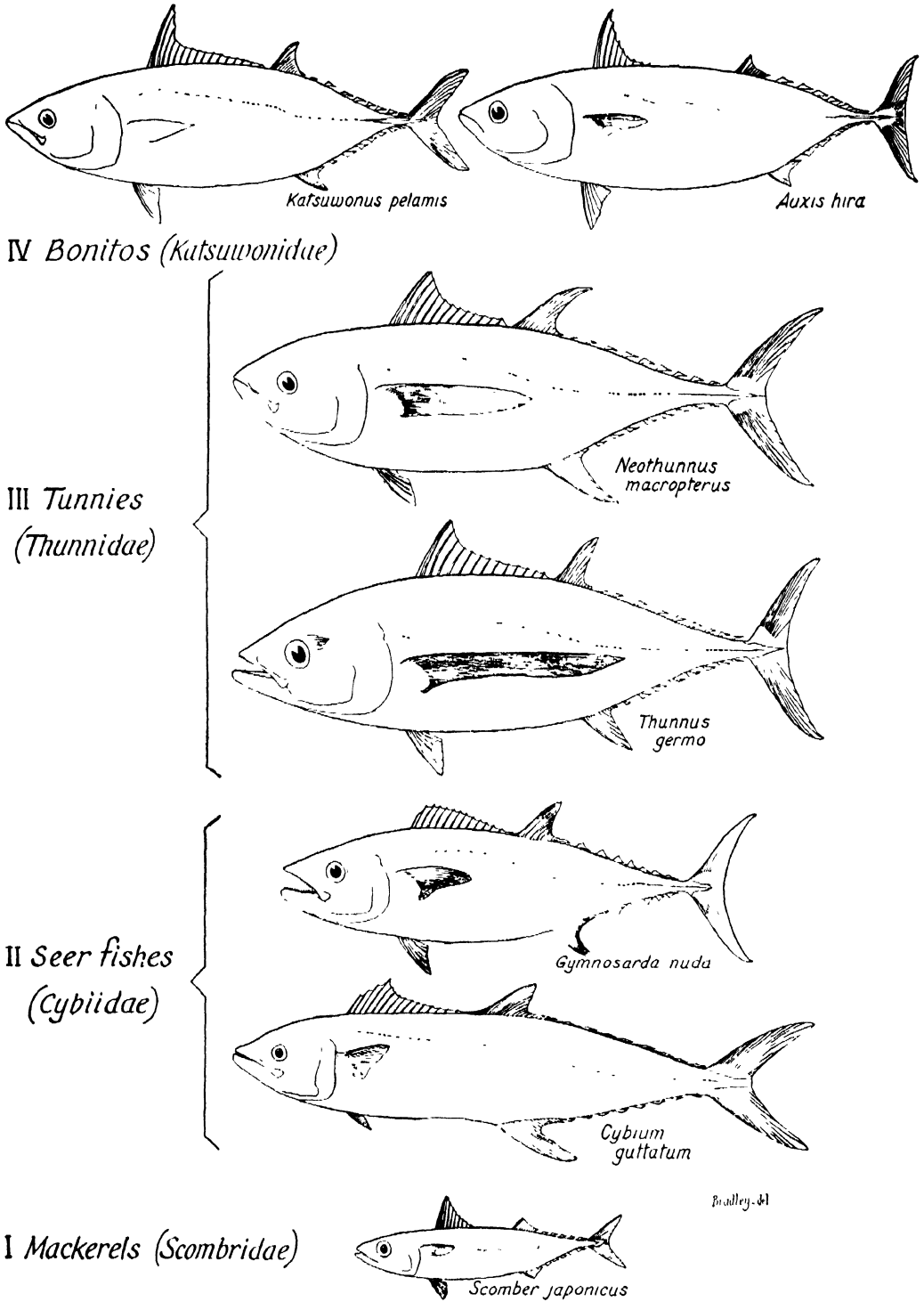
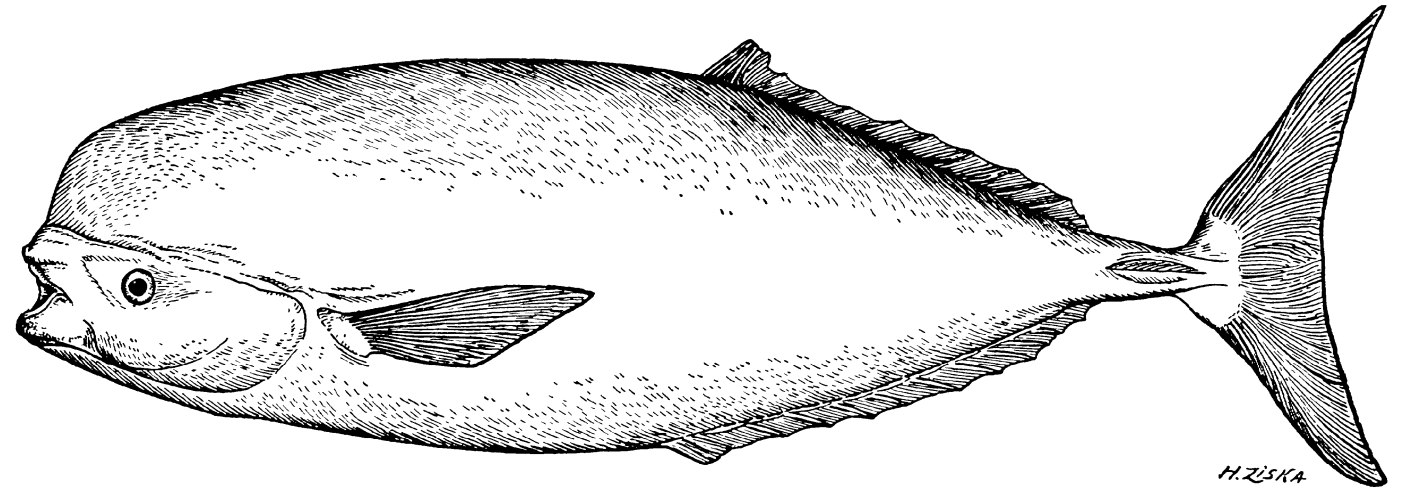


Fig. 9.117. Four grades in the Mackerel tribe. Figures, names and data after Kishinouye.



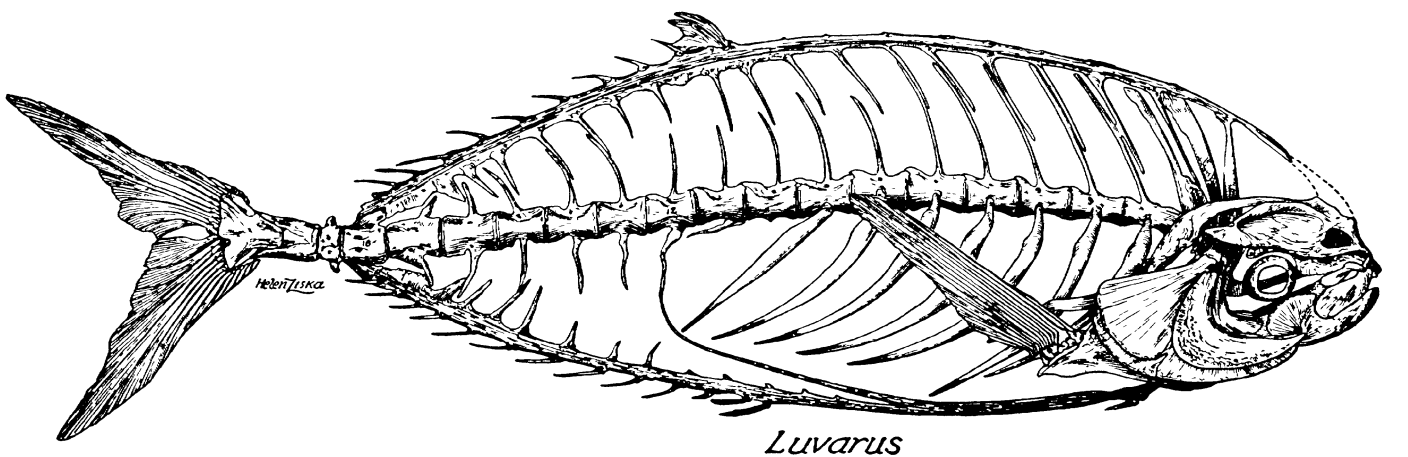


Fig. 9.118 (top). The Louvar. After Gregory and Conrad.
Fig. 9.119. Skeleton of the Louvar. After Gregory and Conrad.

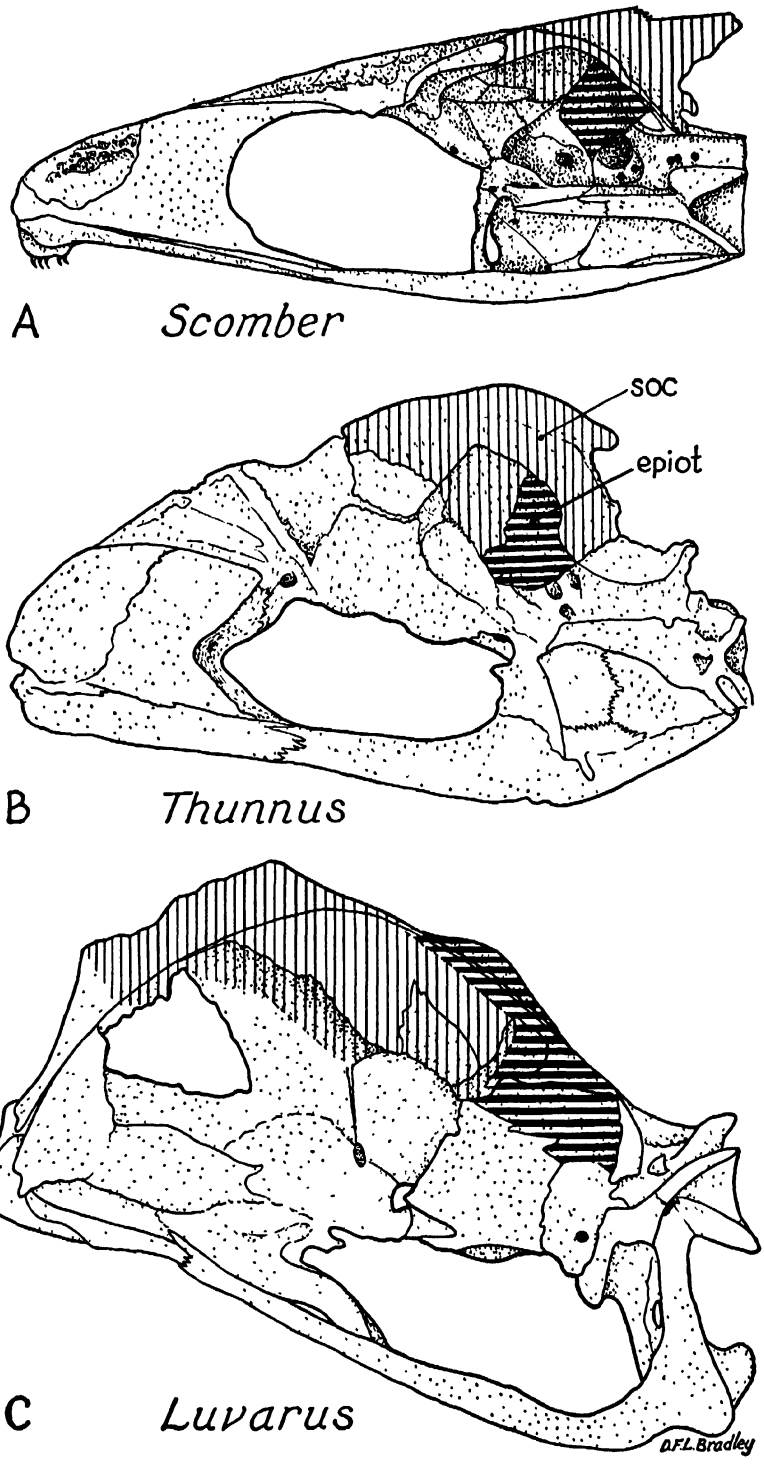


Fig. 9.120. Comparative mesial sections of skulls of Mackerel, Tunny and Louvar, indicating progressive enlargement and forward shift of supraoccipital (vertical lines) and epiotic (horizontal). After Gregory and Conrad.

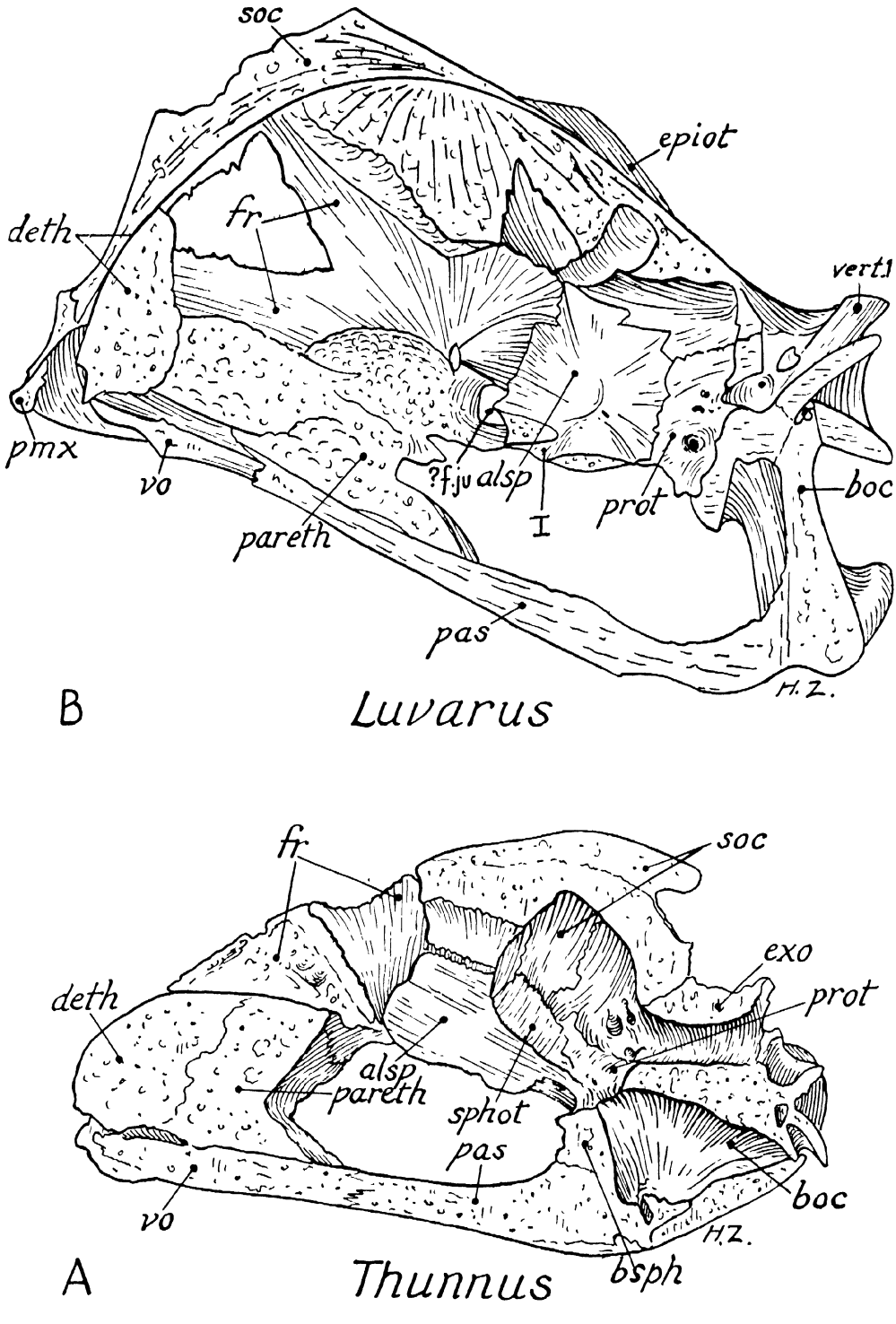


Fig. 9.121. Mesial sections of skulls showing homologous parts in Louvar and Tunny. After Gregory and Conrad (1943).

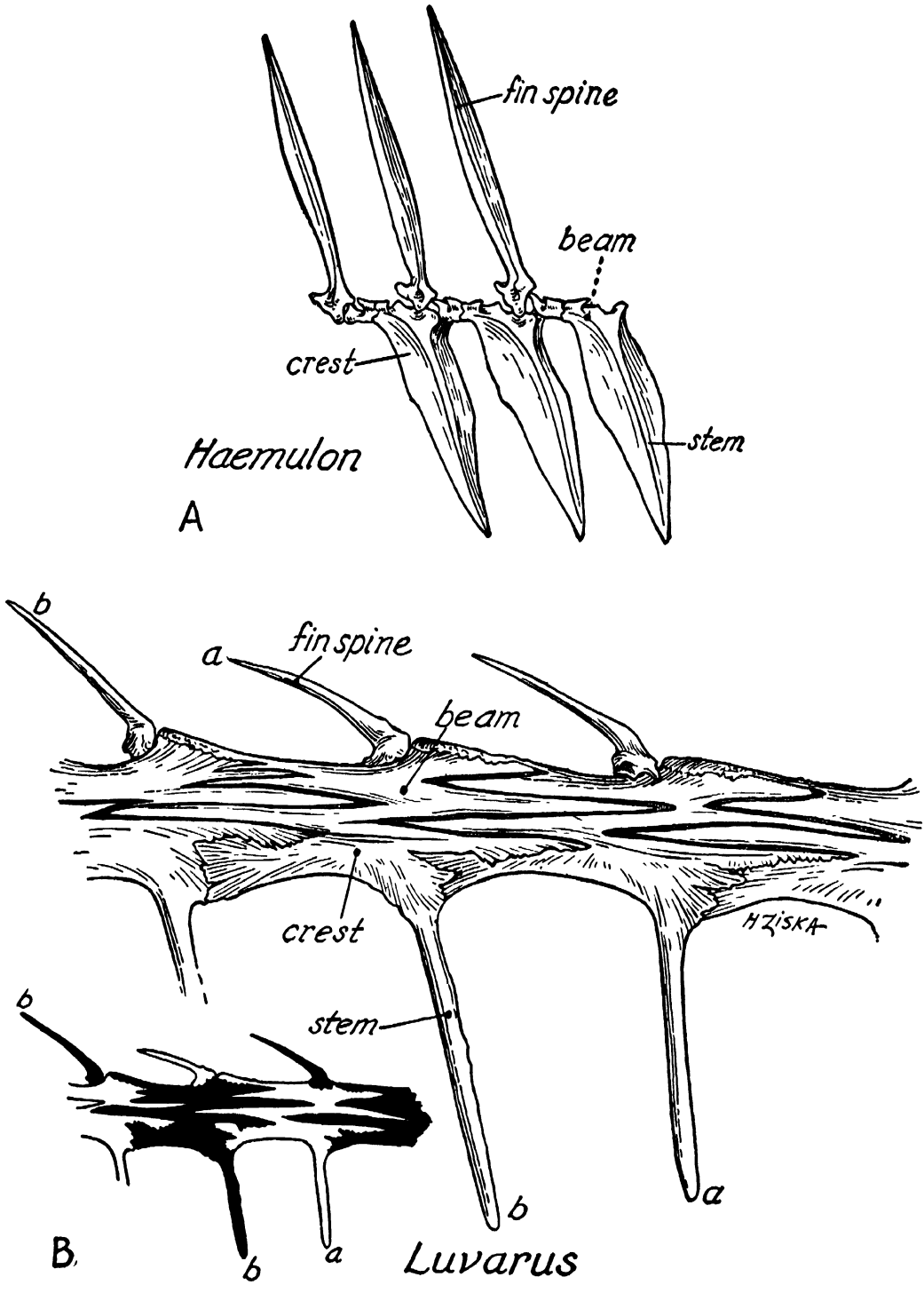


Fig. 9.122. Formation of dorsal truss by zigzag interlocking of portions of the pterygiophores. After Gregory and Conrad.

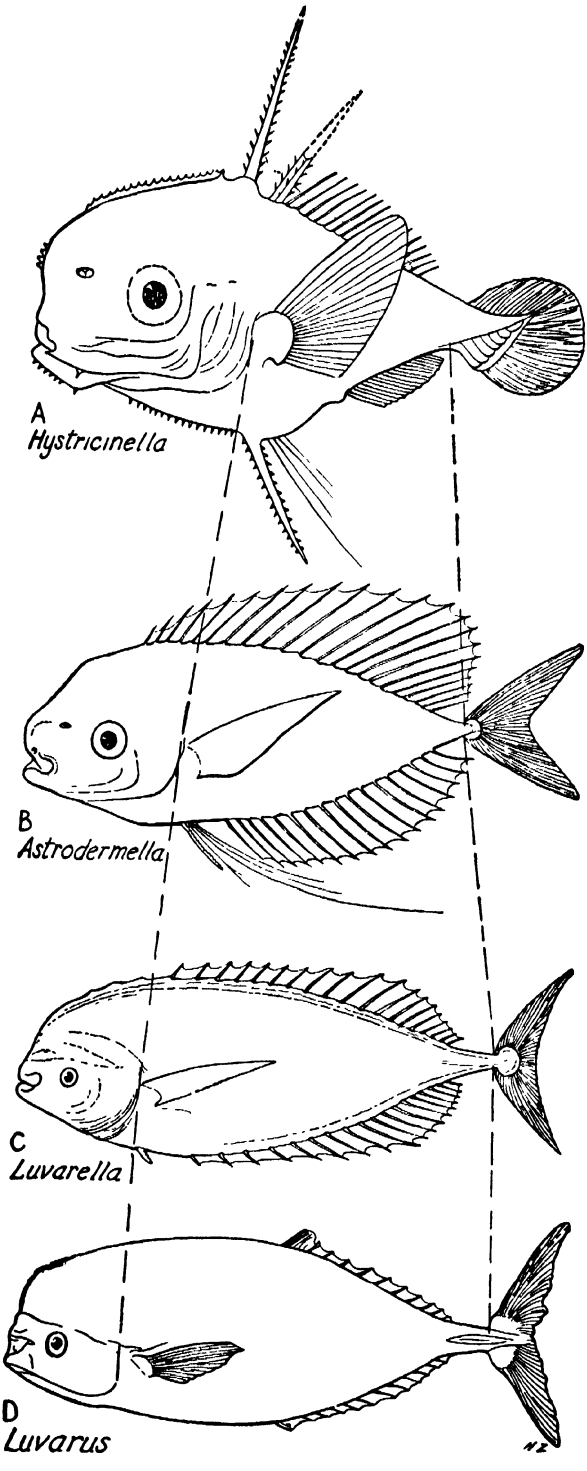


Fig. 9.123. "Hypermetamorphosis" from larval to adult Louvar. All figures reduced to same length in order to show relative decrease in head length and relative lengthening of body. From Gregory and Conrad, after Roule.

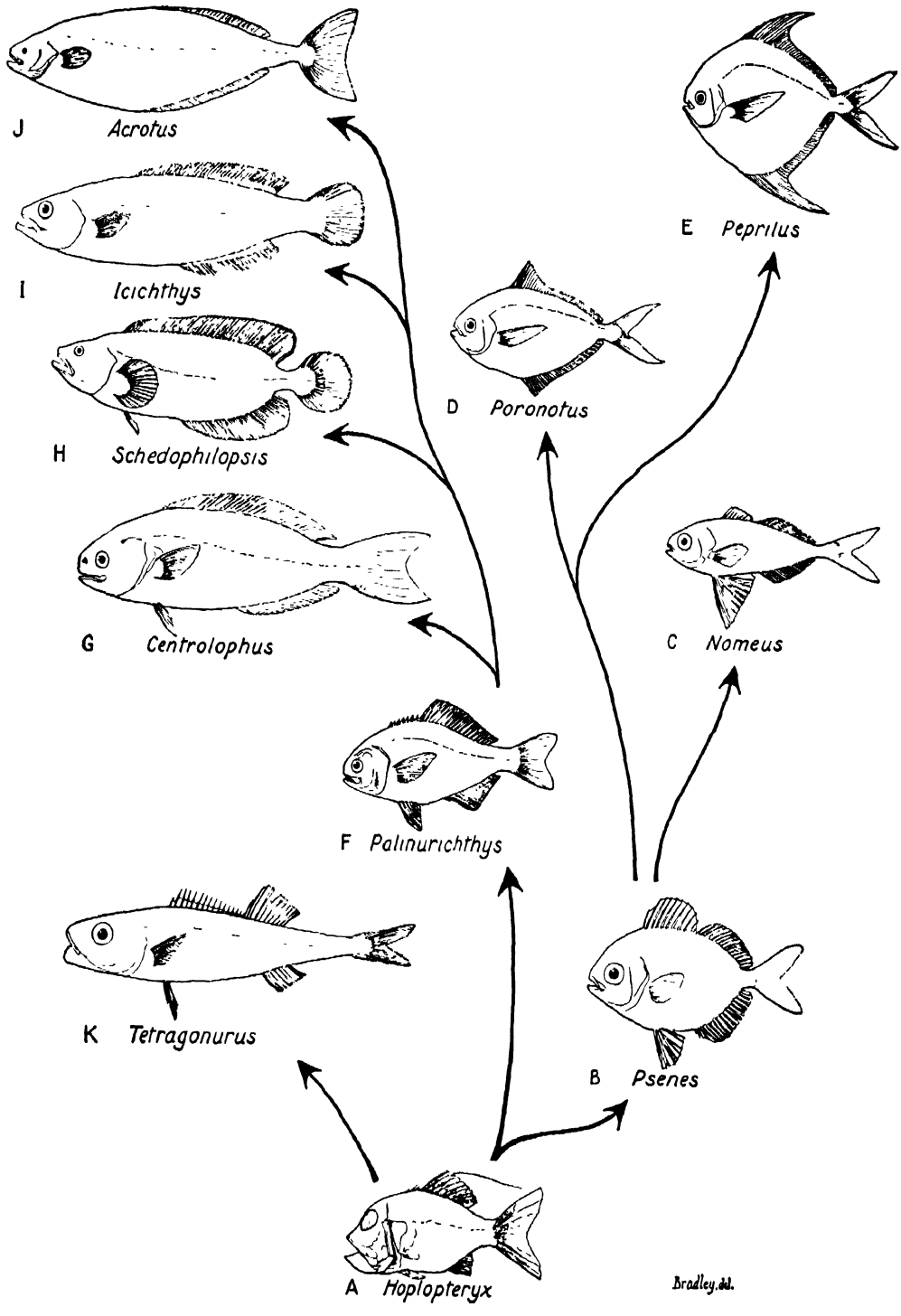


Fig. 9.124. Adaptive branching in the Stromateoids.
Individual figures after Goode and Bean.

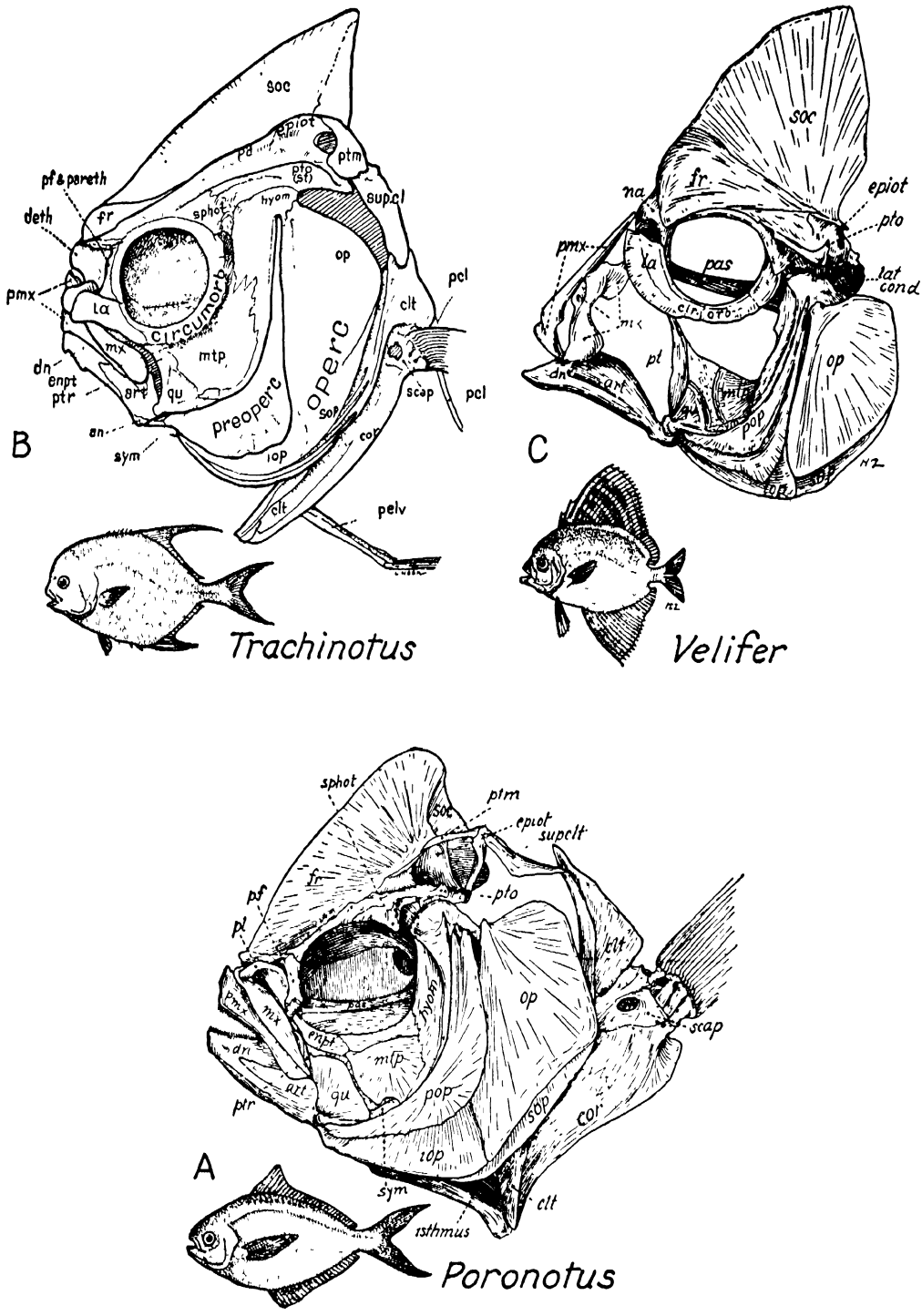


Fig. 9.125. Parallel evolution of similar body form and skull in a Stromateid (A), Carangoid (B) and Allotriognath (C). After Gregory.

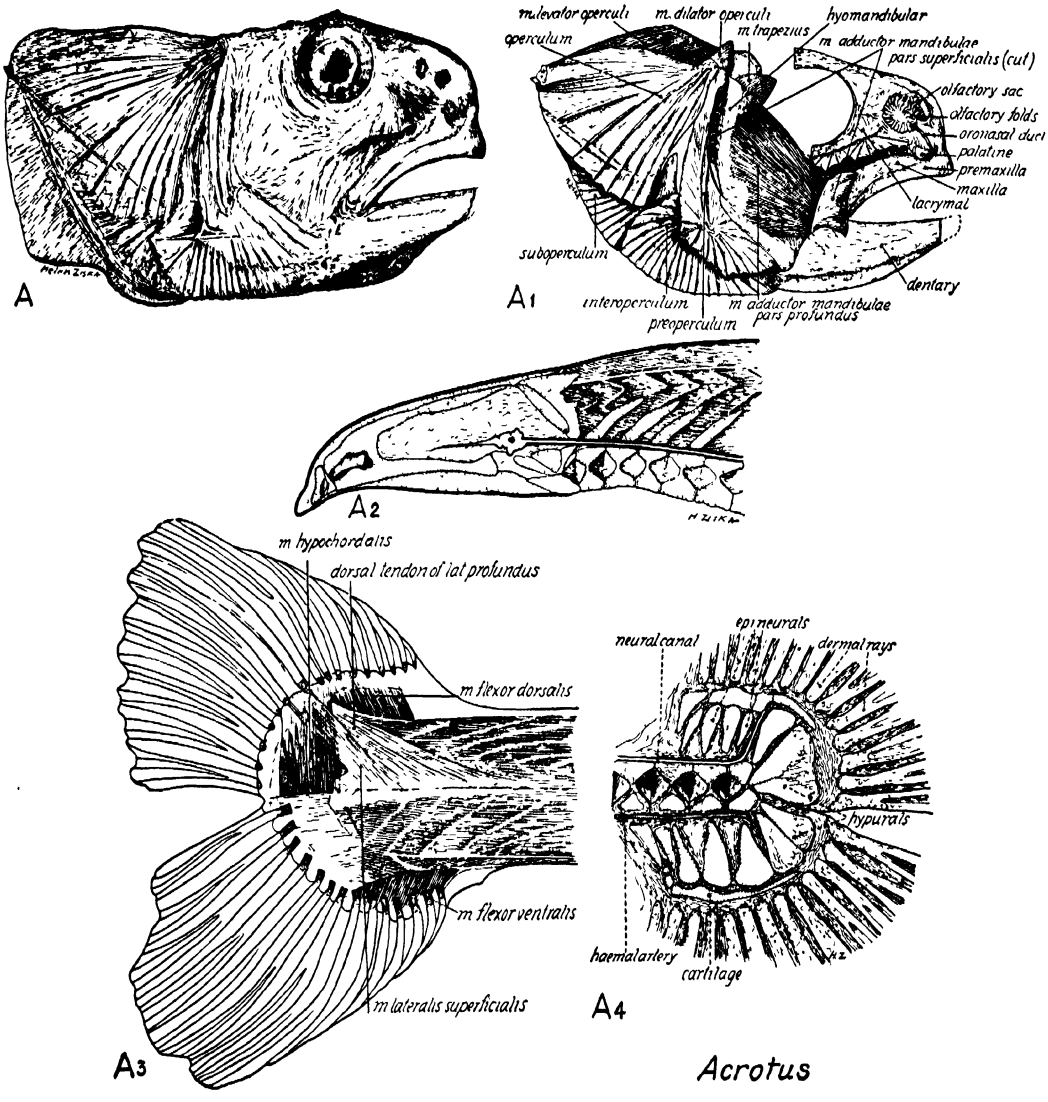


Fig. 9.126. Skeletal parts of deep-sea fish, *Acrotus*.
After H. C. Raven.

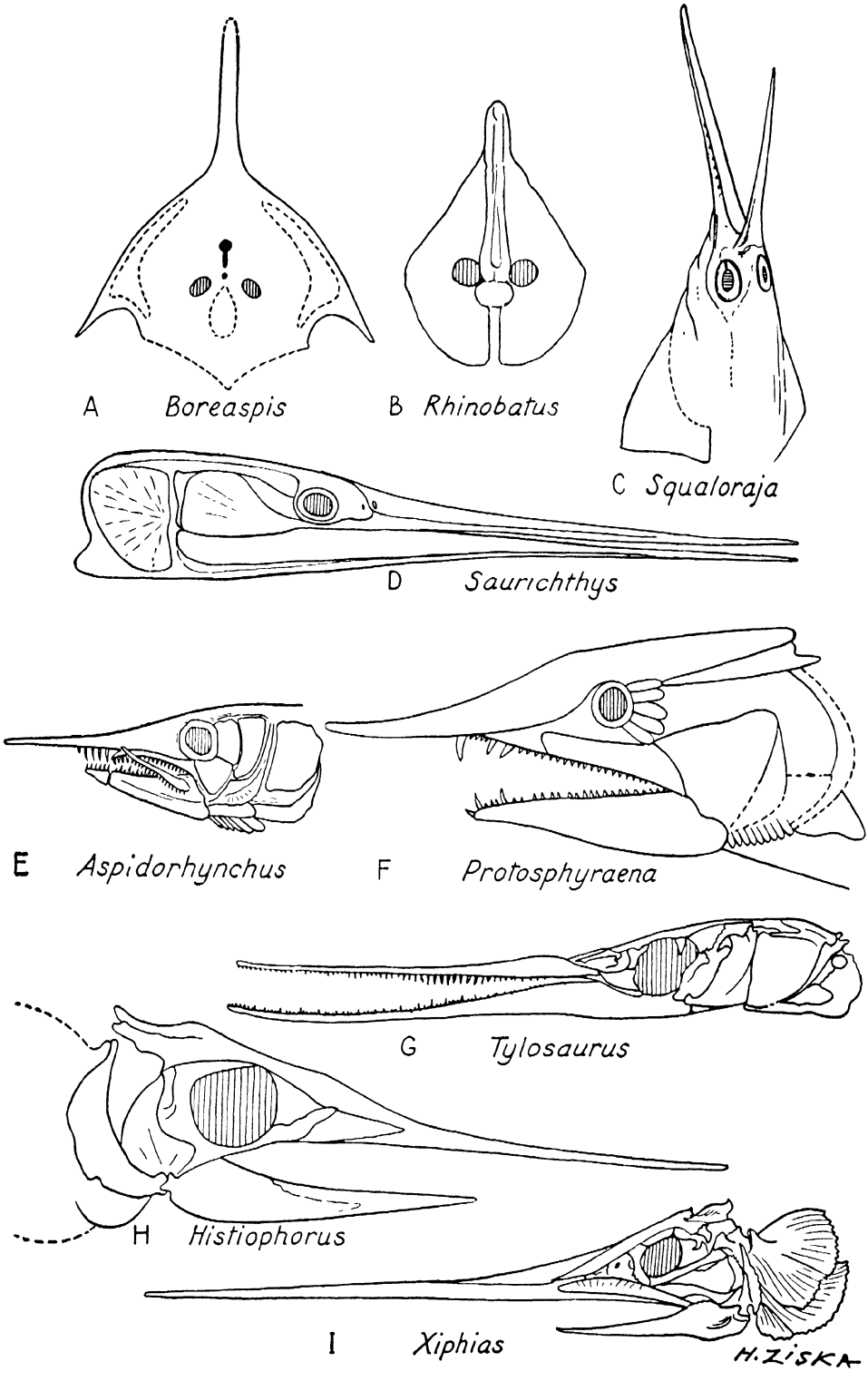


Fig. 9.127. Convergent evolution of "spear" or "sword" snouts in different groups of fishes.

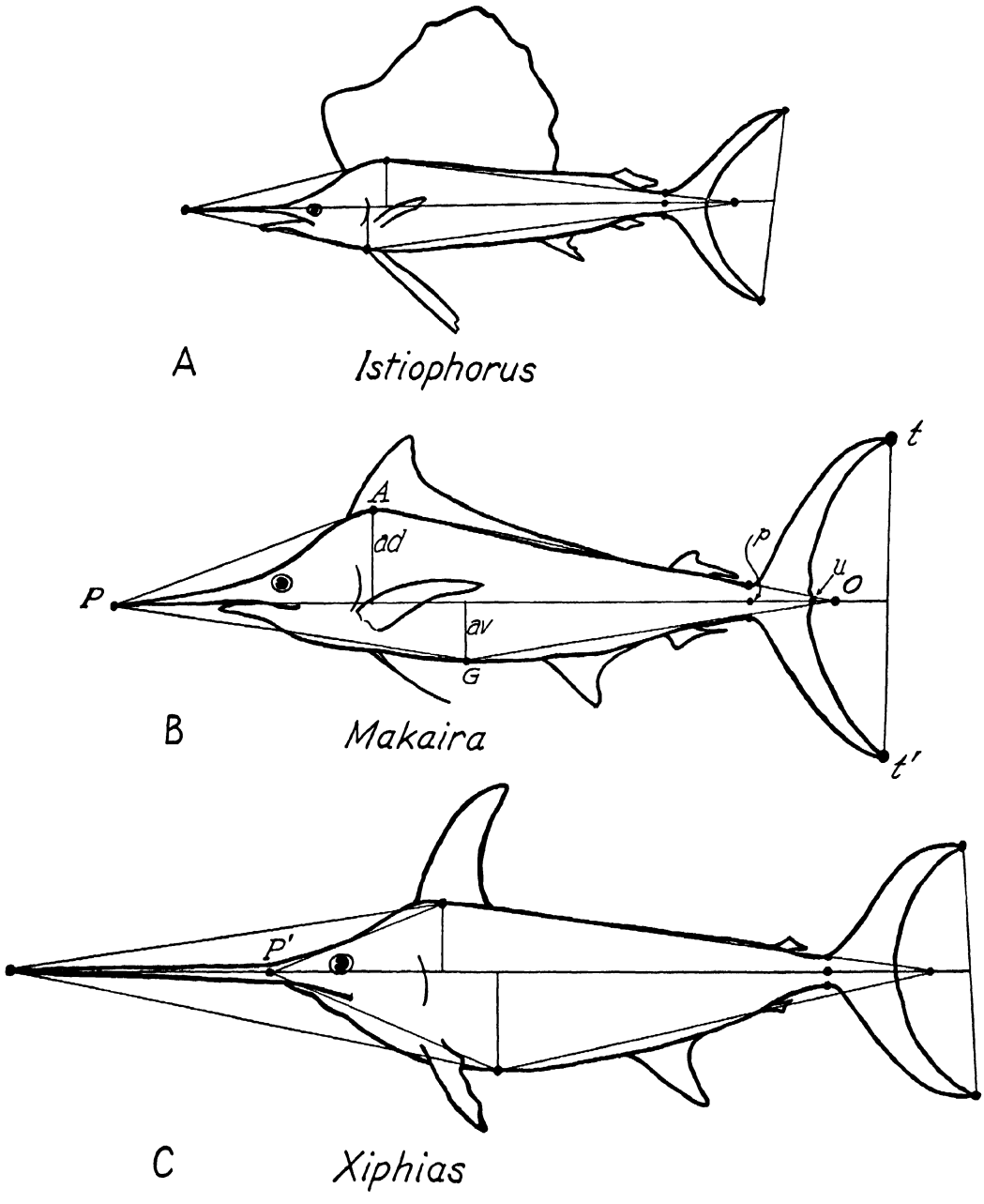


Fig. 9.128. Sailfish (A), Marlin (B) and Swordfish (C). *A*, apex; *G*, gasterion; *P*, prosthion; *p*, pygidion; *tt*, tailspread; *u*, uranion; *O*, opisthion. After Gregory and Conrad.

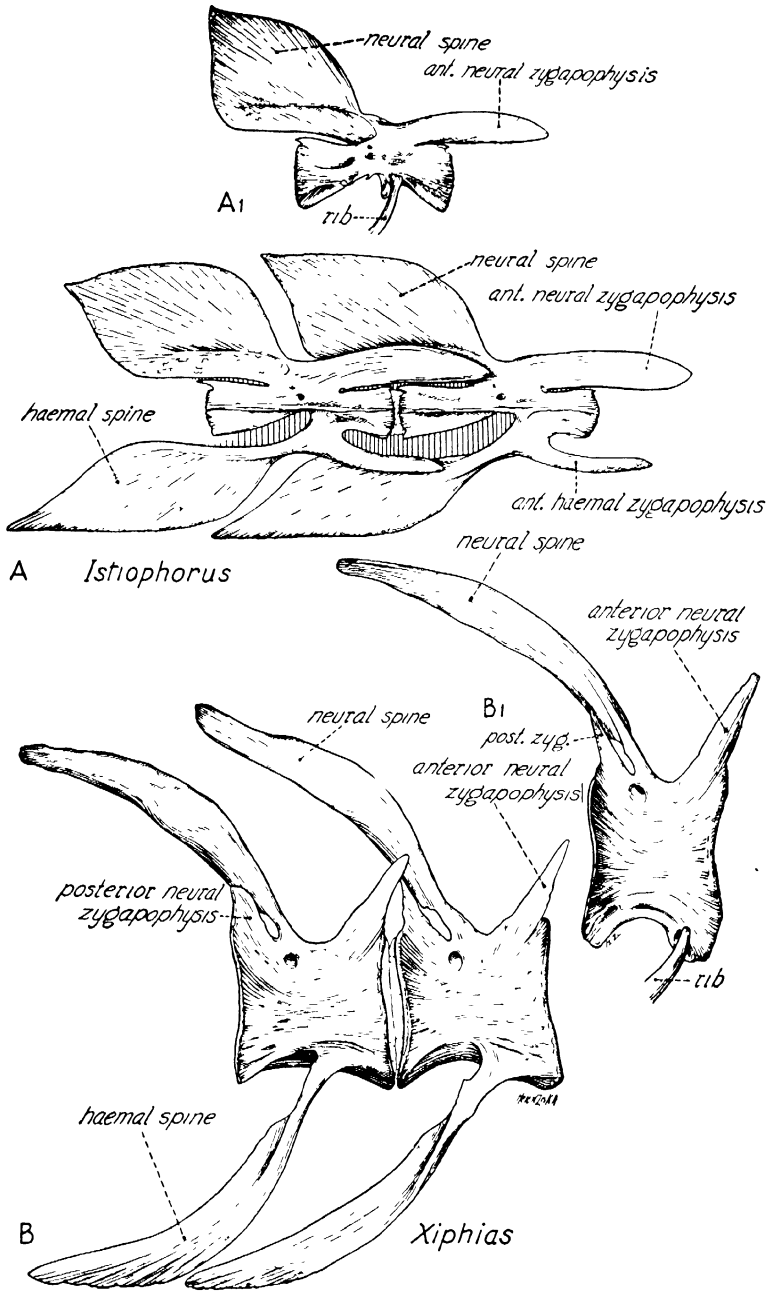


Fig. 9 129. Vertebrae of *Istiophorus* and *Xiphias*. After Gregory and Conrad.

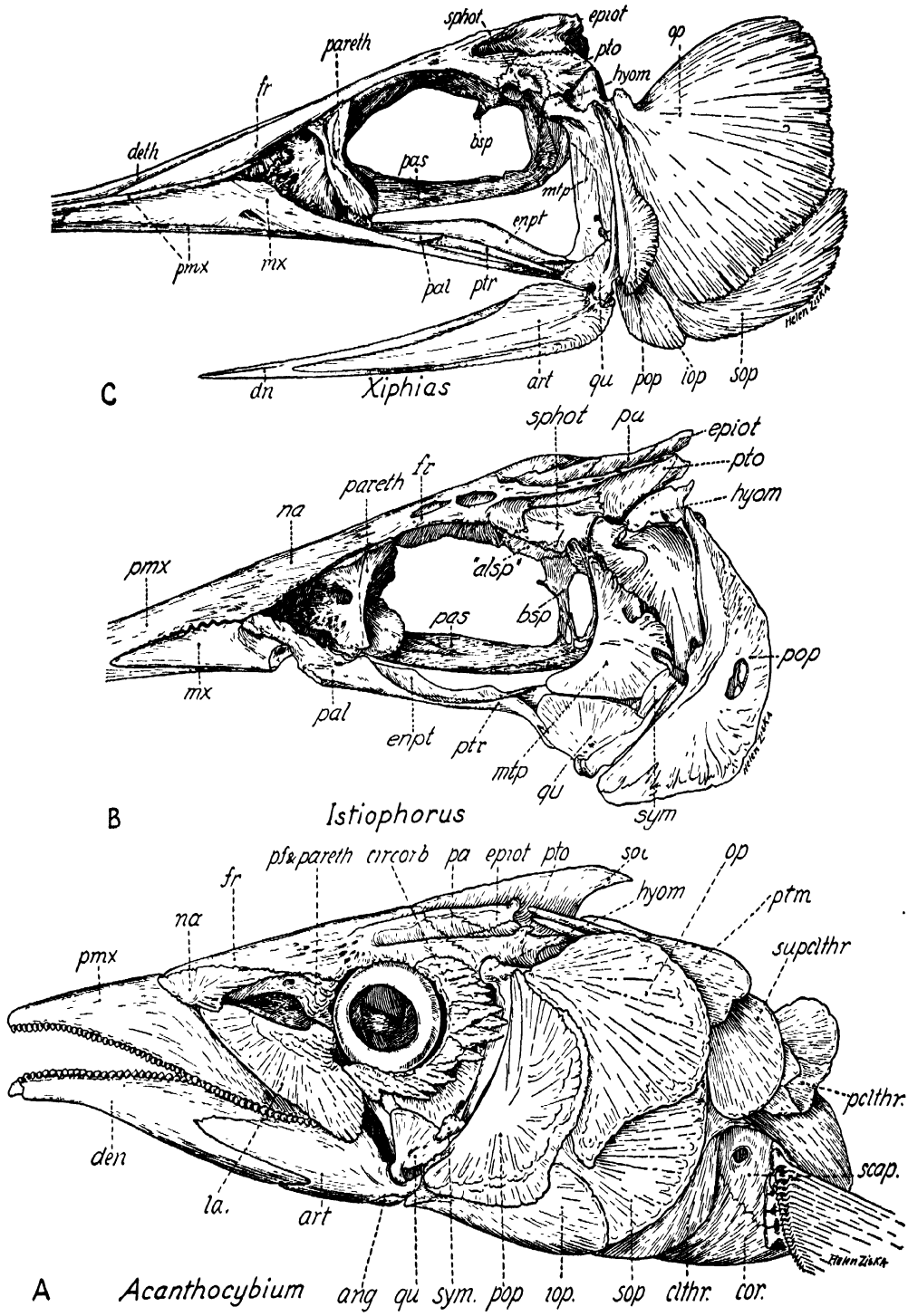


Fig. 9.130. Skulls of Scombrid (A), Sailfish (B) and Swordfish (C). Scales of reduction different. A, after Gregory and Conrad; B, C, after Gregory.

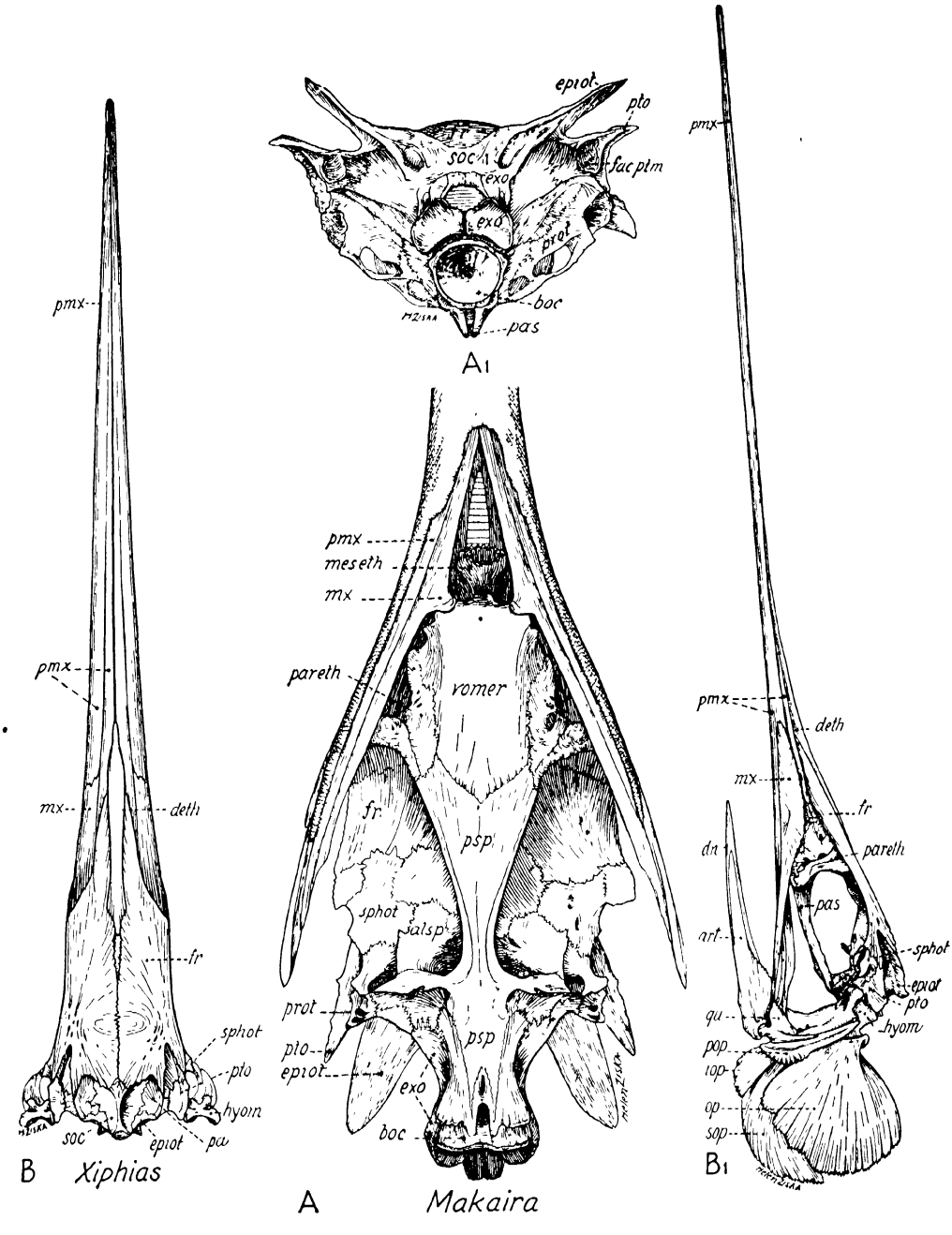


Fig. 9.131. Bracing of the rostrum: against the ethmovomer block (A); against the spongy ethmoid buffer and the frontal region of the skull roof (B, B1); against the backbone by means of the tripartite occipital condyle (A1). From Gudger after Gregory.

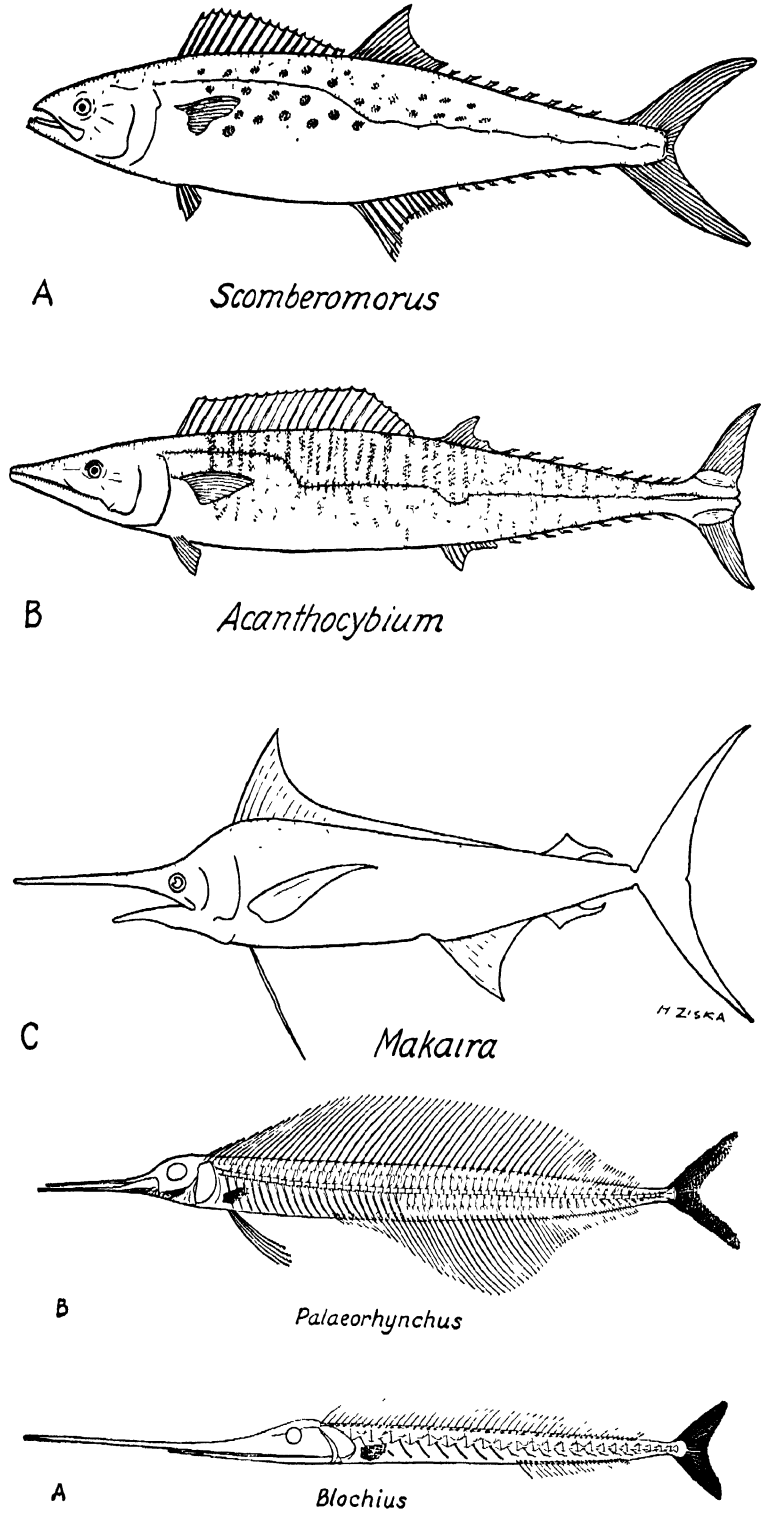


Fig. 9.132 (top). Comparison of Marlin (C) with two Scombroids (B, A). After Gregory and Conrad.

Fig. 9.133. Eocene Swordfish (A) and Oligocene Sailfish (B). After Smith Woodward.

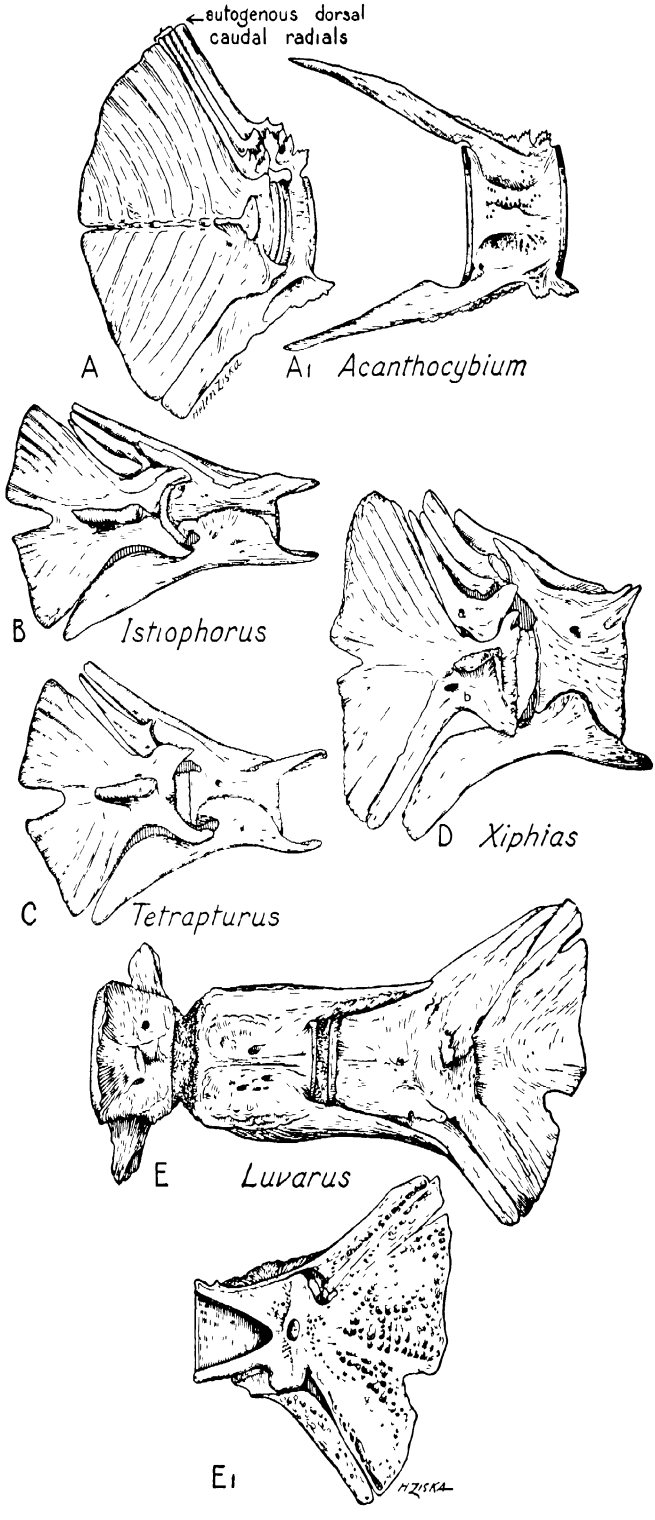


Fig. 9.134. The bony caudal fan in a Scombroid (A), Sailfish (B), Marlin (C), Swordfish (D) and Louvar (E). The marks on the surface of the expanded hypurals have been made by the large and closely appressed bony fin rays.

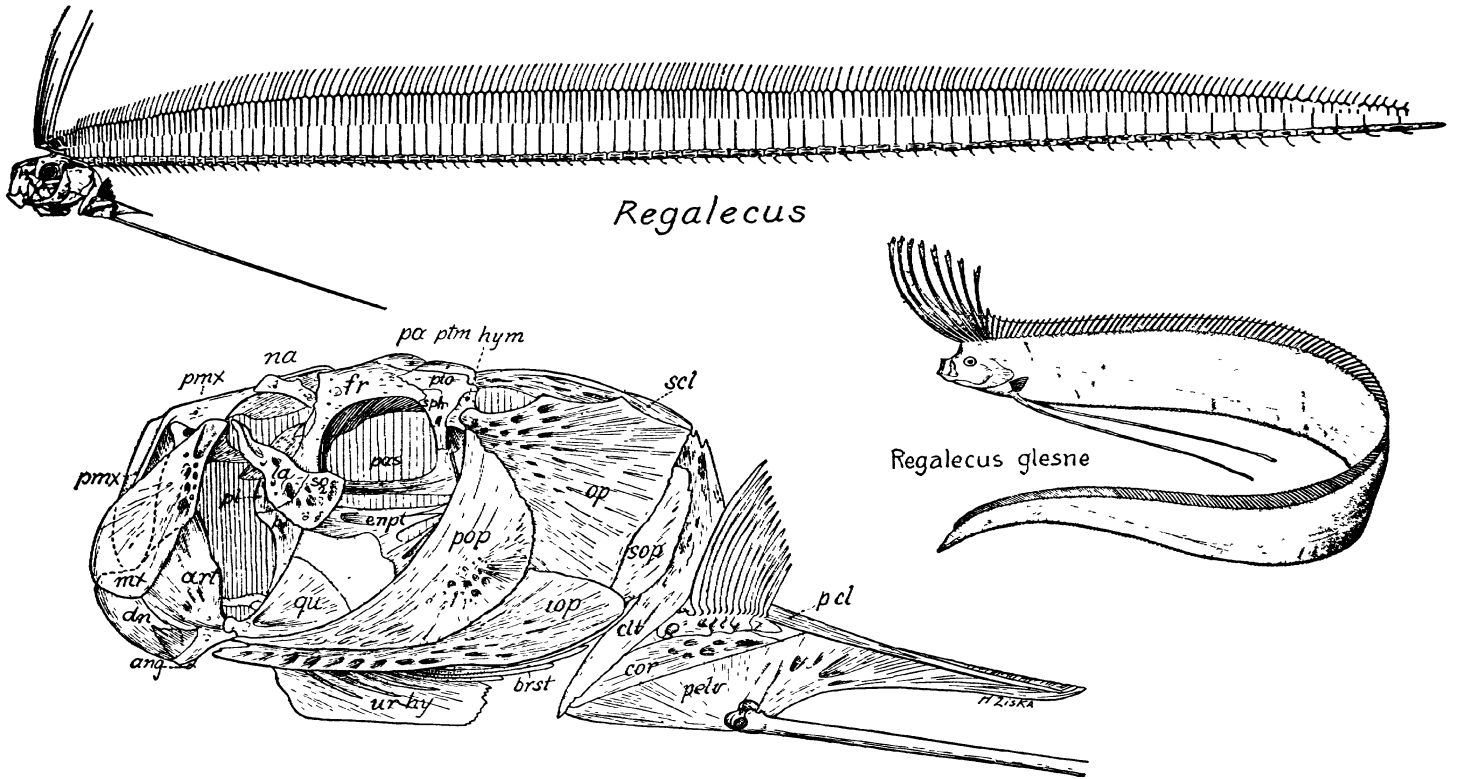


Fig. 9.135a. The "King of the Herrings" of the order Allotriognathi. From Gregory, after T. J. Parker.

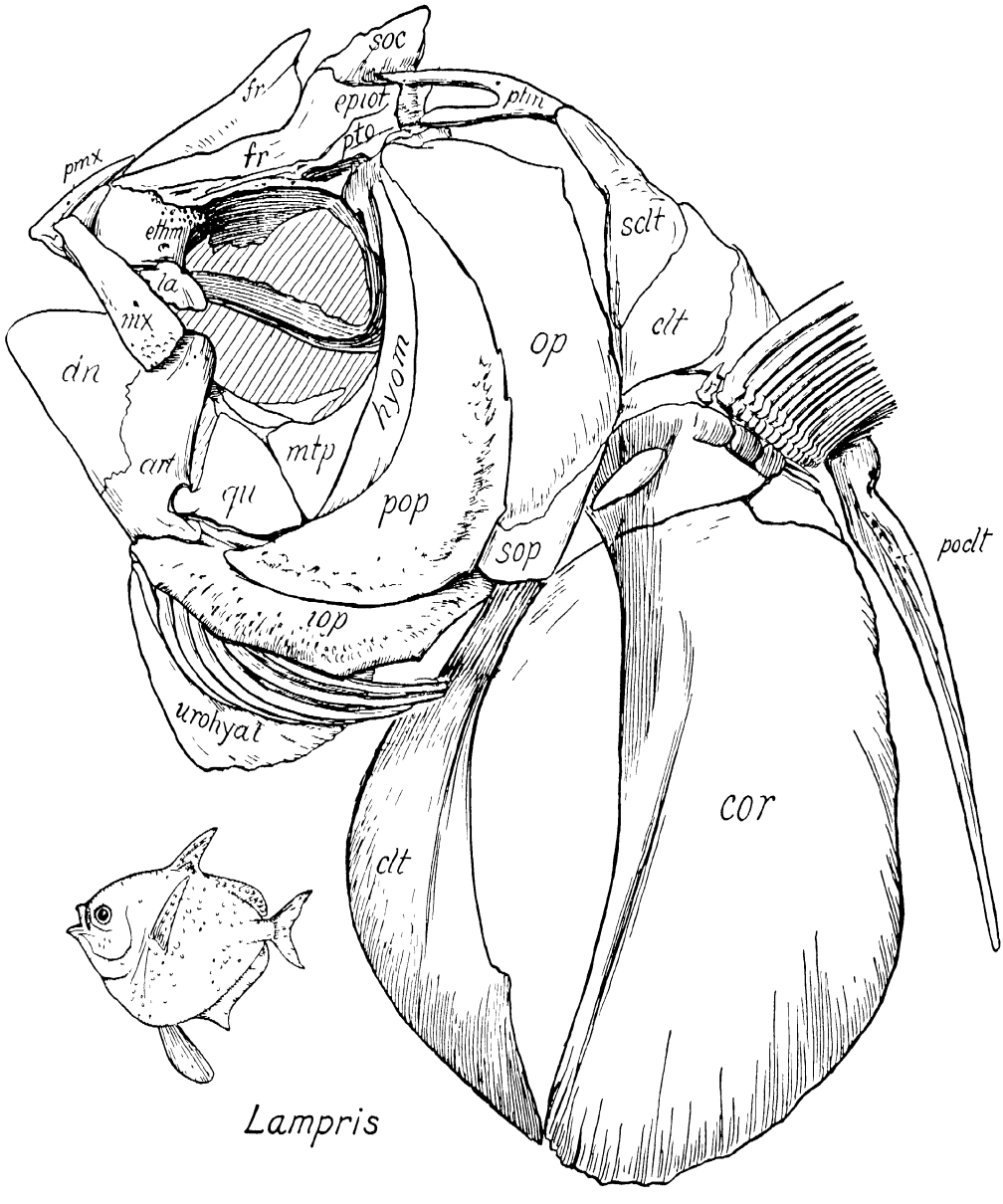
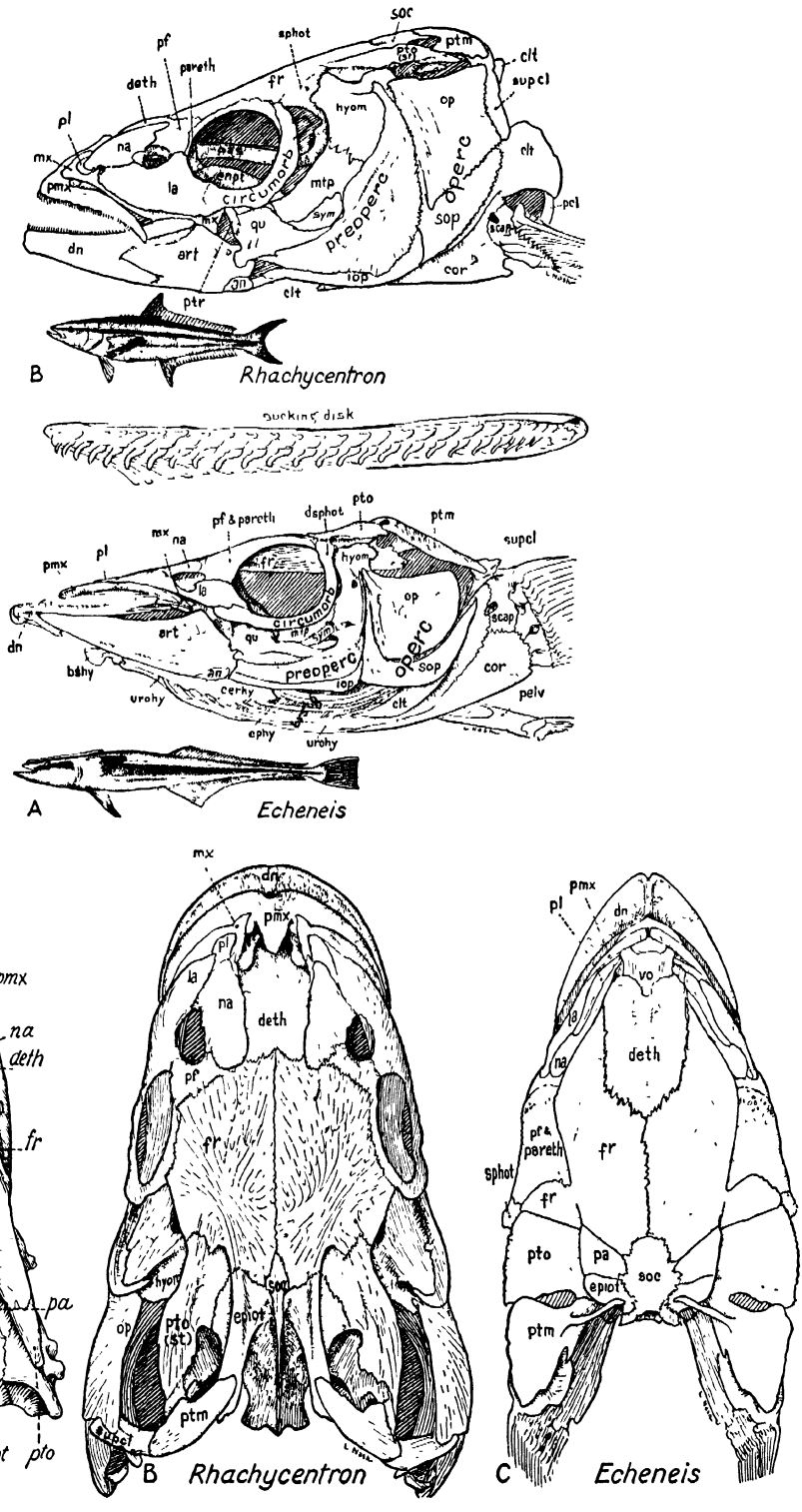


Fig. 9.135b. The "Moonfish." After Gregory.



Figs. 9.136, 137. Comparison of body form and skulls of Sucking-fish (A) and Crab-eater (B). Skull-tops of Mackerel (A), Crab-eater (B) and Sucking-fish (C). After Gregory.

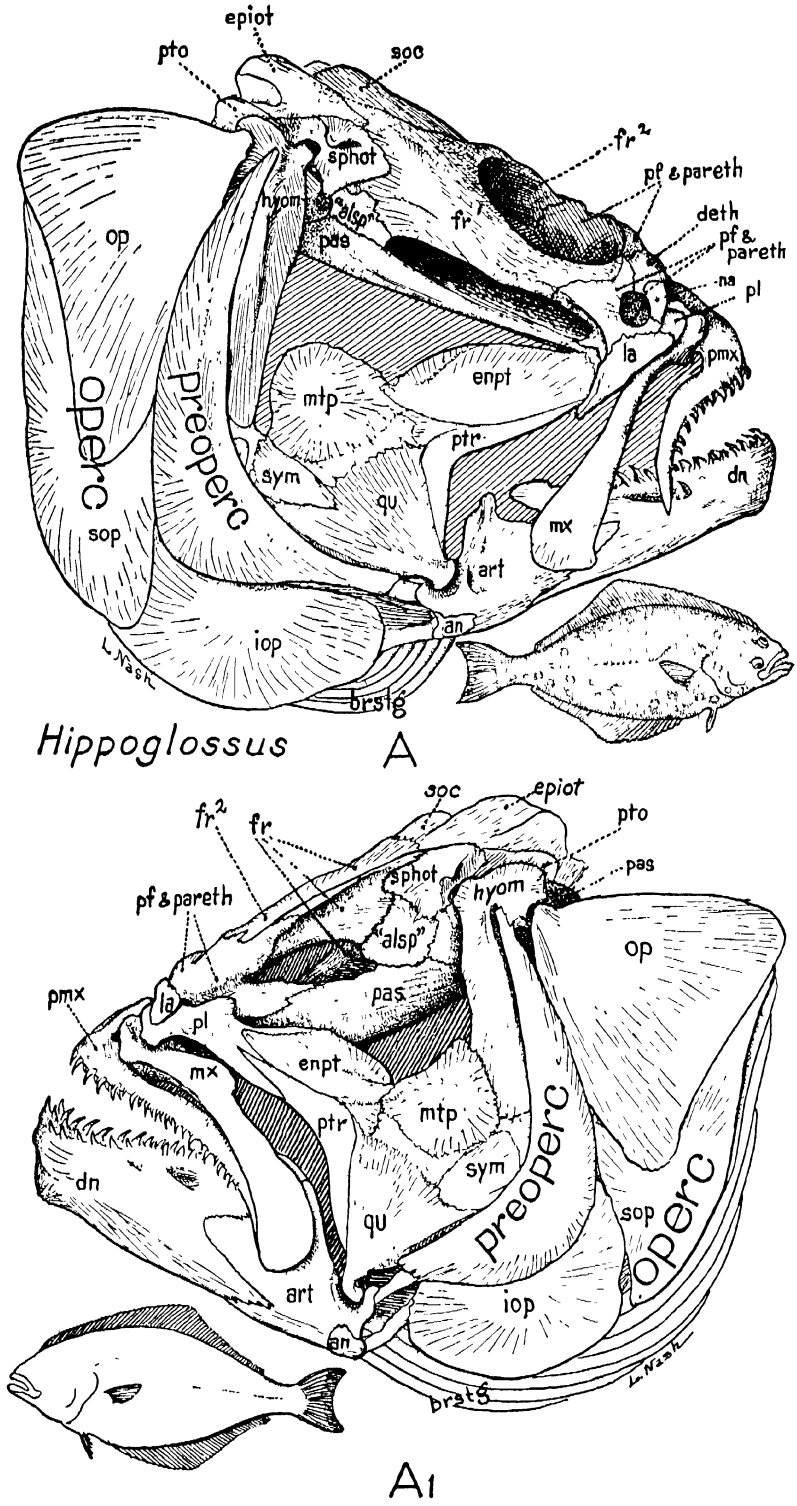


Fig. 9.138. Skull of Flatfish, showing marked asymmetry and readjustment to displacement of eyes to functionally upper side. After Gregory.

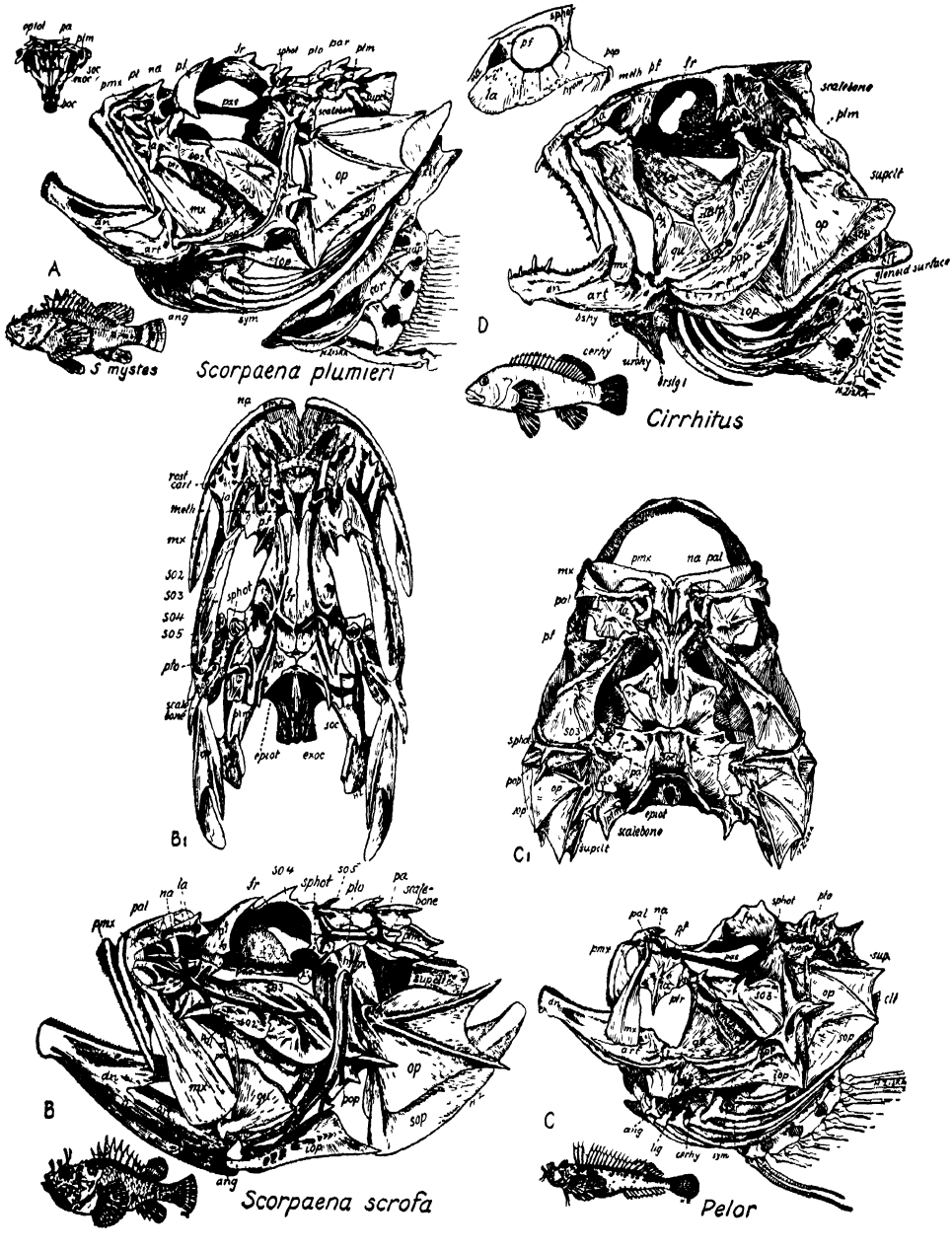


Fig. 9.139. Typical Scorpaenoids (A–C) compared with a cirrhitid Percoid (D). After Gregory.

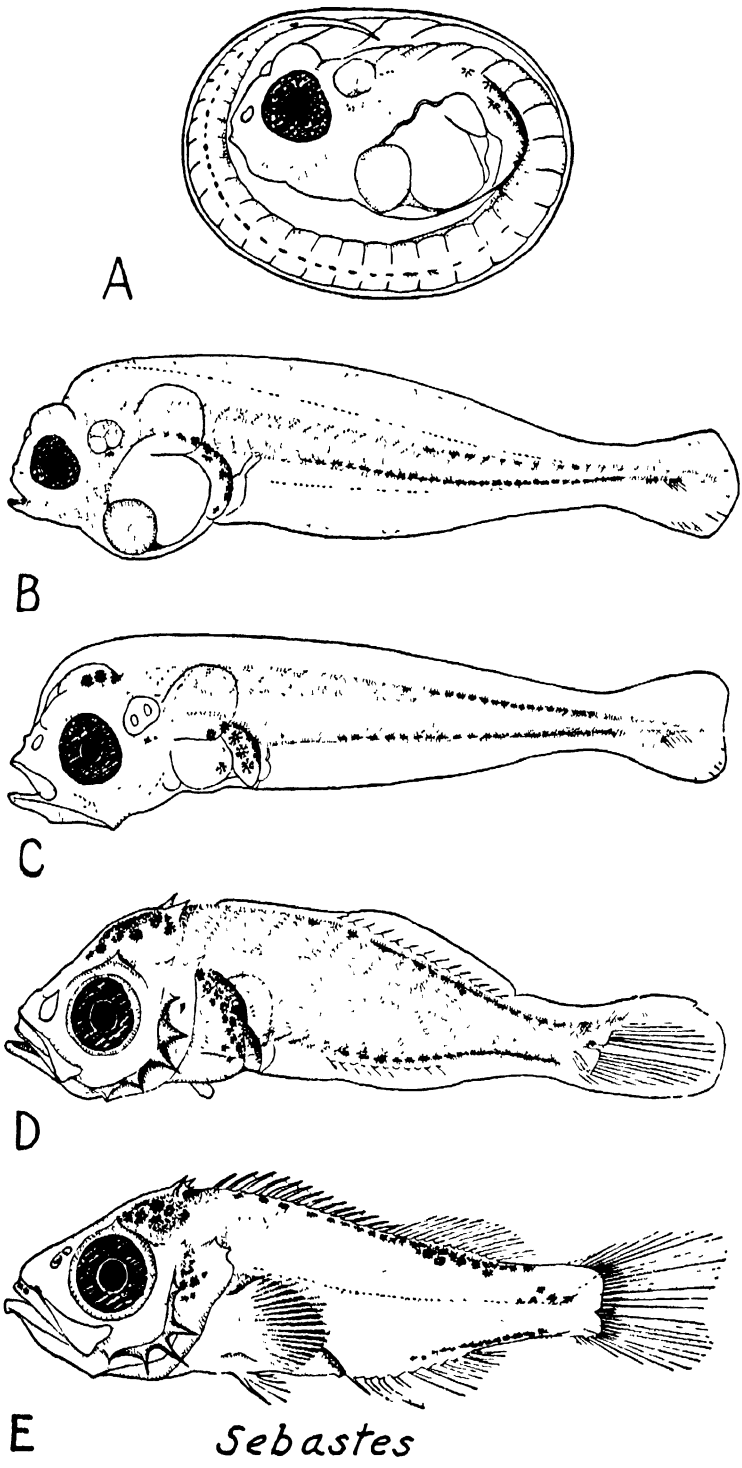


Fig. 9.140. Stages in the development of the Rosefish (*Sebastes marinus*). After Bigelow and Welsh.

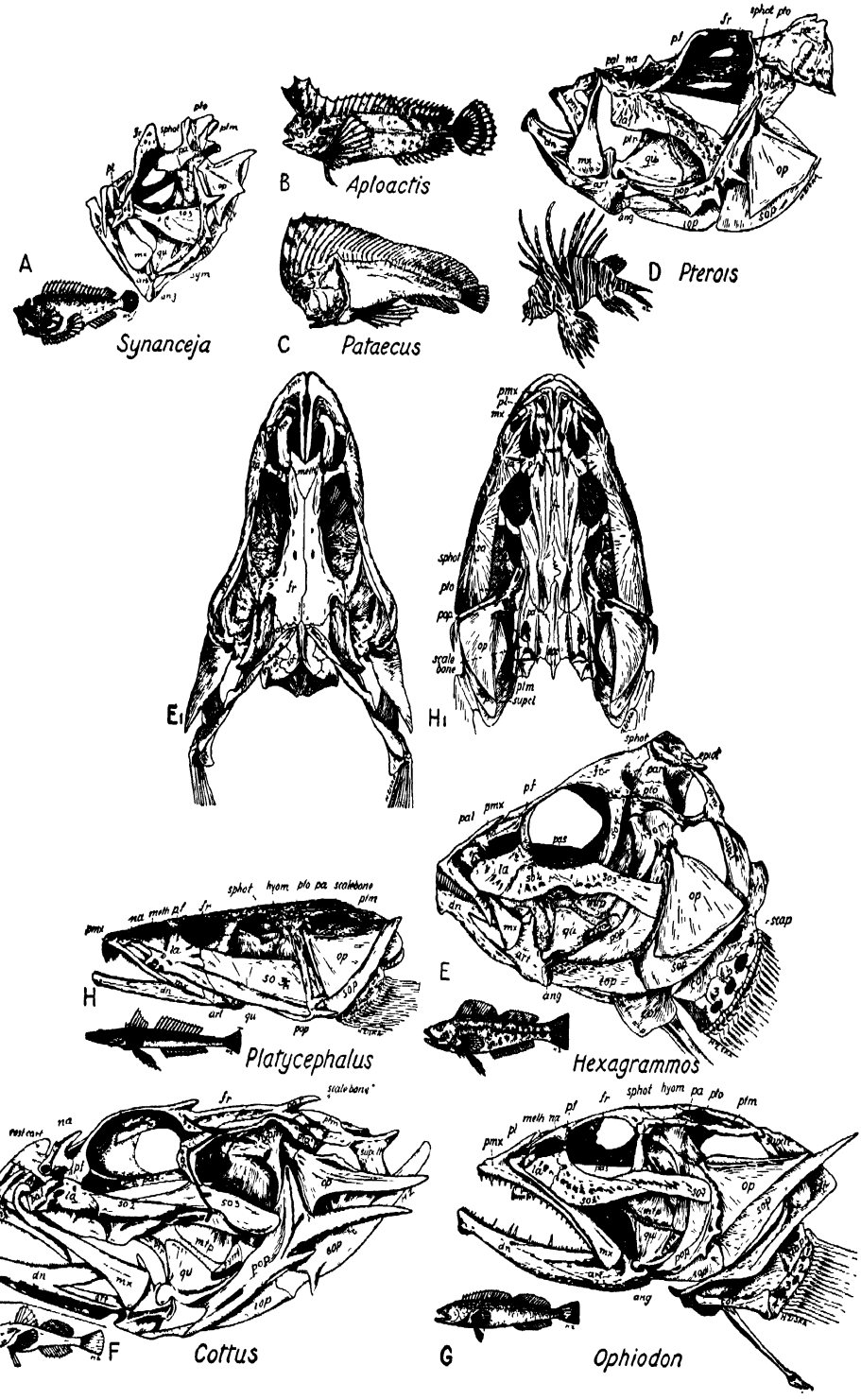


Fig. 9.141. Some fantastic derivatives of the Rosefish type. After Gregory.

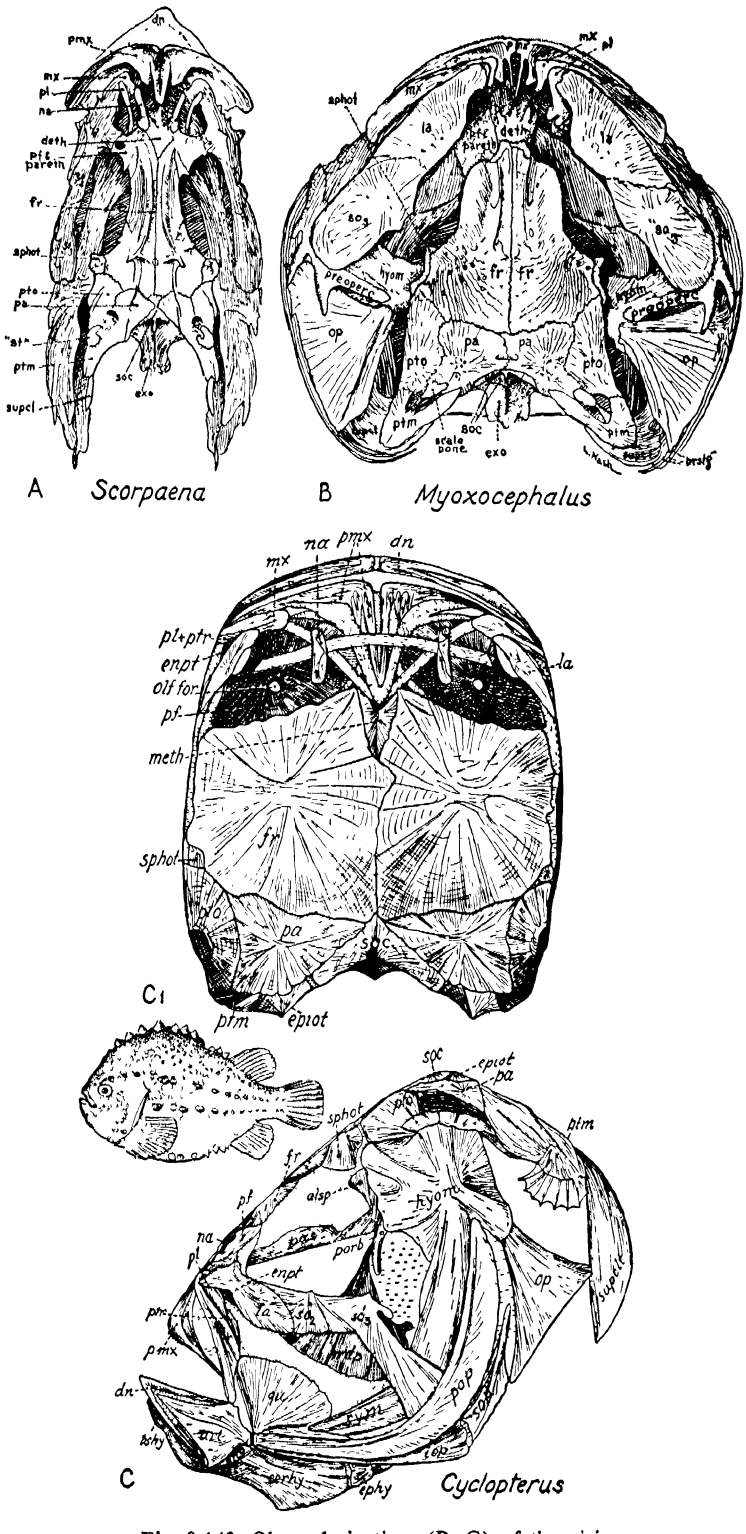


Fig. 9.142. Obese derivatives (B, C) of the vicious Rosefish (A, B). A, B, after Gregory; C, after Uhlmann.

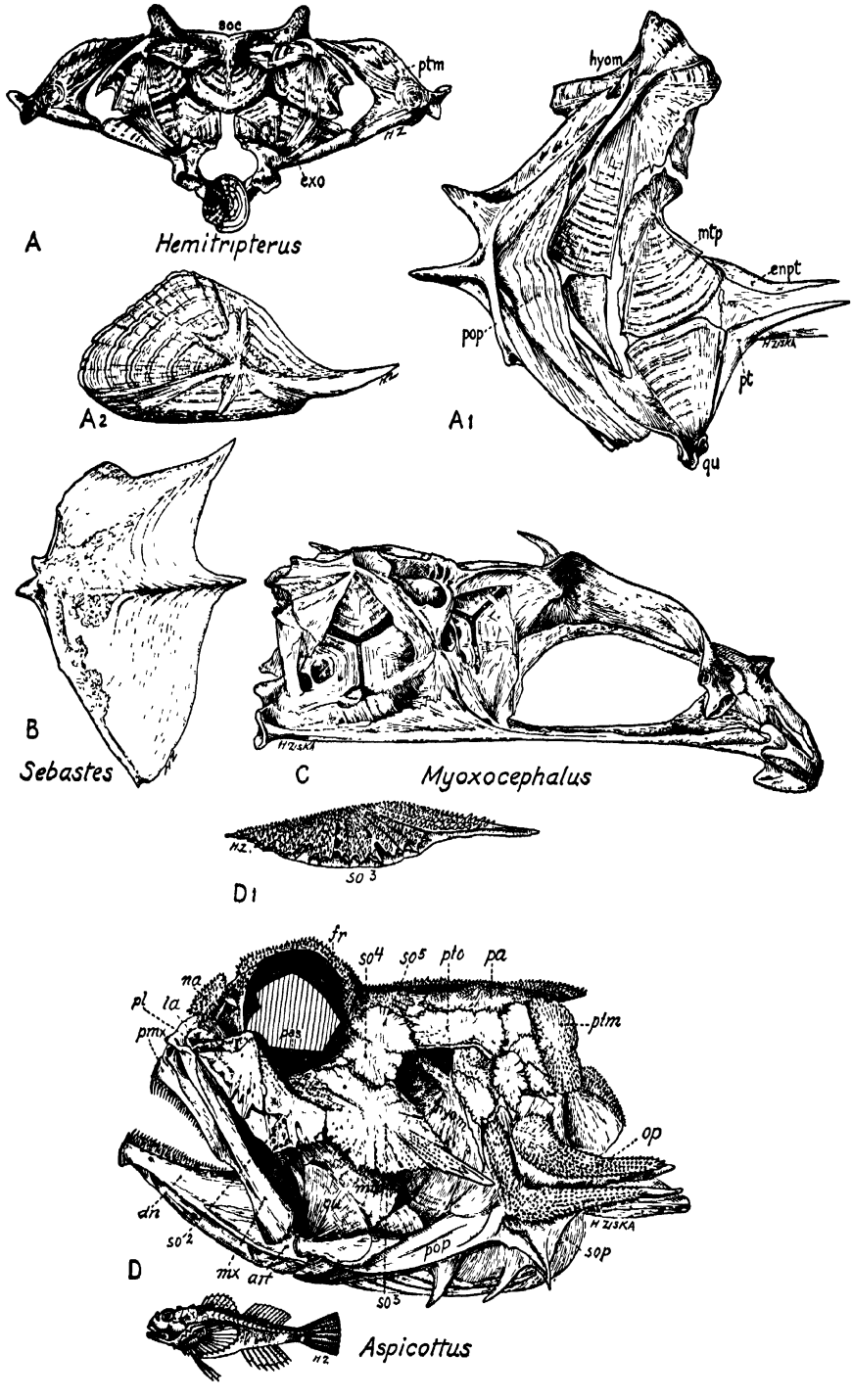


Fig. 9.143. Construction of skull elements in Scorpaenoids. A, occipital view, showing symmetrical arrangement of growth centers; A1, right suspensorium and pterygo-quadrate, showing similar growth lines in both endochondral and dermal bones; A2, right lacrymal enlarged, showing growth center and growth lines; B, left opercle; C, neurocranium, right side, showing triangular arrangement of growth centers and resulting triradiate sutures; D, skull, showing radiating rows of papillae on surface bones. After Gregory.

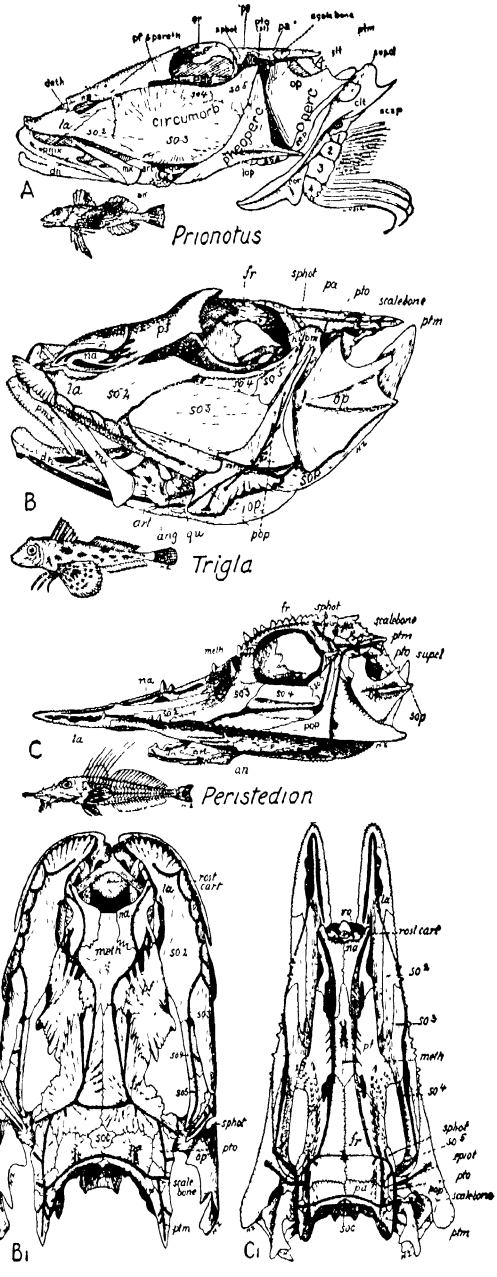


Fig 9.144 Luxuriating polyisomeres on the head-armor of the Gurnards. A–C1 From Gregory; B, B1, C, C1 after Allis.

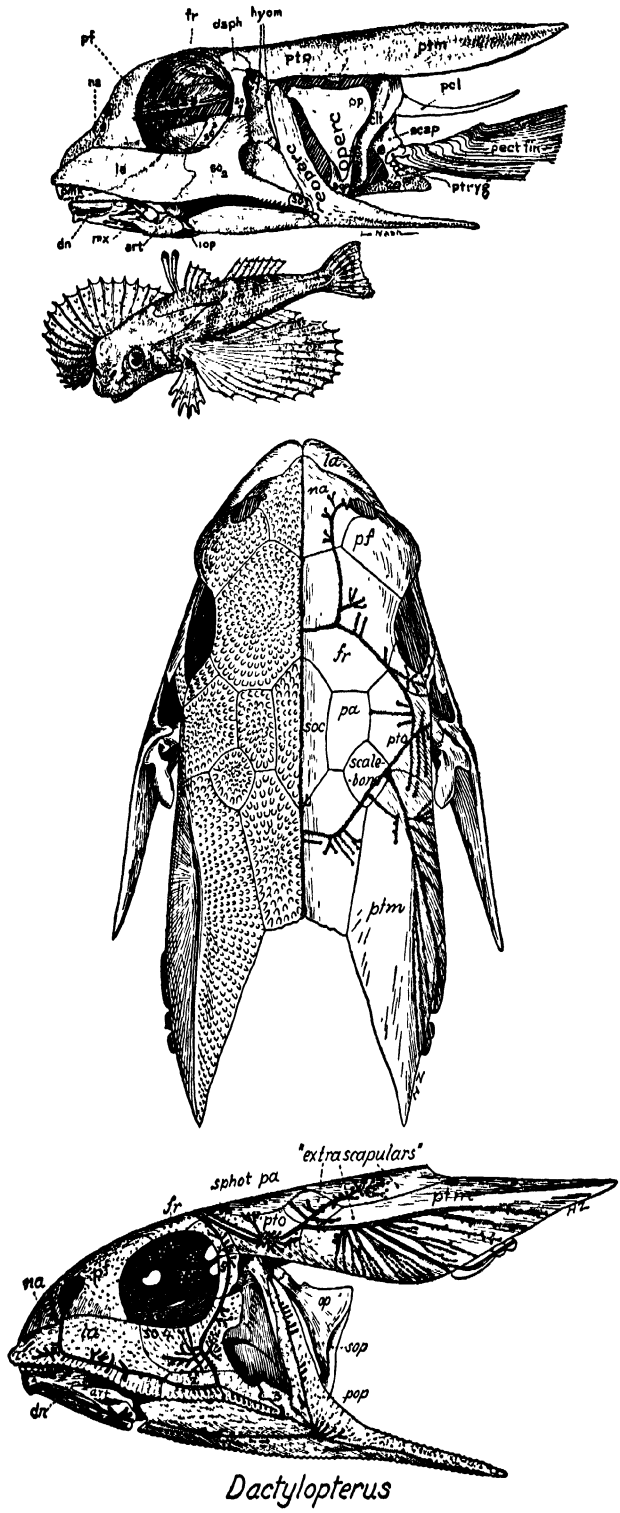


Fig. 9.145. The versatile "Flying Gurnard." From Gregory, after Allis.

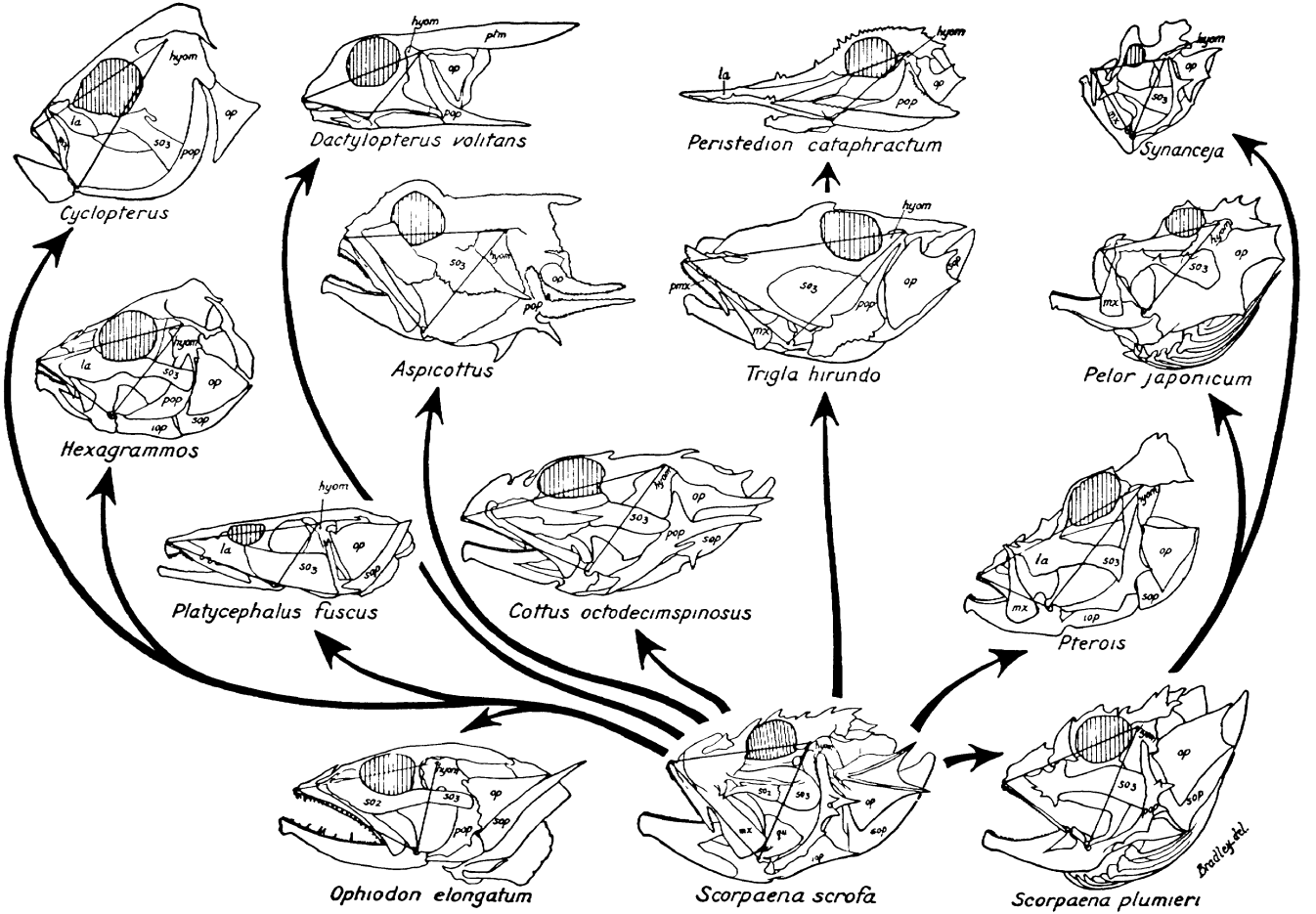


Fig. 9.146. Skull outlines and maxillary-suspensorial triangles of the main branches of the Cheek-armored fishes. Showing the diverse habitus and persistent heritage features.

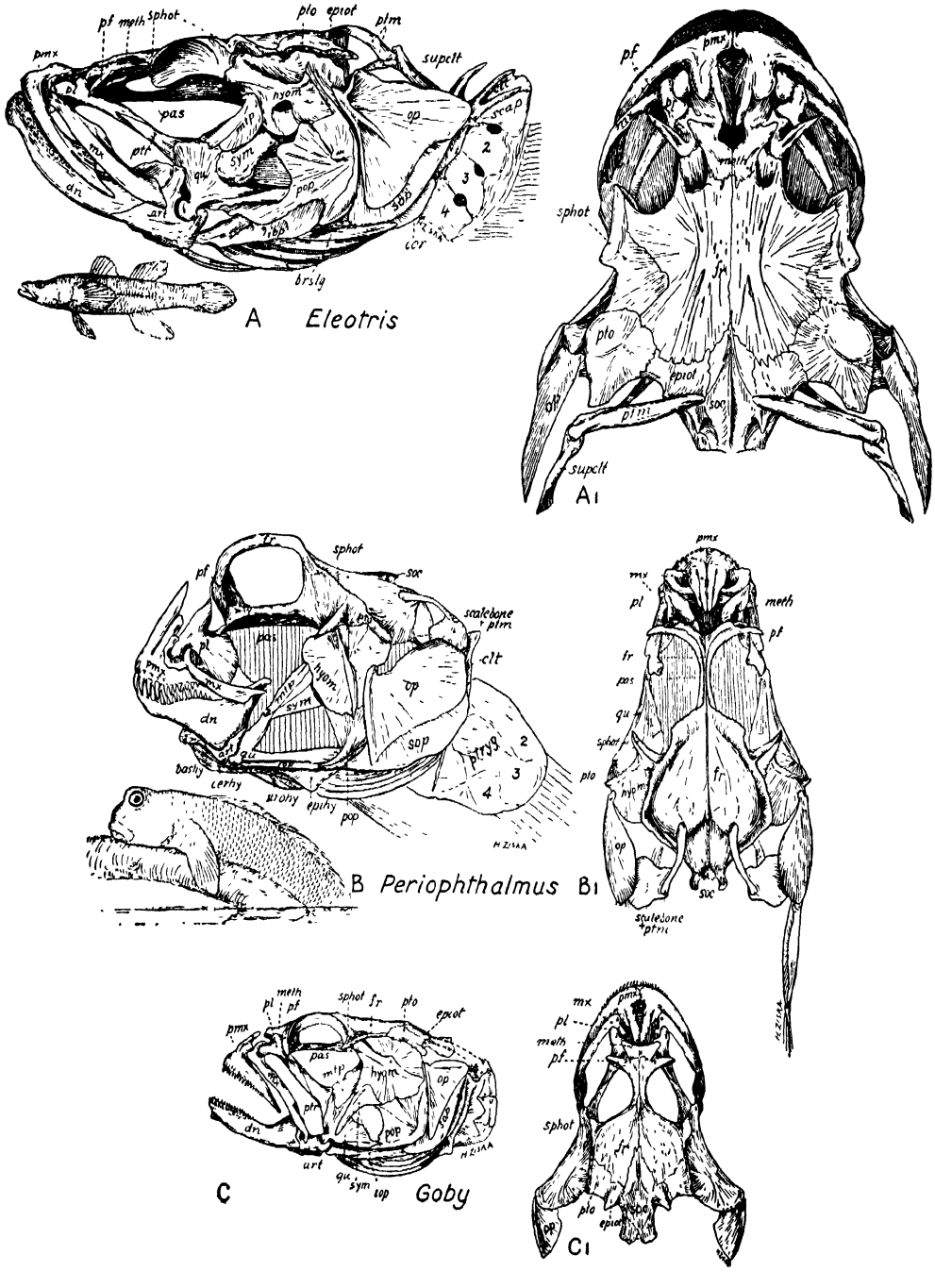


Fig. 9.147. Gobies and their skulls. After Gregory.

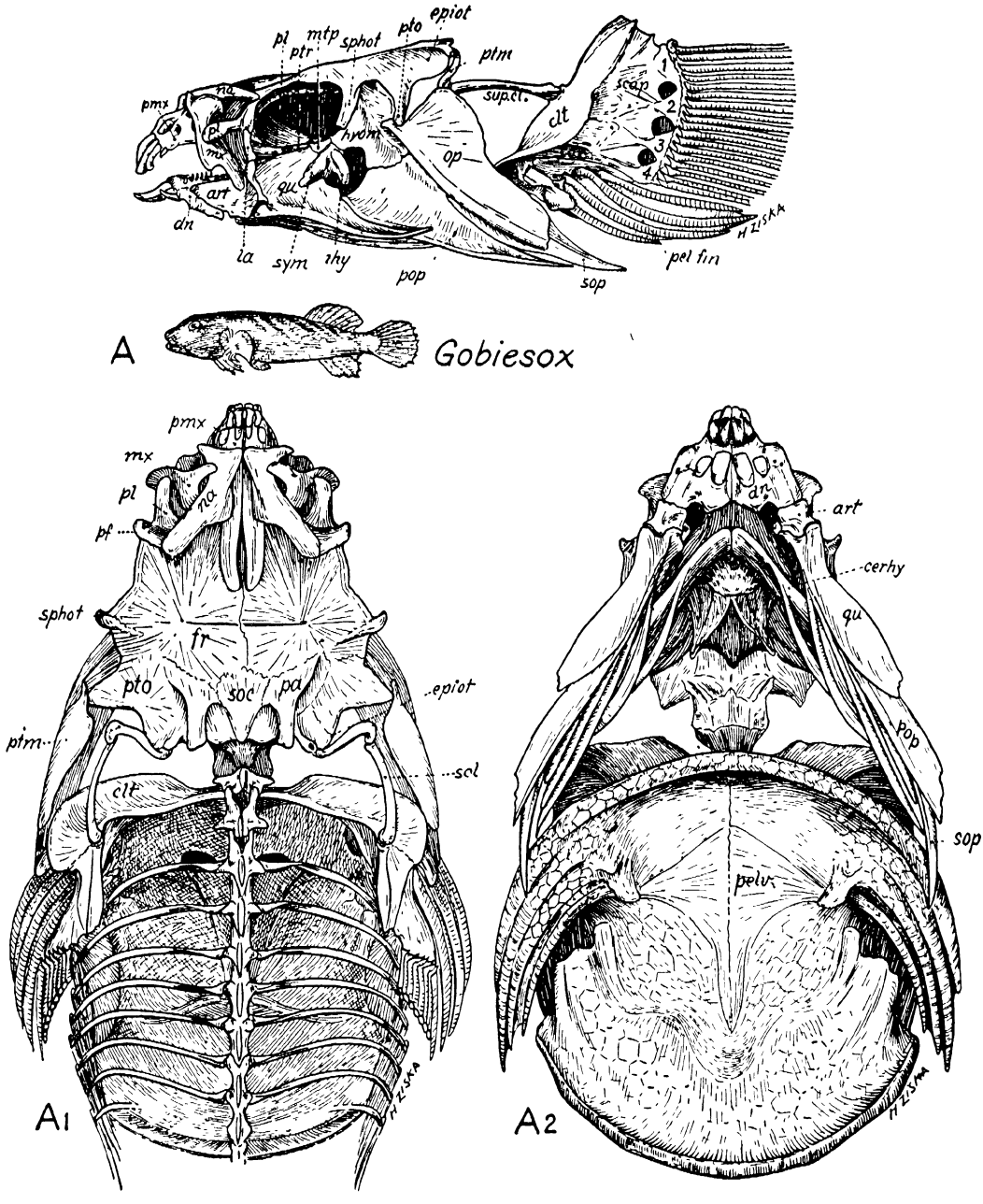


Fig. 9.148. The persistent Cling-fish. After Gregory.

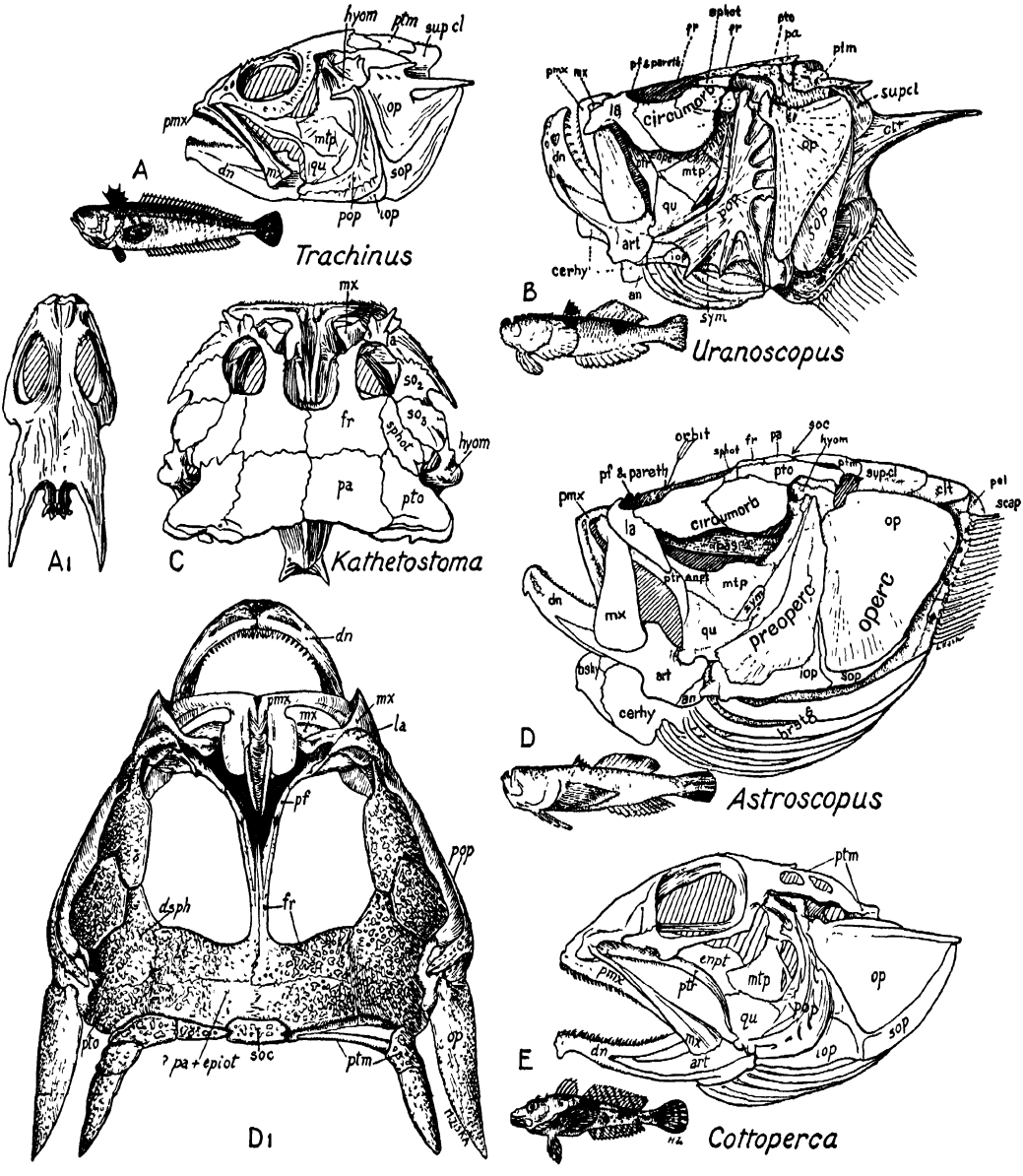


Fig. 9.149. Weaver (A, A1), Stargazers (B, C, D, D1) and Notothenid (E). After Gregory.

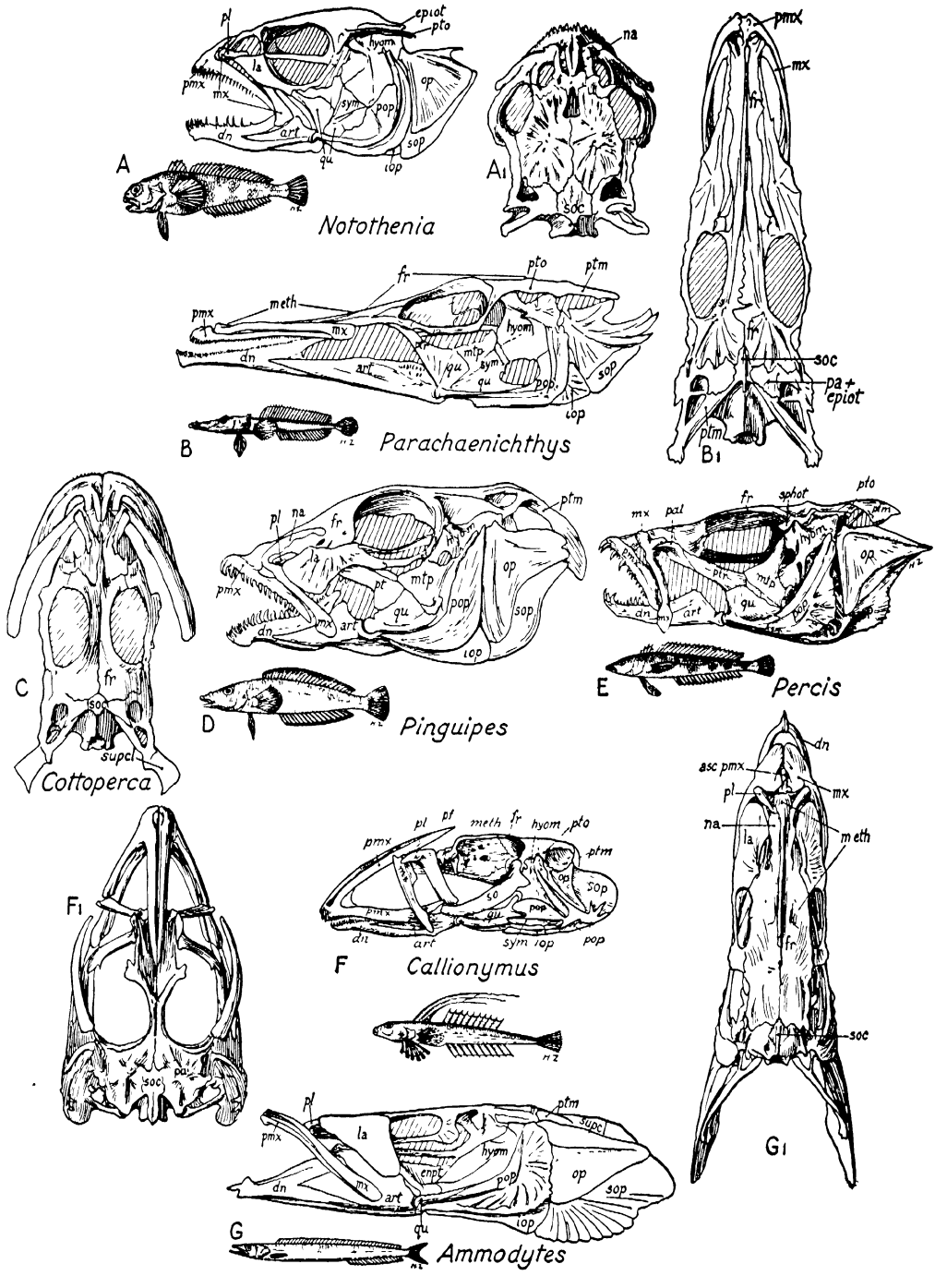


Fig. 9.150. Varied branches of the trachinoid stem. After Gregory.

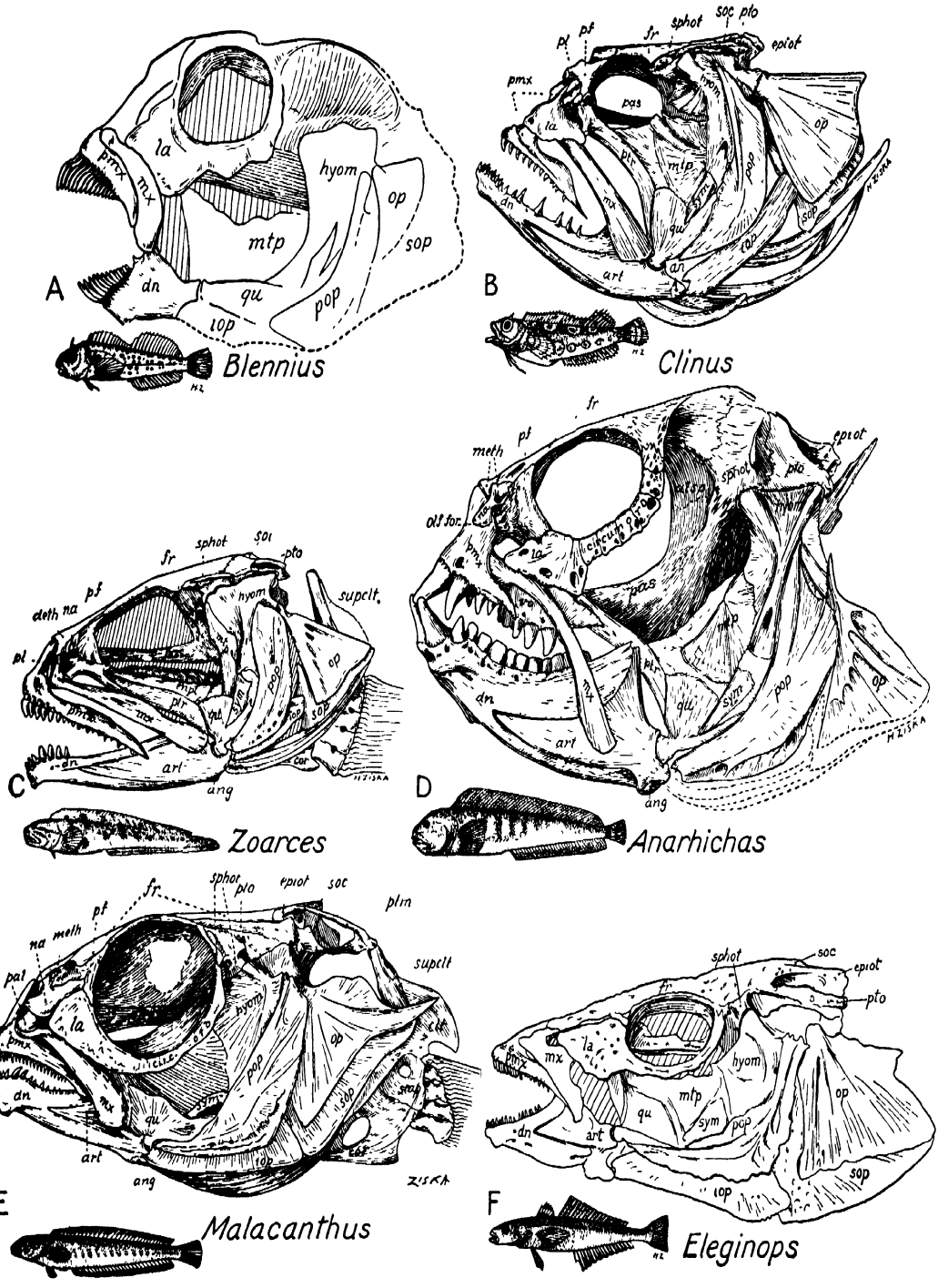


Fig. 9.151. Blennies (A–D) and Blenny-like forms (E, F) of other groups. After Gregory.

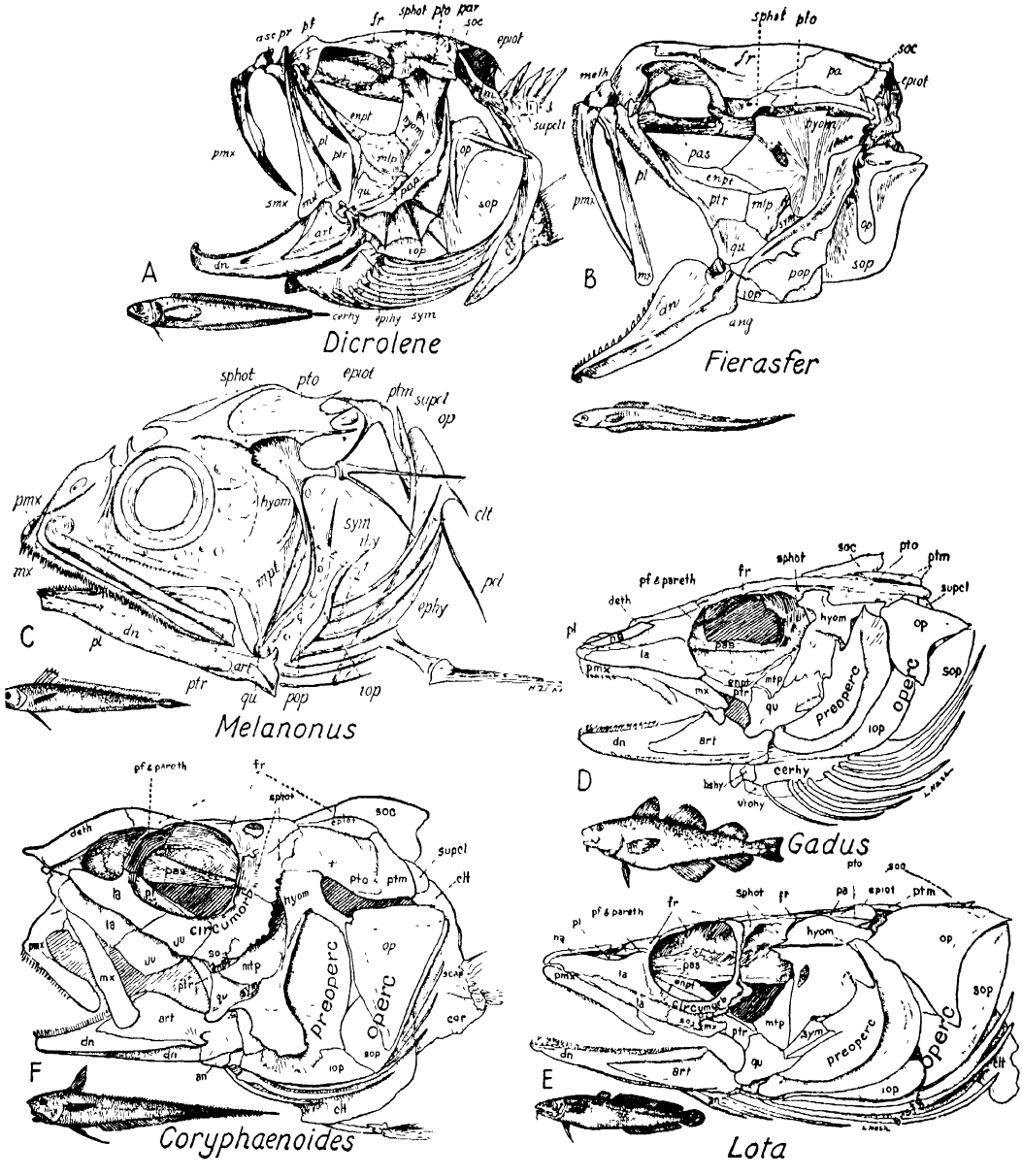


Fig. 9.152. Brotulid (A), Snake-fish (B) Cods (C–E) and Grenadier (F). After Gregory.

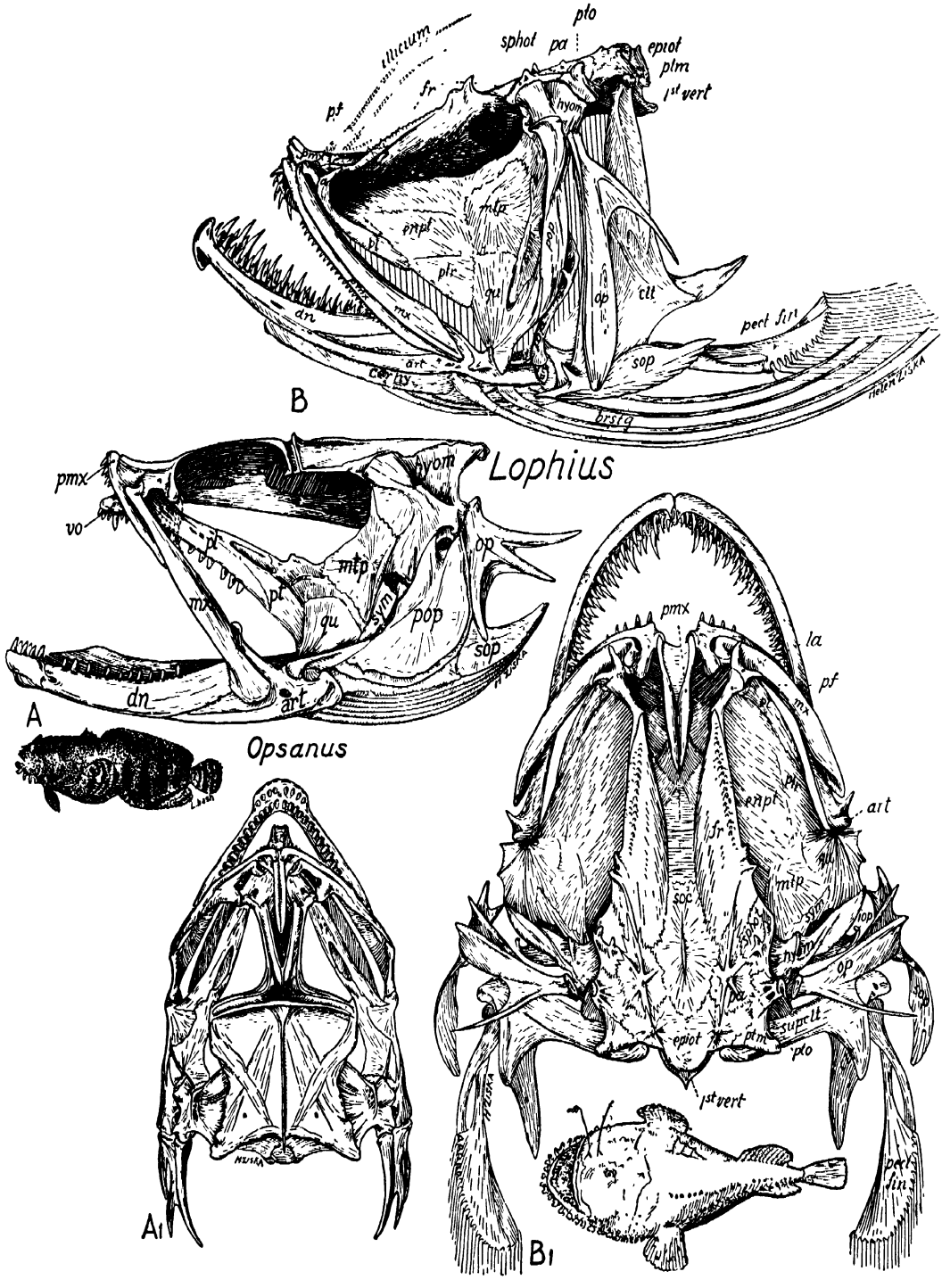


Fig. 9.153. Toadfish (A, A1) and angler (B, B1).
After Gregory.

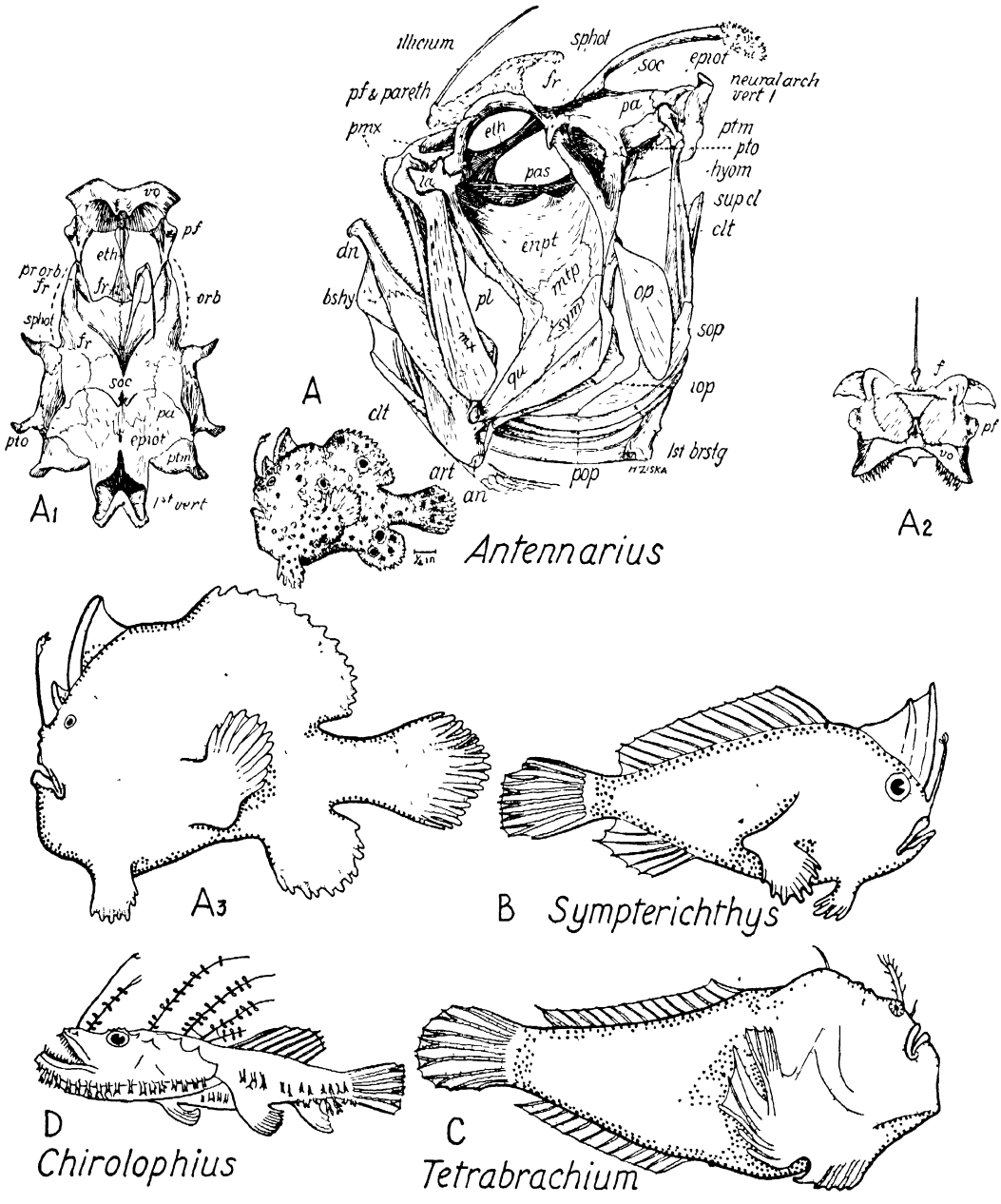


Fig. 9.154. Sargassum fishes and anglers. After Gregory (C from McCulloch).

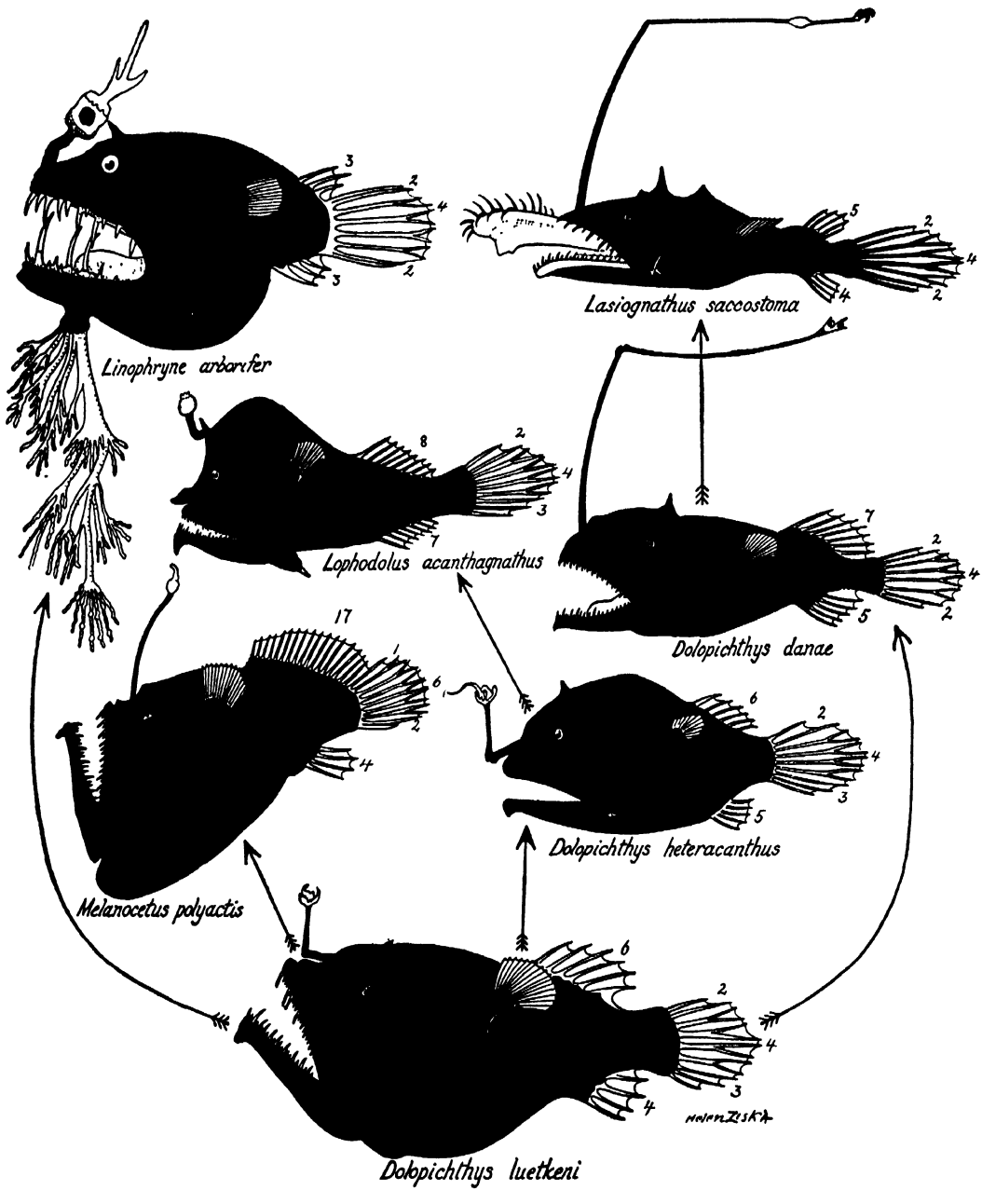


Fig. 9.155. Adaptive branching of deep-sea anglers (Ceratioids). From Gregory; figures based on Regan and Trewavas.

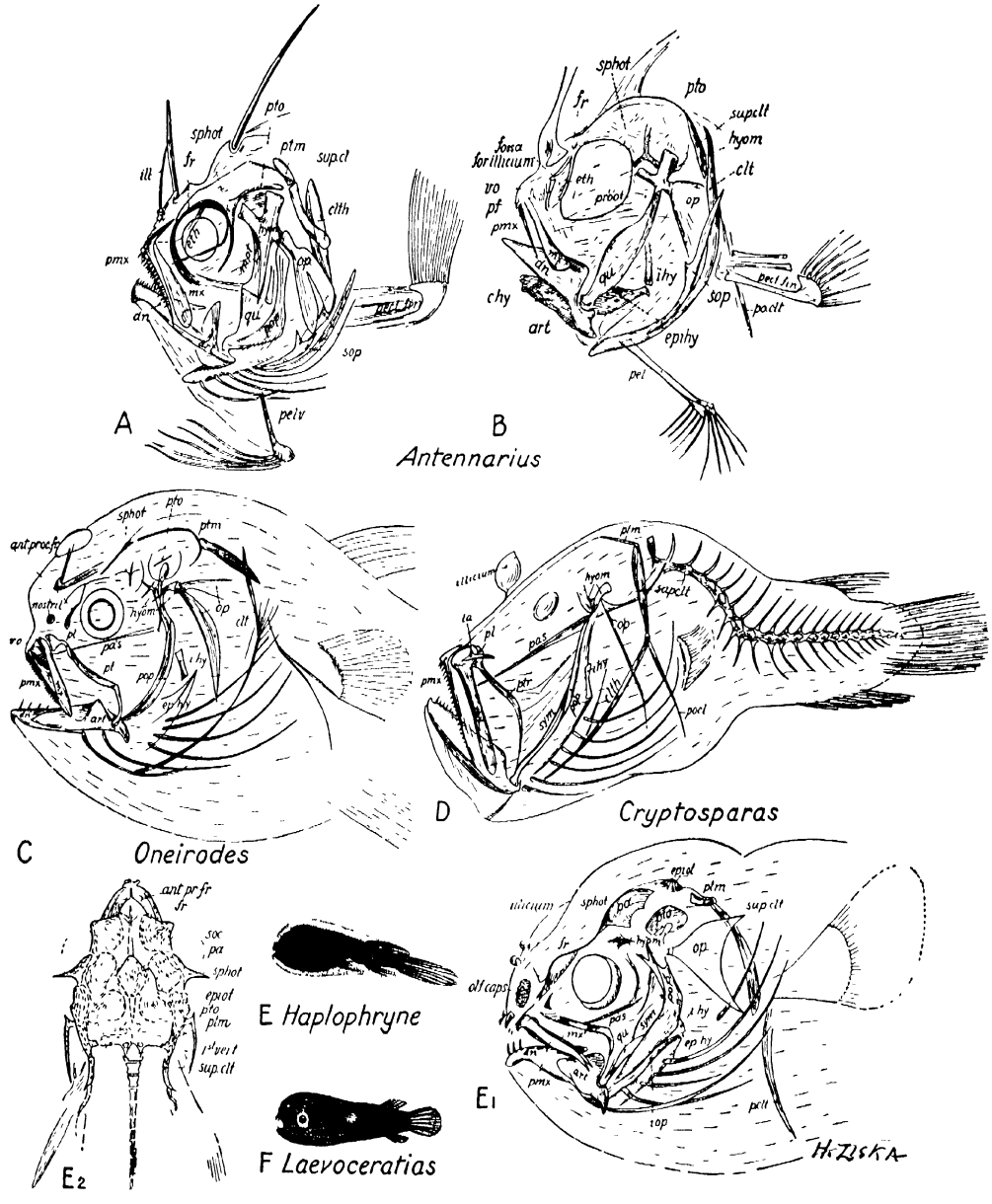


Fig. 9.156. Young Sargasso fishes and Ceratioids with imperfectly ossified skeletons. E, F, Are probably young unattached males with nipping teeth on the lips. From Gregory. E–E2, after Beebe; F, after Parr.

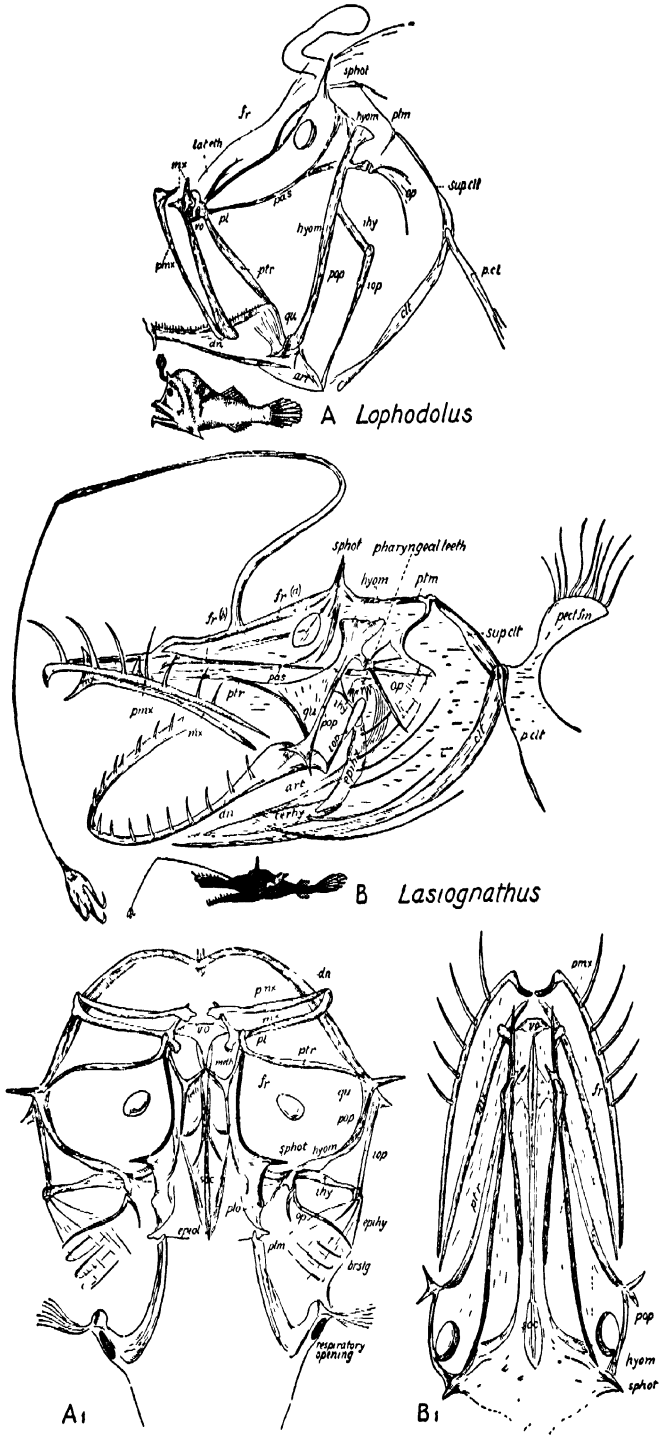


Fig. 9.157. Some bizarre Ceratioids with imperfectly ossified skulls. After Gregory, material from Beebe.

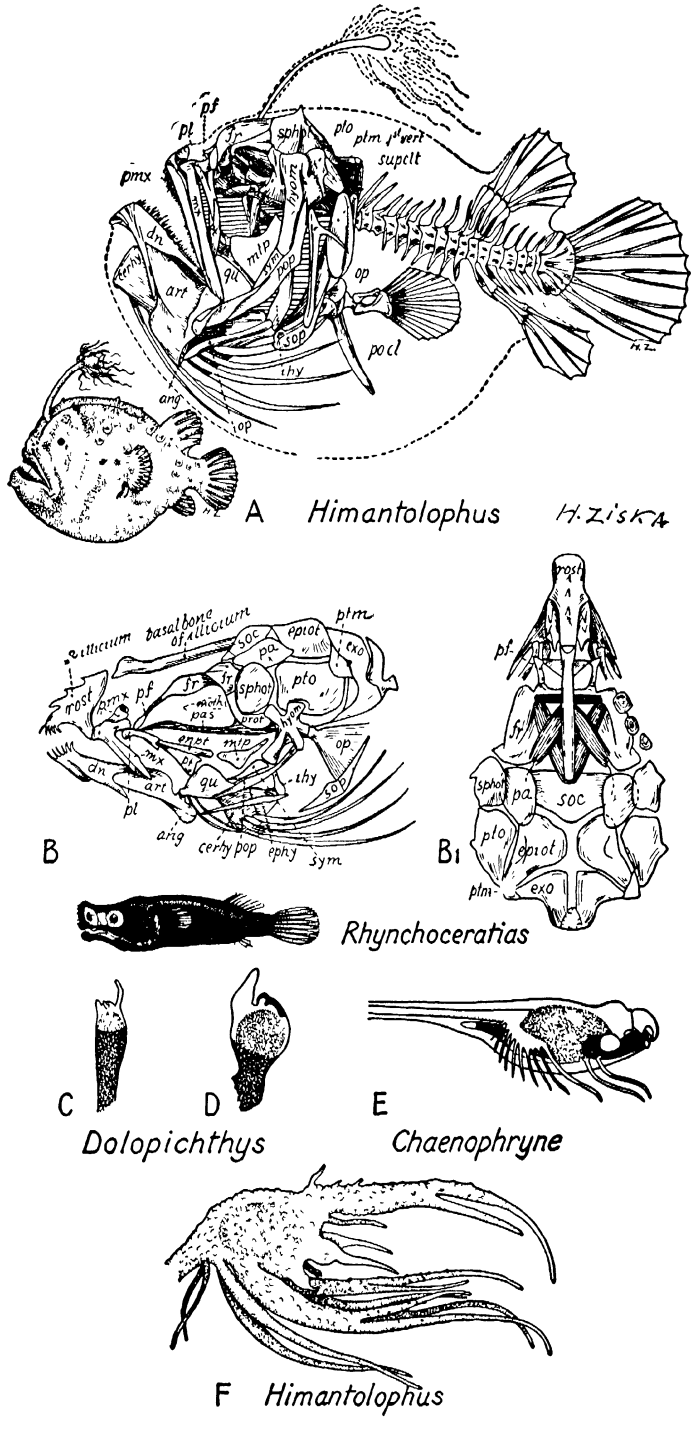


Fig. 9.158. A, A1, Large Ceratioid with a relatively well ossified skeleton, after Lütken. B, B1, A small unattached male with rostral denticles, after Parr. C–F, distal parts of illicia: C, *Dolopichthys simplex*; D, *Dolopichthys microlophus*; E, *Chaenophryne fimbriata*; F, *Himantolophus danae*; all after Regan and Trewavas.

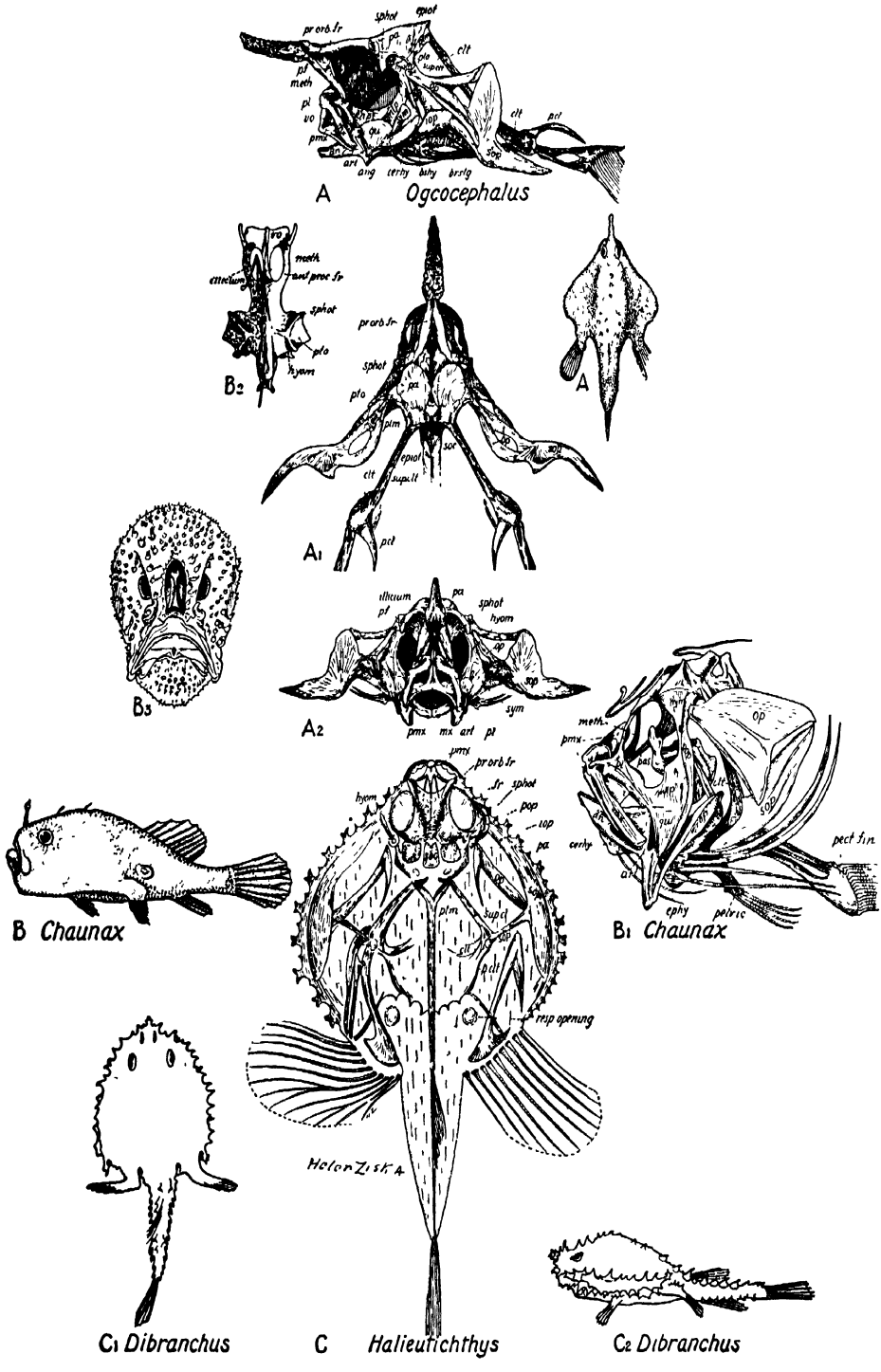


Fig. 9.159. From Chaunax (B, B1) to Sea-bats (A, C). A–A2, C after Gregory; B–C2, after Garman.

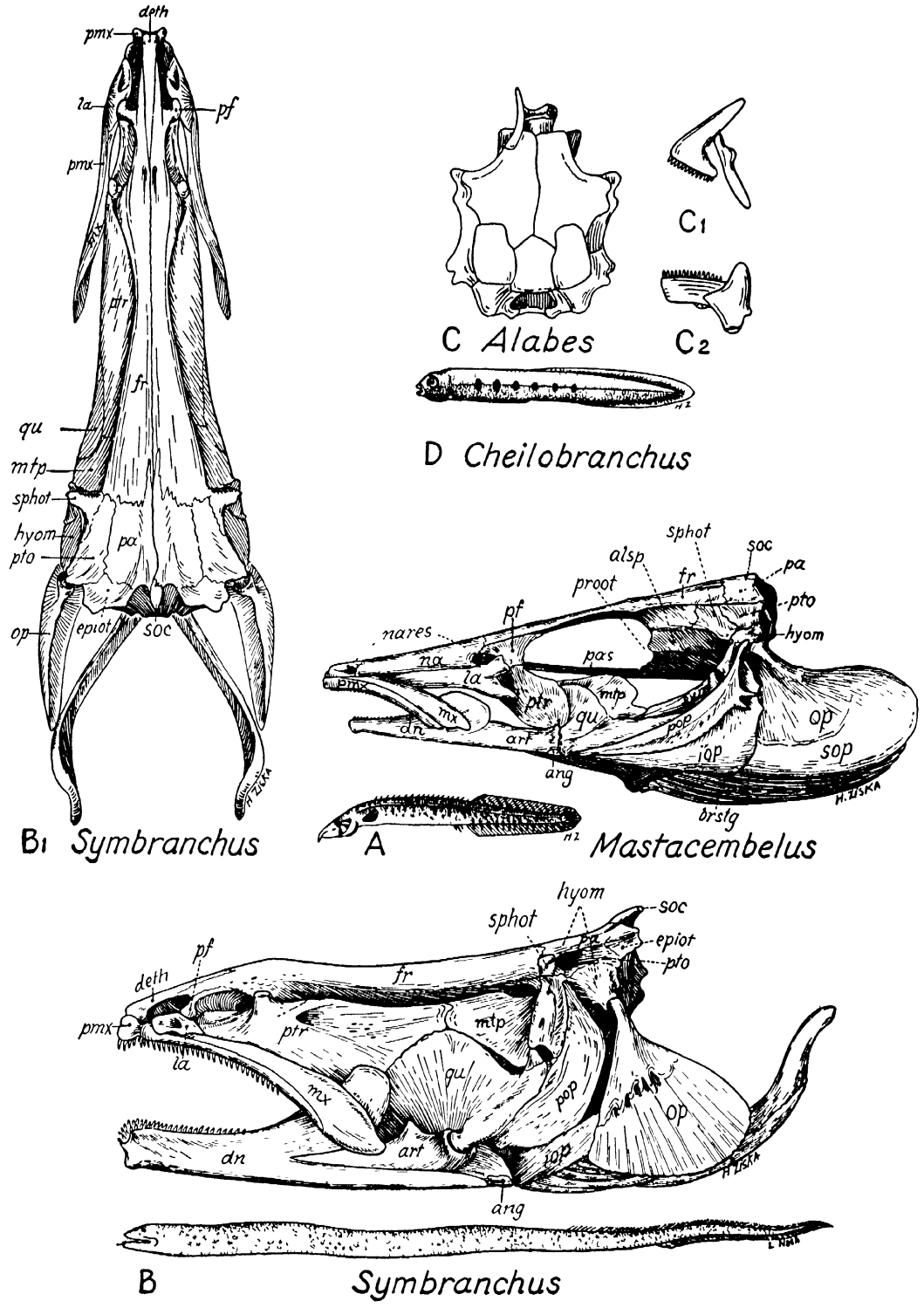
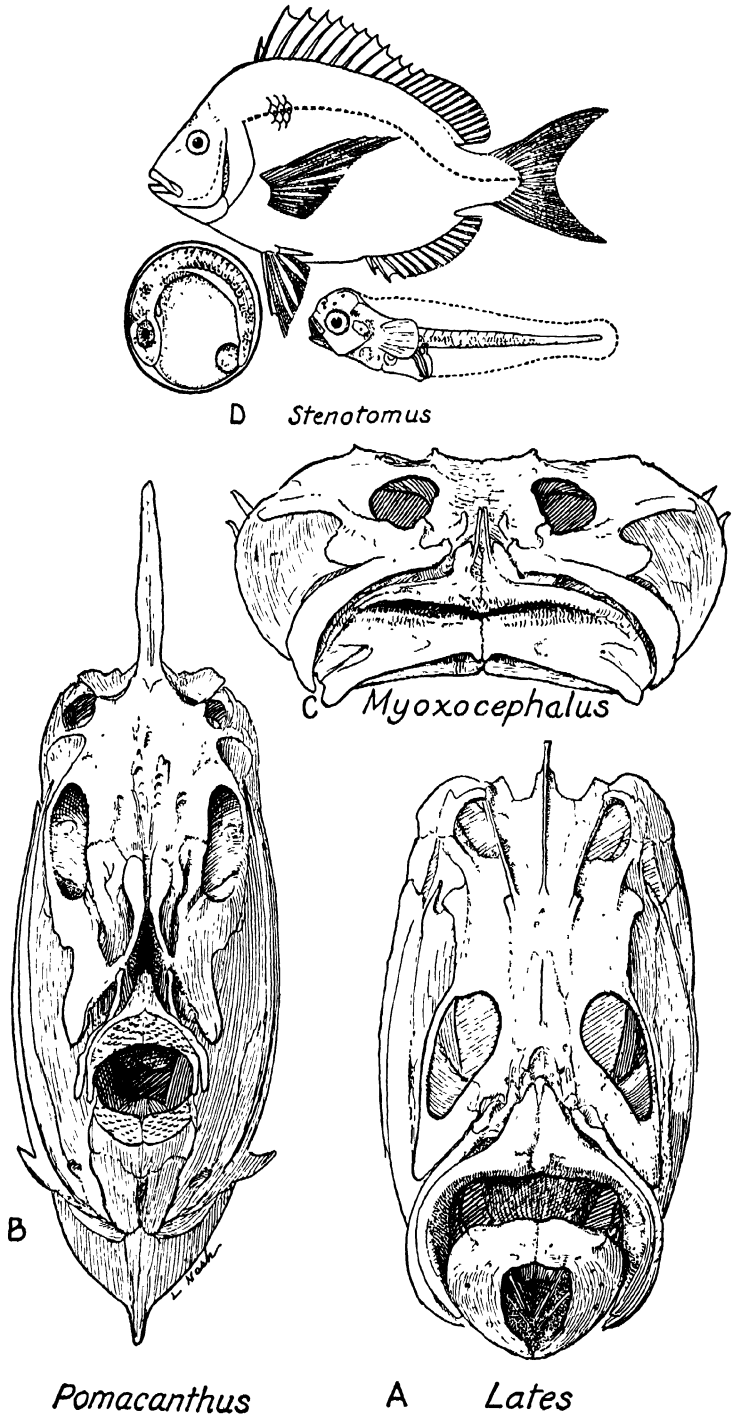


Fig 9.160. Eel-like derivatives of the Percoid stem.
A, B, B1, after Gregory; C, D, after Tate Regan.



Figs. 9.161, 162. Transformation (D) from embryo to larva to adult. Transformation, whether in ontogeny or phylogeny, implies anisomerism ("heterogony"). After Bigelow and Welsh. Front views of skulls of a normal Percoid type (A) and two divergent derivatives (B, C). By emphasis, or anisomerism, of either the vertical or the transverse diameters of a normal subovoid contour (A), (B) has become high, while (C) has been widened or depressed. After Gregory.

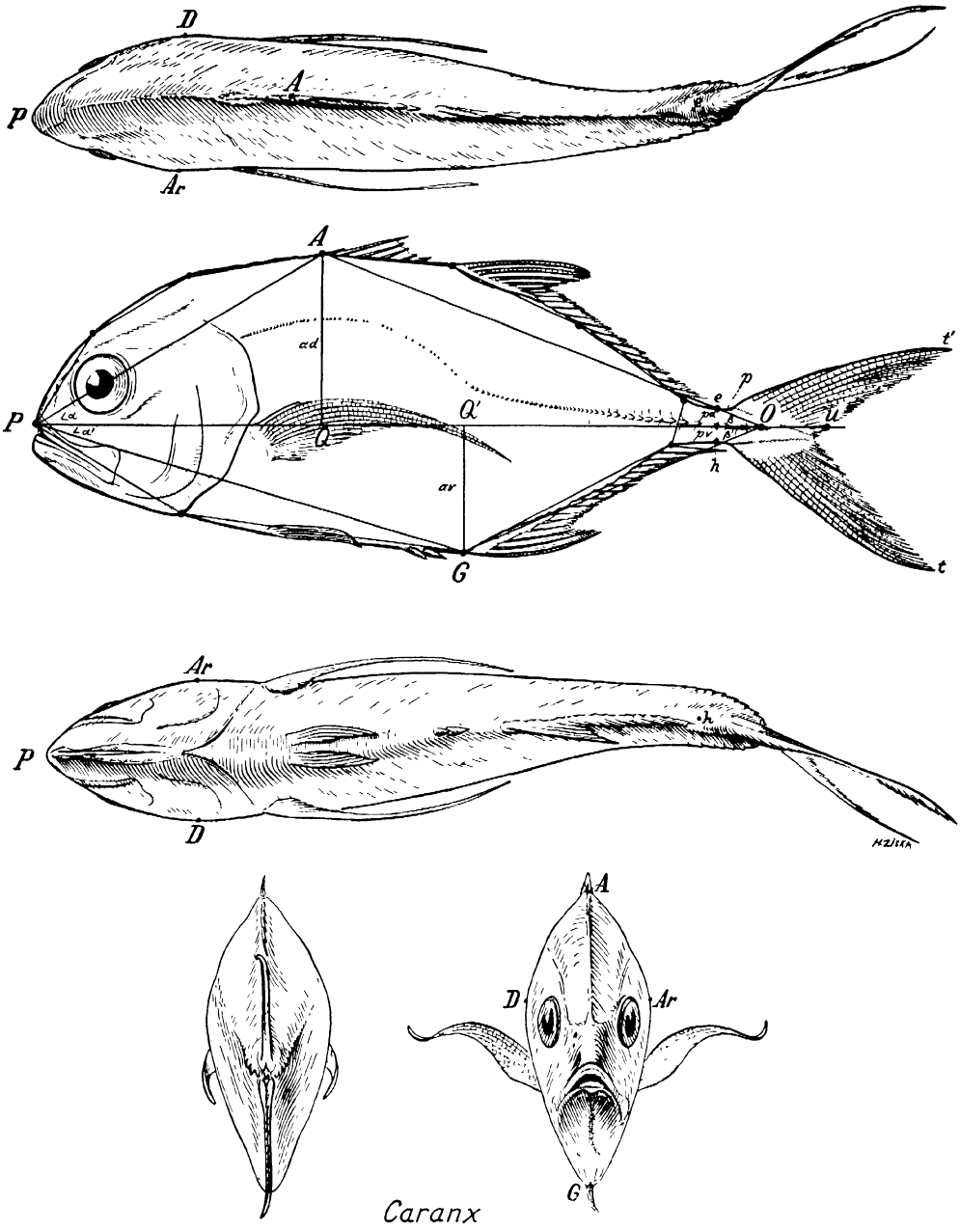
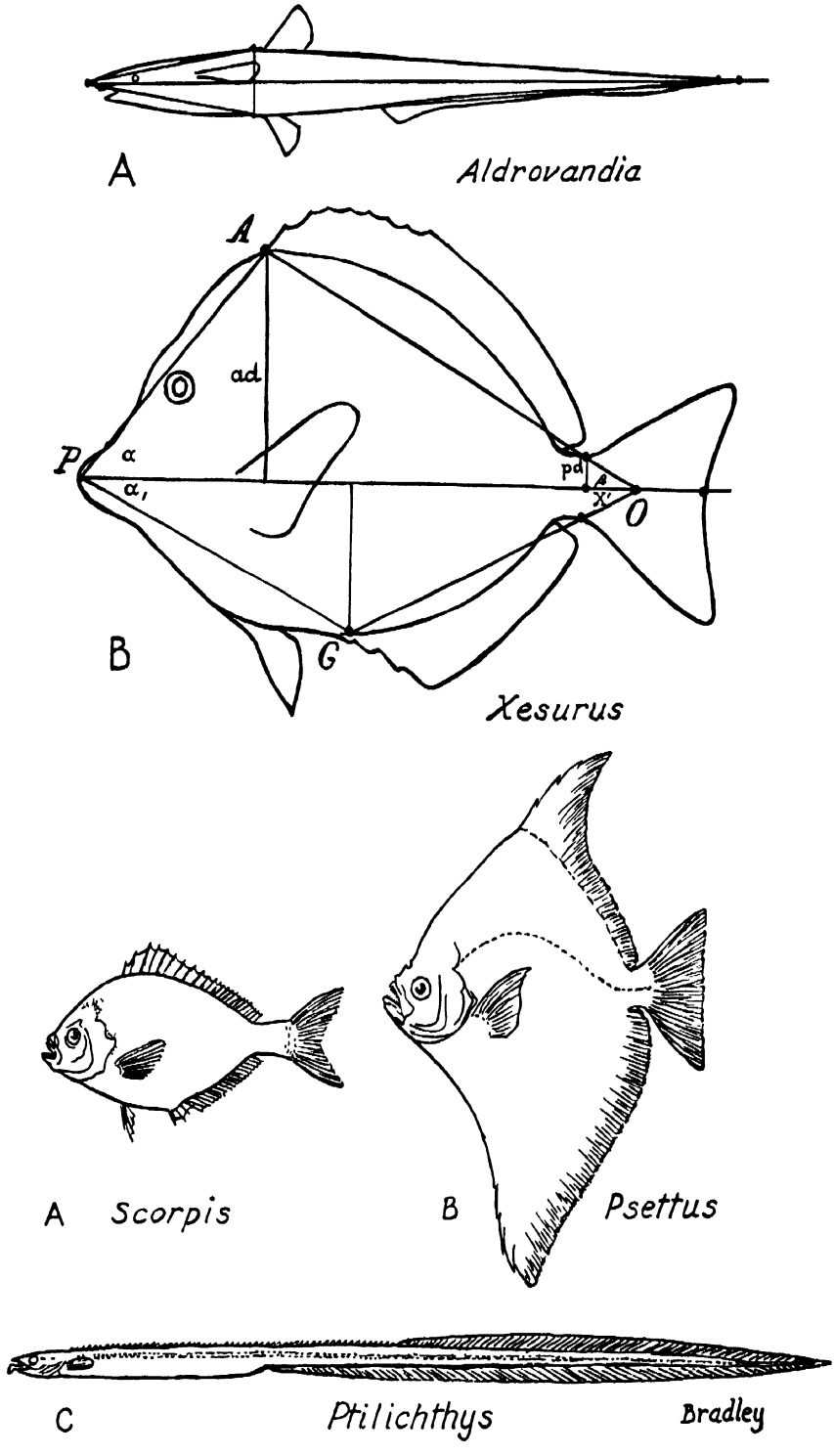


Fig. 9.163. A free-swimming fish (*Caranx*) in its ventral, lateral, dorsal, posterior (caudal), and anterior views. The six main points of reference are: *A*, apex; *P*, prosthion; *G*, gasterion; *O*, opisthion; *D*, dexterion (right); *Ar*, aristerion (left); auxiliary points are: *p*, pygidion; *ep*, epipygidion; *u*, uranion; *ad*, anterior dorsal vertical; *pd*, posterior dorsal vertical, etc ; *DP Ar*, entering angle; *De Ar*, angle of the run. After Gregory.



Figs. 9.164, 165. Streamlining in relation to inscribed rectilinear figures. Divergent anisomerism in the Percoid group, from a primitive, mesosomatic to highly specialized hypsi- and dolichosomatic end stages. After Gregory.

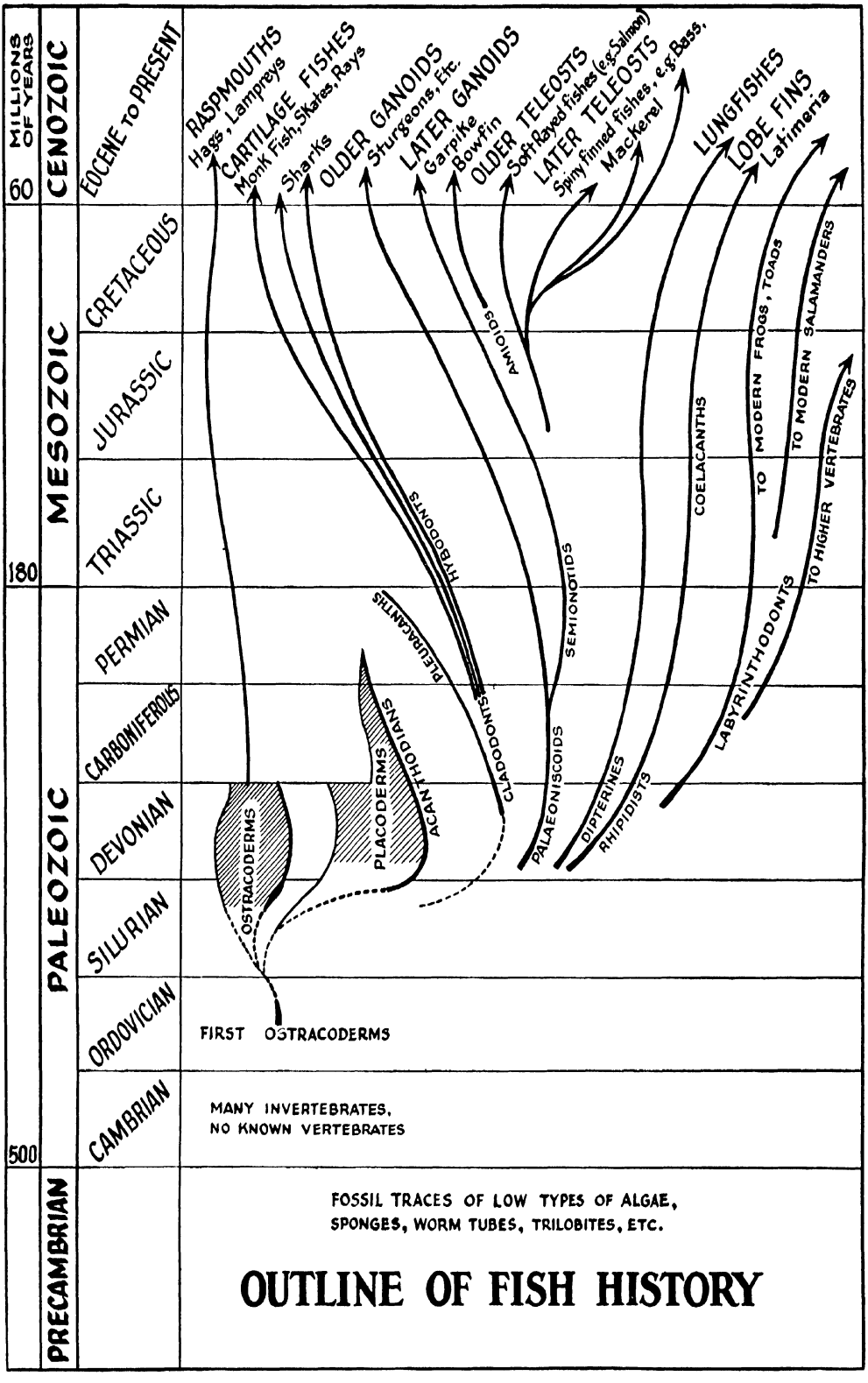

MILLIONS OF YEARS
60
180
500
CENOZOIC
MESOZOIC
PALEOZOIC
PRECAMBRIAN
EOCENE to PRESENT
CRETACEOUS
JURASSIC
TRIASSIC
PERMIAN
CARBONIFEROUS
DEVONIAN
SILURIAN
ORDOVICIAN
CAMBRIAN
RASPMOUTHS
Hags, Lampreys
CARTILAGE FISHES
Monk Fish, Skates, Rays
Sharks
OLDER GANOIDS
Sturgeons, Etc.
LATER GANOIDS
Garpike
Bowfin
OLDER TELEOSTS
Soft-Rayed fishes (e.g. Salmon)
LATER TELEOSTS
Spiny-finned fishes, e.g. Bass,
Mackerel
LUNGFISHES
LOBE FINS
Latimeria
AMIOIDS
HYBODONTS
PLEURACANTHS
CLADODONTS
SEMIONOTIDS
PALAEONISCOIDS
DIPTERINES
RHIPIDISTS
COELACANTHS
TO MODERN FROGS, TOADS
TO MODERN SALAMANDERS
TO HIGHER VERTEBRATES
LABYRINTHODONTS
OSTRACODERMS
PLACODERMS
ACANTHODIANS
FIRST OSTRACODERMS
MANY INVERTEBRATES,
NO KNOWN VERTEBRATES
FOSSIL TRACES OF LOW TYPES OF ALGAE,
SPONGES, WORM TUBES, TRILOBITES, ETC.
OUTLINE OF FISH HISTORY

Fig. 9.166

CHAPTER X

THE AIR-BREATHERS STRUGGLE FOR LIFE (DIPNOANS, LOBE-FINS)

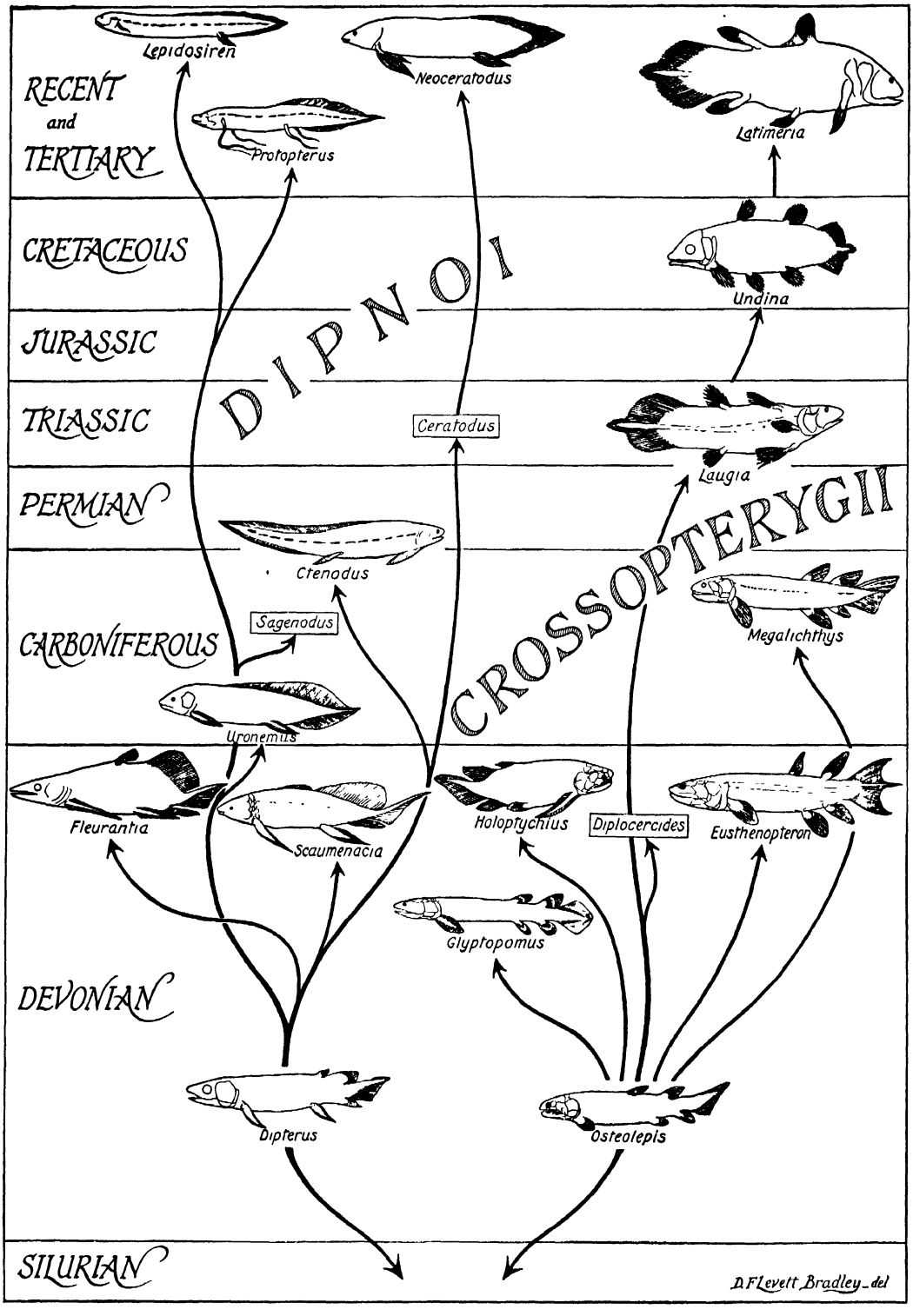


Fig. 10.1. Suggested family tree of the air breathers. Data from many authors, including Pander, Traquair, Dollo, Watson, Hussakof, Graham-Smith and Westoll, Wellburn, Stensiö, Smith Woodward, Schaeffer, J. L. B. Smith.

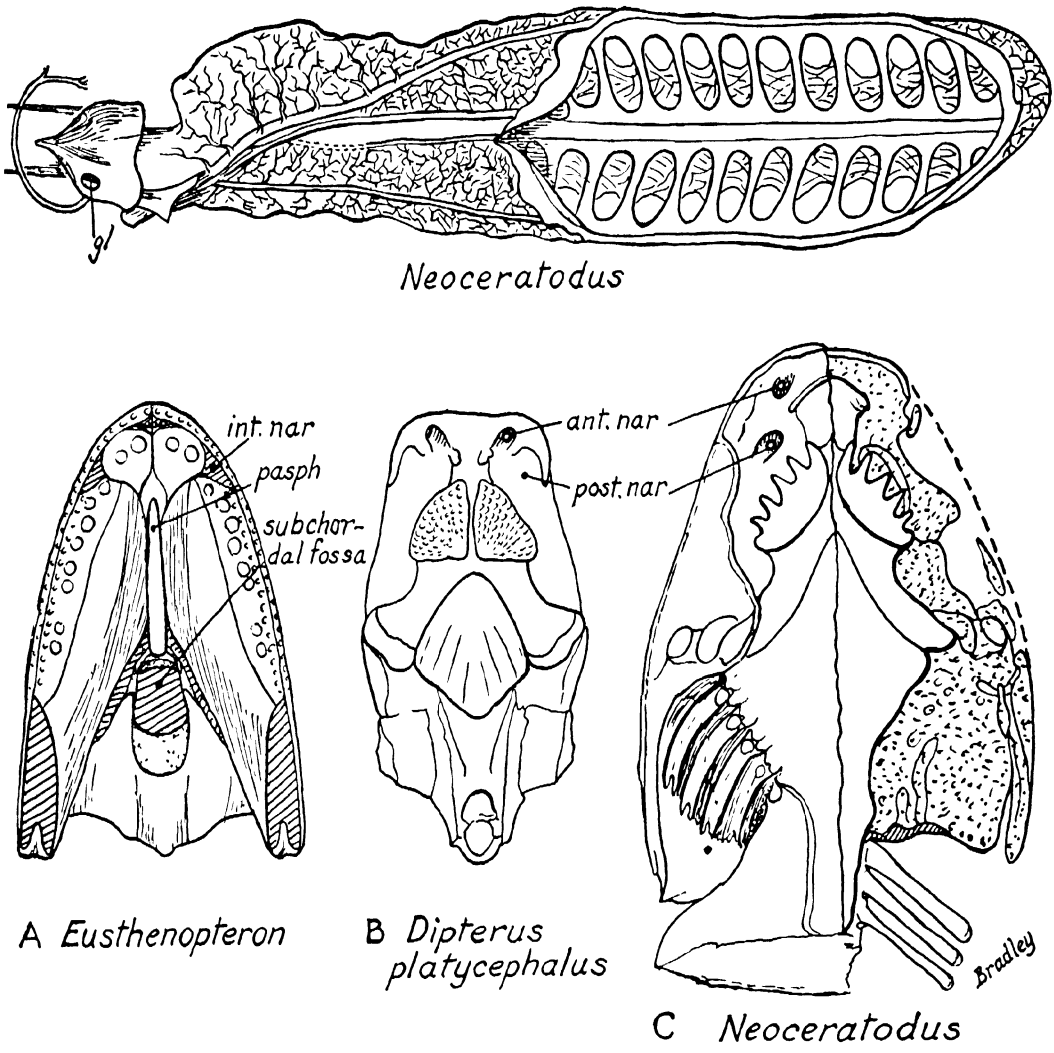


Fig. 10.2 (top). Air-bladder-lung of the Australian lungfish. The oesophagus is cut open to show the glottis (*g*) opening into it. The posterior half of the sac is cut open to show the air cells. From Goodrich after Günther.

Fig. 10.3. The air breather's palate. Under side of the skull in a primitive Devonian crossopterygian (A), a Devonian lungfish (B) and a modern lungfish (C) A, from Watson, after Bryant; B, after Pander; C, after Goodrich. In both groups the olfactory capsule was connected by an internal (or posterior) narial opening with the palatal surface or roof of the mouth, probably to enable the animal to smell its food. In breathing, the air was probably sucked in through the same tube and then forced into the lung through the glottis. This figure also shows the contrast between the long-jawed predaceous (A), and the short-jawed (B, C) type with cutting-crushing dental plates.

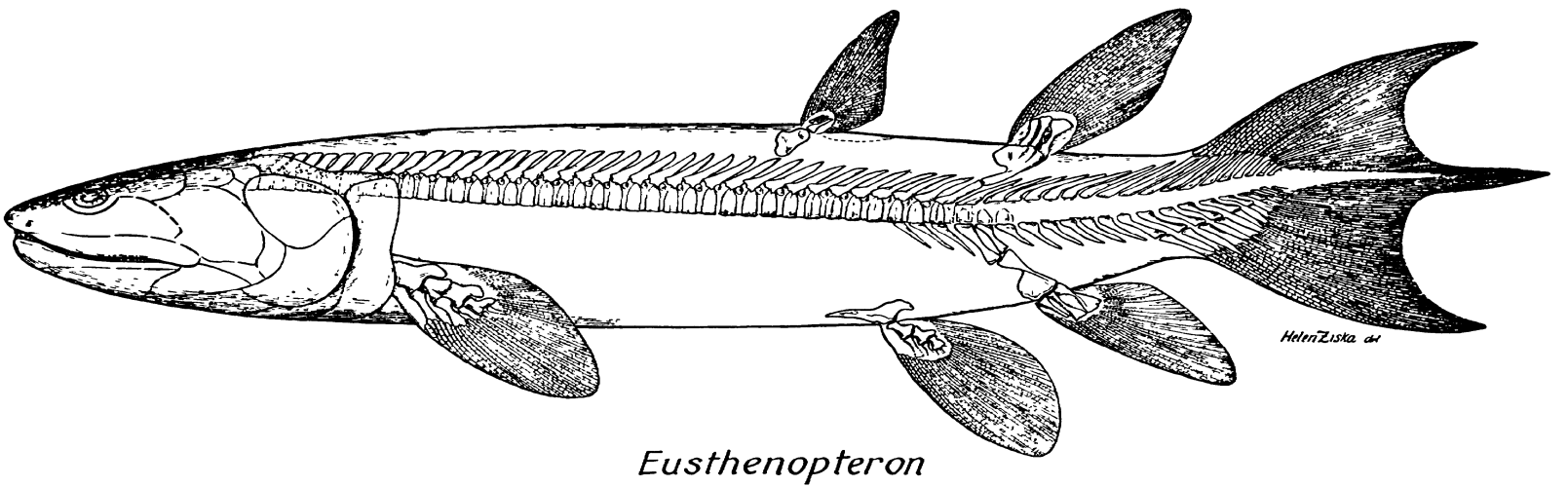
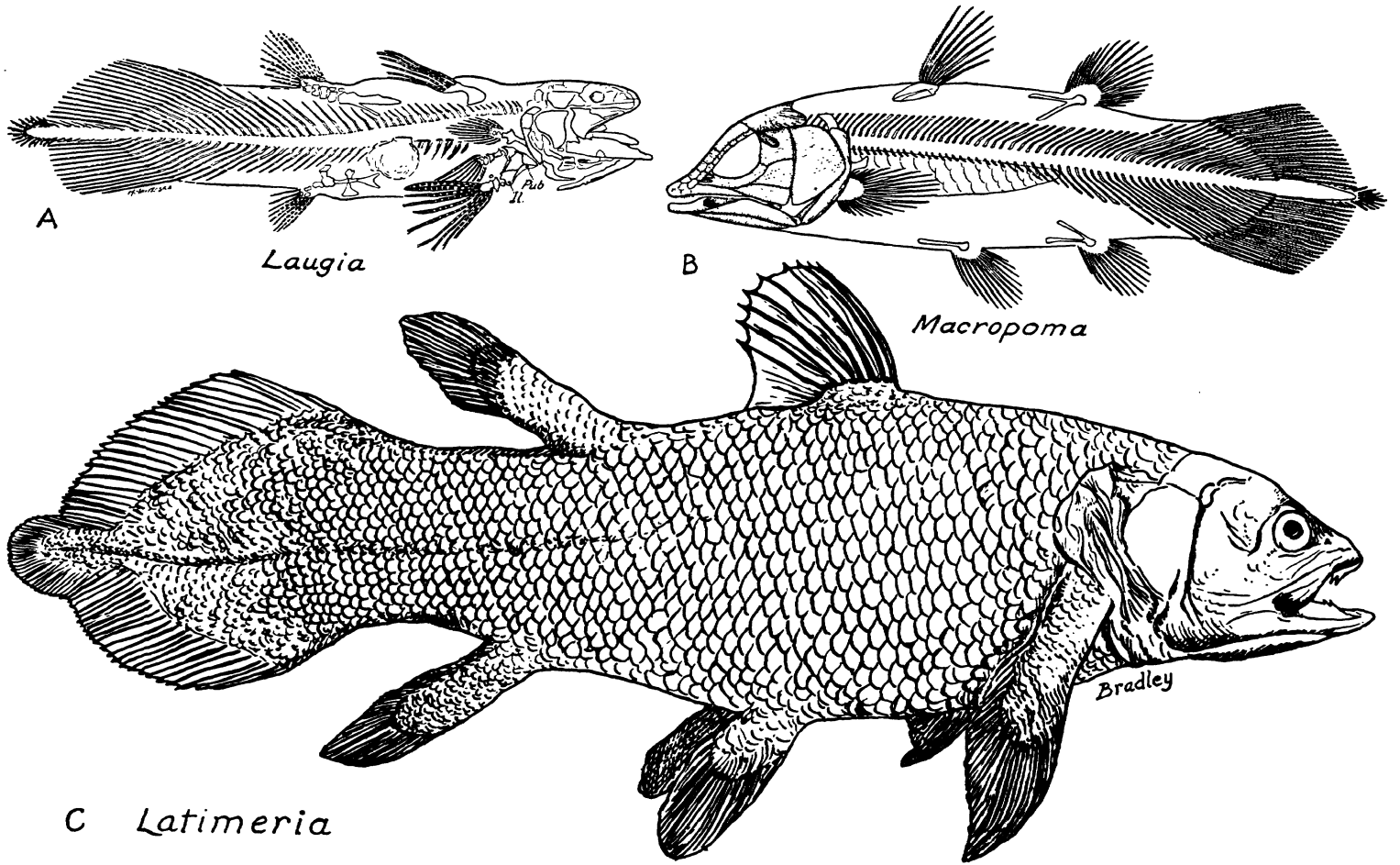


Fig. 10.4. A predatory lobe-fin (*Eusthenopteron*) of Upper Devonian age. Reconstruction (scales omitted) by Gregory and Raven.



Figs. 10.5,6. Coelacanths from the Triassic (A), Cretaceous (B) and Recent (C). In A, the pelvis and pelvic fins have moved forward to a point beneath the pectorals, thus converging toward quick-darting spiny-finned teleosts. C, A living relic of this essentially Cretaceous group, caught off East London, South Africa. A, after Stensiö; B, after Smith Woodward; C, after J. I. B. Smith.

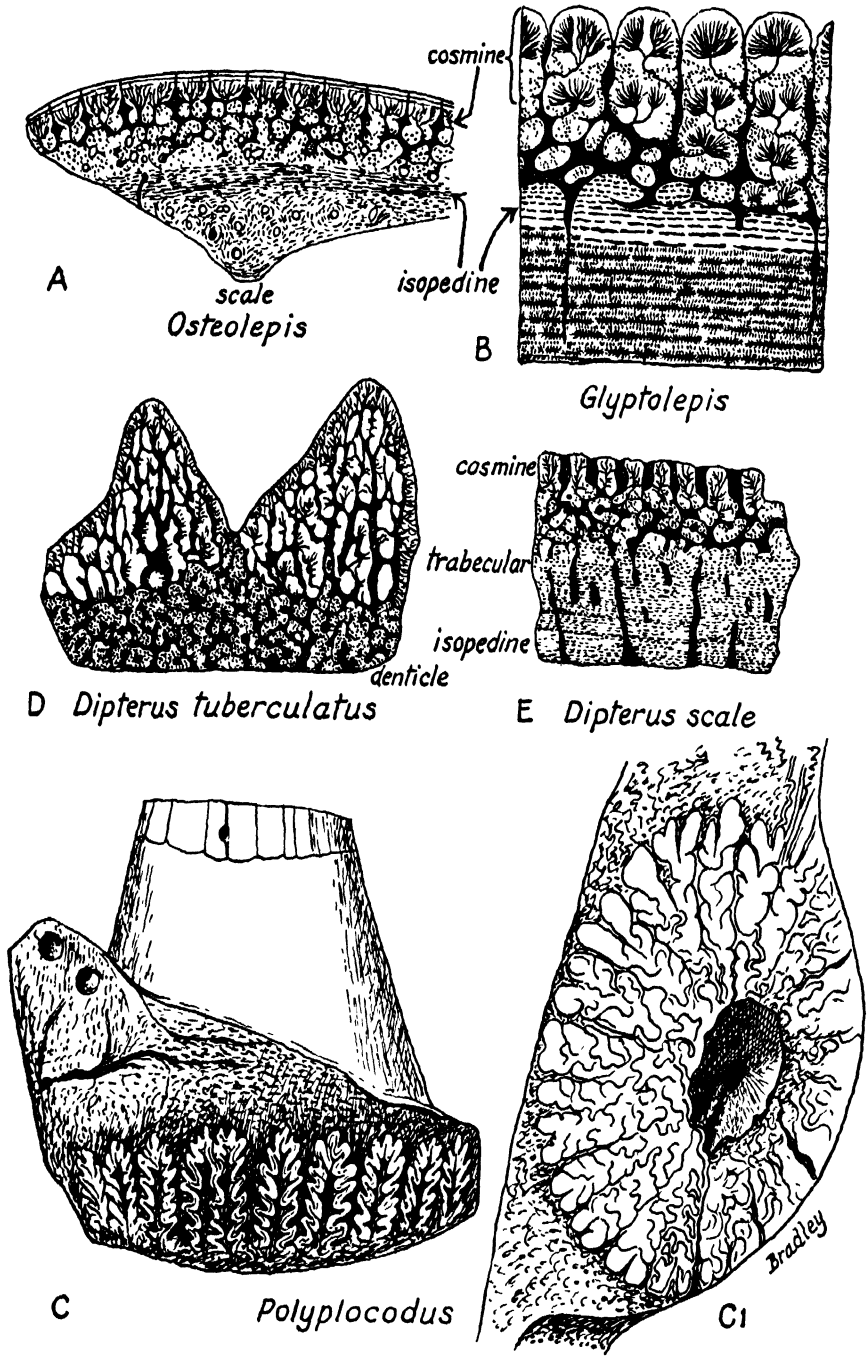
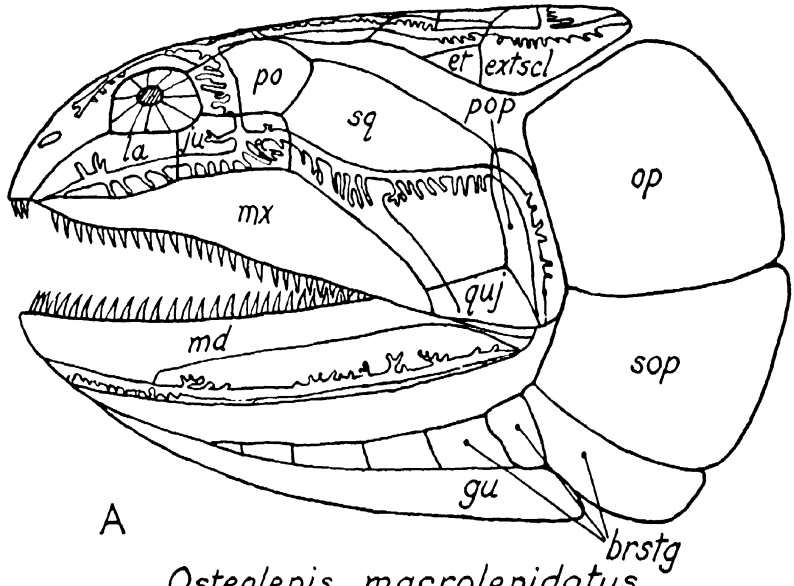
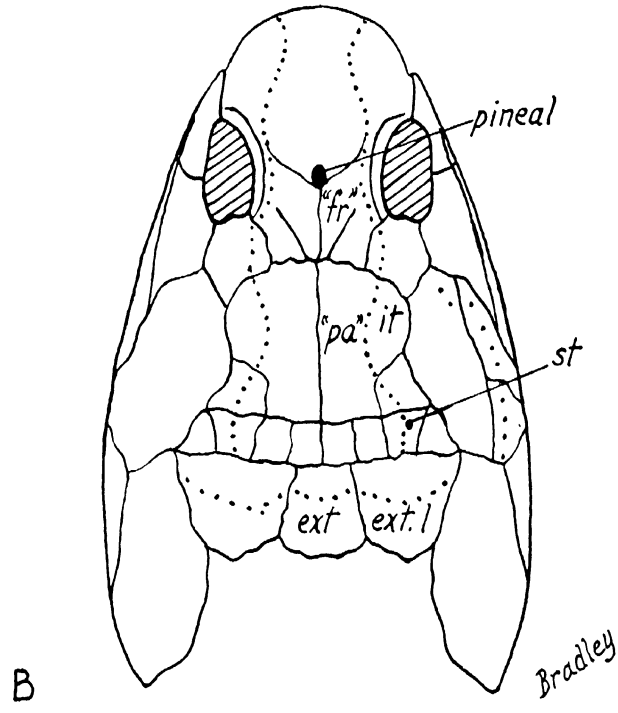


Fig. 10.7. Microsections of crossopterygian (A–C) and dipnoan (D, E) scales (A, B, E) and teeth (C, C1, D). After Pander. In the primitive crossoperygian scale (A) the thin enamel layer is intact, the cosmine layer is single. Loss of enamel and multiplication of the cosmine cells is shown in B. In the primitive dipnoan scale (E) and denticle (D) the bush-like cosmine layer likewise grades down into the vascularized middle layer. In the great laniary teeth of *Megalichthys* and its allies (C, C1) the radiating labyrinthine folds, opening into a central pulp cavity, seem to represent gigantic derivatives of the cosmine and vascular layers.



Osteolepis macrolepidotus



Osteolepis microlepidotus

Fig. 10.8. Skull patterns of the lobe-fins' founder. In A, the course of the lateral line branches is very primitive and fully developed. A, after Säve-Söderbergh; B, after Pander.

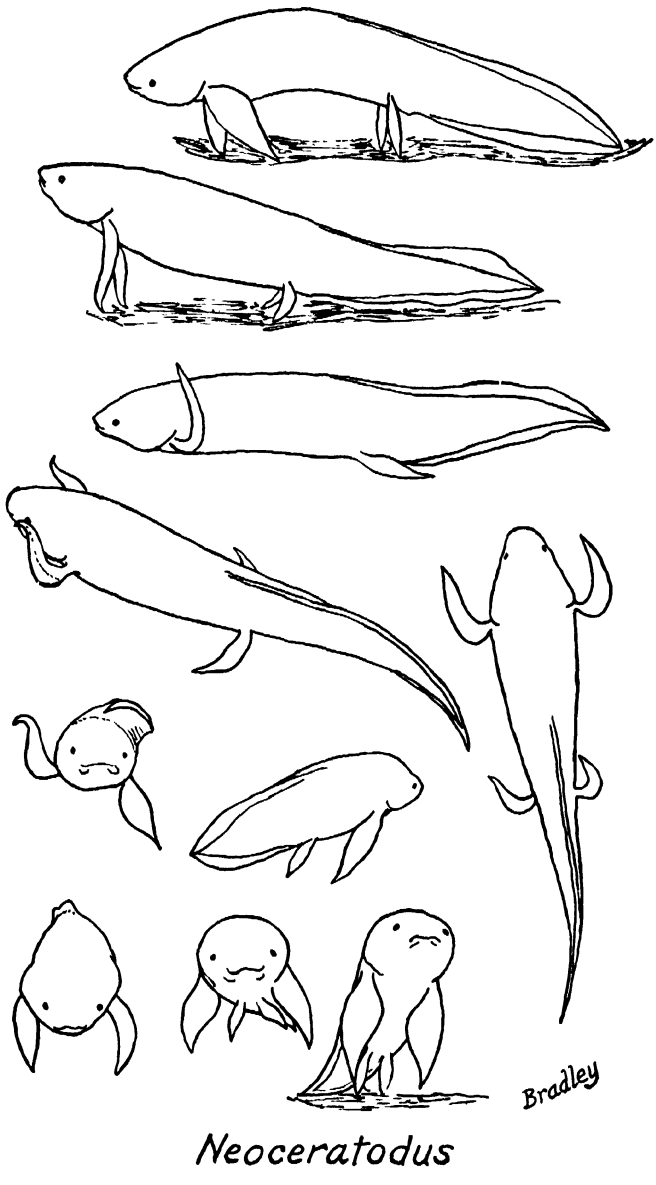


Fig. 10.9. Life poses of an Australian lungfish. From a sketch by Bashford Dean.

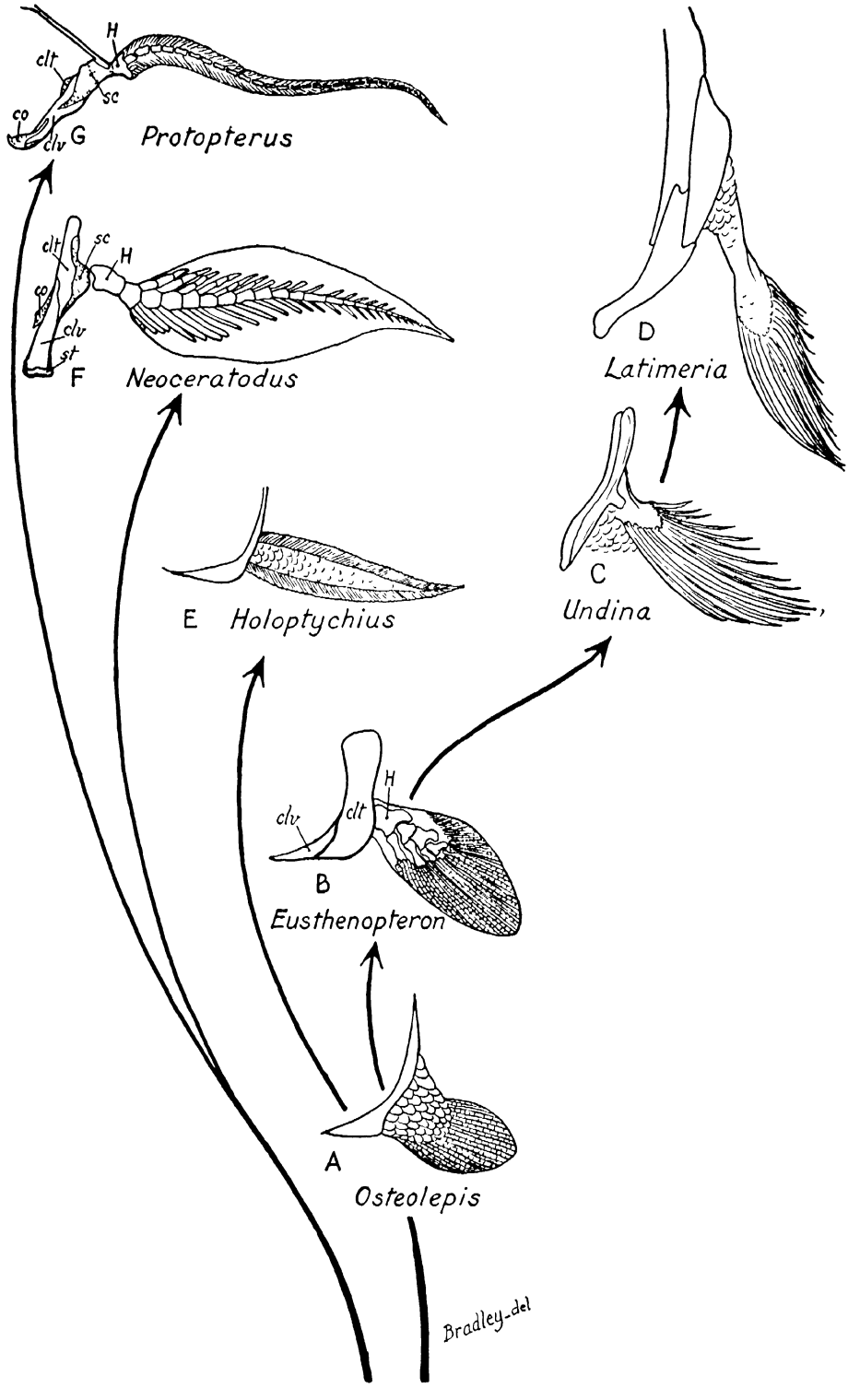


Fig. 10.10. Adaptive divergence in pectoral fin types among the dipnoans and lobe-fins. A, after Goodrich, D, after J. L B Smith; F, after Parker and Haswell; others, original

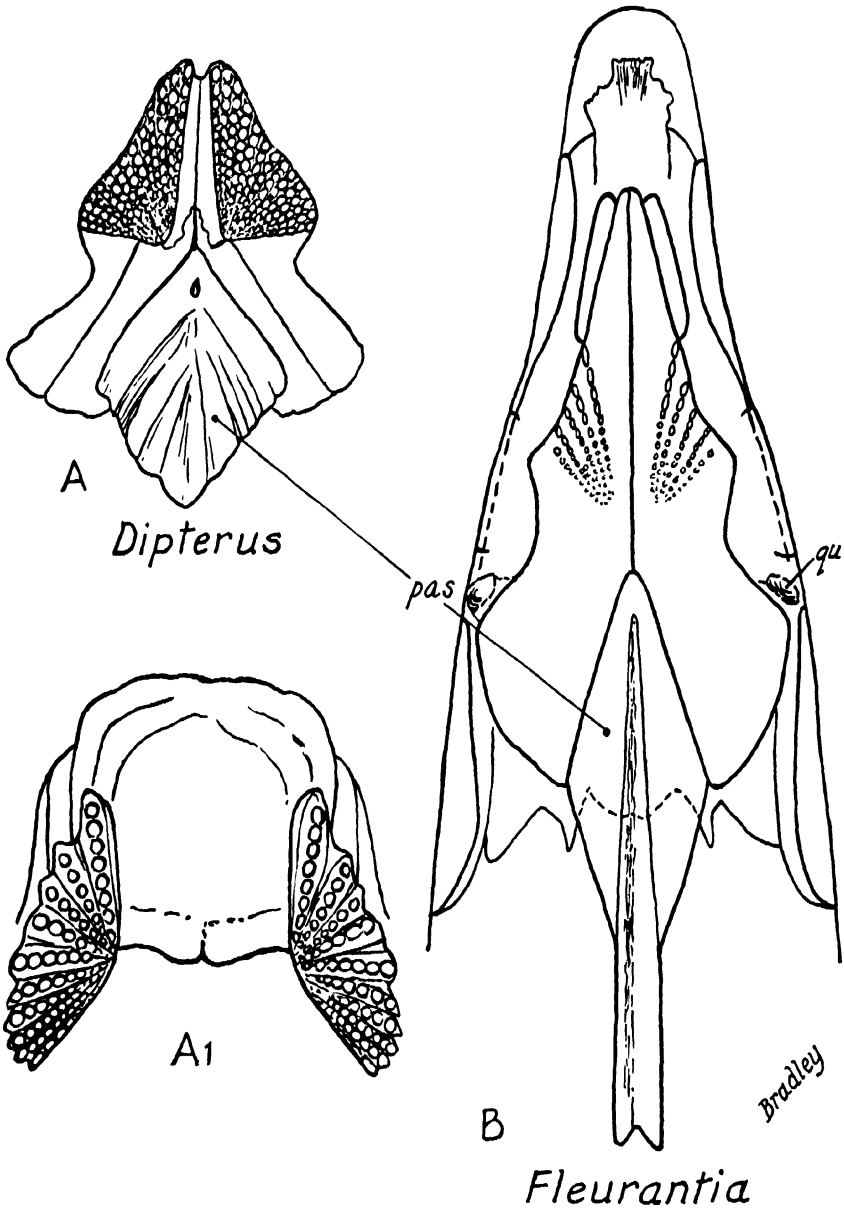


Fig. 10.11. Radiating dental clusters in primitive (A, A1) and retrogressive (B) dipnoans. A, after Pander; B, after Graham-Smith. (A and A1 belong to different species.)

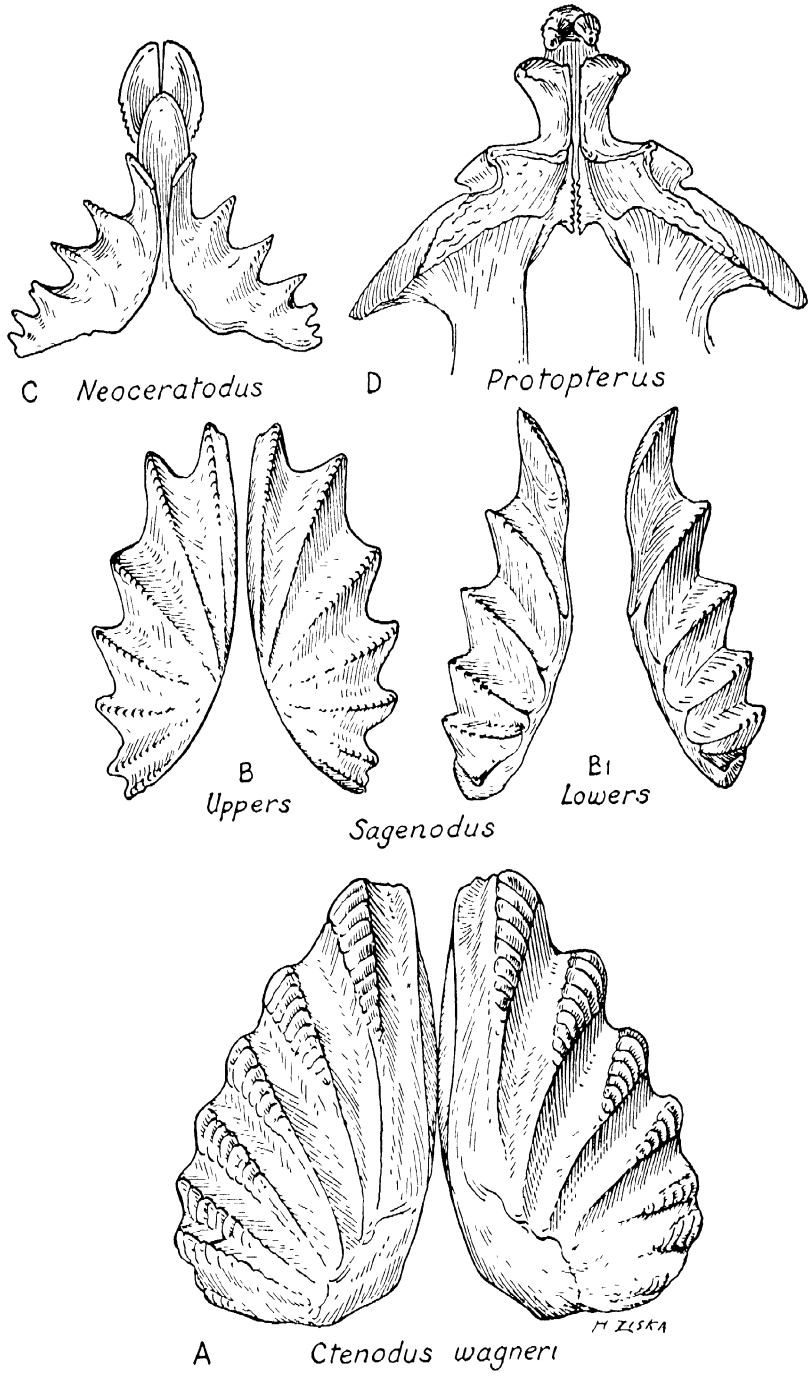


Fig. 10.12. Palaeozoic (A, B, B1) and Recent (C, D) dipnoan tooth plates. The fusion of the tooth rows into a solid mass provides a firm base for them and in turn requires a strongly built palate and massive skull. In *Ctenodus wagneri,* unlike some other species of this genus, the rounded tooth rows seem to be adapted to crushing mollusc shells and crustacean tests. At the other extreme (D) the denticles have fused into shears and the tooth rows are reduced to three on each side.

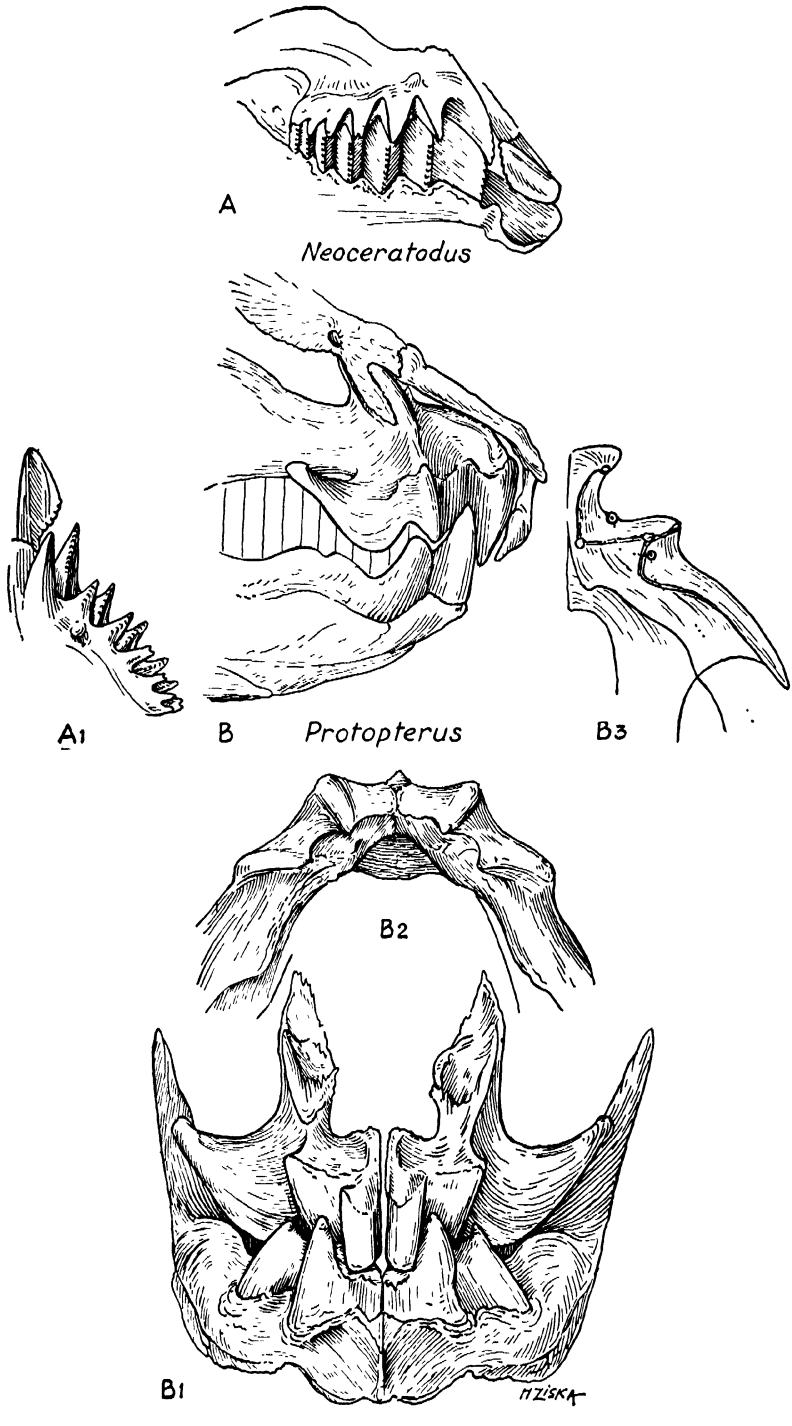
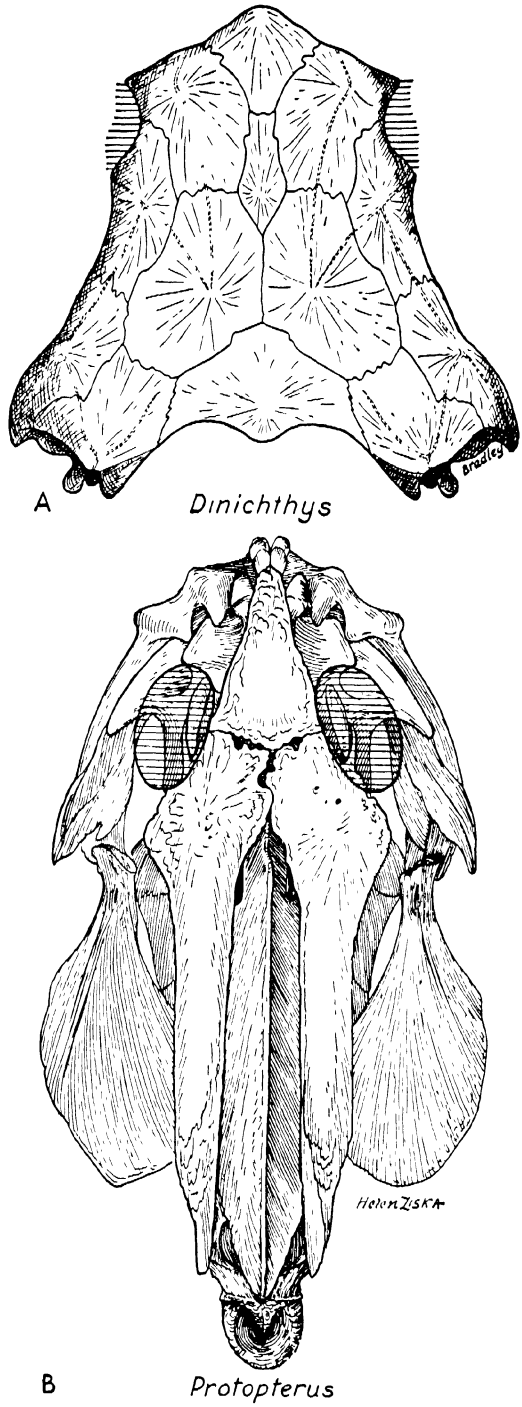


Fig. 10.13. Upper and lower tooth plates in occlusion, showing alternation of upper and lower ridges and grooves. A, right side, showing incisor-like anterior upper tooth and gutter-like lower; A1, left side from below; B, right side, showing incisor-like front tooth, two ridges and long blade representing the dental base of *Sagenodus* (fig. 10.12B); B1, front view; B2, lower jaw, top view; B3, occlusal diagram. Lower dental ridges dotted; circles represent cusps.



Figs. 10.14, 15. Relatively primitive skull pattern of Devonian arthrodire (A) and extremely specialized pattern of modern dipnoan (B). In B, the lateral roof bones have disappeared, exposing the temporal region and leaving only the naso-rostral and possibly the centrals and the occipital crest. A, after Heintz; B, original.

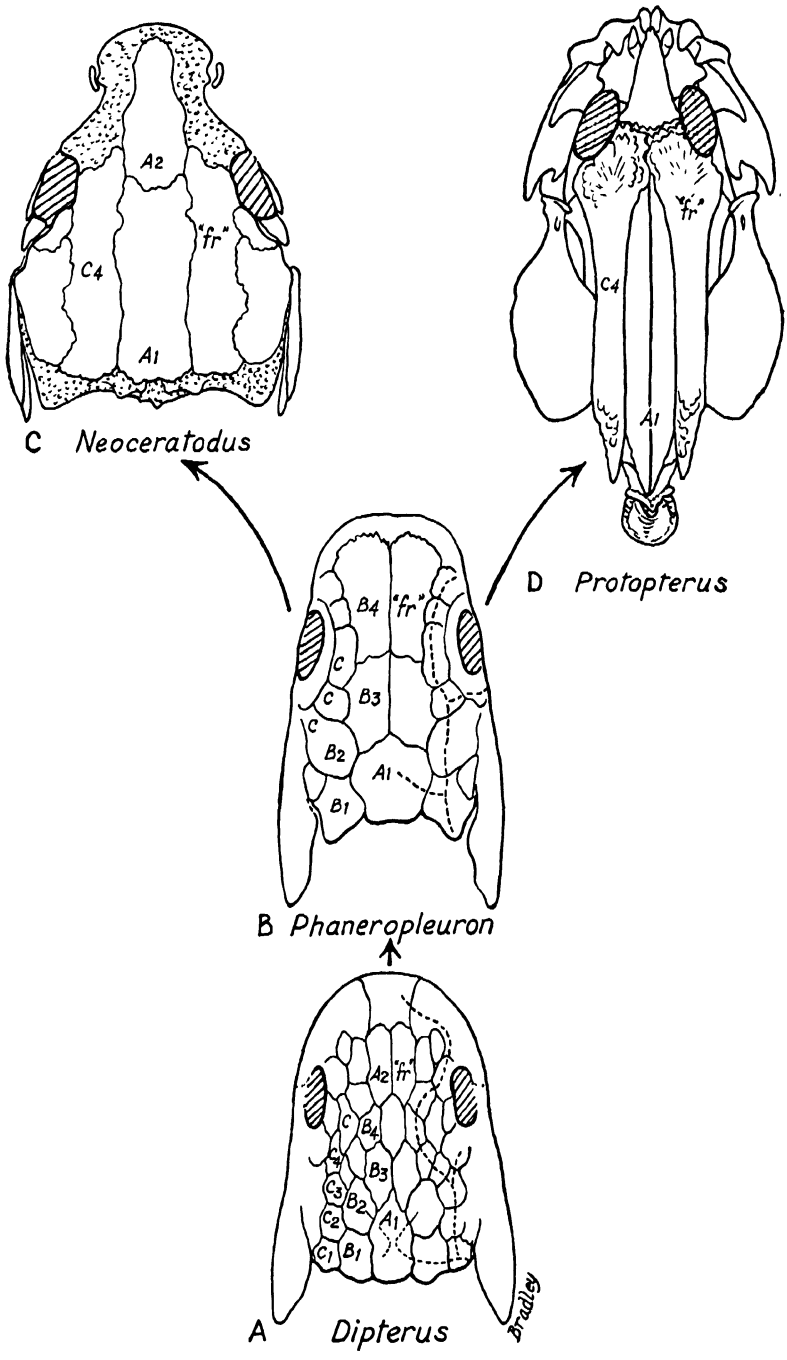


Fig. 10.16. Progressive simplification of the skull roof in dipnoans. The mosaic of small plates in *Dipterus* (A) is probably due to fragmentation of an earlier pattern with continuous skull roof. In B, there has been a marked anisomerism, involving enlargement of certain pieces and elimination of others. C and D show culmination of process in modern dipnoans. Probable homologies in A–C, according to Romer; D, original.

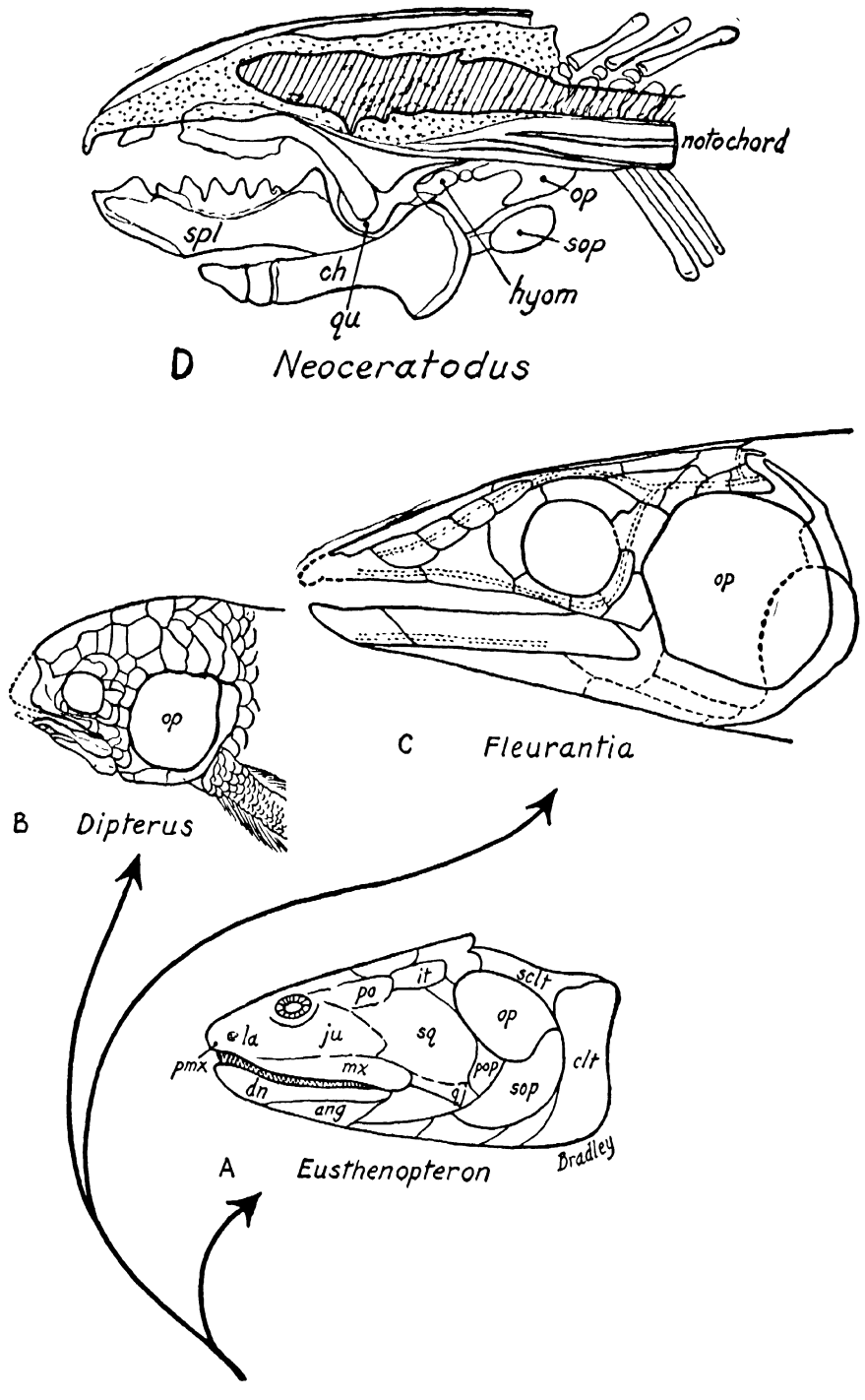


Fig. 10.17a. Mesial sagittal section (D) of Australian lungfish skull, showing the massive cartilaginous endocranium and the thin-shelled dermocranium, the vestigial condition of the hyomandibular and the presence of a strong splenial bone supporting the lower tooth plate. After Goodrich.

Fig. 10.17b. Extreme fragmentation of skull pattern in primitive dipnoan (B) (Pander), secondary simplification in C (Graham-Smith and Westoll), producing a somewhat convergent resemblance to the relatively primitive lobe-fin pattern (A). Data from Bryant, Watson, Stensiö, Gregory and Raven.

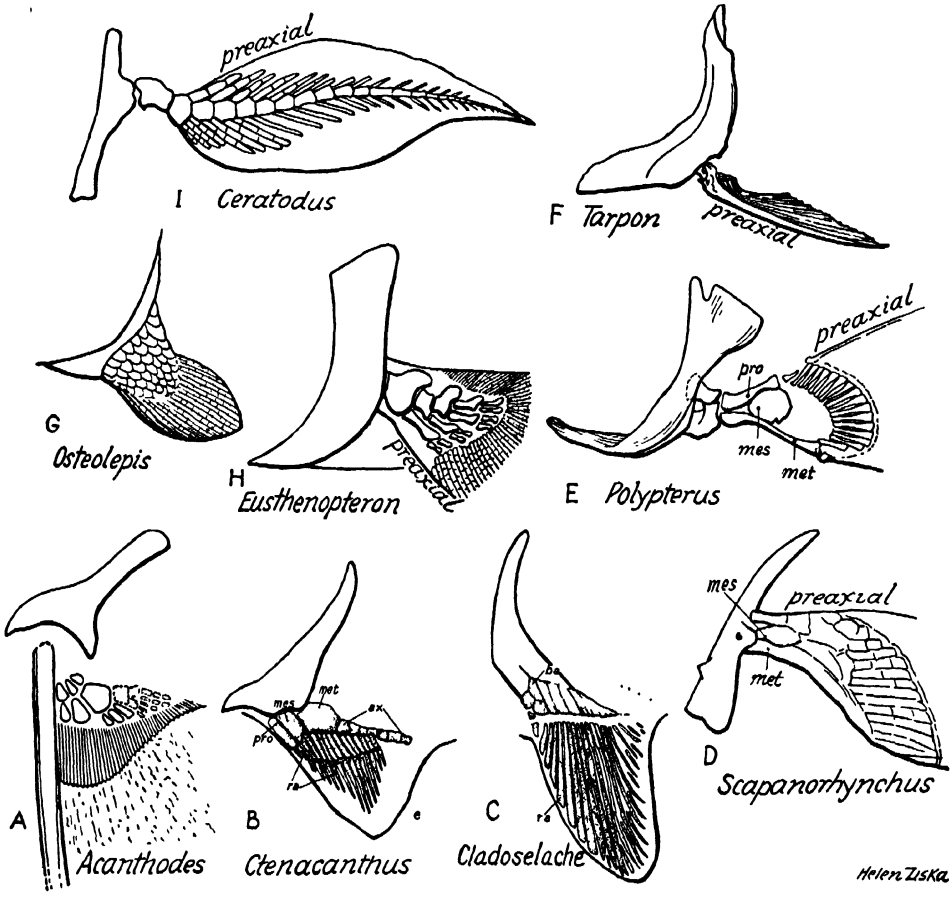


Fig. 10.18. Twisting of the preaxial border of the pectoral fin from the anteroventral (A–C) to the dorsoposterior (E, G–I) position, in different subclasses of fishes. After Gregory and Raven. When the proximal base of the fin is extended anteroposteriorly (B, C), the fin can only be raised, lowered and undulated but not twisted. When the base is narrow and wrist-like (D, E, H), the fin can be twisted so that the preaxial border is turned upward. In the dipnoan (I) the chevron-like arrangement of the muscle segments is associated with a nearly symmetrical arrangement of the radials on either side of the many-jointed axis. A, after Watson; B, after Moy-Thomas; C, after Dean; G, after Goodrich; H, after Bryant; I, after Rabl, in part; others original.

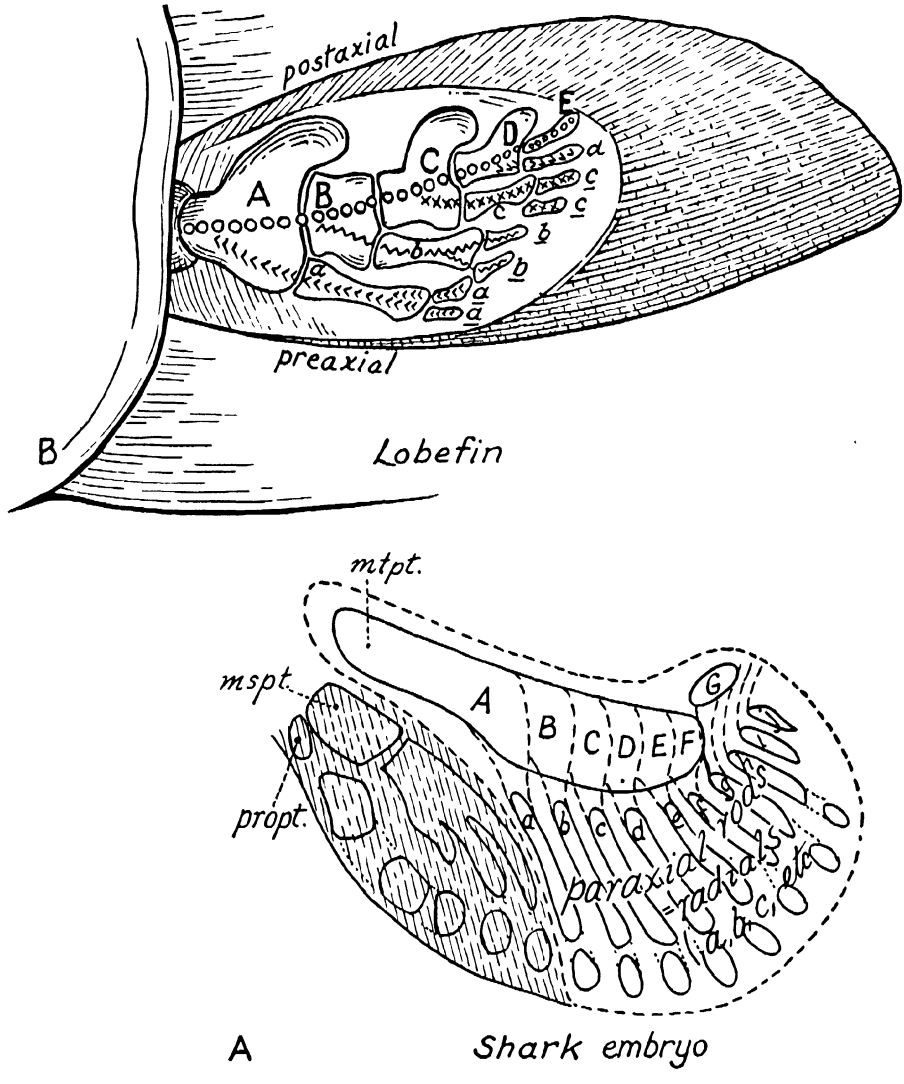


Fig. 10.19. Possible homologies of the axial and radial pieces in crossopterygian (B) and selachian (A). Data from Moy-Thomas (A), Gregory and Raven (B).

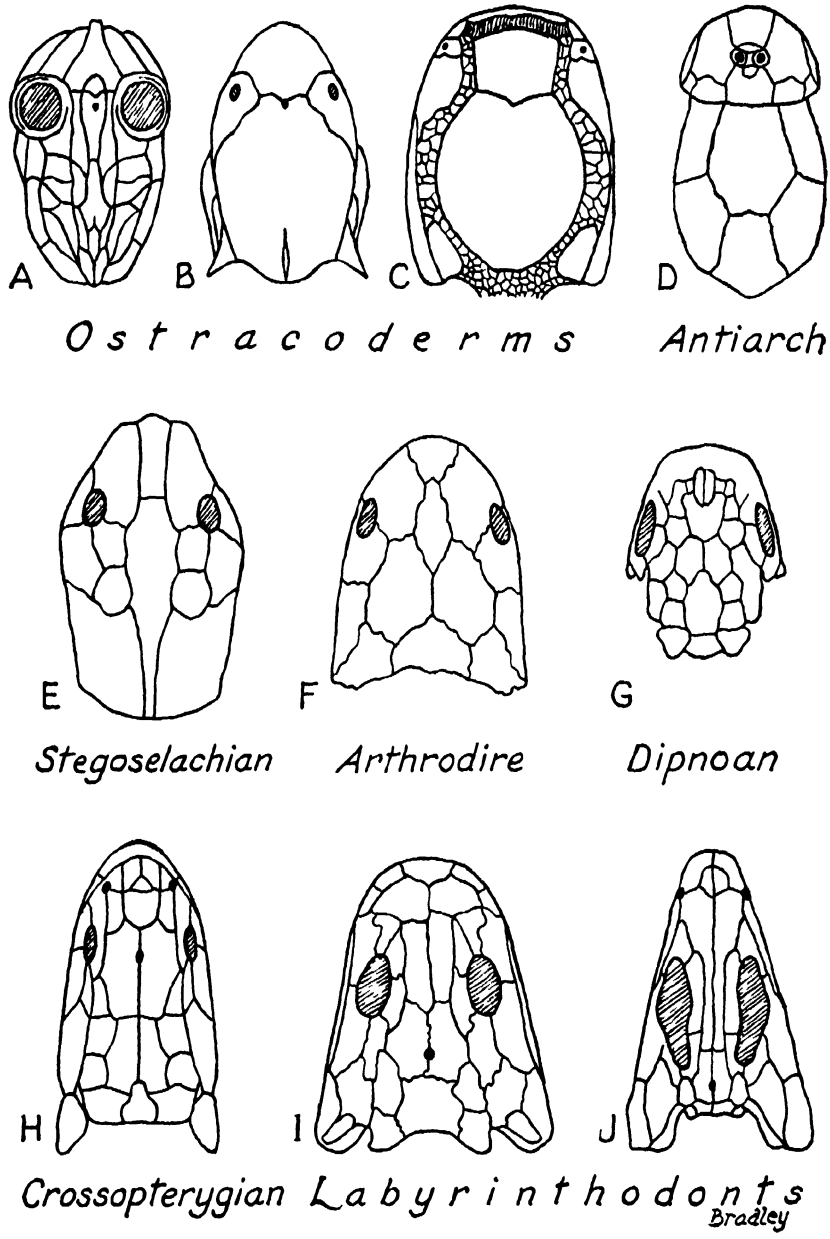
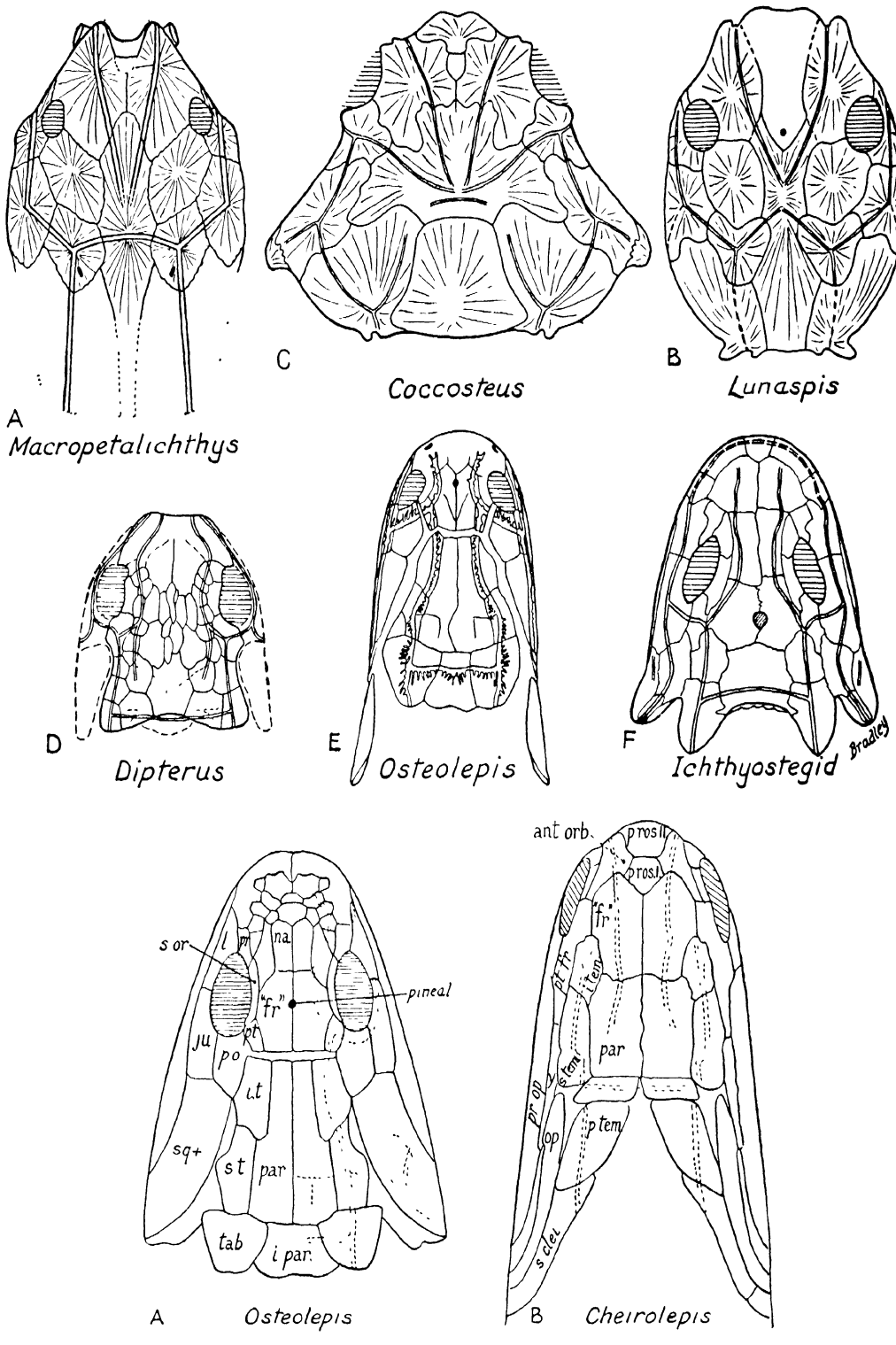


Fig. 10.20. Predominance of median plates in the skull roof of earlier fishes (A–G) and of paired plates in lobe-fins and labyrinthodonts. After Broili.



Figs. 10.21, 22. Homologous lateral line patterns with varying skull roof patterns in placoderms (A–C) and choanates (D–F). A–D, after Stensio; E, F, after Säve-Söderbergh. Basal identity in skull-top plan with marked differences in proportions, in primitive lobe-fin and ganoid. After Watson.

CHAPTER XI

THE AIR-BREATHERS COME UP ON LAND

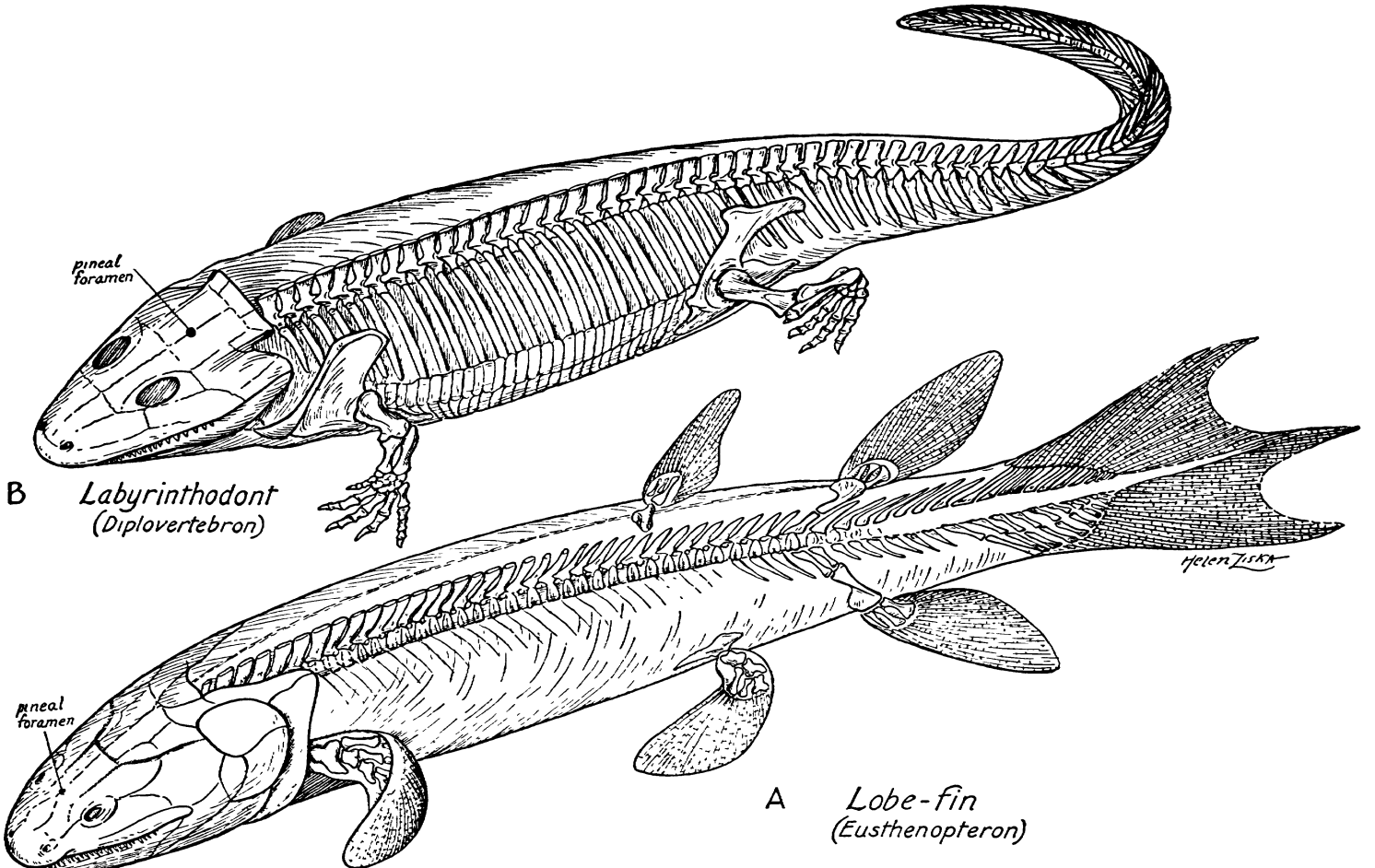


Fig. 11.1 Upper Devonian lobe-fin (A) and Carboniferous amphibian (B). The amphibian has advanced beyond the lobe-fin in many ways, especially in the loss of median fins, transformation of paired paddles into limbs, development of strong ribs, great increase in size of the scapulo-coracoid, loss of posttemporal bar connecting the shoulder-girdle with the skull, increased height and spread of dorsal blade of pelvis.

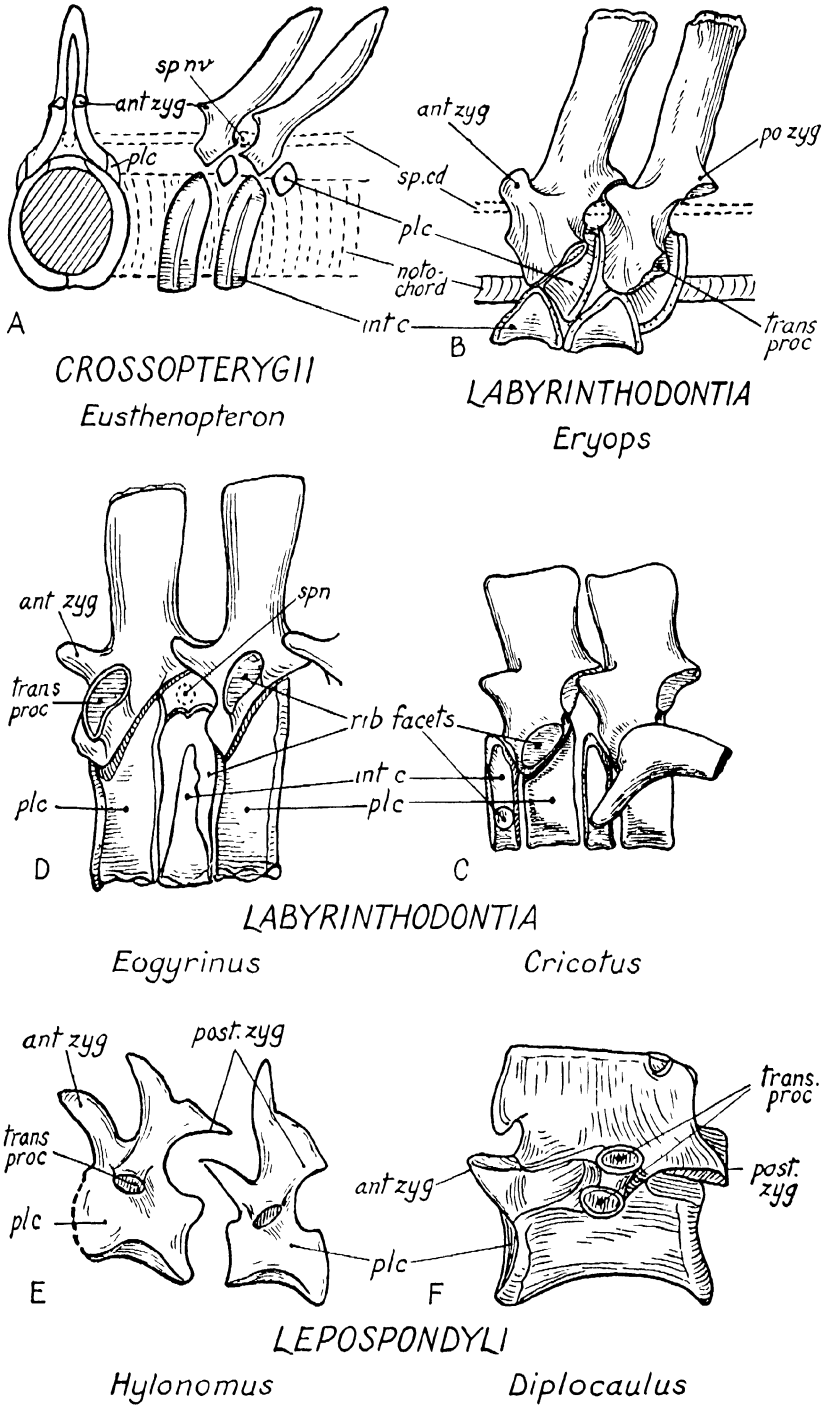


Fig. 11.2. Dorsal vertebrae of Upper Devonian lobe-fin (A) Carboniferous labyrinthodonts (B, C, D) and lepospondyls (E, F). A and B are of the rhachitomous type, with small pleurocentra confined to the dorsal half of the vertebra; C, D, embolomerous vertebrae, with fully developed pleurocentra reaching to the ventral line; E, F, lepospondylous (holospondylous) vertebrae with undivided centra. C, after Watson; E, after Steen; others original.

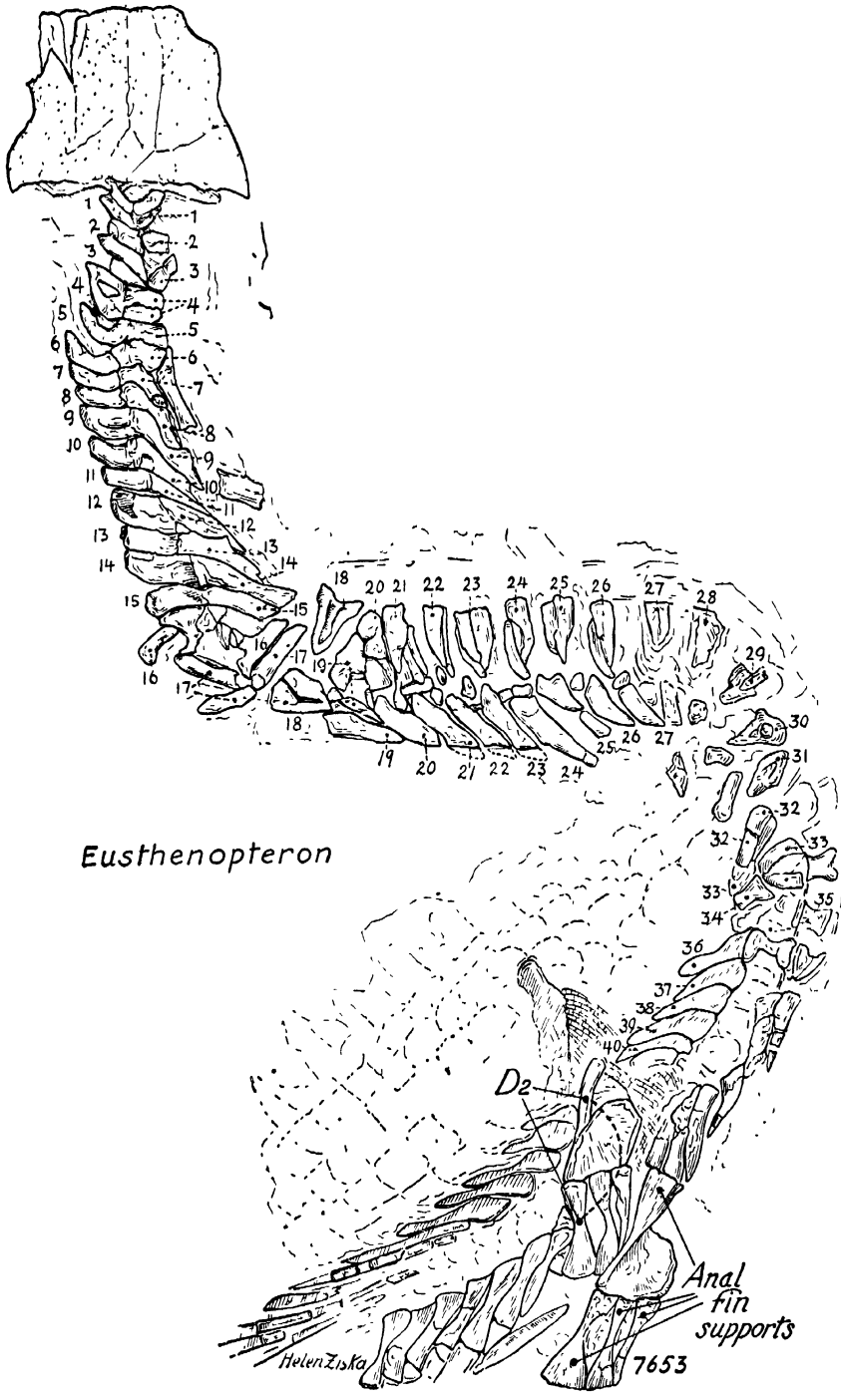


Fig. 11.3. Vertebral column of Upper Devonian lobe-fin *Eusthenopteron*. After Gregory and Raven. Shows crescentic half-centra (intercentra), very small nodular pleurocentra and large neural arches. No ribs are present.

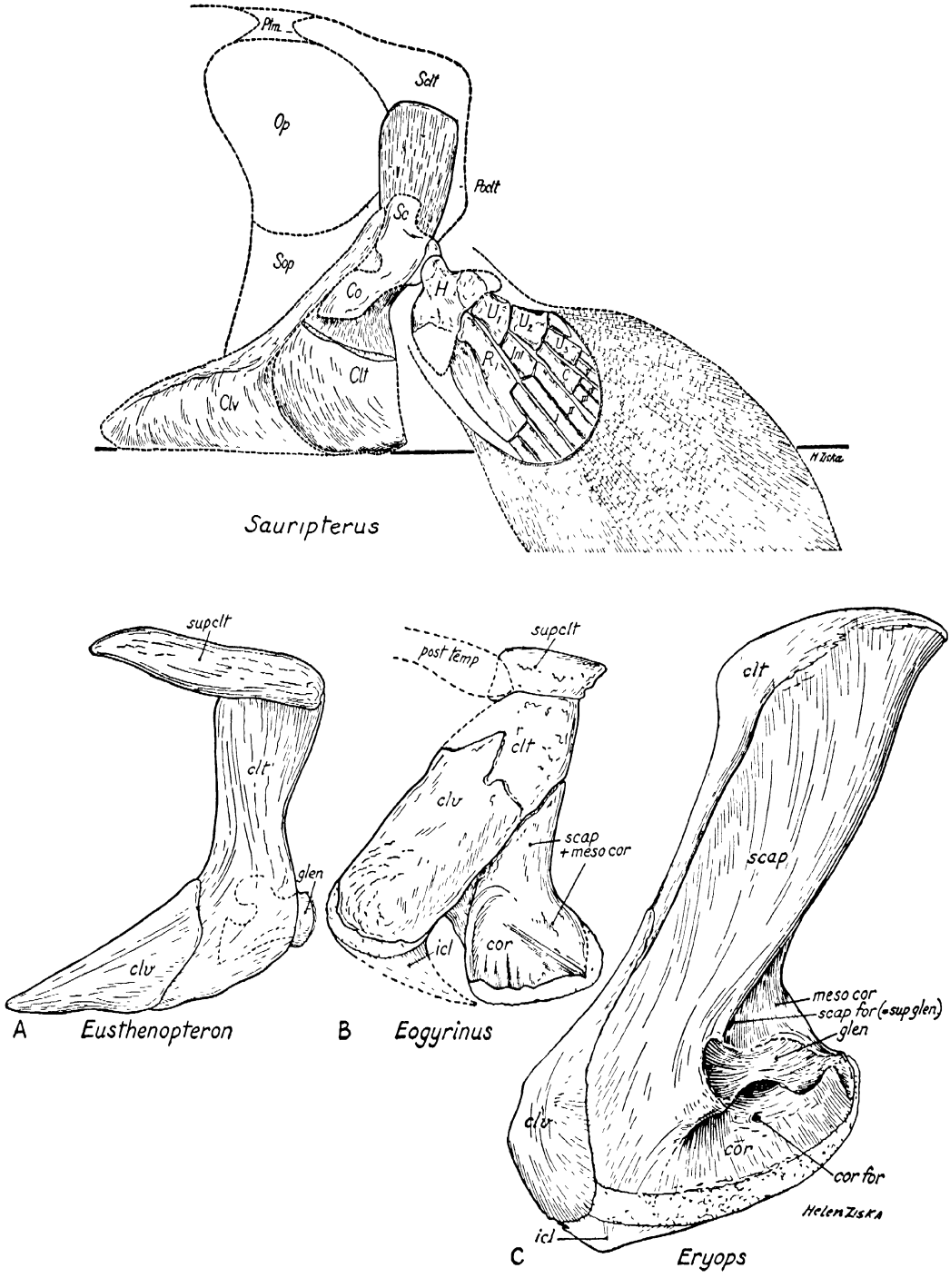


Fig. 11.4 (top). Pectoral girdle and paddle of Upper Devonian lobe-fin *Sauripterus* (cf. fig. 11 8). Restored, after Gregory. Inner view of right side, showing relations of pectoral paddle and girdle to skull. Fig. 11.5. Pectoral girdles (lateral view of left side) of Upper Devonian lobe-fin (A), Upper Carboniferous amphibian (B) and Permo-Carboniferous amphibian (C). A, after Bryant; B, after Watson; C, original. The series shows the great increase in size of the scapulocoracoid and of the glenoid region, together with the marked reduction of the cleithrum in the later stage.

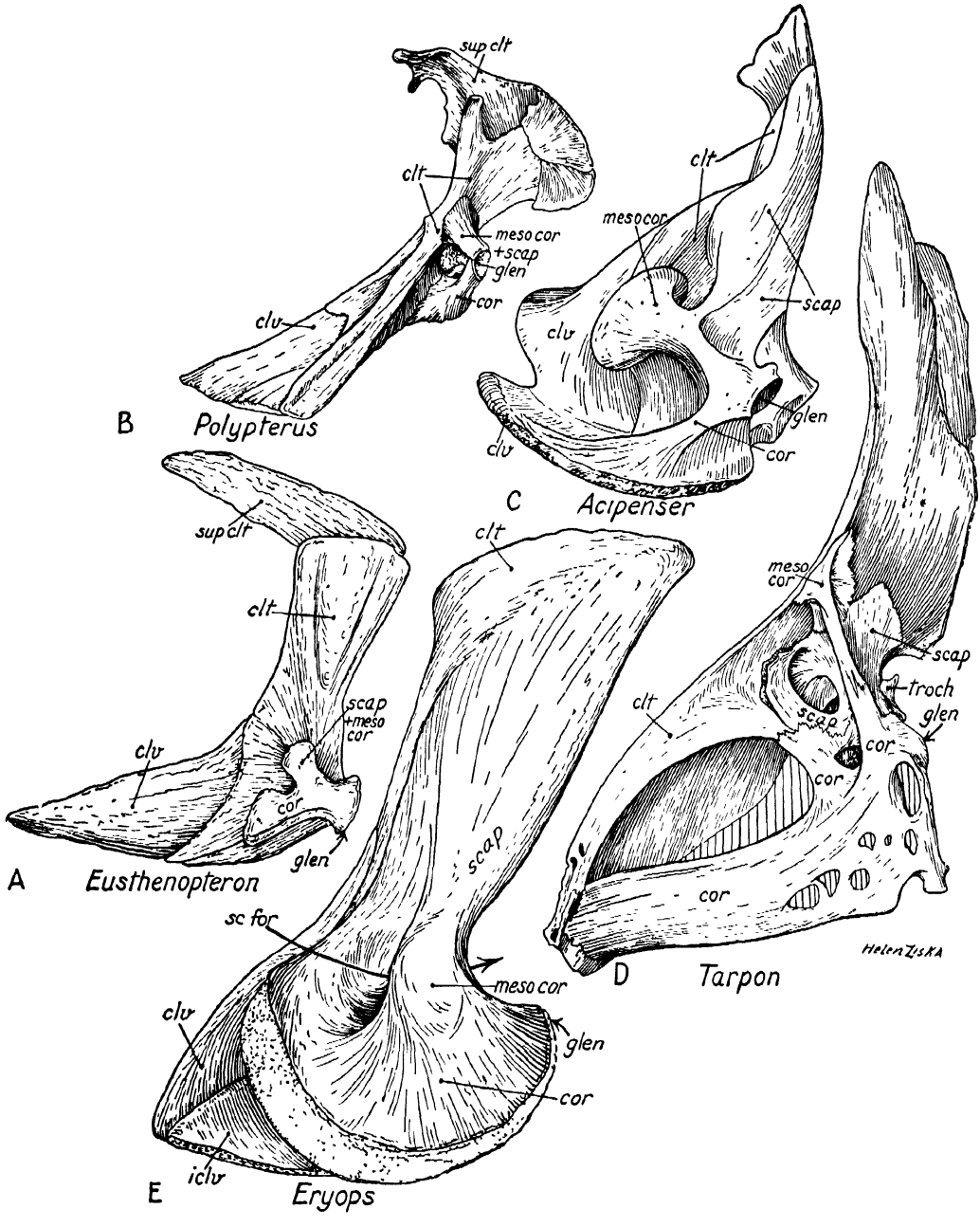


Fig. 11.6. Inner views of right half of pectoral girdle of primitive lobe-fin (A), two surviving ganoids (B, C), a primitive teleost (D) and a Permo-Carboniferous amphibian (E). A, data partly from Bryant; C, data from W. K. Parker; B, D, E, original.

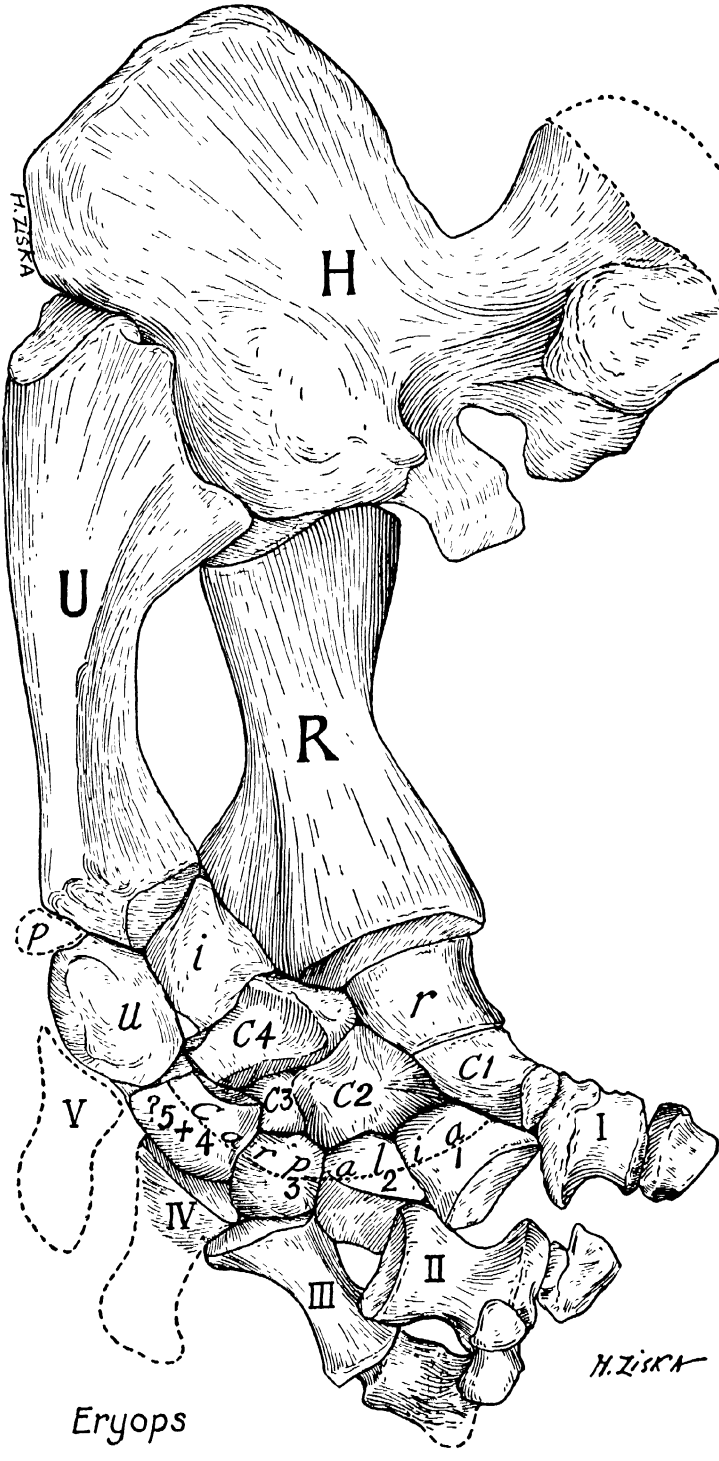


Fig. 11.7. Inner or flexor side of the left arm and hand of a large Upper Carboniferous amphibian. The first, second and third metacarpals (I, II, III) are somewhat displaced away from their proper carpals (1, 2, 3); the missing fifth metacarpal (V) left its facet on the ulnare. The first centrale (C1) has a large facet, apparently for a prepollex, the other metacarpals and carpals converge toward the ulna.

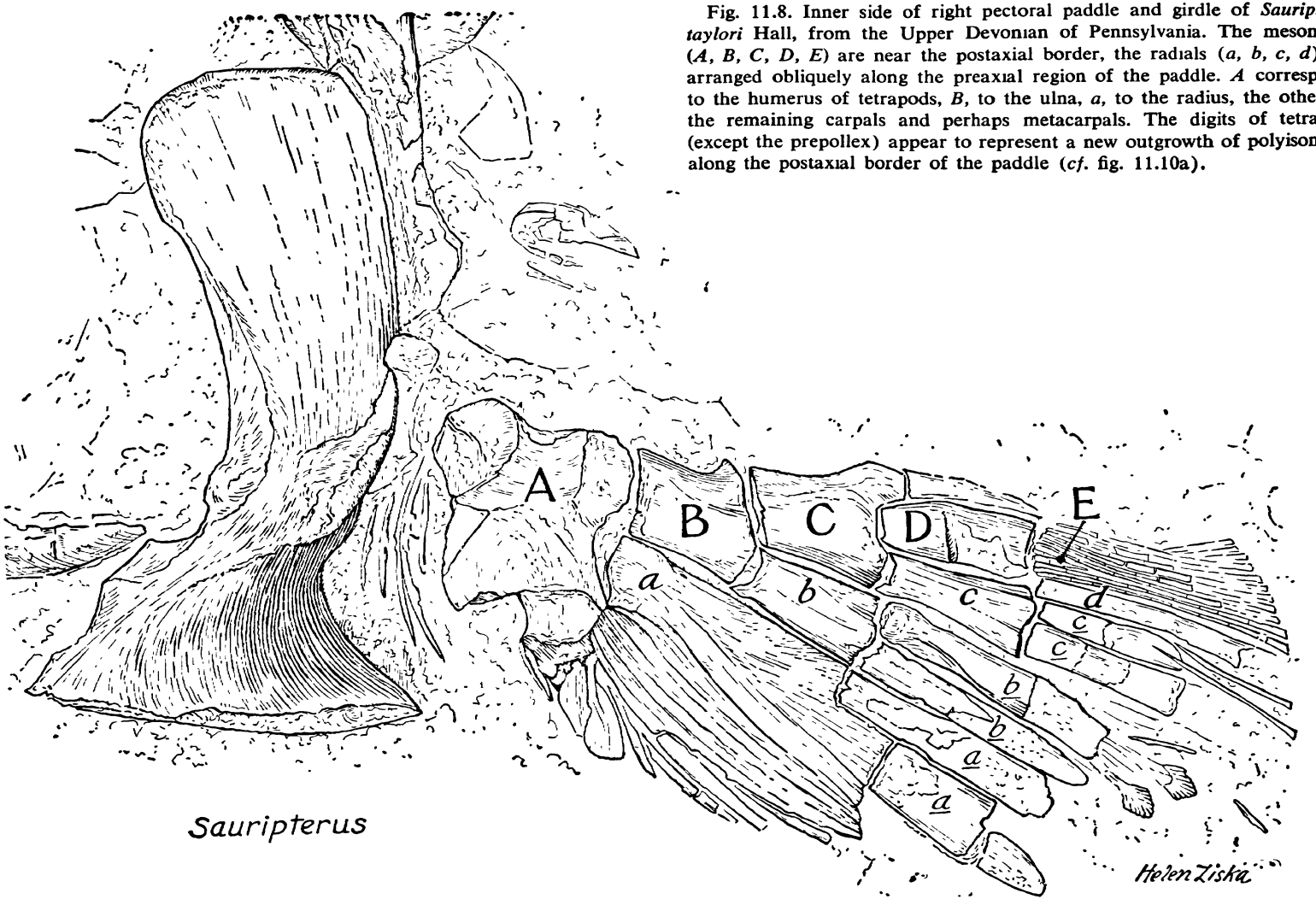


Fig. 11.8. Inner side of right pectoral paddle and girdle of *Sauripterus taylori* Hall, from the Upper Devonian of Pennsylvania. The mesomeres (*A, B, C, D, E*) are near the postaxial border, the radials (*a, b, c, d*) are arranged obliquely along the preaxial region of the paddle. *A* corresponds to the humerus of tetrapods, *B*, to the ulna, *a*, to the radius, the others to the remaining carpals and perhaps metacarpals. The digits of tetrapods (except the prepollex) appear to represent a new outgrowth of polyisomeres along the postaxial border of the paddle (*cf.* fig. 11.10a).

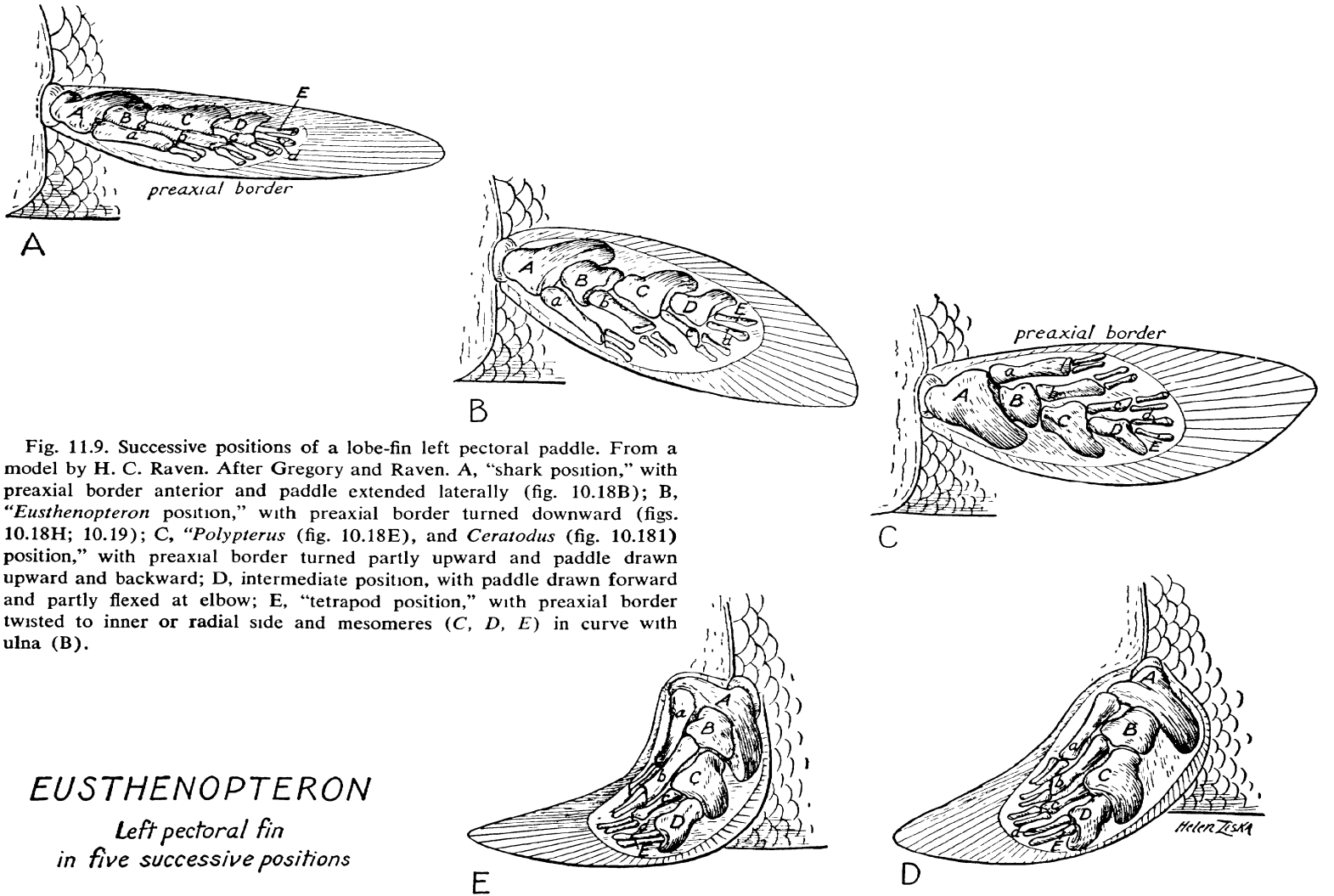


Fig. 11.9. Successive positions of a lobe-fin left pectoral paddle. From a model by H. C. Raven. After Gregory and Raven. A, "shark position," with preaxial border anterior and paddle extended laterally (fig. 10.18B); B, "*Eusthenopteron* position," with preaxial border turned downward (figs. 10.18H; 10.19); C, "*Polypterus* (fig. 10.18E), and *Ceratodus* (fig. 10.181) position," with preaxial border turned partly upward and paddle drawn upward and backward; D, intermediate position, with paddle drawn forward and partly flexed at elbow; E, "tetrapod position," with preaxial border twisted to inner or radial side and mesomeres (*C, D, E*) in curve with ulna (B).

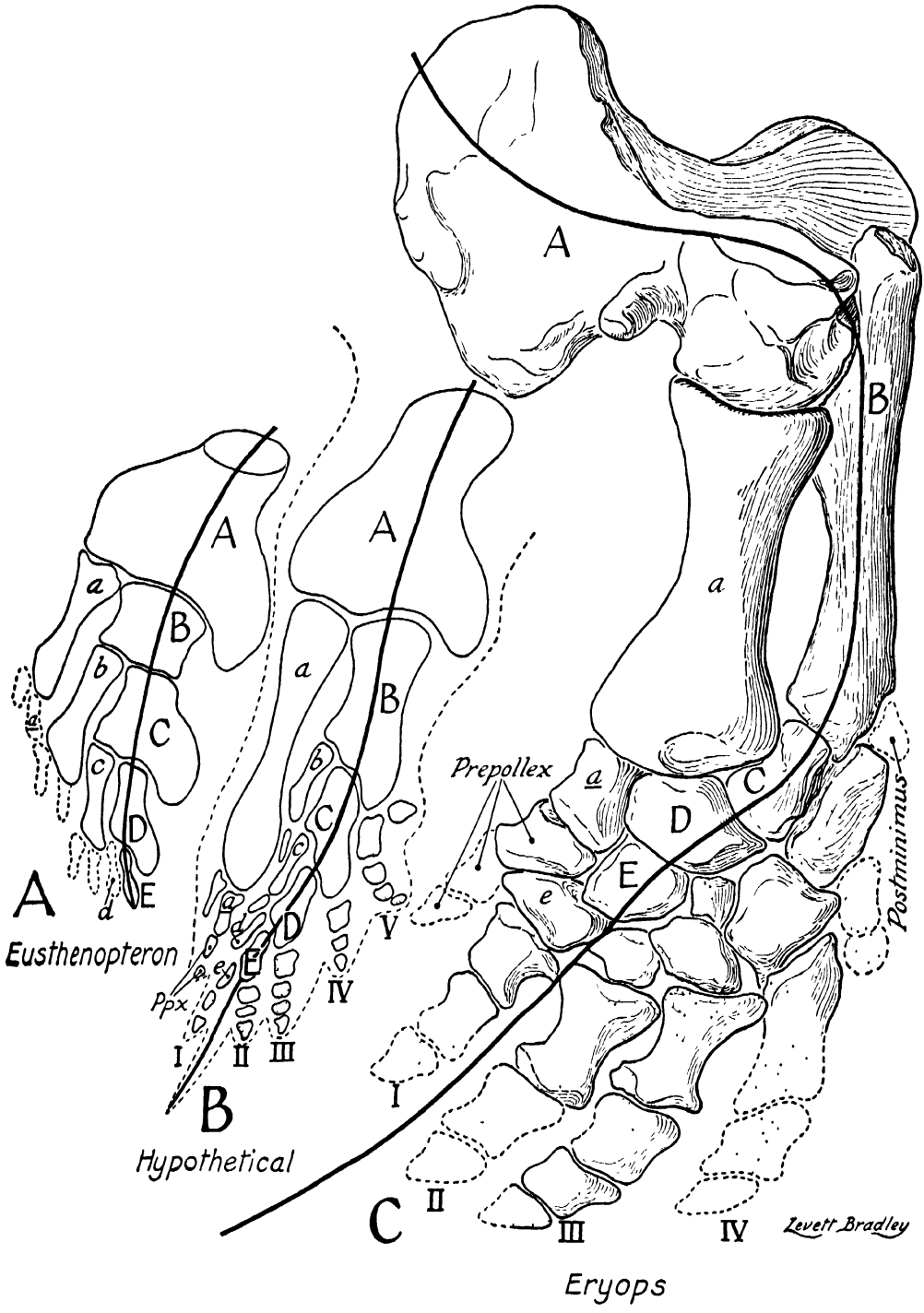


Fig. 11.10a. Supposed homologies of pectoral limb parts between Devonian lobe-fin (A) and amphibian (C). Extensor surface of left hand, to show bending of mesomeral axis (black line) and supposed outgrowth of ulnar, carpals, metacarpals and digits (dotted). After Gregory and Raven. The graphic intermediate (B) is based partly on the data supplied in Holmgren's papers (1933, 1939) on the embryonic stages in the development of the pectoral limbs of modern urodeles.

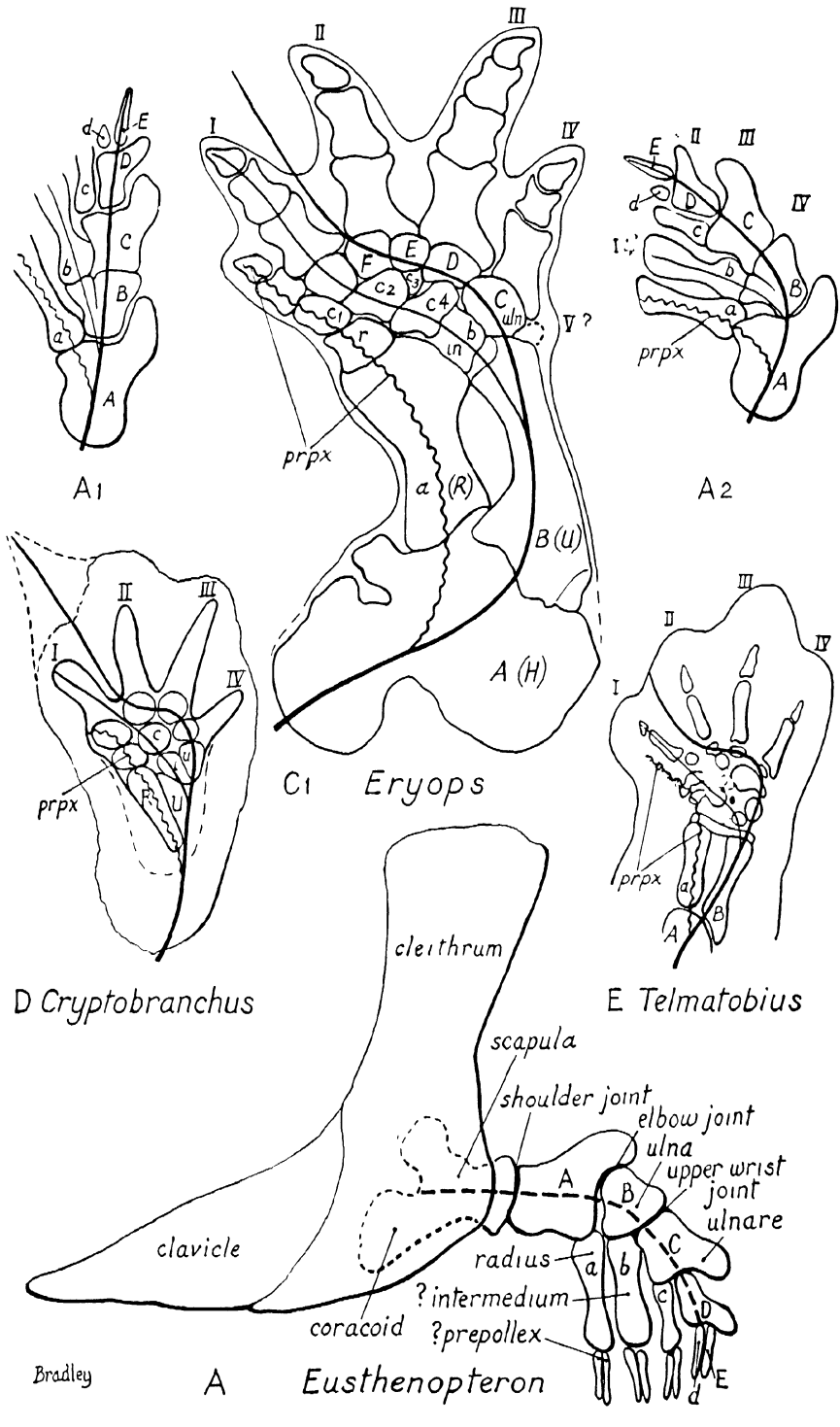


Fig. 11.10b. Flexor surface of left hand. Upper Devonian lobe-fin (A1, A2), Permo-Carboniferous amphibian (C1), larval urodele (D) and larval anuran (E), showing sharp bending of mesomeral axis (black line) in amphibian and possible homologies of parts. D, E, after Holmgren; others original.

Fig. 11.10c (bottom). Extensor surface of left arm, shown as bent but not twisted.

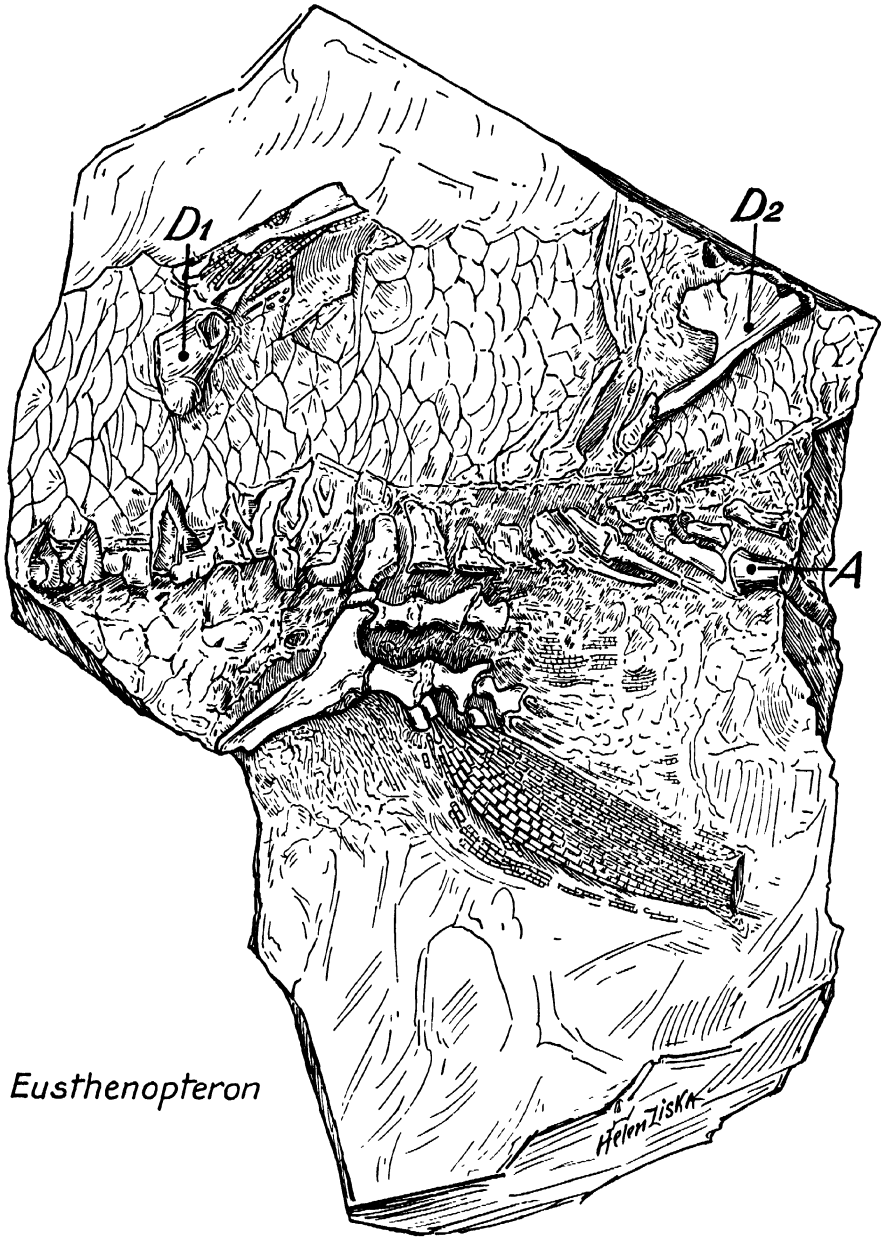


Fig. 11.11. Pelvic region of *Eusthenopteron*, showing the pelvis (left half) and both pelvic paddles, the caudal vertebral column with spaced centra, the supports of the dorsal fins (D1, D2). After Gregory and Raven.

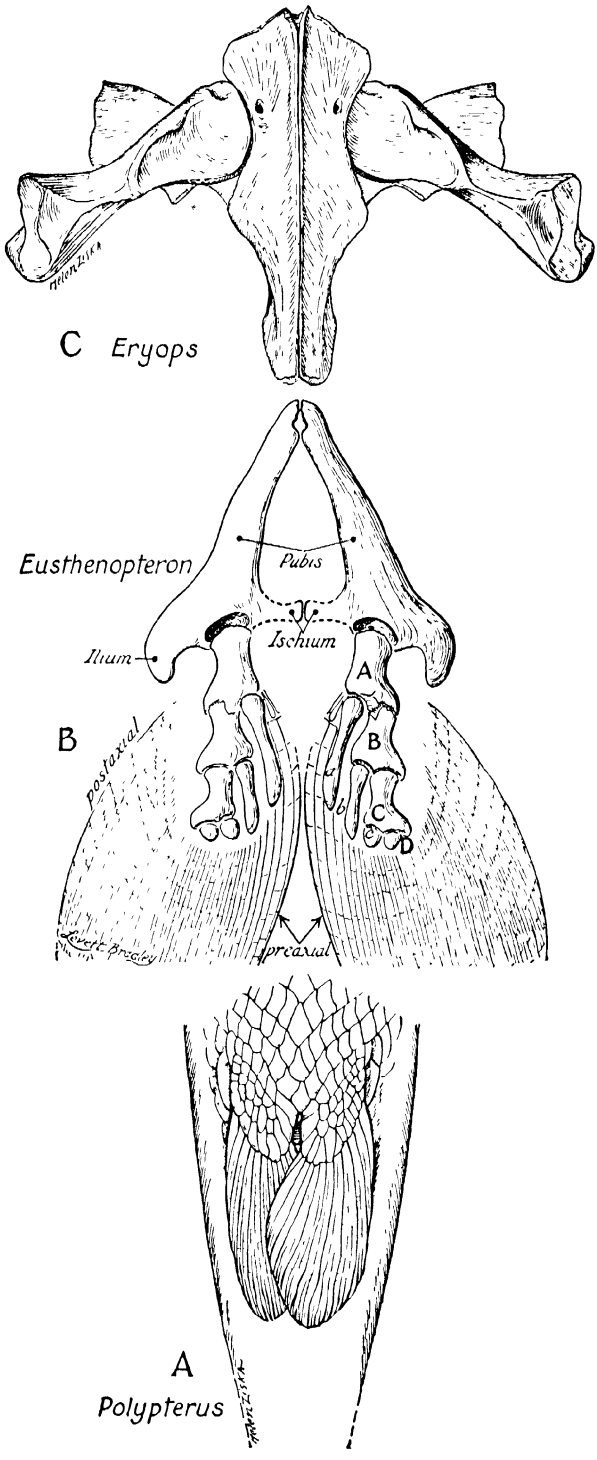


Fig. 11.12. Ventral view of the pelvic region in *Polypterus* (A), *Eusthenopteron* (B) and primitive tetrapod (C). After Gregory and Raven. The pelvic paddles (A, B) are directed caudally, but when paddles changed into limbs, the proximal mesomeres (A) moved around to the outer side of the pelvis (C) to form the femora of primitive tetrapods (C).

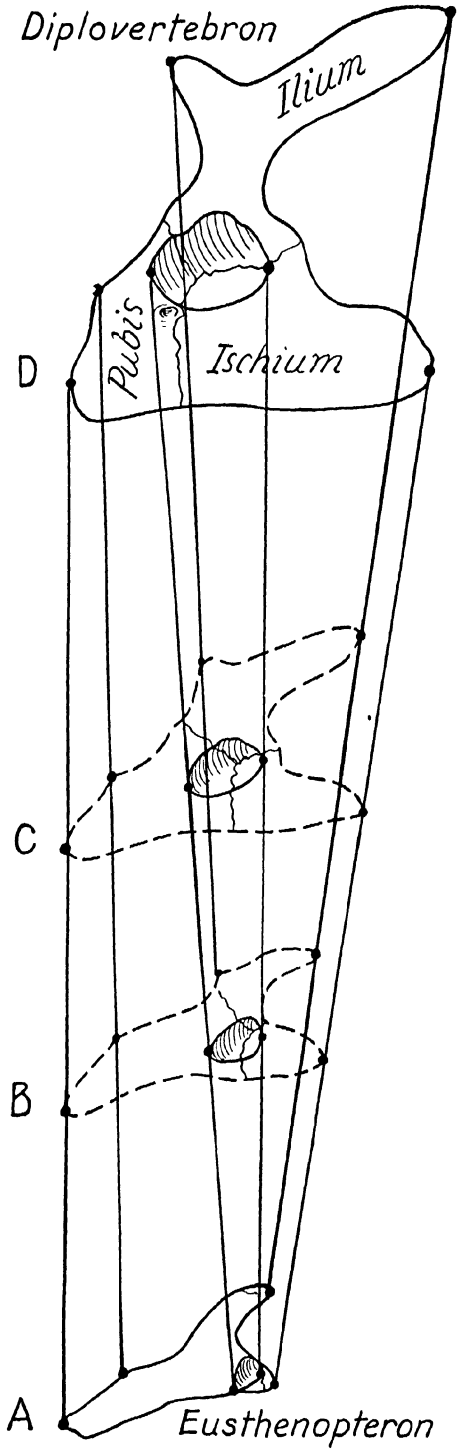


Fig. 11.13. Suggested solution of the problem of the origin of the tetrapod pelvis. After Gregory and Raven. As the femur moved around from the caudal or posteroexternal to the anterolateral position, the parts around it grew radially away from it, giving rise to the three growth centers of the pubis, ilium and ischium.

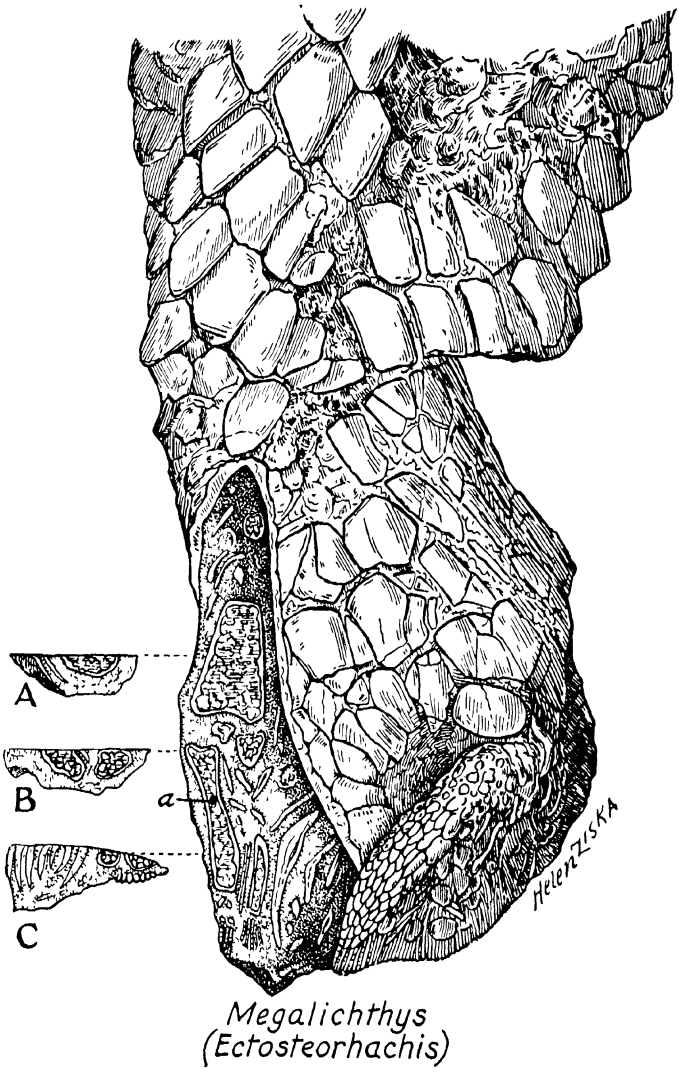


Fig. 11.14. Pelvic region of a progressive lobe-fin (*Megalichthys*), from the Permo-Carboniferous of Texas. After Gregory and Raven. The sections, which were begun by Cope and finished by Raven, show the limb-like skeleton of the muscular pelvic paddles. The stout segment (*A*) may be homologous with the first mesomere (*A*) of the *Eusthenopteron* paddle (Fig. 11.12 B).

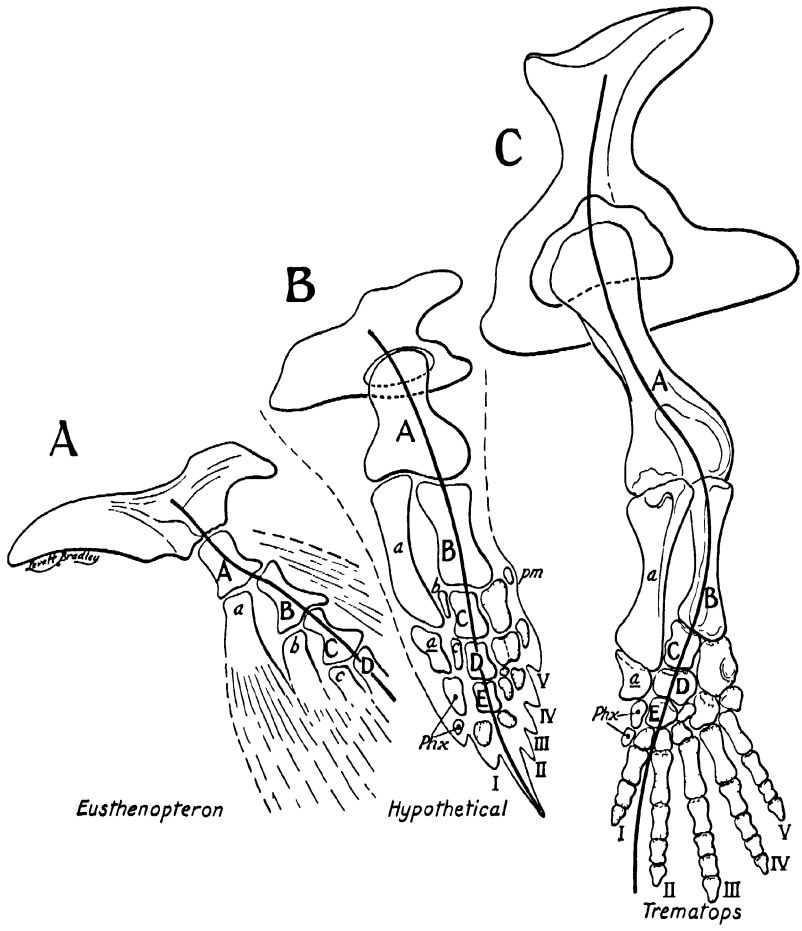


Fig. 11.15. Suggested solution of the problem of the origin of the tetrapod pelvic limb. After Gregory and Raven. A, lobe-fin stage; C, primitive tetrapod stage; B, graphic intermediate or protodactylate stage (based in part on embryology and recent urodele amphibian). *Phx*, prehallux.

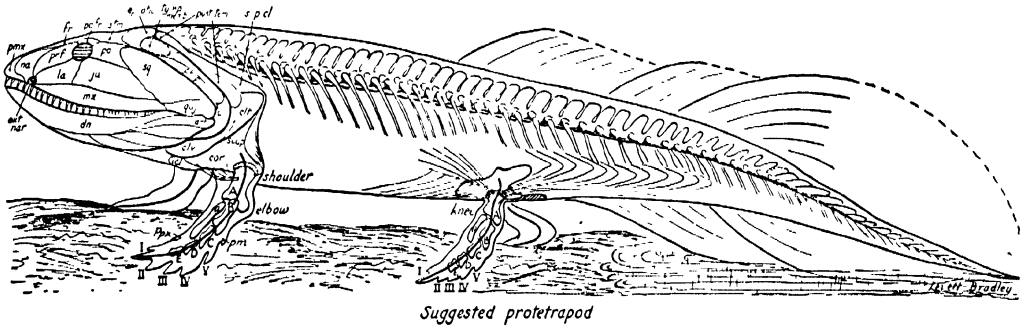


Fig. 11.16. Suggested intermediate between lobe-fin and tetrapod in body form, skull and limbs. Modified from Gregory and Raven. The skull, girdles and limbs combine features of the lobe-fin *Eusthenopteron* and various primitive amphibians. The two dorsal, anal and caudal fins are represented as in a late stage of retrogression, as in certain dipnoans.

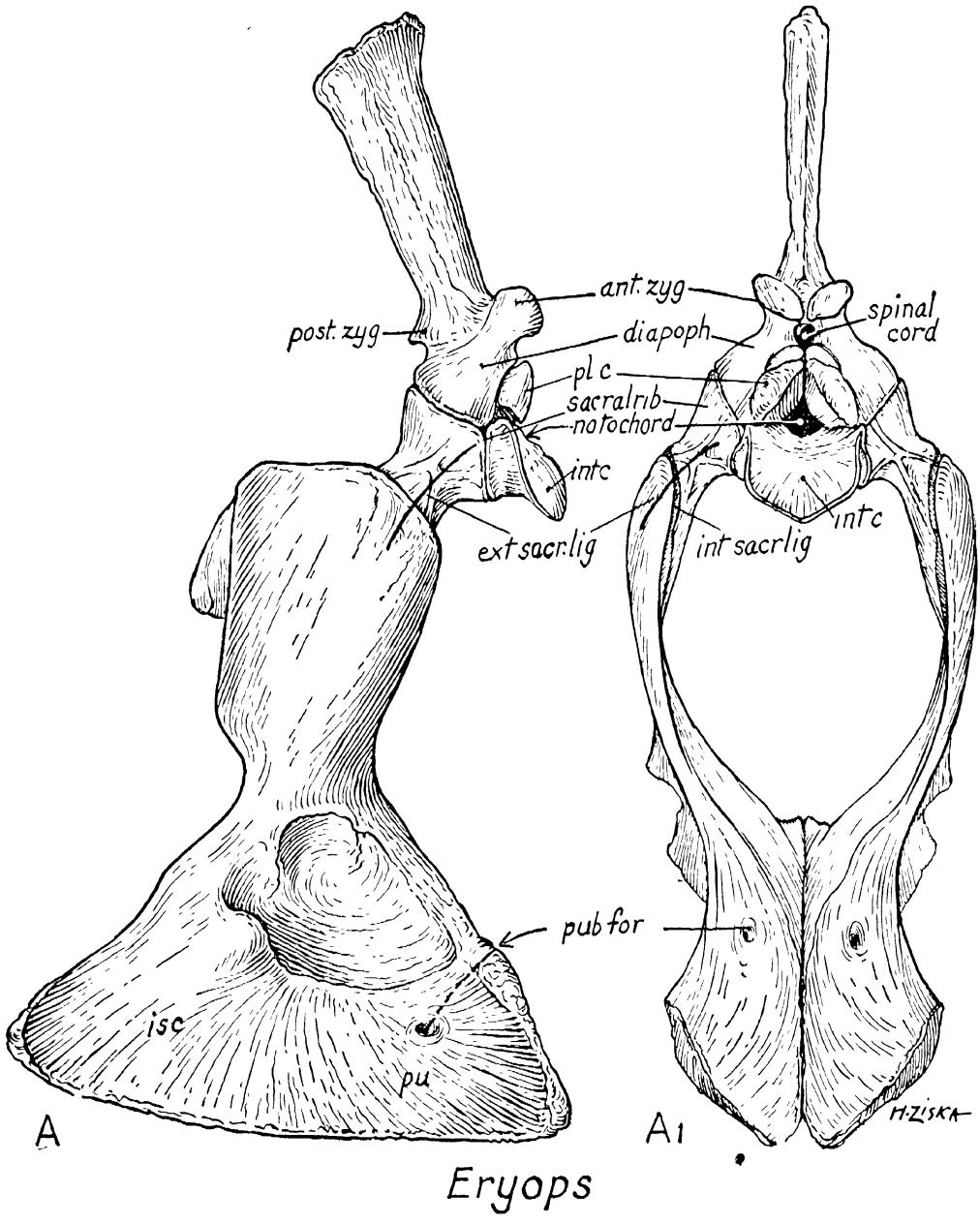


Fig. 11.17. Relations of the sacral region to the pelvis in a fairly primitive amphibian (*Eryops*). A, right side; A1, front. Original. The ilia merely overlapped the enlarged sacral ribs and were connected with them only by ligaments.

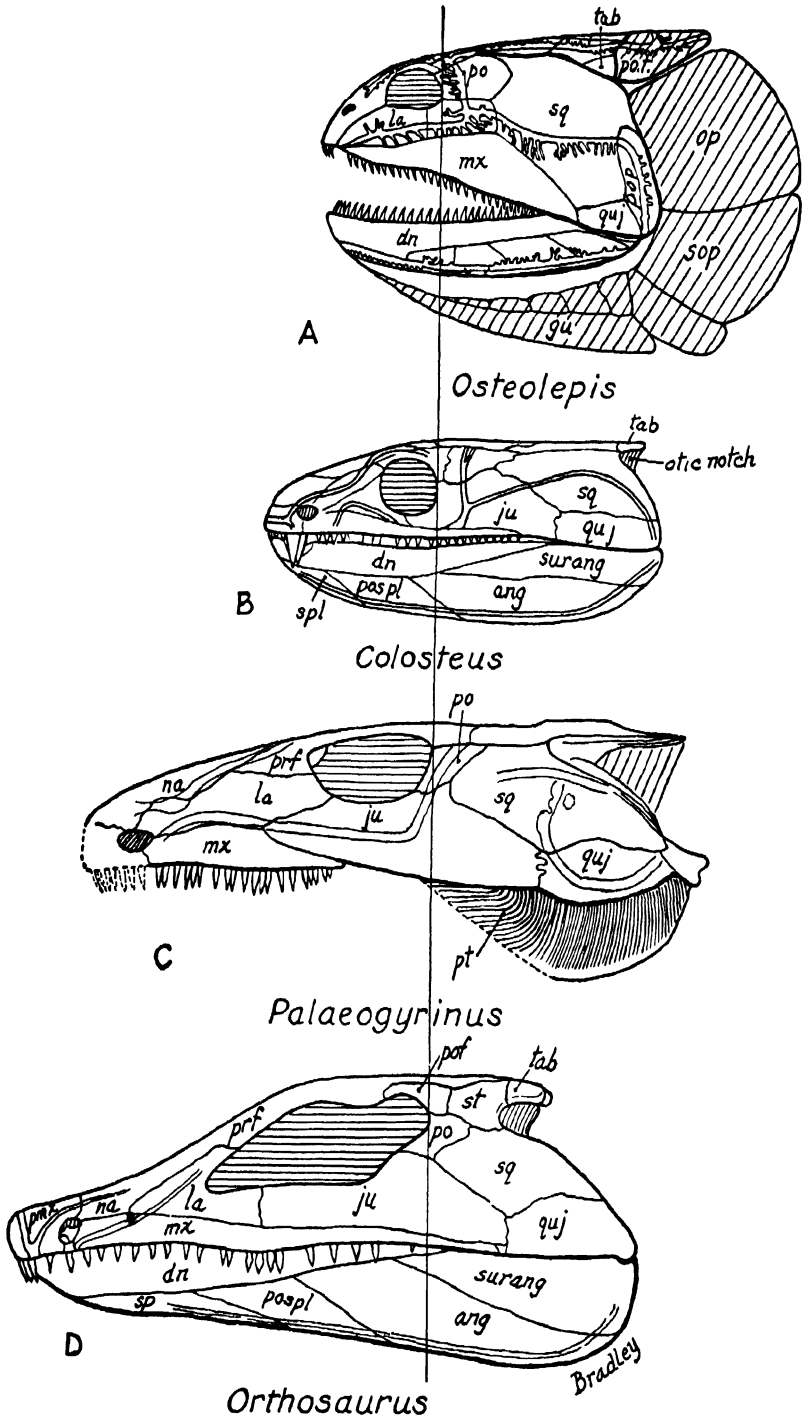


Fig. 11.18. Skulls of lobe-fin (A) and primitive amphibians (B–D). Side view, showing in the Amphibia the elongation of preorbital and shortening of postorbital parts, together with loss of extrascapular-opercular series (oblique lines). A, after Säve-Söderbergh; B, after Romer; C, D, after Watson.

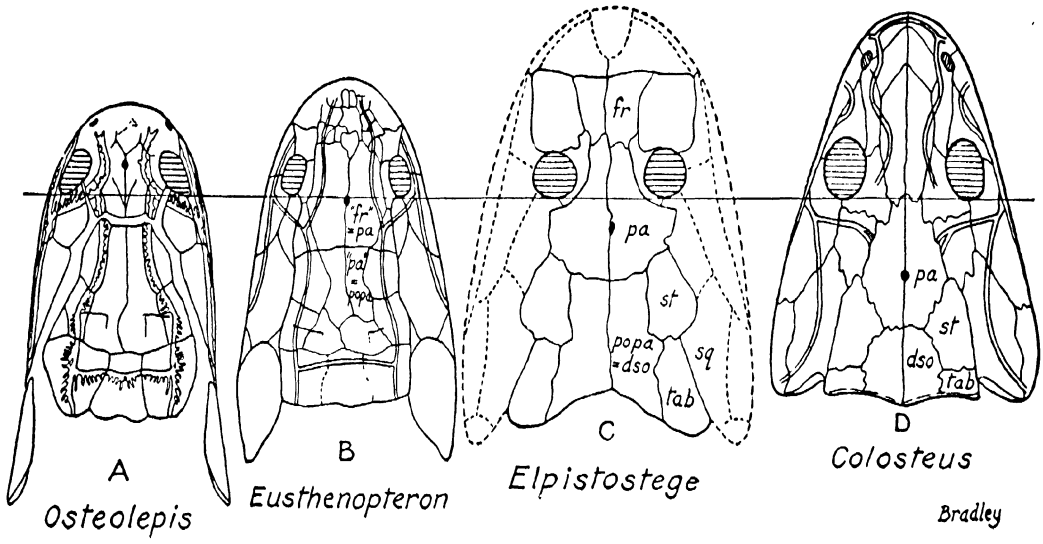


Fig. 11.19. The skull roofs of lobe-fins (A–C) and primitive amphibian (D), showing progressive backward shift of pineal foramen and orbits and shortening of postparietal region. A, Primitive lobe-fin, after Säve-Söderbergh. B, Typical lobe-fin, after Bryant and Stensiö. C, Advanced lobe-fin, after Westoll. D, Primitive amphbian, after Romer. Westoll (1940) has shown that the so-called frontals ("*fr*") of fishes are homologous with the parietals of tetrapods, while the so-called "parietals" ("*pa*") of fishes are homologous with the postparietals (dermosupraoccipitals) of tetrapods.

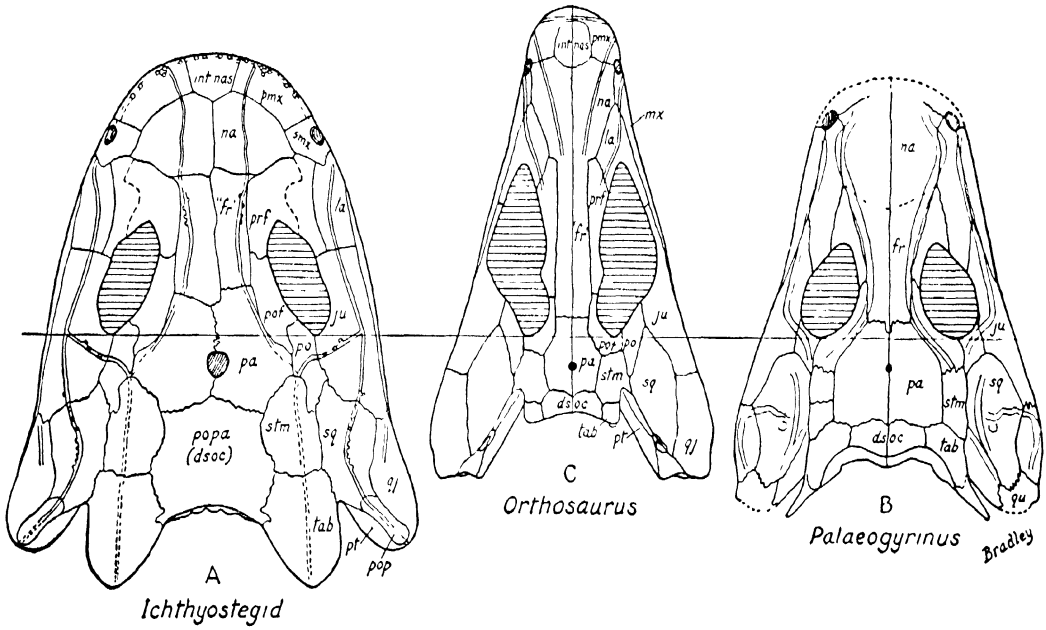


Fig. 11.20. Skull tops of primitive Upper Devonian (A) and Carboniferous (B, C) amphibians. A, data from Säve-Söderbergh and Romer; B, C, after Watson.

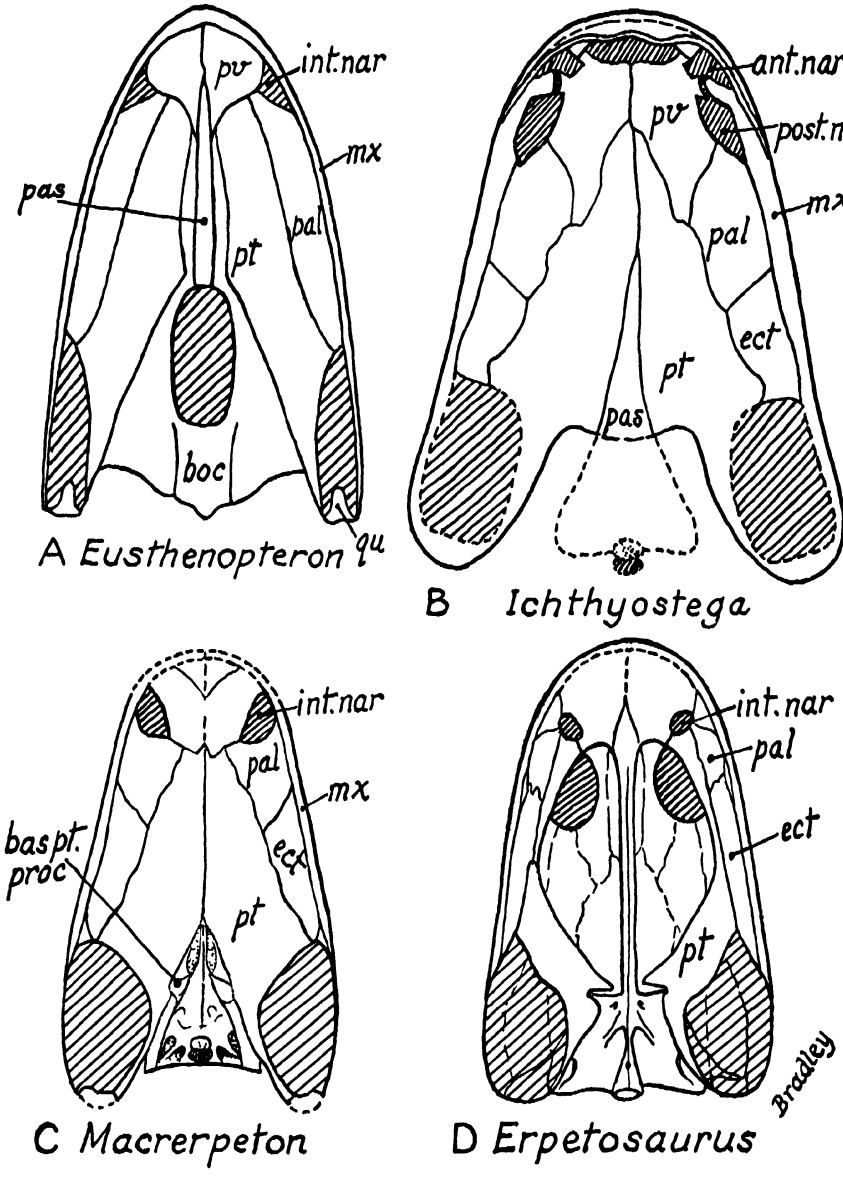


Fig. 11.21. Basal view of the skulls of lobe-fin and early amphibians. In the lobe-fin (A) the parasphenoid and its contacts with the pterygoid are confined to the anterior or ethmo-sphenoid division of the skull; in the primitive amphibian (B) they have moved backward, obliterating the pituitary vacuity; in more advanced stages (C, D) the parasphenoid overlaps the basisphenoid and reaches the basioccipital. Meanwhile the originally wide pterygoids become narrow strips, leaving a large interpterygoid vacuity (D). A, from Holmgren, Stensiö and Watson, mainly after Bryant; B, after Säve-Soderbergh; C, D, after Romer.

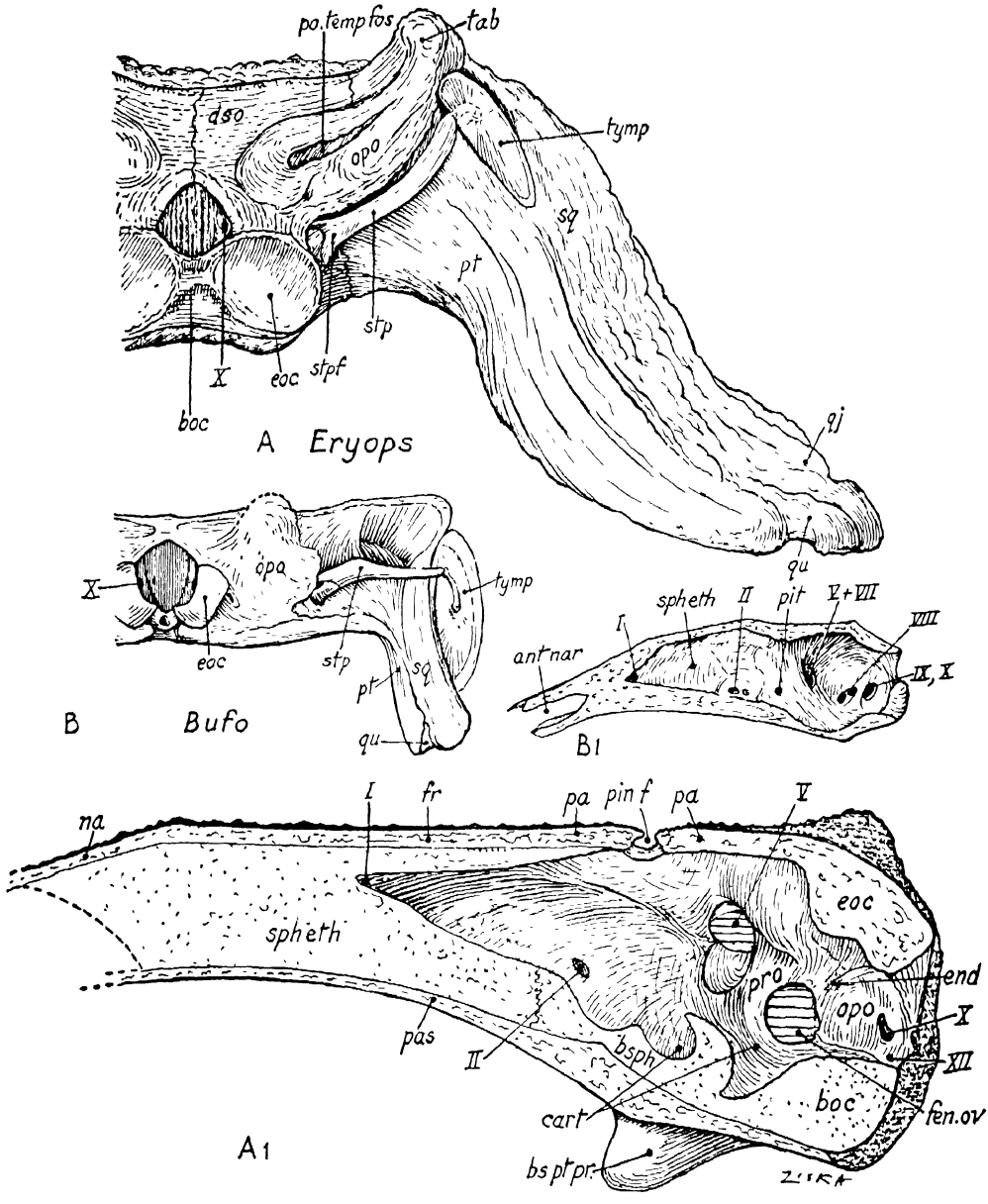


Fig. 11.22a (top). Occipital views of primitive labyrinthodont (A) and modern anuran (B), showing essential identity in the relations of the stapes to the tympanum and skull. Original.

Fig. 11.22b. Braincase of labyrinthodont (A1) and anuran (B1) in sagittal section, showing basic identity in structural plan. A1, Composite drawing from several specimens. Interpretation of bones and foramina after Watson, Broom, von Huene, Sawin, Romer and Witter, Romer and Edinger. *Ant. nar.*, anterior naris; *boc*, basioccipital; *bsp*, basisphenoid; *bspt. pr.*, basipterygoid process; *cart.*, cartilage; *end.*, endolymphatic duct; *eoc.*, exoccipital; *fen. ov.*, fenestra ovalis; *fr.*, frontal; *opo*, opisthotic, *pa*, parietal, *pas*, parasphenoid, *pit.*, pituitary fossa; *pro.*, prootic; *pro. f.*, proötic foramen; *spheth.*, sphenethmoid. *I*, olfactory foramen; *II*, optic; *V+VII*, exit for parts of fifth and seventh nerves; *VIII*, internal auditory meatus; *IX–XI*, exit for glossopharyngeal, vagus and accessory; *XII*, foramina for hypoglossal.

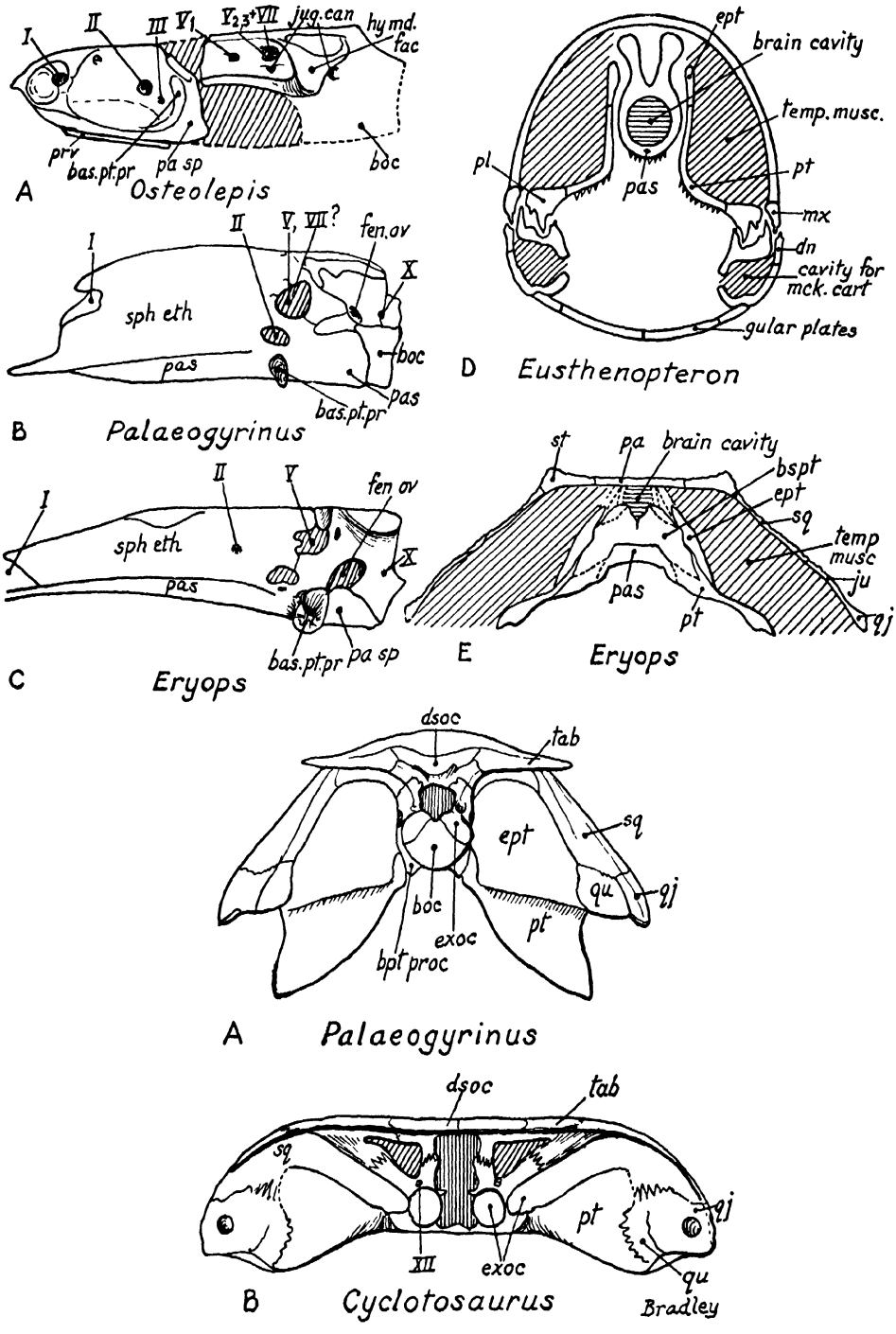
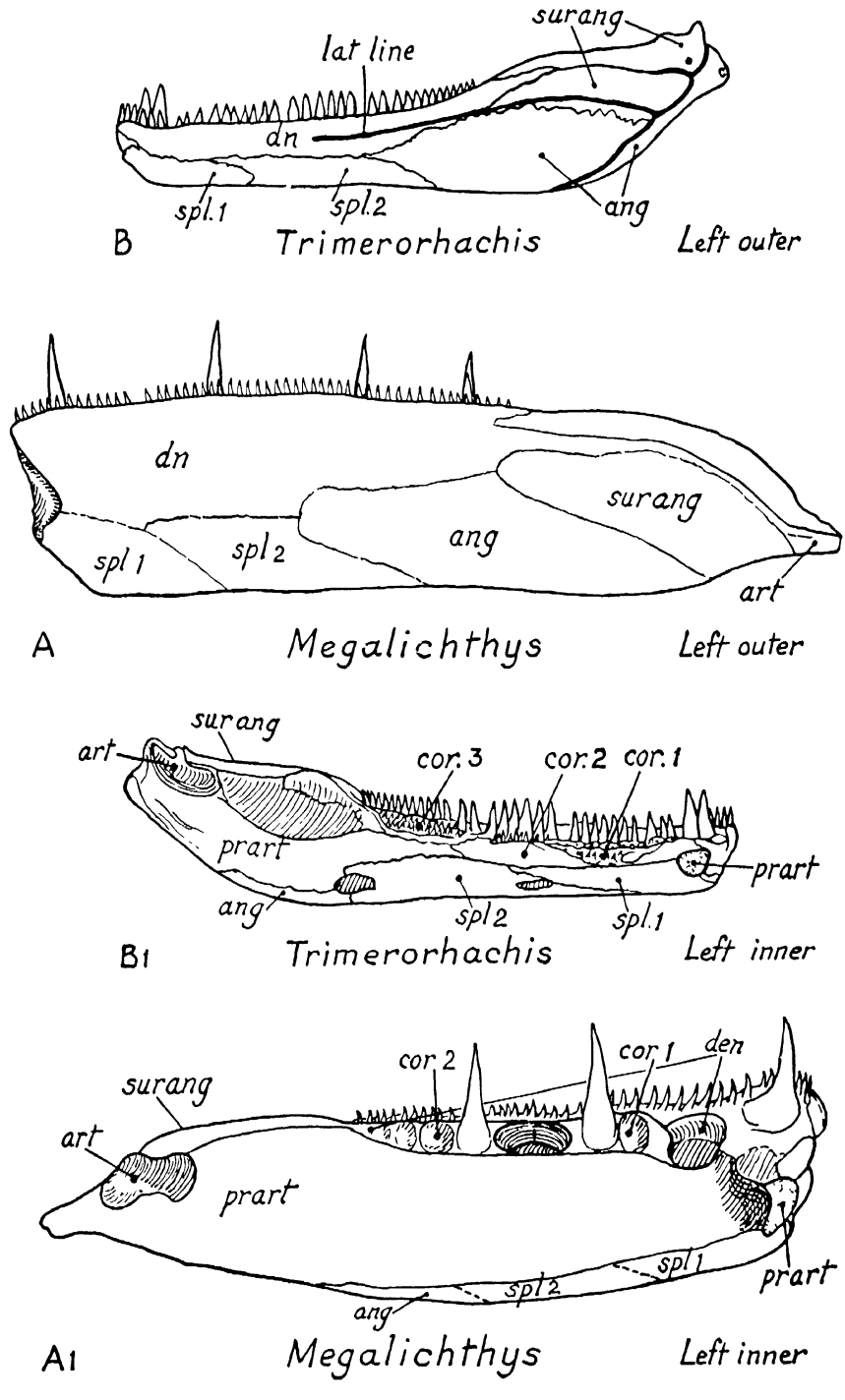


Fig. 11.23a (top). Braincase of lobe-fins (A, D) and labyrinthodonts (B, C, E). Left side views (A–C) after Watson. In A the anterior and posterior divisions of the braincase are separated by a large ventral vacuity and the parasphenoid is confined to the anterior division. In B and C the parasphenoid has extended backward, the vacuity is obliterated and the two divisions are firmly united. The transverse sections (D, E) show essentially similar relations of the epipterygoid and pterygoid to the braincase. D, after Bryant; E, after Sawin.

Although Section D is across the anterior division of the skull, while Section E is across the posterior division of the skull, the parasphenoid is seen in both



divisions (since it has extended backward in E) and the epipterygoid of each side forms a dorsal flange, lateral to the braincase.

Fig. 11.23b (facing page). Occipital views of the skulls of a primitive (A) and a highly specialized Triassic amphibian (B), showing the great widening and flattening of the latter, the transformation of a tripartite to a bipartite condyle. After Watson.

Fig. 11.24. Lower jaws of lobe-fin (A, A1) and primitive amphibian (B, B1) showing essential identity in plan. A, A1, after Watson; B, B1, after Broom and Williston.

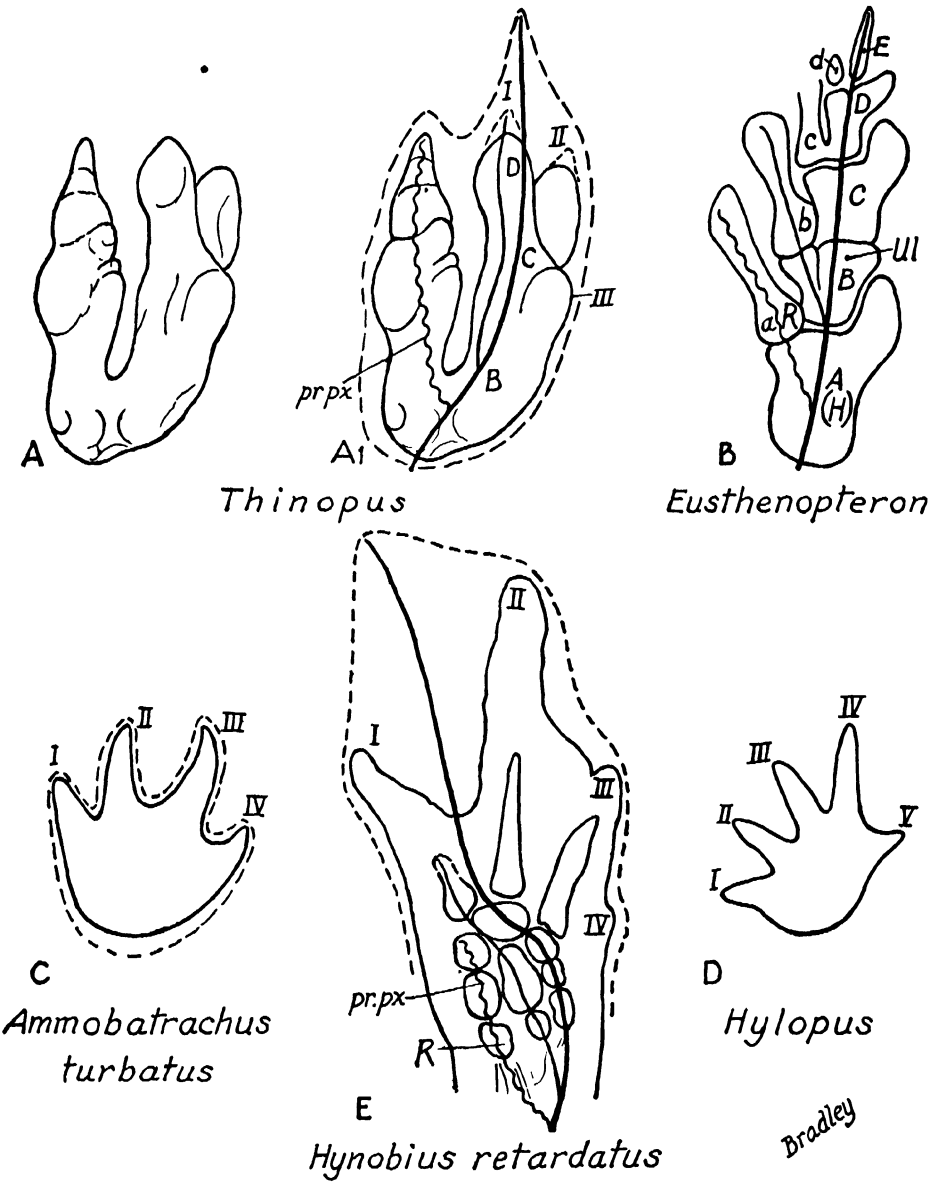


Fig. 11.25. Footprint of Upper Devonian (A, A1) and Carboniferous amphibians (C, D) in comparison with skeleton of pectoral limb of lobe-fin (B) and larval hand of existing urodele (E). A, A1, from cast of original footprint; B, after Gregory and Raven; C, D, after Gilmore; E, after Holmgren. According to D. J. Morton (1926) the digits of *Thinopus* represent Nos. I, IV, V, of the right hind foot, digits II, III, having been squeezed above the level of the others when the foot was sunk in the mud. However, this footprint differs enough from any of those figured by Gilmore (cf. figs. 26, 27, 28) from the Pennsylvanian and Permian of the Grand Canyon to make it difficult to identify the digits with any certainty. It may possibly even represent an intermediate stage between the lobe-fin and the amphibian, as suggested above in A1 and B. Footprints C, D, represent the right forefoot.

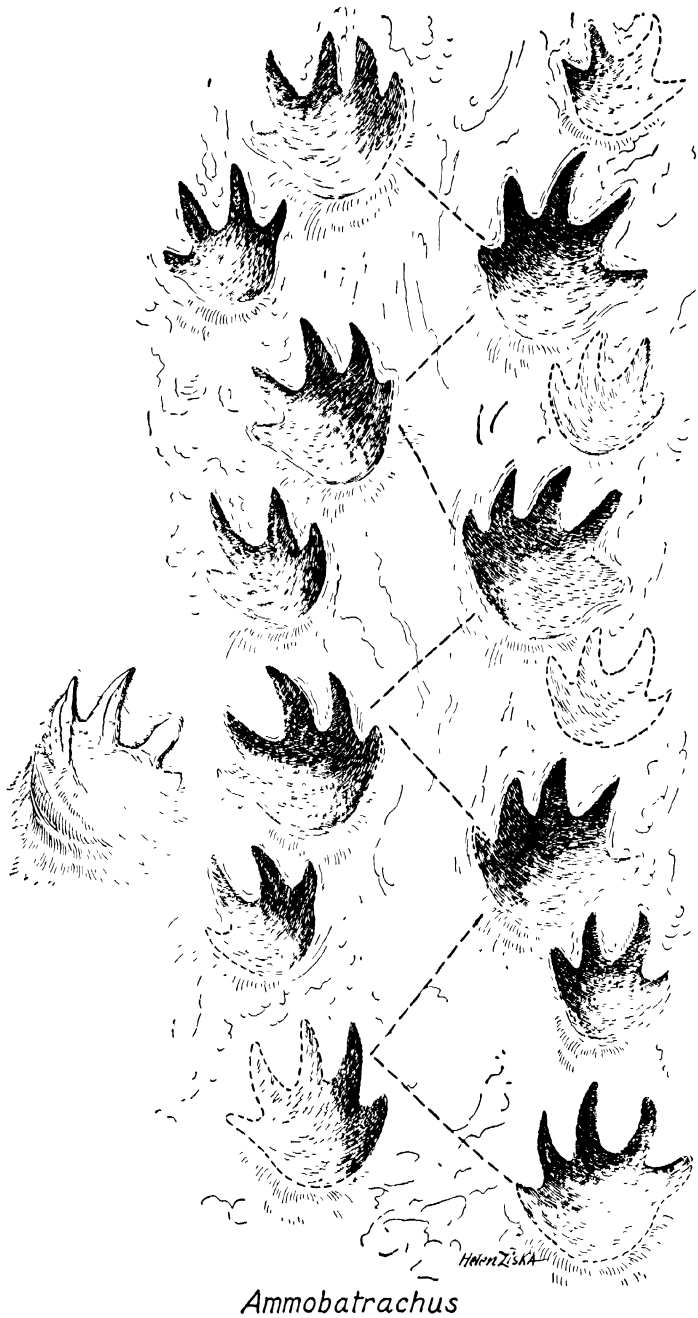


Fig. 11.26. Footprints of a primitive amphibian (*Ammobatrachus turbatus*) from the Pennsylvanian (Carboniferous) of the Grand Canyon, Colorado. After B. Schaeffer, with data from Gilmore. The wide trackway indicates wide eversion of knees and elbows in walking and is consistent with the short footsteps.

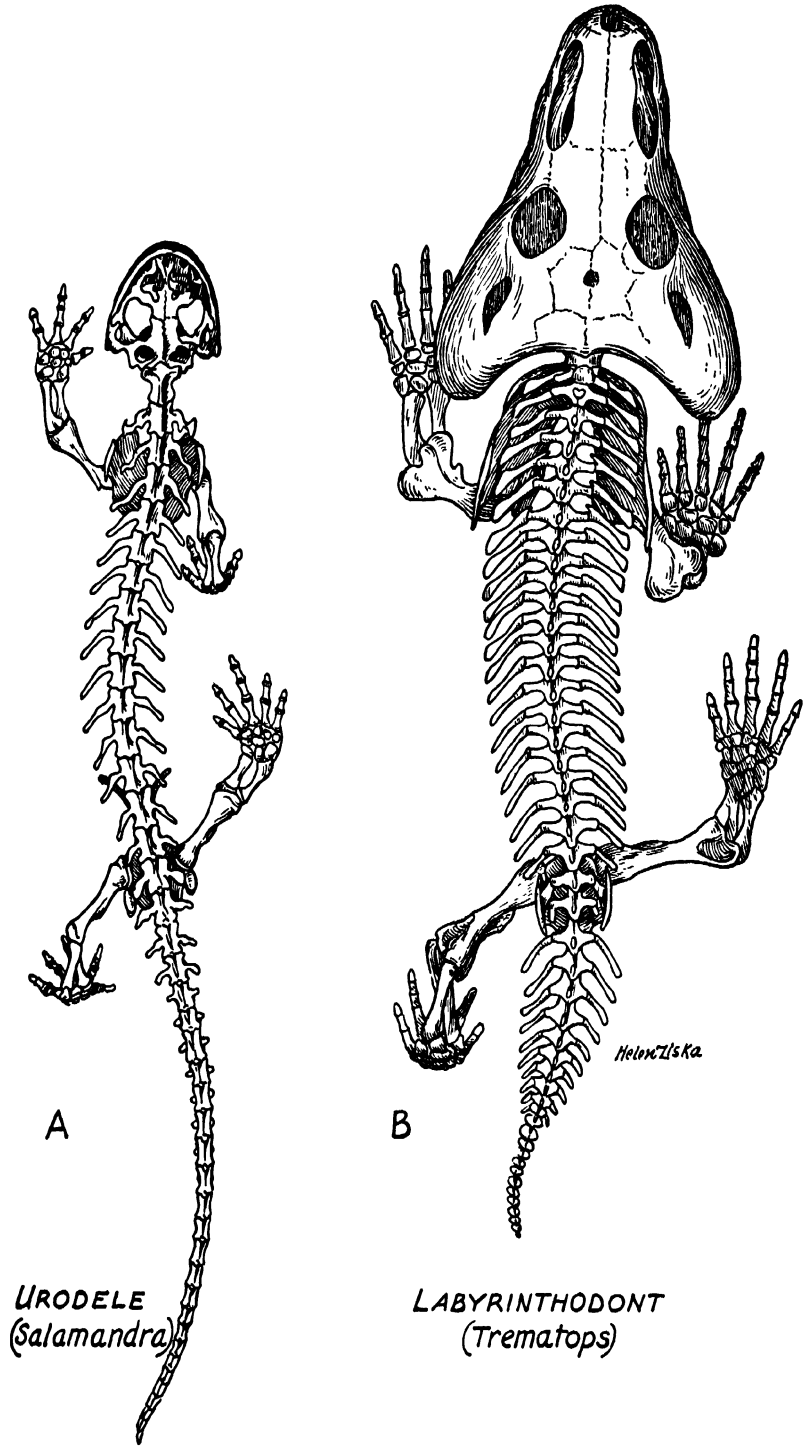


Fig. 11.27. Recent and Permian amphibian skeletons in walking pose. After Schaeffer (1941). The primary method of progression by transverse wriggling, inherited from primitive fishes, is used to extend the stride of the limbs. The forward planting of the feet necessitates the crossing of the tibia by the fibula and a twisting stress on the tarsus.

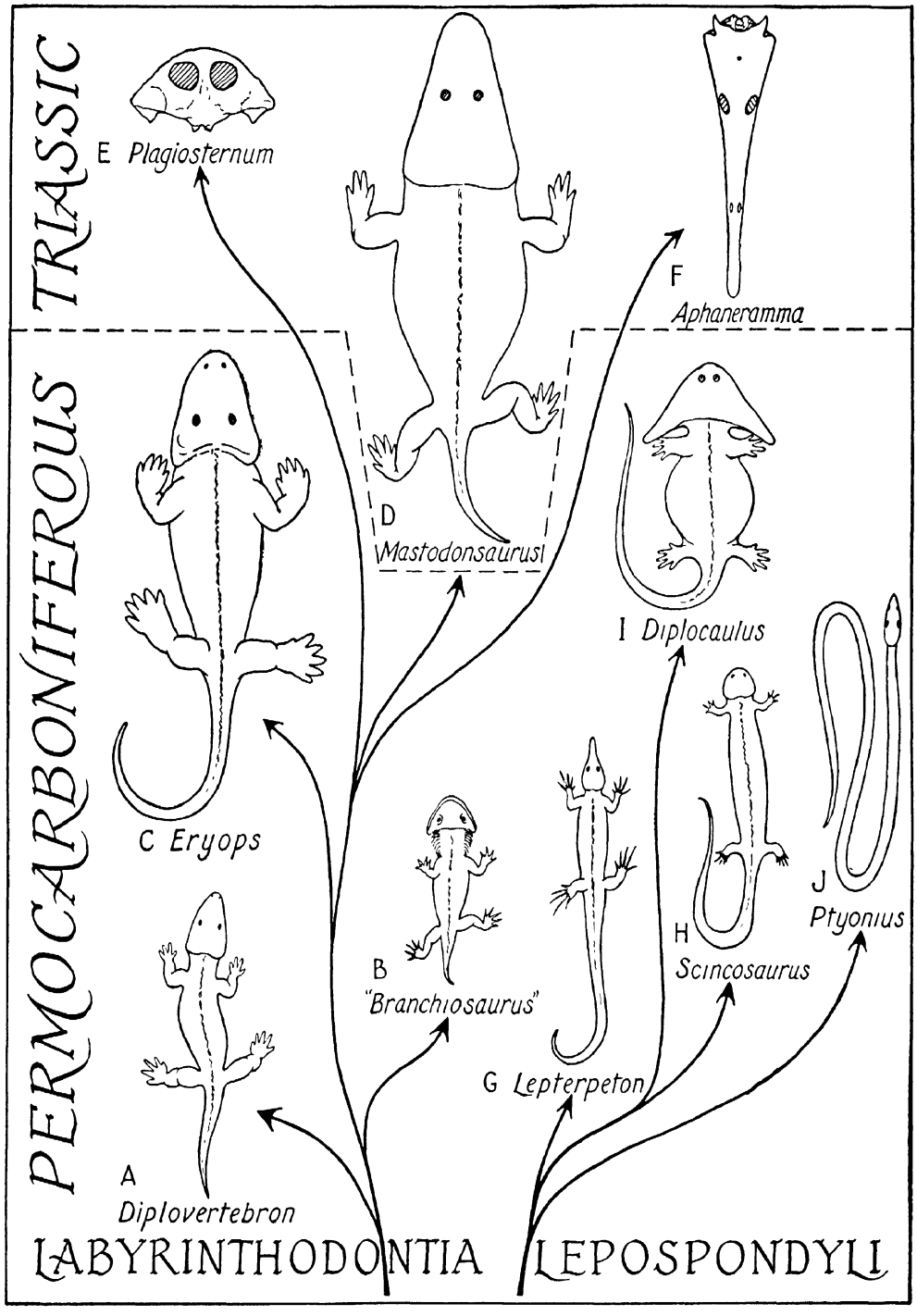
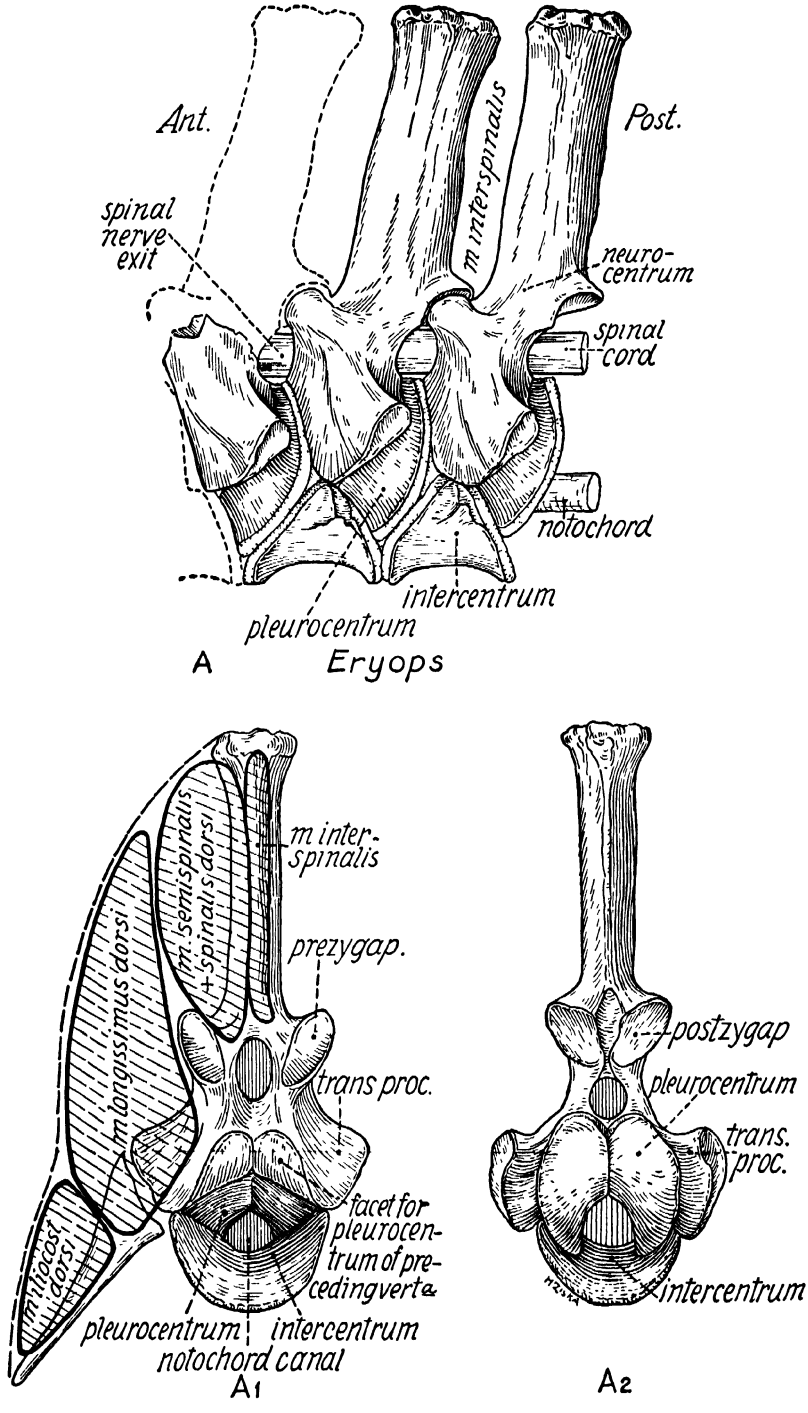


Fig. 11.28. Diverse body and skull forms in earlier Amphibia, illustrating the two main divisions (labyrinthodonts and lepospondyls) and the successive grades in the former (Embolomeri, Rhachitomi, Stereospondyli). The "Phyllospondyli" according to Romer, seem to be the larval stages of labyrinthodonts. The lepospondyls may be a very early branch of the reptiles. The modern frogs and their allies (Anura) appear to be highly specialized derivatives of the Rhachitomi. The urodeles (Caudata) may be derived from some of the Lepospondyli.



Figs. 11.29, 30. Rhachitomous vertebrae of *Eryops* in their relations to the notochord, spinal cord and spinal muscles. After Rockwell, Evans and Pheasant. A, left side view; A1, front view (muscles after Olson); A2, rear view.

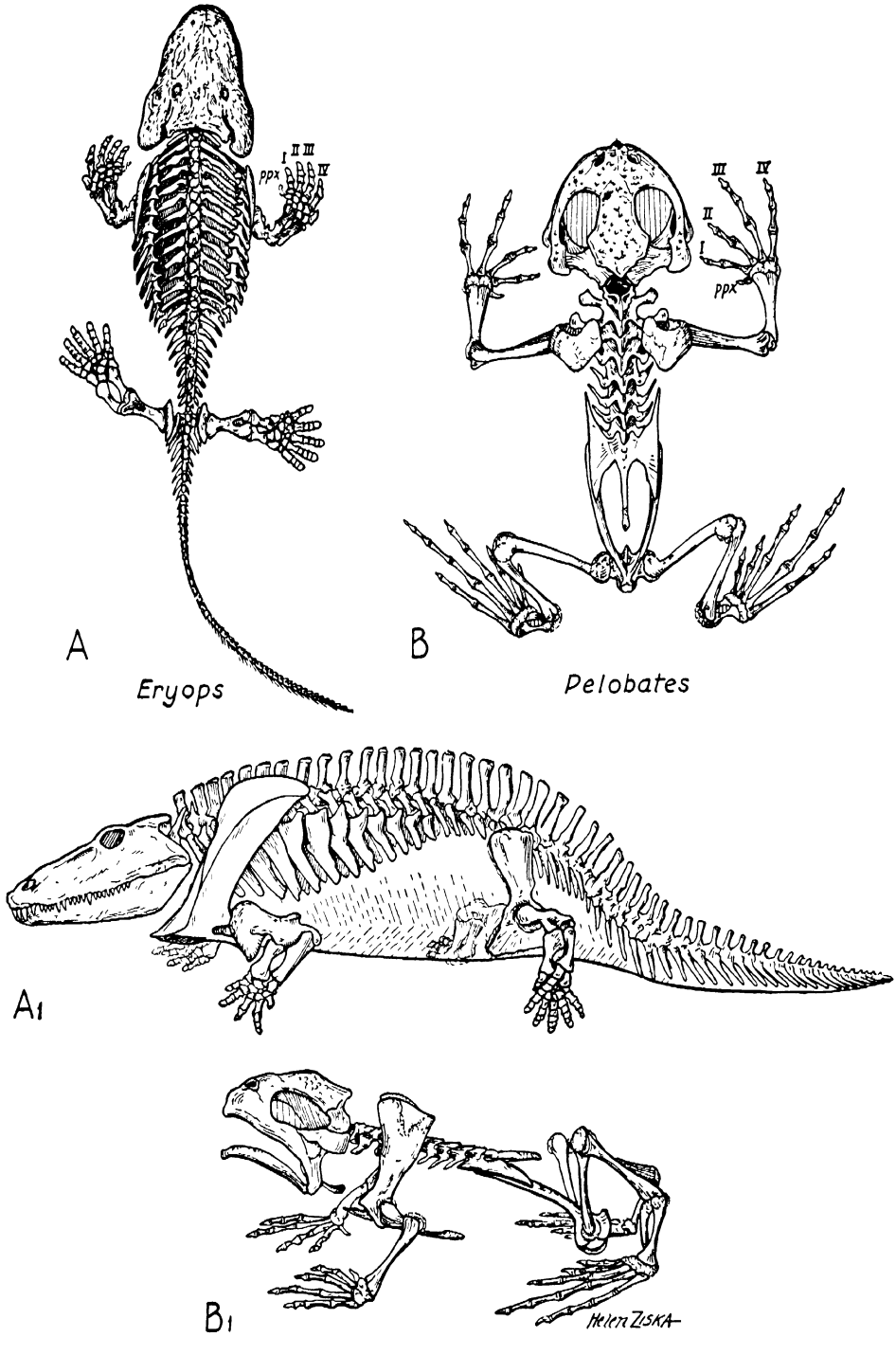


Fig. 11.31. Permo-Carboniferous labyrinthodont and a fairly primitive modern frog. A, A1, Based chiefly on the mounted skeleton in the American Museum of Natural History. The hands are restored from the specimen figured in Fig. 11.7; the arrangement of the tarsals is partly based on that of *Trematops* (Fig. 11.27). The evidence both from fossil footprints (fig. 11.26) and from embryology indicates that the fifth digit of the hand was small or absent, as it is in modern Amphibia. B, B1, In the adult stage of modern frogs the skeleton is extremely specialized for leaping and swimming.

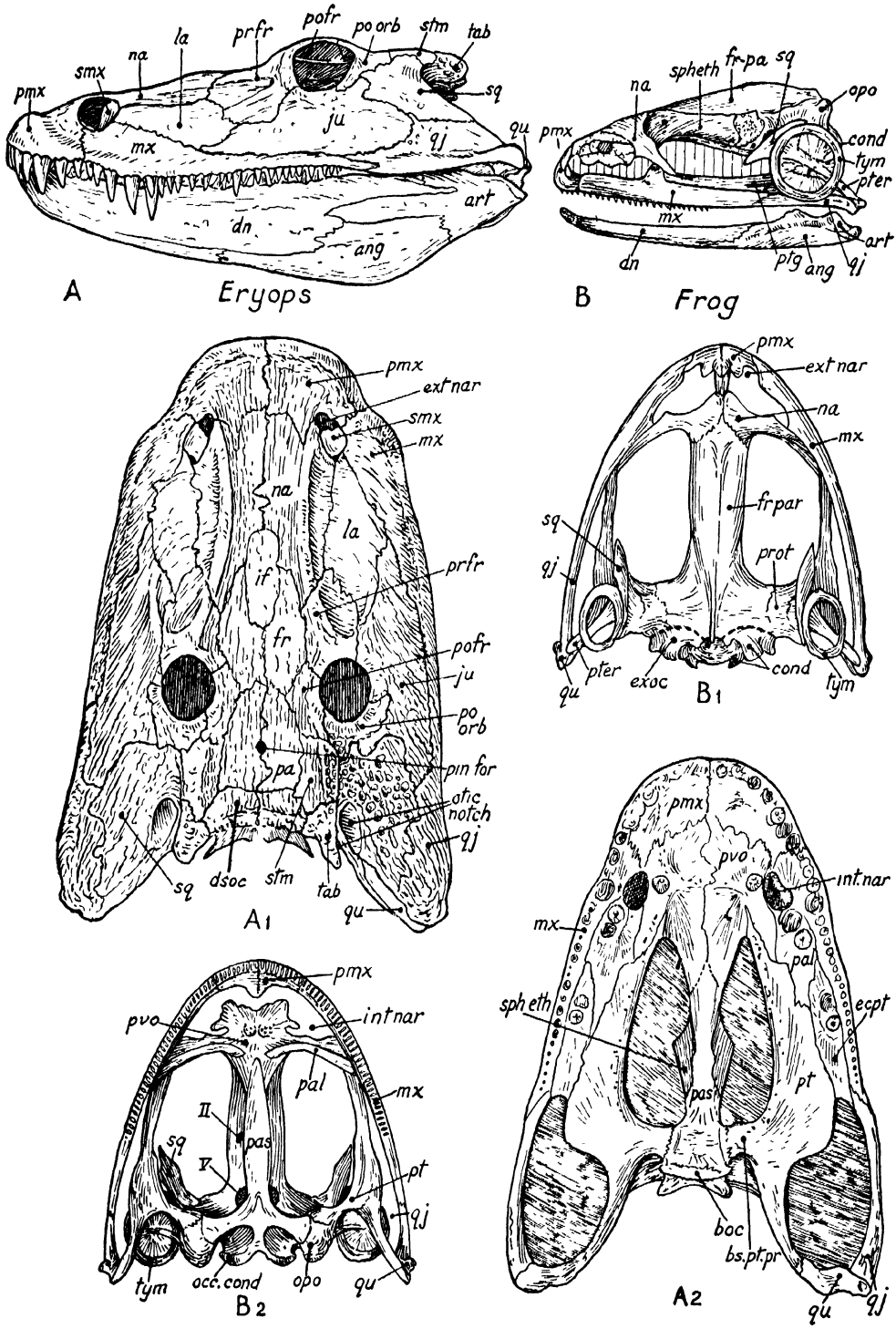
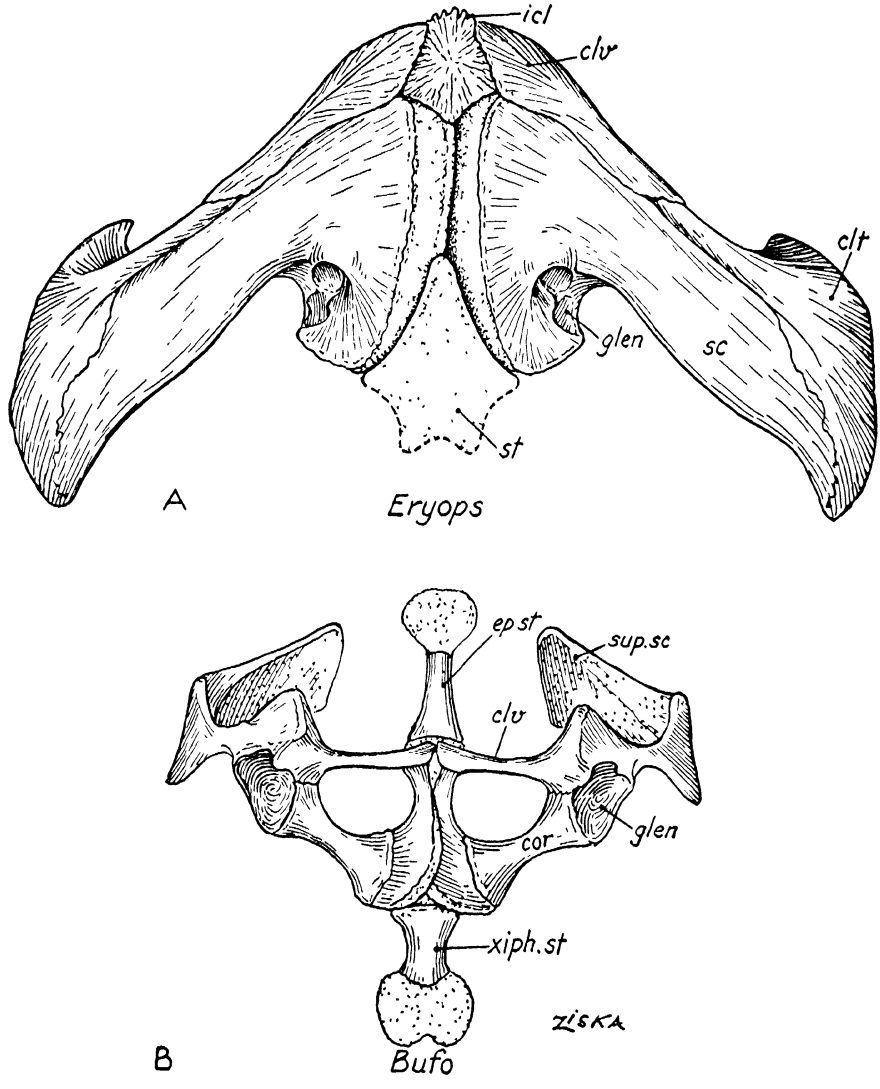


Fig. 11.32. Skulls of Permo-Carboniferous labyrinthodont and modern anuran. Based chiefly on American Museum material, with data on *Eryops* from Broom, Romer and Witter, Sawin. For the occipital view and sections of the braincase see fig. 11.22b.



Figs. 11.33, 34. Pectoral girdle of primitive labyrinthodont and specialized anuran, in ventral view A, Reconstructed from several specimens. Cartilaginous ventral borders of scapulo-coracoid and entire sternum restored. In A the coraco-scapula forms a continuous imperforated plate, the glanoid facet is a warped oval, the cleithrum is relatively large, the clavicles and interclavicle retain their primitive relations. In B the coracoid plate is fenestrated, the glenoid facet is cup-like, the clavicle forms a stiff transverse bar adherent to the coracoid, the interclavicle has disappeared as such and is replaced by an episternum, the sternum has given rise to a xiphisternum, the cleithrum has been replaced by a cartilaginous suprascapula.

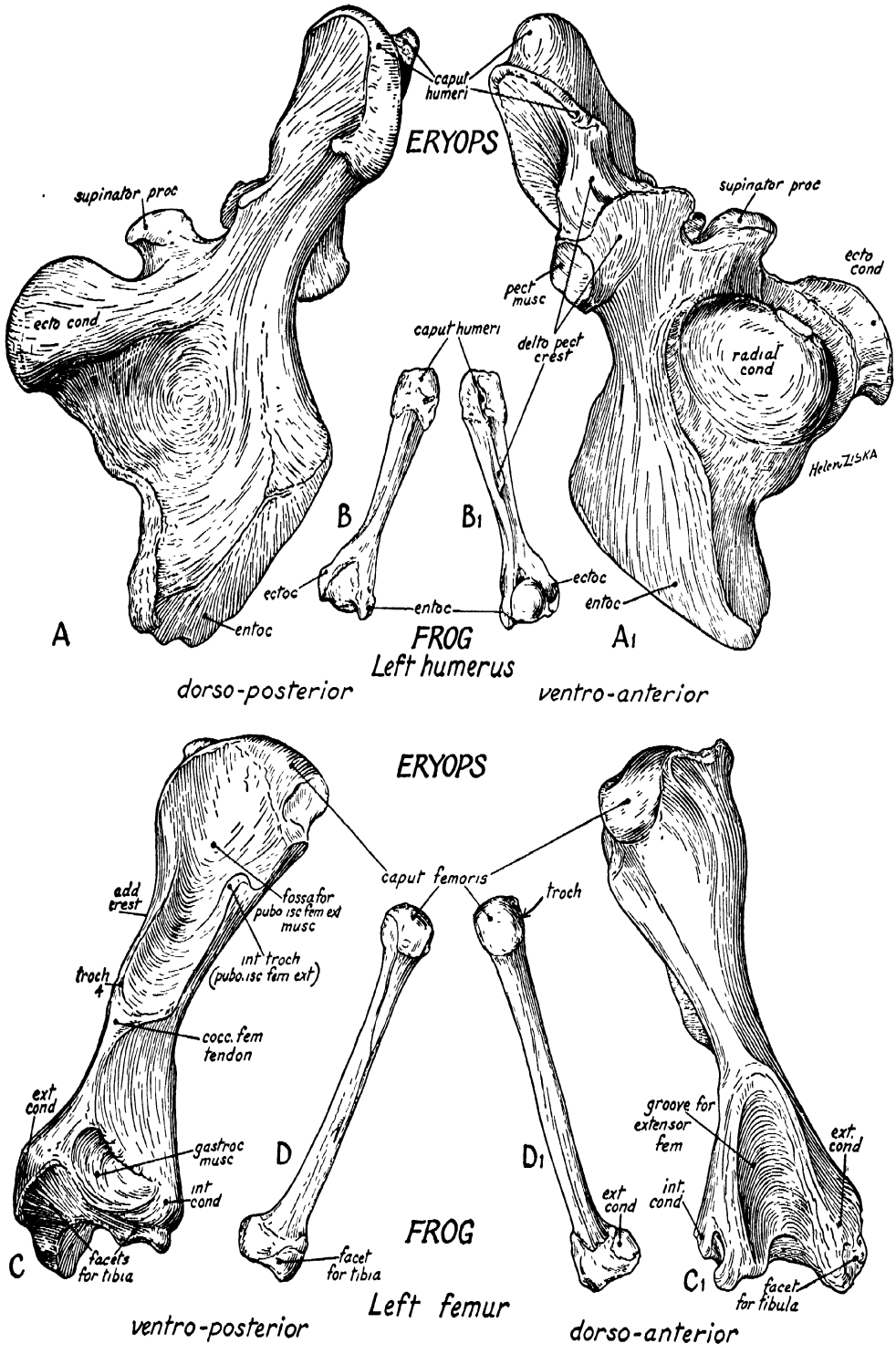


Fig. 11.35. Proximal limb segments of primitive labyrinthodont and modern anuran. Identification of parts of *Eryops* chiefly after Romer (1922) and Miner (1925).

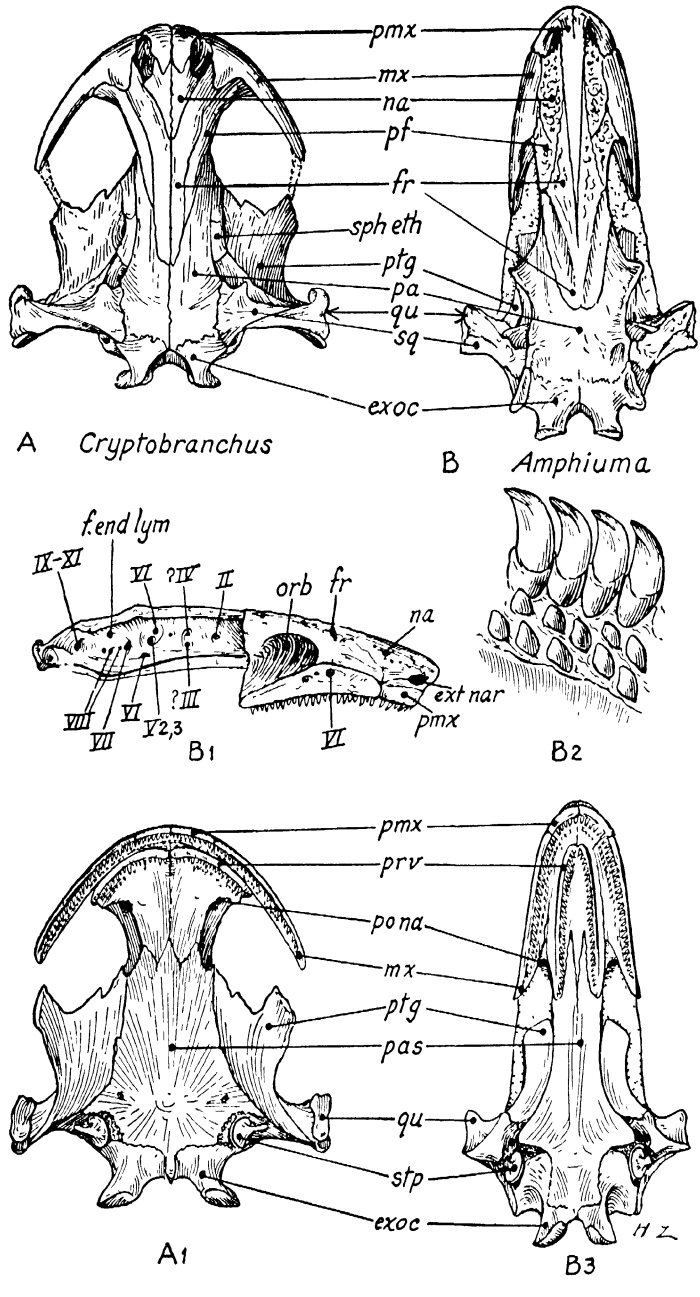


Fig. 11.36. Brachy- and dolichocephalic skulls of modern urodeles. In spite of wide differences in proportions these skulls are variants of the same basic pattern as those of Permian amphibians. *Cryptobranchus* (A) is a wide-skulled derivative of the most primitive existing salamanders (Hynobiidae). *Amphiuma* (B) is a long-skulled, eel-like offshoot of the true salamanders (Salamandridae). The tubular braincase (B1) is comparable with that of other amphibians (fig. 11.22) and is pierced by similar foramina for the cranial nerves (identifications based on data in Francis, 1934, Romer and Edinger, 1942, Romer and Witter, 1942). The three curved rows of teeth in the maxilla (B2) afford reserves in case of breakage.

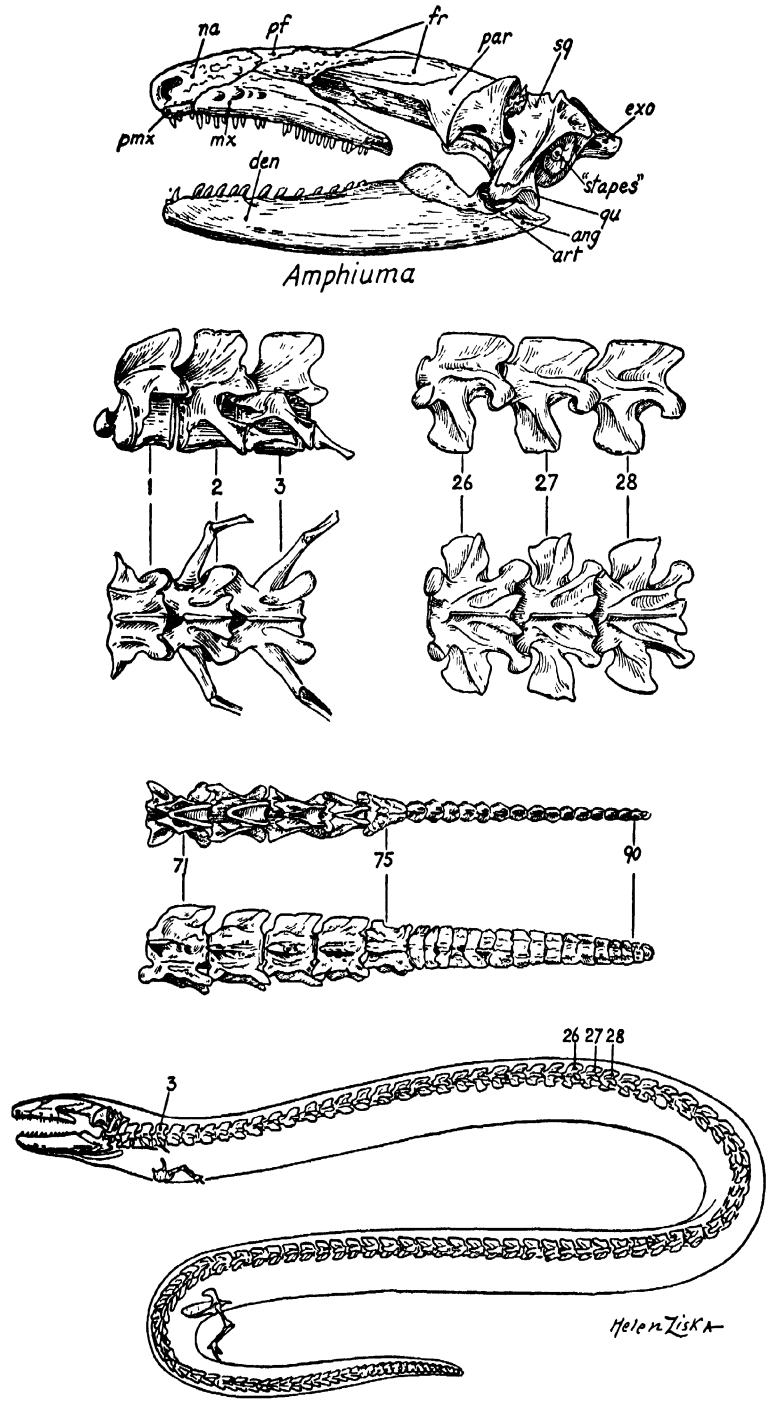


Fig. 11.37. Skeleton of eel-like salamandroid. Original. The long snake-like jaws can open widely to grab the prey, while the very numerous strongly crested vertebrae indicate marked flexibility, power and manoeuverability in purusit. According to Noble (1931, p. 482), the "Congo Eel" of southeastern United States "is a semilarval type derived from the salamandrids and agreeing with them in most characters." It exceeds the mud puppy, *Necturus*, in the elongation of the body and reduction of the legs and converges toward two other eel-like and larva-like forms, *Proteus*, a virtual derivative of *Necturus*, and *Siren*, probably an offshoot of primitive salamanders (hynobiids).

CHAPTER XII

FROM LOWLAND MARSH TO FOREST AND DESERT

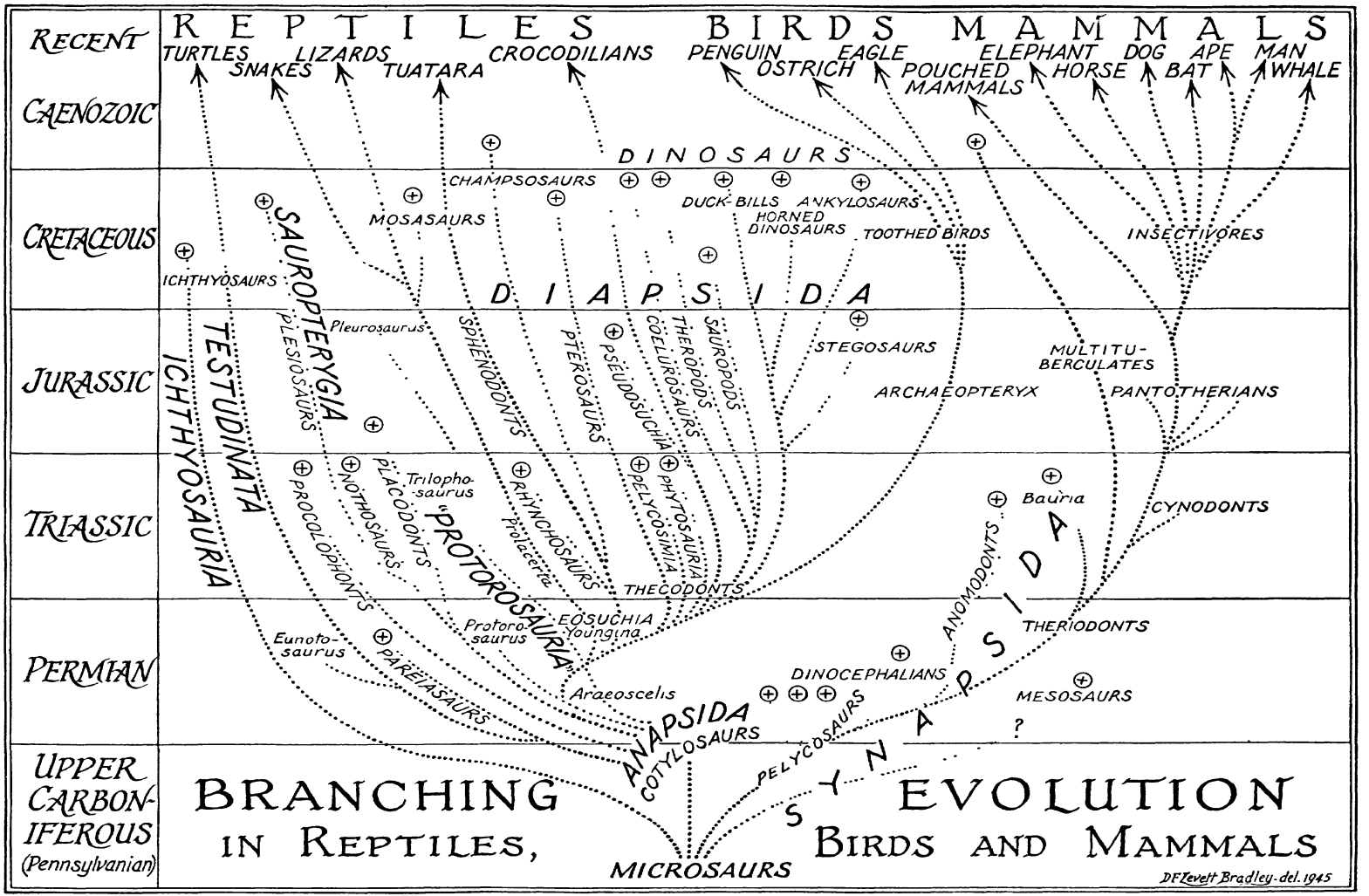

RECENT
CAENOZOIC
CRETACEOUS
JURASSIC
TRIASSIC
PERMIAN
UPPER CARBONIFEROUS (Pennsylvanian)
REPTILES
BIRDS
MAMMALS
TURTLES
SNAKES
LIZARDS
TUATARA
CROCODILIANS
PENGUIN
OSTRICH
EAGLE
POUCHED MAMMALS
ELEPHANT
HORSE
DOG
BAT
APE
MAN
WHALE
DINOSAURS
CHAMPSOSAURS
DUCK-BILLS
ANKYLOSAURS
HORNED DINOSAURS
TOOTHED BIRDS
INSECTIVORES
MOSASAURS
ICHTHYOSAURS
SAUROPTERYGIA
PLESIOSAURS
DIAPSIDA
Pleurosaurus
SPHENODONTS
PTEROSAURS
PSEUDOSUCHIA
THEROPODS
COELUROSAURS
SAUROPODS
STEGOSAURS
MULTITUBERCULATES
ARCHAEOPTERYX
PANTOTHERIANS
TESTUDINATA
ICHTHYOSAURIA
PROCOLOPHONTS
NOTHOSAURS
PLACODONTS
Trilophosaurus
"PROTOROSAURIA"
RHYNCHOSAURS
Protolacerta
PHYTOSAURIA
PELYCOSAURIA
THECODONTS
Bauria
CYNODONTS
ANOMODONTS
Eunotosaurus
PAREIASAURS
Protorosaurus
EOSUCHIA
Youngina
Araeoscelis
ANAPSIDA
COTYLOSAURS
DINOCEPHALIANS
THERIODONTS
MESOSAURS
PELYCOSAURS
SYNAPSIDA
?
MICROSAURS
BRANCHING EVOLUTION
IN REPTILES, BIRDS AND MAMMALS
DF Levett Bradley. del. 1945

Fig 12.1

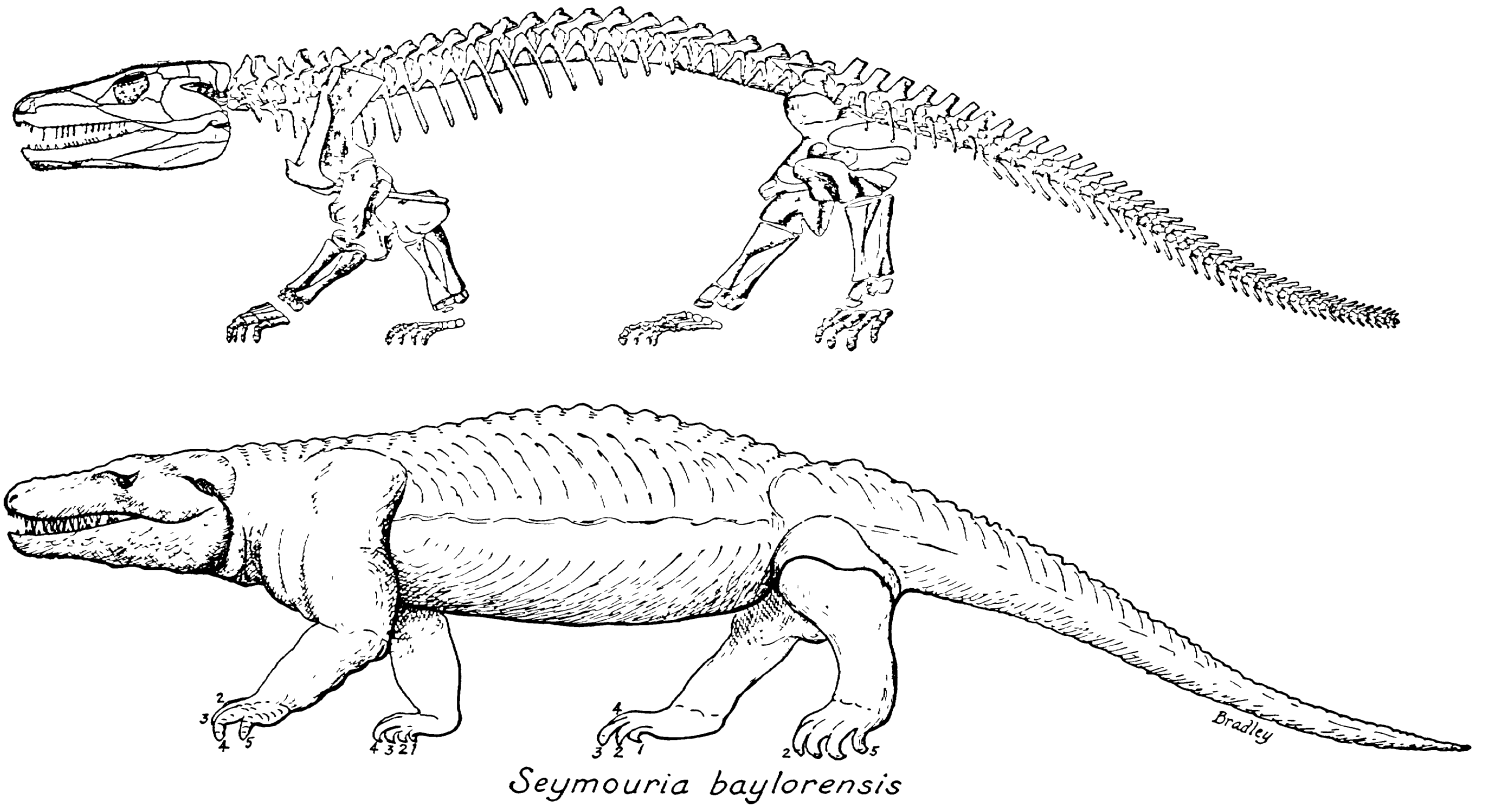


Fig. 12.2. *Seymouria*, progressive amphibian or primitive reptile? A, Restoration of skeleton by T. E. White. Estimated total length, about 2 feet, 8 inches. A1, Sketch, indicating enormously thick upper arm and knee. Original.

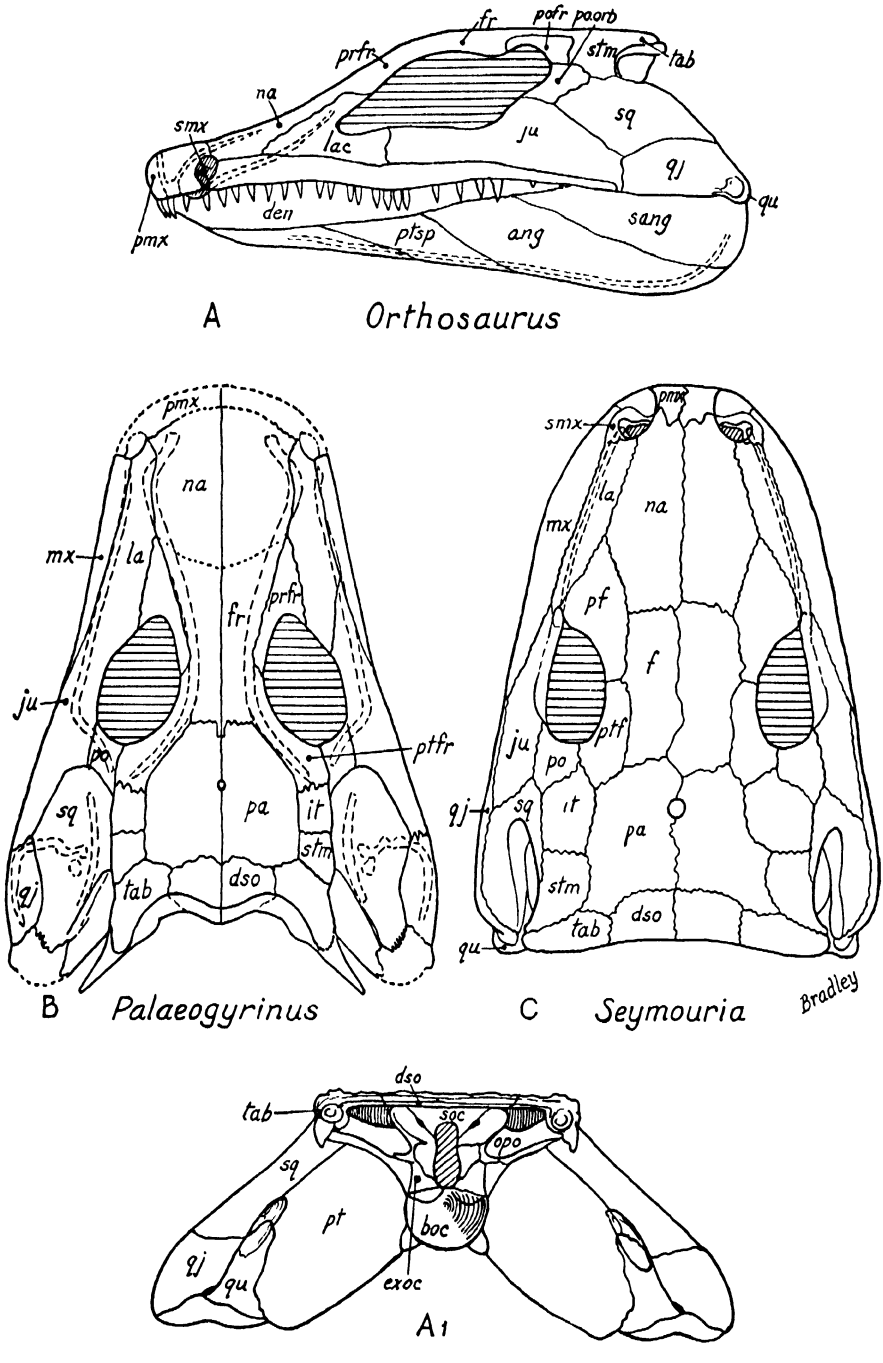


Fig. 12.3. Skulls of *Seymouria* (C), after White; primitive labyrinthodonts (A, A1, B), after Watson. For comparison with fig. 12.4.

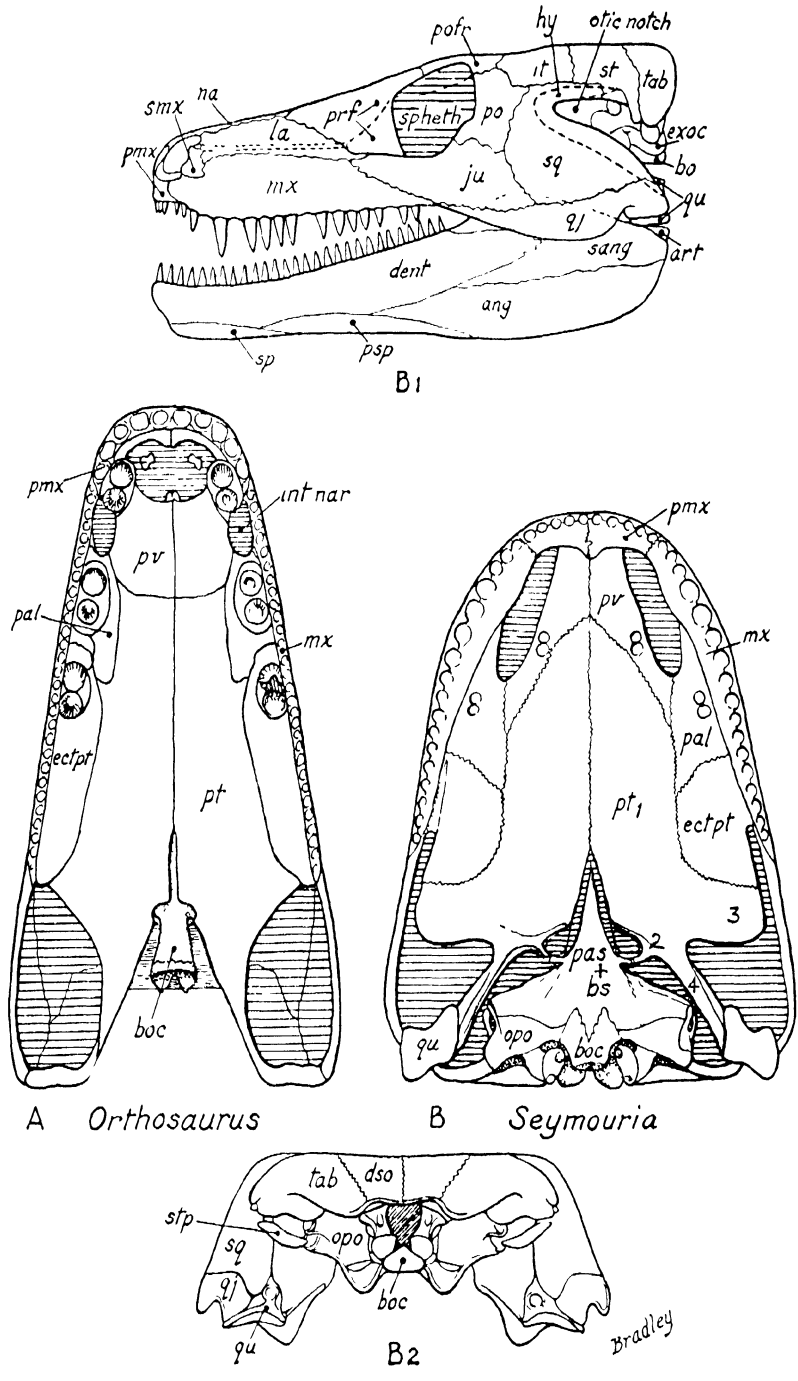


Fig. 12.4. Skulls of *Seymouria* (B, B1, B2), after White; primitive labyrinthodont (A), after Watson.

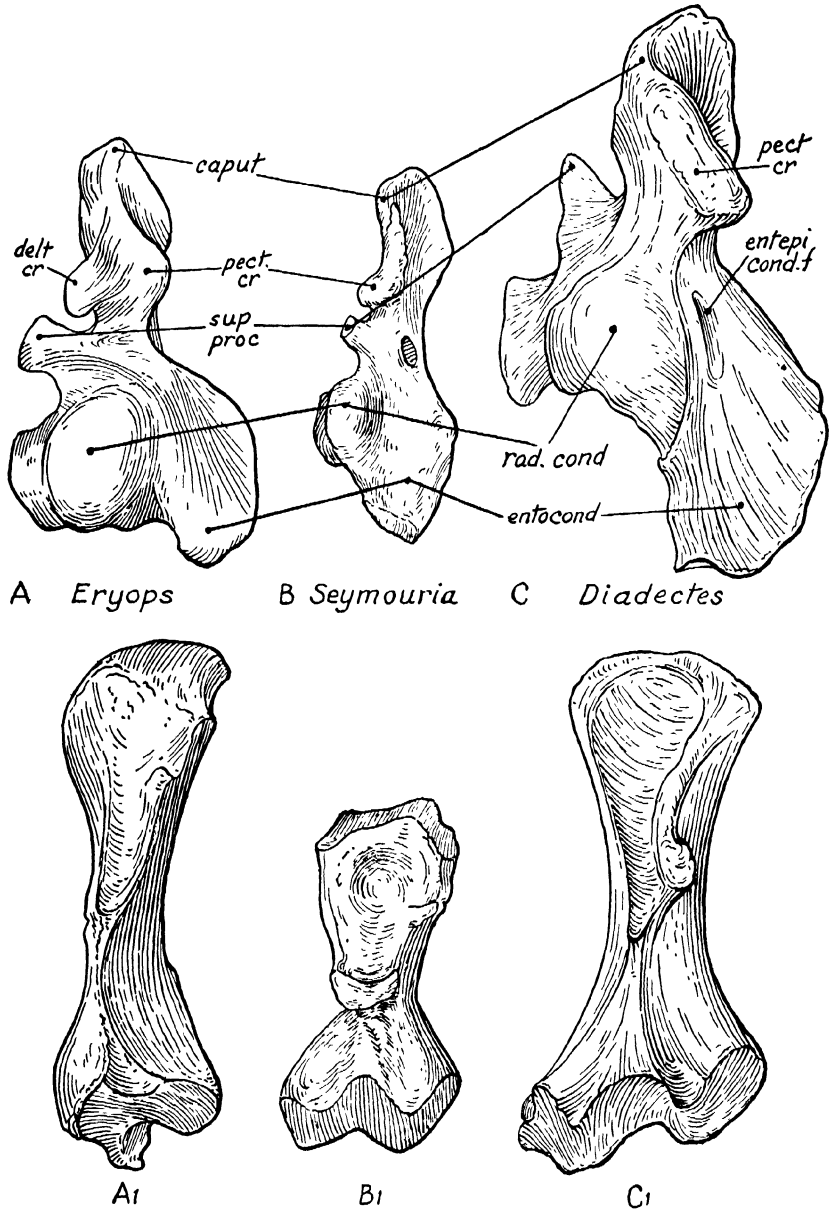


Fig. 12.5a. Right humerus and left femur of *Seymouria* (B, B1), after White; primitive labyrinthodont (*Eryops*, A, A1) and specialized cotylosaur (*Diadectes* C, C1), from specimens

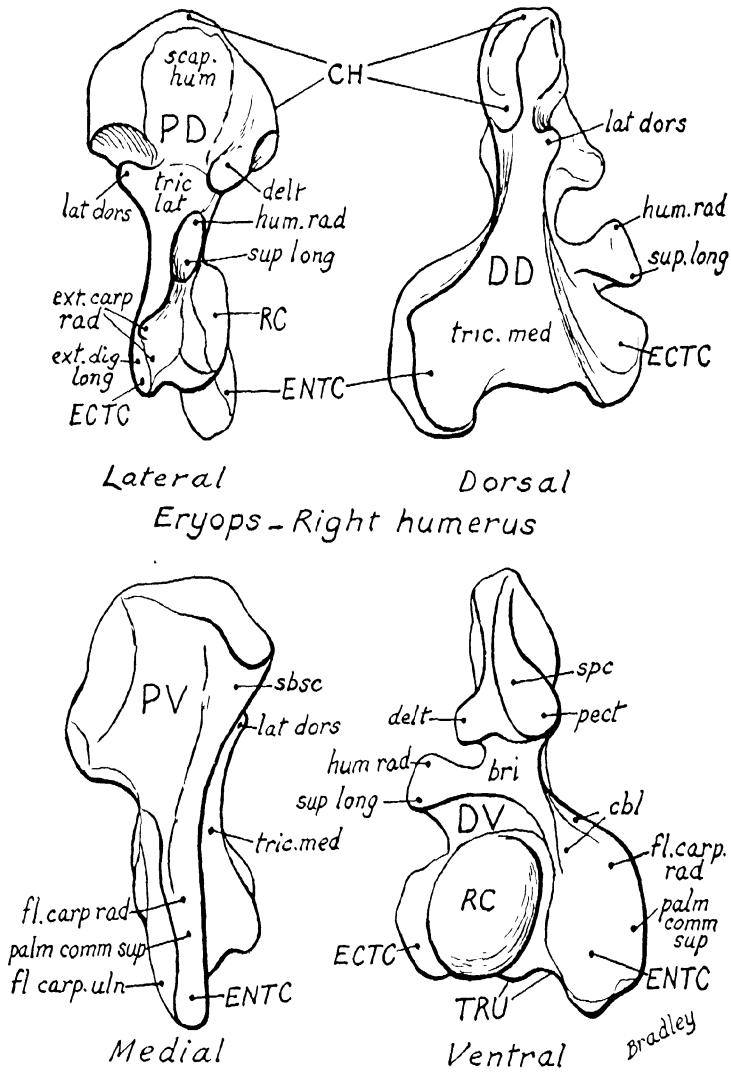


Fig. 12.5b. Humerus of *Eryops*, showing four roughly triangular areas in relation to muscles. Data from Romer, Miner. *PD*, proximal dorsal; *PV*, proximal ventral; *DD*, distal dorsal; *DV*, distal ventral; *CH*, caput humeri; *ECT*, ectocondylar process; *ENT*, entocondylar process; *RC*, capitellum (for radius); *TRU*, trochlearis ulnaris.

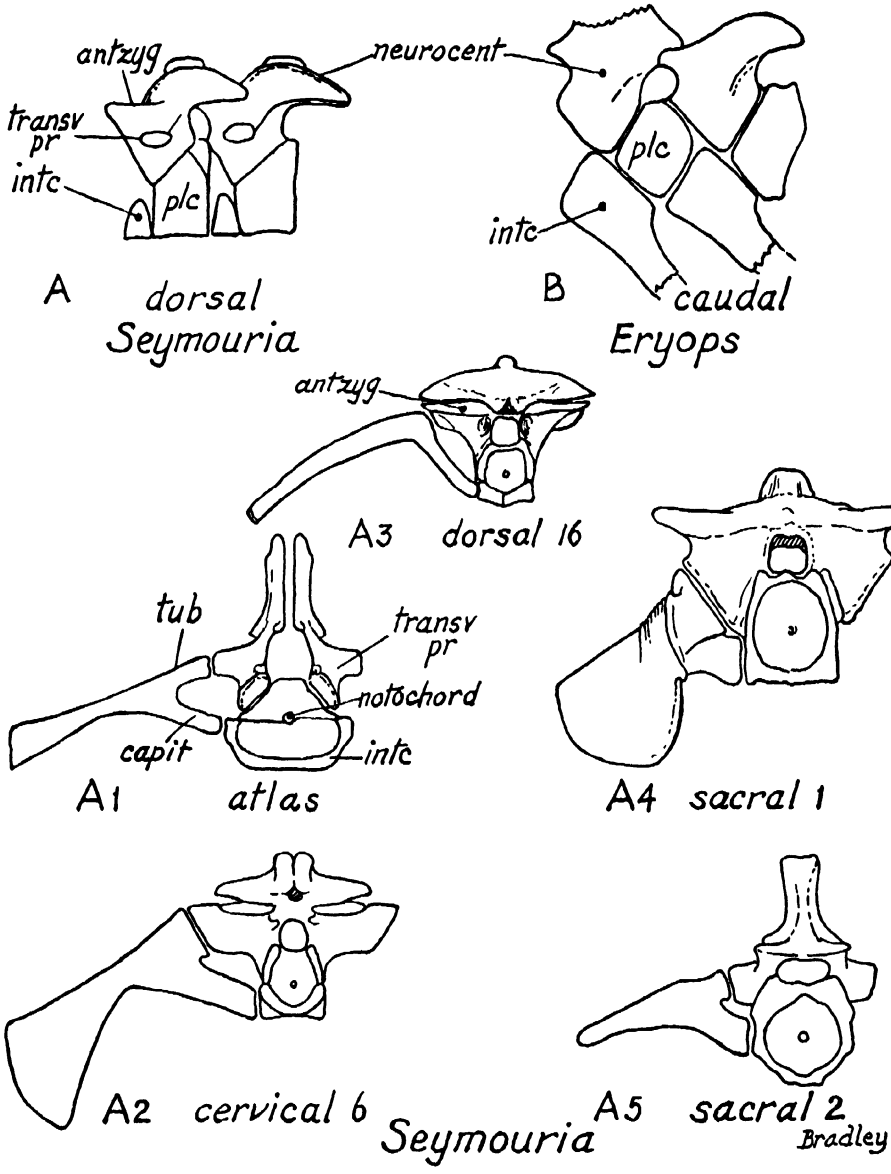


Fig. 12.6. Vertebrae of *Seymouria* (A–A5) and *Eryops* (B), to show homologous parts. A, B, side views, after Williston; A1–A5, front views, after White.

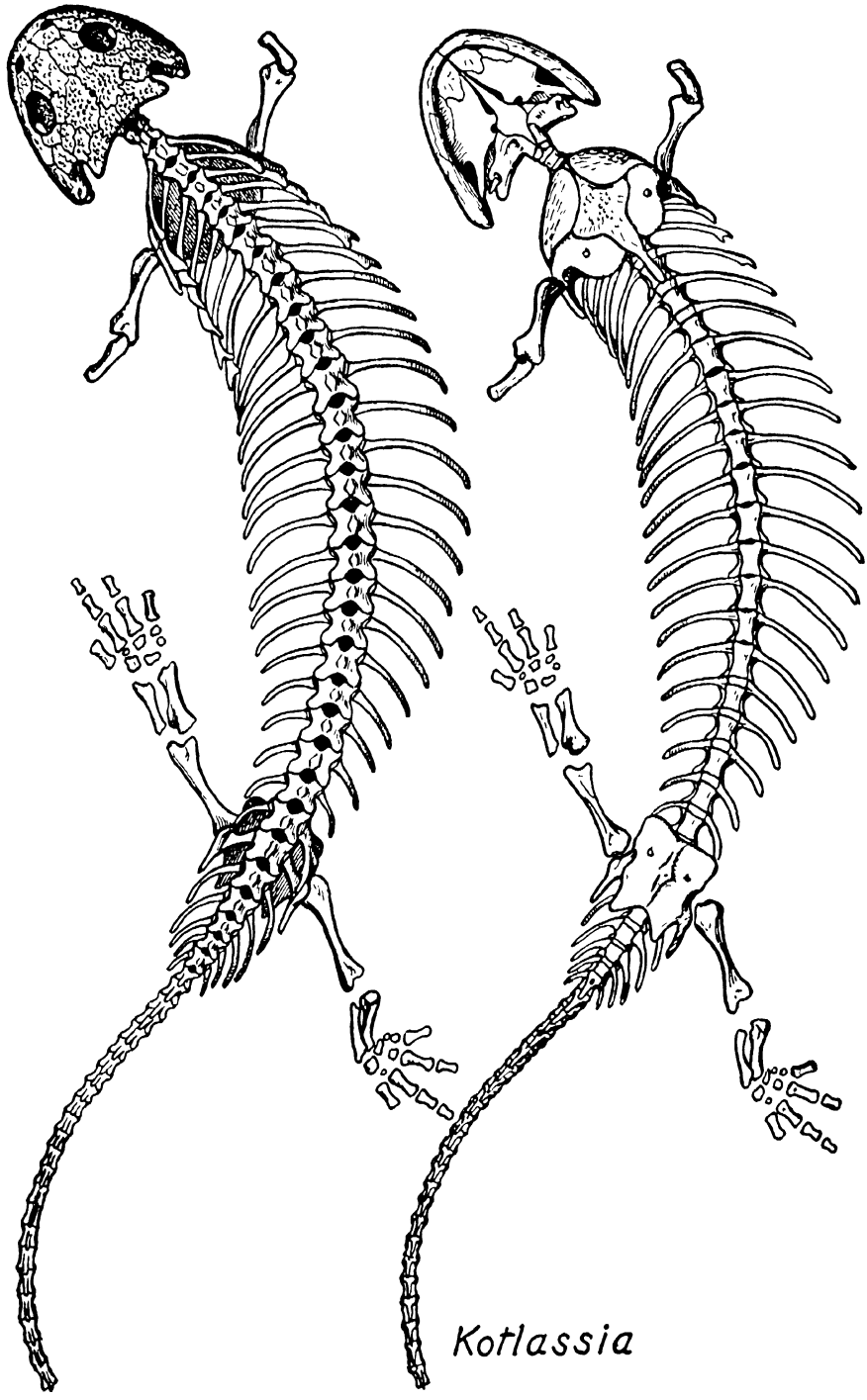


Fig. 12.7. A Russian relative of *Seymouria* After Bystrow.

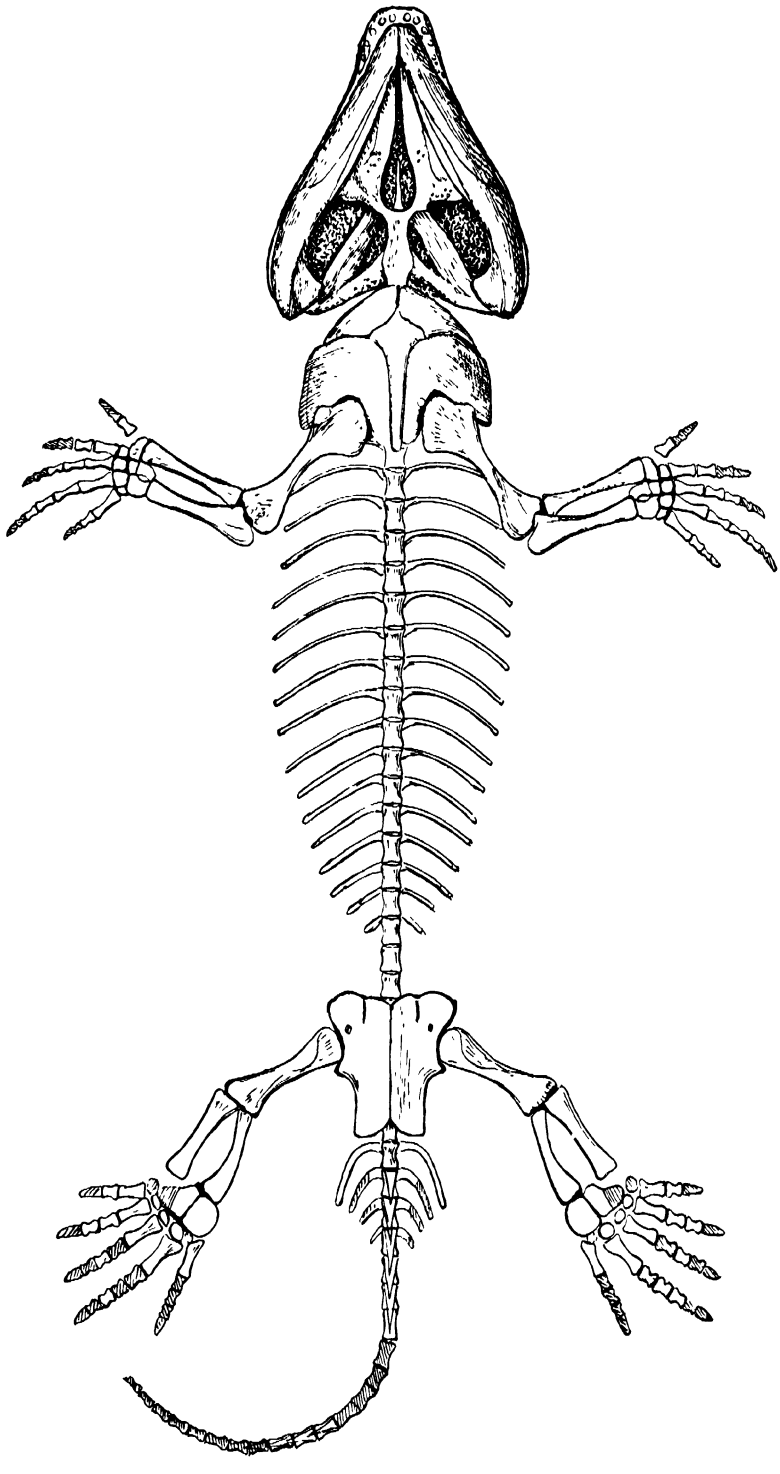


Fig. 12.8. Skeleton of *Captorhinus*, ventral view. After Williston.

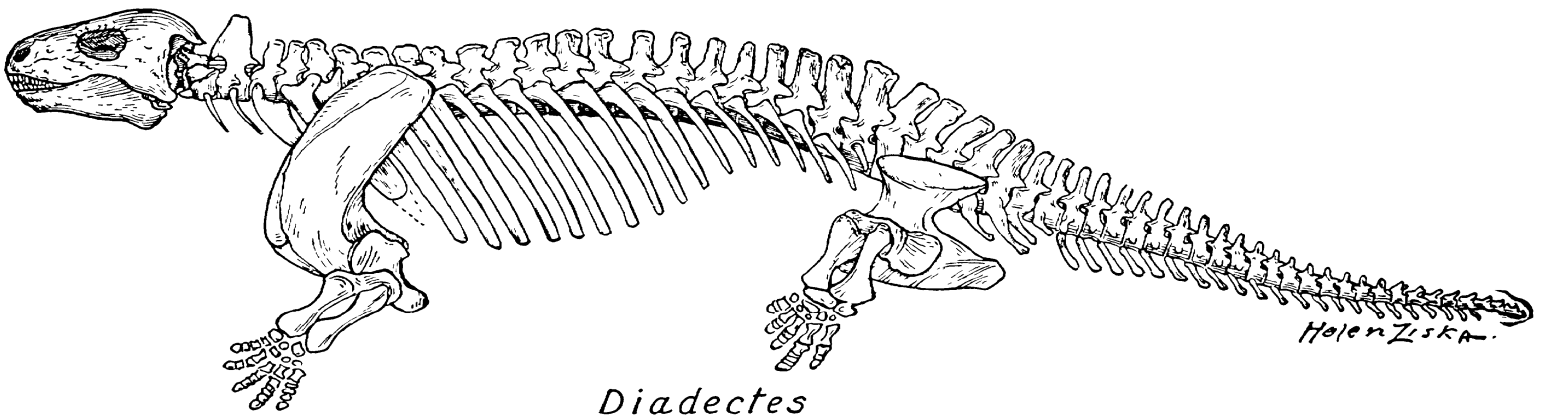


Fig. 12.9. Reconstruction of *Diadectes* skeleton. Length about 1.7 meters. Data chiefly from Case and American Museum specimens.

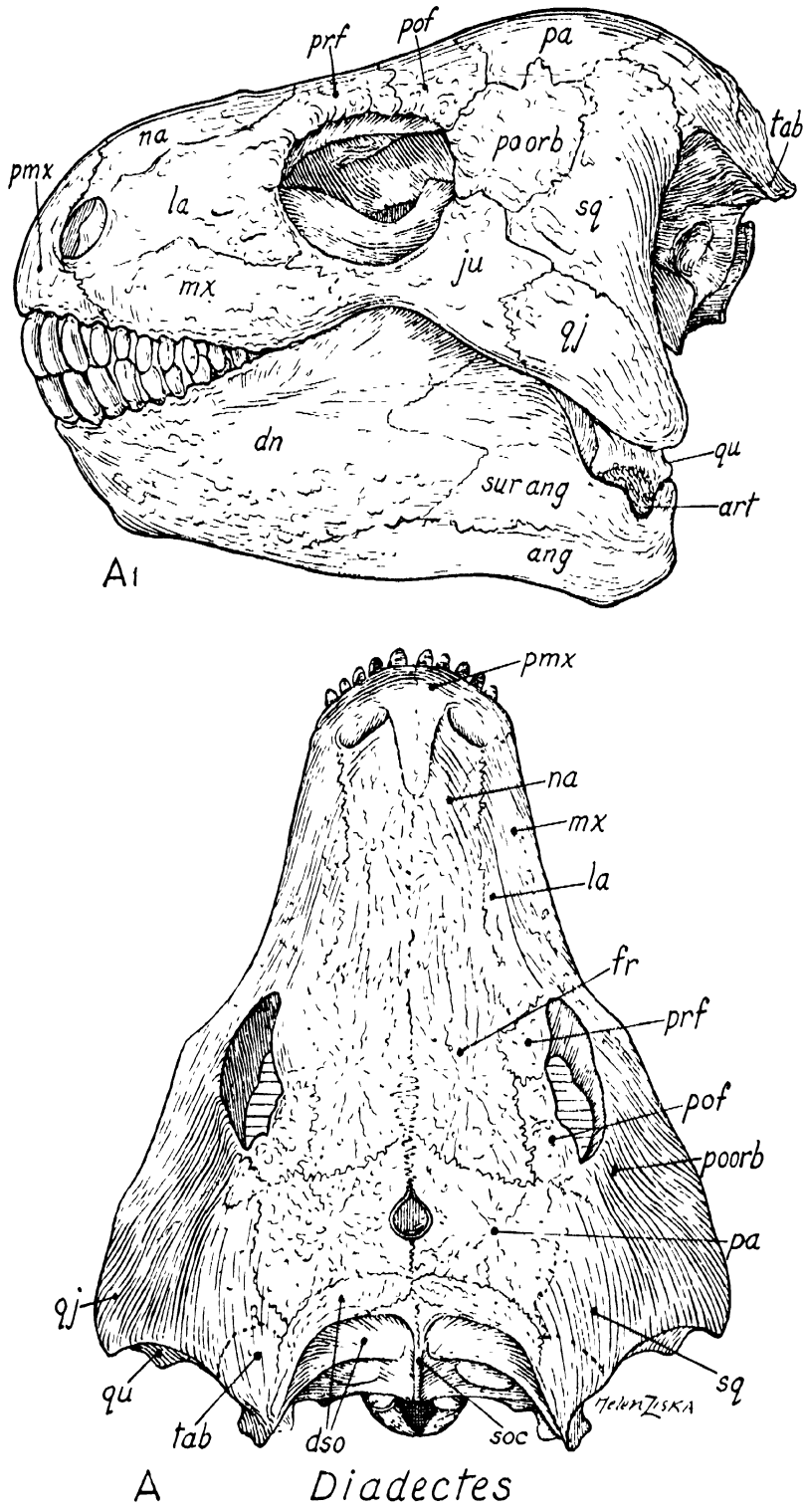


Fig. 12.10. Skull of *Diadectes phaseolinus*. Restored from Amer. Mus. Nos. 4839, 4352, 4370 (teeth). Data on sutures chiefly from Case, von Huene; mandible in part from Wells.

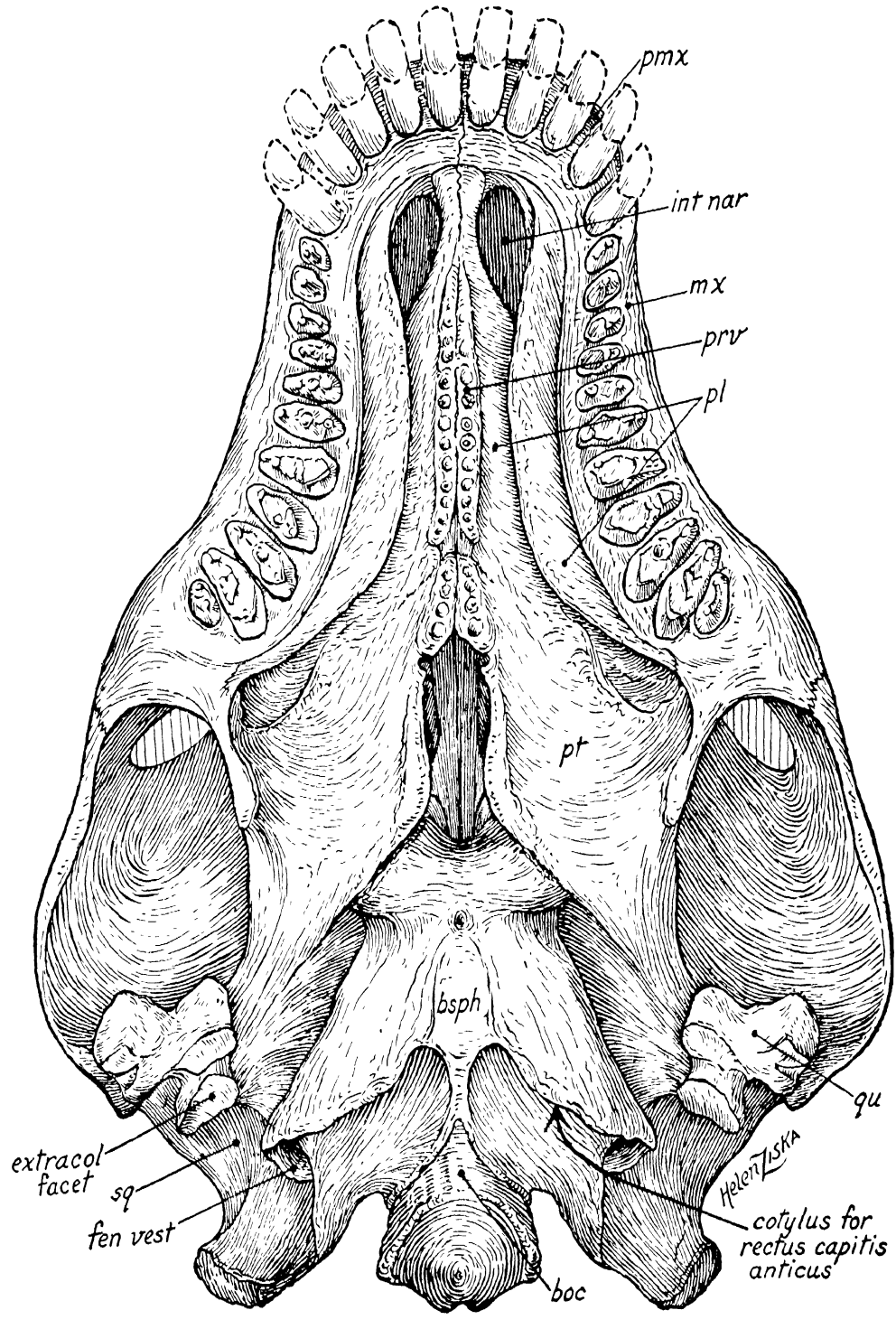


Fig. 12.11. Skull of *Diadectes*, palatal view. Restored from Amer. Mus. Nos. 4370 (teeth), 4839, 4352.

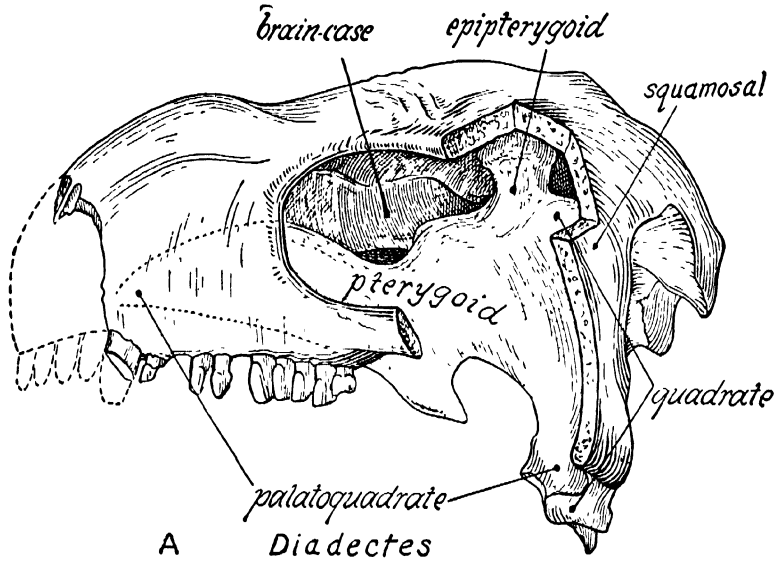


Fig. 12.12a. Relations of the primary upper jaw (palatoquadrate) to the braincase in a primitive reptile. The bony surface mask of the temporal region has been cut away to show the underlying parts.

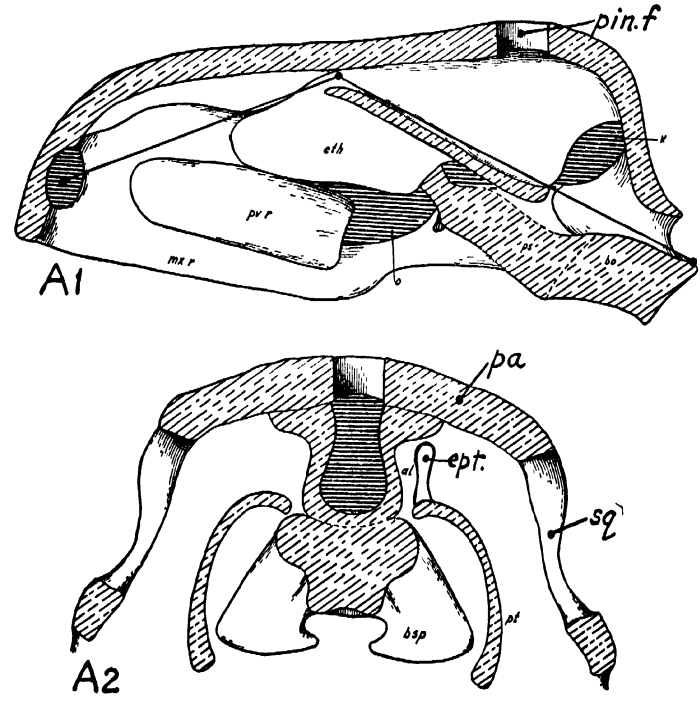


Fig. 12.12b. Skull construction of *Diadectes*. Slightly modified after Case. A, right half of entire skull in sagittal section; A1, cross-section through pineal (epiphyseal) tunnel, showing relation of epipterygoid to brain trough.

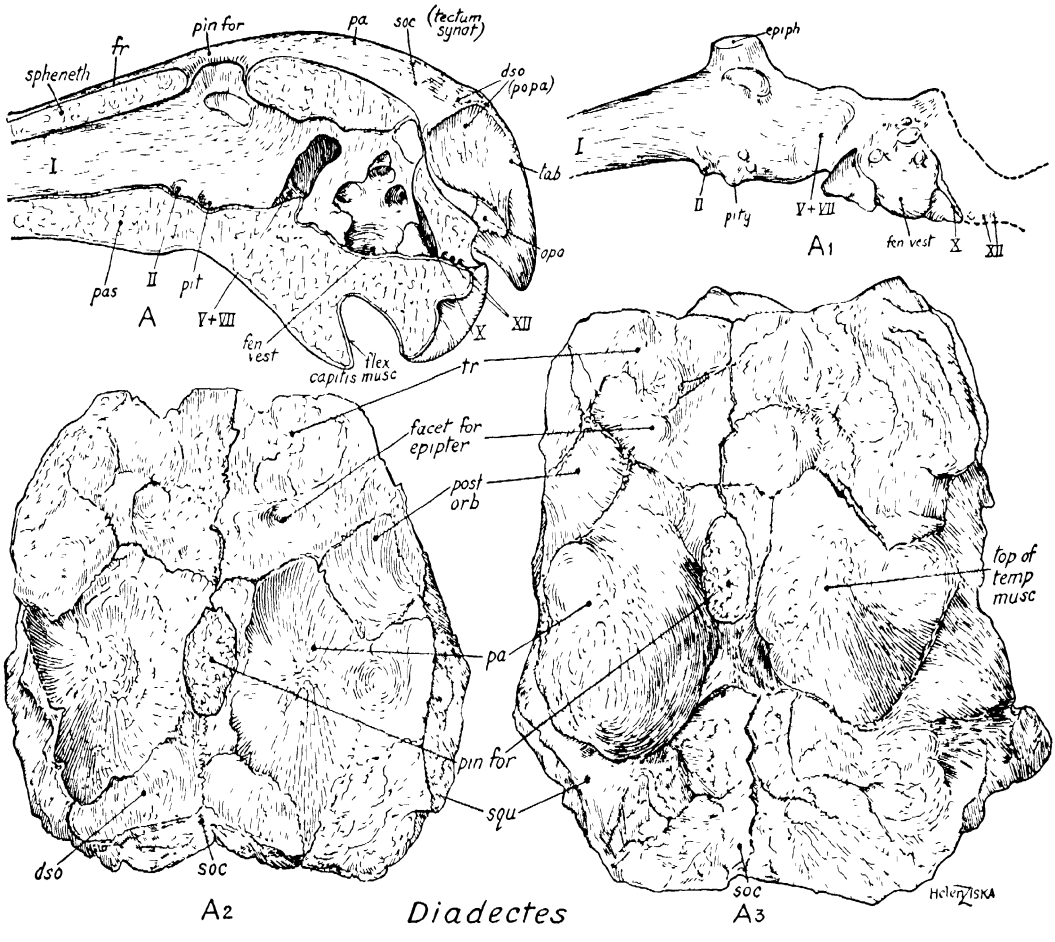


Fig. 12.13. Reconstruction of braincase (A) and endocranial cast (A1) of *Diadectes*. Data from specimens and from Cope, Case, Watson, von Huene. Underside of cranial roof (A2) of *Diadectes*, showing pineal tunnel in relation to neighboring parts. A1, Counterpart (A3) of same, showing on either side of the pineal stalk the large matrix-filled chambers for the temporal jaw muscles (fig. 12.26A). Original.

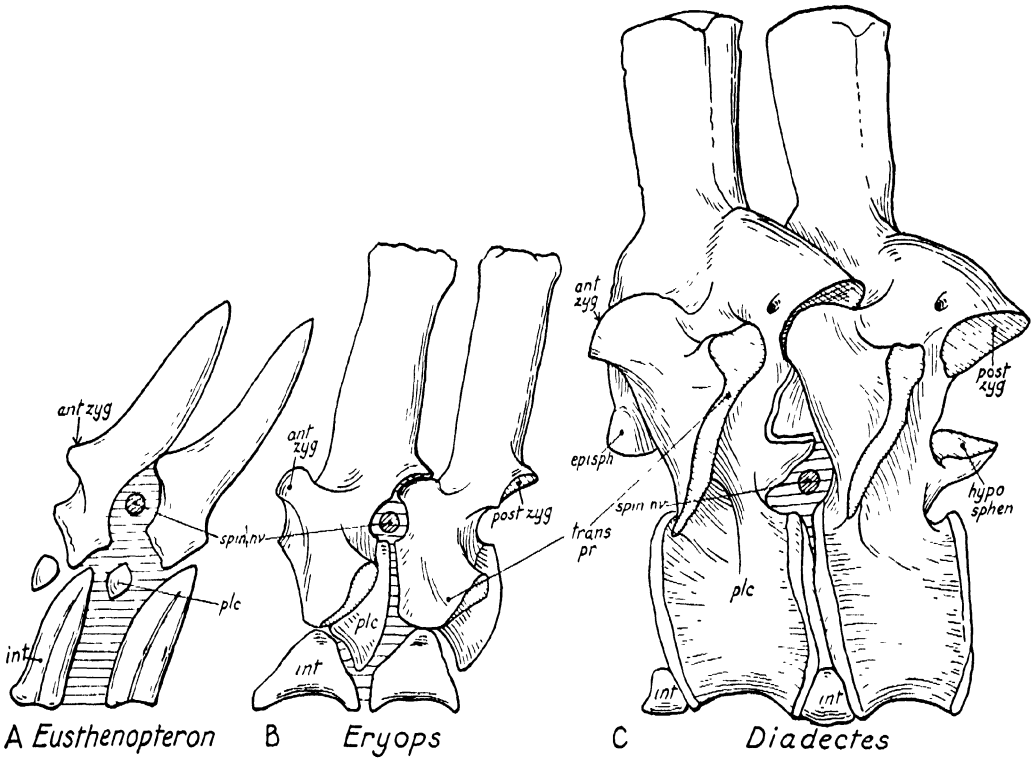


Fig. 12.14a. Increasing complexity of vertebrae and their articulations. Original. In the primitive lobe-fin fish (A) the notochord was dominant and the future centra were represented by thin intercentral crescents (*int*) and incipient pleurocentral nodules (*plc*); the successive neural arches were but slightly if at all in contact and the zygapophyses (*ant zyg*) barely indicated. In the rhachitomous labyrinthodont (B) the notochord was restricted and the intercentral crescents and pleurocentra were much better developed, the large neural arches have established close-fitting anterior and posterior zygapophyses; well developed diapophyses (*trans pr.*) spring from the lower sides of the neural arches for the support of the large ribs. In the giant cotylosaurian reptile (C) each pair of pleurocentra (*plc*) formed a complete centrum, the intercentra were reduced and the swollen neural arches had acquired large zygapophyses and an extra pair of articulations (hyposphenes, episphenes) lying below the zygapophyses. This arrangement greatly strengthened the vertebral column against wrenching thrusts from the massive everted limbs.

Fig. 12.14b (facing page). Dorsal vertebrae of *Diadectes* (A, B) and Python (C). Original. In the cotylosaur (A, B) the centra are amphicoelous (concave at both ends), the diapophyses (for the tubercula of the ribs) are borne by the neural arches, the extra articulations (hyposphenes and episphenes) are below the zygapophyses; in the python the centra are porcoelous (concave in front) with a spherical articular surface on the posterior end; the ribs articulate with large parapophyses on the sides of the centra and the extra articulations (zygosphenes, zygantra) are above the zygapophyses.

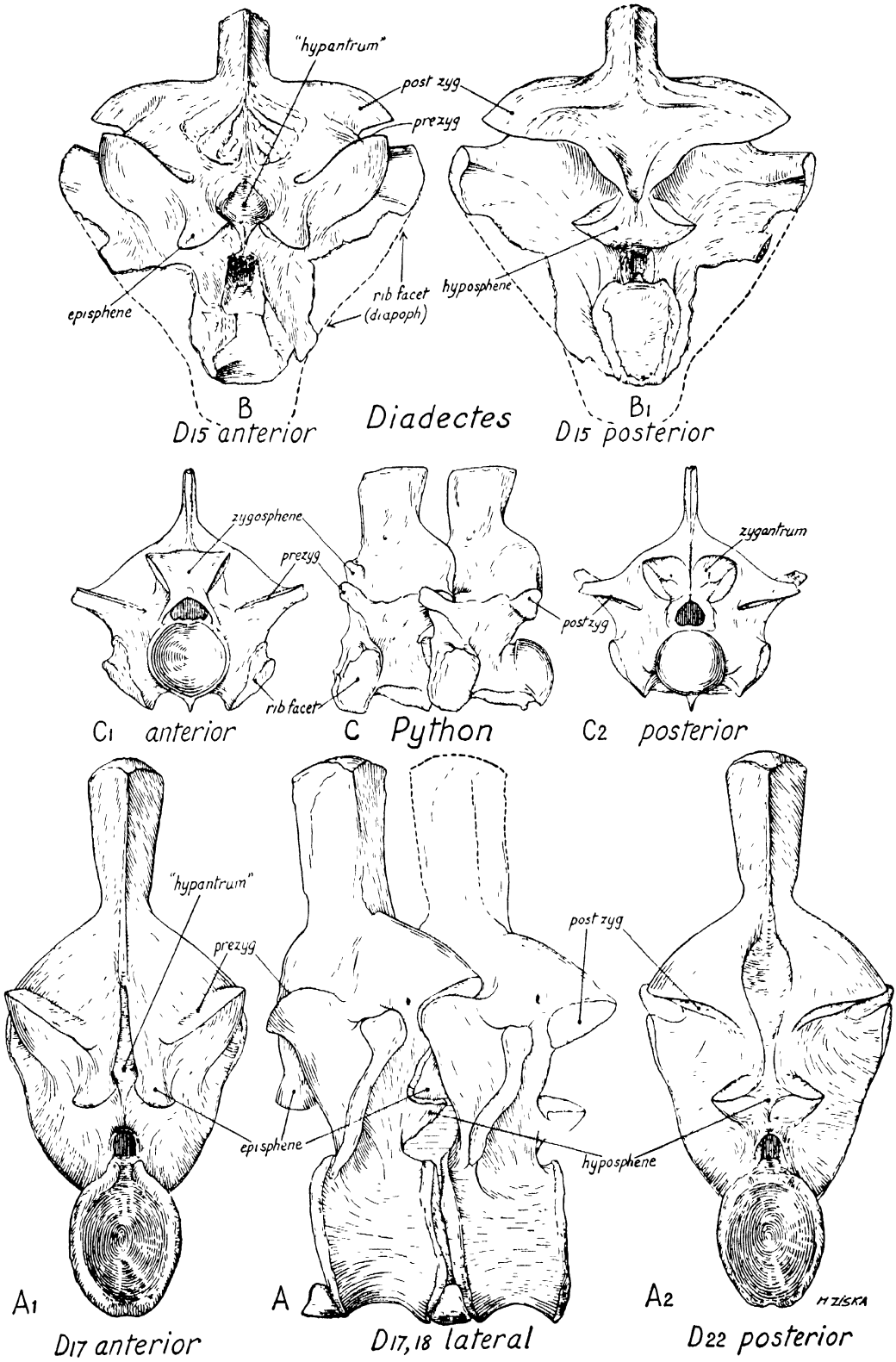

"hypantrum"
post zyg
prezyg
episphene
rib facet
(diapoph)
hyposphene
B
D15 anterior
Diadectes
B1
D15 posterior
zygosphene
prezyg
rib facet
C1 anterior
C Python
zygantrum
postzyg
C2 posterior
"hypantrum"
prezyg
episphene
post zyg
hyposphene
A1
D17 anterior
A
D17,18 lateral
A2
D22 posterior
MZISKA

Fig. 12.14b

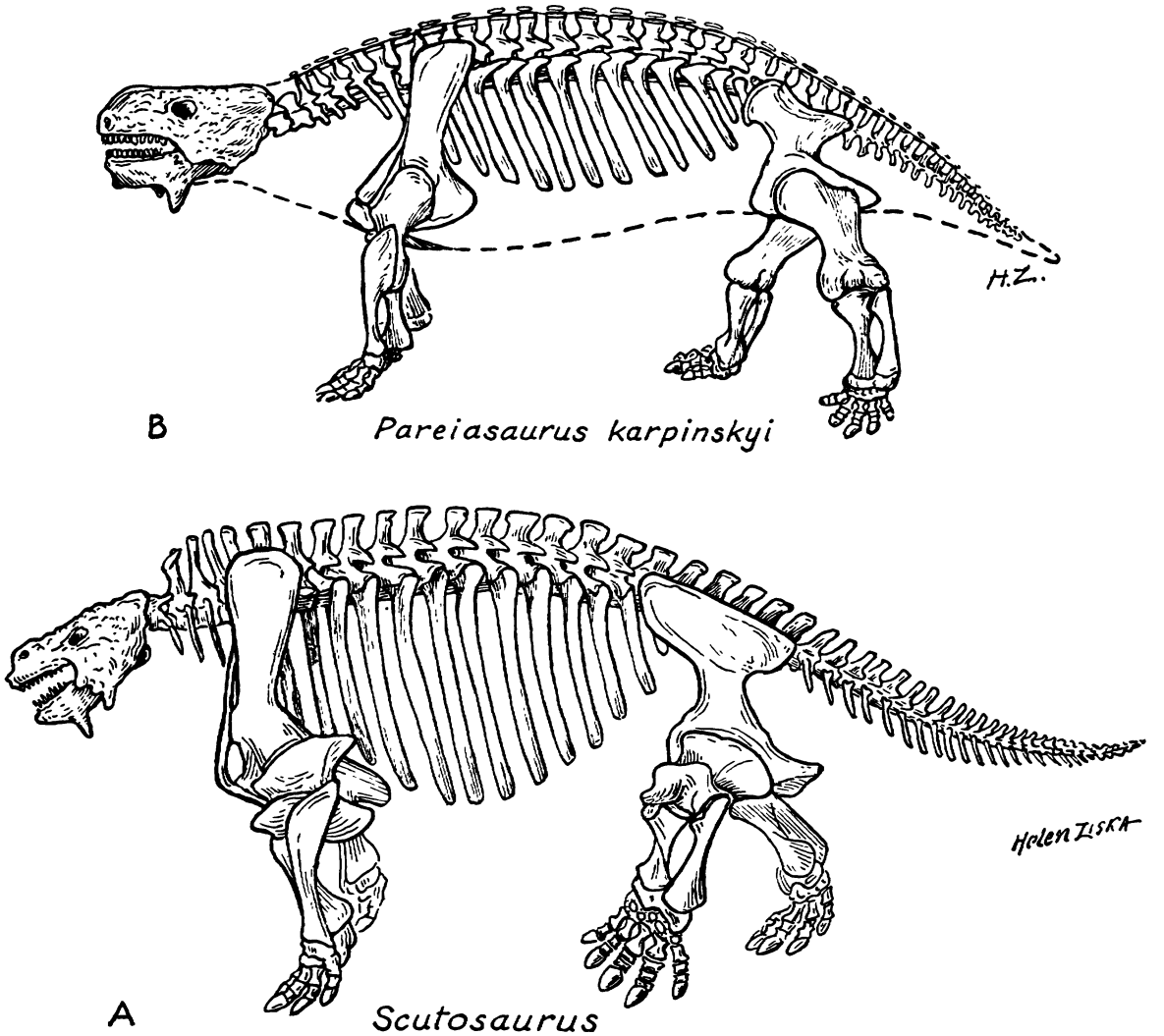
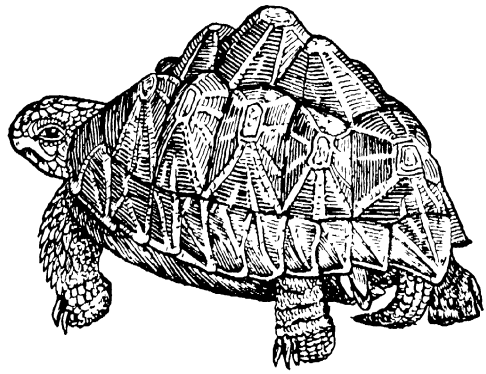
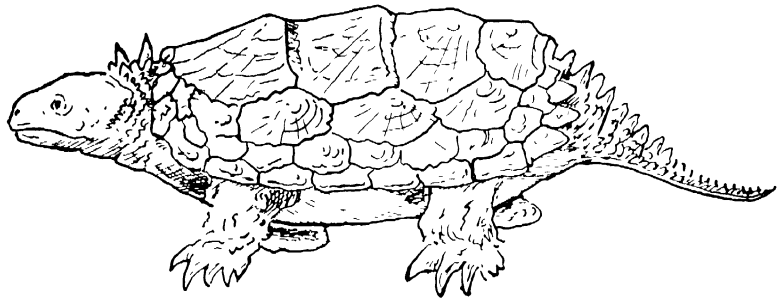


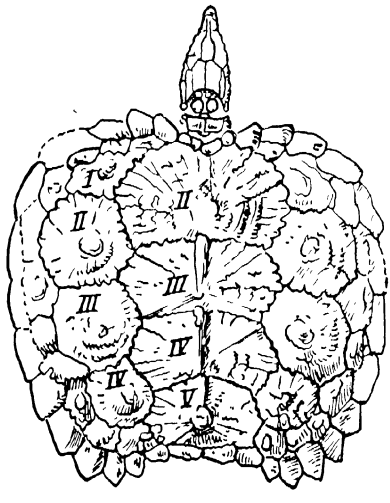
Fig. 12.15. Russian pareiasaur skeletons. A was received in exchange by the American Museum of Natural History and mounted under the direction of Dr. Barnum Brown. Posture of limbs changed in drawing in order to show better the structural patterns of the hand and foot. B, Resembles the central chelonian types (fig. 12.26) in its general form and was likewise protected by a carapace of bony dermal scutes covering the back and sides. Data from Amalitsky's lithographic plate. Previous authors have mostly derived the chelonians directly from the cotylosaurian stem and they seem to have overlooked the very numerous features in which the later pareiasaurs were approaching the chelonian grade (cf. figs. 12.31–12.41).



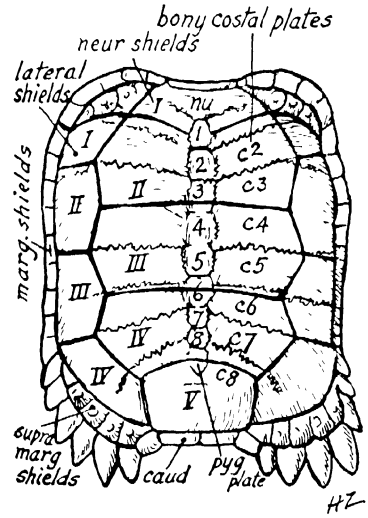
C *Testudo elegans*



A *Triassochelys*



A1



B *Proganochelys*

Fig. 12.16. Modern tortoise (C) and Triassic ancestors (A, B). A, Primitive Triassic chelonian, as restored by Jaekel. A1, Dorsal view, showing the pattern of the horny shields. After Jaekel. B, Relations of the horny shields (roman numbers) to the underlying neural and costal bony plates (arabic numbers). From Zittel, after E. Fraas. C, Modern tortoise with very large horny shields. After Lydekker. The carapace retains the essential pattern of the stem Triassic chelonian, except for the loss of the supramarginal row.

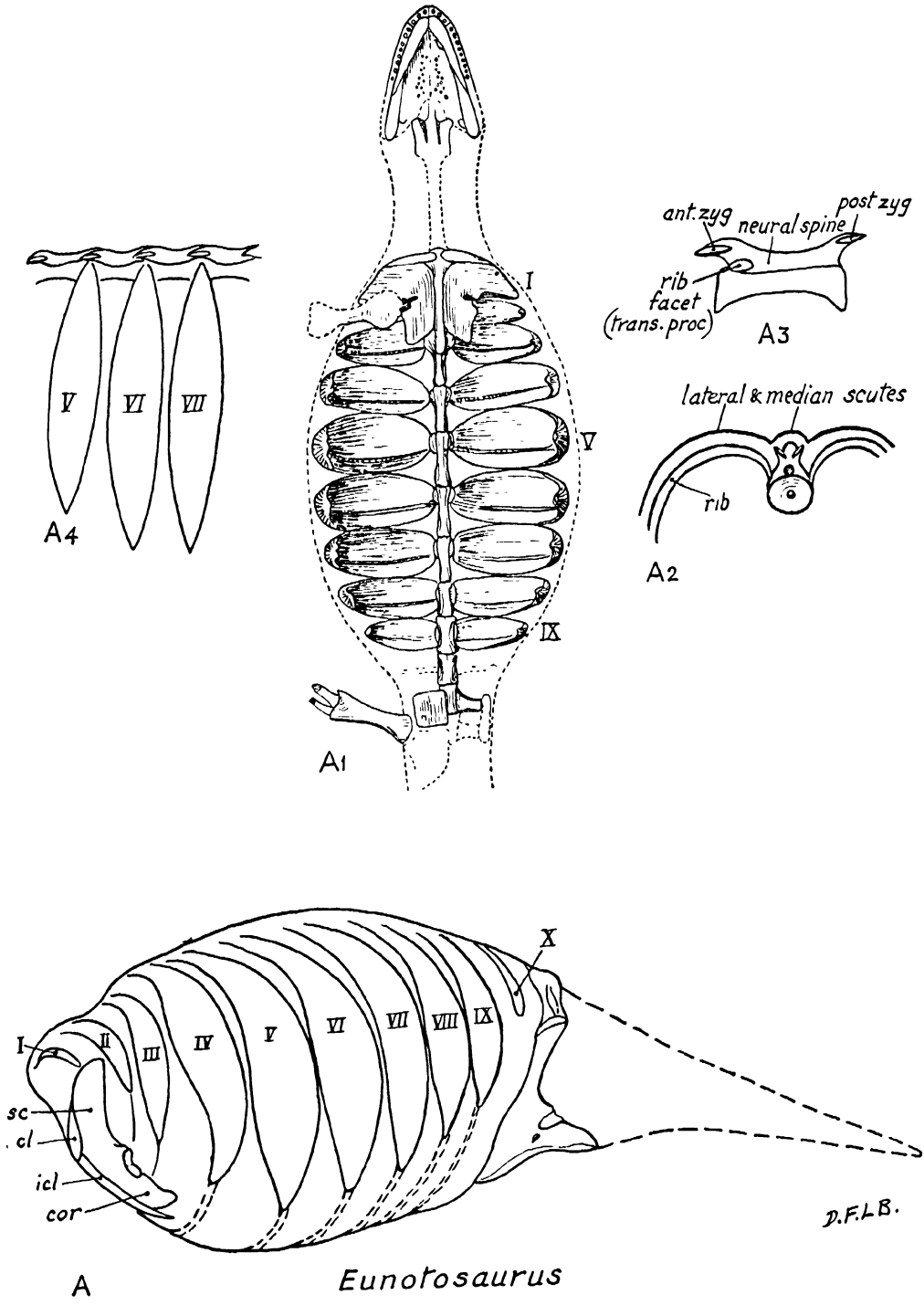
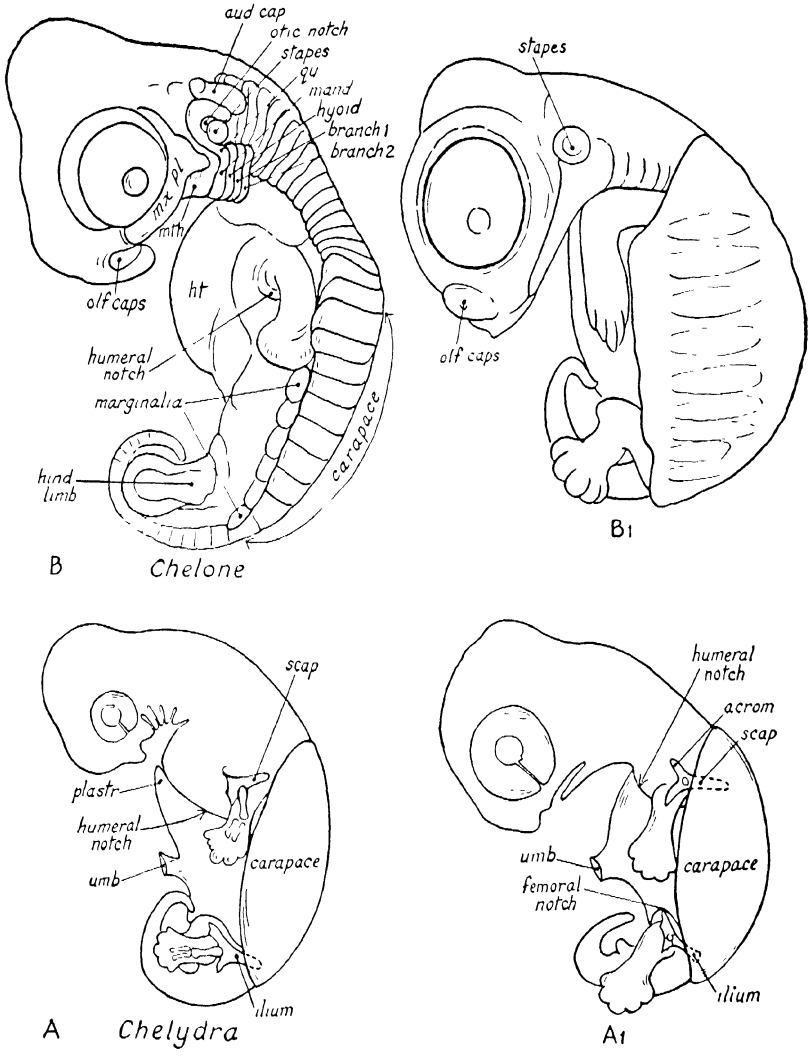

A4
V
VI
VII
A1
I
V
IX
A3
ant. zyg
post zyg
neural spine
rib facet (trans. proc)
A2
lateral & median scutes
rib
A
Eunotosaurus
I
II
III
IV
V
VI
VII
VIII
IX
X
sc
cl
icl
cor
D.F.L.B.

Fig. 12.17



←Fig. 12.17 (facing page). A Permian South African near-tortoise. The general form of the carapace of *Eunotosaurus* was exceedingly tortoise-like but it had barely begun to overlap the shoulder girdle and the expanded thoracic ribs were apparently not enclosed in dermal costal plates (or perhaps the sutures are not shown). The under side of the skull, so far as shown, suggests that of such a pareiasaur as *Dolichopareia* (fig. 12.36A). A, after Watson, A1–A4, tentative reconstructions, data from Watson; B, modified from Amalitsky.

Fig 12.18. How the carapace overspreads the girdles and limbs in embryo turtles. A, A1, after Ruckes; B, B1, after W. K. Parker.

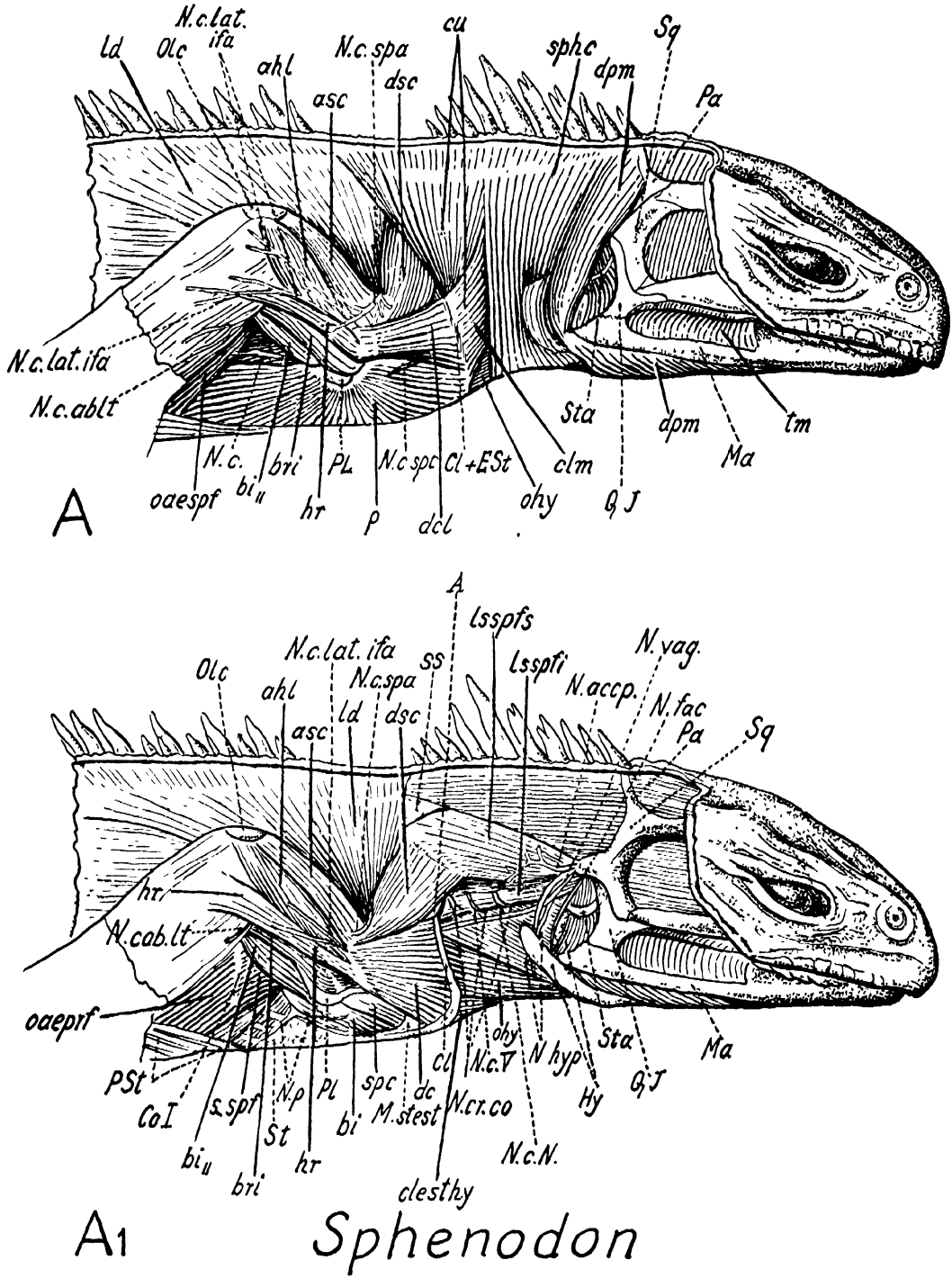
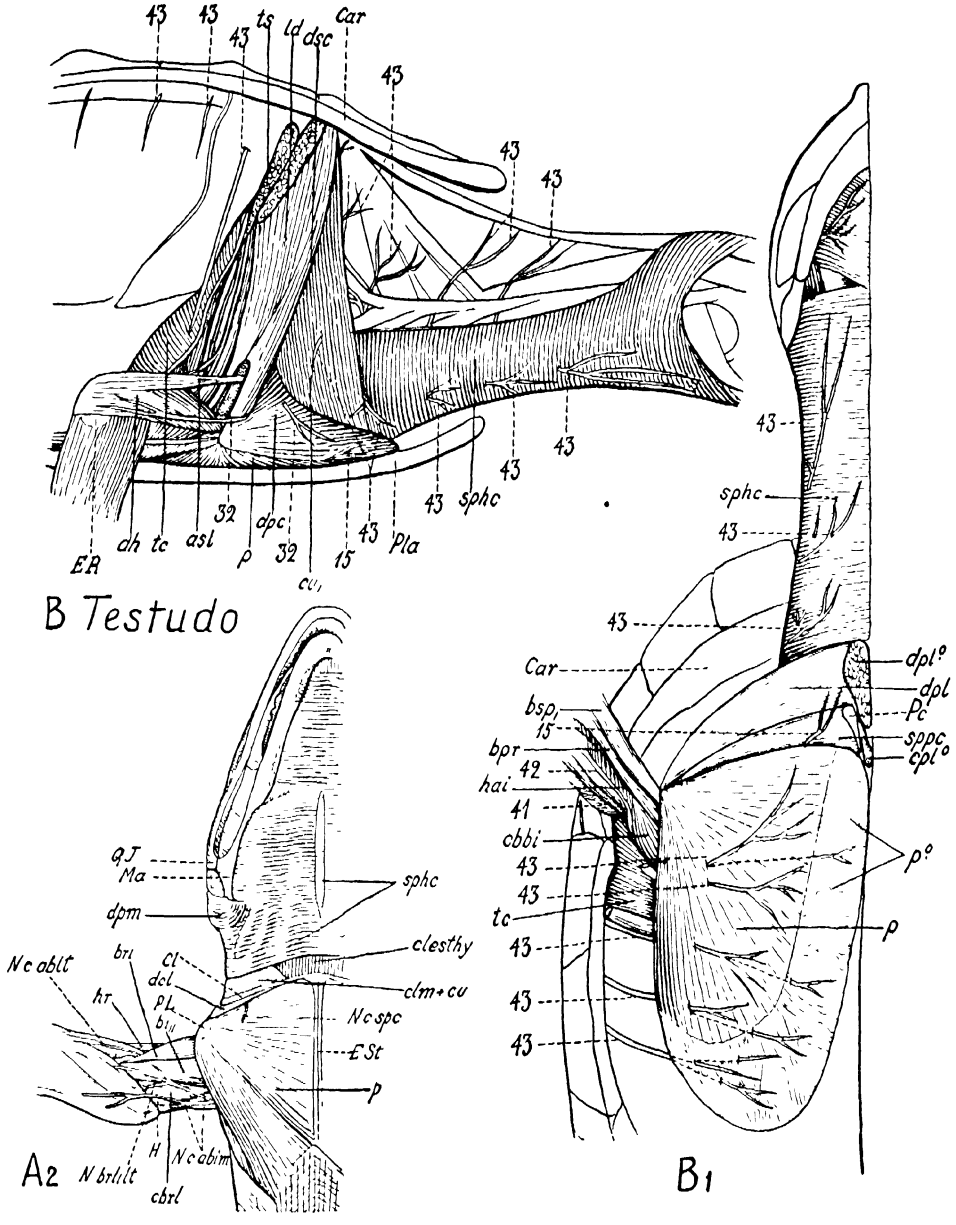


Fig. 12.19a, b. Musculature of the shoulder girdle in a primitive reptile (A, A1, A2,) and a tortoise (B, B1). From Gregory and Camp, after Fürbringer. In the tortoise the dorsal muscles of the shoulder girdle are all crowded on to the scapula which, with its acromial process and the coracoid (figs. 12.31 D, 12.27), forms a strongly muscled pyramid for moving the limb. The greatly enlarged pectoral muscles are firmly based on the median raphe and on the plastron. *Tm.*, temporo-masseter; *hr.*, humero-radialis; *dpm.*,



depressor mandibulae; *ohy.*, omohyoideus; *sphc.*, sphincter colli; *clm.*, cleidomastoideus; *cu.*, cucullaris (trapezius); *dcl.*, deltoides clavicularis; *dsc.*, dorsalis scapulae; *p.*, pectoralis; *ld.*, latissimus dorsi; *oaespf.*, obliquus abdominis externus superficialis; *asc.*, anconeus scapularis (triceps); *bri.*, brachialis internus; *ahl.*, anconeus humeralis lateralis; *bi''*, biceps, distal belly.

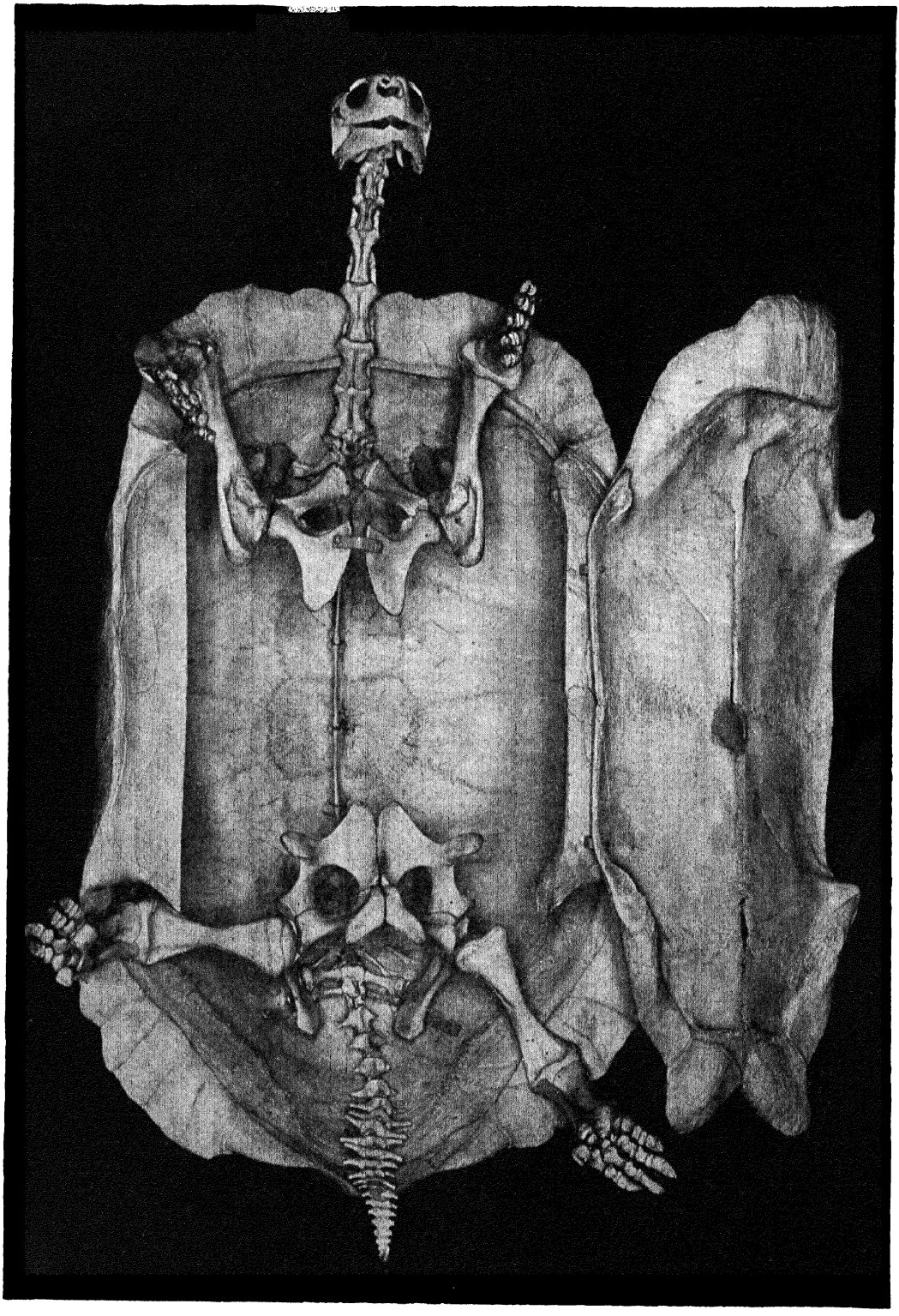


Plate 12.I. Skeleton of *Testudo pardalis.* Ventral view. Amer. Mus. Nat. Hist.

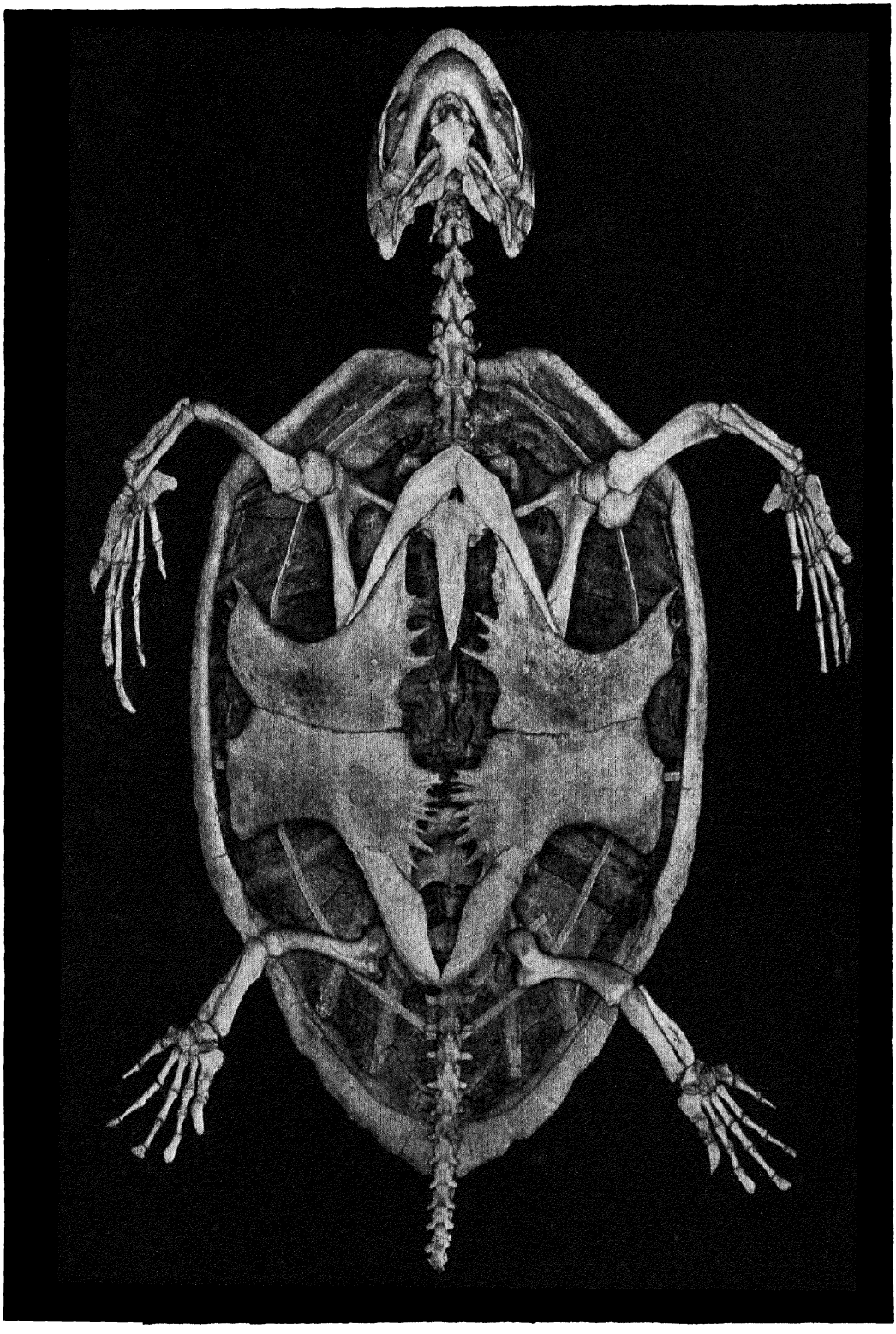


Plate 12.II. Skeleton of *Chelone*. Ventral view.
Amer. Mus. Nat. Hist.

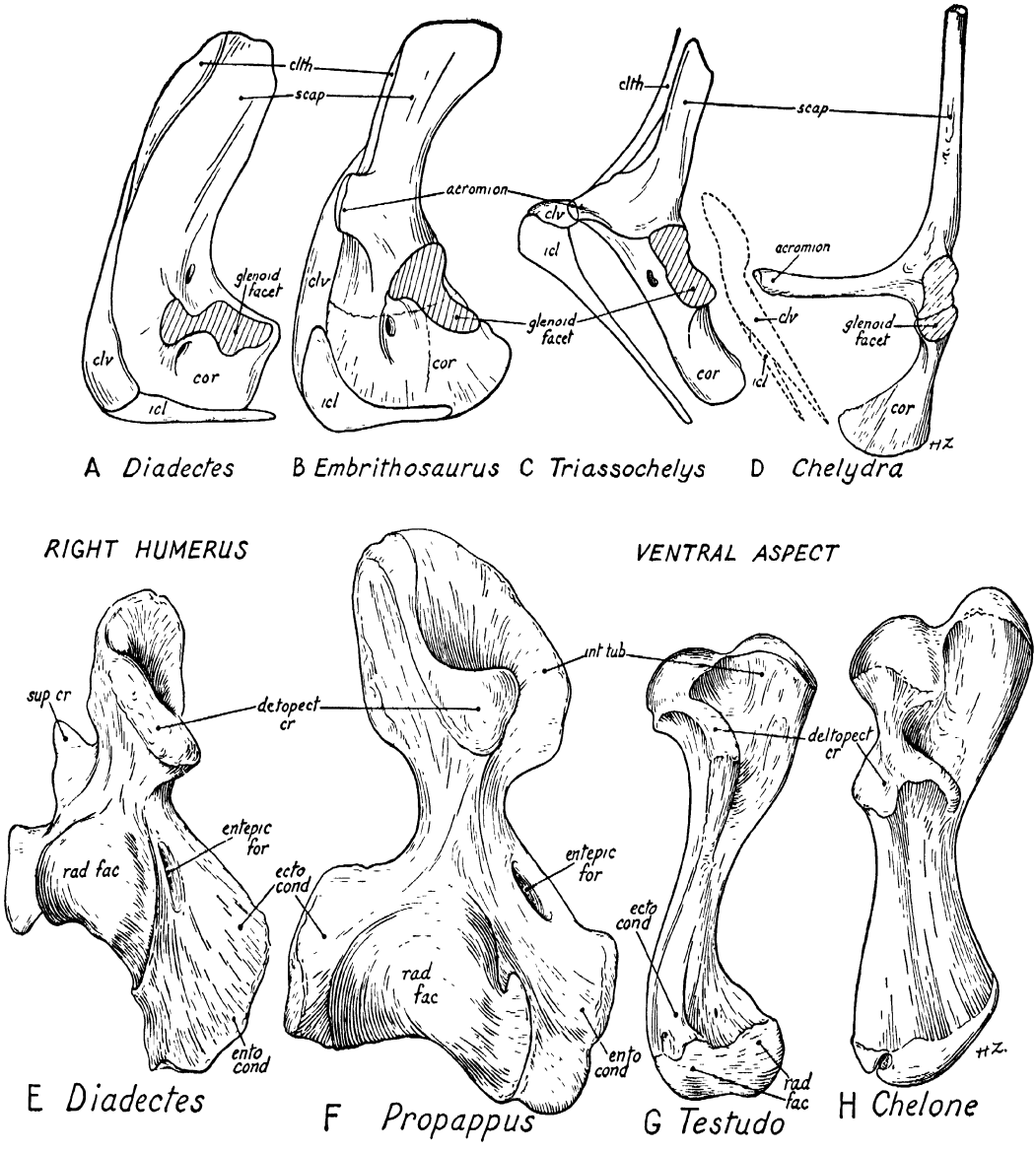

clth
scap
glenoid facet
clv
cor
icl
acromion
glenoid facet
A Diadectes
B Embrithosaurus
C Triassochelys
D Chelydra
RIGHT HUMERUS
VENTRAL ASPECT
sup cr
detopect cr
entepic for
rad fac
ecto cond
ento cond
int tub
deltopect cr
E Diadectes
F Propappus
G Testudo
H Chelone

Fig. 12.20

Fig. 12.20. Pectoral girdles (A–D) and humeri (E–H) of cotylosaur (A, E), pareiasaur (B, F) stem chelonian (C), modern tortoise (D, G), sea-turtle (H). B, after Haughton and Boonstra; C, after Jaekel; others, original.

In the cotylosaur (A) the glenoid facet for the humerus is extended anteroposteriorly in accordance with the outward and upward direction of the humerus.

In the pareiasaur (B) the glenoid is becoming extended ventrally as the humerus is directed more downward. The coracoid is shorter anteroposteriorly than in *Diadectes* and an acromion process has grown out from the anterior border of the scapula, probably for the insertion of one head of the trapezius (Boonstra, Part VIII, p. 495). Thus the pareiasaurian pectoral girdle affords an excellent initial stage leading from the cotylosaurian to the stem chelonian.

In the stem turtle (C) the glenoid is extended dorsoventrally, permitting the globar head of the humerus (G) to roll freely. The acromion is retained and the coracoid plate has been strengthened laterally by a strong column.

In the modern tortoise (D) the acromion has grown forward into a long process and together with the rod-like scapula and coracoid forms a three-branched support for the dorsal muscles of the shoulder-girdle (cf fig. 12.30 B).

In the humerus of *Diadectes* (E) the narrow head permits only a limited gliding, twisting and bending at the shoulder-joint on the laterally-facing glenoid facet of the scapulo-coracoid (A); the shortness of the shaft implies a correspondingly short swing at the elbow; the radial condyle is almost wholly on the ventral surface because the elbow is sharply bent.

The pareiasaurian humerus (F), while retaining the basic cotylosaur plan, has begun to approach the turtle stage in enlarging the caput humeri, in widening the radial facet and in folding the deltopectoral crest toward the internal tuberosity. The sigmoid curve is beginning.

In the tortoise (G) the expanded globular head permits a wide degree of rotation, the sigmoidally curved shaft permits the elbow to be turned forward well in front of the girdle, while the greatly widened radial capitellum permits a wide hinge-like movement at the elbow. The deltopectoral crest is folded over toward the enlarged internal tuberosity.

In the sea-turtle (H) the whole humerus (as part of a swimming paddle) is flattened and widened, the internal tuberosity greatly enlarged, the deltopectoral crest reduced.

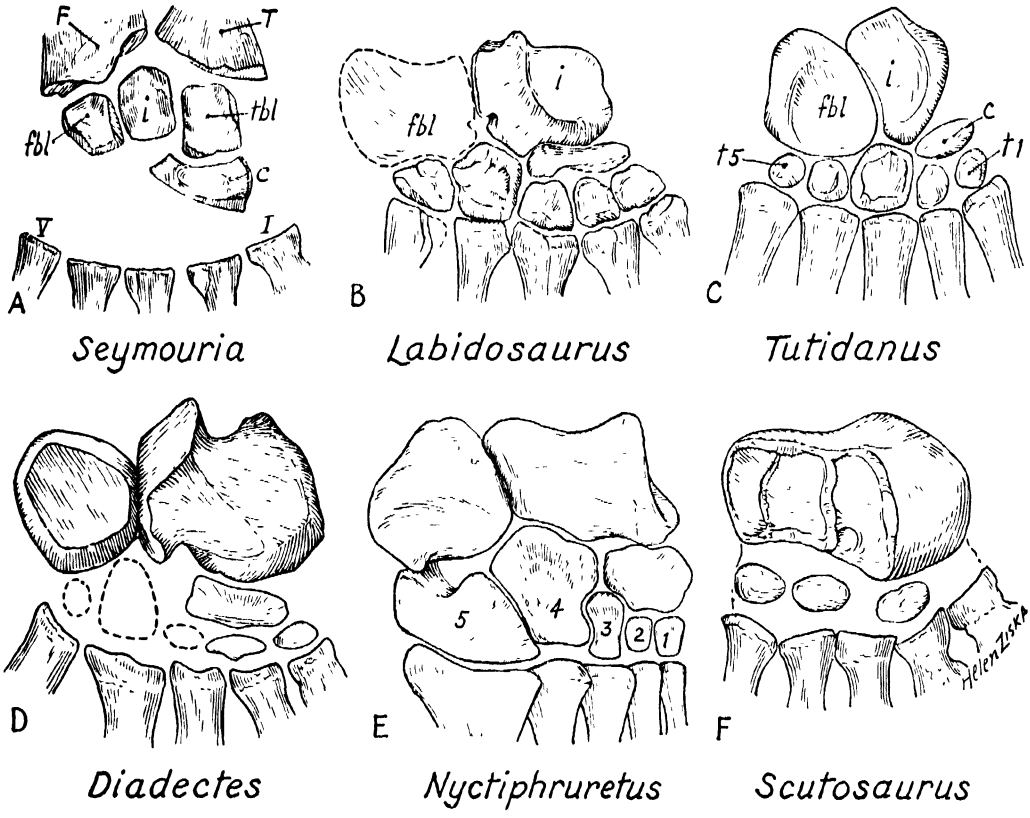


Fig. 12.21. The right tarsus of various cotylosaurs. After B. Schaeffer. The *Seymouria* tarsus is essentially amphibian, retaining a separate tibiale and relatively small astragalus (intermedium) and calcaneum (fibulare). In *Labidosaurus* (B), representing the primitive reptilian type, the bony tibiale has disappeared and the astragalus (*i*) bears a large facet for the tibia. The tarsus of *Tuditanus* (C, "*Eosauravus*") is likewise of very primitive reptilian type. In *Diadectes* (D) the astragalus and calcaneum are greatly enlarged and embedded in cartilage. The rounded tibial facet on the astragalus permitted the tibia to rotate on the astragalus (Romer and Byrne). In the Procolophonia (E) the wide astragalus is appressed to the calcaneum, and in the pareiasaur (F) these two bones unite into a firm base for the massive tibia. In this case the main bending of the tarsus was between the astragalo-calcaneum and the metatarsals. In other words, this joint was "mesotarsal." These and other features of the pareiasaurian tarsus probably indicate their ability to draw in the femora away from the everted position of primitive crawling types.

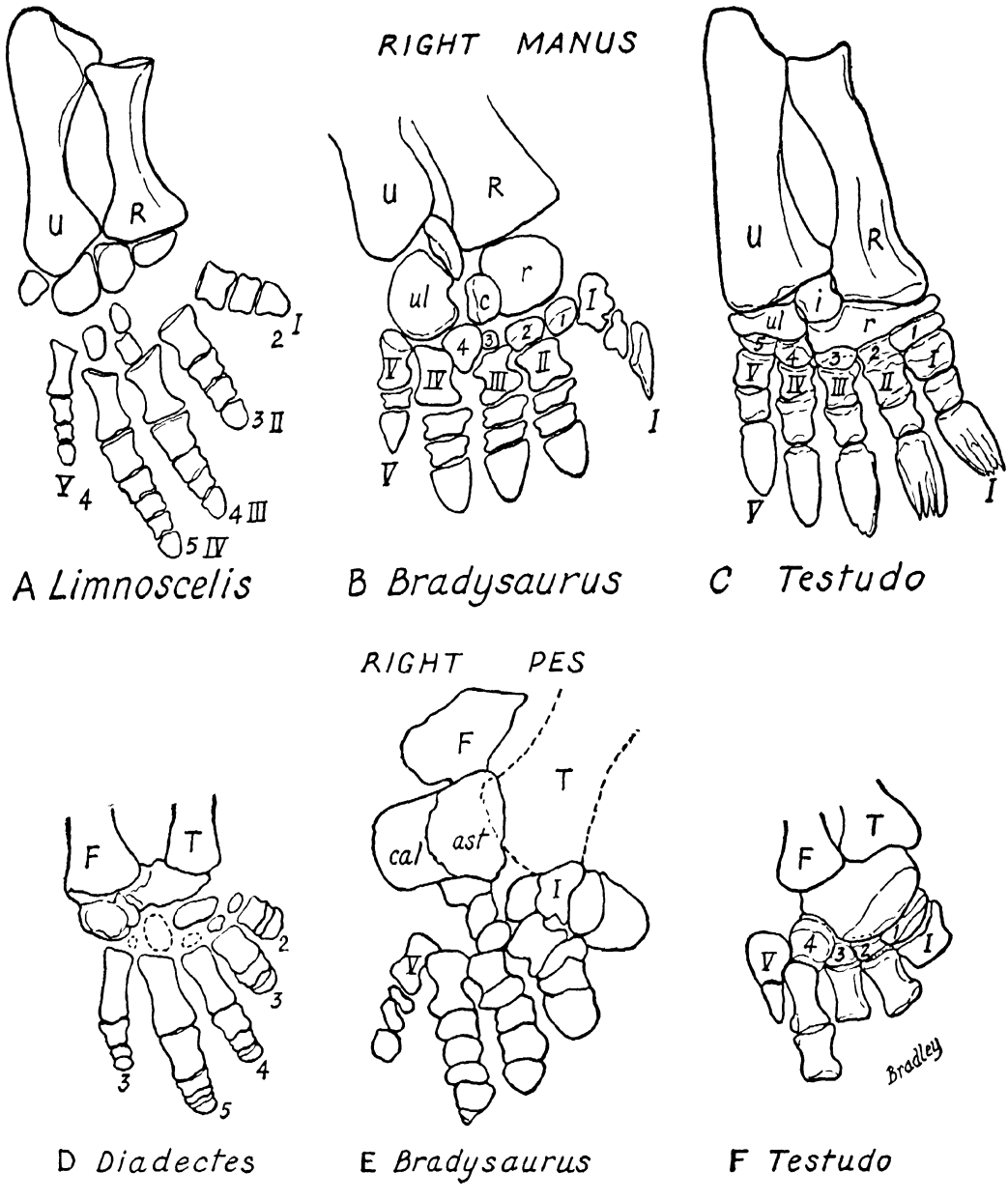


Fig. 12.22. Hands (A–C) and feet (D–F) of cotylosaur (A, D), pareiasaur (B, E) and modern tortoise (C, F). A, C, after Williston; B, E, after Boonstra; D, after Romer and Byrne. The basic identity of all three is very evident. The cotylosaur retains the primitive reptilian phalangeal formula (2,3,4,5,4); in some of the pareiasaurs it is reduced to 2,3,3,3,2, and in the modern tortoise to 2,2,2,2,2. The latter has also further shortened the metatarsals and expanded the radiale. In the pes of the cotylosaur (D) the astragalus and calcaneum are separate, but in the pareiasaur (E) they are united, as in the tortoise (F).

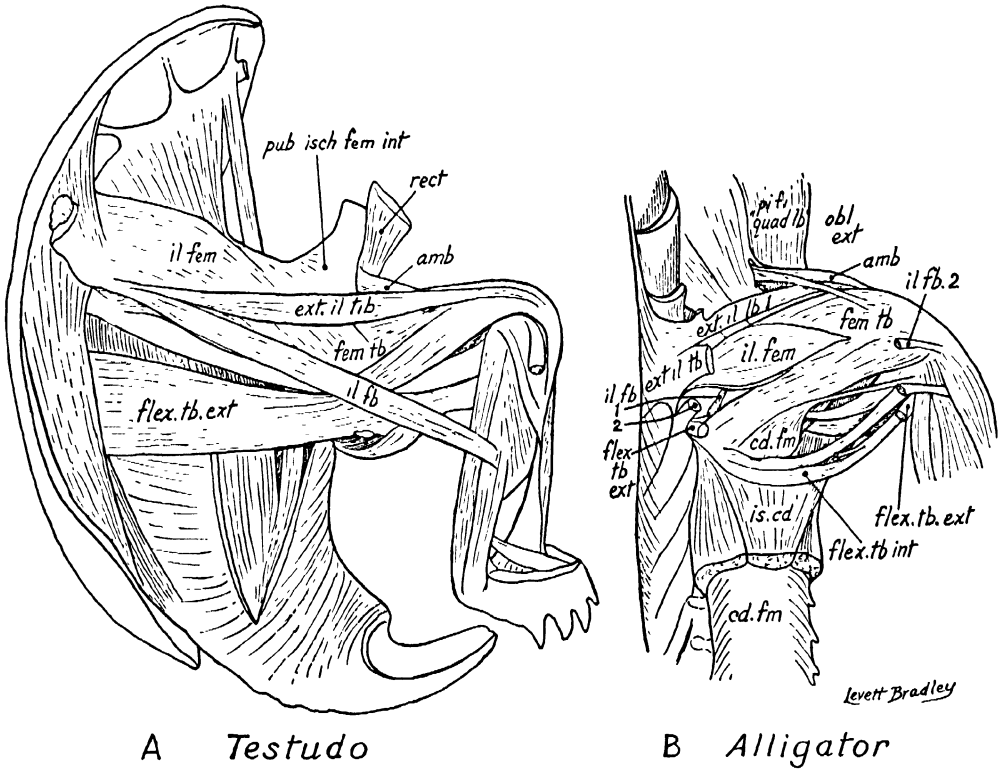


Fig. 12.23a. Surface muscles of pelvis and hind limb in tortoise (A) and alligator (B). After Gadow. *Amb,* ambiens; *cd.fm,* caudifemoralis *ext.il.tib,* extensor ilio-tibialis; *fem.tb,* femoro-tibialis; *flex.tb.ext,* flexor tibialis externus; *flex.tb.int,* flexor tibialis internus; *il.fb,* 1,2, ilio-fibularis, 1,2; *il.fem,* ilio-femoralis; *is.cd,* ischio-caudalis; *pub.isch,fem.int* (*p.i.f.i*), pubi-ischio-femoralis internus; *"quad.lb,"* "quadratus lumborum"; *pub.isch.fem.ext.* (*p.i.f.e.*), pubi-ischio-femoralis externus.

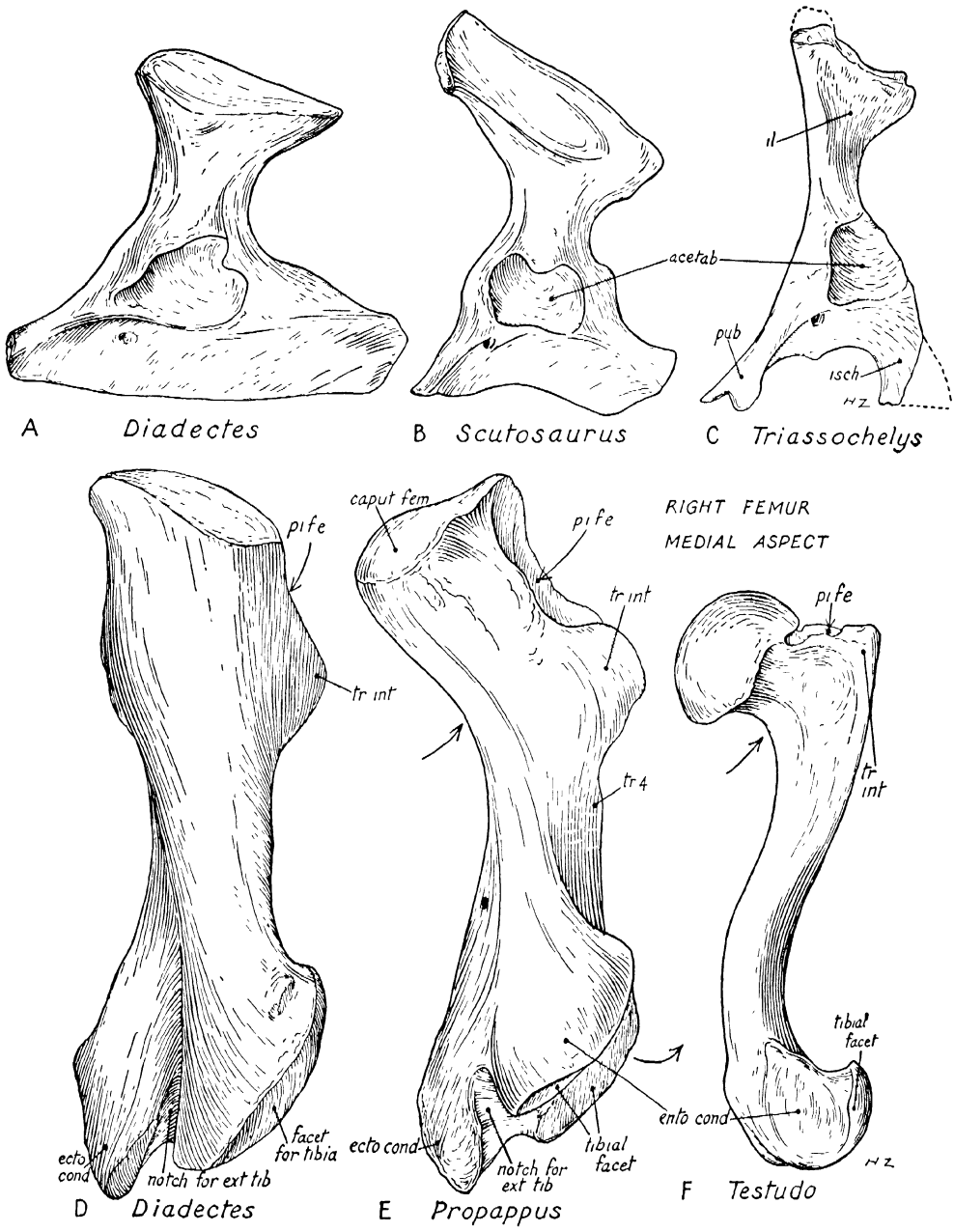


Fig. 12.24. Pelvis and femur of cotylosaur (A, D), pareiasaur (B, E), stem chelonian (C) and tortoise (F). A, B, from specimens; C, after Jaekel. The cotylosaur pelvis (A) is low in proportion to its length, the acetabulum faces outward and is extended anteroposteriorly and slightly forward, the surface for the ilio-caudalis faces laterally. The chelonian pelvis (C) is very high in proportion to its length, the acetabulum is extended dorsoventrally and faces backward and outward. The pareiasaurian pelvis (B) is in an early stage in the change from A to C. In the cotylosaur femur (D) the shaft is nearly straight, the head very narrow and the internal trochanter not very large; the "digital fossa" (*p.i.f.e.*) is on the ventral side. In the pareiasaur femur (E) the head has begun to expand, the internal trochanter is strongly developed and the upper part of the sigmoid curve is beginning (see arrow). In the femur of the tortoise (F) the shaft is strongly sigmoid, the head globular, the internal trochanter very large and the digital fossa (*p.i.f.e.*) has moved up to the proximal end.

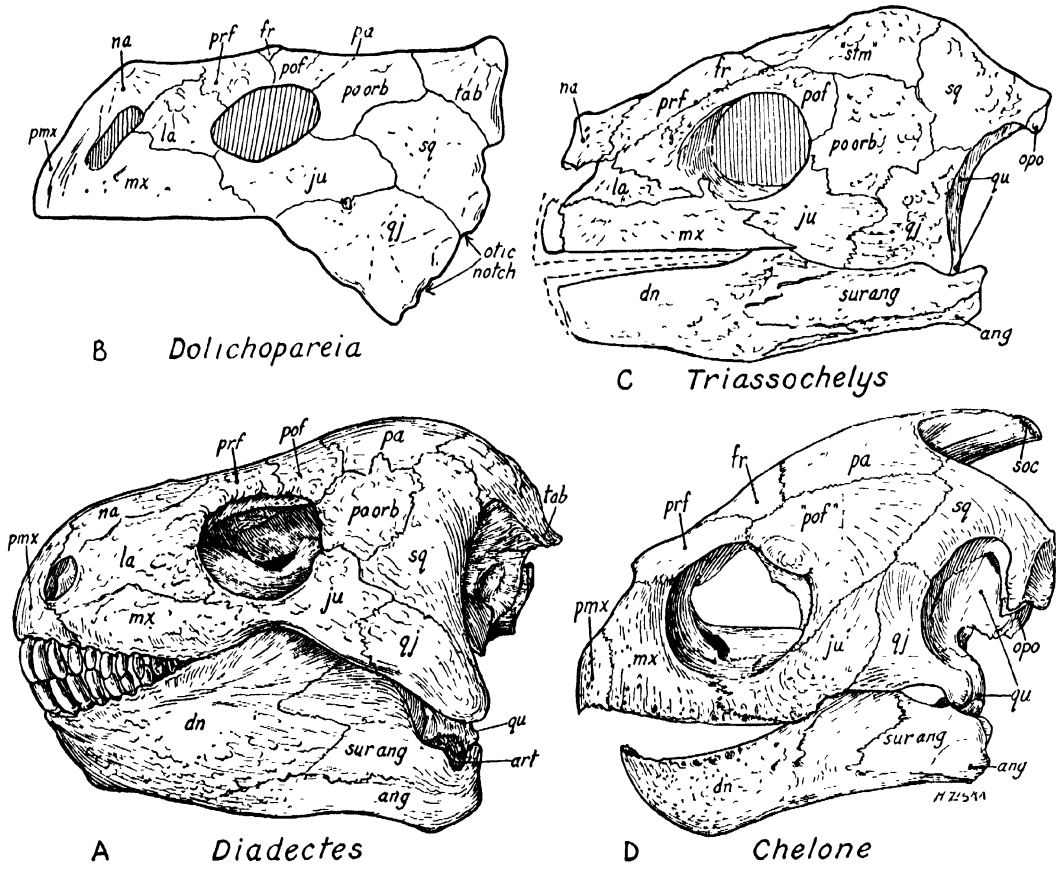


Fig. 12.25. Skulls of cotylosaur, pareiasaur and chelonian. Lateral aspects. A, D, original; B, after Boonstra; C, after Jaekel. The skull roof of the pareiasaur (B) was evidently covered with bony scutes like those of its carapace. These were probably faced with a tough or horny integument, as indicated by the channels for nutrient vessels. The same is true of the Triassic stem turtle (C). In the modern *Chelone* (D) the horny shields leave grooves on the bone. The skull pattern of the pareiasaur (B) seems ideally suited to have given rise to that of the stem chelonian (C) with the following possible exceptions: (1) that in the latter the tabular has *apparently* disappeared and has been replaced by the dorsally extended squamosal, and (2) that in *Triassochelys*, according to Jaekel, there is a large "supratemporal," which is not present (or not recorded) in the pareiasaurs. It is, however, questionable whether this alleged supratemporal (whose supposed suture may conceivably be due to the imprint of a surface plate) is at all homologous with the true supratemporal of labyrinthodonts. Its position suggests that it belongs to the parietal (cf. A). The side views suggest that in the pareiasaur the otic notch if present was slight and that its enlargement in chelonians (C, D) has effected a convergent resemblance to this region in *Diadectes* (A).

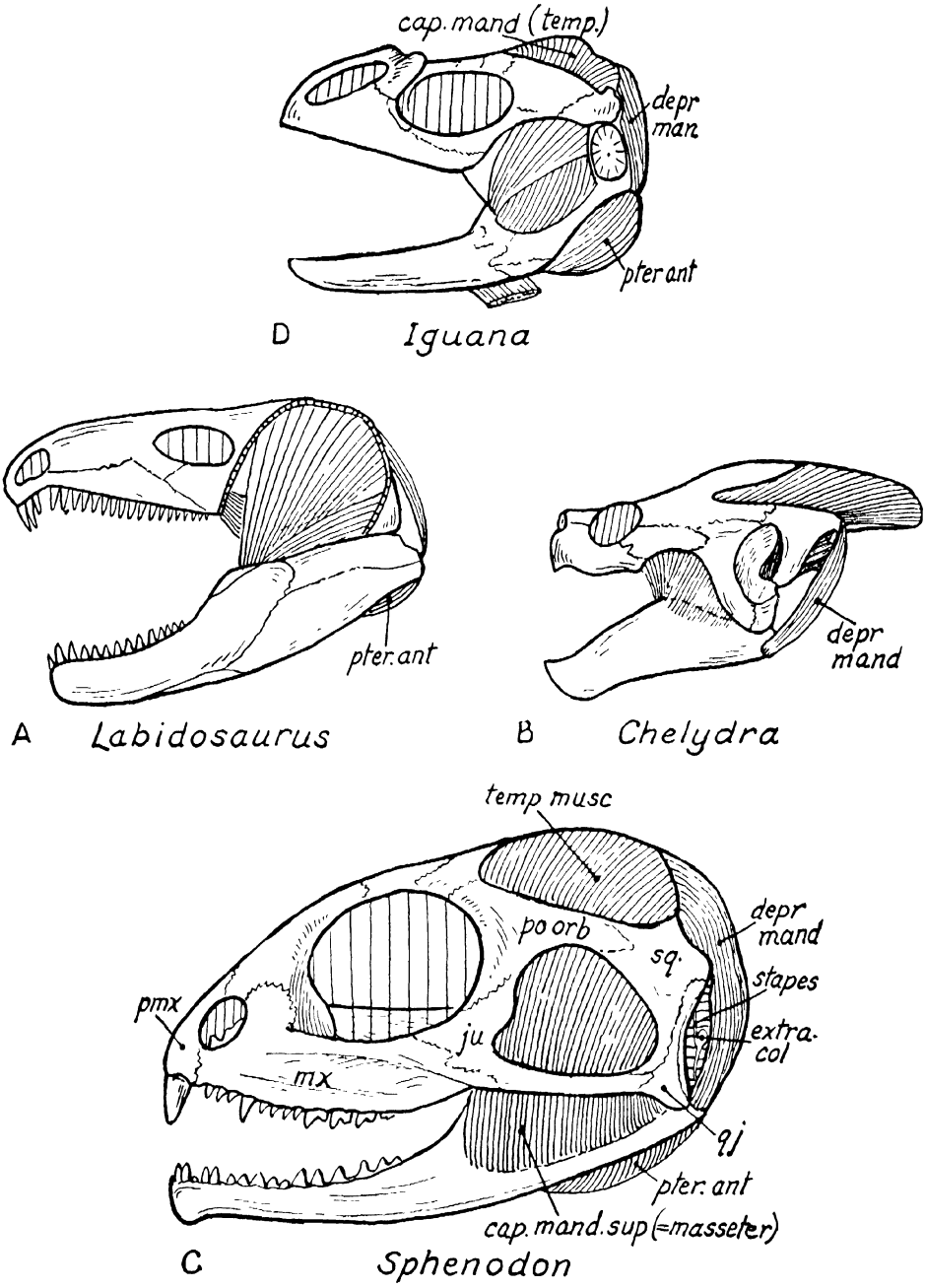


Fig. 12.26. Relations of the jaw muscles to the temporal region in anapsid (cotylosaur) (A), chelonian (B), rhynchocephalian (C) and lizard (D). Mainly after L. A. Adams. In A the temporal roof has been cut away to show the jaw muscles, which it completely covers. In B the jaw muscles (after entering the posttemporal fossae) have emarginated the temporal roof from behind forward. In C they have perforated both the top and the side of the temporal roof, leaving only the upper and lower temporal arches. C also shows the position of the otic notch and its associated stapes, extra-columella and cerato-hyoid, which lie between the depressor mandibulae muscle and the quadrate-squamosal bar.

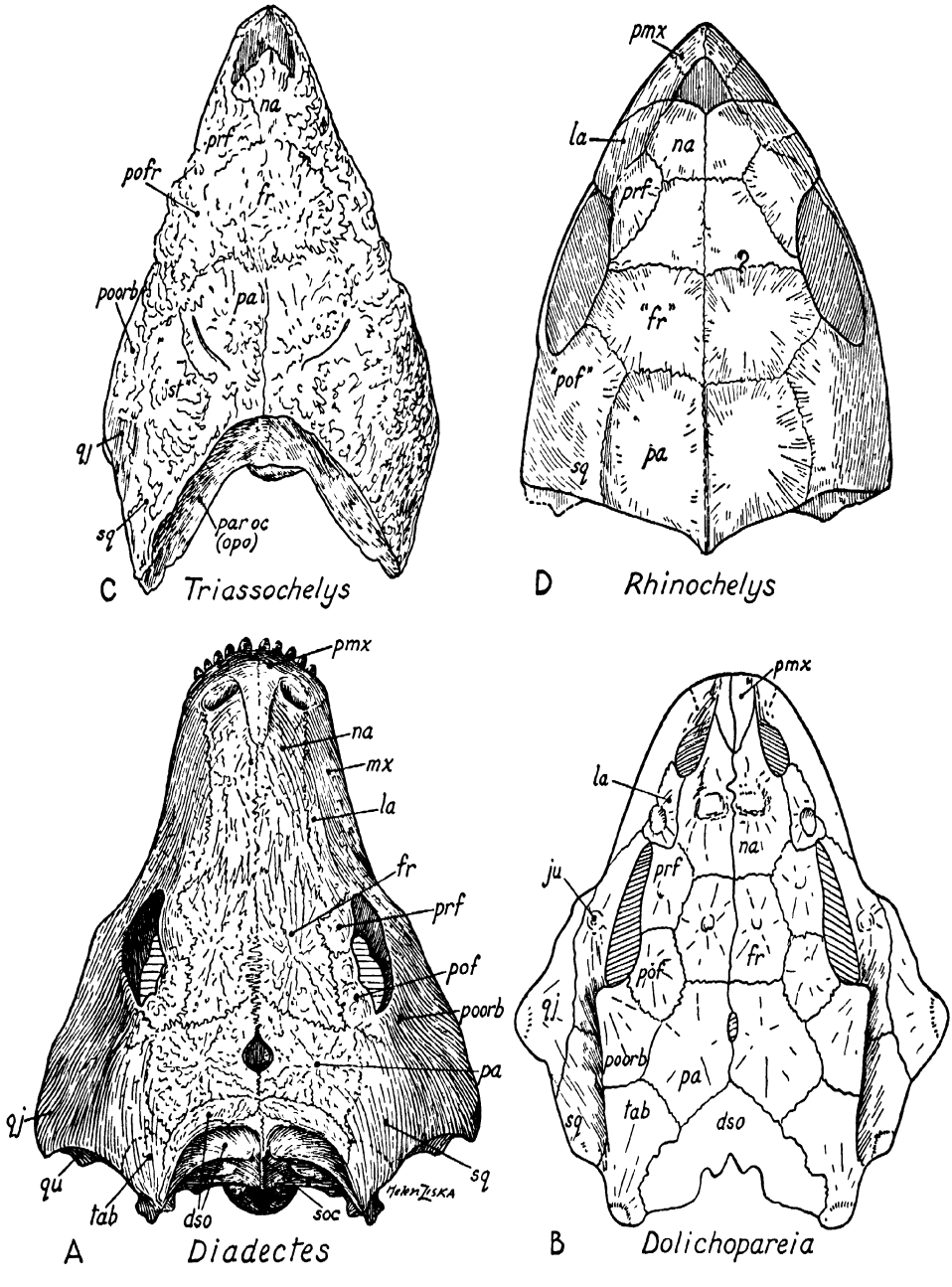


Fig. 12.27. Skulls of cotylosaur (A), pareiasaur (B) and primitive chelonians (C, D). Top view. A, after Gregory; B, after Broom; C after Jaekel; D, after Zittel. In the Jurassic amphichelydian (D) the general contour of the skull has become completely chelonian. Although the nasals are retained, the ascending processes of the premaxillae have disappeared.

→Fig. 12.28 (facing page). Palatal (A, B, C) and occipital (D, B1, C1) views of the skulls in pareiasaur (A, D), stem chelonian (B, B1) and modern chelonian (C, C1) The stem chelonian strongly recalls the pareiasaur, especially in the relations of its well-toothed pterygoid. The progressive expansion of the posttemporal fossae is well shown. A, D, after Boonstra; B, B1, after Jaekel; C, after Gregory.

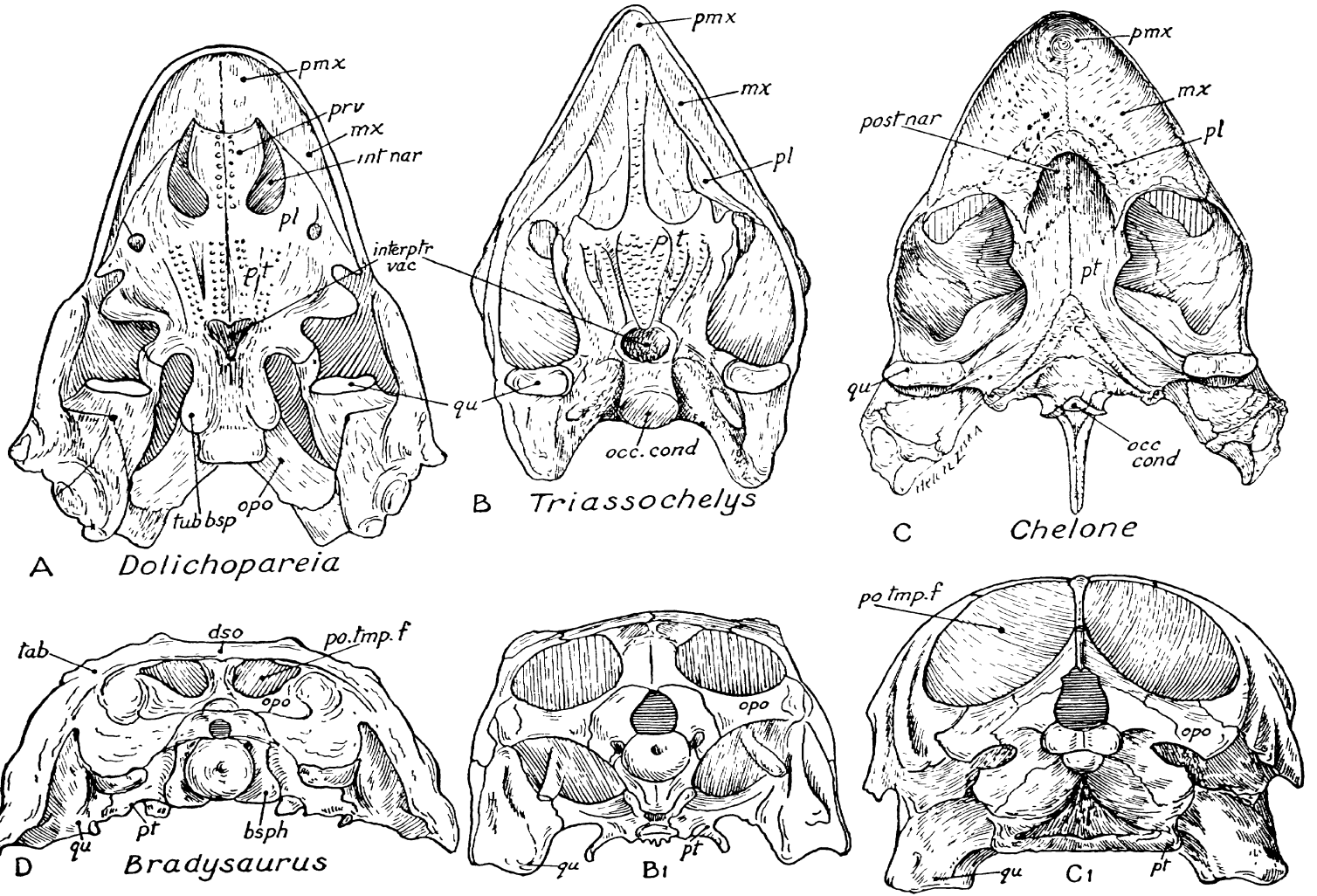

pmx
prv
mx
int nar
pl
pt
interptr vac
qu
tub bsp
opo
A Dolichopareia
pmx
mx
pl
pt
occ. cond
B Triassochelys
pmx
mx
post nar
pl
pt
qu
occ cond
C Chelone
tab
dso
po.tmp.f
opo
qu
pt
bsph
D Bradysaurus
opo
qu
pt
B1
po.tmp.f
opo
qu
pt
C1

Fig. 12.28

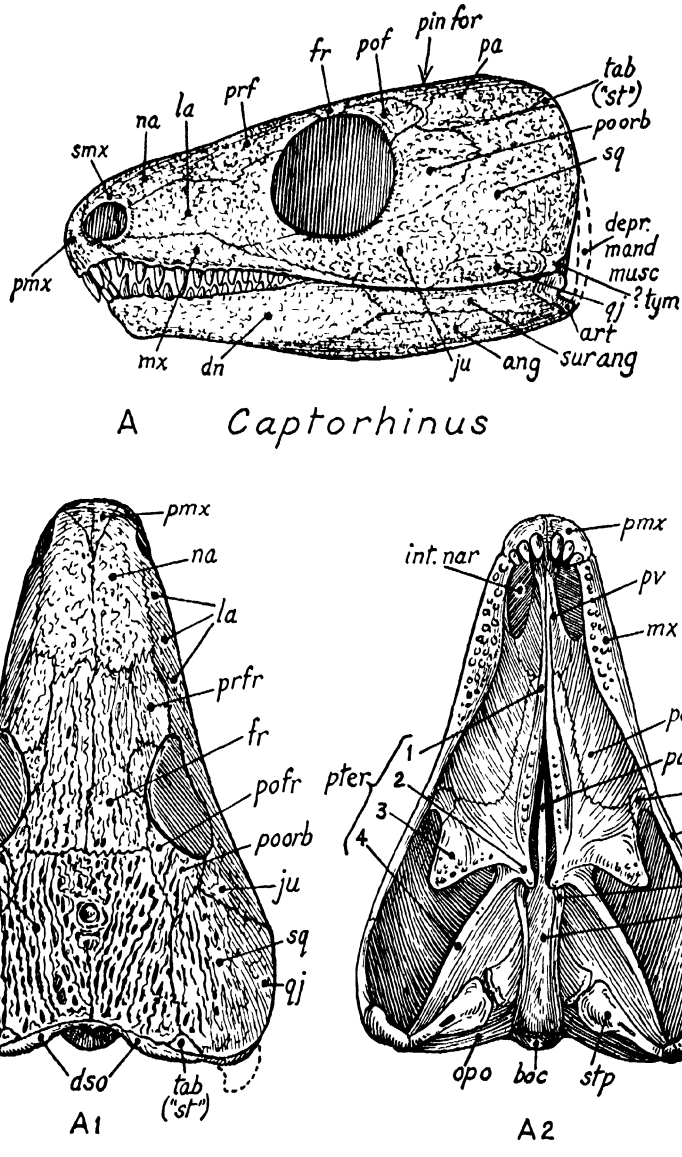


Fig. 12.29. Skull of *Captorhinus*, a primitive cotylosaur. Based on skulls in the American Museum of Natural History. Data for sutures from Case, Williston, Broom, von Huene, Sushkin, and especially Romer and Price.

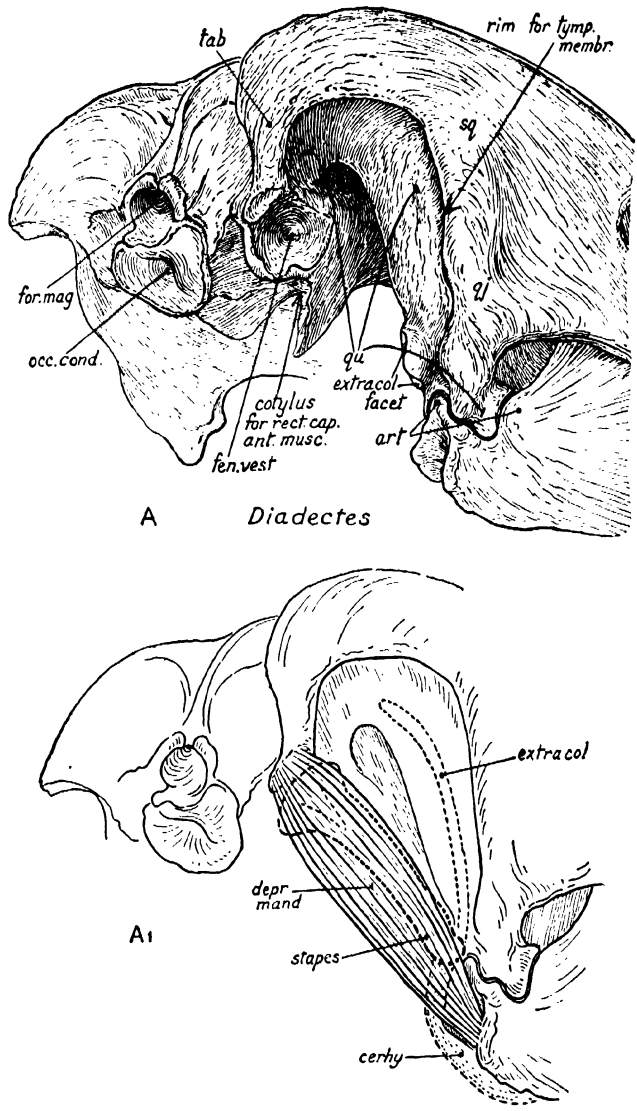


Fig. 12.30. A, Oblique occipito-lateral view of *Diadectes* skull, showing relations of fenestra vestibuli to expanded otic notch and neighboring parts. A1, Attempted restoration, showing probable position of depressor mandibulae muscle and relations of stapes to extracolumella and ceratohyal. The tympanic groove was ear-shaped, narrowing at the bottom.

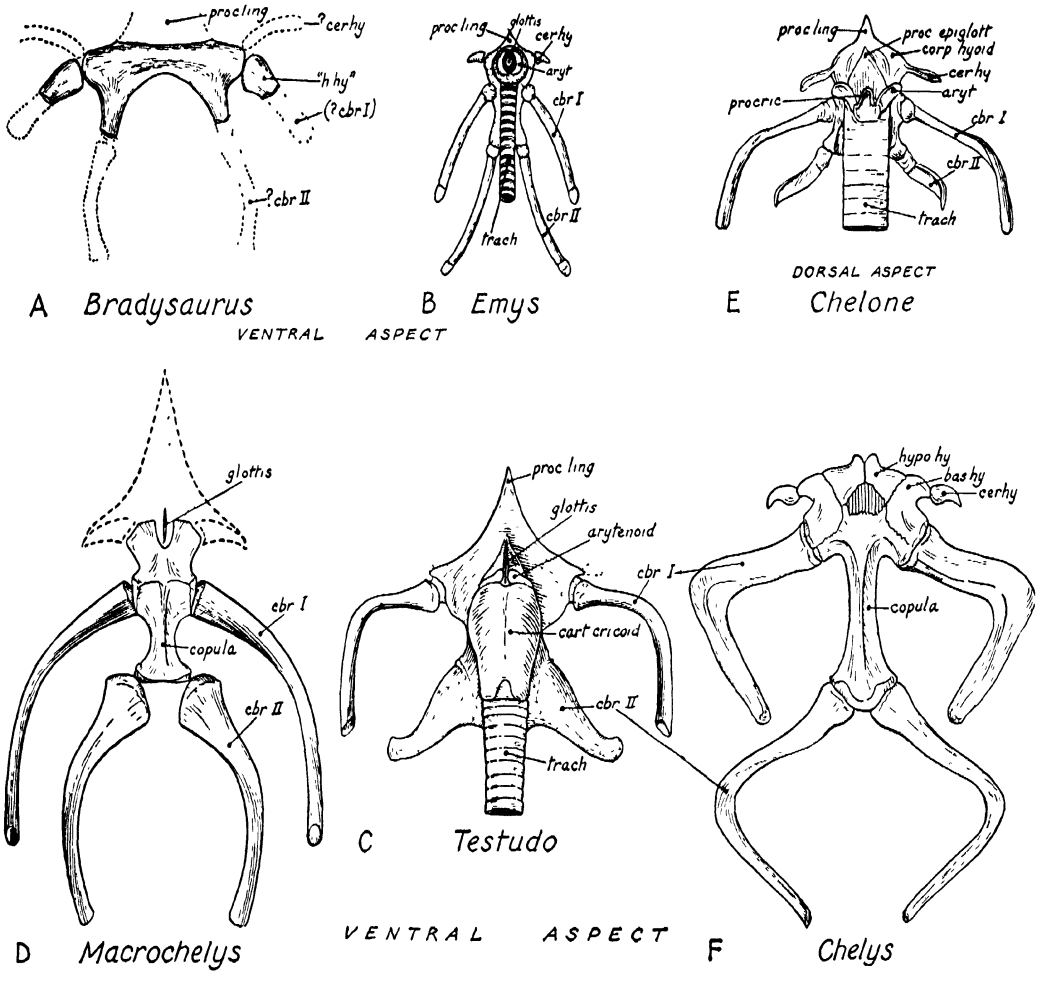


Fig. 12.31. Hyoid bones of pareiasaur (A) and recent chelonians (B–F). A, modified from Boonstra (1932); B, after Wiedersheim (1907); E, after Van Kampen. In the pareiasaur the wide median basal piece may represent both the basihyal and the copula of the chelonians, while the supposed hypohyal may be the first ceratobranchial. In the chelonians the copula has been markedly lengthened, the first and second ceratobranchials are large, the ceratohyal reduced or vestigial (F).

→Fig. 12.32 (facing page). A–C, Parasagittal sections of skulls of cotylosaur (A, A1), pareiasaur (B, B1) and modern chelonian (C). A, A1, C, after Gregory; B, after Boonstra; B1, after Watson. The cranial cavity in the typical cotylosaur and pareiasaur is relatively low and more or less tubular; in the chelonian the middle part of its roof has apparently been dragged upward under the influence of the enormously developed jaw muscles arising from the borders of the sagittal crest. In the latter the margins of the muscular base are stiffened, while the middle part is thinned down and almost translucent—a case of incipient fenestration. The epipterygoid in the typical cotylosaur (A) is strongly developed dorsally and seems to support the cranial roof. In the pareiasaur (B) the abortive dorsal process of the epipterygoid is far beneath the cranial roof. In *Chelone* (C) only the root of the dorsal process of the epipterygoid remains, the function of supporting the cranial roof having been taken over by a descending flange of the parietal. A low separate epipterygoid is present, however, in the snapping turtle (*Chelydra serpentina*).

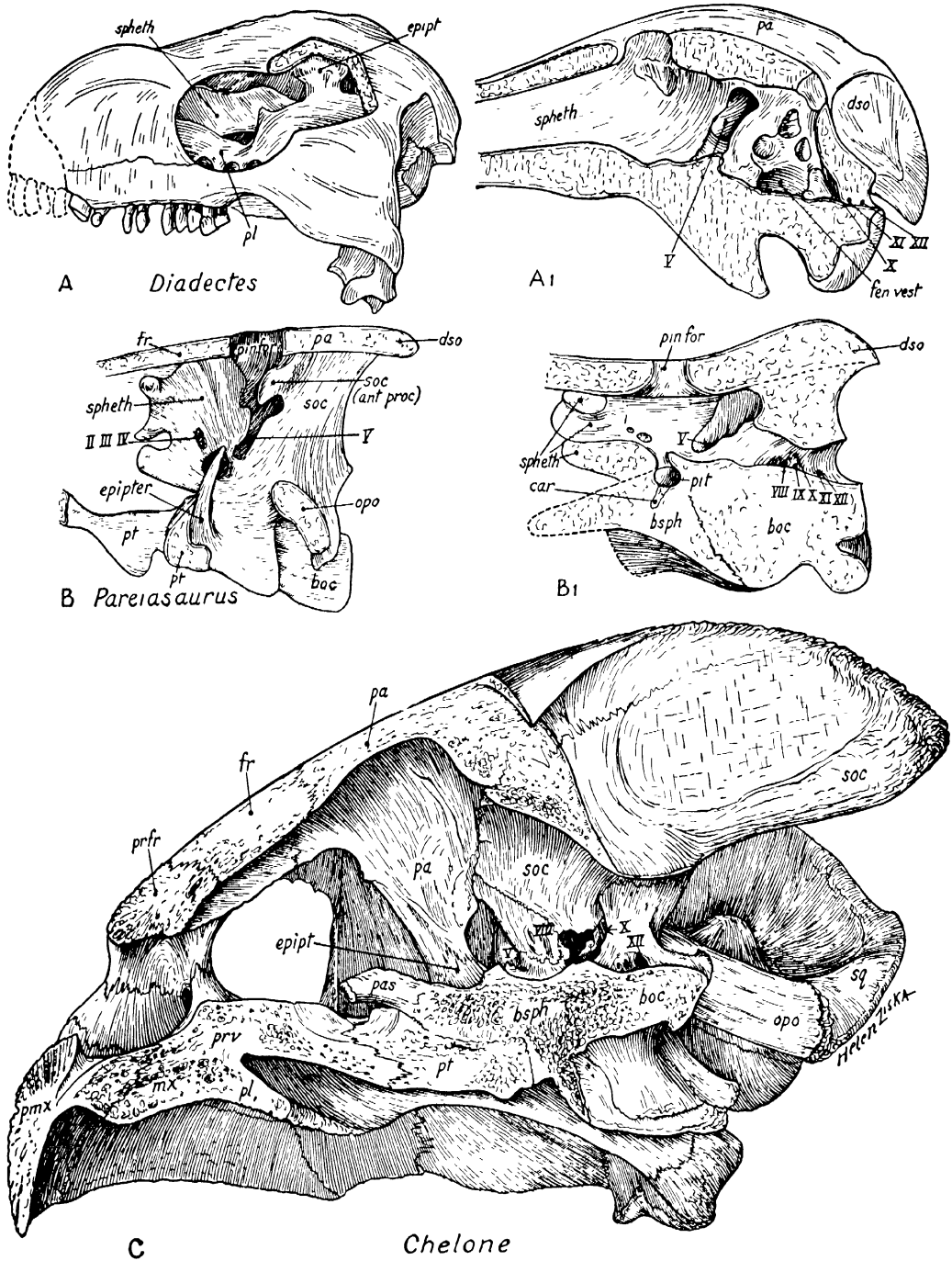

spheth
epipt
pl
A Diadectes
pa
spheth
dso
V
XI XII
X
fen vest
A1
fr
prfr
pa
dso
soc
(ant proc)
spheth
soc
II III IV
V
epipter
opo
pt
pt
boc
B Pareiasaurus
pinfor
dso
V
spheth
car
pit
VIII IX X XI XII
bsph
boc
B1
pa
fr
soc
prfr
pa
soc
epipt
VIII
X
XII
pas
bsph
boc
sq
opo
prv
pt
mx
pl
pmx
C Chelone

Fig. 12.32

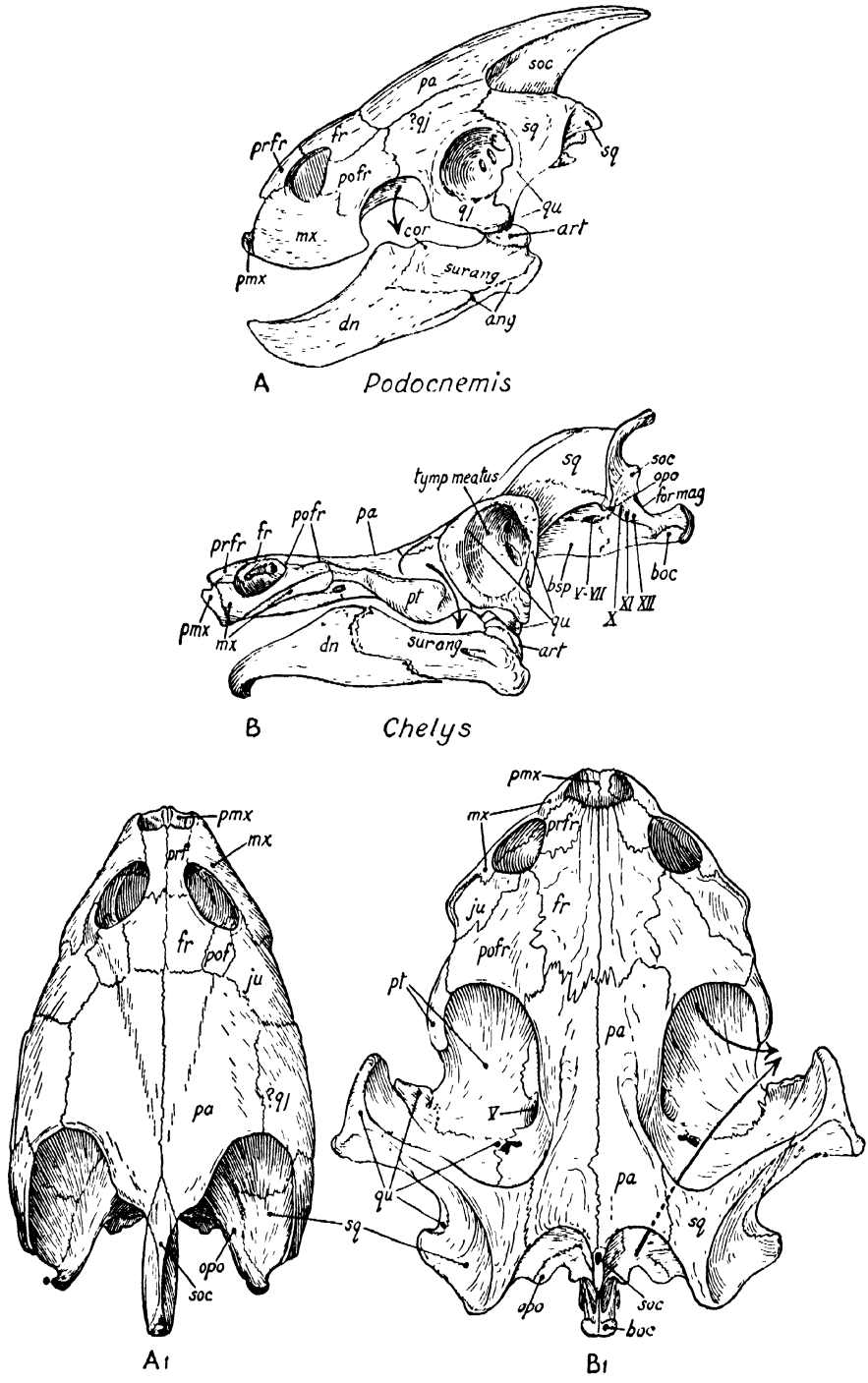


Fig. 12.33. Skulls of Upper Cretaceous (A, A1) and Recent (B, B1) pleurodires. The Upper Cretaceous stage (A, A1) far surpasses the primitive *Triassochelys* (fig. 12.34 G) in (a) the dominance of the supraoccipital, (b) the complete encirclement of the tympanum, and (c) the appearance of a lateral sinus for the adductor mandibulae muscles (cf. arrows). In the modern matamata (B, B1) features (b) and (c) are emphasized in extreme degree but (a) is secondarily reduced. A, A1, after Hay; B, B1, original.

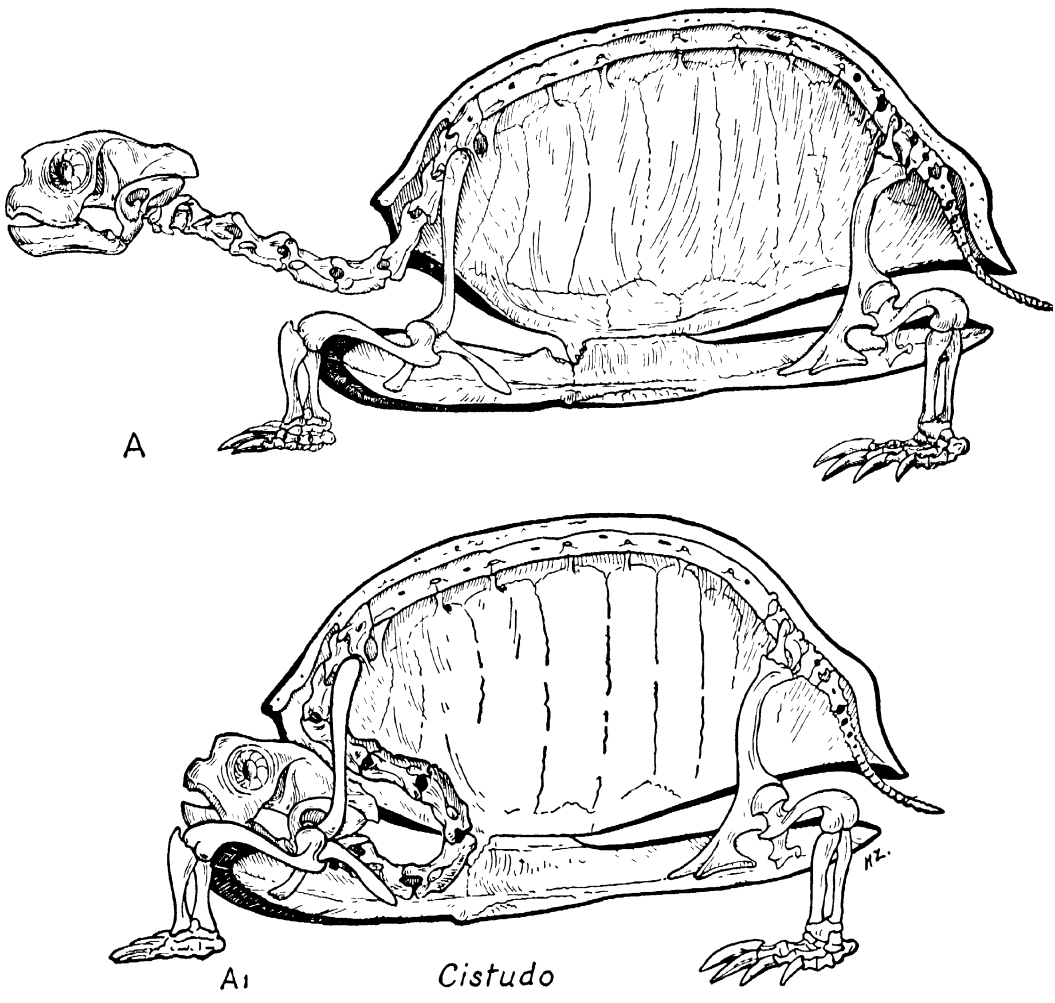
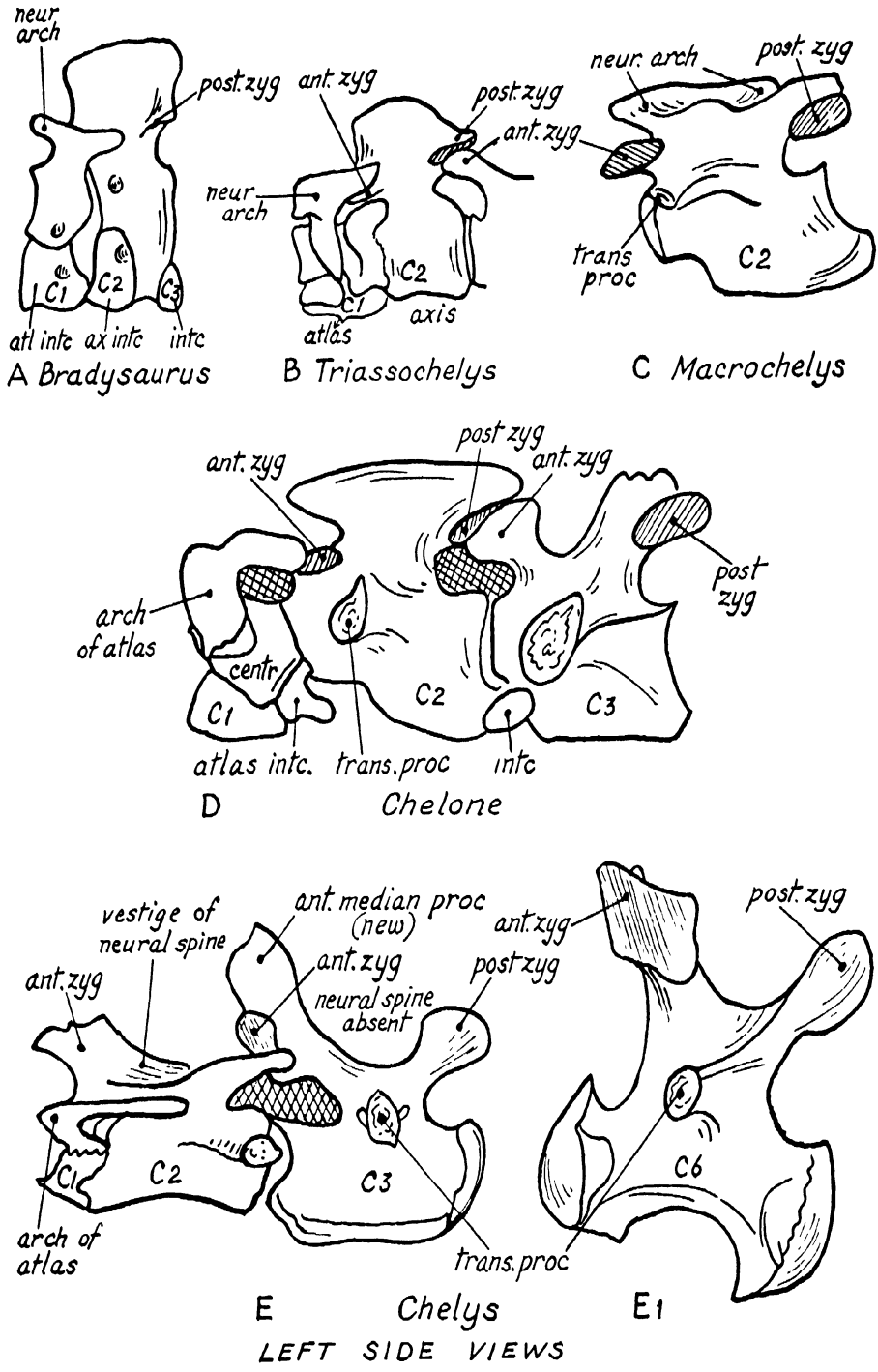
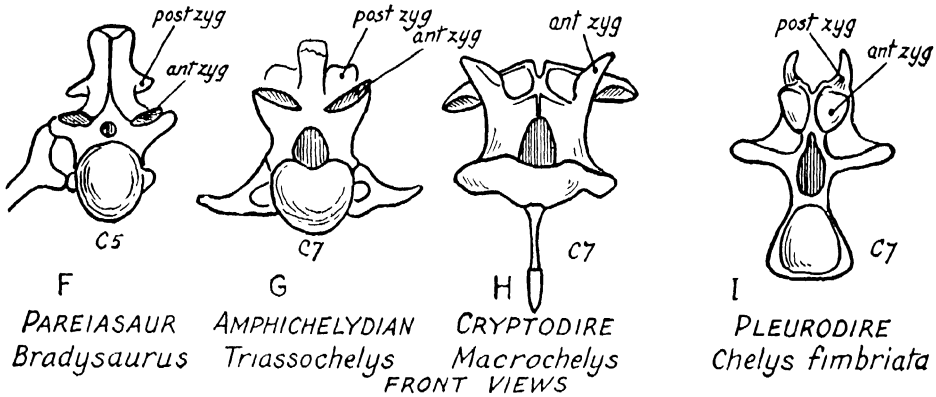
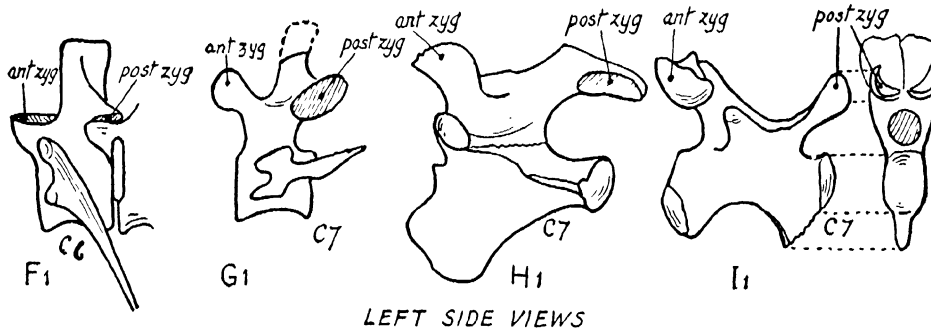


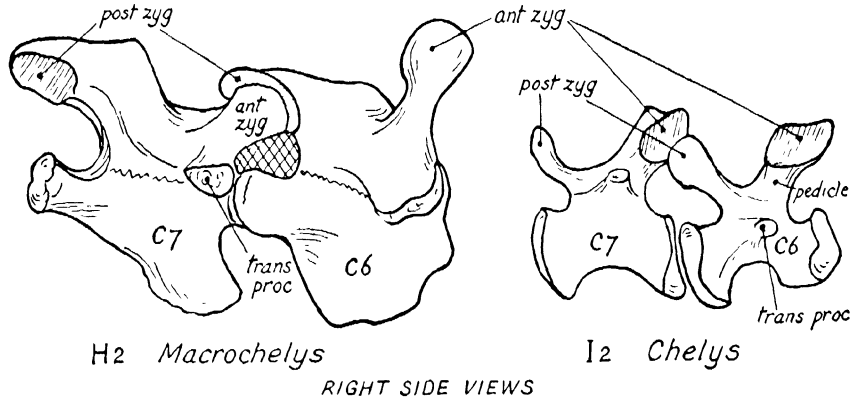
Fig. 12 34. Turtle (A) with neck extended; A1, the same with neck retracted and concealed within the shell (whence *Crypto-dira*, concealed neck).



Figs. 12.35, 36. Cervical vertebrae of pareiasaur (A, F), amphichelydian (B, G, G1), cryptodires (C, D, H–H3), and pleurodire (E, E1, I–13). To show pareiasaurian heritage in the amphichelydian and contrasting characters of articular facets of pre- and postzygapophyses in cryptodire and pleurodire. A, F, F1, after Boonstra; B, G, G1, after Jaekel; others original.


post zyg
ant zyg
C5
C7
ant zyg
C7
post zyg
ant zyg
C7
F
G
H
I
PAREIASAUR
Bradysaurus
AMPHICHELYDIAN
Triassochelys
CRYPTODIRE
Macrochelys
PLEURODIRE
Chelys fimbriata
FRONT VIEWS


ant zyg
post zyg
C6
C7
C7
C7
F1
G1
H1
I1
LEFT SIDE VIEWS


post zyg
ant zyg
C7
trans proc
C6
ant zyg
post zyg
pedicle
C7
C6
trans proc
H2 Macrochelys
I2 Chelys
RIGHT SIDE VIEWS

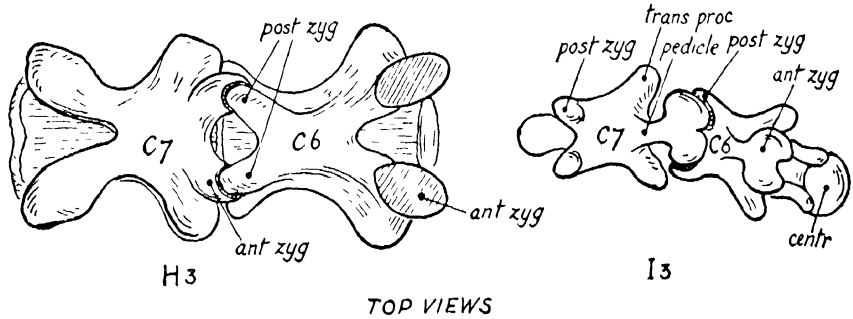

post zyg
C7
C6
ant zyg
ant zyg
trans proc
post zyg
pedicle
post zyg
ant zyg
C7
C6
centr
H3
I3
TOP VIEWS

Fig. 12.36

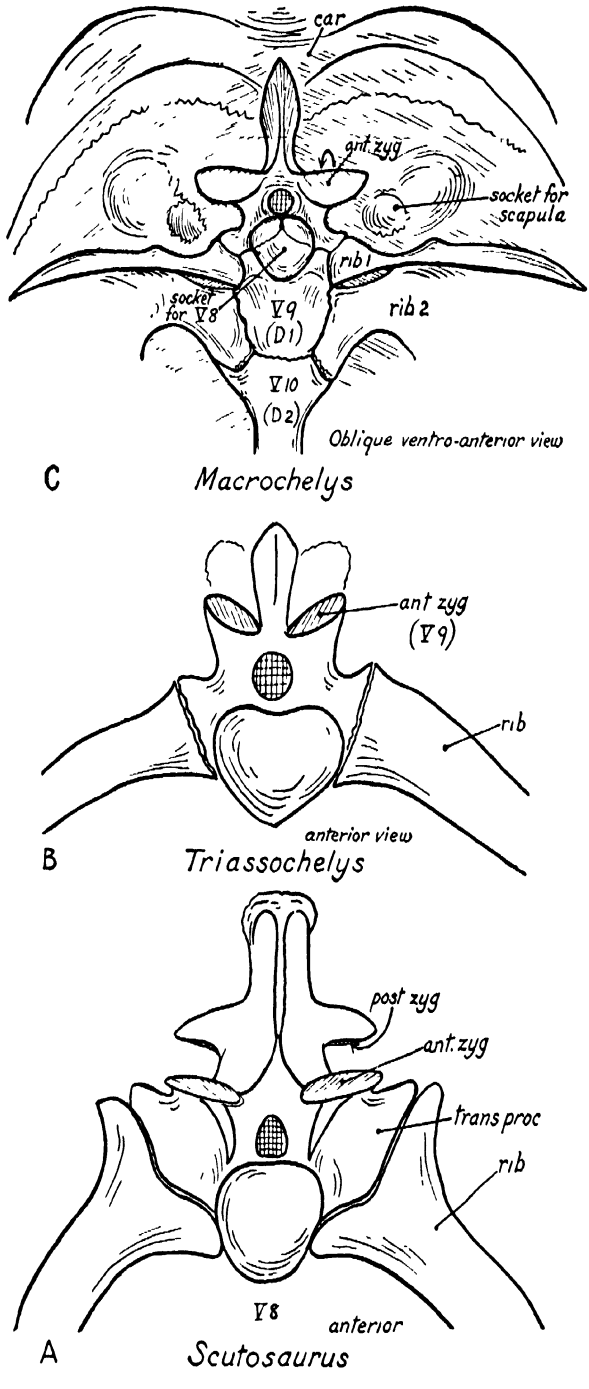


Fig. 12.37. Vertebral fulcrum for the neck. In the pareiasaur (A) the anterior dorsal and posterior cervical vertebrae differ but little from each other and are quite primitive. *Triassochelys* (B) was still primitive. In *Macrochelys* (C) the enlarged zygapophyses of the ninth vertebra form a transversely wide rolling surface for the raising and lowering of the neck, while the large centrum distributes the impact to the next vertebra, to the buttress-like ribs and to the carapace. A, after Boonstra; B, after Jaekel; C, after Gregory.

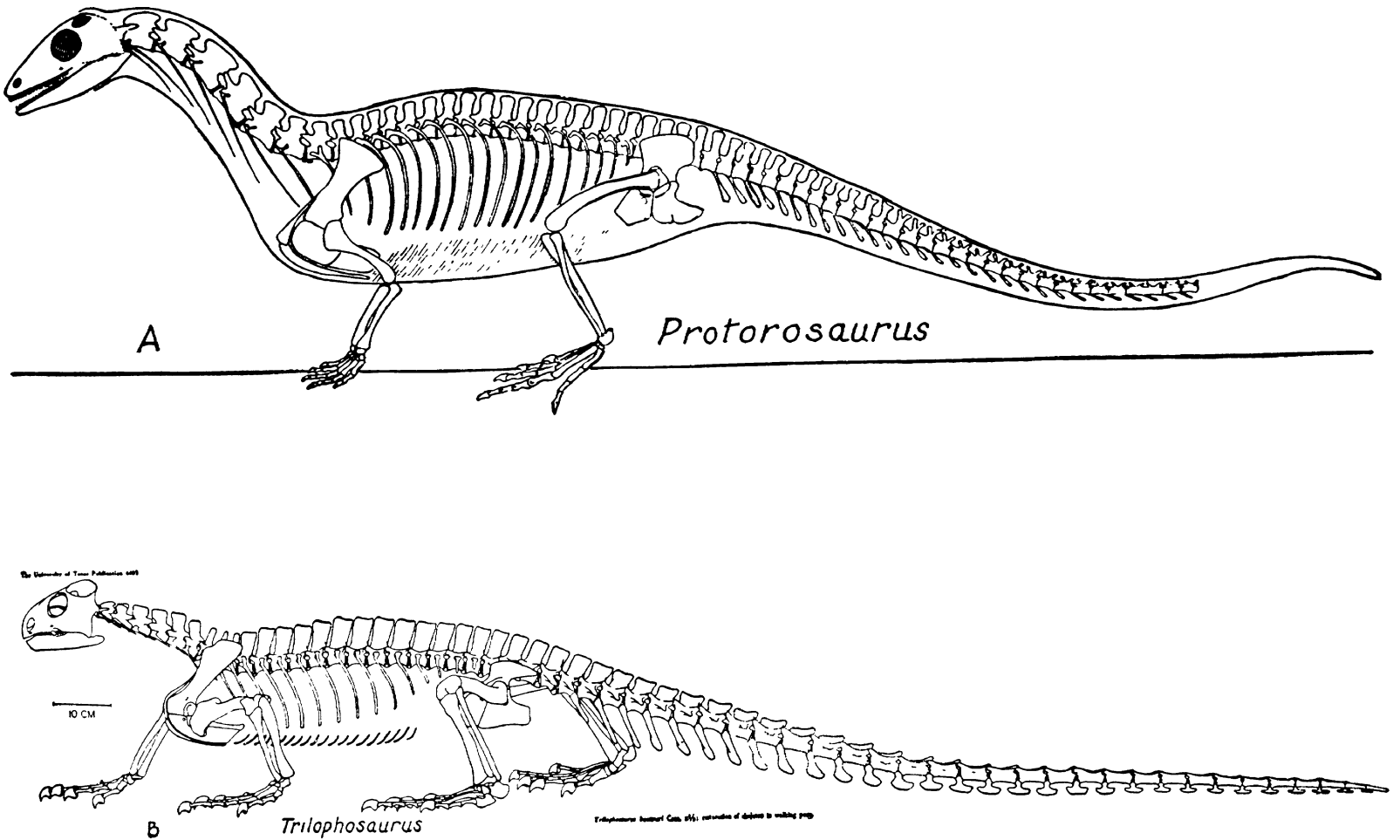


Fig. 12.38a, b. Protorosaurs: A, from the Upper Permian of Europe, after von Huene; B, from the Upper Triassic of Texas, after J. T. Gregory.

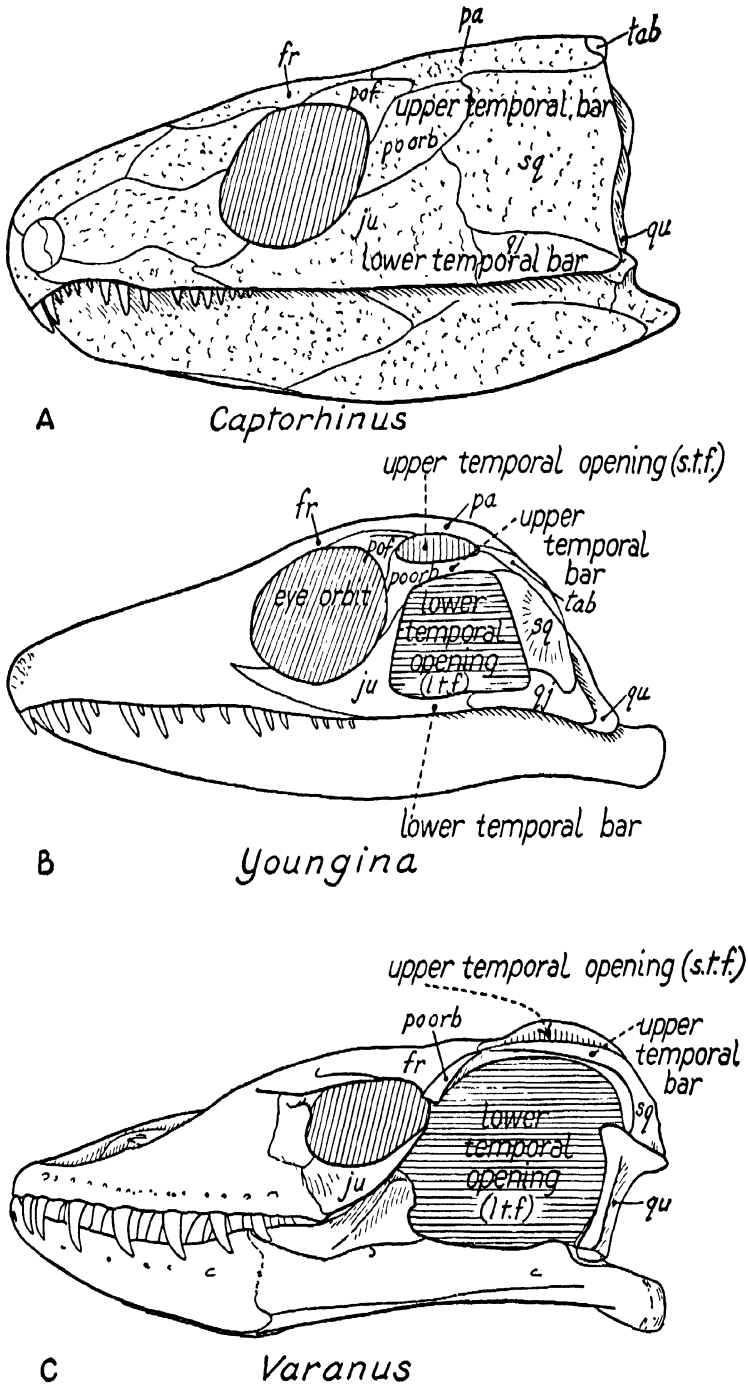


Fig. 12.39. Skulls of: typical anapsid (A), with neither upper nor lower temporal openings; primitive diapsid (eosuchian) with both openings and two bars or arches (B); typical lizard (C), which has lost the lower bar, leaving the upper temporal bar and opening and a lateral embayment (*l.t.f*). *S.t.f*, superior temporal fenestra; *l.t.f*, lateral temporal fenestra. After Gregory.

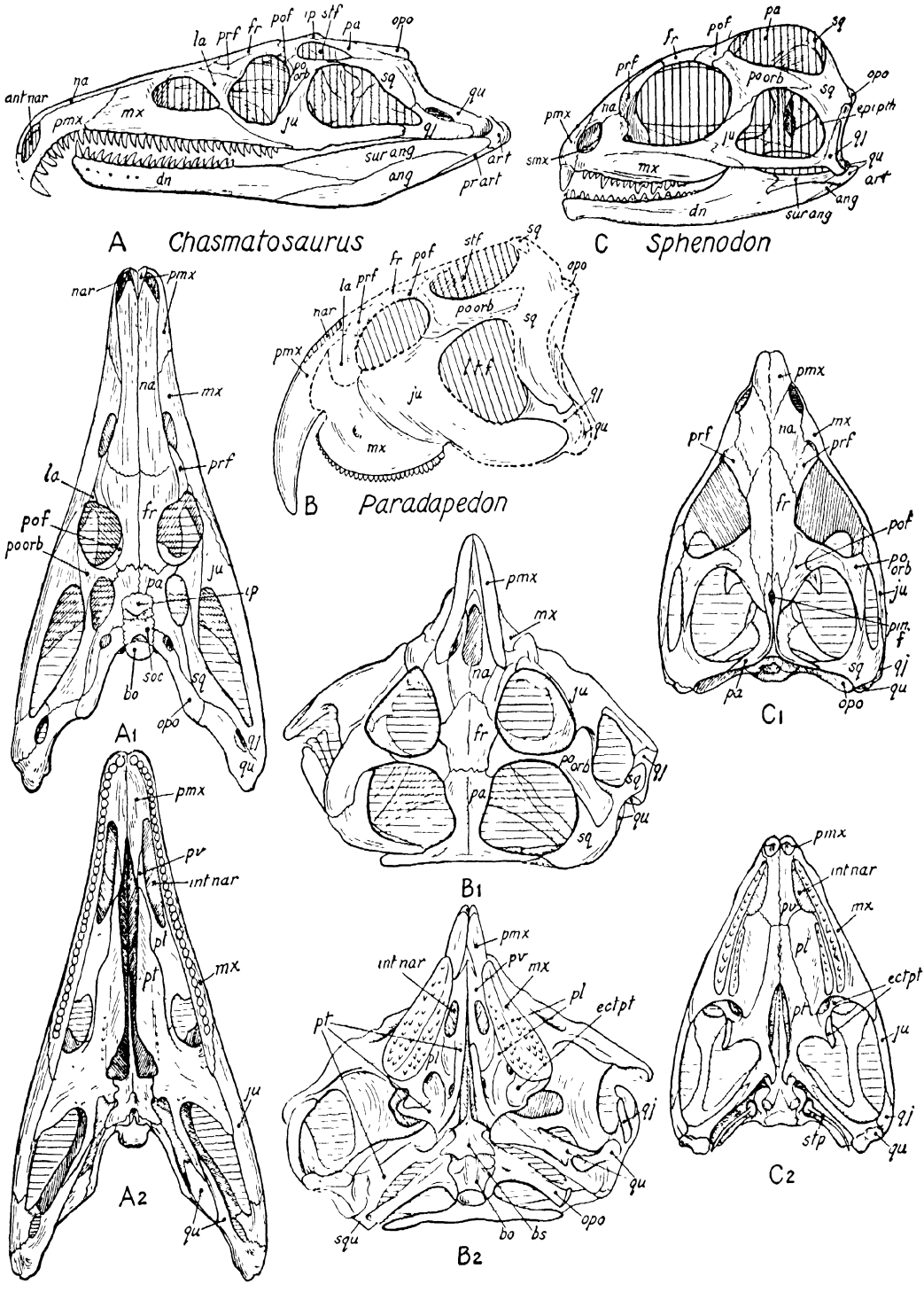


Fig. 12.40. Skulls of Triassic South African erythrosuchian (A), (pseudosuchian), Triassic South American rhynchosaur (B), and New Zealand tuatara (C). A–A2, after Broili and Schröder; B–B2, after von Huene; C–C2, original.

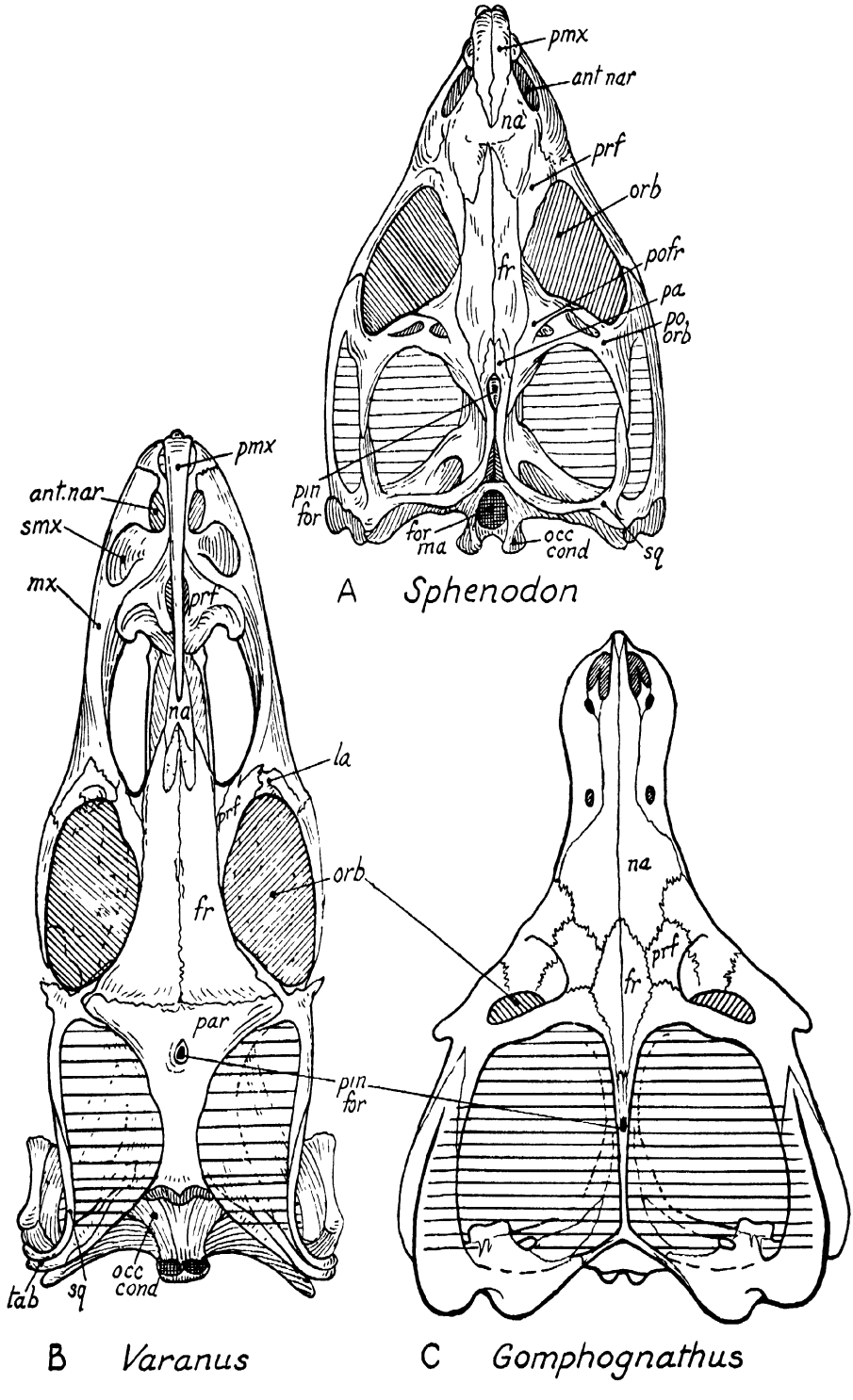
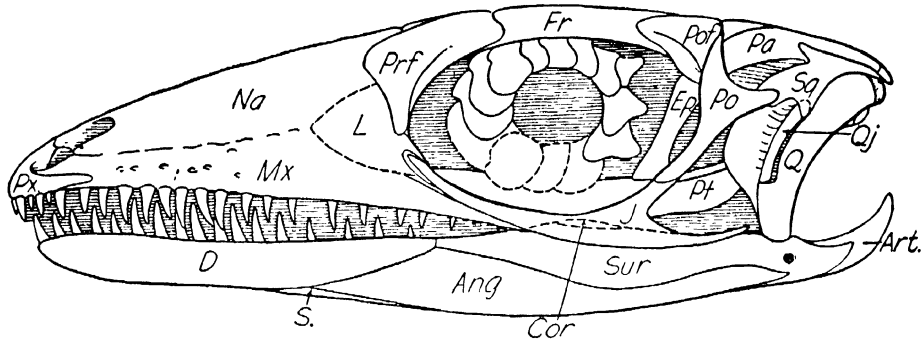
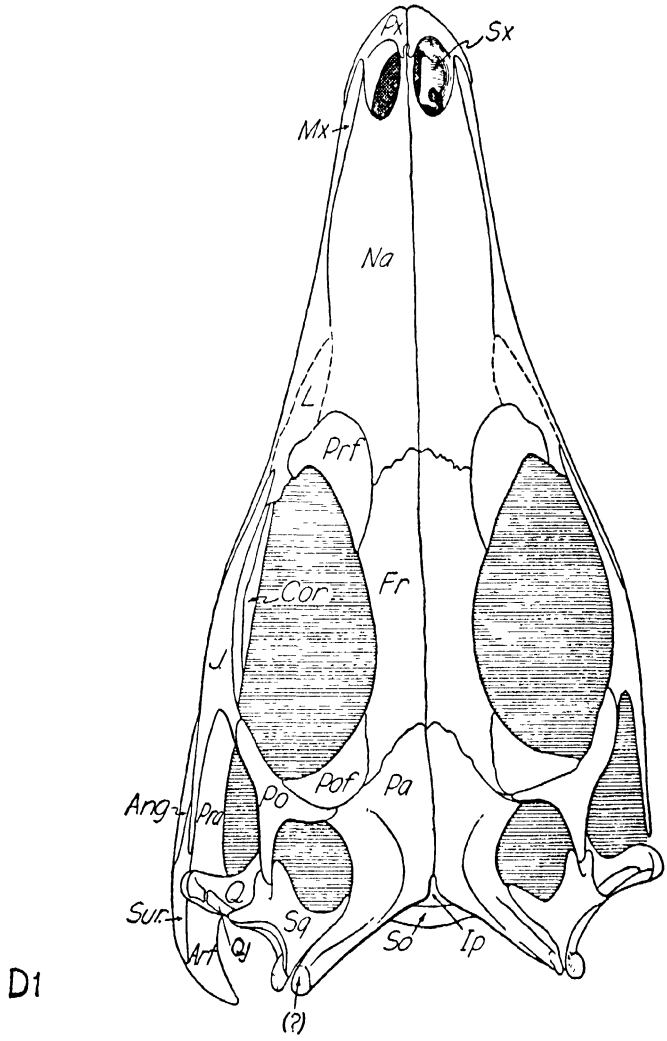


Fig. 12.41a. Skulls of rhynchocephalian (A), lizard (B) and cynodont (C), retaining the pineal foramen. Skull of South African Triassic lizard, after Camp. *Sx*, septomaxilla.



D Prolacerta



D1

Fig. 12.41b. Dorsal view of skull of *Prolacerta broomi*, x2. Reconstructed Septomaxillary (*Sx*) omitted from the left naris. After Camp.

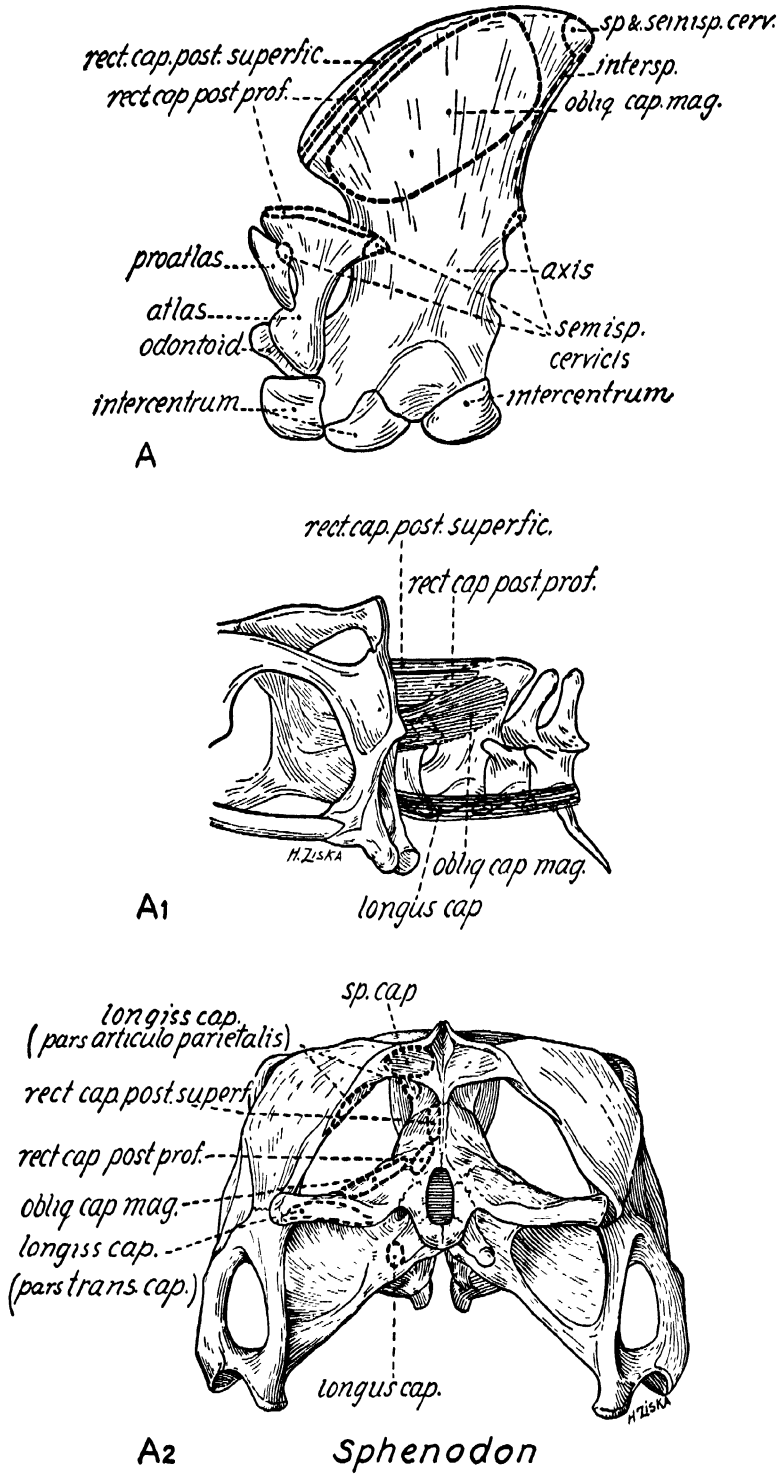


Fig. 12.42. The atlas-axis and its muscles in relation to neck and skull. After Gaynor Evans.

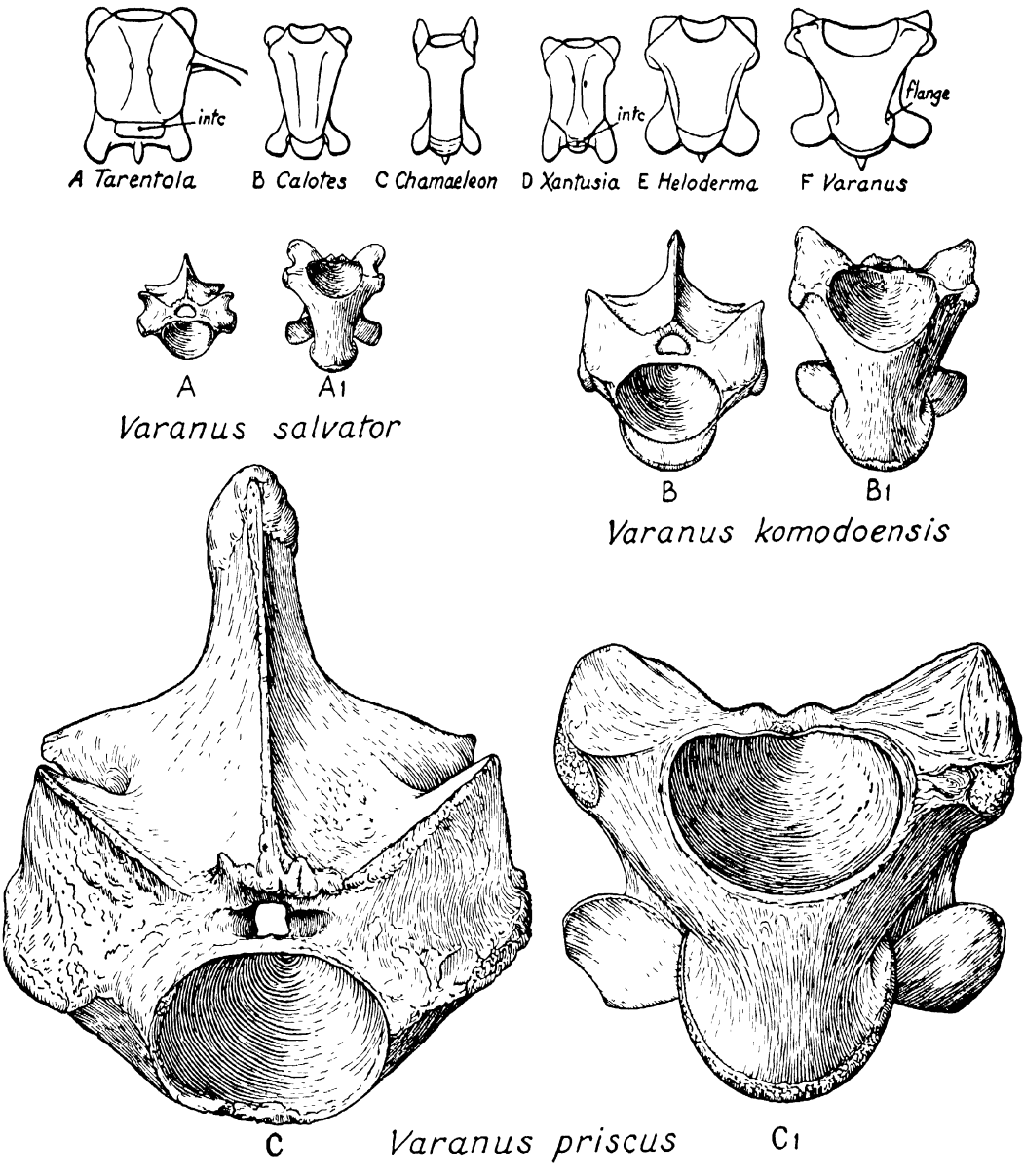


Fig. 12.43 (top). Dorsal centra (ventral view) of lizards. After Camp. Anterior end faces upward. A, Primitive gekko, with squarish centrum, separate intercentrum, small condylar ball. B, Iguanid, centrum elongate, widening anteriorly; intercentrum lost, ball enlarged. C, Chameleon, centrum elongate. D, *Xantusia* (scincomorph), primitive. E, *Heloderma* (Diploglossa), normal procoelous. F, Monitor (Platynota), centra very wide anteriorly, condyles very large, with flanges, cup facing ventrally.

Fig. 12.44. Dorsal vertebrae of ordinary monitor (A, A1), Komodo "dragon" lizard (B, B1) and Pleistocene Australian giant lizard (C). A11 × ½. After Gregory.

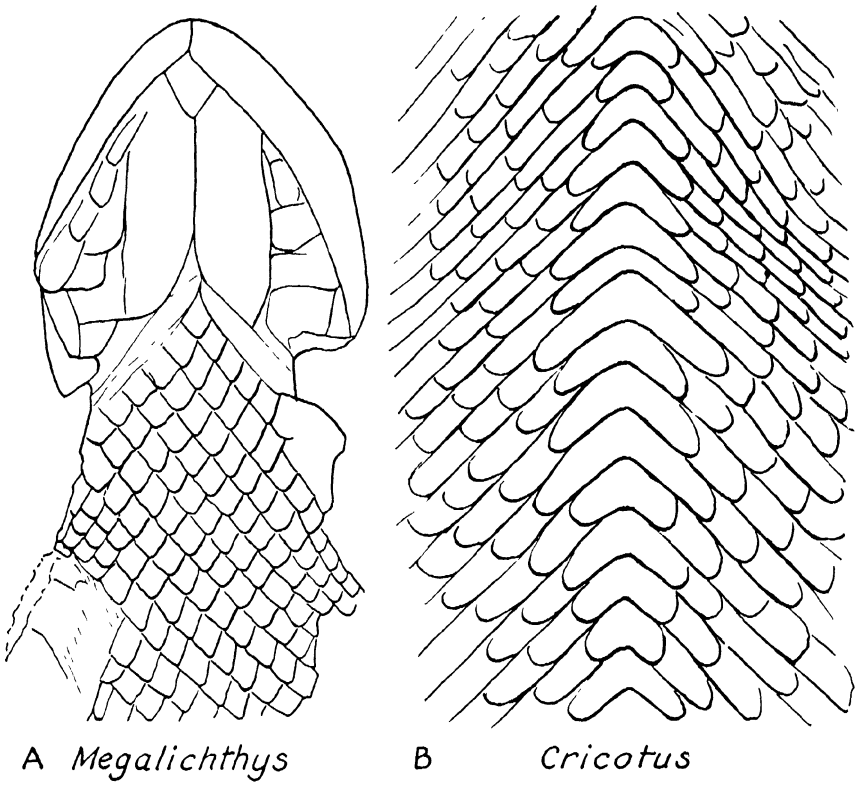


Fig. 12.45. Ventral surface of Permian lobe-fin fish (A), amphibian (B) and microsaur (C). The chevron-like gastralia of the amphibians have presumably been derived from the convergent rows of scales in the lobe-fin. A, B, after Cope and Matthew; C, after Moodie.

→Fig. 12.46 (facing page). Ventral surface of chest in primitive tetrapod (A) and tuatara (B). After Miner. Relatively primitive (C) and degenerate (D) shoulder girdles of lizards. After Camp. The relatively primitive stage with unreduced limbs has advanced beyond the truly primitive reptilian stage (fig. 12.8) in the fenestration of the clavicular and coracoid plates. The degenerate stage (D), with the loss of the pectoral limbs retains only vestiges of the shoulder girdle.

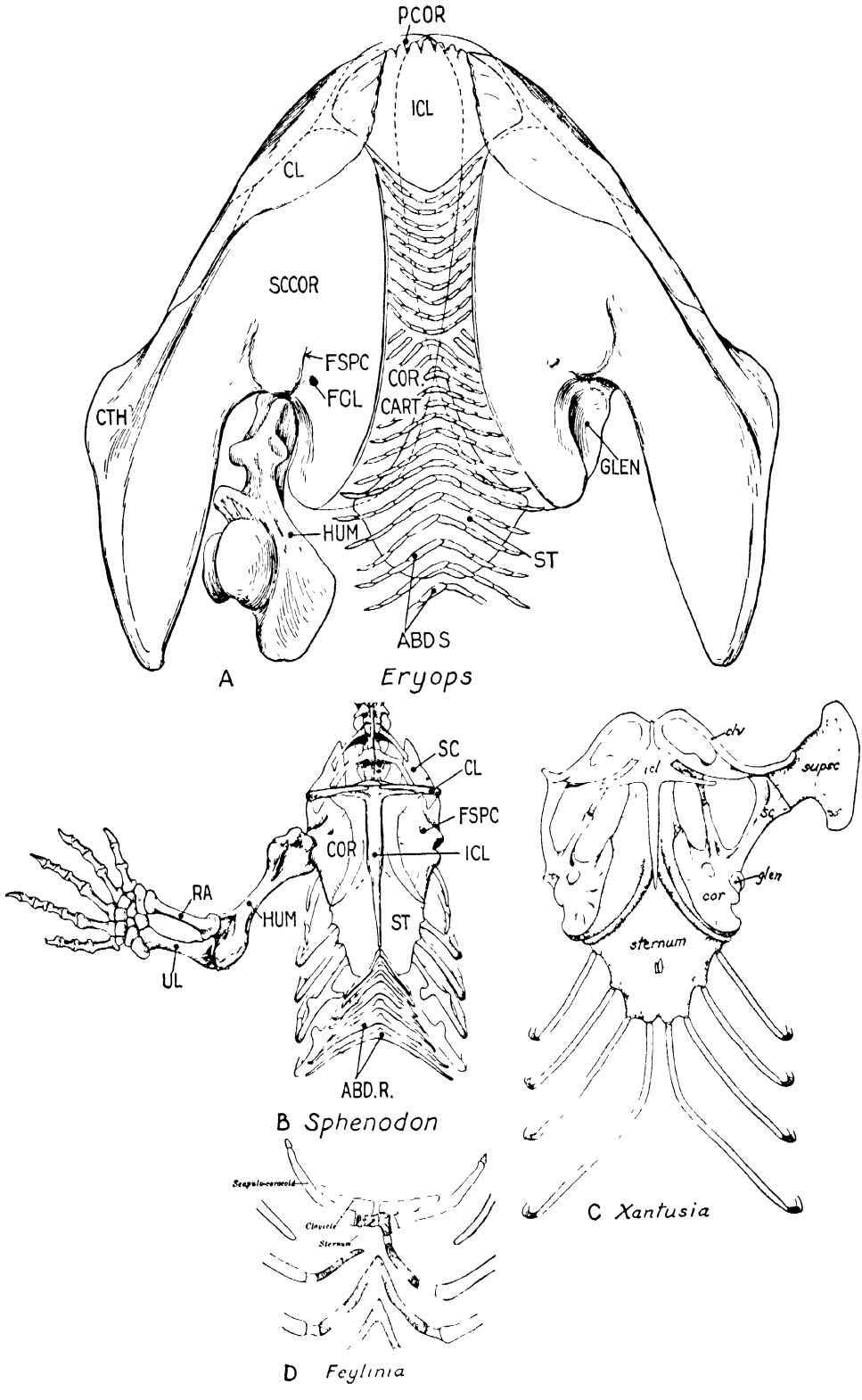

PCOR
ICL
CL
SCCOR
FSPC
FGL
COR.
CART
CTH
GLEN
HUM
ST
ABDS
A Eryops
SC
CL
FSPC
COR
ICL
RA
HUM
ST
UL
ABD.R.
B Sphenodon
clv
supsc
icl
sc
glen
cor
sternum
C Xantusia
Scapulo-coracoid
Clavicle
Sternum
D Feylinia

Fig. 12.46

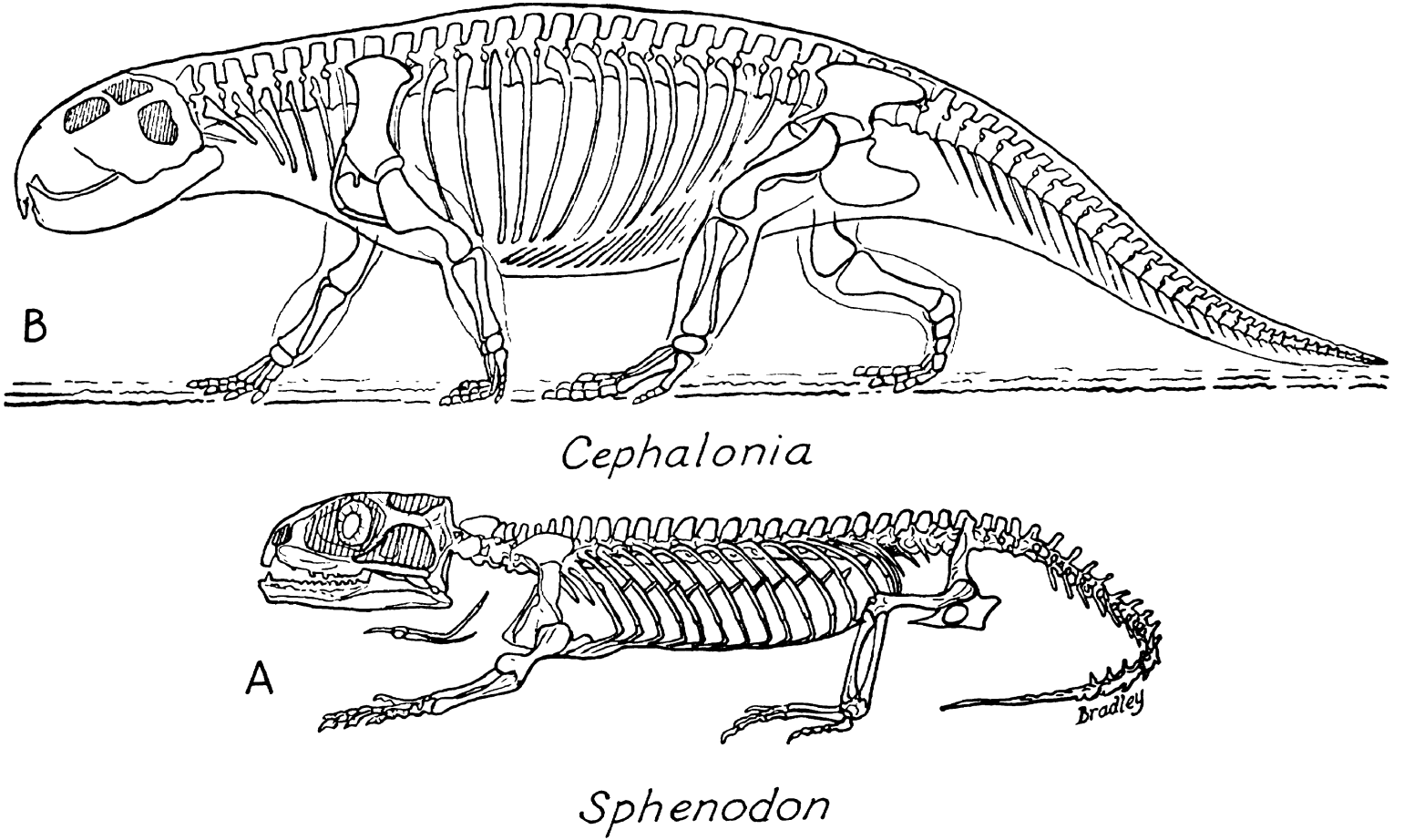


Fig. 12.47. Skeletons of New Zealand tuatara (A) and South American Triassic rhynchosaur (B). A, from Parker and Haswell, after Headley; B, after von Huene.

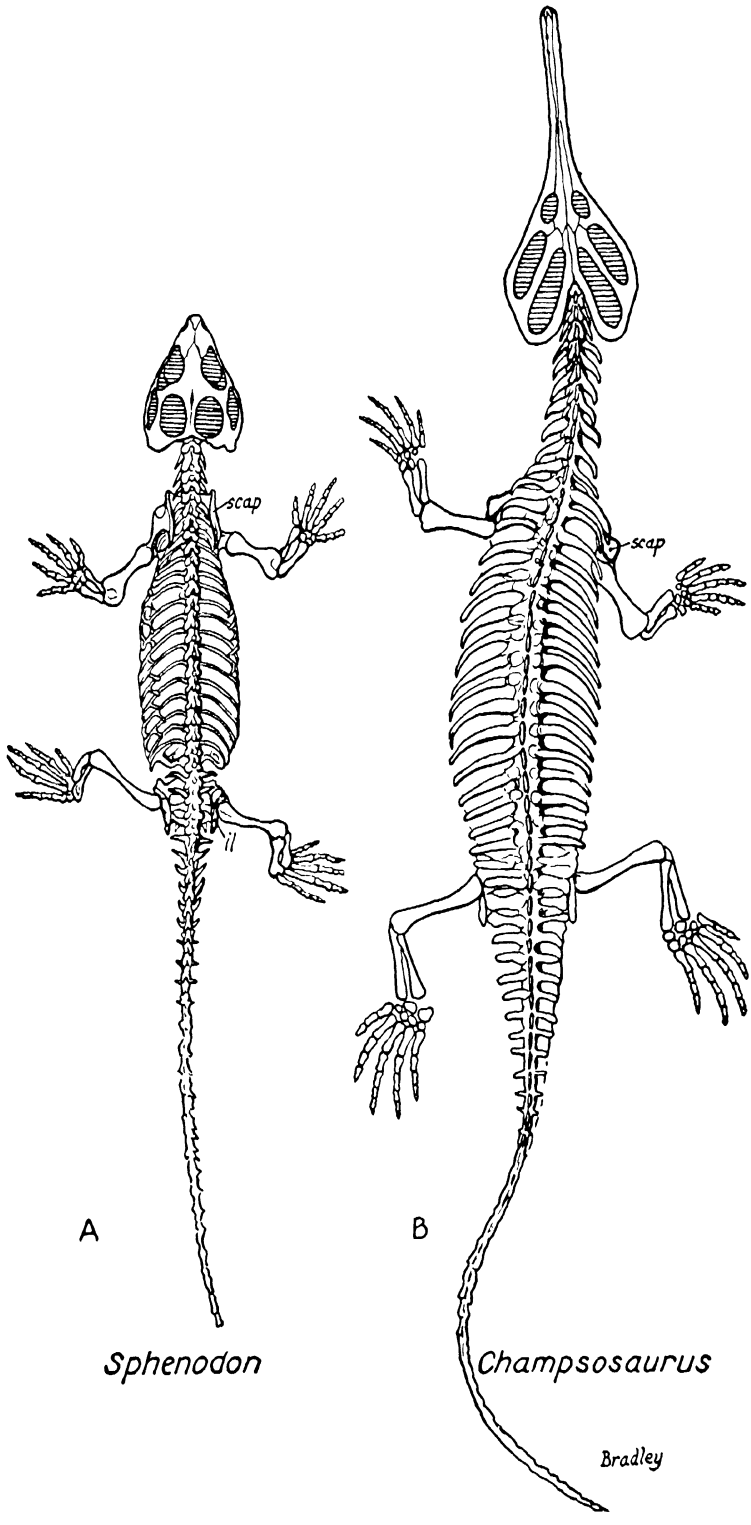
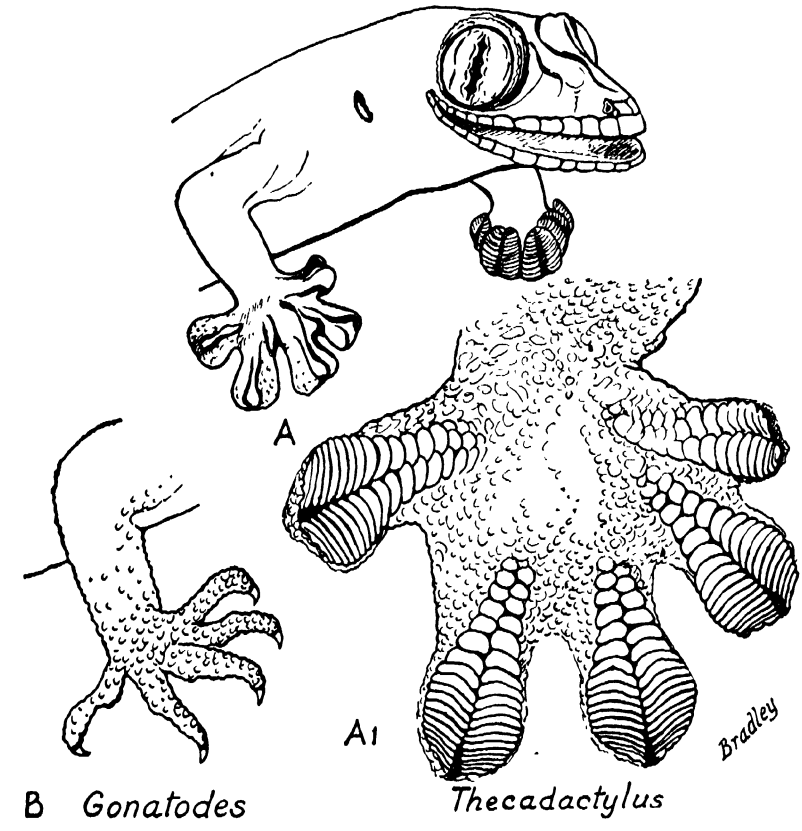


Fig. 12.48. Skeletons of Recent tuatara (A) and Lower Eocene champsosaur (B). B, after Barnum Brown.



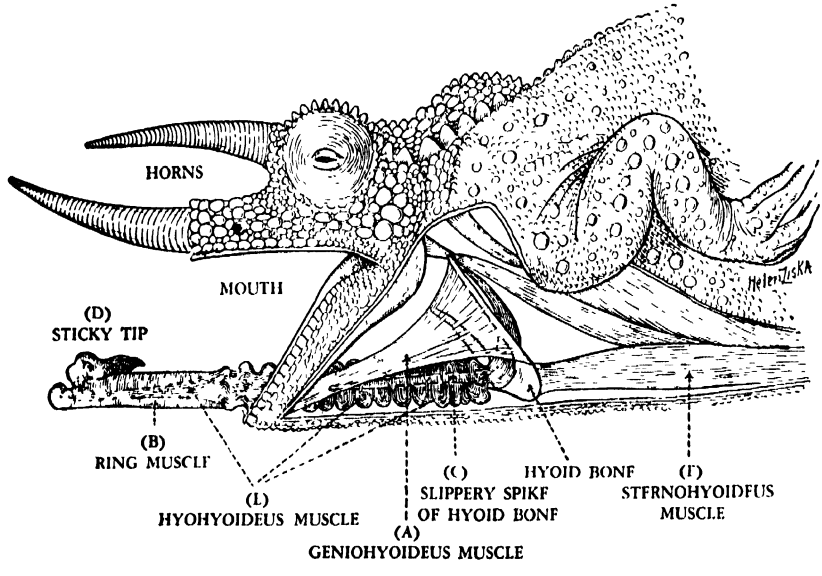


Fig. 12.49 (top). Two South American geckos, one with very primitive feet (B), the other (A, A1) with highly specialized adhesive discs. Both after Beebe. In A, the digits of the left hand are curled backward. The reverse movement squeezes the air from beneath the discs and helps to create a partial vacuum.

Fig. 12.50. Mechanism of the chamaeleon's protrusile tongue. After R. C. Murphy, from a dissection by H. C. Raven. The retraction of the hyoid bone and of the cylindrical tongue piles up a spring-like compression of the latter; sudden release of the tongue and snapping open of the jaw projects the tongue very far in front of the mouth.

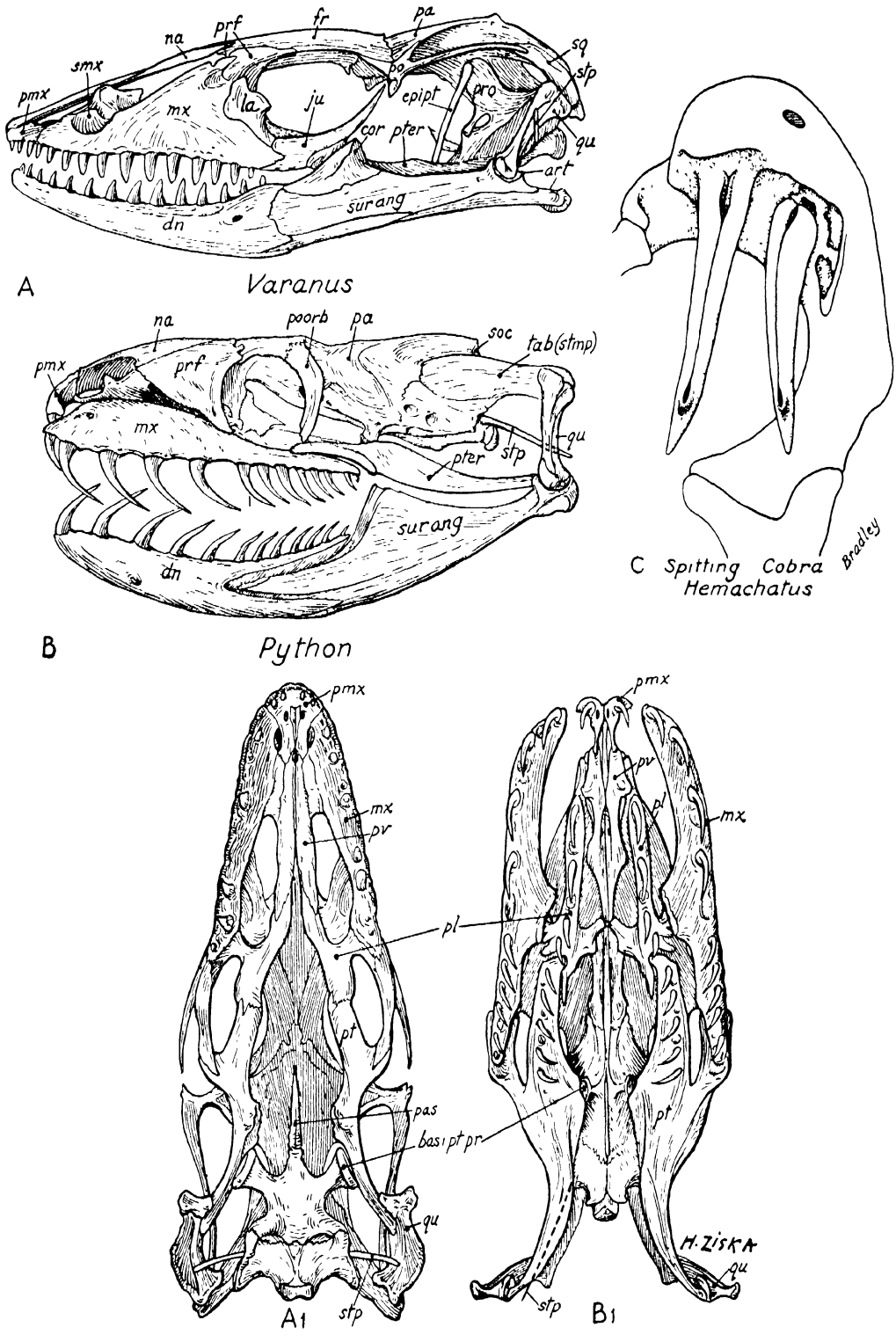


Fig. 12.51. Skulls of monitor (A, A1) and python (B, B1), showing far greater specialization of the latter for the ingestion of large prey. Original. Fangs (C) of the "spitting cobra," showing discharge orifice. After Bogert.

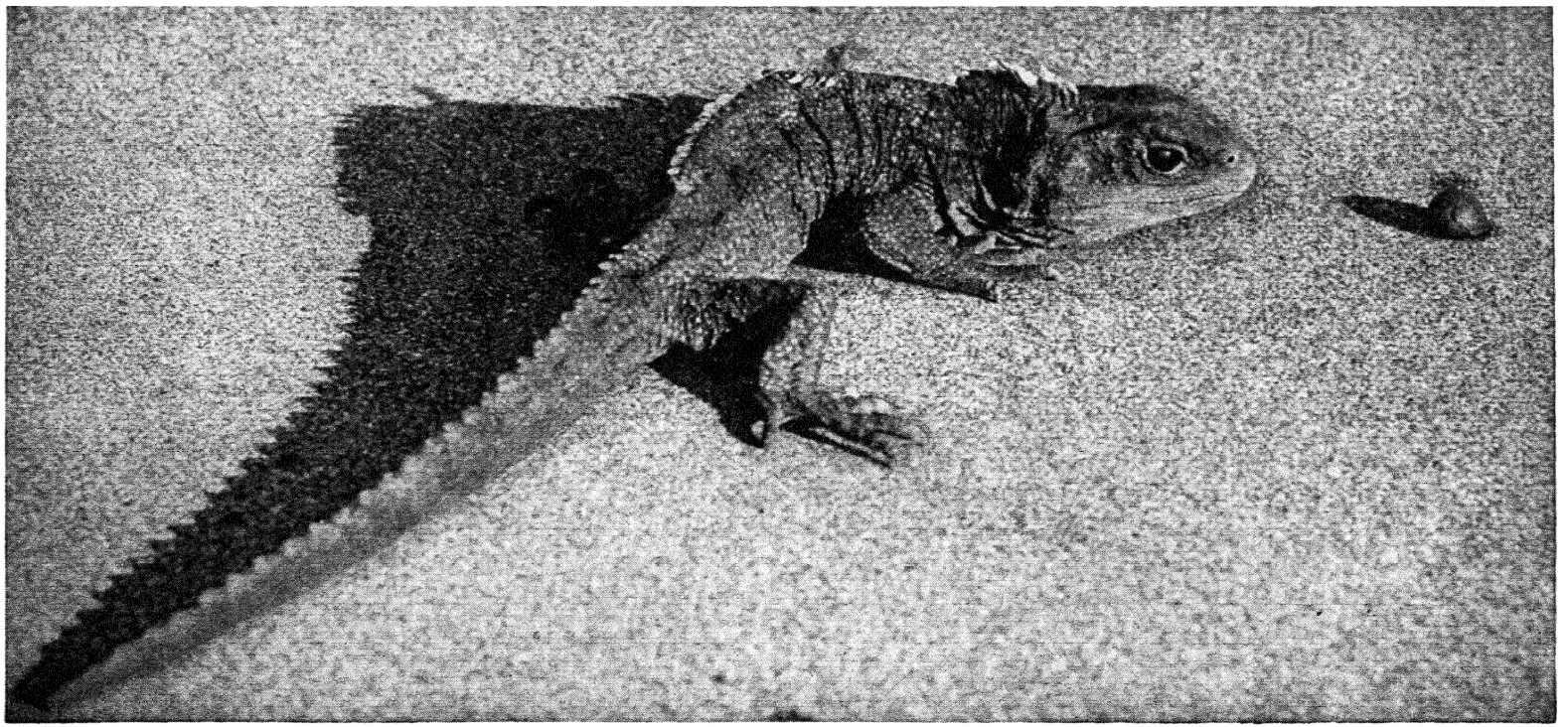


Plate 12.III. Tuatara and snail. Courtesy of W. Baden Powell, Auckland Museum, New Zealand.

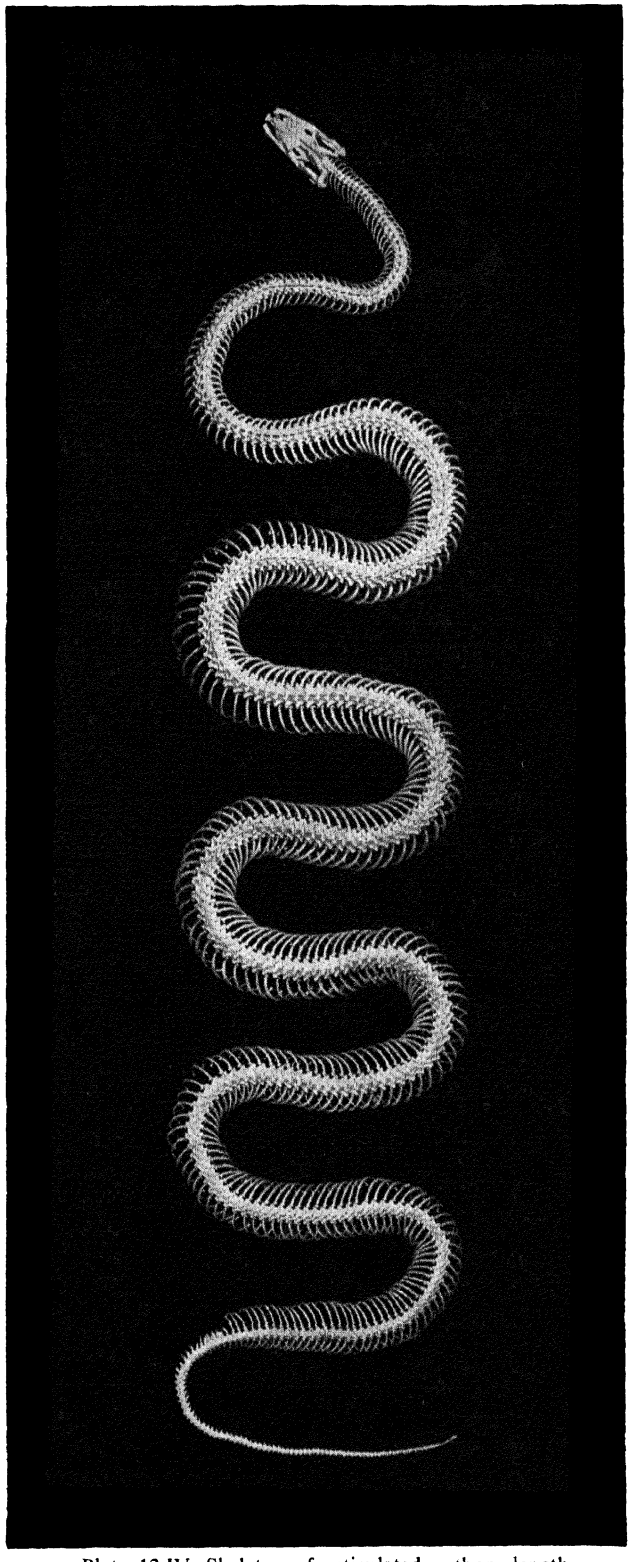
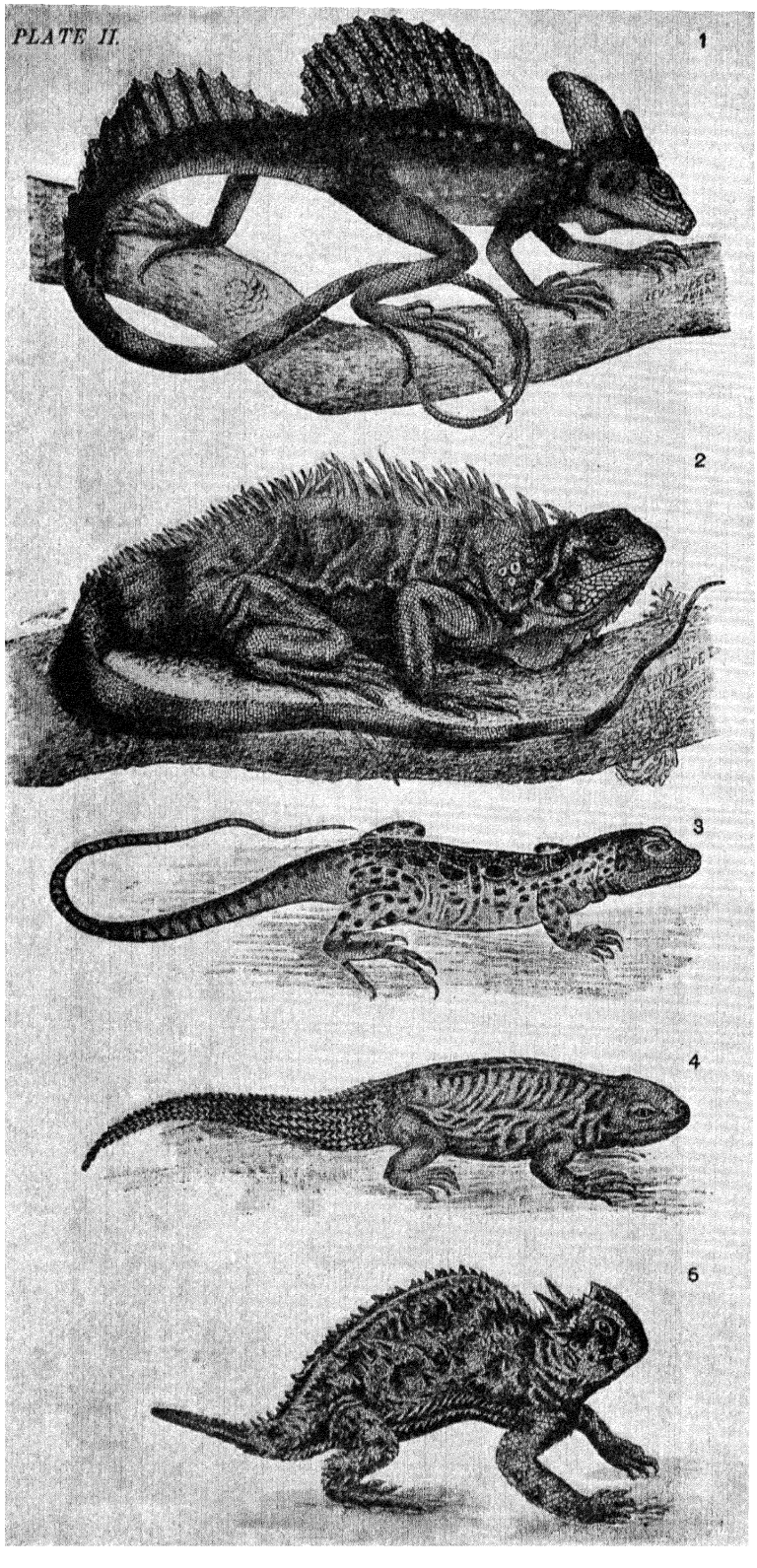


Plate 12.IV. Skeleton of reticulated python, length 22 ft., 9 in. Amer. Mus. Nat. Hist.


PLATE II.
1
2
3
4
5

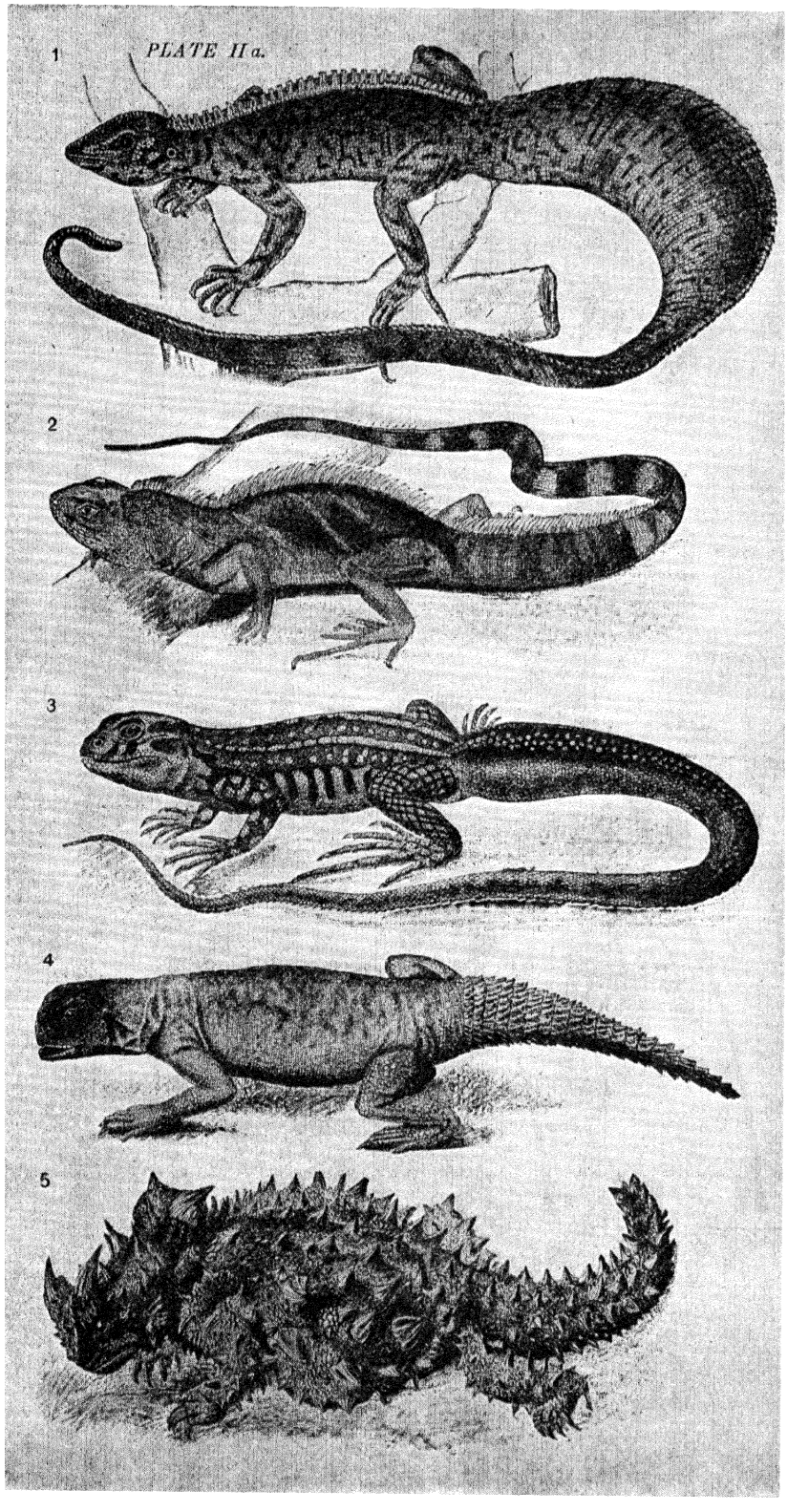
Plates 12.V, VI. Parallelism between New World iguanids and Old World agamids. After Cope.

"Plate II." Figures of Lizards of the family Iguanidae to be compared with a homologous series of Agamidae represented in Plate IIa.

1. *Basiliscus plumifrons* Cope, Costa Rica. From Cope.
2. *Iguana tuberculata* Linn., South America. From the Standard Natural History.
3. *Crotaphytus wislizeni* B.G., Sonoran Region of North America. From Baird.
4. *Phymaturus palluma* Grav., Chili. From Bell.
5. *Phrynosoma cornutum* Harl., Texas. From Standard Natural History.

"Plate IIa." Figures of Lizards of the family Agamidae which form a homologous series with the Iguanidae represented on Plate II.

1. *Lophura amboinensis* Schloss., Amboina. From Wagler.
2. *Physignathus mentager* Günther, Siam. From Günther.
3. *Liolepis bellii* Gray, China. From Duméril and Bibron.
4. *Uromastix spinipes* Cuv., Arabia. From Guérin.
5. *Moloch horridus* Gray, Australia. From standard Natural History.


PLATE II a.
1
2
3
4
5

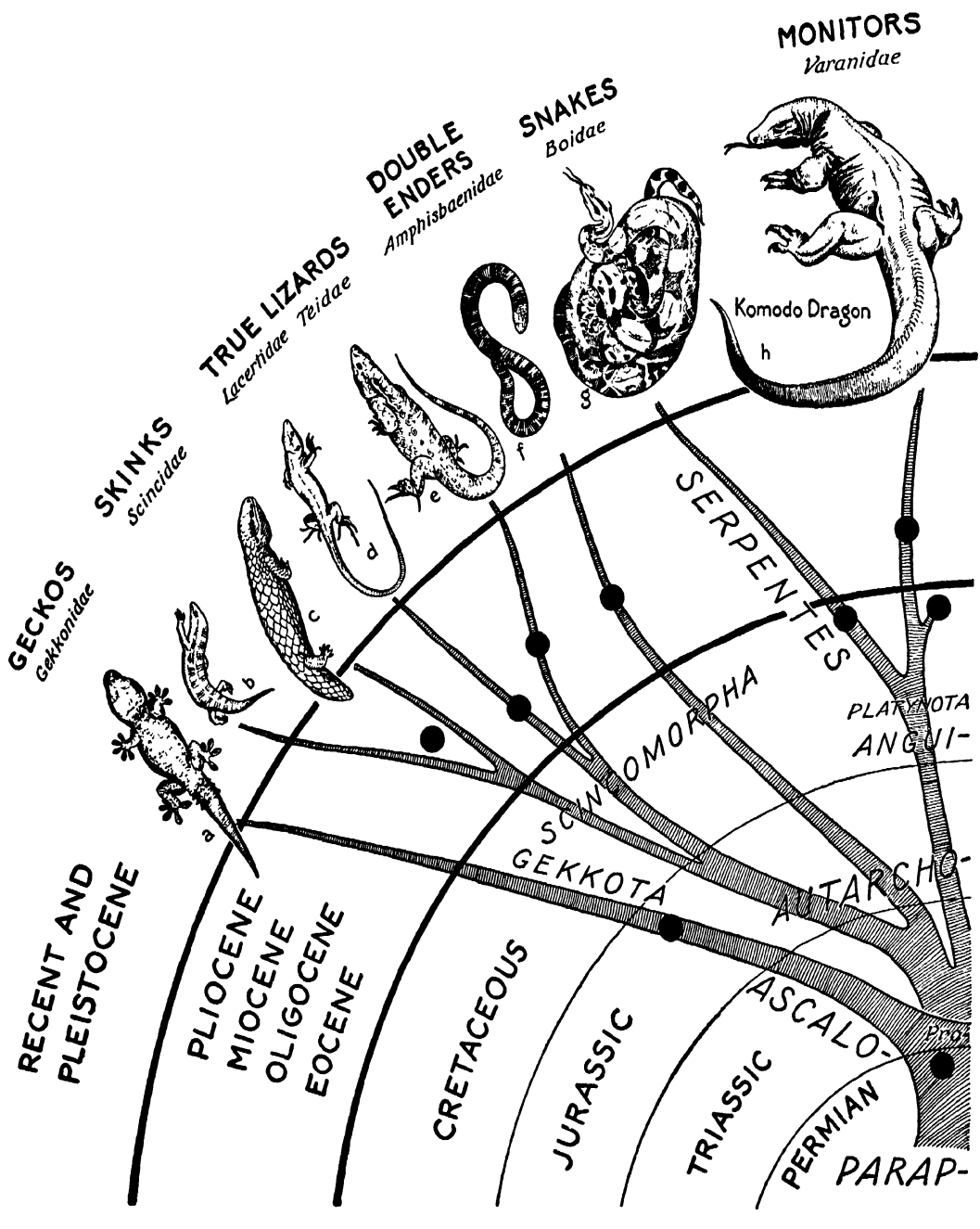
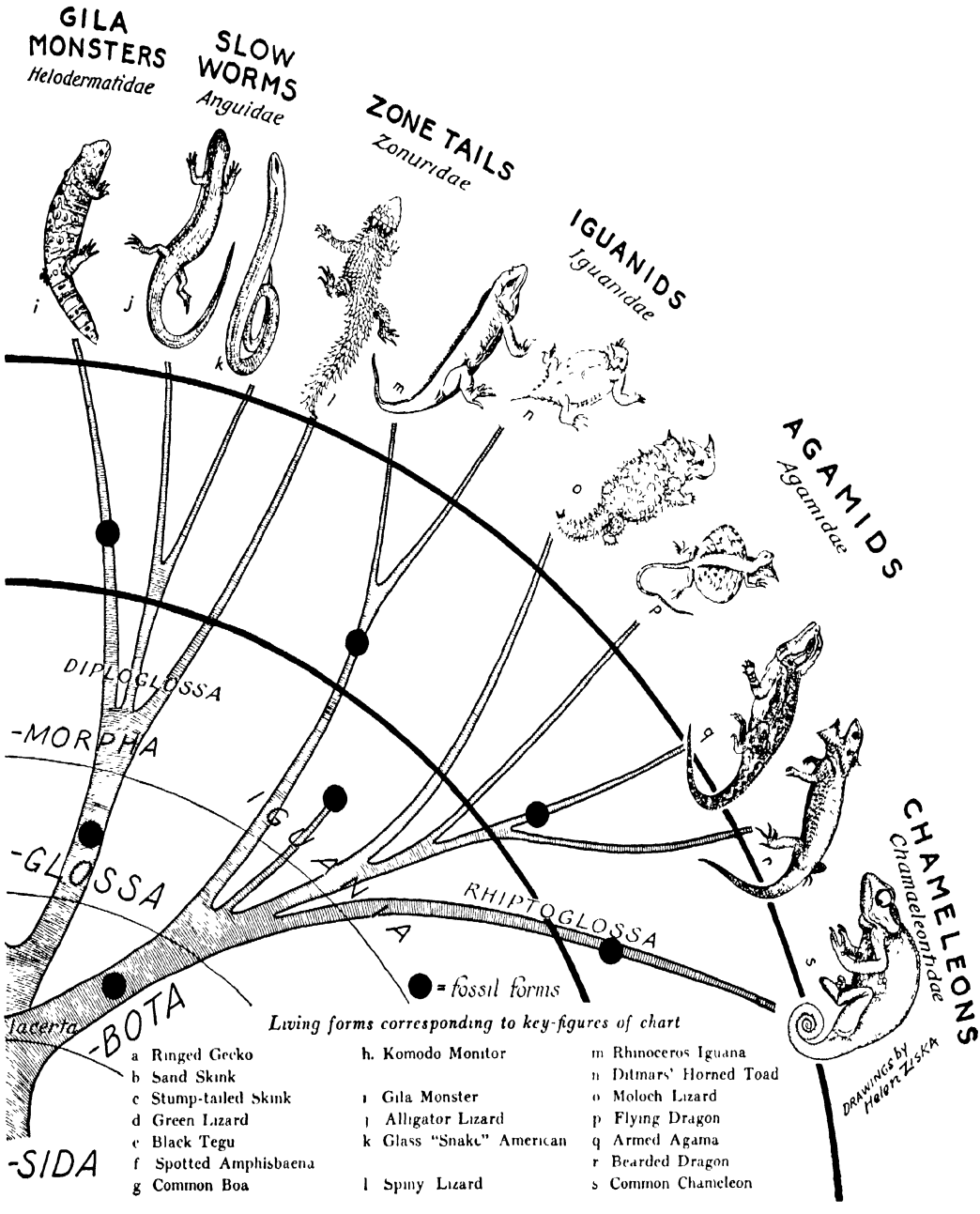


Fig. 12.52a, b. Adaptive branching of the lizards. From Gregory. Classification and phylogenetic data after Camp. Lizards from photographs by Ditmars.



Living forms corresponding to key-figures of chart

a Ringed Gecko
b Sand Skink
c Stump-tailed Skink
d Green Lizard
e Black Tegu
f Spotted Amphisbaena
g Common Boa
h. Komodo Monitor
i Gila Monster
j Alligator Lizard
k Glass "Snake" American
l Spiny Lizard
m Rhinoceros Iguana
n Ditmars' Horned Toad
o Moloch Lizard
p Flying Dragon
q Armed Agama
r Bearded Dragon
s Common Chameleon

Fig. 12.52b

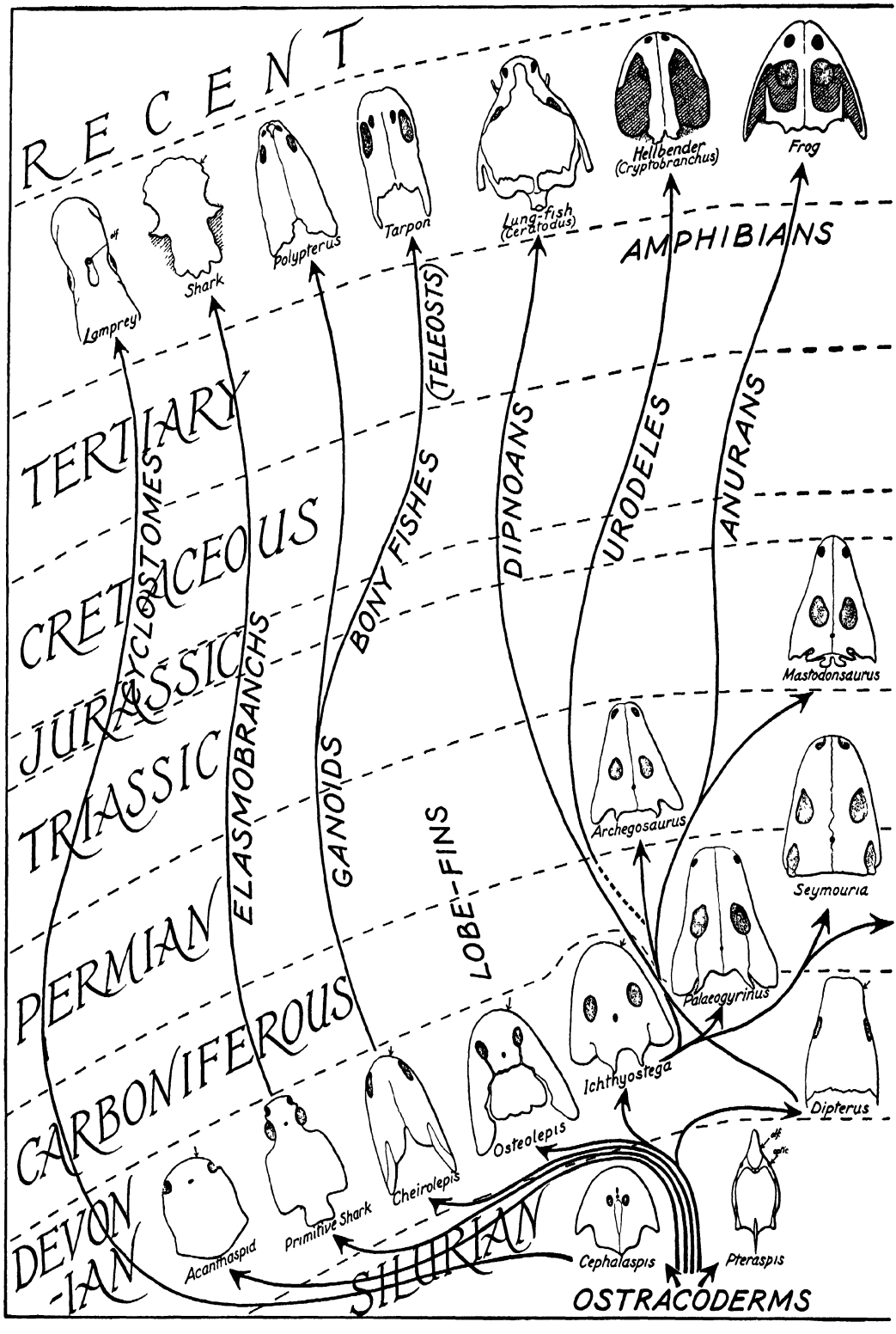

RECENT
TERTIARY
CRETACEOUS
JURASSIC
TRIASSIC
PERMIAN
CARBONIFEROUS
DEVON-IAN
SILURIAN
CYCLOSTOMES
ELASMOBRANCHS
GANOIDS
BONY FISHES (TELEOSTS)
LOBE-FINS
DIPNOANS
URODELES
ANURANS
AMPHIBIANS
OSTRACODERMS
Lamprey
Shark
Polypterus
Tarpon
Lung-fish (Ceratodus)
Hellbender (Cryptobranchus)
Frog
Mastodonsaurus
Archegosaurus
Seymouria
Palaeogyrinus
Ichthyostega
Dipterus
Osteolepis
Cheirolepis
Primitive Shark
Acanthaspid
Cephalaspis
Pteraspis

Fig. 12.53a

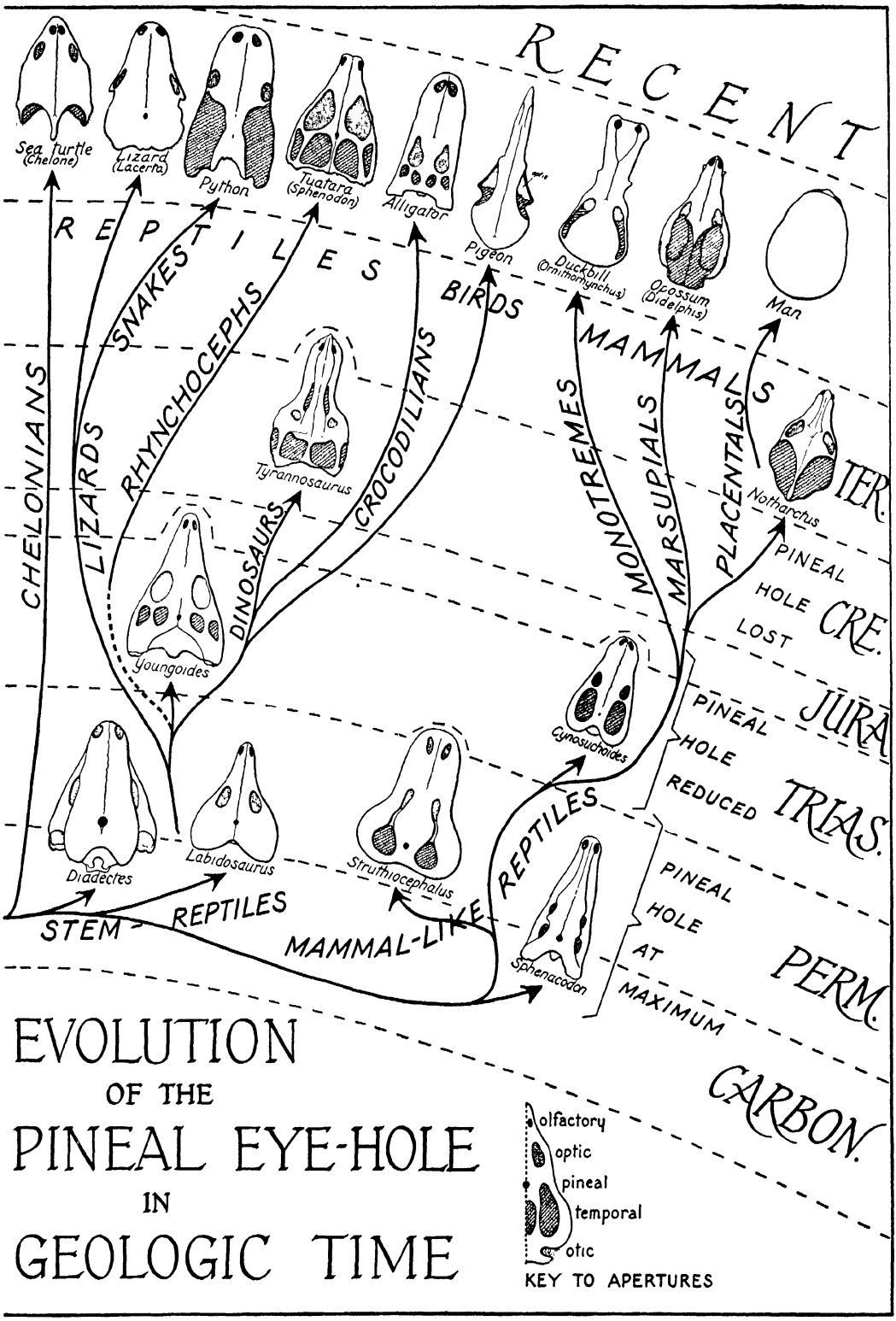

RECENT
Sea turtle (Chelone)
Lizard (Lacerta)
Python
Tuatara (Sphenodon)
Alligator
Pigeon
Duckbill (Ornithorhynchus)
Opossum (Didelphis)
Man
REPTILES
BIRDS
MAMMALS
CHELONIANS
LIZARDS
SNAKES
RHYNCHOCEPHS
DINOSAURS
CROCODILIANS
MONOTREMES
MARSUPIALS
PLACENTALS
Tyrannosaurus
Notharctus
TER.
PINEAL HOLE LOST
CRE.
Youngoides
Cynosuchoides
JURA
PINEAL HOLE REDUCED
TRIAS.
Diadectes
Labidosaurus
Struthiocephalus
REPTILES
STEM REPTILES
MAMMAL-LIKE REPTILES
Sphenacodon
PINEAL HOLE AT MAXIMUM
PERM.
CARBON.
EVOLUTION
OF THE
PINEAL EYE-HOLE
IN
GEOLOGIC TIME
olfactory
optic
pineal
temporal
otic
KEY TO APERTURES

Fig. 12.53b

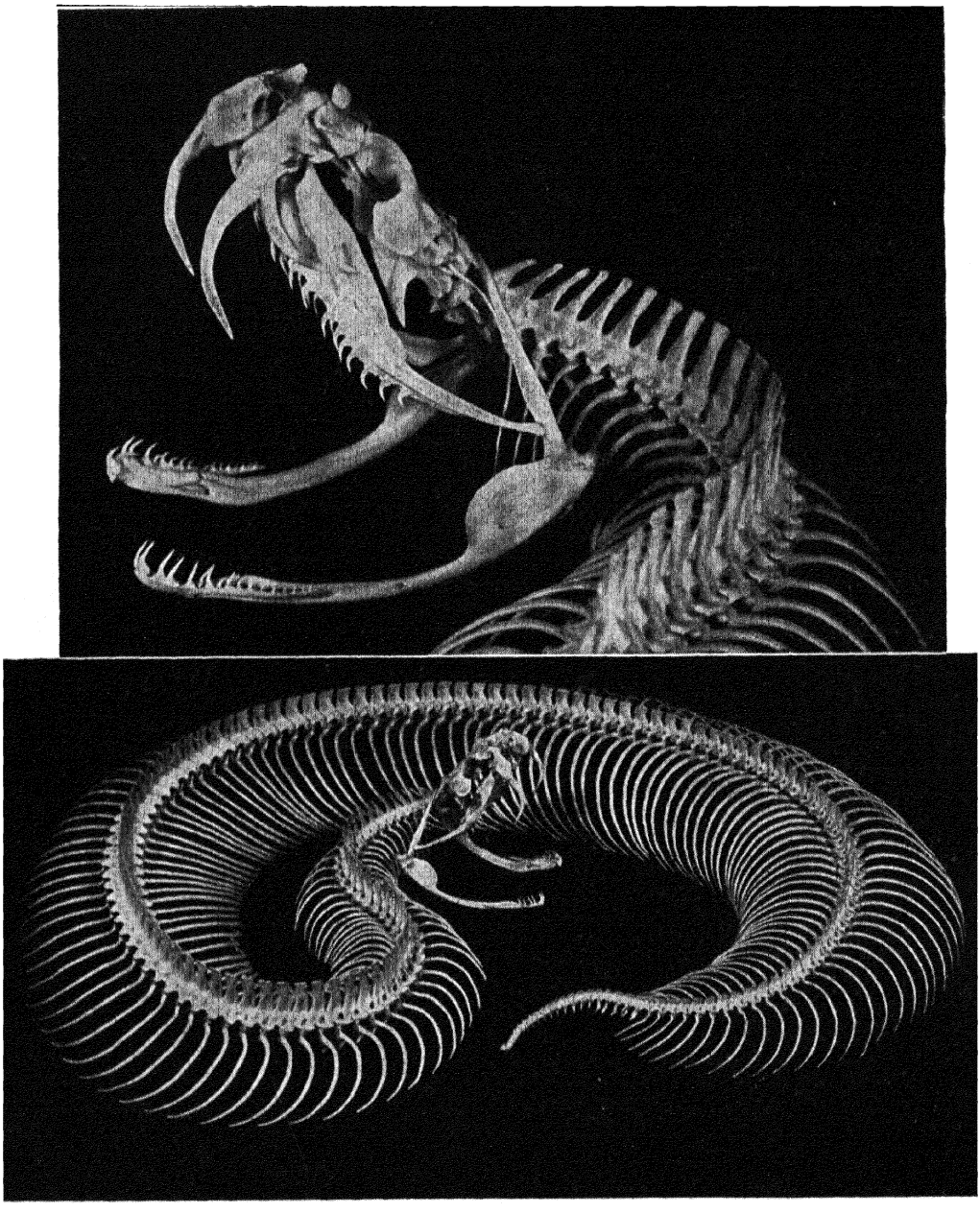
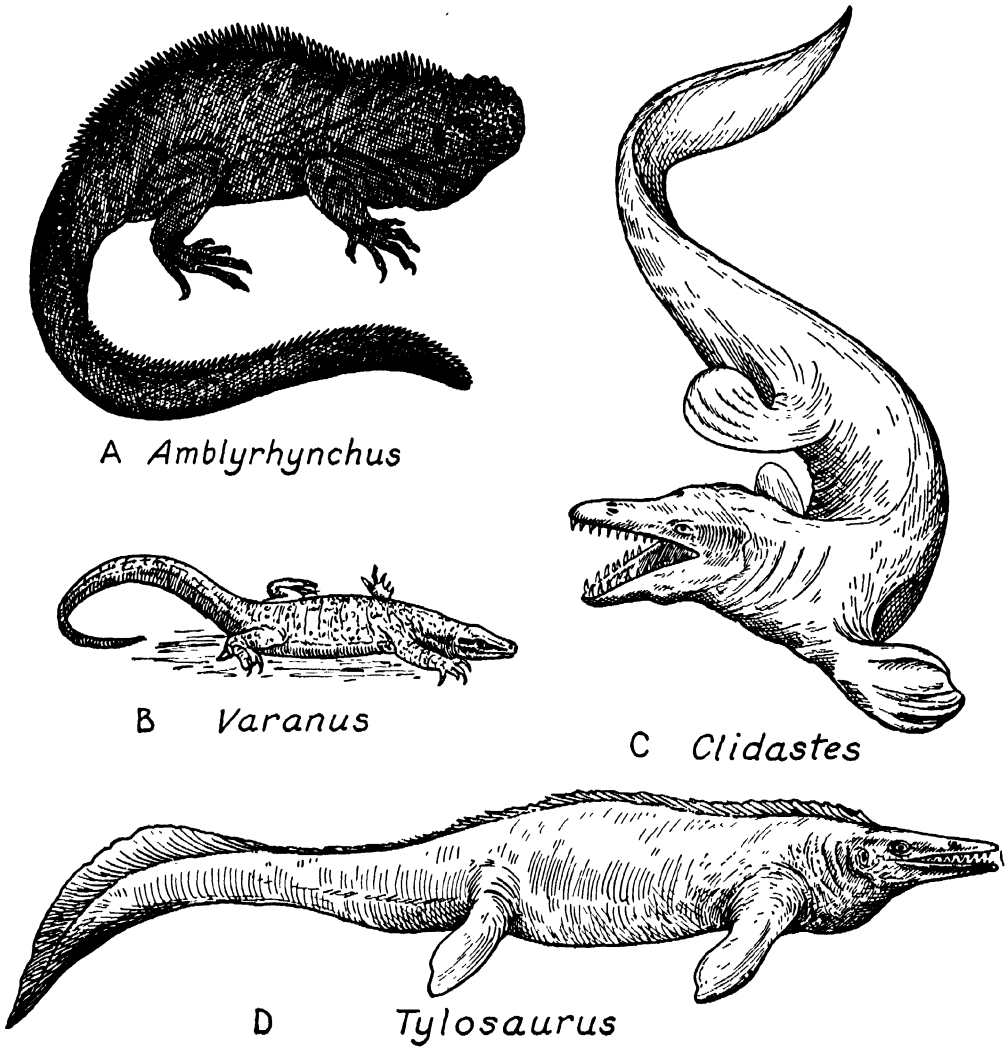


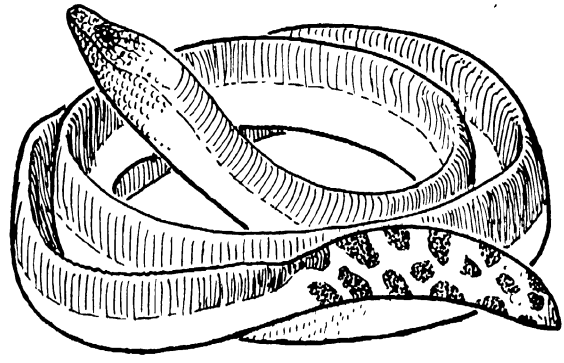
Plate 12.VII. Skeleton of gaboon viper. *Bitis gabonica*. After Bogert. Amer. Mus. Nat. Hist.

CHAPTER XIII

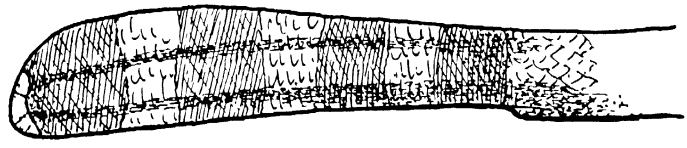
BACK TO THE WATERS AND DOWN TO THE SEA



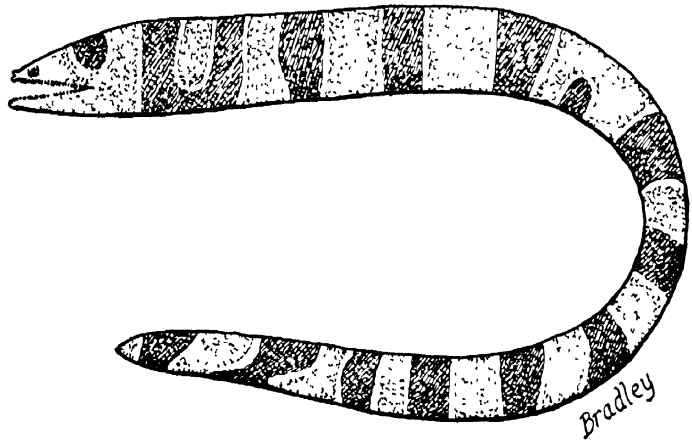
Figs. 13.1, 2. The first step toward marine life. A, An iguanid lizard of the Galapagos Islands, which has acquired the habit of swimming under water after seaweed, without undergoing any obvious modifications of its limbs. After Lydekker. Existing monitor lizard (B), which has preserved the remote ancestral structure of the Cretaceous mosasaurs (C, D). B, from a photograph; C, after Williston; D, after Osborn.



A *Hydrus bicolor*



B *Platurus laticaudatus*



C *Channomuraena vittata*

Fig. 13.3. Flattening of tail in sea-snakes (A, B) and moray (C). A, from Williston, after Brehm; B, after Abel; C, after Jordan and Evermann.

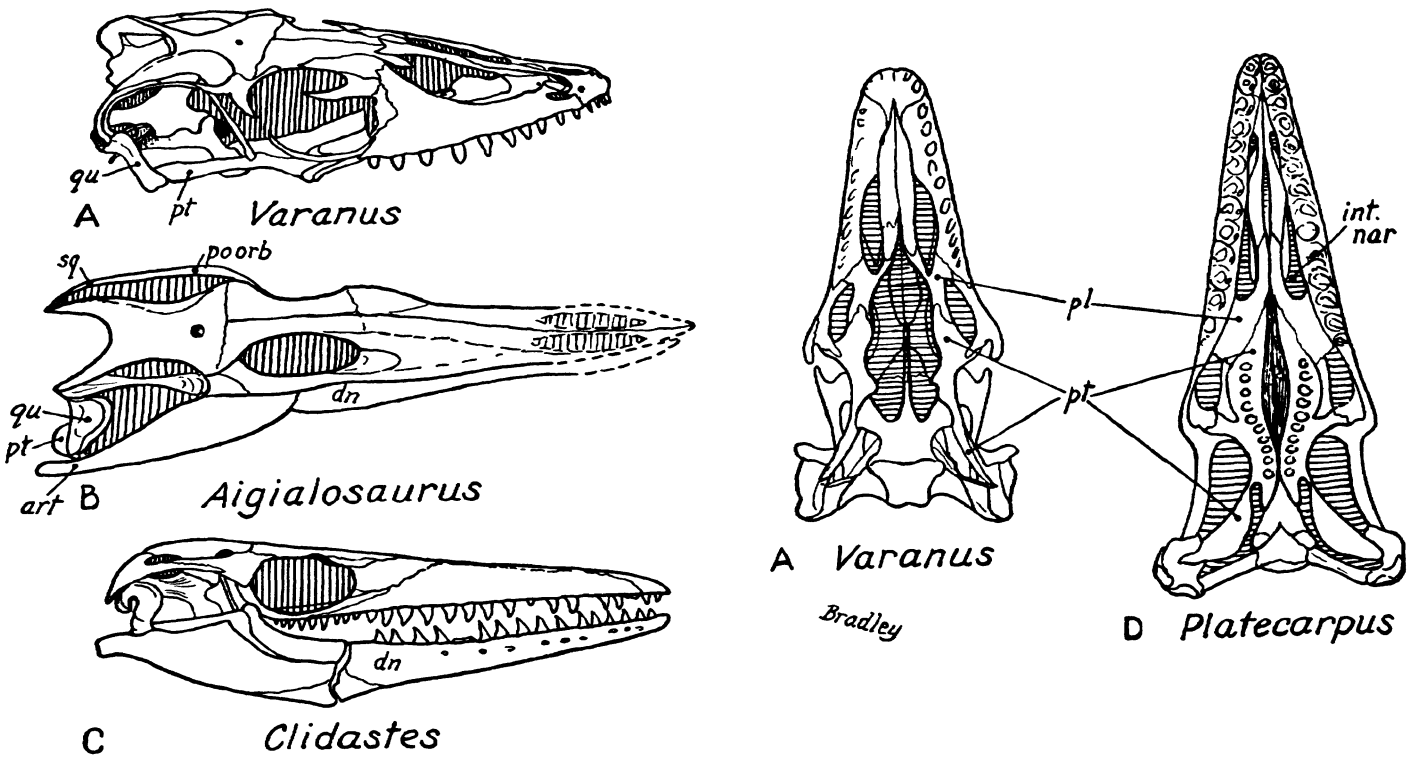


Fig. 13.4. Skulls of recent monitor (A), Lower Cretaceous intermediate (B) and Upper Cretaceous mosasaur (C); palatal views of skulls of monitor (D) and mosasaur (A). A, A, after Zittel; B, after Gorjanovic-Kramberger (but quadrate turned to fit); C, D, after Williston.

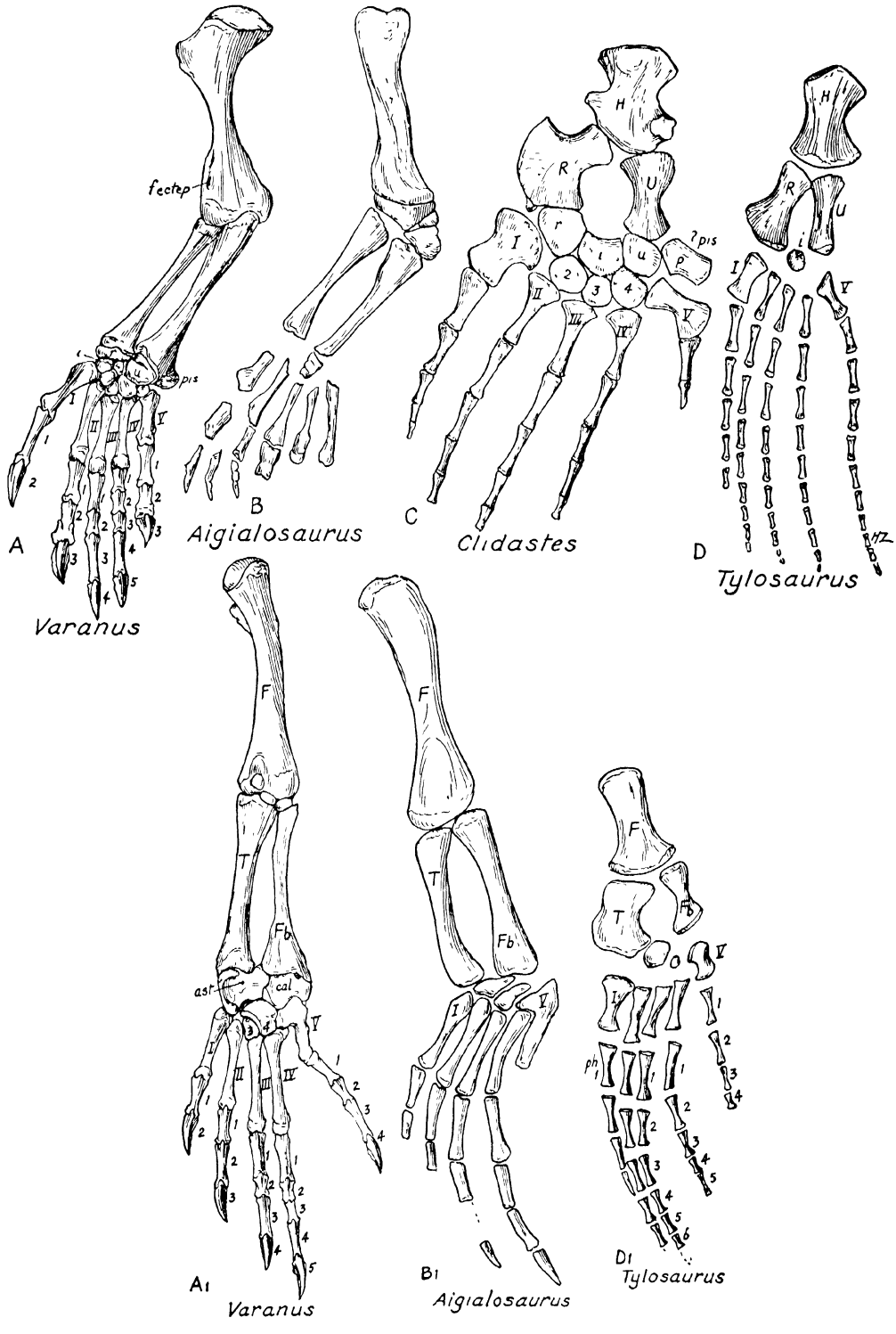


Fig. 13.5. Fore and hind limbs of: existing monitor (A, A1), Lower Cretaceous intermediate (B, B1), wide (C) and narrow (C, D1) mosasaur paddles. Note divergence of fifth metacarpal. The fifth metatarsal is hook-like. Secondary polyisomerism is evident in the phalanges of C, D, D1. A, A1, original; B, B1, after Gorjanovic-Kramberger; C, after Williston; D, after Osborn.

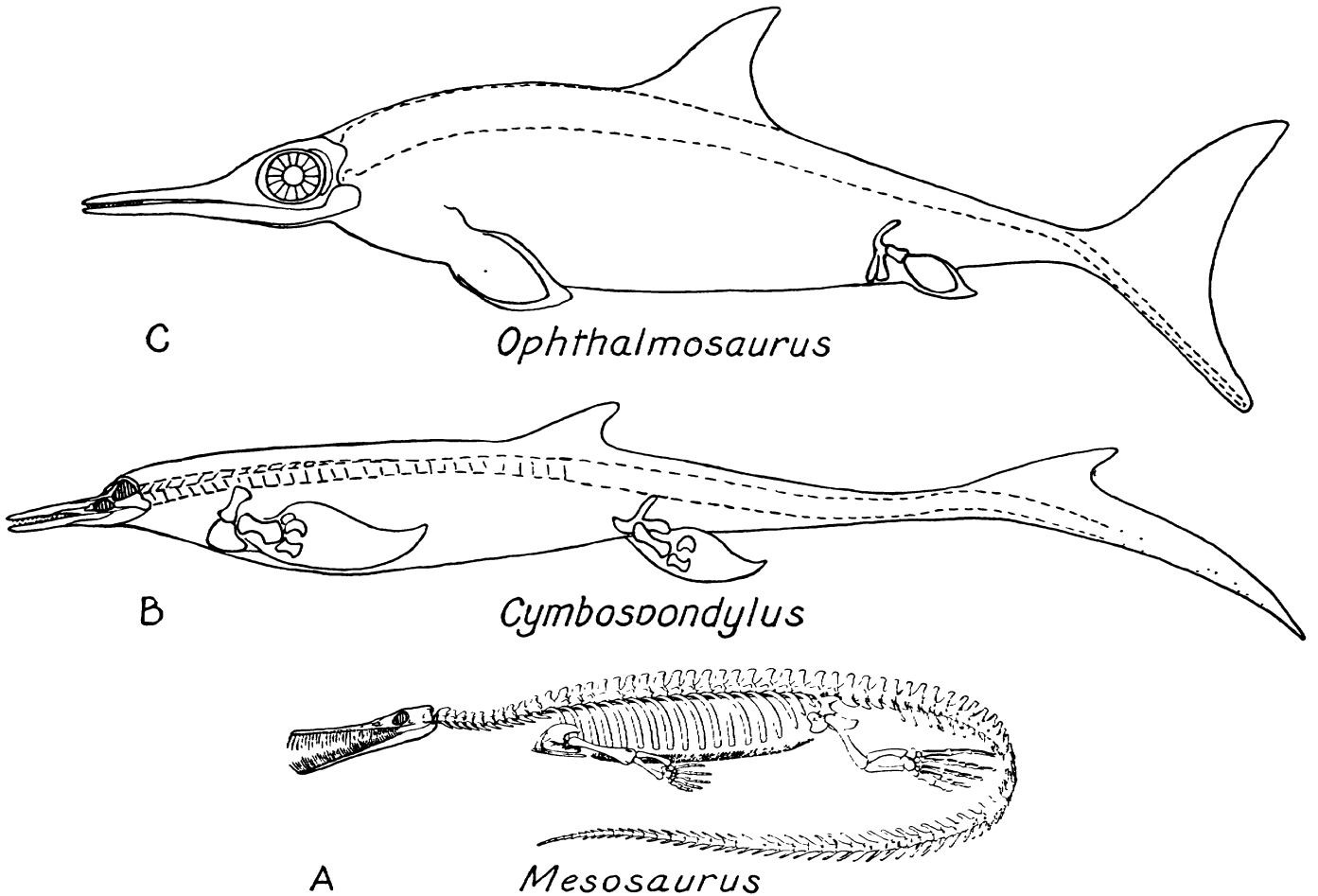


Fig. 13.6. Three structural grades in transformation from lizard-like to fish-like body form. A, Permian proganosaur, restored by McGregor; B, diagram of Triassic ichthyosaur, data from Merriam; C, Upper Cretaceous ichthyosaur with huge eyes and reduced teeth in jaws, based on data from C W. Andrews.

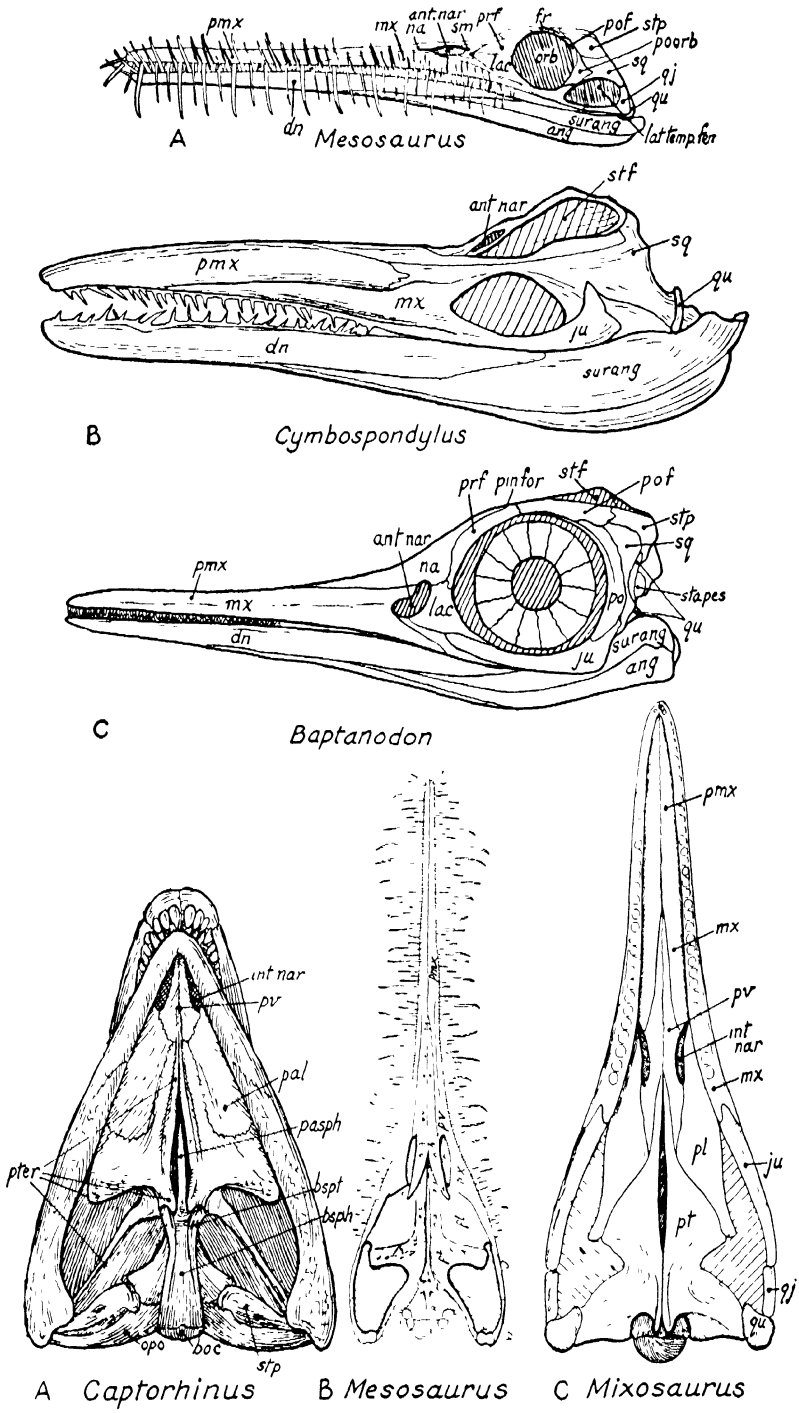


Fig. 13.7a, b. Side views: Permian proganosaur (A) with extremely long delicate teeth and lower temporal opening (*l.t.fr.*); Triassic ichthyosaur (B) with large dorsal temporal opening (*st.f.*); Cretaceous stage (C) with restricted postorbital space and small dorsal temporal opening. A, after von Huene; B, after Merriam; C, after Andrews. Palatal views: cotylosaur (A) with primitive palate; proganosaur (B) with elongate snout but relatively primitive palate; Triassic ichthyosaur (C) with pterygoids prolonged far backward. A, original; B, after von Huene; C, from a model by Repoussi.

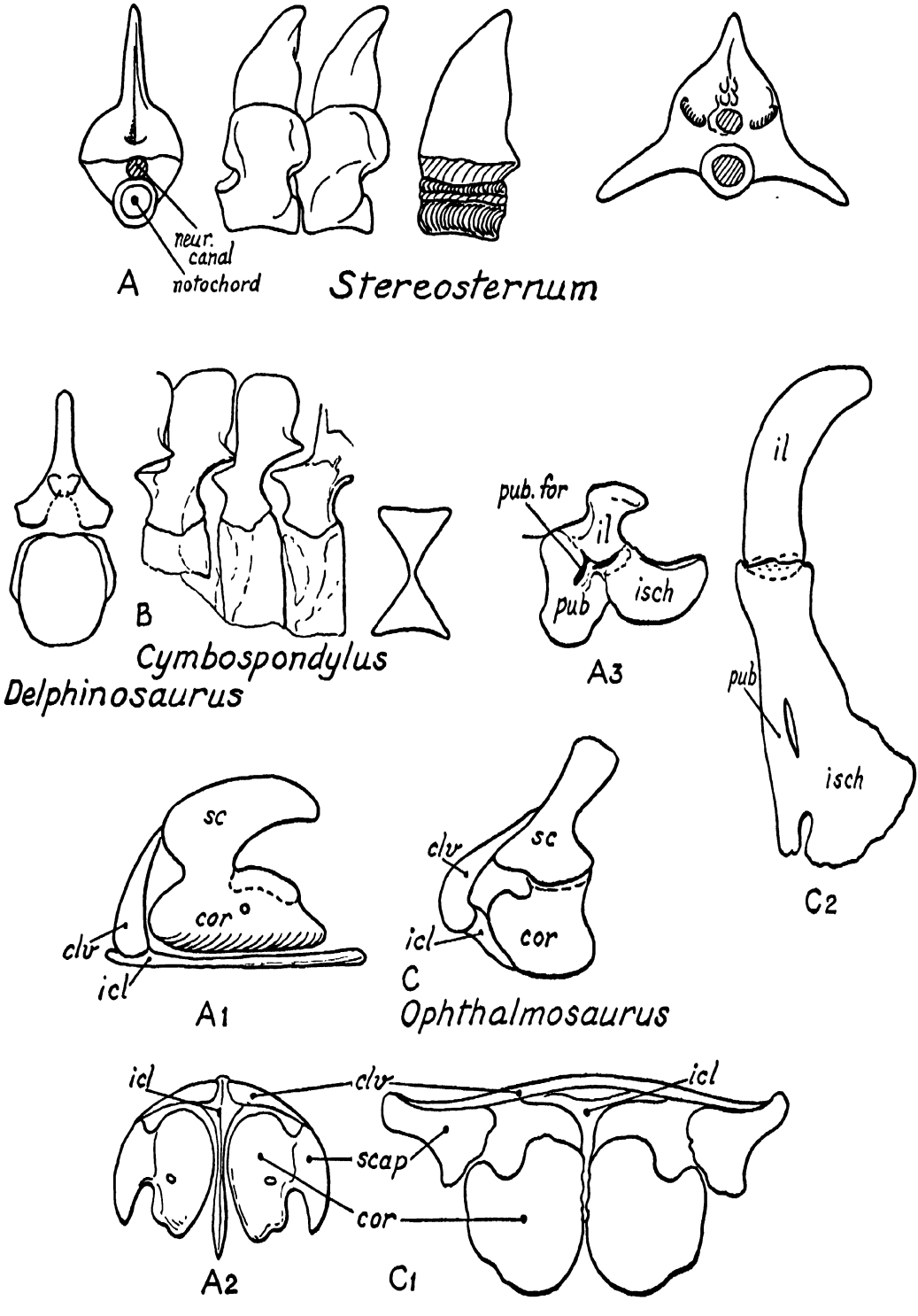


Fig. 13.8. Vertebrae and girdles of proganosaur (A, A1–A3) and ichthyosaurs (B, C, C1, C2). A, after Osborn; A1–A3, after McGregor; B, after Merriam; C–C2, after Andrews.

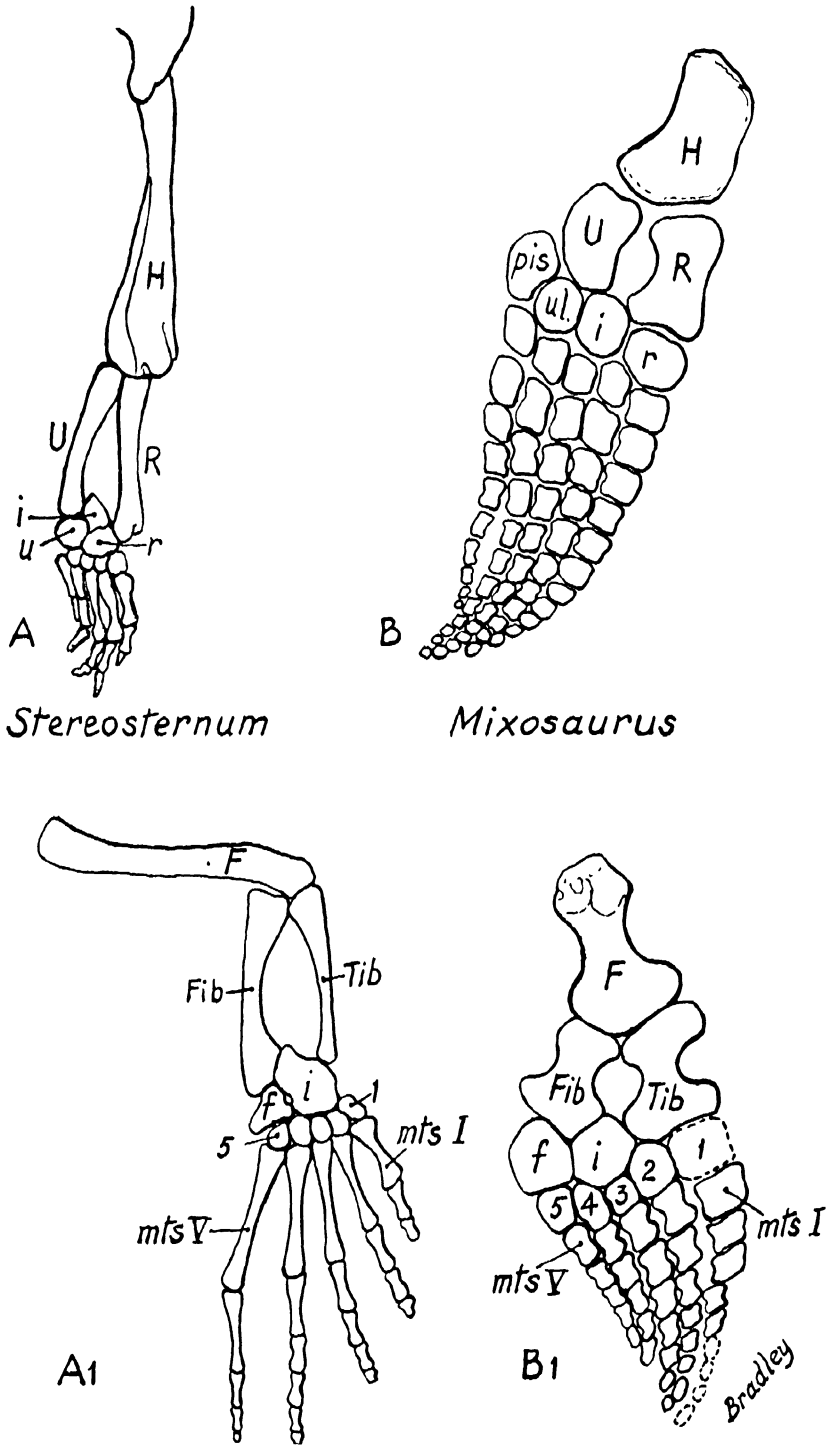
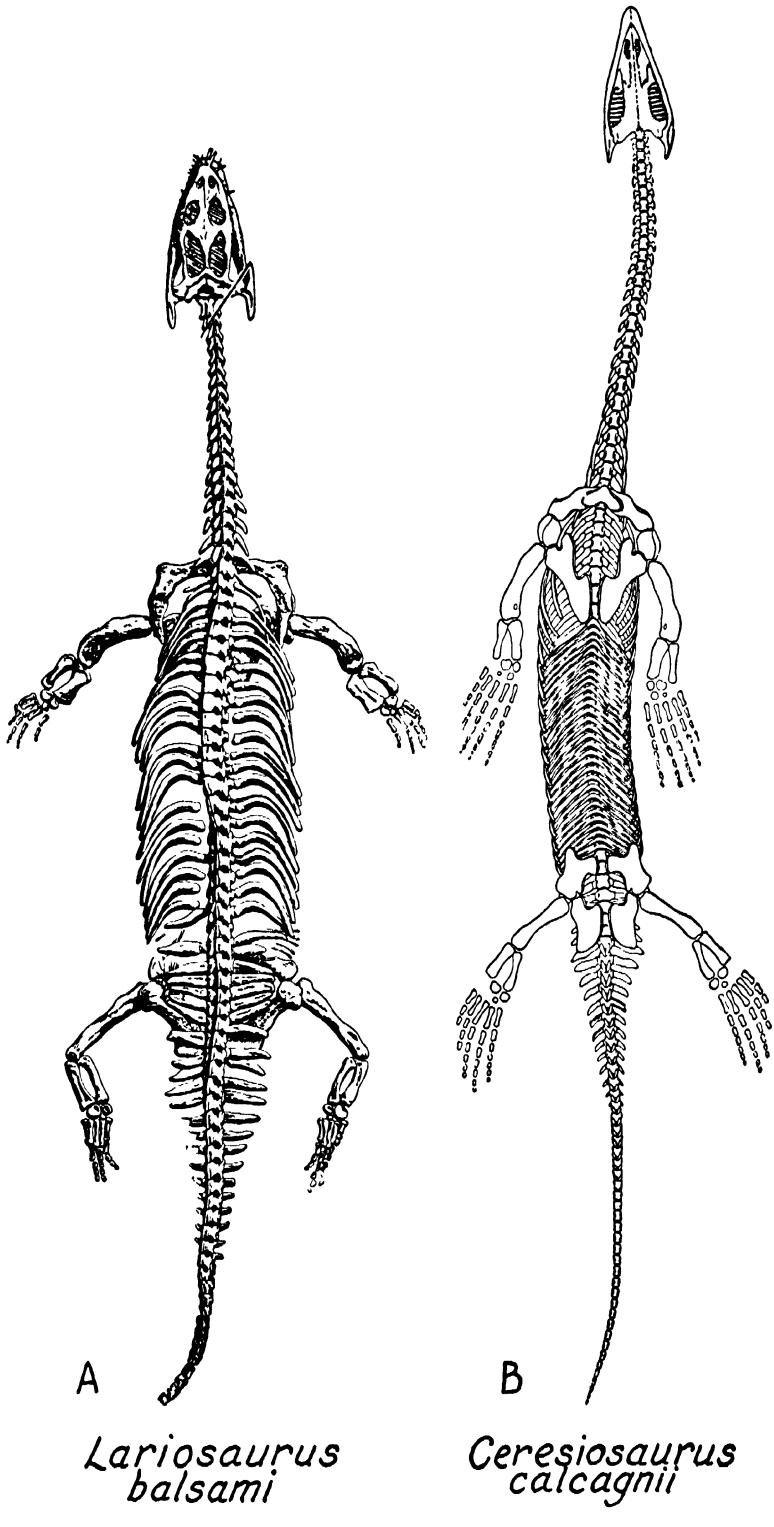


Fig. 13.9. Fore (A, B) and hind (A1, B1) limbs of Permian proganosaur and Triassic ichthyosaur. A, A1, after McGregor; B, B1, after Repoussi.



Figs. 13.10, 11. Progressive adaptation for marine life in Triassic nothosaurs (A, B) and Jurassic plesiosaur (C). (A, C, dorsal, B, ventral view.) A, B, after Peyer; C, from mounted skeleton in the American Museum of Natural History.

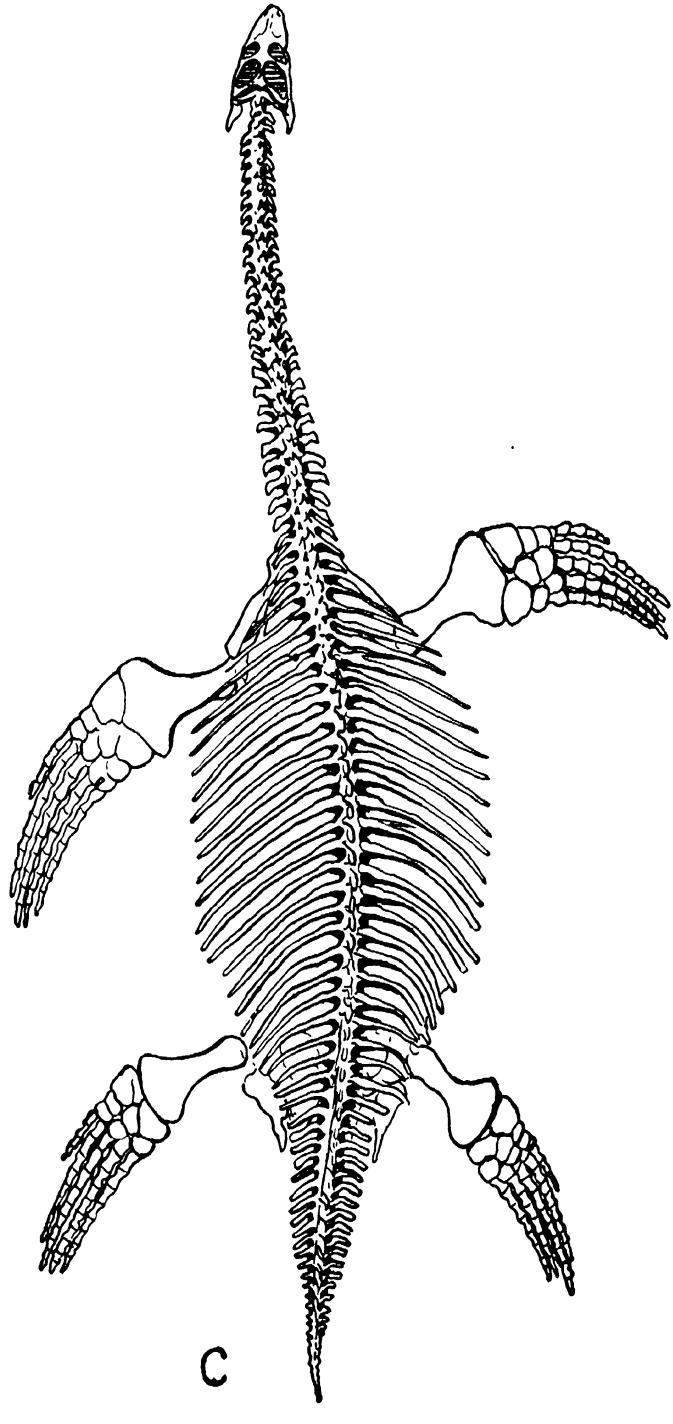


Fig. 13.11

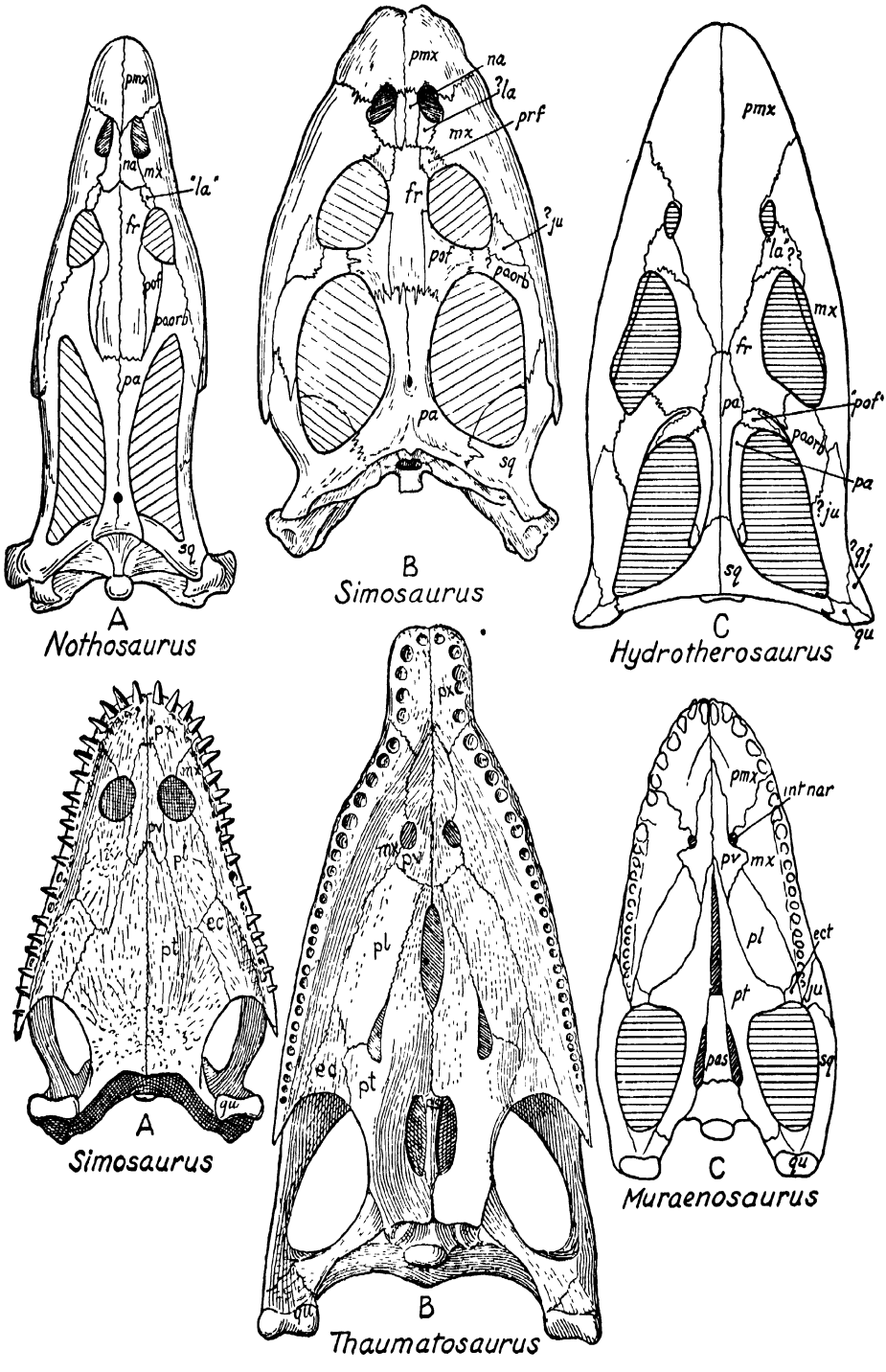


Fig. 13.12 (top). Skulls (dorsal view) of Triassic nothosaurs (A, B) and Cretaceous plesiosaur (C). A, B, after Williston; C, after Welles.

Fig. 13.13. Skulls (palatal view) of: Triassic nothosaur (A), Jurassic pliosaur (B) and Upper Cretaceous plesiosaur (C). The exposure of the parasphenoid in B and C may be secondary. A, B, after Williston; C, after Andrews.

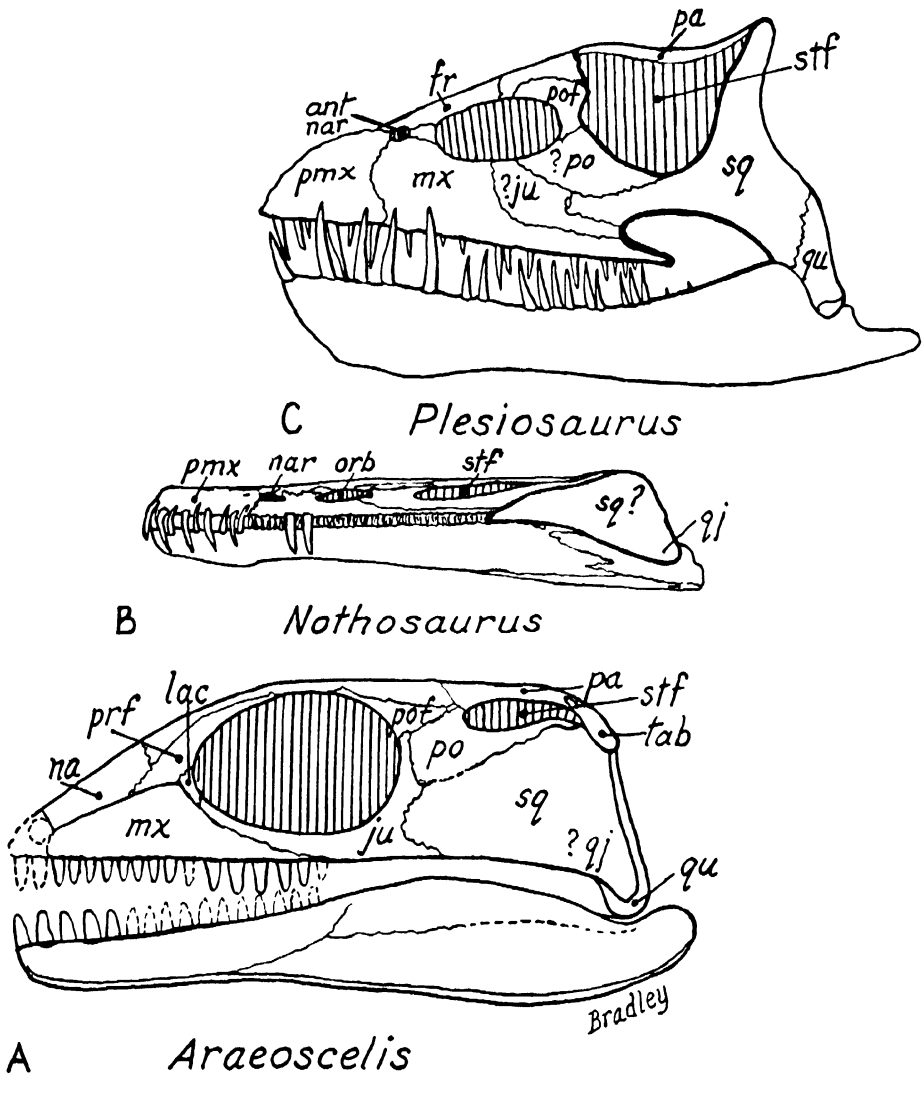


Fig. 13.14. Skulls of Lower Permian "protorosaur" (A), Triassic nothosaur (B) and Jurassic plesiosaur (C). A, is close to the protorosaur type, with a vertically deep squamosal and an upper temporal opening (*stf*); B, a long-jawed fish-catcher; C, a secondarily shortened skull with long teeth. A, B, after Williston; C, after Zittel.

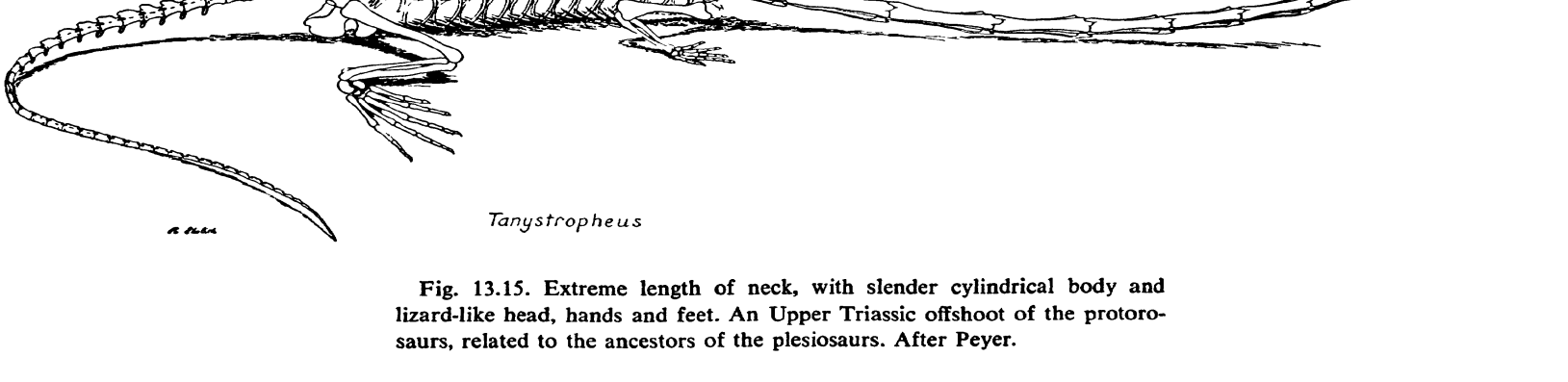


Fig. 13.15. Extreme length of neck, with slender cylindrical body and lizard-like head, hands and feet. An Upper Triassic offshoot of the protorosaurs, related to the ancestors of the plesiosaurs. After Peyer.

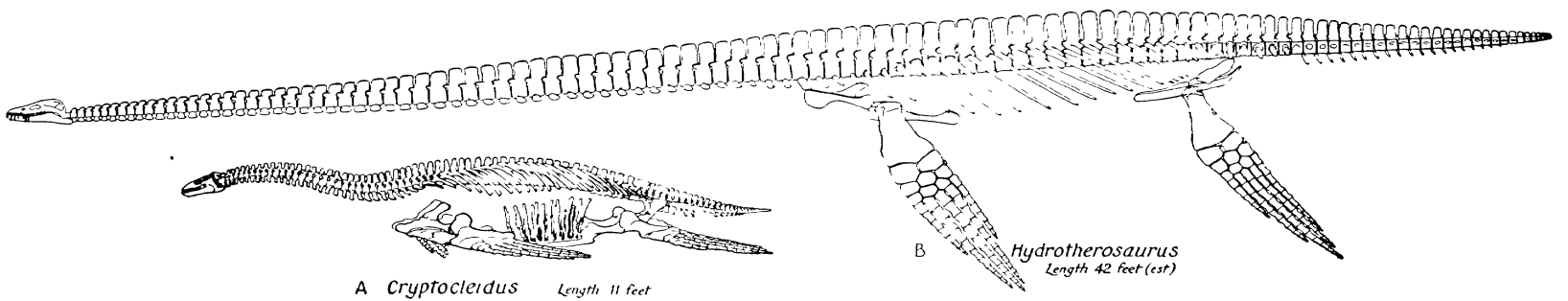


Fig. 13.16. The acme of the plesiosaurs Jurassic and Cretaceous stages. A, from mounted skeleton in the American Museum of Natural History; B, after Welles.

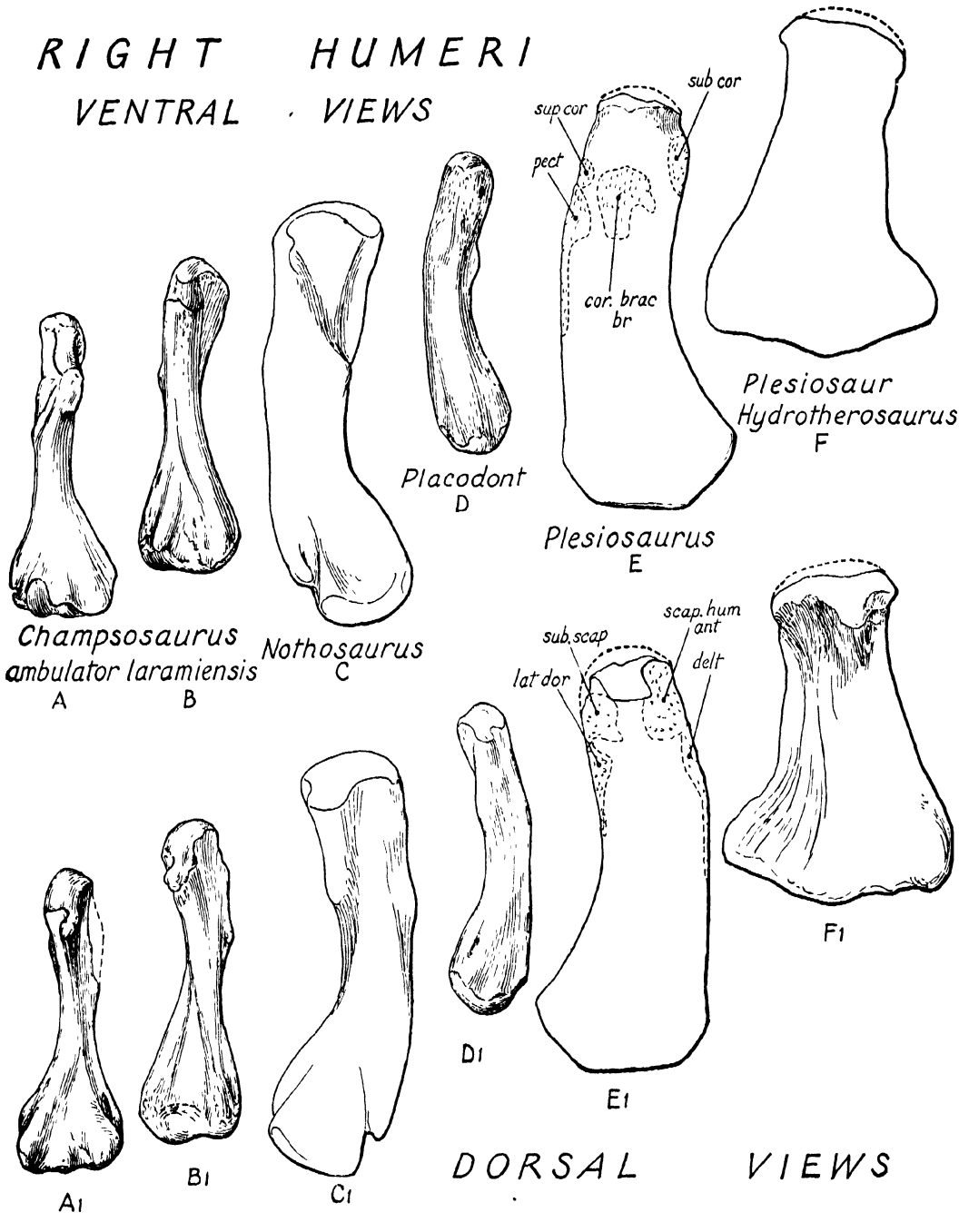


Fig. 13.17. Series of humeri illustrating change from semi-aquatic to extreme aquatic types. A, A1, B, B1, after Barnum Brown; C, C1, D, D1, after von Meyer; E, E1, after Watson; F, F1, after Welles.

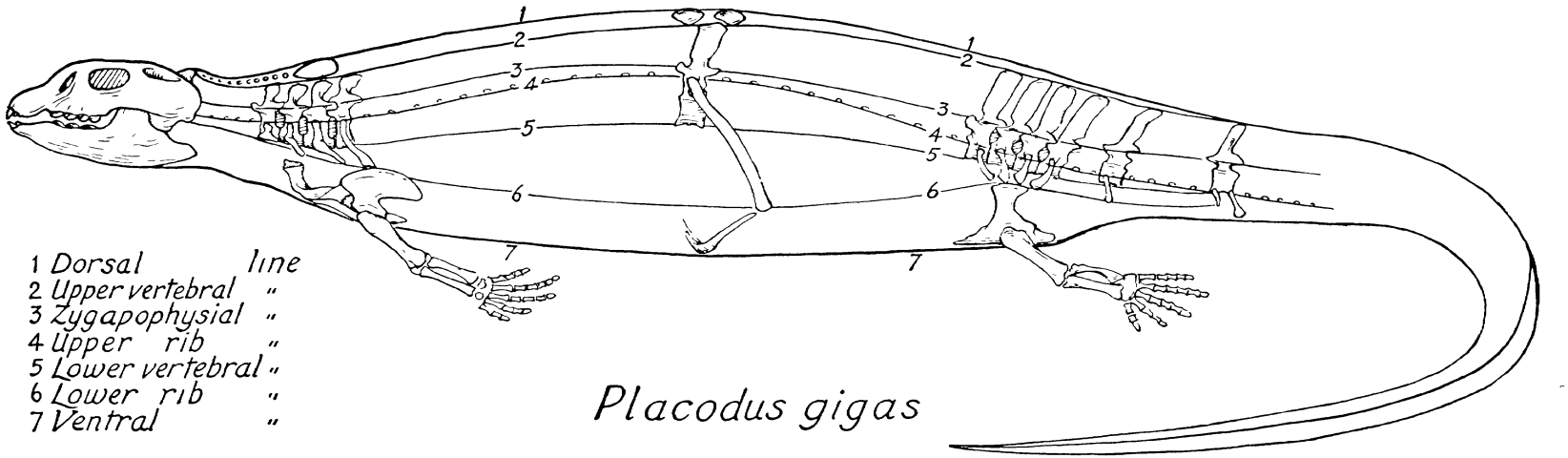


Fig. 13.18. Skeletal contours of a Triassic placodont Based on the mounted skeleton in the Senckenberg Museum, Frankfurt, with data from Dreverman.

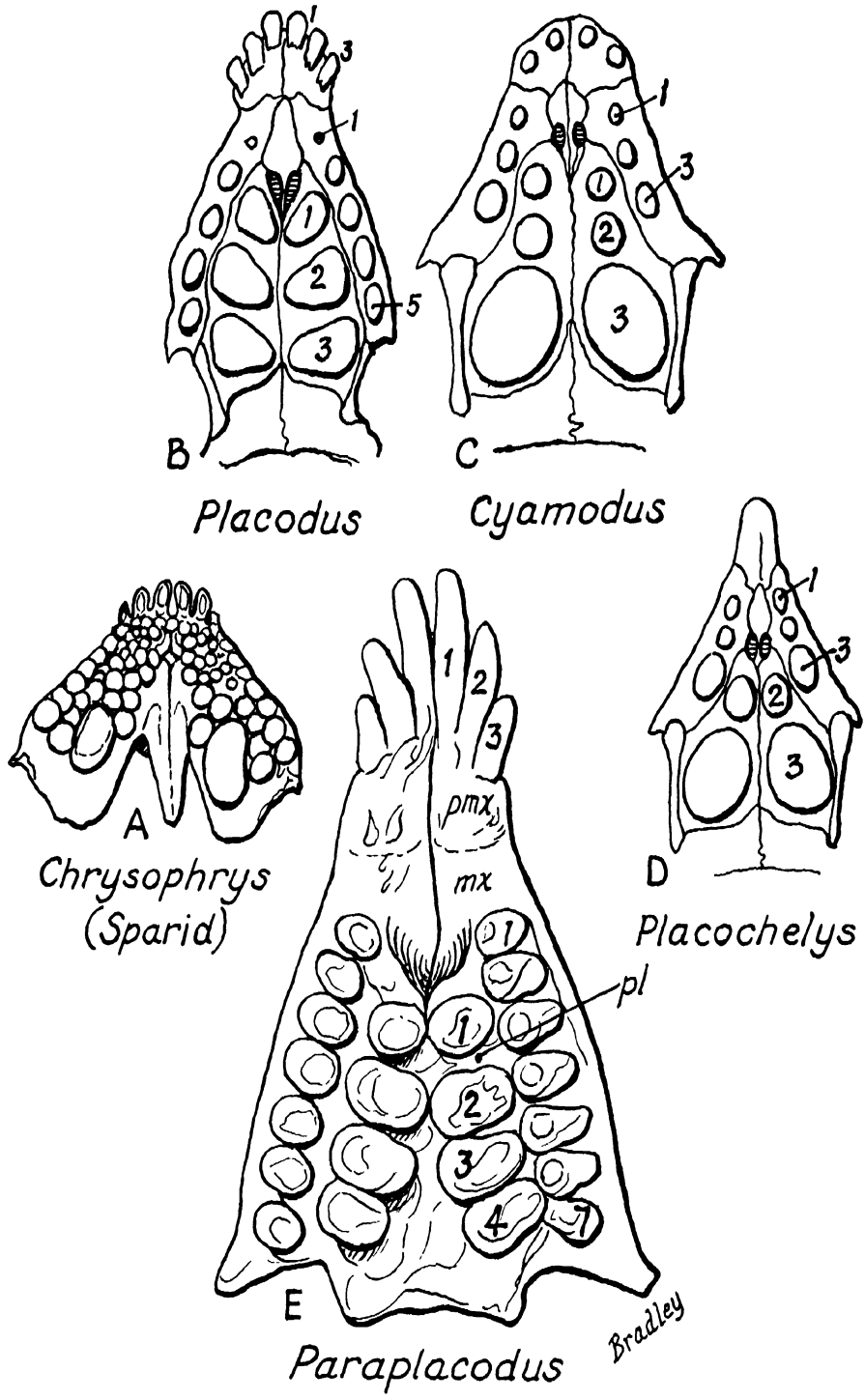


Fig. 13.19. Shell-crushing dentitions of sparid fish and placodont reptiles. Note progressive emphasis of palatal 3. A, after Abel; B–E, after Peyer.

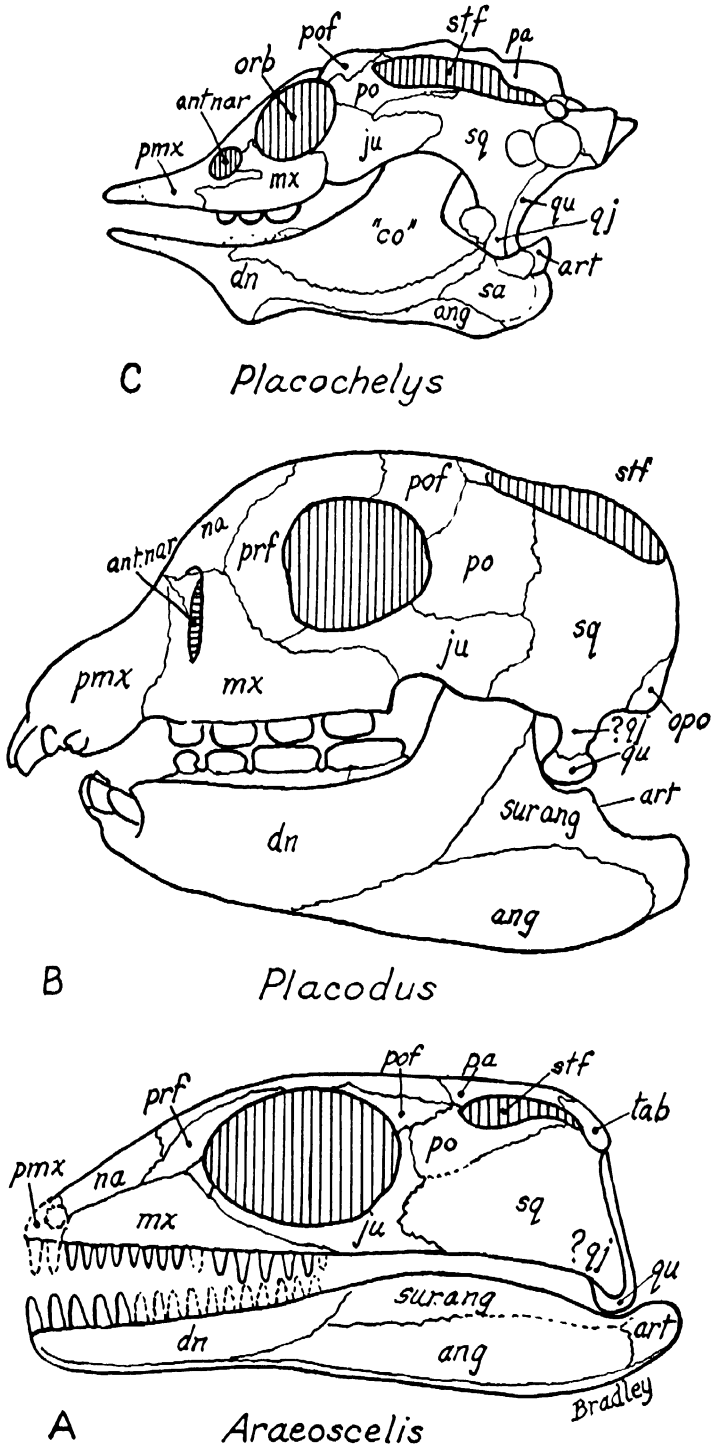


Fig. 13.20. Skulls of relatively primitive Permian protorosaur (A) and Triassic placodonts (B, C). A, after Williston; B, after Dreverman; C, after Jaekel.

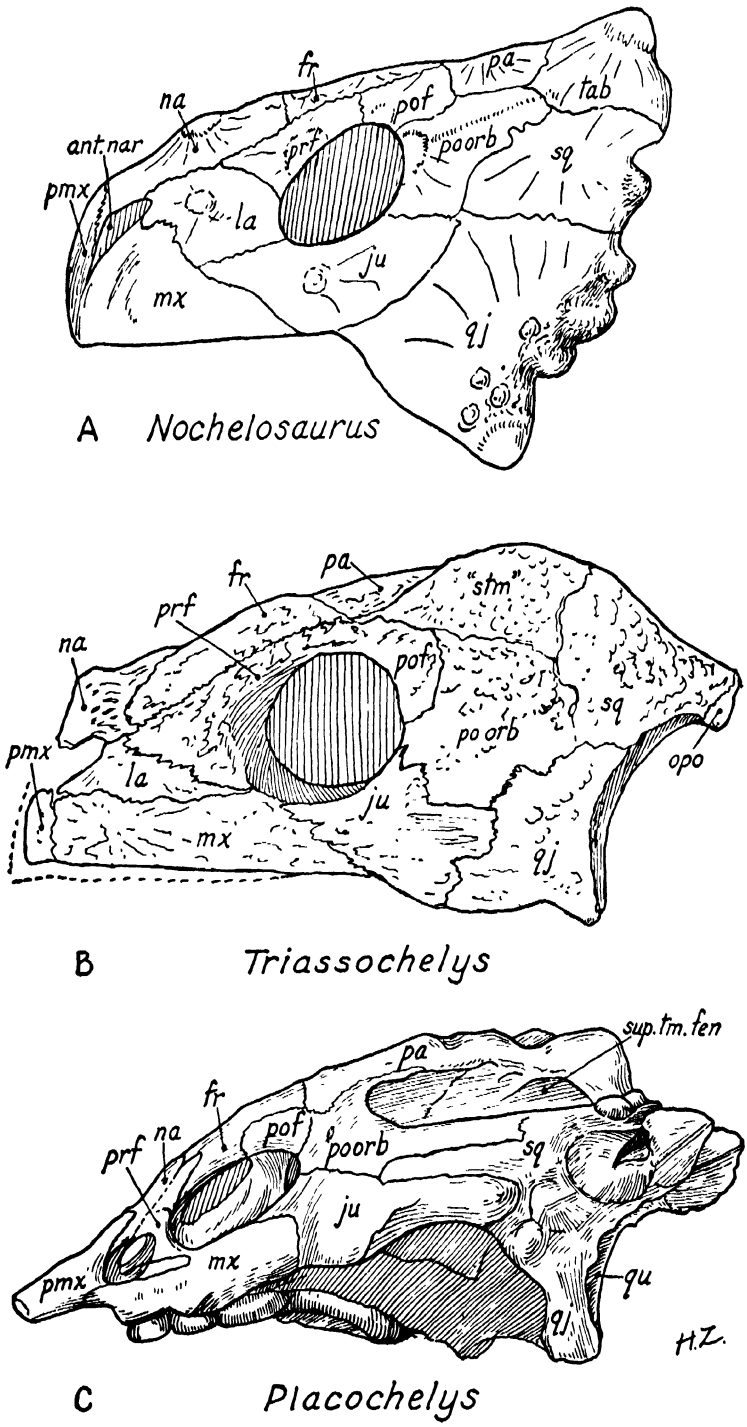


Fig. 13.21. Skulls of pareiasaur (A), primitive chelonian (B) and placodont (C). A, after Boonstra; B, after Jaekel; C, after von Huene.

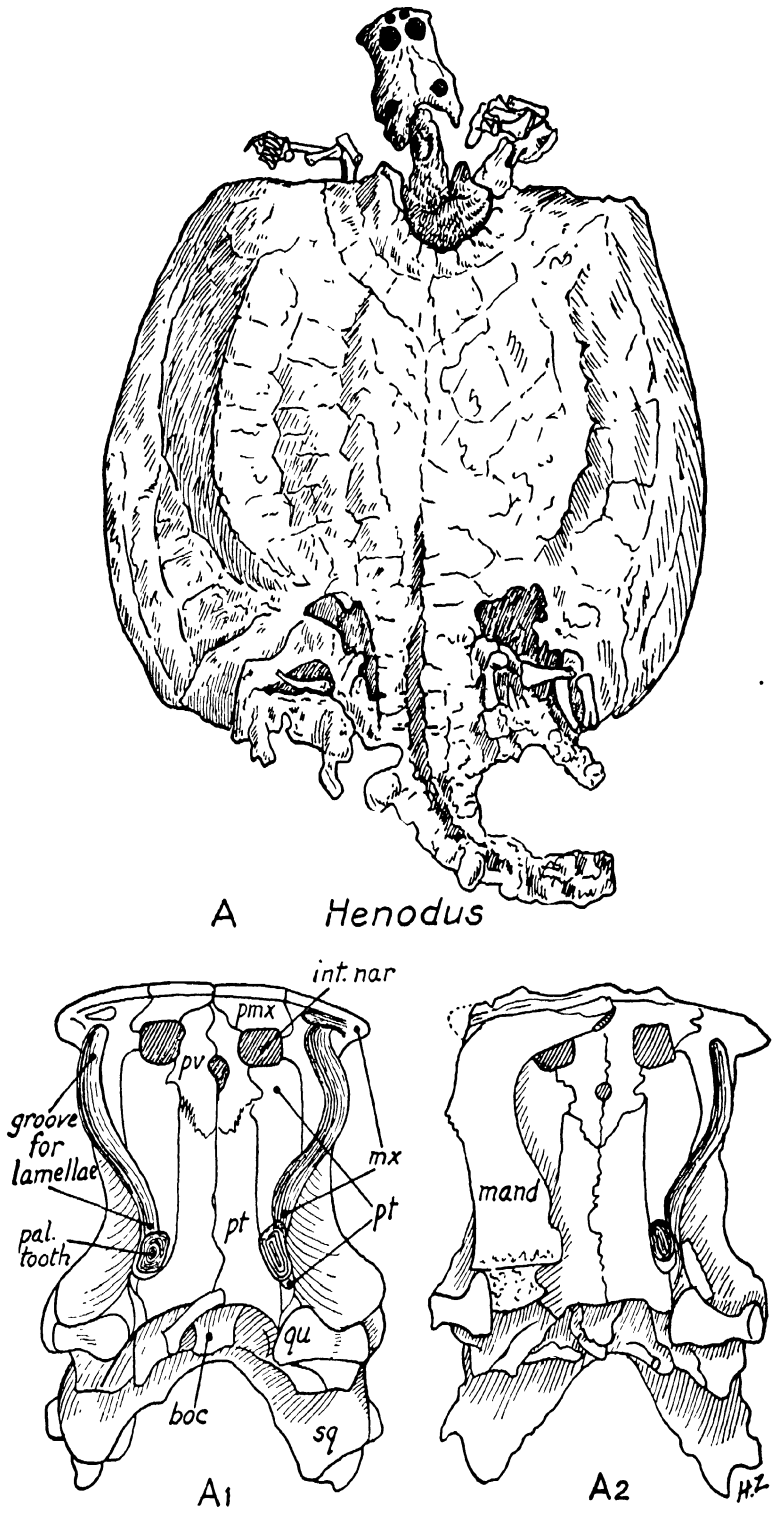


Fig. 13.22. Skeleton and test of turtle-like placodont. After von Huene.

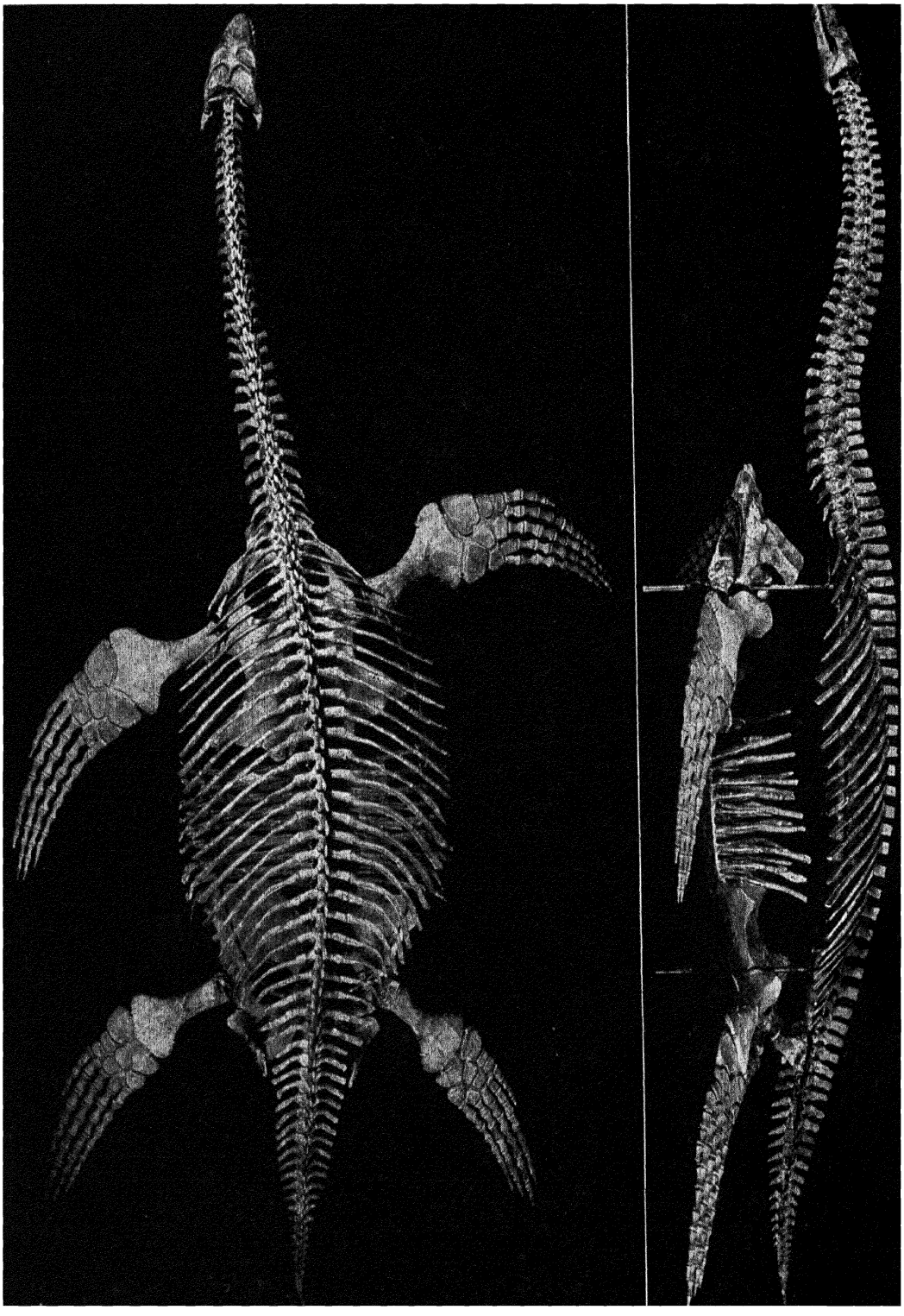


Plate 13.I. Jurassic plesiosaur. Mounted skeleton in the American Museum of Natural History.

CHAPTER XIV

THE REIGN OF THE ARCHOSAURIANS (THECODONTS, CROCODILIANS AND DINOSAURS)

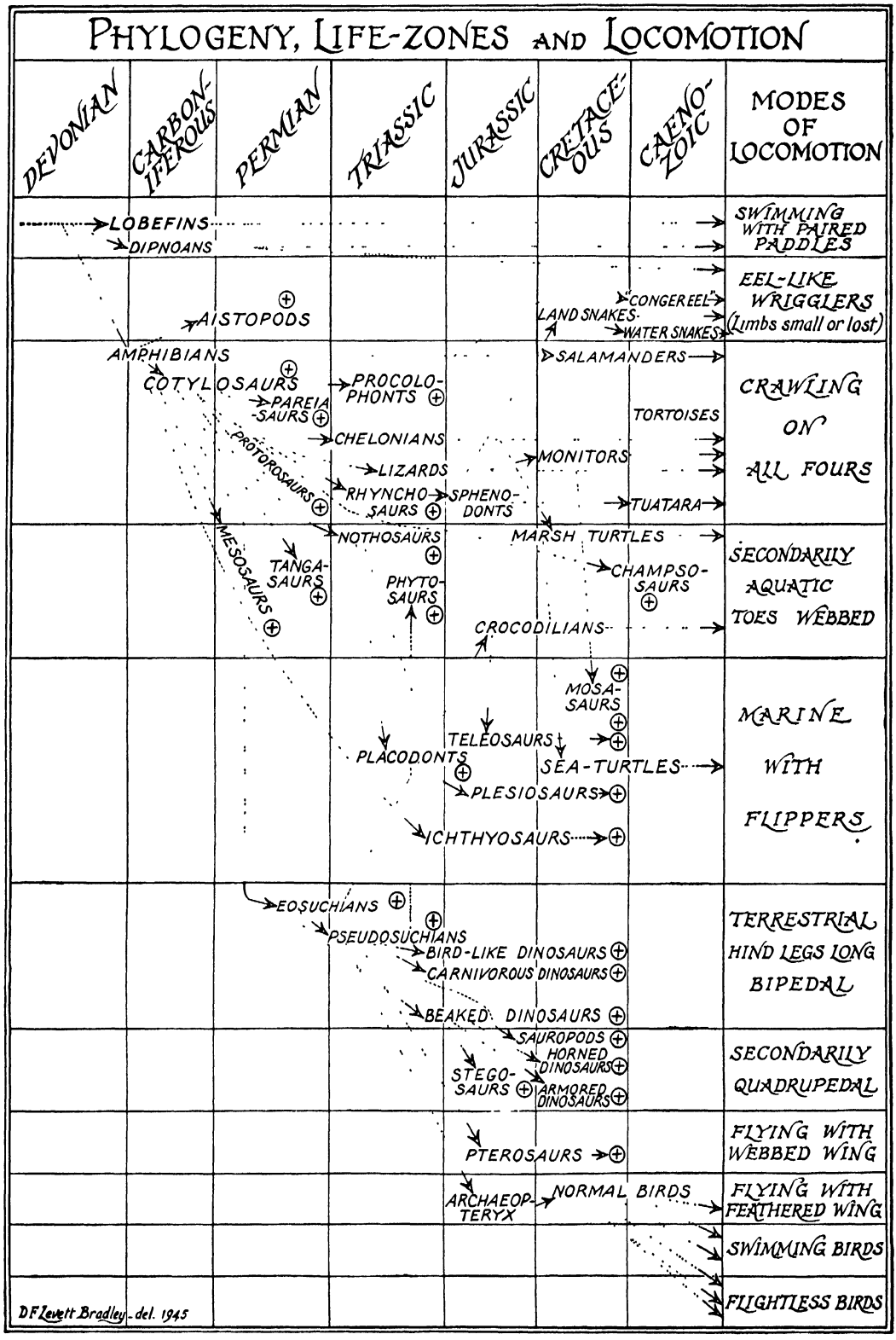

PHYLOGENY, LIFE-ZONES AND LOCOMOTION
DEVONIAN
CARBON-IFEROUS
PERMIAN
TRIASSIC
JURASSIC
CRETACE-OUS
CAENO-ZOIC
MODES OF LOCOMOTION
LOBEFINS
DIPNOANS
SWIMMING WITH PAIRED PADDLES
EEL-LIKE WRIGGLERS (Limbs small or lost)
CONGER EEL
LAND SNAKES
WATER SNAKES
AISTOPODS
AMPHIBIANS
SALAMANDERS
COTYLOSAURS
PAREIA SAURS
PROCOLO-PHONTS
TORTOISES
CRAWLING ON ALL FOURS
CHELONIANS
MONITORS
LIZARDS
PROTOROSAURS
RHYNCHO-SAURS
SPHENO-DONTS
TUATARA
NOTHOSAURS
MARSH TURTLES
MESOSAURS
TANGA-SAURS
PHYTO-SAURS
CHAMPSO-SAURS
SECONDARILY AQUATIC TOES WEBBED
CROCODILIANS
MOSA-SAURS
TELEOSAURS
PLACODONTS
SEA-TURTLES
MARINE WITH FLIPPERS
PLESIOSAURS
ICHTHYOSAURS
EOSUCHIANS
PSEUDOSUCHIANS
BIRD-LIKE DINOSAURS
CARNIVOROUS DINOSAURS
TERRESTRIAL HIND LEGS LONG BIPEDAL
BEAKED DINOSAURS
SAUROPODS
HORNED DINOSAURS
STEGO-SAURS
ARMORED DINOSAURS
SECONDARILY QUADRUPEDAL
PTEROSAURS
FLYING WITH WEBBED WING
ARCHAEOP-TERYX
NORMAL BIRDS
FLYING WITH FEATHERED WING
SWIMMING BIRDS
FLIGHTLESS BIRDS
D F Lovett Bradley del. 1945

Fig. 14.1

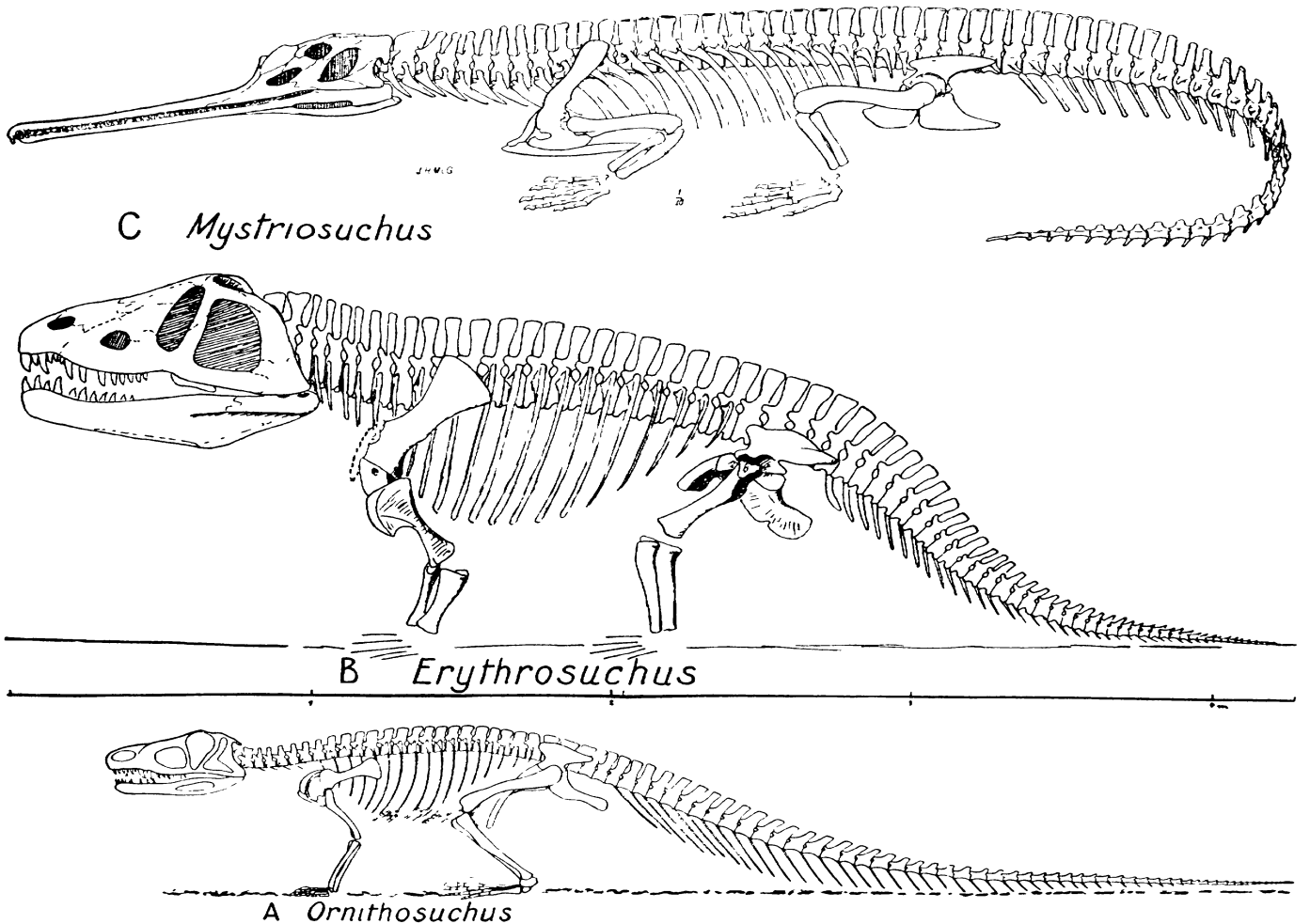
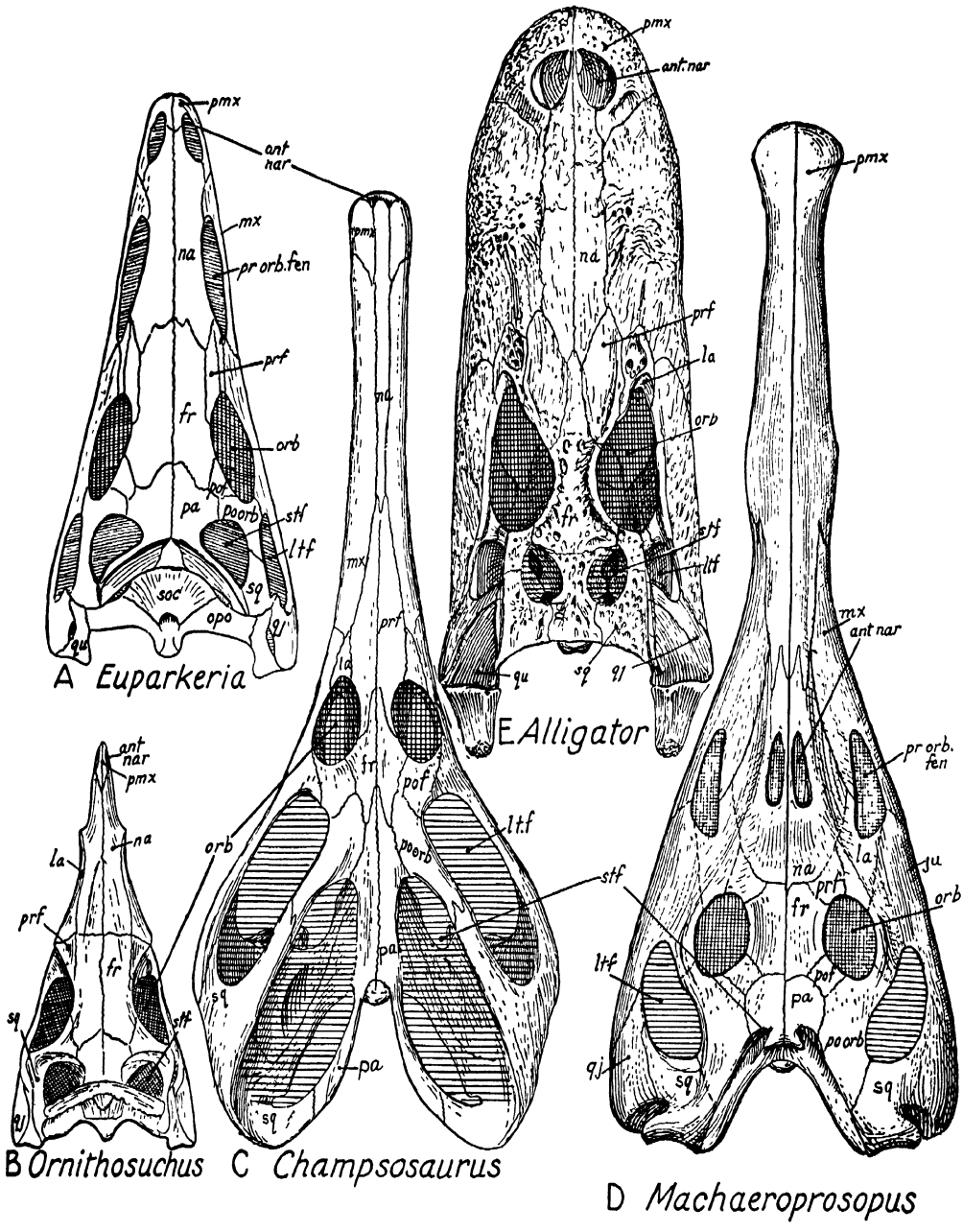


Fig. 14.2. Triassic pseudosuchians (A, B) and a phytosaur (C). A, a swift lizard-like form from Europe; B, a large predator about 13 feet long, with dinosaur-like skull, from South Africa; C, a large phytosaur from Europe. Restorations by von Huene (A, B) and McGregor (C).



Figs. 14.3, 4. Adaptive anisomerism in diapsid skulls. A, after Broom; B, after Newton; C, after Brown; D, E, after Williston. The small, more primitive skulls of the terrestrial pseudosuchians (A, B) in dorsal view are acutely triangular, with rather large orbits and moderately short snout. In the fish-catching forms (C, D) the snout becomes very long and tubular. In the carnivorous alligator (E) the snout has become wide and depressed. The supratemporal fenestrae (*stf*), rather small in the primitives, become very large in C, as do also the lateral temporal fenestrae, but they are reduced in the alligator (E) and become vestigial in the phytosaur (D). The anterior nares, originally terminal (A, B) either remains so (C, E) or shift far backward and upward to the upper surface of the skull (D), as in several other aquatic reptiles.

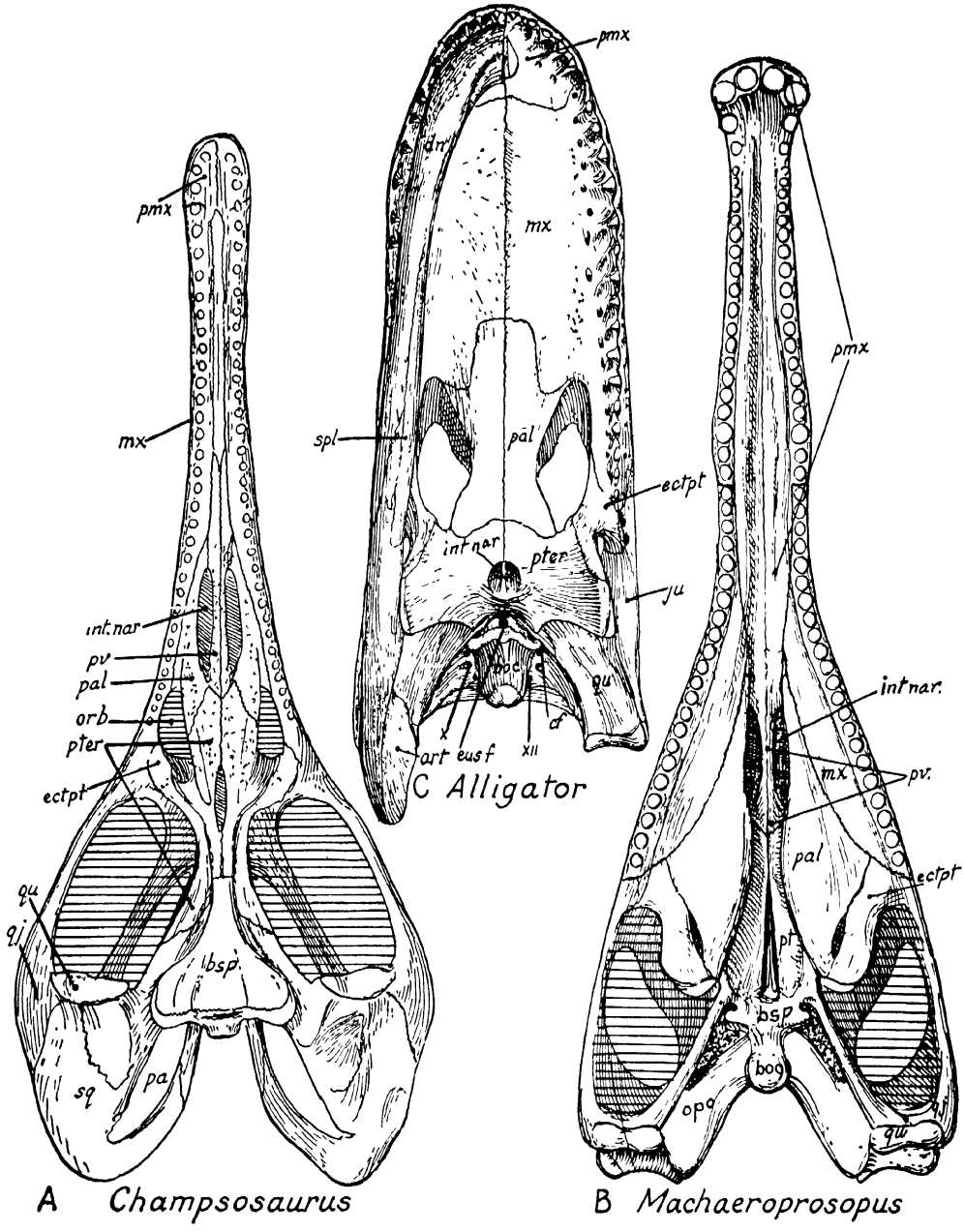


Fig. 14.5. Anisomerism in diapsid skulls (continued). Palatal views. From Williston. In the otherwise specialized rhynchocephalian (A) the bones around the internal nares retain their primitive relations. However, the great enlargement of the temporal and pterygoid muscles have squeezed the opposite pterygoids in to meet in the midline and have developed lateral crests upon them. In the phytosaur (B) the palatines are partly folded under the naso-pharyngeal tube. In the alligator (C) the maxillae, palatines and pterygoids completely surround this tube, thus transferring the internal narial opening to the rear of the backwardly prolonged secondary palate; meanwhile the descending processes of the pterygoids form a strong transverse ventral brace for the widened upper jaws, the ectopterygoids acting alternately as keystones and anchors.

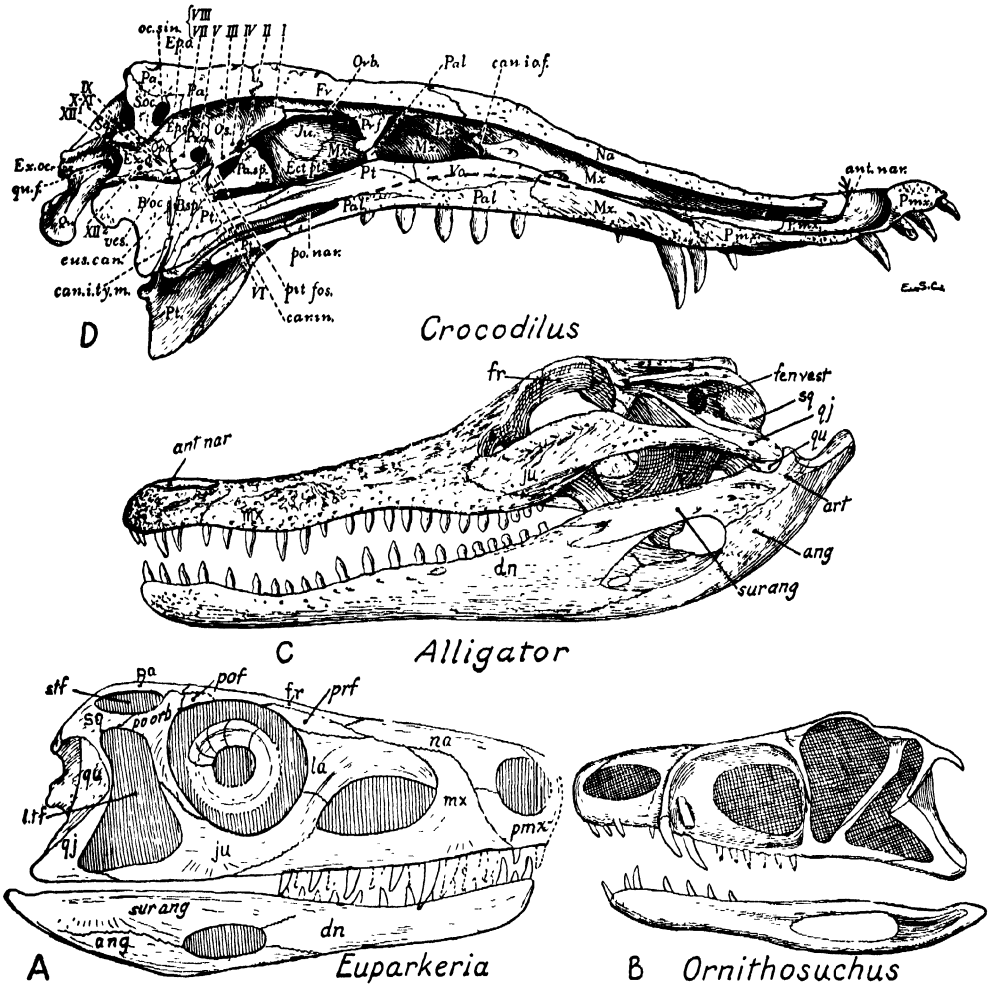


Fig. 14.6. Divergent anisomerism in diapsid skulls (continued). Lateral view (A–C) and parasagittal section (D). A–C, from Williston; D, after Osborn. In the primitive pseudosuchians (A, B) the rear part of the skull is fairly high and so is the lateral temporal fenestra (*l.t.f.*); the lower part of the suspensorium is moderately inclined backward, the jugal arch is nearly level with the cheek teeth. In the specialized alligator (B), on the other hand, the rear part of the skull is depressed, the lateral temporal fenestra vertically shallow, the suspensorium sharply inclined backward, the jugal arched upward above the level of the cheek teeth. The parasagittal section (D) illustrates *inter alia* the enclosed naso-pharyngeal tube, the long anterior pterygoid fossa for the muscle so named (cf. fig. 14.7 B), the median eustachian canal, the strongly built occipital and sphenoid regions. The prolongation of the suspensorium (*qu*) behind the occipital fulcrum not only lengthens the jaw but makes it easy to elevate the head (fig. 14.7) and thus to increase the height of the gape.

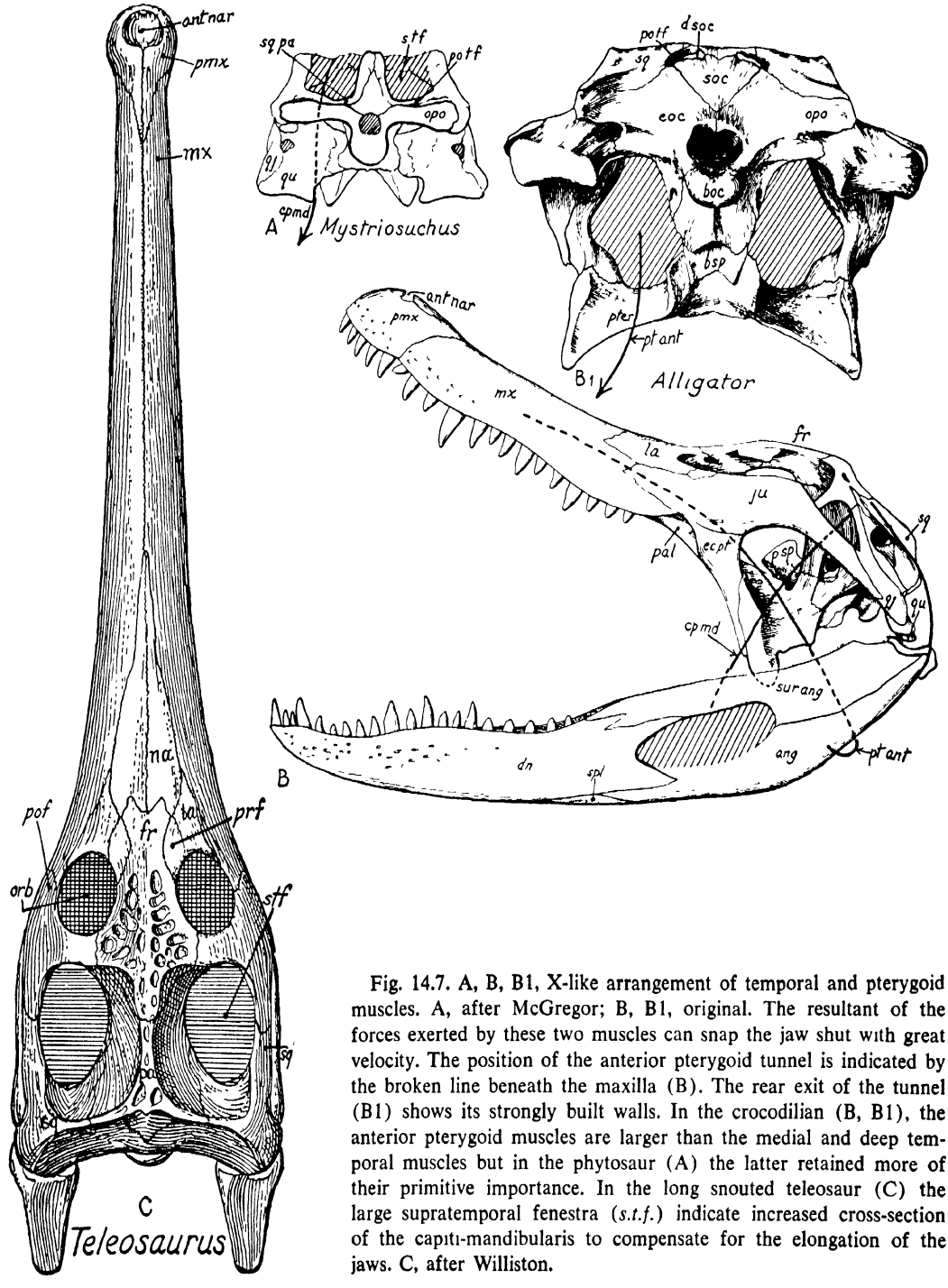


Fig. 14.7. A, B, B1, X-like arrangement of temporal and pterygoid muscles. A, after McGregor; B, B1, original. The resultant of the forces exerted by these two muscles can snap the jaw shut with great velocity. The position of the anterior pterygoid tunnel is indicated by the broken line beneath the maxilla (B). The rear exit of the tunnel (B1) shows its strongly built walls. In the crocodilian (B, B1), the anterior pterygoid muscles are larger than the medial and deep temporal muscles but in the phytosaur (A) the latter retained more of their primitive importance. In the long snouted teleosaur (C) the large supratemporal fenestra (*s.t.f.*) indicate increased cross-section of the capiti-mandibularis to compensate for the elongation of the jaws. C, after Williston.

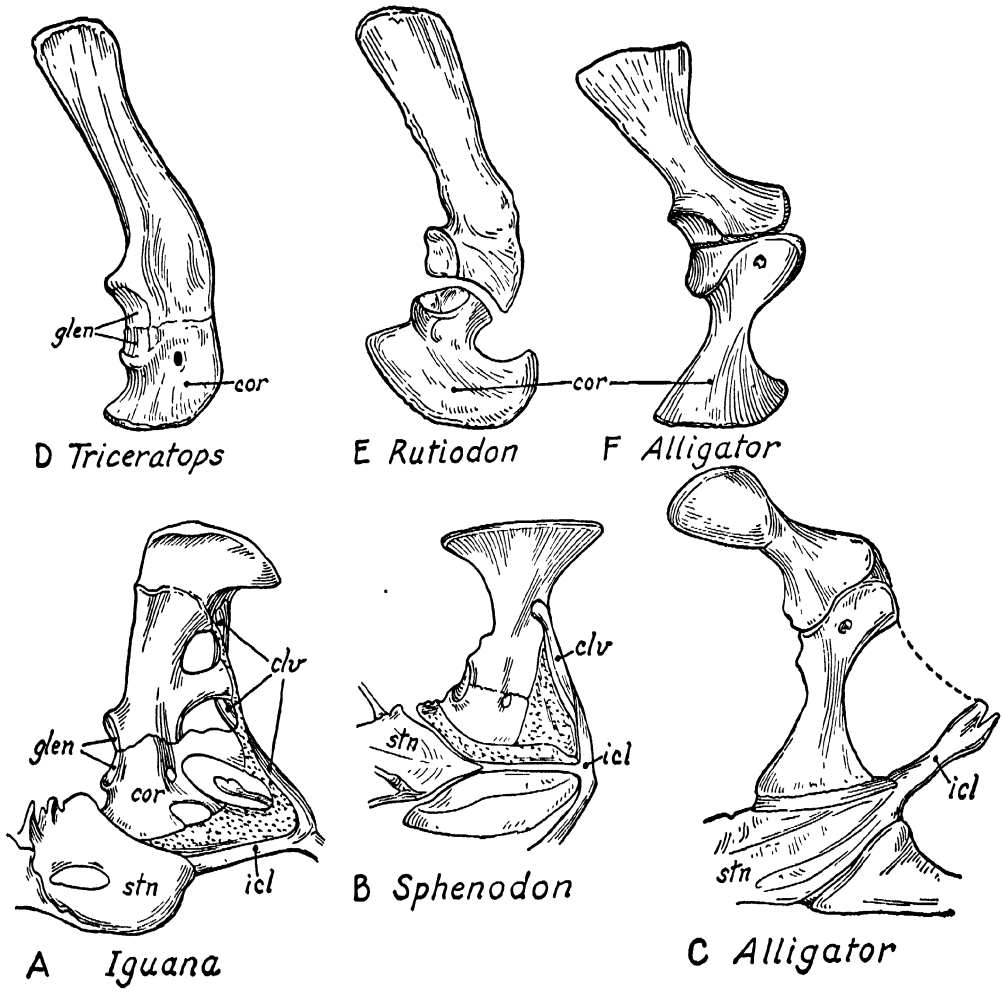

glen
cor
D Triceratops
cor
E Rutiodon
F Alligator
clv
glen
cor
stn
icl
A Iguana
clv
stn
icl
B Sphenodon
icl
stn
C Alligator

Fig. 14.8

Fig. 14.8. The pectoral girdle of parapsid (A) and diapsid (B–F) reptiles, showing the single undivided coracoid and the relations of the scapulo-coracoid to the sternum, interclavicle and clavicle. Medial view (A–C) of the left half of the pectoral girdle, and lateral view (D–F) of the right scapulo-coracoid. A–C, after Gregory and Camp; D, from Williston, after Marsh; E, from Williston, after McGregor; F, after Williston. The pectoral girdle of *Sphenodon* has inherited its primitive stamp from the primitive Permian reptiles. Here the scapulo-coracoid is unfenestrated and the coracoids transversely short, the glenoid facet being not far from the midline. The lizard scapulo-coracoid is well fenestrated in accordance with the subdivision of the dorsalis scapulae and deltoid muscles. The crocodilian coracoid (C) has widened transversely with the width of the chest, so that the glenoid facet for the humerus is far from the midline. The large coracoids are firmly based in sockets on the strong sternum. The long massive blade of this horned dinosaur scapula may be associated with its huge head and long ribs. The coracoids are relatively small, but the sternum as a whole may have been wide. A small clavicle was probably present (cf. Brown and Schlaikjer, 1940, p. 230). In the phytosaur (E) the recurved blade and embayed anterior border of the coracoid suggest those of Crocodilia (F) but are more primitive.

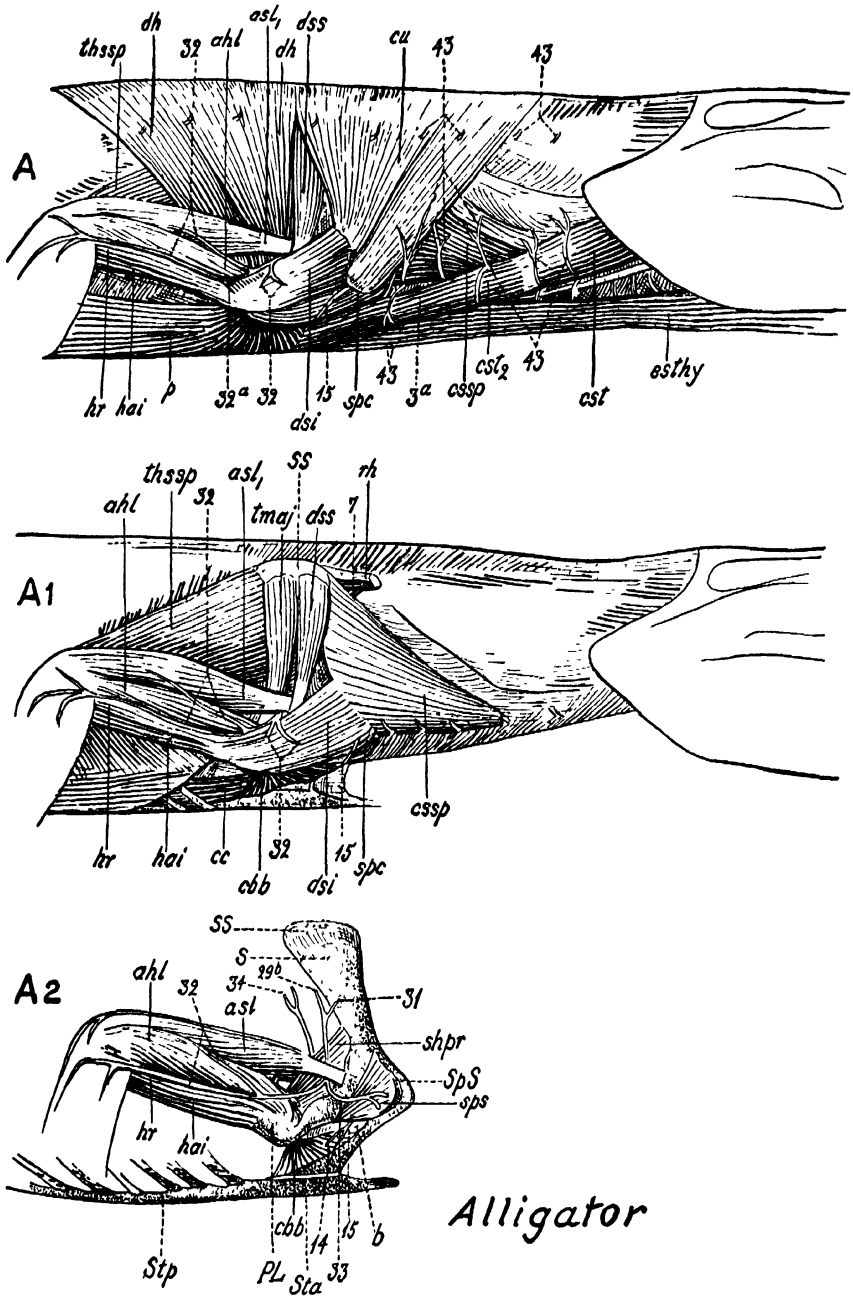
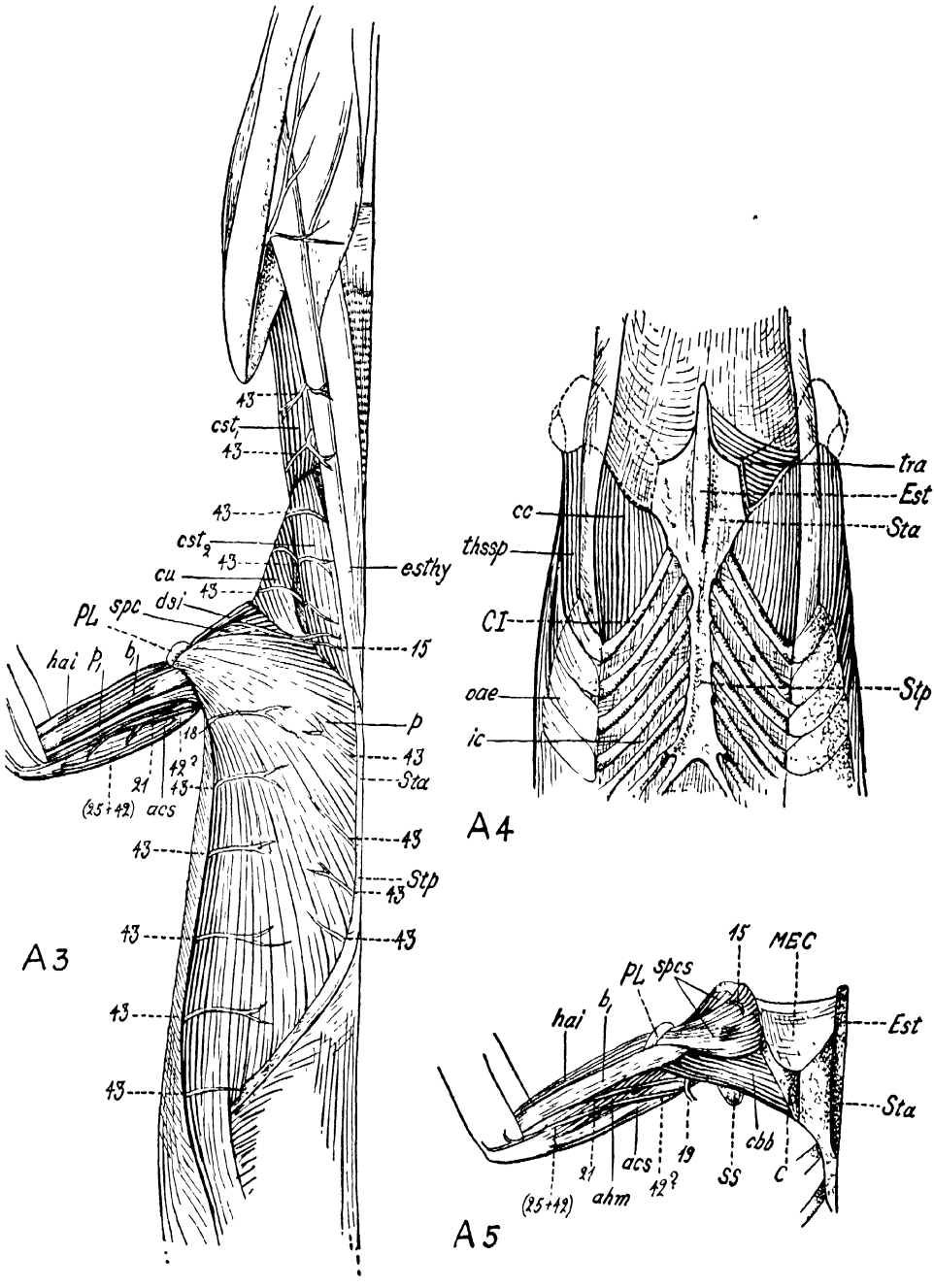


Fig. 14.9a, b. Musculature of the pectoral girdle and upper arm in the alligator. From Gregory and Camp, after Fürbringer. The girdles and limbs of vertebrates are specialized lateral outgrowths of the muscular body wall; their muscles are derived eventually from myomeres, their skeletal cores from osseous deposits in the interspaces between adjacent muscle masses. The pectoral girdle is like a cradle or hayrack, which is folded around the thorax. It is fastened at the bottom of the thorax (A2) by the sternum, interclavicle and clavicles (the latter have been lost in the Crocodilia).



The dorsal branch of the hayrack or cradle is the scapula, which grows upward outside the body wall, carrying with it the cervical and thoracic parts of the serratus musculature (A 1 *cssp, thssp*), an arrangement not unlike a suspension bridge. The pectoral limb muscles are divided (by Romer, 1922, 1944) into: (1) DORSAL GROUP, above the fulcrum or glenoid facet, tending to elevate the humerus, including deltoides clavicularis (*"dsi"*), deltoides scapularis (*"dss"*+ *"tmaj"*), latissimus dorsi (*dh*), triceps ("anconeus," *"ast"*+*"aht"*), subscapularis (*"shpr"*); (2) VENTRAL GROUP, ventromedial to the glenoid facet, tending to depress the humerus, including pectoralis (*"p"*), supracoracoideus (*"spcs"*), coracobrachialis (*"cbb"*), brachialis inferior (*"hai"*) biceps (*"bi"*).

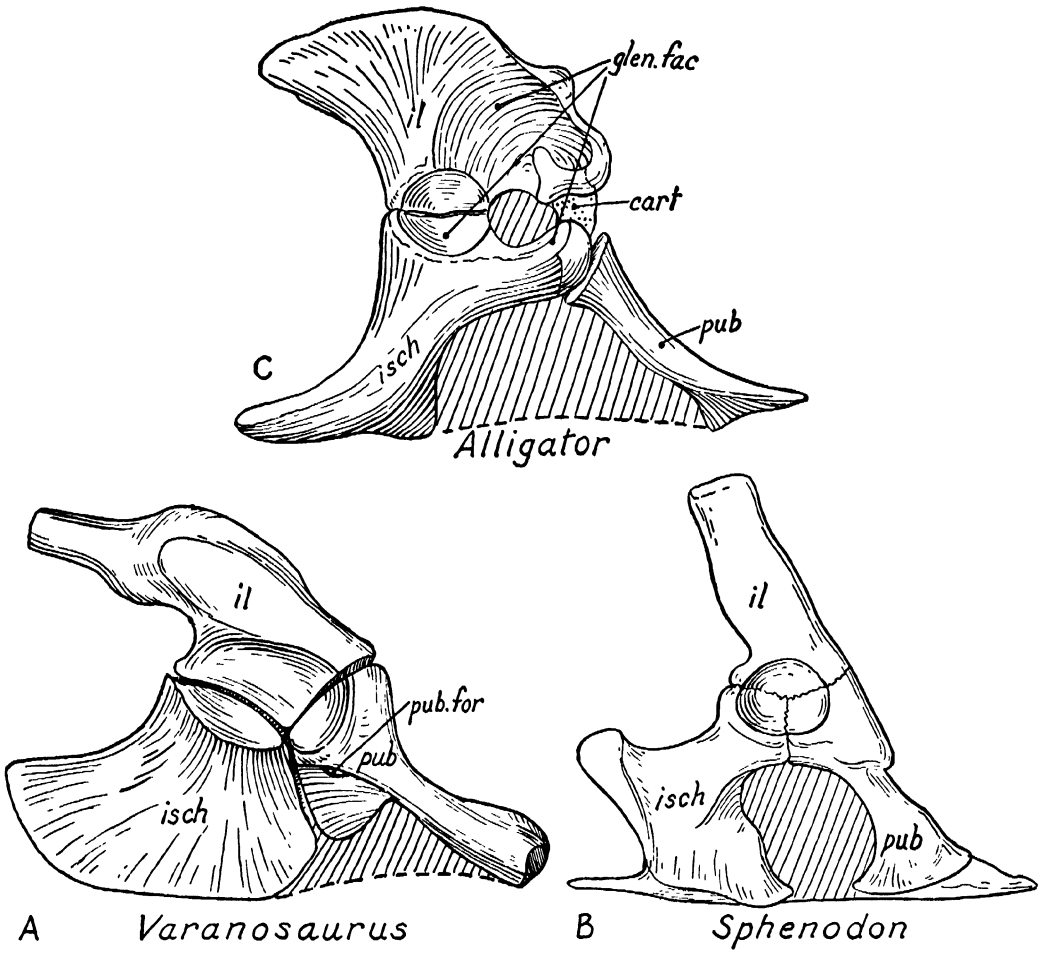


Fig. 14.10. Three grades of evolution of the pelvis. A, C, after Williston; B, from Gregory and Camp. A, Primitive reptilian grade in a Permian pelycosaur: glenoid articular surface tripartite, suture triradiate; pubo-ischiadic fenestra relatively small, anterior; pubic foramen retained; ischium plate-like, massive; gluteal surface of ilium but little expanded; dorso-posterior process of ilium (for ilio-caudalis muscle) prolonged backward. B, Intermediate grade: glenoid tripartite, suture triradiate; pubo-ischiadic fenestra well developed, iliac blade without anterior expansion; ischium large, with prominent tuberosity; iliac blade not expanded. C, Specialized crocodilian grade: acetabulum no longer tripartite, the pubis being excluded from it by a large anterior acetabular process of the ischium; glenoid facet expanded, perforated and otherwise differentiated, its anterior border including a cartilaginous nodule, thought by Williston to represent the remains of the true pubis, the so-called pubis being in his view (Williston) really an epipubis or parasternal plate. But in the very primitive Triassic crocodilian *Protosuchus*, fig. 14.14 B, the pubis is barely excluded from the acetabulum. Nor does the arrangement of the muscles favor the view that these paired bones are not true pubes (cf. Romer, 1923, pl. XXIV). The massiveness of the ilium is in resistance to the great strength of the muscles of the tail and limbs (fig. 14.11 C).

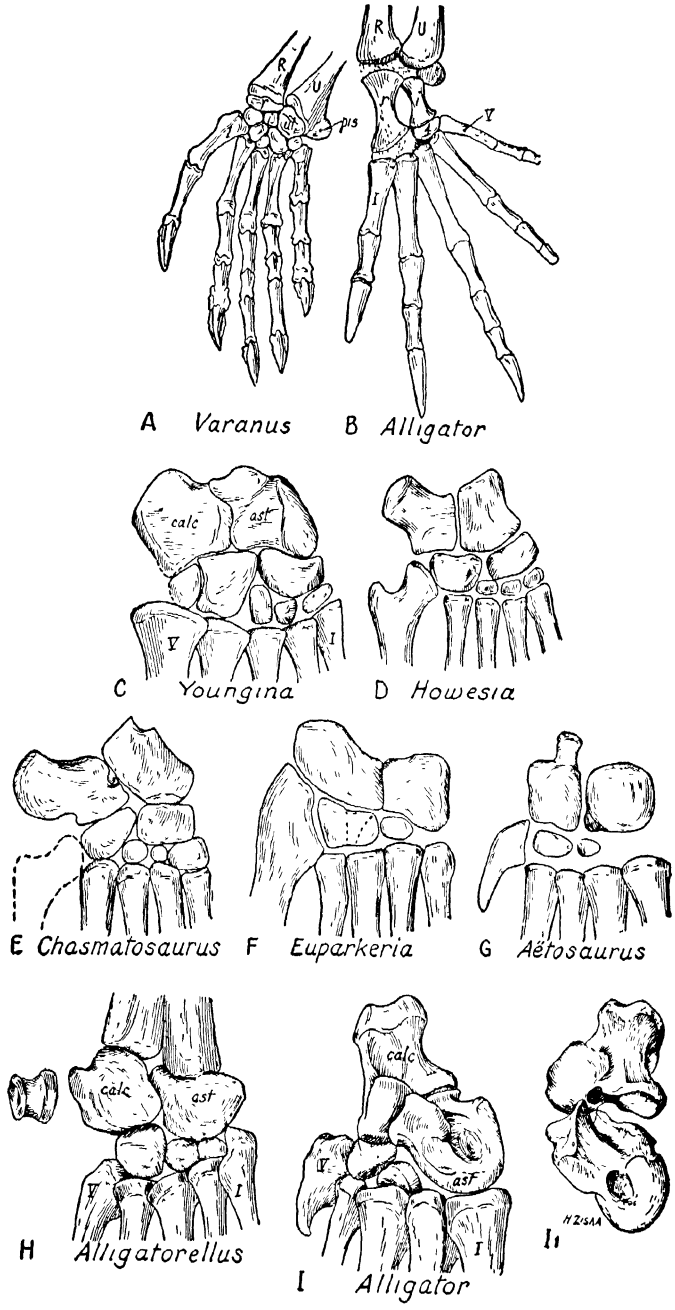


Fig. 14.11. Specialized carpus (A) and tarsus (H, I) of crocodilians compared with those of primitive parapsid (A) and diapsids (C–G). A, B, original; others after Schaeffer. A, B, left manus; C–I, right tarsus. The differential elongation of the radiale and intermedium in the Crocodilia bends the hand backward and spreads the metacarpals and digits, increasing the efficiency of the hand both in swimming and in running. The well turned joints on the astragalus and calcaneum in the alligator (I, I1) contrast with the more primitive, less differentiated conditions of the lizard-like pseudosuchians (C–G). These articular surfaces permit sharp bending and smooth extensive twisting of the tibia and fibula upon the tarsus (Schaeffer).

Fig. 14.12. Musculature of the pelvis and thigh in reptiles. From Gregory and Camp, after Fürbringer. The hind limb, like the fore limb, consists essentially of an outgrowth of muscle segments from the body wall, forming a sort of flexible cone or pyramid surrounding a central bone core. Nevertheless the several muscles of the hind limb are not individually serially homologous with those of the fore limb, although both are derived collectively from serially homologous groups of myomeres innervated by the motor branches of spinal nerves (cf. figs. C1, A, C). Applying the classification of pelvic and hind limb muscles worked out by Romer (1922, pp. 521–523, 595–599) to the study of figs. A–C1, we may note that:

(1) The pelvis serves as an anchor in front to the presacral, spinal and abdominal muscles, and in the rear to most of the caudal muscles (e.g. *il.cd, is.cd*).

(2) The "Primitive Dorsal Group" of limb muscles includes among others the following:
   (a) superficial extensors (*e.il.t.1,2*), ambiens (*amb*), femoro-tibialis (*fm.tb.*), tibialis anticus, etc.
   (b) iliofibularis (*il.fib.*)
   (c) pubo-ischio-femoralis internus (=*ilio-psoas*) (incorrectly named "*qudr lb*" in C, C1), (*p.is.f.int.*, C1), ilio-femoralis (*il.f.*= *glutei*), pubo-ischio-femoralis posterior (*pb.is.fm.post.*)

(3) "Primitive Ventral Group," includes:
   (a) pubi-ischio-tibialis (*pb.is.tb.*), pubo-tibialis (*pb.t*), flexor tibialis internus (*fl.t.int.*).
   (b) adductor ("ischio-femoralis") (*is.fm.*).
   (c) pubo-ischio-femoralis externus (*p.is.f.ext.*)
   (d) gastrocnemius and flexors of foot. The caudi-femoralis (sensu lato, *cd.fm.*) and related caudilio-femoralis pull the leg backward and inward.

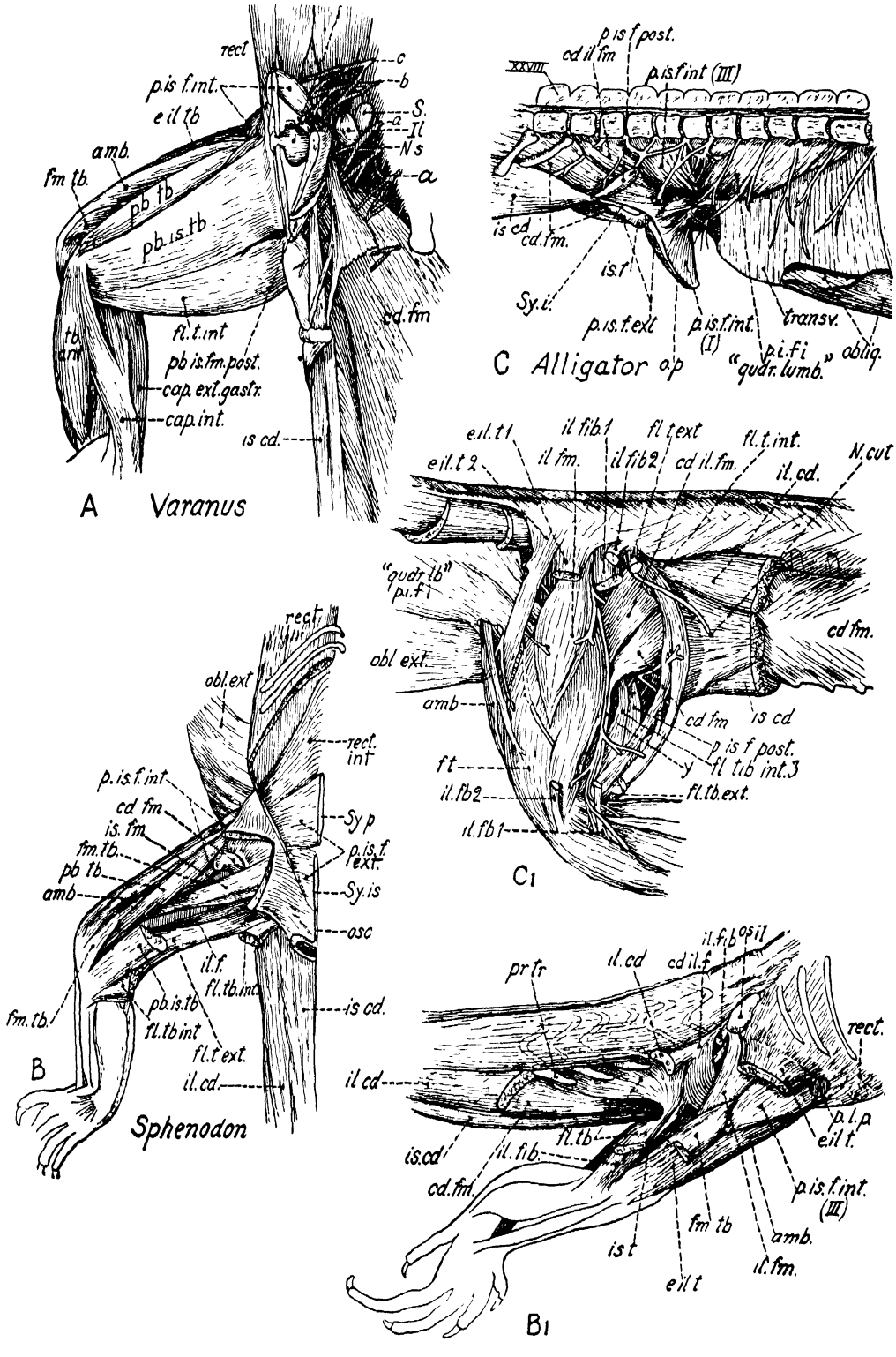

rect
c
b
p.is f.int.
e il tb
S.
a
Il
Ns
amb.
a
fm tb.
pb tb
pb.is.tb
cd.fm
fl.t.int
pb is.fm.post.
cap. ext.gastr.
cap.int.
is cd.
A Varanus
p.is f post.
cd il fm
XXVIII
p.is.f int (III)
is cd
cd.fm.
is.t
Sy.i.
p.is.f.ext
p.is.f.int.
(I)
transv.
p.i.fi
"qudr. lumb."
obliq.
C Alligator o.p
e.il.t1
il fib1
fl t ext
fl.t.int.
N.cut
e il.t 2
il fm.
il fib2
cd il.fm.
il.cd.
"qudr.fb"
p.i.fi
cd fm.
obl ext.
amb
cd fm
is cd
p is f post.
ft
fl t.b int.3
il.fb2
fl.tb.ext.
il.fb1
C1
rect
obl.ext
rect.
int
p.is.f.int
cd fm
Syp
is. fm
p.is.f.
ext.
fm.tb.
pb tb
amb
Sy.is
osc
il.f.
fl.tb.int
pb.is.tb
is cd.
fm.tb.
fl.tb int
fl.t ext
B
il.cd
Sphenodon
il.f.b osil
il.cd
cd il.f
pr tr
rect.
p.l.p
e.il t.
il cd
fl.tb
is.cd
il.fib.
p.is.f.int.
(III)
cd.fm.
fm tb
amb.
is t
il.fm.
e il t
B1

Fig. 14.12

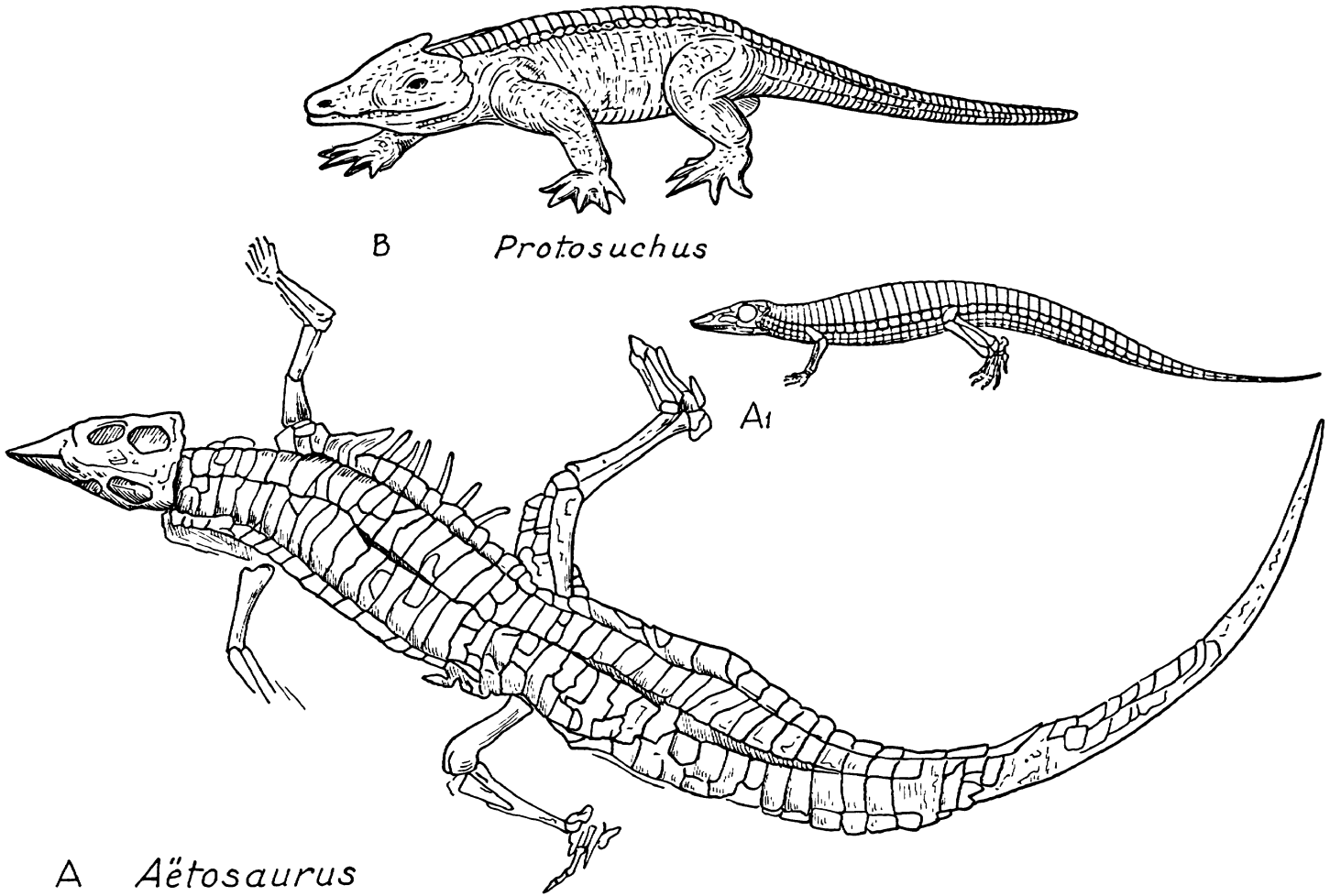


Fig. 14.13. A, An armored aëtosaur from the Trias of Germany. Composed from two of the many individuals figured by O. Fraas. A1, Restoration of *Aetosaurus,* after Marsh. B, A Triassic link between crocodilians and pseudosuchians, restoration after Barnum Brown.

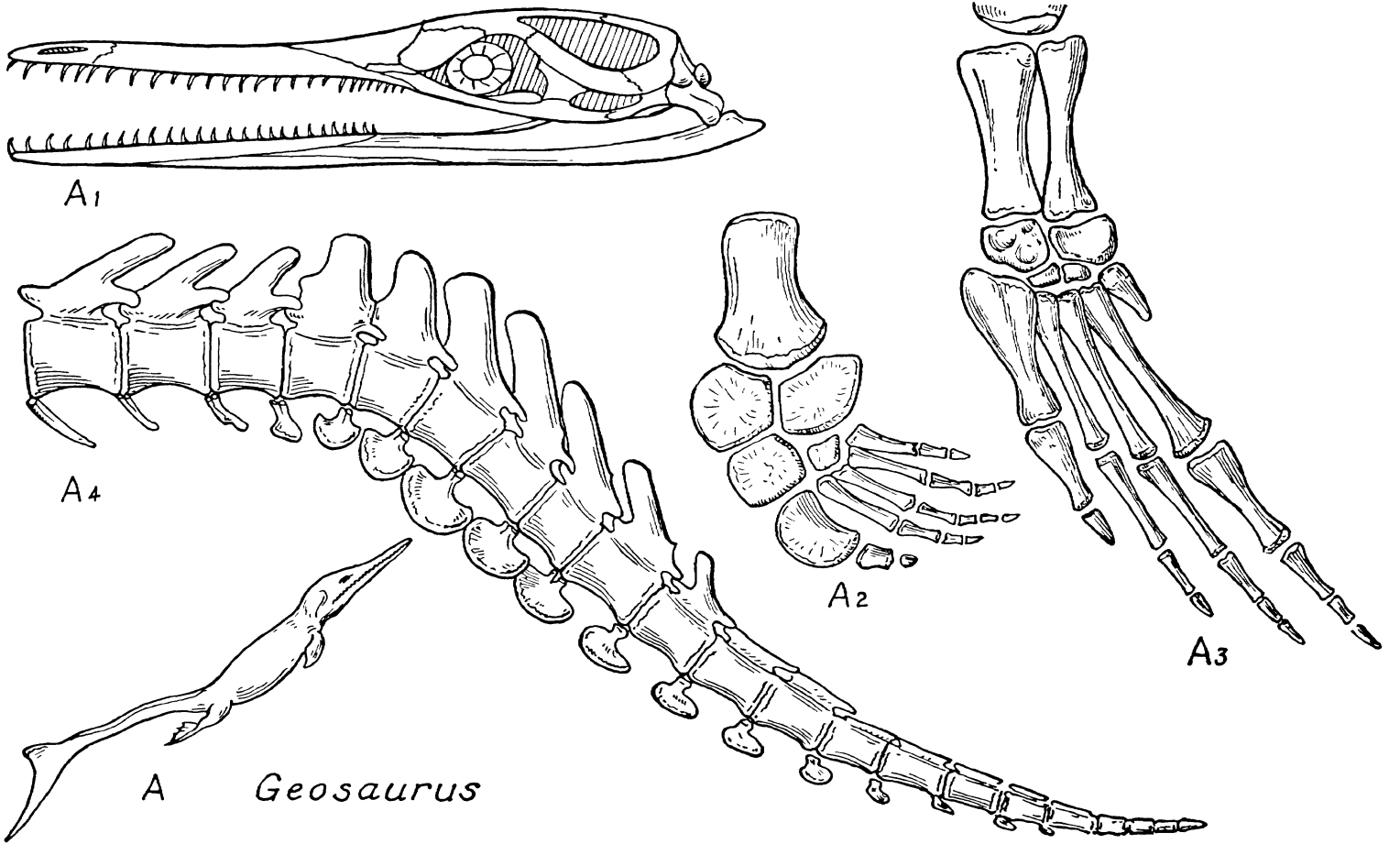


Fig. 14.14. A marine crocodilian of Jurassic age. After E. Fraas. Convergence toward contemporary ichthyosaurs is seen in the general appearance of the fish-catching skull, in the down-turning of the posterior caudal vertebrae to support a dermal caudal fin, in the extreme shortening and widening of the humerus, radius, ulna and radiale. But the phalangeal formula is crocodilian. The hind limb, although less specialized than the fore limb, is becoming paddle-like.

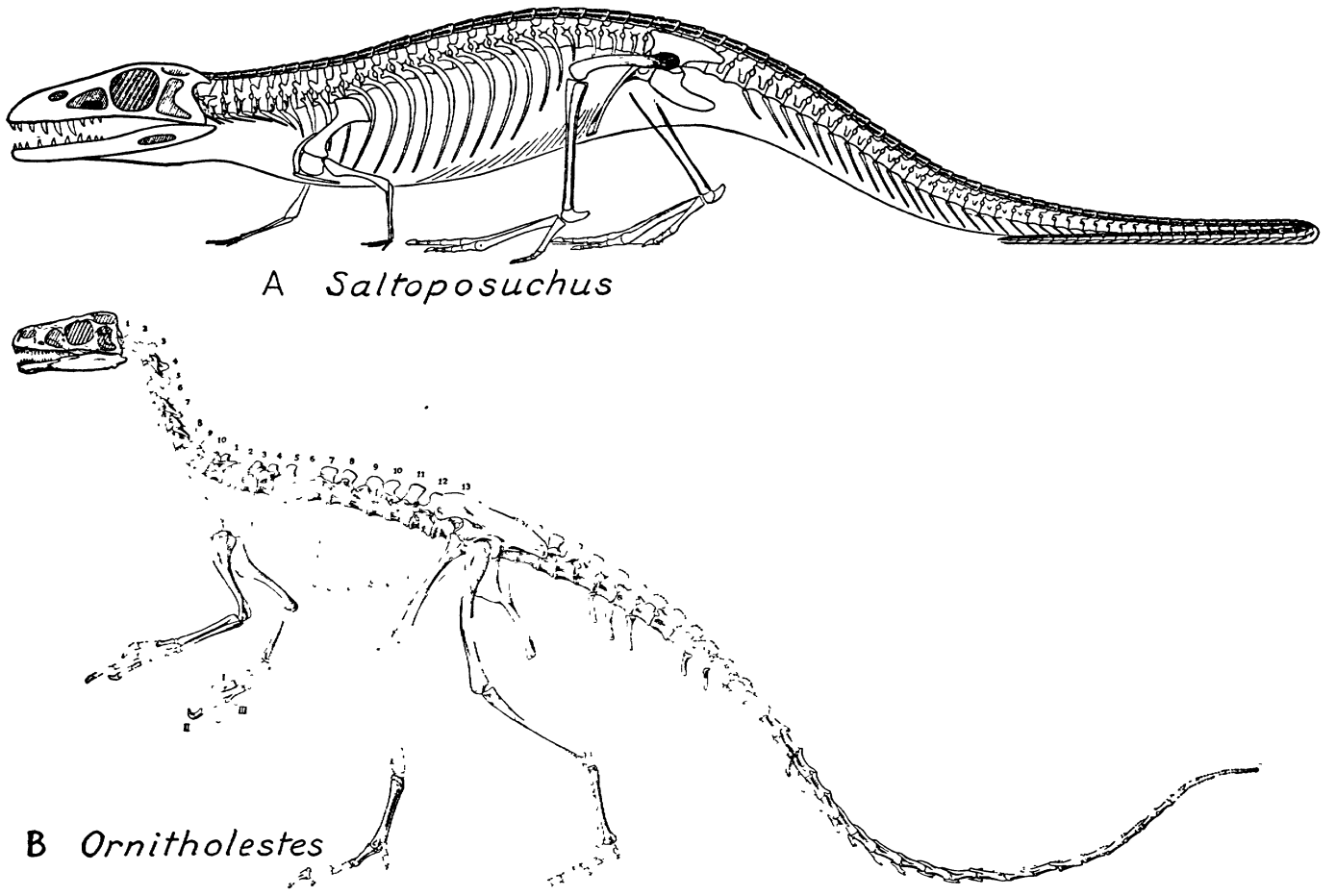


Fig. 14.15. A, Primitive pseudosuchian from the Trias of Connecticut, restored by von Huene. B, Coelurosaurian dinosaur from the Jurassic of Wyoming, after Osborn.

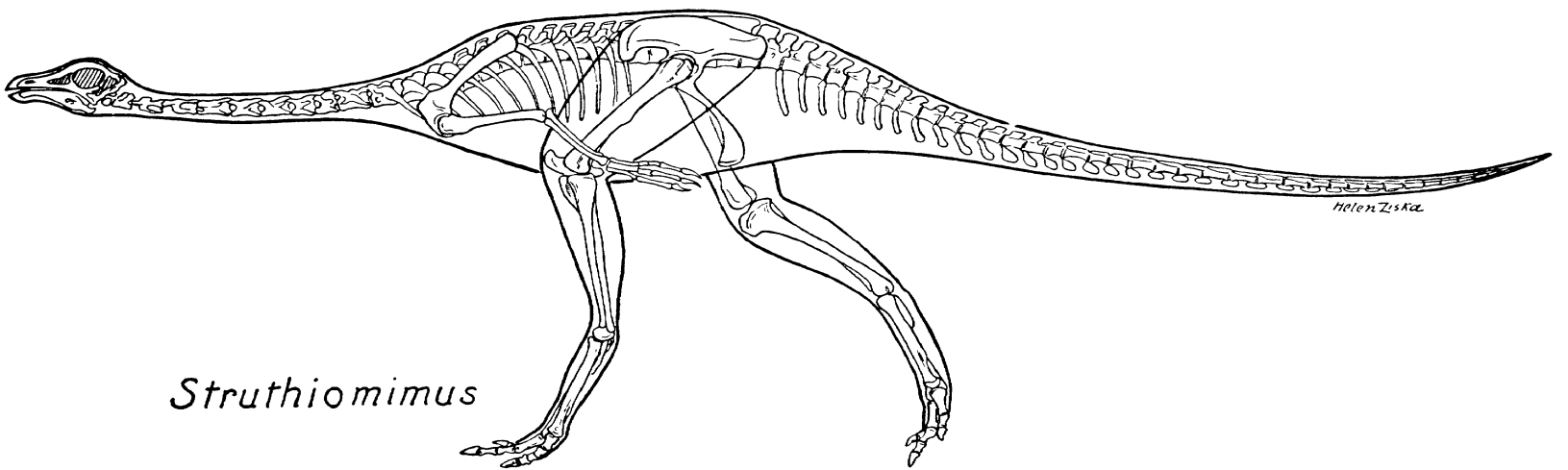


Fig. 14.16. Restoration of the skeleton of *Struthiomimus*; in running pose with body balanced at the hip. After Gregory. In stopping, the head would be raised, the arm bent forward and the tail lowered.

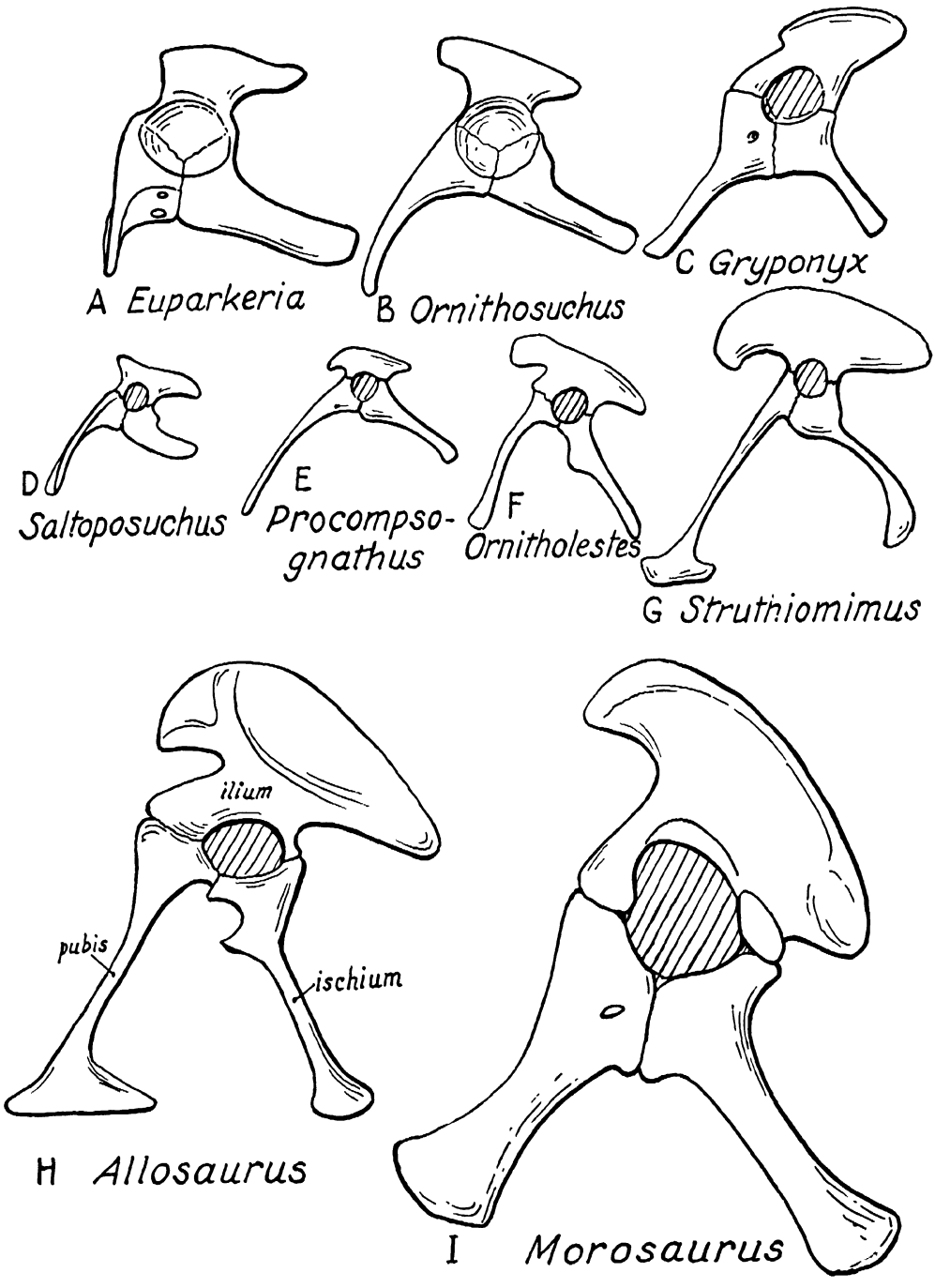


Fig. 14.17. Triramous pelves of Triassic pseudosuchians (A, B, D, E) and of saurischian dinosaurs (C, F–I). A–C, after Broom; D, E, after von Huene; F, G, after Osborn; H, I, after Marsh. In the lizard-like *Euparkeria* (A) the pelvis was close to the primitive Permian type, except for the down-turning of the anterior rim of the pubis and the backward prolongation of the ischium. The large acetabulum is imperforate. In the more swift-running pseudosuchians (B, D, E) the pubis is longer. In the bipedal saurischians (F–H) the pelvis remains triramous, the acetabulum is perforate, the ilium expands. In the gigantic sauropod (I) the enlarged pubis becomes secondarily plate-like.

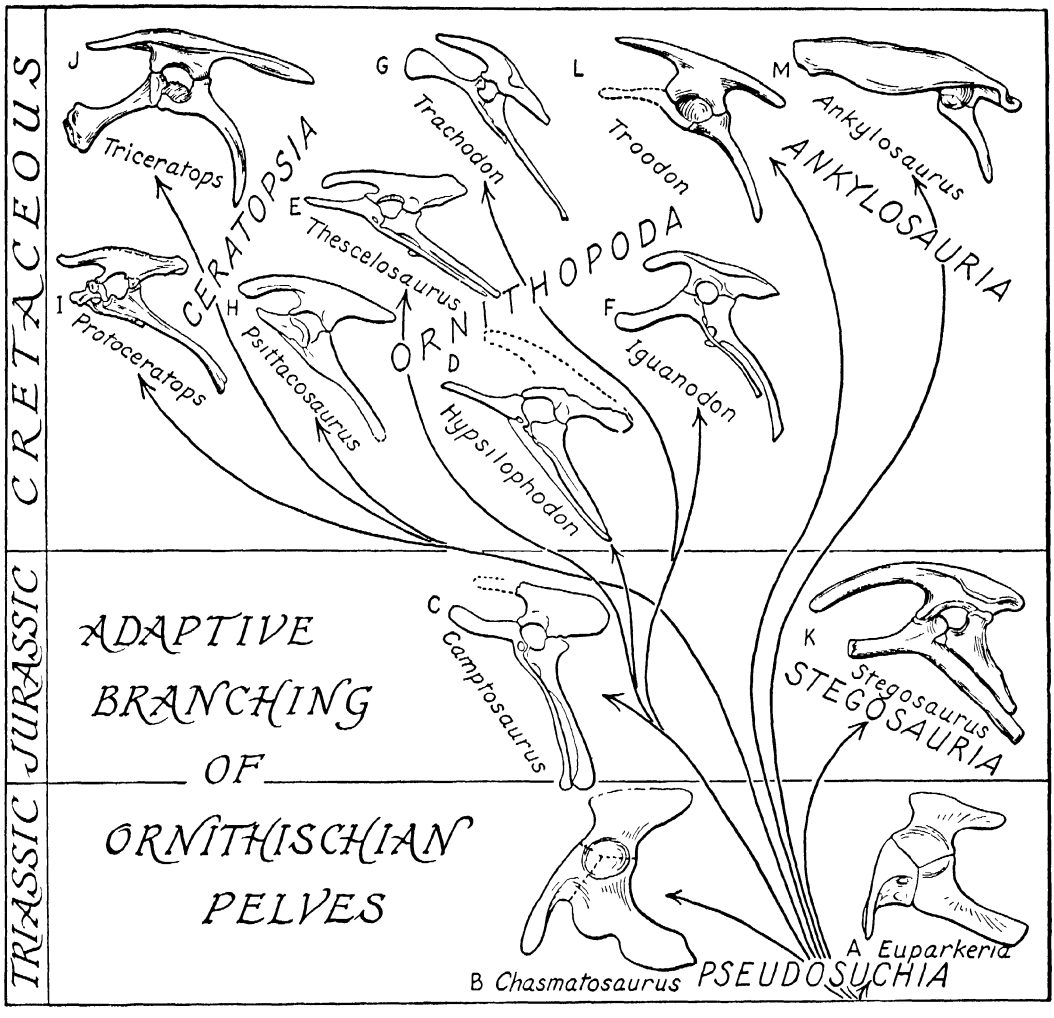


Fig. 14 18. Evolution of the quadriramous pelvis of the ornithischians. A, B, after Broom; C, after Gilmore; D, after Huxley and Romer; E, after Brown; F, from Osborn, after Dollo; G, after Brown; H, after Osborn; I, after Brown and Schlaikjer; J, K, after Marsh; L, after Gilmore; M, after Brown and Romer.

The long posterior ventral rod appears to be the backwardly rotated pubis (fig. 15.15 and Romer, 1927, p. 245), while the anterior ventral process is an outgrowth from the body of the pubis to which the obliquus abdominis was probably attached (fig. 14.35 A2 and Romer, 1927, pp. 242, 263). Romer (1927) has also noted that the backward prolongation of both pubis and ischium probably greatly increased the length of the obturator and ischio-trochantericus muscles (fig. 14.35b). Meanwhile the prolongation of the anterior process of the ilium greatly widened the base for the iliotibialis muscles. The long notch between the ilium and the prepubis was occupied by the iliofemoralis internus (fig. 14.35). The main changes from the relatively primitive stage (C) onward were as follows: (1) reduction of prepubic process in H, I, M; (2) enlargement of prepubic process (G, J); (3) eversion and transverse expansion of dorsal rim of ilium, beginning in K, culminating in J and M.

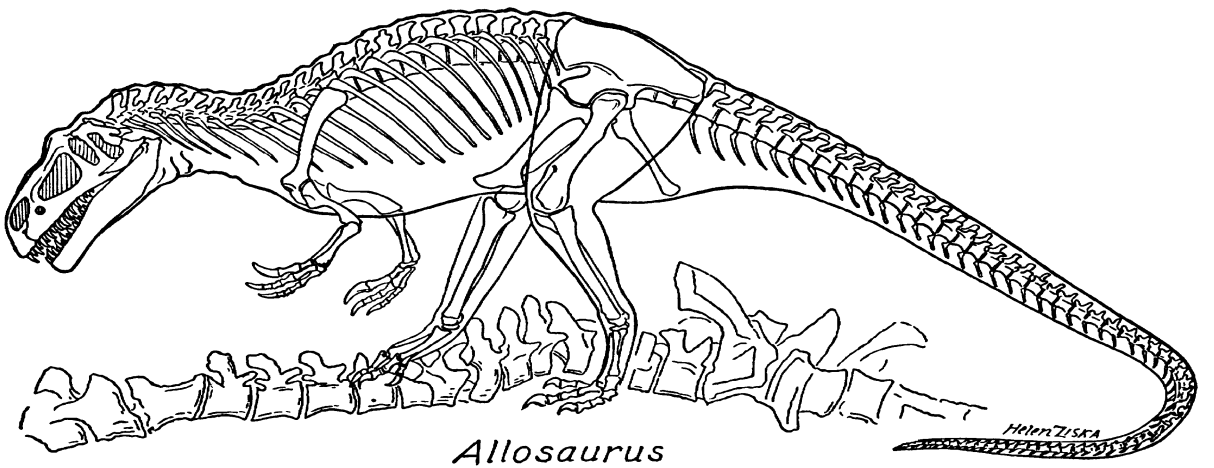


Fig. 14.19. Skeleton of *Allosaurus* (=*Antrodemus*). From mounted skeleton in the American Museum of Natural History. Hands corrected from Gilmore (1920).

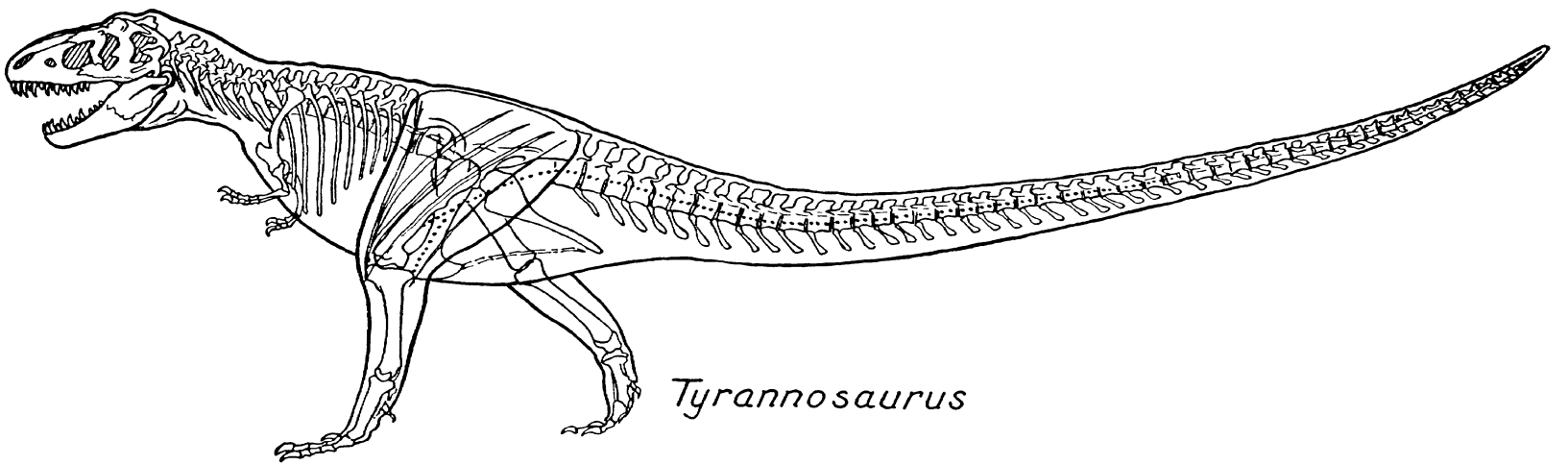


Fig. 14.20. *Tyrannosaurus rex*. New restoration, based on data from Osborn, 1916, but placed in balanced running pose. For data on pelvic musculature of *Tyrannosaurus*, see Romer, 1923.

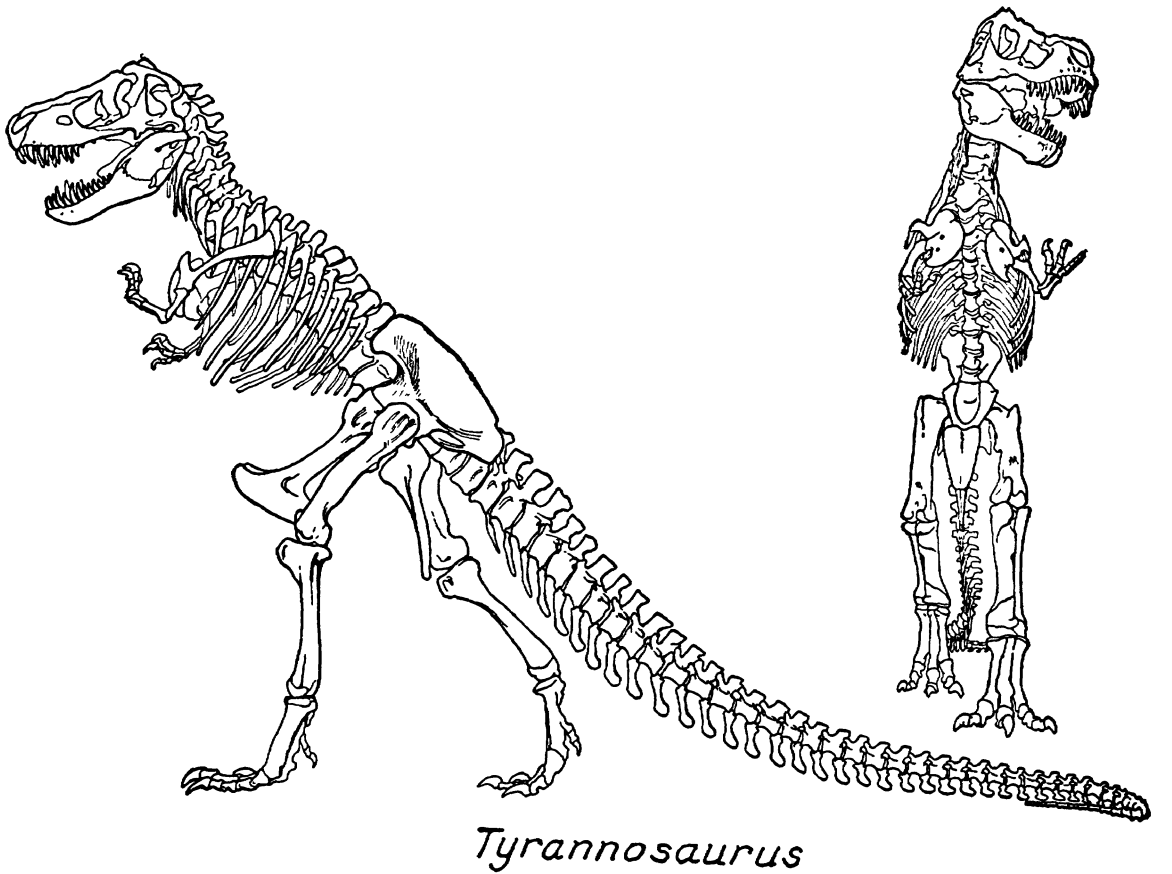


Fig. 14.21a. *Tyrannosaurus* skeleton, as mounted (Osborn, 1916). The same, front view.

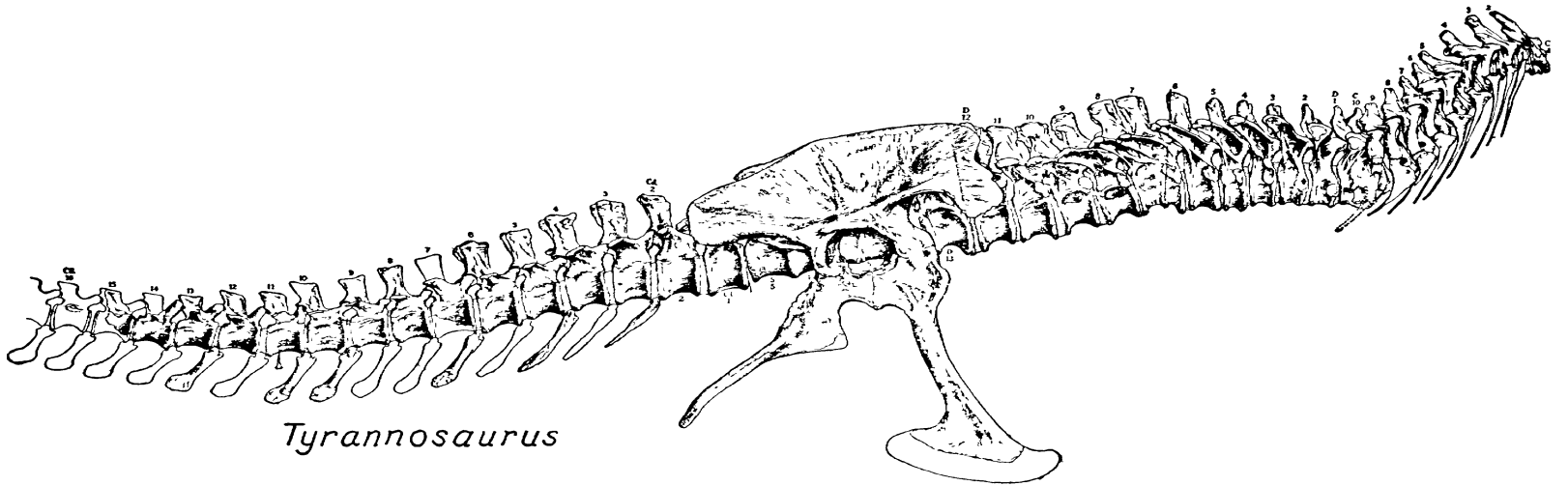


Fig. 14.21b. Vertebral column and pelvis of *Tyrannosaurus*. After Osborn, 1916. The vertebral column, pivoted at the open acetabula, was firmly slung between the opposite halves of the pelvis, the ilia being produced dorsally, parallel to the neural spines (for the musculature of the pelvis, see fig. 14.23 below). In the sitting pose the main weight was probably transmitted through the strong pubic column and its expanded "shoe," which also served as anchor for the powerful obturator (*p i.f e.2*) muscle. The thoracic vertebrae, although strongly braced, retained the pleuroceles of primitive coelurosaurians, although in a reduced condition. The facets for the capitula of the ribs gradually rise from the ventral border of the centrum in *C 10* to the side of the neural arch in *D 12*. Meanwhile the facets for the capitula rise from a point low down on the side of the centrum in *C 8* and far below the zygapophyses to a high level on upcurved diapophyses of *D 11, 12*—indicating a dorsally expanded lung. The cervical vertebrae are shortened, crowded and curved upward to shorten the adverse leverage against the pelvis in carrying the huge head.

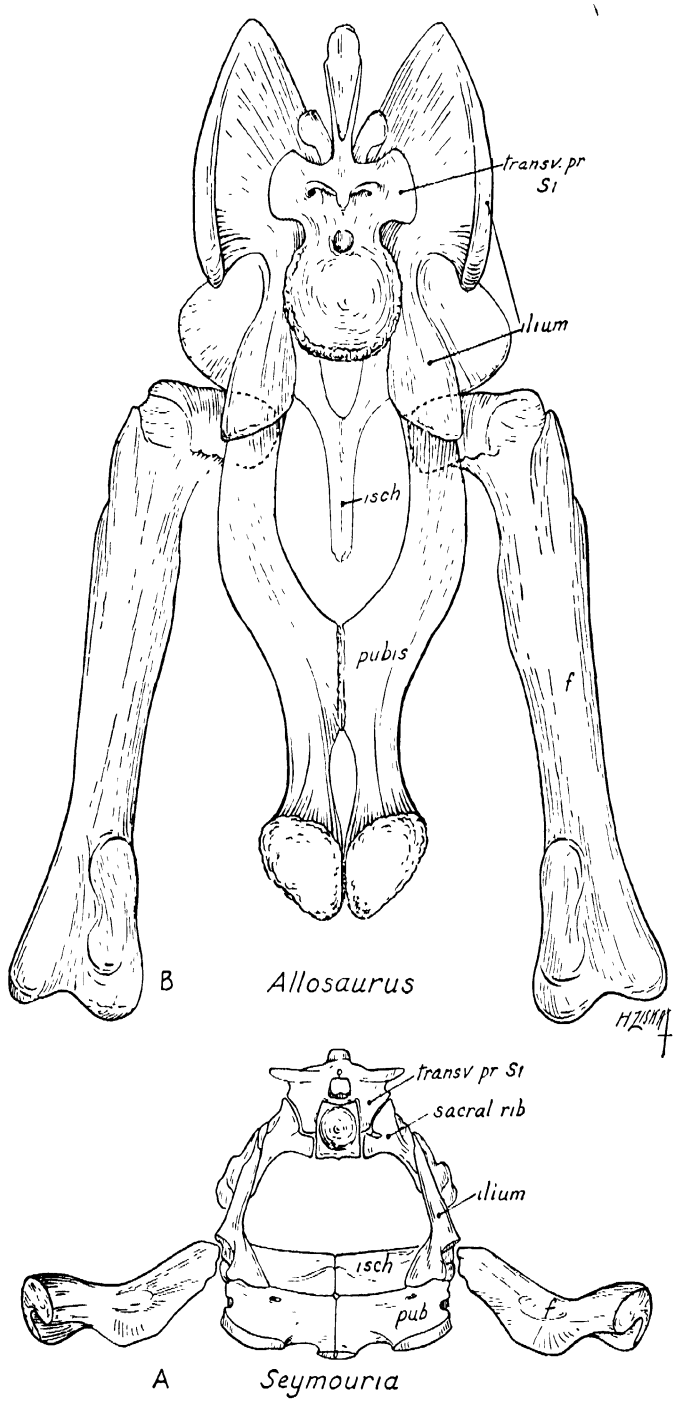


Fig. 14.22. Front view of the pelvis and femora in primitive Permian tetrapod (A) and bipedal saurischian dinosaur (B). A, after T. E. White; B, original. Data from Gilmore and from mounted skeleton. Shows marked contrast between: (A) primitive reptilian crawling gait, with everted femora and only incipient integration of ilium, sacral rib and vertebral column, and (B) highly specialized bipedal gait, with bird-like columnar femora downwardly directed, with opposite heads brought nearer to the midline; complete integration of ilia with sacrum; fenestrated puboischium.

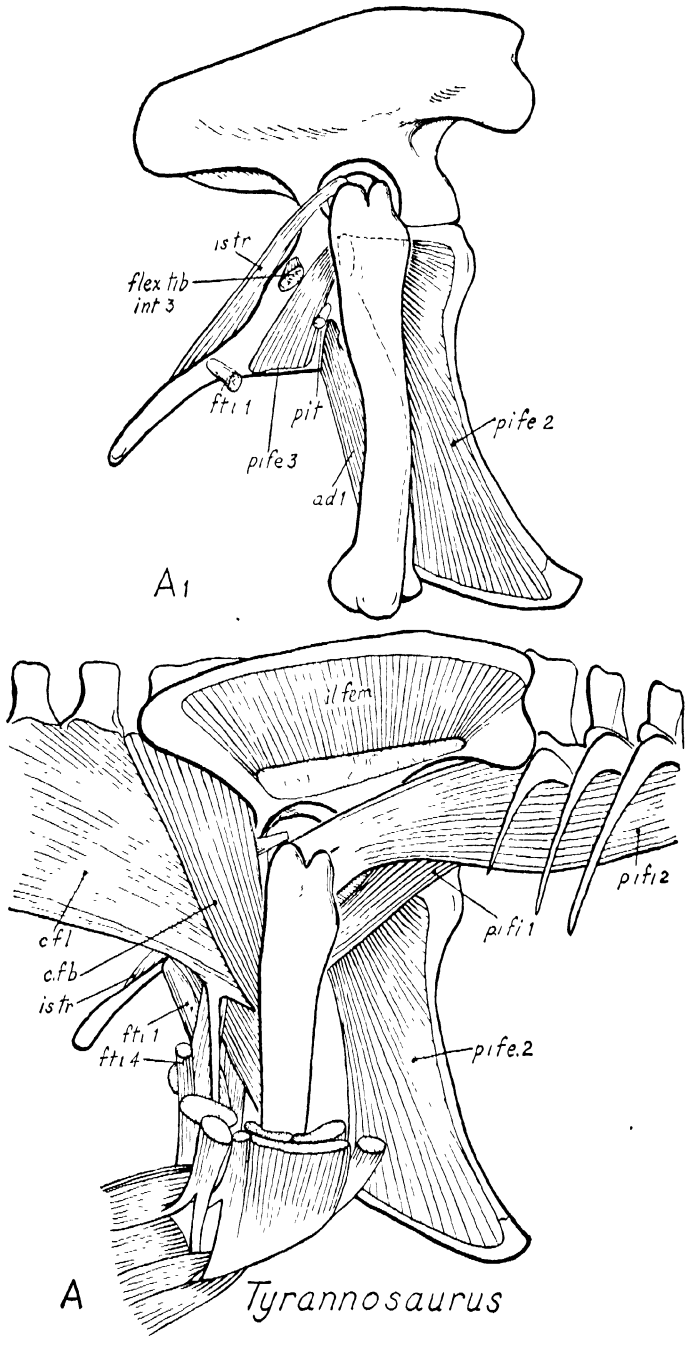


Fig. 14.23. The deeper muscles of the saurischian pelvis. After Romer, 1923. *Ad. 1*, adductor 1; *c.f.l.*, coccygeofemoralis longus, with its side tendon running to the under side of the knee joint; *c.f.b.*, coccygeofemoralis brevis, inserting on the ventro-medial surface of the femur; *flex.tib.int. 3, f.t.i. 1, 3, 4*, flexor-tibialis internus 1, 3, 4; *il.fem.*, iliofemoralis; *is.tr.*, ischiotrochantericus; *p.i.f.e. 2, 3*, pubo-ischio-femoralis externus, 2, 3, inserting on ventro-medial surface of femur; *p.i.f.i., 1, 2*, pubo-ischio-femoralis internus, 1, 2; *p.i.t.*, pubo-ischio-tibialis.

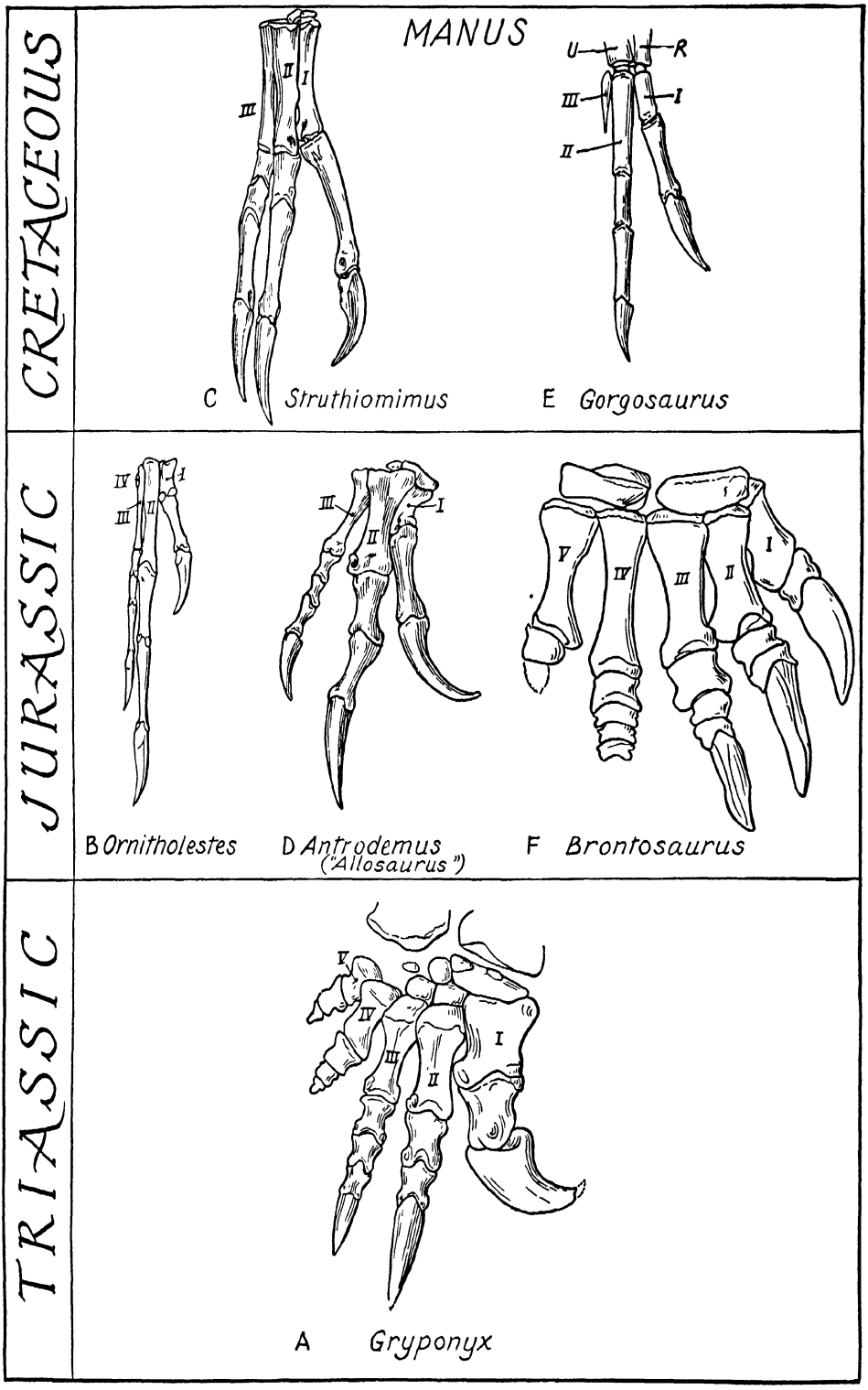


Fig. 14.24a. Manus and pes of saurischian dinosaurs. Ranging from primitive Triassic pentadactylate to highly specialized Cretaceous di- and tridactylate forms. A, after Broom; B, C, after Osborn; D, after Gilmore; E, after Lambe; F, original.

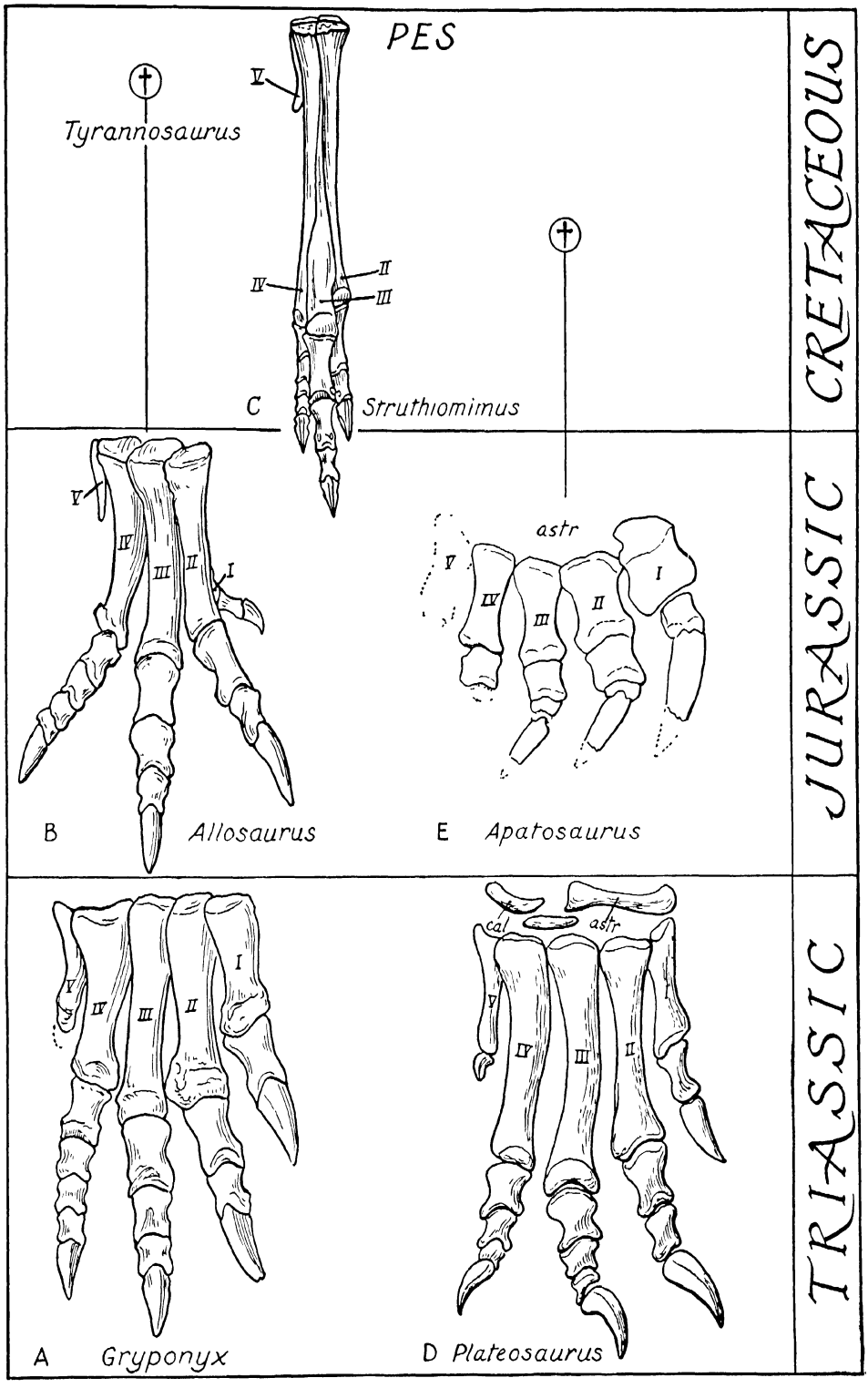
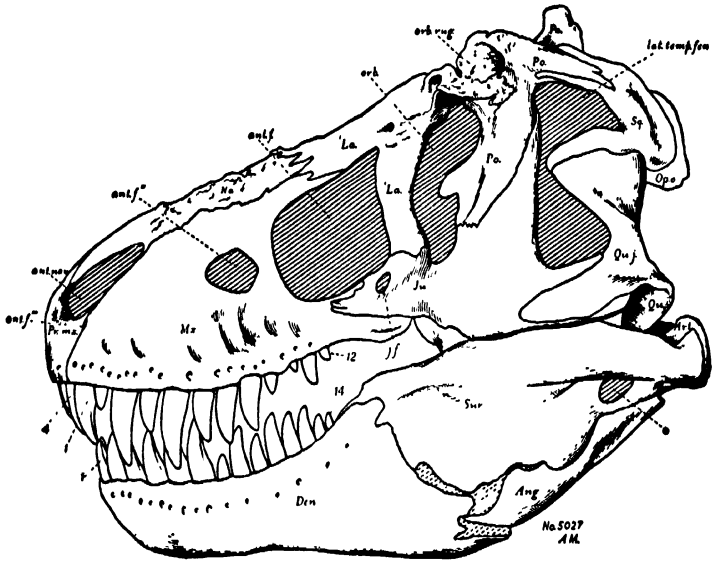
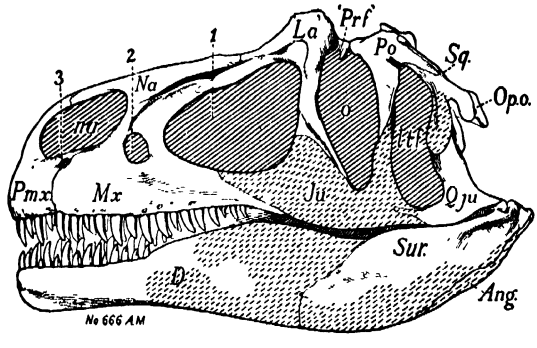


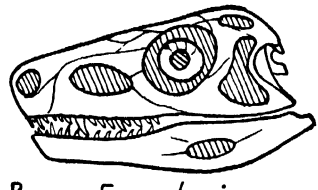
Fig. 14.24b. Manus and pes of saurischian dinosaurs (continued). A, after Broom; B, original; C, after Osborn; D, original; E, after Gilmore.



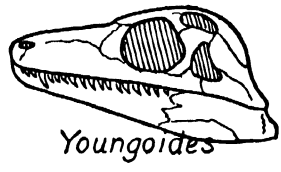
D *Tyrannosaurus*



C *Allosaurus*



B *Euparkeria*



A *Youngoides*

Fig. 14.25. Four structural stages, from lizard-like predator (D). A, after Olson and Broom; B, after Broom; C, D, after Osborn.

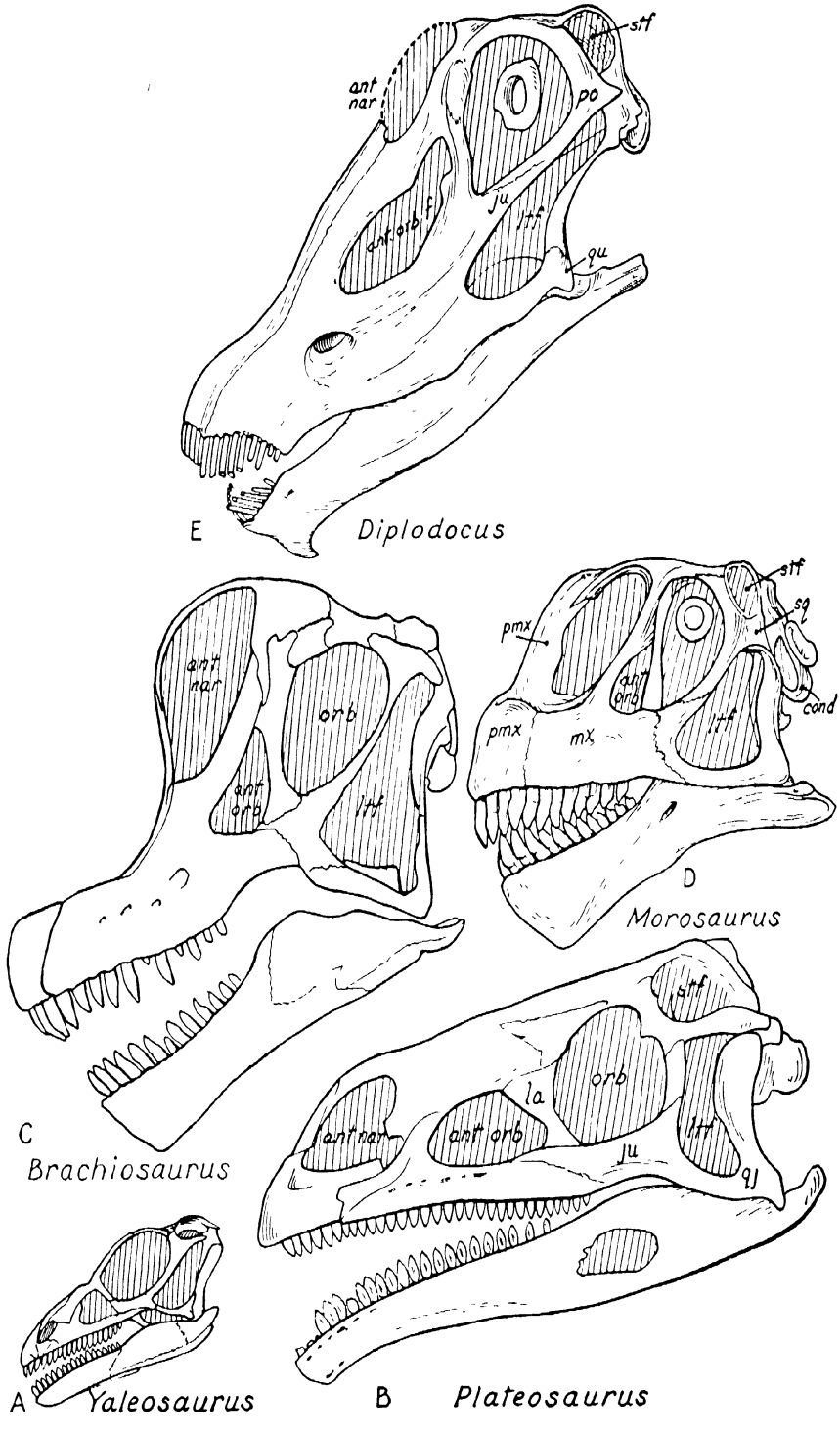


Fig. 14.26. From Triassic coelurosaur to Jurassic sauropods. A, after Marsh; B, after von Huene; C, after Janensch; D, after Gilmore, E, after Hatcher and Holland.

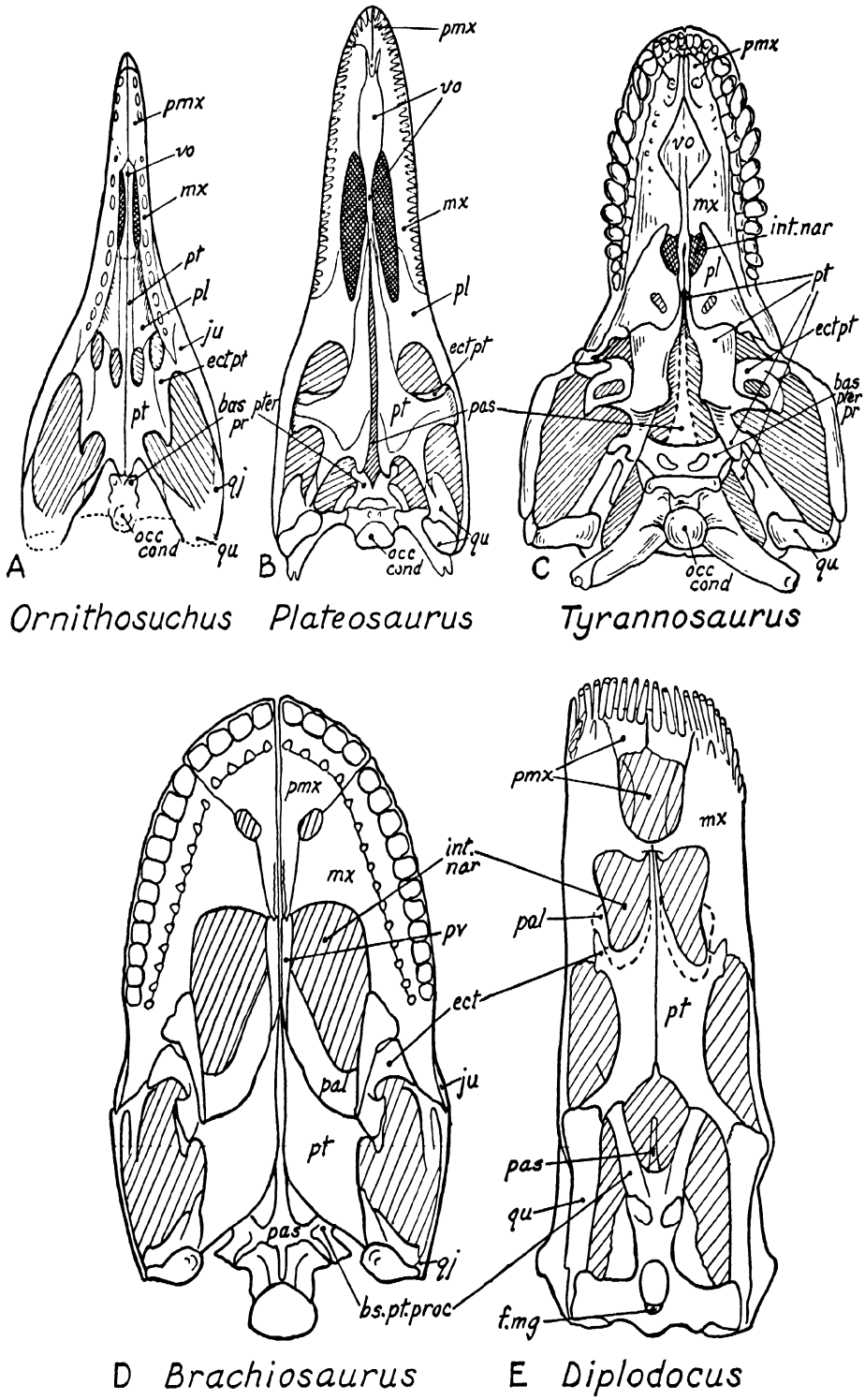


Fig. 14.27. Palatal views of skulls of primitive pseudosuchian (A), primitive saurischian (B), specialized carnivorous dinosaur (C), short-headed sauropod (D), long-headed sauropod (E). A, after Broom; B, reconstruction data from von Huene, Romer; C, after Osborn; D, after Wiman; E, after Marsh, Hatcher, Holland.

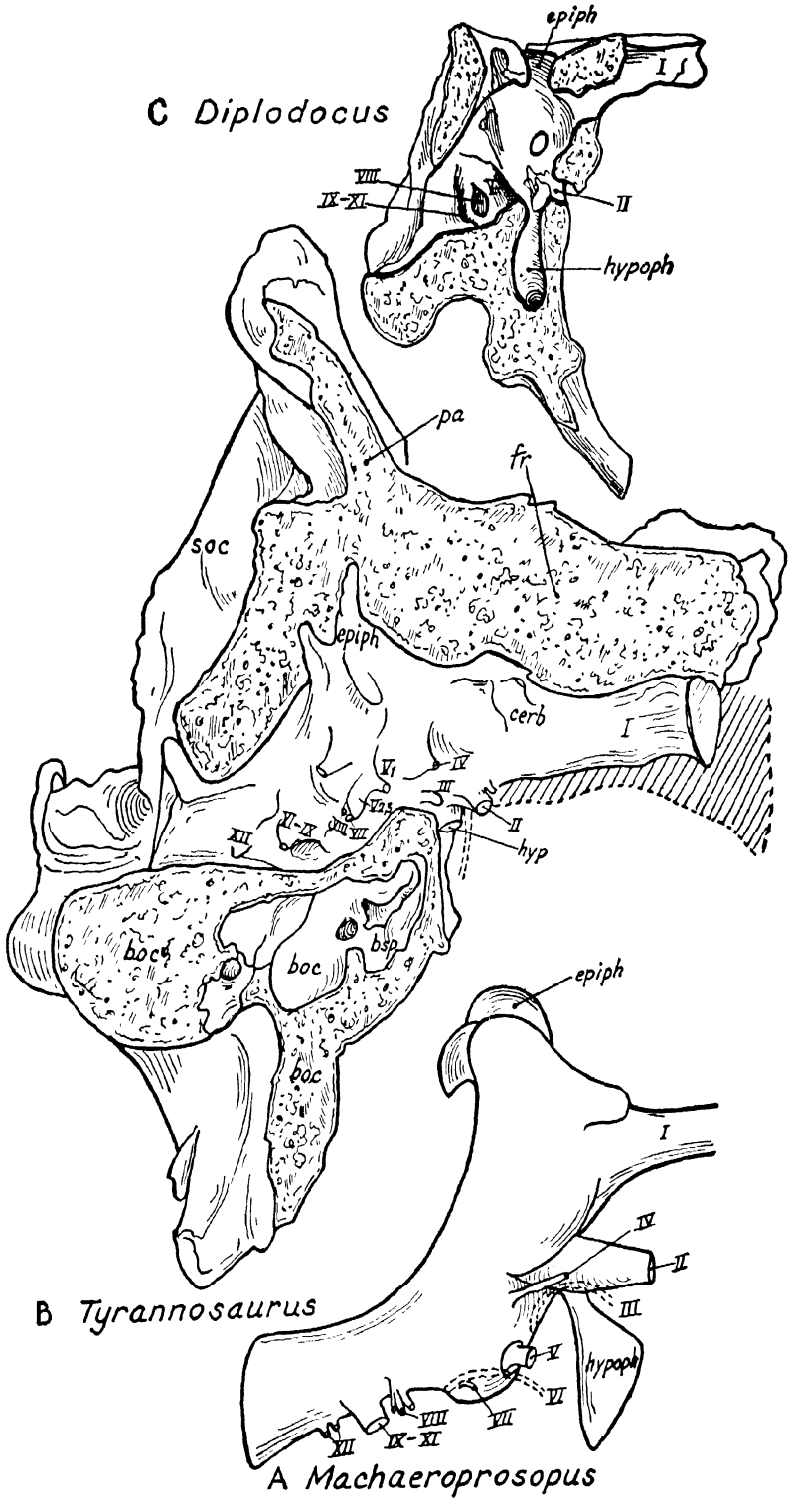


Fig. 14.28. Brain-cast of phytosaur (A); crania and brain-casts of two saunschiandinosours. A, after Camp; B, C, after Osborn. I–XII, roots of cranial nerves.

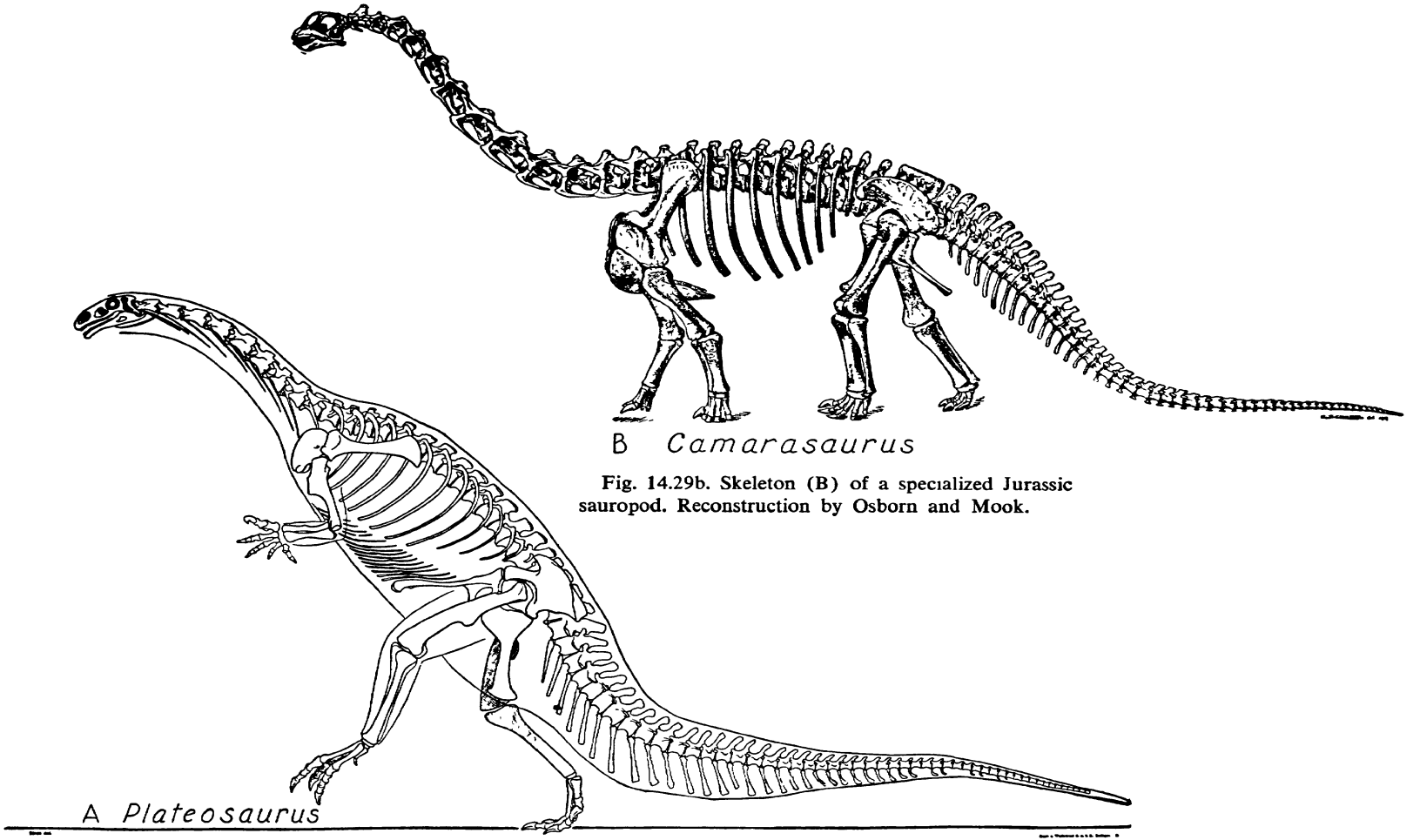


Fig. 14.29b. Skeleton (B) of a specialized Jurassic sauropod. Reconstruction by Osborn and Mook.

Fig. 14.29a. Skeleton (A) of primitive Triassic prosauropod. Restoration by von Heune. A, B, not to same scale.

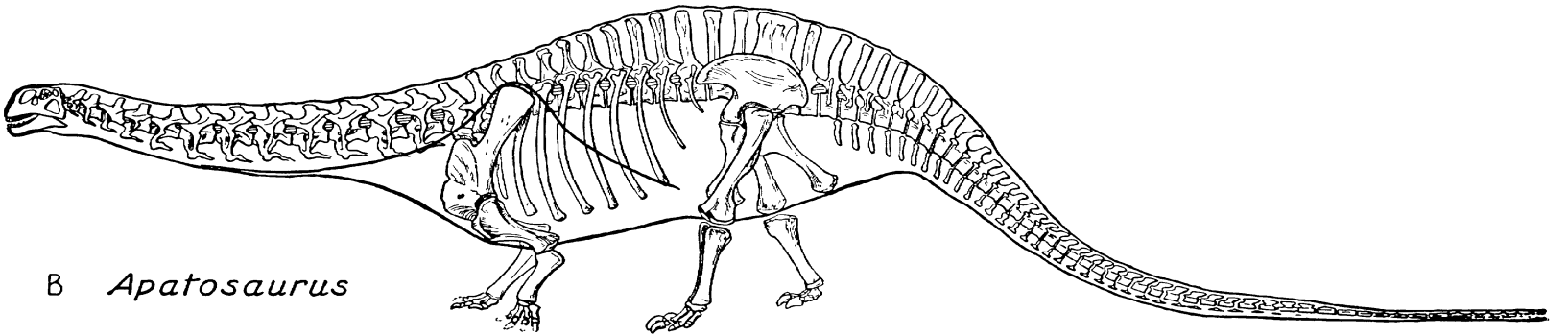


Fig. 14.30b. Skeleton (B) of Jurassic sauropod. After Gilmore, but with modified position of scapulo-coracoid and fore limb. Showing suspension bridge form of pectoral girdle and attached serratus muscles (black line).

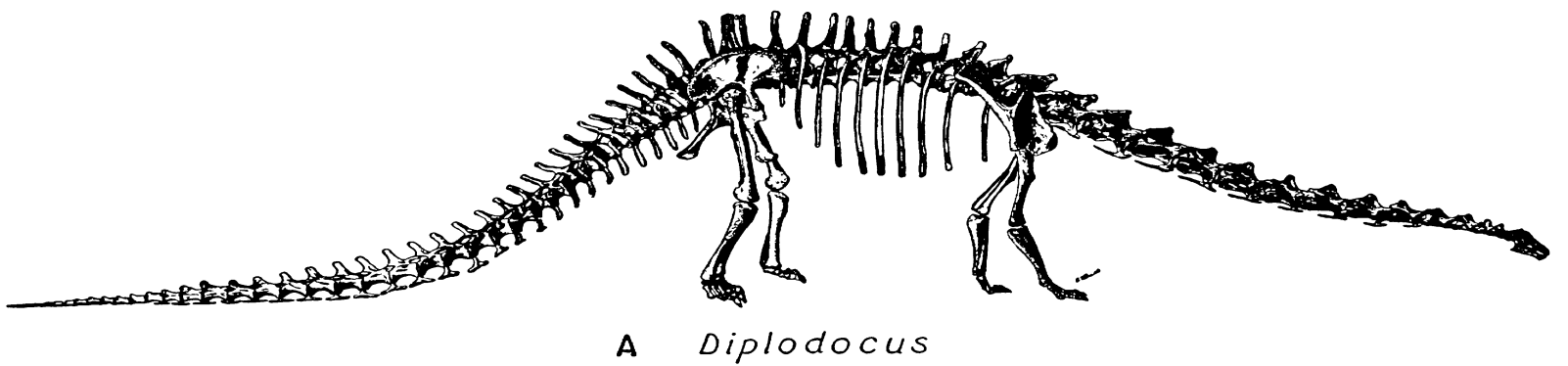


Fig. 14.30a. Skeleton (A) of long-necked Jurassic sauropod. Reconstruction by Hatcher.

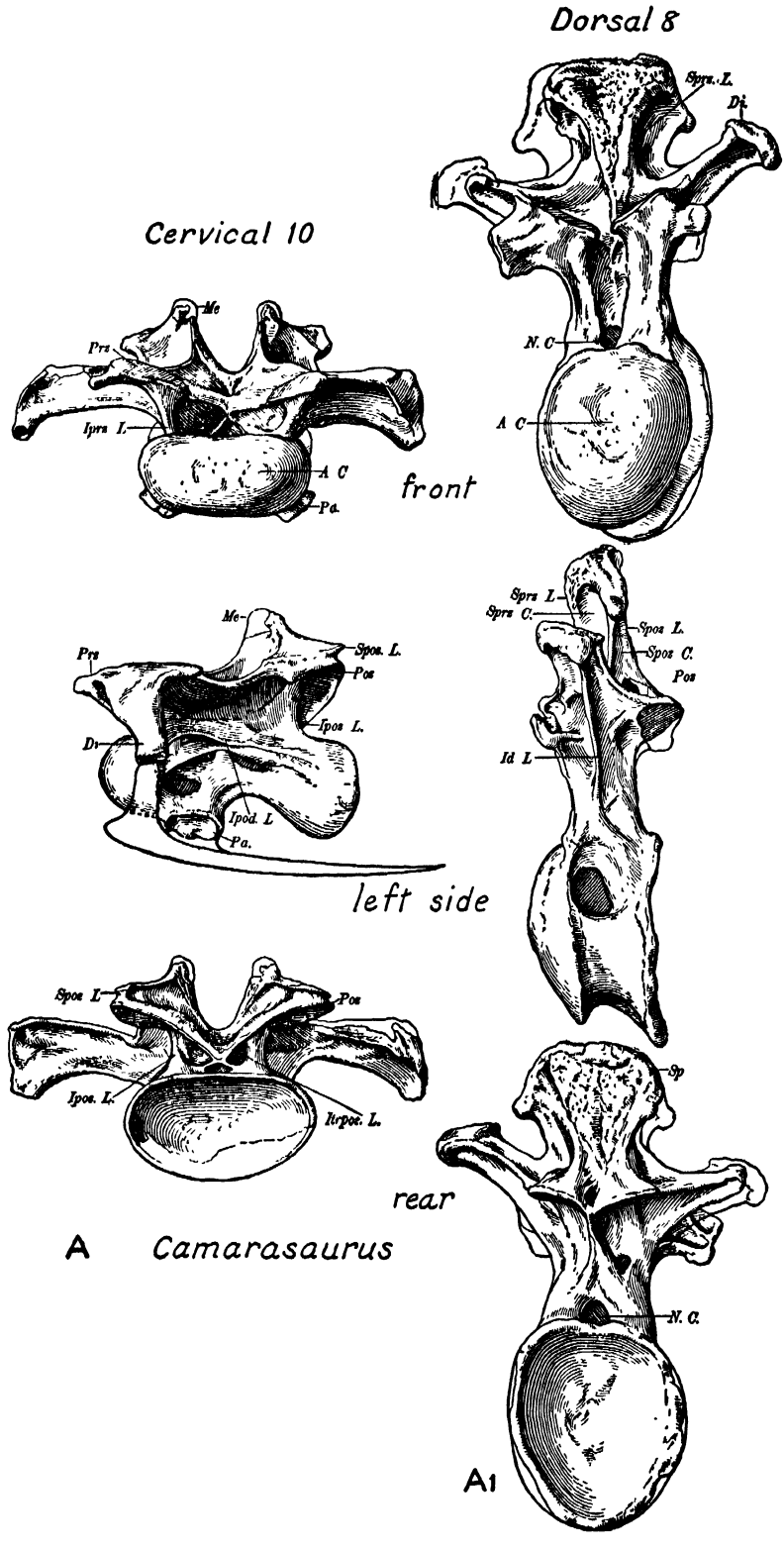

Dorsal 8
Sprs. L.
Di
N. C
A C
Cervical 10
Me
Prz
Iprs L.
A C
Pa.
front
Me
Prz
Spos. L.
Pos
Ipos L.
Di
Ipod. L
Pa.
left side
Sprs L
Sprs C.
Spos L.
Spos C.
Pos
Id L
Spos L
Pos
Ipos. L.
Itrpos. L.
rear
A Camarasaurus
Sp
N. C.
A1

Fig. 14.31a

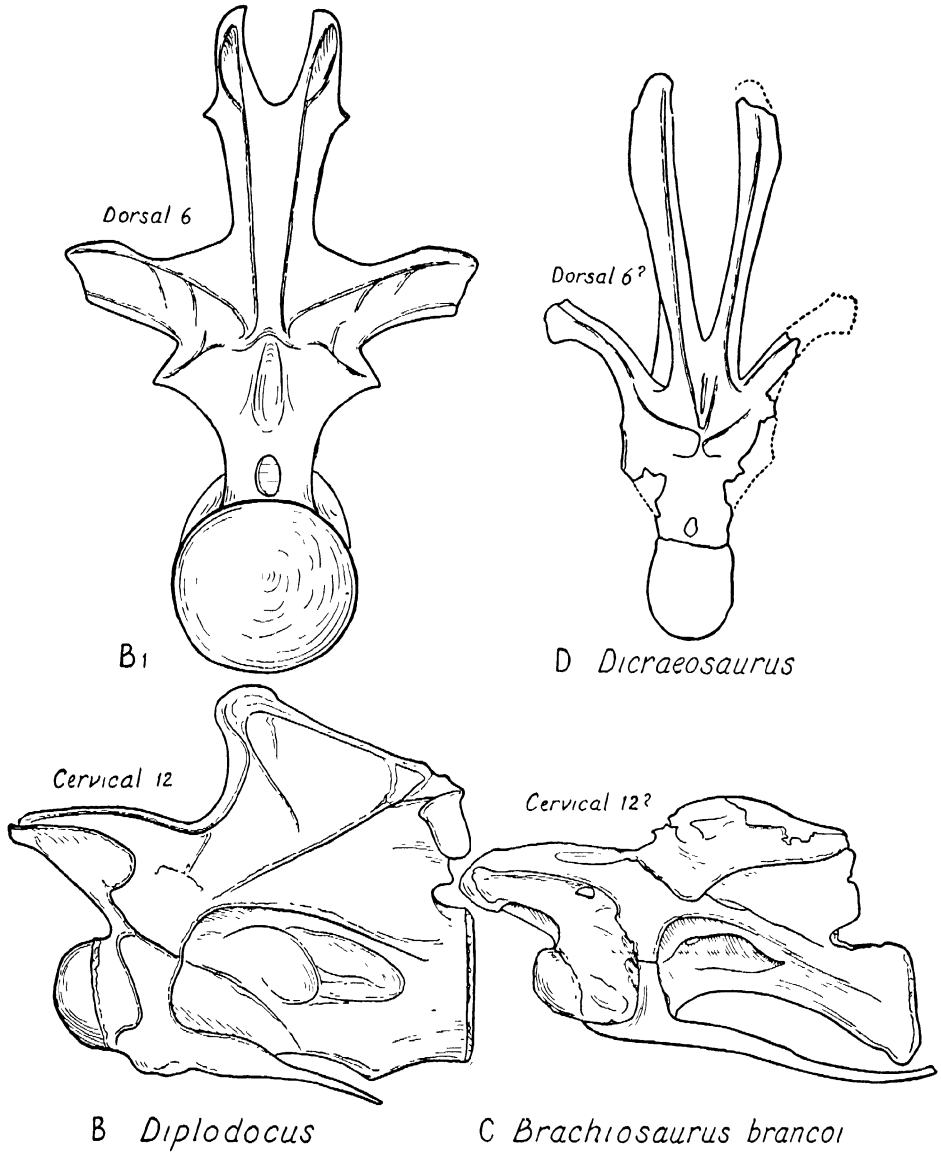


Fig. 14.31a, b. Selected cervical and dorsal vertebrae of sauropods. A, A1, x 1/15, after Osborn and Mook; B, B1 x 1/10, after Hatcher; C, D, x 1/10, after Janensch.

The cervical centra have ball-like anterior and cup-like posterior articular facets, so that adjacent centra could be extended and flexed, abducted and adducted, through fairly wide arcs. Wide oblique anterior and posterior zygapophysial articular surfaces also permitted these movements, while preventing dislocation. Wide transverse processes (diapophyses) received thrusts and pulls from the dorsal processes ("tubercles") of the cervical ribs. The heads of these ribs articulated with the low parapophyses (*pa*) on the bases of the centra, while the wide space between the rib heads and tubercles on the one hand, and the centra on the other, formed a longitudinal arcade probably enclosing some of the lateral neck muscles. The sides of the centra are deeply excavated, presumably for processes from the lungs or air sacks. The various cavities and depressions on the sides of the neural arches presumably indicate the position of the complex spinal, interspinal, lateral and ventral neck muscles. The bony laminae and crests and arches served as attachments of the deep fasciae of the neck muscles, as indicated in the cleft between the supraneural processes (A, B1, D).

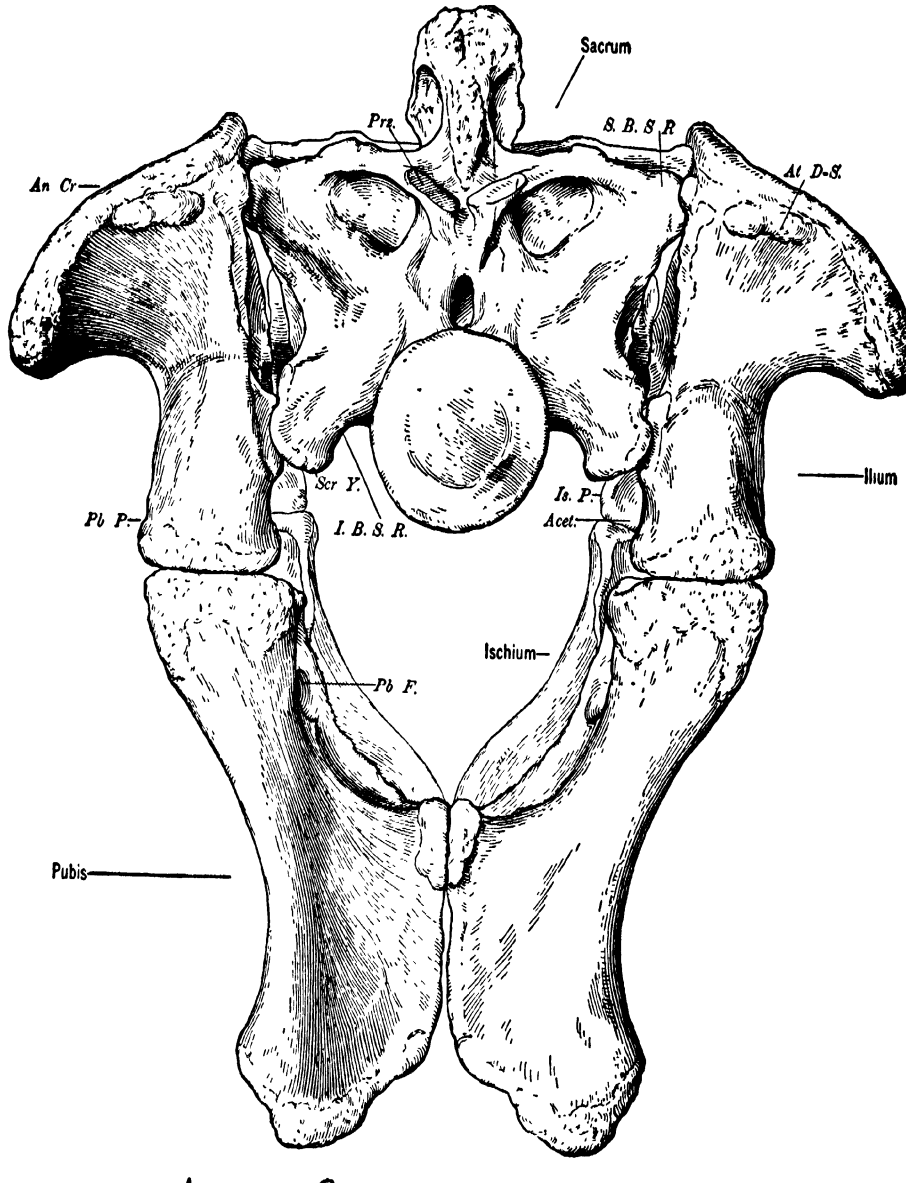
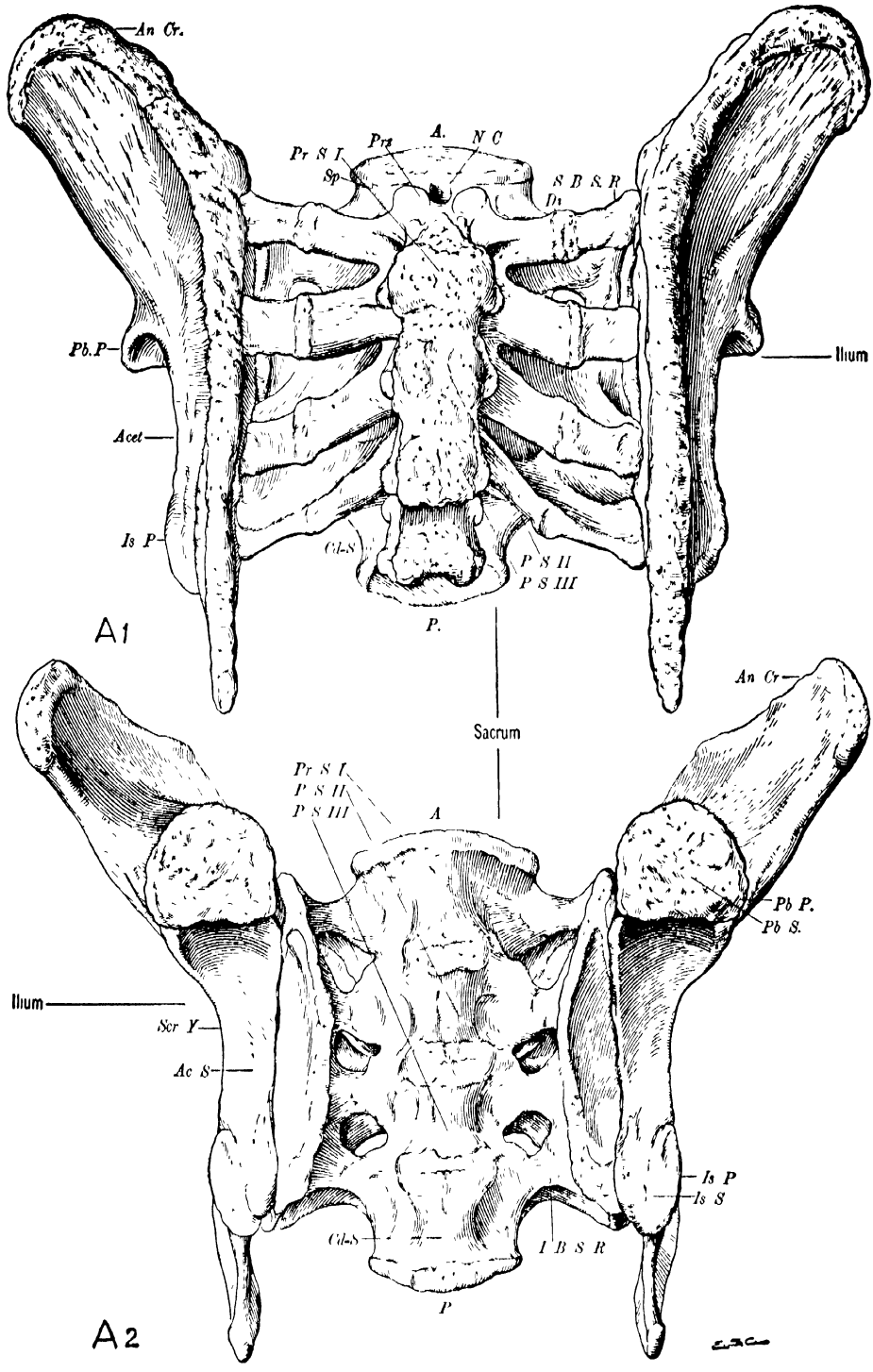


Fig. 14.32a, b. The sacro-pelvis, or fulcrum of the locomotor system of sauropods. After Osborn and Mook. The front view (A) shows the pelvis suspended to the transversely and vertically expanded sacral ribs through their superior and inferior branches (*S.B.S.R.*, *I.B.S.R.*). The top view shows how the four sacral ribs on each side transmit their loads or thrusts to the transverse processes (*Di.*) and thence to the neural arches; also the coalescence of the latter. The under side (A2) shows the coalescence of the inferior branches of the sacral ribs to form the central part of the concave acetabulum, which receives the thrusts of the femur.



Camarasaurus

Fig. 14.32b



Fig. 14.33. Restoration of the skull and neck of the Chinese Cretaceous sauropod *Helopus zdanskyi*. Skull from Wiman.

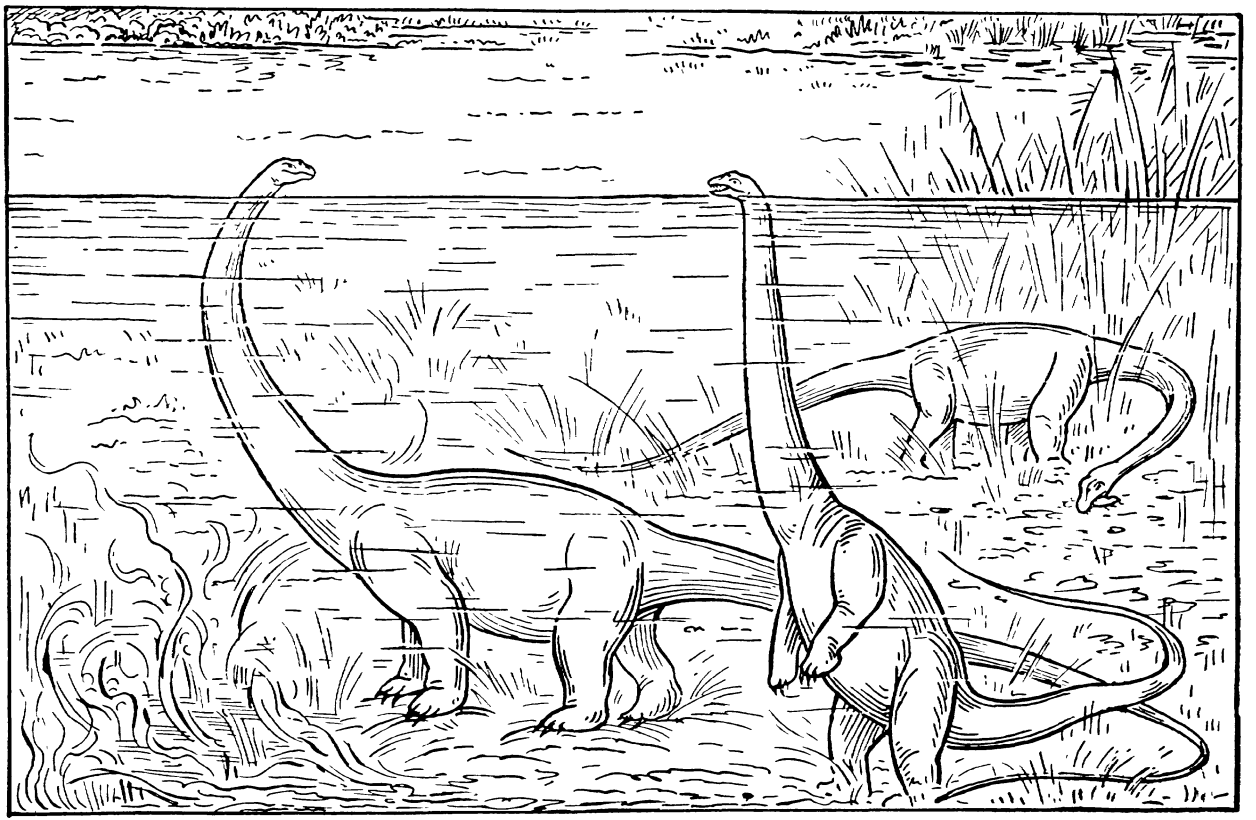
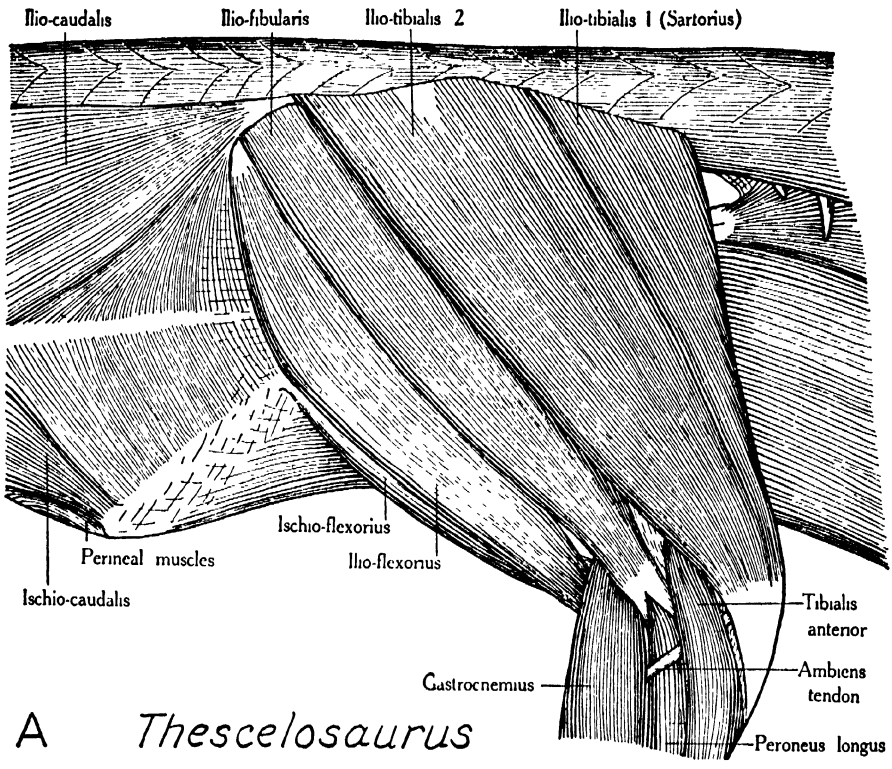


Fig. 14.34. Chinese sauropods—Life restoration. Data from Wiman.


Ilio-caudalis
Ilio-fibularis
Ilio-tibialis 2
Ilio-tibialis 1 (Sartorius)
Ischio-flexorius
Perineal muscles
Ilio-flexorius
Ischio-caudalis
Tibialis anterior
Ambiens tendon
Gastrocnemius
Peroneus longus
A Thescelosaurus

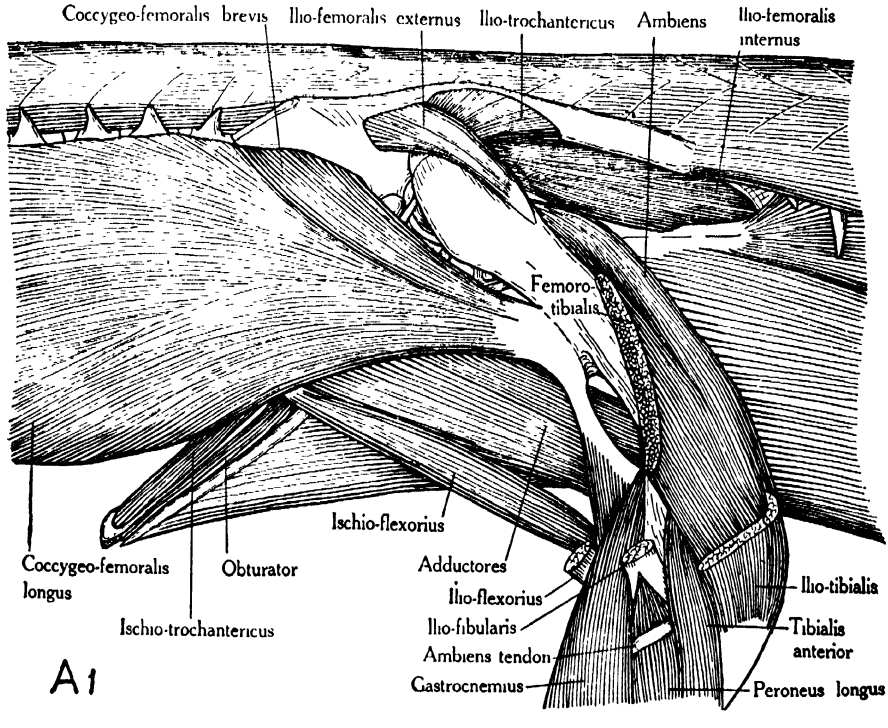

Coccygeo-femoralis brevis
Ilio-femoralis externus
Ilio-trochantericus
Ambiens
Ilio-femoralis internus
Femoro-tibialis
Ischio-flexorius
Coccygeo-femoralis longus
Obturator
Adductores
Ilio-flexorius
Ilio-fibularis
Ambiens tendon
Gastrocnemius
Ischio-trochantericus
Ilio-tibialis
Tibialis anterior
Peroneus longus
A1

Fig. 14.35a

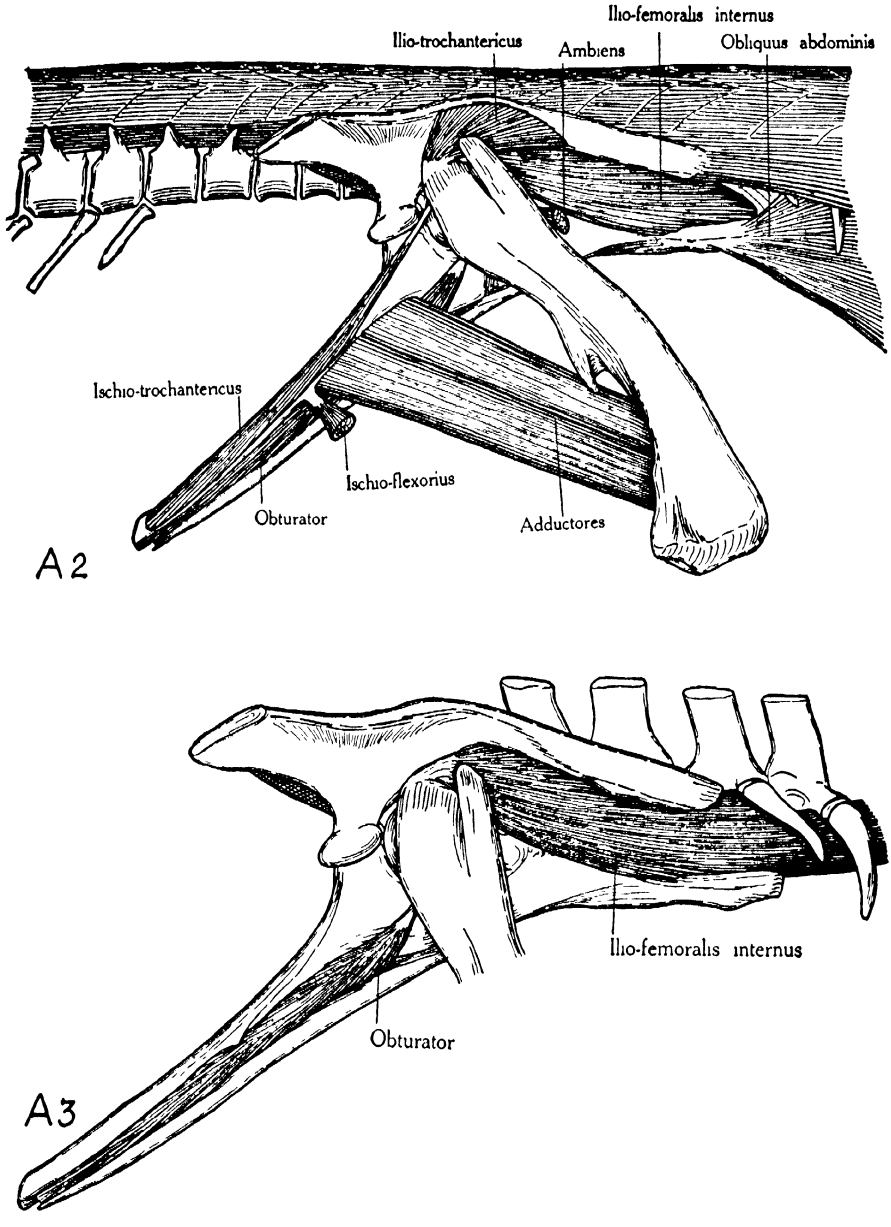


Fig. 14.35a, b. Restoration of the pelvic musculature of an ornithischian dinosaur. After Romer.

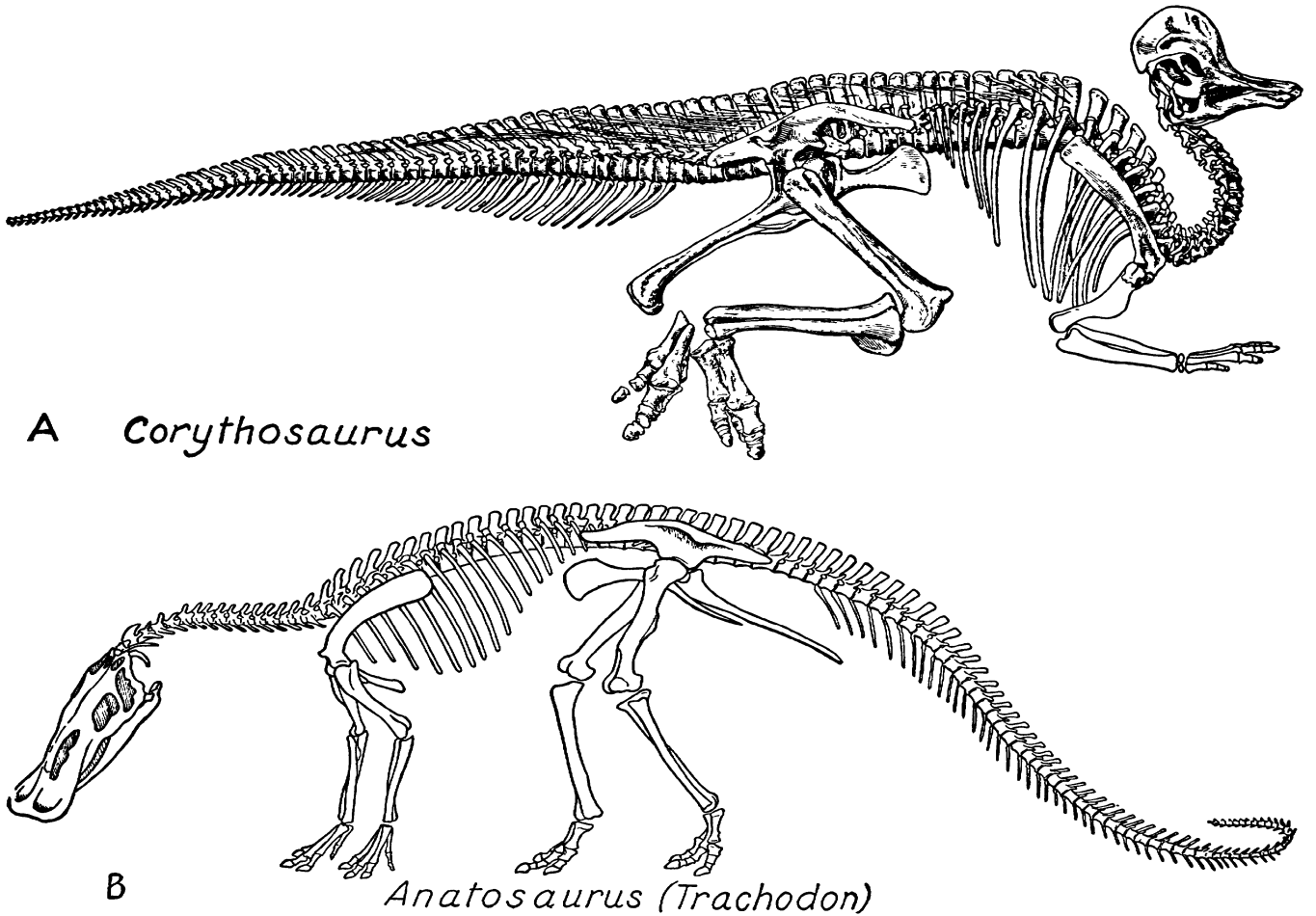


Fig. 14.36. A, Skeleton of casuary dinosaur. After Barnum Brown. B, Mounted skeleton of a duck-billed dinosaur in the American Museum of Natural History. Original.

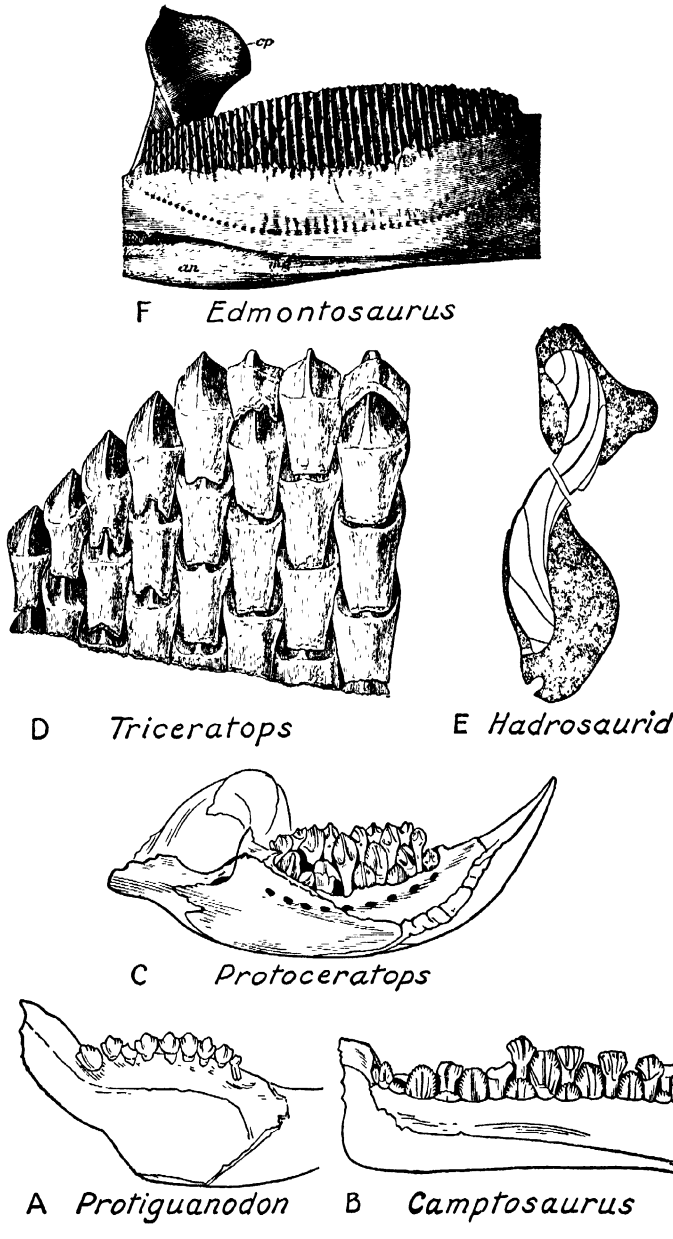


Fig. 14.37. Lower jaw and teeth from primitive ornithischian (A) to highly specialized hadrosaur. In the latter, the multiplication of cheek teeth, reaching an extreme, resulted in the close appression and integration of many hundreds of teeth to form massive grinding plates. A, after Osborn; B, after Gilmore; C, after Brown and Schlaikjer; D, after Hatcher, Marsh and Lull; E, F, after Lambe.

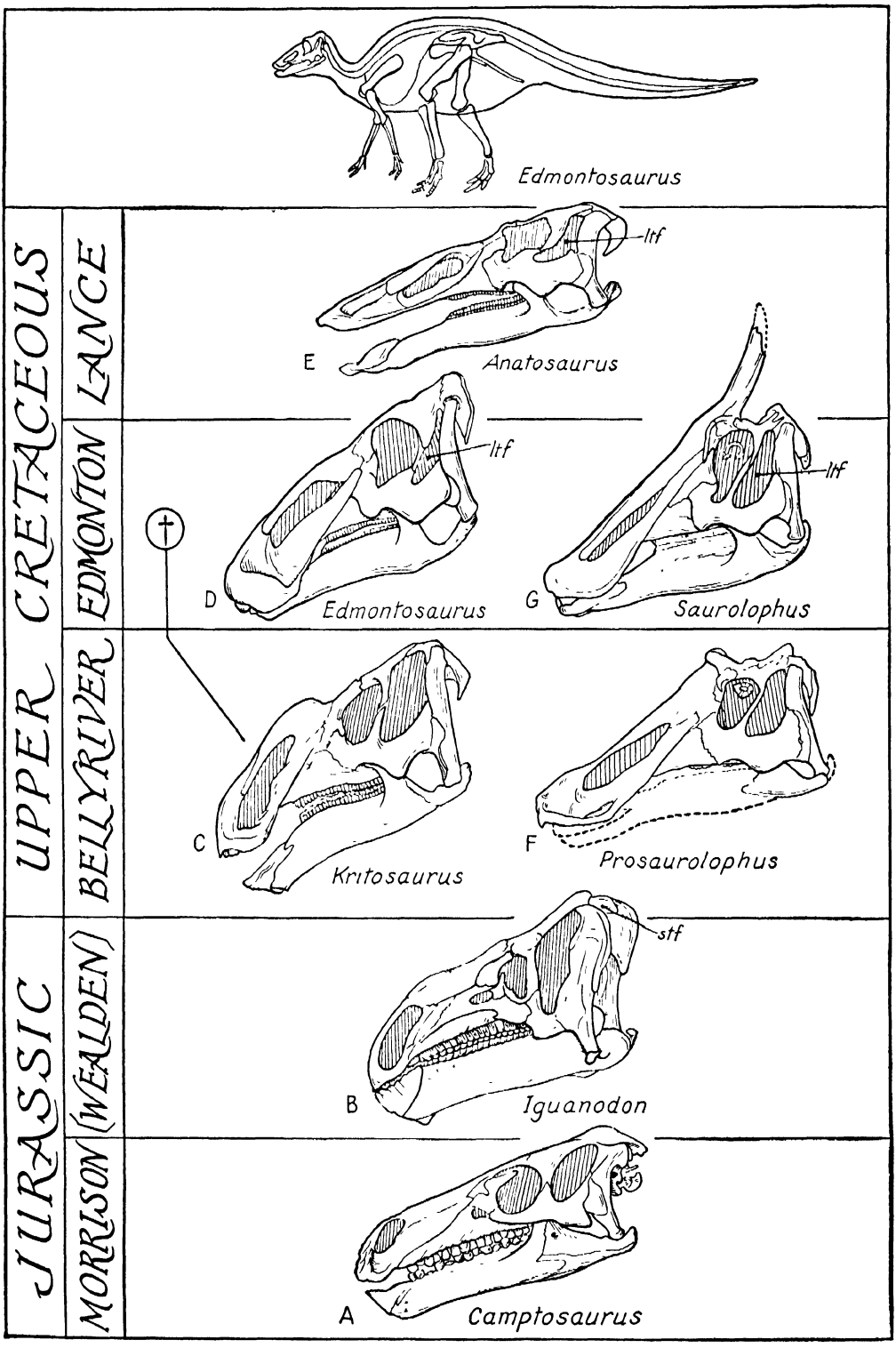


Fig. 14.38a, b. Succession of the hadrosaurs. Data after Lull and Wright (except A, B). (Fig. 14.38b on facing page.)

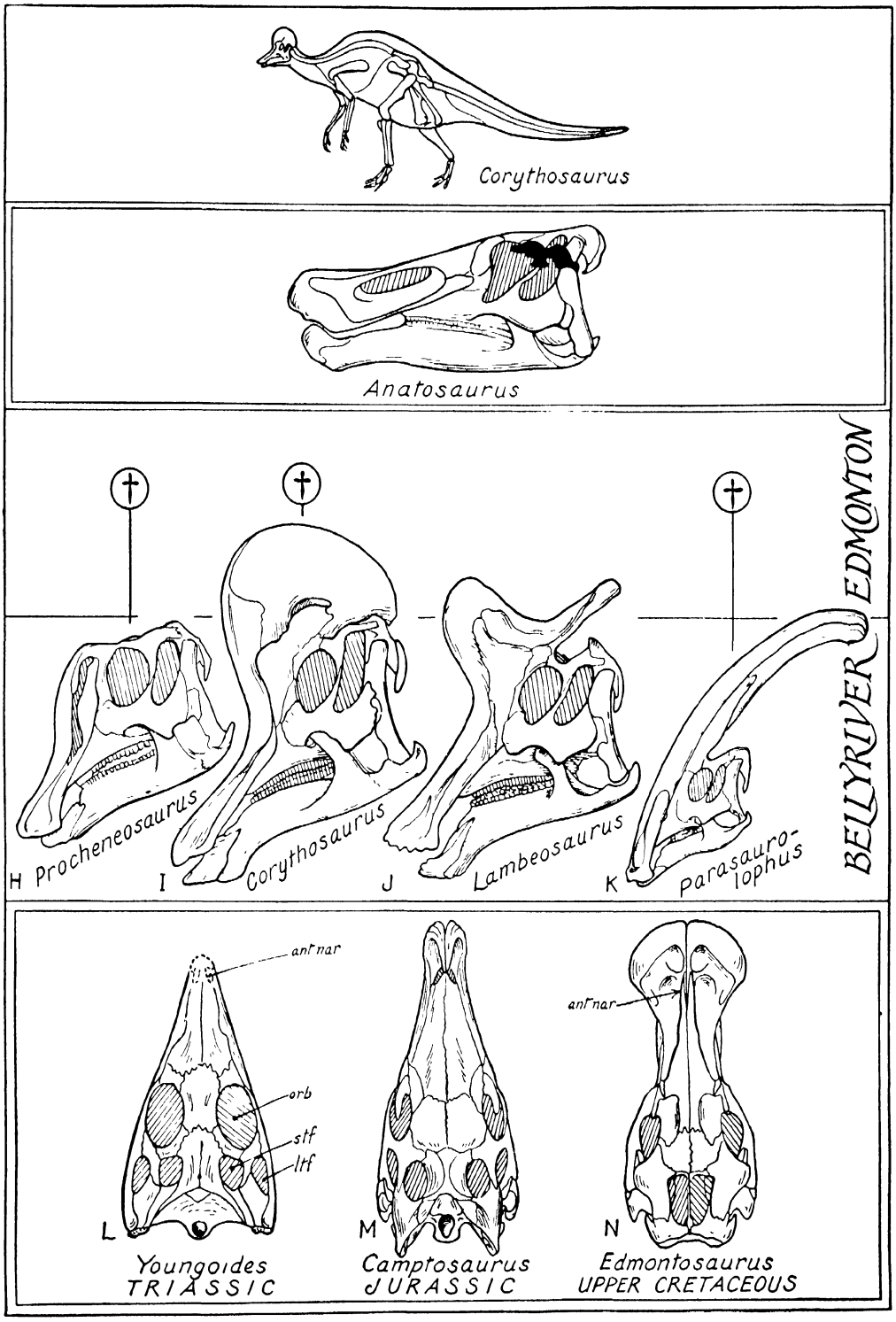


Fig. 14.39 (bottom). From primitive thecodont to broad-billed hadrosaur. L, After Olson and Broom; M, after Gilmore; N, after Lull and Wright. † = extinction.

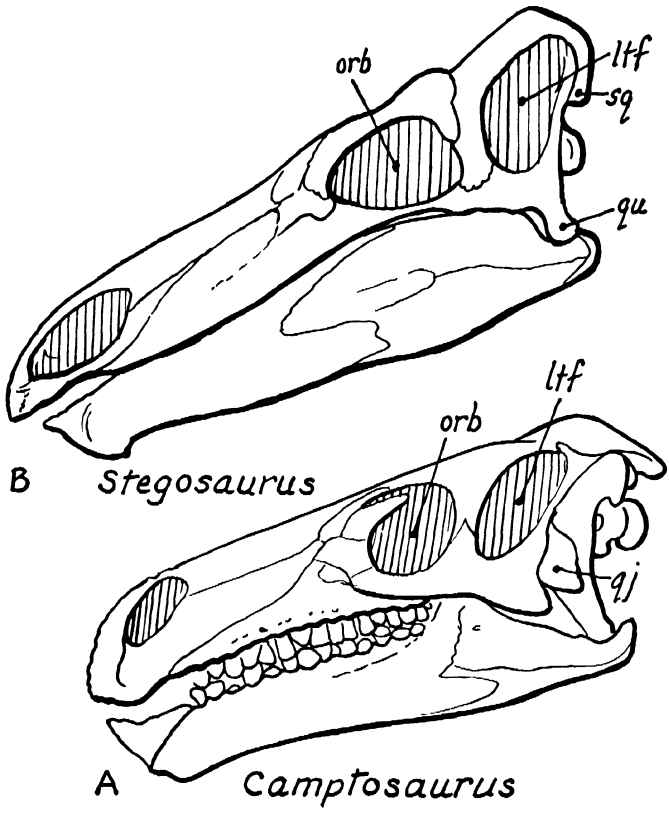


Fig. 14.40 (top). Primitive camptosaur and specialized stegosaur skulls. A, after Gilmore; B, after Marsh.

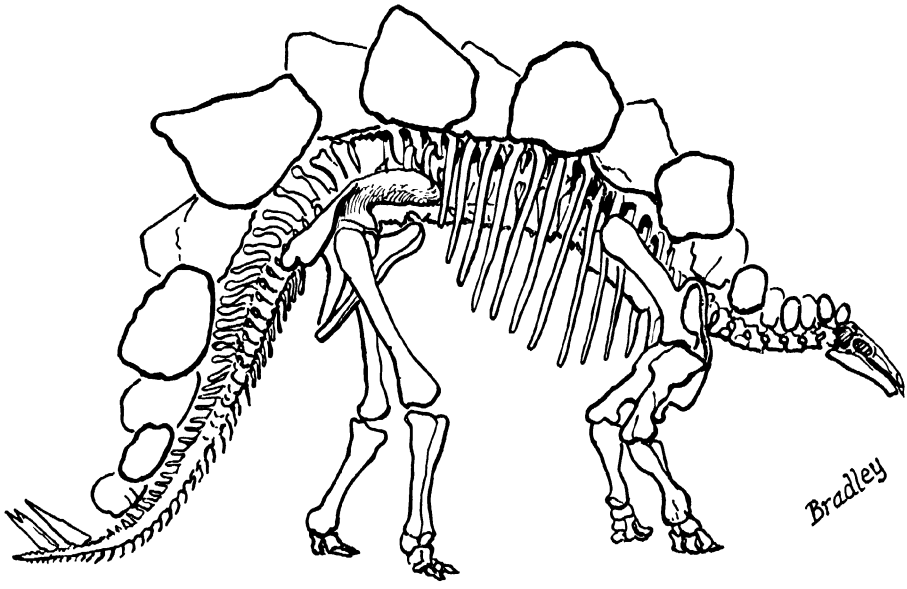


Fig. 14.41. *Skeleton of Stegosaurus stenops,* in the U. S. National Museum. Data after Gilmore.

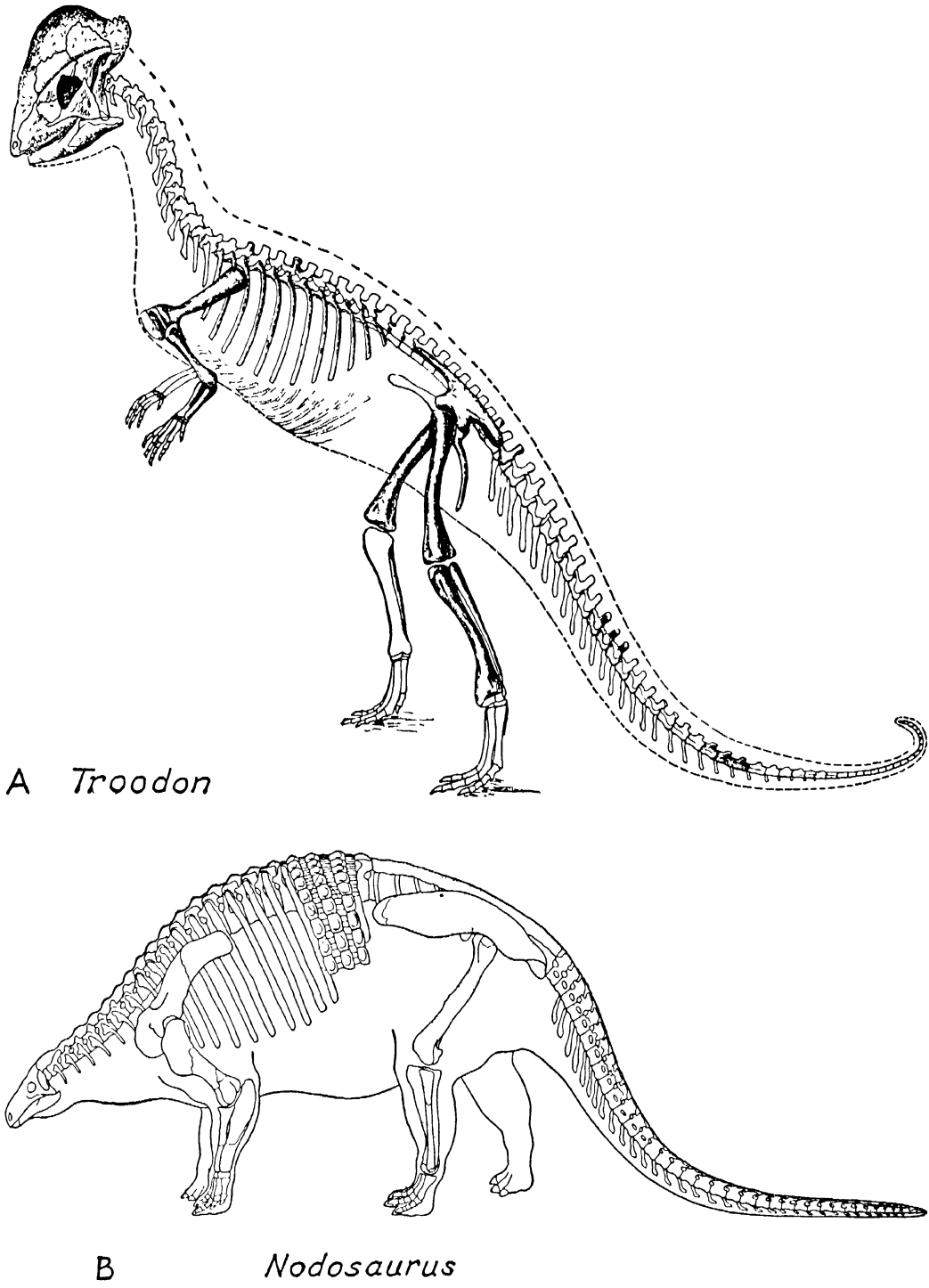


Fig. 14.42. A, Skeleton of small, thick-skulled troödont. After Gilmore. In the marked swelling of the skull roof this form suggests the barrel-shaped armored ankylosaurs (B). B, after Lull. According to Gilmore, *Troodon* retained the general bipedal habitus of the primitive ornithischians (fig. 14.43), but the skeleton looks much too slender to have supported the massive bony head. The nodosaurs (B) and other ankylosaurs were excessively specialized and secondarily quadrupedal. A, B not to scale.

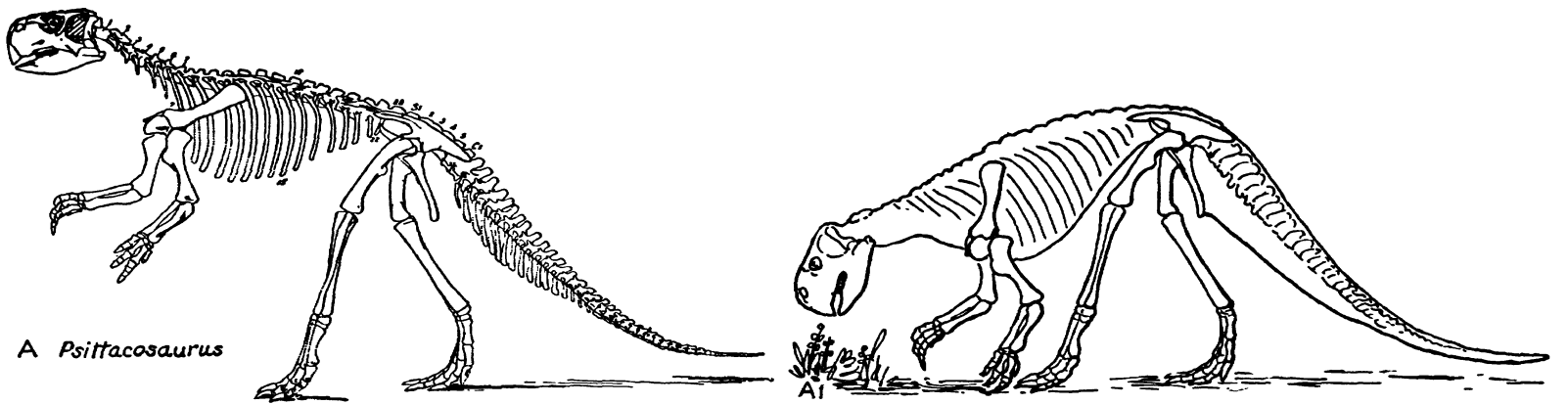


Fig. 14.43. A, Skeleton of the primitive "parrot dinosaur" from the Cretaceous of Mongolia. After Osborn. Although restored in the bipedal pose, the massiveness of the fore arms suggests that a quadrupedal pose (A1), with elevated hips and sharply bent elbows, was also possible, as it was in camptosaurs, hadrosaurs, stegosaurs and ceratopsians, and possibly even in the remote Triassic forerunners of all the ornithischians.

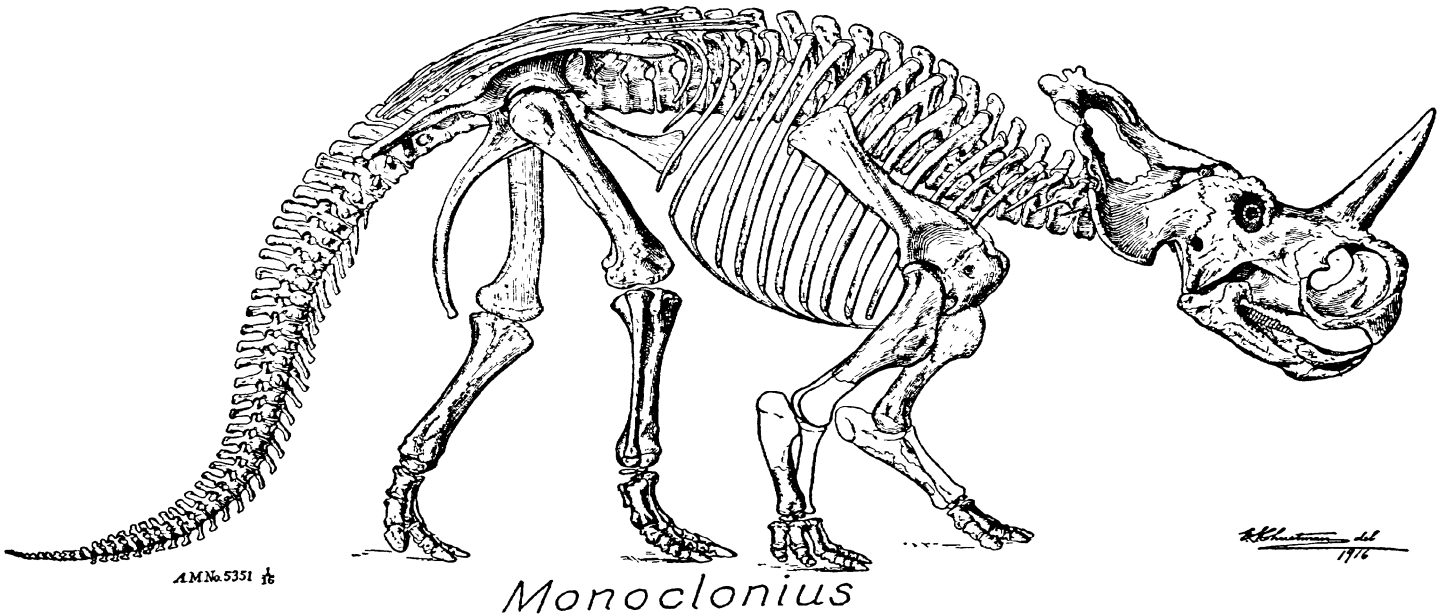


Fig. 14.44. Restoration of an Upper Cretaceous ceratopsian. After Barnum Brown.

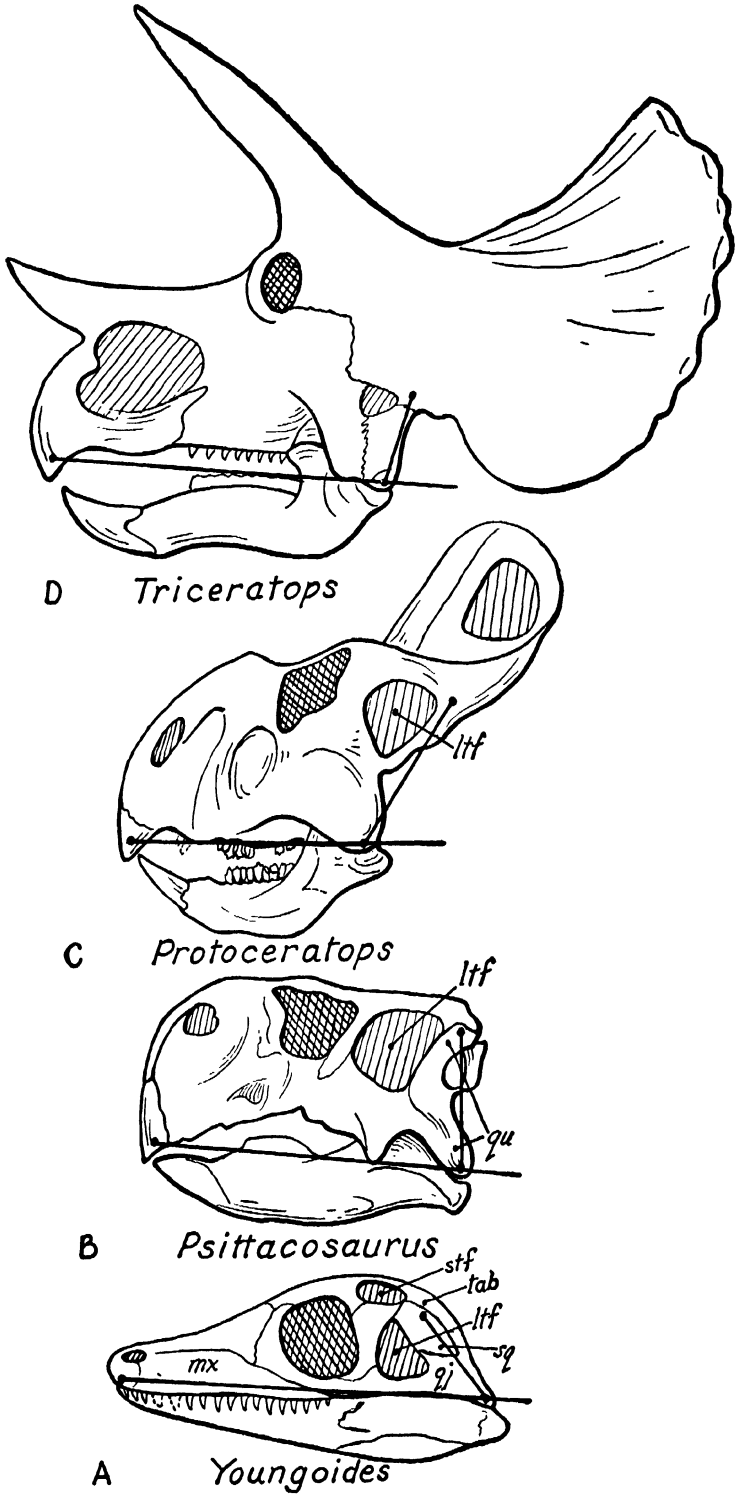


Fig. 14.45. From primitive thecodont to highly specialized ceratopsian. A, after Olson and Broom; B, after Osborn; C, after Brown and Schlaikjer; D, after Marsh. The suspensorium (black line), originally inclined backward (A) in the carnivorous thecodont, gradually swings forward in the herbivorous ceratopsians.

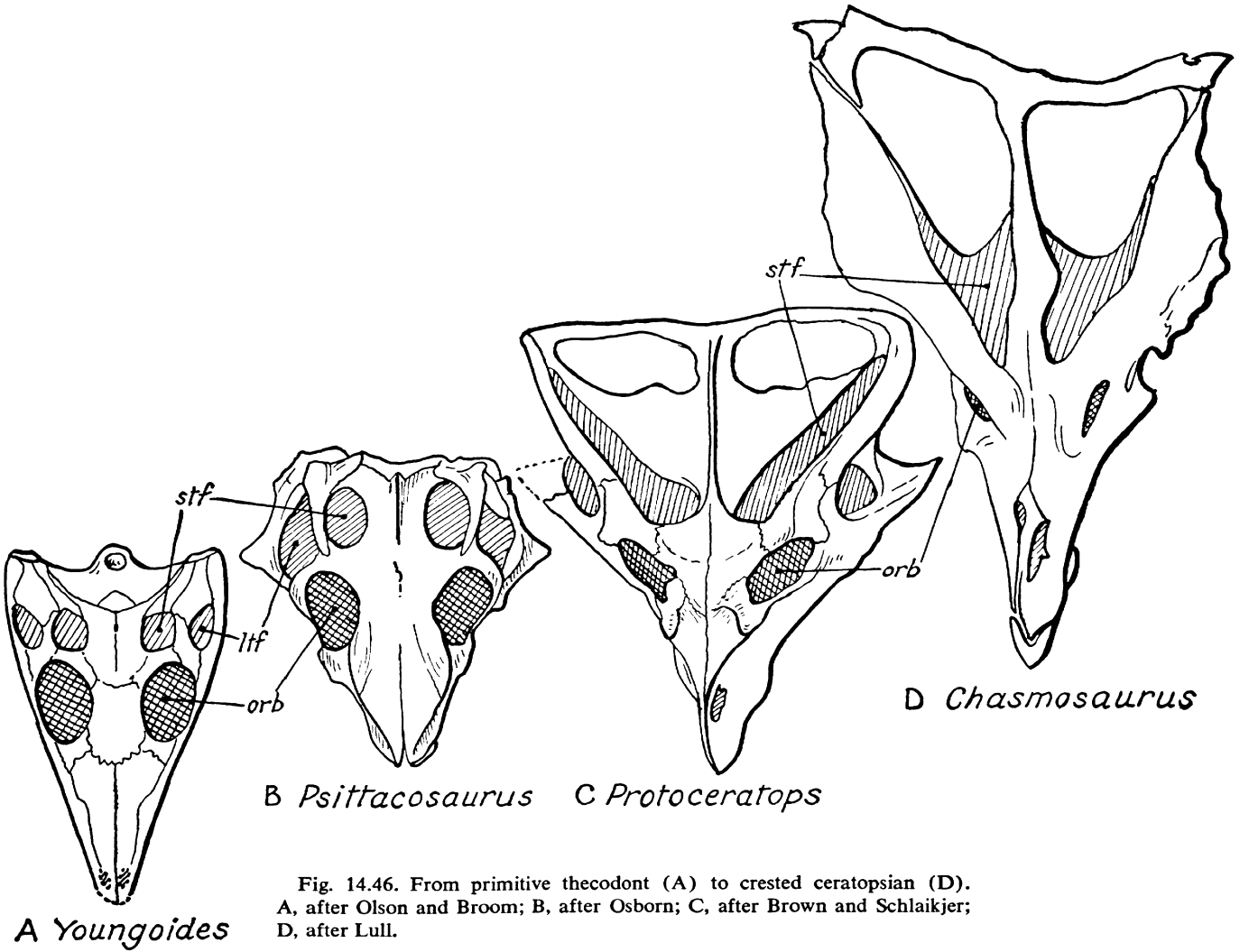


Fig. 14.46. From primitive thecodont (A) to crested ceratopsian (D). A, after Olson and Broom; B, after Osborn; C, after Brown and Schlaikjer; D, after Lull.

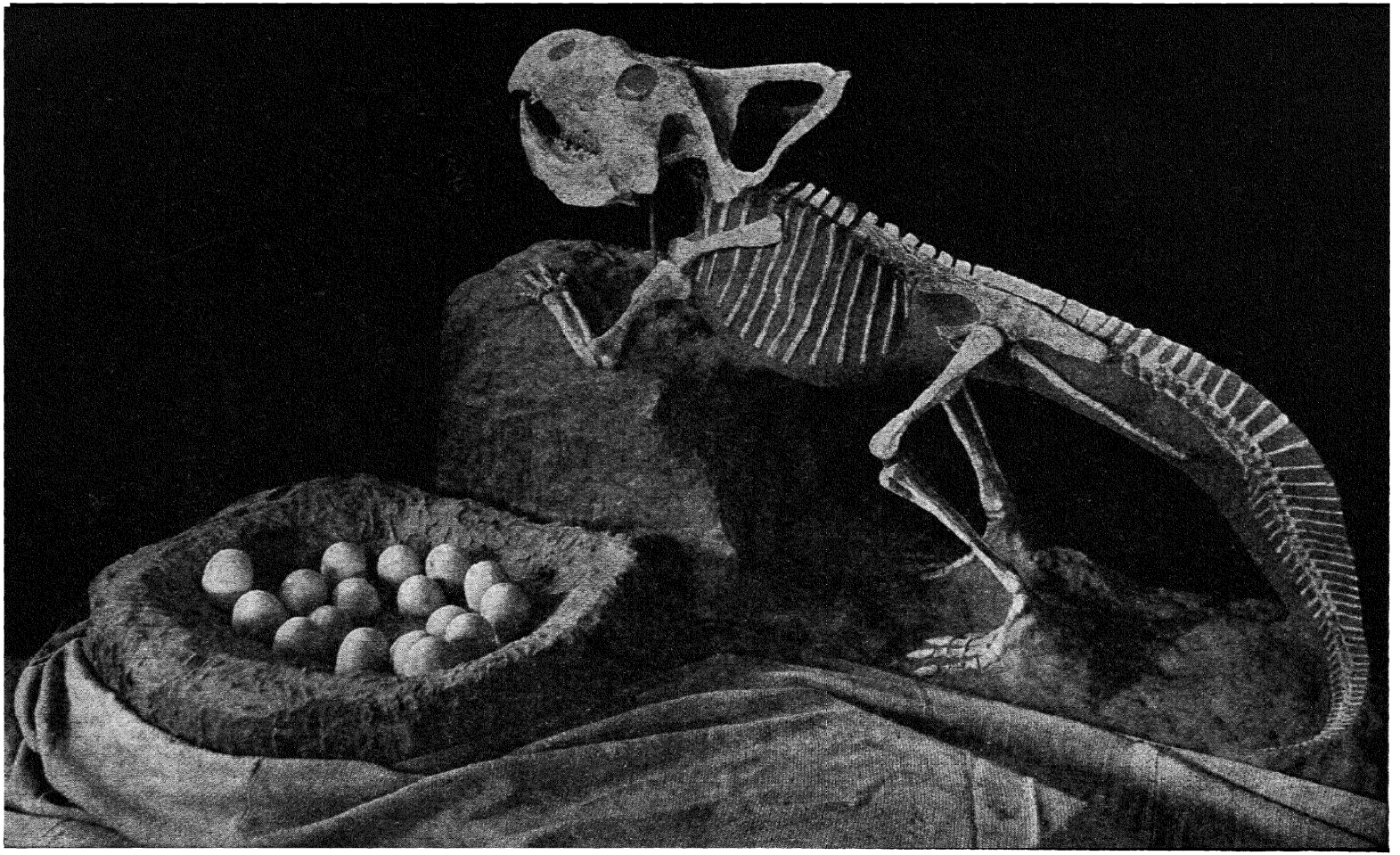


Plate 14.I. Skeleton of ancestral "horned dinosaur" (*Protoceratops grangeri*), and its nest and eggs, from the Cretaceous of Mongolia. Mounted by Charles Lang in the American Museum of Natural History.

CHAPTER XV

BAT-WINGED REPTILES (PTEROSAURS) AND THE FEATHER-WINGED FRAME OF BIRDS

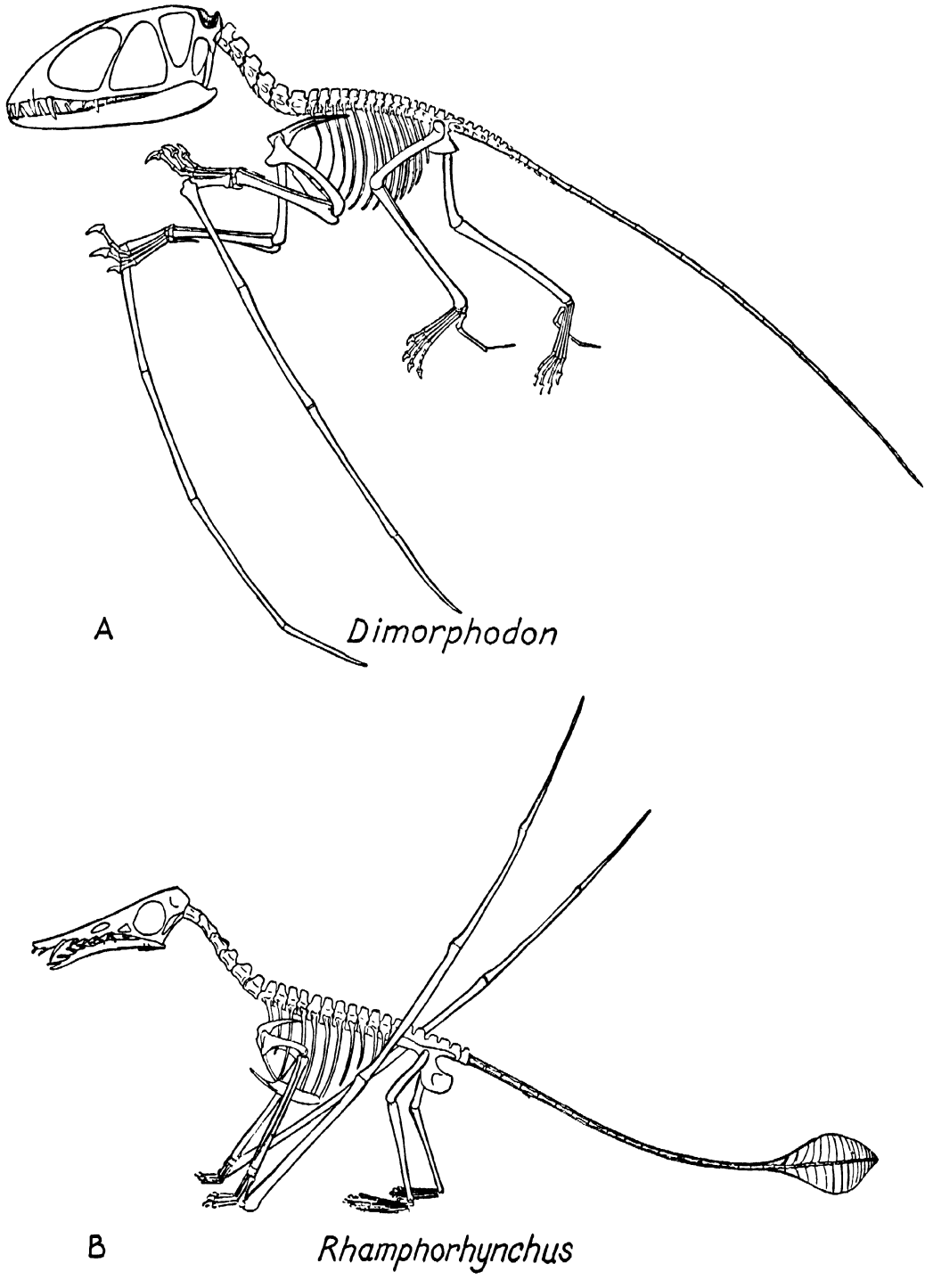


Fig. 15.1. Two primitive Jurassic pterosaurs. A, after Owen; B, after Seeley. Anisomerism of the hands, including extreme lengthening of the fourth digit, at first glance obscures the fundamental thecodont or pseudosuchian heritage preserved in the skeleton of *Dimorphodon*.

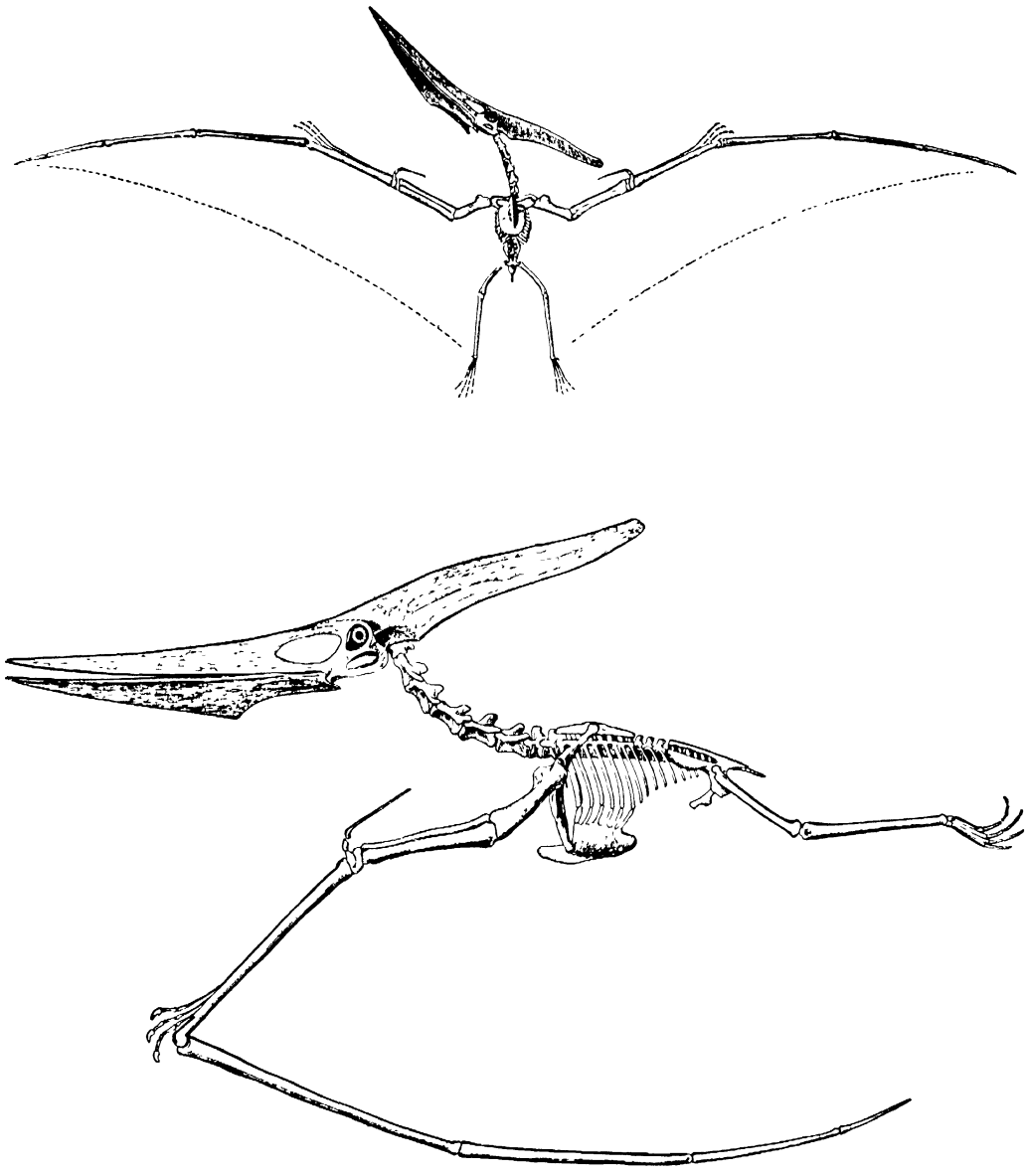


Fig. 15.2. Giant pterosaur from the Upper Cretaceous of Kansas. After Eaton. With a wing spread up to 22 feet, the length of the body (from first dorsal rib to rear end of ischium) was less than one-seventh the effective length of one wing. The head in spite of its huge length (3⅔ times length of body) was exceedingly light and strong.

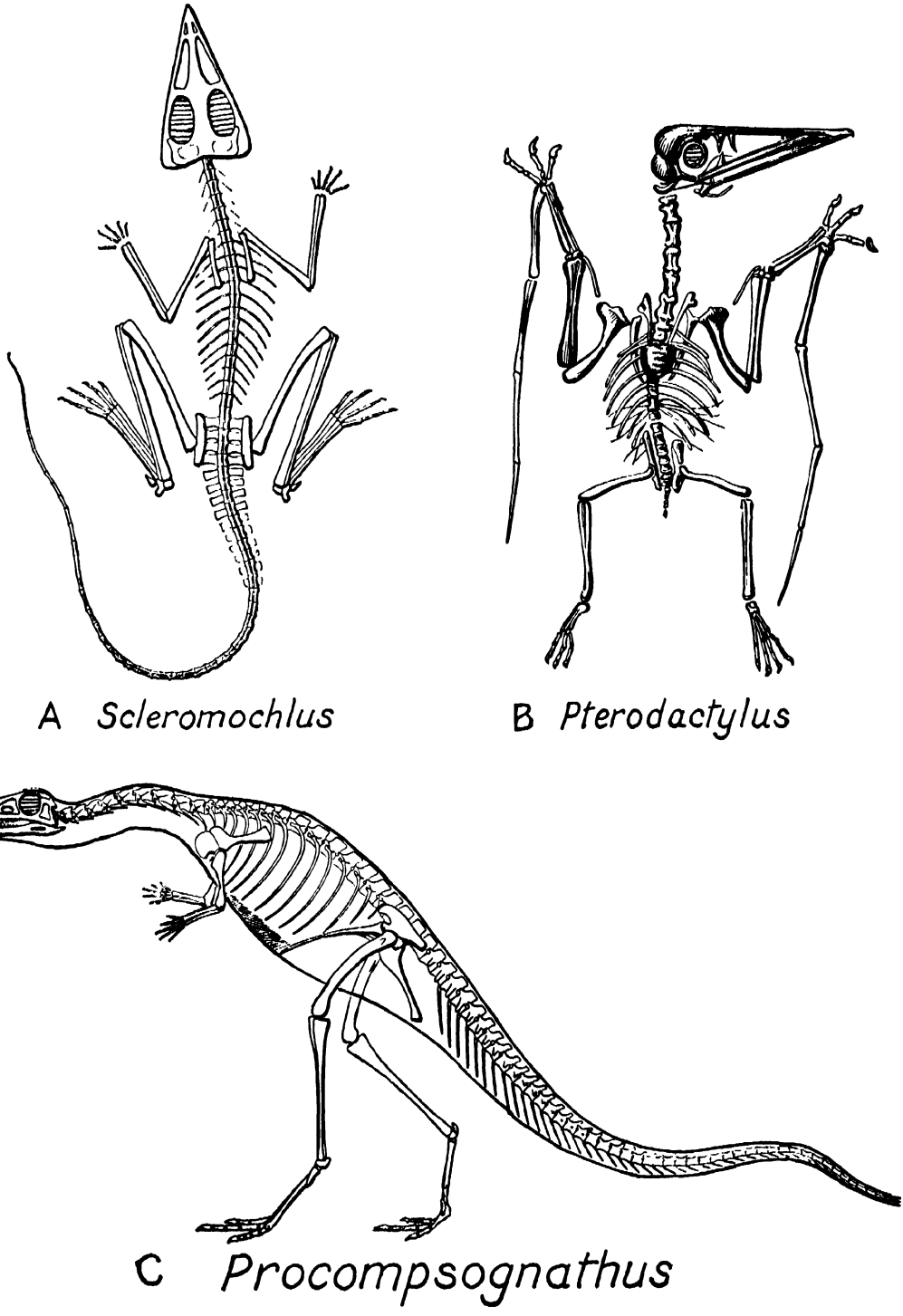


Fig. 15.3. Frog-like Triassic pseudosuchian (A) compared with a pterosaur (B), and a coelurosaur (C). A, after Smith Woodward; B, after Seeley; C, after von Huene. These figures suggest that the pterosaurs, like *Rhacophorus*, the "flying frog," may have been climbers before they became skimmers and fliers

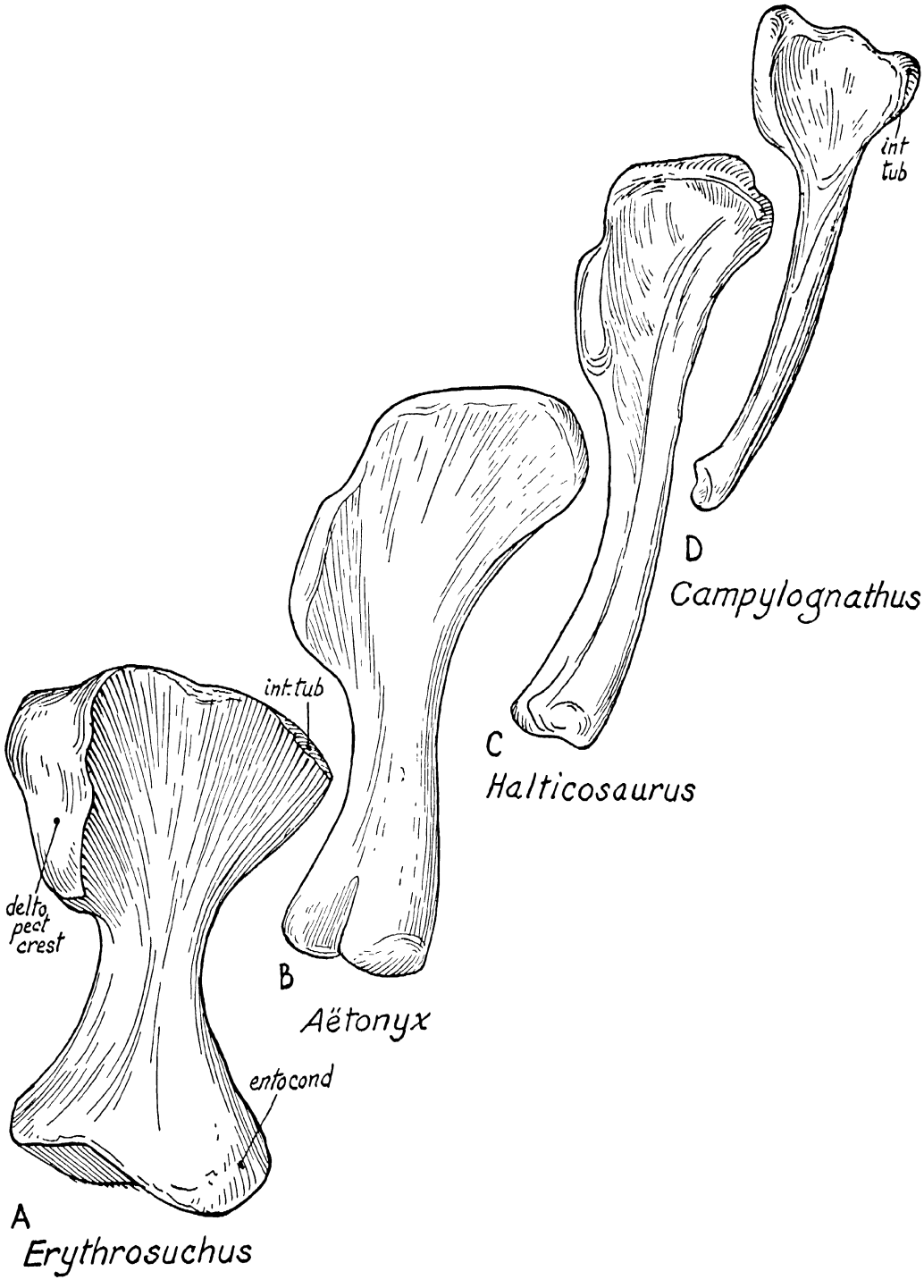


Fig. 15.4. Structural stages in the humerus, from primitive thecodont (A) to pterosaur (D). A, antero-ventral view of right humerus of large crawling reptile with huge brachial and pectoral muscles; B, slightly medial view, primitive bipedal dinosaur with grasping forearms; C, primitive running thecodont with slender and curved humeral shaft; D, pterosau, with slender, forwardly curved shaft, prominent delto-pectoral crest and distinct internal tuberosity. A, B, After Broom; C, after von Huene; D, original.

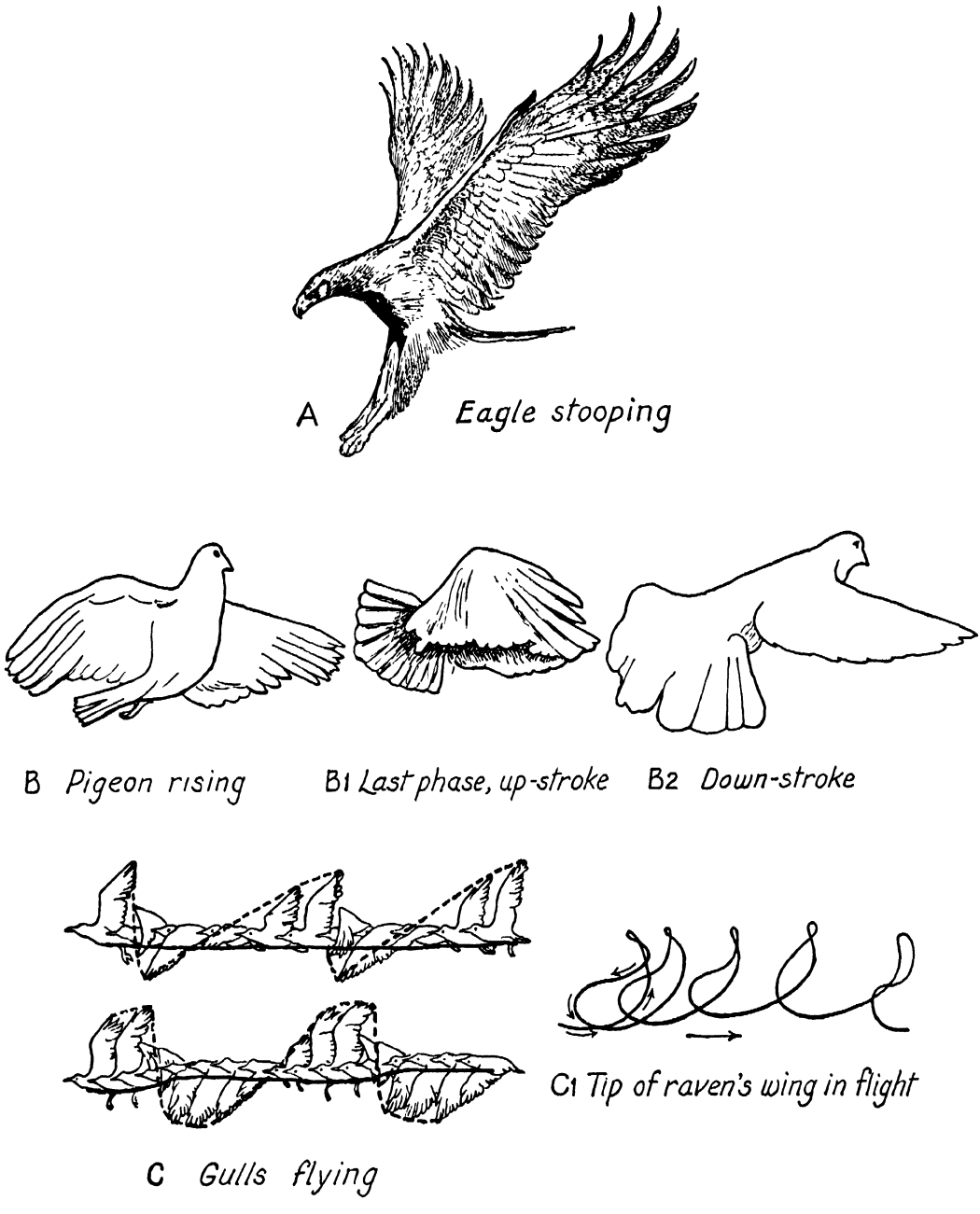


Fig. 15.5 Wing-stroke and flight. From **Warner,** after Marey (A, C) and Headley (B–B2).

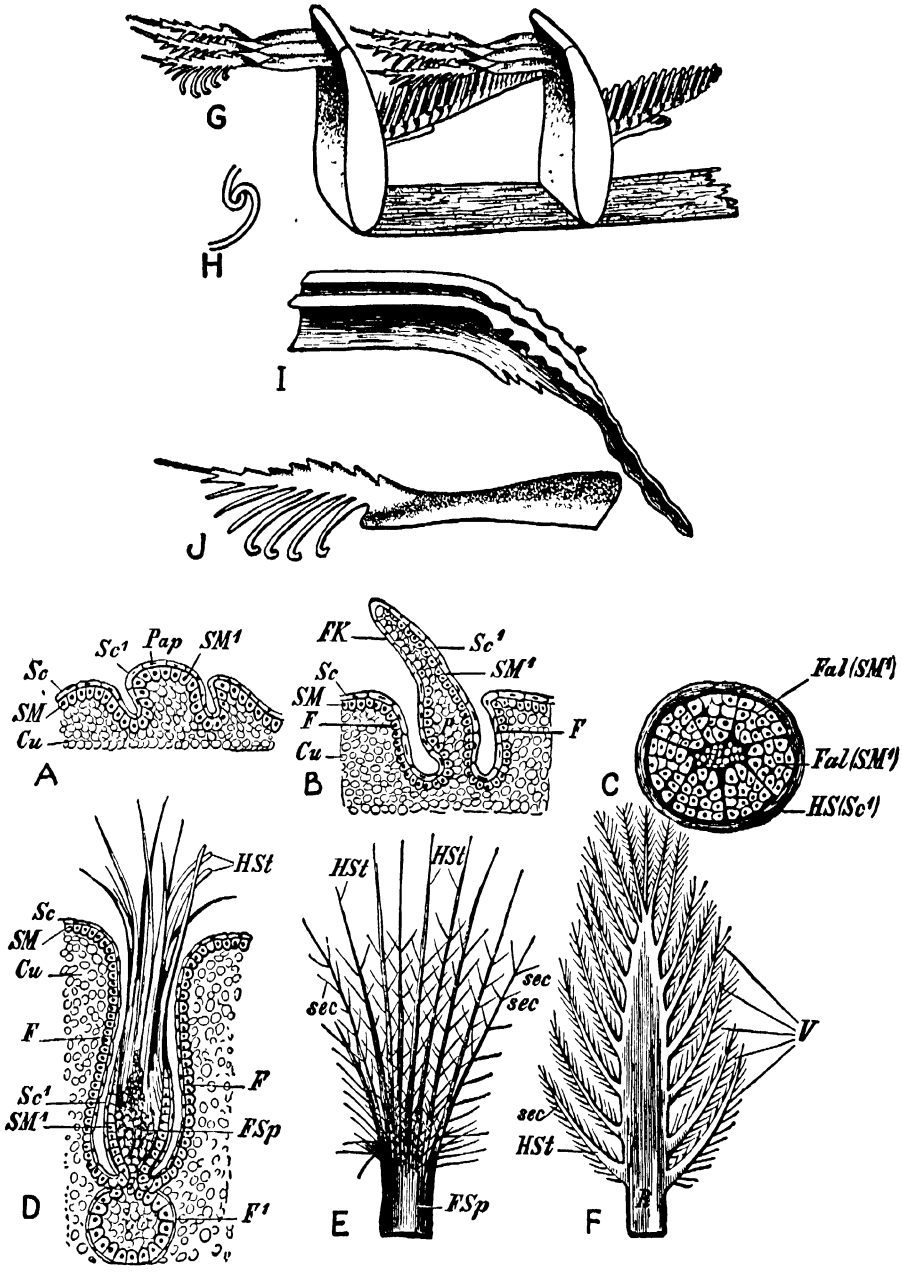


Fig. 15.6. Feathers—the essential organs of bird flight. A–F, from Parker and Haswell, from Wedersheim, after Studer; G–J, from Parker and Haswell, from Headley, after Pycraft. These complex polyanisomeres begin as epidermal papillae (A), not unlike reptilian scales. Each papilla sinks down and develops into a feather-germ. The rapidly proliferating Malpighian layer (C) folds itself into a series of radiating ridges which give rise to the hair-like feather tips of the nestling-down and later to the adult flight feather with its rachis or shaft and minute barbs and barbules (G–J).

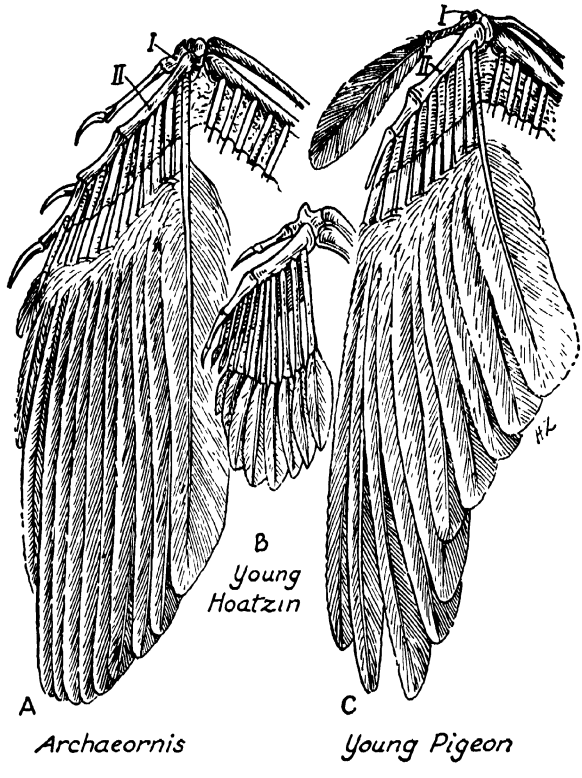


Fig. 15.7 (top). A–C, The highly developed wing feathers of Jurassic *Archaeornis* compared with those of two Recent birds. After Heilmann.

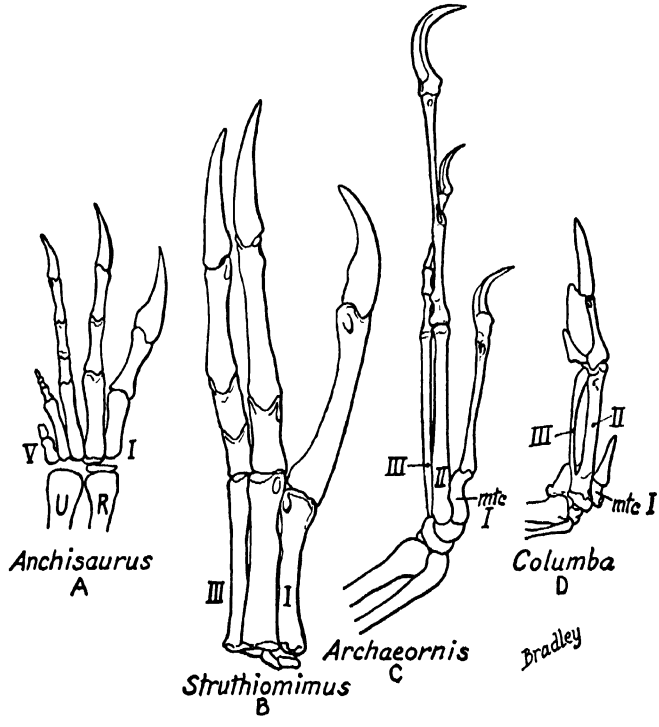


Fig. 15.8. A–D, From pendactyl manus to tridactyl wing. A, after Marsh; B, after Osborn; C, D, after Heilmann.

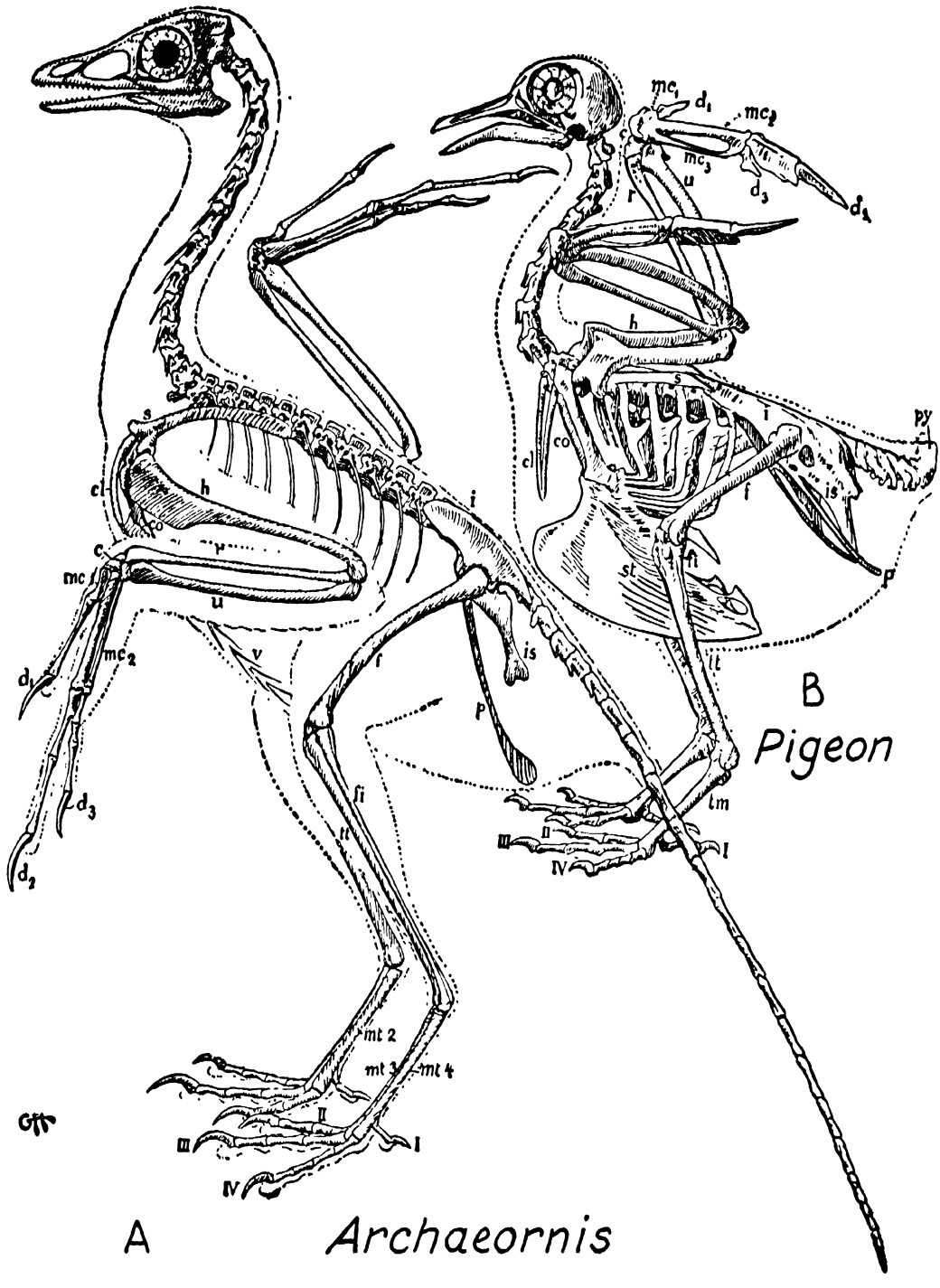


Fig. 15.9. Jurassic *Archaeornis* compared with Recent pigeon. After Heilmann. *Archaeornis*, notwithstanding the reptilian features of jaws, teeth, skull, wings, pelvis and tail, had as a whole attained the lowest known plane among birds and was assuredly nearer in general construction to a modern bird than it was to its running collateral ancestor among the primitive Triassic dinosaurs (fig. 15.3C).

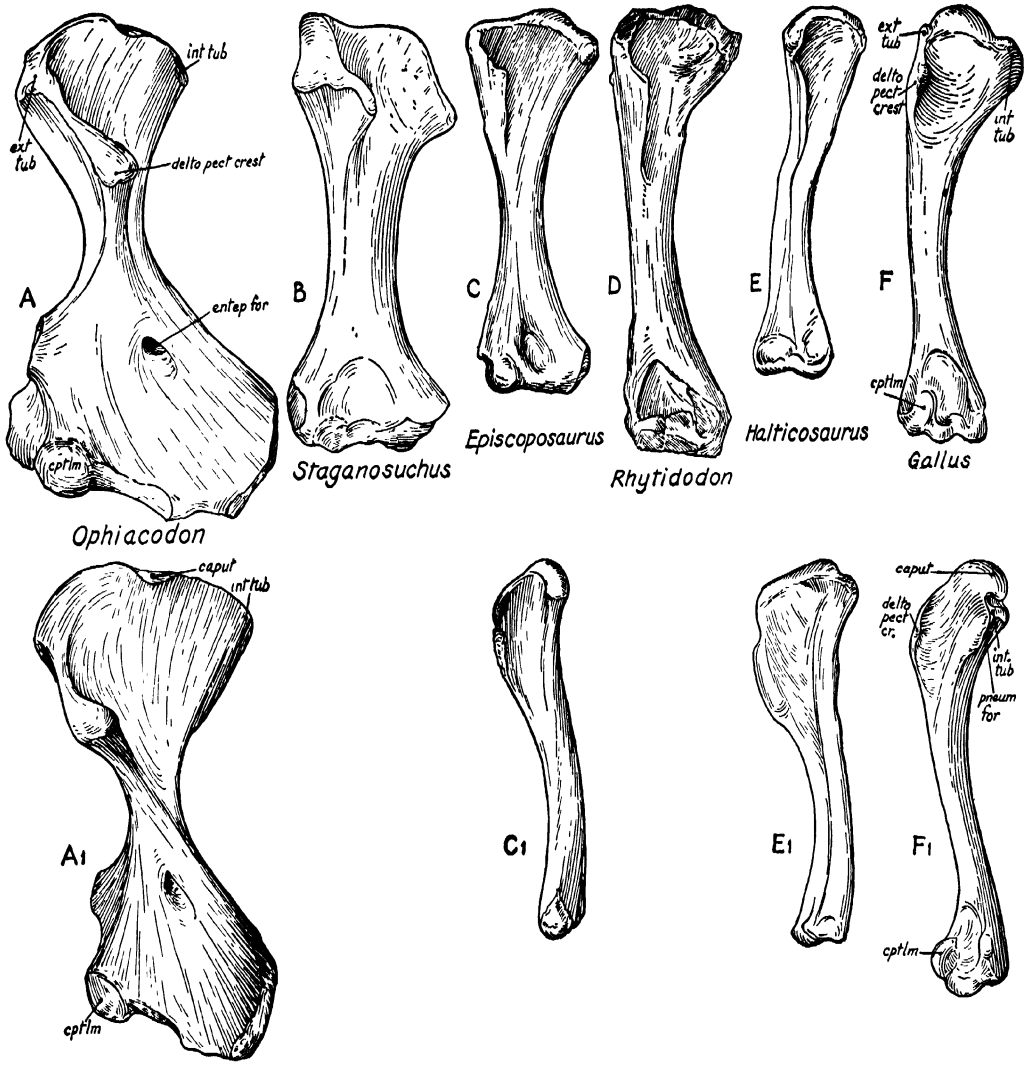


Fig. 15.10. The humerus from Permian reptile to modern bird. Antero-ventral (A–F) and medial (A1–F1) aspects. The primitive pelycosaur (A, A1), although not in the direct line of ancestry to birds, illustrates a stage which crawled on all fours; the great delto-pectoral and wide entocondylar crests indicate equally robust muscles for pulling the arm inward and pronating the forearm. The pseudosuchians (B, C) show intermediate stages leading, on the one hand, to the semiaquatic phytosaur (D) and on the other, to the coelurosaur (E) and bird (F). In the latter the humeral shaft is slender and sigmoid, with well rounded prominent head and distinct internal tuberosity. A, A1, F, F1, original; D, after McGregor; others after von Huene.

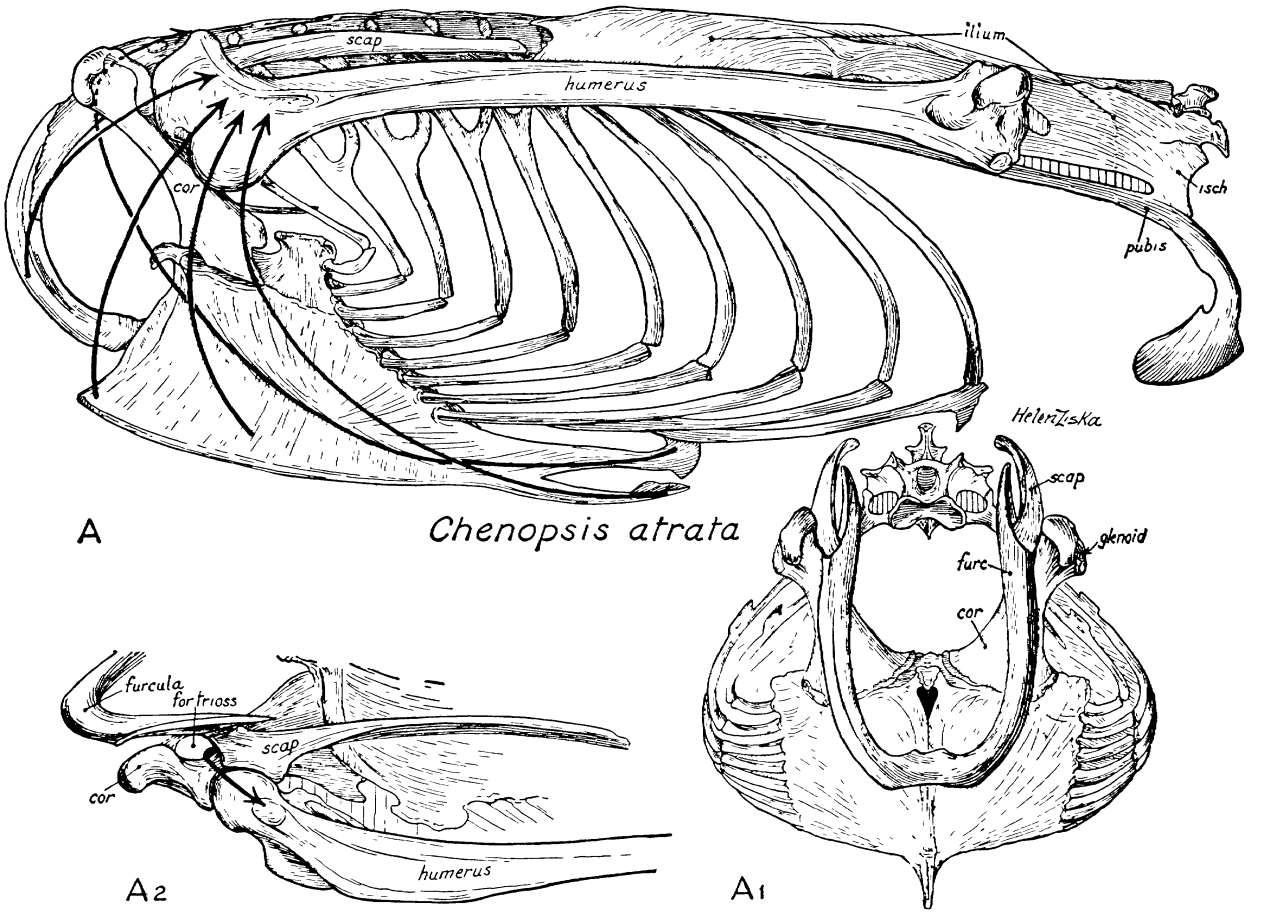


Fig. 15.11. The bony frame for the wings. The great pectoral muscle converges from the strong high-keeled sternum on to the ventral surface of the proximally expanded great tuberosity, which it depresses. The wing is raised by the subclavius, or pectoralis secundus, which passes through the foramen triosseum (A2) to be inserted on the lesser tuberosity. The thrusts of the wing are transmitted through the stout coracoids and furcula to the expanded sternum, which in turn reacts against the spring-like ribs and rigid vertebral column.

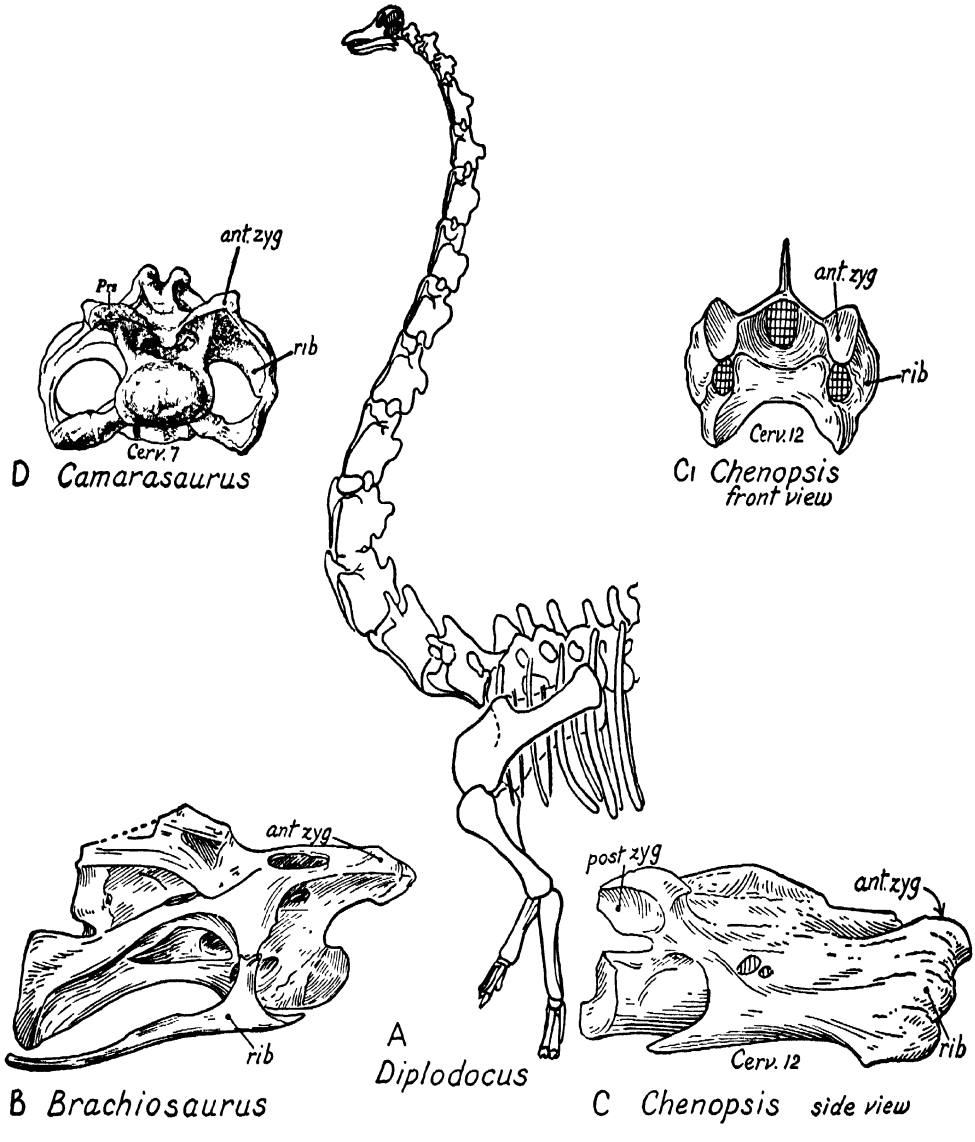


Fig. 15.12. Independent elongation of cervical vertebrae in sauropod dinosaurs (A, B) and swan (C). The high specialization for complex movements of the neck vertebrae in dinosaurs is surpassed in the swan. A, after von Huene; B, after Janensch; C, C1, original; D, after Osborn and Mook.

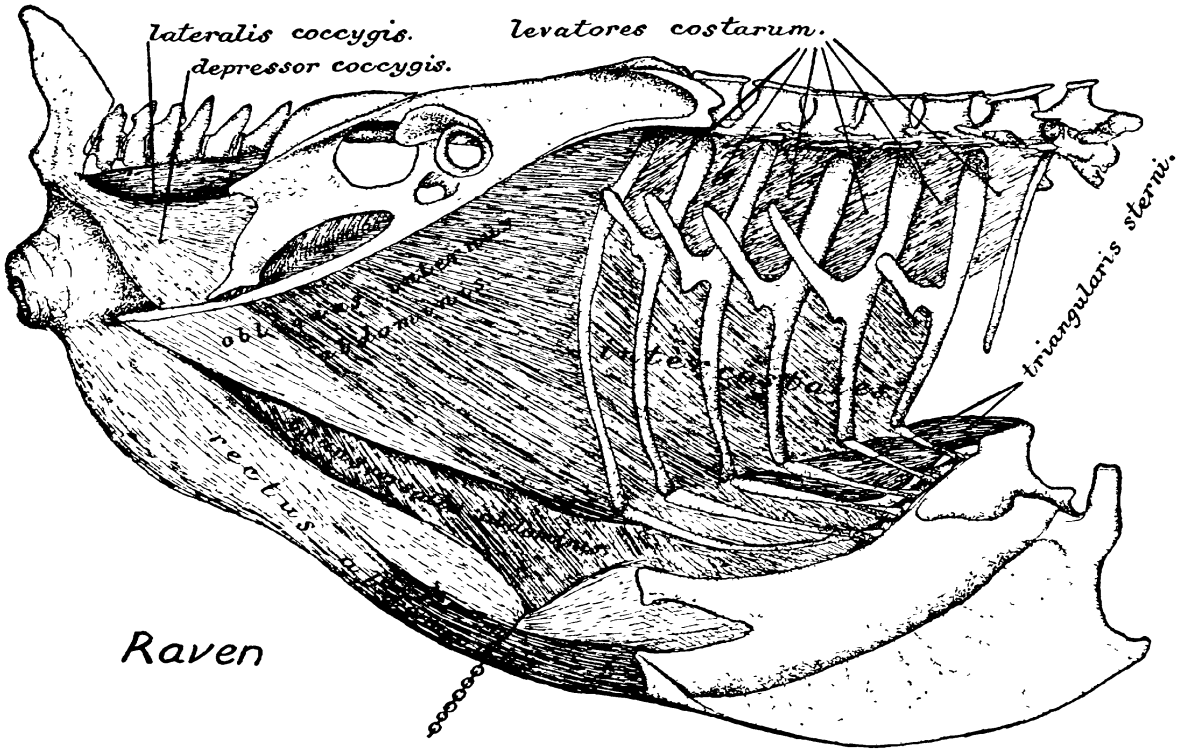


Fig. 15.13. Intercostal, abdominal and coccygeal muscles in relation to sternum and to pelvis. After Shufeldt.

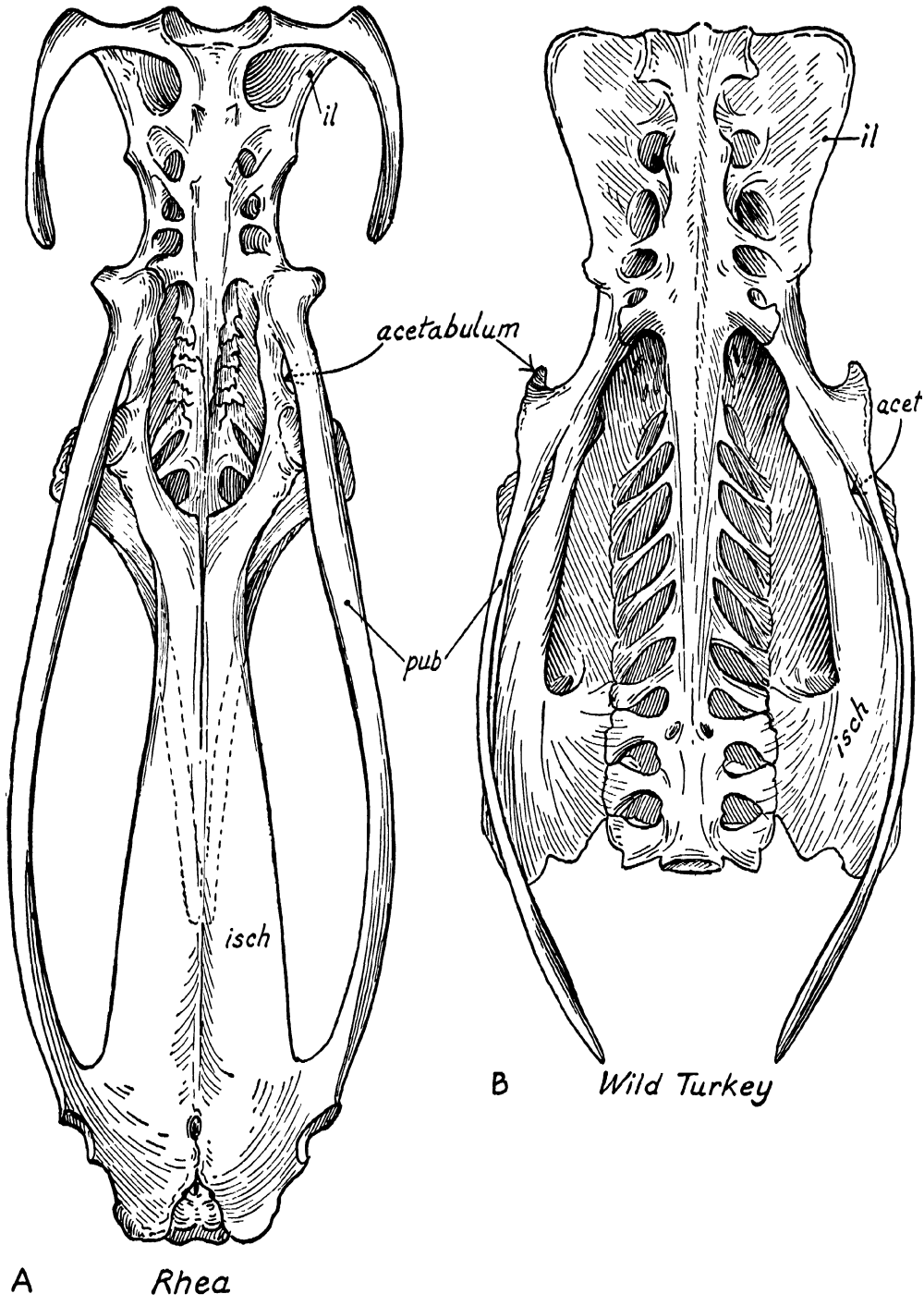


Fig. 15.14. Contrasting length-to-breadth proportions in pelves of *Rhea* (A) and wild turkey (B). Original. In *Rhea*, the opposite ischia, meeting in a long symphysis, together with the strong bowed-out pubes, form a stiff frame for the powerful adductors. The great length of the entire pelvis gives a long reach for the muscles of the thigh. In the turkey the much wider, ventrally open pelvis gives a wide space for abdominal viscera, but the legs are much shorter than in *Rhea*, the wings being useful in sudden flight.

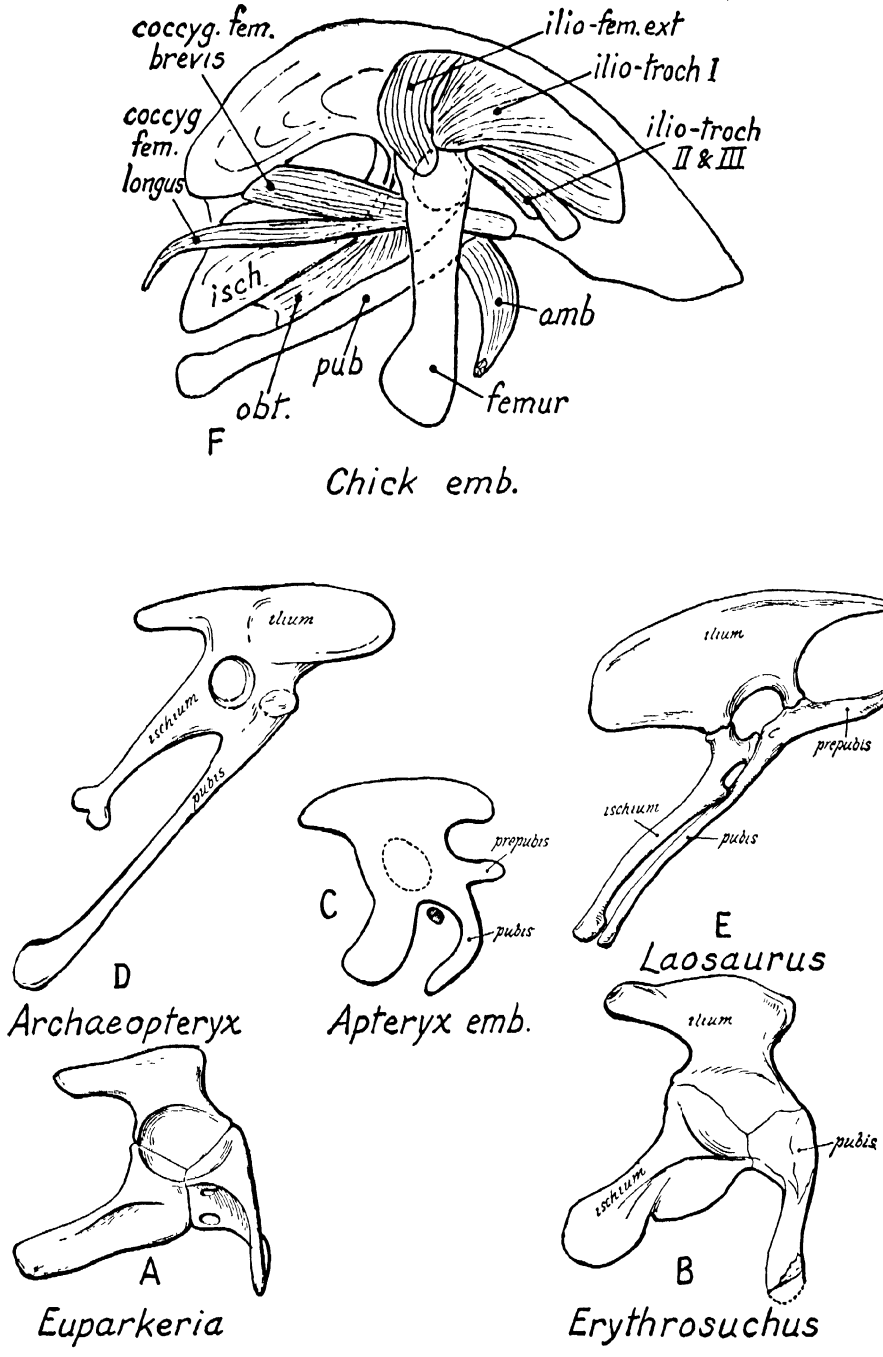


Fig. 15.15. Pelves of Triassic thecodonts or pseudosuchians (A, B), Jurassic ornithischian dinosaur (E), embryo *Apteryx* (C) and Jurassic bird (D), showing (F) the turning of the pubis downward and backward, presumably under the influence of the lengthening obturator muscle (*obt.*); also the outgrowth of the prepubic process (C, E), presumably under the influence of the internal oblique abdominal muscles (cf. fig. 15.13). A, B, after Broom; C, after Parker; D, after Heilmann; E, after Marsh; F, after Romer.

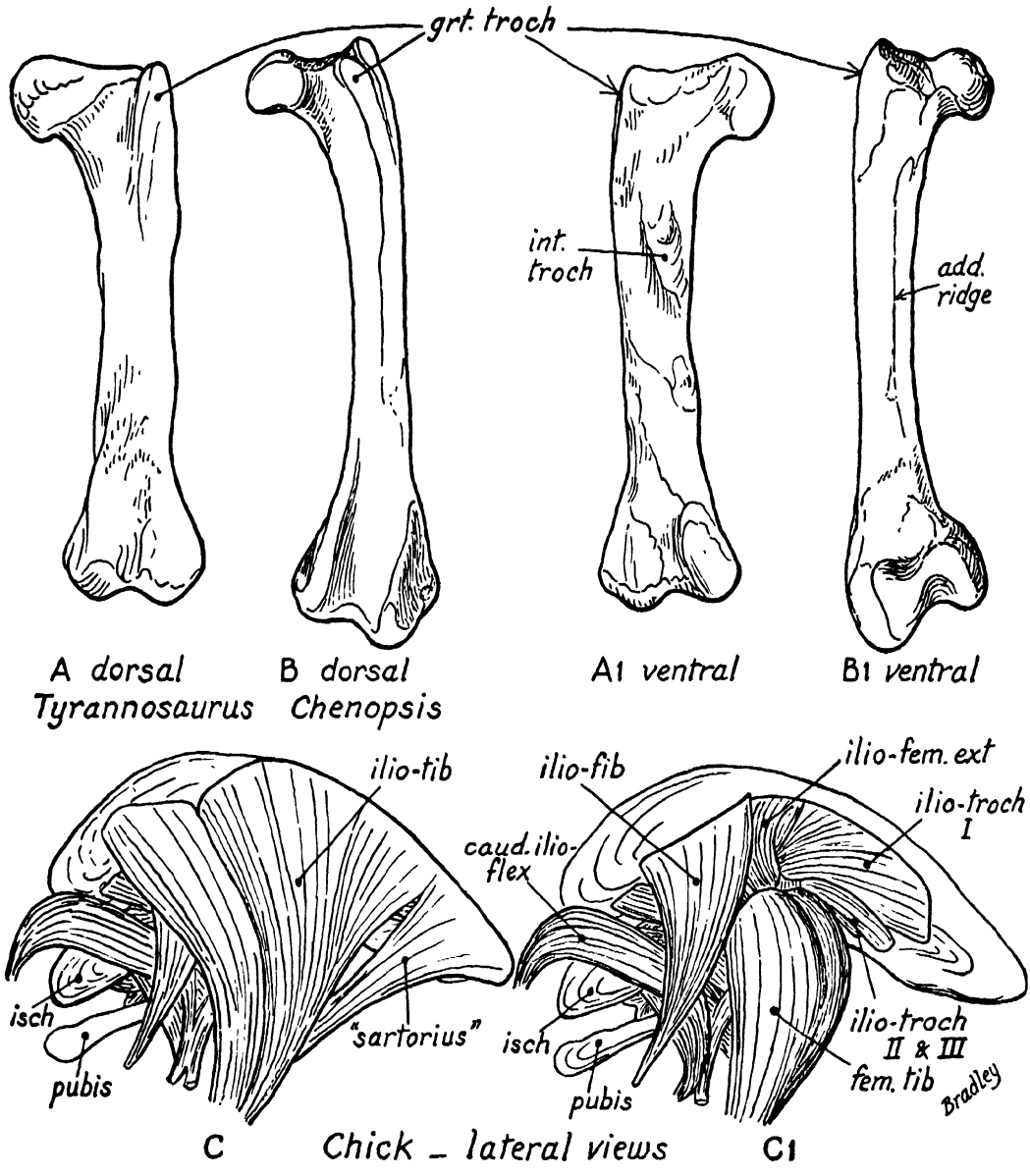


Fig. 15.16. Femora of dinosaur (A, A1) and bird (B, B1), thigh musculature of embryo chick (C, C1). A, A1, after Osborn; B, B1, original; C, C1, after Romer. All functional vertebrate femora are reversible levers, embedded in a great conical muscle mass (C), extending from the pelvis to the lower leg and foot (cf. fig. 15.17).

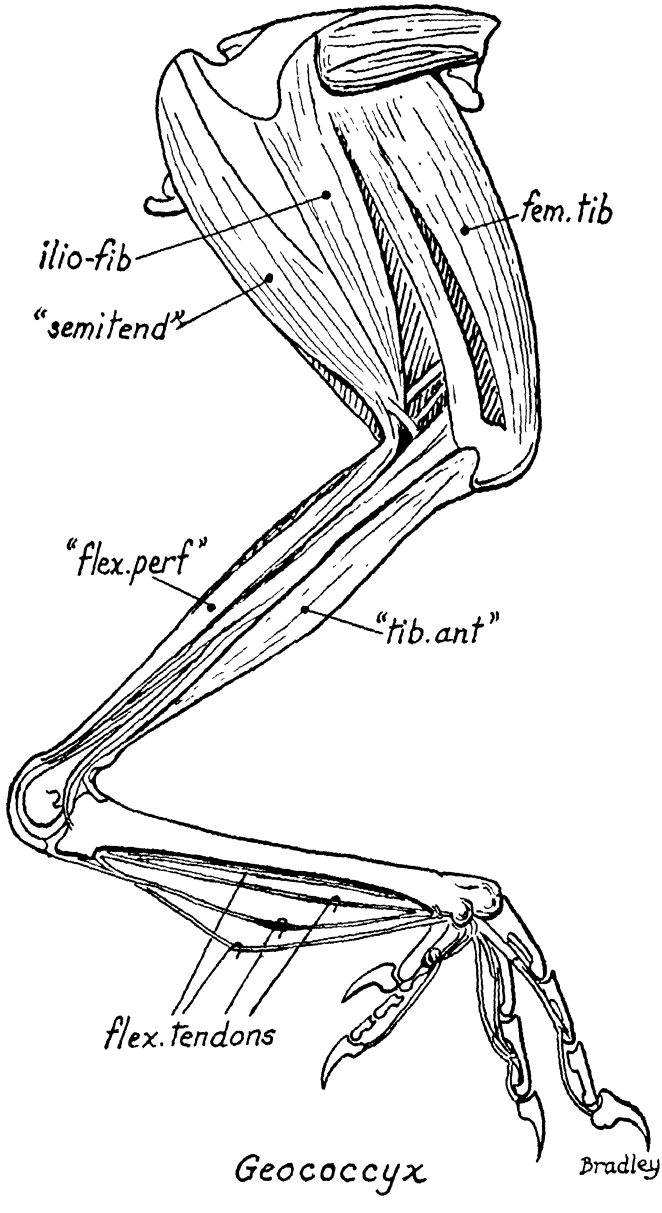


Fig. 15.17. Hind limb of road-runner. After Shufeldt. Showing the flexor tendons of the foot, which pass over the "reversed knee" of the tibio-tarsus, continuing beneath the tarso-metatarsus, to be inserted into the phalanges. In resting Passeres, the weight of the body flexes the limb and automatically tenses the flexors of the digits, thus insuring a firm grasp on the perch. The hinge-like characters of the mesotarsal joint is well shown. For the evolution of this joint, see fig. 12.22.

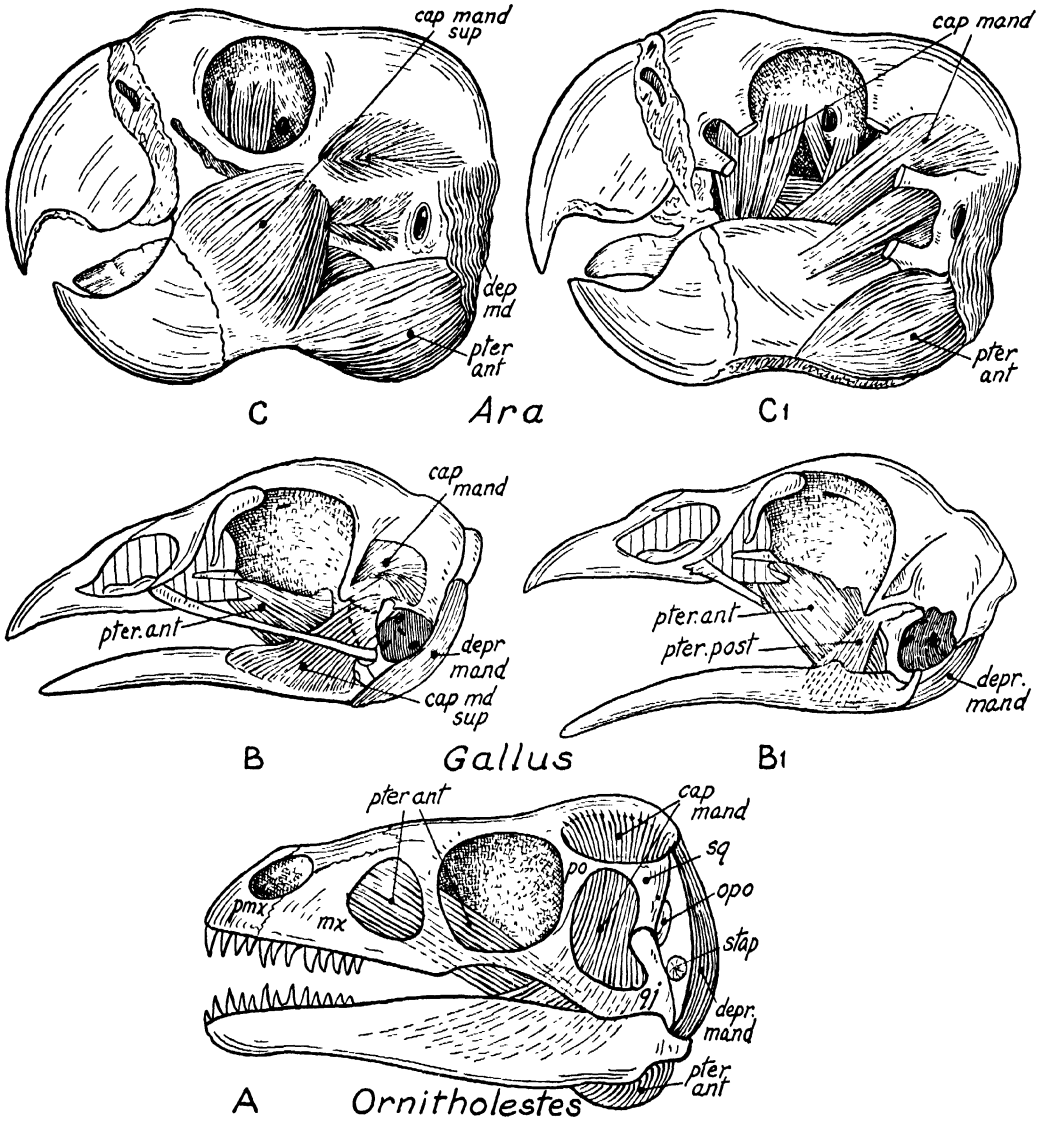


Fig. 15.18. Skulls and jaw muscles of fowl (B), macaw (C) and bird-like dinosaur (A). A, skull modified from Osborn, muscles after Adams; B, B1, after Adams; C, C1, after Gadow. In the saurischian dinosaur, whose jaw muscles can be safely restored in the main from those of the alligator, the anterior pterygoid extended backward and downward, wrapping around the jaw in the rear, while part of the capiti-mandibularis was inserted on the inner side. The depressor muscle, inserted just behind the fulcrum, could very quickly snap the jaw open. The fowl inherits this musculature with minor specializations. In the parrot some of the deeper palatal muscles draw the palate and jaw forward and raise the upper beak, while the powerful capiti-mandibularis and pterygoid muscles close them.

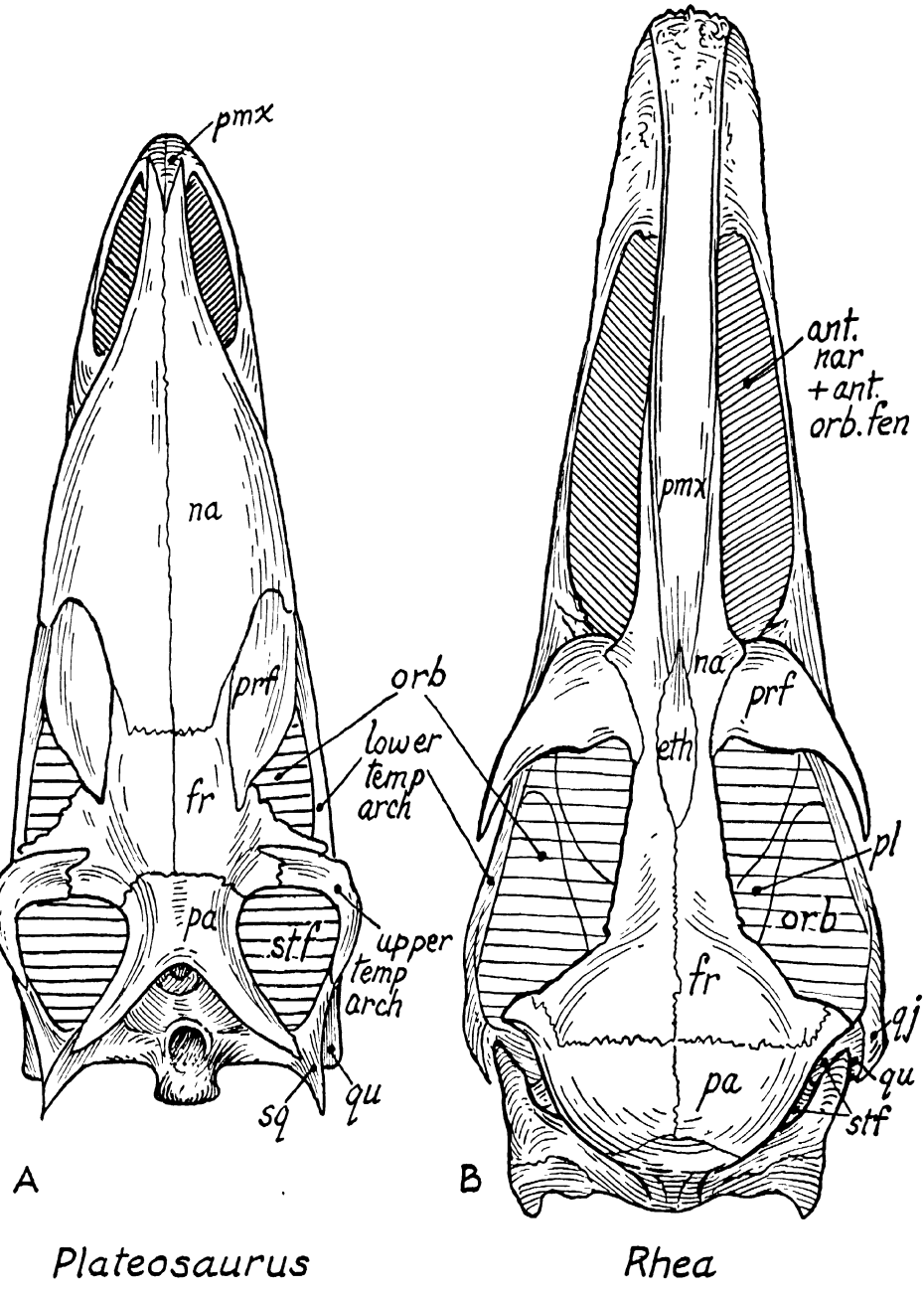


Fig. 15.19. Dorsal view of skulls of saurischian dinosaur and ratite bird. A, after Romer; B, original. A, x 5/13; B, x 1. The dinosaur skull (A), although specialized in its enlarged nasals, retains most of the basic diapsid pattern. In this bird skull (B) the dorsal process of the premaxillae has become enlarged, as well as the preorbital fenestrae, while the nasals are reduced, the postorbito-squamosal or upper temporal arch is lost, the supratemporal fenestrae open into the greatly enlarged orbits and the braincase is expanded.

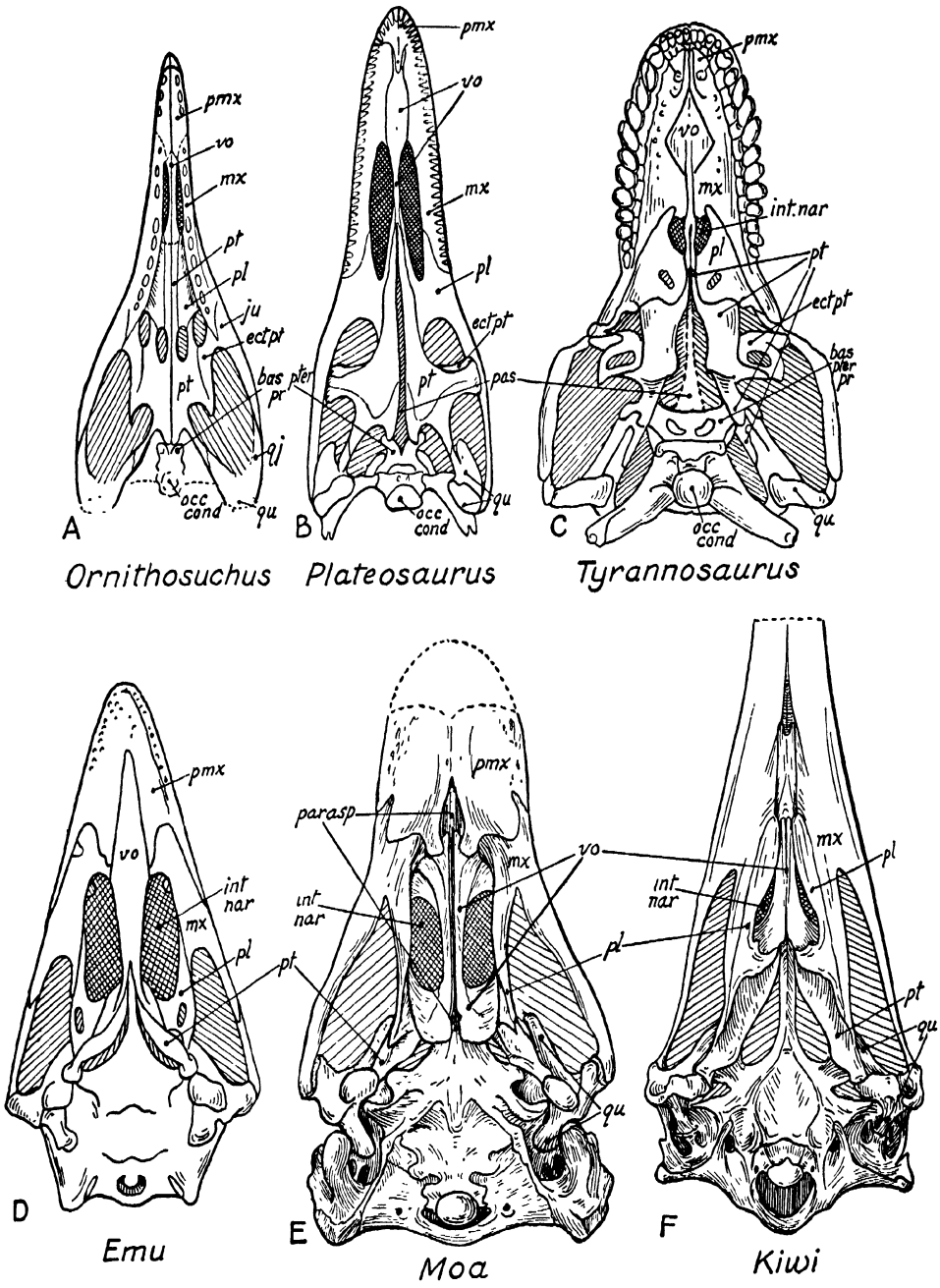


Fig. 15.20a. Avian palatal types and their derivation. A, after Broom; B, modified after Romer, data from von Huene; C, after Osborn; D, after Pycraft; E, after Pycraft; F, original. In the ancestral pseudosuchian (A) and in the saurischian dinosaurs (B, C) the pterygoids are, so to speak, the keystones of the palato-pterygo-quadrate arches, retaining their five processes (anterior, transverse, medial, dorsal (epipterygoid) and quadrate), receiving and withstanding the varied stresses from the moving lower jaws and jaw muscles. In the birds, with the backward extension of the internal nares, the pterygoids lose their five-rayed form and become more or less rod-like. Nevertheless they still serve as struts, transmitting the thrusts from the beak and palate back to the quadrates and to the lateral buttresses of the braincase. With the backward movement of the nares and the reduction of the anterior processes of the pterygoids, the palatines become the side walls of the narial tube.

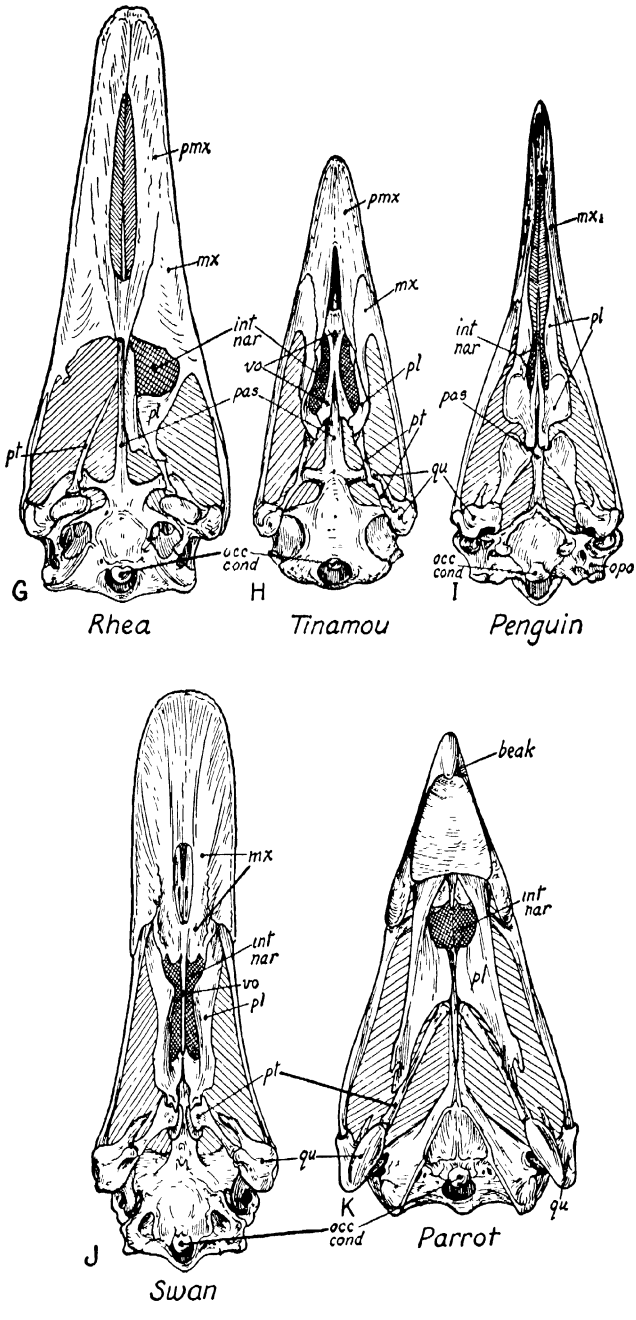
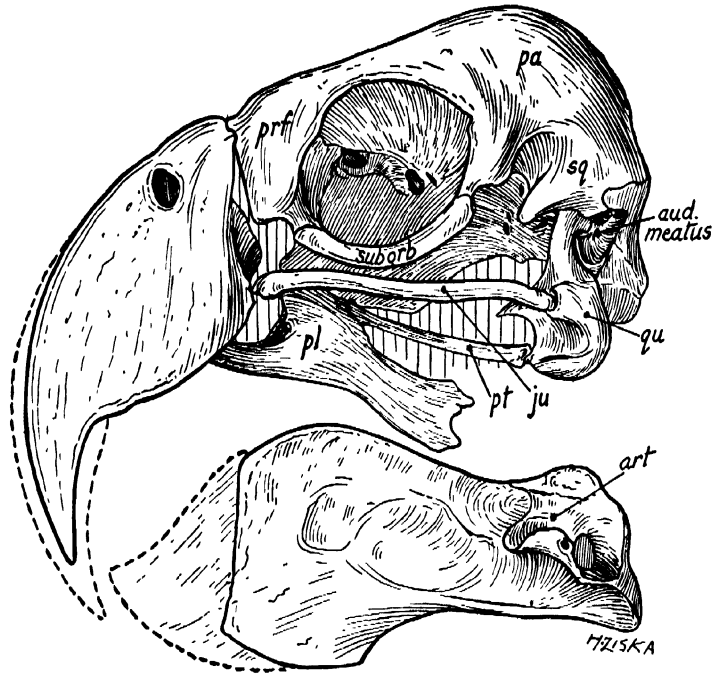
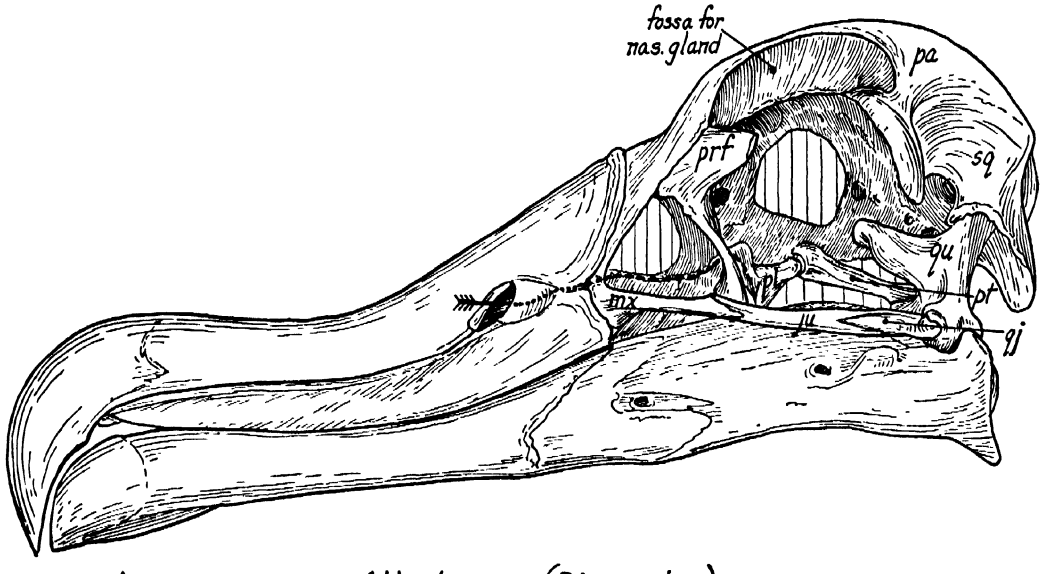


Fig. 15.20b. In the Palaeognathae (D–H) the diminishing palatines retreat as the posterior forks of the vomer extend laterally, losing their contact with the para-basisphenoid rostrum. In the Neognathae (I–K) the palatines retain or enlarge their contact with the cranial rostrum, sometimes (I) forming a secondary median symphysis which tends to compensate the bending stresses received from the beak and jaw muscles. Birds with somewhat movable upper beaks (I, J, K) develop a peg-and-socket (I) or sliding (J, K) contact between the palatines and the pterygoids. H, after Pycraft; F, I–K, original.



B Macaw (Ara)



A Albatross (Diomedea)

Fig. 15.21. Wide contrast in beaks and jaws between fish-eating sea birds (A) and fruit-eating forest bird (B). Original. The long narrow beak and jaws of the albatross are well adapted for snapping at living fish. The upper beak and quadrate are held in place by the nasals, maxilla, prefrontal, frontal, jugal, quadratojugal, squamosal, pterygoid and palatines. In the fruit-eating macaw the jaws are short, the large upper beak is transversely hinged on the tough skull roof; the entire palatoquadrate-jugal complex can be swung forward, raising the upper beak while the mandible slides forward on the longitudinal rim of the quadrate.

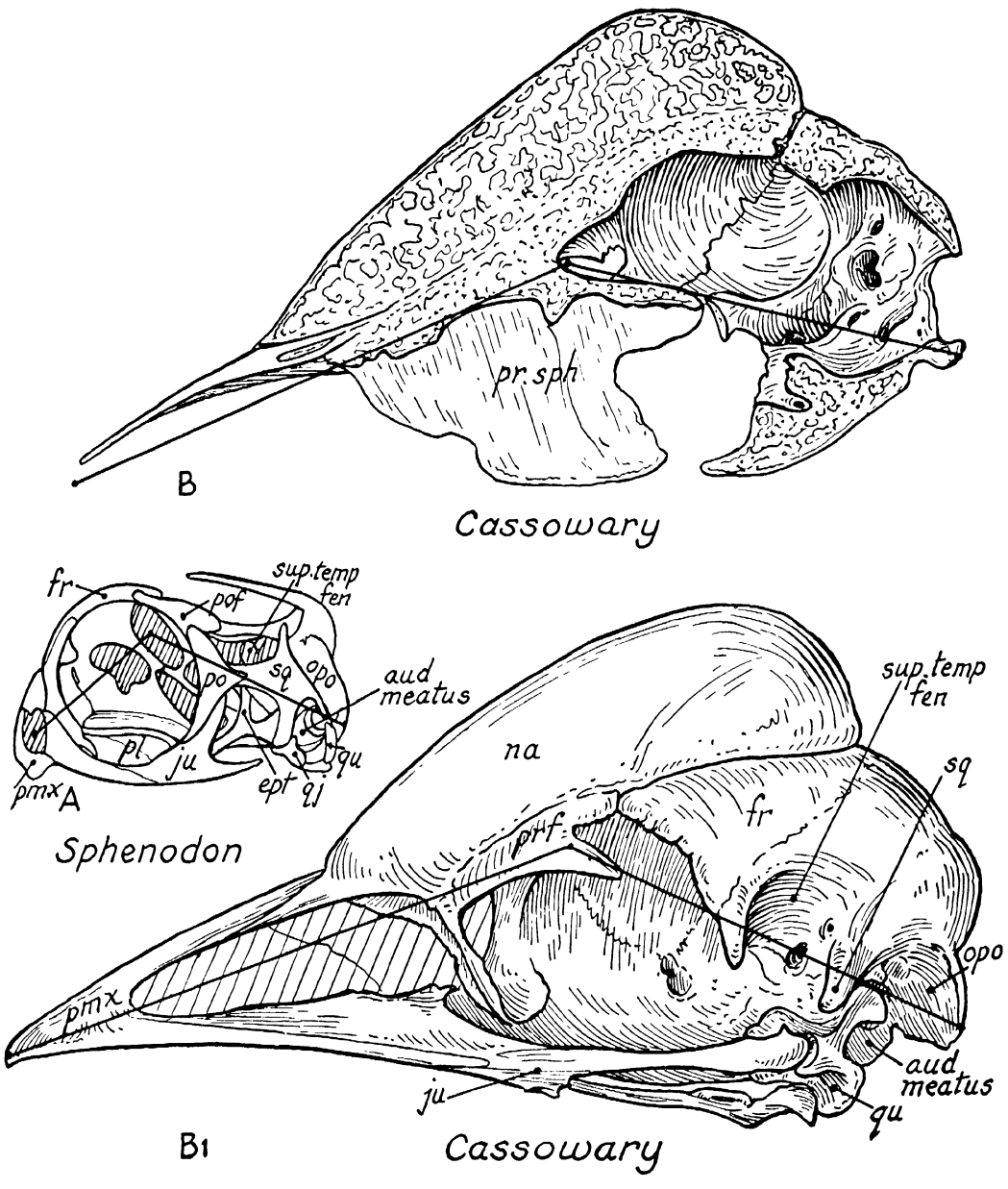


Fig. 15.22. Cranio-facial angle in a young *Sphenodon* (A) and an immature cassowary (B, B1). In reptilian embryos and young (A, A1) the facial axis is sharply inclined to the axis of the brain. A similar condition holds in late embryos and young birds (B, B1). A, after Howes and Swinnerton; B, B1, original.

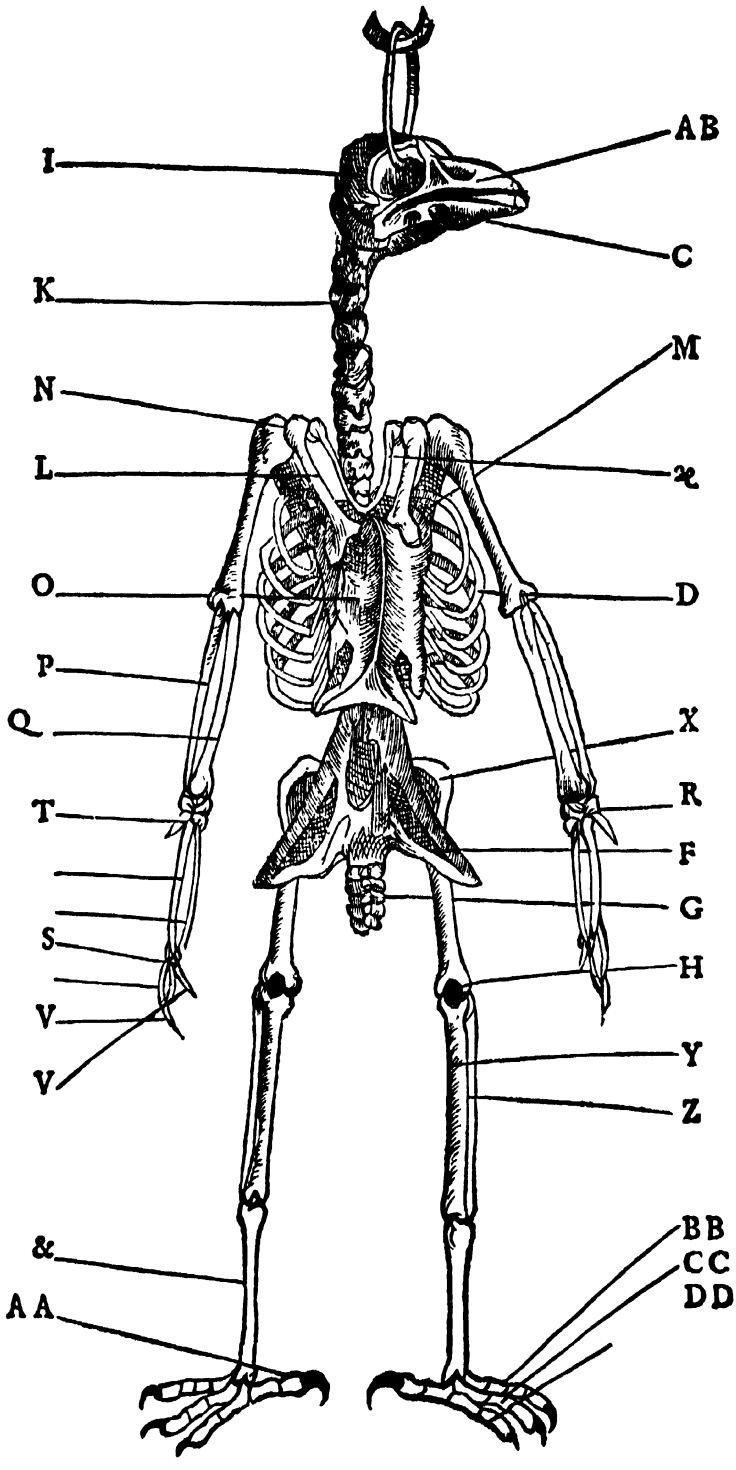


Fig. 15.23a, b. An early comparative study (Belon, 1555) of the skeletons of bird and man, with Belon's suggested homologies of the several parts. From Gudger, after Belon.

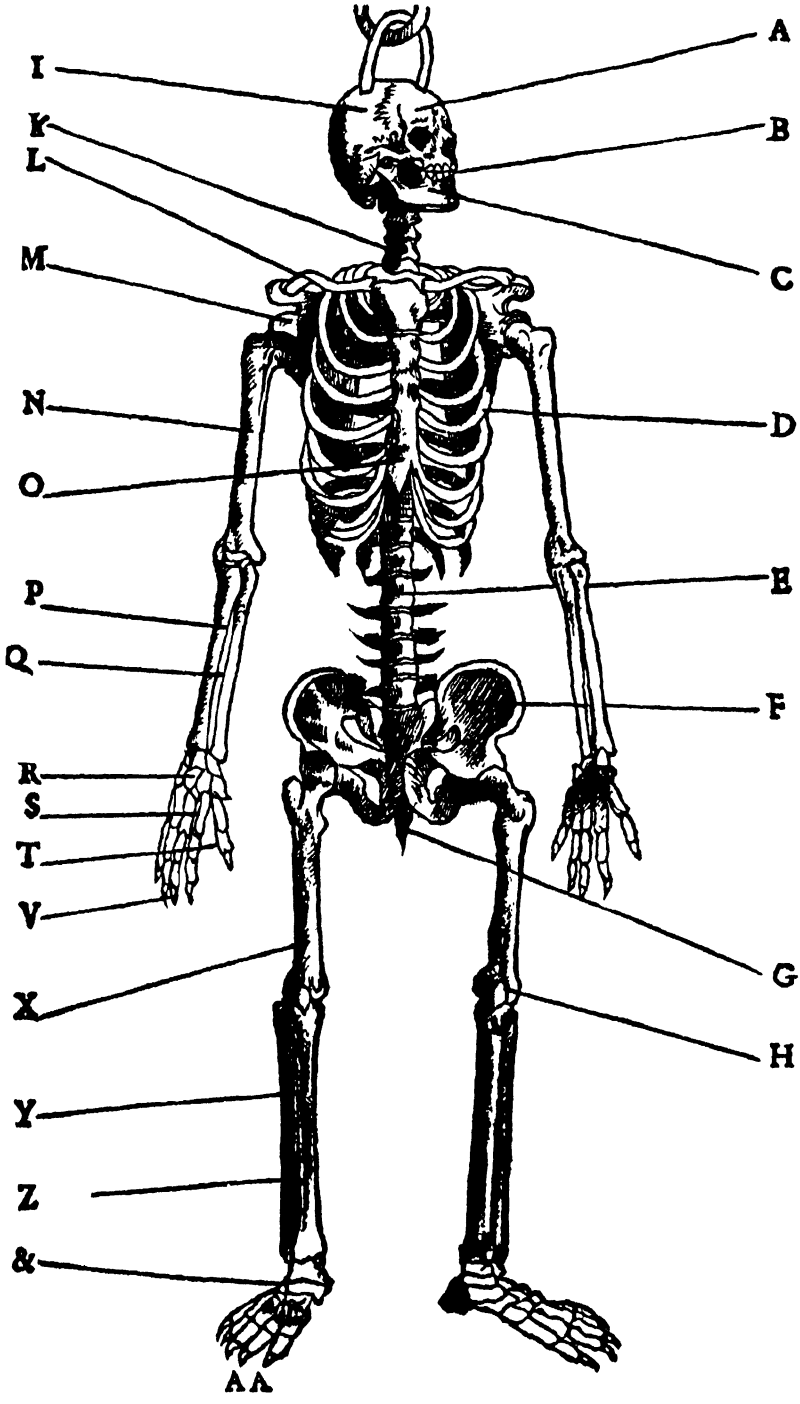


Fig. 15.23b

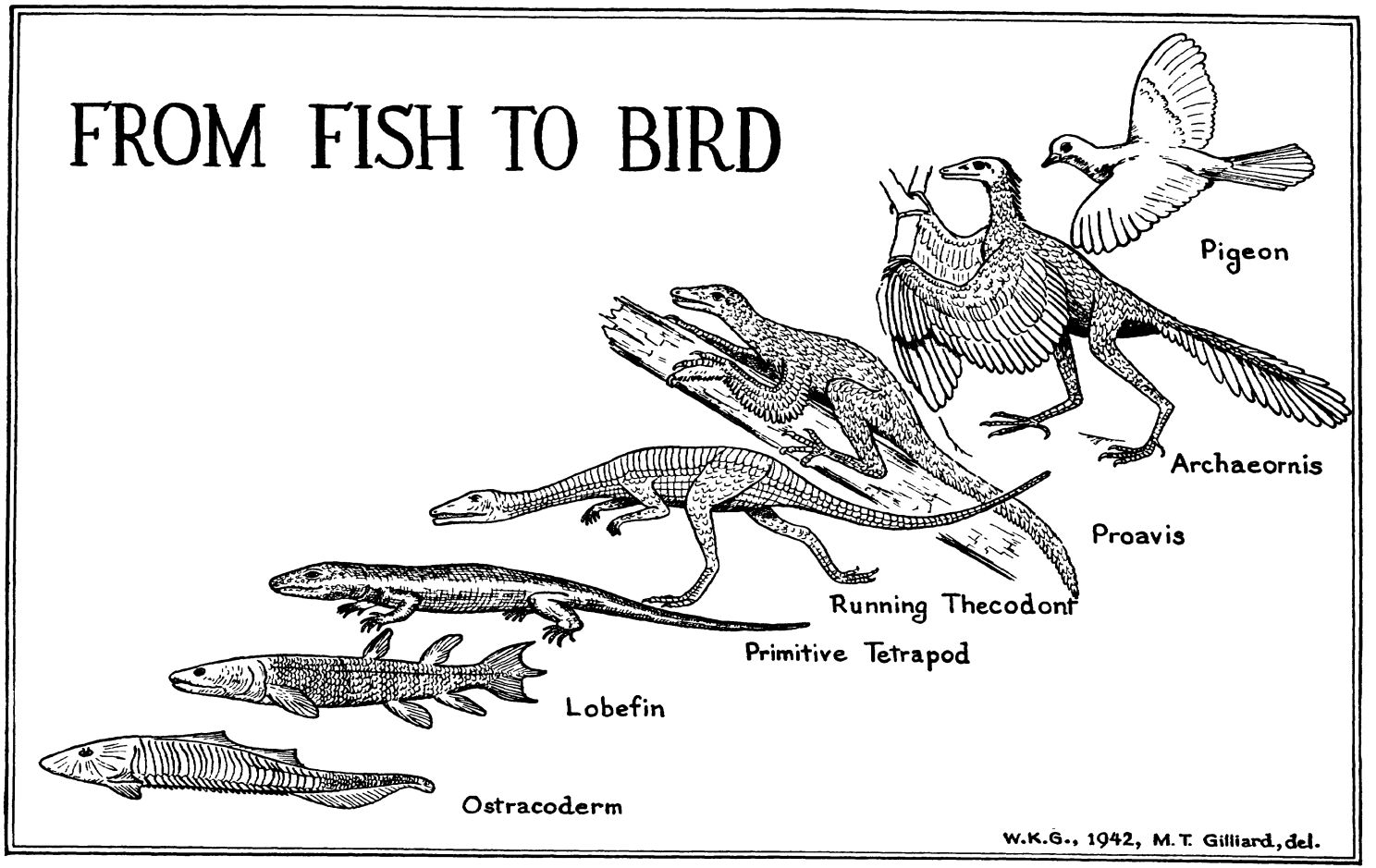
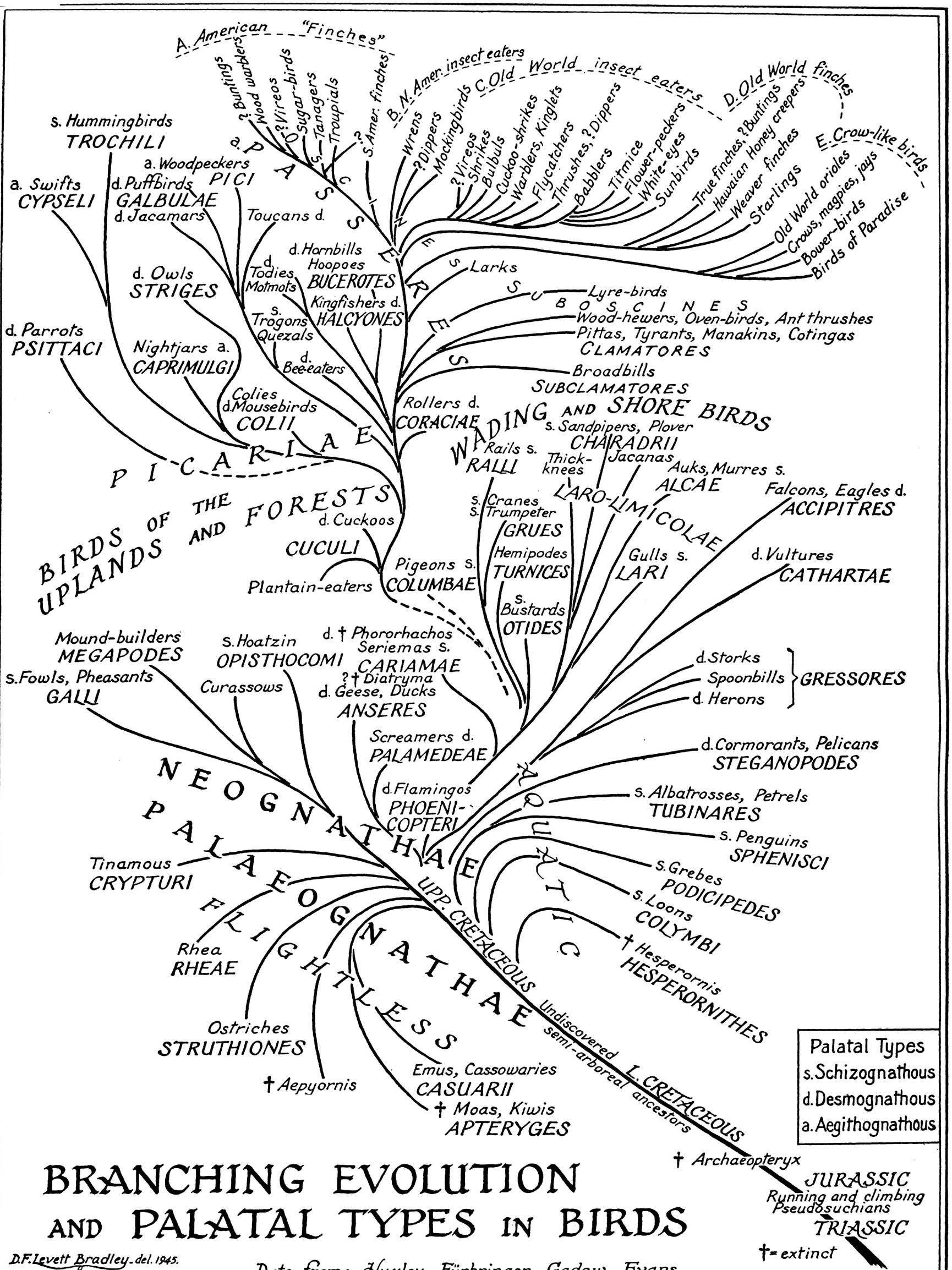


Fig. 15.24. Seven stages in locomotor habitus, from the earliest known mud-grubbing Silurian chordate to the typical bird. The "Proavis," a hypothetical stage, suggests that flight feathers may at first have functioned as arm coverts and holdfasts in climbing. After Gregory.

BRANCHING EVOLUTION AND PALATAL TYPES IN BIRDS



D.F. Levett Bradley. del. 1945.

Data from: Huxley, Fürbringer, Gadow, Evans, Pycraft, Stresemann, Wetmore, Chapin, Mayr, Miller, Zimmer.

CHAPTER XVI

FROM SLINKING REPTILES TO RUNNING MAMMALS: A CRITICAL STAGE IN EVOLUTION

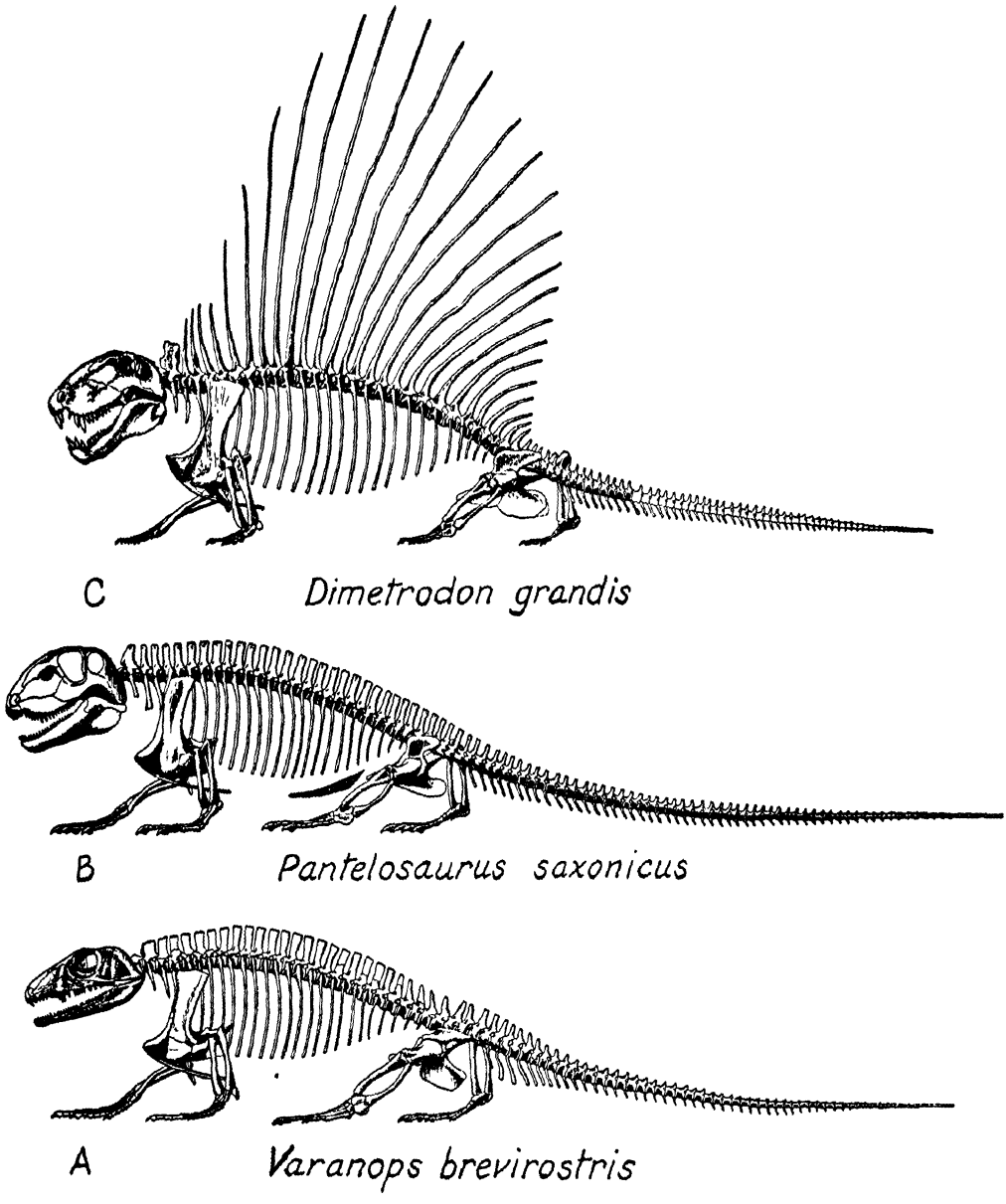


Fig. 16.1. Restored skeletons of pelycosaurs, representing three grades from the lizard-like *Varanops* to the long-spined giant predator *Dimetrodon*. After Romer and Price.

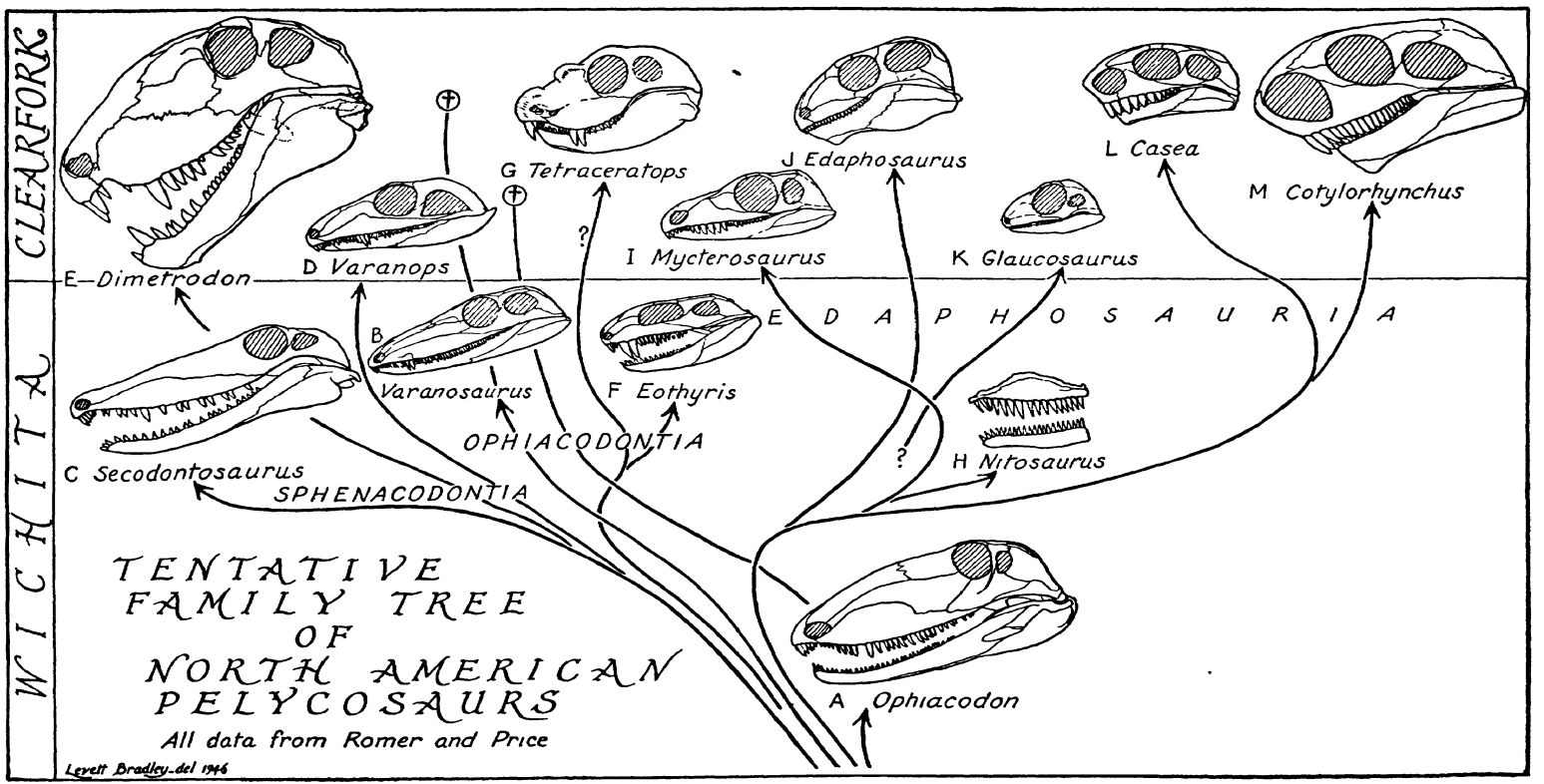

WICHITA
CLEARFORK
E—Dimetrodon
D Varanops
G Tetraceratops
I Mycterosaurus
J Edaphosaurus
K Glaucosaurus
L Casea
M Cotylorhynchus
B
Varanosaurus
F Eothyris
E D A P H O S A U R I A
OPHIACODONTIA
C Secodontosaurus
SPHENACODONTIA
H Nitosaurus
A Ophiacodon
TENTATIVE
FAMILY TREE
OF
NORTH AMERICAN
PELYCOSAURS
All data from Romer and Price
Leyett Bradley-del 1946

Fig. 16.2

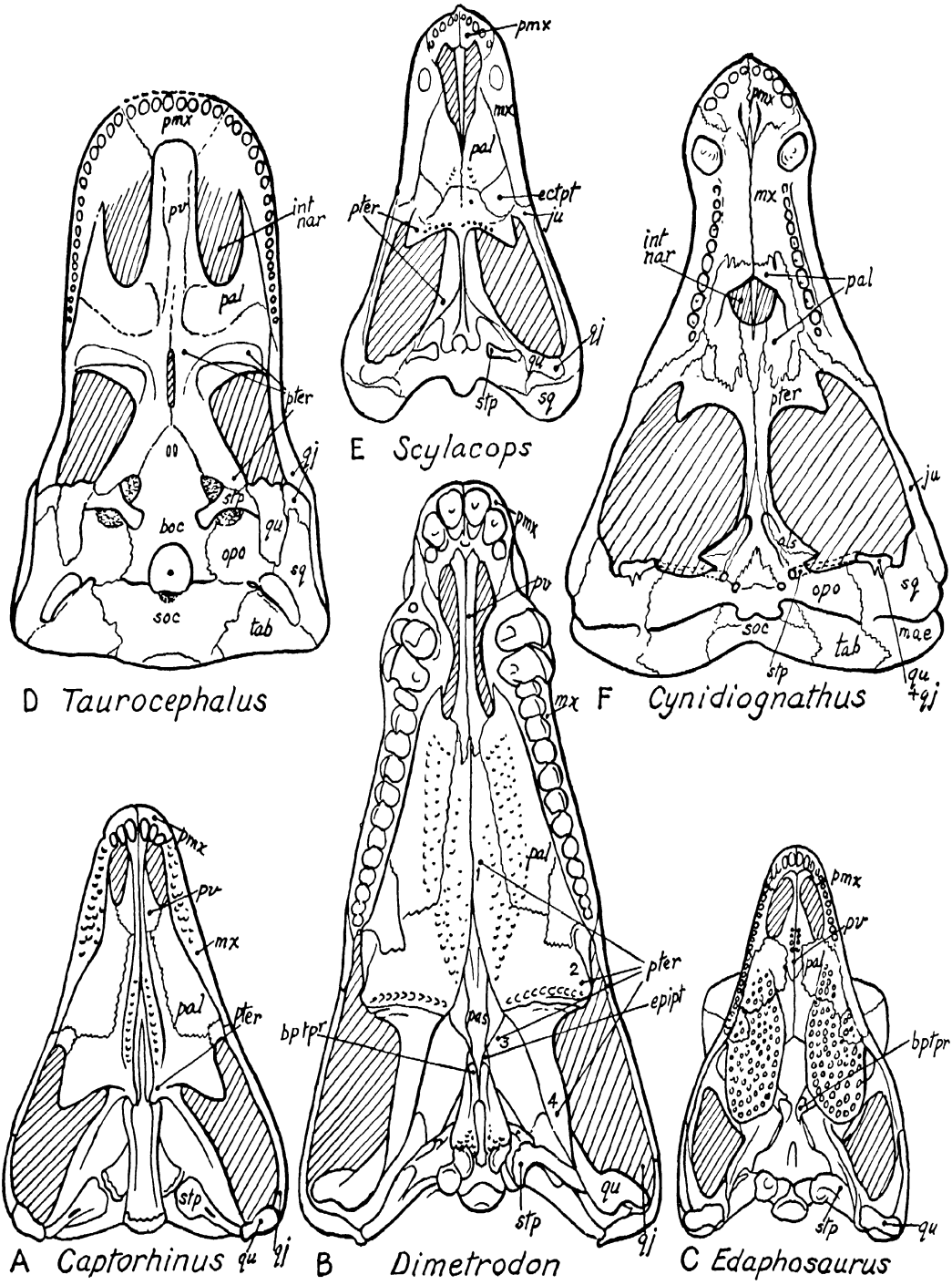


Fig. 16.3. Palatal views of skulls of primitive cotylosaur (A), two pelycosaurs (B, C) and three grades of South African mammal-like reptiles (D, E, F). A, original; B, C, after Romer and Price; D, after Boonstra; E, after Broom; F, after Broili. The primitive "four-way palate brace" is retained by the central pelycosaurs (B) and becomes highly modified in the mammal-like reptiles (D, E, F).

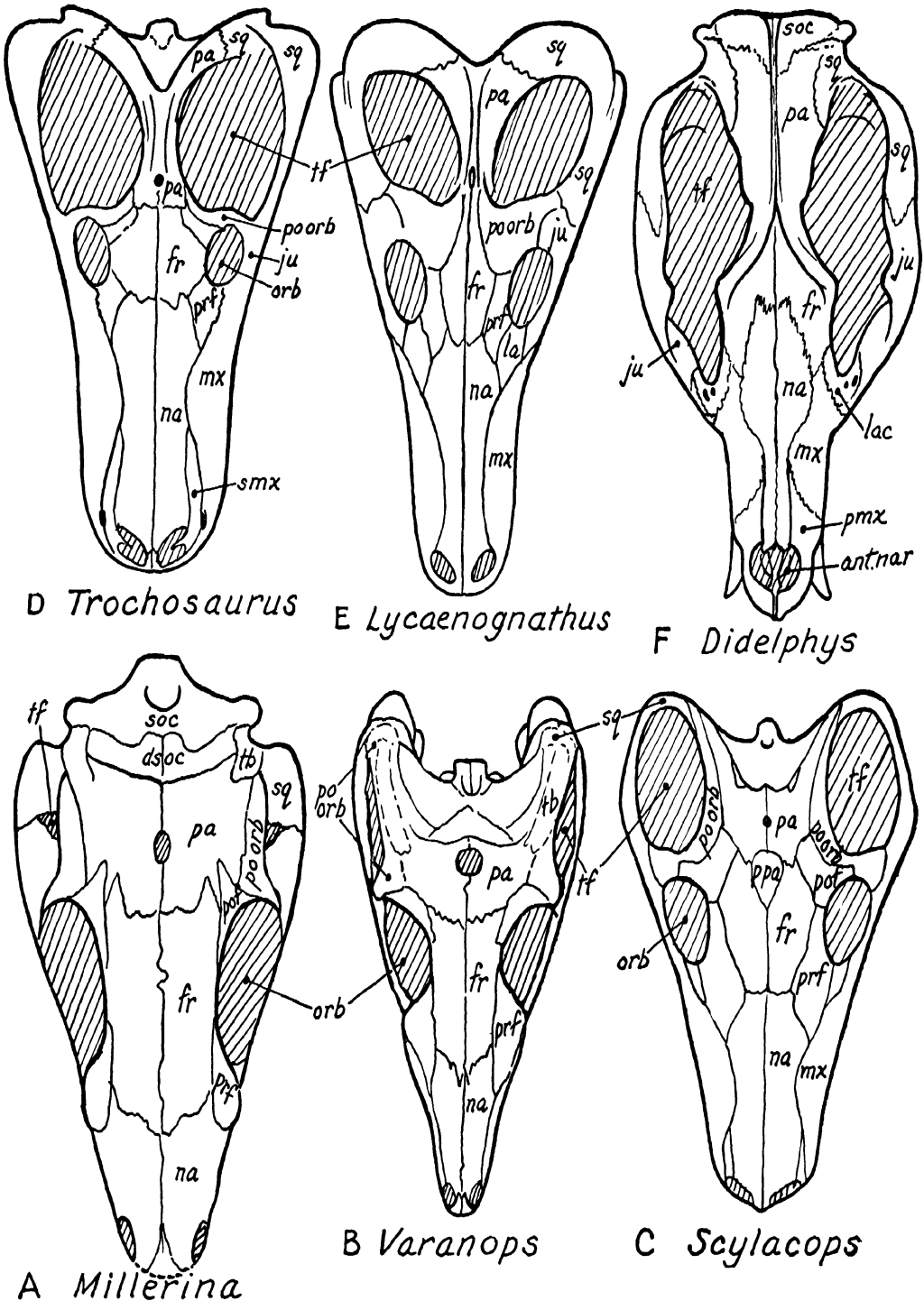


Fig. 16.4a. Dorsal views of skulls in progressive South African captorhinomorph cotylosaur (A), primitive American pelycosaur (B); three grades of South African mammal-like reptiles (C, D, E) and a primitive Recent mammal (F). A, C, E, after Broom; B, after Romer and Price; F, original.

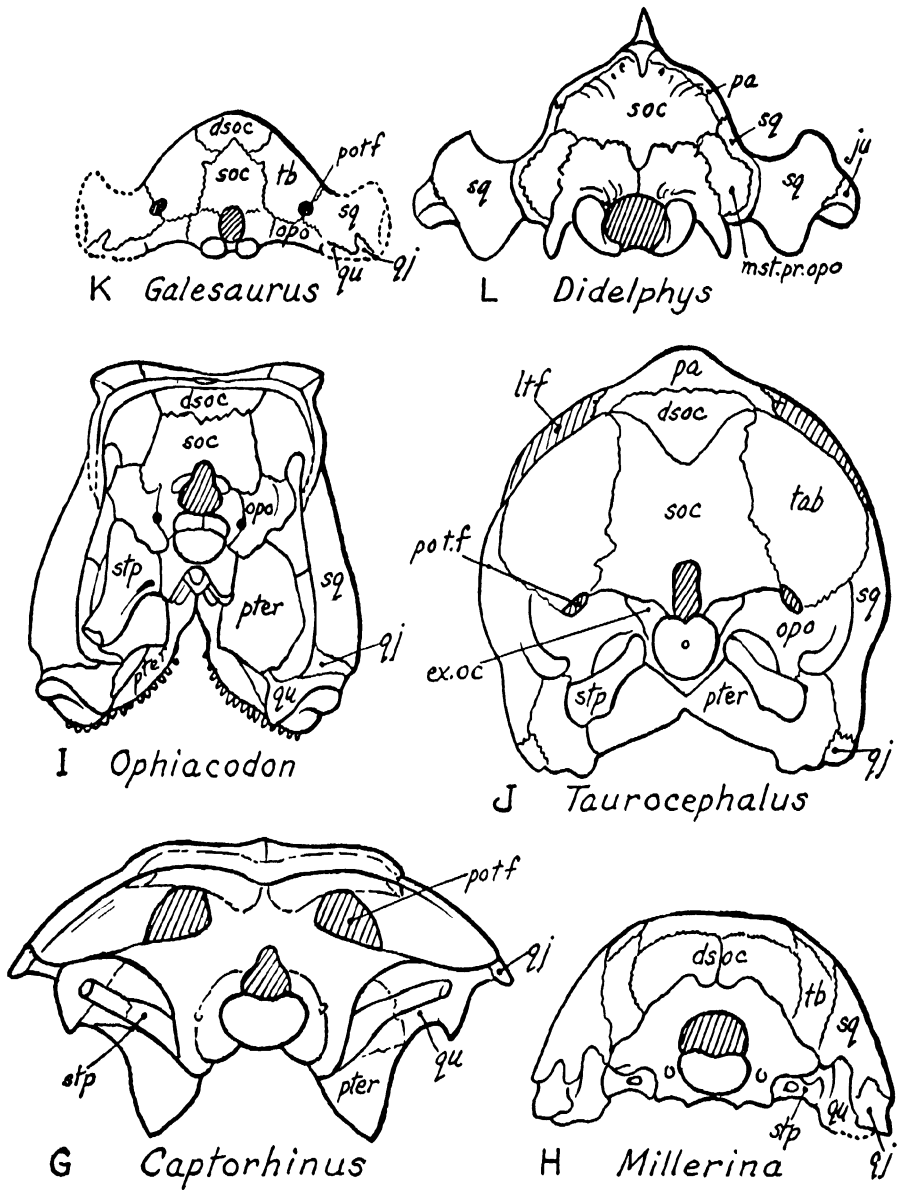


Fig. 16.4b. G–L, Occipital views of skulls in: primitive captorhinomorph cotylosaur (G), South African Permian cotylosaur (H), American pelycosaur (I) and South African mammal-like reptiles (J, K) and primitive recent mammal (L). G, after Sushkin, H, after Broom; I, after Romer and Price; J, after Boonstra; K, after Broom; L, original. The primitive captorhinomorph (A) retains the posttemporal fenestrae, which are reduced or eliminated in more advanced forms. The pelycosaur skull is primitively high and narrow in the occipital view (I) and the quadrate is far below the level of the occipital condyle; this contrasts with the wide low skull of the cyondont (K) and primitive mammal (L).

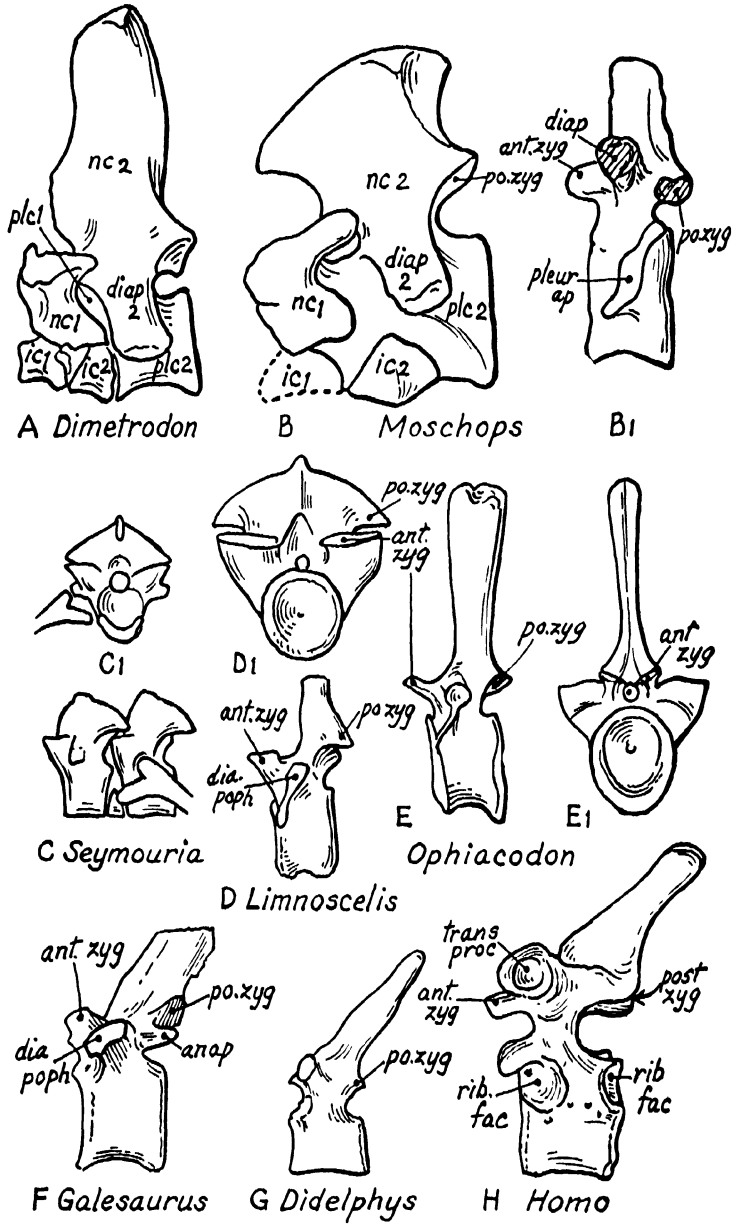


Fig. 16.5. Atlas-axis complex (A, B) and typical dorsal vertebrae: primitive reptiles (A–E), mammal-like reptile (F), primitive mammal (G) and man (H). A, B, after Broom; B1, G, original; C, C1, after T. E. White; D, D1, after Williston; E, E1, after Romer and Price; F, after Broili; H, after Cunningham. The pelycosaur (A) inherits the plan of its atlas-axis complex from still earlier tetrapods and transmits it to the mammal-like reptiles (B). In the dorsal vertebrae of the cotylosaurs the width across the flat anterior and posterior zygapophyses was probably connected with a primitive transversely rocking movement of the column. In the pelycosaurs (E, E1) the zygapophyses have become small and have been squeezed nearer to the midline, facilitating dorso-ventral flexure and moderate lateral bending. These characters were transmitted to the mammal-like reptiles (B1, F) and thence to the mammals (G), including man (H).

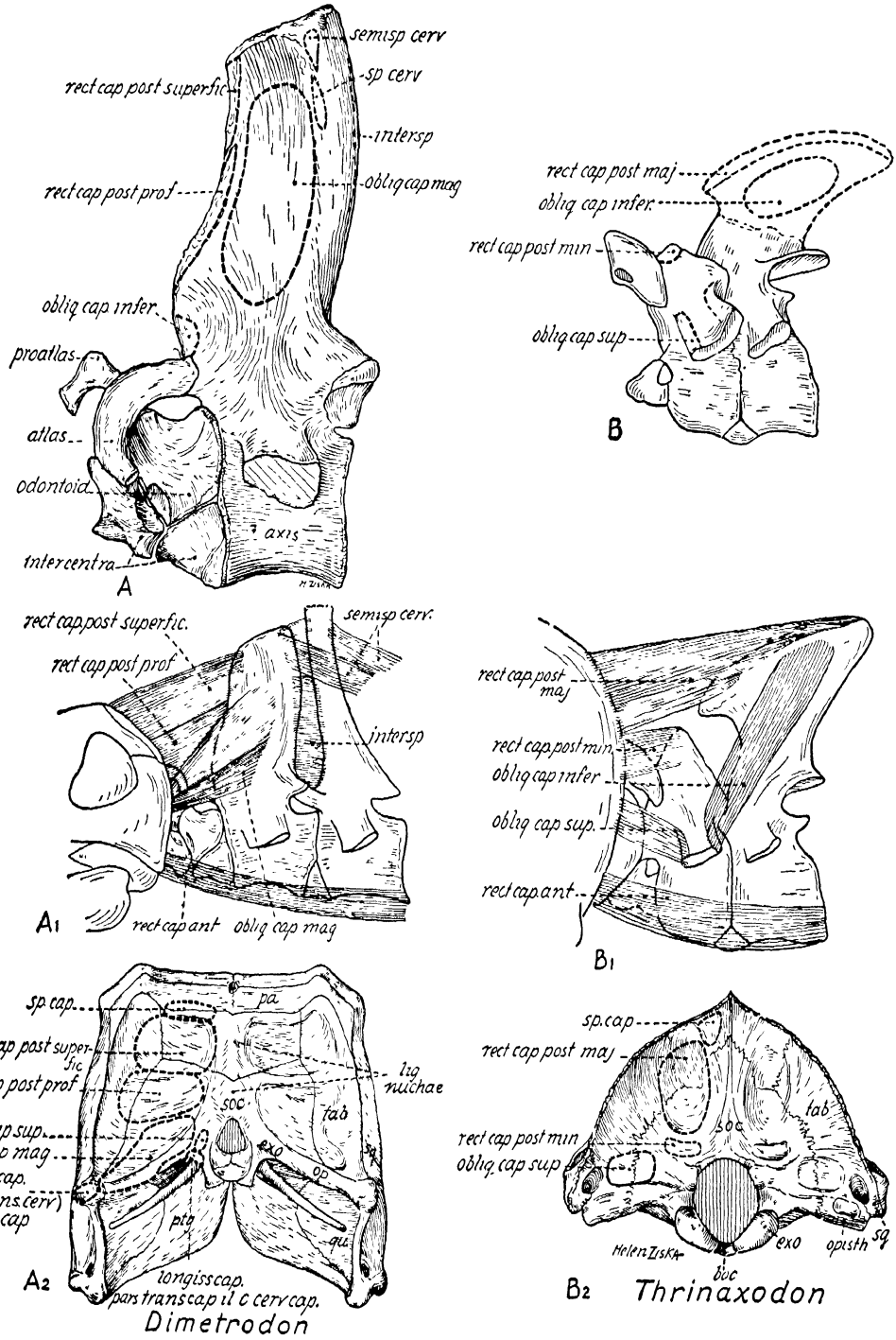


Fig. 16.6a. The atlas-axis complex and its musculature in relation to the occiput. After Gaynor Evans. A, primitive pelycosaur, inheriting its construction from stem reptiles and transmitting its basal features to the mammal-like reptiles; B, advanced mammal-like reptile; C, primitive mammal; D, Man.

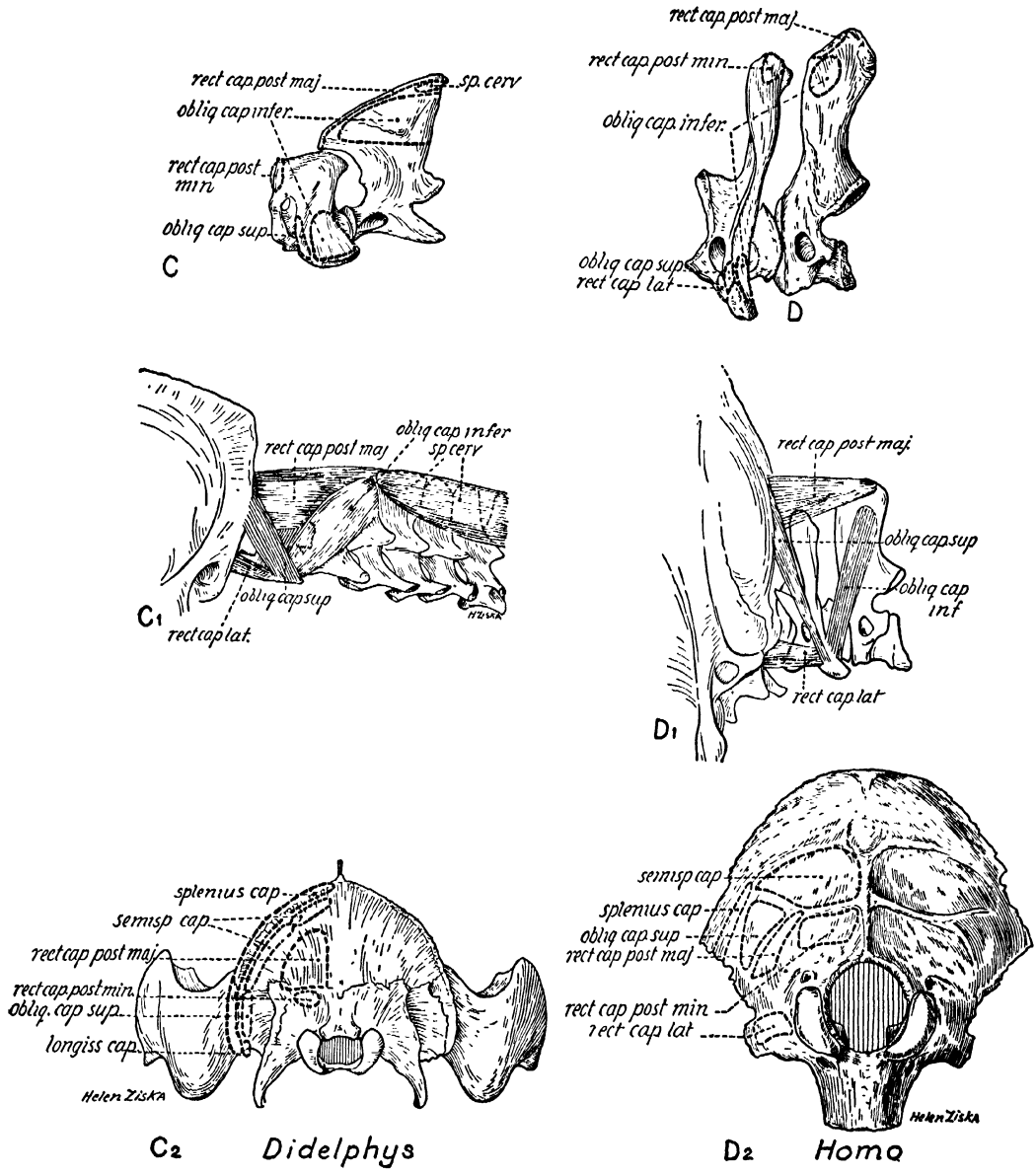


Fig. 16.6b. The elimination of the median neural spine of the atlas secured greater room especially for the muscles that elevate the head (rect. cap. post. maj.). Increased mobility of the head upon the atlas-axis in the mammals was probably accompanied by a marked widening of the transverse processes of the atlas. H. C. Raven (cited by G. Evans, 1939, p. 91) suggested that this widening conditioned a subdivision of the single obliquus capitis muscle into two parts, the obliquus capitis superior and the obliquus capitis inferior.

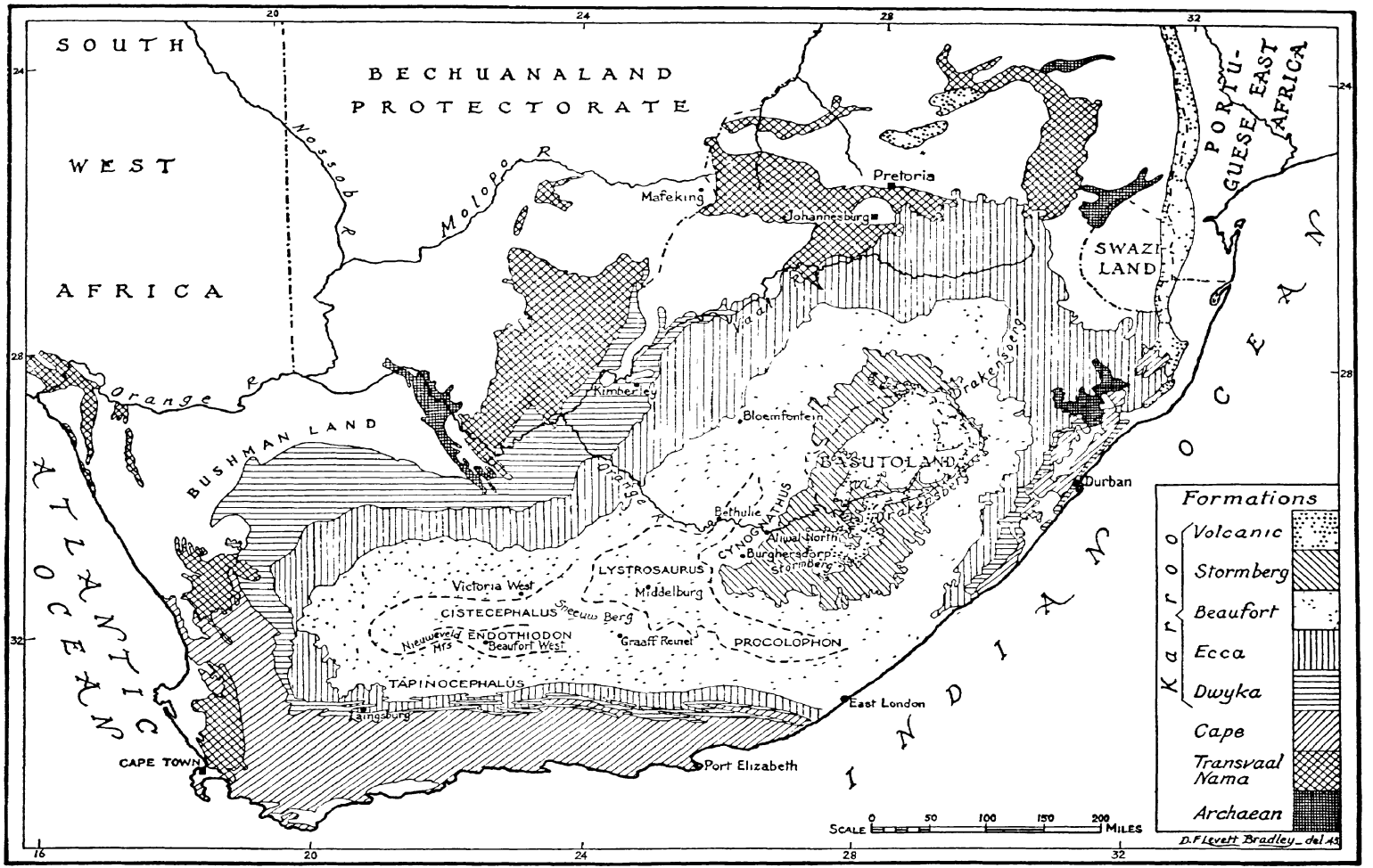
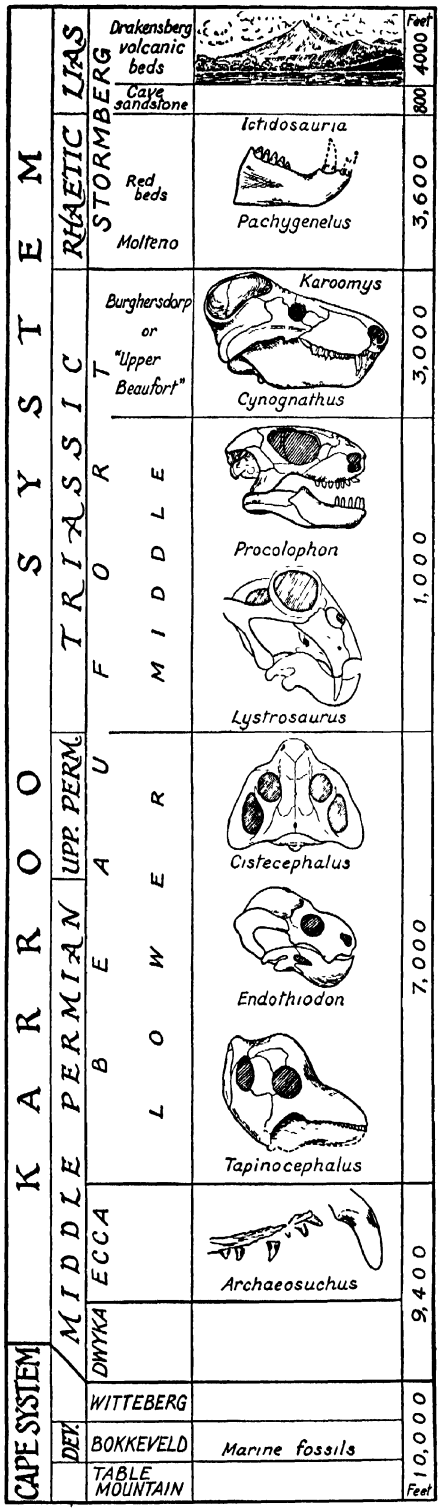


Fig. 16.7a. The great South African geosyncline containing the Karroo and its faunal horizons. Map and geological data from Rogers, DuToit and Haughton; all palaeontological data from Broom.



ICTIDOSAUR ZONE: Ictidosaurians varied but little known. No anomodonts, cynodonts nor bauriamorphs. Pseudosuchians, primitive lizards and dinosaurs present.

UPPER CYNOGNATHUS ZONE: Earliest ictidosuchian, *Karroomys*, cynodonts rare, bauriamorphs replacing them. Large cynodonts, preying upon giant anomodont (*Kannemeyeria*). Huge pseudosuchian (pelycosimian) *Erythrosuchus*. Bauriamorphs varied. Many smaller cynodonts with flat broad heads and flat-topped molars (*Gomphognathus* group). Small cynodonts with carnivorous molars rare. Small pseudosuchians, *Euparkeria*, *Broomiella*. Other small diapsids.

PROCOLOPHON ZONE: *Procolophon*, a small lizard-like cotylosaur. *Prolacerta* and *Paliguana* (eosuchians). Small primitive bauriamorphs. Therocephalians probably extinct.

LYSTROSAURUS ZONE: Numerous small cynodonts, a few specialized therocephalians, at least one small anomodont (*Myosaurus*) and a number of small amphibians. A large aquatic pseudosuchian (*Proterosuchus*). Land anomodonts replaced by semiaquatic *Lystrosaurus* (derived from *?Dicynodon lacerticeps*). Two species of *Dicynodon* at base of zone.

CISTECEPHALUS ZONE: *Cistecephalus*, a specialized anomodont, confined to a thin layer at the very base of this zone. *Rubidgina*, combining features of therocephalians, gorgonopsians and other suborders, near top of zone. Small cynodonts appear; other small forms becoming scarce. Large dicynodonts and gigantic aulacocephalodonts near top; also large specialized therocephalians.

ENDOTHIODON ZONE: During most of the *Endothiodon* times small dicynodons and other anomodonts were common and small gorgonopsians and therocephalians rare. Parieasaurs scarce. At top of Endothiodon zone, small gorgonopsians in considerable numbers. Small dicynodons becoming scarce.

TAPINOCEPHALUS ZONE: Pareiasaurs, dromosaurs, dinocephalians, therocephalians, gorgonopsians, dicynodonts; *Anningia*, a very primitive skull tending to connect therapsids with pelycosaurs and cotylosaurs. In upper *Tapinocephalus* times anomodonts scarce.

ECCA SHALES AND SANDSTONES, mostly barren. Coal in Transvaal and Natal.

Fig. 16.7b. Geologic sequence and succession of fossil reptilian faunas in South Africa. Data from Broom, Rogers, Du Toit, Haughton.

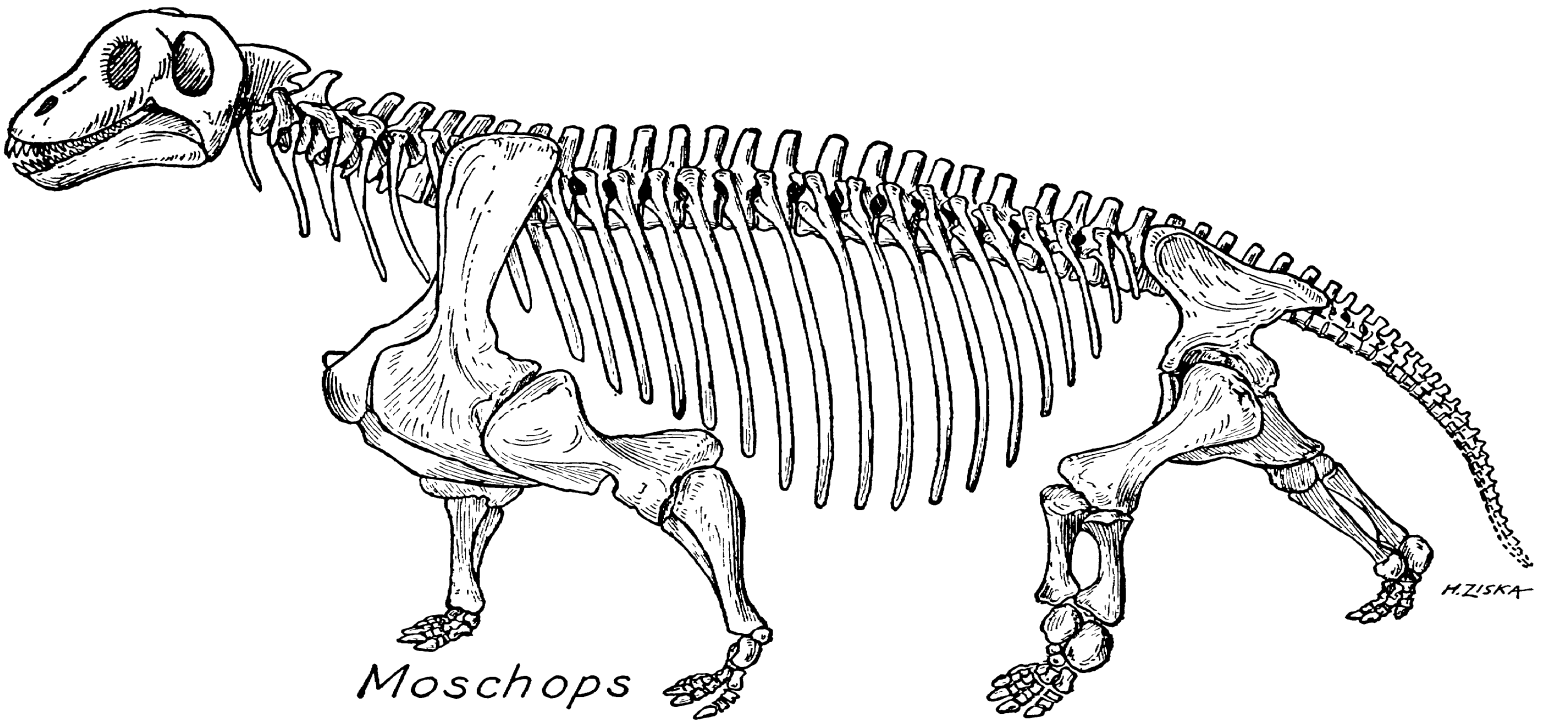


Fig. 16.8. Skeleton of a tapinocephalid dinocephalian. Modified from the mounted skeleton in the American Museum of Natural History, but with data on manus and pes partly from Byrne.

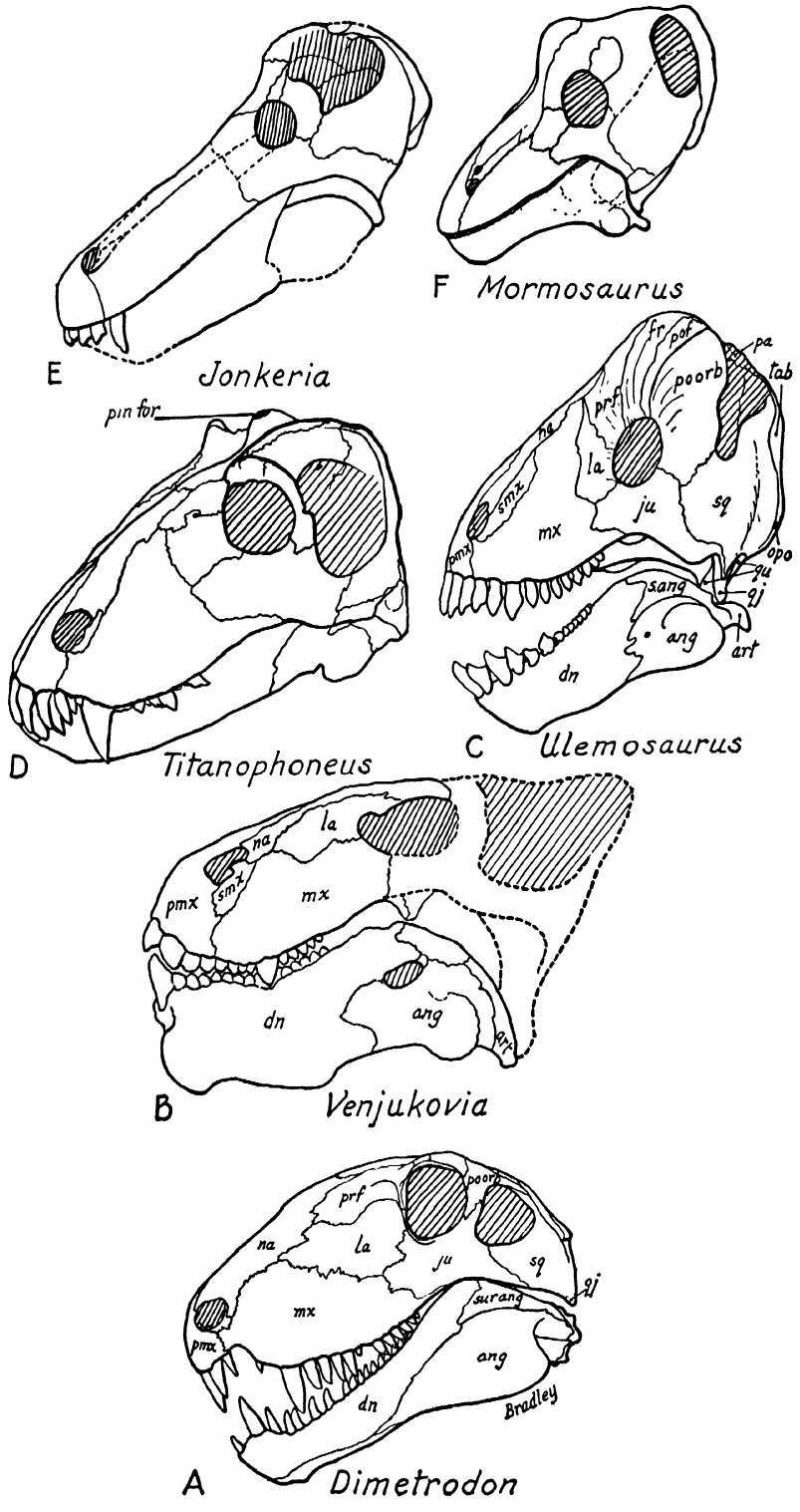


Fig. 16.9. Comparison of skulls of pelycosaur (A), from the Lower Permian of Texas and (B–F) dinocephalians from the Middle Permian of Russia and South Africa. A, after Romer; B–C, after Efremov; E, after Boonstra; F, after Watson.

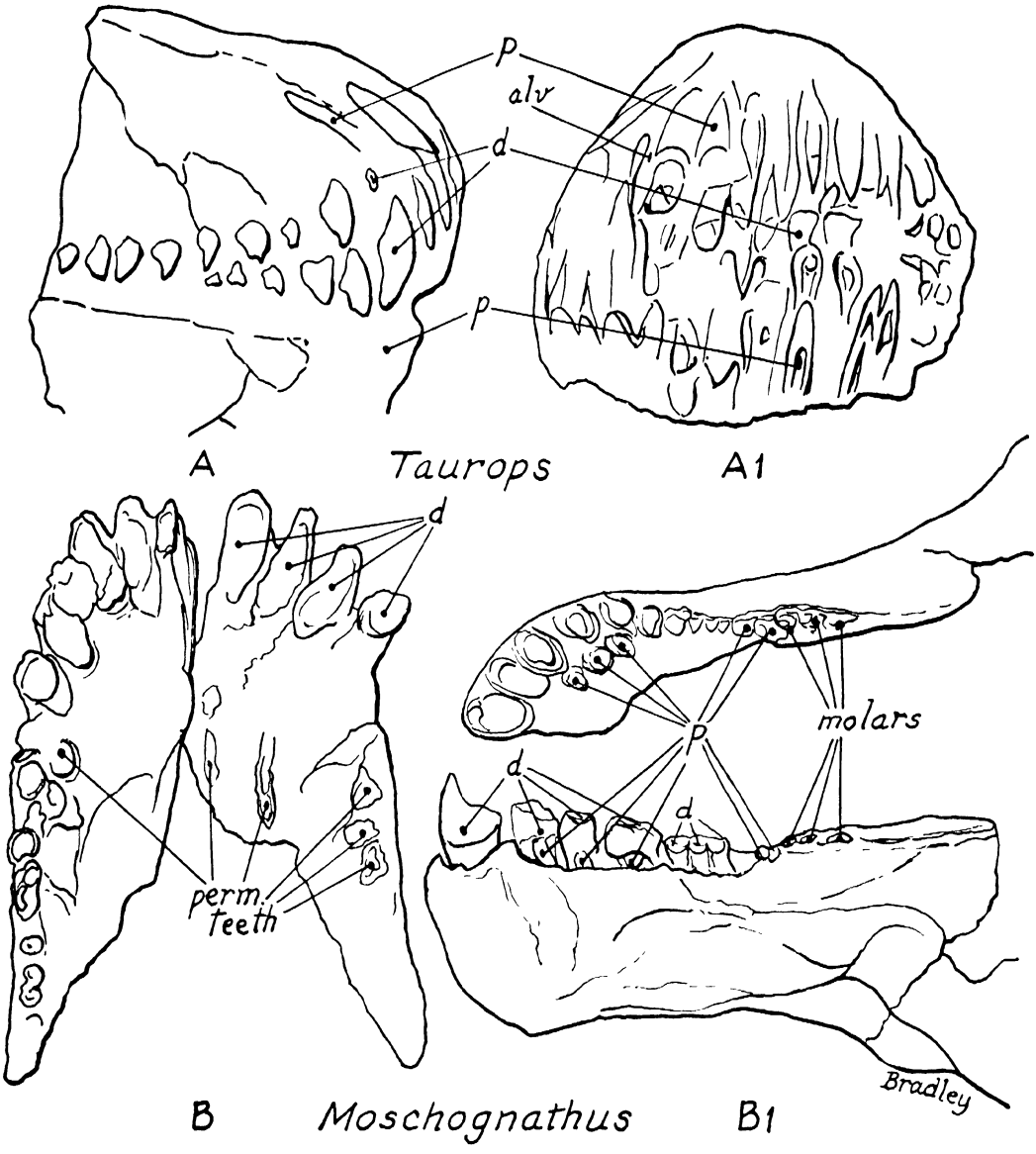


Fig. 16.10. Dentition of tapinocephalid dinocephalians, showing teeth of two sets, "deciduous" (*d*) and "permanent" (*p*). A, after Broom; A1, B, B1, from specimens.

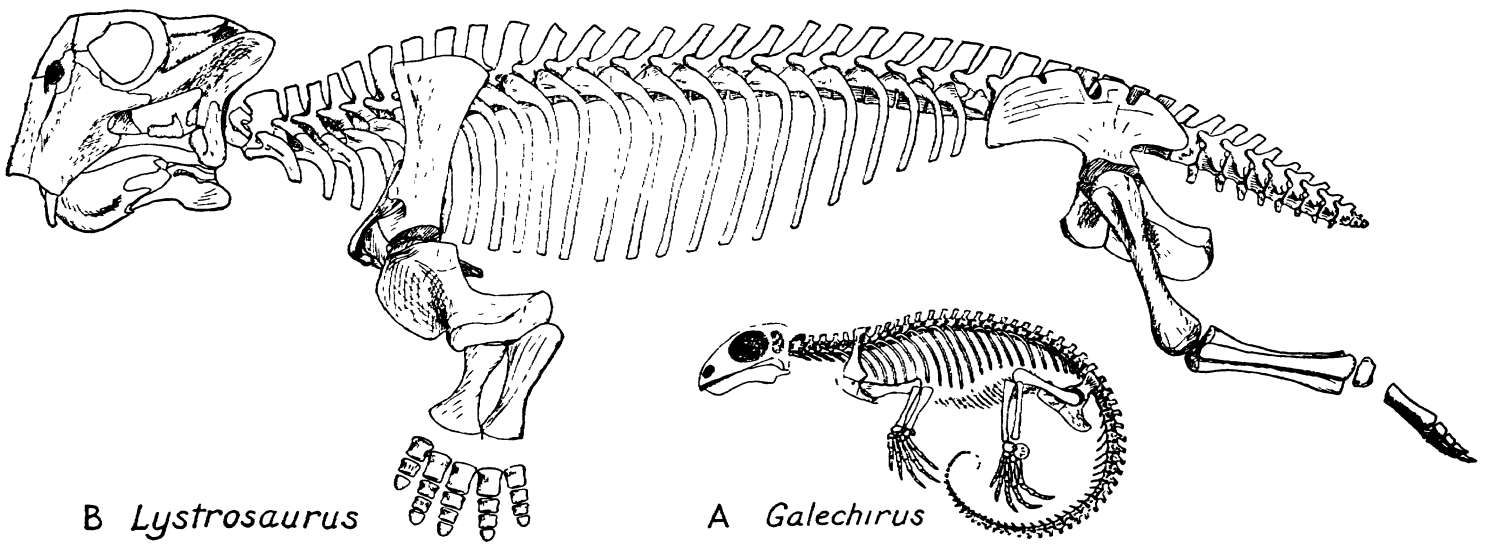


Fig. 16.11a, b. A dromasaurian (A) and two (B, C) anomodont skeletons. The endothiodont (C) seems not far from the primitive Russian *Venjukovia* (fig. 16.9 B); the lystrosaurid (B) is specialized for semiaquatic life. The dromasaurian (A) is very primitive. A, C, after Broom; B, after Watson.

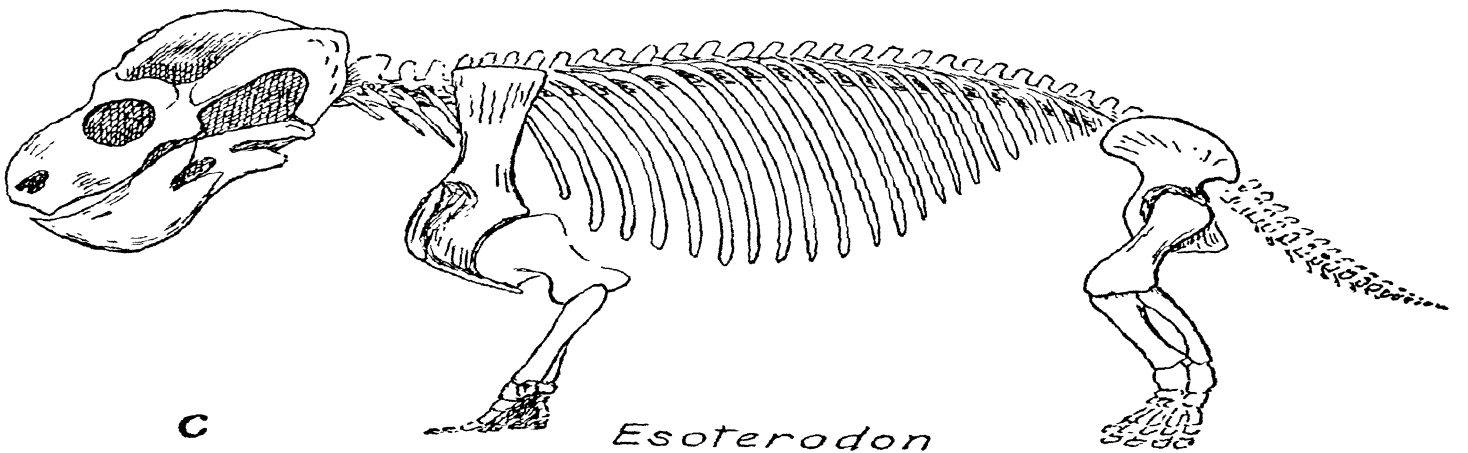


Fig. 16.11b

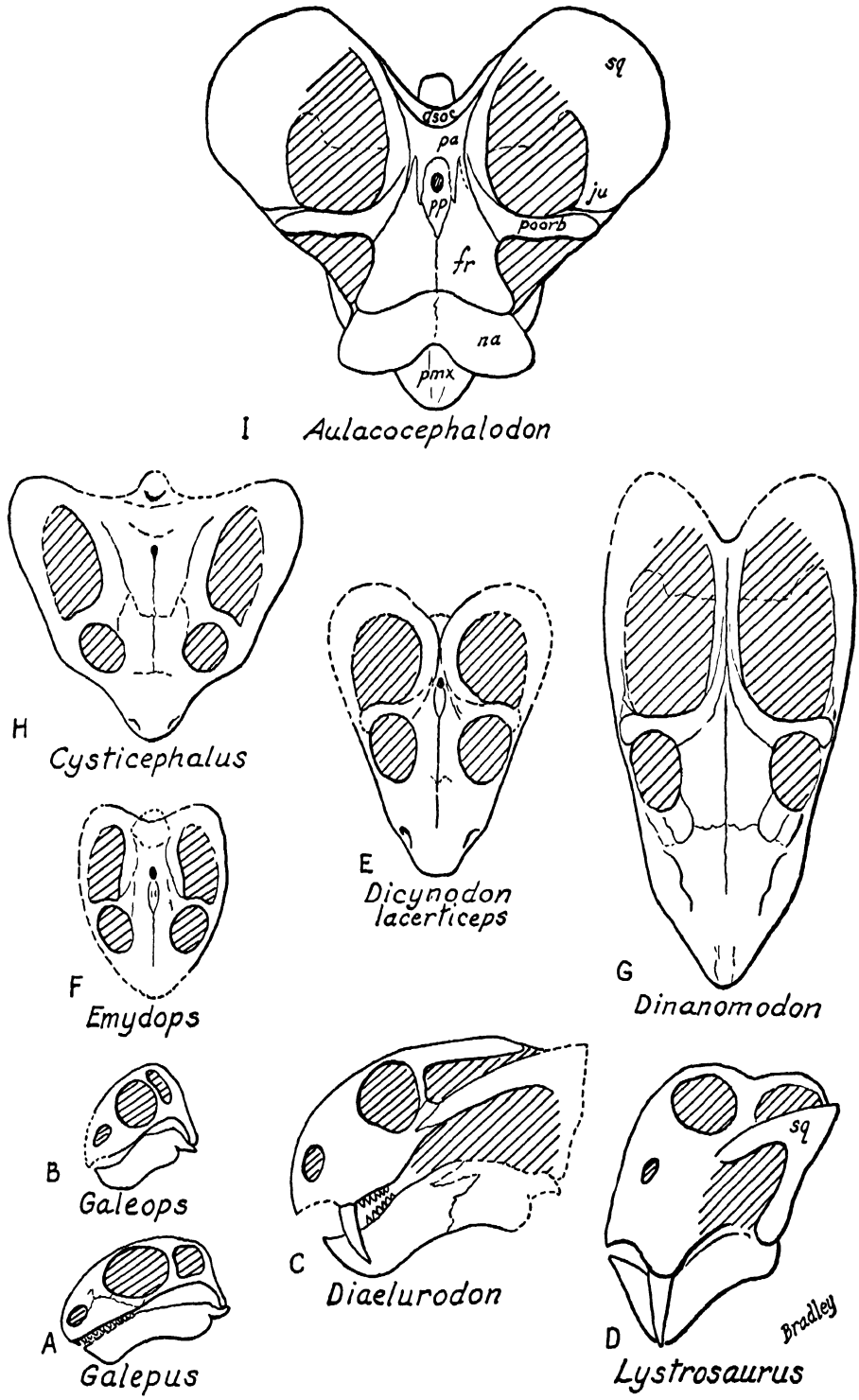


Fig. 16.12. Anisomerous divergence in South African dromasaurian (A) and anomodont (B–I) skulls. Side (A, D) and top (E–I) views. All data from Broom. The skulls range in size from the tiny *Emydops* to *Aulacocephalodon*, with a skull width of nearly 20 inches. Widening of the jaw muscles in the larger forms greatly increased their piercing and shearing power.

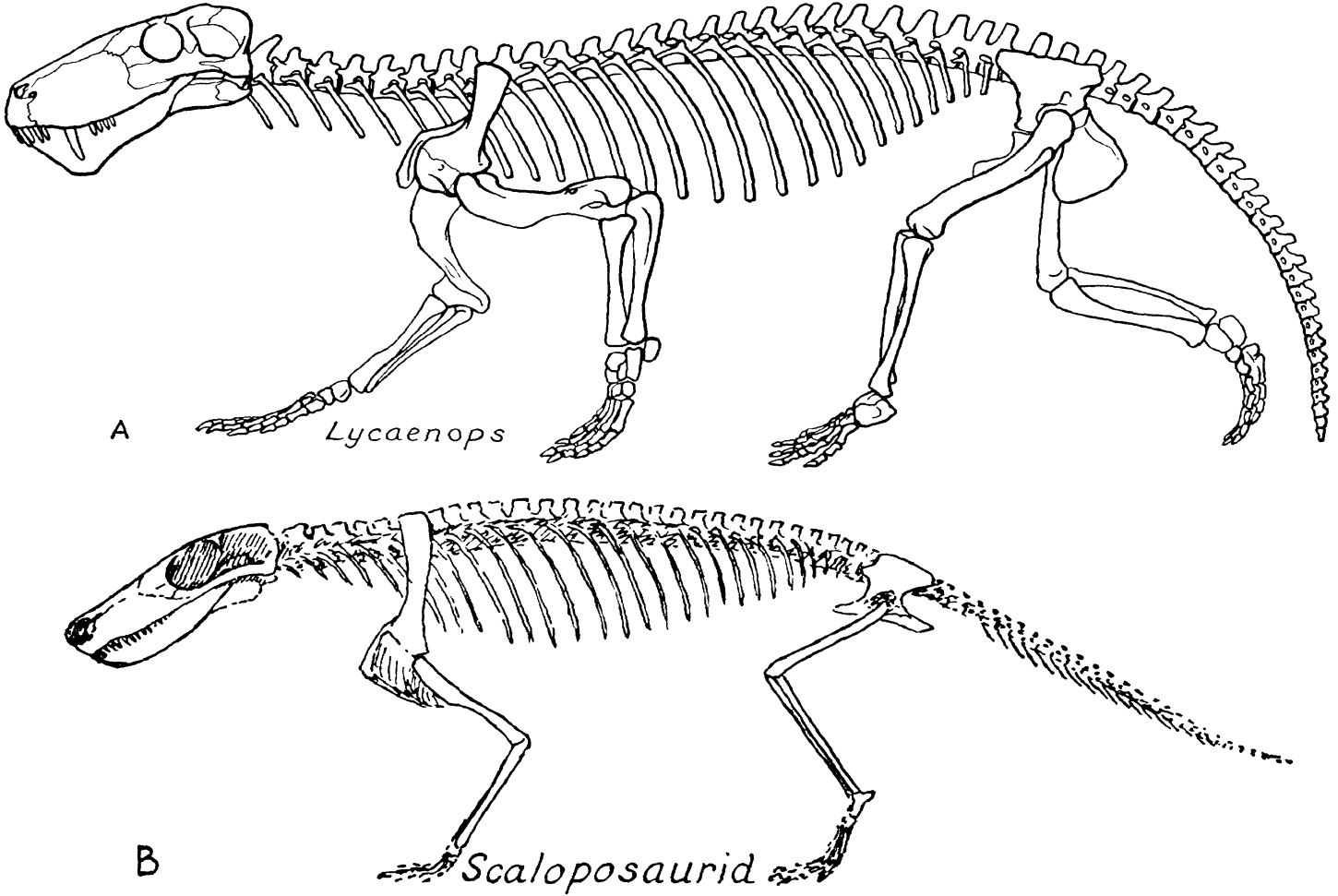


Fig. 16.13. Skeletons of medium-sized gorgonopsian (A) and small therocephalian (B). A, after Colbert; B, from Broom, modified from Watson.

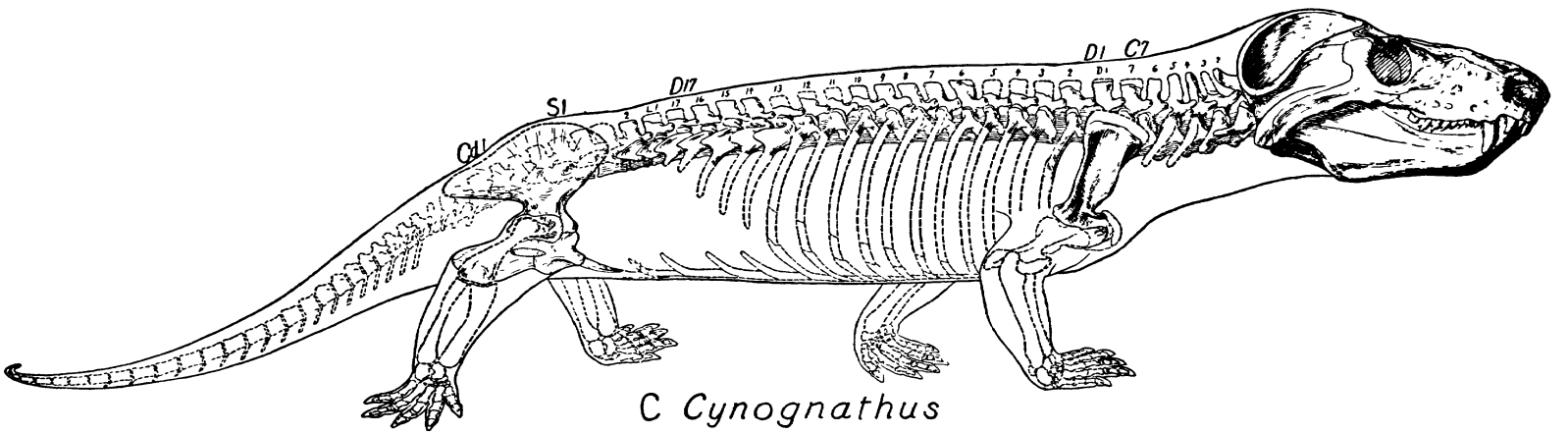


Fig. 16.14. Skeleton of large cynodont, in crawling posture. Modified from Gregory and Camp. Data from Seeley and casts of skull, vertebral column, etc.

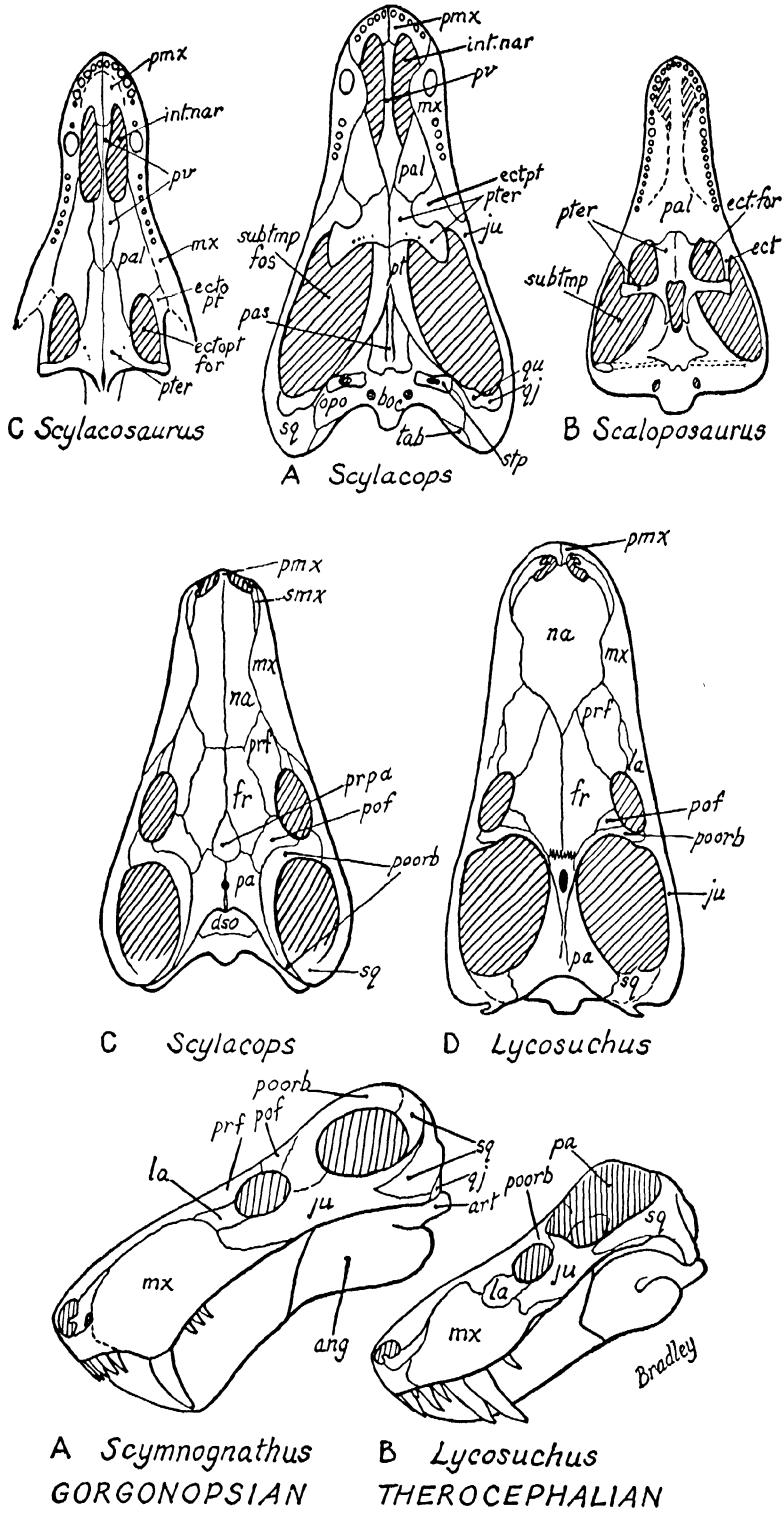


Fig. 16.15a, b. Contrasting characters in gorgonopsian and therocephalian skulls. Palatal views (top); dorsal (C, D) and lateral (A, B) views. After Broom. The gorgonopsian palate (A) lacks the ectopterygoid fenestrae which are prominent in typical therocephalians (B, C).

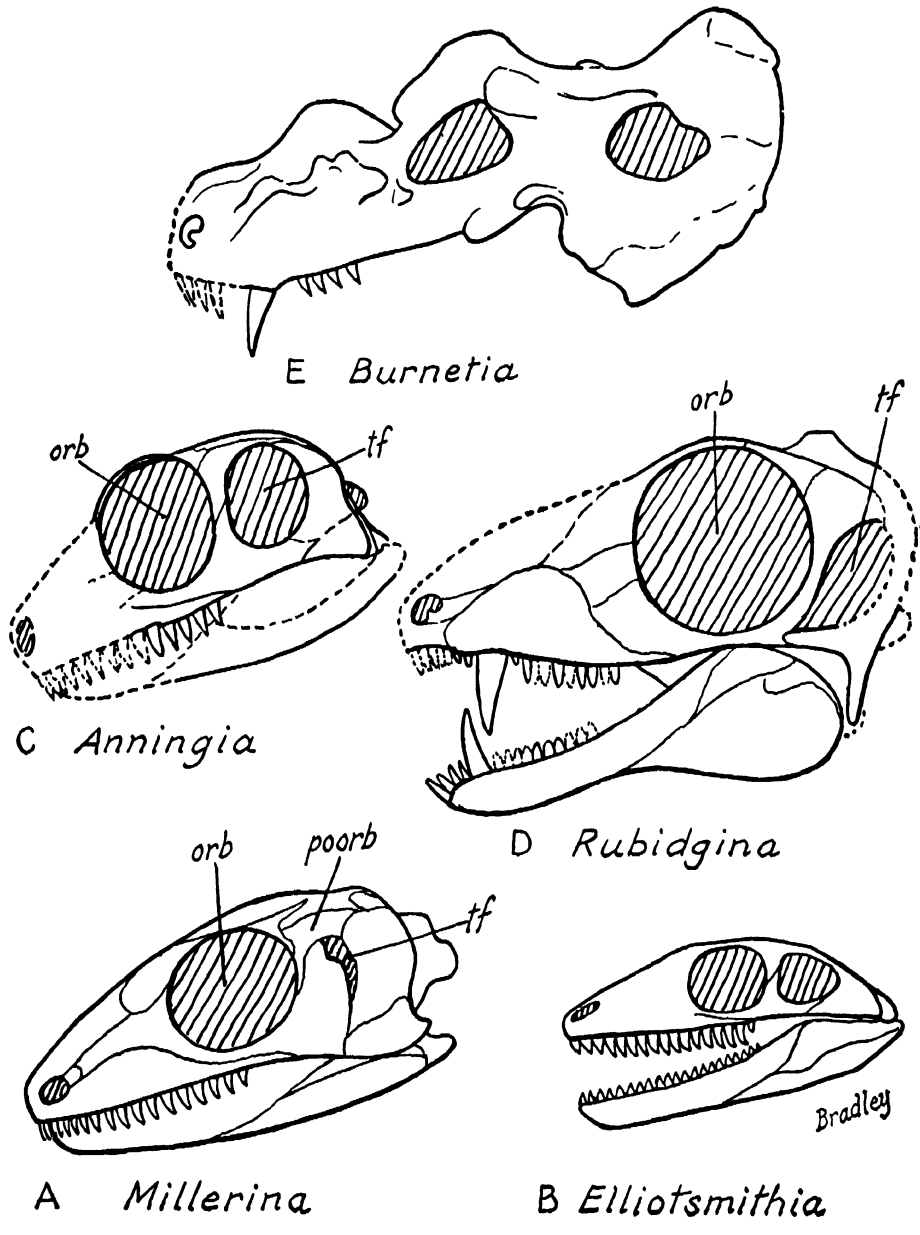
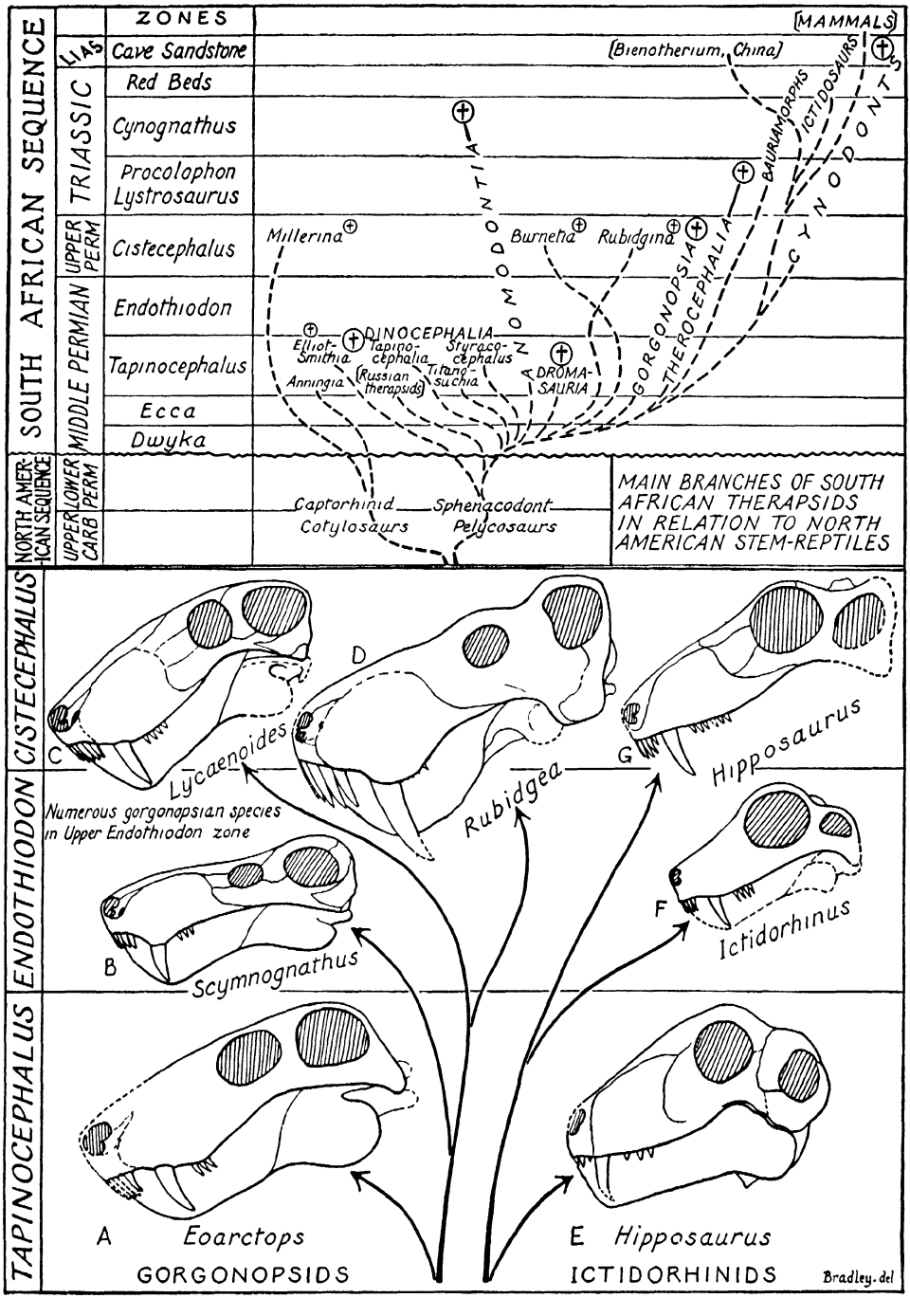


Fig. 16.16. Two "primitives" (A, B), two conservatives (C, D) and a "freak" (E) among Karroo reptiles. A–D, after Broom; E, after Boonstra.



Figs. 16.17, 18. Geologic succession and relationships of South African gorgonopsians After Broom.

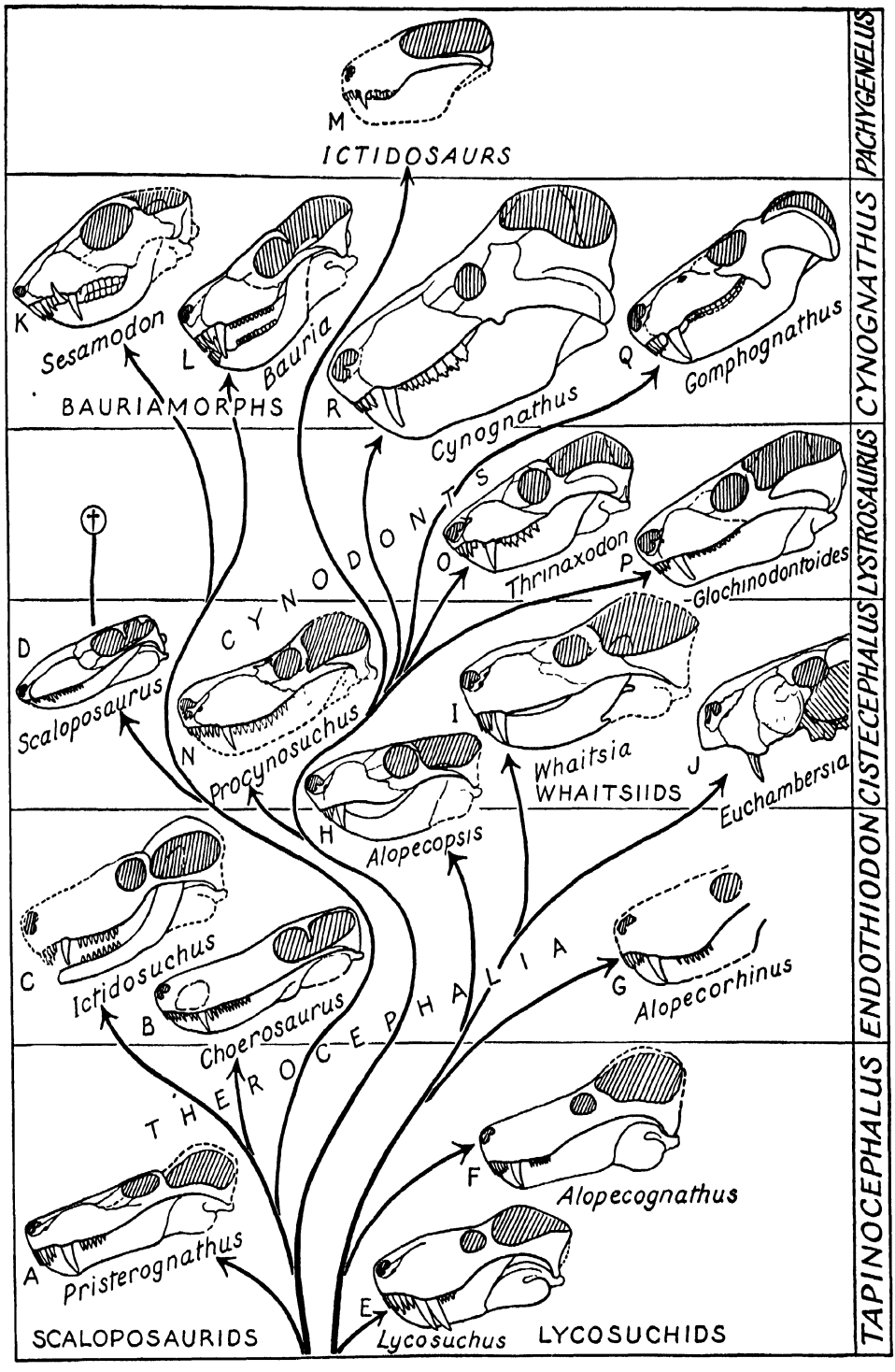


Fig. 16.19. Geologic succession and relationships of South African therocephalians, bauriamorphs, cynodonts and ictidosaurs. Data from Broom, Watson, Haughton, Boonstra.

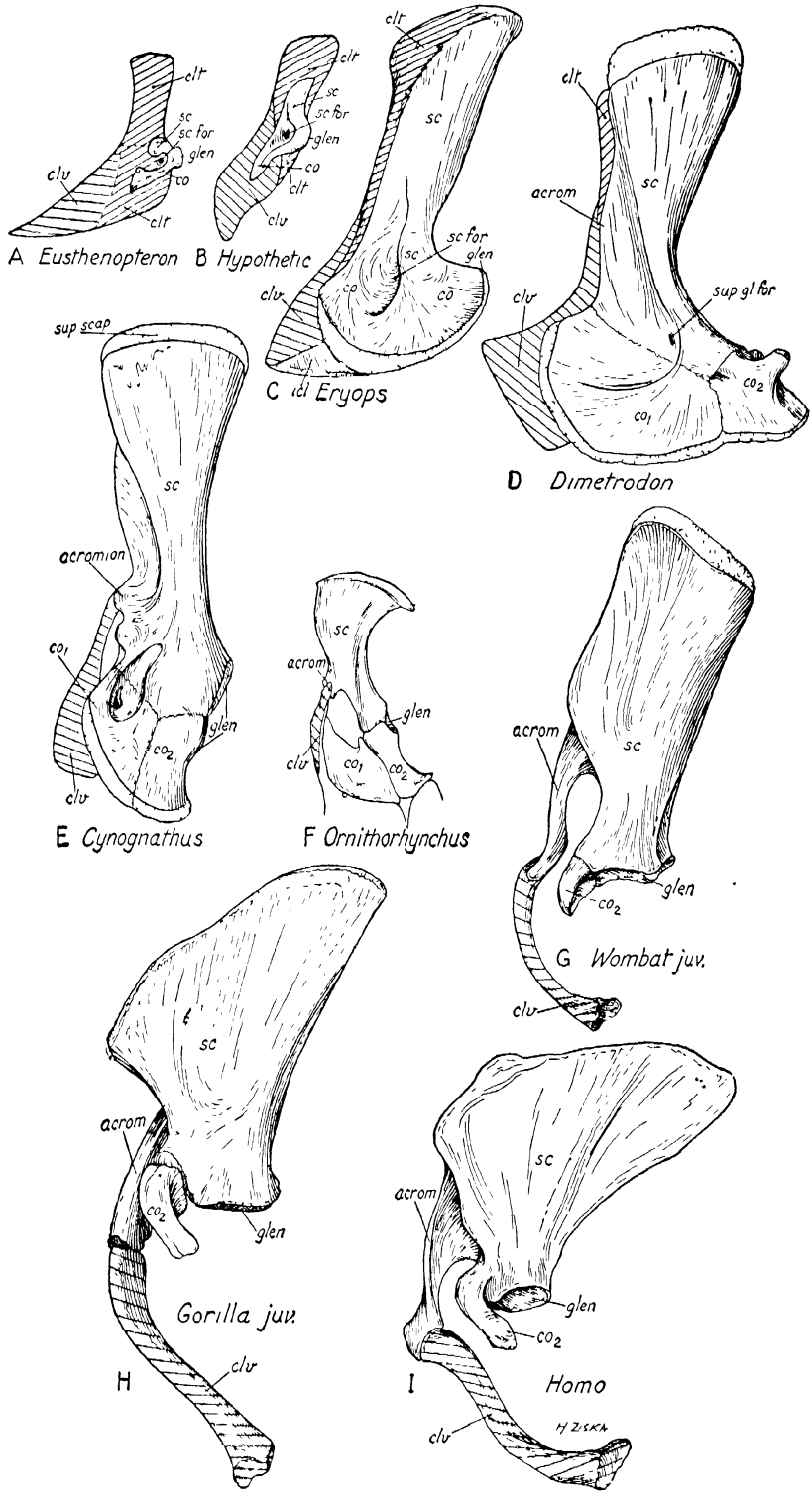


Fig. 16 20 Evolution of scapulo-coracoid and clavicle (inner surface) from Devonian lobe-fin fish (A) to man (I). A, partly after Bryant, B, partly after Watson's *Eogyrinus*; D, after Romer and Price; C, E–I, original. The interclavicle of stages A–F is omitted.

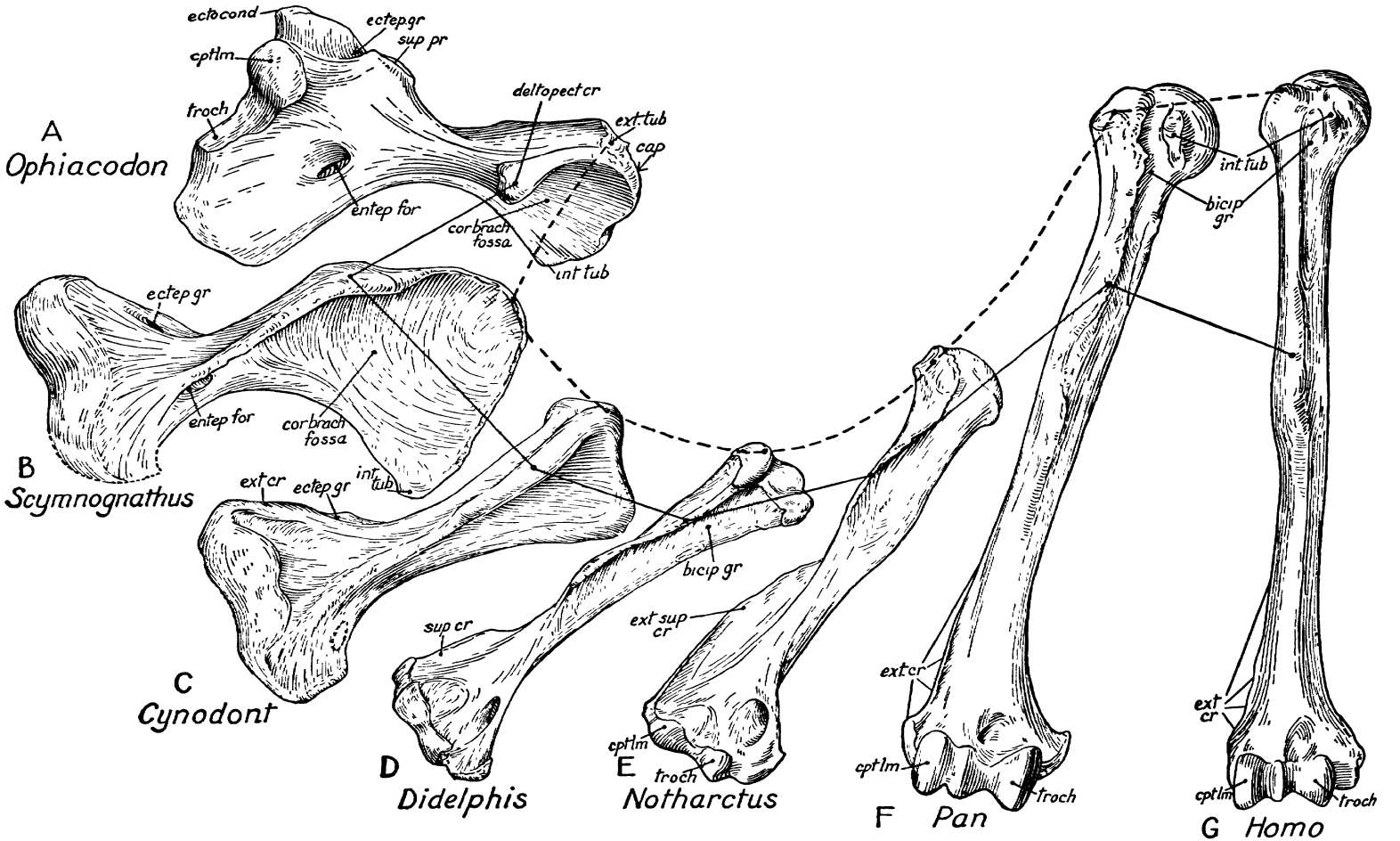


Fig. 16.21. Evolution of the humerus; anteroventral aspect in standing pose, from bent-limbed to erect, bipedal posture. A, Lower Permian pelycosaur; B, Upper Permian gorgonopsian; C, Triassic cynodont; D, recent opossum, representing Upper Cretaceous marsupial; E, Eocene lemuroid; F, recent anthropoid ape; G, man. B, after Broili; others, original.

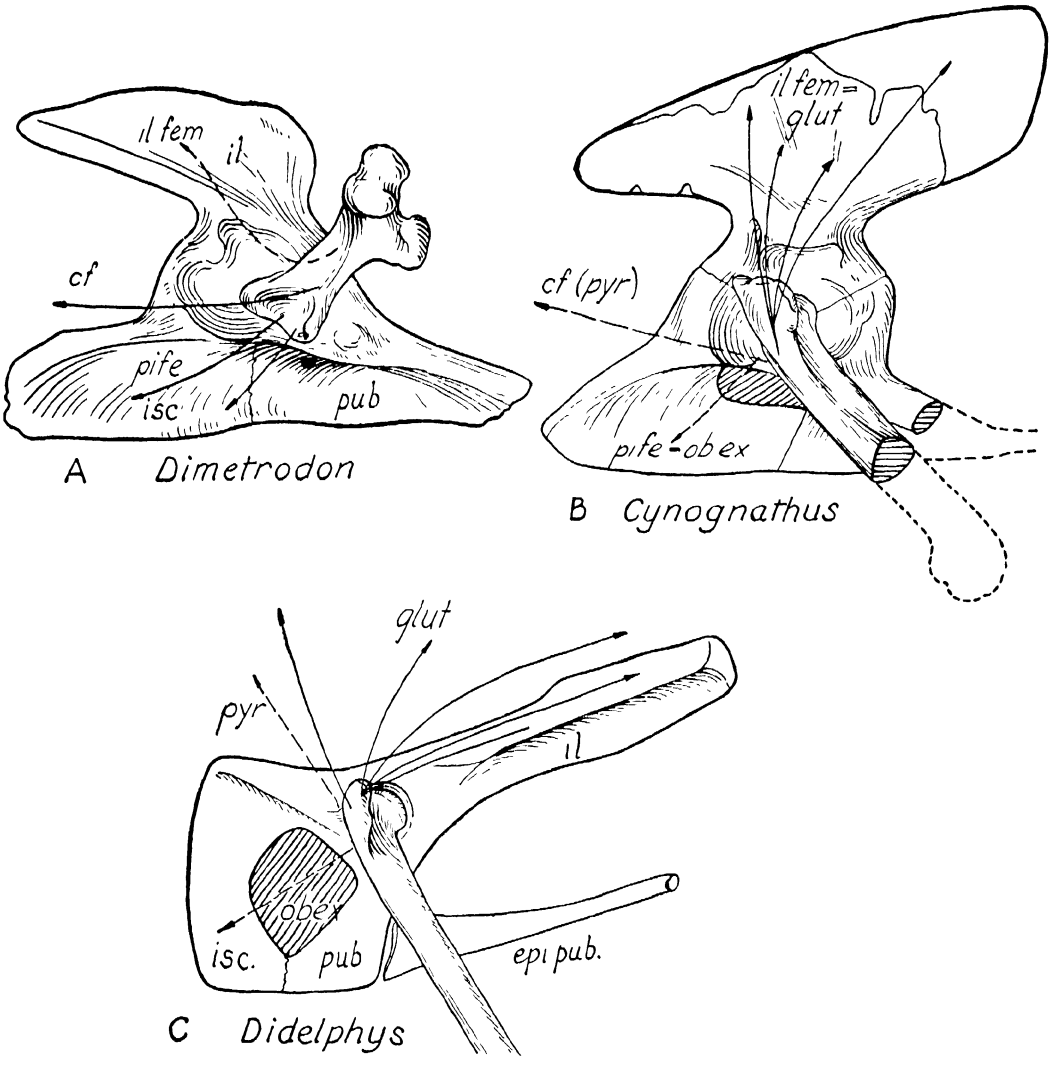


Fig 16 22. Evolution of pelvis and femur, with changes in musculature, from crawling pelycosaur (A) to running mammal (C). After Romer.

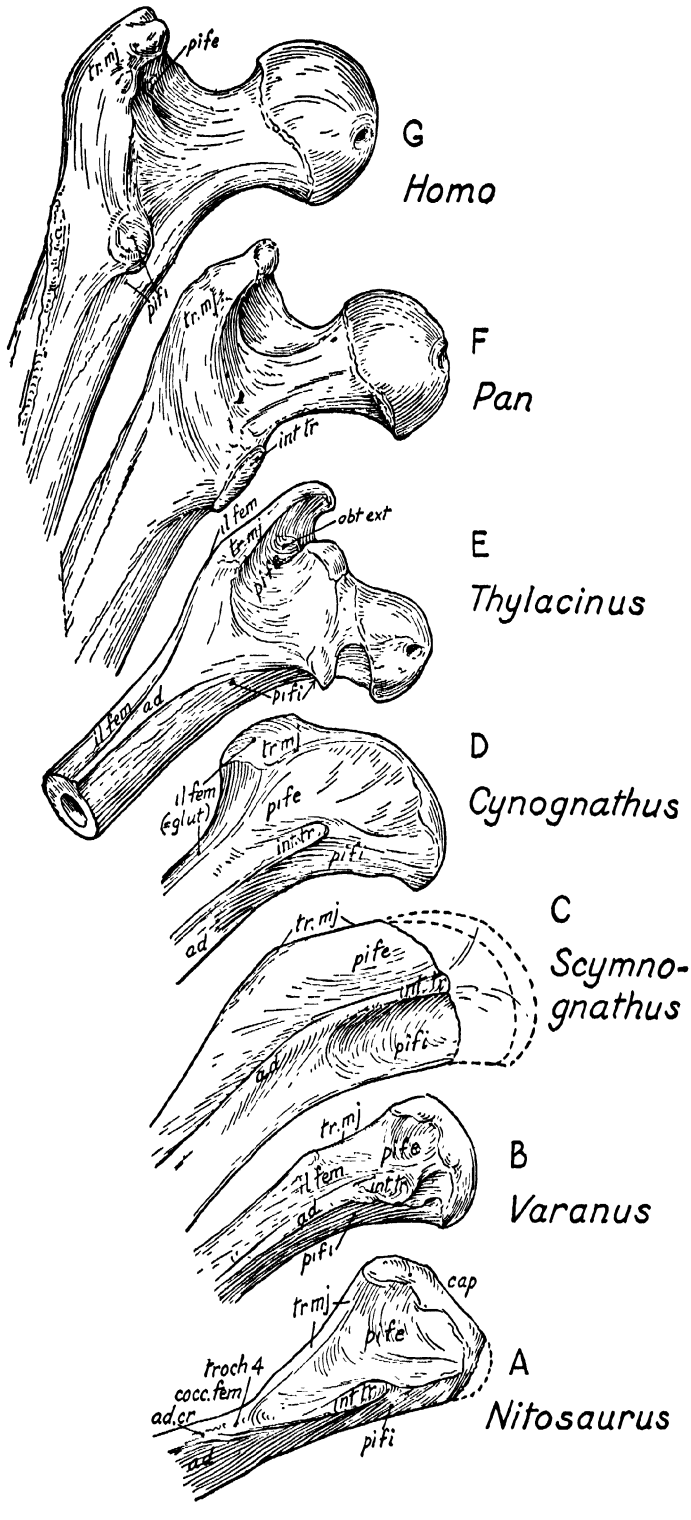


Fig. 16.23. Evolution of the femoral head and trochanters; left femur, rear view of proximal end. All figures from specimens. Data on muscles from Romer.

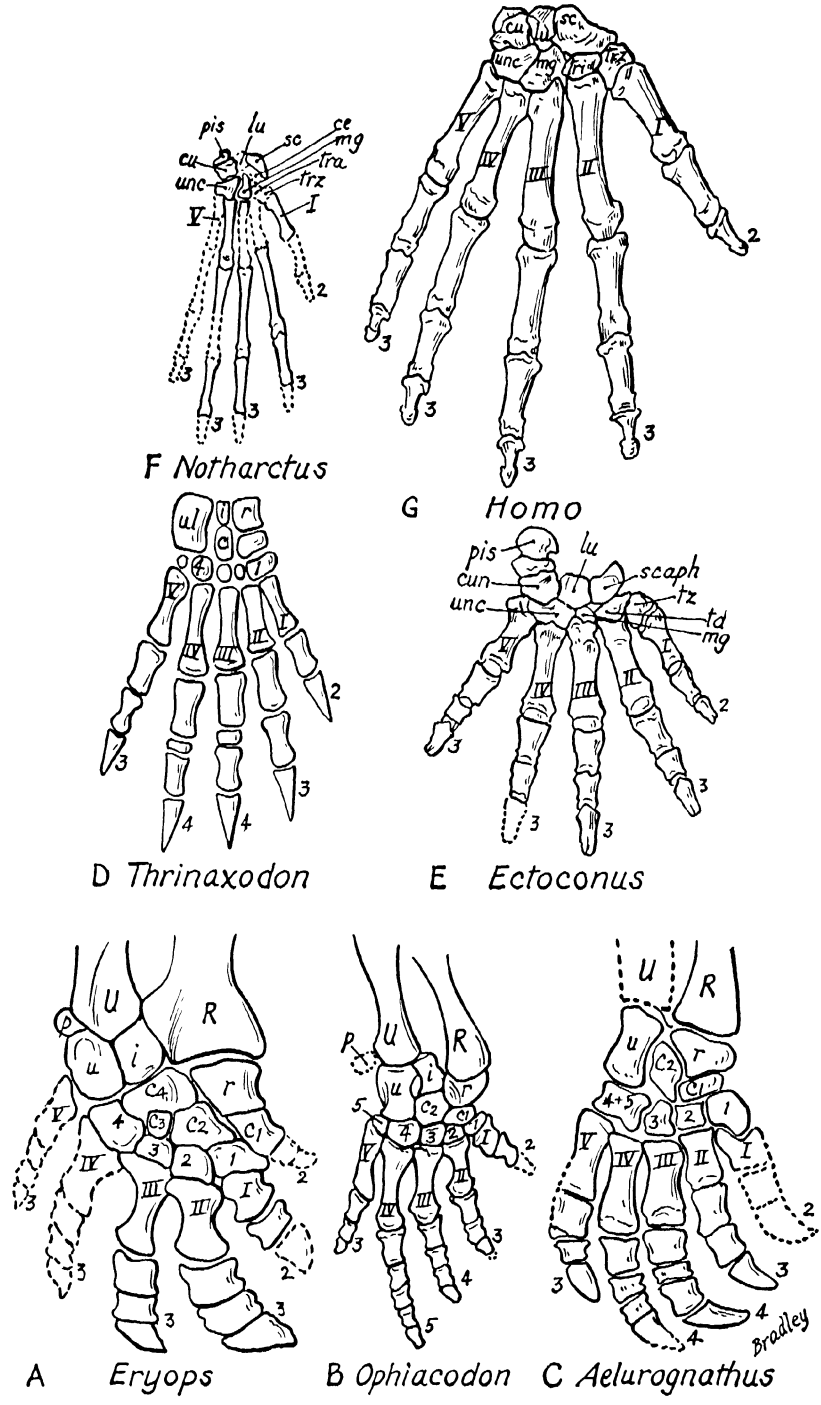


Fig 16.24. Evolution of the hand, from primitive tetrapod (A) to man (G). A, after Gregory and Raven; B, after Williston; C, after Boonstra. D, after Parrington; E, after Matthew; F, G, original. It is usually supposed that the lunar or middle bone of the upper row of the wrist of mammals was derived from the intermedium of reptiles but in Boonstra's gorgonopsian (C) the intermedium is very small, while the second centrale is large and interposed between the radiale and the ulnare as if it were about to become the lunar. In Parrington's small cynodont, however, the intermedium, although small, was present.

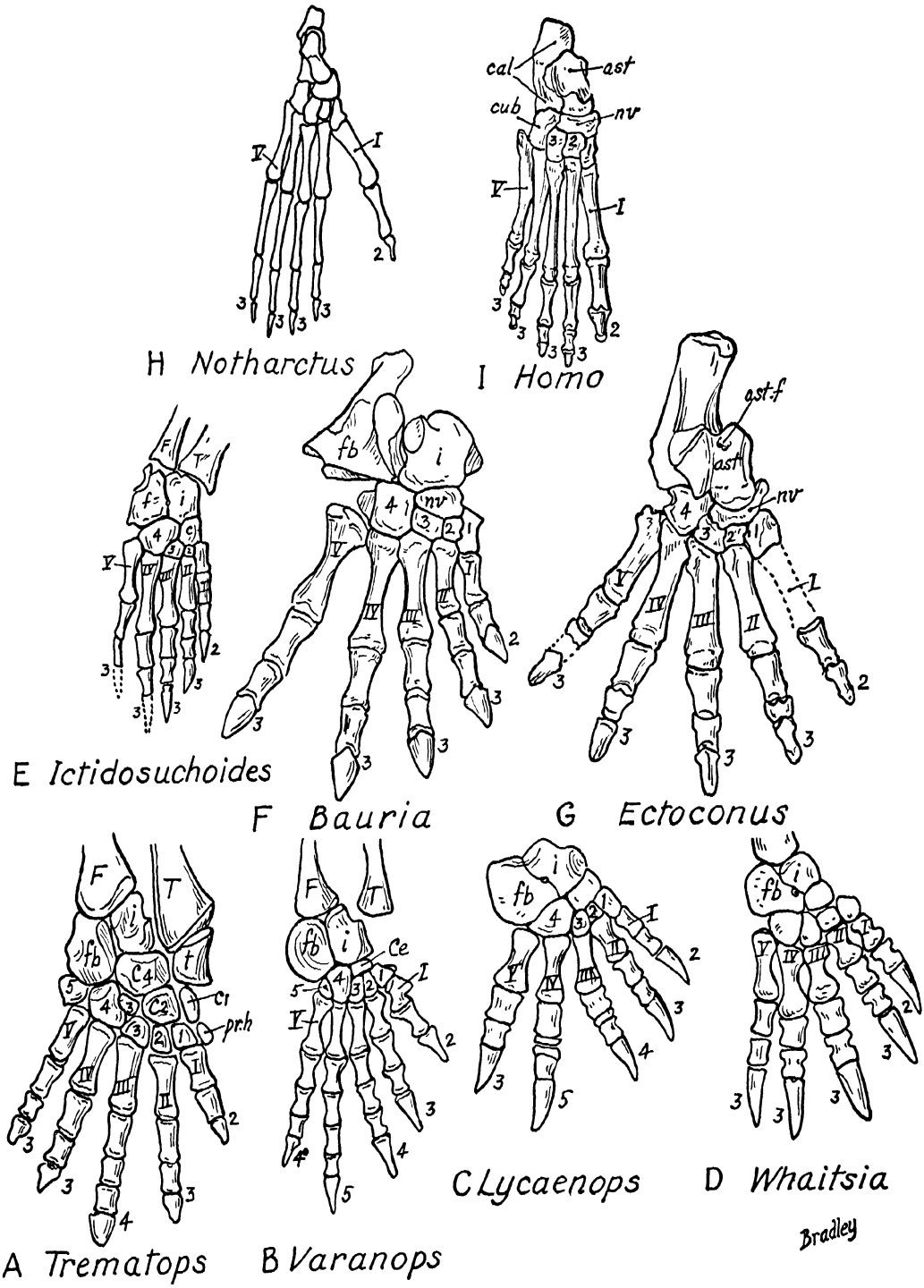


Fig. 16.25. Evolution of the foot, from primitive tetrapod (A) to man (I). A, after Schaeffer; B, after Williston; C–E, after Broom; F, after Schaeffer; G, after Matthew; H, I, original.

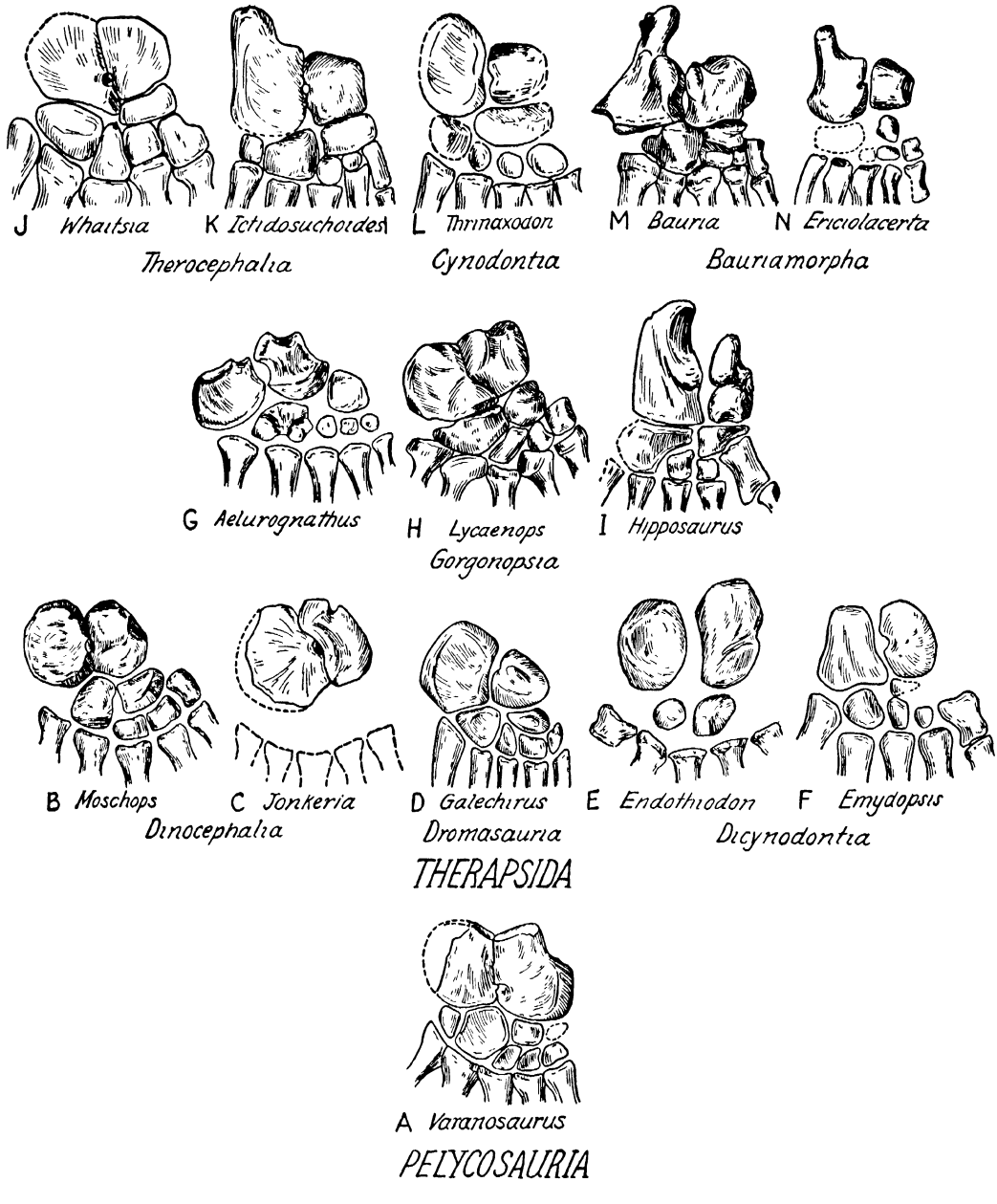


Fig. 16.26. Essential unity of plan in the tarsus of pelycosaur (A) and South African mammal-like reptiles (B–N). After B. Schaeffer. A tuber calcis appears in some of the smaller theroscephalians (L) and the whole tarsus approaches the mammalian grade in the Bauriamorpha (M, N).

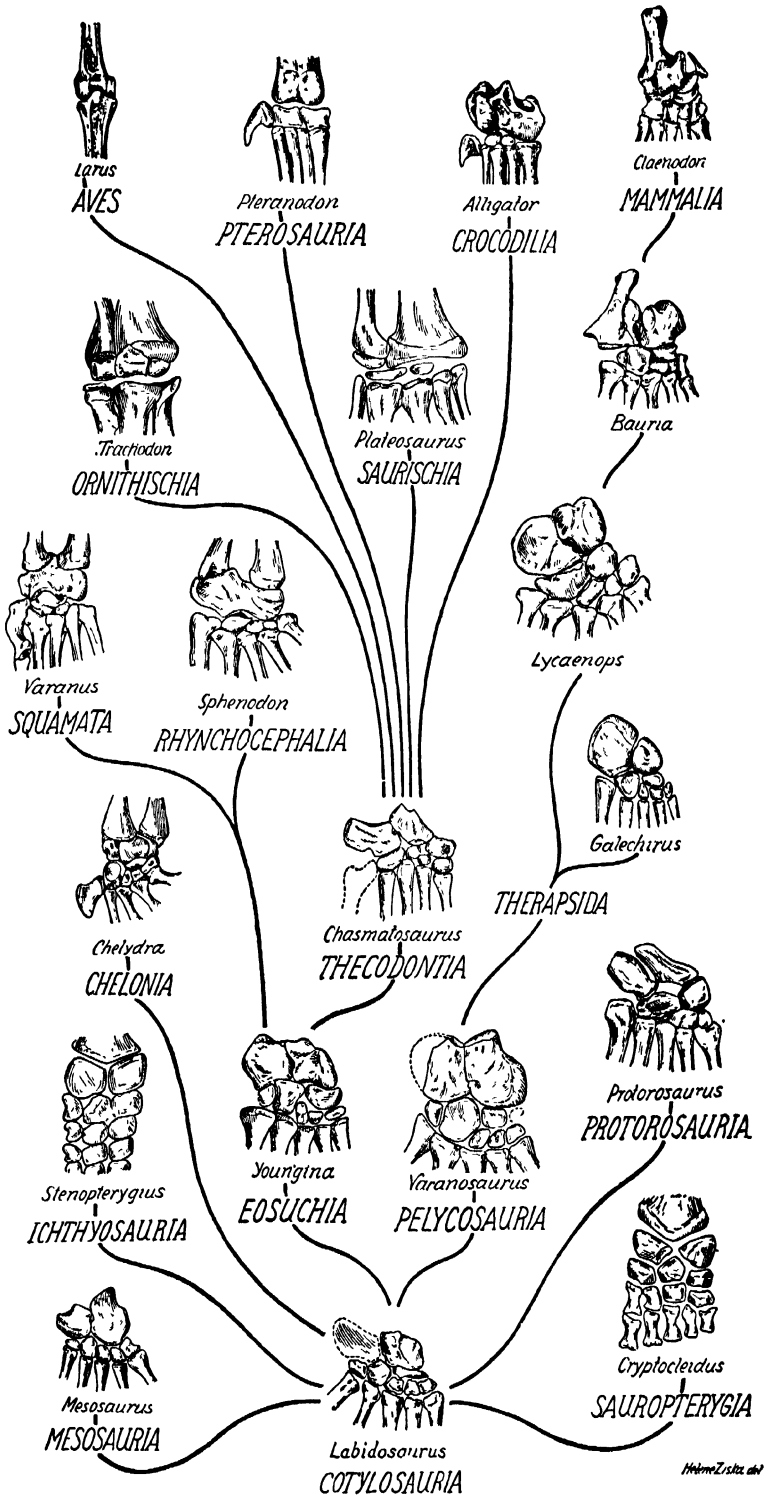


Fig. 16.27. Branching evolution of the tarsal bones, showing the evolution of the mesotarsal joint in typical reptiles and birds and of the crurotarsal joint in mammal-like reptiles and mammals. After B. Schaeffer.

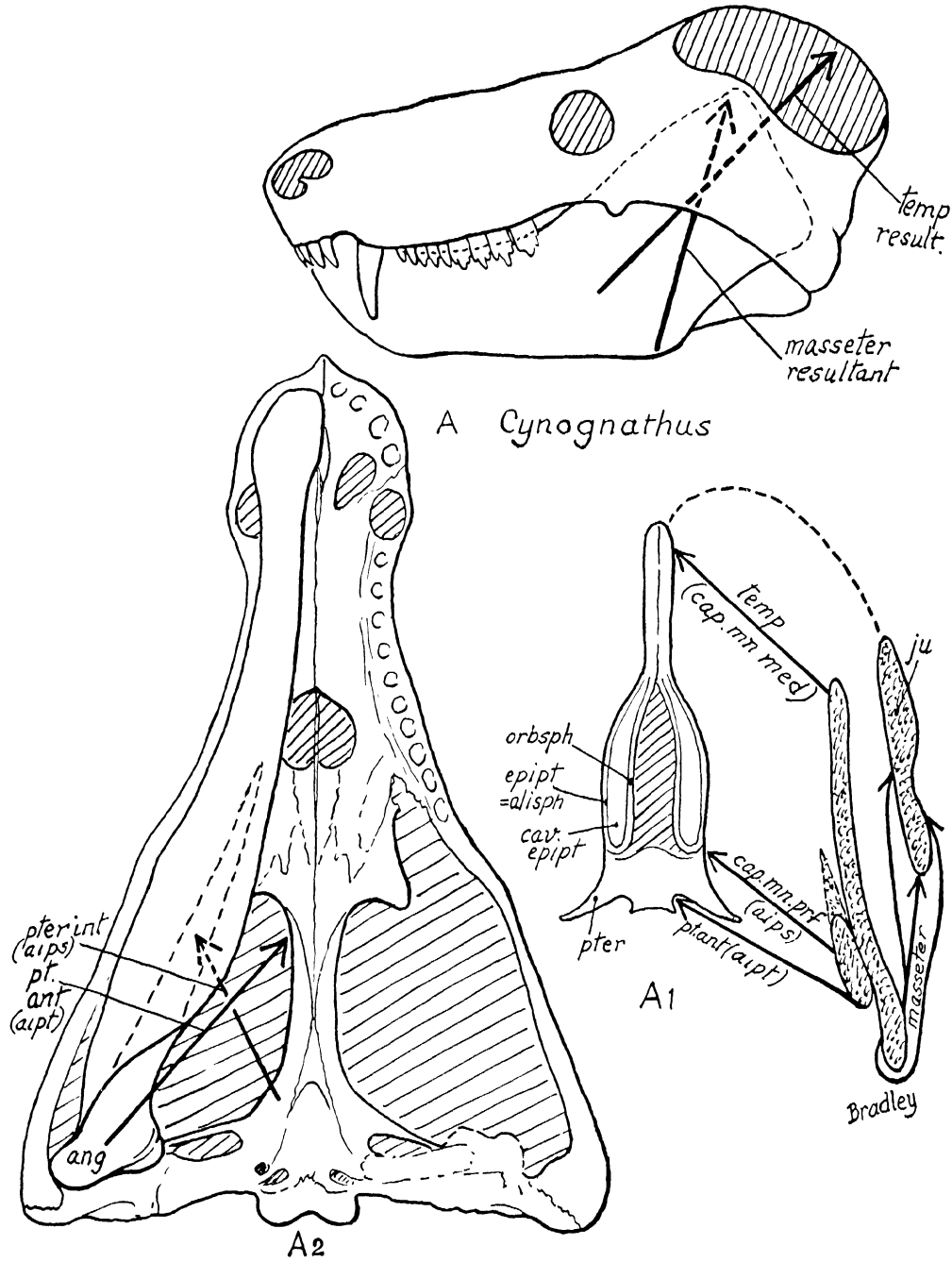


Fig. 16.28. The X–V jaw-trap of therapsids The black arrows indicate the general directions of the pulls of all the parts of the principal jaw muscles Data on muscles from Adams, and Parrington and Westoll (*Aips*), adductor internus pseudotemporalis, (*aipt*), adductor internus pterygoideus.

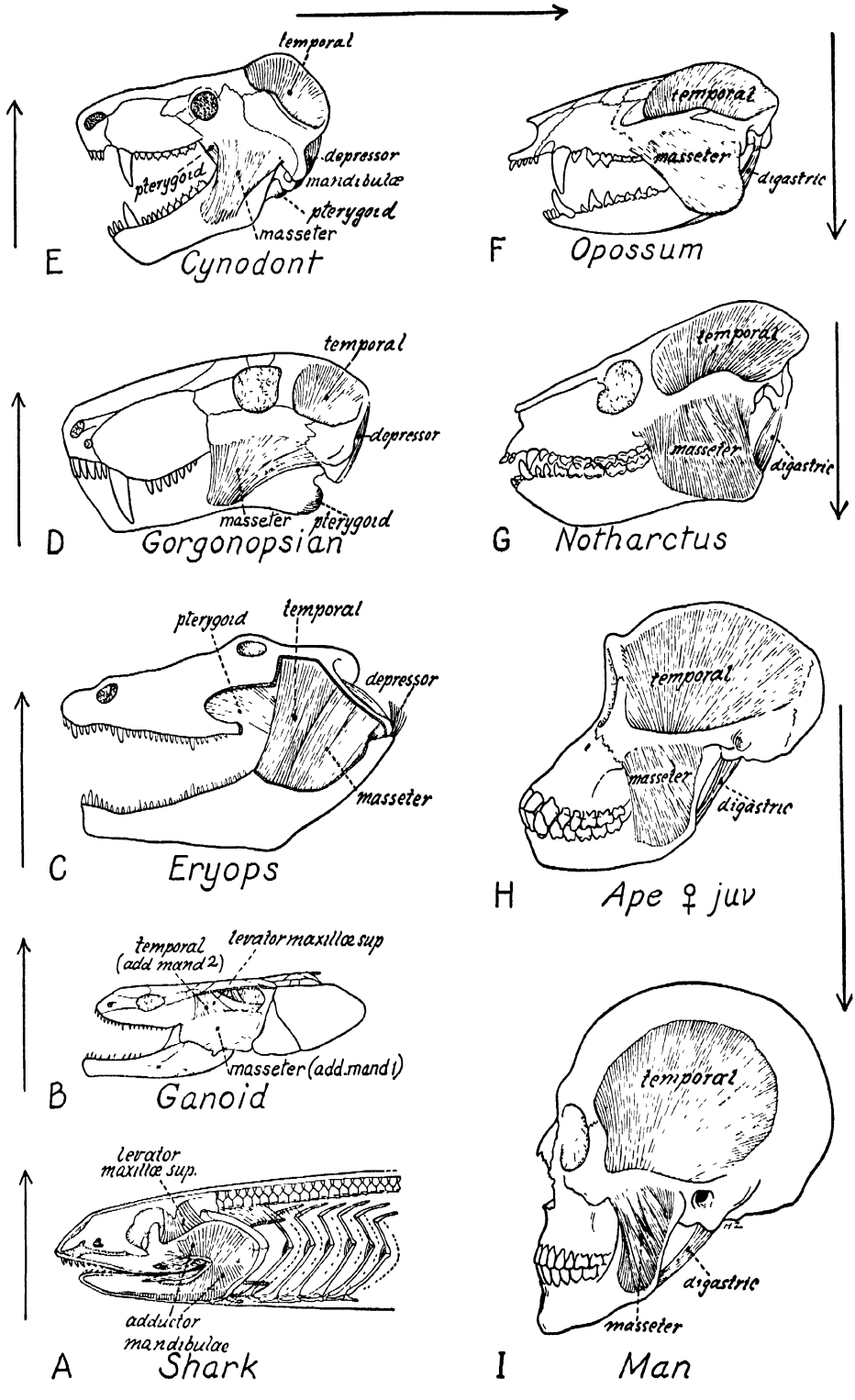


Fig. 16.29. General relations of the temporal and masseter muscles to the jaws and temporal arches from fish to man. Data on muscles mostly from Adams.

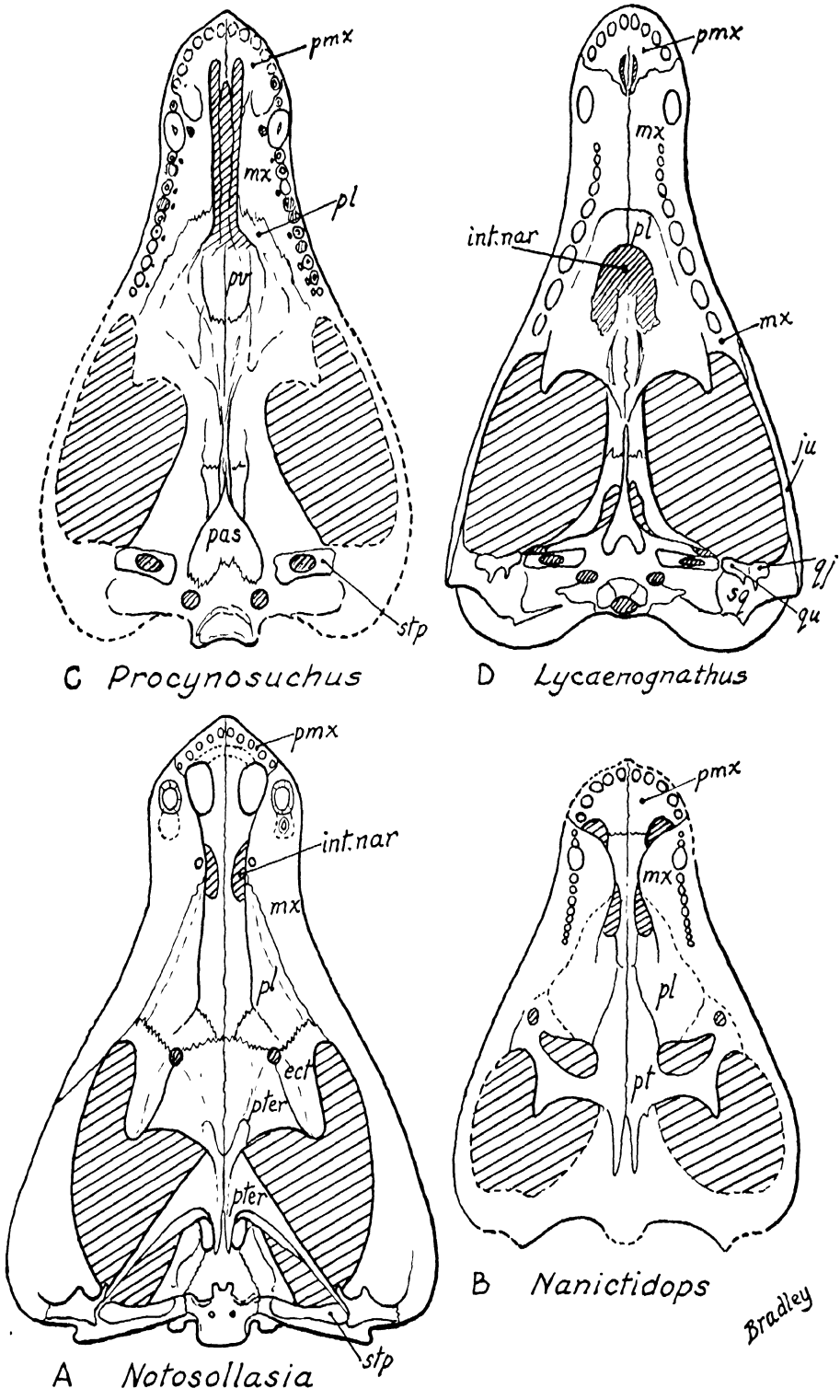


Fig. 16.30. Structural stages in the formation of a secondary bony palate. A, after Boonstra; B–D, after Broom. A, B are therocephalians; C, D cynodonts.

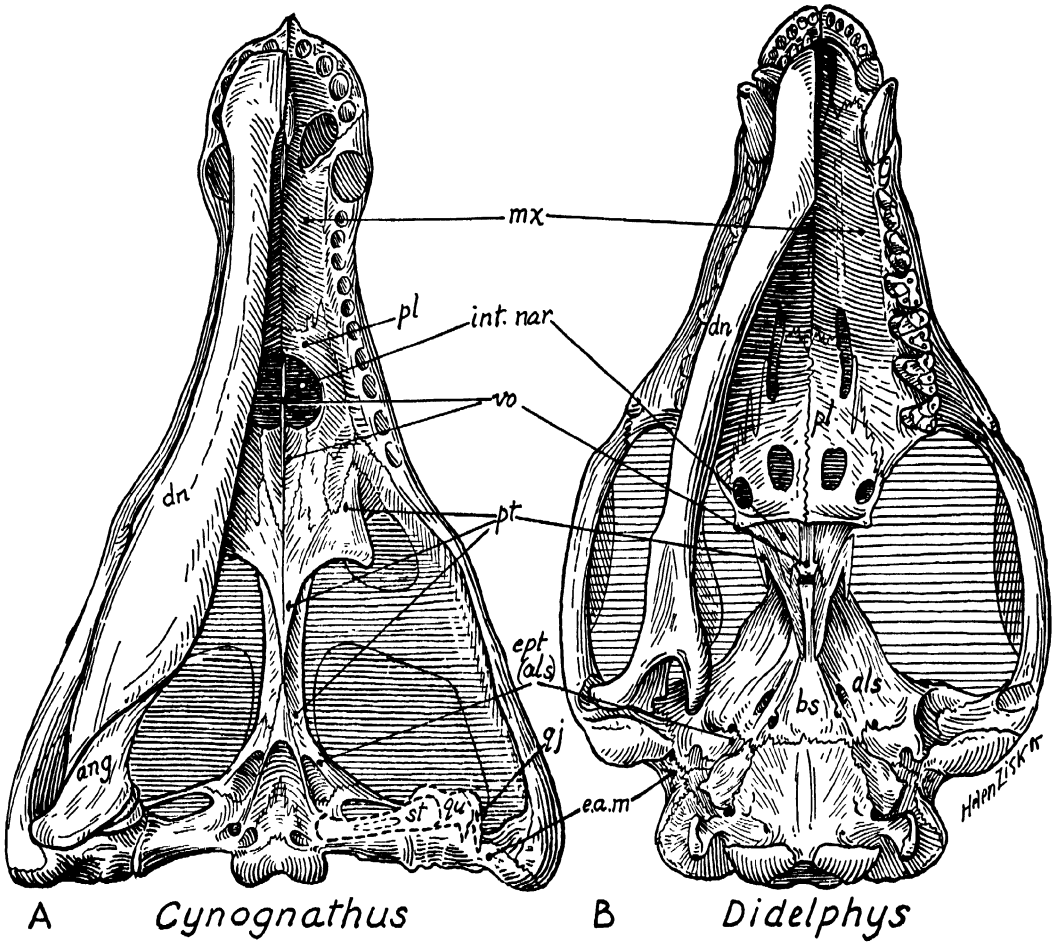
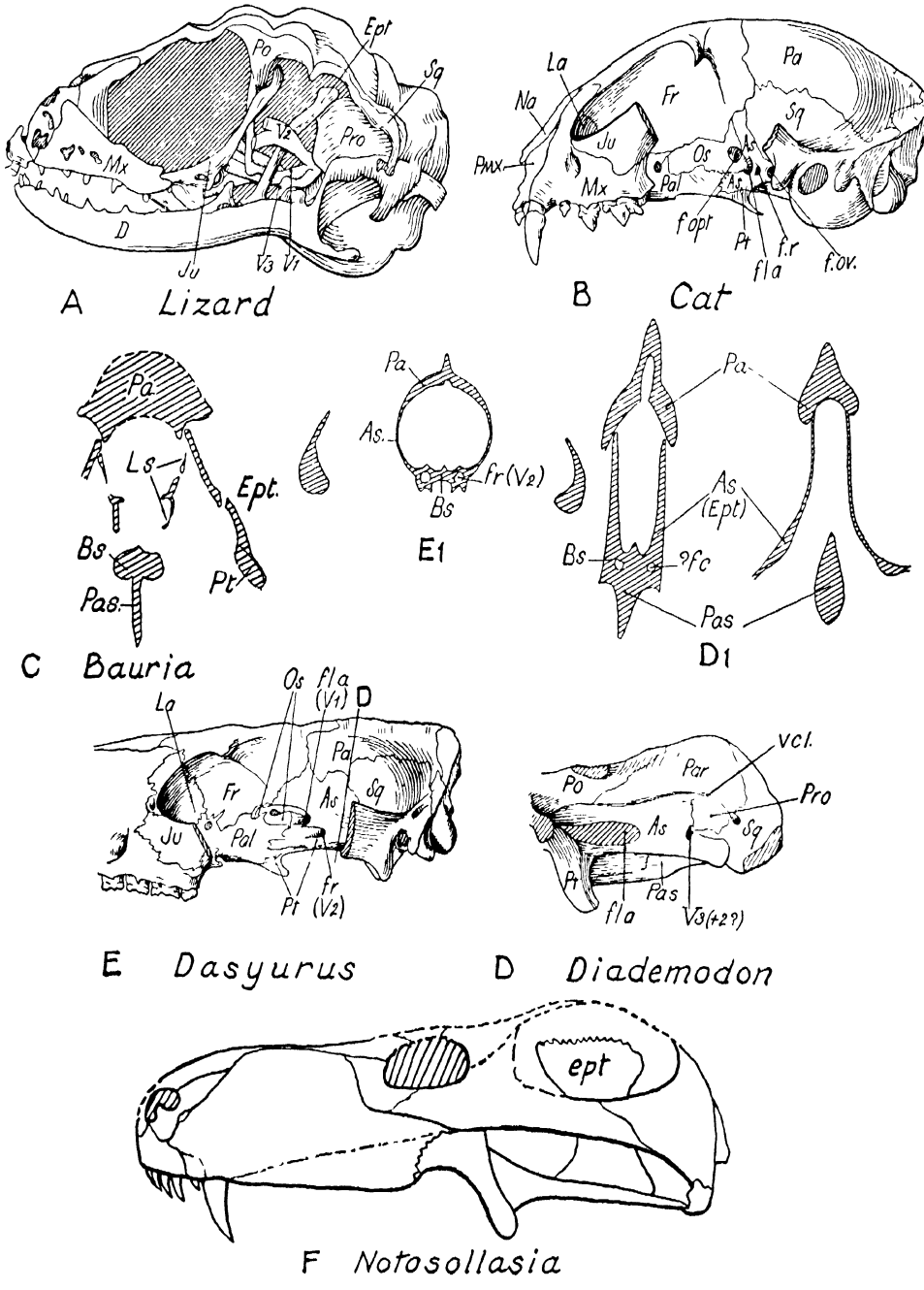


Fig. 16.31. The pterygoid in relation to palate and epipterygoid (alisphenoid) in cynodont (A) and mammal (B). A, after Broili; B, original.



Figs. 16.32, 33. Epipterygoid into alisphenoid. After Gregory and Noble. A, after Pearson; B, E, E1, D1, original, C, after Broom, D, after Watson; F, after Boonstra The epipterygoid (*Epi*, columella cranii) in the lizard (A) bears but little resemblance to the alisphenoid (*As*) of the cat (B), but the therocephalian (F) and still more the cynodont (D) afford transitional stages. In the cross-sections, the bauriamorph (C) retains part of the old sphenethmoid (or laterosphenoid, *L.s*) but the epipterygoid (here broken) supports the parietal roof; in the cynodont (D1) the laterosphenoid has apparently disappeared (at least at these two levels) leaving the epipterygoid (alisphenoid); in the marsupial (E1) the lateral expansion of the brain has pressed the alisphenoid outward.

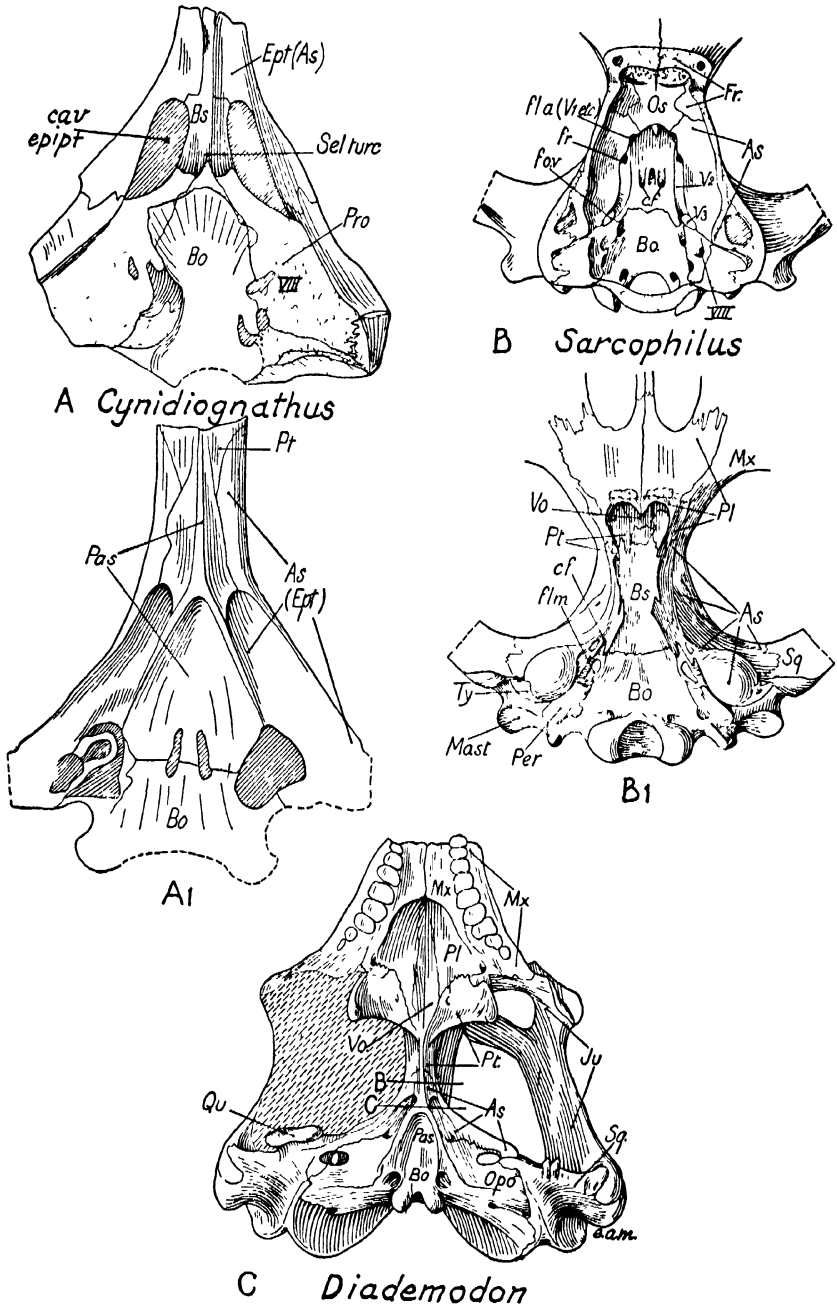


Fig. 16.34. Epipterygoid into alisphenoid (continued). After Gregory and Noble. A, A1, after Haughton; B, B1, original; C, after Watson. In the cynodont (A) the interior and floor of the braincase is seen from the dorsal side. The epipterygoid anteriorly embraces the basisphenoid; posteriorly it diverges laterally to the cavum epiptericum to meet the anterior projection of the prootic. In the marsupial (B) the alisphenoid has inherited its basic features from the epipterygoid but has been pressed laterally by the expansion of the brain. In the ventral view of the cynodont (A1) the greatly enlarged epipterygoids embrace the keeled para-basisphenoid (*Pas*). In the mammal they give rise to descending flanges and to the "alisphenoid bulla" covering the expanded cavity of the middle ear.

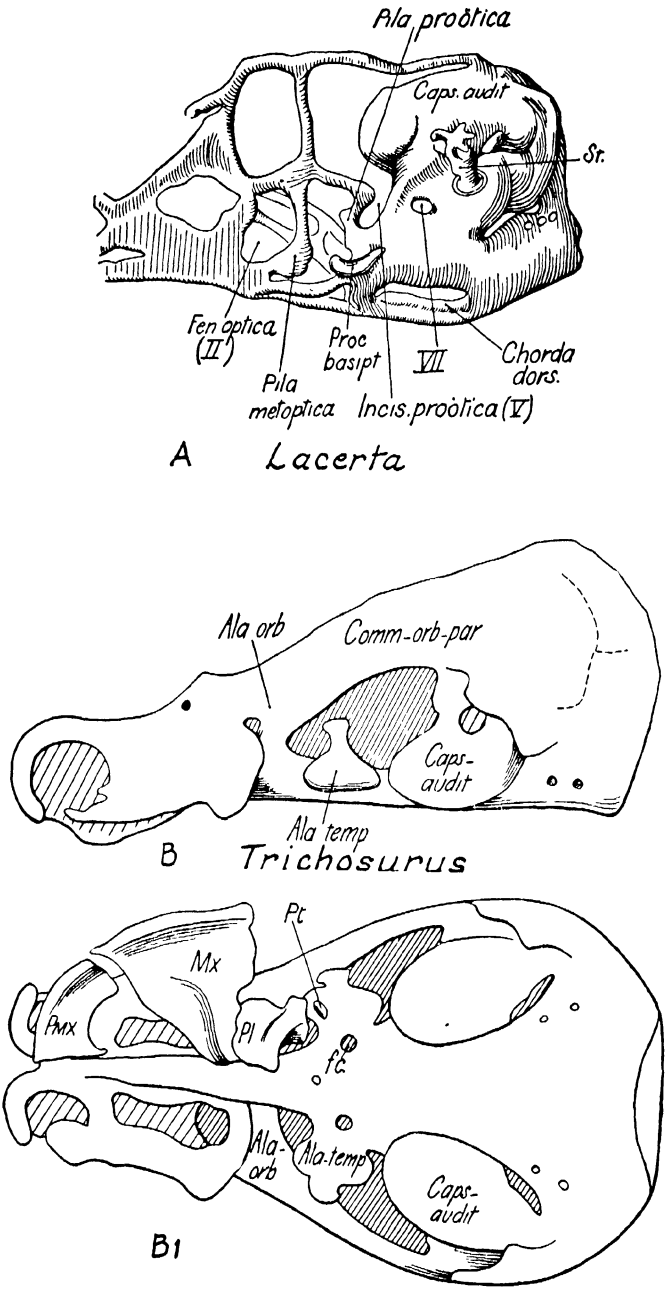


Fig. 16.35. Chondrocrania of embryo lizard (A) and marsupial (B). After Gregory and Noble. A, after Pearson; B, B1, after Broom The basipterygoid process of the embryo lizard resembles, but is probably not homologous with, the mammalian ala temporalis (alisphenoid).

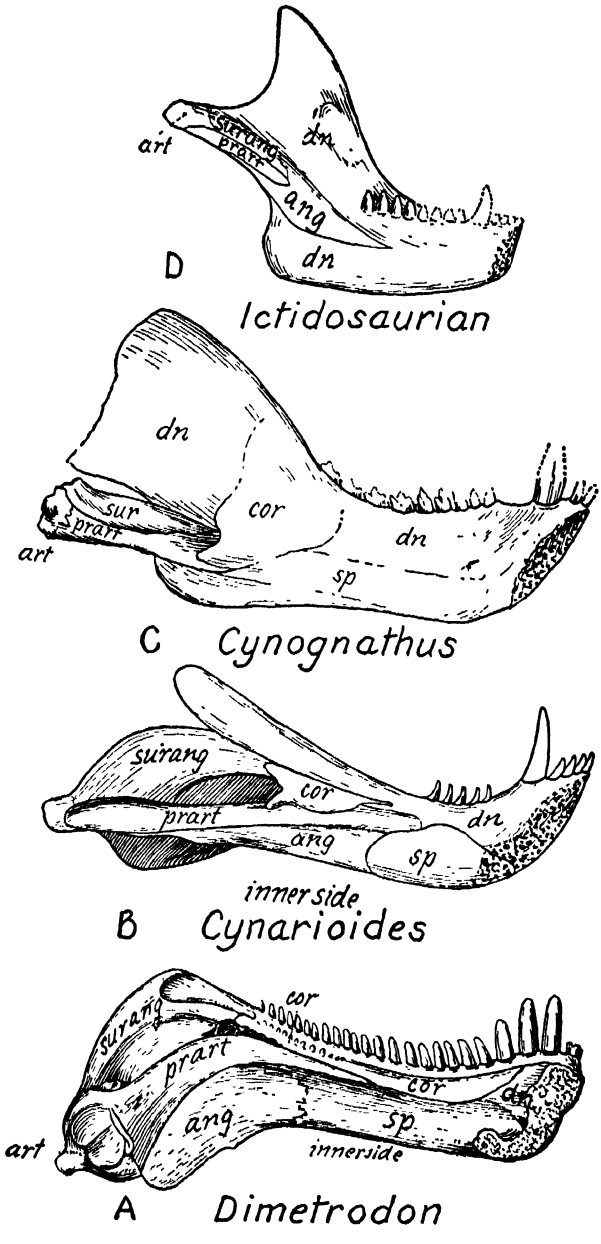


Fig. 16.36. Progressive enlargement of the ascending ramus of the dentary and reduction of the bones behind the dentary in therapsids, from Permian pelycosaur (A) to Upper Triassic ictidosaur (D). A, after Williston; B, D, after Broom; C, after Watson, and Broili.

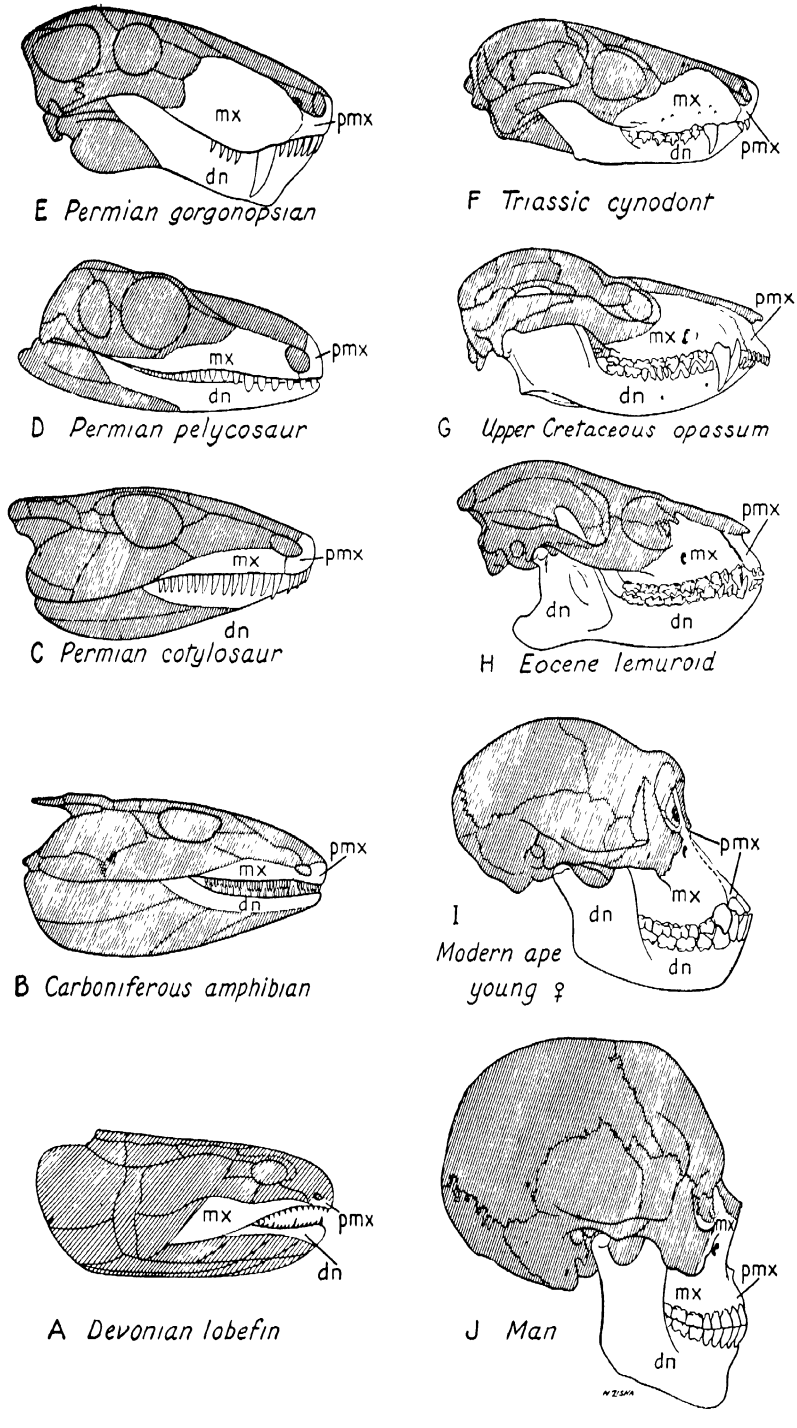


Fig. 16.37. Ten stages in the evolution of the outer or secondary upper and lower jaw bones from Devonian lobe-fin fish (A) to man (J). After Gregory. A, after Traquair, Watson, Bryant; B, after Watson; C, D, after Williston; E, F, after Broom; G, after Gregory; I, original; J, after Cunningham.

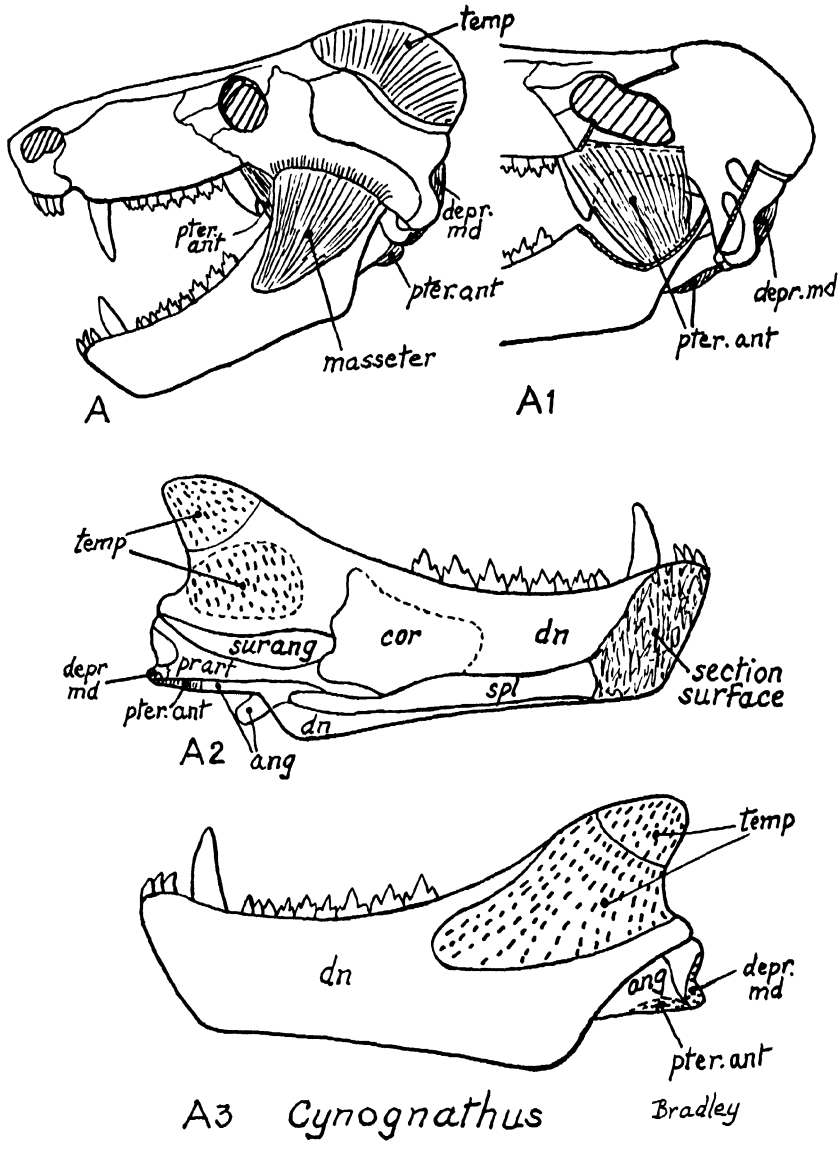


Fig. 16.38. The principal jaw muscles of *Cynognathus*, as restored by Adams. The captimandibularis, or chief jaw muscle of reptiles, included a superficial (=mammalian masseter), medial (= mammalian temporal) and a deep branch (=mammalian pterygoids) inserted on the inner side of the ascending ramus of the dentary. The anterior pterygoid of other reptiles was still present. Presumably these were all innervated by the mandibular nerve (D3). The depressor mandibulae (*D.m.*) was innervated by the seventh nerve. According to Adams, Parrington, and Westoll, this type of musculature was changed into the mammalian type chiefly by the reduction of the reptilian anterior pterygoid, which probably became the tensor tympani, and by the separation of the mammalian internal pterygoid and possibly the external pterygoid from the deepest branch of the capiti mandibularis.

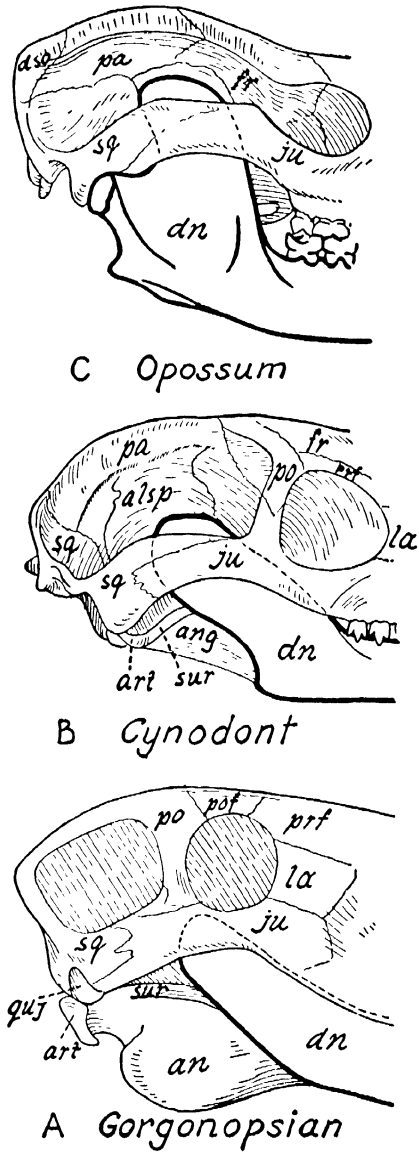


Fig. 16 39. Progressive enlargement of the ascending ramus of the dentary in mammal-like reptiles (A, B) and its ultimate contact with the squamosal to form the new or temporo-mandibular joint in mammals (C), as compared with the old (A) or quadrato-articular joint of reptiles. A, B, after Broom; C, original.

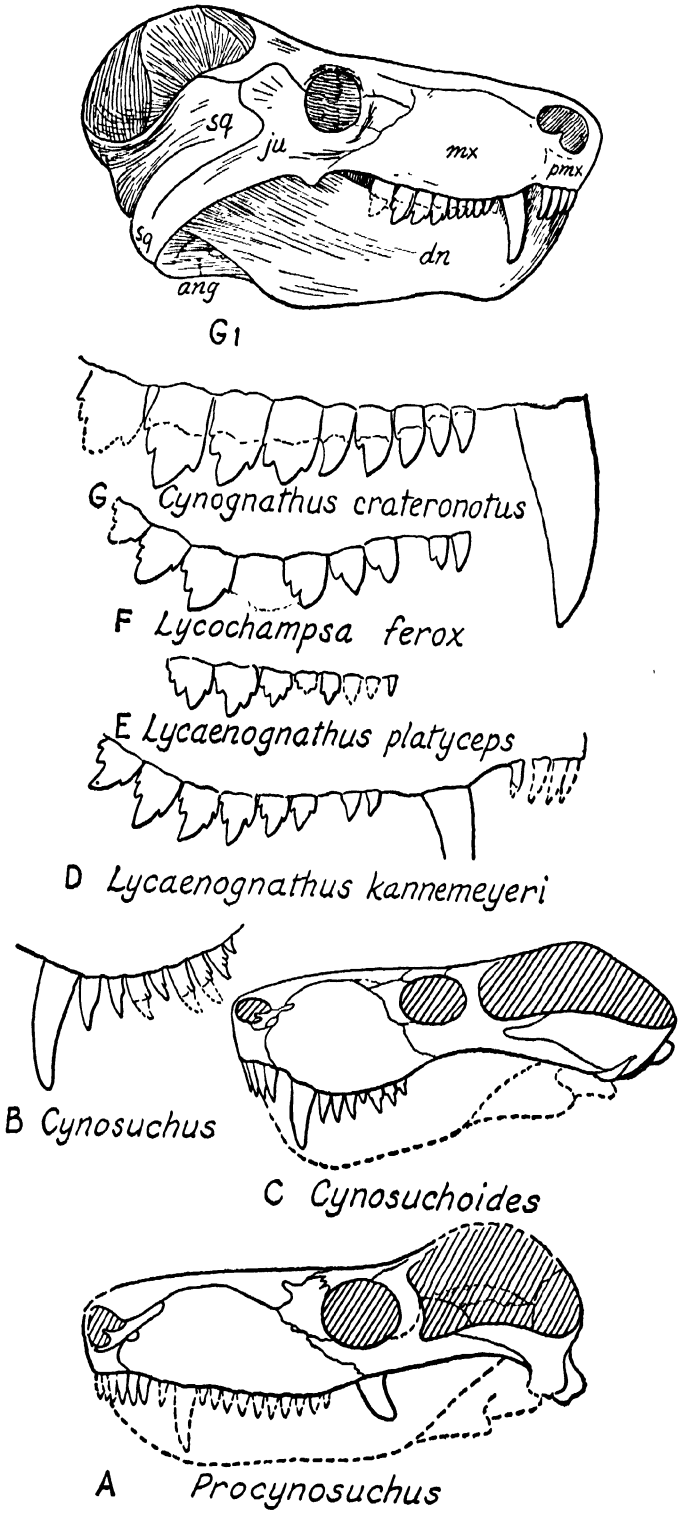


Fig. 16.40. Carnivorous dentition of cynodonts, showing gradual differentiation of premolars and molars and increasing cuspidation of the molars. A, C–G1, after Broom; B, after Haughton.

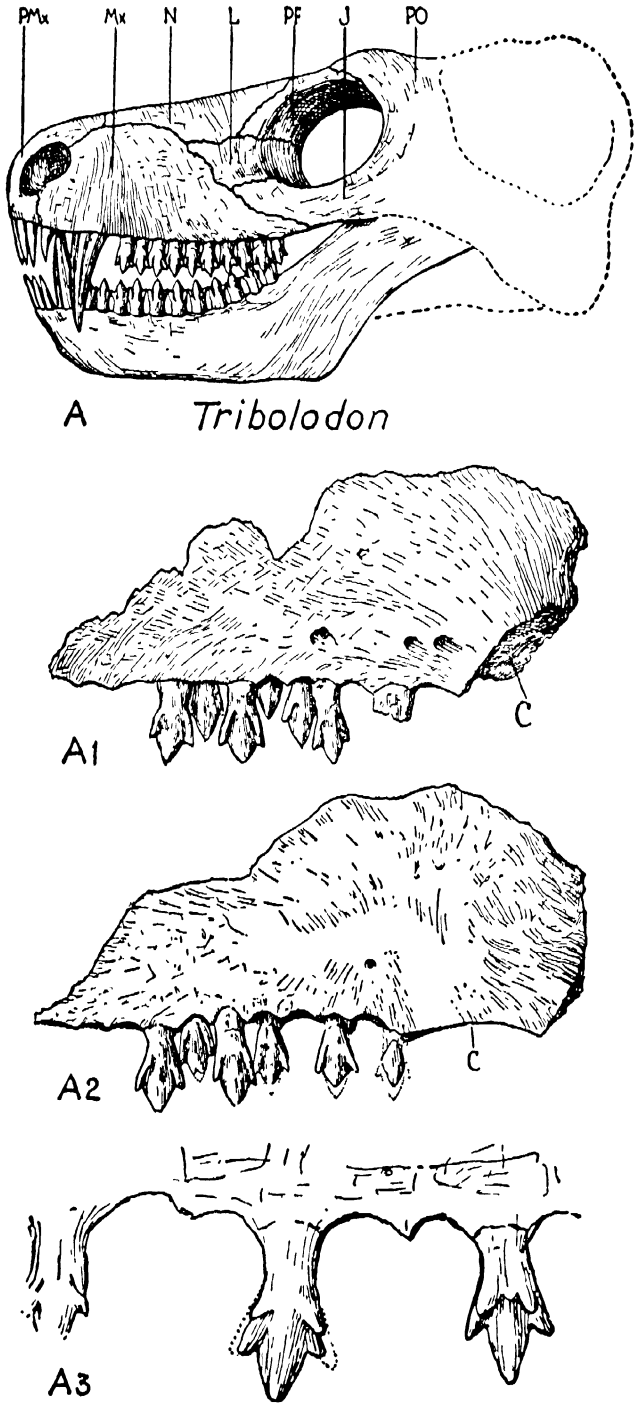


Fig. 16.41. Skull and dentition of a small progressive cynodont, *Tribolodon*, from the Upper Triassic of South Africa After Broili and Schroder.

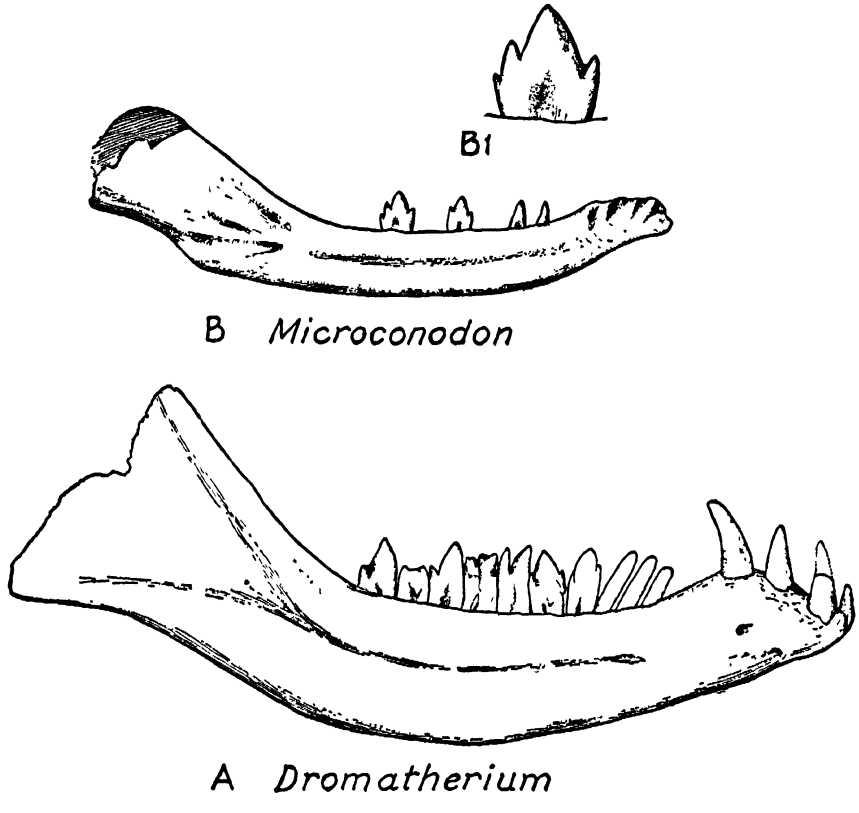


Fig. 16.42. Progressive cynodonts (?) from the Upper Triassic of North America. After Simpson. A, B, × 4; B1, × 12. Both these minute jaws were taken from a coal mine of Upper Triassic age in North Carolina. They were formerly regarded as primitive mammals and may well be near the border between mammal-like reptiles and mammals, but partly because the roots of the molars, although compressed, are not subdivided into anterior and posterior roots, these genera are doubtfully referred to the cynodonts (Simpson).

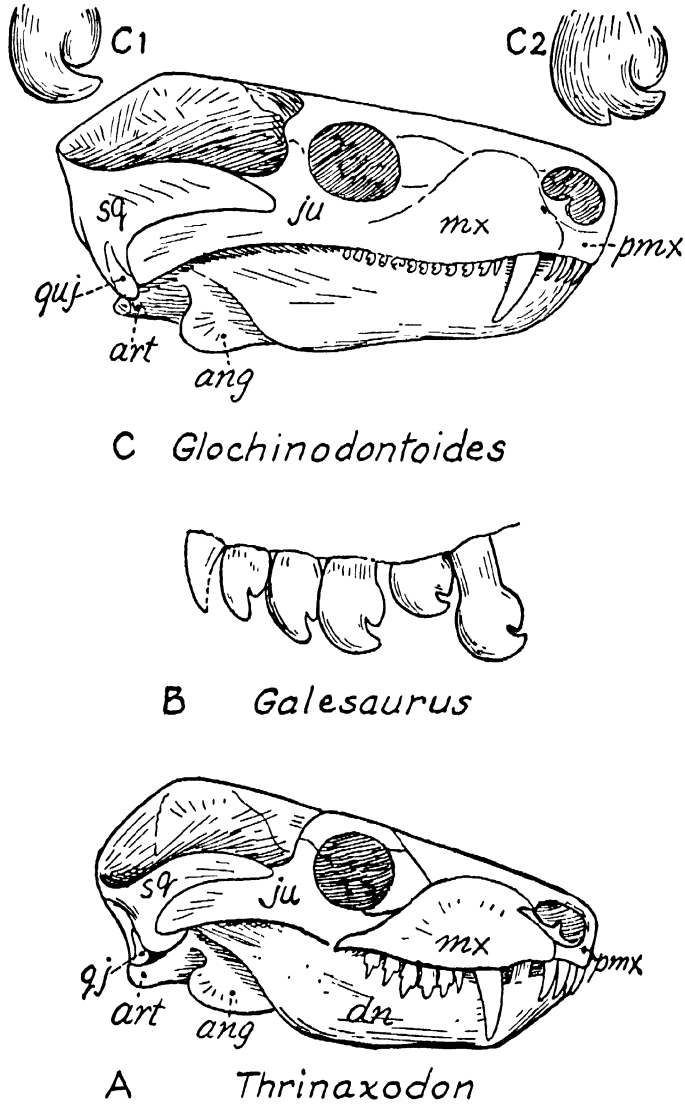


Fig. 16 43 Skulls and teeth of small cynodonts with cuspidate molars. After Broom.

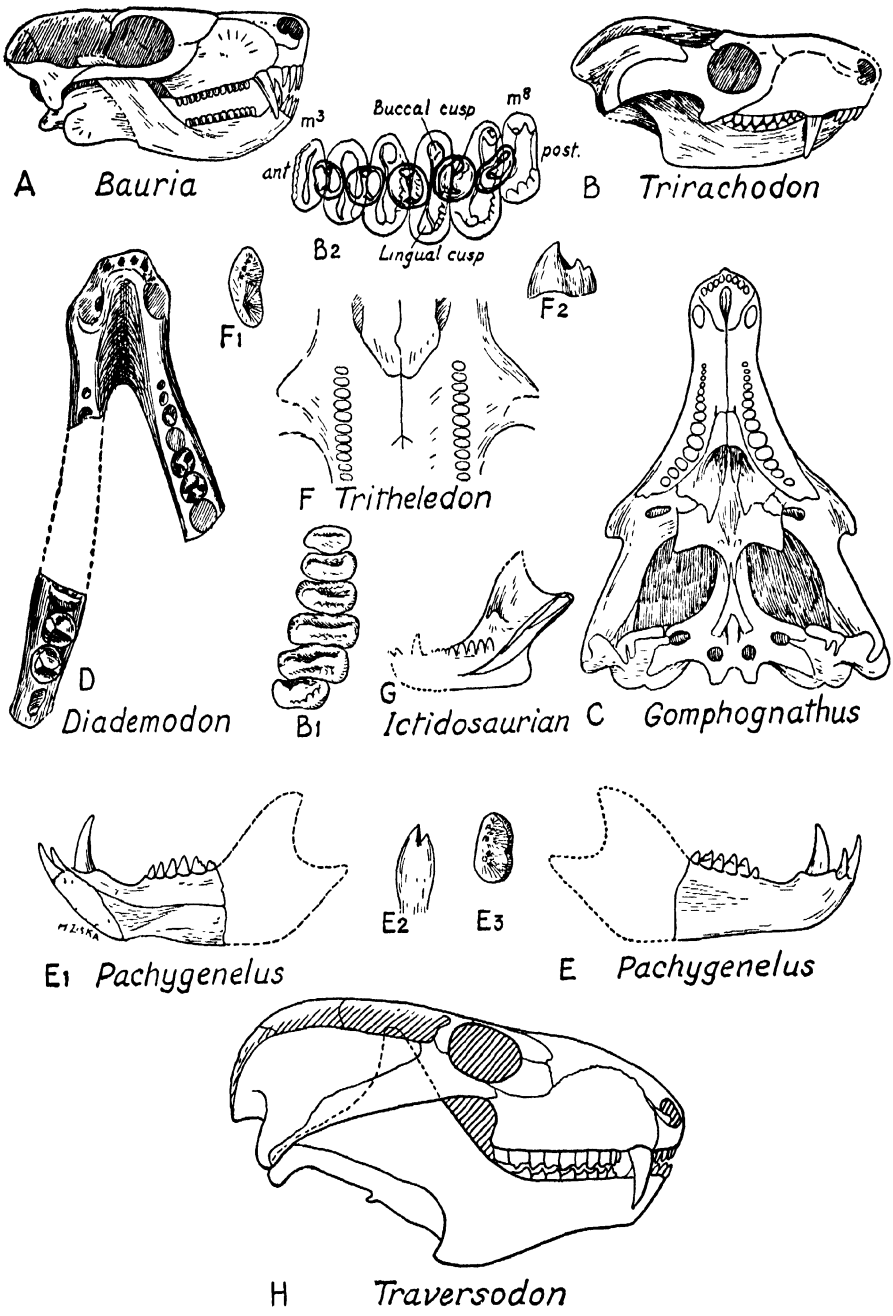


Fig. 16.44. Crushing or grinding adaptations in mammal-like reptiles. A–G, after Broom; H, after von Huene. Although belonging to different suborders, all tend to wear the postcanine series down into a flattened occlusal surface. Some (B, E, F, G) are transversely widened and some (E–E3) also show evidence of transverse reduplication or budding. D, Lower jaw of small diademodont, showing empty alveoli of deciduous incisors, canines and premolars, with tips of succeeding set at bottom. Each lower molar fitted between two uppers (B, G). The highest cusps are on the outer or buccal side of the uppers (F1, F2) and on the inner or lingual side of the lowers (E1–E3).

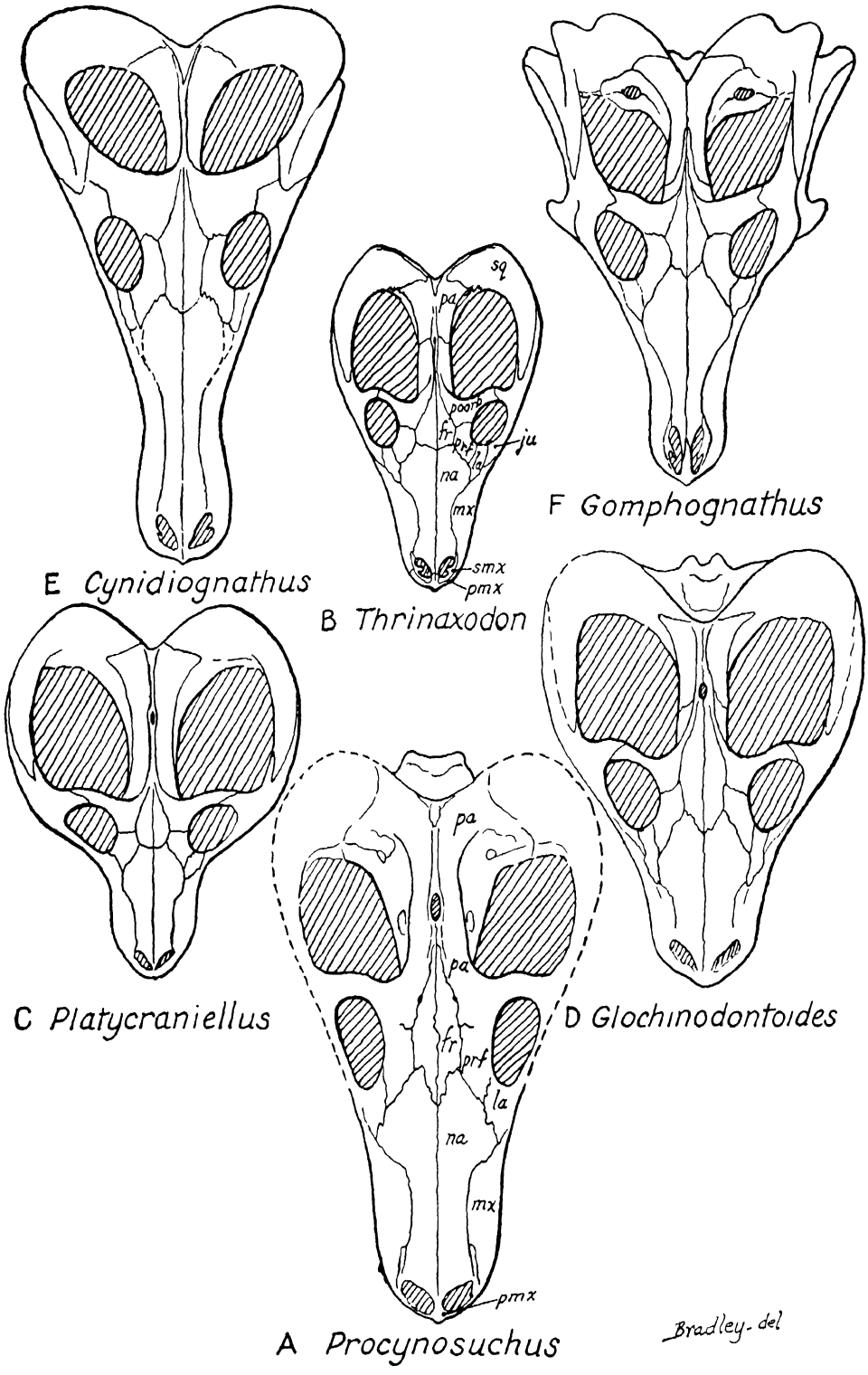


Fig. 16.45. Skulls of cynodonts Dorsal views to show widening of temporal fossae. All after Broom.

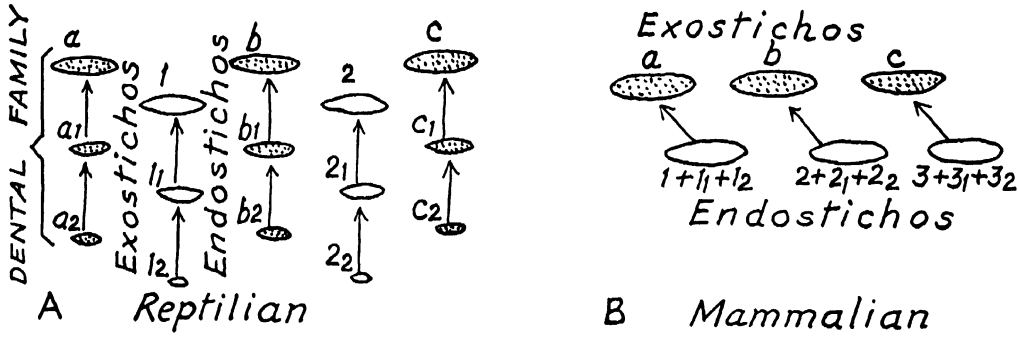


Fig. 16.46. Bolk's theory of the origin and relationships of the successional teeth in reptiles (A) and mammals (B). In reptiles each "dental family" of succesional teeth belongs either to the exostichos (outer set) or endostichos (inner set). In mammals, each single tooth represents a dental family, the exostichos giving rise to the deciduous, the endostichos to the permanent set.

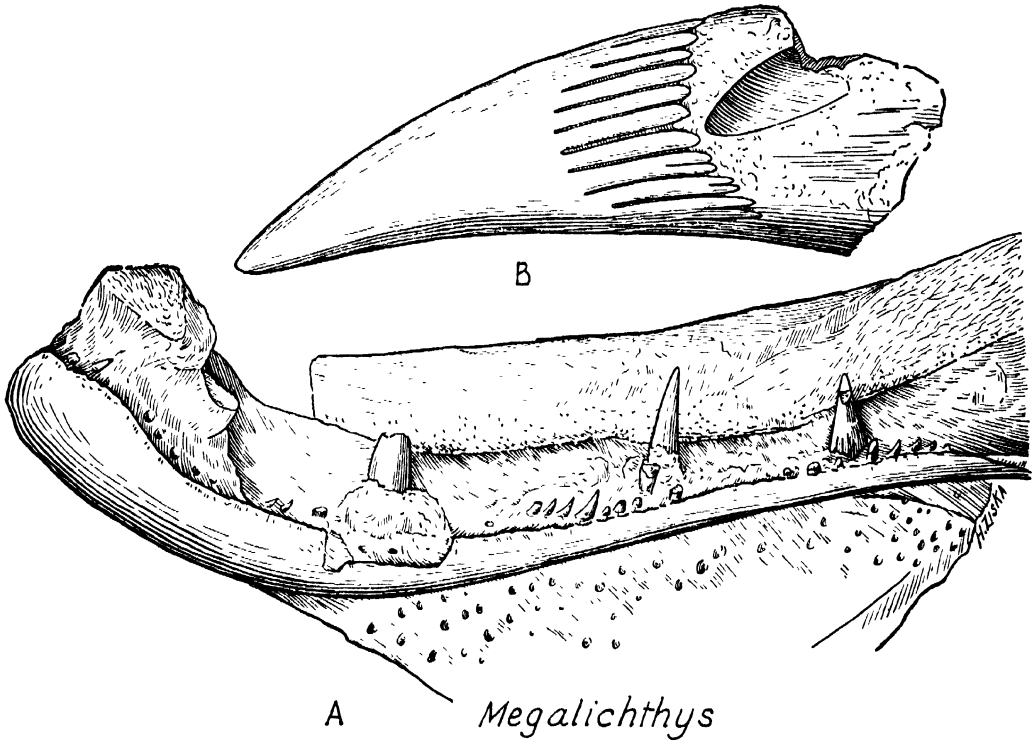


Fig. 16.47. Lower jaw and teeth of an advanced lobe-fin fish of Upper Carboniferous Age. A, lower jaw, showing the outer row (small teeth) and the inner row (tusks); B, single tusk, showing depression caused by presence of succeeding tooth during its formative stages.

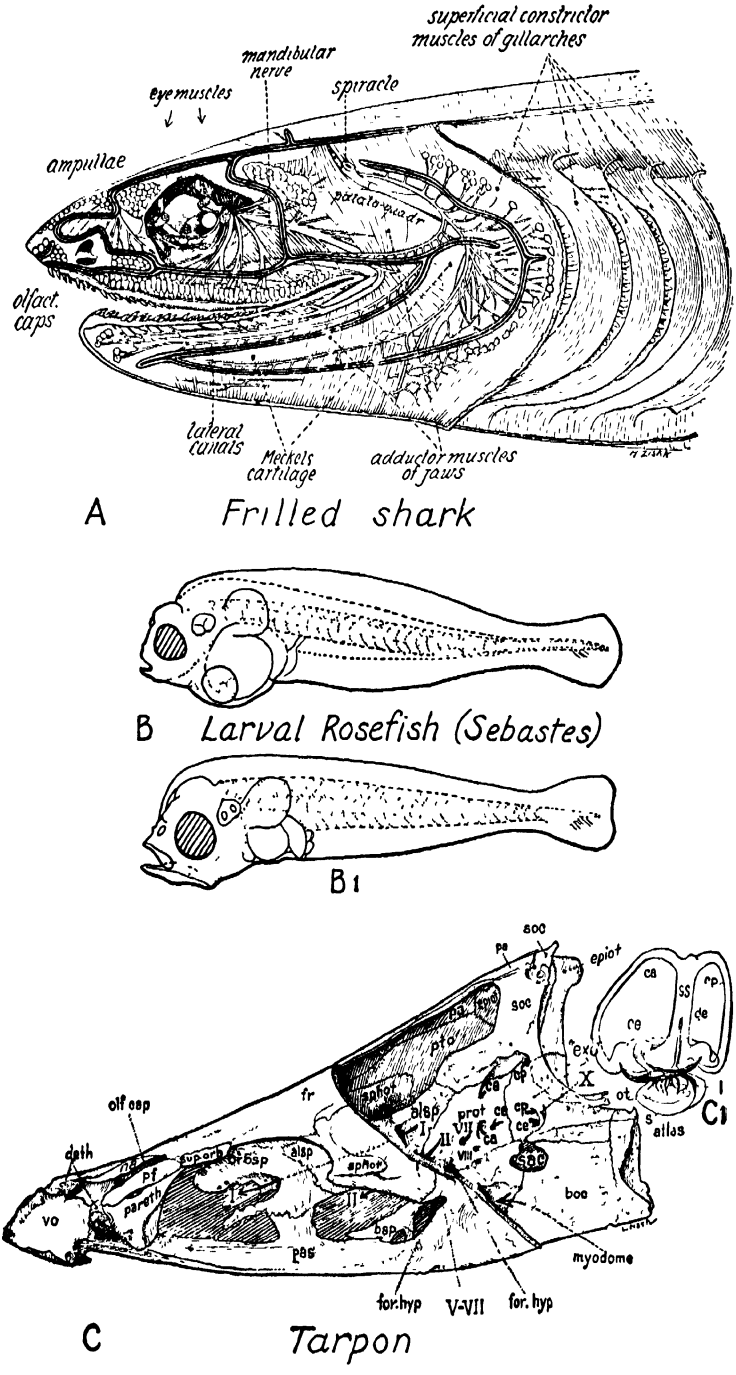


Fig. 16.48. The lateral line system and its derivative, the inner ear. A, after Allis; B, B1, after Bigelow and Welch; C, after Gregory; C1, after Retzius. A, the lateral line system of a shark; B, B1, embryo taleost, showing two stages in the development of the auditory capsule. In B, is shown the tripartite division that predetermines the position of the semicircular canals; B1 shows the *Anlagen* of the anterior and posterior semicircular canals and of the crus communis. The membranous and bony auditory capsules (C, C1) are well protected from shock by the entire construction of the skull.

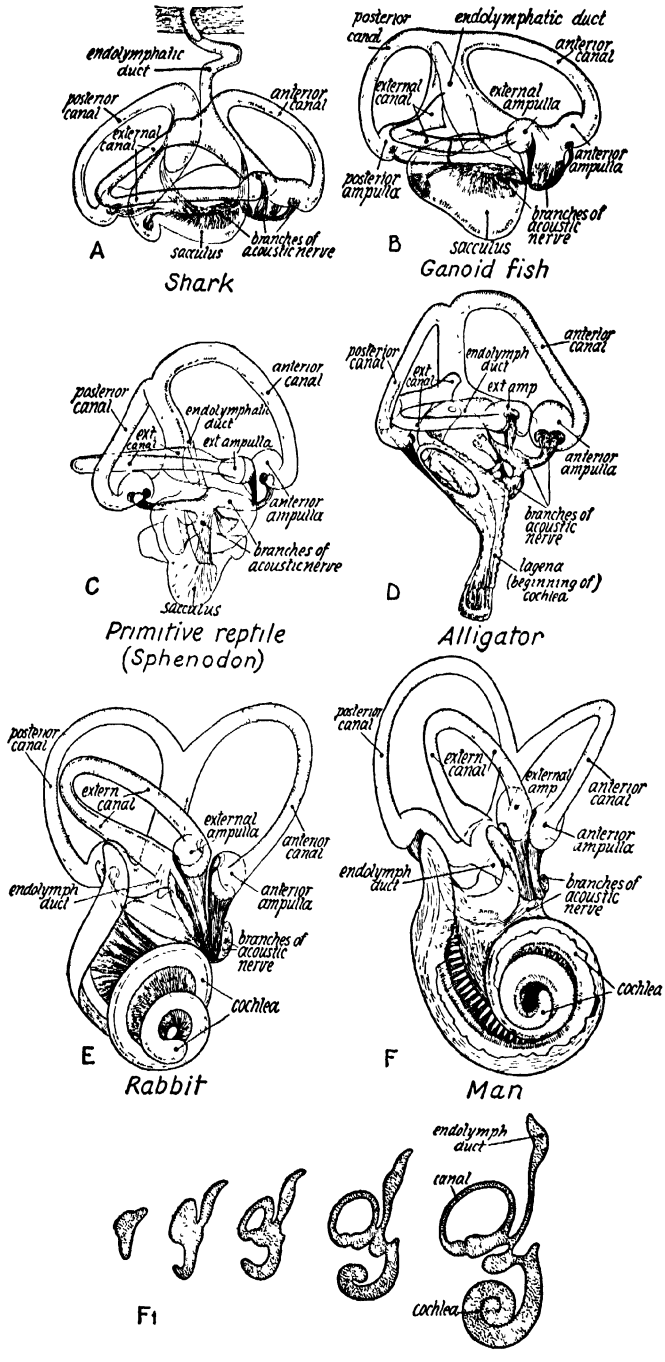


Fig. 16.49. The inner ear from shark to man. (A–F, from Gregory, after Retzius; F1, embryonic development of the inner ear in man, after Streeter. The basic construction is remarkably uniform throughout the series, save for differences in the height of the semicircular canals and the outgrowth of the lagena (D) and its subsequent coiling into a cochlea (E–F). The series F1 shows how the inner ear begins as an invagination from the surface of sensitive ectoderm. Then it sinks inward, leaving the endolymphatic duct as its connection with the surface. The downwardly growing cochlea goes through successive stages of coiling, the earlier stages of development paralleling more or less the primitive reptilian and early mammalian stages of evolution.

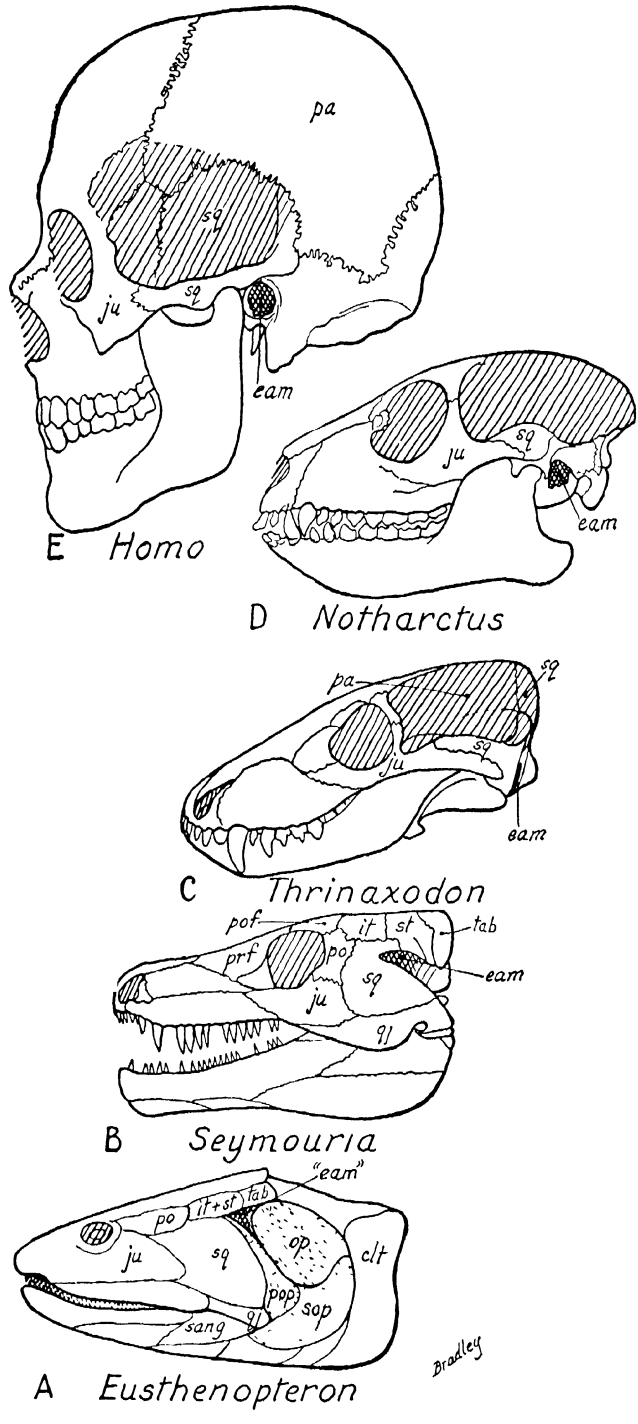


Fig. 16.50. Procession of vertebrate skulls from Devonian lobe-fin fish to man. A, after Bryant, Stensiö *et al*; B, after T. E. White; C, after Broom; D, after Gregory. To show the origin and subsequent shifting of the external auditory meatus (*eam*) from near the upper side (A) to the base of the skull (C). Its later apparent displacement forward (D, E) is due to the upright posture and the backward overgrowth of the temporal pole of the brain in man (E). After Gregory. See also figs. 16.51–63

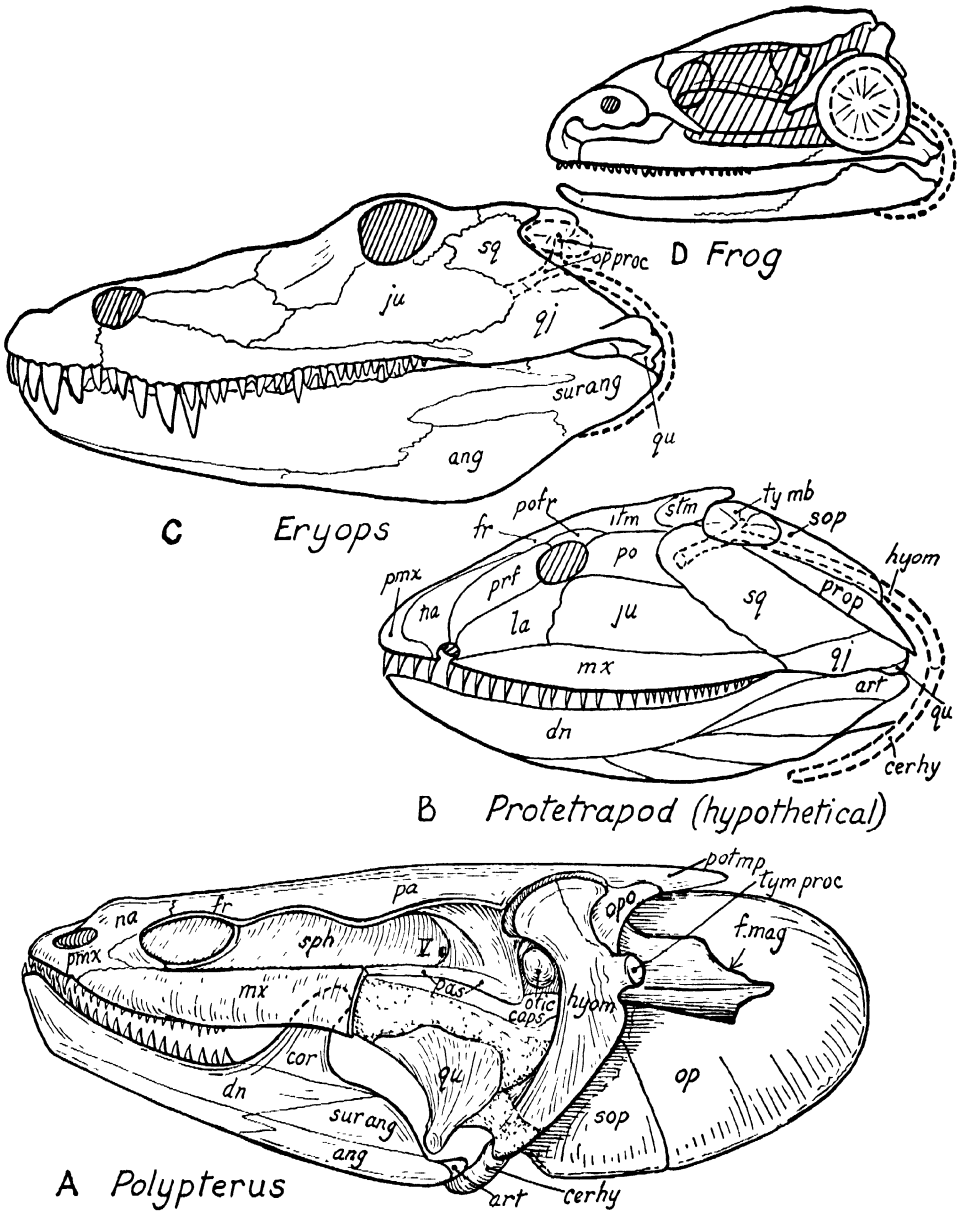


Fig. 16.51. Hyomandibular into stapes. A, composition from specimens, with data from Allis; B, hypothetical, to show the reduction the preoperculum and operculum, formation of the tympanic membrane and transformation of the hyomandibular into the stapes, extracolumella and ceratohyal; C, composite figure, with data from specimens, Sawin, Romer and Witter. Data on hyoid from Eaton, Westoll, after W. K. Parker. In the fish (A) the hyomandibular articulates with the upper side of the otic region above the auditory prominence; in the tetrapods its homologue, the stapes (columella auris) has shifted its ventral process downward and forward to a point below the auditory prominence, which becomes the site of the fenestra ovalis. With the loss of the bony operculum, the membranous residue gave rise to the tympanic membrane and the opercular process of the hyomandibular was perhaps specialized as the extracolumella. The relatively large size of the frog's tympanic membrane is probably the phylogenetic result of acceleration of growth in the embryo stages.

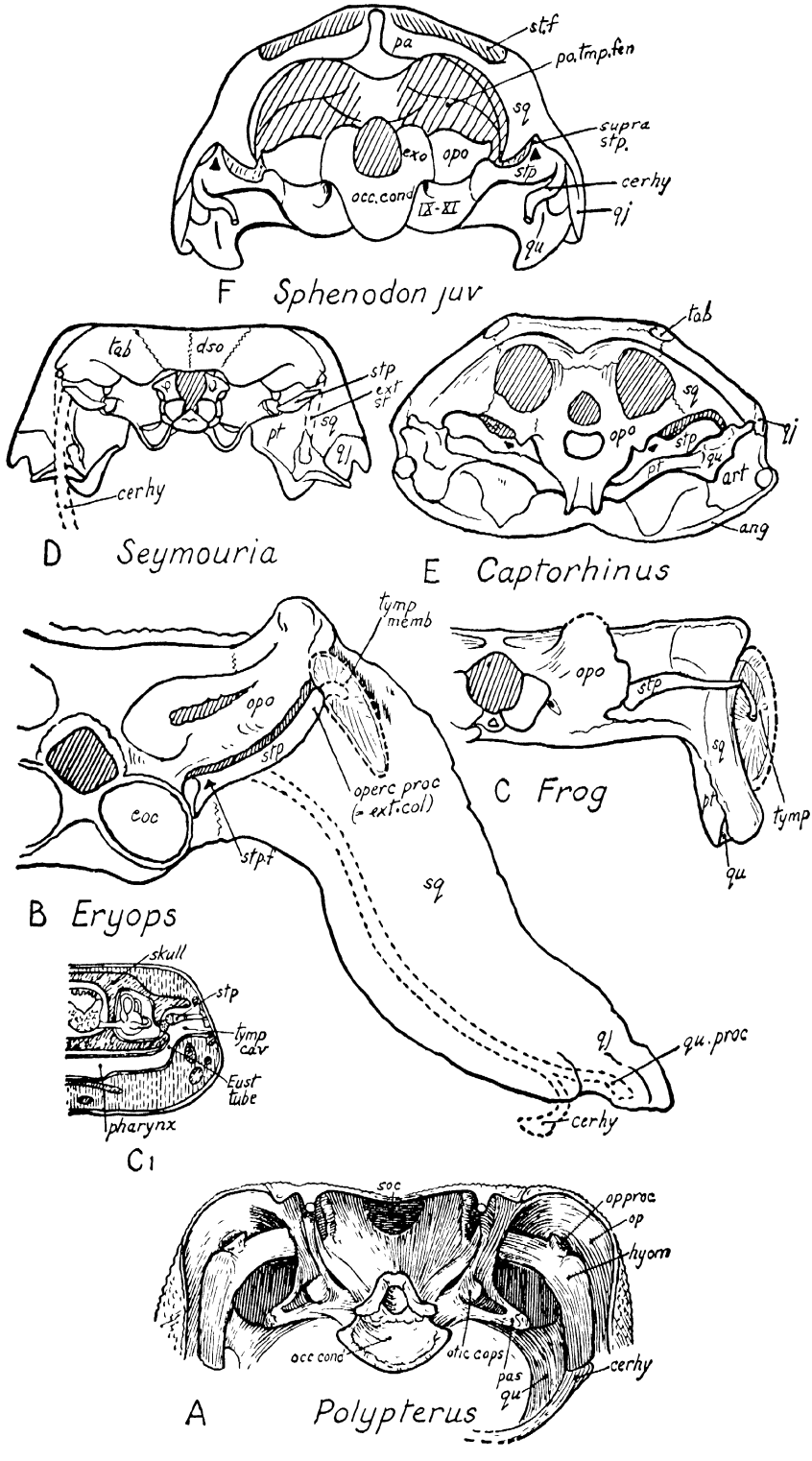

st.f
pa
po.tmp.fen
sq
supra stp.
exo
opo
stp
cerhy
occ.cond
IX-XI
qj
qu
F Sphenodon juv
tab
dso
stp
ext st
pf
sq
qj
cerhy
D Seymouria
tab
sq
opo
stp
qu
qj
pf
art
ang
E Captorhinus
tymp memb
opo
stp
coc
operc proc (= ext.col)
stpt
sq
B Eryops
opo
stp
sq
pf
tymp
qu
C Frog
skull
stp
tymp cav
Eust tube
pharynx
C1
qj
qu.proc
cerhy
soc
occ cond
otic caps
pas
qu
opproc
op
hyom
cerhy
A Polypterus

Fig. 16.52

Fig. 16.52. Hyomandibular into stapes (continued). Occipital views. A, original; B, original but with data on hyoid from Eaton and from Westoll; C, after T. J. Parker and W. N. Parker; C1, original; D, after T. E. White but with ceratohyal dotted on; E, after Sushkin, Romer and Price; F, after Howes and Swinnerton. A, Primitive surviving ganoid fish, with very large hyomandibular above and in front of the otic capsule. Note the opercular process carrying the operculum. B, Permian amphibian (labyrinthodont). The hyomandibular has shifted its ventral attachment downward and inward and has been transformed into a stapes, while the operculum has given place to the tympanic membrane. The opercular process of the hyomandibular has been transformed into the extracolumella (extrastapedial). In certain labyrinthodonts a long groove on the back of the squamosal seems to indicate (Bystrow, Westoll) the direction of the greatly prolonged quadrate branch which is continuous below with the hyoid cornu (stylohyal or ceratohyal). In amphibians (B, C) the stapes usually points outward and partly upward to the center of the tympanic membrane, which is far above the articular region of the quadrate. In adult reptiles, on the other hand, the stapes is usually directed outward and downward (fig. 16.53 A, B) toward the lower end of the quadrate. But in the primitive cotylosaur (fig. 16.52 D) the direction of the stapes was somewhat upward as in amphibians. In the progressive captorhinomorph cotylosaur (E) the direction of the stapes is outward and partly upward as it is in the embryo *Sphenodon* (F).

Fig. 16 53. Relations of the stapes to the quadrate and adjacent parts in pelycosaurs (A, B) and therapsids (C–E). A, B, after Romer and Price; C, D, after Broom; E, from Gregory, modified from Sushkin. In the pelycosaurs (A, B) the very large stapes had inherited the essential features of a hyomandibular, save that its attachment to the skull had shifted to the latero-ventral surface beneath the otic region It was still fastened by cartilage or ligament to the stapedial process of the quadrate, but the tympanic membrane must have been minute or absent and hearing may have been effected by means of bone conduction. In the gigantic dinocephalians (C) the stapes was still massive, but in the small therocephalian (D) it was a delicate rod, bearing at its outer distal end an upturned extrastapedial process. The latter was probably inserted into the small tympanic membrane, whose position and form seem to be indicated by the curved medial border of the squamosal (Broom) In the primitive cynodont (E) the stapes seems to have been connected by one distal process with the quadrate and by another (extracolumella) with the tympanic membrane.

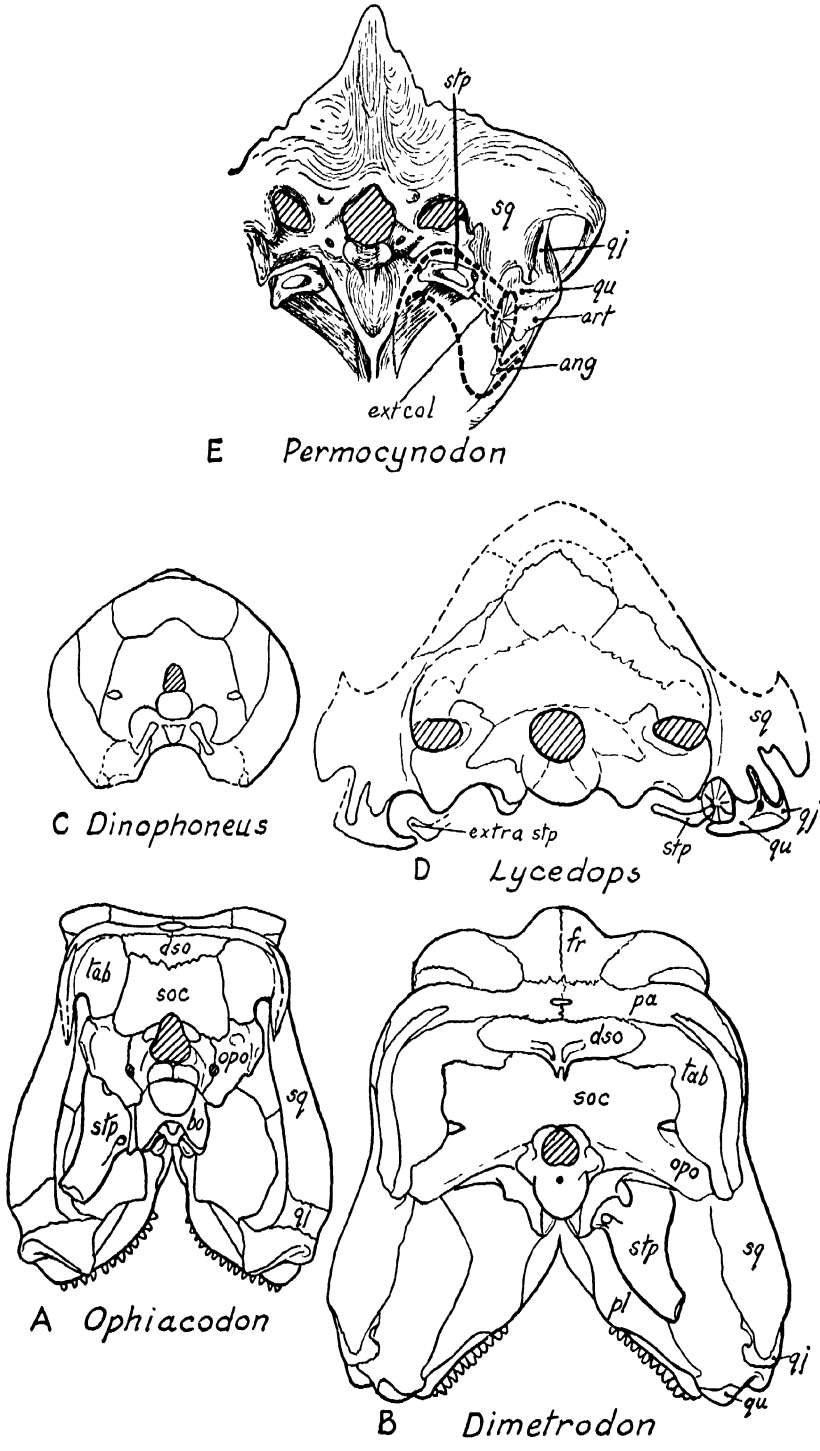

stp
sq
qj
qu
art
ang
extcol
E Permocynodon
C Dinophoneus
extra stp
stp
sq
qj
qu
D Lycedops
dso
tab
soc
opo
sq
stp
bo
qj
A Ophiacodon
fr
pa
dso
tab
soc
opo
stp
sq
pl
qj
qu
B Dimetrodon

Fig. 16.53

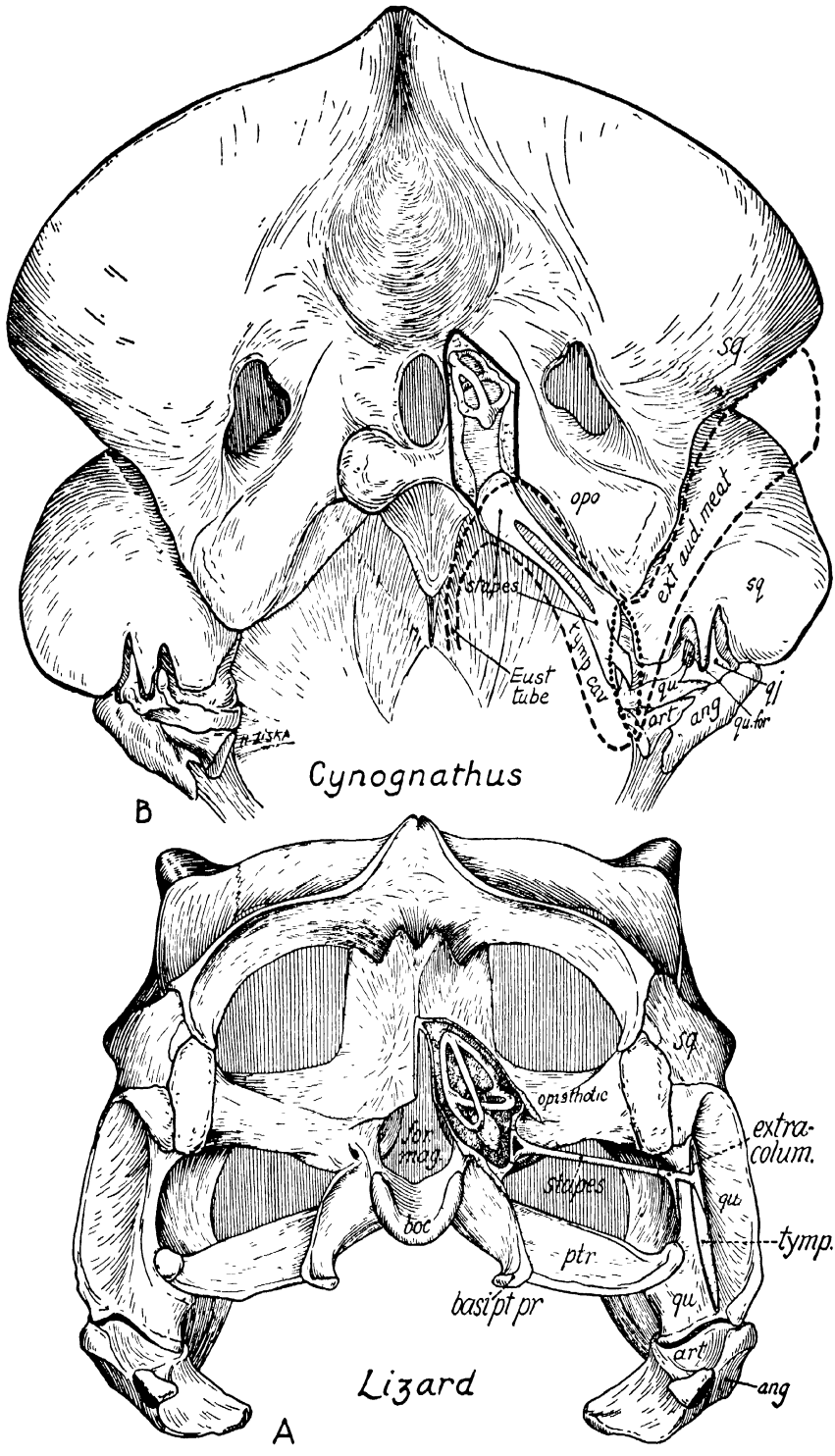


Fig. 16.54 a, b. Relations of the middle ear to the inner ear, lower jaw and skull in typical reptile (A), cynodont (B), marsupial (C) and man (D). Modified from Gregory. Data on inner ear of cynodont from Olson; data on tubotympanal diverticulum partly from Westoll.

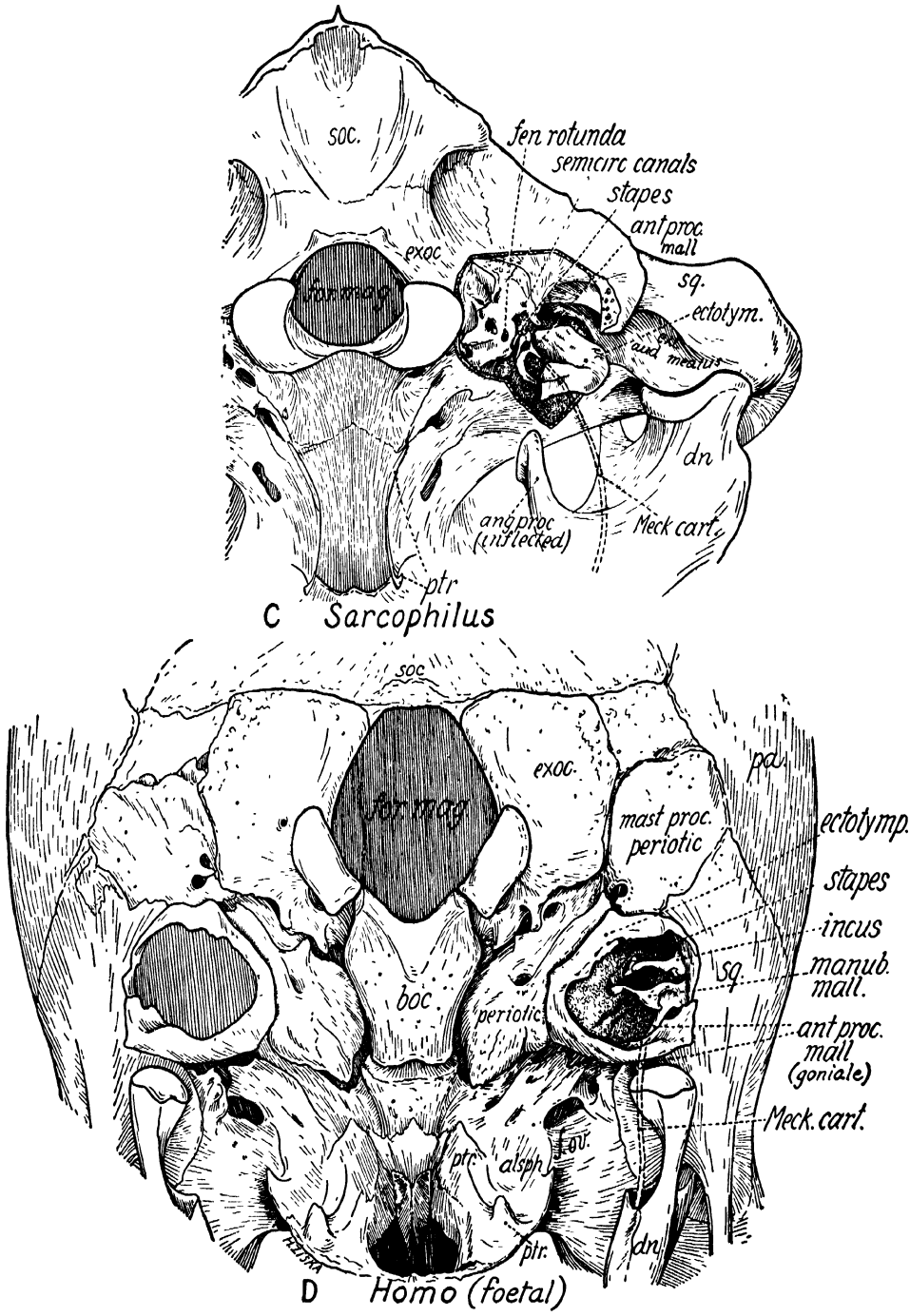

soc.
fen rotunda
semicirc canals
stapes
ant proc mall
exoc.
for mag.
sq.
ectotym.
aud meatus
dn
ang proc (unfleched)
Meck cart.
ptr
C Sarcophilus
soc
exoc.
for mag
pd.
mast proc. periotic
ectotymp.
stapes
incus
manub. mall.
sq.
boc
periotic
ant proc. mall (goniale)
Meck. cart.
ptr.
alsph.
for.
ptr.
dn
D Homo (foetal)

Fig. 16.54b

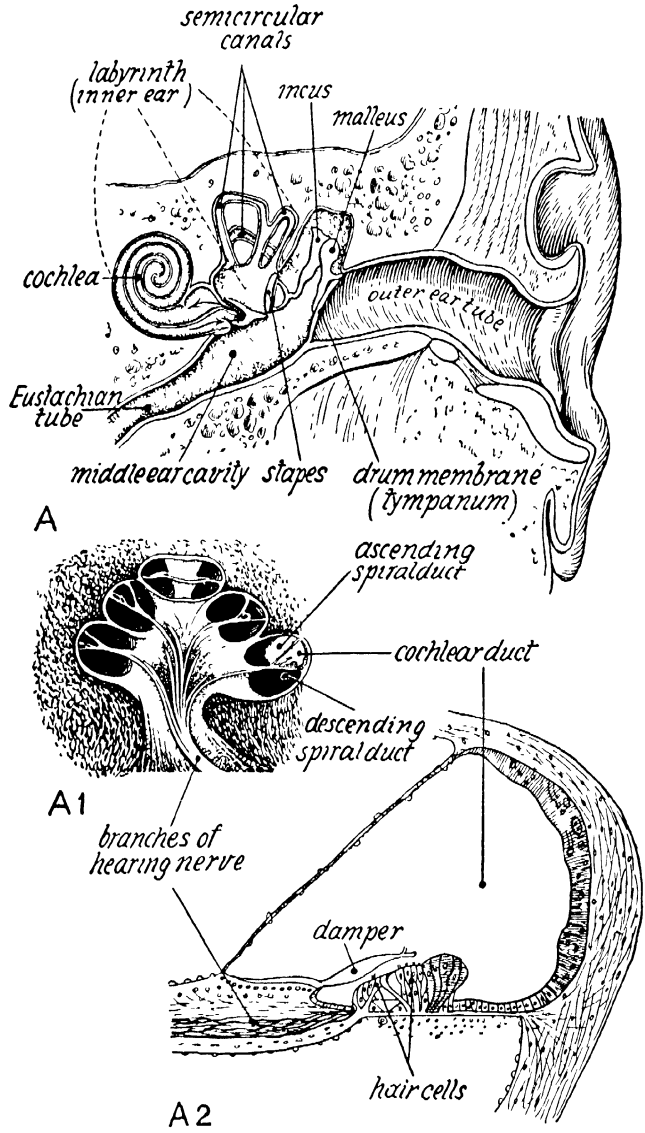


Fig. 16.55a, b. The human organ of hearing. After Cunningham (1903). A, Diagrammatic cross-section of the left side, seen from in front. The tympanum or drum membrane separates the external auditory meatus from the tubo-tympanal cavity of the middle ear containing the auditory ossicles. These ossicles are suspended by several ligaments from the roof and sides of the epitympanic recess or attic. They collectively reduce the amplitude of the vibrations received from the tympanic membrane. The handle of the malleus, embedded in the tympanic membrane, is a lever which transmits the movement of the membrane through the body of the malleus and the cog-tooth articulation to the incus. The latter, through its long process, passes on the vibrations to the head of the stapes, which in turn transmits its pulsations through its foot plate to the endolymph, or fluid that fills the inner ear. These pulsations in the fluid run up the

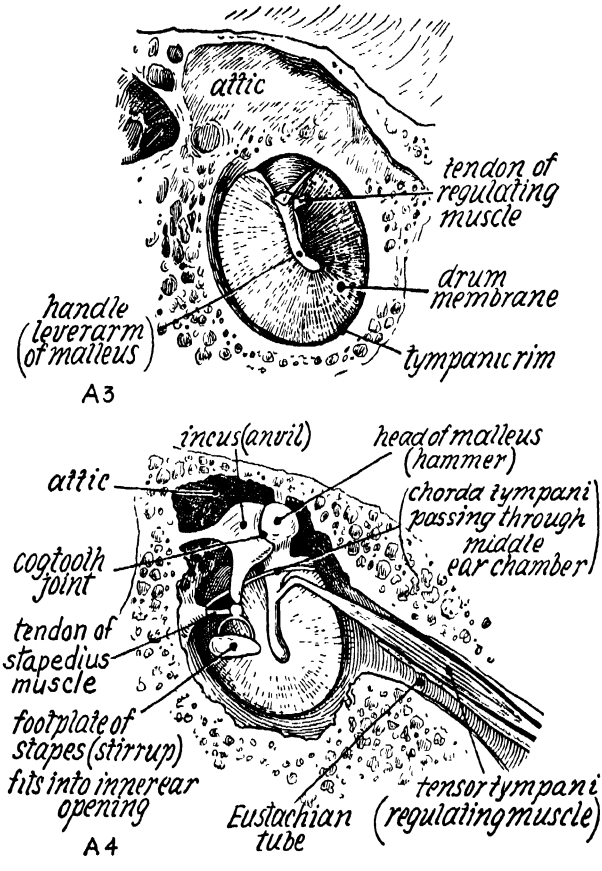


Fig. 16.55b

cochlear duct, disturbing the delicate sensory hairs, which in turn transmit nervous impulses through the acoustic nerve to the auditory parts of the brain.

When the tensor tympani or regulating muscle contracts, it draws inward the handle of the malleus and so renders tense the tymphanic membrane. The stapedius muscle tends to tense the annular ligament which surrounds the foot plate of the stapedius and attaches the latter to the petrous or inner ear-bone. In extremely large movements of the tympanic membrane the forcible dragging of the foot of the stapes out of the fenestra ovalis is prevented by the gliding of the incus upon the malleus at the cog-tooth joint (Cunningham).

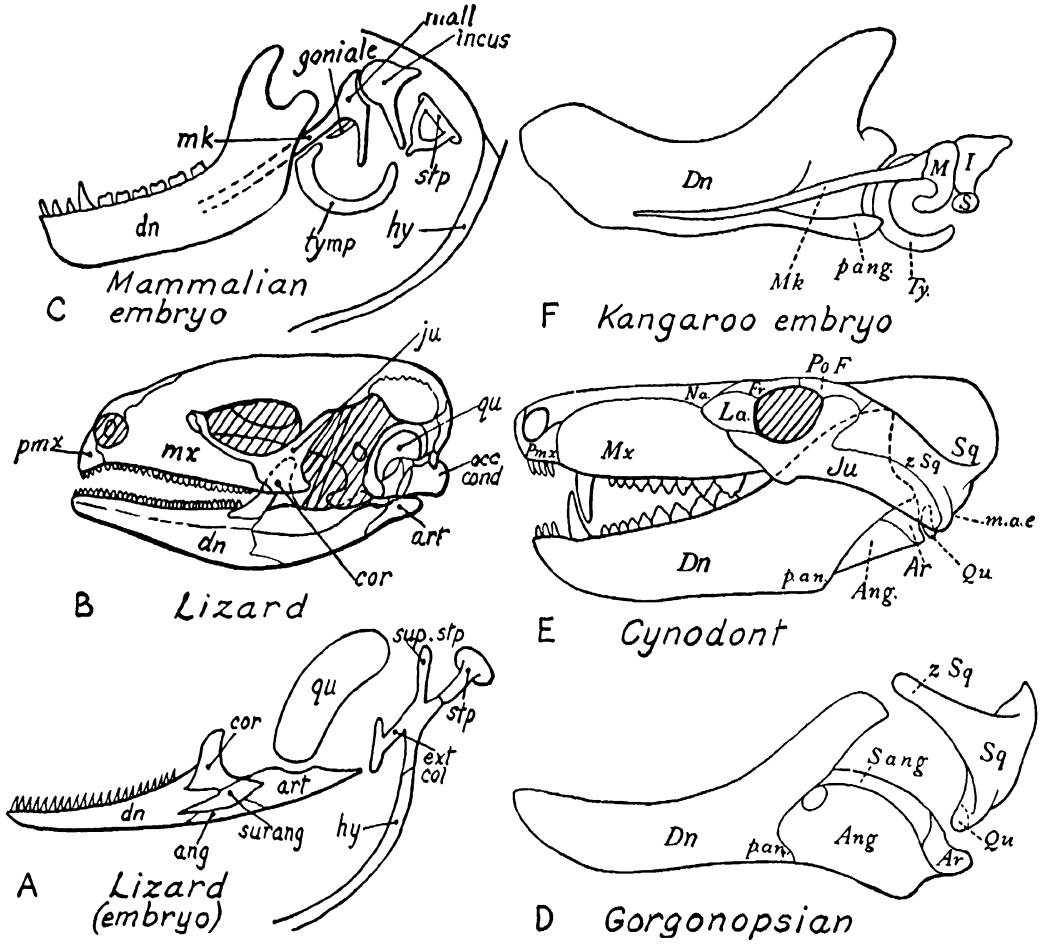


Fig. 16.56. Two different applications of the Reichert theory of the origin of the mammalian incus and malleus. A–C, by Gaupp (1905, 1913), from a streptostylic reptilian stage, best represented today by the lizard; D–F, by Gregory (1910), from a cynodont reptile stage (E) of Triassic age; F, after Bensley.

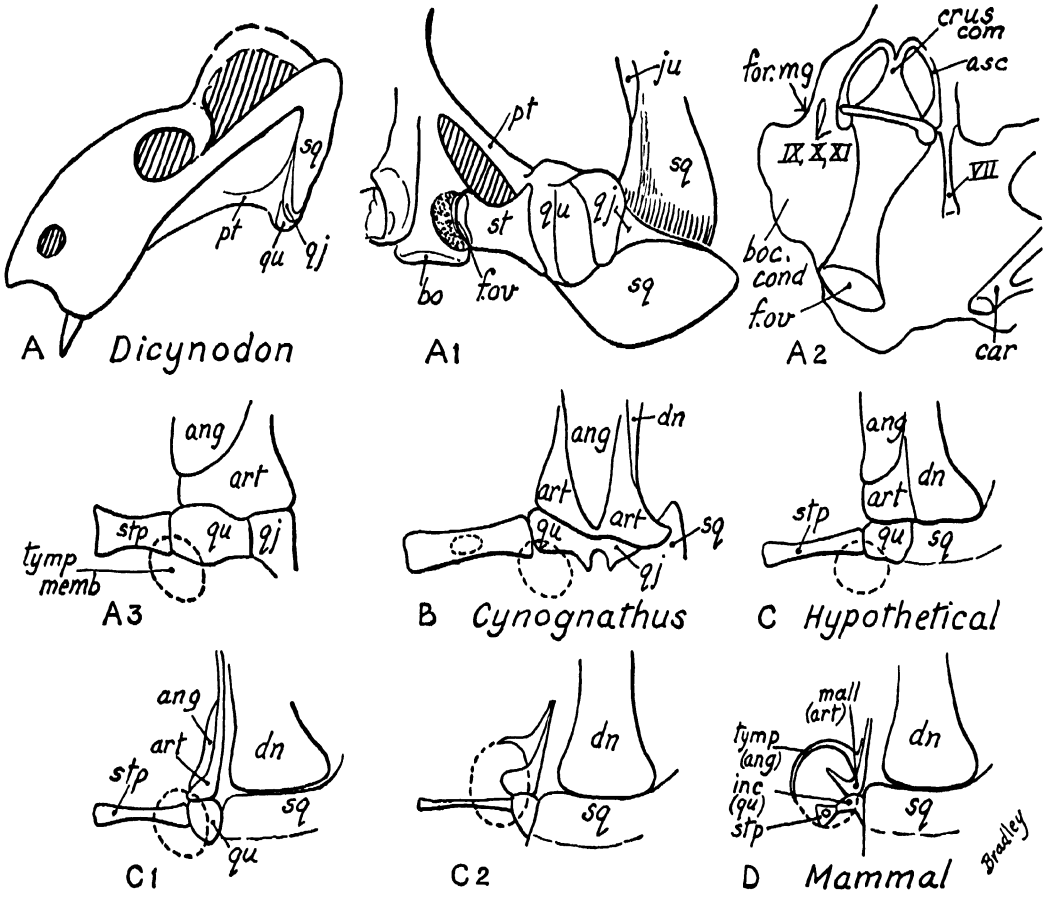


Fig. 16.57. A–A2, Broom's proof that the bone which he had formerly called tympanic was really a stapes; A3–D, Broom's conception of the stages of the transition from *Cynognathus* (B) to mammal (D).

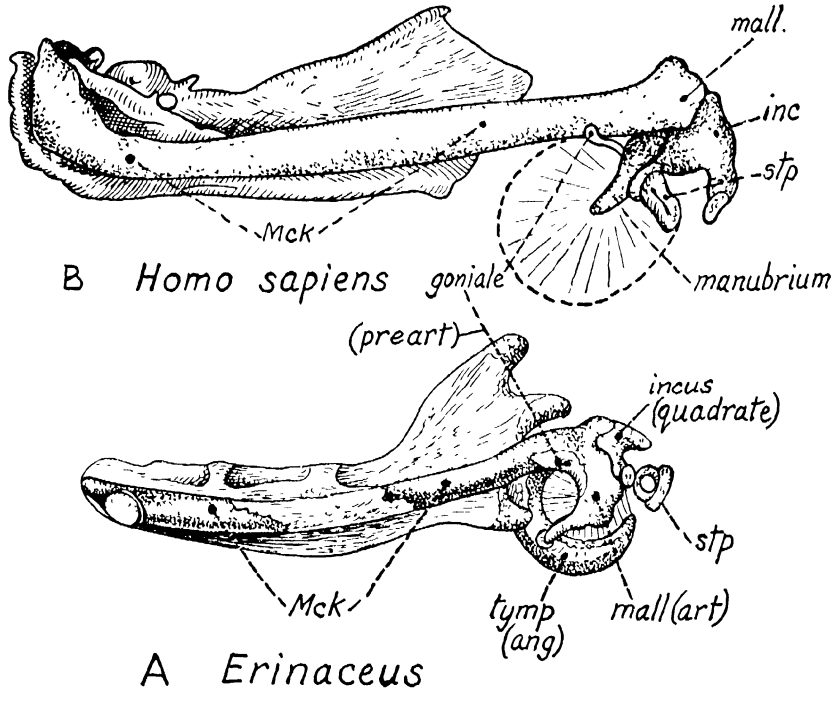


Fig. 16 58 Evidence from embryology for the Reichert-Gaupp theory. A, after W K Parker; B, after Macklin. Showing the derivation of the malleus from the articular portion of Meckel's cartilage in an insectivore (A) and in man (B). After Gregory

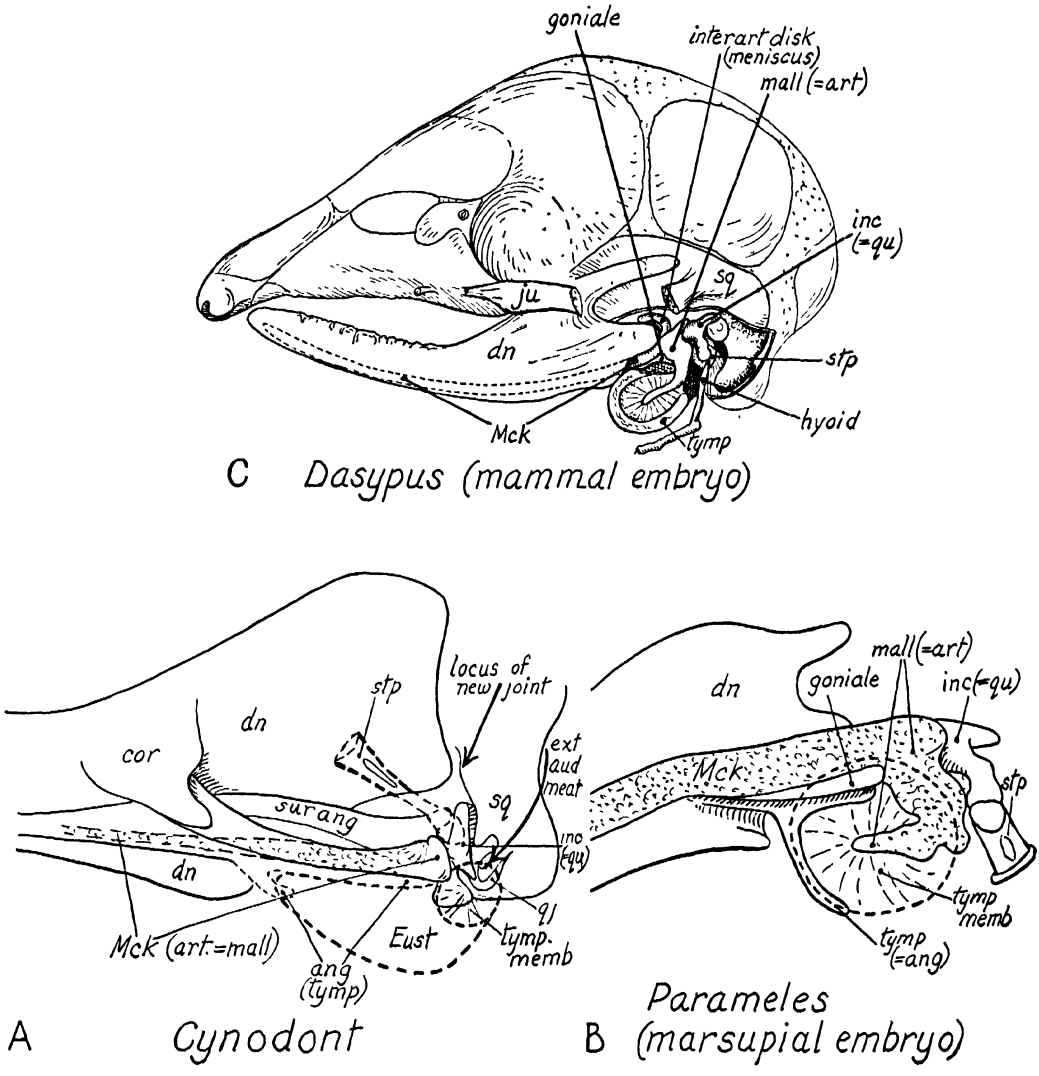


Fig. 16.59. Jawbones into ear bones. Modified from Gregory. A, Medial aspect of right jaw-joint in *Cynognathus* (semidiagrammatic), showing old reptilian jaw-joint (between the articular and the quadrate) still functioning as such, while the ascending ramus of the dentary is nearly in contact with the squamosal (temporal) to form the new temporomandibular jaw-joint. The tympanic membrane, as in fig. 16.54, is represented as separating the membranous external auditory meatus from the supposed auditory diverticulum of the tubo-tympanal (Eustachian) tube. B, Diagram based on Palmer's figure of the malleo-incudal region in a foetal marsupial (*Perameles*). At this stage the tympanic ring (*tymp*) is in the form of a short stem with an expanded fork, which suggests the posteriorly notched angular of cynodonts (A). The goniale or anterior process of the malleus was thought by Gaupp to be the homologue of the prearticular of reptiles but has been shown by later workers (fig. 16 62) to arise as part of the tympanic. The cog-tooth articulation between the malleus and the incus is the homologue of the old jaw-joint between the quadrate and the articular (A). C, Relations of the auditory ossicles to the lower jaw in a foetal armadillo. Composed from several figures in W. K. Parker.

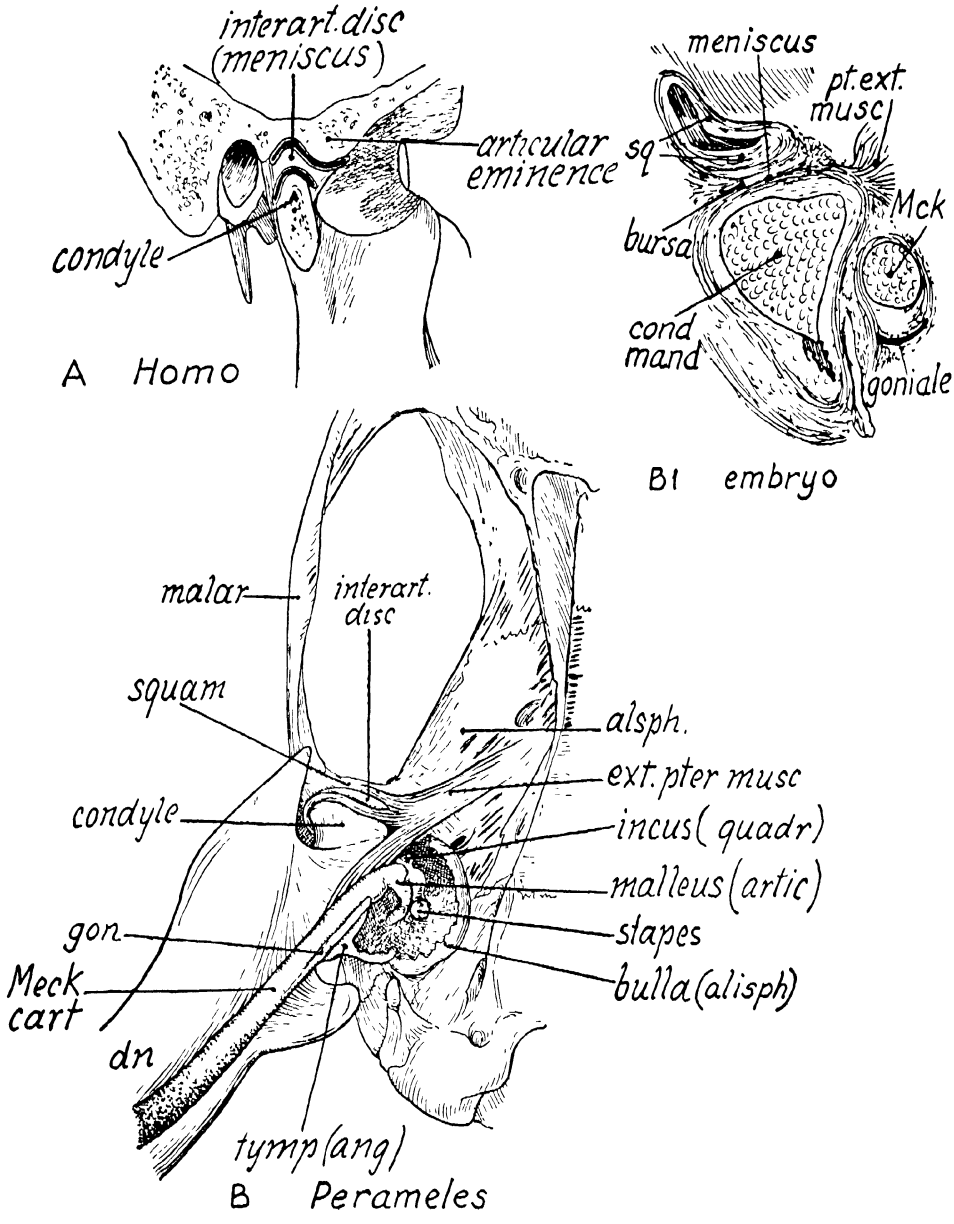


Fig. 16.60. The meniscus or interarticular disc in man (A) and in a marsupial (B, B1). After Cunningham (A), Palmer (B), Gaupp (B1). A, shows the buffer-like character of the meniscus in man; B, reconstruction of the relations of the pterygoid muscles to the lower jaw, including Meckel's cartilage, in an adult marsupial. B1, Relations of the external pterygoid muscle to the mandibular condyle in an embryo marsupial in transverse vertical section. Between the growing mandibular condyle and the squamosal, a bursa or sac forms in the midst of part of the external pterygoid muscle. This sac forms the core or nucleus of the meniscus. The condylar cartilage (*cond.mand.*) is a "secondary cartilage" formed at the growing end of the ascending ramus of the dentary bone. Meckel's cartilage (Meck), on the contrary, is a "primary cartilage" inherited from the earliest vertebrates. The part here shown will give rise to the malleus, while the derm bone beneath it (*goniale*) will give rise to the anterior process of the malleus.

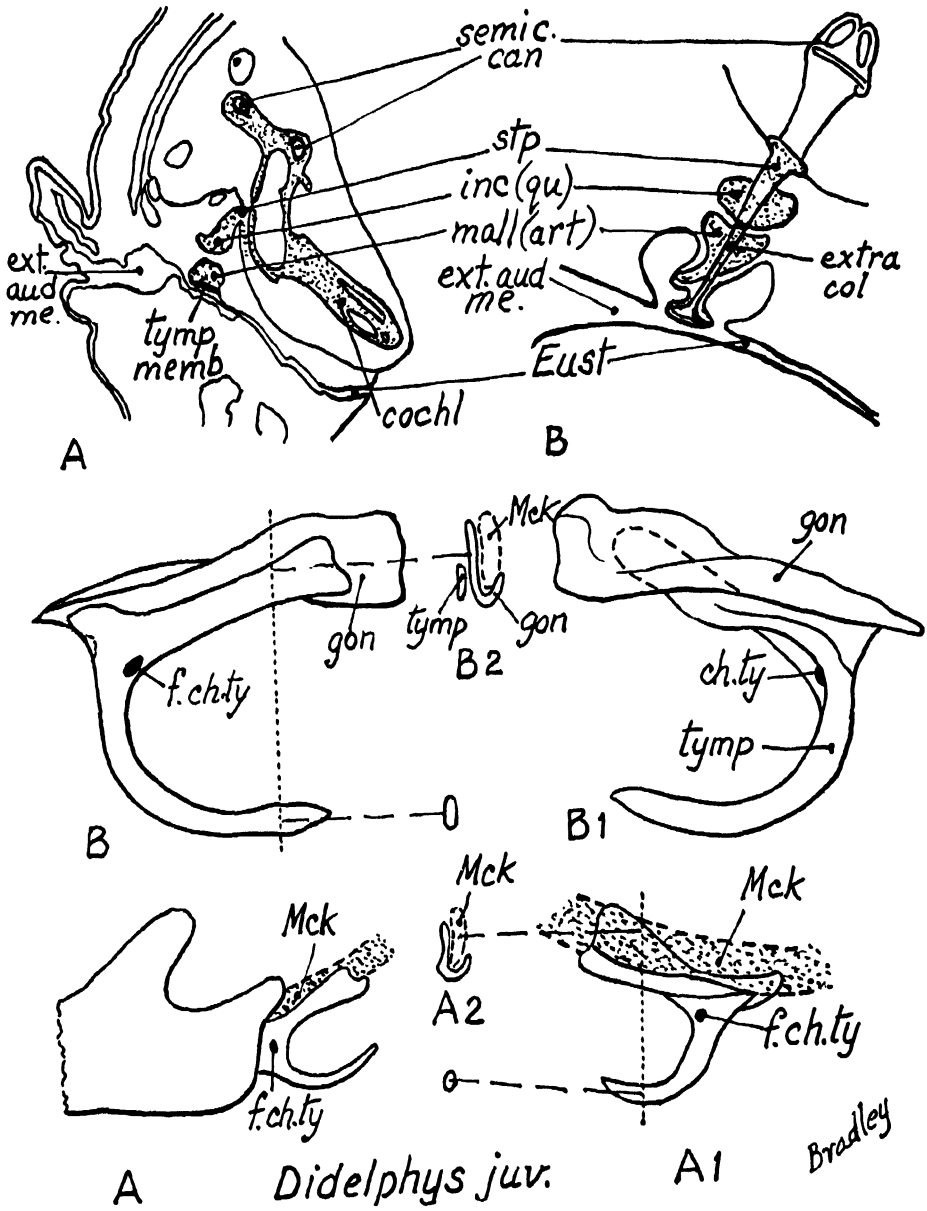


Fig. 16.61 (top). Relations of the tubo-tympanal (Eustachian) canal and its diverticula to the middle and inner ear in a human embryo (A) and inferentially in a mammal-like reptile (B). Modified from Gregory. A, after Minot.

Fig. 16.62. Relations of the tympanic bone to the dentary in a young opossum. Slightly modified from Olson. A, Lateral view of left jaw (15-day pouch young). The tympanic bone has the relations of the cynodont angular. The posterior fork supports the tympanic membrane. A1, Medial view of same, showing the foramen for the chorda tympani nerve. A2, Cross-section (on level of vertical line in A1) showing one undivided bone embracing the Meckel's cartilage. B, B1, Same parts in 22-day pouch young. B2, Cross-section showing tympanic separated from goniale.

Fig. 16.63. Three suggested stages (diagrammatic) in the evolution of the mammalian middle ear from an advanced theriodont (a cynodont). After Westoll. In A, the mandibular recess of the tubo-tympanal (Eustachian) canal has filled the posterior notch or fork of the angular. The surface skin may have already begun to serve as a new drumhead or tympanic membrane, transmitting its vibrations through the angular and small quadrate bones to the stapes. To the latter was attached by way of its extracolumella the dwindling old tympanic membrane inherited from reptilian ancestors. The chorda tympani nerve, looping around the stylohyal, passes above the extracolumella and beneath the quadrate to perforate the goniale, as in reptiles. In stage B, the mandibular recess is becoming larger and the angular bone is nearly all transformed into the tympanic The retroarticular process of the articular is giving rise to the handle of the malleus, the extrastapedial is becoming slender and the old reptilian tympanic membrane and its cavity are closely approaching the new tympanic membrane and the mandibular recess. In stage C, the old and new tympanic cavities and membranes are virtually united, the old membrane becoming Shrapnelli's membrane. (*MEMS.*). Meanwhile the last vestiges of the extracolumella (*E ST.*) are seen in Spence's cartilage (*S C.*) and Paauw's cartilage (*P.C.*). *A.*, articular; *ANG.*, angular; *C M*, caput mallei; *COND*, condyle of dentary, *CR B.*, crus brevis; *CR.L.*, crus longus; *CT.*, chorda tympani; *D*, dentary; *E.ST.*, distal part of extrastapes; *GON.*, gonial; *M C.*, Meckel's cartilage; *MEMS.*, membrana Shrapnelli, *M.M.*, manubrium mallei; *M.TY.*, mammalian tympanum; *M TY.*(D), developing mammalian tympanum; *P.C*, Paauw's cartilage; *P.C.H F.*, posterior "Chordafalte"; *Q*, quadrate (incus of mammals); *RAP*, retro-articular process; *REC M.*, recessus mandibularis; *R.TY*, reptilian tympanum; *S.C*, Spence's cartilage; *SH*, stylohyal, *S.M.*, stapedial muscle; *ST.*, stapes, *TY*, tympanic bone; *VII*, facial nerve.

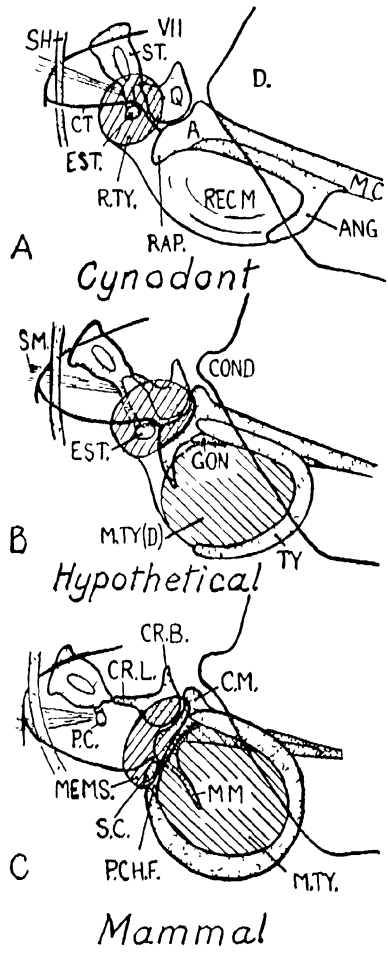


Fig. 16.63

➔Fig. 16.64 (facing page). Gill-bars into ear bones —from fish to man. All figures from de Beer. In the fish (A) even the primary jaws (palatoquadrate, Meckel's cartilage) are in series with and homologous with the hyoid and branchial arches. Here too the hyomandibular or upper part of the second or hyoid arch serves as a suspensor for both the upper and the lower jaws; it also supports the operculum or cover of the gill chamber. In the lower tetrapods (B, C) the hyomandibular has been transformed into the stapes; the lower segment of this arch cooperates with the remnants of the branchial arch to form the skeletal base for the larynx or voice box. In mammals (D–G) the stapes retains its function but the quadrate and the proximal part of Meckel's cartilage were gradually relieved of their jaw fuctions and became the malleus and incus.

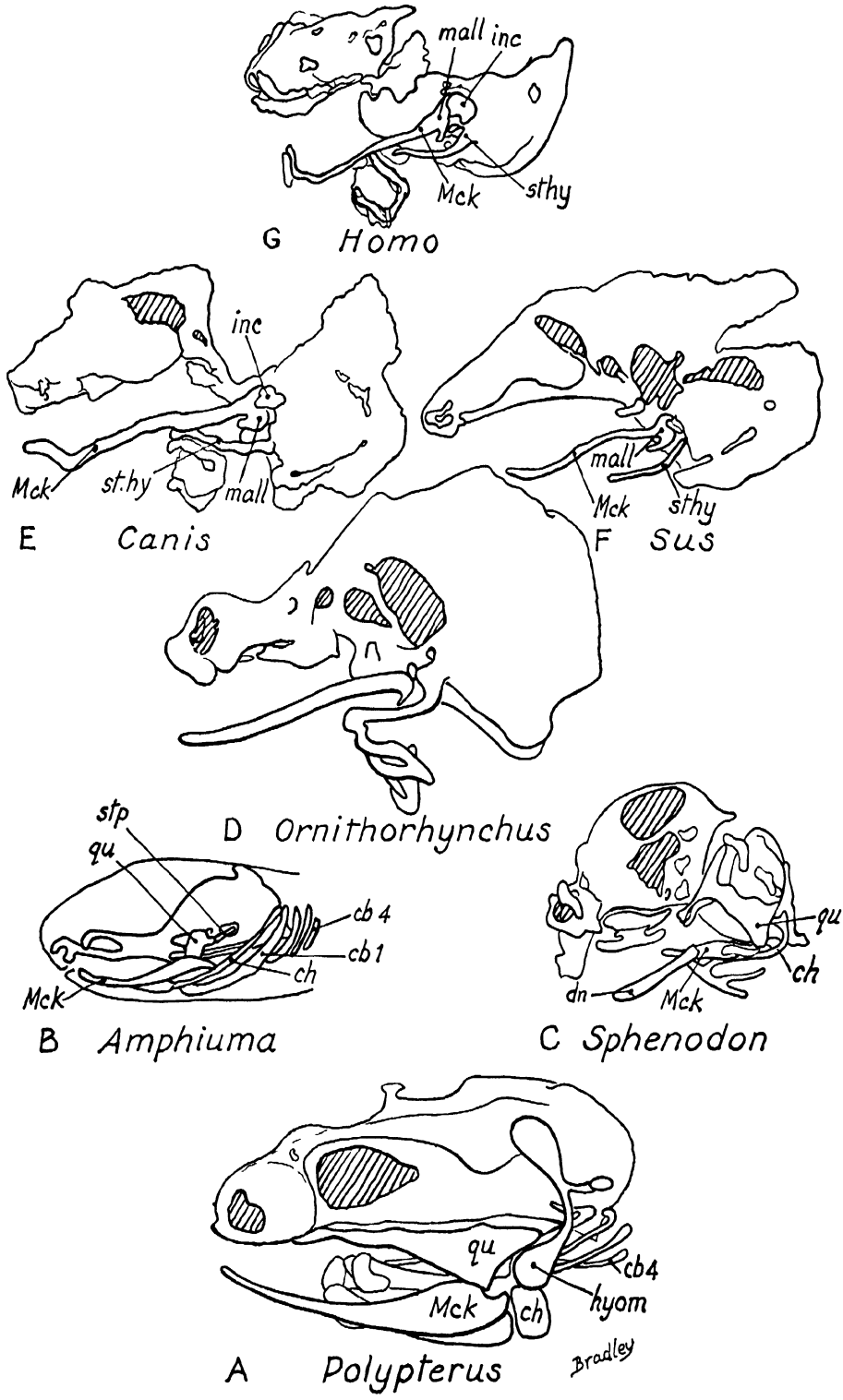

mall
inc
Mck
sthy
G Homo
inc
Mck
st.hy
mall
E Canis
mall
Mck
sthy
F Sus
D Ornithorhynchus
stp
qu
cb 4
cb 1
ch
Mck
B Amphiuma
qu
ch
dn
Mck
C Sphenodon
qu
cb4
hyom
Mck
ch
A Polypterus
Bradley

Fig. 16.64

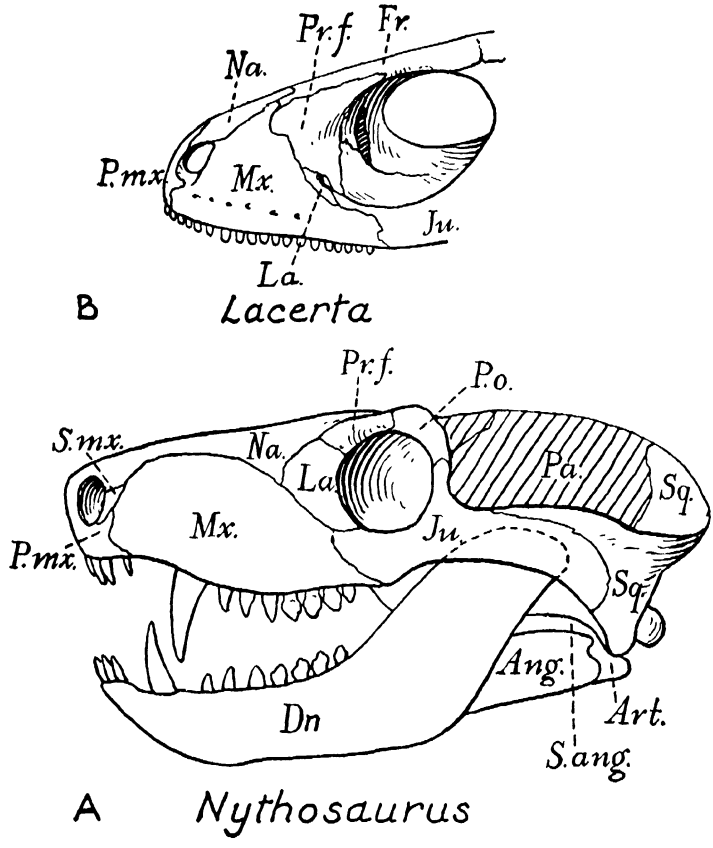


Fig. 16.65. The lacrimal (*La*) of cynodont (A) and lizard (B). From Gregory after Gaupp; B, after Broom. Gaupp transferred the name *lacrimal* to the prefrontal of the lizard and other reptiles, proposing the name *adlacrymal* for the little bone that had been called lacrimal (*La*). But in the cynodont, which is more nearly related to the mammal than is the lizard, the prefrontal and lacrimal are both well developed and the latter has its normal mammalian contacts.

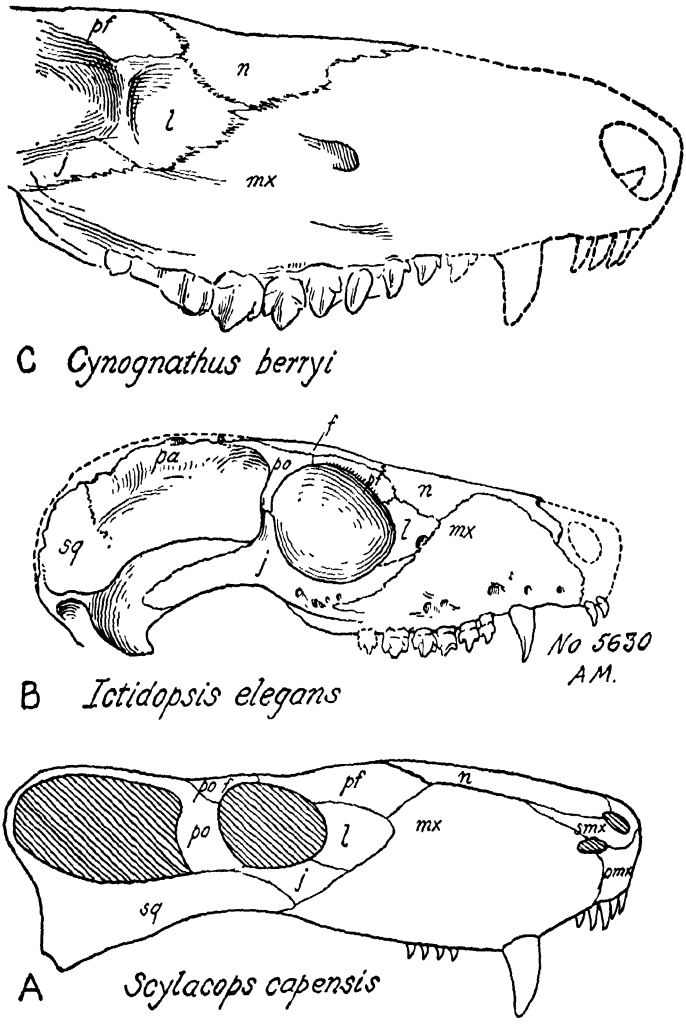


Fig. 16.66. The lacrimal region in a therocephalian (A) and two cynodonts (B, C). From Gregory. A, after Broom; B, from specimen; C, after Seeley.

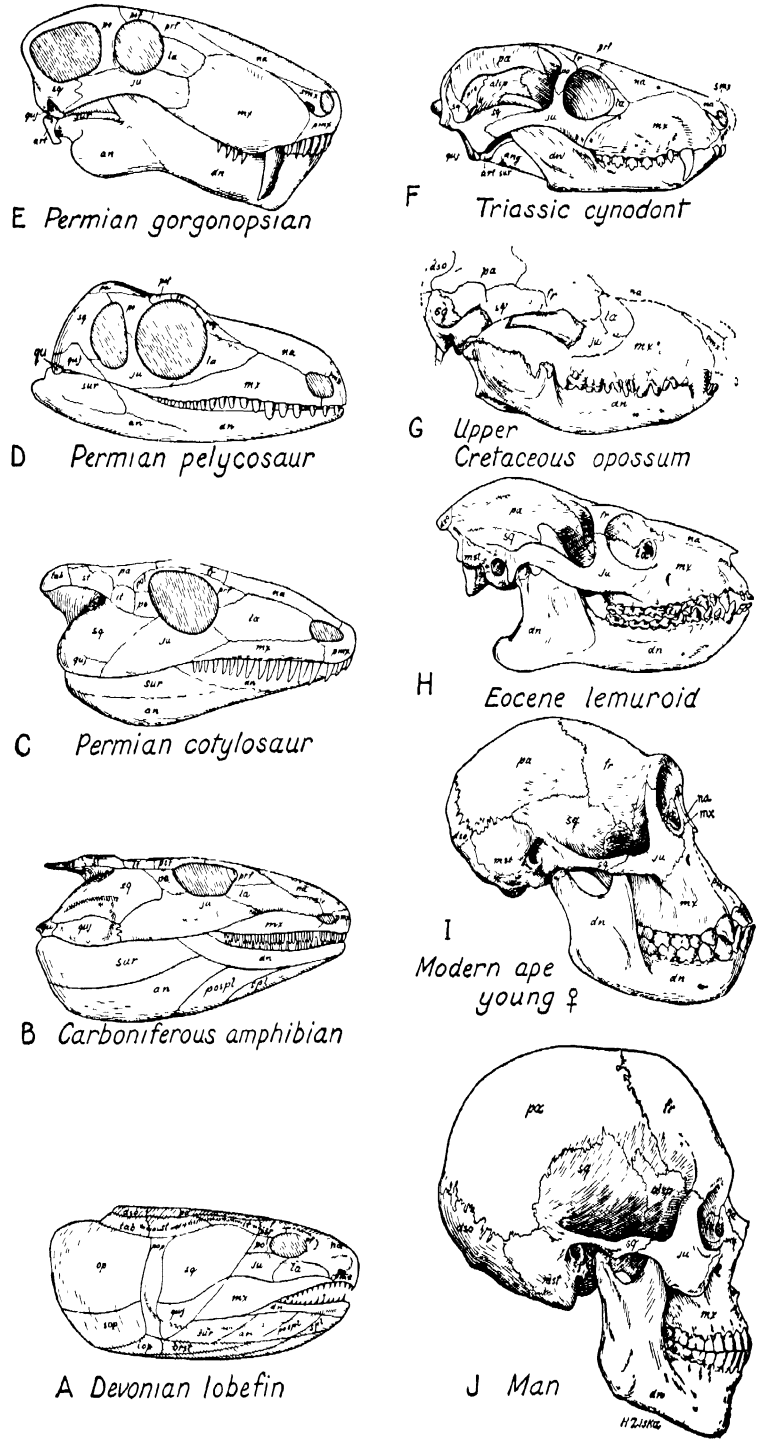


Fig. 16.67. The skull from fish to man in ten structural stages. After Gregory.

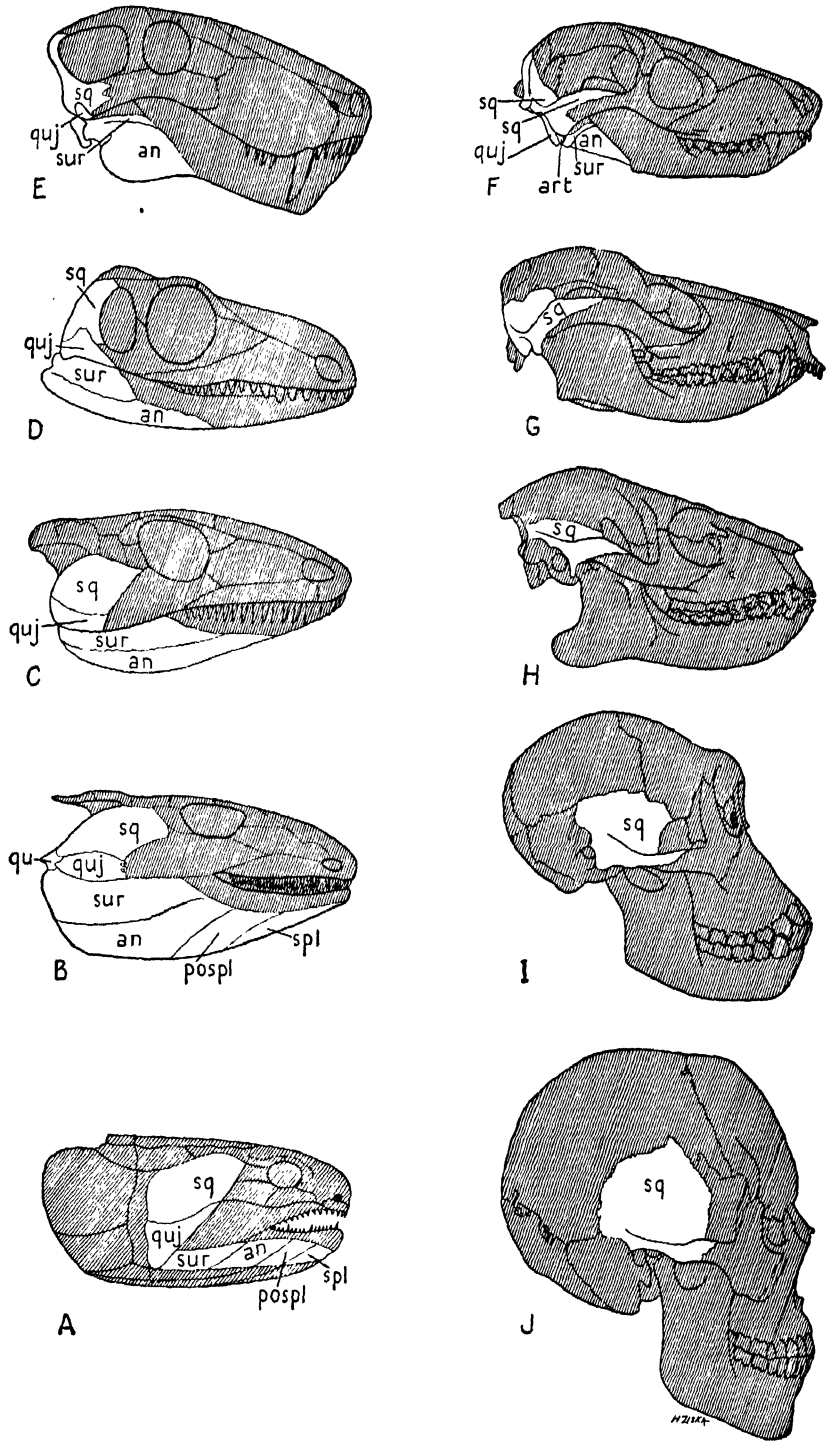


Fig. 16.68. The skull from fish to man (continued). Evolution of the temporo-mandibular bones behind the maxilla and dentary.

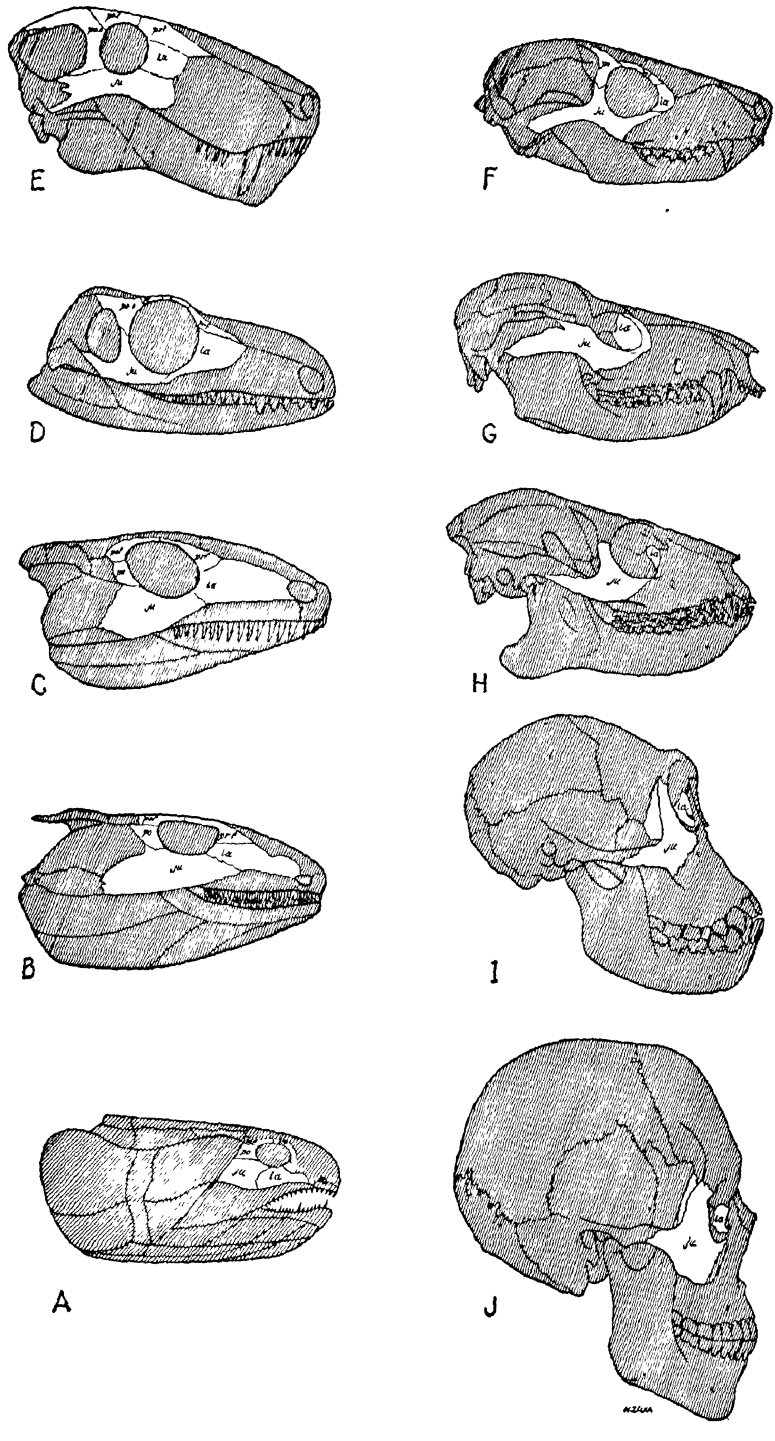


Fig. 16.69. The skull from fish to man (continued). *Evolution of the circumorbital series.* Originally including five or six bones around the orbit, the series loses the postfrontal in the cynodonts and the prefrontals and postorbitals in the mammals. Eventually the lacrimal lost contact with the jugal but remained on the inner corner of the eye.

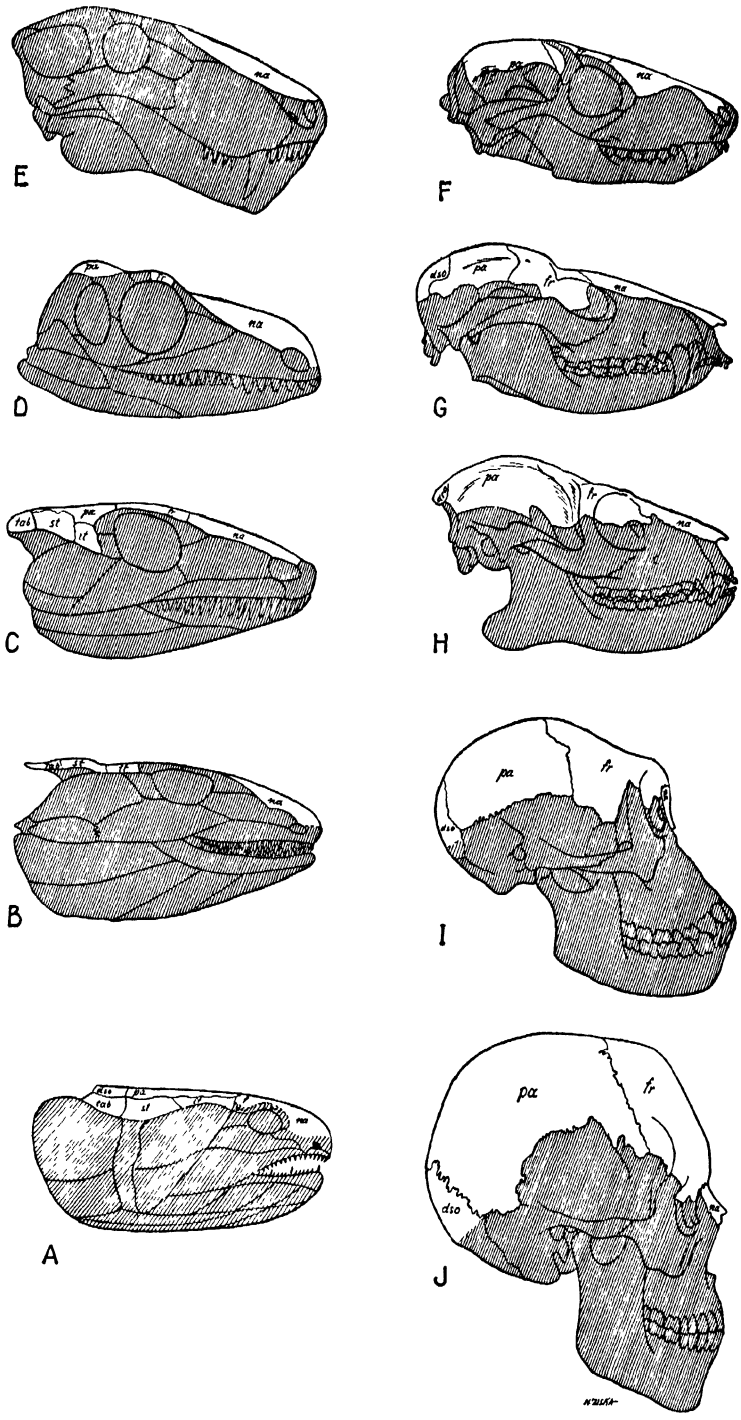


Fig. 16.70. The skull from fish to man (continued). In the fish the lateral margin of the cranial table is covered by a series of three bones (intertemporal, supratemporal, tabular). These persist in the lower amphibians and stem reptiles but disappear in the mammals, thus exposing the parietals and the dermosupraoccipital in the side view. Finally (I) the upgrowth of the brain pushes up and expands the frontals and parietals to form the vaulted dome of modern man (J).

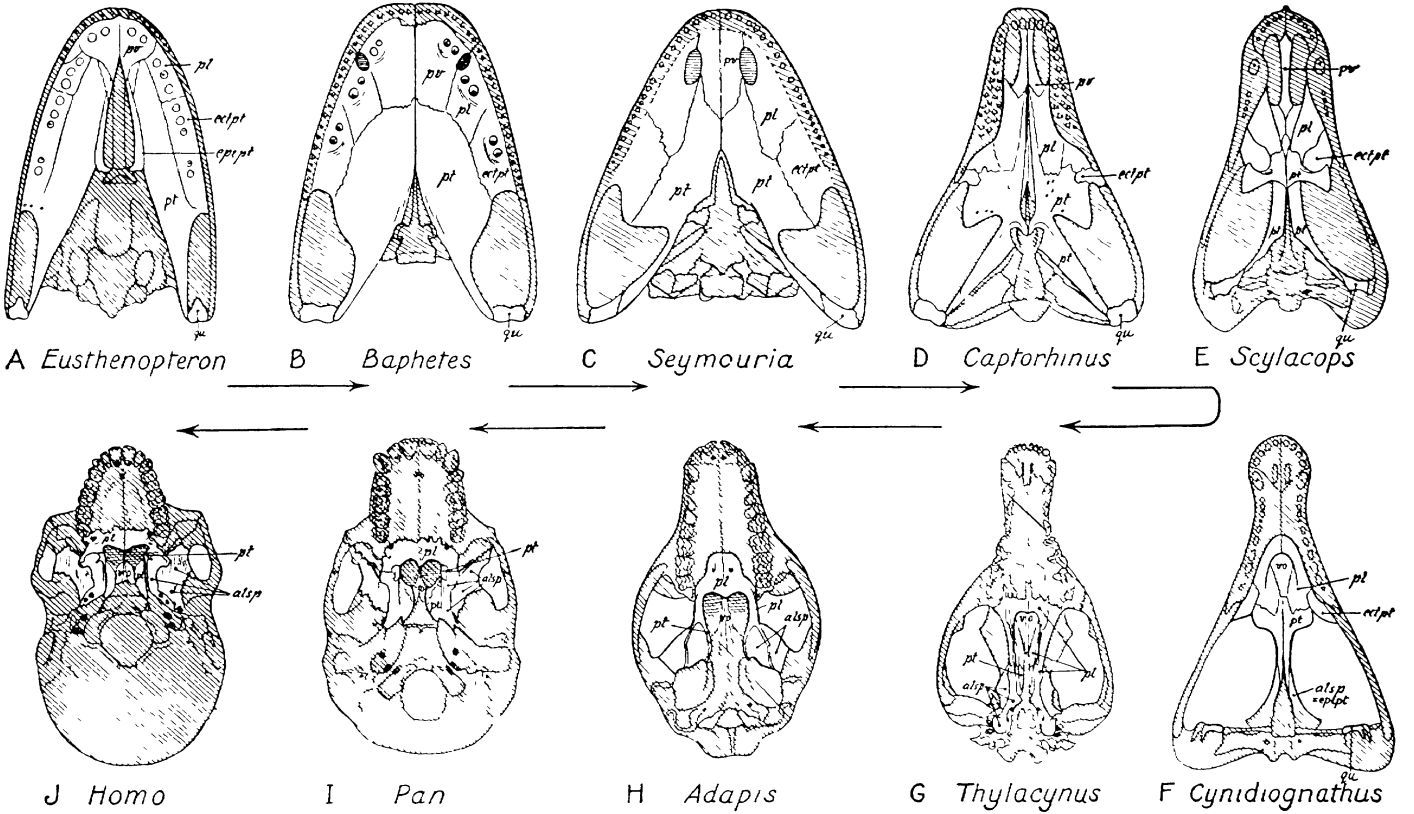


Fig. 16.71. Rise and decline of the pterygo-palato-quadrate arch in vertebrates. After Gregory. A, Devonian lobe-finned ganoid, from Watson, chiefly after W L. Bryant. B, Lower Carboniferous embolomerous amphibian, after Watson. C, Primitive Permo-Carboniferous reptile, from Watson, data from Broili, Williston, Watson. D, Advanced Permian cotylosaurian reptile, data from Broom, von Huene, Sushkin. E, Primitive Middle Permian mammal-like reptile, after Broom. F, Advanced Triassic mammal-like reptile, from Broom, after Haughton. G, Modern marsupial mammal, representing a survivor of Cretaceous marsupial stock, from specimens. H, An Eocene lemuroid primate, after Stehlin. I, Chimpanzee, representing a little modified survivor of the Miocene anthropoid stock, from specimen. J, *Homo sapiens,* represented by aboriginal Australian, survivor of Pleistocene man, after Gregory.

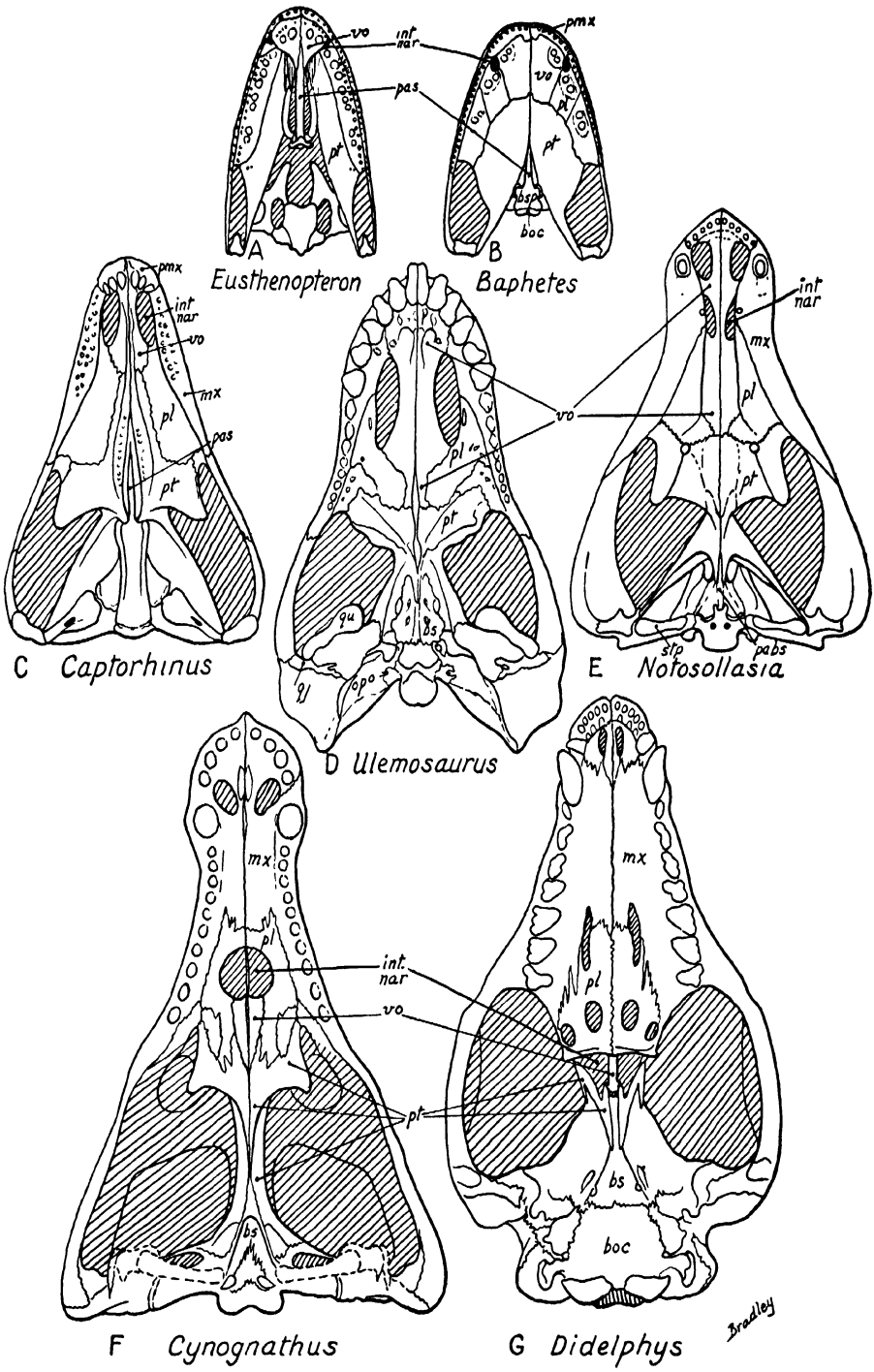


Fig. 16.72. Prevomers into vomers. According to Parrington and Westoll, the so-called prevomer of the fish (A) evolved into the true vomer of cynodonts (F) and mammals, while the parasphenoid, after bearing the stresses of part of the pterygoid system in amphibians and reptiles, became reduced, along with the postdentary bones of the jaw in the mammals.

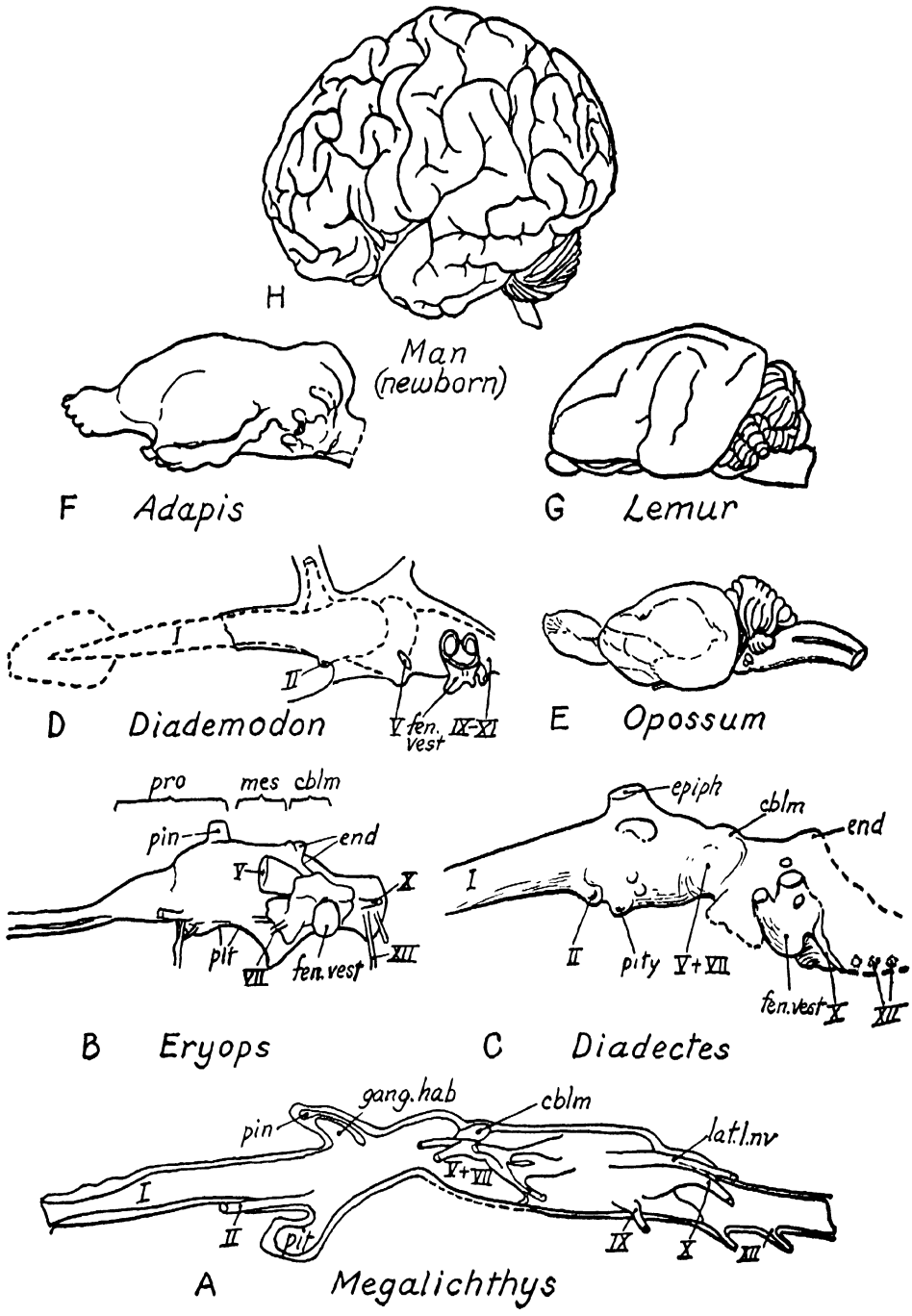


Fig. 16.73. The brain from fish to man. A, after Romer; B, after Sawin; C, original; D, after Watson; E, after Papez; F, after Le Gros Clark; G, H, after Romer. Although the brain did not fill the cavity of the braincase in the earlier forms, the "endocast" of the interior of the braincase approximates more or less to the true brain form. The series does indeed show the relatively long and tubular form of the brain in the primitive lobe-fin fish (A), the early increase in the cerebellum and the delayed lateral outgrowth of the cerebrum (E), which ultimately gives rise to the greatly folded brain of man. *Cblm*, cerebellum; *end*, endocast; *epiph*, epiphysis; *fen.vest.*, fenestra vestibuli; *gang.hab.*, ganglion habenulae; *lat.l.nv.*, lateral line nerve; *mes*, mesencephalon (midbrain); *pin*, pineal stalk (epiphysis); *pity*, pituitary; *I–XII*, cranial nerves.

CHAPTER XVII

THE DARK AGES OF MAMMALIAN HISTORY (MESOZOIC MAMMALS)

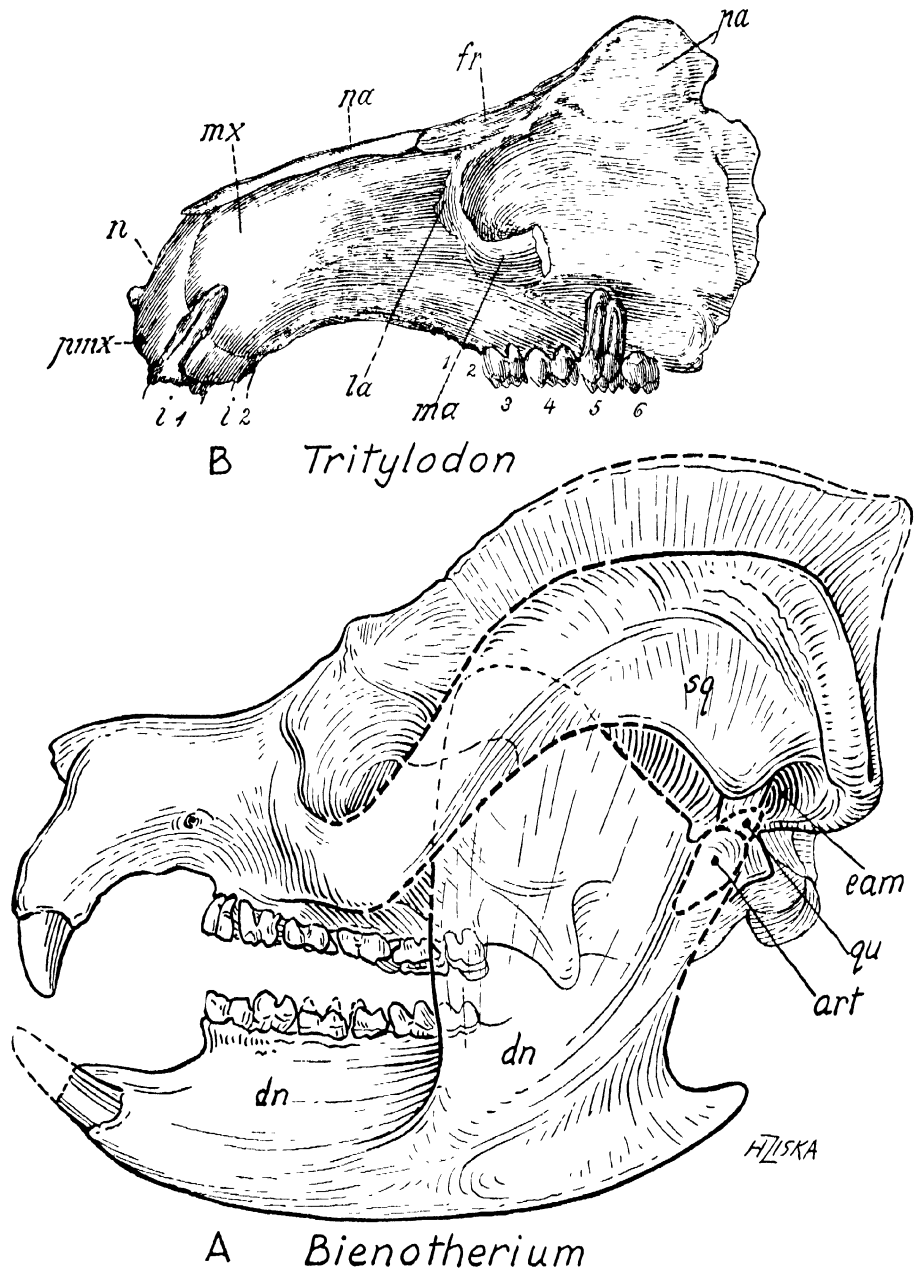


Fig. 17.1. Tritylodont (A) from the Upper Triassic of China, closely related to *Tritylodon* (B) from the Upper Triassic of South Africa. A, From a model made from the originals by Otto Falkenbach under direction of Dr. C. C. Young, with slight modification in the articular region. Natural size. B, The type of *Tritylodon longaevus* Owen from the Rhaetic of South Africa. From Osborn, after Owen. × ⅔.

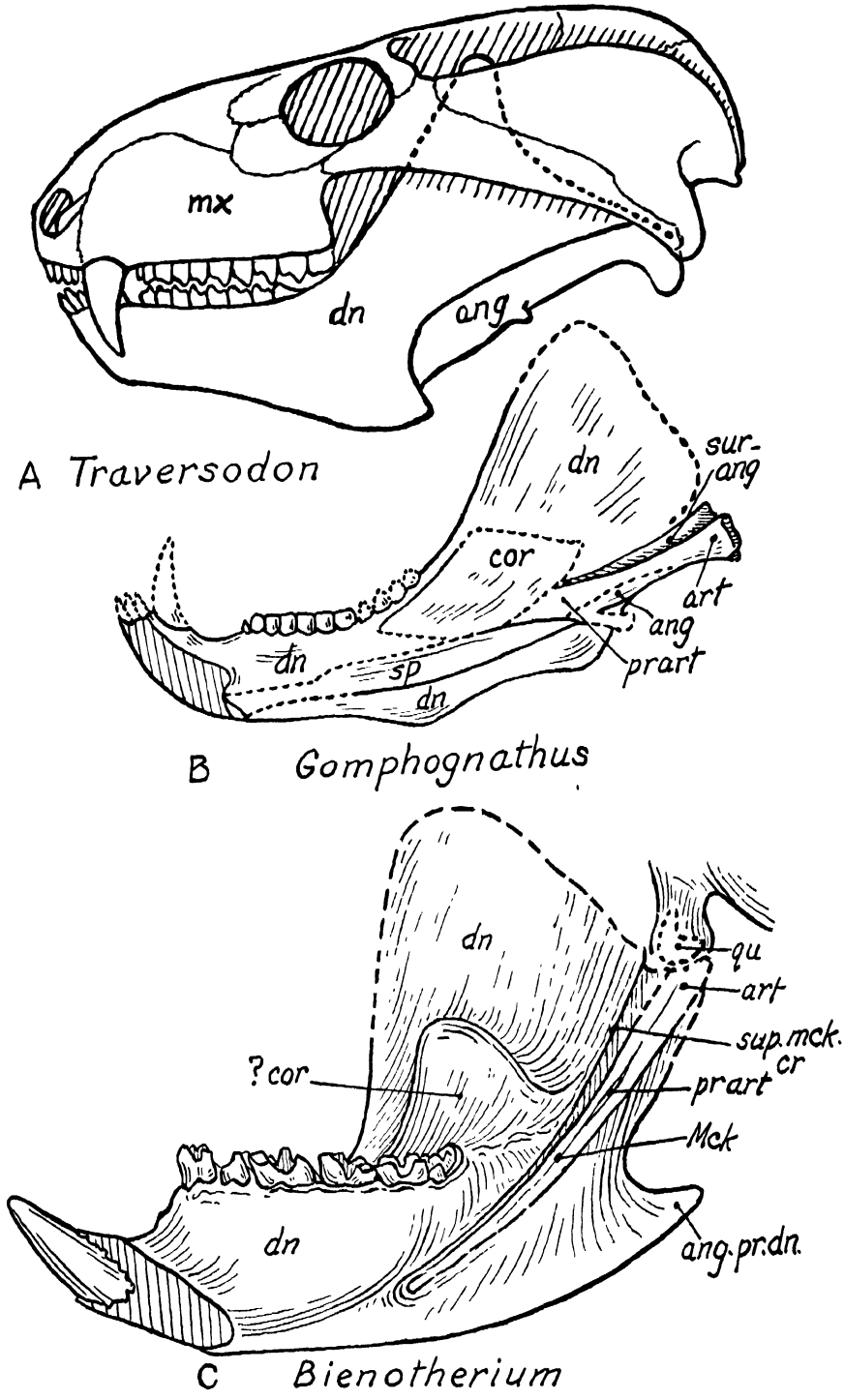


Fig. 17.2. Cynodont skull (A) from the Triassic of Brazil, related to *Gomphognathus* (B) and its allies of the Triassic of South Africa, × ½. After von Huene. Lower jaws of mammal-like reptile (B) and tritylodont (C) Medial aspect of right half. A, B, after Broili and Schröder, × ½; C, from a cast of the type, natural size. The suprameckelian crest of the ascending ramus of the dentary is at least analogous with the subcondylar or pterygoid crest of Triconodonta (cf. Simpson, 1928, p. 76).

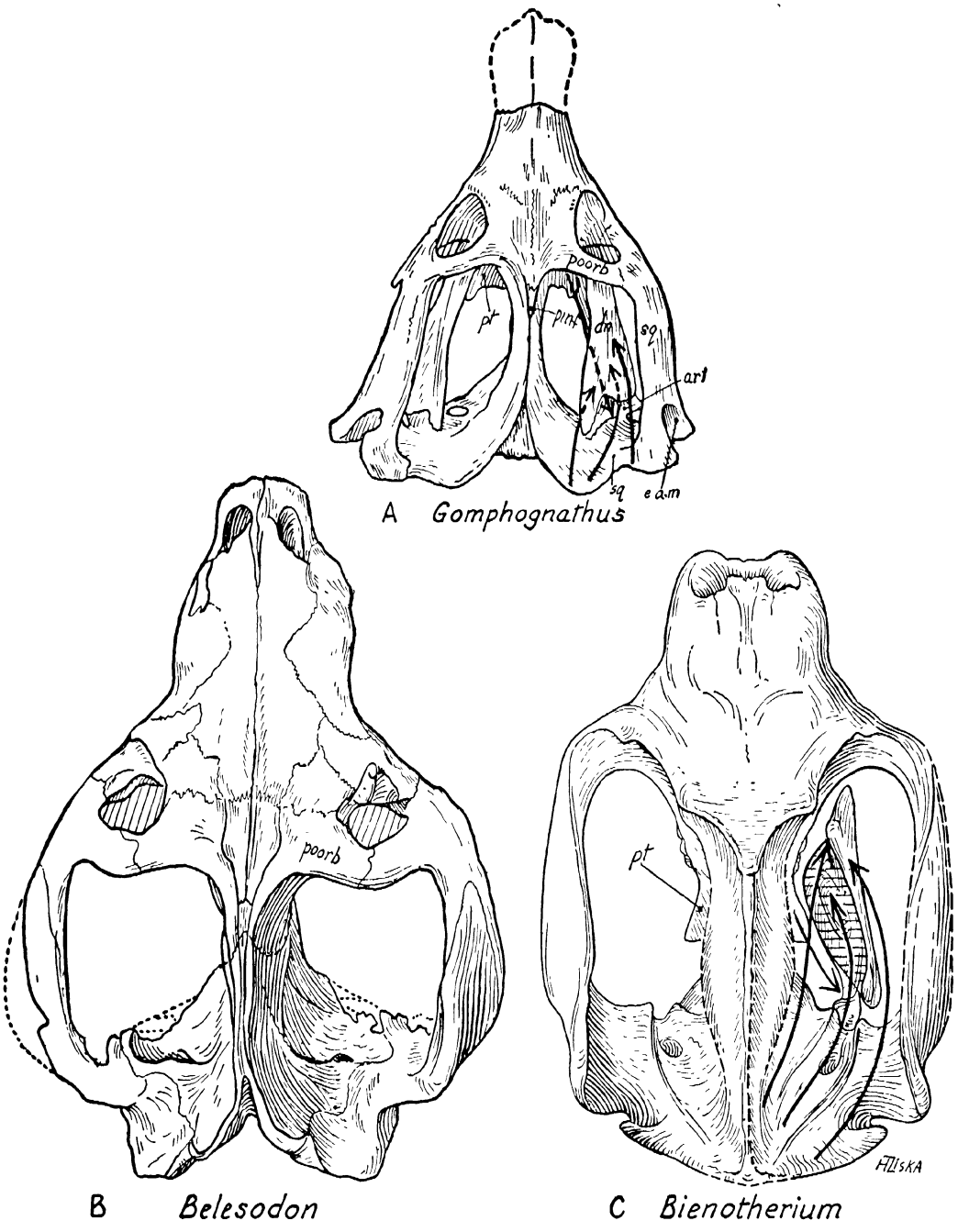


Fig. 17.3. Skulls from the Upper Triassic of South Africa (A), Brazil (B) and China (C), as seen from above. A, after Broili and Schroder, B, after von Huene; C, from a model restoration made under direction of Dr. C. C. Young (See fig. 17.1). The tritylodont (C) has advanced in the mammalian direction especially in the loss of the postorbital bone and the marked anterior extension of the ascending ramus of the mandible. The black arrows indicate the probable position of several divisions of the capti mandibularis muscles. The lateral flange of the pterygoid, together with the curved ridges on the floor of the temporal fossa, suggest the directions of the muscles which pull the jaw upward and inward.

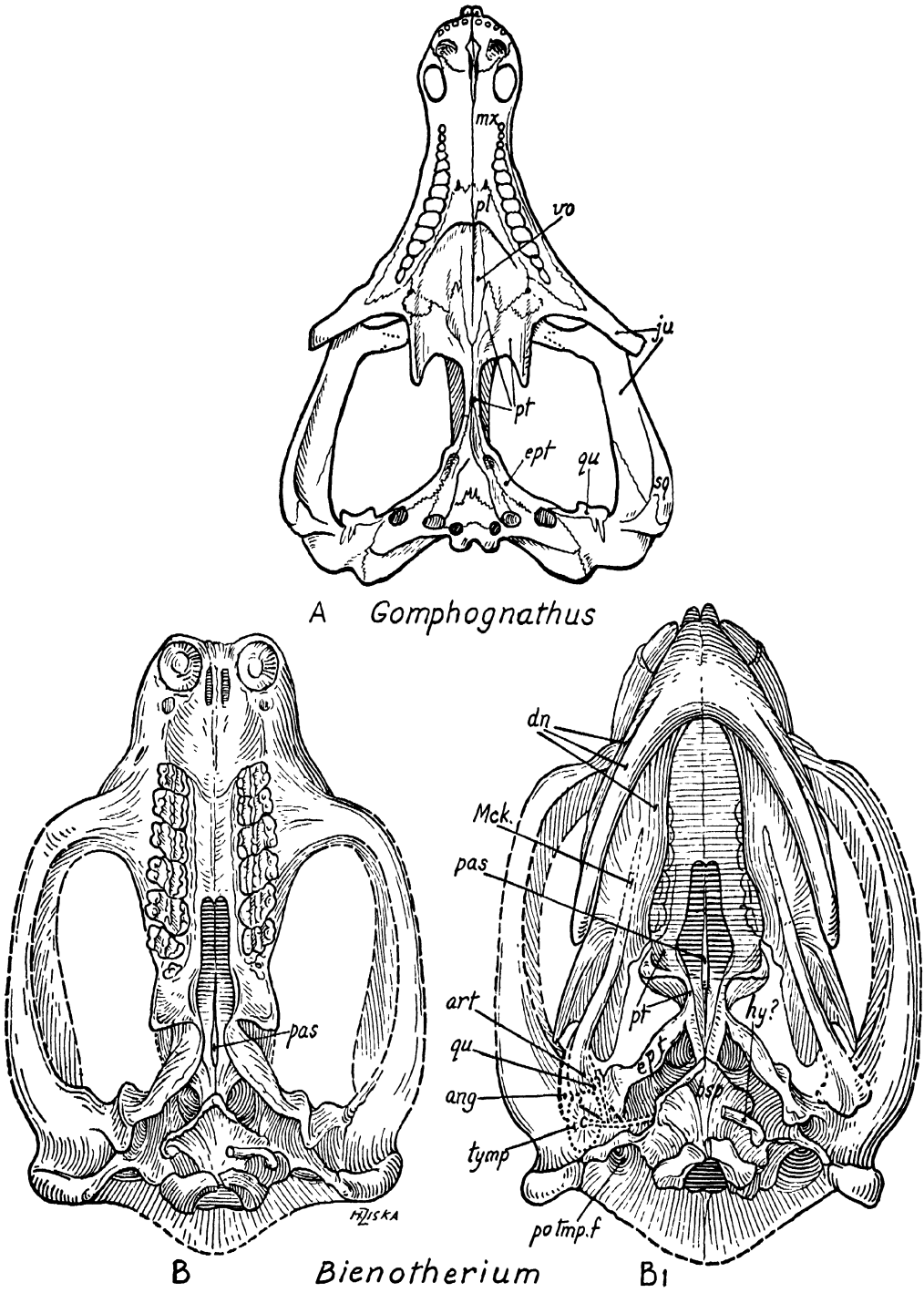


Fig. 17.4. Skulls from the Trias of South Africa (A) and China (B, B1). A, after Broili and Schröder; B, from the model made under the direction of Dr. C. C. Young. Palatal views. In B1, the lower jaw is articulated with the skull and an attempt is made to restore the parts connecting the inner or "reptilian" lower jaw with the skull, which in the mammals become the small bones of the middle ear. The bone marked ? *hy* may possibly be the displaced stapes.

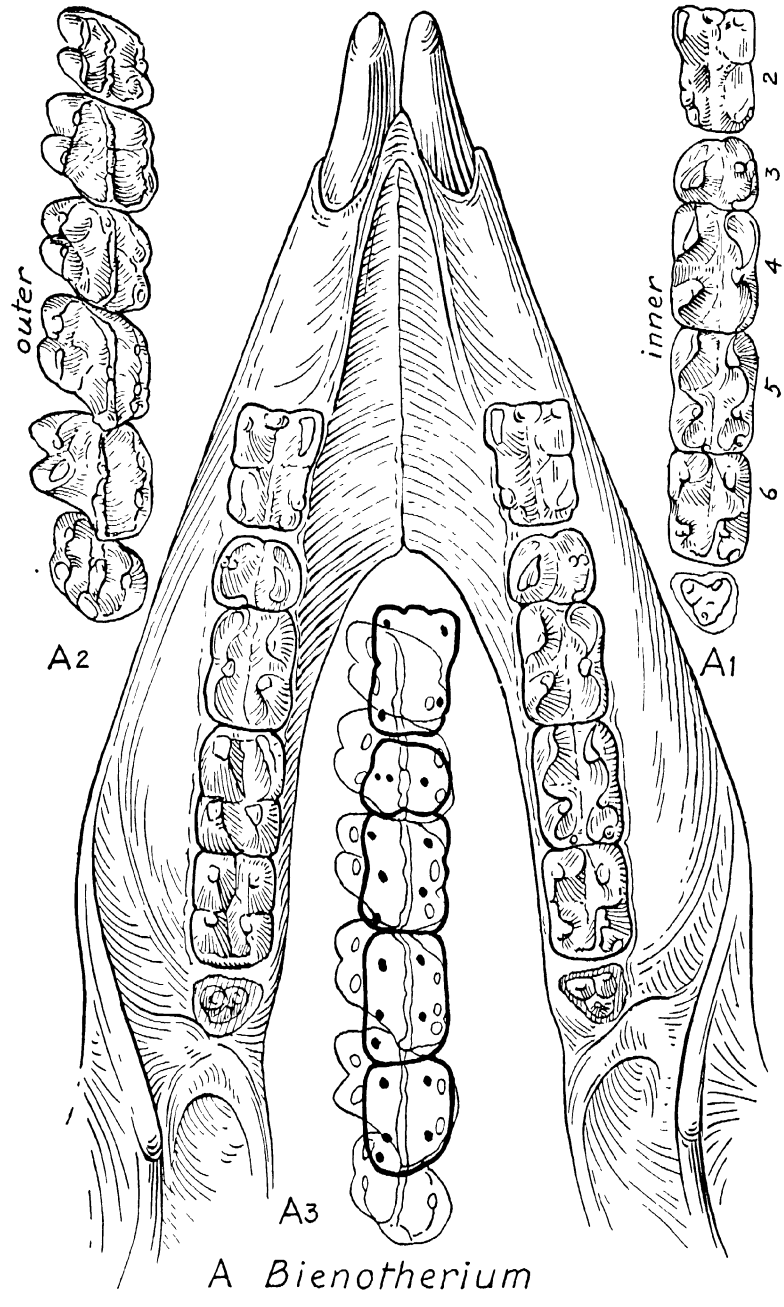


Fig. 17.5. Lower jaw (A) and lower cheek teeth (A1), upper cheek teeth (A2) and occlusion diagram (A3) of Triassic tritylodont from China Based on the model prepared under direction of Dr. C. C. Young The arrangement of the front teeth, the form of the molar cusps and their worn tips indicate that the motion of the jaw was largely vertical, with but little or no transverse slip. This accords with the downward projection of the pterygoid flanges (figs. 7.3C; 7.4B1) facing the broad inner surface of the mandible, which prevent lateral movements. The quadrate-articular joint, although relatively small (fig. 17.2C), was well braced to absorb the oblique anteroposterior thrusts, while the huge dentary was virtually suspended in a muscular sling which exerted great vertical pressure.

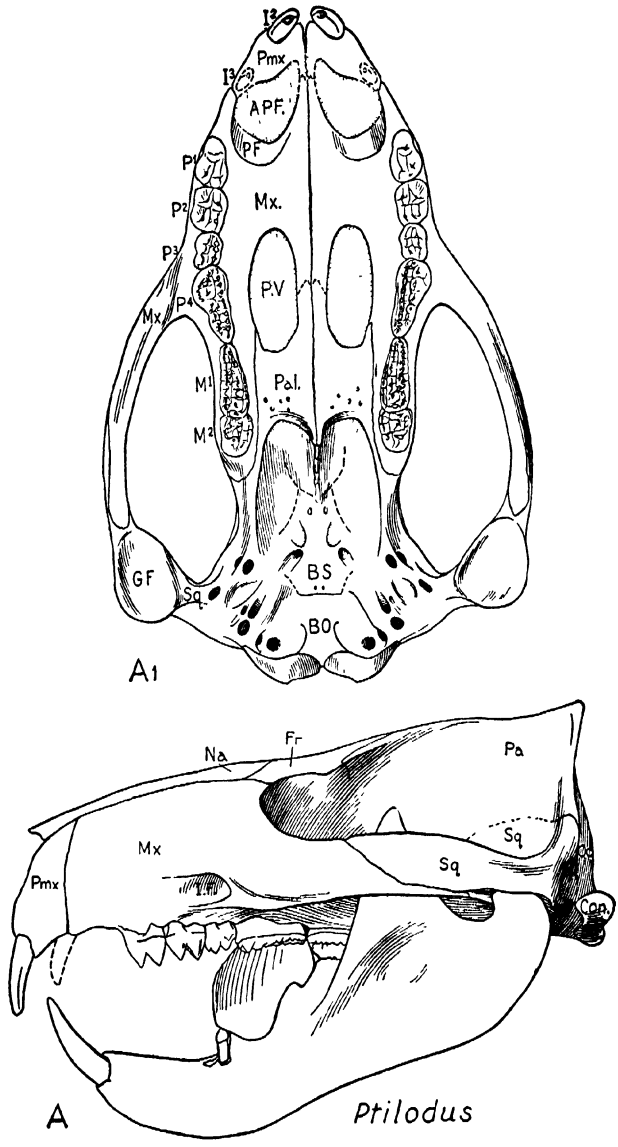


Fig. 17.6. Skull of specialized Paleocene multituberculate for comparison with the much less specialized conditions in the tritylodont. Restorations after Simpson.

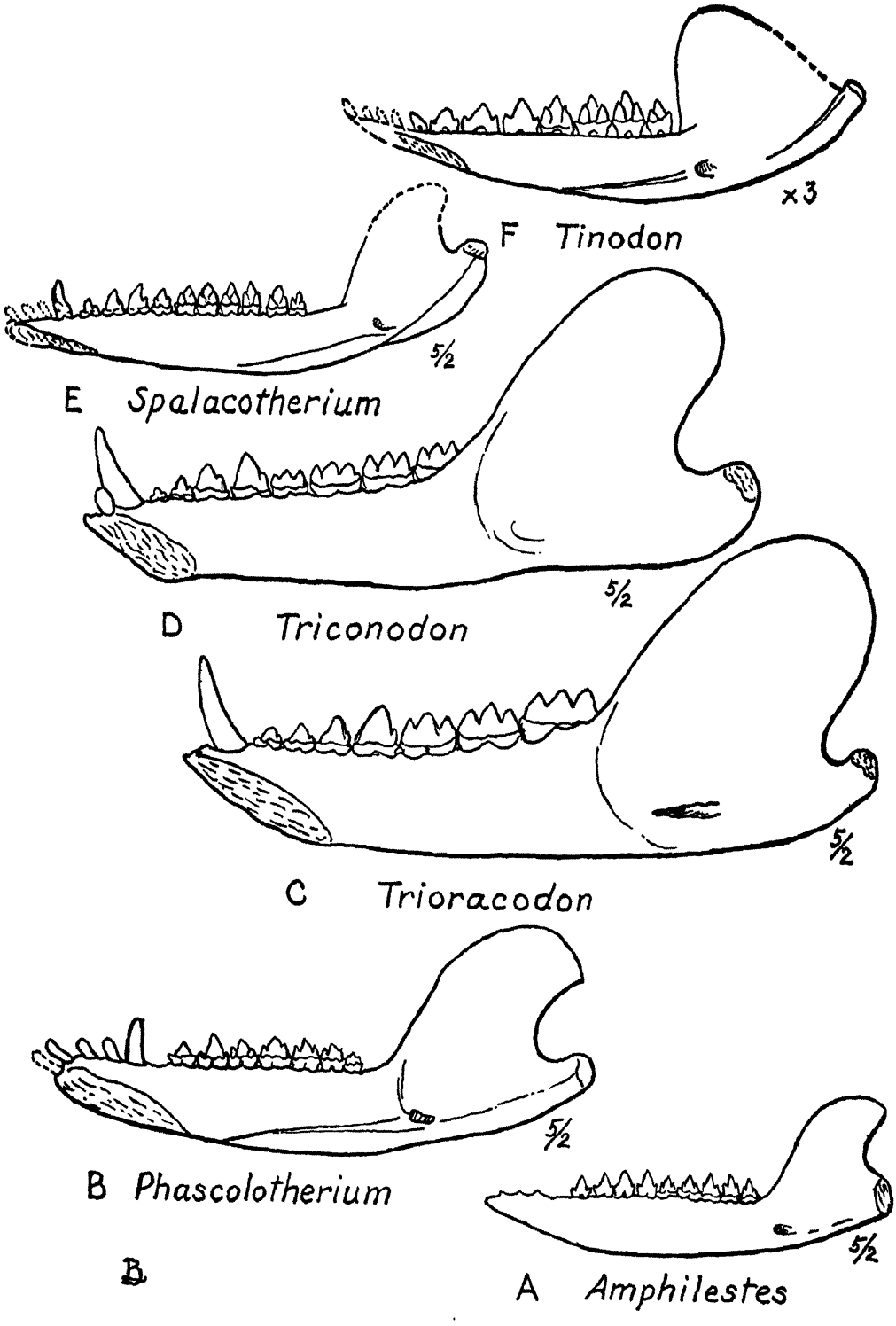


Fig. 17.7. Jaws of triconodonts (A–D) and symmetrodonts (E, F). After Simpson. A and B are from the Stonesfield Slate (Middle Jurassic), D and E, from the Purbeck (Uppermost Jurassic) of England, F, from the Morrison (Uppermost Jurassic) of Wyoming. For size see fig. 17.9.

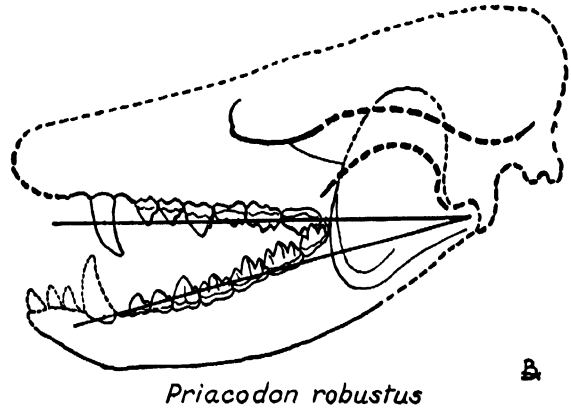


Fig. 17.8. Partial restoration of a triconodont skull, × 3. Chiefly after Simpson but with the rear parts tentatively restored to suggest the probable form of the glenoid facet. The scissors-like relations of the cheek teeth to the fulcrum are indicated by the straight lines.

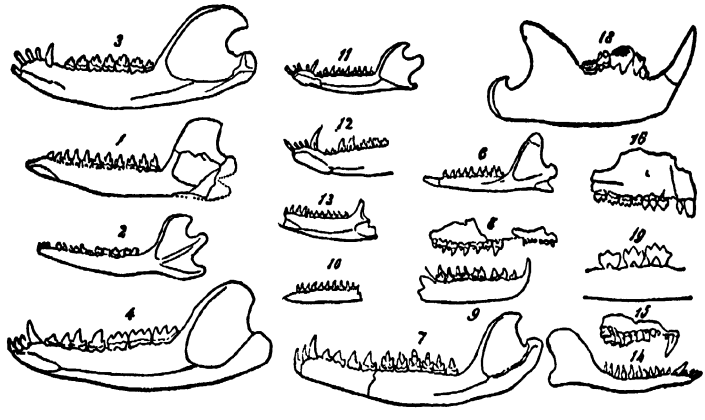


Fig. 17.9. Jurassic mammal jaws. Approximately natural size. After Osborn. The largest were no bigger than those of young kittens, the smallest more minute than the jaws of mice. The types of the British mesozoic mammals, representing the natural size. 1. *Amphilestes.* 2. *Amphitylus.* 3. *Phascolotherium.* 4. *Triconodon mordax.* 6. *Peramus.* 7. *Spalacotherium.* 8. *Peralestes.* 9. *Peraspalax.* 10. *Leptocladus.* 11. *Amblotherium.* 12. *Phascolestes.* 13. *Achyrodon.* 14. *Stylodon.* 15. *Athrodon.* 16. *Bolodon.* 18. *Plagiaulax minor.* 19. *Stereognathus.*

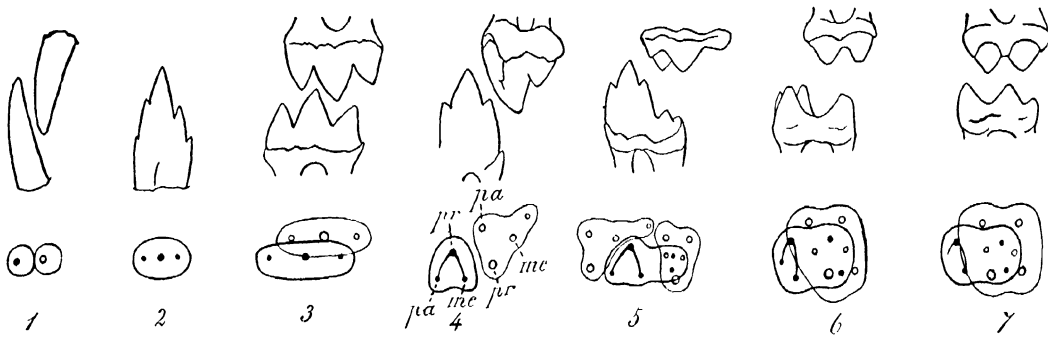


Fig. 17.10. Seven stages in the evolution of mammalian molar teeth, as first conceived by Cope and Osborn. 1, Haplodont, molar crown simple, conical 2, Protodont, main cusp margined by anterior and posterior cuspules. 3, Triconodont, molar crowns compressed oval, with three subequal cusps in anteroposterior line. 4, Tritubercular, the upper and lower crowns folded in opposite directions, the two accessory cusps shifting inward in the lower, outward in the upper. The apex of the triangle, internal in the upper, external in the lower, molars. 5, Tuberculo-sectorial, the lower molars developing a talonid or heel, which articulates with the main internal cusp or protocone of the upper molar. 6, Quadritubercular, lower molars with paraconid reduced or wanting, talonid enlarged, bearing two main cusps (hypoconid, entoconid) as in Eocene ancestors of the hoofed mammals. 7, Quinquetubercular, as in F but with a large fifth cusp or hypoconulid (as in certain Eocene primates). For critical reviews of this theory, see Gregory, 1934, Butler, 1941, Simpson, 1933. *Pa,* paracone; *me,* metacone; *pr,* protocone.

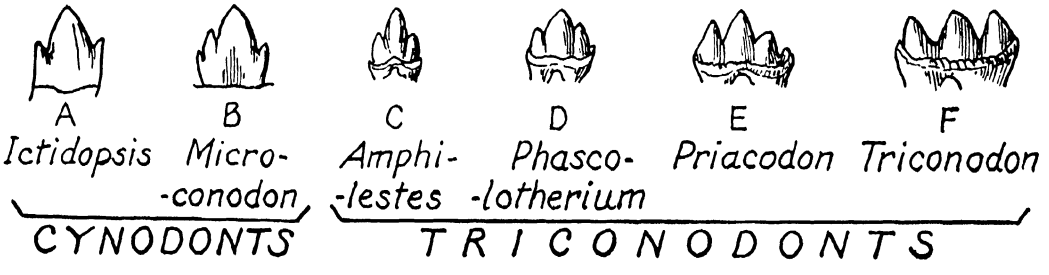


Fig. 17.11. Comparison of lower molars in cynodonts and triconodonts. After Simpson.

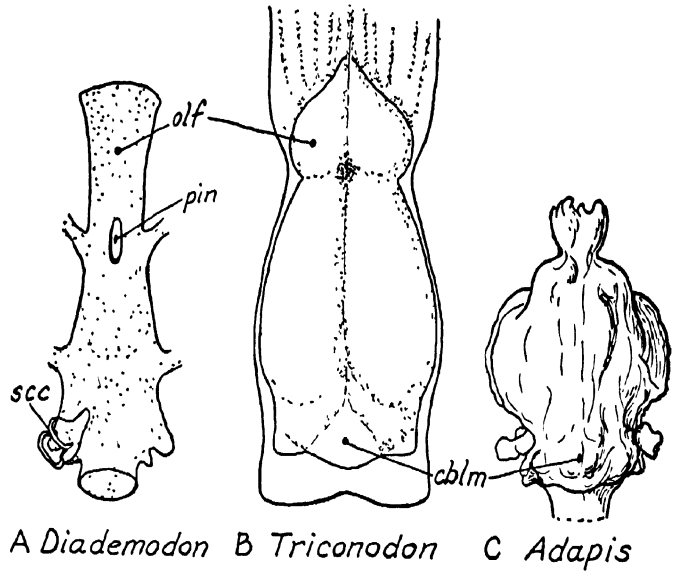


Fig. 17.12. Progressive evolution of the brain, indicated by comparison of endocranial casts (endocasts) of a Triassic mammal-like reptile (A), a Jurassic triconodont (B) and an Upper Eocene primate (C). A, after Watson; B, after Simpson; C, after Le Gros Clark.

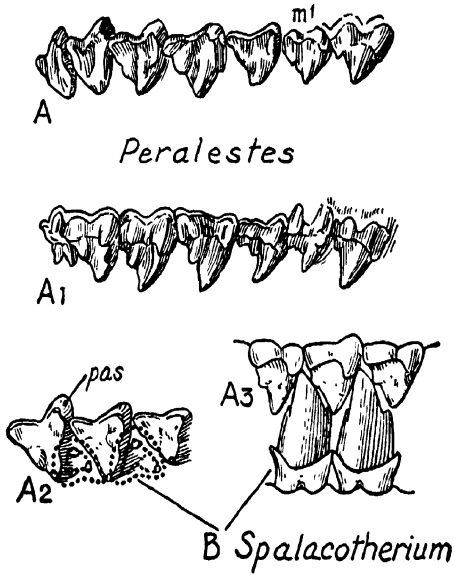


Fig. 17.13. Cheek teeth of symmetrodonts. After Simpson. A, Crown view of upper molars, right side showing a symmetrical triangular contour, with high main cusp, laterally projecting parastyle (*pas.*).

A1, The same, in outer side view, showing strongly developed stylar cusps, small metacone. A2, Occlusal diagram, showing reversed triangles of upper and lower molars, the nearly symmetrical lowers fitting into the triangular notches between the uppers. A3, The same, outer side. The sides of the upper and lower triangles act as shears; the cusps support the blades and break the food. Enlarged.

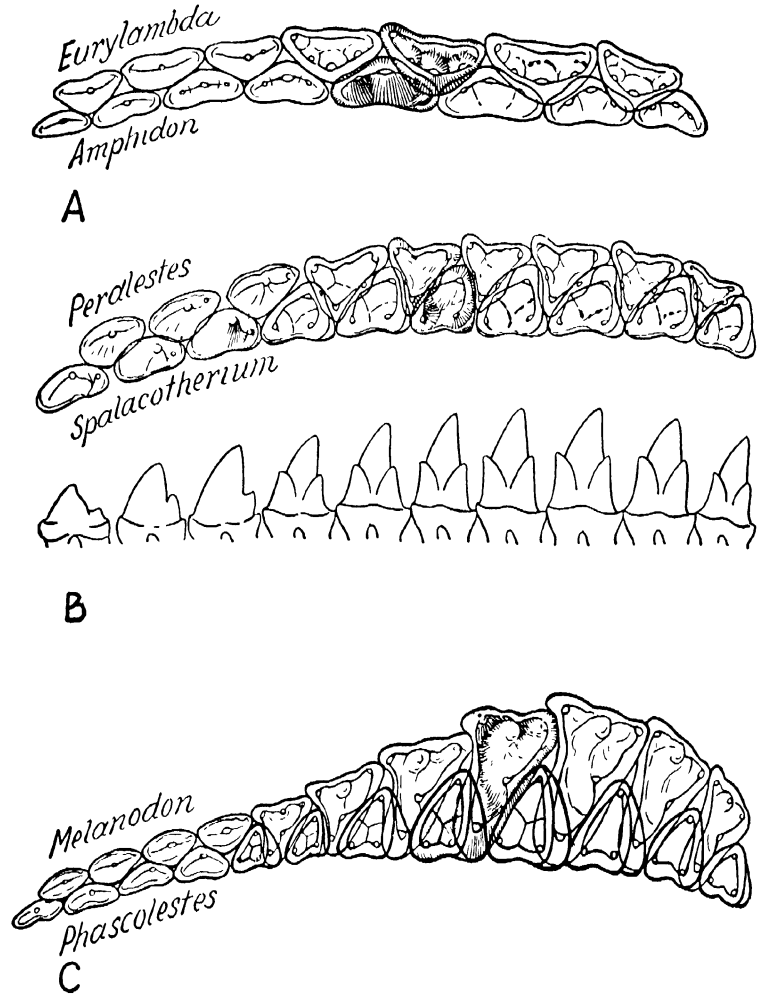


Fig. 17.14. Comparison of Upper Jurassic symmetrodonts (A, B) and pantotheres (C). From Gregory, all data after Simpson. An attempt to restore the upper and lower cheek teeth in series, to indicate their occlusal relations and to illustrate the hypothesis of the origin of reversed triangles by transverse growth of molar tips. Although the series is composed of contemporaneous forms and therefore lacks direct evidence of stratigraphic sequence, yet the dentitions named (A) *Eurylambda* and *Amphidon* may have retained much of their heritage from ancestors related to Middle Jurassic triconodonts and Triassic cynodonts, especially in the relatively simple premolars and in the relations of the secondary cusps to the main cusps. The upper and lower teeth are nearer to being mirror images of each other than in C, in which the upper and lower molars become very different, the uppers being much wider. The lower molars interlock in the interdental spaces between the uppers, especially in B. In C, the small heel or talonid on the lower molars acts as a stop for the main internal cusp of the uppers.

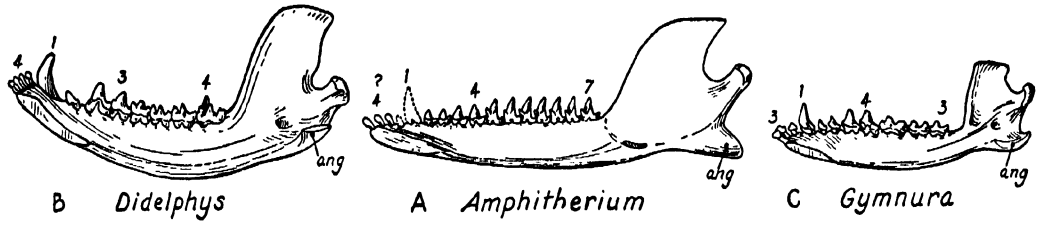


Fig. 17.15. Lower jaws (inner side) of primitive Jurassic pantotherian (A), Recent marsupial (B), and insectivore (C). A, after Simpson. A×2, B,C×⅔. In the primitive pantotherian the dental formula is I_4 C_1 P_4 M_7; the cheek teeth are numerous (11) and small, the angular process (*ang*) not inflected. In the relatively primitive marsupial (B) the dental formula is I_4 C_1 P_3 M_4; the posterior premolars large and the angle inflected. In the relatively primitive placental insectivore (C) the dental formula is I_3 C_1 P_4 M_3; the first molar is enlarged, the angle not inflected.

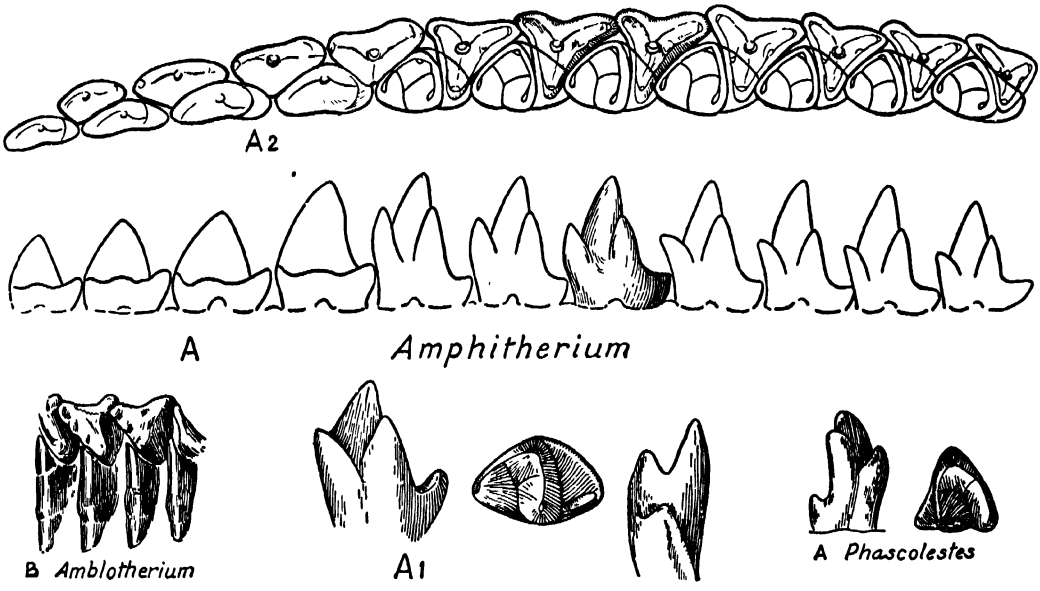


Fig. 17.16 (top). An attempt to restore the unknown upper teeth of *Amphitherium* from comparison with its known lower teeth and with the known occlusal relations in other pantotheres. Modified from Gregory; data from Simpson. The presence of a heel or talonid in the lower molars implies the existence of a well developed internal cusp of the uppers to fit into the talonid basin, while the oblique protoconid-paraconid shear suggests the presence in the uppers of parts corresponding to the metaconule and metacone-metastyle shear.

Fig. 17.17 (bottom). Molars of dryolestid pantotheres. After Simpson. A, Left lower molar, internal and top views, from the Morrison (Upper Jurassic) of Wyoming. Shows very small talonid, which in occlusion overlapped the large internal cusp of the upper molar. Enlarged. B, Right upper and lower molars from the Purbeck (Upper Jurassic) of England. The upper molars show the crown view, the lowers, the external view, but the latter still remain in the interdental notches. A,A_2×12.

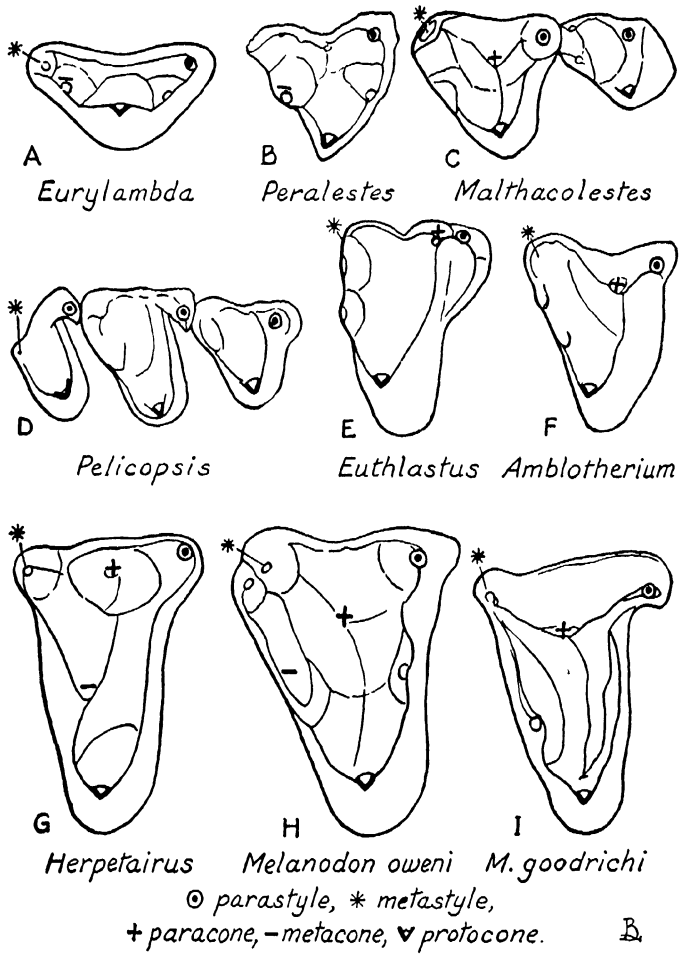


Fig. 17.18. Upper molars of symmetrodonts (A, B) and dryolestid pantotheres (C–I) to show homologies of cusps as here interpreted. Data from Simpson. The naming of the cusps is in accordance with Osborn's (1907) identification of the protocone in "*Dryolestes*."

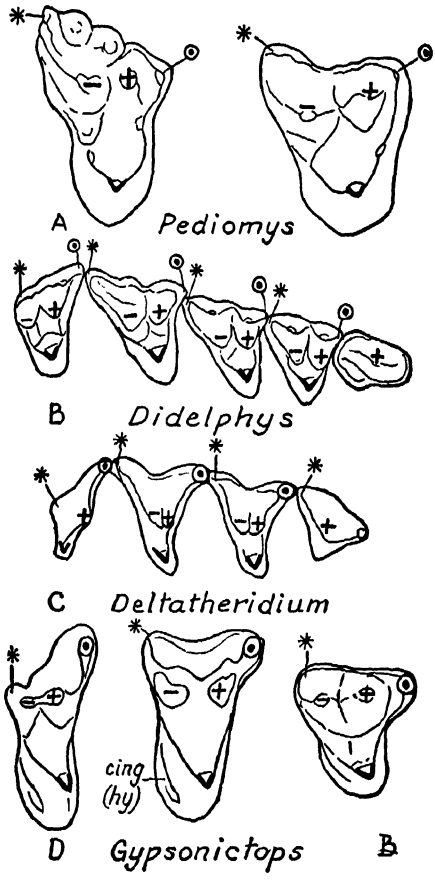
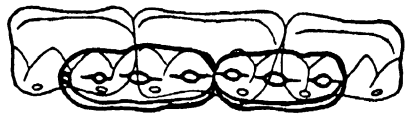
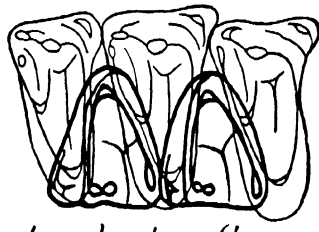


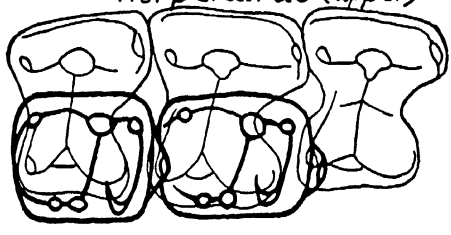
Fig. 17.19. Upper molars of Upper Cretaceous marsupial (A), Recent opossum (B), Upper Cretaceous placental insectivores (C, D). A, D, after Simpson; C, after Gregory and Simpson; B, after Gregory. Main cusp homologies as in fig. 17.18. A different interpretation of the homology of the main internal cusp, by P. M. Butler, is given in fig. 17.22.



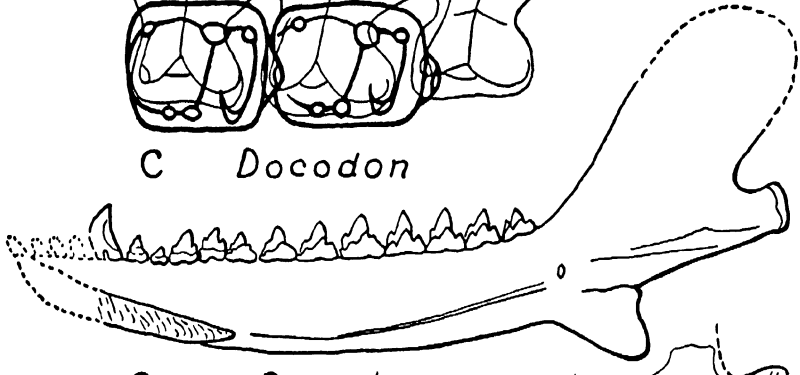
A *Priacodon*



B *Laolestes (lower)*
Herpetairus (upper)



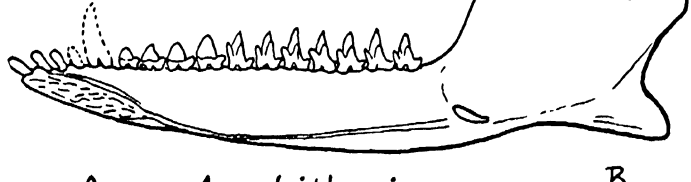
C *Docodon*



C *Docodon*



B *Peraiocynodon*



A *Amphitherium* B

Fig. 17.20 (top). Occlusion diagrams of upper and lower molars of triconodont (A) dryolestid (B) and docodont (C). After Simpson.

Fig. 17.21. Lower jaws (right half, inner side) of primitive (A), intermediate (B) and peculiarly specialized pantotheres (C). After Simpson. Enlarged.

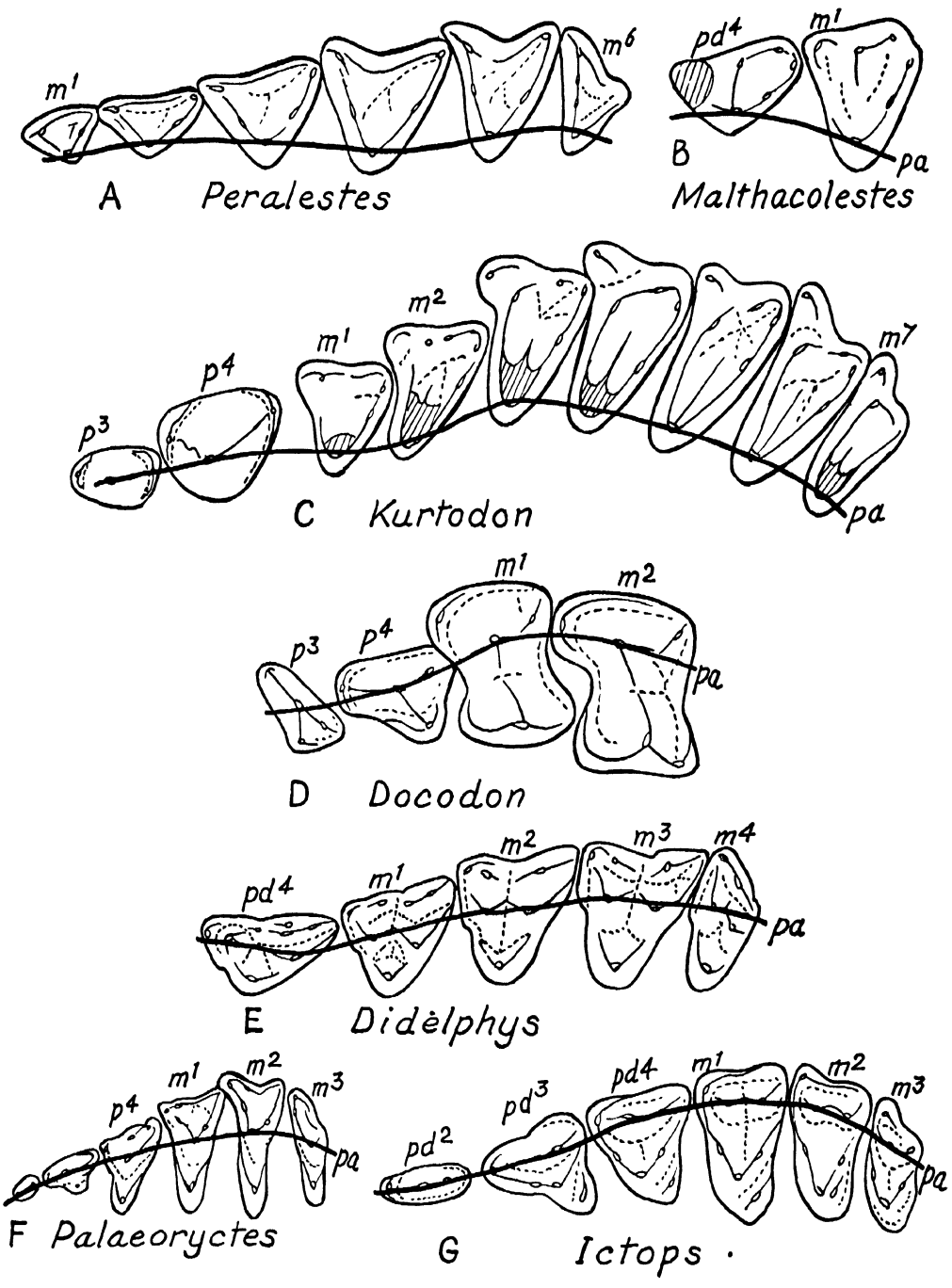


Fig. 17.22. P. M. Butler's reading of the homologies of the main upper molar cusps in symmetrodonts (A), dryolestids (B, C), docodonts (D), primitive marsupial (E) and two placental insectivores (F, G). After Butler. According to this interpretation, the paracone of *Docodon* has retained its primitive position near the outer side of the crown, while in *Kurtodon* it has moved inward to form the inner tip of the crown. But according to the data set forth in fig. 17.20 B, C, the upper molar crown of *Docodon* is fundamentally the same as in the dryolestids, the main internal cusp being homologous in B and C.

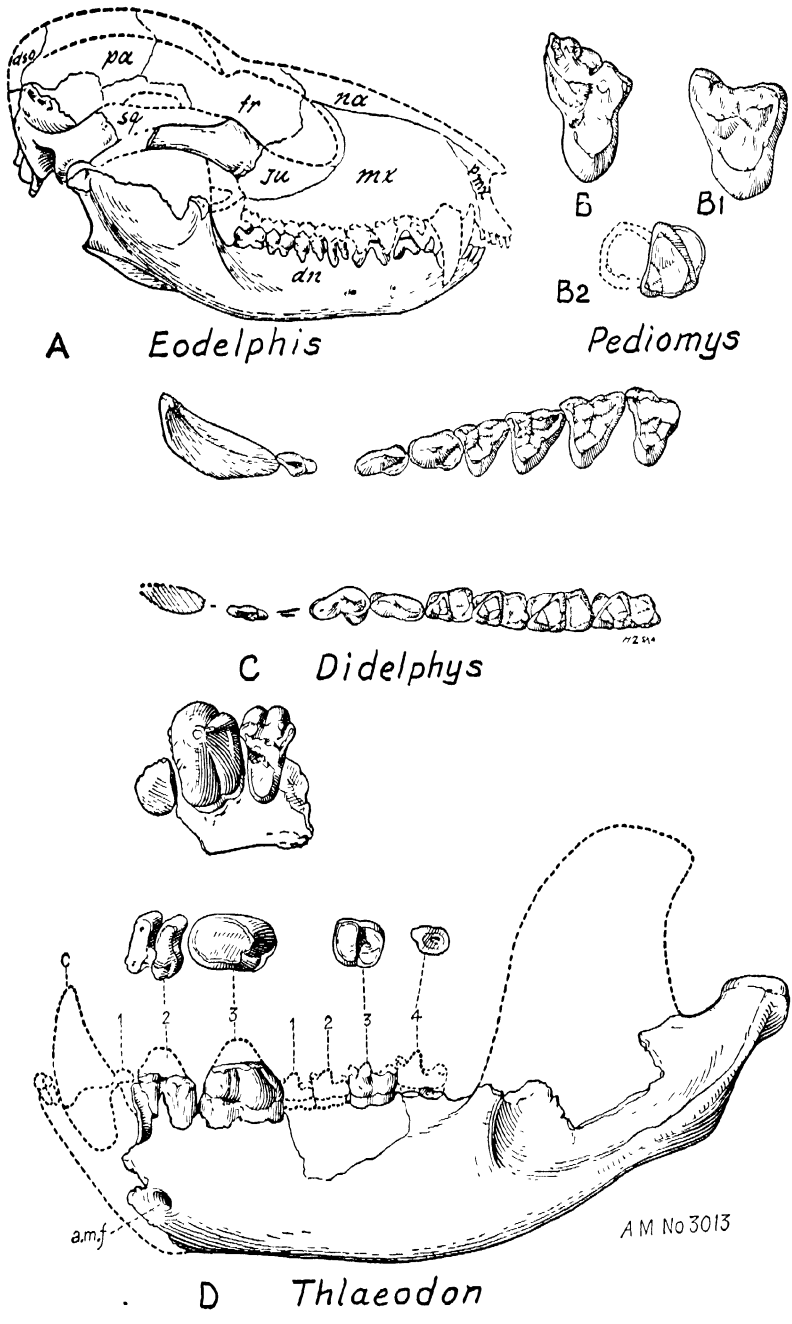


Fig. 17.23. Upper Cretaceous (A–B2, D) marsupials of the American opossum family compared with Recent opossum (C). A, *Eodelphis*, contemporary of the latest dinosaurs. Restoration of skull by Gregory, data from Matthew. B, B1, two left upper molars; B2, left lower molar. From Simpson, after Osborn. B2 shows the anteroexternal cingulum-ledge, which in occlusion receives the tip of the metacone. This peculiar character is found also in the modern opossum (C). C, Upper teeth (left) and lowers (right) of American opossum. D, Lower jaw and some upper teeth of large Upper Cretaceous relatives of the opossum After Matthew.

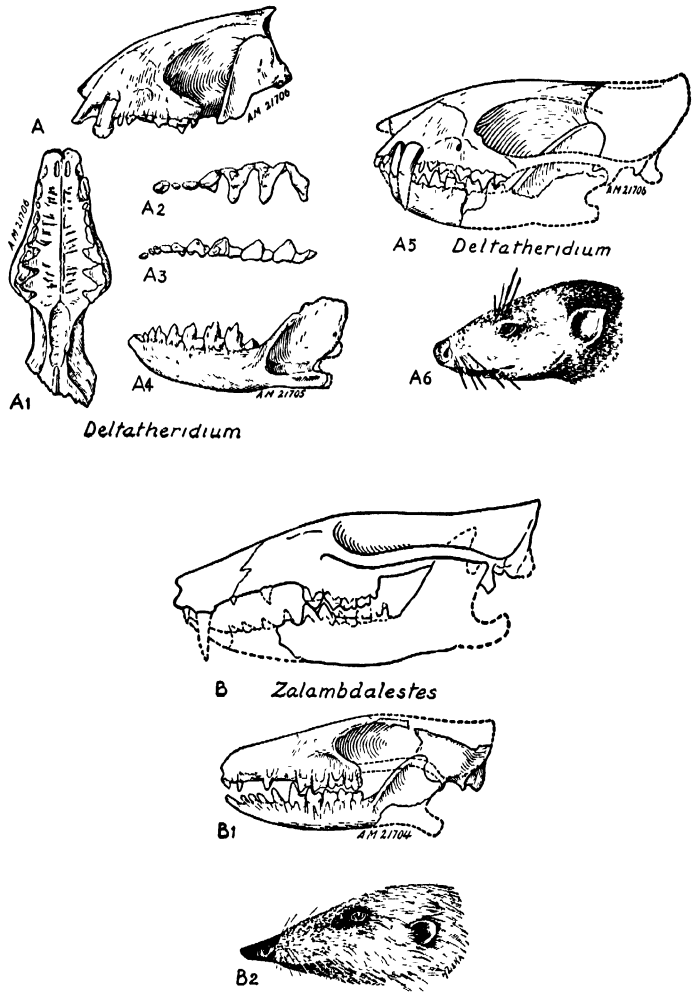


Fig. 17.24. Mongolian Cretaceous insectivores. (A5, B) with restorations of heads (A6, B2). Natural size. After Gregory and Simpson. Skulls partly restored

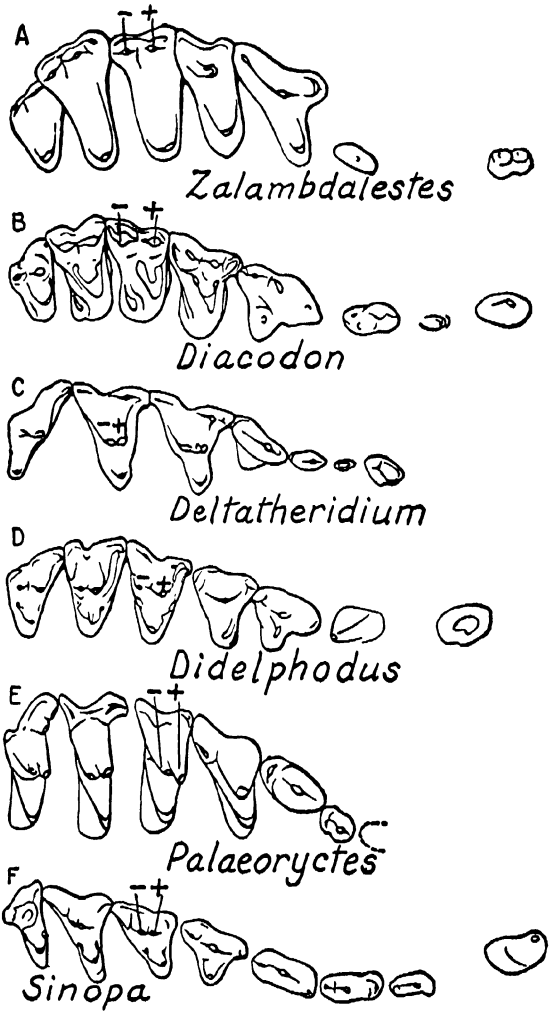


Fig. 17.25. Right upper cheek teeth of Mongolian Cretaceous insectivores (A, C) compared with Eocene (B, D) and Paleocene (E) insectivores and an Eocene carnivore (F). After Simpson. In the leptictids A and B, the paracone (+) and metacone (−) are near the outer border, in C–F, they are near the middle of the molar The series indicates that in A and B the paracone (+) is homologous with the main outer cusp of the premolars, while the internally projecting protocone seems to be homologous with the internal basal projection of the premolars.

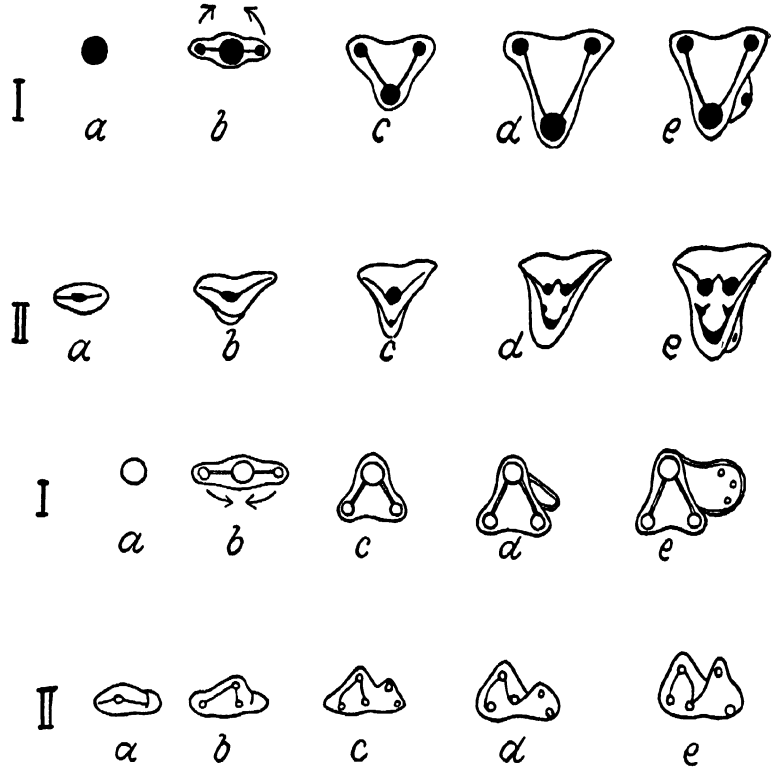
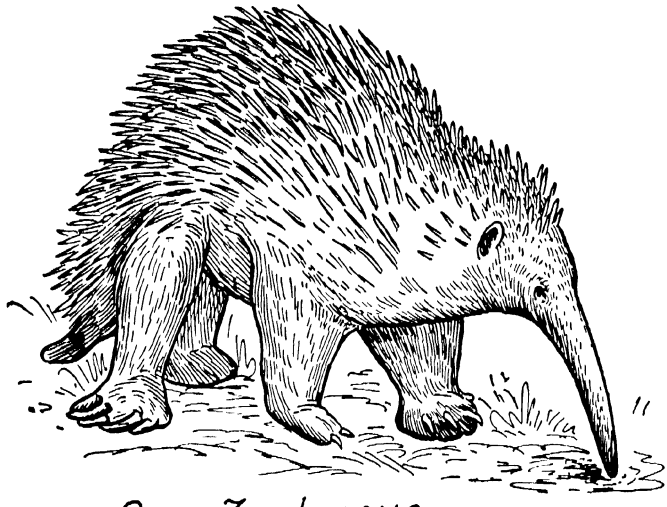


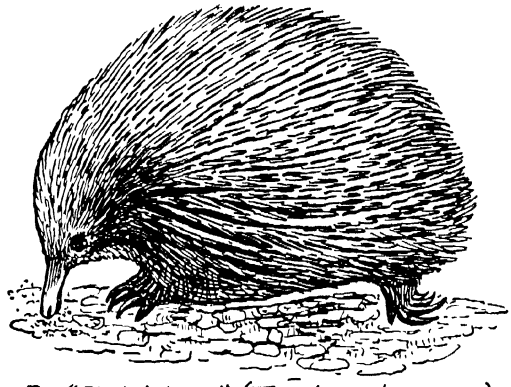
Fig. 17.26. Rival theories (I, II) of origin of triangular upper (I) and lower (II) mammalian molars. I, The Cope-Osborn theory, including rotation or circumduction of the accessory cusps (para-metacones) to the outer side of the upper and the inner side of the lower molars. II, The "Premolar Analogy" theory: in the upper teeth origin of the protocone or internal cusp as a bud from the internal cingulum; in the lower teeth. origin of the paraconid and metaconid *in situ* on the slopes of the protoconid.

CHAPTER XVIII

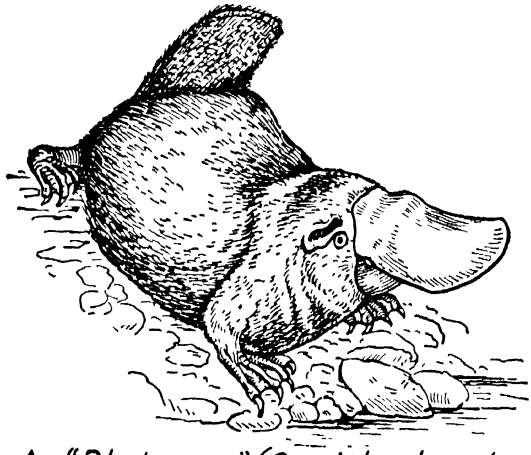
BRANCHING EVOLUTION IN EGG-LAYING AND MARSUPIAL MAMMALS



C *Zaglossus*



B "*Echidna*" (*Tachyglossus*)



A "*Platypus*" (*Ornithorhynchus*)

Fig 18.1. Living monotremes A, B, from H. C. Raven. Courtesy New York Zoological Society. C, from Weber.

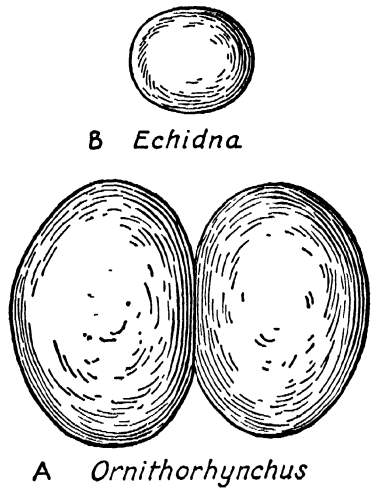


Fig. 18.2. Eggs of monotremes. A. Twice natural size, after Wood Jones; B, natural size, after Semon.

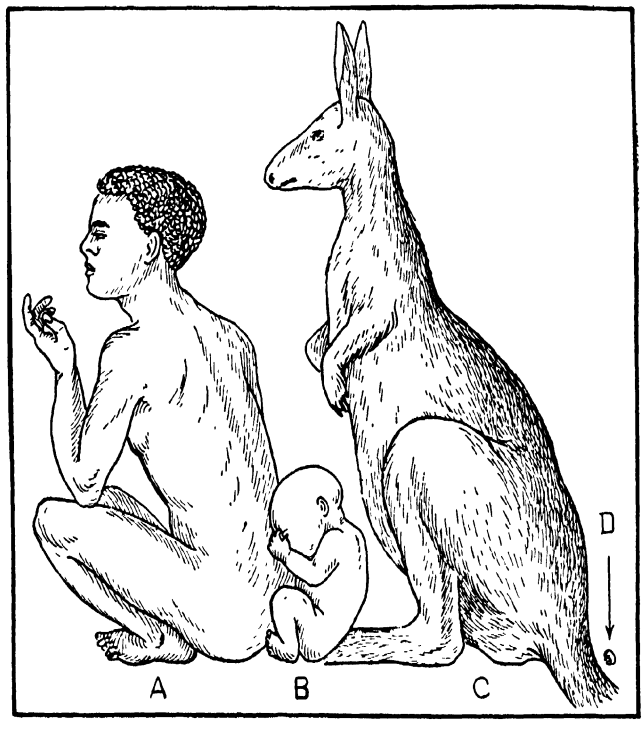


Fig. 18.3. Adults and new-born. After H. C. Raven. Figures drawn to scale, showing the wide differences in body-size between the adult and the young at birth, of man and the kangaroo. A, adult man; B, new-born child; C, adult kangaroo; D, new-born kangaroo.

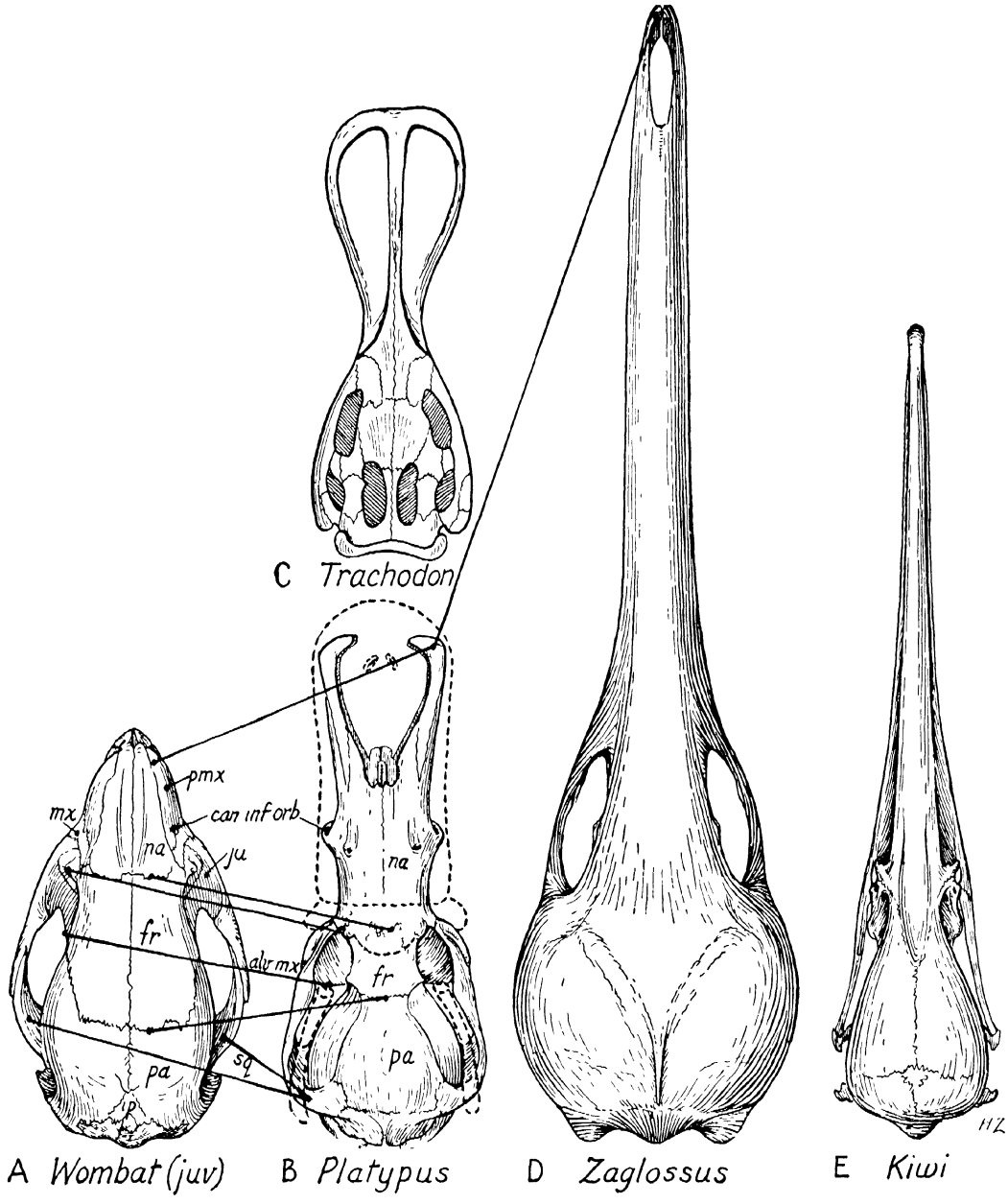


Fig. 18.4. Adaptive divergence (A, B, D) and convergence (B and C; D and E) in skull form. Dorsal views.

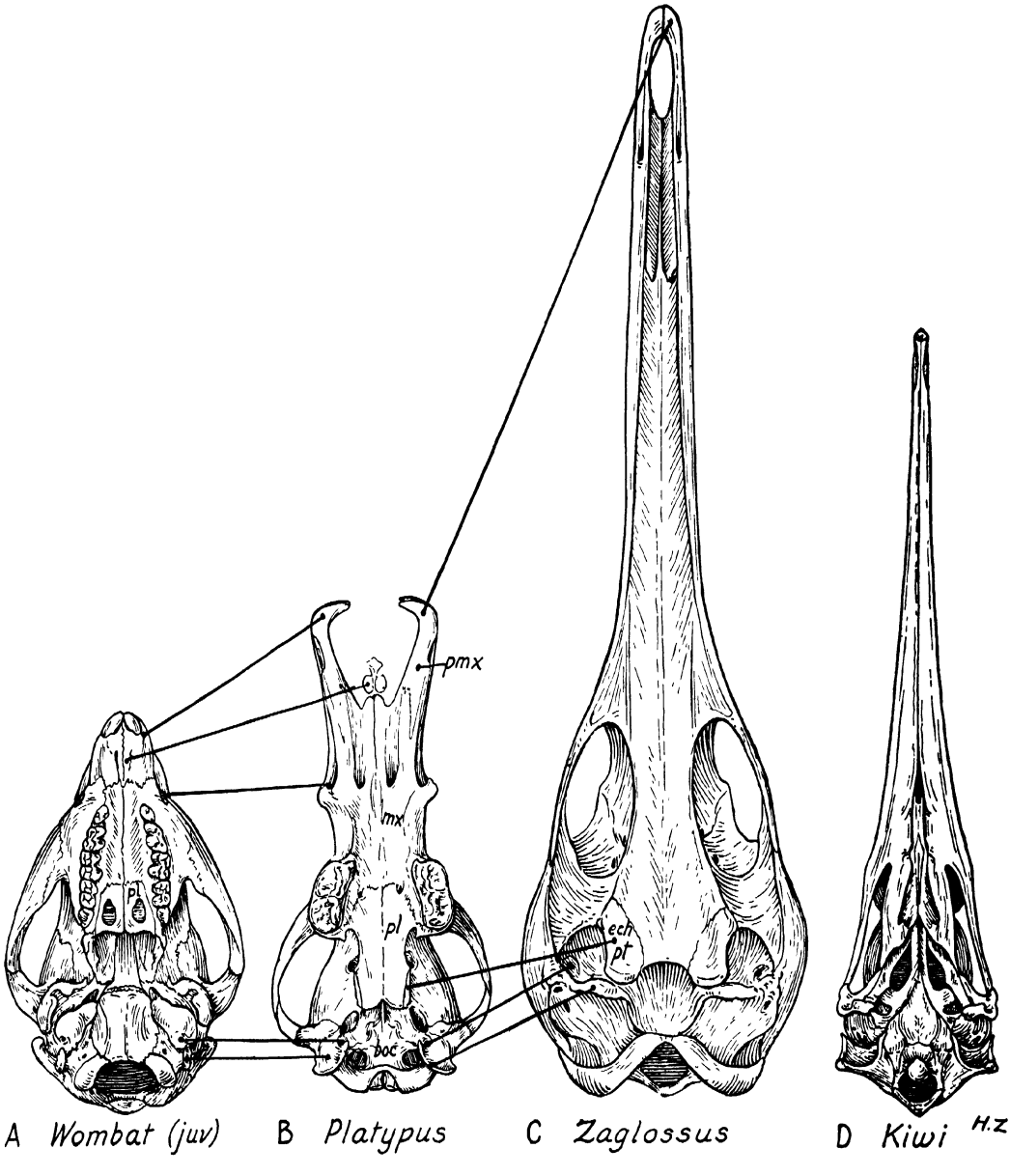


Fig. 18.5. Adaptive divergence (A–C) and convergence (C, D) in skull form. Palatal views. Guide lines indicate great forward growth of bill and backward growth of palate in end stage of monotremes.

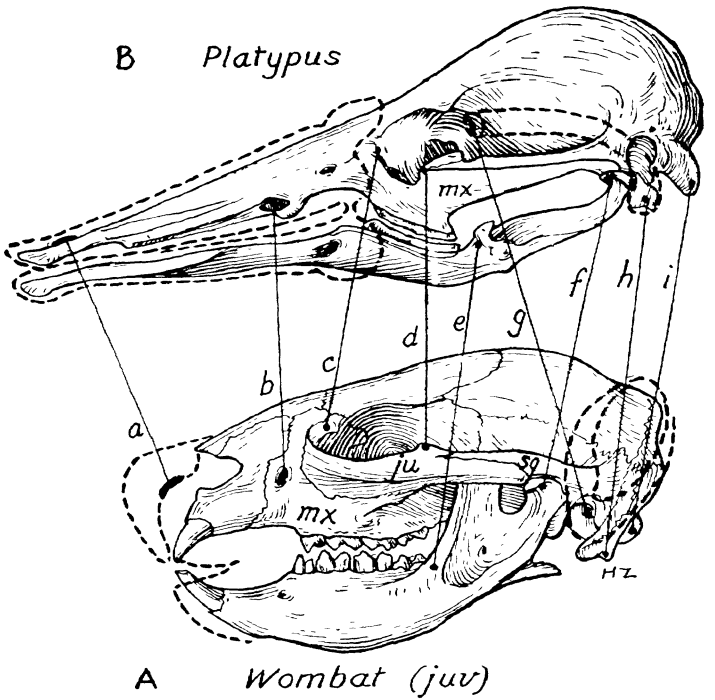


Fig. 18.6. Skulls of young wombat (A), representing a diprotodont marsupial, and platypus (B), the latter showing greater specialization. Broken lines indicate position of rhinarium and "bill"; also of external ears Guide lines connect homologous points and indicate differential shifts in growth rates.

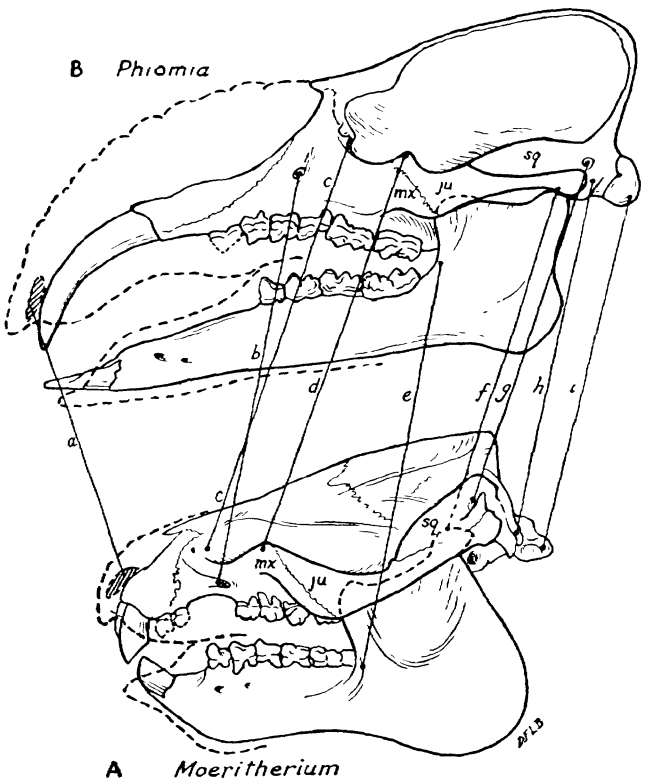


Fig. 18.7. Skulls of primitive (A) and long-jawed (B) proboscideans. After Osborn. Comparison of guide lines with those of fig. 18.6A indicates more or less similar changes and differential shifts in growth rates in passing from more primitive to more specialized stages

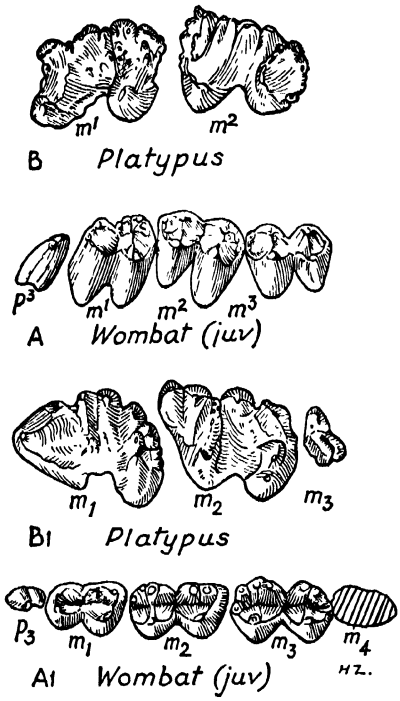


Fig. 18.8. Unworn molar crowns of young wombat (× 2) and platypus (× 4). The platypus molar crowns, although plainly degenerate in detail, seem to retain traces of two main V's separated by deep transverse valleys, as in the wombat. B, B1, after Simpson.

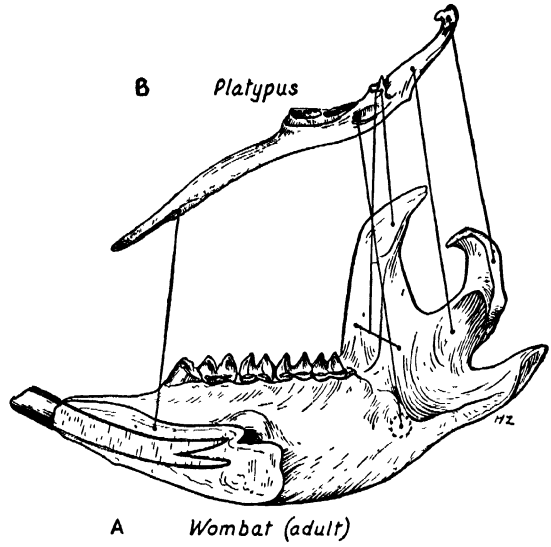


Fig. 18.9. Right half of mandible, medial aspect, showing extreme specialization in the platypus.

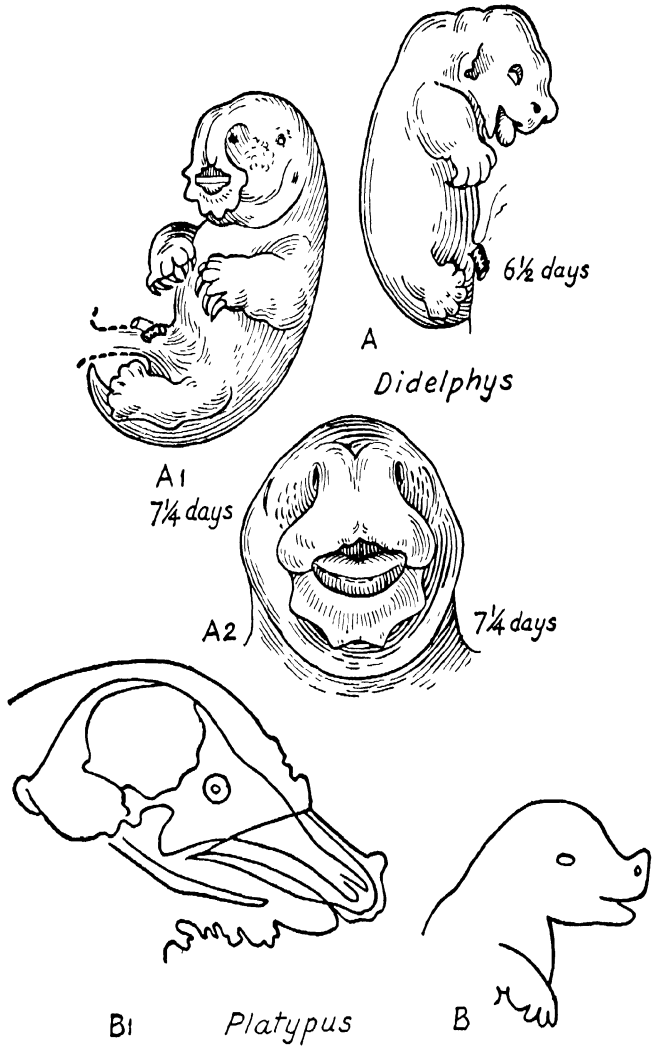


Fig. 18.10. Embryos of platypus and marsupial. In the earlier stage (B) the platypus resembles the marsupial (A); in a later stage (B1) the "duck-bill" features are developing. A, A2, after Selenka; B, B1, after de Beer and Fall.

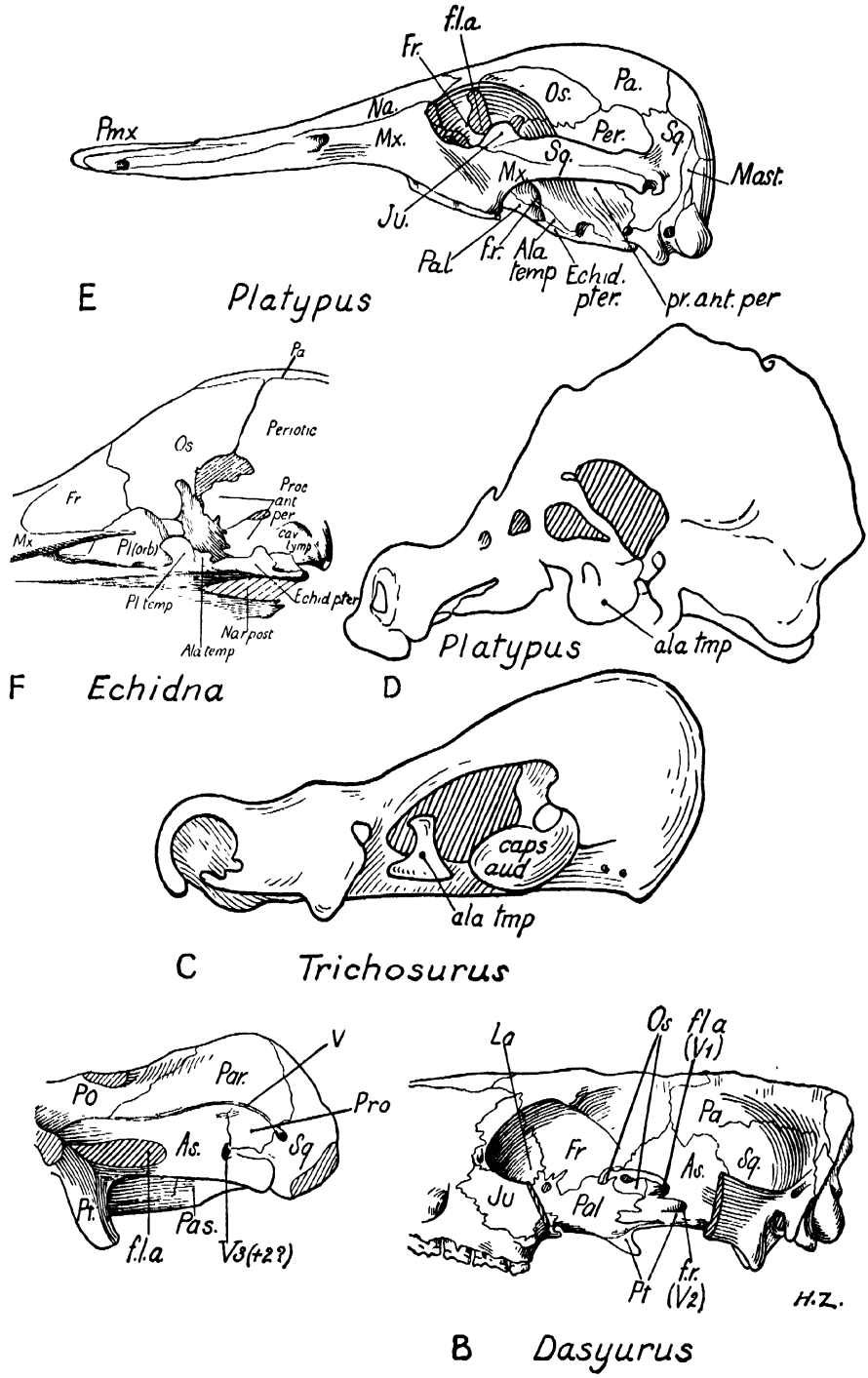


Fig. 18.11. Cynodont (A), marsupial (B, C) and monotreme (D–F) braincases. C and D are from foetal specimens, showing the chrondro cranium. A, F, after Watson; B, E, after Gregory and Noble; C, after Broom; D, after de Beer.

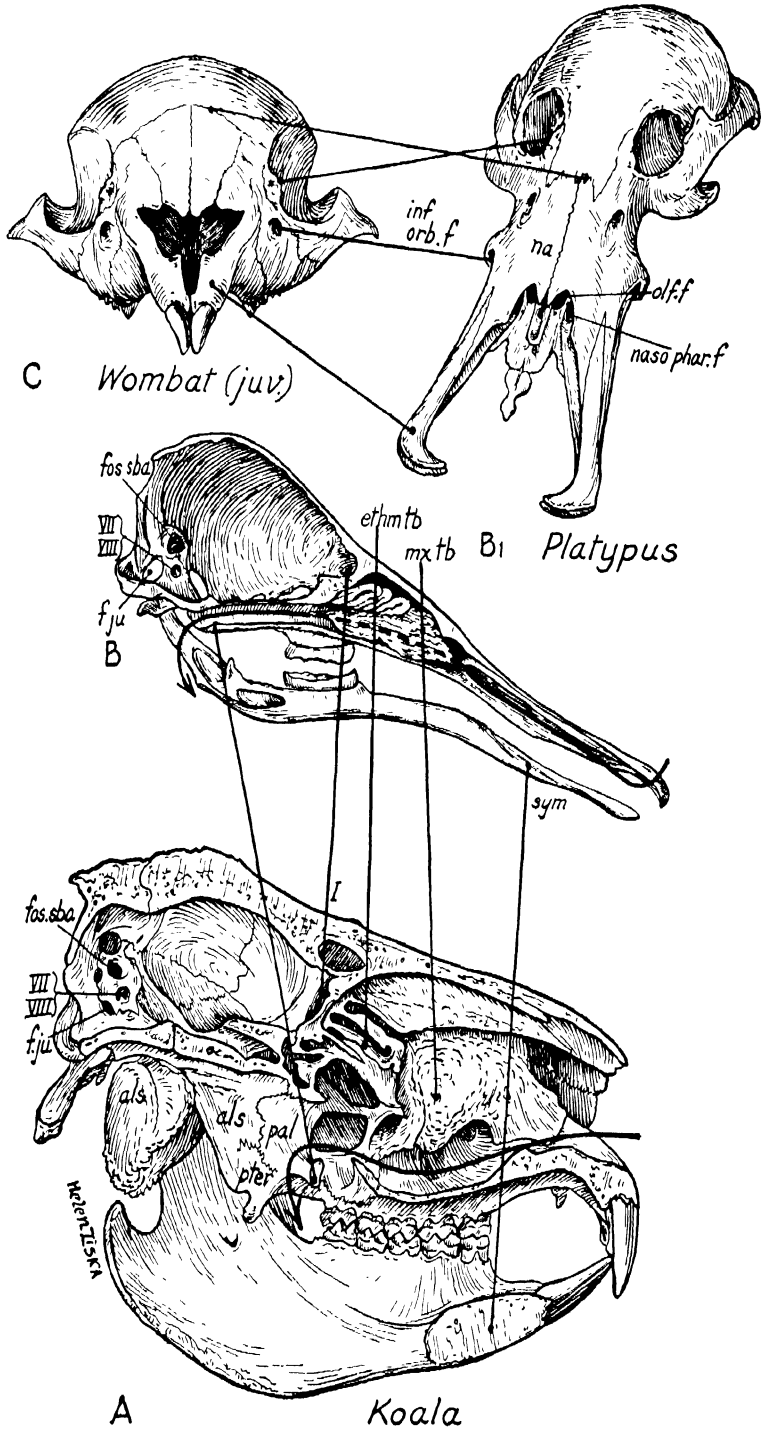


Fig. 18.12. Nasal chamber and nasopharyngeal canal in relation to endocranium. Although highly specialized and superficially bird-like in its cranium and bony bill, the platypus retains mammalion ethmo- and maxillo-turbinals.

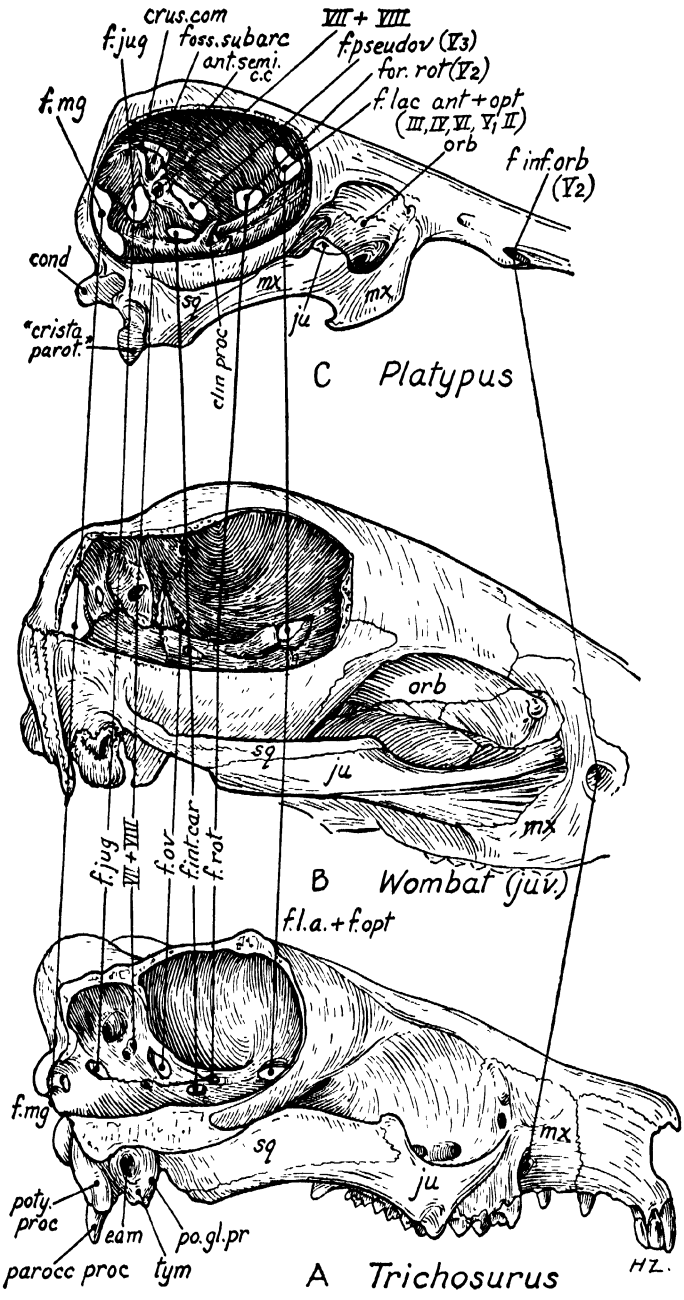


Fig. 18.13. Endocranium and main cranial nerve foramina. In the platypus some of the foramina have expanded into fenestrae but still conform in general to the marsupial pattern.

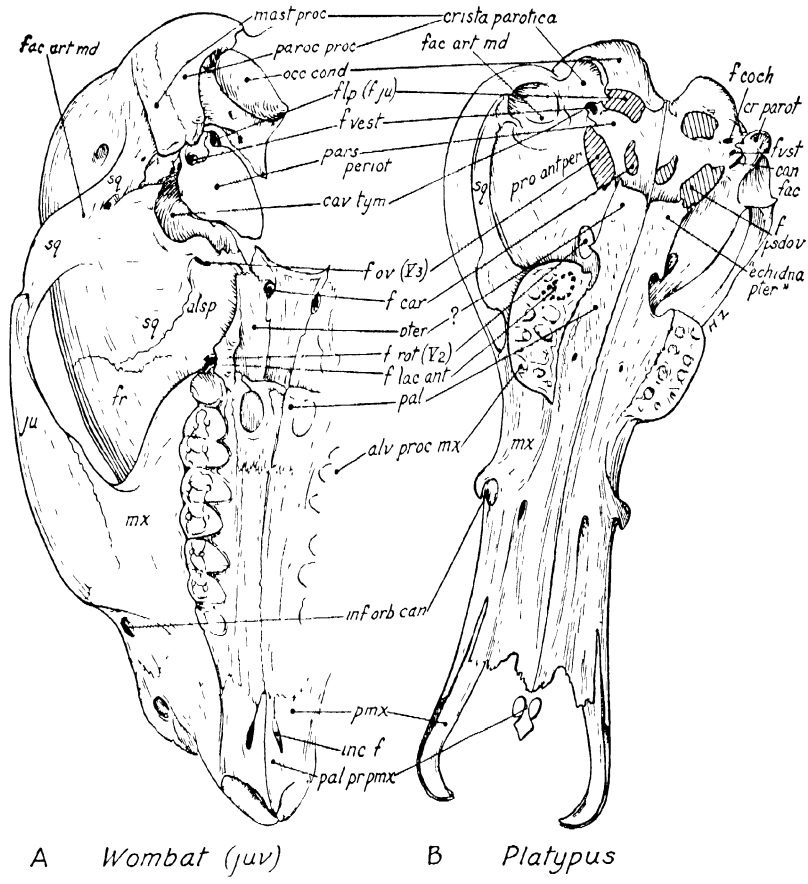


Fig. 18 14 Oblique inferior view of skulls, showing (in B). (1) backward displacement of articular support for mandible (*fac.art md*), (2) crowding and marked diminution of auditory and basioccipital region, (3) backward shift of main foramina (4) The minute epitympanic cavity is overarched by the conjoined mastoid and paroccipital processes which form the "crista parotica"

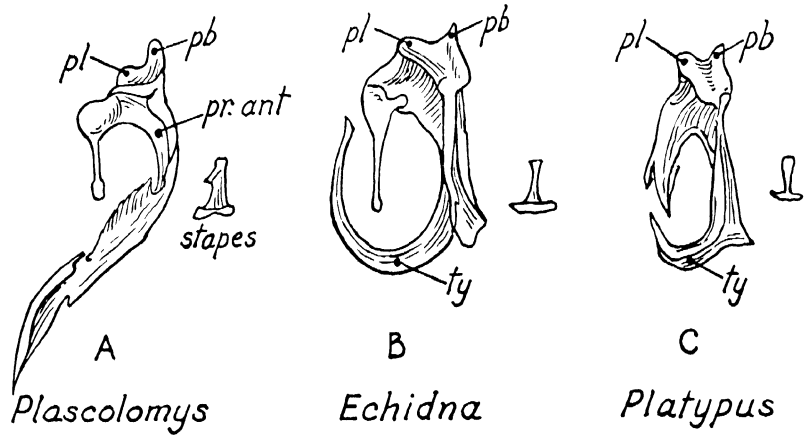


Fig. 18.15. Ossicula auditus. After Doran. Showing essentially mammalian pattern in montotremes. *Pl*, processus longus (of incus); *pb*, processus brevis; *pr ant*, processus anterior (of malleus); *ty*, tympanic.

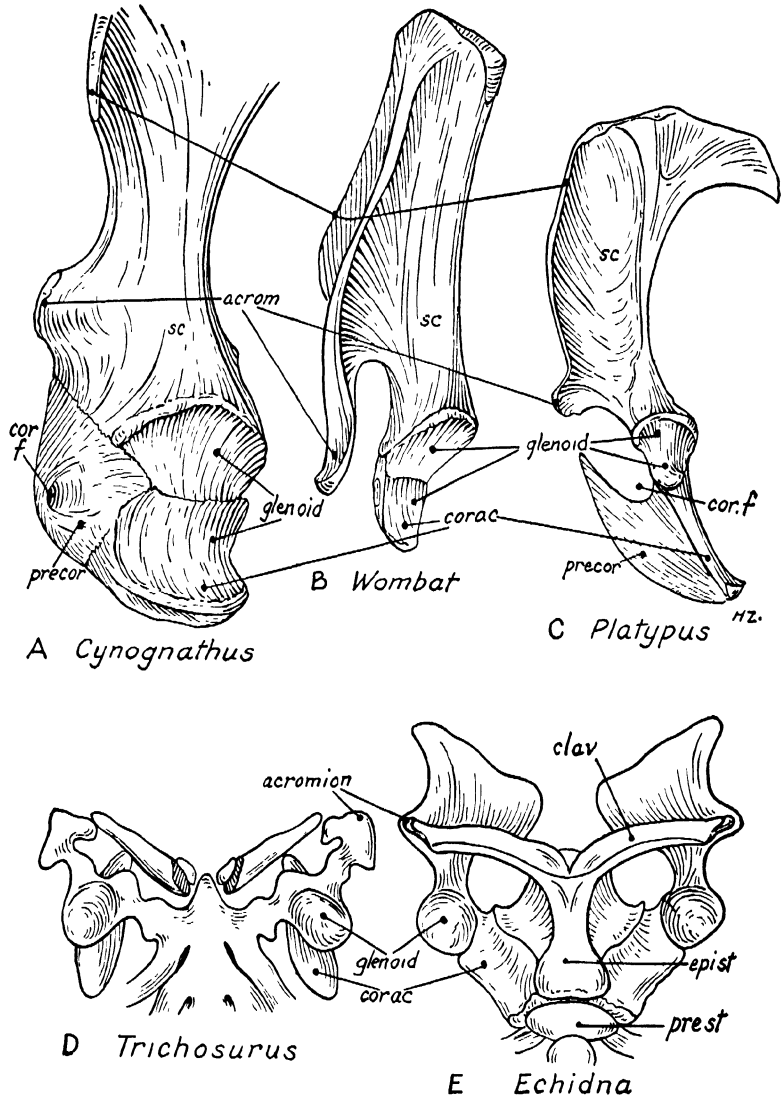


Fig. 18.16. Morphology of the coracoid. D, E, after Broom. In B the dot on the upper anterior margin should have been on the edge of the crest or spine.

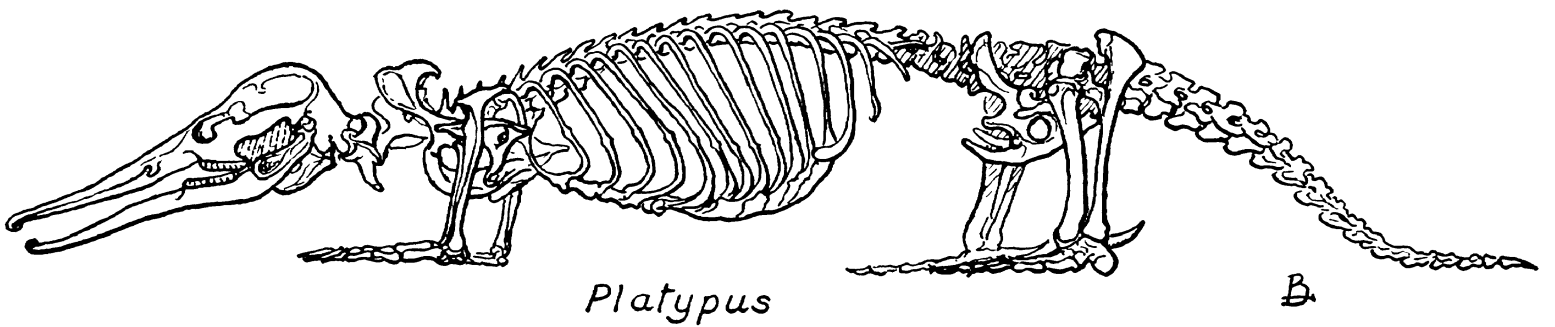


Fig. 18.17. Skeleton of platypus.

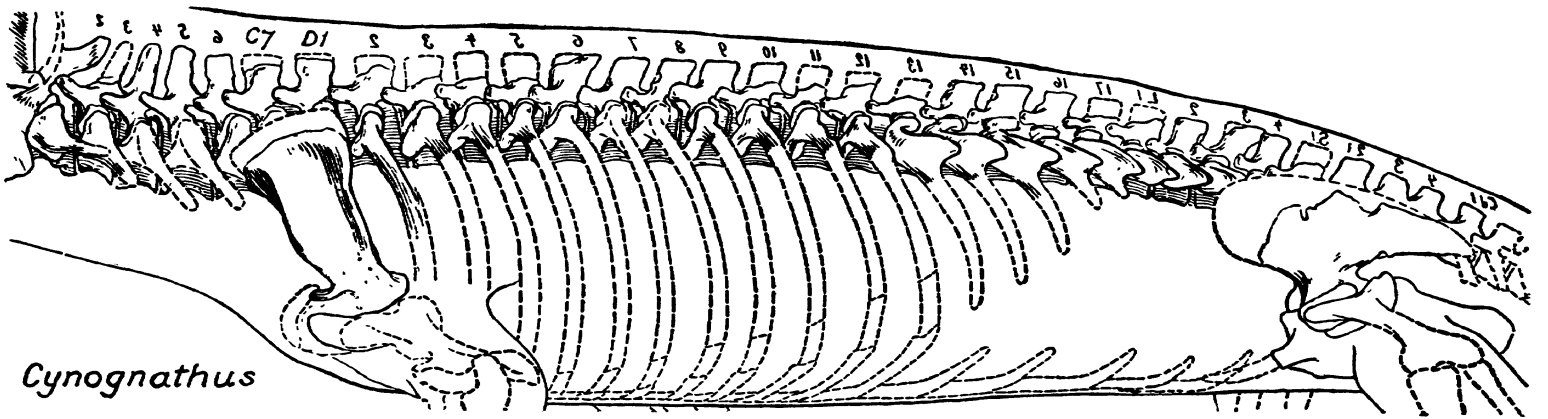


Fig. 18.18. Reconstruction of *Cynognathus* skeleton.

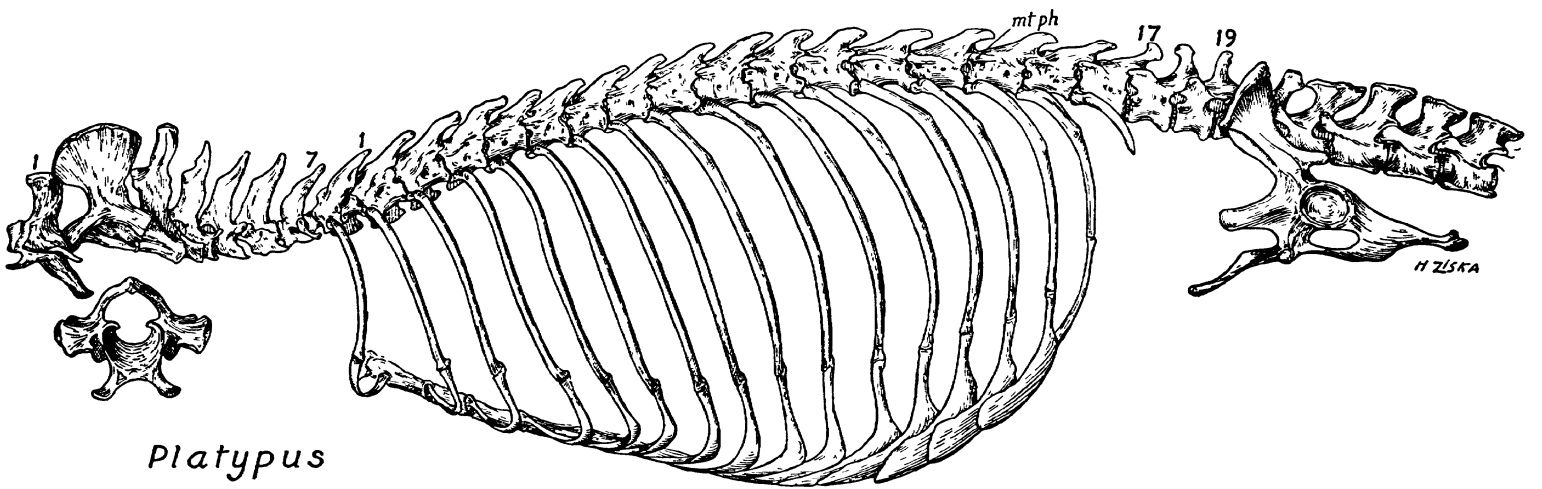


Fig. 18.19. Vertebral column, ribs and pelvis of platypus.

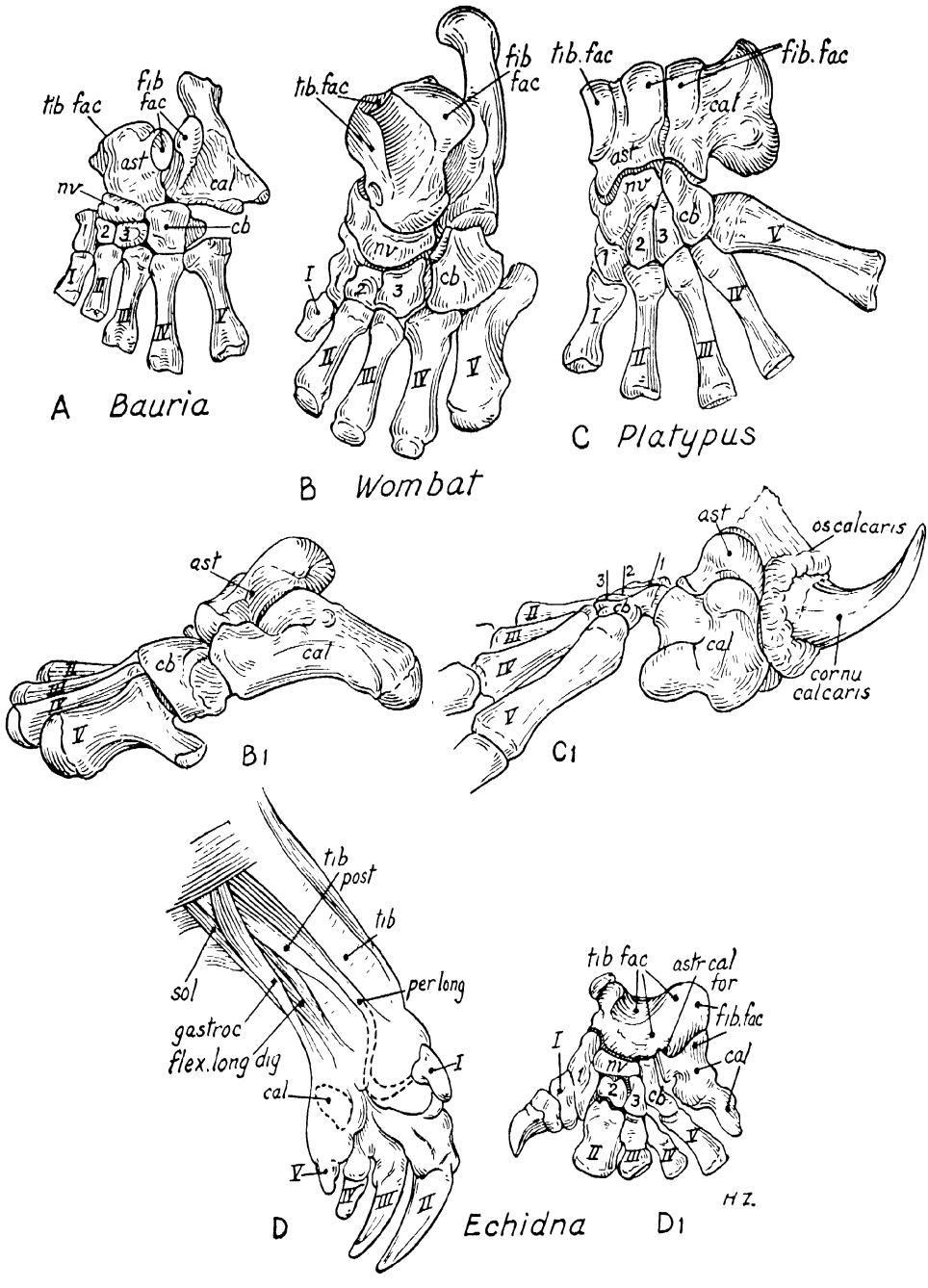


Fig. 18.20. Left hind feet: A, Triassic mammal-like reptile which had almost attained the mammalian grade (p. 339); B, wombat (*Phascolomys*), with bones adapted for digging; C, Platypus, with bones adapted for digging and swimming. B1, C1, Lateral views showing large tarsals adapted for digging; C1 also shows the pulley-like articular surface for the tibia and the fang-like form of the horny spur. D, Posterior side of the left hing leg, showing some of the muscles that draw the foot backward and inward in digging. A, after B. Schaeffer; D, after Mivart; others original.

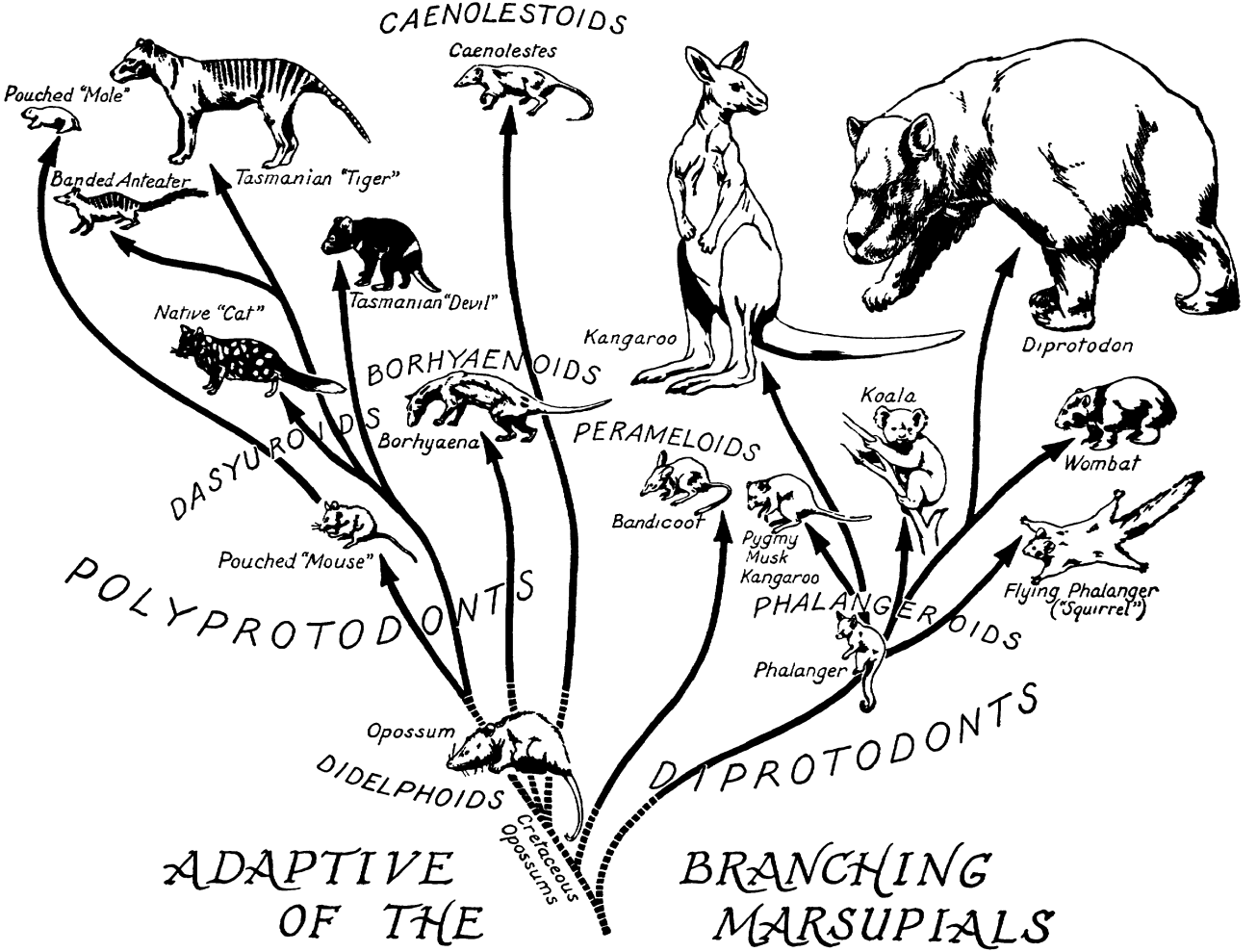


Fig. 18.21. Adaptive branching of the marsupials. After Gregory.

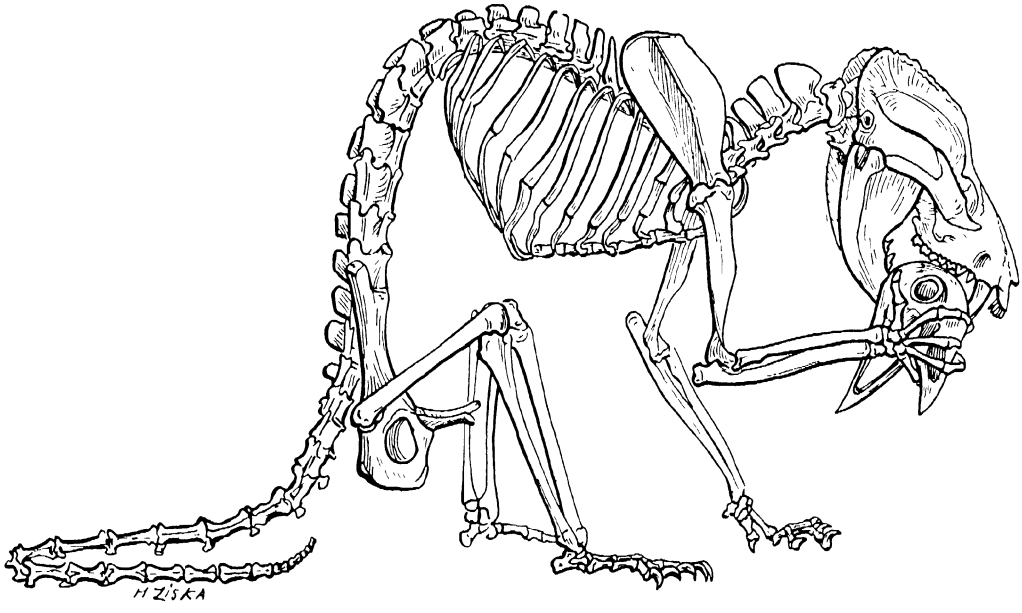


Fig. 18.22. Skeleton of North American opossum. Mounted by S. H. Chubb.

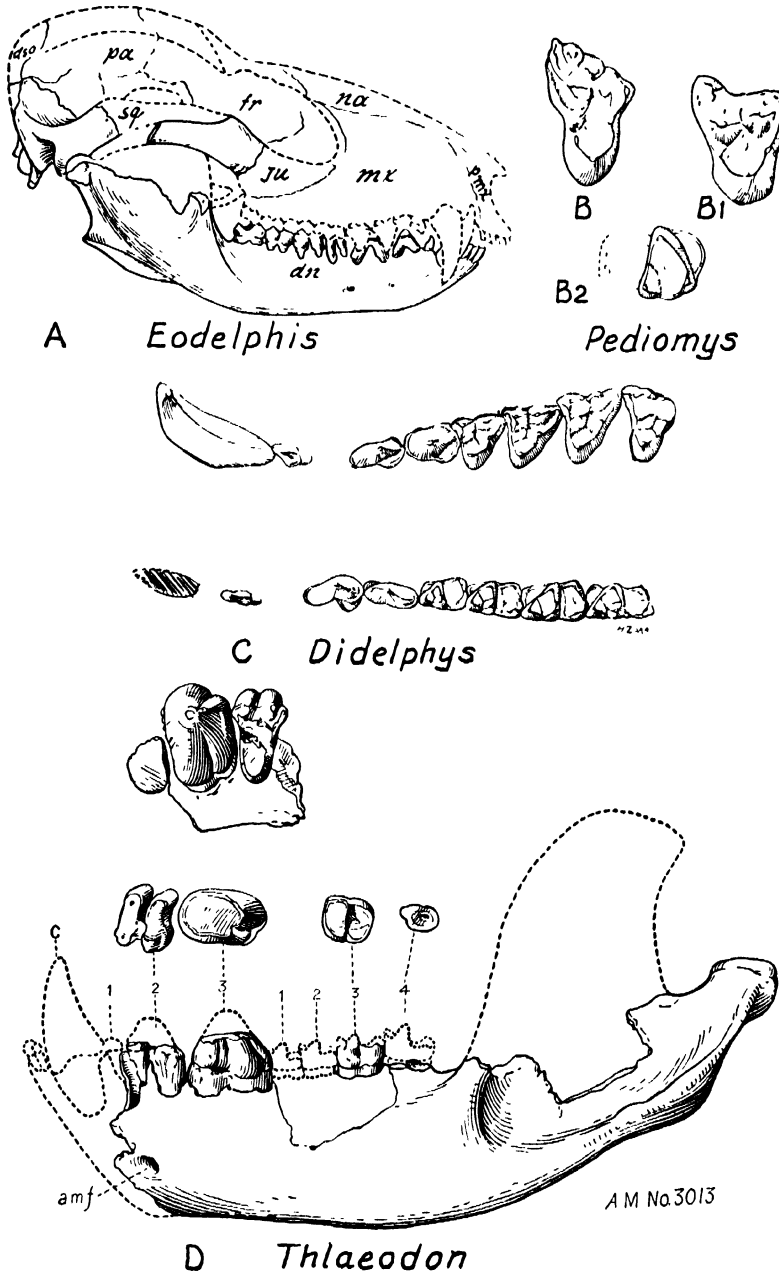


Fig. 18.23. Fossil marsupial skull fragments (A, D) and teeth (B–B2, D) from the Upper Cretaceous of North America. Upper and lower teeth of modern opossum (C).

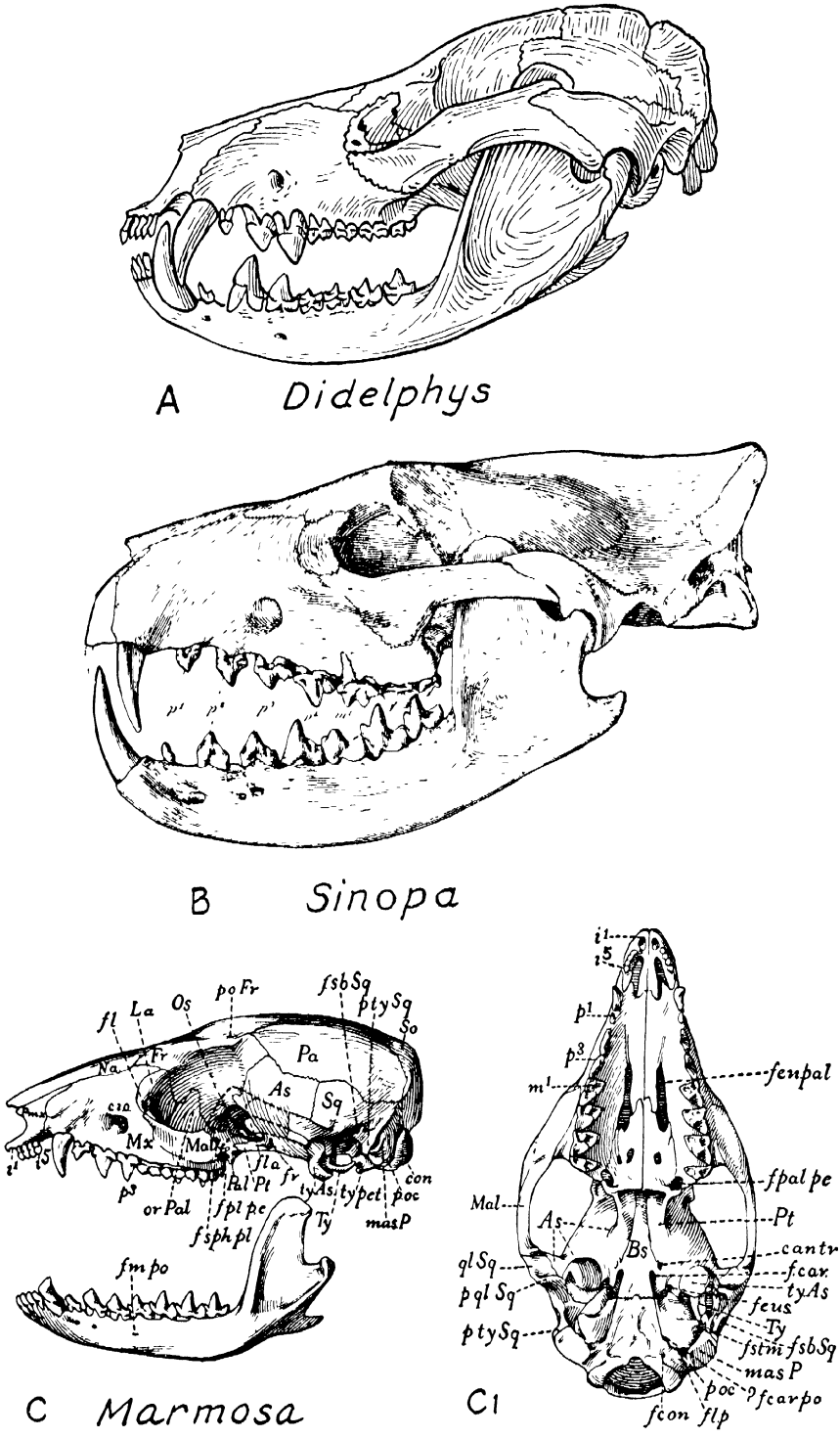


Fig. 18.24. Skulls of opossum (A) and Eocene creodont (B). A, original; B, after Matthew. Skull of small opossum (C, C1) to show marsupial heritage characters After Gregory.

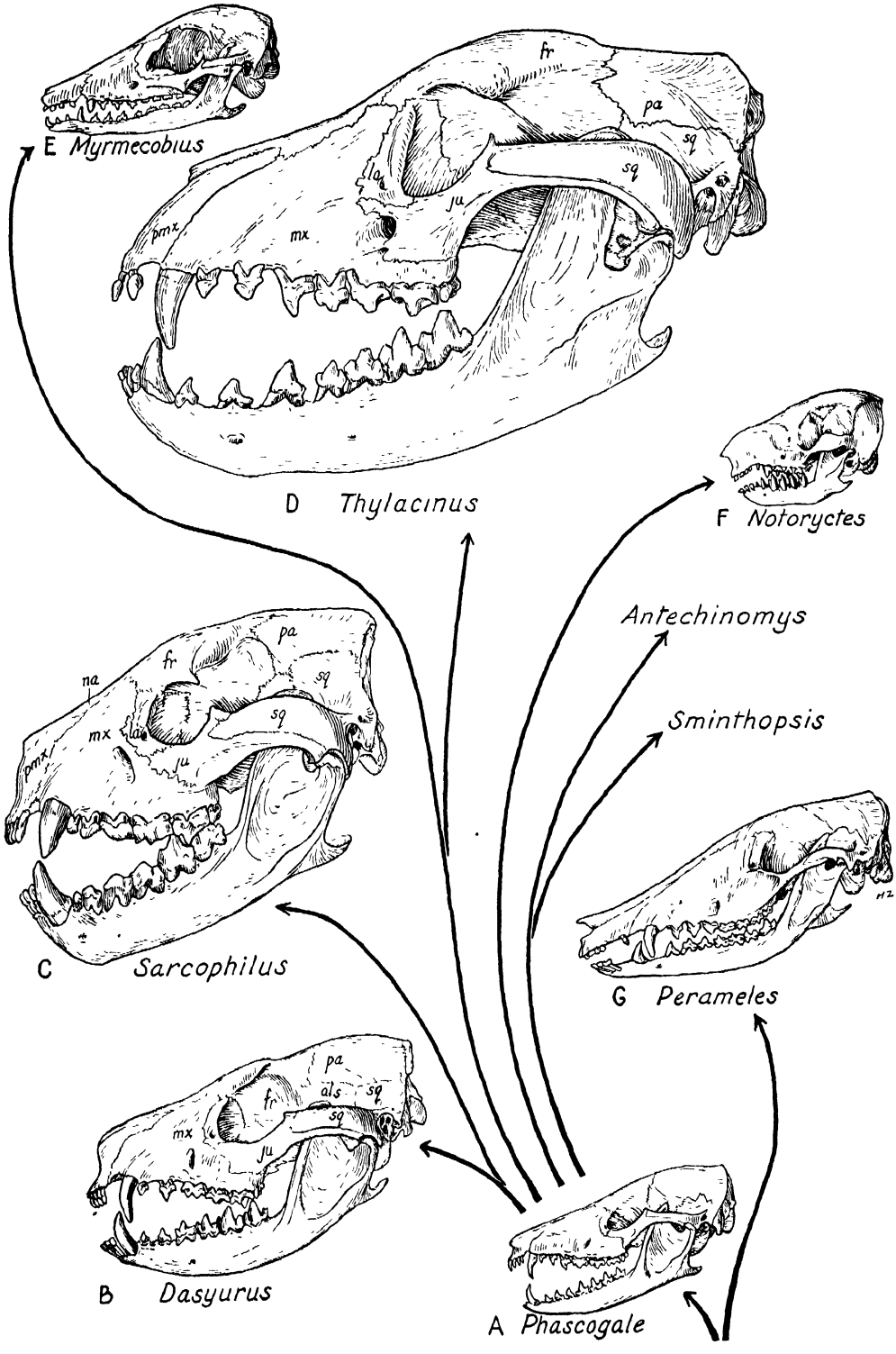


Fig. 18.25. Skulls of Australian polyprotodonts.

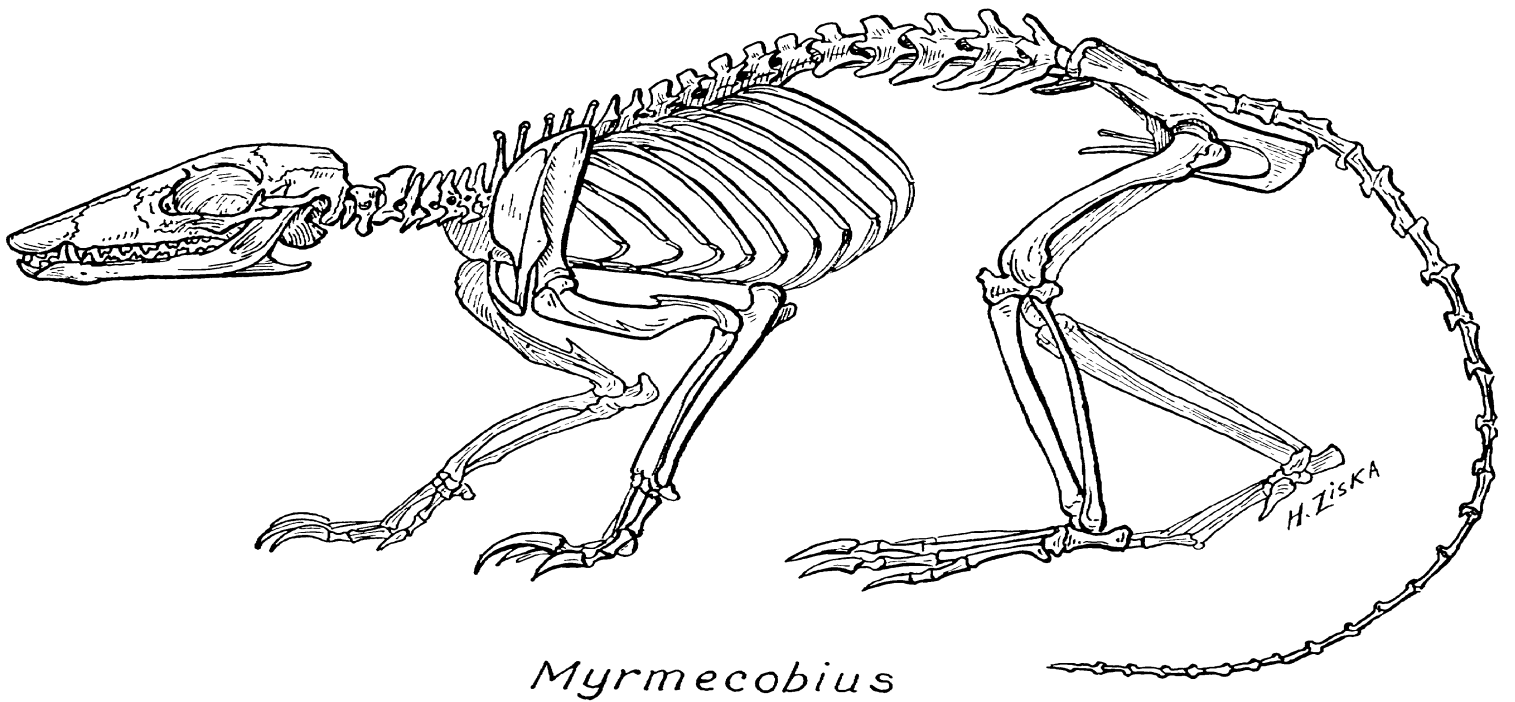


Fig. 18.26. Skeleton of "banded anteater" From mounted specimen.

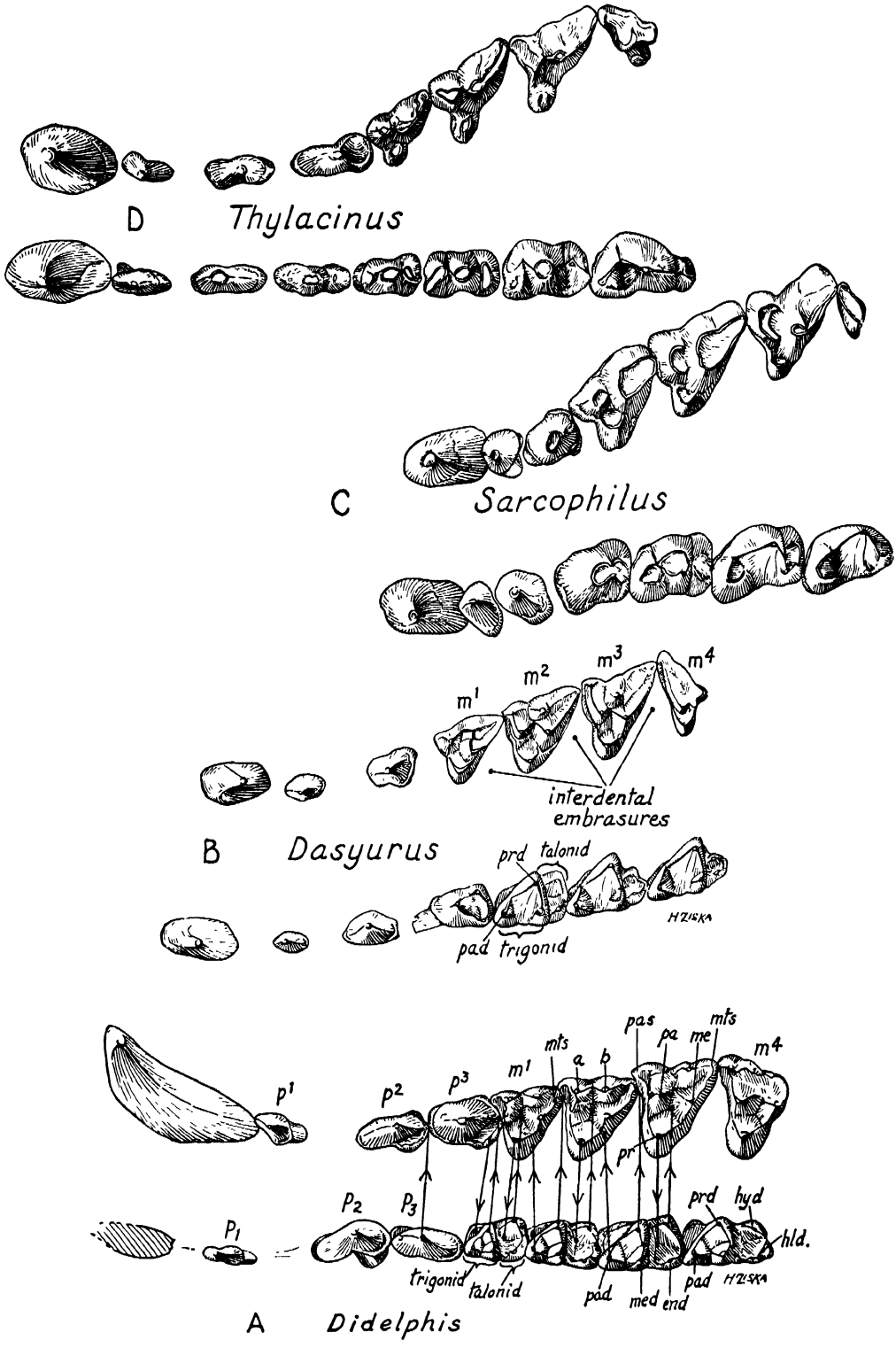


Fig. 18.27. Correlated evolution of upper and lower cheek teeth in progressively shearing dentitions of Australian dasyuroids and in an American opossum.

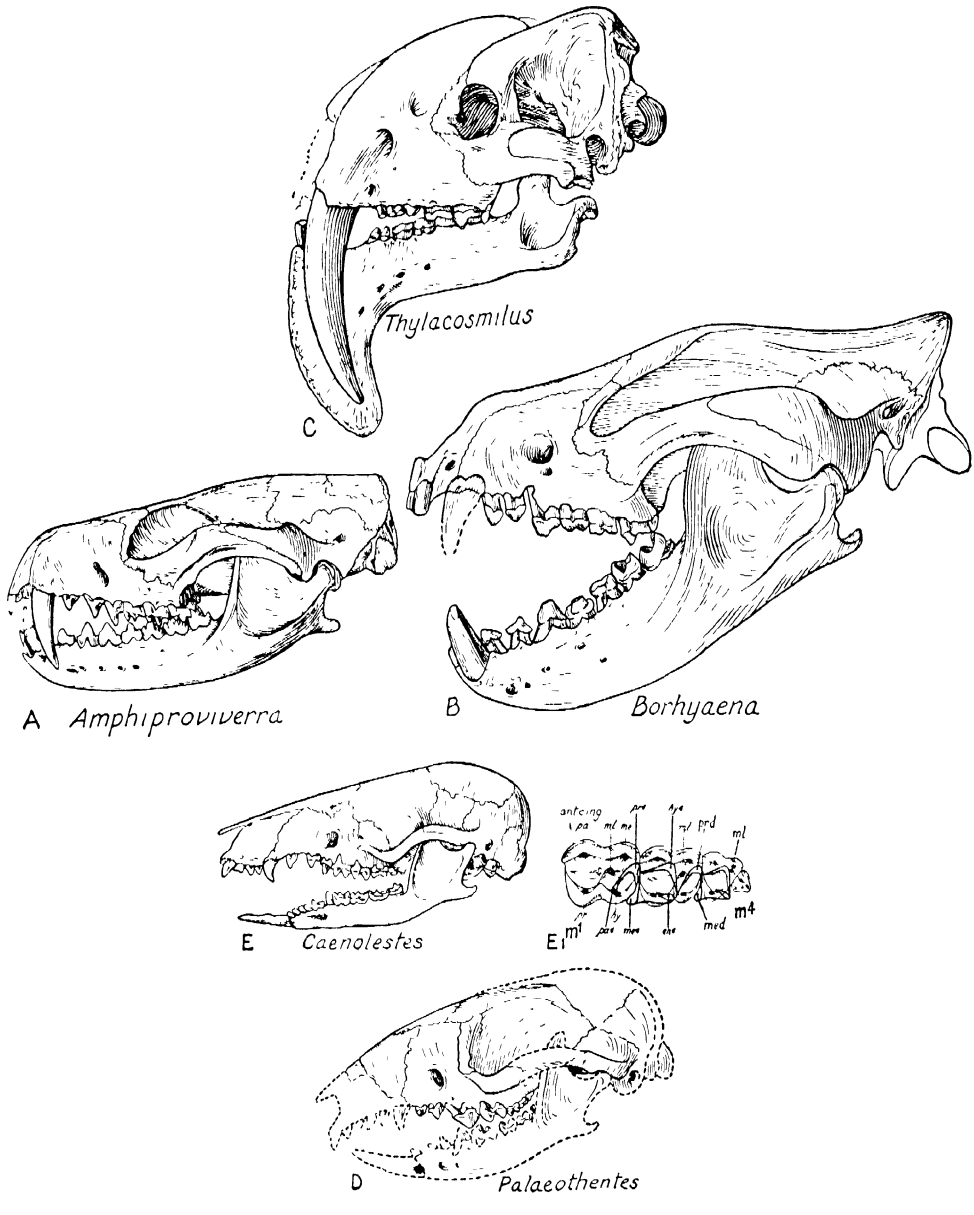


Fig. 18.28. South American marsupial carnivores (A–C) and caenolestoids (D–E1). A, B, E, after Sinclair; C, after Riggs; D, data from Sinclair; E1, after Gregory.

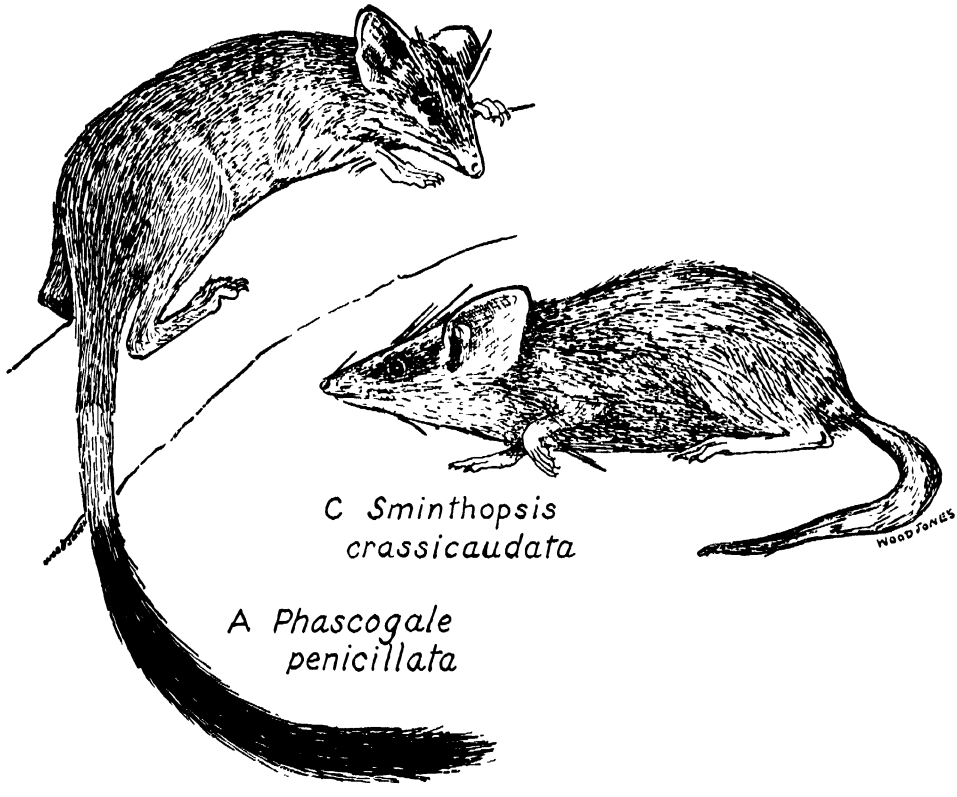


Fig. 18.29a. Small dasyuroids from the Australian central desert. After Wood Jones.

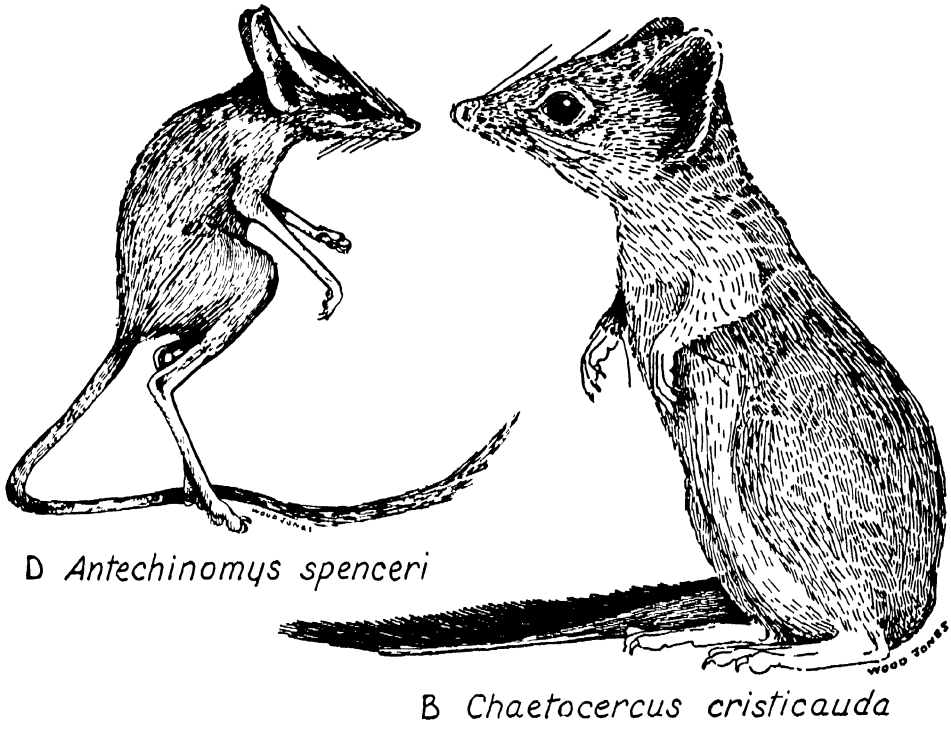


Fig. 18 29b. Small dasyuroids from the Australian central desert (continued). After Wood Jones.

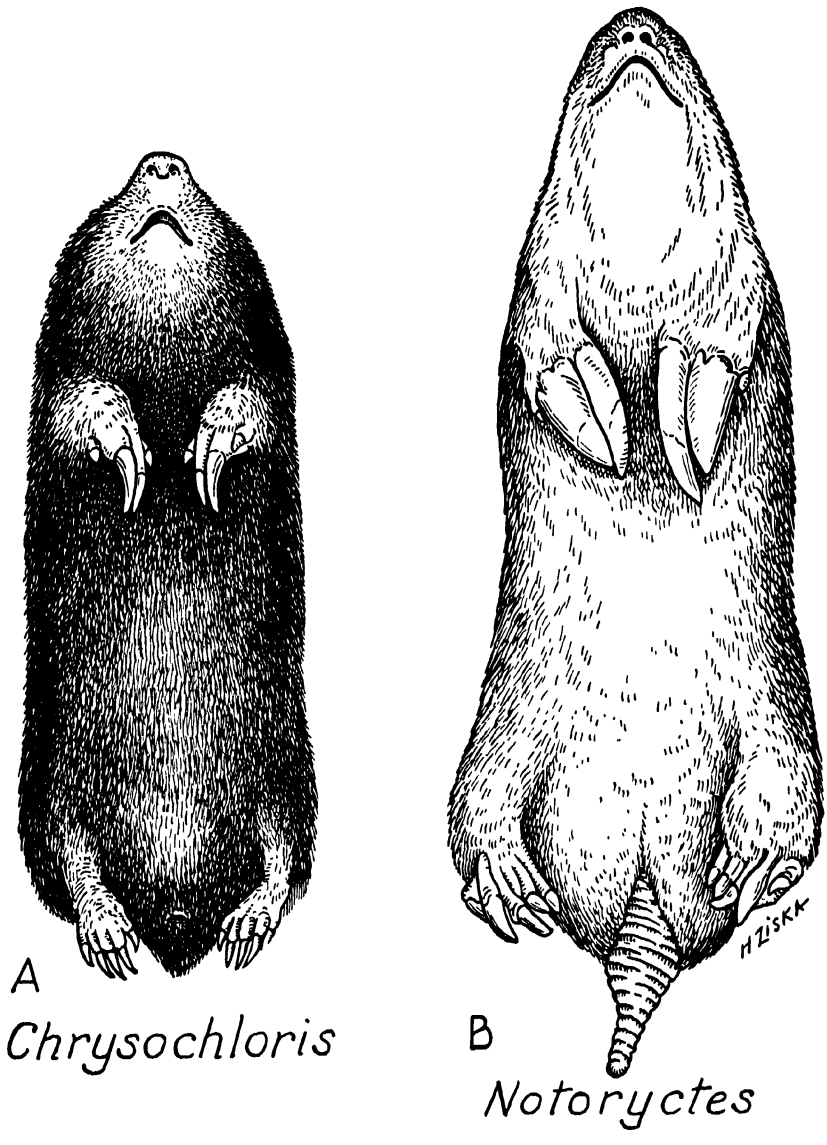


Fig. 18.30. Convergence in body form between the placental Cape Golden mole (A) and the marsupial "pouched mole." From Gregory; A, original; B, after Stirling.

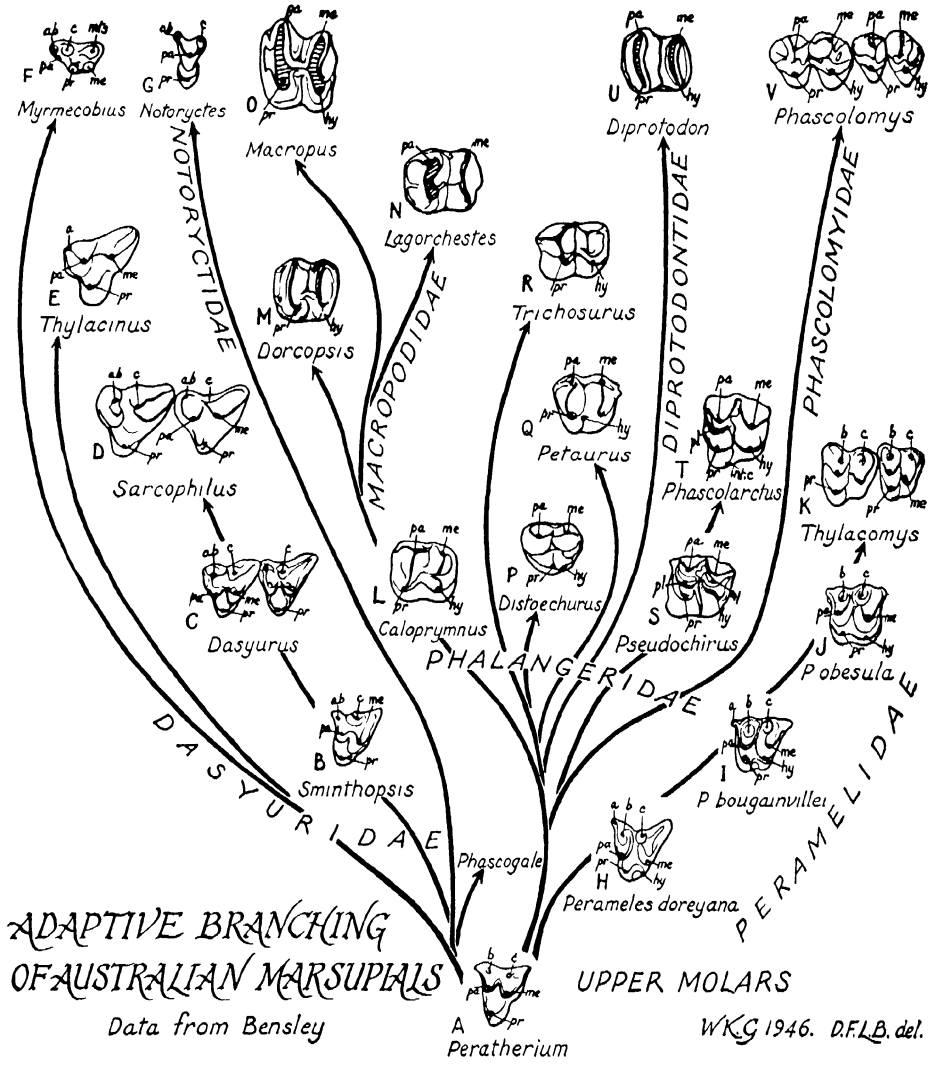


Fig 18.31. Branching evolution of upper molar patterns in Australian marsupials. Data chiefly from Bensley.

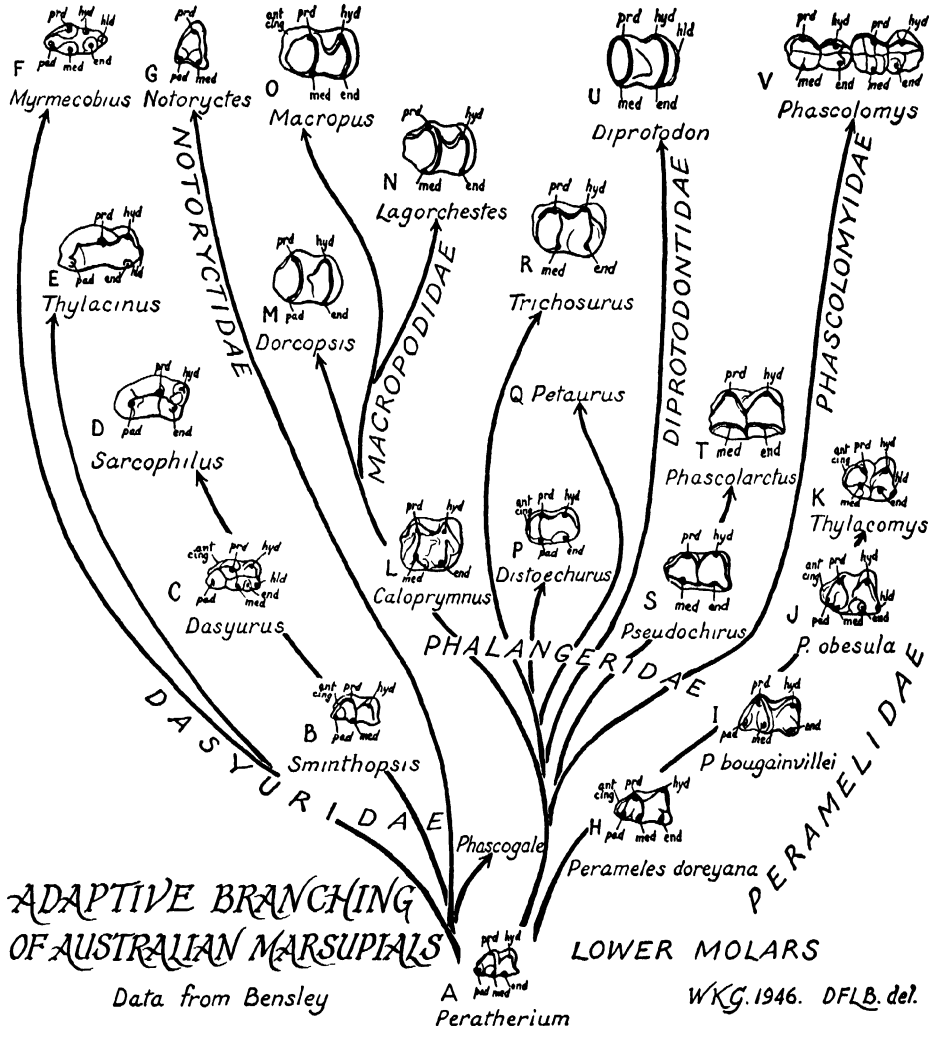


Fig. 18.32. Branching evolution of lower molar patterns in Australian marsupials. Data chiefly from Bensley.

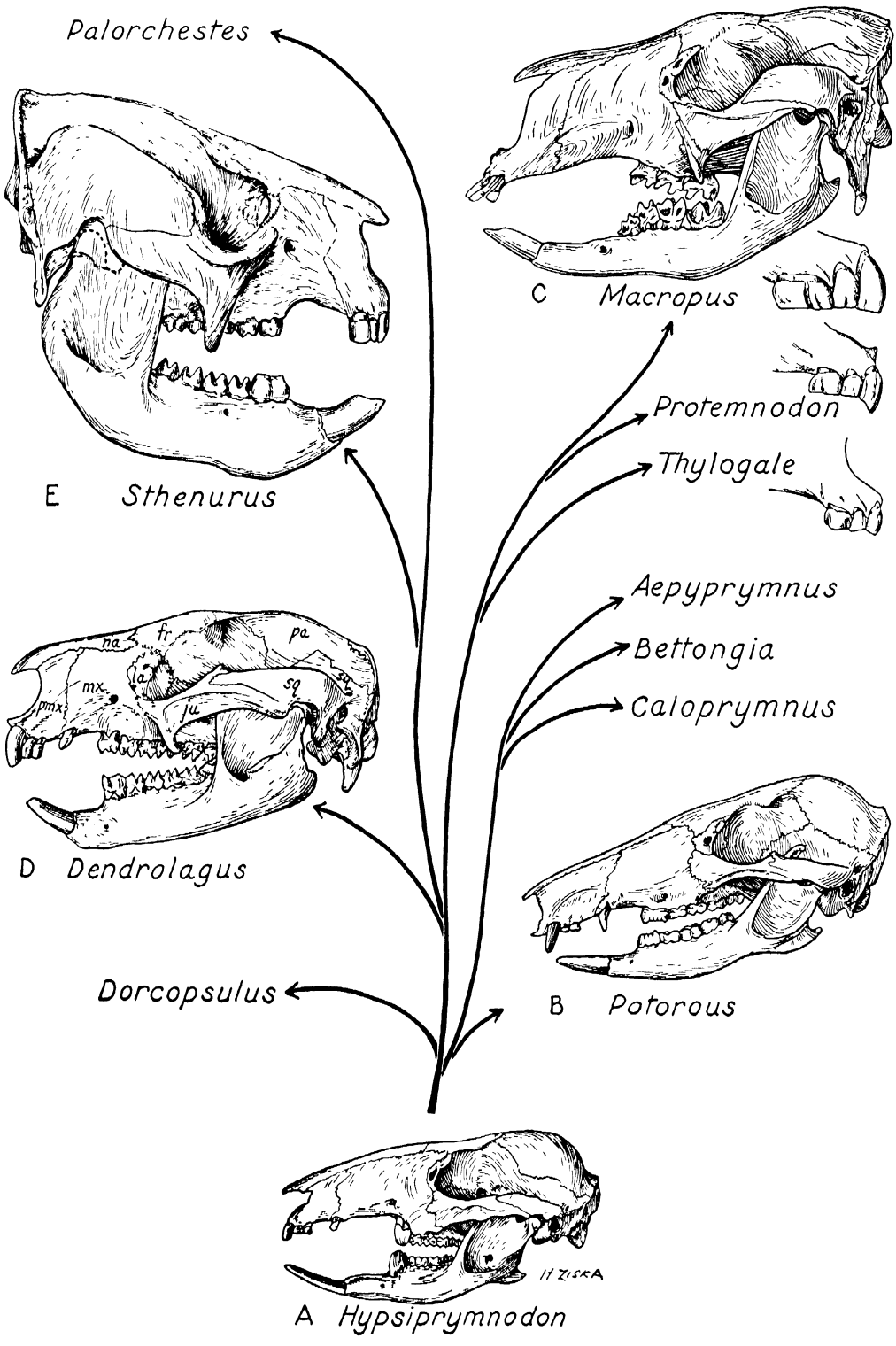


Fig. 18.33. Adaptive branching of the skulls of kangaroos. Phylogenetic data from Raven.

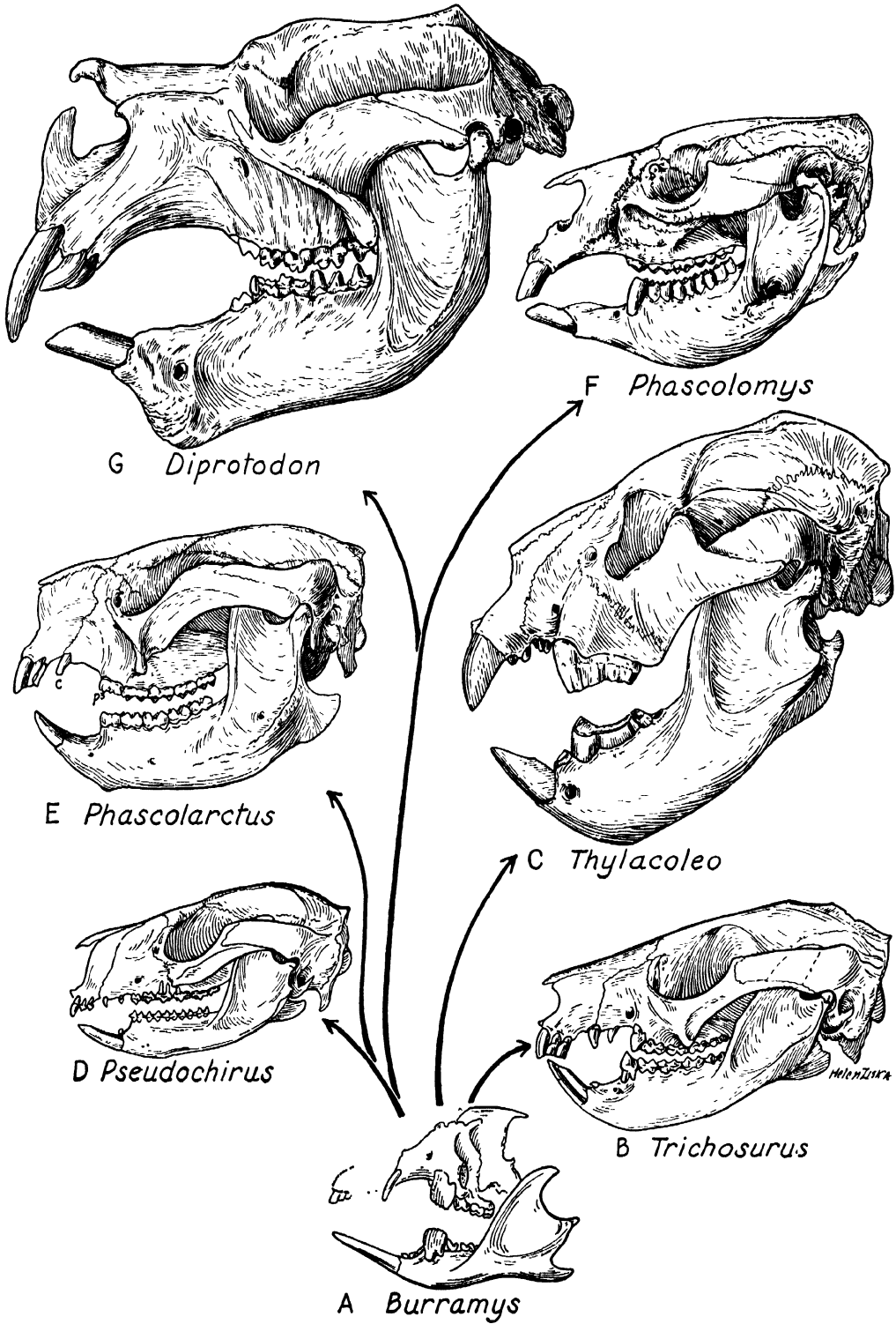


Fig. 18.34. Adaptive branching of the skulls of phalangeroids.

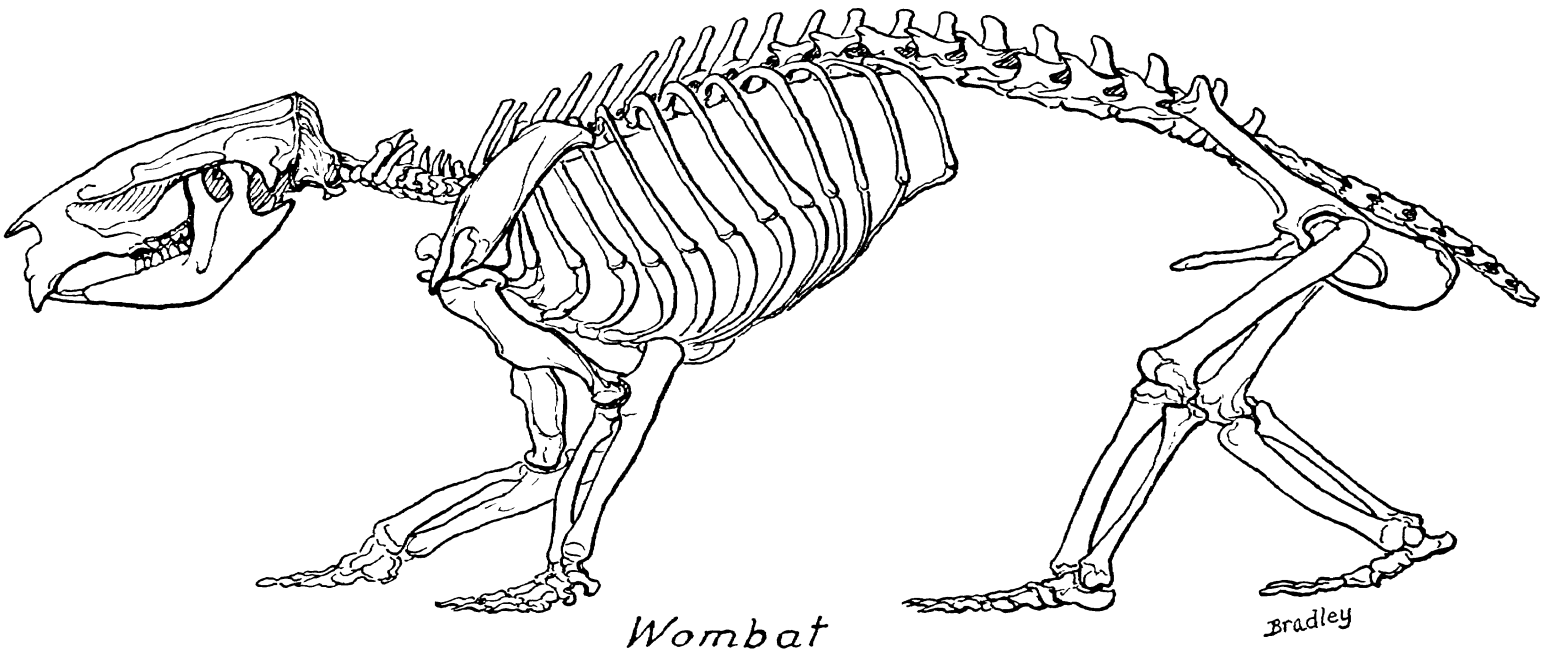


Fig. 18.35. Skeleton of wombat, showing adaptation for digging, especially in the massive limbs and short, wide, well-clawed feet.

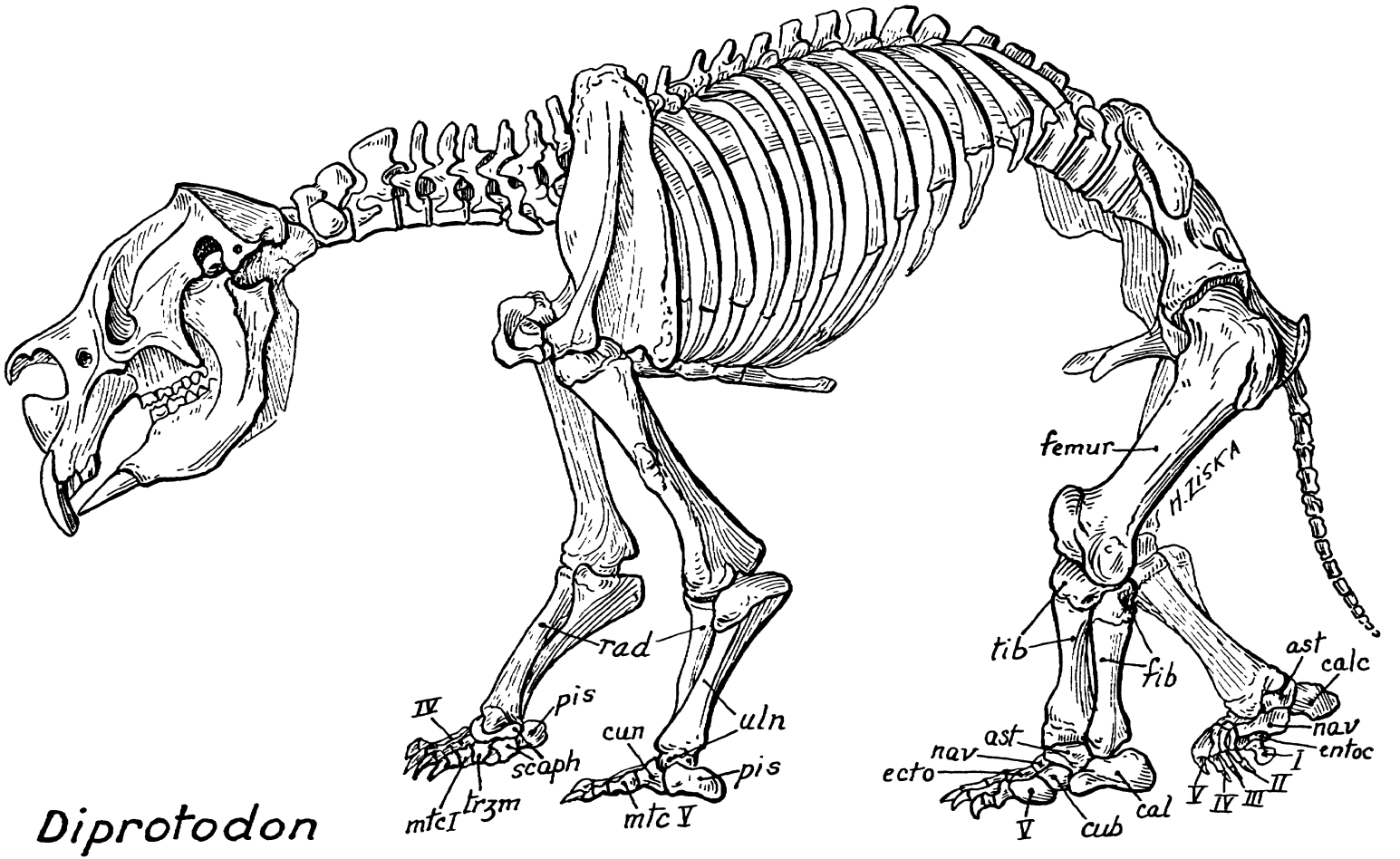


Fig. 18.36. Skeleton of *Diprotodon*. Data from Stirling and Dietz and from casts of bones assembled and mounted in the American Museum of Natural History.

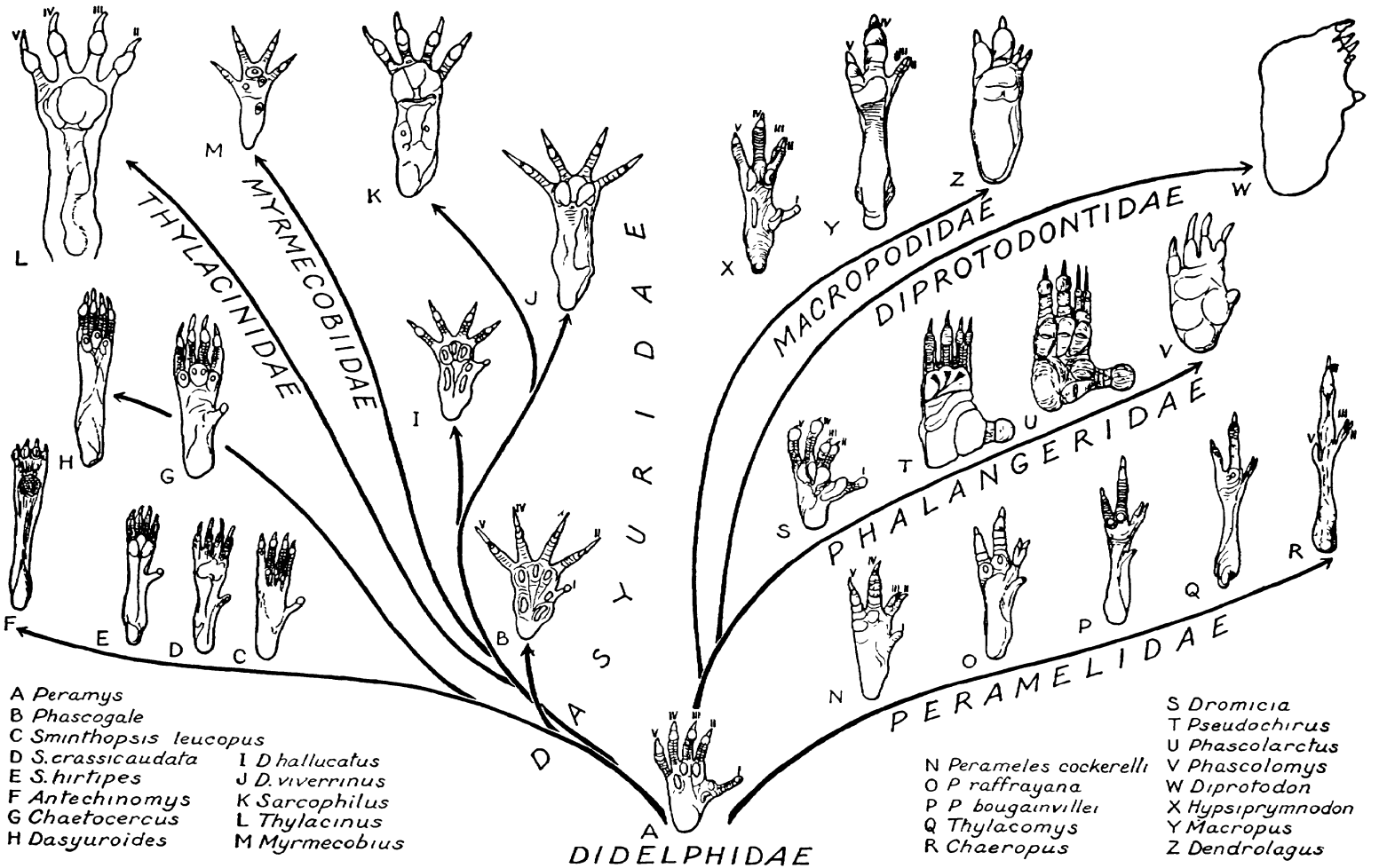


Fig. 18.37. Branching evolution of the hind feet in Australian marsupials. Chiefly after Bensley.

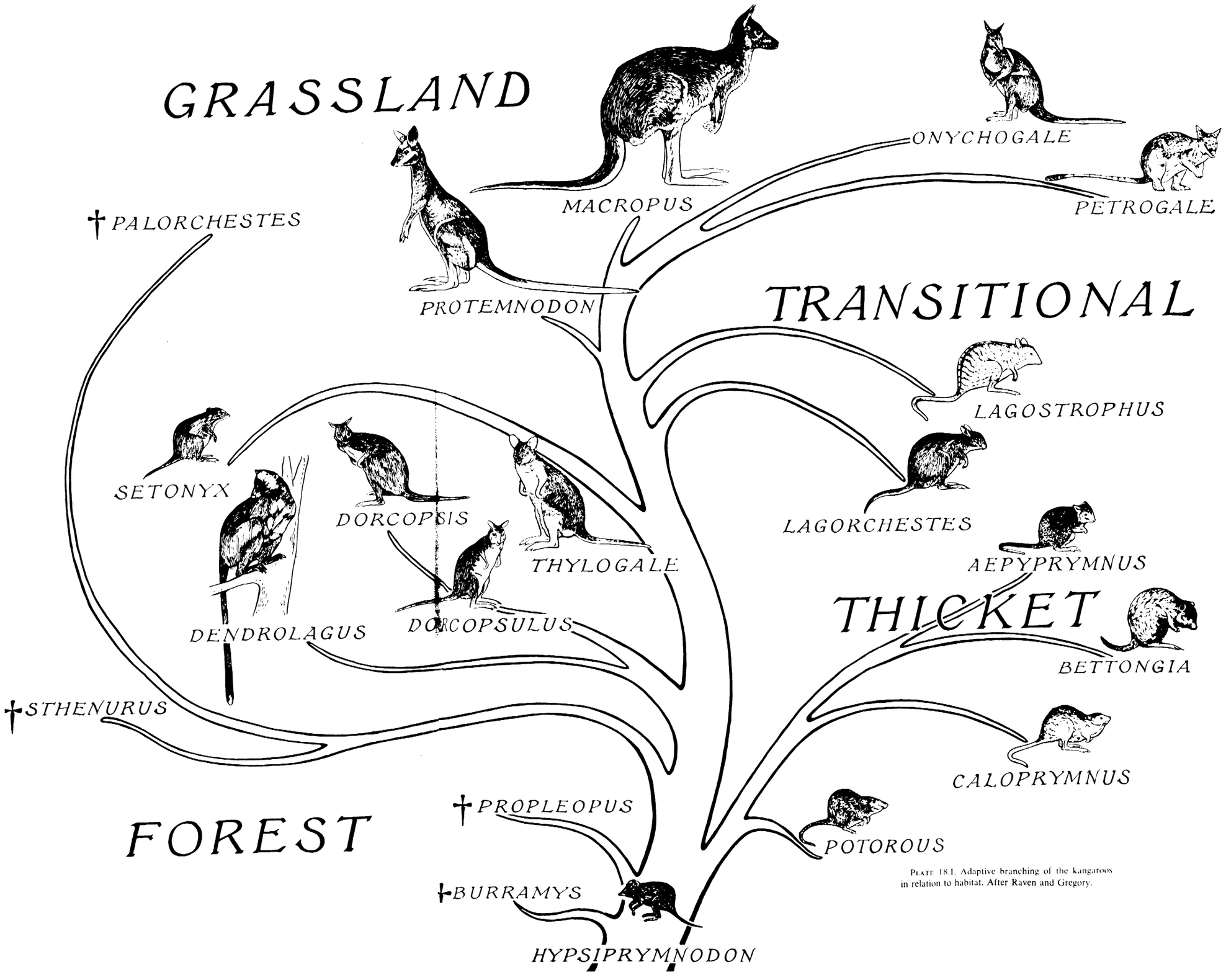
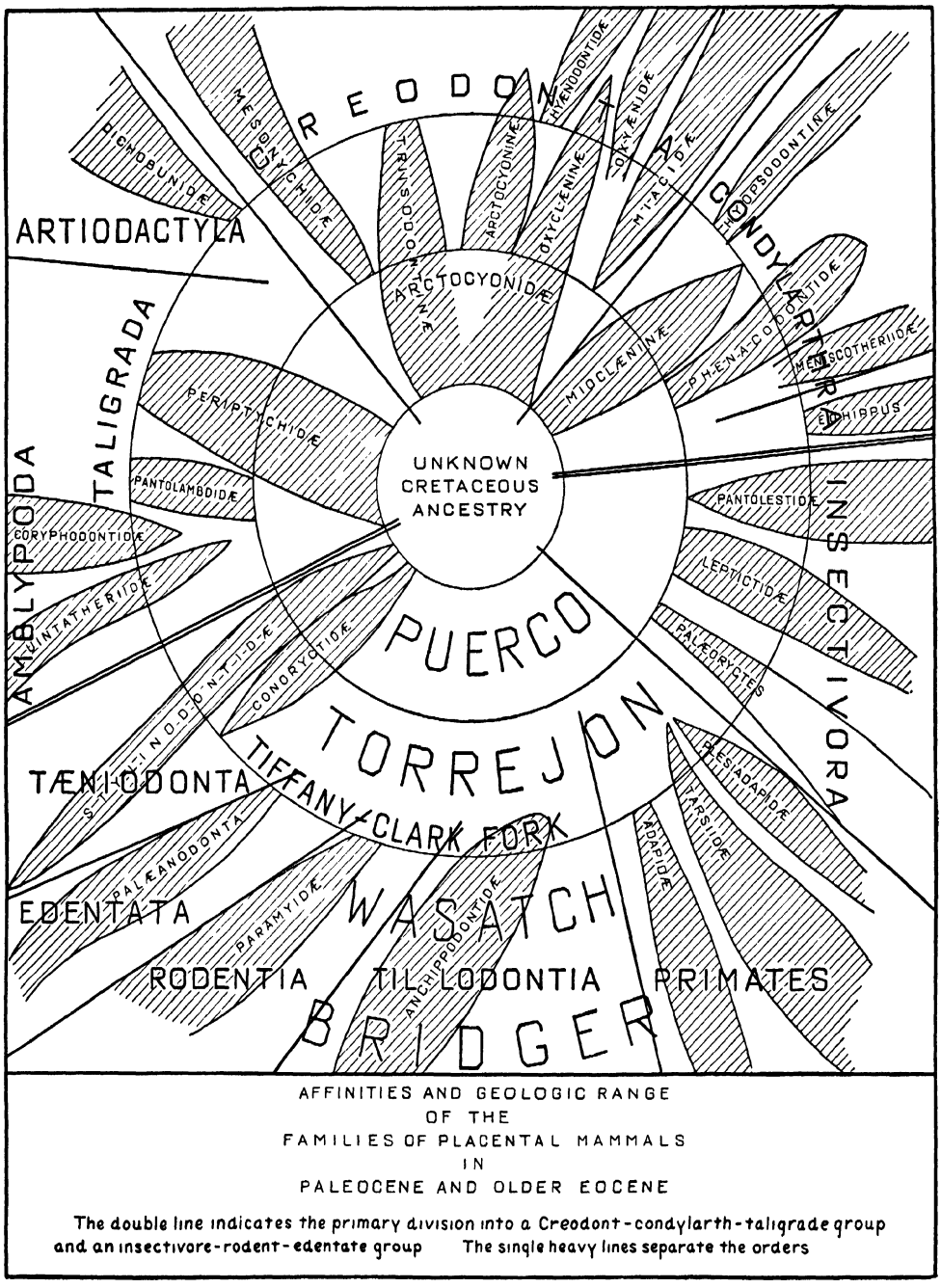


PLATE 18.I. Adaptive branching of the kangaroos in relation to habitat. After Raven and Gregory.

CHAPTER XIX

RISE OF THE PLACENTAL MAMMALS (THE OUTER FORM AND INNER FRAME OF INSECTIVORES, EDENTATES, BATS, RODENTS)



AFFINITIES AND GEOLOGIC RANGE
OF THE
FAMILIES OF PLACENTAL MAMMALS
IN
PALEOCENE AND OLDER EOCENE

The double line indicates the primary division into a Creodont-condylarth-taligrade group and an insectivore-rodent-edentate group The single heavy lines separate the orders

Fig. 19.1. Deployment and dispersal of the placental orders. After Matthew.

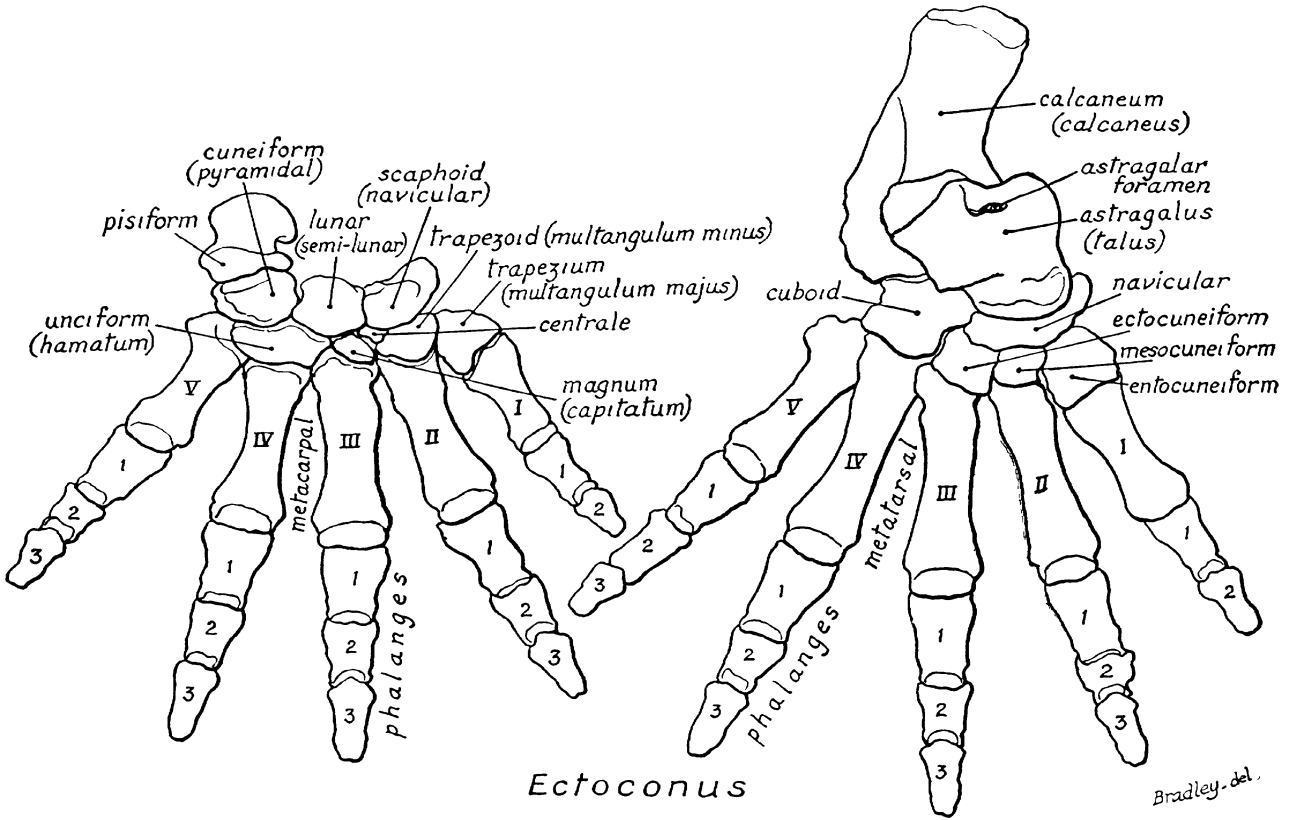


Fig. 19.2. Pentadactylate hands and feet of a representative Paleocene placental mammal. After Matthew. B. N. A. names in parentheses

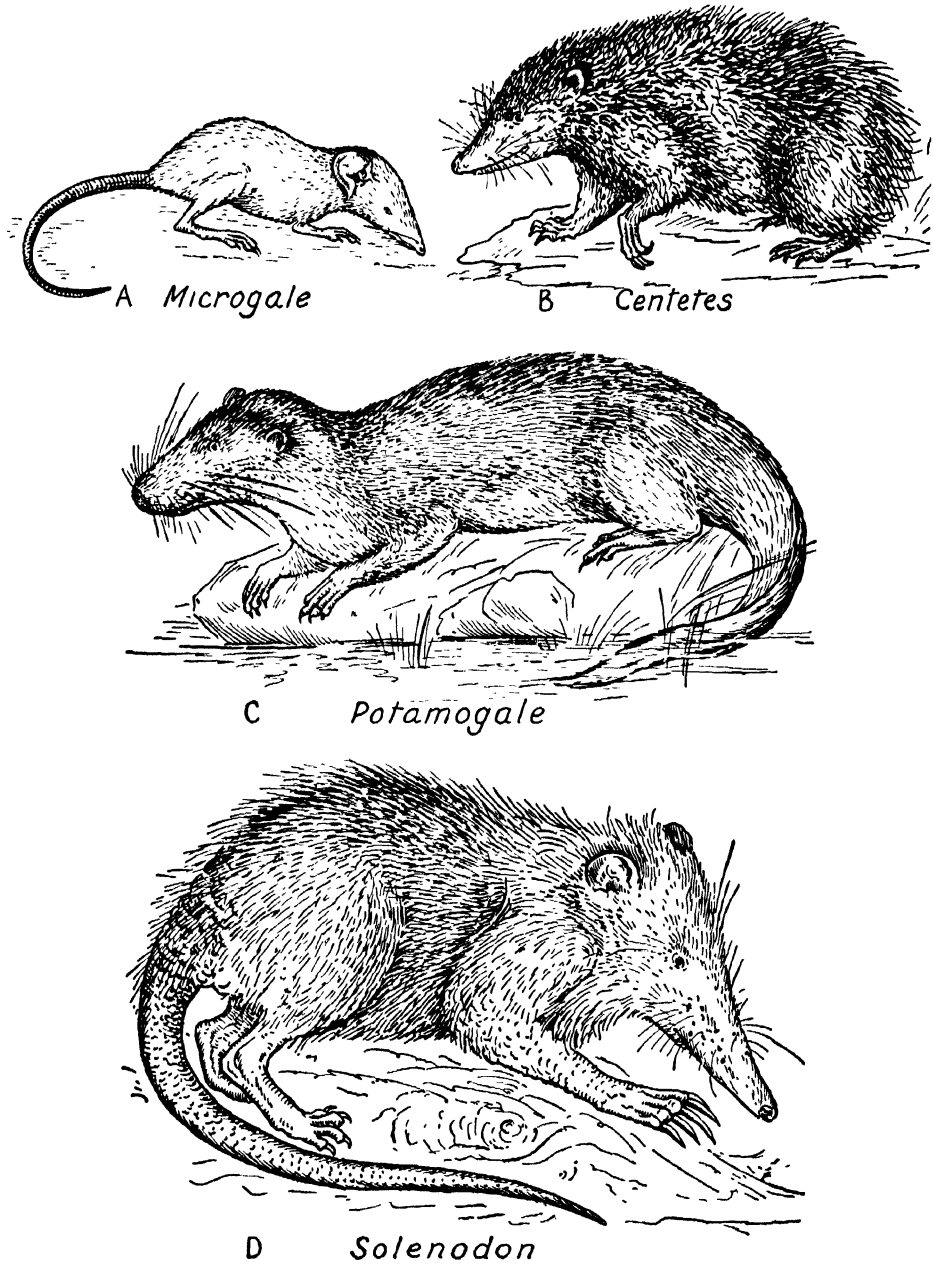


Fig. 19.3. Living zalambdodonts (centetoids) of Madagascar (A, B), Africa (C) and West Indies (D). A, after Leche; B, C, partly after Lydekker; D, after Verrill.

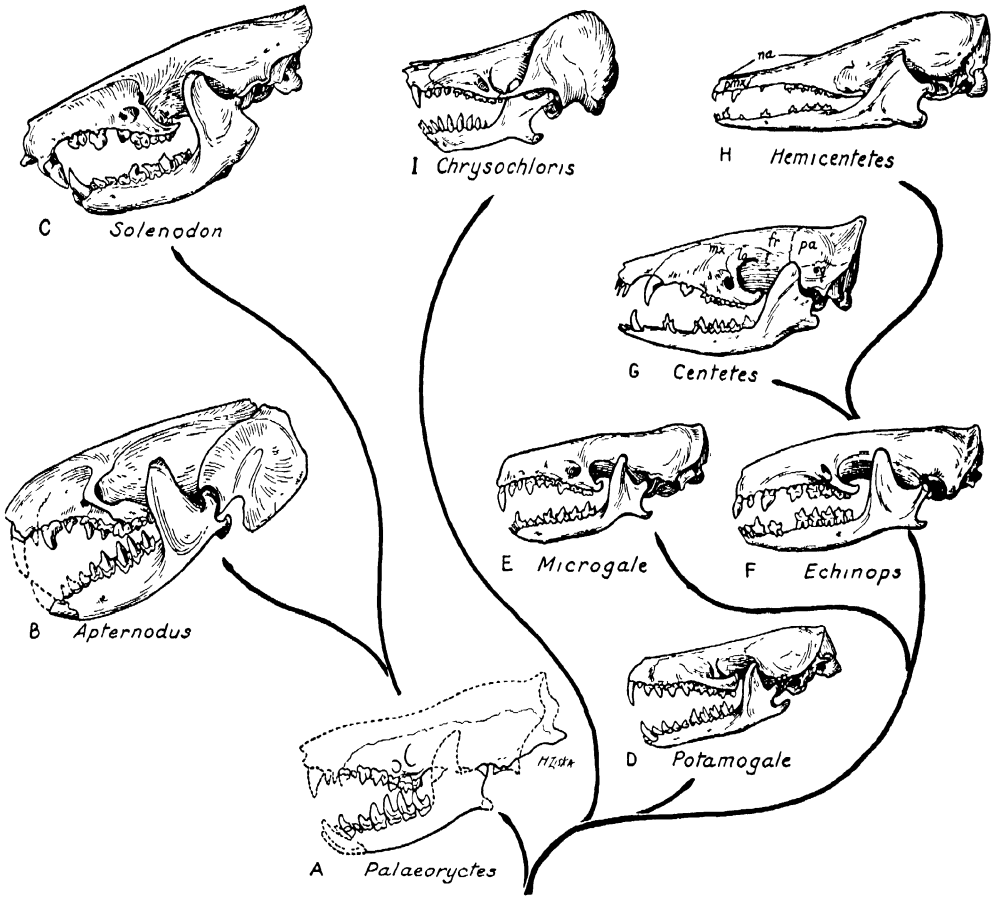


Fig. 19.4. Skulls of zalambdodont insectivores illustrating broadly successive stages. A, after Matthew; B, after Schlaikjer; C, original; D–I, African and Madagascan zalambdodonts from specimens.

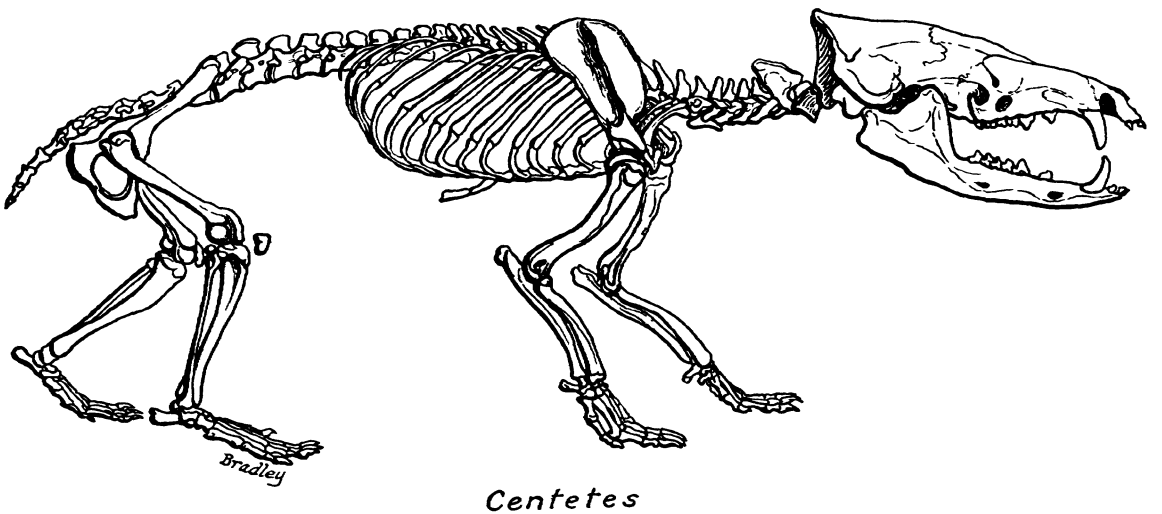


Fig. 19. 5. Skeleton of a large *Centetes.* After De Blainville.

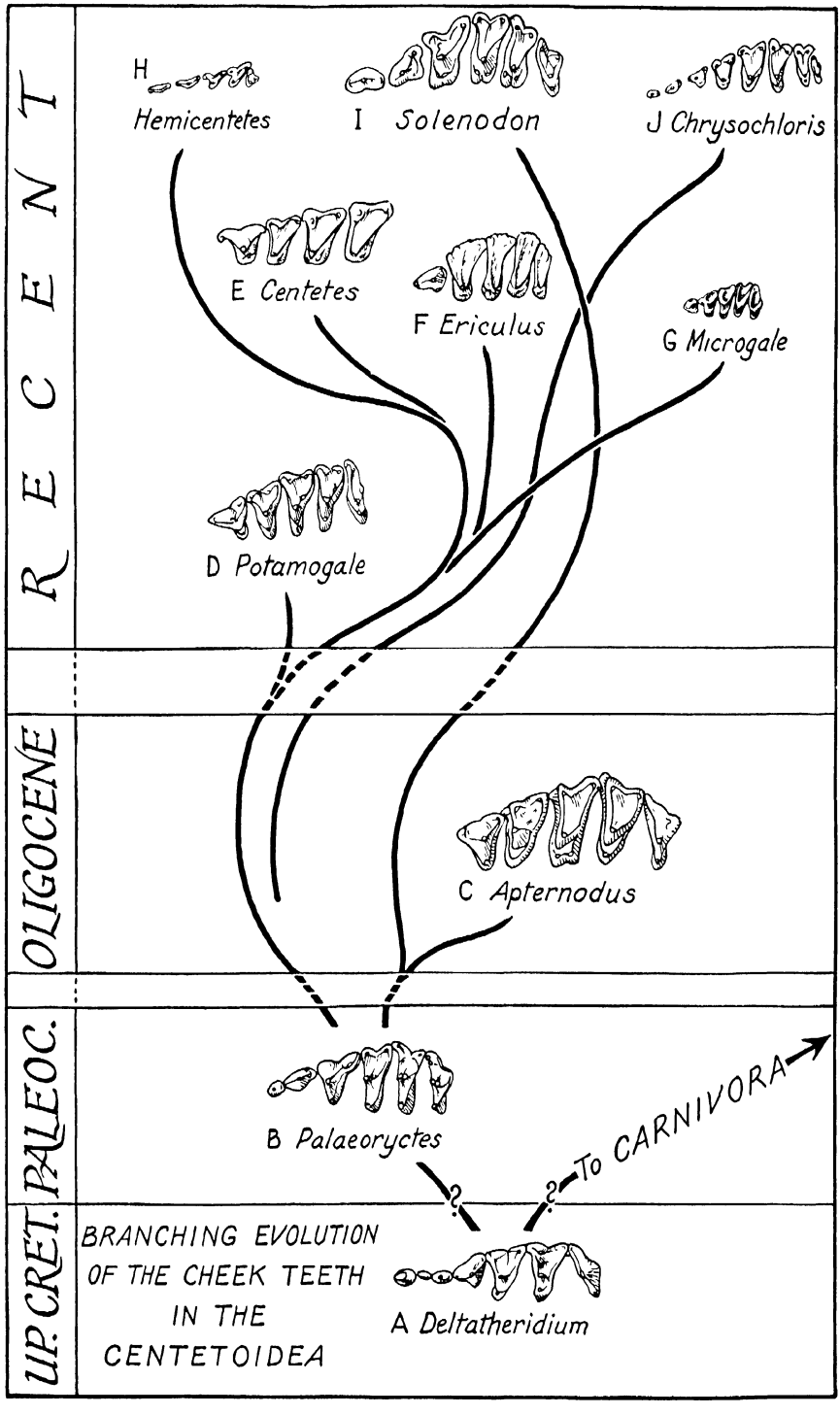


Fig. 19.6. Branching evolution of the upper cheek teeth in zalambdodonts. A, after Gregory and Simpson; B, after Matthew; C, after Schlaikjer; D–J, mostly from originals, partly from Gidley and from Leche.

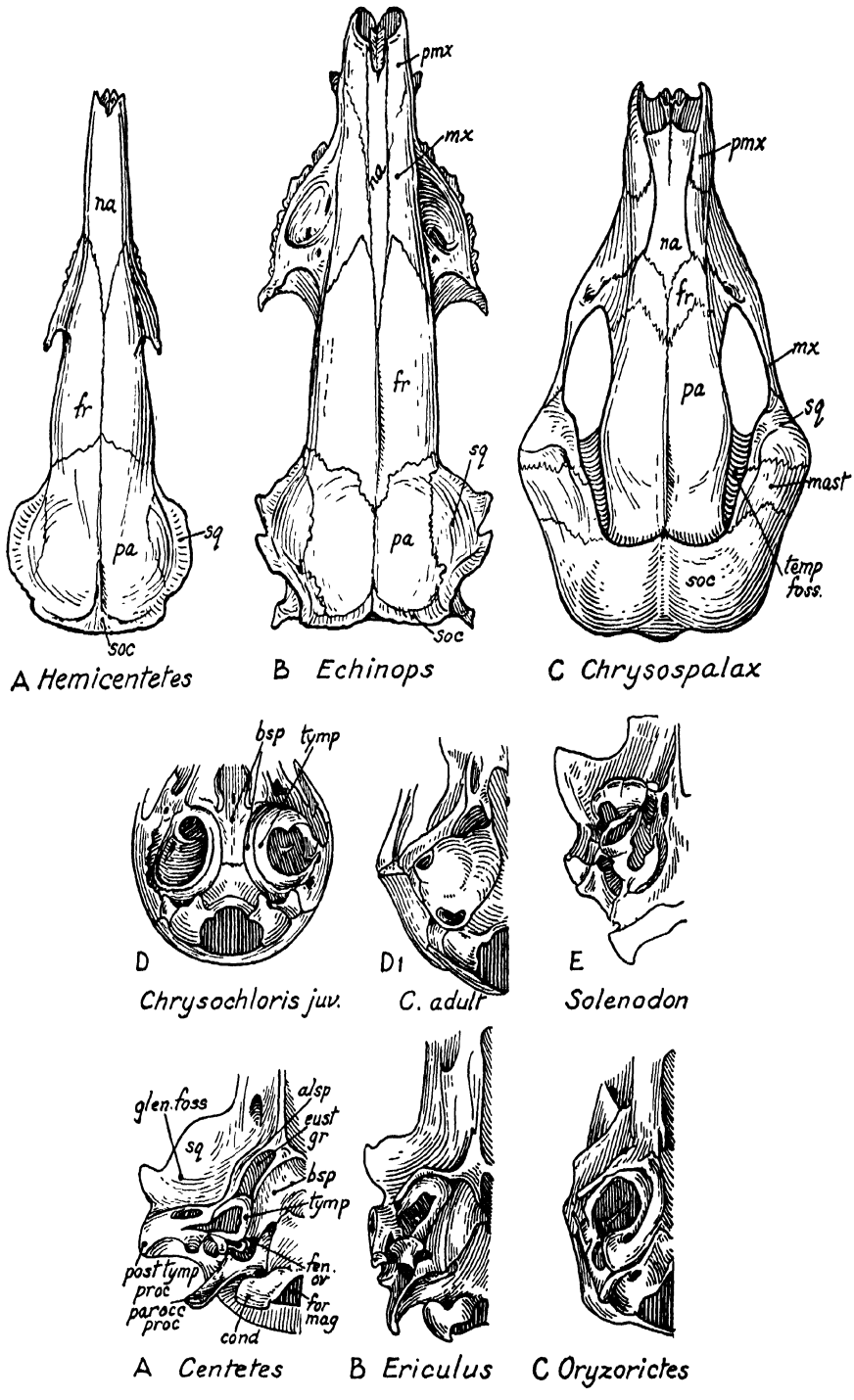


Fig. 19.7 (top). Contrasting skull proportions in recent zalambdodonts. As in many other groups, skull proportions vary from intermediate to very long or very wide.

Fig. 19.8. Auditory region in zalambdodont skulls. After Leche. As in many other groups of mammals, the expanding auditory diverticulum of the tubotympanal canal during ontogeny molds whatever bones it presses against, thus causing them to develop shell-like rims or flanges around part of the Eustachian tube, the tympanic cavity and its derived outgrowths.

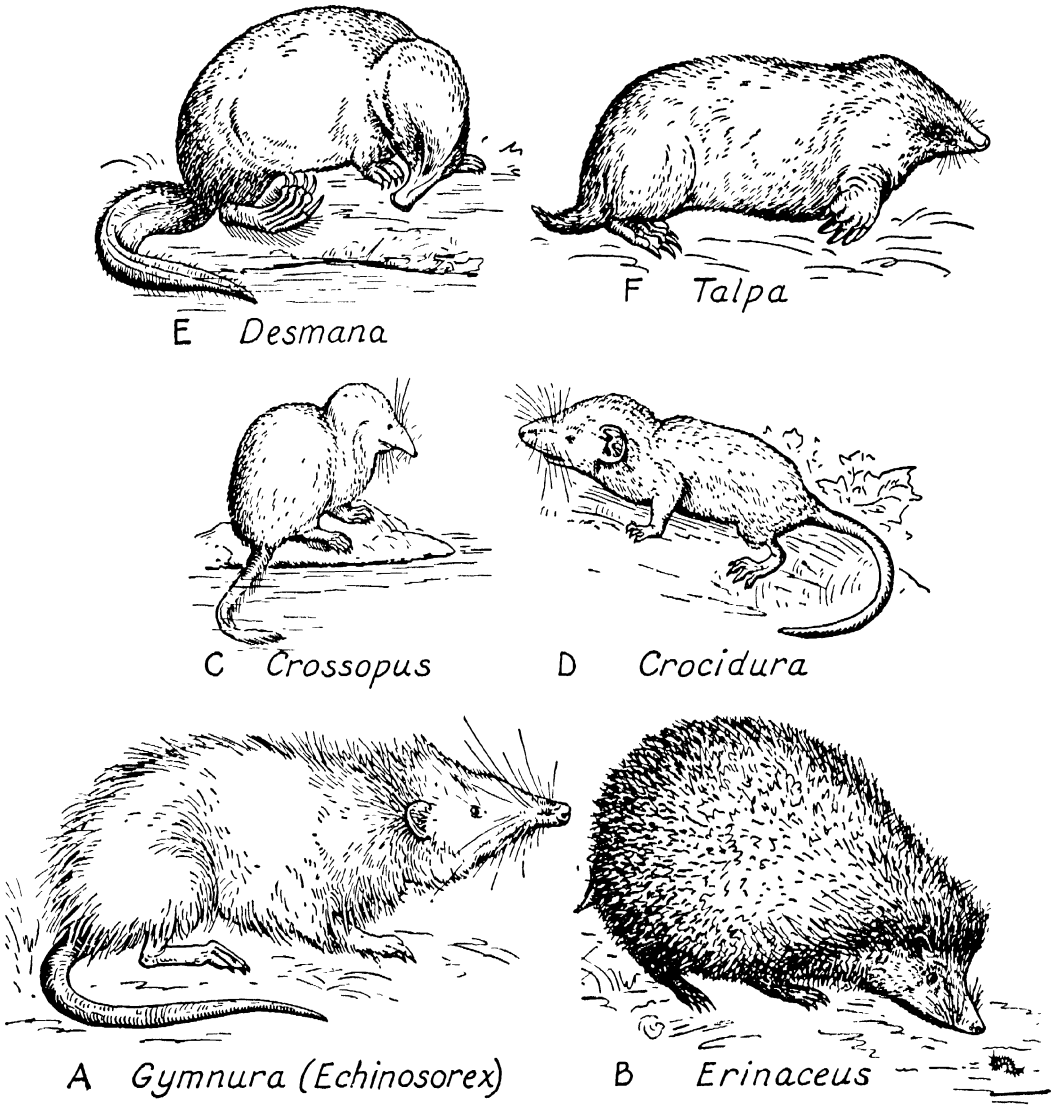


Fig. 19 9. Some Recent hedgehogs (A, B), shrews (C, D) and moles (E, F). A, partly after a photograph by H. C. Raven; B, mounted specimens; C, E, F, after Lydekker; D, after J. A. Allen.

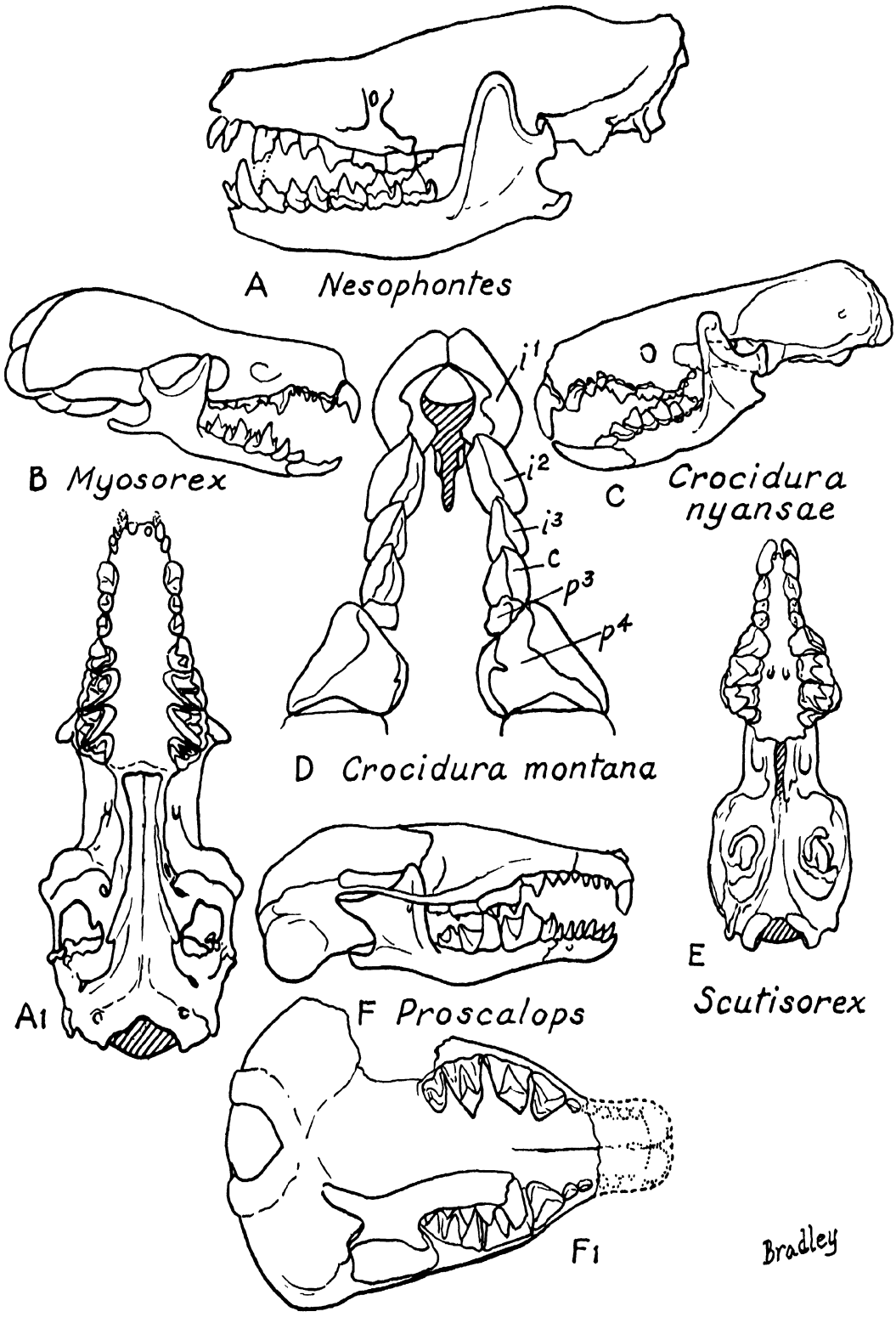


Fig. 19.10. Skulls and dentitions of shrews and moles. Data from Anthony (A, A1), Dobson (B, D), Allen (C, E), Matthew (F, F1)

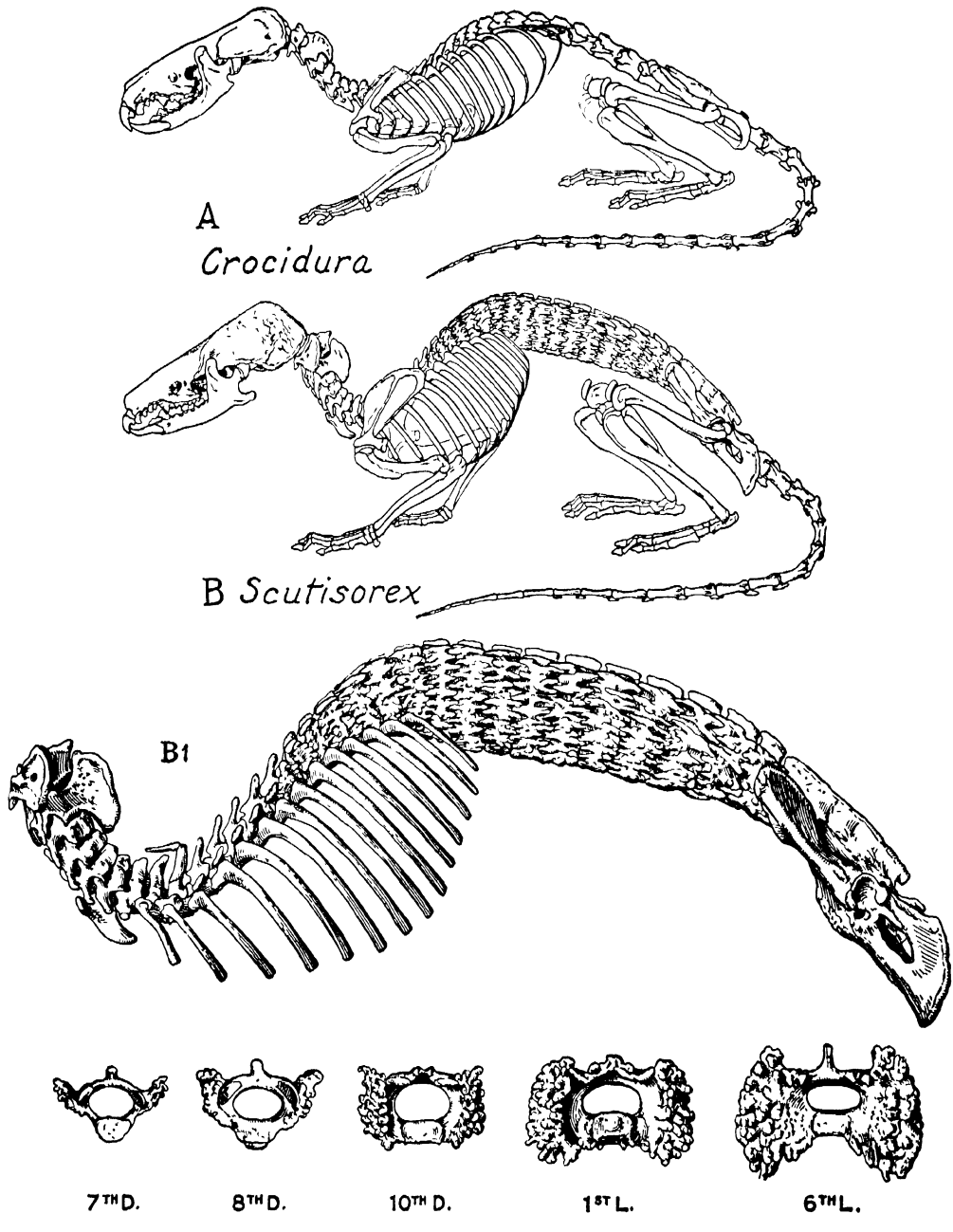


Fig. 19.11. Axial skeletons of ordinary shrew (A1) and of "hero shrew" (B, B1), the latter showing very numerous interdigitating articular processes of the dorsal and lumbar vertebrae After J. A. Allen.

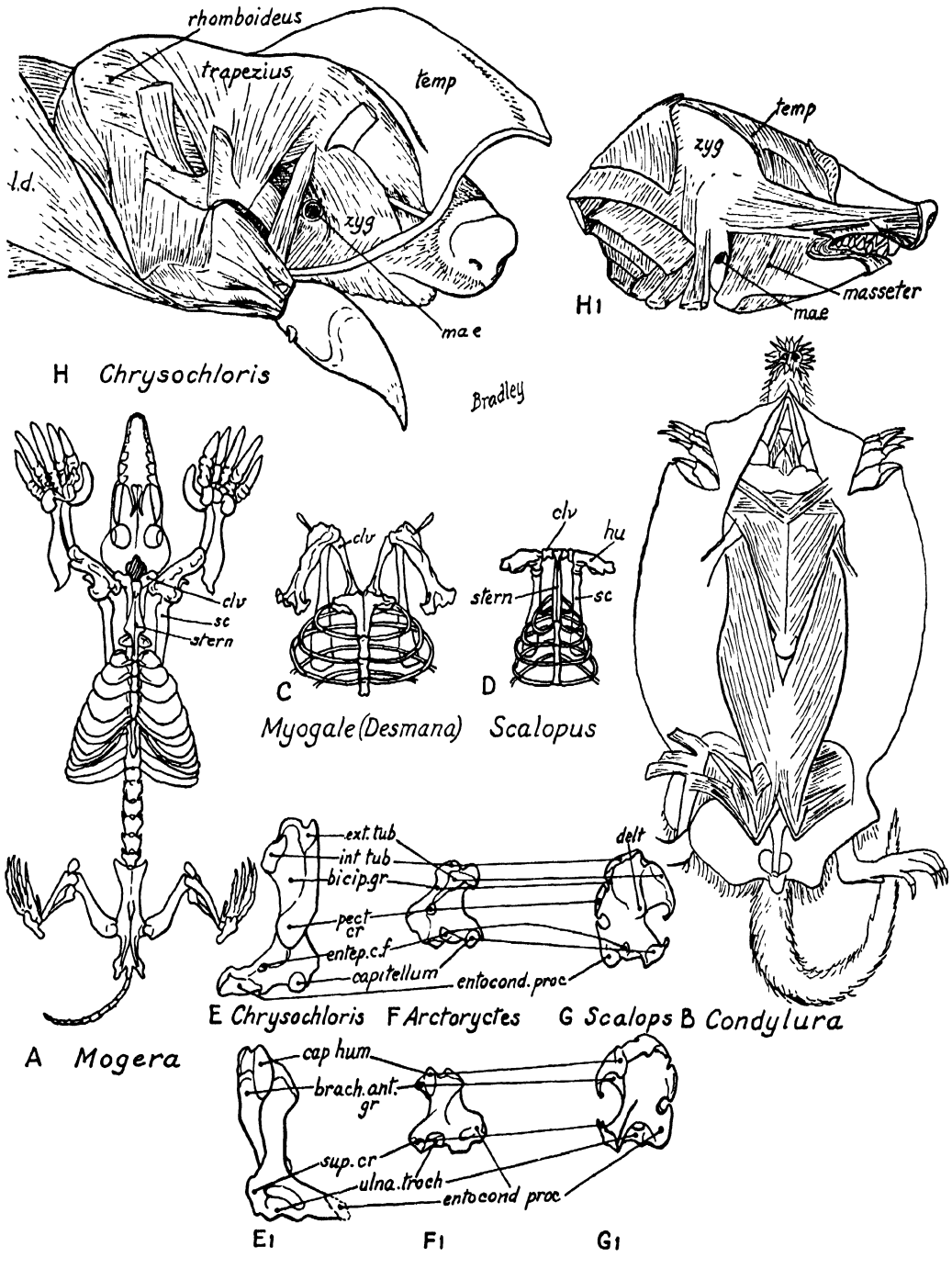


Fig. 19.12. Fossorial adaptations of moles (A–G) and golden-moles (H, H1). A, B, H, H1, after Dobson; C, D, after Kistin; E–G, after Schlaikjer. In the typical moles (A, B) the clavicles have become exceedingly short and wide, simulating the coracoids of *Echidna* and transmitting the powerful thrusts of the pectoral limbs to the strongly braced sternum. The clavicles of the desmans (C) are of more normal mammalian type. The humeri of moles (G, G1) likewise reflect extreme fossorial adaptations in their great width, flatness and shortness, as compared with the less specialized conditions in the Cape Golden moles (E, E1). In the Miocene *Arctoryctes* (F) the humerus is somewhat less specialized than in the modern moles. In H the enlarged muscles of the shoulder cover the neck.

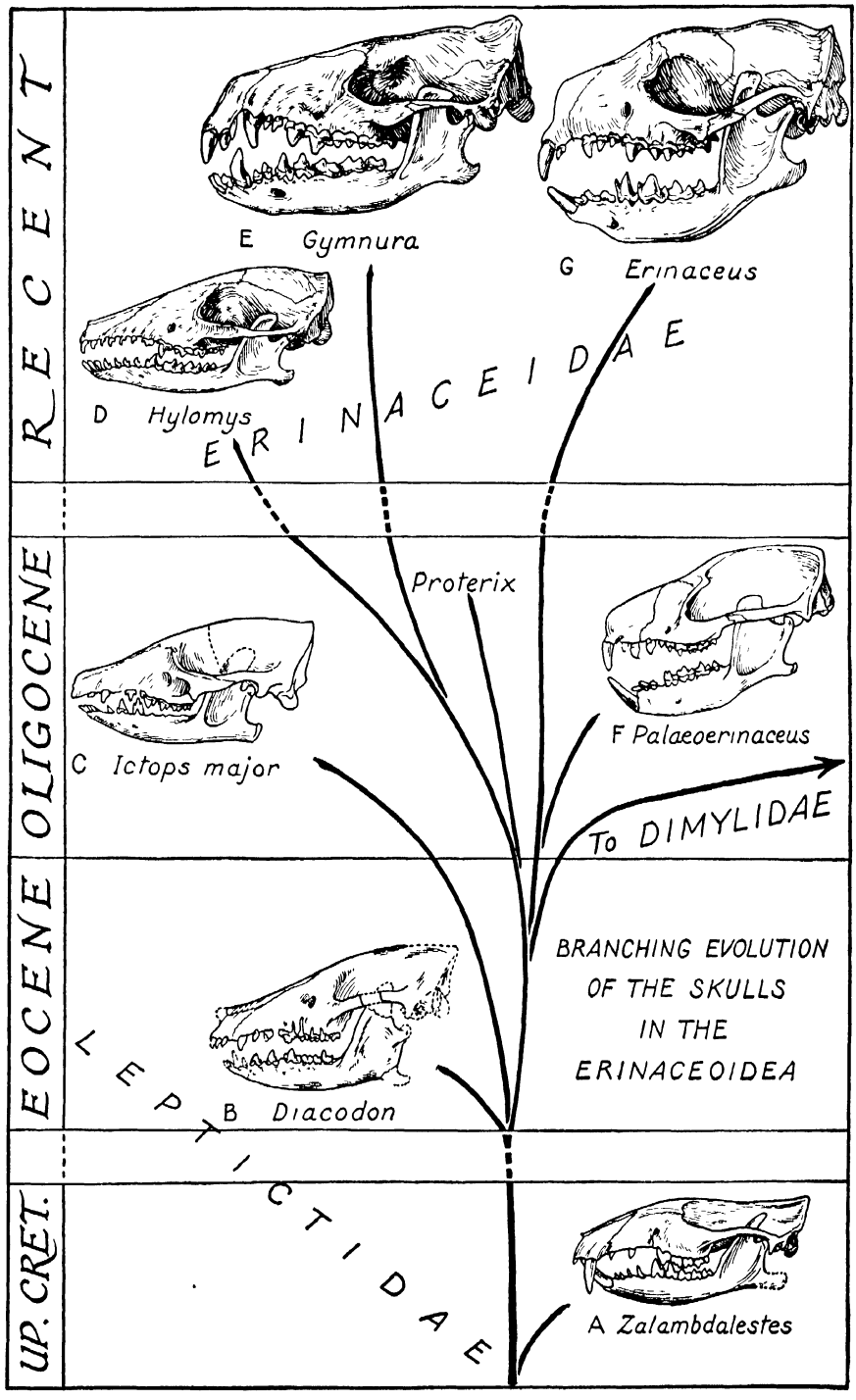


Fig. 19.13. From Upper Cretaceous to Recent erinaceoid insectivores. A, B, after Gregory and Simpson; C, after Matthew and Granger; D, after Earl Douglas; F, after Viret; E, G, original. In general these skulls and dentitions are less peculiar than those of zalambdodonts; e.g, the orbits are less reduced, the skull less tubular, the zygomatic arch is intact (although the jugal is reduced), the nasals remain separate.

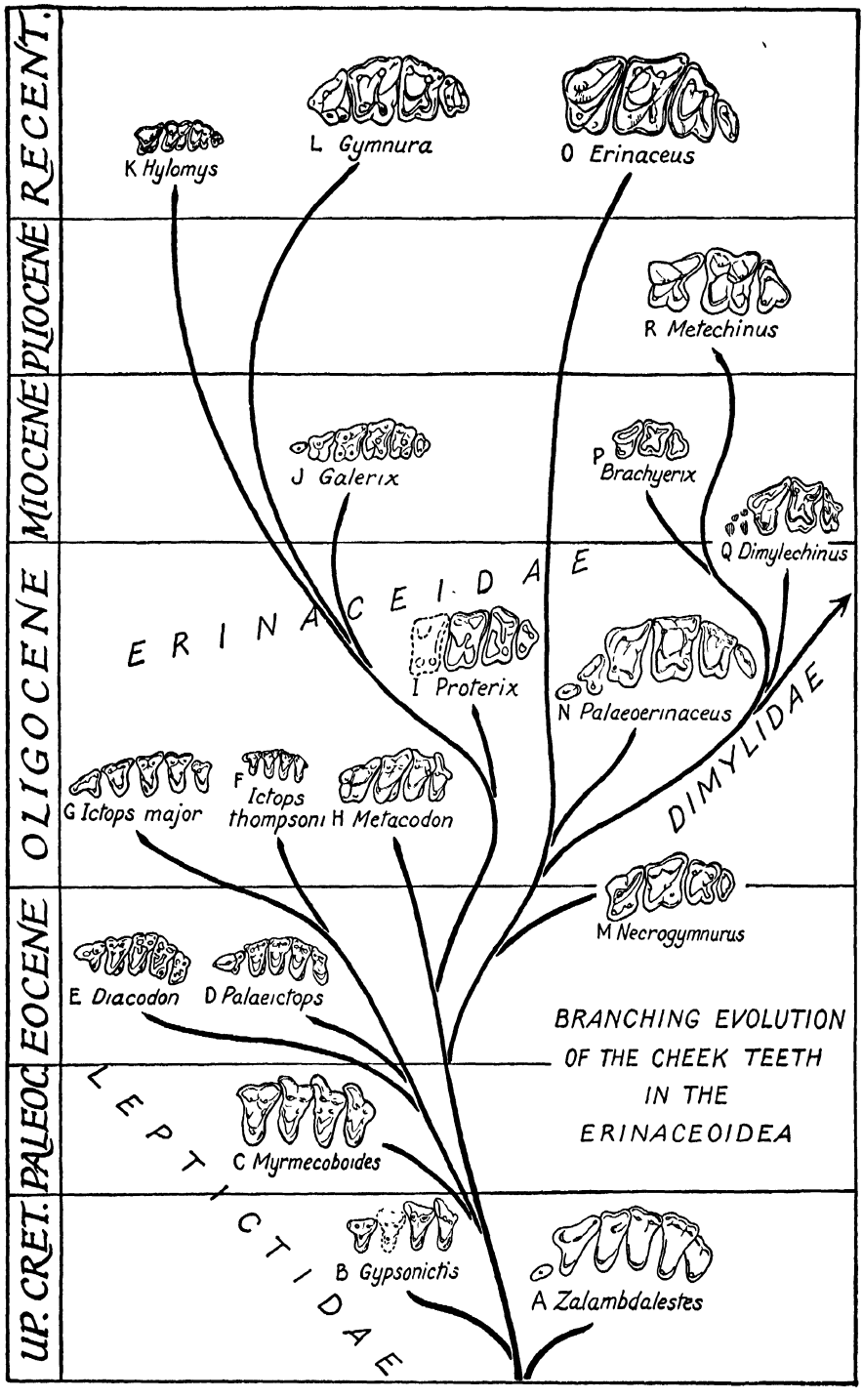


Fig. 19.14. The upper cheek teeth of erinaceoids from Upper Cretaceous to Recent. In contrast with zalambdodont dentitions (fig. 19.6), the para- and metacones remain near the outer margin of the crown, the protocones remain well developed. In earlier stages (A–F) the crowns are wide transversely; in middle and later stages (G–K), the hypocones become larger, the crown more elongated anteroposteriorly. In the true hedgehogs (O) the cross-crests are emphasized, especially in m^2, which is almost bilophodont. Data from: Simpson (A–C), Matthew (D–I), Leche (M), Viret (Q).

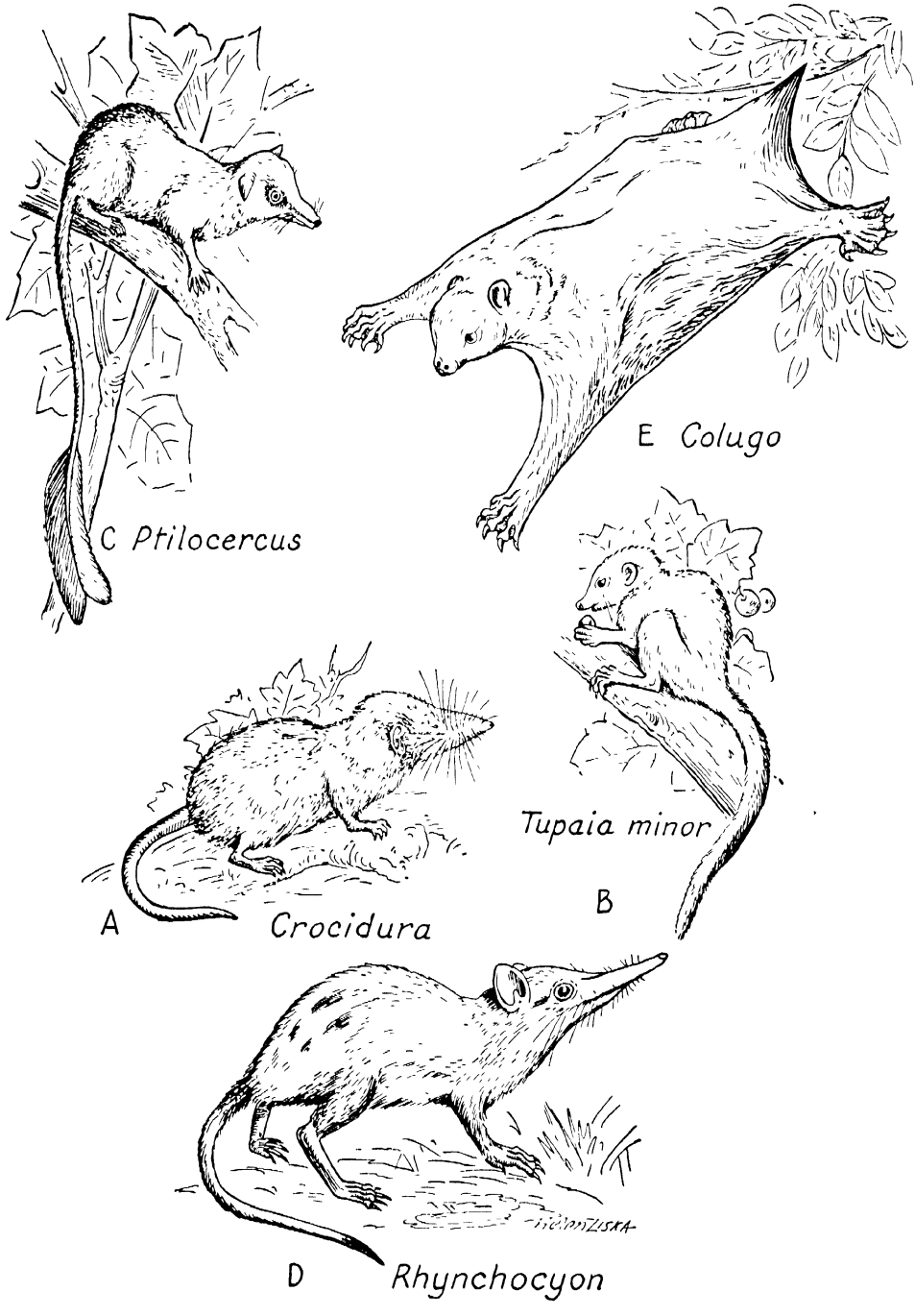


Fig. 19.15. A shrew (A), a tree-shrew (B), the pen-tailed tree-shrew (C), an African jumping-shrew (D), and a "flying lemur" (E). B and C, representing the tupaioids, are related to the lemurs among the Primates. A, D, after J. A. Allen, C, after Flower and Lydekker.

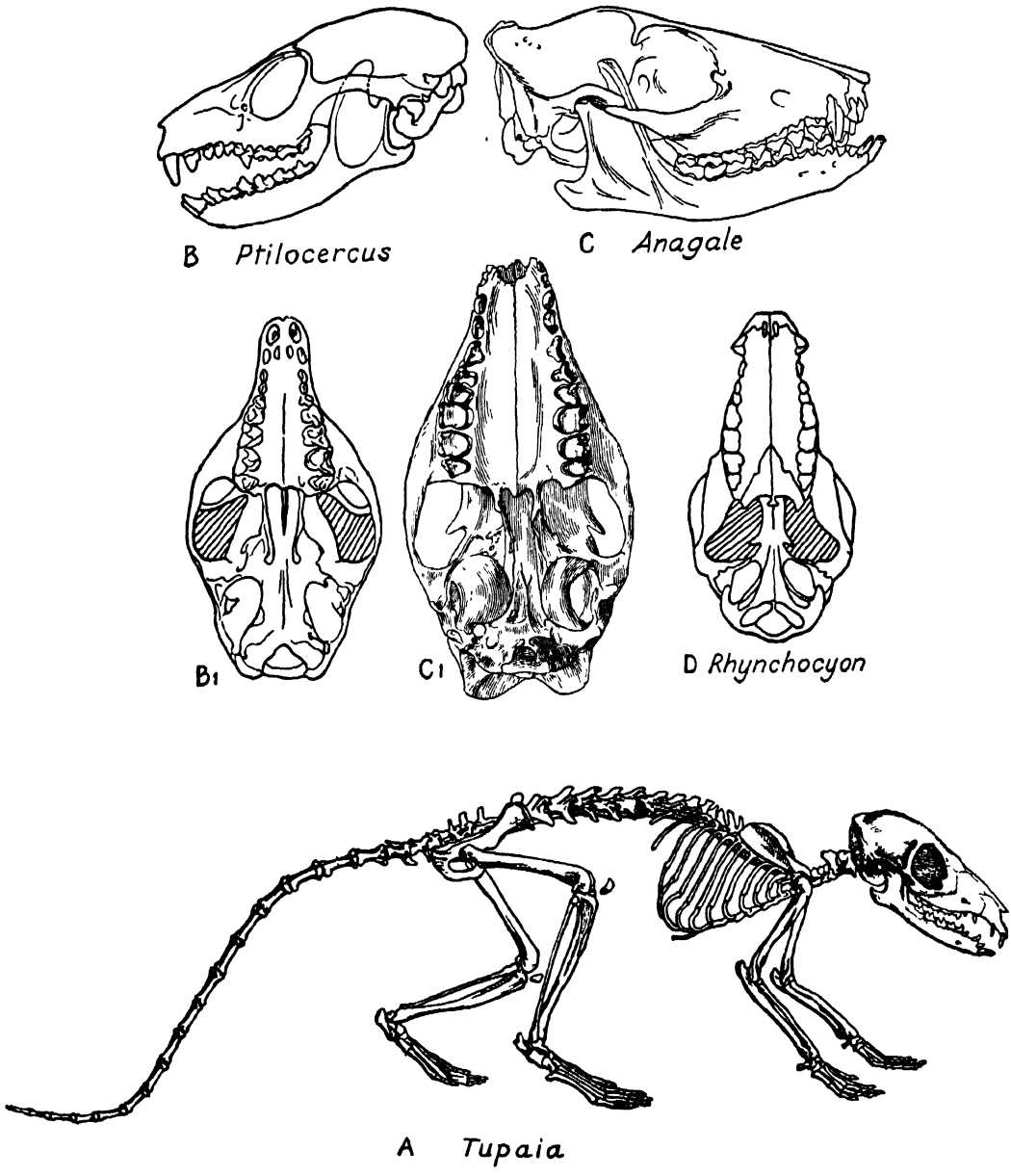


Fig. 19.16. Tupaioids: Recent (A, B, B1, D) and fossil (C, C1). A, from Gregory, after De Blainville; B, B1, after Gregory; C, C1, after Simpson; D, after Gaynor Evans.

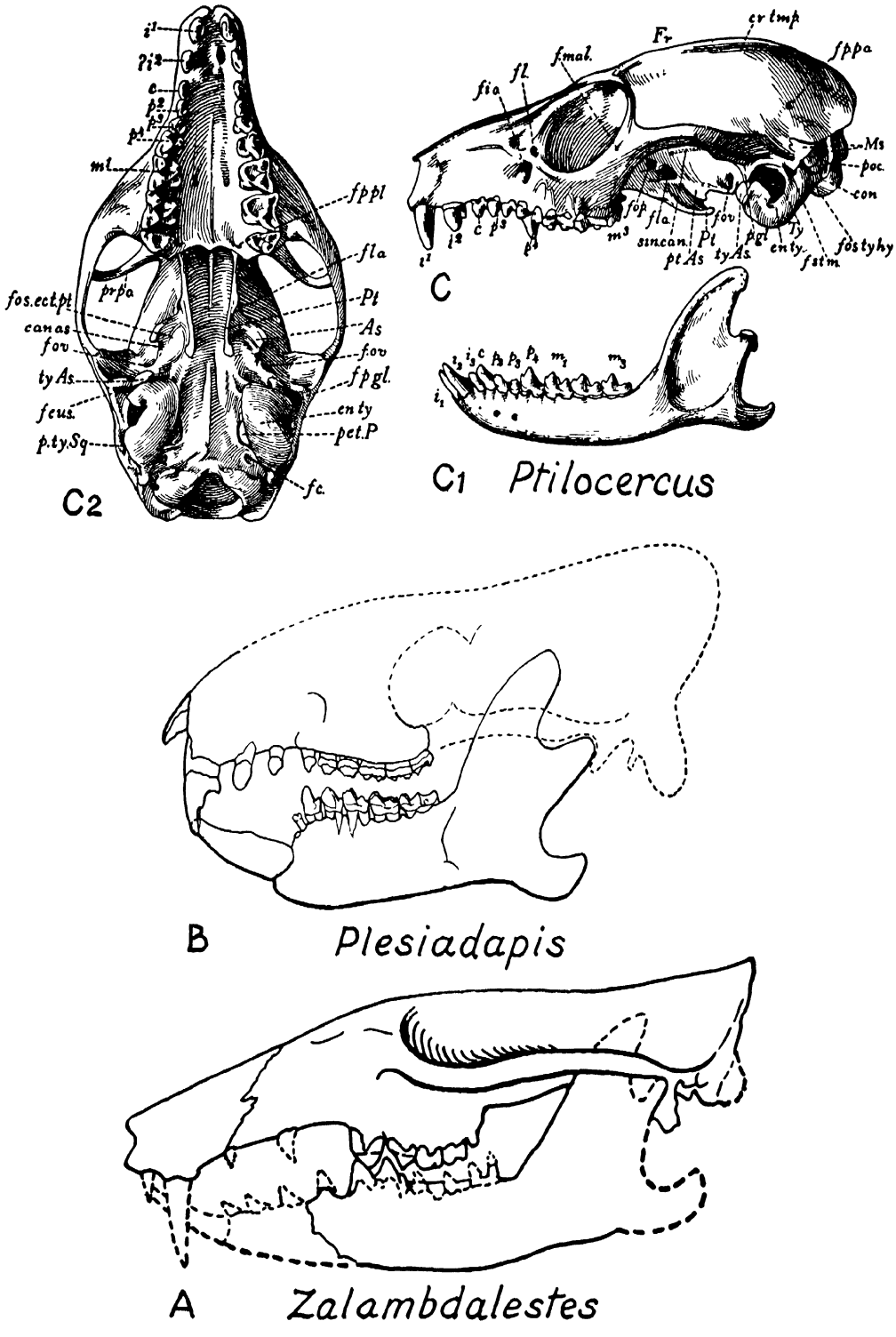


Fig. 19.17. Skulls of Upper Cretaceous insectivore (A), Paleocene lemuroid (B), recent pen-tailed tree-shrew (C, C1, C2). A, after Gregory and Simpson, B, partly restored, data from Matthew and Simpson; C–C2, after Gregory.

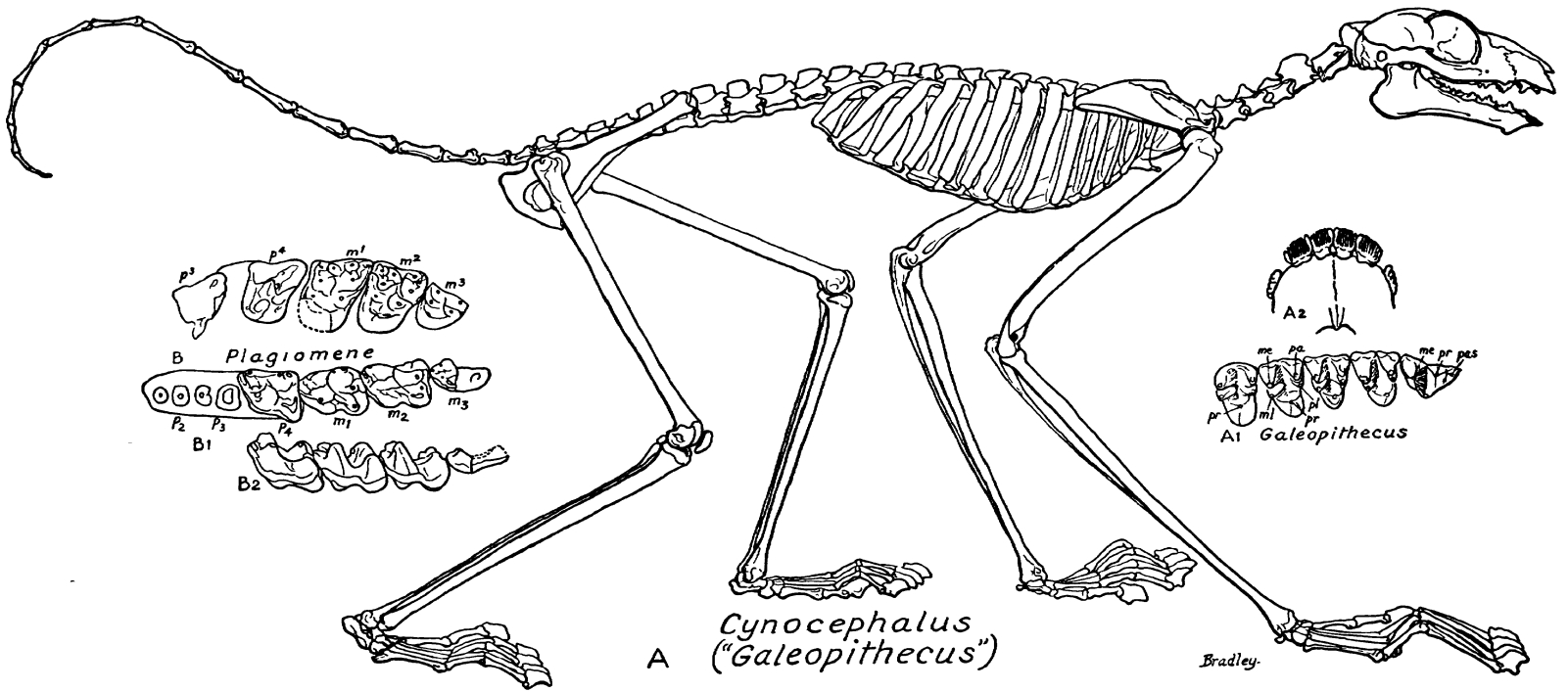


Fig. 19.18. Skeleton and teeth of "flying lemur" (A–A2); teeth of Lower Eocene insectivore (B–B2), possibly ancestral to A. A, A2, after De Blainville; A1, from specimen; B–B2, after Matthew.

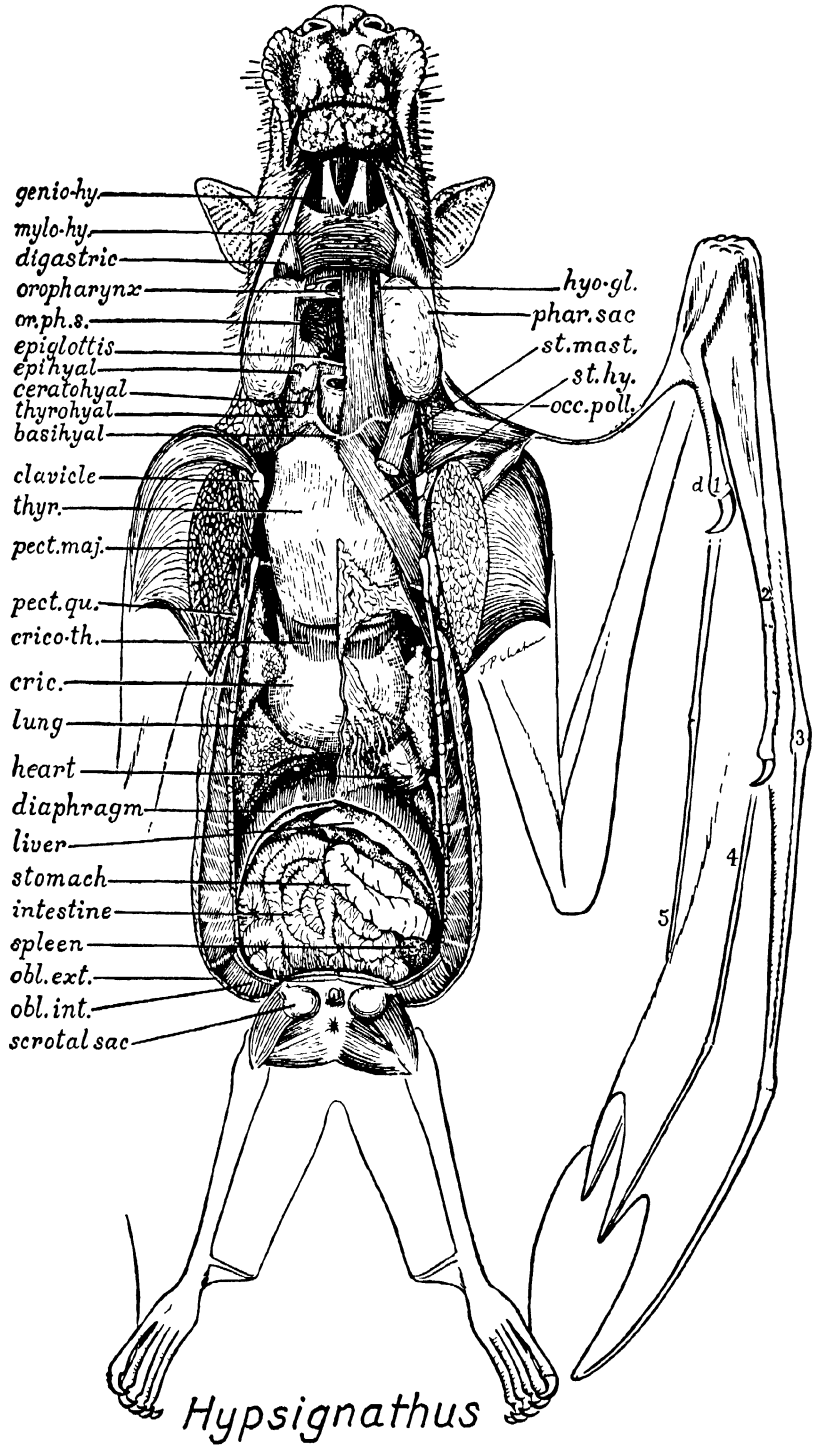


Fig. 19.19. Anatomy of a specialized African fruit bat, showing hypertrophy of the larynx and consequent crowding of the viscera. After Allen, Lang and Chapin.

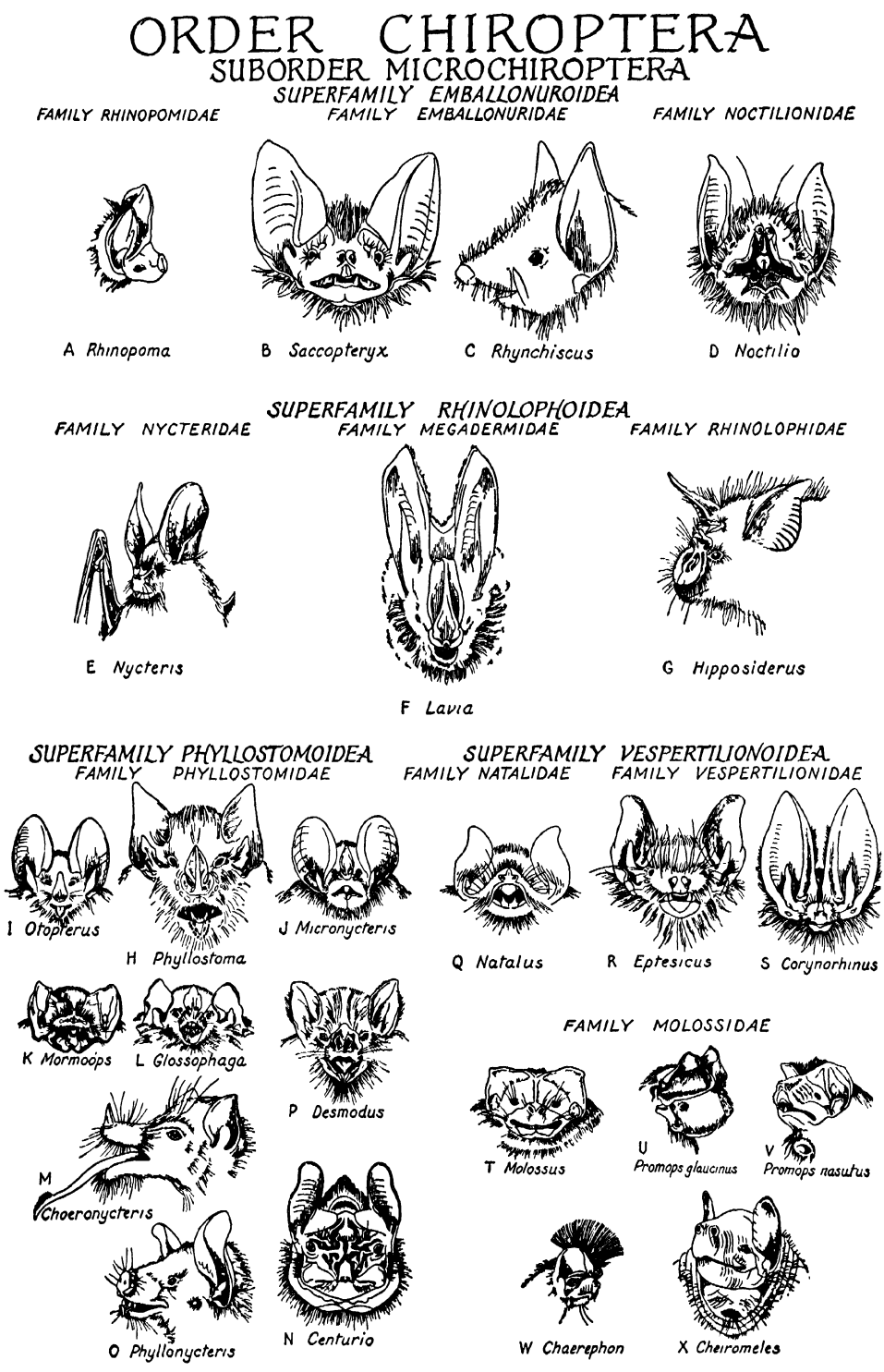


Fig. 19.20. Adaptive modifications of the face among the Microchiroptera. A, after G. M. Allen; A1, X, after Lydekker; B–D, H–S, U–W, after Elliot; E–G, T, after Allen, Lang and Chapin.

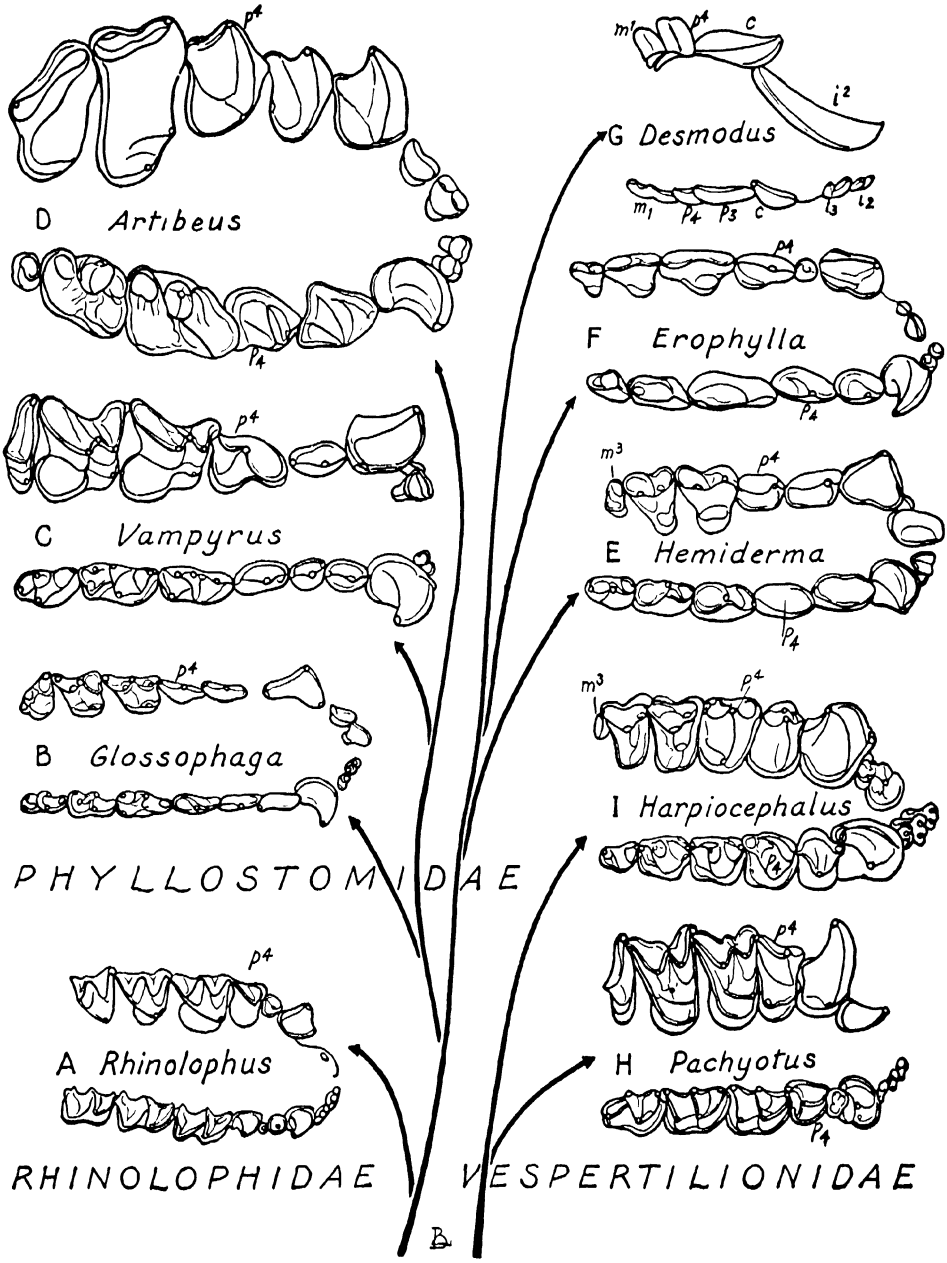


Fig. 19.21. Branching evolution of the upper and lower cheek teeth among the Microchiroptera All drawings and data from Gerrit S. Miller. What may be called the main stem begins with insectivorous types with sharp W-shaped outer cusps (A, H), and culminates in: (1) enlarged molars with crushing conical cusps (D, I); (2) rather small molars with small rounded cusps (B, E), (3) enlarged pointed, blade-like incisors and shearing molars of the blood-sucking vampire bat (G).

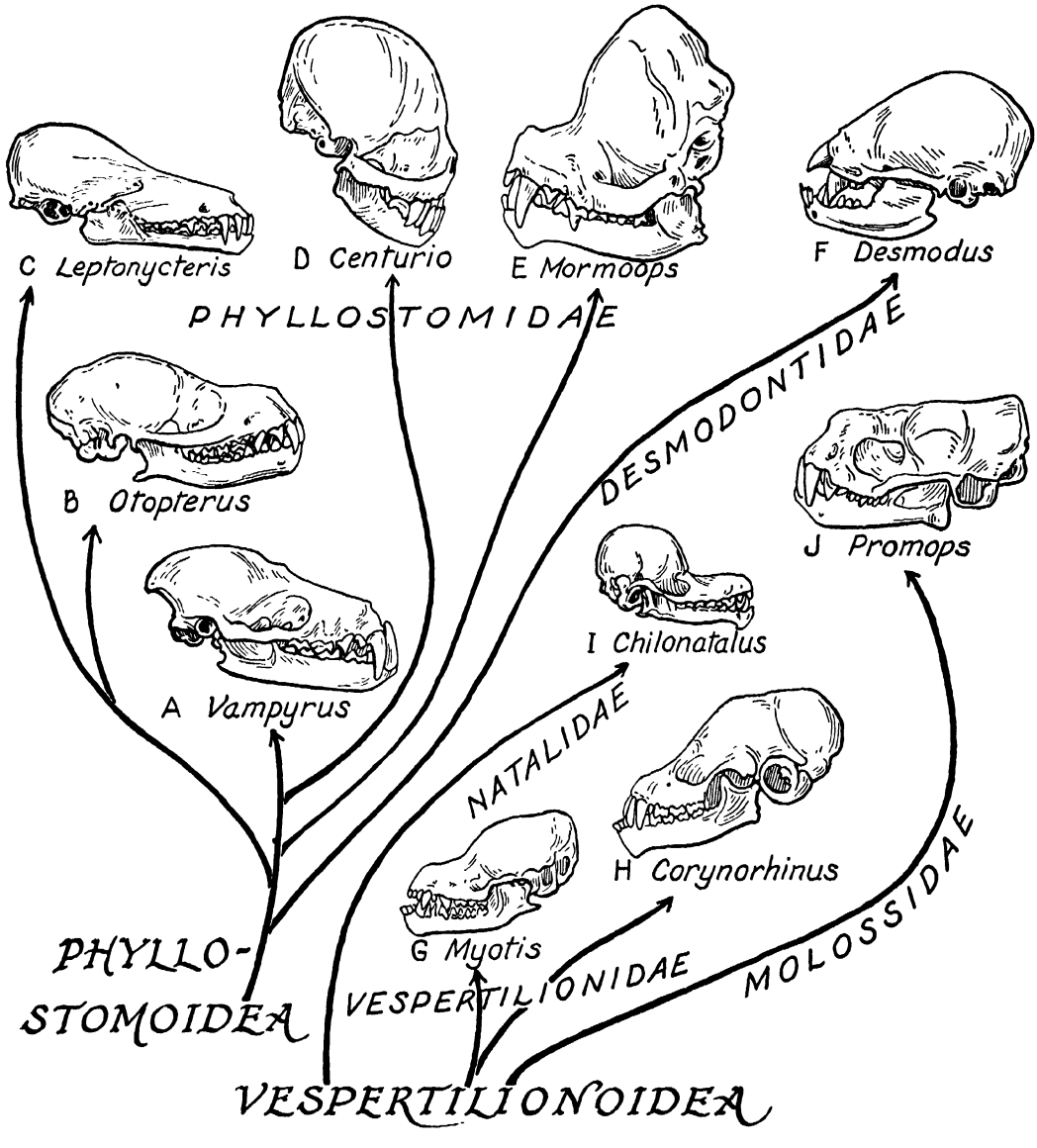


Fig. 19.22. Branching evolution of skulls among Microchiroptera. Figures and data from Gerrit S. Miller.

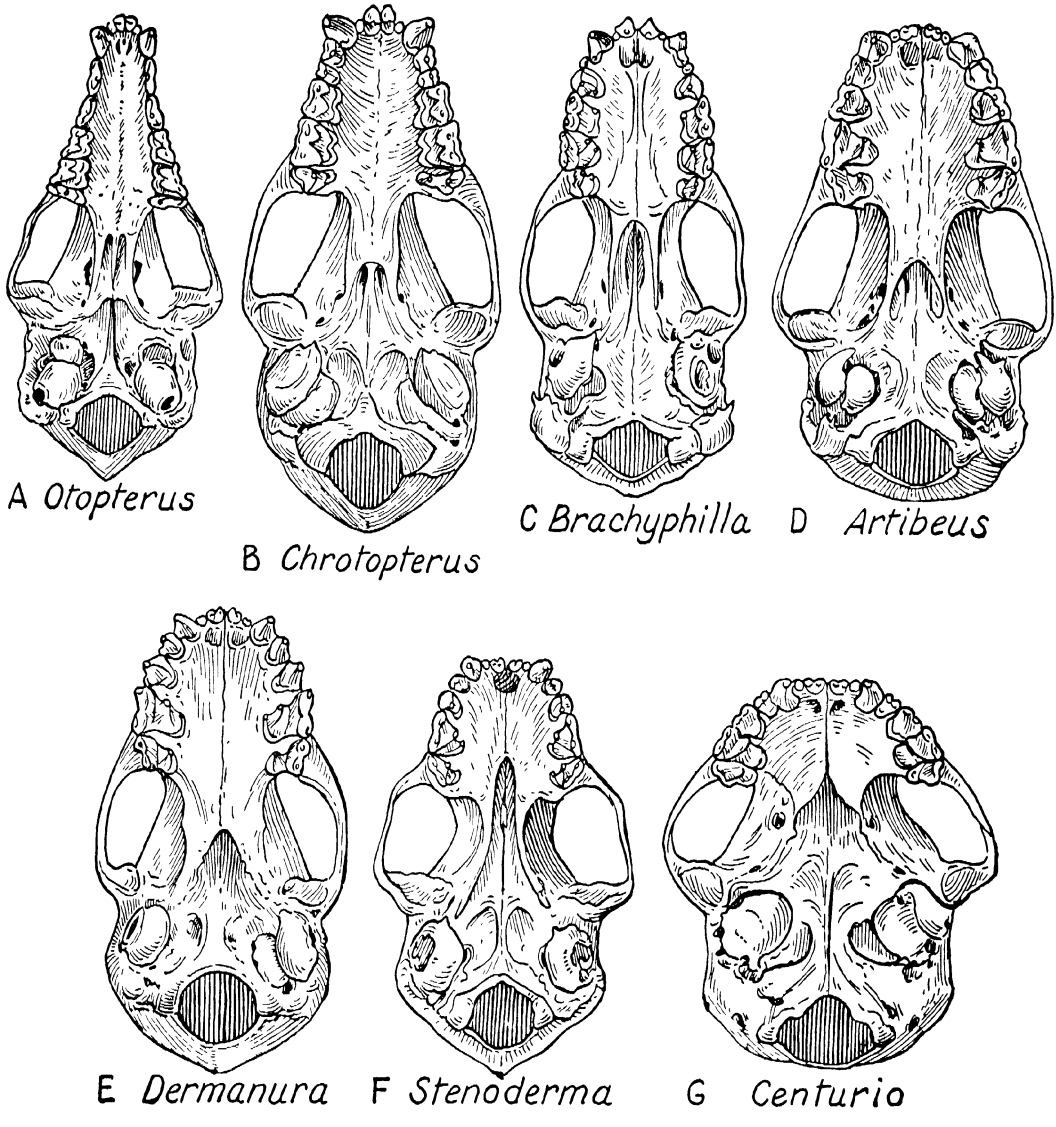


Fig. 19 23. From hyperdolicho- to hyperbrachycephalic skulls among the American leaf-nosed bats (Phyllostomidae). Data and figures after D. G. Elliot.

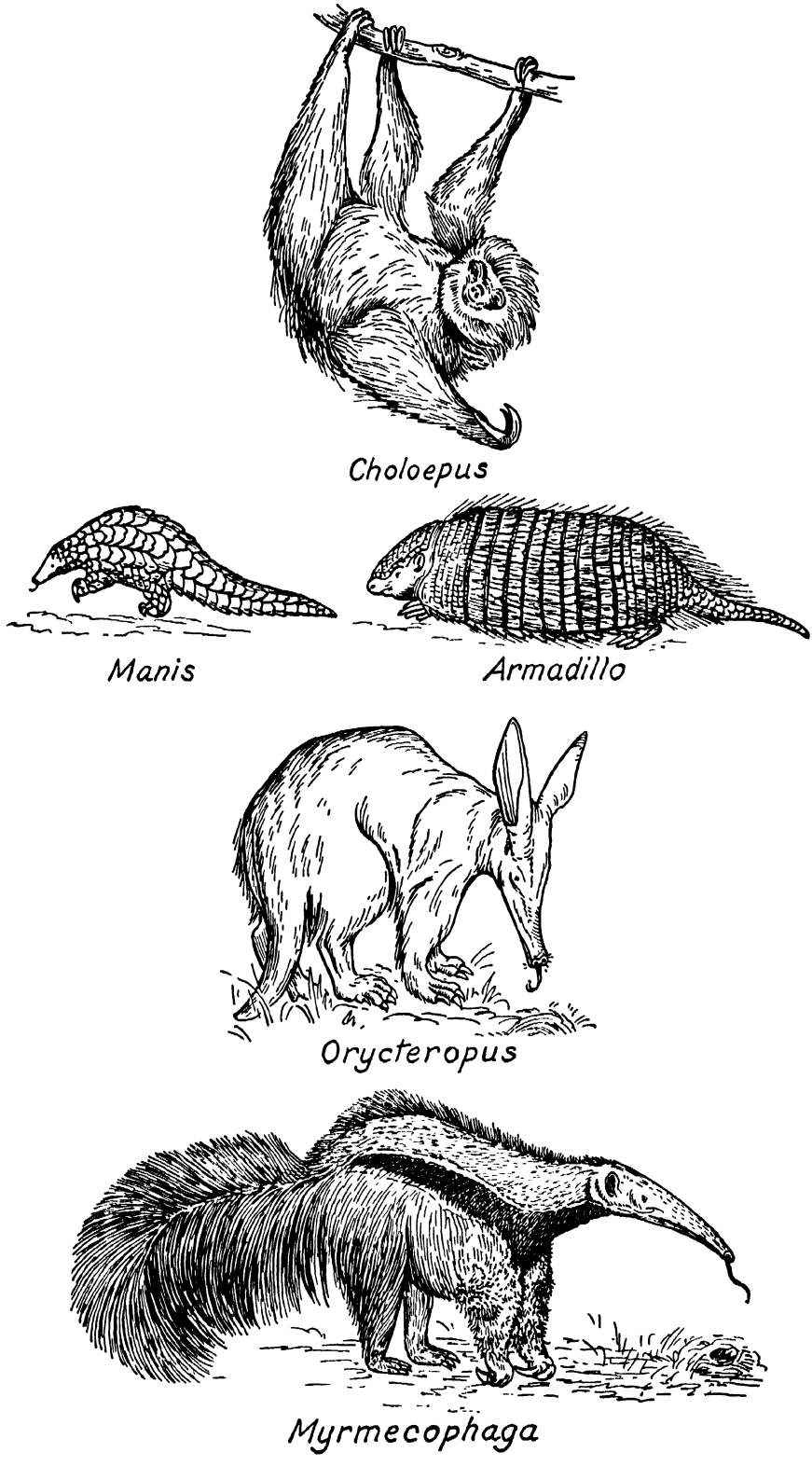


Fig. 19.24. Sketches of Recent 'edentates." By Helen Ziska.

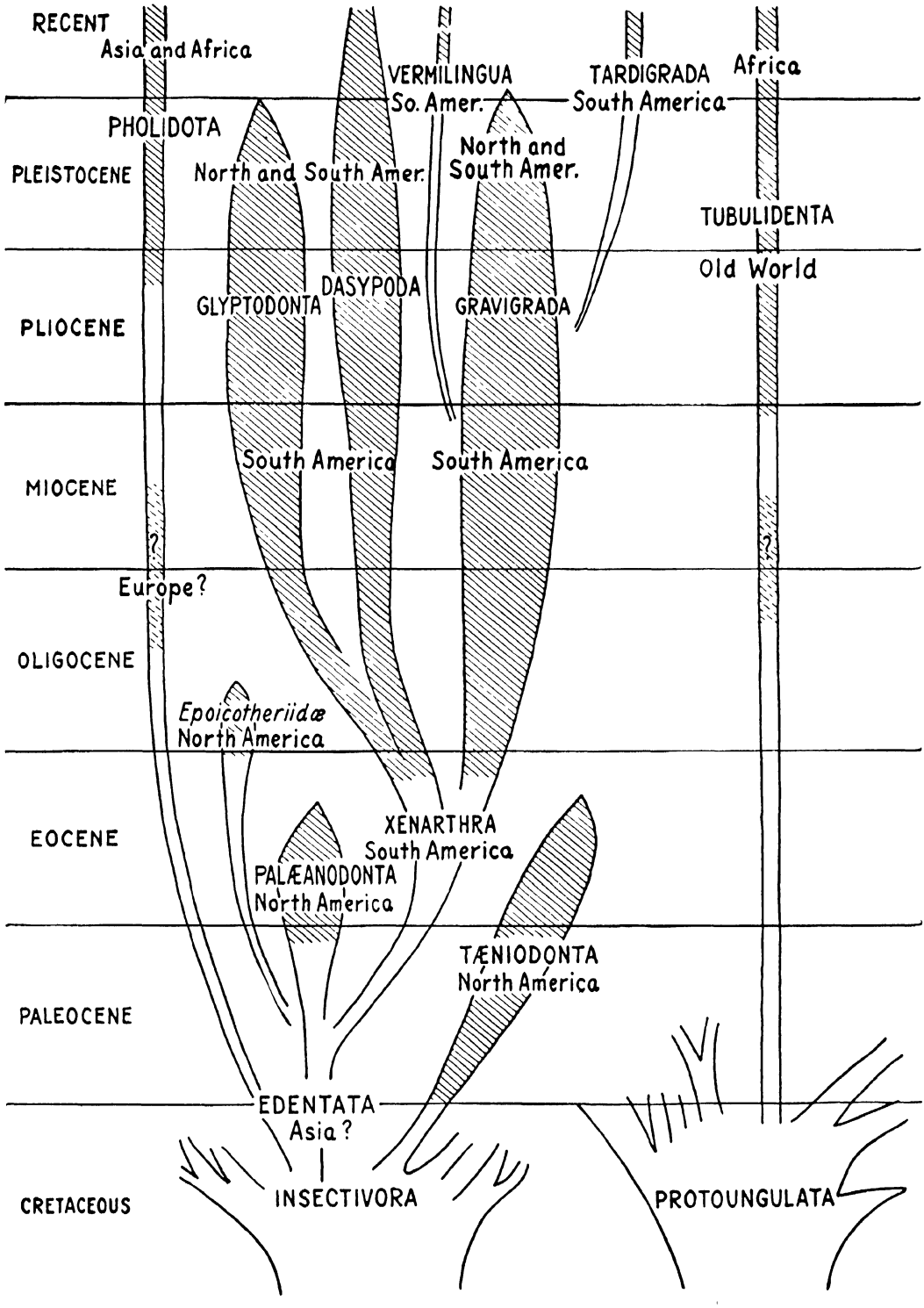


Fig. 19.25. Phylogeny and distribution of edentates and supposed edentates. Cross-lined areas indicate known occurrences. After Simpson

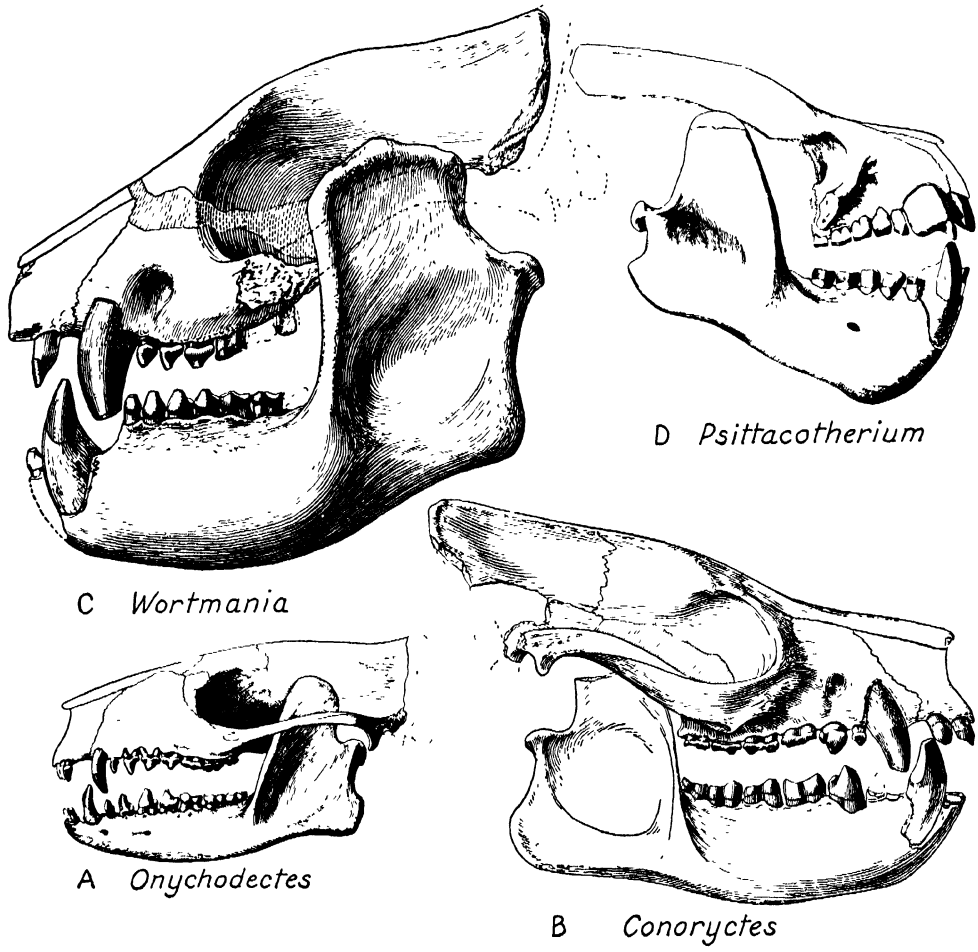


Fig. 19.26. Skulls of Paleocene and Lower Eocene taeniodonts. After Matthew. The least specialized (A) recalls the contemporary primitive carnivores, especially in its fang-like canine teeth; but it retains an older basic insectivore heritage in its general skull form, slender zygomatic arch and relatively primitive cheek teeth. In the specialized stage (D) the face is shortened and the jaws greatly strengthened to support the huge beak-like canines. B, C, are structurally intermediate stages.

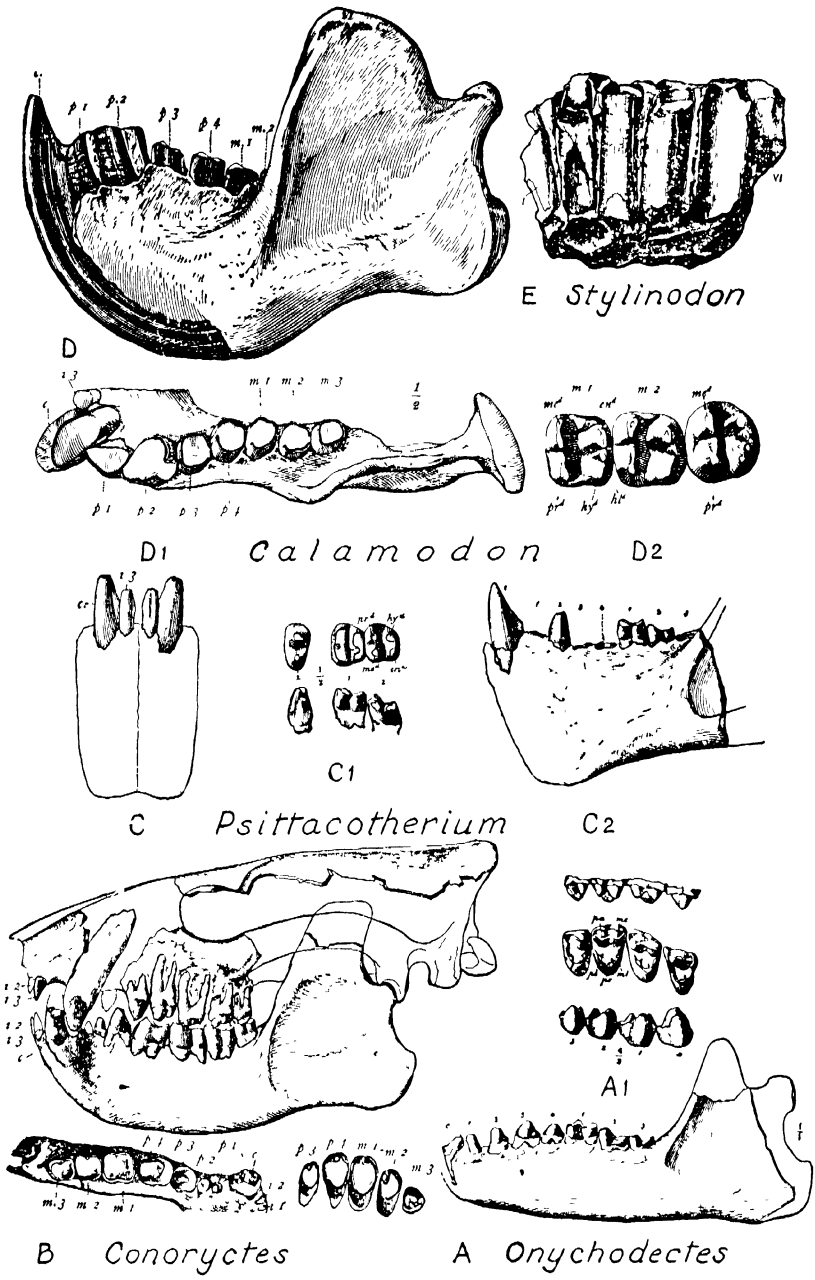


Fig. 19.27. Teeth and jaws of taeniodonts. After Osborn. A, A1, inherit the primitive insectivore dental formula and the basic patterns of the jaws and teeth; but the molar crowns are bunodont (with blunt cusps), adapted for crushing, and the diet may have been omnivorous. In B, the jaws are stouter, the canines larger and the badly worn molars indicate abrasive food. In C1, the low molar cusps are arranged in two transverse pairs, as in D2. In D, the lower canine root has extended far back beneath the cheek teeth; the enamel band stiffens its front face, as in ever-growing incisors of rodents and others. In the highly specialized *Stylinodon* (E), the very high-crowned molars convergently resemble those of aardvarks, rodents, edentates and ungulates.

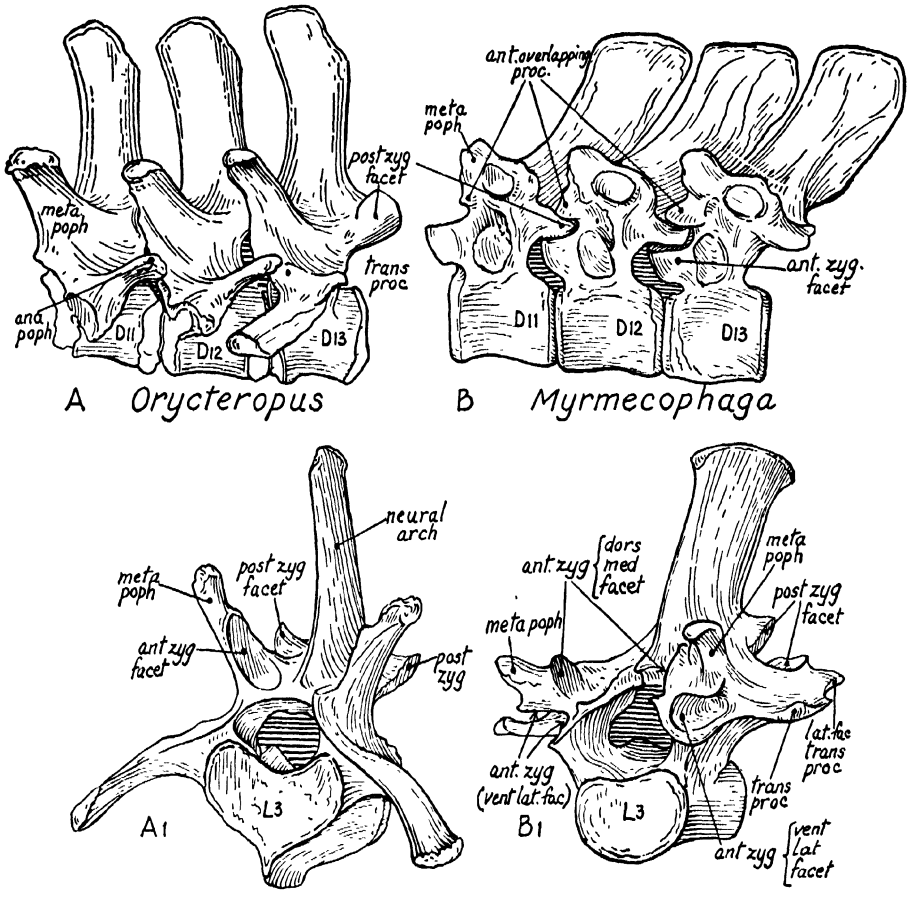


Fig. 19.28. Zygapophysial articulations in tubulidendate (A, A1) and xenarthran (B, B1). From specimens. In the aardvark (A, A1) the zygapophysial facets are large and directed obliquely upward but no extra facets are formed. In the ant-bear (B, B1) the massive, wide zygapophyses of successive vertebrae, supporting the stout metapophyses in the posterior dorsals and lumbars, overlap and interlock with each other, forming extra or xenarthral facets: dorsomedial, ventro-lateral and lateral to the original facets.

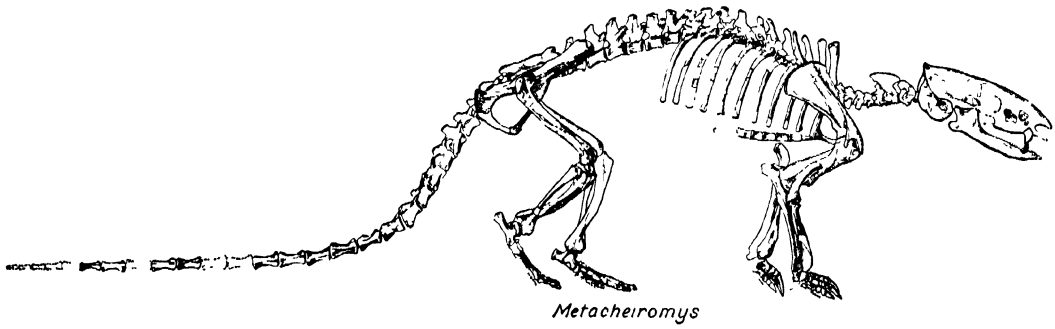


Fig. 19.29. Skeleton of armadillo-like Eocene palaeanodont. After Simpson. Differs from armadillos in lack of xenarthral articulations (? a primitive character) and in loss of cheek teeth.

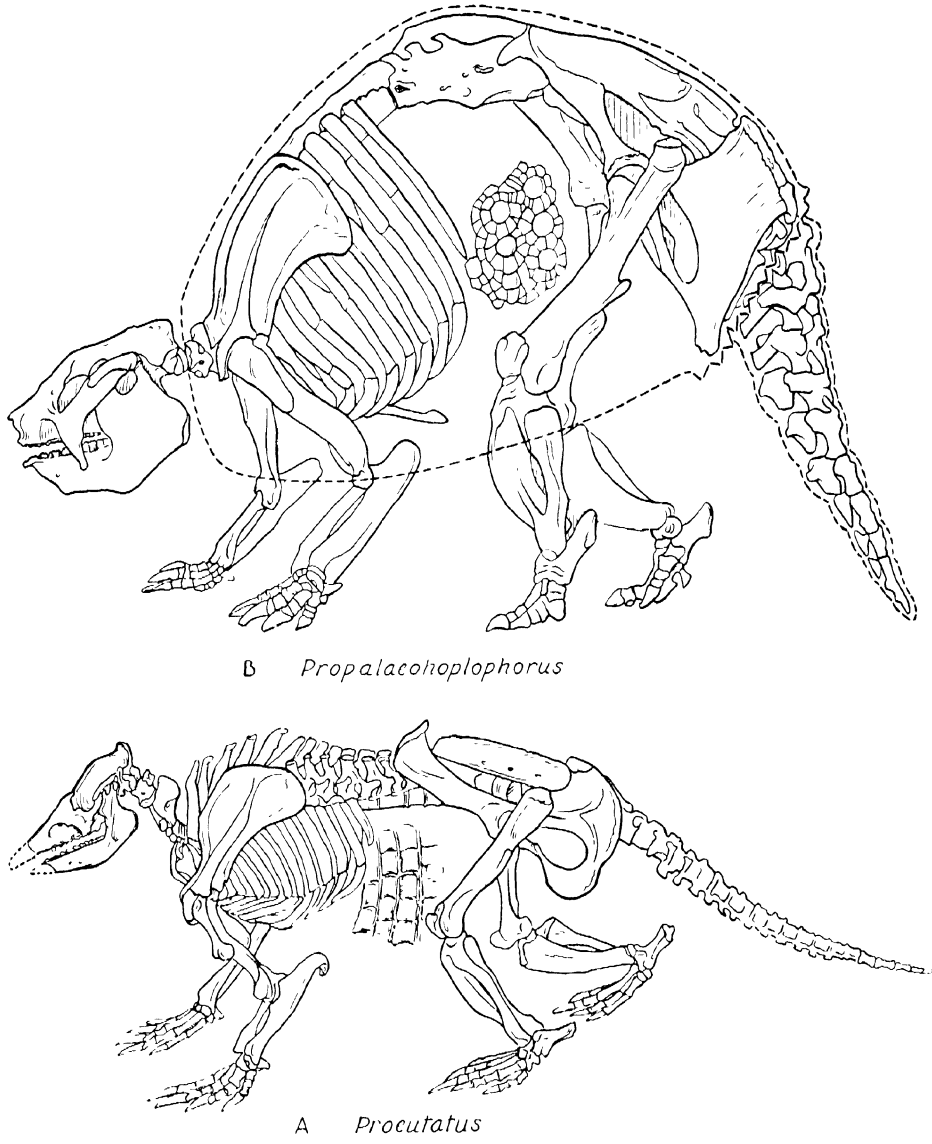


Fig. 19.30. Armadillo (A) and glyptodont (B) from the Santa Cruz (Lower Mocene) of Patagonia. All data from Scott. The armadillo retained a more primitive type of digging skeleton and carapace than did the glyptodont, which was already highly specialized and turtle-like in the immobilization of the vertebrae beneath the carapace.

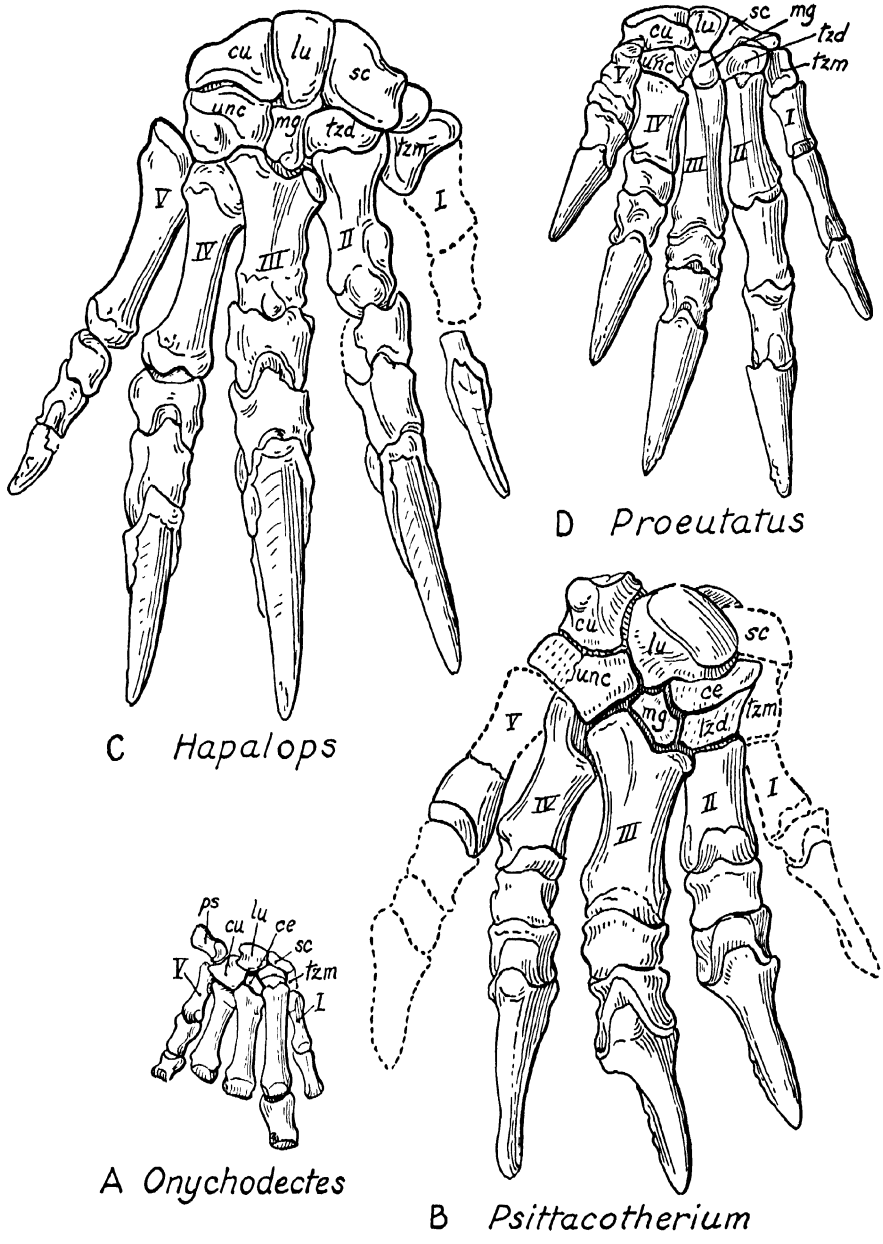


Fig. 19.31. Manus of taeniodonts (A, B) and edentates (C, D). All × ⅔. A, B, after Matthew; C, D, after Scott. All retain most of the basic mammalian pattern, inherited with slight changes from the higher mammal-like reptiles (fig. 16.25 D). Digging habits are indicated by the very strongly built, wide spreading hands, huge claws and strong pulleys on the phalanges (C, D) to prevent dislocation. In the more primitive stages (A, B) the centrale carpi is distinct,* in the others it has probably fused with the adjacent facet of the scaphoid, forming the articular surfaces of the scaphoid with the lunar (in part), magnum and trapezoid (in part). Possible derivation from partly arboreal primitive placentals is suggested by the grasping arrangement of the well clawed hand with divergent first digit (A). In view of the great time-interval between A, B, on the one hand, and C, D, on the other, no very close relationship of the taeniodonts to the edentates is indicated.

* In A, for *ce* read *mg*.

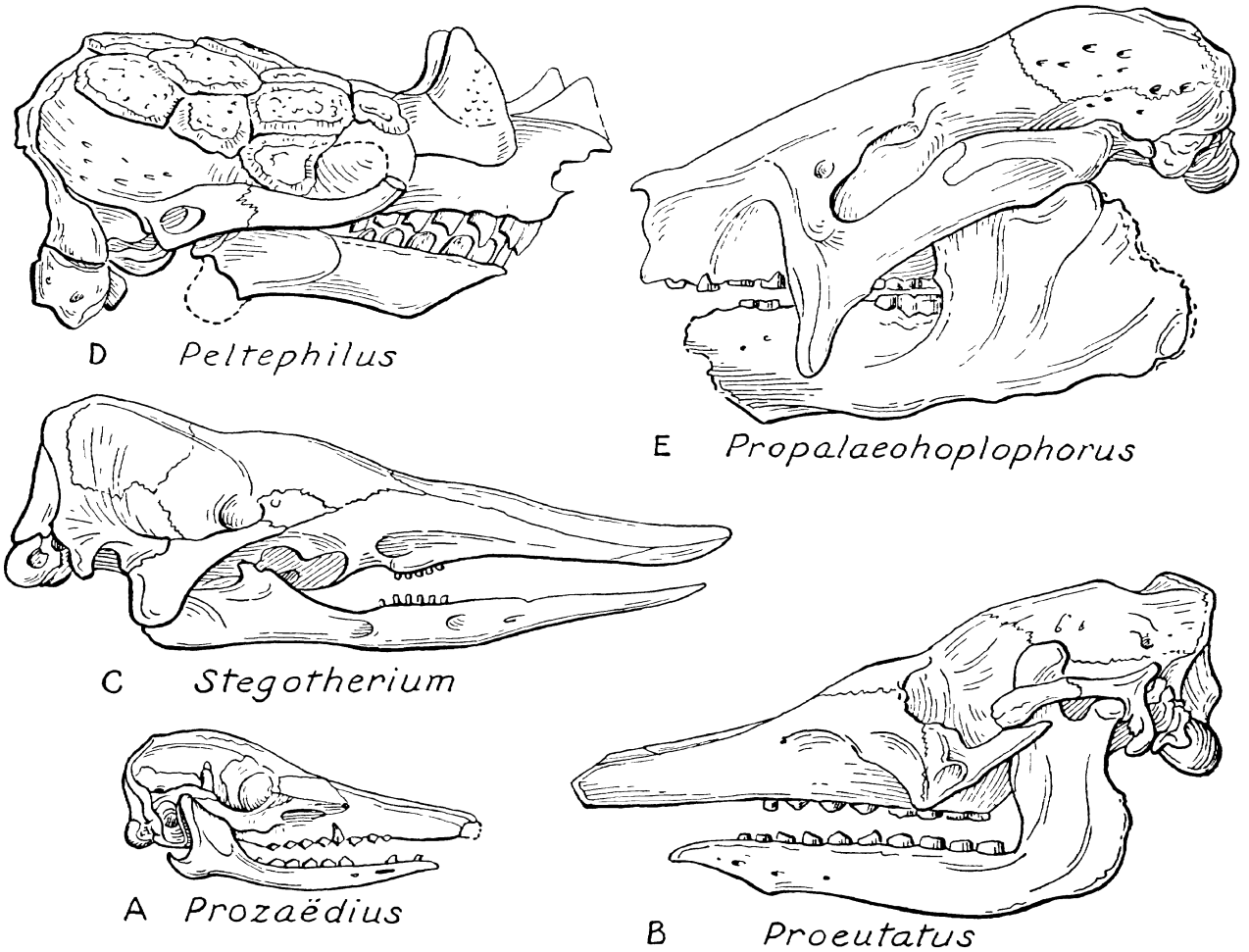


Fig. 19.32. Santa Cruz (Lower Miocene) armadillos (A–D) and glyptodont (E). After Scott. The armadillos were diversified in species and habits from the glyptodonts (E). A was related to the Pleistocene-Recent pichi (*Zaedyus*); B to the nine-banded armadillo; C, D to extinct branches.

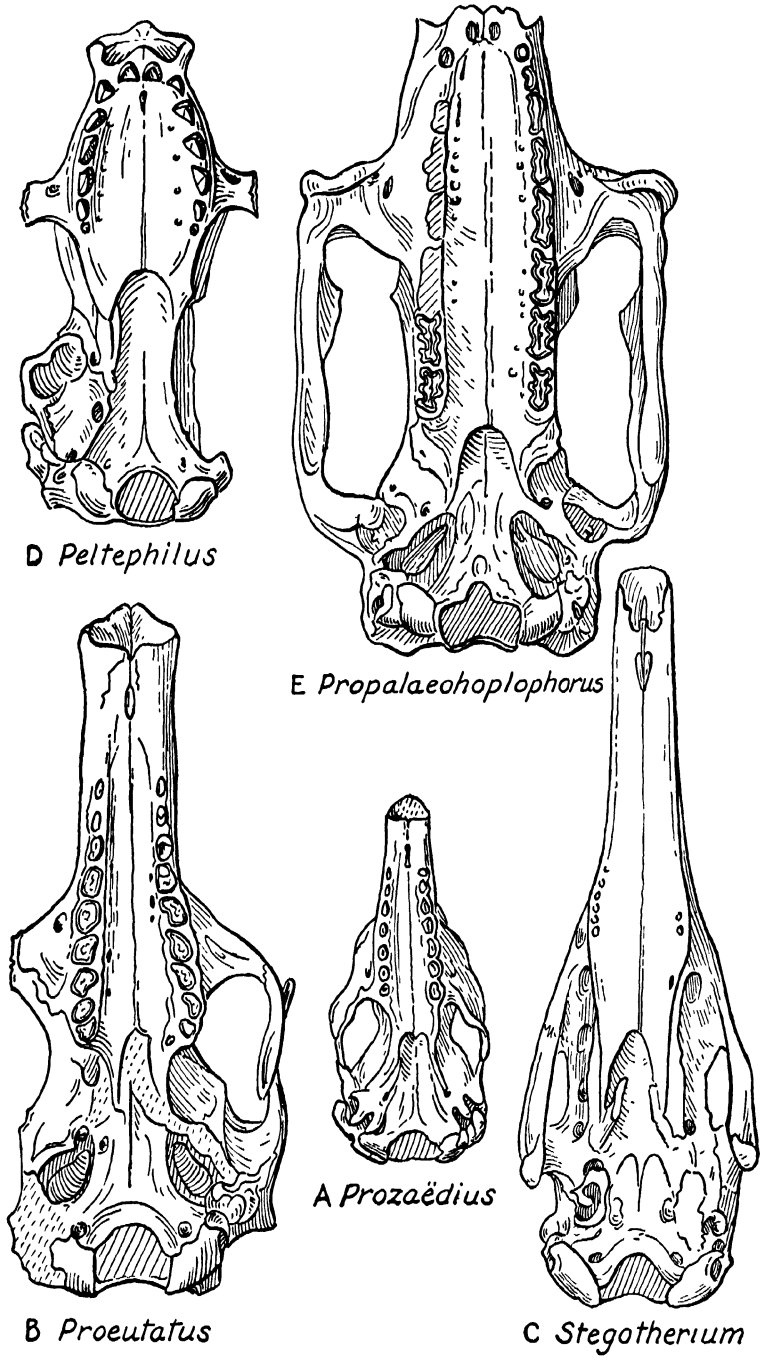


Fig. 19.33. Santa Cruz armadillos and glyptodont (continued). After Scott. Showing wide variation in length of snout and palate, size and shape of teeth, relative stability of cranial base and auditory region. In A–C snout elongate, tubular, incisors and canines lost; cheek teeth numerous; but reduced in C, converging toward an ant-eater habitus. Less specialized features retained in D, with short snout and cutting teeth. Occipital candyles set wide apart (? for bracing snout used in probing). Cheek teeth of glyptodonts (E) herbivorous, in two straight rows, with high crowns strengthened by three transverse folds.

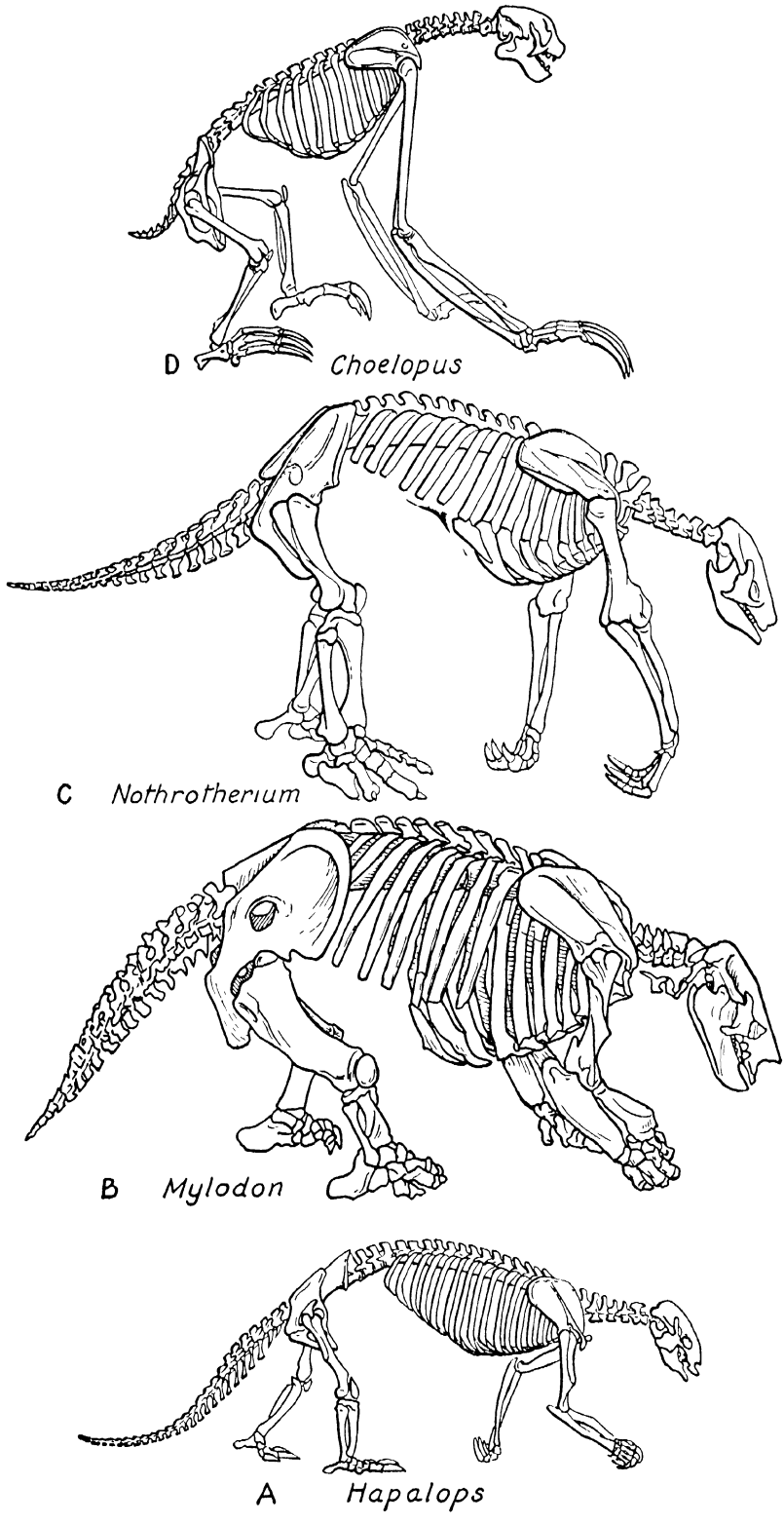


Fig. 19.34. Ground sloths (A–C) and tree sloth (D). A, after Matthew; B, C, after Stock; D, from Parker and Haswell after De Blainville.

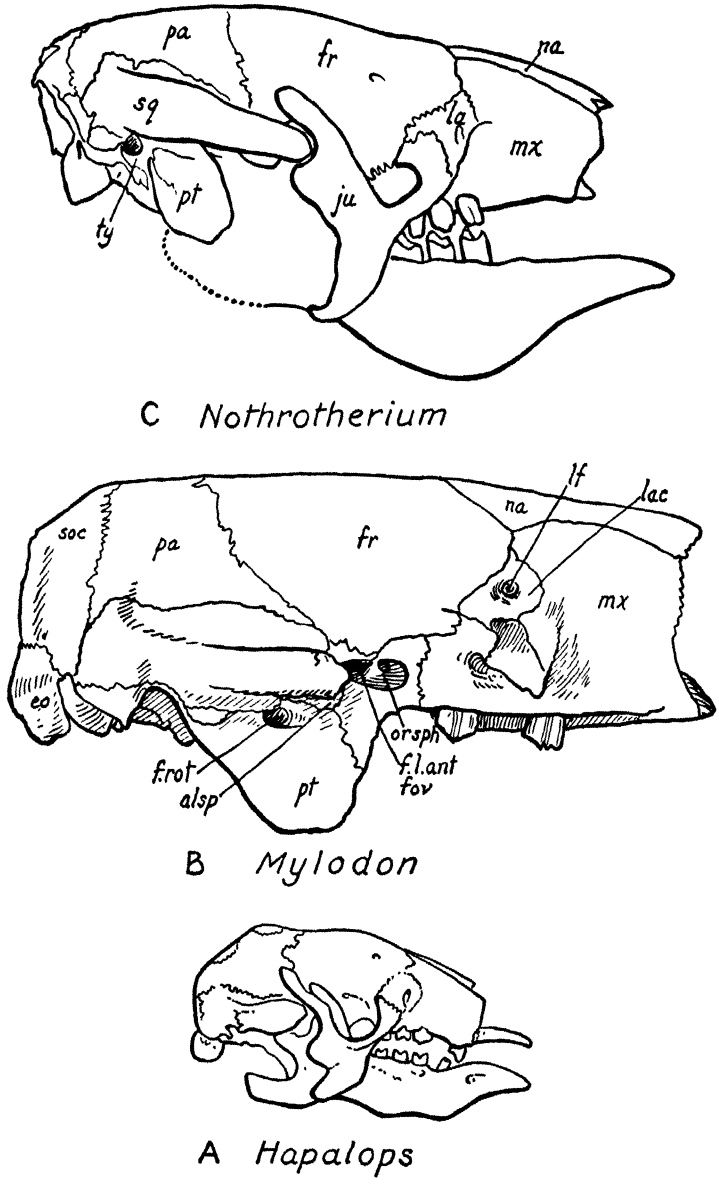


Fig. 19.35. Skulls of Lower Miocene (Santa Cruz) (A) and Pleistocene (California) (B, C) ground sloths. A, after Scott; B, C, after Stock.

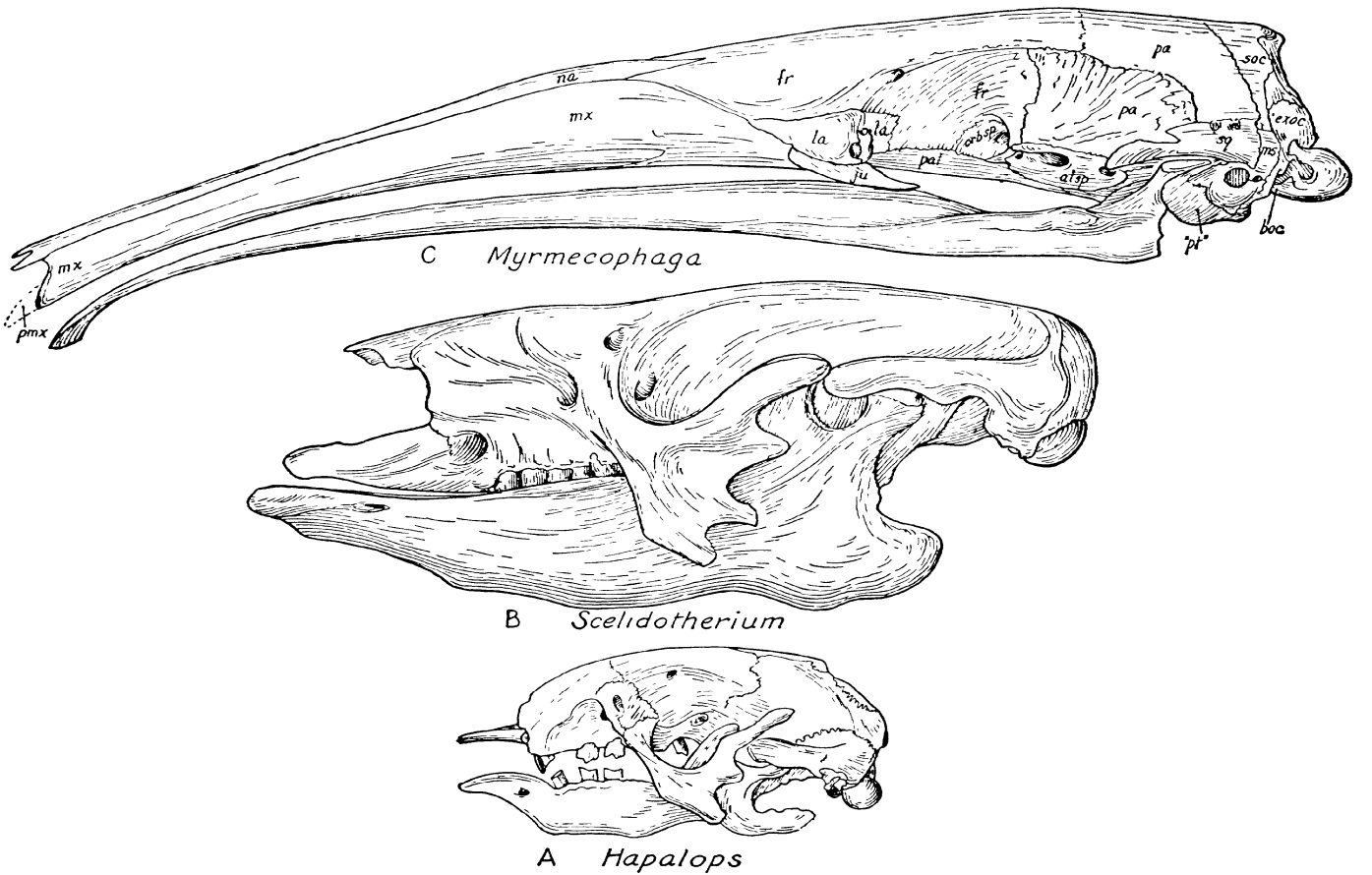


Fig. 19.36. Skulls of Miocene ground-sloth (A), long-skulled Pleistocene ground-sloth (B) and Recent ant-eater (C). Not to scale. A, after Scott; B, after Lydekker; C, original.

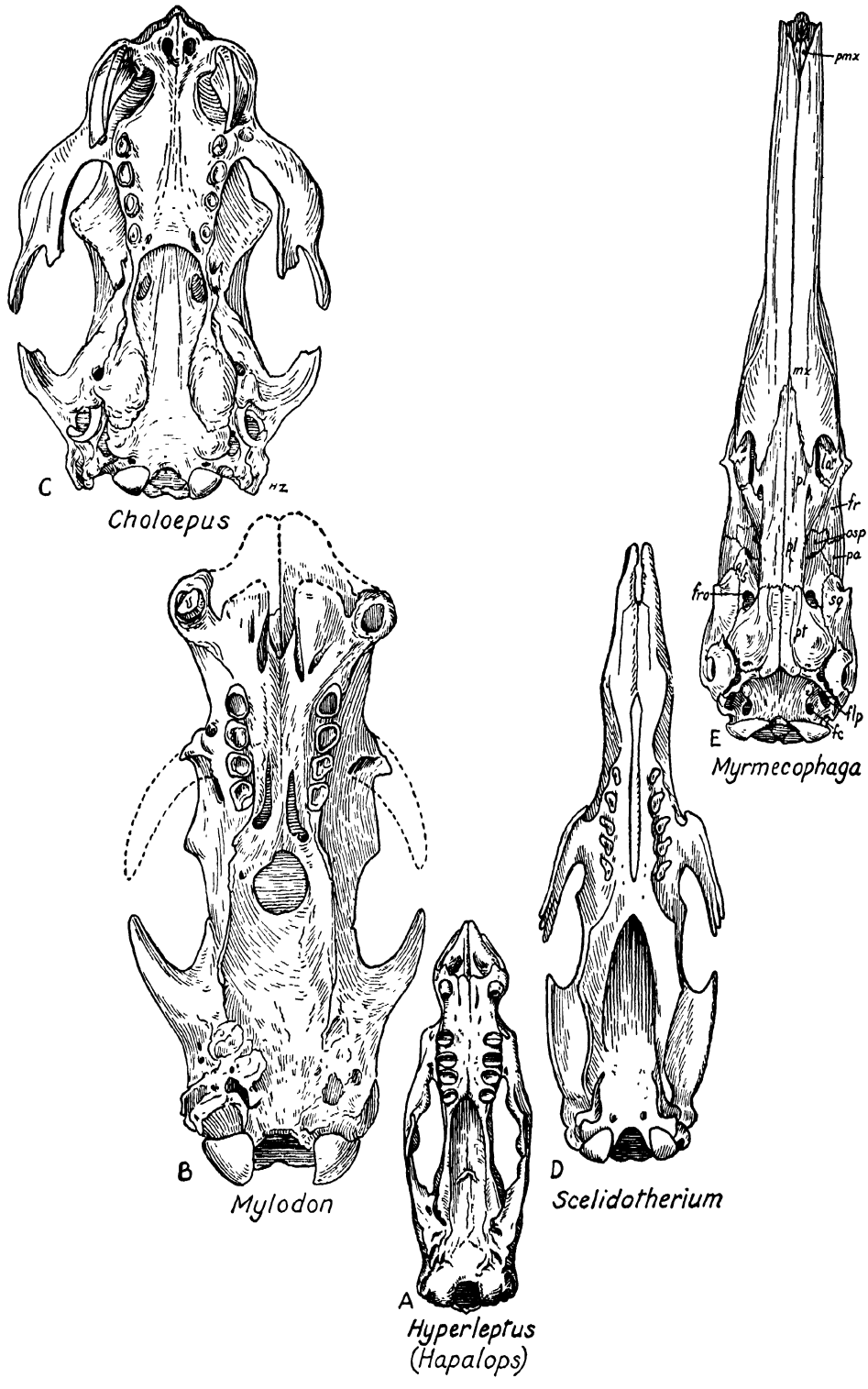


Fig. 19.37. Contrasting skulls of Recent tree-sloth (C) and young ant-eater (E) and their probable derivation respectively from wide- (B) or long-skulled (D) ground-sloths. A, after Ameghino; B, after Lydekker; C, E, original; D, after Burmeister.

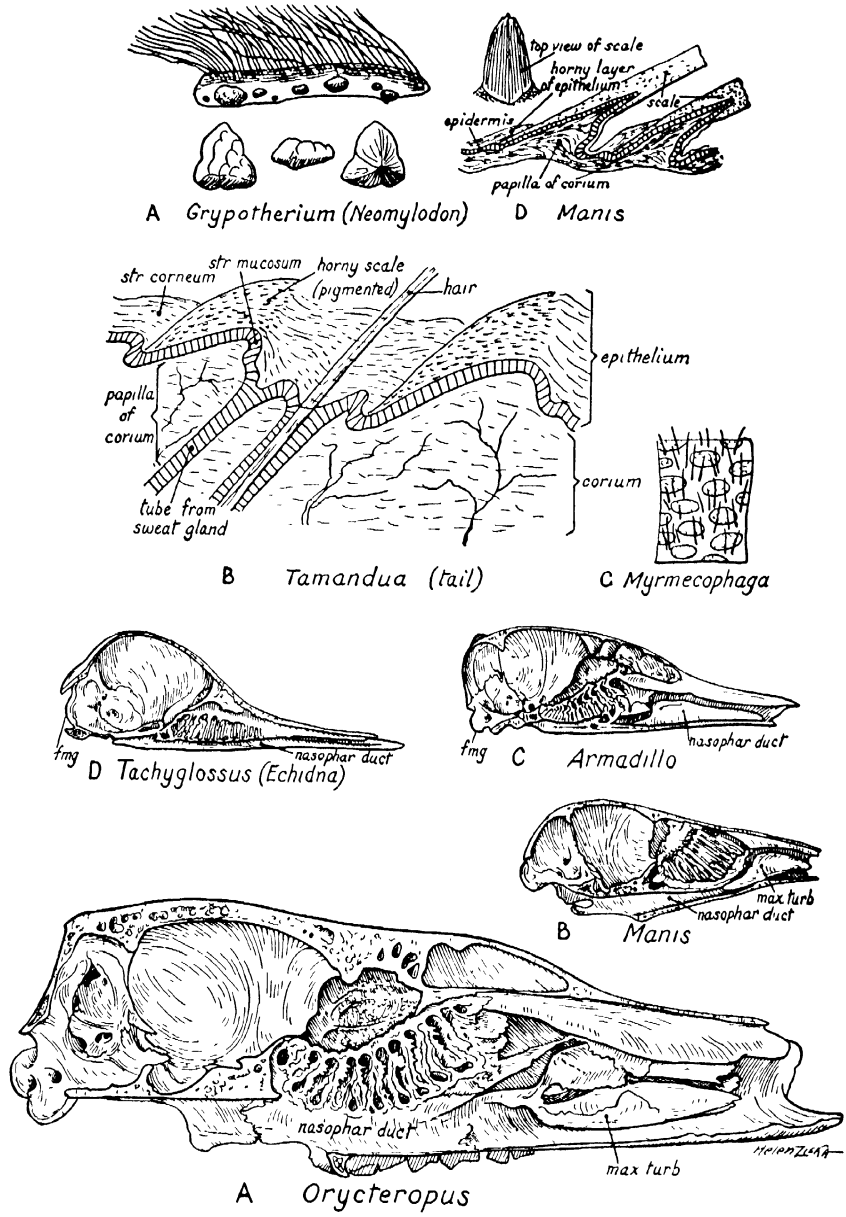


Fig. 19.38 (top). Integument of edentates (A–C) and scaly ant-eater (D). A, from Weber, after Smith Woodward; B–D, after Weber. The leathery skin of the ground-sloth (A) bore many ossicles in its basal layer, three of which are shown enlarged. Vestiges of this condition are found in the skin of Recent tree-sloths, and, in armadillos, well developed ossicles occur in the carapace and around the tail, beneath horny scales. In the tail of the South American ant-eaters (B, C) there are no ossicles but pigmented horny scales. In the scaly ant-eater (D) the scales are very large and simulate reptilian scales; but they appear to represent enlarged hair-papillae covered with hypertrophied horny scales.

Fig. 19.39. Paramesial sections of skulls of ant- or termite-eating mammals, showing great development of ethmoid scrolls, associated with a macrosmatic brain (i.e., with enlarged olfactory parts).

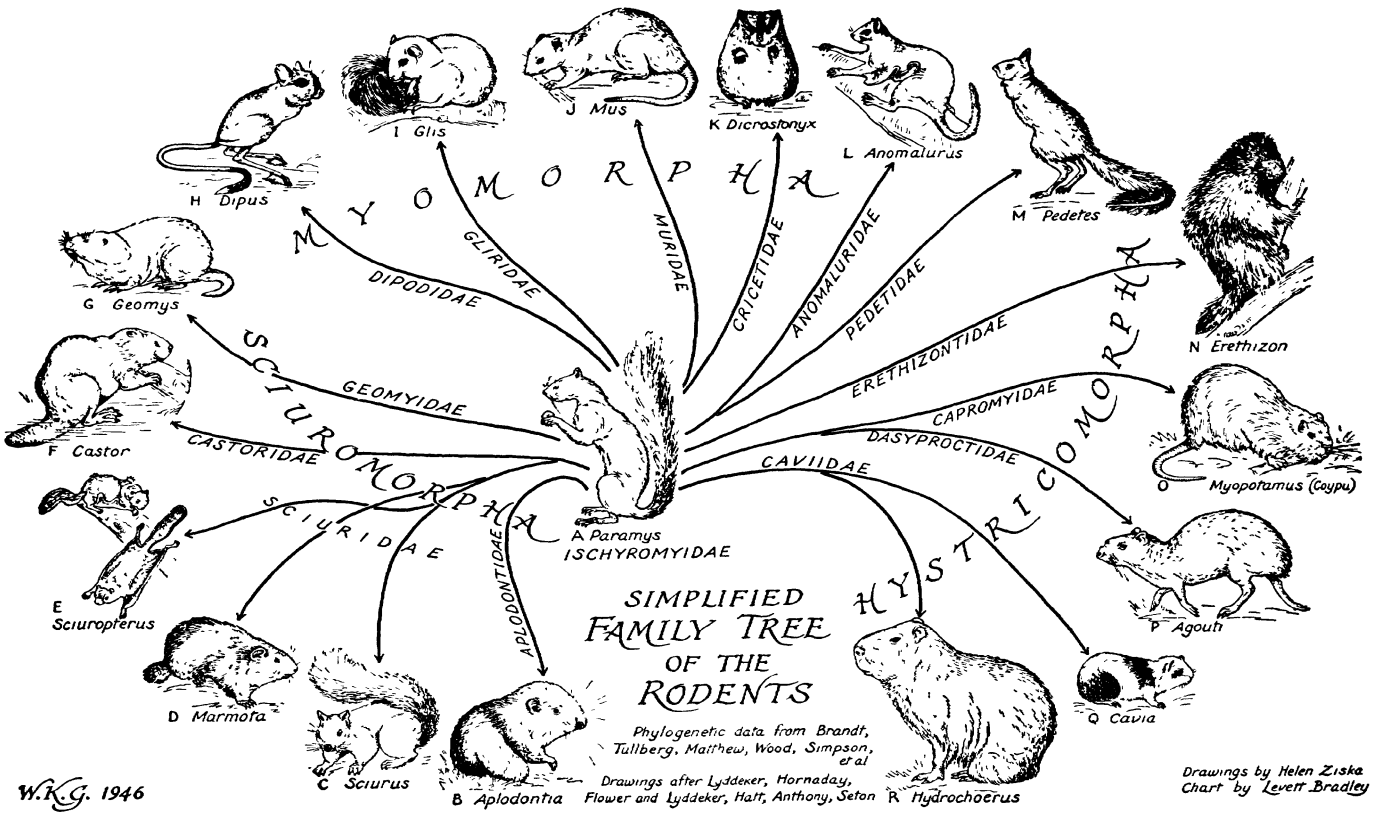

SIMPLIFIED
FAMILY TREE
OF THE
RODENTS
Phylogenetic data from Brandt, Tullberg, Matthew, Wood, Simpson, et al
Drawings after Lyddeker, Hornaday, Flower and Lyddeker, Hatt, Anthony, Seton
Drawings by Helen Ziska
Chart by Levett Bradley
W.K.G. 1946
MYOMORPHA
SCIUROMORPHA
HYSTRICOMORPHA
DIPODIDAE
GLIRIDAE
MURIDAE
CRICETIDAE
ANOMALURIDAE
PEDETIDAE
ERETHIZONTIDAE
CAPROMYIDAE
DASYPROCTIDAE
CAVIIDAE
GEOMYIDAE
CASTORIDAE
SCIURIDAE
APLODONTIDAE
A Paramys
ISCHYROMYIDAE
B Aplodontia
C Sciurus
D Marmota
E Sciuropterus
F Castor
G Geomys
H Dipus
I Glis
J Mus
K Dicrostonyx
L Anomalurus
M Pedetes
N Erethizon
O Myopotamus (Coypu)
P Agouti
Q Cavia
R Hydrochoerus

Fig. 19.40

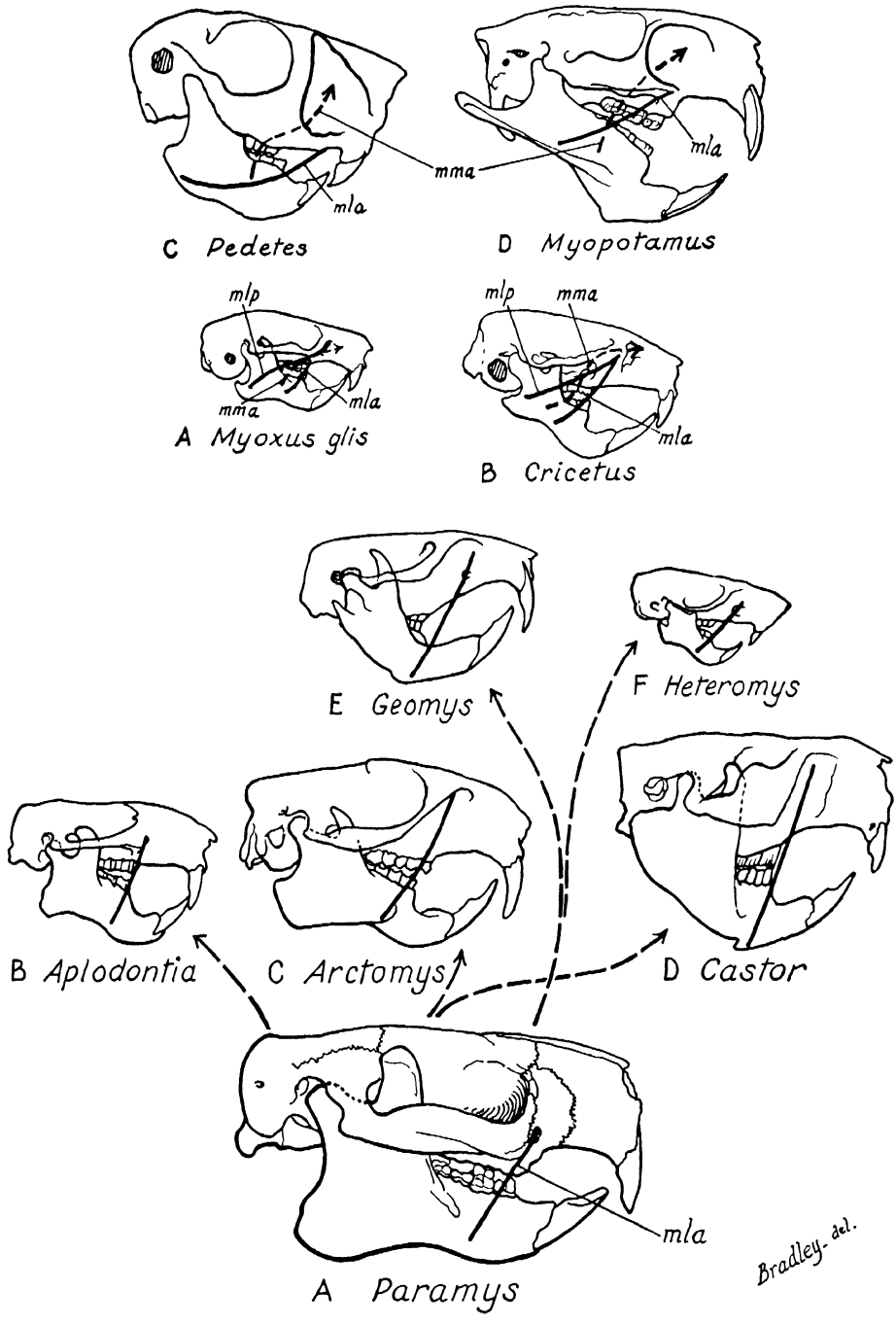


Fig. 19.41 (bottom). Principal skull forms of the suborder Sciuromorpha, showing phyletic branching in relation to upward growth of the anterior slip of the masseter lateralis muscle (*mla*) on the side of the muzzle (C–F). Drawings after Matthew (A) and Tullberg (B–F). Phylogenetic data chiefly from Matthew (1910) and Simpson (1945).

Fig. 19.42 (top). Skulls of dormouse (A), cricetid (B), anomaluroid (C) and hystricomorph (D). After Tullberg. The anterior part of the medial layer of the masseter (*mma*) works its way inward, upward and forward, through the infraorbital canal, finally (C, D) crowding the anterior lateral or superficial branch of the masseter (*mla*) off the muzzle, greatly expanding the infraorbital canal and filling the enlarged preorbital area

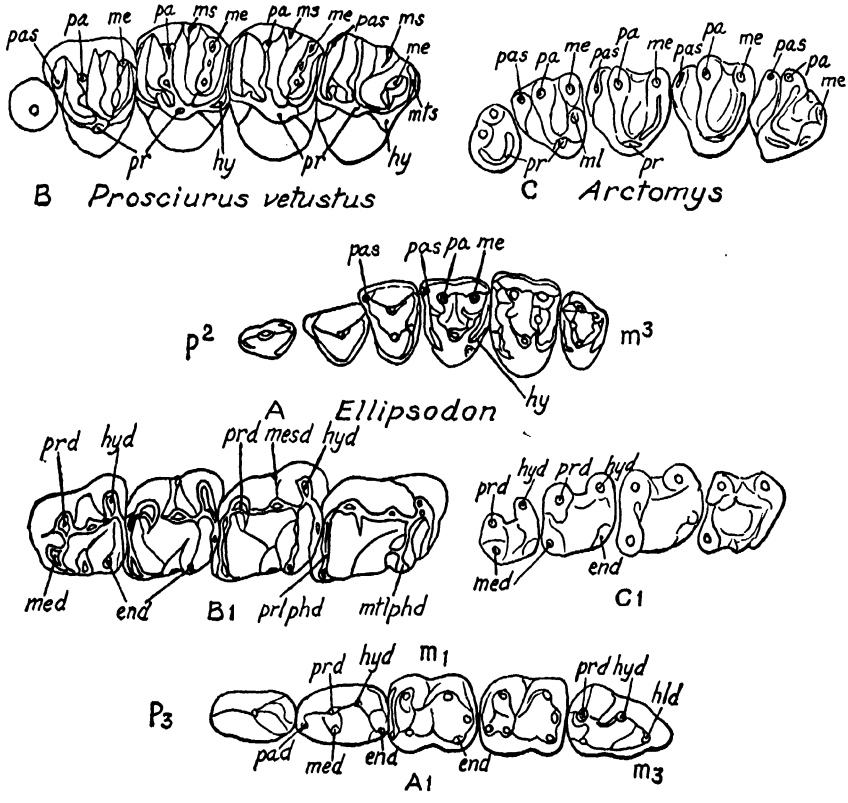


Fig. 19.43. Comparison of upper and lower cheek teeth patterns. A, A1, after Simpson; B, B1, after A. E. Wood; C, C1, original. A, A1, A Paleocene insectivore-condylarth, illustrating a primitive "tritubercular" (A) and "tuberculo-sectorial" (A1) molar stage. B, B1, A relatively primitive Oligocene sciuromorph rodent. The upper molars have developed a mesostyle (*ms*) and cross-crests on the anterior cingulum and on the para- and metacones; the lower molars (B1) have apparently lost the paraconid, developed large talonid basins, with mesostylid (*mesd*) protolophid (*prlphd*) and metalophid (*mtlphd*). C, C1, A Recent marmot with prominent cross-crests, large protocones and deep talonid basins.

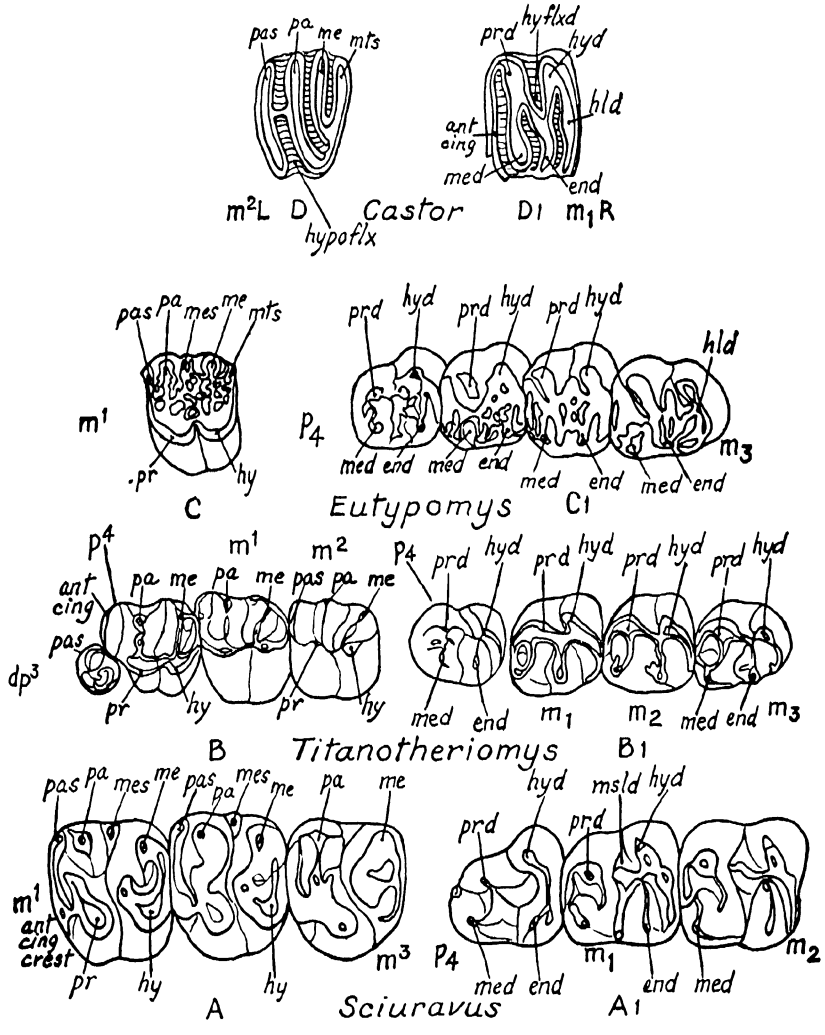


Fig. 19.44. Increasing complexity of upper (A–D) and lower (A1 to D1) molar patterns, from brachyodont Oligocene (A, A1) to ptycho-hypsodont Recent (D, D1) sciuromorphs. A–C, A1, to C1, after A. E. Wood, D, D1 original. *Hypoflx,* hypoflexus; *hyflxd,* hypoflexid.

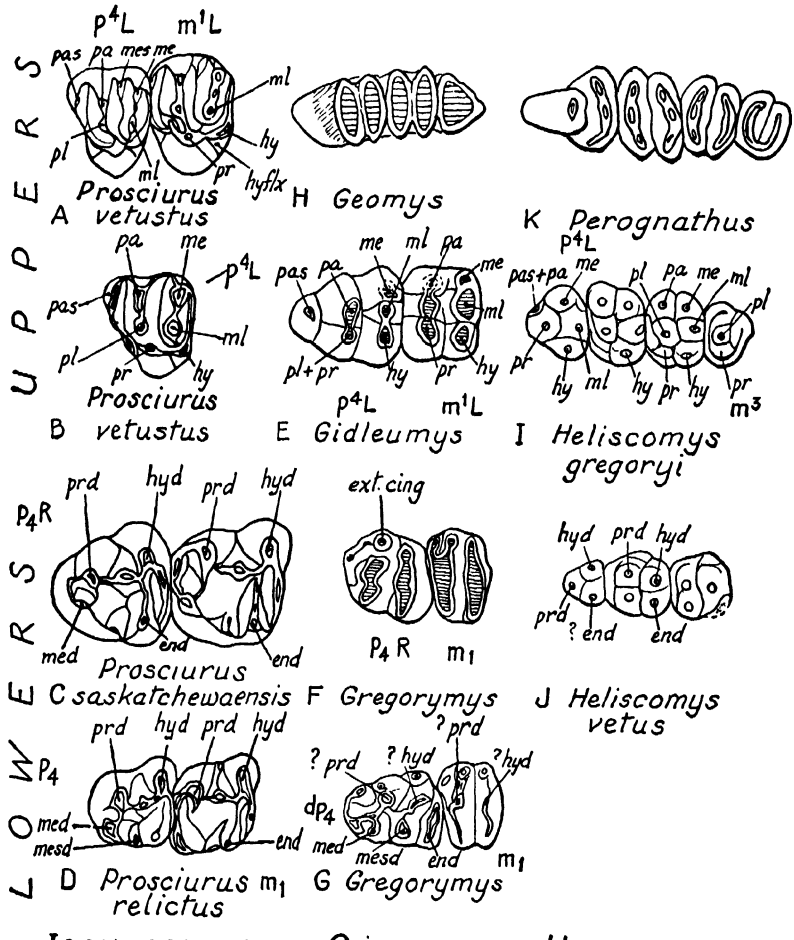


Fig. 19.45. Premolar-molar patterns of Oligocene prosciuroids (A–D) and Oligocene to Recent geomyids (E–H and heteromyids (I–K). All data after A. E. Wood, but with certain tentative changes in cusp names. *Gidleyumys*, a close relative of the *Entoptychus* group of minute Oligocene rodents, foreshadows the geomyids (H) in arranging its main molar cusps in two transverse rows of three cusps each. As the crown becomes higher, the cusps are soon worn off, leaving two cross-crests. *Gregorymys* (F, G), a Lower Miocene heteromyid has large external cusps which may be derived from the external cingulum. In *Heliscomys* (I, J), a minute ancestor of the heteromyids, the six cusps of the relatively low-crowned upper molars seem to be homologous with those of *Prosciurus* (A). With the great heightening of the crown, the cusps tend to fuse into two main cross-crests, sometimes joined into a U.

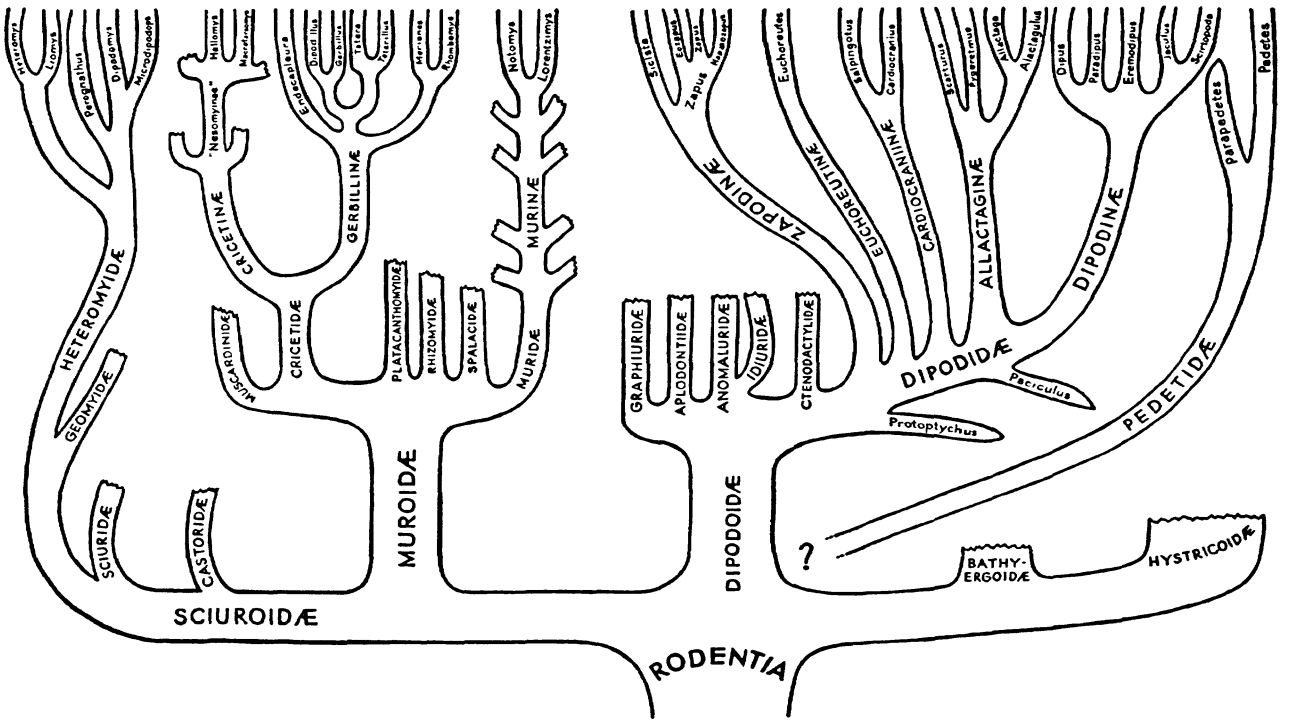


Fig. 19.46. Independent derivation of ricochetal types in different families of rodents. After Hatt Groups which have not produced ricochetal types are shown as broken branches. Fossil genera are placed in closed branches.



Fig. 19.47. Evolution of premolar-molar patterns from primitive Oligocene sciuromorph (A) to Recent Aplodontia (E, E1), and mylagaulids (F–K). After McGrew. Thanks chiefly to Cope, Matthew, Riggs, Stock, McGrew, the curious and very complex premolar-molar patterns of the modern "Mountain Boomer" are linked by several intermediate stages with those of the primitive Oligocene sciuromorph stock. Beginning with *Allomys* (B), the upper molar crowns gradually lengthen anteroposteriorly, emphasizing the W-shaped ectoloph, especially at the mesostyle (*ms*), enlarging the proto- and metaconules, elongating the worn proto-hypocone loops to form anteroposterior lakes and wrinkling the enamel about the intercuspidal lakes. In the later stages the crowns become hypsodont and the elaborate pattern is soon worn off. The lower molar crowns undergo corresponding changes.

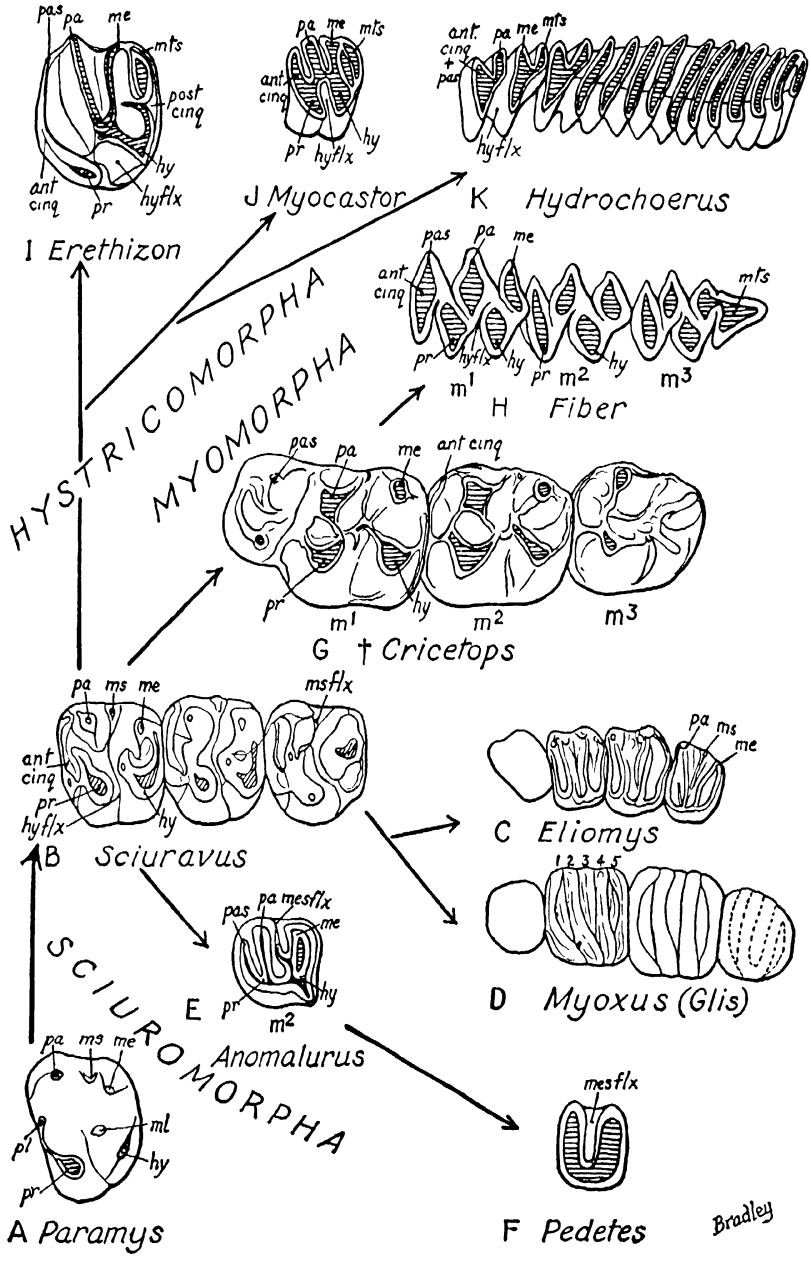


Fig 19.48. Emergent upper molar patterns in the three suborders of true rodents. A, B, after A. E. Wood, C–F, J, K, after Frechkop; G, after Schaub; H, I, original. Reduplication of parts (polyisomerism) is conspicuous in members of different families (D, K). Anisomerism, or emphasis of certain parts, is especially notable in *H*. Negative anisomerism, or reduction of certain parts, is seen in *F*. Some rodent molar patterns display partly convergent resemblances to those of other orders: e.g., many-plated molars in elephants, bilophodont molars (B) in tapirs. There is also parallelism between patterns belonging to different rodent families; e.g., beaver-like (fig. 19.44D) molars of *Myocastor* (J).

CHAPTER XX

ARCHAIC AND MODERNIZED CARNIVORA, INCLUDING SEALS (PINNIPEDIA)

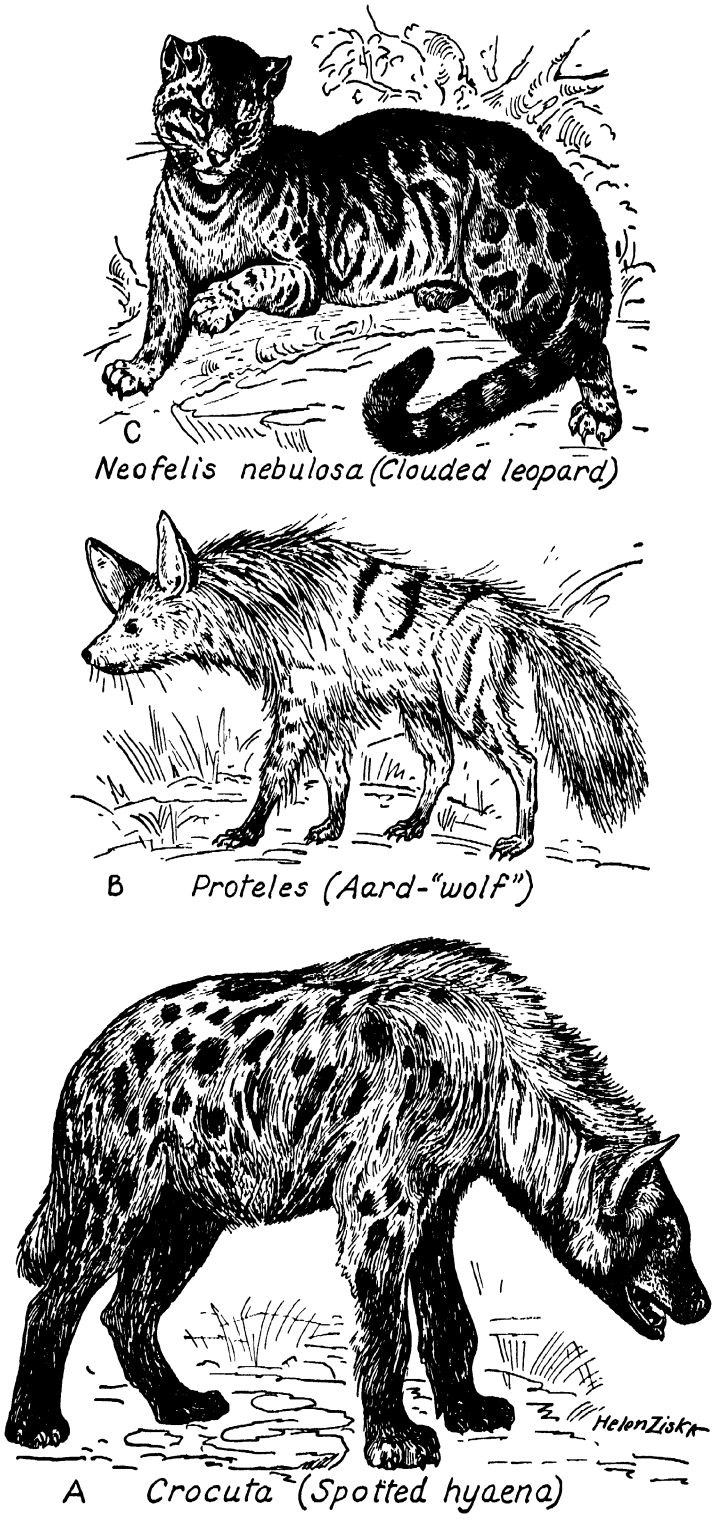


Fig. 20.1. Two flesh-eating predators (A, C) and a "poor relation" (B). A, C, after Lydekker; B, from a specimen mounted by Herbert Lang.

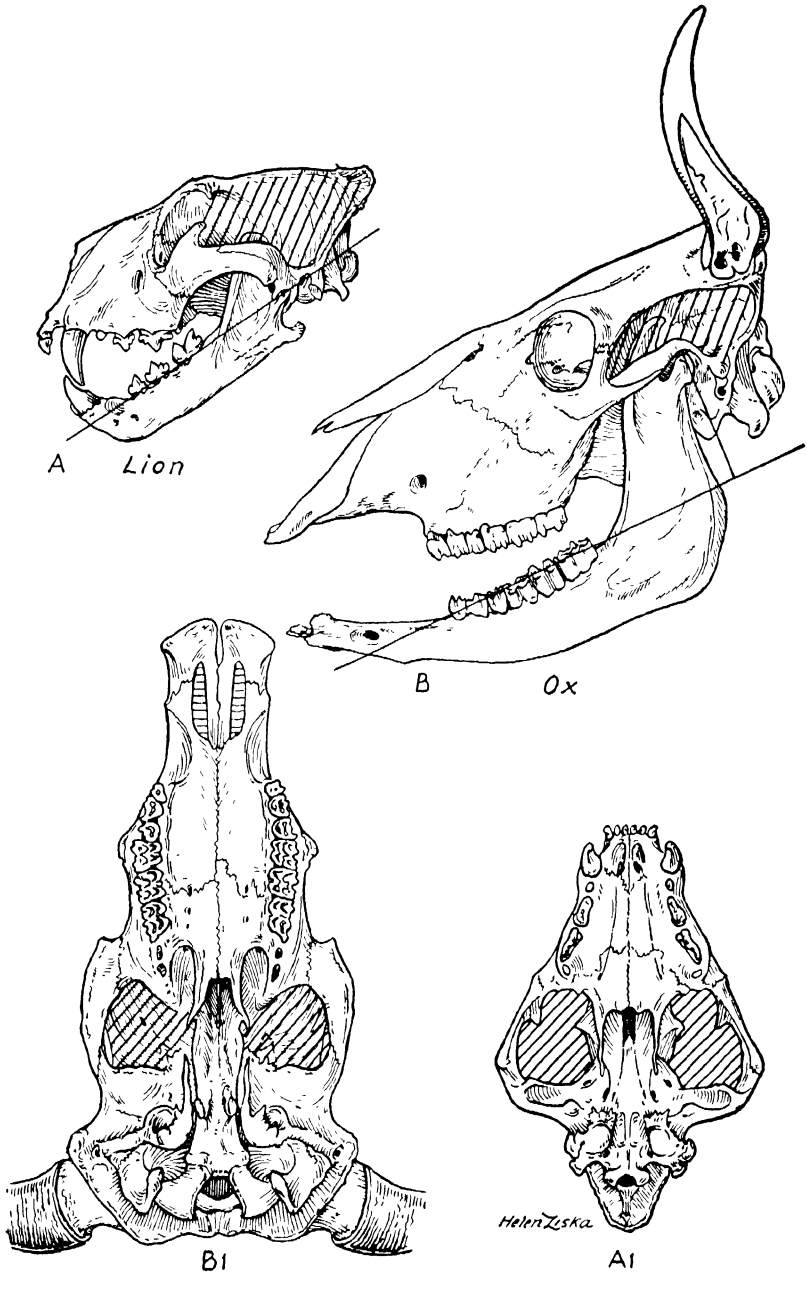


Fig. 20.2. Skulls of lion and ox, to show contrasts in construction correlated with opposite extremes in diet. Temporal muscle area crosshatched.

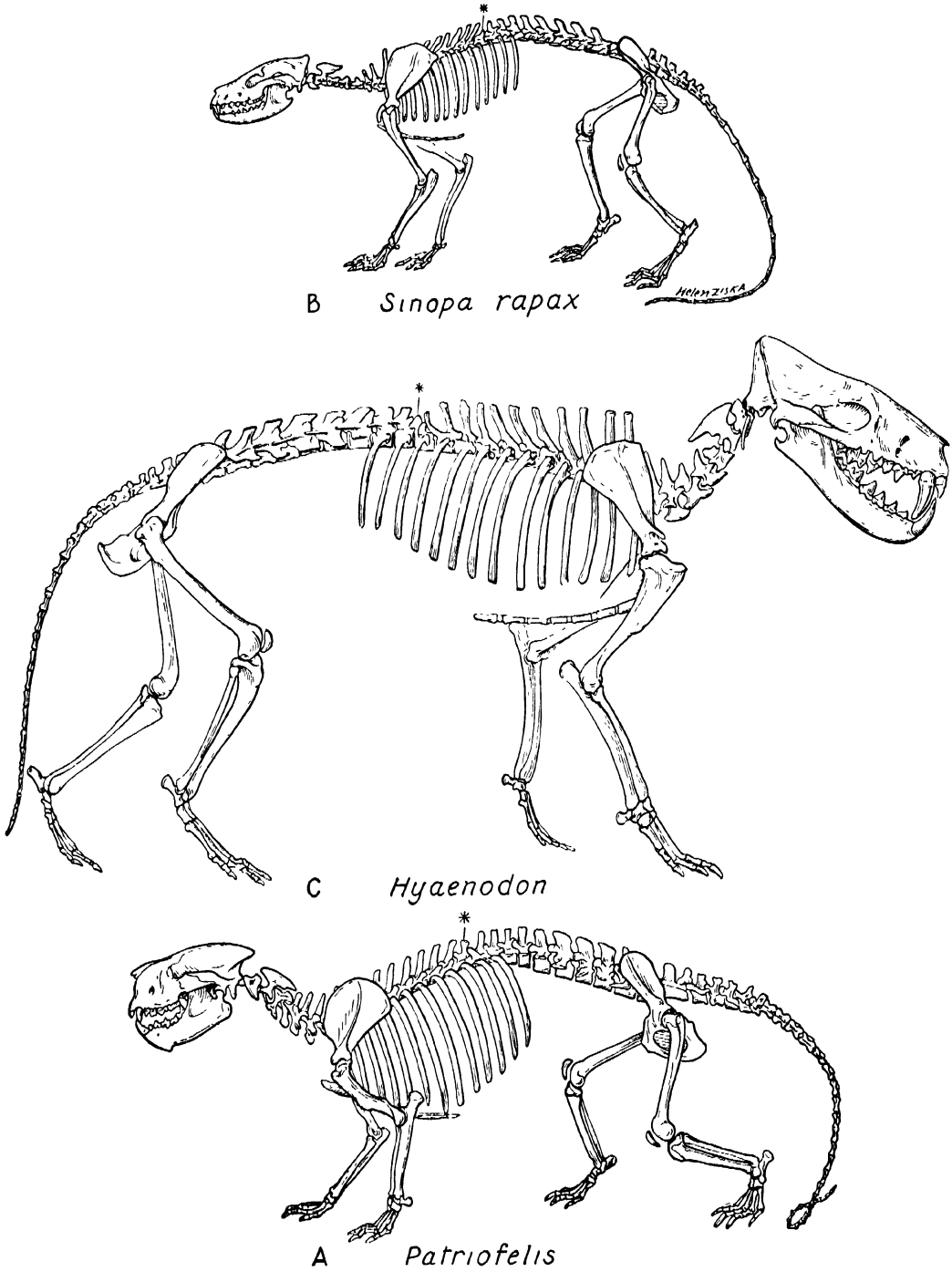


Fig. 20.3. Skeletons of tiger-like oxyaenid (A), fairly primitive fox-like (B) and advanced wolf-like (C) hyaenodonts. A, after Osborn; B, after Matthew; C, after Scott. *Anticlinal vertebra.

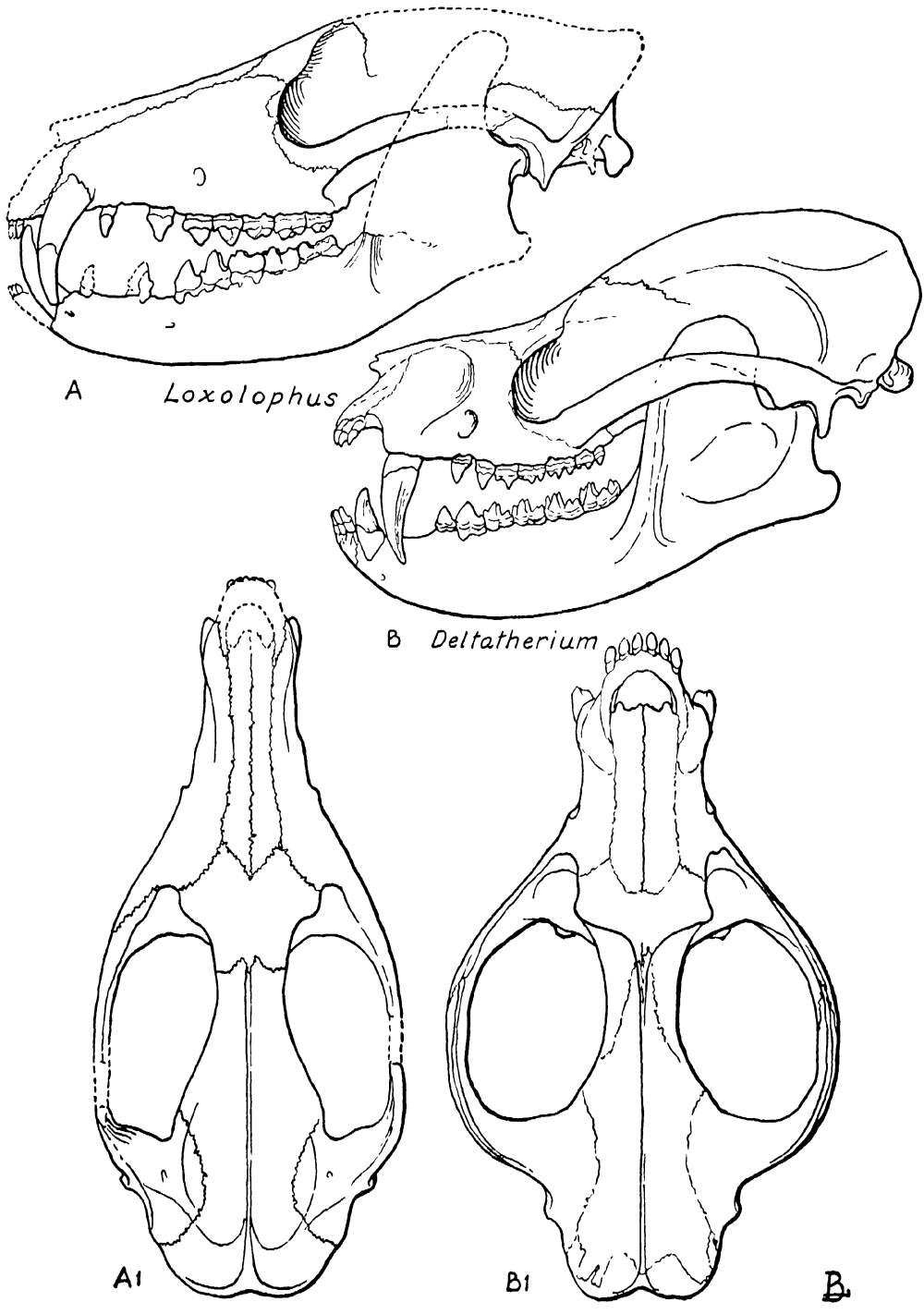


Fig. 20.4. Skulls of two Paleocene oxyclaenid creodonts. After Matthew. A is of central and generalized appearance, related both to typical Carnivora and to primitive Herbivora. B is a primitive predaceous type, not unlike the opossum among marsupials. In the dorsal view, the long muzzle and long temporal fossae (A1) contrast with the short muzzle and transversely widened zygomatic arches of (B1), indicating great piercing and cutting power.

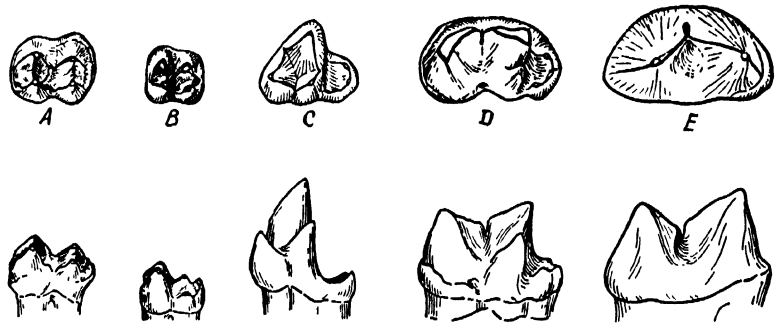


Fig. 20.5. Cope's theory of the origin of the lower sectorial tooth of the Carnivora. Illustrated from fossils known to Cope in 1875 and from two recent forms. Crown view (upper row) and medial view (lower row) of right lower molars. A, *Achaenodon*; B, *Hyopsodus*; C, *Oxyaena*; D, *Hyaena*; E, *Felis leo*.

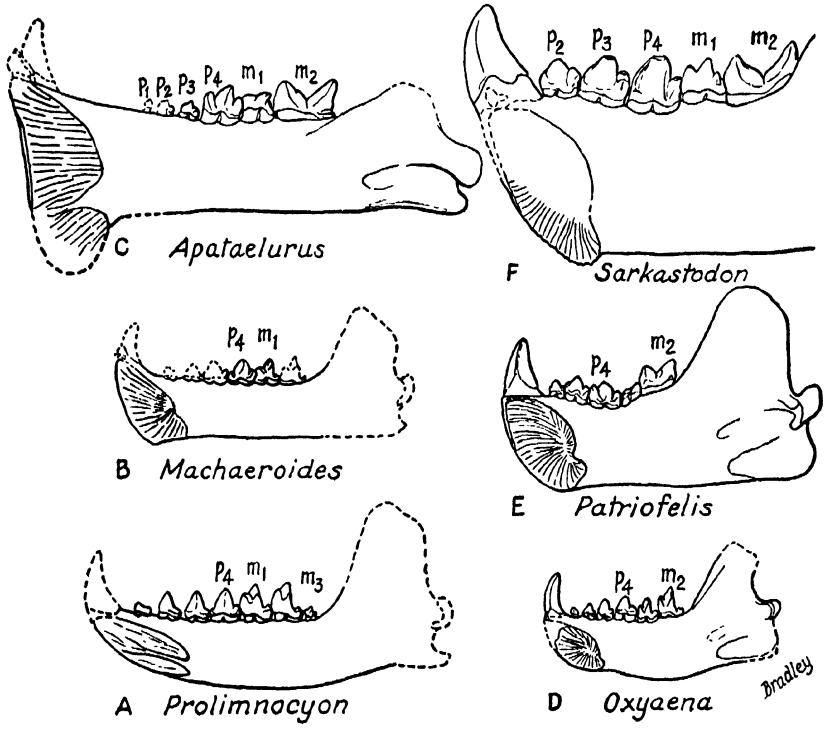
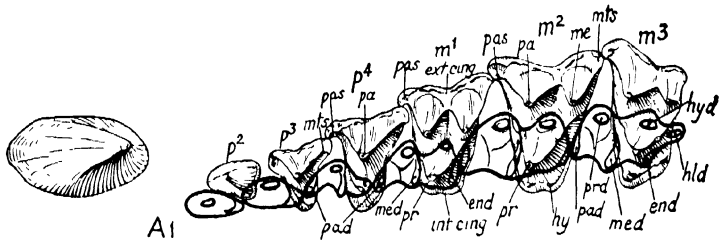
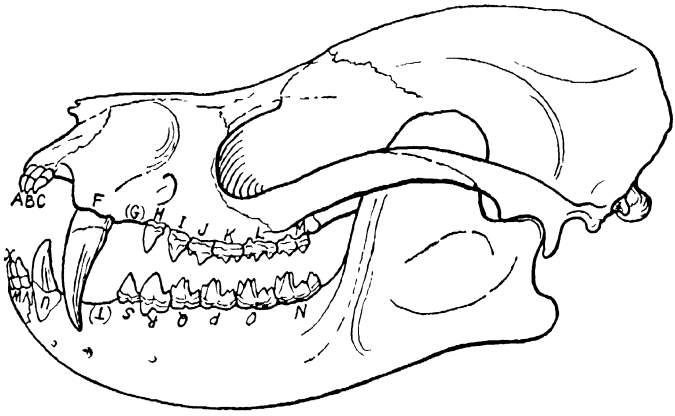
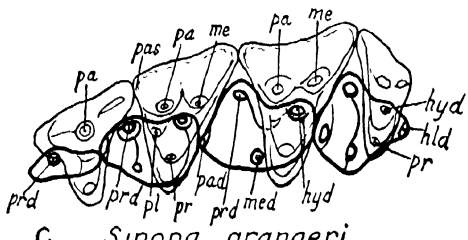
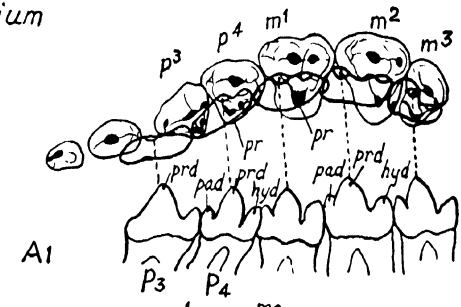


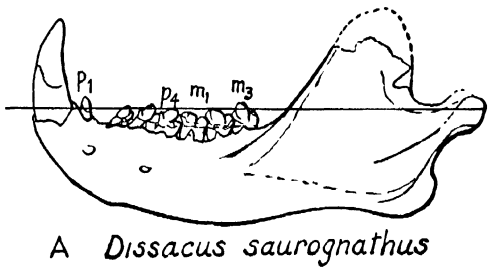
Fig. 20.6. Parallel evolution of shearing m_2 in the "false sabre-tooth" line (Machaeroidinae, A–C) and in the Oxyaeninae (D–F). After Denison. "Sabre-tooth" forms have also been evolved quite independently in the Miocene South American marsupial *Thylacosmilus* (fig. 18.24 C) and in the true or fissiped sabre-tooths of the Oligocene of North America (fig. 20.30).











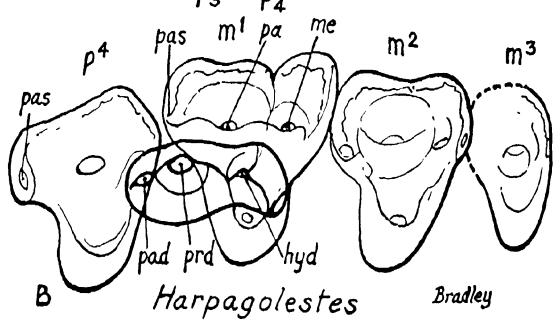


Fig. 20.7 (top). Skull and cheek teeth of a sharp-toothed oxyclaenid (A, A1), illustrating inverse relations of upper and lower teeth in articulation.

Fig. 20.8. Jaw and dentition of mesonychids (A–B) and hyaenodont (C). In the mesonychids the hypoconid (*hyd*) remained medial on the crown, as it is in the premolars, but became enlarged; whereas in the hyaenodonts (C), as in most other placental mammals, the hypoconid (*hyd*) was lateral in position and the talonid acquired a basin lingual to the hypoconid for the reception of the protocone of the upper molar.

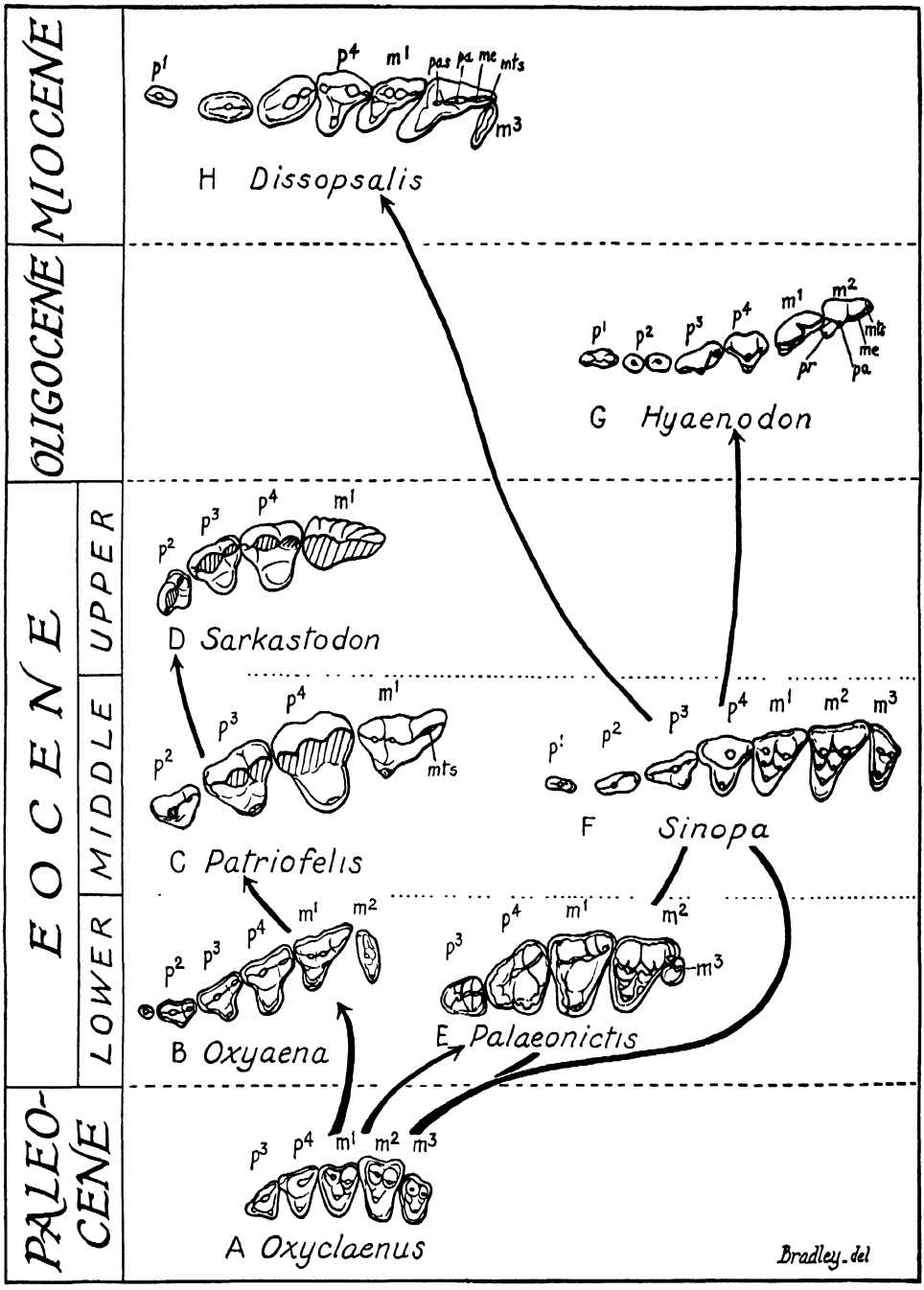


Fig. 20.9. Left upper teeth of typical oxyaenids (A, B–D) and hyaenodonts (E–G) in geologic sequence. A, E, after Matthew; B–D, after Denison; F, after Scott; G, H, after Colbert. In the primitive oxyclaenid (A) the metacone-metastyle cutting blades are small but present, especially on p^4, m^1, m^2. In the oxyaenids these blades become dominant on m^1, which grows very long, while m^3 disappears and m^2 is greatly reduced or wanting. In the hyaenodonts these blades become increasingly prominent on both m^1 and m^2. Thus in *Hyaenodon* there are increasingly long blades on p^3, p^4, m^1, m^2. *Dissopsalis* was a side branch from the *Sinopa-Tritemnodon* stage (Colbert).

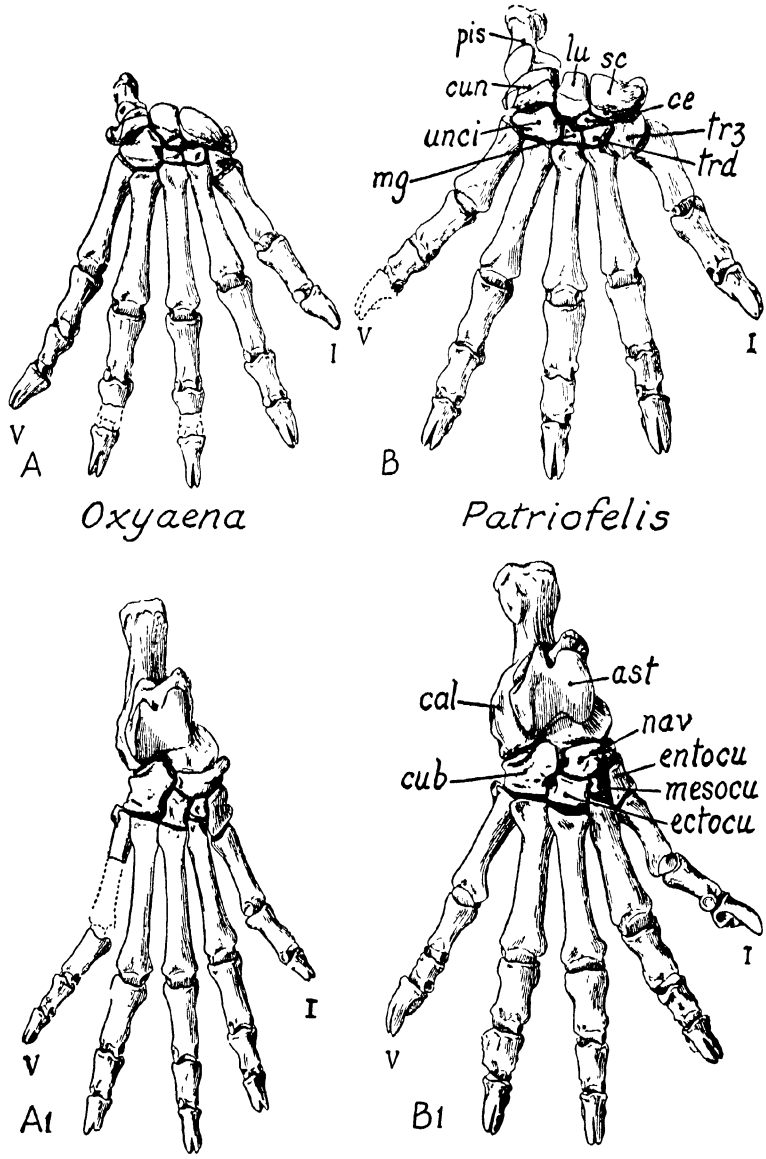


Fig. 20.10. Hands and feet of *Oxyaena* and *Patriofelis*. After Denison. Showing the scaphoid, lunar and centrale not fused into a scapho-lunar-centrale bone. The other Oxyaenidae and the more primitive Hyaenodontidae of the subfamily Limnocyoninae have essentially similar hands and feet

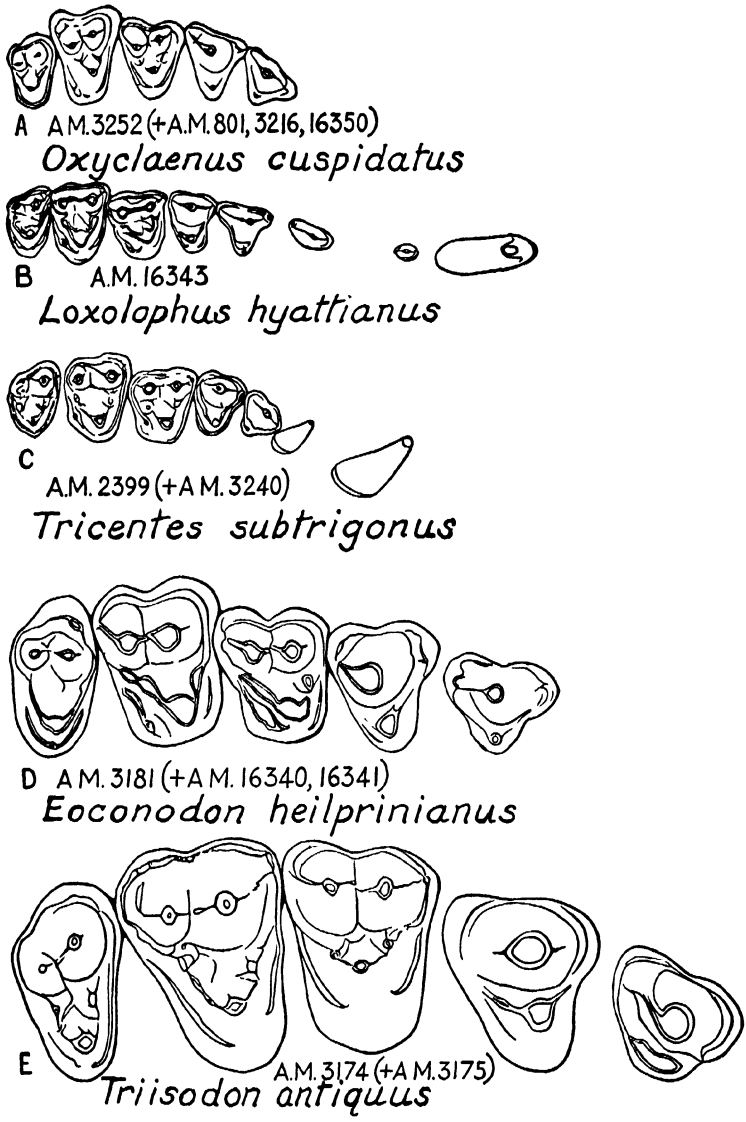


Fig. 20.11a, b. (a) Right upper (A–E) and (b) lower (A–G) cheek teeth of blunt-toothed arctocyonids (oxyclaenids). After Matthew. The transverse diameters of the crowns increase from p^2–m^2. M^3 is limited posteriorly by the temporal muscle. The lower cheek teeth are narrower transversely than the uppers, thus increasing their piercing and cutting power. The greater breadth of the upper teeth provides a firm base for the food.

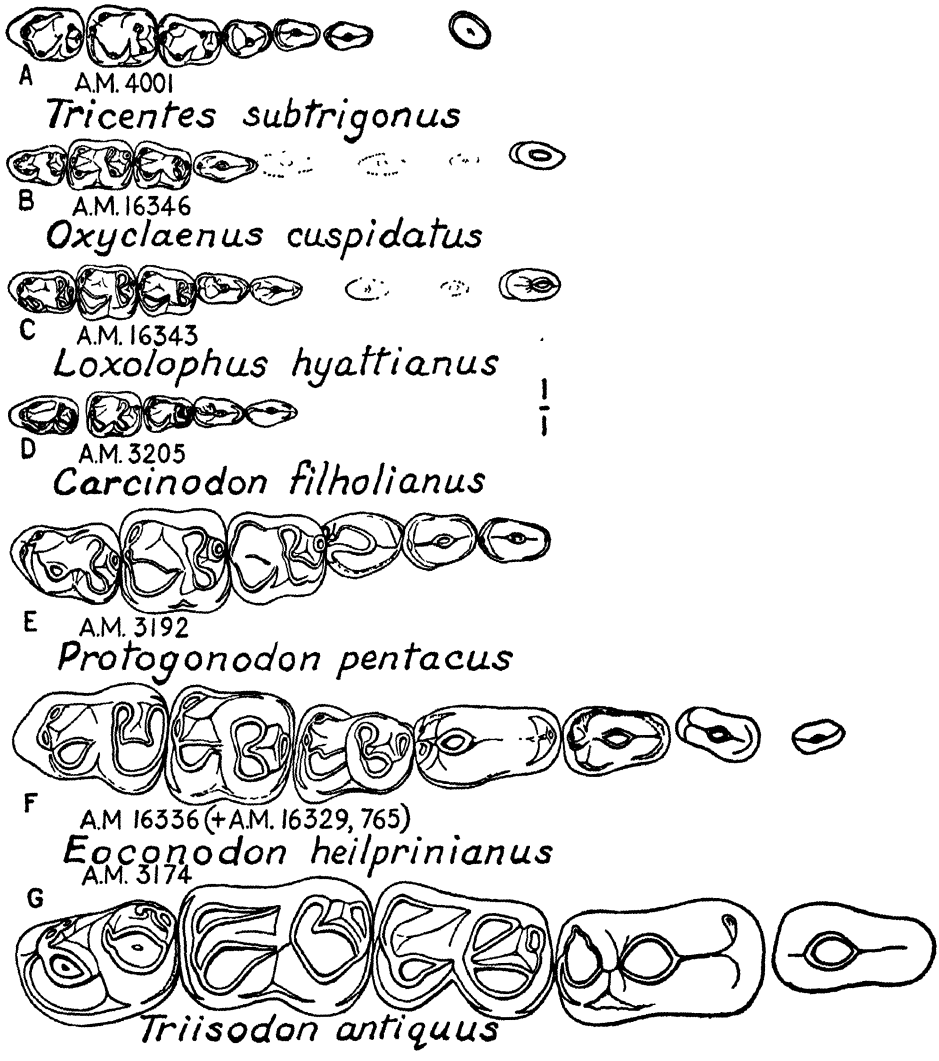

A
A.M. 4001
Tricentes subtrigonus
B
A.M. 16346
Oxyclaenus cuspidatus
C
A.M. 16343
Loxolophus hyattianus
D
A.M. 3205
Carcinodon filholianus
E
A.M. 3192
Protogonodon pentacus
F
A.M 16336 (+A.M. 16329, 765)
Eoconodon heilprinianus
A.M. 3174
G
Triisodon antiquus

Fig. 20.11b

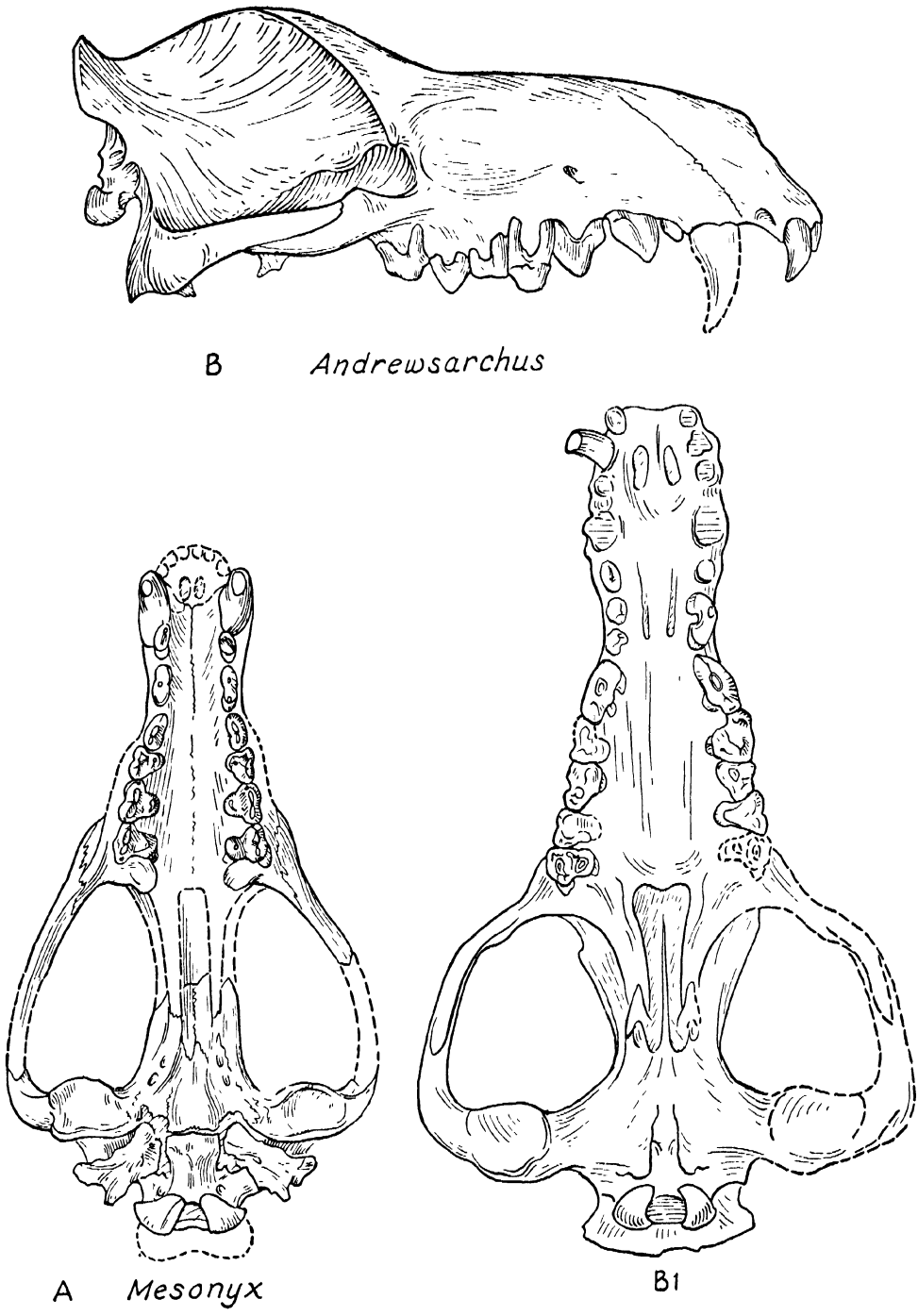
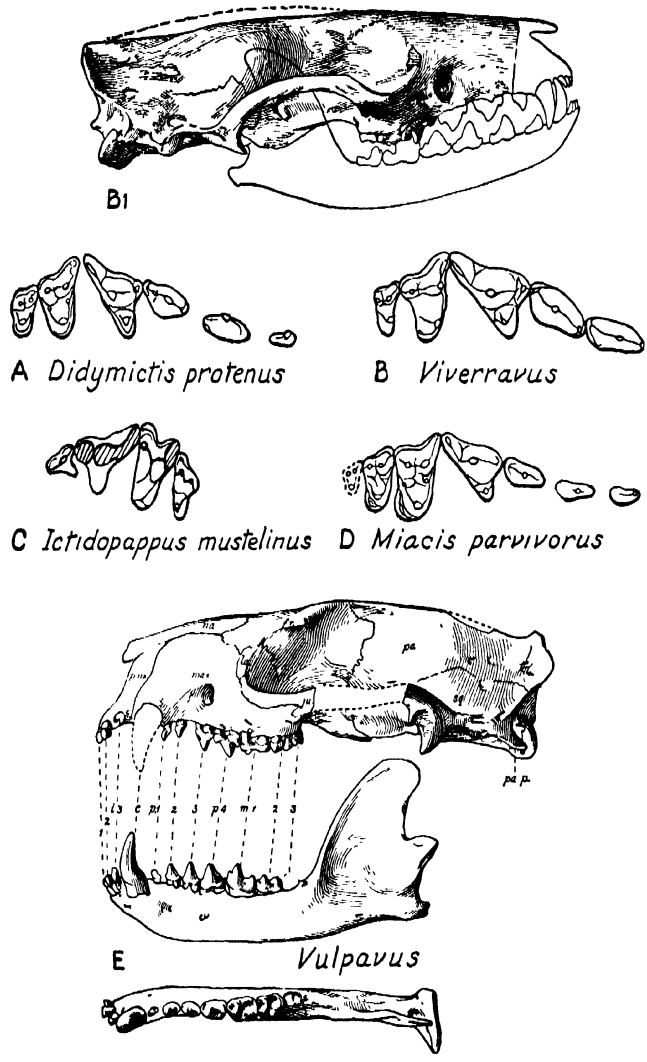


Fig. 20.12. Skulls of relatively primitive (A) and super-giant (B, B1) mesonychids. The posterior position of the zygomatic base and the great length of the jaw implies ability to open the mouth very widely and to kill by a quick snap of the large canines and incisors. A, after Matthew; B, from the type skull; B1, after Osborn.



Figs. 20.13–15. Primitive miacids from the Paleocene (A, C) and Eocene (B, B1, D, E). C, after Simpson; others, after Matthew.

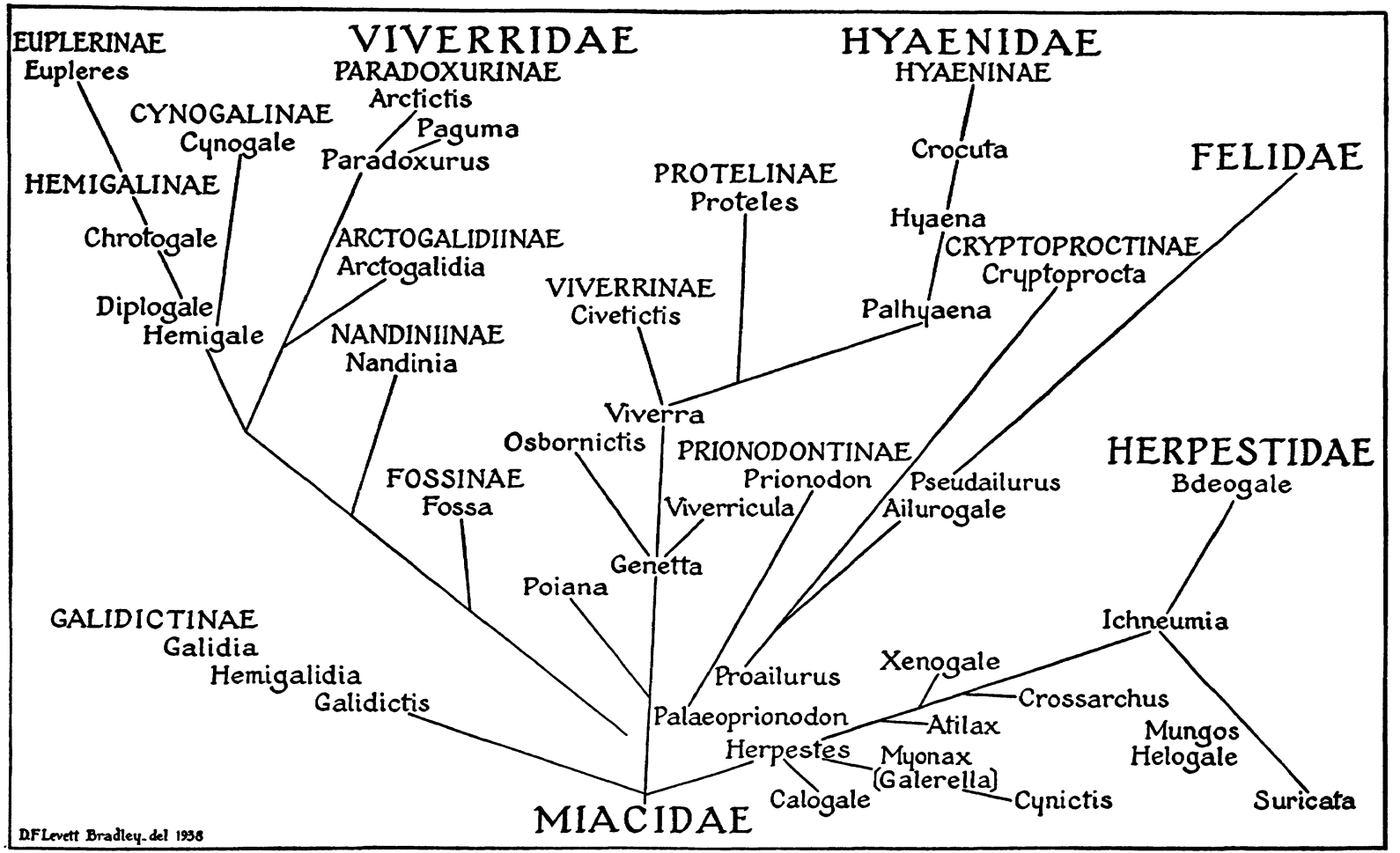


Fig. 20.16. Classification and phylogeny of the cat-like (aeluroid) Carnivora. After Gregory and Hellman.

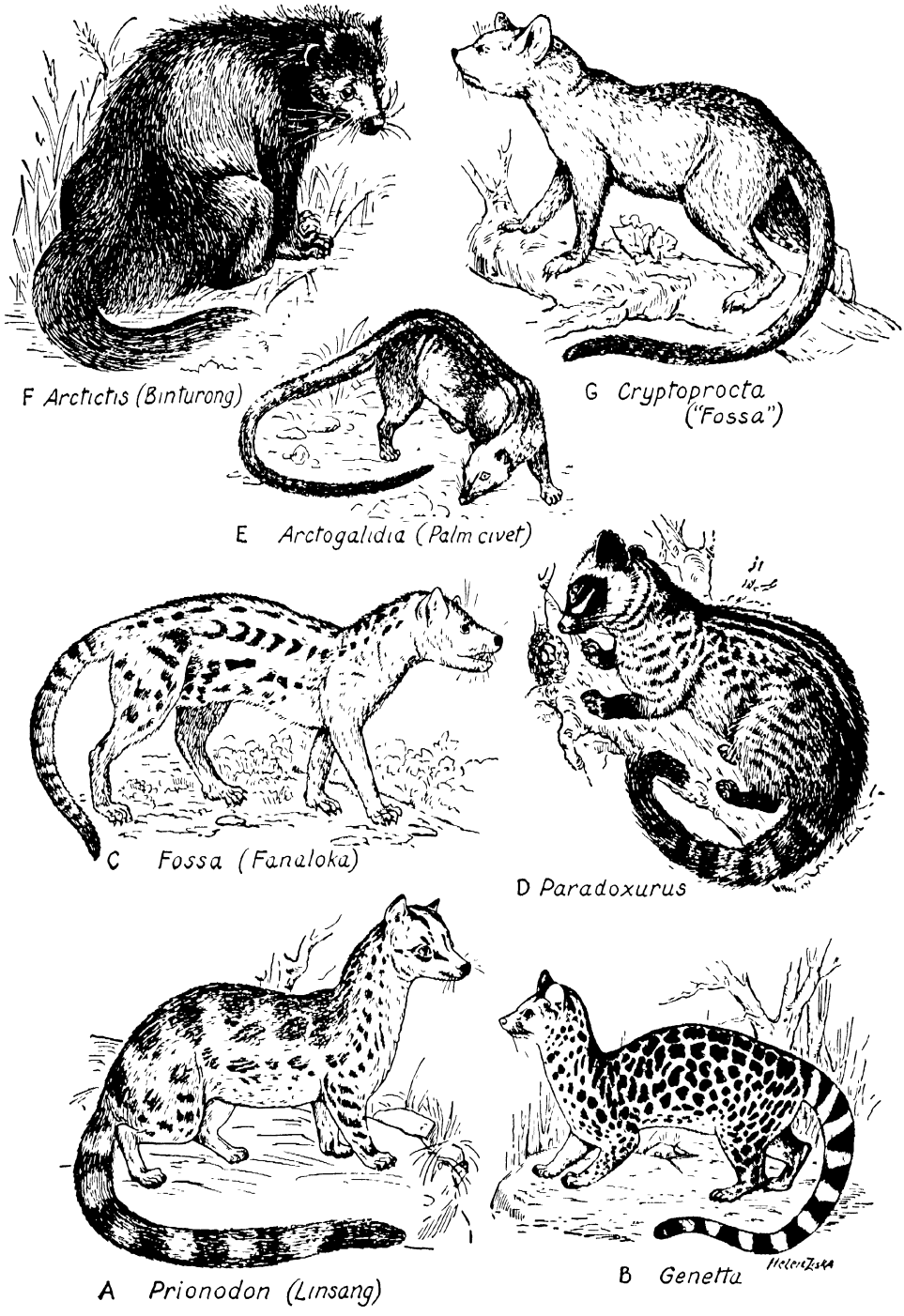


Fig. 20.17. Recent civets and related forms. A, D, E, after Lydekker; B, after J. A. Allen; C, original, based mainly on pelage collected by A. L. Rand; G, from young mounted specimen in the American Museum of Natural History; F, from photograph now lost.

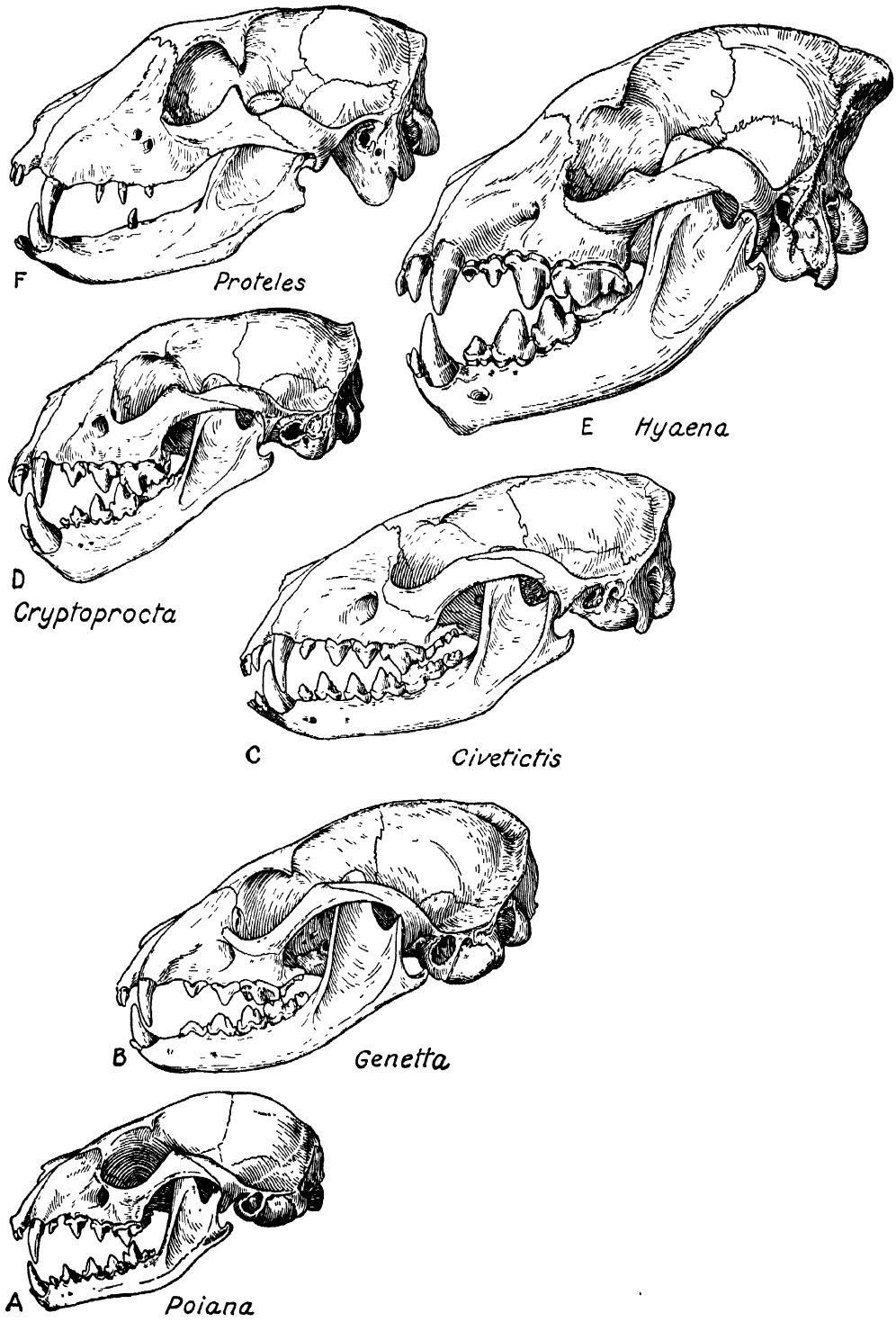


Fig. 20.18. Skulls of civets (Viverrinae, A–C) and their allies, from primitive shear-toothed (A) to diversely specialized stages (D–F). After Gregory and Hellman.

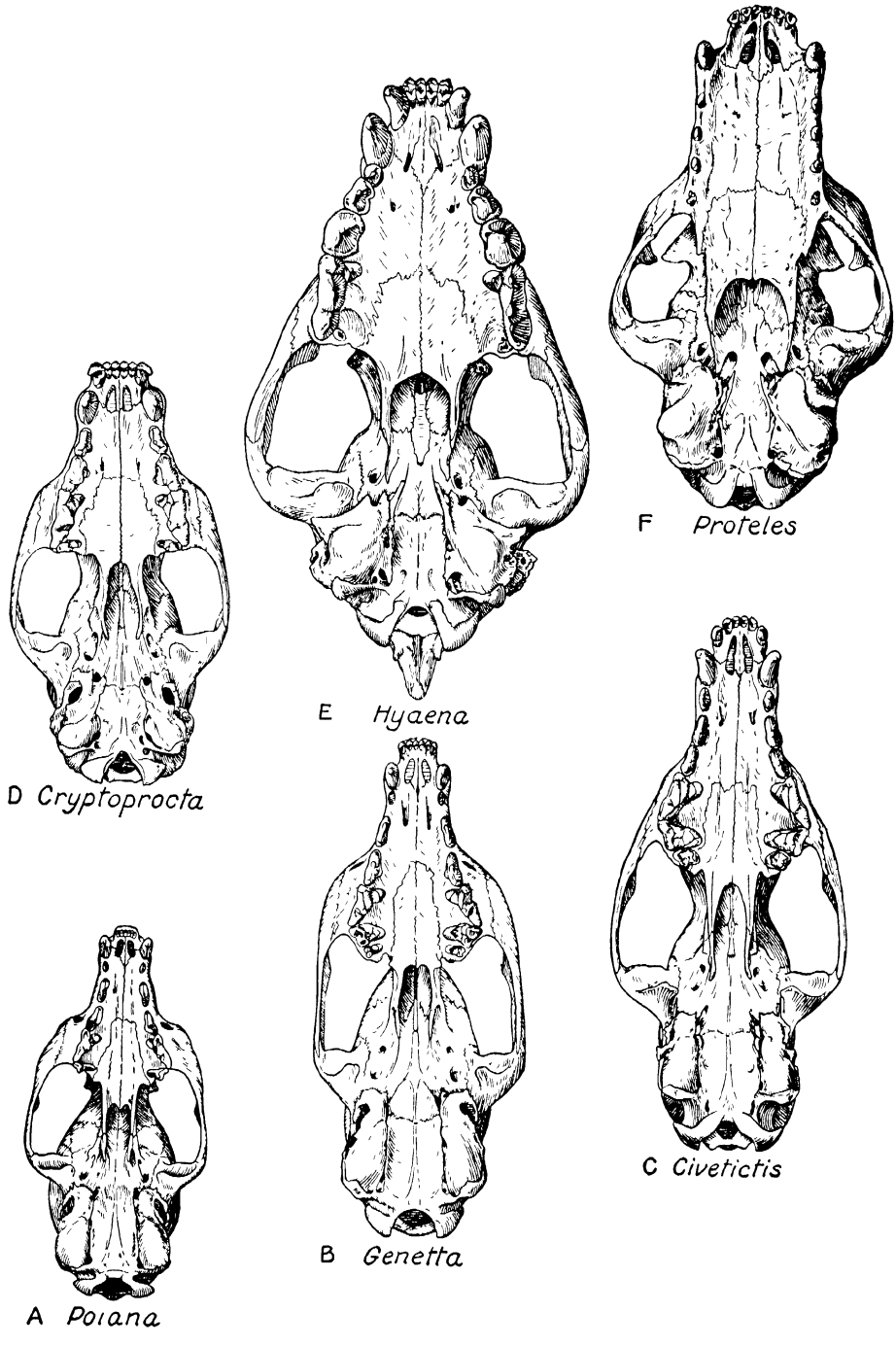


Fig 20.19. Skulls of civets and their allies (continued). After Gregory and Hellman.

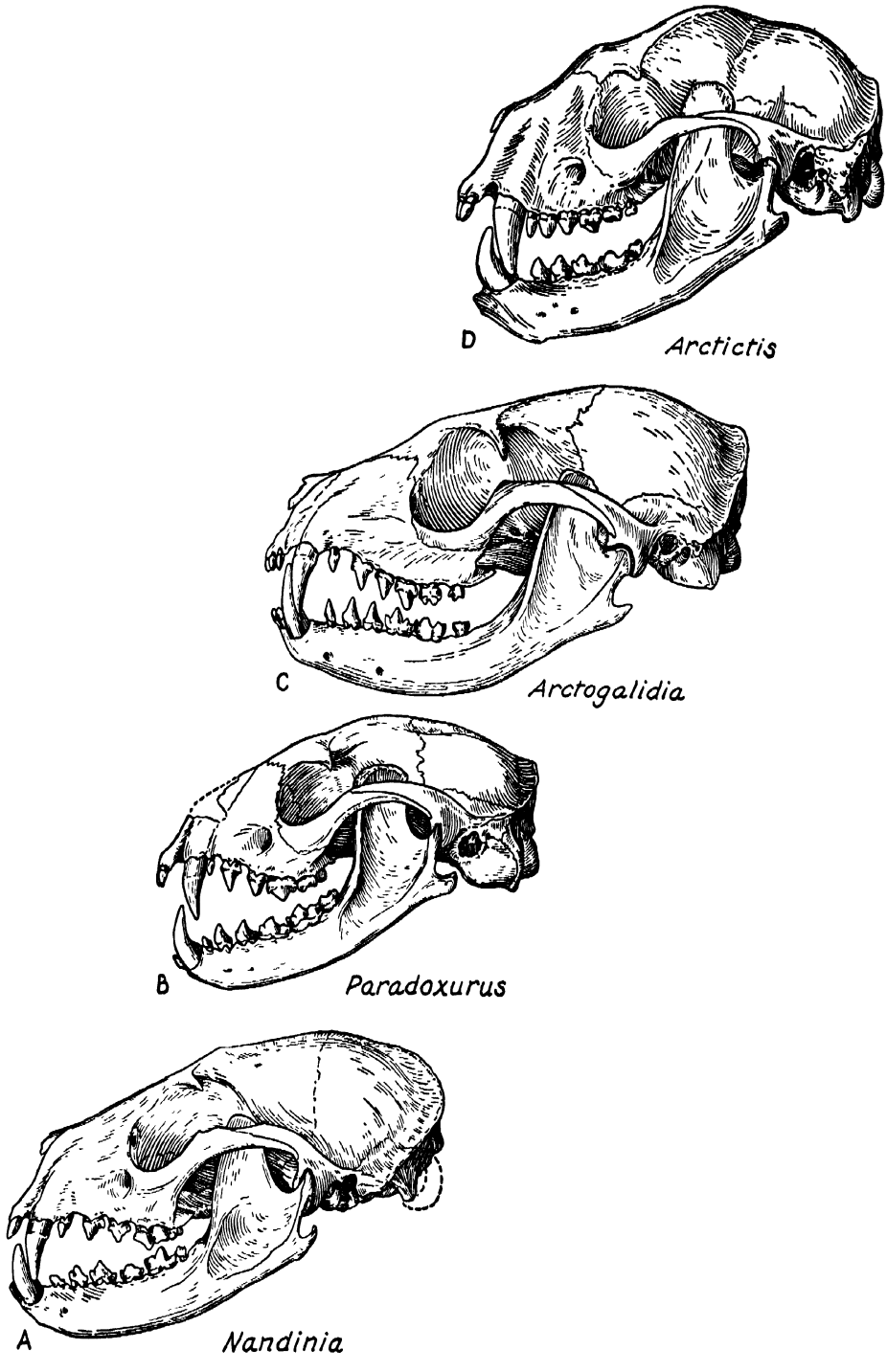


Fig. 20.20. Skulls of civets and their allies (continued). After Gregory and Hellman.

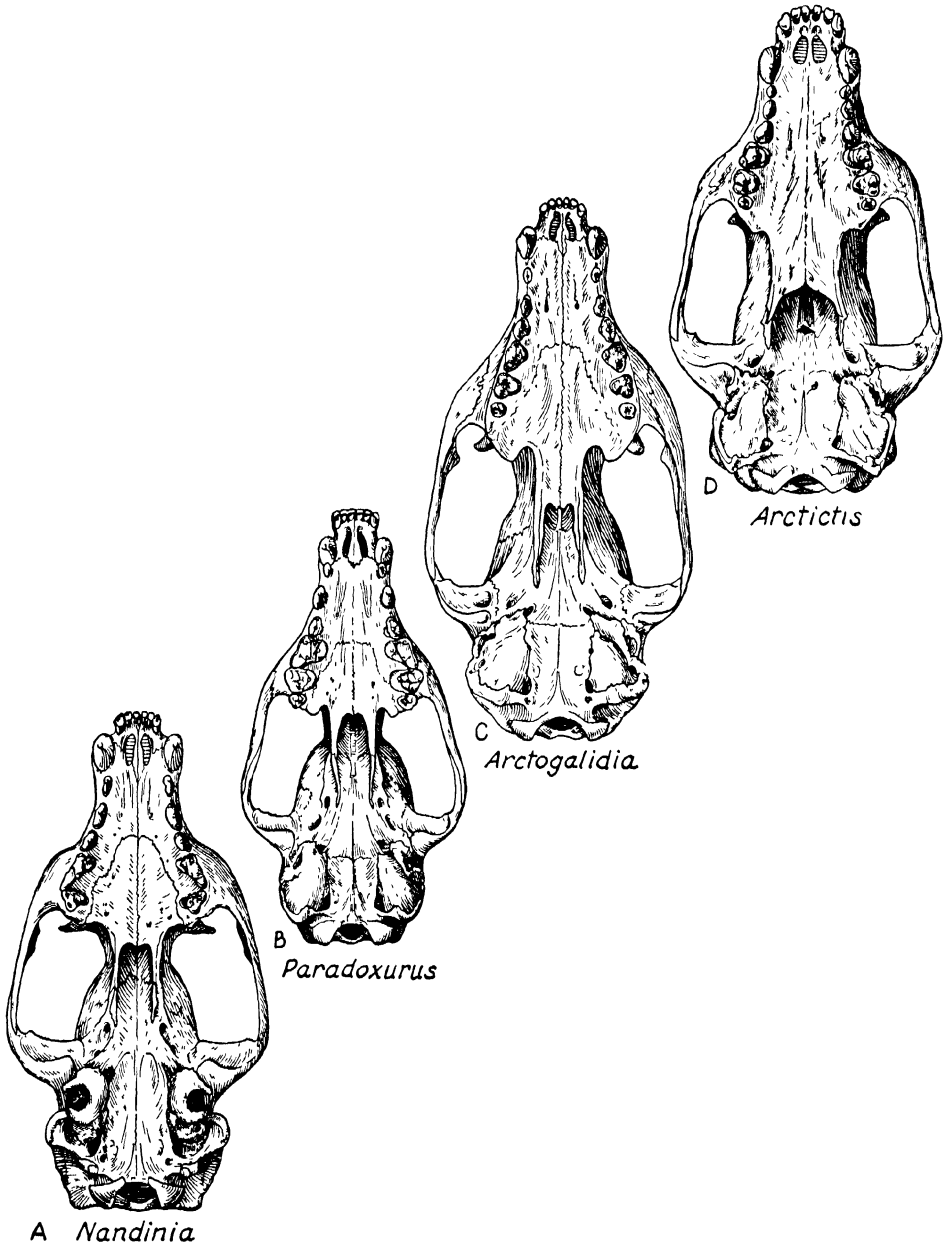


Fig. 20.21. From shear-toothed to blunt-cusped palm civets. After Gregory and Hellman.

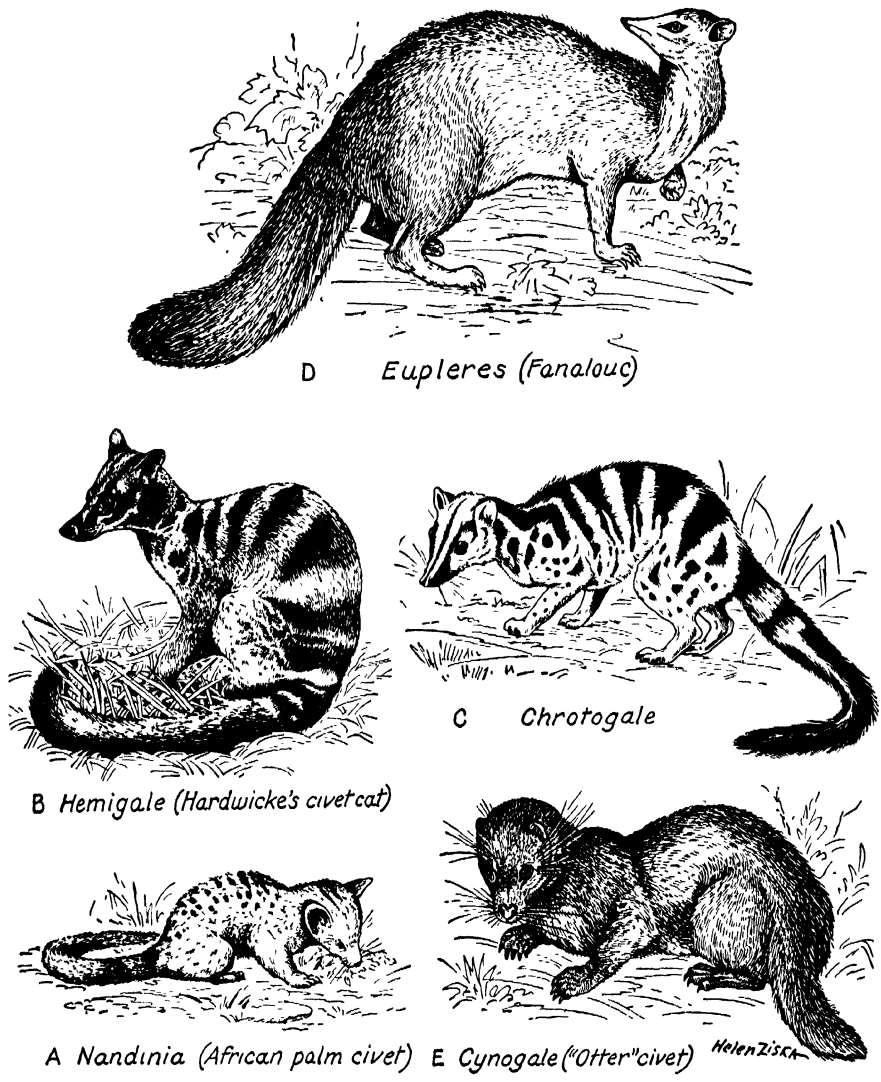


Fig. 20.22. The hemigalines; diversely specialized members of the civet family. A, after J. A. Allen; B, E, after Lydekker; C, after Osgood; D, after Gervais.

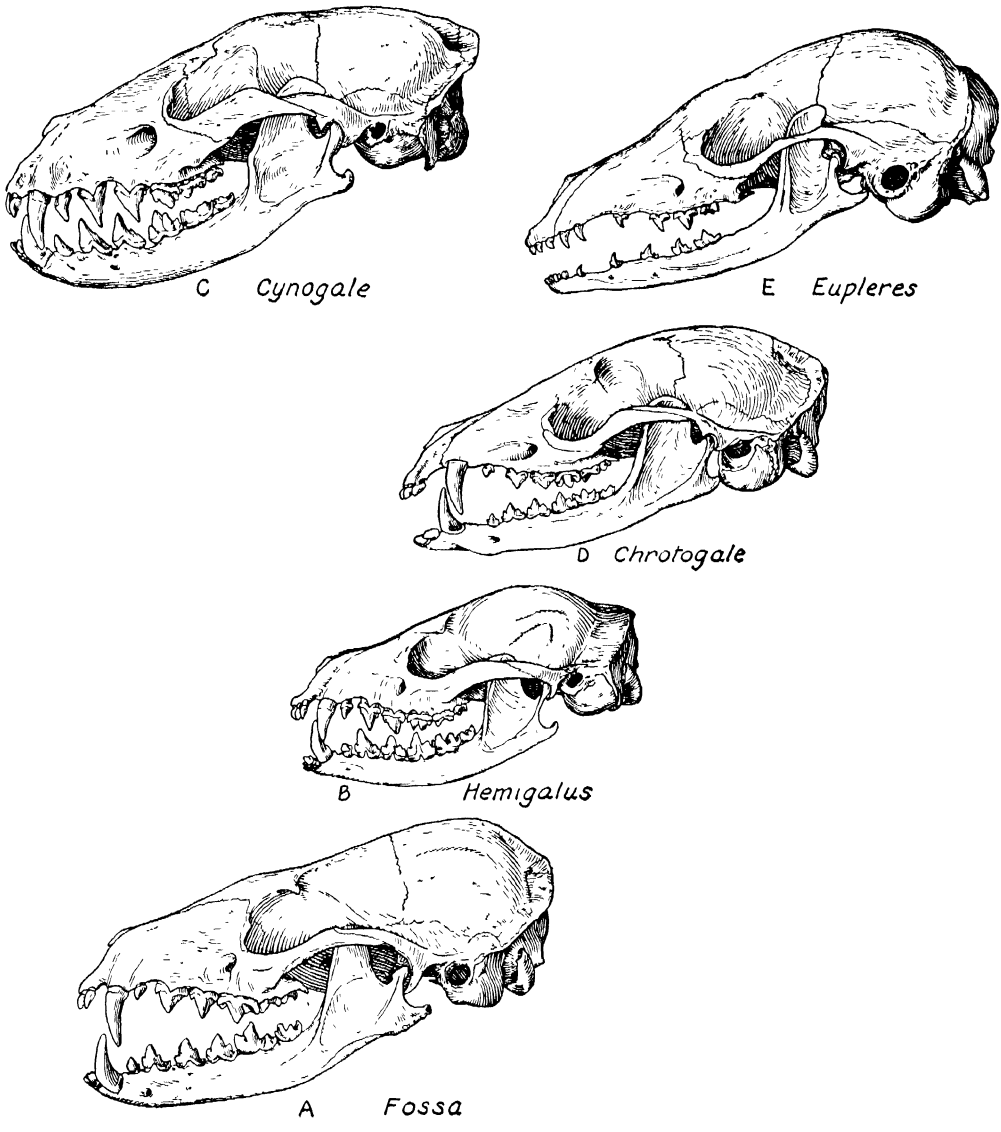


Fig. 20.23. Skulls of the relatively primitive fanaloka or "Malagasy civet" (confusingly named "*Fossa*") and of the hemigalines. After Gregory and Hellman.

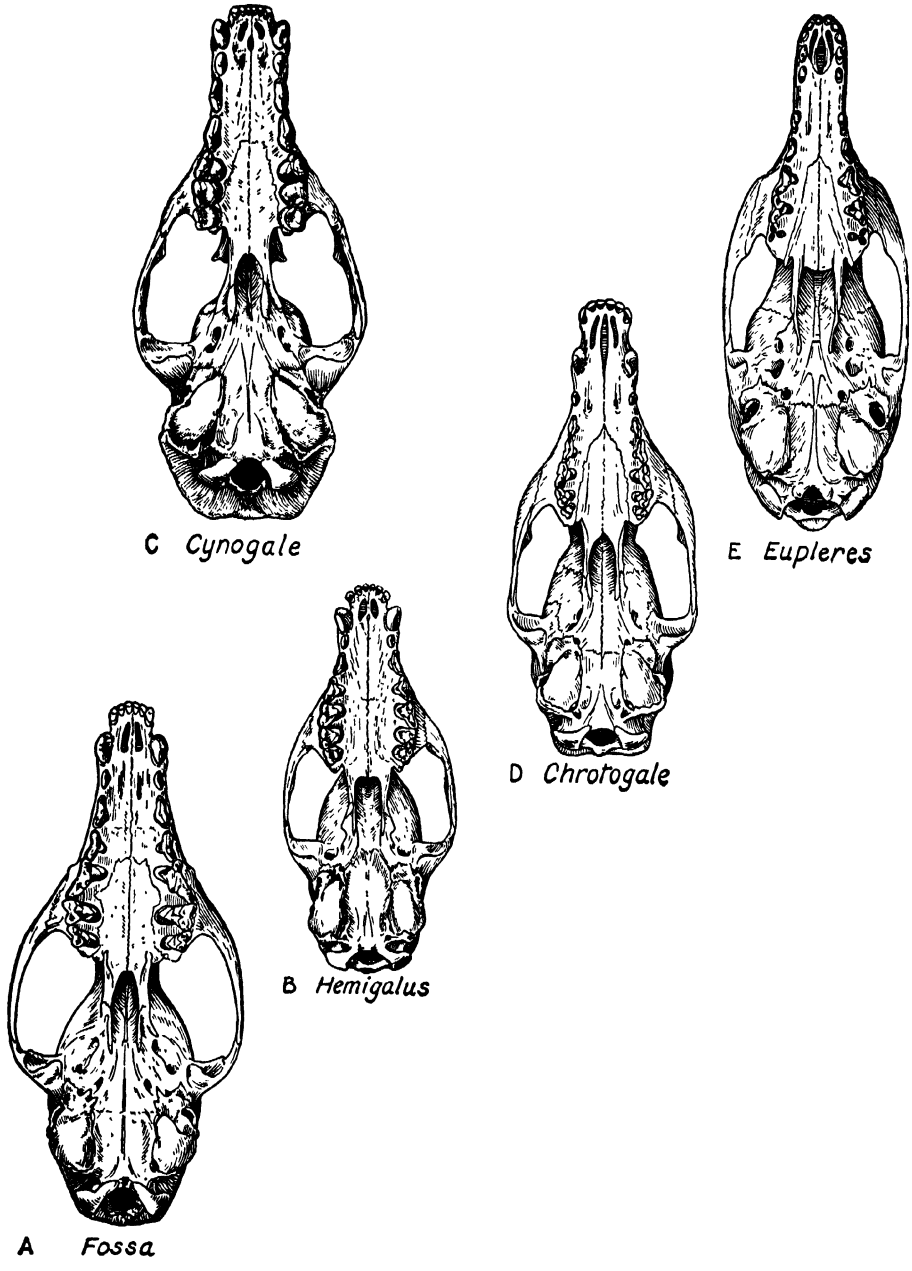


Fig. 20.24. Skulls of the relatively primitive fanaloka and the hemigalines (continued). After Gregory and Hellman.

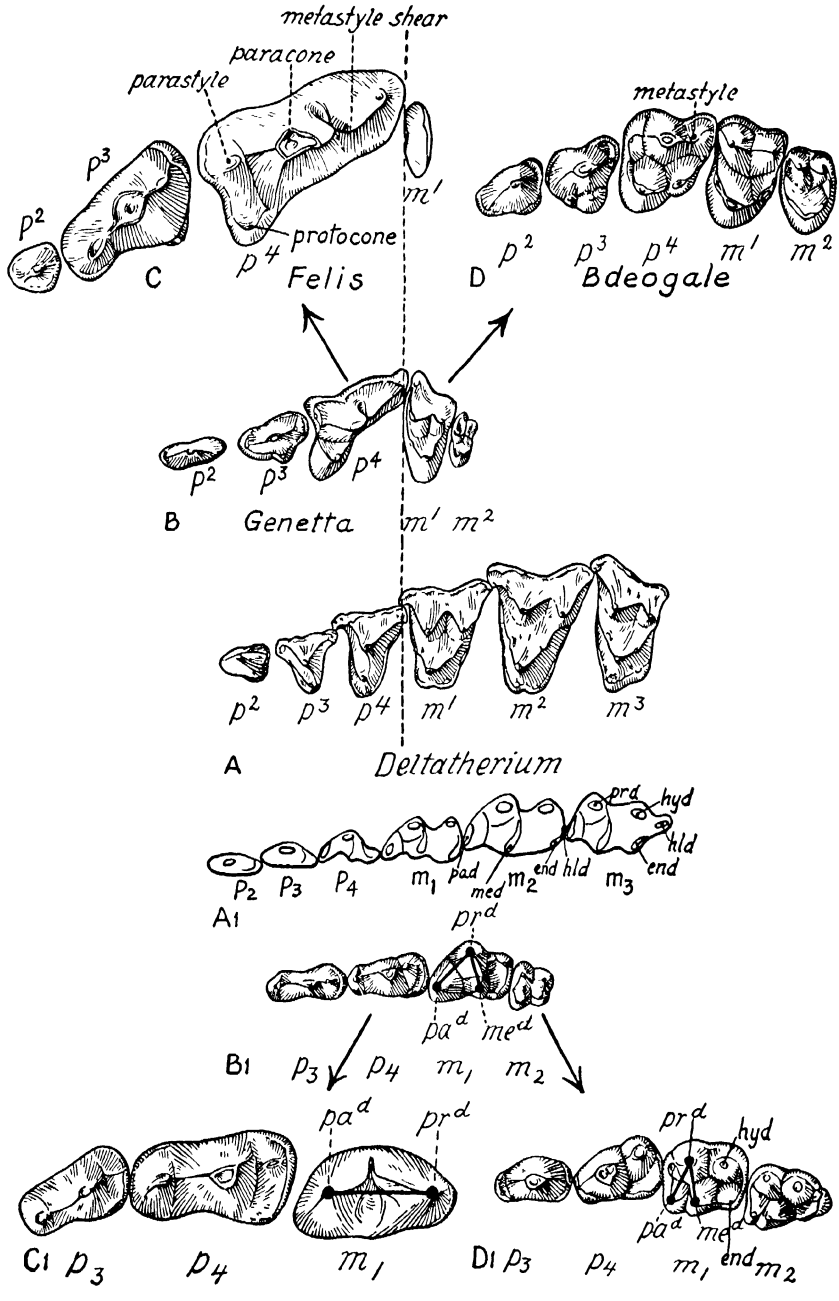


Fig. 20 25 From primitive tritubercular molars (A) to shear-teeth (C) or crushing teeth (D). After Gregory and Hellman.

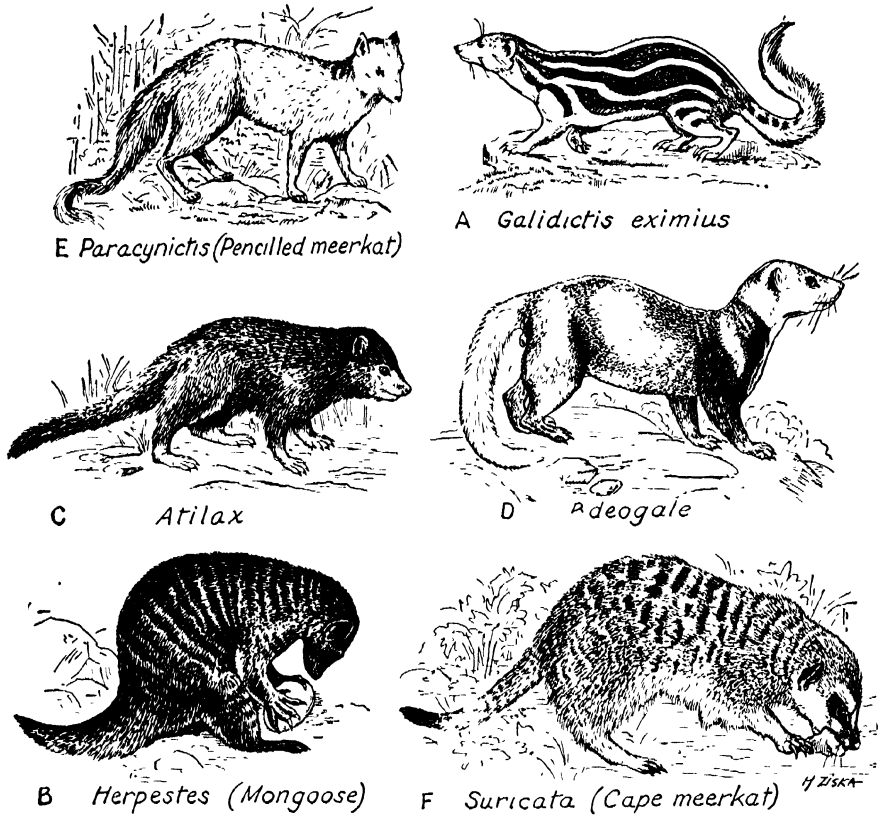


Fig. 20.26. The "Malagasy mongoose" (A), the true mongoose (B) and its specialized African relatives (C–E). A, after Pocock; B, after F. Finn; C, D, after J. A. Allen; E, after Donald Carter; F, after Lydekker.

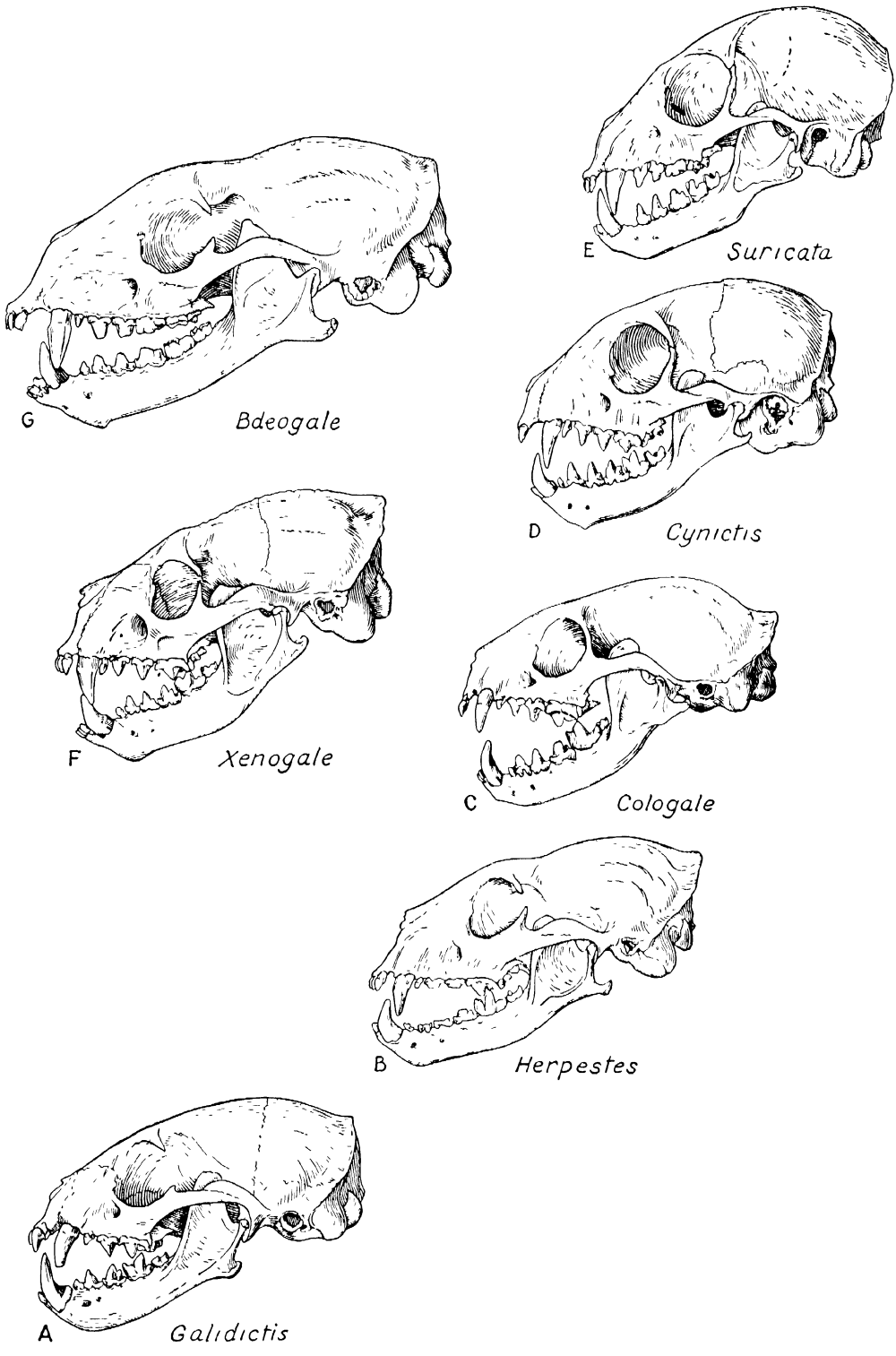


Fig. 20.27. Skulls of the Malagasy mongoose (A), the true mongoose (B) and its specialized African relatives (B–G) After Gregory and Hellman.

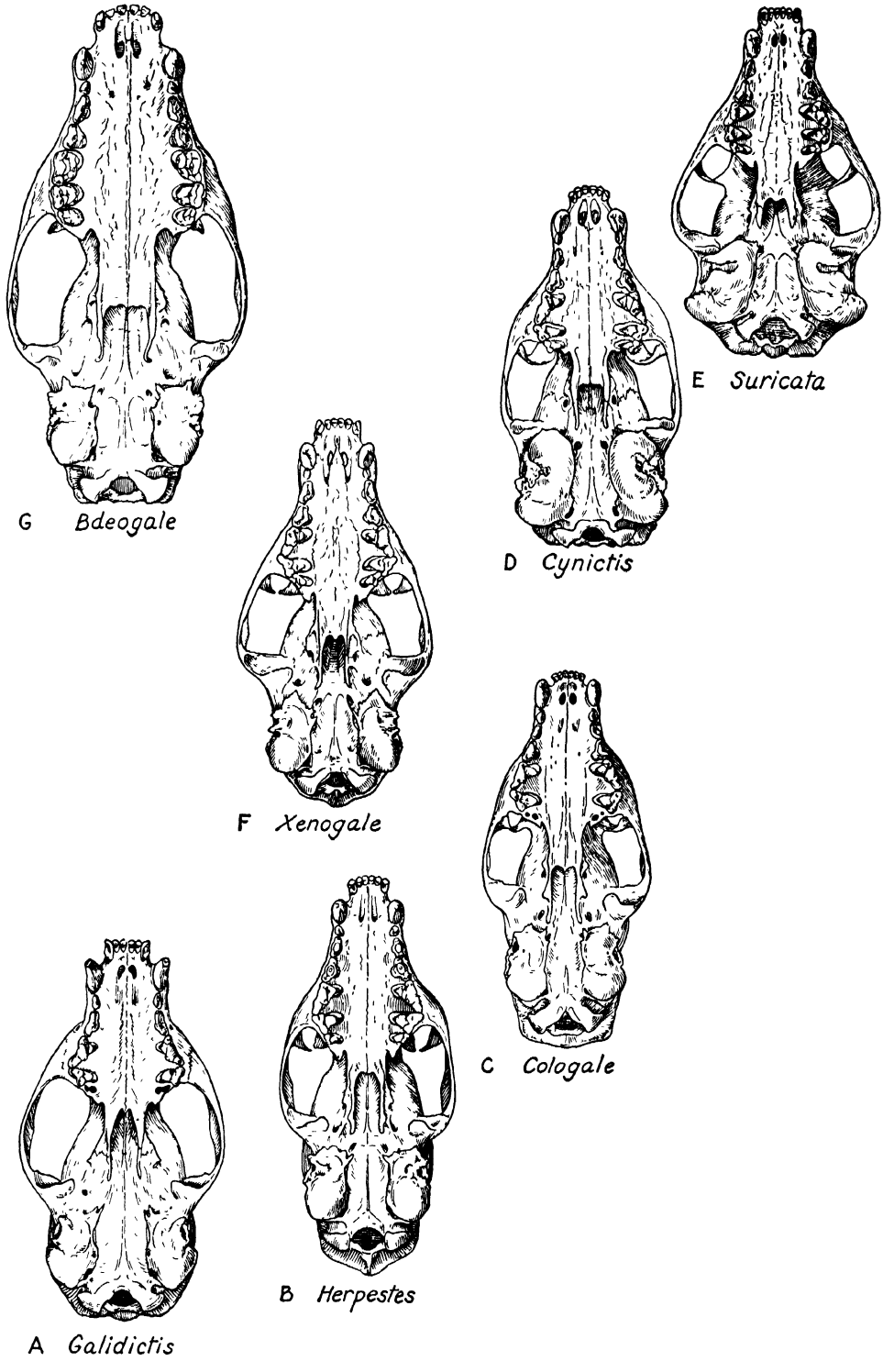


Fig. 20.28. Skulls of the Malagasy mongoose, the true mongoose and its specialized African relatives (continued). After Gregory and Hellman.

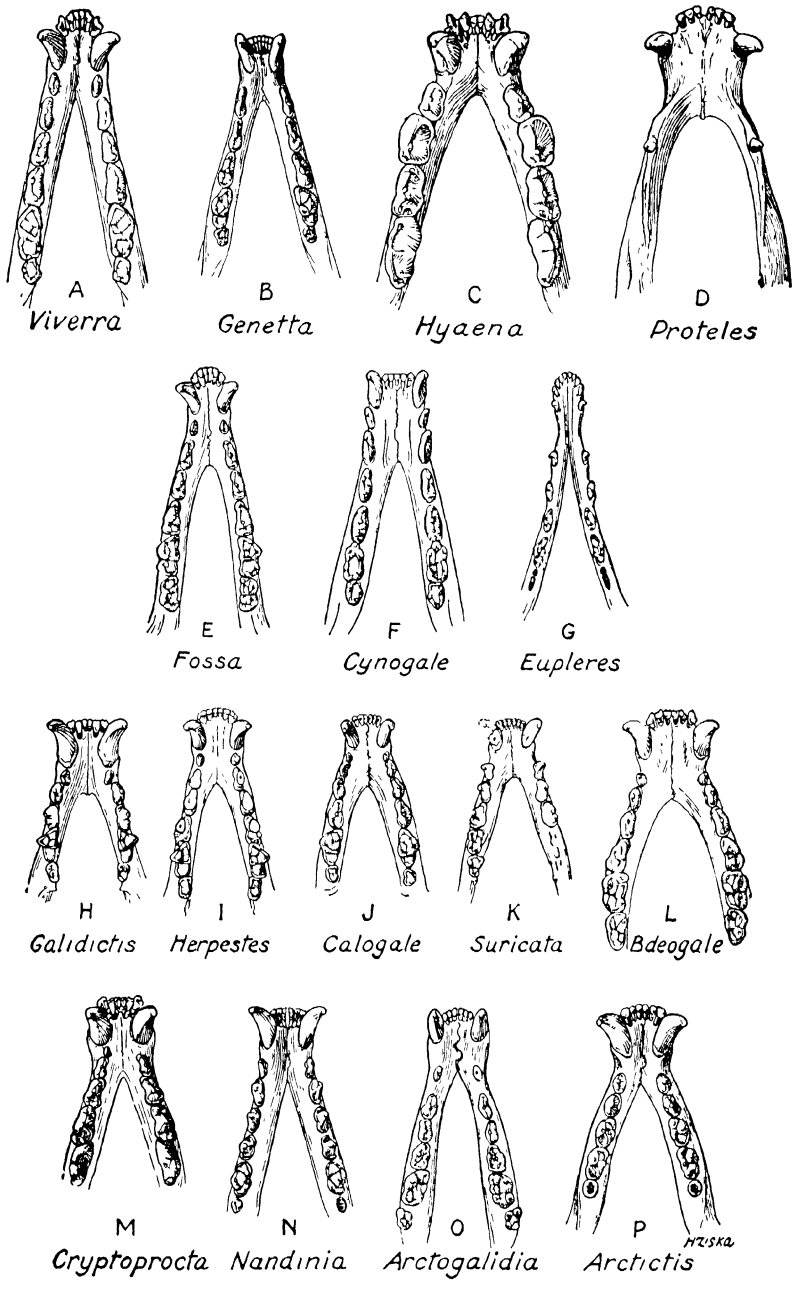


Fig. 20.29. Lower jaws and teeth of primitive viverrids and their diversely specialized derivatives. After Gregory and Hellman.

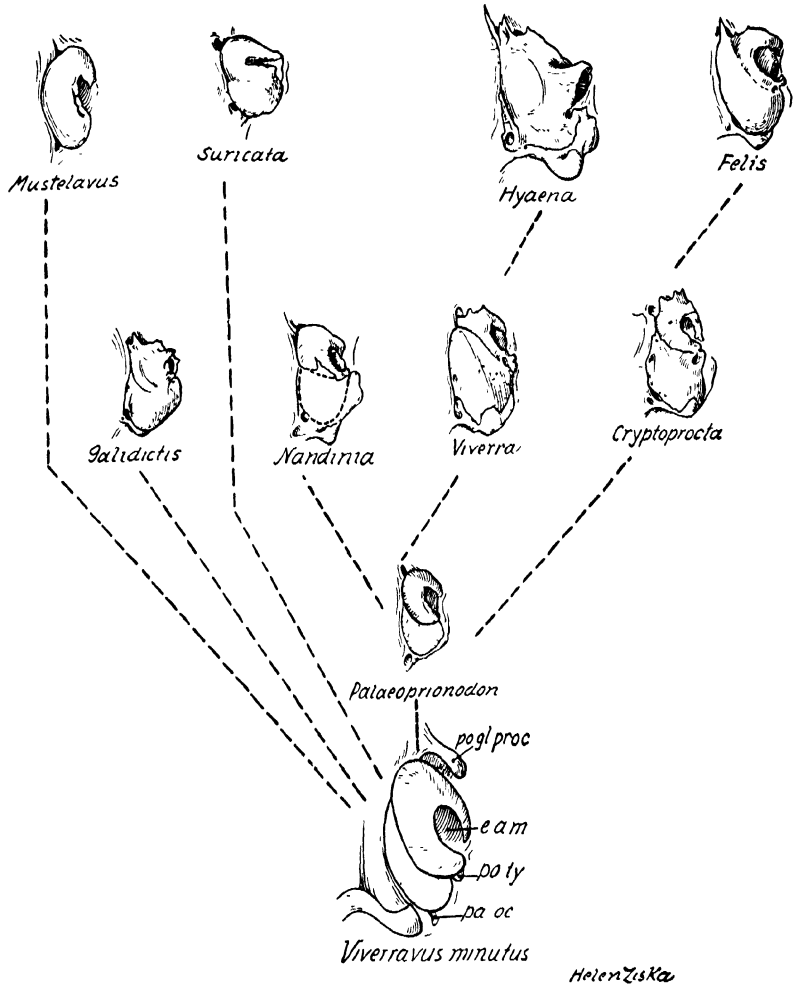


Fig. 20.30. Divergent evolution of the auditory bullae in fissiped carnivores, showing reciprocal emphasis of the ento- (stippled) and ectotympanic elements. After Gregory and Hellman. *E.a.m.*, ear opening; *pa.oc.*, paroccipital process; *po.gl.proc*, postglenoid process; *po.ty.*, posttympanic process.

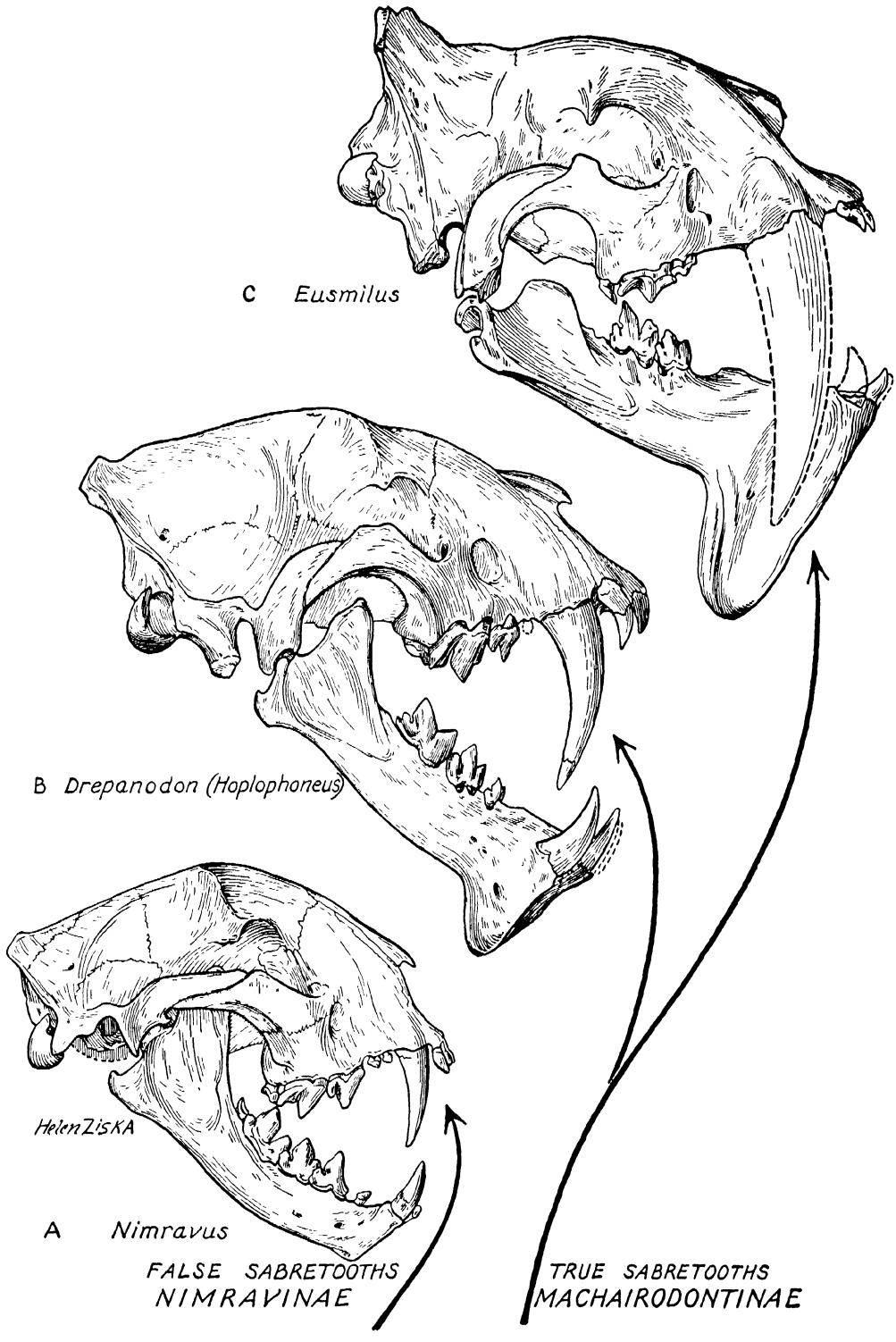


Fig. 20.31. "False" and "true" sabre-tooths from the White River Oligocene. After Scott and Jepsen.

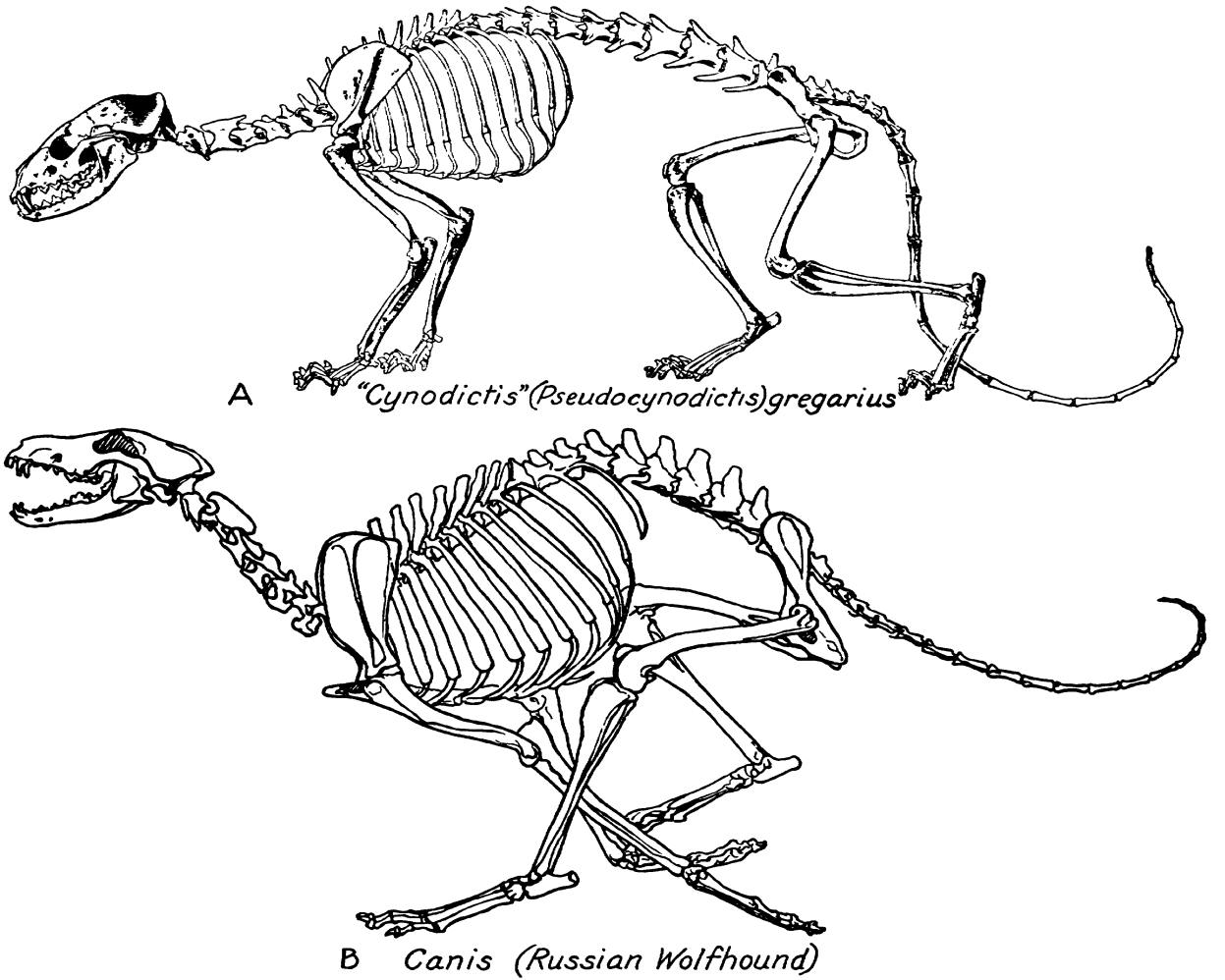


Fig. 20.32. Primitive civet-like ancestral dog (A) of the Oligocene epoch and one of its modern derivatives. A, after Matthew; B, from skeleton mounted by S. H. Chubb.

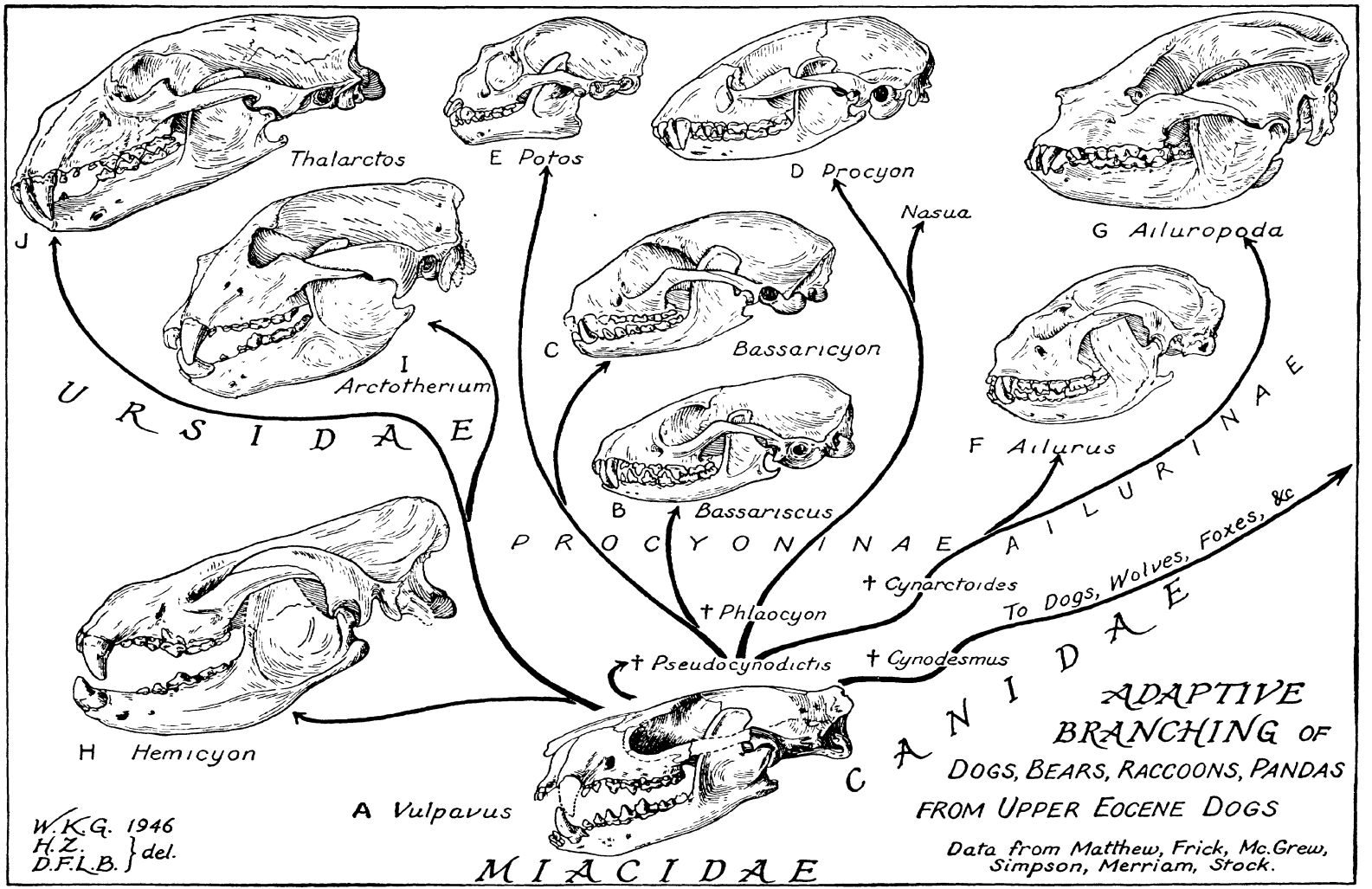

Thalarctos
E Potos
D Procyon
Nasua
G Ailuropoda
J
I
Arctotherium
C
Bassaricyon
URSIDAE
B
Bassariscus
F Ailurus
PROCYONINAE
AILURINAE
† Cynarctoides
To Dogs, Wolves, Foxes, &c
† Phlaocyon
† Pseudocynodictis
† Cynodesmus
CANIDAE
H Hemicyon
A Vulpavus
C
MIACIDAE
ADAPTIVE BRANCHING OF DOGS, BEARS, RACCOONS, PANDAS FROM UPPER EOCENE DOGS
Data from Matthew, Frick, Mc.Grew, Simpson, Merriam, Stock.
W.K.G. 1946
H.Z.
D.F.L.B. } del.

Fig. 20 33

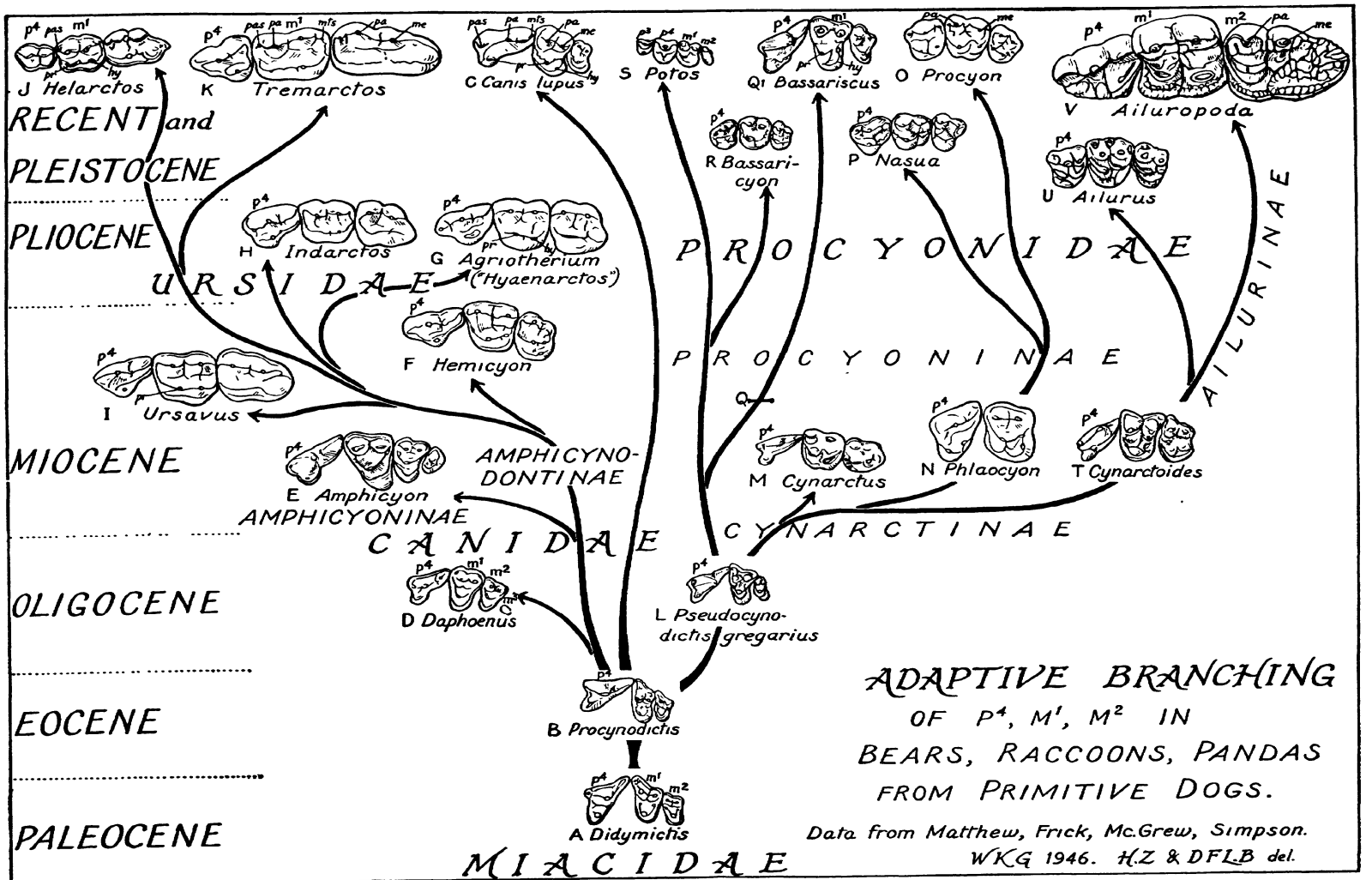

RECENT and PLEISTOCENE
PLIOCENE
MIOCENE
OLIGOCENE
EOCENE
PALEOCENE
J Helarctos
K Tremarctos
C Canis lupus
S Potos
Q1 Bassariscus
O Procyon
V Ailuropoda
R Bassari-cyon
P Nasua
U Ailurus
H Indarctos
G Agriotherium ("Hyaenarctos")
URSIDAE
PROCYONIDAE
PROCYONINAE
AILURINAE
F Hemicyon
I Ursavus
AMPHICYNO-DONTINAE
E Amphicyon
AMPHICYONINAE
CANIDAE
M Cynarctus
N Phlaocyon
T Cynarctoides
CYNARCTINAE
D Daphoenus
L Pseudocyno-dictis gregarius
B Procynodictis
A Didymictis
MIACIDAE
ADAPTIVE BRANCHING
OF P4, M1, M2 IN
BEARS, RACCOONS, PANDAS
FROM PRIMITIVE DOGS.
Data from Matthew, Frick, Mc.Grew, Simpson.
WKG 1946. H.Z & DFLB del.

Fig. 20 34



Fig. 20.35. Raccoons and pandas (H–D, after D. G. Elliott; E, F, from photographs.

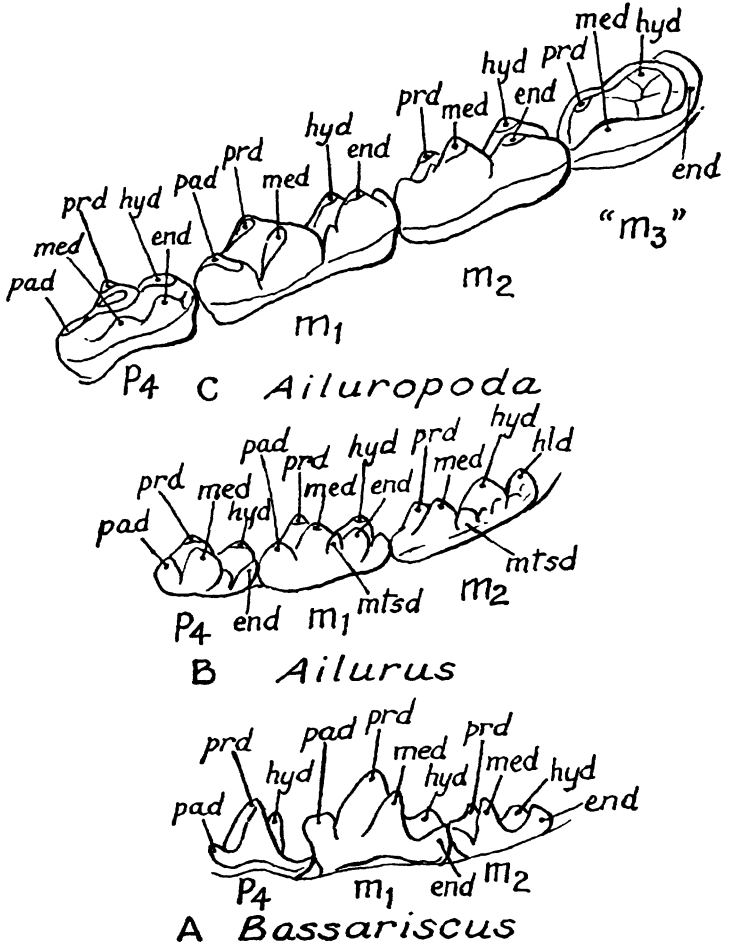


Fig. 20.36. Lower cheek teeth seen from the inner side, showing progressive loss of shearing and increase of crushing characters, from primitive procyonid to giant panda.

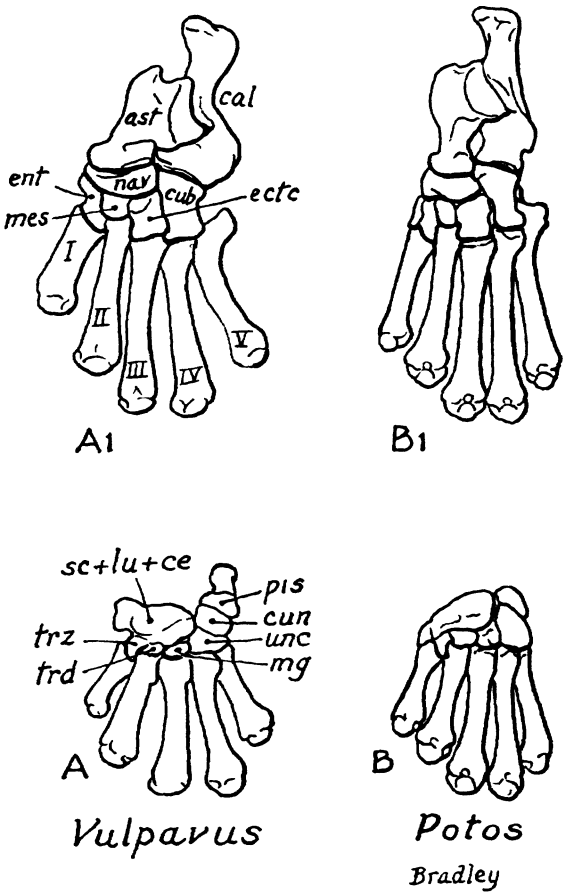


Fig. 20.37. Comparison of left hand and left foot of Eocene miacid (A, A1), inheriting traces of arboreal characters, and modern kinkajou, a highly specialized, secondarily arboreal derivative of the procyonid stock (B, B1). All data from Matthew.

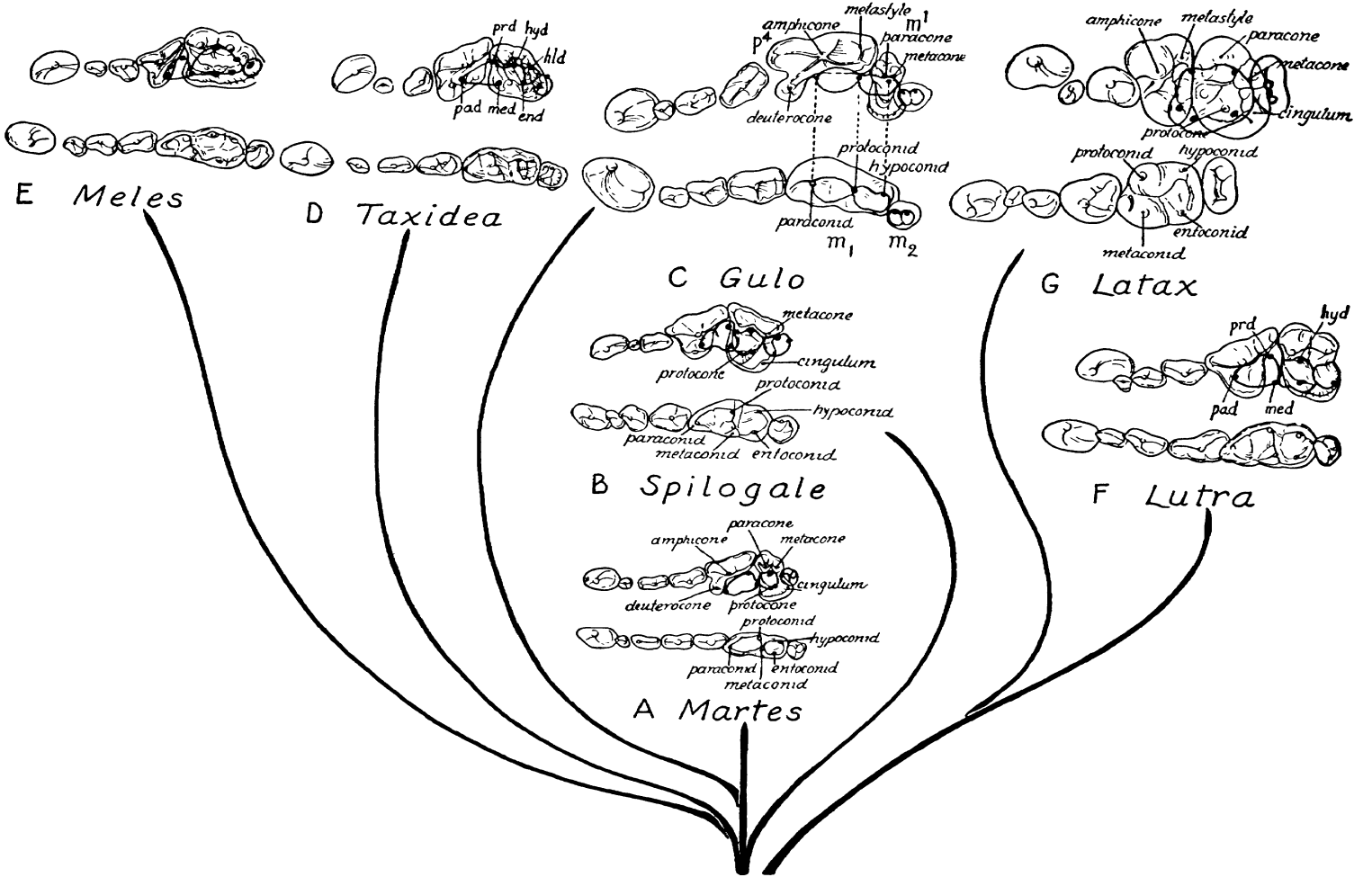


Fig. 20.38. Adaptive branching and occlusion diagrams of the upper and lower teeth in Mustelidae.

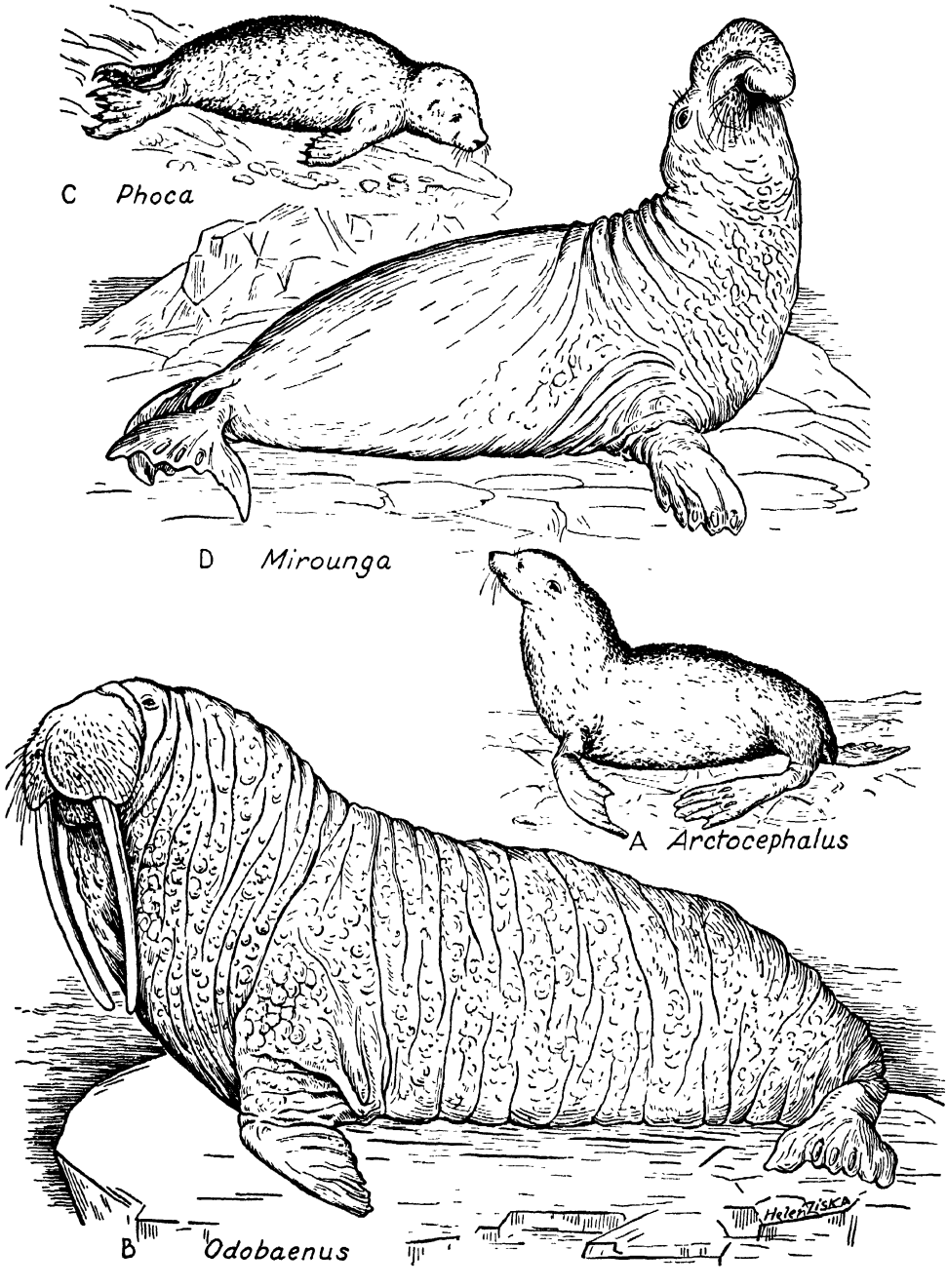


Fig. 20.39. Recent eared seal (A) and its specialized relative, the walrus (B), compared with earless seal (C) and its highly specialized relative, the sea-elephant (D).

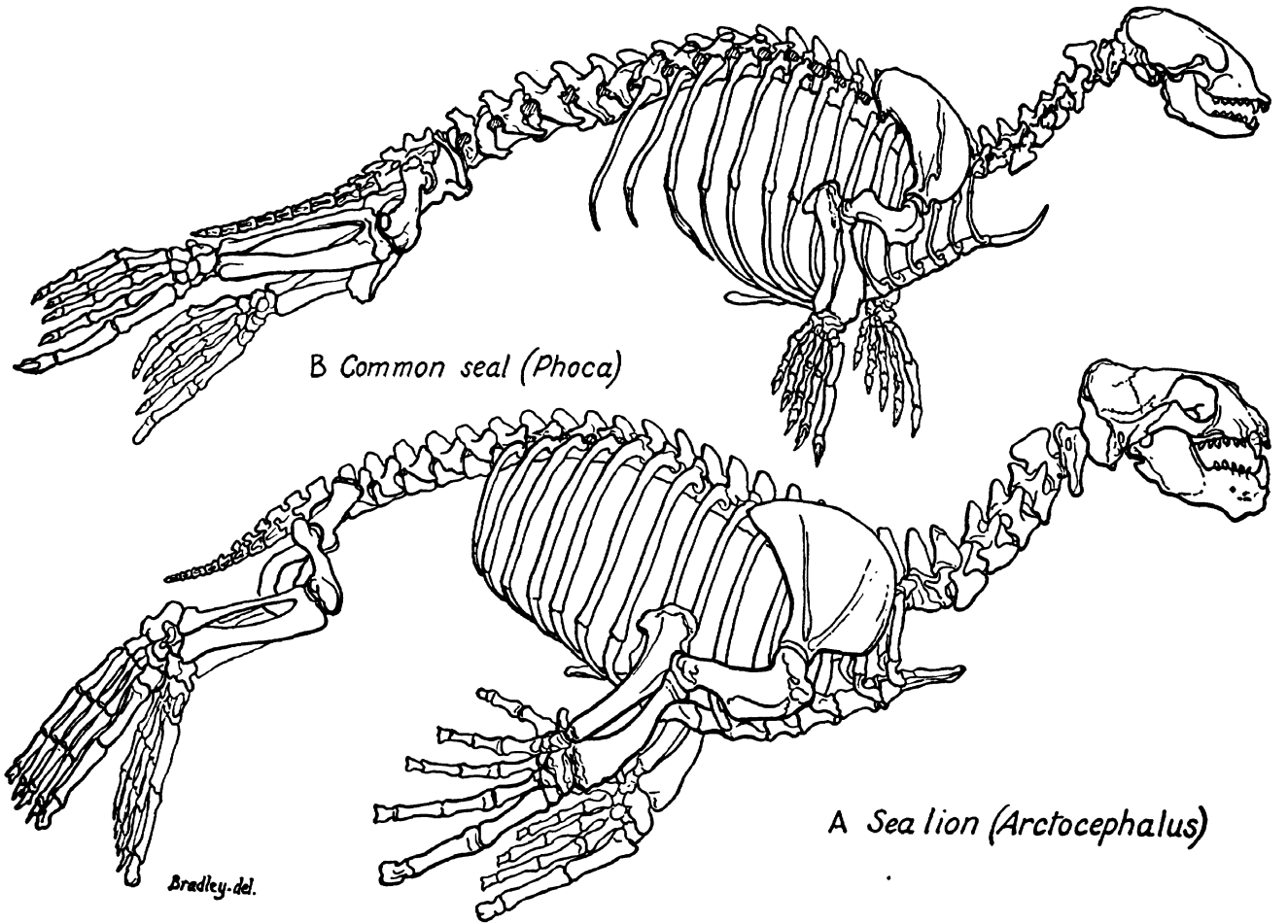
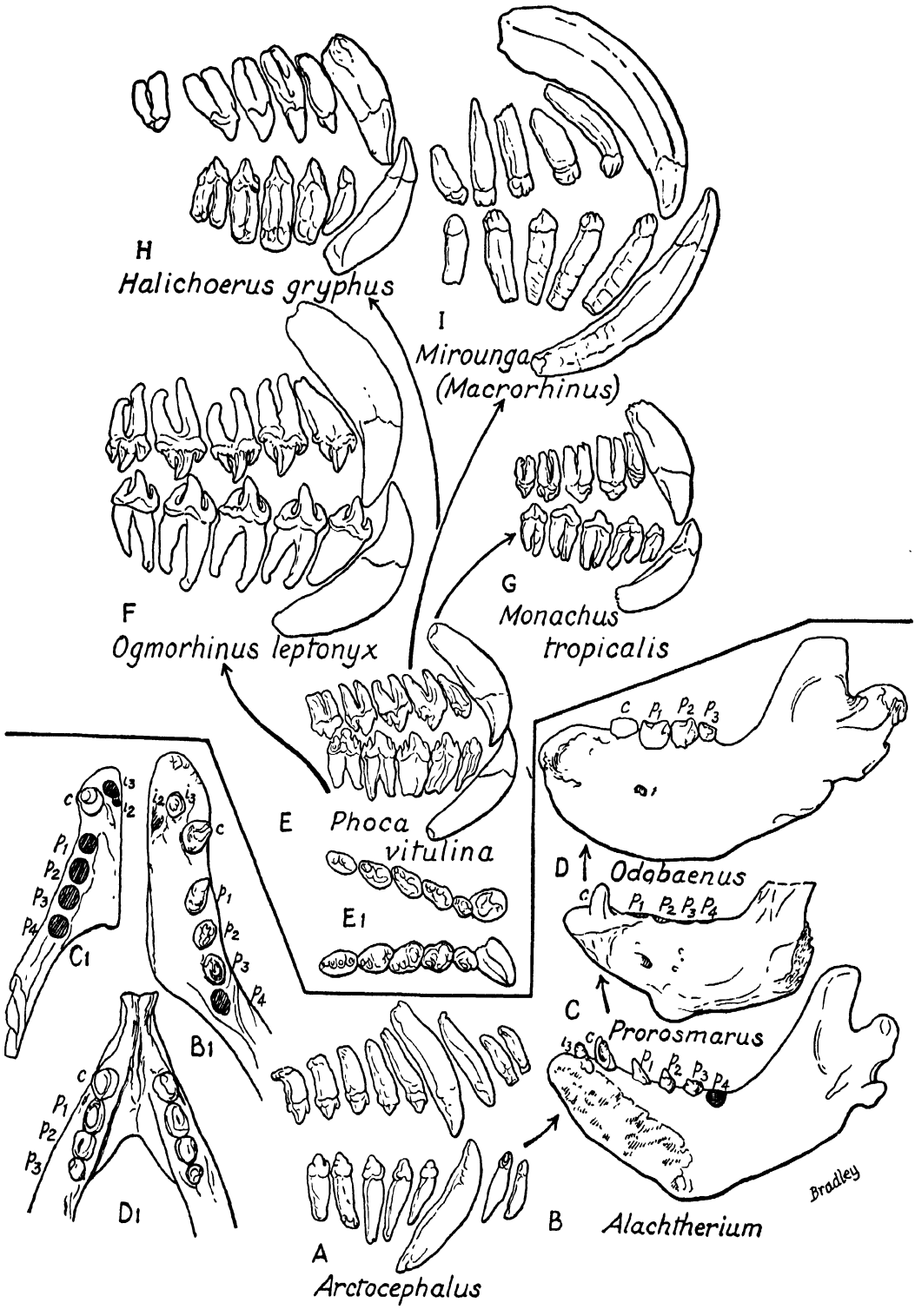


Fig. 20.40. Skeletons of seals, representing two widely different families: Otariidae (A); Phocidae (B). After De Blainville.



Figs. 20.41, 42. Jaws and dentitions of otariids (A, B, B1), odobaenids (C, C1, D, D1) and phocids (E–I). A, E–I, after De Blainville; B, B1, after Van Beneden; C, C1, after Berry and Gregory.

CHAPTER XXI

OUTER FORM AND INNER FRAME AMONG THE HOOFED MAMMALS (UNGULATA)

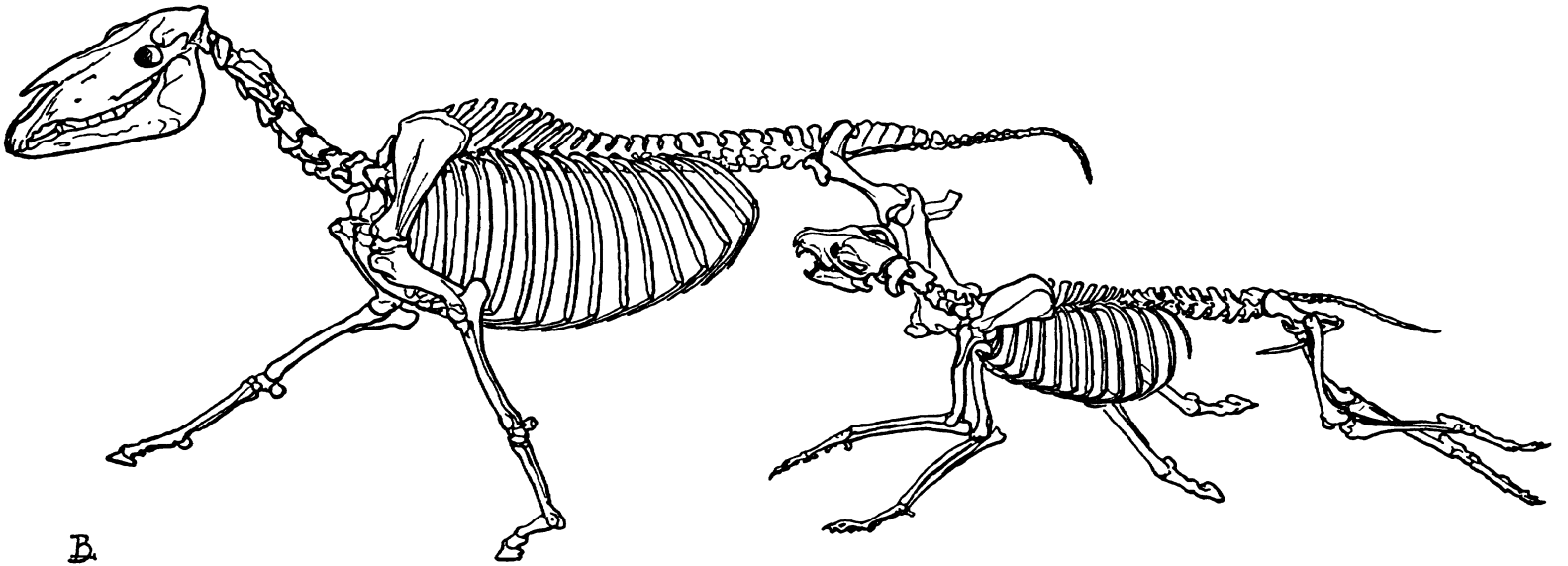


Fig. 21.1. Skeletons of wild horse (*Equus przewalskii*) and wolf. Mounted by S. H. Chubb.

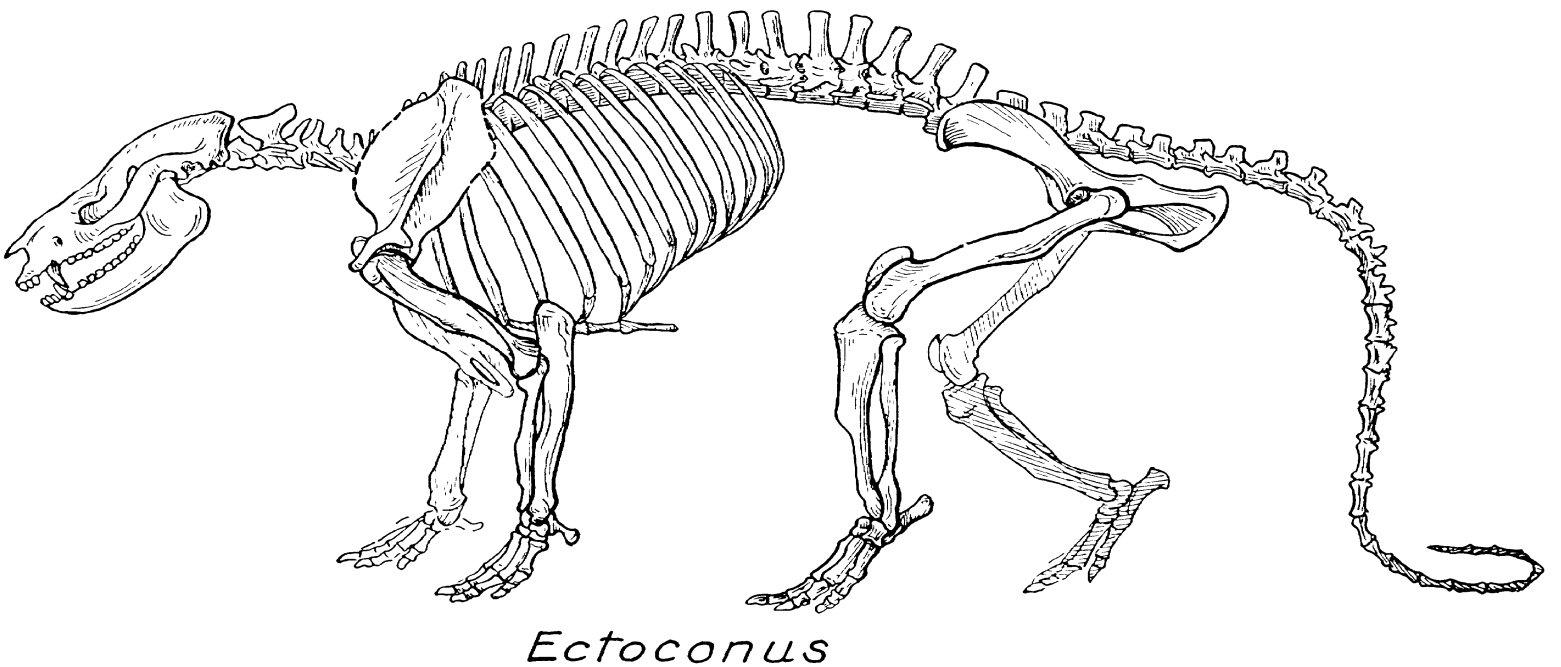


Fig. 21 2. Skeleton of Paleocene taligrade. Data from mounted skeleton in the American Museum of Natural History.

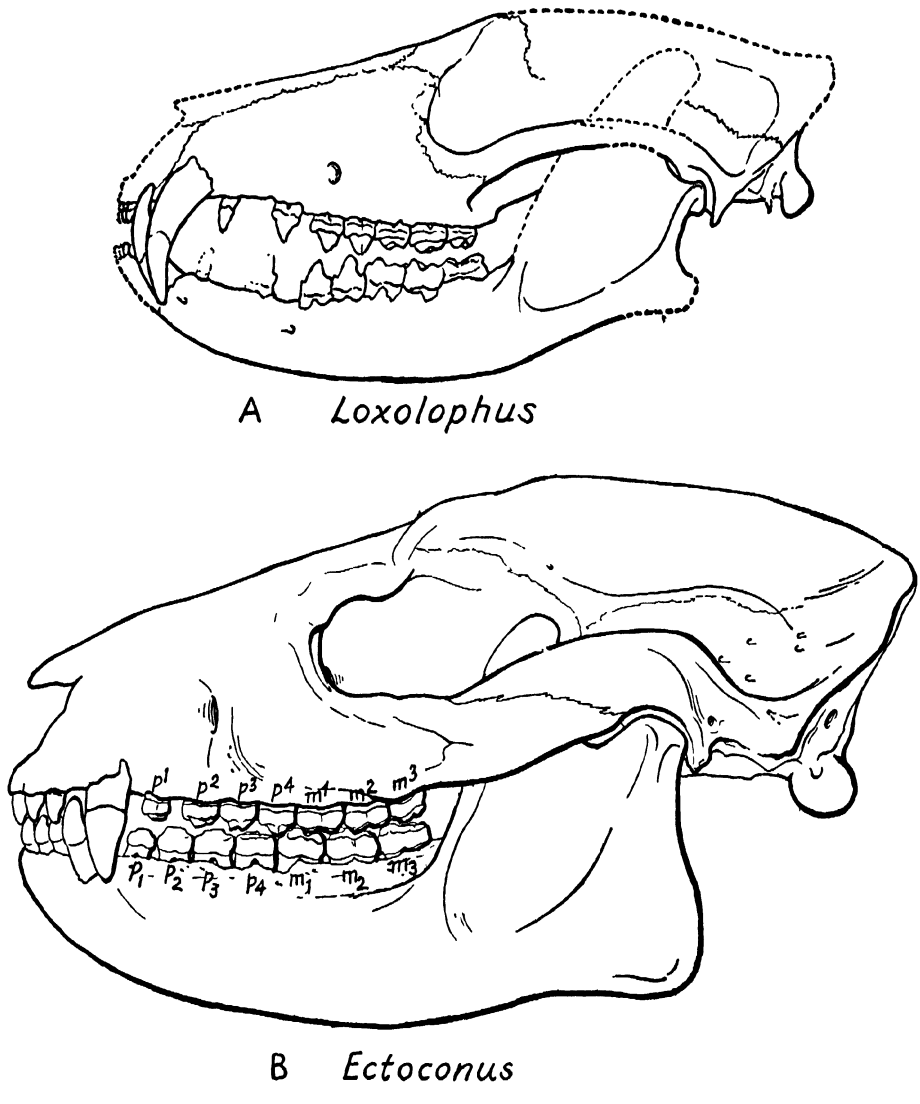


Fig. 21.3. Skulls of Paleocene creodont (A) and taligrade (B). Both retain the primitive dental formula for placental mammals: I $\frac{3}{3}$ C $\frac{1}{1}$ Pm $\frac{4}{4}$ M $\frac{3}{3}$. After Matthew.

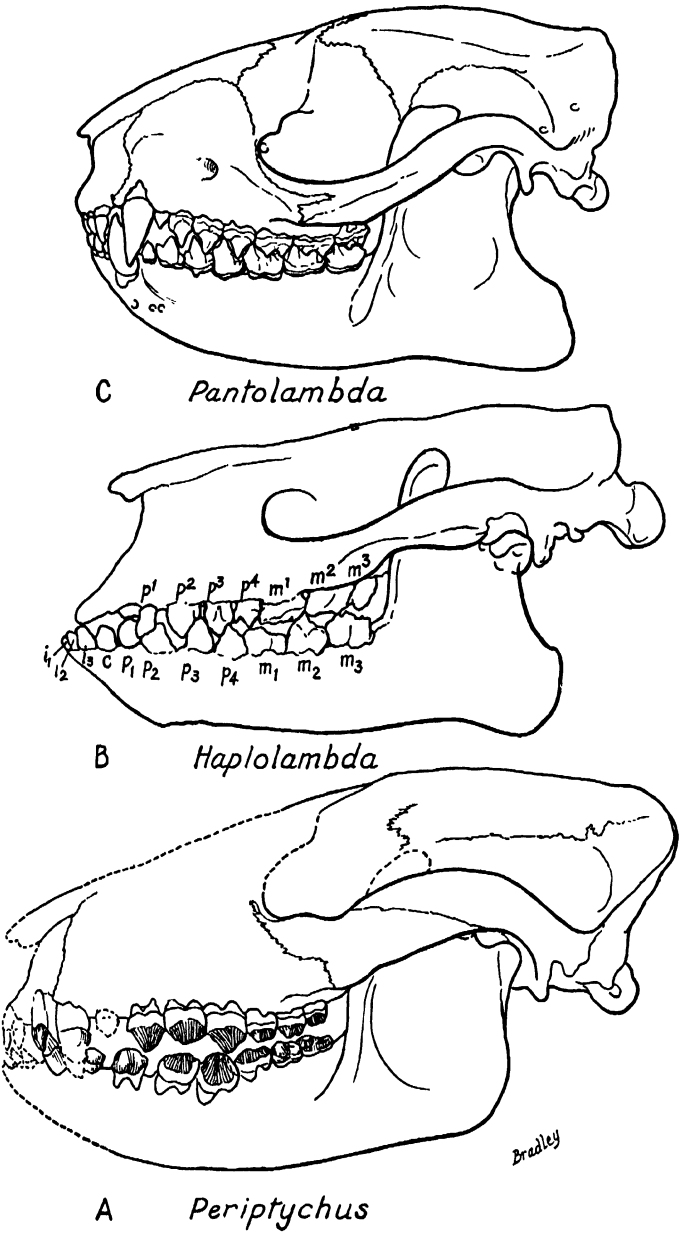


Fig. 21.4. Skulls of Paleocene taligrade (A) and pantodonts (B, C). A, C, after Matthew; B, after Patterson.

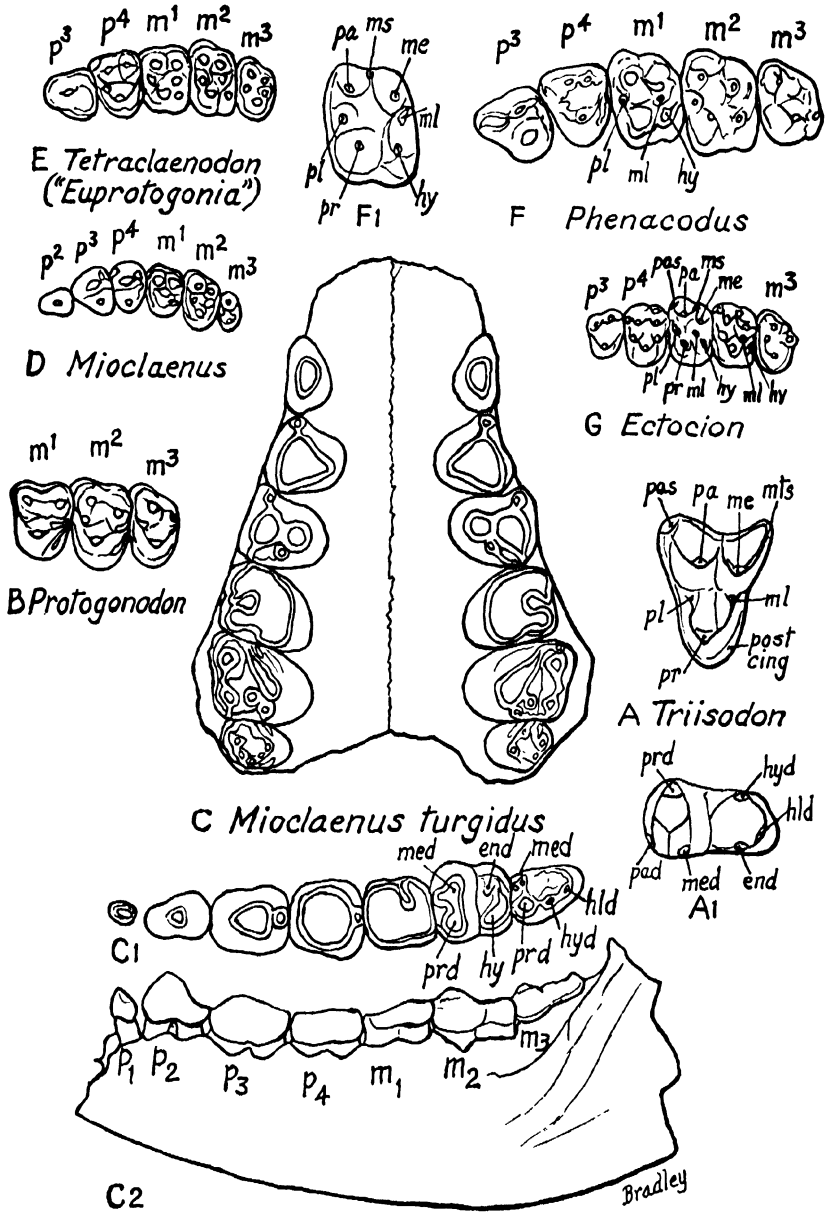


Fig. 21.5. "Tritubercular key" (A) to upper and lower molar patterns of primitive Paleocene and Eocene hoofed mammals. Data from Osborn, Matthew, Granger. The primitive creodont upper molar (A) shows: (1) three main cusps, proto- (*pr*), para- (*pa*), meta- (*me*) cones; (2) accessory conules, protoconule (*pl*), metaconule (*ml*); (3) peripheral cusps, parastyle (*pas*), metastyle (*mts*) and (4) posterointernal cingulum (*post.cing.*). In earlier herbivorous mammals (C–E) the tritubercular (tribosphenic) or triangular upper molar gradually assumed the "quadritubercular" pattern (F, G) as the posterointernal cingulum (*post.cing*) gave rise to the hypocone (*hy*). In lower molars of early herbivores (C1) the anterointernal cusp, paraconid (*pad*) was ususally minute or had disappeared, leaving four main cusps, protoconid (*prd*), metaconid (*med*), hypoconid (*hyd*), entoconid (*end*). C2 shows the side and crown views of the left, A1, of the right lower molar pattern. From these elements were evolved the complex molar patterns of later herbivores.

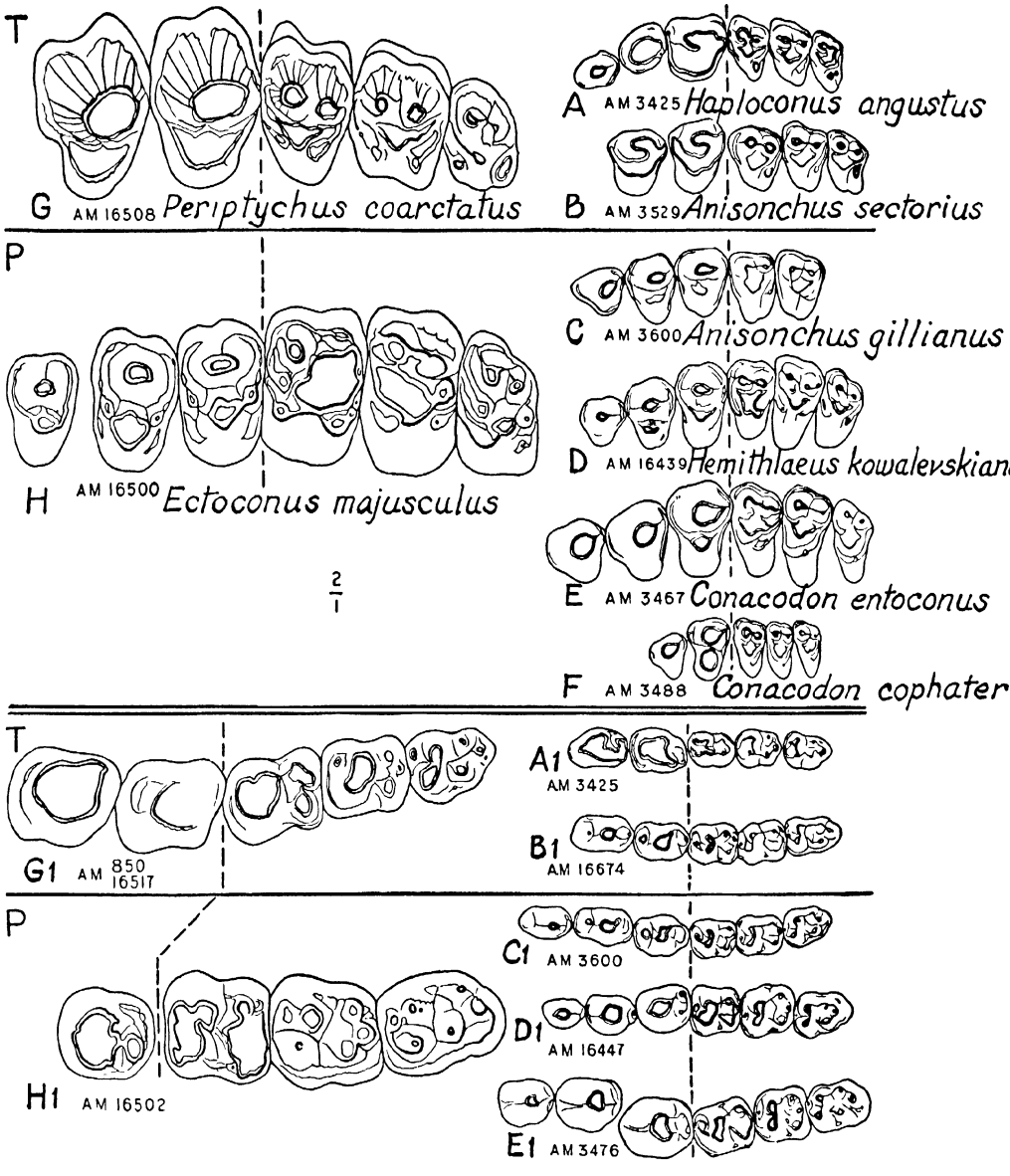


Fig. 21.6. Left upper (A–H) and lower (A1 to H1) cheek teeth of taligrades. After Matthew. P, Puerco (Lower Paleocene); T, Torrejon (Middle Paleocene).

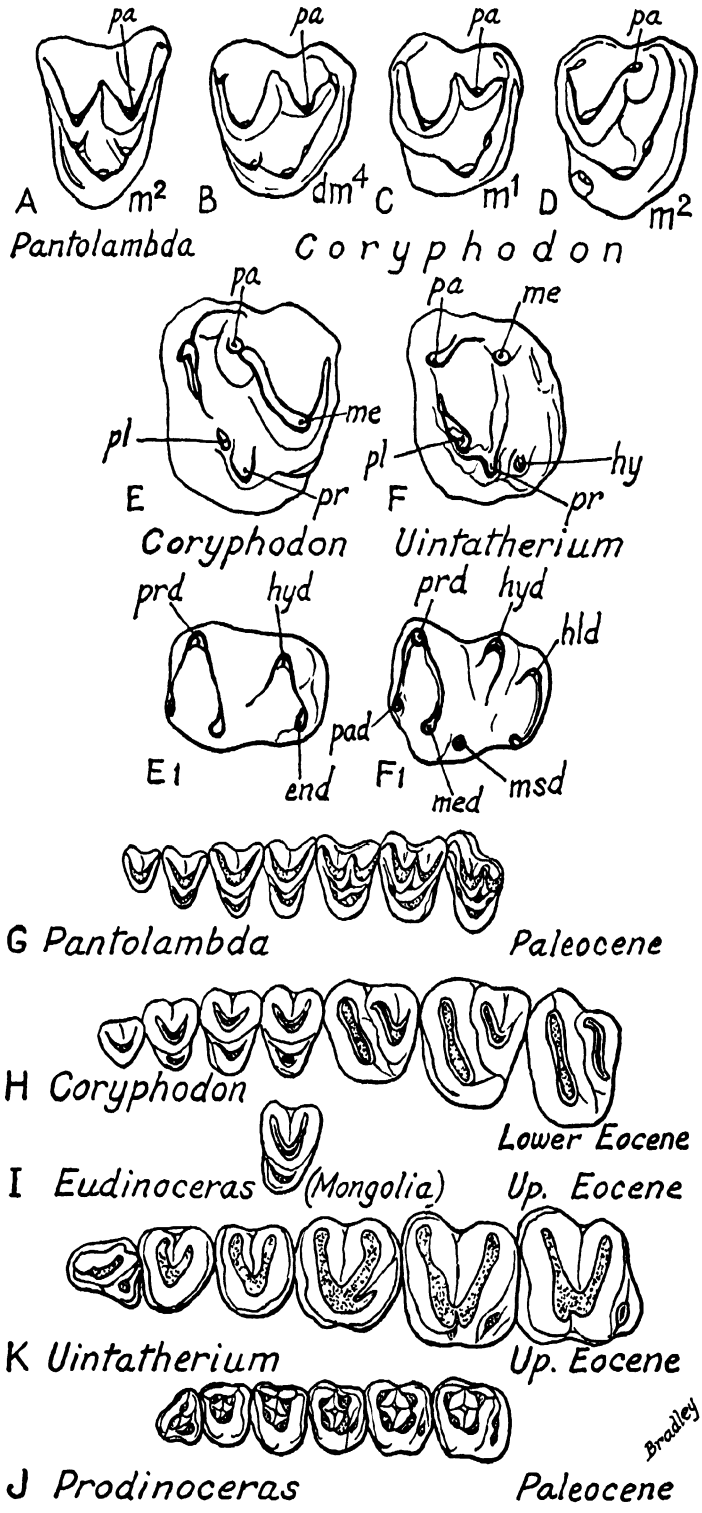


Fig. 21.7. Evolution of molar patterns in pantodonts (A–E, G, H) and Dinocerata (F, F1, J, K). A–F1, after Simpson; G–K, after Matthew.

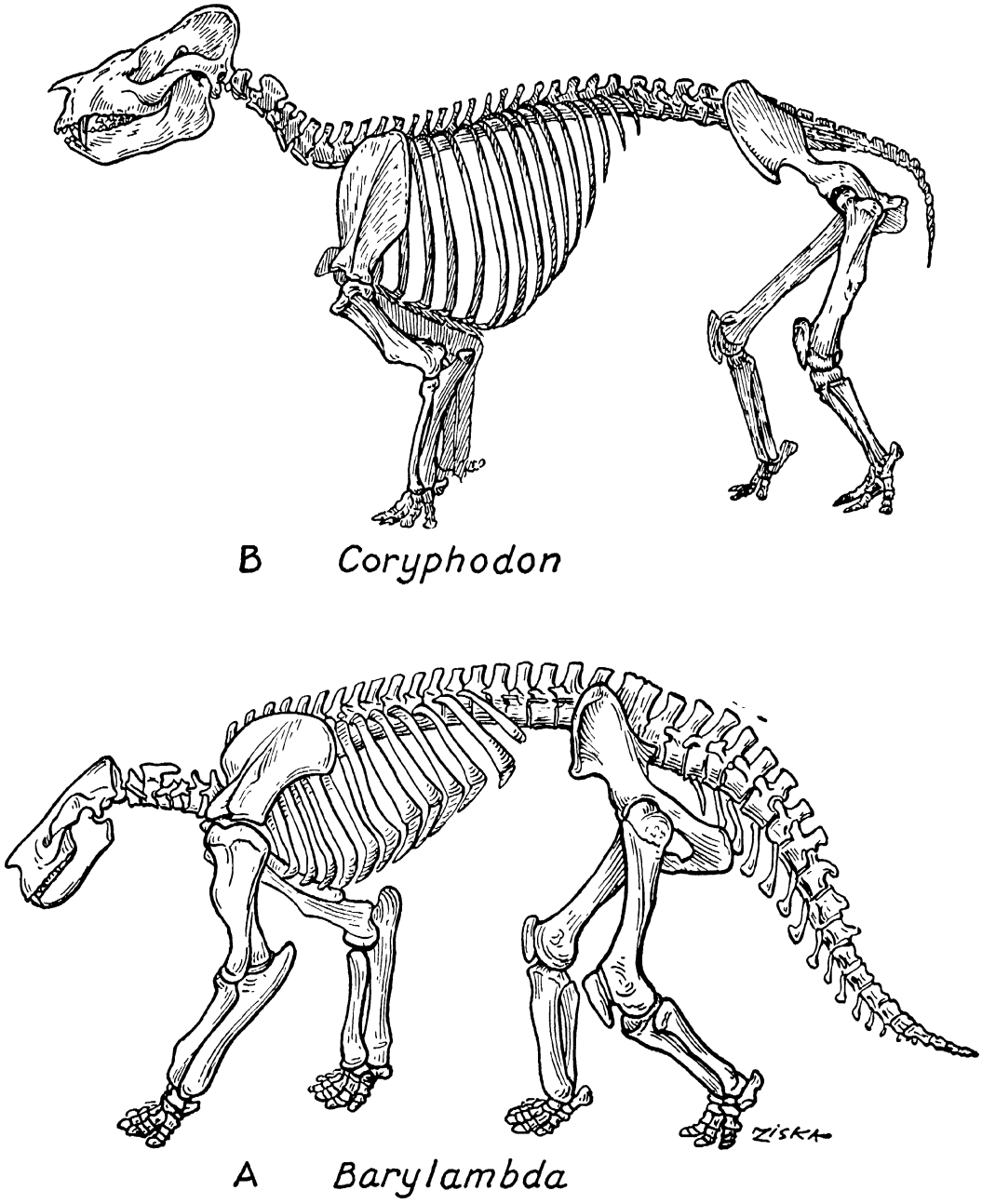


Fig. 21.8. Skeletons of Paleocene (A) and Lower Eocene (B) pantodonts. A, after Patterson; B, mainly after Romer.

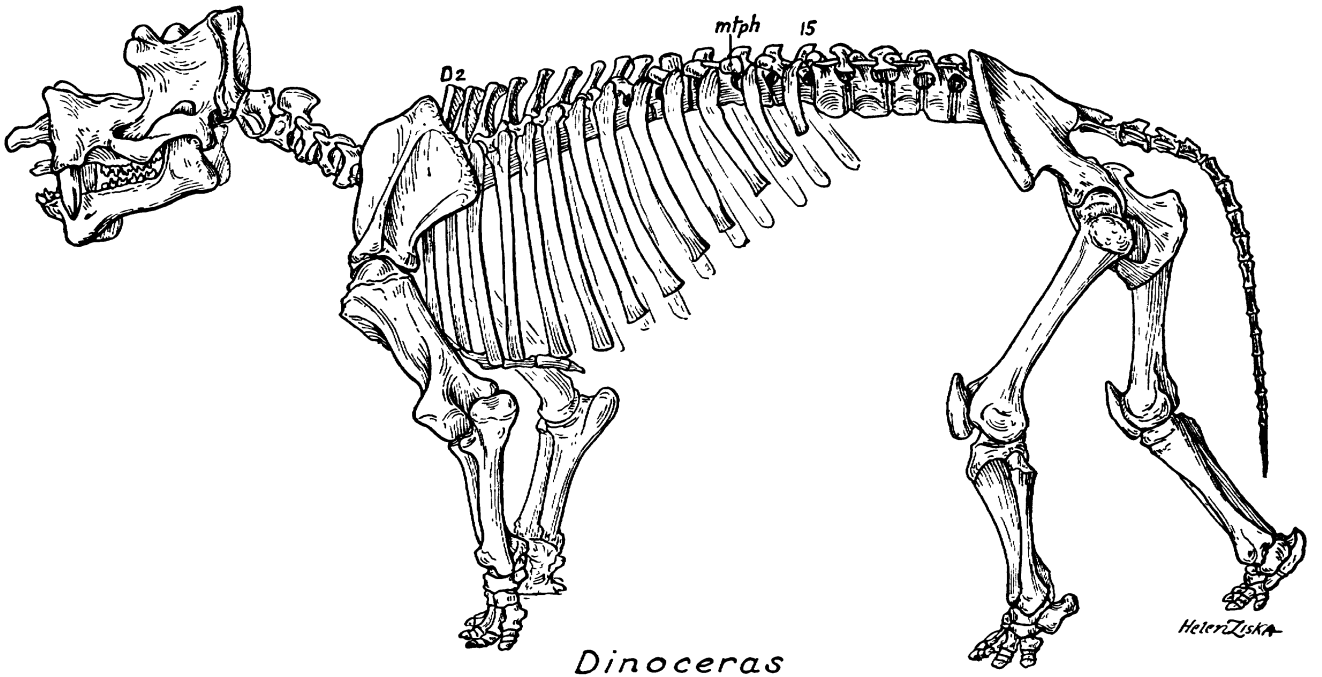


Fig. 21.9. Skeleton of Middle Eocene uintathere. Data from mounted skeleton in the American Museum.

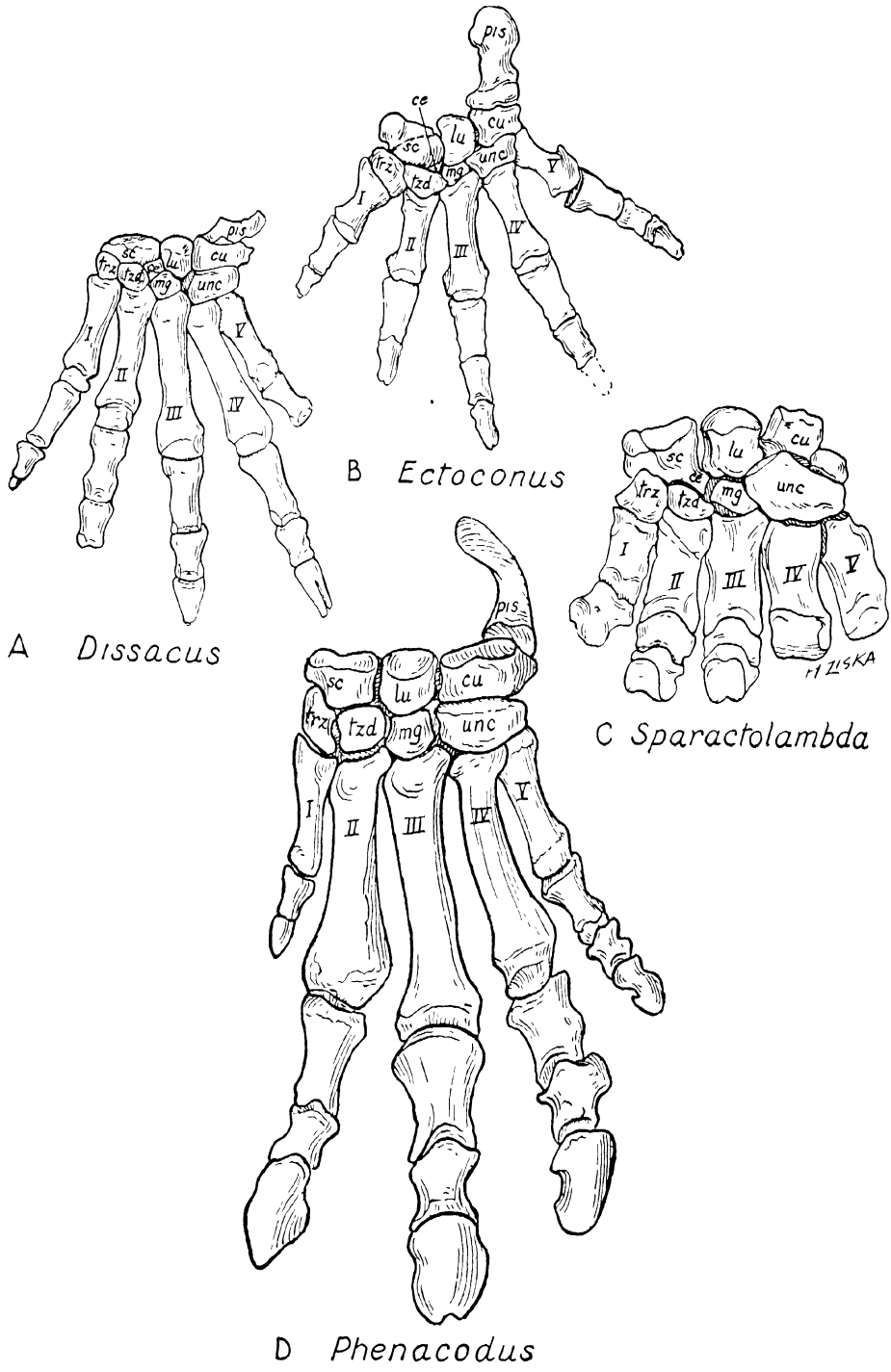


Fig. 21.10. Left forefoot of primitive Paleocene creodont (A), taligrade (B), pantodont (C) and condylarth (D). In D, the wrist and hand are drawn as if unrolled or flattened, to show the full width of the carpals and metacarpals. A, B, after Matthew; C, after Patterson; D, original.

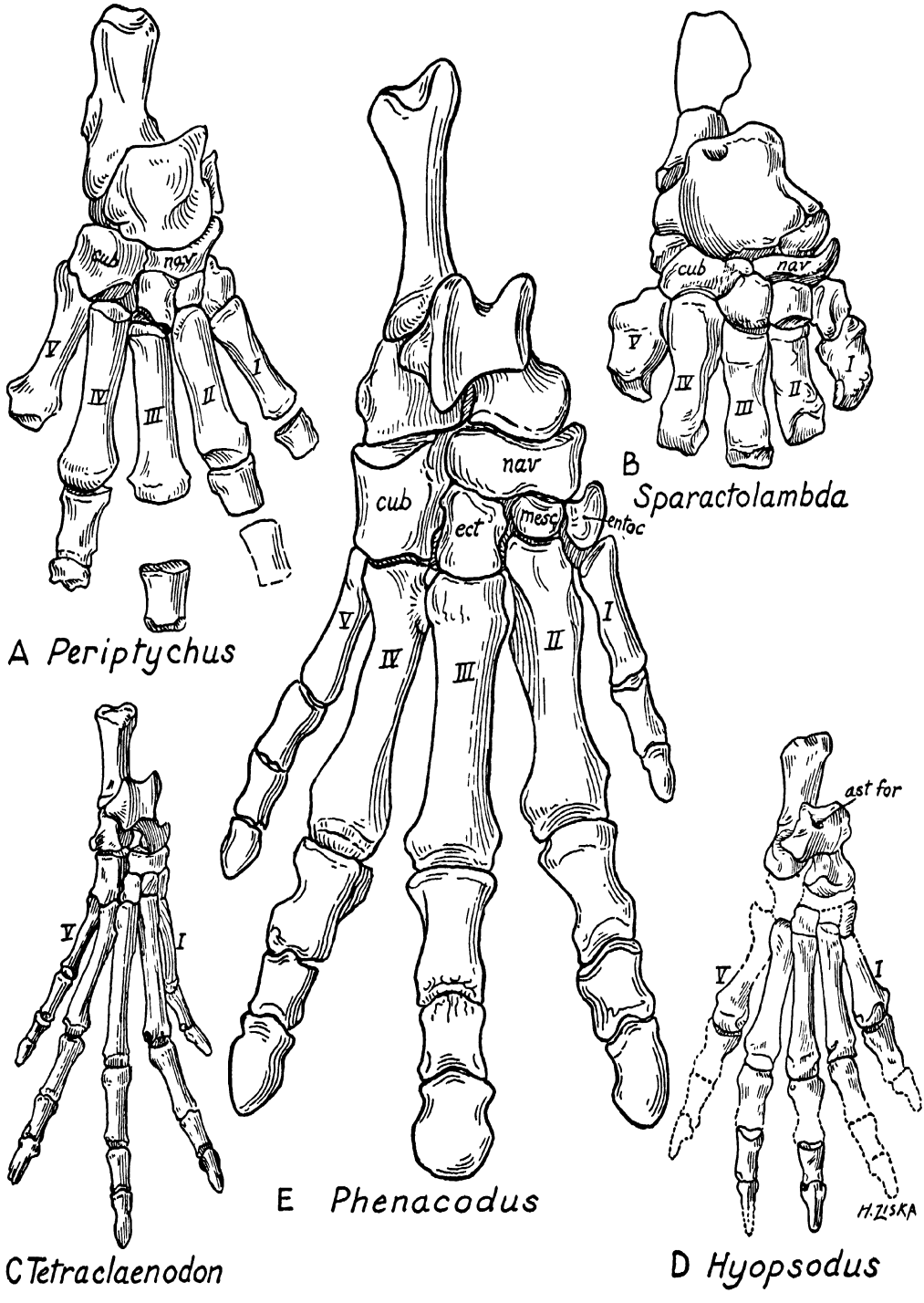


Fig. 21.11. Right hind feet of taligrade (A), pantodont (B) and condylarths (C–E). A and D are probably the least specialized and represent the spreading hand and relatively short digits of the most primitive Paleocene placental mammals. B is a derived graviportal type, with flattened astragalus and very wide short metacarpals and digits (not shown). C is a slender subcursorial form. A, C, after Matthew; B, after Patterson, D, after Matthew and Granger; E, from cast of mounted foot but unrolled or flattened to show full width of all bones.

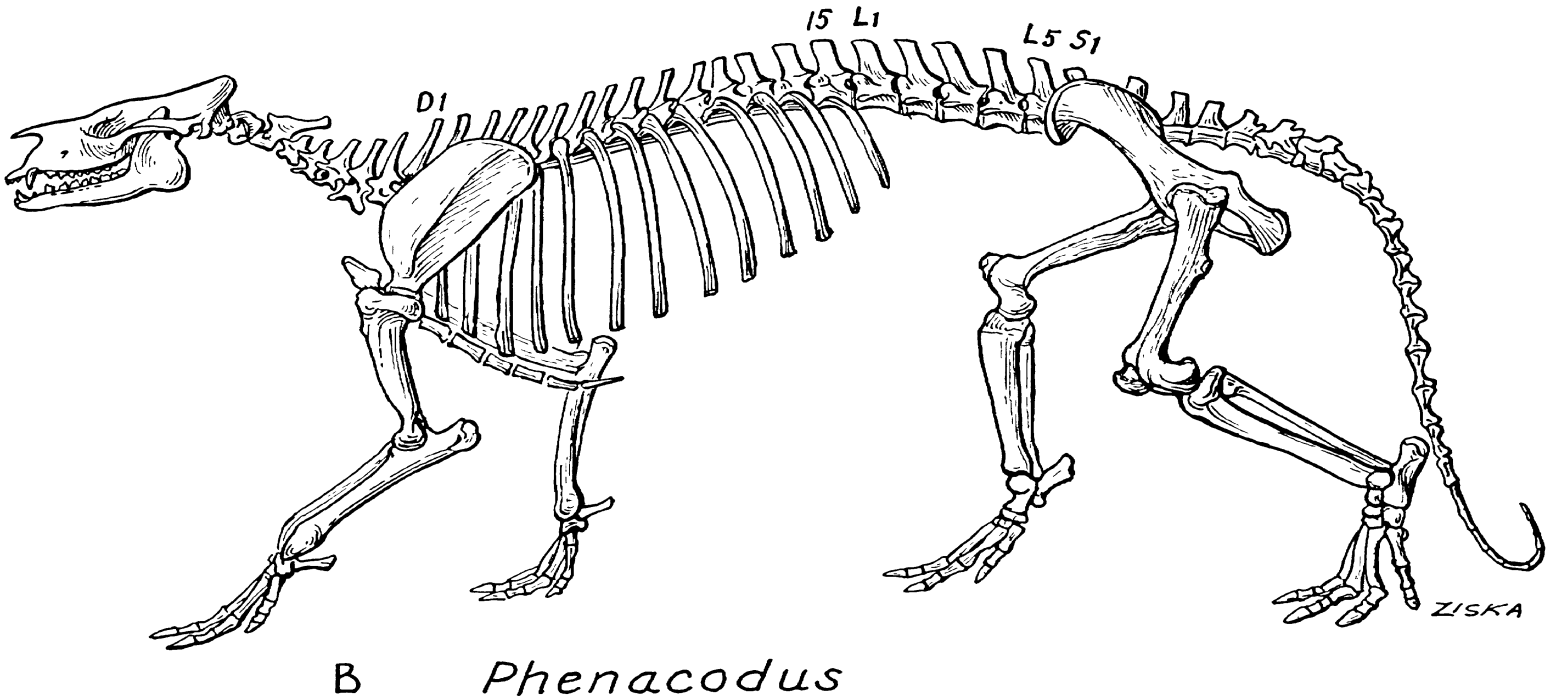


Fig. 21.12 Skeleton of *Phenacodus primaevus* Cope. Data mainly from mounted skeleton.

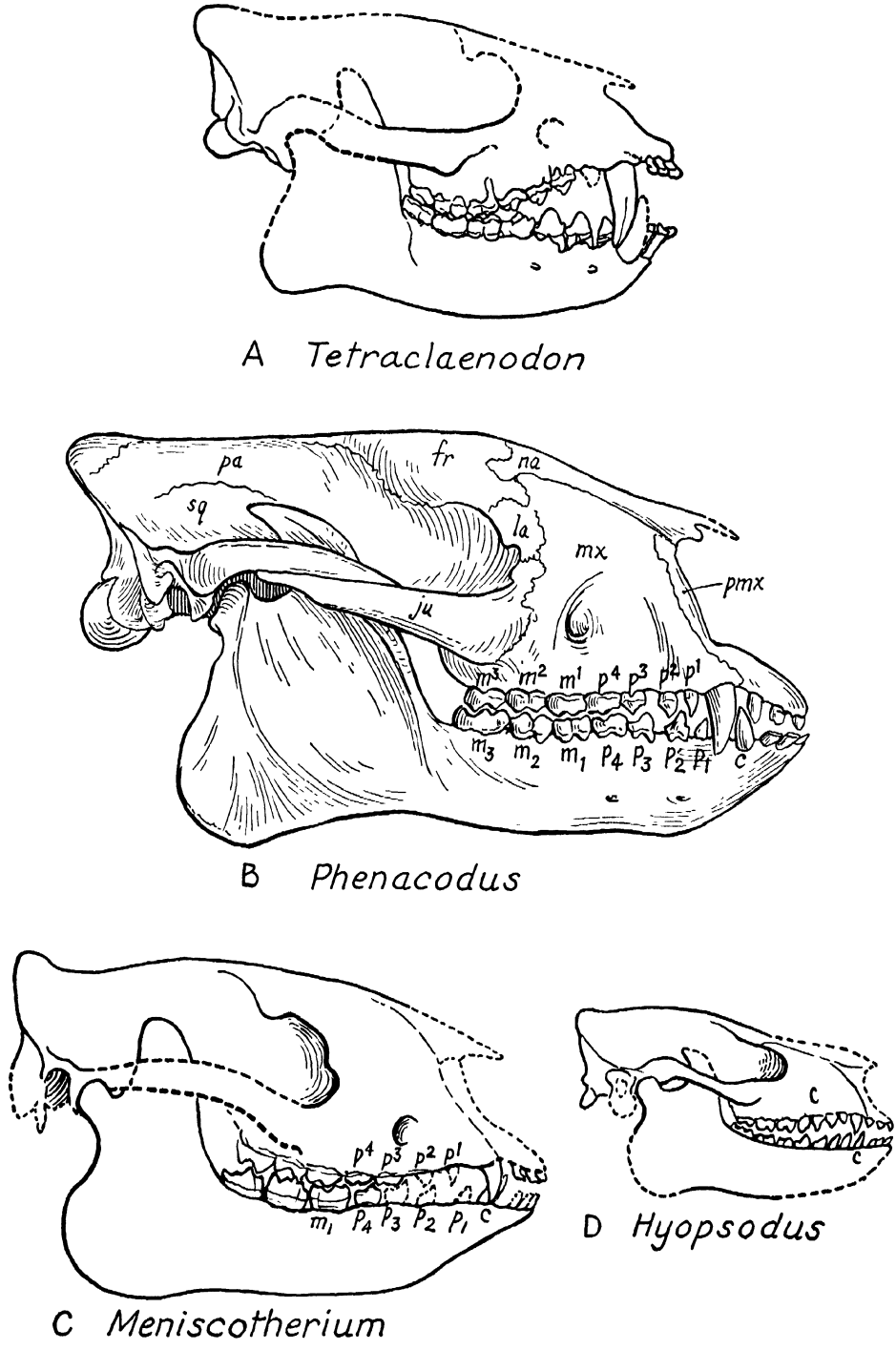


Fig. 21.13. Skulls of condylarths. A, after Matthew; B, reconstruction from photographs of a fine skull of *Phenacodus primaevus* in the School of Mines, Rapid City, South Dakota; C, D, reconstructed from American Museum fossils, data partly after Osborn and Matthew.

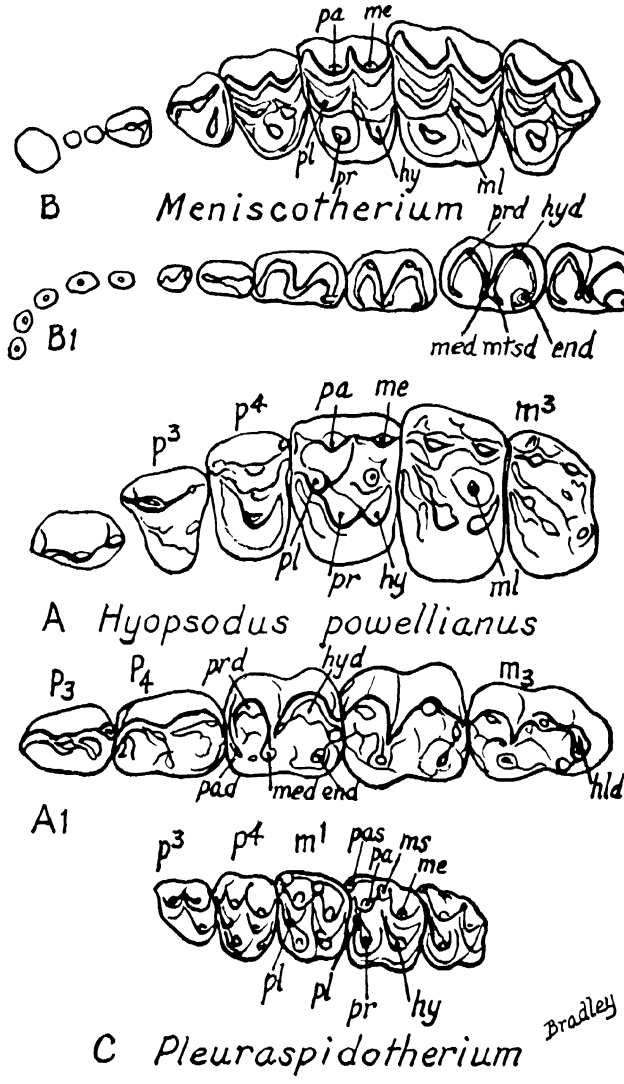


Fig. 21.14. Keys to condylarth molar patterns (cf. fig. 21.5). In C, from the Paleocene of Europe, the proto- and metaconules (*pl, ml*) form small oblique crosscrests (protoloph, metaloph) as in primitive perissodactyls. A, after Matthew; B, after Osborn; C, after Teilhard de Chardin.

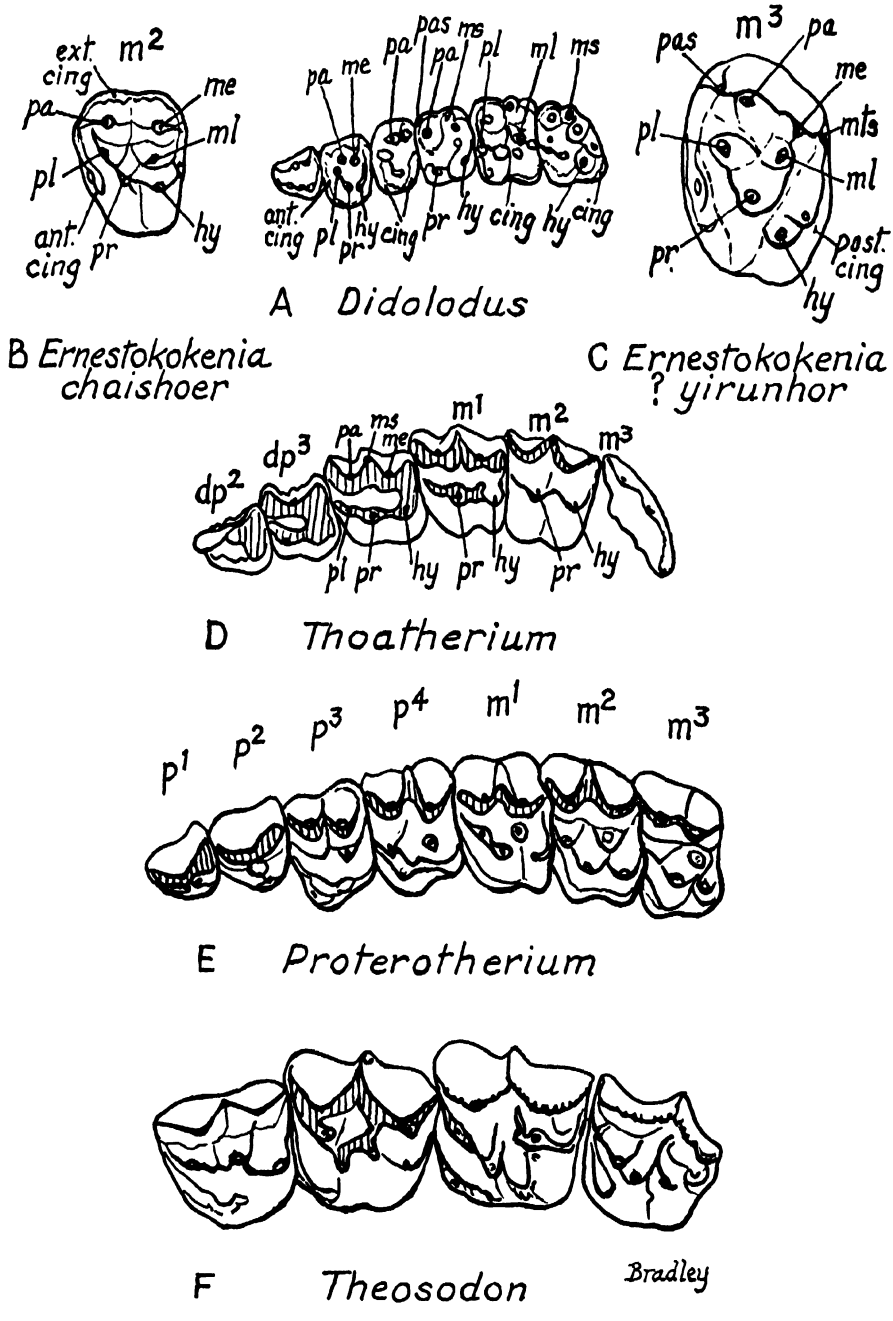


Fig. 21.15. Tritubercular key to litoptern molar patterns. Data from: Scott (A, D, E, F); Simpson (B, C).

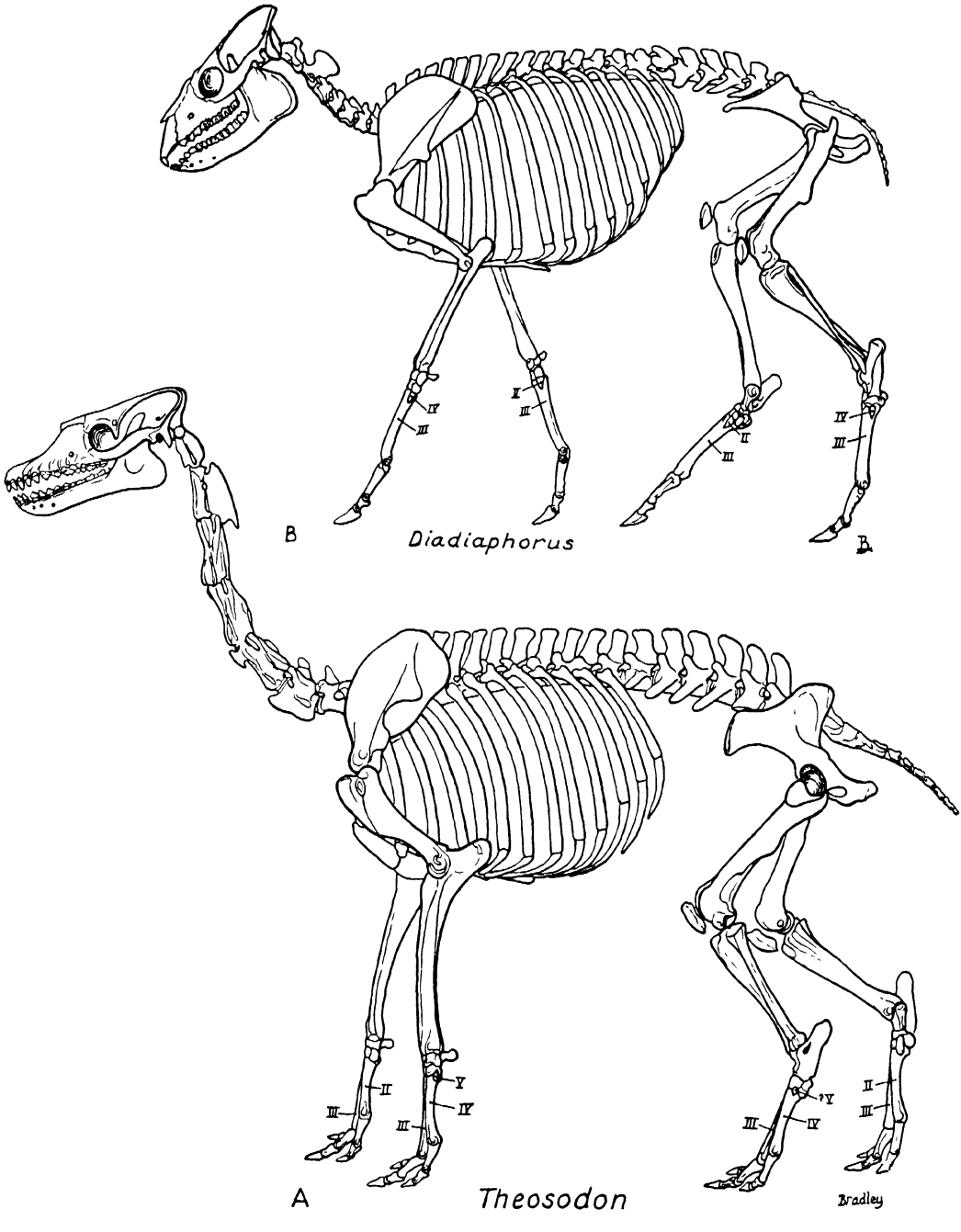


Fig. 21.16. Skeletons of llama-like (A) and horse-like (B) litopterns. After Scott.

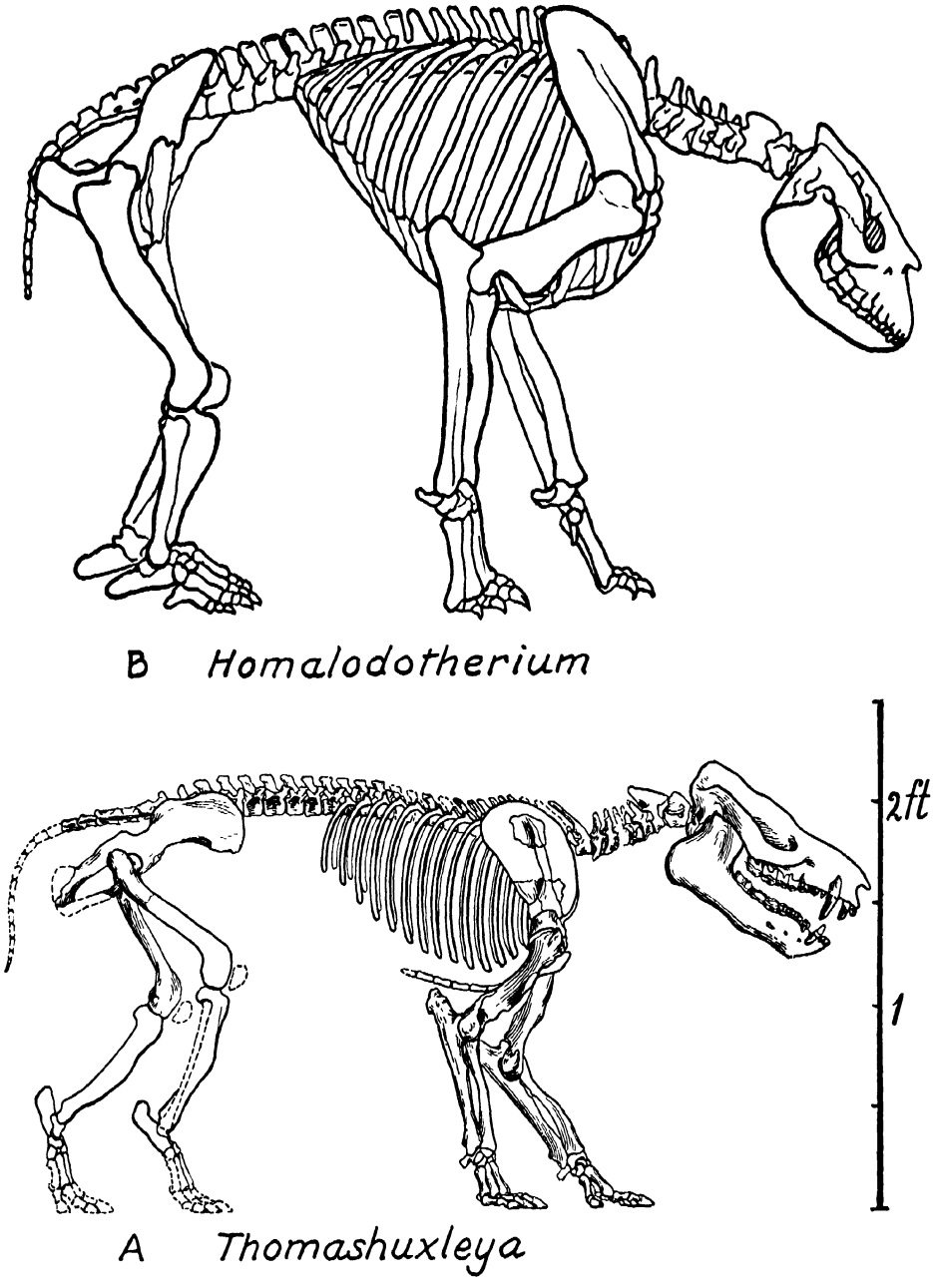


Fig. 21.17. Skeletons of notoungulates. A is smaller and far less specialized than B and comes from a much older (Lower Eocene) horizon. A, after Simpson; B, after Scott.

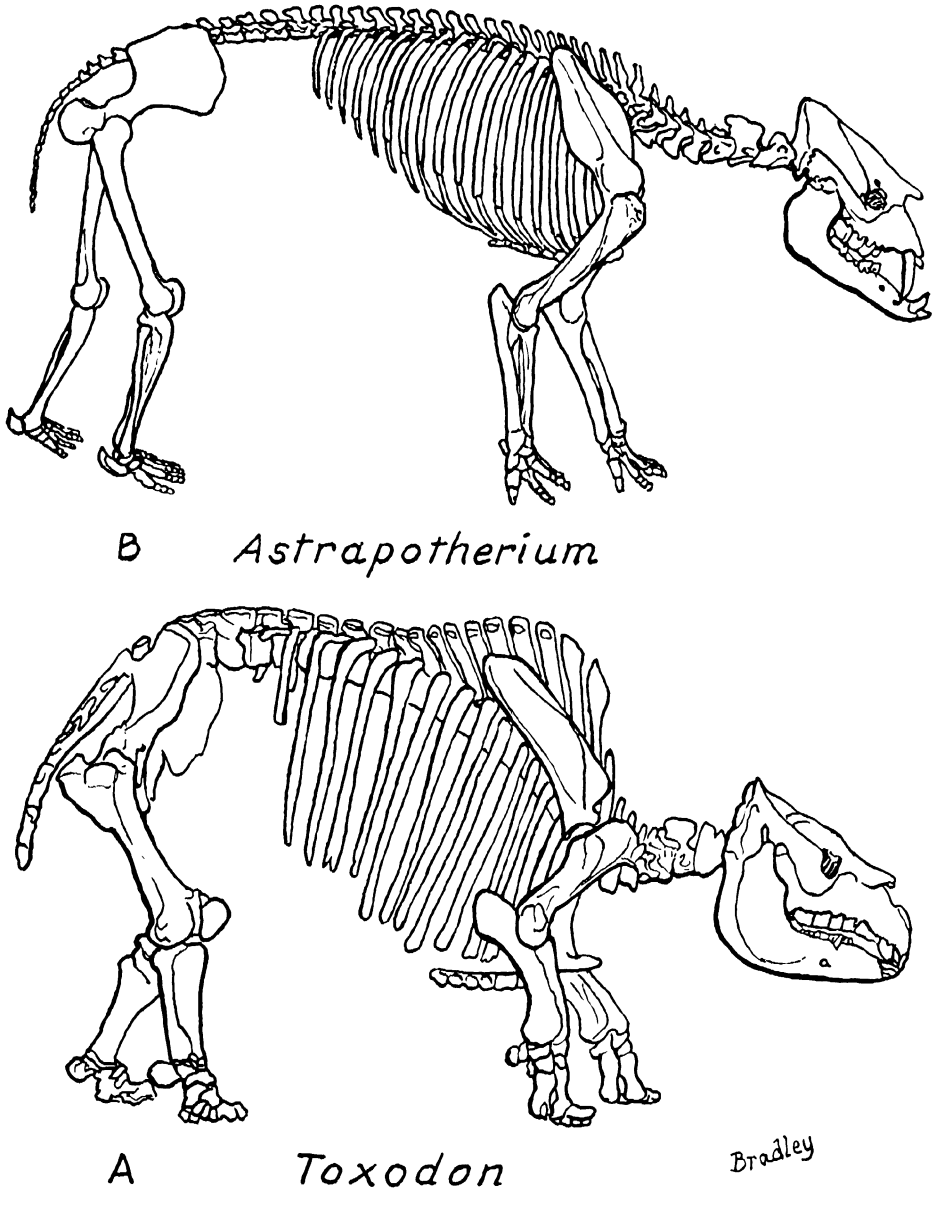


Fig. 21.18. Skeletons of Pleistocene toxodont (A) and Lower Miocene astrapothere (B). After Scott.

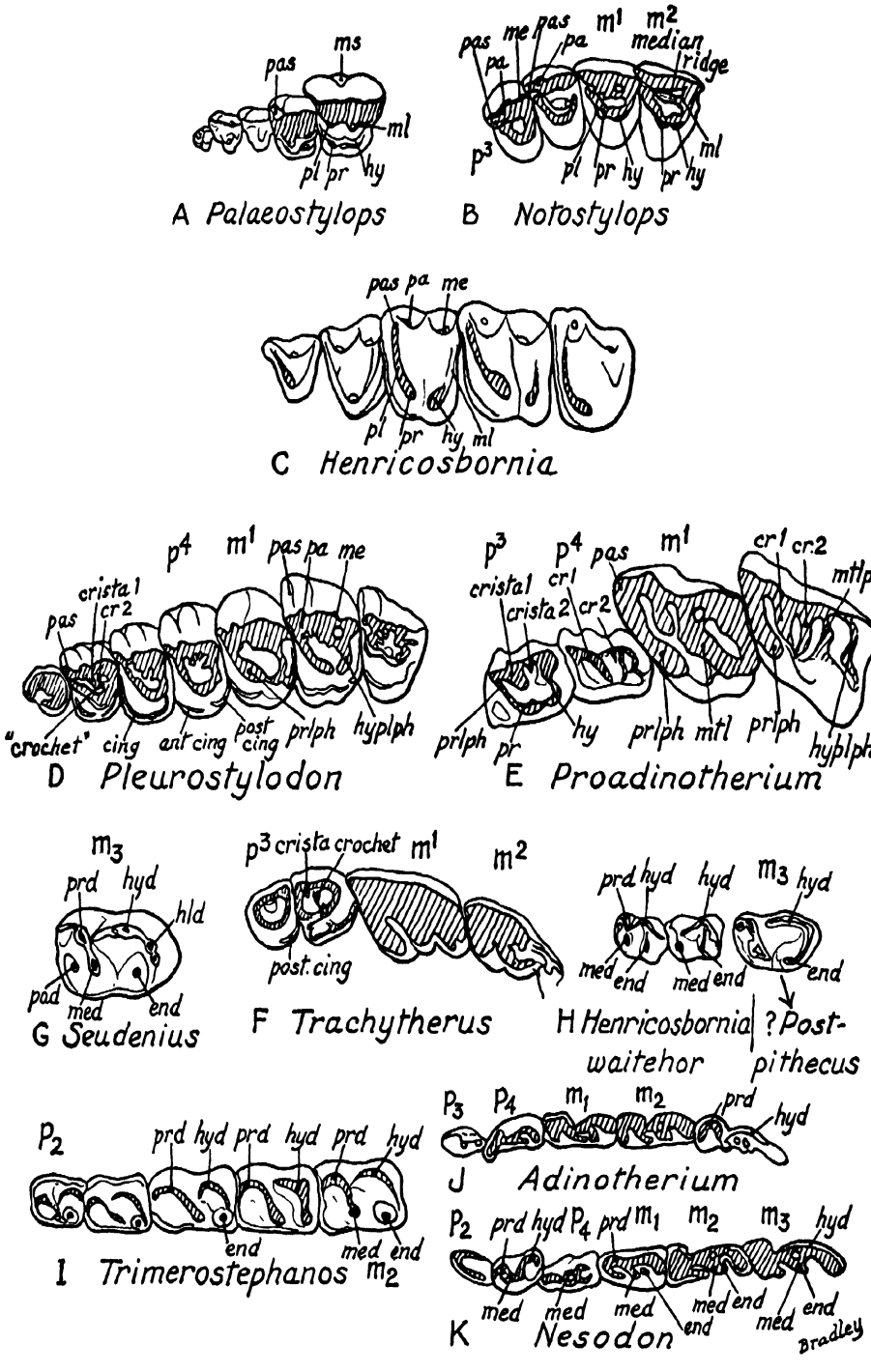


Fig. 21.19. Tritubercular key to notoungulate molars. Data from Patterson (A, B, D–F), Simpson (G, H), Loomis (I), Scott (J. K). C, Original from American Museum specimens. The suborders (Simpson, 1945) represented are: Notioprogonia (A–C, G, H); Toxodonta (D, E, I–K); Typotheria (F).

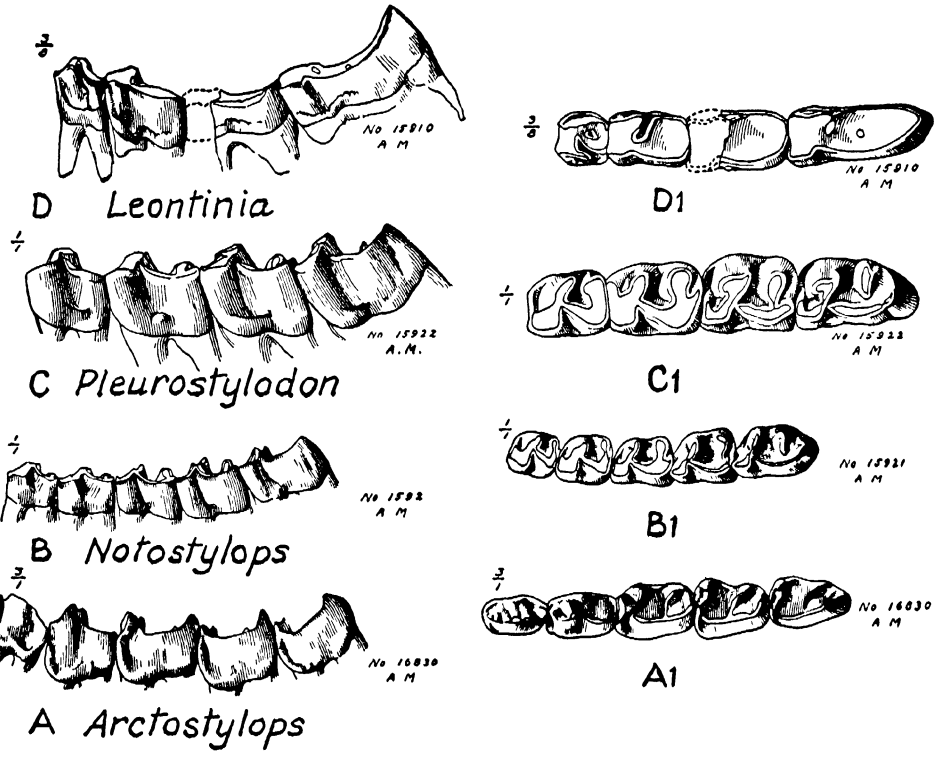


Fig. 21.20. Left lower cheek teeth of notoungulates: from the Lower Eocene of North America (A, A1), the Lower Eocene of South America (B, B1, C, C1) and the Lower Oligocene of South America (D, D1). After Matthew. The North American form agrees with its nearest South American relatives in basic patterns especially in the flattening and blade-like form of the hypoconids and in the distinctness of the entoconid (A1, B1).

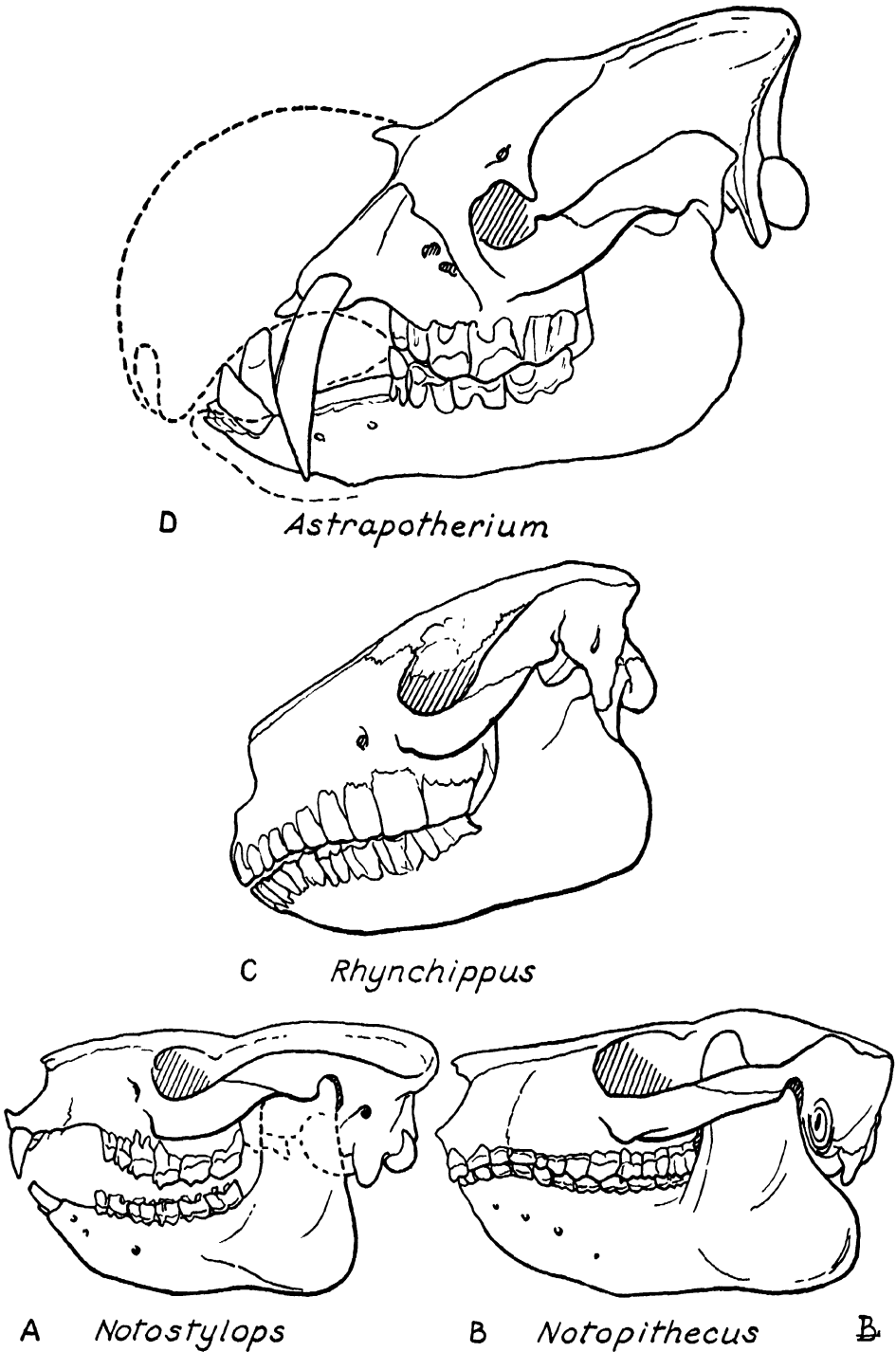


Fig. 21.21. Skulls of notoungulates (A–C) and astrapothere (D). A, B, after Simpson; C, D, after Scott.

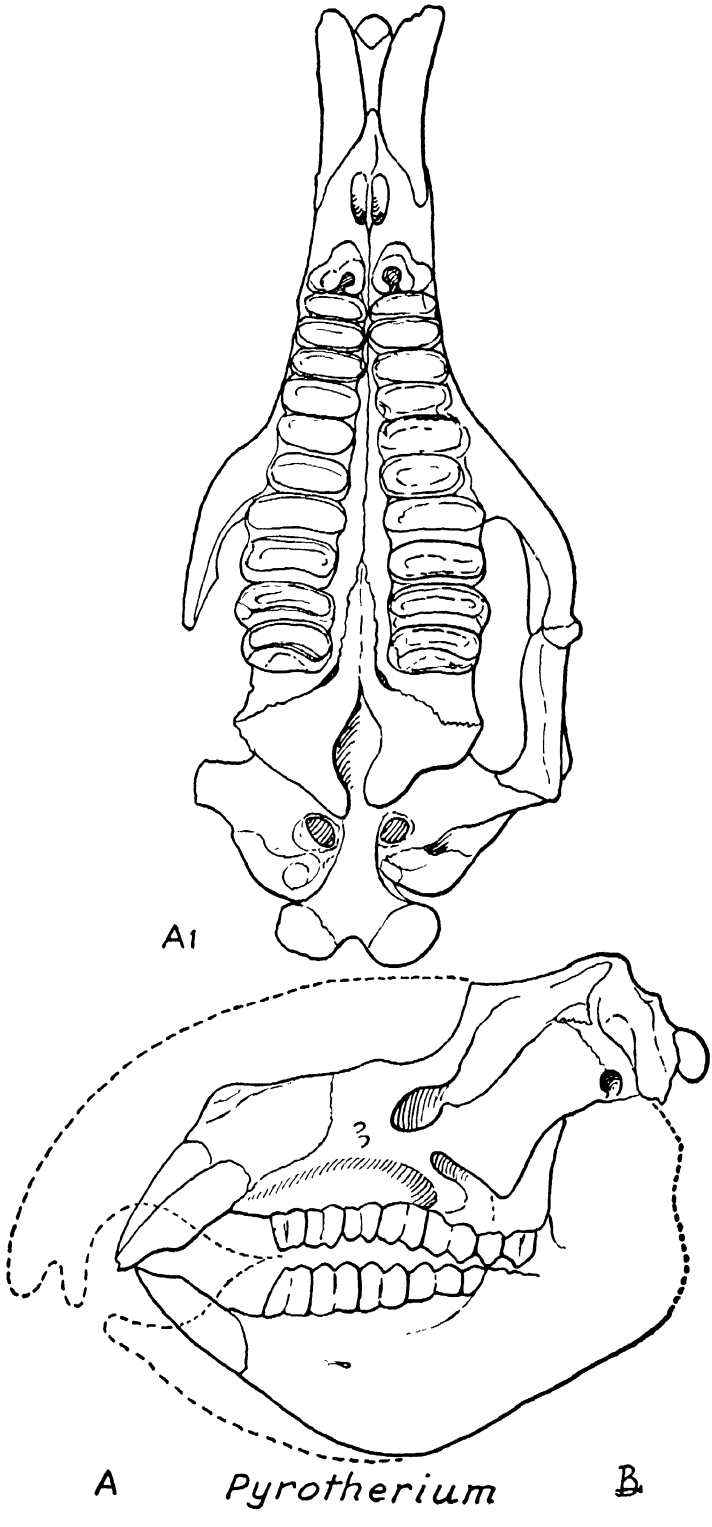


Fig. 21.22. Skull of *Pyrotherium*, showing the marked recession of the nasals and the bilophodont molars, producing a superficial resemblance to the Proboscidea. After Loomis.

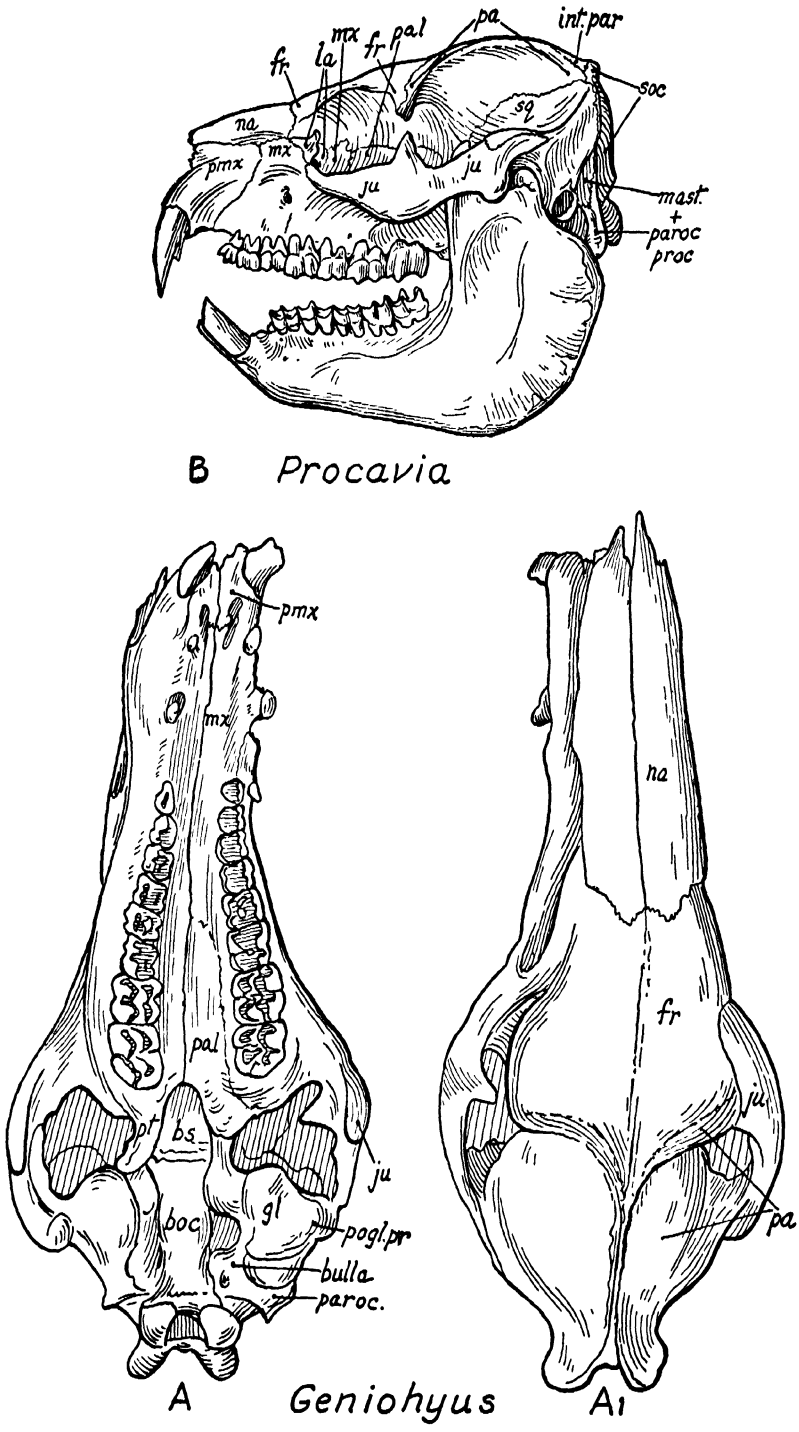


Fig. 21.23. Oligocene (A) and modern (B) hyracoid skulls. A, data from Matsumoto; B, original.

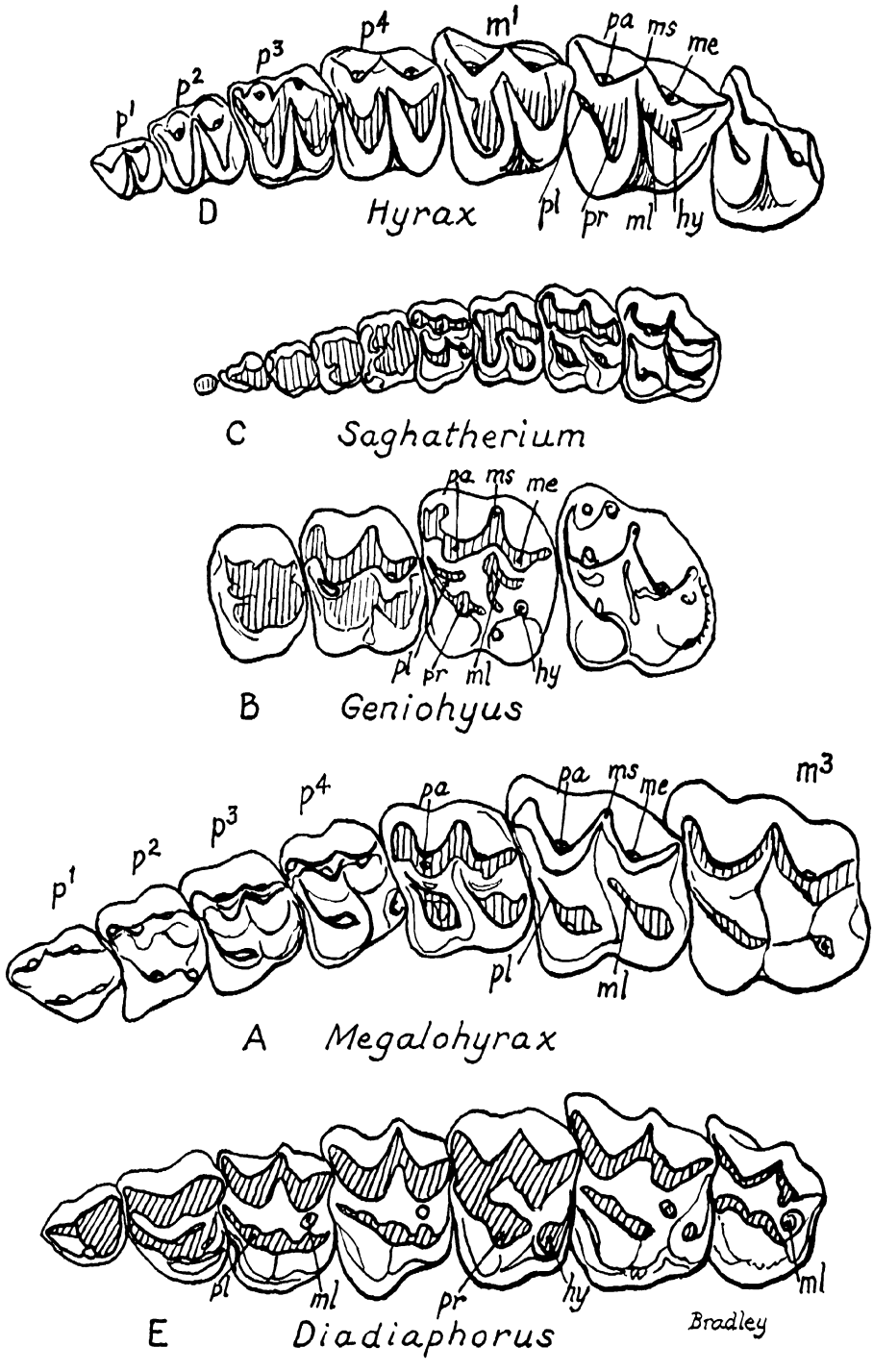


Fig. 21.24 Egyptian Oligocene (A–C) and Recent African (D) hyracoid upper premolar-molar series, compared with Lower Miocene Patagonian litoptern (E). A, after C. W. Andrews; B, C, after Matsumoto; D, original; E, after Scott.

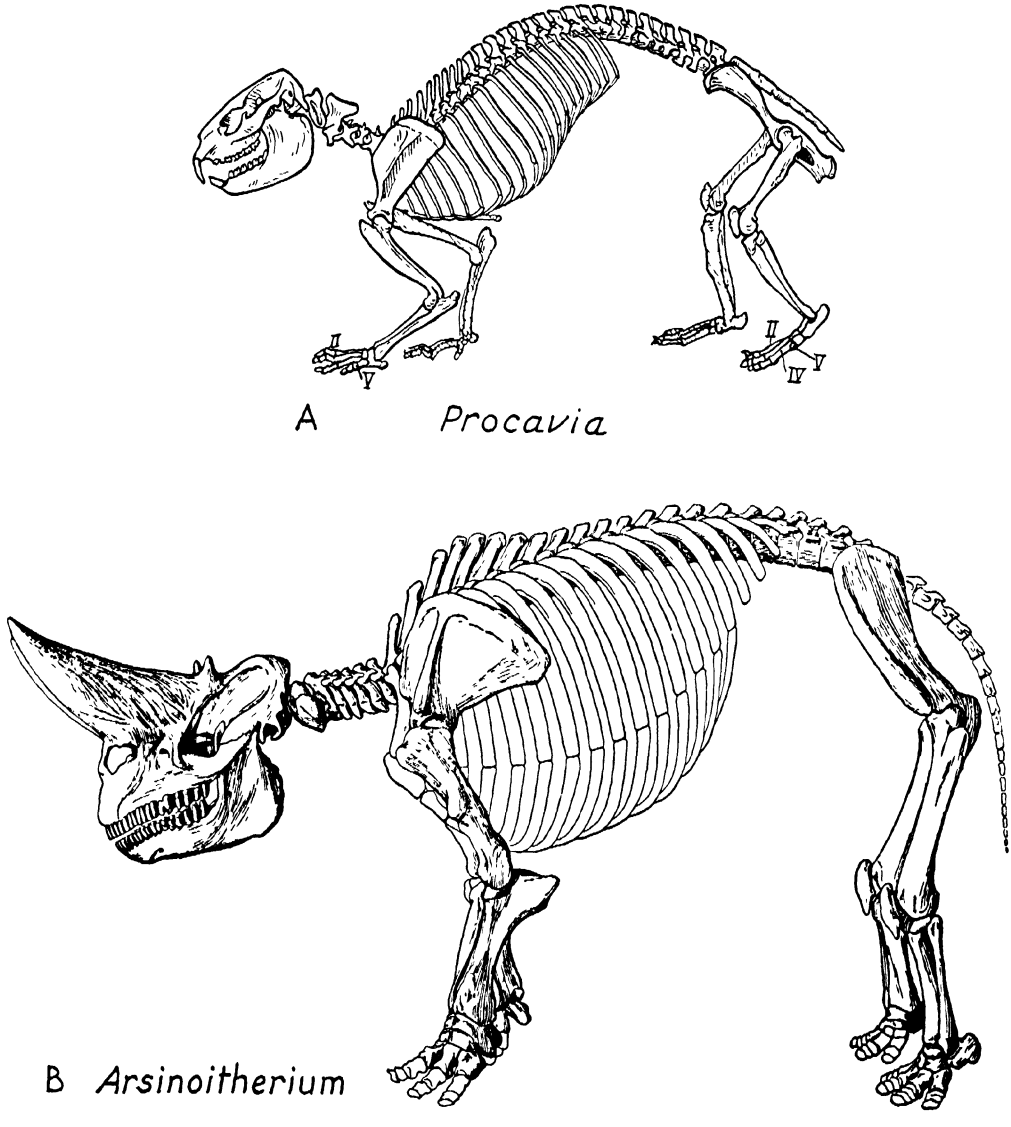


Fig. 21.25. Relatively primitive ambulatory skeleton of modern hyracoid (A) and graviportal skeleton of Lower Oligocene Egyptian arsinoithere (B). A, original; B, after C. W. Andrews.

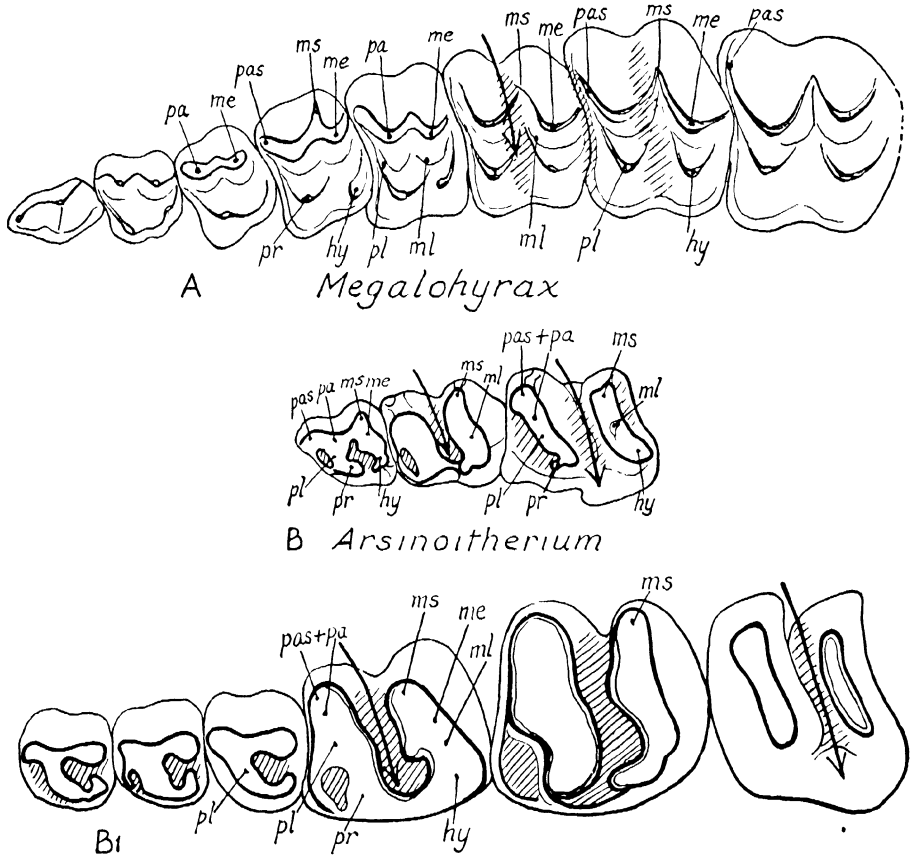


Fig. 21 26 Tritubercular key to upper premolar-molar patterns of Lower Oligocene Egyptian hyracoid (A) and arsinoithere (B, B1) to illustrate C. W. Andrews' theory of origin from a primitive hyracoid type (A). Arrows indicate flexures and reentrant valleys.

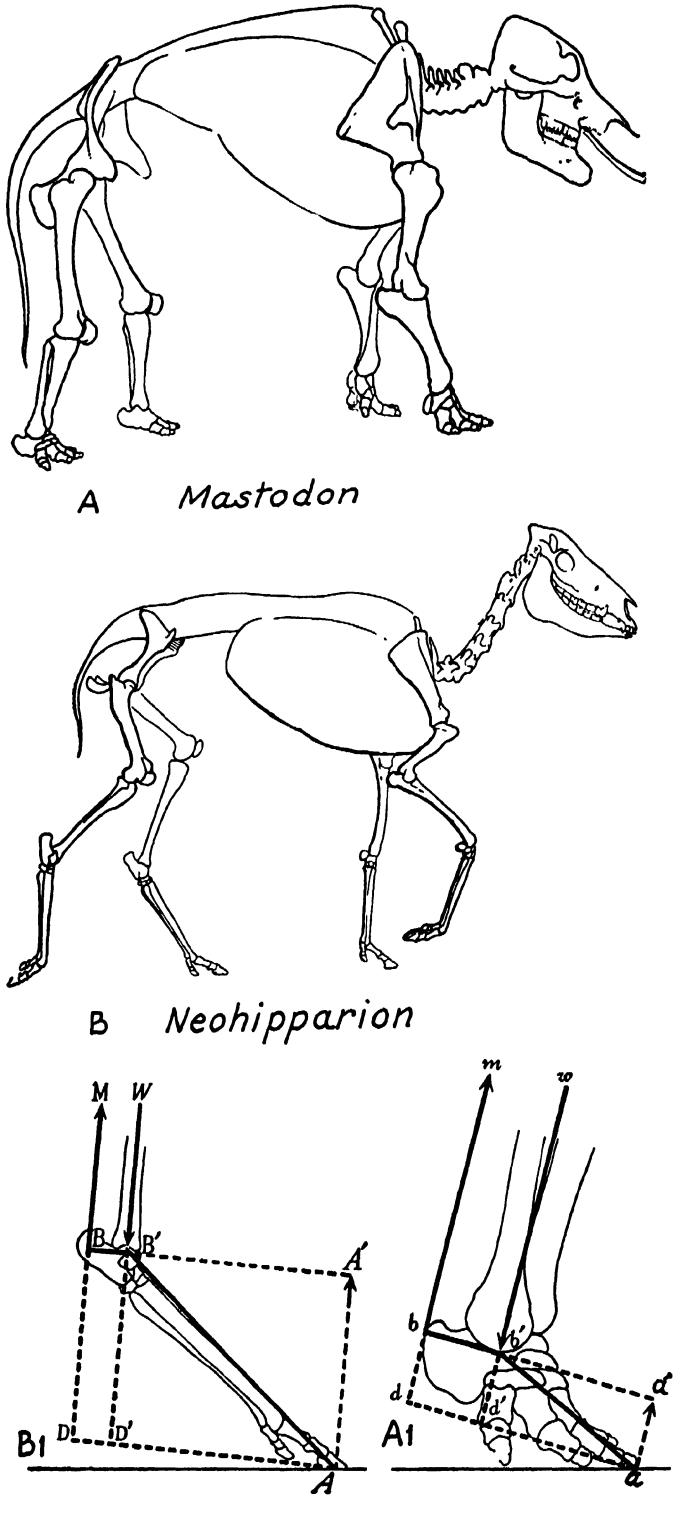


Fig. 21.27. Contrast of extreme graviportal (A, A1) and cursorial (B, B1) types of limbs and girdles. After Gregory.

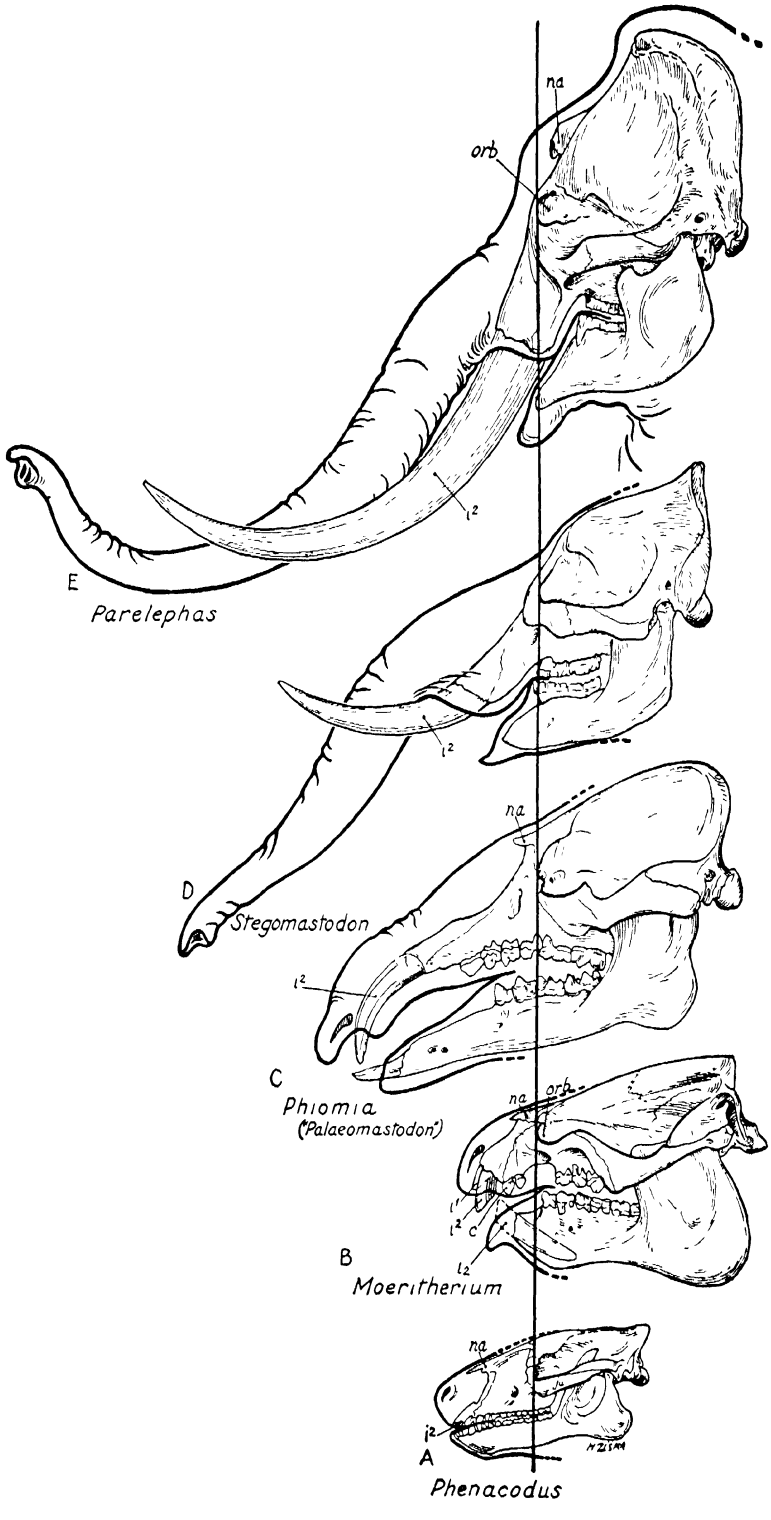


Fig. 21.28. Structural series, showing recession of nasals, forward growth of nostril-upper lip, and transformation of skull and dentition from primitive condylarth to highly specialized mammoth. A, original; B–E, skulls after Osborn.

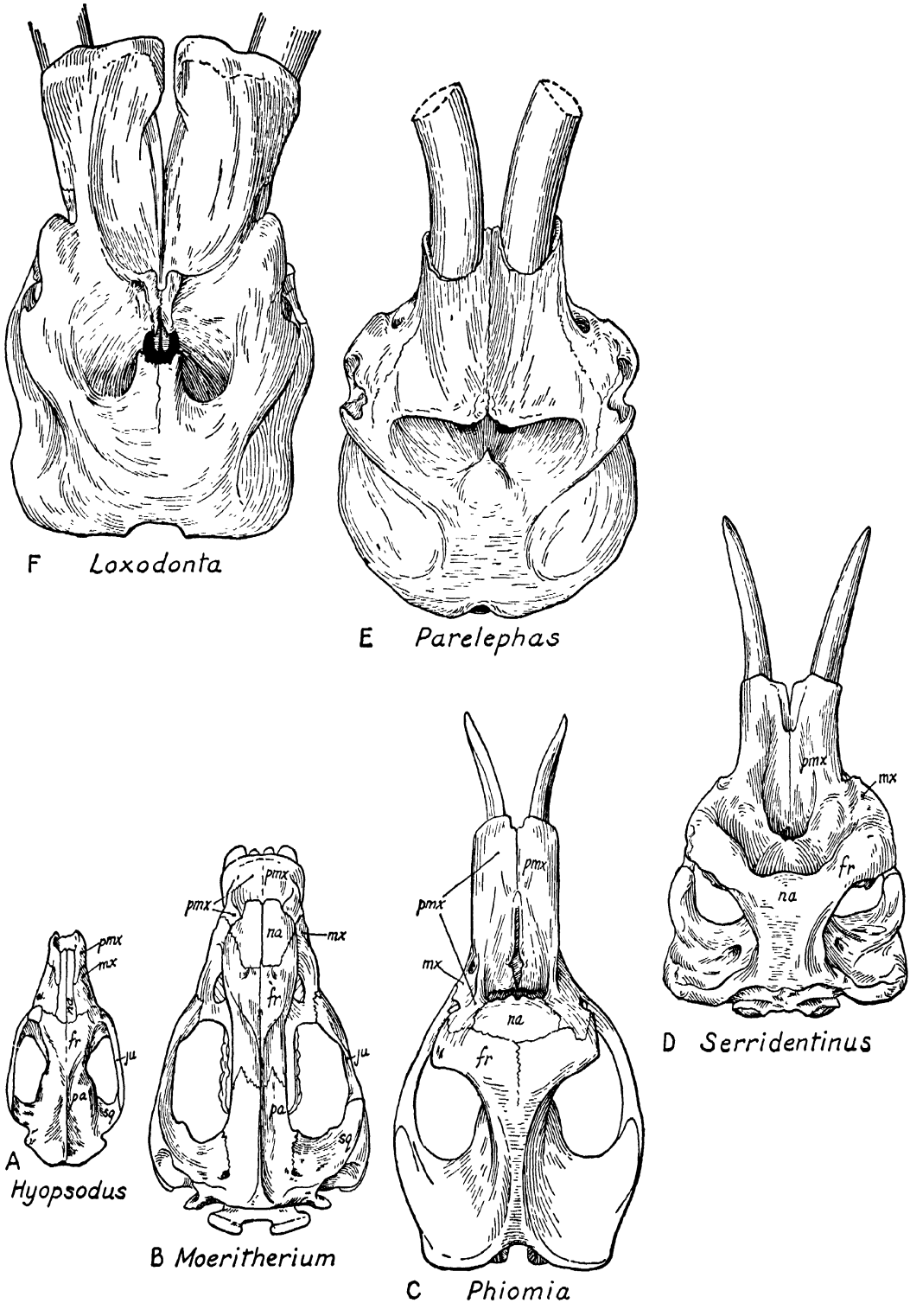


Fig. 21.29. Structural series of skulls (top view) from primitive Eocene condylarth to Recent African elephant. A, after Matthew; B–F, after Osborn.

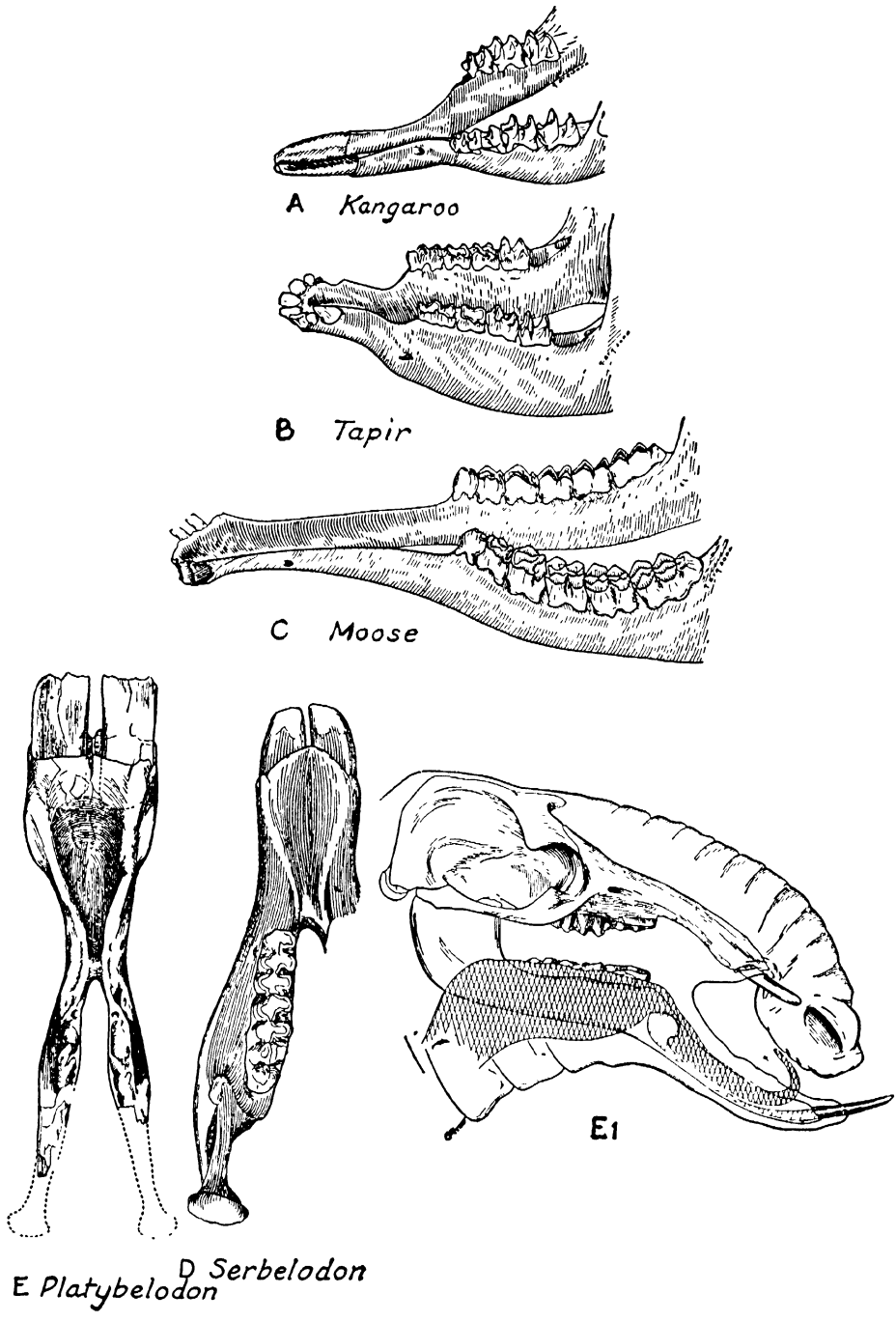


Fig. 21.30. The sublingual groove of the lower jaw (A–C) and its function in long-jawed mastodonts (D–E1). After Gregory. In E1 the protrusile half of the tongue lies in the symphysial basin.

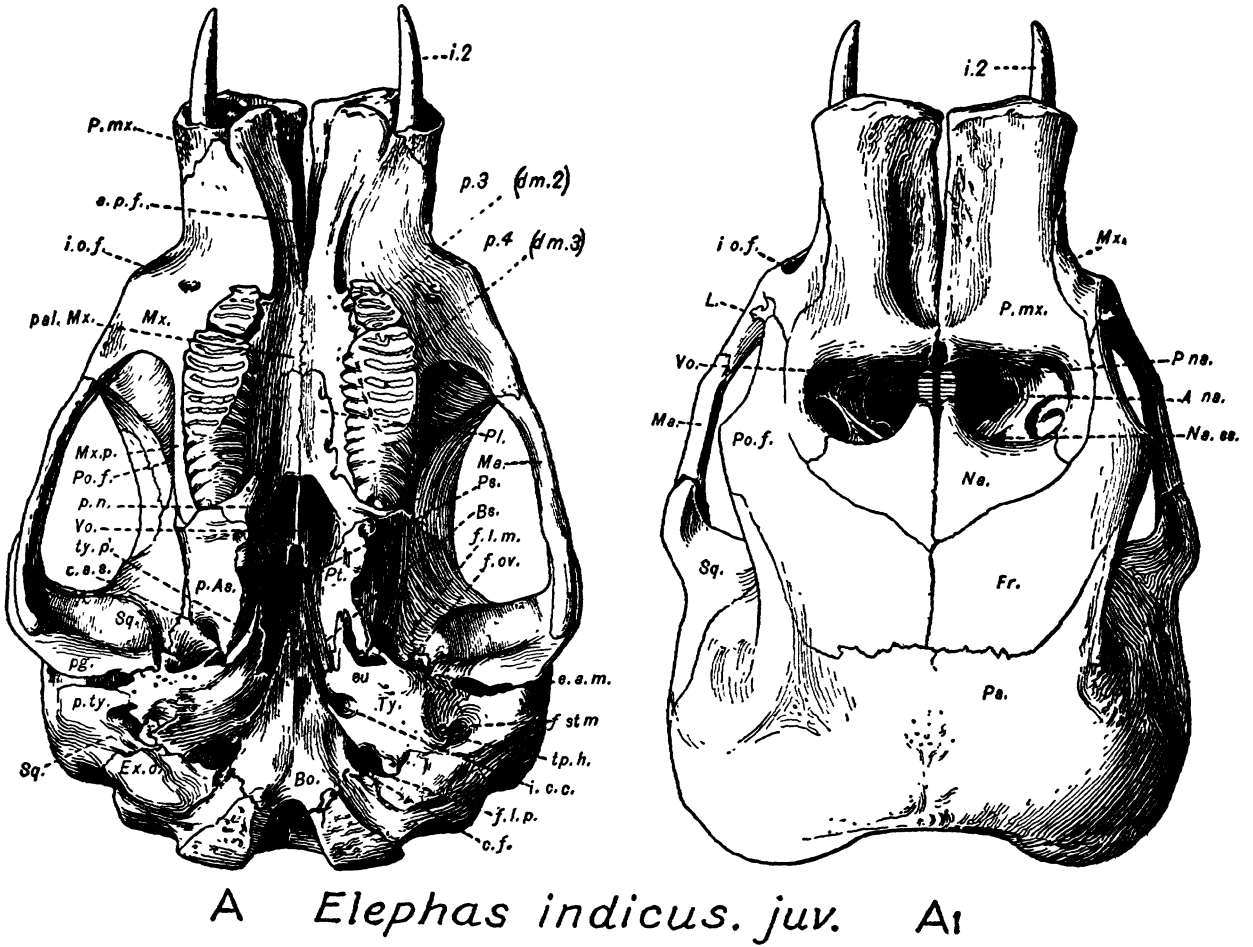


Fig. 21.31. Young Indian elephant skull, showing constituent polyanisomeres and adaptive bracing. After Gregory. A, Inferior view. For abbreviations, see Vol. I, p. 422.

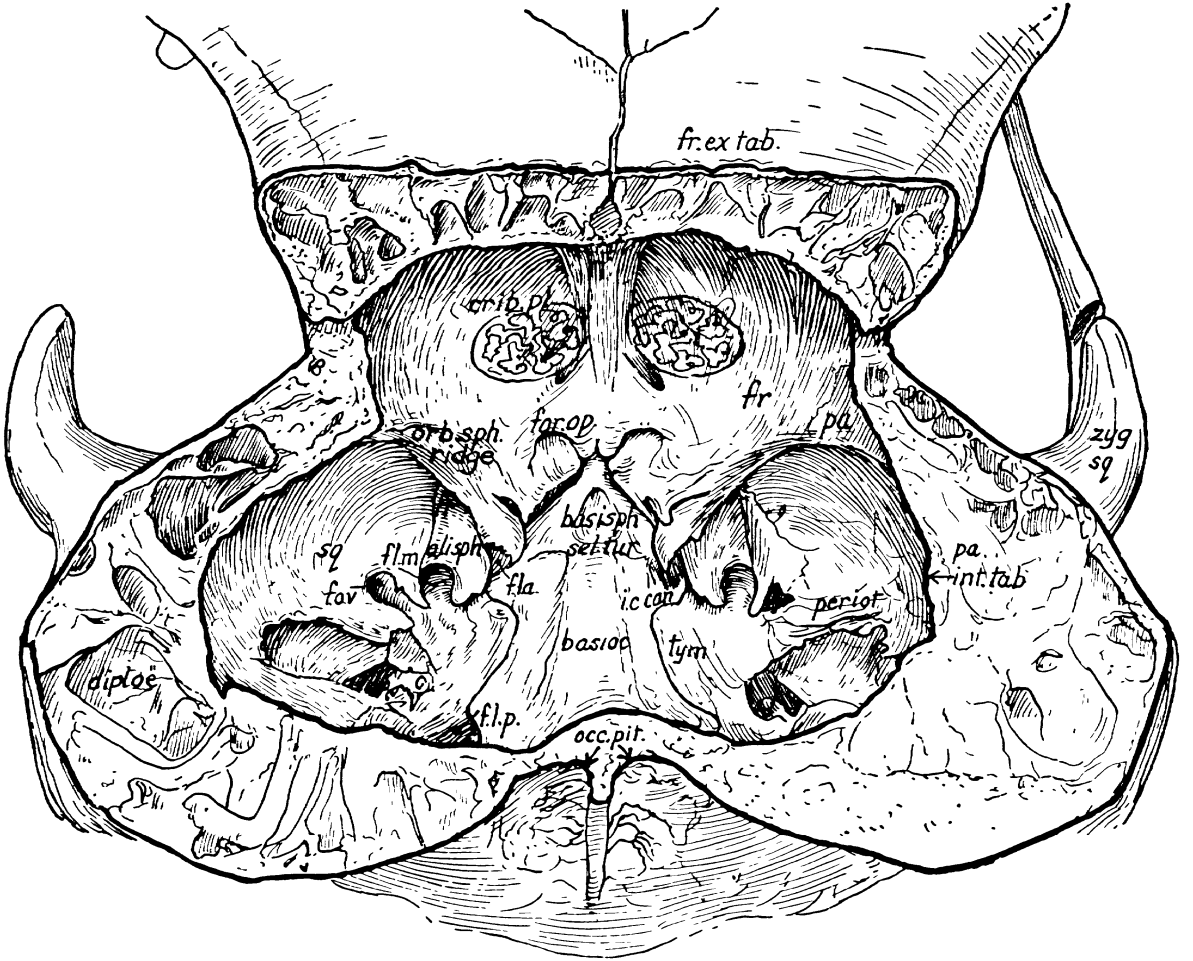


Fig. 21.32. Cranium of young Indian elephant after resection of roof, showing keystone position of spheno-occipital base. After Gregory.

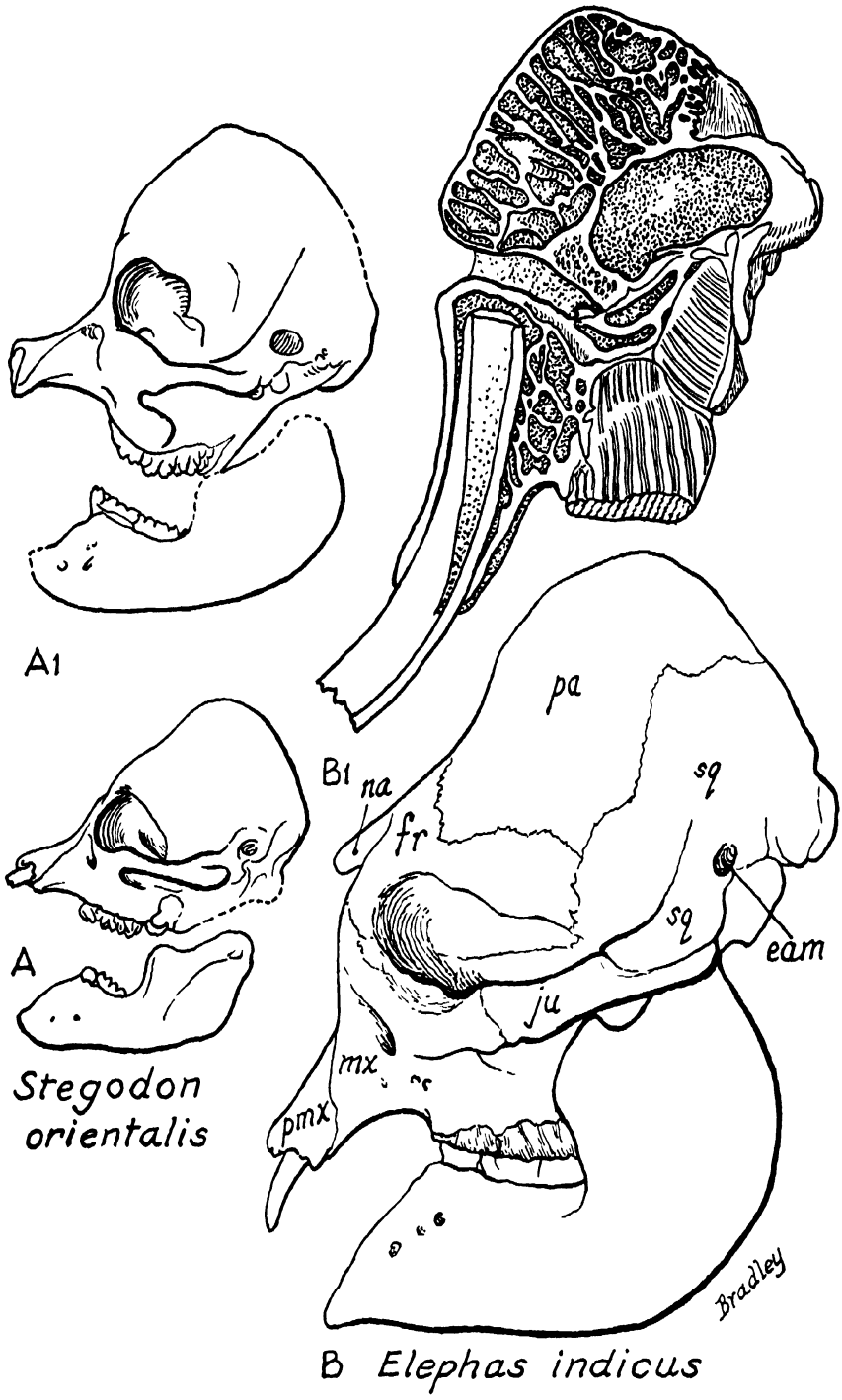


Fig. 21.33. Doming of the elephant skull, due to great thickening of the fronto-parietal region (B1) with development of air-filled bone-cells and trabeculae. The baby and young stegodonts (A, A1) strongly resemble the young modern elephant (B). A, A1, B, after Osborn; B1, after Zittel.

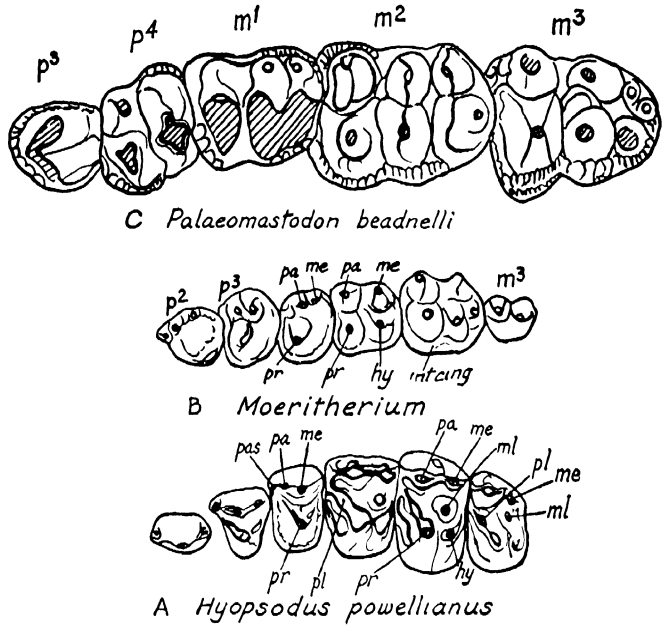


Fig. 21.34a. Tritubercular key to molar patterns of proboscideans. Data from Matthew (A), C W. Andrews (B, C).

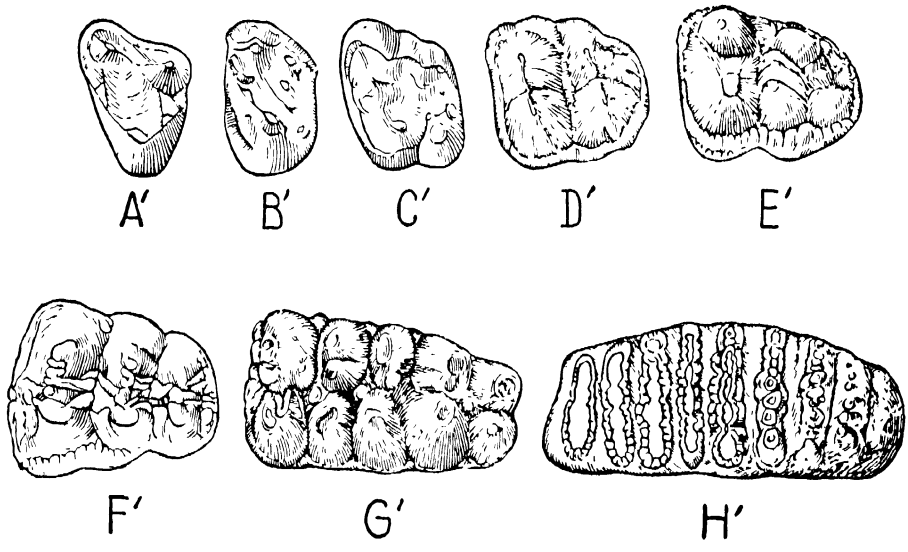


Fig. 21.34b. Primary (A′–C′) and later (D′–H′) polyisomeres in proboscidean molars. From Gregory. Data after W. D. Matthew (A′–C′), C. W. Andrews (D′, E′), Osborn (F′), Falconer (G′, H′). A′–C′, hyopsodonts; C′, *Phenacodus*; D′, *Moeritherium gracile*; E′, *Palaeomastodon minor;* F′, *Serridentinus anguirivalis*; G′, *Mastodon sivalensis*; H′, *Stegodon bombifrons.*

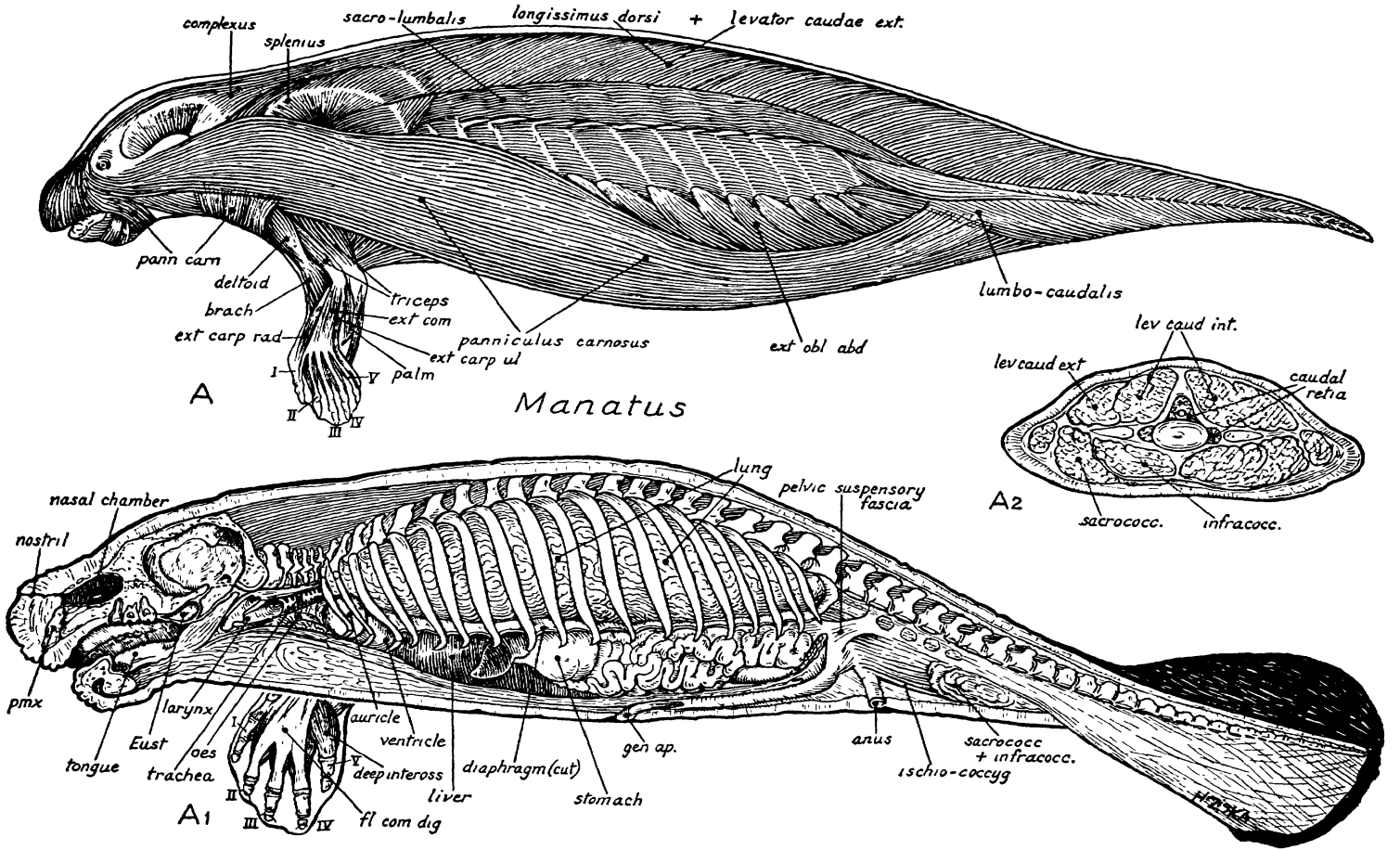


Fig. 21.35. Anatomy of the manatee. Redrawn after Murie. Especially noteworthy are the great development of the panniculus and facial muscles, the backward extension of the lungs, the nearly horizontal position of the diaphragm, the absence of hind limbs, the loss of the sacrum. The vestigial pelvis is not shown.

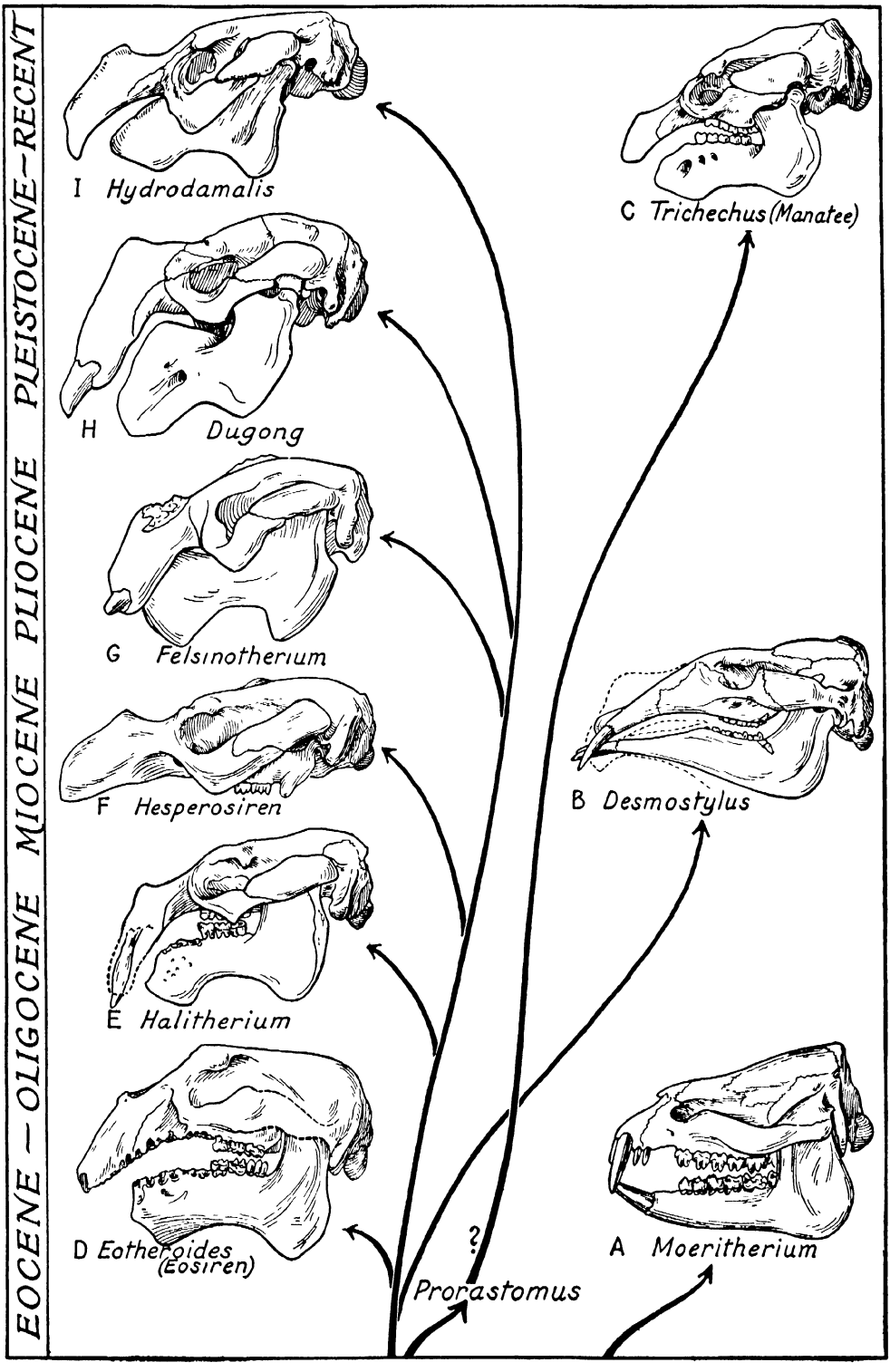


Fig. 21.36. Succession of the Sirenians: Skulls. Data from Depéret, C. W. Andrews, Simpson, Vanderhoof (B).

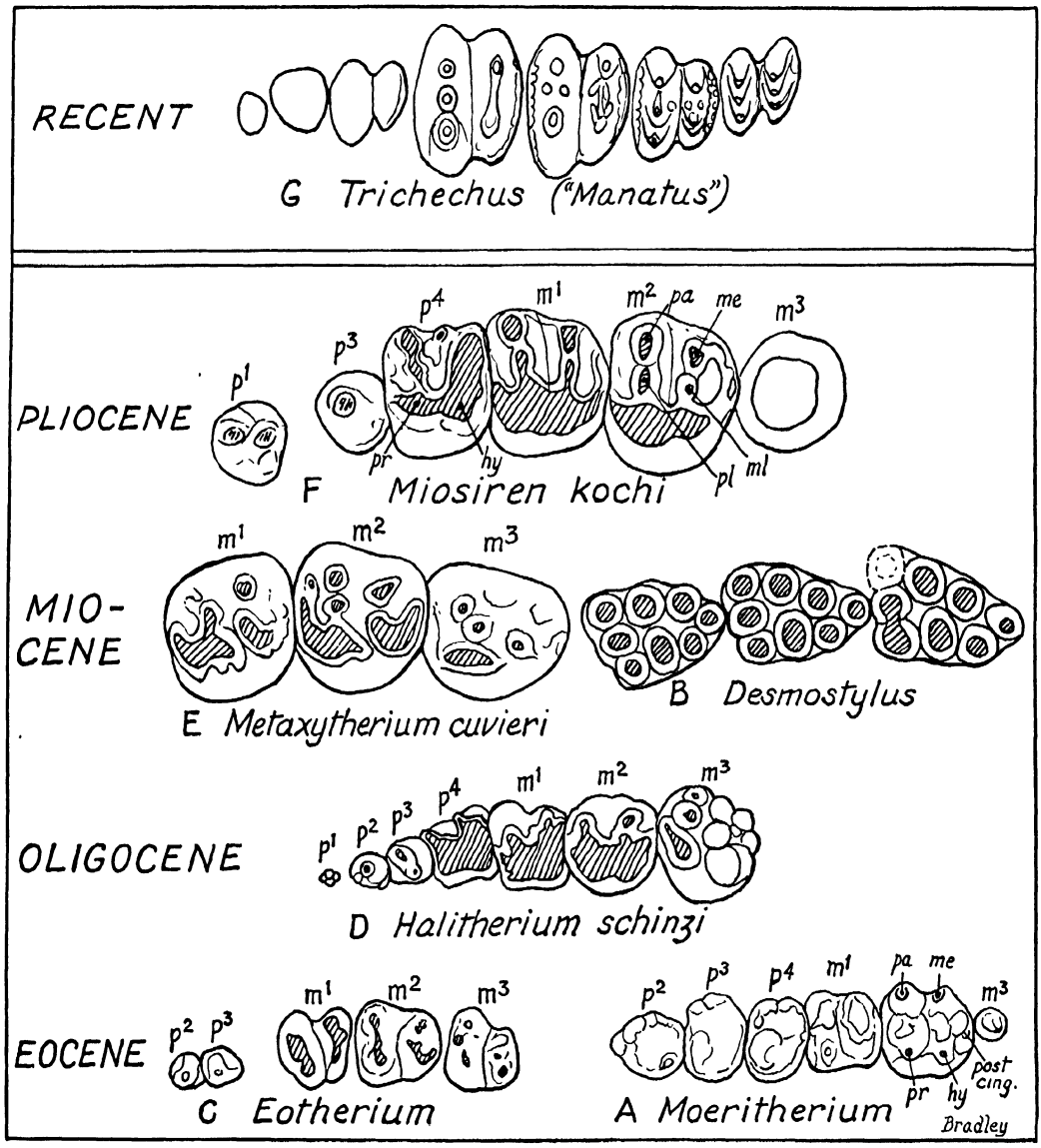


Fig. 21.37. Succession of the Sirenians: Upper cheek teeth. Data from Depéret (C–F), Vanderhoof (B), C. W. Andrews (A). In the typical sirenians (C–G), the cuspules (*p'*, *m'*) often joined the four main cusps to make two transverse ridges (G), somewhat as in tapirs; but in *Desmostylus* (B) all the cusps grew up into cylindrical columns and the crown became elongated anteroposteriorly. Here the third transverse row and the posterior cusp may have grown up from the posterior cingulum, as in the Proboscidea (A).

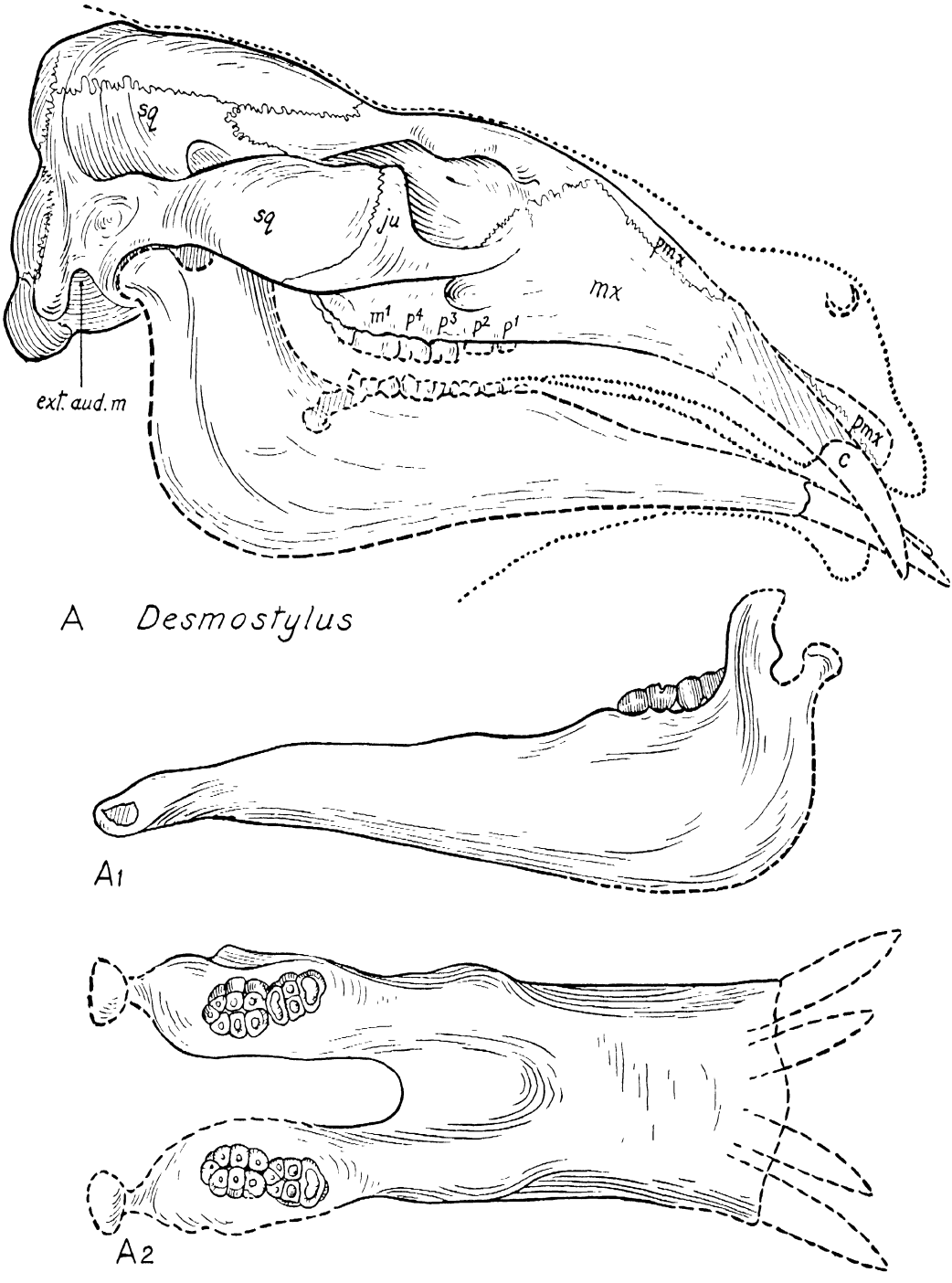


Fig 21 38. Tentative reconstruction of *Desmostylus* skull. Data from Tokunaga and Iwasaki, Vanderhoof. In the relatively young skull the rear molar, which is but partly erupted, is probably one of the true molars (Vanderhoof); the tooth in front of it may be either p^4 or a deciduous molar. The lower jaw (A1, A2), belongs to an old adult in which two true molars are in place.

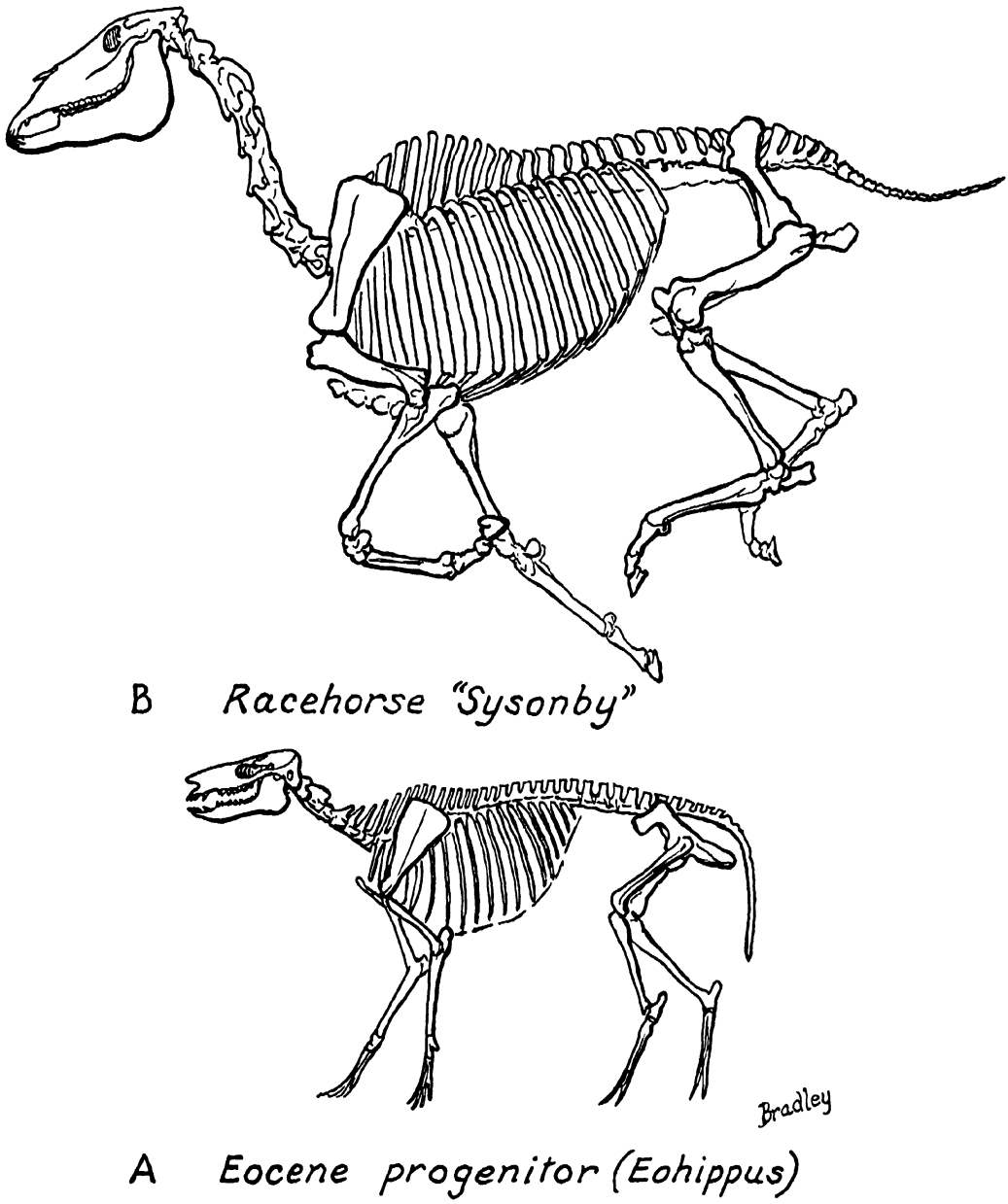
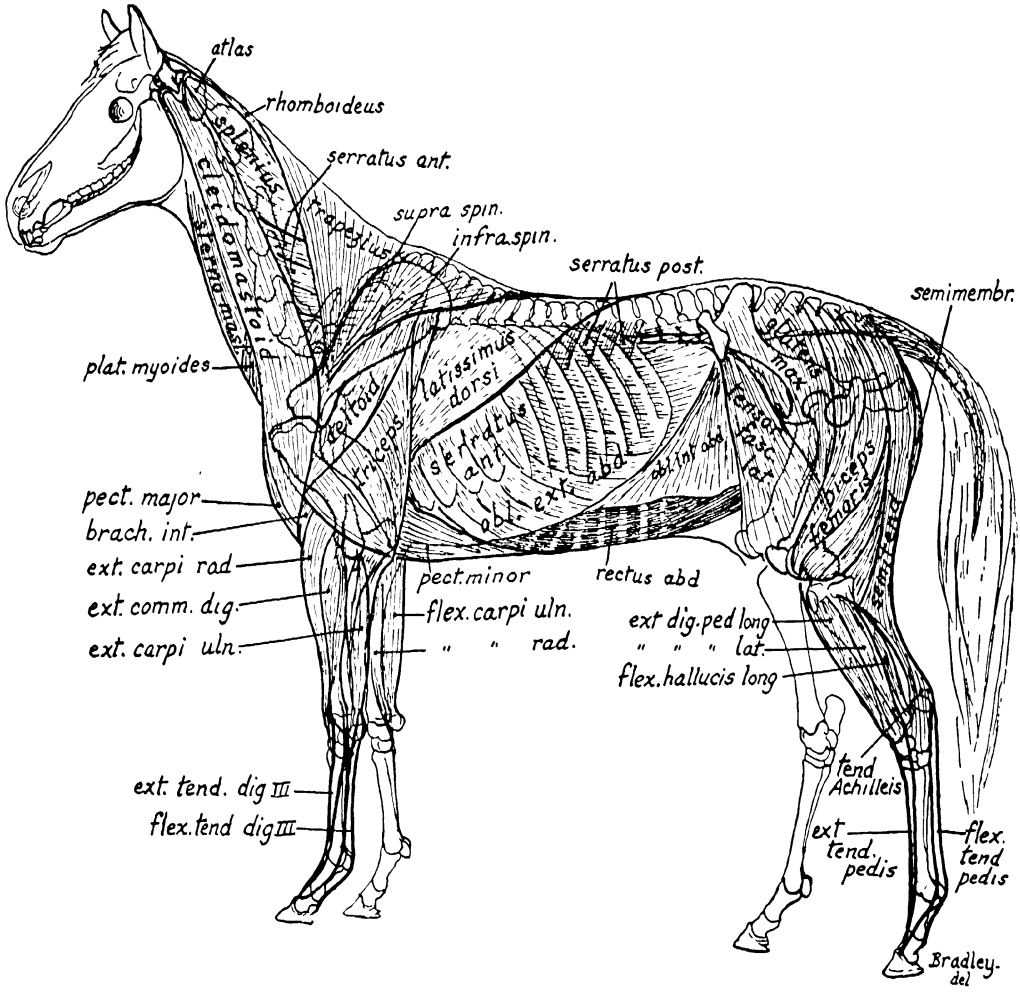


Fig. 21.39. Modern race horse (B) and primitive Lower Eocene perissodactyl (A). From American Museum specimens. A, skeleton mounted by S. H. Chubb; B, data from fossil skeletons.



Figs. 21.40, 41. (see following page). Diagrams indicating relations of the main locomotor muscles to the skeleton. Data from Schmaltz. In spite of its high specializations, the locomotor system of the horse, like that of other mammals, has inherited many basic features from the earliest tetrapods (cf. Chapters XI, XII). Among the relatively primitive metameric muscles which cooperate with the limb muscles are: *longissimus capitis, semi-spinalis capitis, multifidus spinae, longissimus dorsi* and the muscles of the tail; also *splenius, serratus anterior, serratus posterior,* the intercostal and abdominal muscles. The profound morphological contrasts between the anterior and the posterior girdles and appendages are likewise inherited from the earliest tetrapods.

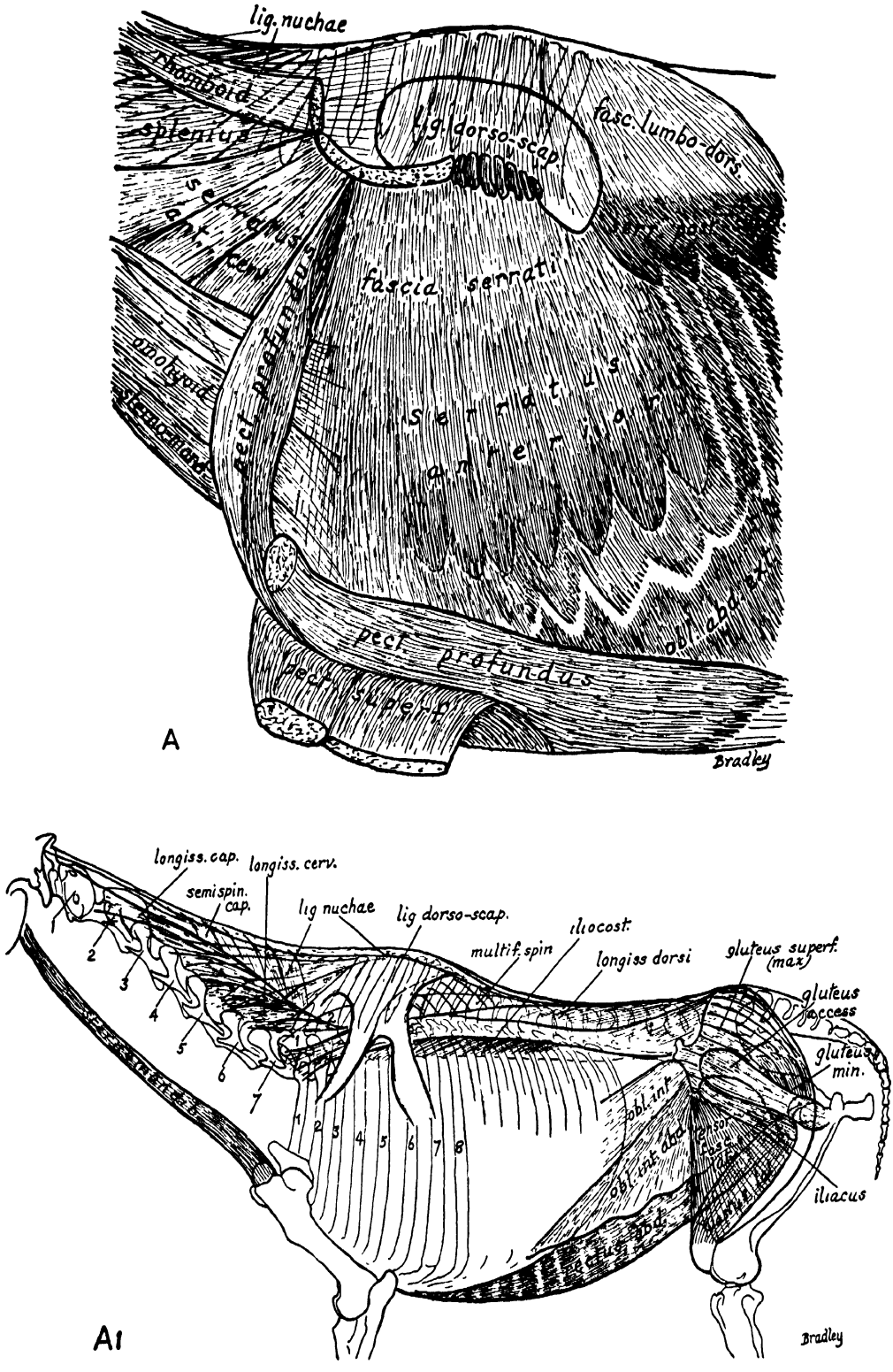

lig. nuchae
rhomboid
splenius
serratus ant. cer.
lig. dorso-scap.
fasc. lumbo-dors.
fascia serrati
serratus ant.
pect. profundus
anconeus
pect. profundus
pect. superf.
obl. abd. ext.
A
Bradley
longiss. cap.
longiss. cerv.
semispin. cap.
lig nuchae
lig dorso-scap.
iliocost.
multif. spin
longiss dorsi
gluteus superf. (max)
gluteus access
gluteus min.
obl. int.
obl. int. abd.
iliacus
A1
Bradley

Fig. 21.41

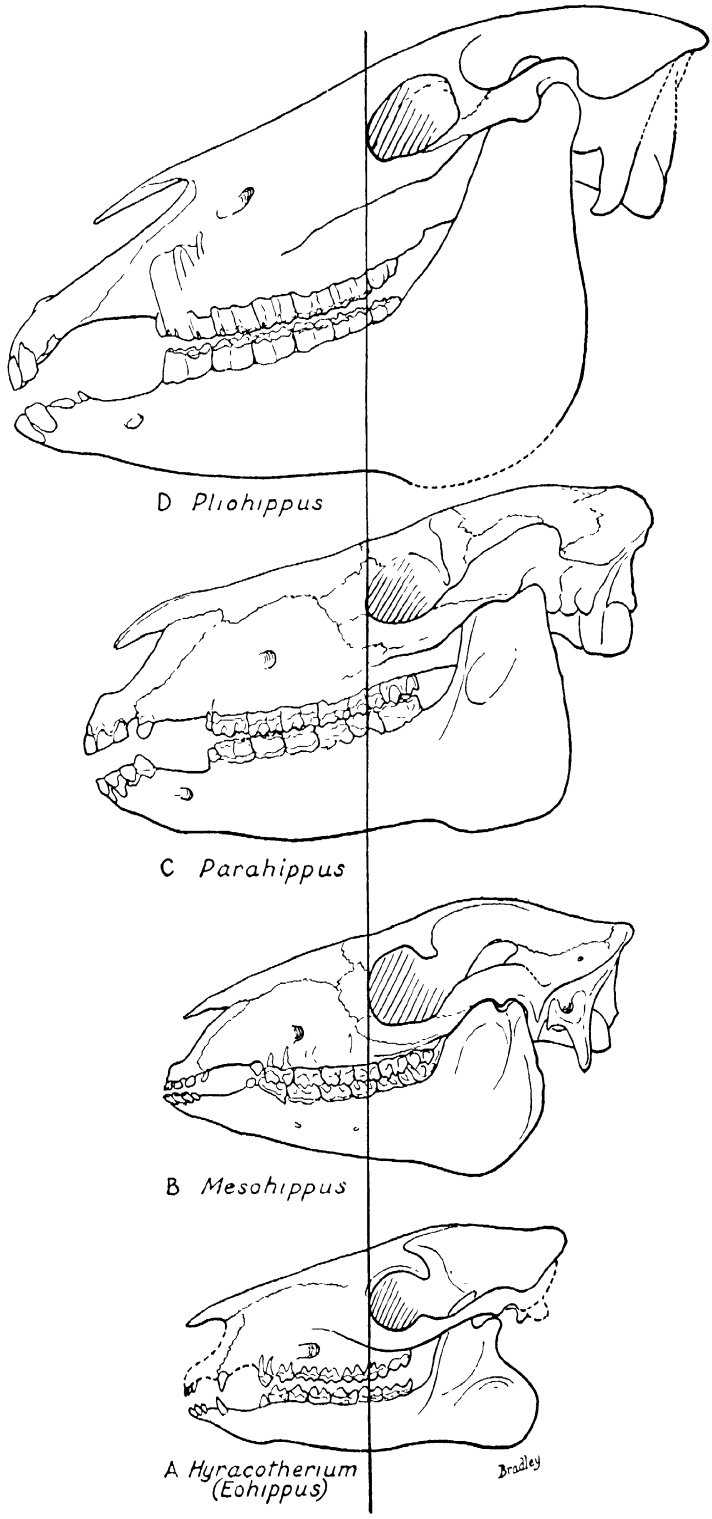


Fig. 21.42. Structural series of equine skulls, showing progressive lengthening of bony face and heightening of ascending ramus of lower jaw (to increase vertical space for high-crowned molars). A, revised restoration based on data from Owen, Forster-Cooper and American Museum specimens; B–D, after Osborn.

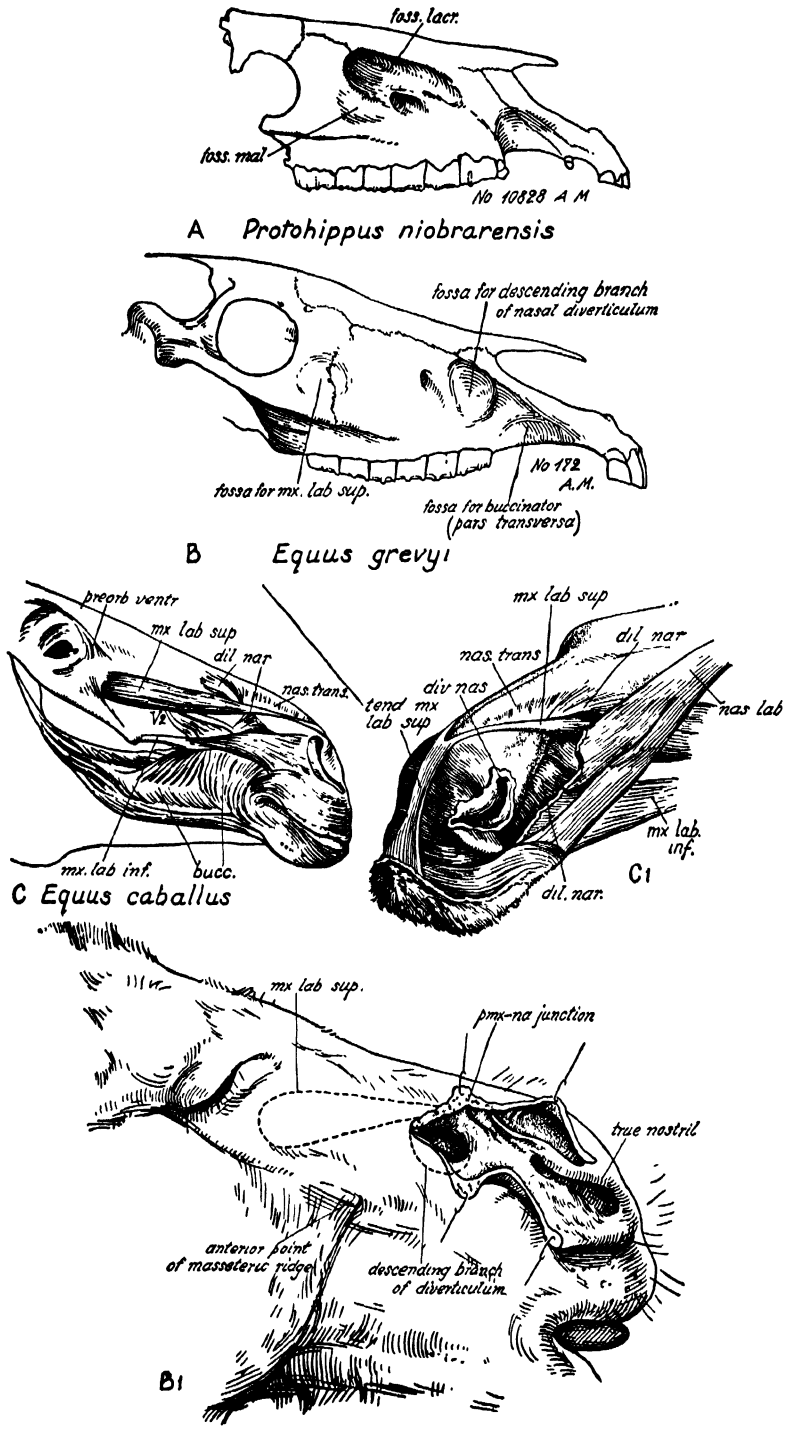


Fig. 21.43. Muscles of the lips and nose in equines (B1, C, C1) in relation to the nasal diverticula and to the prelacrimal fossae of fossil horses (A). After Gregory.

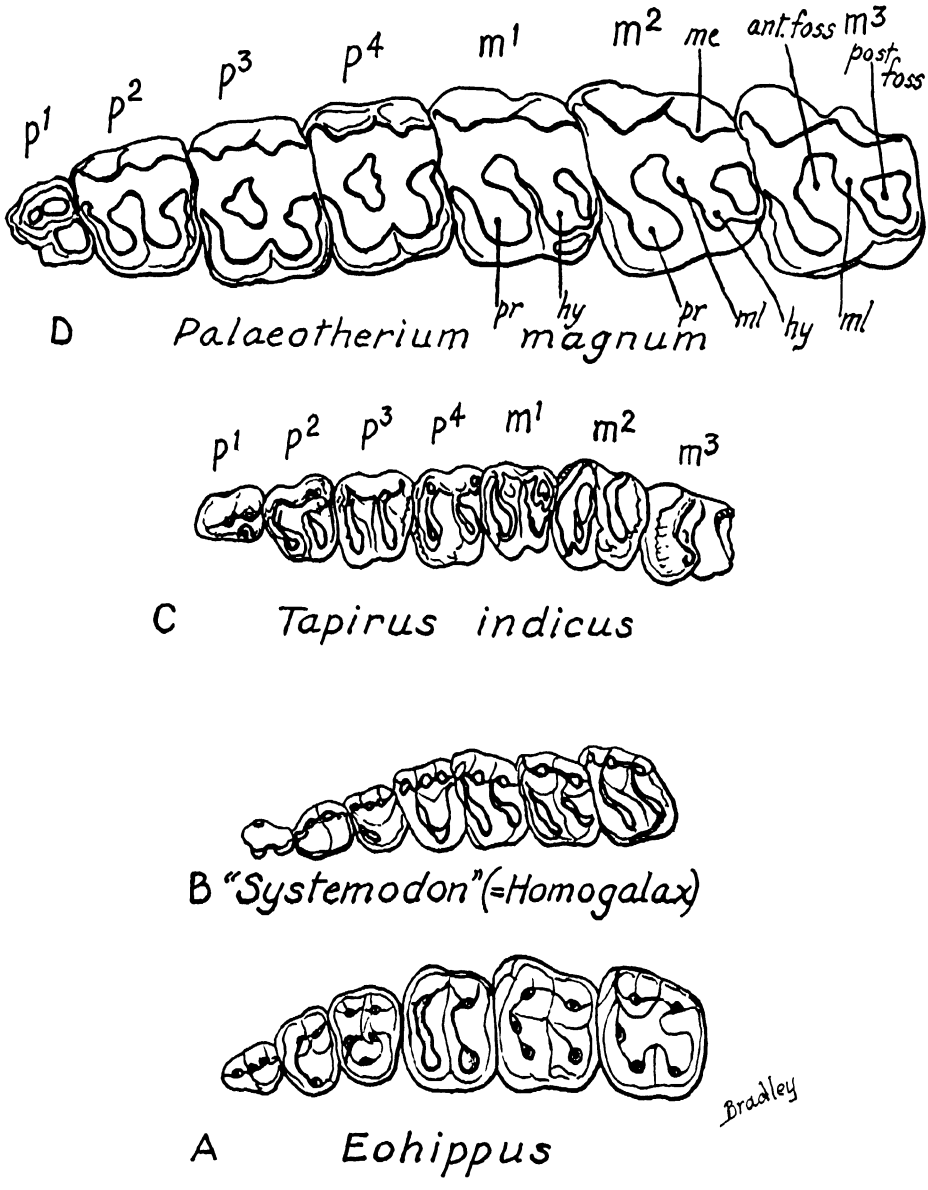


Fig. 21.44. Tritubercular key to upper premolars and molars of primitive perissodactyls (A, B), Eocene palaeothere (D), and Recent tapir (C), showing "molarization" of premolar patterns in C, D.

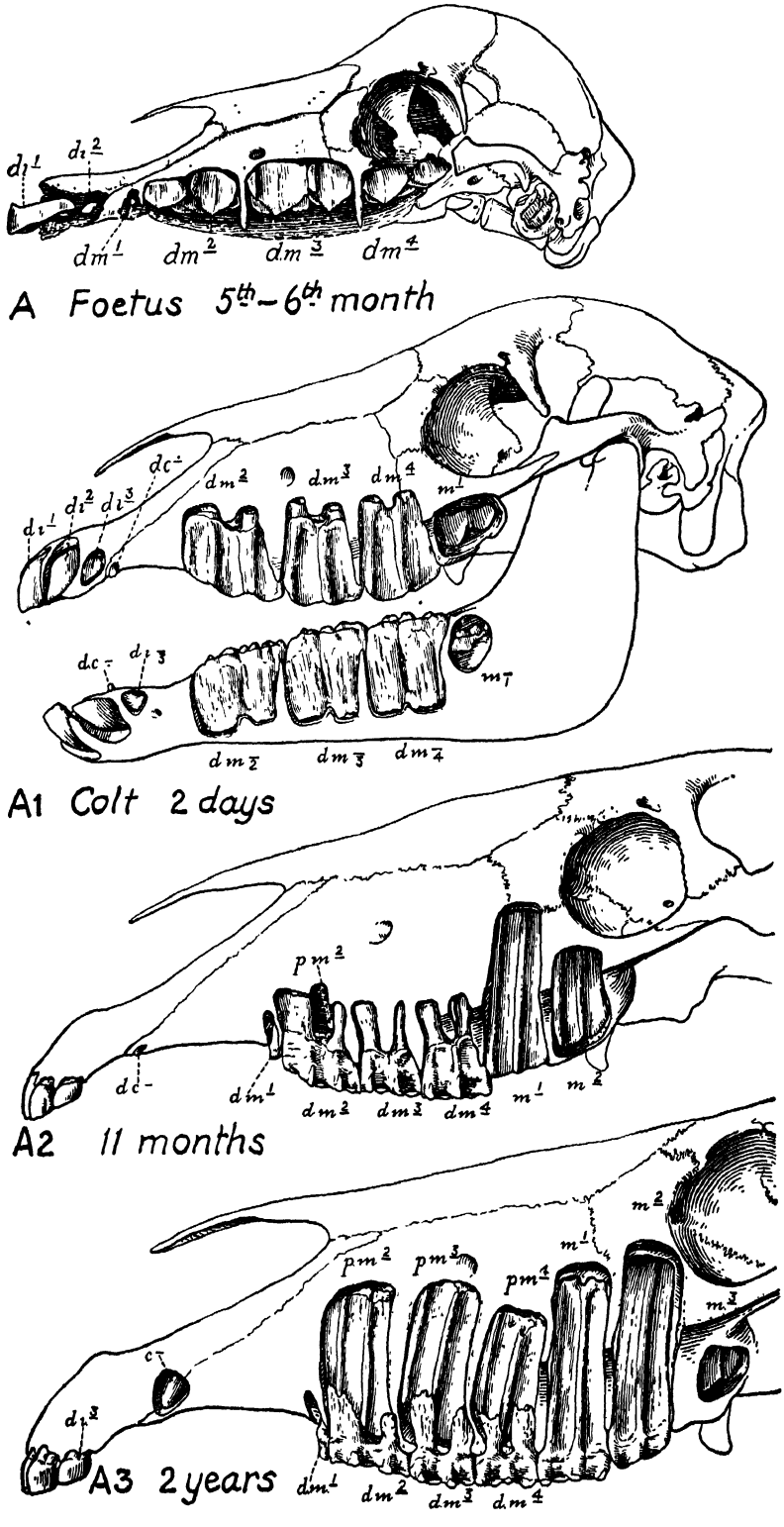
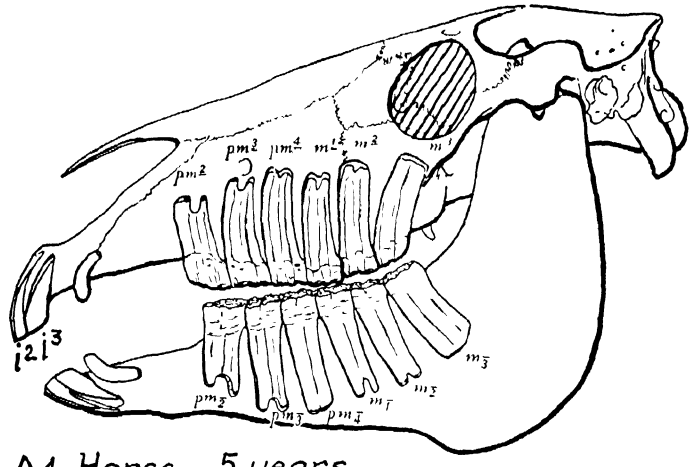
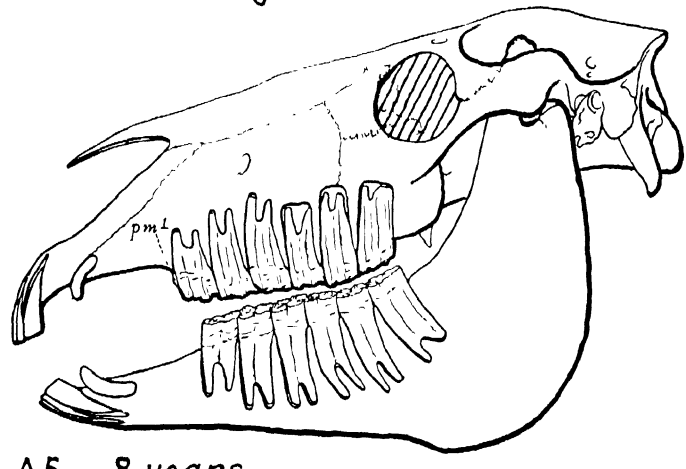


Fig. 21.45a, b. Successive stages in the growth, replacement and wear of the upper premolars and molars in the horse. After Chubb.





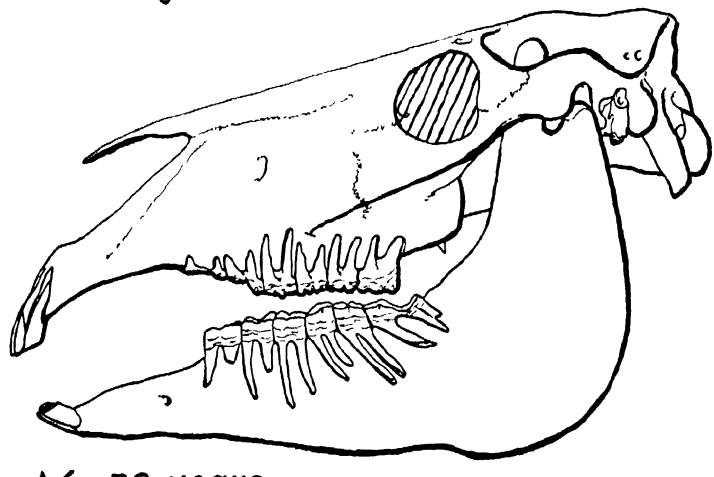


Fig. 21.45b

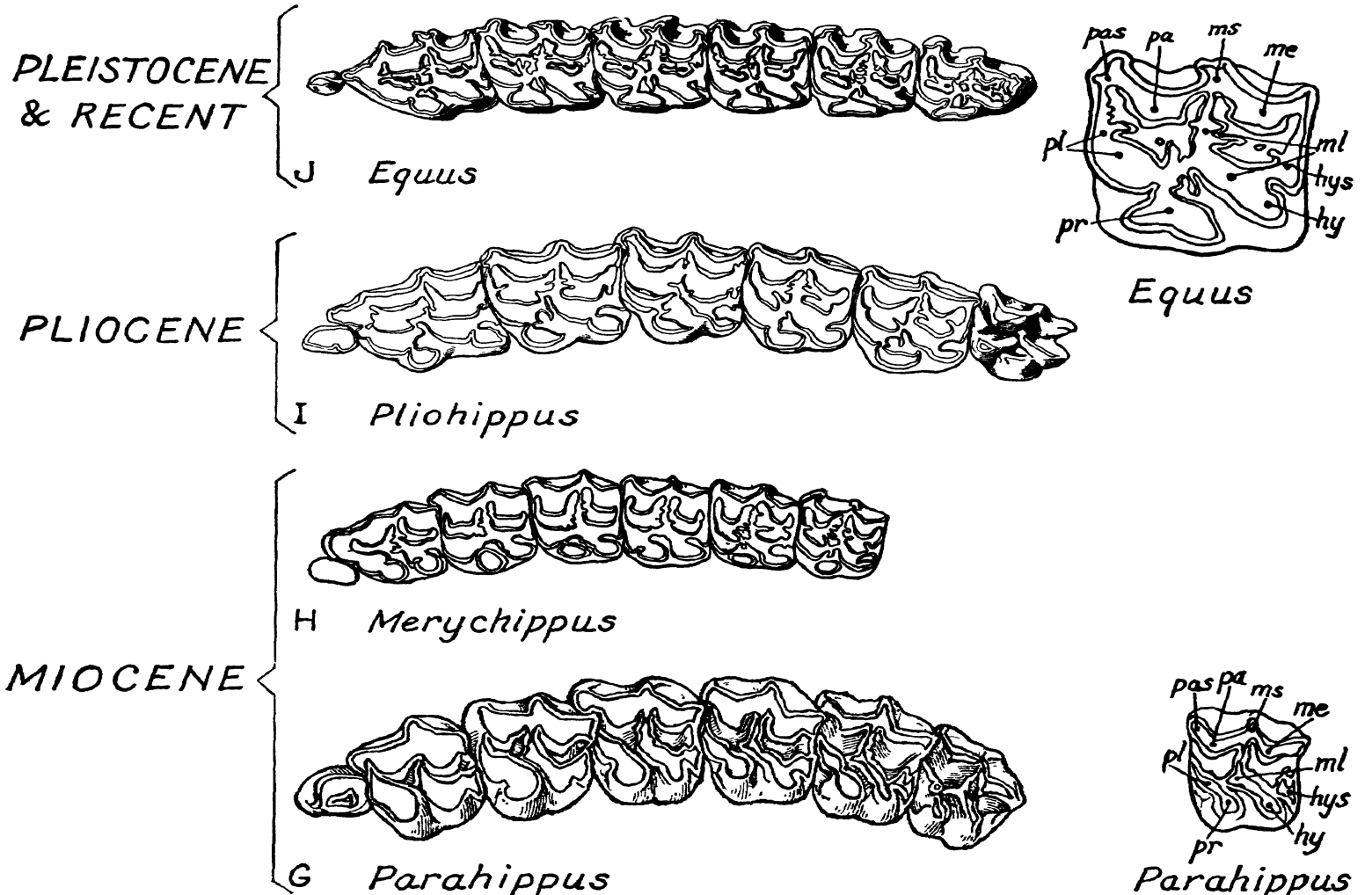

PLEISTOCENE & RECENT
J Equus
pas
pa
ms
me
pl
ml
hys
pr
hy
Equus
PLIOCENE
I Pliohippus
MIOCENE
H Merychippus
G Parahippus
pas
pa
ms
me
pl
ml
hys
pr
hy
Parahippus

Fig. 21.46a

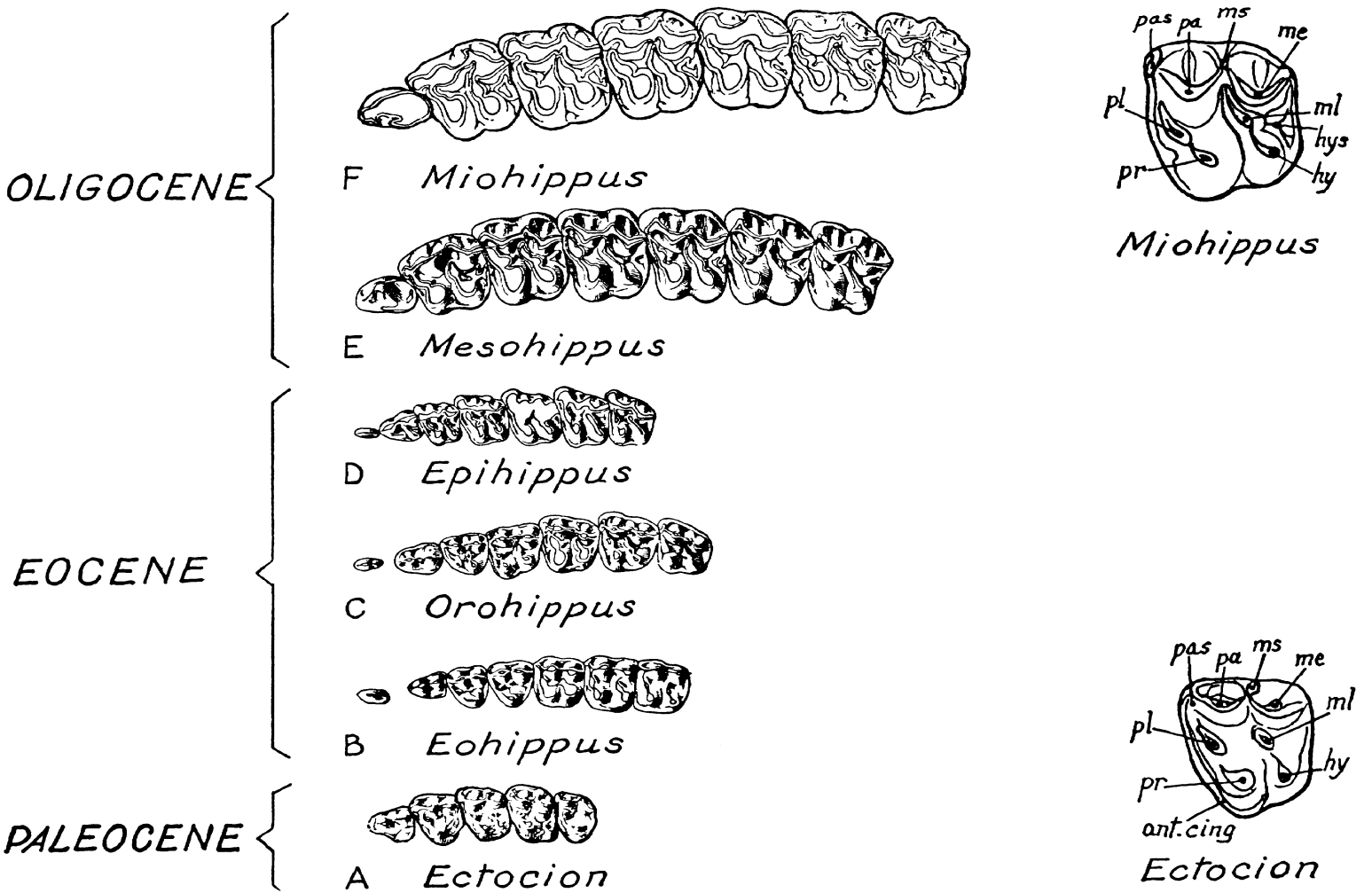


Fig. 21.46a, b. Tritubercular key to upper premolar-molar patterns from Paleocene condylarth (A) to Recent horse (J). Data from Matthew.

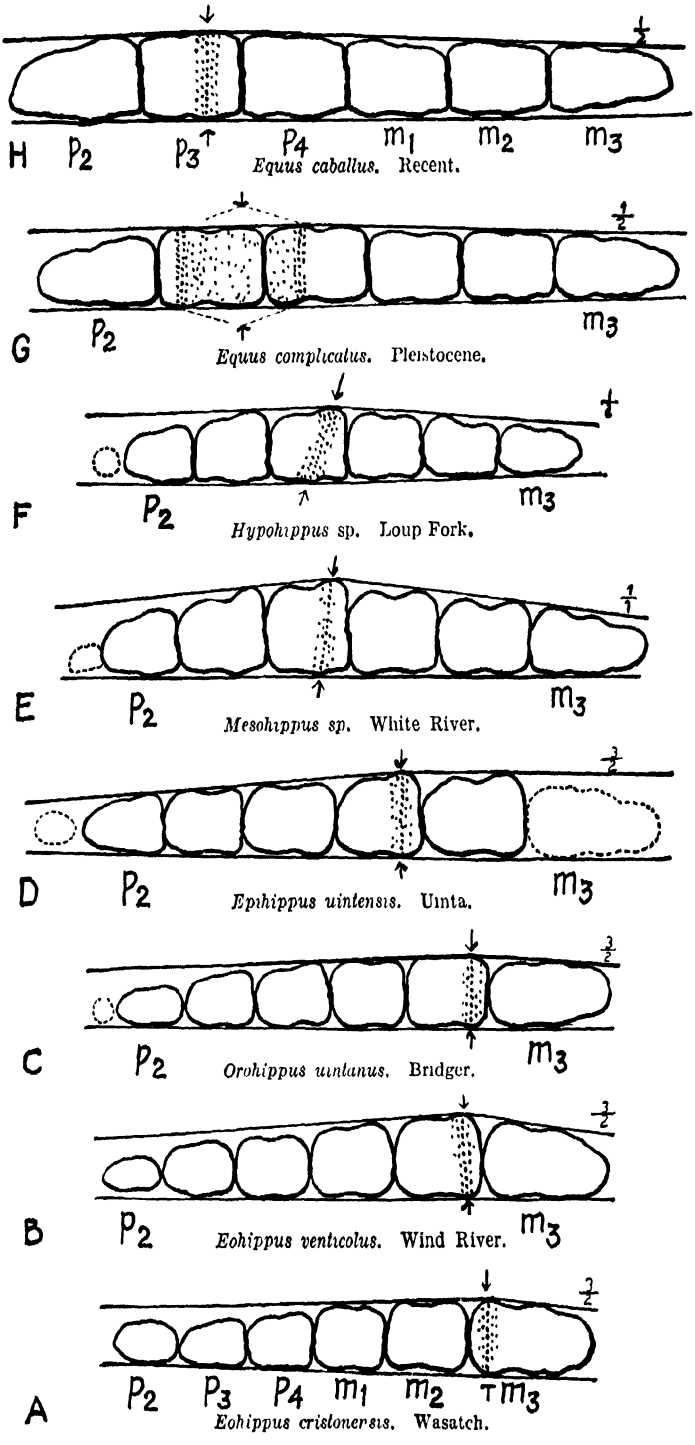


Fig. 21.47a. Contours of lower premolar and molar crowns in Equidae from successive ages. After Granger. The area of greatest width gradually shifts forward from the anterior part of m_3 to the posterior half of p_2.

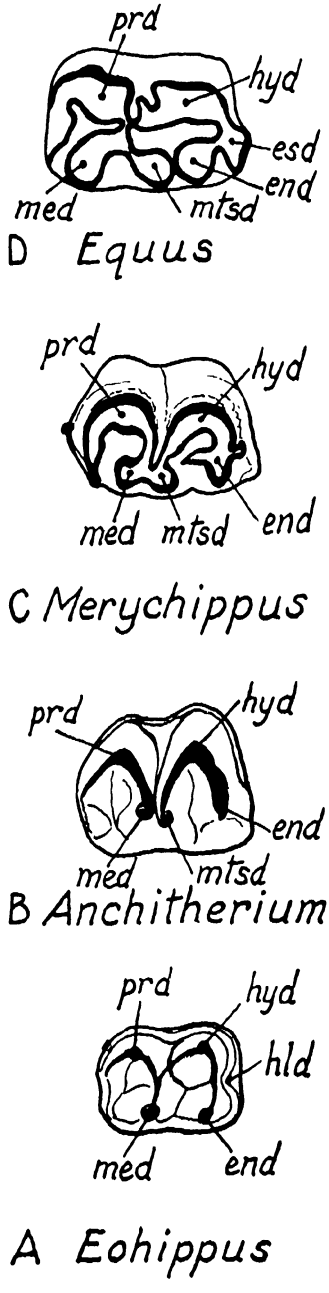


Fig. 21.47b. Tritubercular key to lower premolar-molar patterns. Data from Osborn, Stirton.

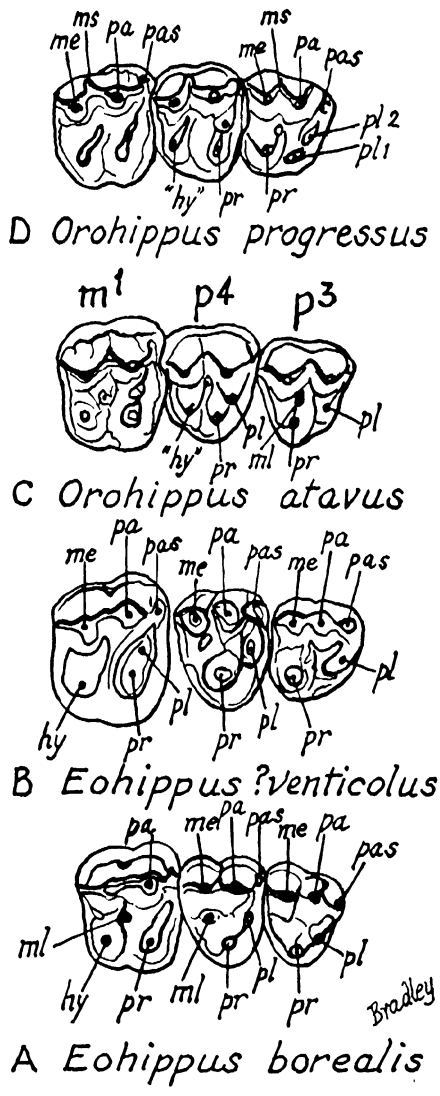


Fig. 21.47c. Tritubercular key to progressive molarization of third and fourth upper premolar and first upper molar patterns in Eocene Equidae. After Granger. The "protocone" in p^4 remained on the anterointernal corner but in p^3 it was gradually displaced to the posteroninternal corner as the enlarging protoconule took its place.

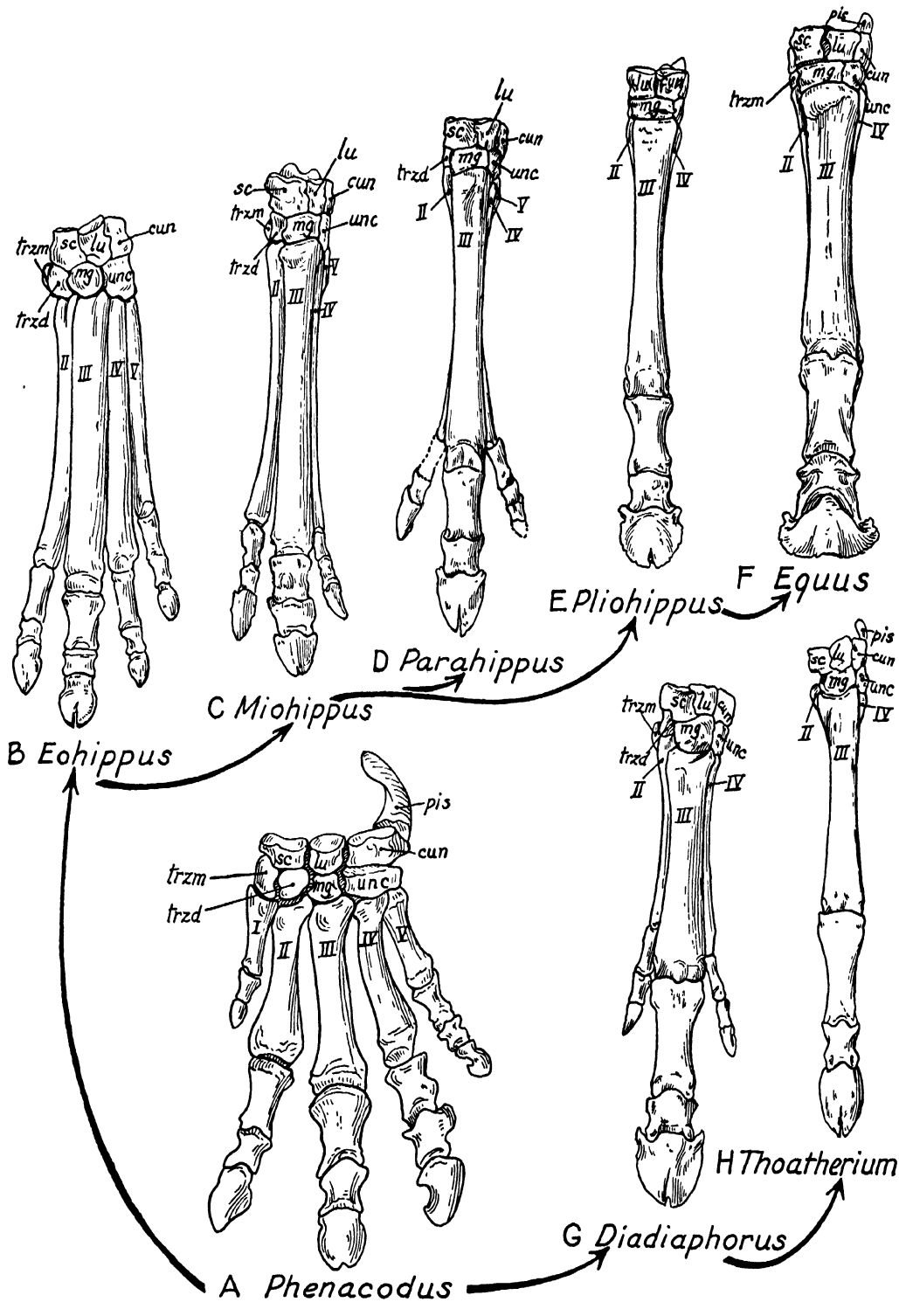


Fig. 21.48. Evolution of the hand (left) in Eocene to Recent horses (B–F) and Miocene South American pseudo-horses (G, H), presumably from a five-toed condylarth (A). A, from a mounted cast (Amer. Mus.), drawn as if unrolled or flattened, to show contacts of elements; B–E, after Matthew; F, original; G, H, after Scott.

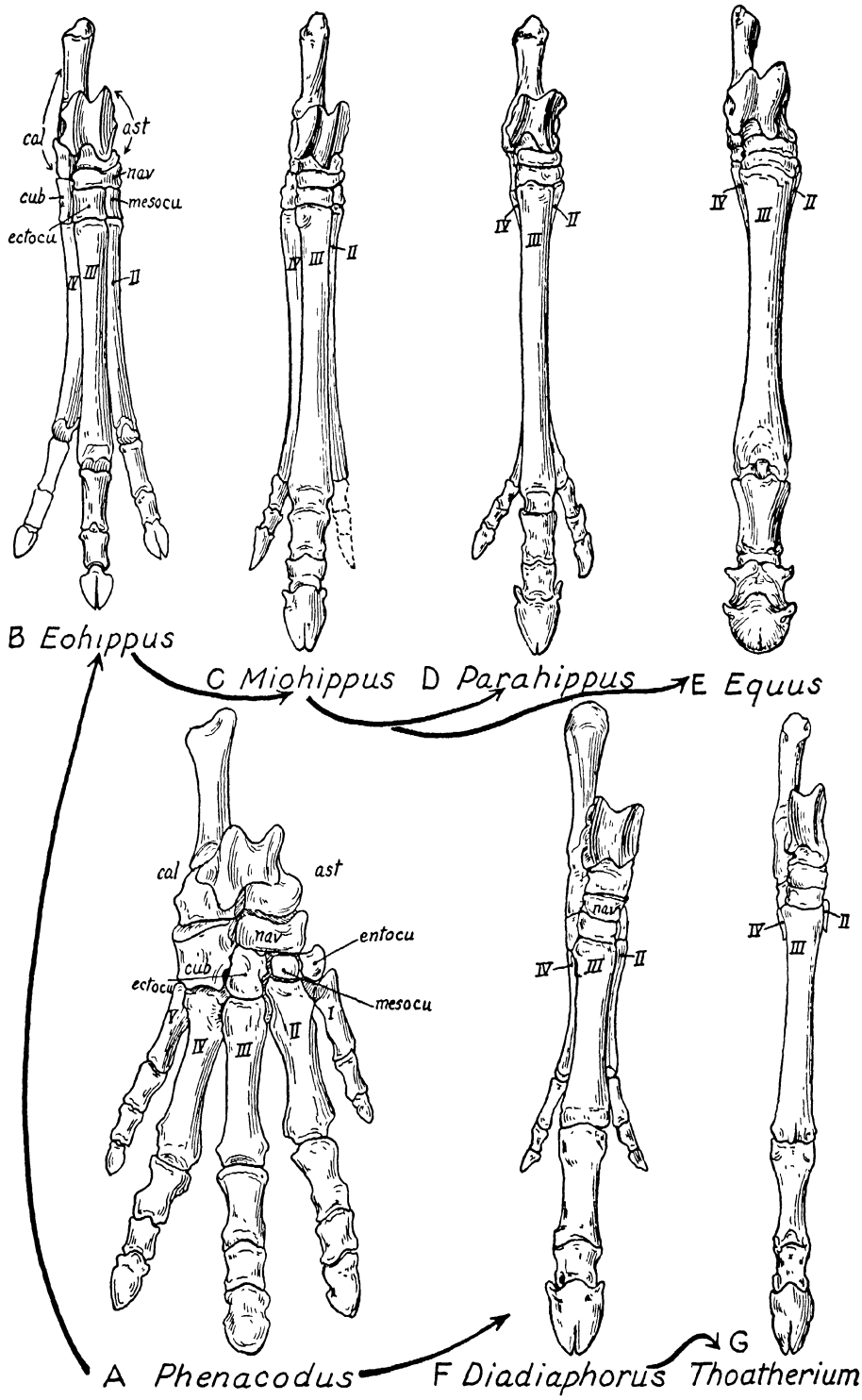


Fig. 21.49. Evolution of the hind foot (right) in Eocene to Recent horses (B–E) and Miocene South American pseudo-horses (F, G), presumably from a five-toed condylarth (A). B–D, after Matthew; A, E, original; F, G, after Scott; A, from a mounted cast (Amer. Mus.) drawn as if flattened or unrolled to show contacts of elements.

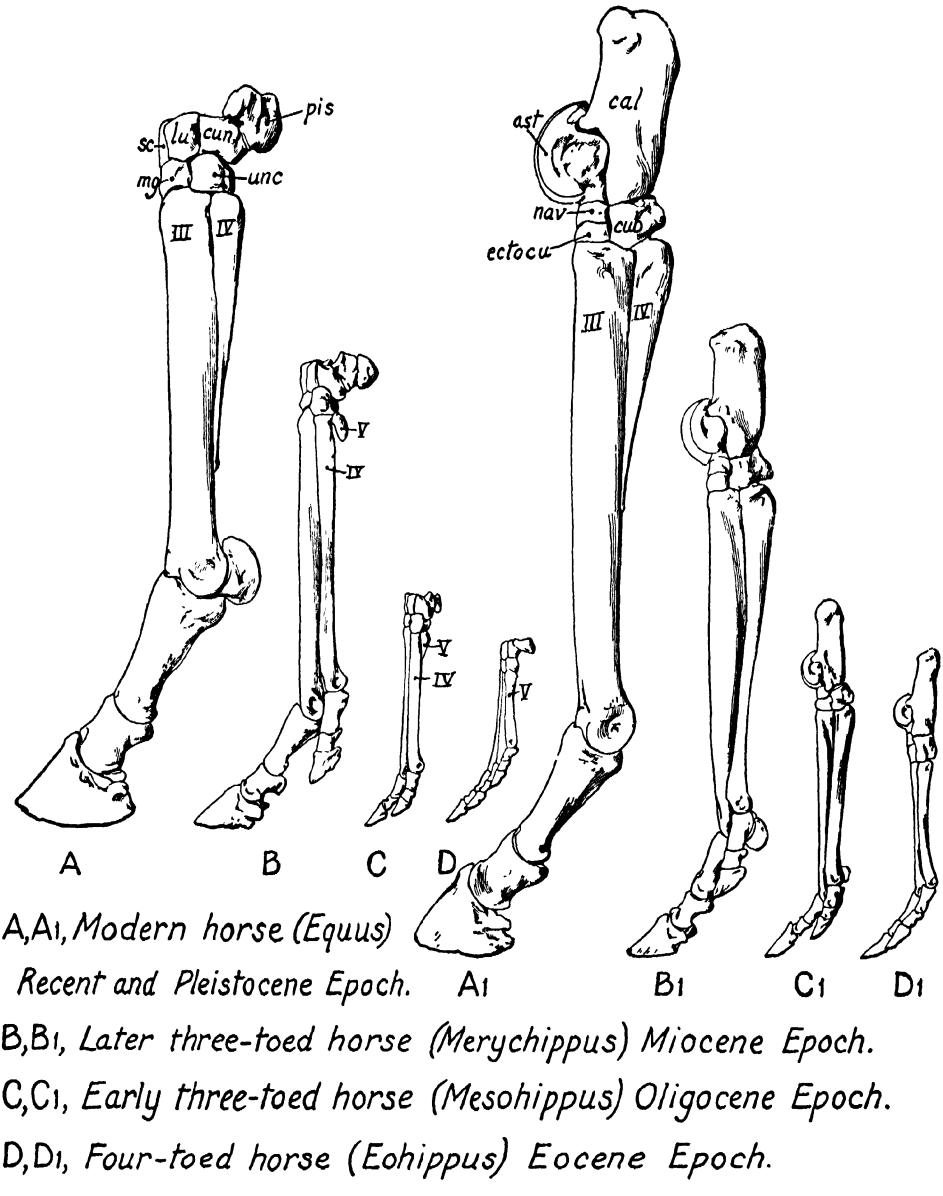
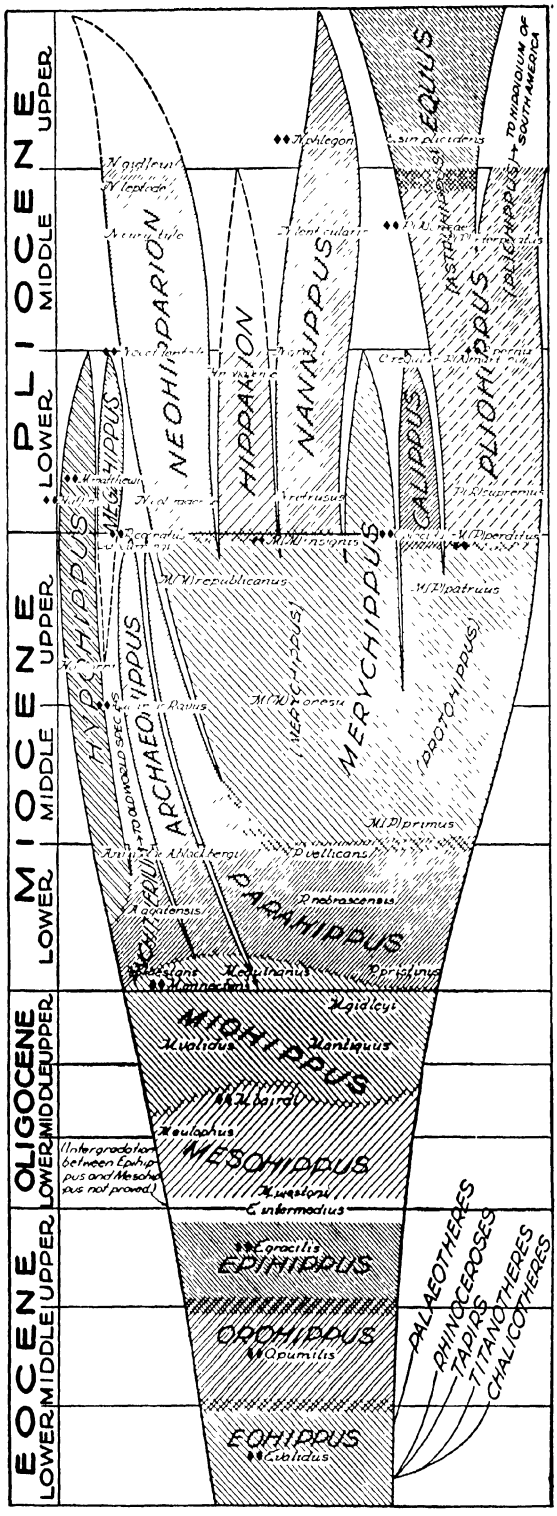


Fig. 21.50. Left fore (A–D) and hind (A1 to D1) foot of equids, arranged in descending series. After Matthew. The outer or fifth metacarpal and digit is retained only in the fore foot of *Eohippus* (D). In C and B only a nubbin of this element is left. In the latest stage (A) the fourth metacarpal (*IV*) is reduced to a splint the third (*III*) having become completely dominant.



Phylogenetic chart showing the apparent relationships and geographical distribution of the North American Equidae

Fig. 21.51. Geologic succession and branching of North American equids. After Stirton.

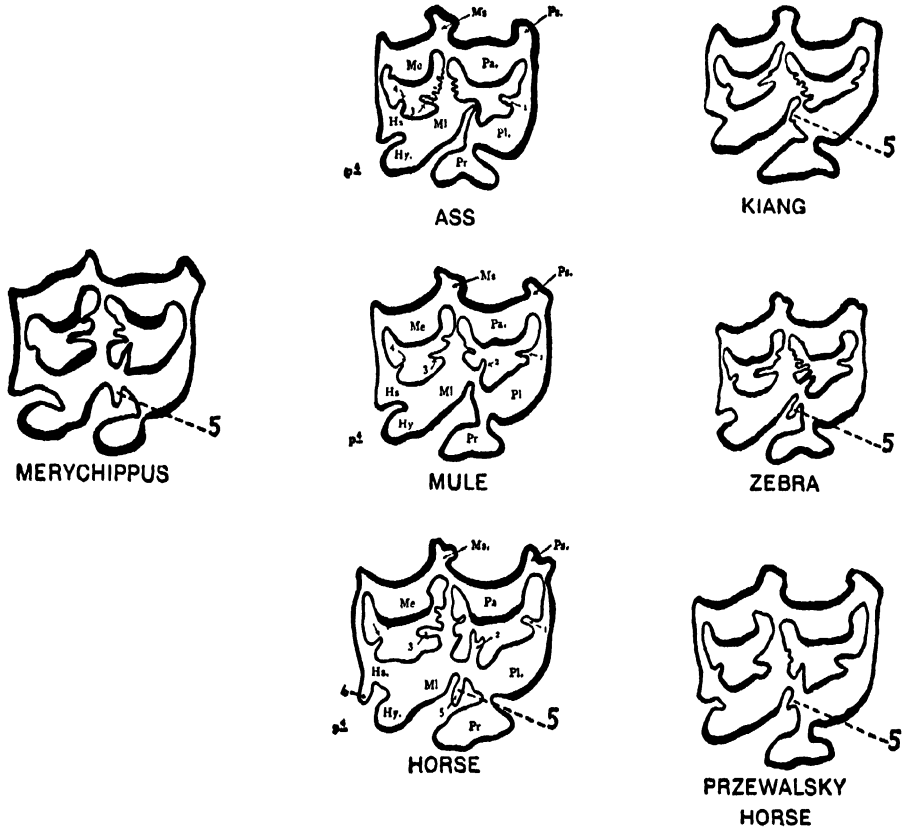


Fig. 21.52. The "pli caballin" (5) in the upper molars of equids. After Osborn. This minute fold is present in the Miocene *Merychippus* and in the true horses, the zebra and the kiang, but absent in the ass and the mule.

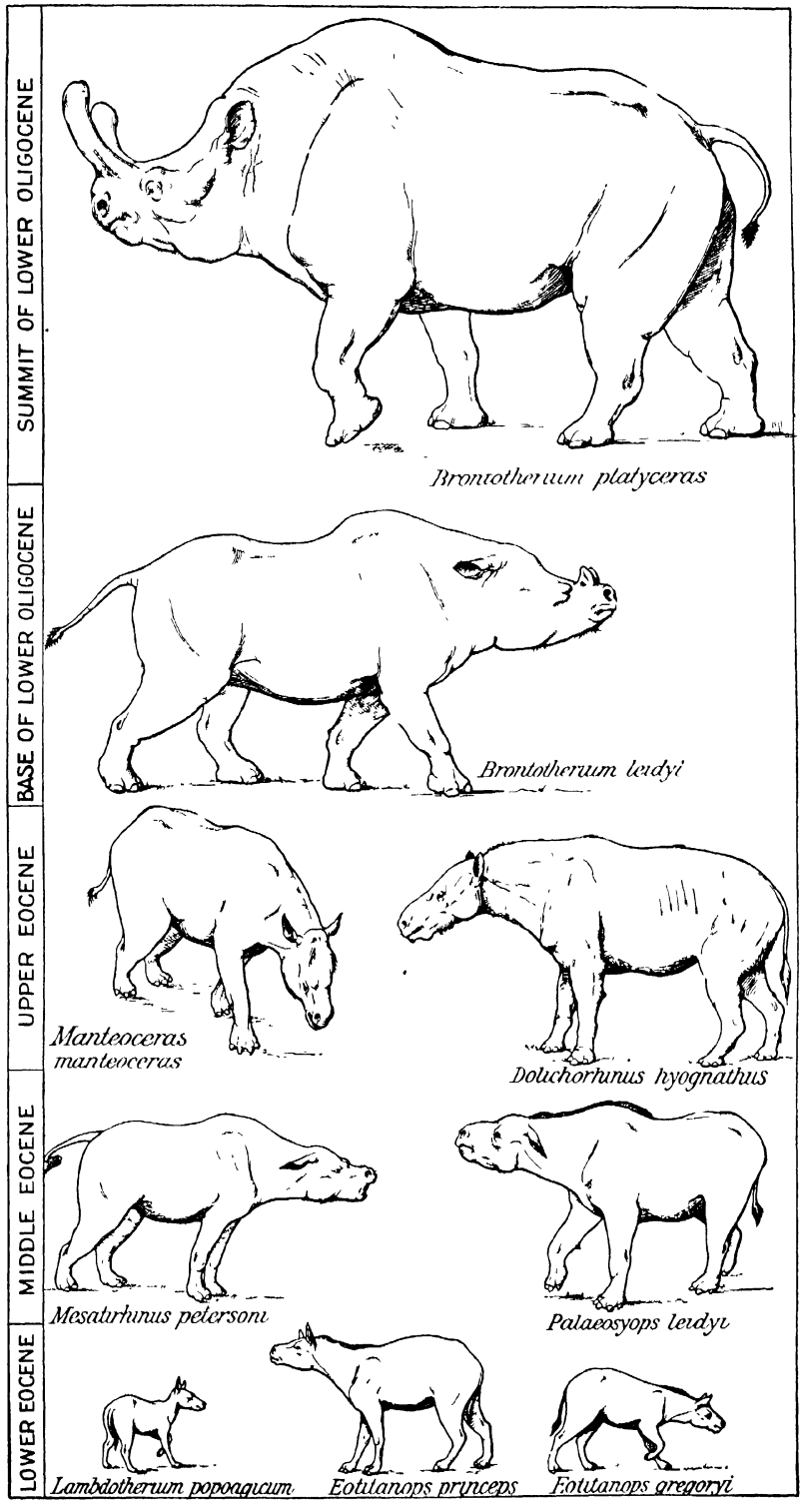


Fig. 21.53. Pictorial history of the titanotheres from late Lower Eocene to Lower Oligocene. After Osborn.

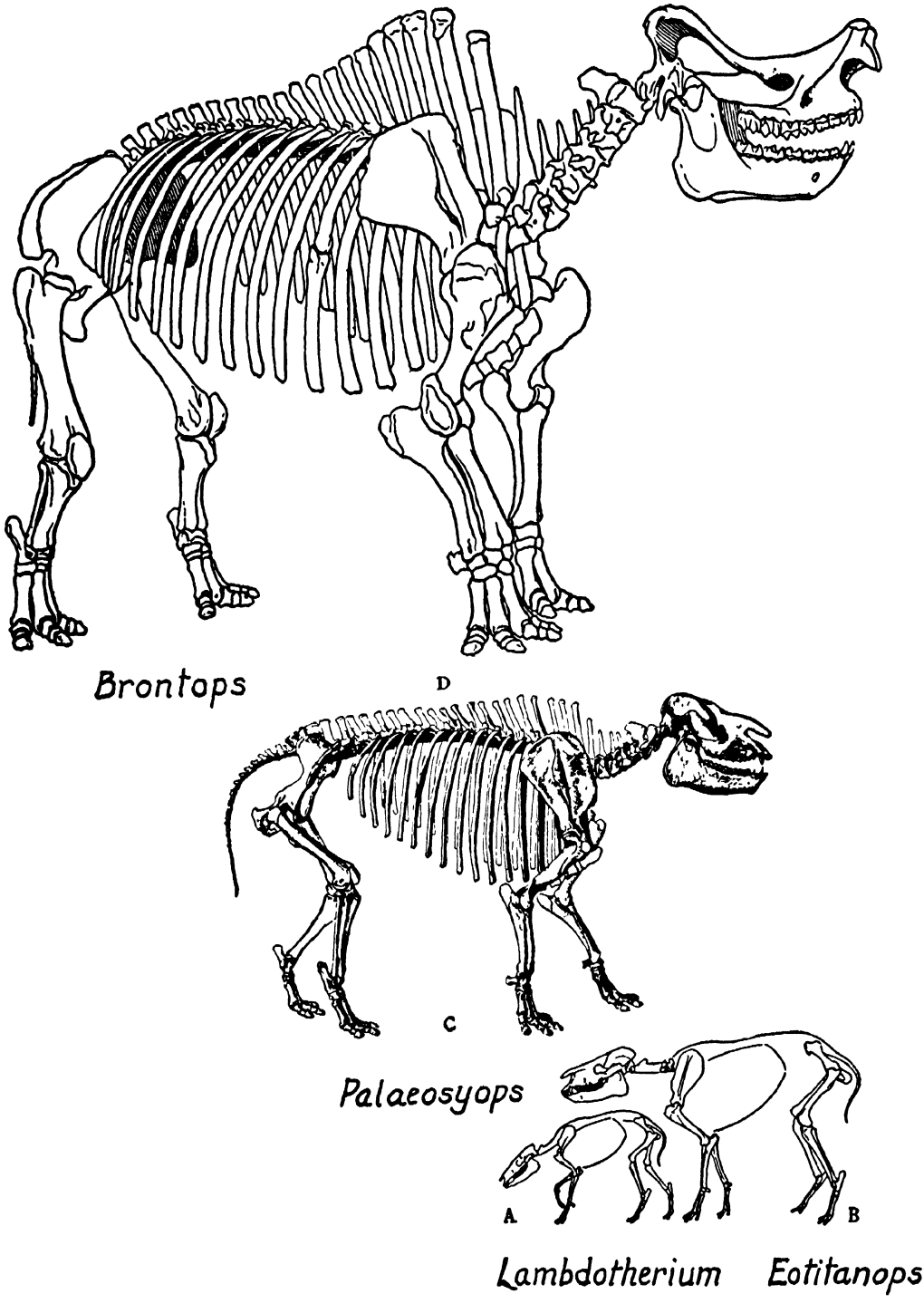


Fig. 21.54. Four structural stages in the evolution of the titanothere skeleton. After Osborn.

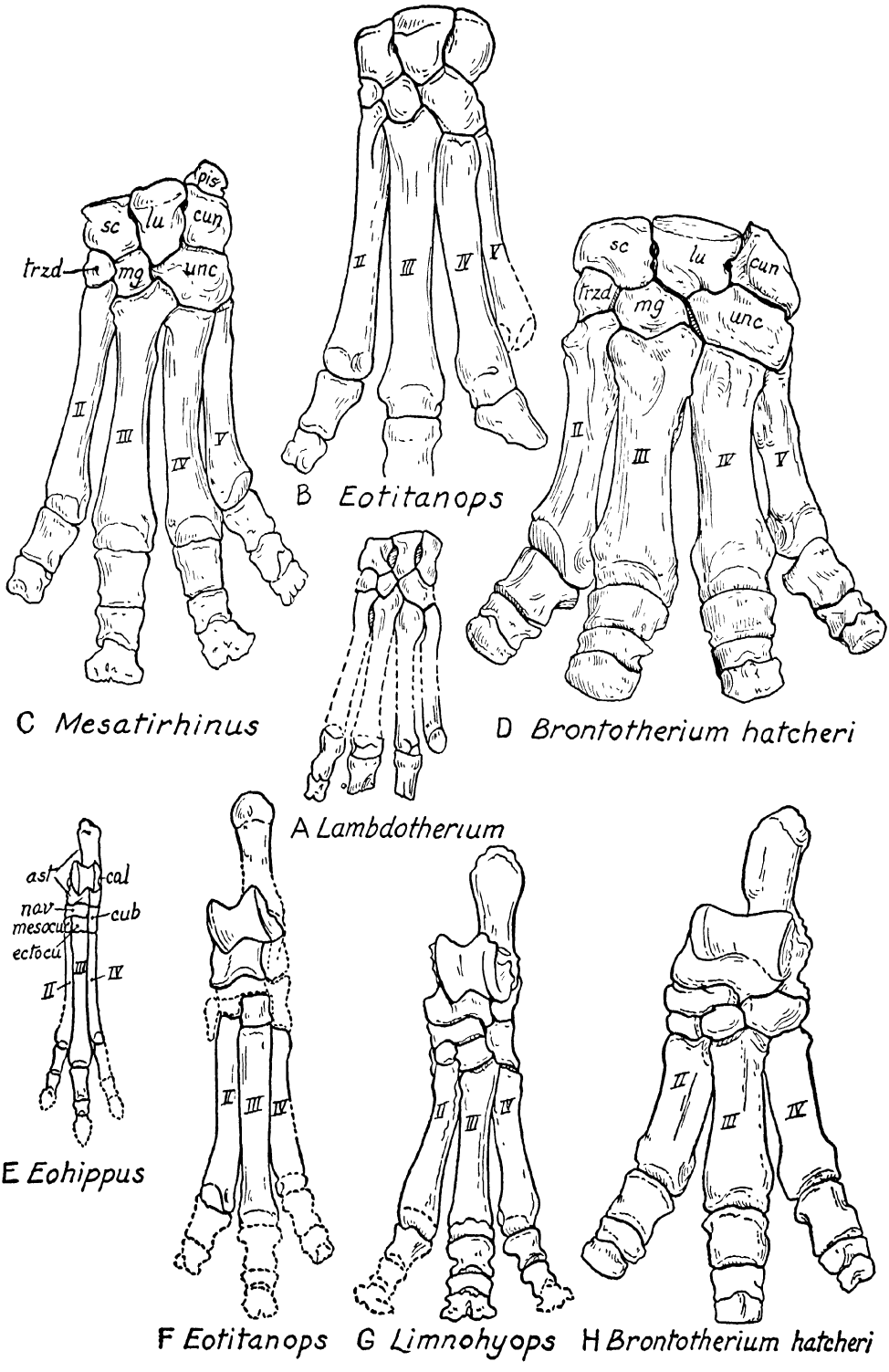


Fig. 21.55. Progressive widening of fore (A–D) and hind (F–H) feet of titanotheres. The primitive "horse" (E) retains the slender three-toed foot of basal perissodactyl type. Data from Osborn.

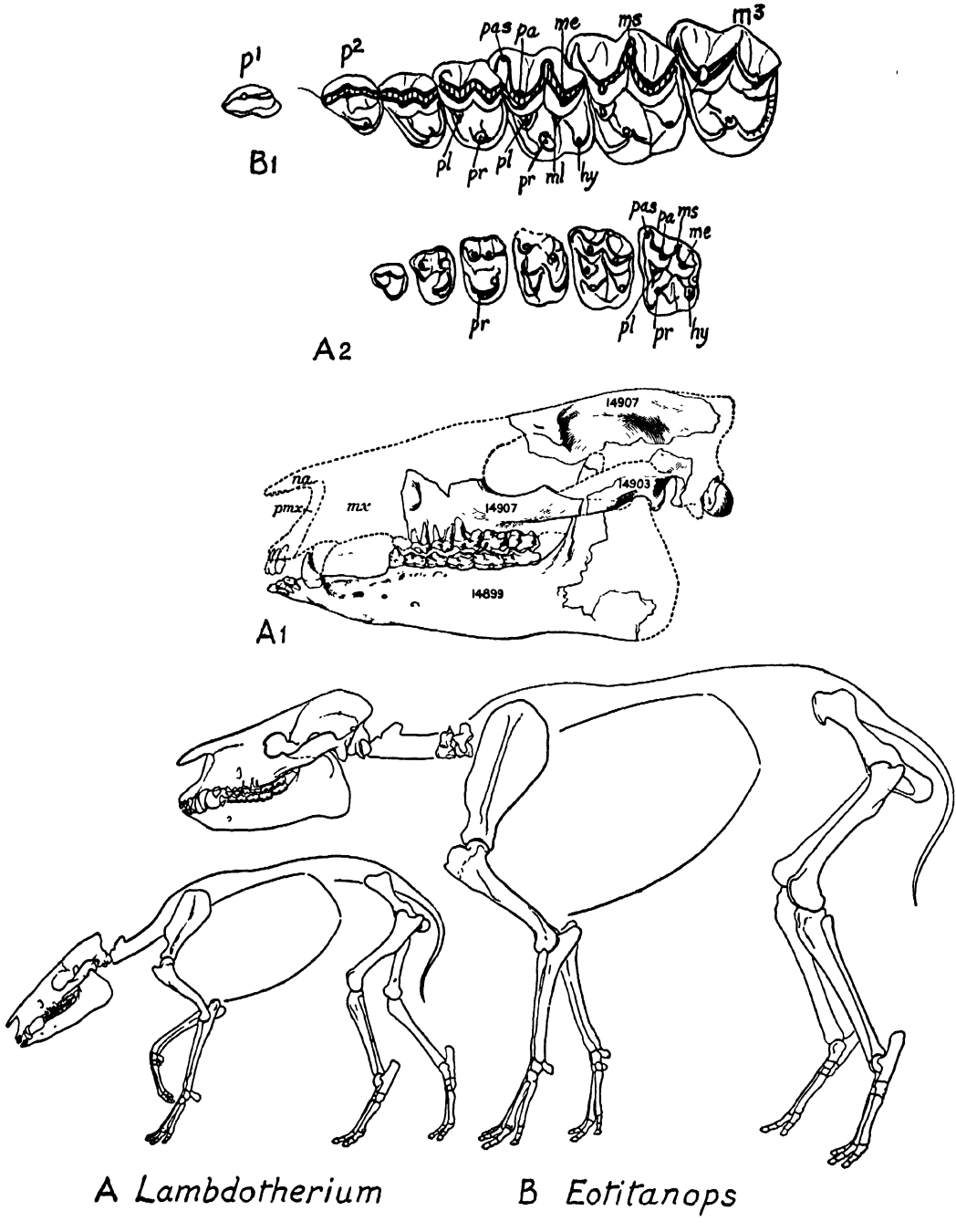


Fig. 21.56. Lower Eocene ancestors of the titanotheres. After Osborn.

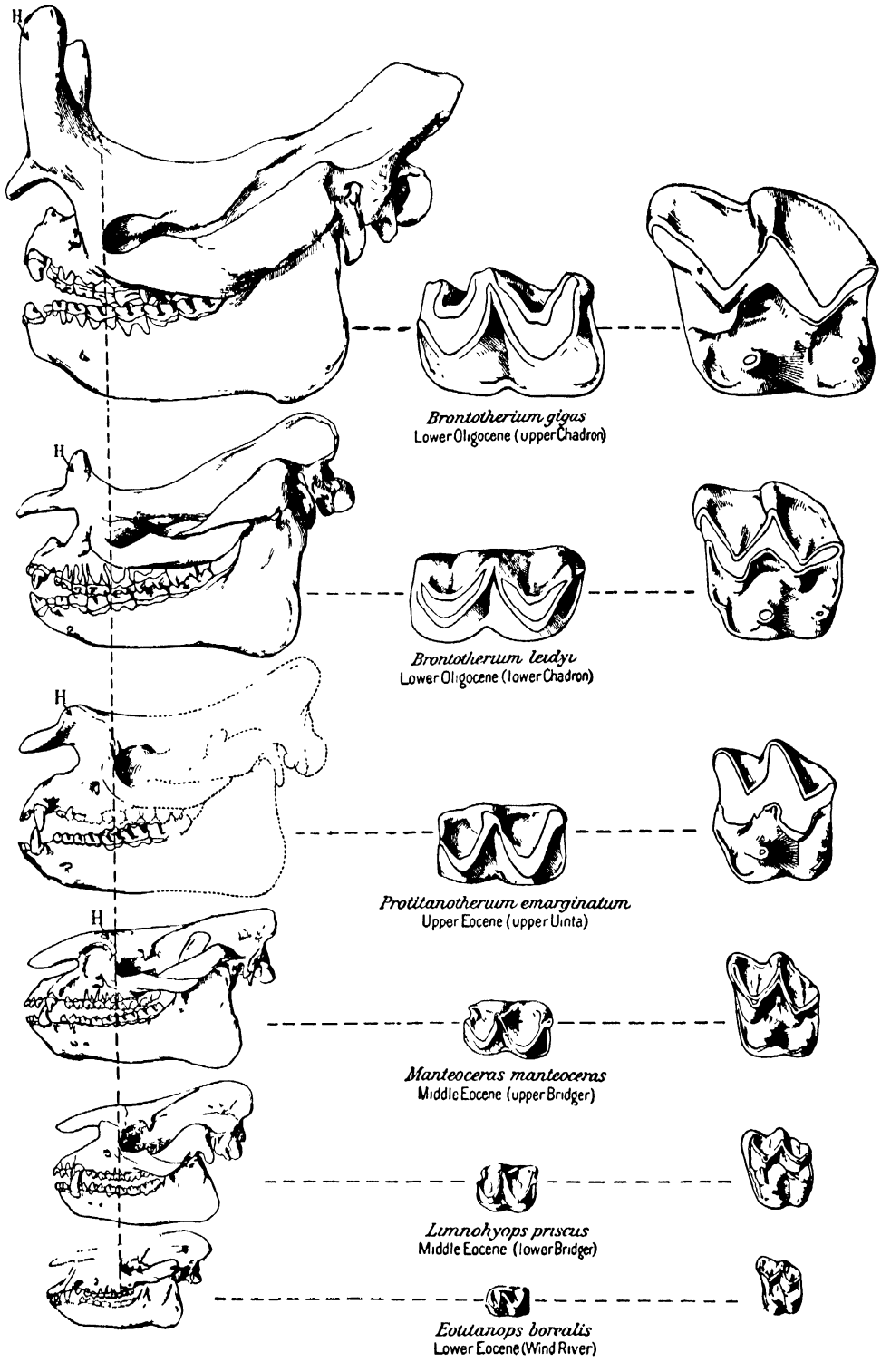


Fig. 21.57. Evolution of the skull and molar patterns in titanotheres. After Osborn.

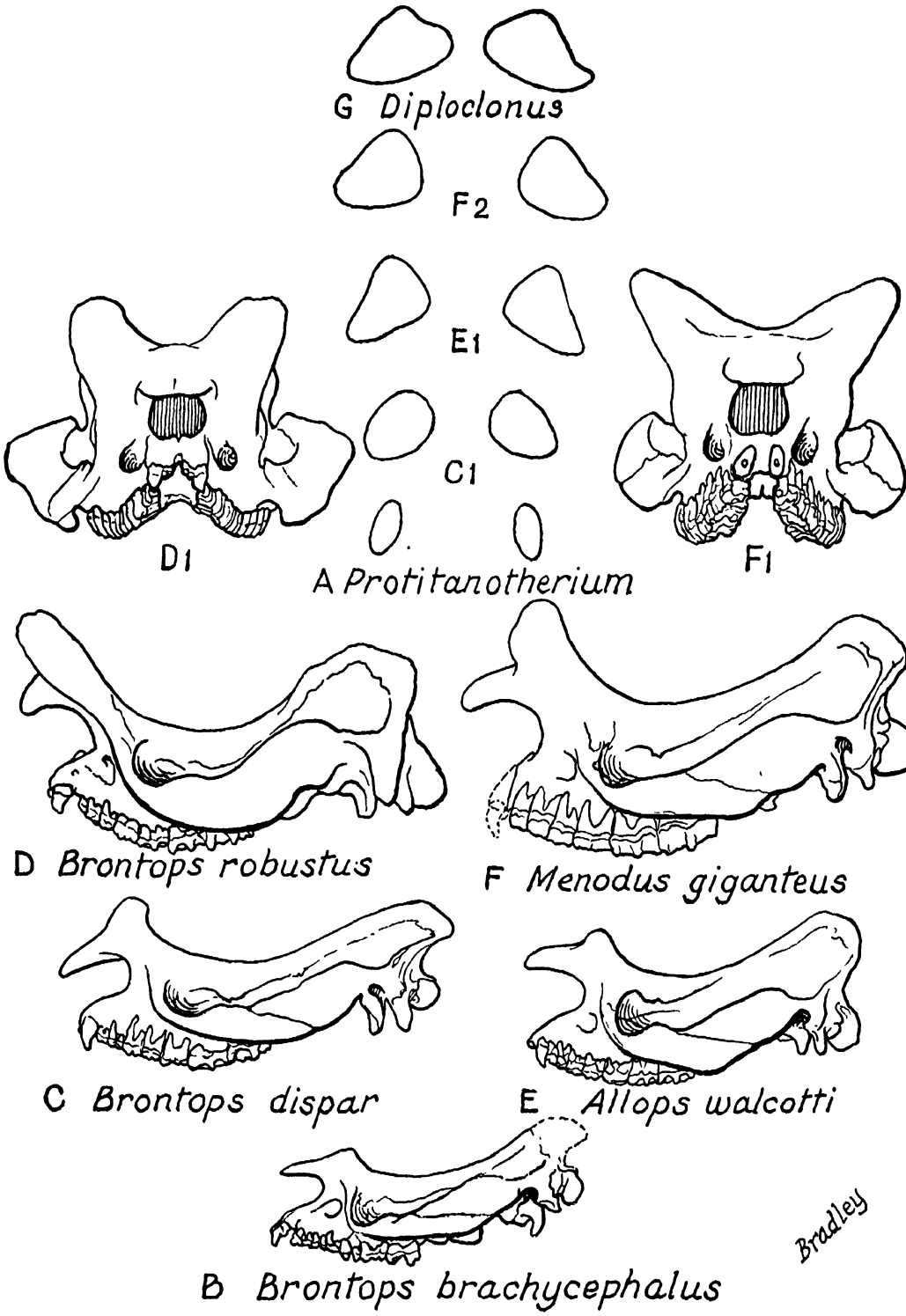


Fig. 21.58a, b. Constrasting skull characters of Lower Oligocene titanotheres. After Osborn.

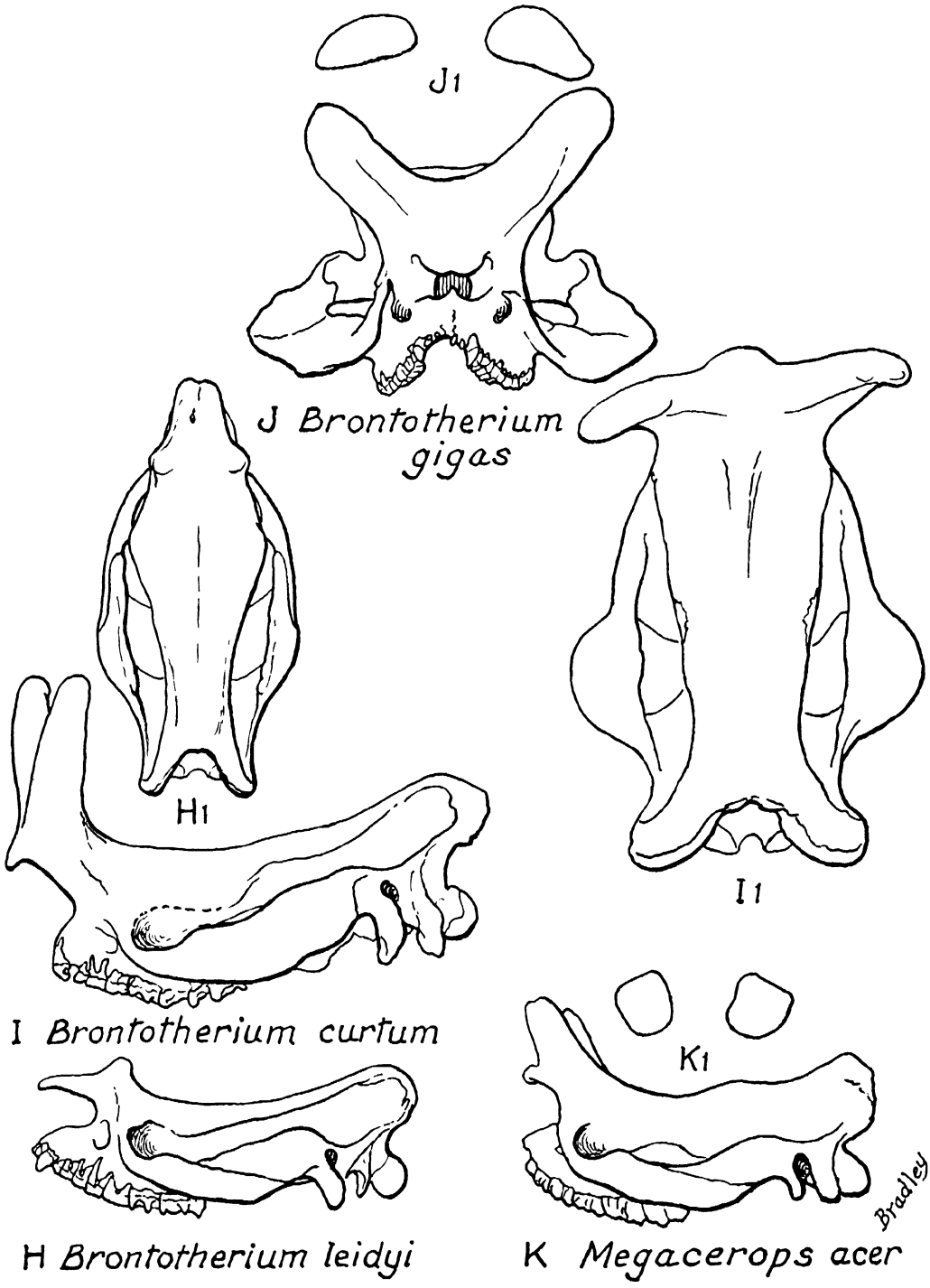

J1
J Brontotherium gigas
H1
I1
I Brontotherium curtum
K1
Bradley
H Brontotherium leidyi
K Megacerops acer

Fig. 21.58b

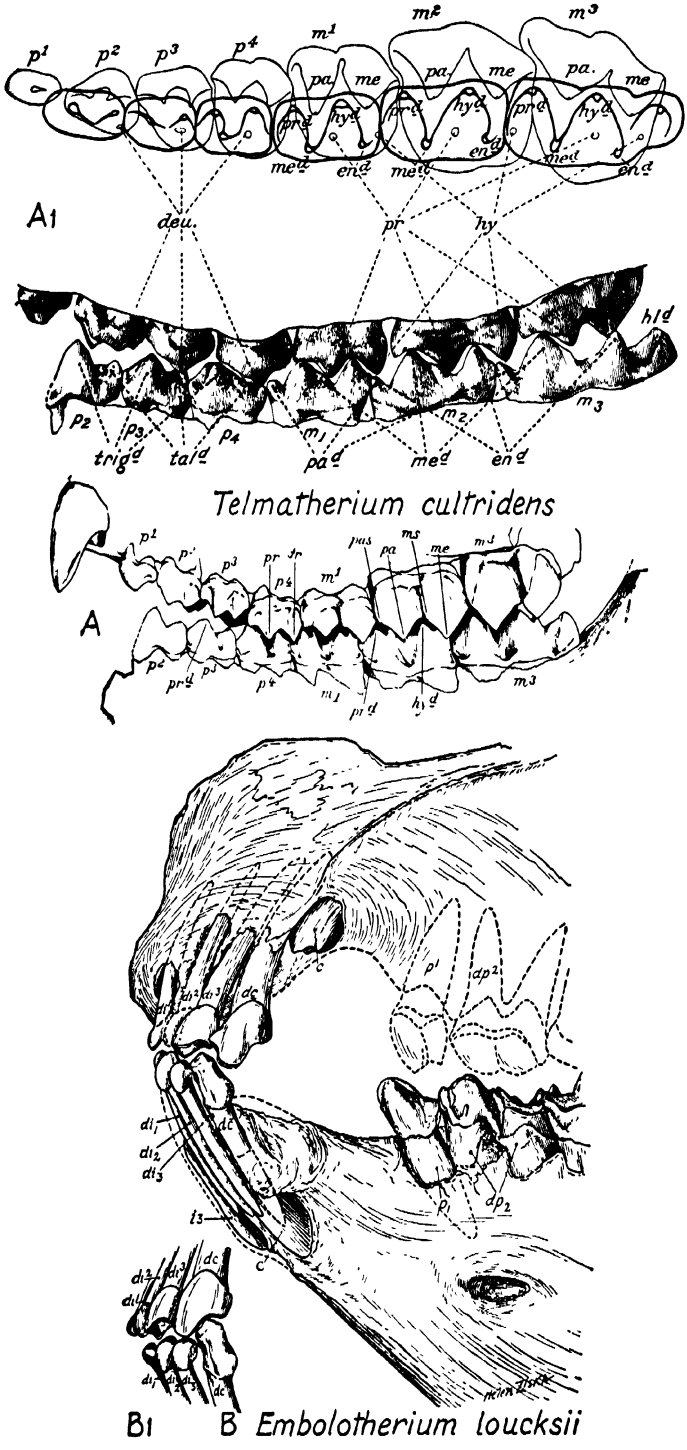


Fig. 21.59. Occlusal relations of upper and lower teeth in titanotheres. A, A1, from Osborn, after Gregory; B, B1, after Granger and Gregory. *Deu*, deuterocone, internal cusp of upper premolars.

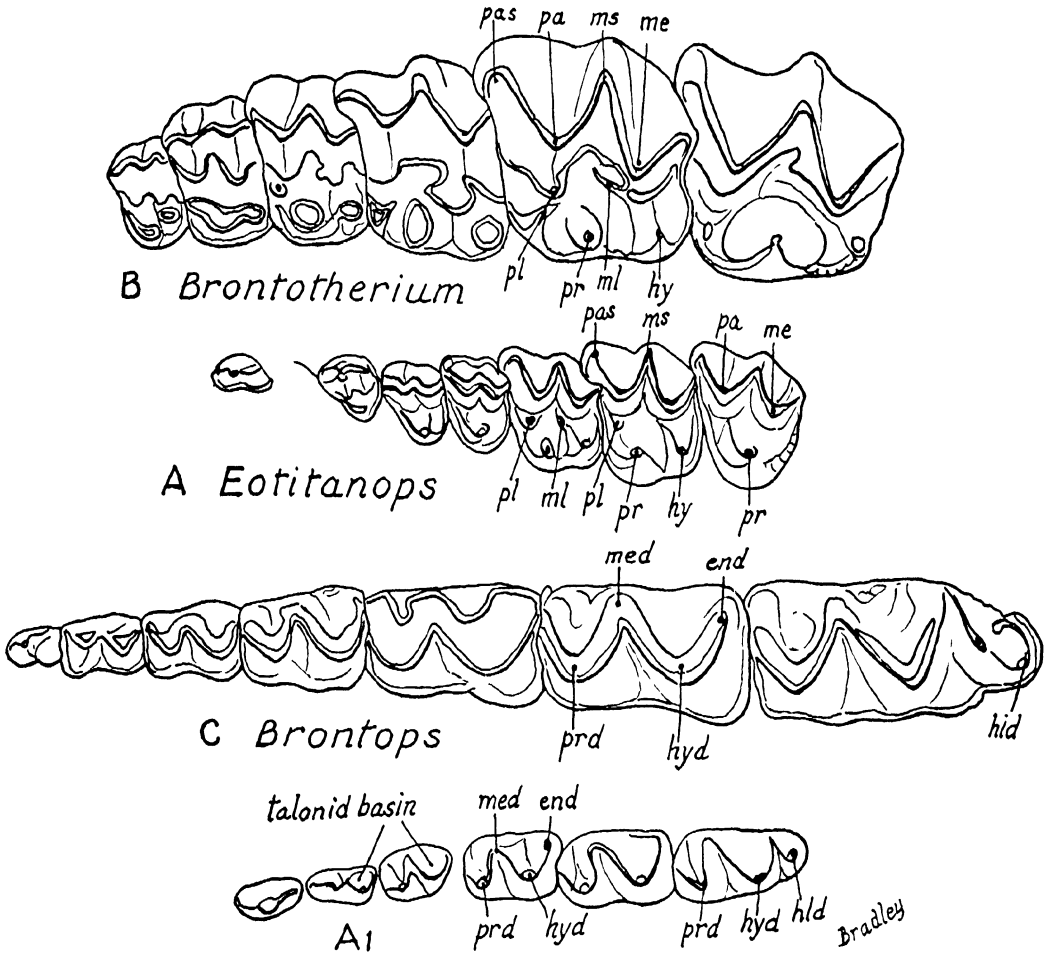


Fig. 21.60. Lower Eocene (A, A1) and Lower Oligocene (B, C) premolar-molar patterns of titanotheres, showing increase in size in the later stage and advance in molarization of the premolar patterns. After Osborn.

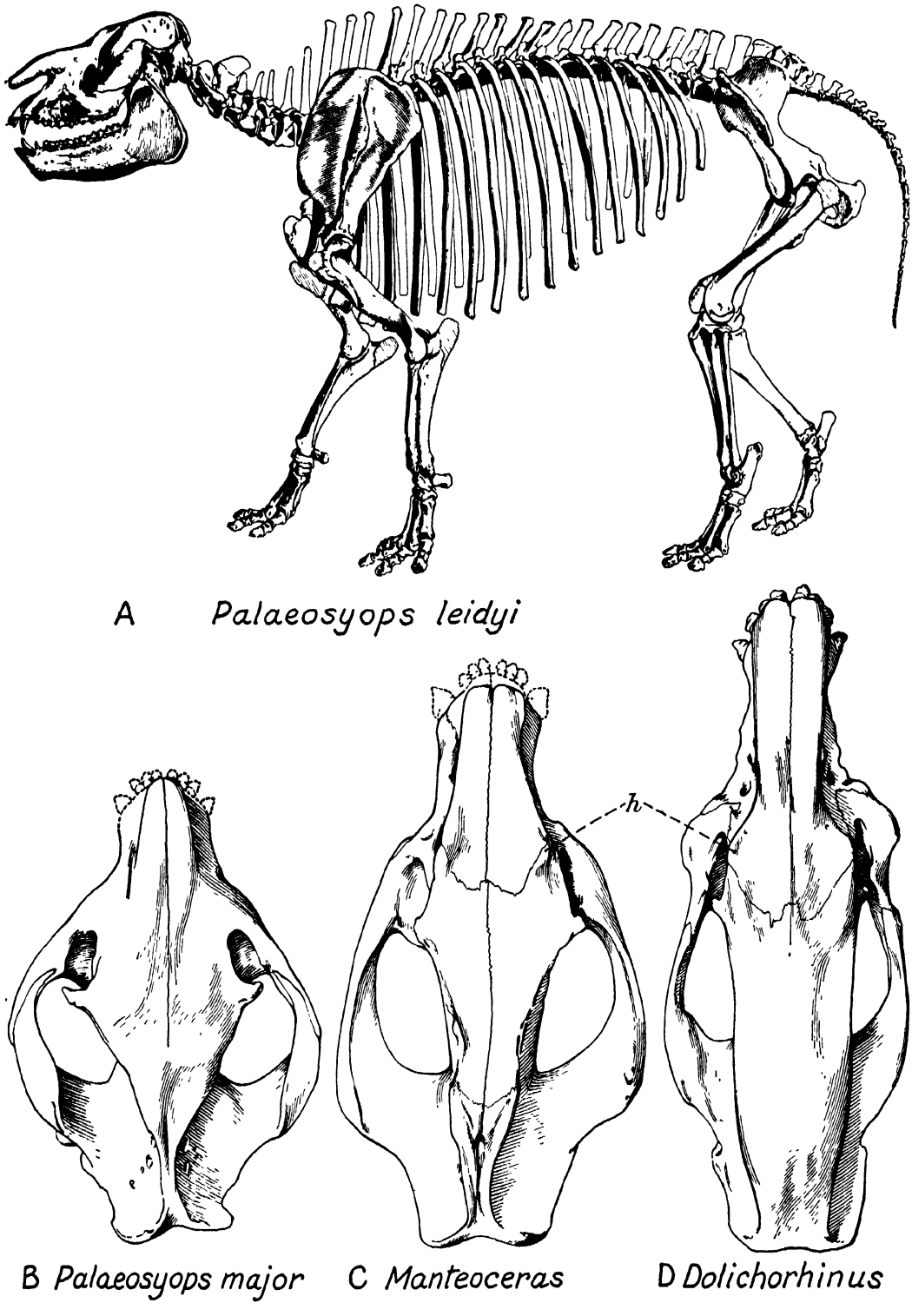


Fig. 21.61. Skeleton of Middle Eocene titanothere (A) and skulls of brachy-, meso- and dolichocephalic Eocene titanotheres (B–D). After Osborn.

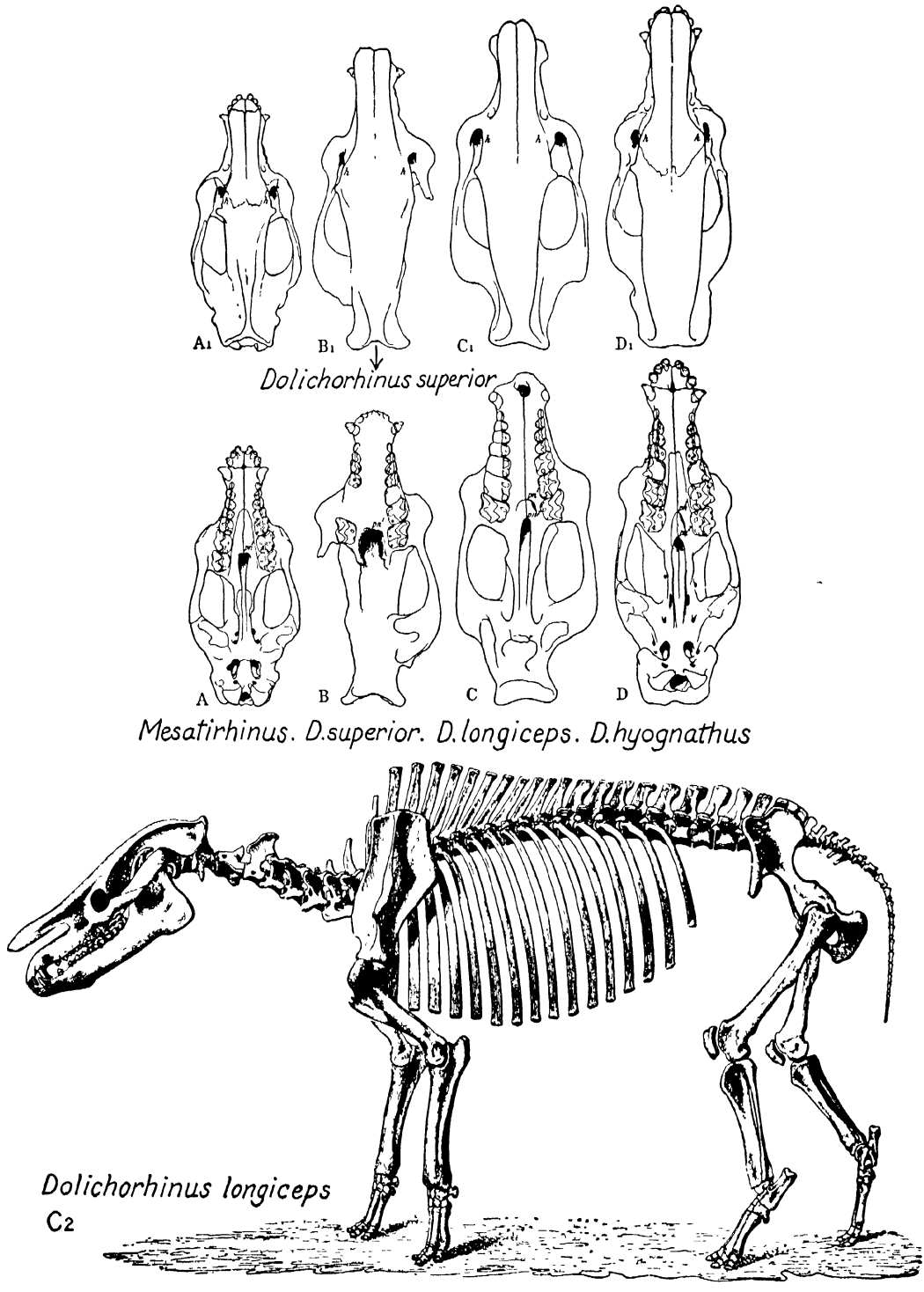


Fig. 21.62. Long-skulled Eocene titanotheres. A–D, after Osborn; C2, after Peterson.

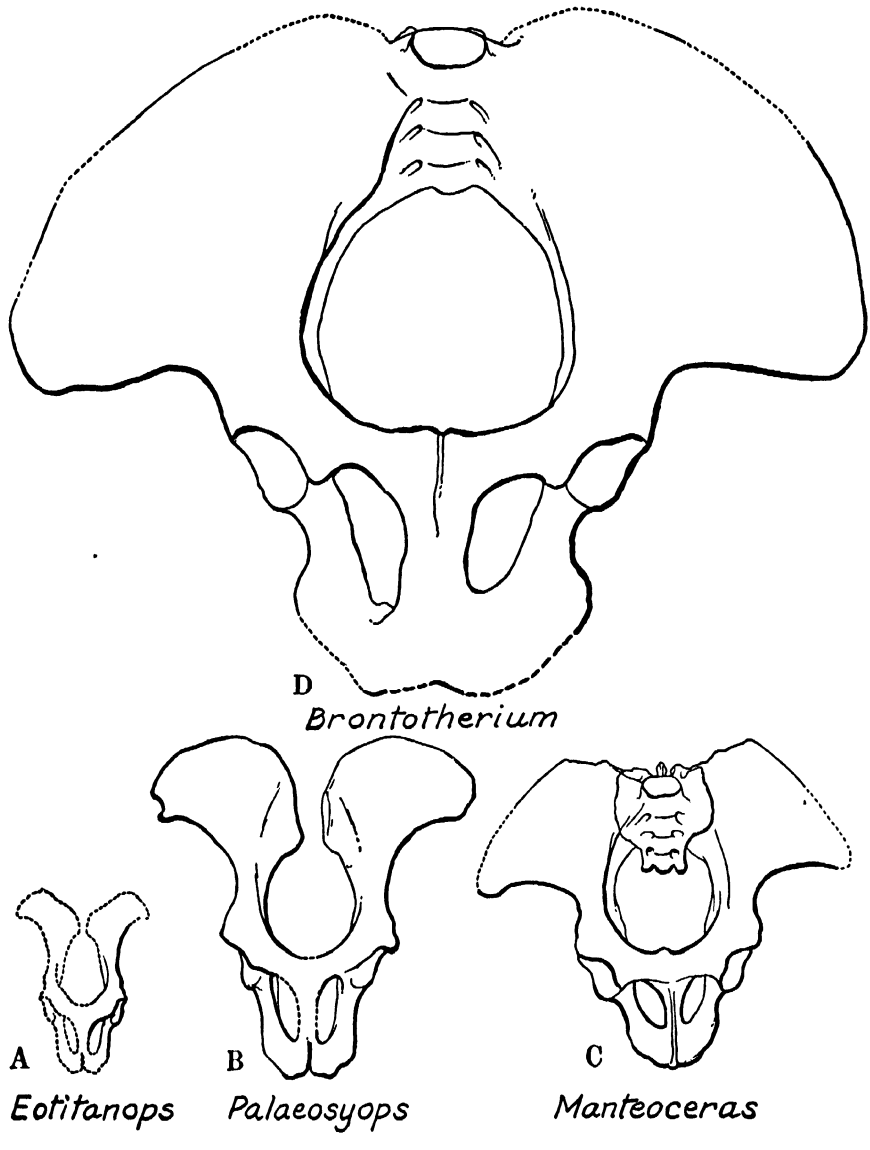


Fig. 21.63. Progressive widening of the pelvis in titanotheres. After Osborn.

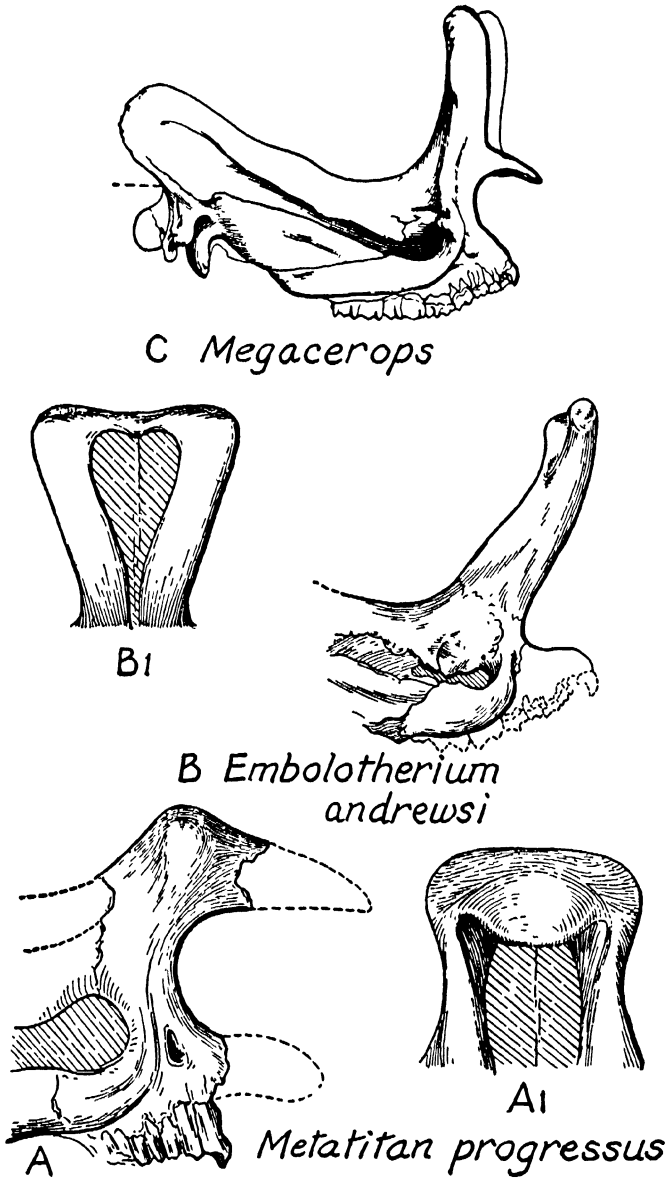


Fig. 21.64. Mongolian (A, B) Upper Eocene, and North American (C) Lower Oligocene, titanotheres. A–B1, after Granger and Gregory; C, after Osborn. The "horns" of B and C look similar but the free part of the nasals, well developed in C, seem to have become vestigial in B and B1.

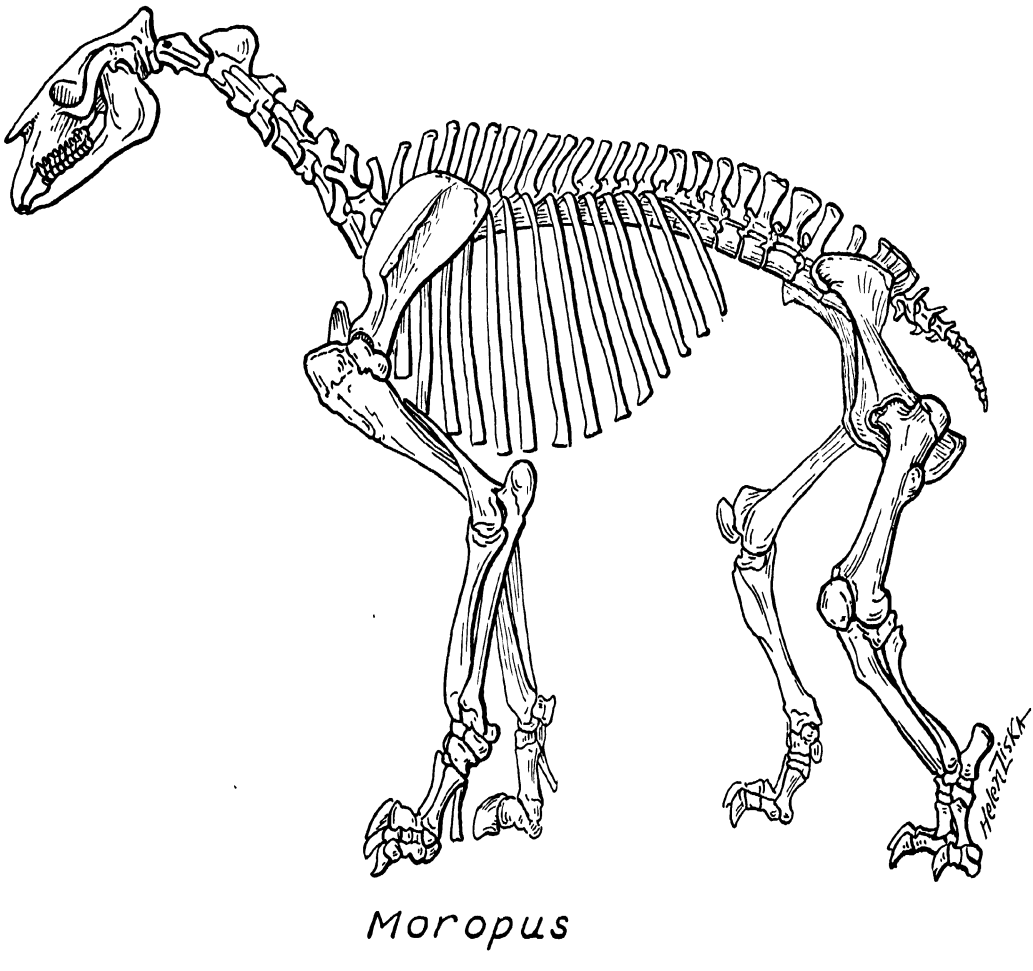


Fig. 21.65. Skeleton of Lower Miocene chalicothere. Data from mounted skeletons in Pittsburgh Museum, University of Nebraska, University of Wyoming, and American Museum of Natural History.

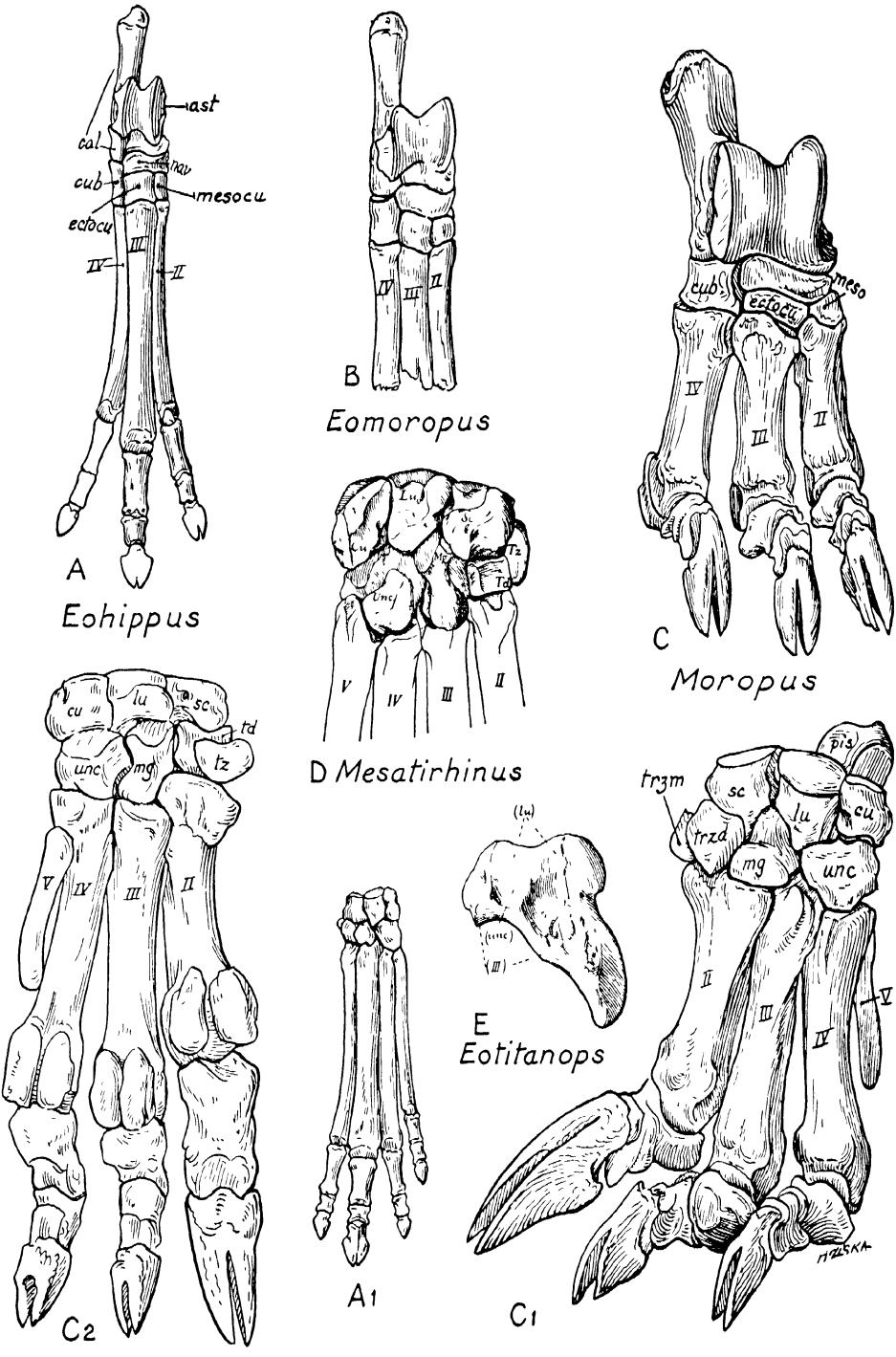


Fig. 21.66. Left fore-foot (C1, C2) and right hind foot (C) of a Miocene chalicothere, compared with other perissodactyls. The magnum (*mg*) is the key-stone of the carpus. A, A1, after Matthew; B, D, E. after Osborn; C, C1, C2, after Holland and Peterson.

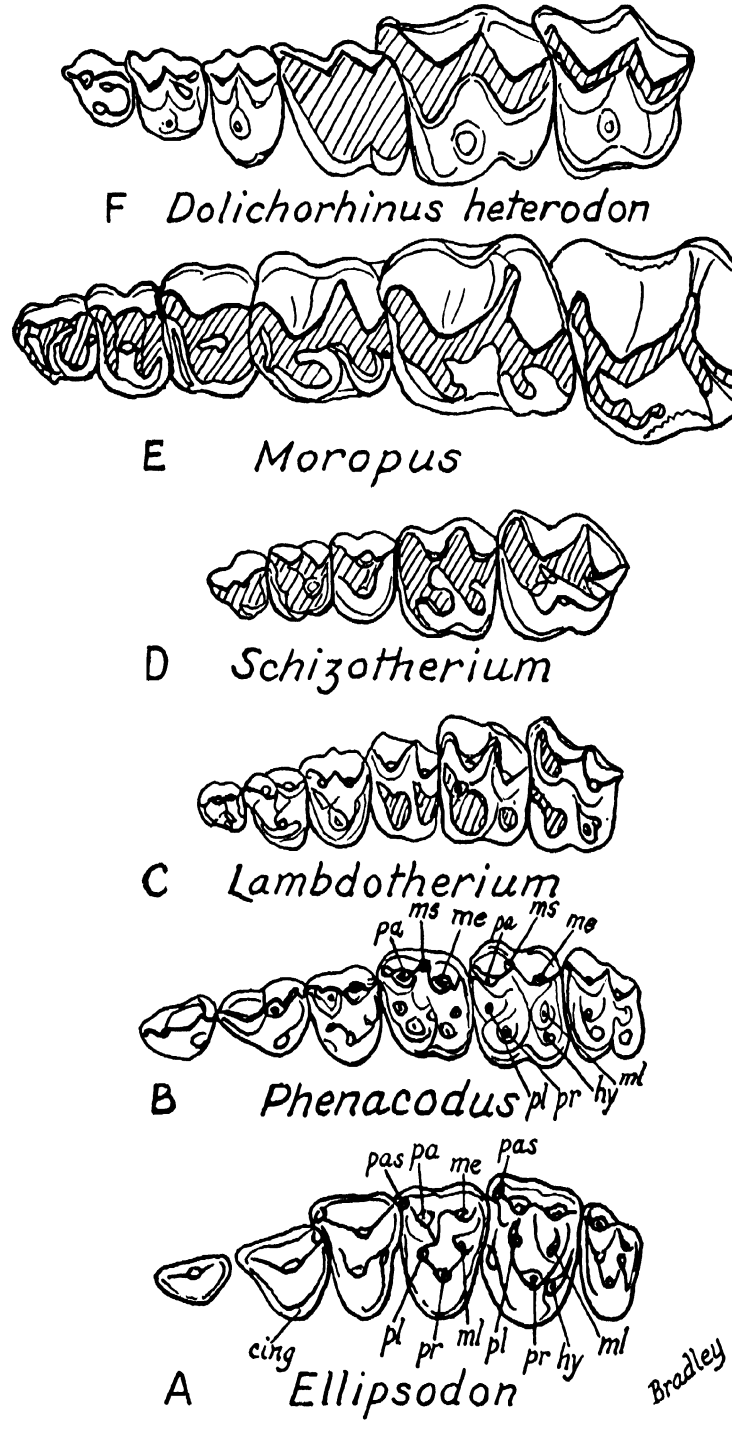


Fig. 21.67. Comparative premolar-molar patterns. A, primitive Paleocene condylarth, after Simpson; B, Lower Eocene condylarth, after Matthew and Granger; C, Lower Eocene titanothere, after Osborn; D, Oligocene chalicothere, after Osborn; E, Lower Miocene chalicothere, after Holland and Peterson; F, Upper Eocene titanothere, after Osborn.

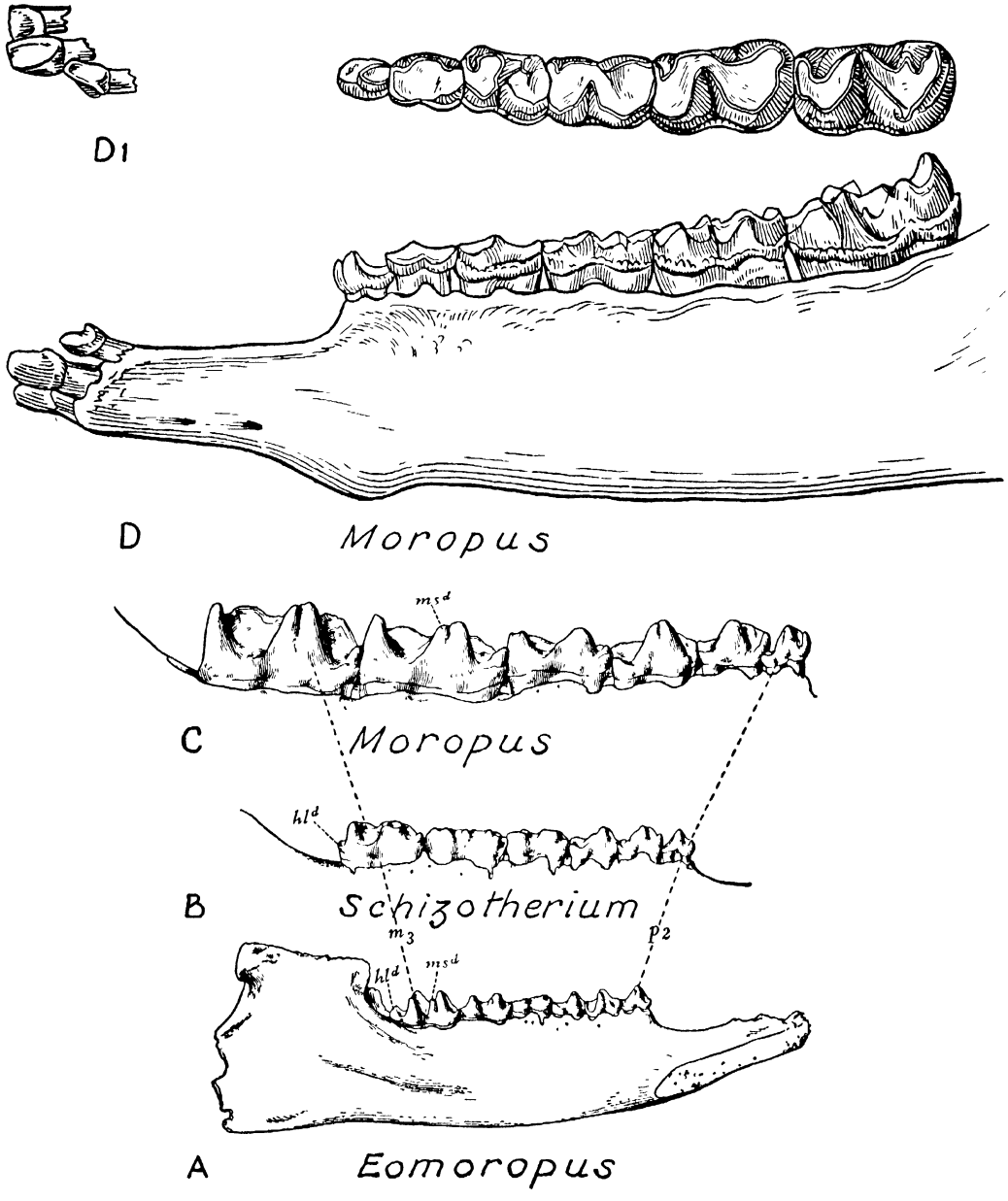


Fig. 21.68. Lower jaw and teeth of Upper Eocene (A), Oligocene (B) and Lower Miocene (D) chalicotheres. A–C, after Osborn; D, D1, after Holland and Peterson.

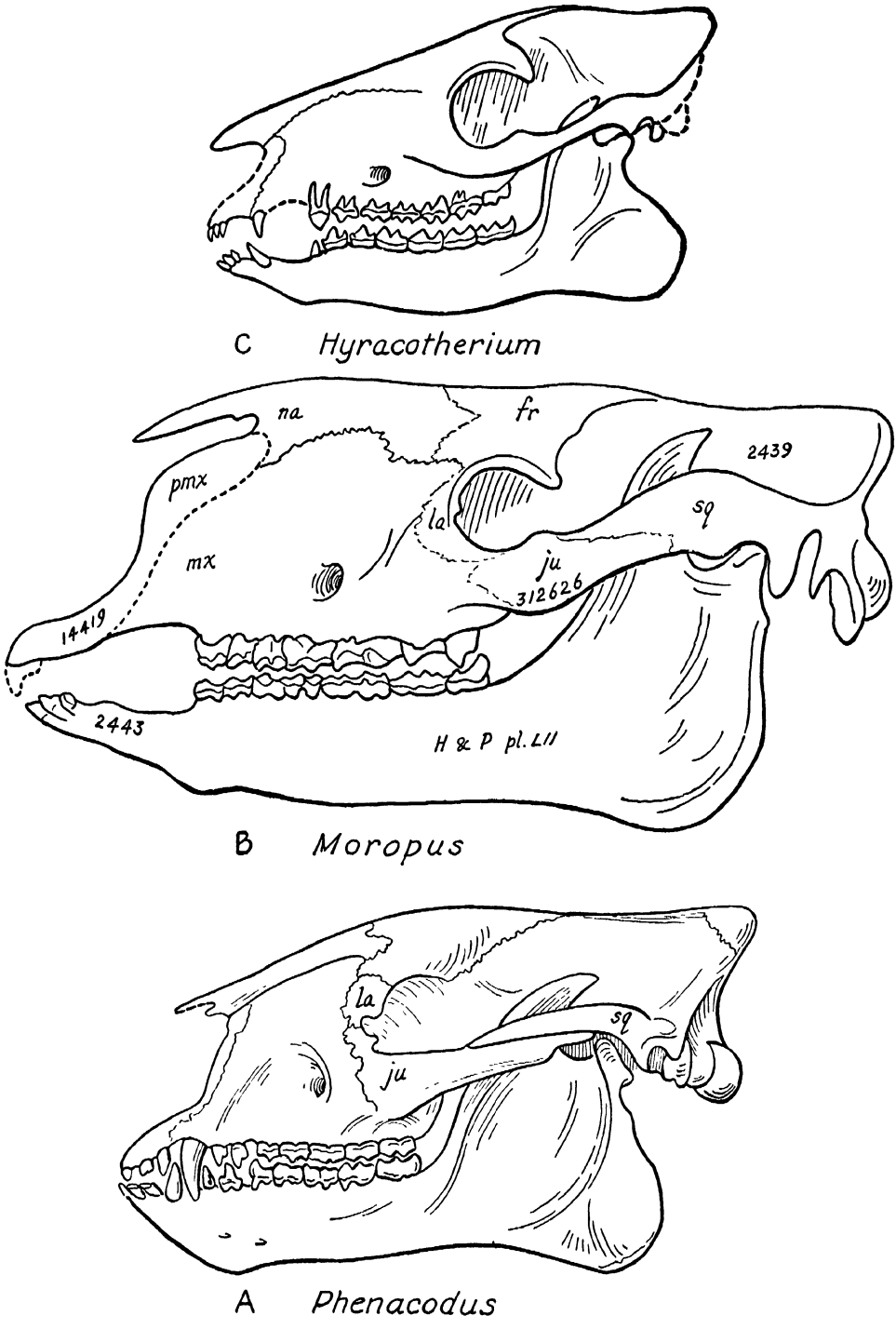


Fig. 21.69. Skulls of Lower Eocene condylarth (A), Lower Eocene perissodactyl (C) and Lower Miocene chalicothere (B). A, data from photograph of well preserved skull in School of Mines, Rapid City, South Dakota; B, data from American Museum specimens and Holland and Peterson; C, data from Owen, Forster Cooper, and fossils.

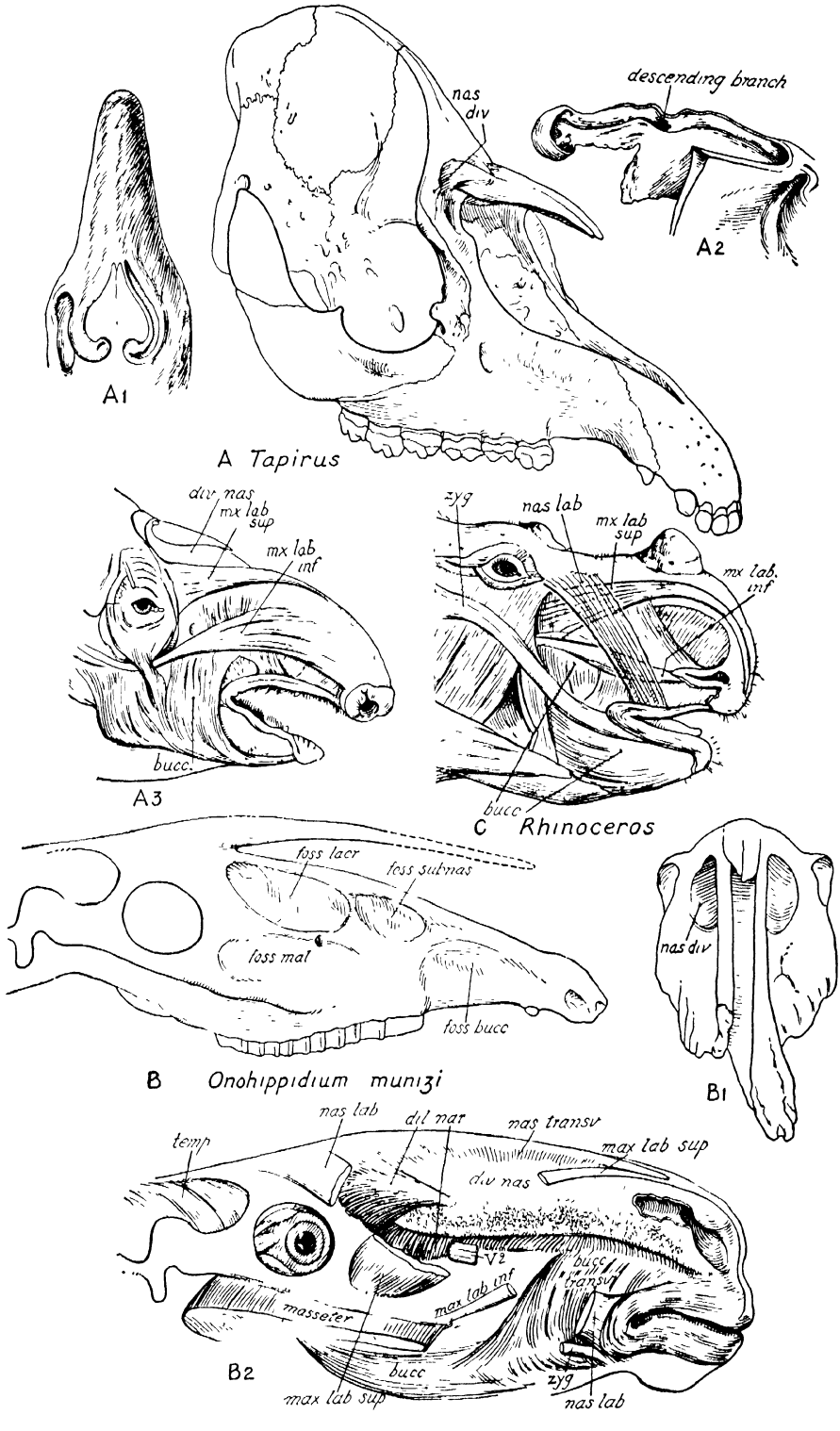


Fig. 21.70. The naso-preorbital region in perissodactyls. After Gregory. Data for A1, A2, from Murie; data for A3, from Boas and Pauli; data for B, from Lydekker; data for C, in part from Beddard and Treves, in part from preserved specimen.

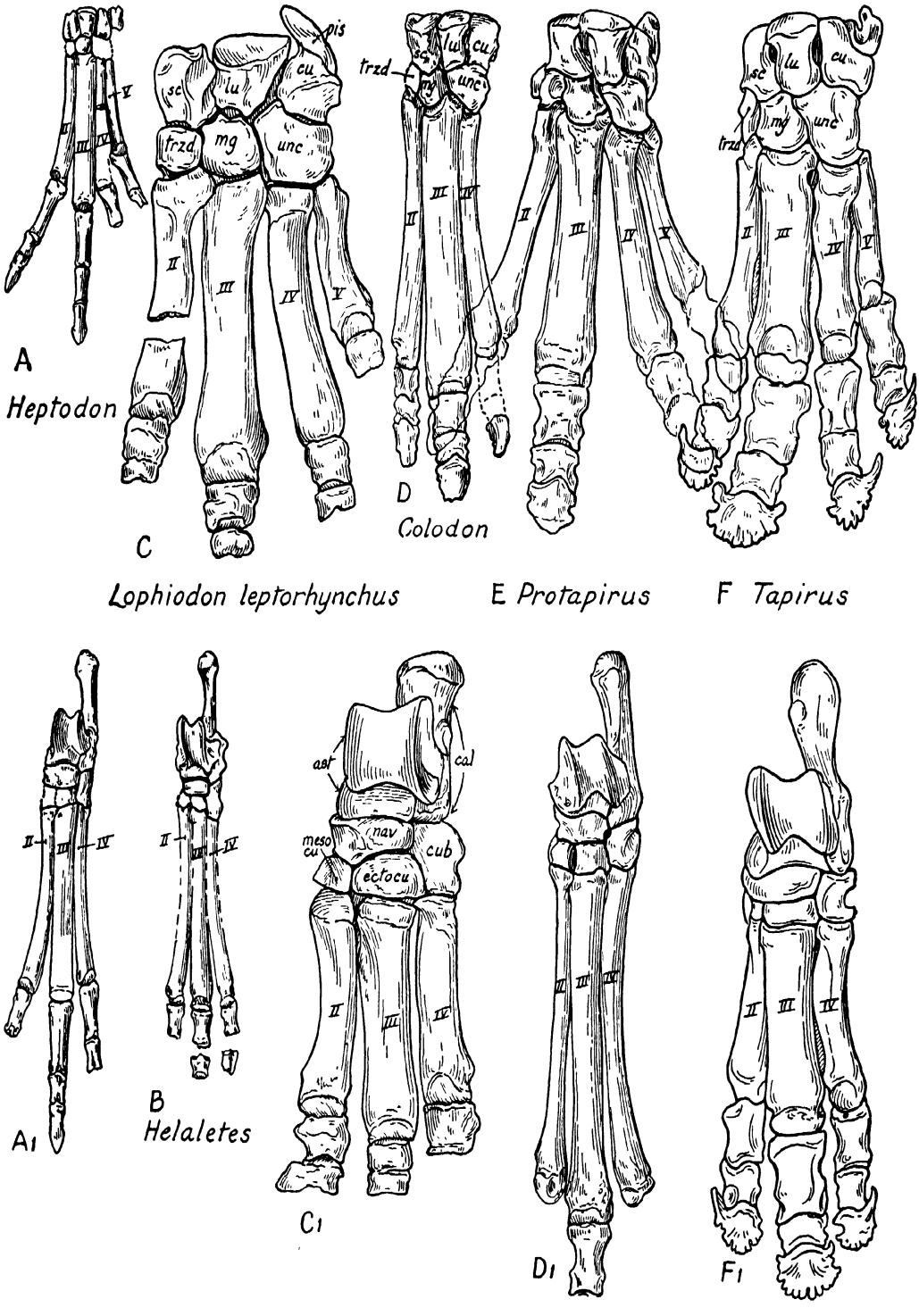


Fig. 21.71. Fore and hind feet of tapiroid perissodactyls. A, after Osborn; B, after Peterson; C, C1, after Depéret; D, D1, E, after Scott and Jepson; F, F1, after De Blainville.

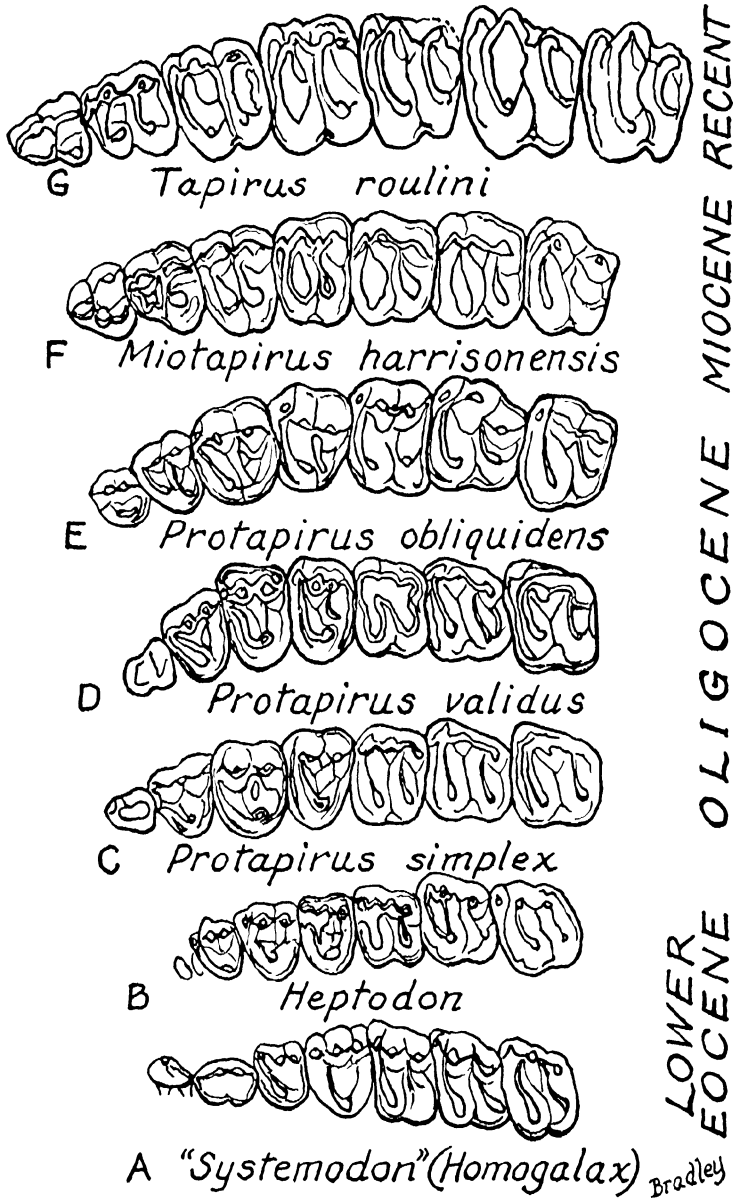


Fig. 21.72. Upper premolar-molar patterns of Eocene to Recent tapiroids. A, after Osborn; B–G, after Schlaikjer.

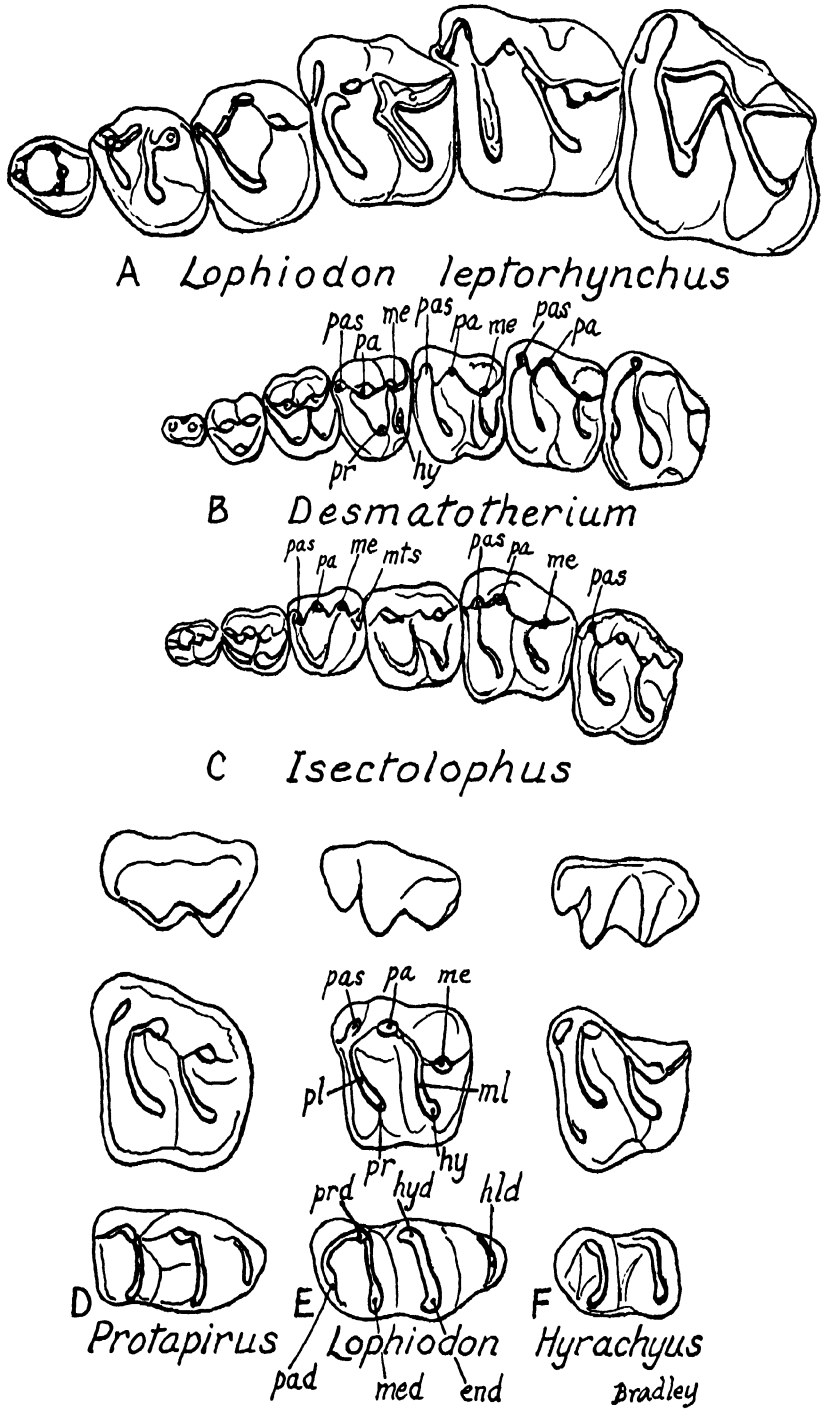
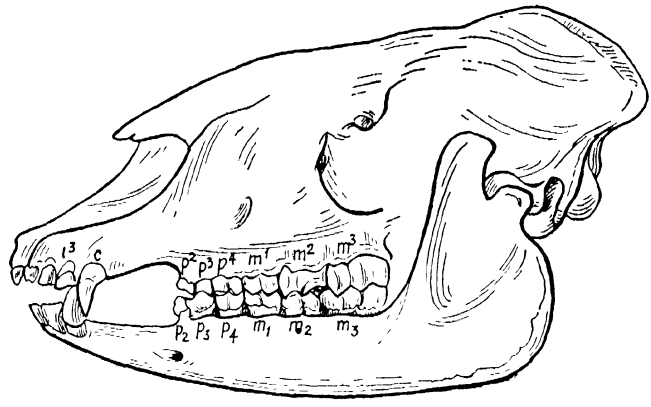
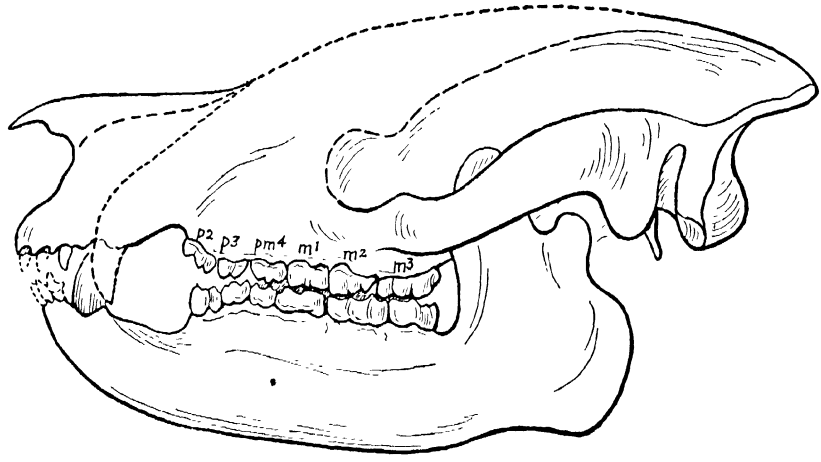


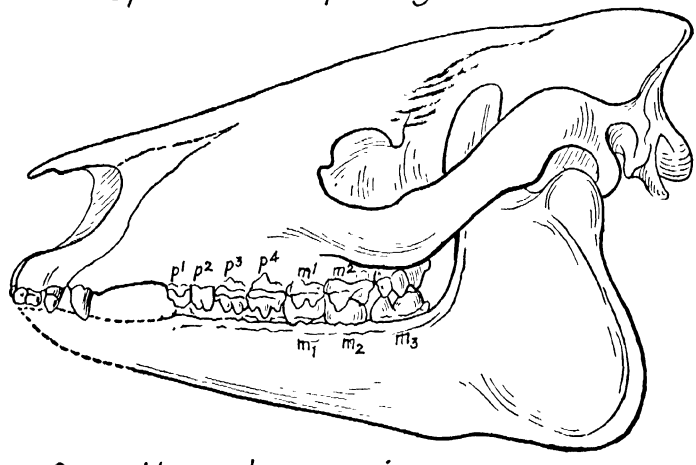
Fig. 21.73. Molar patterns of tapiroids (A–E) and primitive Eocene rhinoceros (F). A, after Depéret; B, C, after Scott; D–F, after Osborn



A *Plagiolophus*



B *Lophiodon leptorhynchus*



C *Hyrachyus princeps*

Fig. 21.74. Skulls of Eocene palaeothere (A) tapiroid (B) and hornless rhinoceros (C). A, B, adapted from Depéret; C, data from H E. Wood II. In C, the remarkably small muzzle is not due to crushing of fossil

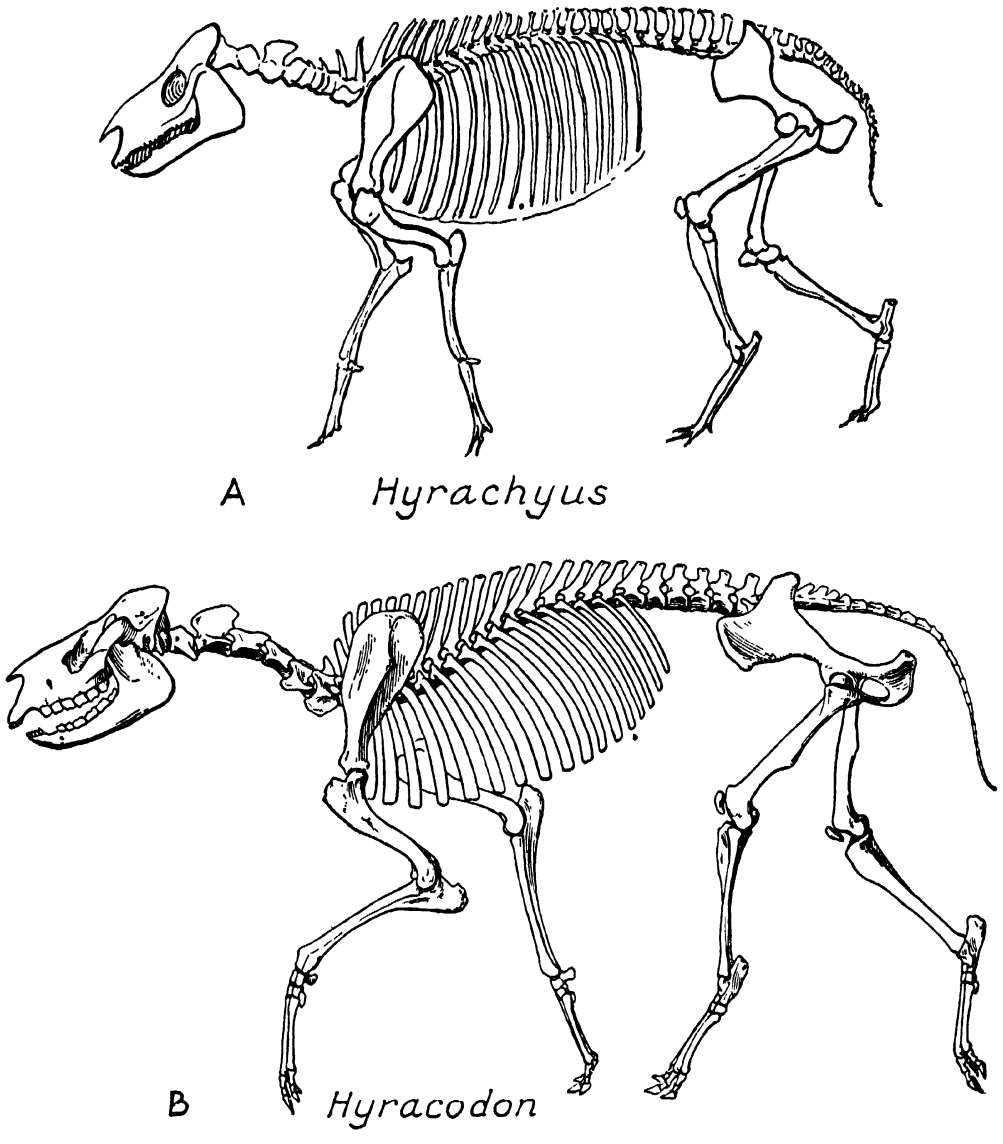


Fig. 21.75. Skeletons of Middle Eocene and Lower Oligocene hornless rhinoceroses. A, data from Osborn, Scott; B, after Scott. Not to scale. Measurements (after Romer): A, skull length about 11½ inches; B, total length about 5 feet.

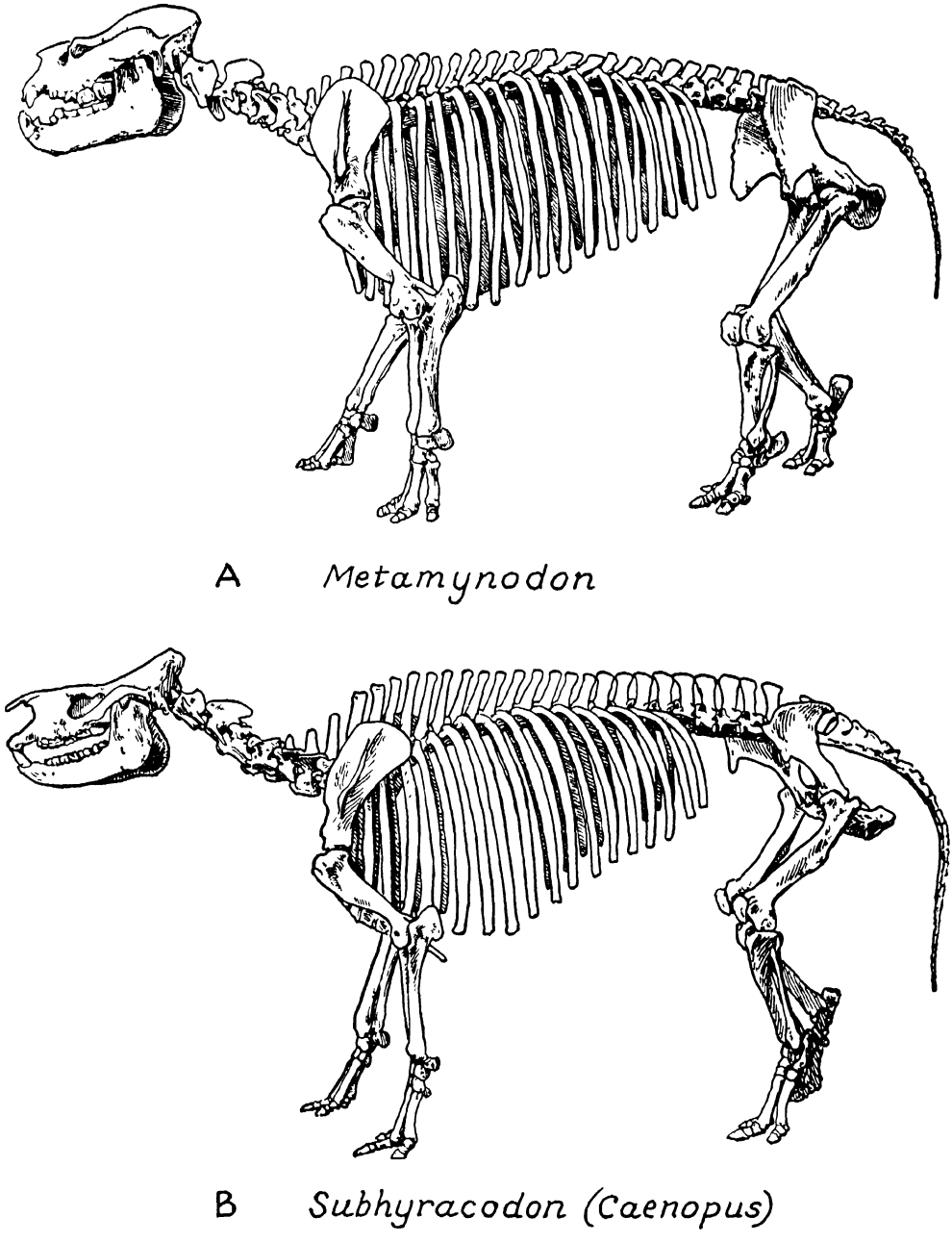


Fig. 21.76. Skeletons of generalized true rhinoceros (B), and aberrant semi-aquatic rhinocderotoid (A), after Scott. Not to scale. Total lengths (after Romer): A, about 14 feet; B, about 8 feet.

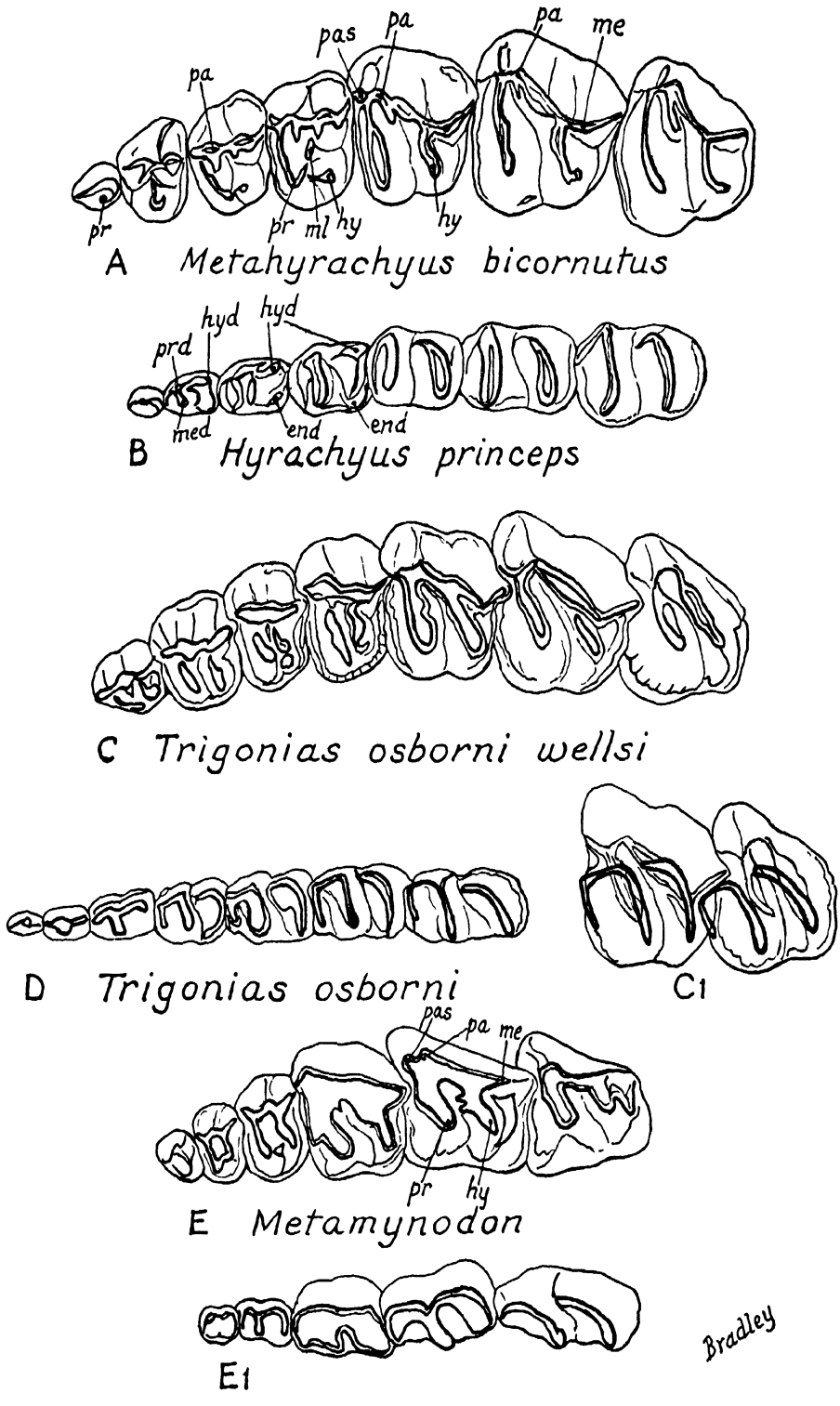


Fig. 21.77. Dental mechanism of rhinoceroses. A–D, after H. E. Wood, II; E. E1, after Scott. The occlusal diagram (C1) shows the lower molar crests cutting obliquely across the upper crests.

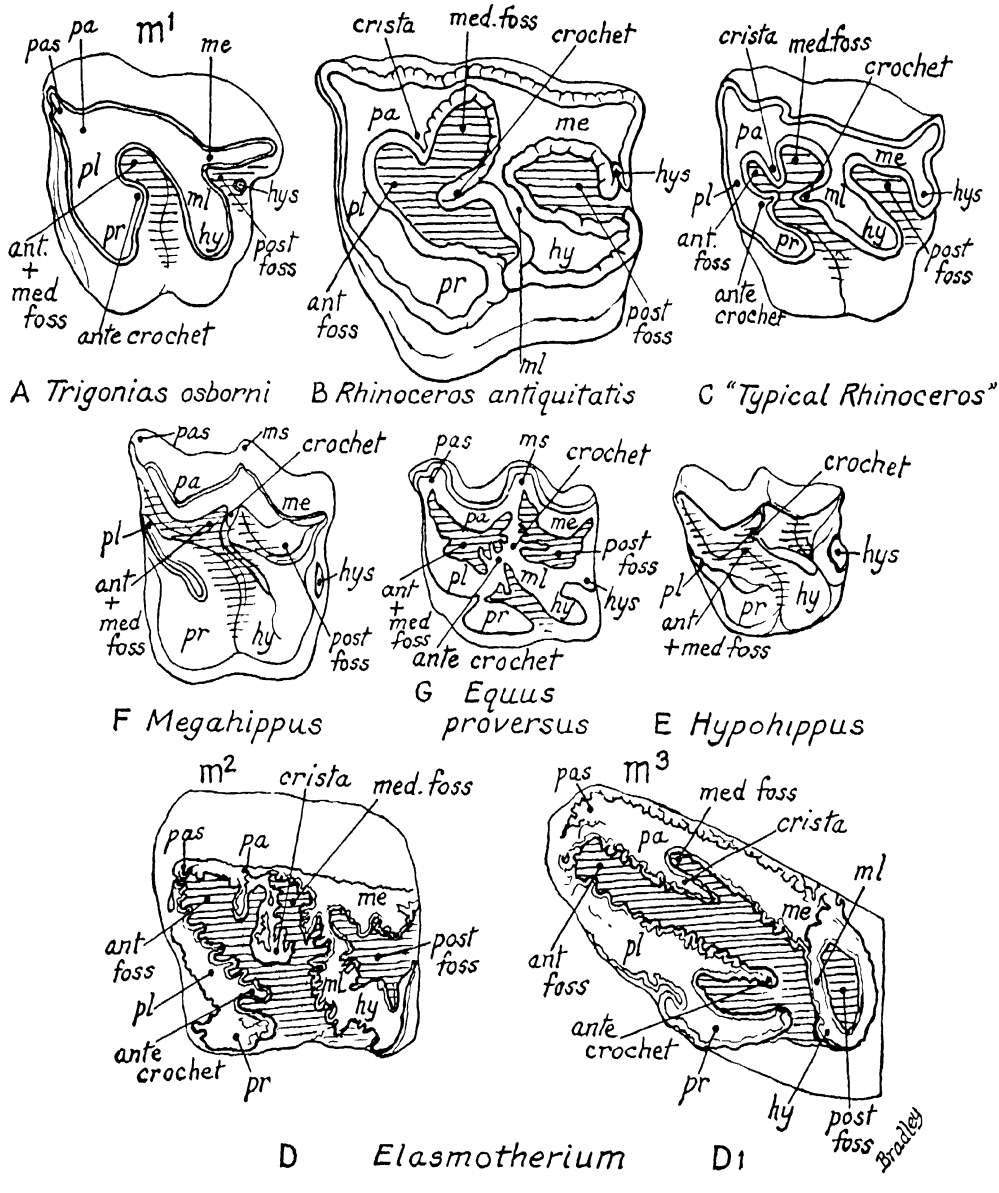


Fig. 21.78. Fossettes and folds in upper molars of rhinoceroses (A–D1) and horses (E–G) A, after Gregory and Cook; B, from Flower and Lydekker, after Falconer, C, after Osborn; D, D1, after Borissiak; E–G, after Stirton.

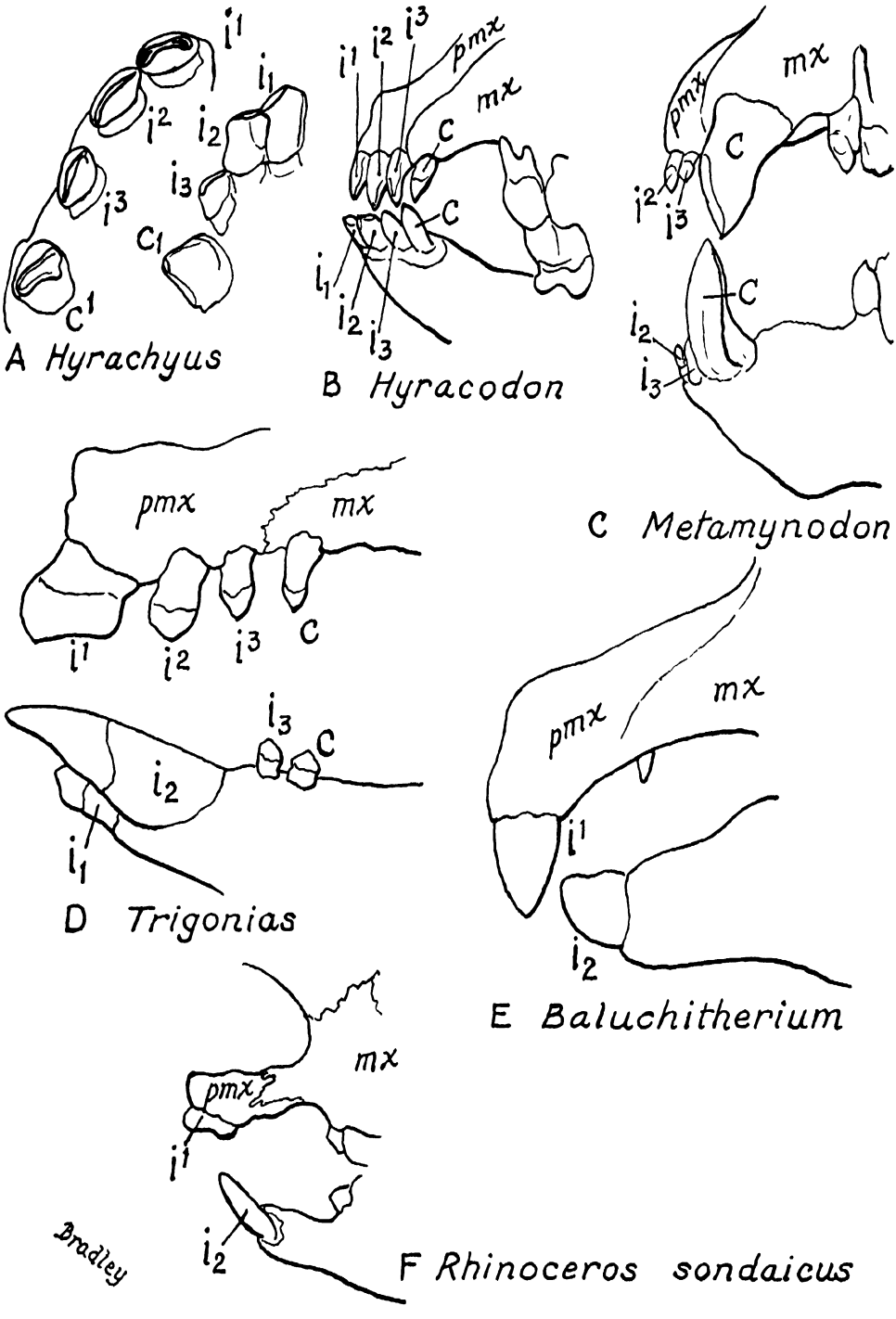
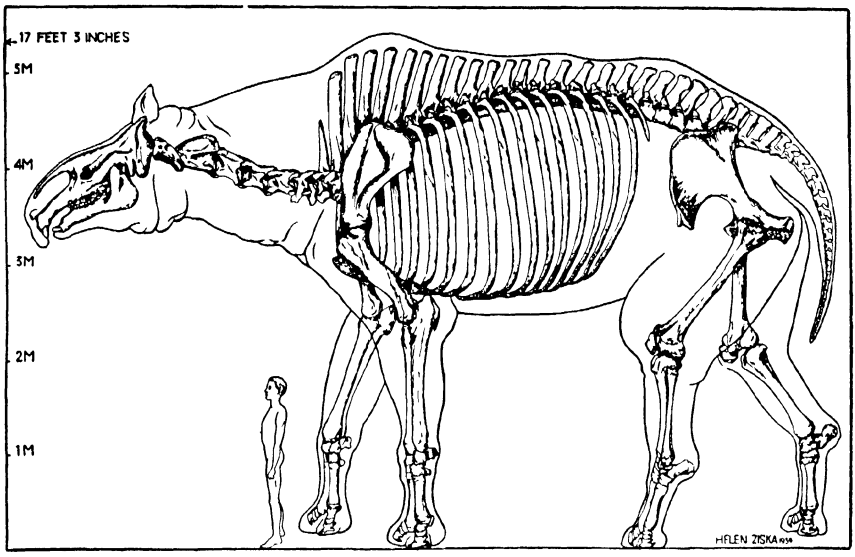
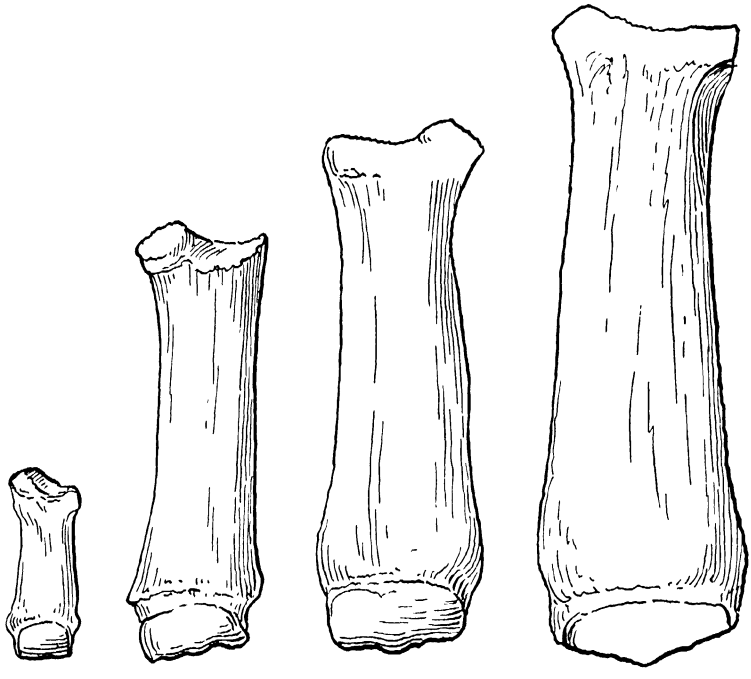


Fig. 21.79. Form and homologies of incisor and canine teeth in rhinocerotoids. A, after H. E. Wood II; B, C, after Scott; D, after Gregory and Cook; E, after Granger and Gregory; F, after Osborn.



The restoration of the skeleton of Baluchitherium, as completed by Walter Granger and William K. Gregory. Drawing by Mrs. Helen Ziska



The small bone shown at the left in the photograph above is the middle metacarpal bone from a modern white rhinoceros. The others are the corresponding bones from a small, a large, and a super-giant Baluchitherium. The largest of these is twenty-five inches in length

Fig. 21.80. Restoration of skeleton and third metacarpal of giant baluchithere. After Granger and Gregory.

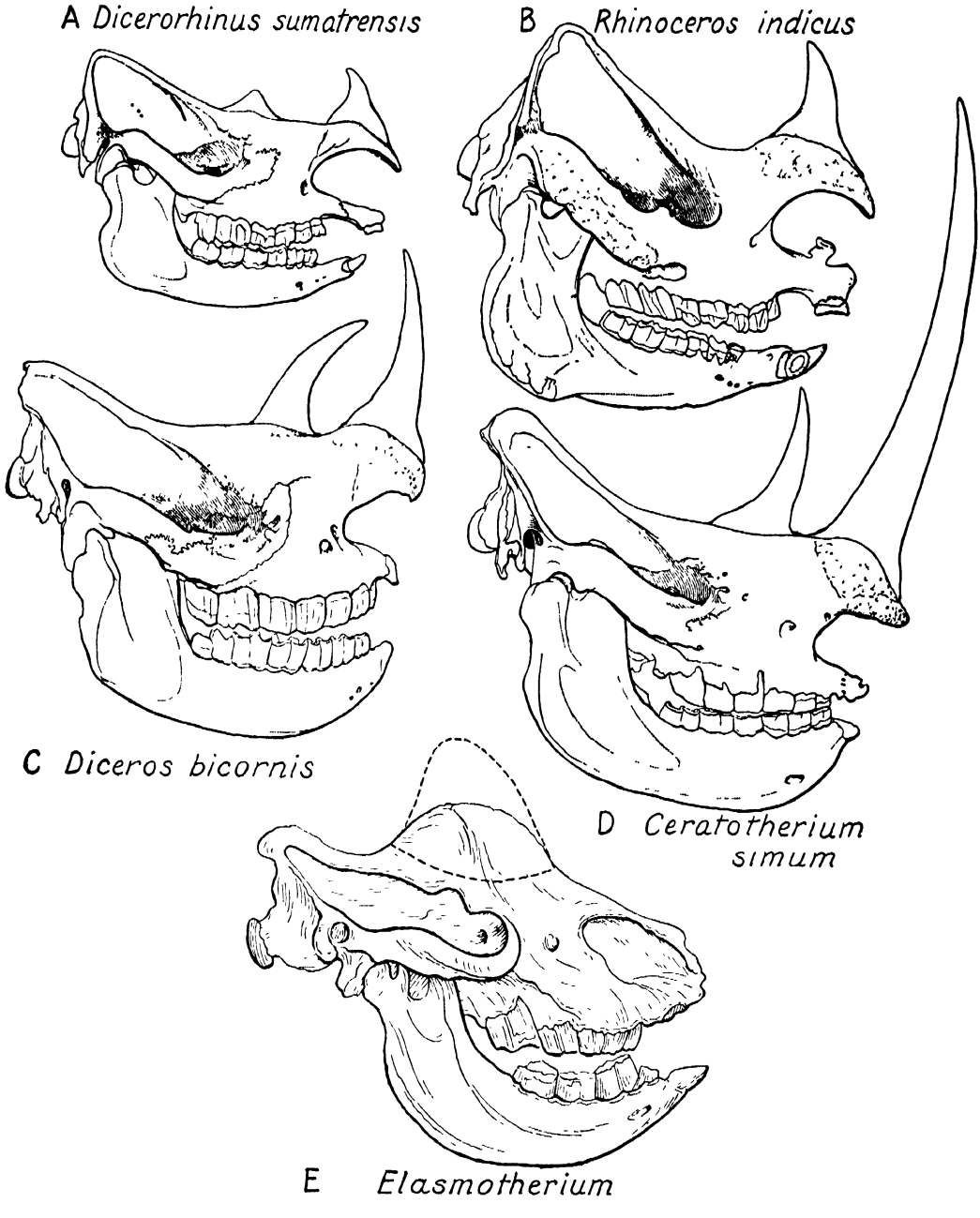


Fig. 21.81. Skulls of Recent (A–D) and Pleistocene (E) rhinoceroses. A–D, after Osborn, horns from specimens; E, after Brandt, horn outline hypothetical.

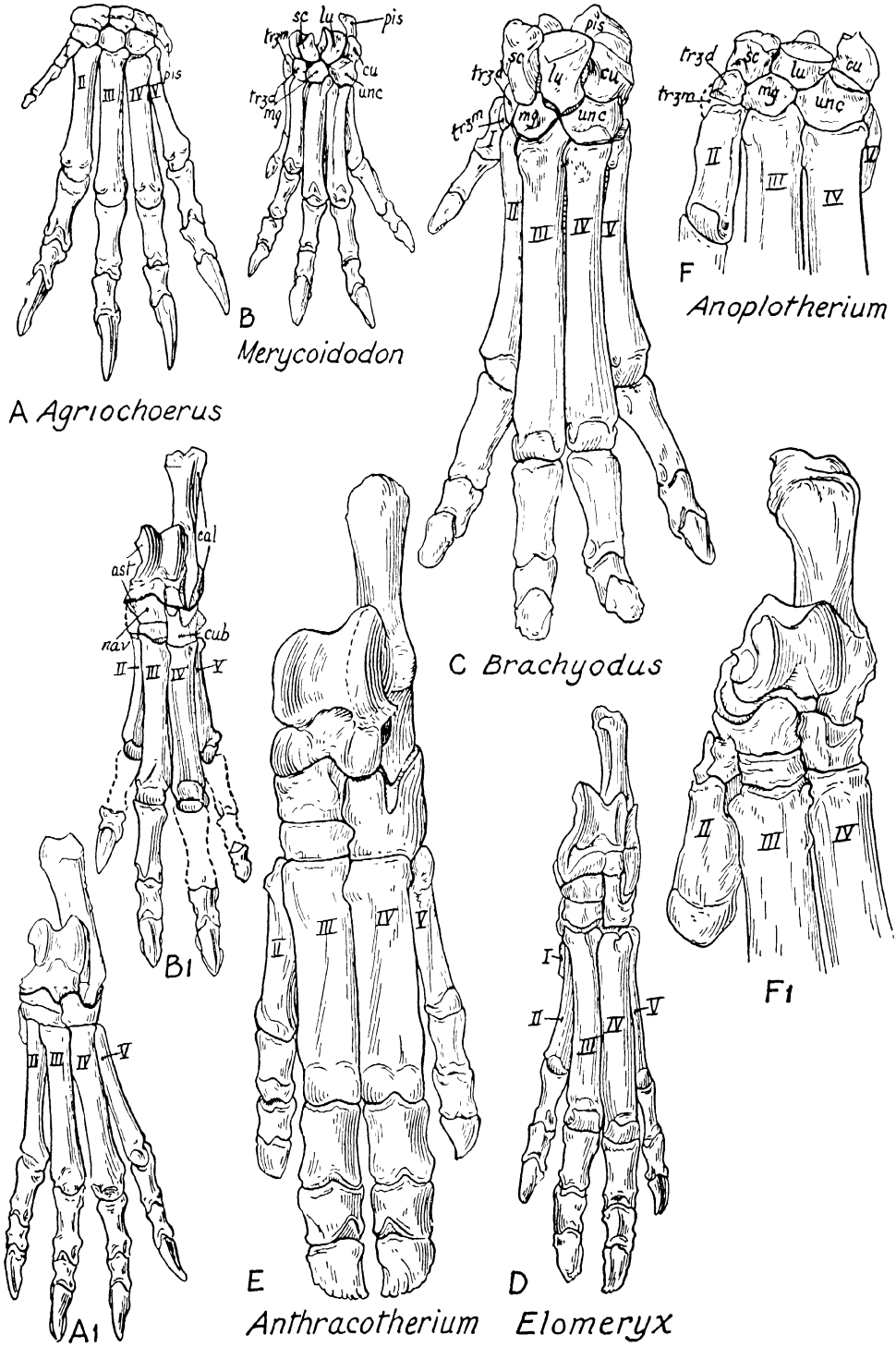


Fig. 21.82. Left fore and left hind feet of relatively primitive artiodactyls. A, B, D, A1, B1, after Scott and Jepsen; C, after Stehlin; E, F, F1, after Kowalevsky.

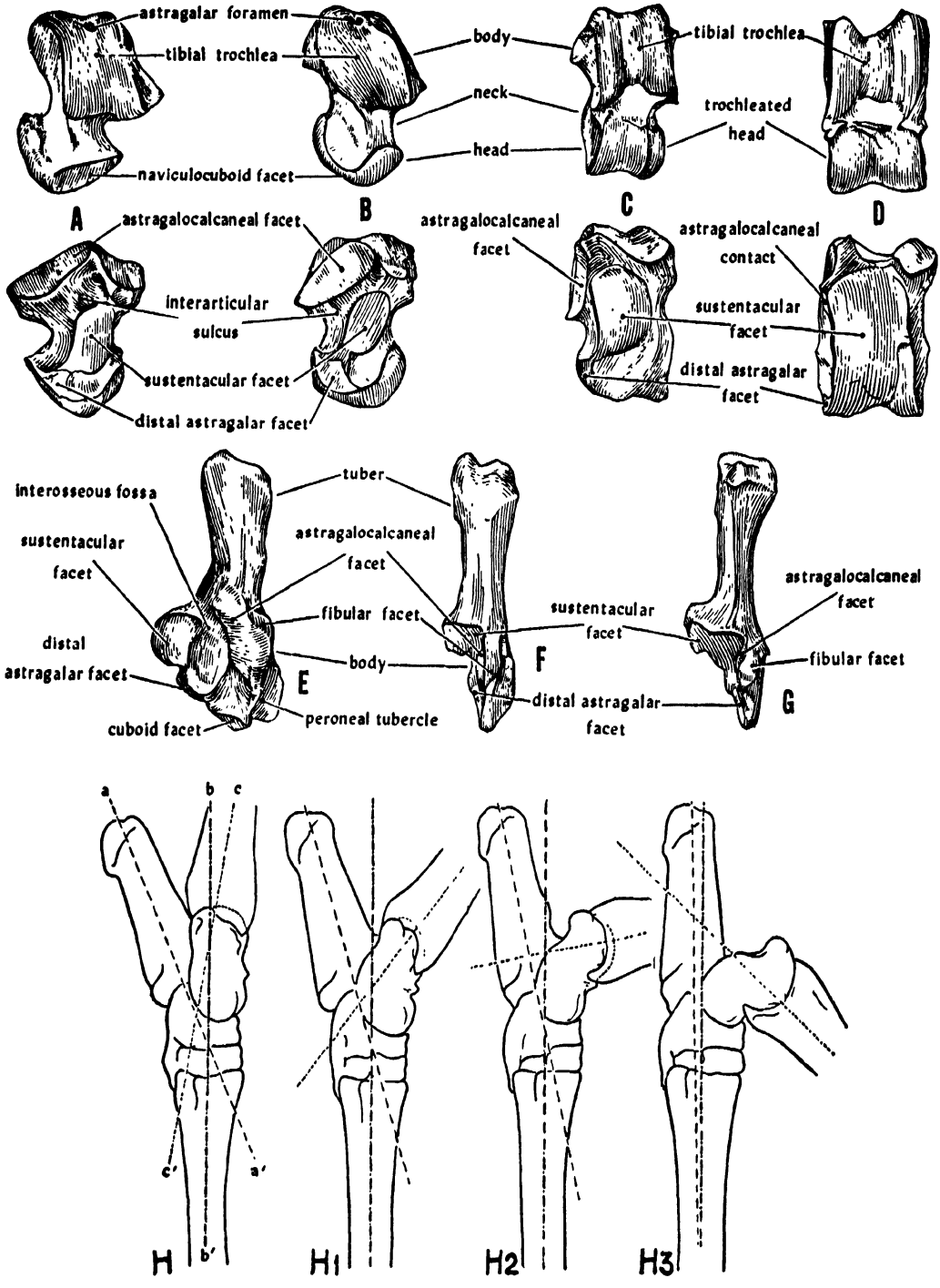


Fig. 21.83. Mechanism of tarsus in relatively primitive mammals (A, B, E) and artiodactyls (C, D, F–H3). After Schaeffer. A, E, Paleocene creodont (*Claenodon*); B, *Choeroclaenus*; C, F, primitive Eocene artiodactyl (*Diacodexis*); D, modern sheep (*Ovis*); H–H3, shows wide extension and flexion of artiodactyl tarsus.

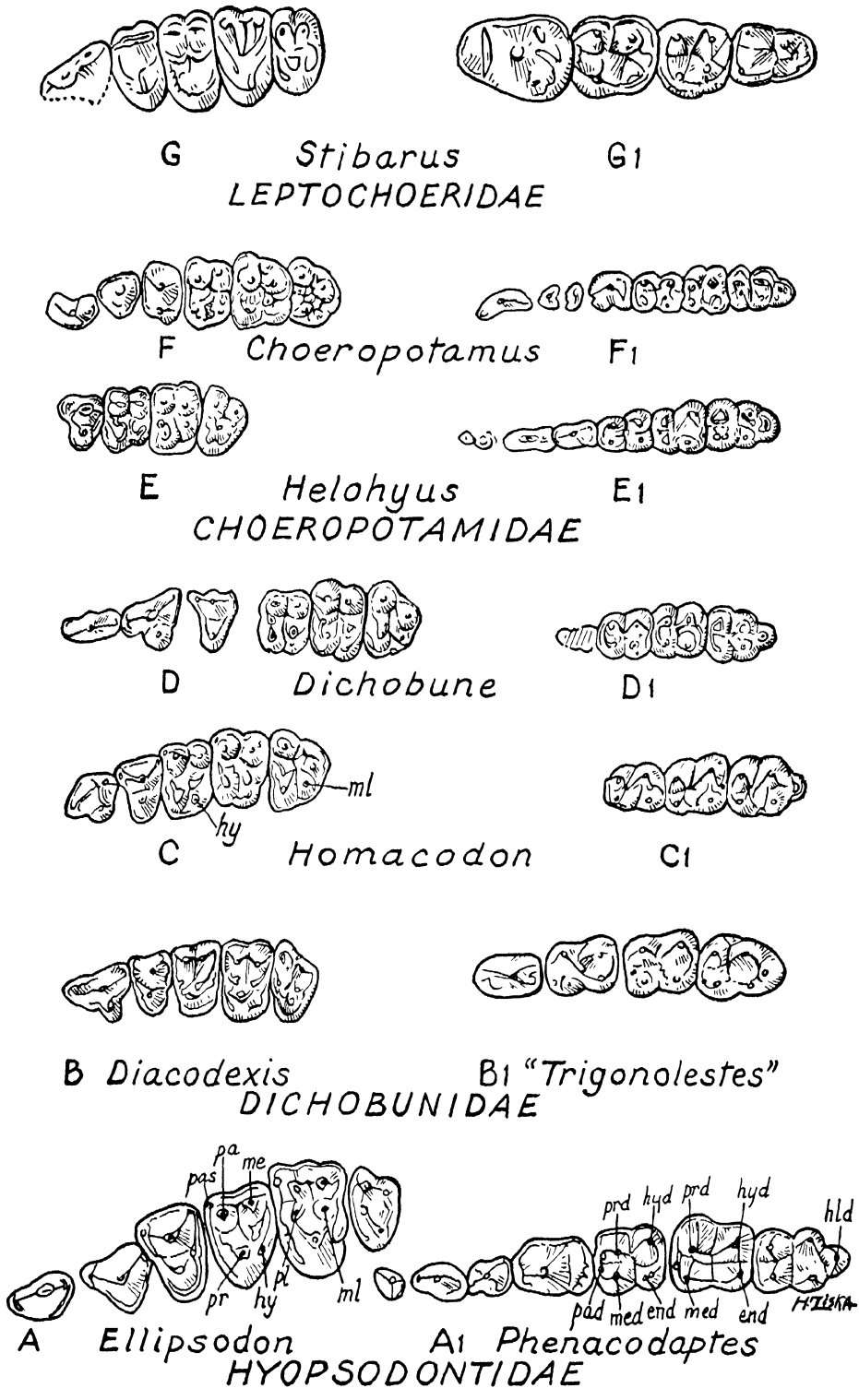


Fig. 21.84. Upper and lower molar patterns of primitive Paleocene condylarths (A, A1), Eocene dichobunids (B–D), choeropotamids (E, F) and Lower Oligocene leptochoerids. A, after Simpson; A1, after Jepsen; B, C, after Sinclair; D–F, after Stehlin; G, after Scott and Jepsen.

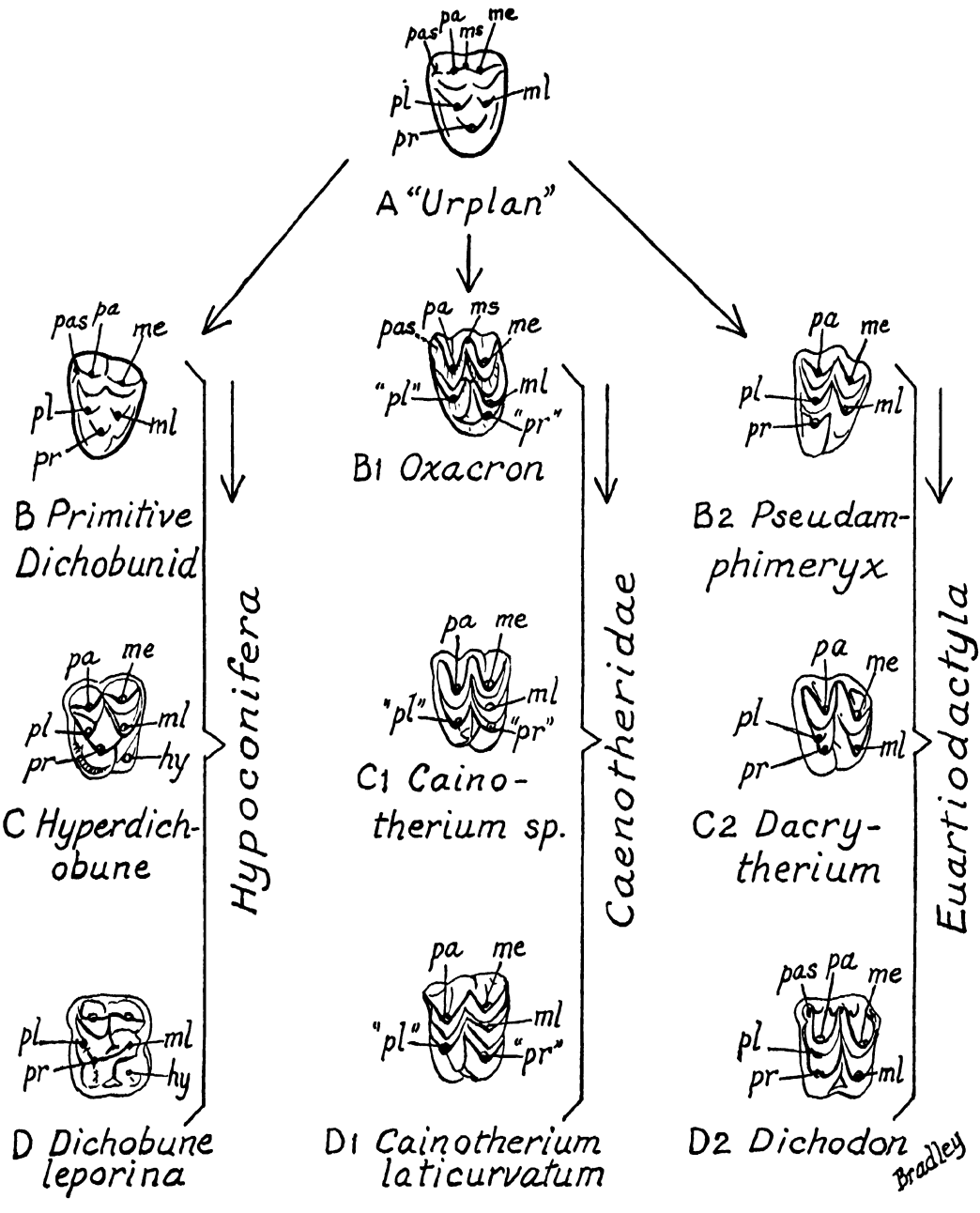


Fig. 21.85. Divergence of upper molar patterns of Eocene and later artiodactyls from an inferred ancestral pattern (A). After Stehlin.

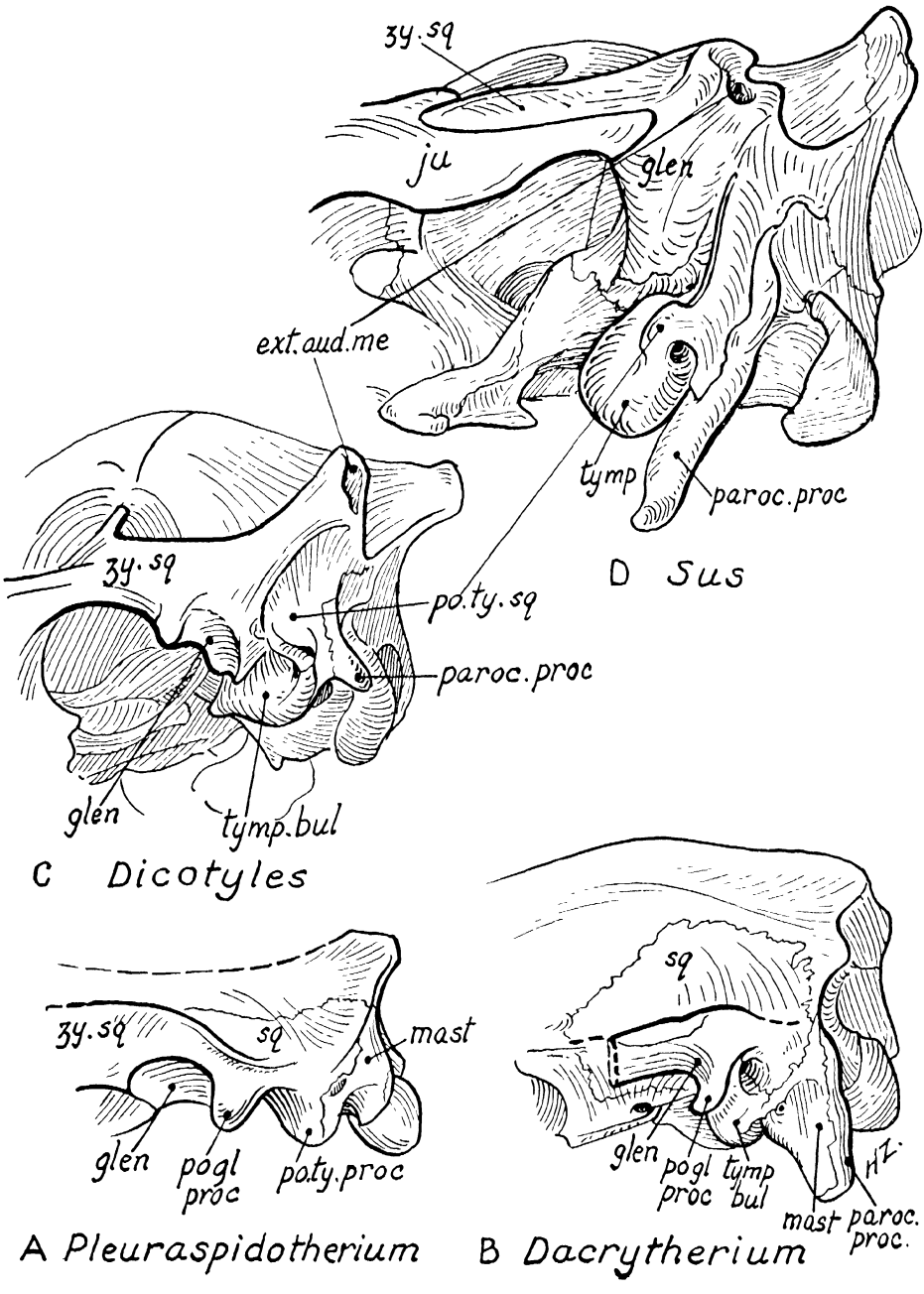


Fig. 21.86. Exposed mastoid process of periotic complex in primitive Paleocene condylarth (A) and an Eocene anoplothere (B); mastoid reduced or wanting in Recent peccary (C) and pig (D). After H Pearson

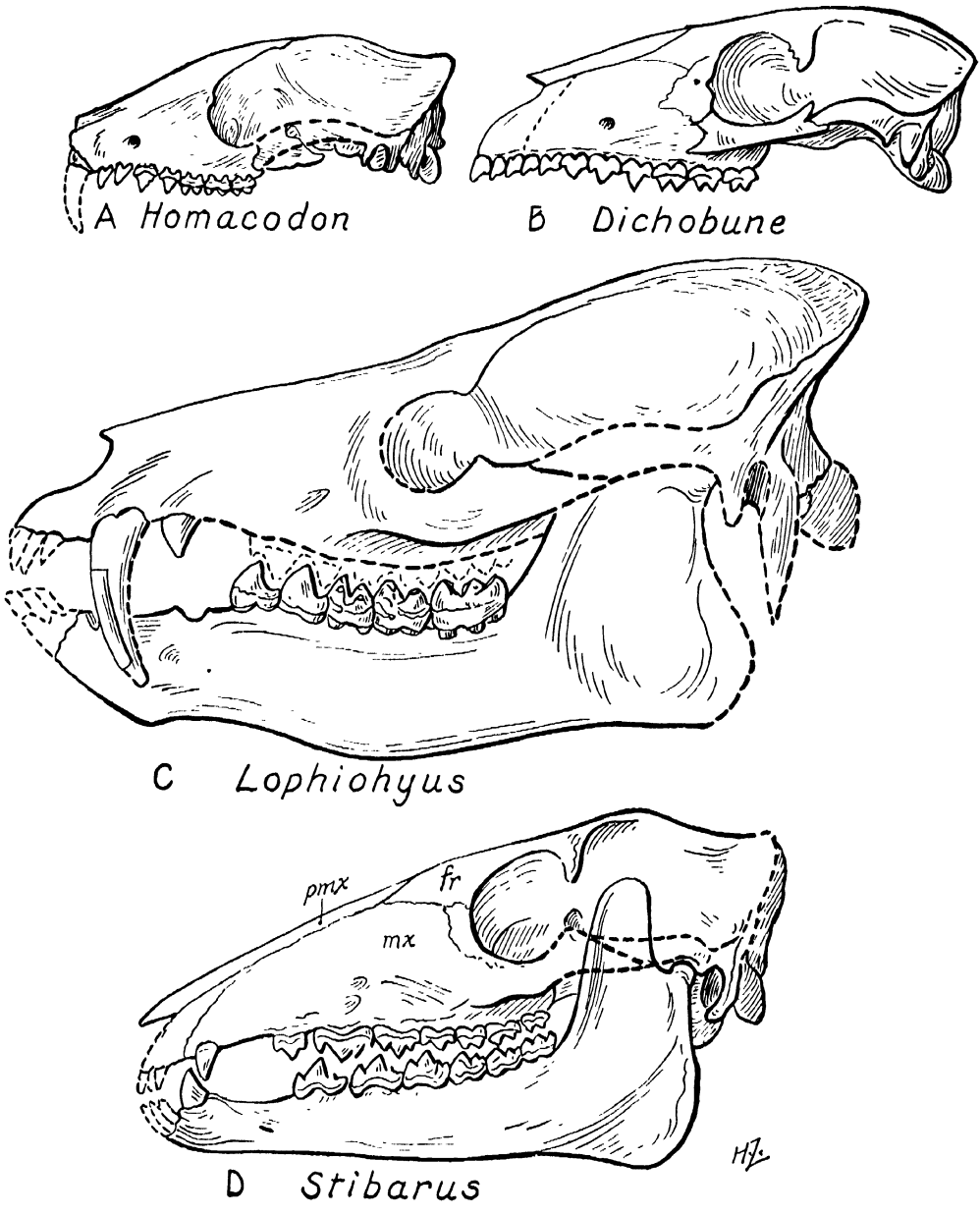


Fig. 21.87. Skulls of relatively primitive Eocene (A–C) and Lower Oligocene artiodactyls. A, after Sinclair; B, after Stehlin; C, data partly from Sinclair; D, after Scott and Jepsen.

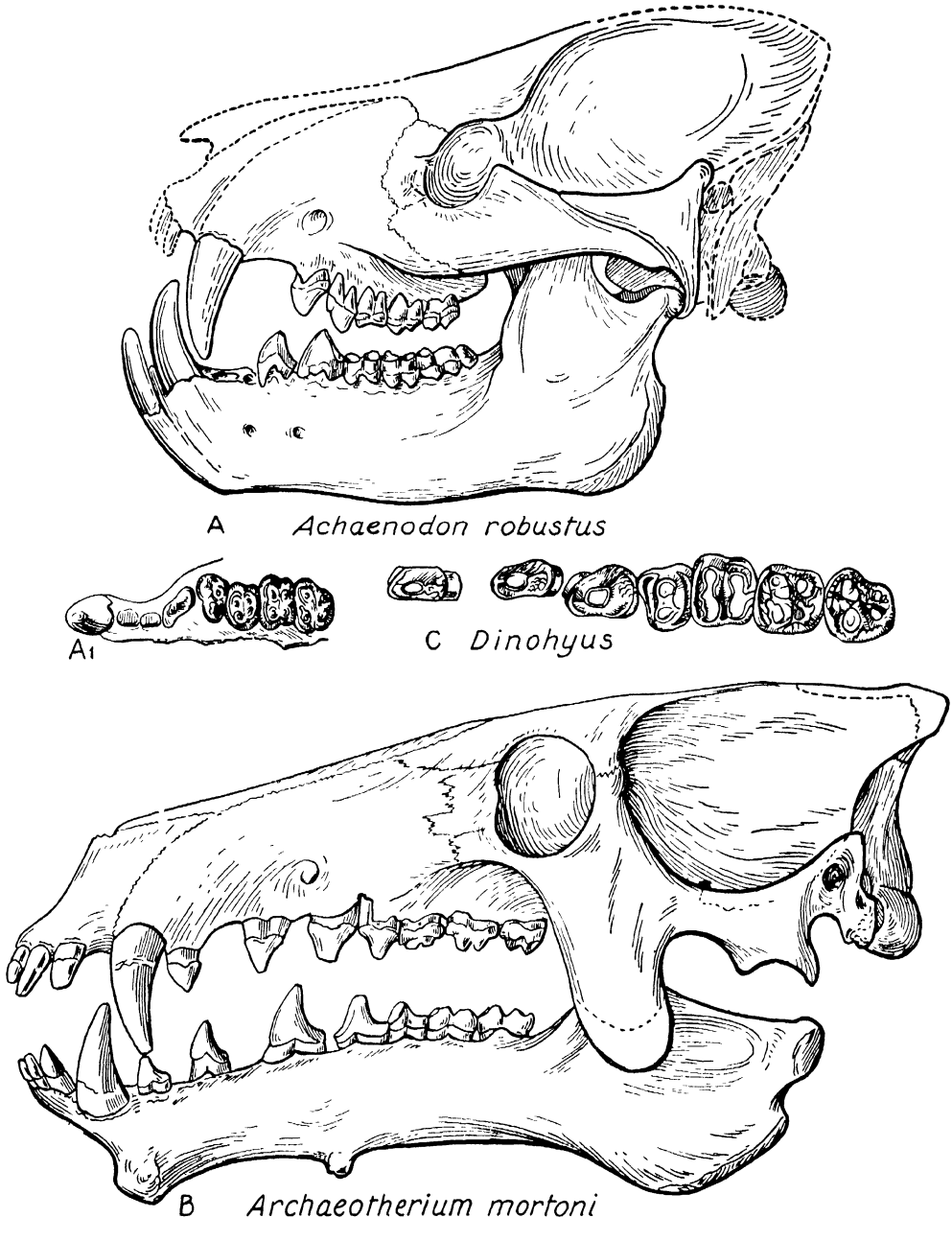


Fig. 21.88. Skulls and teeth of relatively primitive Upper Eocene achaenodont (A, A1), specialized Oligocene (B) and Lower Miocene (C) entelodonts. A, A1, after Scott and Osborn; B, C, after Holland and Peterson.

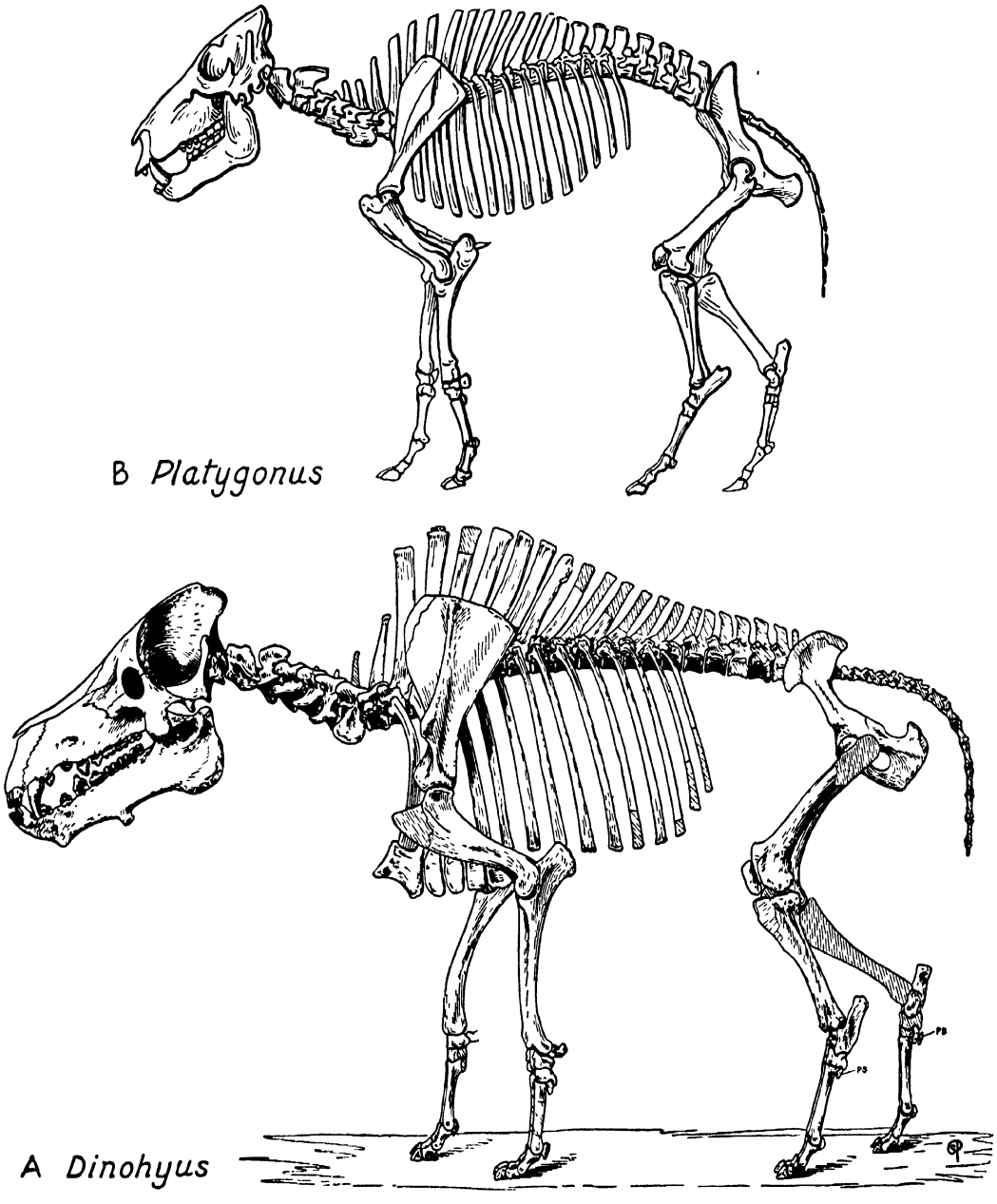


Fig. 21.89. Skeletons of Lower Miocene entelodont (A) and Pleistocene peccary (B). A, after Holland and Peterson; B, after Hay. Not to scale.

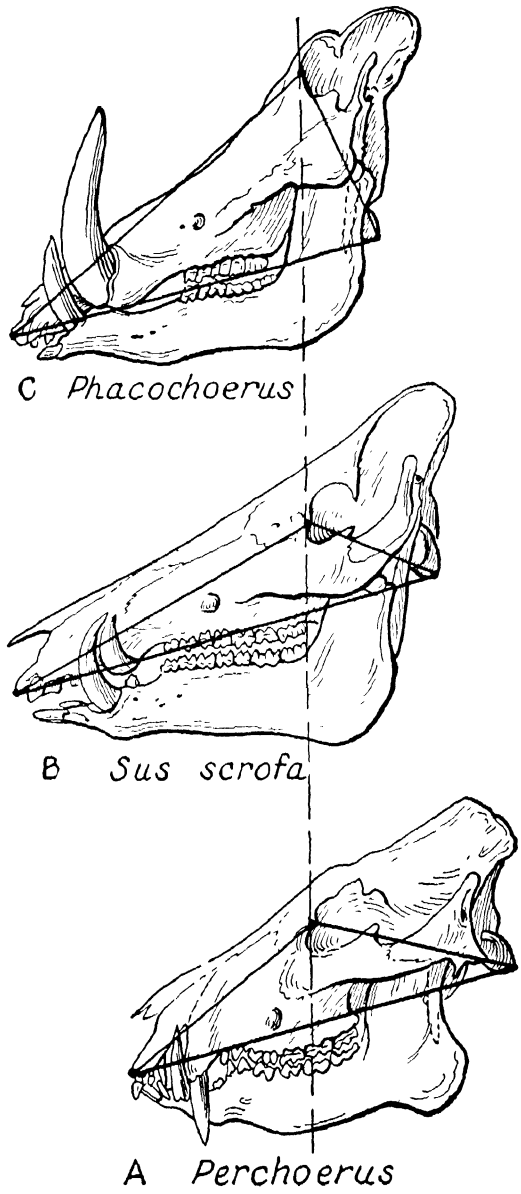


Fig. 21.90. Skulls of Oligocene (A) and Recent (B, C) suoids, showing progressive elevation and dorsal retreat of orbits. Data from H. Pearson (A), De Blainville, Colbert, and specimens.

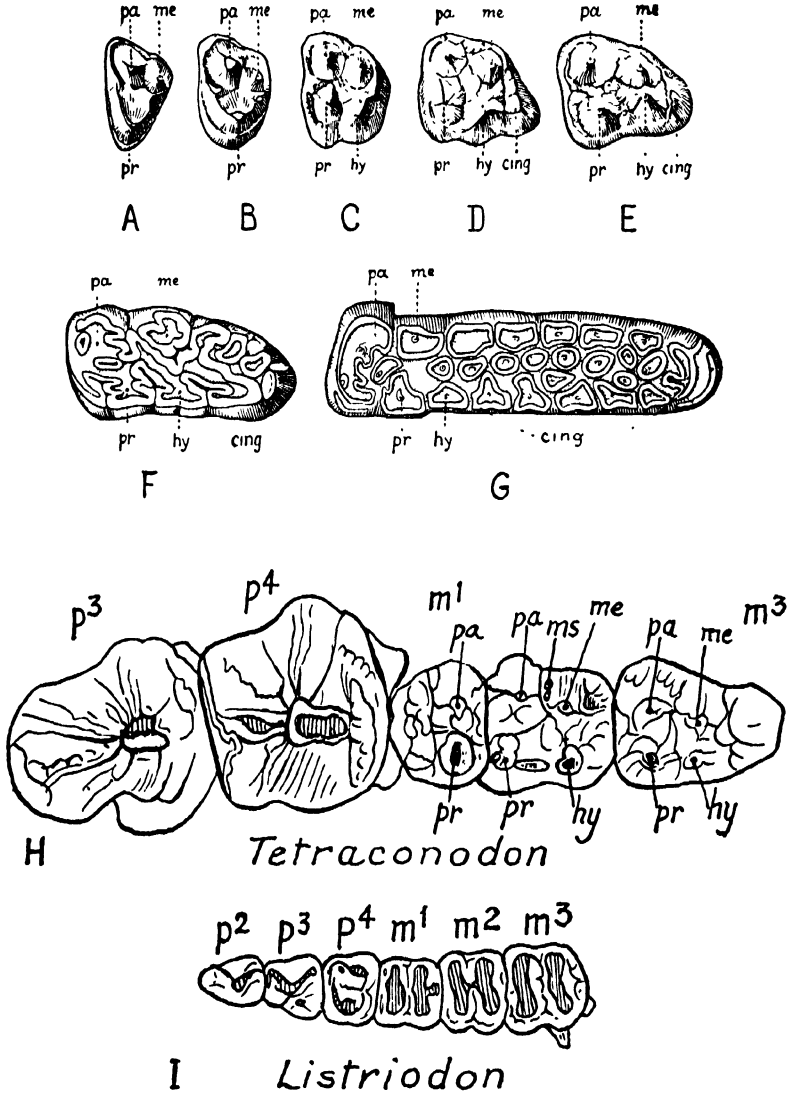


Fig. 21.91. A–G, Third left upper molars, indicating progressive secondary polyisomerism, with lengthening of anteroposterior diameter and addition of ridges and conules in the later forms. All reduced to same width. After Gregory, 1934.

A, *Chriacus baldwini*, after Osborn.

B, *Protogonodon pentacus*, after Osborn and Earle.

C, *Palaeochoerus typus*, after Stehlin

D, *Palaeochoerus waterhousi*, after Stehlin.

E, *Dicoryphochoerus* sp, after Colbert.

F, *Sus falconeri*, after Lydekker.

G, *Phachochoerus* sp.

H, Giant suid from Siwaliks (late Tertiary) of India, with greatly enlarged p^3, p^4, after Colbert.

I, Tapir-like teeth of another Indian suid, after Colbert.

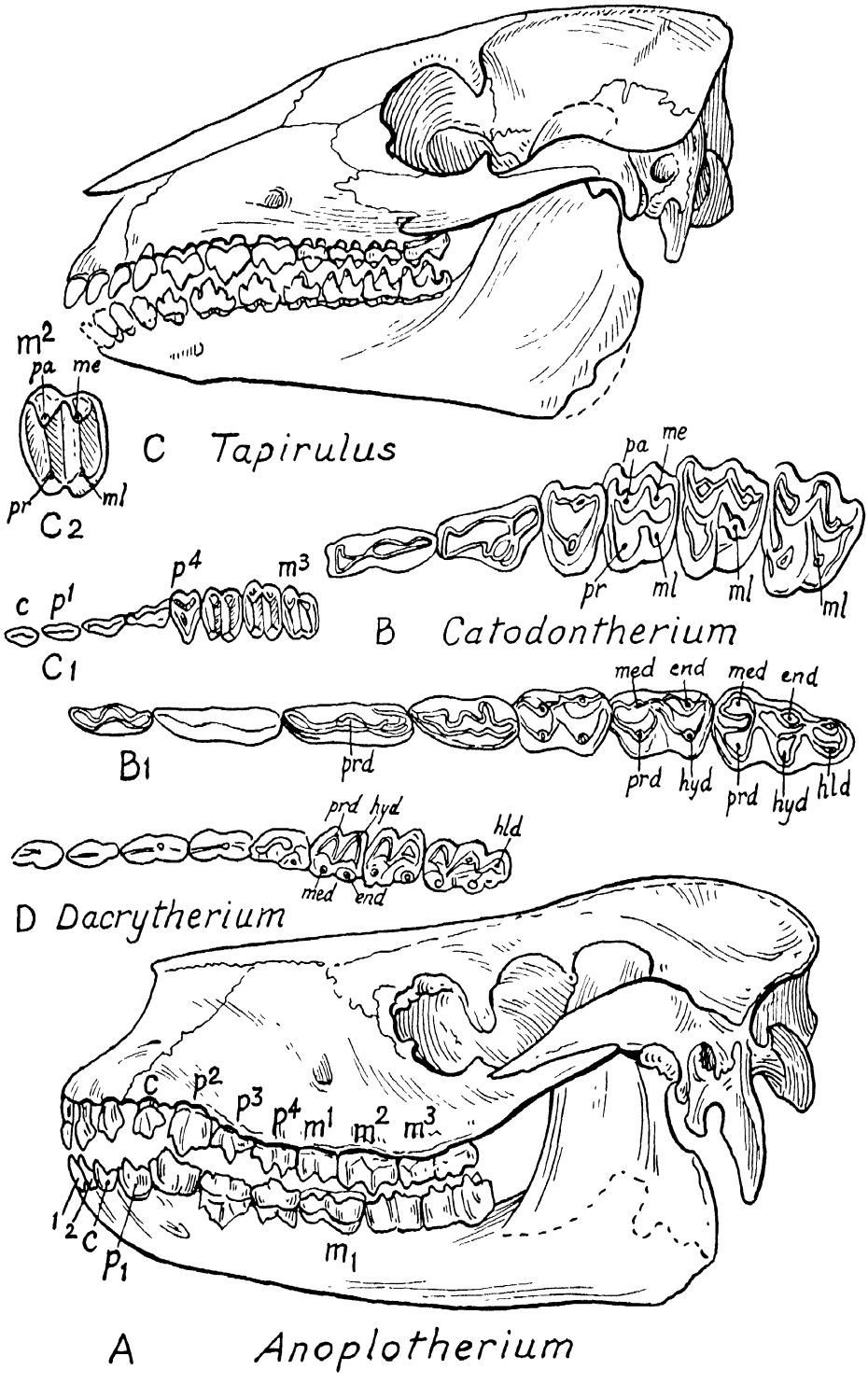


Fig. 21.92. Skulls and teeth of Eocene anoplotheres.
A, data from De Blainville, Zittel; B–D, after Stehlin.

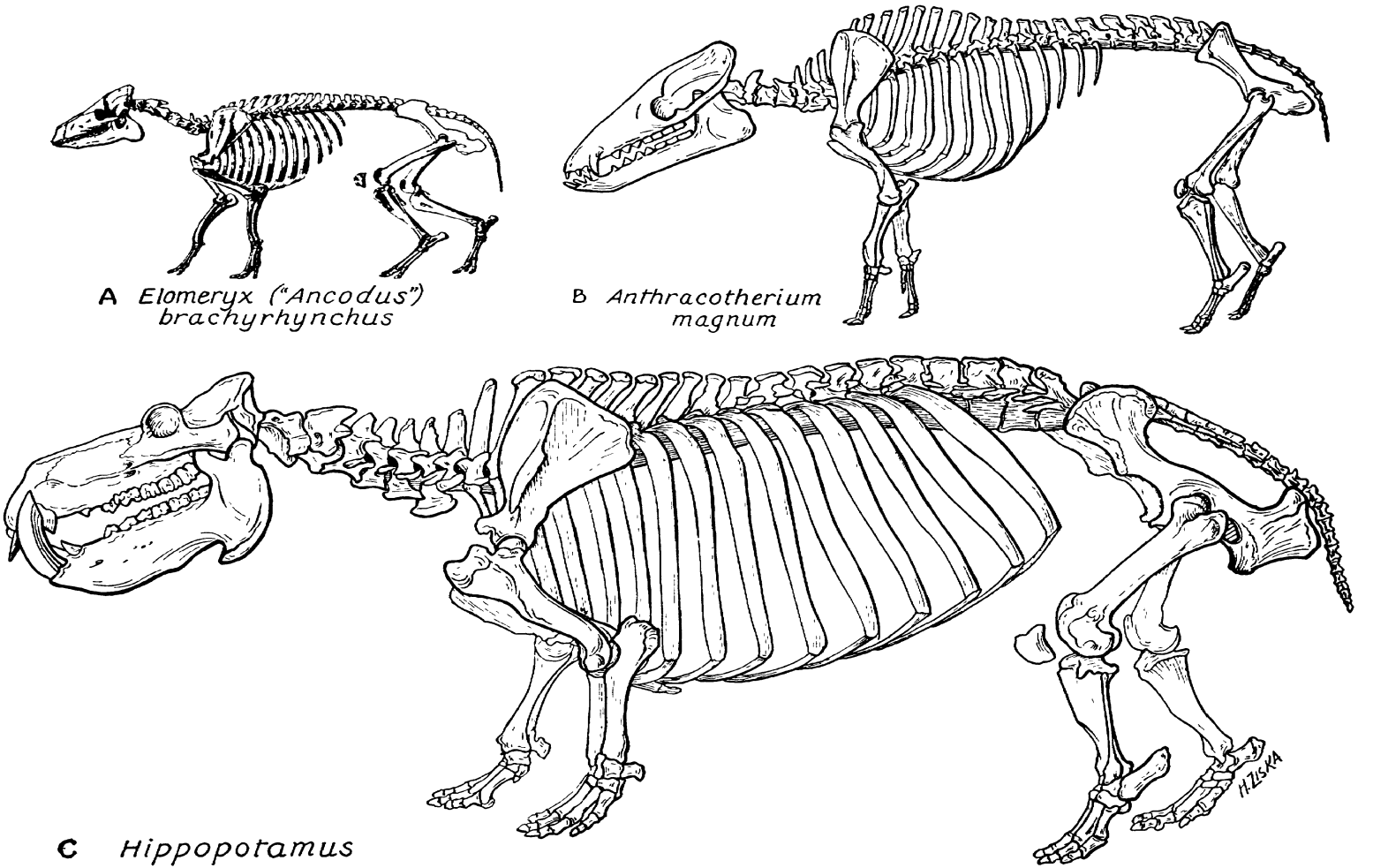


Fig. 21.93. Skeletons (not to scale) of Oligocene anthrocotheres (A, B) and a Recent hippopotamus. A, after Scott; B, data from Kowalevsky; C, after De Blainville.

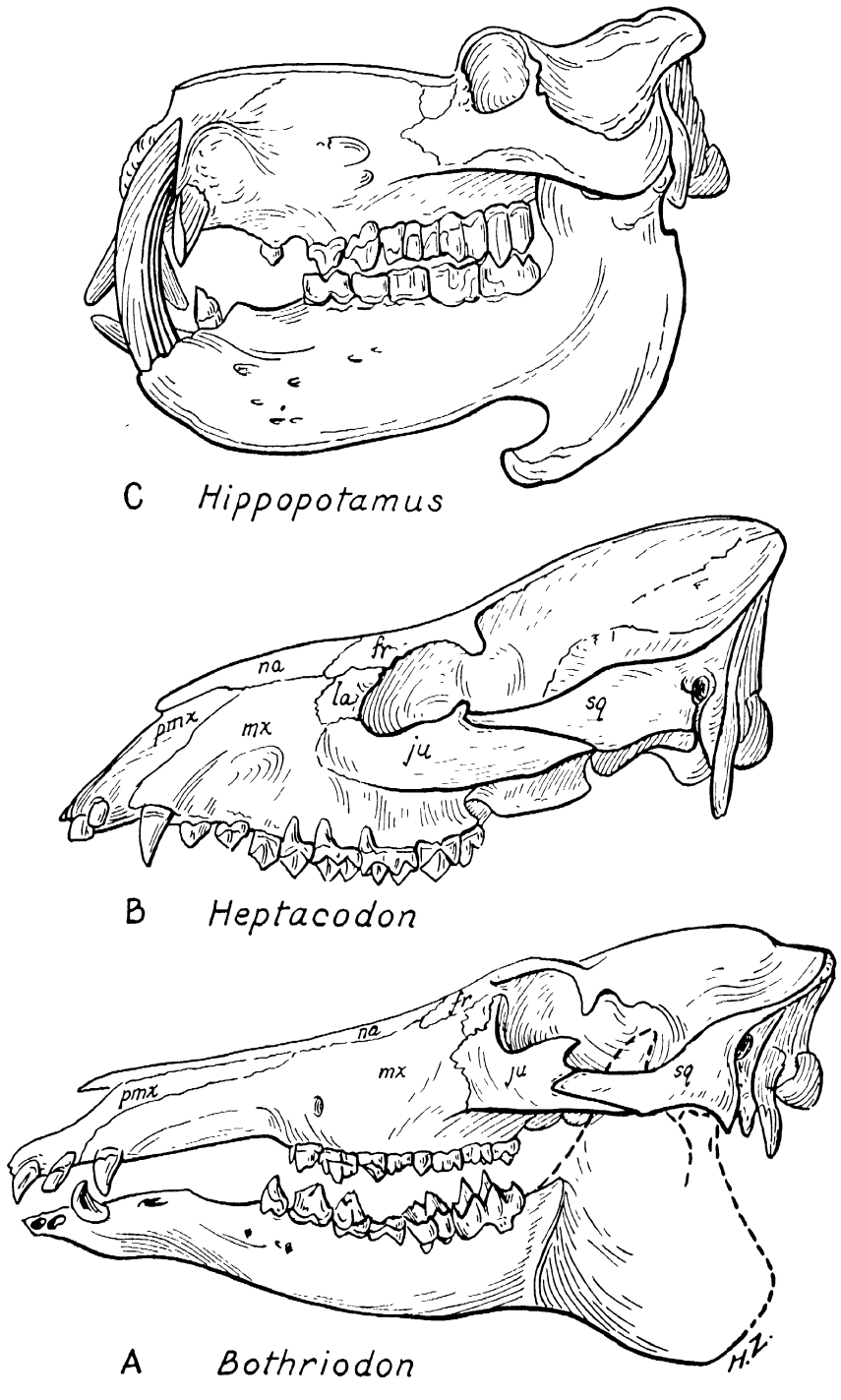


Fig. 21.94. Skulls of Oligocene anthracotheres (A, B) and Recent hippopotamus (C). A, B, after Scott; C, after De Blainville.

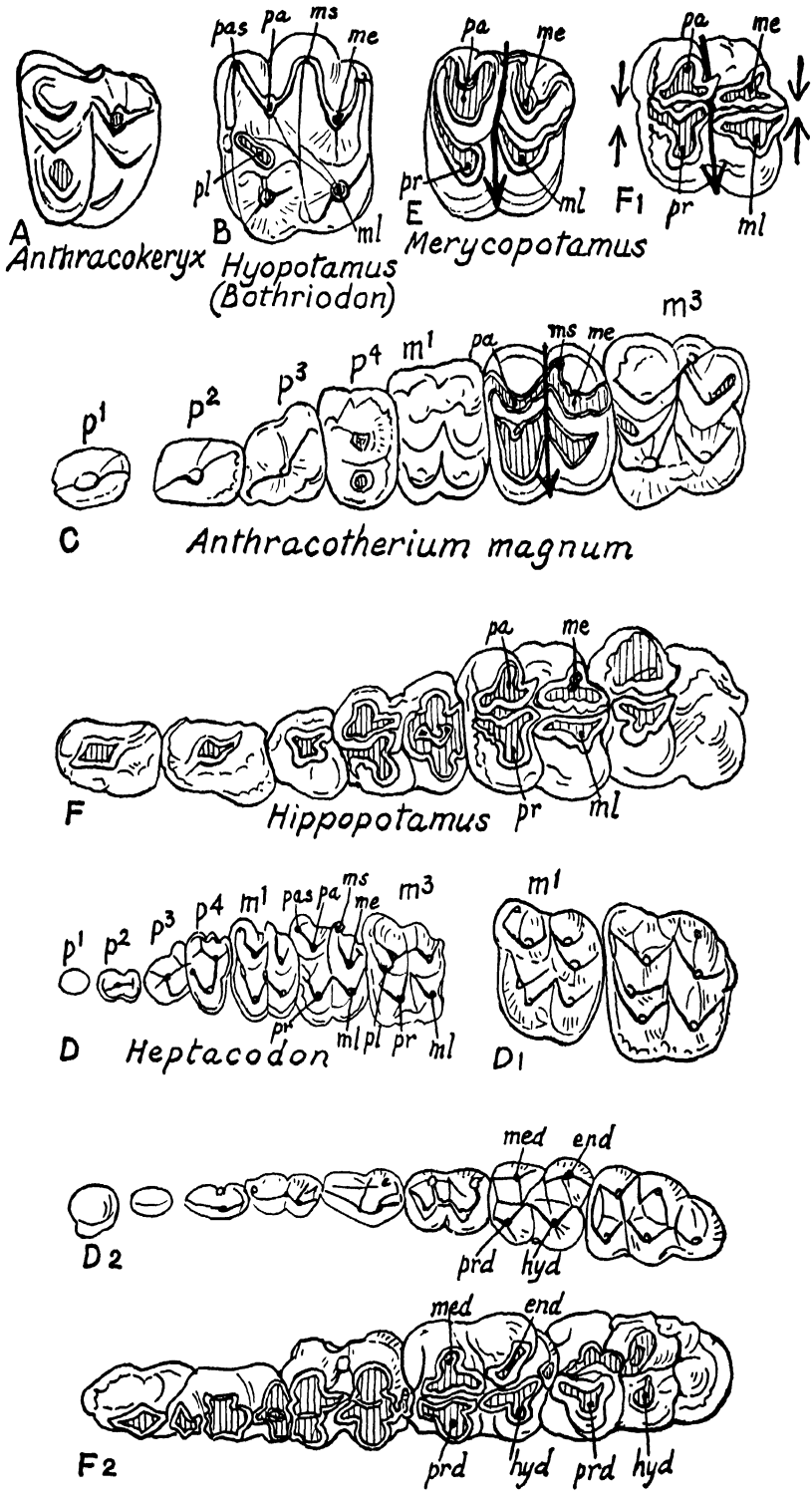


Fig. 21.95a. Teeth of anthracotheres (A–E); hippopotami (F, F1, F2). A, B, E, from specimens; C, F, F1, F2, after De Blainville; D, D1, D2, after Scott and Jepsen.

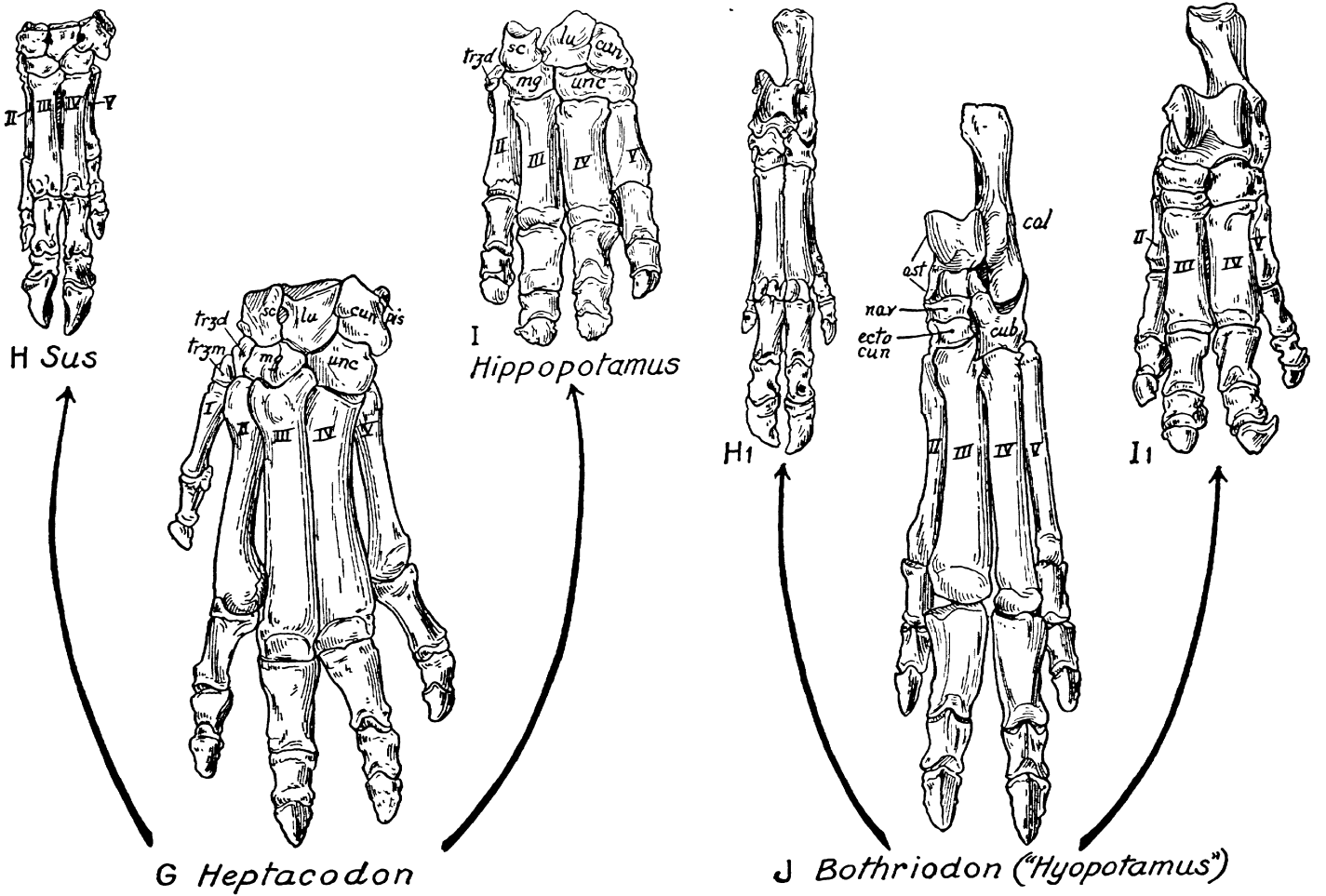


Fig. 21.95b. Left fore (H, G, I) and hind (J, H1, I1) feet of Oligocene anthracotheres (G, J), Recent pig (H, H1), and hippopotamus (I, I1). G–J, after Scott and Jepsen.

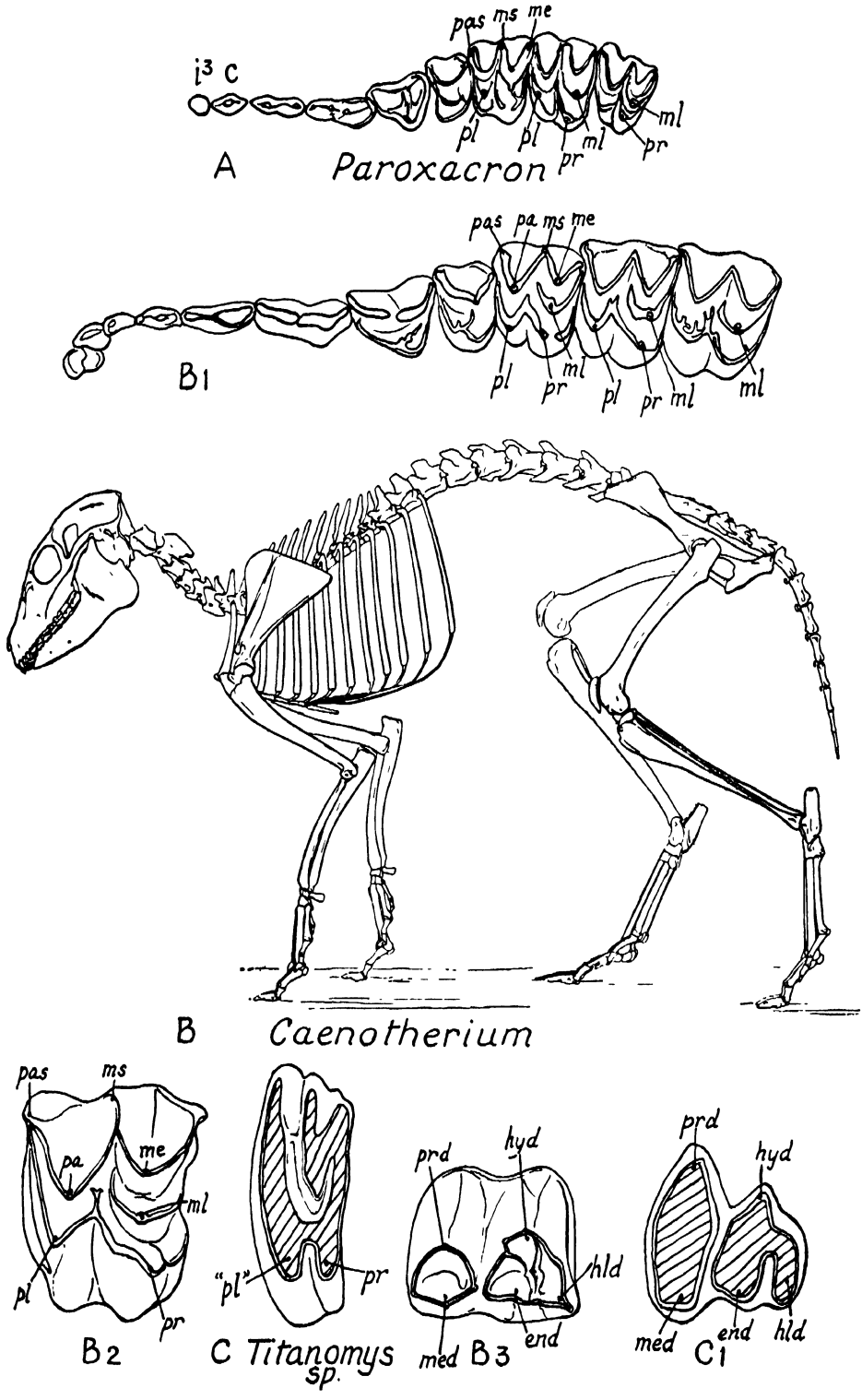


Fig. 21.96. A–B3, teeth and skeleton of caenotheres; C, upper, C1, lower, molar patterns of Oligocene lagomorph rodent. After Hürzeler.

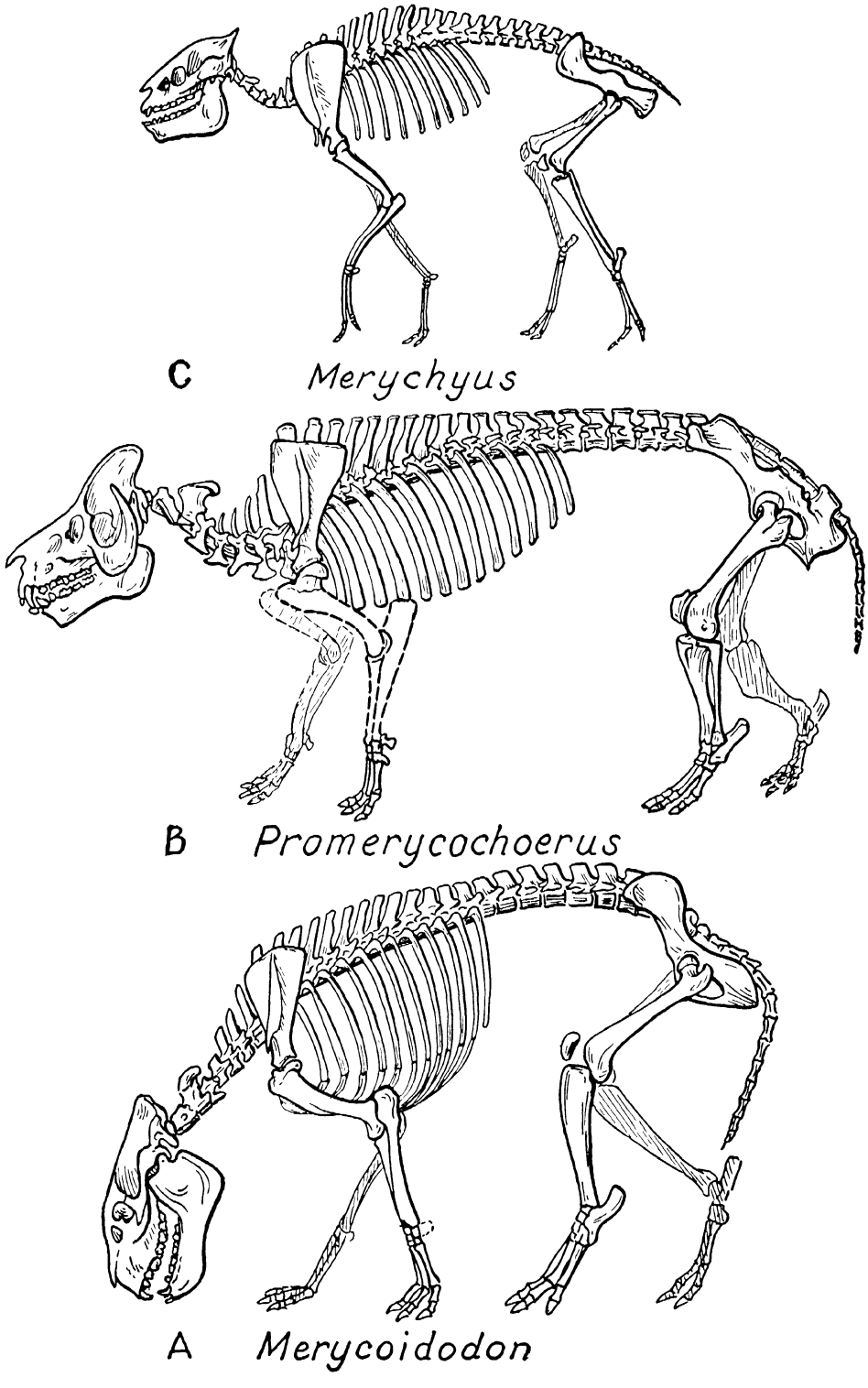


Fig. 21.97. Skeletons of oreodonts. Data from Thorpe, Loomis, Peterson, Scott, and Jepsen.

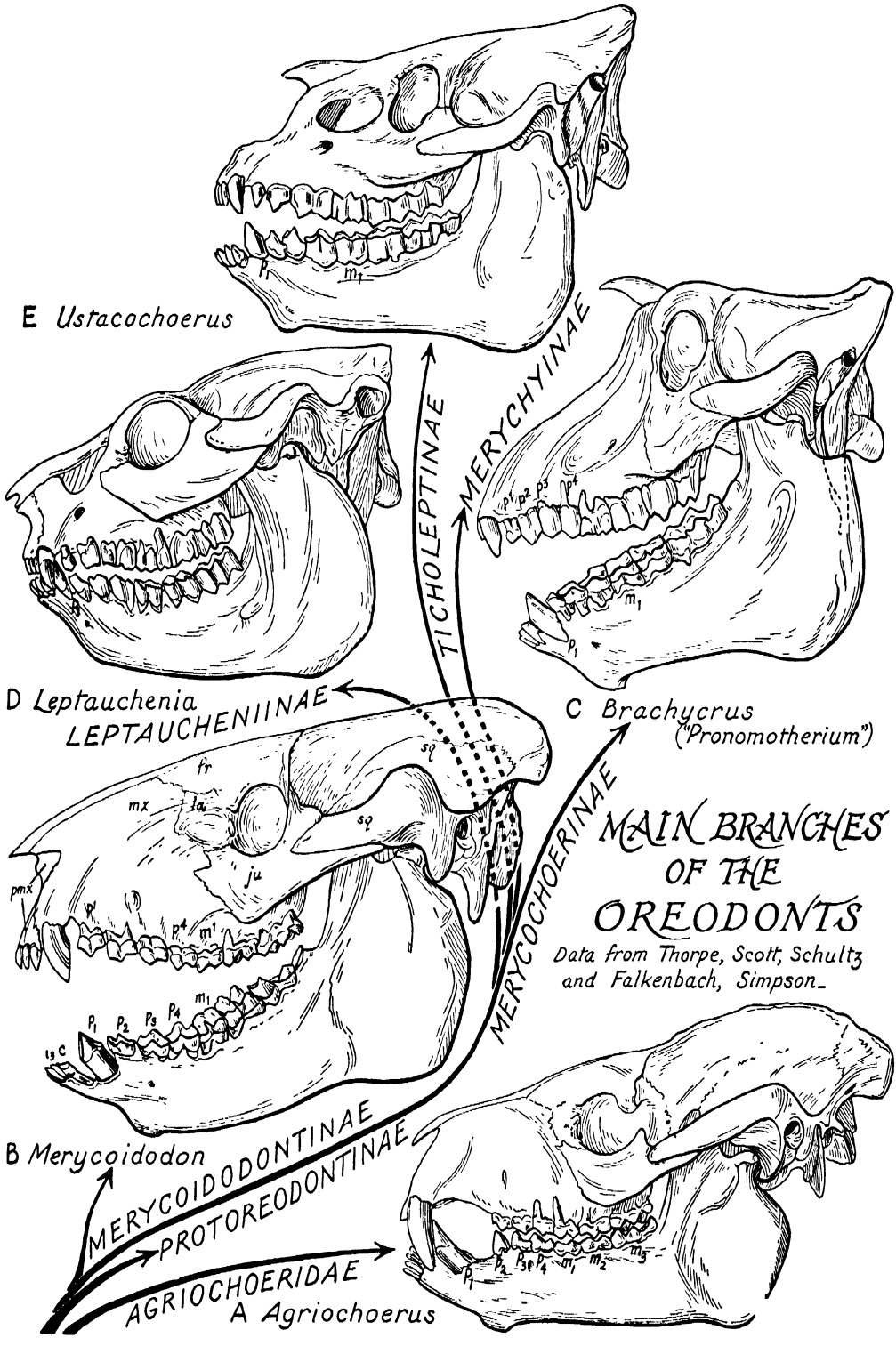

E Ustacochoerus
TICHOLEPTINAE
MERYCHYINAE
D Leptauchenia
LEPTAUCHENIINAE
C Brachycrus
("Pronomotherium")
MERYCOCHOERINAE
MAIN BRANCHES
OF THE
OREODONTS
Data from Thorpe, Scott, Schultz
and Falkenbach, Simpson.
B Merycoidodon
MERYCOIDODONTINAE
PROTOREODONTINAE
AGRIOCHOERIDAE
A Agriochoerus

Fig. 21.98

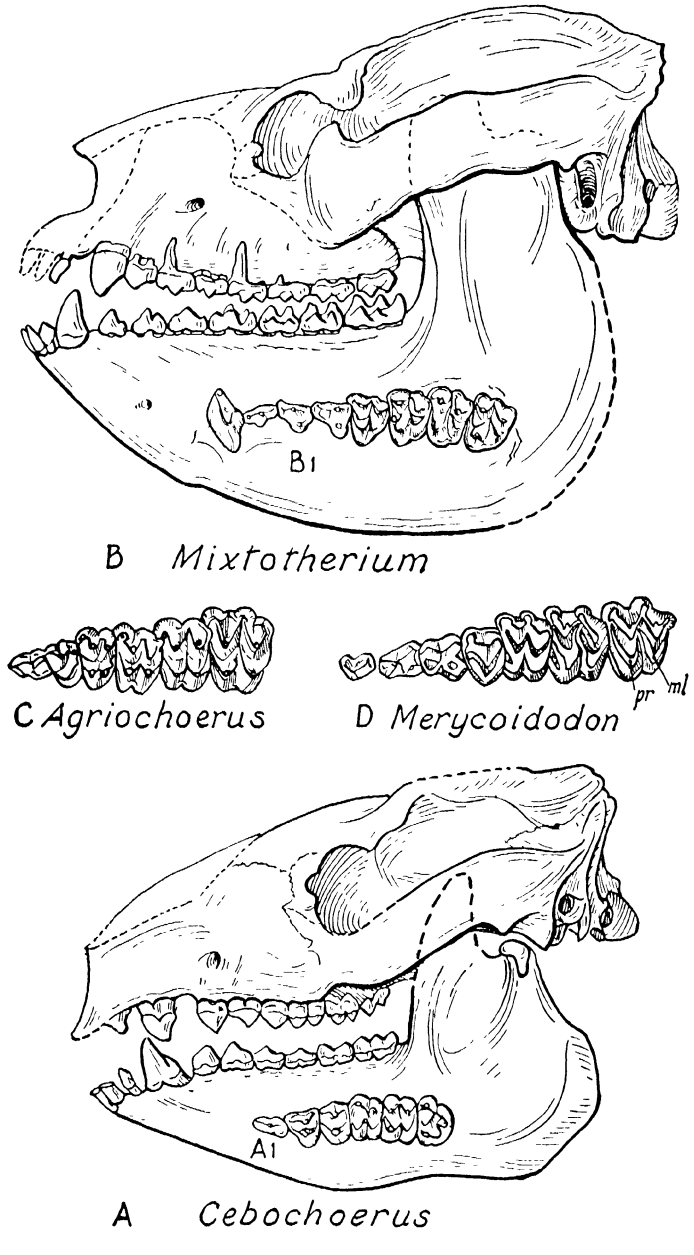


Fig. 21.99. A, B, Skulls and teeth of European dichobunids and teeth of North American oreodonts. A, A1, B, B1, after Stehlin; C, D, after Scott and Jepsen.

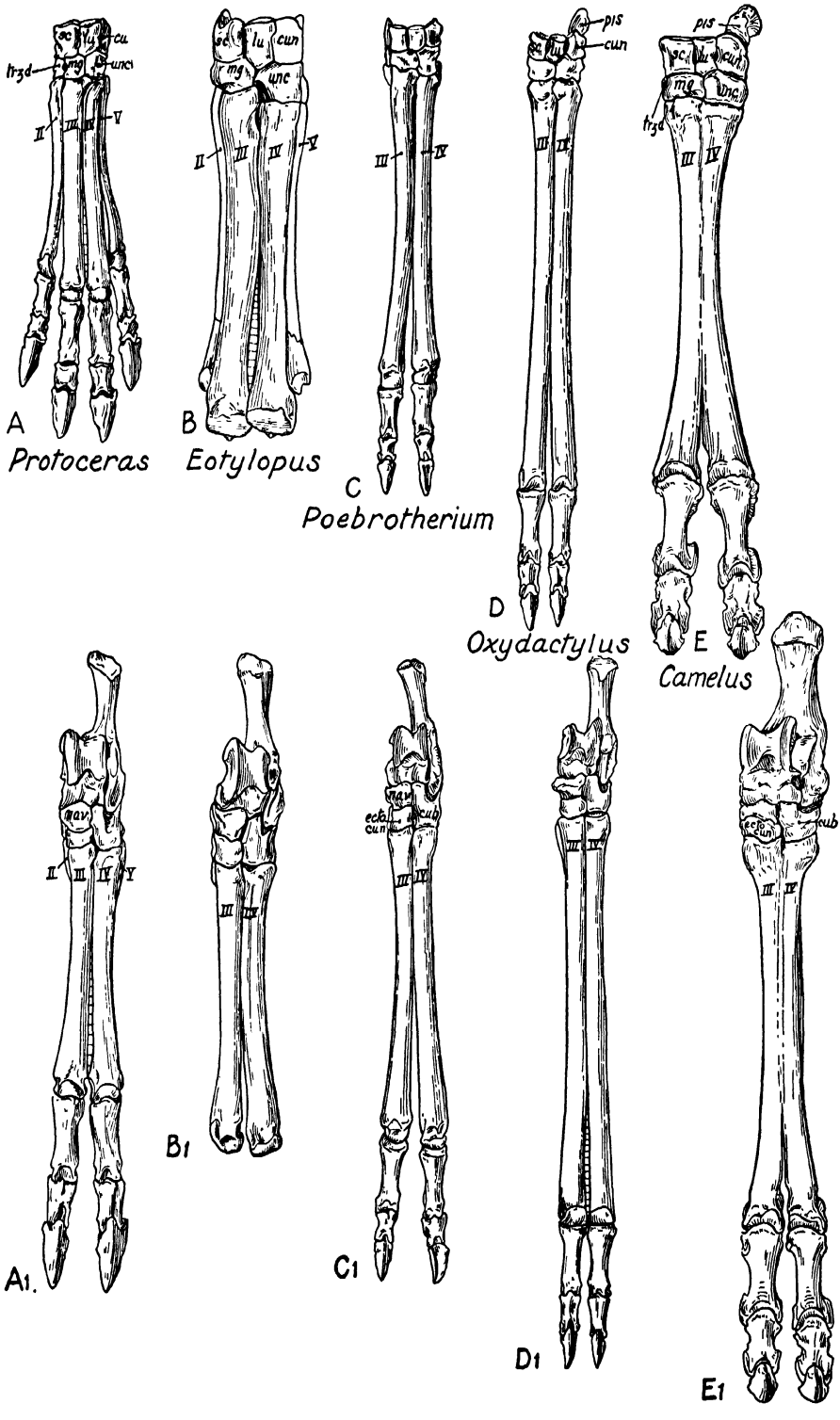


Fig. 21.100. Left fore (A–E) and hind (A1 to E1) feet of artiodactyls. Not to scale. A–C1, after Scott and Jepsen; D, D1, after Peterson; E, E1, original.

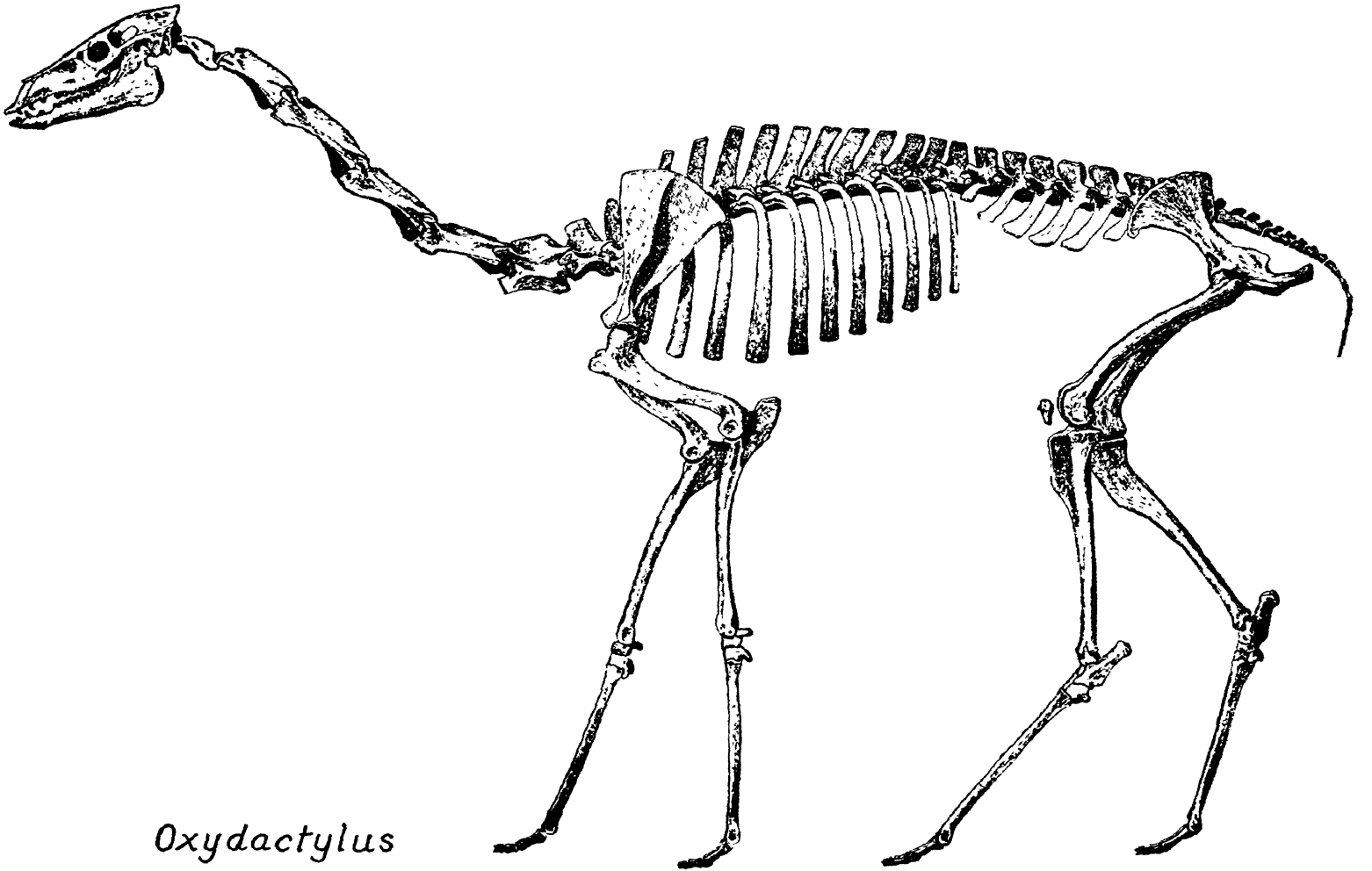


Fig. 21.101. Skeleton of Lower Miocene camel, *circa* 1/12. After Peterson.

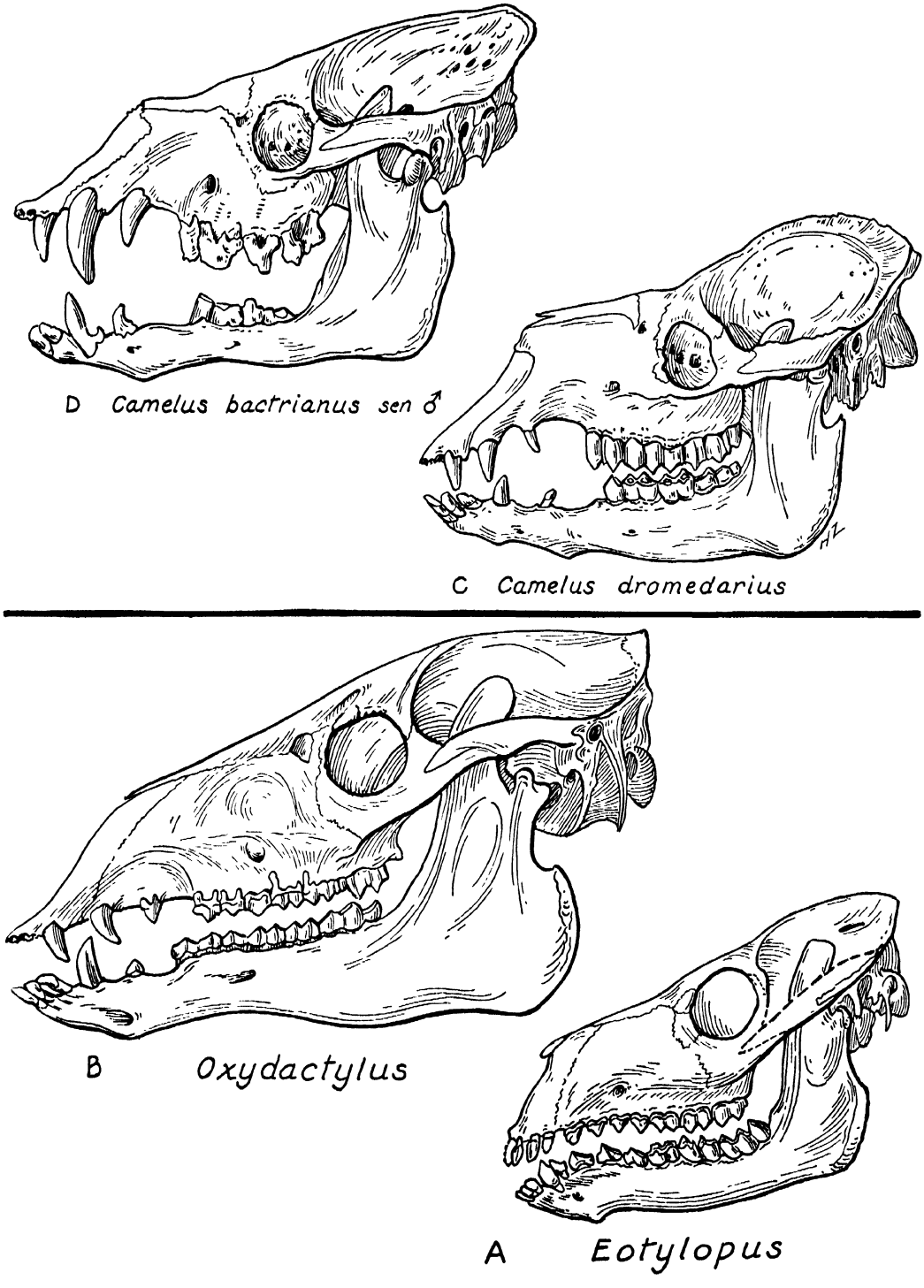


Fig. 21.102. Skulls of primitive Lower Oligocene camel and specialized Lower Miocene camel. Not to scale. A, after Scott and Jepsen; B, after Peterson; C, D, specialized and Recent camel skulls, after De Blainville. D, shows signs of extreme old age.

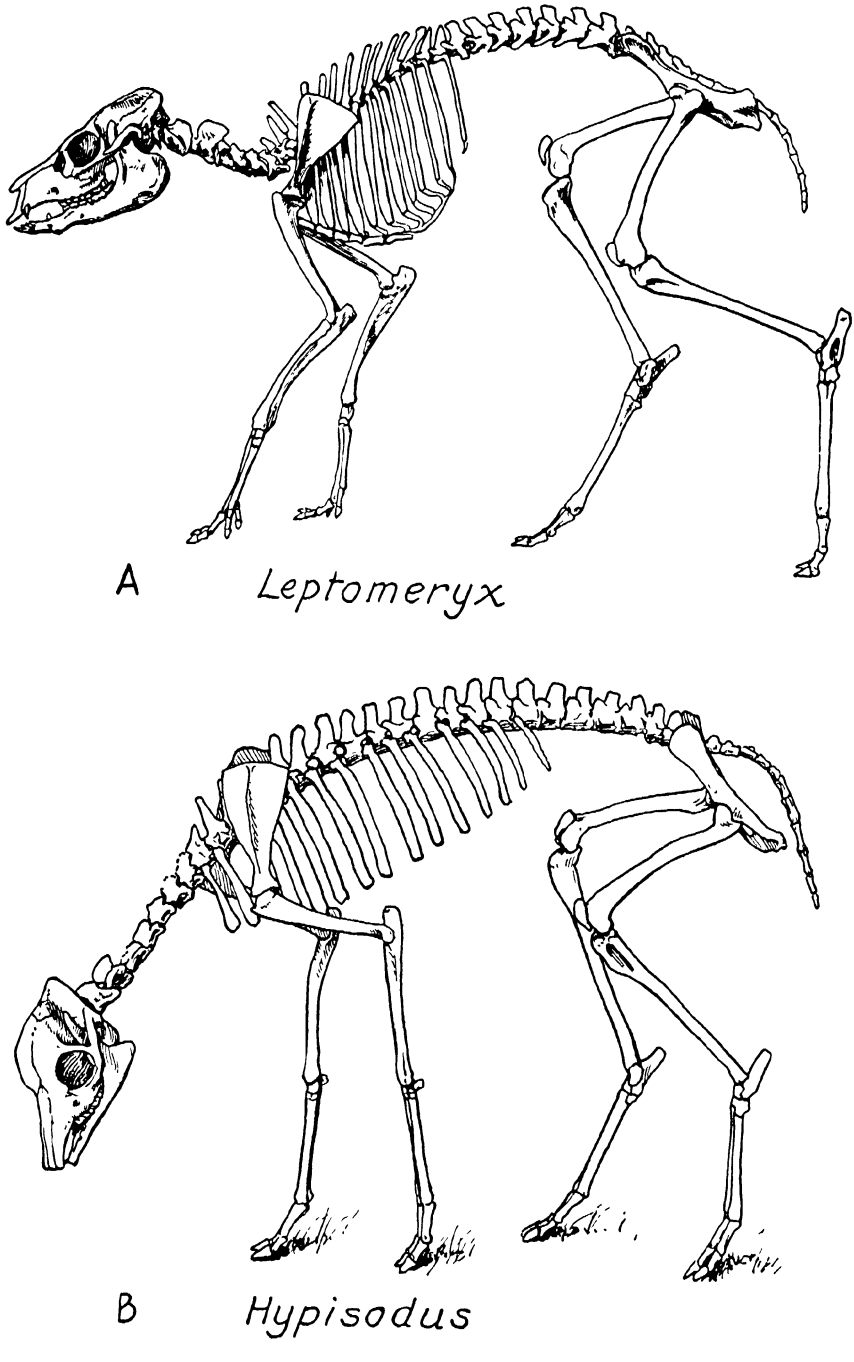


Fig. 21.103. Small Oligocene hypertraguloids. After Scott. A, may be near the common ancestors of the deer-giraffe-bovid group. B, has specialized high-crowned molars and rather camel-like legs.

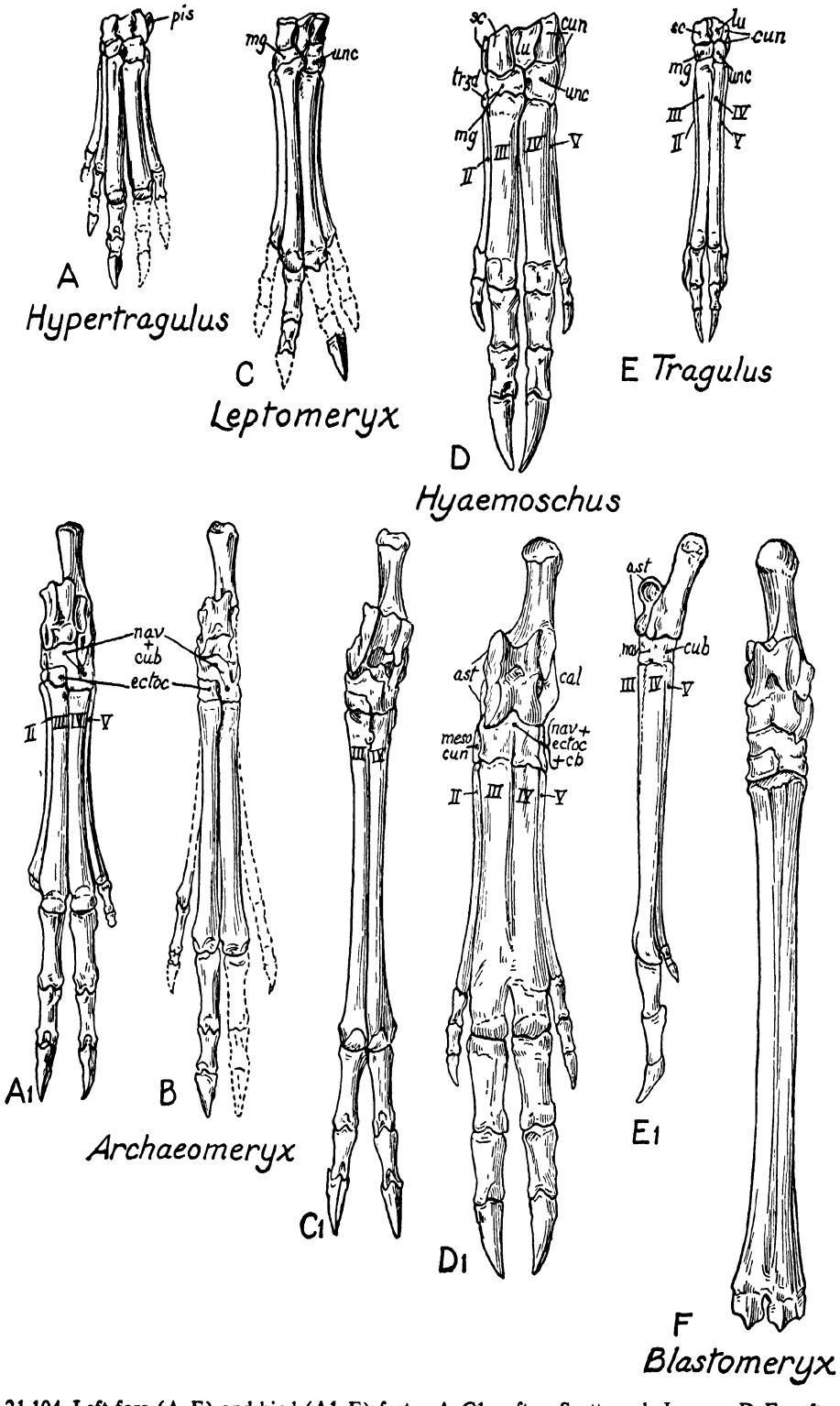


Fig. 21.104. Left fore (A–E) and hind (A1–F) feet of Oligocene (A, A1, B, D) hypertraguloids; Recent traguloids (D, D1, E1), and primitive cervoid (F). A–C1, after Scott and Jepsen; D–E, after Milne Edwards; F, after Frick.

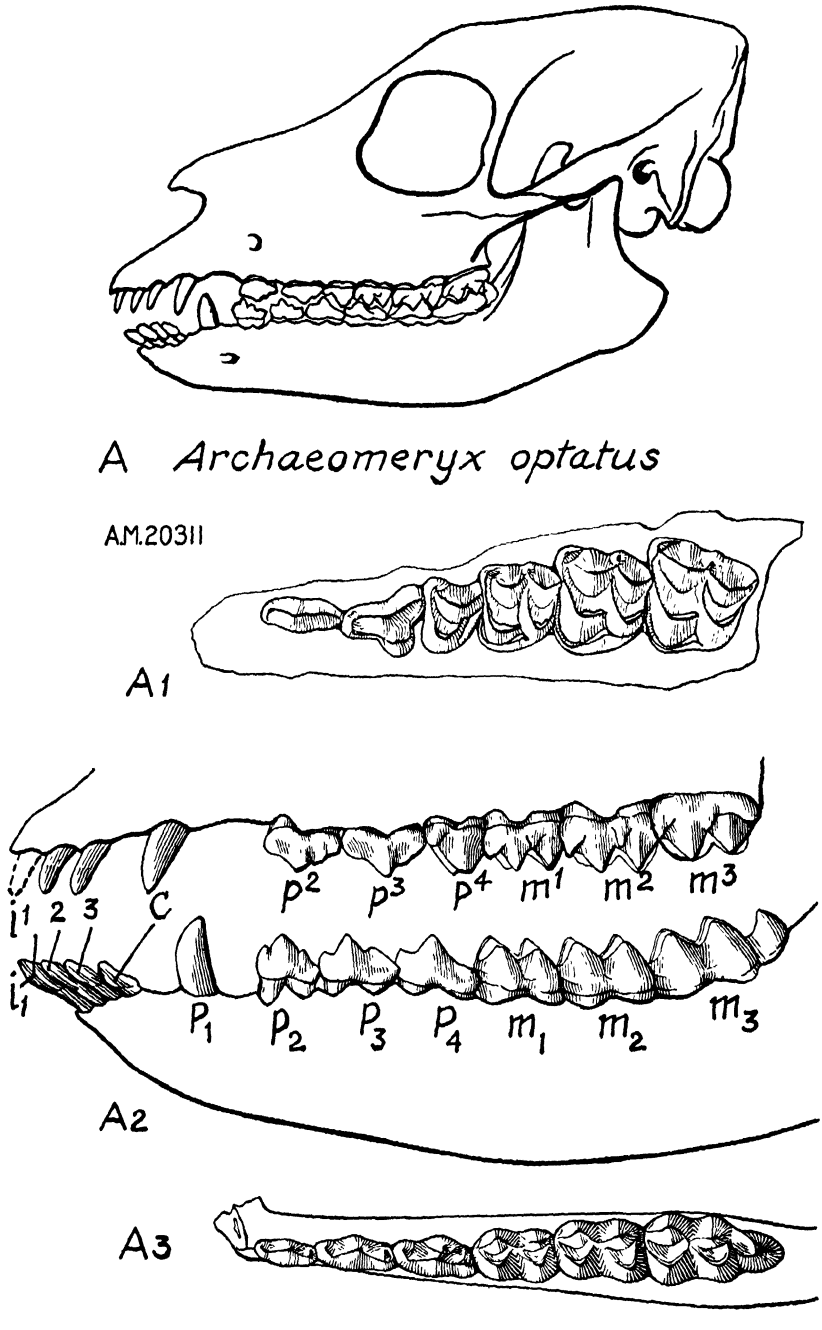


Fig. 21.105. Skull and teeth of primitive traguloid from the Upper Eocene of Mongolia. After Matthew and Colbert.

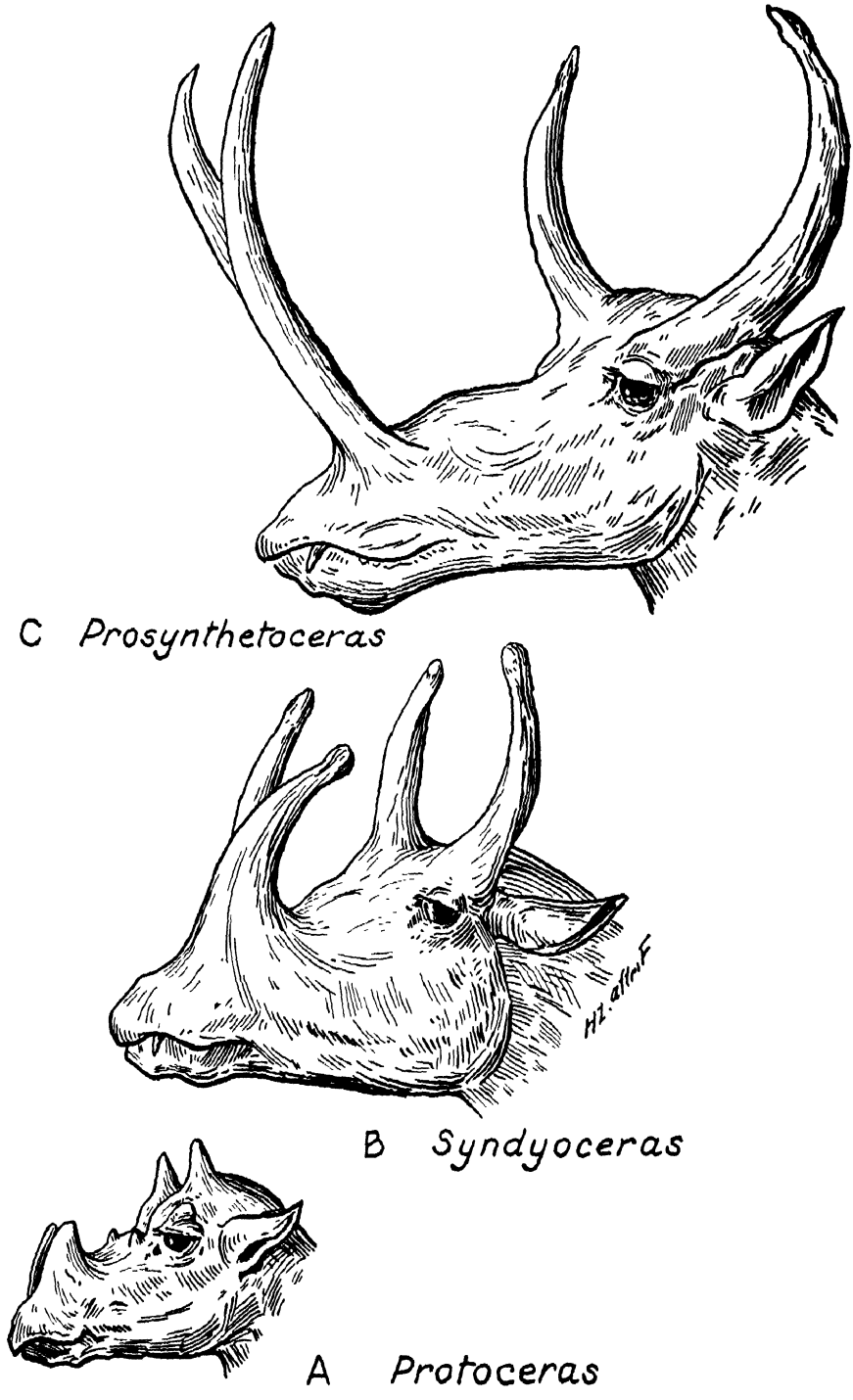


Fig. 21.106. Heads of relatively primitive (A) and specialized (B, C) protoceratids. After Frick.

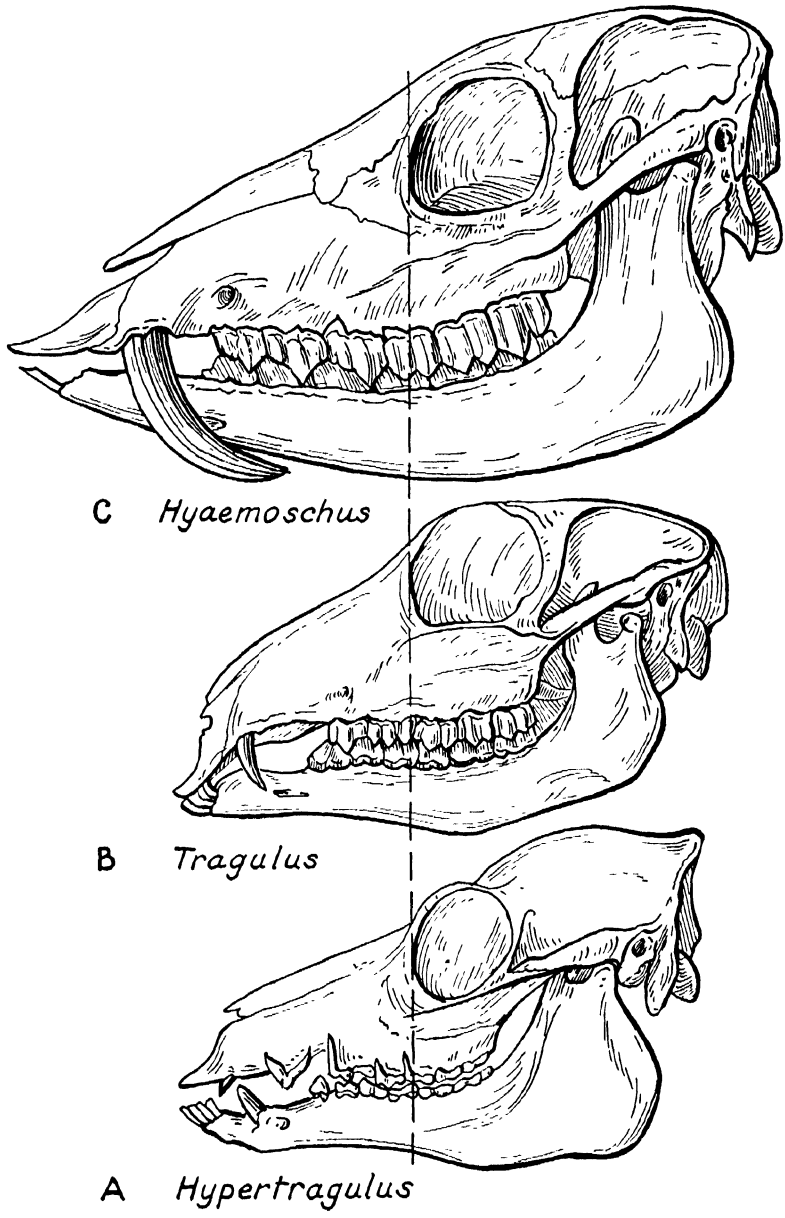


Fig. 21.107. Skulls of Oligocene hypertraguloid and Recent traguloids. A, after Frick; B, C, after Milne Edwards.

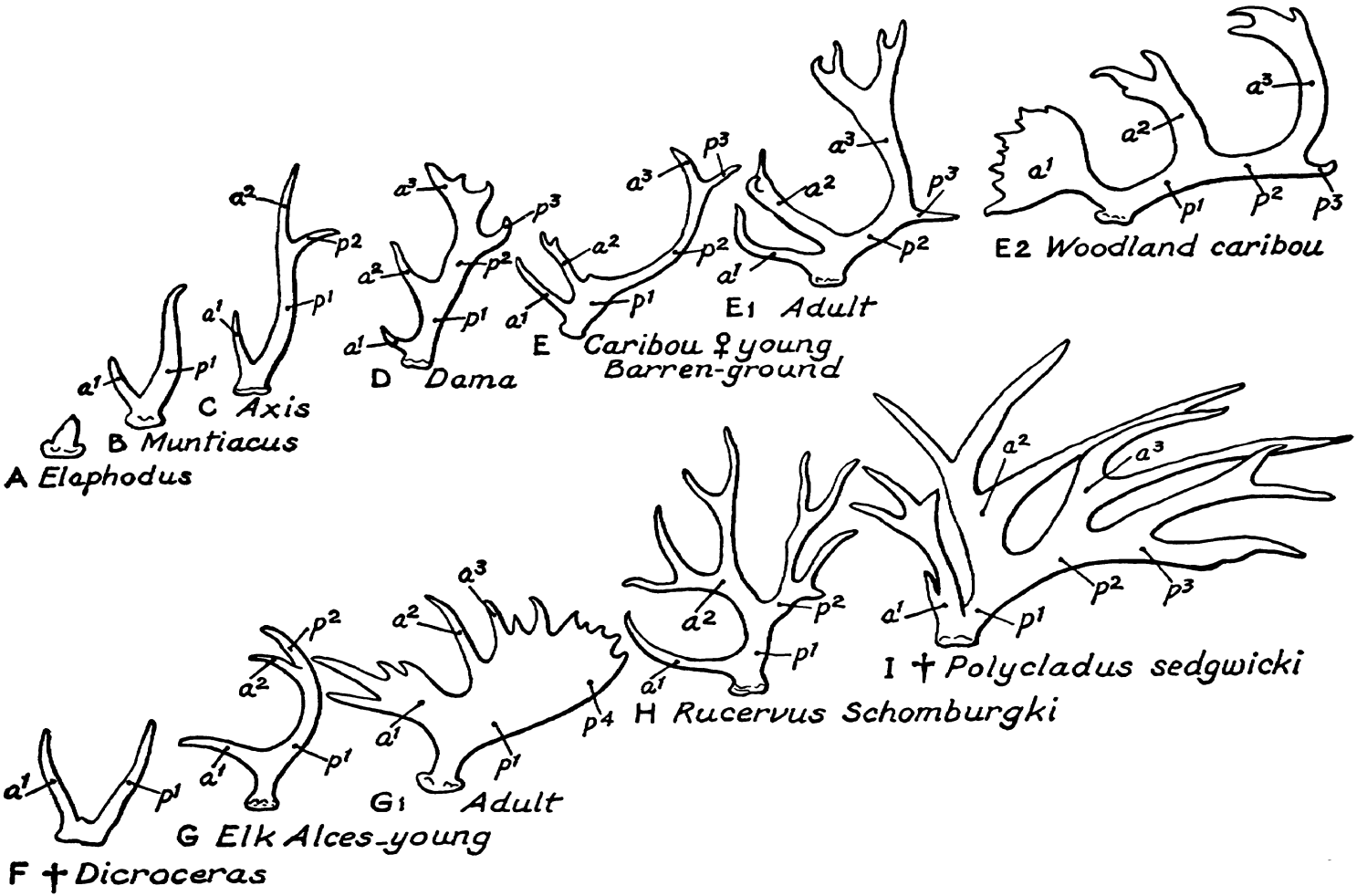


Fig. 21.108. Branching of antlers and homologies of tines in deer. After Pocock.

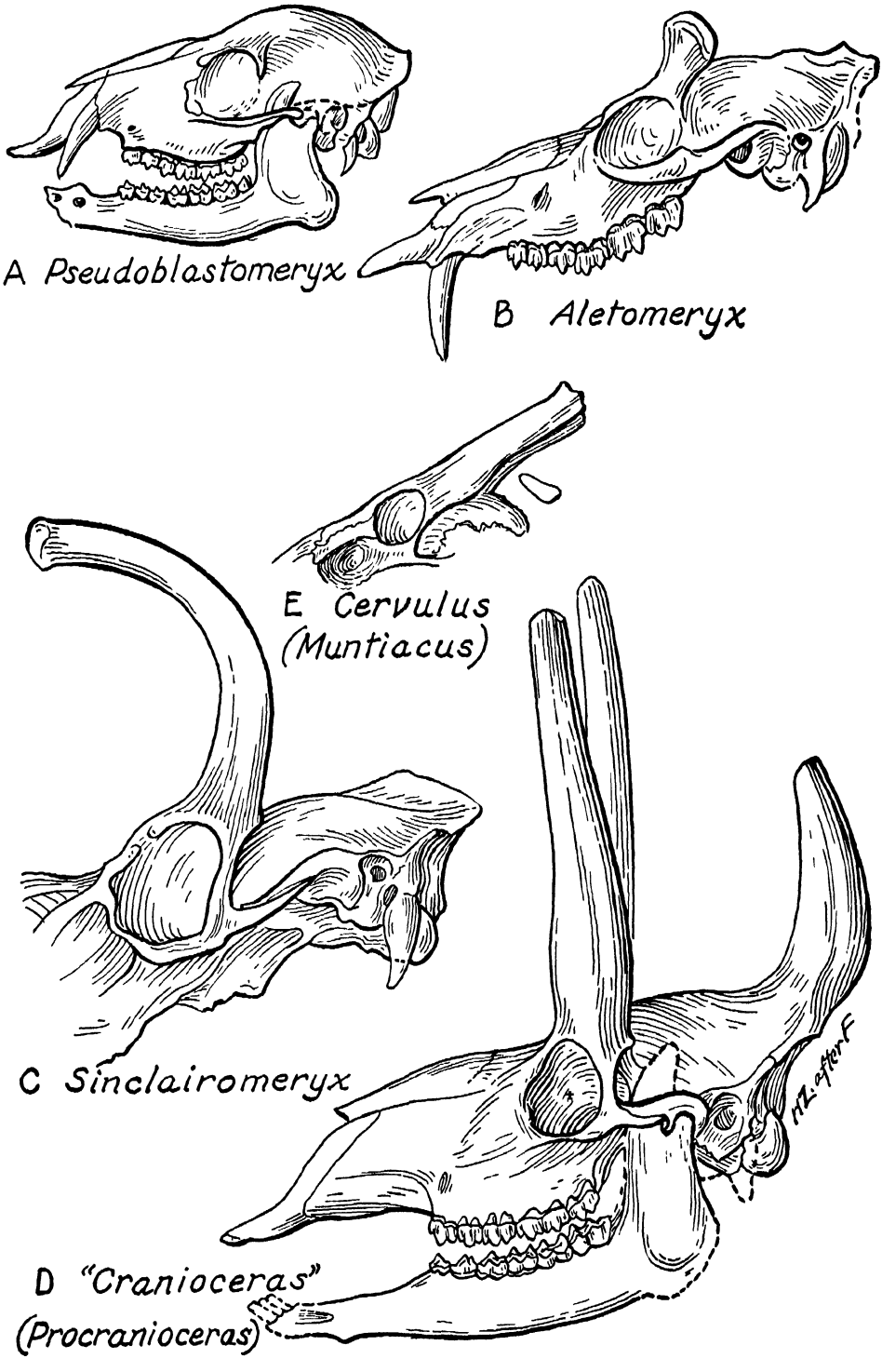


Fig. 21.109. Skulls of primitive (A) intermediate (B) to specialized extinct side branches (C, D) of the Cervoidea. After Frick. B, C, D, in some features resemble the musk-deer (E) but their cheek teeth suggest relationships with the giraffes (cf. fig. 21.112C, D).

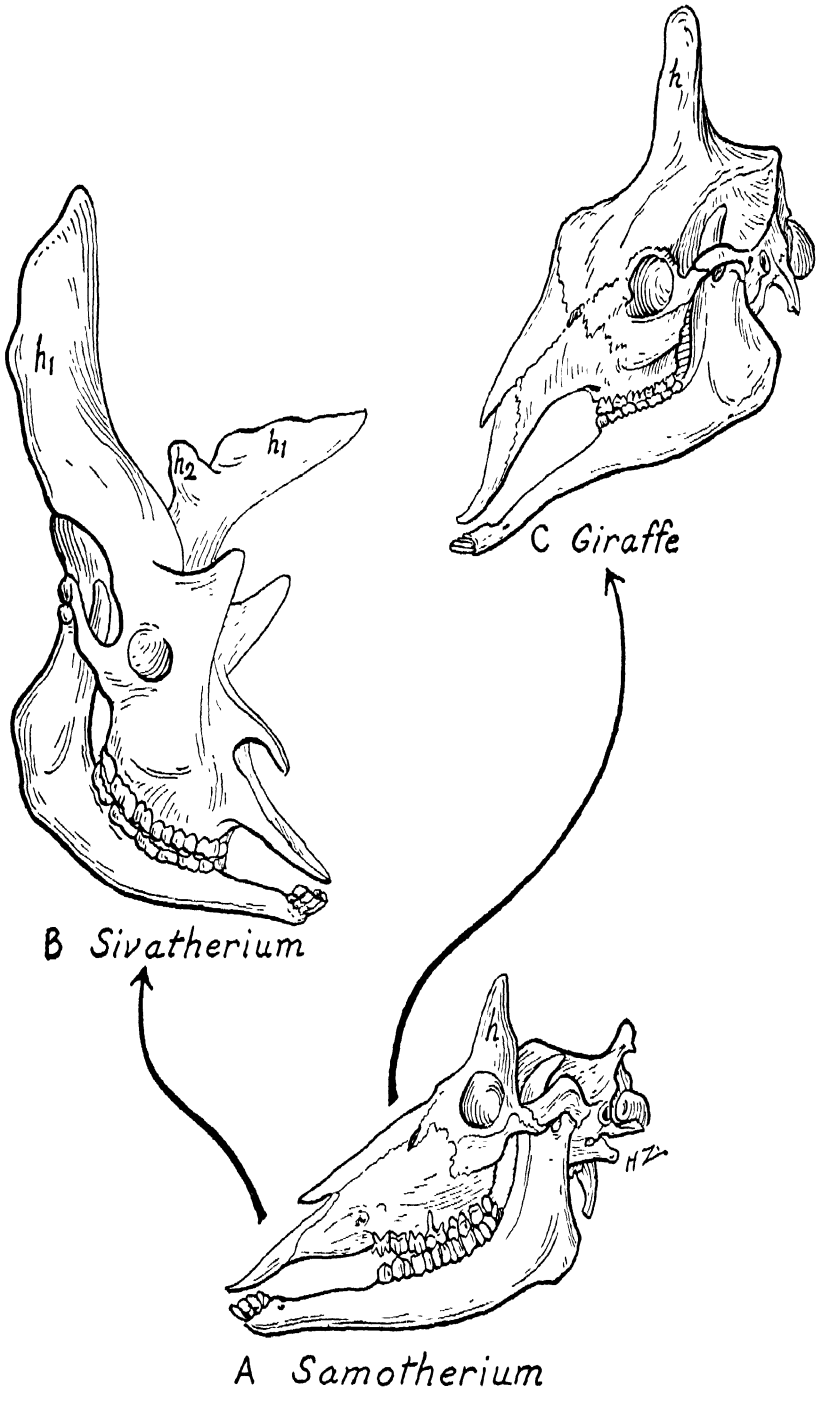


Fig. 21.110. Pliocene (A), Pleistocene (B) and Recent giraffe skulls. Data from Colbert.

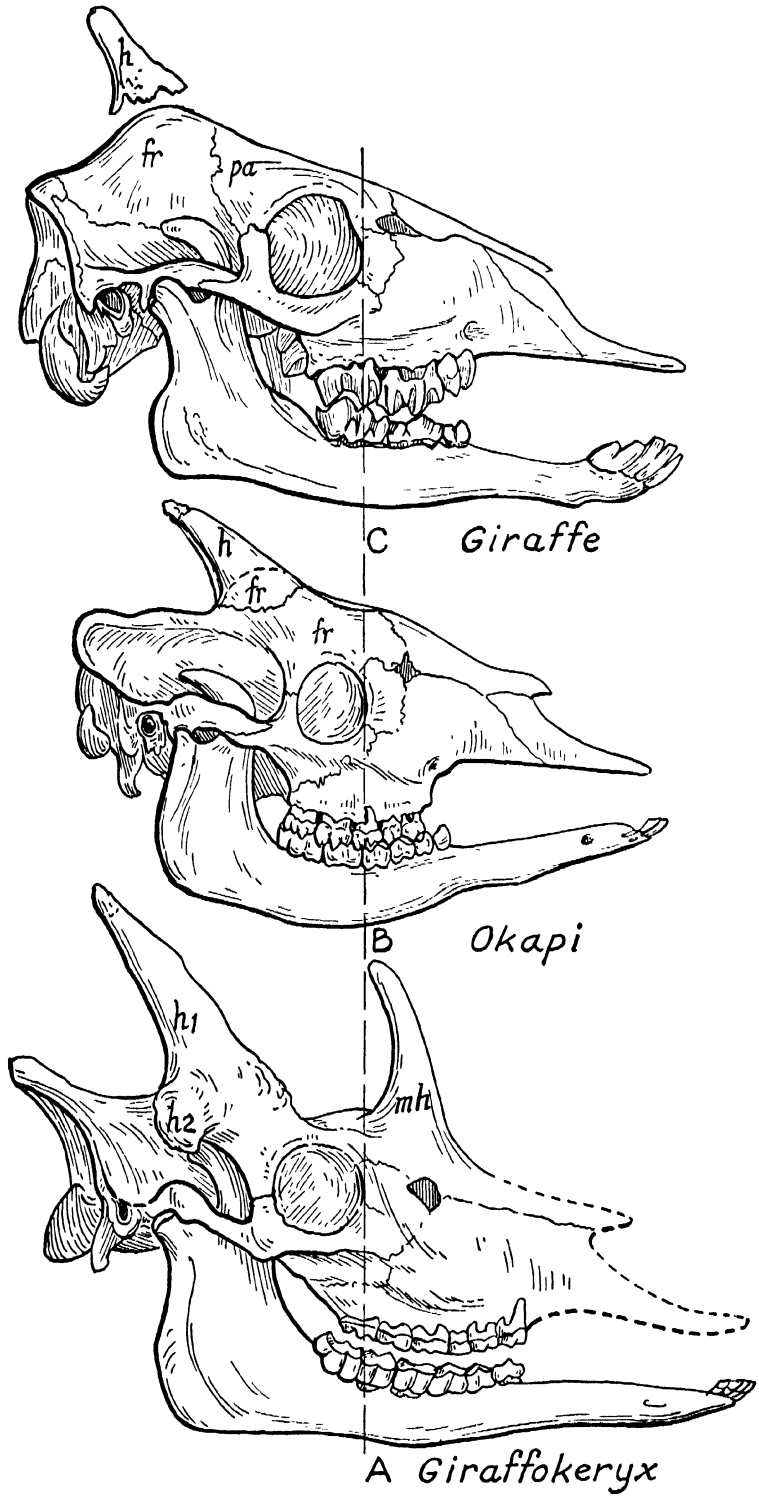


Fig. 21.111. Skulls of Pliocene (A) and Recent (B, C) giraffes. A, after Colbert; B, after Lankester; C, after Forsyth Major.

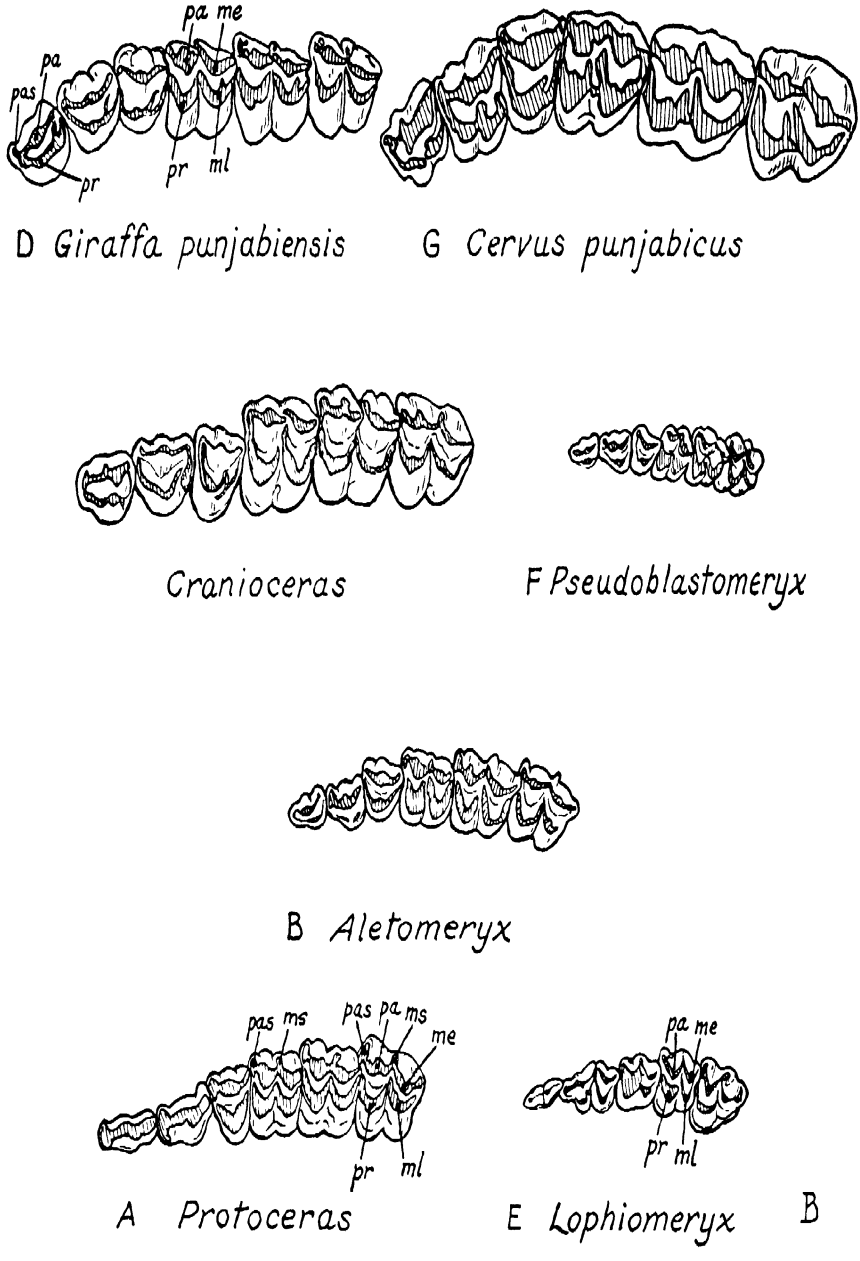


Fig. 21.112. Upper cheek teeth of Oligocene (A, E) and later ruminants (cf fig. 21.109). A–C, F, after Frick; D, after Colbert; E, after Matthew; G, after Barnum Brown.

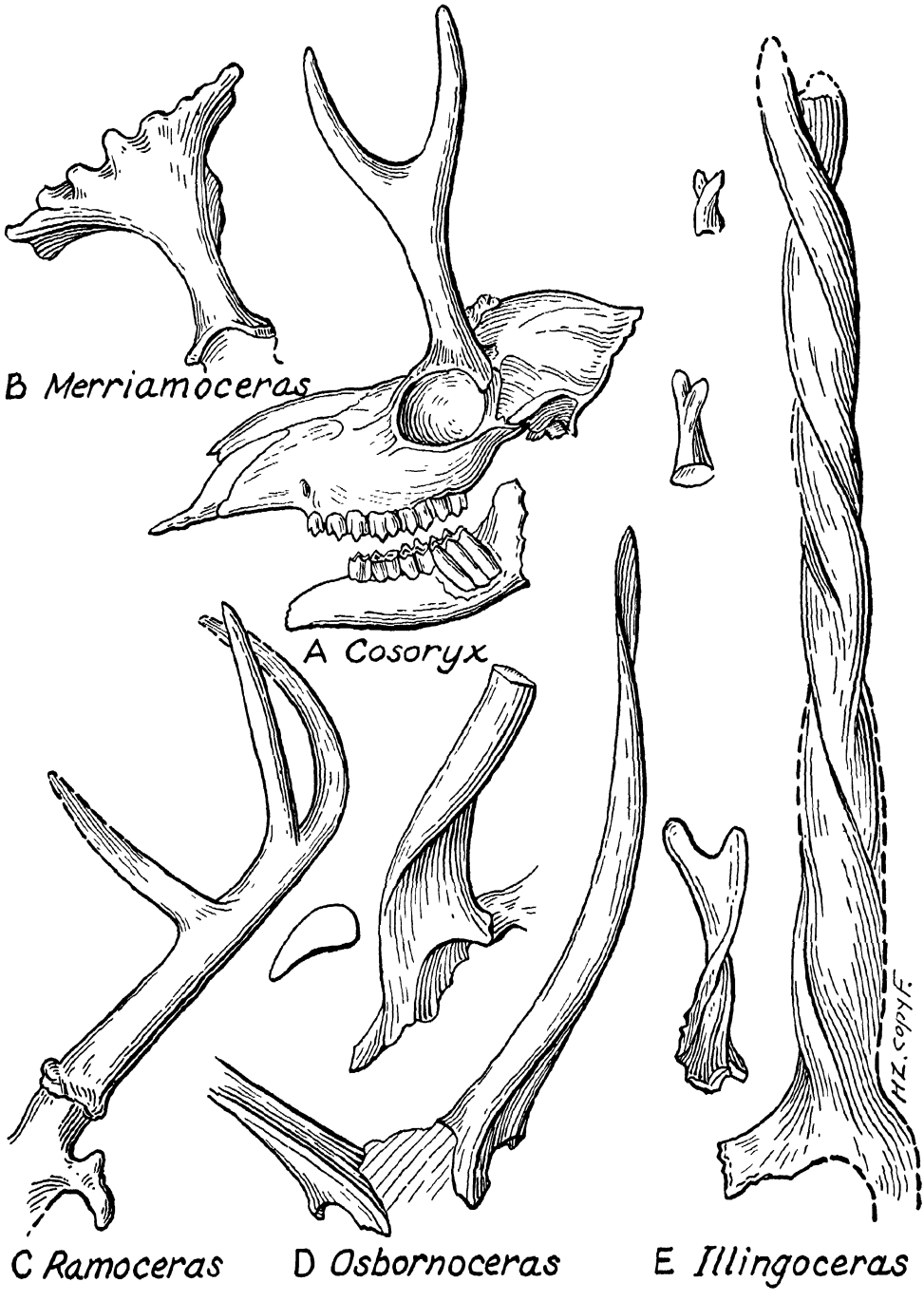


Fig. 21.113. Relatively primitive (A, B) and diversely specialized (C–E) antilocaprids. After Frick.

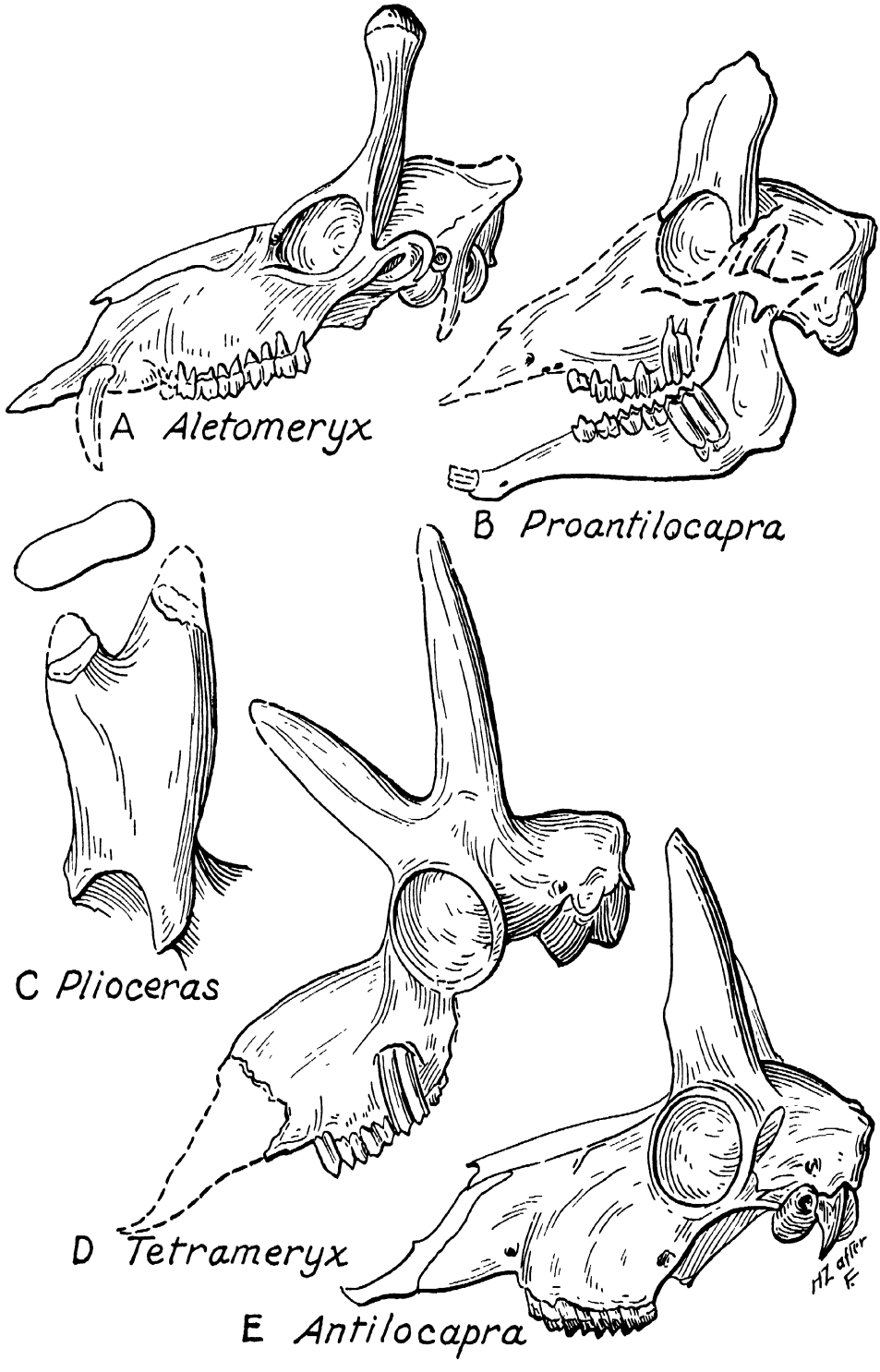


Fig. 21.114. Primitive musk-deer (A) and specialized antilocaprids. After Frick (cf. fig. 21.109).



Fig 21.115. Development of skull and horns in domestic cattle. From Osborn. Specimens prepared by S. H. Chubb.

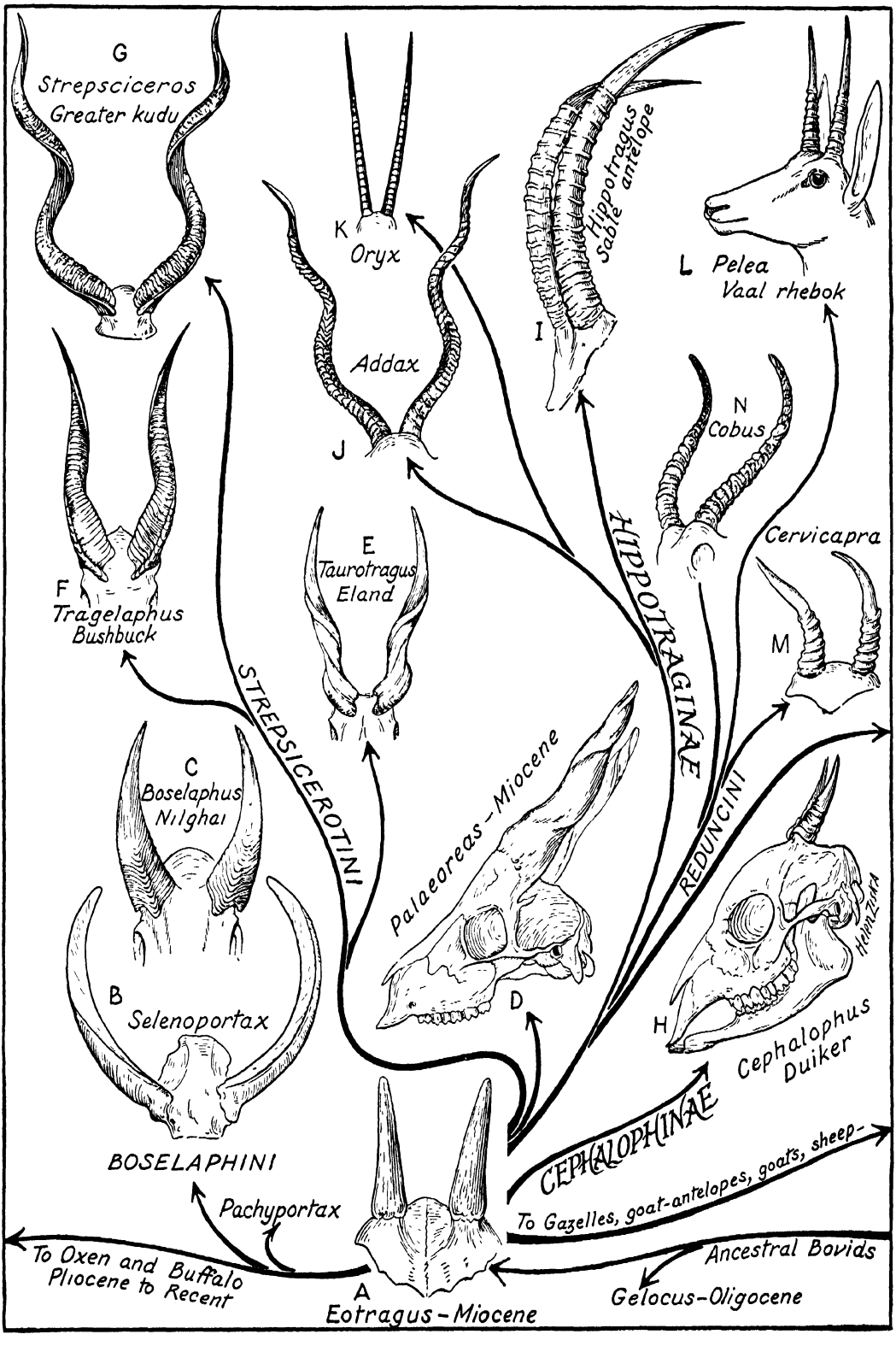

G
Strepsciceros
Greater kudu
K
Oryx
Addax
J
Hippotragus
sable antelope
I
L Pelea
Vaal rhebok
N
Cobus
Cervicapra
M
F
Tragelaphus
Bushbuck
E
Taurotragus
Eland
HIPPOTRAGINAE
STREPSICEROTINI
REDUNCINI
C
Boselaphus
Nilghai
B
Selenoportax
Palaeoreas-Miocene
D
H
Cephalophus
Duiker
Heinz Ziska
BOSELAPHINI
CEPHALOPHINAE
Pachyportax
To Gazelles, goat-antelopes, goats, sheep-
To Oxen and Buffalo
Pliocene to Recent
Ancestral Bovids
A
Eotragus-Miocene
Gelocus-Oligocene

Fig. 21.116a

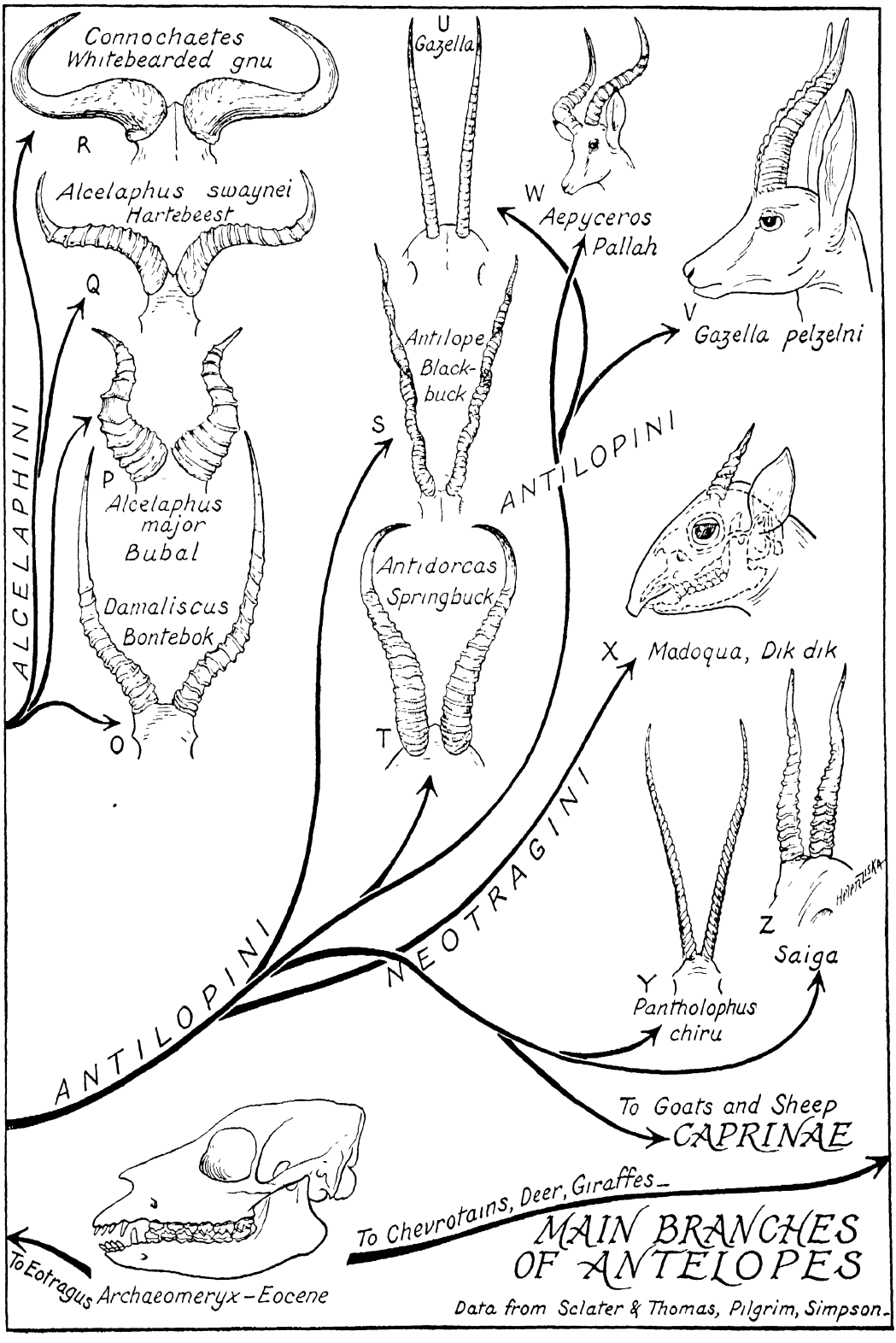

Connochaetes
Whitebearded gnu
R
Alcelaphus swaynei
Hartebeest
Q
P
Alcelaphus
major
Bubal
Damaliscus
Bontebok
O
ALCELAPHINI
U
Gazella
Antilope
Black-
buck
S
Antidorcas
Springbuck
T
ANTILOPINI
W
Aepyceros
Pallah
V
Gazella pelzelni
X
Madoqua, Dik dik
NEOTRAGINI
Y
Pantholophus
chiru
Z
Saiga
ANTILOPINI
To Goats and Sheep
CAPRINAE
To Chevrotains, Deer, Giraffes
To Eotragus
Archaeomeryx – Eocene
MAIN BRANCHES
OF ANTELOPES
Data from Sclater & Thomas, Pilgrim, Simpson.

Fig. 21 116b

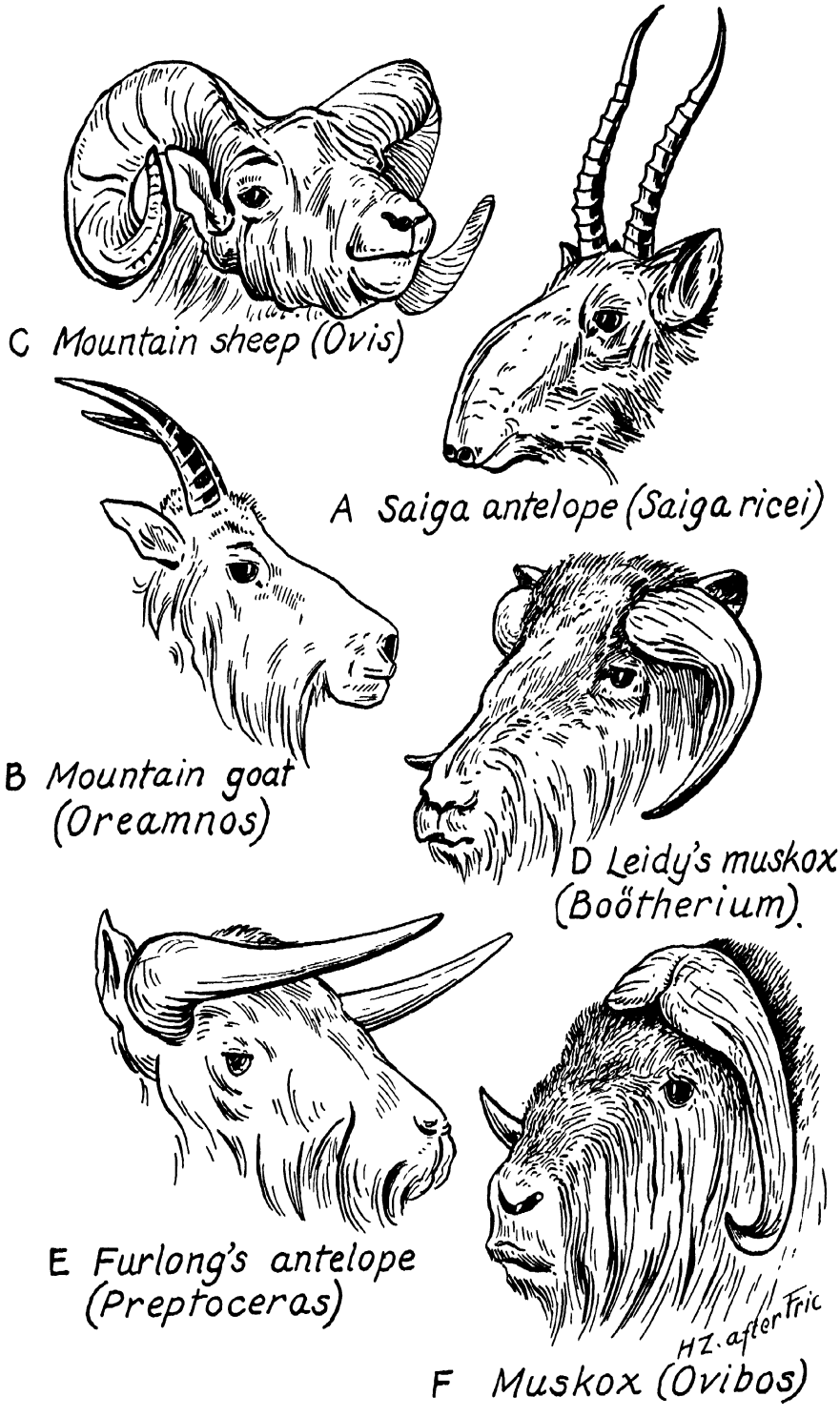


Fig 21.117. Heads of Pleistocene and Recent wild sheep and musk oxen After Frick.

CHAPTER XXII

FISH-LIKE BY CONVERGENCE (CETACEA)

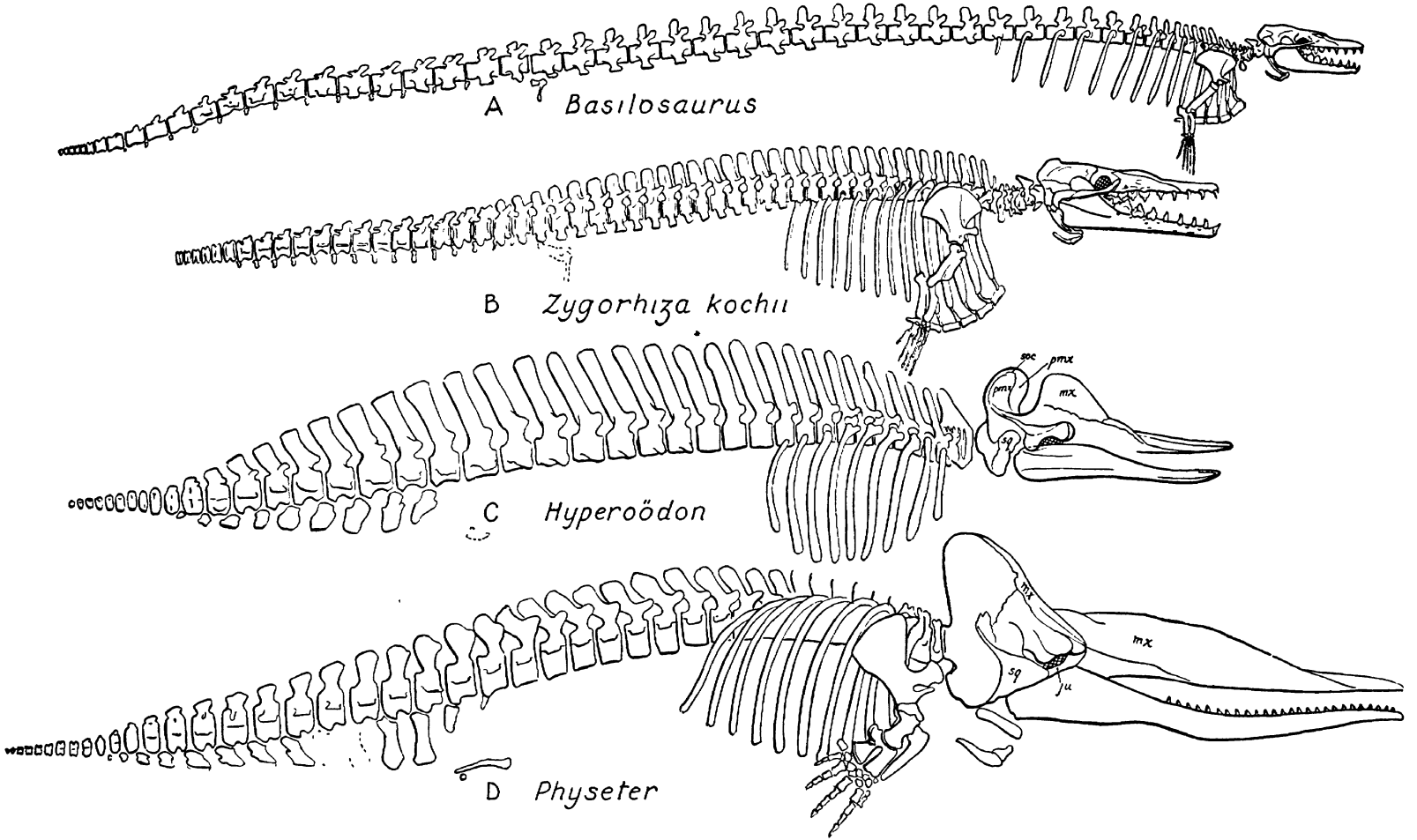


Fig. 22.1. Skeletons of Eocene archaeocetes (A, B) and Recent odontocetes (C, D). In A, B, the skull is much less specialized than in C, D, but the rest of the skeleton has nearly reached the odontocete stage. A, B, after Kellogg; C, D, after van Beneden and Gervais.

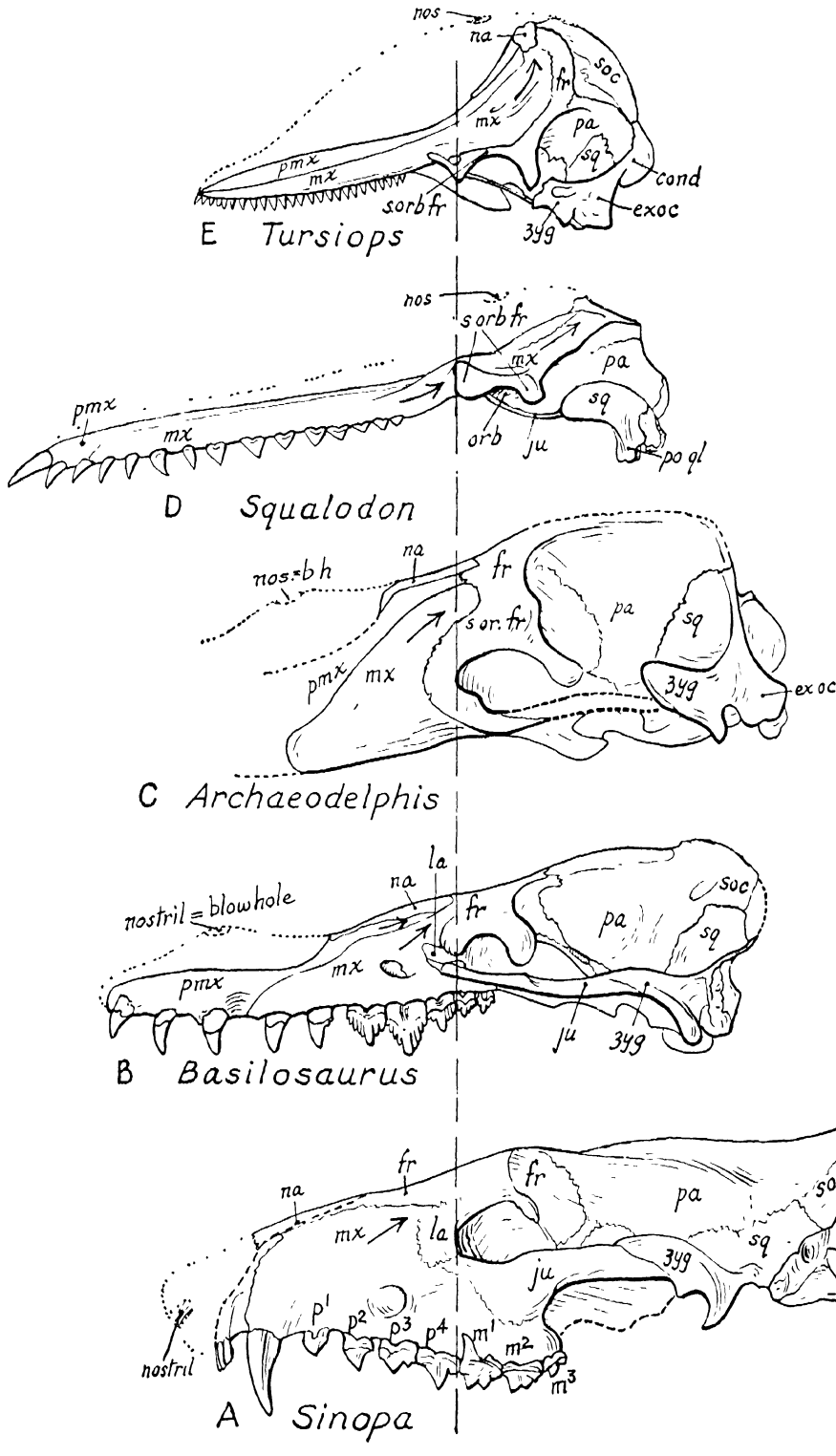


Fig. 22.2. Structural skull series, side view, from primitive creodont (A) to modern dolphin (E). Showing retreat of nostrils, nasals; upward and backward growth of premaxillae, maxillae; (in E) forward extension of supraoccipital. A, after Matthew; B, D, E, after Kellogg; C, after G. M. Allen.

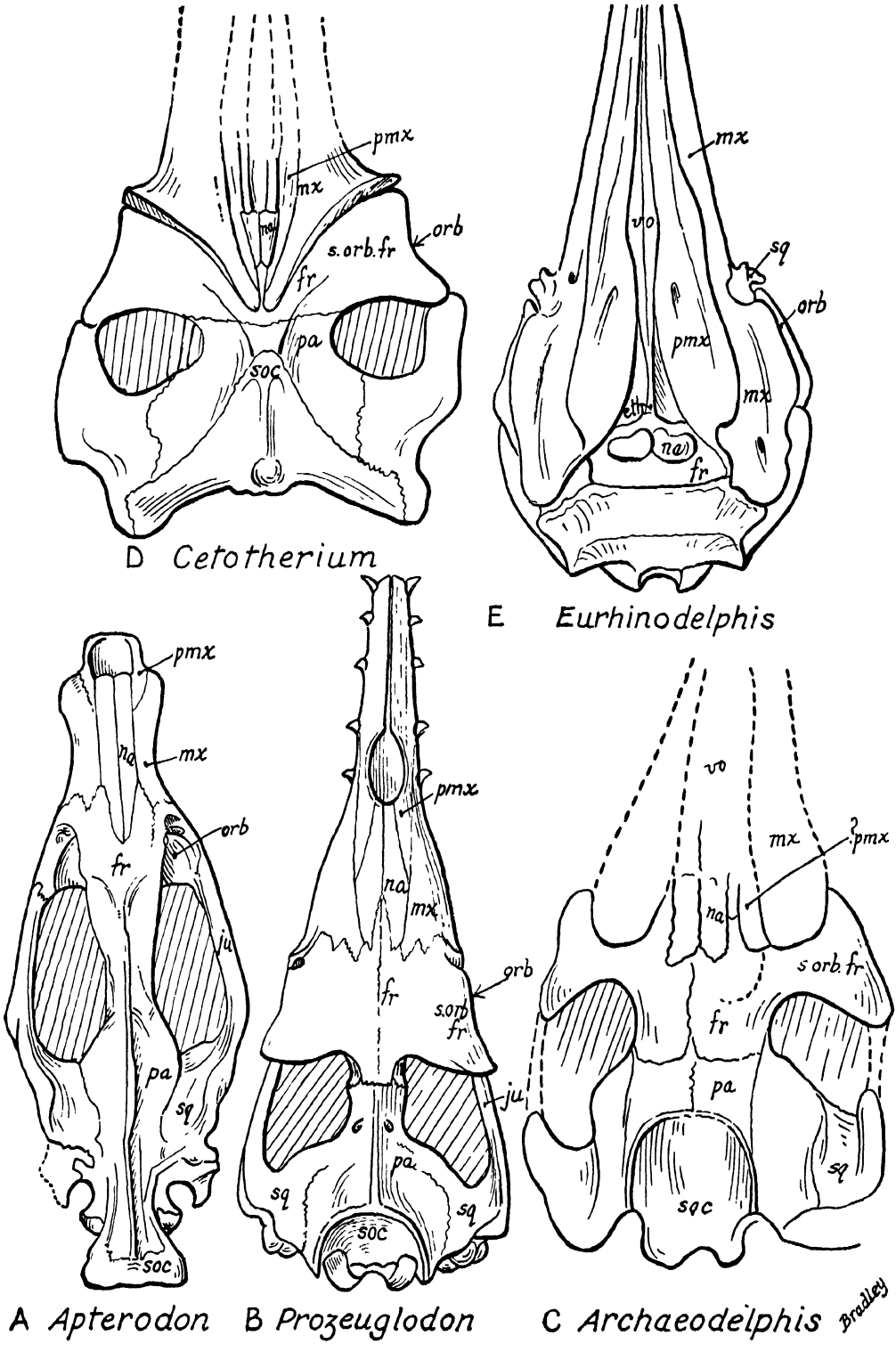


Fig. 22.3. Structural skull series, top view, from relatively primitive creodont (A) to Miocene whalebone whale (D) and toothed whale (E). A, after Osborn; B, after Kellogg; C, after G. M. Allen; D, E, after van Beneden and Gervais.

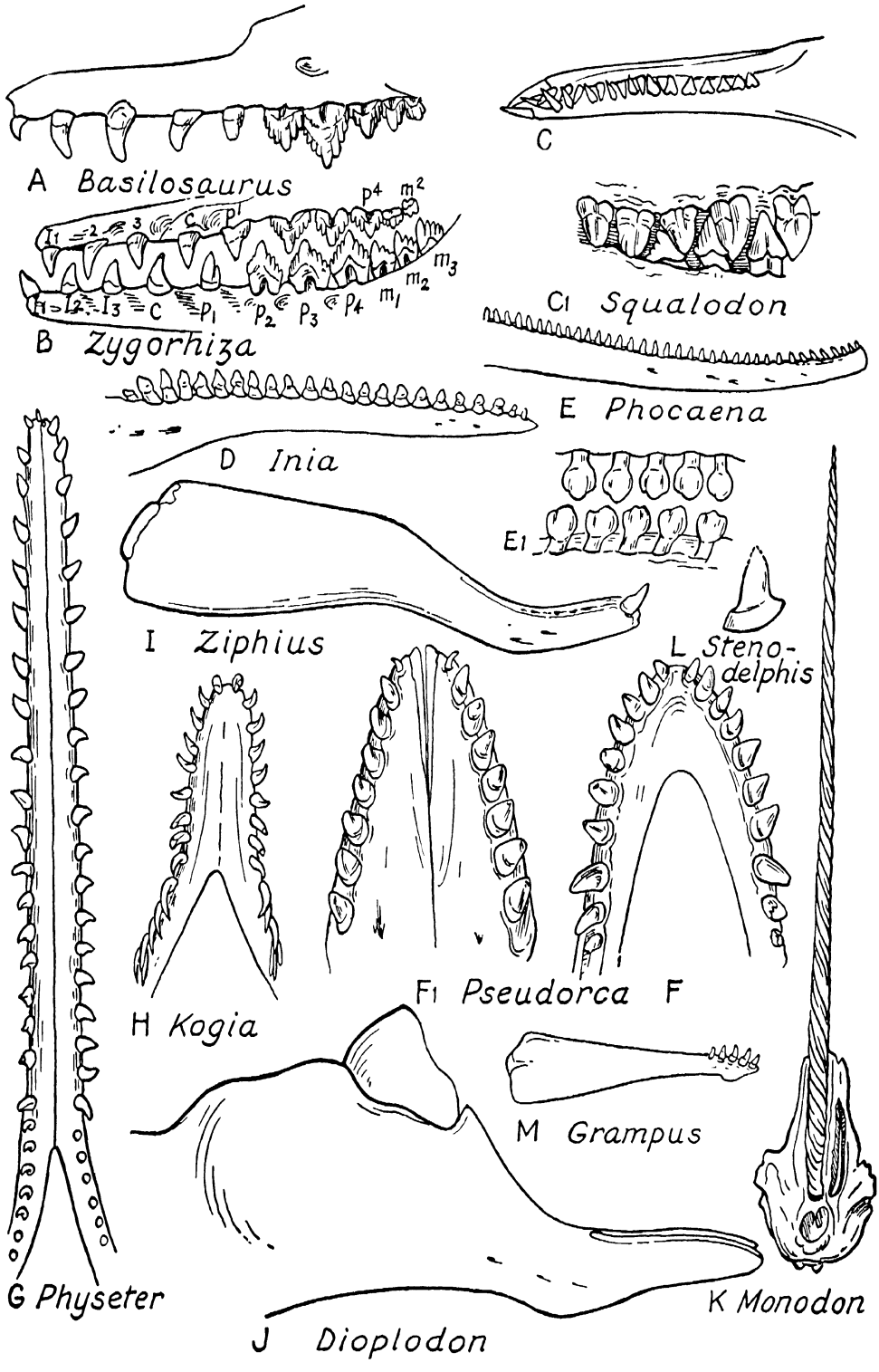


Fig. 22.4. Adaptive branching in the dentition from Eocene archaeocete (A, B) to highly specialized odontocetes (I–K). A, B, after Kellogg, C–J, after van Beneden and Gervais; K, after Flower and Lydekker.

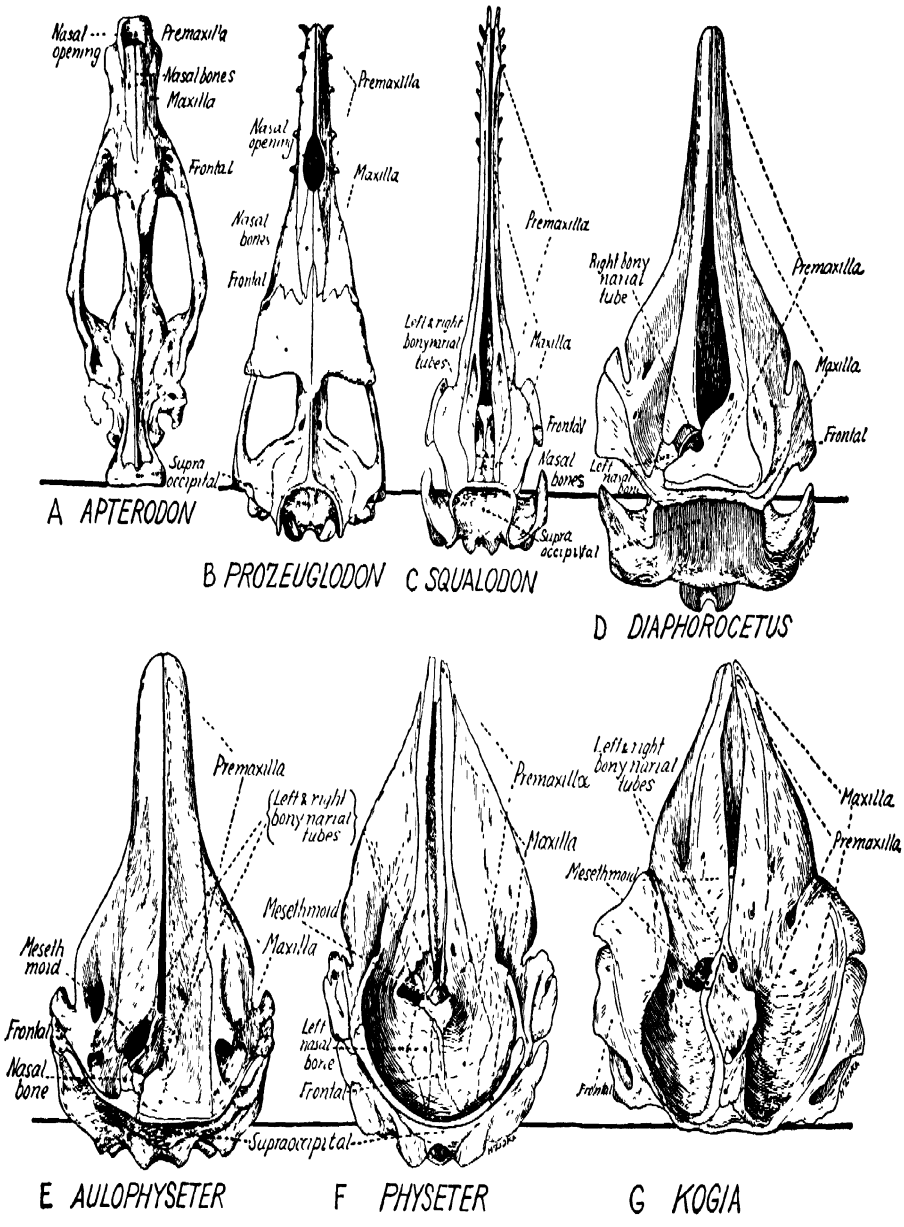


Fig. 22.5. Structural skull series, top view, from relatively primitive creodont (A) to highly specialized odontocete (G). A, after Osborn; B–G, after Kellogg. Showing progressive shortening of the rostrum, widening of the cranium, asymmetrical enlargement of right premaxilla, reduction of the right and enlargement of the left narial tube. After Raven and Gregory.

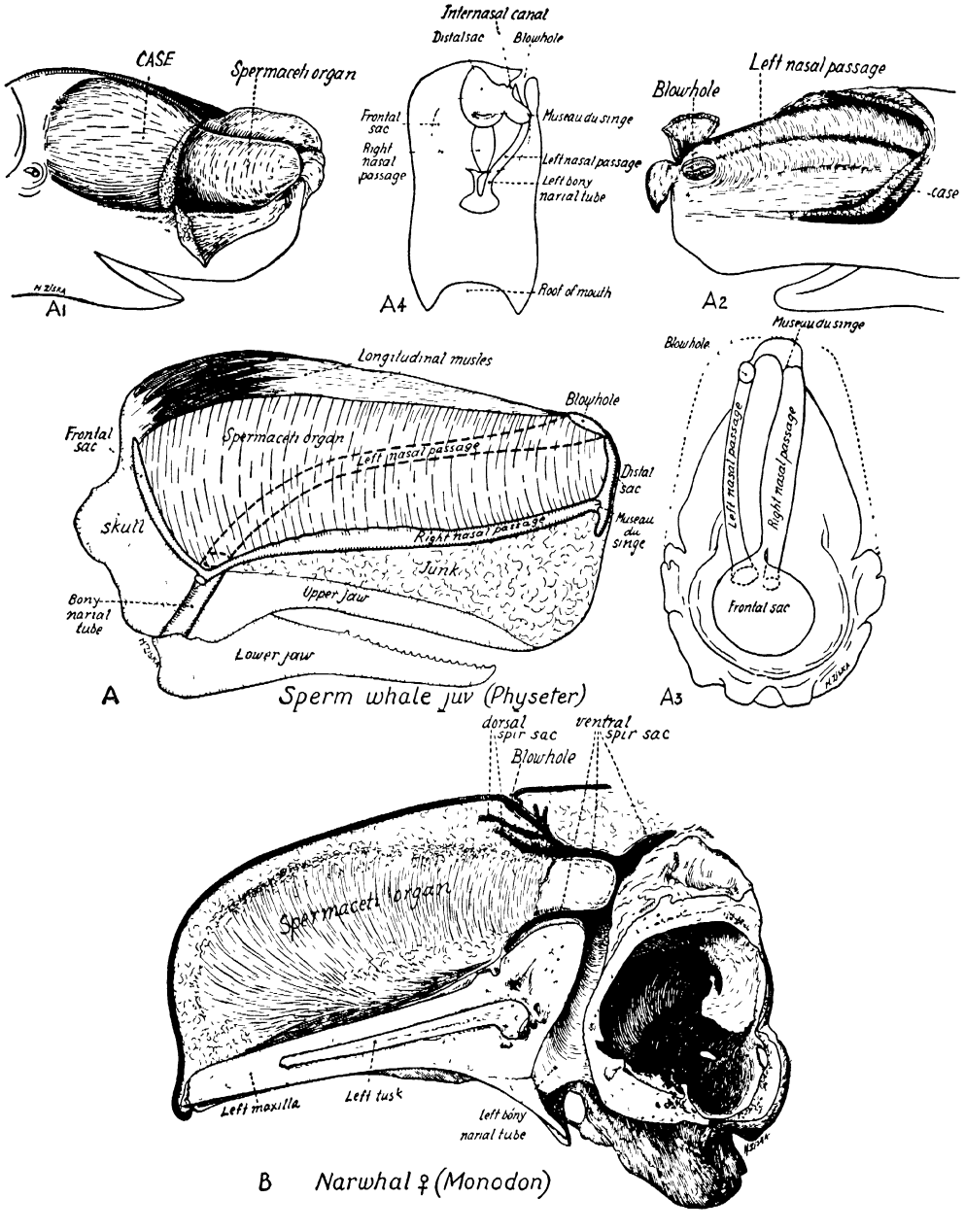


Fig. 22.6. Morphology of the nasal "melon," or primitive spermaceti organ, of the narwhal and its relatively simple nasal tubes (B) in comparison with the enormous spermaceti organ and complex nasal tubes of the sperm whale (A–A4). After Raven.

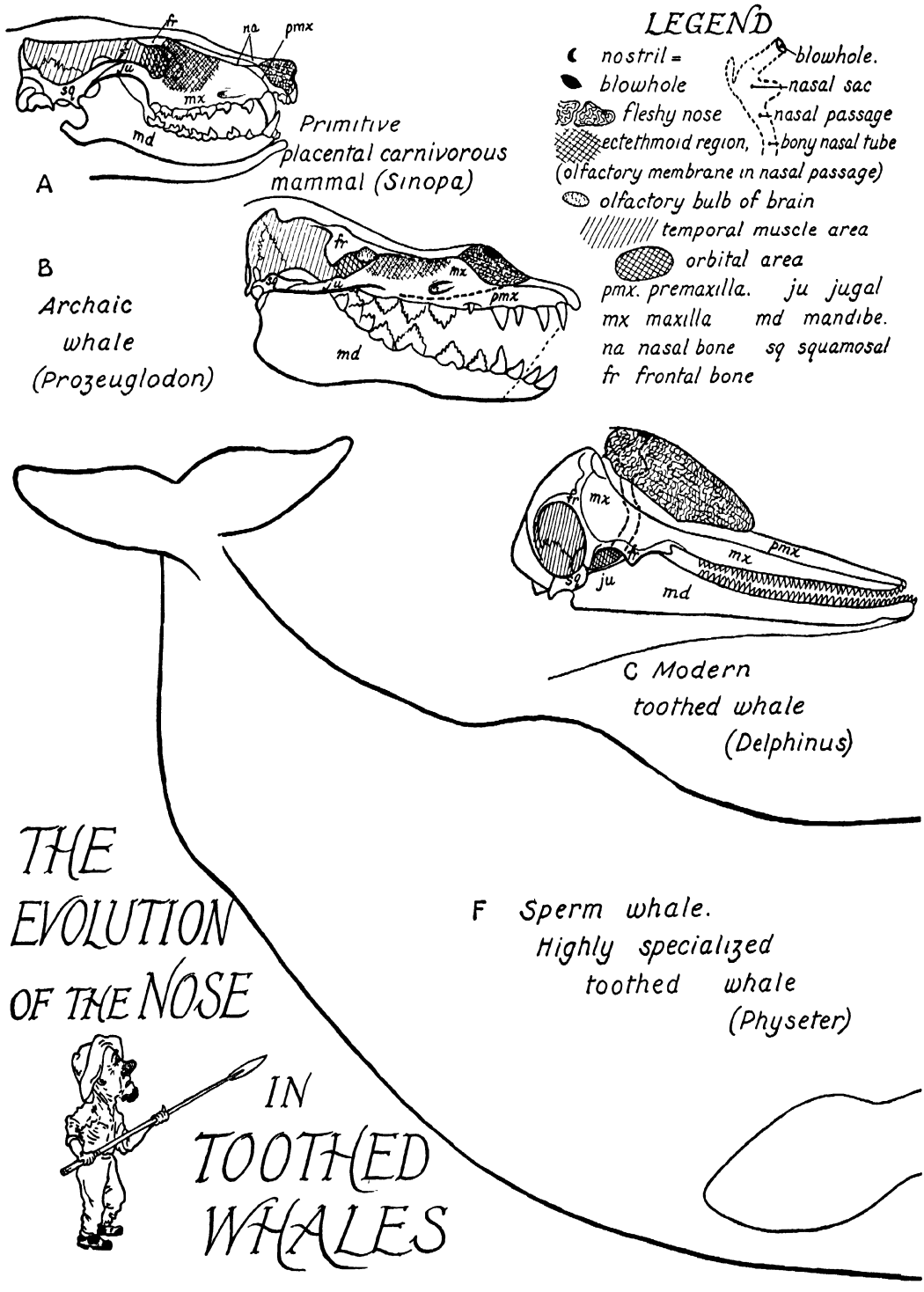
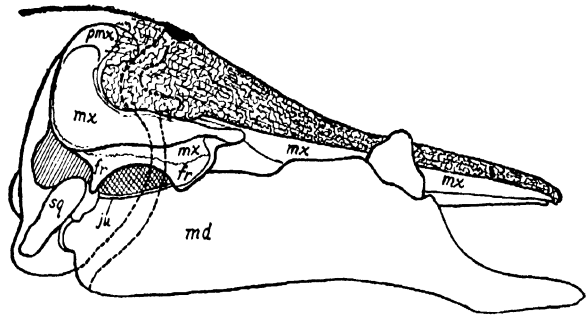
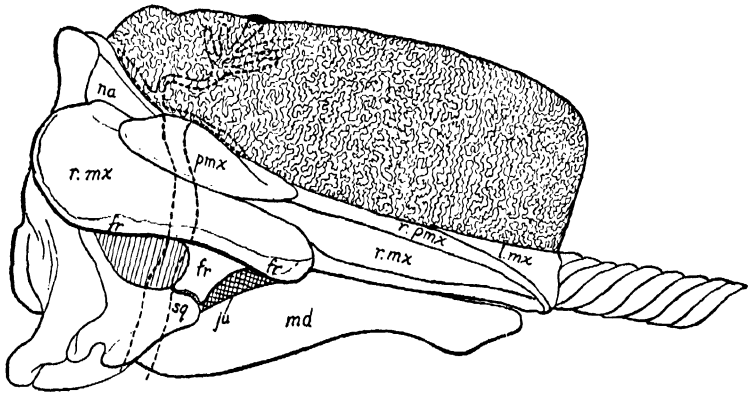


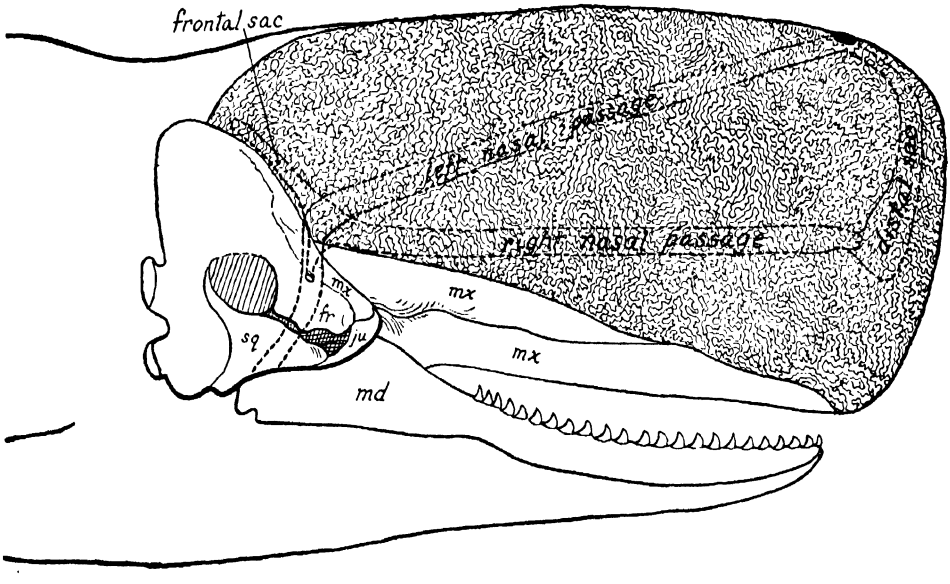
Fig. 22.7. Evolution of the nose in odontocetes. After Raven. Structural series, showing the early reduction and loss of the olfactory organs (A, B), the elevation of the nasal passage and nostrils (C), the



E *Beaked whale - specialized toothed whale - (Hyperoödon)*



D *Narwhal - specialized toothed whale - (Monodon)*



finally enormous increase of the external muscular part of the nose (A–F). In the sperm whale (F) the nostrils (blowhole) are secondarily moved forward and the nasal passages greatly prolonged.

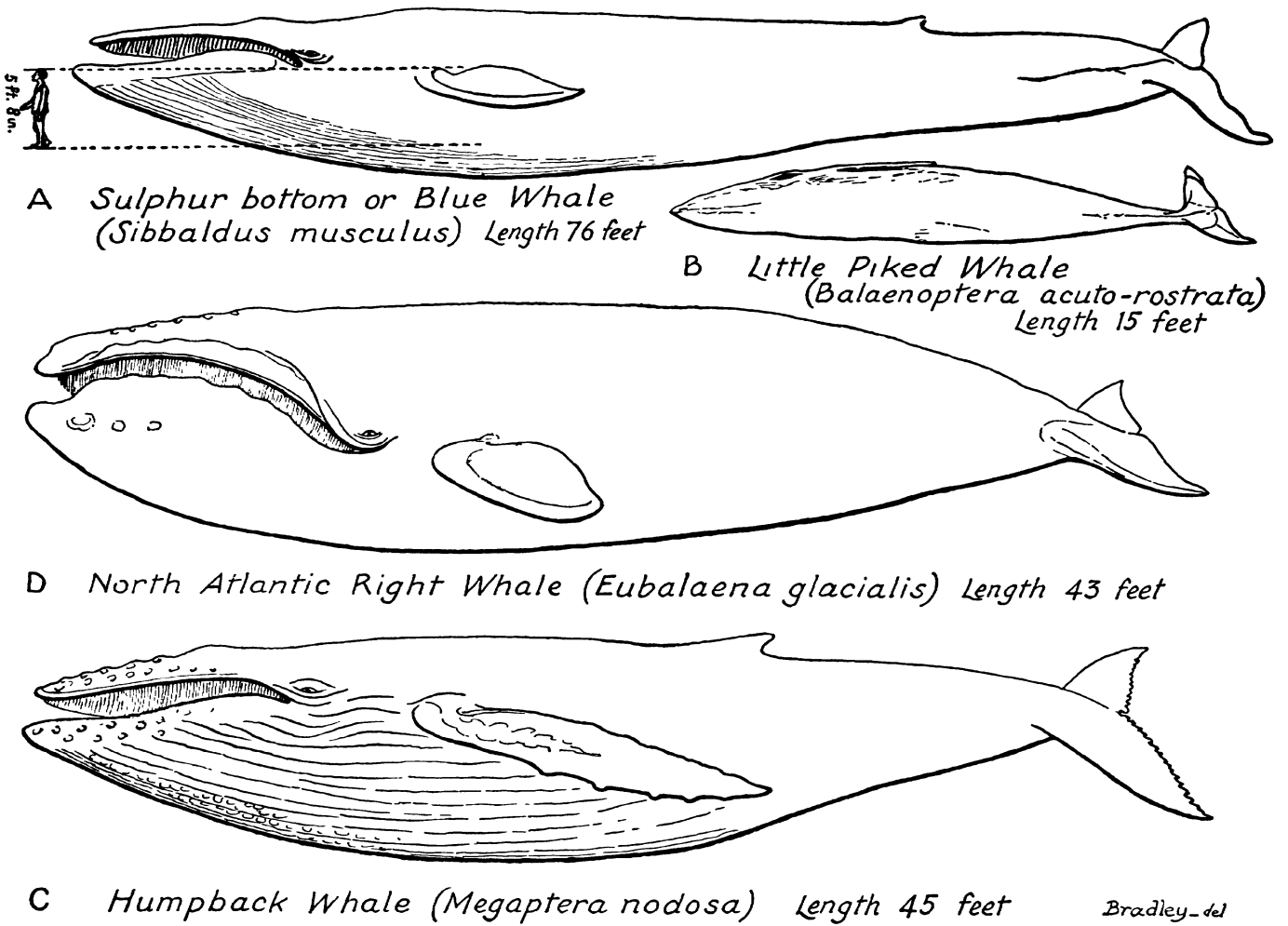


Fig. 22.8. Giant (A, C, D) and pygmy (B) whalebone whales. A, C, D, after G. M. Allen; B, after True.

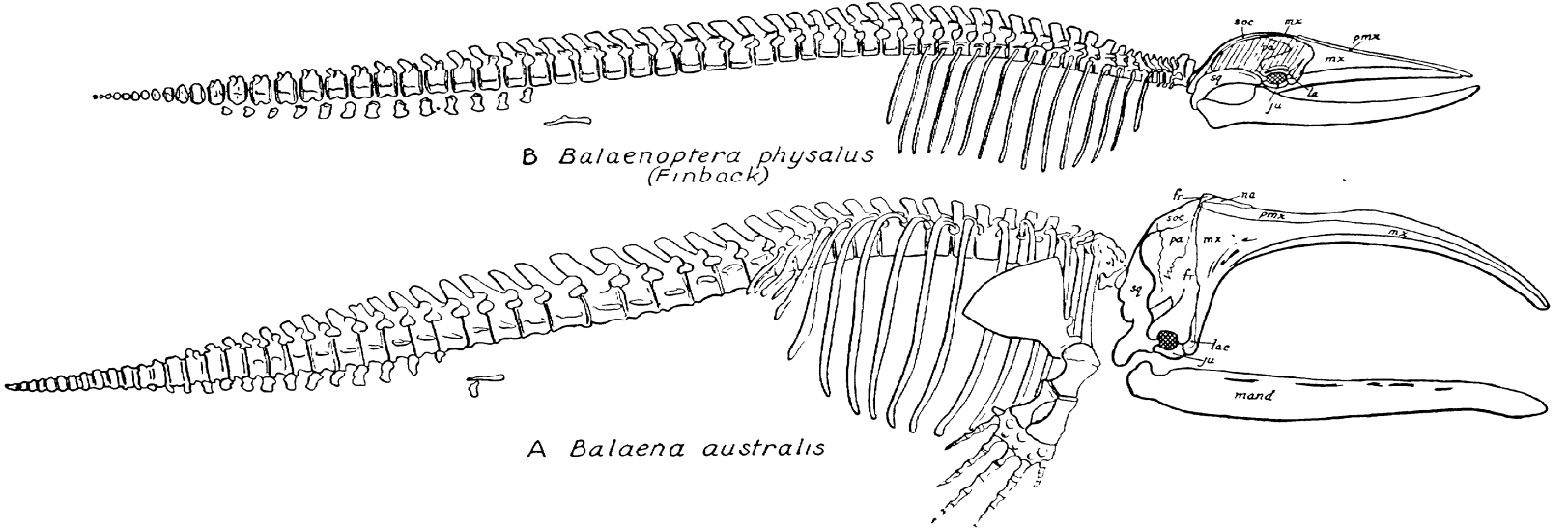
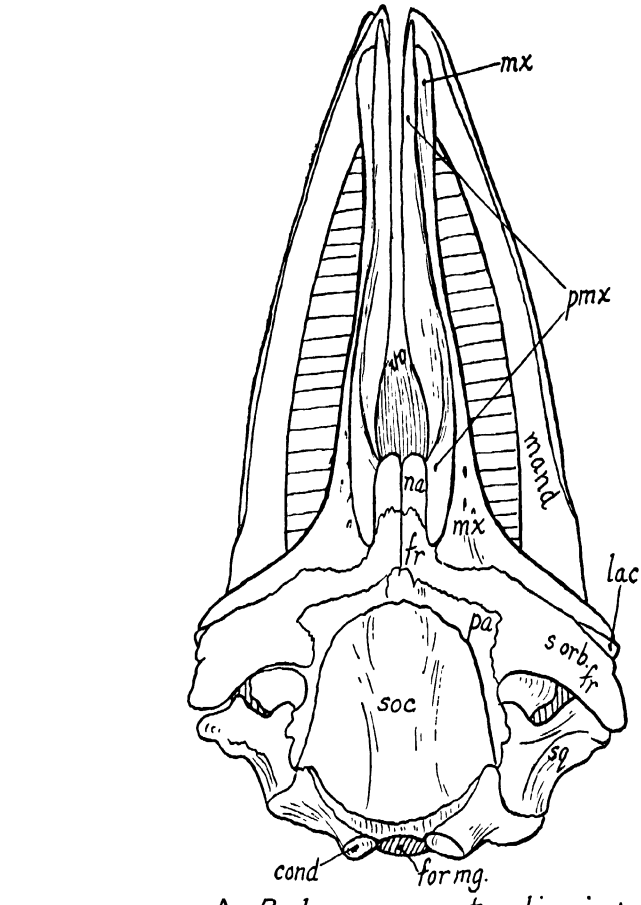
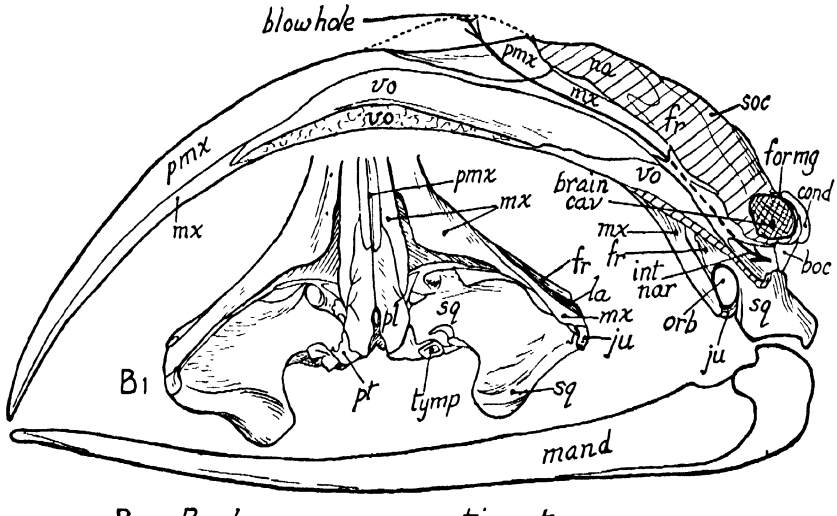


Fig. 22.9. Skeletons of whalebone whales. After Van Beneden and Gervais. Temporal muscle area hatched.



A *Balaena australis. juv.*



B *Balaena mysticetus*

Fig. 22.10. Skulls of whalebone whales. A, top view; B, right half of skull, partly sectioned, showing relations of the braincase to the rostrum; B1, basal view showing backward prolongation of the palate and internal nares. A, after Van Beneden and Gervais; B, B1, from Weber, after Eschricht and Reinhardt.

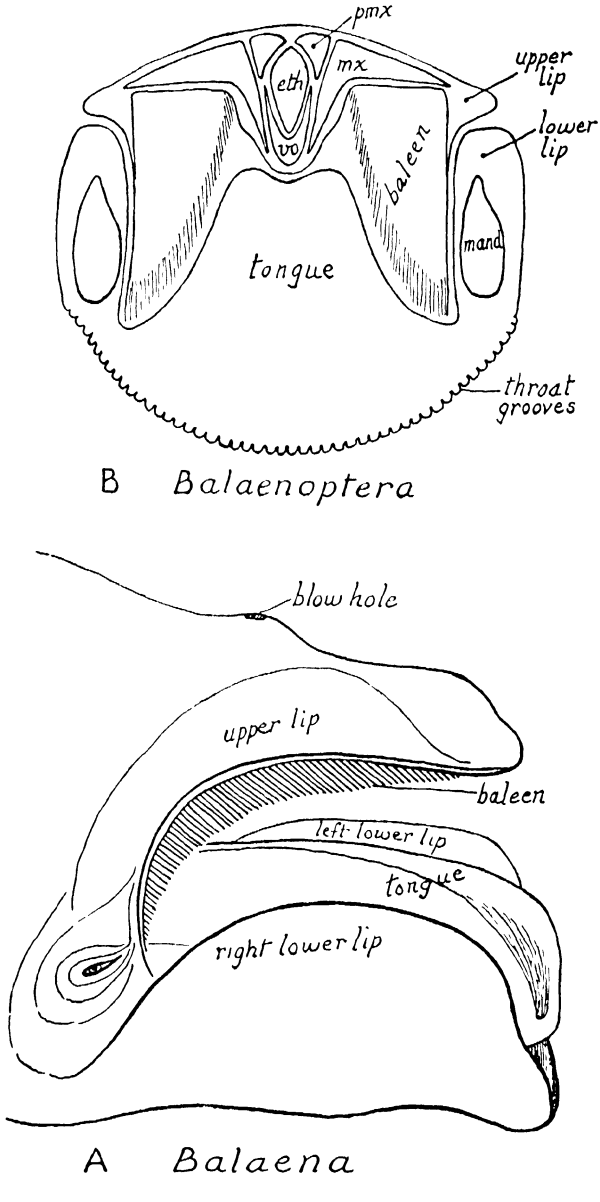


Fig. 22.11. Relations of the tongue and lips to the baleen plates and skull bones in Balaenoptera From Weber, after J. Delage

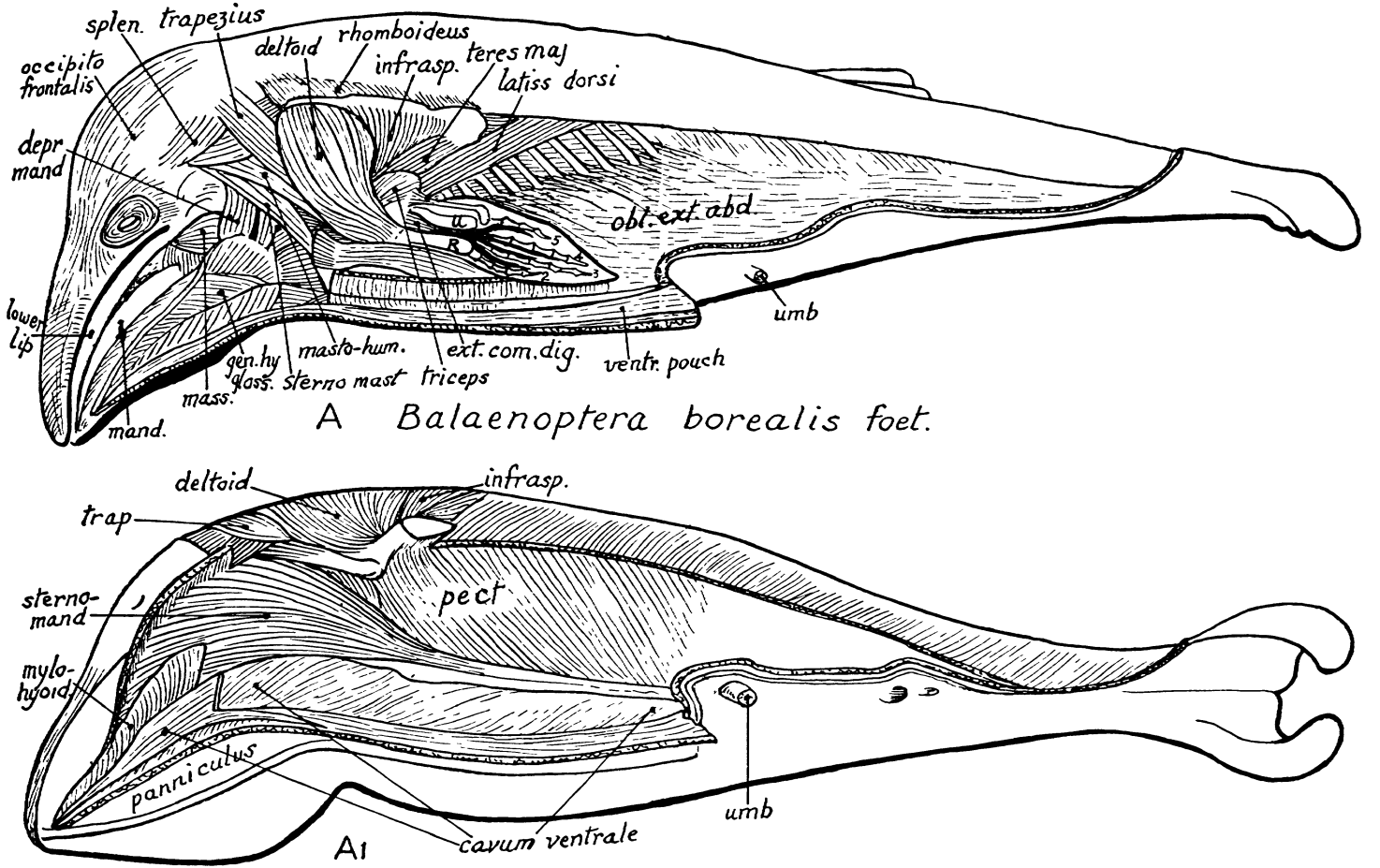

splen.
trapezius
deltoid
rhomboideus
occipito frontalis
infrasp.
teres maj
latiss dorsi
depr mand
obl. ext. abd
umb
lower lip
gen. hy
glass.
masto-hum.
ext. com. dig.
ventr. pouch
mass.
sterno mast
triceps
mand.
A Balaenoptera borealis foet.
deltoid
infrasp.
trap
sterno-mand
pect
mylo-hyoid
panniculus
umb
cavum ventrale
A1

Fig. 22.12a

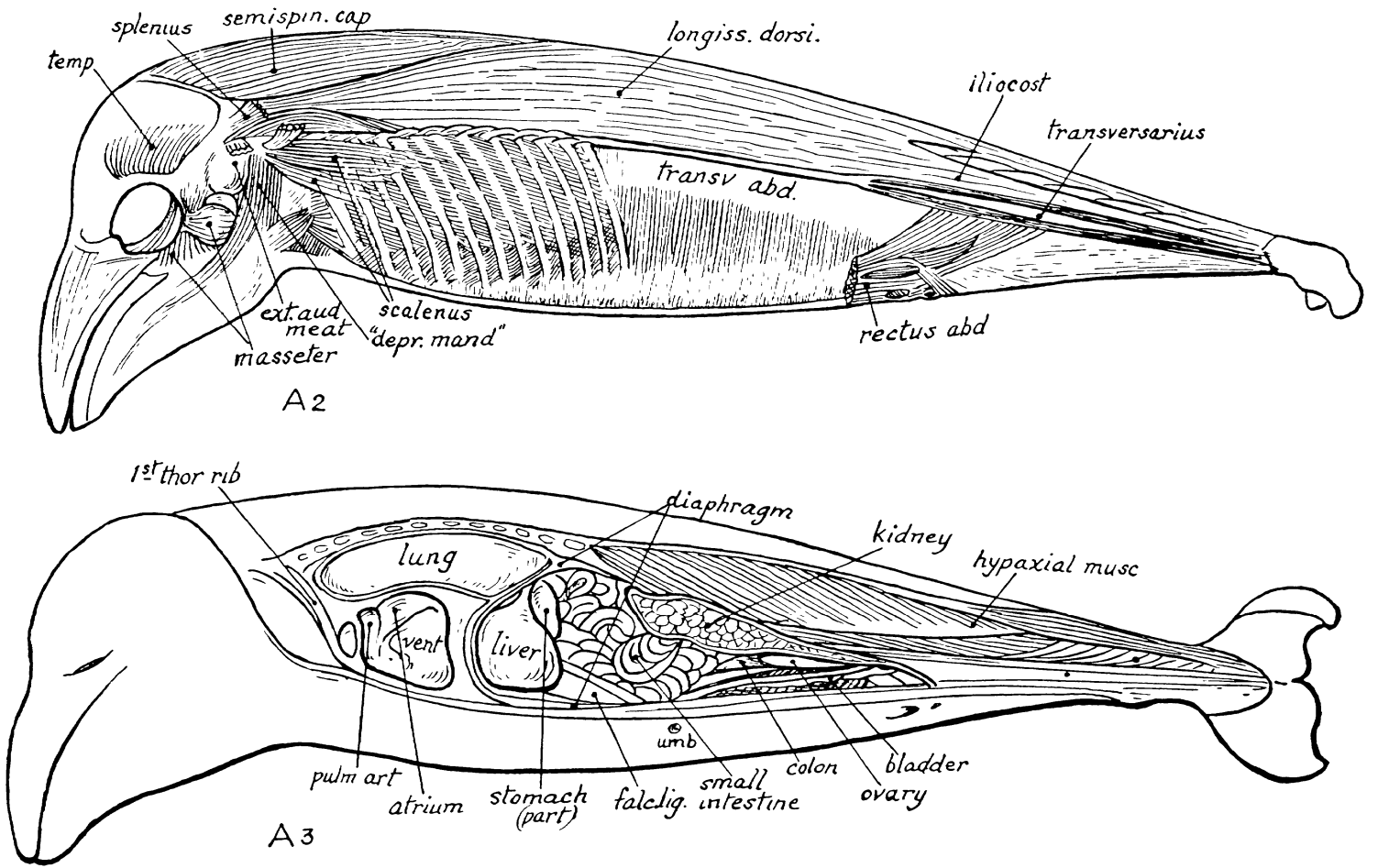


Fig. 22.12a, b. Anatomy of foetal whalebone whale. After Schulte. A, side view, showing facial and limb muscles; A1, oblique ventral view after removal of limb; A2, showing jaw muscles and immense development of dorsal axial muscles; A3, visceral anatomy, showing relatively huge heart and the small left lobe of the liver. The diaphragm retains its normal mammalian position.

CHAPTER XXIII

ORIGIN, RISE AND DEPLOYMENT OF THE PRIMATES

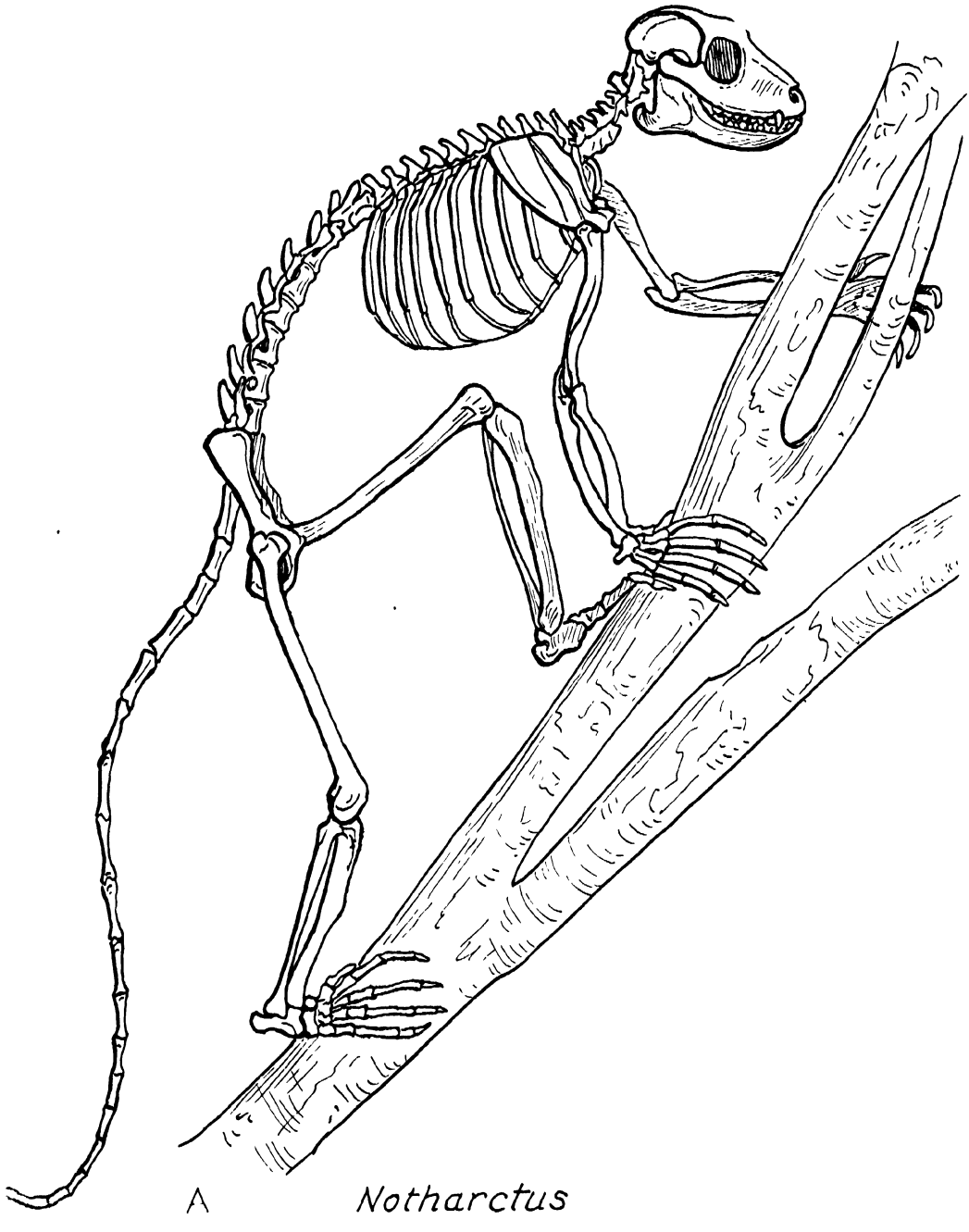


Fig. 23.1a, b. Mounted skeletons of lemurs: A, from the North American Eocene; B, Recent, from Madagascar. A, after Gregory; B, after Grandidier and Milne-Edwards.

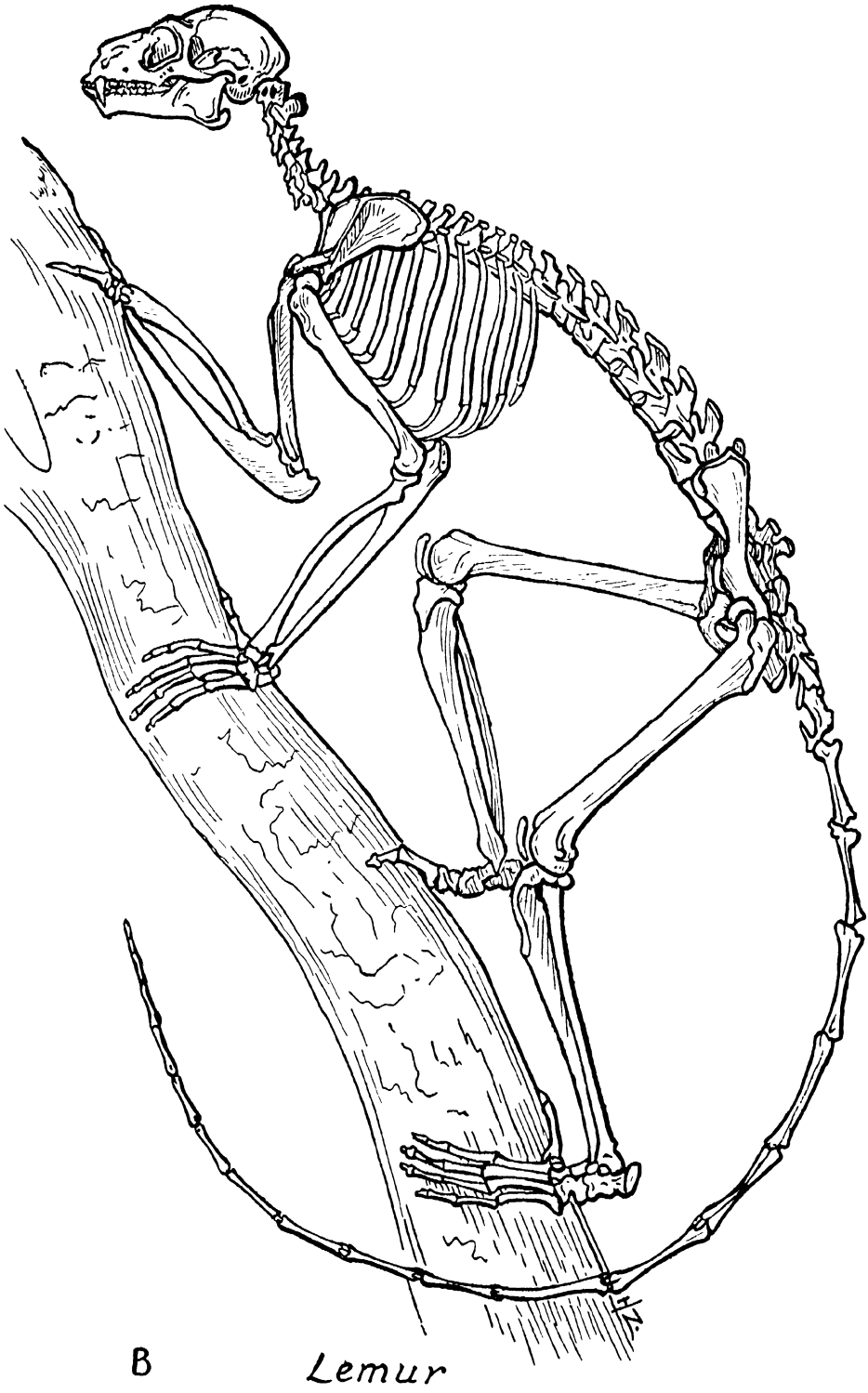


Fig. 23.1b

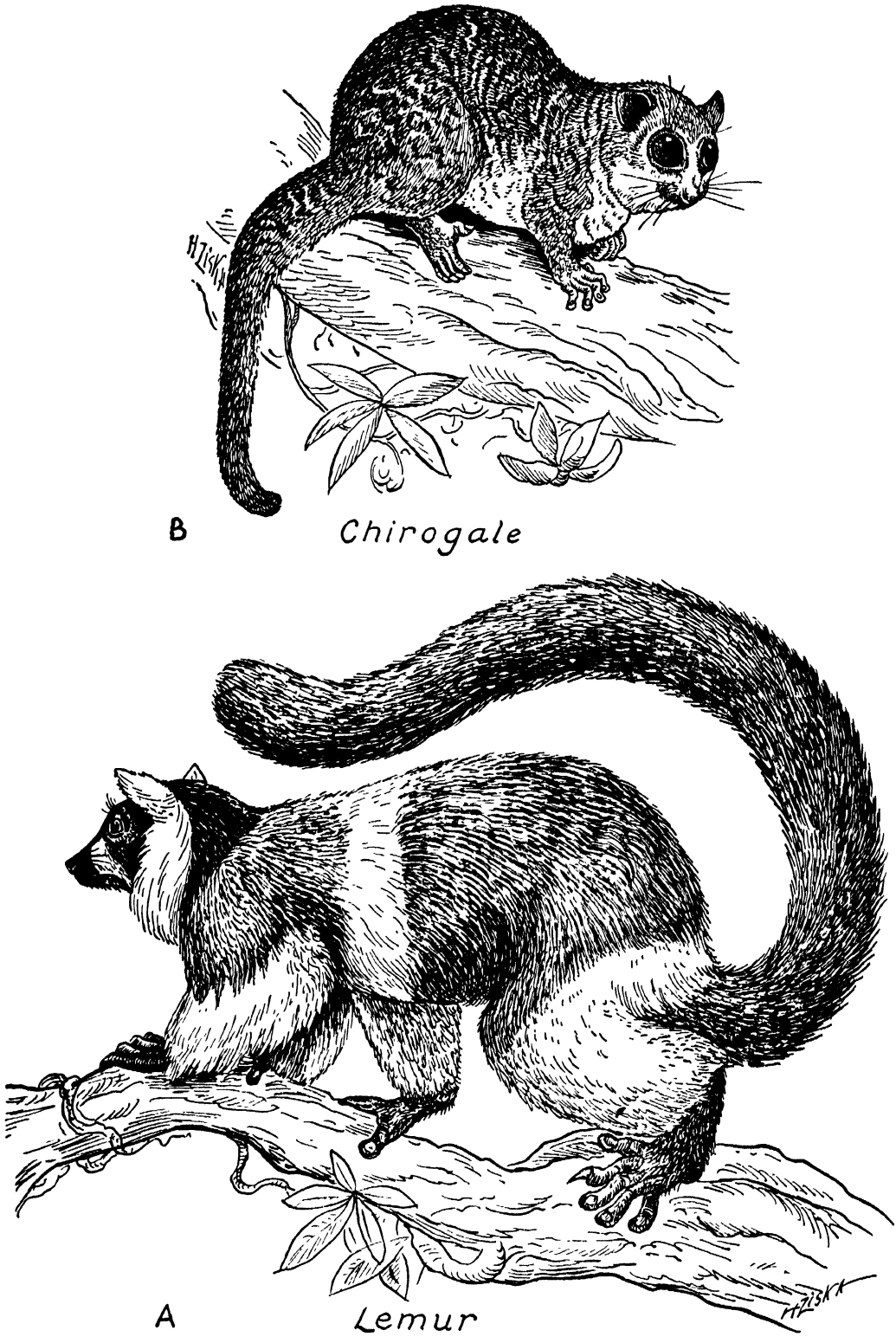


Fig. 23.2. Two existing Madagascan lemurs. A, after Milne-Edwards; B, after Elliot.

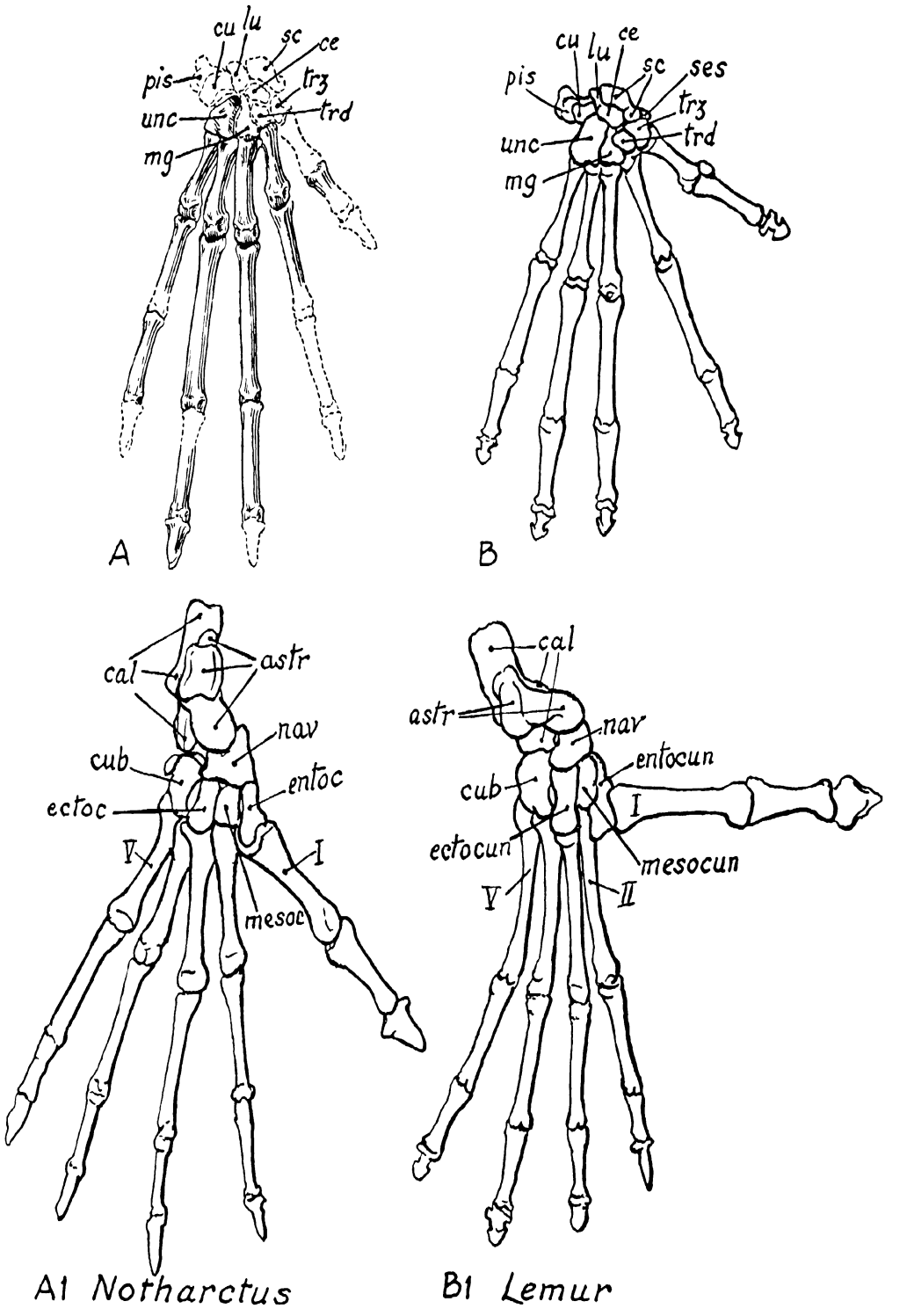


Fig 23.3. Right hand (A) and right foot (A1) of Eocene and modern (B, B1) lemuroids. After Gregory.

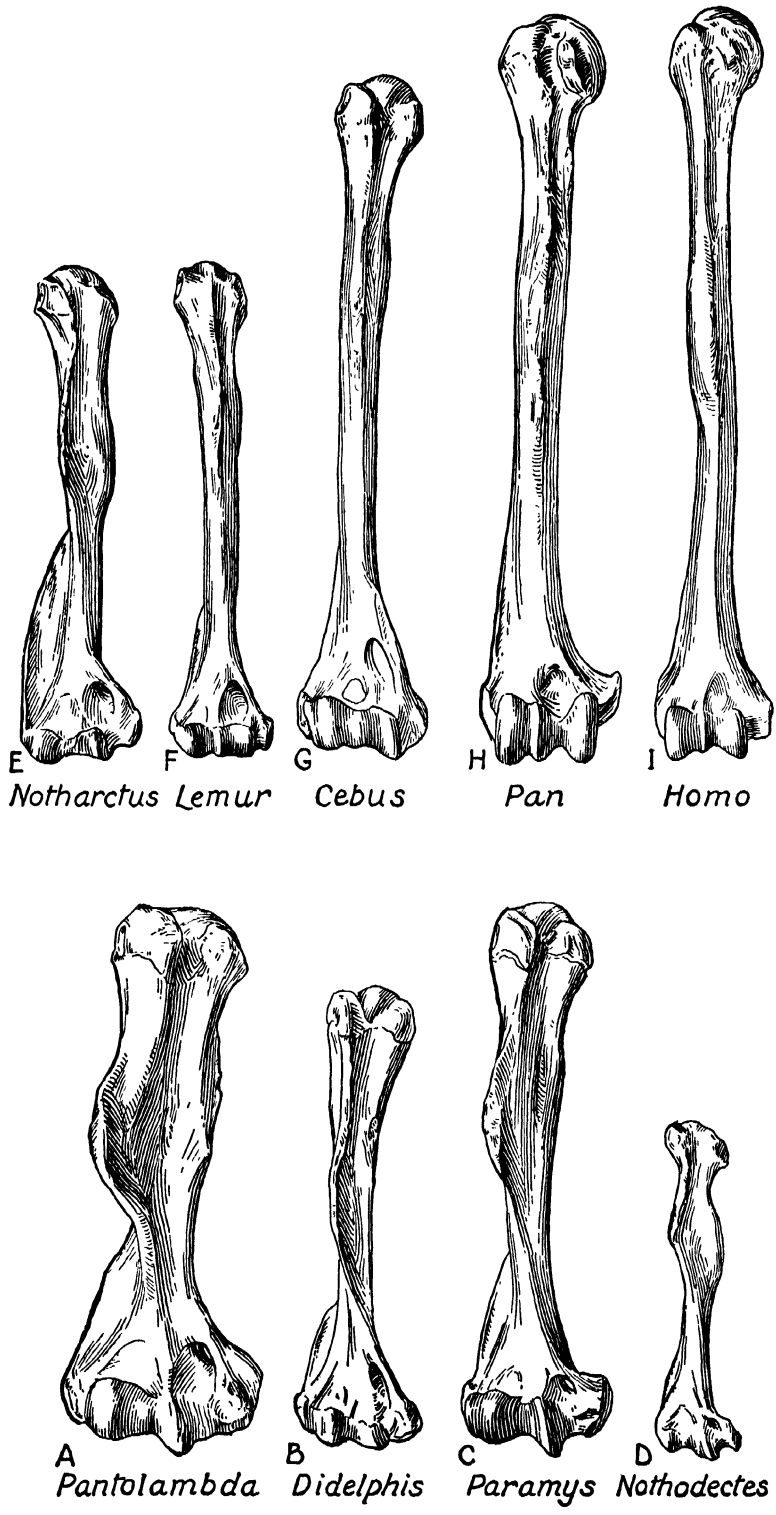


Fig. 23.4. Right humerus: of primitive mammals (A–D), of Eocene lemuroid (E) and living primates (F–I). Not to scale. After Gregory.

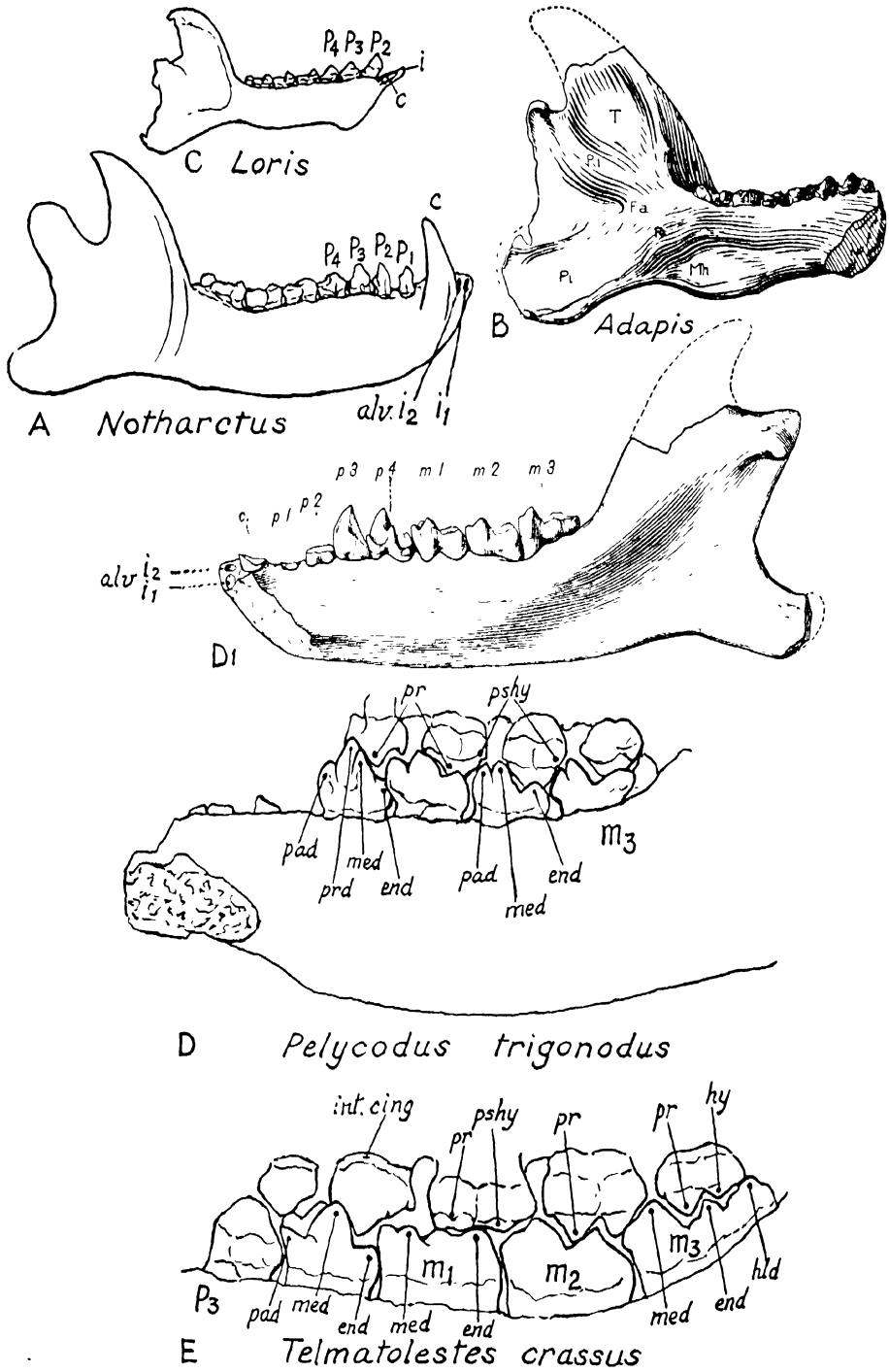


Fig 23.5. Lower jaws of Lower Eocene (A), Upper Eocene (B) and modern (C) lemurs, the latter showing reduction and procumbency of lower canines and incisors. B, Inner view of lower jaw showing large area for internal pterygoid muscle, *P.i.* A, C, after Gregory; B, after Stehlin. Lower and upper cheek teeth (D, E) in occlusion (lingual aspect), showing interlocking and overlapping of upper and lower teeth. D1, after Osborn; D, E, after Gregory.

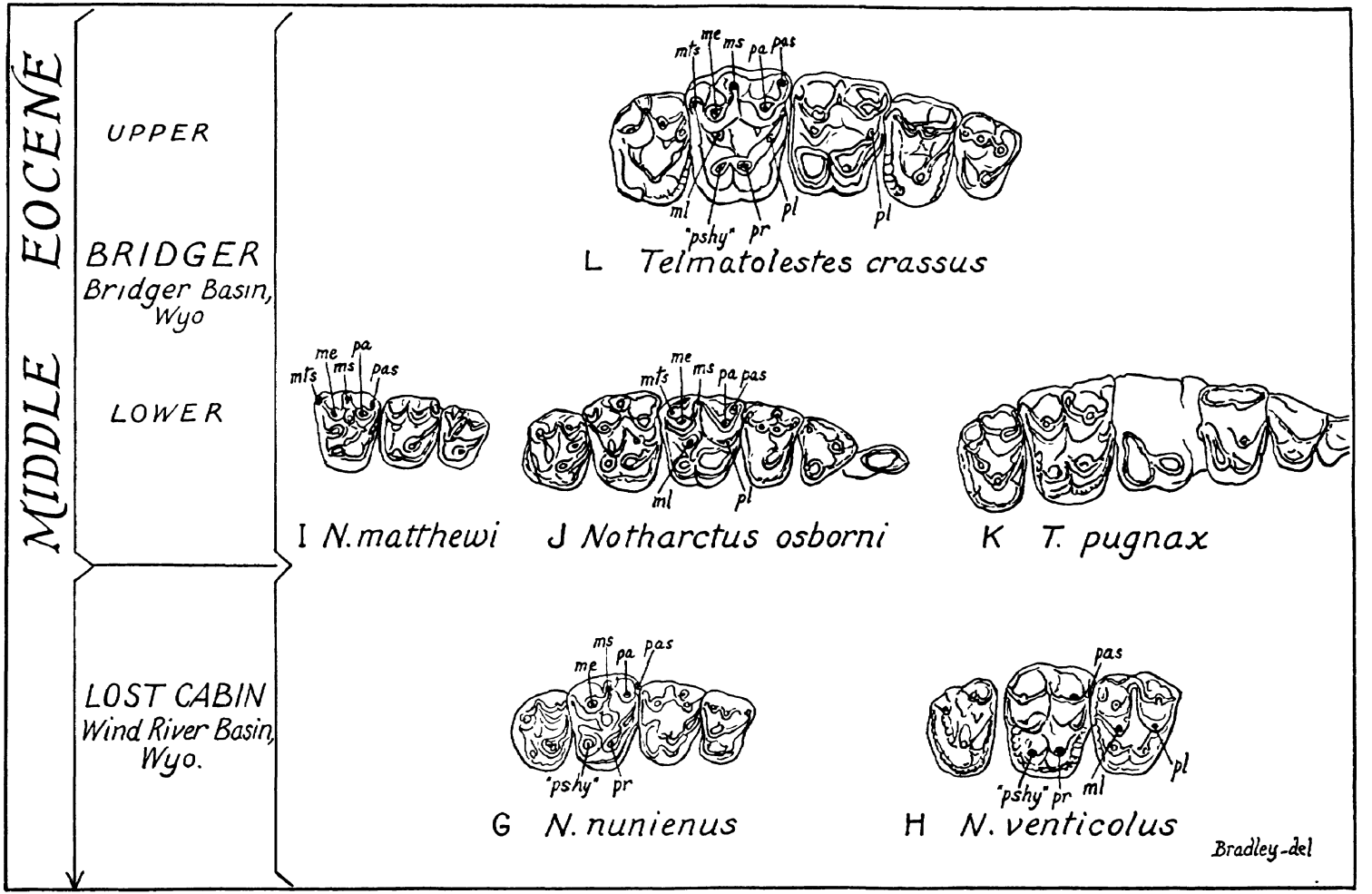
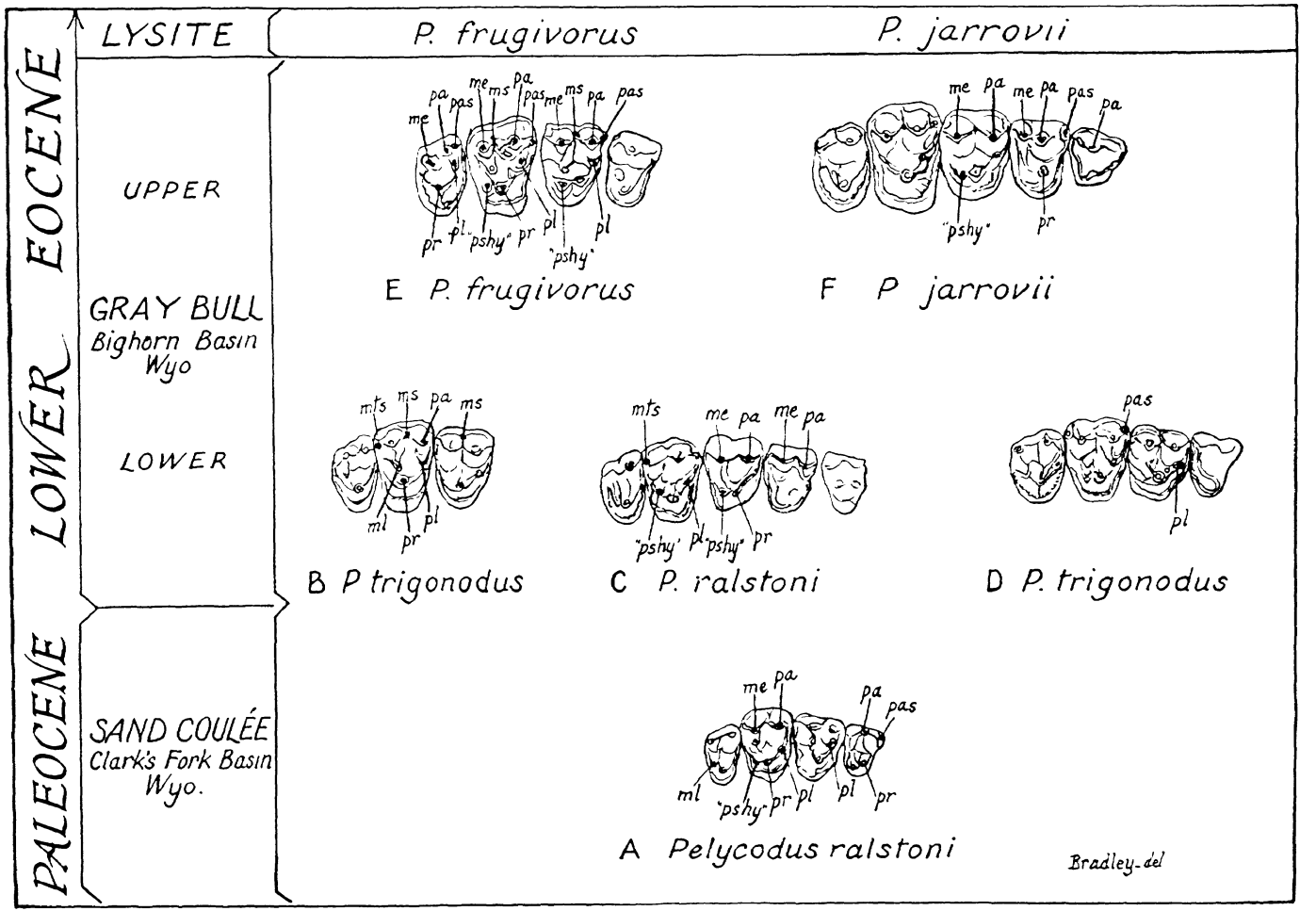

MIDDLE EOCENE
UPPER
BRIDGER
Bridger Basin, Wyo
LOWER
LOST CABIN
Wind River Basin, Wyo.
me ms pa pas mts ml "pshy" pr pl
L Telmatolestes crassus
I N. matthewi
J Notharctus osborni
K T. pugnax
G N. nunienus
H N. venticolus
Bradley-del

Fig. 23.6a



Figs. 23.6a, b Evolution of upper right premolar and molar patterns in Eocene Notharctinae. Data from Matthew, Gregory.

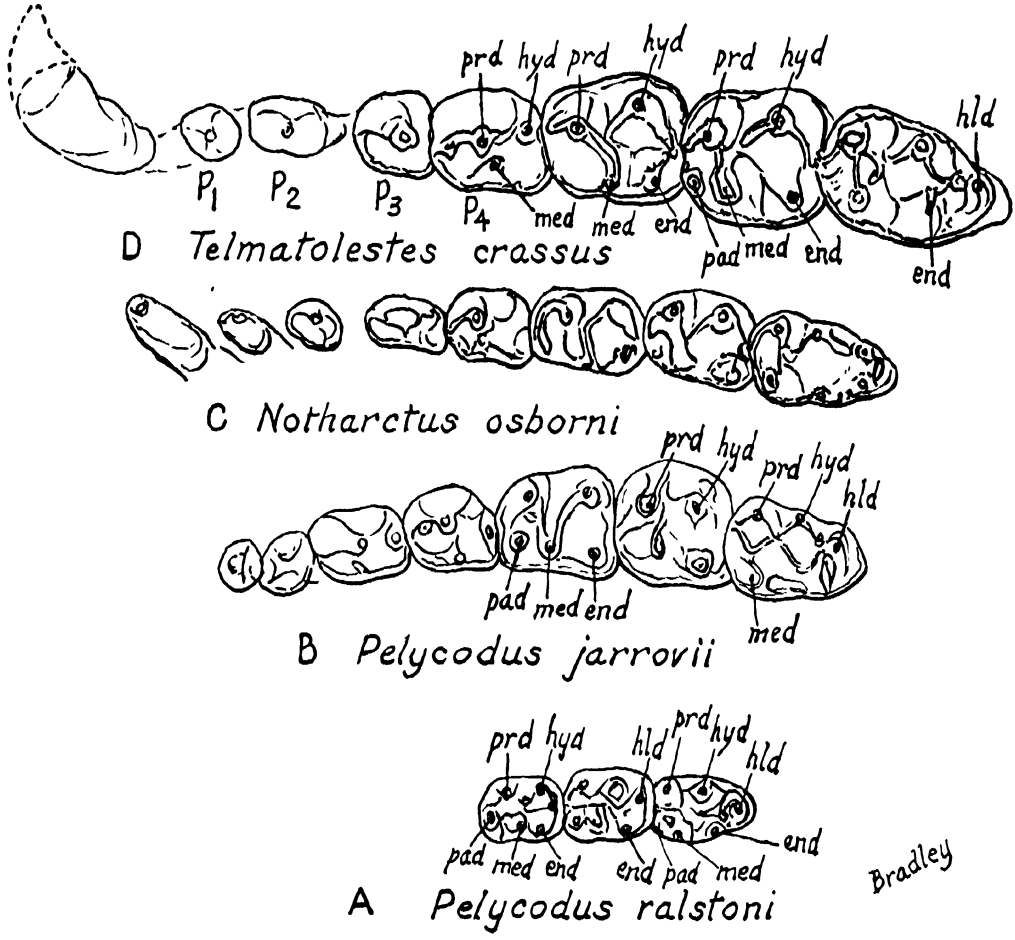


Fig. 23.7. Evolution of lower right cheek teeth in Notharctinae. After Gregory.

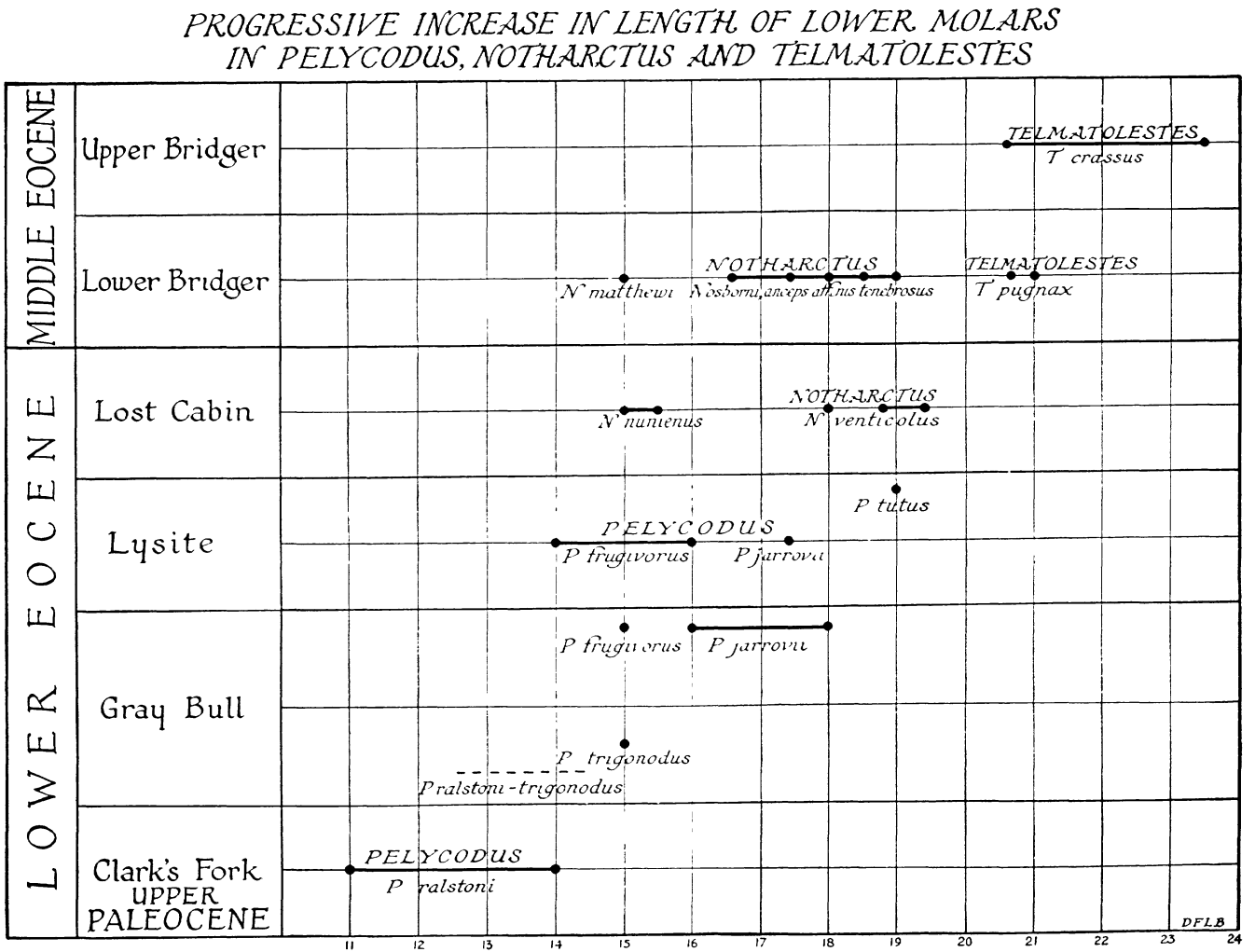

PROGRESSIVE INCREASE IN LENGTH OF LOWER MOLARS
IN PELYCODUS, NOTHARCTUS AND TELMATOLESTES
MIDDLE EOCENE
LOWER EOCENE
Upper Bridger
Lower Bridger
Lost Cabin
Lysite
Gray Bull
Clark's Fork
UPPER
PALEOCENE
TELMATOLESTES
T crassus
NOTHARCTUS
N matthewi
N osborni, anceps affinis tenebrosus
TELMATOLESTES
T pugnax
NOTHARCTUS
N nunienus
N venticolus
P tutus
PELYCODUS
P frugivorus
P jarrovii
P frugivorus
P jarrovii
P trigonodus
P ralstoni-trigonodus
PELYCODUS
P ralstoni
DFLB
11
12
13
14
15
16
17
18
19
20
21
22
23
24

Fig. 23.8

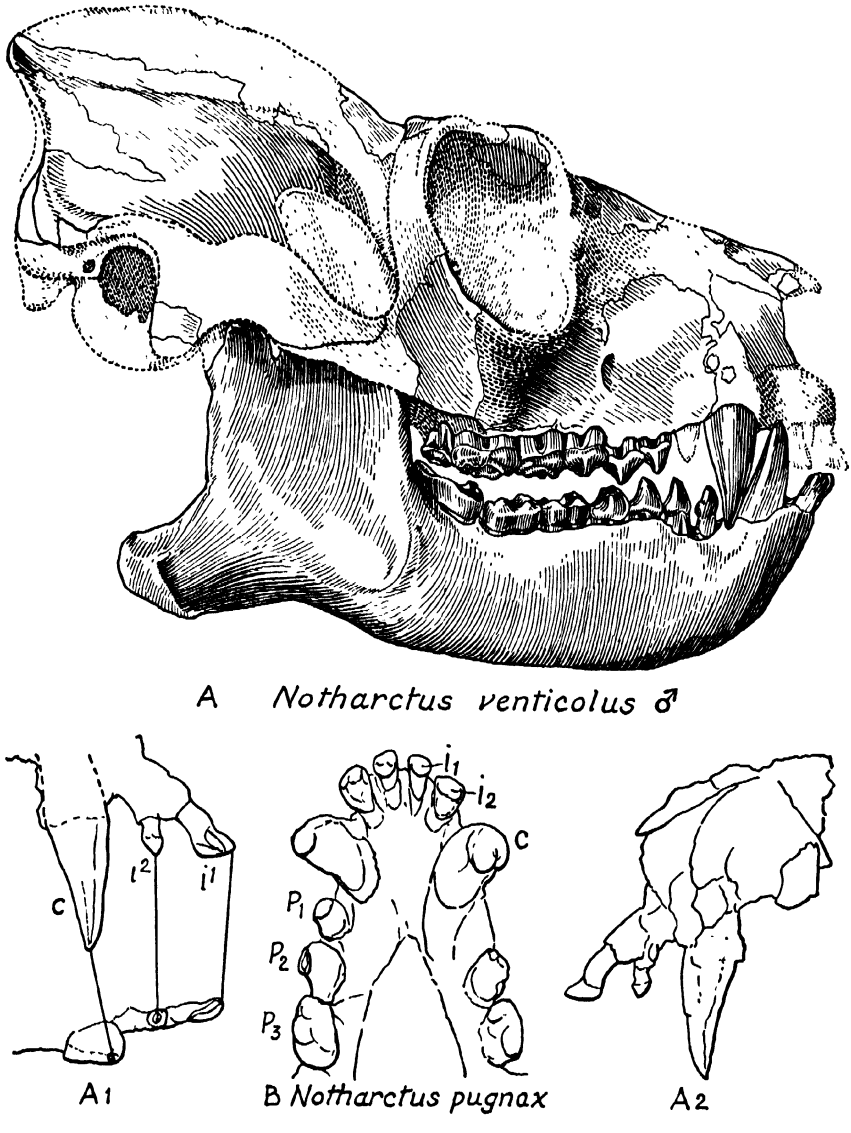


Fig. 23.9. Partly restored skull of Eocene lemuroid, with incisors and canines. After Gregory.

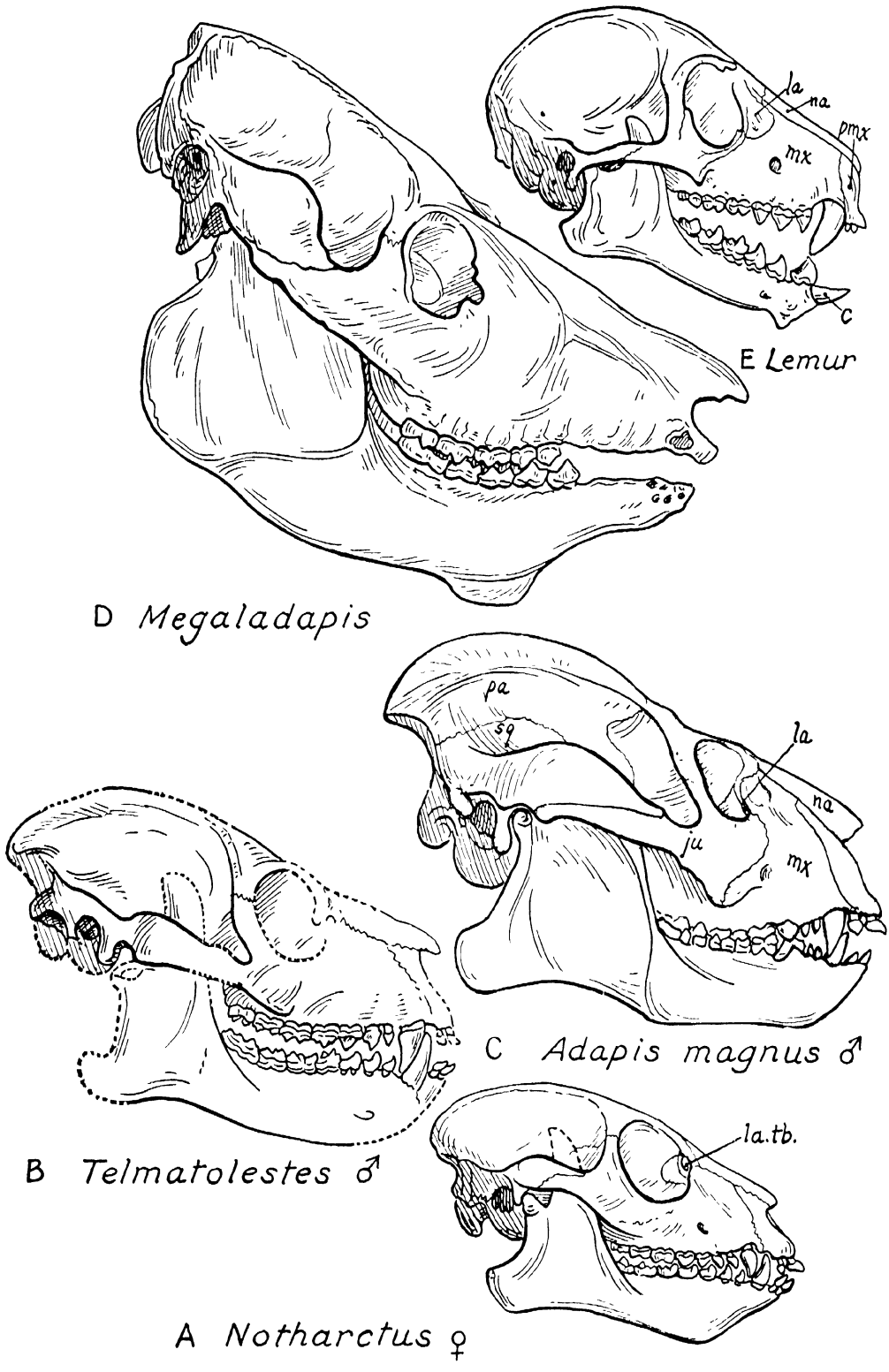


Fig. 23.10. Skulls of Eocene Notharctinae (A, B), Adapinae (C), extinct (D) and Recent (E) Malagasy lemurs. A, B, after Gregory; C, after Stehlin; D, after Standing; E, after Milne Edwards

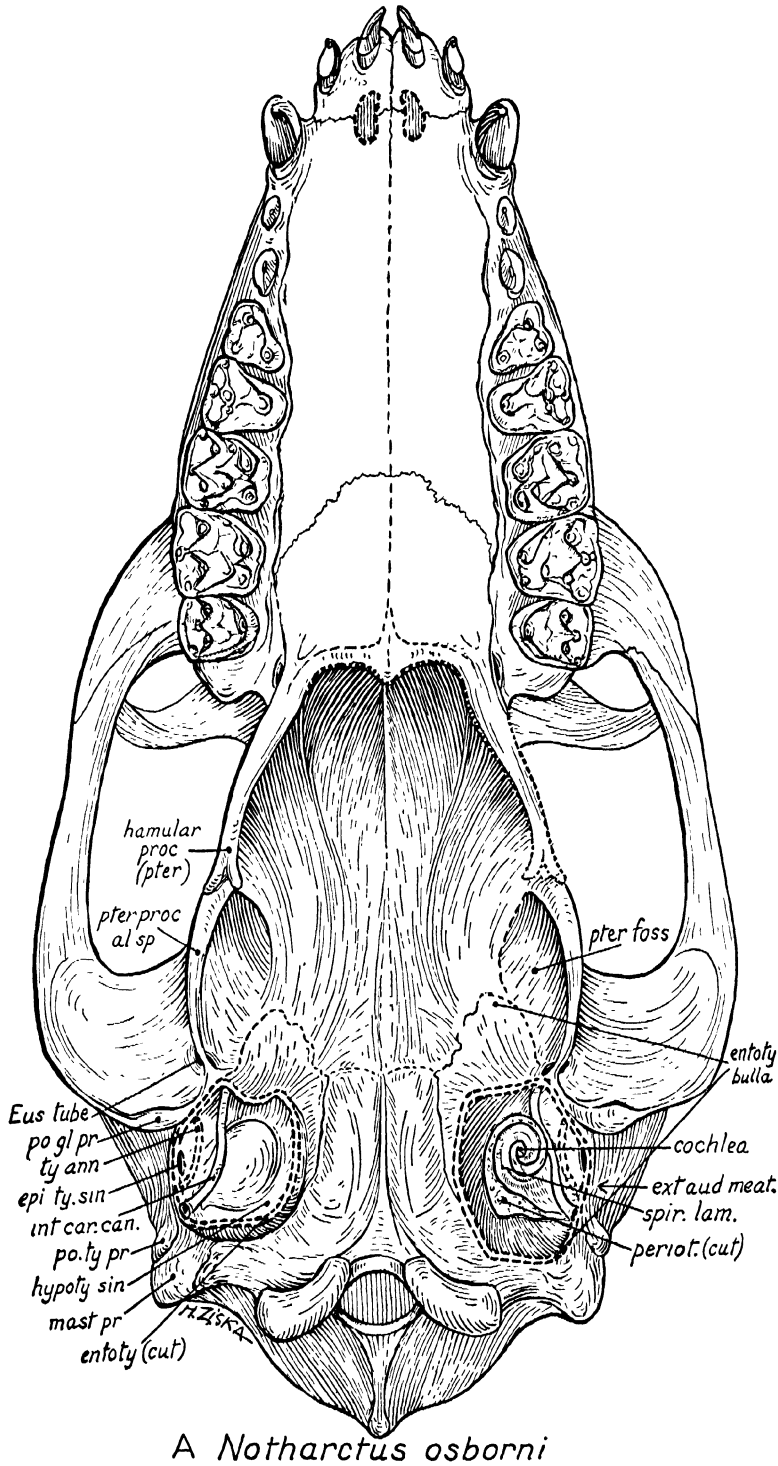


Fig. 23.11a, b. Reconstruction of skull, in palatal aspect, of notharctine (A), adapine (B), and modern lemur (C). A, original; B, C, after Stehlin.

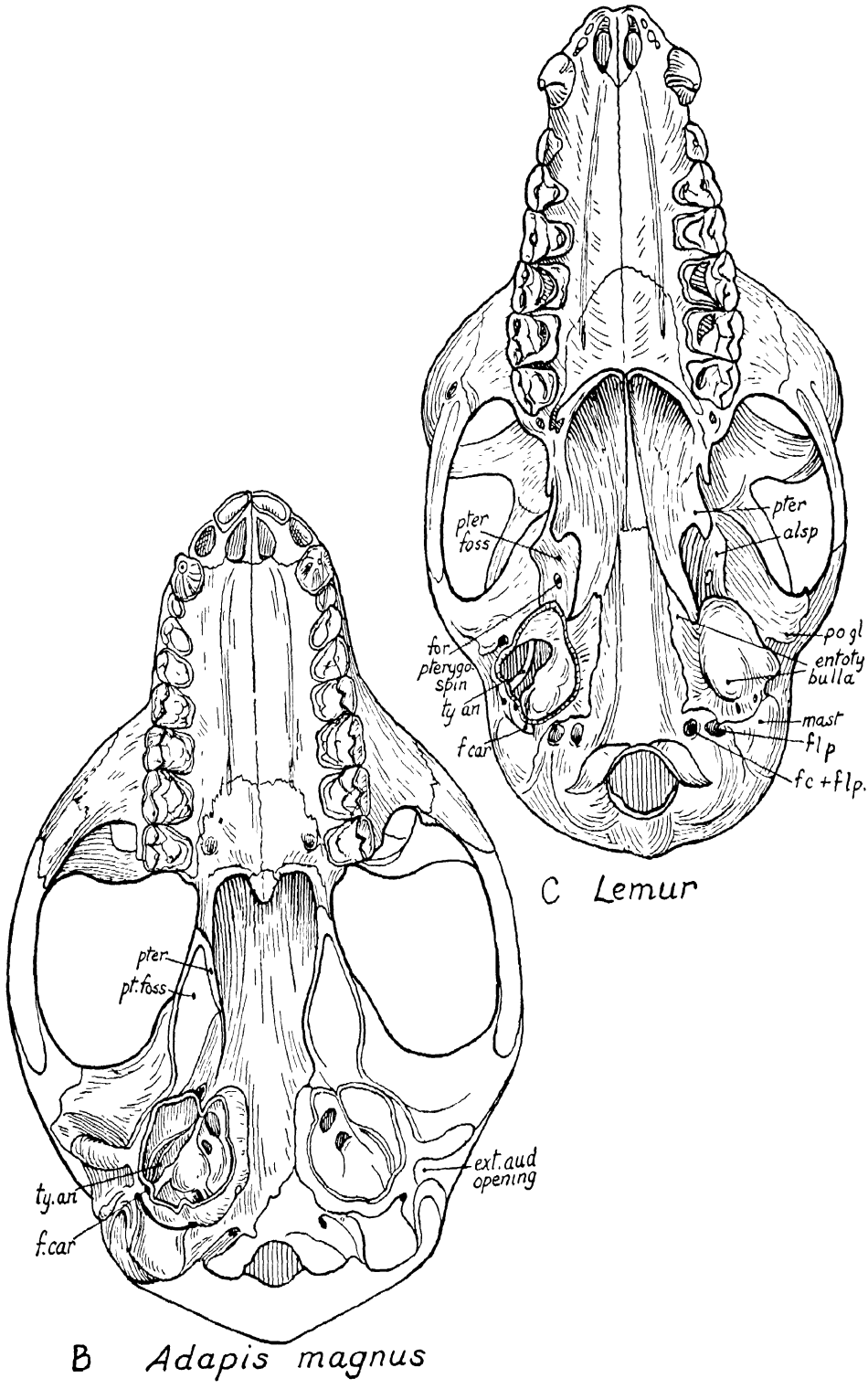

pter
pter foss
for pterygo spin
ty an
f car
pter
alsp
po gl
entoty bulla
mast
f l p
f c + f l p.
C Lemur
pter
pt. foss
ty. an
f. car
ext. aud opening
B Adapis magnus

Fig 23.11b

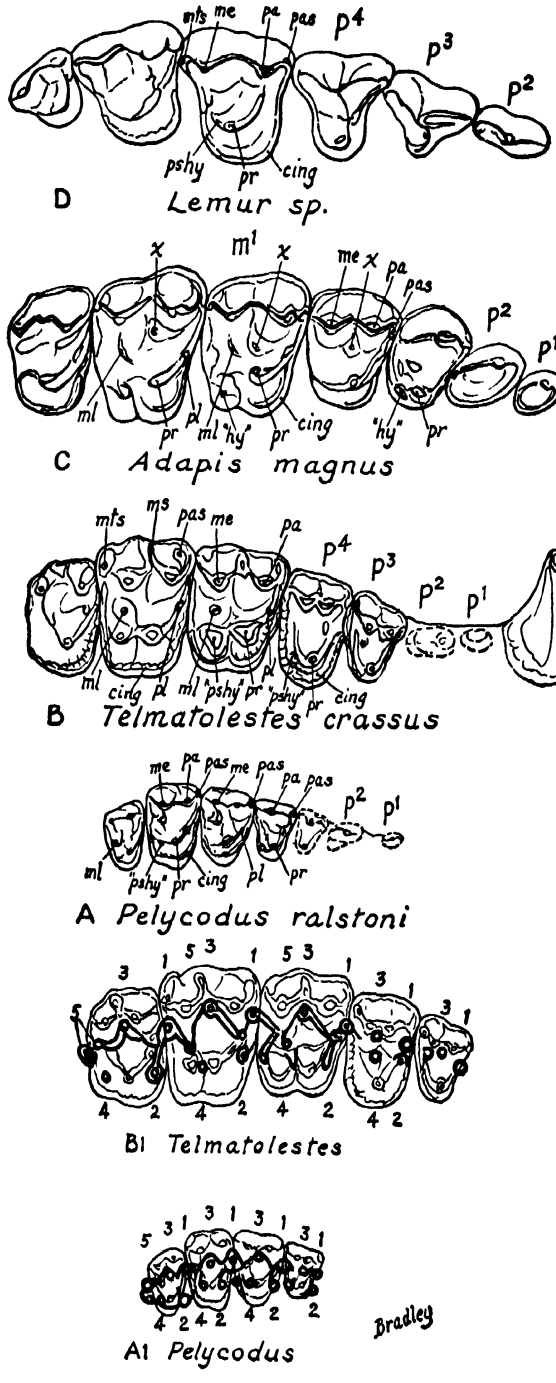


Fig. 23.12. Upper premolar-molar series of lemuroids, indicating progressive complication (A, B) followed by simplification (C, D). Occlusal diagrams (A1, B1) of Eocene notharctines. 1, 3, 5, cusps on outer side; 2, 4, on inner side of lower molars. After Gregory.

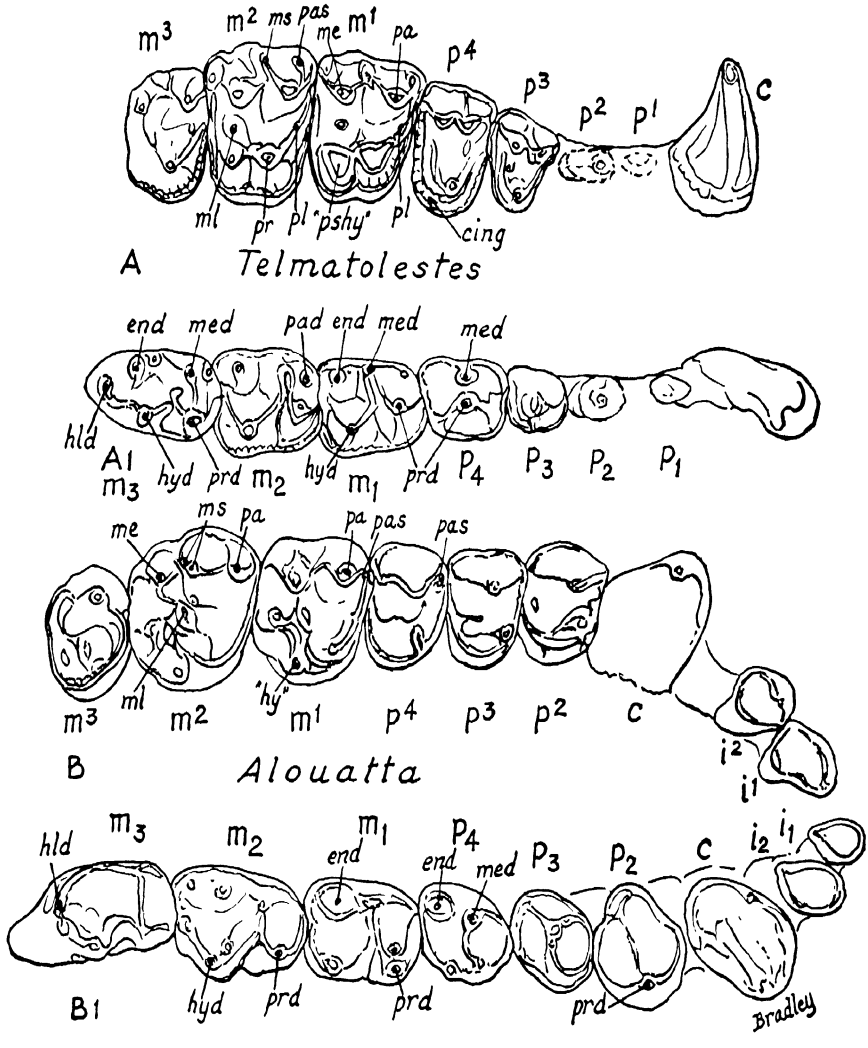


Fig. 23.13. Comparison of upper and lower teeth of Eocene notharctine (A, A1) and modern South American howler monkey (B, B1). After Gregory.

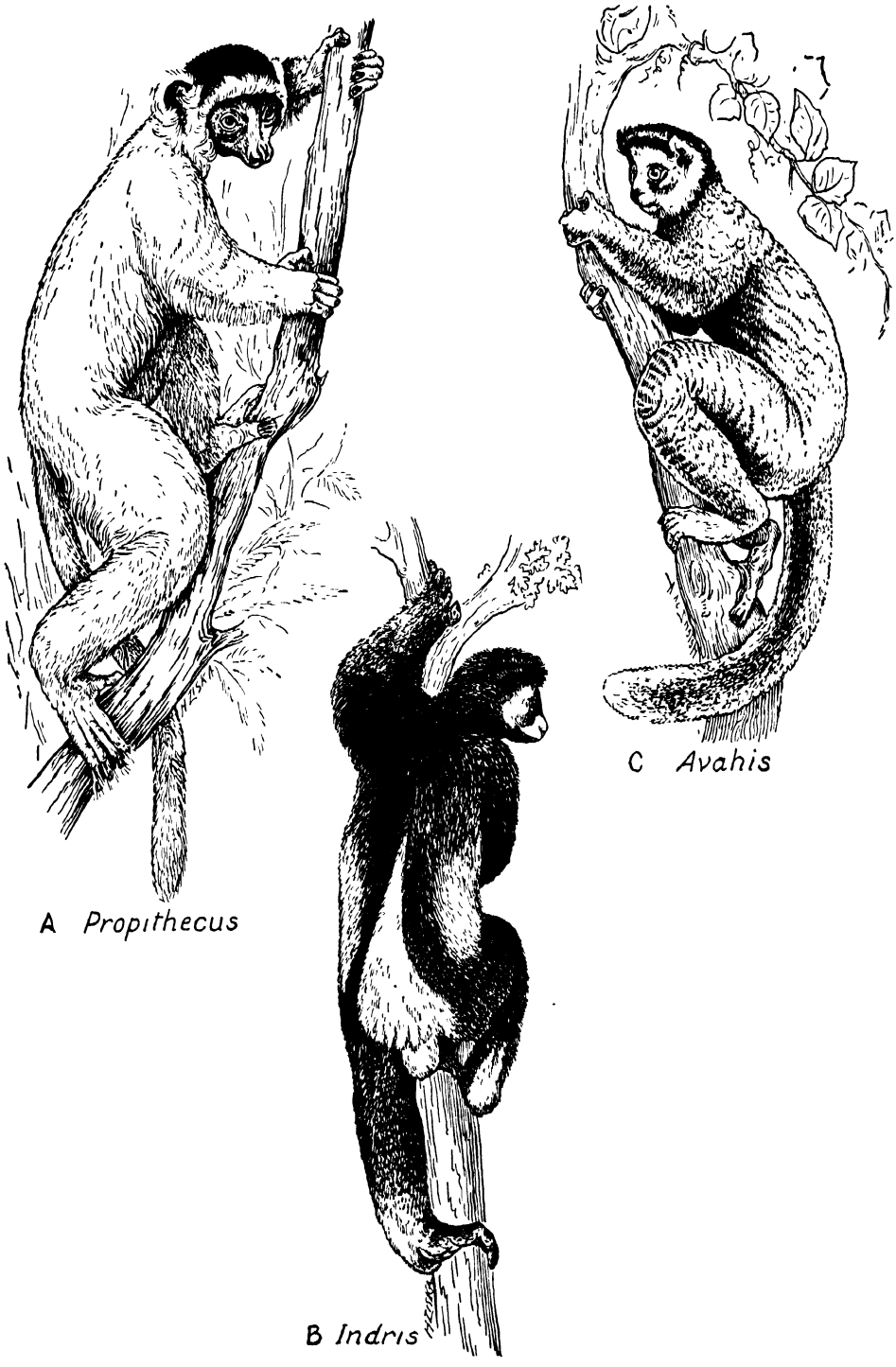


Fig. 23.14. Recent indrisid lemurs of Madagascar.
After Milne Edwards.

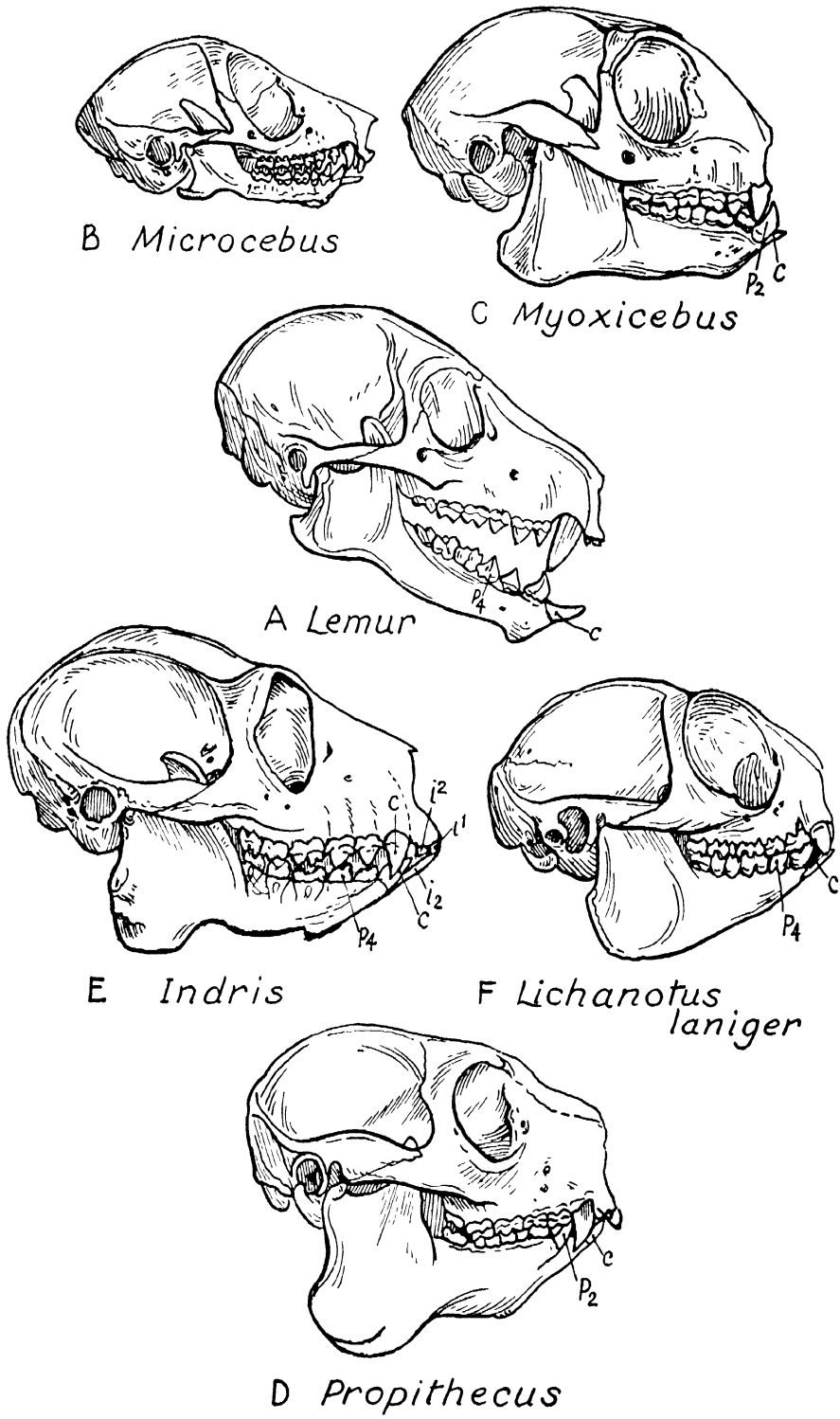


Fig. 23.15 Skulls of recent lemurids (A–C) and indrisids (D–F). After Milne Edwards.

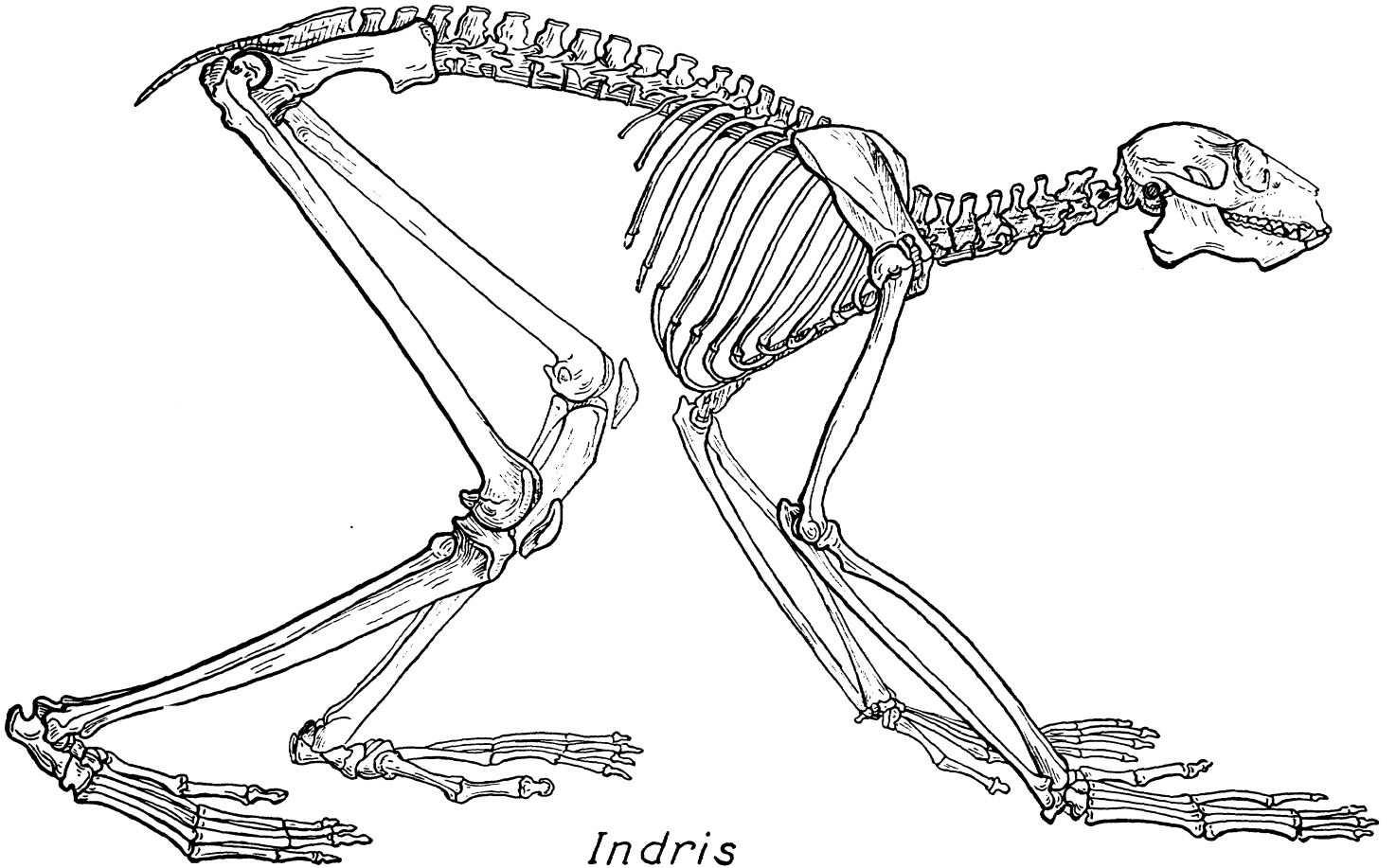


Fig. 23.16. Skeleton of a short-tailed indrisid. After De Blainville.

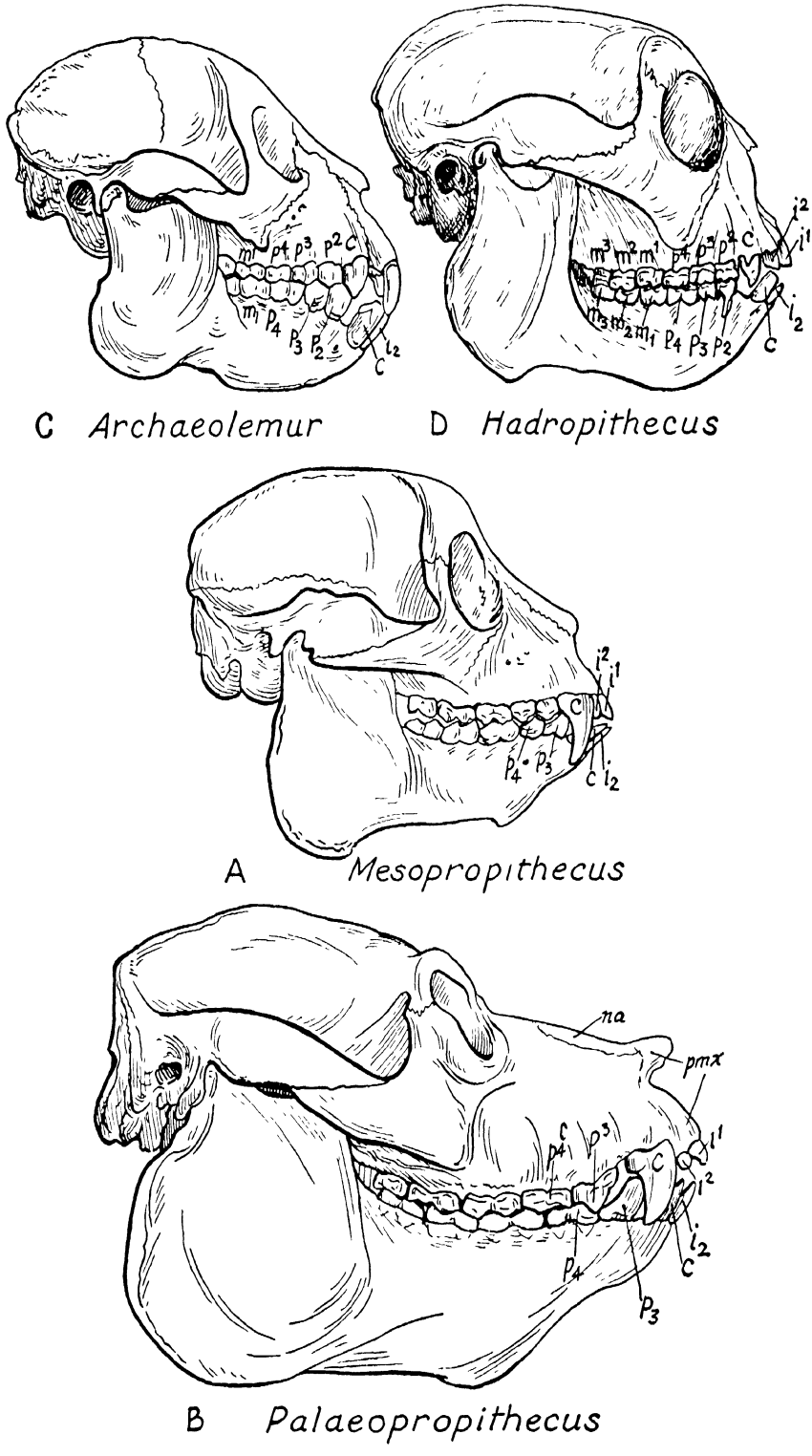


Fig. 23.17. Skulls of indrisids and archaeolemurids.
A–C, after Standing; D, after Lamberton.

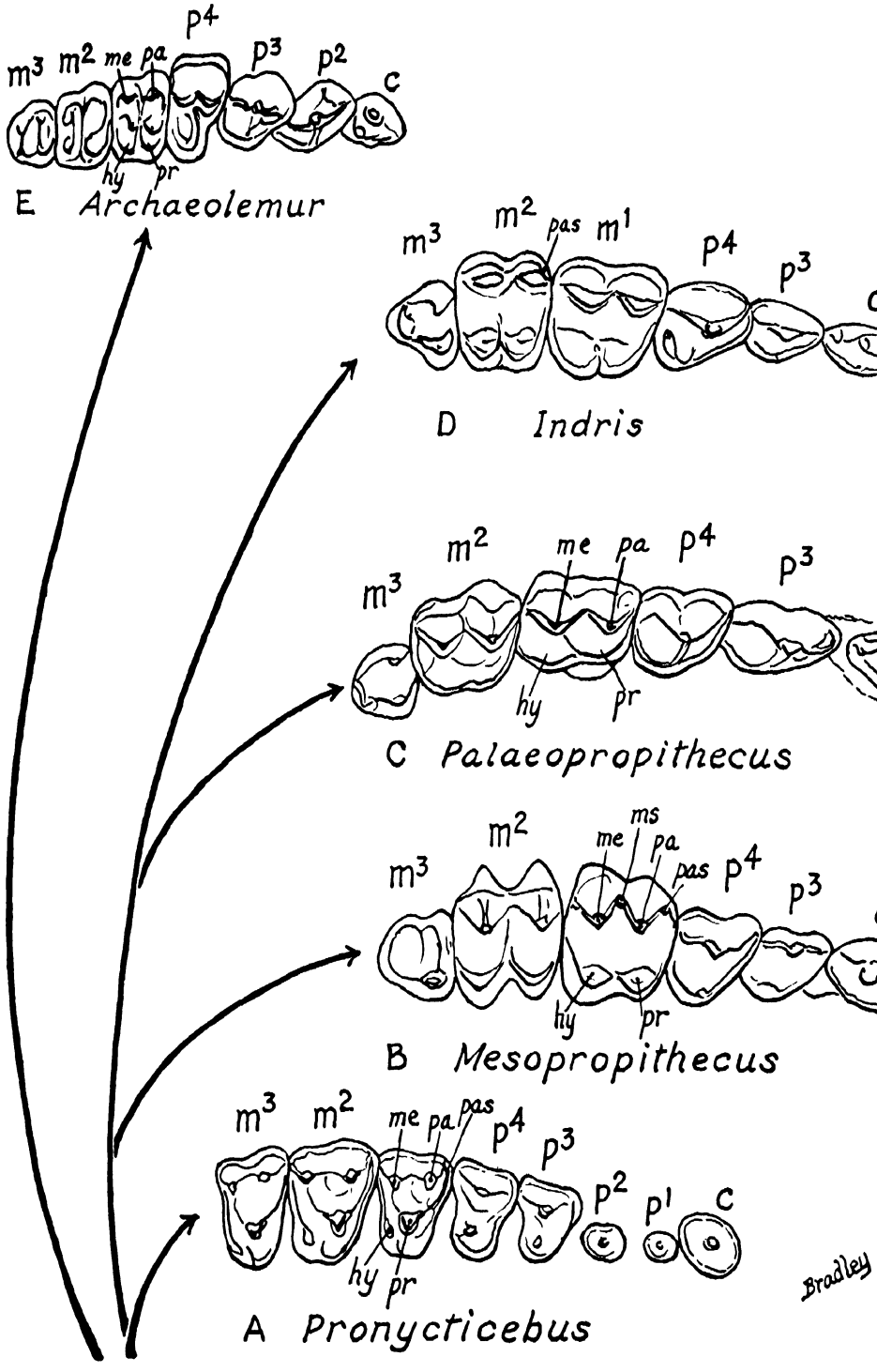
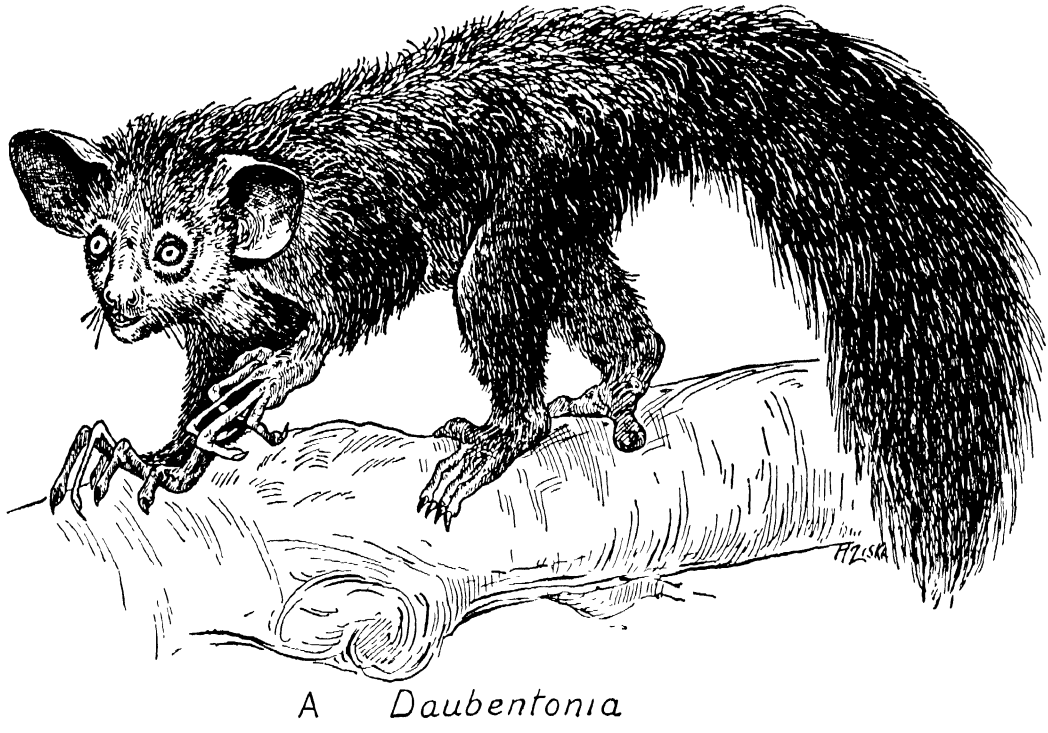


Fig. 23.18. Upper cheek teeth of primitive lemuroid (A), indrisids, and archaeolemurids. A, after Grandidier; B–E, after Standing.



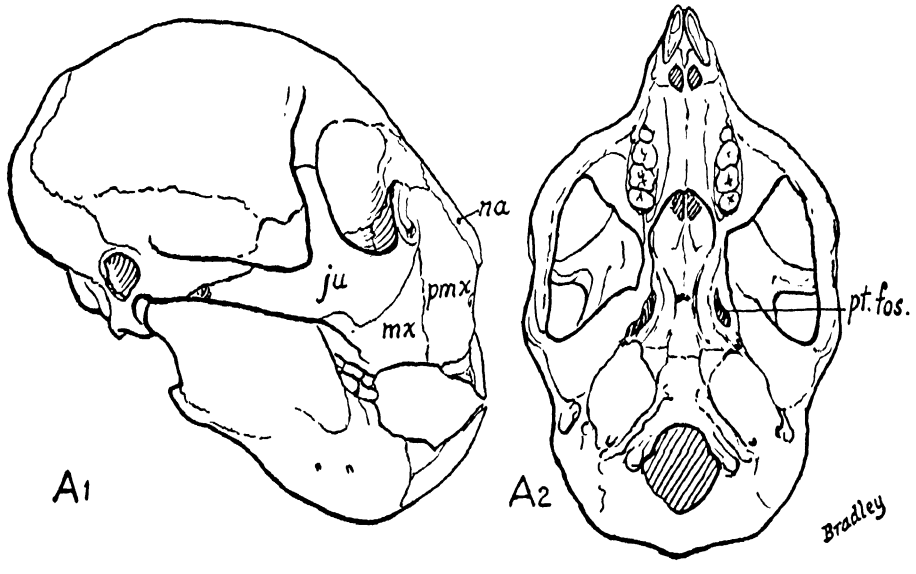


Fig. 23.19. The strange aye-aye and its skull. A, after Owen; A1, A2, after Elliot.

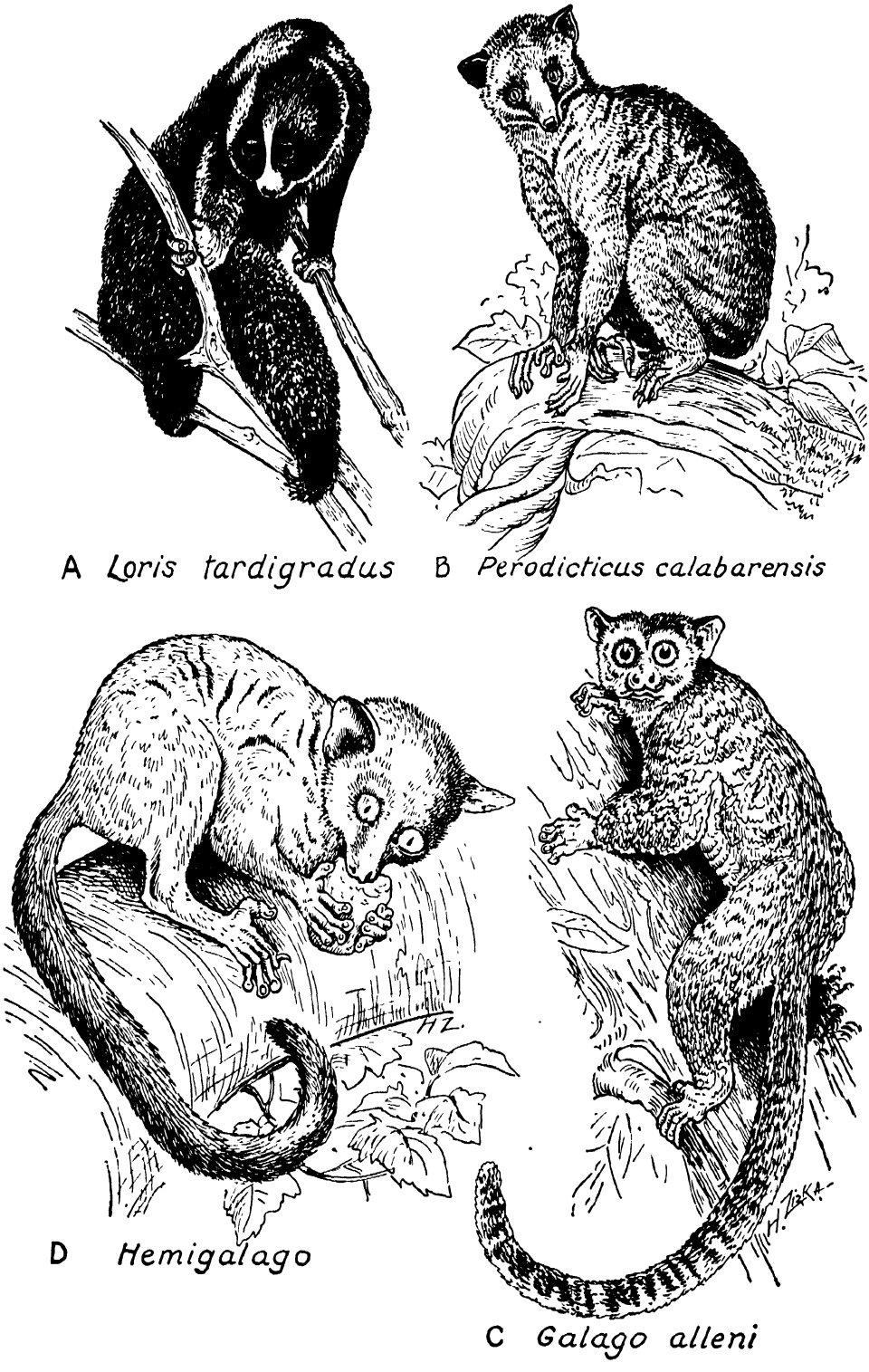


Fig. 23.20. Slow lemurs (A, B) and galagos (C, D).
Animals from Elliot.

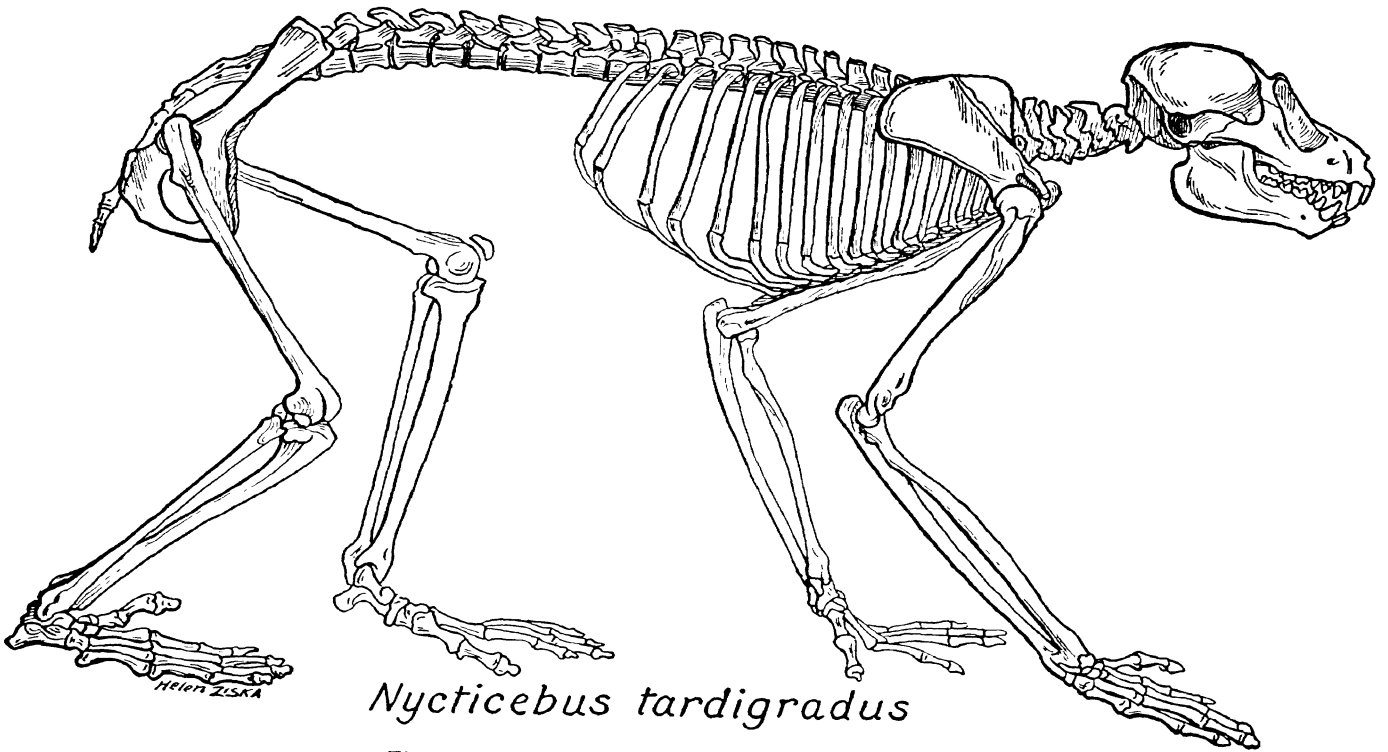


Fig. 23.21. Skeleton of slow lemurs. After De Blainville.

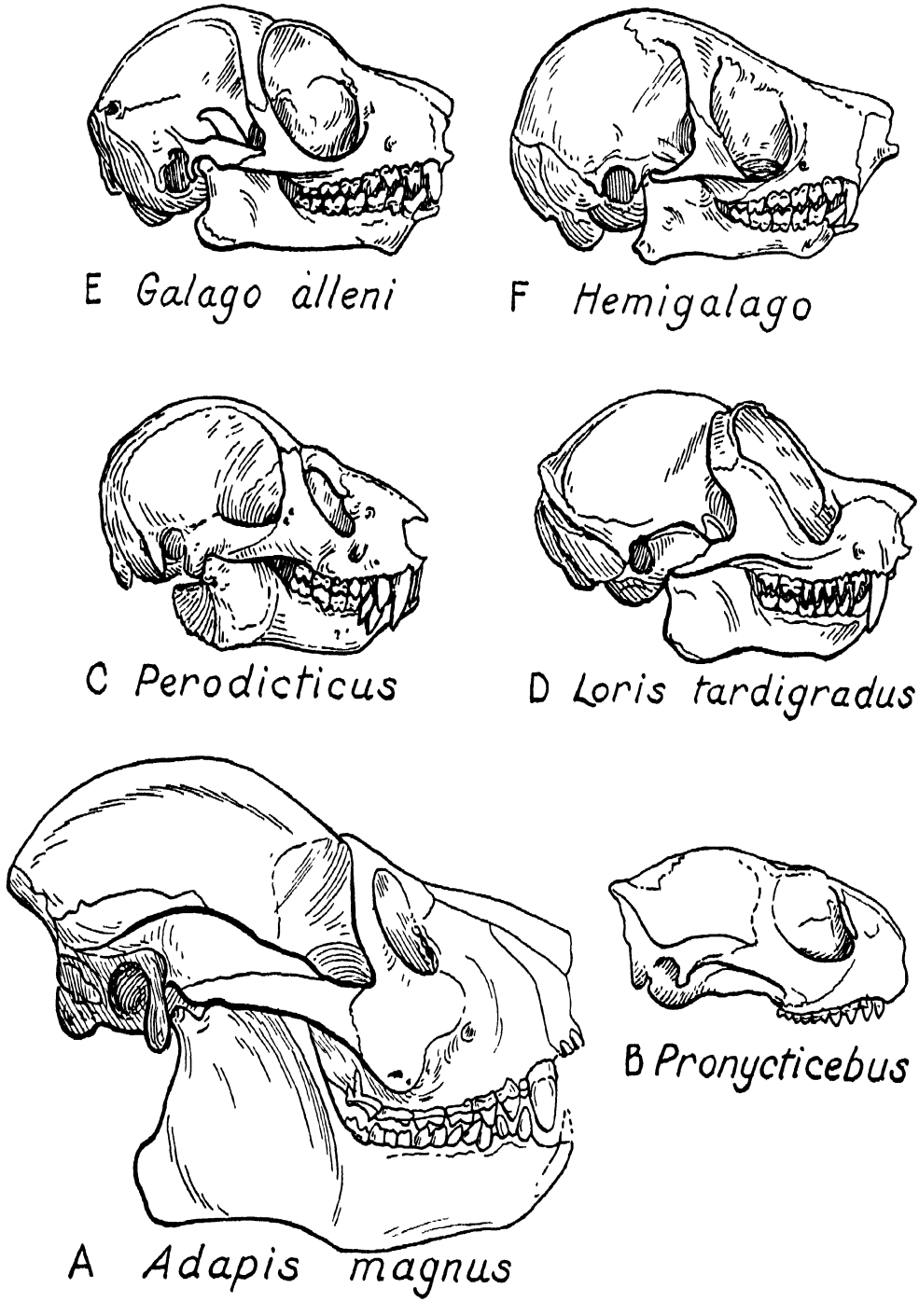


Fig. 23.22. Skulls of Eocene adapids (A, B), modern lorisids (C, D) and galagos (E, F). A, after Stehlin; B, after Grandidier and Milne Edwards; C–F, after Elliot.

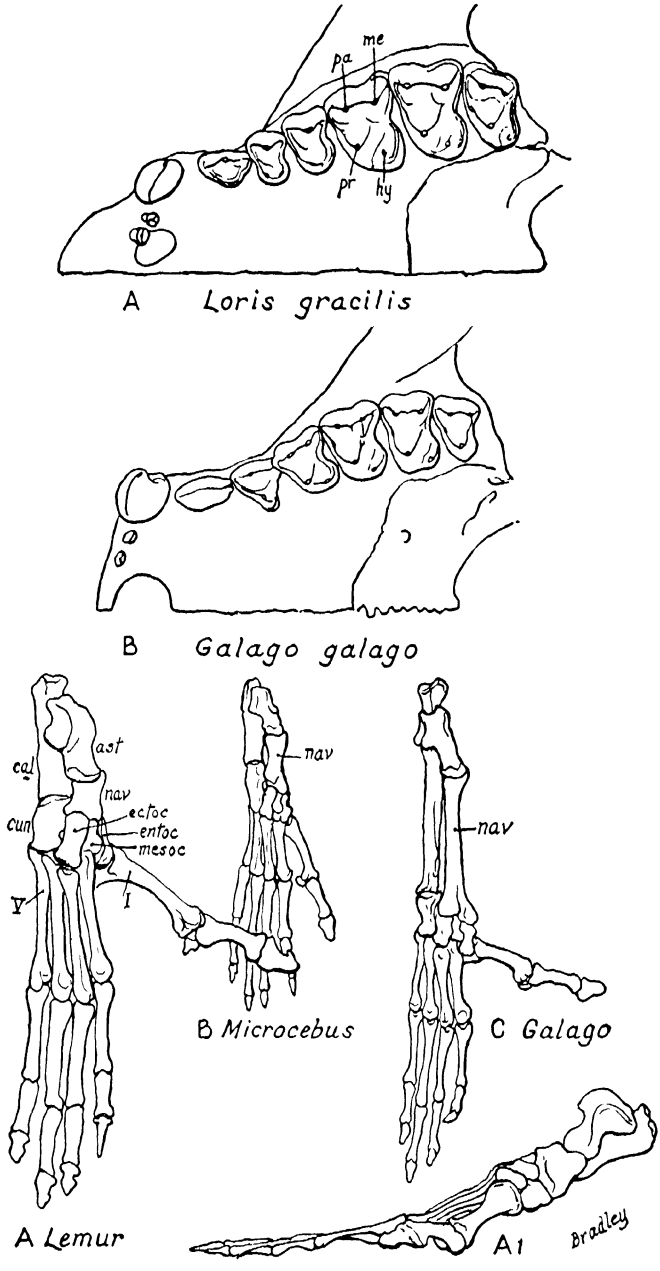


Fig. 23.23 (top). Upper teeth of slow lemur (A) and galago (B). After Stehlin.

Fig. 23.24. Feet of modern lemurs, to show large divergent hallux and elongation of navicular and distal end of calcaneum, reaching an extreme in *Galago*. After De Blainville.

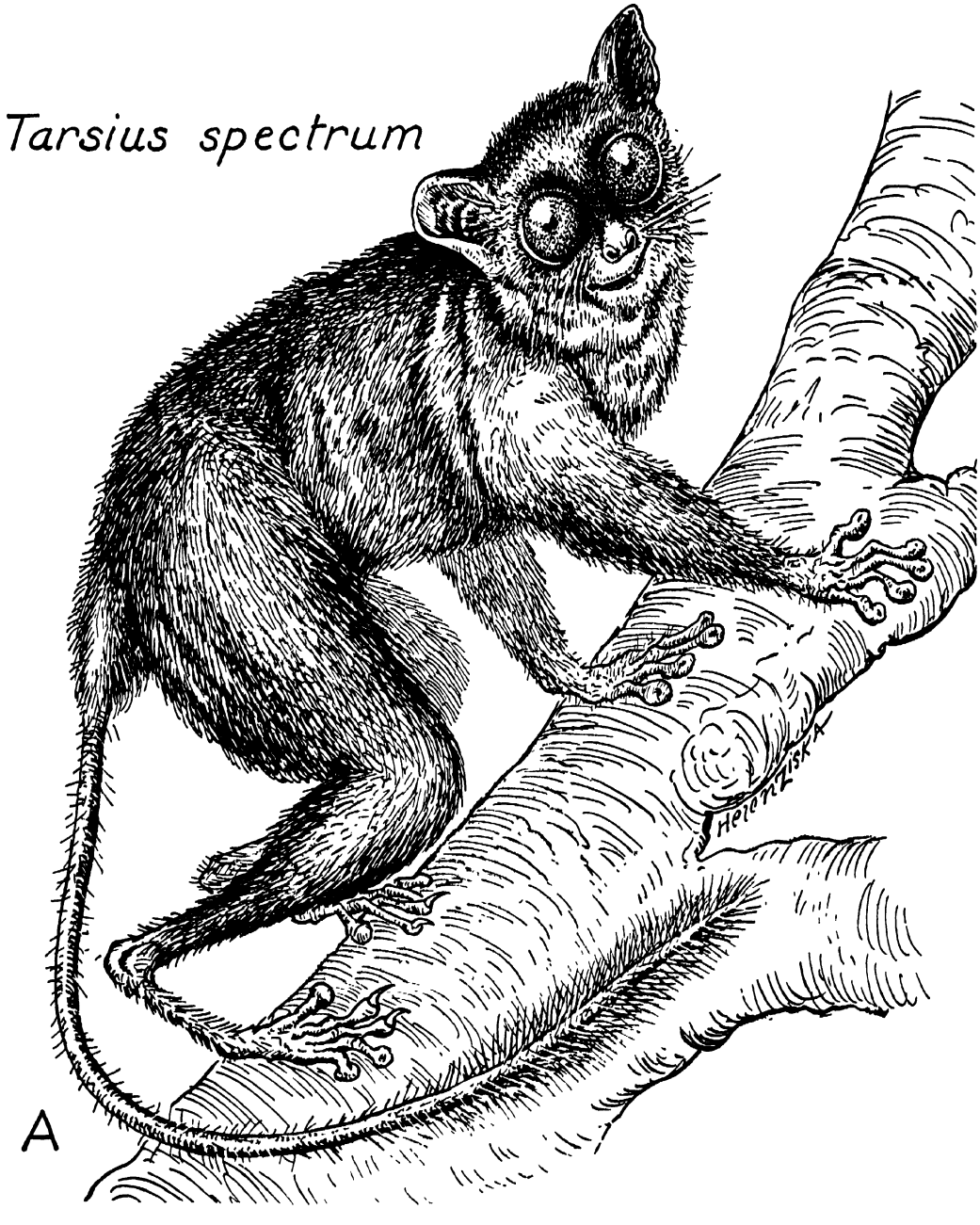


Fig. 23.25. The spectral tarsier. Data on animal from photographs by H. C. Raven and others.

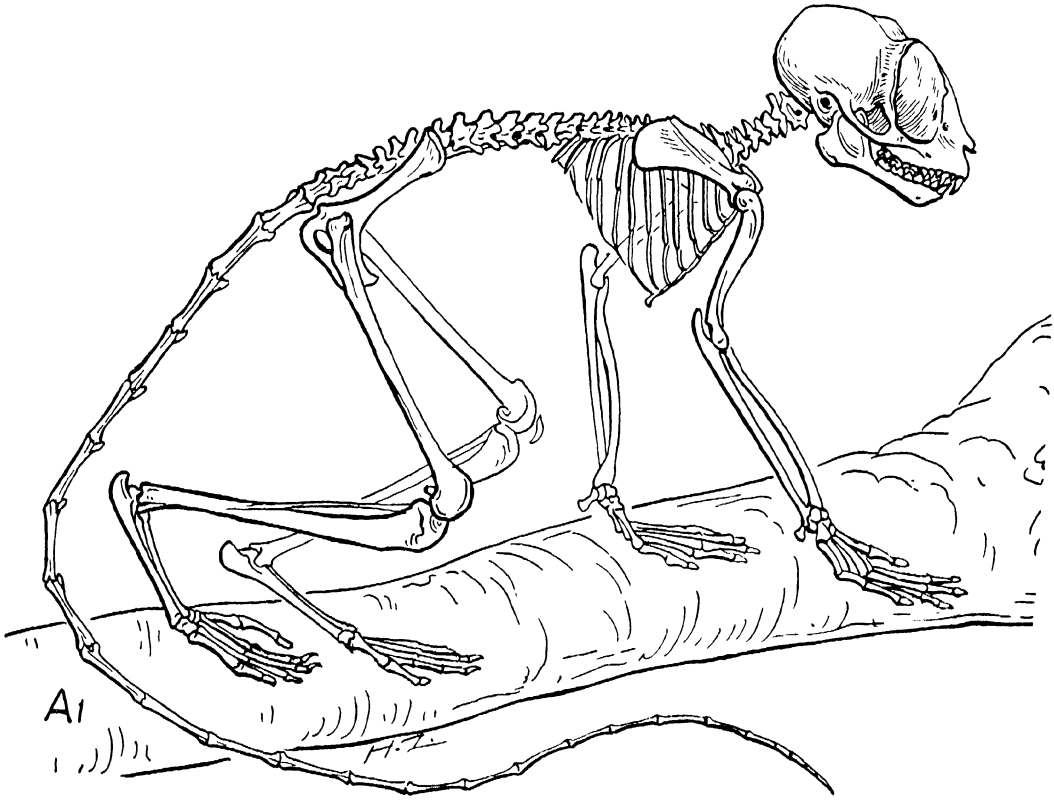


Fig. 23 26. Skeleton of spectral tarsier. After De Blainville.

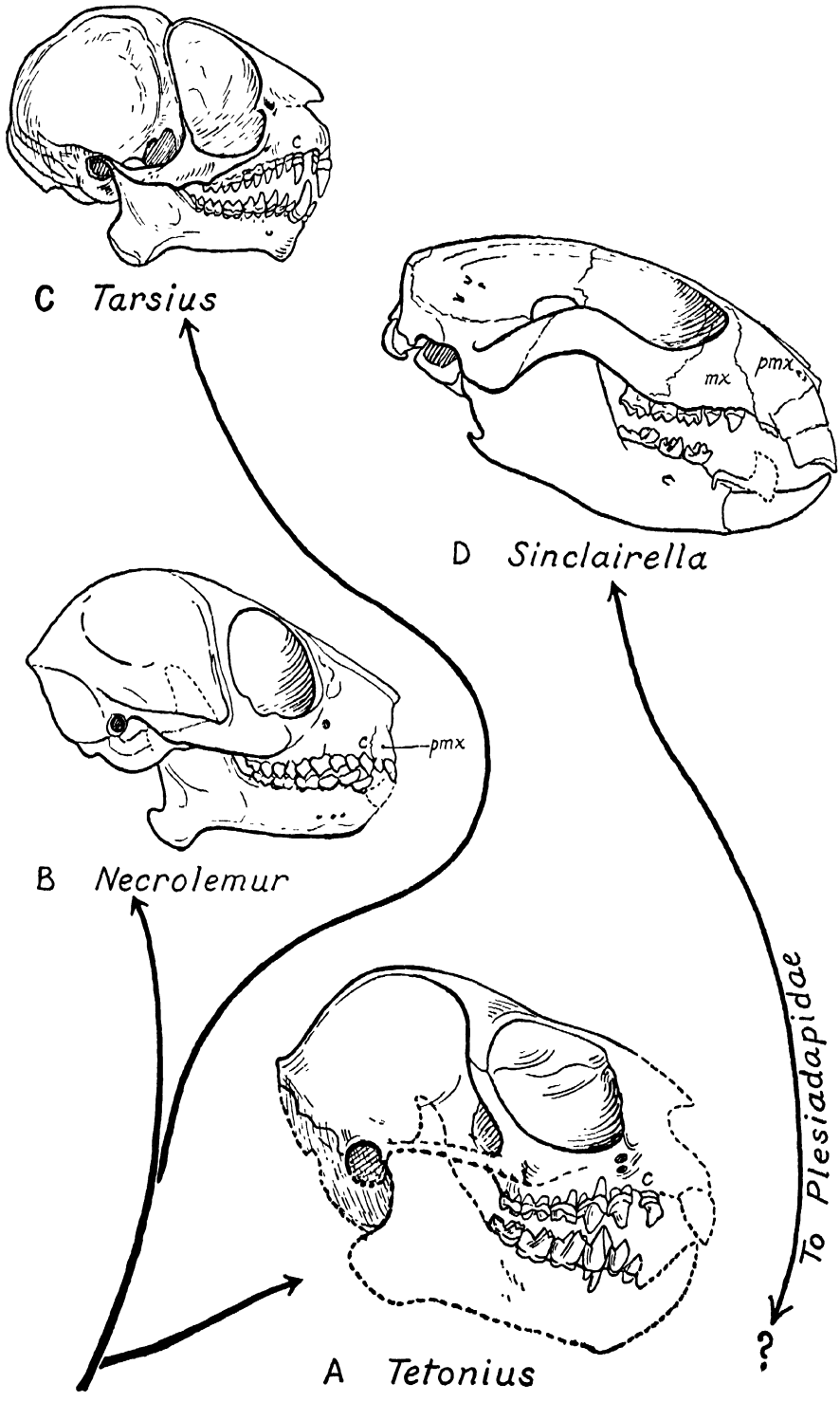


Fig. 23.27. Skulls of tarsioids (A–C) and apatemyid (D). A, after Matthew; B, after Stehlin; C, after Gregory; D, after Jepson.

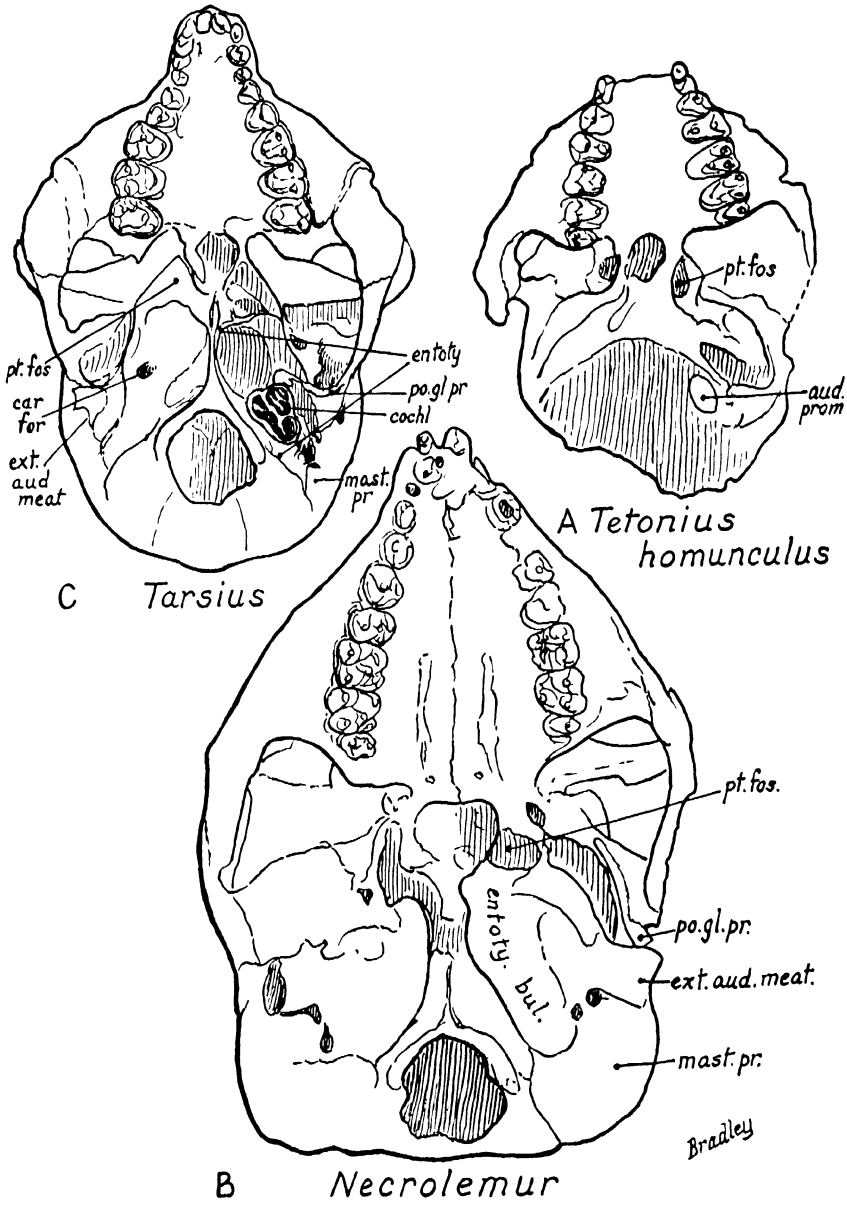


Fig. 23.28. Skulls of Lower Eocene (A), Upper Eocene (B) and modern (C) tarsioids, basal aspect. After Gregory. A, C, × 2; B, × 8/3.

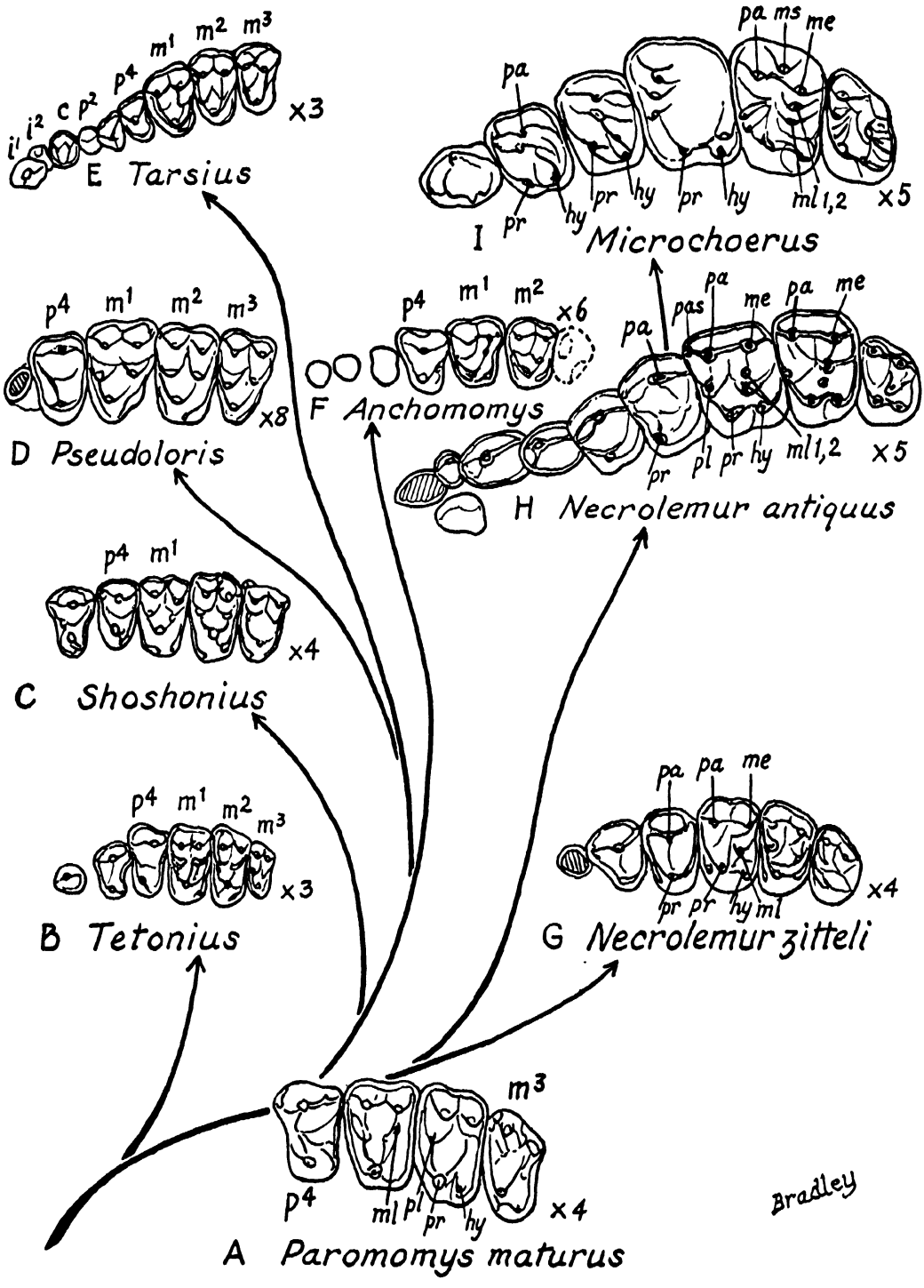


Fig. 23.29a. Phylogeny of Paleocene (A) to Recent tarsioids; upper cheek teeth. A, after Simpson; B, C, after Matthew; D, F, G–I, after Stehlin; E, after Gregory.

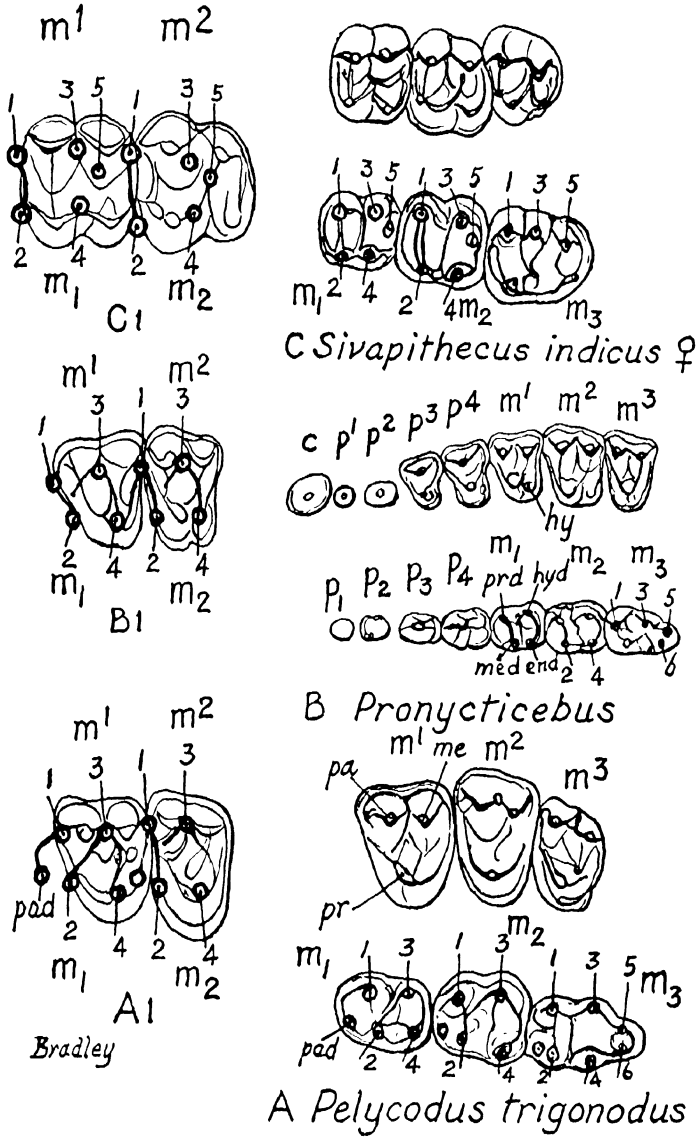


Fig. 23.29b. Tritubercular key to evolution of cheek teeth: A, Lower Eocene primitive lemuroid; B, Upper Eocene progressive lemuroid; C, Lower Pliocene central anthropoid. Data from: A, Matthew; B, Grandidier; C, original; *1*, protoconid; *2*, metaconid; *3*, hypoconid; *4*, entoconid; *5*, hypoconulid. In occlusion diagrams (A1, B1, C1) position of lower cusps in thick circles and lines.

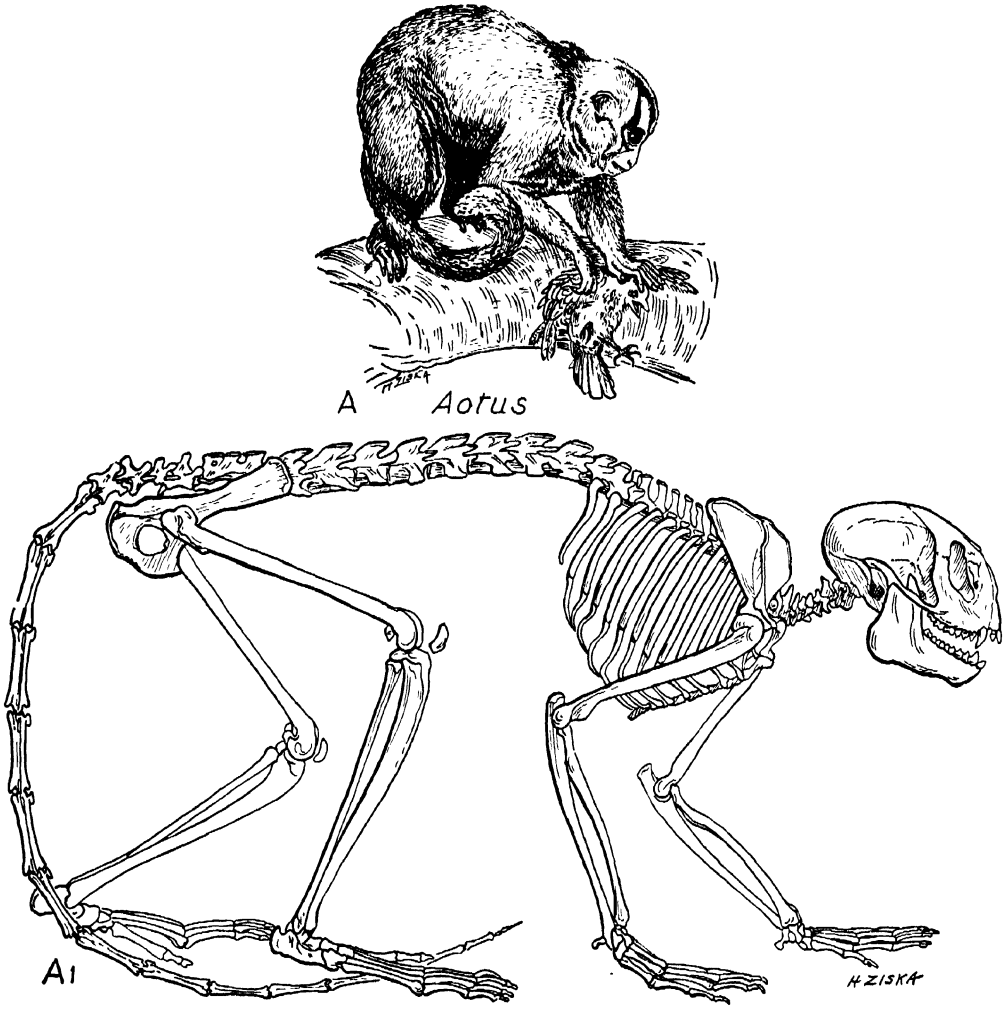


Fig. 23.30. The dourocucouli, a primitive South American monkey. A, after Lydekker; A1, after De Blainville.

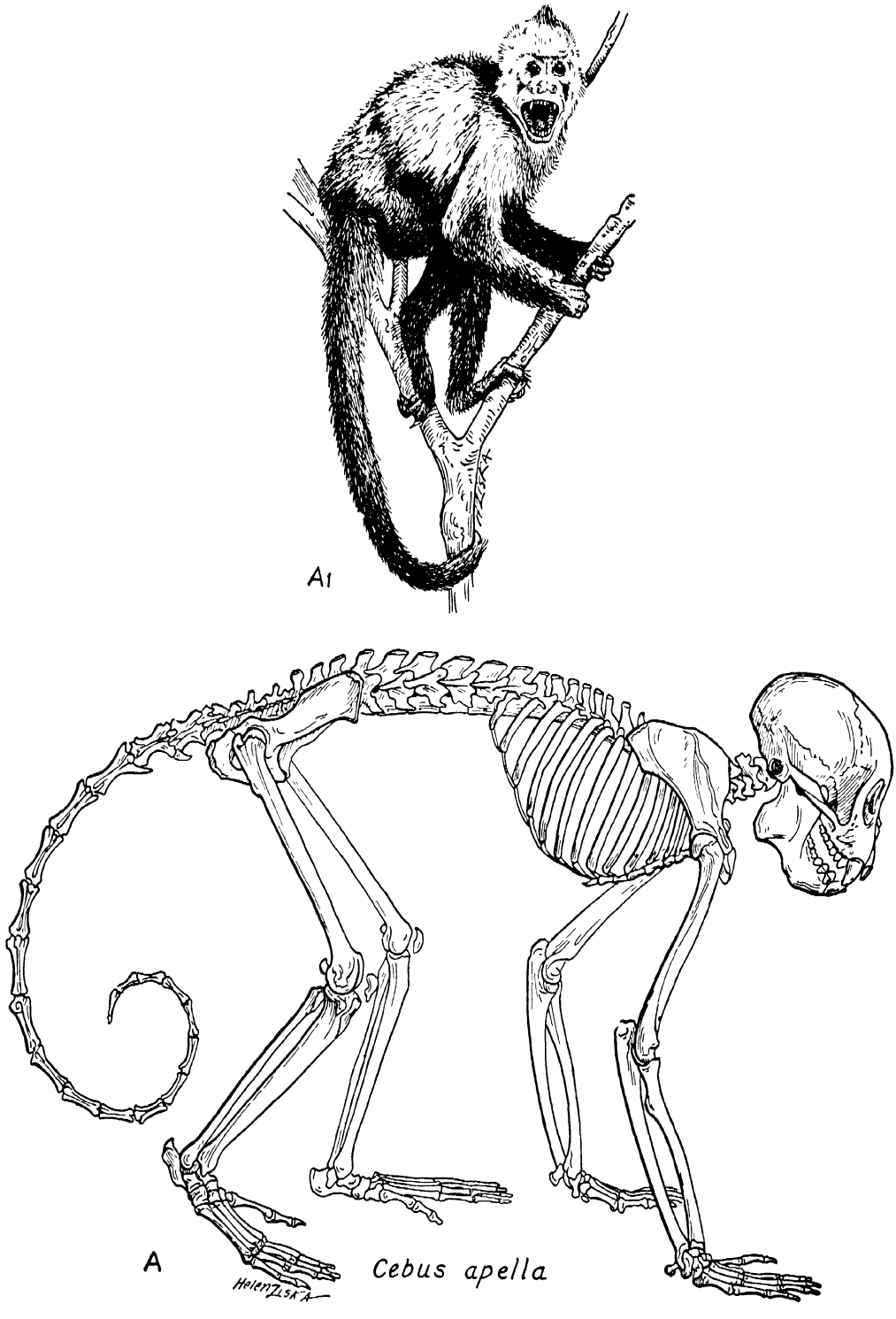


Fig. 23.31. The typical South American monkey.
A, after De Blainville; A1, after Lydekker.

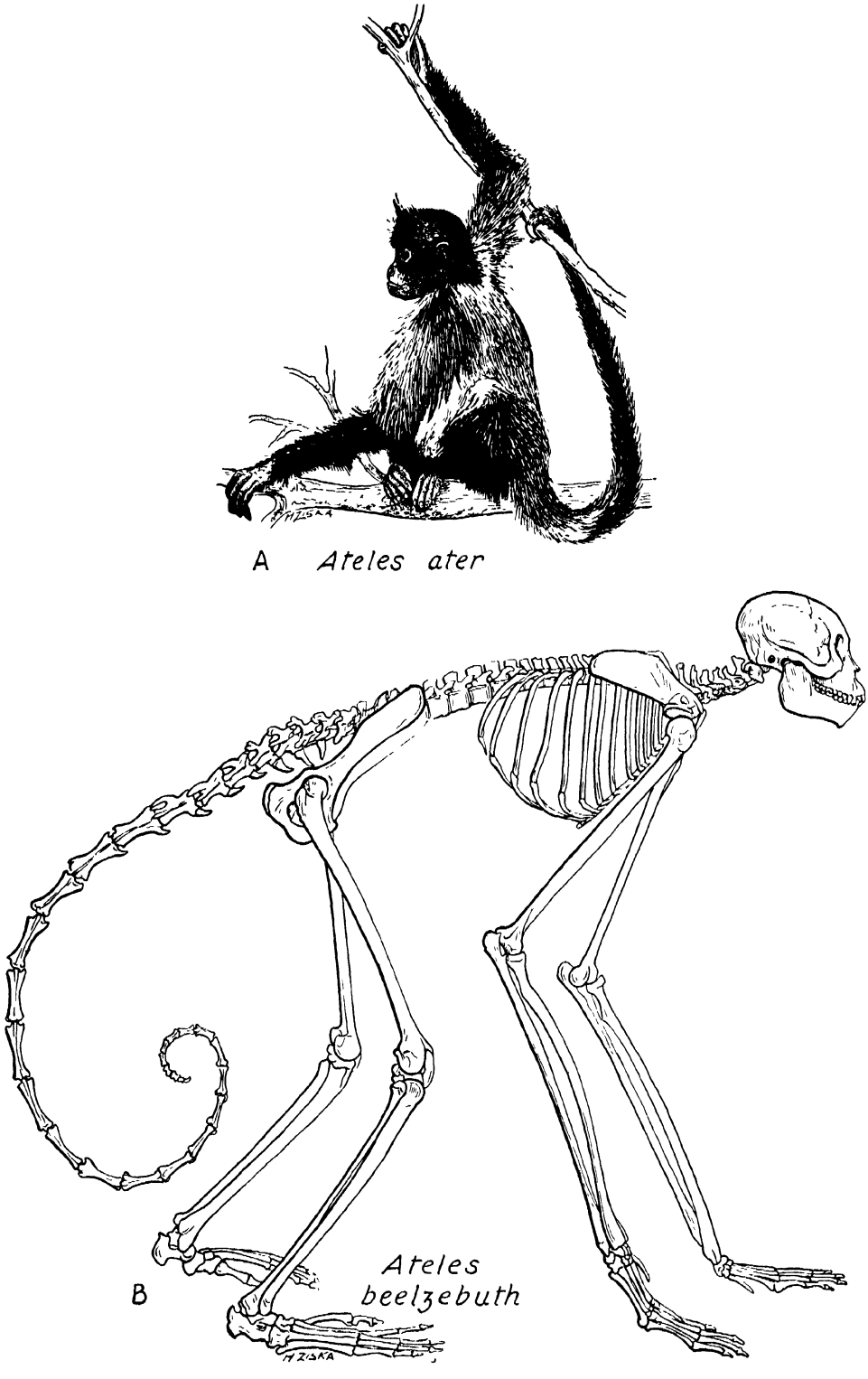


Fig. 23.32. The spider monkey, a highly specialized South American monkey. A, after Elliot; B, after De Blainville.

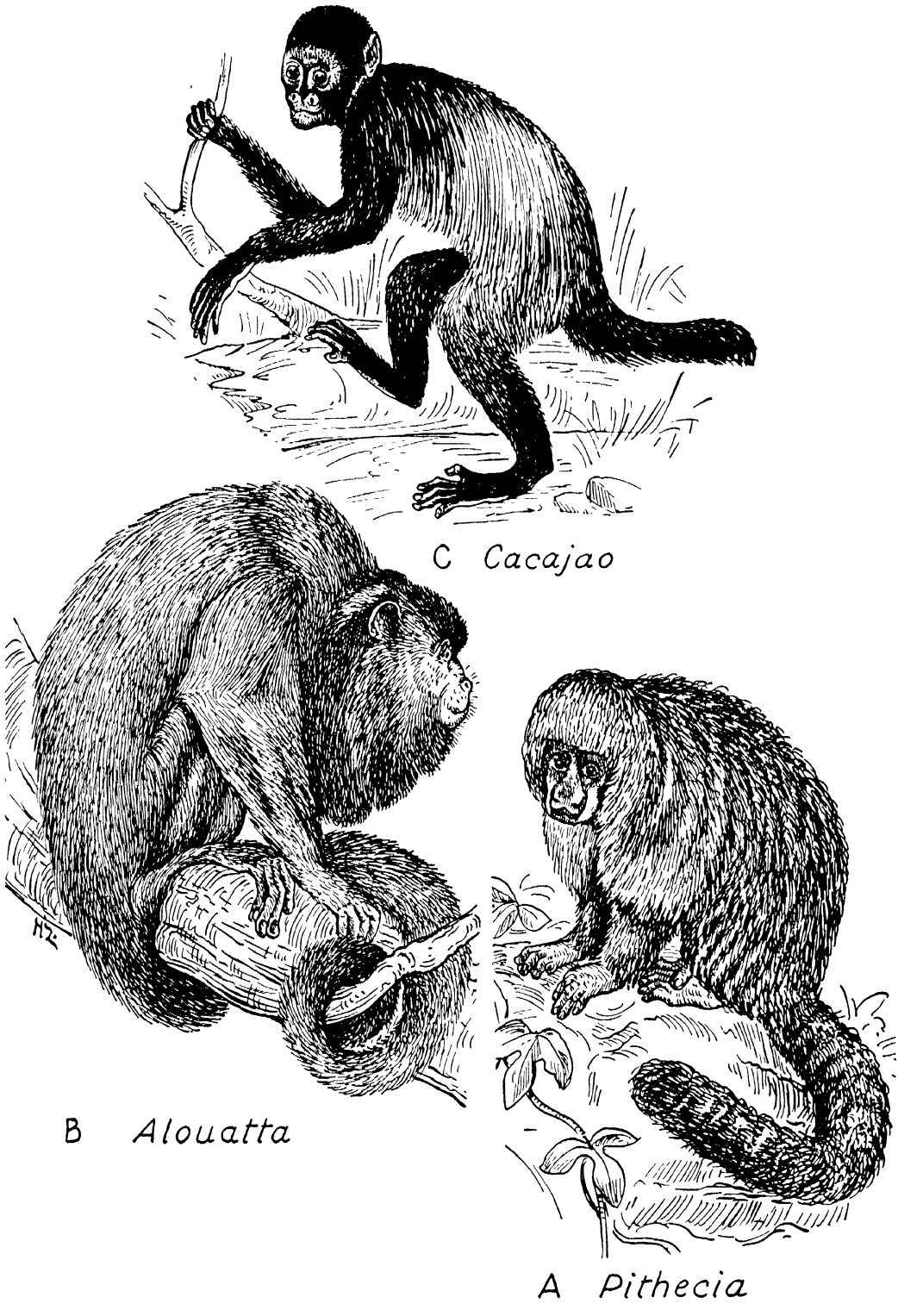


Fig. 23.33. Diversely specialized South American monkeys. A, C, after Elliot; B, after Lydekker.

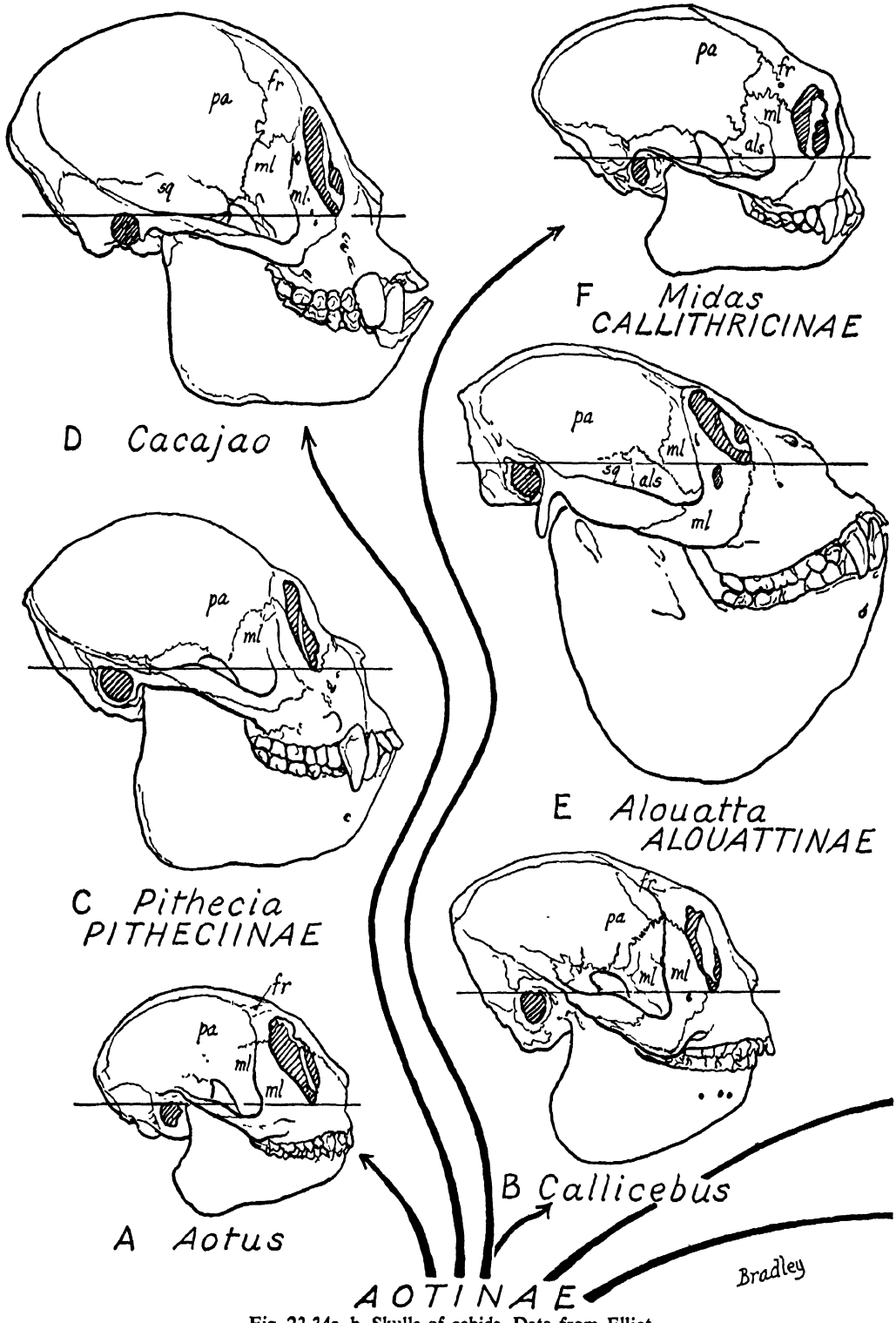


Fig. 23.34a, b. Skulls of cebids. Data from Elliot.

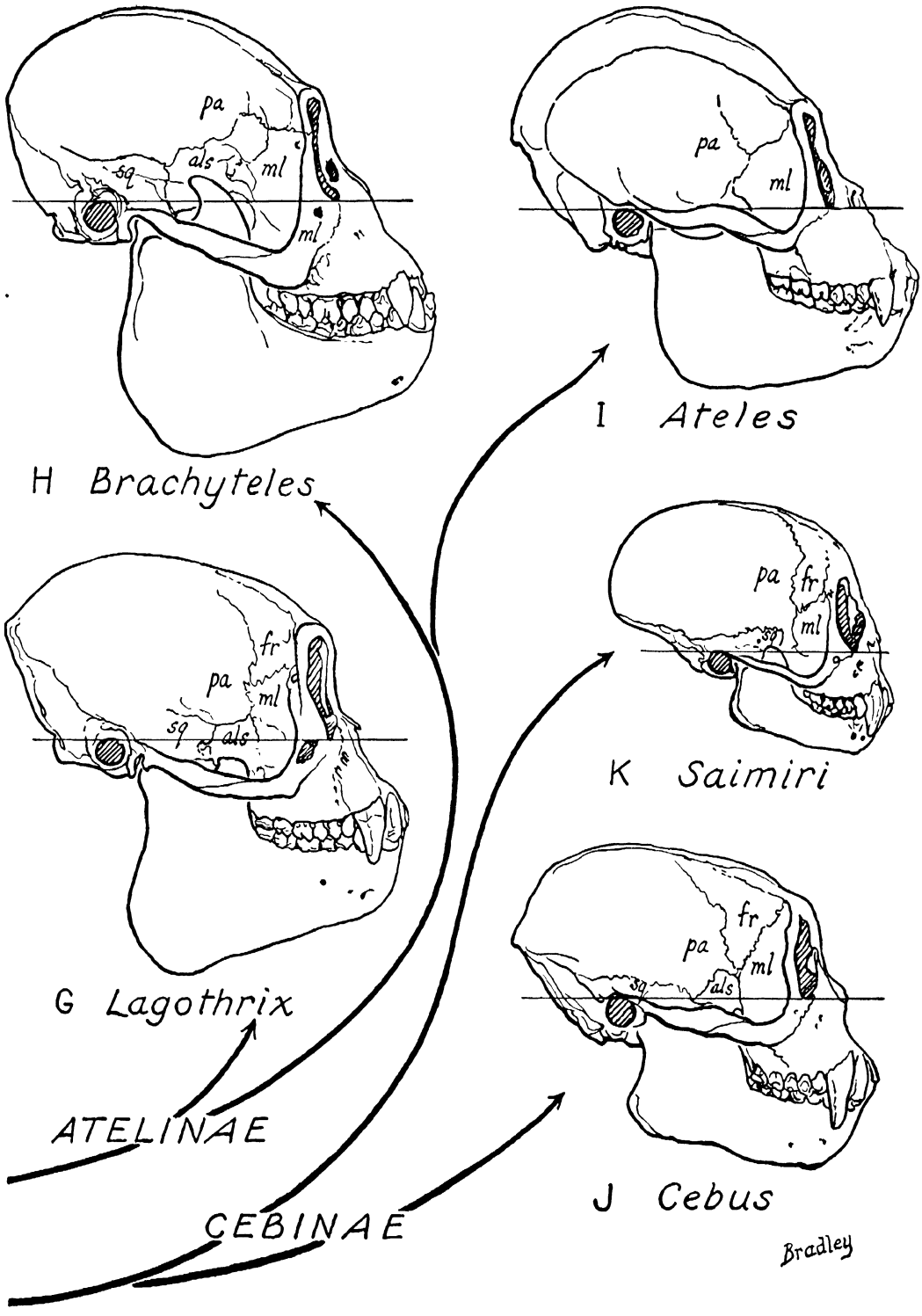

pa
als
sq
ml
ml
H Brachyteles
pa
ml
I Ateles
fr
pa
ml
sq
als
G Lagothrix
pa
fr
ml
sq
K Saimiri
fr
pa
ml
sq
als
J Cebus
ATELINAE
CEBINAE
Bradley

Fig. 23.34b

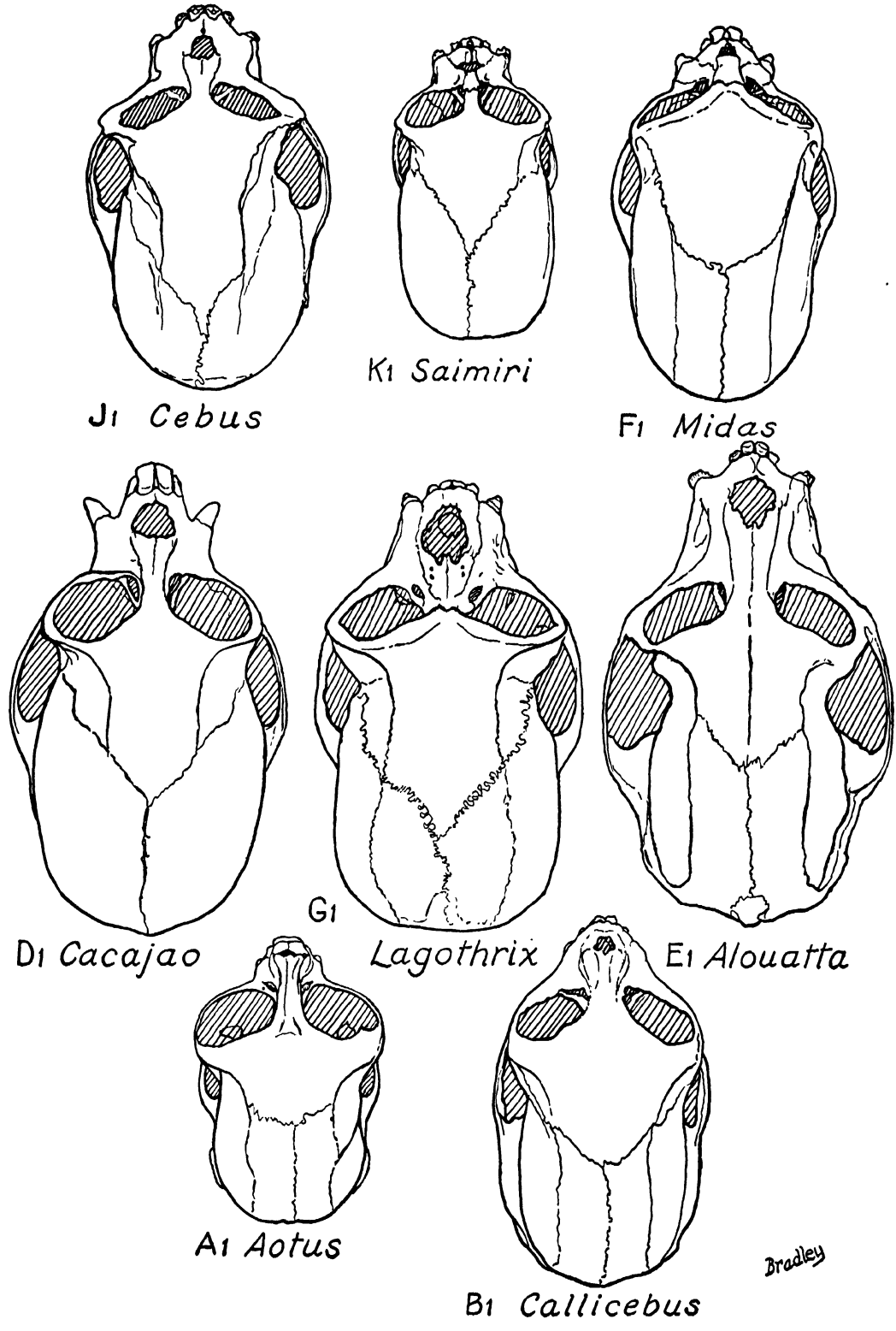


Fig. 23.34c. Skulls of cebids (continued). Data from Elliot.

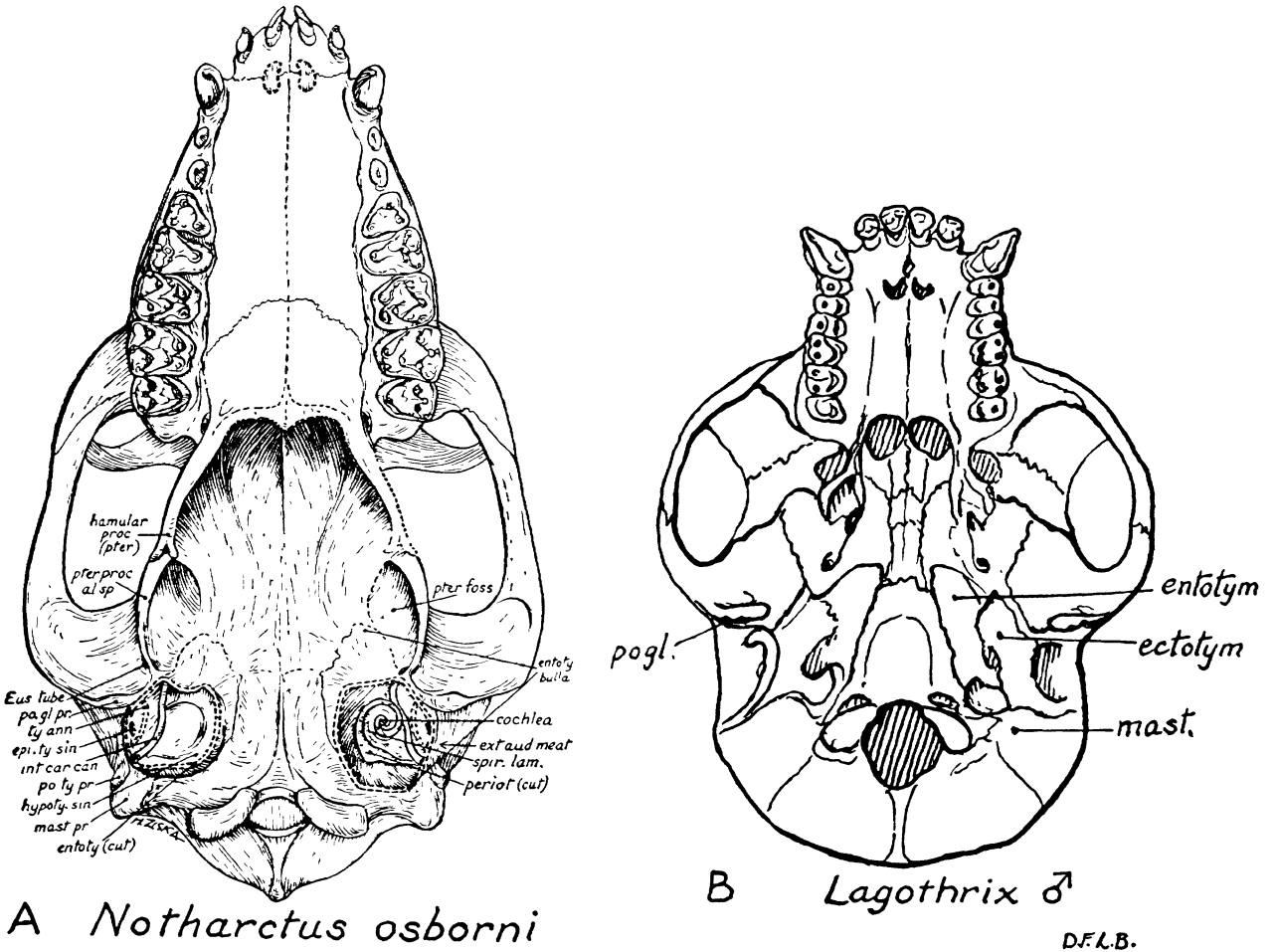


Fig. 23.35. Skulls, palatal aspect, of Eocene lemuroid (A) and South American monkey (B). A, original: B, data from Elliot.

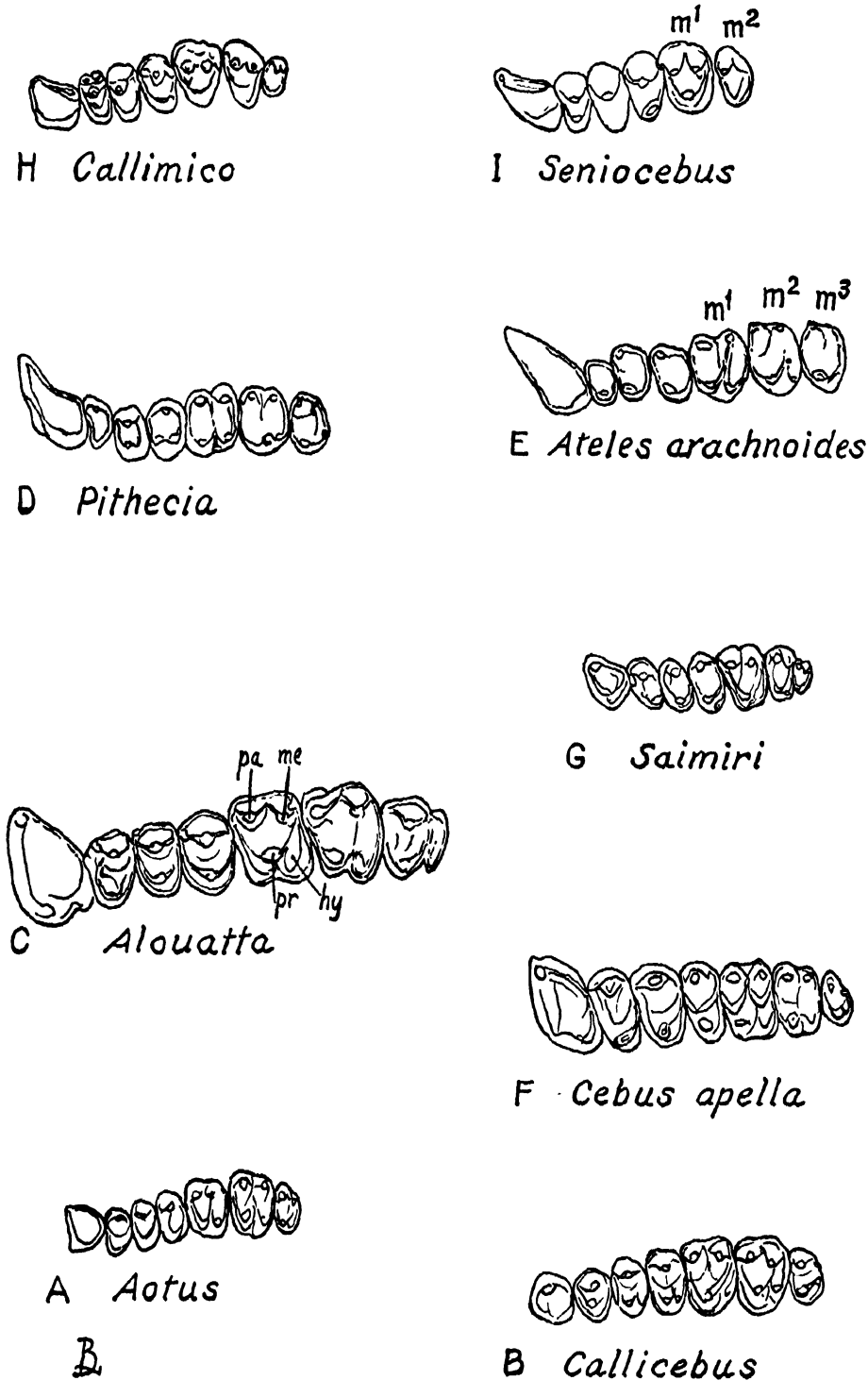


Fig. 23.36. Upper molar patterns of South American monkeys. After Gregory.

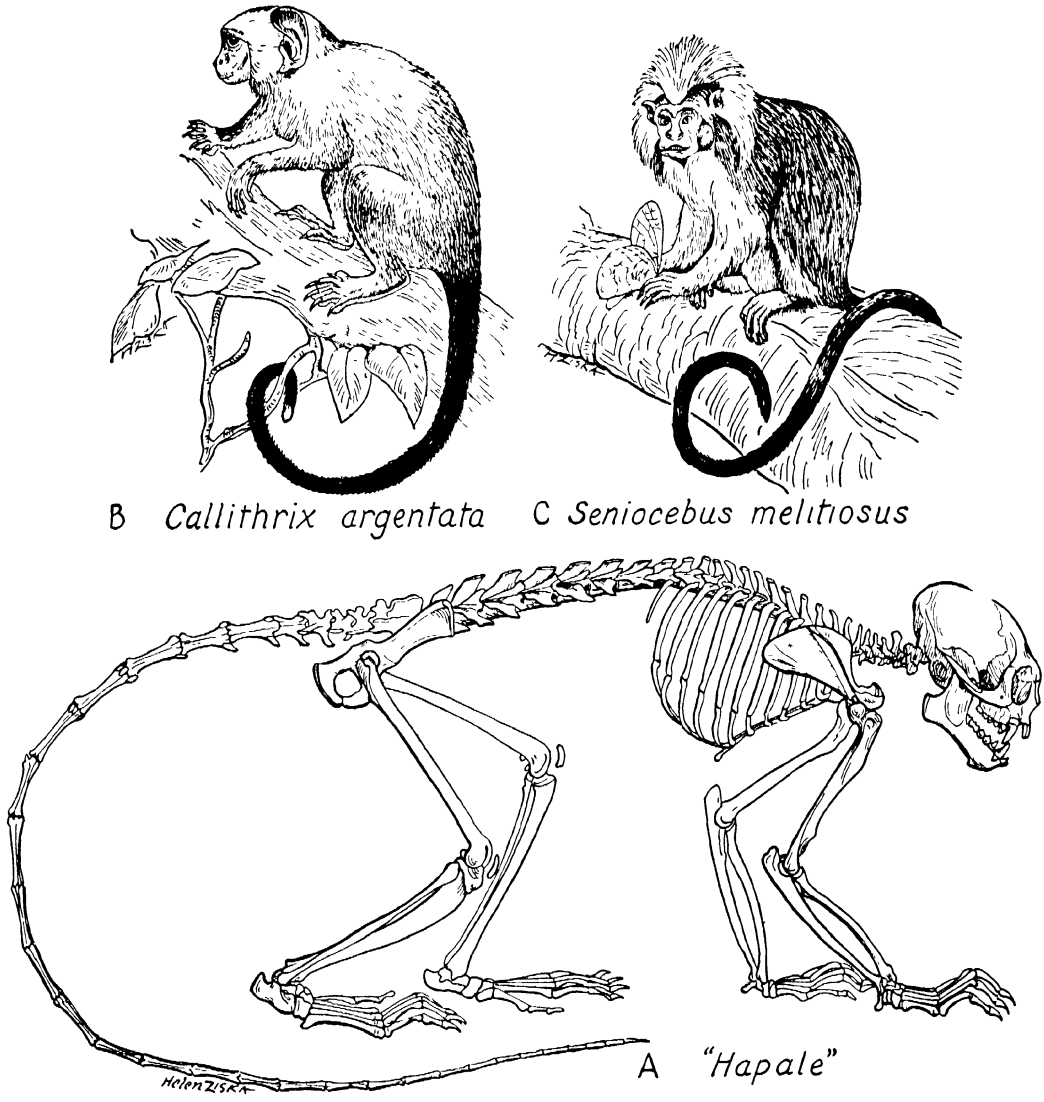


Fig. 23.37. Marmosets. A, after De Blainville; B, C, after Elliot.

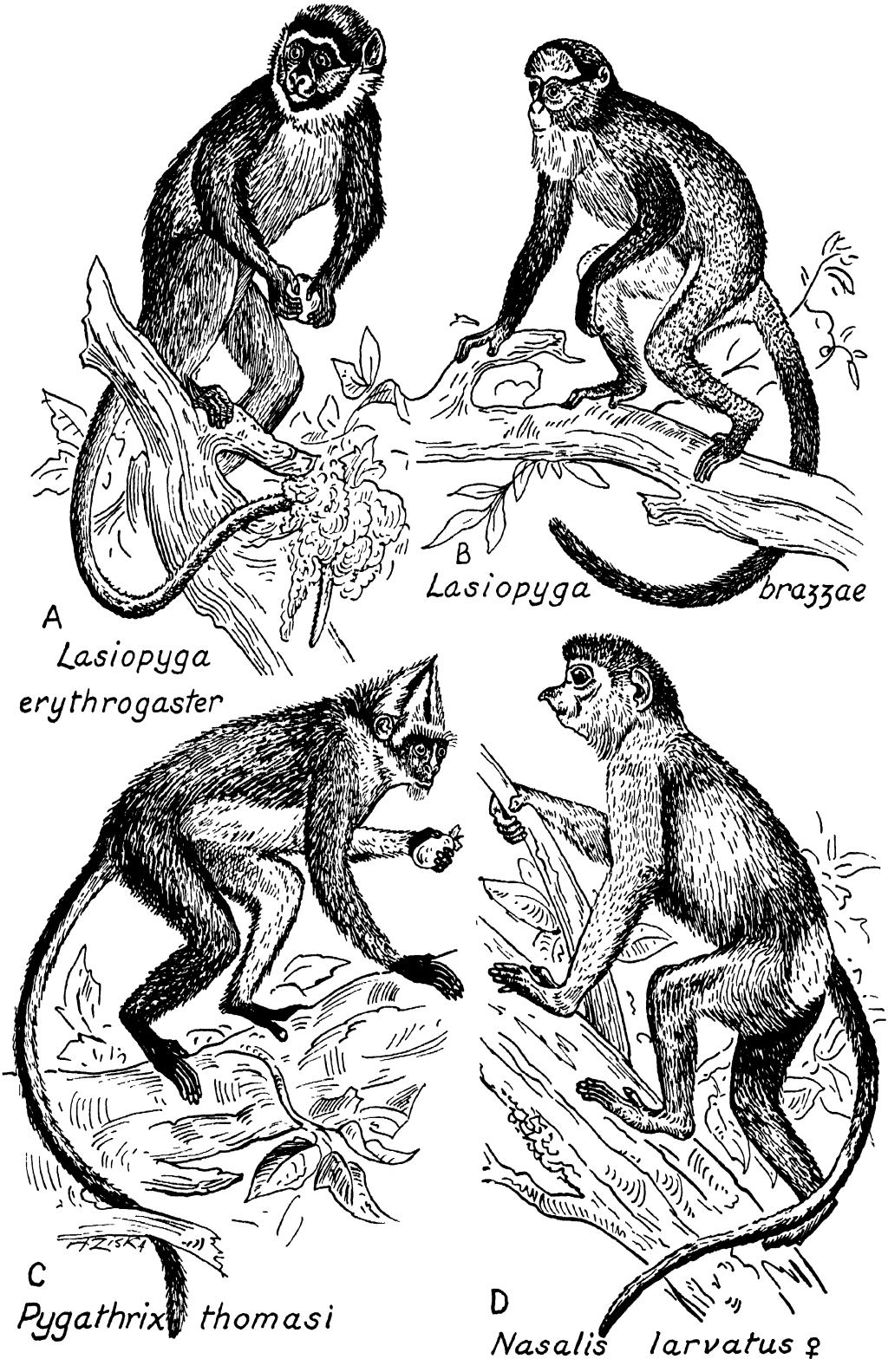


Fig. 23.38. Old World monkeys of the subfamilies Cercopithecinae (A, B) and Colobinae (C, D). After Elliot.

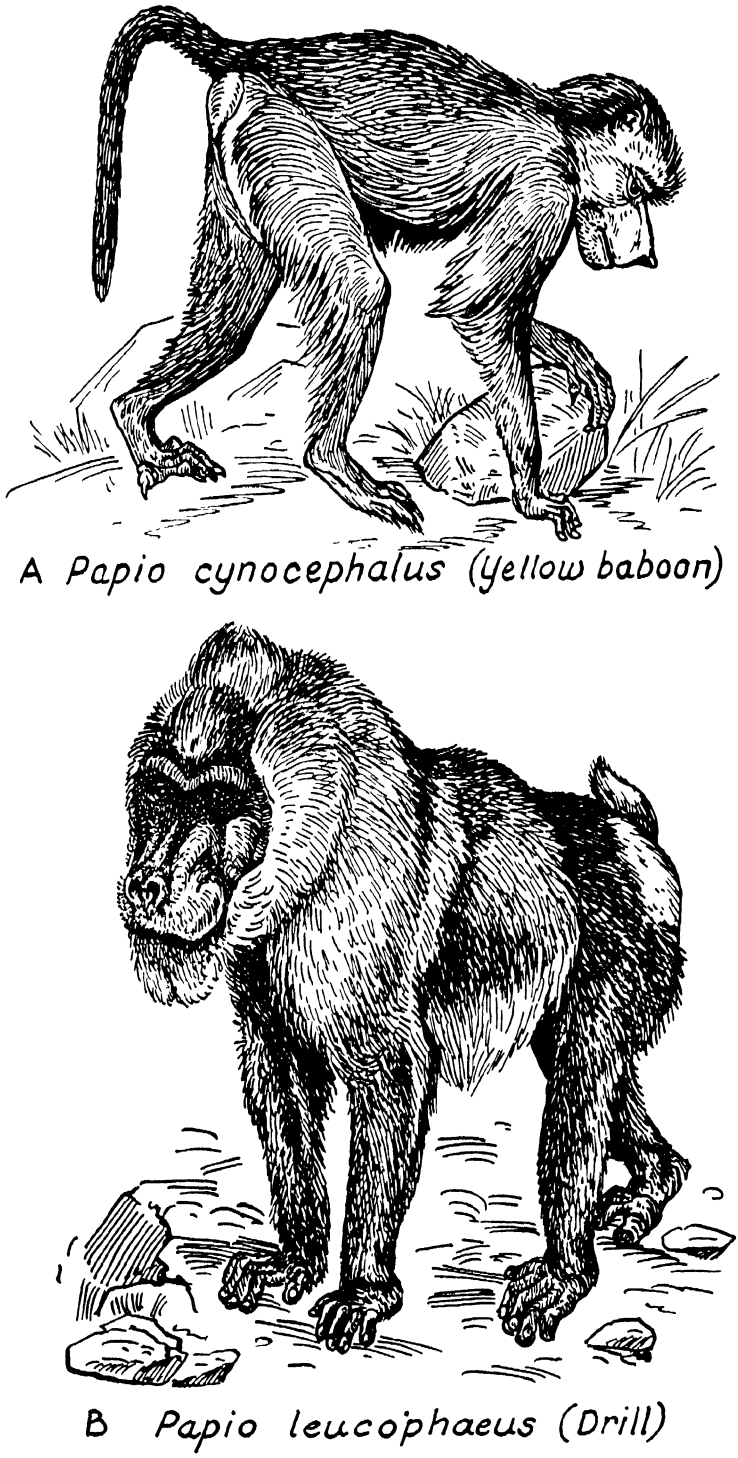


Fig. 23.39. Baboon and Drill. After Lydekker.

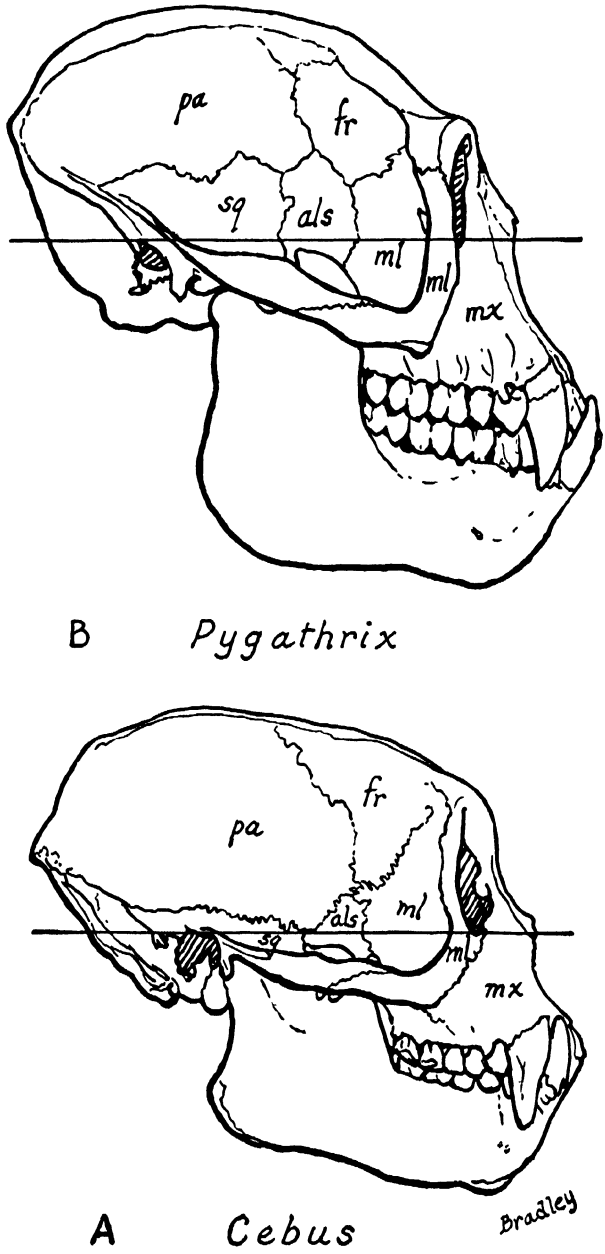


Fig. 23.40. Contrasting skull characters of typical New World (A) and Old World (B) monkeys. Data from Elliot.

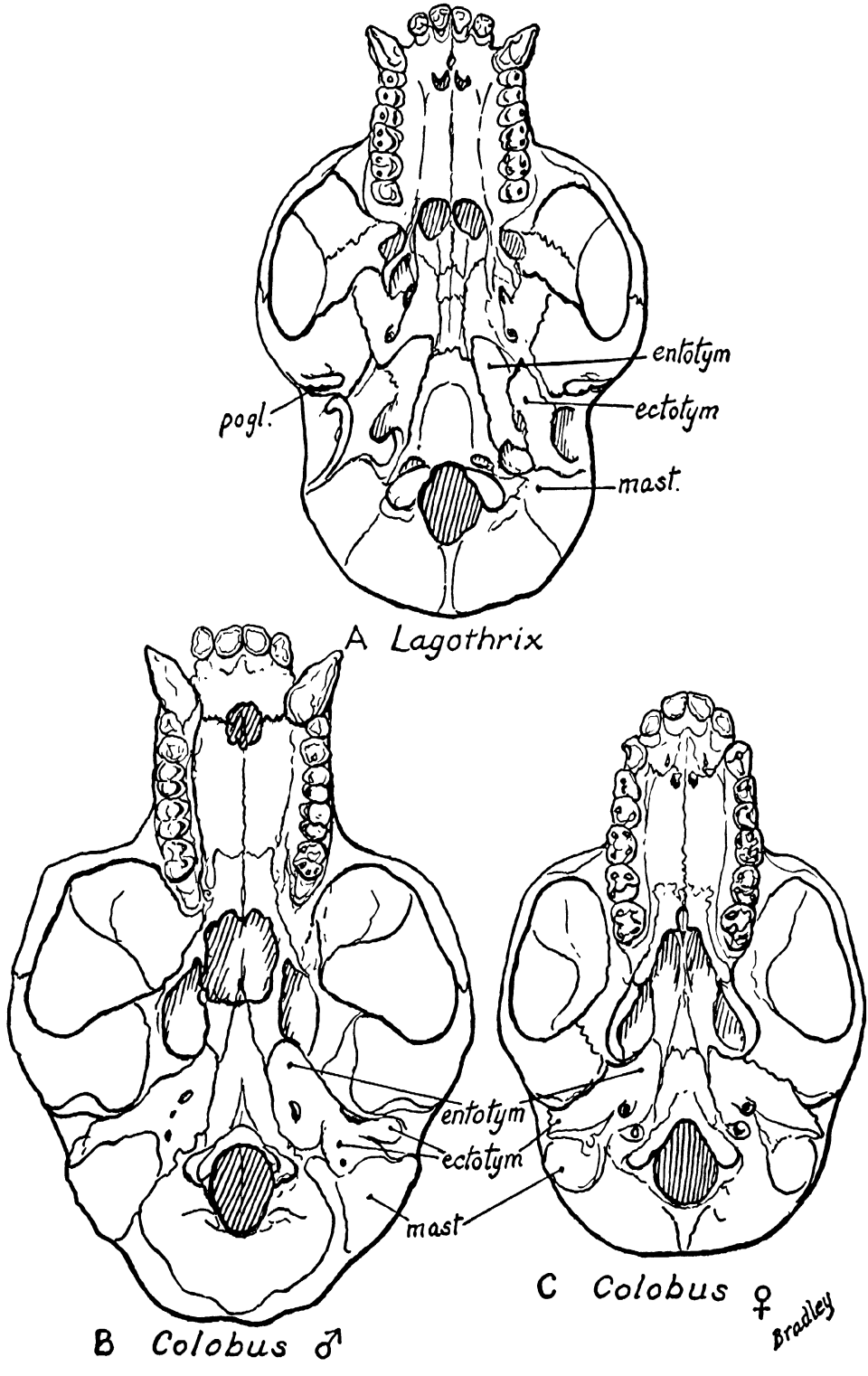


Fig. 23.41. Contrasting skull characters of typical New World (A) and Old World (B, C) monkeys. Palatal aspect. Data from Elliot.

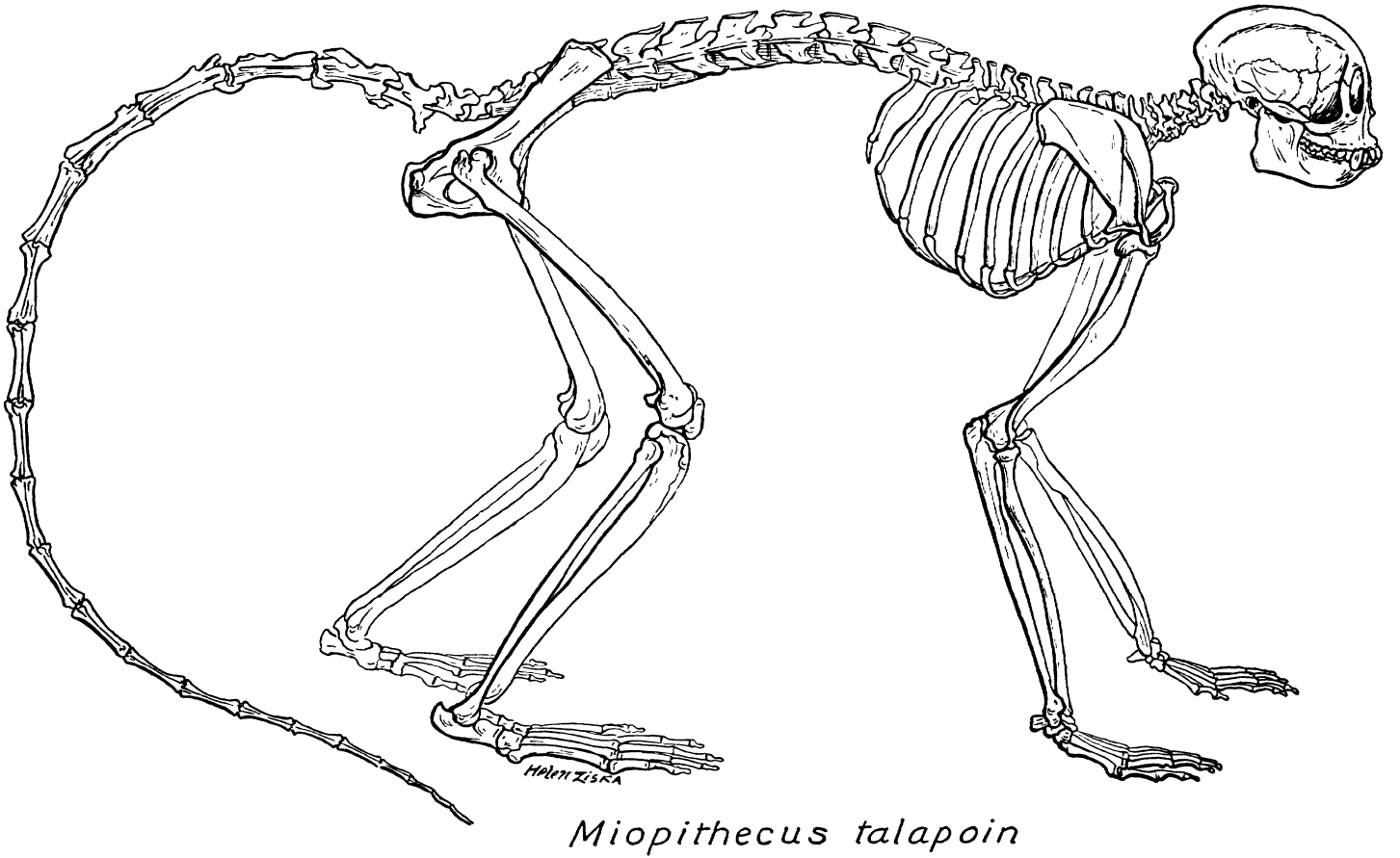


Fig. 23.42. Skeleton of relatively primitive Old World monkey. After De Blainville.

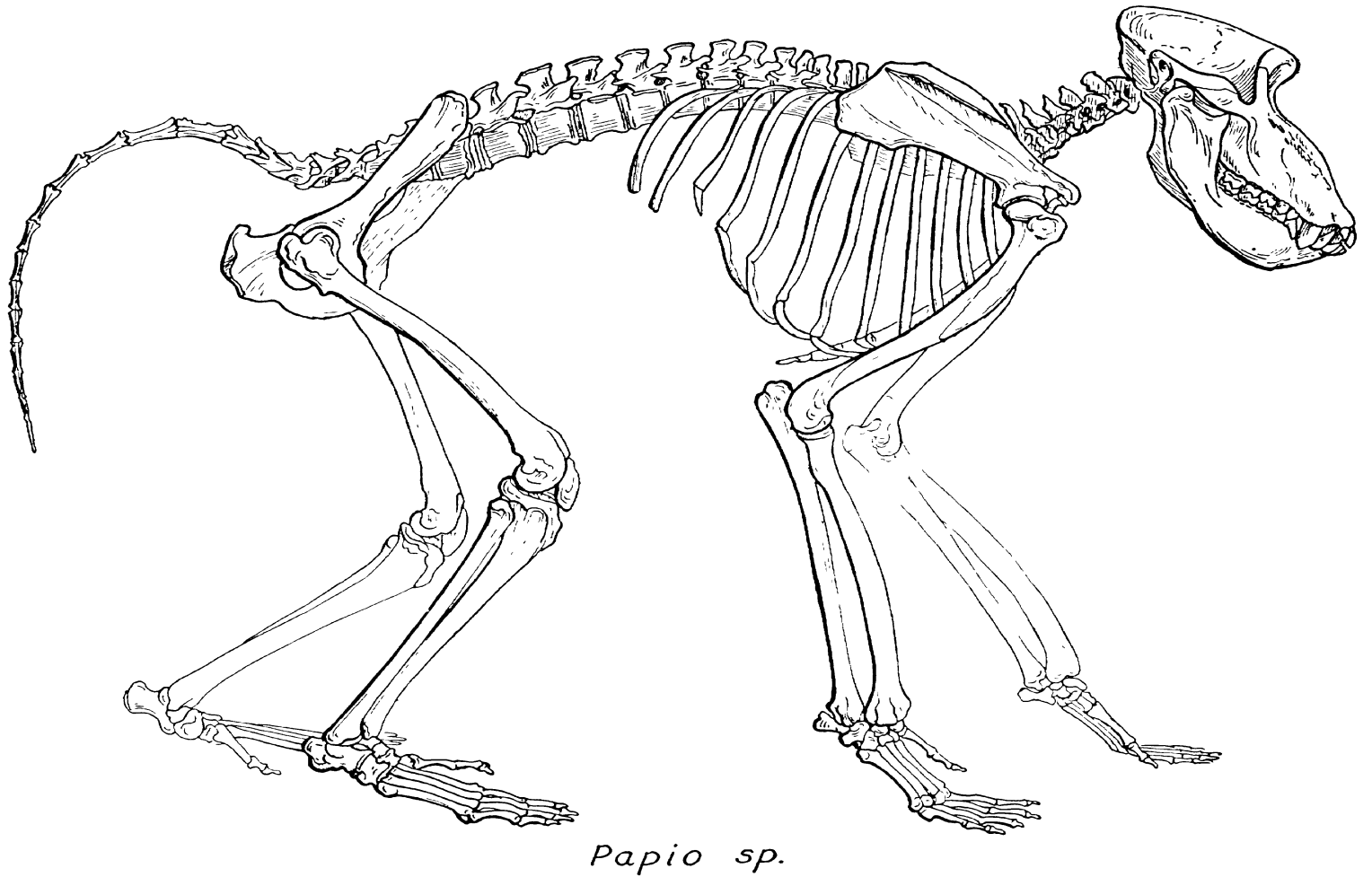


Fig. 23.43. Skeleton of specialized dog-like baboon. After De Blainville.

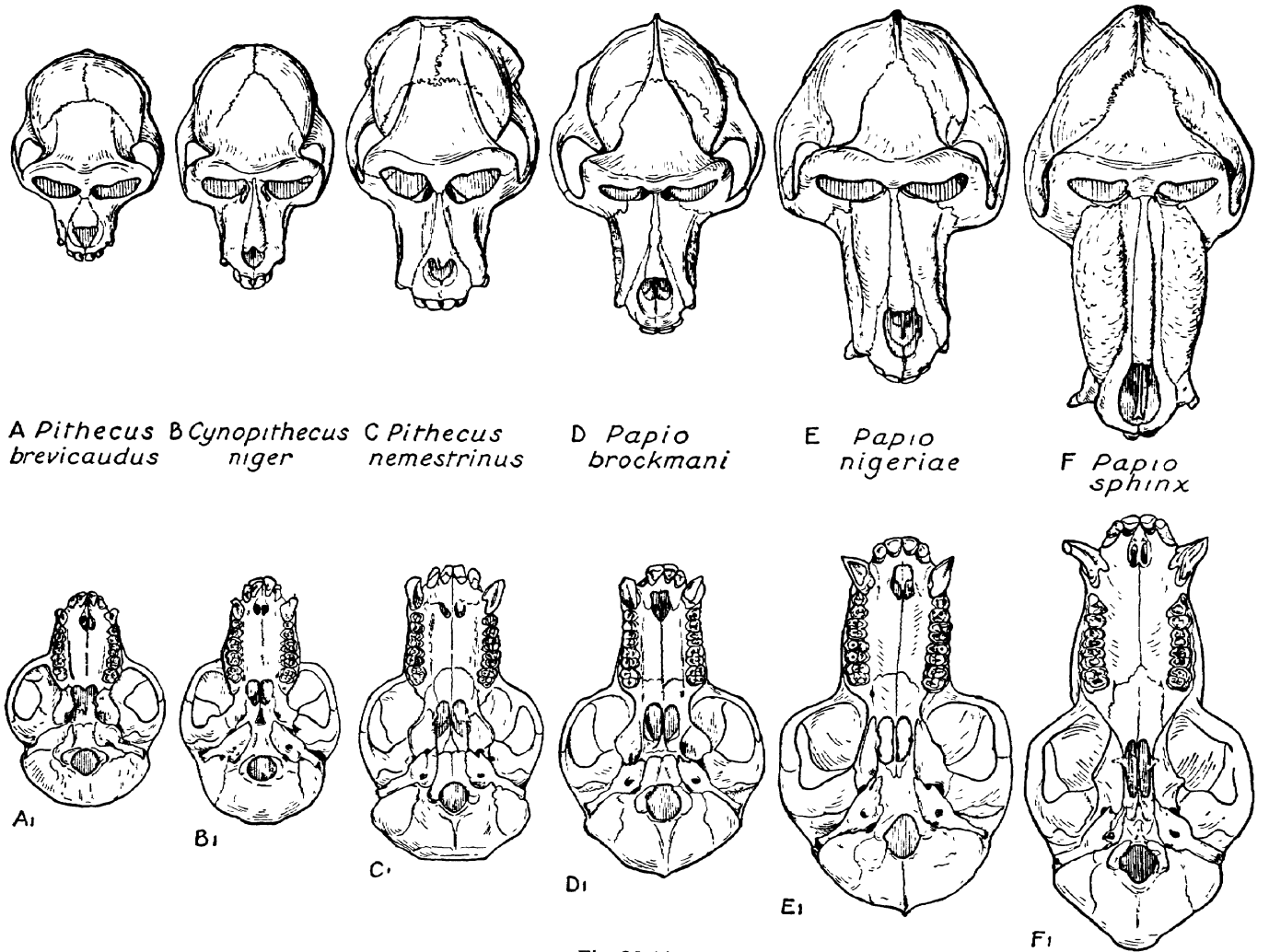

A Pithecus brevicaudus
B Cynopithecus niger
C Pithecus nemestrinus
D Papio brockmani
E Papio nigeriae
F Papio sphinx
A1
B1
C1
D1
E1
F1

Fig. 23.44a

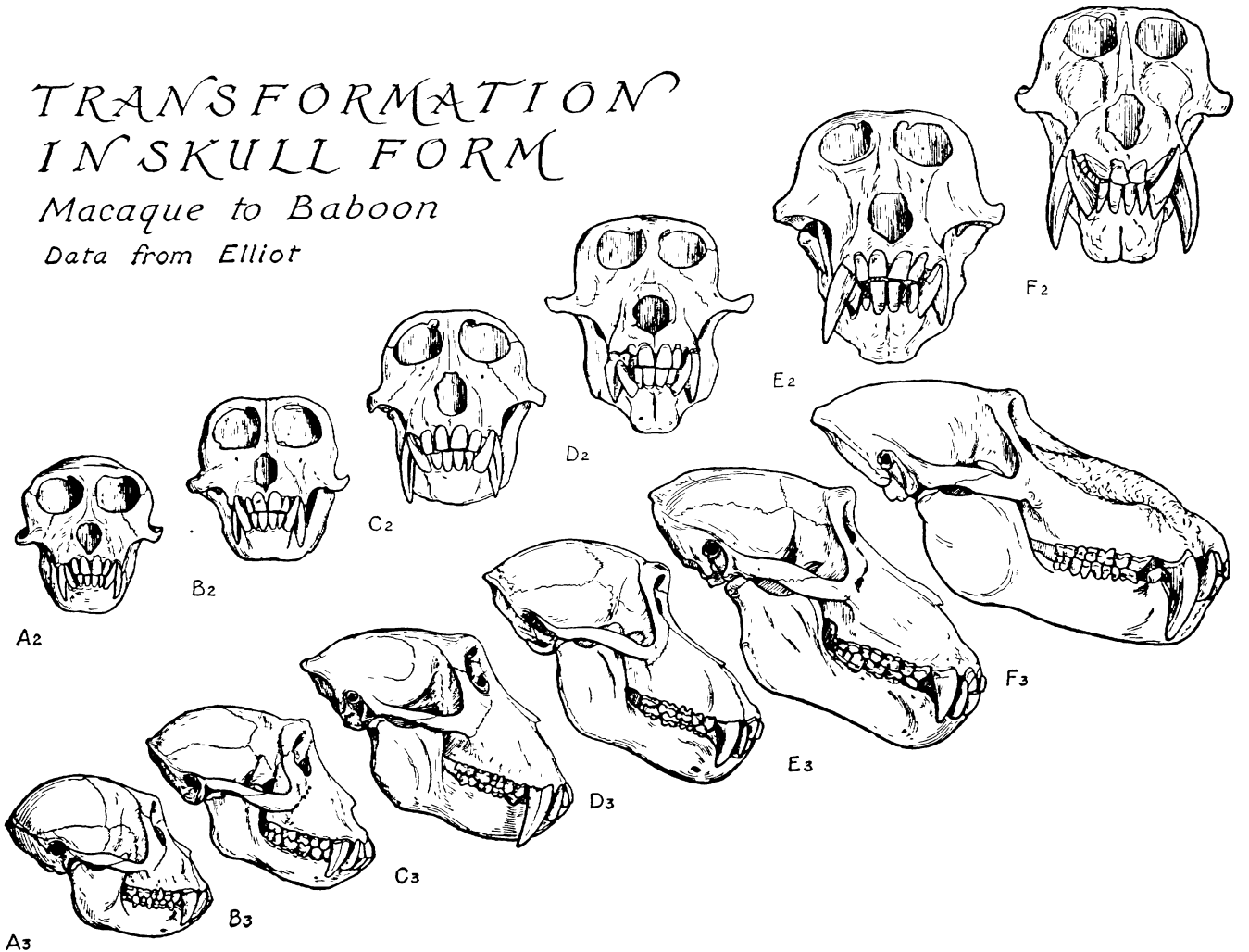
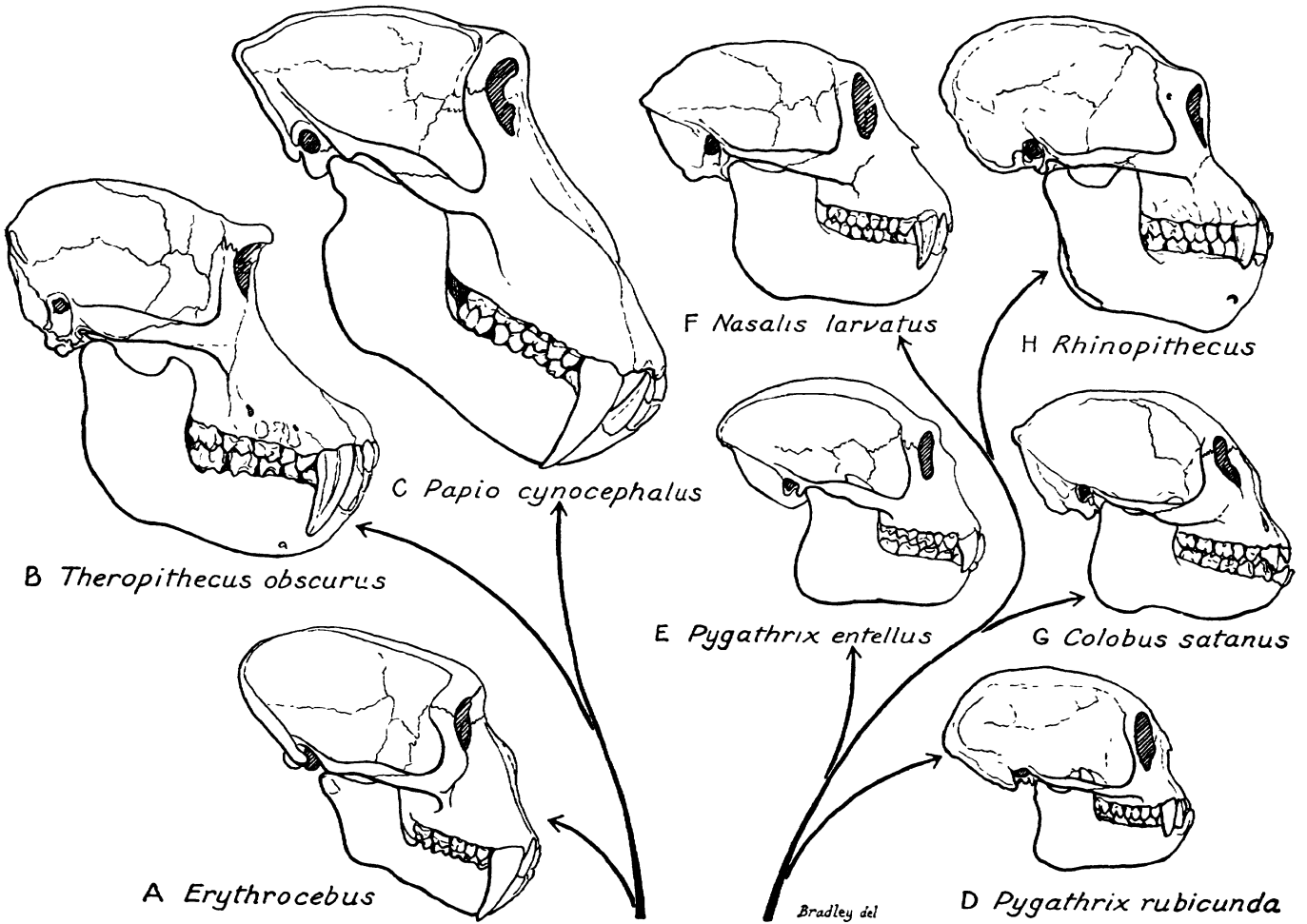

TRANSFORMATION
IN SKULL FORM
Macaque to Baboon
Data from Elliot
A2
B2
C2
D2
E2
F2
A3
B3
C3
D3
E3
F3

Fig. 23.44b



Figs. 23.45, 46. Contrasts in face and cranium between ground-living (A–C) and tree-living (D–H) monkeys. Data from Elliot.

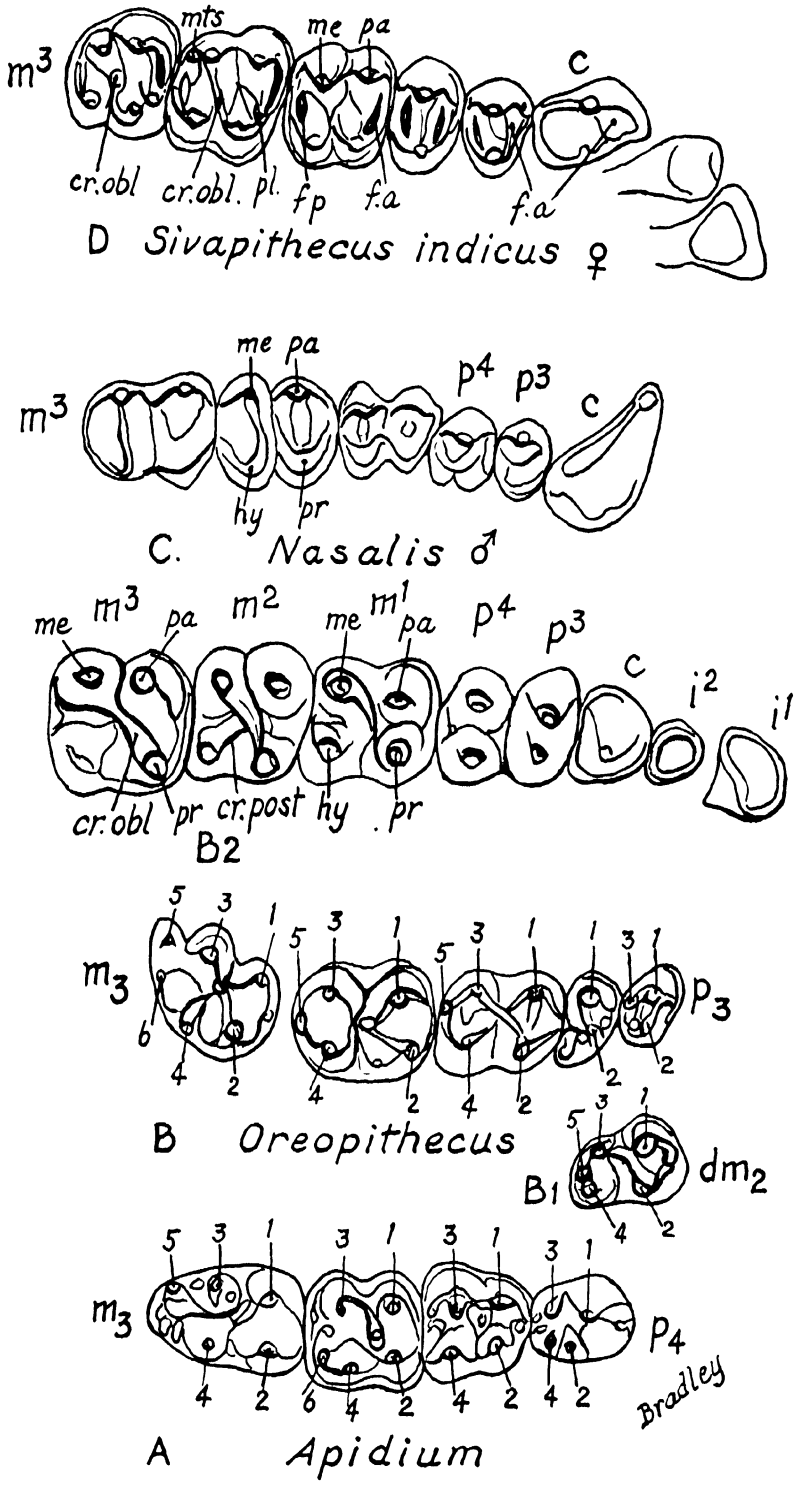


Fig. 23.47. Lower (A, B, B1) and upper (B2, C, D) molar patterns. A, supposed primitive catarrhine monkey from Upper Eocene of Egypt; B–B2, peculiar catarrhine from Lower Pliocene of Italy; C, modern herbivorous catarrhine; D, anthropoid ape from Lower Pliocene of India. Data from: A, Osborn; B, B1, B2, Schwalbe, and cast; C, D, Gregory, and cast.

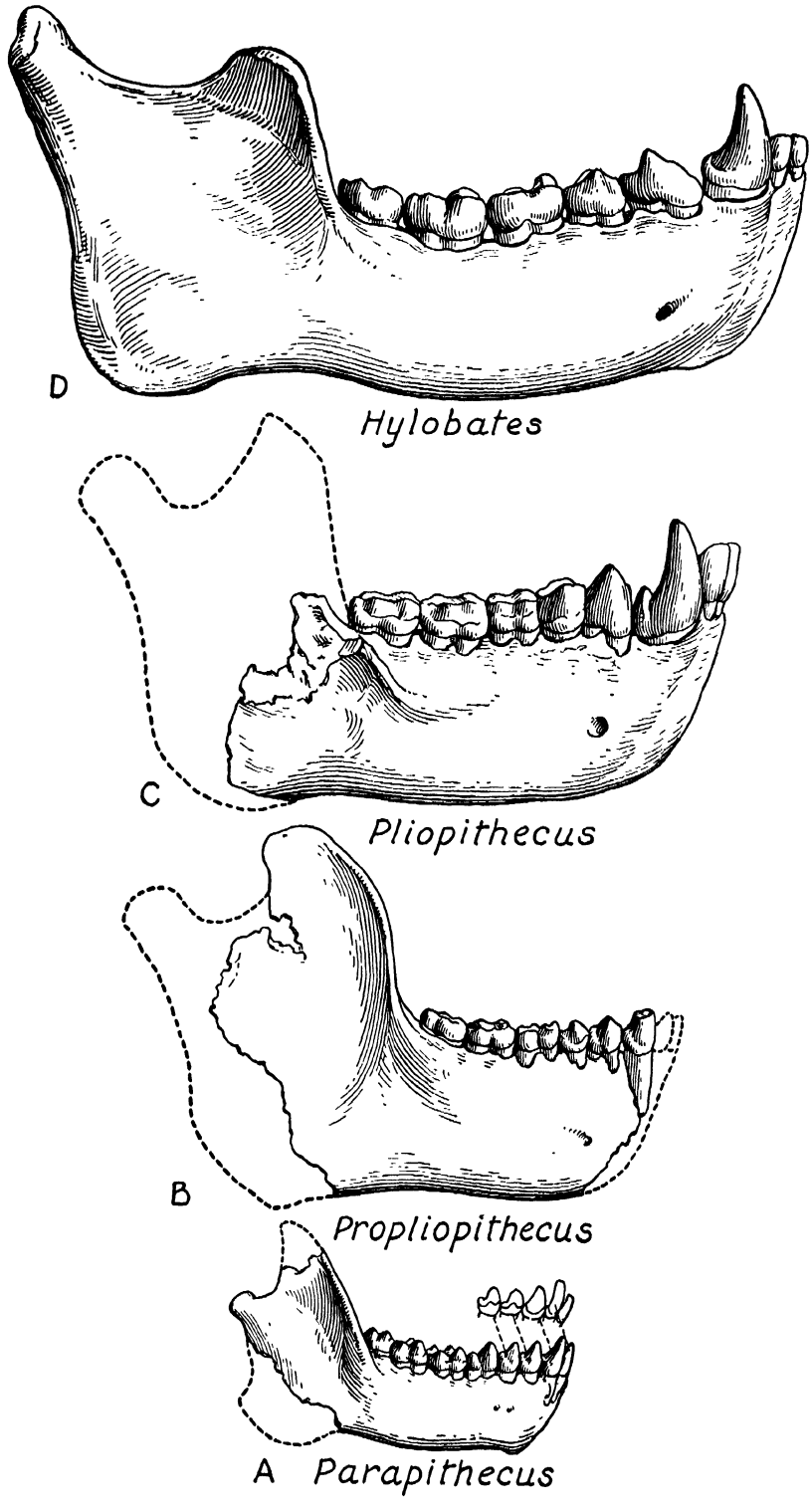


Fig. 23.48a, b. Jaws of fossil and recent gibbons. From Gregory. Data from: A, A1, B, Schlosser, and cast; C, C1, De Blainville, Hoffman, and cast; D, D1, specimen.

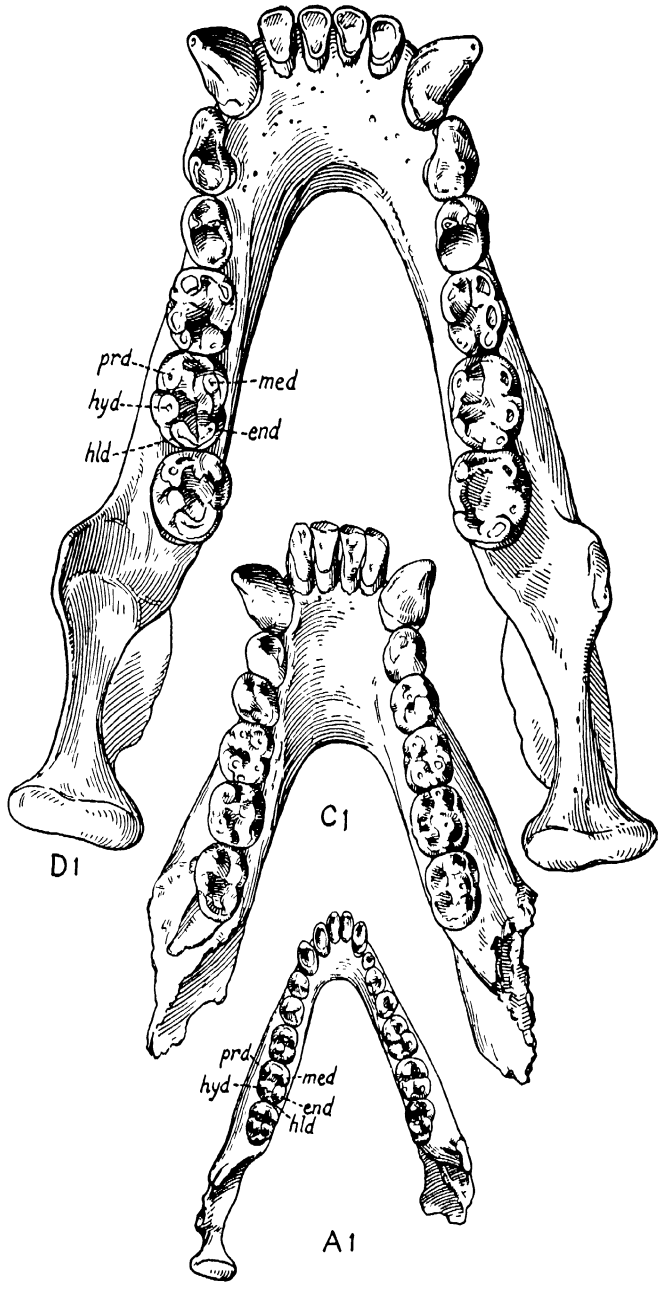


Fig. 23.48b

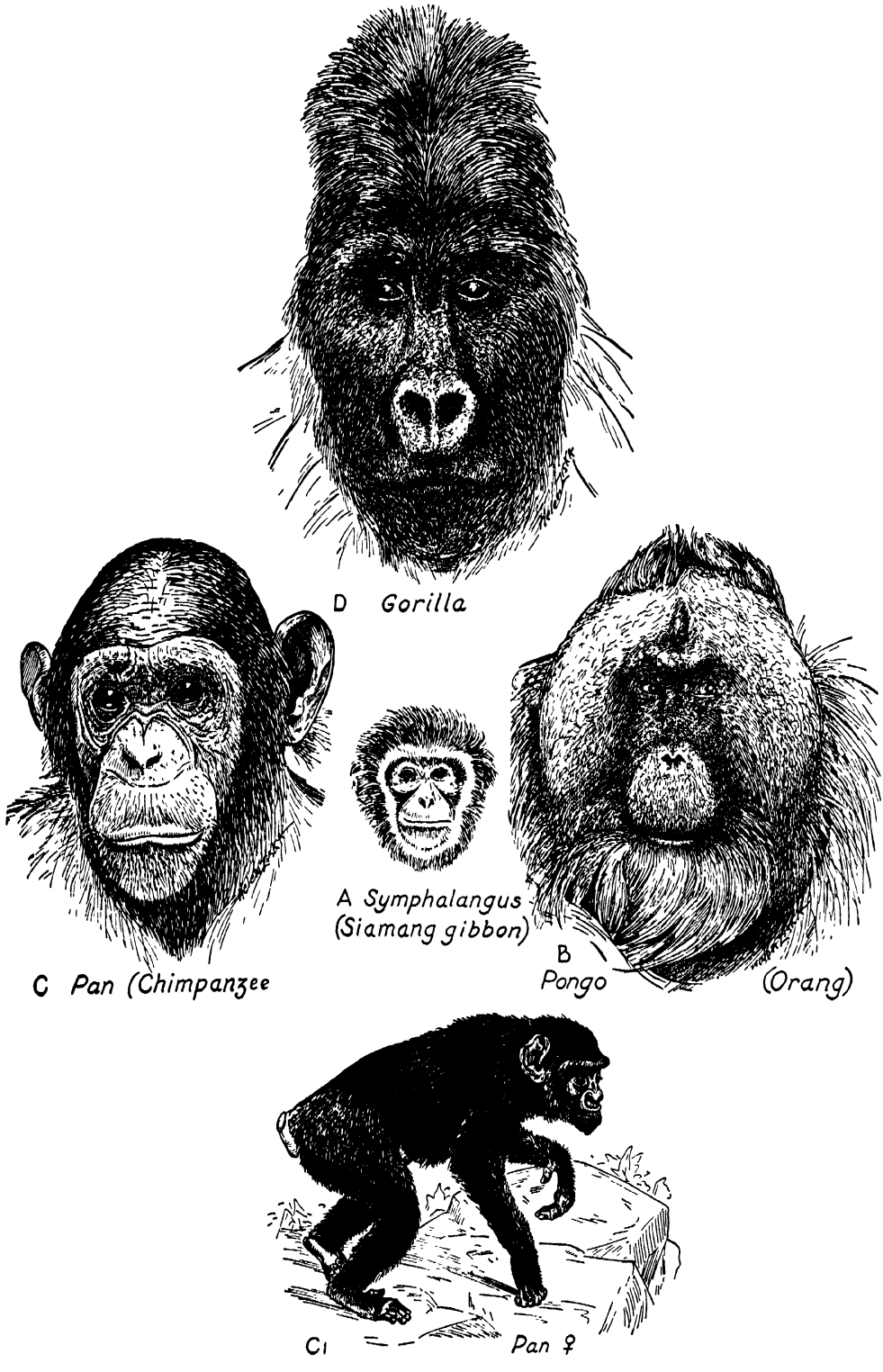


Fig. 23.49. Faces of apes. Data from: A, C, Elliott; B, Bluntschli; D, Gregory and Raven. Female chimpanzee (C1) after Lydekker.

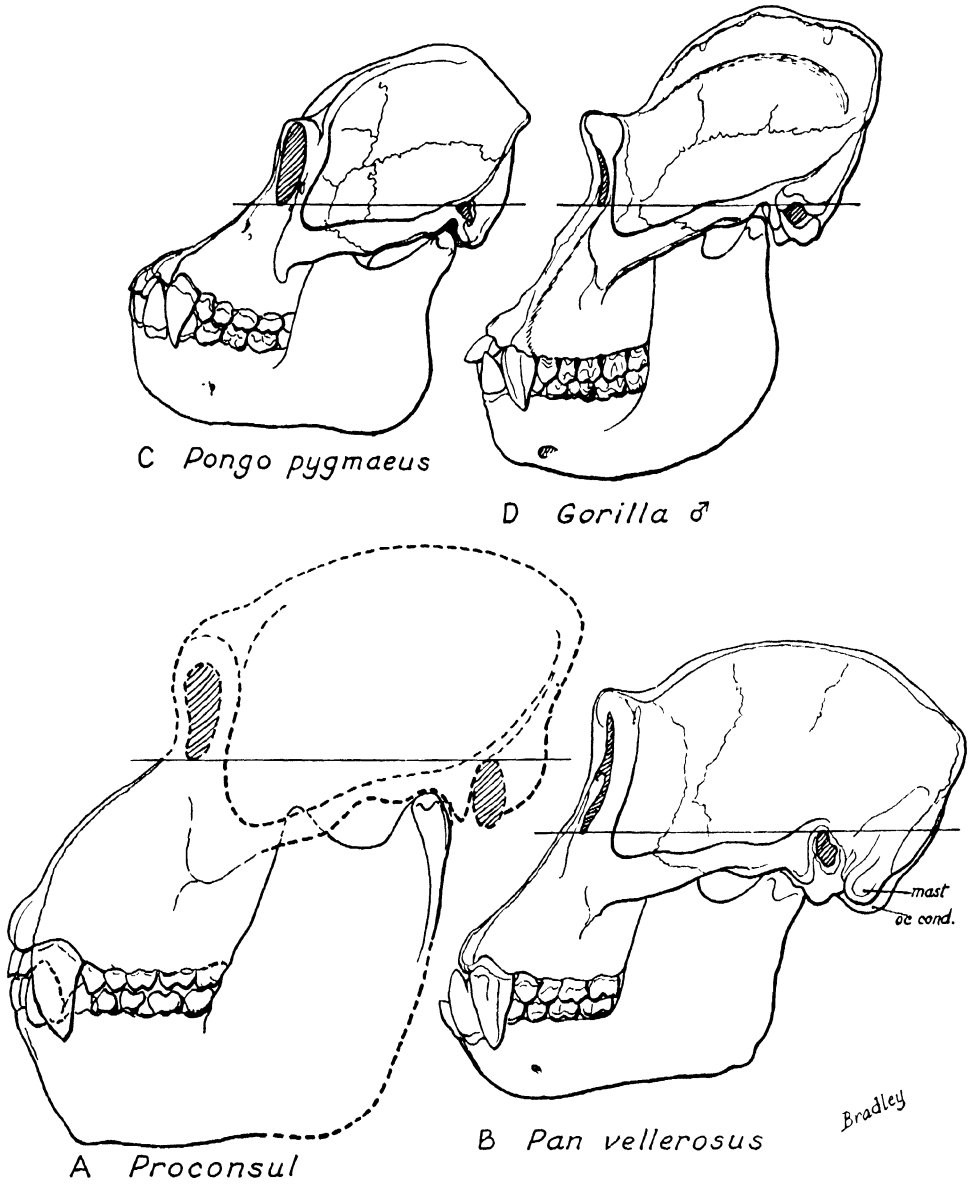


Fig. 23.50. Skull outlines of *Proconsul* and modern apes. A, preliminary restoration, data from MacInnes and Leakey, Le Gros Clark, and casts; B–D, from Elliot.

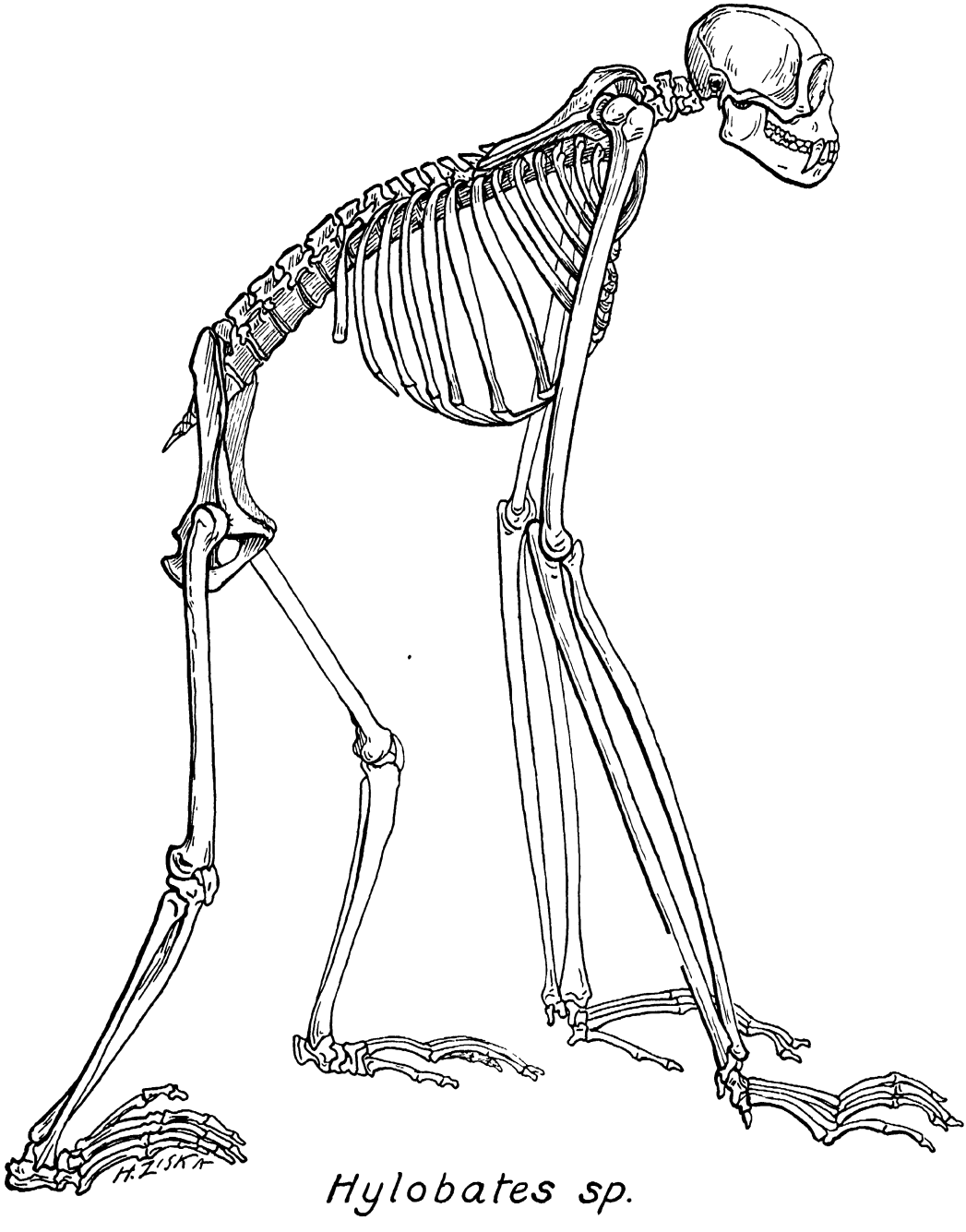


Fig. 23.51. Gibbon skeleton. After De Blainville.

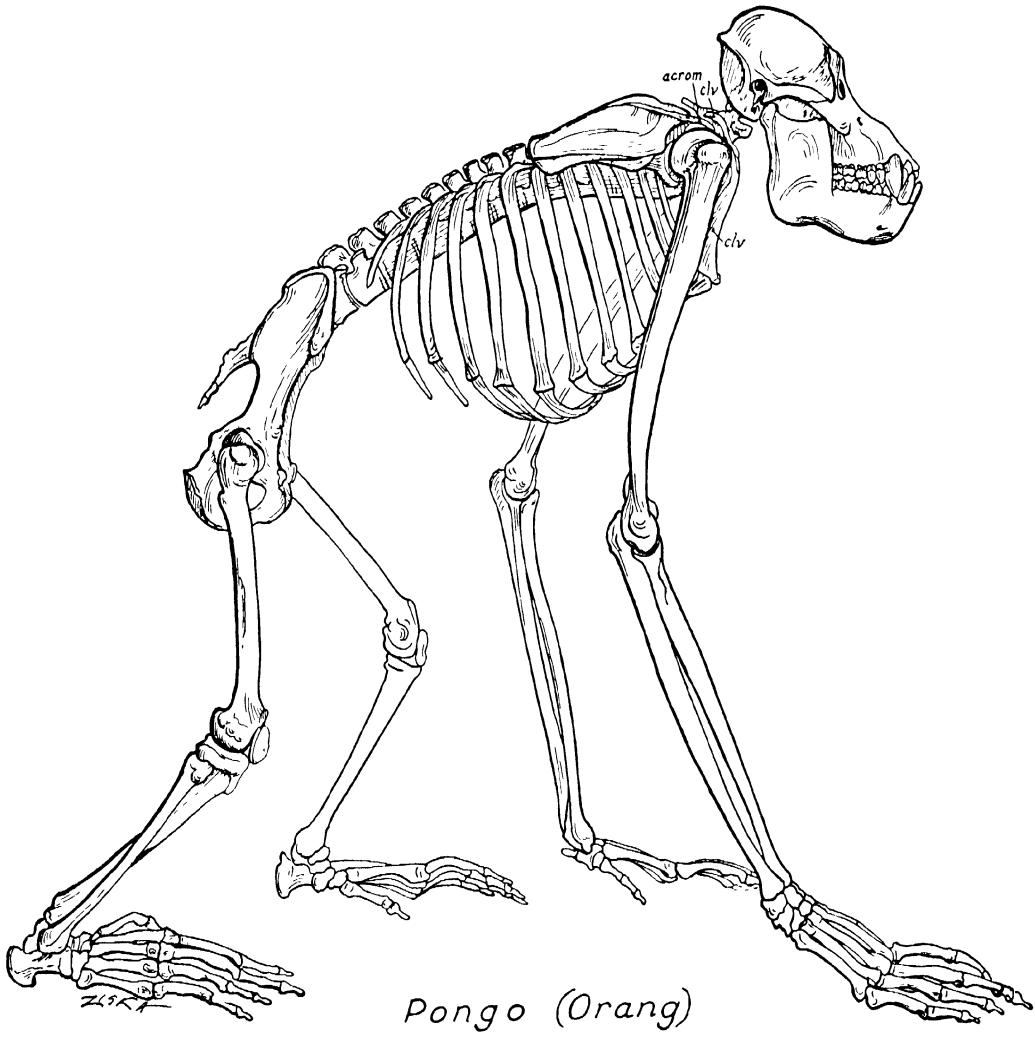


Fig. 23.52. Orang skeleton. After De Blainville.

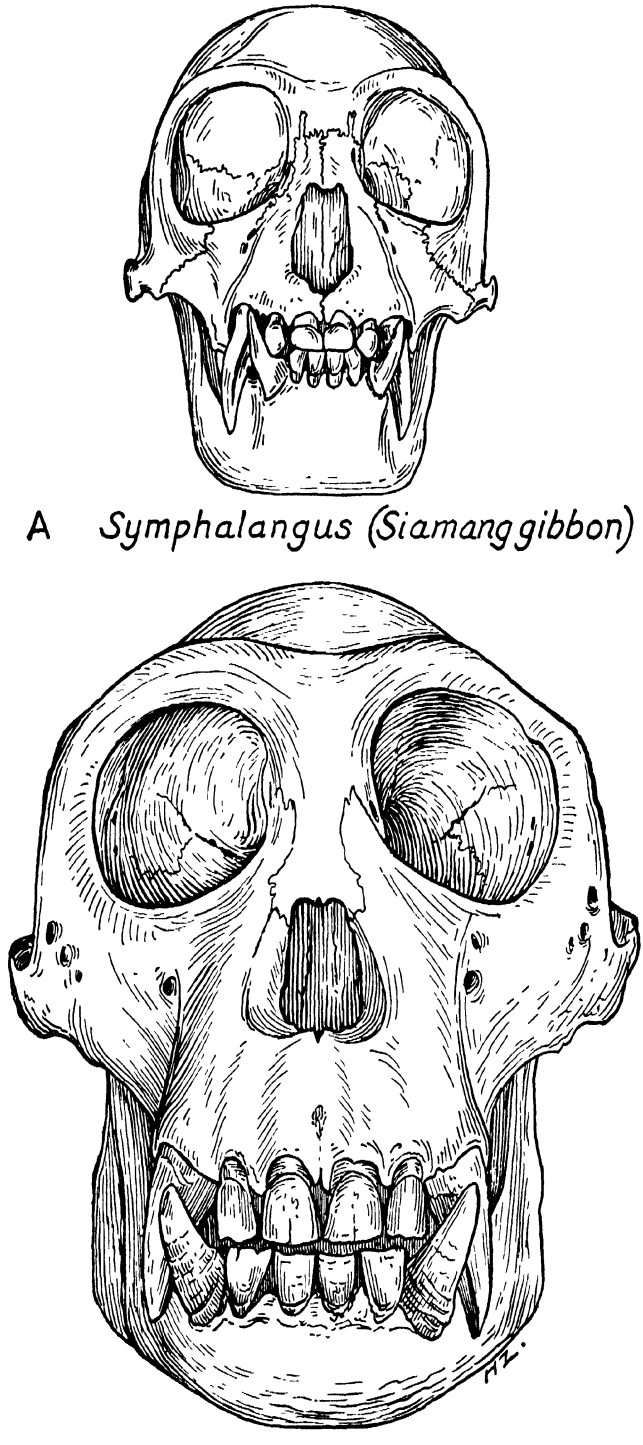


Fig. 25.53. Front view of gibbon (A) and chimpanzee (B) skulls to show basic identity in structural patterns. Data from Elliot.

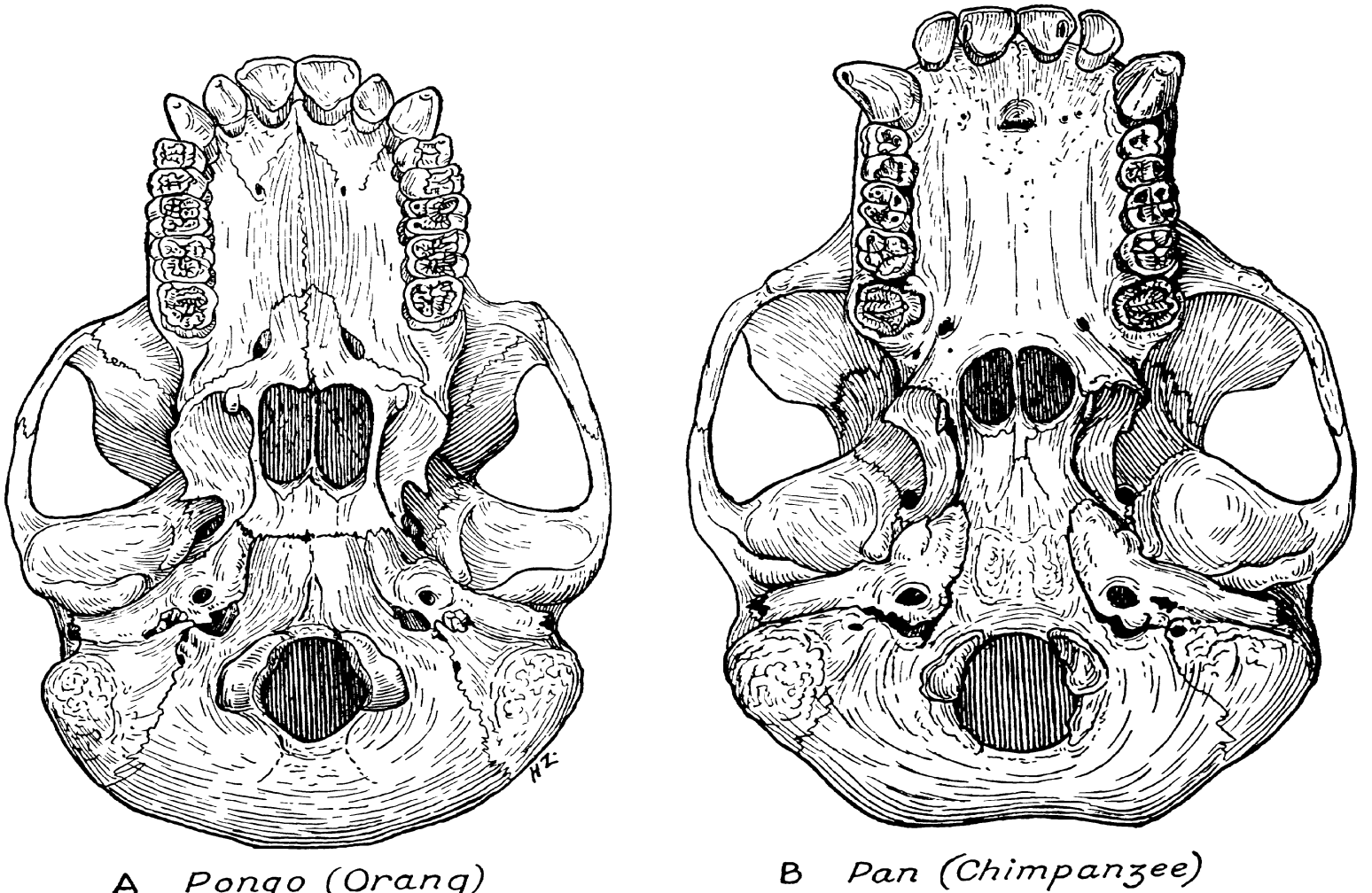


Fig. 23.54. Skulls, under side, of orang and chimpanzee. Data from Elliot.

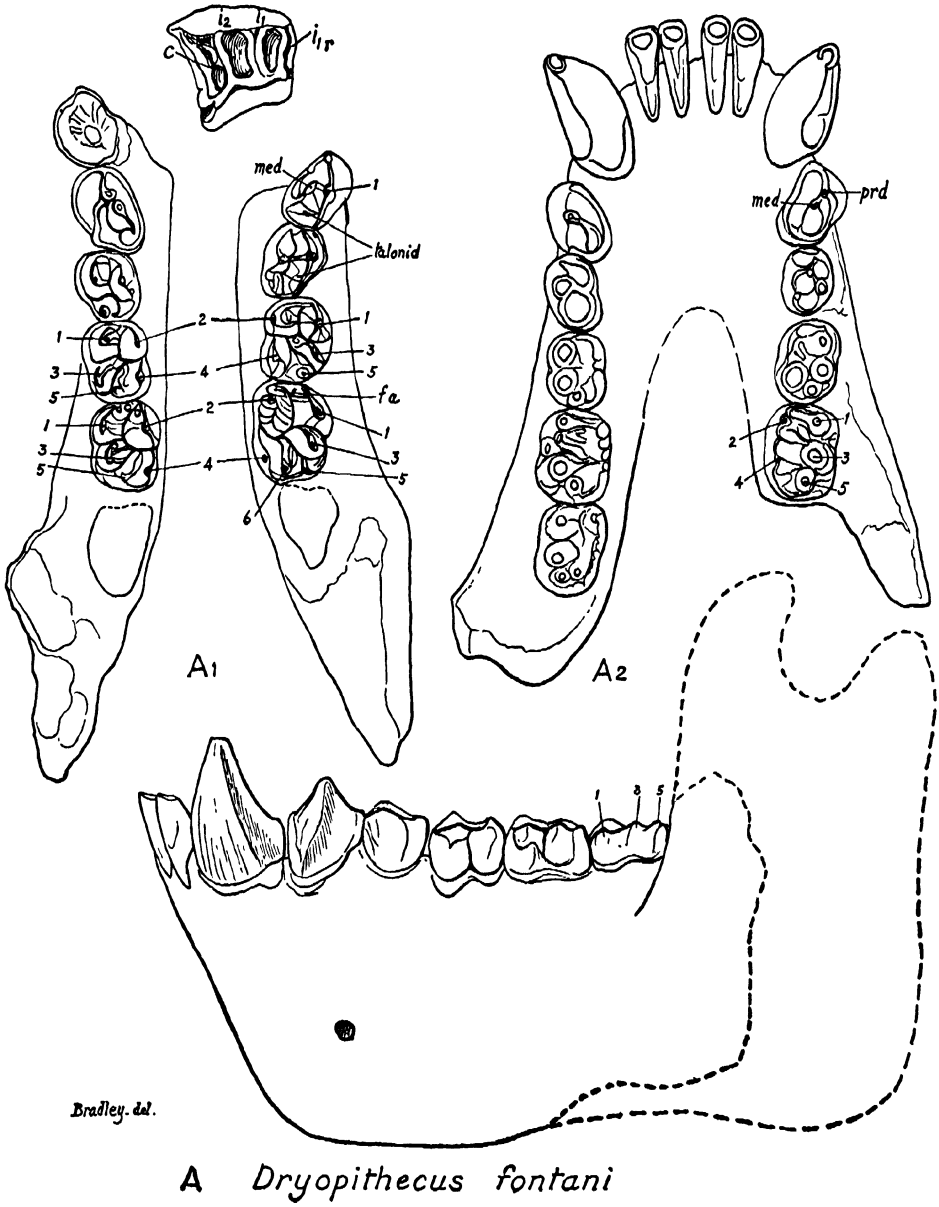


Fig. 23.55. Lower jaw and teeth of *Dryopithecus fontani*. Data from Gervais, Gaudry, casts, photographs (kindness of Dr. G. H. R. von Koenigswald).

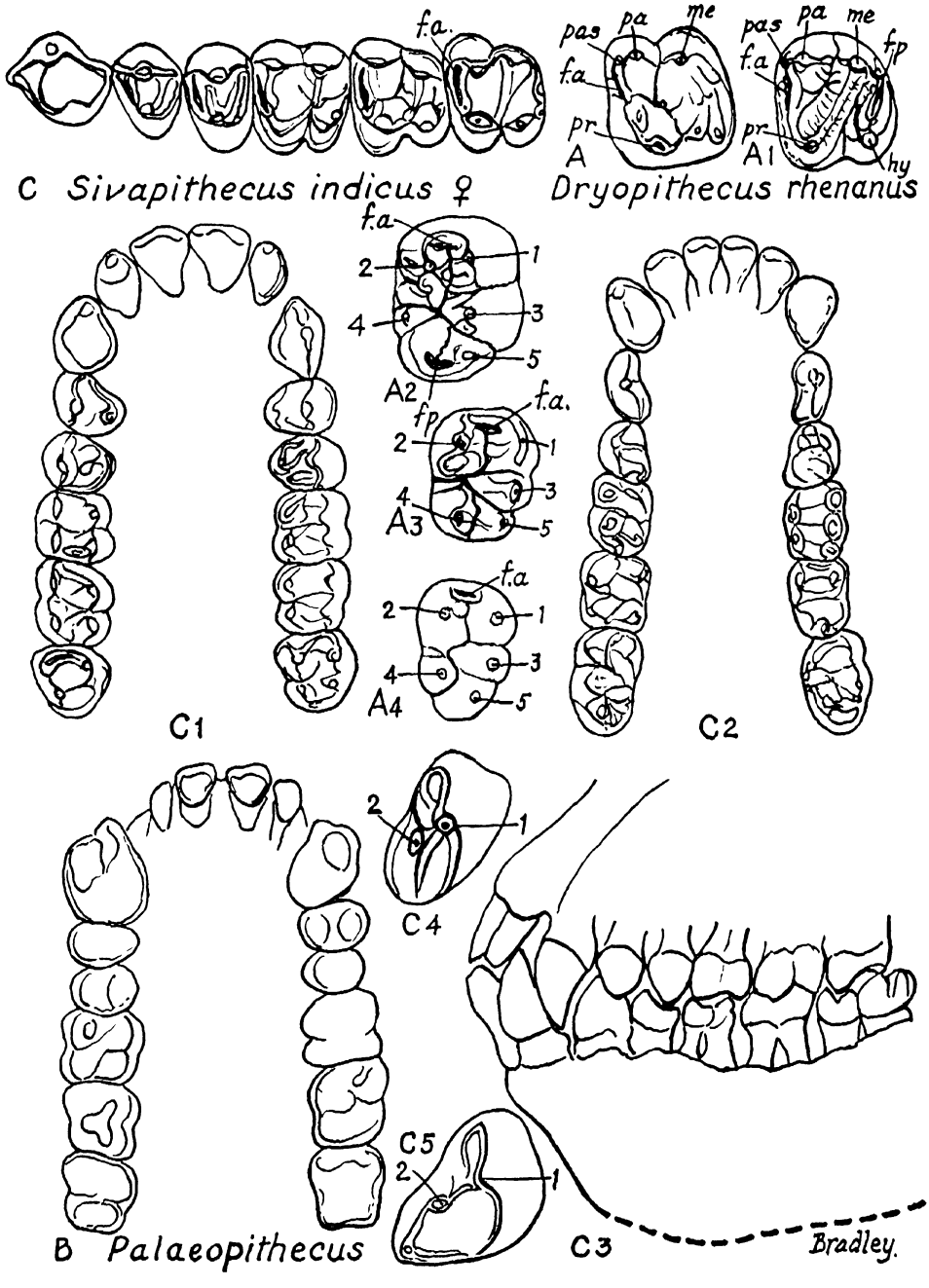


Fig. 23.56. Dental arches, jaws and teeth of dryopithecine apes. Data from: A–A3, McGregor (enlarged photograph); B, Lydekker; C–C3, Gregory, Hellman, and Lewis; D, Gregory and Hellman; D1, Pilgrim. *f.a.*, fovea anterior; *f.p.*, fovea posterior.

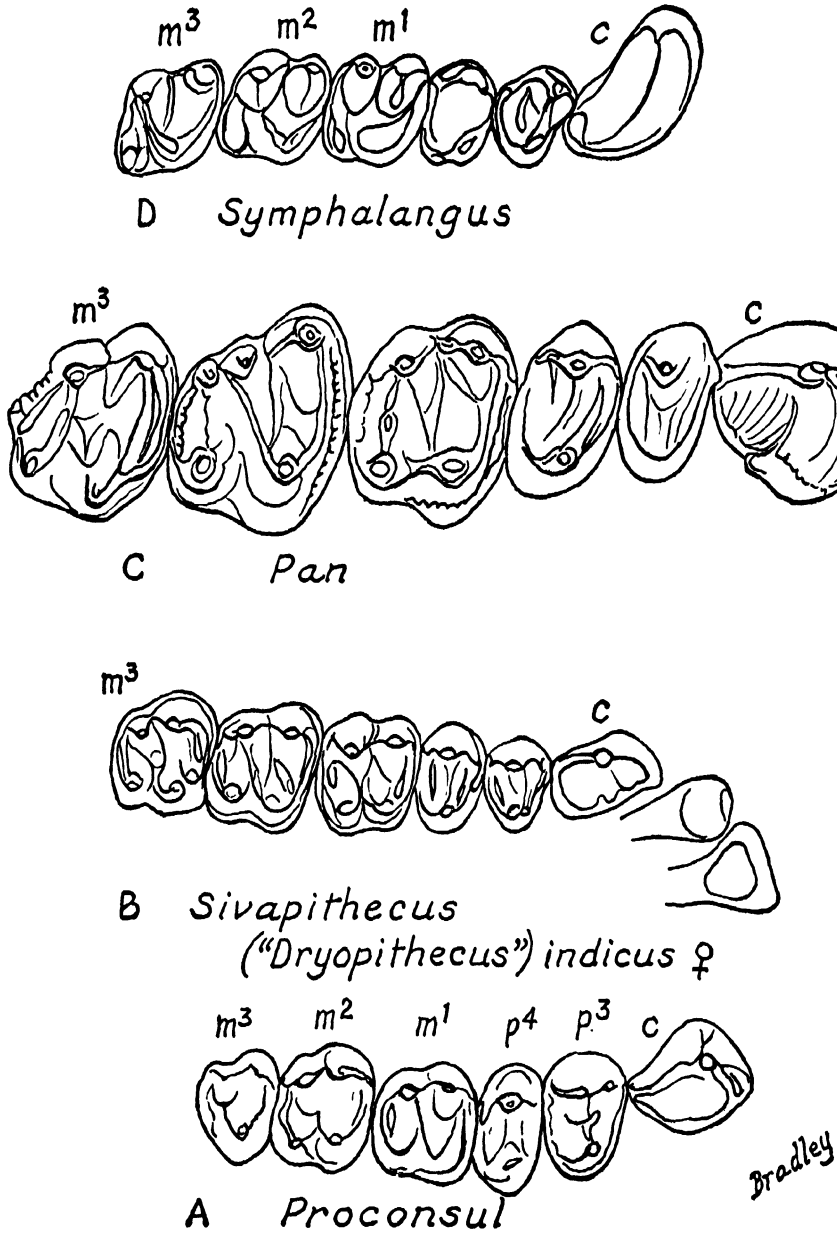


Fig. 23.57. Comparative series of upper molars of anthropoids. Data from: A, Hopwood, and cast; B, Gregory, Hellman and Lewis, and cast; C, D, specimens.

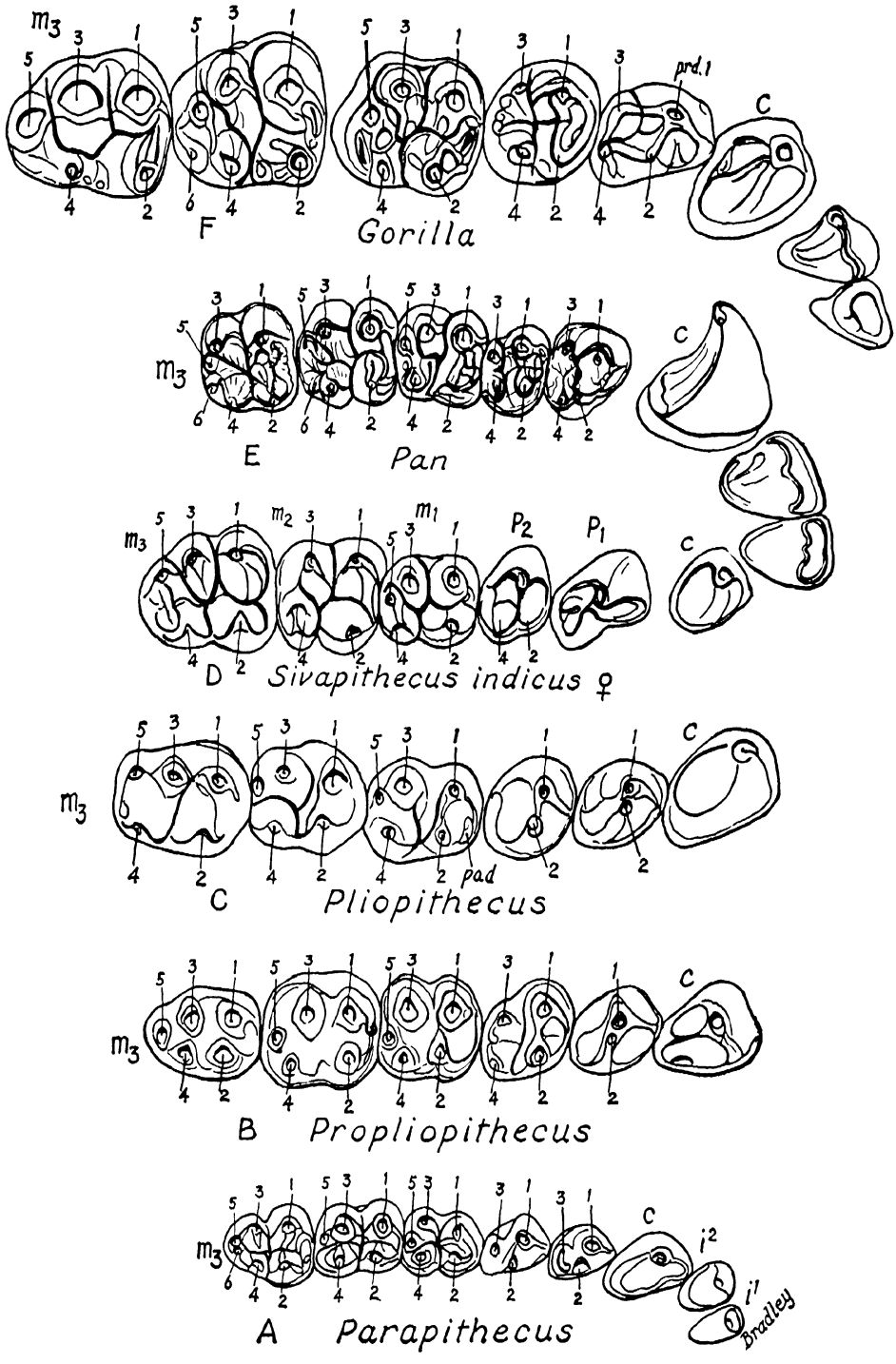


Fig. 23.58. Lower teeth of fossil and recent anthropoids. Data from: A, Schlosser, Mollison, Abel, and cast; B, Schlosser, McGregor (photograph); C, De Blainville, and cast; D–F, Gregory and Hellman, and specimens. Scales: A, B, 20/9; C, 16/9; D, E, F, 2/9.

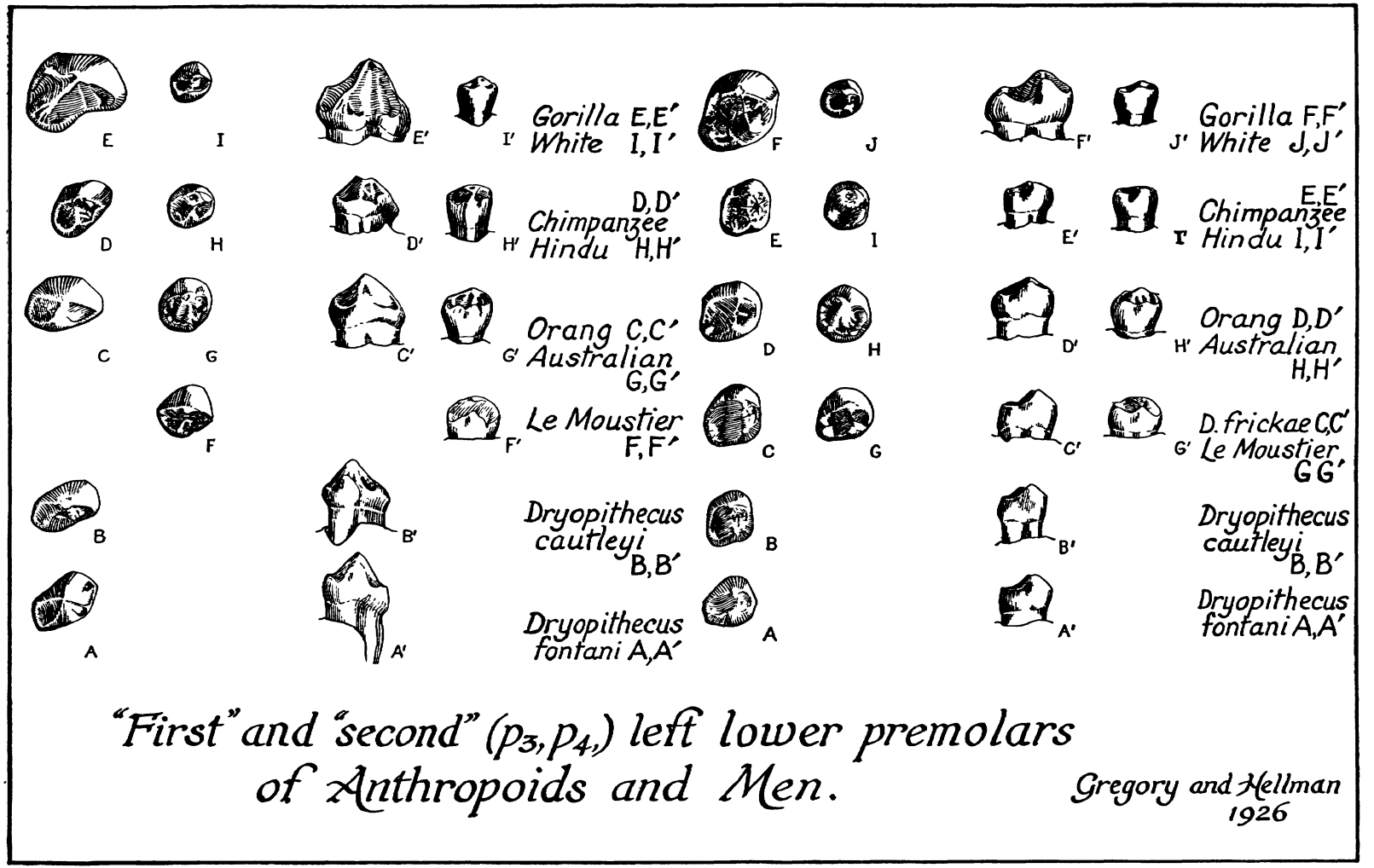

E
I
E'
I'
Gorilla E,E'
White I,I'
F
J
F'
J'
Gorilla F,F'
White J,J'
D
H
D'
H'
Chimpanzee D,D'
Hindu H,H'
E
I
E'
I'
Chimpanzee E,E'
Hindu I,I'
C
G
C'
G'
Orang C,C'
Australian G,G'
D
H
D'
H'
Orang D,D'
Australian H,H'
F
F'
Le Moustier F,F'
C
G
C'
G'
D. frickae C,C'
Le Moustier G,G'
B
B'
Dryopithecus cautleyi B,B'
B
B'
Dryopithecus cautleyi B,B'
A
A'
Dryopithecus fontani A,A'
A
A'
Dryopithecus fontani A,A'
"First" and "second" (p_3, p_4,) left lower premolars of Anthropoids and Men.
Gregory and Hellman 1926

Fig. 23.59

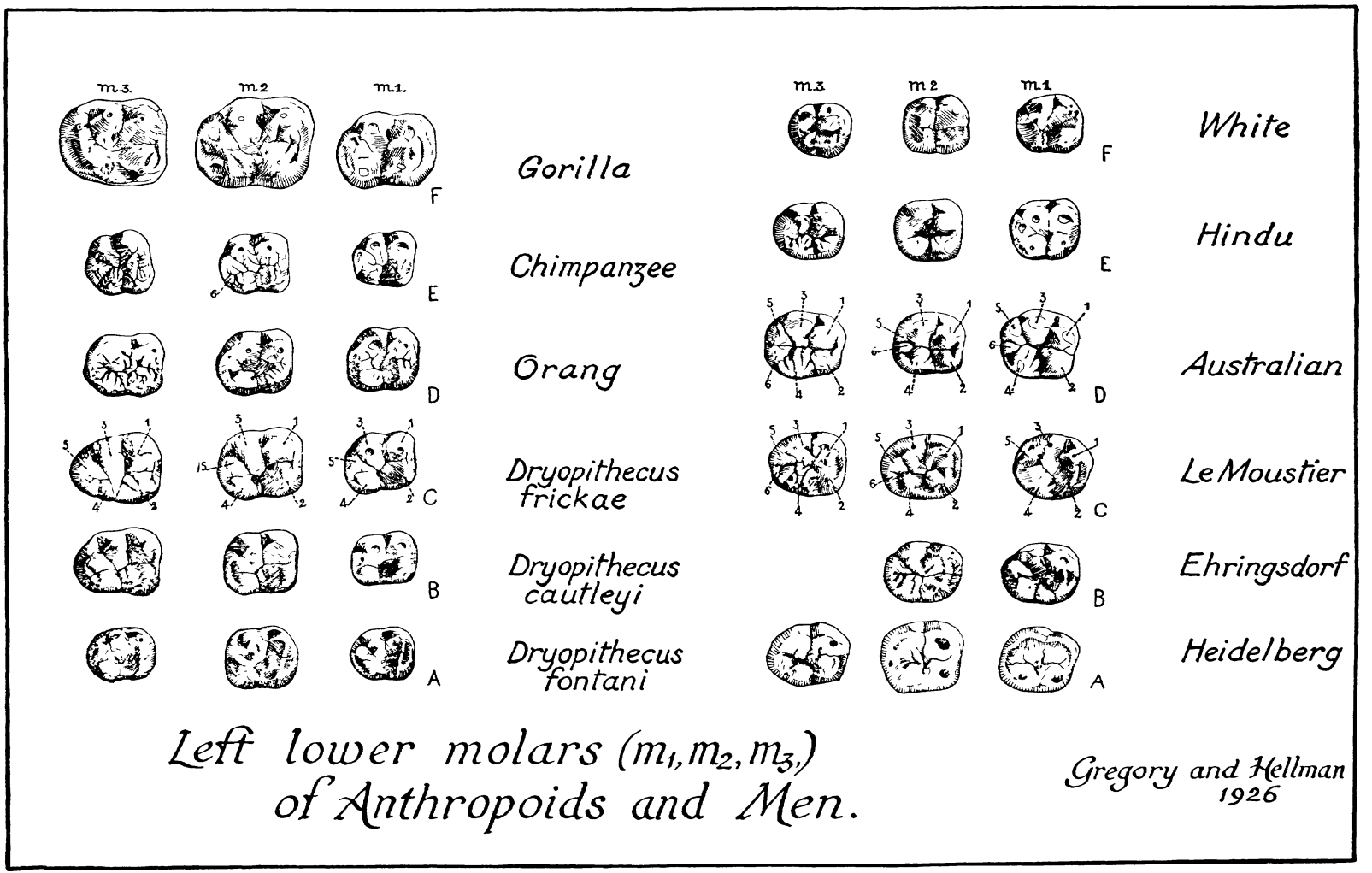

m.3.
m.2.
m.1.
F
E
D
C
B
A
Gorilla
Chimpanzee
Orang
Dryopithecus frickae
Dryopithecus cautleyi
Dryopithecus fontani
White
Hindu
Australian
Le Moustier
Ehringsdorf
Heidelberg
Left lower molars (m_1, m_2, m_3) of Anthropoids and Men.
Gregory and Hellman 1926

Fig. 23.60

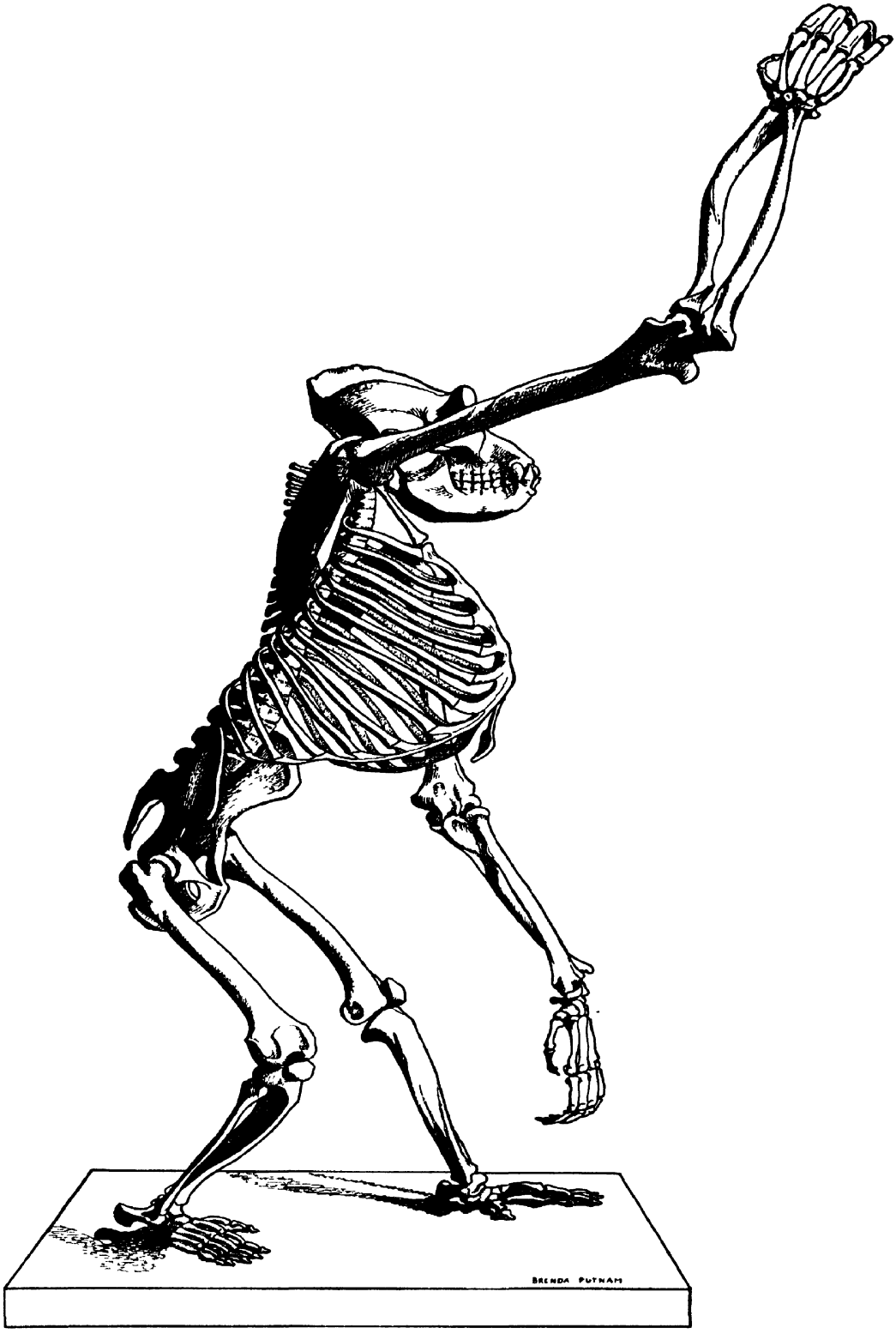


Fig. 23.61. Gorilla skeleton, mounted under direction of Dr. John Eric Hill and Miss Brenda Putnam.

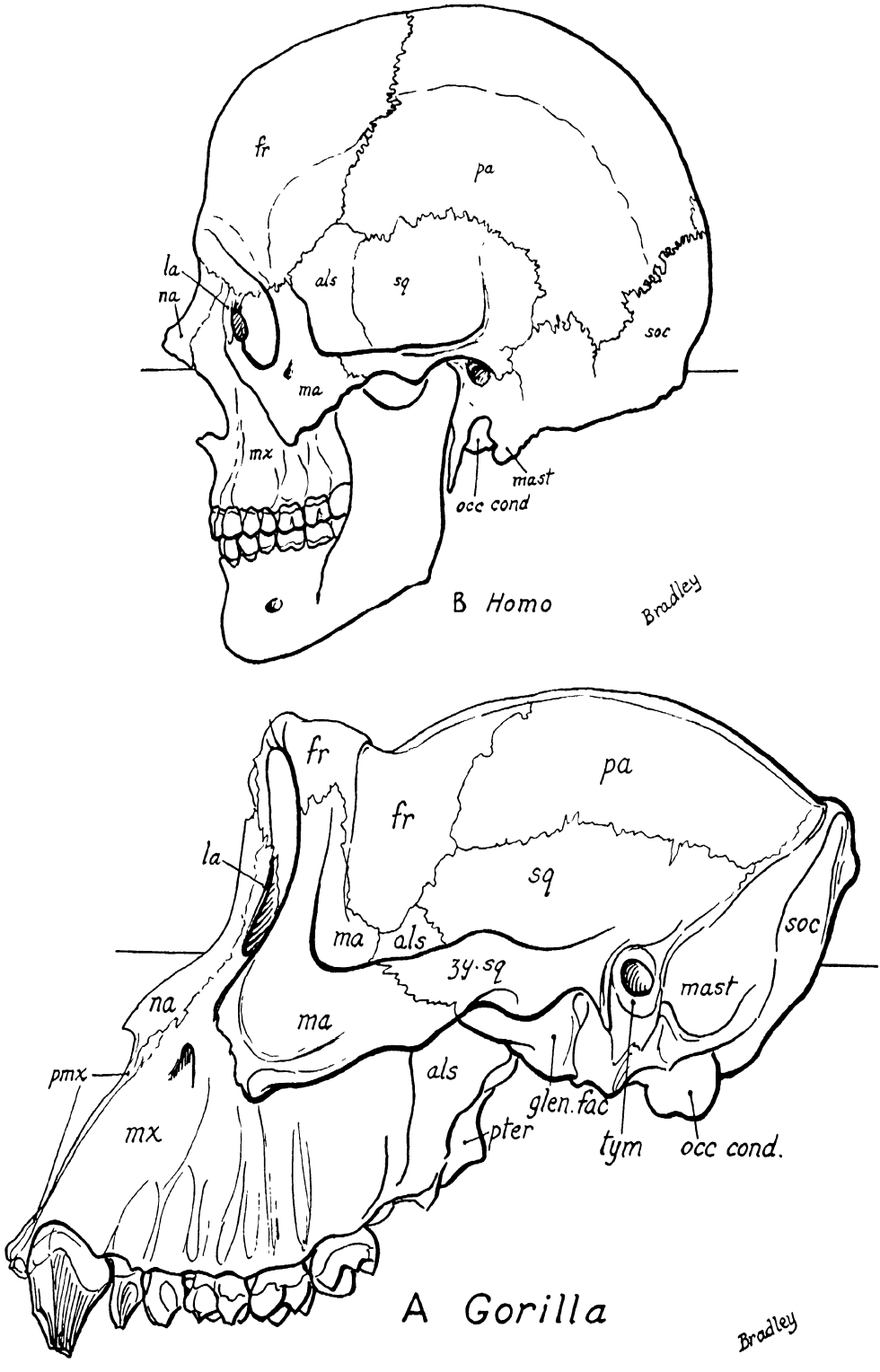


Fig. 23.62. Extremes in skull form, showing contrasts in pterion region. Original.

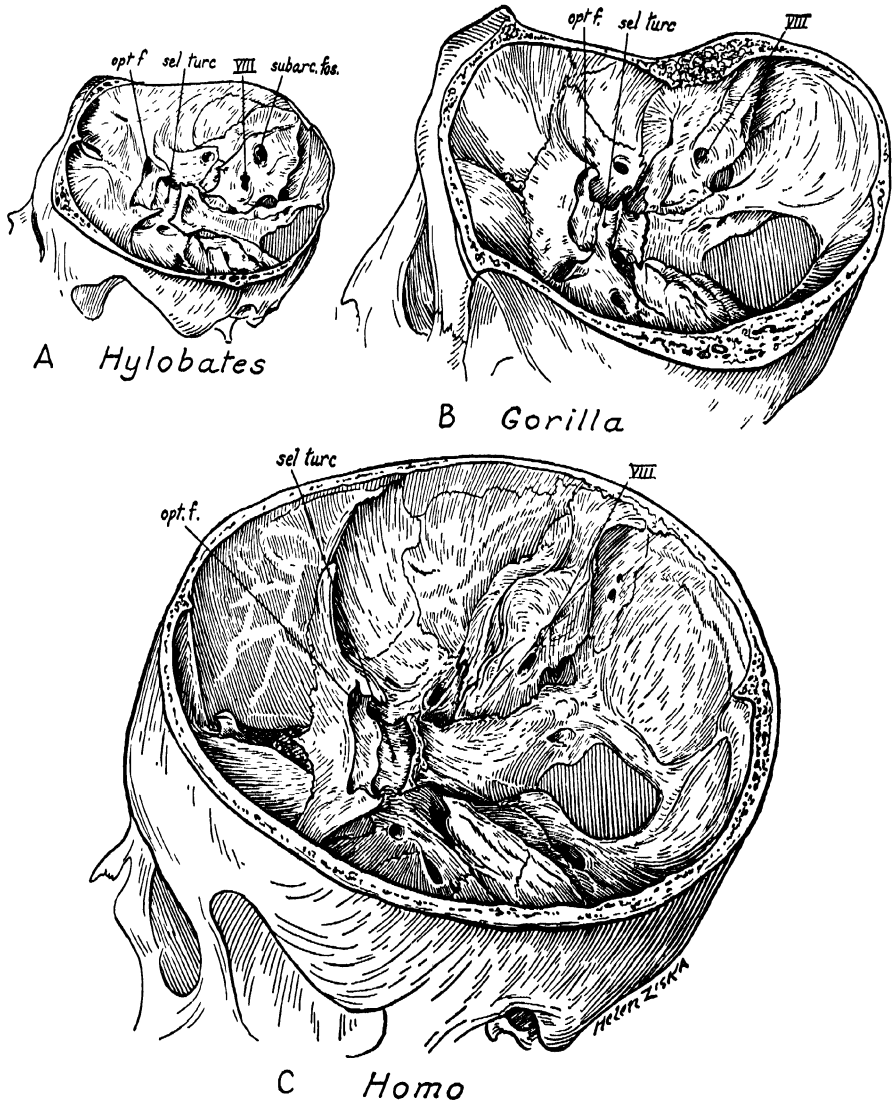


Fig. 23.63. Presence of fossa subarcuata in gibbon and absence in higher apes and man. Original.

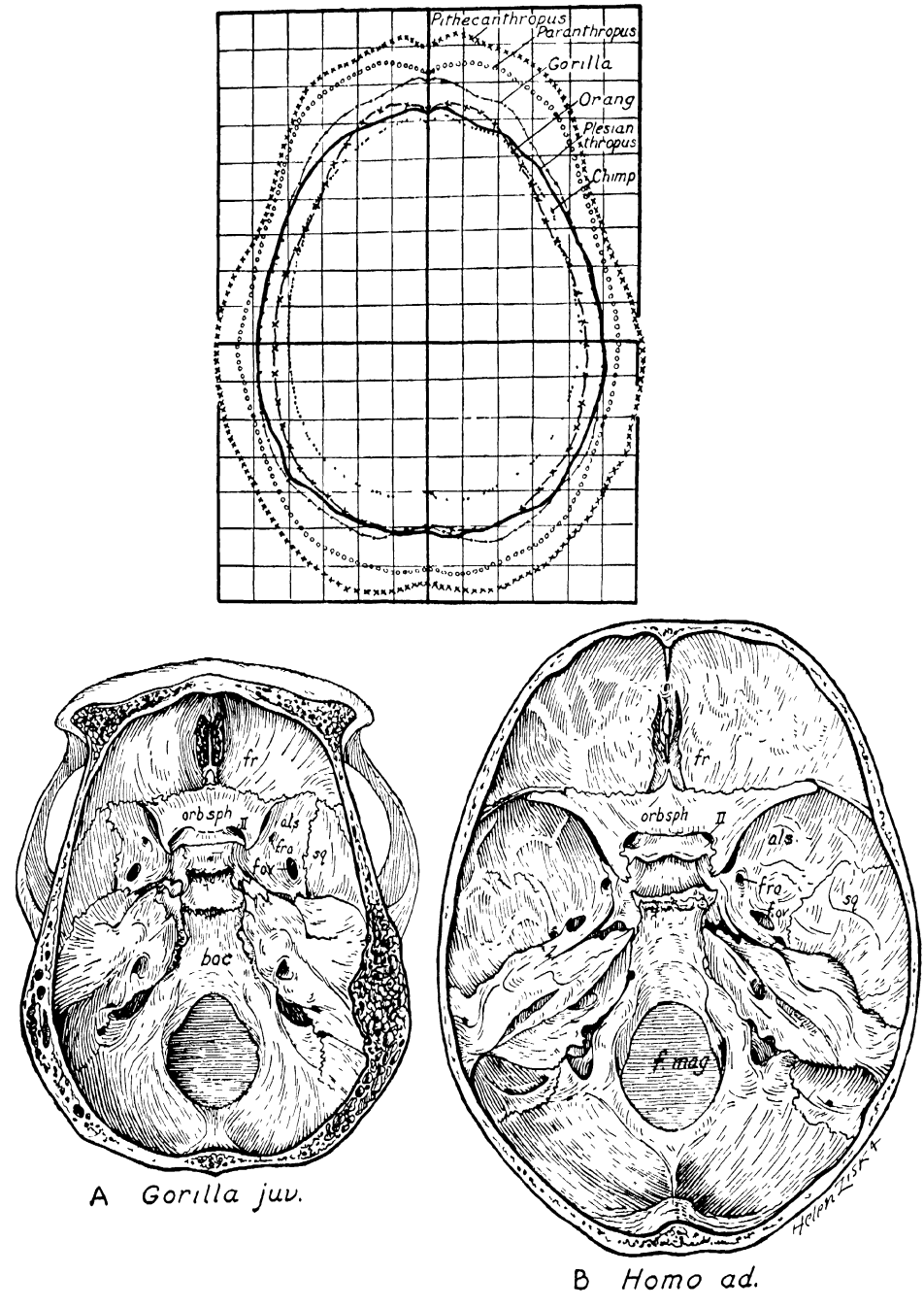


Fig. 23.64. Contours of brain-casts. After Schepers. Interior of crania (A, B), showing relatively primitive conditions in immature gorilla. In the adult gorilla the opposite frontals meet in front of the orbitosphenoid and overlap the contact between the orbitosphenoid and the ethmoid.

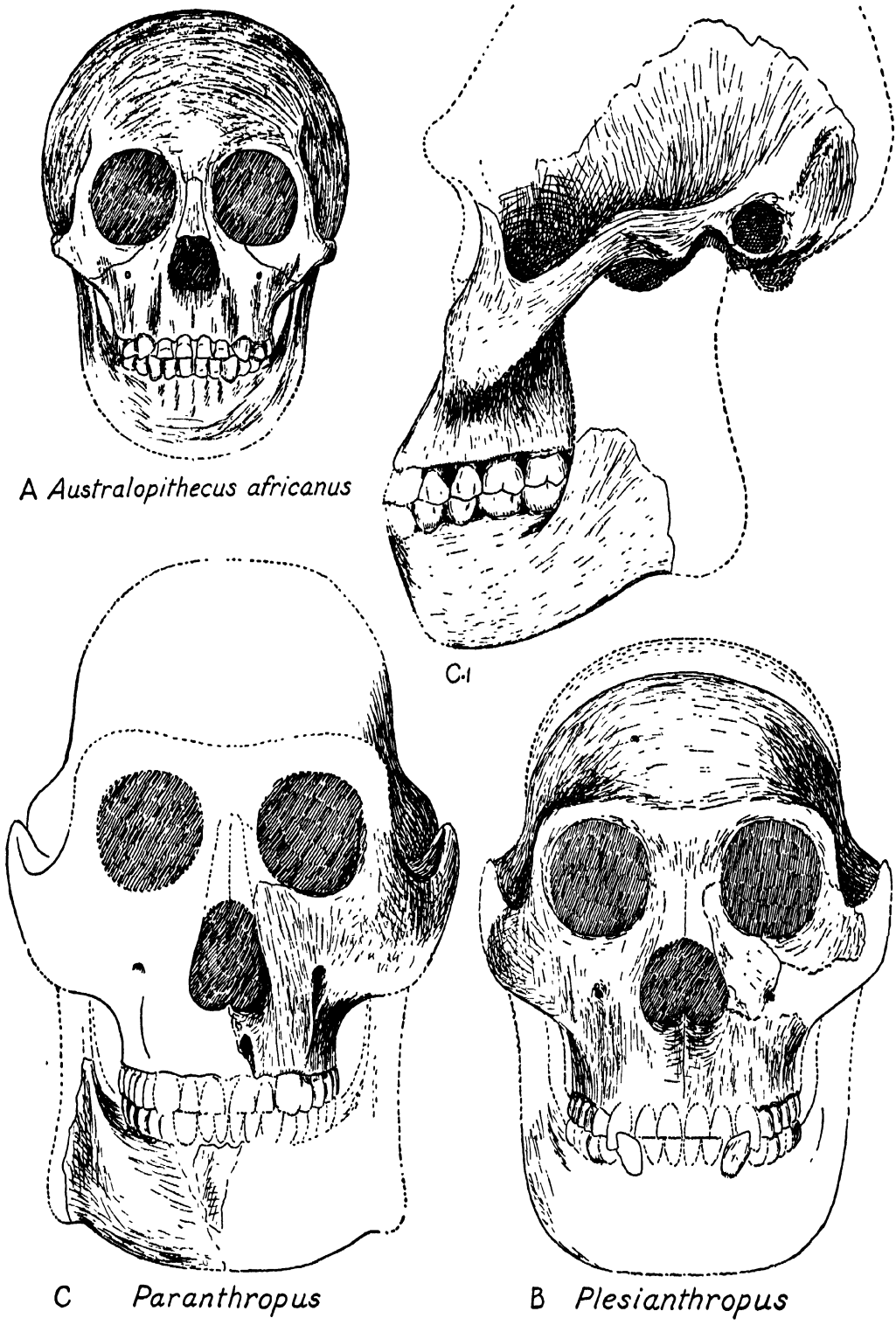


Fig. 23.65. Skulls of South African ape-men. Restorations by Broom.

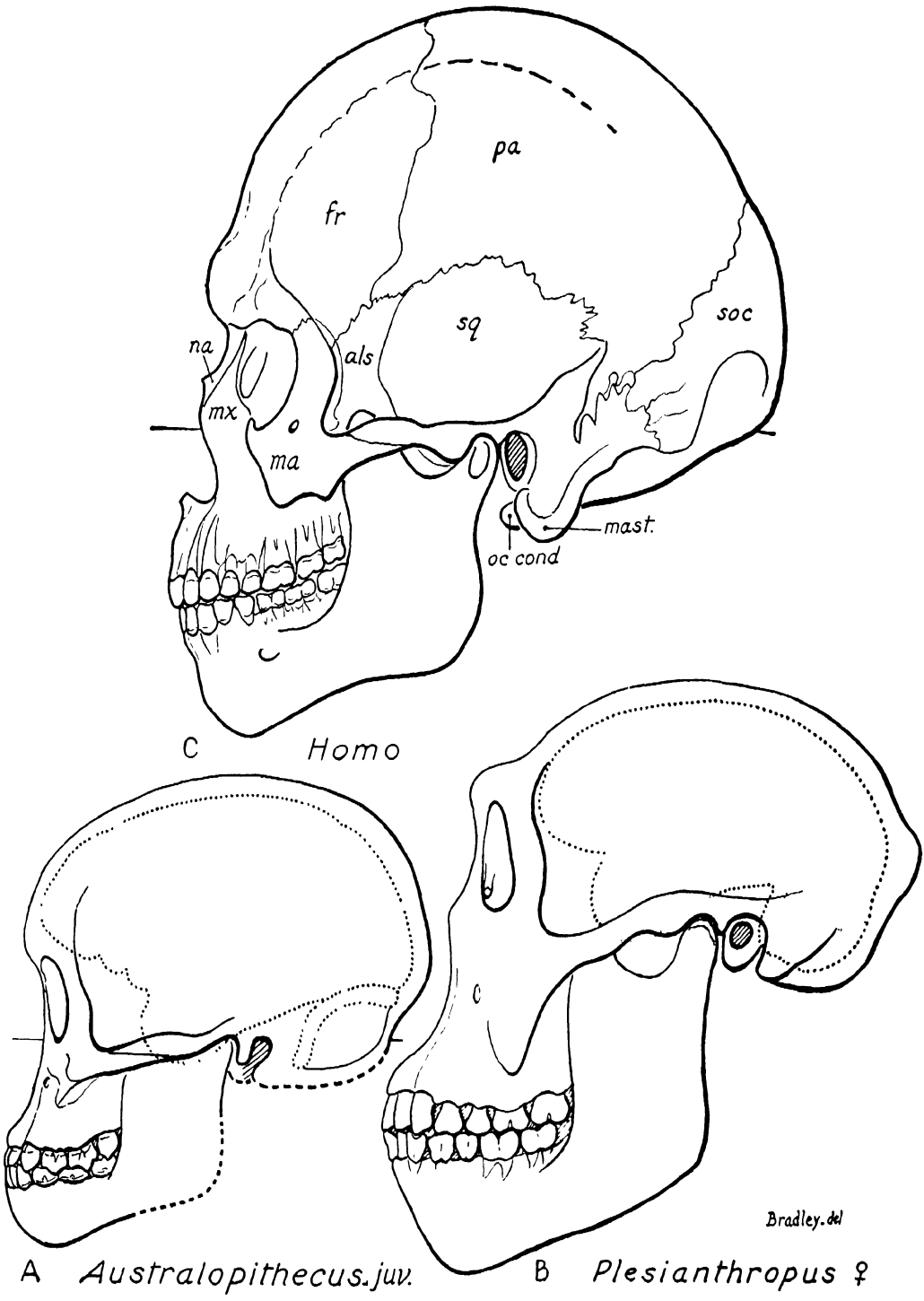


Fig. 23.66. Skull contours of South African apemen (Australopithecinae, A, B) and Tasmanian aboriginal (C). A, after Dart; brain contours, after Schepers; B, provisional reconstruction, data from Broom, and casts; brain-cast contour (dotted line) from Schepers; C, original.

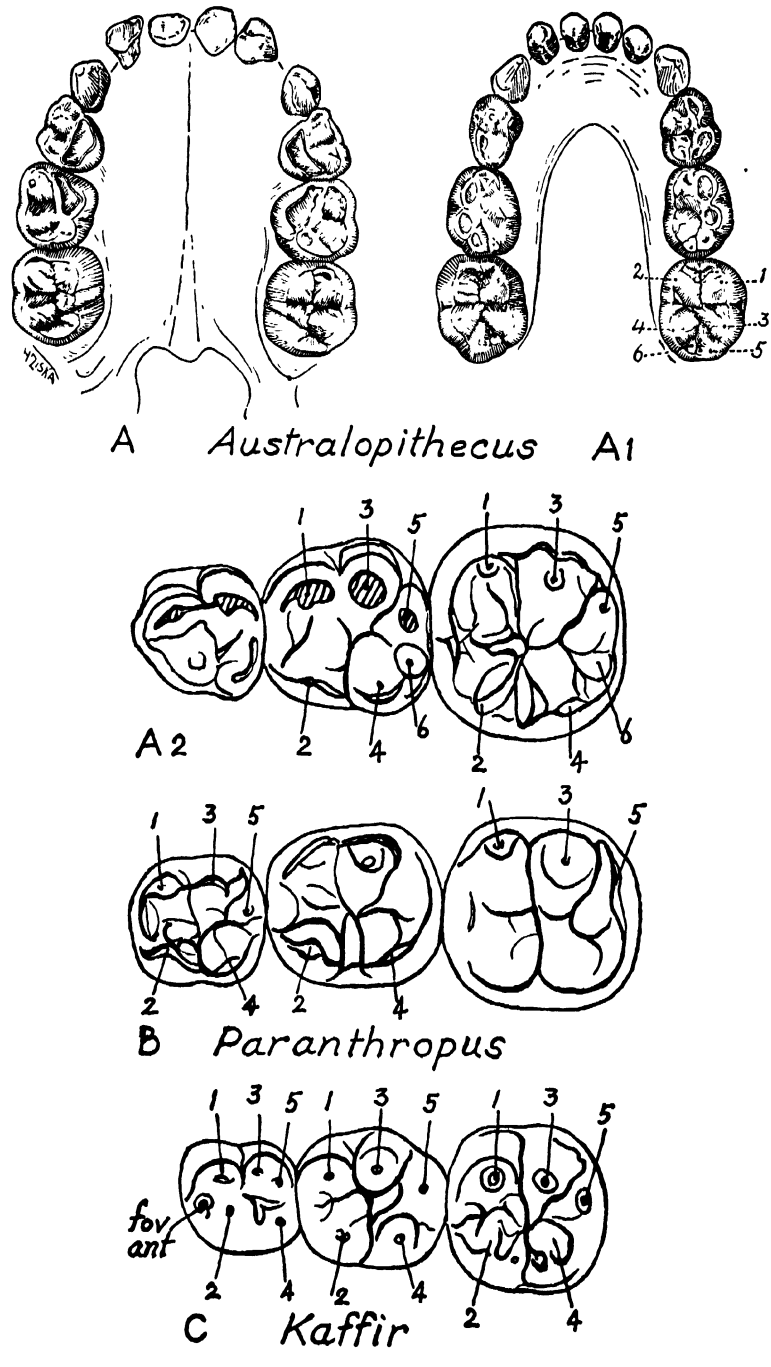


Fig. 23.67. Dental arches and deciduous molars of extinct South African ape-man (Australopithecinae, A, B) and man (Kaffir). A, A1, after Gregory, data from Dart; B, data from Broom.

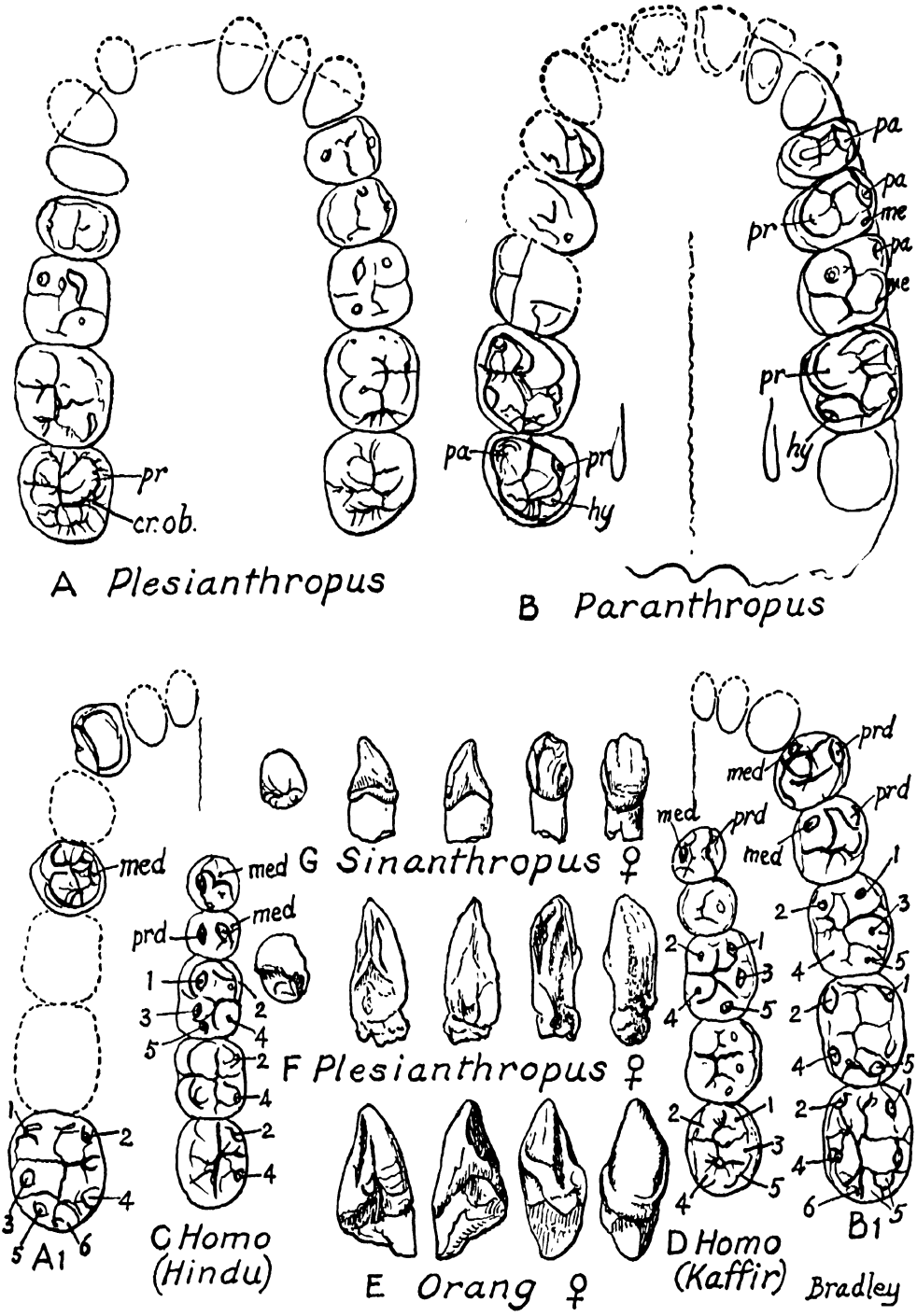


Fig. 23.68. Upper (A, B) and lower (A1, B1) dental arches of South African ape-men (A, A1, B, B1), Kaffir (D). After Broom. Left lower cheek teeth of Hindu (C), original. Left lower canines (E–G): occlusal, distal, mesial, lingual, buccal views, after Weidenreich.

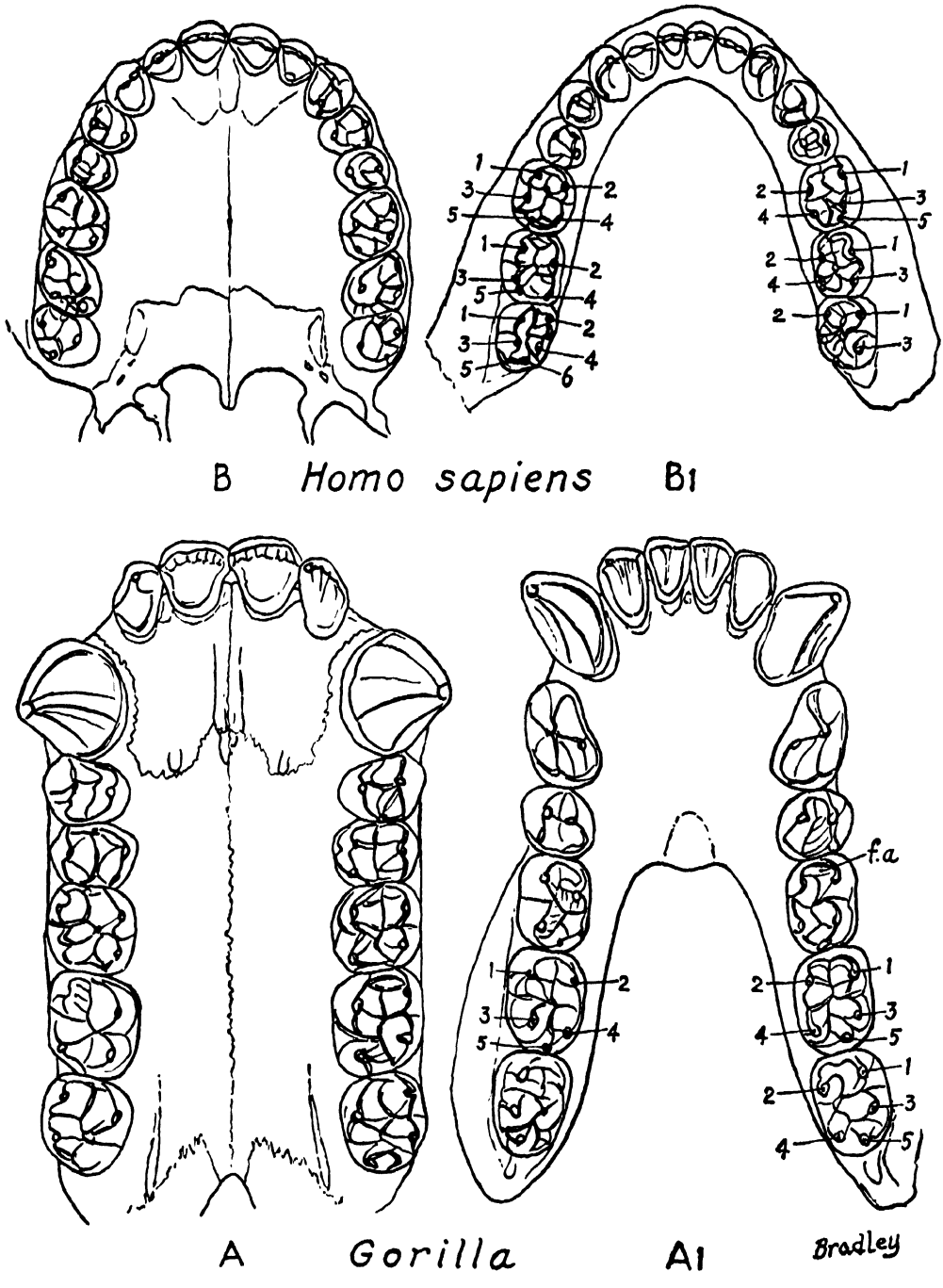


Fig. 23.69. Extremes in dental arch form. From Gregory, after Röse.

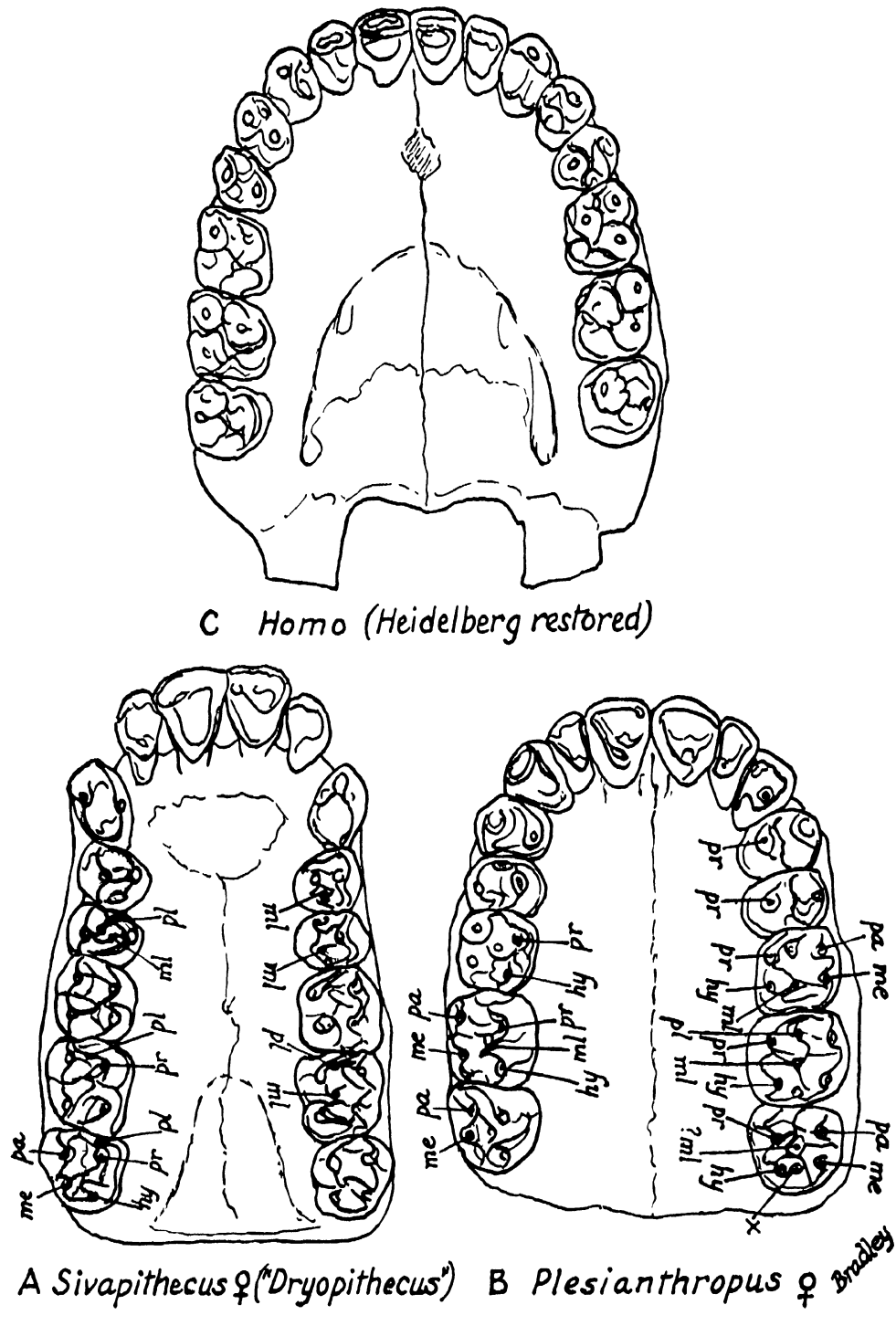


Fig. 23.70. Upper dental arches of Lower Pliocene Indian ape (A), South African Pleistocene ape-man (B) and European Pleistocene man. A, B, after Gregory and Hellman; C, restored to fit lower teeth by McGregor.

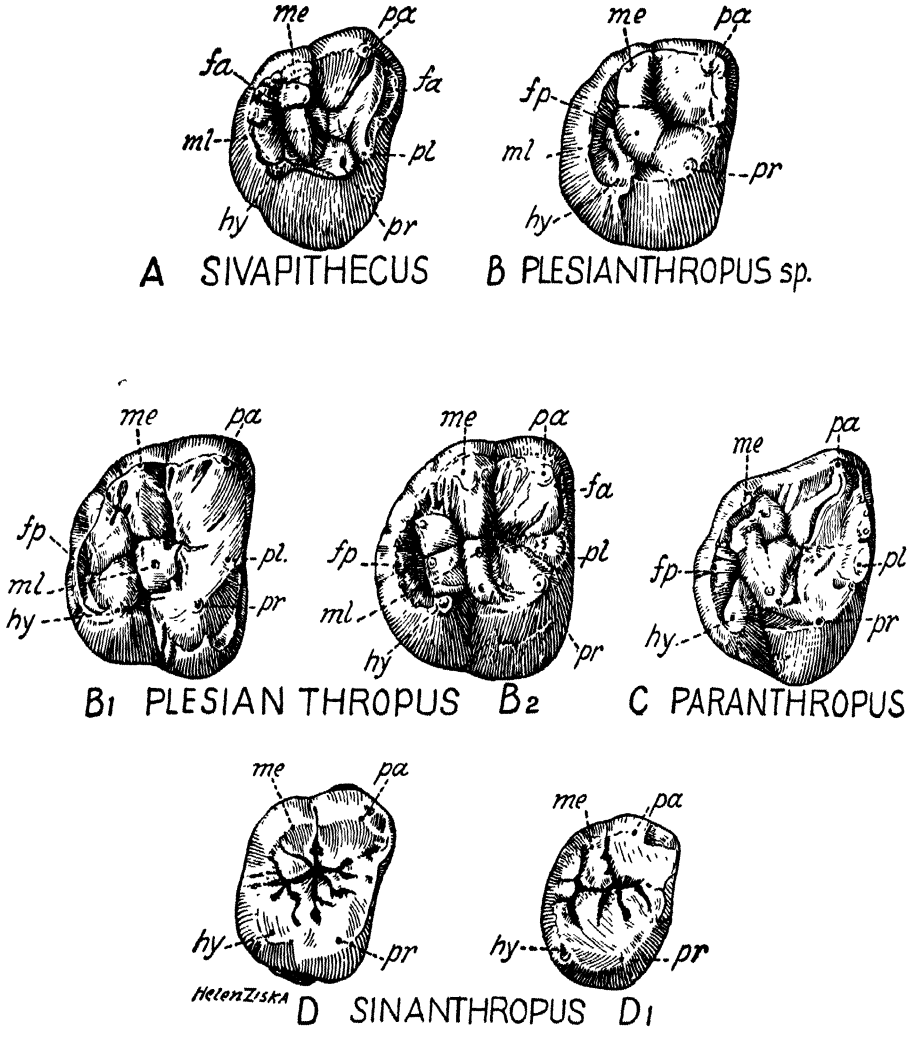


Fig. 23.71. Third right upper molars of fossil ape, ape-men (B–C) and men. A–C, original; D, D1, after Weidenreich.

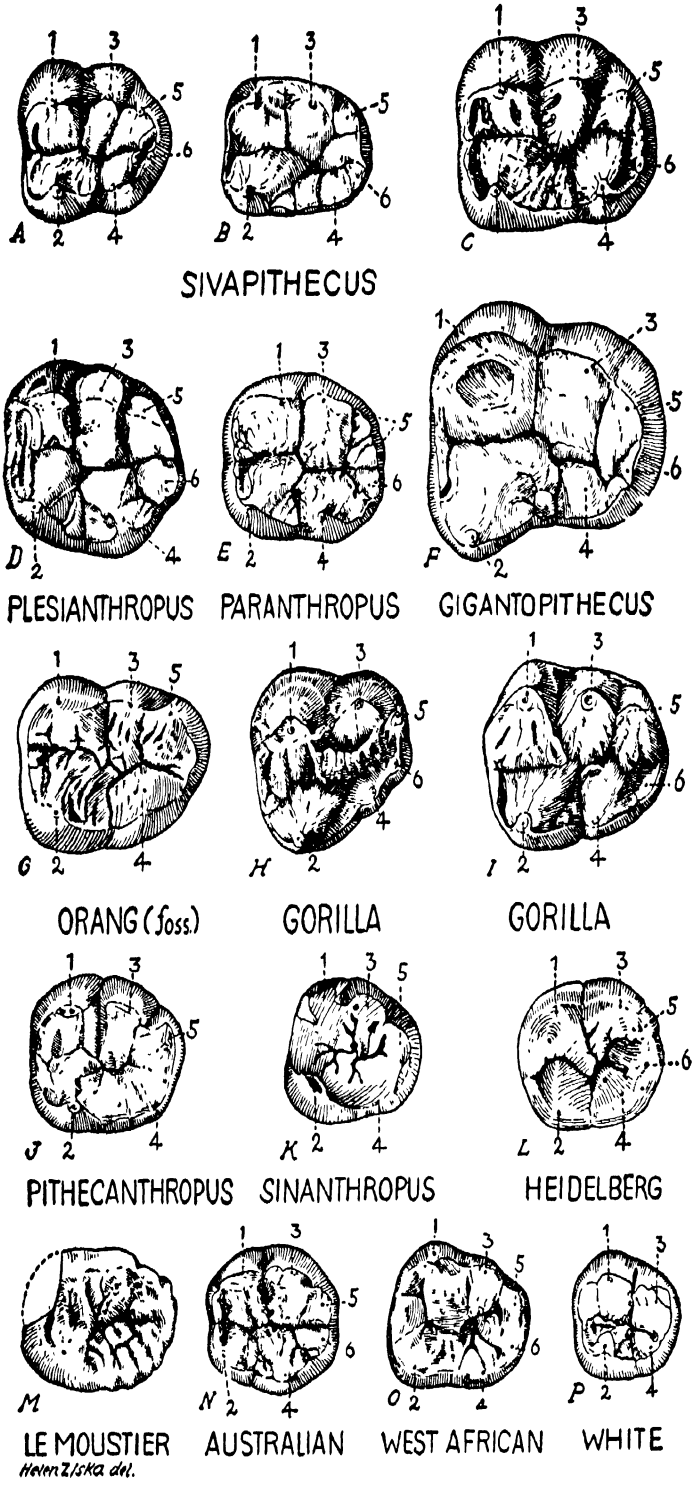


Fig. 23.72. "Dryopithecus pattern" of third right lower molar and some of its derivatives. After Gregory and Hellman. Data also from: A–C, Pilgrim; D, E, Broom; F–J, von Koenigswald; K, M, Weidenreich.

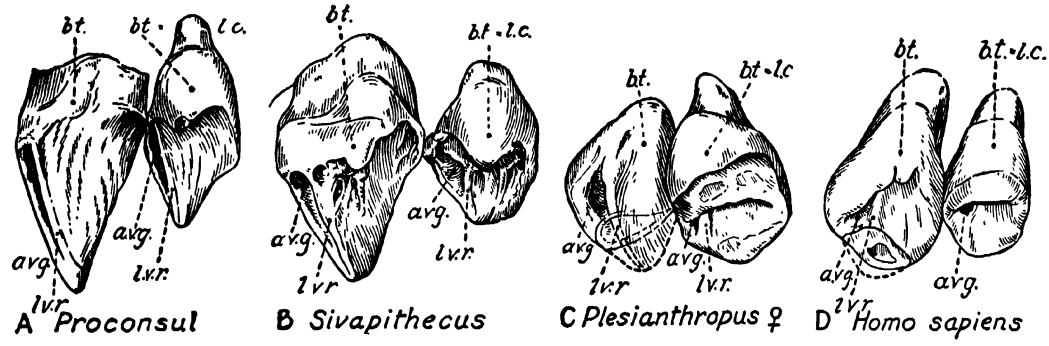


Fig. 23.73. A–D, Upper canines and first premolar, inner aspect. Data from: A, Hopwood, and cast; B, Gregory and Hellman; C, Broom, and cast; D, Hellman, and specimen. *A.v.g.*, anterior vertical groove; *l.v.g.*, lingual vertical ridge; *b.t.=l.c.*, buccal tubercle= lingual cusp.

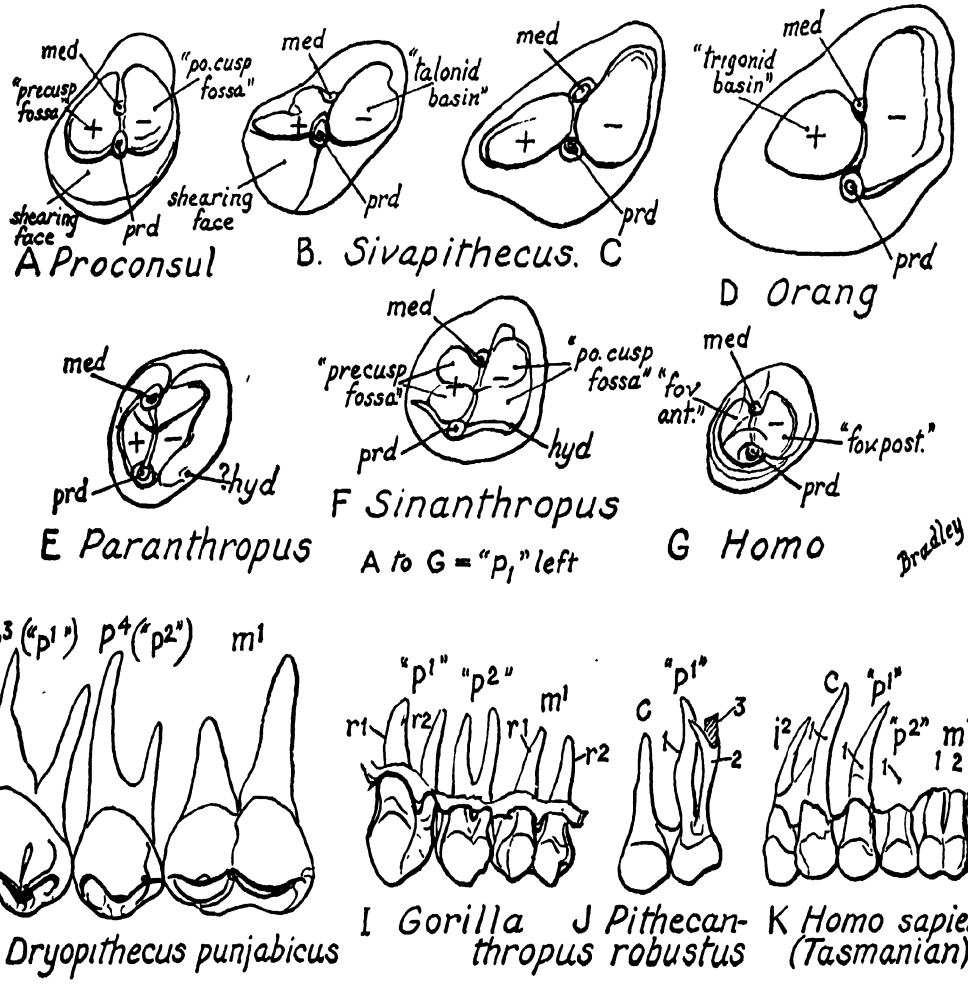


Fig. 23.74. A–G, Left lower first premolar in anthropoids and man. A–D, G, original; E, data from Broom; F, data from Weidenreich. H, upper premolars and m^1 of Pliocene Indian ape, showing two buccal roots on all three teeth, after Pilgrim; I, modern gorilla, original; J, p^1 with two buccal roots, after von Koenigswald; K, modern man, both premolars with single buccal root, original.

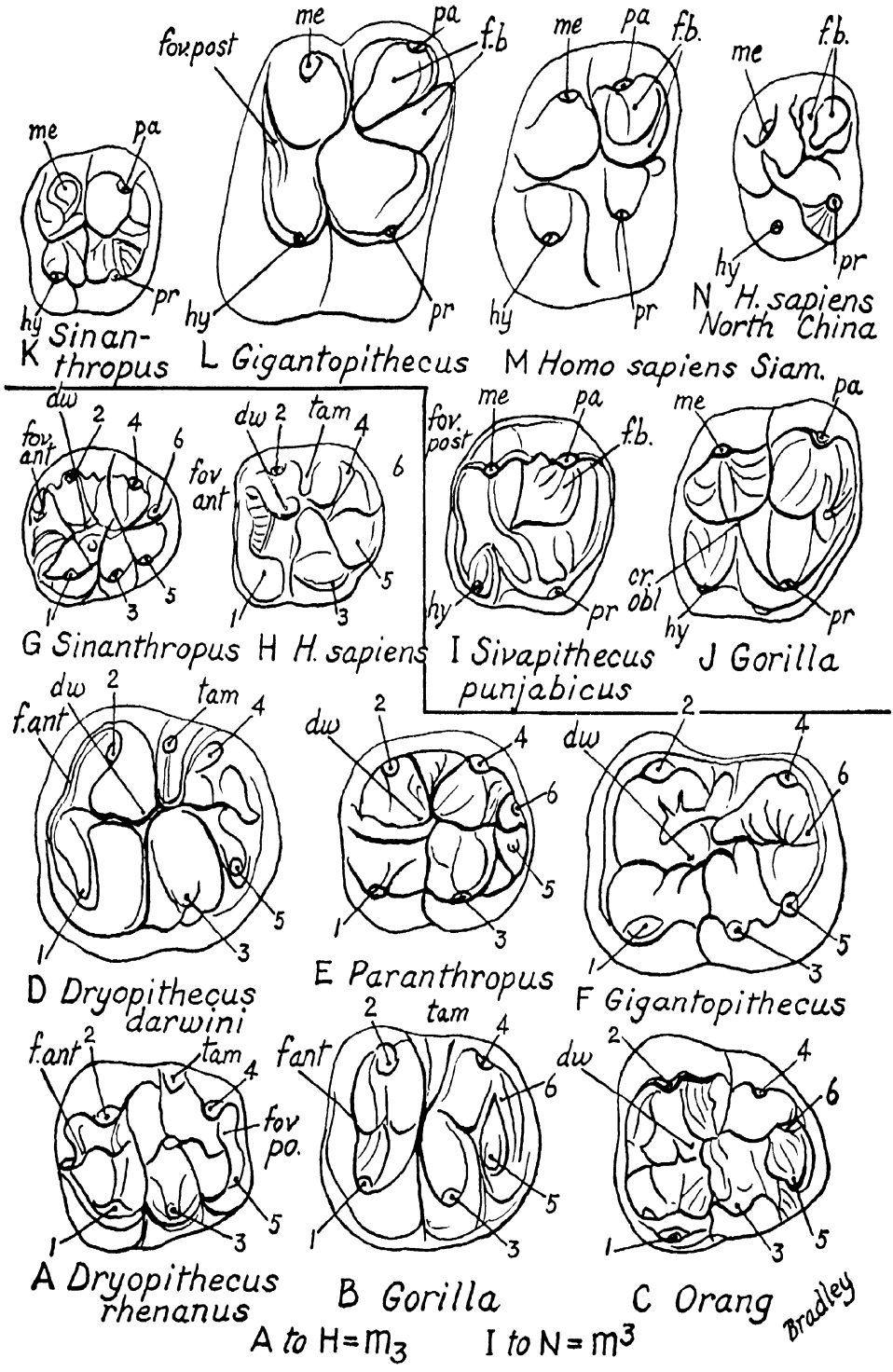


Fig. 23.75. Lower (A–H) and upper (I–N) molar patterns. Chiefly after Weidenreich. *f.b.*, "flower bud" pattern; *tam*, tuberculum antero-mediale; *d.w.*, deviating wrinkle; *fov.ant.*, fovea anterior.

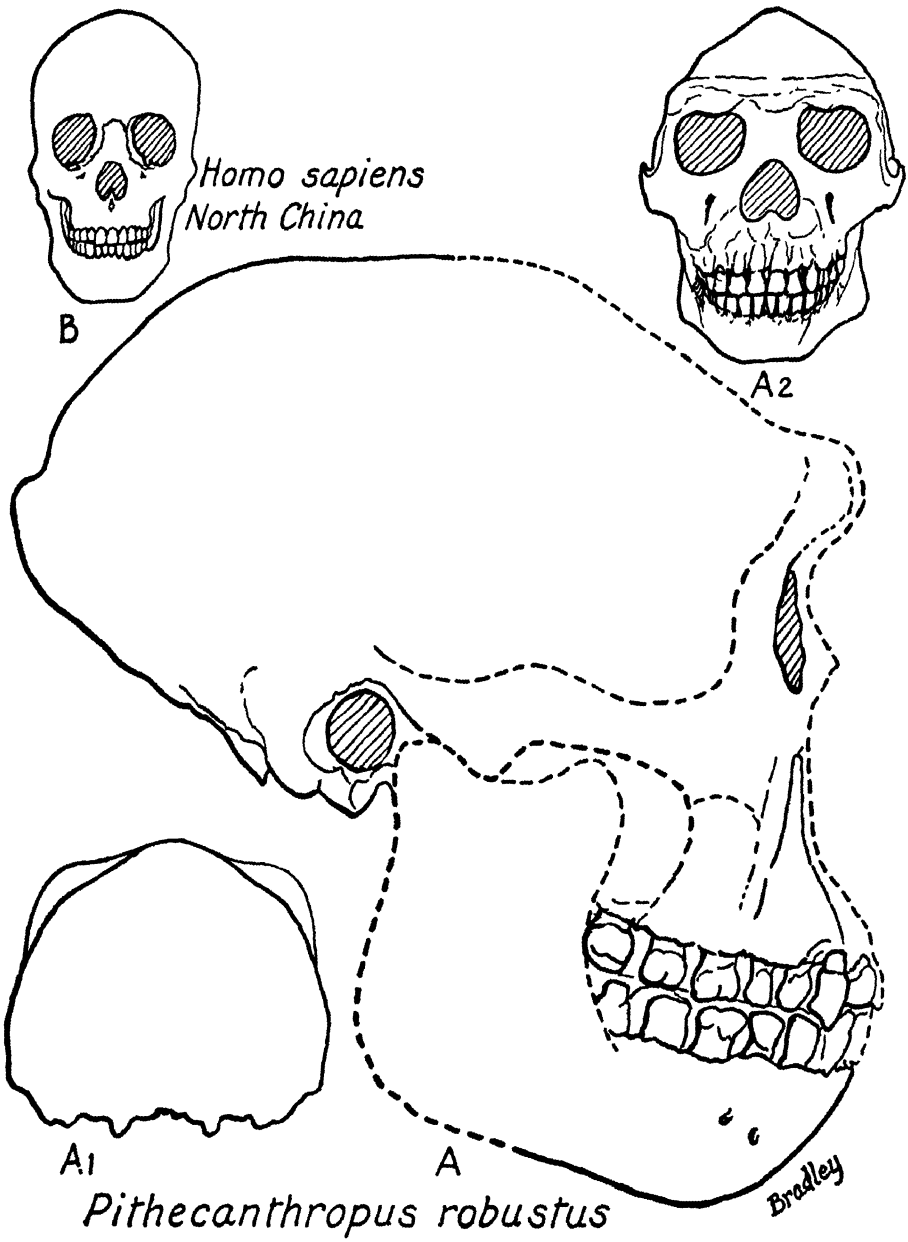


Fig. 23.76. Skulls of Javan fossil man and modern man. After Weidenreich. A1, Occipital view.

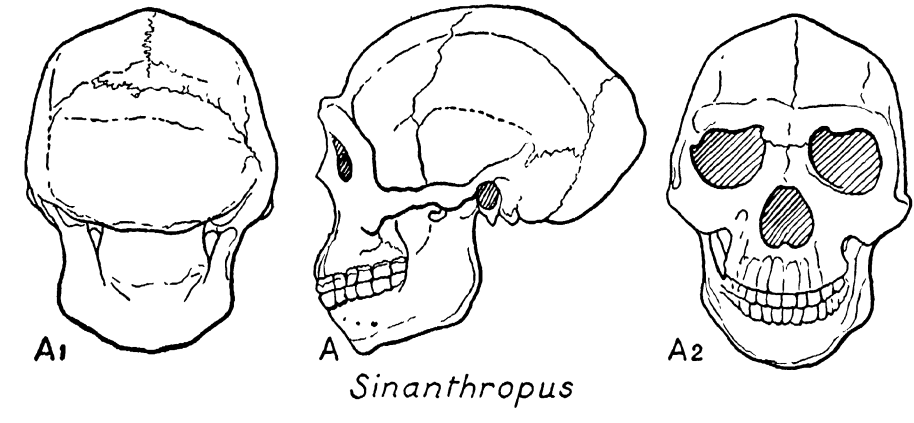


Fig. 23.77a (top). Skull of Peking man (A–A2). After Weidenreich.

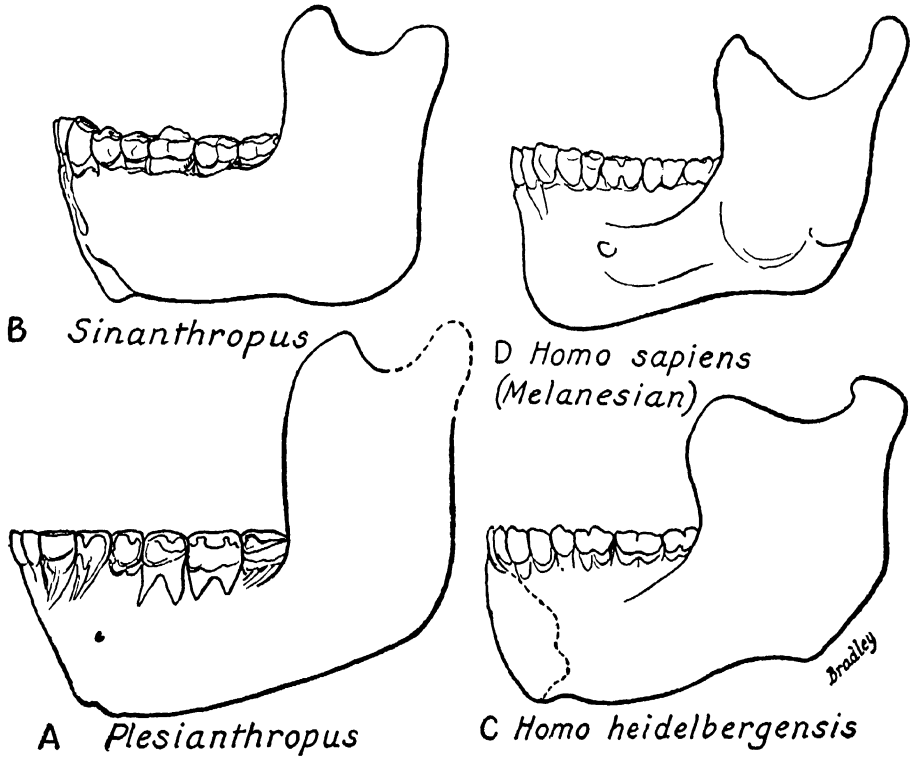


Fig. 23.77b. Lower jaw contours of ape-men and men. A, after Broom; B, after Weidenreich; C, data from Schoetensack, and casts.

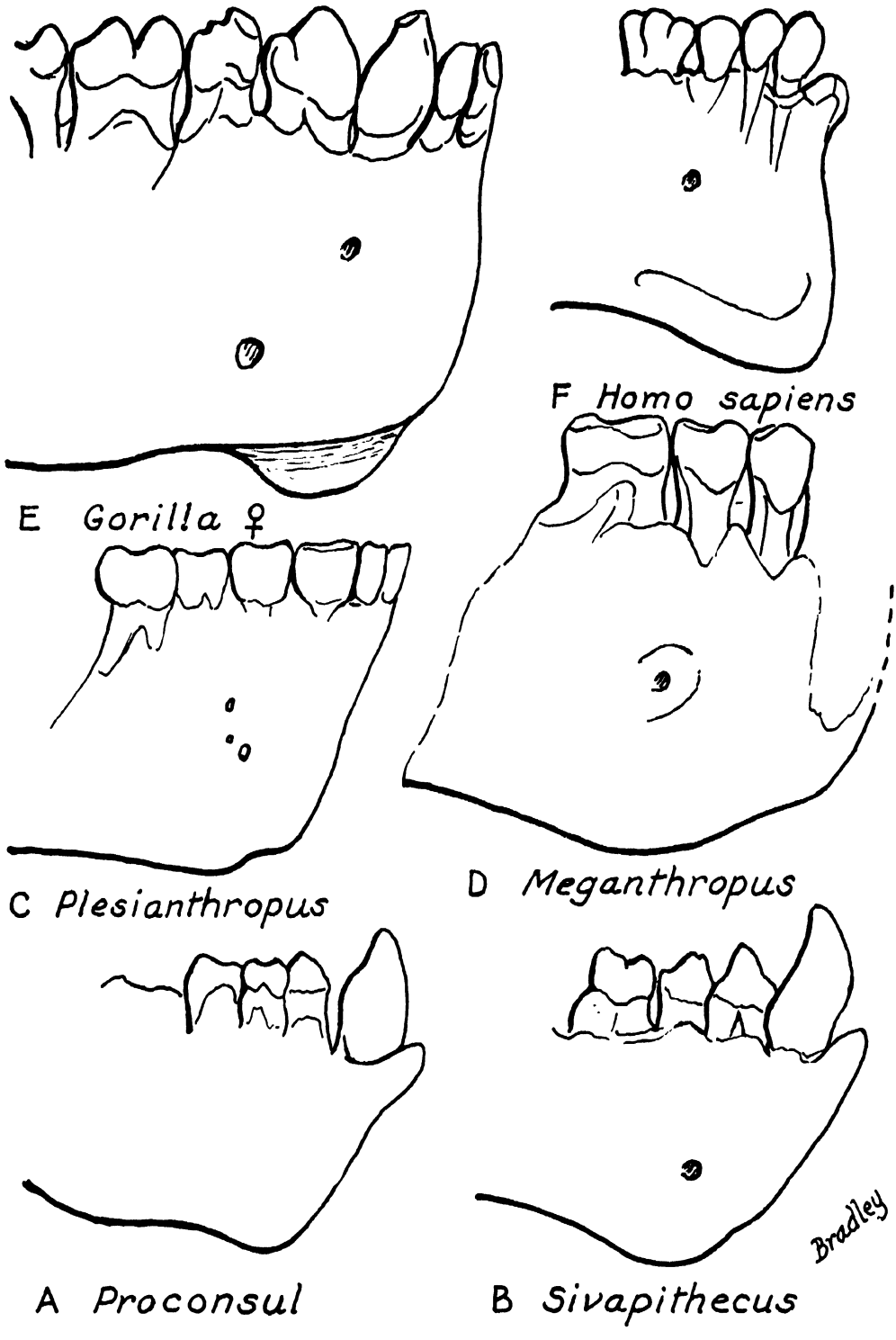


Fig. 23.78. Lower jaws of *Meganthropus*, anthropoids and man. A, data from Leakey; B, data from Gregory and Hellman; C, after Broom, 1947; D, after von Koenigswald and Weidenreich; E, F, original. Natural size.

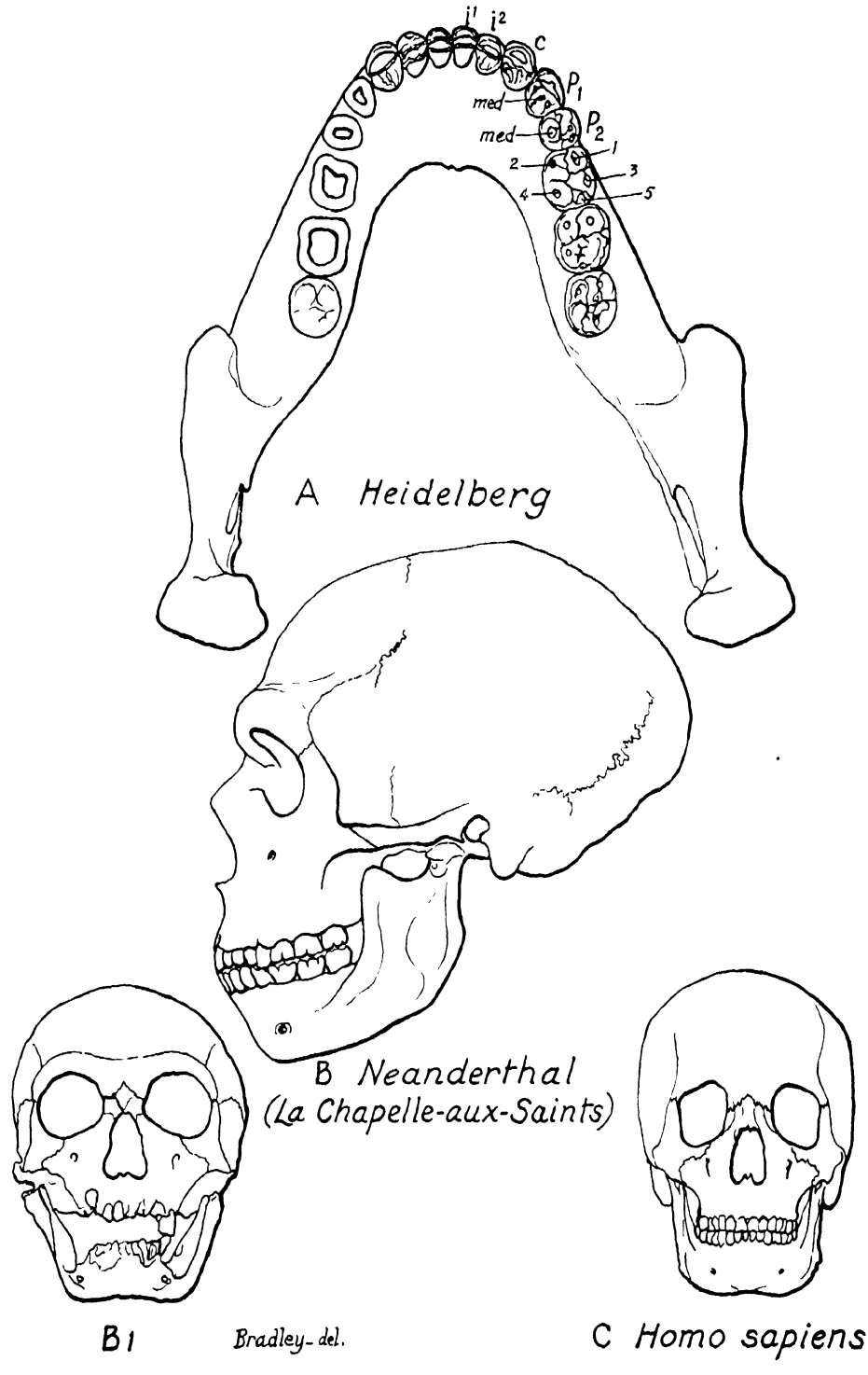


Fig. 23.79 Heidelberg (A), Neanderthal (B, B1), modern man (C). A, from Schoetensack; B, B1, C, after Boule.

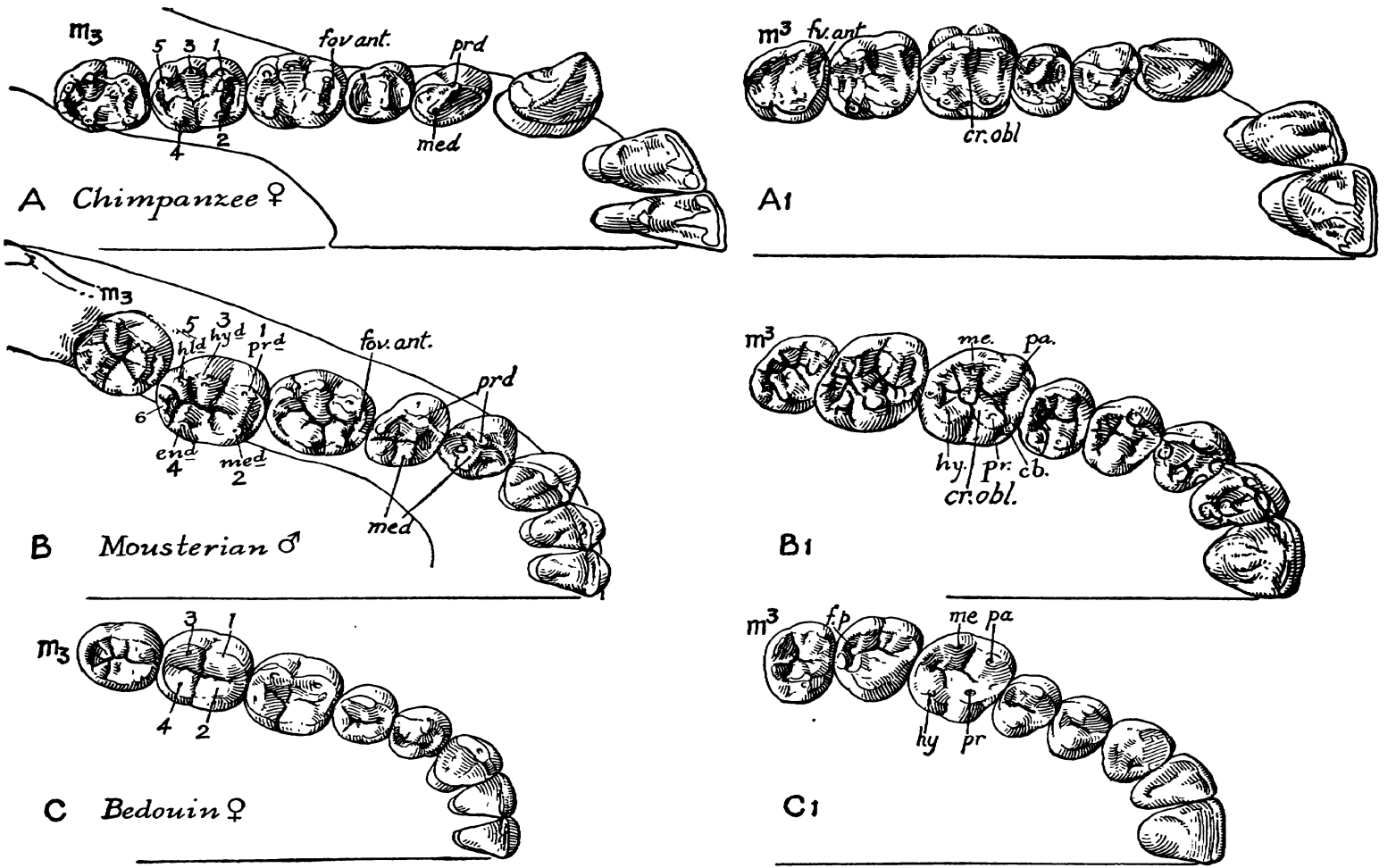


Fig. 23.80. Lower (A, B, C) and upper (A1, B1, C1) tooth patterns showing progressive reduction in size and complexity in molar patterns. After Gregory.

CHAPTER XXIV

MAN'S DEBT TO THE PAST

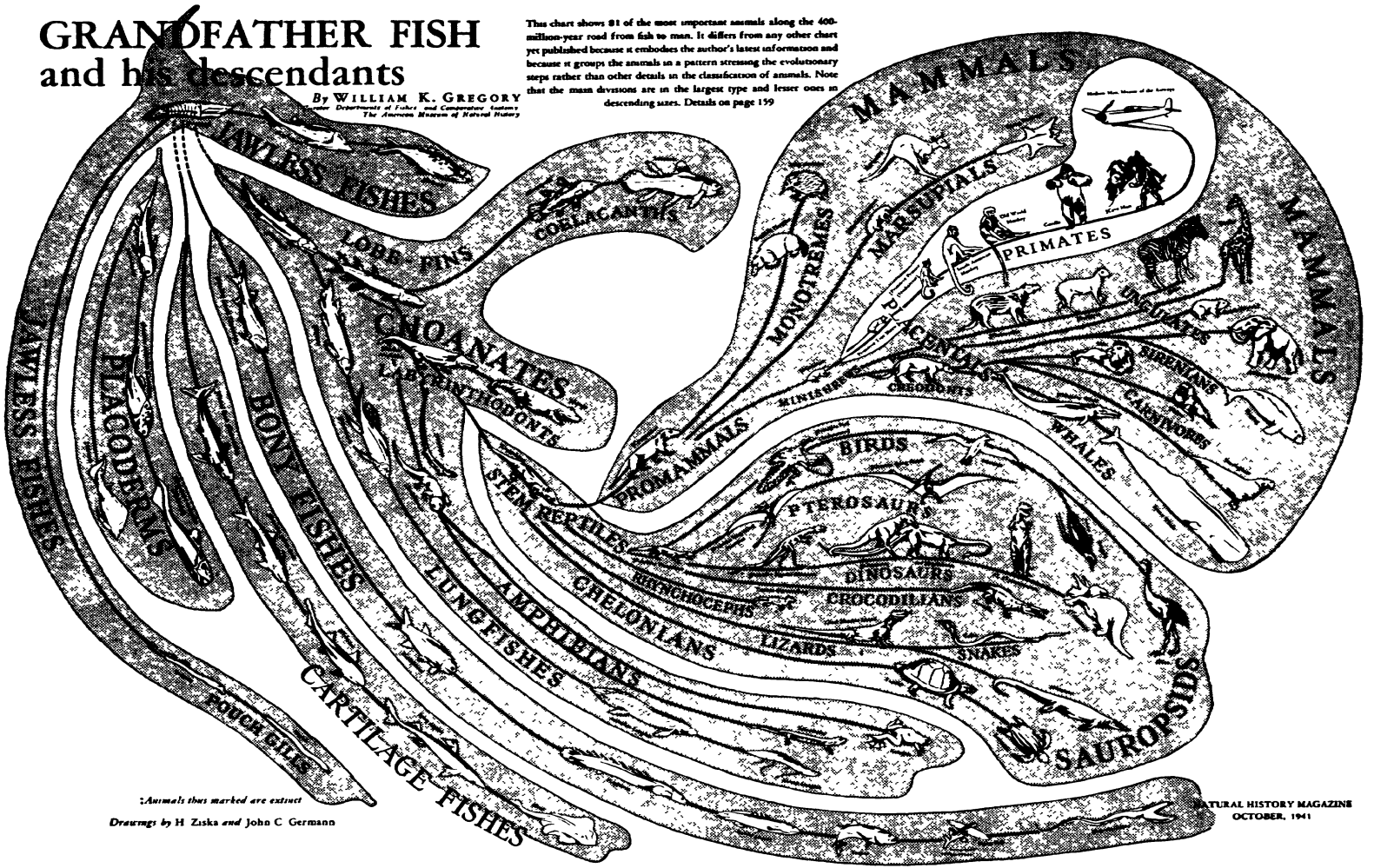

GRANDFATHER FISH
and his descendants
By WILLIAM K. GREGORY
Curator Department of Fishes and Comparative Anatomy
The American Museum of Natural History
This chart shows 81 of the most important animals along the 400-million-year road from fish to man. It differs from any other chart yet published because it embodies the author's latest information and because it groups the animals in a pattern stressing the evolutionary steps rather than other details in the classification of animals. Note that the main divisions are in the largest type and lesser ones in descending sizes. Details on page 159
JAWLESS FISHES
LOBE FINS
COELACANTHS
CRAWLING FISHES
PLACODERMS
CHONDRICHTHYANS
LABYRINTHODONTS
BONY FISHES
CARTILAGE FISHES
LUNGFISHES
AMPHIBIANS
STEM REPTILES
CHELONIANS
MAMMALS
MONOTREMES
MARSUPIALS
PRIMATES
PLACENTALS
INSECTIVORES
RODENTS
CREODONTS
CARNIVORES
PROSIMIANS
WHALES
BIRDS
PTEROSAURS
DINOSAURS
RHYNCHOCEPHS
CROCODILIANS
LIZARDS
SNAKES
SAUROPSIDS
FISH GILLS
*Animals thus marked are extinct
Drawings by H Ziska and John C Germann
NATURAL HISTORY MAGAZINE
OCTOBER, 1941

Plate 24.I

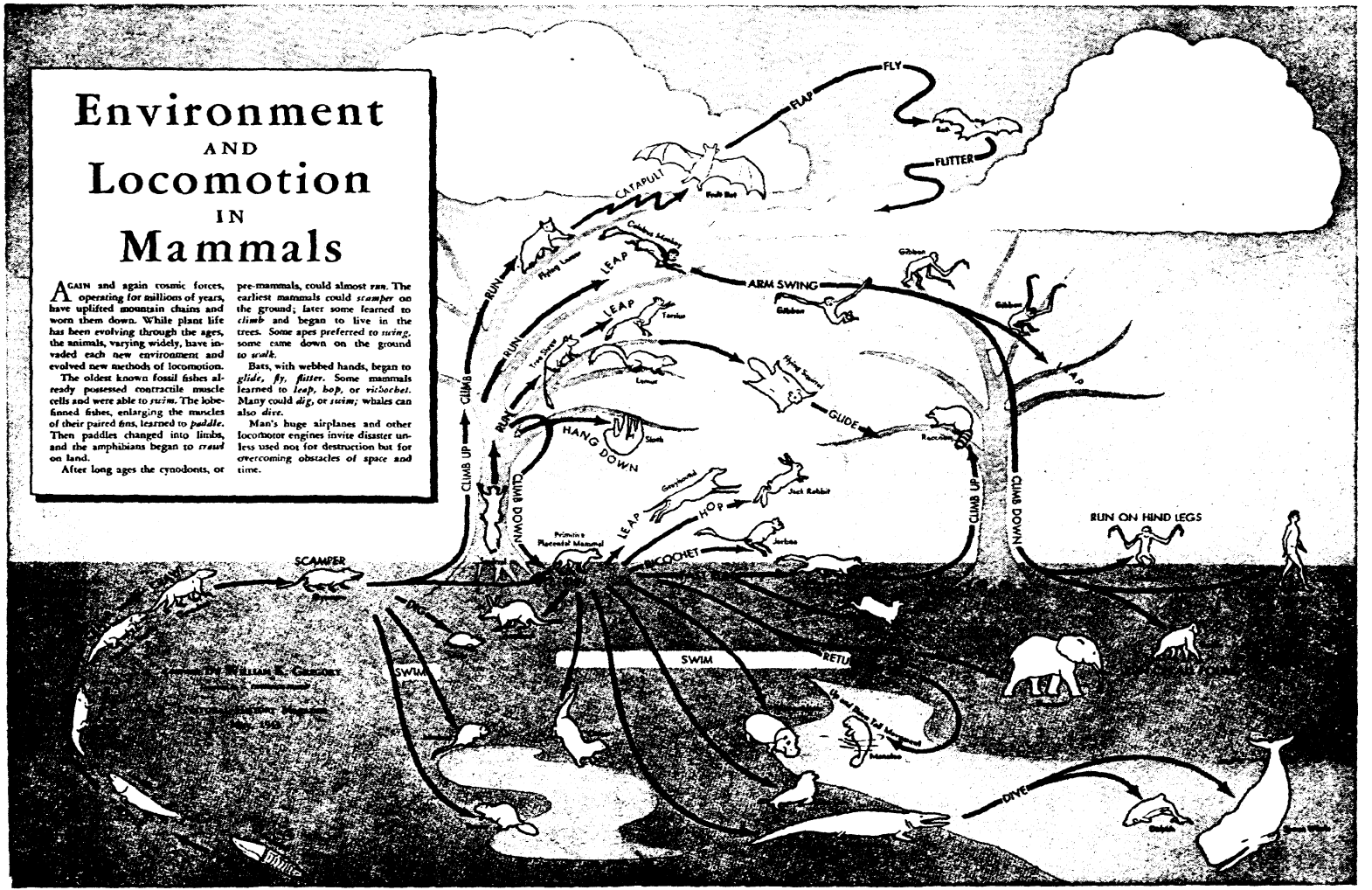

Environment
AND
Locomotion
IN
Mammals
AGAIN and again cosmic forces, operating for millions of years, have uplifted mountain chains and worn them down. While plant life has been evolving through the ages, the animals, varying widely, have invaded each new environment and evolved new methods of locomotion.
The oldest known fossil fishes already possessed contractile muscle cells and were able to swim. The lobe-finned fishes, enlarging the muscles of their paired fins, learned to paddle. Then paddles changed into limbs, and the amphibians began to crawl on land.
After long ages the cynodonts, or pre-mammals, could almost run. The earliest mammals could scamper on the ground; later some learned to climb and began to live in the trees. Some apes preferred to swing, some came down on the ground to walk.
Bats, with webbed hands, began to glide, fly, flitter. Some mammals learned to leap, hop, or ricochet. Many could dig, or swim; whales can also dive.
Man's huge airplanes and other locomotor engines invite disaster unless used not for destruction but for overcoming obstacles of space and time.
FLY
FLAP
FLITTER
CATAPULT
RUN
LEAP
ARM SWING
CLIMB UP
CLIMB DOWN
HANG DOWN
GLIDE
HOP
RICOCHET
SCAMPER
SWIM
RETURN
RUN ON HIND LEGS
DIVE

Plate 24.II

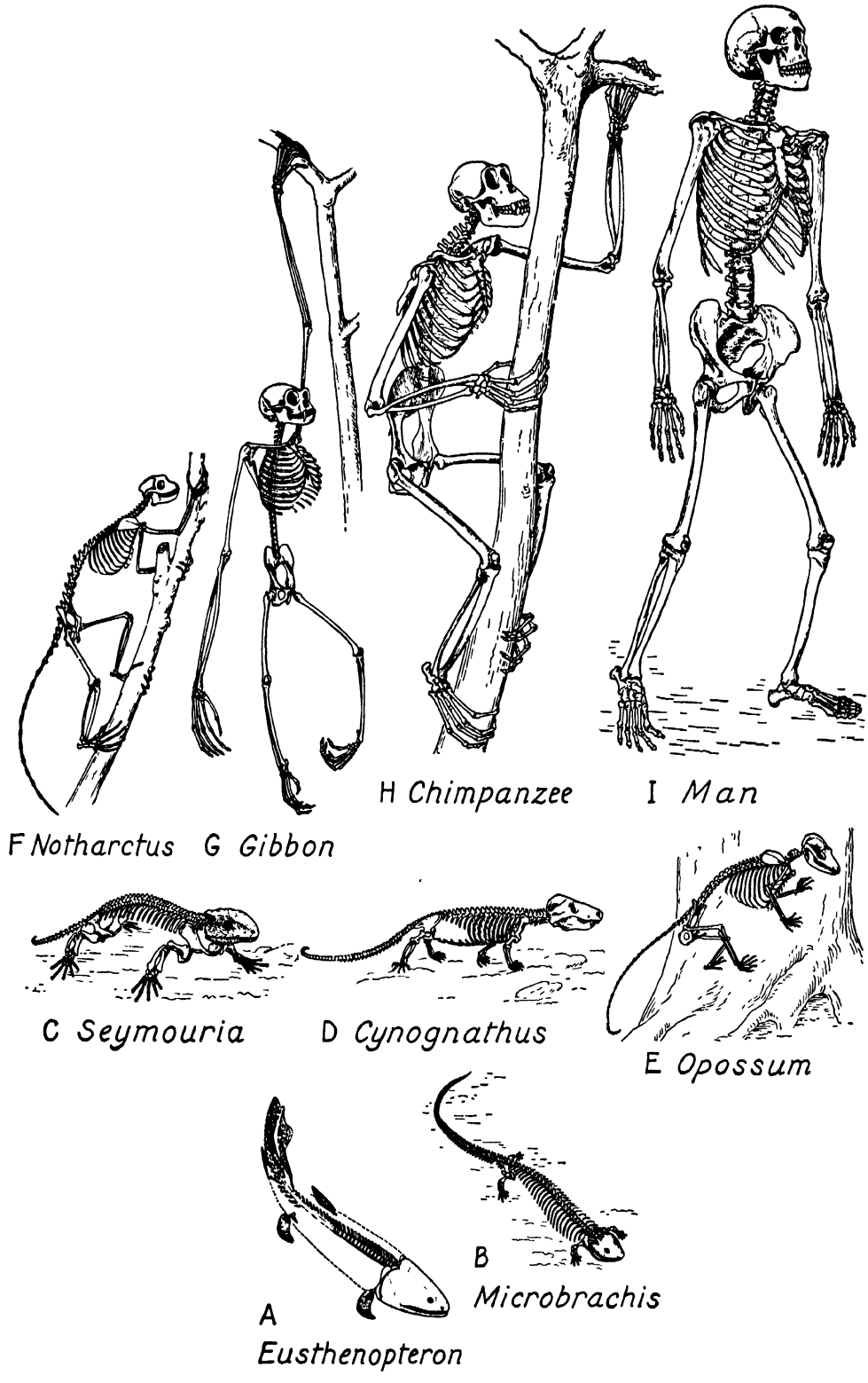


Fig. 24.1. Structural sequence of skeletons from fish to man. After Gregory.

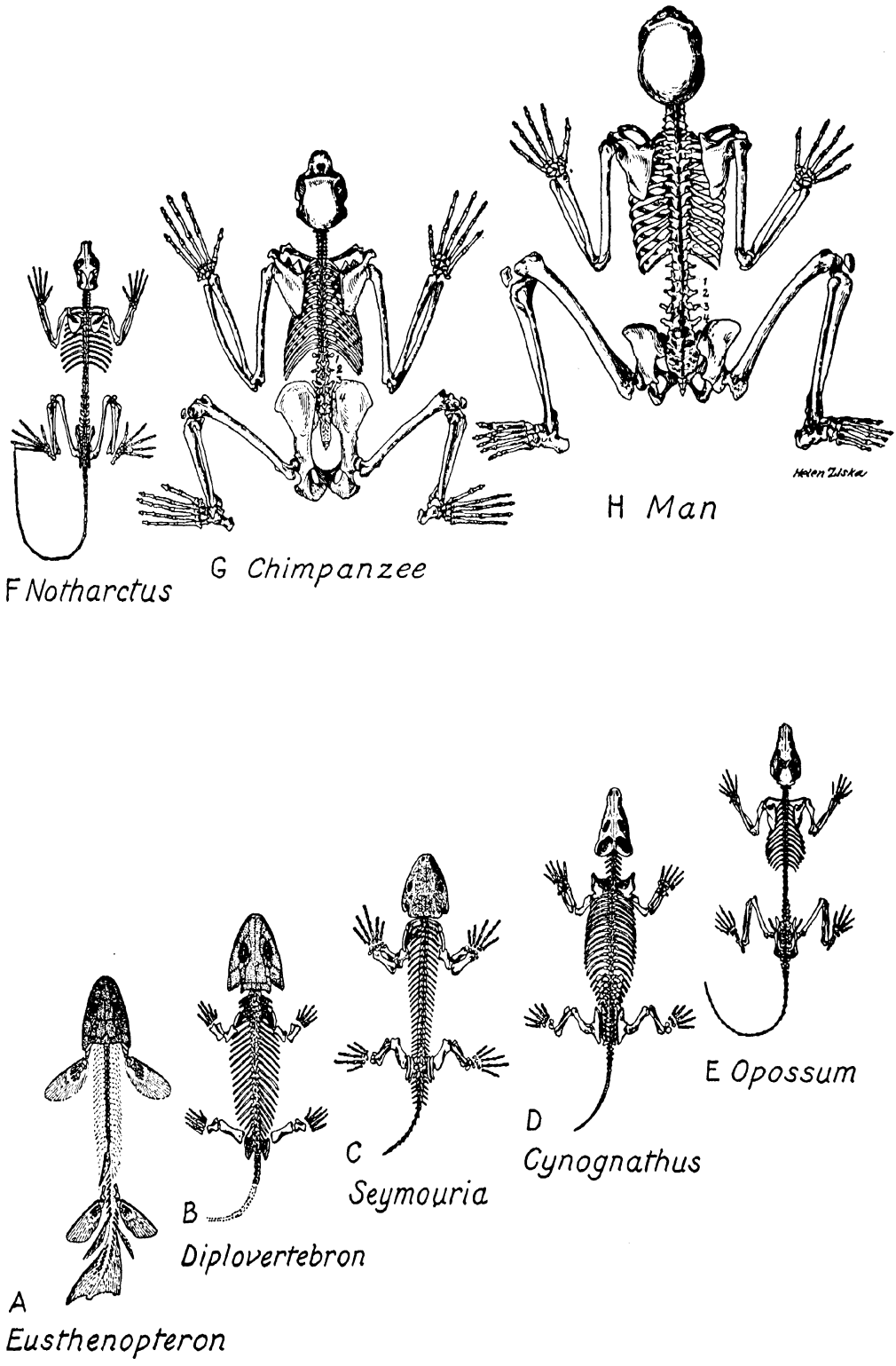


Fig. 24.2. Structural sequence of skeletons from fish to man (continued). After Gregory.

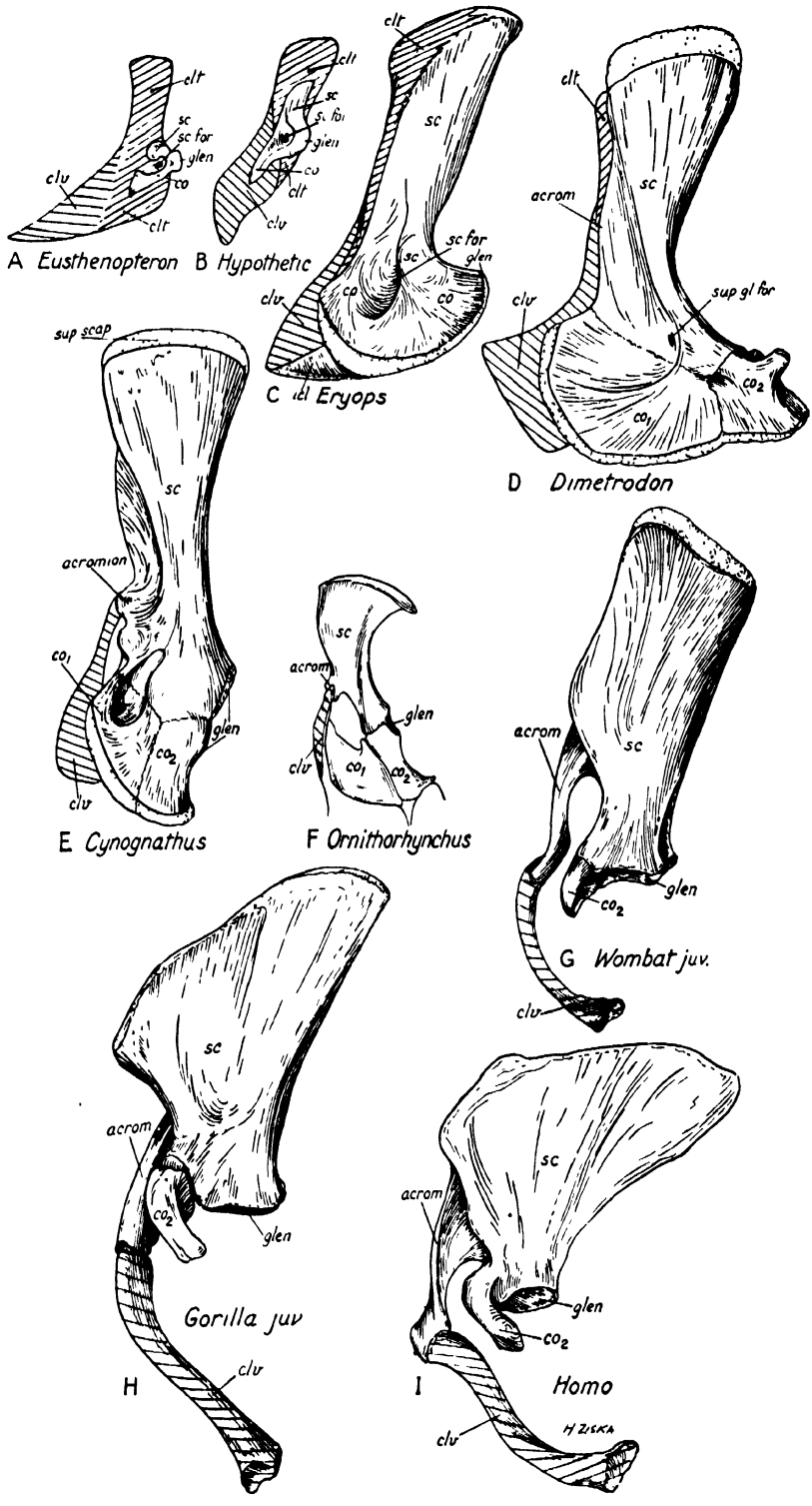


Fig. 24.3. The coraco-scapula, from fish to man. Original.

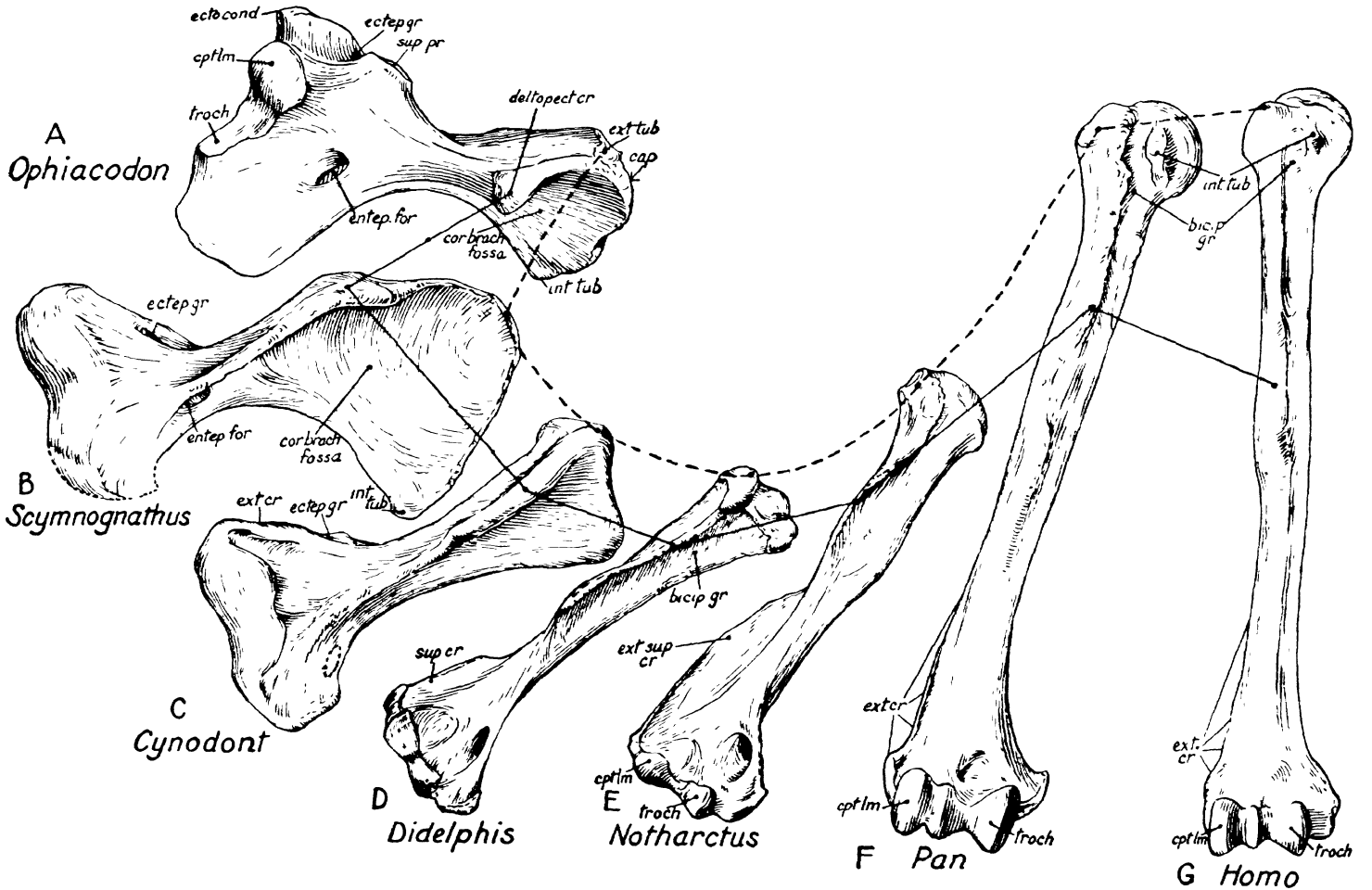


Fig. 24.4. The humerus from primitive pelycosaur to man. After Gregory.

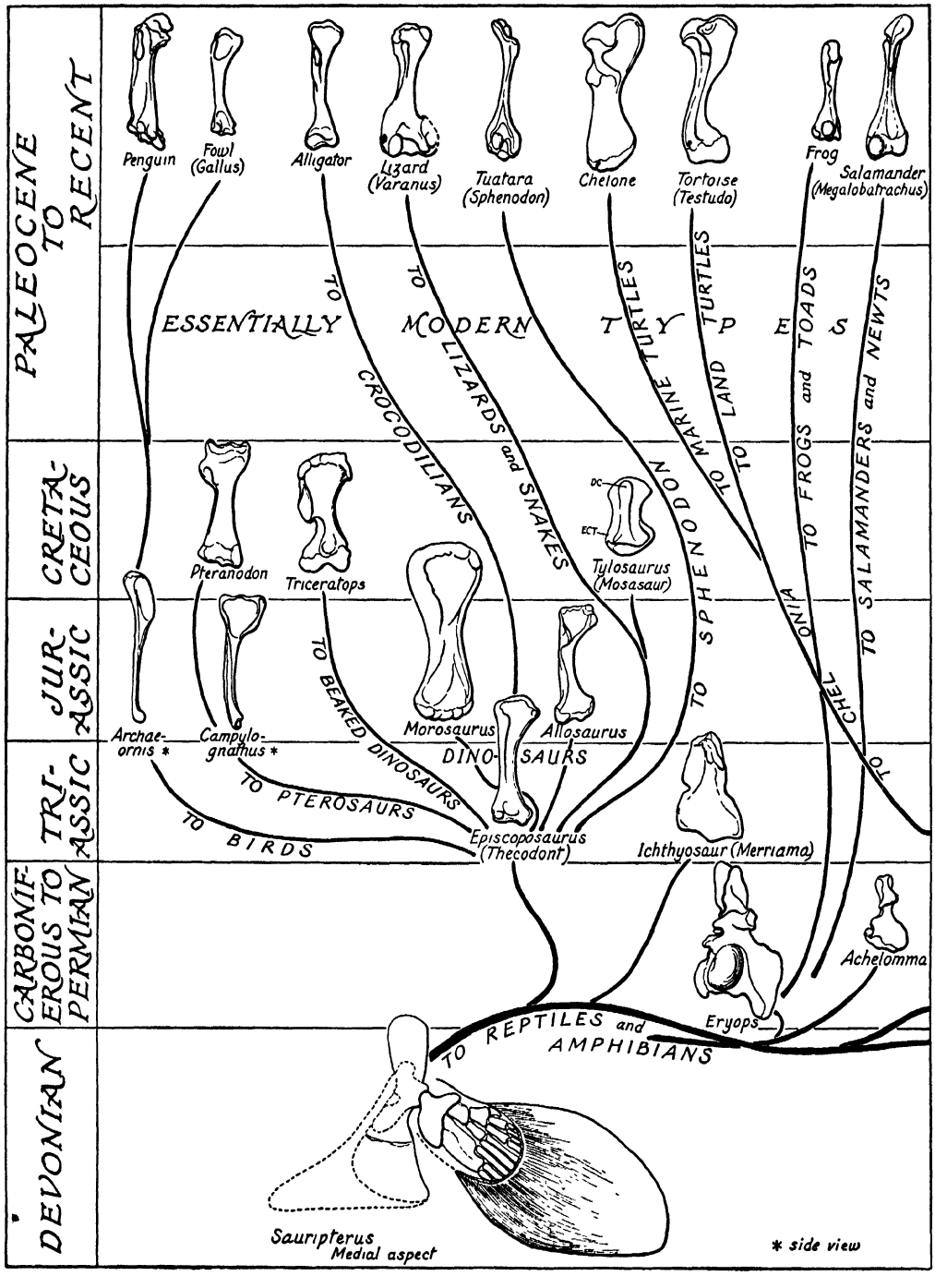

PALEOCENE TO RECENT
CRETACEOUS
JURASSIC
TRIASSIC
CARBONIFEROUS TO PERMIAN
DEVONIAN
Penguin
Fowl (Gallus)
Alligator
Lizard (Varanus)
Tuatara (Sphenodon)
Chelone
Tortoise (Testudo)
Frog
Salamander (Megalobatrachus)
ESSENTIALLY MODERN TYPES
TO CROCODILIANS
TO LIZARDS and SNAKES
TO SPHENODON
TO MARINE TURTLES
TO LAND TOADS
TO FROGS and TOADS
TO SALAMANDERS and NEWTS
Pteranodon
Triceratops
DC
ECT
Tylosaurus (Mosasaur)
Archaeornis *
Campylognathus *
TO BEAKED DINOSAURS
Morosaurus
Allosaurus
DINOSAURS
TO PTEROSAURS
TO BIRDS
Episcoposaurus (Thecodont)
Ichthyosaur (Merriama)
Achelomma
Eryops
TO REPTILES and AMPHIBIANS
Sauripterus
Medial aspect
* side view

Fig. 24.5a

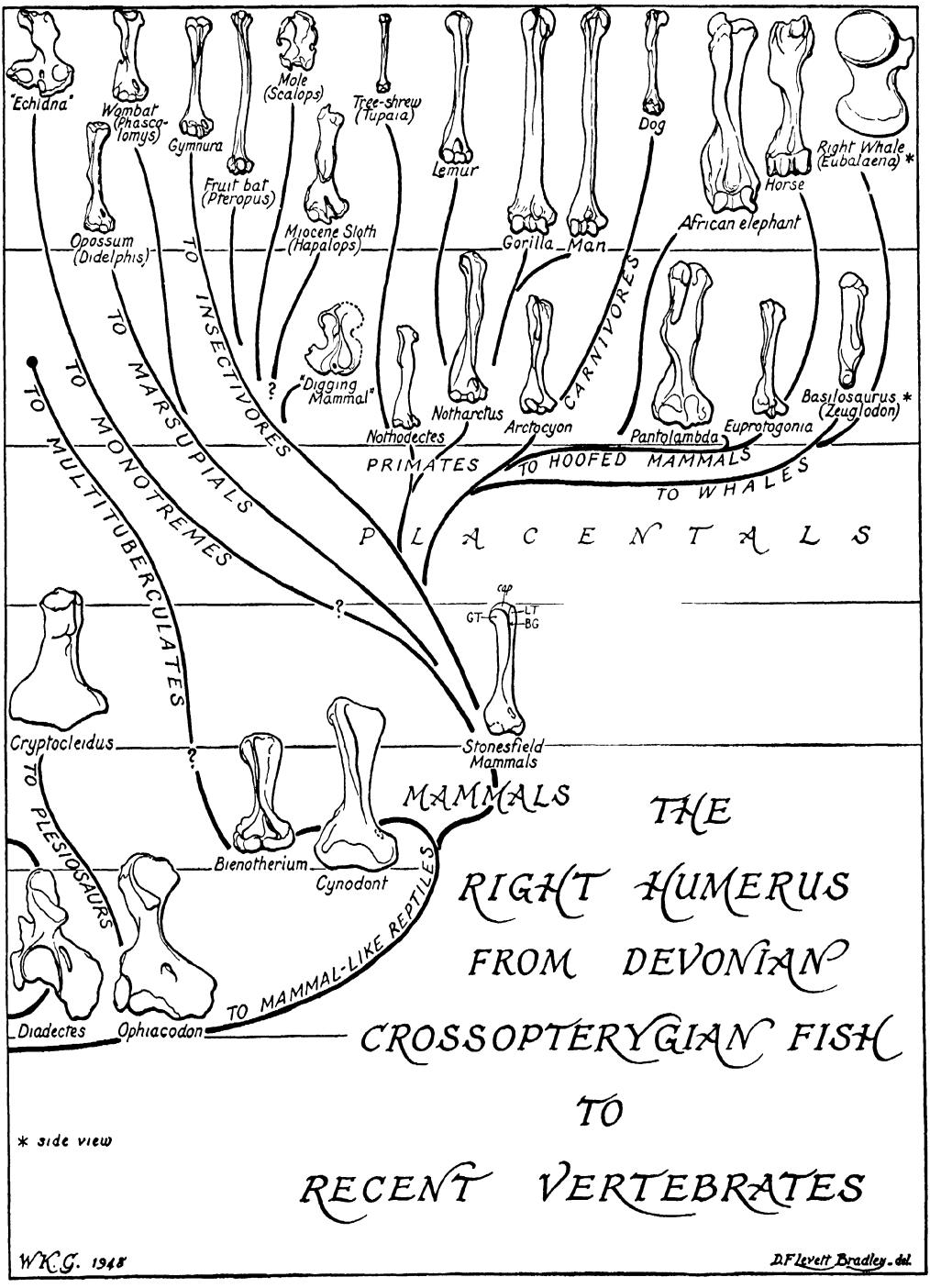

"Echidna"
Wombat (Phascolomys)
Gymnura
Mole (Scalops)
Tree-shrew (Tupaia)
Lemur
Dog
Right Whale (Eubalaena) *
Fruit bat (Pteropus)
Horse
Opossum (Didelphis)
Miocene Sloth (Hapalops)
Gorilla
Man
African elephant
"Digging Mammal"
Notharctus
Arctocyon
Pantolambda
Euprotogonia
Basilosaurus * (Zeuglodon)
Nothodectes
TO INSECTIVORES
TO MARSUPIALS
TO MONOTREMES
TO MULTITUBERCULATES
CARNIVORES
PRIMATES
TO HOOFED MAMMALS
TO WHALES
PLACENTALS
cap
GT
LT
BG
Cryptocleidus
Stonesfield Mammals
TO PLESIOSAURS
Bienotherium
Cynodont
MAMMALS
THE RIGHT HUMERUS FROM DEVONIAN CROSSOPTERYGIAN FISH TO RECENT VERTEBRATES
TO MAMMAL-LIKE REPTILES
Diadectes
Ophiacodon
* side view
WKG. 1948
D.F.Levett Bradley. del.

Fig. 24.5b

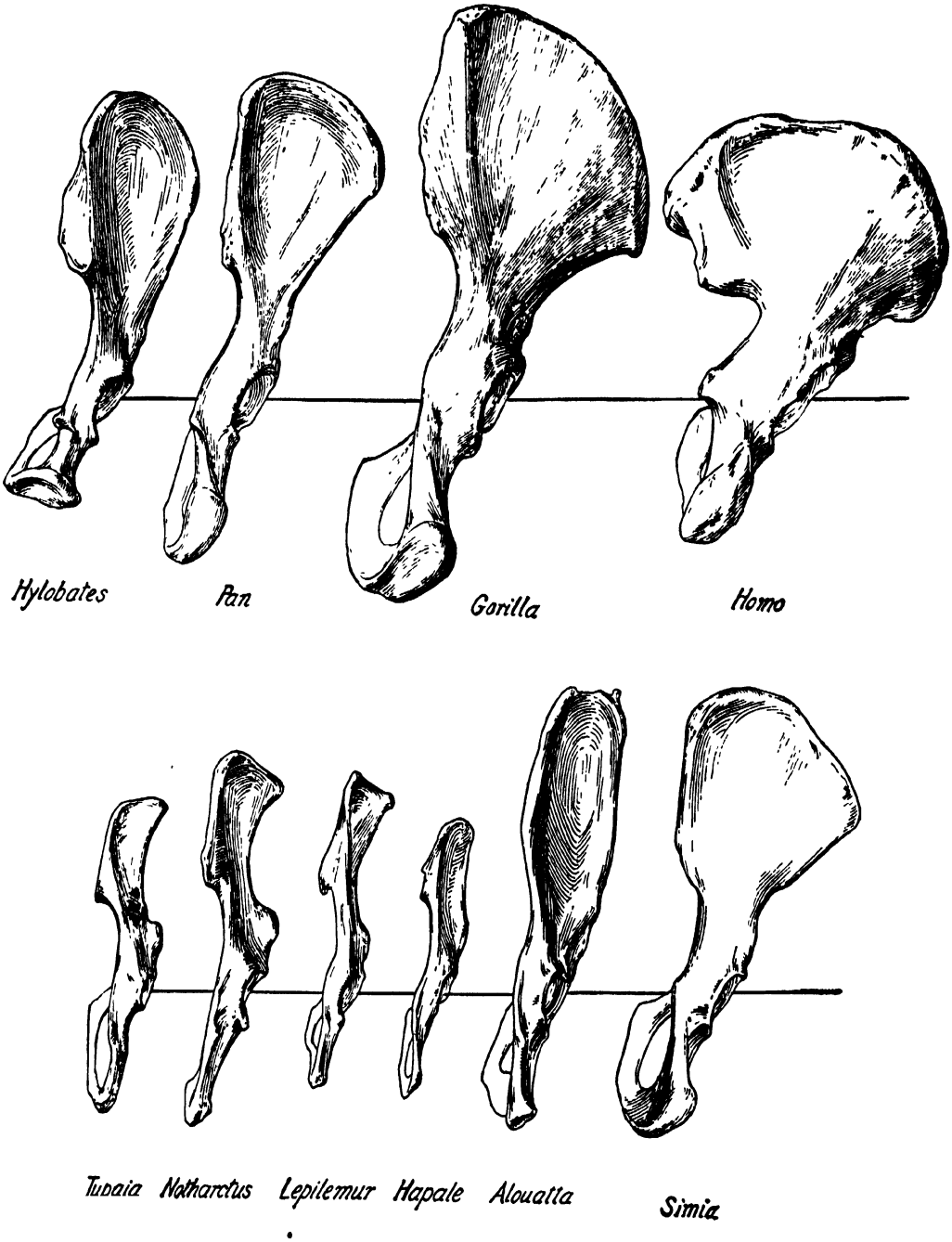


Fig. 24.6. Progressive widening of the ilium in primates. After Gregory.

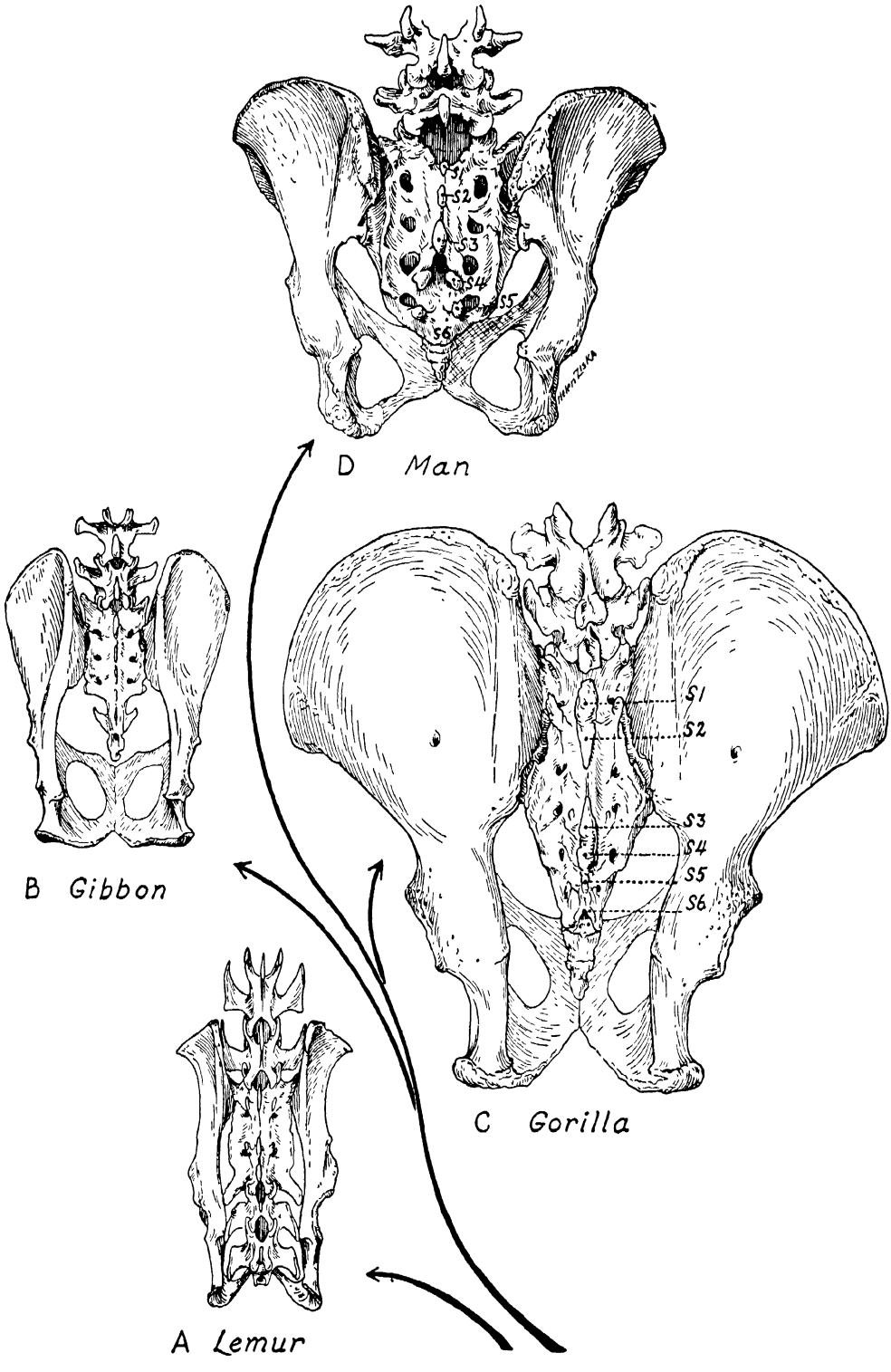


Fig. 24.7. Progressive widening of the sacrum and pelvis in primates. After Gregory.

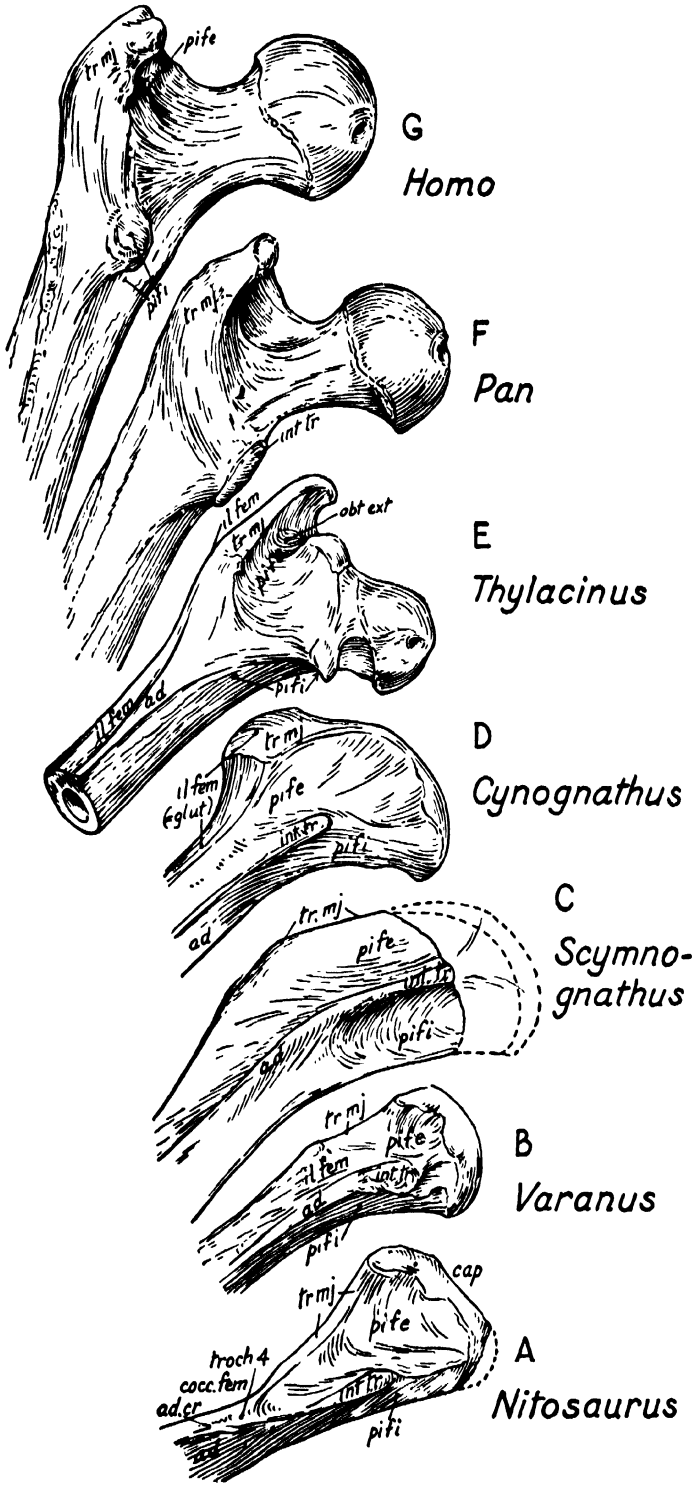


Fig. 24.8. The femur, rear view of proximal end, from primitive pelycosaur to man. Original.

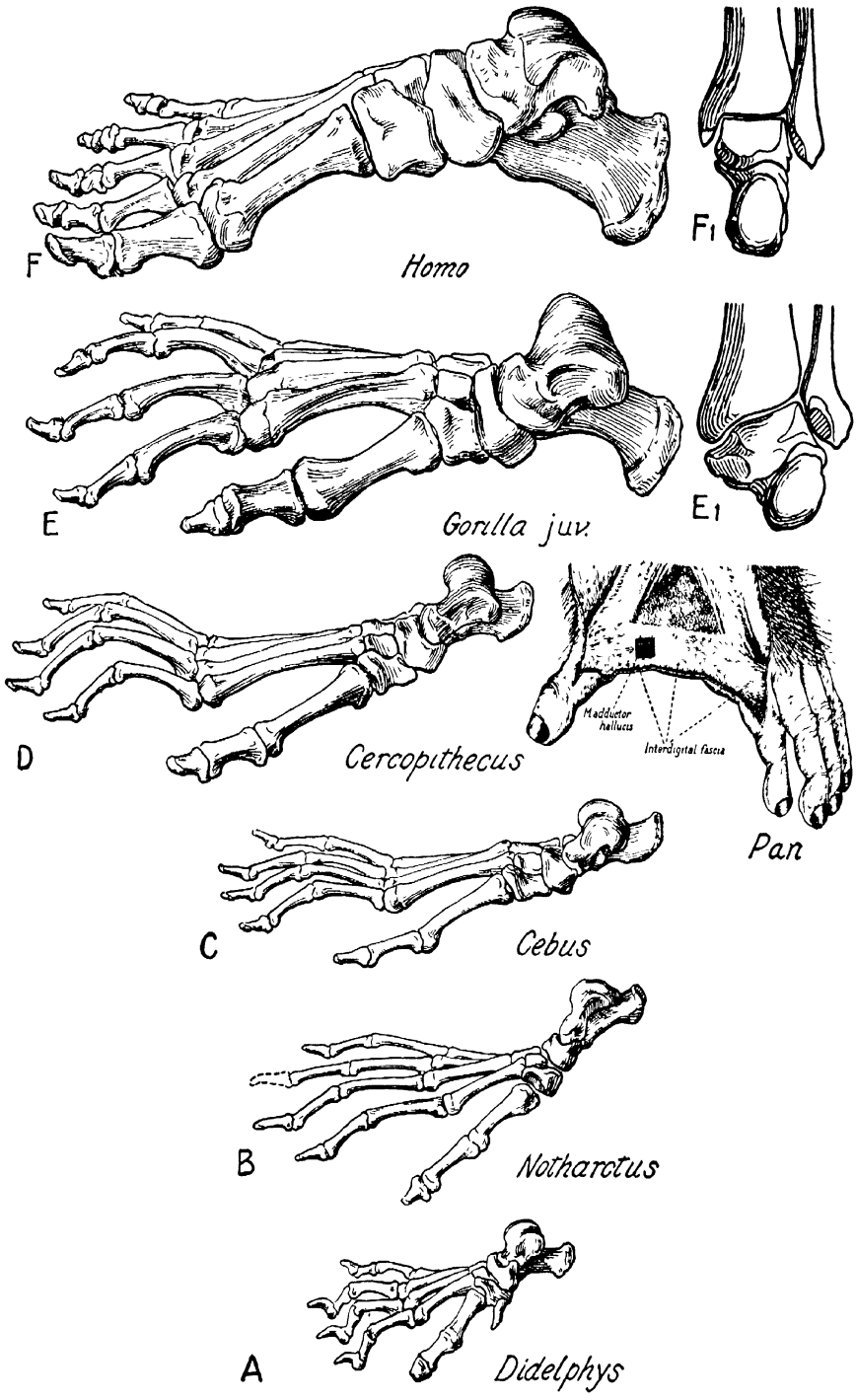


Fig. 24.9. Structural stages in the evolution of the human foot. After Gregory. Rear view of ankle joint (E1, F1), from Weber after Topinard. Foot (left) of chimpanzee showing relations of tissues between first and second metatarsal, after Raven.

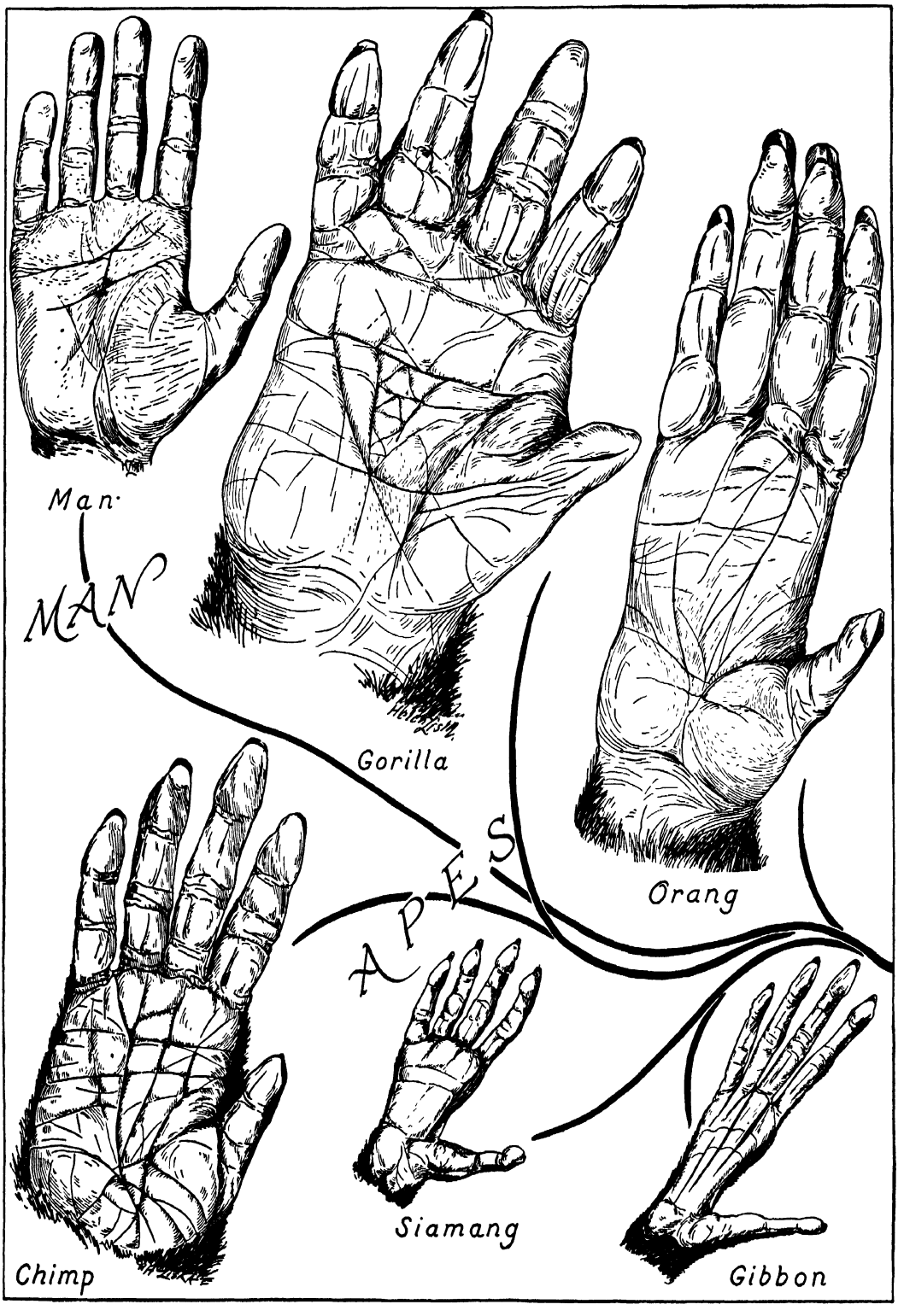


Fig. 24.10a

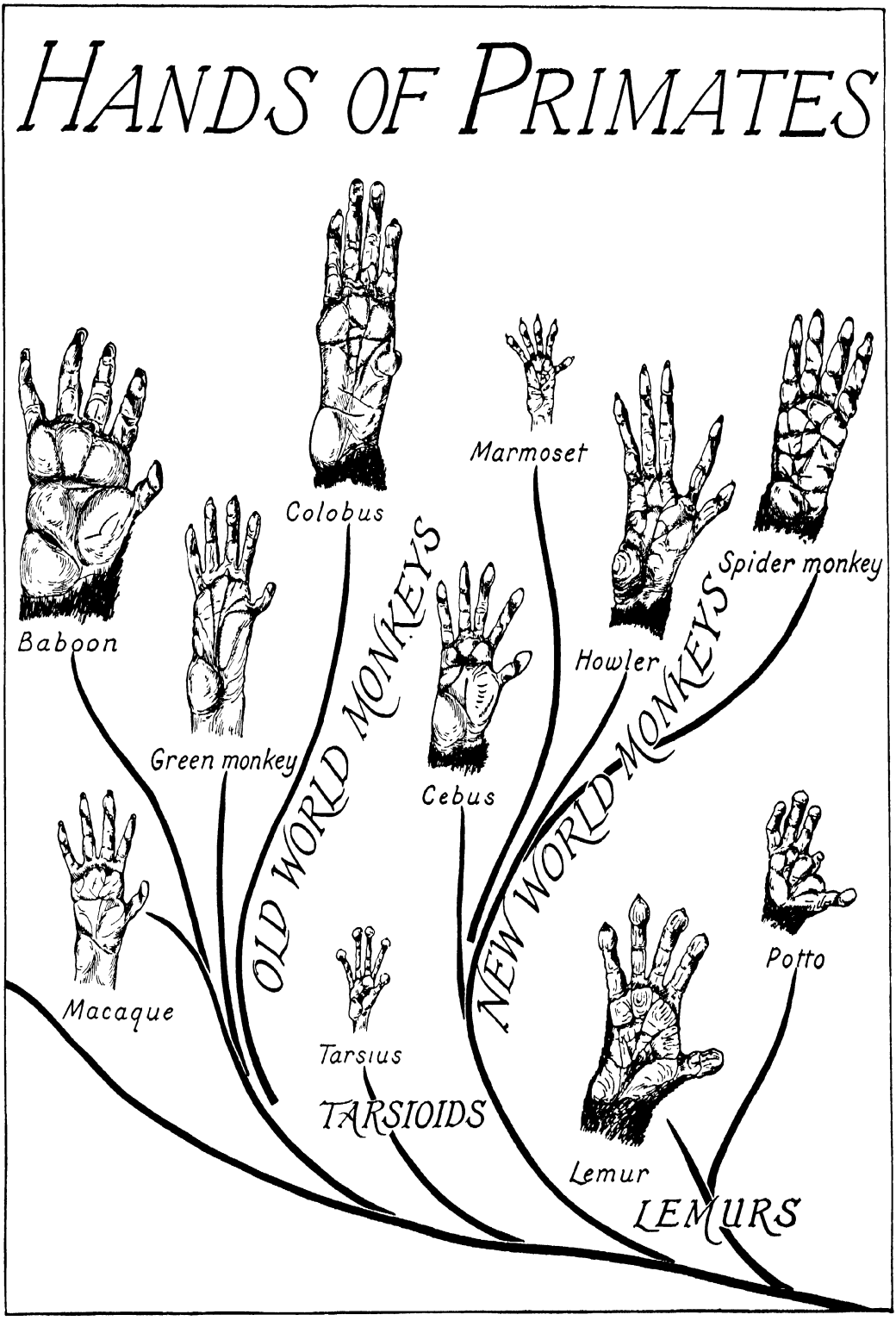

HANDS OF PRIMATES
Baboon
Colobus
Marmoset
Howler
Spider monkey
Green monkey
Cebus
OLD WORLD MONKEYS
NEW WORLD MONKEYS
Macaque
Tarsius
TARSIOIDS
Potto
Lemur
LEMURS

Fig. 24.10b

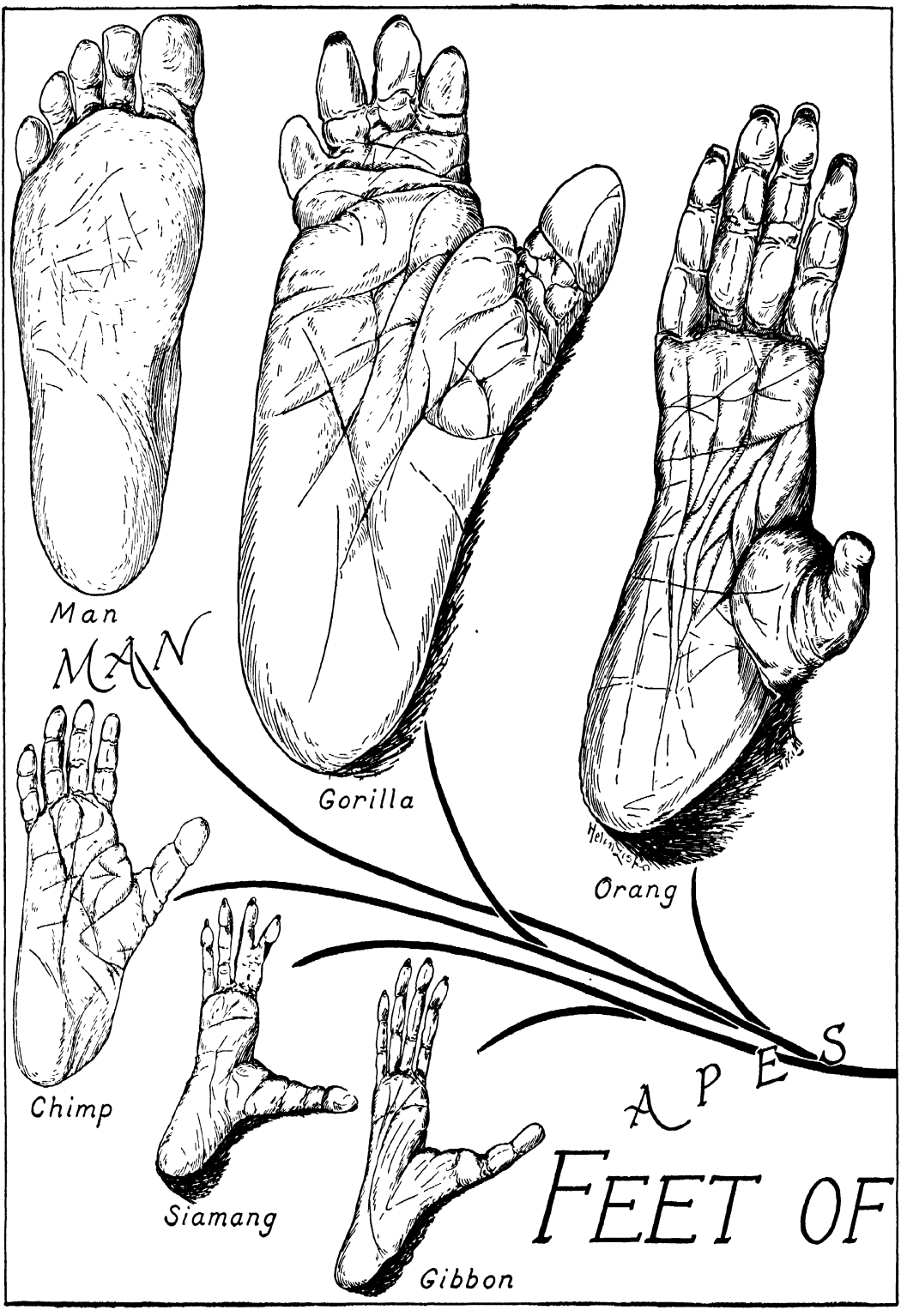


Fig. 24.11a

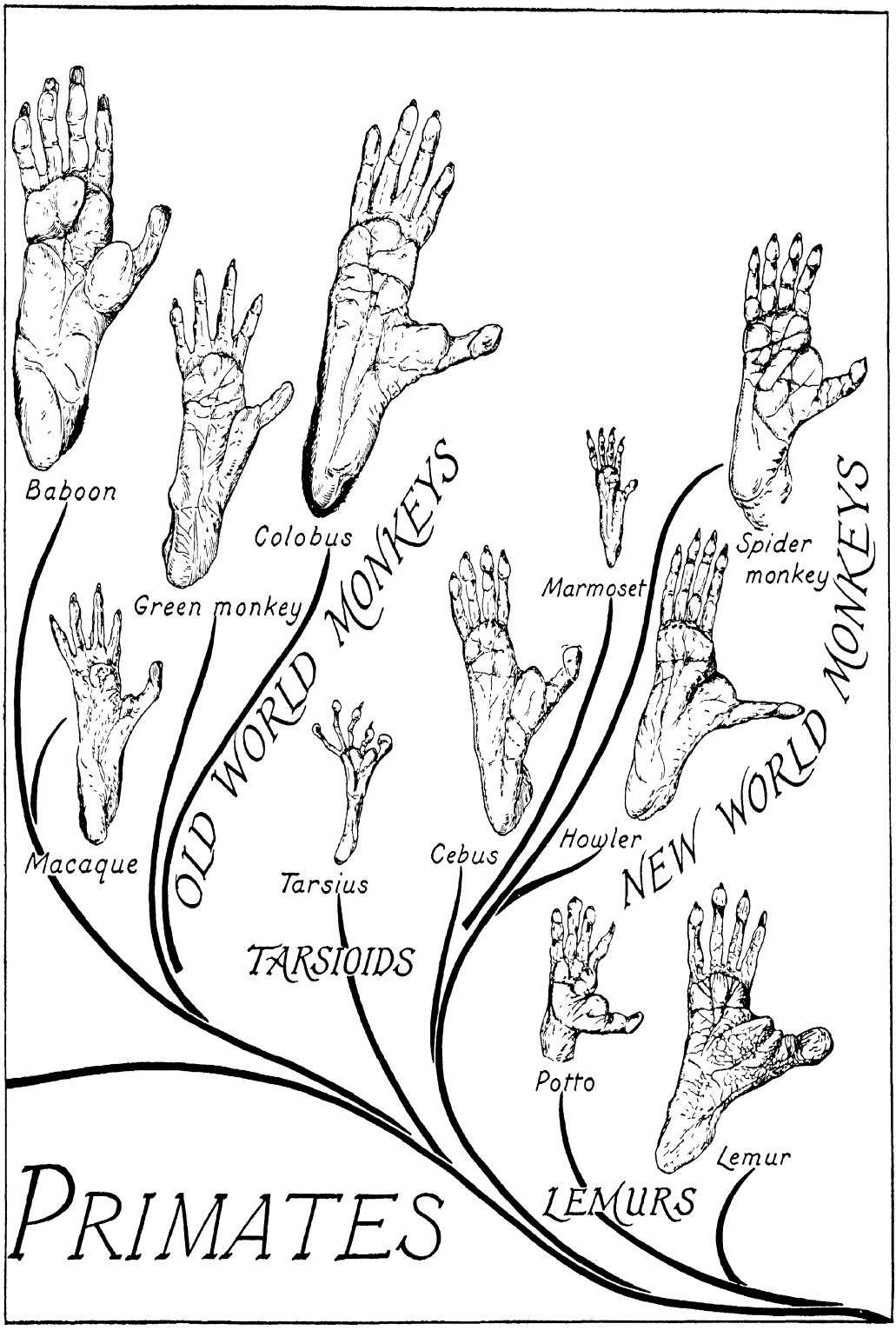
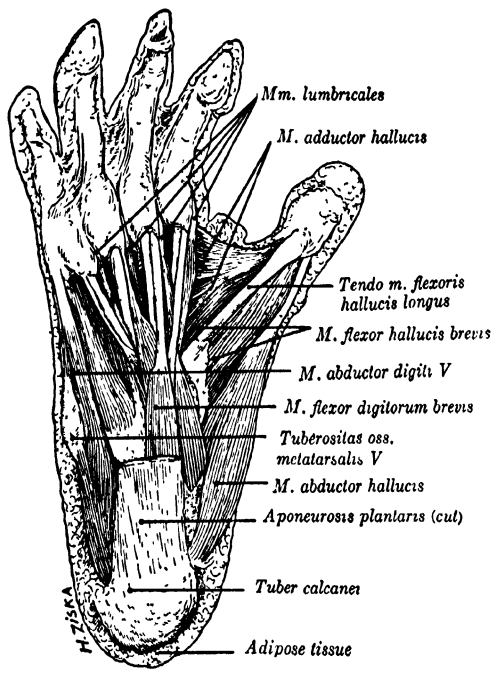
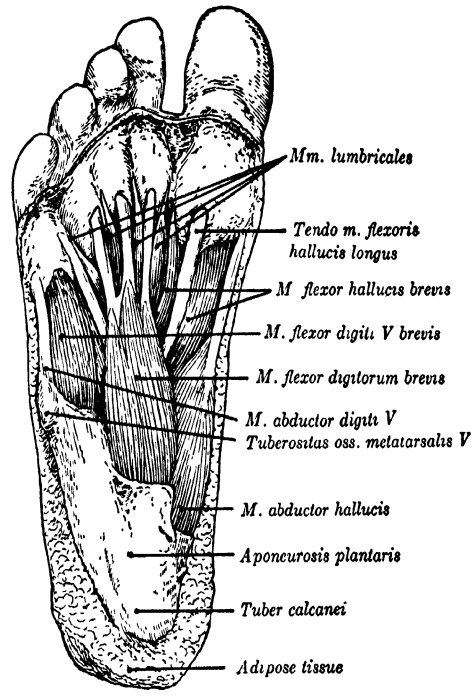

Baboon
Colobus
Green monkey
Macaque
OLD WORLD MONKEYS
Tarsius
TARSIOIDS
Marmoset
Spider monkey
Cebus
Howler
NEW WORLD MONKEYS
Potto
Lemur
PRIMATES
LEMURS

Fig. 24.11b

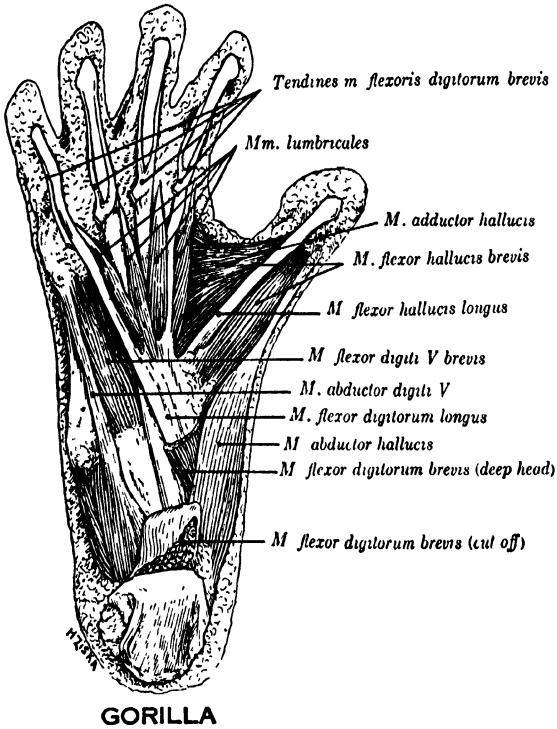


GORILLA

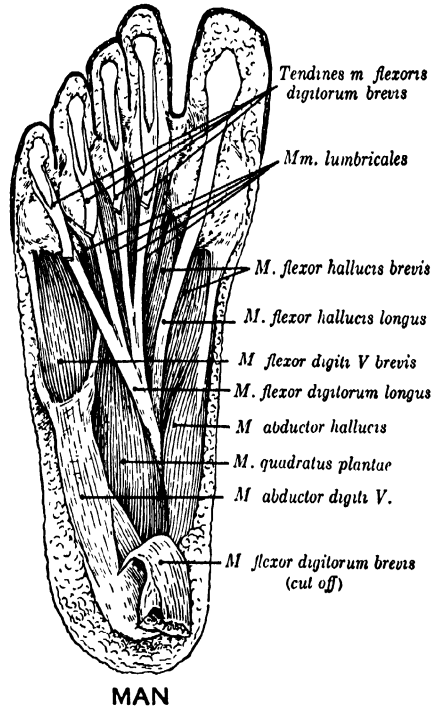


MAN

Dissections of plantar musculature, superficial layer.



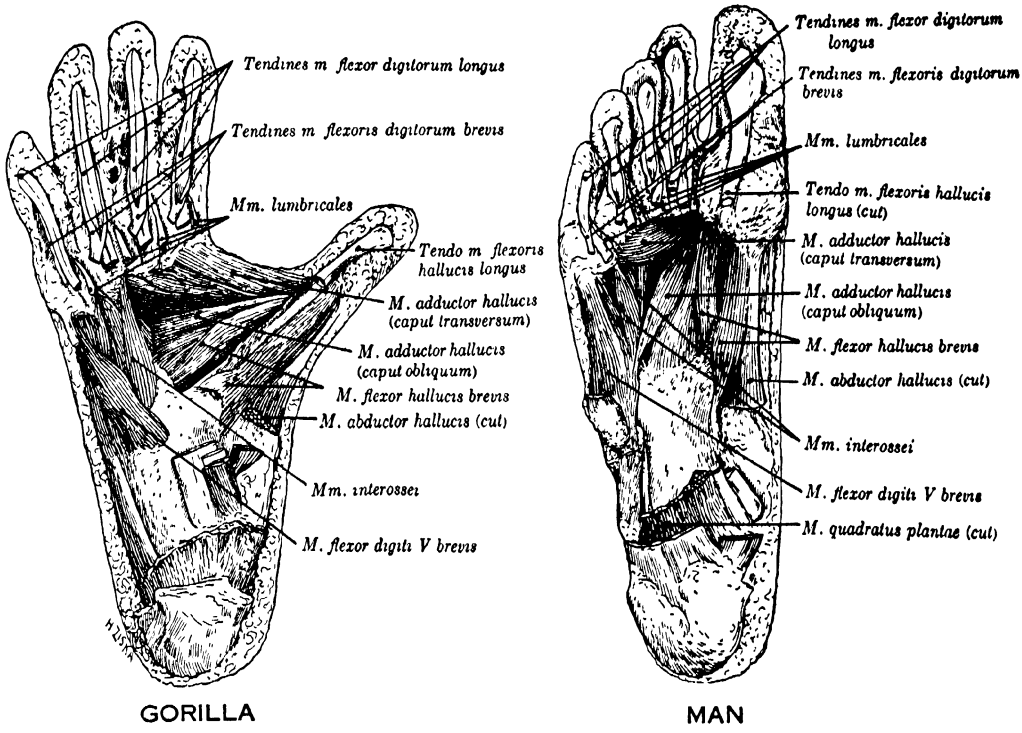
GORILLA



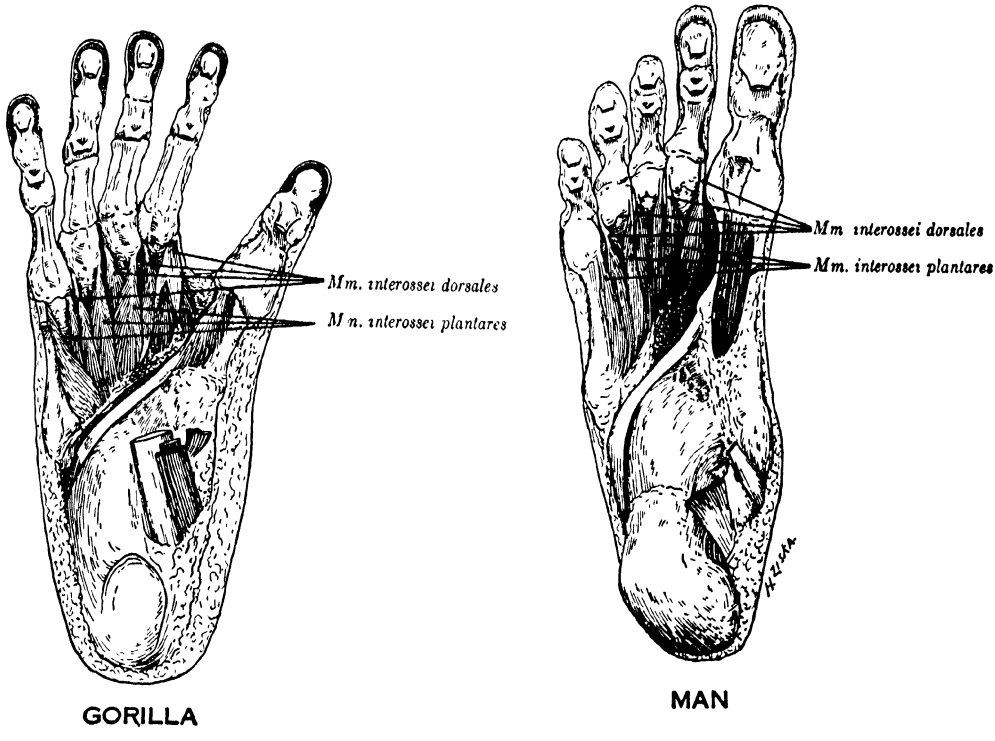
MAN

Dissections of plantar musculature, second layer.

Figs. 24.12a, b. Dissections of the foot of gorilla and man. After H. C. Raven.



Dissections of plantar musculature, third layer.



Dissections of plantar musculature, deep layer.

Fig 24.12b

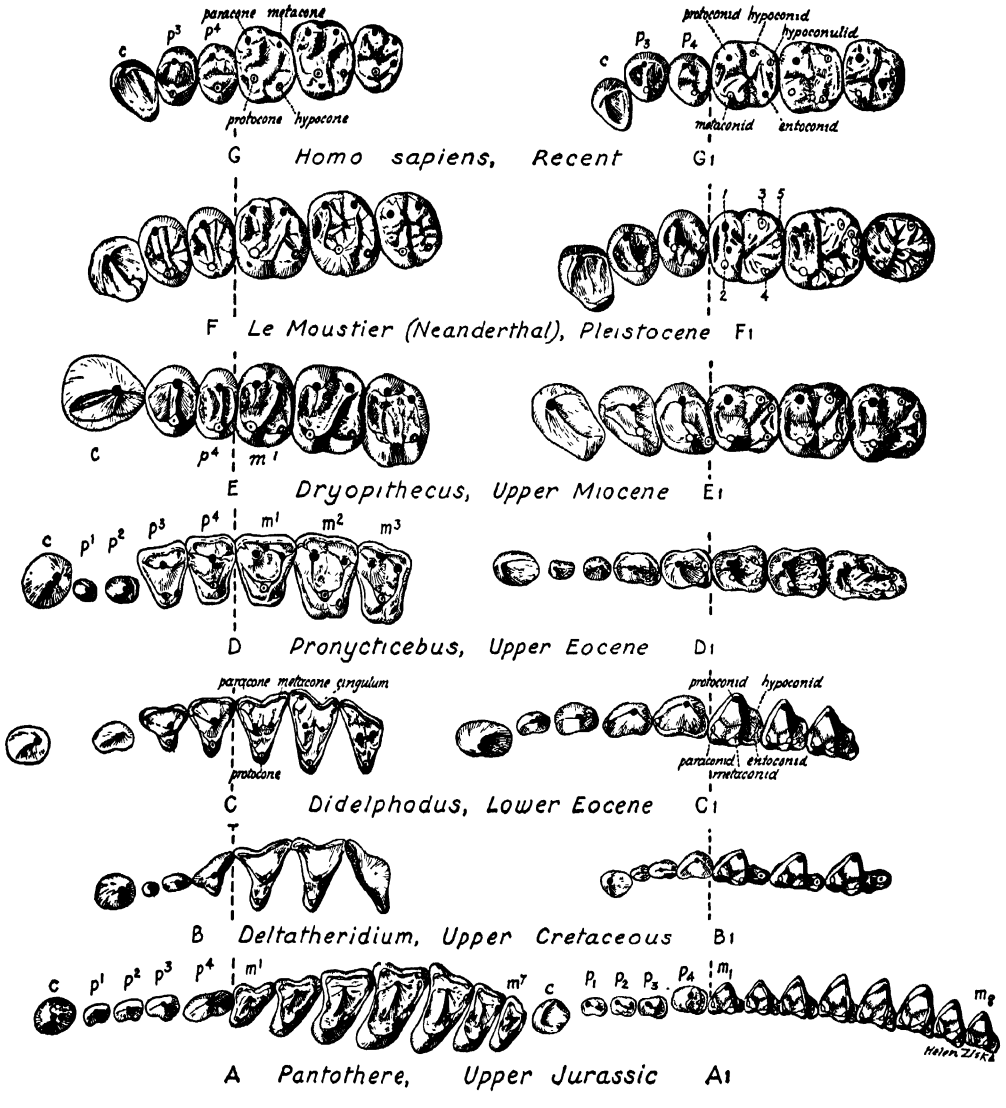


Fig. 24.13. Eight structural stages in the evolution of the dentition from Jurassic pantothere (A) to modern man (G). After Gregory. Data also from: A, G. G. Simpson; B, Gregory and Simpson; C, Matthew; D, Milne Edwards; E–G, Gregory and Hellman; F, McGregor.

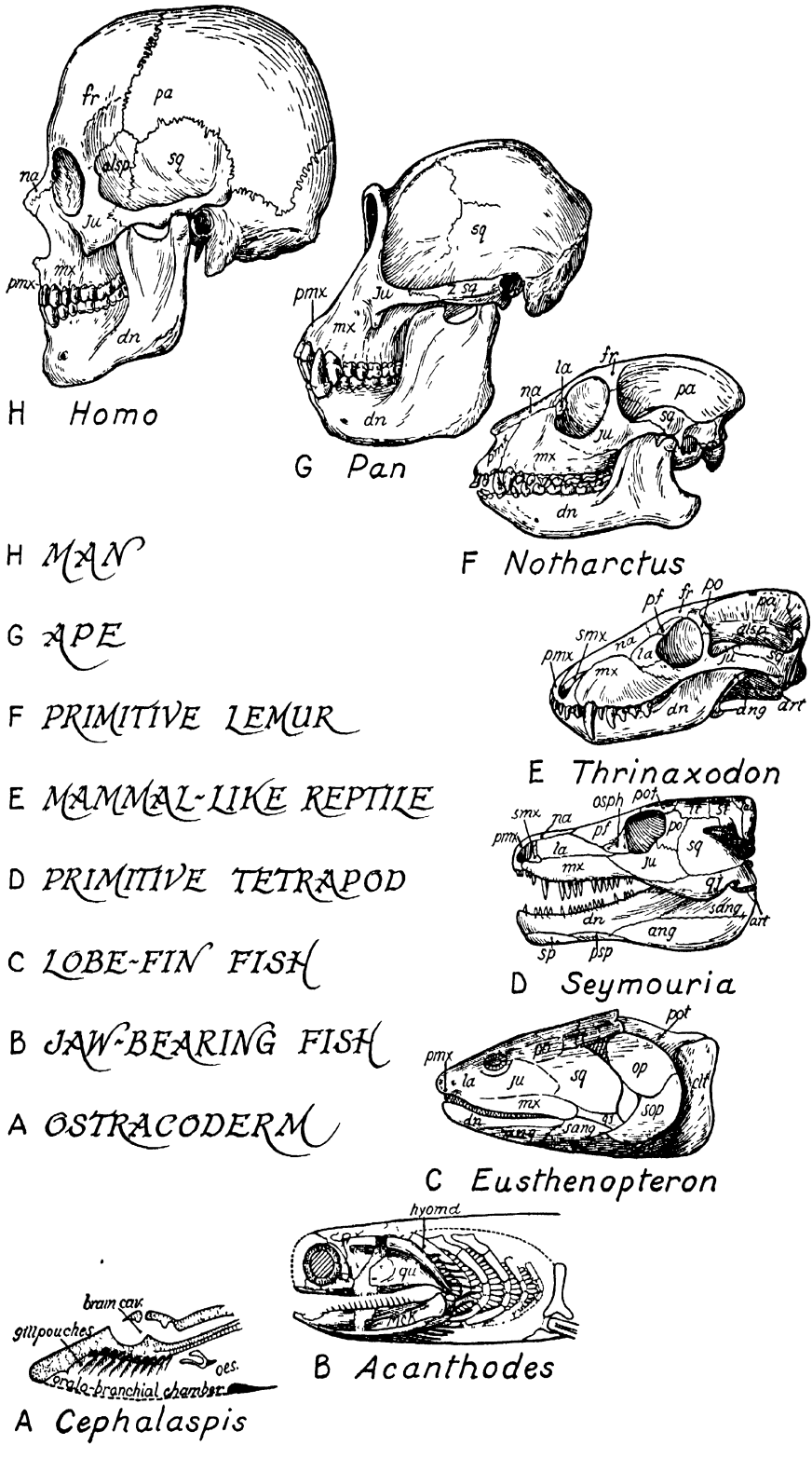

H Homo
G Pan
F Notharctus
E Thrinaxodon
D Seymouria
C Eusthenopteron
B Acanthodes
A Cephalaspis
H MAN
G APE
F PRIMITIVE LEMUR
E MAMMAL-LIKE REPTILE
D PRIMITIVE TETRAPOD
C LOBE-FIN FISH
B JAW-BEARING FISH
A OSTRACODERM
fr
pa
sq
na
alsp
Ju
mx
pmx
dn
la
pf
po
smx
osph
pot
ang
art
sang
sp
psp
op
sop
hyomd
qu
brain case
gill pouches
oes.
orala-branchial chamber

Fig. 24.14

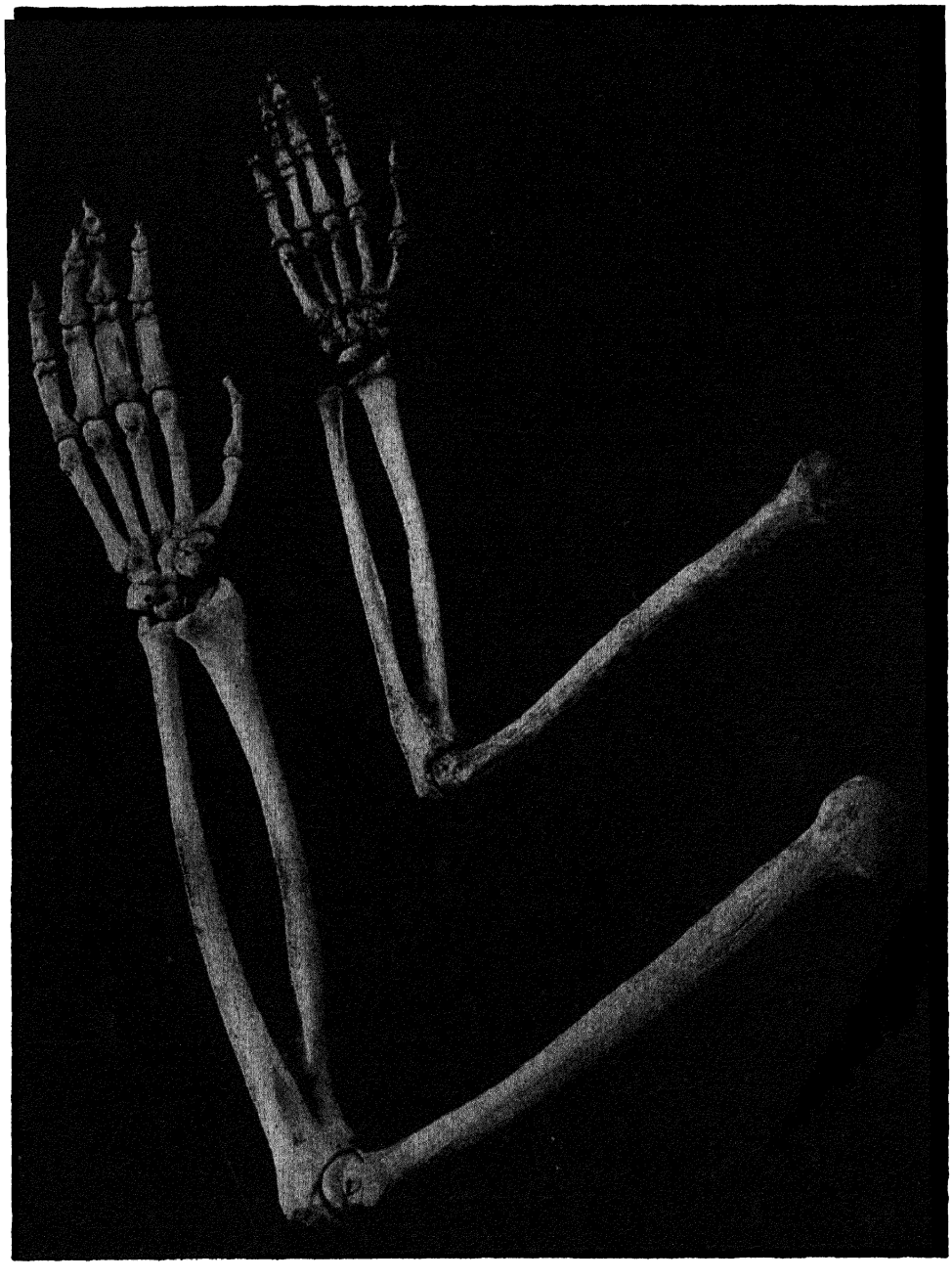


Plate 24.III. Arm and hand of gorilla and man.
After Gregory.

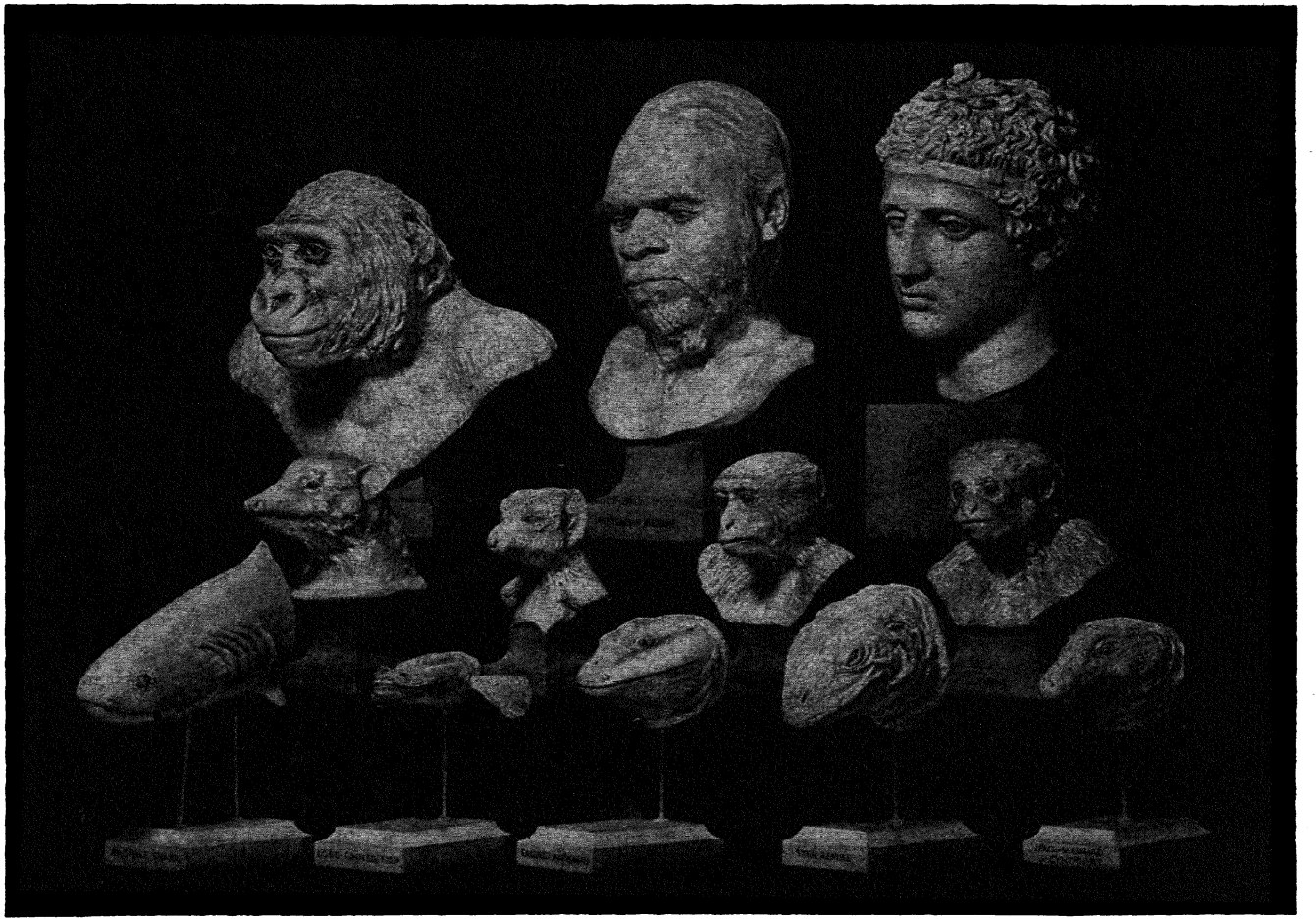


Plate 24.IV. Structural sequence from fish to man. Lower row: ancient shark, lobe finned fish, earliest amphibian, stem reptile, pre-mammal (cynodont). Second row: opossum, lemur, old world monkey, siamang (Gibbon). Upper row: young gorilla, Australian aboriginal, Greek athlete. After Gregory.